Proceedings of the
Forty-Seventh

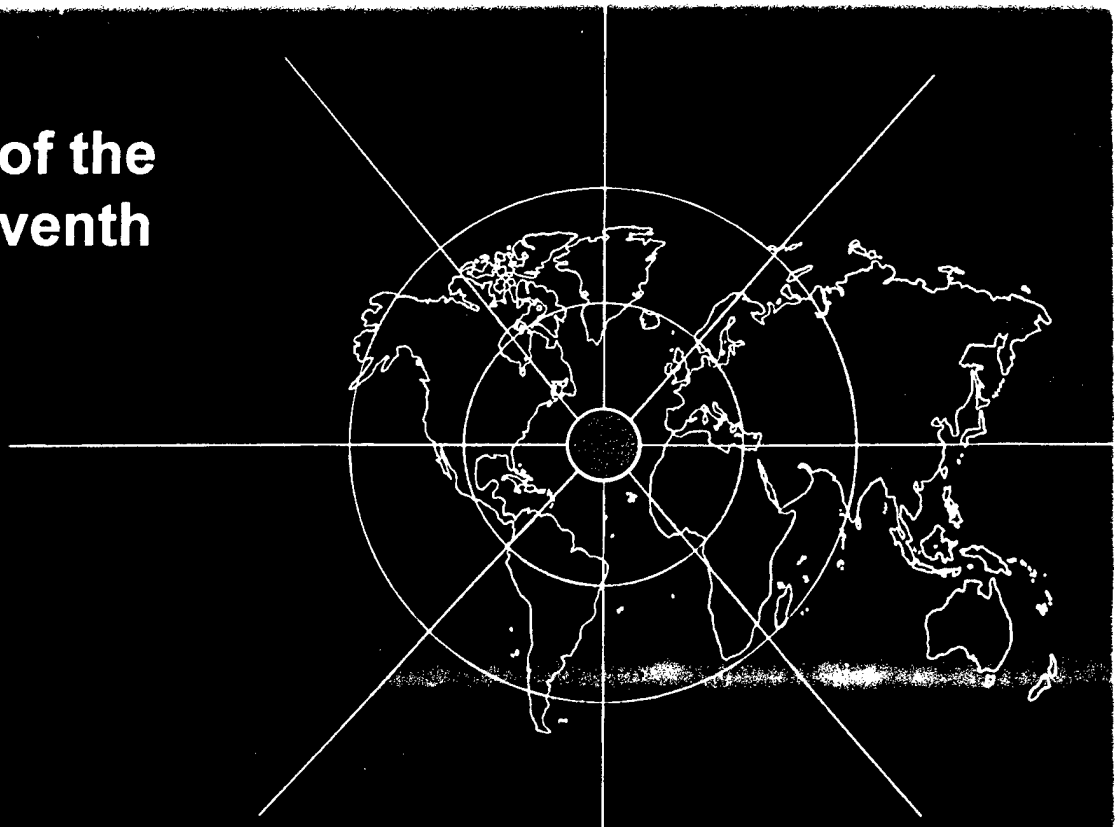

INTERNATIONAL WIRE AND CABLE SYMPOSIUM

NOVEMBER 16 THRU 19, 1998

Sponsored by
International Wire and Cable Symposium, Inc. (IWCS)
Eatontown, New Jersey
http://www.iwcs.org/iwcs/

With Participation by
US Army Communications-Electronics Command (CECOM)
Fort Monmouth, New Jersey

Supporting Associate
Europacable, Brussels, Belgium

Reproduced From
Best Available Copy

PROCEEDINGS OF 47TH INTERNATIONAL WIRE AND CABLE SYMPOSIUM

Sponsored by
International Wire and Cable Symposium, Inc. (IWCS)
Eatontown, New Jersey
Website: http://www.iwcs.org/iwcs/
Email: iwcs@monmouth.com

With Participation by
US Army Communications-Electronics Command (CECOM)
Fort Monmouth, New Jersey

Supporting Associate
Europacable, Brussels, Belgium

PHILADELPHIA MARRIOTT HOTEL
PHILADELPHIA, PENNSYLVANIA
NOVEMBER 16, 17, 18 AND 19, 1998

19981230 111

APPROVED FOR PUBLIC RELEASE: DISTRIBUTION UNLIMITED

DTIC QUALITY INSPECTED 3

MISSION

The International Wire and Cable Symposium provides a forum for the exchange of technical information amongst suppliers, manufacturers, and users on technological advancements in materials, processes, and products used for voice, data and video signal transmission systems.

TECHNICAL PAPERS

		Tuesday, November 17
9:00 am	PLENARY SESSION	The Future of Telecommunications
		Track 1-- Fiber
1:00 pm	SESSION 1	Fiber Optic Cable Design I
1:00 pm	SESSION 2	Fiber & Cable Manufacturing
		Track 2 -- Materials
1:00 pm	SESSION 3	Polymeric Materials for Cable Construction I
		Track 3 -- Copper
1:00 pm	SESSION 4	Metallic Cables in Telecommunications Networks
		Wednesday, November 18
		Track 1 -- Fiber
8:30 am	SESSION 5	Fiber Optic Cable Design II
8:30 am	SESSION 6	Plastic Optical Fibers
		Track 2 -- Materials
8:30 am	SESSION 7	Polymeric Materials for Cable Construction II
		Track 3 -- Copper
8:30 am	SESSION 8	Super Conductivity - Invited
		Track 1 -- Fiber
2:00 pm	SESSION 9	Submarine Cables
2:00 pm	SESSION 10	Fiber Ribbon
		Track 2 -- Materials
2:00 pm	SESSION 11	Fiber & Systems; Testing & Field Evaluation
		Track 3 -- Copper
2:00 pm	SESSION 12	Broadband Services – Panel Discussion
4:00 pm	SESSION 13	Poster Papers
		Thursday, November 19
		Track 1 -- Fiber
8:30 am	SESSION 14	Aerial Cables
8:30 am	SESSION 15	Optical Connectors
		Track 2 -- Materials
8:30 am	SESSION 16	Polymeric Materials for Cable Construction III
		Track 3 -- Copper
8:30 am	SESSION 17	LAN Designs
		Track 1 -- Fiber
1:00 pm	SESSION 18	Fiber Optic Cable Installation
1:00 pm	SESSION 19	Fiber Optic Components & Splicing
		Track 2 -- Materials
1:00 pm	SESSION 20	Cable Design, Fiber Reliability & Fiber Optic Components
		Track 3 -- Copper
1:00 pm	SESSION 21	Copper LANS: Installation & Testing

PAPERS

The papers in this volume were printed directly from unedited reproducible copies prepared by the authors. Responsibility for contents rests upon the authors and not the symposium committee or its members. All rights reserved by the International Wire and Cable Symposium, Inc., 174 Main Street, Eatontown, New Jersey 07724.

PROCEEDINGS/PUBLICATIONS
INTERNATIONAL WIRE AND CABLE SYMPOSIUM (IWCS)

Proceedings - Bound - Available from IWCS

39th IWCS Proceedings - 1990 - $15.00
40th IWCS Proceedings - 1991 - $25.00
44th IWCS Proceedings - 1995 - $40.00
46th IWCS Proceedings - 1997 - $30.00
47th IWCS Proceedings - 1998 - $50.00
46th & 47th IWCS CD - $10.00

Copies of original proceedings not listed above can be reproduced for $75.00 per copy plus shipping.

Publications - Bound - Available from IWCS

Index of IWCS Papers (1983-1990); PUB #1001RP-1991 - $15.00
PIC Insulation Testing Field Experience; PUB #1003RP-1992 - $25.00
Fiber Optic Cables; PUB #1004RP-1992 - $25.00

Extra Copies of the 1998 Proceedings can be obtained for: 1 - $50; 2 - $100; 3 - $150; 4 - $190; 5 - $230; 6 - $270; 7 - $310; 8 - $350; 9 - $390; 10 - $430; 11 and above - $430 plus $30 for each additional copy.

Shipping/Handling:

Proceedings	Publications	CDs
$ 7.50 per copy USA only	$ 4.00 per copy USA Only	$ 3.00 per copy USA Only
$20.00 per copy Surface Mail (overseas - 4 to 6 weeks)	$10.00 per copy Surface Mail (overseas - 4 to 6 weeks)	$ 7.00 per copy Canada
$35.00 per copy Airmail (Europe)	$15.00 per copy Airmail (Europe and Asia)	$10.00 per copy Air/Surface Mail
$40.00 per copy Airmail (Asia)		

Payment: Make a check or bank draft payable in U.S. Dollars drawn on a U.S. Bank, to the INTERNATIONAL WIRE & CABLE SYMPOSIUM, INC. or use your VISA/MC/AMEX by providing number and expiration date and forward request to: International Wire and Cable Symposium, Inc., 174 Main Street, Eatontown, NJ 07724. Telephone inquiries may be directed to Ms. Pat Hudak (732) 389-0990. Prices are subject to change.

Photocopies are available for complete sets of papers for 1964 through 1997. Information on prices and shipping charges should be requested from the: US Department of Commerce, National Technical Information Service (NTIS), Springfield, Virginia 22161, Telephone: (703) 487-4650

Include Title, Year and "AD" Number

13th Annual Wire Cable Symposium (1964)	- AD 787164
15th Annual Wire Cable Symposium (1966)	- AD A006601
16th International Wire Cable Symposium (1967)	- AD 787165
17th International Wire Cable Symposium (1968)	- AD 787166
18th International Wire Cable Symposium (1969)	- AD 787167
19th International Wire Cable Symposium Proceedings 1970	- AD 714985
20th International Wire Cable Symposium Proceedings 1971	- AD 733399
21st International Wire Cable Symposium Proceedings 1972	- AD 752908
22nd International Wire Cable Symposium Proceedings 1973	- AD 772914
23rd International Wire Cable Symposium Proceedings 1974	- AD A003251
24th International Wire Cable Symposium Proceedings 1975	- AD A017787
25th International Wire Cable Symposium Proceedings 1976	- AD A032801
26th International Wire Cable Symposium Proceedings 1977	- AD A047609
27th International Wire Cable Symposium Proceedings 1978	- AD A062322
28th International Wire Cable Symposium Proceedings 1979	- AD A081428
29th International Wire Cable Symposium Proceedings 1980	- AD A096308
30th International Wire Cable Symposium Proceedings 1981	- AD A110859
31st International Wire Cable Symposium Proceedings 1982	- AD A125662
32nd International Wire Cable Symposium Proceedings 1983	- AD A136749
33rd International Wire Cable Symposium Proceedings 1984	- AD A152119
34th International Wire Cable Symposium Proceedings 1985	- AD A164384
35th International Wire Cable Symposium Proceedings 1986	- AD A180828
36th International Wire Cable Symposium Proceedings 1987	- AD A189610
37th International Wire Cable Symposium Proceedings 1988	- AD A200903
38th International Wire Cable Symposium Proceedings 1989	- AD A216023
39th International Wire Cable Symposium Proceedings 1990	- AD A233634
40th International Wire Cable Symposium Proceedings 1991	- AD A244038
41st International Wire Cable Symposium Proceedings 1992	- AD A259235
42nd International Wire Cable Symposium Proceedings 1993	- AD A279242
43rd International Wire Cable Symposium Proceedings 1994	- AD A293473
44th International Wire Cable Symposium Proceedings 1995	- AD A303506
45th International Wire Cable Symposium Proceedings 1996	- AD A324572
46th International Wire Cable Symposium Proceedings 1997	- AD A338941
Kwic Index of Technical Papers, International Wire Cable Symposium (1952-1982)	- AD A027588

MESSAGE FROM THE PRESIDENT/DIRECTOR

During the final stages of preparing for the symposium, I become excited with the expectation and anticipation for another great symposium. The symposium offers the very best in new developments, new applications and evaluation of a technology where the requirements are constantly changing and the demands for improved performance are always present. The concept of wire/cable being the backbone for many of our telecommunication and electronic needs has little interest for many that enjoy the benefits of its use. Therefore, it is exciting and stimulating each year to read or witness the presentation of papers that you think for the moment represents the ultimate in design or development and at future symposiums realize that what you read or heard was only the beginning of potential new and novel ideas or concepts. This is what makes IWCS such a great and interesting symposium. The large international participation in both attendance and technical presentations also extend the interest and significance of the symposium, since it provides attendees the opportunity to keep abreast of new wire/cable development and applications worldwide.

This year's technical program maintains the concept of three distinct tracks devoted to fiber optic cables, copper cables and materials. A special invited session on High Temperature Super-Conductivity (HTS) and a panel discussion on Broadband Services is also included which should be of interest to many attendees. The opening or plenary session on Tuesday will follow last year's initial concept of one prominent speaker. Dr. Arno Penzias, Nobel laureate and former Vice Chairman and Chief Scientist of Lucent Technologies will speak on the Future of Telecommunication. Dr. Penzias' talk should be informative and provide info on information technology as we look and plan for the future.

Committee member Dr. Marek Kapuscinski of NORDX/CDT, James A. Caballero of Synergistics Industries and Leo Chattler of DCM Industries, Inc. are retiring from the committee this year. On behalf of the committee I extend to Marek, Jim and Leo, our sincere thanks and appreciation for their dedication and support of the symposium's program and objectives.

As always, the IWCS Committee and CECOM, Fort Monmouth extend to each and every attendee and supporter of the symposium, a hearty welcome and thanks for your continued support. Your comments and/or suggestions are always appreciated. It is only with your support that we can continue each year to bring you the latest in new and advanced information in wire/cable technology.

This should be another great symposium from start to finish and I can assure you, that the committee is planning now for a greater show next year (1999) when we return to Atlantic City after more than twenty-five years.

Elmer F. Godwin
President/Director

HIGHLIGHTS OF THE 46TH IWCS

International Wire and Cable Symposium
November 17, 18, 19 and 20, 1997
Philadelphia Marriott Hotel, Philadelphia, Pennsylvania

Announcements/Greetings

Elmer F. Godwin
President/Director, IWCS
Eatontown, NJ

James R. Leech
IWCS Chairman
Union Carbide Corp
Somerset, NJ

Guest Speakers Plenary Session

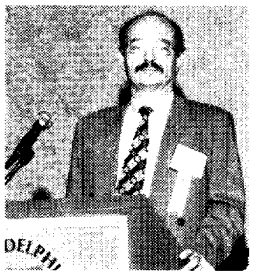

DR. MAREK KAPUSCINSKI
Chairman, Plenary Session, NORDX/CDT
Quebec, Canada

DR. ROBERT W. LUCKY
Bellcore
Morristown, NJ

Luncheon Speaker

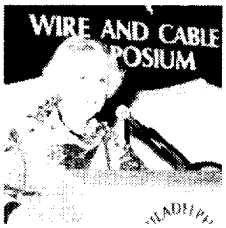

DR. YVONNE KAYE
Philadelphia, PA

Scholarship Recipients

Xavier Mann Of IWCS
(on right) presenting Scholarship check to
Janet Armstrong of Rutgers University

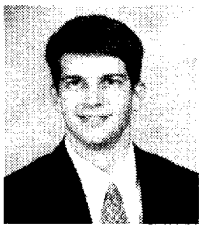

Billy Oates
Attending
Georgia Institute of Technology

Michael Rich
Attending
Georgia Institute of Technology

Award Winners

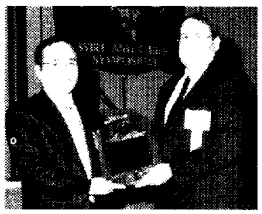

Outstanding Technical
Jim Leech of IWCS (on right) making presentation
to **Matsuhiro Miyamoto**, Fujikura Ltd, Chiba, Japan
(who is also aaccepting for
Mitsuru Kamikatano and Osamu Ogawa)

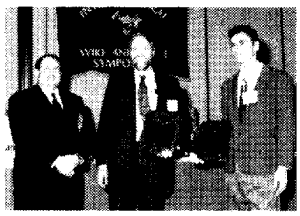

Outstanding Poster Paper
Jim Leech of IWCS (on left) making presentation
to Jan Bjorkman (middle) of Telia Network Services,
Farsta, Sweden and **Dr. Torbjorn Svensson**
(right) of Telia Research AB, Haninge, Sweden

Best Presentation
Jim Leech of IWCS
(on left) making presentation to **Dr. Priya L. Tabaddor**
Lucent Technologies, Bell Labs
Norcross, GA

IWCS Retiree

Elmer F. Godwin of IWCS (on left)
presenting a Retirement
Certificate to **Dr. John Mellis**
British Telecom Laboratories
Ipswich, United Kingdom

Registration

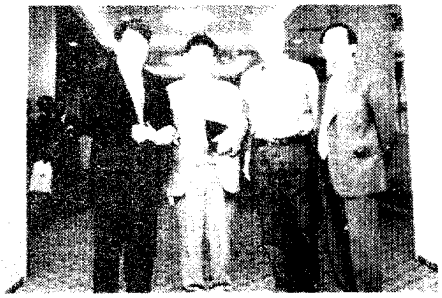
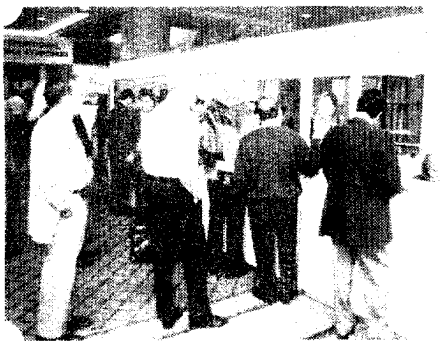

Educational

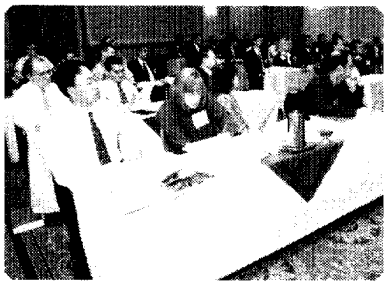

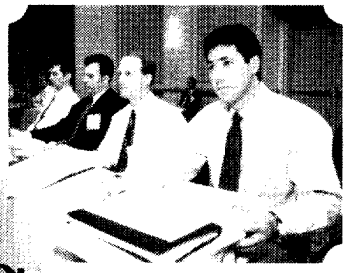

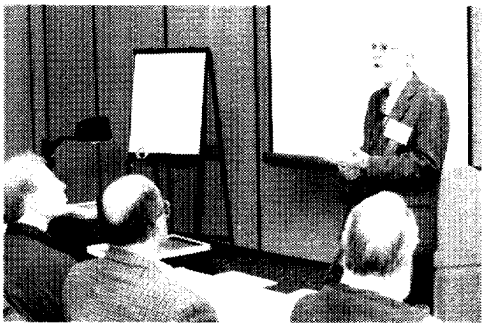

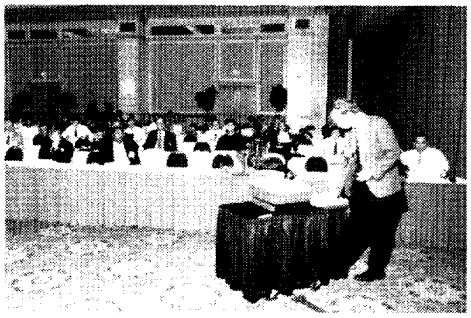
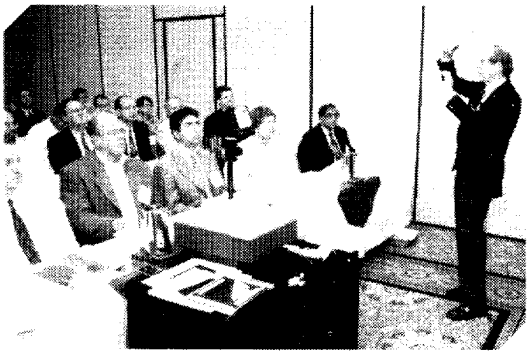

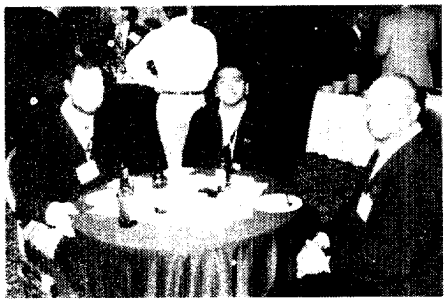

Hospitality
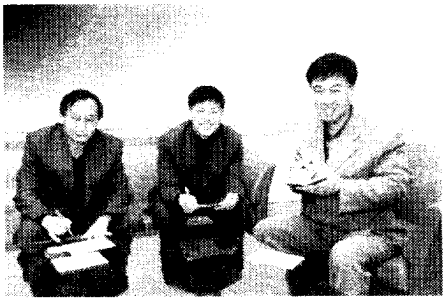

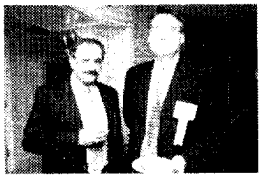

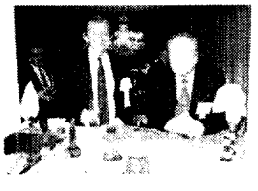

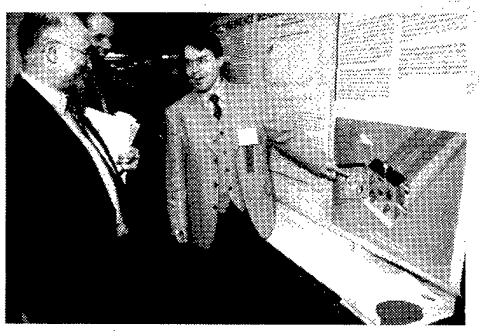

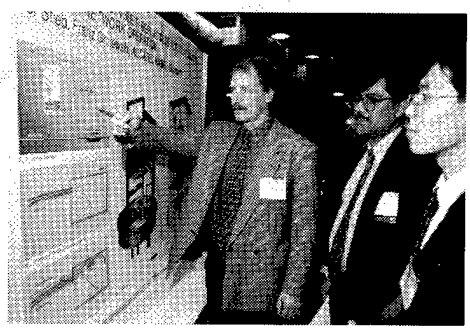

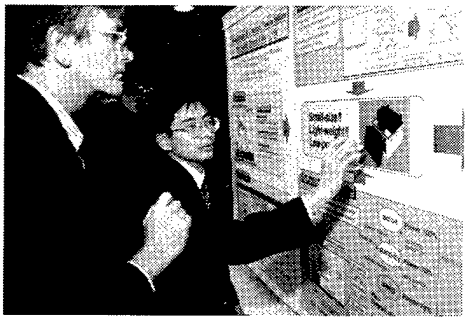

IWCS 1997

Posters

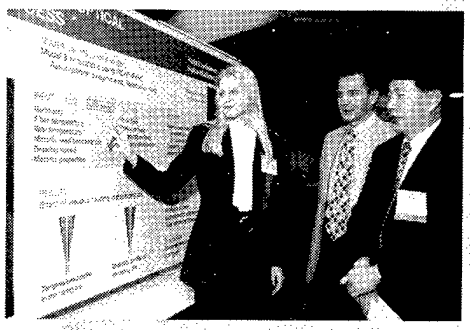

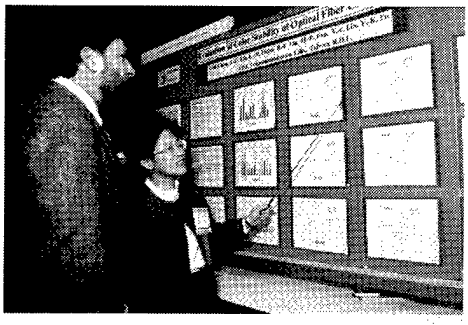

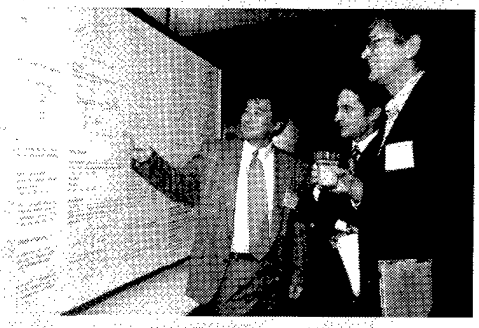

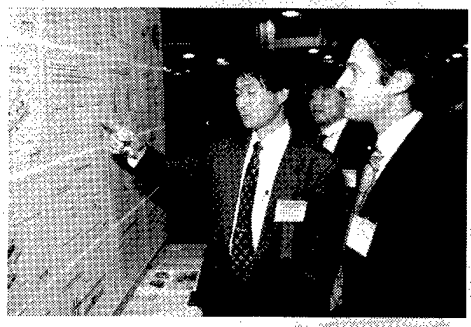

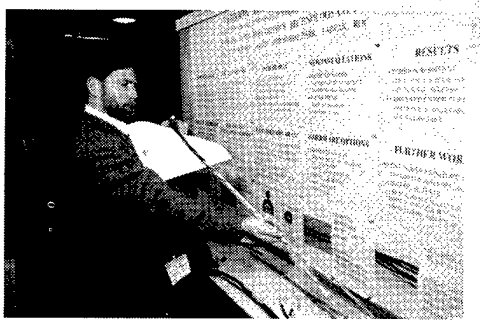

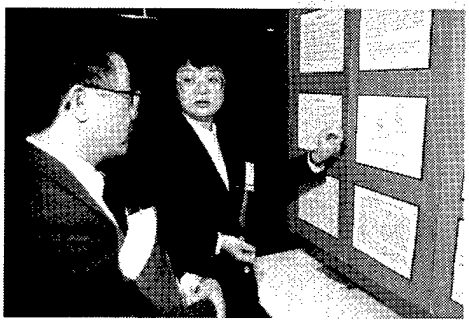

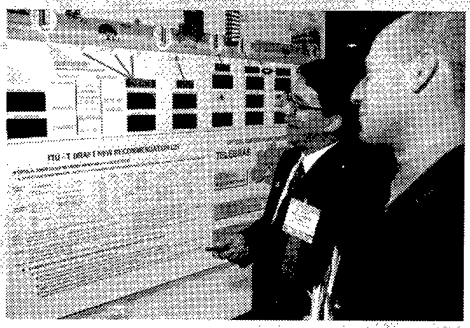

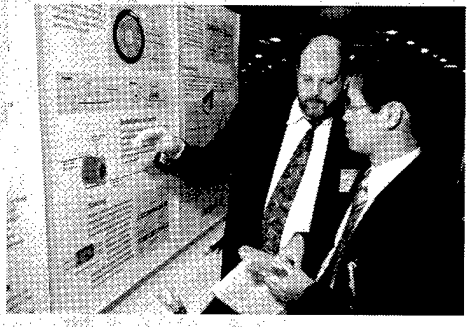

AWARDS

		Best Presentation
Outstanding Technical Paper		
H. Lubars and J. A. Olszewski, General Cable Corp. — "Analysis of Structural Return Loss in CATV Coaxial Cable"	1968	N. Dean, B.I.C.C.—"The Development of Fully Filled Cables for Distribution Network"
J. P. McCann, R. Sabia and B. Wargotz, Bell Laboratories — "Characterization of Filler and Insulation in Waterproof Cable"	1969	J. D. Kirk, Alberta Government Telephones—"Progress and Pitfalls of Rural Buried Cable"
D. E. Setzer and A. S. Windeler, Bell Laboratories — "A Low Capacitance Cable for the T2 Digital Transmission Line"	1970	Dr. O. Leuchs, Kable and Metalwerke—"A New Self-Extinguishing Hydrogen Chloride Binding PVC Jacketing Compound for Cables"
R. Lyenger, R. McClean and T. McManus, Bell Northern Research — "An Advanced Multi-Unit Coaxial Cable for Toll PCM Systems"	1971	S. Nordblad, Telefonaktiebolaget L. M. Ericsson—"Multi-Paired Cable of Nonlayer Design for Low Capacitance Unbalance Telecommunications Network N. Kojima, Nippon Telegraph and Telephone—"New Type Paired Cable for High Speed PCM Transmission"
J. B. Howard, Bell Laboratories — "Stabilization Problems with Low Density Polyethylene Insulations"	1972	S. Kaufman, Bell Laboratories—"Reclamation of Water-Logged Buried PIC Telephone Cable"
Dr. H. Martin, Kabelmetal — "High Power Radio Frequency Coaxial Cables, Their Design and Rating"	1973	R. J. Oakley, Northern Electric Co., Ltd.—"A Study Into Paired Cable Crosstalk"
D. Doty, AMP Inc. — "Mass Wire Insulation Displacing Termination of Flat Cable"	1974	G. H. Webster, Bell Laboratories—"Material Savings by Design in Exchange and Trunk Telephone Cable"
T. S. Choo, Dow Chemical U.S.A. — "Corrosion Studies on Shielding Materials for Underground Telephone Cables"	1975	J. E. Wimsey, United States Air Force—"The Bare Base Electrical Systems"
N. J. Cogelia, Bell Telephone Laboratories and G. K. Lavoie and J. F. Glahn, US Department of Interior — "Rodent Biting Pressure and Chemical Action and Their Effects on Wire and Cable Sheath"	1976	Michael DeLucia, Naval Ship Research and Development—"Highly Fire-Retardant Navy Shipboard Cable"
T. K. McManus, Northern Telecom Canada Ltd. and R. Beveridge, Saskatchewan Telecommunications, Canada — "A New Generation of Filled Core Cable"	1977	William L. Schmacher, AMP Inc.—"Design Considerations for Single Fiber Connector"
F. Suzuki, S. Sato, A. Mori and Y. Suzuki; Sumitomo Electric Industries, Ltd., Japan — "Microcoaxial Cables Insulated with Highly Expanded Polyethylene By Chemical Blowing Method"	1978	Richard C. Mondello, Bell Labs.—"Design and Manufacture of an Experimental Lightguide Cable for Undersea Transmission Systems"
S. Masaki, Y. Yamazaki and T. Ideguchi, Nippon Telegraph and Telephone Public Corporation, Japan — "New Aluminum Sheath Cable Used for Electromagnetic Shielding"	1979	I. Wadehra, IBM Corporation—"Performance of Polyvinyl Chloride Communication Cables in Modified Steiner Tunnel Test"
P. Kish and Y. BeBorgne, Northern Telecom Canada Limited, Montreal, Canada — "General Crosstalk Model for Paired Communication Cables"	1980	J. J. Refi, Bell Laboratories—"Mean Power Sum Far-End Crosstalk of PIC Cables as a Function of Average Twist Helix Angle"
C. J. Arroyo, N. J. Cogelia, Bell Laboratories, and B. J. Darsey, Western Electric — "Thermal Behavior of Experimental Plenum Cable Sheaths Determined in a Radiant Heat Chamber"	1981	G. S. Anderson, Belden Corporation—"Installation of Fiber Optic Cable on 457 Meter Tower"
R. H. Whiteley, Raychem Ltd. — "A Comprehensive Small Scale Smoke Test"	1982	A. Yoshizawa, The Furukawa Electric Co., Ltd.—"Structure and Characteristics of Cables for Robots"
V. A. Fentress, Raychem Corp. and D. V. Nelson, Stanford University — "Fracture Mechanics Evaluation of the Static Fatigue Life of Optical Fibers in Bending"	1983	J. R. Bury, Standard Telecommunication Laboratories, Ltd., Hailow, England—"Development of Flame Retardant, Low Aggressivity Cables"
M. Fujise and Y. Iwamoto, KDD Research & Development Laboratories, Tokyo, Japan — "Self-Core-Alignment Arc-Fusion Splicer Based on a Simple Local Monitoring Method"	1984	William E. Dennis, Dow Corning Corporation, Midland, Michigan—"Hydrogen Evolving Tendencies of Cable Fillers and Optical Fiber Coatings"
James A. Krabec and John W. Kincaid, Jr., Belden Technical Research Center — "Advances in the Optimization of Multi-Layer Shield Design"	1985	Stephen Hornung, British Telecom Research Laboratories—"Manufacture and Performance of Fibre Units for Installation by The Viscous Drag of Air"
Simon D. Dadakarides and Bruce B. Lusignam, Stanford University — "Magnetically Loaded Cables"	1986	Dave Fischer, Superior Cable Corp.—"Progress Towards the Development of Lighting Test for Telecommunication Cables" John C. Chamberlain, Siecor Corp.—"Zero Halogen Fire Retardant Fiber Optic Shipboard Cable"

Outstanding Technical Paper	*Outstanding Poster Paper*	*Best Presentation*
1987 Stephen B. Pierce — Conel Laboratories — "Digital Transmission on Customer Premises Wiring"	William Wood — Bell Communication Research — "Performance Analysis of Optic Fiber Cleavers"	Richard Rossi — General Cable Company — "Cable Sheathing Design and Performance Criteria"
1988 Martin C. Light Jr., James A. Moses, Mark A. Sigmon and Christopher A. Story — Siecor Corp. — "Design and Performance of Telecommunication Cable Optimized for Low Fiber Count"	Dr. R. Raman — Contel Laboratories — "Loss at Dissimilar Fiber Splices"	Janice B. Haber — AT&T Laboratories — "Single-Mode Media and Apparatus for Fiber to the Home"

Outstanding Technical Paper	*Outstanding Poster Paper*	*Best Presentation*
1989 Michel Plasse, Lise Desroches and Paul-Andre Guilbert — Northern Telecom Canada Limited — "High Performance Twisted-Pair Cable for LAN Systems"	Werner Bernard and Susan C. Grant — Siecor Corporation — "Fiber Optic Drop Cables in the Subscriber Loop"	Michel de Vecchis — Les Cables de Lyon — "Results on a Large Scale Installation of a Fibre Optic Distribution Network"
1990 Trevor N. Bowmer, Russell J. Miner, Irene M. Plitz, Joseph N. D'Amico and Lal M. Hore — Bellcore — "Thermal Stability Tests for Polyolefin Insulations"	Steve Lischynsky, Helmut Lukas, Robin McIntyre and Grant Pacey — Bell-Northern Research Ltd. — "New Technology for a Single Mode Mechanical Splice"	Harold W. Friesen — AT&T Bell Laboratories — "An Improved Characteristic Impedance Measurement Technique"
1991 Shigeru Tomita, Michito Matsumoto, Tetsuro Yabuta and Takuya Uenoya — NTT — "Preliminary Research into Ultra High Density and High Count Optical Fiber Cables"	G. Scott Glaesemann — Corning Inc. — "The Effect of Proof Testing on the Minimum Strength of Optical Fiber"	Sue V. Wolfe — STC Submarine Systems — "Structure and High Voltage DC Behaviour of Submarine Cable Mouldings"
1992 Nathan E. Hardwick III and Kris Kathiresan — AT&T Bell Laboratories and J. G. Hartley — Georiga Institute of Technology — "Analysis of Fiber Optic Cable Design Conditions in Vicinity of Steam Lines — Ruptured and Pristine"	Svend Hopland and Albert Klykken — Norwegian Telecom — "Installation of Submarine Fiberoptic Cables in Rugged Coastal Terrain"	Peter Latoszynski — Telecom Australia — "Development of Co-Extruded Polyethylene/Polyamide 12 Insect Resistant Telecommunications Cable"
1993 Dr. Yoshinori Namihira and Toshio Kawazawa — KDD R&D Laboratories; and Naoki Norimatsu — KDD Company, Limited — "PMD Reduction of Optical Fiber Cables for Transoceanic Optical Amplifier Submarine Cable Systems"	Willem Griffioen — PTT Research — "Mechanical Lifetime of Optical Fibers"	Timothy S. Dougherty — AT&T Network Cable Systems — "The Temperature of Aerial Plant and Its Effect Upon Foam-Skin Insulation Life" and Wolfgang Wenski — Kabelmetal Electro GmbH — "First Large Scale FITL Installation: Experience From Opal '93"
1994 Toshio Kurashima, Kazuo Hogari, Satoshi Matsuhashi, Dr. Tsuneo Horiguchi, Dr. Yahei Koyamada and Yutaka Wakui — NTT Access Network Systems Laboratories; and Hiroshi Hirano — NTT Technical Assistance & Support Center — "Measurement of Distributed Strain in Frozen Cables and Its Potential for Use in Predicting Cable Failure"	Dr. Sverker Forsberg — Swedish University of Agricultural Sciences; and Jan Björkman — Telia AB — "Release of Lead from Lead-Sheathed Telecom Cables in Soil"	Barry J. Keon — Telstra — "The Effects of Optical Fiber Coating and Ink Materials on the Corrosion of the Glass Surface"
1995 Jean Luc Lang and Jean-Francois Libert — Alcatel Submarine Network; David I. Curtis and Peter Worthington — STC Submarine Systems Ltd. — "Optical Performance of Submarine Cables in Optically Amplified High Bit Rate Systems"	Richard S. Wagman, Gregory A. Lochkovic and Kevin T. White — Siecor Corporation — "Component Optimization for Slotted Core Cables Using 8-Fiber Ribbons"	Dr. Dan L. Philen — AT&T Bell Laboratories — "Optical Fiber for Amplified Undersea Systems"
1996 Mitsuru Kamikatano and Matsuhiro Miyamoto — Fujikura Limited; and Osamu Ogawa — Tokyo Electric Power Company — "A Time-Varying Optical Fiber Strain Measurement by Using Brillouin Ring Amplifying System"	Jan Björkman — Telia Network Services; and Dr. Torbjörn Svensson — Telia Research AB — "Ageing of Fibres and Ribbon in Water and Filling Compound"	Dr. Priya L. Tabaddor — Lucent Technologies Incorporated, Bell Laboratories — "An Evaluation of Protective Polymer Coatings for Optical Fiber Applications"
1997 Debra A. Simoff, Dr. Mark A. Paczkowski, Dr. Daryl Inniss, Dr. Thomas A. Strasser, J. Renee Pedrazzani, Dr. Rolando P. Espindola, Dr. Robert M. Atkins, Katherine T. Nelson, Valerie J. Kuck, John M. Borick and Jennifer Aspell — Lucent Technologies; and Regina Ragan — California Institute of Technology — "Coatings Having Enhanced UV Transpar-ency for the Fabrication of Optical Fiber Gratings"	Katja Lyytikäinen — Nokia-Maillefer Oy — "Numerical Simulation of Optical Fiber Coating Process"	Dr. Neil R. Haigh — BICC Cables Limited — "Applicability of All-Dielectric Self Supporting Cable Systems to Very High Voltage Overhead Power Lines"

ELMER F. "ACE" GODWIN SCHOLARSHIP

1994

Sara Ransom, Massachusetts Institute of Technology, Freshman — Materials Science Engineering Major

Jurron Bradley, Vanderbilt University, Senior — Chemical Engineering Major

1995

Jason Chang, Princeton University, Freshman — Chemistry Major

Fionna Murray, Virginia Tech, Junior — Mechanical Engineering Major

1996

Anthony Tindall, Cornell University, Freshman — Mechanical Engineering Major

John Belle, North Carolina State University, Sophomore — Electrical Engineering Major

1997

Michael Rich, Georgia Institute of Technology, Freshman — Electrical Engineering Major

Billy Oates, Georgia Institute of Technology, Senior, Mechanical Engineering and Math Major

Janet Armstrong, Rutgers University, Ph.D. Candidate, Ceramic Engineering Major

47TH INTERNATIONAL WIRE AND CABLE SYMPOSIUM (IWCS)
SYMPOSIUM COMMITTEE

IWCS STAFF

ELMER F. GODWIN
(President/Director)
GEF Associates
3A Buttonwood Drive
Shrewsbury, NJ 07702
Tel: (732) 389-0990 (Office)
Fax: (732) 389-0991 (Office)
E-mail: iwcs@monmouth.com

IRVING KOLODNY
(Director's Assistant)
31 Maple Run Drive
Jericho, NY 11753
Tel & Fax: (516) 932-0699
E-mail: ikolodny@msn.com

MICHAEL A. DELUCIA
(Director's Assistant)
1775 Crofton Parkway
Crofton, MD 21114
Tel & Fax: (410) 721-5588
E-mail: mdelucia@clark.net

PATRICIA HUDAK
(Administrative Assistant)
174 Main Street
Eatontown, NJ 07724
Tel: (732) 389-0990
Fax: (732) 389-0991
E-mail: iwcs@monmouth.com

1998 OFFICERS

JOHN R. SICOTTE
(Chairman)
Corning Incorporated
35 W. Market St; MP-RO-02
Corning, NY 14831
Tel: (607) 974-4447
Fax: (607) 974-7041
E-mail: sicottejr@corning.com

MICHEL ROUSSEAU
(Vice-Chairman)
Alcatel
54, RUE La Boétie
75008 Paris, France
Tel: +33-1-4076-2909
Fax: +33-1-4076-1423
E-mail: michel.rousseau@accyd.alcatel.fr

XAVIER MANN
(Secretary)
Fitel Lucent Technologies
One Lucent Drive
Carrollton, GA 30117
Tel: (770) 838-5278
Fax: (770) 836-8820
E-mail: xmann@fitel.com

DR. HOWARD WICHANSKY
(Treasurer)
Cdr, US Army CECOM
ATTN: AMSEL-RD-ST-WL-AW
Fort Monmouth, NJ 07703-5203
Tel: (732) 427-4713
Fax: (732) 427-2150
E-Mail: wichansk@doim6.monmouth.army.mil

1998 COMMITTEE MEMBERS

NILS ARTLÖVE
Telia AB
123 86 Farsta
Sweden
Tel: +46-8-713-1212
Fax: +46-8-713-2926
E-mail: Nils.A.Artlove@telia.se

JEAN BAER
Essex Group, Inc.
1710 Wall St, PO Box 1750
Fort Wayne, IN 46801-1750
Tel: (219) 461-5641
Fax: (219) 461-5660
E-mail: baer_jeanie@essexgroup.com

JAMES A. CABALLERO
Synergistics Industries (NJ) Inc.
10 Ruckle Avenue
Farmingdale, NJ 07727
Tel: (732) 938-5980
Fax: (732) 938-6035
E-mail: caballerojim@worldnet.att.net

RUSSELL S. DANIELS
Equistar Chemicals, LP
One Houston Center, Suite 1600
1221 McKinney St; PO Box 2583
Houston, TX 77252-2583
Tel: (713) 309-4958
Fax: (713) 652-4687
E-mail: russell.daniels@equistarchem.com

HIROTOSHI HONDO
The Furukawa Electric Co, Ltd.
Information & Electronics Laboratory
5-1-9 Higashiyawata
Hiratsuka, Kamagawa, 254, Japan
Tel: +81-3-3286-3495
Fax: +81-3-3286-3708
E-mail: hondo@ie.inf.furukawa.co.jp

DR. MAREK KAPÚSCÍSKI
NORDX/CDT
2345, Boulevard Des Sources
Point Claire, Quebec
Canada H9R 5Z3
Tel: (514) 822-7328
Fax: (514) 822-7985
E-mail: marek.kapuscinski@nordx.com

INGE B. KOVACS
Consultant for Polycheck Ltd
180 Durham Court
Hackettstown, NJ 07840
Tel: (908) 852-1610
Fax: (908) 852-1518
E-mail: ibkovacs@goes.com

JAMES R. LEECH
Union Carbide Corp.
Weston Canal Center
PO Box 450
Somerset, NJ 08875-0450
Tel: (732) 271-7935
Fax: (732) 271-7949
E-mail: leechjr@ucarb.com

FRED NARAYAN
Phelps Dodge International Corp.
2121 Ponce de Leon Blvd.
Coral Gables, FL 33134
Tel: (305) 447-4322
Fax: (305) 447-4321
Email: fnarayan@phelpsd.com

JOHN R. SACH
Pirelli Cables & Systems NA
710 Industrial Drive
Lexington, SC 29072
Tel: (803) 951-4020
Fax: (803) 957-8654
E-mail: John.Sach@us.pirelli.com

JOHN P. VARACHI, JR
Bellcore
445 South St; Rm MCC 1J142G
Morristown, NJ 07960-6438
Tel: (973) 829-4920
Fax: (973) 829-5965
E-mail: jvarachi@notes.cc.bellcore.com

ADVISORY

DR. PETER R. BARK
Siecor
P.O. Box 489
489 Siecor Park
Hickory, NC 28603
Tel: (828) 323-6205
Fax: (828) 323-6264
E-mail: peter.bark@siecor.com

LEO CHATTLER
DCM Industries, Inc.
2930 Faber Street
Union City, CA 94587
Tel: (510) 429-9500
Fax: (510) 429-1250
E-mail: leochattler@dcmindustries.com

DAVE FALLOWFIELD
TELUS Communications Inc.
6B, 10020 100 Street NW
Edmonton, Alberta
Canada T5J 0N5
Tel: (403) 493-4928
Fax: (403) 493-3115
E-mail: david.fallowfield@telus.com

DIETER S. NORDMANN
(European Representative)
Alcatel Contracting
P.O. Box 160; Kabelkamp 20
D30179 Hannover, Germany
Tel: +49-511-676-2020
Fax: +49-511-676-3042
E-mail: Nordieter@aol.com

MANUEL R. SANTANA
Lucent Technologies
Bell Laboratories
2000 NE Expressway; Rm 1D32
Norcross, GA 30071
Tel: (770) 798-2754
Fax: (770) 798-4654
E-mail: msantana@lucent.com

CONSULTANTS

DR. REINER J. GERDES
TransTel Group Inc.
5555 Oakbrook Pkwy, Suite 110
Norcross, GA 30093
Tel: (770) 368-8343
Fax: (770) 368-8382
E-mail: rgerdes@transtelgroup.com

DR. RAYMOND E. JAEGER
SpecTran Corporation
50 Hall Road
Sturbridge, MA 01566
Tel: (508) 347-2261
Fax: (508) 347-8626
E-mail: cmaruk@spectran.com

HANS A. MAYER
Olex Cables
(A Division of Pacific Dunlop Ltd.)
207 Sunshine Road
Tottenham, VIC 3012
Melbourne, Australia
Tel: +61-3-9281-4240
Fax: +61-3-9314-9919
E-mail: hmayer@olexau.pacdun.com

47th GOLD SUSTAINING CONTRIBUTORS

Akzo Nobel Aramid Products Inc.
801-F Blacklawn Road
Conyers, GA 30012-5187

Alcatel
30, rue Pierre Bérégovoy
92111 Clichy Cedex
France

AlphaGary Corporation
170 Pioneer Drive
Leominster, MA 01453

ASI/Silica Machinery
7525 Ethel Avenue
North Hollywood, CA 91605

Bellcore
445 South Street
Morristown, NJ 07960-6438

Chase & Sons
19 Highland Avenue
Randolph, MA 02368

CommScope, Inc.
1375 Lenoir-Rhyne Blvd.
Hickory, NC 28603

DSM Desotech
1122 St. Charles Street
Elgin, IL 60120

DuPont
5401 Jefferson Davis Highway
Richmond, VA 23234

Elf Atochem North America, Inc.
2000 Market Street
Philadelphia, PA 19103-3222

Equistar Chemicals, LP
1221 McKinney, Suite 1600
PO Box 2583
Houston, TX 77252-2583

Ericsson Cables AB
Telecom Cables Division
Kabelvägen 1
824 82 Hudiksvall
Sweden

Essex Group, Inc.
1710 Wall Street
Ft. Wayne, IN 46801

Facile Holdings, Inc.
185 6th Avenue
Paterson, NJ 07509

Fujikura Ltd.
1-5-1 Koto-ku, Kiba
Tokyo, 135
Japan

The Furukawa Electric Co. Ltd.
6, Yawata-Kaigandori
Ichihara, Chiba, 290
Japan

Fusion UV Systems, Inc.
910 Clopper Road
Gaithersburg, MD 20878-1357

Hitachi Cable, Ltd.
5-1-1 Hitaka-Cho, Hitachi-Shi
319-1414 Japan

Information Gatekeepers
214 Harvard Avenue, Suite 200
Boston, MA 02134

Kroschu-Kabelwerke
Kromberg & Schubert GmbH u. Co
Spitzenstr. 37
42389 Wuppertal
Germany

Lucent Technologies
2000 NE Expressway
Norcross, GA 30071

Mitsubishi Cable Industries, Ltd.
New Kokusai Bldg
4-1 Marunouchi 3-chome, Chiyoda-Ku
Tokyo, 100-8303
Japan

Neptco
PO Box 2323
Pawtucket, RI 02861

Nextrom Ltd.
65 Basaltic Road
Concord, Ontario
Canada L4K 1G4

Nippon Telegraph and Telephone Corp.
1-7-1, Hanabatake
Tsukuba, Ibaraki, 305-0805
Japan

NOVA-BOREALIS Compounds LLC
176 Thomas Road
Port Murray, NJ 07865

Olex Cables
A Division of Pacific Dunlop, Ltd.
207 Sunshine Road
Tottenham, Melbourne
Victoria 3012, Australia

Optical Fibres
Second Avenue
Deeside Industrial Park
Deeside, Flintshire CH5 2NX
United Kingdom

Owens Corning
One Owens Corning Parkway
Toledo, OH 43659

GOLD SUSTAINING CONTRIBUTORS

Penreco
138 Petrolia Street
Karns City, PA 16041

Plasma Optical Fibre
PO Box 1136
5602 BC Eindhoven
The Netherlands

Siecor
1928 Main Avenue, SE
Hickory, NC 28602

Siemens AG
ÖN NK E AT
Schertlinstr. 17
81359 München
Germany

SpecTran Communication Fiber Technologies
50 Hall Road
Sturbridge, MA 01566

The Stewart Group Inc.
259 Steelcase Road West
Markham, Ontario
Canada L3R 2P6

Sumitomo Electric U.S.A., Inc.
21221 S. Western Avenue, Suite 200
Torrance, CA 90501

Telia AB
S-123 86 Farsta
Sweden

UBE Industries (America), Inc.
666 Fifth Avenue
New York, NY 10103

Union Carbide Corporation
39 Old Ridgebury Road
Danbury, CT 06817-0001

Watson AFA Industries
74 Railroad Avenue
Paterson, NJ 07509

Weber & Scher Mfg. Co., Inc.
1231 US Highway 22 East
PO Box 366
Lebanon, NJ 08833-0366

Witco Corporation
5777 Frantz Road
Dublin, OH 43017

TABLE OF CONTENTS

TUESDAY MORNING—9:00 AM–11:00 AM

Grand Ballroom (Salons G/H), Fifth Floor

Announcements/Greetings

Elmer F. Godwin, President/Director, IWCS, Inc., Eatontown, NJ

John R. Sicotte, Chairman, IWCS, Corning Inc., Corning, NY

Dr. Marek Kapuscinski, Chairman, Plenary Session, NORDX/CDT, Quebec, Canada

PLENARY SESSION: THE FUTURE OF TELECOMMUNICATIONS

Speaker: Dr. Arno Penzias, Recently retired Vice President and Chief Scientist, Lucent Technologies (formerly Bell Labs.)

TUESDAY AFTERNOON—1:00 PM–4:50 PM

Salon E

TRACK 1—FIBER

SESSION 1: FIBER OPTIC CABLE DESIGN I

Chairperson: Manuel R. Santana, Lucent Technologies, Bell Labs., Norcross, GA

Development of Miniature Optical Fiber Cords—*F. Nakajima, N. Ishii, Y. Watanabe, S. Takagi,* Furukawa Electric Co., Ltd., Ichihara, Japan 4

New Indoor/Outdoor Tight Buffered Fiber LSZH Distribution Cable—*B. M. Blell,* CommScope, Inc., Claremont, NC 10

Development of Cross-Functional Totally Dry Optical Fiber Cable for Outdoor, Riser, and Plenum Applications—*D. A. Keller, J. Rosko, R. Yoder,* Alcatel-Berk-Tek, Fuquay-Varina, NC; *B. Risch, S. Munday,* Alcatel Cable, Claremont, NC 17

Finite Element Modeling of Optic Fiber Cable Crush Performance—*J. B. Stevens, P. Elisson, B. Risch, C. Bastide,* Alcatel OFCCC, Claremont, NC 25

Development of 2000-Fiber Cable with SZ-Stranded U-Grooves and Slotted Rod—*H. Iwata, M. Okada, J. Sogame, H. Akimoto, S. Tomita, Y. Dei,* NTT Access Network Systems Labs., Ibaraki, Japan 34

Design of Ultra-High Density and High Count 2000 Optical Fiber Cable for Easy Branching—*D. Iwakura, I. Kobayashi, M. Hara, H. Kanzaki, H. Hiramatsu, Y. Kamikura,* Furukawa Electric Co., Ltd., Chiba, Japan 41

Development of New Slotted Rod Cable Composed of Foamed Polyethylene Slotted Rod—*I. Kobayashi, R. Takaoka, E. Konda, F. Hosoi, H. Hiramatsu, Y. Kamikura,* Furukawa Electric Co., Ltd., Chiba, Japan 49

Very High Transmission Density Cables Including Multicore Fibers—*M. Garcia, S. Richter, V. Bourget,* Alcatel OFCCC, Claremont, NC; *G. Orcel, A. Tardy,* Alcatel FOCC, France; *J. C. Bizeul, J. P. Louboutin,* France Telecom (CNET), France; *J. P. Bonicel,* Alcatel TPLE, France 57

TUESDAY AFTERNOON—1:00 PM–4:50 PM

Salon F

TRACK 1—FIBER

SESSION 2: FIBER & CABLE MANUFACTURING

Chairperson: John P. Varachi, Jr., Bellcore, Morristown, NJ

PCVD: The Ultimate Technology for Production of High Bandwidth Multimode Fibres—*A. H. van Bergen, T. Breuls,* Plasma Optical Fibre B.V., Eindhoven, The Netherlands 66

Characterization of Meltdown Profile During Fiber Draw—*D. S. Vaidya, G. D. Mihalacopoulos,* SpecTran Corp., Sturbridge, MA 73

Numerical Simulation of Optical Fiber Cooling During the Drawing Process—*M.-G. Gossiaux, J.-F. Bourhis, G. Orcel,* Alcatel, Conflans Ste. Honorine, France 81

Study on Cure Behavior of UV Curable Resins for High Speed Drawing—*K. Moriura, M. Nagai, H. Kuzushita, K. Tsuji, T. Kinoshita,* Mitsubishi Cable Industries, Ltd., Hyogo, Japan 85

Multivariate Statistical Process Control Techniques for Cable Manufacturing—*H. M. Bush,* Lucent Technologies, Norcross, GA 92

Logistic Regression Techniques for Modeling Defects in Cables—*H. M. Bush, H. P. Debban,* Lucent Technologies, Norcross, GA 103

TUESDAY AFTERNOON—1:00 PM–4:50 PM

Salons A/B

TRACK 2—MATERIALS

SESSION 3: POLYMERIC MATERIALS FOR CABLE CONSTRUCTION I

Chairperson: Inge B. Kovacs, Consultant for Polycheck Ltd., Hackettstown, NJ

The Low Smoke Halogen Free Option to Chlorosulfonated Polyethylene Low Voltage Insulation and Jackets—*K. E. Cope,* Pirelli Cables and Systems North America, Columbia, SC 111

Effects of Phenolic and Nonphenolic Additives on the Electron Beam Crosslinking of an Ethylene Vinyl Acetate Copolymer—*J. A. Lupia,* Ciba Specialty Chemicals, Tarrytown, NY 117

Characterizing and Selecting Superabsorbing Cable Components—*J. D. Gruhn,* Neptco Inc., Pawtucket, RI 126

Functional Performance of Ocean Water Blocking Tapes—*N. I. Patel,* Siecor Corp., Hickory, NC 136

Novel Halogenfree Flame Retardant Polyolefins Intended for Internal Wiring—Properties and Flame Retardant Mechanism—*B.-Å. Sultan,* Borealis AB, Stenungsund, Sweden; *K. Ericsson, T. Hjertberg,* Chalmers University of Technology, Gothenburg, Sweden; *M. Hirvensalo, M. Hänninen,* Borealis Polymers Oy, Porvoo, Finland 147

Rheology of Semiconductive Black Compounds with Low Carbon Black Content—*C. D. Lee,* Equistar Chemicals, Cincinnati, OH 161

TUESDAY AFTERNOON—1:00 PM–4:50 PM

Salons C/D

TRACK 3—COPPER

SESSION 4: METALLIC CABLES IN TELECOMMUNICATIONS NETWORKS

Chairperson: Fred Narayan, Phelps Dodge International Corp., Coral Gables, FL

Cost Driven Innovative Solutions for the Local Loop—*P. Matthijsse,* KPN Telecom-Network Services, The Netherlands 170

Improving Range and Bandwidth of TELCO Loop Plant—*R. A. Combellack,* Nortel (Northern Telecom), Ontario, Canada 176

Performance of Coaxial Distribution Cables Under Mechanical Stress—*L. M. Hore, W. McLaughlin, K. V. Hsing,* Bellcore, Morristown, NJ 184

Coupling Attenuation: Correlation Between Near and Far Field Measurements—*M. Pelt, D. Hess,* Alcatel Cabling Systems, Brussels, Belgium 192

Powerline Telecommunication PLC—*R. Kallenborn,* GHMT mbH, Bexbach/Saar, Germany 201

TUESDAY EVENING

Exhibit Hall, Fourth Floor

Hospitality Hour—6:30 PM–8:00 PM

Suppliers Forum—6:30 PM–8:30 PM

Admission by badges issued to all registrants

WEDNESDAY MORNING—8:30 AM–11:30 AM

Salon E

TRACK 1—FIBER

SESSION 5: FIBER OPTIC CABLE DESIGN II

Chairperson: Michel Rousseau, Alcatel Cable, Clichy Cedex, France

Development of the Dry Type Water Blocking Optical Cables with SZ-Slotted Core and 2-Fiber Ribbons—*H. Watanabe, N. Okada, M. Yamanaka, M. Miyamoto,* Fujikura Ltd., Chiba, Japan 208

Study on Strain Characteristics of Fiber Ribbons in a SZ-Grooved Spacer Caused by Cable Bending—*A. Makiyama, J. Ohta, A. Nishimura,* Sumitomo Electric Industries, Ltd., Yokohama, Japan 215

Study of the SZ-Stranded 2000-Fiber Cable with 8-Fiber Ribbons for Underground Access Networks—*N. Okada, Y. Sato, A. Yamasaki, M. Miyamoto,* Fujikura Ltd., Chiba, Japan 220

Development of Low Skew Optical Fiber Cable—*F. Hosoi, M. Kosaka, M. Hara, Y. Kamikura,* Furukawa Electric Co., Ltd., Chiba, Japan; *S. Toda, T. Watanabe, O. Suzuki,* Fujitsu Ltd., Kanagawa, Japan 227

Characteristics and Long-Term Reliability of Several Types of Thin Optical-Fiber Cord—*T. Shimomichi, E. Ino, K. Ishida, K. Oohashi, M. Miyamoto,* Fujikura, Ltd., Chiba, Japan 233

WEDNESDAY MORNING—8:30 AM–11:30 AM

Salon F

TRACK 1—FIBER

SESSION 6: PLASTIC OPTICAL FIBERS

Chairperson: Dieter S. Nordmann, Alcatel Cable, Hannover, Germany

Performance and Reliability of Graded-Index Polymer Optical Fibers—*L. L. Blyler, Jr., T. Salamon, W. R. White, M. Dueser, W. A. Reed, C. S. Koeppen, C. Ronaghan, P. Wiltzius, X. Quan,* Lucent Technologies, Murray Hill, NJ 241

Recent Advances of Plastic Optical Fiber—*M. Nishiguchi, M. Hattori, S. Takagi,* Furukawa Electric Co., Ltd., Chiba, Japan 248

Plastic Optical Fiber and Optical Link Module for Short Haul High-Speed Transmission—*M. Hattori, M. Nishiguchi, S. Takagi,* Furukawa Electric Co., Ltd., Chiba, Japan 257

How to Meet the Reach Specification of the ISO 11801 with POF—Comparison of the Attenuation Windows/Advantages of Green Light Sources—*O. Ziemann, T. Ritter, B. Gorzitza,* Deutsche Telekom AG, TZ Darmstadt, Berlin, Germany, and FHTW Berlin, Germany 264

New POF-Cable Generation with Corrugated Micro Tube (CMT) in Bus Systems for Automobiles—*W. Scheideler, H. Steinberg,* Alcatel, Floss, Germany; *P. E. Zamzow,* Alcatel Kabel, Hannover, Germany ... 271

WEDNESDAY MORNING—8:30 AM–11:30 AM

Salons A/B

TRACK 2—MATERIALS

SESSION 7: POLYMERIC MATERIALS FOR CABLE CONSTRUCTION II

Chairperson: Hans A. Mayer, Olex Cables (A Division of Pacific Dunlop Ltd.), Melbourne, Australia

Impact of Contaminants on Wire Coating Process—*M. A. Macip-Boulis,* Alcatel NA Cable System, Inc., New Holland, PA 281

Oscillatory Flow of Polypropylene and Its Effect on Conductor Eccentricity—*J. S. Borke,* Equistar Chemicals, LP, Cincinnati, OH 294

Thermal Aging Effects on Coaxial Cable's Transmission and Its Life Expectancy—*L. M. Hore, O. Chavez,* Bellcore, Morristown, NJ 299

Novel Material and Extrusion Technology for Highly Expanded Insulation of Coaxial Cables—*K. Ishihara, Y. Kawasaki, T. Sakamoto,* Nippon Unicar Co. Ltd., Kawasaki, Japan; *S. Maki,* Union Carbide Canada Inc., Quebec, Canada 307

Gas Injection Compound for High Frequency Insulation Applications—*H. Eklind, H.-B. Martinsson,* Borealis AB, Stenungsund, Sweden; *L. Westling, E. Brunner,* Nova-Borealis LLC Compounds, Port Murray, NJ 317

Analysis of the Processing of Foamed Polyethylene for High Performance Coaxial Cable Applications—*T. Chen, J. R. Leech,* Union Carbide Corp., Somerset, NJ; *R. E. Ginger, S. G. Maki,* Union Carbide Corp., Quebec, Canada 325

WEDNESDAY MORNING—8:30 AM–11:30 AM

Salons C/D

TRACK 3—COPPER

SESSION 8: SUPER CONDUCTIVITY—INVITED

Chairperson: John Sach, Pirelli Cables & Systems North America, Lexington, SC

A Decade of HTS Material Advances—*P. C. W. Chu,* University of Houston, Houston, TX 335

Status of Superconducting Electric Power Developments in the USA and Worldwide—*J. G. Daley, C. E. Platt,* U.S. Department of Energy, Washington, DC 337

HTS Wire Technology: Present and Future—*K. Sato,* Sumitomo Electric Industries, Ltd., Osaka, Japan 345

Role of HTS Cables in High Current Capacity Network—*M. Rahman, S. Norman, M. Nassi, P. Ladié,* Pirelli Cavi e Sistemi SpA, Milano, Italy 353

Vision for Applications of HTS Transformers—*V. R. Ramanan, S. J. Dale,* ABB Power T&D Company Inc., Raleigh, NC; *G. N. Riley, Jr., L. J. Masur,* American Superconductor Corp., Westborough, MA. 360

WEDNESDAY AFTERNOON—11:30 AM–2:00 PM

Grand Ballroom, Salons G/H, Fifth Floor

AWARDS LUNCHEON

Speaker: Dr. Lowell Catlett, Professor, New Mexico State University, New Mexico

Admission by badges issued to all registrants

WEDNESDAY AFTERNOON—2:00 PM–4:35 PM

Salon E

TRACK 1—FIBER

SESSION 9: SUBMARINE CABLES

Chairperson: Hirotoshi Hondo, The Furukawa Electric Co., Ltd., Kanagawa, Japan

High Fiber Counts in Aerial and Submarine Optical Cables with Metal Tube Design—*C. Unger,* NSW GmbH, Nordenham, Germany; *G. Zeidler,* Siemens AG, München, Germany 365

New 160 Gigabit WDM Challenge for Submarine Cable Systems—*JF. Libert, JL. Lang, J. Chesnoy,* Alcatel Submarine Networks, Calais, France 375

Study of Abrasion Resistance Behaviour for Different Submarine Cable Protection Methods—*Y. Charles, I. Houghton, J.-F. Libert, P. Worthington,* Alcatel Submarine Networks, Calais, France 385

Evaluation of Mechanical Properties of Various Fiberoptic Submarine Cables in Both Elastic and Plastic Regions—*T. C. Chu, R. J. Rue,* Tyco Submarine Systems Ltd., Holmdel, NJ 394

WEDNESDAY AFTERNOON—2:00 PM–4:35 PM

Salon F

TRACK 1—FIBER

SESSION 10: FIBER RIBBON

Chairperson: Nils Artlöve, Telia AB, Farsta, Sweden

Ribbon Concept from the Manufacturing Process to the Field—*B. Arvidsson,* Ericsson Cables, Hudiksvall, Sweden; *J. Björkman,* Telia Network, Farsta, Sweden; *J. Tanskanen,* Nextrom, Vantaa, Finland 404

Review on the Correlation of the Optical Loss with Ribbon Twist—*G. W. Seo, Y. H. Jeon, S. H. Kim, K. J. Lew, J. H. Oh, D. Y. Shin,* Daewoo Telecom Co. Ltd., Incheon, Korea, and Samsung Chemical Paint Co. Ltd., Kyonggi-do, Korea 411

Non-Destructive Measurement System of Fiber Alignment for the Optical Fiber Ribbon—*K. Hashimoto, Y. Tamura, M. Shigehara, T. Hattori, I. Tsuchiya,* Sumitomo Electric Industries, Ltd., Yokohama, Japan 420

New Microbending Test Methods for Fiber Optic Ribbons—*W. Rutzen,* Siemens AG, Nordenham, Germany 427

Analysis of a Modular 24-Fiber Ribbon for the Distribution Network—*S. A. McCreary, W. E. Beasley, S. R. Stokes, R. G. Lindsay, Jr.,* Sumitomo Electric Lightwave Corp., Research Triangle Park, NC 432

WEDNESDAY AFTERNOON—2:00 PM–4:35 PM

Salons A/B

TRACK 2—MATERIALS

SESSION 11: FIBER & SYSTEMS; TESTING & FIELD EVALUATION

Chairperson: Dr. Howard Wichansky, US Army Communications-Electronics Command (CECOM), Fort Monmouth, NJ

Attenuation, Chromatic Dispersion and Polarization Mode Dispersion Parameters of 40,000 KM of Standard Monomode Fibers in the Optical Network of "Deutsche Telekom AG"—*H. Gruhl, J. Vobian,* Deutsche Telekom AG,TZ, Darmstadt, Germany 440

Optical Cable Identification System Based on Optical Interference of Back-Scattered Lights—*K. Tsujikawa, K. Matsuno, K. Arakawa, K. Yoshida,* NTT Technical Assistance & Support Center, Tokyo, Japan 450

Approach of Low PMD Non-Zero Dispersion Shifted Single-Mode Fiber & Cabling to Achieve 40Gb/s Data Transmission—*K. Ohsono, S. Hinoshita, K. Tan, Y. Suzuki, Y. Nasuno,* Hitachi Cable, Ltd., Hitachi-shi, Japan 457

Effect of Transient Load on Optical Cable During Lifetime—*W. Griffioen,* KPN Research, Leidschendam, The Netherlands 462

Verification of Optical Fiber and Cable Reliability—*K. Houser,* Corning Inc.; *S. Chahanovich,* Pirelli Cables and Systems North America 468

WEDNESDAY AFTERNOON—2:00 PM–4:35 PM

Salons C/D

TRACK 3—COPPER

SESSION 12: BROADBAND SERVICES—PANEL DISCUSSION

Chairperson: Leo Chattler, DCM Industries, Inc., Union City, CA

Moderator: Dr. Jo Walling, NORDX/CDT, Quebec, Canada

Hybrid Fiber-Wireline Access Technologies—*T. Yeap,* University of Ottawa, Ontario, Canada 475

Loop Plant Environment Affecting XDSL Deployment and Performance—*C. F. Valenti,* Bellcore, Morristown, NJ 476

High Performance Twisted Pair PIC Distribution Cable (HPTP)—*J. I. Green,* Norcom/CDT, Ontario, Canada 477

FSAN Initiative: Accelerating the Introduction of Broadband Services to the Home—*C. Taylor,* Nortel Technology, Ottawa, Canada 480

ADSL Deployment for Broadband Services to the Home—*R. Stein,* Paradyne Corp., Largo, FL 481

WEDNESDAY AFTERNOON—4:00 PM–6:30 PM

EXHIBIT HALL, FOURTH FLOOR

SESSION 13: POSTER PAPERS

Chairpersons: Dr. Reiner J. Gerdes, TransTel Group Inc., Norcross, GA

Dieter S. Nordmann, Alcatel Cable, Hannover, Germany

Combination Furnace for Drawing Large Optical Fibre Preforms at High Speed—*M. Rajala, K. Asikkala,* ABR Innova Oy, Helsinki, Finland; *M. Mäkinen, T. Tuurnala, E. Peltoluhta,* Nextrom Oy, Vantaa, Finland 483

Design of Ribbon Aerial Cable Stranded by Copper-Cladded Steel Wire—*S. C. Park, J. C. Cho, Y. I. Lee, H. J. Kang,* Taihan Electric Wire Co., Ltd., Kyungki-do, Korea 489

UV Curable Materials with High Adhesion to Copper—*M. Mase, H. Abe, Z. Komiya, T. Ukachi,* JSR Corp., Tsukuba, Japan 495

Thermal Analysis of Buffer Tube Gels in Loose Tube Fiber Optic Cables—*M. T. Costello,* Witco Corp., Dublin, OH; *A. Eckard, W. J. Thalman,* Witco Corp., Oakland, NJ 501

Long Term Hydrolytic Aging Study of a Block Copoly-(Ether Ester) Undersea Cable Buffer—*D. A. Simoff, C. A. Pryde, C. Gieniewski,* Lucent Technologies, Murray Hill, NJ 507

Fiber Group Index Measurements Using Optical Low Coherence Reflectometry—*G. Marradi, P. G. Peretta, S. Cattelan,* SIRTI, Milano, Italy 513

Remote and Automatic 4,000-Fiber Optical Testing System—*H. Katayose, K. Sakuma, K. Yasuhara, Y. Numura,* Fujikura Ltd., Chiba, Japan 517

Minimize Network Installation Costs by Setting Appropriate Maximum Splice Loss Values—*P. Lindskog,* Ericsson Cables AB, Sundbyberg, Sweden; *B. Sundström,* Ericsson Components AB, Kista, Sweden; *J. Tyrcha, R. Sundberg,* Stockholm University, Stockholm, Sweden 522

Optical and Mechanical Characteristics of Optical Cable after Field Aging and Storage—*T.-C. Chang, W.-J. Chen, C.-M. Hsiao, H.-F. Lin, H.-P. Hsu, Y.-C. Lin, Y.-K. Tu,* Chunghwa Telecom Co., Ltd., Taiwan, R.O.C. 527

Fast Multi-Channel Optical Transmittance Testing for Optical Cable Qualification—*A. J. Barlow, D. Deogan, M. Rendle, T. G. Arnold,* EG&G Fiber Optics, Wokingham, UK 536

Study on Mid-Span Accessibility for Ultra High Count SZ-Type Optical Fiber Cable—*H. Ishikawa, Y. Suetsugu, G. Morikawa,* Sumitomo Electric Ind. Ltd., Yokohama, Japan 542

Reliability of Self-Supported Jelly-Filled Cables for Aerial Trial—*C.-H. Hsieh, H.-F. Lin, S.-H. Chou, R.-C. Wang, Y.-H. Hwang, C.-C. Pei, H.-P. Hsu, Y.-C. Lin, Y.-K. Tu,* Chunghwa Telecom, Taiwan, R.O.C. 548

Delivering Fiber-to-the-Desk: A New Low-Cost Solution—*D. J. Rutterman,* Siecor, Hickory, NC 554

Development of High-Count Intra-Office Optical Fiber Cable with 8-Fiber Ribbon Cords, Fan-Out Fibers and SC2-Connectors—*N. Tuchiya, K. Kouda, Y. Nagase, H. Tamura, M. Yoshida,* Toyokuni Electric Cable Co., Ltd., Saitama, Japan 558

Unique Sheathing Solution for Halogen Free, Low Smoke, Fire Retardant Fibre Optic Cables—*D. Sawyer, J. Preston, P. Holland,* Scapa Polymerics Ltd., Manchester, UK; *V. Watson, J. Rhodes,* Pinacl Communication Systems Ltd., Denbighshire, UK 563

Quickly Assembling Technique for MT Connector—*K. Takayama, M. Shiino,* Furukawa Electric Co., Ltd., Chiba, Japan 569

Development of Single-Mode 2-Fiber Mini-MPO Connector Using Injection-Molded Ferrule—*Y. Arai, N. Shimoji, K. Takayama, K. Maeno,* Furukawa Electric Co., Ltd., Chiba, Japan 574

Study on Jointing Work on the Ground for Aerial Optical Cable Installation—*K. Kohga, H. Oizumi, M. Ueda, T. Kaneko,* Mitsubishi Cable Industries Ltd., Hyogo, Japan 579

Novel Method for True Splice Loss Analysis by Using One-End Optical Time-Domain Reflectometer Incorporated with the Microbender—*C.-C. Lee, T.-J. Liaw, F.-Y. Tsai, C.-S. Wang, Y.-K. Tu,* Chunghaw Telecom Lab., Taiwan, R.O.C. 583

Effect of Preparation Conditions on the Strength of Fusion Splices I: Use of AFM Imaging—*J. D. Mann, O. S. Gebizlioglu, C. R. Kurkjian,* Bellcore, Morristown, NJ 589

Anti-Rodent Type Portable Fiber Optic Cable for Safety Operation—*H. Miyano, M. Katayama, H. Tanji,* Sumitomo Electric Industries, Ltd., Yokohama, Japan 597

THURSDAY MORNING—8:30 AM–12:00 NOON

Salon E

TRACK 1—FIBER

SESSION 14: AERIAL CABLES

Chairperson: Xavier Mann, Fitel Lucent Technologies, Carrollton, GA

Vibrational Properties of All-Dielectric, Self-Supporting (ADSS) Fiber Optic Cables—*C. Militaru,* Alcoa Fujikura Ltd., Spartanburg, SC 602

The Phenomenon of Aeolian Vibrations for ADSS Cables—*A. Ginocchio, E. Consonni,* Pirelli Cavi e Sistemi SpA, Milano, Italy; *R. Sutehall,* Pirelli Communication Cables, Newport, UK; *G. Diana, F. Resta,* Politecnico di Milano, Italy; *A. Manenti,* Universitá degli studi di Brescia, Italy 612

All Dielectric Self-Supporting Cables: Mechanical Features and Aeolian Vibration—*A. Cigada, M. Falco, M. Vanali,* Politecnico di Milano, Italy; *E. Consonni, P. Marelli,* Pirelli Cavi e Sistemi SpA, Milano, Italy; *R. Sutehall,* Pirelli Communication Cables Ltd., Newport, UK 621

New Generation of Optical Module: A Composite Loose Tube—*F. Legros, E. Kertscher, B. Buluschek,* SWISSCAB, Yvonand, Switzerland 631

Development of High Count Optical Wrap Cable Around Overhead Ground Wire—*N. Okada, Y. Higashide, Y. Rintsu, A. Ishikawa, S. Ibuki,* Furukawa Electric Co., Ltd., Chiba, Japan; *S. Tanaka,* Chubu Electric Power Co., Inc., Aichi, Japan 636

Fibre Optic Lashed Cables on High Voltage Lines—*R. Böhme, R. Girbig, G. Hög,* Alcatel Kabel AG & Co., Mönchengladbach, Germany 642

THURSDAY MORNING—8:30 AM–12:00 NOON

Salon F

TRACK 1—FIBER

SESSION 15: OPTICAL CONNECTORS

Chairperson: Dr. Peter R. Bark, Siecor, Hickory, NC

SC-DC/SC-QC Connector—*K. M. Wagner, J. P. Luther, D. L. Dean,* Siecor, Hickory, NC 650

Development of MT Type Connector Using an Injection Molded Ferrule and a Quick Assembly Technique—*M. Takaya, T. Katagiri, S. Nagasawa, Y. Murakami,* NTT Access Network Systems Labs., Ibaraki, Japan 658

Field-Installable Connector for Optical Fiber—*K. Takizawa, T. Arikawa, Y. Tamaki, H. Yokosuka,* Fujikura Ltd., Chiba, Japan 666

Optical Connectors Reliability at Four Different Climatic Conditions: Relevant Measurements and Most Common Failure Modes—*S. Bianco, D. Suino, M. Ughetti,* CSELT, Torino, Italy; *F. Montalti,* Telecom Italia, Roma, Italy 672

Optical Fiber Cord with SC-type Optical Connector Integrated with Fiber Bragg Grating—*K. Morita, S. Suzuki, Y. Morishita, K. Kiyotake, K. Sugi, K. Muta,* Showa Electric Wire & Cable Co., Ltd., Kanagawa, Japan 682

THURSDAY MORNING—8:30 AM–12:00 NOON

Salons A/B

TRACK 2—MATERIALS

SESSION 16: POLYMERIC MATERIALS FOR CABLE CONSTRUCTION III

Chairperson: James R. Leech, Union Carbide Corp., Somerset, NJ

Moderator: Kenneth E. Bow, Dow Chemical Co., Midland, MI

Development of Functionality of Aramid Yarns as Optical Fiber Cable Reinforcement—*H. A. M. Stuut, O. Grabandt, J. H. van Leeuwen,* Aramid Products VoF, Arnhem, The Netherlands 688

Advanced Impact Polypropylene Buffering Material for Superior Long Term Hydrolytic and Thermo-Oxidative Stability—*B. G. Risch, J. Auton, O. Tatat,* Alcatel, Claremont, NC 698

Controlled Jacket Bond Coated Steel Armoring for Fiber Optical Cables—*F. Achille, K. E. Bow, W. F. Busch,* Dow Chemical Co., Midland, MI 705

A New Approach to Fiber Strength Reliability Mechanism Against Heat-Damp Aging—*H. Suzuki, I. Seki, S. Hinoshita, H. Shimane, K. Yamada, T. Yamazaki,* Hitachi Cable, Ltd., Hitachi-shi, Japan 714

Mechanics of Delamination Resistance Testing—*P. L. Tabaddor, C. J. Aloisio, C. H. Plagianis, C. R. Taylor,* Lucent Technologies Inc., Norcross, GA; *V. Kuck, P. G. Simpkins,* Lucent Technologies Inc., Murray Hill, NJ 725

Moisture Penetration Through Optical Fiber Coatings—*J. L. Armstrong, M. J. Matthewson,* Rutgers University, Piscataway, NJ; *C. R. Kurkjian,* Bell Communications Research, Morristown, NJ 732

Optical Cable Recycling—*T. Konaka, M. Shima, T. Hara, S. Nishi, I. Imoto,* Nippon Telegraph and Telephone Corp., Ibaraki, Japan 740

THURSDAY MORNING—8:30 AM–12:00 NOON

Salons C/D

TRACK 3—COPPER

SESSION 17: LAN DESIGNS

Chairperson: Jean Baer, Essex Group, Inc., Fort Wayne, IN

Modeling UTP Cabling: Return Loss, CAT 5 and Beyond—*J. W. Kincaid, P. Z. Vanderlaan,* Belden Wire and Cable Co., Richmond, IN 748

Development of Equal Level Far-End Crosstalk (ELFEXT) and Return Loss Specifications for Gigabit Ethernet Operation on Category 5 Copper Cabling—*C. T. Di Minico,* Cable Design Technologies Corp., MA; *P. Kish,* NORDX/CDT, Montreal, Canada 758

Power Sum, Integral Power Sum and Vector Sum-Crosstalk—*M. Belanger, J.-F. Richard, J.-H. Walling,* NORDX/CDT, Montreal, Canada 768

High Grade Copper Data Cables and Connecting Hardware for Generic Cabling—*H. G. Haag, P. E. Gregor, M. Voigt, D. Seidel,* Alcatel Kabel AG & Co., Berlin, Germany 776

Effects of Production-Specific Interference Signals on Transmission Characteristics of 600 MHZ Data Cables—*A. Obst, J. Bör,* GHMT mbH, Bexbach, Germany and Kerpenwerk GmbH & Co., Stolberg, Germany 785

THURSDAY AFTERNOON—1:00 P.M.–4:50 PM

Salon E

TRACK 1—FIBER

SESSION 18: FIBER OPTIC CABLE INSTALLATION

Chairperson: James A. Caballero, Synergistics Industries (NJ) Inc., Farmingdale, NJ

Technology and Evolution of Optical Cables in Brazil—*P. J. P. Curado, R. Arruda,* CPqD, Campinas, SP, Brazil 793

Veni, Vidi, Probáví (I Came, I Saw, I Qualified): Air Blown Fiber is Tested Against the Standards—*T. L. Dixon, K. Quistorff,* Sumitomo Electric Lightwave Corp., Research Triangle Park, NC 801

Optical Fiber Distribution in Central Offices and Testing Methods for Commercial FTTH System—*K. Tomita, K. Yoshioka, N. Nakao, N. Tomita,* Nippon Telegraph and Telephone Corp., Chiba, Japan..... 808

A Very Innovative Technology for Right of Way Application—*J. P. Bonicel,* Alcatel, TPLE, France; *H. Costa-Elias,* SANEF, France; *P. Vertuaux,* ADPS, France; *P. Gaillard,* Alcatel, USA; *R. Newman,* MKI, France; *M. Rivard,* Marais, France..... 815

Optical Fibre Cable Links Within Drink Water Pipes as an Alternative Telecommunications Route Technology—*P. E. Gregor, H. G. Haag,* Alcatel Kabel AG & Co., Mönchengladbach, Germany; *W. Braun,* Kellner Telecom, Korntal-Münchingen, Germany..... 825

Retention of Strength in Optical Fibres Under Strain in a Warm, Moist Field-Installed Environment—*P. Ostojic, D. Coulson, K. Clarke, A. W. Kruijshoop,* Telstra Corp., Victoria, Australia 832

High Dense Optical Fiber Unit for Extending Flexibility of Air Blown Fiber System—*Y. Taira, N. Suzuki, J. Hanai, S. Takaoka, M. Saeki, H. Kato,* Sumitomo Electric Industries, Ltd., Yokohama, Japan 837

Modular Design and Evaluation of Blowable Acrylate Multi-Fibre Units—*D. Pendleton, S. R. Dodd, A. P. J. Cadden,* Optical Fibres, Flintshire, UK..... 845

THURSDAY AFTERNOON—1:00 PM–4:50 PM

Salon F

TRACK 1—FIBER

SESSION 19: FIBER OPTIC COMPONENTS & SPLICING

Chairperson: Dieter S. Nordmann, Alcatel Cable, Hannover, Germany

Lifetime of High-Strength Spliced Fibers—*M. Zimnol,* Ericsson Cables AB, Sundbyberg, Sweden; *B. Sundström,* Ericsson Components AB, Kista, Sweden; *T. Svensson,* Telia Research AB, Farsta, Sweden 850

High Quality Fiber Optic Splices and Significantly Improved Splice Loss Measurement Accuracy—*B. Zamzow, G. Ruegenberg,* Siemens AG, Munich, Germany; *M. Anderson,* Siecor Corp., Hickory, NC; *H. Krupp,* RXS Kabelgarnituren GmbH, Hagen, Germany 854

New Chemical Stripping Method for Obtaining High Strength Splices of UV Colored Optical Fibers—*S. Siddiqui, L. R. Pritchett, J. R. Szwec, C. R. Taylor, R. J. Brown, Jr., H. C. Chandan,* Lucent Technologies, Inc., Norcross, GA..... 864

Effect of pH on the Strength and Fatigue of Fused Silica Optical Fiber—*A. T. Taylor, M. J. Matthewson,* Rutgers University, Piscataway, NJ..... 874

Mechanical Behavior and B-Value of an Abraded Optical Fiber—*T. Volotinen,* OFCON Optical Fiber Consultants AB, Hudiksvall, Sweden; *A. Breuls,* Plasma Optical Fibre, Eindhoven, The Netherlands; *N. Evanno,* France Telecom CNET, Lannion, France; *K. Kemeter,* Siecor GmbH, Neustadt, Germany; *C. Kurkjian,* Bellcore, Morristown, NJ; *P. Regio,* CSELT, Torino, Italy; *S. Semjonov,* FORC, Moscow, Russia and Bellcore, Morristown, NJ; *T. Svensson,* Telia Research, Farsta, Sweden; *S. Glaesemann,* Corning Inc., Corning, NY 881

Splice Loss in Non-Zero Dispersion-Shifted Fibers—*M. E. White, S. A. Cooper,* Corning Inc., Corning, NY..... 891

Analysis of Multimode Fiber Behavior with Laser Sources in the Development of the Gigabit Ethernet Fiber Optic Specifications—*J. S. Abbott, M. J. Hackert, D. E. Harshbarger,* Corning Inc., NY; *D. G. Cunningham,* Hewlett-Packard, UK; *C. T. Di Minico,* Cable Design Technologies Corp., MA; *I. H. White,* University of Bristol, UK..... 897

Optimizing the Embedded Fiber Plant Using Dense Wavelength Division Multiplexing—*P. L. Scrivener,* Pirelli Telecom Systems Division, Lexington, SC 908

THURSDAY AFTERNOON—1:00 PM–4:50 PM

Salons A/B

TRACK 2—MATERIALS

SESSION 20: CABLE DESIGN, FIBER RELIABILITY & FIBER OPTIC COMPONENTS

Chairperson: Dr. Peter R. Bark, Siecor, Hickory, NC

Optimization of Loose Tube Cable Designs: The Next Step—*P. Gaillard, O. Tatat,* Alcatel OFCCC, Claremont, NC; *K. Nothofer, Dr. A. Weiss,* Alcatel TPLE, Germany; *D. Benzel,* Alcatel TPLE, France ... 913

Development of Optical Fiber Ribbon Units for Fiber Blowing—*M. Kosaka, I. Kobayashi, F. Hosoi, H. Kanzaki, H. Hiramatsu, Y. Kamikura,* Furukawa Electric Co., Ltd., Chiba, Japan 921

Modeling of Proof Test Level Flaws Using Cube Corner Indents—*S. L. Semjonov, M. M. Bubnov,* Russian Academy of Sciences, Moscow, Russia; *G. S. Glaesemann,* Corning, Inc., Corning, NY; *C. R. Kurkjian,* Bellcore, Morristown, NJ..... 928

Break Source Analysis: Alternative Mirror Measurement Method—*L. K. Baker, G. S. Glaesemann,* Corning Inc., Corning, NY..... 933

Characteristics of Tin-Codoped Germanosilicate Fiber Bragg Gratings Written Through an UV-Transparent Coating—*T. Nakai, K. Imamura, Y. Sudo, Y. Imada,* Mitsubishi Cable Industries, Ltd., Hyougo, Japan..... 938

Analysis and Research of Chirped Bragg Fiber Grating Theory on Dispersion Compensation—*Z. Liu-Juan, Z. Zhi-Min, X. Long-Pan,* Huazhong University of Science and Technology, Wuhan, R.O.C.; *Z. Dao-Wen,* Jiang Xi Normal University, Jiangxi, R.O.C.; *L. Shuihuo, L. Bing, Z. Zisen,* Wuhan Research Institute of Posts and Telecommunication, Wuhan, R.O.C. 944

Packaging Solutions for a Multiwavelength in Fiber Bragg Grating Based Chromatic Dispersion Compensator—*F. Pozzi, R. Vinzio, A. Marcone,* Sirti S.p.A., Cassina dé Pecchi, Italy..... 950

Development of Flat Flexible Erbium-Doped Fiber-Coil Sheets (EDF-Sheets)—*K. Kondo, M. Yoshida, K. Imamura, T. Kawamura, Y. Sudo, Y. Imada,* Mitsubishi Cable Industries, Ltd., Hyougo, Japan; *A. Toyohara,* NEC Corp., Kanagawa, Japan 959

THURSDAY AFTERNOON—1:00 PM–4:50 PM

Salons C/D

TRACK 3—COPPER

SESSION 21: COPPER LANS: INSTALLATION & TESTING

Chairperson: Dr. Marek Kapuscinski, NORDX/CDT, Quebec, Canada

A New Technique for Measuring the Parameters of Channels, Cables, and Connecting Hardware—*C. R. Curry,* Leviton Telcom, Bothell, WA 965

How EFT Disturbances Affect Fast Ethernet Performance in Multichannel Plastic and Metal Racways—*M. Michalak,* Wiremold Co., West Hartford, CT..... 973

EMC Within Systems and Installations—*D. Wilhelm, Dr. P. Schulz,* GHMT mbH, Bexbach/Saar, Germany 980

Balance Measurements on UTP and STP Cables—*J.-H. Walling, O. Saad,* NORDX/CDT, Montreal, Canada 988

Implementation of IEC 61196-1 Shielded Screening Attenuation Test Method—*J. W. Kincaid, C. W. Dole,* Belden Wire and Cable, Richmond, IN..... 999

OPENING SPEAKERS

JOHN R. SICOTTE
Chairman, IWCS
Corning Incorporated
Corning, New York

John R. Sicotte is the director for Corning's International Operations group. His responsibilities include export sales and commercial support of optical fiber customers and joint ventures outside of North America.

Sicotte joined Corning in 1978 as an engineer in the Manufacturing and Engineering Division. He joined the Telecommunications Products Division in 1982. Subsequently he has held positions in sales, marketing and engineering management.

Sicotte holds a bachelor's degree in civil and environmental engineering from the University of Rhode Island, Kingston and a master's degree in business administration from Syracuse University.

He is a member of the Society of Photo-Optical Instrumentation Engineers and is Chairman of the Board of Trustees of the International Wire and Cable Symposium.

DR. MAREK KAPUSCINSKI
Chairman, Plenary Session
NORDX/CDT
Quebec, Canada

Marek Kapuscinski graduated from Leeds University in England in 1974 with a Ph.D. in Polymer Physics. In 1976, he joined Nortel's Communications Cable Division, which was acquired by Cable Design Technologies in 1996, being renamed NORDX/CDT. After several years in Technology and Product Management, his current position is Quality Manager for Copper LAN products. He is a member of ASTM, SPE and ICEA.

PLENARY SESSION

"THE FUTURE OF TELECOMMUNICATIONS"

DR. ARNO PENZIAS

Recently Retired Vice President and Chief Scientist
Lucent Technologies (Formerly Bell Labs)

Nobel Prize winner Dr. Arno A. Penzias is involved in a broad range of research on productivity enhancements, information management and increased synergy between people and computers.

He says the convergence of computers and people is the key to how we work, what we do for a living, where the economy is going and what your company must do to stay alive. Calling this merger the start of the Harmony Era, he brings you brilliant insight on:

- Giving the customer greater value through personalization
- Vertical integration
- Integrating work throughout your organization ... and throughout your partners' organizations to their customers

His research is detailed in his book *Harmony: Business, Technology and Life After Paperwork.* In it, he charts the course of the information revolution and its likely impact on us all. The book follows his highly acclaimed book, *Ideas and Information: Managing in a High-Tech World,* which addresses the application of information technology to create positive change for the future. He has also written more than 100 scientific articles and numerous patents.

While tailoring his program to your needs, he addresses:

- An inside look at cyberspace technology that helps solve problems the way people do
- The impact of information technology on your organization
- Opportunities for increased productivity and improved competitiveness through networking
- The coming "Harmony Era" in which business and technology will provide new sources of economic value
- A look at life on the Internet and what it means to you

Formerly vice president and chief scientist at AT&T Bell Laboratories, before it was spun off into Lucent Technologies, Penzias was instrumental in building the firm's reputation for scientific excellence. His scientific career began in 1961 when he joined Bell Laboratories. He conducted research in radio communication and related areas and took part in pioneering communications satellite experiments. He is known for his work in radio astronomy, especially his part in the discovery of evidence supporting the Big Bang theory of the origin of the universe, work for which he shared the 1978 Nobel Prize for Physics.

Penzias earned a Bachelor of Science degree from City College of New York in 1954. After serving two years as an officer in the U.S. Army Signal Corps, he earned his master's and doctorate degrees at Columbia University. He has earned many honors and lectureships, among them some twenty honorary degrees. He is a member of the National Academy of Sciences and the National Academy of Engineering, as well as the corporate boards of Arthur D. Little and Duracell, Inc.

LUNCHEON SPEAKER

DR. LOWELL CATLETT
Professor, New Mexico State University
New Mexico

Dr. Lowell Catlett, a full-time professor at New Mexico State University is an exciting futurist whose knowledge of technologies and their implications on the way we will live and work is addressed in his varied and upbeat presentations. His vast knowledge astounds corporate and association audiences both nationally and internationally. His presentations are thought-provoking and highly-entertaining.

Dr. Catlett received his doctorate in Economics from Iowa State University, and has twice received the Don C. Roush Award for Excellence in Teaching. He is also a recipient of the prestigious Burlington Foundation Faculty Achievement Award for Outstanding University Teaching. In 1994 he was one of two Western Regional recipients of the NASULGD's Excellence in College and University Teaching in the Food and Agricultural Sciences Award.

Lowell recently received the College of Agriculture and Home Economics Advisor of the Year as well as Teacher of the Year at New Mexico State University.

He is a consultant to the U.S. Departments of Agriculture, the Interior, Defense and Labor. He has also been a consultant to many Fortune 500 companies.

Development of Miniature Optical Fiber Cords

Fuminori Nakajima, Nobuhisa Ishii, Yasuhiro Watanabe, Seiji Takagi

The Furukawa Electric Co.,Ltd. Opto-Technology Laboratories
Ichihara, Chiba-ken, Japan

ABSTRACT

The number of the intra-office optical wiring counts is expected to increase by several times than that of present system in correspondence to the rapid spread of the services which call for high speed transmission by fibers. But as the room for accommodation in the termination modules (FTM) is restricted, reduction of the cord diameter comes to be more important. This paper describes two types of novel miniature optical fiber cords. Cord of the 1mm diameter with the loose type structure was designed for the effective wiring instead of a conventional cord of 1.7mm diameter. The prototype 1mm diameter cord proved to have good mechanical and optical characteristics.

Moreover, ultra thin (0.25mm$^{\phi}$ in diameter) tight type cord was developed for the accommodation of larger counts up to several ten thousands. The optical performance of the tight type cord proved to have satisfactory characteristics for wiring.

1. INTRODUCTION

As subscriber networks evolve into the optical fiber networks rapidly, intra-office wiring systems are expected to become higher in density by several times in FTTH (fiber to the home). At present, 2,000 or less fiber terminations of the 1.7mm diameter loose type cords are accommodated in the FTM. In order to accomplish terminations of 4,000 optical fiber cords, diameter of each cord should be reduced to as thin as 1mm. [1][2][3]

A 1.7mm cord consists of a polyamide buffered fiber of 0.9mm in diameter, the aramid yarns and a PVC (polyvinyl chloride) jacket. To reduce the cord diameter, the thinner buffered fiber, the less yarns and the thinner sheath are required, but the thinner buffered fiber tends to make anti crush performance lowered, while the less yarn cause tensile strength deteriorate and the thinner sheath leads to poor flexural rigidity. The cord of poor flexural rigidity would bring about the increase transmission loss when the cord was pulled at right angle against the connector rubber boots because the cord of poor flexural rigidity is easily broken during handling.

At the first section, the development of 1mm diameter loose type cord, which includes investigation on the above effects of three factors, is presented. In the next section, the higher density wiring 0.25mm diameter cord designed and produced to accommodate the fibers for the future service and the efficient connection is presented. The 0.25mm diameter cord has such advantage as that it facilitates making a ribbon fiber for the high-density wiring, but has such disadvantages as that it is difficult to make it to a loose type cord. Ultra thin cord was designed as tight type by putting tensile strength member yarn into the buffered fiber outer coating layer.

2. DESIGN OF 1mm$^{\phi}$ LOOSE TYPE CORD

During the process to reduce diameter of the cord , we made examination on some factors, which influence effects on making buffered fiber, a flexural rigidity and a strength member.

Buffered fiber diameter

An available buffered fiber diameter was investigated for a 1mm cord because a 0.9mm polyamide buffered fiber was found to be not suitable and the using of a thinner buffered fiber

lowers the anti crush performance. The investigated buffered type fiber is what consists of an over-coating layer of UV resin on the 0.25mm UV buffered fiber due to advantageous manufacturing. Results of the anti crush test on over-coated fibers were shown in Table.1. The observed excess loss for the 1mm cord was at a level of 0.1dB/km or less at the wavelength of 1.55μm. By the results obtained, the effective diameter of the buffered fiber proved to be 0.4mm or more.

Table.1 Relationship between over-coated buffered fiber diameter and the excess loss caused by crush test at 4.9N/mm

Buffered fiber diameter	Result at 1.31μm	Result at 1.55μm
0.25mm$^{\phi}$	Break	Break
0.40mm$^{\phi}$	0.03 dB	0.05 dB
0.50mm$^{\phi}$	0.01 dB	0.02 dB
0.60mm$^{\phi}$	0.00 dB	0.01 dB
0.70mm$^{\phi}$	0.00 dB	0.00 dB

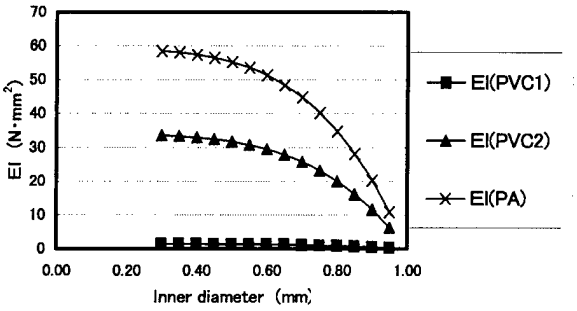

Fig-1. Relationship between 1mm cord sheath inner diameter and flexural rigidity

Flexural rigidity

Conventional PVC was applied to 1mm cord sheath at the beginning but it could not accomplish the requirement on flexural rigidity. A factor that effects mainly to the flexural rigidity of 1mm cord was material and thickness of the cord sheath. Each flexural rigidity of some thermoplastic resin was calculated for the diameter of 1mm cord. These results are shown in Fig.1, where the EI (PVC1) is a flexural rigidity of the conventional PVC which has 29MPa of Young's modulus, the EI (PVC2) is a high modulus type which has 690MPa and EI(PA) is polyamide which has 1200MPa. As inner diameter of the sheath is required to be 0.8mm or less in order to avoid deformation to flatten and for the efficient manufacturing, polyamide sheath is used for the sheath for 1mm cord because flexural rigidity of the 1mm cord is higher than that of a conventional 1.7mm cord, whose flexural rigidity was about 30N·mm^2.

Strength member yarn

An aramid yarn was applied for the strength member of the cord. The amount of the yarn and the packing ratio of the yarn, which determines the cross sectional area of the yarn in that layer, were studied. The result on the relationship between the relaxation and the packing ratio or the amount is shown in Fig-2, where relaxation of aramid yarn relaxation is indicated as a cross point on the vertical axis. If the packing ratio of yarn was the same, smaller amount of yarn leads to less relaxation than that of the larger one. While the amount of yarn were the same, the high packing ratio makes a brief relaxation. Although reducing the amount of yarn caused to lower tensile strength, it was known that a small amount and a high packing ratio could improve the tensile strength to a degree.

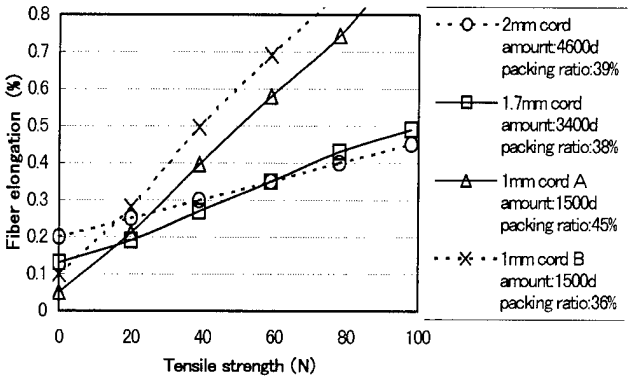

Fig-2. Relationship between the tension and the fiber elongation

Performance on the Loose type 1.0mm$^{\phi}$ cord

Based on the above preliminary study, a performance of the 1mm diameter cord was evaluated. The cross sectional view of the cord is shown in Fig-4, which consists of a 0.5mm UV coated buffered fiber, aramid yarn of 1500 denier and polyamide sheath whose Young's modulus is 1200MPa. The properties of the developed loose type 1mm cord are shown in Table.2. Also, evaluation data on 1mm cord was investigated for long term reliability including the heat aging test (85℃) (Fig-5) and the humidity and heat aging test (85℃, 85%) (Fig-6). As a result, the developed 1mm cord proved to have sufficient performance for the installation in intra-office wiring of higher density.

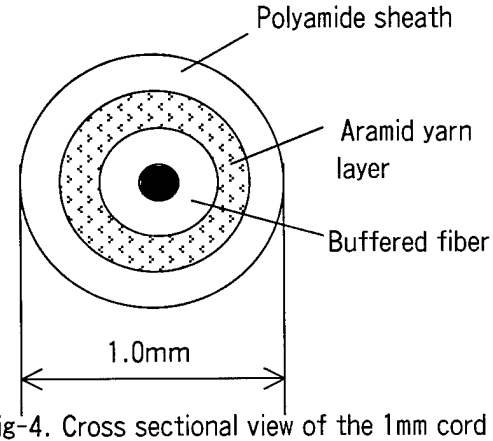

Fig-4. Cross sectional view of the 1mm cord

Table. 2 Properties of a 1mm cord

Items	Description
Diameter of buffered fiber	0.5mm$^{\phi}$
Amount of aramid yarn	1500denier
Packing ratio	45%
Transmission loss 1.31 μm	0.34 dB/km
Transmission loss 1.55 μm	0.20 dB/km
Crush test (4.9N/mm)	0.01dB*
Excess bending loss (ϕ30mm,10turn)	0.02dB/turn*
Thermal cycling test (-10~40℃,5cycles)	0.1dB/km>*
Flexural rigidity (30mm$^{\phi}$) [4]	40 N·mm^2
Fiber elongation (69N)	0.65 %

*: measured at 1.55 μm

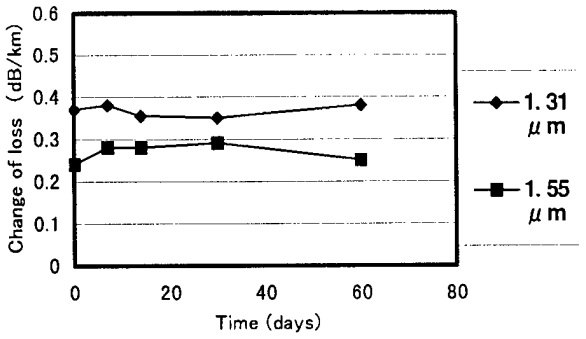

Fig-5. Heat aging properties of the 1mm cord at 85℃

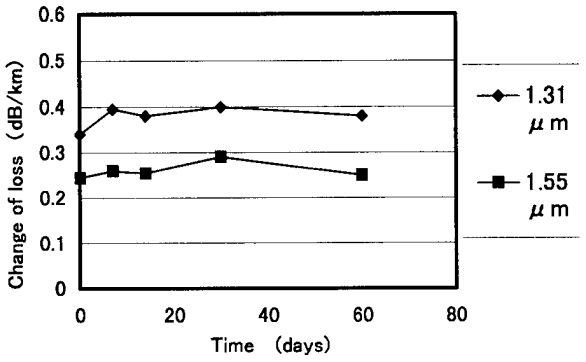

Fig-6. Humidity and heat aging properties of the 1mm cord at 85℃, 85%

3. 0.25mm$^{\phi}$ TIGHT TYPE CORD

In order to know the most suitable structure of the thinner diameter buffered fiber, loss and mechanical characteristics of the ultra thin tight cord of the 0.25mm diameter were studied on buffered fibers of different diameter, yarns of different tensile strength and the coated resins. From the results listed in table 3, the most appropriate construction of the proved to be 0.25mm in diameter and that with strength yarn. But as there remains an anxiety of the transmission loss increase when thinner buffered fiber is applied, we carried out a variety of evaluations. From the number of evaluations, diameter of 160 μm and 180 μm are seen to be most suitable for the buffered fibers.

Table.3. Tight type cord structure and performance

	1	2	3	4	5	6
Diameter of buffered fiber	160 μ m	180 μ m	160 μ m	180 μ m	160 μ m	180 μ m
Strength member yarn	E Glass 302denier	E Glass 252denier	Aramid 211denier	Aramid 140denier	Polyalyrate 219denier	Polyalyrate 194denier
Prepreged volum ratio	46%	47%	55%	45%	59%	64%
Transmission loss 1.31 μ m 1.55 μ m	4.41dB/km 1.55dB/km	1.89dB/km 3.11dB/km	1.28dB/km 3.58dB/km	2.04dB/km 2.56dB/km	1.56dB/km 4.61dB/km	0.36dB/km 0.57dB/km
Strength of 2% fiber elongation	46 N	41 N	59 N	45 N	49 N	45 N

The applied strength member yarns were commercial fiber glass, aramid yarn and polyalyrate yarn.

The coated resins we studied were thermosetting polyester at the beginning because of that it allows easy pregnation into the yarns. But as the polyester resin suffers from the high speed manufacturing, UV cure urethane system was chosen finally. The structure of designed 0.25mm tight cord is schematically shown in Fig-7, while the cords performance of several tight type are shown in Table 3. As a result, the tight cord of 180 μm buffered fiber was found to be remarkably superior in a transmission loss than that of 160 μm in diameter. The applied polyalyrate yarn proved to show a satisfactory transmission loss.

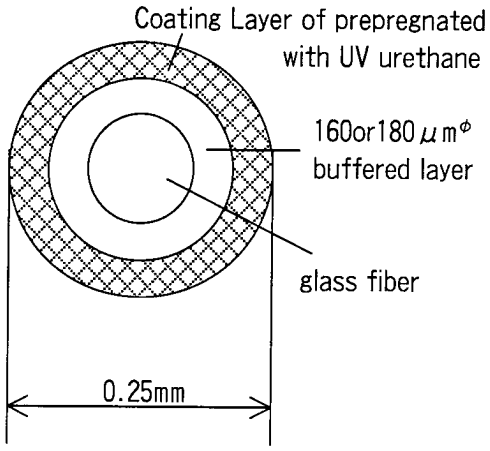

Fig-7. Cross sectional view of tight type cord

0.25mm$^{\phi}$ UV immersed tight cord

The 0.25mm $^{\phi}$ UV immersed tight cord was designed on above results including that of the 180 μm buffered fiber and polyalyrate yarn with UV cured resin suitable for high speed manufacturing.

That evaluated data on the cord is shown in Table.4 while the cross sectional view is shown in Fig-8.

The 0.25mm tight type cord proved to have satisfactory transmission characteristics.

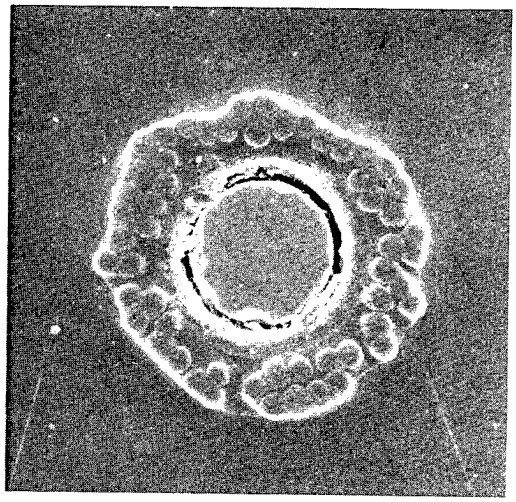

Fig-8. Cross sectional photo. of 0.25mm$^{\phi}$ tight cord

Table.4. Structure and performance of 0.25mm$^{\phi}$ tight type cord

Diam. of buffered fiber	180 μm
Strength member	Polyalyrate yarn
Amount of yarns	180denier
Pregnated resin	UV resin
Transmission loss	
1.31 μm	0.35 dB/km
1.55 μm	0.25 dB/km
Tension (2% fiber elongation)	38 N
Flexural rigidity (30mm$^{\phi}$)	4.9N·mm^2
Excess bend loss (30mm$^{\phi}$,10turns)	0.03dB/turn*
Thermal cycle test (-10~40℃,5cycles)	0.07dB>*
Crush test (Increasing 1dB)	2.9 N/mm*

*: measured at 1.55 μm

4. CONCLUSIONS

The miniature optical fiber cords were developed after the increase of needs caused by the increase of intra-office network wiring. We investigated on the performance of thinned cord of 0.25mm OD in detail. We developed loose type 1mm diameter cord which has satisfactory performance also. A 0.25mm$^{\phi}$ tight type cord which had strength yarns for realizing the same diameter as the conventional buffered fiber was developed for the higher density terminations.

REFERENCES

[1]M.Tachikura,Y.Enomoto,S.Uruno, H.Takemoto,N.Tomita and H.Takasugi,; "OPTICAL FIBER DISTRIBUTON SYSTEM IN CENTRAL OFFICES FOR THE FTTH ERA" Proc.of 46th IWCS pp.859-866,1997.

[2]M.Sato,M.Tachikura,N.Tomita and S.Iwano; "A 1-mmϕ miniature optical fiber cord adaptable for MU-type connectors" ,Proc.of 45th IWCS, pp.374- 380, 1996.

[3]M.Sato,M.Tachikura and N.tomita; "Design of Miniature Optical Fiber Cord" ;Technical Digest of first Optoelectronics and Communications Conf.(OECC), pp.278-279,1996.

[4]M.Tachikura, H.Takemoto and N.Tomita,; "Miniature optical fiber cords with high flexural rigidity" , Technical Digest of 2nd Optoelectronics 8 Communications Conf. (OECC), pp.526- 527, 1997.

Fuminori Nakajima

The Furukawa Electric Co.,Lit.
6,Yawata Kaigandori Ichihara, Chiba,
290-8555,Japan

He received his M.E. degree in Material Engineering from Nagaoka University of Technology in 1992. He joined The Furukawa Electric Co.,lit. in 1992 and has been engaged in research and development of materials for optical fiber cables. He is now a research engineer of Opto-technology laboratory.

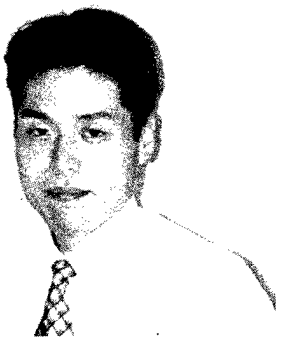

Yasuhiro Watanabe

The Furukawa Electric Co.,Lit.
6,Yawata Kaigandori Ichihara, Chiba,
290-8555,Japan

He received his M.E. degree in Mechanical Engineering from Kanazawa institute of technology in 1993. He joined The Furukawa Electric Co.,ltd. in 1993 and has been engaged in design of equipment. He is now a research engineer of Opto-technology laboratory.

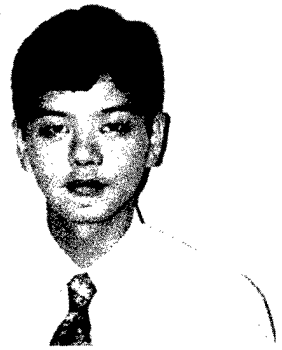

Nobuhisa Ishii

The Furukawa Electric Co.,Lit.
6,Yawata-Kaigandori Ichihara, Chiba,
290-8555,JAPAN

He received his M.E. degree in Applied Chemistry from Waseda University in 1987, then joined The Furukawa Electric Co., Ltd. and has been engaged in the development of the materials for optical fiber cable. He is now a senior research engineer of Opto-Technology Laboratory.

Seiji Takagi

The Furukawa Electric Co., Ltd.
6,Yawata-kaigandori Ichihara, Chiba,
290-8555 JAPAN

He was born in Osaka, Japan in 1951. He received his M.E. degree in Industrial Chemistry from Kyoto University in 1976. He joined The Furukawa Electric Co., Ltd. in 1976. He is now a general manager of research department of Opto-Technology Laboratory.

NEW INDOOR/OUTDOOR TIGHT BUFFERED FIBER LSZH DISTRIBUTION CABLE

Bernard M. Blell

CommScope, Inc
Claremont, North Carolina

ABSTRACT

This paper describes a line of Low Smoke Zero-Halogen (LSZH), Indoor/Outdoor, UL Riser Rated (Type OFNR), distribution style cables which can accommodate up to twenty-four 900 micron Tight Buffer Fibers. The buffer and jacket material is UV Stable, flame retardant, resistant to moisture absorption, and allows the optical fiber to perform well in temperatures down to -40°C. These attributes make the cable suitable for use in an indoor and outdoor environment.

This unique cable design maintains the flexibility, small size and weight of an indoor distribution cable while providing the operating temperature range, water blocking, and UV resistance of an outdoor cable construction.

The cable performance characteristics and design features are discussed, as are the results from the qualification testing performed at CommScope and Underwriters Laboratory (UL). Installation, applications, and results from a field trial performed in conjunction with Indianapolis Power and Light Company will also be presented.

INTRODUCTION

Traditionally, there have been two categories of fiber optic cable designs common to the industry: the Outside Plant (OSP) Gel-Filled Loose Tube design (which includes both Stranded Loose Tube and Central Tube), and the premises Tight Buffer Fiber cable designs popular in the indoor cabling arena. The gel-filled cables maintain the loose or "ribbonized" fibers in a relatively strain free environment which is absolutely necessary for long-haul applications where the cable is permanently exposed to the extremes of the outside plant environment. The industry accepted standard for the performance of such cables is Bellcore GR-20-CORE which clearly specifies the Mechanical, Environmental, and Physical requirements for cables which are to be placed in the Outside Plant environment. The allowable attenuation change per fiber throughout the barrage of testing is minimal: 0.05 to 0.10 dB for Singlemode fiber (SMF) @ 1550 nm. These tight attenuation specifications reflect the true needs of a long haul (>> 2 km) OSP fiber optic cable.

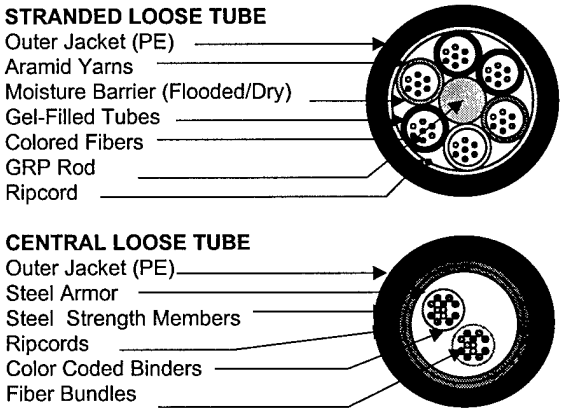

Figure 1. Stranded Loose Tube and Central Loose Tube Outside Plant (OSP) Cables

On the other hand, premises fiber cable installations consist of relatively short cable runs (generally << 2km). The majority of installations are high-fiber count Riser backbone or low-fiber count fiber to the desk (FTTD) applications. Typical installations are not longer than 300 meters. Many other cable designs exist in the indoor cable category with most manufacturers offering both the tight buffer as well as the gel-filled Riser cable designs. The performance requirements for the tight buffer cable designs are listed in Bellcore GR-409-CORE, which describes

the generic requirements for the performance of Premises fiber optic cables. Since these cables are meant for indoor applications, the National Electric Code (NEC Article 770) specifies that they must meet the appropriate flammability listing. These cables can be Riser or Plenum rated as dictated by the location in the building where they are to be installed. If not rated, the cable must be terminated within 50ft. (15.2m) of entrance into the building. The mechanical and environmental requirements are for the most part less stringent for the premises than for the outdoor cables. The attenuation change allowed during testing (0.20 to 0.30 dB for SMF @ 1550 nm) is more generous due to the nature of the operating systems. For these applications, the use of traditional PVC tight buffer fiber is adequate.

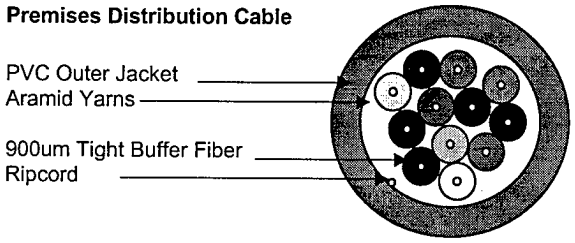

Figure 2. Tight Buffer Fiber Indoor Cable

In recent years the fiber optic cable industry has released several new Indoor/Outdoor cable designs. Most all of these are based on an existing non-flooded Stranded or Central tube core with a flame retardant jacketing material allowing them to pass UL 1666. These are true outside plant cables which can be brought into the building beyond the 50-ft threshold dictated by the NEC.

However, these cables hold the same limitations of their OSP sister designs once they have entered the building; they are large, stiff, messy, and costly to terminate. For these reasons CommScope has developed a tight buffered fiber distribution cable which is suitable to be run between buildings. This small OD, highly flexible cable, qualified for an operating temperature range of –40°C to +70°C, is waterblocked using Arid-Core™ technology, and is UV resistant. The option of direct termination to the 900-micron tight buffer results in cost savings of approximately $500, per end, for a 12f-cable, when compared to traditional OSP loose tube cables. An additional benefit of this design is the use of LSZH materials for buffer and jacketing which eliminates the emission of corrosive and toxic gasses in the event of a fire.

Cable performance characteristics include mechanical and environmental design specifications, cable constructions and weights. Design features describe the ease of sheath entry, ease of stripability and potential cost savings associated with direct termination of the 900 micron tight buffer fiber.

CONSTRUCTION

The 250-micron acrylate coated glass fiber is up-jacketed with a Flame Retardant Polyethylene (FRPE) up to 900 microns.

The tight buffer fibers are stranded around a Glass Reinforced Plastic (GRP) central strength member up-coated with the same FRPE material. Additional tensile strength, cushioning, and water blocking of the cable core is achieved by use of Aramid Yarns which are impregnated with Super-Absorbent Polymers. These Aramid yarns allow for superior water-blocking of the cable core without the use of core-wrap tapes or flooding compounds thereby making the cable very craft-friendly to the installer.

An outer jacket made from the same FRPE material is extruded over the cable core to provide the final layer of protection from the outside or premises environment. The jacketing material is UV stable and moisture resistant. Its flame resistance allows for the UL Type OFNR cable rating. The cushioning layer of Aramid yarns provides sufficient de-coupling of the cable jacket to the cable core to allow for excellent attenuation performance through the cable operating temperature range of -40°C to + 70°C. This cable design is a significant improvement over traditional tight buffer PVC or LSZH cable designs, which are typically not water-blocked, UV stable and/or do not have as wide an operating temperature range. The cable core and jacket are de-coupled and a ripcord is built into the cable allowing for ease of entry to the cable core while minimizing the potential for damage to the tight buffer fibers.

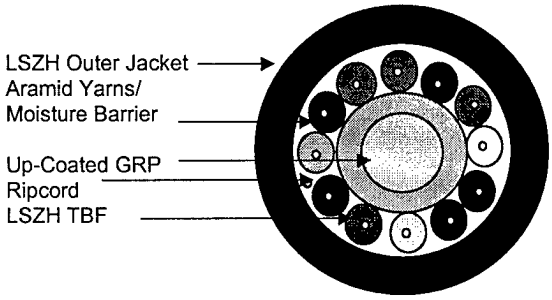

Figure 3. Indoor/Outdoor Tight Buffer Fiber (TBF) LSZH Riser Distribution Cable

QUALIFICATION

The cable was tested for compliance to Bellcore GR-409, Issue 1 requirements for riser cables and Bellcore GR-20, Issue 1 test conditions and criteria for water-blocking and UV resistance. A summary of these test results is presented as are the results form the UL 1666 burn test.

Attenuation Change:

Maximum Allowable Change in attenuation per Bellcore GR-409 is: 0.2 dB for 90% of fibers measured & 0.3 dB 10% of fibers measured. After Heat Aging: 0.6dB/km Max. change is allowed. All measurements performed on Singlemode Fiber (SMF) at 1550nm.

Mechanical Testing:

24f Ind/Out Distribution	*Units*	*EIA/TIA-455-xxx*	*Bellcore GR-409 Requirements*	*Actual Test Conditions*	*Maximum Attenuation*	*PASS/ FAIL*
Hot/Cold Bend	mm	FOTP-37A	254	254	0.14dB max 0.04dB ave	PASS
Tensile Rating Loaded	N	FOTP-33A	1320	2640 GR-20	0.03 dB	PASS
Tensile Residual	N	FOTP-33A	330	660	0.03 dB	PASS
Compression	N/cm	FOTP-41A	100	220 GR-20	0.05 dB	PASS
Impact	Nm	FOTP-25A	5.88 Nm X 20 cycles	5.88 X 25 Cycles	0.07 dB	PASS
Flex	mm	FOTP-104A	254 mm X 25 cycles	254 mm X 25 cycles	0.02 dB	PASS
Twist	deg.	FOTP-85A	+/-180deg.	180 deg.	0.04 dB	PASS

Environmental Testing:

Temp. Cycling	°C	FOTP-3A	-20°C to +70°C	-40°C to +75°C	0.10dB max 0.05dB ave	PASS
Heat Aging	°C	FOTP-3A	85°C for 1 week 0.60 dB/km Max.	85°C/1 week -40°C /+75°C	0.21dB max 0.12dB ave	PASS
Cable Freeze	°C	FOTP-98A	-10°C, 50m Coil @ 20 in. dia.	-10°C, 50m Coil, 20in.	0.08 dB	PASS

Table 1. Mechanical and Environmental Test Results

Additional Test Results:

TEST	*Criteria*	Test Method	*Requirements*	*Actual*	*Results*	*PASS/ FAIL*
Water Penetration	hrs.	FOTP-82	1 meter column/24 hrs.	1 meter column/24 hrs.	72 hrs 7.6 cm Penetration	PASS
UV Resistance	hrs.	FOTP-89A	720 hrs. QUV >90% retention tensile X elong	1000 Hrs. Black Jacket	>95% retained tensile x elongation	PASS
UL	OFNR	1666	12 feet 850 °F	UL 1666	4' 6" and 460 °F.	PASS

Cable Materials:

Plastic Compounds	N/A	EPA's TCLP	No lead based stabilizers or cadmium-based materials	Vendor Guarantee	No Lead based stabilizers or cadmium-based materials	PASS
Cable Jacket tensile strength and elongation	Mpa, %	FOTP-89A	13.8 Mpa (2000psi) 100% elongation	110°C/1 week aging	After Aging 13.8 Mpa 160%	PASS
Jacket Shrinkage	%	FOTP-86	5%	110°C/1 week aging	1%	PASS

Table 2. Additional Test Results and Cable Jacket Materials

CABLE DESIGN CHARACTERISTICS

Fiber Count (distribution)	Tensile Rating (N) Loaded / Residual		Cable OD (mm)	Minimum Bend (cm) Loaded / Unloaded		Cable Weight (kg/km)
2	1200	400	3.6	7.2	3.6	16
4	1350	445	4.0	8.0	4.0	22
6	1350	445	5.3	10.6	5.3	30
12	1800	600	7.4	14.8	7.4	56
24	2700	710	9.9	19.8	9.9	72

Table 3. Cable Design Characteristics

Indoor/Outdoor Applications

This new LSZH TBF cable is also a riser rated cable and can extend into a building to any area except plenum spaces.
Standard outside plant cable must be terminated (or encased in metallic conduit) within fifty feet of the building entrance creating a transition point between the outside plant cable and inside plant cable. This new cable can run from the exterior directly to the first cross-connect bypassing the need for a transition point.

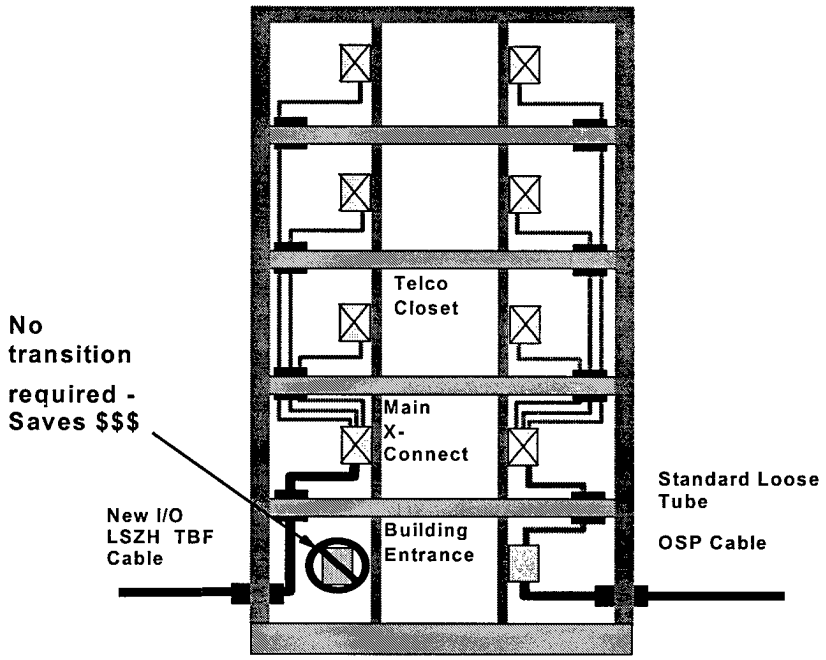

Figure 4. Potential for InstallationCost Savings

Although designed for outside plant conditions, this cable retains the ease of installation of a tight buffer cable. Side by side, the TBF cable looks identical to a standard distribution style fiber optic cable. The 900 micron buffered fibers can be directly connectorized thereby elliminating breakout kits or pigtail splicing typically required by loose tube cable. The Arid Core™ water blocking system is a completely dry technology so there is no flooding compound or gel to clean.
Installation is fast and easy providing a labor savings over other indoor/outdoor cables.

Fire Safety

Another benefit of this new TBF cable is the ability to meet the U.L. requirements for riser rating without the use of halogenated compounds. This means the cable is listed Optical Fiber Nonconductive Riser (OFNR) and is also a Low Smoke Zero Halogen (LSZH) cable. Cables with halogens such as chlorine (e.g. PVC) or fluorine (e.g. PVDF) emit potentially hazardous toxins and substantial amounts of smoke when they burn. Indeed, the vast majority of fire related victims succumb to smoke and gases, not flames or heat.

While human safety is the foremost concern, protecting the expensive and delicate telecommunication and other electronic equipment found in today's workplace is another consideration. Along with being toxic, the gasses released when halogenated compounds burn

are corrosive and can attack the metallic contacts and other platings destroying the functionality of key components. So even if a fire is well contained, property loss from smoke and corrosivity can be substantial.

LSZH cables can dramatically minimize these dangers. They contain no halogens and have reduced smoke production when burned. As testament to the significance of the safety factor for LSZH cables, they are the product specified for use for U.S. Navy ships and Department of Transportation projects (e.g. tunnels) where it is essential that people and equipment have a high degree of survivability.

Property	Test Method	Unit	Typical Value
Limiting Oxygen Index (LOI)	ASTM D2863	%	39
Acid Gas Generation	MIL-C-24643	%	0.47
Toxicity Index	NES-713	-	1.4
Acidity of Combustion Gases (pH)	IEC-754-2		4.5

Table 6. FRPE LSZH Material Combustion Properties

CABLE FIELD TRIAL

In May of 1997, The Indianapolis Power & Light (IPL) Company asked CommScope to provide a fiber optic cable link in downtown Indianapolis. This was to be an underground link between the communications vault beneath the IPALCO Enterprises, Inc. Corporate Center at One Monument Circle, and another vault at 25 Meridian Street South.

The connection was to enable IPL to utilize an Electronic Technologies, Inc. Network Protector Relay via a DYMEC RS232 serial port master slave at 9600 baud by means of an optical fiber converter (2179 protocol) to continually monitor relay status at the Meridian Street location.

IPL had some very specific requirements for the cable construction. A fiber optic cable was necessary because the cable would be run through existing four-inch ducts already occupied by 3 X 350 MCM (13.2 KVA) lead-jacketed primary power cables. These close quarters meant that the cable had to have a small diameter, light weight, and high degree of flexibility. Even though the installation was in ductwork, the cable had to be robust enough for outdoor use.

For this application CommScope provided a 300m long sample of Indoor/Outdoor LSZH TBF Cable with a total of 4 fiber FDDI grade multimode fibers. Upon installation, the cable was stripped and connectorized with Siecor ST Unicam™ connectors. An OTDR was used to verify the installed fiber attenuation reading. The OTDR confirmed an acceptable 0.9 dB loss at 1300 nm over the connectorized 300m installed length (all four fibers measured the same). To date, cable and assembly have performed well within IPL expectations.

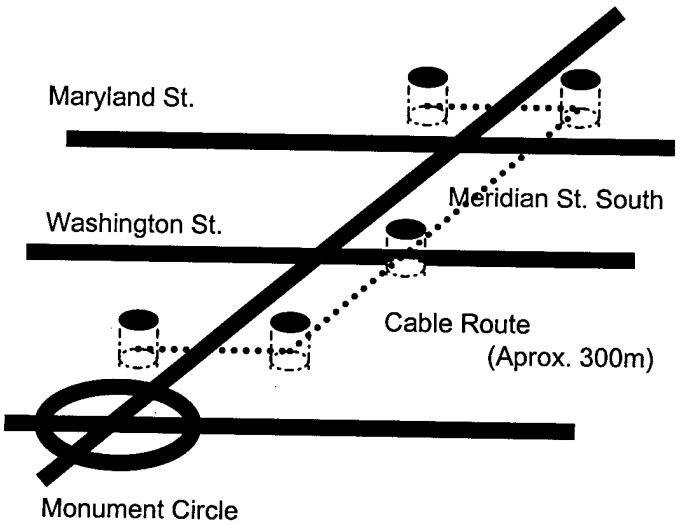

Figure 5. IPL Field Trial Project Map

CONCLUSIONS

Traditional PVC tight buffer cables are generally not suitable for outside plant applications. The absence of water blocking systems can allow water and/or vapor to migrate the length of a cable compromising long term reliablility. PVC Tight buffer cables also exhibit poor performance at temperatures below -20° C. Low temperatures can cause brittleness in the buffer and ultimately put the fiber at risk due to increased fiber strain. From a cable jacket view point, the PVC materials used with tight buffer cable do not exhibit the same protective properties as the polyethylene (PE) jackets used on standard outside plant cables. PVC jackets are softer and abrade more during installations, they also age faster than PE.

Challenged with the limitations presented by standard tight buffer cable, CommScope, Inc. has developed a new line of tight buffer cables that are designed specifically for the indoor/outdoor applications found in most LANs. The major changes incorporated into the design include the switch from PVC's to FRPE (LSZH) for the buffer and jacket, and the development of an Arid-Core™ water blocking system. The final design provides a cable that can meet the operating temperature window and moisture resistance of a loose tube cable yet maintains the key advantages of a tight buffer cable i.e. ease of installation and a riser rating (OFNR).

REFERENCES

(1) Bellcore GR-409-CORE, Generic Requirements for Premises Fiber Optic Cable, Issue 1, May 1994

(2) Bellcore GR-20-CORE, Generic Requirements for Optical Fiber and Fiber Optic Cable, September 1994

ACKNOWLEDGEMENTS

I would like to thank Adrian Brewer, Joe Lichtenwalner, Scott Stevens, Will Thompson, Ray Yeager, Sandra Young, and Rob Wessels for their support and enchoragement in the development of this product and the writing of this paper. Many thanks also to The Indianapolis Power and Light Company Installation, and Communication & Control crews for their support with the field trial of this new cable design.

AUTHOR

Bernard Blell was born in Belgrade, Yugoslavia in 1967. He received his BS in Aerospace Engineering from North Carolina State University in 1991 and Master of Engineering Degree in 1995, also from NCSU. Bernard is the Engineering Manager for Fiber Optic Product Development at CommScope, Inc. where he has been employed since 1996. From 1993 to 1996 he worked as a Product Design Engineer for Sumitomo Electric Lightwave Corp. in RTP, NC.

DEVELOPMENT OF CROSS-FUNCTIONAL TOTALLY DRY OPTICAL FIBER CABLE FOR OUTDOOR, RISER, AND PLENUM APPLICATIONS.

David A. Keller[1], Jack Rosko[1], Brian Risch[2], Randy Yoder[1], Scott Munday[2]

1) Alcatel-Berk-Tek, Fuquay-Varina, N.C., 2) Alcatel Cable, Claremont, N.C.

ABSTRACT

Outdoor-Riser Cables were the start of meeting the demand for Cross-Functional Cable performance capabilities.

Point to point building plenum links across an outside plant environment illustrates the benefits of having a cable designed for Indoor and Outdoor use. The design should be as fire resistant/retardant meeting the highest rated cable flammability. The cable link should also meet outside performance and environmental stability requirements.

The development of a Cross-Functional Totally Dry Optical Fiber Cable for Outdoor, Riser and Plenum Applications required meshing GR-20-CORE, GR-409-CORE and UL 910 requirements.

Flame retardant, UV resistant plastics, water swellable materials, and flexible strength elements are combined to optimize compression and cold bend performance.

Gel-filled and dry tubes were explored, with the totally dry version being the choice for accessibility, cable preparation, and UL 910 performance.

Bare fiber exposure water ingress was investigated for attenuation increase and fiber tensile strength degradation.

A Cross-Function Totally Dry Optical Fiber Cable was developed which meets UL 910, GR-20-CORE and GR-409-CORE requirements.

INTRODUCTION

Campus Cables consist of Outdoor, Riser, Outdoor-Riser and Plenum Rated Designs which link, point to point,[3] to and from a plenum environment, across a riser and an outside plant environment. Newly installed indoor cables should be as fire resistant and retardant as possible to lower the aggregate flammability of new or existing installations [2].

The highest rated cable flammability test is the UL 910 Plenum, as illustrated from Chapin, Caudill, & Hoover[2]:

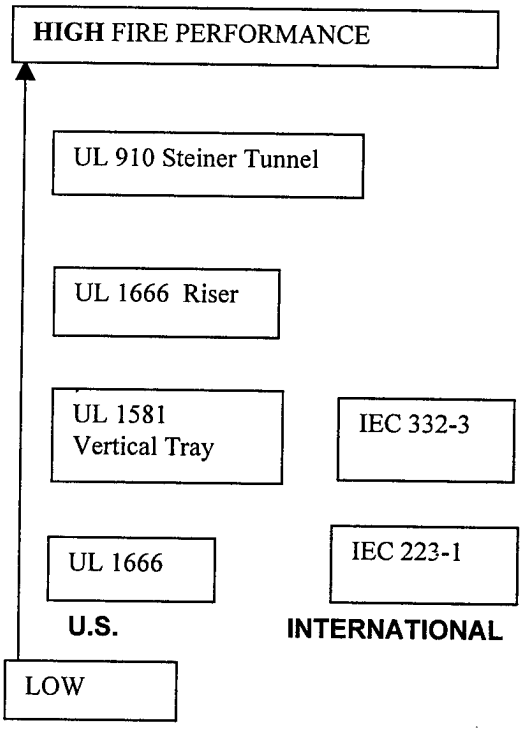

An Outdoor-Riser Cable, having a higher fuel content, and effected by fire from other sources, could further enhance the magnitude and propagation of the fire, as compared to a Plenum Rated cable[1].

For convenience, some customers have used indoor plenum cables, which were not UV stabilized or designed against water ingress, for outdoor applications. The regulatory environment demands strict compliance with regard to fire hazards, but allows the customer to take their own risk with regard to outdoor performance and environmental stability.

The fire enhancement risk versus the environmental performance risk trade-off generated the need for the Development of a Cross-Functional Optical Fiber Cable for Outdoor and Plenum Applications.

The work performed in 1997-1998, as outlined in this paper, illustrates some of the steps required to realize this objective.

DESIGN REQUIREMENTS

Current customer demand requires particular requirements of GR 20-CORE and/or GR-409-CORE to be met without exception; however there is a certain amount of latitude allowed[3], based on applications, regarding:

1) OD and Flexibility of Design
2) UL Riser or Plenum Rating
3) Tensile Rating
4) Allowable Compression Resistance
5) Cold Bend Performance.

The first step taken to realize a Cross-Functional Totally Dry Optical Fiber Cable for Outdoor, Riser and Plenum Applications was to optimize an Outdoor/Riser solution which was upgradable to Plenum performance.

RISER OPTIMIZED

The current Uni-Lite Design was converted to a reduced diameter design. This more flexible, modified design is illustrated as follows

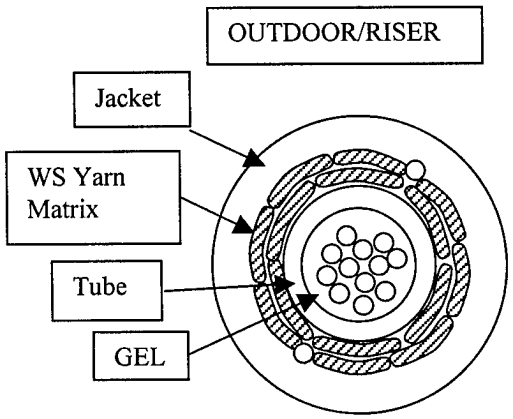

UL 1666

The UL 1666 Riser 12 ft. vertical shaft flame test has five points of measurement:

1) 12 ft Maximum temperature of 850 F.
   12 ft Maximum height:
   2) Flame
   3) Melting
   4) Charring
   5) Ash

Results from the UL 1666 testing of two existing Riser materials are normalized and presented.

Riser Jacket material 2 (JR2) consistantly passed the UL 1666 test as illustrated by the following chart:

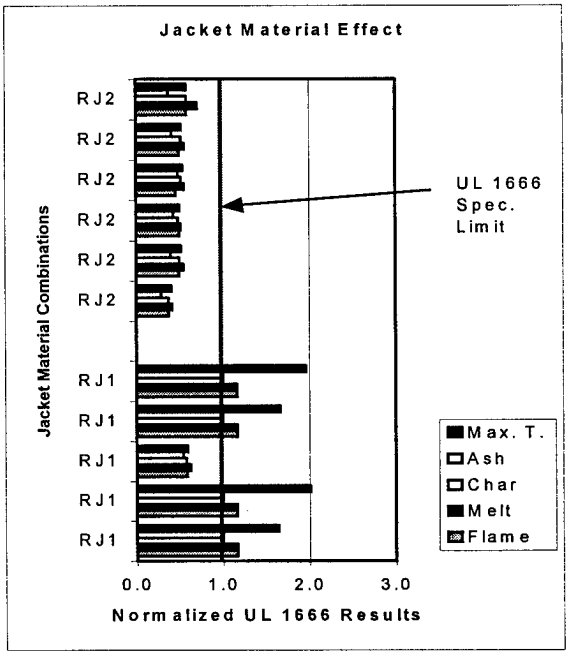

Yarn-Matrix B has a greater fuel contribution than Yarn-Matrix A as illustrated by the following chart:

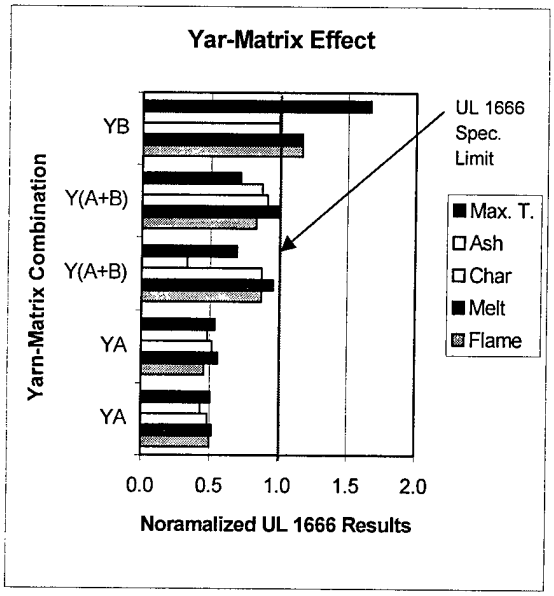

Yarn-Matrix A (YA) performed well with R2 while use of Yarn-Matrix B (YB) was limited to a low percentage in order to allow a "passing" result on the UL 1666 Riser test.

Riser Tube materials RT1, RT2, RT3 were expected to have a significant fuel content variance, but their low volumetric fuel contribution, resulted in only a slight effect relative to UL1666.

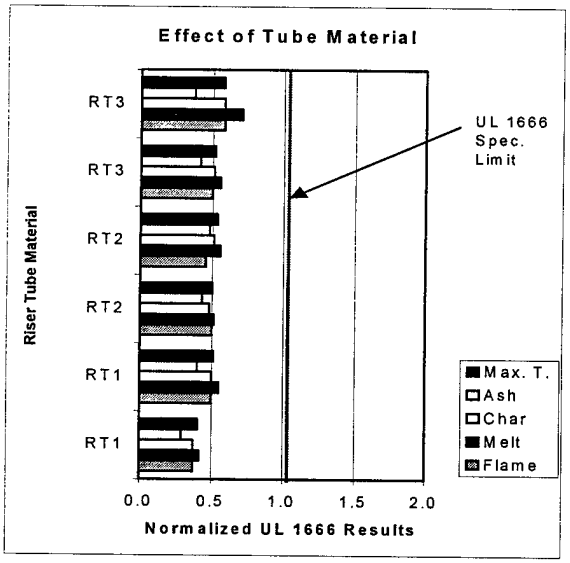

COMPRESSION

Isolating the tube material and thickness for compression performance illustrates effect of material mechanical properties as follows:

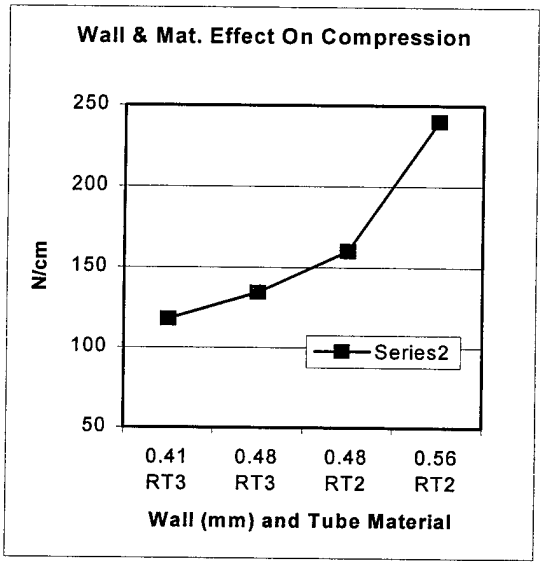

Increasing wall thickness and selecting material RT3 in place of RT2 dramatically increased the compression performance of the tube.

Increased thickness of the Jacket (RJ2) and a mix of YA and YB both generated an increase in compression resistance. YB exhibited slightly increased adhesion properties. YB was mixed with YA by increased percentages, denoted by samples A, B, & C, as illustrated in the chart below:

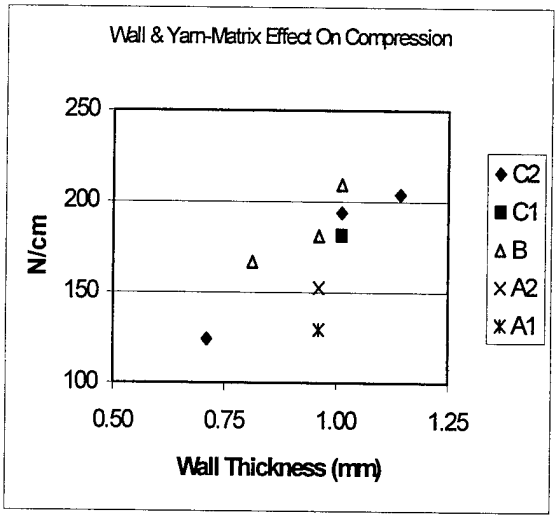

OUTSIDE-PLENUM DEVELOPMENT

Upgrading the Uni-Lite RD to Plenum Rating, required rethinking the material selection to meet the meshing of GR-20, GR-409 and UL 910 specifications.

UL 910 fuel content limitations indicated a preference for a dry tube without gel.

This combined with accessibility and cable splicing preparation for splicing, resulted in a choice to develop a totally dry plenum indoor and outdoor cable.

The resulting design exceeded the friendliness and relative performance of the Riser design. The tube material is very flexible, routes easily and unobtrusively in connection housings, and is clean and free of gel.

Water swellable yarn matrix strength members were used between the jacket and tube, as in the reduced diameter Riser design. A plenum flame retardant and UV Resistant material was used for the jacket material. Water swellable powder was used to prevent water ingress inside the plenum flame retardant tube.

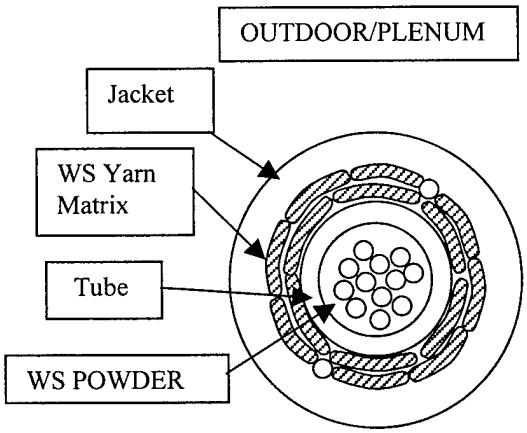

UL 910

A 7.6 m long x .3 m wide array of cables are strung from a horizontal ladder in the (UL 910) Steiner Tunnel. A 90kW gas burner supplies direct flame to 1.5 meters length of the array. Ventilation is supplied from the burner end at a rate of 73m per minute.[2]

In the following chart, sets of horizontal columns illustrate the effect of a dry versus a gel-filled tube. The columns display normalized results for the max flame, peak and average smoke from the UL 910 cable tests, performed in the Steiner Tunnel.

The first two sets of columns (from the bottom) represent materials which are equal or superior to the Riser materials mentioned previously; however, they fail the UL 910 test by a 2.5 – 4.0 factor, while improved Plenum materials and a dry tube resulted in a consistently UL 910 passing design.

This comparison illustrates how the greater UL 1666 Riser rated cable's fuel content, when effected by fire from other sources, could further enhance the magnitude and propagation of flames as compared to the more fire retardant and resistant UL 910 rated cables.

Of five Plenum designs submitted, P3, P4, P5 met UL 910 requirements as illustrated in the following chart:

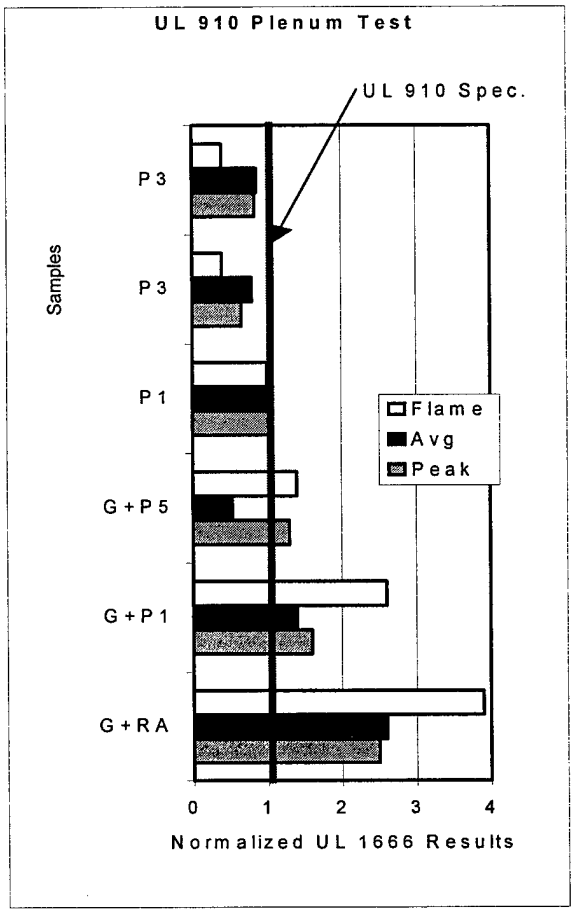

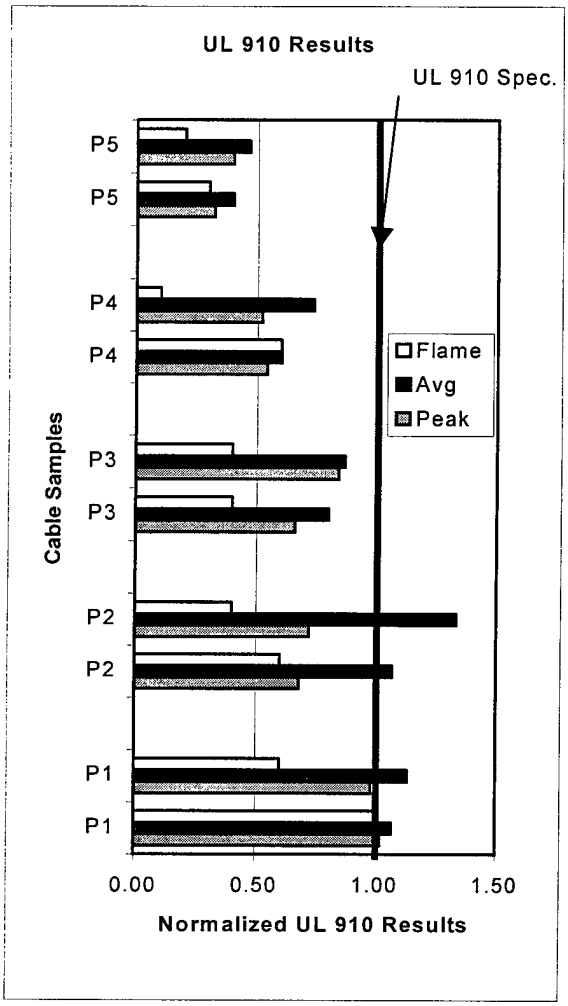

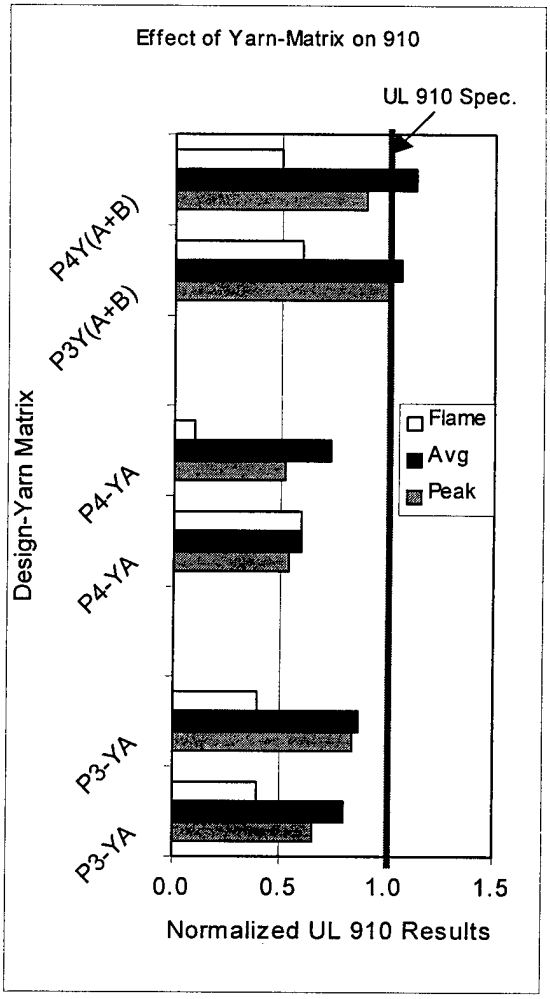

Note the variability in the Peak, Average, and Flame results between the three sets of columns. The grouped normalized test results seem to provide some consistency while individual measures do not.

Yarn-matrix elements have different fuel contents as any other materials and must be considered in the final design.

The Yarn-Matrix fuel contribution was investigated.

Yarn-Matrix YA utilized in the samples 1-4 (bottom to top) met UL 910, while Yarn-Matrix YB, generated results which failed to meet UL 910 (sets 5 and 6) as illustrated in the following chart:

DRY INTERIOR TUBE

As stated previously, the dry tube containing water swellable powder provided for improved performance in the UL 910 test.

The dry tube itself generated some questions as to how the fiber would perform when subjected to water ingress into the tube.

A 300 m tube containing optical fibers and WS Powder was respooled and a 12 mm access slice was created at every 30 m.

The length was then coiled and immersed in water for 24 hrs, measured for attenuation increase, frozen; and measured again. No increase in attenuation was noted.

After 30 days of 23 C water immersion, the fibers were measured. No increase in attenuation was noted.

As the most aggressive test, bare fibers (without tube and without water swellable powder) were immersed in 85 C water for 45 days. No attenuation increase was noted.

Three fiber samples were subjected to 85 C immersion in water and their tensile strengths were measured:

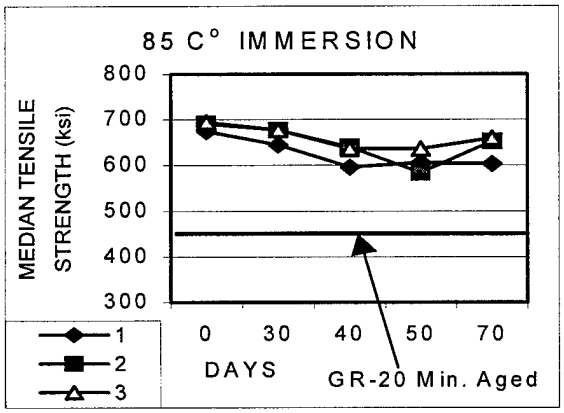

Here we see a slight decrease in strength, but we are well within the limitation set by GR 20-CORE

OUTDOOR-PLENUM COMPRESSION AND COLD BEND

Design P3 & P4 performed acceptably in compression, as compared to targets set by Ellwanger, Nave, & McDowell[3]. The Outdoor/Plenum Design was further modified to P6 in order to pass 20x & 10x Bend at –20 C° in the cold bend test and generates improved compression to 120 N/cm as illustrated in the following charts:

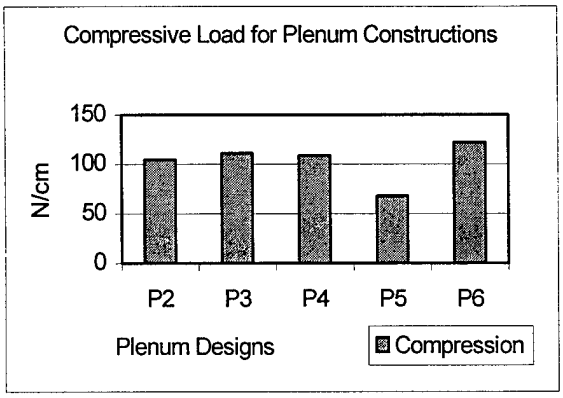

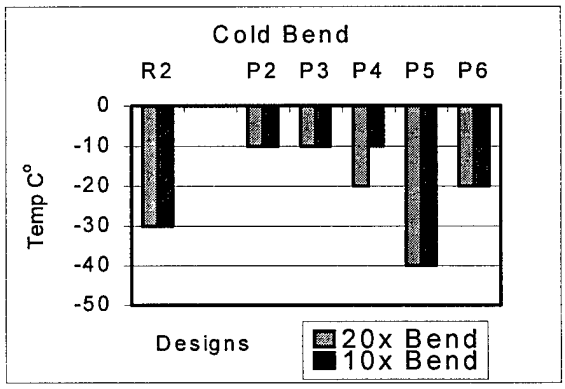

TEST RESULTS

UL 1666 Riser, UL 910 Plenum, GR 409-CORE and GR 20-CORE results are tabled (revised[4] as follows:

UL 1666 RISER RESULTS:

Parameter	Max.	Results
Flame	12 ft	6/5-6 ft-in
Melt	12 ft	6-2/6-8 ft-in
Char	12 ft	5-10/6-3 ft-in
Ash	12 ft	5-2/5-10 ft-in
Temp	850 F	429/456 F

UL 910 PLENUM RESULTS

Parameter	Max.	Results
Flame	5 ft	2/2
Peak Smoke	0.5	0.33/.42
Avg. Smoke	0.15	0.12/0.13

GR-20 AND GR-409

TEST	GR-20	GR-409	Outdoor-Riser Results	Outdoor-Plenum Results
Low Temp. Bend	20 x -30C	20 x -20 C	20 x -30 C	20 x -20C
Impact Resist.	25 cyc 2.2 N·m	25 cyc 2.2 N·m	25 cyc 5.9 N·m	25 cyc 2.2 N·m
Comp. Strength	220 N/cm	100 N/cm	175 N/cm	110 N/cm
Tensile Strength	2660 N	1320 N	1335N	1335N
Twist	10 cyc 2 m	10 cyc 2 m	10 cyc 2 m	10 cyc 2 m
Cyclic Flexing	25 cyc	25 cyc	25 cyc	25 - 300 cyc
Temp. Cyc -Age	-40 +70C & 85 C Age	-20 +50C & 85 C Age	-40 +70C & 85 C Age	-40C to +70C & 85 C Age
Water Pen	24 hr unaged 1 hr aged	N/A	24 hr unaged 1 hr aged	24 hr unaged 1 hr aged

CONCLUSIONS

1) The modified outdoor/riser cable failed the plenum burn by a 3-4 factor, illustrating the importance of the UL 910 plenum rating.

2) The material fuel characteristics of the Yarn matrix effects the overall cable flammability in both the UL 1666 Riser and the UL 910 Plenum test..

3) The Yarn-matrix adhesive relationships effects compression performance of the total cable.

4) The optimization of compression and cold bend is on-going.

5) The dry interior tube, having water swellable powder, is performing very well, and our tests are continuing.

6) The Outdoor/Riser & Outdoor-Plenum, successfully meet specific GR-20-CORE and GR-409-CORE requirements with modifications to Tensile, Cold Bend and Compression.

REFERENCES

1. Siegfried Richter, Rudiger Schmidt," TESTING OF CABLES DESIGNED FOR FIRE RESISTANCE A COMPARISON OF U.S. AND EUROPEAN STANDARDS" International Wire and Cable Symposium, 1997, pp 752-760.

2. J. T. Chapin, L. Caudill, J. R. Hoover, "COMPARISON OF FIRE BEHAVIOR OF COPPER AND FIBER OPTIC CABLE IN LARGE AND FULL SCALE FIRE TEST FACILITIES" International Wire and Cable Symposium, 1997, pp 775-784.

3. Michael R. Ellwanger, Samuel D. Nave, Harvey R. McDowell III, "HIGH FIBER COUNT INDOOR/OUTDOOR FAMILY OF RIBBON CABLES" NFOEC Proceedings, 1996, pp 371-380.

4. Allan Kaiser, John C. Smith, "INDOOR/OUTDOOR FIBER OPTIC CABLE" NFOEC Proceedings, 1996, pp 347-355.

AUTHORS

David A. Keller, ALCATEL BERK-TEK, 100 Technology Park Lane, Fuquay-Varina NC 27526, USA.

David received his B.S. in Mechanical Engineering from the University of Kentucky in 1983 while working in materials research for Continental Can. After receiving his B.S. he worked for General Motors, Siecor , and Philadelphia Insulated Wire. He held positions in product and process development before and after joining Alcatel-Claremont, NC. in 1987. In

May 1993, He moved to Bezons, France to develop cables at Alcatel's OFCCC, returning to Claremont in Dec, 1995. In Sept, 1997 he moved to Alcatel-Berk-Tek's Data-Cable Division and holds the position of Senior Product Development Engineer for optical fiber Riser and Plenum cables.

Jack Rosko, ALCATEL BERK-TEK, 100 Technology Park Lane, Fuquay-Varina NC 27526, USA. Jack Rosko received his BSEE Degree from Union College in Schnectady, NY. He has worked for Berk-Tek since 1991 and is now Research & Development manager. Mr. Rosko has been involved in Fiber Optic Cable Design and Development since 1979. His previous work experience has been with Siecor, Phalo OSD, and Sumitomo Electric.

Brian G. Risch Alcatel Cable, 2512 Penny Road, Claremont, NC, 28610 USA Brian is a Senior Materials Scientist at Alcatel–Claremont's Optical Fiber Cable Competence Center (OFCCC). He holds a B.A. degree in Physics from Carleton College and a Ph.D. in Materials Science and Engineering from Virginia Polytechnic Institute and State University. His research was in polymer crystallization and structure property relationships in polymers. Directly after he worked for ORD laboratories in optical polymers developing polyurethane and polythiourethanes for high performance ophthalmic lens applications. Since 1996 Brian has worked for Alcatel's OFCCC in thermoplastic materials with specialization in processing and crystallization behavior of polyolefins.

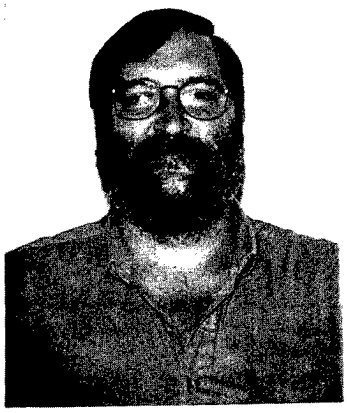

Randy L. Yoder ALCATEL BERK-TEK, 100 Technology Park Lane, Fuquay-Varina NC, 27526 USA. Randy started working for Berk-Tek in 1980 in the Copper Data Cable Division in New Holland, Pa. His professional experience has included all areas of Process Development of Data Cables and Manufacturing Process Control, with specific expertise in flame retardant thermoplastic extrusion processing. In October of 1997 he moved to Alcatel-Berk-Tek's Optical Fiber Data-Cable Division and holds the position of Senior Product Development Technician for Optical Fiber Riser and Plenum cables.

Scott Munday, Alcatel Cable, 2512 Penny Road, Claremont, NC, 28610 USA. Scott Munday received his A.A.S. degree in Mechanical Engineering Technologies from Catawba Valley Community College in 1992. He joined Alcatel in 1993 and held the position of Cable Development Engineering Technician. In 1997 he moved to the Quality Assurance Department, and now holds the position of Quality Assurance Technician. His responsibilities include managing the test schedules for newly developed cable designs, product qualifications, and requalification testing of standard designs.

FINITE ELEMENT MODELING OF OPTIC FIBER CABLE CRUSH PERFORMANCE

J. Boyet Stevens[1], Peter Elisson[1], Brian Risch[1], Christian Bastide[1]

[1]Alcatel OFCCC, Claremont, NC

ABSTRACT

When optic fiber cable elements undergo crush loading, they can collapse and induce attenuation in the enclosed fibers. A clear understanding of the mechanisms of crush failure is necessary to design application-optimized, cost-effective and robust optic fiber cables. To this end, we analyzed the elastic-plastic deformations of thermoplastic cable elements using finite element modeling.

INTRODUCTION

Cable Crush Performance Modeling

The level of crush performance required for various cable designs depends on the application and expected service loads. Some crush tests are used to demonstrate that a cable will suffer no increase in attenuation while transversely loaded between two parallel plates. Other standard crush tests require that a cable must show no added loss ***upon release*** of the load (typically the load requirement for this type of test is higher). These two test definitions may have different implications about the mechanism of crush failure. For a cable to pass the "attenuation-under-load" test, the fibers must have sufficient space in the cavity while the cable is loaded, and the transverse load transmitted to the fibers must not cause excessive loss. Failure upon load release indicates that there must have been sufficient load transmitted to the fibers so as to break them or cause significant coating damage or permanent strain. Plastic materials used in optic fiber cables tend to recover very well after load release and therefore do not likely impart significant loads to the fibers after the crushing load is released. Some standardization activity in recent years has included some reductions in crush performance specifications for optic fiber cables. It is therefore important to understand the mechanical behavior of cable units subject to crush load so their designs can be optimized for the given application.

While the small, linearly elastic deformations of a plastic cable element subject to crush loading are predicted well by elasticity theory, the evolution of plastic strain, viscous relaxation and nonlinear contact effects can dominate the crush behavior of optic fiber cables.[1] Cable elements subject to transverse load always undergo finite deformations and absorb energy via viscoelastic-plastic work. As plastic work commences, the flow of stress may be redirected and cause subsequent redistribution contact stresses. The nature of these stresses influences the residual deformed shape and thereby effects the loading of the contained optic fibers. The crush resistance of a loose tube structure has been empirically characterized [2,3] in terms of tube pitch and core compactness.

We used the nonlinear finite element code ABAQUS to calculate the plastic post-buckling of various cable elements and configurations. The cable elements considered for this analysis were a buffer tube, a central cavity cable unit, and a loose tube cable.

Models Developed

The optic fiber cable components simulated in this study are shown in Figure 1.

Buffer Tube. An optic fiber buffer tube is made of a suitable plastic material and contains optic fiber units and some water-blocking compound. The crush response of a buffer tube can be used as a rough gauge of its mechanical performance in a cable. The crush model described here does not include the fibers or filling compound.

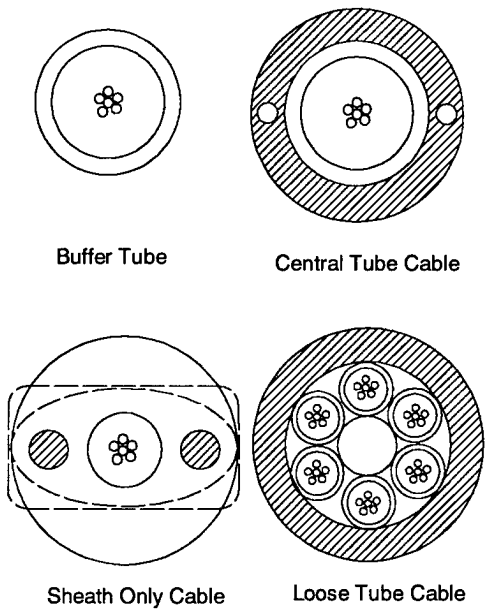

Figure 1 - Cable Constructions Considered for Crush Simulations

A simple 2D finite element model was created to validate the constitutive relations and contact conditions fairly simple configuration. The basic load deflection response is predicted well within the valid range of the material stress-strain data and is characteristic to the crush response of most cable structures. The curve consists of an initial elastic regime, followed by a structural yielding and a secondary linear region. Finally, the slope of the load deflection curve increases rapidly indicating the tube (or other cable component) has collapsed.

Central Cavity Cable. The basic central cavity cable unit includes a single sheath, or jacket, of plastic material, containing a cavity for optical fiber sub-units. The sheath may also contain embedded rigid or flexible strength members to boost tensile performance. The inclusion of a central buffer tube in this design would yield a typical central tube optic fiber cable design. The crush performance of this cable construction is critical since the buffering elements typical to optic fiber cables (tubes, intermediate jackets etc.) are not present. As such, the crush response of the sheath alone will be a conservative gauge of central tube cable response. In the present study, we determine the thermo-visco-plastic post-buckling deformations of a central cavity cable construction with embedded strength elements. Circular and noncircular shapes were considered in this case. The aspect ratio, a/b, and conic factor ρ, characterize the general exterior shape of the sheath in a continuous fashion from circular to rectangular (Figure 2). A conic factor of 0.414 yields an elliptical section (or circular if a/b=1) while a conic factor of greater than 0.414 lends a hyperbolic shape to the corners. The combination of these two factor influences the way the compressive load will be transmitted from the loading plates to the surface of the cable.

Loose Tube. The well-known loose tube construction consists of a number of fiber optic buffer tubes stranded about a central

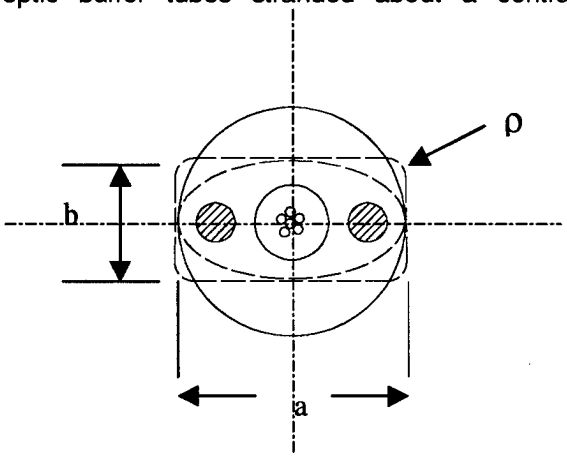

Figure 2 - Central-Cavity Unit Geometry

strength member (CSM) with a plastic outer sheath. Strength yarns, tapes and other elements may be included in the cable to provide sufficient stiffness, water-tightness and core protection. The 3D finite element model discussed herein includes only the tubes, the CSM and the sheath.

Crush Failure Mechanisms and Definitions

The failure of the crush test is essentially defined by the performance of the contained optic fibers. Therefore the task of modeling the crush performance of a cable involves first determining the elastic-plastic deformations of the cable under load, then calculating the lateral forces transmitted to the fiber and finally predicting the attenuation in the fibers due to those loads. The latter endeavor is very difficult because the loads transmitted to the fibers would likely be statistical function of the fiber/unit placement in the tube. The mechanical response studied herein is that of the various cable elements without the influence of the fibers. The

inclusion of the fibers in the crush simulation would introduce many contact surfaces and complicate the analysis considerably. In the present analysis, the load required to collapse defines crush failure. Experiments suggest that typically a cable element subject to a crushing load will begin with an initial elastic response then undergo structural yielding and a more compliant secondary response. When the bore of the cable element finally collapses, the response stiffens again and the fibers become constrained by the walls of the tube. It is generally somewhere between the load to cause structural yield and the load to cause fiber constraint that we begin to observe increase in attenuation the fibers. Residual attenuation in the fibers after load release is generally observed only if the cable was loaded well beyond the fiber constraint load. Experimental observations confirm that, for low fiber count tubes, although the collapse of the cable may occur, the subsequently loaded fibers may still pass the attenuation requirements upon load release. Therefore it is necessary to understand both the initial compressive response of cable elements as well as the collapse.

Theory

Basic equations. The basic equations governing the motion of a continuum - the balance of mass, momentum and energy - are solved to determine the deformations of a plastic cable unit subject to crush loading. [4]

$$\frac{d}{dt}(\rho J) = 0 \qquad \rho_0 \frac{d\mathbf{v}}{dt} = Div\mathbf{T} \tag{1,2}$$

$$\mathbf{T}\mathbf{F}^{\mathrm{T}} = \mathbf{F}\mathbf{T}^{\mathrm{T}} \qquad \rho\frac{de}{dt} = tr(\mathbf{T}\frac{d\mathbf{F}}{dt}) \tag{3,4}$$

$$\mathbf{F} = \frac{d\mathbf{x}_A}{d\mathbf{X}_A} \tag{5}$$

Here, x_A gives the present position of a material particle that occupied place $\mathbf{X}_A$ in the reference configuration, ρ its mass density and ρ_0 its mass density in the reference configuration. The particle velocity is **v**, **T** is the first Piola-Kirchoff stress tensor and **F** is the deformation gradient, the Jacobian, J=det**F**, and **e** is the specific internal energy. The deformations are assumed to be adiabatic and the plastic flow is governed by hardening data gathered in uniaxial compression and tension experiments. Equations 1 and 2 are the balance of mass and momentum and 3,4 and 5 are the balance of moment of momentum, energy and the definition of the deformation gradient respectively. The cable crush process is considered to be adiabatic and temperature generated by plastic deformation is not calculated in the analysis. Therefore there is no need to explicitly solve the balance of energy. The energy balance is important however in the explicit analyses of the loose tube cable to ensure that inertial effects do not dominate the solution.

The cable material is considered a linear, isotropic elastic-plastic material with kinematic strain hardening. Both elastic-plastic and Drucker-Prager models were used to describe the plastic. No viscoelastic effects are included thus far, so no hold times are considered during the loading. The loading scenario - a cable unit or assembly transversely loaded at a constant rate between two rigid plates, is typical of quality control experiments. The loading is unidirectional and monotonic so no unloading is considered in the simulation.

Analytical Approach

Finite Element Methods - Domain, Mesh and Boundary Conditions. Plane strain symmetry is assumed for the buffer tube crush and central cavity crush simulations. It is only necessary to mesh a 2D cross section for these. Examples of initial mesh used in these problems are shown in figure 3. Due to the symmetry of these problems, only one quarter of the cross-section was considered and appropriate symmetry boundary conditions were imposed.

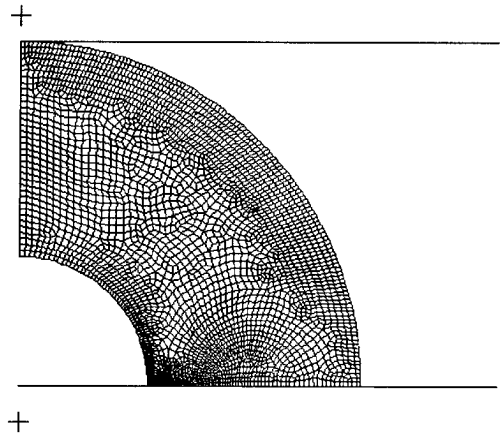

Figure 3 - Finite element mesh for the circular shaped cable

The domain shown in Figure 3 was meshed using 4-noded, linear quadrilateral 2D plane strain continuum elements. Only one Gauss point was used for integrating the stresses. The section geometry is defined first parametrically in Pro/Engineer and then imported in to PATRAN to create the mesh and boundary conditions. The mesh density, element shape, Jacobian ratio, and connectivity are optimized using PATRAN. The element density is graded such that the mesh is very fine in areas we expected rich solution gradients. One such point is at the lateral extremities of the bore where the tube collapse will initiate and also where most of the plasticity will occur. Another region where the solution gradients could be large is at the interface between the jacket material and the glass reinforced plastic (GRP) strength member. The rigid walls are defined in ABAQUS using the analytic rigid wall feature. This means there are no explicit elements defining the wall but just the simple geometry. The lines defining the wall were then used to impose non-inter-penetration conditions. Half of the crush load magnitude is used because of the quarter symmetry. The rigid surfaces are considered to be smooth with no friction developing between the load platens and the plastic sheath. In reality, the friction is of course non-zero, however, including the small friction effect in the contact specification has little effect on the solution and costs additional computation time. In the loose tube model, friction between the tubes and jacket was included. [5,6]

Contact conditions. Kinematically consistent contact algorithms were used to impose the contact conditions in all of the described crush simulations. In the buffer tube and central cavity, 2D rigid boundaries are defined to represent the rigid loading plate and to simulate the internal contact between the tube walls. When a plastic tube collapses, folds in the inner wall may result. The details of the simulated folds can be quite mesh dependent. Several mesh distributions and densities were tried to verify that the overall solution did not depend on the folding behavior. The contact definitions for the loose tube calculation are more numerous and complex. The contacts in this case are imposed between shell elements and other shells or rigid surfaces. The contact searching and calculations tend to dominate the computer time for this analysis.

Explicit and implicit solving methods. Both explicit and implicit solvers were used in the crush simulations. The type of solver used determines the type of equations we will solve. An implicit solver assumes that the acceleration term in the balance of momentum is zero and solves for static equilibrium. The tube and sheath only crush problems were solved this way because they do not involve many contact planes. The loose tube simulation was done using an explicit solver, which is suitable for problems involving many contact planes. The explicit solver solves the complete equations of motion, which are a matrix representation of the well-known Newton's second Law, F=ma.

Discussion of results

Buffer tube crush simulation. This 2D simulation was the first step of the modeling process to validate material models and the finite element methods used to handle contact and other issues. The simulated crush response matched well with the experiments within the ranges of the constitutive model.

Central cavity crush simulation. The mechanical process of collapse is tantamount to the buckling of a curved beam with arbitrary cross-section. The simulations show that the collapsed shapes of the various cable sections are similar except in the way the inner cavity closes. In the case of the circular section, the hole collapses catastrophically forming a straight line of contact between the bottom and top surface of the cavity. The load versus deflection curve shows a distinct stiffening at this point indicating that fibers contained would be constrained and possibly damaged. The elliptical cable responds with a lower structural yield, however due to favorable load redistribution, the load required to collapse the cavity is much higher than the circular case. The deformed shapes of the circular, elliptical and rectangular sections are shown in Figure 4.

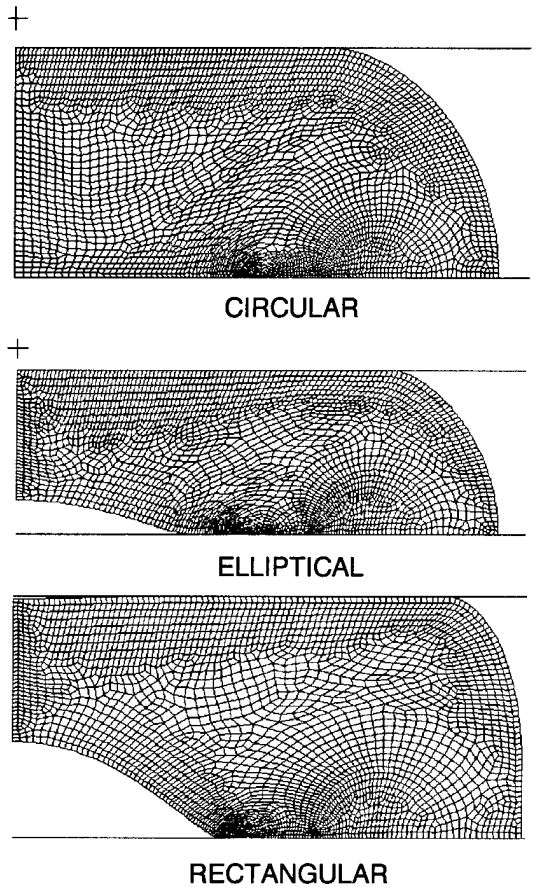

Figure 4 - Deformed mesh for the circular, elliptical and rectangular cross-sections

Elliptical shaped sheaths increase the crush performance by more than 100% in the direction perpendicular to the plane of the radial strength members. The early yielding causes redistribution of the loads, engaging the lateral portions of the plastic sheath and embedded RSMs and delaying the collapse of the bore. The result is a very orderly collapse and greatly increased load to cause fiber constraint. While the structural yield is a good indicator of crush performance for a typical buffer tube with relatively thin walls, it does not necessarily indicate the crush performance of a thick walled tube or a thick walled cable element described in this study. For these types of structures, the yield of the structure may be low while the load required to collapse the bore may still be high.

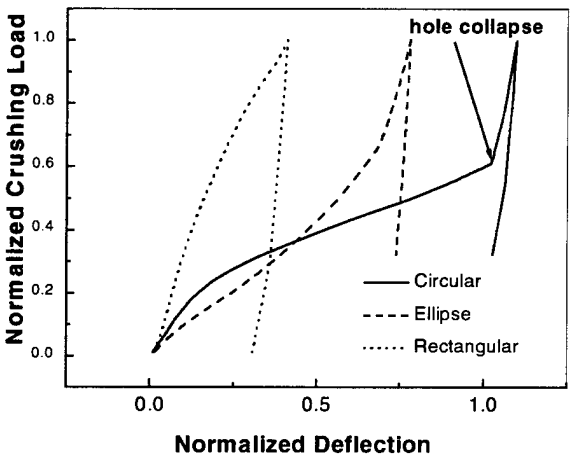

Figure 5 Load vs. Deflection crush response of the circular, elliptical and rectangular

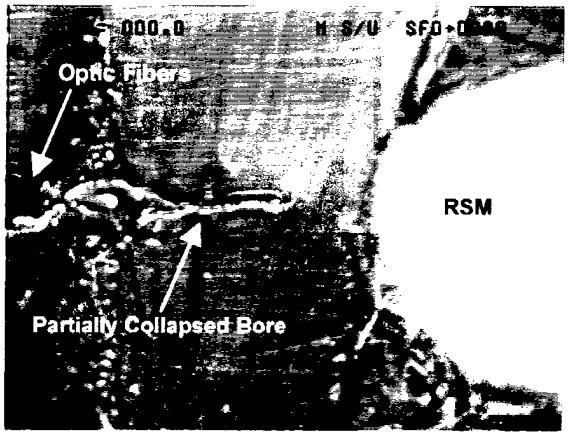

Figure 6 - Micrograph of a partially collapsed elliptical central-cavity cable

In addition to the reduced cross-sectional area, the moment of inertia is lower for the elliptical and rectangular sections than for the circular one. Therefore, by simply changing the shape, the cable design can have greatly improved crush resistance, lower weight and better unidirectional flexibility.

The rectangular cross-section demonstrates superior performance compared to the elliptical one. The load transmitted from the loading plates to the cable is quickly distributed laterally away from the bore and hence does not cause a collapse of the bore at all. The loads required to completely collapse the rectangular cable are more than twice that of typical crush requirements. The load versus deflection curves for the three different shaped sections is shown in Figure 5. The load-deflection curve for the circular case shows the telltale stiffening associated with tube collapse. The sharp increase in the slope there indicates a very sudden unstable collapse compared to the elliptical or rectangular cases that show little or no unstable collapse.

Laboratory crush experiments confirm the model very well. The deformed shape of the elliptical cable compares well with the observed experimental deformation shown in Figure 6. The figure illustrates the partial collapse of the bore similar to the deformed mesh shown in Figure 4.

The transverse compression performance (i.e. compression loading direction parallel to the plane of the containing the RSMs) is only slightly reduced according to both experiment and modeling for the circular case. The stiffening of the load-deflection response is a little more severe under transverse loading. The deformed shape of the transverse case tends to exhibit more of a pinching behavior due to the RSMs. In practice, the elliptical cable cannot be loaded in the transverse direction (along the major axis of the ellipse) because prior to reaching the structural yield load, the cable will flip over such that the load aligns with the minor axis. The rectangular section will not likely flip over like the elliptical one unless the aspect ratio is very high. However if the aspect ratio is 1 and the rectangular shape becomes square, the compressive response will be nearly equal in both directions.

Loose Tube Crush Simulation

The components of a five around one loose tube cable structure: the tubes, jacket and central strength member were meshed using general shell elements. These allow for three displacements and three rotations at each node as well as change in thickness and the integration points. Although the structure is generally S-Z stranded, only the helical part is considered in this model. The jacket shrinkage is accounted for in the initial stress-state of the model. The mode of deformations observed in the loose tube crush simulation is verified by experimental observation. The deformed and undeformed experimentally observed deformation is shown in Figure 8. The entire cable structure is deformed from an originally circular shape to an ellipse (Figures 7 and 8). The tubes crossing over the central strength member are pinched in those locations and the sides of the core bulge out and deform the jacket. Clearly, increasing the thickness of jacket material will increase the compression resistance by adding more material to support the load but also by constraining the tubes from bulging out. As the tubes pass over the top and bottom of the cable, they undergo periodic pinching between the jacket wall and the central strength member as shown in Figures 9 and 10. The tubes on the sides of the cable bulge out and deform the jacket as shown in Figure 11. The grayscale contours shown represent the Von Mises stress distribution in the sheath.

The plastically deformed bands observed at the point where any tube passes between the central strength member evidence the pinching

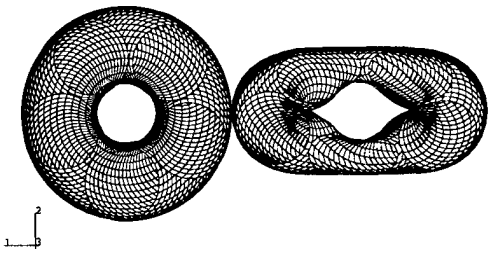

Figure 7 Predicted deformed shape of the crushed loose tube cable

Figure 8 - Observed deformation in a loose tube cable subject to crush

effect (Figures 9 and 10). Near the pinched regions local surface buckling causes dimples to form in the tube thus reducing the available space for the fibers.

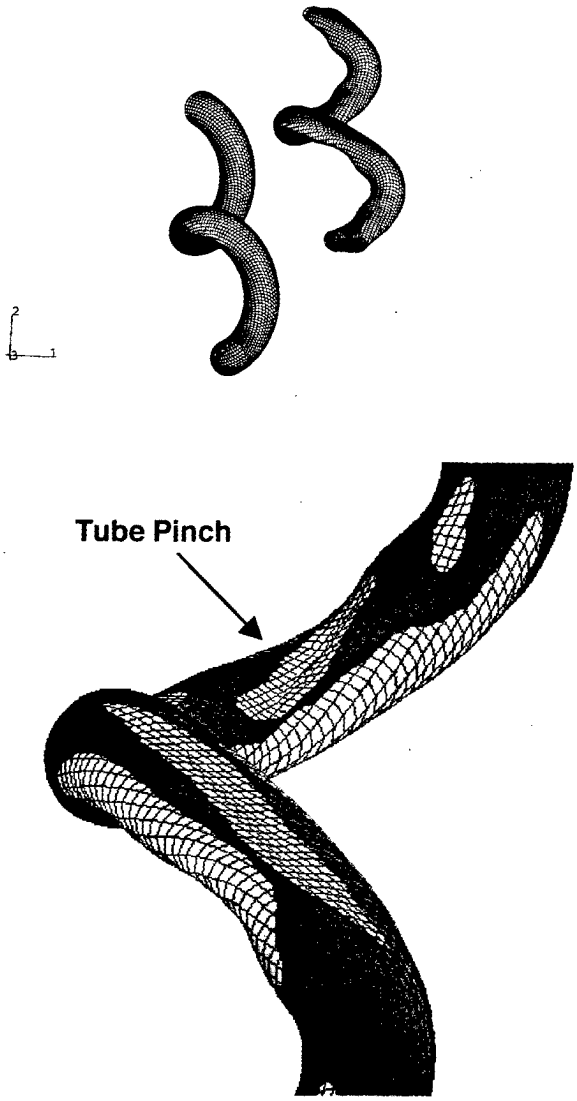

Figure 9 - Deformed and undeformed shapes and the stress distribution in the pinched region of a tube.

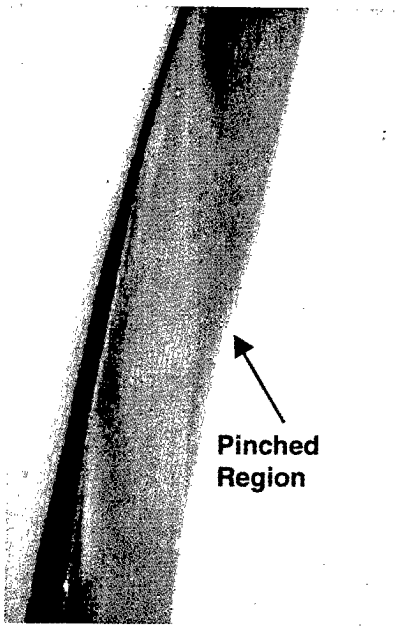

Figure 10 - Pinched tube from a loose tube compression specimen

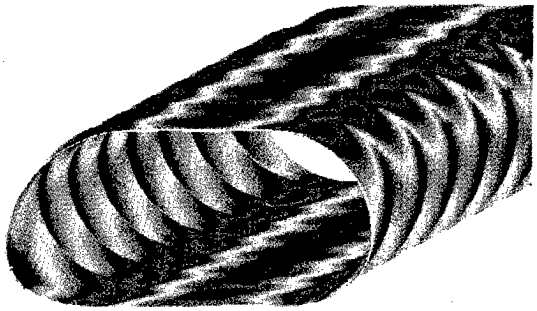

Figure 11- Stress distribution in the plastic sheath during crush loading.

CONCLUSIONS

The crush of fiber optic cables and cable components has been studied using a combination of finite element analysis and experiments. The modeling has been done on three basic cable components, namely the buffer tube, the central cavity design and the loose tube design. Buffer tube modeling was used to verify and calibrate the application of simple elastic-plastic material models for use in more complex cable simulations such as the loose tube cable. The central cavity cable simulations and experiments demonstrate excellent crush resistance. The presence of embedded radial strength members has little effect on the crush performance. The exterior shape of the cable has a dramatic influence on the crush response and can be used to reduce the amount of jacket material while increasing the crush performance.

The loose tube crush simulations demonstrate the fundamental mechanisms of deformation. Current work is ongoing to evaluate the relative influence of various design parameters on the cable crush resistance and to relate the compressive forces transmitted to fiber optic units to the induced loss. The research reviewed here demonstrates the fundamental mechanisms of crush response. Finite element modeling has proven to be a valuable supplementary tool for the design and analysis of optic fiber cable structures.

REFERENCES

[1] N. Mitsunaga, U. Katsuyama, Y. Ishida, Optical Cable Deformation Characteristics under Lateral Load, Report IEEE J, J64-B No. 2, Feb. 1981, pp. 142-149.

[2] C.L. Hogg, P. Huang, Crush Resistance Paramaters of Loose Tube Optical Fiber Cables and the Application to Cable Design, 16th Australian Conference on Optic Fiber Technology Proceedings, pp390-3, Dec. 1991.

[3] P. Neveux, W. Hatton, Designing Compression Resistance in Loose Tube Cables, IWCS Proceedings 1987, pp. 656-661.

[4] C. A. Truesdell and W. Noll, The nonlinear field theories of mechanics, in: S. Flugge, ed.:Hadnbuch der Physik, Vol. III/s (Springer-Verlag, Berlin, 1965).

[5] ABAQUS 5.7 Standard Theory Manual

[6] ABAQUS 5.7 Explicit Theory Manual

AUTHORS

J. Boyet Stevens was born in 1964 and is the Computer Modeling Group Leader at Alcatel Telecommunications Optical Fiber Cable Competence Center. He holds a B.S. degree in Engineering Science and Mechanics and a M.S. degree in Engineering Mechanics from Virginia Polytechnic Institute and State University. His experience includes finite element modeling and characterization of composite materials for aerospace and ballistic applications. Since 1997, Boyet has been working for Alcatel Telecommunications Claremont Optical Fiber Cable Competence Center (OFCCC) on finite element modeling of various optic fiber cable designs involving finite plastic deformations and contact.

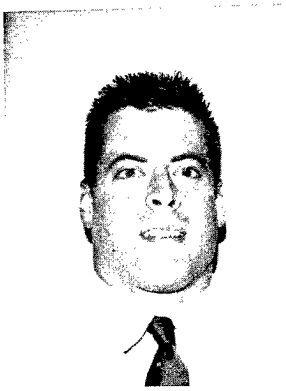

Brian G. Risch is a Senior Materials Scientist at Alcatel Telecommunications Optical Fiber Cable Competence Center. He holds a B.A. degree in Physics from Carleton College and a Ph.D. in Materials Science and Engineering from Virginia Polytechnic Institute and State University. His Ph.D. research was in the area of polymer crystallization and structure property relationships in polymers. Directly after he finished his Ph.D. he worked for ORD laboratories in the area of optical polymers developing new polyurethane and polythiourethanes for high performance ophthalmic lens applications. Since 1996 Brian has worked for Alcatel Telecommunications Claremont OFCCC in the area of thermoplastic cable materials. His specialization has been in the area of processing and crystallization behavior of polyolefins for cable applications.

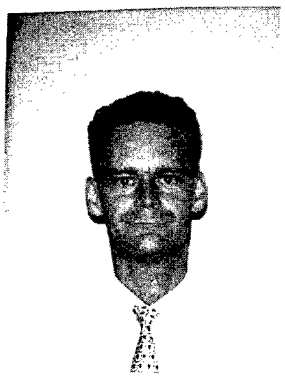

Peter Ellison is a design engineer at Alcatel Telecommunications Optic Fiber Cable Competence Center. He holds a Master of Science degree in Electrical Engineering from Chalmers University of Technology, Sweden, and has been involved in cable research and development since 1988.

Christian Bastide was born in 1957. He joined Alcatel Cable after his graduation from Grenoble University with the DEA (physics) degree and with a thesis (microbending loss in optical fiber, Alcatel Alsthom Research) in 1985. He has been engaged in research and development of optical fiber cables. He is an engineer of the cable design Group of Optical Fiber Cable Competence Center.

Development of 2000-fiber Cable with SZ-stranded U-grooves and Slotted Rod

Hideyuki Iwata, Masaru Okada, Jiro Sogame, Hiroyuki Akimoto, Shigeru Tomita, Yutaka Dei

NTT Access Network Systems Laboratories

Hanabatake, Tsukuba, Ibaraki, 305-0805 JAPAN

Phone +81(298)52-2522
Fax +81(298)60-6130
Email address: iwata@ansl.ntt.co.jp

ABSTRACT

In this paper, we describe the design and performance of 2000-fiber cable with an SZ stranded slotted rod and a U-groove. This structure is suitable for use with the mid span access technique which allows easy branching because fiber ribbons can be easily extracted from a slotted rod without cutting it.

We also studied reducing the cable jacket friction coefficient by adding lubricant to the polyethylene cable jacket which enabled us to reduce the required cable installation force.

This cable will assist the economical construction of optical access networks for fiber to the home (FTTH).

INTRODUCTION

The cost of optical fiber cable must be reduced in order to construct optical access networks economically for FTTH. In addition, the characteristics must allow a reduction in the total cost including that incurred in joining and installation work.

Cable branching through the use of mid span access technologies enables efficient access networks to be economically constructed when the service demand is unpredictable.

An increase in the number of fibers in a duct achieved through the use of a multiple installation technique will allow the effective use of existing ducts.

We reported on 1000-fiber single slotted rod cable and 3000-fiber cables at a past IWCS [1,2]. Between 1000 and 3000 fiber cables are needed to achieve the above levels of performance.

In this paper, we describe the design and performance of 2000-fiber cable with SZ stranded U-grooves and a slotted Rod.

CABLE STRUCTURE FOR MULTIPLE INSTALLATION

Currently we install additional cable alongside existing cable in a 75 mm diameter duct. For this we use an additional inner duct and the multiple installation technique.

The maximum fiber count when one additional duct is used is 1600 with this method.

We studied a way of installing an additional cable without the need for an additional duct. The current and proposed approaches are shown in Fig.1(a) and (b), respectively.

a) Cable diameter in a duct

Figure 2 shows the calculated model of one and two additional cables installed in a duct. The relationship between the radius of the additional and existing cables when two cables are installed in a duct is given by

$$r_{c2}=r_{dc}-r_{c1} \qquad \text{----------(1)}$$

where the inner radius of a duct r_{dc} is less than 73/2 mm for a cable capable passing through a bent duct.

We also assumed that when two additional cables are used they both have the same radius, and the relationship between rdc, rc1, rc2 and rc3 is expressed by the following equation.

$$r_{c2}=r_{c3}=\frac{2(r_{dc}+x)^2}{\{r_{c1}+2(r_{dc}+x)\}} \qquad \text{----------(2)}$$

where x is the distance between the center of the duct and the line which connects centers of two additional cables. The cable radius (rc1,rc2,rc3) is including the pulling head thickness.

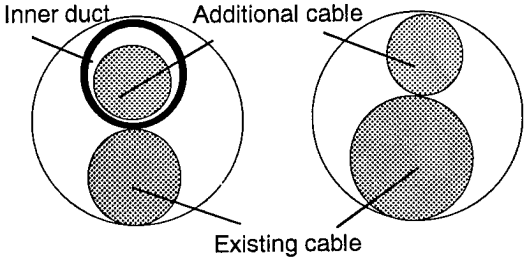

(a) Current method (b) New method

Figure 1 Multiple installation method

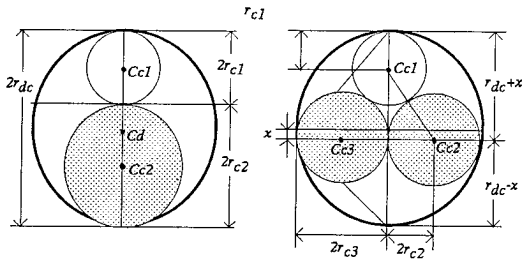

Figure 2 Calculated model of additional cables in a duct

b)The fiber count N for cable structures

b.1) Single slotted rod cable

The diameter of a single slotted rod cable with ten stacked 8 fiber ribbons in a slot is given by [2]

$$D_S=2\left(\sqrt{\left\{S_h+\frac{\left(\frac{w}{\cos\left(\pi-\frac{\pi}{N_S}\right)}+S_W\right)}{2\tan\left(\frac{\pi}{N_S}\right)}\right\}^2+\left(\frac{S_W}{2}\right)^2}+B_t+S_t\right) \quad \text{----------(3)}$$

Where w is rib thickness, St is sheath thickness, Bt is water blocking tape thickness, Sh is slot height,Sw is slot width and Ns is slot number.

b.2) Multi slotted rod cable

The diameter of a multi slotted rod cable with ten stacked 8 fiber ribbons in a slot is given by [3]

$$D_m=2\left(\left(D_s-B_t-2S_t\right)\left(\frac{1}{\sin\left(\frac{\pi}{N_m}\right)}-1\right)+D_s+2\left(B_t+S_t\right)\right) \quad \text{----------(4)}$$

Where Nm is slotted rod number.

b.3) Single slotted rod/U-groove cable

The diameter of a single slotted rod/ U-groove cable with ten stacked 8 fiber ribbons in a slot is given by[2]

$$D_u=2\left(\sqrt{\left(U_h+\frac{U_w}{2\tan\left(\frac{\pi}{N_u}\right)}\right)^2+\left(\frac{U_w}{2}\right)^2}+\left(2B_t+S_t\right)\right) \quad \text{----------(5)}$$

Where Uw is U-groove unit width, Nu is groove number and Uh is U-groove unit height.

Figure 3 shows the cable diameter for three different cable structures with 8 fiber ribbons calculated using these equations. Based on these results, the relationship between the fiber count N for three different cable structures and cable diameter is given by approximate equations (6),(7) and (8)

$$N_s=\frac{D_s-12.5}{0.016} \quad \text{----------(6)}$$

$$N_m=\frac{D_m-27}{0.009} \quad \text{----------(7)}$$

$$N_u=\frac{D_u-20}{0.0095} \quad \text{----------(8)}$$

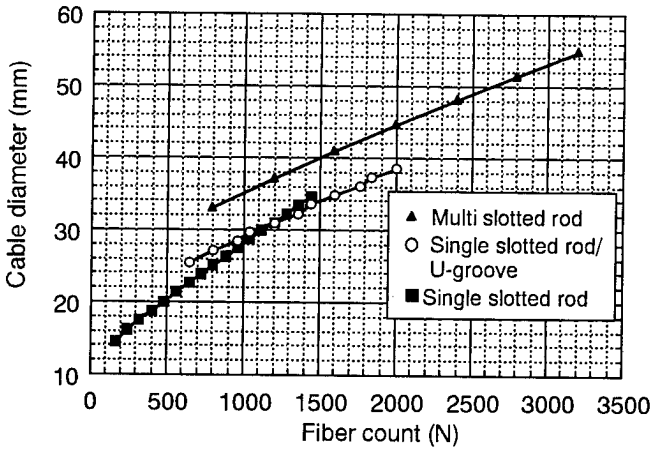

Figure 3 Cable diameter for three different cable structures with 8 fiber ribbons

Figure 4 shows the fiber count in a duct with one additional cable calculated using equations (1),(6) and (8). Based on the results, the maximum fiber count N in a duct is from 1600 to 2600.

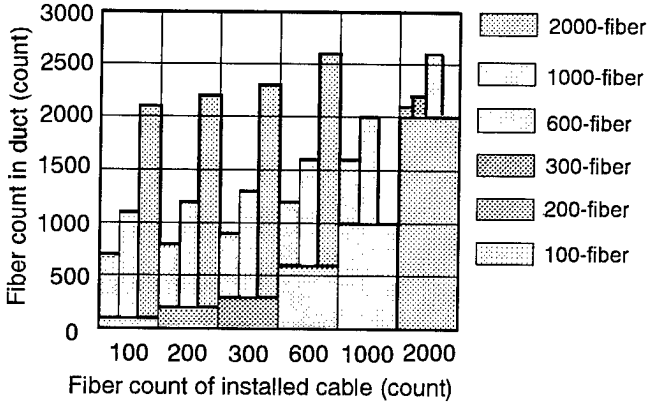

Figure 4 Fiber count in a duct with one additional cable

Figure 5 shows the fiber count in a duct with two additional cables calculated using equations (2), (6) and (8). Based on these results, the maximum fiber count N in a duct is from 600 to 2600.

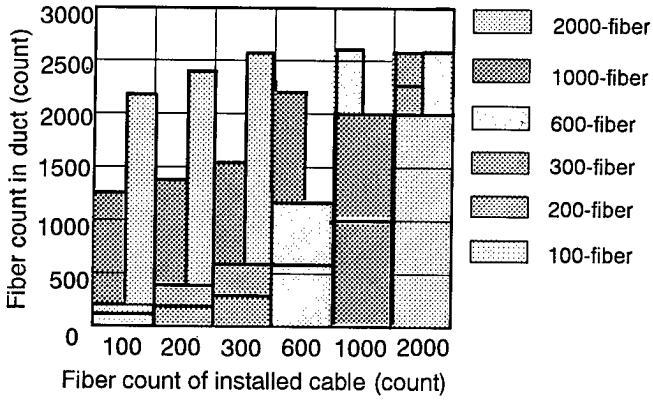

Figure 5 Fiber count in a duct with two additional cables

CABLE STRUCTURE FOR BRANCHING

A conventional high count fiber cable structure with a large outer diameter would make it difficult to extract fiber ribbons easily from a slotted rod for cable branching. Therefore, there is a danger of the optical fiber loss increasing during cable and fiber handling. Our SZ cable structure allows easy cable branching via the mid span access technique. The cable branching time is much shorter than with the conventional method.

For ease of branching, a certain excess length of fiber ribbon is needed for identification and joining work. The use of a conventional identification tool requires a 20 mm space between the slotted rod and the fiber ribbon. The sag length is determined by the reverse angle, the distance between a slotted rod and the ribbon in the slots, and the reverse pitch.

a) Fiber sag length for branching point

The sag length is different depending on the point at which the cable jacket is removed when the removed length is less than twice the reverse pitch.

When the center of the removed length of the cable jacket is the reverse pitch point, the sag length S1 is expressed as this equation.

$$S_1 = \sqrt{\left(\int_0^{\theta}\sqrt{1+\left(\frac{a\Phi'}{2}\cos\theta\right)^2}d\theta\right)^2 - \left(\frac{L}{2}\right)^2} \qquad \text{----------(9)}$$

$$\theta = \frac{L\pi}{2P} \qquad \text{----------(10)}$$

where a is the distance between the center of the rod and the fiber ribbon in a slot. P is the reverse pitch, Φ is the reverse angle and L is the removed length of cable jacket.

Conversely, when the center of the removed length of the cable jacket is between the reverse points, the sag length S2 is expressed as these equations.

Where the locus of an optical fiber ribbon assembled in an SZ slotted rod is assumed to be a sine wave.

$$S_2 = \sqrt{\left(\int_0^{\theta}\sqrt{1+\left(\frac{a\Phi'}{2}\sin\theta\right)^2}d\theta\right)^2 - \sqrt{\left(\frac{L}{2}\right)^2+\left(\frac{a\Phi}{2}\sin\theta\right)^2}^2} \qquad \text{----------(11)}$$

Figure 6 shows the calculated results of sag length versus cable jacket removal length and removal cutting point.

Here the reverse pitch was 500 mm and the distances between the center of the slotted rod and the fiber ribbon in the slot were 8 and 15 mm.

Based on the results, when the length of cable jacket to be removed was shorter than twice the reverse pitch, the sag length was different depending on the position of the central cable jacket removal point.

We could obtain sufficient sag length by increasing the distance between the center of the slotted rod and the fiber ribbon in the slot.

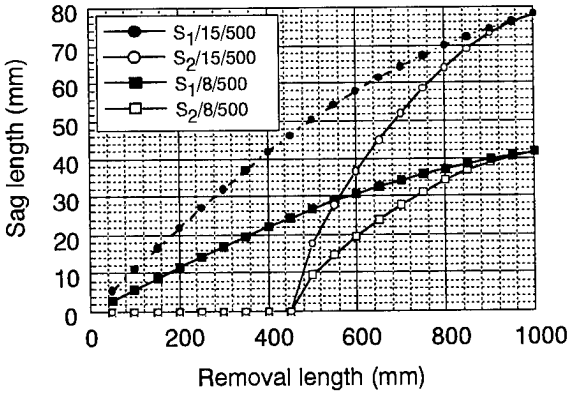

Figure 6 Calculated results of sag length versus cable jacket removal length and removal cutting point.

Next, we calculated the sag length for different reverse pitches.

Figure 7 shows the calculated results of sag length versus cable jacket removal length and removal cutting point.

Here the reverse pitch was 350, 400, 450, and 500 mm and the distance between the center of the slotted rod and the fiber ribbon in the slot was 8 mm.

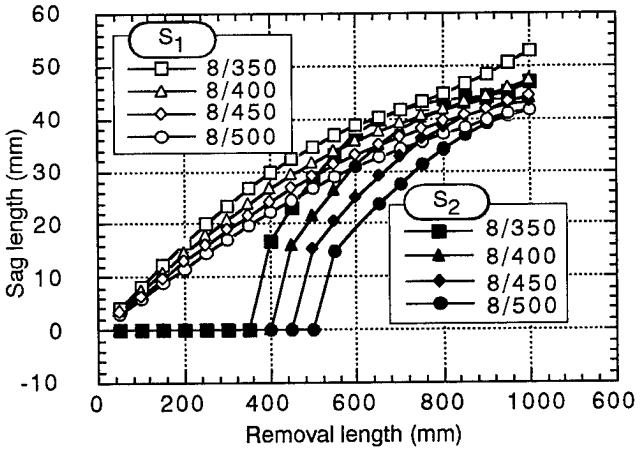

Figure 7 Calculated results of sag length versus cable jacket removal length and removal cutting point.

Based on these results, when the length of cable jacket to be removed was 700 mm, the sag length was more than 20 mm for each position for all reverse pitches. We should select a short reverse pitch to obtain sufficient sag length. But we must consider the fact that a reduction in the reverse pitch increases the optical fiber strain and bending in the fiber ribbon.

2000-FIBER PROTOTYPE CABLE

a) Structure

A cross-sectional view of the prototype 2000-fiber cable is shown in Fig.8. This cable has fifteen SZ-stranded U-grooves which are stranded around an SZ-stranded slotted rod with ten slots.

Ten stacked 8-fiber ribbons are contained in each U-groove and slot. The cable diameter is 40 mm, which is the same as the formerly used 1000 -fiber multi slotted rod cable. Therefore, the currently used installation tools can be used with this cable. Two prototype cables evaluated. In one, the reverse pitches of the slotted rod and U-grooves were both 300 mm, in the other they were 350 and 500 mm, respectively.

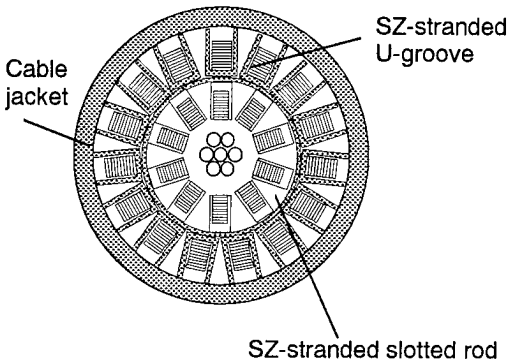

Figure 8 Structure of 2000-fiber prototype cable

b) Performance

Table 1 shows the attenuation, mechanical and temperature characteristics for the two types of cable. The attenuation performance was similar to that of currently used optical cable. The optical loss changes were measured for temperatures between -30 and +60 ℃ with the cable off the reel.

The optical loss of the top corner fibers in a U-groove increased less than 0.2 dB/km.

The mechanical performance at a wavelength of 1550 nm in bending, lateral pressure , tensile and squeezing tests was found to be similar to that of current cable.

Table 1 Prototype cable performance

Test item	Result	
	Inner	Outer
Attenuation at 1550 nm	<0.25 dB/km	
Temperature cycle at 1550 nm:-30～+70℃	<0.05 dB/km	
Bending: 200 mmR	No loss increase	
Lateral pressure: 30 N/mm	No loss increase	
Tension: 0.25%	No loss increase	
Squeeze: 0.2 % R=600 mm	No loss increase	

c) Strain distribution of fiber in the cable

Figure 9 shows the fiber strain on and after applying a maximum pulling force of 7840N to trial 2000-fiber SZ-stranded cable and 1000-fiber helically stranded cable measured by B-OTDR.

Here the open circles show the fiber strain for helically stranded cable. The filled circles show the fiber strain in an SZ stranded U-groove unit. and the open squares show the fiber strain in the SZ-stranded single slotted rod.

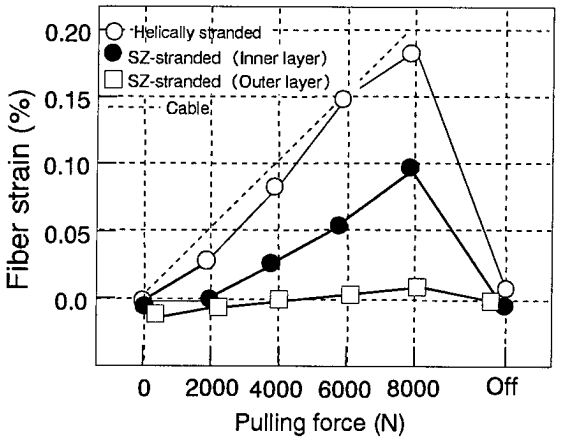

Figure 9 Fiber strain on and after applying a pulling force

Based on the results, the fiber strain in the helically slotted rod was as same as the applied cable elongation pulling force. The fiber strain in the SZ-stranded slotted rod was half that for cable elongation.

In addition, the fiber strain in the SZ-stranded U-groove caused no elongation. Figure 10 shows the slot locus of helically stranded rod and an SZ-stranded rod expanded into a plane. The tensile fiber strain in the SZ-stranded rod was smaller than in the helically stranded rod because the equivalence bending radius decrease reduced the applied force in the fiber ribbon. In the same figure, it looks that the increase in the distance between the center of the slotted rod and the fiber ribbon reduced the fiber strain.

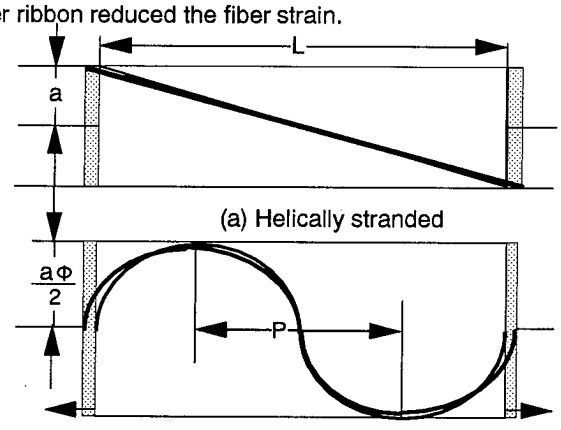

a: Distance between center of slotted rod and fiber ribbon in slot
L: Lay length
P: Reverse pitch
Φ:Reverse angle

Figure 10 Slot locus of helically and SZ stranded rod expanded into a plane

d) Mid span access performance

d.1) Fiber ribbon sag length

Figure 11 shows a photograph of the cable with a 7 00 mm length of its jacket removed. Figure 12 shows the relationship between the measured sag length and reverse pitch for an outer SZ-stranded U-groove. When the outer reverse pitch was 900 mm the sag length was more than 20 mm but in some cases it was less than 20 mm dependig on the position from which the cable jacket was removed.

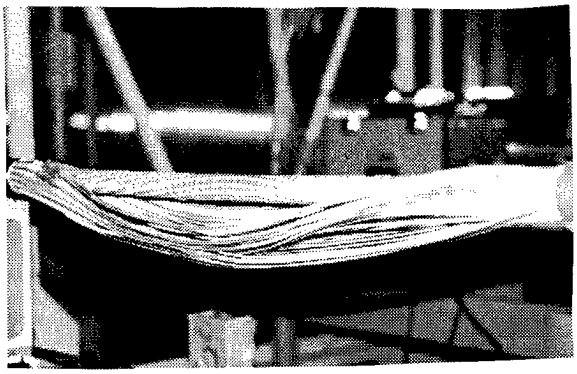

Figure 11 Photograph of cable with cable jacket removed

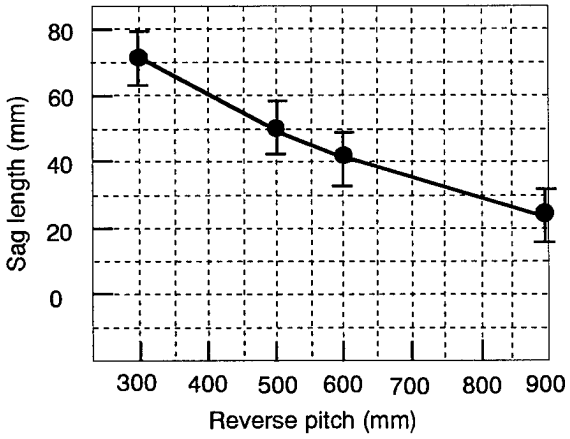

Figure 12 Sag length with mid span access

d.2) Handling performance at mid span access

We measured the optical loss change at a wavelength of 1550 nm while working on mid-span access.

Figure 13 shows the handling characteristics. The procedure is divided into seven stages, removing the cable jacket, removing water blocking tapes, extracting ribbons from U-groove, cutting the U-grooves, removing water blocking tapes, extracting ribbons from slot and cutting the slotted rod.

The maximum optical loss change for both cutting the U-groove and removing the slotted core was about 1 dB , but there were no loss changes with the other procedures.

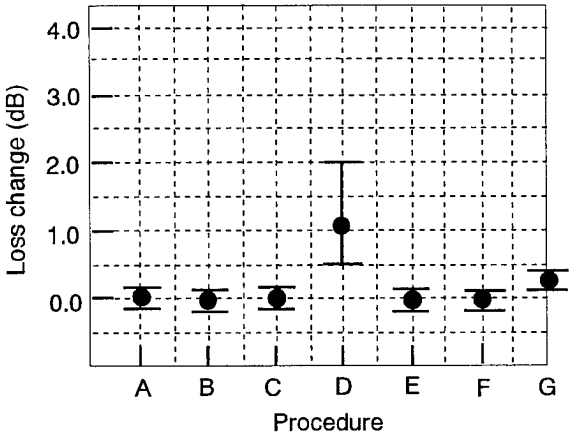

A:Removing jacket
B:Removing water blocking tapes
C: Taking out ribbons in U-groove
D: Cutting U-groove
E: Removing water blocking tapes
F: Taking out ribbons in slot
G: Cutting slotted rod

Figure 13 Handling characteristics

Figure 14 shows a photograph after cutting slotted rod for mid span access.

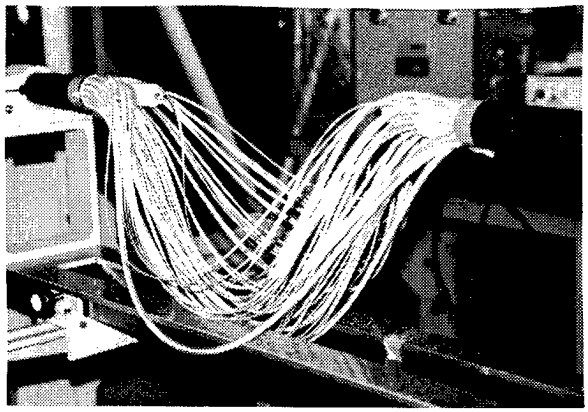

Figure 14 Photograph of cutting slotted rod for mid span access.

CABLE JACKET

A reduction in the cable jacket friction coefficient means that the length of cable that can be installed is longer than for conventional cable. This also means a reduction in the required cable pulling force.

The reduction in the cable jacket friction coefficient makes it possible to install additional cable easily into an existing duct already containing cable. We investigated the effect on the cable jacket friction coefficient of adding lubricant to the polyethylene cable jacket .

Table 2 shows the static and dynamic coefficients of friction when using a sheet sample between standard and lubricated cable jacket material, between lubricants, and between lubricant and PVC. The test method we used were ASTM D-1894 and 1895.

Table 2 Static and dynamic coefficients of friction for cable jacket material

	Coefficient of friction	
	Static	Dynamic
Standard/ lubricated	0.60	0.45
Lubricated/ lubricated	0.25	0.15
Lubricated/ PVC	0.50	0.35

Table 3 shows the pulling force needed to draw a 2000-fiber cable into a duct containing a 600-fiber cable. The cable jacket friction coefficient of the 2 000-fiber cables depends on whether or not lubricant is added to the polyethylene cable jacket. When we added lubricant to the polyethylene cable jacket of an existing 600-fiber cable in a 15 m long test duct made of PVC, there was a decrease of 30% in the pulling force required for the additional cable.

Table 3 Pulling force of additional cable

	Additional 2000-fiber cable	
	Standard	Low
Existing 600-fiber cable	14 kgf	11 kgf

Figure 14 shows the recovery the dynamic coefficient of friction after rubbing the surface of lubricant material sheet. The coefficient of friction recovered in about a week. It shows that we can expect to have same pulling force characteristic in a week after the installation.

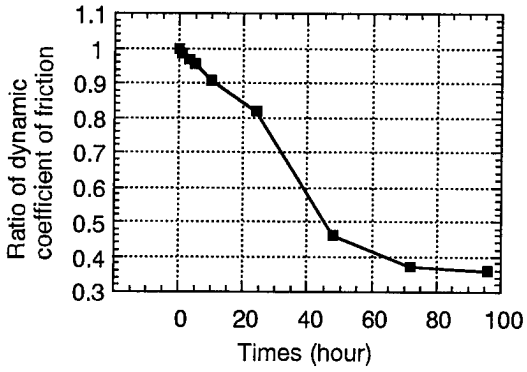

Figure 14 Recovery the dynamic coefficient of friction after rubbing the surface

CONCLUSION

We studied on design and performance for 2000-fiber cable. These SZ structures provide ease of branching without having to cut the slotted rod. The cable branching time is much less than that with the conventional method.

Also we added lubricant to the polyethylene cable jacket of these cable, there was a decrease of 30% in the pulling force required for the additional cable.

Our cable provides good levels of performance and is promising with regard to upgrading the access network for FTTH.

ACKNOWLEDGMENTS

The authors wish to thank K.Nishimura, H.Shirakawa and A.Hirooka for continuous encouragement.

REFERENCES

[1]H.Iwata, M.Tsutsumi, E.Nakamura, N.Matsumoto, S. Hayami, S.Nagasawa and T.Tanifuji, "Pre-connectorized 1000-fiber single slotted core cable" 44th IWCS, pp. 627-634 (1995).

[2] H.Iwata et al., "Development of 3000-fiber cable using 16-fiber ribbons" 45th IWCS, pp. 638-644 (1996).

[3] H.Iwata et al., "Pre-connectorized high density optical fiber cable technology" IEICE Trans.Com.vol.E80-B,no. 4,pp540-550 (1997).

Hideyuki Iwata

NTT

Access Network

Systems Laboratories

Tsukuba, Ibaraki,

305-0805 , JAPAN

Hideyuki Iwata is a research engineer. He was born in 1965 and received B.E. and M.E. degrees in electronic engineering from Yamagata University in 1989 and 1991, respectively.

He joined NTT in 1991. Since 1993 he has been engaged in research on high-density underground and aerial optical fiber cable. Mr. Iwata is a member of IEICE of Japan.

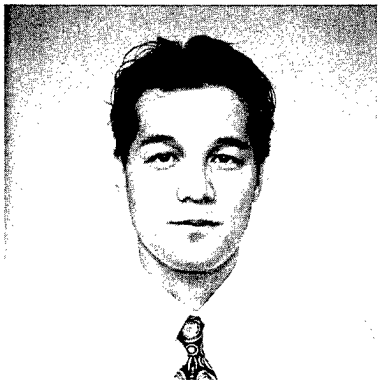

Hiroyuki Akimoto

NTT

Access Network

Systems Laboratories

Tsukuba, Ibaraki,

305-0805 , JAPAN

Hiroyuki Akimoto is engineer. He was born in 1965 and graduated from Miyako National Collage of Technology in 1989. He joined NTT in 1989. Since 1 997 he has been engaged in research on aerial optical fiber cable.

Masaru Okada

NTT

Access Network

Systems Laboratories

Tsukuba, Ibaraki,

305-0805 , JAPAN

Masaru Okada is an engineer. He was born in 1970 and graduated from Kisarazu National Collage of Technology in 1991. He joined NTT in 1991.

Since 1995 he has been engaged in research on aerial optical fiber cable.

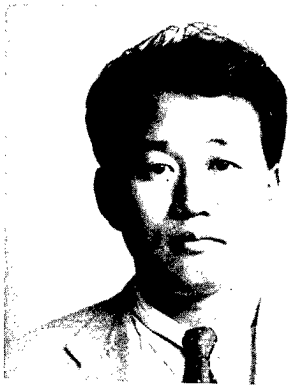

Shigeru Tomita

NTT

Access Network

Systems Laboratories

Tsukuba, Ibaraki,

305-0805 , JAPAN

Shigeru Tomita was born in 1960 and received B.E. and Ph.D. degrees in electrical engineering from Nihon University in 1983 and 1992, respectively.

In 1983 he joined NTT Laboratories, where he has been engaged in research on optical fiber cable.

Dr. Tomita is a member of the Institute of Electronics, Information and Communication Engineers of Japan.

Jiro Sogame

NTT

Access Network

Systems Laboratories

Tsukuba, Ibaraki,

305-0805 , JAPAN

Jiro Sogame was born in Ehime Prefecture, JAPAN, in1968. He received the B.E and M.S degrees in mechanical engineering from Ehime University in 1993. He joined NTT in 1993. He has been engaged in developing underground optical fiber cable installation technology.

Yutaka Dei

NTT

Access Network

Systems Laboratories

Tsukuba, Ibaraki,

305-0805 , JAPAN

Yutaka Dei was born in 1955 and received B.E. degrees in from Hokkaido University in 1978.

In 1978 he joined NTT. He is engaged in research and development on optical fiber cable and installation technology .

Design of ultra high density and high count 2000 optical fiber cable for easy branching

Daisuke Iwakura, Ichiro Kobayashi, Masami Hara, Hideaki Kanzaki
Hideyo Hiramatsu , Yasuhiro Kamikura

Opto-Technology Laboratory
The Furukawa Electric Co.,Ltd

Abstract

We designed ultra-high density and high count optical fiber cables which have good mid-span branching characteristics.

In order to realize good mid-span branching, we designed a cable structure with SZ slotted –rod for the internal layer and SZ –stranded U-grooves for the external layer . We investigated in detail the amount of ribbon slack which is one of the important parameters to indicate the feasibility of mid-span branching. It will be reported in this paper that the reverse pitch under 510 mm for external layer and under 380mm for internal layer are necessary to obtain sufficient ribbon slack of more than 20mm at any point where cable sheath is removed for 700mm. We manufactured a 2000-fiber count cable to actually evaluate the mid-span branching characteristics. The reverse pitch was 500mm for external layer and 350 mm for internal layer. By removing the cable jacket for 700mm , ribbon slack length of more than 20mm were obtained for both layers. And good initial transmission loss was also obtained .

1.Introduction

In order to realize FTTH , economical construction of access network will be one of the most important targets in developing new cables. For example it may be demanded of cables to be installed easily in the existing duct along with the already existing cables. And good mid-span branching characteristics may be also an important requirement.

In Japan in order to construct FTTH network ,high count optical fiber cable such as 2000-fiber count cables may be demanded in the subscriber networks .

Since it is very difficult to meet both demands of ultra high fiber density and easy mid-span branching with the conventional single slotted rod design, we investigated a new cable design .

2. High fiber density and easy mid-span branchig

Fig.1 depicts the relationship between fiber counts and fiber density of single slotted rod type(fig .2) and double layer type(fig3). In either design, a 10 layer stack of 8 fiber ribbons is accommodated in each slot.

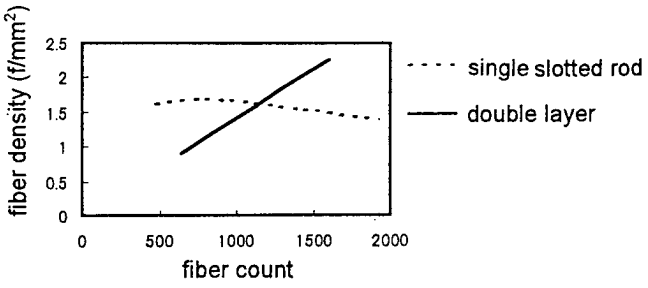

fig.1 theoretical investigation of fiber density .

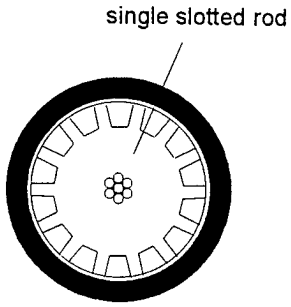

fig.2 single layer structure

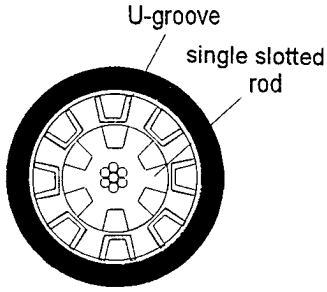

fig.3 double layer structure

For the fiber count over 1200, double layer structure can realize higher fiber density than single layer structure.

Next the structure to allow easy mid-span branching was considered. In the case of mid-span branching of multi layer structure , it is necessary that external layers can be removed easily without damaging the fibers. For this reason, we adopted SZ-stranded u-groove structure for external layer (fig.4). For internal layer we adopted the SZ slotted rod design so that fiber ribbons can be easily extracted from the slots without cutting the slotted rod .(fig.5)

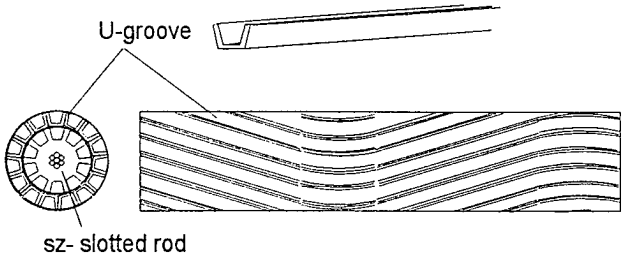

fig.4 structure of external layer (u-groove)

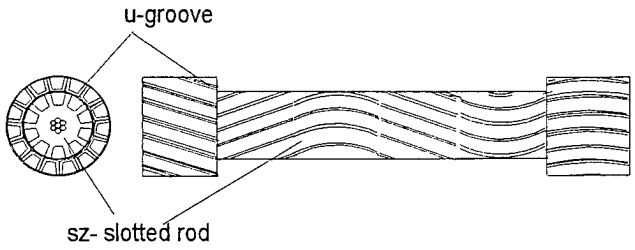

fig.5 structure of internal layer (SZ-slotted rod)

Generally the use of a conventional fiber identification tool requires a 20mm space between the surface of the slotted rod and the extracted ribbon fiber.(fig.6)

We designed the cable so that slack length of more than 20mm can be secured at arbitrary point of cable .

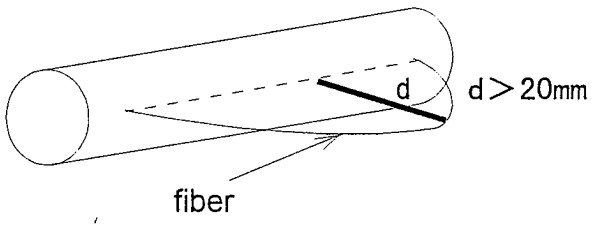

fig.6 necessary slack length

In the following sections of this paper , the calculation method of the slack length will be explained first. The relationship between slack length and extraction length divided by reverse pitch will be investigated. We will then explain the design concept of 2000-fiber count cable to attain sufficient ribbon slack for mid-span branching. We will show that the calculated and the measured ribbon slack coincide quite well, thus optimal reverse pitch was successfully obtained. Finally we will show the characteristics of the trial cable.

3 Calculation of slack length

Examination of fiber slack length of SZ-stranded structure has been reported in some papers[1,2,3]. In this paper we present more detailed calculation considering cable core diameter and the

position of sheath removal. The slack length of the extracted fiber is very much affected by the position and extraction length . Extraction length is defined as cable length from which fibers are extracted. For example , in **fig.7** and **fig.8,** although extracting length L is same, the effective slack length d is very different. In fig.7, both ends of extracted ribbon, A and B, are on the same plane. On the other hand in fig.8, A and B are shifted by angle α, so the slack length d_α is smaller than d_0 by the length D indicated in fig.8. In the case of high fiber count cable such as cables over 1000-fiber count R0(radius to the fiber) becomes larger and therefore the value of D also becomes larger . In this report we calculated slack length considering the value D. Next we will explain formulas used to calculate the slack length.

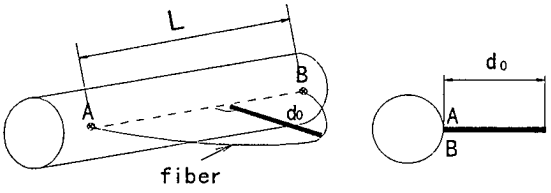

fig.7 long slack condition

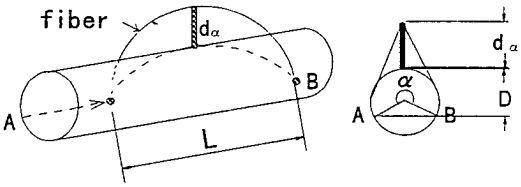

fig.8 short slack condition

Fig.9 is the development of SZ locus .In this model, P is SZ reverse pitch 、θ is reverse angle and R0 is radius to ribbon fiber . Calculation was made for two extreme cases of different sheath removal positions. One case is when the center of the sheath removal corresponds to the reverse point (in this case, slack length is indicated as d1 in the formulas.) Maximum slack is expected in this case. The other case is when the center of the sheath removal corresponds the center between reverse points. (in this case slack length is indicated as dD2 in the formulas). (fig.10) Minimum slack is expected in this case

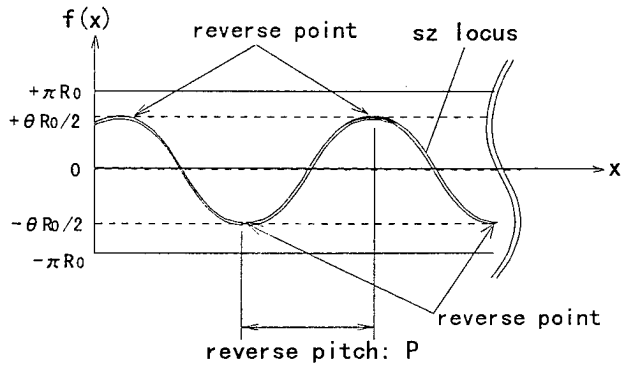

fig.9 Development of SZ locus

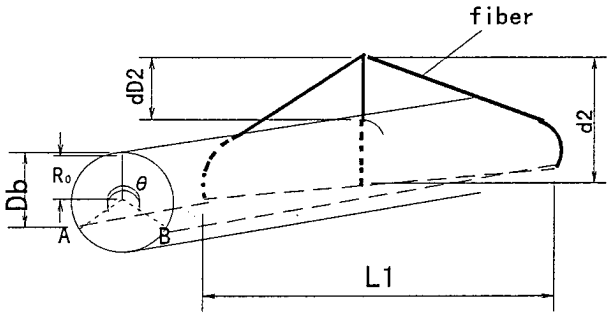

fig.10 calculation model

Case1: when reverse point is the center of sheath removal

$$f(x)=\frac{R0}{2}\theta\cos(\frac{\pi x}{p}) \qquad (1)$$

$$s1(L)=\int_{\frac{-L}{2}}^{\frac{L}{2}}\sqrt{1+\left(\frac{d}{dx}f(x)\right)^2}\,dx \qquad (2)$$

$$d1(L)=\sqrt{\left(\frac{s1(L)}{2}\right)^2-\left(\frac{L}{2}\right)^2} \qquad (3)$$

Case2: when the center between reverse point is the center of sheath removal

$$g(x) = \frac{R0}{2}\theta\cos(\frac{\pi x}{p} - \frac{\pi}{2}) \quad (4)$$

$$s2(L) = \int_{\frac{-L}{2}}^{\frac{L}{2}} \sqrt{1 + \left(\frac{d}{dx}g(x)\right)^2}\, dx \quad (5)$$

$$Da(L) = \frac{R0}{2}\sin(\frac{\theta}{2}\sin(\pi\frac{L}{2p})) \quad (6)$$

$$Db(L) = \frac{R_0}{2}\left(1 - \cos\left(\frac{2}{R0}g\left(\frac{L}{2}\right)\right)\right) \quad (7)$$

$$l_1(L) = \sqrt{(L)^2 + \left(2Da\left(\frac{L}{2}\right)\right)^2} \quad (8)$$

$$d2(L) = \sqrt{\left(\frac{s2(L)}{2}\right)^2 - \left(\frac{l1(L)}{2}\right)^2} \quad (9)$$

$$dD2(L) = d2(L) - Db(L) \quad (10)$$

Fig.11 shows the result of calculation of d1 and dD2 for different values of L (extraction length) /P(reverse pitch) in the case of two different R0 (5,10mm).

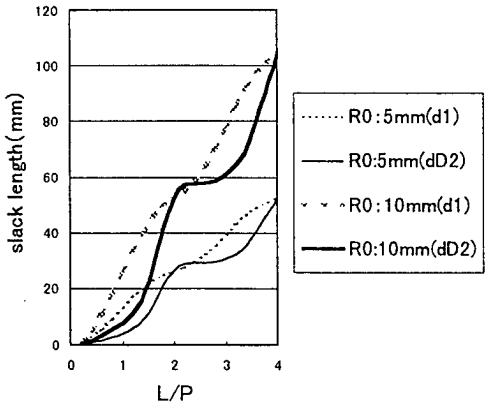

Fig.11 theoretical investigation of slack Length

fig.11 shows that the slack length differs very much depending on the values of L/P,R0 and sheath removal position. And when L/P=2n(n is integer), the slack length becomes independent of sheath removal position. This can be easily understood from the formula (7) (Db(L)=0 at L=2nP). This suggests that the fiber slack can be obtained stably by setting the extraction length L equal to 2Pn

4 Ribbon extraction from external layer

In case of double layer structure, it is important that the external layer can be easily removed. Since ribbon fibers are accommodated in the u-groove, care should be taken not to bend the u-groove excessively. (especially at the removed sheath edge). We measured the attenuation increase of ribbon fibers in u-groove segment when the segment is bent at the point X (mm) from the edge of the removed sheath on the assumption that such bend can occur during the branching work. In the experiment, 10 pieces of 8-fiber ribbons were stacked in a segment. The segment was bent at X :30mm、40mm、and 50mm. The radius of bend R ranged from 20mm to 45mm. The set up of experiment is shown in fig12. The result are shown in fig.13.

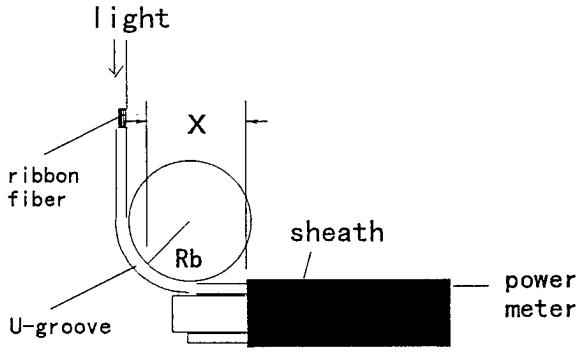

fig.12 set up of experiment

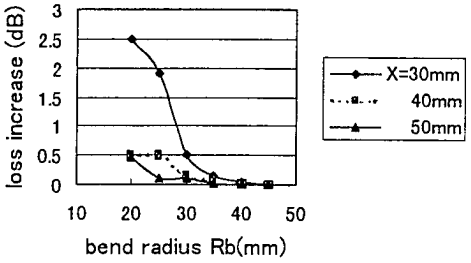

fig.13 fiber loss increase vs. bend radius

Fig.13 shows that the loss increase is negligible at X=50 if bending radius R is larger than 30mm. Higher loss increase is observed for smaller X. This is because U-groove is distorted more easily by the sheath edge when the bending point is close to it. So it was decided to leave about 50mm of outer layer segment from the edges of sheath. In this case, when the length of removed jacket is L_E(mm), the length of exposed inner layer L_I is expressed as follows.

External layer : L_E mm

Internal layer : $L_I = (L_E - 100)$mm

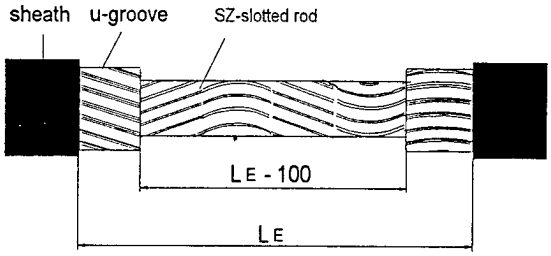

fig14 cable after the removed of external u-groove

5 Design of 2000-fiber count cable

5-1 Design of cross section

Fig.15 shows the cross section of 2000-fiber count cable. The inner layer is SZ-slotted rod with 10 slots. The external layer is SZ stranded 15 pieces of u-groove . Cable diameter is 40mm. In this cable, the ribbons are accommodated in the slot or groove with ribbons parallel to the slot bottom at the center between reverse points. At the reverse points, ribbon's side faces the slot bottom[4,5].(fig.16)

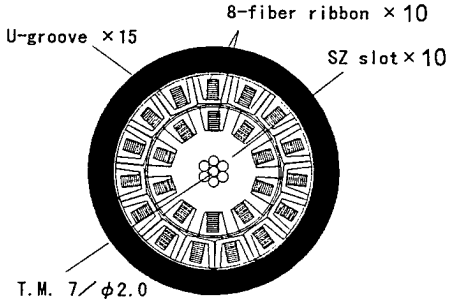

fig.15 Design of cross section of 2000-fiber count

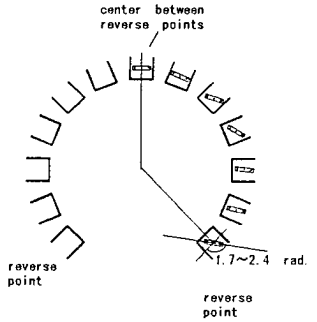

fig.16 accommodation condition

5-2 Design of reverse pitch

We calculated the slack length of the cable design of fig.15. The value of R0 is 28mm for external layer and 16mm for internal layer. Fig.17 shows the relationship between L/P and slack length d1 and dD2 in the case of external layer. Fig.18 shows the relationship in the case of internal layer.

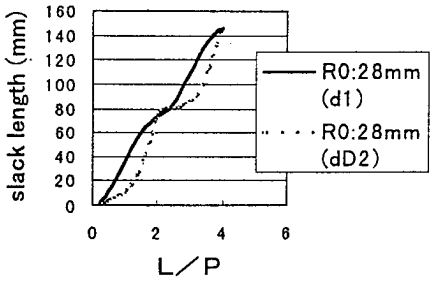

Fig.17 calculation result of slack length (external layer)

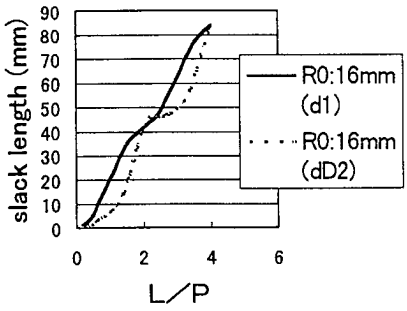

fig.18 calculation result of slack length (internal layer)

According to the results of calculation, L/P must satisfy the following relationship in order to secure the slack length of more than 20mm at arbitrary point.

External layer: $L_E/P > 1.38$ ①
Internal layer: $L_I/P > 1.59$ ②

According to the relationships of ①, ②, If the maximum sheath removal length L_E is assumed to be 700mm, the reverse pitch must satisfy the following relationships .

External reverse pitch <510mm ③
Internal reverse pitch <380mm ④

6 Examination of trial cable

6-1 Slack length

We made trial 2000 fiber count cable based on the above mentioned investigation. Reverse pitches were selected as follows.

External reverse pitch : 500mm
Internal reverse pitch : 350mm

We measured the relationship of L/P and slack length with the trial cable . Fig.19 shows the calculated and measured results of external layer . Fig.20 shows the results of internal layer. The results of case1 and case2 of chapter3 are shown. As for the experimental results, maximum and minimum values are plotted

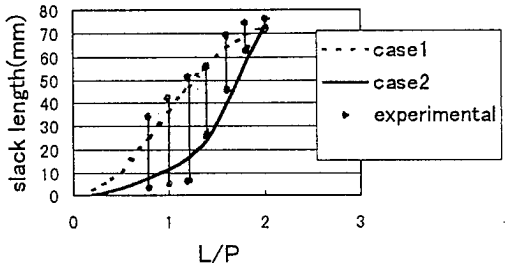

fig.19 Experimental investigation of slack length (external layer)

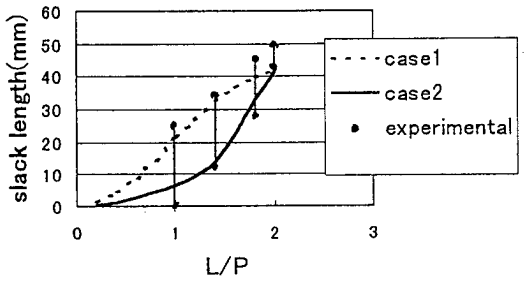

Fig.20 Experimental investigation of slack length (internal layer)

Experimental data well agree with calculated values.

In the case of sheath removal length of 700mm, external reverse pitch of 500mm(700/500:1.4) is sufficient to obtain necessary slack length(>20mm). On the other hand ,for the internal layer where L_I = 600mm, the reverse pitch of 350mm (600/350=1.71) is also sufficient to secure necessary slack length.

6-2 Initial transmission loss

We measured the initial transmission loss characteristics of trial cable at 1550nm and 1310nm. The average transmission loss is shown in table 1.

Table1 :Average loss of trial 2000 fiber cable

n=5 dB/km

	1550nm	1310nm
external	0.21	0.34
internal	0.21	0.34

Good results were obtained.

7 Conclusion

We designed double layer 2000-fiber count cable with particular consideration on easy mid-span branching characteristics. The target was set to secure ribbon slack of more than 20mm at arbitrary branching point. we designed the cable with SZ stranded u-groove (reverse pitch is 500mm) for the external layer, and SZ-slotted-rod (reverse pitch is 350mm) for the internal layer. With the trial cable we confirmed good mid-span branching characteristics and good initial transmission loss. we will further examine mechanical and environmental characteristics.

References

(1) H.Iwata "Design of high count optical fiber cable suitable for mid-span access. IEIEC B-10-3 1997

(2) H.Iwata "Design of Aerial Optical Fiber Cable System Suitable for Easy Branching" IWCS 1997

(3) Y.Ishibashi "Development of Aerial Optical Fiber Cable with Greater Length of Cable Compared to supporting Wire" IWCS 1997

(4) D.iwakura "Development of stacked ribbon SZ-slotted rod cable. IWCS 1997

(5) D.Iwakra "Studies on relation between strain of fibers and state of stacked fiber ribbons in SZ-siotted rod cable." IEICE B-10-13 1997 (in japanese)

Daisuke Iwakura
The Furukawa Electric Co.,Ltd.
6,Yawata Kaigandori Ichihara, Chiba 290, Japan

Daisuke Iwakura received his M.E.degree in Engineering from Electro-Communications University in 1993. He joined The Furukawa Electric Co.,Ltd. in 1993 and has been engaged in research and development of optical fiber cables. He is now a research engineer of Opto-Technology Laboratory

Ichiro Kobayashi
The Furukawa Electric Co.,Ltd.
6,Yawata Kaigandori Ichihara, Chiba 290, Japan

Ichiro Kobayashi received his B.E.degree in Physics from Chuo University in 1986. He joined The Furukawa Electric Co.,Ltd. in 1986 and has been engaged in the development of the optical fiber and cables. He is now a senior research engineer of Opto-Technology Laboratory He is a member of the Institute of Electronics, Information and Communication Engineers of Japan.

Masami Hara
The Furukawa Electric Co.,Ltd.
6,Yawata Kaigandori Ichihara, Chiba
290, Japan

Masami Hara received his M.E.degree in Physics from Osaka University in 1987. He joined The Furukawa Electric co.,ltd. in 1987 and has been engaged in research and development of optical fiber cables. He is now a senior research engineer of Opto-Technology Laboratory. He is a member of the Institute of Electronics, Information and Communication Engineers of Japan.

Hideyo Hiramatsu
The Furukawa Electric Co.,Ltd.
6,Yawata Kaigandori Ichihara, Chiba
290, Japan

Hideyo Hiramatsu received his B .E.degree in Electronic Engineering from Kyoto University in 1984. He joined The Furukawa Electric co.,ltd. in 1984 and has been engaged in research and development of optical fiber cables. He is now a senior research engineer of Opto-Technology Laboratory. He is a member of the Institute of Electronics, Informationand Communication Engineers of Japan.

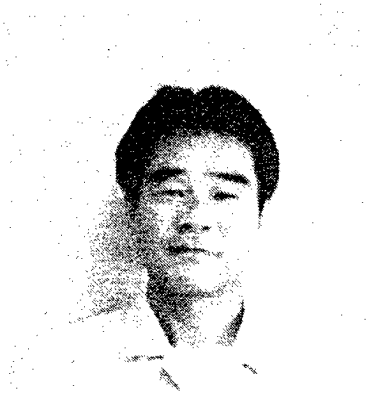

Hideaki Kanzaki
The Furukawa Electric Co.,Ltd.
6,Yawata Kaigandori Ichihara, Chiba
290, Japan

Hideaki Kanzaki joined The Furukawa Electric Co.,Ltd. in 1969 and has been engaged in research and development of optical fiber cables. He is now a senior research engineer of Opto-Technology Laboratory. He is a member of the Institute of Electronics, Information and Communication Engineers of Japan.

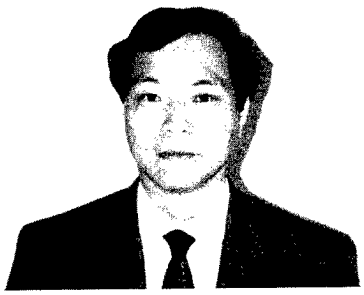

Yasuhiro Kamikura
The Furukawa Electric Co.,Ltd.
6,Yawata Kaigandori Ichihara, Chiba
290, Japan

Yasuhiro Kamikura received his B.E. degree in Electronic Engineering from Tokyo University in 1975 . He joined The Furukawa Electric Co.,Ltd. in 1975 and has been engaged in the development of optical fiber and cables. He is now a general manager of Opto-Technology Laboratory. He is a member of the Institute of Electronics,Information and Communication Engineers of Japan.

DEVELOPMENT OF NEW SLOTTED ROD CABLE COMPOSED OF FOAMED POLYETHYLENE SLOTTED ROD

Ichiro KOBAYASHI Ryuji TAKAOKA Eiji KONDA
Fumiki HOSOI Hideyo HIRAMATSU Yasuhiro KAMIKURA

OPTO-TECHNOLOGY LABORATORY THE FURUKAWA ELECTRIC CO.,LTD.
ICHIHARA, CHIBA , JAPAN

ABSTRACT

As the use of optical fiber cables penetrates into access networks, optical fiber cables which ease cable installation and fiber jointing will be demanded. The reduction of cable weight will be demanded so that longer cable length can be installed into conduit as a result of lower friction between the cable and conduit. The improvement of cable flexibility will also demanded to enable operators to take out the ribbons from the slot during the mid span branching. In order to satisfy these demands, we designed and manufactured new slotted rod cable using composed of foamed polyethylene slotted rod. As a result of the evaluation of the trial cables, We confirmed that new slotted rod cable is light in weight and good in flexibility, and have sufficient mechanical characteristics.

INRTODUCTION

In the near future, to provide broadband and high quality multimedia services, economical construction of optical access networks will be needed. We have already developed downsized optical fiber cables which can reduce the cable cost. In order to realize more economical optical access network, not only reduction of cable cost but also reduction of installation cost will be demanded. Therefore, we designed manufactured and evaluated new optical fiber cables to meet such demand.

ANALYSIS OF CABLE WEIGHT REDUCTION

The installed cable length :L is expressed as expression (1) by using installation force :F, friction coefficient between cable and duct : μ and cable weight :W

$$L = F / (\mu w) \quad **********(1)$$

The reduction of the friction coefficient and cable weight can extend the cable length which can be installed into conduit for the same maximum installation force.

Fig.1 shows a cross section of 1000 fiber cable and fig.2 shows its weight. Because the weight of a tensile strength member and slotted rod polyethylene are the major factors of the cable weight, reduction of these parts can reduce the

whole cable weight efficiently.

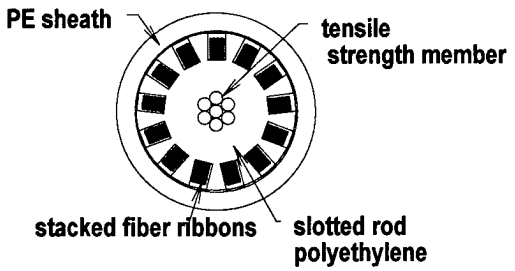

Fig.1 Cross section of 1000 fiber cable

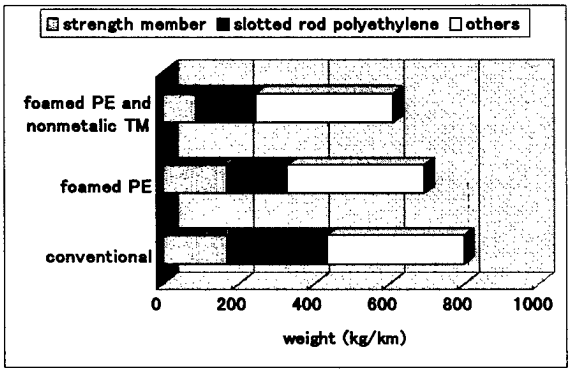

Fig.2 Mass comparison of 1000 fiber cable

Replacing the steel central strength member with FRP and employing a new slotted rod composed of foamed polyethylene can reduce the weight of slotted rod significantly. These approaches can reduce the cable weight by about 20%.

In order to realize these light cable, we designed and manufactured a new slotted rod composed of foamed polyethylene.

DESIGN OF FOAMED POLYETHYLENE SLOTTED ROD

We studied the cell content and structure of the slotted rod with foamed polyethylene layers so as to reduce the cable weight and improve cable flexibility without deteriorating the mechanical characteristics.

Cell content

We defined the volume percentage of the foam in the foamed polyethylene as cell content. Foamed polyethylene with 0 percent cell content means solid polyethylene. When a slotted rod is composed of foamed polyethylene with α% cell content, a Young's modulus: E' and a specific gravity: ρ' of the foamed polyethylene is expressed as follows.

$$E' = (1-\alpha/100)E \cdots\cdots\cdots (2)$$

$$\rho' = (1-\alpha/100)\rho \cdots\cdots\cdots (3)$$

E is a Young's modulus of solid polyethylene and ρ is a specific gravity of solid polyethylene

When the cell content changes from 0 percent to 80 percent, changes of cable characteristics of 1000 fiber cable are as follows.

Reduction of cable weight. Fig.3 shows the relation between the cell content and the cable weight when the cell content changes from 0 percent to 80 percent. As the cell content increases, the cable weight reduces.

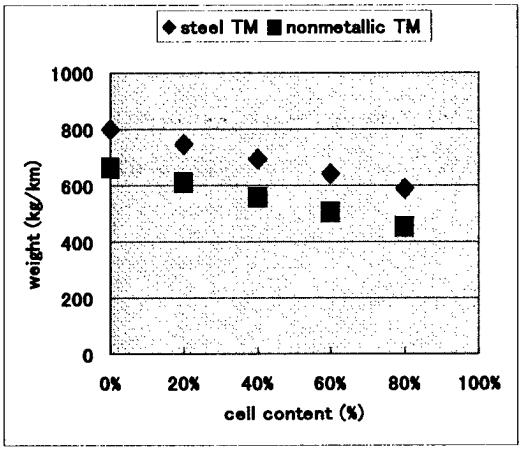

Fig.3 Relation between cell content and cable weight of 1000 fiber cable

Cable flexibility. Fig.4 shows a measurement method of cable flexibility. One end of the cable is fixed and the other end is loaded by force :F. As a result, the cable end is bent in length :Y. We defined the length :Y as cable flexure. The length :Y is expressed approximately by equation (4).

$$Y = (500^3 F) / (3 E I) \cdots\cdots (4)$$

E is Young's modulus of the cable, I is a cross- sectional secondary moment of the cable[4]

Cable flexure :Y is inverse by proportional to flexural rigidity :EI

Fig.5 shows the relation between cell content and the flexural rigidity of 1000 fiber cable when the cell content changes from 0 percent to 80 percent. As the cell content increases, the flexural rigidity becomes smaller and the cable flexibility is improved.

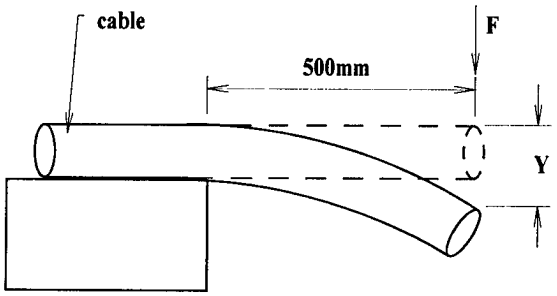

Fig.4 set up of cable flexure measurement

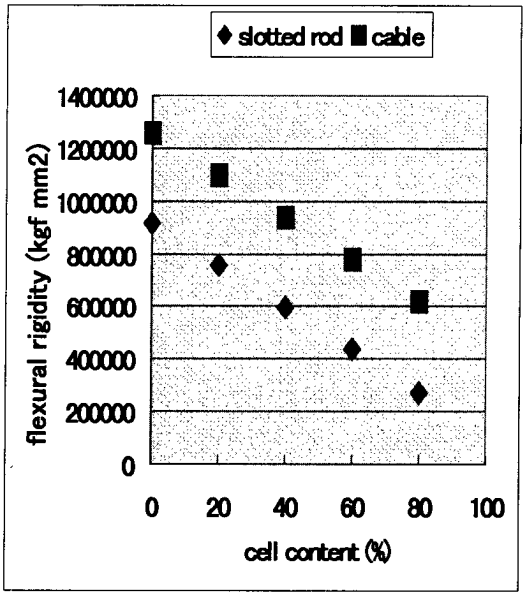

Fig.5 Relation between cell content and flexural rigidity

Mechanical characteristic. As the cell content increases, Young's modulus of foamed polyethylene becomes smaller. As a result, mechanical characteristics of the cable may deteriorate. Therefore, to find the sufficient cell content which does not worsen the cable mechanical characteristics, we manufactured trial slotted rod cables composed of foamed polyethylene slotted rod and evaluated them in mechanical characteristics.

Table 1 summarizes the relation between the cell content and the cable characteristics.

Table1 relation between cell content and cable characteristics

	cell content		
	0 %(solid)	⟷	100%
reduction of cable weight	small	→	large
flexibility	bad	→	good
mechanical characteristics	good	←	bad

Table2 relation between structure of slotted rod and cable characteristics

structure of slotted rod	inner layer	solid	foamed	foamed
	outer layer	solid	solid	foamed
reduction of cable weight		small	→	large
flexibility		bad	→	good
mechanical characteristics		good	←	bad

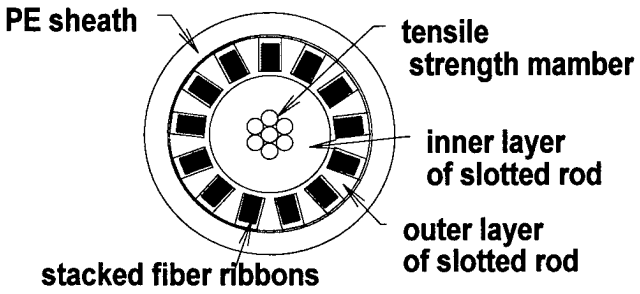

Fig.6 cross section of two layers slotted rod cable

Structure of foamed polyethylene slotted rod

We assumed that a slotted rod is composed of two layers namely inner layer and outer layer and each layer is made either of foamed polyethylene or solid polyethylene. And we compared slotted rods having different combination of solid and foamed polyethylene for both layers from the point of view of weight reduction and flexibility improvement of the cable. Fig.6 shows the cable structure composed of two layer slotted rod and table 2 summarizes the comparison results.

Reduction of cable weight. Because a slotted rod composed of foamed inner and outer layer have more foams than other slotted rod, the reduction of cable weight is largest.

Cable flexibility. Because a slotted rod composed of foamed inner and outer layer have more foams than other slotted rod, the cable flexibility is most improved.

Mechanical characteristic. Because Young's modulus of foamed outer layer is less than that of solid outer layer, the slotted rod having foamed outer layer may deteriorate in mechanical characteristic.

Although slotted rod having foamed inner and outer layer is most suitable for the reduction of cable weight and improvement of cable flexibility, its mechanical characteristics may deteriorate. Therefore, to find the trade off between the improvement in weight reduction and flexibility and the deterioration of the mechanical characteristics, we manufactured

several slotted rods which are different in cell content and structure, and evaluated their mechanical characteristics.

CABLE CHARACTERISTICS

Slotted rod structure

We manufactured four kinds of slotted rod with 13 slots for 1000 fiber cable. Two of them are composed of foamed inner and solid outer layer. And the other two slotted rods are composed of foamed inner and outer layer. Two levels of cell content were examined. One is 20 percent and the other is 40 percent. These structures are shown in Fig.7 .

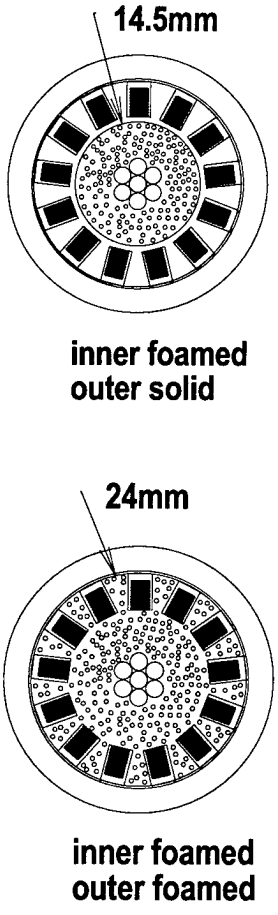

Fig.7 cross section of trial cables

Reduction of cable weight

Fig.8 shows a comparison of cable weight. Because the slotted rod cable composed of foamed inner and outer layer have more foams than other slotted rod cables , the reduction of cable weight was larger. And the weight reduction is larger for higher cell content. We confirmed that a slotted rod cable composed of foamed inner and outer layer with 40 percent cell content reduced the cable weight by about 100 kg/km.

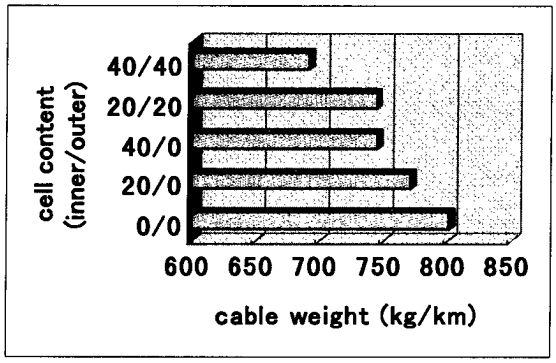

Fig.8 cable weight reduction of 1000 fiber cable

Improvement of cable flexibility

Fig.9 shows evaluation results of cable flexibility. Because a slotted rod composed of foamed inner and outer layer have more foams than other slotted rod, the cable flexibility is most improved. And the improvement by slotted rod having foamed polyethylene with 40 percent cell content was larger than the improvement by slotted rod having foamed polyethylene with 20 percent cell content. We confirmed that a slotted rod cable composed of foamed inner and outer layer with 40 percent cell content improved the cable flexibility about by 40%. The improvement is limited when only inner layer is foamed.

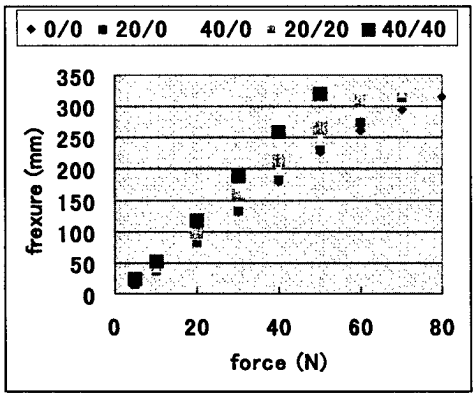

Fig.9 test result of cable flexibility

Compressive strength

Fig.10 shows the evaluation results of compressive strength. The change of outside diameter of the cable when loaded up to 9.8kN was measured. Slotted rod cables having foamed inner layer were weaker than conventional cable having solid inner layer. A slotted rod cable composed of foamed inner and outer layer with 40 percent cell content was weakest among the trial cables. Loss increases occurs when the change of outside diameter exceeded over 2.5mm.

Though the slotted rod cable composed of foamed inner and outer layer with 40 percent cell content was weakest among the trial cables , loss increase did not occur under 4 kN/100mm. It is considered that slotted rod cable composed of foamed polyethylene slotted rod have sufficient mechanical characteristics.

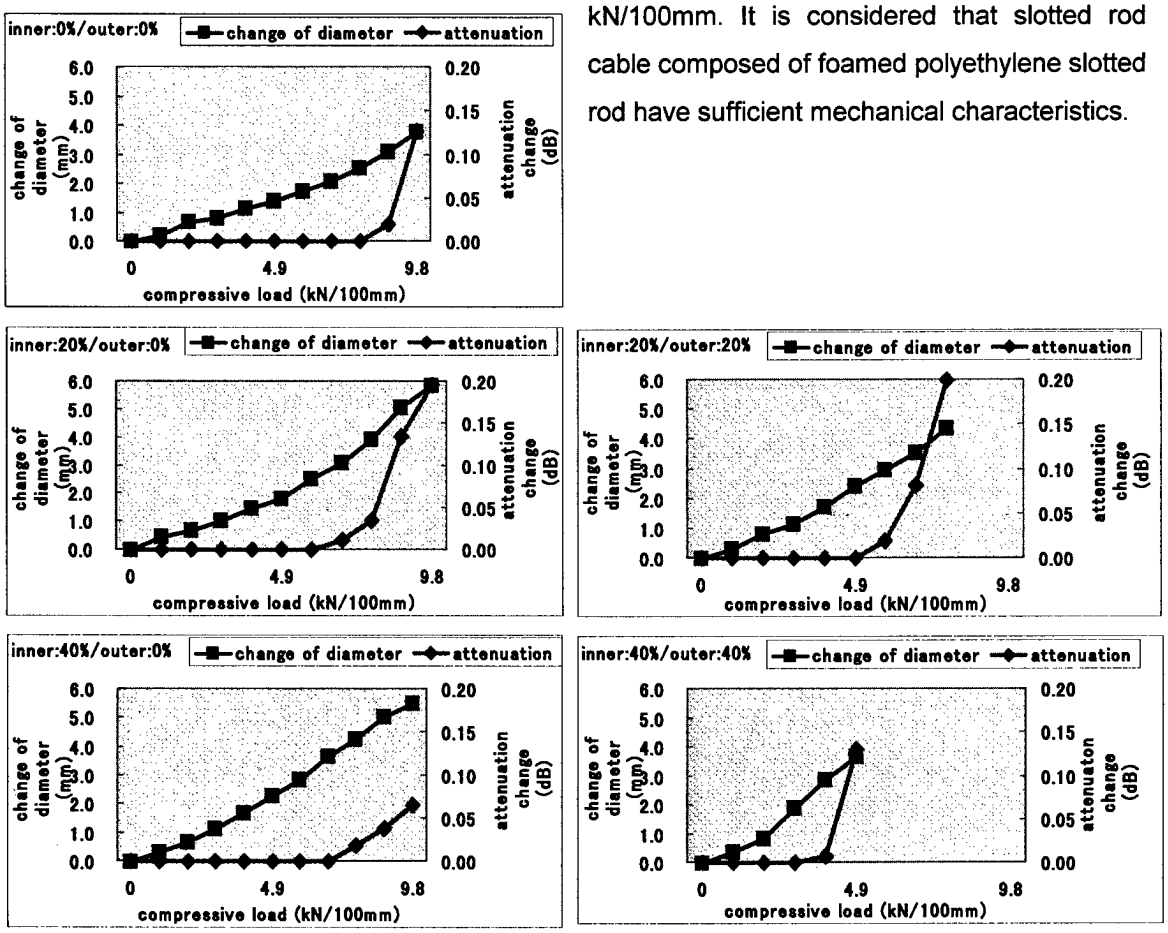

Fig.10 test result of compressive strength

CONCLUSION

We designed and manufactured new slotted rod composed of foamed polyethylene. The features of the cable using the new slotted rod are light in weight and excellent in flexibility. From the results of the evaluation of trial 1000 fiber cables, We confirmed that the new slotted rod cable composed of formed polyethylene slotted rod with 40 percent cell content reduced the cable weight by about 100kg/km, improved cable flexibility by about 40%, and had sufficient mechanical characteristics.

Adoption of the foamed polyethylene and FRP to the slotted rod can provide lightest optical fiber cable and reduce the installation cost. It is hoped that expansion of optical fiber cables in access networks will be accelerated by use of this new slotted rod cable.

REFERENCE

(1) Hideyuki Iwata et. al 「Study on advanced function of optical fiber cable for access」 technical report of IEICE SSE97-177,OSC97-106

(2) Masaru Okada et al 「Study on foamed polyethylene slotted rod」 proceedings of the 1998 IEICE GENERAL CONFERNCE

(3) Fumiki Hosoi et. al 「development of downsized slotted rod optical fiber cables」 45th international wire and cable symposium 1996

(4) Toshirou Miyoshi et al 「DAIGAKU KISO ZAIRYOURIKIGAKU 」 JIKYOUSHUPANNKABUSHIKIKAISHA

(5) Hideyuki Iwata et. al 「 Advanced technology of high density optical fiber cable」 Proceedings of the EuroCable Conference 1998

AUTHORS

Ichiro Kobayashi

The Furukawa Electric co., ltd.

6,Yawata Kaigandori, Ichihara,
Chiba, 2908555,Japan

Ichiro Kobayashi received his B.S. degree in Physics from Chuoh university in 1986. He joined The Furukawa Electric Co., LTD. in 1986 and has been engaged in the development of the optical fiber and cables. He is now a senior research engineer of Opto-Technology Laboratory. He is a member of the Institute of Electronics ,Information and communication Engineers of Japan.

Ryuji Takaoka

The Furukawa Electric co. ,ltd.

6,Yawata Kaigandori , Ichihara,
Chiba ,2908555,Japan

Ryuji Takaoka received his M.E .degree in Mechanical Engineering from Keio University in 1996. He joined The Furukawa Electric co., ltd. in 1996 and has been engaged in research and development of optical fiber cables. He is now a research engineer of Opto-technology laboratory.

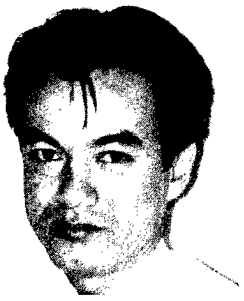

Eiji Konda

The Furukawa
Electric co., ltd.

6,YawataKaigandori
Ichihara,Chiba,
2908555,Japan

Eiji Konda joined The Furukawa Electric co., ltd. in 1977 and has been engaged in research and development of materials and optical fiber cables. He is now a engineer of Opto-technology laboratory.

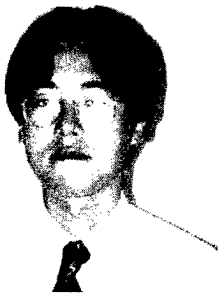

Fumiki Hosoi

The Furukawa
Electric co., ltd.

6,YawataKaigandori
Ichihara,Chiba,
2908555,Japan

Mr. Hosoi received his M.E. degree in Physics engineering from Tokyo University in 1995. He joined The Furukawa Electric Co., Ltd and has been engaged in research and development of optical fiber cable. He is now a research engineer of optical fiber transmission research department, opto-technology laboratory

Daisuke Iwakura

The Furukawa
Electric co., ltd.

6,YawataKaigandori
Ichihara,Chiba,
2908555,Japan

Daisuke Iwakura received his M.E. degree in Engineering from Electro-Communications University in 1993.He joined The Furukawa Electric co., ltd. in 1993 and has been engaged in research and development of optical fiber cables. He is now a research engineer of Opto-technology laboratory

Hideyo Hiramatsu

The Furukawa Electric co., ltd.

6,Yawata Kaigandori, Ichihara, Chiba
2908555,Japan

Hideyo Hiramatsu received his B.E. degree in Electronics Engineering from Kyoto University in 1984. He joined The Furukawa Electric co., ltd. in 1984 and has been engaged in the development of optical fiber cables and devises. He is now a senior research engineer of Opto-Technology Laboratory.

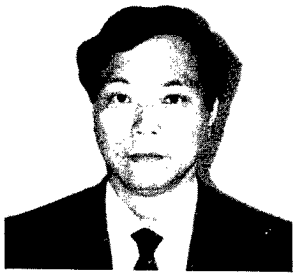

Yasuhiro Kamikura

The Furukawa Electric co.,ltd.
6,Yawata Kaigandori ,Ichihara,Chiba
2908555,Japan

Yasuhiro Kamikura received his B.E.degree in Electronic Engineering from Tokyo University in 1975. He joined The Furukawa Electric co., ltd. in 1975 and has been engaged in the development of optical fiber and cables. He is now a general manager of Opto-technology laboratory. He is a member of the Institute of Electronics, Information and communication Engineers of Japan.

VERY HIGH TRANSMISSION DENSITY CABLES INCLUDING MULTICORE FIBERS

Marta Garcia (1), **Stefan Richter** (1), **Vincent Bourget** (1)

Gerard Orcel (2), **Andre Tardy** (2), **Jean C. Bizeul** (3), **Jean P. Louboutin** (3), **Jean P. Bonicel** (4)

(1) **ALCATEL OFCCC, Claremont NC** (2) **ALCATEL FOCC, France**

(3) **France Telecom (CNET), France** (4) **ALCATEL TPLE, France**

ABSTRACT

Consumer and business desire for high bandwidth communications is increasing the pressure to bring high capacity transmission systems deeper into the network. Technological advances in high bit rate, TDM and WDM systems are making a significant impact on long-haul optical communications systems, but point-to-point services in the access and distribution part of the network are still facing physical space and cost constraints. In order to feed fiber in the loop, higher fiber density cables are required. One way to increase transmission density is to replace standard monocore fibers with Multicore fibers (MCF), which are fibers having multiple waveguide cores and essentially no dimensional difference with respect to the standard SM fibers. This paper introduces MCF in different cable structures with a perfect synergy between fiber and cable manufacturer and telecom operator. These MCF cables are presented as functionally equivalent to standard monocore fiber cables in terms of attenuation and mechanical performances, with a strong advantage on cable densification.

INTRODUCTION

Developing new networks involves taking many global economic aspects into account. Initial and progressive investments, equipment or ancillary infrastructures, operating costs, reliability, maintenance and management costs must be considered. This has to be done in keeping with rules offering the best upgrading possibilities at the lowest cost.

When defining optical distribution networks for residential users, two approaches may be envisioned:

- Using a minimum optical infrastructure, namely **passive optical network** (PON). The very wide bandwidth of fibers is shared out among the *n* users (from 4 to 32) and so is the cost of the optical structure. However, this solution forces multiplying the necessary line transmission rate by *n*. The related insertion loss of optical couplers is a disadvantage with respect to the optical budget of the line. The management of such a network, compared to the point-to-point systems may also be a big concern.

- Using simple, standard optical and digital equipment as far as possible. This equipment, which is generally developed by data communication equipment manufacturers, is connected to an optical fiber dedicated to each user (**point to point** Fiber To The Home -FTTH). This is an attractive solution from a technical viewpoint, but it is rather costly, since it typically requires new optical cables with 1000 or more fibers.

In order to reduce infrastructure costs (cable installation, fiber splicing, active equipment etc.) several ideas have been proposed, including using new and cheaper laying methods (blowing technique, pushing instead of pulling, using existing ducts as multicable ducts etc.), and increasing the cable length to minimize the splice points. In any case, it is clear that this new approach requires the use of light, high-density

cables in order to reduce the installation cost and infrastructure.

At this point, the concept of **Multicore fibers** becomes more important, offering the possibility to reach two important objectives, namely:

- Reducing the cost of optical waveguides
- Developing very high-density optical cable designs, hence optimize the use of ducts in the operator's network [1].

MULTICORE FIBERS

The idea of an optical fiber carrying *n* different waveguides is very attractive, since the concept of increasing the transmission capacity by maintaining the same dimensions (so multiplying by *n* the fiber density) is one of the main ways to decrease cost [2].

Fiber Geometry

The geometry of an ALCATEL 4-core fiber [3] is characterized by a rotational axis, which is the fiber axis, and by the distribution of core axes at the vertices of a regular polygon (see Figure 1). The distance between 2 cores is around 51.8 µm, so that fan-out devices with 125 µm ferrules can be used. A mean core spacing of 51.9 µm, with a standard deviation of 0.8 µm, characterizes the dispersion evaluated on 40 samples issued from different draws. In addition, the standard deviation on the outer diameter during a draw is 0.2 µm, which illustrates the good precision and stability of the process.

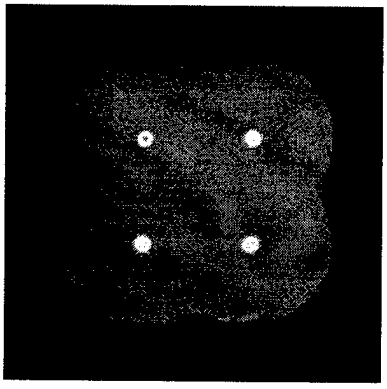

Figure 1: End view of 4-core fiber

Design of a Multicore Fiber

The fiber was designed to minimize microbending losses and crosstalk at both transmission windows. The cut-off wavelength is set at 1.3 µm. Increasing the core refractive index difference, Δn, gives a more strongly confined guided mode and results in lower crosstalk and microbending losses. One of the cores has a distinct index profile for identification purposes. It shows a ring profile while the others exhibit a step index structure. The core index difference for the step index profile is of 6.2×10^{-3}. The ring profile is designed to give a power confinement similar to other guides, which requires a peak Δn of 0.01.

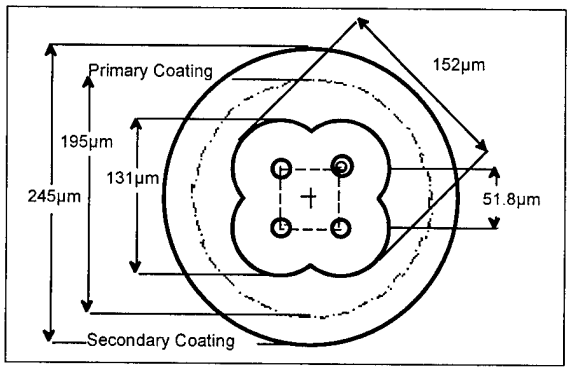

Figure 2: MC Fiber schematic cross section

Alcatel Manufacturing Process

The manufacturing process of a MCF starts with the production of single core preforms made by Alcatel's APVD (Advanced Plasma Vapor Deposition) process. The APVD process allows obtaining straight primary preforms with a precise diameter. The Multicore preform is made by square packing of four optical preforms with an extra rod inside the central interstice to minimize the air gap.

Drawing of the fiber by a rod-in-tube technique (Figure 3) is performed under vacuum to facilitate flowing of material and to obtain a good bonding between the glass components.

The draw parameters must be optimized to control surface tension effects and to prevent shape distortion. The shape of the MCF results from the flowing of the structural components in the draw furnace and thus depends on the draw tension and speed. The draw conditions are determined so no air gap is left inside the fiber and the shape of the cores is maintained.

The MCF structure is symmetrical due to the constant primary preform diameter and the concentricity of the sleeve tube with the preform at the center of the array.

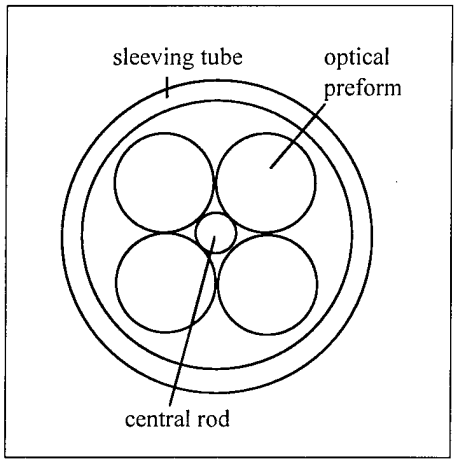

Figure 3: structural components of the MCF preform

Optical Performances

Approximately two hundred kilometers of 4-core fibers have been manufactured according to the defined process. The transmission measurements in both windows with respect to the index profile type are given in Table 1. The step index profile gives losses close to the performance of conventional fiber. The guides with ring index profile systematically show 0.05dB/km extra, due to the higher germanium content required to get the 0.01 index difference. Single core fibers with the same profile exhibit similar optical losses.

Wavelength	core with step index profile	core with ring index profile
1310 nm	0.375±0.01 dB/km	0.445±0.015 dB/km
1550 nm	0.225±0.01 dB/km	0.285±0.015 dB/km

Table 1: Average attenuation from 200km Multicore fibers

The crosstalk taken into account in this study is the coupling to nearest neighbors. Let's consider a guide *j*. Then, let's suppose that a monochromatic signal of a certain power is launched in an adjacent guide to guide *j*.

The crosstalk affecting guide *j* can be represented as:

$$Dj = 10 * \log P'j$$

where P'j is the percentage of power detected at the output of guide *j*. Typical crosstalk of a 10 km long Multicore fiber is less than –50 dB at 1550nm and is negligible (< -70dB) at 1310nm. Crosstalk is low because of the relatively large core spacing and good optical confinement of these fibers. Although this parameter can also depend on the fiber conditioning and length, it was found to be only a few dB variations for distances up to 30km and between loose and tight coil (30 g tension) conditions.

Polarization mode dispersion was found to be less than 1ps/√km for step index profile cores and slightly larger for the ring index profile core. However, this special core is not optimized yet, so reduced values may be obtained.

MCF Splicing

The Multicore fiber concept offers a very high degree of core organization due to the precise core pattern geometry. It also offers the advantage of mass-splicing ability. Fusion splicing of 4-core fibers was tested with an automatic fusion-splicing machine devoted to polarization maintaining fibers. This commercial machine has rotary alignment capability and optical means to detect the rotational position of the fiber. The average loss of 0.2 dB (std.dev. = 0.12 dB) obtained in the automatic mode is directly related to the Multicore geometry quality and instrument splicing ability.

For local network applications, mechanical splicing is of great interest because of its ease of use in field operations. The basic element in the 4-core fiber splice is the four-rod assembly, which has the advantage of defining a square-shaped channel useful to index the Multicore fiber. Figure 4 shows a cross-section view of the splice. The rods of 0.3 mm diameter, made of silica glass, are held in place by a shrinkable sleeve. The splice is used first in the open position. The channel is large enough to allow free movement of the fiber but forbids any excessive rotation leading to a false core indexing. Shrinkage of the sleeve causes the fibers to be compressed into both axial and angular positions, which puts them into the proper alignment.

For laboratory testing, sections of fibers issued from the same preform were used. The splice loss distribution for 40 splices gives a mean value of 0.17dB and a standard deviation of 0.10 dB.

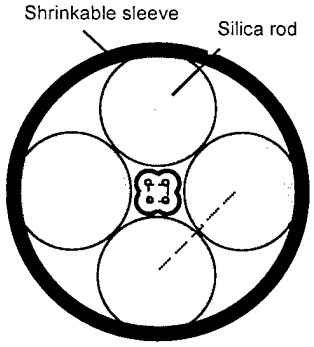

Figure 4: Schematic of the splice concept

Other mechanical splicing techniques have been evaluated, such as minimizing splicing loss with local injection/detection measurement test set. Light is launched into the 4 cores with a random proportion through the lateral surface of a bent fiber. The same technique is used to capture the signal at the other end of the splice. Optimizing fiber alignment minimizes this signal loss.

MULTICORE FIBER CABLES

Fiber Density

Fiber density is continuously asked to be increased, due to the need for higher transmission capacity. For this reason, new cable designs including higher fiber count in a reduced cross-section are requested [4].

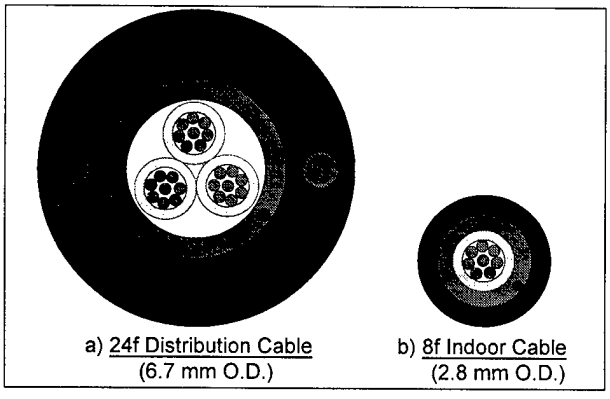

Figure 5: New Compact Distribution Cable Designs

We have reduced the cable cross-section by selecting a very compact design (small cable diameter, low weight, improved flexibility...) like the Distribution Cable designs shown in Figure 5. Comparing to a standard 24f loose tube design, this compact 24f cable is 155% more dense (0.56 vs 0.22 of/mm^2). However, introducing MCFs instead of standard SM fibers can further increase this density. Since every MCF has 4 cores (4 waveguides), this number multiplies the transmission capacity too. Figure 6 shows the fiber density (in fibers per mm^2) for several fiber counts (12 to 144 fibers), in different cable structures:

-. Loose Tube design
-. Central Tube design
-. Compact Distribution design
-. Same design including MCF.

By using MCF, we increase the "core density" in the compact 24f distribution cables by 195% (1.65 vs 0.56 of/mm^2) and, comparing this design to standard 24f LT cable, the increase is 650%. These numbers are even bigger when high fiber count cables are considered, as shown in Figure 6.

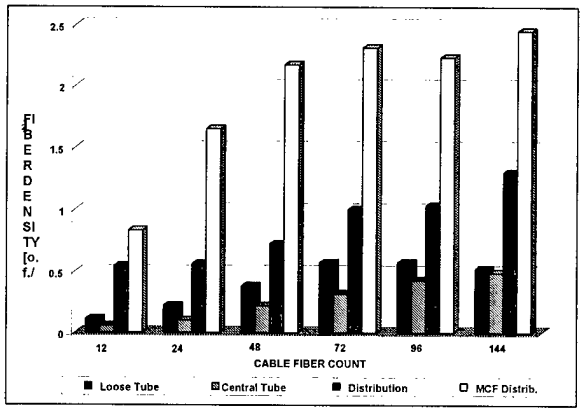

Figure 6: Increase in Core Density by using different cable designs / MCF

In order to prove the ability to manufacture these compact cables including MCF, 10 km of different cables were made by ALCATEL: 4 of them (**A3**, **A4**, **A5**, **A6**) were Distribution Cables with 24f (Figure 5-a), including 8 MCF and 16 SM Colorlock™ fibers. Another design (**E4**) contained 8 MCF and was conceived as an indoor design (Figure 5-b).

Finally, we manufactured a drop cable including 2 tight-buffered MCF (**F1**). All these MCF cables were included in a simulated network created by France Telecom / CNET Laboratories from a Central Office to several potential subscribers called Predemonstrator. Figure 7 shows the way these MCF cables lay in the network.

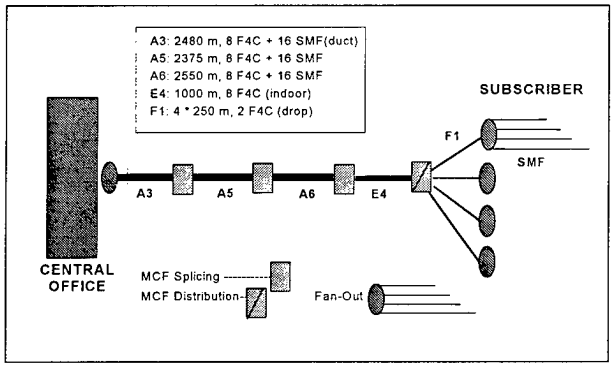

Figure 7: Predemonstrator including MCF cables

Cable Manufacturing

In the compact designs considered, the buffer tubes are made out of a low modulus polymeric material containing up to 8 multicore fibers. During buffering, MCFs were processed with the same parameters and equipment as the standard single mode fibers. Most of the tubes were manufactured without letting the operators know that the fibers were special, in order to avoid any special treatment. During the following process steps the fibers were loaded with the same forces as single mode fibers. None of the fibers failed. However, this fact is not surprising since, during the fiber manufacturing process it was proved that the average strength is close to 70N while a standard 125 μm SM fiber typically breaks around 60N. All fibers for cabling were screen tested at 0.5%.

Checking the optical attenuation followed each production step, in order to detect if the fibers were excessively stressed. Figure 8 shows the mean value of the optical attenuation at 1550nm of all fibers/cores excluding the ring marked cores.

The slight attenuation increase after coloring shown in Figure 8 is due to winding effects. Apart from that, there was no significant change in the optical attenuation through processes.

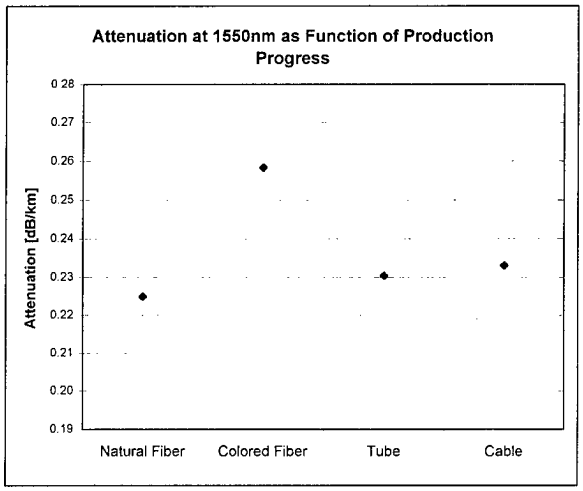

Figure 8: Attenuation in MCF as Function of Production Progress

MCF Cables Handling/Splicing

Multicore fibers are very easy to handle. Strippability is very good, almost like standard SM fibers. Cleaving requires some training before getting optimum results. This is reached by placing the brightest face of the fiber (the side which contains two cores) on the top of the cleaver. This bright face can be easily detected by rotating the fiber under a light source.

Several methods have been used to connect the four cores to equipment. All of them used fan-out devices built by CNET with Alcatel MCF. Among all these connection methods, the following were preferred:

- **Three axes alignment system:**

Allows -3 axes controlled- mechanical splice. This friendly method was mainly used for OTDR measurement.

- **Fusion splice**:

A traditional ribbon fusion splicer was successfully used by rotating one of the fibers and controlling at the same time the geometry in two planes, up to the perfect match between the geometry of the two fibers. During the splicing, the arc duration was slightly increased compared to a standard SM fiber splicing. The splice loss was then controlled by an OTDR. Depending on the quality of the fiber cut and the fiber geometry, we achieved splice loss lower than 0.1 dB. This second method can be used for both transmission and OTDR measurements.

The necessary time to splice two Multicore fibers is, after some training, very close to the time required to splice two standard SM fibers.

We mainly used the *alignment system* to do the OTDR measurements on the cable, and the *fusion splice method* for all the other tests, including the thermal test.

Test Procedures and Results:

All tests were performed according to FRANCE TELECOM specifications for duct and indoor cables. Table 2 shows the test results together with the testing conditions for each mechanical and environmental test.

The specification requires the optical fibers to be looped during some mechanical tests. In order to compare, one loop was created with Colorlock™ fibers, and another one with one core of each Multicore fiber. The attenuation values mentioned in Table 2 for the mechanical tests are given in dB per fiber core for the Multicore fiber circuit only.

Thermal test: This environmental test is very close to the Bellcore test, but the cycles were adapted to show any potential problem at intermediate low temperatures.

Duct cables:
20°C / -40°C / +70°C / -40°C / +70°C / 20°C
Indoor cables:
20°C / -30°C / +60°C / -30°C / +60°C / 20°C

The displayed values for the thermal test represent the average attenuation changes within the mentioned temperature range. All cycles were similar to Bellcore GR20, except for the E4 and F1, where GR20 is not applicable.

- Tensile test: This test is done on a 200m sample. Cable elongation and fiber attenuation meet the requirements, meaning a cable elongation limited (< 0.3%) and an attenuation change not larger than 0.05dB at a maximum load of 2 times the cable linear weight.

	CABLE REFERENCE		
TEST	**A3 (24f duct)**	**E4 (8f indoor)**	**F1 (duplex)**
Tensile (dB)	600N 0.3% cable <0.05	160N 0.2% cable <0.05	200N 0.22% cable <0.05
Crush (dB)	220N/cm <0.05	50N/cm <0.1	50N/cm <0.05
Impact (dB)	5N.m <0.05	2N.m <0.05	2N.m <0.05
Bend (dB)	Bend radius: $10*D_{cable}$ <0.05	Bend radius: $10*D_{cable}$ <0.05	Bend radius: $10*O.D_{cable}$ <0.05
Torsion (dB)	10 cycles (+/-1 per m) <0.05	10 cycles (+/-1 per m) <0.05	10 cycles (+/-1 per m) <0.05
Kink	No physical damage $D=5*OD_{cable}$	No physical damage $D=5*OD_{cable}$	No physical damage $D=5*OD_{cable}$
Thermal (dB/km)	(-30C;+70C) SMF: 0.03 MCF: 0.12	(-30C;+60C) MCF: 0.06 (-20C;+60C) MCF: 0.02	(-30C;+60C) MCF: 0.05 (-20C;+60C) MCF: 0.02B

Table 2. Test Results on MCF cables

Considering the critical tests for this type of light designs: crush, impact, bending, torsion, or kink, (tests involving around 6 meters of cable) the behavior of these cables is remarkable:

- Crush test: applying Bellcore GR20 issue1 for cable **A3**, MCF can withstand a very high load without showing an excessive attenuation increase ($\Delta\alpha$<0.06dB at 2200N). Its behavior is very similar to standard fibers.
- Impact test: MCF also showed a good resistance to impact test, even at loads higher than those required in GR20.
- Twist test: again, this test is stricter than BELLCORE GR20 is. However, no weak points were revealed from either a cable design or a MCF point of view.
- Thermal test: this test showed some small differences between SM and MC fibers. In cable **A3**, the standard SMF performed well even at temperatures below -40°C, while MCF were acceptable just down to -30°C. However, we have to consider that the operating temperature range for this type of cables is generally -10°C to +60°C.

When considering the indoor cable **E4**, the attenuation behavior of the MCF is acceptable, with an average attenuation increase of 0.06dB/km at-30°C. The performance of MCFs also decreases at temperatures below -20°C. However, the specification for indoor designs requires operating temperatures from –5C to +60C.

In all the cases, the behavior of the MC fibers at temperatures up to 70°C is very good.

Tests conclusions

Multicore fibers, integrated into some new distribution cables, show a very good behavior versus a qualification-type battery of tests. In general, MCFs exhibit the same behavior under tests as standard Colorlock™ fibers, which already exceed existing standards.

PREDEMONSTRATOR FEATURES

As mentioned before, Figure 7 presents the architecture of the Predemonstrator built by CNET using Alcatel cables. However, we have not shown so far anything related to this network itself. How do these 10 km MCF cables link customers? How is the transmission system like? That is what Figure 9 is presenting. The Predemonstrator includes 8 bi-directional STM1 Transmission double full duplex [5] per four-core fiber (F4C). Each core presents the same structure as a G652 fiber in terms of core size and refraction index difference.

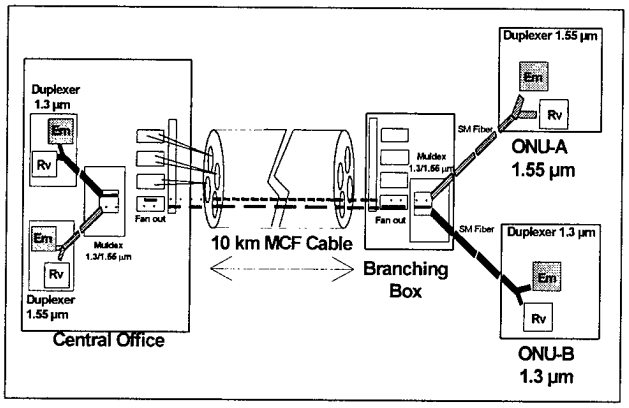

Figure 9: 8-bidirectional STM1 double full duplex

This Predemonstrator includes 10 km of MCF cables connecting the Central Office with the Branching Box by means of mechanical and fusion splices. In order to link the Branching Box to each customer, one standard SM G652 Fiber (from 50 to 150 m) is spliced to each of the cores of every MCF. The bit rate in our trial was STM1, 155 Mbits/s.

Each 4-core fiber involves (according to Figure 9):

- 2 fan-out devices: 1 to Central Office and 1 to Branching Box
- 8 customers: 4 at 1.3 µm and 4 at 1.55 µm
- 8 WDM (1.3/1.55 µm): 4 to the Central Office and 4 to the Branching Box
- 8 transceivers (Em and Rv): 4 customers at 1.55 µm and 4 customers at 1.3 µm

Figure 9 represents how this Point-To-Point system operates, by showing the interaction between two subscribers (one transmitting at 1.3 µm and the other at 1.55 µm) through one single core in one MCF. In this Predemonstrator there are 4 cores per MCF and 8 MCF per cable, resulting in a transmission capacity of 64 Bi-directional STM1 Transmission Double Full Duplex (in other words, 64 customers with just 8 MCF or up to 192 STM1 customers with a 24 MCF cable).

MEASUREMENT RESULTS

The **power loss** from Central Office to subscriber was measured at both wavelengths. Including the equipment loss, plus 2 WDM, 2 fan-outs, 3 fiber splices, power loss in 10 km fibers, and 5 connectors, the attenuation at 1.3 µm was 16 dB. At 1.55 µm, it was 14.5 dB. The **Crosstalk** at 1.3 µm was -60 dB (Measured from the central office to the branching box) and -44 dB at 1.55 µm [6]. The **Bit Error Rate** was measured as 10^{-11} STM1 (155 Mbits/s) at both wavelengths. Other parameters checked were the emitted/received power of the transceivers:

- 1.3 µm Transceiver:
  Emitted power: -3 dBm
  Minimum **REC power** for 10^{-9} BER: -35 dBm
- 1.55 µm Transceiver:
  Emitted power: -7 dBm
  Minimum **REC power** for 10^{-9} BER: -35 dBm

These results show good Multicore fiber behavior in terms of power loss and an acceptable error rate. However, for longer fiber lengths, it will be necessary to perform some other tests. This may be done during the last trimester of the year.

CONCLUSIONS

This paper has proven the feasibility of manufacturing cables with Multicore fibers. These fibers do not need to be treated as special fibers during manufacturing processes, and results after the qualification tests show these cables have good performance. This proves that MCF can be considered as the next generation of fibers for high-density networks.

A point-to point network has been presented in order to include these MCF cables into a real system and the results are very promising. High transmission capacity systems can be achieved with these high-density cable designs including MCF, at a low installation cost.

Finally, considering the lower cost per core of Multicore fibers compared to standard single mode (G652) and taking into account installation cost savings (due to possible micro civil works), this technology may represent the future of FITL network systems.

REFERENCES

[1] "Evolving technologies of optical infrastructure to optimize the FTTH deployment scenarios", D Boscher IWCS 97

[2] "Ultra high density cables using a new concept of bunched multicore monomode fiber", G Le Noane IWCS 94

[3] "Manufacturing and Characterization of Multicore Fibers", J.F. Bourhis et al. IWCS'97, Philadelphia

[4] "Multicore Fiber and Cable for Subscriber Network", A. Tardy and al. AMTC'98, Atlanta

[5] "Feasibility of 155 Mbit/s double full duplex link at 1.3µm 155µm on bunched multicore monomode fiber", D Boscher 8thO/H AN Atlanta 97

[6] "Automatic bench for measuring parameters of multicore fiber", JC Bizeul and al OPTO 95 Paris

AUTHORS

Marta Garcia
Alcatel OFCCC
2512 Penny Road PO 39
Claremont, NC 28610

Marta Garcia received her Physics degree with a specialty in Microelectronics in 1992, from the "Facultad de Ciencias" at the University of Cantabria (Spain). In 1994, she joined Alcatel Cable Iberica, working as a Product Engineer. Since April 1997 she is part of the Alcatel Optical Fiber Cable Competence Center (OFCCC) in Claremont, NC, working as a project leader for the Design Technology Group.

Stefan Richter
Alcatel OFCCC
2512 Penny Road PO 39
Claremont, NC 28610

Stefan Richter (33) studied materials science at the "Technische Universität" in Berlin (Germany). He received the degree Dipl.-Ing. in 1994. The same year he joined Alcatel with the BETEFA (special cables for telecommunication) as a production engineer. In 1995 he changed to the position as development engineer for optical fiber cables with Alcatel Kabel (Kabelrheydt). Since 1997 he is assigned to the Process Technology Group of the Optical Fiber Cable Competence Center in Claremont, NC.

Vincent Bourget
Alcatel OFCCC
2512 Penny Road PO 39
Claremont, NC 28610

Vincent Bourget received his engineering degree from the "Ecole Nationale Superieure de Ceramiques Industrielles" in 1992. He joined Alcatel in 1993 and was involved in preform design and CVD process for dispersion shifted fibers. Since 1996 he is part of the Alcatel Optical Fiber Cable Competence Center (OFCCC) in Claremont, NC, working as Characterization Group Manager

Andre Tardy
Alcatel Fibres Optiques
53, rue Jean Broutin
78700 Conflans
France

A Tardy received his engineering degree in 1966 from the *Institut National des Sciences Appliquées*. He joined CGE, which later became Alcatel, working on optical fiber connection and testing systems. His current interests are distribution fiber and components

Jean Claude Bizeul
France Telecom
CNET/DTD/IBL
22307 Lannion cedex
France

Jean Claude BIZEUL was born in 1948. In 1973 he joined the CNET (Centre National d'Etudes des Télécommunications) France Telecom research center. He was engaged in reseach on process fabrication and characterization of optical multimode and SM fibers. In 1988 he is involved in optical fiber and cable measurements group. From 1997 he is responsible of measurements, reliability, optical monitoring unit. He represents France Telecom in UIT/T especially on optical transmission study group.

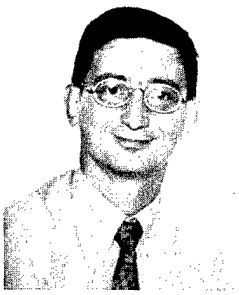

Gerard Orcel
Alcatel Fibres Optiques
53, rue Jean Broutin
78700 Conflans
France

Gérard Orcel received his Ph.D. degree from the University of Florida in 1987. He held positions at GelTech and Spectran before joining Alcatel in 1992. Since then, he has been involved in preform design, CVD and draw technology and coating development.

Jean Pierre Louboutin
France Telecom
CNET/DTD/IBL
22307 Lannion cedex
France

Jean Pierre LOUBOUTIN was born in 1954. Doctor in solid physics, he joined the CNET (Centre National d'Etudes des Télécommunications), France Telecom research center, in 1982. He is in charge of studies and specifications on optical cables. From the beginning of 1998 he is recognized as optical cable expert

Jean Pierre Bonicel
Alcatel
30, rue Pierre Beregovoy
78700 Conflans
France

Jean-Pierre Bonicel (46) received his engineering degree from the *Institut des Sciences de l'ingénieur de Montpellier* (ISIM) in 1976. He joined Les Cables de Lyon, now Alcatel, in 1977. After being Manager of the Alcatel Optical Fiber Cable Competence Center (Claremont, NC), he now is Product Marketing Manager for the Telecom Product Line in Europe (TPL-E).

PCVD: THE ULTIMATE TECHNOLOGY FOR PRODUCTION OF HIGH BANDWIDTH MULTIMODE FIBRES

Andries H. van Bergen, Ton Breuls

Plasma Optical Fibre B.V., Eindhoven, The Netherlands

ABSTRACT

In this paper the recent progress of the PCVD process for manufacturing multi mode graded index fibres is presented. It includes the increase in deposition rates together with further increased preform sizes while maintaining the high deposition efficiencies. It also underlines the excellent capability of PCVD to manufacture high-quality optical multi-mode fibres due to it's precise control of the refractive index profile .

INTRODUCTION

One preform technology for the manufacturing of optical fibres is Plasma-activated Chemical Vapour Deposition (PCVD). Already for many years the high deposition efficiency of (doped) silica together with the precise control of the refractive index profile offered by the PCVD process has resulted in the manufacture of singlemode as well as high bandwidth multi-mode fibres [1]. Although PCVD is capable for precise refractive index control of any single-mode and multimode fibre in all varieties this paper will exclusively discuss multimode fibres.

Multi-mode fibres have observed a growing interest due to following applications [2]:

- LAN networks like:
  Ethernet (Fast + Gigabit), Fibre Channel, FDDI, etc.
- FTTD.
- New cheap laser sources like VCSEL 850 nm.

A way to increase the production rate and resulting preform fibre length of PCVD singlemode fibres has been published earlier [3]. In this paper the recent progress in the increase of deposition rates together with further increased preform sizes for the production of PCVD multi-mode fibres will be given.
Moreover we will show that the excellent capability of PCVD to manufacture high-quality optical multi-mode fibres with high deposition efficiencies will be maintained while increasing the deposition rate. The fibres types meant here are the 50/125 µm as well as the 62.5/125 µm graded index multi-mode fibres.
Another advantage of the PCVD process is the ease to change the refractive index profile. It will be shown that this is very advantageous for making specialty (multi-mode) fibres.

PRINCIPLES PCVD PROCESS

The operating principle of PCVD can best be explained by means of figure 1, which shows an overview of a PCVD preform manufacturing setup.

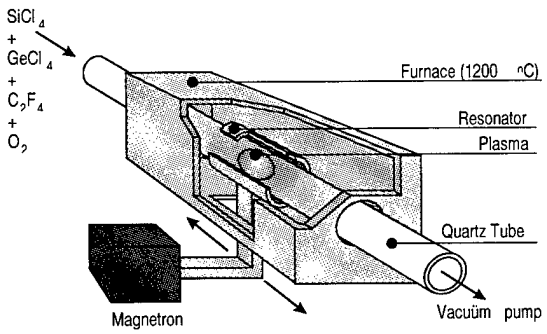

Figure 1: Setup PCVD deposition

The substrate tube for PCVD deposition is mounted between a gas supply system and a pump. During the process the desired gas mixtures, a combination of $SiCl_4$, $GeCl_4$, C_2F_6 and O_2 are fed into the tubes at a specific low pressure. Inside the silica tube a moving non isothermal plasma is generated in a microwave cavity operating at 2.45 GHz which transverses along the tube. In this plasma reactions are stimulated and deposition of the desired glass components on the inner wall of the substrate tube occurs. The deposition at the inner wall of the substrate tube takes place heterogeneously resulting directly in pure or doped silica glass without soot formation. During deposition the substrate temperature is kept constant at a temperature at about 1200 °C by a stationary furnace over the whole unit. The substrate tube itself is rotated.
Other inside tube processes rely on energy transfer through the wall of the substrate tube. In the PCVD process the microwave energy required to maintain the plasma and to stimulate the reactions is coupled directly into the gasphase. Which means that the deposition is not influenced by heat transfer problems like in other deposition processes. Therefore the transverse speed of the resonator can be high (4 - 24 m/min), which allows the deposition of very thin layers (micron thickness). Together with the fact that during each run the gas composition may be changed implies that a refractive index structure consisting of several thousand layers with high radial resolution, accuracy and reproducibility can be made.

PCVD PROCESS DEVELOPMENT

During the development phase quantitative optimalisation criteria were derived from experimental data and process modeling of the PCVD process. These criteria give the "process window" which has to be respected when changing the process. As a result of this work the deposition rate and preform sizes (as well radial as deposition length) have increased while maintaining the deposition accuracy, yield (both SiO2 and GeO2) and the resulting product characteristics.
Furthermore microwave cavities (called resonators) are developed which can be used for bigger substrate tubes (increase of preform deposition diameter) and attributes to the ability to increase the deposition speed.

Deposition Optimalisation Criteria

- The inner wall temperature of the substrate tube, resulting from plasma power and stationary furnace temperature should be kept constant.
- The applied plasma power must be proportional to the deposition rate.
- The residence time of the reactive gas in the plasma zone must be kept constant to get the same deposition yield of SiO2.
- The deposition pressure must be below 30 mbar. Above 30 mbar another regime of higher soot formation exist, due to a lower SiO2 deposition yield.
- To maintain the same materials structure and deposition efficiencies the ratio between the gasflows of Oxygen and Chloride gases must be kept constant.
- The resonator transverse speed has to be proportional to the deposition rate. This means that the deposited layer thickness as well as the dynamic thermal wall load is constant.

Microwave cavities (resonators)

When developing resonator cavities the following design criteria have to be taken care of:

- Operating frequency is 2.45 GHz
- The microwave coupling efficiency from cavity to the plasma should be fairly independent of the different process conditions and inner substrate tube diameters.
- The applied amount of microwave power must not influence the microwave coupling efficiency.
- The inner diameter of the resonator must be large enough to allow the use of bigger substrate tubes
- The resulting plasma has to be rotationally symmetric which means an equal microwave field strength along the plasma.
- One must be able to apply microwave powers from 1 up to 8 kWatt

In figure 2 a scheme of such a resonator is given. Figure 3 shows an experimental setup of a resonator.

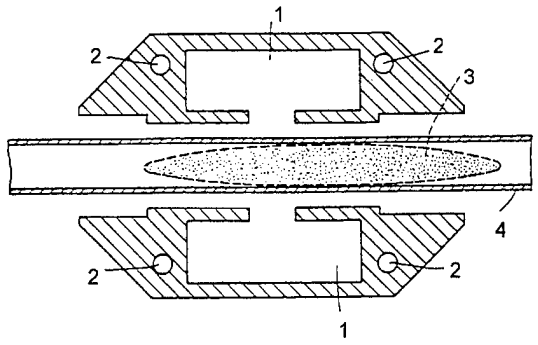

1 Resonance cavity
2 Cooling
3 Plasma
4 Substrate tube

Figure 2: Scheme of a resonator

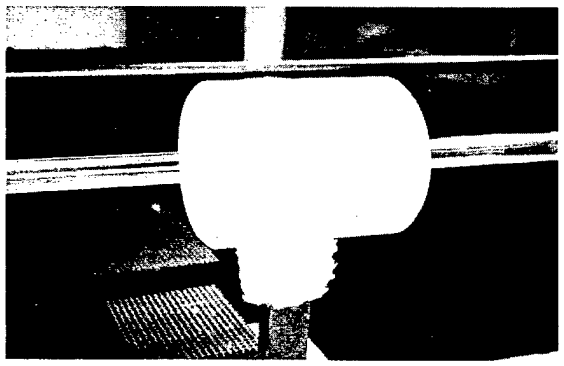

Figure 3: Experimental resonator setup

This design work which consisted of experimental electromagnetic studies resulted in a second generation of resonators [4]. With these cavities it is possible to carry out the PCVD deposition process at an inner wall diameter of 30 mm as well as 16 mm. A third generation resonator [5] cavities will allow us even to go up to 40 mm inner wall diameters. In current studies microwave setups are researched / projected which allows to use substrate tubes of more than 60 mm, [5].

PCVD PROCESS FEATURES

With the help of the design optimalisation criteria and the new generation of resonator microwave cavities a further improved PCVD process for making multi mode graded index preforms has been developed which will be introduced in production shortly.

Deposition rate

In the improved PCVD process the deposition rate has been increased upto 2.5 to 3 gr/min without influencing the yield and the optical properties [6].
Due to a theoretical description of the PCVD process [7], [8], [9] and experimental investigations it turned out that the geometrical taper length at the gasflow entrance linearly increases with the total gasflow. Minimizing of the total gasflow together with an optimalisation of the resonator cavity transverse speed profile at the gas entrance resulted in a minimized taper length which is independent of the deposition rate.

Preform sizes

It is obvious that larger resonator cavities can result in larger deposition diameters which give more optical fibre length per m preform. It has been demonstrated that 133 km multi-mode 50/125 µm and 83 km multi-mode 62.5/125 µm graded index fiber per meter of PCVD preform length can be accomplished.
An advantage of using a microwave plasma (which is coupled directly into the gasmixture) is the low substrate wall temperature because no heat transfer has to take place. As a result this permits the application of large deposition lengths. At the moment the deposition lengths are in the order of 1.2 to 1.5 meter.
Figure 4 contains the effects of deposition diameter and length on preform sizes for multi-mode 50/125 µm graded index fibres

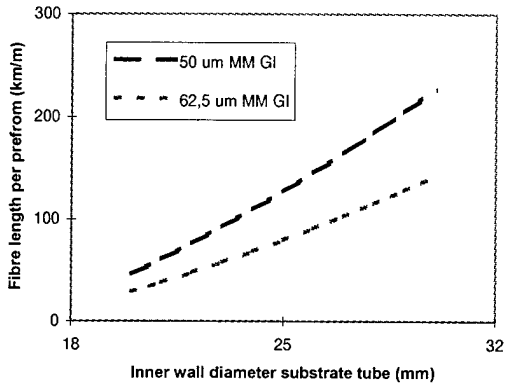

Figure 4: Preform size as a function of deposition geometry

Yield SiO_2

As stated in the process criteria the yield of SiO_2 is mainly affected by process pressure (figure 5), microwave power and residence time of the gases in the plasmazone.

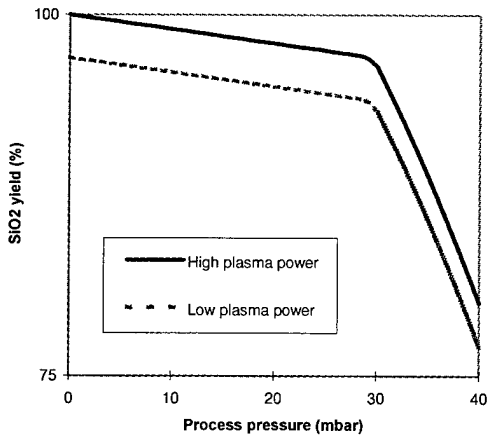

Figure 5: SiO_2 yield

If the criteria are applied the yield of SiO_2 will be above 95 %.

GeO_2 incorporation efficiency

The most important parameter affecting the GeO_2 incorporation efficiency is the temperature of the inner wall of the substrate tube. The GeO_2 incorporation efficiency decreases 2 % per 10 °C [6].
It means that increasing the microwave power without changing the temperature of the stationary furnace causes the GeO_2 incorporation efficiency to the decrease.
So the temperature of the stationary furnace should be lowered while increasing the deposition rate, the microwave power.
Figure 6 contains the refractive index change as a function of $GeCl_4$ dopant concentration in the gas phase.
The figure shows that the incorporation efficiency of GeO_2 is independent of the $GeCl_4$ concentration in the gasphase.

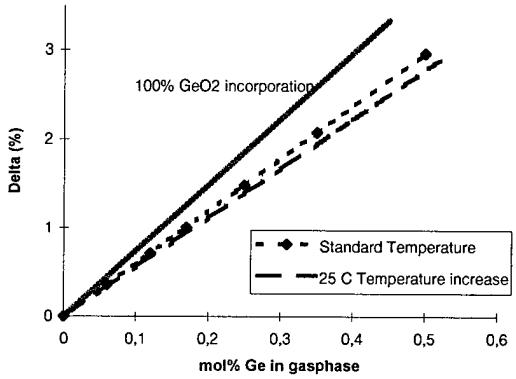

Figure 6: GeO_2 incorporation efficiency

At the moment even at high deposition rates a GeO_2 incorporation efficiency of more than 80 % is reached. Furthermore the highest GeO_2 dopant level reached until now in the PCVD process is approximately 40 mol% which means a refractive index change of more than 3%.

Deposition accuracy

In the PCVD principles it was already stated that the deposition has a very high refractive index deposition accuracy. The reason is that in the several thousand layer structure during each run (layer) the gasmixture at the entrance can be changed combined with the fact that the GeO_2 incorporation efficiency is independent of this gasmixture.

The most important parameter to maintain the same accuracy at higher deposition rates is to increase proportionally the resonator transverse speed.
In figure 7 a preform refractive index profile is given, the applied deposition rate is 2.5 gr/min. Figure 9 shows a 3d plot of the resulting refractive index profile in the fibre.

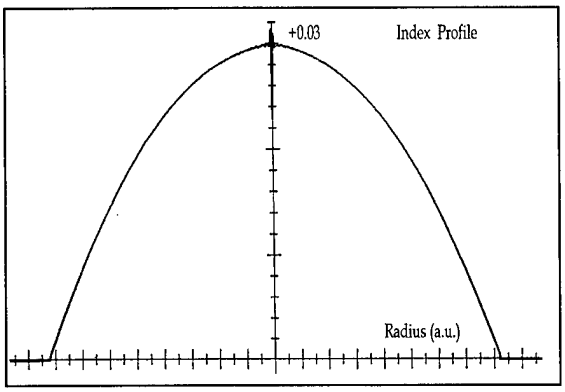

Figure 7: Refractive index profile 62,5 µm preform

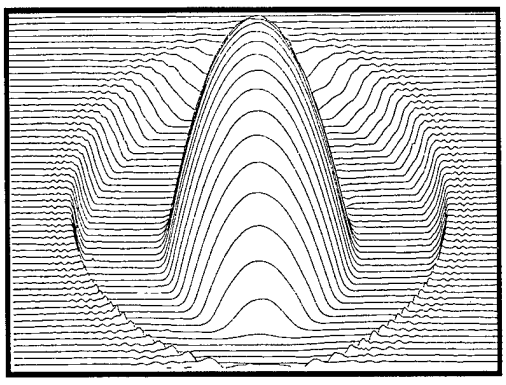

Figure 8: Refractive index profile 62,5 µm fibre

PCVD MULTI MODE FEATURES

Optical properties

Resulting from the deposition accuracy the manufacturing of high quality bandwidth multi mode fibres is possible.
In table 1 the mean bandwidth values of both the multi-mode 50/125 µm and the multi-mode 62.5/125 µm graded index fibres are presented.

Table 1: mean bandwidth

(mHz*km)	850 nm	1300 nm
50/125 µm	600	1200
62.5/125 µm	300	800

Specialty multi mode fibres

The high deposition accuracy makes it possible to make almost any refractive index profile.
For multi mode fibres it means that the alpha of the graded index profile can easily be adjusted, see figure 9. Therefore it is possible to manufacture multi mode fibres for specific transmission windows by adjusting the deposited index profiles.

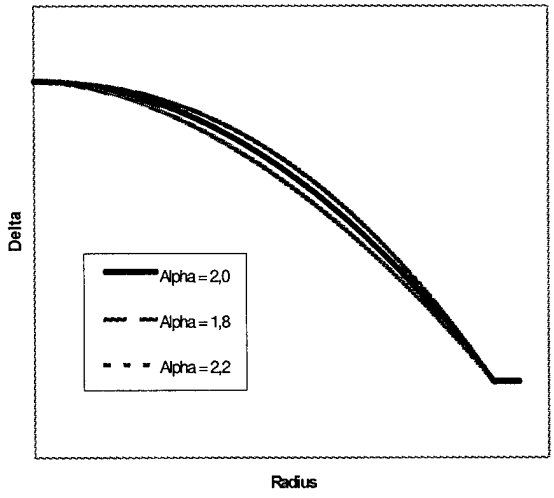

Figure 9: Alpha adjusting of graded index profile

Figure 10 shows the consequences for adjusting the alpha of the graded index profile.

The resulting bandwidth for two cases are given. One with a refractive index profile (= alpha) optimized for 850 nm and one optimized for 1300 nm.

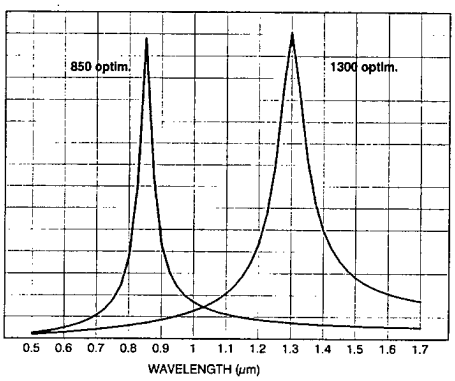

Figure 10: Calculated modal bandwidth

It's clear that by adjusting the alpha of the graded index profile the multi-mode fibre can be bandwidth optimized for each desired window.
In a future publication it will be shown how this is done for a 850 nm optimized MM 62.5 GI fibre.

CONCLUSIONS

The PCVD process is a future prove technology ready to manufacture at both 50/125 μm end 62.5/125 μm multi-mode graded index preforms with:

- high deposition rates
- increased preform sizes
- high deposition and incorporation efficiencies
- high quality optical properties, for example bandwidth
- the possibility to adjust deposited index profiles to optimize for specific data transmission windows (discussed in detail in a future presentation)

REFERENCES

[1] H. Lydtin: PCVD: a technique suitable for large-scale fabrication of optical fibres, J. of Lightwave Technol. Vol LT4 No 8, 1986.
[2] J.W. Leclercq: "Trends in european multi-mode fibre markets", KMI, 1998.
[3] A.H. van Bergen and A.H.E. Breuls: "Large, all synthetic, PCVD preform manufacturing", EFOC/LAN, 1992.
[4] A.H. van Bergen, A.H.E. Breuls and M. van Stralen: patent pending.
[5] A.H. van Bergen, A.H.E. Breuls and M. van Stralen: patent pending.
[6] P. Geittner, H.J. Hagemann, J. Warnier and H. Wilson: "PCVD at high deposition rates", J. of Lightwave Technol. Vol LT-4 No. 7, 1986.
[7] F. Weling: :"A model for the plasma-activated CVD-process", J. Appl. Phys. Vol. 57, 1985
[8] R. Smabers: "Procestechnologische modelstudie naar de mogelijkheden tot verhoging van de effectieve voorvormlengte", Master Thesis, 1991.
[9] F. Gooijer: Private communications, 1998.

AUTHORS

Andries van Bergen
Plasma Optical Fibre B.V.
Eindhoven
The Netherlands

Andries van Bergen was born in Winschoten, The Netherlands, in 1962. He received his M.Sc. degree in chemical engineering in 1986. In the same year, he started working at the Philips Glass Division (Eindhoven, The Netherlands) in the process and product development of optical fibres. At the moment he is a senior project leader in the research and development group of Plasma Optical Fibre B.V. , which is now part of the Draka Holding Group.

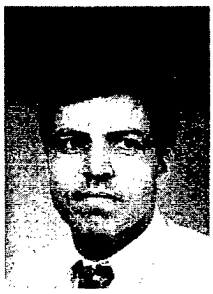

Ton Breuls
Plasma Optical Fibre B.V.
Eindhoven
The Netherlands

Ton Breuls was born in Urmond, The Netherlands, in 1956. He received his M.Sc. degree in applied physics in 1982. He worked at PTT research Leidschendam, The Netherlands from 1982 to 1984. In 1984 he joined the Philips Glass Division, Eindhoven, The Netherlands. Since 1987 he has been working in the process and product development of optical fibres. Since 1990 he has been manager of the research and development group of Plasma Optical Fibre B.V. , which is now part of the Draka Holding Group.

CHARACTERIZATION OF MELTDOWN PROFILE DURING FIBER DRAW

Durgesh S. Vaidya and George D. Mihalacopoulos

SpecTran Corp., Sturbridge, MA.

ABSTRACT

While drawing optical fiber, prediction of the shape of glass deformation and the meltdown length are important towards selection of the draw furnace and optimization of the downstream environment that provides gradual cooling of the fiber prior to the application of coating. Glass preforms were drawn under various conditions of draw speed, heat zone length, furnace gas flow rate, and draw tension. The variation in diameter of the meltdown with distance along the draw path for each condition was measured experimentally. A simple double-sigmoid formulation comprising merely three parameters is proposed to describe the shape of the meltdown and is found to provide very good agreement with experimental data. Correlations are provided for the dependence of these parameters on the process variables. The dependence of the meltdown length on the process parameters is also discussed.

INTRODUCTION

Optical fiber is manufactured by inserting a glass blank (preform) into a high temperature environment such as a resistance or an induction furnace, and pulling the melting mass at a rate such that the diameter of the drawn waveguide thins out to about a few hundred microns. The current worldwide demand for multimode and singlemode fiber is expected to increase at a rapid rate. The need to cope with this growth in demand while minimizing production costs has necessitated the capability to draw preforms of progressively larger sizes and at progressively higher draw rates. In order to avoid deterioration of the optical transmission characteristics and mechanical strength of the fiber in a high-productivity draw process, the melting glass needs to be subjected to optimal conditions of temperature, draw tension and gas flow rates in the draw furnace. Upon reaching its final diameter, the fiber needs to be cooled gradually before the application of a polymer coating. Thus, investigation of the glass deformation phenomenon during meltdown becomes essential towards selection and optimization of the draw furnace. Also, estimation of the axial distance over which the melting mass reaches its target diameter—the meltdown length—under a variety of conditions would greatly aid the design of the fiber-cooling stage downstream of the draw furnace.

Previous theoretical studies pertaining to the shape of the meltdown region involved either an analytical-numerical (e.g. reference 1) or a finite element methodology (e.g. reference 2). The former method provides good qualitative characteristics but suffers from numerical inaccuracy owing to the approximations involved in the formulation of the radiative heat transfer term from the element to the preform. The latter method overcomes this limitation but requires detailed information of all the process parameters and transport properties particularly at high temperatures. Both methods require the meltdown length to be explicitly specified to complete the boundary conditions necessary to obtain solutions to the mass, force and energy balances. The availability of a simple, empirical formulation would greatly aid the calculation and prediction of the meltdown. This in turn could be translated to the design/optimization of the draw process as mentioned in the previous paragraph. We propose such a formulation in the next section. The validity of the approach has been tested by comparison with experimental data for the effect, on the meltdown shape, of 4 process parameters viz., draw speed, length of the heat zone of the furnace element, furnace gas flow rate, and draw tension.

FORMULATION

During the drawing of optical fiber, the preform elongation region (referred to as the meltdown region) is characterized by a steep diameter variation near the top region of the heat zone (referred to as the neckdown region), but a more gradual variation near the region where the glass approaches the target fiber diameter (referred to as the drawdown region). In other words, the change in glass dimension in the neckdown region occurs over a length quite distinct from that in the drawdown region. We approximate this asymptotic variation of the glass diameter at each extremity as a sigmoid of the form,

$$\delta_p(\xi) = \frac{1}{1+\exp(\xi/\alpha_p)} \tag{1a}$$

$$\delta_f(\xi) = \frac{1}{1+\exp(\xi/\alpha_f)} \tag{1b}$$

In the above equation, the quantity δ_p denotes the diameter variation of glass in the neckdown region normalized with that of the nominal diameter of the preform and the symbol ξ represents the distance along the length of the draw tower made dimensionless by a suitable characteristic distance. The parameter α_p denotes the dimensionless characteristic distance over which diameter variations of glass occur in the neckdown region. Symbols with the subscript 'f 'denote the corresponding quantities in the drawdown region. We shall refer to the symbols α_p and α_f as the neckdown length and the drawdown length respectively. Given the asymptotic behavior towards each end of the meltdown region, the diameter variation over the entire region, $\delta(\xi)$, can be represented by the Churchill-Usagi interpolation approximation as:

$$\delta(\xi) = \left\{\left[\delta_p(\xi)\right]^{1/p_0} + \left[\delta_f(\xi)\right]^{1/p_0}\right\}^{p_0} \tag{2}$$

The quantity p_0 is a measure of the distance over which the transition between the asymptotes occurs, and will be referred to as the transition index. Thus if the two asymptotes have identical behavior the transition index goes to zero. Equations (1)—(2) will be referred to as the double-sigmoid formulation.

The variation of the meltdown shape under draw conditions has thus been reduced to merely three empirical parameters. In the subsequent sections, we attempt to correlate these parameters with changes in draw speed, length of the heat zone associated with the furnace element, furnace gas flow rate, and draw tension. The parameters at each draw condition were evaluated by a least-square fit to the experimental meltdown profiles using MATLAB 5. The calculations were performed on a Hewlett-Packard Pentium-pro 180 computer and the computational time for convergence was less than 20 seconds for all cases.

EXPERIMENTAL PROCEDURE

Singlemode preforms (8.3μm core/125μm cladding) were drawn under various conditions with the entire matrix of experiments listed in a normalized form in Table 1. In all cases studied,

Process condition → ***Effect being studied ↓***	*Draw speed*	*Heat zone length*	*Furnace gas flow rate*	*Draw tension*
Draw speed	0.1,1, 1.5,2	1	1	1
Heat zone length	1	0.7,1,1.2	1	1
Furnace gas flow rate	1	1	0.5,1,7	1
Draw tension	1	1	1	0.1,1, 3.5,5

Table 1: Matrix of experimental conditions investigated in the present study. The highlighted regions indicate the specific effect on the meltdown profile.

the final cladding diameter was controlled to within ±1μm of the mean value. After establishment of steady state, the fiber was cut, the preform quickly withdrawn from the furnace and meltdown profiles measured using a high-resolution laser micrometer assembly. In the study of the effect of furnace gas flow rate, the highest value corresponded to the case beyond which the deviations in the fiber diameter were greater than 1μm. Likewise in the data pertaining to various draw tensions, the lowest value represents the case below which the fiber vibrations would prevent accurate monitoring of the diameter. The highest value corresponded to the case beyond which the fiber would break

during the draw run. Also, care was taken to minimize the recoil of the fiber upon relaxation of the draw tension especially at high values.

RESULTS AND DISCUSSION

Figure 1(top) illustrates the fit to experimental data obtained via the double-sigmoid formulation for the effect of draw speed at the lowest and the highest draw speed respectively. The agreement between the actual and best-fit curves is very good and for the most part the experimental and calculated curves are indistinguishable. Throughout this note, only the comparison of the meltdown shapes at the lowest and the highest value of the process variable are presented in the interest of visual clarity; the agreement at intermediate values was observed to be equally good. The best-fit parameters for all draw speeds tested are presented in Figure 1(middle). The meltdown length was calculated by solving for the distance where the diameter reaches a value of 125 μm and its variation with draw speed is presented in Figure 1(bottom).

Results for the effect of heat zone length, furnace gas flow rate, and draw tension are presented in Figures (2)—(5) respectively. In all cases, the best-fit double-sigmoid curve follows the experimental data closely over the entire region of axial distance.

As can be seen in Figure 1 (top), at low speeds the additional elongation due to the downward pulling action is not significant. Therefore, the entire meltdown profile assumes a shape quite similar to a single sigmoid. This translates to a low value of the transition parameter p_0. Also, the neckdown length becomes close in value to that of the drawdown length. As the draw speed increases, the neckdown elongates resulting in an increase in both the neckdown and drawdown lengths. However, the effect of additional elongation due to the downward pulling action is more pronounced in the drawdown region than in the upper region. Hence the values of α_f become significantly higher than that of α_p. The transition region also undergoes stretching owing the higher speeds leading to an increase in the parameter p_0 with draw speed. The variation in all three parameters as well as the meltdown length is seen to be linear with draw speed. For a 20-fold increase in draw speed, the meltdown length is observed to increase by a factor of about 3.

Figure 2(top) illustrates the meltdown profiles as a function of the heat zone length. As can be seen from Figure 2(middle), an increase in the heat zone length leads to a gradual increase in the neckdown length and the drawdown length for the entire range considered. The transition index on the other hand does not vary significantly up to a point beyond which it undergoes a rapid increase. Longer heat zone translates to a longer transition zone over which the preform has to reach the fiber diameter. This is evident in Figure 2(top) where the profile associated with the longest heat zone appears to be stretched more than its counterpart over the entire range of axial distance. The increase in the meltdown length, nevertheless, remains linear and is shown in Figure 2(bottom).

As Figure 3(top) demonstrates, increasing the furnace gas flow rate by a factor of 14 leads to only a minor change in the meltdown profile and primarily in the drawdown region. This translates to a negligible change in both the neckdown length and the drawdown length and only a small change in the transition index. The meltdown length increases by a mere 10% for such a large increase in the flow rate. This indicates that the contribution of the furnace gas to the interfacial force and convective heat transfer is significant only in the lower region of the meltdown.

Study of variation in meltdown profiles with draw tension reveals an interesting trend. The neckdown length does not vary significantly even over a 30-fold increase in the draw tension. The tensile pulling effect however leads to an oscillatory variation in the drawdown length and the transition index. This is indicative of the crossing of meltdown profiles as is evident in Figure 4(top); the only instance amongst all the cases discussed so far. The meltdown profile at high tension starts out thicker but in the transition zone thins out more than its counterpart at low tension. The transition zone intermittently increases and decreases as the tension is increased and consequently the index p_0 oscillates. It is however surprising to find that the drawdown length as well as the meltdown length oscillates with tension since one would expect them to monotonically increase with increasing tensile force.

CONCLUSION

The empirical double-sigmoid approximation furnishes meltdown profiles that are in very good agreement with experimental data over a wide range of processing conditions. The computation time and formulation effort required for generating the diameter variation of drawn preform is substantially small compared to analytical-numerical or finite element methods. The meltdown length is seen to vary linearly with draw speed, heat zone length and furnace gas flow rate. This dependence can be used in the specification of the boundary condition in a finite element simulation of the draw phenomena. Despite the simplicity of the formulation presented in this study, full-scale numerical simulations are essential for obtaining the dependence of transport properties on both the axial and radial distances. The temperature distribution of glass in both axial and radial directions, for instance, is relevant towards understanding and minimizing draw-induced defects that lead to an increase in transmission losses.

The evidence that the meltdown length oscillates with increasing tension is important as it alters the fiber temperature at the entry of the coating applicator, particularly at high draw speeds. This aspect should not be overlooked in optimization of coating design.

ACKNOWLEDGEMENT

The authors would like to express their sincere gratitude to Brenda Wentzell for conducting the draw runs and characterizing the experimental meltdown shapes. We are also thankful to SpecTran Corp. for their permission to present and publish these results.

REFERENCES

[1] Paek U.C. and Runk R.B., "Physical behavior of the neck-down region during furnace drawing of silica fiber", J. Appl. Phys., **49**(8), 1978.

[2] Roy Choudhary S., "Thermal transport in the optical fiber drawing process", Ph.D. Dissertation, Rutgers, The State University of New Jersey, 1995.

AUTHORS

Durgesh S. Vaidya
SpecTran Corp., 50 Hall Road, Sturbridge, MA 01566,USA.

Durgesh S. Vaidya is a Scientist in the R&D department at SpecTran Corp. He received his B.Tech. in Chemical Engineering from IIT-Mumbai, India in 1991, and a Ph.D. in Chemical Engineering from The State University of New York at Buffalo, NY in 1997. He specializes in experimental and computational aspects of heat, momentum and mass transfer phenomena, and is involved in applying these to Fiber Draw development at SpecTran.

George D. Mihalacopoulos
SpecTran Corp., 50 Hall Road, Sturbridge, MA 01566, USA.

George Mihalacopoulos was a Scientist in the R&D department at SpecTran Corp. He received his B.S. in Electrical and Computer Engineering from the National Technical University of Athens, Greece in 1990, a M.Sc. in Applied Mathematics and a Ph.D. in Electrical Engineering from Brown University, Providence, RI, in 1996. After joining SpecTran in 1995, he was responsible for the development of control algorithms, and automation systems for many manufacturing processes at SpecTran, especially in Fiber Draw. He is currently completing his military duty in Greece.

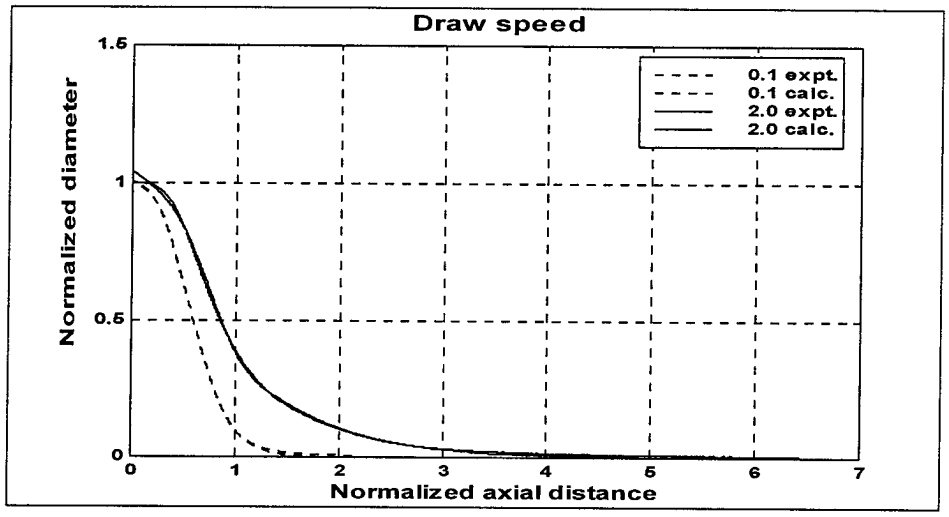

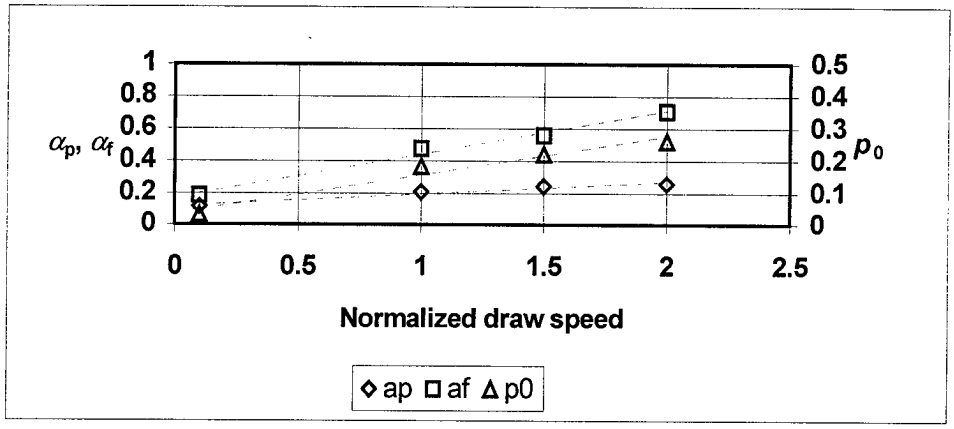

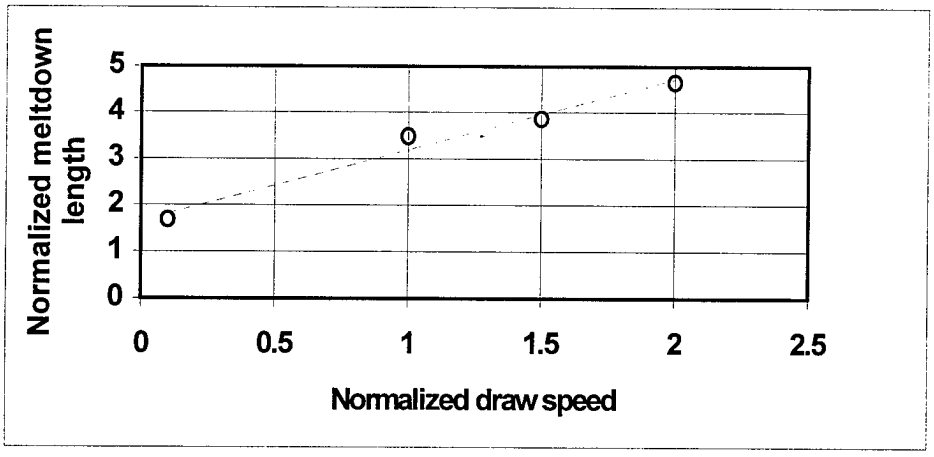

Figure 1: Effect of draw speed on meltdown profile (top), fitting parameters (middle), and meltdown length (bottom).

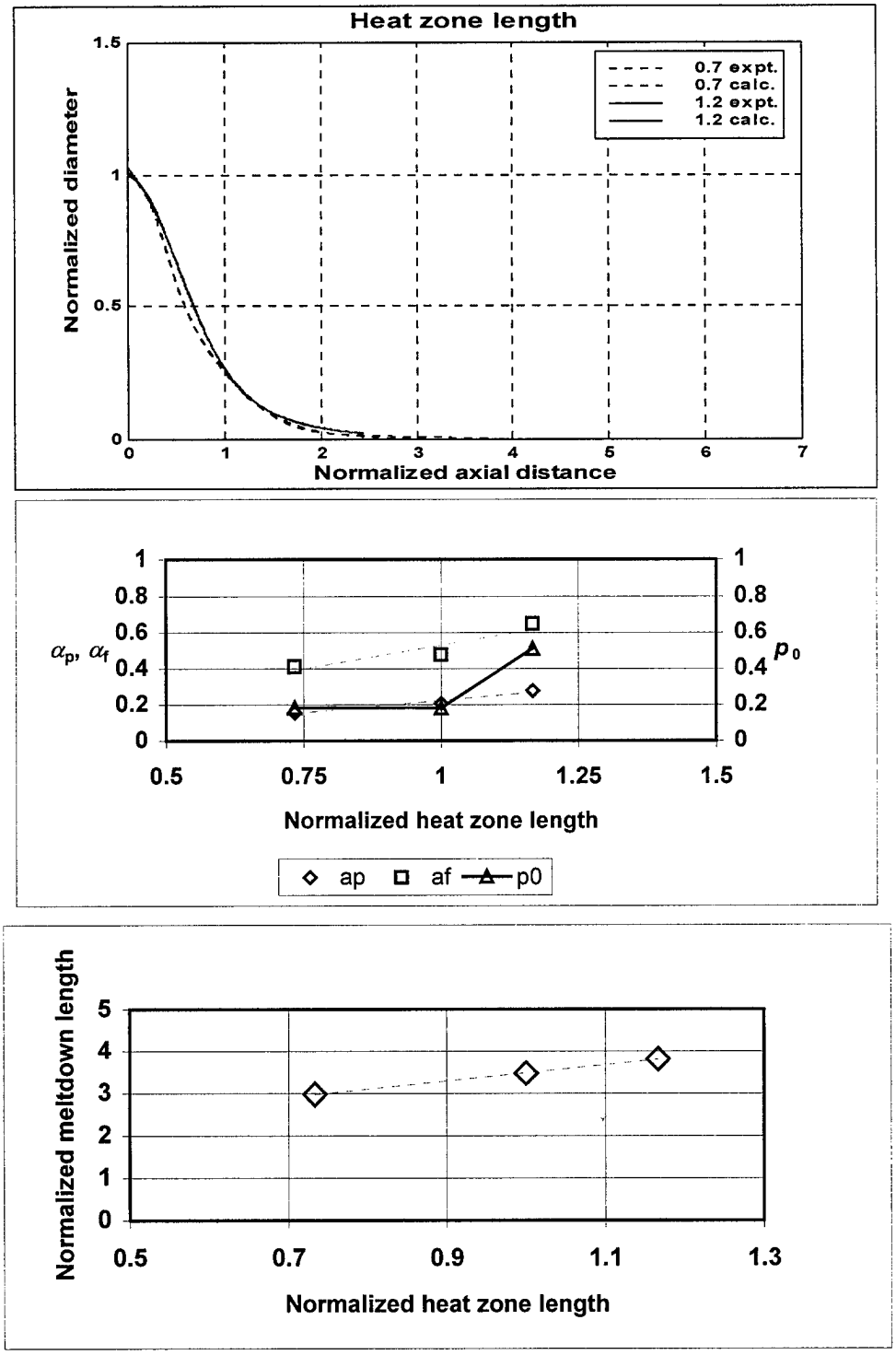

Figure 2: Effect of length of the heat zone of the element on meltdown profile (top), fitting parameters (middle), and meltdown length (bottom).

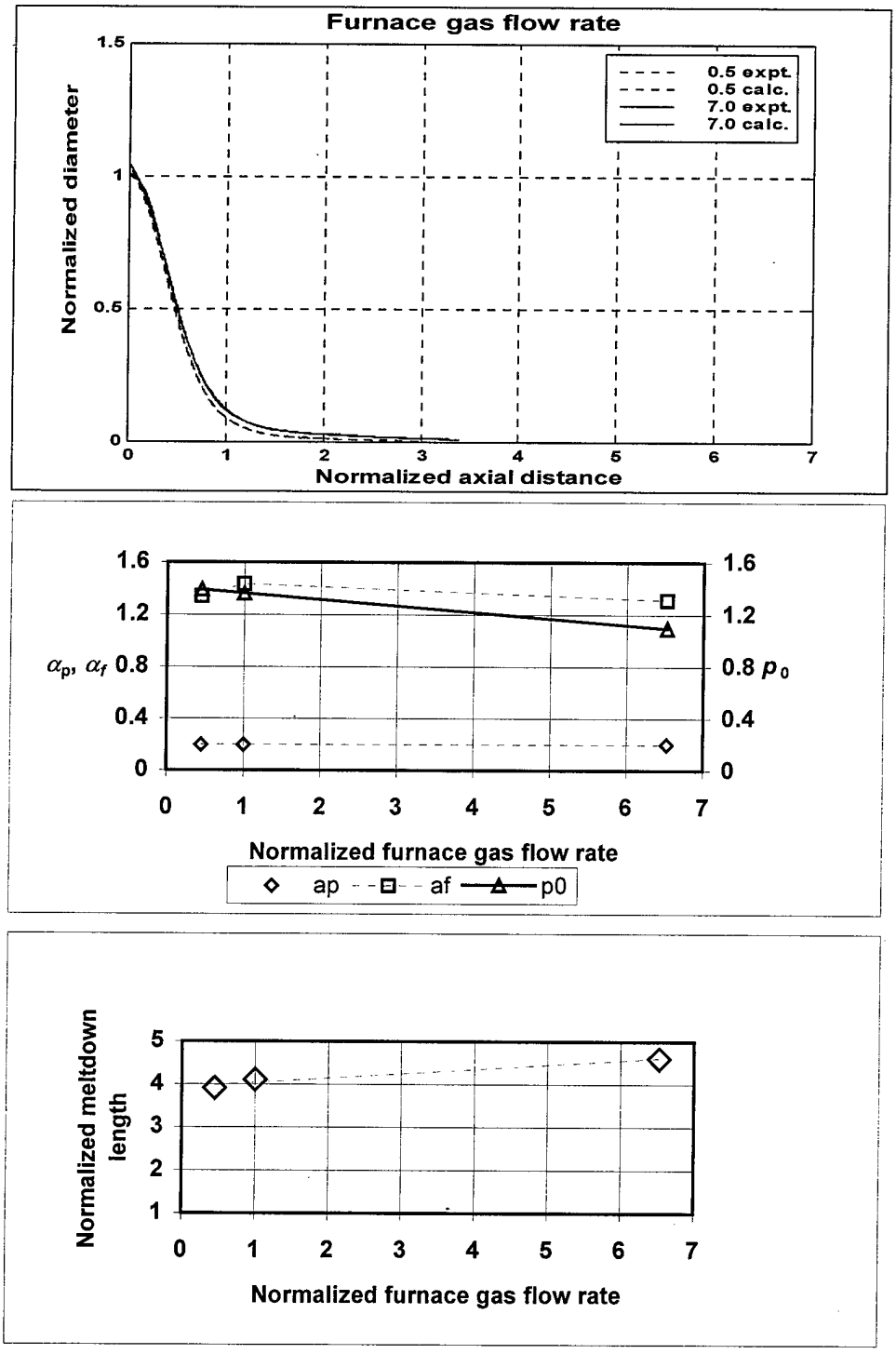

Figure 3: Effect of furnace gas flow rate on meltdown profile (top), fitting parameters (middle), and meltdown length (bottom).

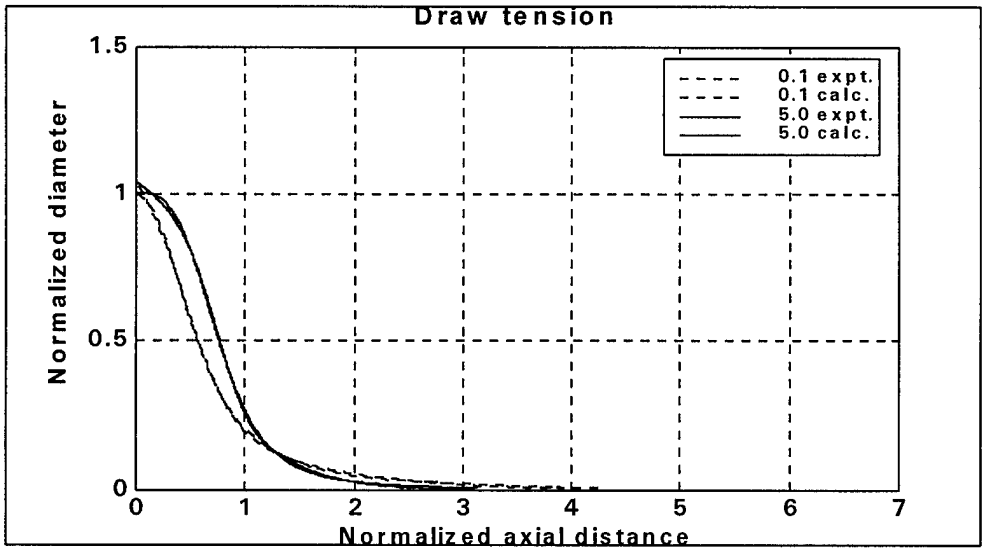

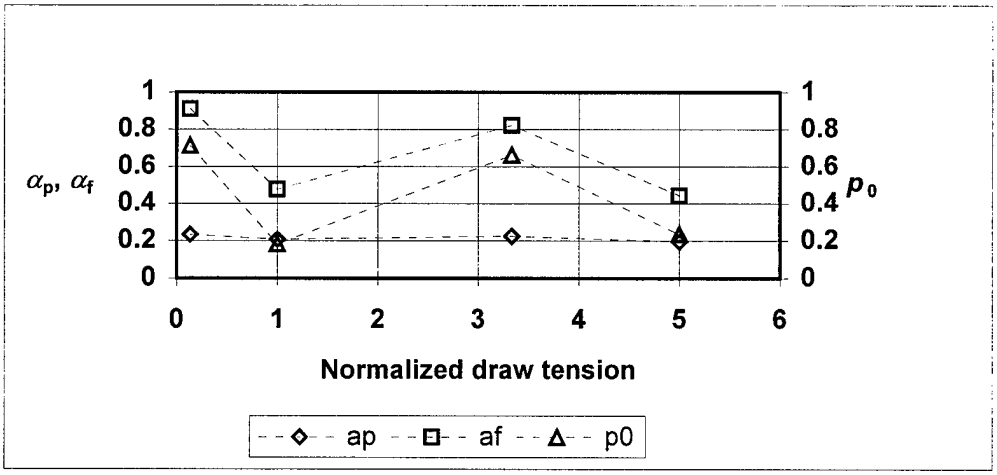

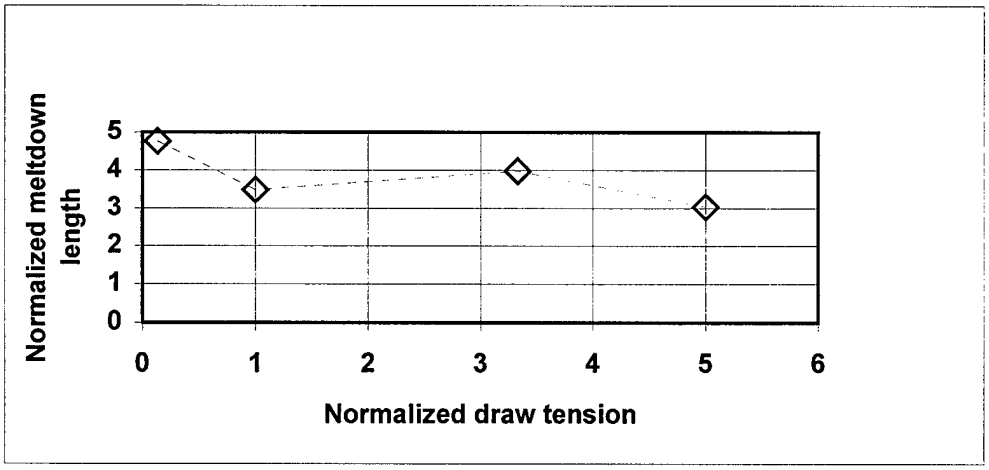

Figure 4: Effect of draw tension on meltdown profile (top), fitting parameters (middle), and meltdown length (bottom).

NUMERICAL SIMULATION OF OPTICAL FIBER COOLING DURING THE DRAWING PROCESS

Marie-Gabrielle GOSSIAUX, Jean-François BOURHIS, Gérard ORCEL

Alcatel, 53 rue Jean Broutin, 78700 Conflans Ste Honorine, France

Abstract

Higher production rates require higher draw speeds. As a consequence, the fiber reaches the coating cup at higher temperatures which could alter the quality of the coating. One approach to deal with this issue is to control the fiber temperature by using a cooling tube. The present work is a 2D numerical simulation of the fiber temperature in a water-cooled tube, in which a gas is injected to increase heat transfer.

The full governing conservation equations are integrated by a finite volume method using a computer code. The numerical predictions were validated by experiments. This paper describes the results of a parametric study which points out the key process parameters regarding cooling efficiency.

Introduction

The last stage of the manufacture of optical fibers is the drawing process. During this operation, the fiber cools from around 1600°C outside the draw furnace to ambient temperature. Its final optical properties are known to be sensitive to the cooling schedule. Moreover, during drawing the glass fiber is coated with a resin to protect it. A too high temperature difference between the fiber and the resin alters the quality of the coating. For these reasons it is important to know and to control the cooling schedule of the fiber during the drawing process.

Nowadays, higher production rates require larger preforms and higher draw speeds. The glass is heated at higher temperatures and the fiber has less time to cool if the draw tower height remains the same. The fiber reaches the coating cup at higher temperatures which may not be acceptable. The two possible approaches to deal with this issue is either to build taller draw towers, which is very expensive or to force cool the fiber. Today, the draw speed is so high that the cooling tube approach is preferred. Numerical simulation is a powerful tool to help designing and optimizing such tubes.

In the past, several authors proposed analytical and empirical analyses to describe the cooling of the fiber.[1,2]These works describe the natural cooling of the fiber with an exponential law derived from the analytical integration of the energy equation written in the glass in which thermal conduction terms have been neglected.The various approaches differ in the way the heat transfer coefficient is estimated. However, none of them solves the momentum equation in the air around the fiber. All works dealt with slow draw speeds and thin fibers.

More recently, other authors proposed numerical simulations of the natural and forced cooling of fibers. One author used the Karman-Polhausen technique to solve the boundary layer equations of the air around the fiber. The temperature profile of the fiber was estimated for thick fibers and slow draw speeds.[3] Another author simulated the forced cooling of the fiber in a tube in which the wall is cooled and helium is injected by solving numerically the equations of energy and momentum.[4]

The present study consists in a two-dimensional numerical simulation of the fiber temperature profile in a tube with a smooth, water-cooled wall and in which gas is injected to increase the heat transfer. The full governing conservation equations are integrated by a finite volume method using a computer code. Experimental results were used to validate the numerical predictions. A parametric study was performed to quantify the effects of the different parameters of the model on the cooling efficiency.

Model

Geometry

The geometry is cylindrical with the fiber moving along the axis of the tube. The gas is injected sideways. The system is axisymmetric and can be modeled in 2D. Figure 1 is a schematic drawing of the mesh. An extended volume is taken into account at the exit of the tube so the outlet boundary condition is moved away from the gas injection port.

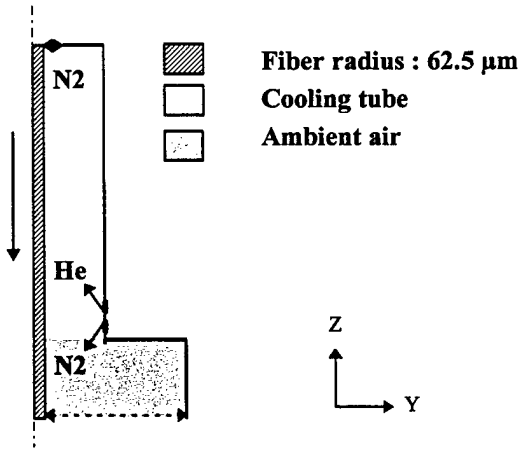

figure 1 : Schematic drawing of the model.

For a short and thin cooling tube, the geometry is extended above the tube in order to allow the hydrodynamic boundary layer to develop around the fiber before entering the tube. It isn't necessary for longer tubes because the effect remains local and doesn't affect the heat transfer calculation.

Computer code

A general computational fluid dynamics (CFD) coupled with heat transfer analysis software package PHOENICS was used. It is based on the Finite Volume Method. The numerical integration of the conservation equations uses the implicit algorithm SIMPLEST. In each cell volume, the fluxes through the faces are evaluated and balanced. Only orthogonal grids are acceptable with this method. The number of cells for the grid was matched to the dimensions of the tube.

Model governing equations and assumptions

The conservation equations solved numerically in the gas phase are the equation of continuity and equation of species continuity, the equation of motion and the equation of energy. In the glass fiber, only the equation of energy is solved. All the equations in the gas phase and in the glass fiber are solved simultaneously.

The fiber of constant diameter is supposed to be pure silica and moving at constant speed. The cooling tube is at constant temperature and a no-slip condition is assumed at the surface of the tube and fiber. The gases are considered incompressible and to form an ideal mixture. The gas flow is taken laminar and Newtonian and in a steady state. The other main assumptions are that the viscous dissipation term (equation of energy) and the thermal diffusion term (equation of species continuity) are neglected, and the heat transfer by radiation is expressed as a heat loss.

Simulation results

Five variables are solved in the gas phase : relative pressure, temperature, helium mass fraction and the two components of the velocity. Only the temperature is solved in the fiber. A typical result is shown figure 2, where the flow pattern and helium concentration (here constant) are represented at the top of the cooling tube.

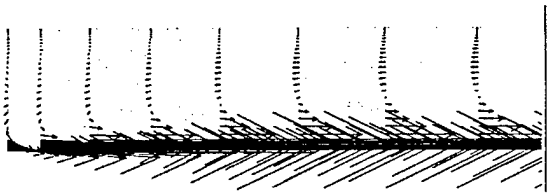

figure 2: flow pattern at the top of the cooling tube

There are 3 main phenomena in the flow pattern within the cooling tube :

- a boundary layer around the fiber created by the motion of the fiber where the main heat transfer is achieved with the fiber.
- an upward flow created by the bottom injection of the helium and amplified by the natural convection induced motion.
- a downward flow located along the tube wall.

In the injection zone, nitrogen recirculates and then is opposed to the boundary layer. For large diameter cooling tubes (such as 40 mm), even a 20 l/min N_2 flow is not powerful enough to break the boundary layer. When the tube ID is smaller N_2 flows of less than 10 l/min can renew the boundary layer. This results locally in a modification of the heat transfer between the fiber and the gas boundary layer due to the variation of the helium concentration.

Another interesting result is the effect of an helium flow increase. Simulation results show that the gas velocity in the boundary layer is not greatly affected. Fiber cooling is more efficient essentially because of helium enrichment of the boundary layer.

All the simulation results on long, large ID cooling tubes demonstrate that the driving parameter of the heat transfer for such geometry is the concentration of helium in the boundary layer especially in the hottest zone of the cooling tube. The higher it is, the more efficient the cooling is.

Model validation

The only parameter which can be easily measured is the fiber temperature. This can be done by IR thermography. The radiation emitted by the fiber is measured and its temperature can be computed knowing the emissivity of the fiber.

Fibers were drawn with different cooling conditions and the fiber temperature was recorded at the inlet of the primary coating cup for each condition. The measured and computed temperatures are reported in figure 3 for various He flows in the cooling tube. The model shows the same trend as the experimental data. From around 5 l/min, the fiber temperature at the primary coater reaches an asymptotic value. Above this value, the increase of the helium flow has no impact on the fiber temperature. This behavior is explained by the fact that the gas in the tube is pure helium and the optimum heat exchange corresponding to the case of the laminar cooling of a solid in a moving helium boundary layer is then reached. The helium concentration field computed for each flow validates this assumption.

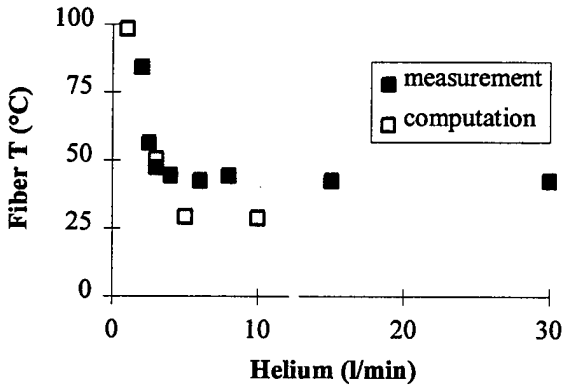

figure 3 : computed and measured temperature values as a function of the He flow

A 10°C of discrepancy remains between the measurements and the computations for the asymptotic value. It can be due to the uncertainty of the measurement or to the assumptions and the inputs of the model. However, the model is entirely satisfactory for prediction or design purposes.

Parametric study

The model was used to quantify the effects of the main process parameters on fiber cooling. It is first necessary to define a parameter to compare the cooling efficiency obtained for different draw conditions.

First, the Reynolds number was computed in each cell of the gas. The maximum value obtained in the simulations ranges from 40 to 150 which comforts the laminar flow assumption.

The dimensionless number used to characterize the cooling efficiency is the Stanton number, St. It is defined as the ratio between the heat exchanged at the fiber-gas interface and the heat advected in the fiber. It can be expressed as :

$$St = h/(\rho c_p V)_{fiber} \quad (1)$$

where h is the heat transfer coefficient between the fiber and the gas, ρ the specific mass, c_p the specific heat ant V the draw speed. The variations of the Stanton number are directly representative of the variations of the heat transfer coefficient along the fiber in the cooling tube.

The parameters studied are the inlet fiber temperature, tube characteristics, and helium gas flow. They are listed in table 1. The reference tube for these simulations is 40mm in diameter and 7.5m in length and the reference conditions are given in line 2 of table 1.

Table 1 : parameters tested in this work

Tube length	Tube ID	Wall T	Inlet Gas T	He flow	N2 flow	Inlet Fiber T	
m	mm	°C	°C	l/min	l/min	°C	
7.5	40	18	22	6	7	**1690**	1
7.5	***40***	***18***	***22***	***6***	***7***	***1350***	2
7.5	40	18	22	6	7	**750**	3
2	40	18	22	6	7	1350	4
2	**6**	18	22	6	7	1350	5
7.5	40	**10**	22	6	7	1350	6
7.5	40	18	22	**20**	7	1350	7
7.5	40	18	**5**	6	7	1350	8

The bold cells indicate which parameter was modified compared to the reference point.

The cooling efficiencies as represented by the Stanton number, are reported in figure 4 for the various draw conditions described in table 1. All the results can be explained in terms of helium concentration near the glass surface. Several

parameters are able to increase the cooling efficiency of the tube. The following conclusions can be drawn from this study :

1. The most sensitive parameter is the tube diameter. When the diameter decreases, the concentration of He near the glass surface increases for a constant flow.
2. The second most important parameter is the He flow. When it increases, the gas velocity increases and helium rises higher in the tube. Heat exchange is favored at higher temperature where it is more efficient.

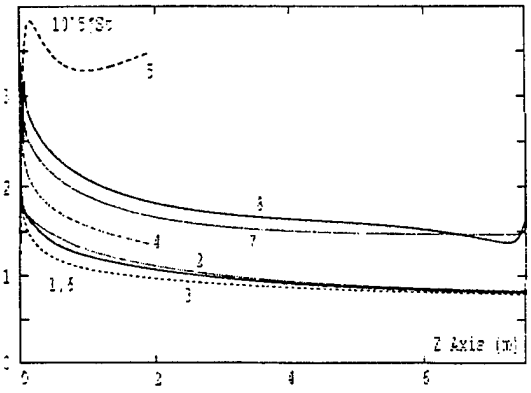

Figure 4 : cooling efficiencies for various process parameters (report to table 1 for curve reference)

The effect of these main parameters on the fiber temperature is presented in figure 5. It is interesting to note that a significant gain in tower height can be achieved by properly designing the cooling tube.

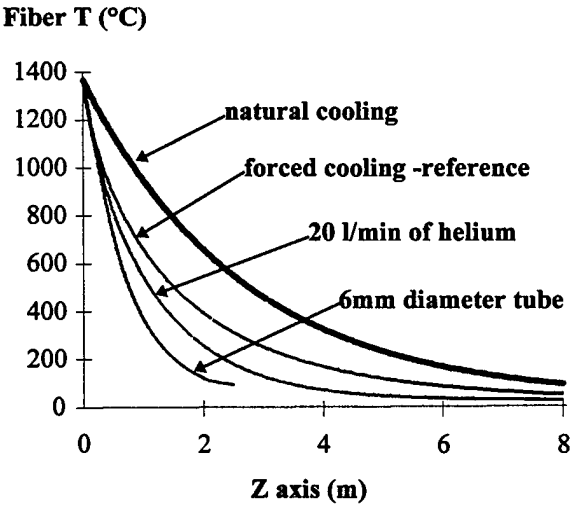

figure 5 : computed fiber temperature as a function of the cooling conditions

CONCLUSIONS

In this study a numerical model was used to simulate the gas flow and the temperature field in a cooling tube used in the manufacturing process of optical fibers. The main parameters for a better cooling efficiency are the tube diameter and the helium flow. These simulation results illustrate the potential of such an approach for the design of new cooling tubes or for the prediction of new operating conditions.

References

(1) L.R.Glicksman, Glass Tech. **9**, 131-138 (1968)
(2) U.C.Paek and C.M.Schroeder, J.Appl.Phys. **50**, 6144-6148 (1979)
(3) H.Papamichael and I.N.Miaoulis, J.Mater.Res. Vol.**6**,
(4) T.Vaskopoulos, C.Polymeropoulos and A.Zebib, Int.J.Heat Transfer. Vol.**38**, No.11, 1933-1944 (1995)

Biographies

Marie Gabrielle Gossiaux graduated from ENSIC in 1990 and received a Ph.D. in chemical engineering from ENS des Mines de St Etienne in 1993. She joined Alcatel in 1993 to work on the simulation of materials and processes. Her current interest is the modeling of fluid dynamics in furnaces.

Jean-François Bourhis joined Alcatel in 1990 and received his Ph. D. in Optoelectronics in 1992 while working on passive integrated optics waveguides and associated pigtailing techniques. His current interest is in Optical Fiber Drawing Technologies.

Gérard Orcel received his Ph.D. degree from the University of Florida in 1987. He held positions at GelTech and SpecTran before joining Alcatel in 1992. Since then, he has been involved in preform design, CVD and Draw technologies and coating development.

STUDY ON CURE BEHAVIOR OF UV CURABLE RESINS FOR HIGH SPEED DRAWING

Kumiyo Moriura, Masaaki Nagai, Hirokazu Kuzushita, Kouji Tsuji, Takaharu Kinoshita

Mitsubishi Cable Industries, LTD
8,Nishinocho, Higashimukaijima, Amagasaki, Hyogo, 660-0856 JAPAN

ABSTRACT

To find a suitable coating material (UV curable resin) of optical fibers for high speed drawing, the curing behavior of the primary coating under low UV doses and high temperature atmosphere were investigated.

As a result, we found that under conditions of low UV doses and high temperatures, the cure degree of the resin largely declines and that such declining degree matches the curing behavior of fibers drawn in high speed. We also found that under such conditions the curing degree is mostly determined by the oligomer of the resin. By high speed drawing tests using the new resin which contains the most suitable oligomer ,we proved that the coatings have sufficient curing degree even under drawing speed twice as fast as usual. We also confirmed that the fiber using the new coating had good fiber properties and long-term reliability.

INTRODUCTION

As an excellent communication medium, there is a growing demand for optical fiber cables. Speeding up the drawing process is an useful measure to meet the demands and can also hold down the cost of optical fibers.

UV curable resins are generally used as coating materials of optical fibers. The curing degree of the resin is an important factor which could change other physical properties such as Young's modulus and adhesion between glass and primary coating, also influencing fiber properties and long-term reliability. As the cure degree of these resin might be change largely depending on the curing conditions, maintaining the curing degree in a certain range is one of the most important factors to achieve high speed drawing.

Under high speed drawing, one of the problems is lower UV dose due to shorter exposure time under the UV lamp. In addition, it can be predicted that the temperature of the resin curing atmosphere is higher due to the use of high power lamps to make up for lower UV dose.

We investigated the curing behavior of resins under low UV doses and high temperatures, and suggested a fiber coating suitable for high speed drawing.

EXPERIMENT

Resin

In the experiment, we chose primary coating materials said to have relatively slow curing speeds on account of low closslinking density. The used resins are shown in Table 1. The resins are all urethane acrylate. The kind of oligomers and the concentration of the photo initiator were taken as parameters. Because the former makes up 50% of the resin component and the latter has a large influence on the curing speed of resin . Each resin was designed to have 2.5% Young's

Table 1. Primary Coatings used for experiments

Coating	A	$A_{0.8}$	$A_{1.7}$	B	C	D	E
Variety of oligomer	X	X	X	X	Y	Y	Y
Concentration of photo initiator[1)]	1	0.8	1.7	1	1	1	1

1)Concentration of photo initiator are expressed with relative value as A's concentration is 1

Table 2. The combinatin of primary and secondary coatings used for drawing

Fiber	①	②	③	④	⑤	⑥
primary coating	A	B	C	D	E	-
secodary coating	Z	Z	Z	Z	Z	Z

modulus in a range of 0.10 to 0.15kg/mm^2.

Sheet experiment

Using sheets, we evaluated the curing behavior of the resin under low UV doses and high temperatures which are conditions of high speed drawing.

Fabrication of the sheet samples

A resin sheet was fabricated in the below method, taking the UV dose and temperature as parameters.

1)Resin was coated 30 μ m^t thick on glass plate with a spinner.

2)The resin surface was covered with a 50 μ m^t thick PET film.

reason: to prevent resin component volatilization.

to prevent curing inhibition of the resin surface by oxygen

3)The samples were left in an oven for 10 minutes at temperatures ranging from 25 to 150°C

4)Immediately after taking out from the oven , the samples were cured under UV dose of (10 to 500mJ/cm^2) using a metal halide lamp. The UV dose was controlled by conveyer speed.

Cure degree

We evaluated the gel fraction as an indication of the cure degree. Gel fraction was calculated by applying the value obtained by extraction using methyl ethyl ketone to the below equation:

$$\text{Gel fraction (\%)} = \frac{\text{weight(after extraction)}}{\text{weight(before extraction)}} \times 100$$

Because each resin has a different saturation point, the absolute value of the gel fraction cannot be compared by itself. Therefore the gel fraction of each resin cured at 25°C-500mJ/cm^2 was represented by a relative value of 100.

Drawing experiment

Drawing was experimented to see if the results obtained by the sheet experiment could be applicable to commercial lines.

Materials

The combinations of primary and secondary coatings using a test drawing are shown in Table 2. Except for the change of primary coatings, the drawing conditions are the same.

Cure degree of the primary coating

First the total gel fraction of primary and secondary coating was evaluated by extraction using methyl ethyl ketone. Next, we assumed that "the gel fraction of the secondary coating drawn under same conditions are constant," and calculated the gel fraction of the primary coating by proportionally distributing the total gel fraction to coated area ratio of primary and secondary coatings. The gel fraction value of fiber 6 which only had a single coating of the secondary coating on the glass fiber was used as that of the secondary coating.

To study the change in the gel fraction, it is necessary to know the saturated gel fraction of the resin. We evaluated the gel fraction of the primary coating after re-irradiating each fiber with 1000mJ/cm^2 of UV rays, using the UV device used to make the sheets. (We confirmed that the gel fraction of the secondary coating is not effected by this re-irradiation.)

The gel fraction of the fibers are represented by relative values where 100 is the saturated gel fraction.

RESULTS AND DISCCUSIONS

Relations of the gel fraction and UV dose / curing temperatures

UV doses of the gel fraction vs. temperature of resin A is shown in Figure 1. The gel fraction declines with the decrease of UV dose and with the rise in temperatures. The gel fraction declines largely at temperatures above 60°C and UV doses below 100mJ/cm^2.

Decline of gel fraction and resin component

Correlation with the oligomer

Approximately 50% of the UV resin is made from high molecular weight component called oligomers. The oligomer which forms the backbone of the resin is an important component which determines many physical properties of the resin. Because the oligomer is so dominant, it is thought to have a large influence on the curing behavior. Therefore, we investigated the relationship between the oligomer and the gel fraction of a resin cured with low UV dose and in high temperature atmosphere (150°C-10mJ/cm^2). Results are shown in Figure 2. To distinguish the declining trend of the gel fraction, in the experiment we selected severe conditions unthinkable in commercial drawing. The degree

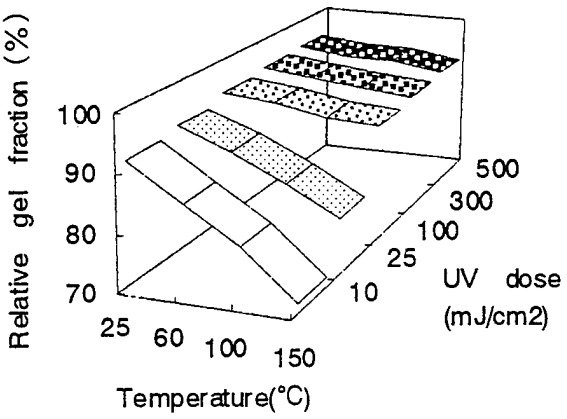

Fig.1. Relative gel fraction of coating A ,cure temperature and UV dose

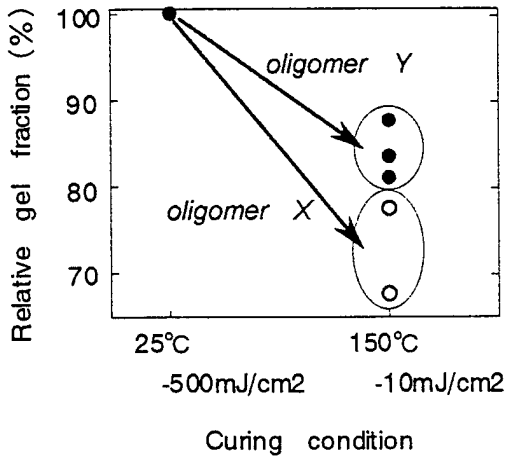

Fig.2. Relation of the oligomer and the gel fraction decline of curing sheets under low UVdoses and high temperature.

of decline differs depending on the resin. However, resin with Y as the oligomer has less declining trends under low UV doses and high temperatures conditions than those with X as the oligomer.

Correlation with the photo initiator concentration

Though the photo initiator concentration makes up only a small portion of the UV resin component, the curing speed is largely effected by type and concentration of the photo initiator. Therefore we experimented with the photo initiator concentration as the parameter, using resin $A_{0.8}$, A, and $A_{1.7}$. Results are shown in Figure 3. As concentration of photo initiator increases, curing sheets under low UV doses and high temperatures tend to get larger gel fractions. Namely, we can see that there is correlation between the photo initiator concentration and cure degree of sheets. But between resin A(photo initiator content :1) and resin $A_{1.7}$(photo initiator content :1.7), there is little difference in gel fraction. Therefore, the method of increasing photo initiator content is not an effective for the purpose of improvement of cure degree under low UV doses and high temperatures.

Fiber drawing

Figure 4 shows comparison of gel fraction between drawn fibers and sheets. Resins with large gel fractions under low UV dose/high temperature conditions, were sufficiently cured when they were drawn. We confirmed that the cure degree of the resin under this condition is correlated to the curing behavior during drawing. Therefore, in the case of searching for a resin suitable for high speed drawing, it is effective to test the curing behavior of resin under low UV doses and high temperatures.

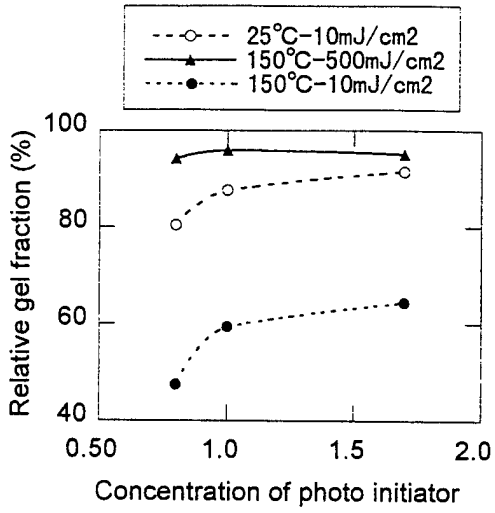

Fig.3. Relationship between concentration of photo initiator and gel fraction of sheets which were cured under various conditions.

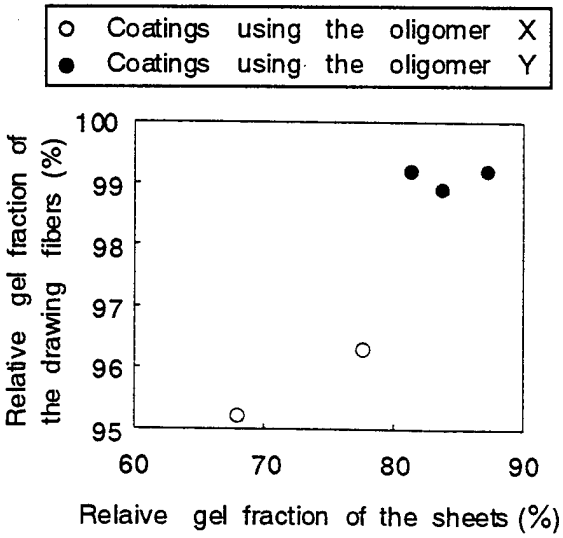

Fig.4. Relation between gel fraction of the drawing fibers and the sheets . The sheet samples were cured at high temperature(150°C) and low UV dose(10mJ/cm2).

Table 3. Fiber properties and long-term reliability of high speed drawing fibers which were colored and made into a four-fiber ribbon.
(Resin C was used as primary coating.)

Test Performed	Condition	Change in transmission loss (at 1.55μm)
Temperature dependence	-40C～+85°C	max.0.03dB/km
Heat Aging	+85°C/240Hr	max.0.01dB/km
Temperature-Humidity	+85°C/95%/2000Hr	max.0.01dB/km
Jelly immersion	+80°C/2000Hr	max.0.04dB/km

HIGH SPEED DRAWING EXPERIMENT

From the above results, we tested high speed drawing using resin A which uses oligomer X and resin C which uses oligomer Y as the primary coatings. Besides the drawing speed all conditions relating to resin curing were the same(resin temperature, lamp power, number of lamps, etc.) . Results are shown in Figure 5. As predicted by the sheet tests, the gel fraction of resin A largely declines as the drawing speed becomes faster. On the other hand, resin C which has Y as the oligomer maintains its gel fraction in even high speed.

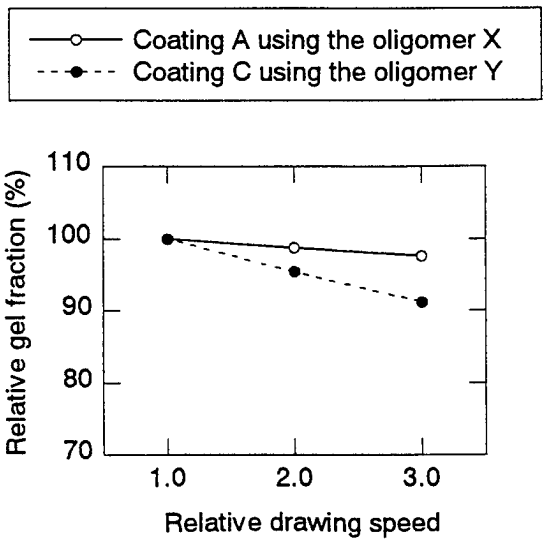

Fig.5. Relationship between drawing speed and gel fraction of drawing fibers

Further, we evaluated fiber properties and long term reliability of four-fiber ribbon, which was made of high speed drawing fibers (middle, drawing speed 2) using resin C .Results are shown in Table 3. The results show good fiber properties.

CONCLUSIONS

To evaluate suitable optical fiber coatings of optical fibers (UV curable resin) for high speed drawing, we investigated curing behavior of the primary coating, focusing on the temperature and UV dose. The results obtained are as follows:

1. Gel fractions of resins decline largely when cured under low UV doses and high temperature conditions
2. The curing behavior under low UV doses and high temperature matches that of high speed drawing.
3. The new resins using a suitable oligomer show no decline of gel fraction even under high speed drawing.
4. The fiber using the new resin shows good fiber properties and long-term reliability.

AUTHORS

Kumiyo Moriura
Mitsubishi Cable Industries, Ltd.
8,Nishinocho, Higashimukaijima, Amagasaki, Hyogo,
660-0856 JAPAN

Moriura received a B.E. degree in Chemistry from Osaka-City University in 1994. Then she immediately joined Mitsubishi Cable Industries, Ltd. And she has been engaging in the research and development of plastic materials for optical fiber cables. She is now a engineer of Materials Research Dept.

Hirokazu Kuzushita
Mitsubishi Cable Industries, Ltd.
8,Nishinocho, Higashimukaijima, Amagasaki, Hyogo,
660-0856 JAPAN

H. Kuzushita received B.E. and M.E. degrees in Industrial Chemistry from Kyoto University in 1977 and 1979 respectively. Then he immediately joined Mitsubishi Cable Industries, Ltd. And he has been engaging in the research and development of plastic materials for communication cables. He is now a chief engineer of Materials Research Dept.

Masaaki Nagai
Mitsubishi Cable Industries, Ltd.
8,Nishinocho, Higashimukaijima, Amagasaki,
Hyogo,660-0856 JAPAN

M. Nagai graduated from Kobe Technical College majoring in Chemistry in 1973. Then he joined Mitsubishi Cable Industries, Ltd. And he has been engaging in the research and development of plastic materials for communication and power cables. He is now a senior chemist of Materials Research Dept.

Kouji Tsuji
Mitsubishi Cable Industries, Ltd.
4-3, Ikejiri, Itami, Hyogo, 664-0027 JAPAN

Kouji Tsuji graduated from Nagoya Electronics and Communication college majoring in electronics in 1985. Then he immediately joined Mitsubishi Cable Industries, Ltd. And he has been engaging in the research and development of optical fiber cables. He is now a engineer of Optical Fiber Cable Telecommunication Engineering Dept.

Takaharu. Kinoshita
Mitsubishi Cable Industries, Ltd.
4-3, Ikejiri, Itami, Hyogo, 664-0027 JAPAN

T. Kinoshita received a B.E. degree in Physics from Osaka-City University in 1992. Then he immediately joined Mitsubishi Cable Industries, Ltd. And he has been engaging in the development of light guide. He is now a engineer of Optical Fiber Manufacturing Section.

MULTIVARIATE STATISTICAL PROCESS CONTROL TECHNIQUES FOR CABLE MANUFACTURING

Helen M. Bush

Lucent Technologies
Norcross, Georgia

ABSTRACT

Cable manufacturing has special circumstances which can make traditional $\bar{x}$ charts a poor choice for quality control. Small sample sizes, correlated variables, and small, varying batch sizes complicate the SPC choices. Multivariate charts are ideal for monitoring several correlated variables and are recommended for cable processes such as extrusion. These methods use the correlation of the variables to detect out of control situations that using multiple individual charts would not. The traditional multivariate quality control method is Hotelling's T^2 chart, which can be used when the variables are normally distributed. New nonparametric methods presented here can be used when the variables have an unknown distribution. The nonparametric methods are simple to program and can be easily automated.

INTRODUCTION

Statistical process control (SPC) is widely used as a tool for process improvement. SPC is a means to monitor key process variables and should provide direction and focus for process improvement. How an SPC program is planned and implemented can be the difference between having an effective tool for process improvement or a waste of time and resources.

Control charts are commonly used SPC tools. A typical control chart depicts the average value of a measured variable over time. When observations plotted on the chart appear to be random and centered about a single mean with constant variance, the process is said to be *in control.* *Control limits* are also shown on the chart, and any sample average exceeding a control limit is said to indicate that the process is *out of control*, or that a process shift, a change in the process mean or variance, has taken place. Non-random patterns, such as many observations in a row above or below the *centerline*, the overall average, also indicate an out of control situation. Out of control situations are opportunities to learn what affects the process. Investigations launched after an out of control signal can lead to the elimination of *root causes* and hence to a decreased process variance and fewer defective products.

The purpose of this paper is provide instructions for developing and using an SPC plan that will have an impact on cable manufacturing processes. In the next section, the characteristics of cable manufacturing that must be considered when designing a control plan are presented. In the following sections, different control schemes appropriate for cable manufacturing are described and compared. The last section is a step by step example of designing a control plan for a cable process. A guideline for choosing the program most suitable for different manufacturing scenarios is also presented.

SPC CHARACTERISTICS FOR CABLE MANUFACTURING

The typical textbook manufacturing scenario consists of large numbers of identical units being manufactured continuously. These units may be manufactured in large lots or batches. A small random sample from the lot is collected and measured, and the average of the sample is added to an $\bar{x}$ control chart. However, cable manufacturing is not an ideal setting for a typical SPC application. Several characteristics constrict and complicate the choices for an SPC scheme. These characteristics are discussed in the sections below.

Cable Samples

Knowledge of the distribution of the variables is traditionally vital to designing a control plan. When the distribution of the data is known, one can calculate the probabilities of certain events. Two important events are making Type I and Type II errors. A Type I error is concluding that the process is out of control when in fact it is not, and a Type II error is failing to recognize a specific out of control situation. In practice the desired probability of a Type I error dictates where the control limits are set. The Central Limit Theorem states that as the sample size becomes infinitely large, the distribution of linear combinations of any variable becomes normal. Therefore a general rule of thumb is to assume that sample averages are normally distributed if the sample size is at least 10 (smaller sizes can often be sufficient as well). When this assumption can be made, control charts can be designed for a desired probability of a Type I error.

In cable manufacturing, batches are not usually large and may be as small as a single cable. Some measurements may be taken as the cable is being manufactured. If this is the case, then the solution is to treat each cable as a batch and randomly sample throughout the length of the cable. However, some measurements may be impossible to take without cutting the cable open. In this case, the cable is limited to a maximum of two observations: one from either end of the cable. The collection of these measurements is not a random sample, but one may use an end measurement or the average of the two as a single statistic for the cable. Samples this small may not have a known distribution, and other procedures may need to be employed in order to design an effective control scheme.

Multiple Variables

The quality of a cable depends on several, if not many, variables. Each of p variables may be measured per sample. Let the vector $\mathbf{x}_i$ denote the ith observation in a sample of measurements for the p variables where

$$\mathbf{x}_i = (x_{i1}, x_{i2}, \ldots, x_{ip}). \qquad (1)$$

The sample average is then denoted

$$\bar{\mathbf{x}} = (\bar{x}_1, \bar{x}_2, \ldots, \bar{x}_p). \qquad (2)$$

Monitoring many variables can be cumbersome if one chart is displayed per variable. Additionally, these variables are often heavily correlated. Consider an extrusion process. It is not difficult to imagine that if the jacket diameter is known to be below average then the wall thickness is also likely to be below average. There is also a problem of designing a scheme with multiple correlated variables. One can set limits on a control chart so that the probability of a false alarm is known, say α. However, the total probability of a false alarm, the probability of a false signal from *any* chart, is unknown, but has a maximum value of

$$\alpha_T \leq 1 - \prod_{i=1}^{p} (1 - \alpha_i), \qquad (3)$$

where p is the number of variables, and α_i is the probability of a false alarm on the ith chart. As the number of variables to monitor increases, so does the chance of an overall false alarm. If the number of variables p is large, then either α_T is too large or the individual probabilities are so small that the charts are ineffective. *Multivariate charts* are used to solve this problem. One statistic is calculated from all variables. If the distribution of the multivariate statistic is known, then a control scheme can be designed with a desired false alarm rate. Having one chart both eliminates the burden of having many charts to examine and greatly simplifies the design phase.

An advantage of using multivariate statistics is that they use the correlation of the variables to construct control limits. Consider Figure 1 below of a bivariate situation. The plot indicates a positive correlation between the two variables. If individual charts are constructed, then the control limits would be the dashed lines on the plot. Any point inside the square made by the four limits is considered to be in control. If a multivariate chart is constructed, then the control limits are represented by the elliptical shape. In this case, any point within the ellipse is considered to be in control. The ellipse is determined by the mean, variance and correlation of both variables, while traditional limits are determined by the mean and variance of each individual variable. Note that an observation that plots in the lower right or upper left hand corner of the square would be considered in control from the individual charts, but out of control with the multivariate chart.

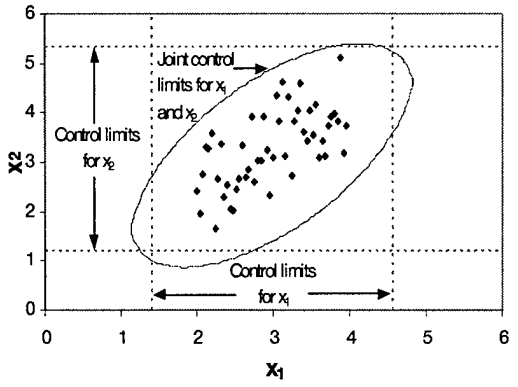

Figure 1: Control limits for bivariate data

Product Mix

The product mix may also change quickly in cable manufacturing. Again, this may or may not have an adverse effect on designing a control program. Different products may have different specifications, including nominal values. Should observations from different populations be pooled together on one chart? The answer is no, unless certain conditions exist. If the variances of the observations from the different populations are the same (this is not an unreasonable condition) then the user should monitor the difference between the observation and the nominal value. If the nominal value for variable y is μ the control statistic is then x, where

$$x_i = y_i - \mu. \quad (4)$$

If the mean of the variable is its nominal, or target value, then the variable x should have mean 0 and constant variance σ^2. It is customary to separate observations from different product mixes on a chart with vertical bars. This is also useful in studying differences between different products.

Specifications and Control Limits

Though not unique to cable manufacturing, a common misunderstanding in SPC applications is the difference between specifications and control limits. It is important to realize the difference between the two. Control limits are calculated quantities that are functions of the process mean, variance, and desired probability of a false alarm, α. An observation that exceeds the control limits indicates that the process mean or variance has changed. It does not reflect the acceptability of a product. Specifications are limits set by engineering, and observations that exceed the specifications are deemed defective, unfit for sale. The specifications are *independent* of the process parameters. It is possible to be in control and beyond the specifications, and it is possible to be out of control and within specifications. When the process is within specifications the product may be sold, and an intelligent decision must be made as to whether or not or how to adjust the process to a state of control. It may not be wise to automatically make an adjustment that slows the process down.

MULTIVARIATE SPC METHODS FOR LARGE SAMPLE SIZES

When sample sizes are "large", one can assume that the sample average of each variable is normally distributed. This is a reasonable and well-known assumption. How a "large" sample is defined, depends on the underlying distribution of the data, but generally, a sample size of 10 or more is sufficient for the sample averages to meet the normal distribution criteria. If the user is uncertain, one may perform a test described in the next section that determines if it is sound to assume the data is normally distributed. Now assume that m samples of size n are obtained. For each sample, a vector of averages is obtained.

$$\bar{\mathbf{x}}_i = (\bar{x}_{i1}, \bar{x}_{i2}, \ldots, \bar{x}_{ip}) \quad \text{for } i = 1, \ldots, m. \quad (5)$$

One can then calculate a vector of the average of the sample averages,

$$\bar{\bar{\mathbf{x}}} = (\bar{\bar{x}}_1, \bar{\bar{x}}_2, \ldots, \bar{\bar{x}}_p). \quad (6)$$

The test statistic, Hotelling's T^2, is then

$$T_i^2 = n(\bar{\mathbf{x}}_i - \bar{\bar{\mathbf{x}}})' \mathbf{S}^{-1} (\bar{\mathbf{x}}_i - \bar{\bar{\mathbf{x}}}), \quad (7)$$

for i=1,...,m where S is the sample covariance matrix[2]. The upper control limit presented by Alt[3] is

$$UCL = \frac{p(m+1)(n-1)}{n(mn-m-p+1)} F_{\alpha,p,mn-m-p+1}. \quad (8)$$

The term $F_{\alpha,p,n-p}$ is a statistical term and represents the 1-α percentile of an F-distribution with p and n-p degrees of freedom. Several statistical software packages will calculate the statistics and the control limit automatically. The user need only supply the data and specify the desired probability of a false alarm, α. It is important to note that not all quality control software packages contain multivariate charts, so the cable manufacturer must be careful to select a package that does.

MULTIVARIATE SPC METHODS FOR SMALL SAMPLE SIZES

Normally Distributed Data

When it is not possible to have large samples, it may still be possible to use Hotelling's T^2 statistic if the data happens to be normally distributed. One can test this assumption with a hypothesis test. The simplest way of doing this is to jointly test if each variable is normally distributed, i.e.,

$$H_0 : \bar{x}_i \sim \text{Normal}(\mu_i, \sigma_i^2)$$
$$H_1 : H_0 \text{ not true}$$

for i = 1,...,p. There are several methods for performing this test. Two common methods are a chi-squared goodness of fit test, and the Kolmogorov-Smirnov test. Most statistical packages can perform both tests. The chi-square goodness of fit test is described here.

First, estimate the mean and variance of the m sample averages.

$$\hat{\mu}_i = \bar{\bar{x}}_i = \frac{\sum_{j=1}^{m} \bar{x}_{ij}}{m} \qquad (9)$$

$$\hat{\sigma}_i^2 = s_i^2 = \frac{\sum_{j=1}^{m} (\bar{x}_{ij} - \bar{\bar{x}})^2}{m-1} \qquad (10)$$

Next, arrange the data into a histogram of k intervals where $6 \le k \le 12$. The number of observations that fall in the ith category are denoted O_i. Now determine the number of observations that are *expected* in each interval, E_i. This is done using the parameter estimates and the standard normal tables (or a probability calculator). If the null hypothesis is true, then

$$\chi_0^2 = \sum_{i=1}^{k} \frac{(O_i - E_i)^2}{E_i} \sim \chi_{k-3}^2. \qquad (11)$$

If $\chi^2_0 < \chi^2_{.05,k-3}$, (the p-value > .05) then one may conclude that the assumption of normality is reasonable and proceed with using Hotelling's T^2 charts. Note that if the sample size is equal to one, then Hotelling's test statistic is basically the same, where

$$T_i^2 = n(x_i - \bar{x})' \mathbf{S}^{-1} (x_i - \bar{x}), \qquad (12)$$

and the control limit changes slightly to

$$UCL = \frac{p(m+1)(m-1)}{m(m-p)} F_{\alpha,p,m-p}. \qquad (13)$$

Non-Normally Distributed Variables

When the variables do not have a normal distribution, then alternative methods must be used. *Nonparametrics* is the field of study dedicated to analyzing data independent of the underlying distribution of the variables. This means that nonparametric techniques can be used on any data set no matter how the data is distributed. Generally, these methods are preferable only when the distribution of the data is unknown.

Assume there exists an initial pool of m observations from the process with some mean and covariance structure. The purpose of using control techniques is to determine if a new observation has the same underlying distribution as the observations in the initial pool. The nonparametric procedures produce a set of scores

$$\mathbf{S} = (S_0, S_1, \ldots, S_m) \qquad (14)$$

for each observation in the initial pool and for the new observation. The score S_i describes the position of x_i relative to the other observations in the pool, and the score S_0 is the score for the new observation and reflects its position relative to the pool. In general, the lower the score, the closer an observation is to the "center" of the

pool of observations. Let R_i denote the ranking of S_i among the scores. As the size of the initial pool increases, the distribution of the ranks approaches a uniform(1,m+1) distribution. If the ranks are uniformly distributed, then the p-value associated with the new observation is then

$$\text{p}-\text{value} = \frac{m+2-R_0}{m+1}. \qquad (15)$$

In order to design a control scheme the user must choose the desired probability of a false alarm α. Recall that the smaller this probability is the less likely a true out of control situation will be detected. Therefore the costs of failing to detect an out of control situation and the costs of a false alarm must be weighed when making the decision. Generally, the false alarm rate is between .01 and .001 with .0027 being the false alarm rate for a standard "3σ" control chart. The next step is to compare the false alarm rate to the number of observations in the initial pool. If the pool size is larger than $1/\alpha$, then the user may conclude that the process is out of control when the p-value of the new observation is less than α. If the pool size is smaller than $1/\alpha$, then another step must be taken.

Exponentially weighted moving average (EWMA) statistics are popular for control charts and are a solution to having small pools relative to the false alarm rate. EWMA statistics are moving averages where the more recent an observation is, the higher its weight on the average is.

Let the EWMA statistic at time t be denoted as

$$z_t = \lambda v_t + (1-\lambda) z_{t-1}, \qquad (16)$$

where λ is the percentage weight of the most recent observation ($.05 \le \lambda \le .30$), and v_t is the p-value of the new observation at time t. The mean and variance of the EWMA statistic are

$$E(z_t) = \frac{m+2}{2(m+1)} \qquad (17)$$

$$V(z_t) = \frac{\lambda(1-(1-\lambda)^{2t})}{2-\lambda}\left(\frac{m(m+2)}{12(m+1)^2}\right) \qquad (18)$$

when the process is in control[4]. By the Central Limit Theorem, it can be assumed that the EWMA statistics are normally distributed. Therefore, one may conclude that the process is out of control if

$$\frac{|z_t - E(z_t)|}{\sqrt{V(z_t)}} > Z_{\alpha/2}, \qquad (19)$$

where $Z_{\alpha/2}$ is the $(1-\alpha/2)$ percentile of the standard normal distribution. To plot this on a graph, the control limits would be

$$E(z_t) \pm Z_{\alpha/2}\sqrt{V(z_t)}. \qquad (20)$$

Note that to have a "3σ" control chart, $Z_{\alpha/2}$ is set to 3. One property of EWMA charts is that they are generally slower to detect wildly out of control situations, but faster to detect slight changes in the process. The EWMA chart requires a "warm-up" period, meaning that it is unlikely that an out of control situation will be detected on the very first sample. Simulations performed on the procedure verified that the assumptions are reasonable, and the desired false alarm rate is achieved[5].

What remains is the method for obtaining the scores for the observations. The procedures developed by Bush[6] are divided into two general categories: functional algorithms and linkage algorithms. In the sections below, the categories and two examples of each are presented.

SCORE CALCULATIONS

Functional algorithms

The score for an observation obtained with the functional algorithms are functions of that observation and every other observation in the pool. Two functional algorithms are presented here.

Central Statistic Method. The score for this method is the Mahalanobis distance from an observation to a central statistic, such as the overall mean or median. The Mahalanobis distance measures distance in multivariate space and differs from a traditional Euclidean distance in that it incorporates the covariance structure of

the variables into the measure. It equalizes the effects of variables with large and small variances, and two highly correlated variables contribute less than two relatively uncorrelated variables to the overall score[7]. If the mean vector is chosen for the central statistic, the scores are

$$S_i = (\mathbf{x}_i - \bar{\mathbf{x}})'\mathbf{S}^{-1}(\mathbf{x}_i - \bar{\mathbf{x}}), \quad (21)$$

where S is the sample covariance matrix. The observations most distant from the mean vector will have the largest scores.

Total Distance Method. The score for this method is the total distance from an observation to every other observation in the pool where

$$S_i = \sum_{j=1}^{m} (\mathbf{x}_i - \mathbf{x}_j)'\mathbf{S}^{-1}(\mathbf{x}_i - \mathbf{x}_j). \quad (22)$$

Like the central statistic method, observations on the perimeter of the distribution will have larger scores, but an added advantage of this method is that observations in sparsely populated regions will also have large scores. Observations in dense areas will have smaller scores because the contributions to the score from the observation to the others in the same region will be very small.

Linkage Algorithms

Linkage algorithms are based on the concept of chaining observations together. The chain begins at the center of the distribution and branches to all the observations in the pool. Observations are added in succession until all are part of the chain, and the score statistic is the order in which an observation is added. Therefore low scores indicate the observation is added early, and high scores show it was added late. The criterion for selecting the next observation to be added is that it is the closest observation to the chain. It is important then, to define how to measure the distance from an observation to a chain of observations. The members already in the chain should have a large influence over the selection of the next observation added. Therefore the distance to the chain is a function of the distances to all or some of the observations already in the chain. The initial point in the chain is the overall mean of the pool. The rule is to add observation x_i to the chain if the total Mahalanobis distance from x_i to any k observations already in the chain is the minimum among all such distances. The variable k is selected by the user. Three cases are discussed in more detail below.

Single Link. When $k = 1$, the observation added to the chain is the closest observation to any one observation already in the chain. This case is called the *single link algorithm*, and is illustrated in Figure 2 below. For simplicity, fifteen observations are added to a chain. The observations have been standardized so that the Mahalanobis distances and the Euclidean distances are the same. The order in which the observation is added is shown above each observation. The links are also shown, represented by lines connecting the observations. The initial point is the overall mean at (0,0). The first observation added is the one closest to the mean. The second observation is closest to the first observation added, and is therefore linked to the first observation. The third observation added is linked to the central statistic. Note that once an observation is linked, its nearest neighbors are also soon to join.

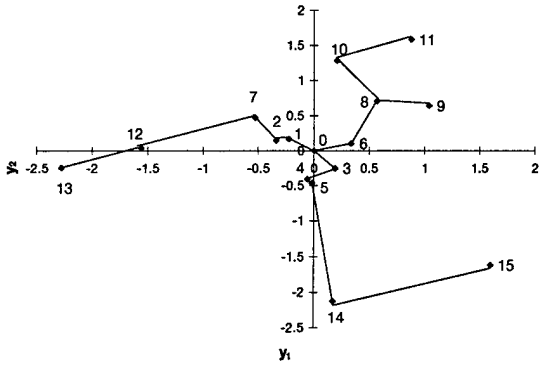

Figure 2: Example of Single Link Algorithm

Double Link. When k=2 the observation joined to the chain has the smallest total Mahalanobis distance to any *two* observations already in the chain. Figure 3 illustrates the double link algorithm with the same 15 observations. Note that each observation is linked to two others.

Total Link. With the *total link* algorithm the distance from an observation to the chain is the sum of all distances to observations in the chain. Here, k=g where g equals the number of observations in the chain at any given point. In the first step, the observation to join is the closest

to the central statistic. The second observation to join has the minimum distance to the two in the chain. The third observation to join has the minimum distance to the three in the chain, etc.

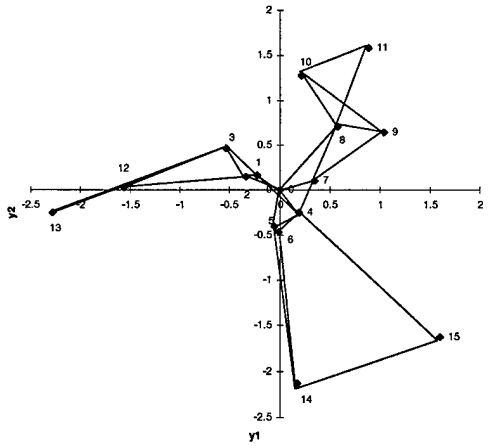

Figure 3: Example of Double Link Algorithm

Functional vs. Linkage algorithms

The functional and linkage algorithms were simulated with the purpose of comparing the performances to determine if one of the methods is superior to the others[8]. A method would be judged superior if for a given probability of a false alarm, it detected true out of control situations more quickly for all tested data distributions. No method was superior in all cases. Different methods tended to work better for different distributions of the variables. However, in no case did one procedure perform significantly "worse" than the others. In general, the functional algorithms perform well when the data is symmetric, and the linkage algorithms perform well when the data is skewed. The central statistic method is the easiest to implement and the fastest computationally, however, that may not be an important issue.

An example of the design and implementation of a control scheme for a fictional extrusion process is presented in the sections below.

EXAMPLE

Getting started

Suppose an extrusion process for a cable has specifications on the outer diameter and the inner diameter (only two variables are used in the example for simplicity of illustration). The engineer responsible for SPC decides to simultaneously monitor both variables with a multivariate control chart. Assume it is not possible to measure both variables during production, so a sample from each cable is taken at the end of production. These variables have always been measured for each cable, but a couple of months ago a new tooling design for the extruder was installed. Data from before the change may be considered to come from a different process, so only data collected after the design change was implemented may be used to establish the control charts. One-hundred cables have been made since the change. Two cable designs are made on the line in question, which require different specifications for the two variables.

The first step is to resolve the issue of having two specifications. The nominal values for the variables are different for the two designs, but the standard deviations are about the same. The variables are then transformed by subtracting their respective nominal values as described in Equation 4. Figure 4 below is a plot of the transformed outer diameter variable over time. The vertical bars designate when the different products were run. Note that the data appears to be random with respect to the different designs. If there were noticeable differences between the sections, then further transformations would be necessary. The plot of the transformed inner diameter x_2 is not shown here, but it too appears to be random with respect to the sheath design.

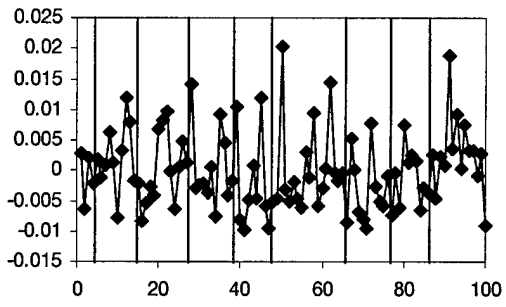

Figure 4: Transformed Outer Diameter, Variable x_1

The second step is to determine the desired probability of a false alarm. An out of control signal does not mean that the process must be stopped. If a measurement exceeds the specifications for the variable, then the cable may be scrapped, *but the process may be out of control and still be within specifications*! Plots

of each of the variables against their specifications indicate no problem with large variability. In fact for this example, the process capability is estimated to be very high. Therefore, it is possible that the mean or variance may change without producing defective cables. In other words, when the process does go out of control, there will be time to adjust it before the change affects the acceptability of the cable. If the cost of a false alarm were high (production would be slowed down) then the situation would call for a small probability of a false alarm, and had the specifications been tighter, a larger probability would have been desired. Because neither is the case here, a "typical" value of .0027 is selected (this is equivalent to using "3σ" limits on traditional charts). False alarms are expected to occur one in every 370 samples.

The next step is to select a control scheme. The sample size is not large (n=1) therefore a chi-squared goodness of fit test should be performed to determine if the data can be assumed to be normal. Figure 5 below is a histogram of the data. A normal distribution is fit to the data and is also shown. The data does not indicate that the distribution is symmetric, much less normally distributed. The observed vs the expected values were compared for the nine intervals in the histogram, and the p-value for the chi-squared goodness of fit test is 0.004 which indicates there is sufficient evidence that the data is not normally distributed.

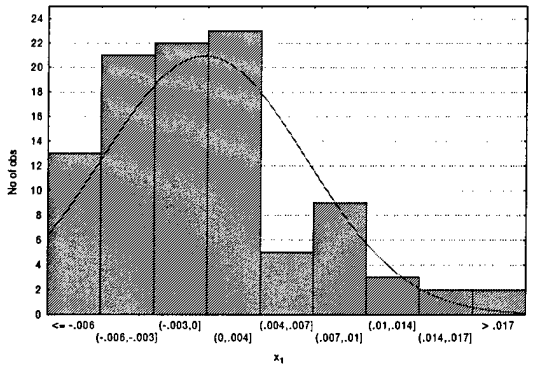

Figure 5: Histogram of x_1

Because the data is not normally distributed, a nonparametric procedure must be used. While any method is appropriate, the single link method is selected. The central statistic for the procedure is the sample average vector, $\bar{\mathbf{x}} = (0,0)$. Recall that the variables were transformed in the first step to make this so. The sample covariance matrix is then calculated.

$$\hat{\mathbf{S}} = \begin{bmatrix} 4.03\times10^{-5} & 3.98\times10^{-5} \\ 3.98\times10^{-5} & 1.51\times10^{-4} \end{bmatrix} \quad (23)$$

A new observation is collected $\mathbf{x}$ = (0.009, -0.02). In order to use the single link algorithm, the Mahalanobis distance from one observation to another must be calculated. A sample calculation of the distance from the central statistic to the new observation is shown below.

$$MD = (\mathbf{x}_{new} - \bar{\mathbf{x}})'\mathbf{S}^{-1}(\mathbf{x}_{new} - \bar{\mathbf{x}}) =$$

$$= [.009 \quad -.020] \times \begin{bmatrix} 4.03\times10^{-5} & 3.98\times10^{-5} \\ 3.98\times10^{-5} & 1.51\times10^{-4} \end{bmatrix} \times \begin{bmatrix} .009 \\ -.020 \end{bmatrix}$$

$$= 9.5. \quad (24)$$

The algorithm is applied to the data, and the results are shown below in Figure 6. The new observation is marked with an "X" on the chart, and the score each observation received through the procedure is shown above or beside the observation.

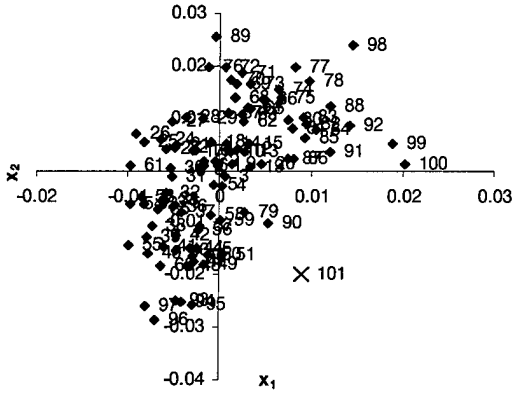

Figure 6: Scores for example data from SLINK method

Note that the scores of the observations on the perimeter of the distribution are the highest. The new observation is isolated with respect to the others, and has the highest score. The p-value for the new observation calculated from Equation 15 is 0.0099. If α had been selected to be 0.01 or greater, the process would be declared to be out of control. However, α is 0.0027, not 0.0099. Therefore the EWMA procedure must

be used. But for the sake of illustration, consider Figure 7 below which shows the same data with their respective individual control limits for α = .0099. Note that the new observation is nestled well within both sets of limits, and neither individual chart shows cause for suspicion.

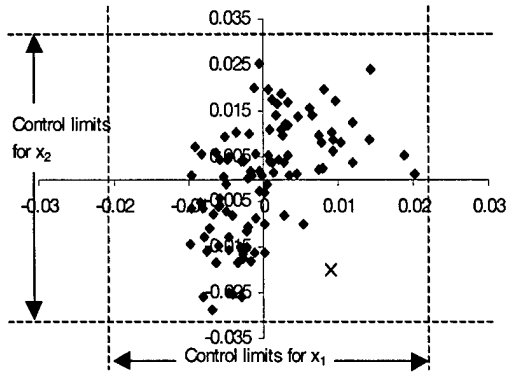

Figure 7: Individual control limits for example data

The weight factor λ is set to 0.20. The statistic is a function of z_{t-1}, and it is common practice to set the initial value $z_0 = E(z_t)$. The EWMA statistic at t=1 is

$$z_1 = .2(.0099) + .8\left(\frac{102}{2(101)}\right) = .40594 \quad (25)$$

Now suppose the new system has run in an control state for 15 new cables. The p-value at t = 2 is 0.7723. The statistic is z_2 = .2(.7723) + .8(.4059) =0.4792. The EWMA statistic for each cable is calculated and plotted on a chart. Assume the process has been in control, but at t=16, the mean of both variables decreases, due to a blockage in the extruder which slightly decreases the amount of material extruded. The shift is detected at t = 21, and the results are shown in Figure 8. Had any variable been below the specifications, the process would have been stopped and investigated immediately. When the alarm did signal, an investigation was launched, and the problem was resolved *before* the quality of the cable was compromised.

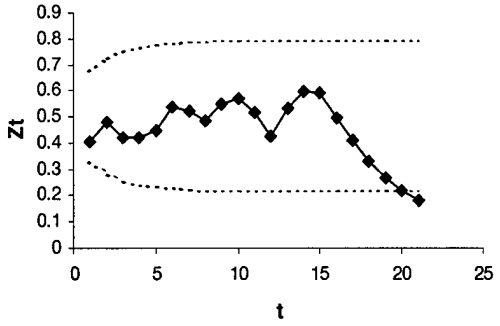

Figure 8: EWMA chart

A flowchart has been provided in Appendix A to aid the cable manufacturer with a multivariate SPC design.

CONCLUSION

Cable manufacturing is definitely not a textbook case when it comes to quality control. Small sample sizes, multiple correlated variables, and many changeovers all complicate the design of the SPC scheme. With careful planning and an understanding of these issues, the SPC engineer can design a plan to suit the cable company's own needs. A traditional Hotelling's T^2 chart may be used, or the new nonparametric methods may be appropriate. In either case, an effective SPC program is vital to making timely process improvements.

REFERENCES

1. Montgomery, Douglas C., 1991. *Introduction to Statistical Quality Control.* John Wiley and Sons, New York.
2. Montgomery.
3. Alt, F. B., 1985. "Multivariate Quality Control" in *Encyclopedia of Statistical Sciences*, Kotz and Johnson (eds.) vol. 6, Wiley, New York.
4. Bush, Helen M. 1996. *Nonparametric Multivariate Quality Control.* A thesis from the Department of Industrial and Systems Engineering, Georgia Institute of Technology.
5. Bush.
6. Bush.
7. Johnson, Richard A. and Wichern, Dean W., 1992. *Applied Multivariate Statistical Analysis.* Prentice Hall, Englewood Cliffs.
8. Bush.

APPENDIX A
Cable SPC Flowchart

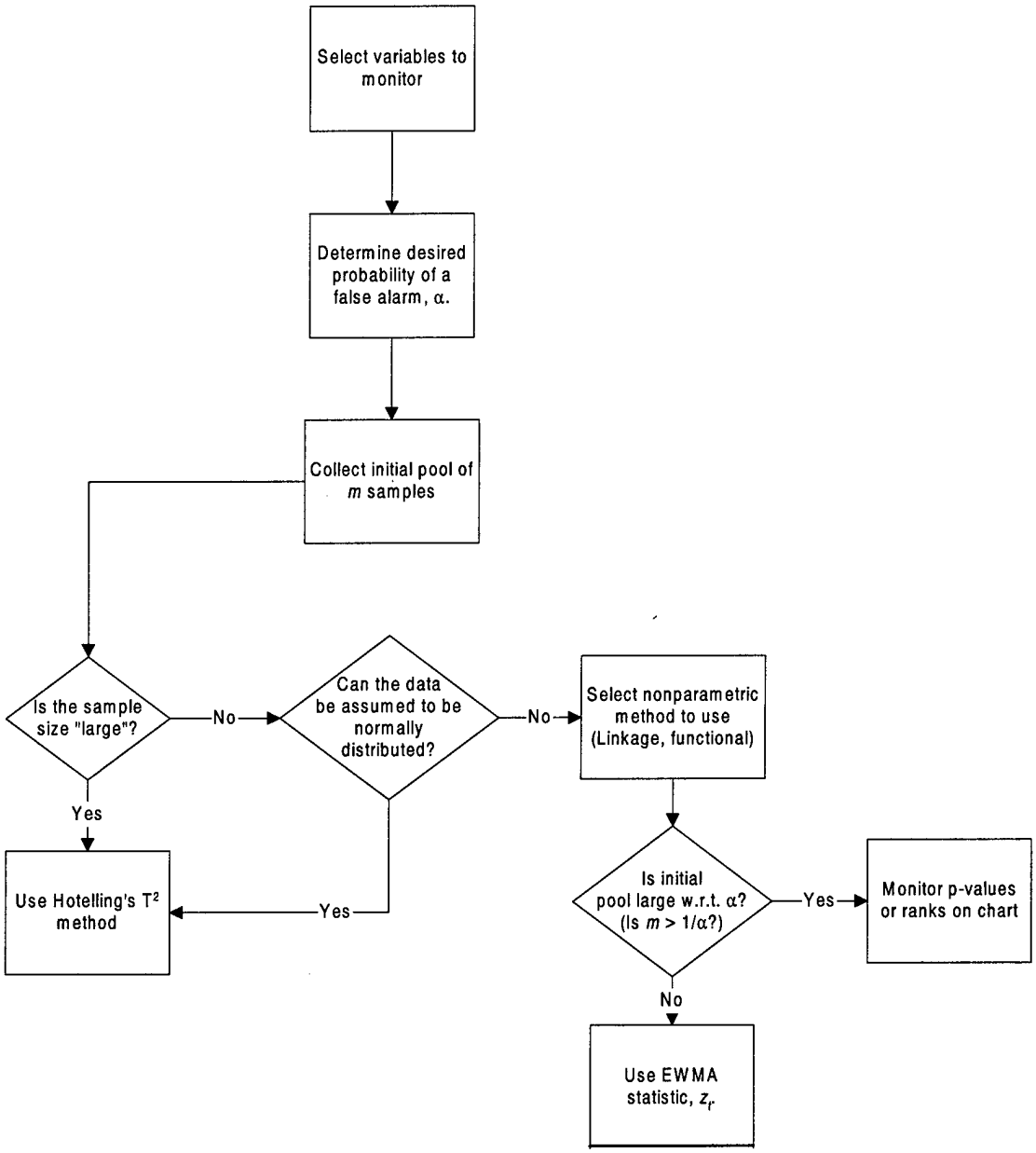

Helen Bush is a Member of the Technical Staff at Lucent Technologies in the Outside Plant Cable group. Her projects focus on process improvement, and her primary responsibilities include designing and executing data analysis, statistical process control, data modeling, design of experiments, and simulation modeling.

Helen graduated from the Georgia Institute of Technology in 1996 with a Ph.D. in Industrial Engineering specializing in engineering statistics, and her thesis is in nonparametric multivariate quality control. Helen taught several undergraduate courses while she was at Georgia Tech, including *Introduction to Statistical Process Control*, and *Engineering Statistics*. She received her Masters degree from the Georgia Institute of Technology in 1993 in Statistics and her Bachelors degree from Mississippi State University in Industrial Engineering in 1992.

LOGISTIC REGRESSION TECHNIQUES FOR MODELING DEFECTS IN CABLES

Helen M. Bush and H. Paul Debban

Lucent Technologies
Norcross, Georgia

ABSTRACT

Logistic regression is a statistical technique used to build models that describe binary data. A binary variable has two possible outcomes usually thought of as a "success" or a "failure". A good example of an important binary random variable in cable manufacturing is whether or not a cable is defective. Traditional regression techniques assume that the response variable has a continuous domain such as weight or length. However, in cable manufacturing it is of interest to model the presence or absence of certain defects in order to find which variables are correlated to the defects and to determine *how* the variables are correlated. A model quantifies those effects and is a powerful tool in root cause analysis.

INTRODUCTION

Consider a cable manufacturer who wishes to analyze fiber breaks. A simple analysis reveals that fiber color, buffering line, line speed, and sheath type are correlated with fiber breaks. If the analysis stops at this point, he may begin to implement four separate programs to solve four separate problems. However, if he jointly explores these factors and their interactions, he may discover one problem that is simultaneously reflected by several variables. One problem causes all four variables to be significantly correlated with fiber breaks. A model of fiber breaks where color, line number, line speed, and sheath type and their interactions are the predictor variables is an effective way of looking at these variables jointly. This paper provides the framework and instructions for using logistic regression techniques to build such a model. In the next section, some basic concepts related to variables in numeric models are presented. The second section illustrates why traditional linear regression modeling is not suitable for modeling binary response variables. Logistic regression models are presented in the third section as the appropriate choice, and the example introduced in this section is continued in the final section.

SOME BASIC CONCEPTS

Model building serves a two-fold purpose: to *identify* variables that are correlated with the response variable and to *quantify* the effects of those variables. It is helpful to know that a variable has an effect on cable defects, but it is valuable to understand the nature of that effect. Models show these effects in equation form and explore the relationship between a single *dependent* or *response* variable, y and k *independent* or *regressor* variables, $x_1, x_2, \ldots, x_k$. The relationship between the response and independent variables may be known and is characterized by a mathematical equation, where

$$y = \phi(x_1, x_2, \ldots, x_k). \qquad (1)$$

The true function ϕ is usually unknown and is estimated using regression techniques. The analyst selects the functional form of the model which may or may not have the same form as ϕ. Let $\hat{y}$ denote an estimate of the response variable for a given set of inputs. Then the regression equation has the form

$$\hat{y} = f(x_1, x_2, \ldots, x_k). \qquad (2)$$

Response and independent variables may be classified as *continuous* or *categorical.* Continuous variables such as weight, temperature, and pressure have a continuous

domain over some interval. Categorical or *discrete* variables are set in categories and may or may not be numeric in nature. Typical examples of categorical variables are sex, geographic location, and size.

An important categorical variable in production is whether or not a cable is defective. This is a binary variable, having two possible outcomes and may be represented with a 0 (nondefective) or a 1 (defective). The remaining sections of this paper focus on modeling cable defects. These defects may be a specific type of defect or a group of defects. Though modeling factors important to cable defects is the subject here, the principles examined can apply to any situation with a binary response variable.

WHY NOT LINEAR REGRESSION?

Linear regression is used to estimate polynomial models. The simplest example of a linear model is

$$y = \beta_0 + \beta_1 x . \qquad (3)$$

The term β_0 is the equation *constant*, or the y intercept, and β_1 is the *slope* or *rate of change* of y with respect to x. A simple polynomial model is

$$y = \beta_0 + \beta_1 x_1 + \beta_2 x_2 + \beta_{12} x_1 x_2 . \qquad (4)$$

This equation has two linear terms and one interaction term. The interpretation of the interaction parameter β_{12} depends on the types of variable x_1 and x_2 are. If they are both continuous, it represents the change in y with respect to the change in the product of both variables. If they are binary variables, it represents the difference in the average of y in the presence of a specific condition (both variables equal one).

Linear regression techniques are well documented and are ideal to use for building these and other polynomial models. It is not even necessary to purchase special statistical software to estimate a model with linear regression, for many standard spreadsheet software packages have linear regression tools built-in. However, the best equation to describe the response variable is not always in polynomial form. Consider modeling cable defects. The response variable is either 0 or 1, therefore predicted values for y should remain between 0 and 1. With a polynomial model, the predicted variables are not restricted to these bounds. This is illustrated in Figure 1 below where an actual probability distribution is modeled using a simple linear regression.

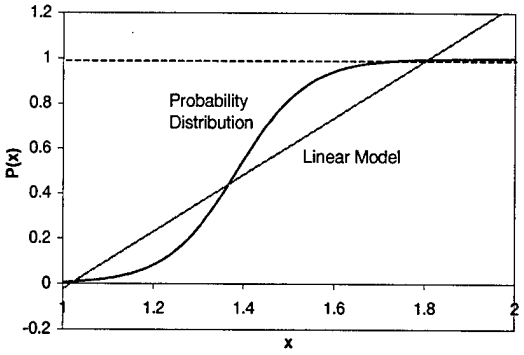

Figure 1: Linear model fit to probability distribution

For small or large values of the regressor variable, the model fit exceeds the boundaries of 0 and 1. Also, the fit is poor. For small values of the independent variable the model overestimates the probability, and for large values it underestimates it. This is because the linear model assumes a constant slope over the range of x. Probabilities do not tend to exhibit this tendency. Rather, probability distributions are typical of the example above, where there are ranges of rapid change and ranges of slow change. Clearly this is not an acceptable model for this probability distribution. The non-linear model presented in the next section overcomes the problems linear regression models have when modeling binary data.

LOGISTIC REGRESSION MODELS

The Logistic Regression Function

A model that fits binary data well must, at a minimum, be bound by 0 and 1 and be flexible in shape and slope. A function with an S-shaped curve is

$$p(x) = \frac{e^{\beta_0+\beta_1 x}}{1+e^{\beta_0+\beta_1 x}} \qquad (5)$$

and is called the *logistic regression function*. The parameter β_1 determines the slope of the S-shape. As the magnitude of β_1 increases, so does the slope. When β_1 is positive, the probability of a defect (y=1) increases as x increases, and when β_1 is negative, the probability of no defects (y=0) increases with x. When β_1 equals zero, then the response variable is independent of x.

When there is more than one regressor variable in the model, the function looks like

$$p(x) = \frac{e^{\beta_0+\beta_1 x_1+\beta_2 x_2+\ldots+\beta_k x_k}}{1+e^{\beta_0+\beta_1 x_1+\beta_2 x_2+\ldots+\beta_k x_k}}. \qquad (6)$$

Note that any polynomial terms such as an interaction may also be included in this function.

The Odds Ratio and the Logit

Gamblers relay probabilities in terms of *odds*. A "2 to 1" odds ratio for an event means that the probability the event will occur is 2/3. The probability of an event from a given odds ratio for the event expressed as "*a* to *b*" is $a/(a+b)$. In general, the odds of an event is the ratio of the probability that it will happen to the probability that it will not. The odds ratio for making response 1 is

$$\frac{p(x)}{1-p(x)} = e^{\beta_0+\beta_1 x}. \qquad (7)$$

The log of the odds ratio is linear. This term is called the *logit*.

$$\log\left(\frac{p(x)}{1-p(x)}\right) = \beta_0 + \beta_1 x \qquad (8)$$

When there is only one response variable, a helpful tool is to plot the empirical logits against x. The independent variable should at least be on an interval scale. If x is continuous, group the data into ranges. Let n_i be the number of observations in the ith range of x. Let w_i denote the total number of "successes" (times when y = 1). The empirical logit is then defined as

$$\log\left(\frac{w_i+\frac{1}{2}}{n_i-w_i+\frac{1}{2}}\right). \qquad (9)$$

A logistic regression function will work well if a plot of the empirical logits appears linear with respect to x.

Estimating the Logistic Regression Function

It is recommended to use a statistical software package that has logistic regression tools to estimate models. The user may want to compare many models before he or she selects the "best" one, and if estimated by hand, the task is time consuming and complicated, for the parameter estimates require an iterative solution. A brief description of the estimation procedure follows, but it is recommended to consult a text for more details if writing a program to do these calculations[1,2]. If using a statistical software package, it is permissible to skip to the next section.

A common procedure for deriving estimation equations is to find the maximum likelihood estimator (MLE). The reader who is unfamiliar with MLE procedures may consult any standard statistical text[3]. The first step is to find the joint probability mass function of a sample of the dependent variable. Let x_i represent the ith combination of settings of k regressor variables, where

$$\mathbf{x}_i = (x_{i0}, x_{i1}, \ldots, x_{ik}), \qquad (10)$$

$i = 1,\ldots,I$, and $x_{i0} = 1$ (x_{i0} is required to estimate the constant parameter, β_0). The total number of settings, I, may equal the total number of observations if the explanatory variables are continuous. If they are discrete, then the maximum value for I is the product of the number of levels for each variable. For example, if there are two variables at two levels each, then the total number of possible settings is 2X2=4. The object is to use the model to estimate the probability that a cable will be defective for a given set of inputs. The response matrix, y_i is the counts of defective cables at each fixed x_i level. Let n_i represent the total number of trials at the ith level. Then each y_i is an independent

binomially distributed random variable, and the joint probability mass function of all of the y_i ($y_1,\ldots,y_I$) is a multiple of the product of their binomial functions.

$$\prod_{i=1}^{I} p(x_i)^{y_i}[1-p(x_i)]^{n_i-y_i}$$

$$=\prod_{i=1}^{I}[1-p(x_i)]^{n_i}p(x_i)^{y_i}[1-p(x_i)]^{-y_i}$$

$$=\left(\prod_{i=1}^{I}[1-p(x_i)]^{n_i}\right)\prod_{i=1}^{I}\exp\left[\log\left(\frac{p(x_i)}{1-p(x_i)}\right)^{y_i}\right]$$

$$=\left(\prod_{i=1}^{I}[1-p(x_i)]^{n_i}\right)\exp\left[\sum_{i=1}^{I}y_i\log\left(\frac{p(x_i)}{1-p(x_i)}\right)\right] \quad (11)$$

Substituting $\sum_j \beta_j x_{ij}$, $j = 0,\ldots,k$ for the ith logit $p(x_i)/(1-p(x_i))$ and noting that

$$1-p(x_i)=\frac{p(x_i)}{e^{\sum_{j=1}^{k}\beta_j x_{ij}}}=\frac{e^{\sum_{j=1}^{k}\beta_j x_{ij}}}{e^{\sum_{j=1}^{k}\beta_j x_{ij}}\left(1+e^{\sum_{j=1}^{k}\beta_j x_{ij}}\right)}$$

$$=\frac{1}{1+e^{\sum_{j=1}^{k}\beta_j x_{ij}}}, \quad (12)$$

the log likelihood of Equation 11 is

$$L(\beta)=\sum_j\left(\sum_i y_i x_{ij}\right)\beta_j-\sum_i n_i\log\left(1+e^{\sum\beta_j x_{ij}}\right). \quad (13)$$

The maximum likelihood estimates of the β_j are obtained by taking the derivative of the above equation and setting it equal to 0. The derivative is

$$\frac{dL}{d\beta}=\sum_i y_i x_{ij}-\sum_i n_i x_{ij}\left[\frac{e^{\sum\beta_j x_{ij}}}{1+e^{\sum\beta_j x_{ij}}}\right]. \quad (14)$$

Therefore the likelihood equations are

$$\sum_i y_i x_{ij}-\sum_i n_i p(x_i)x_{ij}, \quad (15)$$

for $j = 1,\ldots,k$.

The likelihood equations must be solved in an iterative manner, and an initial "guess" must be supplied for each parameter. There are several techniques for solving non-linear equations. Though their details are outside the scope of this paper, it is recommended to use the Newton-Raphson method if performing these calculations on a spreadsheet.

Evaluating a Fitted Model

It is a simple task to evaluate whether or not a fitted model is significantly superior to using no model at all. The *independence model* is formed when the response variable is based on its average independent of x, where $\hat{y}=\beta_0$. Let $L_1(\beta)$ denote the value of the likelihood function of the independence model and let $L_2(\beta)$ denote the likelihood value of a fitted model. Assume the fitted model has k+1 parameters. Then

$$-2[\log(L_1-L_2)] \quad (16)$$

has a chi-square distribution with k degrees of freedom. Again, if using a software package, this task will be automatically performed. A low p-value associated with the statistic indicates the significance of the fitted model. In practice a p-value less than .05 is considered significant.

Confidence Intervals

Let the estimated logit be designated

$$\hat{L}=\mathbf{x}\hat{\beta}. \quad (17)$$

The covariance matrix of $\hat{\beta}$ is

$$\mathrm{Cov}(\hat{\beta})=\left(\mathbf{x}'Diag[n_i\hat{p}(x_i)(1-\hat{p}(x_i))]\mathbf{x}\right)^{-1} \quad (18)$$

The approximate 1-α percent confidence interval for the logit is then

$$\hat{L}\pm Z_{\alpha/2}\hat{\sigma}_{\hat{L}}, \quad (19)$$

where $\hat{\sigma}_L$ is $\mathbf{x}\mathrm{Cov}(\hat{\beta})\mathbf{x}'$. To obtain a confidence interval for $p(\mathbf{x})$, use the transformation on the endpoints of the above confidence interval

$$\hat{p}(\mathbf{x}) = \frac{e^{\hat{L}}}{1+e^{\hat{L}}}. \qquad (20)$$

EXAMPLE

Consider again the manufacturer who has determined that line speed, line number, fiber color, and sheath type are correlated with fiber breaks on the buffering lines. The manufacturer does not understand the nature of these correlations nor by how much these factors affect fiber breaks. He decides to build a model to quantify these relationships. There are three lines used to make cables. Each line has a fast speed and a slow speed. The line speed is determined by the sheath design and the cable diameter. Line A tends to run at its fastest speed more often, and line C tends to run at its slower speed. There are two sheath designs, metallic and non-metallic. Finally, there are three fiber colors, red, white, and blue. The data is summarized in Appendix A.

Goodness of Fit Tests

Assume that these variables were deemed significant from previous analyses. This can be done with a chi-square goodness of fit test for contingency tables. The test is performed here with the example data for the lines. These tests can be automatically performed with a standard statistical software package, but the steps are shown here for illustration. The first step is to summarize the data as in Table 1 below.

Table 1: Broken fibers and sample sizes by line

Line	Broken Fibers	n	% Broken
A	162	8220	1.9708
B	201	9660	2.0807
C	48	3600	1.3333
total	411	21480	1.9134

The second step is to calculate the expected number of broken fibers if fiber breaks are independent of the line. The overall estimate of percent broken fibers is p=1.91%. If that is the case, then the expected number of broken fibers is the number of fibers processed on that line multiplied by p. For example, the expected number of fiber breaks on line C is 3600*.0191 = 69. The chi-squared statistic, χ_0^2 is

$$\chi_0^2 = \sum_i \frac{(O_i - E_i)^2}{E_i}, \qquad (21)$$

which has a chi-squared distribution with I-1 degrees of freedom. If there is a large difference between the observed and the expected values, then the statistic will be large, signifying that the break rates differ between the buffering lines. The last step is to calculate the probability of obtaining a value at least as large as χ_0^2 if the break rates are the same. If that probability is small, then it is unlikely that the break rate is independent of line number. The remaining part of this exercise is summarized below in Table 2.

Table 2: χ^2 calculations

Line	Broken Fibers	n	% Broken	E	χ^2
A	162	8220	1.97	157.3	0.14
B	201	9660	2.08	184.8	1.41
C	48	3600	1.33	68.9	6.33
total	411	21480	1.91	411	7.89

The chi-squared statistic is 7.89, and the corresponding p-value is .02. This probability is low enough to merit further investigation into the relationship between break rates and buffering lines.

Selecting the Model

The nature of the model is unknown, so several models are estimated and compared. In general it is advisable to select a simpler model over a complicated one. Therefore to start, models without any interactions are examined. The next step is to add interaction terms if none of the simple models are completely satisfactory. Let "A", "B", "S", "D", "R", and "W" designate line A, line B, line speed, sheath design, red colored fiber, and white colored fiber respectively. The variables with three categories were split into two because the software package used to estimate the models assigns numeric values to all

variables, even categorical ones. It is a common practice in linear regression to split a categorical variable with m levels into m-1 variables with two levels each. However, not all packages require such a conversion. Note that the blue fibers did not disappear from consideration. The effect of the blue fibers is seen when both R=0 and W=0. The results of a sample of fitted models are in Table 3 below.

Table 3: Model comparison

Model	χ^2	dof	p-value
A + B + S + D + R + W	10.6	6	0.100
S + D	0.6	2	0.741
A + B	4.4	2	0.110
A + R + S	6.3	3	0.096
A + R	5.7	2	0.056
AR	11.7	1	0.00061
AR + B	16.1	2	0.00033

The first model contains all terms and has a p-value of about 10%. Several things can be done to improve the model such as adding interaction terms and eliminating terms that either do not belong or are redundant. Simpler models are tried next. The model with line speed and sheath design has a very poor fit. This may not necessarily be because neither variable is still correlated to breaks. Rather, the two variables are redundant, and the presence of both variables in the model produces a poor fit. Recall that line speed depends on the sheath design. The model with just line A and red colored fibers has the best fit of all the simple models with a p-value just above .05. In practice this may be considered an acceptable stopping point, but the cable manufacturer decides to explore the possibility of highly significant interaction terms. The models with the best fits have the line A, red fiber color interaction. The term by itself is an exceptional model, but adding the line B term reduces the p-value in half. There are several schools of thought on selecting the "best" of several models with low p-values. Some recommend to choose the simplest model whose p-value is below a certain threshold value, while others profess it is logical to add any term that appears to improve the model fit. A word of caution is added. Check the model diagnostics to be sure that the parameter is statistically significant to the model. If it is, include it. If the models are estimated by hand, a simple t-test can be performed on any one parameter using the $\mathrm{Cov}(\hat{\beta})$ matrix to determine if a parameter is statistically significant from 0.

Assume the cable manufacturer determined that both parameters are significant. The fitted model is

$$\hat{p}(x) = \frac{\exp(-4.13 + .585AR + .230B)}{1 + \exp(-4.13 + .585AR + .230B)}. \quad (22)$$

Note that both β_{AR} and β_B are positive. This means that on line A red fibers have a higher probability of breaking, and all fibers on line B have a slightly higher probability of breaking than other fibers.

Not all variables that are correlated with fiber breaks ended up in the model. Of the original four, only line number and color have been selected. Some variables may have been redundant, such as sheath design which is confounded with line speed and possibly even line number. Other variables may be correlated with fiber breaks and not redundant, but their effect on fiber breaks may be weak compared to that of other variables, in which case the user can't distinguish it from a variable that does not belong.

Now that the manufacturer has a model, what is to be done about reducing fiber breaks? By how much can he expect to decrease the break rate if he finds the special causes on lines A and B? Table 4 below summarizes the data and gives the point estimate and confidence interval for the probabilities of dropping a cable at line B, at line A with a red fiber, and all other cases.

Table 4: Probability estimates and confidence intervals

	phat	95% Confidence Interval
A-red	0.0281	(.0274, .0288)
B	0.0199	(.0197, .0201)
other	0.0159	(.0156, .0161)

There is much to gain in this example by finding and removing the special causes of breaks. The special causes associated with lines A and B increase the average break rates by 77% and 25% respectively.

In this example, the source of breaks on line A was quickly traced to the spindle assigned to the red fiber spools. The problem was fixed at little expense, and procedures were put into place to prevent the same problem from occurring on other lines.

The problem with line B was more difficult to diagnose, because the manufacturer did not know where to start the investigation. The line was thoroughly canvassed, and an examination of the guide sheaves revealed physical damage that nicked fibers every so often. The sheaves were replaced, and again procedures were developed to prevent the problem from happening again.

The final step in this analysis is to start collecting data after all the process improvements have taken place. Once a sufficient amount of process data has been collected, the analysis should begin again, and a new model will be created. The next analysis may find problems that were small compared to the ones associated with lines A and B, or it may find a new root cause to fiber breaks.

CONCLUSION

Statistical models can be powerful tools in process improvement. They simplify the root cause detection process and prioritize the importance of solving different process problems. Logistic regression is a model building tool ideal for analyzing defects in cables. Unlike linear regression models, logistic regression models are bound by 0 and 1, the natural bounds of a binary response variable. Linear regression models perform best when the response variable is continuous over some domain. A key advantage of creating a model for these situations is that models can explore interactions between the independent variables. One could examine the relationship of each independent variable with the dependent variable one at a time, but what one ends up with is a list of factors that influence the dependent variable, not an understanding of how they influence it *together*. That understanding is the key to efficient root cause detection analysis.

REFERENCES

1. Agresti, Alan, 1990. *Categorical Data Analysis*. John Wiley and Sons, New York.
2. Hosmer, David W. and Lemeshop, Stanley, 1989. *Applied Logistic Regression*. John Wiley and Sons, New York.
3. Hines, William H. and Montgomery, Douglas C., 1990. *Probability and Statistics in Engineering and Management Science*. John Wiley and Sons, New York.

APPENDIX A
Data Table for Example

Line	Speed	Sheath	Color	Drops	ni
A	Fast	1	red	26	1000
A	Fast	1	white	13	1000
A	Fast	1	blue	16	1000
A	Fast	2	red	26	800
A	Fast	2	white	11	800
A	Fast	2	blue	17	800
A	Slow	1	red	12	500
A	Slow	1	white	5	500
A	Slow	1	blue	6	500
A	Slow	2	red	15	440
A	Slow	2	white	8	440
A	Slow	2	blue	7	440
B	Fast	1	red	21	1200
B	Fast	1	white	19	1200
B	Fast	1	blue	26	1200
B	Fast	2	red	11	520
B	Fast	2	white	13	520
B	Fast	2	blue	11	520
B	Slow	1	red	22	800
B	Slow	1	white	16	800
B	Slow	1	blue	19	800
B	Slow	2	red	16	700
B	Slow	2	white	12	700
B	Slow	2	blue	15	700
C	Fast	1	red	3	400
C	Fast	1	white	5	400
C	Fast	1	blue	4	400
C	Fast	2	red	10	600
C	Fast	2	white	9	600
C	Fast	2	blue	11	600
C	Slow	1	red	1	100
C	Slow	1	white	1	100
C	Slow	1	blue	1	100
C	Slow	2	red	1	100
C	Slow	2	white	1	100
C	Slow	2	blue	1	100

Helen Bush is a Member of the Technical Staff at Lucent Technologies in the Outside Plant Cable group. Her projects focus on process improvement, and her primary responsibilities include designing and executing data analysis, statistical process control, data modeling, design of experiments, and simulation modeling.

Helen graduated from the Georgia Institute of Technology in 1996 with a Ph.D. in Industrial Engineering specializing in engineering statistics, and her thesis is in nonparametric multivariate quality control. Helen taught several undergraduate courses while she was at Georgia Tech, including *Introduction to Statistical Process Control*, and *Engineering Statistics*. She received her Masters degree from the Georgia Institute of Technology in 1993 in Statistics and her Bachelors degree from Mississippi State University in Industrial Engineering in 1992.

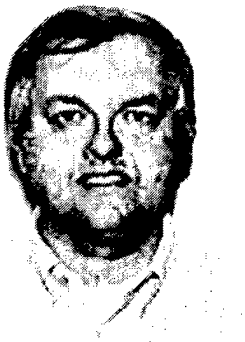

Paul Debban is a Distinguished Member of Technical Staff in the Outside Plant Cable Engineering Group at Lucent Technologies in Norcross, GA. He joined Western Electric in 1980 after receiving a BSME from the University of Nebraska-Lincoln. He has worked in the fiber optic cable manufacturing group since 1981. He has been awarded one patent.

THE LOW SMOKE HALOGEN FREE OPTION TO CHLOROSULFONATED POLYETHYLENE LOW VOLTAGE INSULATION AND JACKETS

Kyle E. Cope

Pirelli Cables and Systems North America, Columbia, South Carolina

ABSTRACT

Material selection for low voltage insulation and jackets is becoming more important. Due to its excellent chemical and flame resistance, chlorosulfonated polyethylene (CSPE) has experienced a long history of beneficial use in applications such as control, power and distribution circuits which operate in a wet or dry environment. Many cables using CSPE carry a UL RHW-2 designation stating they have been approved for operation in a 90°C wet environment. Some CSPE uses have been as a low voltage insulation component of EPCP (EPR insulation with CSPE outer layer) cable, as a central office power wire insulation and as a cable jacketing material. However, the trend towards using more environmentally friendly materials has led the wire and cable industry to supply additional options. These materials provide low smoke, halogen free, flame retardant, low acid gas generation and moisture resistant properties.

INTRODUCTION

During a fire, if large amounts of smoke are produced, human safety can be compromised. This occurs not only from smoke inhalation, but due to large volumes of smoke clouding exit signs. In addition, toxic gases in the smoke can be dangerous. A design is proposed utilizing low smoke halogen free materials as part of a two layer insulation system. Each layer is formulated to provide appropriate physical, mechanical, electrical and other properties.

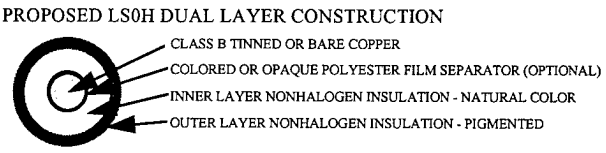

Figure 1: Design Breakdown

Cables utilizing a CSPE jacket or outer insulation can be very difficult to install over long lengths. The tacky, rubbery nature of CSPE is responsible for a high level of friction between the material and other cables in the environment. The proposed design adds a sheath system to the outer layer which greatly reduces the coefficient of friction, making installation easier.

As stated earlier, CSPE layers can also release high levels of toxic smoke when burned. The proposed design not only has lower levels of toxicity, but yields significantly lower smoke levels. The non-halogenated nature of the insulation reduces the corrosive by-products which can damage nearby electrical equipment.

The proposed cable meets UL-44 for RHH/RHW-2 insulation and also carries LS, SUN RES, OIL II, VW-1, CT and CSA FT-4 markings. RHW-2 is a UL designation which states that the insulation is acceptable for use in wet or dry environments of 90°C. The benefits of these low smoke halogen free compounds should be compared to chlorosulfonated polyethylene before choosing a material to use as a low voltage insulation or jacket.

There are numerous low voltage power distribution applications where CSPE has been specified. The fact that CSPE has a long history in these applications can make it difficult to

remove the material from wire specifications. However, if a material is made available which has similar performance to CSPE with added environmental and safety benefits, installations may be better served by examining LSOH materials.

BENEFIT COMPARISON

The use of chlorosulfonated polyethylene in wire and cable is centered around two main benefits: chemical resistance and flame resistance. These properties make the material very viable for use in cable insulation and jackets.

Before the benefits and drawbacks of CSPE are discussed, it is beneficial to examine the repeat units in CSPE.

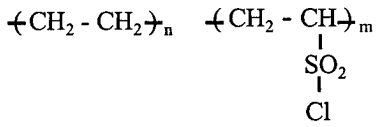

Figure 2. Repeat Units of CSPE

The obvious feature is the SO_2 and Cl group hanging off the backbone of the ethylene monomer. There is typically one chlorosulfonyl group for each 200 backbone carbon atoms[1]. It is this group which gives CSPE its chemical resistant and flame retardant properties.

Chemical/Oxidative Resistance

As shown in Figure 2, the fact that the repeat units are saturated (no carbon-carbon double bonds) gives the material excellent resistance to ozone and other oxidative reactions which attack double bonds. Double bonds are very reactive, so oxygen reacts with them very readily - resulting in quicker oxidation.

In addition, the large chlorine atom gives the rubber a degree of polarity so CSPE shows excellent resistance to hydrocarbon based chemicals such as petroleum oil.

Table 1: Physical and Oil Resistance Properties

	LSOH Insulation*	UL 44 Reqt.
Unaged Physical Properties		
Tensile Strength, MPa	13.3	10.3 min.
Elongation, %	163	150 min.
After 60 days/75°C IRM-902 Oil		
Retained Tensile Strength, %	80	65 min.
Retained Elongation, %	74	65 min.

* Insulation taken from 14 AWG wire

The proposed LSOH insulation is also saturated. Property retention and resistance to oil are also excellent, allowing the insulation to carry UL's Oil II rating.

Flame Resistance

A discussion on flame retardancy is not needed as there is a vast source of information on the subject[2]. Simply put, when a material burns, combustion takes place. This combustion reaction results in the formation of free radicals which in turn combine with available fuel to continue the combustion process. Halogenated materials, such as CSPE, do an excellent job acting as radical scavengers, thereby slowing the combustion reaction and giving the material a measure of flame retardancy.

The oxygen index test (ASTM D2863) is a popular measurement of polymer flammability. The test measures the amount of oxygen (in %) necessary to keep a polymer sample burning vertically downward. There are specific testing conditions which are constants (such as gas flow rates) so that comparative testing between materials can be made. As seen in the table, the subject insulation has a similar oxygen index to CSPE.

Table 2: LSOH and CSPE Oxygen Index Comparison

	LSOH Insulation		CSPE Insulation
	Inner	Outer	
Oxygen Index, %	28	>50	33-35

CSPE can be compounded a number of different ways in order to give specific heat resistance, weathering, moisture or electrical properties. Such compounding is beyond the scope of this paper, but commercial suppliers of CSPE such as DuPont-Dow's Hypalon® can supply the necessary formulation information to meet the specific application.

With these benefits aside, CSPE does have drawbacks which give the material some limited application in the wire and cable industry.

CSPE DRAWBACKS COMPARED TO NEW INSULATION

Disposal

The basic reaction used to produce CSPE is as follows:

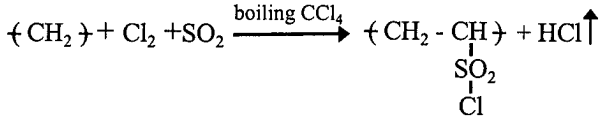

Figure 3. CSPE Reaction

As the reaction shows, carbon tetrachloride (CCl_4) is needed. Carbon tetrachloride is considered an air contaminant under the Occupational Safety and Health Act (OSHA). Therefore, ventilation should be used where CSPE cable is in use to prevent the build up of off-gassed CCl_4 in an enclosed area. The proposed insulation uses no CCl_4.

Many insulation formulations use lead oxide. Lead provides long term wet stability, but can lead to special disposal problems for the user if the final cured insulation has lead levels above EPA limits as measured by TCLP (Toxic Characteristic Leaching Procedure) for lead.

The proposed LSOH insulation passes a TCLP test. This means the cable insulation is not considered a hazardous waste and does not need special disposal.

Acid Gas Corrosion

When CSPE burns, the reaction releases Hydrochloric Acid (HCl) gas which can damage electrical equipment such as motherboards or switches. Certain customer copper power wire specifications have corrosive gas limits which restricts the range of applications where CSPE insulation can be used.

The proposed LSOH insulation has an acid gas equivalent of 0.56%. A popular upper limit to this test is 2%, making the proposed LSOH insulation acceptable to be used for central office power wires or wherever sensitive and expensive electronic equipment are present. Acid gas corrosion is measured per MIL-C-24643 Para. 4.7.25

Smoke Evolution

In addition to giving off HCl when burned, CSPE releases smoke rapidly and is a safety hazard as this smoke can block the location of emergency exits during a fire. Also, the toxicity of the smoke makes it dangerous if inhaled.

If a cable carries an "LS" rating from UL, it has met the requirements for a low smoke article. However, all low smoke designs are not alike. CSPE can release a great deal of smoke in a short amount of time. As the table below shows, in the maximum time of the test (20 minutes), the subject insulation materials released much less smoke than CSPE. Even more dramatic is the rate at which smoke is released from CSPE. The smoke density at 4 minutes is nearly 70% less for the proposed LSOH insulation materials. The data shown for the layers is not additive. Smoke values for a full wall of insulation would be between the two smoke numbers with the inner layer contributing more because of layer thickness.

Table 3: LSOH and CSPE NBS Smoke Chamber Comparison

	LSOH Insulation		CSPE Insulation
	Inner layer	Outer Layer	
Flaming Mode			
Ds at 4 min.	5	25	95
Ds at max.	119	194	393
Non-flaming Mode			
Ds at 4 min.	71	47	200
Ds at max.	201	224	497

Smoke measurements were made using an NBS smoke chamber and following the procedures of ASTM E662.

Toxicity

The toxicity index was measured per MIL-C-24643 Para. 4.7.29 and is a measure of the toxic gases, such as carbon monoxide, ammonia, hydrochloric acid and sulfur dioxide which can be released when a material is burned. The total ppm of gases are measured and an index is calculated. When testing CSPE materials, toxicity indexes of 8.1 were measured. This is mostly due to the chlorine and sulfur contents of the rubber. Compared with the proposed LSOH insulation, which has an index of 3.02, this is very significant. The subject insulation contains very low levels of halogen (i.e. 0.02 %) and contains no sulfur.

Shelf-Life

Moisture can slightly crosslink CSPE insulations. Jackets, which do not need lead for long term electrical stability may also pick up water more readily. If uncrosslinked CSPE raw material is exposed to the atmosphere for an extended period of time, processing will quickly become very difficult. Experience has shown that the shelf life of raw material CSPE with lead to be about 3-4 months.

The proposed LSOH insulation has a shelf life of approximately 12 months. Mechanical water absorption (MWA) testing performed according to UL 1581, (section 1040 from First Edition) shows that a low lead CSPE insulation has a high degree of moisture absorption. This may be explained by the low lead level and chlorine allowing for a more "open" structure for moisture absorption.

Table 4: LSOH and CSPE Water Absorption Comparison

	LSOH Insulation	CSPE Insulation
MWA, mg/m^2	5	54

Friction Behavior

CSPE has a very rubbery feel to it. This means it will feel tacky, an undesirable property when trying to install long lengths of cable. As presented previously[3], as the coefficient of friction increases, the force necessary to move the cable can increase drastically.

Table 5: Pulling Force to Overcome Static Friction

Weight of Cable in Tray	Proposed Design	CSPE Insulation
	$\mu_s = 0.73$	$\mu_s = 1.76$
0.5 kN	0.37 kN	0.88
1.0 kN	0.73 kN	1.76
1.5 kN	1.10 kN	2.64
2.0 kN	1.46 kN	3.52
2.5 kN	1.83 kN	4.40

The addition of a braid assists the installation, but is an added expense and a smoke adding component. Tests have shown the static coefficient of friction for CSPE to be 1.76 when pulled over another CSPE cable. When the subject insulation was pulled over itself, a static coefficient of friction of 0.73 was recorded.

The cable is tested using a modified ASTM D 1894 setup. A track is constructed of the material over which the cable will be pulled. This may be aluminum or steel based on an empty tray, or it may be the test cable itself if the tray is filled with similar cable.

The test cable is then placed horizontally over the test track and the cable end is attached to a load cell of a mechanical tester. The cable is pulled via a cord which moves over a pulley to change the direction of the force. As the cable is pulled, the load cell measures the load exerted on the cable. Only the insulation surface and the track are in contact.

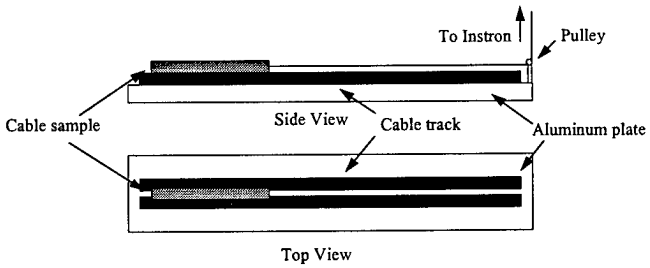

Figure 4 - Friction Testing Layout

The subject insulation has a very low friction sheath system as part of the cable insulation. This system does not add any flammability to the cable nor does it add any smoke component to the cable as a braid can do. The addition of this system can reduce the coefficient of friction of the insulation by approximately 35-55%[4].

OTHER COMPARISONS

Abrasion/Scoring

Abrasion and scoring are two important tests when it comes to evaluating the integrity of the insulation for pulling cable into trays. As the cable is pulled into the tray, it can encounter sharp edges in the tray as well as edges from the opening of the tray. Ruggedness tests evaluated according to ICEA S-81-570 show that the abrasion resistance of the cable with the proposed LSOH insulation is almost three times as high as the cable insulated with CSPE. Scoring results show very similar performance between the two cables.

Table 6: Ruggedized Properties for Cable Tray Installations

	CSPE Insulation	Proposed Non-Braided Design
Abrasion, # cycles	36	113
Scoring, # cycles	3	8

Flexibility

Cable flexibility of a braided 750 KCM CSPE cable compared to an unbraided cable with the proposed LSOH insulation is shown in Table 7, The flexibility is similar which is important when trying to install cable over long lengths. The cable flexibility can be measured by performing a 3-point bend test such as a modified ASTM D 740 test method. Using a mechanical testing machine, the maximum load to bend a cable around a prescribed bend radius was measured. In this case, the higher the force, the more difficult the cable is to bend. The use of a braid will decrease flexibility slightly. Testing using a Class I strand in place of the Class B strand would show a similar trend, with lower forces.

Table 7: Flexibility of 750 KCM Power Cable with Separator Tape

	CSPE Insulation w/braid	Proposed Non-Braided Design
Flexibility, N	925	743

Colorability

CSPE compounds which are cured using sulfur based accelerators cannot be colored if lead oxide is also used. As stated earlier, the addition of lead to the compound is often needed to meet wet insulation resistance requirements. The reaction between sulfur and lead creates black lead sulfide and hence renders the CSPE material black and non-colorable. The subject insulation is fully peroxide cured and colorable with no impact on insulation resistance properties.

OTHER INSULATION DATA

Long Term Insulation Resistance (LTIR)

Earlier versions of this LSOH material were only compliant in 75°C wet environments. In order to increase the wet rating, a modification to the formulation was made which made it more ionically stable.

Figure 5 shows excellent insulation resistance in 90°C water. The cutoff point for initial analysis of the data is after 12 weeks per UL 44, Sect. 39. As the figure shows, the insulation resistance continues to rise up to 30 weeks.

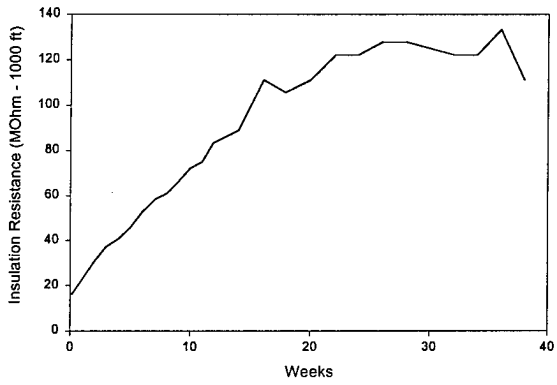

Figure 5 - LTIR Data for 14 AWG LSOH Wire

FUTURE WORK

To date, there are few specifications which either describe or classify low smoke halogen free materials. ICEA T-33-655 is an example of one that does. Other specifications such as CSA C22.2 No. 239 and ICEA S-73-582 are in the publication stages. Cable users are encouraged to look ahead at these specifications and see what impact they may have on their cable material choices.

CONCLUSIONS

Chlorosulfonated polyethylene has many positive properties such as flame and chemical resistance. However, the proposed LSOH insulation has equal flame retardance and is oil resistant as well.

The drawbacks to CSPE, including smoke and environmental factors, are greatly improved with the proposed LSOH insulation. With the low friction sheath system, braided cables are no longer needed to assist in cable pulling.

Some of the environmental aspects of CSPE discussed in this paper can be improved by modifying specific CSPE formulations. However, the inherent chemistry of CSPE will limit the amount of advancement that can be obtained from these materials. Also the rubbery/pliable nature of the material will give it a high coefficient of friction which will be hard to overcome.

CSPE has a long history of use in the cable industry and it can be difficult to change well entrenched specifications. However, in the interest of moving forward with new materials which have been developed, each application which uses CSPE should be evaluated to determine what are the actual properties needed and then evaluating if these new LSOH materials will fit, keeping in mind the added safety benefits of low smoke, no halogens, and improved installation ability.

REFERENCES

[1] Rodriguez, Ferdinand. Principles of Polymer Systems (New York: Hemisphere, 1989) 442.

[2] Warren, P.C. Polymer Stabilization, ed. W. Lincoln Hawkins (New York: Wiley-Interscience, 1972) 313.

[3] Cope, Kyle "Non-halogenated, Non-braided, Easy to Install Central Office Power Wire" IWCS 1997

[4] Ibid.

AUTHOR

Kyle Cope received a B.S. in Materials Science and Engineering from Drexel University in 1993. He is Senior Engineer for Materials Development in the RD&E Center of Pirelli Cables and Systems North America headquartered in Columbia, South Carolina. His main focus is on the engineering of materials for use in energy and fiber optic cables.

Kyle Cope
Pirelli Cables and Systems North America
710 Industrial Drive - Lexington, SC 29072

THE EFFECTS OF PHENOLIC AND NONPHENOLIC ADDITIVES ON THE ELECTRON BEAM CROSSLINKING OF AN ETHYLENE VINYL ACETATE COPOLYMER

Joseph A. Lupia

Ciba Specialty Chemicals, Additives Division, Tarrytown, NY 10591 USA

ABSTRACT

This paper examines the effect of phenolic and nonphenolic additives on Electron Beam Crosslinking of an ethylene vinyl acetate copolymer. Due to the ever increasing requirements of thermal and light stability on polyolefins used in the wire & cable and pipe industries, crosslinking is becoming a useful technique in extending the physical lifetimes of polymers.

Peroxides are often used to crosslink polymers, however negative interactions with additives used to properly stabilize these compounded resins often suffer by the chemical severity of these conditions. The effect is two fold: 1) The additives can chemically react with the radicals generated and become deactivated. 2) The degree of crosslinking can decrease as result of these radical species being consumed by the additive. This often leads to the use of additional crosslinking agent which can further deactivate additives and lead to higher formulation costs.

Electron Beam crosslinking is an alternative which eliminates the need and handling of chemical crosslinking agents. Electron Beam allows crosslinking of finished articles which can simplify processing and can often decrease overall formulation costs. As in any crosslinked system selecting the appropriate additive package is critical to meeting mechanical and physical properties as well as oxidative stability. This paper will describe the Electron Beam crosslinking process and evaluate the general effects of irradiation on the performance of several classes of additives including; phenolics, phosphites and hindered amines. Thermal and light stability data, gel content and OIT results will be reviewed in an attempt to better understand the effect of additives on Electron Beam crosslinking.

INTRODUCTION

Manufacturers of wire & cable grade polyolefins and their downstream product manufacturers are usually interested in new developments in stabilization technology that may help to improve physical and aesthetic properties of their products[1]. Representative examples of improvements might include: improved maintenance of MW during processing, lower YI color, improving thermal stability, improving light stability, enhanced additive compatibility (especially in filled systems), reduced taste and odor (Pipe), as well as suppressing the formation of imperfections due to polymer chain-scission or crosslinking.

The development of new products that deliver this type of recognizable improvements usually require the discovery of new chemistries. These new chemistries are typically brought forward through a series of developmental stages. Along the way, the utility of the new product is measured and compared to what is commercially available, or "state of the art." Among the various stages of this developmental cycle, the testing of the new chemistries must progress from standard experiments, where melt flow rates, color maintenance, oxidative induction times (OIT) and retention of physical properties are the key measures, to real end use applications, such as Wire and Cable.

Accordingly, the point of this study was to examine the relative effectiveness of some of these new chemistries in comparison to traditional systems in a wire and cable grade crosslinkable resin. This involved measuring

various combinations of traditional phenolic antioxidants, such as; AO-1, AO-2, and metal deactivator MD-1 with traditional melt processing additives, such as phosphite; P-1 in comparison to a variety of new stabilizer systems containing phenolic antioxidants in combination with hindered amine stabilizers such as HAS-1, HAS-2 and HAS-3. These systems were compounded and injection molded into microtensile bars which in turn were subjected to electron beam crosslinking at two separate dose rates; 10 and 15 megarads. All these systems were evaluated using gel content, oxidative induction time and retention of elongation tensile data on both thermal and xenon exposed samples. By using this approach in our laboratories, we would hopefully be in a better position to elucidate what effect various additive and co-additive packages may have on key criteria evaluated by polymer producer as well as the manufacturer. The measures of performance in these experiments were percent gel, oxidative induction time, initial YI color, YI color after crosslinking, polymer physicals after crosslinking, color maintenance during oven aging and xenon exposure as well as an assessment of physical property maintenance during oven and xenon aging.

SYSTEM CONSIDERATIONS

Irradiation Crosslinking Principles

Ionizing radiation is a distinct and efficient means of bringing about controlled beneficial changes in polymeric systems. These beneficial changes include increases in modulus, tensile and impact strength, hardness, deflection and service temperature, stress-crack resistance, abrasion resistance, creep and fatigue resistance, and barrier properties[2]. This technology is especially versatile, since the changes are achieved in the solid-state, as opposed to alternative thermochemical methods which typically take place in hot, molten polymer. Likewise, radiation processing requires a lower expenditure of energy than other conventional chemical processes.[2]

In the case of electron beam irradiation, highly energetic electrons strike at or near the C-H bonds in target molecules, and give up enough energy to the molecule to break some of the bonds, releasing hydrogen, and leaving the molecule with excited carbon atoms (free radicals). When this process occurs at two adjacent molecules or nearby sites, excited carbon atoms can release excitation energy forming a chemical bond, known as a crosslink, between them. The amount of electron beam radiation absorbed by the target is referred to as the dose, which is defined in terms of kiloGrays (1 kGy=1000 J/kg) or MegaRads (1 MRad=1,000,000 erg/g).[3] The degree or efficiency of crosslinking depends on certain complex secondary chemistries involving, among others, polymer additives, including radical-"scavenging" anti-oxidants and stabilizers.

Commercially, e-beam crosslinking is performed using medium to high energy (2.5 to 10 MeV), high power (50+ kW) accelerators, which are equipped with a variety of material handling systems, and are capable of significant throughput.[5] The accelerator creates a beam of electrons ca. 1 inch in diameter and energizes it to near light speed. The beam passes through a scanhorn, where a magnet scans it back and forth at ca. 200 Hz, creating a curtain of electrons 4-6 feet wide.[4] Products are passed under the scanhorn using conveyors, carts, reel-to-reel equipment, or other specialized handling means. Worldwide, there are approximately 700-800 electron beam accelerators in industrial use today.[6]

Stabilization Principles

As a brief review[7], the autoxidation cycle for unstabilized olefin polymers is shown in Figure 1. In this cycle, which is representative of various stages of the life cycle of the polymer, the polymer is subjected to a variety of damaging stresses. Representative examples include high temperatures and shear rates associated with the sequential melt compounding steps as the product is transformed from reactor powder (or melt) to pellet to formulated compound to finished article. In addition to temperature and shear, the polymerization catalyst residues, oxygen trapped inside the system, and other types of impurities can also play a role in promoting the further degradation of the polymer.

During these repeated thermal histories, free radicals are initiated via C-C and C-H bond breaking. Once the free radical cycle is initiated, the resultant carbon centered free radicals not only react with other polymer molecules, but also feed on the oxygen that is

entrained in the system, leading to the formation of peroxy radicals. The peroxy radicals react further with the polymer generating hydroperoxides; concomitantly, a new carbon centered free radical site is also formed. The carbon centered free radical feeds back into the beginning of Cycle I.

The formation of unstable hydroperoxides, which can be decomposed by heat, UV light, catalyst residues, or other metallic impurities, ultimately leads to the formation of alkoxy and hydroxy radicals, as depicted in Cycle I. Oxygen centered radicals can react further with the polymer, leading to the formation of more carbon centered free radicals, which continue to feed into Cycle I. The reactions leading to the formation of free radicals along the polymer chain inevitably leads to polymer chain linking and/or chain scission reactions in an entropic effort to quench the free radical chemistry.

These chain linking and chain scission reactions, which can take place simultaneously, can result in fundamental changes to the molecular architecture of the polymer in regard to molecular weight (MW), MW distribution (MWD), as well as the nature of chain branching on the polymer backbone. Most, if not all of these changes are unwelcome in that they can change the physical properties, melt processability and the ultimate utility of the polymer during its life cycle. Considering the costs associated with the design that had already been put into the development of the polymer regarding the catalyst and the polymerization process, it is usually quite undesirable for any of these random indiscriminate changes in the molecular architecture of the polymer (remodeling) to take place.

In order to eliminate these negative reactions that lead to the unwelcome remodeling of the molecular architecture of the polymer, a variety of stabilization chemistries have been developed[8,9] and commercialized over the last four decades. In the early days, a phenolic antioxidant, with or without a melt processing stabilizer, such as a phosphite or phosphonite, were typically used in various loadings and ratios to meet most end use applications. The role of the phenolic antioxidant is scavenging the oxygen centered free radicals, such as alkoxy, hydroxy and peroxy type species, while the role of the phosphite is to decompose the hydroperoxides before they split back into oxygen centered free radicals. The utility of these chemistries is illustrated in Figure 1.

Where limitations were encountered in the desired level performance, the judicious re-selection of the phenolic antioxidant and/or phosphite, combined with adjustments in the concentration and ratio of the stabilizers could usually resolve the problem.

In addition to phenolic antioxidants and phosphorus based melt processing stabilizers, acid acceptors (or scavengers) can also be used, to fine tune the system as well to assure that these stabilizers function synergistically.[10]

There have also been entirely new approaches to polymer stabilization. One such new stabilization chemistry, denoted as NOH-1, is based on the hydroxylamine functionality, which can serve as a very powerful hydrogen atom donor and free radical scavenger[11] and hydroperoxide decomposer.[12] Accordingly, the hydroxylamine can be repeatedly positioned in Figure 1 as a broadly applicable melt processing stabilizer to inhibit the autoxidation cycle.

Hindered Amine Stabilizers

Hindered amine stabilizers (HAS) are very effective and efficient stabilizers for polyolefins. They do not absorb UV radiation, but act to inhibit degradation of the polymer, which has already formed free radicals. Several theories have been advanced to explain the mechanism of stabilization by HAS. These include; free radical termination and peroxide decomposition.

The most remarkable characteristics of HALS is their high light stabilizing efficiency. Significant levels of stabilization are achieved at relatively low concentrations. Among the theories explaining HALS high efficiency and longevity are a cyclic process, outlined in Figure 2, wherein the HALS are regenerated, rather than consumed, during the stabilization process.

These theories suggest that the hindered amine oxidizes to form nitroxyl radicals (**NO**$^{\cdot}$) which in turn react with polymer free radicals (**R**$^{\cdot}$) to form an alkoxy amine, a non-free radical species. The alkoxy amine, in turn, can then terminate peroxy radicals formed during degradation as shown in step 3 of Figure 2, and during this process regenerate the nitroxyl species which can go through the cyclic process again and again.[13]

The radical trapping effectiveness of HAS is similar to that of hindered phenolic

antioxidants. Continuing studies have indicated that oligomeric HAS such as HAS-1, HAS-2 and HAS-3 are effective long term

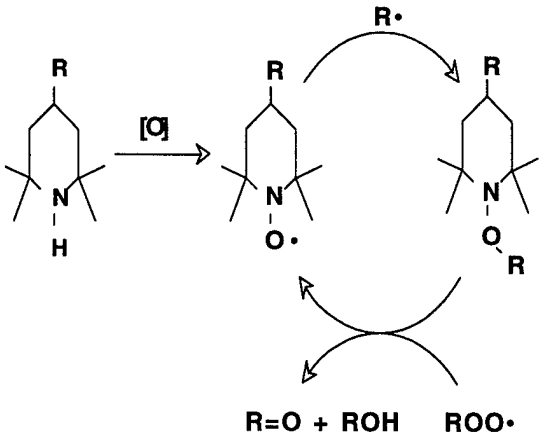

Figure 2: Hindered Amine Cycle

thermal stabilizers and when used at temperatures below 135°C can outperform traditional hindered phenolic antioxidants. Figure 3 demonstrates areas where HAS contribute to both light stability and outstanding thermal stability.

The improved thermal stability of HAS based systems is evident at the test temperature of 90 °C (195 °F), which reflects, for most practical purposes, the upper limit of actual application conditions. At temperatures greater than 135 °C, which may be used in some accelerated test methods, the effectiveness of HALS as thermal stabilizers is usually not observed. Combinations of phenolic antioxidants and HALS can give the broadest range for thermal stabilization.

Results and Discussion

One concern of the electron beam crosslinking process is its effect on phenolic antioxidants. It is well documented that the vis breaking process[14] in polypropylene controlled rheology consumes phenolic AO and often times additional peroxide needs to be added to achieve the desired melt flow. Also in chemically crosslinked systems the antioxidant often suffers during the crosslinking process. To address these issues in electron beamed samples, analytical extraction of phenolics; AO-1, AO-2 and AO-3, were determined on samples before and after irradiation. The following table (Table 1) summarizes recovery data for samples. Surprisingly little effect was observed between irradiated and unirradiated samples at higher concentrations (>2.0%). At concentrations of less than 0.2% The majority of the AO was consumed and in most cases no AO was recovered. Also evaluated were the oxidative induction times (OIT) of samples before and after irradiation. Table 2 summarizes these results for samples at low and high concentrations. In the case of the phenolics it was observed that a substantial loss in the ability of the phenolic to influence the oxidative induction time was observed and that in every case the OIT before irradiation was considerable and reduced by as much as 90% after irradiation. The impact on OIT for hindered amine was surprising, typically hindered amines give low initial OIT values which was observed, however after irradiation the OIT for the hindered amine stabilizers increased by as much as 20 minutes in the case HAS-1. This observation suggests that the hindered amine may have undergone some transformation during the irradiation process. When comparing recoveries of the HAS it is noted that low recoveries are observed(<25%) one possible theory is that the hindered amine has been oxidized and may be bound into the polymer.

Initial % AO-1	Pellets	15 MR Tensile
0.1	0.03	<0.005
0.2	0.06	<0.005
2.4	2.2	1.8
AO-2		
0.1	0.05	<0.005
0.2	0.06	0.01
MD-1		
0.1	0.05	<0.005
0.2	0.10	<0.005
HAS-1		
0.1	0.06	0.005
HAS-2		
0.1	0.04	0.005
HAS-3		
0.1	0.05	0.005

Table 1: Effect of irradiation on recovery of AO-1 and HAS

Initial % AO-1	OIT @ 200 °C	OIT after 15 MR
0.1	31	5
0.2	62	7
2.4	ND	ND
AO-2		
0.1	68	7
0.2	98	8
MD-1		
0.1	73	7
0.2	183	26
HAS-1		
0.1	4	24
HAS-2		
0.1	1	1
HAS-3		
0.1	6	11

Table 2: Effect of irradiation on oxidative induction time of AO-1 and HAS

Tensile elongation was determined on samples as a criteria for aging, as of time of this paper no differentiation was observed. The final data will be presented at the conference. When comparing the initial elongation an interesting observation was made. Samples containing phenolic antioxidants had greater elongation then those containing hindered amine alone. Table 3 contains these values for the various phenolics and hindered amines evaluated. This observation is believed to be a result of the phenolic interfering with the E-beam process thereby reducing the degree of crosslinking under a constant irradiation. The hindered amine on the other hand does not interfere with the E-beam process and allows for higher degree of crosslinking observed via this elongation data.

At the time of the conference further data regarding thermal and light stability of crosslinked systems will be discussed and recommendations for E-Beam crosslinked systems will be made.

Initial % AO-1	10MR	15 MR
0.1	698	682
0.2	747	688
AO-2		
0.1	733	710
0.2	775	700
MD-1		
0.1	743	754
0.2	726	720
HAS-1		
0.1	415	395
HAS-2		
0.1	705	647
HAS-3		
0.1	488	519

Table 3: Effect of irradiation on tensile elongation of samples containing AO-1 and HAS

CONCLUSIONS

Based on our initial data several conclusion can be made. Phenolic antioxidants at low concentration get consumed by the E-Beam process and drastically effect OIT. Hindered amine stabilizers give an unusual boost to OIT after irradiation, although the values are very low, this information may help us to propose a mechanism as to what happens to hindered amines during crosslinking. Hindered amines also have a unique effect on elongation. In the case of HAS-1 and HAS-2 a considerable decrease in the % elongation was observed, this may imply that the HAS interfere less with the E-Beam process giving rise to more highly crosslinked system, or that the HAS acts to catalyze the crosslinking process and may become bound into the system itself, possibly acting as a crosslinking agent. At the time of the presentation further performance data will be reviewed regarding these types of systems.

ACKNOWLEDGEMENTS

The development of new stabilization chemistries and new products is the result of a lot of hard work by many people. The authors wish to thank our colleagues and technologists for their contributions, at the Ciba Specialty Chemical sites around the world. We would also like to thank our worldwide management for their continued support and their commitment. Special thanks go to I. Avila for the extrusion and testing work used in this paper.

Acknowledgment is also made to Michael Stern and Thomas M. Knobel of E-BEAM Services, Inc. for assistance with e-beam processing of samples, as well as informative discussions relative to irradiation processing of polymeric materials.

REFERENCES

[1] J. R. Pauquet, R. V. Todesco, W. O. Drake, Proceeding of the Forty-Second IWCS, (1993), p. 77-86,

Th. Schmutz, E. Kramer, H. Zweifel, G. Dorner, Proceeding of the Polyolefins X International Conference, (1997), p. 372-383

[2] Gehring, J., Zyball, A., Radiat. Phys. Chem., 46 (1995) pp. 931-936.

[3] V.S Ivanov , Radiation Chemistry of Polymers, VSP, Utrecht, The Netherlands, (1982).

[4] J. H. Bly , Electron Beam Processing, International Information Associates, Yardley, PA, (1988).

[5] Minbiole, P.R.., Radiat. Phys. Chem., 46 (1995) pp. 421-428.

[6] Machi, S., Radiat. Phys. Chem., 46 (1995) pp. 399-410.

[7] F. Gugumus, in "Plastic Additives", Chapter 1; 3rd Edition., Hanser Publisher, New York, 1990.

[8] Moss, S, Pauquet J-R., Zweifel, H., "Degradation and Stabilization of Polyolefins during Melt Processing", International Conference on Advances in the Stabilization and Degradation of Polymer, Lucerne 1991, Conference Preprints (A. Patsis, Ed.).

[9] Zweifel, H., Moss, S., "Degradation and Stabilization of High Density Polyethylene during Multiple Extrusion", Polymer Degradation and Stability, 25(1989),217-245.

[10] Pauquet, J.R., King, R., Kröhnke, C., "Revolutionary Stabilizer Systems for Polyethylene", Polyethylene '97 Maack Conference, Milan, May 1997

[11] Smith, P.A., Gloyer, S.E., J. Org. Chem., 40 (1975), pp. 2508-2512.

[12] DeLaMare, H.E., Coppinger, G.M., J. Org. Chem., 28 (1963) pp. 1068-1070.

[13] E.T. Denisov , in "Developments in Polymer Stabilization" , Ed.: G. Scott , Applied Science Publishers, London , Vol. 5 , 37 (1982)

[14] Stadler, U., King, R. E. III, Proceeding of the 1997 Lucerne Conference

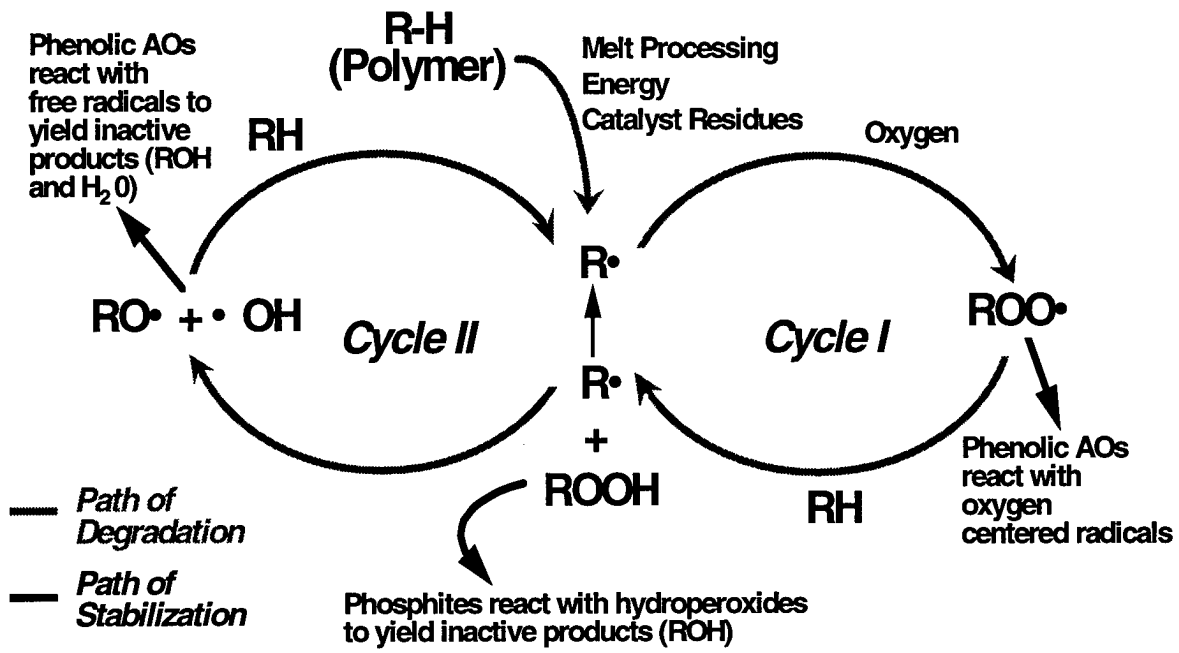

Figure 1: Simplified thermo-oxidative degradation cycle for unstabilized polyolefins including Disruption of the Polymer Degradation Cycle with Phenolics & Phosphites

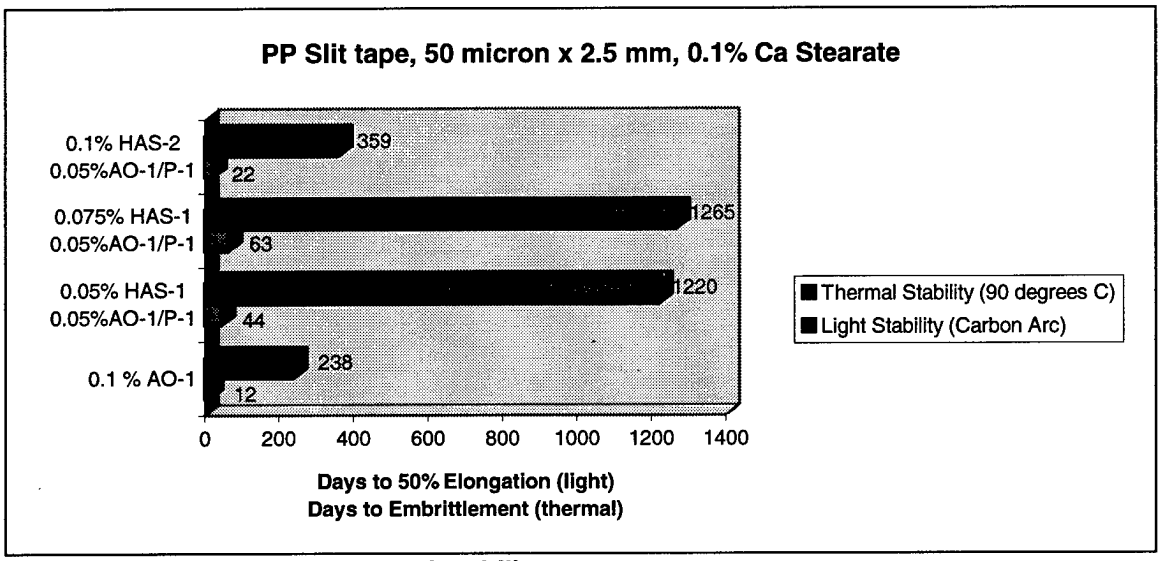

Figure 3: Effect of HAS on thermal stability

Appendix 1. Description of Stabilization Chemistries.

Code	Class	Tradename	Structure	Function
AO-1	Phenolic	Irganox® 1010	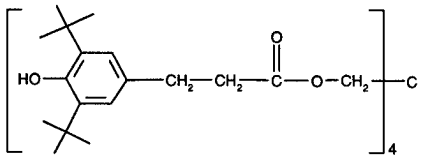	Melt Processing; LTTS: Long Term Thermal Stability; OIT
AO-2	Phenolic	Irganox 1035	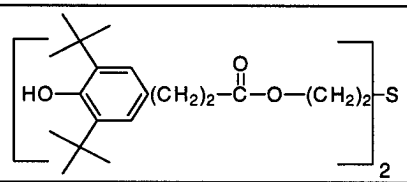	Melt Processing; LTTS; OIT
MD-1	Phenolic Metal Deactivator	Irganox MD1024	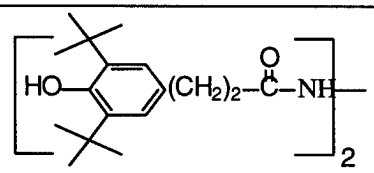	Melt Processing; OIT: Oxidative Induction Time; Metal Deactivator
P-1	Phosphite	Irgafos® 168	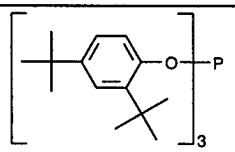	Melt Processing;
HAS-1	Hindered Amine	Chimassorb® 944	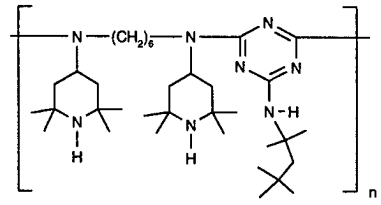	UV Stability; LTTS
HAS-2	Hindered Amine	Tinuvin® 622	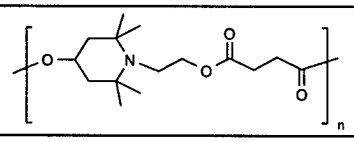	UV Stability; LTTS
HAS-3	Hindered Amine	Chimassorb 119	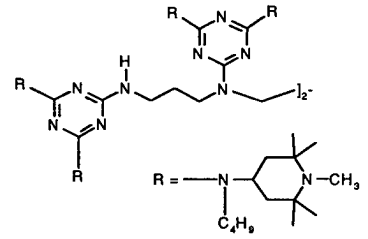	UV Stability; LTTS

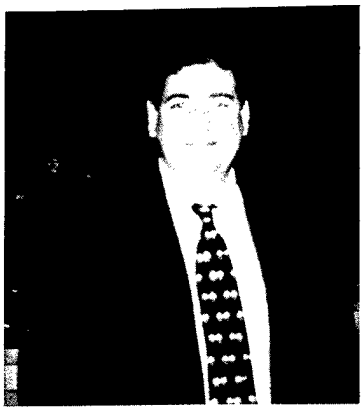

Joseph Lupia joined the Additives Division of Ciba Specialty Chemical in 1994, where he is a Senior Scientist with the Polymer Additives Group located in Tarrytown, New York. He is a member of the Technical Service and Development group where he supports developmental projects for several key customers. He received his B.S. in Biochemistry from The University of Scranton and Ph.D. in Synthetic Organic Chemistry from Seton Hall University.

Ciba Specialty Chemicals
540 White Plains RD
P.O. Box 2005
Tarrytown, NY 10591-9005

Characterizing and Selecting Superabsorbing Cable Components

Joel D. Gruhn

Neptco Incorporated, Pawtucket, Rhode Island

ABSTRACT

Selection of superabsorbing waterblocking materials has often been accomplished by empirical "design of experiment" methods because key engineering attributes of these materials are not sufficiently available. As a result, superabsorbing cable materials may be over specified, or alternatively, cables may be at risk for water penetration after sufficient aging.

We have developed a simple method for design with these materials that predicts their short and long term performance in waterpaths found in fiber optic cables. This method describes cable waterpaths as capillaries with time dependent flow coefficients (Poiseuille laminar flow).

Performance of superabsorbent tape and yarn format materials is characterized in four aspects - the ultimate swell volume per unit length of cable, the swelling time constant, the gel shear strength and the shear adhesion levels toward cable materials. Test methods have been developed for each of these characteristics and data representing the current range of properties is presented.

The minimum gel strength and adhesion needed to block a capillary of given dimension has been explored. The effects of wet accelerated aging of polyacrylic acid based superabsorbent powders on these two properties are evaluated.

The method has been used to estimate the water penetration distance in typical cable tests and the potential for long term creep in the water penetration front.

INTRODUCTION

Dry Core Cables

Over the past few years, many fiber optic cables have been introduced which feature a "dry core" construction. These cables incorporate water-blocking components, commonly tapes, yarns, or coatings, to prevent longitudinal water transit in the cable core. As dry core cables have become accepted, the dry core cable components have rapidly replaced the traditional petroleum based cable filling compounds which were previously applied in bulk in an attempt to completely fill the interior spaces of the cable. In contrast, the dry core cable components utilize novel polymers capable of rapidly absorbing water and forming a hydrogel which swells to fill the free volume of a cable waterpath.

The multiple advantages of dry core designs are now widely recognized. In addition to a welcome craft friendliness due to the absence of sticky grease, they provide a significant reduction in time need to prepare a cable for splicing, a decrease in cable weight, less risk of loss of good adhesion between the outer reinforcing yarns and the sheath, and no need for rags, solvents and cleaners to prepare the cable for splicing. [1 2 3]

Waterswellable Components

To realize these benefits, a wide variety of tapes, yarns, powders, coatings, and specialty compounds - all incorporating some form of superabsorbent polymer (SAP) - have also been introduced. In many cases the waterswellable component is simply a passive carrier of the SAP, chosen to be compatible with other cable manufacturing processes.

More recently introduced products have tended toward greater material efficiency and economy by reducing the quantity of carrier material, or eliminating carriers altogether and pre-applying the SAP directly onto reinforcing or binding materials otherwise already present in the cable.

Superabsorbent Polymers (SAP)
Most commonly, SAP's are derivatives of materials used in diapers, personal care and hygiene products. They are often based on lightly cross linked polyacrylates, such as partially sodium neutralized acrylic acid, derivatives of materials used in the personal care and hygiene products. However other lightly crosslinked polymers based on poly(acrylamide), poly(ethylene oxide), and other hydrophilic monomers, as well as their co-polymers are also useful, particularly with water of high ionic strength.

For a material to be truly defined as a superabsorbent it must be capable of swelling at least 20 times it's own volume. Commercial powders are capable of swelling volume ratios in excess of 500 times in low ionic strength water and over 50 times in seawater.

System Developmental and Optimization
Because of the relatively recent introduction of first generation waterblocking products, they are not yet truly optimized. The engineering science needed to apply them is still too much in a state of infancy. The task has just begun to define the terms and build the database. The designer has too little information on which to base a selection or application. There has not yet been sufficient time for the end user to generate significant long term field experience.

The basic chemistry of SAP's continues to be actively developed. Over 1000 patents are granted by the US Patent Office for superabsorbent polymer chemistry and articles made from superabsorbents. (Figure 1)

In addition, the type, density and location of cross-links on the polymer are at the designer's option. It is possible to trade properties of swell speed, swell volume and gel strength to achieve new materials with different balances of properties tailored specifically to large or small cross-sectional area waterpaths.

The active SAP may be supplied in many forms - a continuous coating, a pattern coating, a fine coarse or porous powder, or a staple fiber. The finished components may also take a variety of forms. For example, a quantity of SAP powder

Superabsorbant Patents Granted

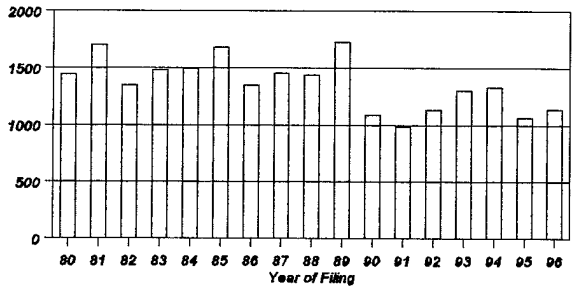

may be laminated between two layers of non-woven fabric to form a tape. Alternatively, the same SAP may be bound onto the outer surface of a single non-woven layer with a water soluble adhesive.

Without question the driving force in many instances is further economic efficiency of the waterblocking system. A petroleum based compound is at a theoretical disadvantage as compared to a superabsorbent gel composed largely of "free" water, both gels possessing similar physical properties. The economic potential of SAP's is being realized in fiber optic cables - replacing refined oil as the predominant waterblocking material. Other types of cables are also sure to be protected by SAP materials as total costs ultimately fall below the cost of petroleum based products.

Cable Testing - Short Term (24 hours)
Overall, the optimization task is guided by the need to pass standardized industry water penetration tests which have evolved from earlier tests for filled metallic cables. The principal test for fiber optic cables in the US is ANSI/EIA/TIA-455-82B, FOTP-82, Fluid Penetration Test for Fluid Blocked Fiber Optic Cable. Similar tests are published by Bellcore in GR-20-CORE and by ASTM as D4565. In Europe, a number of similar specifications apply. These tests have as common features, a standpipe for supplying water at a standard head pressure, a valved connection between the standpipe and a length of test cable, and a time duration over which the cable shall not leak. (Figure 2) The EIA/TIA-455 standard specifies a 1 meter cable sample length, a 1 meter water head, and a 24 hour test duration.

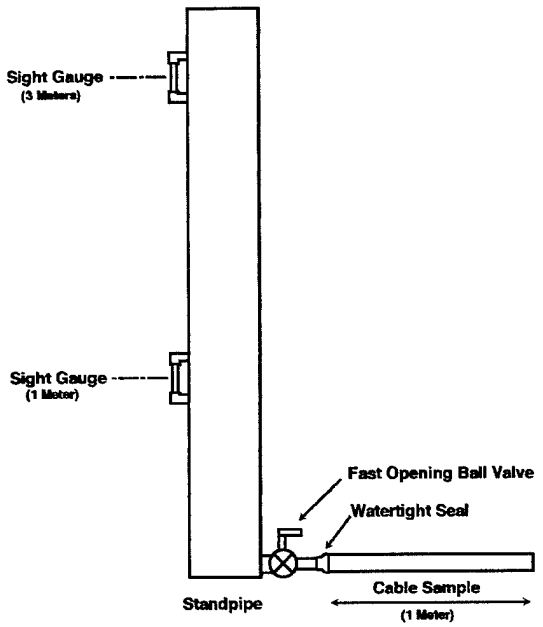

Figure 2. FOTP-82 Waterpenetration Test Apparatus

Cable Testing - Long Term

Cable testing to assure performance over 40 years even under isothermal, isostatic conditions requires significant extrapolation of artificial aging data. Ideally this extrapolation is supported by models relating long term effects of physical and environmental stresses to the effects of shorter term exposures.

Modeling

Our goal is to guide the selection and optimization of waterblocking components. If we correctly model the cable, water and gel as a fluid dynamic system, getting the details of water flow, SAP swelling, and gel stability within the cable, we will have a basis for further optimization and cost reduction of the cable and component designs. The idea is to put just the minimum amount, of the most economical type of waterswellable material, capable of forming the necessary strength gel, exactly where it is needed to ideally waterblock the cable, and be confidant of the cost efficiency and long term stability of the design.

Regardless of the chemistry of the SAP or the particular form in which it is introduced into the cable, it is the dynamic mechanical performance of the waterswellable materials when first brought into contact with water that determines how well (and if) the cable will be water blocked, and with what margin it will pass the standard test. And it is the physical properties of the resulting gel that determine the stability of the point of maximum water penetration and assurance of longer term waterblocking under a continuous head pressure of water.

Accordingly, two models have been explored - a short term model that describes water entry into the cable replicating the GR-20-CORE apparatus, and a long term model that assumes a uniform visco-elastic gel within a capillary subject to a constant head of pressure.

Short Term Water Penetration Model

The purpose of a short term model is to predict the initial penetration of water into the cable. For reasonably fast SAP's, waterblocking will occur in the first few seconds after water is introduced. Our method has been to provide a numeric simulation of the FOTP-82 test and compare the results of the model with tests made on physical cables.

Capillary Flow in Cables

In previous work[4] we reported on a model which predicts the time to water blockage and distance of initial water penetration. For all but the largest capillaries and highest pressures, the initial entry of water is laminar and viscosity dominated. The Hagen-Poiseuille[5] Law may then be used to calculate water penetration.

$$Q = \frac{\pi r^4 (P_1 - P_2)}{8 \mu L} \qquad (1)$$

In this equation Q is the flow rate of water in a section of the cable of length L, r is the equivalent hydraulic radius of the capillary, (P_1-P_2) is the pressure drop over the section, and μ is the viscosity of water.

The various spaces within cables that may serve

as pathways for water migration have a considerable range of characteristic cross-sectional dimensions.

Typical water pathways are:

Waterpath	Effective Dia. (mm.)
Around GRP and Fiber Optic Buffer Tubes	1 - 2 mm.
Between Power cable screening wires	0.5 - 3
Edge of Sheathing Overlap	0.2 - 0.5
Along Strength Yarns, along preferred axis reinforcements	0.1 - 0.5
Along film edges	0.02 - 0.15
Between glass or aramid filaments in unfilled yarns	0.005 - 0.03

The largest capillaries found in common fiber optic cables are those surrounding the buffer tubes (Figure 3) In real cables the waterpath does not have a circular cross-section and we must substitute the equivalent hydraulic radius, r_e . The initial hydraulic radius may be calculated fromcable design dimensions with standard fluid dynamic approximations for non-circular ducts, or it may be directly measured on sample cables made without waterswellable components.

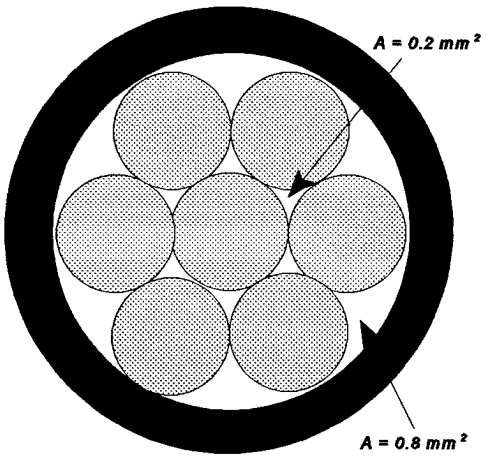

Figure 3 The Loose Tube Geometric Model

The inclusion of superabsorbing components will convert r_e from a parameter to function of time, and hence distance, along the cable, r_e (t,x). Ultimately, when the superabsorbing materials have filled the waterpath volume, r_e will be reduced to zero. Reasonably good agreement may be achieved in computer modeling water penetration using the following empirically validated assumptions:

- The volumetric swelling of superabsorbent materials per unit length of cable may be modeled as an exponential function, having the form

$$V_{Gel} = V_{max} (1 - e^{-t/t_s}) \qquad (2)$$

where t_s is the time constant for swelling and V_{max} is the ultimate swell volume. For this reason it is useful to have manufacturers data on volumetric swelling rate over the first 1-10 seconds of water contact taken continuously on an instrumented swell cup apparatus.

- Due to the fact that SAPs are granular materials, the water is blocked when the largest particles first block the waterpath. This is sooner than when the waterpath is completely filled with gel. For uniform distributions of particulate SAP's, the effective blocking volume is from 150-250% of V_{gel}.

- The effective flow radius may then be modeled until the path is blocked as:

$$r_e = r_{e,initial} \cdot \left(\frac{V_{waterpath} - 2V_{Gel}}{V_{waterpath}} \right)^{1/2} \qquad (3)$$

$$for\ V_{waterpath} > 2V_{Gel}$$

Long Term Model

Cables are designed to be permanent and service lifetimes are assumed to be 40+ years. As waterblocking components are developed, the desire to use faster swelling, lower cost SAPs that

are effective at lower usage rates will tempt designers to use of lower gel strength materials.

The purpose of the long term model presented here is to predict the stability of the wet gel front under continuous hydrostatic pressure, estimate minimum gel strengths required for the various waterpaths, to identify other variables that govern long term stability and to further direct comments on the types of tests that may provide a better lifetime estimation of waterblocking components.

Newtonian Filler

The simplest representation of a weak gel column is when the gel is a high viscosity fluid. For these Newtonian fluids, the shear stress τ is directly proportional to the velocity gradient (du/dy) .

$$\tau = \mu \frac{du}{dy} \qquad (4)$$

This model also applies in the limit where gel crosslinking is very low.

Considering equation 1, allowing L to be a function of time, and integrating over time gives for the penetration

$$L(t) = \frac{r}{2}\left(\frac{P}{\mu}\right)^{1/2} t^{1/2} \qquad (5)$$

The relatively high viscosity needed to block cable capillaries against a 1 meter water head is plotted in Figure 4.

Bingham Gel

Adding a finite shear strength to the Newtonian model results in a closer approximation to a true gel. Such semi-solid materials are known as Bingham-plastic fluids[6]. They require the application of a shear stress τ_p to cause any deformation. At stresses below τ_p they behave like solids, and at stresses above τ_p a plot of τ versus the applied shear is linear.

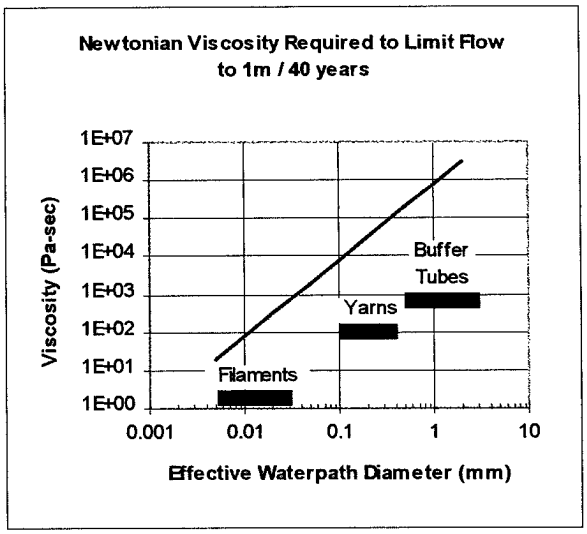

Figure 4

Their shear stress is represented by:

$$\tau = \tau_p + \mu_p \frac{du}{dy} \qquad (6)$$

Examples of Bingham fluids are catsup, toothpaste, latex paint, and wet concrete. These fluids all have a particulate structure capable of interlocking at zero shear and have a particle size smaller than the scale of interest.

In the case of an SAP gel, the interlocking particles are the swollen, semi-solid granules of the gel. The size of the swelled particles may be inferred from the size distribution of the original SAP - they are presumed to scale uniformly, scaling as the cube root of the swell ratio.

The particles are only nominally solid in that the shear forces required to rupture the particles are greater than typical shear forces between particles, or frictional forces against GRP, buffer tubes, other internal cable surfaces.

Flow of Bingham fluids in capillaries includes a central plug that flows as a solid, surrounded by a zone that is in shear flow[7].

For a cylindrical capillary the shear stress at the wall surface, τ_w, is

$$\tau_w = \frac{r\,P}{2\,L} \qquad (7)$$

There are two conditions for gel blockage. The condition for no shear within the gel is

$$\tau_p \geq \tau_w \qquad (8)$$

And representing the static friction of the gel against the capillary wall as τ_f, the condition for no slip against the wall, ie. no plug flow, is

$$\tau_f \geq \tau_w \qquad (9)$$

Over the dimensions of our model cable geometry, the gel strength and frictional shear strength needed to withstand a 1 meter water head undefinedly is as given in Figure 5.

Note that to block water within the largest openings requires that both τ_p and τ_f be greater than ~5 Pa.

Results

Four SAP's were chosen for this study. All four were commercial materials offered for sale as cable waterblocking grades. All wet measurements were made on materials pre-swelled to 50% of the Free Swell Capacity. The properties of the respective materials is summarized in Table 1.

SAPs type C and D are from the same manufacturer, and are reported to be the same chemistry, but are from different manufacturing lots and particle size distributions. The differences observed in Free Swell Capacity are normal manufacturing lot variations. The principal difference between these two materials is the presence a fraction of larger particles, as indicated by the tail on the large end of the dry size distribution for Type C, Figure 6.

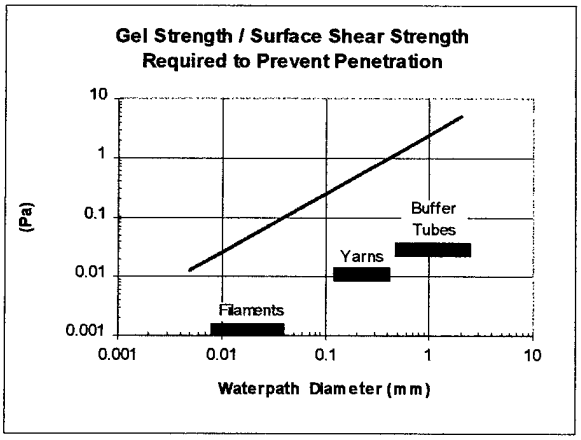

Figure 5

Polymer	Chemistry of Base Polymer	Free Swell Cap. (g/g)	Swell Ratio Tested (50% g/g)
SAP A	potassium polyacrylate/ acrylamide copolymer	294	147
SAP B	potassium polyacrylate/ acrylamide copolymer	229	114
SAP C	poly (sodium acrylate) homopolymer	432	216
SAP D	poly (sodium acrylate) homopolymer	443	221

Table 1

All materials had dry particle size distributions measured by sieving that resulted in the bulk of particles between 100 and 300 microns.

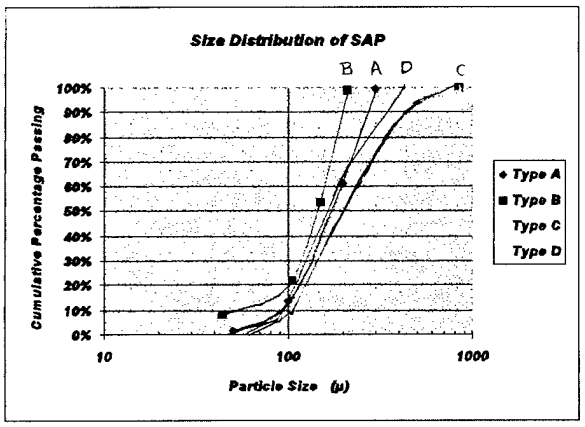

Figure 6

Measurement of Gel Strength, τ_p

Bingham plastics may have their yield strengths measured by a wide variety of techniques[8910] Measurements on samples of wet particulate gels are often taken under conditions of steady shear; they are essentially a data point taken on a flowing material, inappropriate for a long term static strength measurement. Alternatively, gel strength may be reported as the elastic modulus of a block of the un-ground gel, such as the Bloom number used for natural gelatins. Outside the cable industry a number of strength indices are made with the use of special purpose texture measuring equipment without relating the values to customary engineering units[11].

For this analysis we wanted to report on the zero shear yield of the wet gel - an indication of the adhesive interaction between gel surfaces. A normal cone and plate viscometer was found to not be well suited for this measurement, due to the loss of gel particles from the sampled volume. The method selected was simple and inexpensive - slump height measurements made on cylindrical samples[12].

The slump test consists of filling an open cylindrical sleeve with the test material, evenly raising the cylinder, and allowing the material to collapse under its weight. Ideally, the final slumped material will have two zones, a cylindrical upper portion, and a conically shaped lower portion of material that has undergone shear. The height of the slumped material may be related directly to the maximum yield stress. The cylinder dimensions chosen were a 32 mm diameter and a 50 mm height.

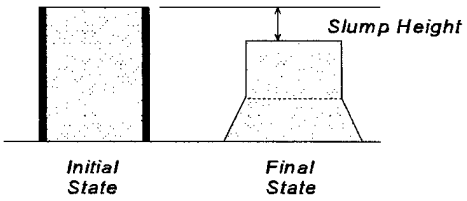

Figure 7

Gel yield strengths, the average of three determinations, are given as Table 2.

Material	Gel Strength (Pa)
SAP A	140
SAP B	58
SAP C	69
SAP D	70

Table 2 Gel Strength of Selected Super-absorbent Gels

Gel Adhesion to Cable Surfaces, τ_f

When hydrostatic pressure is applied to a gel blockage, the pressure forces must be transmitted via shear forces acting at the gel/cable material interface. For hydrophobic cable materials, this interface may be the weakest mechanical link supporting the gel block.

Shear strengths were measured for the SAP's at pressures of 50 Pa against plane surfaces of four typical fiber optic cable materials spanning a range of hydrophobic/hydrophilic polarity.

In increasing order of adhesion the surfaces were:

- Unfilled natural LDPE
- Polyethylene Terepthalate (PET) Film
- Epoxy - Fiberglass
- Spunbonded Polyester Non-woven

All SAP samples failed in shear at the interface against the LDPE, PET, and epoxy surfaces without significant gel transfer to the opposing surface. A strong effect of surface polarity was observed suggesting interaction between polar groups on the surface and the SAP.

All SAP samples failed cohesively against the non-woven surface at the gel yield strength, indicating that the strength of adhesion to the non-woven was greater than the yield strength of the gel. This is due to the porous, fibrous texture of the non-woven surface allowing mechanical keying to take place.

Surface	Gel Type	Adhesion (Pa)
Epoxy-fiberglass	A	88
"	B	49
"	C	26
"	D	55
Polyethylene	A	55
"	B	26
"	C	13
"	D	19
PET	A	111
"	B	51
"	C	23
"	D	36

Table 3 Adhesion Strength of Un-aged SAP

Wet Aging of SAP Gels

Previous studies have shown that the effect of dry aging on cable water penetration is nominal[1314].

Crosslink density determines much of the physical properties of the swollen gel. In order to swell to high volumetric swell ratios, SAP's must be manufactured with low levels of crosslinking and the long term stability of these crosslinks is important.

Two of the SAP's in this study were subjected to accelerated thermal aging at 85°C for 72 hours at 50% of volumetric free swell.

Yield Strength Retention

As a polymer wet ages, crosslinks may potentially be lost due to hydrolysis. Should this occur, the individual grains of SAP may lose a measure of physical strength, and possibly gain potential free swell capability. The effect on the overall yield strength of a mass of gel particles is determined as much by attractive forces between the particles as the modulus of the particles themselves.

Overall yield strength retention after aging was:

Aged Shear Strength Retention			
Polymer Type	Initial Shear Strength (Pa)	Aged Shear Strength (Pa)	Retention %
SAP A	140	36	26%
SAP B	58	39	67%

Table 4

Retention of Adhesion After Aging

Some reduction of adhesion was seen in all cases, most particularly by SAP A against LDPE. However in all cases the polymers retained a higher shear strength and adhesion level than required to block the largest capillaries.

Gel Type	Surface	Adhesion		
		Initial	Aged	Retention
SAP A	Epoxy-glass	88	36	41%
"	LDPE	55	8	15%
"	PET	111	36	32%
SAP B	Epoxy-glass	49	39	92%
"	LDPE	26	19	73%
"	PET	51	36	71%

Table 5 Adhesive Shear Strength of Aged SAP (85°C/ 72h)

Acknowledgments

The assistance of Phillip Shows, Craig Bahlman Calvin Shell, and Karen Blizzard is gratefully acknowledged.

1. Bringuier, Anne G., Dry Waterblocking Technology in Optical Fiber Cable, BICSI 1998

2. Davis, Jim, Demaree, Robert, Performance of Swellable Materials in High Ionic and Seawater Environments, pp. 211-219. NFOEC 1997

3. Gaillard, P., C. McNutt, J. Holder, A. Bouvard, O. Tatat, Significant Improvement of Loose Tube Cable Spliceability Based on New Cable Dry Design, IWCS 1996, pp. 353-358.

4. Gruhn, Joel D., Dr. Stuart Fairgrieve, Predicting the Waterblocking Performance of Super-Absorbing Cable Components. FOCUS 1997

5. Green, Don W., ed., Perry's Chemical Engineer's Handbook, 6th Ed., p. 5-26, McGraw-Hill, New York

6. Bennett, Carroll O., Momentum, Heat and Mass Transfer, p. 21-27, McGraw-Hill, New York, 1974

7. Bird, R. Byron, Dai Gance, Barbara J. Yarusso, The Rheology and Flow of Viscoplastic Materials, The University of Wisconsin, Rheology Research Center, Madison, WI, June 1981.

8. McKinley, Mark J., Dan P. Sheridan, 4500670: Composite Mixtures for Improving Gel Strength of Water Absorbent Gels, U.S. Patent Office, February 19, 1985.

9. Lodge, A.S., Basic Concepts in Polymer Rheology, Rheological Measurements and Their Application in Polymer Characterization, The University of Wisconsin, Rheology Research Center, Madison, WI, March 1980.

10. ASTM D 217 Standard Test Methods for Cone Penetration of Lubricating Grease, The American Society for Testing and Materials, June 1994

11. Applications Studies Illustrating How to Quantify The Texture of Your Products, Texture Technologies Corp.

12. Pashias, N., D.V. Boger, J. Summers, D.J. Glenister, A Fifty Center Rheometer for Yield Stress Measurement, Journal of Rheology, Transactions of the Society of Rheology, v. 40, Issue 6, pp. 1179-1189.

13. Clyburn, Clinton E. III, Anne G. Bringuier, A Dry Core Loose Tube Cable for Outside Environments, International Wire & Cable Symposium Proceedings 1995, pp. 29-36.

14. Anne G. Bringuier, Clinton E. Clyburn III, Reliability of Dry Waterblocking Materials, International Wire & Cable Symposium Proceedings 1996, pp. 779-787.

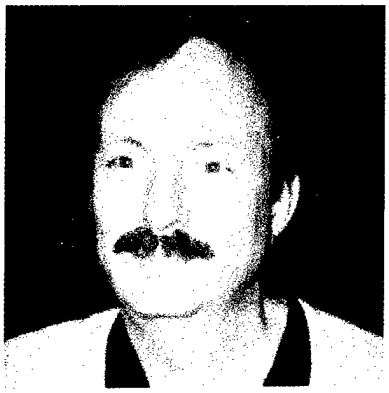

Joel D. Gruhn received a BEE degree from the University of Minnesota in 1970. He is Vice President of Product Engineering for NEPTCO Incorporated of Pawtucket RI

FUNCTIONAL PERFORMANCE OF OCEAN WATER BLOCKING TAPES

Naren I. Patel

Siecor Corporation, Hickory, North Carolina

ABSTRACT

It has been a long established practice to minimize entry and migration of water in telecommunication cables by flooding the interstices within the cables with 'greasy' filling and flooding compounds. While that practice continues, use of super water absorbent polymers (SAPs) is gradually replacing the cable flooding compounds in many cable designs. Small SAP molecules absorb large quantities of water and, in the process, swell and create a pressure dam within the cable preventing further ingress and migration of water. However, unlike the 'greasy' filling and flooding compounds, the swelling efficiency of a SAP is significantly altered by the presence of certain ionic species potentially present in ocean water.[1]

This paper provides experimental data of swell rates and swell heights of different ocean water swellable tapes in waters of different ionic contents, and compares those data with the actual water blocking performance of cables containing the same tapes. The penetration distances in the cables do not correlate with the maximum swell heights or the swell rates measured in the laboratory. Only the functional performance of a cable is of ultimate value to the providers and customers of telecommunications services.

INTRODUCTION

Background

Demand for 'craft-friendly' optical fiber cables in applications where fibers are accessed, spliced, connectorized and terminated frequently is rapidly growing. Cable handling advantages of using dry cables over flooded cables for common duct, aerial and buried applications are well documented.[1-8] Davis and Demaree investigated the time needed for cable end access of both flooded and loose tube cables incorporating SAPs. Dry cables required less time, which is the primary benefit driving their growing use.

Dry cables contain SAPs that combine with intruding water to form a gel. The volume of gel is far greater than the combined volume of the SAP and water. When a gel is formed inside a cable, it fills cavities in the cable creating a pressure dam to prevent entry of additional water and to slow down further migration. The quickness with which a SAP forms gel, and the quantity or volume and quality of that gel, are important considerations in selection of SAP for cabling applications. The construction of a cable also plays a major role in the determination of the quantity, quality and precise location of the SAP needed for optimum water blocking performance.

The volume of a gel depends upon the chemical composition of the SAP and upon ions present in the water. Certain ionic species retard and restrict gel formation affecting the reliability of water blocking performance of dry cables. Ocean waters are solutions of a large variety of ions that could alter swell performance of SAPs. The ionic content of 'ground water' to which cables are exposed varies from location to location.[4, 6] Installation of dry cables in coastal areas where they can be exposed to ocean water or ground water contaminated with the ocean water has recently received some attention.[1] The current project was undertaken to investigate this situation. Water blocking performance of cable samples tested in simulated ocean waters was compared to the gel swell characteristics of water blocking tapes used for making those cables.

Super Absorbent / Water Swellable Polymers

The chemical composition and cross links in SAPs control their water swelling

performance. The SAPs used for blocking fresh or ocean waters are derived from acrylic acid, but their chemical compositions vary. The water absorbency of most common cross linked polymers of partially neutralized acrylic acid diminishes in the presence of polyvalent cations; hence, they can be used for blocking fresh water but not ocean water. Comparatively, absorbency of cross-linked poly(chloro-trimethylaminoethyl-acrylate) or PTMAEA-Cl is affected less by cations, including those present in ocean water, and therefore, it can be used more effectively for blocking both ocean water and fresh water. Since water absorbency and the resultant swelling are lowered for PTMAEA-Cl, additional SAP is required for making ocean water blocking tapes effective. This extra SAP is useful because it combines with and depletes more cations from the intruding water. Ocean water thus depleted of harmful (to gel formation) cations now behaves more like deionized water and permits the gel to swell more and faster, inhibiting further migration. For SAPs of the same chemical formula, the density and location of cross links within a polymer molecule dictate the water blocking effectiveness. Cross-links make polymer molecules less soluble in water, increase gel strength, and reduce initial absorbency. If the cross links are minimal, the gel "dissolves" partially in the ionic water, becoming watery and mushy.

Water Blocking Tapes

Typically, water blocking tapes are made by applying SAP onto, or between, one or more layers of a substrate (typically a web made of polyester or acrylic). At least one of those layers must be porous so that the intruding water can easily come into contact with the SAP. Bonding agents or adhesives are used to keep the SAP on the tape. They act as a barrier between the SAP and intruding water, thus delaying and restricting gel formation. Since the ocean water blocking tapes have more SAP, they require more adhesive. That additional adhesive retards the swell rate of the gel, and as a result, they swell more slowly even in fresh water than the regular fresh water blocking tapes. However, in time, they swell more and block the ingress of water more effectively.

Cables Studied

The cables tested in this study consisted of a ten-position single layer of grease filled buffer tubes wrapped together by a water blocking tape. Ten-position cables, (which indicates that the cable contained 10 buffer tubes), were studied because the water penetration distance data obtained for that design predicts the water blocking performance of that tape in most other loose tube cable constructions. Six-Position cables were also evaluated to provide comparison with the findings of Davis and Demaree. During the investigation, water blocking properties of five tapes, Tape A - Tape E, in 6 or 10 position cables were evaluated.

Simulated Ocean Waters

Solutions of Aquamarin® and Instant Ocean® aquarium salts in deionized water were used to simulate ocean water. Aquamarin and Instant Ocean are available commercially. They represent a variety of ionic species present in ocean water, seen in Tables 1 and 2. Water blocking performance of cables and swell characteristics of tapes by themselves were tested using those solutions. Diluted 25%, 50% and 75% Aquamarin and Instant Ocean solutions were used to mimic brackish or ground water in coastal areas.

TESTING METHODS

Laboratory Testing:

The cup and plunger method (illustrated in Figure 1), a laboratory test normally used for evaluating swell performance of incoming water blocking tapes was selected for measuring the swell heights and swell rates. A disk, 80 mm in diameter, of the tape specimen was placed swell side up covering the bottom of the testing cup. Kimwipe® tissue of the same size was placed over the tape layer, and the perforated plunger of the instrument was placed directly over the Kimwipe. A Digimatic indicator mounted on a "height stand" recorded the initial position of the plunger as zero height. One hundred milliliters of the testing solution was poured into the cup and the real-time change in the position of the plunger was recorded continuously. As the tape swelled, the plunger was pushed upward; thus, the change in the height of the plunger indicated the swell height of the tape. The

same measurements were also made using deionized water. The maximum swell height was reported as the swell height (mm) for the tape/solution system. The swell rate was the ratio of the swell height to the time interval for reaching that height (mm/sec). Three samples of each tape were tested, and the average values were reported.

Cable Testing:

The standard testing setup described in TIA/EIA FOTP 82 that is normally used for evaluating outdoor cables for their water blocking performance was used for the aforementioned dry cables prepared for this project (illustrated in Figure 2). Cable samples were exposed to a one meter head of testing solution for a period of 24 hours. Lengths of samples were selected so that the maximum solution penetration distance for each sample could be measured for comparative evaluation. In order to get consistent results, the samples were placed as flat as practical during the entire test.

TESTING DATA

Five water swellable tapes, Tapes A - E, were evaluated in the laboratory for gel swell performance. Those data are graphically presented in Figures 3 through 11. A six-position cable was made using only Tape A. Ten-Position cables were made with every tape. With the exception of Tape A in both six-position and ten-position cables, the same tape was used over and under the buffer tubes. Tape A, which was recommended for blocking only the fresh or ground water, was applied over the buffer tubes and a water swellable yarn was used to block passage of water under the tubes. At least five samples of each cable were tested for their water blocking performance using one meter head of the appropriate testing solution for a period of 24 hours. At the end of testing, cables were dissected and the longest path of water travel over or under the buffer tubes was reported as the water penetration distance. Those data are reported in Table 3.

DISCUSSION

As was anticipated, all tapes swelled faster and higher in deionized water. In other experiments, Tape B swelled more in every ocean water solution, but it did not provide the best water blocking protection to the cables. Tapes E and D were clearly superior in their water blocking performance in cables, but their swell heights were not even close to that of Tape B. Tapes B and C provided almost the same protection to the cables, but their swell heights and swell rates were vastly different. **These results are at odds with the conclusion reached in a previous publication, that "the penetration distance in a dry cable depends on the swelling speed and ultimate swollen size of its components.". That conclusion feeds a common misconception that the SAPs, which swell more and faster, are the better candidates for use in cables.**

Upon closer examination, the gel that swelled rapidly to a large volume, appeared watery and mushy. It seems conceivable that after some time, water under pressure will pass right through that gel and migrate further into the cable. Low cross-linked SAPs will swell faster and swell more, but they will be partially soluble permitting further migration of water in cables. On the other hand, overly cross-linked molecules will fail to swell and fail to stop migration of water. Only the optimum cross linking in SAP molecules is likely to provide an effective solution (no pun intended!) to the problem. Alternatively, a higher density of cross links only at the surface of the SAP molecule will make the SAP swell slowly letting water reach the innermost areas of the SAP molecule without letting the molecule disintegrate. These gels will be granular, and the whole granule will move under water pressure forming an effective water blocking dam. That could be an explanation for the mediocre water blocking behavior in cables of Tape C, and excellent water blocking performance of Tape E. Comparative ratings of simulated ocean water blocking performance of tapes in ten-position cables, on a scale 1 (best) to 5 (worst), are given in Table 4.

All the tapes swelled more rapidly in deionized water than in ionic waters. Tape E had a relatively lower swell rate in every ionic solution than the other tapes. However, it consistently exhibited the best cable water blocking performance. This confirms that using swell rate is not a reliable predictor of the tape's water blocking potential in cable form. Our experiments could not collaborate the

findings of Gruhn and Fairgrieve. More adhesive used in making ocean water blocking tapes retarded the rate of gel growth, but eventually those tapes swelled, and blocked migration of water more effectively in cables than the fresh water tape, Tape A, did.

Testing of six-position cables with Instant Ocean solutions, like Davis and Demaree, did not provide any additional insight for the water blocking mechanism in cables. Six-position cables allowed far shorter water penetration distances than the comparable ten-position cables did. This reinforced our belief that the results of experiments with the ten-position cable design effectively predicts the water blocking performance of a water blocking tape in most other loose tube cable constructions.

CONCLUSION

The swelling efficiency of a SAP is significantly altered by the presence of certain ionic species potentially present in ocean waters. An intuitive perception that those SAPs which swell more and faster are the better candidates for use in cables was not supported by experimental data in our investigation. The measured penetration distances in cables did not correlate with the maximum swell heights or the fastest swell rates of SAP tapes. Based on those data, we concluded that: The actual penetration distance in a dry cable does not depend on the swelling speed or ultimate swollen size of water blocking tapes alone. As a result, the functional performance of a cable should not be estimated from the swell speed or ultimate swollen size data for a particular water blocking tape. *Only the functional performance of a cable is of paramount value to the providers of telecommunications services in coastal areas.*

ACKNOWLEDGMENTS

I gratefully acknowledge the contributions of Hilde Hagemeister, Wesley Nicholson, and Roger Peterson in carrying out the experimental work of this project; express my sincere thanks to Bill Jackman, Alan Parsons and Dean Yamasaki for their keen interest and support; and to the management of Siecor for encouraging me to present this paper.

REFERENCES

[1] J. Davis and R. Demaree, "Performance of Swellable Materials in High Ionic and Seawater Environments", Proceedings of 1997 National Fiber Optic Engineers Conference, Volume 1, pp. 211-219.

[2] M. Fukuma, N. Akasaka and S. Suzuki, "Dry Type Water-Blocking Optical fiber Tape Cable with Slotted Core", Proceedings of the 36th International Wire and Cable Symposium, pp. 350-356, 1987.

[3] M. Kawase, "Reliability of Waterproof Optical Fiber Cables", Proceedings of the 42nd International Wire and Cable Symposium, pp. 637-644, 1992.

[4] A. Bringuier and C. Clyburn III, "A Dry Core Loose Tube Cable for Outside Environments", Proceedings of the 44th International Wire and Cable Symposium, pp. 29-36, 1995.

[5] R. Gravely III and S. Stokes, "An Improved Loose Tube Cable with Dry Water Blocking Elements", Proceedings of the 11th Annual National Fiber Optic Engineers Conference, pp. 367-375, 1995.

[6] A. Bringuier and C. Clyburn III, "Development of a Loose Tube Cable with Non-Flooded Core for Outdoor Plant Environment", Proceedings of 1995 National Fiber Optic Engineers Conference, pp. 376-386.

[7] A. Bringuier and C. Clyburn III, "Reliability of Dry Waterblocking Materials", Proceedings of the 45th International Wire and Cable Symposium, pp. 787-644, 1996.

[8] J. Gruhn and S. Fairgrieve, "Predicting the Waterblocking Performance of Super-Absorbing Cable Components", 6th Annual Wire and Cable Focus, 1997.

Table 1, Constituents of Aquamarin	
MgCl2	KBr
CaCl2	H3BO3
SrCl2	NaF
KCl	NaCl
NaHCO3	Na2SO4

Table 2, Composition of Instant Ocean[1]	
Major Ion	Concentration (ppm)
Cl^-	18,740
Na^+	10,454
SO_4^{2-}	2,631
Mg^{2+}	1,256
Ca^{2+}	400
K^+	401
HCO_3^-	194

Table 3, Maximum Solution Penetration Distance in Cables (cm)						
	6-Position Cable	10-Position Cables				
Testing Solution	**Tape A**	**Tape A**	**Tape B**	**Tape C**	**Tape D**	**Tape E**
25 % Aquamarin	x	337	119	173	x	47
50%	x	885	115	x	x	31
75%	x	x	213	225	x	41
100%	x	x	219	241	165	55
25 % Instant Ocean	86	263	116	x	x	50
50%	173	791	153	197	x	61
75%	x	x	196	217	x	54
100%	412	x	228	227	160	64

Table 4, Performance Ratings of Tapes in Cables Scale: 1 (Best) to 5 (Worst)					
Testing Solution	**Tape A**	**Tape B**	**Tape C**	**Tape D**	**Tape E**
Aquamarin	5	3	4	2	1
Instant Ocean	4	3	3	2	1

Figure 1, The Cup and Plunger Testing Apparatus

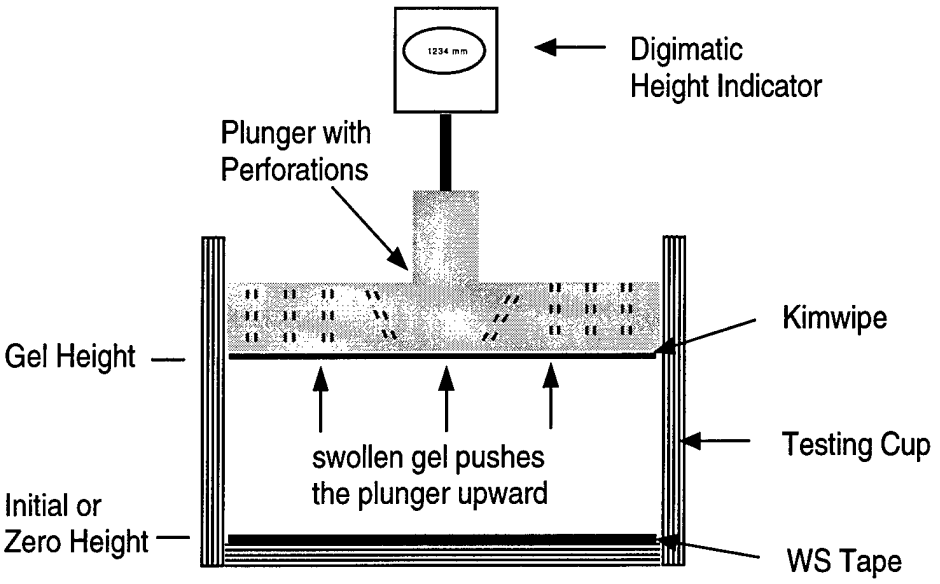

Figure 2, One Meter Head Test Setup

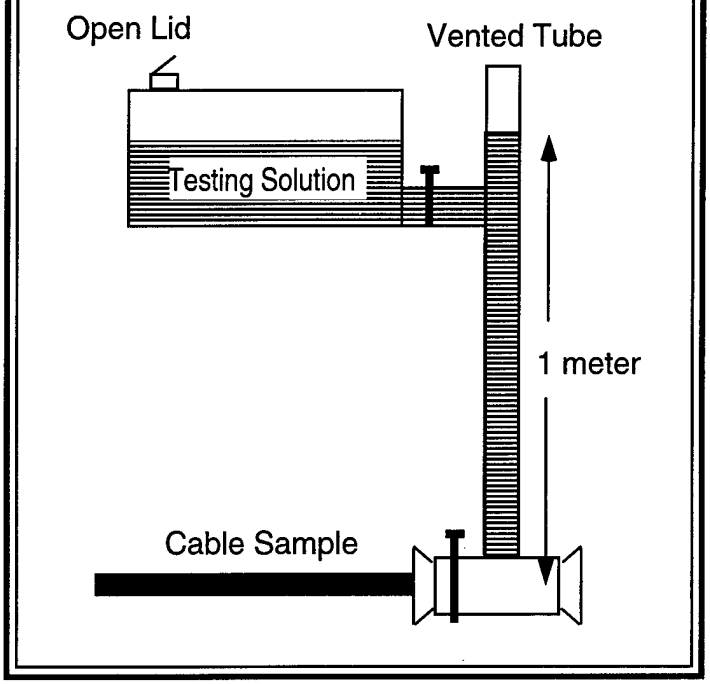

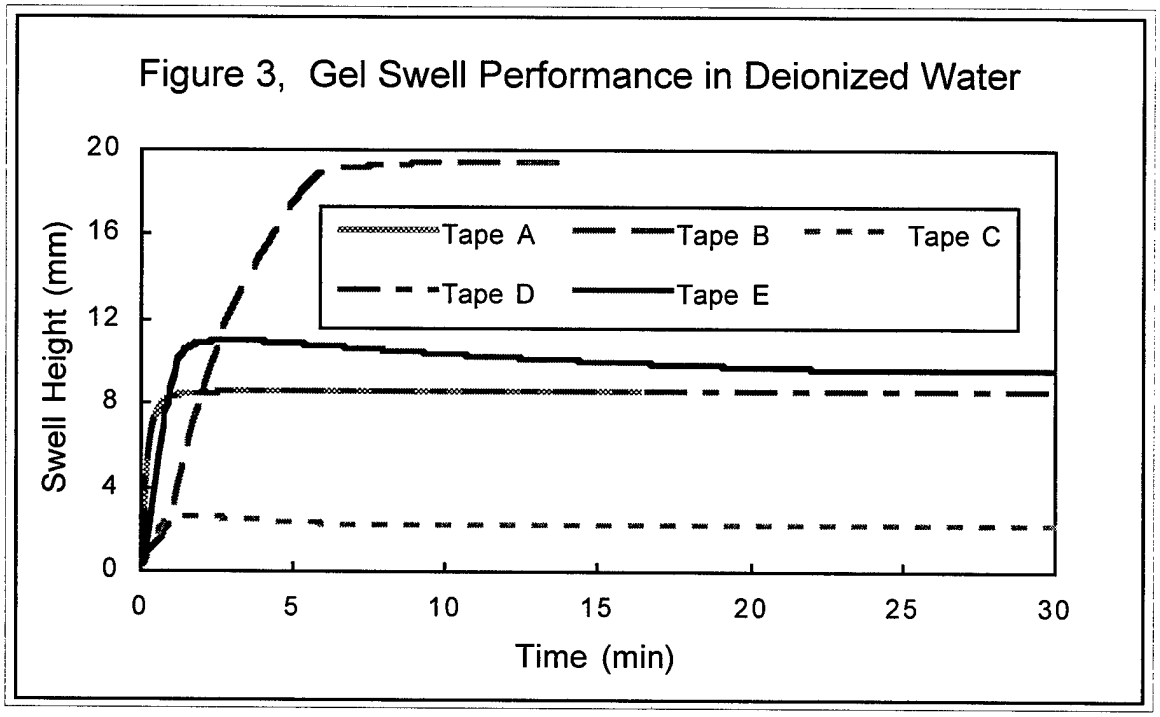
Figure 3, Gel Swell Performance in Deionized Water
Swell Height (mm)
20
16
12
8
4
0
0
5
10
15
20
25
30
Time (min)
Tape A
Tape B
Tape C
Tape D
Tape E

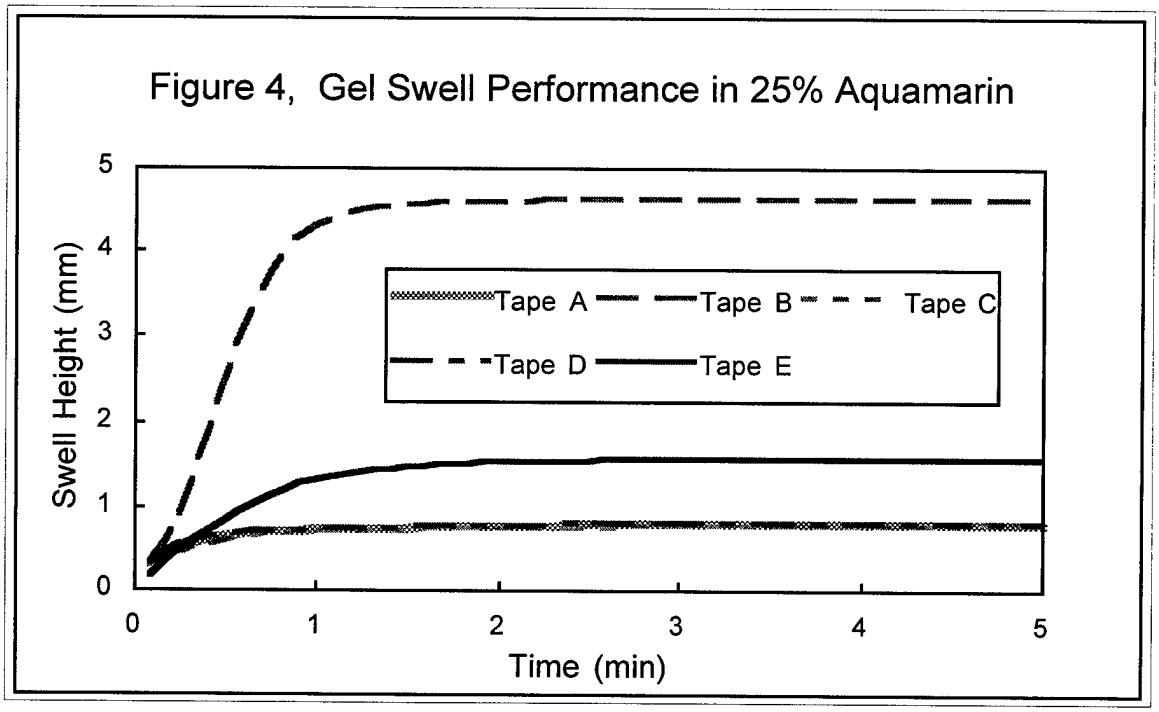
Figure 4, Gel Swell Performance in 25% Aquamarin
Swell Height (mm)
5
4
3
2
1
0
0
1
2
3
4
5
Time (min)
Tape A
Tape B
Tape C
Tape D
Tape E

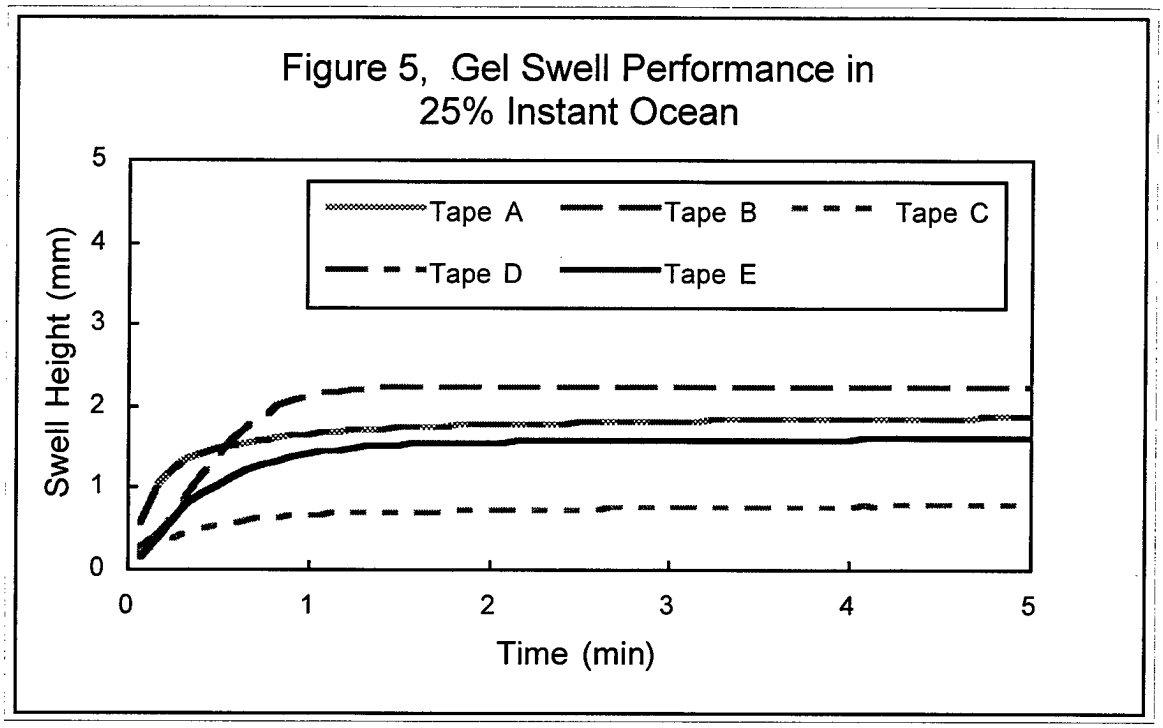
Figure 5, Gel Swell Performance in 25% Instant Ocean
Tape A
Tape B
Tape C
Tape D
Tape E
Swell Height (mm)
Time (min)
0
1
2
3
4
5

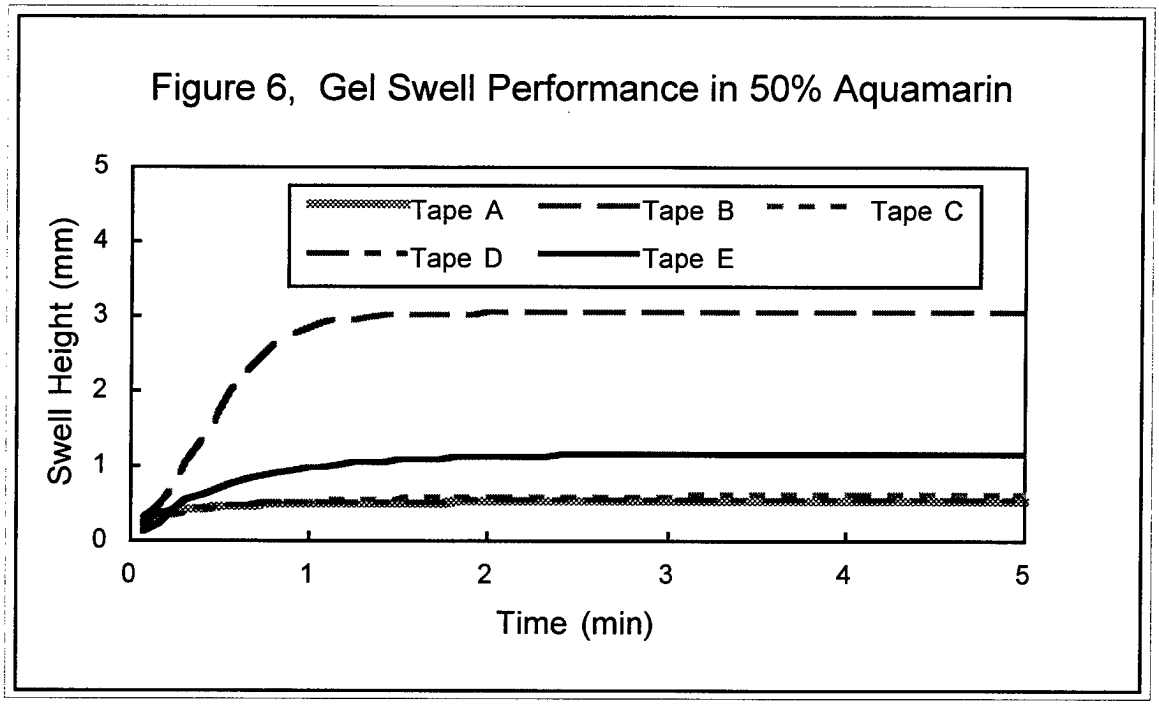
Figure 6, Gel Swell Performance in 50% Aquamarin
Tape A
Tape B
Tape C
Tape D
Tape E
Swell Height (mm)
Time (min)
0
1
2
3
4
5

Figure 7, Gel Swell Performance in 50% Instant Ocean

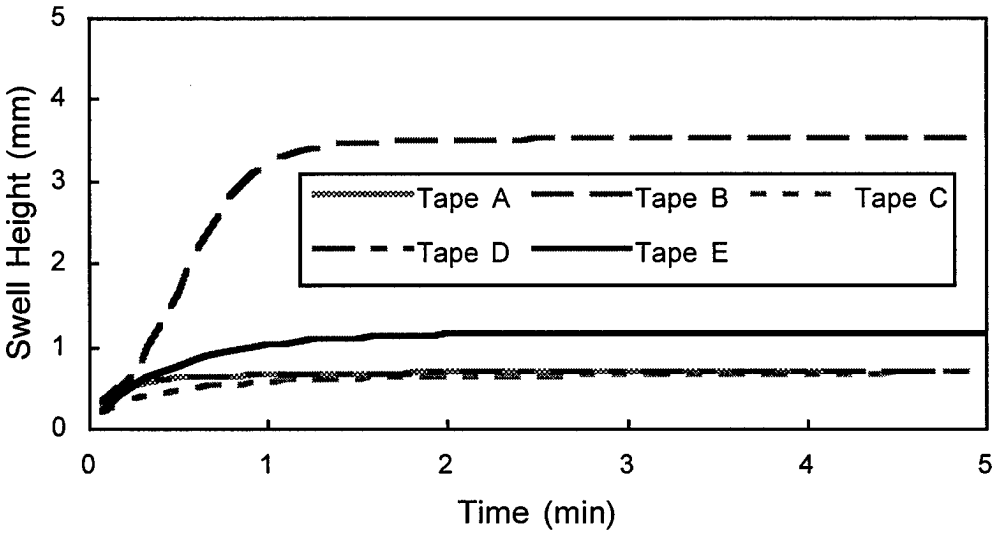

Figure 8, Gel Swell Performance in 75% Aquamarin

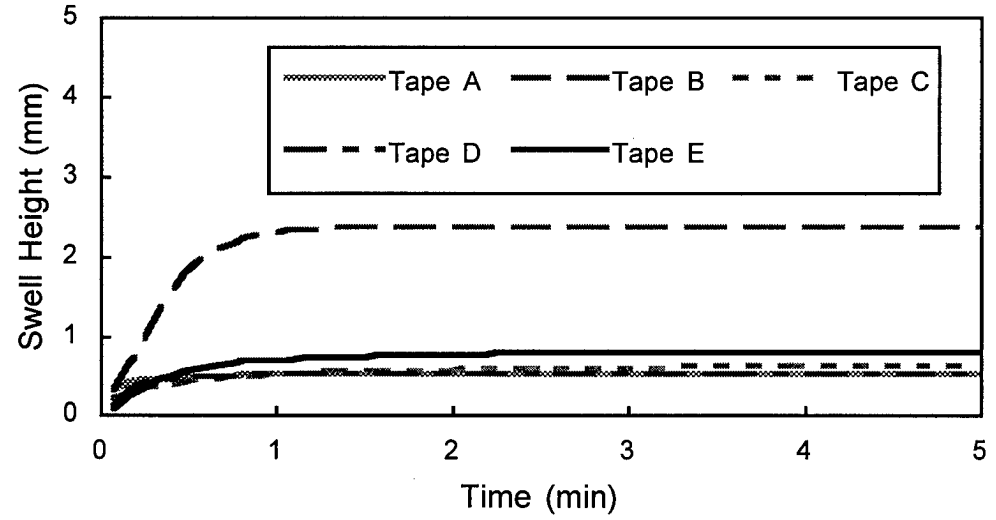

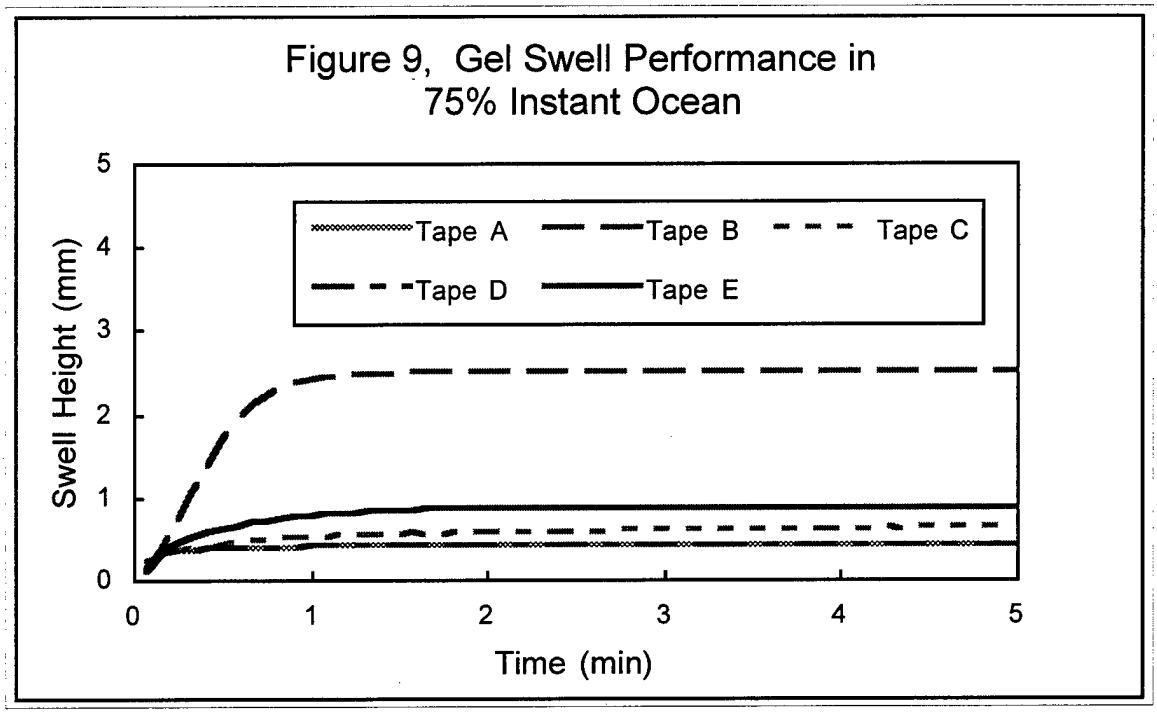
Figure 9, Gel Swell Performance in
75% Instant Ocean
Swell Height (mm)
Time (min)
Tape A
Tape B
Tape C
Tape D
Tape E
0
1
2
3
4
5

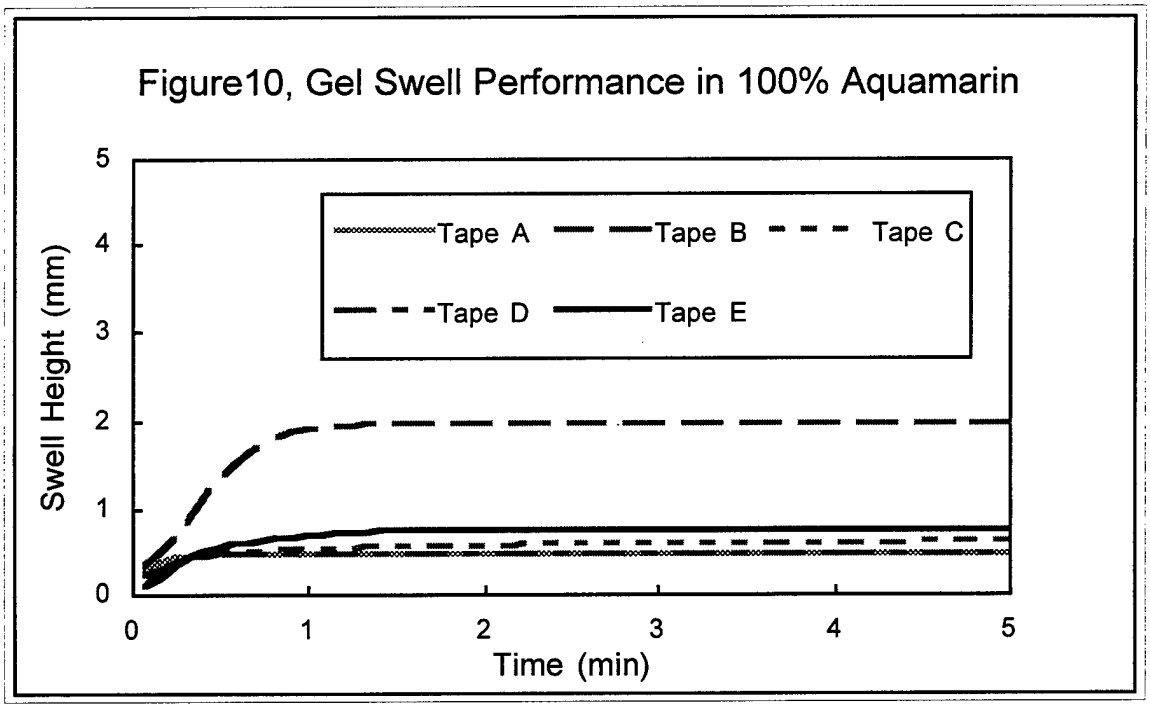
Figure10, Gel Swell Performance in 100% Aquamarin
Swell Height (mm)
Time (min)
Tape A
Tape B
Tape C
Tape D
Tape E
0
1
2
3
4
5

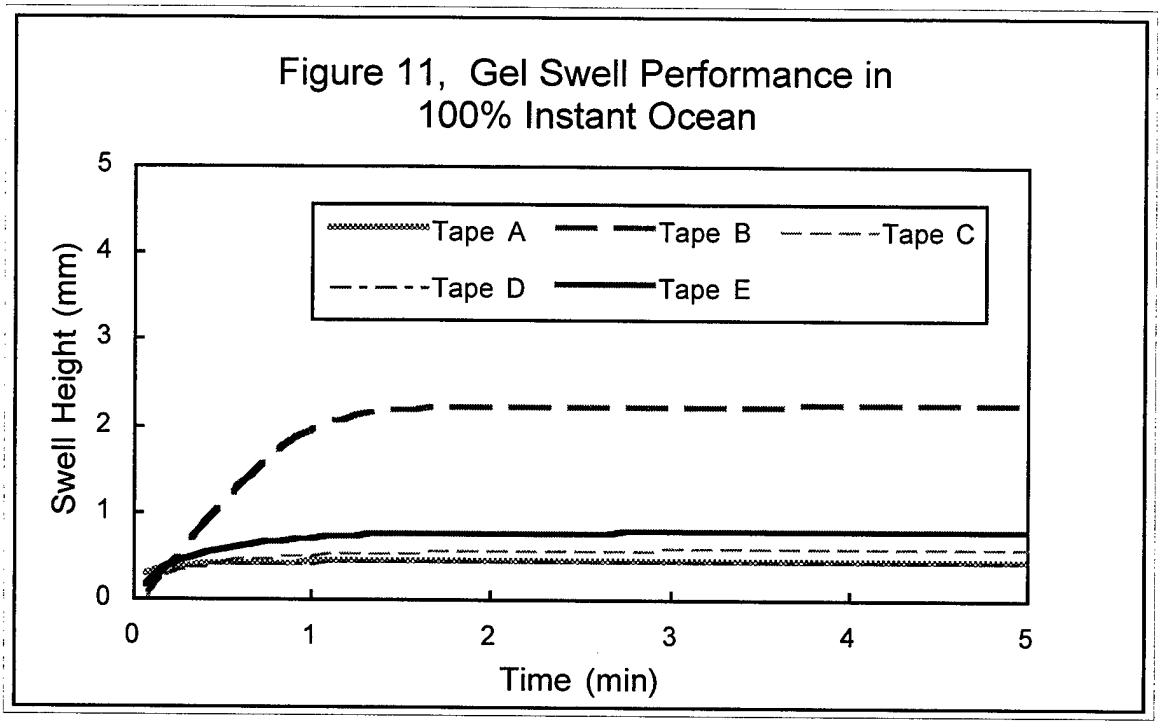

Naren I. Patel
Siecor (RD)
PO Box 489
Hickory, NC 28603-0489

Naren Patel joined Siecor in 1979, and is the Staff Materials Specialist in Research, Development and Engineering. He received his B.S. degree in Chemistry from Gujarat University, B.S. (Textile Chemistry) from the Department of Chemical Technology of Bombay University, India, and Ph.D. from the University of Leeds, U.K. Prior to joining Siecor, he had served as the Director of Quality Control, and Director of Research and Development in the Textile Industry.

NOVEL HALOGENFREE FLAME RETARDANT POLYOLEFINS INTENDED FOR INTERNAL WIRING - PROPERTIES AND FLAME RETARDANT MECHANISM

Bernt-Åke Sultan[1], Karin Ericsson[2], Matti Hirvensalo[3], Thomas Hjertberg[2], Marjo Hänninen[3]

[1]Borealis AB, Skill Center Wire&Cable, Stenungsund, Sweden
[2]Chalmers University of Technology, Department of Polymer Technology, Gothenburg, Sweden
[3]Borealis Polymers Oy, Porvoo, Finland

ABSTRACT

The physical and electrical properties, burning characteristics and flame retardant mechanism of a novel flame retardant technology are presented in this paper. This technology, based on the addition of a relatively low amount of calcium carbonate (20-40%) and a small amount of a silicon elastomer to a traditional oxygen containing ethylene copolymer, ethylene butyl acrylate (EBA), known as Casico, is becoming of increasing importance for internal standard cables especially. Its properties are compared with a PVC compound, which is still the dominant material used for internal wires, and a traditional aluminium hydroxide based Low Smoke Zero Halogen (LSZH) compound.

Cone calorimeter tests on plaques show that Casico has similar burning characteristics as the more traditional LSZH material based on highly filled aluminium hydroxide polyolefins with respect to heat release rate, heat of combustion, smoke formation, corrosivity and carbon monoxide formation. Casico shows the longest ignition time of all the materials investigated, being nearly three times longer than PVC and about 60% longer than the hydrate based material.

PVC has a very short ignition time and generates very dense smoke already in the initial phase of the fire. The burning gases are corrosive and contain five times the amount of carbon monoxide compared with polyolefins. The advantage of PVC is its lower heat of combustion.

Recently performed full scale experiments comparing Casico and PVC based building wires have confirmed these results.
Due to the low filler content and the non-polar character of the polymer used Casico shows outstanding physical, low temperature and wet electrical performance. The use of copolymers makes the flexibility similar to that of PVC. The low density of the compound results in lighter cables.

The studies performed in order to increase understanding of the flame retardant mechanism of Casico show that;

Ester pyrolysis of the acrylate containing copolymer results in a reaction between the chalk and the polymer. This leads to ionomer formation and the formation of non-combustible carbon dioxide and water, which dilute and reduce the combustible gases. The formed gases effervesce and generate a heat insulating foamed structure. A hard skin layer consisting mainly of non-combustible silicon oxide is formed which holds the structure together and reduces the amount of combustible gases transported to the flame front.

INTRODUCTION

Polyolefins have become the dominant materials for external cables due to their outstanding electrical properties and balance of physical and barrier performance combined with a competitive cost structure.

The proportion of the cable system close to the consumer is however much larger. Nearly all of these cables are currently PVC based, and because they are installed indoors flame retardancy is a key issue.

It is true that PVC has a relatively low calorific value. But when exposed to fire it gives off dense smoke, toxic gases and corrosive combustion products.[1]

In order to reduce their calorific value, polyolefin based compounds heavily loaded with aluminium hydroxide were introduced during the 1980's. These traditional Low Smoke Zero Halogen (LSZH) compounds work well in a fire situation but their cost structure and processing limitations have restricted their use mainly to the industrial power cable segment and, with exceptions, some limited progress in building wire applications[1].

Building wire applications fall into three categories; mains (220/240 volt) wiring, telephone cables and data cables. In most European countries mains wiring and telephone cables have PVC insulation and jacket and data cables have PVC jacket and polyolefin insulation.

There is also an interest in finding competitive LSZH solutions for the building wire segment, not only because of the negative burning characteristics of PVC, but also because of its rather restricted low temperature properties and the problem of plasticizer migration, which disturbs the properties of surrounding materials and restricts the life of PVC cables. PVC is also a somewhat unstable polymer, giving off corrosive by-products even during extrusion conditions. This causes corrosion problems of the manufacturing equipment and a quite rapid discoloration of the compound, making special cleaning routines necessary. The negative environmental impact of PVC is a further concern.

Over the past two years however, the situation has changed. Volume sales of a new technology of polyolefin based LSZH materials for the wiring of buildings have seen rapid growth. It is apparent that cost effective replacement of PVC for data distribution and mains wiring has become a reality.

The purpose of this paper is to present the properties of this novel technology, known as Casico, in comparison with PVC and traditional LSZH materials. The present understanding of its flame retardant mechanism is also covered.

EXPERIMENTAL

Materials

To compare the properties of Casico with alternative flame retardant technologies used for internal wiring, the samples described in Table 1 were used

Table 1. Samples used for comparative studies of physical, electrical and burning characteristics

Sample	Description
PVC-1	Typical PVC used as building wire jacket comprising about 20% plasticizer (DOP), 20% chalk, lead stabiliser and titanium dioxide
ATH-14	Ethylene vinyl acetate/HDPE mixture filled with 58% aluminium hydroxide
MH-22	Ethylene vinyl acetate copolymer filled with 58% magnesium hydroxide

To understand the flame retardant mechanism of Casico the burning properties, analysis of remaining ash, thermal and thermo-oxidative degradation behaviour, the samples described in Table 2 were studied.

Table 2. Materials used to study the flame retardant mechanism of Casico. The commercial Casico samples, 02-Casico, 04-Casico and 07-Casico were also used to study the physical, electrical and burning characteristics of Casico.

Sample	30 w-% CaCO3	5 w-% Silicon elastomer	EBA-1 Normal BA content	EBA-2 High BA Content	LDPE	PP
02-Casico	x	x		x		x
04-Casico	x	x	x			
07-Casico	x	x		x		
LD-Casi	x	x			x	
02-Caco	x			x		x
04-Caco	x		x			
07-Caco	x			x		
02-Sico		x		x		x
04-Sico		x	x			
07-Sico		x		x		

02-Casico, 04-Casico and 07-Casico are commercial samples. The remainder were specially prepared for this study.

Fire tests

Limited Oxygen Index (LOI) determination was performed using Stanton Redcroft oxygen index apparatus according to the standard ISO 4587. Test samples (6.5x100mm, thickness 3mm) were cut from pressed plates.

Cone calorimeter (Stanton Redcroft) tests were performed according to ASTM E 1354-90, on 3mm thick 100x100 mm plaques. Unless otherwise specified, a heat flux of 35 KW/m^2 was used.

Thermogravimetry

Thermo Gravimetric Analysis (TGA) was made using a Perkin Elmer TGA-7 with a gas flow of 50 ml/min. I mm thick plaques were used.

Thermal Treatment in Tubular Oven

For visual observation of degradation and to study structural changes of the polymeric material during thermal treatment, a tubular oven (1200x65 mm), made of glass, was used. It is designed for adequate control of temperature and atmosphere, and contains a low temperature section for conditioning and cooling of the samples. The treated samples (15x50mm) had a thickness of 1 mm and were placed on glass microscope slides during treatment. The oven is described elsewhere in more detail.[2]

Microscopy

The treated samples were studied using a Wild Heerburg M8 Zoom stereo microscope and JEOL JSM 820 Scanning Electron Microscope (SEM). The samples were carbonised and plated with gold prior to analysis.

Chemical Analysis

To determine the type and amount of elements present in the samples a PGT EDS Energy Dispersive X-ray Spectrometer (EDS) was used.

For infrared analysis an FTIR Nicolet 730 spectrometer was used. The samples were ground and then mixed with potassium bromide (KBr), and studied as tablets. Silicone absorptions were registered at 805 and 900-1150 cm^{-1} .

FLAME RETARDANT TECHNOLOGIES FOR POLYOLEFINS - PHYSICAL, ELECTRICAL AND BURNING CHARACTERISTICS COMPARED WITH PVC

The usual technique for making flame retardant polyolefin compounds for wire & cable applications is by high loadings (50-65%) of aluminium hydroxide, table 3. Two more novel flame retardants, chalk and magnesium hydroxide, are also shown. By combination with the right polymer system, optimal flame retardancy is achieved, Table 4.

Table 3. Inorganic additives used as flame retardants for polyolefins in cable applications

Type	Dec. Temp. °C	Price DEM/kg	Addition %
$CaCO_3$	± 700	0.4	20 - 40
$Al(OH)_3$	± 200	1.7	50 - 65
$Mg(OH)_2$	± 300	3.5 - 5.0	50 - 65

Table 4. Optimal combinations of filler and polymer

$CaCO_3$	PE-copolymers, Silicon elastomer[1)]
$Al(OH)_3$	EVA/HDPE
$Mg(OH)_2$	PE-copolymers PP

Note: The synergy between Silicon Gum and PE copolymers is a patented technology of Borealis[1)] (EP0393959B1)

Aluminium hydroxide starts to decompose at 200°C. This limits the extrusion temperature to about 160°C, which is below optimum conditions. As can be seen from Table 3 the more novel flame retardants do not have this limitation. Due to the broader processing window and the development of effective filler coating systems, magnesium hydroxide based formulations have, in spite of high filler loadings, a comparable processability to unfilled PE and ordinary PVC compounds. Consequently they can be extruded on normal PVC and PE extruders without any major modification. The extrusion speed will be similar to that of unfilled PE and PVC. Magnesium hydroxide is, however, too expensive to be a realistic alternative to PVC for building cables.

A more cost effective solution is to combine a relatively small amount of chalk, 20-40%, and a small fraction of silicon gum with traditional polar ethylene copolymers, preferably ethylenethylacrylate (EEA) or ethylenebutylacrylate (EBA). This novel patented technology is known as Casico, an acronym for this technology based on its composition i.e. **Ca**lcium carbonate, **Si**licon elastomer and traditional oxygen containing ethylene **Co**polymers.[3] Over recent years, these types of material have become increasing important as a replacement of PVC in standard cables, e.g. building wires according to VDE 0250 pt 215. They are also used as jacket and insulation for flexible-, 1 kV-, control-, medium voltage- and communication cables. Another major application is data cable jacketing.

The characteristics of these different flame retardant systems are presented below in comparison with PVC.

Physical and electrical properties

The typical range of physical properties is described in Table 5. Due to the modest amount of filler needed in Casico technology the weight of the material is reduced by 20 to 25% compared with PVC and hydrate filled materials, resulting in lighter cables, reduced volume cost and improved flexibility compared with the more highly filled materials. Elongation is normally a borderline parameter for aluminium hydroxide materials. The greatest elongation is achieved by Casico as well as the best low temperature properties.

Casico also has the best wet (Figure 1) and electrical properties (Table 6), which are retained even after extended periods of immersion in hot water, Figure 2.

Table 5. Typical physical properties

	Unit	Casico	ATH-14	MH-22	PVC
Density	kg/m^3	1150	1400-1500	1400-1500	1400-1500
Tensile Strength	MPa	10-15	10-15	10-15	10-20
Elongation	%	400-600	125-250	400-600	200-300
Flexural Modulus	kg/m^3	100-200	500-800	500-800	50-200
Limited Oxygen Index	%	30-40	30-45	30-45	20-30
Brittleness temp.	°C	<-60	-10 - -20	–	-10 - -20

Table 6. Electrical properties

Product	Volume resistivity (10^{16} Ωcm) Mean	Dissipation factor (10^{E-4}) Mean	Rel. permittivity (ε) Mean
Casico	1.0	39	2.92
MH-22	0.5	44	4.00
ATH-14	0.008	1310	6.07
PVC-1	0.008	701	6.02

IEC 94, 50 Hz, 23°C, 500 VDC applied, 1 mm press moulded plaques

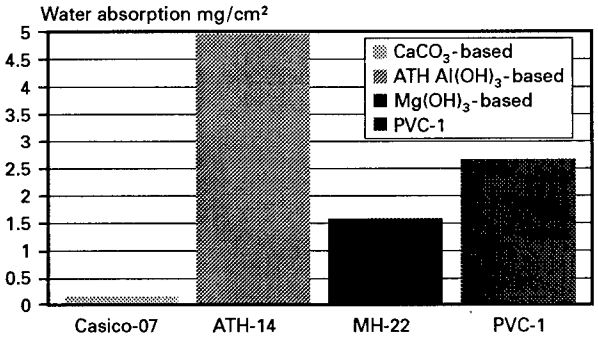

Figure 1. Water absorption

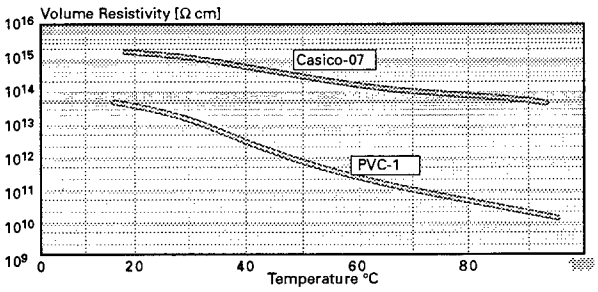

Figure 2. Volume resisitivity after storage in water (14 days, 1mm² conductor, 0.7 mm insulation thickness).

Burning characteristics

The burning characteristics of Casico are compared with those of PVC and hydrate filled LSZH compounds in Figure 3, Figure 4 and Table 7. PVC has the shortest ignition time, and the lowest heat release rate and heat of combustion of all materials investigated (see Figure. 3 and Table 7). Non-flame retardant low density polyethylene (LDPE) has a longer ignition time but a very short and intensive heat release. By adding ATH , burning intensity is reduced. The Casico compound has a similar heat release as the ATH filled compound. Casico has the longest ignition time of all materials investigated, being nearly three times longer than the PVC compound

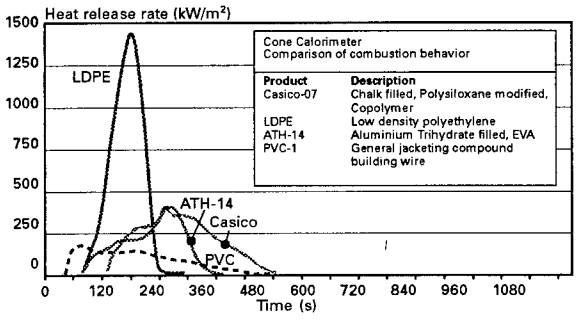

Figure 3. Heat release rate - flame retardant polyolefins in comparison with PVC and LDPE.

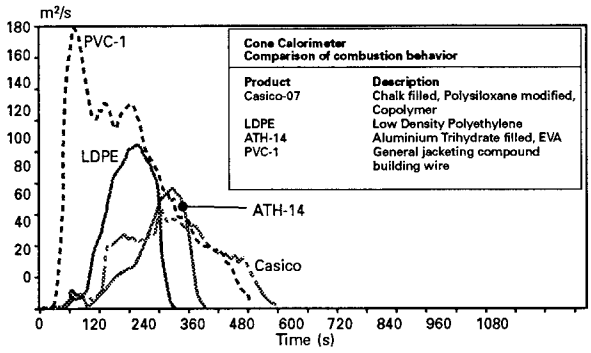

Figure 4. Rate of smoke production for flame retardant polyolefins in comparison with PVC and LDPE

Table 7. Cone calorimeter data

	RHR (max) (kW/m²)	RHR (ave) (kW/m²)	Ign. time (s)	HC (MJ/dm³)	SEA (m²/dm³)	CO (kg/dm³)	CO_2 (kg/dm³)
LDPE	1420	520	82	38.2	392	0.021	2.67
ATH-14	410	135	80	25.8	391	0.018	1.62
Casico-07	410	105	130	27.6	472	0.023	1.74
PVC-1	170	95	47	14.7	1240	0.096	0.96

Light obscuration is presented in Figure 4. In the initial phase of the fire the PVC sample gave off a dense smoke, which was formed even before the PVC sample ignited.

All polyolefin based compounds gave similar carbon monoxide formation, Figure 5. The carbon monoxide level was approximately five times higher for the PVC sample.

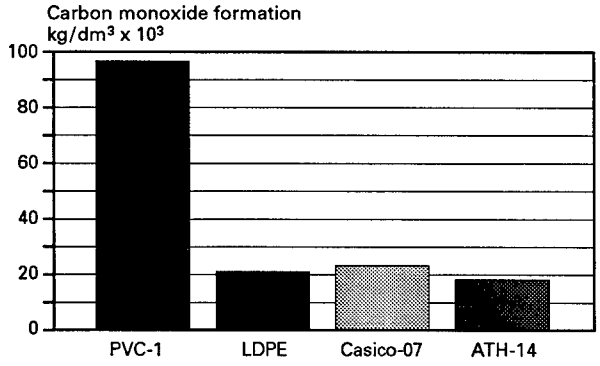

Figure 5. Carbon monoxide formation during combustion in the cone calorimeter.

The pH and conductivity of the different flame retardant systems have been measured according to IEC 754-2 Figure 6 and 7.

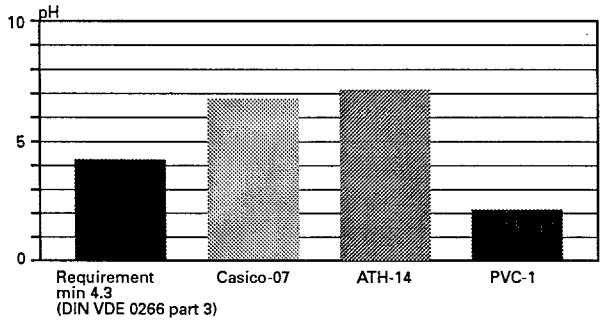

Figure 6. Acidity of combustion fumes (IEC 754-2)

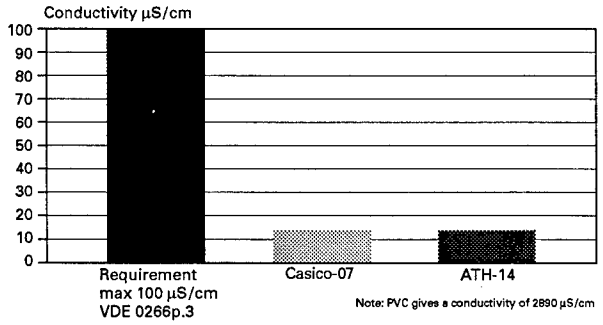

Figure 7. Conductivity of combustion fumes (IEC 754-2)

The pH of combustion fumes from the polyolefin compounds is about 6 and the conductivity about 10uS/cm. The smoke from PVC has a pH of about 2 and a conductivity of 2890uS/cm. These results are expected. The degradation products from polyolefins and its additives are not corrosive. Contrastingly, a typical PVC compound intended for cable applications will generate about 250g/kg compound of hydrogen chloride (HCl) when heated or burnt. This fits well with the measured pH.

The smoke density of the different materials have also been investigated using the NBS smoke chamber, Figure 8. In the flame phase PVC reaches the maximum smoke density 350 in approximately 6 seconds. The results correspond with the result from the cone calorimeter i.e. the polyolefin based compounds show much lower smoke densities. The Casico system appears to produce somewhat less smoke in the non-flaming mode than the hydrate filled compound.

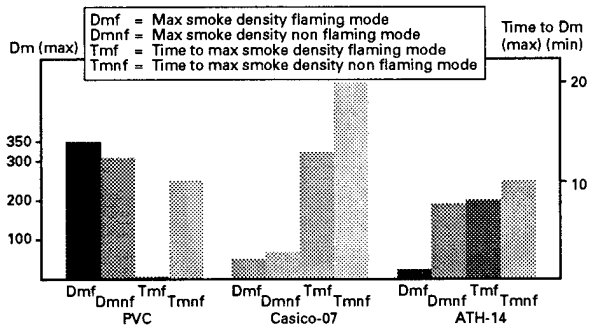

Figure 8. NBS smoke chamber data (ASTM E 662-83)

The scenario for fire fatalities starts with disorientation due to smoke and irritant combustion fumes such as HCl, which is a strong acid and thus a powerful irritant . Escape becomes difficult and fatalities follow due to asphyxiation or inhalation of poisonous fumes. Carbon monoxide (CO) is the component in most fire gases that causes the greatest threat to life[4]. According to the US Fire Administration, 80% of the damage to health and life is due to smoke, while only 13% is due to heat and the remaining 7% due to other causes.[5] It is also known that the acidic gases evolved when cable materials are burned cause extensive damage to electrical and electronic equipment. The cost of corrosion damage often far exceeds the cost directly attributable to the fire.[6,7]

In a fire situation the primary concern is escape. PVC has the shortest ignition time of all the materials investigated and generates dense smoke even before ignition. Furthermore, it generates high levels of acid gas and carbon monoxide at an early stage in the fire. By contrast, escape from a fire involving Casico or ATH based materials is made easier due to good visibility, the absence of acid gas and lower toxicity. PVC has the lowest heat of combustion of the materials investigated, but the better electrical properties of polyolefins have enabled cable down-sizing (VDE 0250, pt 215) i.e. a smaller amount of combustible material which in practice compensates for this difference.

Large scale fire tests comparing building wires based on Casico technology and PVC confirm the results from the plaque tests presented above.[8] The PVC cable caught fire quickly and burned with a steadily decreasing intensity . In comparison the Casico cable was much more difficult to ignite and burned with an intensity that increased during the later stages of the fire. Smoke production differed dramatically. The PVC cable immediately generated large amounts of smoke that decreased over time. The initial visibility was so poor that the flames could hardly be observed on the video camera located less than three meters from the fire. In the full scale test, the Casico cable also produced far less carbon monoxide.

PRESENT UNDERSTANDING OF THE FLAME RETARDANT MECHANISM OF CASICO

The influence of the different components on burning characteristics

To increase understanding of the influence of the different components in Casico technology, the LOI's of the formulations have been measured.

Table 8. Limited Oxygen Index (LOI) of formulations measured in order to investigate the flame retardant mechanism of Casico

Compound	LOI, %
Casico-02	34
Casico-04	40
Casico-07	37
LD-casi	22
02-Caco	24
04-Caco	22
07-Caco	20
02-Casi	20
04-Casi	19
07-Casi	19

It is clearly apparent that compounds containing the full Casico formulation show the highest flame retardancy, which confirms the finding in the original Casico patent.[3]

By replacing the copolymer with an ordinary LDPE the LOI is reduced by up to 18%. Acrylate content also seems to have an influence on burning properties, the lower BA containing copolymer giving the highest LOI.

Addition of chalk to copolymers without the silicon elastomer also gives a dramatic reduction in LOIs - reaching between 20-24% depending on the polymer system used.

Addition of silicon elastomer to the copolymers without chalk reduces flame retardancy even further to a level of 19-20%.

Thermogravimetry (TGA)

To explain the above findings thermogravimetric analysis has been performed on some of the above formulations. The objective of this study was to investigate weight loss rate in a temperature range below self-ignition temperatures.

Initial studies were performed at a heating rate of 10°C/min in both nitrogen and oxygen atmospheres. The samples chosen were 02-Co, 02-Casico, 02-Caco and 02-Casi.

The results are presented in Figure 9.

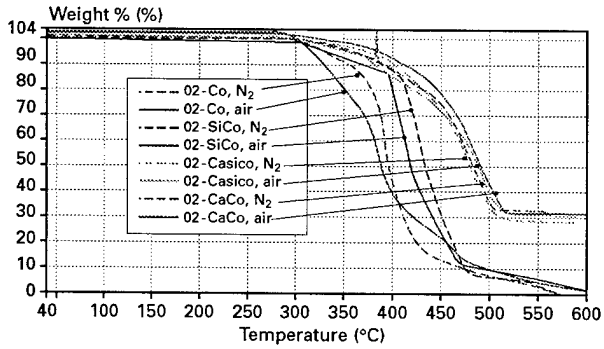

Figure 9. TGA analysis at a heating rate of 10°C/min in nitrogen and air for 02-Co, 02-Casico, 02-Caco and 02-Casi.

For all samples, significant degradation leading to the observed weight losses appeared to commence at around 300°C. An astonishing difference in the rate of the weight loss was seen amongst the tested samples. Addition of silicon elastomer, and especially chalk alone or in combination with silicon elastomer cause a dramatic reduction in the rate of weight loss.

Due to the oxygen and its autocatalytic oxidation of the polymer the rate of weight loss is higher both for the pure polymer (02-Co) and the combination of polymer and silicone elastomer. This difference appears to be smaller for the samples containing chalk.

As expected, chalk containing samples give a residue of about 30%

Further studies were performed in isothermal conditions. 02-Casico was studied at 300, 400 and 500°C, Figure 10.

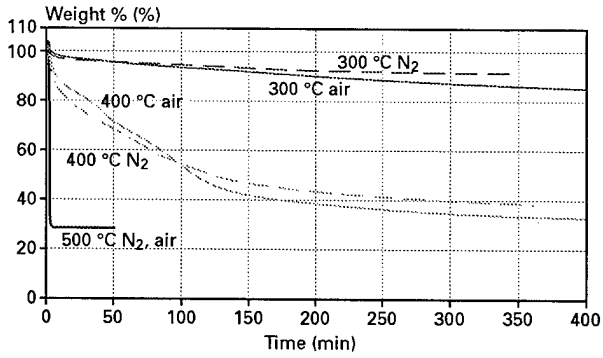

Figure 10. Isothermal TGA studies of 02-Casico at 300, 400 and 500°C in air and nitrogen.

At 500°C weight loss is very rapid and probably due to self-ignition. At 300 and 400°C weight loss is much slower than normal for a polyolefin and the influence of oxygen is surprisingly small, confirming the results presented in Figure 9.

Isothermal TGA studies of 02-Casico, 02-Caco, 02-Sico and 02-Co presented in Figure 11 and Figure 12 clearly show the reduction in weight loss achieved by the addition of chalk and silicon elastomer, and especially the combination of chalk and silicon elastomer, to the copolymers.

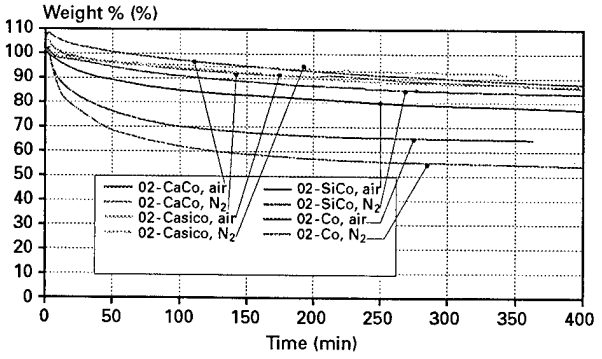

Figure 11. Isothermal TGA studies at 300°C in air and nitrogen for 02-Casico, 02-Caco, 02-Sico and 02-Co.

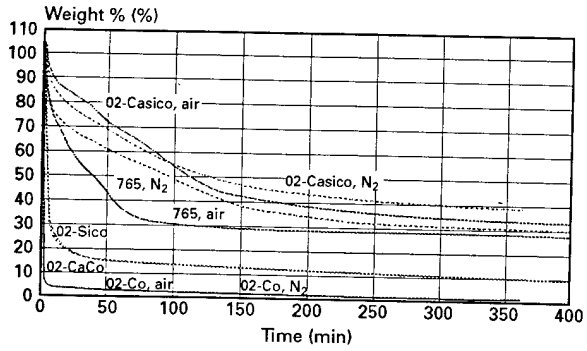

Figure 12. Isothermal TGA studies at 400°C in air and nitrogen for 02-Casico, 02-Caco, 02-Sico and 02-Co.

Thermal and thermo-oxidative stability of the pure silicon elastomer was also studied in isothermal TGA experiments, Figure 13.

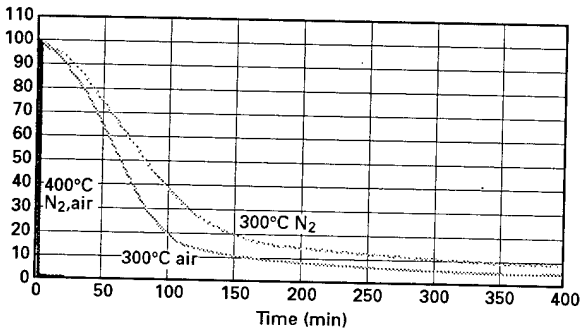

Figure 13. Isothermal TGA studies of pure silicon elastomer at 300 and 400°C in air and nitrogen.

The silicone elastomer degrades somewhat faster than the copolymer itself, compare with 02-Co in Figure 11 and 12.

The reduced weight losses observed by the combination of chalk and especially chalk and silicon elastomer will influence the rate at which volatile and combustible chain fragments reach a flame front. This may provide one explanation for the flame retardancy observed.

To make visual observations during thermal treatment the tubular oven was used for degrading larger (1 x 15 x 50 mm) samples. The samples (02-Casico, 02-Caco, 02-Sico and 02-Co) were treated in a nitrogen atmosphere at 300°C for 1 hour.

During treatment it was observed that that all samples effervesce, generating a cellular structure characterised by large bubbles. After a time the effect subsides and the bubbles stabilise. Only the formulation containing all the components, 02-Casico, kept some of its original shape.

After treatment the samples, together with the glass slides, were cooled in liquid nitrogen and divided in two. In this way excellent cross section surfaces were obtained. Stereo microscopic investigation showed that only the formulation with all the components contained a cellular structure with large bubbles, while the other materials contained only a few, very small bubbles, Figure 14

Figure 14a. 02-Casico

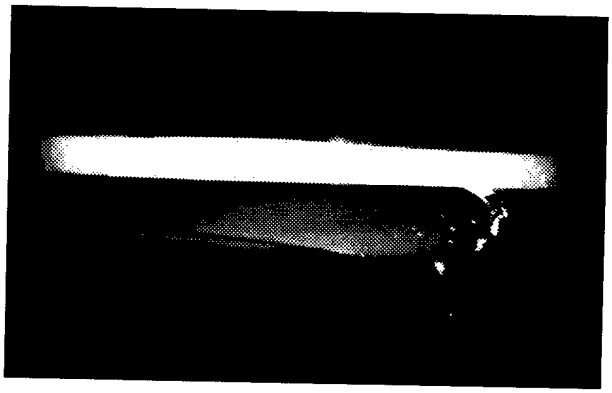

Figure 14b. 02-Sico

Figure 14. Microscopic (optical) pictures of samples treated in nitrogen at 300°C for 1 hour.

Cross sections of 02-Co, 02-Caco and 02-Sico all show similar surfaces with no cellular structure.

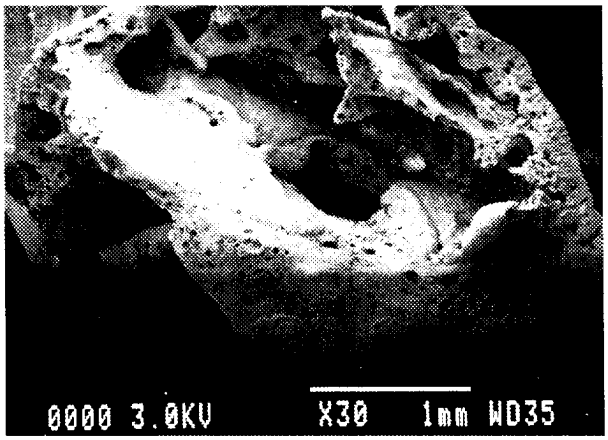

Figure 15a. Cross section (SEM)

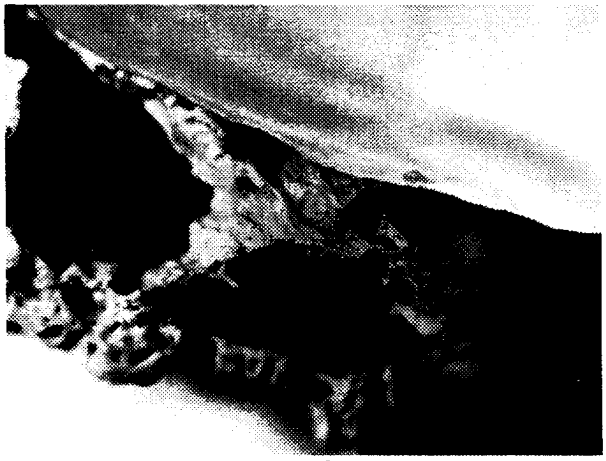

Figure 15b. Skin layer (optical microscope 30 x magnification)

Figure 15 Microscopic pictures of ash from 04-Casico after complete burning in cone calorimeter

As can be seen from Figure 15 the voids remain in the ash after burning. A skin layer containing far fewer and smaller voids is also observed, Figure 15b. The sample containing no copolymer LD-casi had a thicker and more dense skin layer than the copolymer containing samples. The higher the acrylate content the more voids were observed in the skin layer.

Infra Red (IR) Studies of Ash and Samples Thermally Treated in Tubular Oven

A comparison between the two tubular oven treated materials containing silicone, 02-Casico and 02-Sico show that the silicon vanishes completely from the chalk free sample, while it is mainly retained in 02-Casico, see figure 16.

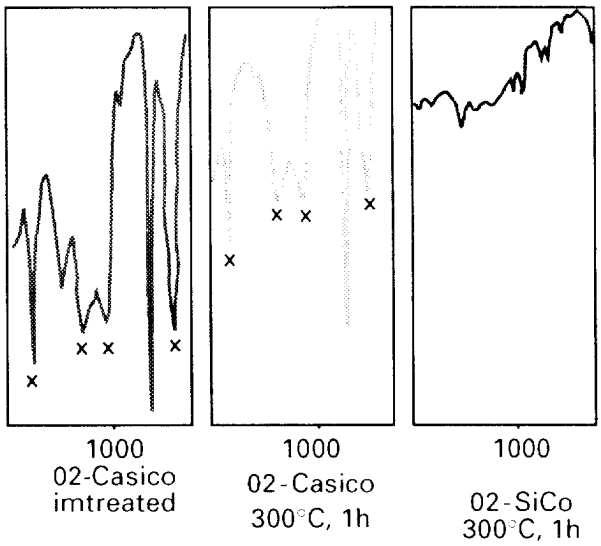

Figure 16. IR studies of 02-Casico and 02-Sico treated for one hour at 300°C in nitrogen in the tubular oven compared with an untreated sample. Marked peaks are typical silicone absorption bands.

The presence of chalk appears to stabilise or bind the silicone elastomer.

It is well known that acrylate containing ethylene copolymers, excluding ethylene (methyl acrylate) copolymers, undergo ester pyrolysis during thermal treatment.[2] For EBA, ester pyrolysis results in the formation of butene with a carboxylic residue remaining in the polymer chain, see Figure 17.

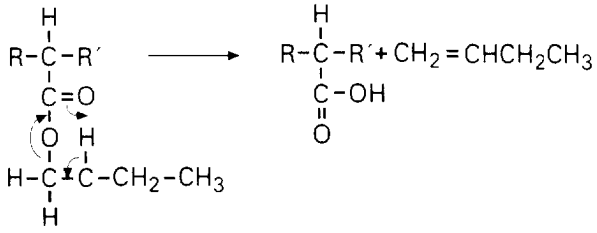

Figure 17. Ester pyrolysis of EBA.[2]

IR studies of the carbonyl region confirms this for 02-Co, The ester peak at 1735 has diminished and a new peak typical for a carboxylic acid unit absorbing at 1705 cm^{-1} is formed, see Figure 18.

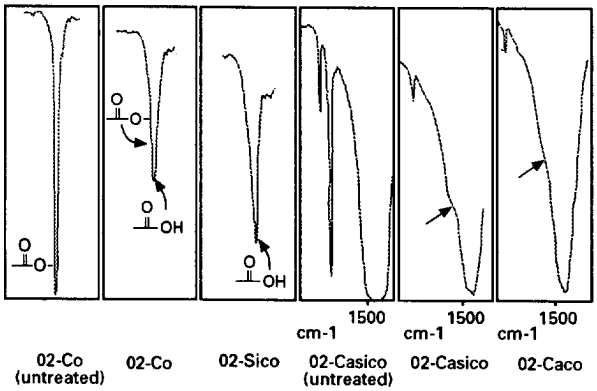

Figure 18. IR studies of thermally treated (300°C, 1h) 02-Co, 02-Casico, 02-Sico and 02-Caco in comparison with untreated samples.

The expected carboxylic acid formation is also observed for the silicon containing sample, 02-Sico.

With the chalk containing samples however, neither the carboxylic acid nor the ester peak is visible. Instead a broadening of the CaCO3 peak at 1560 cm-1 is observed. An ionomer with calcium has probably been formed, according to the process suggested in Figure 19.

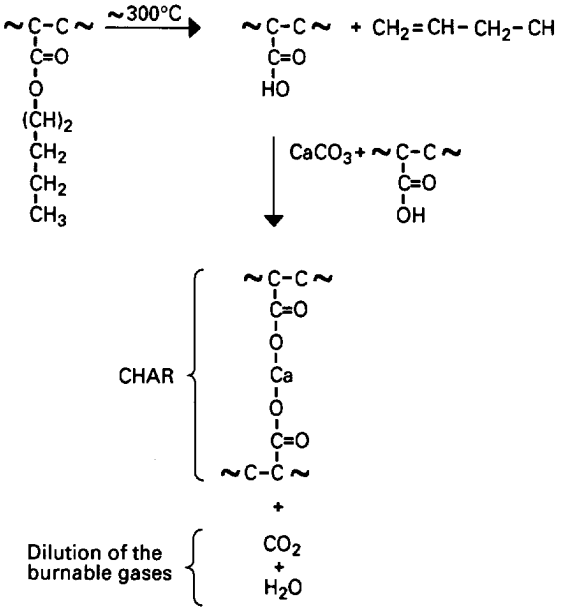

Figure 19. Ionomer formation during thermal treatment of EBA in the presence of $CaCO_3$.

The above findings might be the explanation for the significant reduction of weight loss observed by the TGA when the copolymer is degraded in the presence of chalk. Instead of leaving the sample as volatile and combustible chain fragments, the polymer fragments are bound to the chalk leaving non-combustible carbon dioxide and water which dilute the combustible gases.

Scanning Electron Microscope (SEM)/EDS Studies

The IR results imply that when thermally treated for one hour at 300°C, silicone leaves the sample completely when CaCO3 is not present. This finding is confirmed by SEM/EDS analysis. In the 02-Sico sample virtually no silicone is observed in the top coat. Conversely, large quantities remain in the top coat of the 02-Casico sample. It was further observed that the Si content varies in different parts of the surface.

Cross sections of ash formed in the cone calorimeter of 07-Casico were also studied by SEM/EDS. Calcium carbonate was the main component. Silicon could be identified in all samples and was present in the same amounts at both the top and bottom of the cross section. In the upper skin layer more silicon was identified in comparison with the majority of the samples.

Electron Spectroscopy for Chemical Analysis (ESCA)

ESCA is a very surface sensitive analytical technique with a penetration depth of 20-50 Å i.e. the chemical composition of the outermost 10-25 atomic layers.

Table 9. ESCA analysis of thermally treated (300°C, N2, 1 hour) samples and the skin layer formed when burned in a cone calorimeter at 35 KW/m².

Sample	Si, atomic-%	O, atomic-%	C, atomic-%	Si/C	O/Si
02-Casico 300°C, 1h	19.5	21.9	58.6	0.33	1.1
02-Sico 300°C, 1h	5.2	9.7	85.1	0.06	1.9
07-Casico - light ash	33.4	63.2	3.4	9.8	1.9
07-Casico - grey ash	33.6	62.2	4.2	8.0	1.9
07-Casico - dark ash	23.2	52.0	24.8	3.7	2.2
LD-Casi - light ash	33.1	60.6	6.3	5.3	1.8
LD-Casi - grey ash	32.1	61.0	6.9	4.7	1.9
LD-Casi - dark ash	32.6	60.2	7.3	4.5	1.8

When treated at 300°C for one hour, IR and SEM implies that silicone leaves the material completely when there is no calcium carbonate present. ESCA shows however that some silica remains in the uppermost atomic layers, Table 9. No $CaCO_3$ is observed in either of these samples. For 02-Casico, more Si is present, and the silica is apparently connected with three carbon atoms and one oxygen atom, indicating that a reaction between the silicon gum and the polymer has taken place. For the non-chalk containing sample much less silica is observed and it appears that the surface layer consists mainly of a hydrocarbon layer and some SiO_2.

ESCA analysis of ash remaining after cone calorimeter treatment at normal conditions (35kW/m²) for the skin layer of 07-Casico and LD-Casi is also presented in Table 9. The skin consists of areas with different colorations - the black areas seem to be thicker than the lighter areas but not as hardened. The darker the ash, the more carbon is present. As can be seen in Table 9 the uppermost skin layer of both the copolymer and LD based compounds have an even higher silicon content than the samples treated at 300°C - over 30% for all lighter areas. Calculating the O/Si ratio, it can be seen that SiO_2 seems to form the skin with some carbon.

CONCLUSIONS

Cone calorimeter tests on plaques show that Casico has similar burning characteristics as the more traditional LSZH material based on highly filled aluminium hydroxide polyolefins with respect to heat release rate, heat of combustion, smoke formation, corrosivity and carbon monoxide formation. Casico shows the longest ignition time of all the materials investigated, being nearly three times longer than PVC and about 60% longer than the hydrate based material.

PVC has a very short ignition time and generates very dense smoke already in the initial phase of the fire. The burning gases are corrosive and contain five times the amount of carbon monoxide compared with polyolefins. The advantage of PVC is its lower heat of combustion.

Recently performed full scale experiments comparing Casico and PVC based building wires have confirmed these results[6]. Due to the better electrical properties of the Casico cables the insulation thickness is reduced. As a result, the Casico cable shows a similar heat formation as the PVC cable.

Due to the low filler content and the non-polar character of the polymer used Casico shows outstanding physical, low temperature and electrical performance even after storage in water. The use of copolymers makes the flexibility similar to that of PVC. The low density of the compound results in lighter cables.

The studies performed in order to increase understanding of the flame retardant mechanism of Casico show that the optimal flame retardancy of Casico is achieved at an intermediate level of acrylate content in the copolymer in combination with a small amount of silicon elastomer and approximately 30% chalk. The combination of all three components is necessary to reach optimal flame retardancy.

Ester pyrolysis of the acrylate containing copolymer results in a reaction between the chalk and the polymer leading to ionomer formation and the formation of non-combustible carbon dioxide and water, which dilute and reduce the combustible gases. The formed gases effervesce and generate a heat insulating foamed structure.

When heated in presence of the filler, the silicon elastomer forms a hard skin layer holding the surface structure together and reducing the amount of combustible gases transported to the flame front. The skin layer consists mainly of non-combustible silicon oxide and a small amount of carbon.

REFERENCES

1. Robinson, J.E., "The Cost Effective Replacement of Halogenated Materials for the Wiring of Buildings", Eurocable 97, Manchester, UK, June 1997
2. Sultan, B-Å., Ph.D. Thesis, "Thermal Degradation and Adhesion studies of Ethylene Copolymers" , Department of Polymer Technology, Chalmers university of Technology, Gothenburg, Sweden, 1993
3. Borealis patent EP0393959B1
4. Ness, DEM., Scott G.J., "Living with Fire Smoke Toxicity Problems in a Critical Industry, In Fire Toxicity of Plastics, Rapra Technology Limited, UK, May 1989
5. Troitzsch, J., International Plastics Flammability Handbook, Carl Hanser Verlag, Munchen, Germany, 1983, p.500
6. Bottin, M-F., "Acidity and Corrosivity Measurements of Fire Effluent", International Wire & Cable Proceedings, 1990, p. 205-213
7. Grune, G.L., "Wire & Cable Material Selection Criteria for the 90's", International Wire & Cable Proceedings, 1990, p. 634-642
8. Fagrell, O., Robinson, J. E., Low Cost Building Wire in a Large Scale Fire, Plastics in Telecommunication VIII Proceedings, London, Sept 1998

BIOGRAPHIES

Bernt-Åke Sultan was born 1957. He has a M.Sc. degree in Chemical Engineering from Chalmers University of Technology, Gothenburg, Sweden. He took his Ph.D. at the same university in the Department of Polymer Technology and worked on the thermal stability and adhesion properties of ethylene copolymers. Since 1984 he has worked at Borealis (former Unifos and Neste Chemicals) on the development of polymers and compounds for cable applications. Today he manages the group responsible for the development and technical service of Borealis low voltage, telecommunication and jacketing materials.

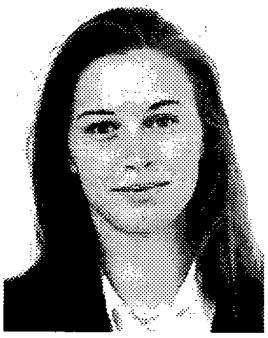

Karin Ericsson has recently graduated from Chalmers University of Technology with a M.Sc. degree in Chemical Engineering. Part of her diploma work on the flame retardant mechanism of Casico is included in this paper. Karin now works at SAAB Automobile, Trollhättan, Sweden.

Matti Hirensalo was born 1944. He graduated with a M. Sc. degree in polymer chemistry from the University of Helsinki in 1973. From 1973 to 1991 he worked at Nokia cables as a researcher, laboratory manager and research manager. Since 1991 Matti has worked at Borealis (former Neste Chemicals) research center in Porvoo Finland, primarily on the development of materials for cable applications. Today he manages Borealis' general flame retardant laboratory.

Marjo Hänninen graduated in 1995 from the University of Tampere with a M.Sc. degree in material engineering. Part of her diploma work on the flame retardant mechanism of Casico is included in this paper. Today Marjo is employed by Enso Laminating Papers, Kotka, Finland.

Thomas Hjertberg is a professor at the Department of Polymer Technology, Chalmers University of Technology. He graduated with a M.Sc. degree in Chemical engineering in 1974 and obtained a Ph.D. degree in 1982 for his studies on the thermal stability of PVC. Since then he has mainly been focusing his work on conductive polymers, surface modifications, degradation, stabilisation, and crosslinking of polymers.

RHEOLOGY OF SEMICONDUCTIVE BLACK COMPOUNDS WITH LOW CARBON BLACK CONTENT

Chun D. Lee

Equistar Chemicals, LP. Cincinnati, Ohio

ABSTRACT

In certain wire and cable applications, semiconductivity or low surface/volume resistivity is required. This is accomplished primarily through the addition of high structural carbon black to a natural resin. Typically, to produce a compound with acceptable resistivity, the carbon black (CB) content will range from 20 to 40 wt%. This amount of CB loading can result in two difficulties: 1) high melt viscosity; and 2) poor CB dispersion.

This paper describes rheological methods which can be used to characterize and to design semiconductive compounds with reduced CB loading (<15%) while retaining good resistivity, viscosity and CB dispersion.

It was found from dynamic rheology that semiconductive compounds show viscosity up-turns at low frequencies (< 0.5 rad/sec). This "up-turn" is believed to be a CB particle-particle network structure, which is critical to CB dispersion as well as conductivity. Rheological methods are presented to characterize the up-turn and a model is proposed supporting the correlation between "up-turn", dispersion, and conductivity.

INTRODUCTION

In certain wire and cable applications, semi-conductivity or low surface/volume resistivity is required. This is accomplished primarily through the addition of high structural carbon black to a natural resin. Typically, to produce a compound with acceptable resistivity, the carbon black (CB) content will range from 20 to 40 wt% [1-4]. This high amount of CB loading can result in two difficulties: 1) high melt viscosity and 2) poor CB dispersion.

Since rheology can be used to help understand polymeric structures and flow properties [5-9], it can also be a useful tool to investigate carbon black filled compounds. For example, it has been noted in the literature [10] that the addition of carbon black into polymer matrix results in unusual rheological behavior, i.e.. viscosity up-turn at low frequencies. However, little information has been published on the correlation between the noted "up-turn" and the issues faced in designing semi-conductive compounds.

This paper describes the rheological characterizations of semi-conductive compounds and supports the correlations between low and high frequency viscosity to dispersion, conductivity and processability. In addition, a morphological model of semi-conductive compounds is proposed.

EXPERIMENTAL

1. Materials

Table 1 describes the types of carbon black (CB) fillers (**A** through **D**), with their particle sizes, and filler loading. Small amounts of additive (0.5 wt% calcium stearate) and antioxidant (500 PPM of Irganox 1010) were added to the compounds. The carrier resins used were conventional 6 MI, Low Density PE (LDPE I through III) resins produced by different polymerization processes.

2. Compound preparation

A Farrel OOC Banbury mixer (2400 CC) was used to produce the semiconductive compounds for this investigation. At the initial mixing stage, the mixture of carbon black, resin, antioxidant, and calcium stearate was loaded into the mixing

chamber maintained at 95 ^{o} F. Ram pressure was applied to the chamber at 40 psi. Flux was achieved after approximately 40 seconds, the ram raised and the throat was cleaned for 15 seconds. The pressure was reapplied to the chamber and mixing was continued for at least 3 minutes to reach 340 ^{o}F. The Banbury drop was pelletized through a 25-mm single screw extruder to produce the final compound.

3. Compound characterization

a) Rheological measurements

Steady state shear viscosity measurements were carried out on an Instron Capillary Rheometer equipped with an 8-mm die and a L/D of 20 at 210 ^{o}C. Bagley and Rabinowitsh corrections [11,12] were not made.

The dynamic rheological measurements were conducted on a Rheometrics RDA-II equipped with parallel plates. The measurements were conducted at 190, 210, and 240 ^{o}C using a frequency sweep from 100 to 0.0398 rad/sec with a strain of 5%. All compounds reported in this paper had unusual rheological behavior with viscosity up-turn at low frequencies. The up-turns were quantified by a G^*_o parameter (zero frequency dynamic modules) which can be derived from G' and G" values. The parameter G^*_o was obtained by plotting $(\omega)^{0.5}$ versus $(G^*)^{0.5}$ data, where G^* is defined as $((G')^2 + (G")^2)^{0.5}$. The extrapolation of this to $\omega = 0$ yields $(G^*_o)^{0.5}$. As an example, Figure 1 shows the dynamic data of polypropylene impact copolymers with different degrees of viscosity up-turns at low frequencies [13]. Copolymer **A** shows a normal rheological behavior: with gradual viscosity increases with decreased frequencies, whereas copolymers **B, C, & D** show the usual viscosity up-turns at low frequencies. Plots for an intercept values of $(G^*)^{0.5}$ vs. $(\omega)^{0.5}$ from dynamic data (figure 2) indicate that the higher up-turn leads to higher G^*_o. This method is analogous to the Casson [14] plot, which is used to determine the yield stress from steady state data.

b) Dispersion quality measurement

The pressure rise test (PRT), which is analogous to the screen pack plugging method, was used to evaluate the dispersion quality of the compounds. A Haake Rheomix 90 single screw extruder (25 -mm diameter) was used. The heated die had a breaker plate containing a 60-60-325-60-mesh screen pack arrangement. Zones 1 through 3 were heated to 235 ^{o}C and the die was heated to 305 ^{o}C. The extruder screw was run at 150 RPM. The pressure rise (PR) in psi was determined by subtracting the first 5 minutes reading from the final 20 minutes reading.

c) Surface/volume resistivity measurements

Surface resistivity (inverse relation to surface conductivity) was determined following ASTM D991. Film samples were produced by a 120-mm slot die under the same conditions using a Haake single screw extruder. The die gap was set at 0.76 mm at 485 ^{o}F, and a molten web was stretched to approximately 0.025-mm thickness using Haake film take-up equipment. Also, compression molded plaques were prepared following ASTM D991 using slow and rapid cooling processes for volume resistivity measurements.

RESULTS AND DISCUSSION

Figure 3 shows the steady-state shear viscosity for compounds **A-10-I** and **C-10-I.** Each were made from the same carrier resin and loaded with 10 % CB, but with different CB types. The observed viscosity difference between these two compounds results from the different CB types used. Also note that each compound shows similar shear thinning behavior (decreased shear viscosity with increased shear rates).

Figure 4 shows the dynamic data for the carrier LDPE and its corresponding CB compound, **A-14-I**. As expected, the addition of CB results in two observations: a) increased viscosity with similar shear thinning behavior at high frequencies (> 10 rad/sec); and b) low frequency (< 0.1 rad/sec) viscosity up-turn. This viscosity up-turn is a result of the formation of a network structure due to filler/filler interaction within PE matrix [15,16,17].

Figure 5 shows the dynamic data of the

compounds, **A-10-I, B-10-I, C-10-I,** and **D-10-I.** Each was made from the same carrier resin, LDPE-1 and 10% CB loading, but with different types of CB. The viscosity at high frequencies and the degree of viscosity up-turn at low frequencies varies depending on the type of CB. For an example, type **D** carbon black in compound **D-10-I** shows the highest viscosity and up-turn. **D-10-I** also has the best dispersion and conductivity, as indicated in Table 2, G^*_o. This data supports that the higher the relative "up-turn", the better the dispersion and conductivity. It should also be noted that due to the high viscosity of compound **D-10-I,** it could not be drawdown into a thin (0.025-mm) film and consequently, was not further evaluated. These observations indicate that the type of CB, at similar loading, has a significant impact on dynamic viscosity.

Figure 6 shows the dynamic data of compounds **A-10-I** and **A-10-III**. Both compounds were produced with type **A** carbon black, but with different carrier resins: LDPE-I for **A-10-I** and LDPE-III for **A-10-III**. Both compounds have identical complex viscosity at high frequencies above 50 rad/sec. However, at low frequencies, below 0.1 rad/sec, compound **A-10-III** shows the higher up-turn (G^*_o= 560) than **A-10-I** (G^*_o= 510). It is believed that this higher up-turn results from the increased degree of network structure associated with this particular LDPE type. It is also believed that the increased degree of network structure in **A-10-III,** resulted in higher surface conductivity (9 logohm for **A-10-III** compared to 12 logohm for **A-10-I**).

As noted in the literature [16], the conductivity of CB filled materials results from the presence of CB network structure. Interestingly, rapid cooled (with a cooling rate of approximately 200 ^{o} C/minute) compression molded specimens showed almost no conductivity (> 15 logohm) on both compounds **A-10-I** and **A-10-III** (Table 2). Literature states [18] that the difference in conductivity between slowly and rapid cooled specimens is the result of different crystalline morphologies produced in the carrier resin.

A-10-I also had higher PRT (610 psi) than compound **A-10-III** (490 psi) indicating poor filler dispersion (Table 2). The poor dispersion of CB in compound **A-10-I** (compared to **A-10-III**) appears to correlate with the lower degree of CB network structure present (as indicated by lower up-turn). Also, as expected, increasing the CB loading to 14% (**A-14-I**) resulted in even poor dispersion as indicated by PRT. In summary, Table 2 supports the correlation between higher "up-turn" (as indicated by G^*_o) and improved dispersion of CB filled materials.

A model morphology is presented in Figure 7 to help understand the correlation between rheological parameters (mainly up-turn) to dispersion and conductivity. In this model, **(A)** depicts poor conductivity (less network structure) and poor CB filler dispersion (more agglomerates). **(B)** depicts improved conductivity (more network structure) with good dispersion (fewer agglomerates). It is proposed that these model structures can be detected by the rheological methods discussed.

It is also interesting to note that these network structures appear to be predominately a physical phenomenon. What is meant by this statement is that the degree of up-turn is reduced in samples that have been re-extruded **C-10-I** (figure 8), indicating the network structure is fragile but reversible in nature [19].

Last, the network structure formed in these semi-conductive compounds was effected by temperature (Figure 9 for compound **B-10-I).** As expected, viscosity at high frequencies decreased with increased temperature. However, unexpectedly, viscosity up-turn increased with increased temperature. This unusual behavior observation may be a result of increased mobility of the CB particles at higher temperature leading to increased network structure.

CONCLUSIONS

Dynamic rheological measurement can be used to observe low frequency viscosity up-turns of semi-conductive compounds at low levels (~10%) of carbon black loading, whereas no unusual behavior was observed in steady-state capillary shear viscosity. There was observed a direct correlation between the degree of low frequency viscosity up-turn to conductivity and dispersion. This low frequency up-turn is a result of a CB network structure and appears to be a useful tool to predict compound conductivity as well dispersion quality.

REFERENCES

1. J. Accorsi and E. Romero, *Plastics Engineering*, April, 29 (1995).
2. D.R. Parris, L.C. Burton, and M.G. Siswanto, *Rubber Chem. Technol.*, **60**, 705(1987).
3. L.C. Burton, K. Hwang, and T. Zhang, *Rubber Chem. Technol.*, **62**, 838(1989).
4. A. Medalia, *Rubber Chem. Technol.*, **59**, 432(1986).
5. J.M. Dealy, K.F. Wissbrun, Melt Rheology and Its Role in Plastics Processing: Theory and Applications, Van Nostrand Reinhold, New York (1997).
6. P.J. Carreau, D. DeKee, R.P. Chhabra, Rheology of Polymeric Systems: Principles And Applications, Hanser, New York (1997).
7. C.D. Han, "Rheology in Polymer Processing", Acedemic Press, New York (1976).
8. C.D. Han, "Multiphase Flow in Polymer Processing", Acedemin Press (1981).
9. R.J. Cembrola, *Polymer Eng. Sci*, **22**, 601(1982).
10. M. Gerspacher, C.P. O"Farrell, and H.H. Yang, *Elastomers*, November, 23 (1990).
11. E.B. Bagley, *J. Appl. Phys*, **28**, 624 (1957).
12. B. Rabinowitsh, *Z. Phys. Chem.*, A**145**, 1 (1929).
13. C. Lee, R. Shroff, & M. Shanker, presented in 69th Annual Conference of Society of Rheology, Columbus, Ohio(1997).
14. N. Casson," in "Rheology of Dispersion Systems", Pergamon Press, New York (1959).
15. N. Minagawa and J.L. White, *J.Appl. Polym. Sci.*, **20,** 501(1976).
16. Y. Chan and J.L. White., *Polym. Eng. Sci.*, **19,** 617 (1979).
17. R.D. Sherman, L.M. Middlemen, and S.M. Jacobs, *Polymer, Eng. Sci*, **23,** 36 (1983).
18. H. Kawamoto et al., Carbon Black Composites, E. K. Sichel. Ed., Marcel Dekker, New York (1982).
19. C.D. Lee, unpublished data (1998).

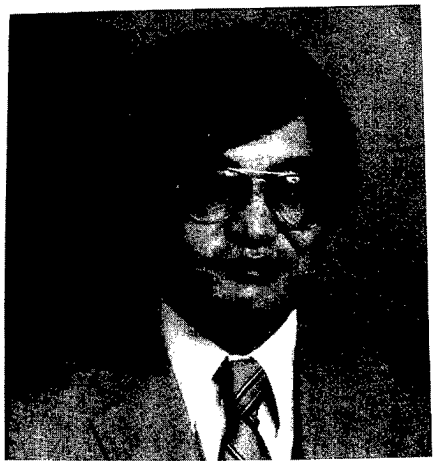

Chun D. Lee is responsible for w/c product development in w/c group at Equistar Technology Center, Cincinnati, Ohio. He joined Equistar Chemicals, LP in 1984. He has a M. S. degree in Chemical Engineering from Ohio University and a Ph.D. degree in Polymer Engineering and Science from Case Western Reserve University, Cleveland, Ohio.

Chun D. Lee
Equistar Chemicals, LP
11530 Northlake Dr.
Cincinnati, OH 45249

Table 1. Composition for the compounds investigated for this paper.

compound	CB type	particle size [nm]	CB content [wt%]	carrier resin
A-10-I	A	18	10	LDPE-I
A-10-II	A	18	10	LDPE-II
A-10-III	A	18	10	LDPE-III
A-14-I	A	18	14	LDPE-I
B-10-I	B	20	10	LDPE-I
C-10-I	C	23	10	LDPE-I
D-10-I	D	35	10	LDPE-I

Table 2. Rheological, dispersion, and resisitivity data for the compounds.

compound	G^* [dyne/cm^2]	η^* 100X10^{-3} [poise]	dispersion [psi]	surface resistivity [log-ohm]	volume resistivity [log-ohm]
A-10-I	510	4.05	610	>15	-
A-10-II	400	4.10	940	>15	-
A-10-III	560	4.00	490	>15	-
A-14-I	9400	5.51	880	>15	>15
B-10-I	13400	5.72	360	9.5	>15
C-10-I	22800	6.60	160	6.1	-1.24
D-10-I	38000	9.51	120	-*)	0.92

*) Could not produce 1 mil film for surface resistivity measurement due to poor processability.

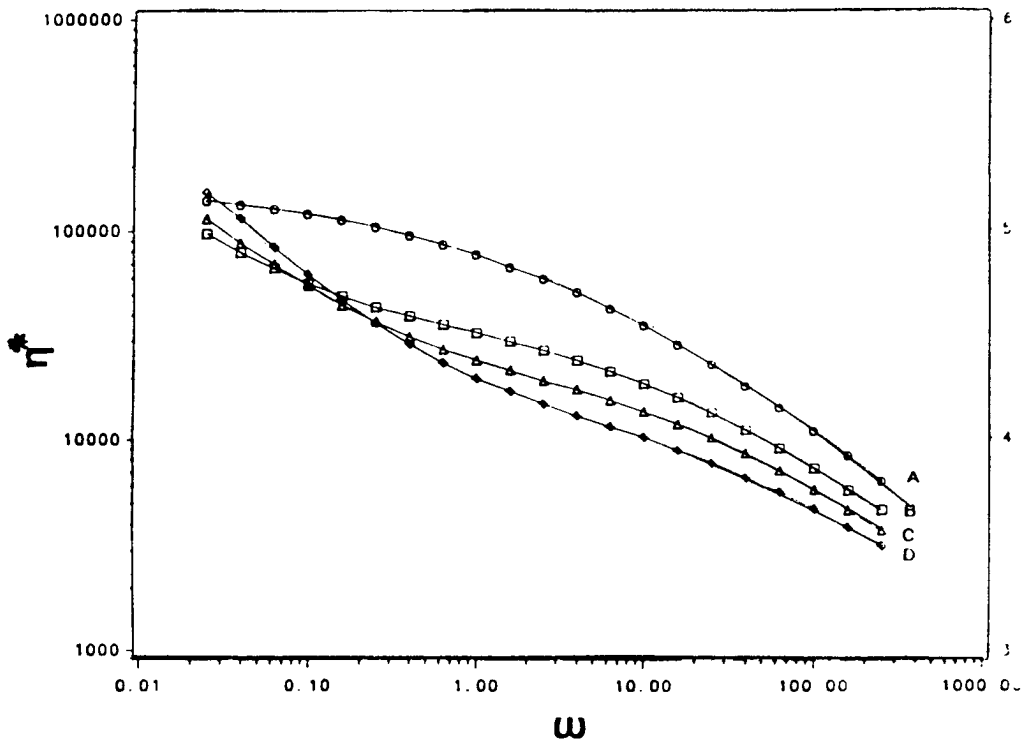

FIG.1. DYNAMIC RHEOLOGICAL DATA OF PP COPOLYMERS A,B,C,& D WITH DIFFERENT MFR.

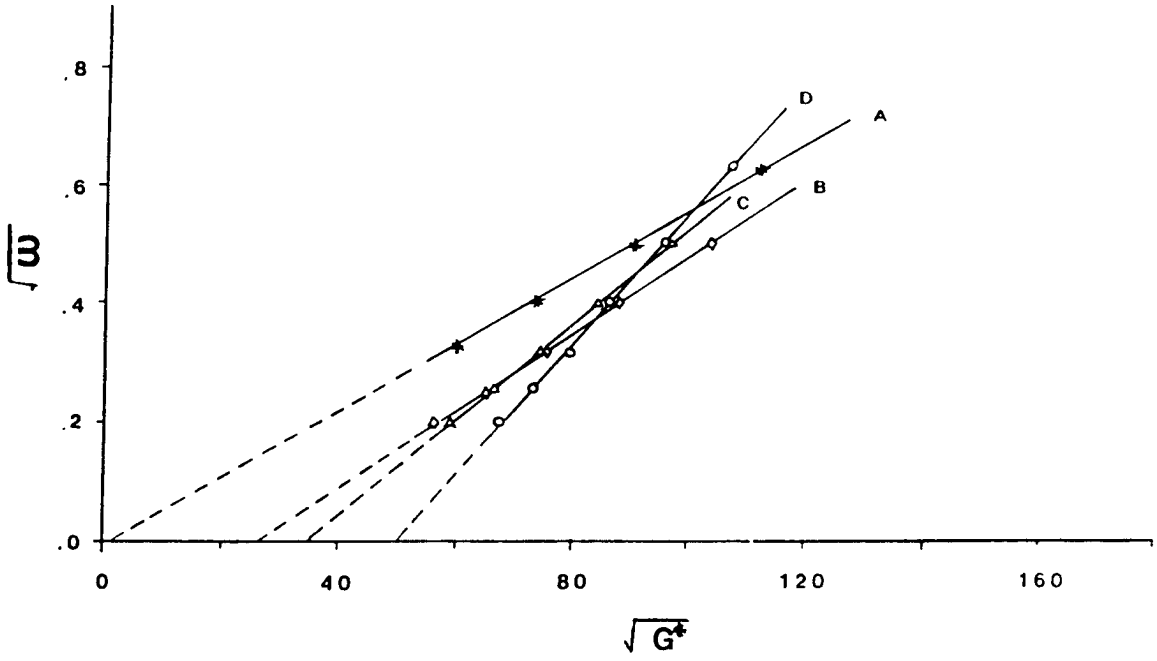

FIG.2. MODIFIED CASSON PLOT OF THE COPOLYMERS A,B, C, & D OF FIG.1.

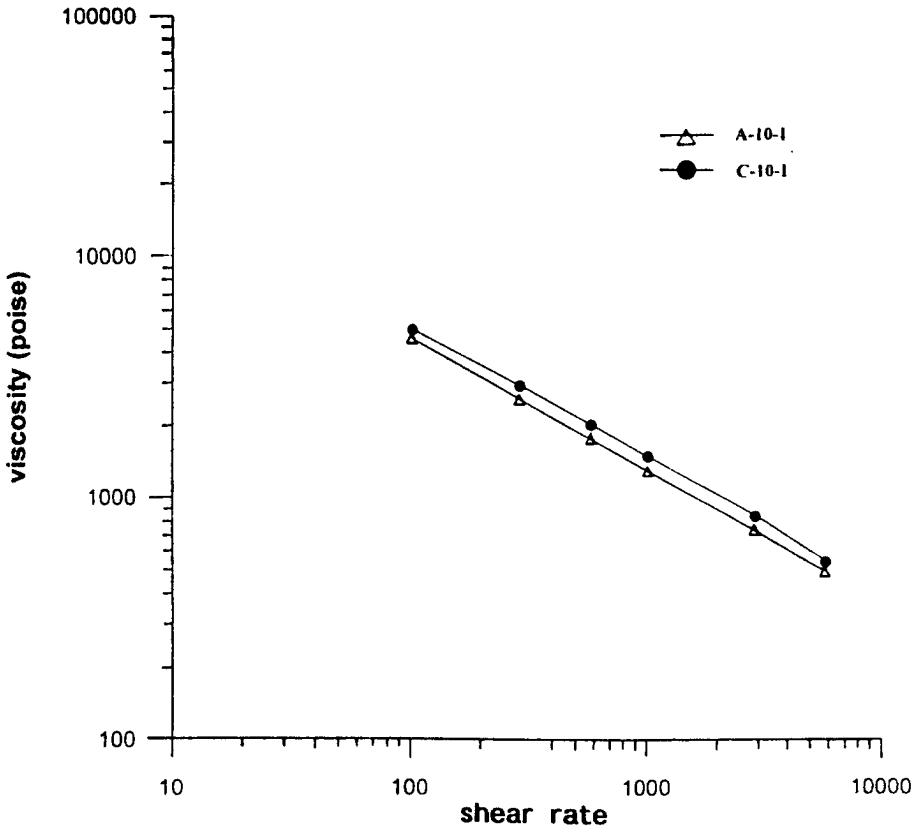

FIG.3. SHEAR VISCOSITY DATA FOR COMPOUNDS.

FIG.4. Rheology for the carrier PE & its compound

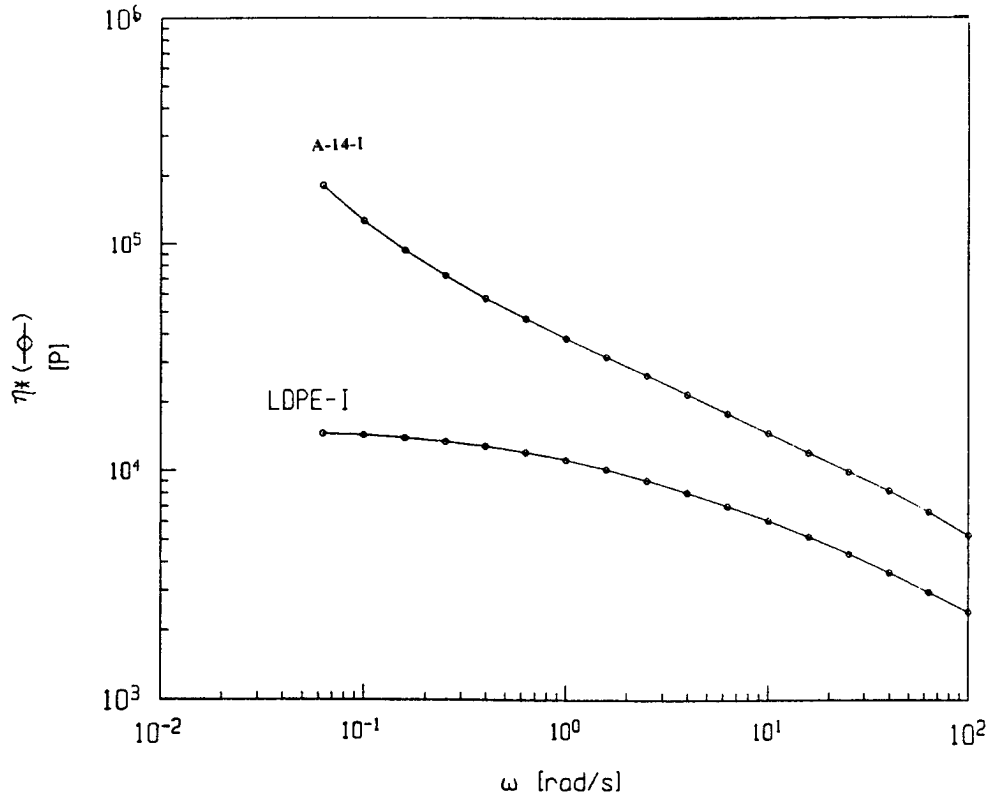

FIG.5. Rheology for the compounds with different CBs

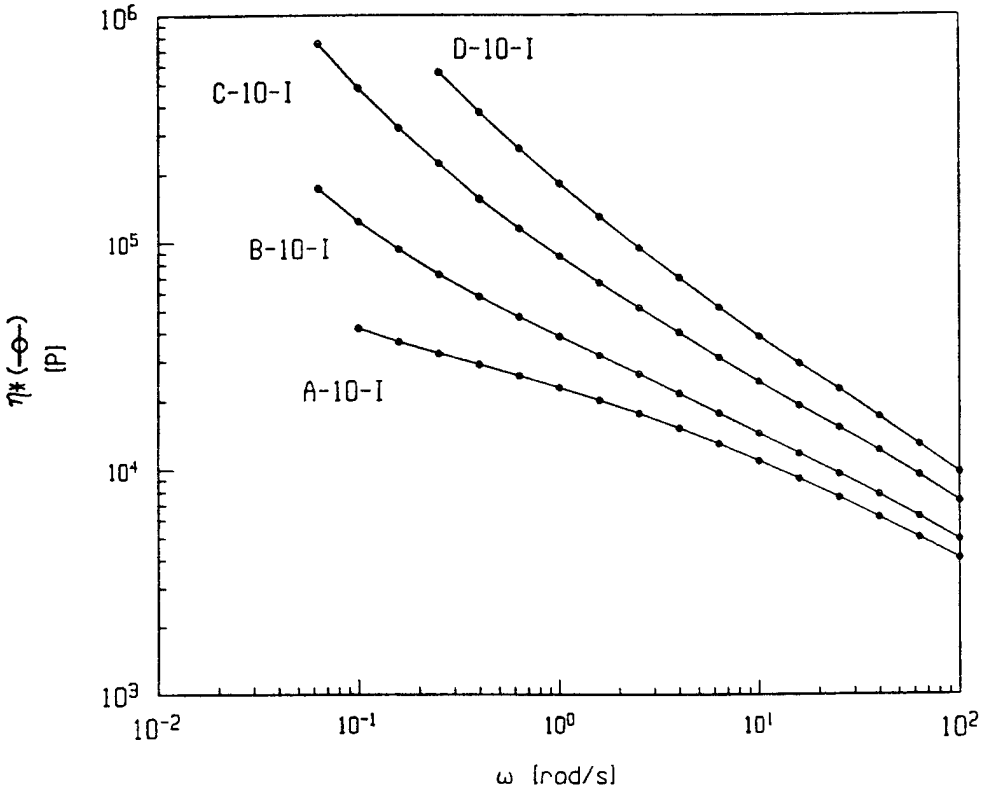

FIG.6. Effect of resins on upturn with 10% loading

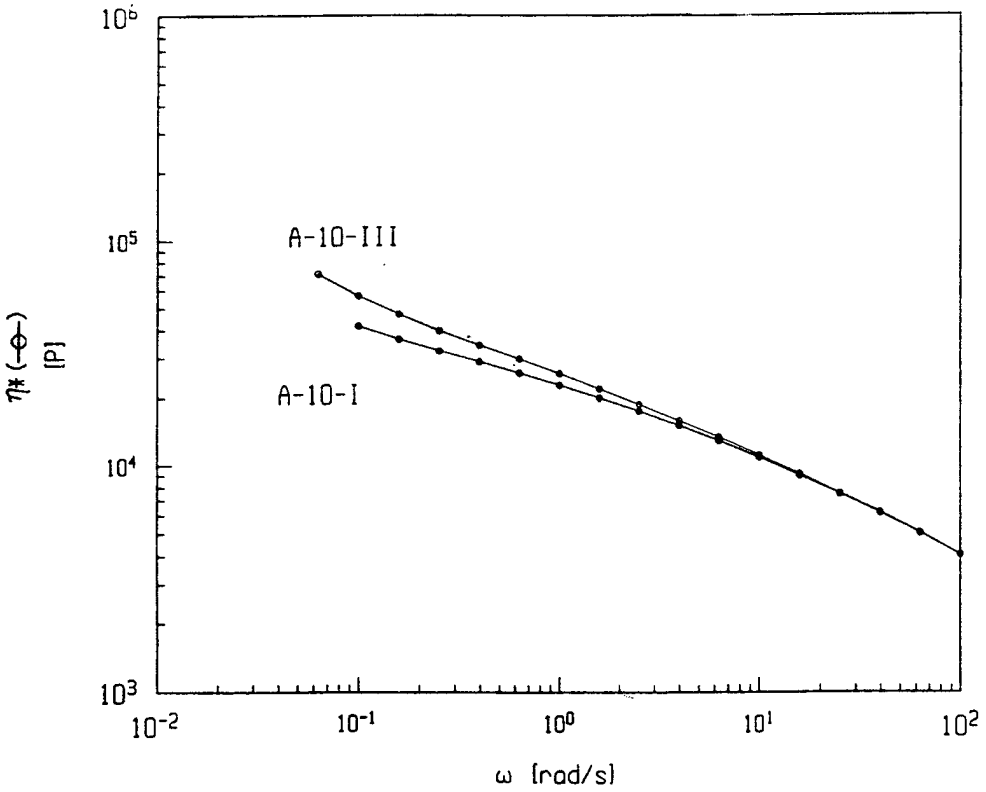

FIG.7. Proposed morphology of particle/particle(polymer) interaction for poor filler dispersion (A) with no conductivity & good dispersion (B) with conductivity

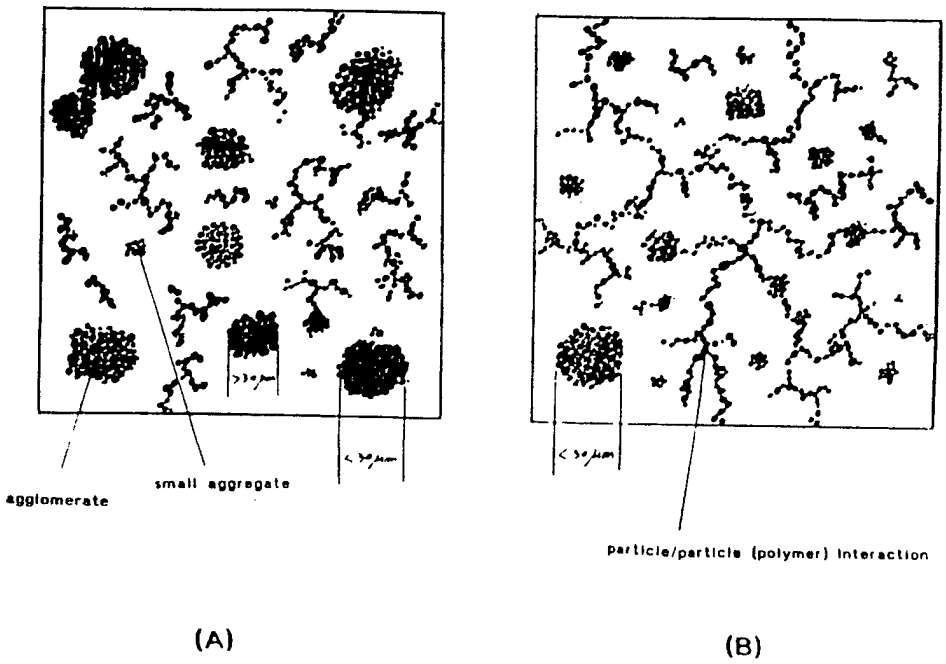

FIG.8. Effect of processing on upturn for the compound

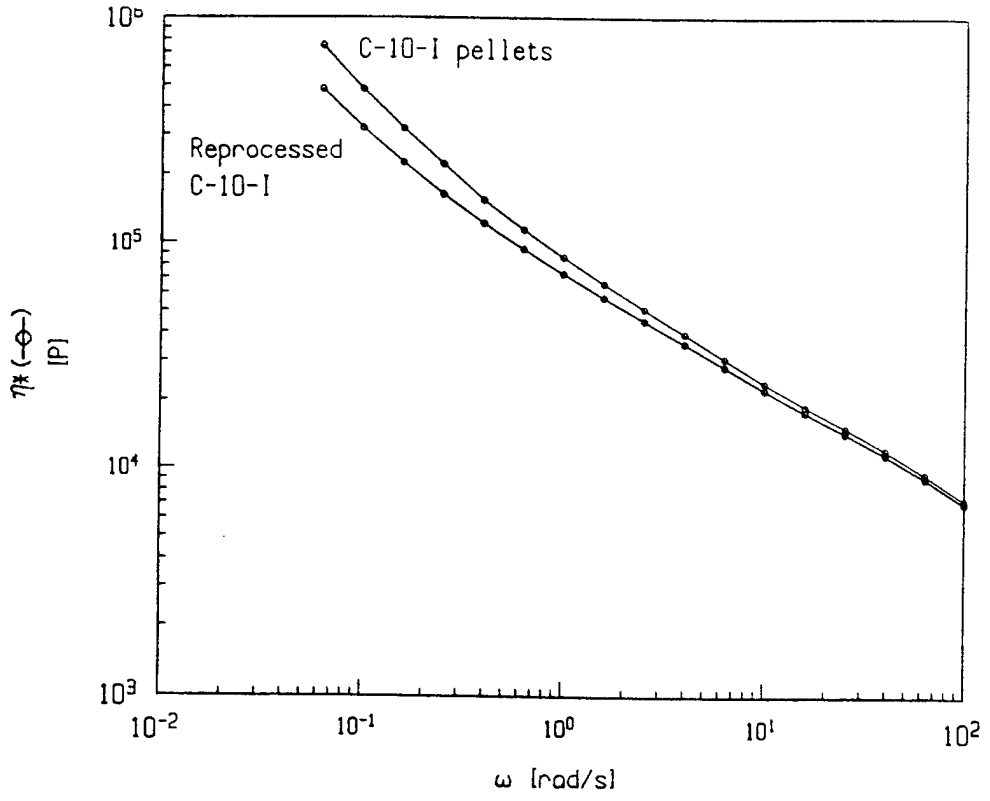

FIG.9. Effect of temperature on upturn for the B-10-1 compound

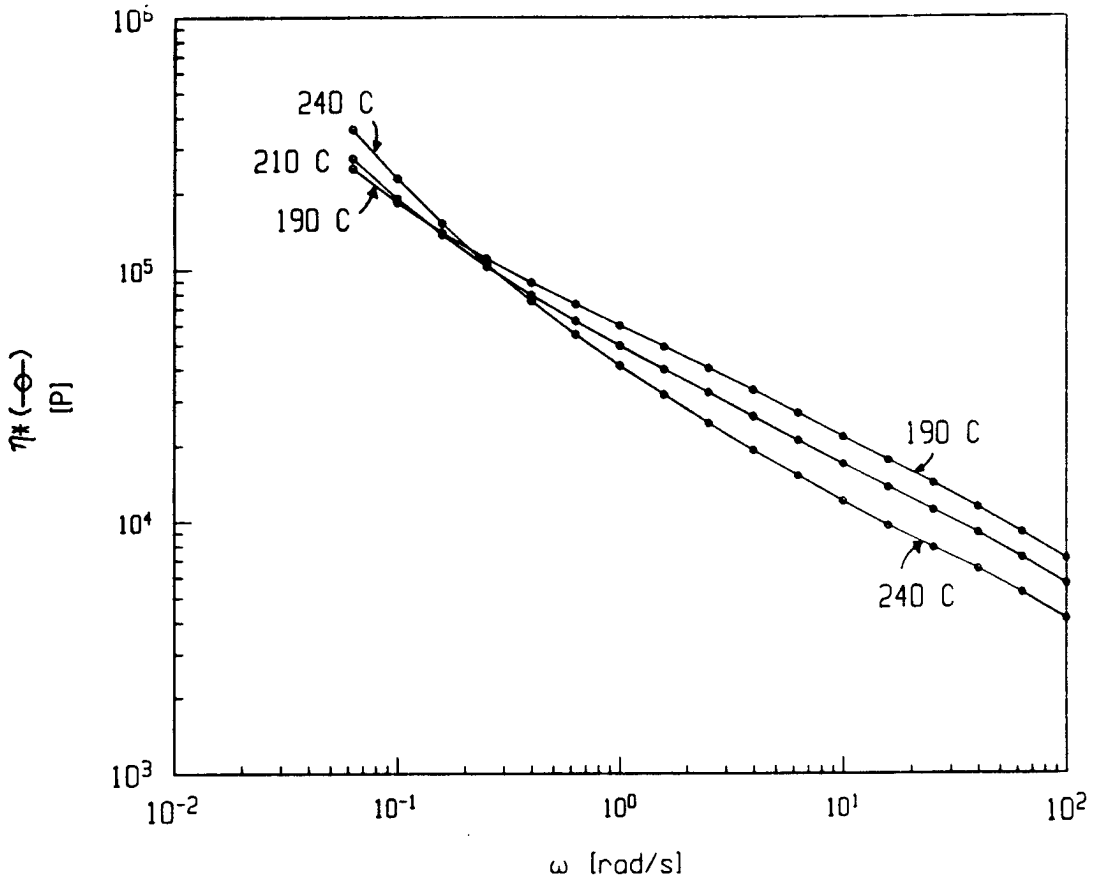

COST DRIVEN INNOVATIVE SOLUTIONS FOR THE LOCAL LOOP

Pieter Matthijsse

KPN Telecom - Network Services, The Netherlands

ABSTRACT

Cost-reduction being the main driver, KPN Telecom started a major innovation project in the local loop area. Chosen architecture was copper with an option for future migration to fibre. The project is based on specifying the network in terms of cost per line and general functionalities, exploiting the competitive forces and applying total network concepts and turn-key deliveries.
The industrial partners, which have a dominant influence in the project, have been selected on their preparedness to go into a "development race" with one winner only who gets the contract for the delivery of access networks. Current offers reasonably fulfill the cost and futureproofness requirements which shows that cost-efficient "no-dig" solutions for later introduction of fibre networks seem realistic. Turn-key aspects require firm attention however. The ultimate technology and the development of new organizational and logistic processes will be ready next year.

INTRODUCTION

In the new competative telecommunication environment KPN Telecom, the main telecom operator in the Netherlands, is faced with the urgent need for cost reduction in the local loop. Apart from an overall target on cost reduction as required by our shareholders, an additional effort is required here to compensate for

- the decrease in occupation efficiency of the access network due to the emerging loss of market share to the new competitors and
- the regulator impressed change in cost assignment in which the cost of the local line has to be paid for directly by the customers, without cross subsidy from the traffic related income.

In strong contrast to this dynamic scenario, primarily driven by political regulation [1], there is the solid and massive cost structure of the current copper local loop, built in several decades with a technical life time of sometimes over 50 years and a cost flexibility like an old elephant. Although there are plenty of new competing technologies these are applicable only for the 1 to 2 % yearly reconstructions or new lines in our network and not for the "sunk lines" in the installed base. So indeed, to divert this giant slowly from its current course into a new one will be a real challenge. In the meantime we have to serve our customers both with market oriented prices for the current services and with the new broadband services they require.
For the existing copper network enrichment with xDSL based technologies is the solution for the short and mid term period. Studies are going on whether or not for the longer term a thin optical overlay network can be afforded. Key factors are the cost of last fibre drop and the possible synergy with the overlay access networks (CityRings) for business customers.
In this paper the focus will be on the passive local loop extension in existing and new areas. Although this represents 1 to 2 % of our network only, it represents a major part of our yearly investment in infrastructure and it also is an investment into the future. As for the customer, the focus will be on the residentials. No underlying system technology will be treated.

COST INDICATORS FOR THE CURRENT LOCAL LOOP

The technical architecture of the local loop in the current KPN Telecom network is depicted in fig. 1, together with some key figures. The great majority of the customer premises is connected with

one single pair of copper with the MDF. To enable additional lines, the copper capacity at the customer side is 200 %, i.e. one quad enters the house, in the primary cable the capacity is reduced to 110 to 140 %, dependent upon growth rates and age of the specific area. The network is, up to now, completely passive and underground (apart from the current cable distribution cabinets (CDC)). Cables are steel armoured and burried directly in the ground. More than 70 % of the new cable installations still consist of paper insulated and lead shielded cable. The rest is PE insulated and Alu-shielded cable.

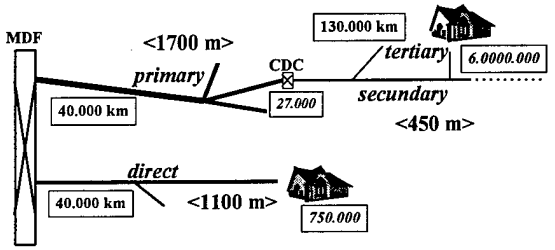

Fig 1: Network architecture and some key figures for the current KPN Telecom local loop

Although a first start with optical feeder networks and Digital Loop Carrier systems has been made some years ago, this has been stopped due to financial and technical reasons. The number of customers connected is negligible.

Investment cost

Distincting between green field areas and extentions or reconstructions in already built areas, table I gives an indication of the relative investment costs in the copper outside plant. Further cost distinction has been made for cable, splicing materials, digging and splicing labour and directly related own personnel overhead (planning, engineering and construction management).

From Table I it can be concluded that:

1. more money, in absolute value, is involved in network extentions or reconstructions than in greenfield area investments.
2. for green field areas the costs for cable and digging are dominant.
3. for extensions/reconstructions costs for digging, splicing and personnel overhead are more significant. This is caused by both small-scale effects and the embedding in already existing areas
4. cost per line in new areas is significantly lower than for new lines in already built areas.

Table I Breakdown of yearly investment cost (%) for new areas (**new**) and extensions/reconstructions (**old**). Rough number of new lines are 120.000 and 80.000 per year respectively

	new	***old***
cable	15	10
splicing material	2	3
digging	15	17
splicing	5	14
personnel overhead	7	13
TOTAL	43	57

Irrespective of the threat of a reducing market share a 100% connection density at first installation is still applied, this being much cheaper then connecting KPN Telecom customers only. Calculated cross-over point is far below 50% market share.

Operational cost

As for operational cost, i.e. maintenance, connecting and moving lines, a rough cost breakdown is given in fig 2. Major cost factors are maintenance, IT and network mutations. The total expenses related to operational cost is about 2/3 of the total expenses related to investment in the current copper loop. From the financial point of view this clearly asks for strong emphasis on reduction of operational cost. This is not the subject of this paper however.

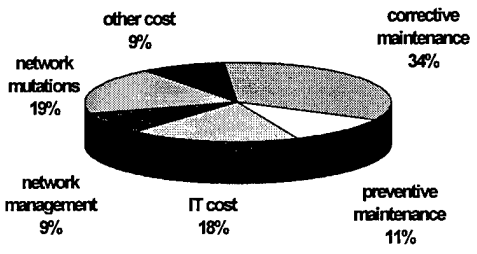

Fig 2: Cost breakdown of operational cost for KPN Telecom copper network (MDF manipulations not included)

Cost reducing measures

Measures taken in recent years to reduce both investment and operational cost and the positive experience of which will be applied also in the new network are:

- Reduce investment in extensions as much as possible by exploiting the installed base on copper lines. The rapid introduction of ISDN in our network certainly has a positive effect here. Use of pair gain is on a very restricted scale only due to the connected limitation in services and the non-allowance of combining customers on one single copper pair. Narrow band radio isn't used at all due to the rather high cost of first introduction, expected high operational cost per installed line and the restrictions for broadband.
- Since two years the application of cable distribution cabinets in new built areas is limited strongly. Only in areas where a highly dynamic growth pattern is expected they are used. Main effect is a strong reduction in operational cost related with these cabinets i.e rewiring and rework due to errors, security, vandalism etc...Of course, a rigid planning of spare capacity positions in the network has to be done on beforehand. In conjunction with this the capacity in the secondary strings has been reduced to a minimum value of 125 %.
- Strong emphasis on "cleaning" and quality assurance of the network and network administration to reduce cost of rework and increase speed of customer connection or change of service.

DRIVERS TO THE FUTURE: CHOICE FOR COPPER

From a cost perspective the drivers for a new local loop are rather simple

i) decrease investment cost per line,
ii) increase flexibility of cost structure and
iii) prevent desinvestment in a too early stage of the local loop life-cycle.

Together with the requirement that the operational cost may not exceed the current level and preferably get lower, this was the challenge to be met.

Comparing the variety of different available solutions ranging from conventional twisted pair, via coax, radio and FTTx to modern satellite based solutions, the conclusion was made that for the access network in our home market a mixture of

- copper twisted pair,
- installation in plastic ducts and
- upgradebility to fibre

is the ultimate solution. It is however beyond the purpose of this paper to elaborate further on all decisive considerations. Supporting building blocks in this decision making process, like the JetNet ® concept, have been presented already before at this conference [2].

The mentioned mixture of solutions is expected to allow us to reduce cost now and in the future and to upgrade the network to a high service potential (fibre) when and if services are required and payed for which are beyond the ADSL capability. Due to the splitting of cost in ducting and removable copper cable, flexibility in assets is obtained as the ducting is useable also for newly installed fibre cables. Also parallel operation of copper and fibre is possible in this way.

A point of special attention is the cost reduction obtained by cost sharing in digging obtained by cooperation with the many others digging in the Dutch soil. Transfer from the steel armoured copper cable to a more or less "standardized" PE duct tubing strongly facilitates these combi-installation.

FLASN PROJECT

To cope with the challenge mentioned in the former section, KPN Telecom started an innovation project called FLASN (**FL**exibel **A**cces**S** **N**etwork) in which a dominant role of the cable and installation industry is expected. The resulting network is called "FLASHNET". The principles underlying this project are:

i) specify the required network in terms of cost per line and general functionalities,
ii) exploit the competitive forces in the open market and
iii) go for total network concepts and turn-key deliveries instead of being the network integrator and installator yourself.

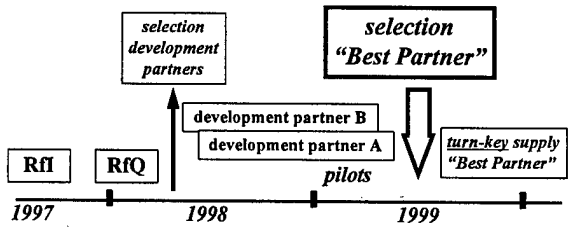

Fig.3 Time schedule for the FLASN project

Based on these principles a tender procedure has been initiated in the autumn of 1997 via the required EC rules. The result of the first phase, a request for information responded by 7 major industries, confirmed that the principle looks viable. In the second phase a request for quotation (RfQ) was issued specifying the network and the turn-key requirements in a rather general way. As much as possible "Dutch" specifications were avoided although interworking with the currently installed base, both in technical and in operational sense, sometimes puts some constraints on this. Strong requirements were set on the overall cost price per line. Some of the general requirements were:

- 20 % reduction of the investment cost per line for new areas without use of upperground cables or cabinets.
- broadband capabilities of the new copper lines at least as good as the currently installed lines.
- migration to fibre connection of the individual customer premises without need for digging trenches.
- definition of control items and accompanying fixed prices on a high abstraction level enabling regular installations of the majority (say > 85 %) of new lines based on simple call out procedures.
- capability to cope with all normally existing geographical and customer network varieties
- applicable in non-FLASHNET environments. For extensions and/or reconstructions the maximum cost target is set on break-even compared with the current level
- no increase in operational cost per line.

Three companies fullfilled the general requirements, two of which have been selected and invited for the next phase of the project in which the network, the components, the accompanying building processes and the turn-key processes have to be developed. This latter in a co-development with KPN Telecom. Both contenders will show in a representative pilot, to be built in the spring of 1999, their capabilities. Throughout the project regular cost up-dates have to be reported with respect to several important cost parameters, i.e. i) investment cost per line in green fields, ii) investment cost for extensions, iii) investment cost for fibre up-grade and iv) representative figures for network dependent operational cost.
As a last step and based on the results of the pilot phase, the definite selection for the "best partners" FLASHNET concept will be made. If in a later stage a second supplying partner will be chosen, this partner has to supply the selected network concept. The rough timeschedule of the whole project is depicted in fig 3.

SUPPLIER INITIATED INNOVATION

Comparing the different solutions offered in the RfQ phase, rather different *technical* solutions have been offered within the constraints of the general requirements. Main aspects are:

- in the primary feeder network use of cable-in-ducts with duct diameters varying from 6 cm up to 10 cm diameter. Number of copper pairs vary from 300 up to 600. In all proposals a spare tube for later migration to fibre and/or extension of the copper network was added. In some proposals also an armoured copper cable was added for the first part of the feeder network. Both pre-ducting of the cable at the production plant and cables which were installed in pre-installed ducts have been offered. Most offered cables will be installed by applying the blown-in technology. No paper insulation or lead shielding has been offered.
- copper wire diameters of both 0.5 mm (installed base value) and smaller values have been offered for either the whole network or distinguishing for the primary and the secondary/tertiary part. Reported impact on cable cost varies considerably.
- number of customers (10 to 24) and design of underground multi-customer joints (integrated copper/fibre, modular, dimensions, mechanical behaviour, ease of making additional connections). In all cases the number of splicing points is much lower than in the current network. Main driver is the need to reduce the number of splices when migrating to a fibre network.
- design of the ducted customer connection cable. Both pure copper and hybride solutions were offered with different approaches for the longitudinal watertightness.
- clearness of the future fibre migration scenario. Main differences were in the complexity of connecting the first customers and in the ratio first installed cost vs cost per later fibre connection.
- vision on and use of advanced planning and engineering systems for the design and administration of the network. Here big differences appeared between the respondees. As this aspect can have a big impact on ope-

rational cost it will be studied further in the current co-development phase.

As for the the *turn key* delivery process not much innovation was offered. Most of the respondees were traditional cable manufacturers and no installation or construction companies. Although they are used to work with turn-key projects as "time and work limited tasks", apparently it is difficult to transfer into the telecom operators skin. The turn-key delivery of access networks or extensions is a result of a continuous activity which involves rough forecasting on building sites, area survey, continuous networking between the operator, municipalities, constructors, cable suppliers, etc.... Innovation can be found in much closer coordination with other operators or installation and construction companies, hiring and providing "right of ways", benchmarking with other constructors, etc.. In the current co-development phase, it is therefore agreed that, as a first step, both contenders start from the current model in which the KPN Telecom Operator and the KPN Telecom Constructor work together. Applied control items are on the level of e.g. i) a completely installed connection to a new dwelling, ii) a unit length of primary feeder cable with indicated capacity, etc... For these control items a yearly fixed price and fixed conditions with respect to delivery time and characteristics are agreed. Once developed, it is expected that from the resulting possibilities for choice between the internal constructor and the "best partner" further improvements for the operator will result.

COST EVALUATION

The main driver for this project being cost reduction, in this section a further evaluation of the offered solutions is described shortly without releasing the confidential company data.
Total cost is defined here as the cost per line when implementing the offered solutions on a given reference service area containing 720 newly built houses on precisely indicated locations. This reference service area has been defined in such a way that it is representative for an average green field situation in the Netherlands. The major characteristics were: i) minimum feeder and secundary network capacity of 125 %, ii) 200% connection per home, iii) all homes connected, iv) no upperground components. Other parameters as network architecture, technology etc.. were free within the general constraints mentioned above and laid down in the RfQ.

The outcome of the evaluation of the offers showed that the total cost per line, provided a reasonable production volume per year was committed, ranged from 75 to 85 % referred to the current level. Overall, this result was just within the project target for short term cost reduction in the new areas. Note that the potential for later cost reduction when migration to fibre gets actual has not been accounted for.

In the requested quotations, the respondees were asked to split the total cost in i) material, ii) installation and iii) overhead. The results are indicated in Table II. Note that percentages are given here and that the average absolute values of each of the cost components are different. Rough contribution ratio is 45% / 45% / 10% for the material, installation and remaining cost respectively.

Material
Compared with the material cost level for the current network solution, the different offers were within a range of +/- 10 %. This means that the additional material cost for making the network upgradable, which is the main difference, is no dominant factor. Although the offered multi-customer joints are more expensive than the traditional ones, the number of jointing points is reduced considerably in all offered architectures. The small variance also indicates that reducing material cost significantly in this mature technology area is not very easily obtained. Effects of armoured vs ducted cables is not visible.

TABLE II Cost contribution per line (%) in decreasing order for the reference service area referred to the current KPN Telecom cost level (=100 %).

	best	middle	worst
material	88	108	109
installation	66	69	94
remaining cost	19	43	57

Installation
The differences were much bigger here. Mentioned technical reasons for installation cost reduction are in the lowering of splicing cost originating from the longer cable installation lengths, the reduction of the number of splicing points in the tertiary network and the highly sophisticated splicing

and installation technologies. Increased possibilities for combi-installation was hardly mentioned as an installation cost reducing reason. An aspect which is still open is the cost reduction which results from delay of investments gained by the operator. Transferring from armoured copper cables to cable-in-ducts opens the possibility to pre-invest in ducts only instead of in complete cables in cases where network building or extension is not sure yet, but where a "golden possibility" for installing ducts is present.

Remaining cost

This part involves all overhead cost directly related with the network installation like sub-contracting, engineering, trench management, quality assurance, etc... . Here the differences with the current situation were surprisingly high and very deviating. From the presentations in the RfQ phase of the project it appeared clearly that this was strongly related with the different views on how to manage turn-key installations including risk management when high level interfaces are used. This subject is treated thoroughly in the current co-development phase.

CONCLUSION

At the current time the FLASN project is well on its way. Both selected partners have shown in their offers the potential for obtaining our goals with respect to cost reduction and network flexibility. "No-dig" solutions for later up-grading of the network in the Dutch environment seem very well possible in a cost-effective way. It also shows however that the technology innovation does not lead to a material cost reduction but apparently to a reduction in (future) installation and overhead cost. Based on the experience in this area with other extensive networks (e.g. SDH or switching) this may involve a risk. It also is an opportunity however to enforce the position of classical cable suppliers into complete passive network suppliers which can innovate here more easily due to the lack of long history of traditional way of working and the potential of synergy along other axes than obtained up to now.

The offered proposals and the current outlook in the co-development phase also shows that cost reduction can be an efficient driver for stimulating innovation. The ultimately selected network and installation technology together with the developed new organizational and logistic processes will be ready next year.

ACKNOWLEDGEMENTS

The author wishes to acknowledge the FLASN project team for the support and Hans Knijnenburg and Willem Griffioen in particular for their valuable contributions to this paper.

REFERENCES

[1] A.Lenfant; "Competition in the Local Loop: A Regulatory Prospect"; Proc. 11th ISSLS (1996), pp 20-25.

[2] W.Griffioen, H.Nijstad, A.T.M.Grooten, A. van Wingerden, G.Brown, D.F. Hawkins, G.Plumettaz; "A new, extremely versatile access network cabling concept for migration to optical fibre". Proc. 45th IWCS (1996), pp 485-489

BIOGRAPHY:

Pieter Matthijsse was graduated at the Eindhoven Technical University in Theoretical Electrical Engineering in 1971. After his PhD study in Fourier Optics at the Applied Sciences Faculty at the Leuven University in Belgium he joined KPN Research in 1976 and worked on fibre characterization and splicing and optical network technology. From 1985 on he was responsible for PCVD fibre production technology development at Philips Optical Fibre in Eindhoven. In 1991 he returned to KPN Telecom where, in several responsibilities, he worked on access network development. Full address: KPN Telecom - Network Services; PO Box 30150, 2500 GD The Hague, The Netherlands; email: p.matthijsse@kpn-telecom.nl

IMPROVING RANGE AND BANDWIDTH OF TELCO LOOP PLANT

Richard A. Combellack

Nortel (Northern Telecom)
Ottawa, Ontario
Canada

ABSTRACT

Increasing use of the Internet and demand for high speed data services is requiring telephone companies to deliver more bandwidth than the existing copper plant was designed for. New systems, such as variants of Digital Subscriber Line (DSL), go a long way to overcoming the limitations of the plant, but even these may run into barriers caused by loop impairments and noise.

There are many mechanisms which can cause metallic noise (Tip to Ring), most of which involve longitudinal signals (Tip and Ring to Ground) being converted into metallic signals and vice versa. This involves unbalanced impedances to ground along the loop.

Reduction of loop attenuation or adjustment of impedances to improve performance of wire plant is difficult. Longitudinal signal attenuation can, however, easily be increased, thus reducing metallic noise.

A simple, passive device is being designed to enable telephone companies to improve data transmission rates on marginal loop plant.

INTRODUCTION

The use of the Internet is increasing rapidly and customers are demanding ever faster means of downloading ever larger files. Local exchange carriers, therefore, increasingly need to be able to provide means of delivering data at rates very much higher than can be compressed into a typical telephone channel bandwidth (3 to 4 kHz.).

This challenge is being met very successfully by the new range of Digital Subscriber Line (DSL) products which are now becoming available. Use of such systems does have some limits in that if too many high frequency systems are carried in the same cable binder group they will tend to interfere with each other, and themselves, and will thus be unable to deliver the maximum theoretical data rate over the longer loops. External radio signals in the same frequency band can also inject significant longitudinal signals into the pairs.

One of the limitations is caused by skin effect which increases attenuation as frequency increases.

Metallic (or transverse or differential) signals are the signals which appear between Tip and Ring, the two wires of a pair. Ideally these signals, measured to ground, on Tip and Ring would be equal in amplitude but inverted. The arithmetic average of the two voltages to ground would thus be zero. In the real world this is often not zero and this is referred to as a longitudinal (or common mode) signal. These occur, largely, because of impedance unbalances to ground along the two wires of the pair and at terminal equipment present at the ends of the pair. This causes metallic signals to be converted into longitudinal signals and longitudinal signals into metallic signals. These unwanted metallic signals, originating externally, from radio stations etc. or internally, from other systems in the same cable or even from the wanted signal on the same pair (self cross-talk), can be as large as or even larger than the wanted metallic signals.

Reducing attenuation throughout the system is impractical. Limiting the effect of longitudinal

impedance imbalances is feasible by application of longitudinal chokes so as to reduce the longitudinal currents flowing in the system.

Proper application of these chokes will mean that a loop carrying a high frequency transmission system will interfere less with adjacent systems; will be less susceptible to interference from adjacent systems and will be less susceptible to the effects of external signals such as those from radio transmitters. Radiation from the telephone system will also be reduced.

When used appropriately these simple devices will enhance both available bandwidth and range for high frequency transmission systems over existing wire plant.

Some International Standards are being written so as to ensure that high frequency systems (e.g. VDSL) are designed to, in effect, notch out certain frequency bands, e.g. amateur radio bands. This limits the analog bandwidth available to the telecommunication system. Since only a relatively small number of systems will actually be located close to amateurs etc. this results in severe constraints on the design of the system. If inexpensive and effective means were available to mitigate this effect when it does occur the standards could, and should, be relaxed. Use of the choke system described here is expected to provide a suitable means of mitigating these effects. This would result in it being permissible to launch higher signal levels than presently allowed thus extending the range of high frequency systems even further.

This paper presents the results of a simulation study, with laboratory measurements, of the mechanisms involved in cross-talk and how the effects of cross-talk and radiated signals from radio stations may be reduced. The results of this work will be applicable to all of the DSL systems but particular attention has been given to VDSL, which might require effective transmission of up to 10 MHz. along the loop. The work reported here has been done with 26 AWG cables as these have the worst high frequency attenuation characteristics. The same principles apply to other wire gauges

CROSS TALK MECHANISMS

Background information

Consider first a single pair of wires in a metal shield. The effects of multiple pairs will be discussed later in the paper.

In order to understand the complex interactions between the many characteristics of a loop transmission system which affect the cross talk performance a list of "factors" as presently understood has been prepared and is shown in Appendix A. Of these the more important are :-

The attenuation of longitudinal signals is much less than that of metallic signals.

The velocity of longitudinal signals is less than that of metallic signals.

Longitudinal balance worsens at 6 dB/octave over the frequency band of interest.

At least two, widely separated, points or regions with significant imbalance are required for cross-talk to occur to a level likely to cause interference.

Cross-talk mechanism

It is evident, from simulations reported in the Appendix, that for self cross-talk to be significant there must be at least two points at which longitudinal imbalance occurs. Consider a perfectly balanced pair of wires with imbalanced capacitances to ground at each end. A metallic signal applied at one end will immediately generate a smaller longitudinal signal at the sending termination. Both metallic and longitudinal signals will be transmitted towards the far end and the metallic signal amplitude will fall at a faster rate than will that of the longitudinal signal. The longitudinal signal will travel slower than the metallic signal and will thus be out of phase with it at most points. At some point the longitudinal signal amplitude will exceed that of the metallic. At this point, or at any point further from the source, encountering another point of imbalance will cause another, probably out of phase and certainly delayed, metallic signal to appear. This second imbalanced point marks the maximum possible range of the loop at the particular frequency when the metallic signal which arrived via the longitudinal path equals

the normal, wanted metallic signal. The effective signal to noise ratio at this point will be zero dB. At higher frequencies or longer ranges the net signal seen at the terminal will switch from the wanted metallic to the metallic converted from the longitudinal path. There may appear to be a possibility of the transmission line continuing to operate at higher frequencies beyond this point using only the signal which came via the longitudinal path. This is not practical, however, because there will probably be unacceptable interference from other pairs in field use. There certainly will be a band of lower frequencies which will suffer severe distortion.

Effect of location of Imbalances

The configuration described above is a very simple arrangement and does not include the effects of structural cable pair imbalances. Investigations, using simulation, indicate that for any particular cable pair the worst situation always occurs when the distance between the two imbalances is at a maximum as this allows the amplitude of the longitudinal signal to converge with that of the metallic signal. This applies whether the imbalances are on the pair or at the terminals. It has also been found that only the first and last few hundred metres of imbalance along the cable (wherever this might occur) are significant. A spreadsheet has been used to investigate the effects of the location of the two imbalances. Using a 26 AWG cable with a known point balance of 80 dB (at 1 kHz.) located at both ends of a 2 mile (3220 m) cable pair the signal to noise at the far end is 16 dB at 500 kHz. Locating the two imbalances at the mid point of this cable gives 16 dB S/N at about 4 MHz. This means that this source of noise becomes insignificant so the range limit is due only to the metallic attenuation (to about 1.5 MHz. In this case). These findings strongly suggest that the balance of the first and last few hundred metres of cable as well as the balance of the terminals at each end are the most critical as far as Far End Cross-talk (FEXT) is concerned. Imbalance in the middle section of the cable will, of course, cause cross-talk but this will be of a much lower level than any caused at the ends.

Longitudinal Choke

Insertion of a device which has a very high impedance to longitudinal signals will reduce cross-talk significantly. It needs to be, in the one pair case, anywhere along the loop downstream of the first imbalance and upstream of the second. If located close to an unbalanced termination with a high longitudinal impedance a means must be found to reduce the longitudinal impedance downstream to allow the desirable longitudinal attenuation to occur. The device consists of a choke with two parallel wound coils which are very closely coupled together. The wire must be at least 26 AWG to prevent the devices acting as fuses. The self capacitance of each coil must be kept low so as to ensure that the longitudinal impedance over the frequency band of interest remains as high as possible. This also implies that a high quality core material is needed. The prototype has a self capacitance of each coil of a little more than 1 pF and has an impedance at 1 MHz. of about 10 k Ω. This device will attenuate longitudinal signals at 1 MHz. by about 35 to 40 dB, when correctly terminated. This, if properly located, will improve cross-talk performance by the same amount (35 to 40 dB). Attenuation is less at lower frequencies but is not needed since the balances will be higher and cross-talk less of a concern. At frequencies above 1 MHz. the attenuation increases up to the self resonant frequency and remains high up to over 10 MHz. The device introduces very little metallic attenuation at any frequency.

The equivalent circuit of the basic longitudinal choke is shown in Figure 1.

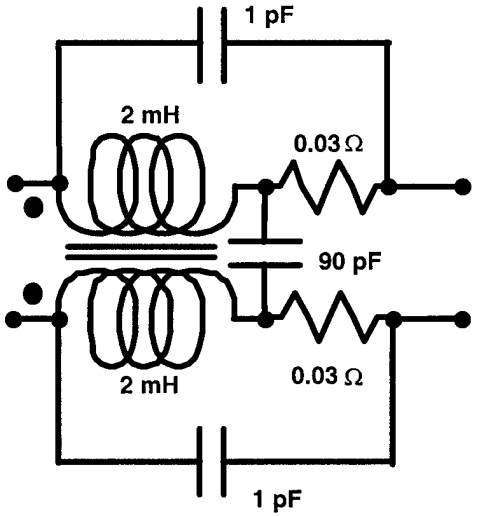

Figure 1. Circuit of Longitudinal Choke

Effect of Opening the circuit

Insertion of the longitudinal choke in the circuit causes a serious mismatch of impedances along the transmission line. This can cause significant reflections to occur which will tend to increase longitudinal voltage on the upstream, unbalanced, part of the loop. This can worsen the effective longitudinal balance. This effect may, when necessary, be overcome by using the same transformer and two external capacitances. The circuit of this device is shown in Figure 2.

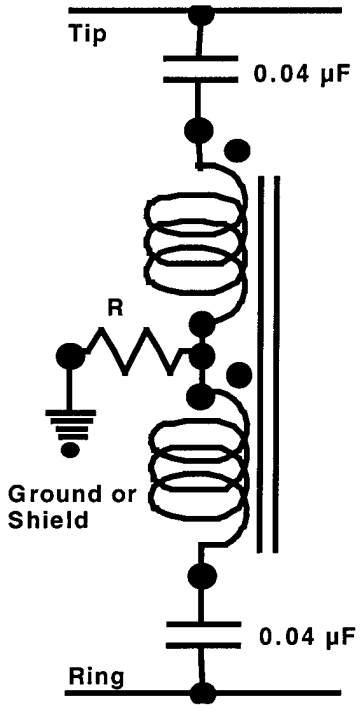

Figure 2. Longitudinal Impedance Matching Transformer Circuit

The various self capacitances have not been shown in Figure 2 in the interest of clarity. The capacitances which are shown are added to ensure that the device does not short out the dc voltage and low (voice band) frequencies on the line. These capacitances must be well balanced at lower frequencies. R should be about 215 Ω. This arrangement does cause significant metallic attenuation at frequencies around 12 kHz. because it becomes series resonant. This will not matter for VDSL since VDSL uses higher frequencies. ISDN and other lower frequency systems, as well as some signaling systems, might be harmed by this resonance but it is possible to move the resonant frequency or even to operate without the matching device if a reduction in cancellation of longitudinal signals is acceptable. To make the system symmetrical it would be desirable that one of the longitudinal matching devices be connected on each side of the longitudinal choke. This is also useful in cases where there is little or no loop between the choke and any termination which has a high longitudinal impedance as it presents a low longitudinal impedance downstream and ensures maximum attenuation of longitudinal signals.

Radio Interference

Broadcast and amateur radio transmitters can induce significant longitudinal signals into wire pairs, particularly in the unshielded drop wiring of overhead plant. The amplitude of such signals can be much greater than that of cross-talk longitudinal signals and so present a serious challenge. Proper use of the chokes and impedance matching devices described in this paper can also make significant improvements to system performance in this respect. The reverse also applies and longitudinal signal levels, at high frequencies, on telephone lines are reduced thus limiting radiated interference from the loop.

Location of Chokes

In general, as already indicated, the new devices should be located downstream of the source of longitudinal signal and upstream of the most remote point at which the longitudinal signal is turned back into a metallic signal. Since we are concerned with two way systems this may require use of more than one device. In particular it appears that there may be significant advantages if chokes are used at both ends of the drop since drops are often unscreened and may be exposed to radio signals which will cause significant longitudinal pick up. This will not affect any cross-talk occurring in the drop itself but will minimize the effects of any imbalance of the termination as well as that of the wires in the cable. It will also reduce the level of longitudinal signals being introduced into the cable itself.

Multiple Pairs

The discussion so far has been about a single pair of wires contained in a shield. Cables typically contain numerous pairs and many of the other pairs are located close to each other and thus have a high level of magnetic and capacitive coupling between them. Metallic signals on any one pair tend not to interfere directly with metallic signals on other pairs because the two directional nature of the metallic signals in each pair tends to cancel signals induced in other pairs. Longitudinal signals, however, couple very well between adjacent pairs and this is the primary reason for pair to pair cross-talk. The discussion above relating to a single pair applies to multiple pairs with one very important addition. If another pair is assumed to be running in parallel with the sending pair the longitudinal signal originating at the first imbalance will appear, with little attenuation, in the second pair and will be transmitted along the second pair. If a choke is applied to the sending pair to reduce its longitudinal signal only marginal system cross-talk performance will be achieved. This is because the longitudinal signal in the second pair will couple back into the sending pair within 10 metres or so downstream of the choke and will reappear only slightly attenuated at the far end. Chokes will therefore be needed at the same point in all pairs which can couple tightly to the pair being considered.

Typical Simulation Results

The following graphs show the outputs of a number of PSpice™ runs to show how use of the new chokes will improve the performance of VDSL like systems under a range of typical circumstances.

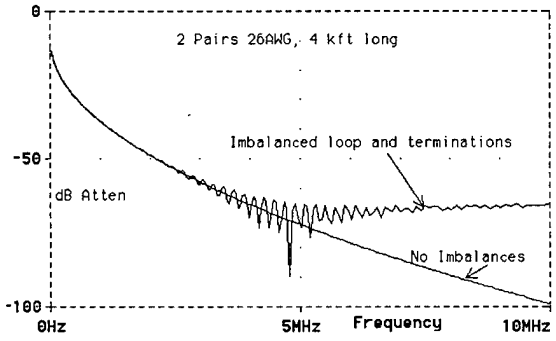

Figure 3. 4 kft loop, 2 pairs, Imbalanced at end

Figure 3. shows the end to end attenuation of a 4 kft (1.219 km.) 26 AWG cable which contains two, tightly coupled, pairs. There is imbalance at both ends of the sending pair as well as at both terminations. The other pair is perfectly balanced everywhere. It shows (by oscillation or ripples on the trace) that the metallic signal via the longitudinal path is becoming significant at about 3 MHz. and completely dominant above 5 MHz. In the absence of cross-talk noise this particular cable pair would have been usable up to about 10 MHz.

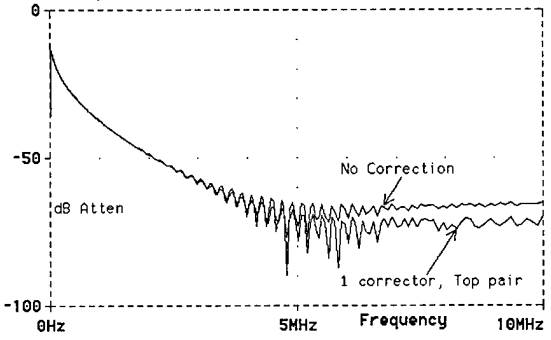

Figure 4. 1 corrector in top pair

Figure 4. shows the effect of one corrector located in the sending pair. This does not much improve the system performance.

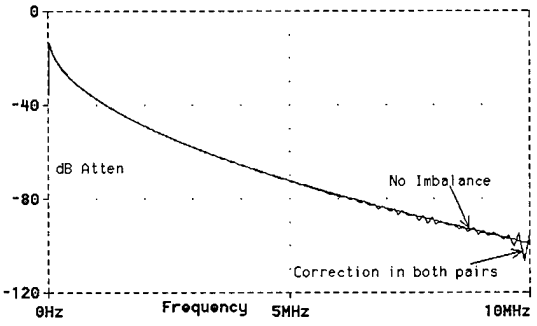

Figure 5. 1 corrector in each pair

The marked improvement caused by using a corrector in each pair is evident in Figure 5. The system is now usable up to nearly 10 MHz. There are signs (trace ripples) that the metallic via longitudinal signal is becoming significant at 10 MHz.

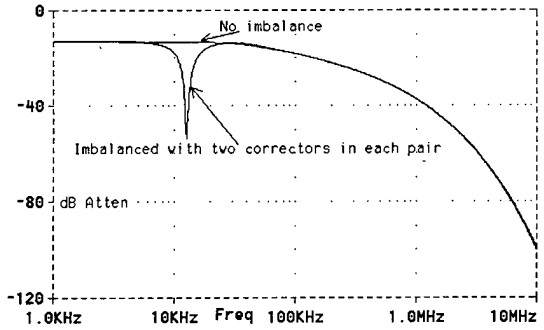

Figure 6. 2 correctors in each pair, log scale

Figure 6. shows how much high frequency performance improvement may be expected from use of two devices in each pair. The logarithmic frequency scale is used here to show the resonant trapping effect of the longitudinal impedance matching devices. The system performance will be virtually indistinguishable from that of a perfectly balanced system, except at around 12 kHz.

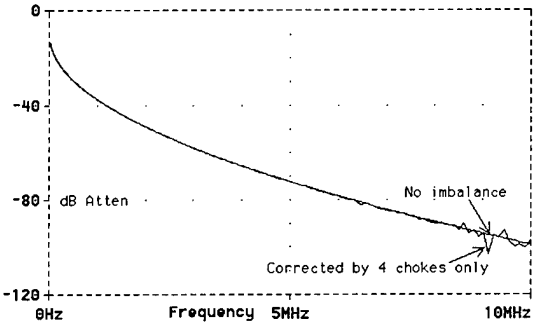

Figure 7. 2 Chokes only in each pair

For cases where the trapping action of the longitudinal corrector is not acceptable a slightly reduced performance may be obtained by using only the longitudinal choke part of the corrector. Figure 7. shows the predicted performance with two chokes in each pair. The results are very similar to Figure 5. where we had one full corrector in each pair. In both cases the system would be usable at frequencies up to nearly 10 MHz. Improved performance could be achieved by using more than two chokes in each pair, if required.

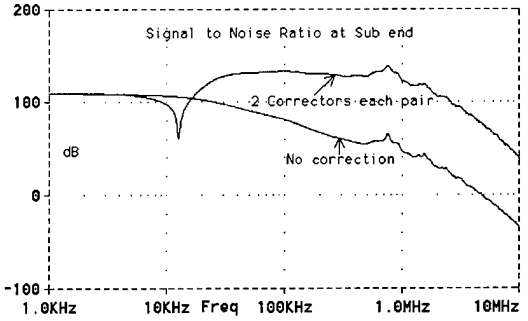

Figure 8. Effect of Correctors on S/N ratio

Figure 8. shows the effect of 2 full correctors on each pair on the Signal to Noise ratio at the customer premises. In this case we are considering that the sending end of the sending pair has poor balance in its terminal and in the first quarter of the cable. The receiving pair has a well balanced Central Office end but has poor balance at the subscriber end. It is not carrying any signal itself. The two traces are of the difference in the metallic signals appearing at the far end of the two pairs and gives a reasonable approximation of the likely Signal to Noise ratio in any one pair. It can be seen that the S/N falls to 20 dB at about 3 MHz. if no correction is used. With the two correctors applied the S/N ratio at 3 MHz. increases to about 95 dB, a 75 dB improvement. This also confirms that the system would be usable at frequencies right up to the point where the end to end attenuation becomes the limiting factor (10 MHz. in this case).

STILL TO DO

While simulations and laboratory trials have proved promising, it is still necessary to determine the scale of improvement which is achievable under actual field conditions, with a range of high frequency signals carried in the plant.

CONCLUSIONS

- For cross-talk to be significant there must be at least two sections of cable or terminations which have poor longitudinal balance.

- The further apart the first and last imbalanced regions are the worse becomes the far end cross-talk.

• Longitudinal signals travel slower than metallic so when turned back into metallic will often be out of phase and will, if of sufficient amplitude, cause peaks and troughs in the signal level at the far end. At high frequencies or long ranges the metallic signal which came via the longitudinal path will dominate the wanted, or direct, metallic signal.

• Longitudinal signals are attenuated less than metallic so, while they may start much smaller than metallic, will converge in amplitude if they travel far enough.

• Insertion of one or more longitudinal chokes in each pair of a cable binder group will greatly improve far end cross-talk performance. It will also improve immunity to radio signals under most circumstances.

• Opening the longitudinal circuit can cause longitudinal reflections and standing waves. Use of a simple longitudinal impedance matching device can minimize this effect, when necessary.

• The high loss nature of telephone loops means that, while use of the longitudinal characteristic impedance matching device is desirable, it is not essential in many cases.

• When the new devices are widely applied it should be feasible to relax the regulatory requirements which presently limit high frequency telephone signal levels. This will permit an even greater increase in range.

ACKNOWLEDGMENTS

Doug Bannard, Power Group, Nortel, Ottawa, who built the prototypes used in this work.

APPENDIX A

There are many factors which interact to influence cross talk levels. The following list shows the factors considered while carrying out the investigation reported here :-

At frequencies exceeding about 10 kHz. skin effect causes significant increase in loop resistance, which increases end to end loop attenuation.

At low (< 100 kHz.) frequencies twisted pairs do not behave as ideal transmission lines.

At high frequencies (> 250 kHz.) they do behave very nearly as ideal, albeit lossy, lines. At mid frequencies there is a range over which the inductive reactance becomes dominant, compared to the resistance, even though resistance increases with frequency.

Characteristic metallic impedance, at high frequencies, is $Z_{0m} = \sqrt{(L/C)}\ \Omega$.

Attenuation, at high frequencies, is
$A = 8.686 * R/(2 * Z_0)$ dB/unit length.

Velocity, at high frequencies, is $Vel = 1/\sqrt{(L*C)}$.

At 1 MHz. Z_{0m} = about 100 Ω.

At 1 MHz. a longitudinal signal injected into both wires of the pair sees the pair as a single wire. This wire is half the length of the loop wire. The return path is through the cable shield.

The cable shield has much less resistance than the wire.

The net per unit length resistance for the model of the longitudinal transmission line is thus significantly less than that of the metallic transmission line.

The net per unit length inductance of the longitudinal transmission line is significantly higher than that of the metallic line because the inductive coupling between wires and shield is less than that between wires.

The net per unit length inductance of each wire of the longitudinal transmission line is also significantly higher than that of the metallic line because the inductive coupling between the wires means that longitudinal currents in each wire increases the effective inductance of the other, coupled, wires to longitudinal signals.

The net per unit length capacitance of the longitudinal transmission line is similar (slightly lower) to that of the metallic line.

It would thus be expected that the longitudinal characteristic impedance (Z_{0l}) of each wire to shield would be higher than Z_{0m}.

It would be expected that the longitudinal attenuation would be significantly less than the metallic attenuation.

It would be expected that the velocity of the longitudinal signal would be less than that of the metallic signal.

A 1 mile (1610 m) length of 26 AWG twisted pair PIC cable typically has a metallic attenuation of about 42 dB and a Z_{0m} of 103 Ω at 1 MHz. The velocity of the metallic signal is about 65% of the speed of light.

Simulation results indicate that the longitudinal characteristics of each of the two wires to the shield are:-

Longitudinal attenuation is only about 7.1 dB/mile (4.4 dB/km), when correctly terminated (less if terminated in a high impedance).

Z_{0l} is about 430 Ω

Treating the pair as a single transmission line to ground and including the metallic source impedance gives an end to end longitudinal attenuation (across the longitudinal terminating resistance) of about 10 dB/mile (6.4 dB/km) at 1 MHz. If the far end is not terminated longitudinally the end to end longitudinal attenuation is even less.

The longitudinal characteristic impedance of the pair is 215 Ω , which is significantly higher than Z_{0m} at 1 MHz.

The velocity of the longitudinal signal along the pair is about 34% of the speed of light, which is about half of the velocity of the metallic signal.

Longitudinal imbalance tends to be a capacitive effect and thus worsens as frequency increases (at 6 dB/octave) up to a maximum value which depends on whether we are concerned with longitudinal to metallic transformations or vice versa (about 6 dB m to l and -6 dB l to m).

All of the above factors must be taken into account when attempting to simulate the performance of wire loops with respect to cross-talk performance.

BIOGRAPHY

Alan Combellack was born in England, many years ago. He obtained his qualifications via the IEE Part 3 examination. He spent 6 years in the RAF as an Engineer Officer; 6 years with what is now British Aerospace as a design Engineer on Missile systems. The last 24 years have been with BNR/Nortel working on various telephony related activities. Alan likes to garden, when the Canadian climate permits; is trying to learn to play golf without too much embarrassment; reads a lot; maintains his old car, when absolutely essential; makes his own wine and actually enjoys working with his computer. He is married and has one 29 year old son, who is still living at home.

R.A. Combellack,
Dept. 0M23, Mailstop 041,
PO Box 3511, Station C,
Ottawa, Ontario,
Canada
K1Y 4H7.

PERFORMANCE OF COAXIAL DISTRIBUTION CABLES UNDER MECHANICAL STRESS

Lal M. Hore, William McLaughlin, and Kai V. Hsing

Bellcore
445 South Street, Morristown, New Jersey 07960-6438

ABSTRACT

This paper examines the performance of coaxial distribution cable which is subject to various mechanical stresses. A preliminary study was conducted in 1996[1]. This study was further necessary to verify the Bellcore specified requirements under these stresses[2]. It is important to determine if a cable can perform adequately when it encounters a situation such as being runover by a truck, accidentally having a toolbox dropped on it, or being bent unnaturally by accident. Simulating those events, the effects of compressive loads and tension on the cable's ability to transmit broadband signals are investigated as well as the cable's ability to withstand bending. It was found that the cable's resistance to compression is related to the thickness of it's outer aluminum conductor. When the cables were deformed by 15% of their original diameter, the performance was severely impaired. However, the cables were quite resistant to damage resulting from high tension forces and performed quite well. It was also discovered that cables are more vulnerable to failure when subject to environmental temperature extremes. High temperatures reduced resistance to impact while low temperatures increased the likely hood of damage resulting from bending.

INTRODUCTION

Coaxial distribution cable is used extensively by the CATV industry and is used to cover the long distances between the fiber node and the curb. It is composed of a copper-clad aluminum center conductor, over which is a concentric dielectric. This dielectric can either be polyethylene foam or spaced polyethylene discs, in which the air spaces also act as a dielectric. A thin aluminum shield acting as an outer conductor is placed over the dielectric. The shield is constructed either as a seamless tube that is extruded over the dielectric then swaged down on the dielectric, or it is made from an aluminum sheet which is wrapped around the dielectric, welded together then swaged down to size. A black polyethylene jacket is then extruded over this shield. Polyethylene is used because of it's low moisture permeability. Six different cables from three manufactures were used in this study. The cables ranged in outer diameter size from 0.50 inch to 0.75 inch. The cables were of various dielectric types and shield construction. Table 1 provides the specifications for each of the cables in this study.

Table 1 - Cable Sample Specifications

Cable Sample	Dielectric Structure	Aluminum Shield Structure	Diameter (inches)
A	Disc and air	Extruded	0.500
B	Foam	Welded	0.540
C	Foam	Extruded	0.565
D	Foam	Extruded	0.700
E	Foam	Welded	0.715
F	Disc and air	Extruded	0.750

Samples B, C, D, E, and F were exposed to the outside environment for two years.

COMPRESSION TESTING

Test Procedure

A nine inch length of cable was compressed at a rate of 0.05 in./min. between two parallel plates using an Instron Machine while at room temperature (65° F). A HP 8753D network analyzer was connected to the sample which measured the following electrical characteristic as the cable was compressed: attenuation, structural return

FIGURE 1 - Compression Loads vs. Percentage Deformation

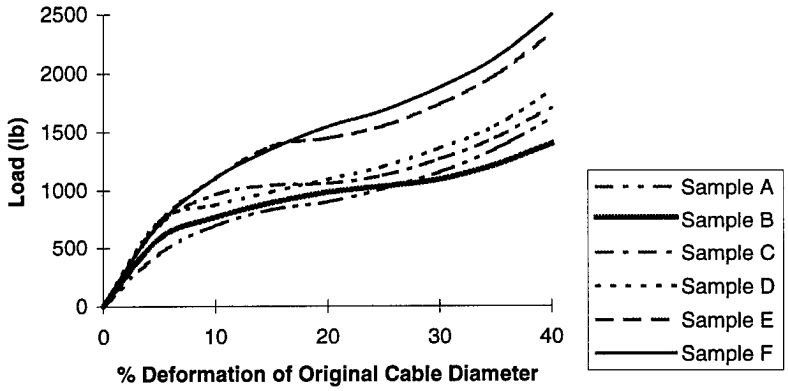

loss (SRL), and characteristic impedance. The test continued until the cable was compressed by 40% of its original diameter.

Physical Performance of the Cables

The physical results of the compression test are shown in Figure 1. Initially, it may appear that a cable's resistance to compression is directly related to the diameter of it's aluminum outer conductor however, closer examination reveals that the thickness of the outer conductor (see Table 2) is the actual controlling factor.

Table 2 - Thickness of Aluminum Outer Conductor

Cable Sample	Thickness of Aluminum Outer Conductor (in.)
A	0.02 (w/ 0.029 dielectric sleeve)
B	0.0135
C	0.023
D	0.022
E	0.035
F	0.025 (w/ 0.053 dielectric sleeve)

It is also evident that the strength of samples A and F are dependent upon the thickness of the dielectric sleeve which lines the inside of the aluminum outer conductor. Samples A and F are only periodically supported along the length of the cable by the spaced polyethylene discs whereas other cables receive continuous support along the length of the cable from the foam dielectric. Though sample F does not have the thickest outer conductor, it has a thick dielectric sleeve. Thus, it is inferred that that cables with the foam dielectric are more resistant to compression if all other characteristics are the same. It is also worthwhile to note that, the relationship between load and percentage deformation (strain) is initially linear indicating that cable deformation was elastic up until a deformation of approximately 5%. Beyond this, the deformation becomes plastic and is therefore permanent.

Electrical Performance of the Cables

The attenuation, structural return loss, and characteristic impedance were measured over a frequency range of 5 MHz to 1 GHz. The attenuation is a measure of the degradation of the strength of the signal as it propagates along the cable in proportion to the strength of the signal at the source. The longer the cable, the greater the decay. Also, as the frequency increases, the attenuation decreases due to the greater losses associated with higher frequencies. It is this loss of signal strength that necessitates the use of amplifiers in coaxial networks and determines how far apart they may be placed in the network. The structural return loss is a measure of the signal strength that is reflected back along the cable length in the opposite direction of the transmitted signal. It is caused by changes in the cable's dimensions and effective dielectric constant. Structural return loss is measured as a proportion of the reflected signal strength to the strength of the signal at the source. The characteristic impedance is a measure of

the cable's total resistance to carrying the signal.

Attenuation

The attenuation at deformations of 0%, 15%, and 25%, respectively, for sample A, is provided in Figures 2A, 2B, and 2C. Attenuation for each case is virtually identical. This indicates that attenuation is not significantly affected by compression.

Structural Return Loss

The SRL at deformations of 0%, 15%, and 25%, respectively, for sample D are shown in Figure 3A, 3B, and 3C. It was observed that SRL increased as deformation became more severe. It was also found that the SRL was quite high for higher frequencies (940 to 1000 MHz).

It is interesting to note that, for nearly every sample of the six cables tested, the SRL first failed the minimum industry requirements of 30 dB at 15% deformation. Only 3 out of 18 samples did not fail the requirement for SRL and all three of these did fail the requirement for SRL at 20% deformation. In addition, the load that was needed to obtain the 15% deformation varied widely among the six cables and even among the three samples of the same cable, as one may see from table 4.

The amount of deformation is the determining factor for increases in SRL. Once the outer conductor looses its shape and is no longer concentric with the center conductor, the cable can not carry the signal without significant reflections which weaken the signal transmitted at the source.

Characteristic Impedance

The characteristic impedance was normal for all samples before deformation. However, once deformation reached 10%, most samples displayed an unacceptable characteristic impedance. At 15% deformation, all samples had a characteristic impedance which indicated performance problems. The compressive load needed to achieve a 10% deformation can be found in Table 3.

Table 3 - Compression Load 10% Deformation

Cable Sample	sample 1 (lb)	sample 2 (lb)	sample 3 (lb)
A	678	680	724
B	755	776	772
C	977	950	972
D	910	855	861
E	1017	1193	1112
F	1081	1110	1130

Thus it can be seen that at loads as low as 700 lb, the cable can be damaged such that performance is severely affected.

BEND TESTING

The construction of coaxial cable causes it to have a certain degree of stiffness. This rigidity makes the cable prone to failure from bending. Therefore the various manufacturers of the cables have rated the cables and specified a minimum bend radius before failure will occur. The six samples were subject to this criteria while placed under various environmental conditions. The specified minimum bend radii can be seen in table 4.

Table 4- Minimum Bend Radius

Cable Sample	Bend Radius (in.)
A	6
B	4
C	5
D	7
E	5
F	8

Test Procedures

Samples were bent around a fixed mandrel with a radius equal to the minimum specified bending radius and to 25% below the minimum specified bending radius. The samples were bent 180° around the mandrel and then straightened on a hard flat surface. The sample went through this procedure four times. Each time, the procedure was done at a 90° interval to the previous bend.

Figure 2A - Attenuation at 0% Deformation for Sample A

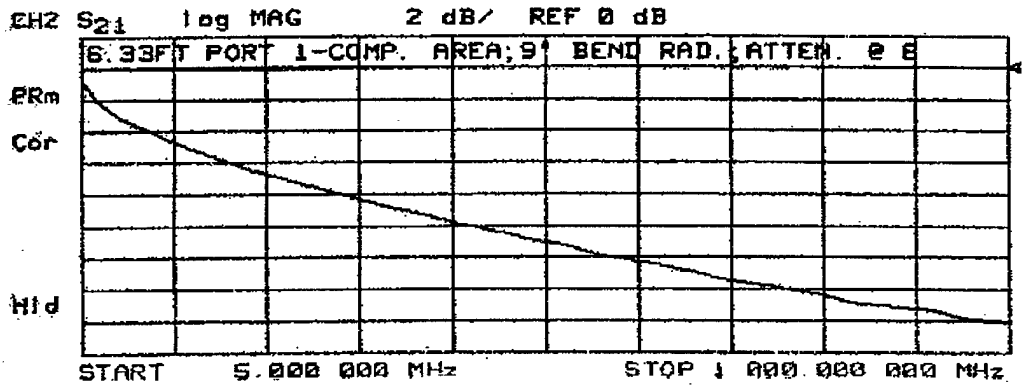

FIGURE 2B- Attenuation at 15% Deformation for Sample A

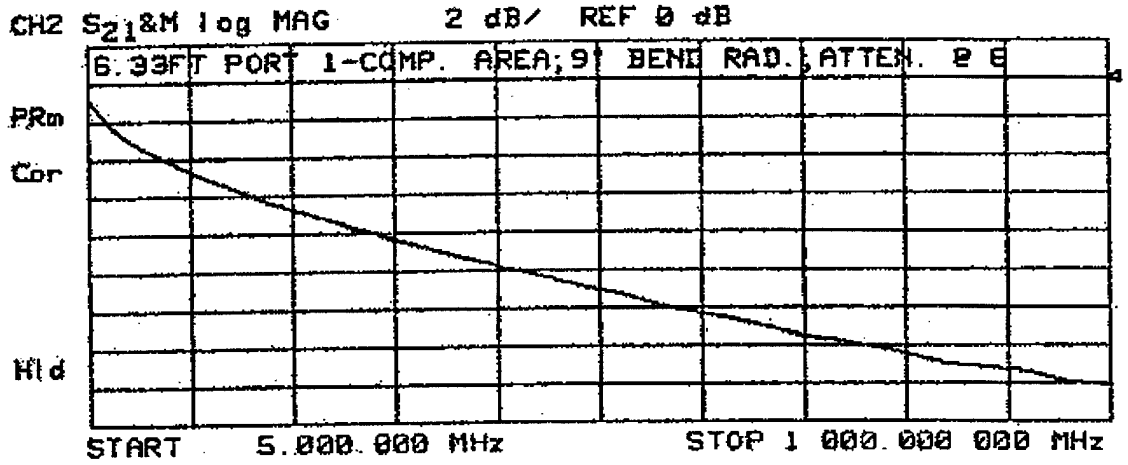

FIGURE 2C- Attenuation at 25% Deformation for Sample A

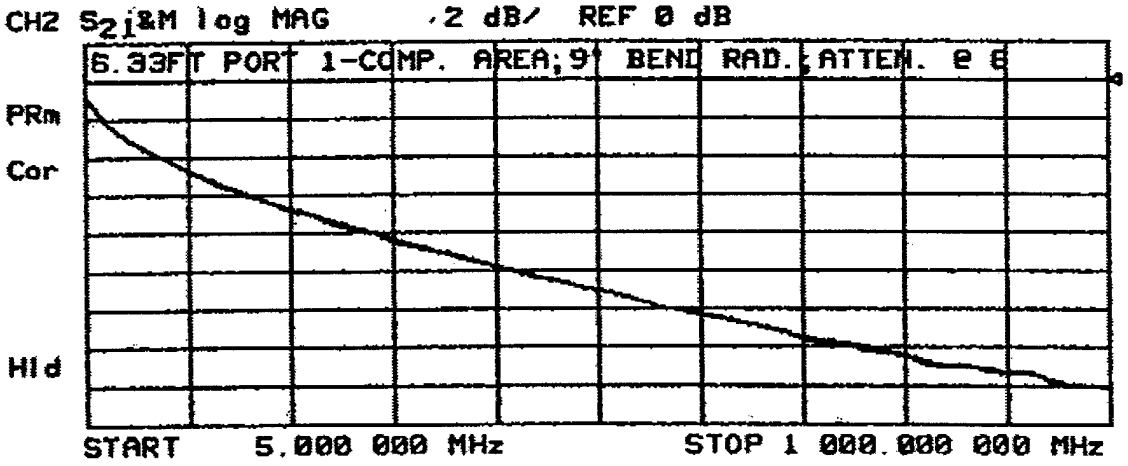

FIGURE 3A - SRL at 0% Deformation for Sample D

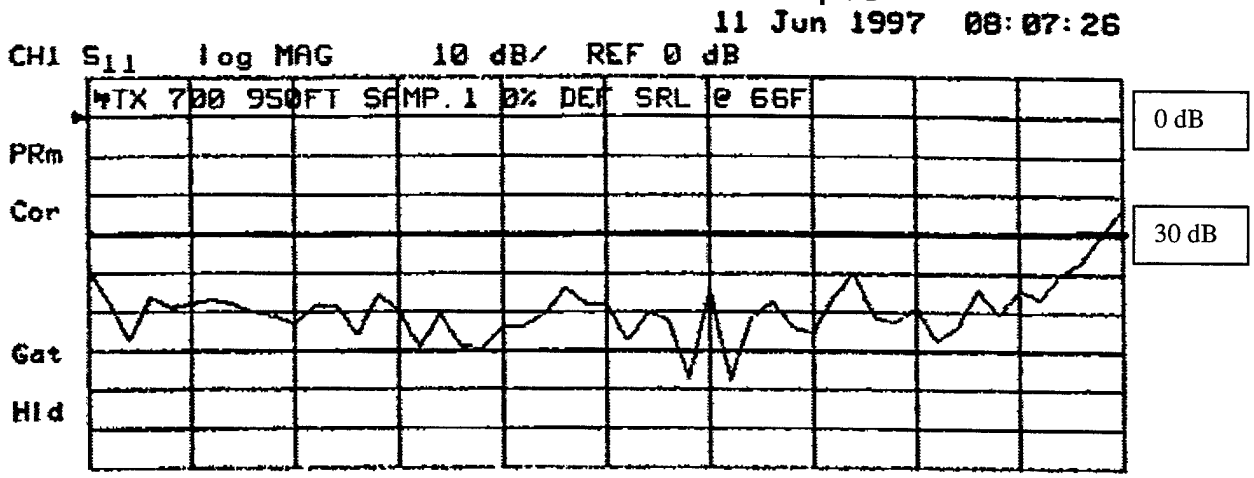

FIGURE 3B - SRL at 15% Deformation for Sample D

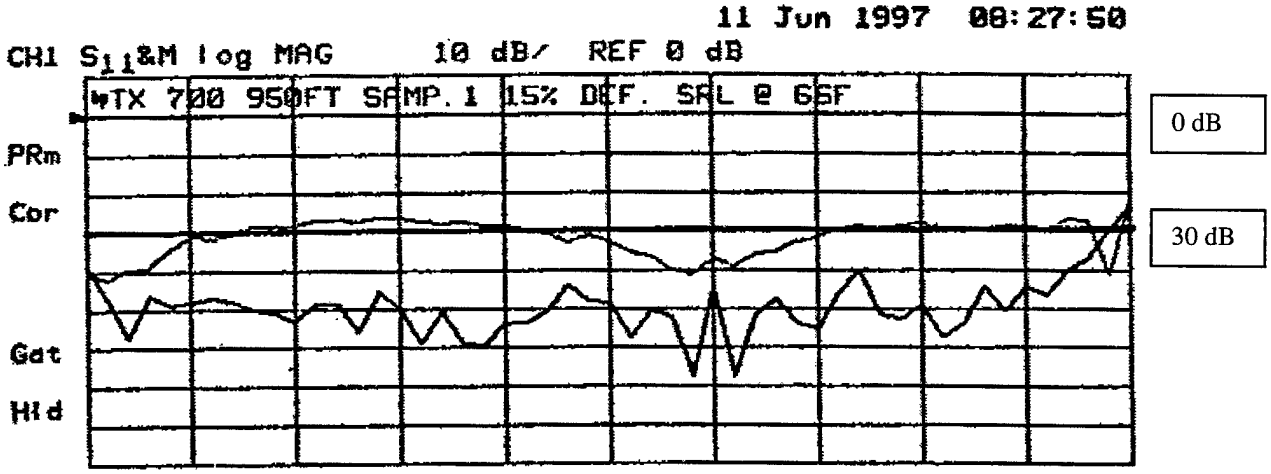

FIGURE 3C - SRL at 25% Deformation for Sample D

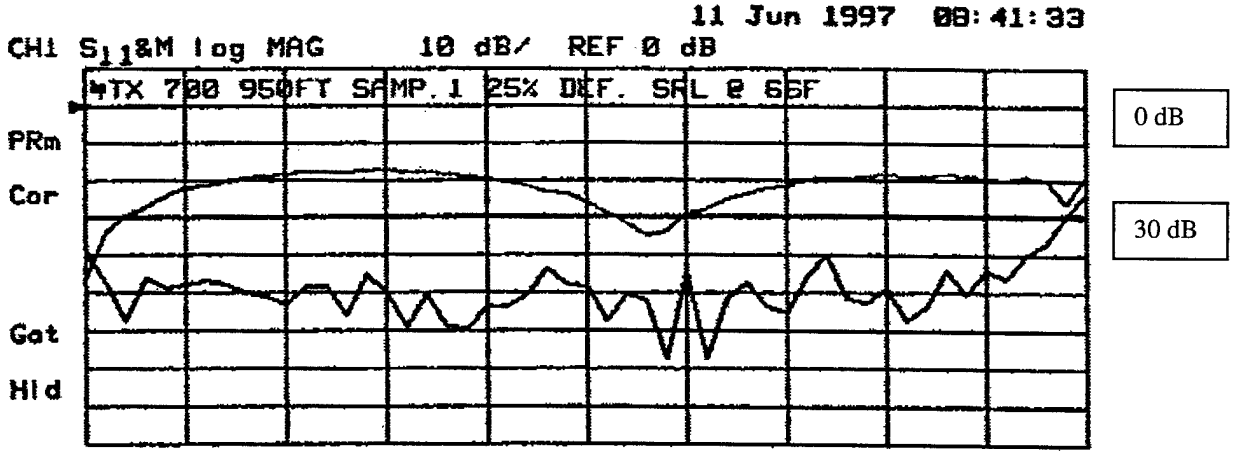

The entire procedure was done by hand and took one minute to complete. The test was performed at -40° C, -10° C, 20° C, and 50° C. Prior to the bend test, the samples were preconditioned to the operating test temperature for four hours.

Physical Results

Table 5 provides the results of the test. Specifically, it documents whether the samples had any kind of visible failure.

Table 5 - Bend Test Results

Cable Sample	Temperature	Failure Observation
A	NA	No failures
B	50° C	kink
C	NA	No Failures
D	50° C	Kink → Crack
E	50° C	Kink → Crack
F	-40° C	Sudden crack

The results indicate that cables with foam based dielectric components failed at warm temperatures (50° C) where as cables with disc air dielectrics failed at low temperatures (-40° C). Due to the temperature extremes, the samples which failed at low temperatures suffered sudden and severe failures indicating that the construction materials, specifically the aluminum outer conductor, became brittle at the lower temperature. On the other hand, cables which failed at warmer temperatures tended to break gradually. In the case of samples D and E, the cables first displayed kinks which eventually developed into cracks. Even cables which initially appeared to have no signs of failure (sample B) were later found to have microscopic ripples in the aluminum shell which eventually led to cracks. This indicates that the cables with foam based dielectrics are more susceptible to failure resulting from creep at warmer temperatures. This is quite problematic since cables placed in the field frequently sit in direct sunlight. On a sunny day, the temperature at the surface of the aluminum shield can easily raise to 65° C.

Thus, the samples which displayed cracks (D, E, F) are unable to transmit a signal without significant leakage and degradation due to the broken outer conductor. However, samples which displayed little evidence of this type of breakage (sample B) would most likely have electrical characteristics which would not hinder performance. Yet, the small cracks in the shield can still allow RF signal ingress and regress. If signal ingress occurred, RF waves from the environment can interfere with transmissions in public airspace. If signal egress occurred, RF leakage from the cable can be strong enough to interfere with other transmissions in the public airspace. This intrusion of cable transmissions into the airwaves is forbidden. Cable operators must periodically demonstrate compliance with FCC regulations regarding signal egress.

IMPACT TESTING

It can only be assumed that cables will have things (i.e. toolbox) dropped on them when they are placed in the field. Thus it is important to test a coaxial distribution cable's ability to withstand impact.

Test Procedure

A two foot length was subject to a three ft.-lb impact. The samples were tested at -40° C, -10° C, 20° C, and 50° C. The samples were preconditioned for four hours at the respective test temperatures.

Physical Results

Initial inspections of the samples after impact found no evidence of any cracking in the outer jacket or outer conductor of any of the cables. The only clearly visible relics of the impact were two small dents made undoubtedly by the edges of the impact weight. Only two test specimens suffered dents large enough to potentially cause problems with the electrical characteristics (based on results of compression testing). Samples A and B were deformed by approximately 10%-15%, an amount large enough to cause problems with the characteristic impedances and the structural return losses of the cables. It was observed that these dents occurred at a temperature of 50° C. At high temperatures, coaxial distribution cables lose some stiffness and

become more ductile thus making them more susceptible to damage resulting from impact.

STATIC LOAD TESTING

The cables tested were rated by their manufactures to withstand a certain amount of pulling force. Table 6 lists these values. If these cables are to be pulled at these forces, it is of interest to see the effects while the cables are under these tension and whether there will be any residual effects after the tension is removed.

Table 6 - Maximum Pull Force

Cable Sample	Max. Pull Force (lb)
A	270
B	220
C	350
D	475
E	340
F	500

Testing Procedure

A static load testing frame was used for this test. 20 ft. lengths of cable were tested. Each length was setup in the testing frame and then connected to a HP 8753D Network Analyzer. Weight was added until the cable was under the appropriate pulling force. The cable was left under tension for 15 minutes. The electrical characteristics: attenuation, structural return loss, and characteristic impedance were measured before, during and after loading.

Physical Results

The specified pulling force was well beneath the yield strength of the cable thus there was no residual elongation resulting from this short term loading.

Electrical Results

Due to the relatively low tension that these cables were placed under, it was not surprising to find that the electrical characteristics were not adversely affected by the static load test with the exception of the SRL results of both foam and disc dielectric cables. Table 7 shows percent change of the various electrical characteristics before, during, and after the loading for sample D. The amount of SRL change ranged from 8.31% to 12.7% for all samples during and after loading.

Conclusions

Despite it's fragile appearance, coaxial distribution cable is a fairly robust medium for the transmission of broadband RF signals. However, there are a few factors to consider if one is to use this medium:

1. Coaxial distribution cable is more prone to failure when placed in environmental temperature extremes.
2. Exceeding the manufacturers specified values for minimum bend radius will result in failure of the cable even at moderate temperature (20° C).
3. Compressing a cable by as little as 10% of it's original diameter can lead to levels of structural return loss and characteristic impedance which will adversely affect transmission performance.
4. A three ft-lb impact can cause significant damage to the cable particularly at elevated temperatures.
5. Pulling coaxial cable at the manufacturers specified minimum puling force is unlikely to cause any type of damage or be detrimental to the cables performance.

Table 7 – Percentage Change in Electrical Parameters of Sample D

Status	Frequency	Percentage Change Attenuation	Percentage Change SRL	Percentage Change Characteristic impedance
Before Loading	303.5 MHz	0%	0%	0%
	900.5 MHz	0%	0%	0%
During Loading	303.5 MHz	0.42%	-0.18%	0.05%
	900.5 MHz	0.26%	-5.05%	-0.29%
After Loading	303.5 MHz	0.38%	-2.03%	0.13%
	900.5 MHz	0.38%	-0.88%	-.027%

With these conclusions in mind, it is necessary to take the proper precautions when installing, servicing, or working near coaxial distribution cable.

REFERENCES

1. "Strength Characteristics of Coaxial Cable" SR-4103, Issue 1, J. N. D'Amico, et al., Bellcore, October 1996.

2. "Generic Requirements for Coaxial Distribution Cable", GR-1399-CORE, Bellcore, July 1994.

Authors

Lal M. Hore

Lal is currently responsible for the preparation of Bellcore's Generic Requirements for Outside Plant Cables and the development of broadband transmission requirements for coaxial cables and other outdoor and indoor wire and cable products. As a Project Director, he is also responsible for the analysis of various wires and cables. After receiving a M.Sc. Tech degree in applied physics from the University of Calcutta and a Dr. Tech Degree from the technical University of Budapest in Electrical Engineering, he joined Bell Northern Research in 1970 to design and develop communications cables. In 1972 Lal moved to General Cable Company where he worked as a manager in the Communications Cable Section and next as a Staff Project Manager in the Applications Engineering Section until 1987 when he joined Bellcore.

Dr. Hore has authored numerous technical papers on dielectric materials and telecommunications wire and cable and holds a number of patents on telecommunications cables.

William Mclaughlin

William received his B.S. degree in Mechanical Engineering from the University of Notre Dame in South Bend Indiana in 1996. He worked at Bellcore in 1996 and 1997 as a summer intern.

Kai V. Hsing

Kai received his B.S. in Mechanical Engineering from Carnegie Mellon University in 1997. He joined Bellcore in 1997 as associate consultant upon completion of his undergraduate studies.

COUPLING ATTENUATION: CORRELATION BETWEEN NEAR AND FAR FIELD MEASUREMENTS

Michiel Pelt, David Hess

ALCATEL CABLING SYSTEMS, Brussels, Belgium

ABSTRACT

A new test standard emerges to evaluate the EMC performance of cables and cable assemblies. With this test method called coupling attenuation balanced and unbalanced cables are investigated. The results are compared with radiated immunity tests inside a semi-anechoic chamber. Using simple antenna theory agreement between both test methods is illustrated. This enables to draw conclusions about the correctness of coupling attenuation.

INTRODUCTION

A long time industry has been looking for a simple test methods to evaluate the EMC performance of symmetrical cables, connectors and cable assemblies. Over the years multiple parameters have been introduced into standards like balance, transfer impedance, screening attenuation, etc. However these parameters describe only partly the radiation and susceptibility properties. Balance describes the conversion between differential and common mode currents on a symmetrical pair. Transfer impedance describes the relation between the common mode voltage and the current on the outside of the screen. However a system engineer is only interested in the combined effect of balance and screening as this determines the noise induced on the cable and the Bit-Error Rate.
As cables and connectors are passive devices, the radiation from a cable and the susceptibility to external fields are reciprocal. Therefor the electromagnetic performance of a passive device can be presented by a single parameter which is the relation between the injected power on the cable and the radiated power. Such a parameter expresses the electromagnetic isolation between a signal pair and its electromagnetic environment.
Today a new test method called coupling attenuation is proposed within the European standardization organization CENELEC. It measures the relation between the injected power and the maximum power of the radiating currents at either near or far end. The power of the radiating currents are measured using a current transformer around the device under test. This makes coupling attenuation a near field test method which may not give a correct indication of the EMC performance. An electric or magnetic field in the neighborhood of a device does not necessary radiate in the far field. To that aim far field tests have been done to demonstrate correlation with coupling attenuation.
In order to make the correlation as precise as possible the experiments have been simplified as much as possible. First the correlation has been focused on cables. Introducing connectors or patch panels adds a supplementary uncertainty to the measurements. Secondly the far field tests have been limited to radiated immunity inside a semi-anechoic room according to IEC 61000-4-3[1]. In this way uncertainties are avoided arising from rotating the device under test, changing antenna height, etc.
The coupling attenuation test method is described extensively inside the emerging draft standard prEN 50289-6[2]. The cabling set-up inside the semi-anechoic room is described in reports from ISO/IEC JTC1 SC25 WG3[3,4]. Therefor both test methods will not be explained in detail in this paper.
The effect from balance and screening will be investigated on the same unbalanced and balanced cables using both test methods.

This enables to verify the correlation between the test methods by applying some simple antenna theory.

COUPLING ATTENUATION

Test procedure

The electromagnetic performance of an unbalanced cable is the effect of the screen. The electromagnetic performance of a symmetrical cable is the combined result of both balance and screening. The coupling attenuation of each cable is expressed in dB as:

$$a_c = 10.LOG_{10}\left(\frac{P_1}{\max[P_{2,n};P_{2,f}]}\right)$$

where

P_1 input power of inner circuit
$P_{2,n}$ maximum near end peak power of outer circuit
$P_{2,f}$ maximum far end peak power of outer circuit

To measure this parameter the cable is fed with power P_1. Due to the electromagnetic coupling between the cable and its environment surface waves are exited and propagated in both directions along the screen surface. A surface current transformer is used for picking up the power of the surface waves with an absorber to suppress unwanted common mode currents. On the basis of the measured surface currents - $P_{2,n}$ or $P_{2,f}$ - it is possible to calculate the maximum peak power in the secondary system formed by the screen of the cable (or the cable itself) and the environment.

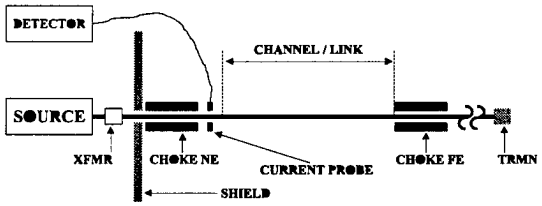

Figure 1: Schematic presentation of coupling attenuation

The cable under test is laid on a non-metallic table and connected to the generator via an impedance matching balun. The stationary absorbing clamp is placed as near as practically possible from the reflector plate for a near end measurement. For a far end measurement the absorbing clamp and the absorber are interchanged.
The power of the output of the absorbing clamp is measured for a linear frequency sweep from 30 MHz up to 1000 MHz in steps of 2.425 MHz. As the injected power injected is known the coupling attenuation can be calculated taking into account the attenuation of the set-up. For a symmetrical cable the test method is repeated for each individual pair.

Experimental results

Three different cables were measured with coupling attenuation: A coaxial cable to observe the effect of the screen, a UTP to observe the effect of the balance and a FTP (dual foil) to observe the combined effect of balance and screen.

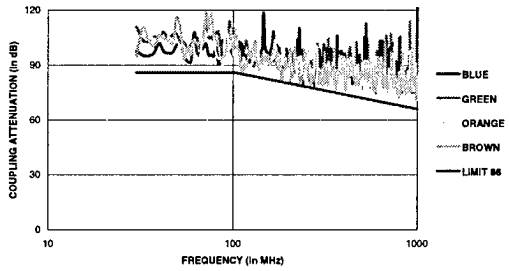

Figure 2: Coupling attenuation of a dual foil twisted pair cable

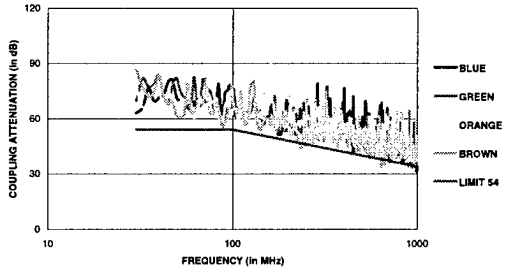

Figure 3: Coupling attenuation of an unshielded twisted pair cable

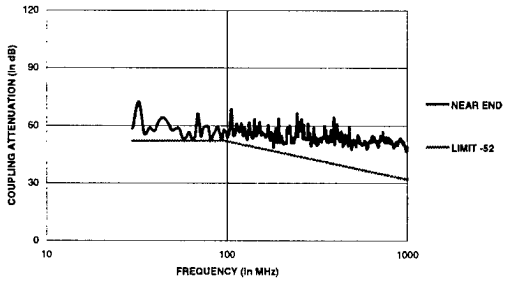

Figure 4: Coupling attenuation of a coaxial cable

The electromagnetic isolation provided by the dual foil cable is higher than for the other measured cables. The coupling attenuation of the FTP is 32 dB better than the UTP and 34 dB better than the coaxial cable.
For the symmetrical cables the recorded traces of the individual pairs remain close to a limit curve which is constant up 100 MHz but decreases with 20 dB/ decade from this frequency. This arises as electromagnetic isolation provided by the screen is independent on frequency whereas isolation provided by the balance decreases with 20 dB / decade. The level of the limit curve is a single parameter used to characterize the coupling attenuation over the entire frequency range. The same approach is proposed within the emerging draft standard for coupling attenuation.
For the unbalanced cable the isolation remains constant with frequency as the balance equals zero. The same limit curve is used to characterize the coupling attenuation over the entire frequency range although the recorded trace is nearly flat. Hence the electromagnetic isolation of the unbalanced cable increases by 20 dB/decade in comparison with the balanced cables.

RADIATED IMMUNITY

A cabling set-up is radiated inside a semi-anechoic room as specified in the radiated immunity standard ISO/IEC 61000-4-3. The transmitting antenna is placed 3 m from the cabling set-up and generates an unmodulated field of about 3 V/m. The frequency range is covered by a biconical antenna from 30 to 200 MHz and with a log-periodic antenna with two amplifiers from 200 MHz to 500 MHz and from 500 to 1000 MHz.

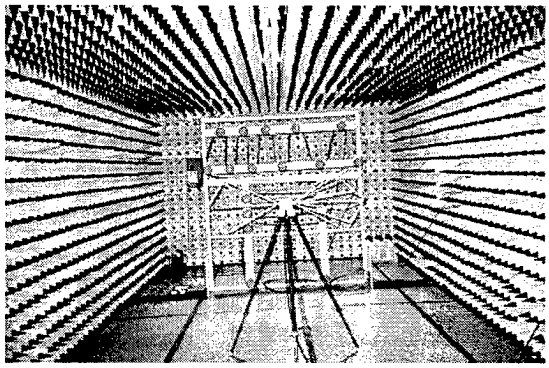

Figure 5: Picture of cabling set-up inside semi-anechoic chamber

Cabling set-up

All radiated immunity testing must be performed in a configuration as close as possible to the installed case. However for cabling there is no standardized cabling set-up to get reproducible test results. Moreover in order that it is useful for EMC tests, the set-up should not suppress or enhance certain frequency ranges, and the direction to the test set-up and polarization of the receiving antenna should not be critical.
Therefor ISO/IEC JTC1 SC25 WG3 proposed to CISPR G a set-up during the London meeting in June 1996[4]. It consists of a 10 cm thick wooden frame on which 70 m cable is wound on the front side and on the back side. The cable is routed on both sides by circular non conducting cable supports with a bending radius of 5 cm.

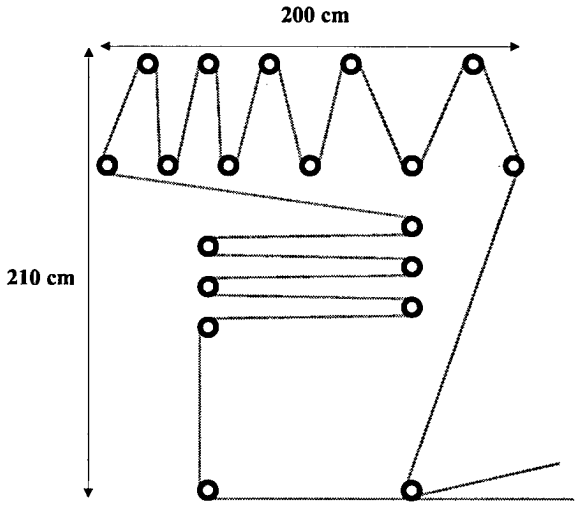

Figure 6: Position cable supports on wooden frame of cabling set-up

The properties of the cabling set-up as radiating element were investigated and compared to the emission of a dipole antenna[3,4]. It was concluded that the minimum attenuation is obtained when the cabling set-up is perpendicular to the direction of the antenna. Moreover the relative gain is quite constant over the frequency range and the set-up has no dominant polarization or directional characteristics. These results made us decide to construct an identical set-up.

Incident field

For radiated immunity testing of equipment the incident field is 80% amplitude modulated. However for linear passive devices like cables this is useless and only gives arise to more intricate calculations when correlating both test methods.
To achieve a constant field inside a semi-anechoic chamber the power fed to the antennas has to be adjusted continuously at each frequency. This makes a radiated immunity test extremely time consuming. Besides there is no reason to keep the incident field constant in order to characterize passive devices. The amount of power induced on the cable is directly related to the power density of the incident field. As cables are linear devices this ratio is totally independent of the field strength.
Therefor the power fed to the antenna was kept constant over the frequency range of each amplifier. As a consequence the incident field was not constant as function of frequency but altered due to the antenna factors and the characteristics of the semi-anechoic chamber.
Nevertheless particular care shall be taken to ensure the uniformity of the generated fields especially at lower frequencies. Because it is impossible to establish a uniform field close to an earth reference plane - i.e. the wall of the semi-anechoic chamber- the calibrated area is established at a height no closer than 0.8 m from the walls. Therefor the anechoic chamber must be sufficiently large for the cabling set-up. As the dimensions of the chamber equals 13.4 m x 4.7 m x 3.0 m this will not affect the measurements.
A "uniform area" is defined as a hypothetical vertical plane of the field in which variations are acceptably small. The size depends on the size of the device under test. For the cabling set-up the defined area is the part of the wooden framework 80 cm above the ground plane. Hence the two cable supports close to the ground plane are excluded from the measurements.

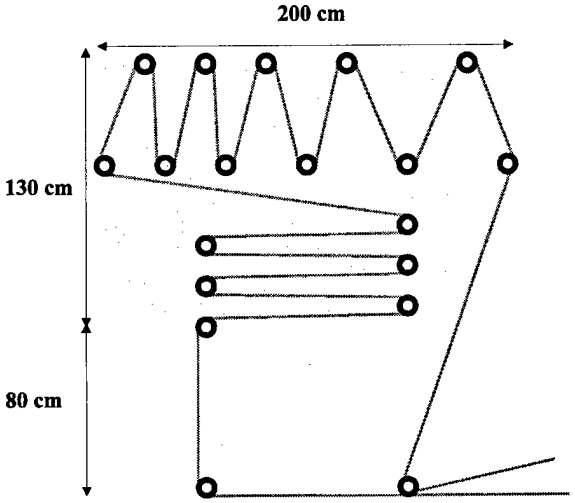

Figure 7: Defined area for which uniformity is required

The uniformity was verified over the defined area with an isotropic handhold field tester at five different locations along the area of interest, i.e. in the center and in corners of the defined area. At each location the field was measured in steps of 50 MHz up to 500 MHz and in steps of 100 MHz up to 1000 MHz for both the horizontal and vertical polarization state.

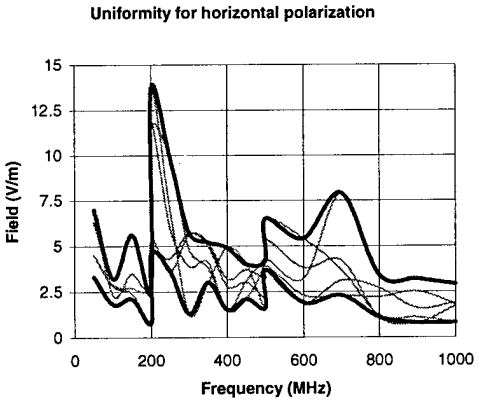

Figure 8: Uniformity of the horizontal field component - Dark traces indicates the maximum and minimum values at different locations; Light traces indicate field at each location versus frequency.

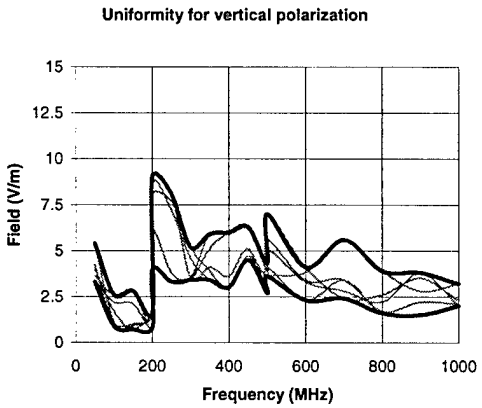

Figure 9: Uniformity of the vertical field component - Dark traces indicates the maximum and minimum values at different locations; Light traces indicate field at one location versus frequency.

According to the radiated immunity standard a field is considered uniform if its magnitude over the defined area is within - 0 dB to + 6 dB of a nominal value over 75 % of the surface. The tolerance of 6 dB is considered to be the minimum achievable in practical test facilities. By eliminating 17 % of the recorded values for the horizontal polarization and by eliminating 11 % of the recorded values for the vertical polarization all the remaining values are within 0 dB to 6 dB limit over the defined area. Hence the field generated by an antenna placed 3 meters from the device under test is uniform. For equipment testing the minimum field strength is of importance, i.e. the magnitude of field over the defined area which corresponds to the 0 dB value. This is logical because an incident field with a higher magnitude will certainly interfere with the equipment. However when characterizing passive devices it is the average incident field of all recorded values that is of interest.

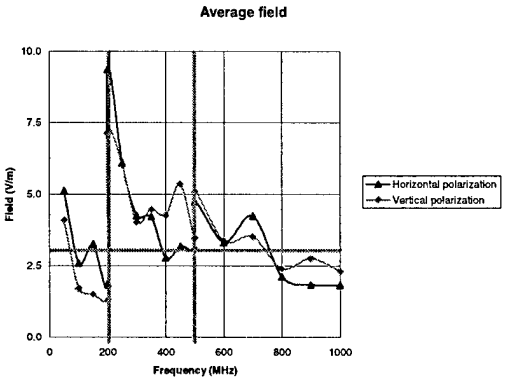

Figure 10: The average field strength over the defined area

The average field strength varies strongly from 1.8 V/m up to 9 V/m. When averaging over frequency the field strength varies slightly around 3 V/m.
Observe that the that the traces for horizontal and vertical polarization are very close to each other. This indicates the polarization insensitivity of the cabling set-up.
When an amplifier is changed, i.e. at 200 MHz and 500 MHz, the uniform field inside the semi-anechoic chamber changes drastically because the antenna is fed with different power levels.

Monitoring noise power

The signal induced on the cable is measured outside the semi-anechoic chamber with a spectrum analyzer (bandwidth 100 kHz). To measure the balanced cables an impedance matching balun is inserted with a balance of 40 dB from 30 MHz to 1000 MHz. This is the same balun as used during the coupling attenuation tests and was put inside a small metallic box fixed to the wall inside the semi-anechoic chamber. The common mode rejection ratio was further improved with ferrite blocks just in front of the balun like for the coupling attenuation tests.

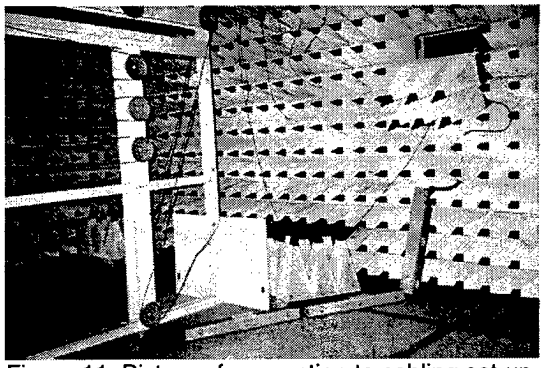

Figure 11: Picture of connection to cabling set-up inside the anechoic chamber

Experimental results

In figures 12-13 the induced noise is shown for horizontal and vertical polarization of the antenna. For all cables the traces for the horizontal polarization are very close to the traces of the vertical polarization. This indicates again the polarization insensitivity of the cabling set-up.

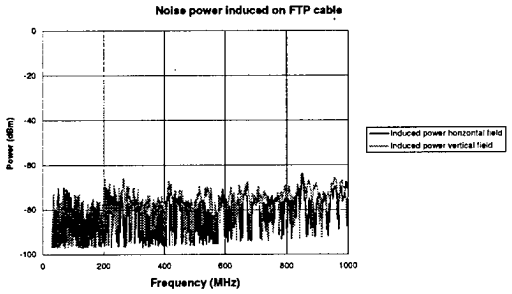

Figure 12: Noise power induced on a dual foil twisted pair cable

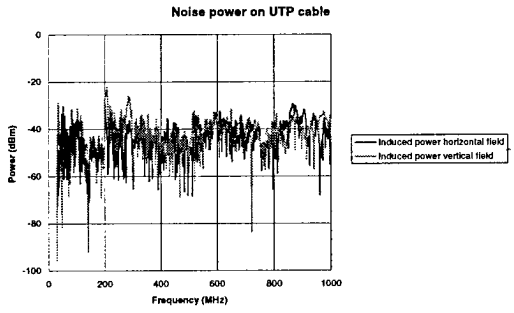

Figure 13: Noise power induced on an unshielded twisted pair cable

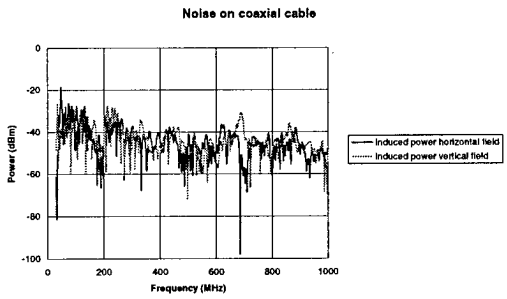

Figure 14: Noise power induced on a coaxial cable

Besides for the unbalanced cable the induced noise seems to be independent of frequency. This is not in contradiction with coupling attenuation as will be explained in next section. The traces for the dual foil cable are about 30 dB lower than the traces of the UTP cable. This difference was also observed with previous test method and applies also to the coaxial cable. However for the unbalanced cable the induced noise decreases with 20 dB/decade with respect to the symmetrical cables. This was also confirmed with previous test method.

CORRELATION FAR FIELD - NEAR FIELD

Theoretical calculations

The induced noise power by a field of 3 V/m can be calculated using simple antenna theory. The amount of energy an antenna picks-up from the an incident field depends on the antenna aperture. The latter is given by following equation:

$$G(\theta,\varphi) = \frac{4.\pi.A_f(\theta,\varphi)}{\lambda\lambda}$$

where

$G(\theta,\varphi)$	antenna gain
$A_f(\theta,\varphi)$	antenna aperture
λ	wavelength

The gain of the cabling set-up have been investigated by comparing the radiation from the cabling set-up with a resonant dipole antenna[3,4]. It was concluded that the relative gain of the cabling set-up referred to a dipole was quite constant over the frequency range of interest and very close to that of a

resonant dipole (gain = 1.64). Using this value the amount of power captured by the cabling set-up is found by multiplying the magnitude of the incident field with the effective aperture. For a constant field of 3 V/m over the entire frequency range the captured power is shown in figure 15.

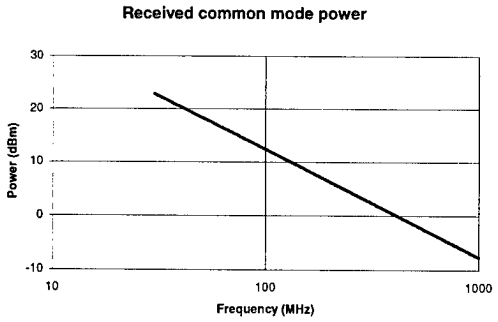

Figure 15: Power picked up from a 3 V/m field

Due to the wavelength dependence of the antenna aperture the power picked-up from the field decreases with 20 dB per decade. Part of the captured power is converted into signals that interfere with the data transfer due to non-infinite balance or non-zero transfer impedance. This electromagnetic isolation provided by the design of the cable is expressed by its coupling attenuation. The behavior of coupling attenuation versus frequency is approximated by the limiting curve which fits very closely to the recorded values for the symmetrical cables. The limit curve is constant up to 100 MHz after which it decreases with 20 dB/decade.

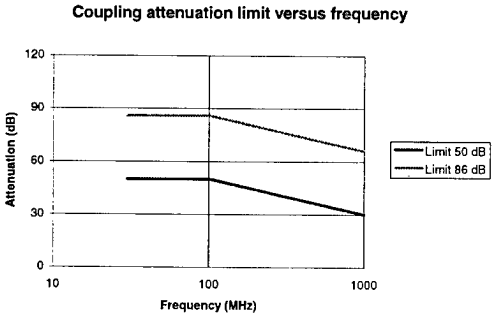

Figure 16: Approximation of coupling attenuation versus frequency

To find the power induced on the cable the attenuation provided by the design of the cable has to be subtracted from the power captured by the cabling set-up.

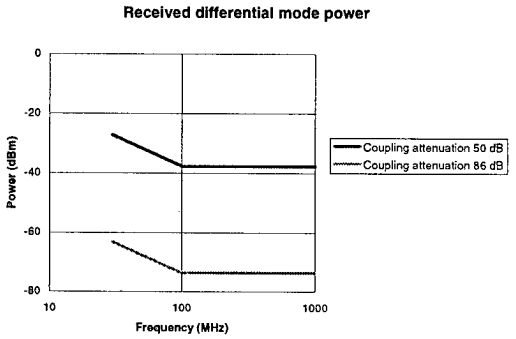

Figure 17: Noise induced on cables with different coupling attenuation by 3 V/m

The induced noise power is flat from 100 MHz like observed in the radiating immunity experiments for the symmetrical cables. This arises as both the received common mode power and the limit curve for coupling attenuation decrease with 20 dB/decade.

Correlation between both test methods

In previous sections it was shown that the uniform incident field was not constant. However when averaging over frequency a value very close to 3 V/m was obtained. For this reason the induced noise power is calculated for 3 V/m for the values of coupling attenuation found in the first section.

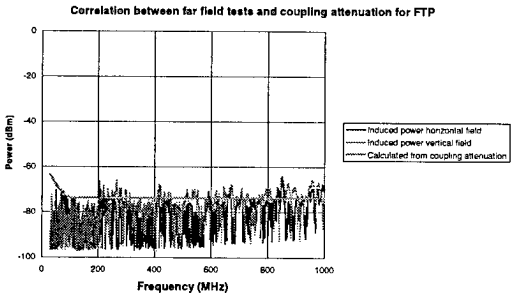

Figure 18: Correlation for dual foil twisted pair cable

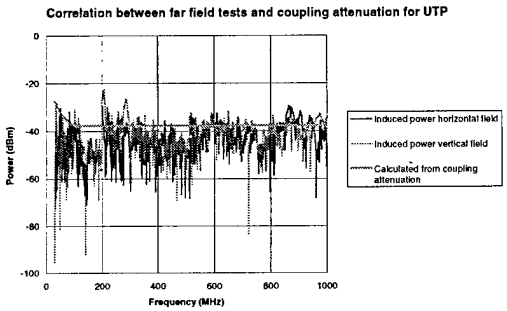

Figure 19: Correlation for unshielded twisted pair cable

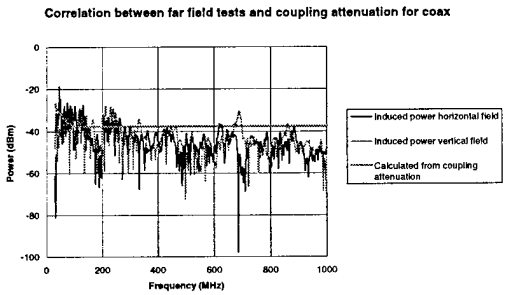

Figure 20: Correlation for coaxial cable

It can be observed that the values vary about 6 dB above and below the calculated noise power. This is acceptable as the accuracy of coupling attenuation and the incident field equals 6 dB. High peaks or dips occur especially at those frequencies where the average field is extremely high. For instance when changing the amplifier at 200 MHz the average field is 1.8 V/m at the end of the frequency range of the first amplifier whereas 9.0 V/m at the beginning of the frequency range of the second amplifier. This generates a dip just below 200 MHz and a peak just above 200 MHz on all graphs above.

Also the effect of approximating the coupling attenuation versus frequency by a limit curve can be observed at the low frequencies. When looking at the recorded data for coupling attenuation only the coaxial cable intersects the limit curve below 100 MHz. For the balanced cables this is not the case and therefor they are lower than the calculated noise power.

A more precise comparison between both test methods is beyond the scope of this paper. This would imply taking into account the field distribution over the cabling set-up, the coupling attenuation versus frequency (not approximating it by a limit curve), the change of the antenna gain versus frequency, etc. Nevertheless satisfactory agreement between both test methods is found.

CONCLUSIONS

A near field emission measurement called coupling attenuation is compared with a radiated immunity test inside a semi-anechoic chamber by measuring the EMC performance of balanced and unbalanced cables. Both test methods are well recognized and specified in the emerging draft standard prEN 50289-6 and in IEC 61000-4-3.

The electromagnetic isolation provided by the screened cable was higher than for the other measured cables. The differences in coupling attenuation between the various cables was equal to the differences in induced power for the radiating immunity test. The coupling attenuation of the symmetrical cables decreased by 20 dB/decade whereas the coupling attenuation of the coaxial cable was fairly independent of frequency. Similar observations were made for the radiating immunity test where the induced power on the symmetrical cables was independent on frequency but the induced power on the unbalanced cables decreased by 20 dB/decade. The experimentally observed resemblance between both test methods was demonstrated theoretically using simple antenna theory.

Moreover it allowed to calculate the noise power caused by a field - with an arbitrary field strength - and induced on a cable - with an arbitrary coupling attenuation. By calculating the noise power for the field used during the radiating immunity tests and the values of coupling attenuation measured very nice agreement was found between both test methods.

In conclusion the results obtained with coupling attenuation are confirmed by the radiated immunity tests. Not only differences in coupling attenuation between the various cables confirmed the results with far field test method but also the calculation of the induced noise power from the incident field. So both relative and absolute agreement is found between both test methods.

REFERENCES

[1] ISO/IEC 61000-4-3, *"Electromagnetic compatibility (EMC) - Part 4: Testing and measurement techniques - Section 3: Radiated, radio-frequency, electromagnetic field immunity test"*, International Standard, ISO, 1995.

[2] prEN 50289-6D, "*Generic specification for electrical test methods for cables used in analogue and digital communication and control systems - Part 6D: Coupling attenuation, absorbing clamp method*", European draft standard, CENELEC, 1998.

[3] E. Bech, *"Evaluation of proposed generic cabling set-up to be included in EMC testing of information technology equipment based on electromagnetic field tests"*, Working document ISO/IEC JTC1 SC25 WG3 /BARCELONA/48, 1997.

[4] ISO/IEC JTC1 SC25 WG3 / N465, *"Liason letter to IEC CISPR G concerning a standard cabling set up for inclusion in CISPR 24"*, Liason report, ISO, 1997.

AUTHORS

Michiel Pelt
Alcatel Cabling Systems
Competence Center
Bd. Paepsemlaan 16
B-1070 Brussels, Belgium
Tel (32) 2 556 0850, Fax (32) 2 556 49 50
Michiel_Pelt@compuserve.com

Michiel Pelt obtained his degree of engineer in applied physics at the Free University of Brussels in 1992. The following years he continued to work as researcher in photonics and produced 10 papers which were published on various international recognized conferences within the optical society. The last four years he is responsible for the research on EMC of structured cabling systems within Alcatel Cabling Systems. He presented already various tutorials on BICSI conferences and papers on European EMC conferences and IWCS. Pelt is a member of different standardization committees within CENELEC which deal with topics related to EMC as TC 215/WG2 and TC 46X/WG3.

David Hess
Alcatel Cabling Systems, NA
5 Great Valley Pkwy
Malvern, Pennsylvania 19355, USA
Tel (1) 610 651 78 10
Fax (1) 610 651 78 11
dhchess@compuserve.com

David Hess, Malvern, PA, has worked for more than 22 years in product design and development in the fields of electronic and optical data communication cabling. He is currently employed as Vice President of Product Marketing with Alcatel. He participates on various data communication and interface standards committees in TIA/EIA, ANSI, and ISO/IEC. He has been active on the TIA TR41.8.1 Premises Cabling Committee since 1989 and on the ISO/IEC JTC1 SC25 WG3 Premises Cabling Committee since 1994. Hess has a B.S. degree in mathematics from Pennsylvania State University and is member of IEEE and BICSI.

Powerline Telecommunication PLC

Ralf Kallenborn

GHMT mbH, Bexbach/Saar, Germany

Abstract

In principle, it is possible to transmit data rates in the megabit per second range via power supply lines. However, the available bandwidth largely depends on the installation structure as well as on the age and type of the cables. By developing methods of measurement which allow to analyze low-voltage distribution networks with respect to their transmission parameters, the required foundation will be provided in order to develop powerful new procedures for the transmission of data along low-voltage networks.

This lecture presents measuring procedures which allow to detect sources of errors and faults when data are transferred through a low-voltage network. A number of examples and test records are also provided in order to explain these methods.

Market Situation

Why is powerline telecommunication so promising?

The information and service era, that has already started, is characterized by the fact that the demand for accesses to the global information highways is increasing exponentially. The number of – currently – about 60 million Internet users e.g. is rising each year by more than 100% while (compared with this number) there are more than 750 million telephone connections worldwide. In Europe, approximately 10% of all households have a PC, and 50% of these have Internet accounts.

The main reasons why users at the moment do not want an Internet access are the insufficient transmission rates and the high costs of the offered accesses.

On account of the worldwide liberalization of telephone and data services, the number of telecommunication providers is certainly increasing. However, bridging the so-called "last mile" – is still carried out almost exclusively by formerly state-owned telephone companies which therefore also control the setting of prices.

The existing power supply networks of regional and municipal utilities would now be an ideal alternative allowing to bridge the gap between the available backbone lines of competing network providers and end users.

Market Opportunities

Due to the worldwide liberalization of the power and telecommunication markets, the chances of alternative providers are rising to establish themselves as true competitors of already existing – and to date monopolist – companies. In particular, electric utilities are interested in the newly emerging markets because they have recognized that the power supply market stagnates and, accordingly, the demand for a further extension of power station and network capacities is dropping as well. The introduction of PLC offers entirely now perspectives to them as well as to any provider of power supply networks. Power-related services can then be extended from simple, unidirectional rate-changing devices, etc. to high-quality, bi-directional services for customers providing added value. Stationary changeovers to overnight rates will be replaced by dynamic rates similar to the customary phone rates. In addition, PLC offers power utilities the opportunity to enter the market of telecommunication services.

Infrastructure

The dominating infrastructure on the various voltage levels has a decisive influence on their suitability for PLC.

On account of its mostly unmeshed lines as well as its transmission properties, the high-voltage level is, in principle, suited for the transfer of high bit rates. The disadvantages of

the high-voltage level are, however, the missing connections to the individual households and the optical fibers that are installed in parallel in the overhead earth wires. Although the utilization of the high-voltage level would be possible for PLC, it will not be required because of the existing optical fiber infrastructure which provides a full coverage.

The medium-voltage level is rather unsuited for PLC due to its highly meshed infrastructure.

The most efficient voltage level for a PLC utilization comprises local power supply distribution networks with the benefits of direct connections to the customers and short line lengths.

Development of PLC

The utilization of power supply networks for the transmission of information is certainly nothing new. Already in the twenties, there were centralized telecontrols, i.e. so-called ripple controls, for streetlights, loads, remote meter reading, and rate changing on the various levels of a power supply network.

Unidirectional audio-frequency ripple control systems are used on the medium-voltage and low-voltage levels with frequencies of up to 3 kHz and transmission levels of up to 1 MW.

Carrier transmission is used on high-voltage lines with frequencies ranging from kilohertz to gigahertz at a transmit power of several watts.

In the in-house area, the baby phone allowing voice transmissions of severely restricted quality has also been known for several years.

The control of devices in domestic areas as well as in industrial networks started 20 years ago through systems such as X-10 (50 bit/sec). Today there are several applications with transfer rates of up to 100 kbit/sec.

Within the frequency range that has been approved for data transmissions (Europe: 3 – 148.5 kHz; U.S.A. and Japan: up to 500 kHz), systems are available for both in-house and outdoor applications which offer transfer rates of up to 27 kbit/sec.

The utilization of the frequency range beyond 148.5 kHz and 500 kHz respectively that to date has not been released yet is also within easy reach. Transfer rates of more than 1 Mbit per second have already been realized.

Obstacles

Hence there is no lack of applications. Prior to the rollout, several obstacles must still be eliminated, however. The first group of problems could be described as "*missing standardization*" while the second group comprises "*technical and physical problems*".

- Lacking standardization

The most urgent need for action within the first group concerns the assignment of frequencies from 148.5 kHz to 20 MHz which are required for PLC. Prior to the definite assignment of the necessary frequency range, regulatory authorities, manufacturers of PLC applications, and measuring laboratories must find a way which ensures the EMC of both emissions and immissions. The immunity to interference of domestic appliances, medical applications, etc. must be examined through comprehensive series of measurements. In addition, the coexistence of long, medium and short waves, emergency call systems, PLC, as well as ADSL/XDSL must be considered.

- Technical and physical problems

One of the main technical and physical obstacles is the time, site and frequency variance of the network impedance. The time and frequency variances are caused by connections and disconnections of household appliances, machines, etc. The site-specific variance results from the differing number of parallel winding phases at various parts of the network (e.g. the impedance on the transformer level is equal to the image impedance divided by the number of outbound phases).

A special feature of low-voltage networks is the finely meshed structure and the resulting propagation of the signals along various paths. A signal that is e.g. supplied on the transformer level propagates on up to 10 outbound winding phases and is reflected at various distances in dependence on impedance changes. The signal which was originally sent to household A is therefore received several times, attenuated, and with considerable delays – firstly because of the large number of possible paths and, secondly, because of the manifold reflections (cf. Figure 11). This leads to interference, i.e. reinforcements and quenching which can be recognized in the measuring curves by the surging attenuation values for several frequen-

cies. This effect of multi-path propagation is known as "fading" from mobile radiocommunications. Each section of a line is characterized by two typical attenuation curves – determined by the wiring and cabling arrangement – for the transmit and receive directions which are relatively constant as a function of time. The directional dependence can clearly be seen from Figure 11.

The high level of "contamination" of the network through interference signals additionally complicates the utilization of this medium for the transmission of information. Within low-voltage networks, basically the following sources of interference can be expected:

1. Noise
2. Radiant interference power received by radio facilities
3. Switched inductors (bursts)
4. Atmospheric discharges (surges)
5. Network-specific phenomena
   - Voltage rises / drops
   - Voltage failures
   - Overvoltage
   - Harmonics / ripple-control signals

Solutions

In order to master all these complex problems, measuring procedures will be required which allow to evaluate the transmission characteristics of both de-energized and energized networks. The developed measuring procedures will presented in the following.

The frequency range under review has been selected in such a way that the requirements applying to data transfers with high bit rates in the Mbit/sec area are complied with and the physical properties of the cable infrastructure simultaneously support these requirements. Thus a frequency range between 150 kHz and 20 MHz has proved to be suitable.

Measuring Procedures

Measurements in de-energized condition

In order to be able to evaluate the high-frequency characteristics of the actual cabling structure, low-voltage cables which are today customarily used for connections from the transformer substation to households are examined with respect to:

- image attenuation a_v;
- near-end crosstalk (NEXT) a_n;
- impedance Z_w (wave impedance);
- reflection characteristics a_r (return loss);
- phase velocity v_p.

Examinations carried out in Germany have shown that spur lines of the type without concentric conductor (cf. Figure 1 a) are mostly used for the connection of households. Such lines consist of four-wire, unshielded cables with an approximately symmetric structure as well as a PVC insulation and do not include any concentric conductor.

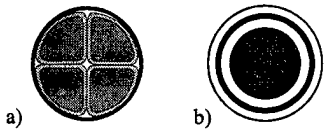

Figure 1: Typical low-voltage cable

To save weight and costs, aluminum is the preferred material for conductors. The distribution downstream of the transformer is effected via aluminum cabling with a cross section of 95 mm² or more. The standard cross section of household spur lines which amounts to 50 mm² can also be larger (depending on the load and the length) although such larger cross sections are not required in most cases.

This type of cables without a concentric conductor is used in many cases. Other concentric cable types (cf. Figure 1 b) are no longer installed but are still used.

- Cable measurements

Both cable types 4 x 50mm² (144 m) and 4 x 95mm² (200 m) were tested with respect to the above-mentioned parameters.

The return losses of both cables were always lower than 10 dB (cf. Figure 6).

The measured impedances are in the order of the wave impedances indicated in Figure 2. The phase velocity (cf. Figure) is slightly higher than the quantity mainly determined by the insulation material PVC ($\varepsilon_r = 4$) and amounts to approximately:

$$v_p \approx \frac{c_0}{\sqrt{\varepsilon_r}} = 1{,}5 \cdot 10^8 \text{ m/s}.$$

	4 x 50 mm²	4 x 95 mm²
Z_w/Ω (side by side)	45	40
Z_w/Ω (opposite)	58	50
NVP = v_p/c_o	0.54	0.58

Figure 2

The slightly higher NVP value of the cross section of 95 mm² is caused by the larger thickness of the wire insulation and the resulting increase of the capacitance per unit length.

Measurements of the near-end crosstalk attenuations (NEXT) showed that opposite wire pairs meet the requirements of cable category 3 while side-by-side wire pairs, however, distinctly miss them (cf. Figure 3). The reason for the considerably better values of opposite pairs consist in the favorable arrangement (similar to a star-quad stranding) which causes field lines to be extinguished between the two pairs.

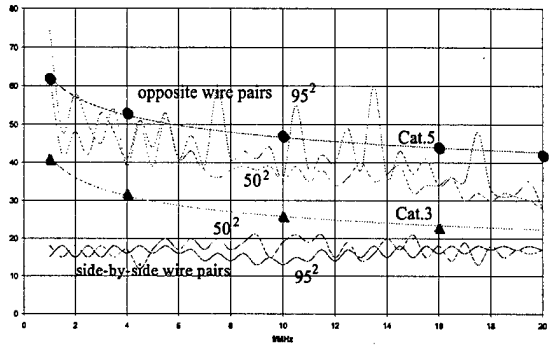

Figure 3: NEXT

Measurements of image attenuation showed that the Category 3 limits are met for all possible combinations of both types – with the results being better for the cable with the cross section of 95 mm² (cf. Figure 4).

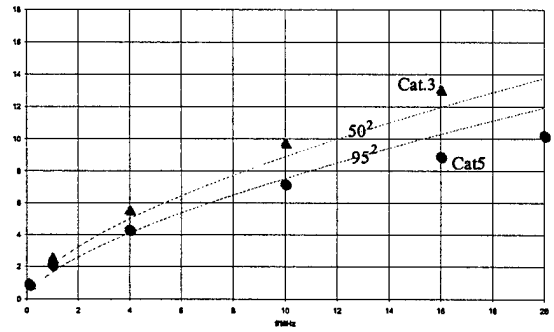

Figure 4: Image attenuation per 100 m

- Cable and coupling box

Using the cable type NAYY-J, a test section with the cross sections 50 mm², 95 mm² and a customary junction box was set up (cf. Figure 5) and tested with respect to its transmission characteristics.

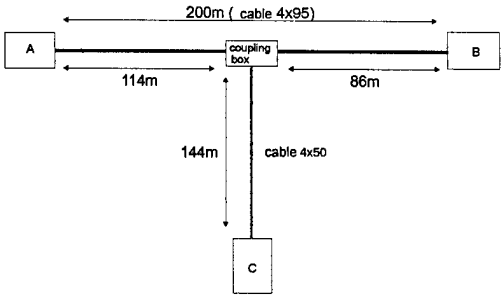

Figure 5: Measuring arrangement in the lab

Compared with non-branched lines, the image attenuations (with the installed service junction box) were higher by about 5 dB across the entire frequency range. The respectively open spur line was terminated with the wave impedance. This constant increase of the attenuation which is not dependent on the frequency is caused by the splitting-up of output (attenuation of 3 dB). The remaining 2 dB can be explained through reflections on the cable box.

The values of the return loss of the branched configuration showed a degradation of up to 20 dB in the low-frequency range and asymptotically approached the line reflections for high frequencies (cf. Figure 6). This curve is caused by the attenuation of the comparatively long line up to the junction which tends to hide the reflection influence of the box for high frequencies.

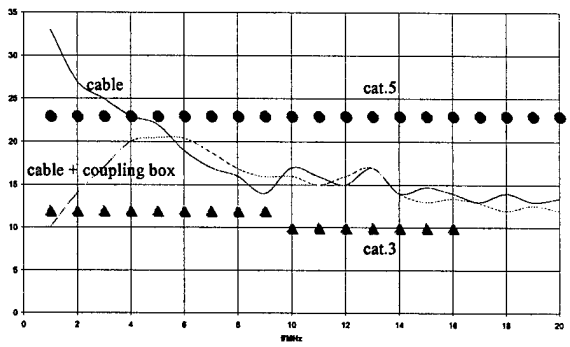

Figure 6: Return loss

The changes of the impedance along the line length for various terminating elements can best be represented by means of a TDR[1] measurement. Figure 7 indicates, by way of an example, the impedance as viewed from the

1 Time Domain Reflectometer

service junction box HAK1 with various terminating elements of HAK2 and HAK3.

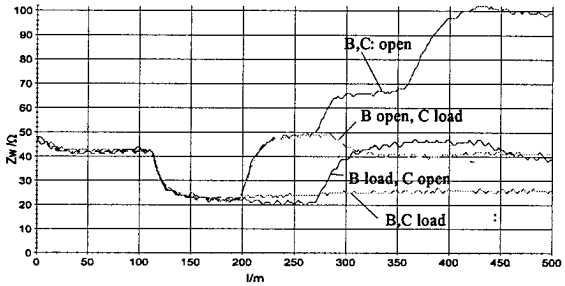

Figure 7: Impedance with various terminating elements

Measurements in energized condition

In order to evaluate the transmission characteristics of the energized low-voltage network, a measuring procedure had to be developed which allows to determine the attenuation and the signal-to-noise ratio of the respective energized network segment.

The network coupling required for this purpose must protect the measuring device against the network frequency and mains-borne overvoltage; it must have a transmission function which is nearly independent of the frequency in the frequency range to be tested, and it must adjust the impedances of the measuring devices and generators to the network impedance.

The adjustment to the network impedance as well as the protection against low-frequency "interference" including the network frequency is provided by a bandpass (cf. Figure 9). There have been problems regarding the adjustment to the constantly changing impedance of the network. However, the bandpass which was used had been dimensioned in such a way that its operating loss was always lower than 3 dB at a changing network impedance of 10 to 200 Ω (cf. Figure 8).

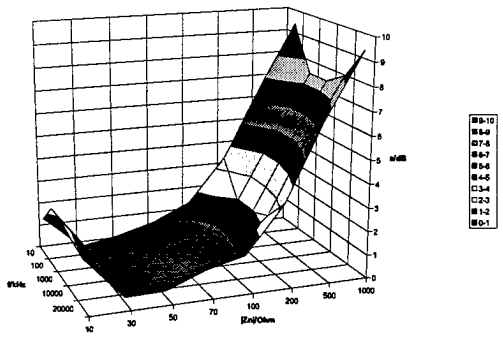

Figure 8: Coupling attenuation

In order to be able to restrict transient overvoltages occurring in the network which may amount to several kilovolts to values of a few volts (in accordance with the requirements applicable to the powerline area), staggered protective elements, i.e. so-called hybrid overvoltage circuits, are used ranging from coarse protection to fine protection. The energetic coordination between coarse, medium and fine protection is carried out by suitable inductors (cf. Figure 9).

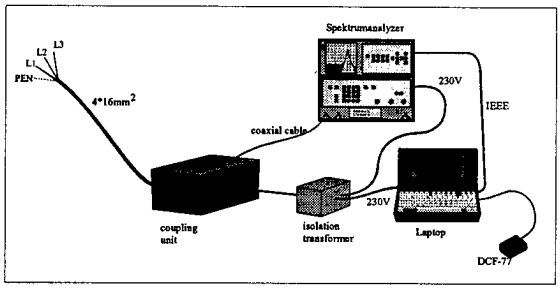

Figure 9: Coupling to the network

In order to determine the attenuation and the signal-to-noise ratio, the same measuring arrangement is used. The transmitting side consists of a signal generator and a control computer which supplies a well-defined level via the coupling element to the network. On the receiving end, a spectrum analyzer simultaneously measures – via the same coupling element to the network – the receive level (cf. Figure 10). The attenuation is then equal to the difference of transmit and receive levels. The synchronization of transmitter and receiver is ensured by time signal sender DCF-77.

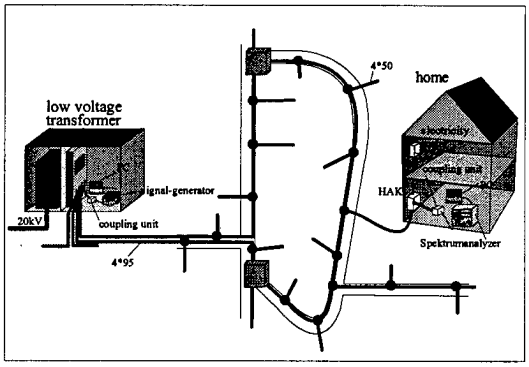

Figure 10: Measuring arrangement

The two measuring curves in Figure 11 clearly show that they are dependent on time, frequency, and direction. The distinct frequency-selective increases of the attenuation of up to 40 dB are caused by the meshed structure of the installation network and the resulting possibility of multipath propagation of the signals. Due to the differing line lengths and propaga-

tion times, interferences occur which give rise to attenuation increases.

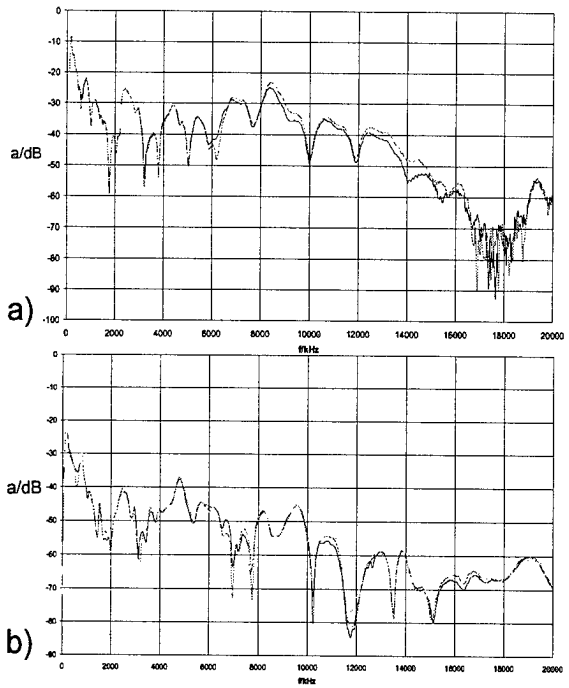

Figure 11: Attenuation
a) A -> B; b) B -> A

The measurements of the signal and noise levels which are required in order to calculate the signal-to-noise ratio must be carried out in very short intervals as the noise level varies very much as a function of time. An interval of one second has been realized between the signal level and the noise level.

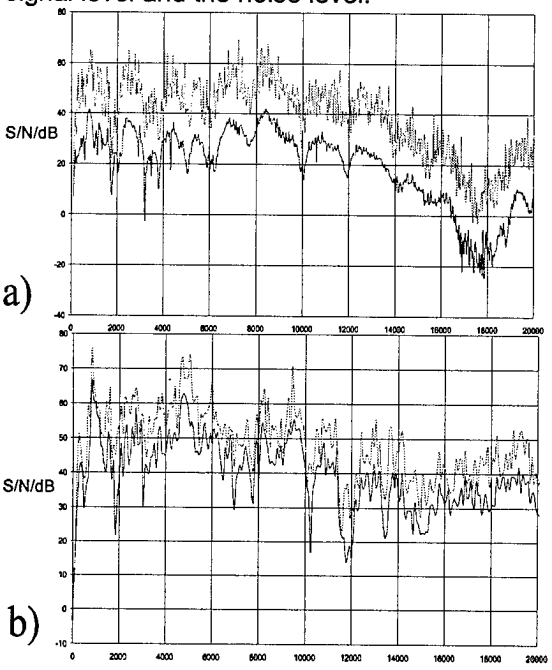

Figure 12: S/N
a) B; b) A

In order to be able to record short interfering pulses, max hold measurements of the interference spectrum are additionally registered for a longer period of time. In connection with the attenuation measurements, a worst-case signal-to-noise ratio can then be indicated.

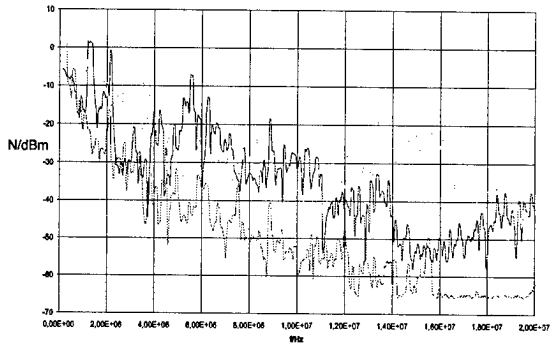

Figure 13: Interference spectra

CONCLUSION

Powerline Telecommunication is a technology which will certainly have distinct reinvigorating effects on the telecommunication and power supply markets. As soon as the regulatory authorities have granted the utilization of the corresponding frequencies, power utilities as well as operators of municipal networks will be able to extend power-related services and also offer telecommunication services. The presented measuring procedures can be used to establish the basis for future standards, to determine the suitability of low-voltage networks for PLC, and to detect faults in existing PLC networks. It is also planned to include tests regarding the strength of interference fields and interference voltages in order to support the EMC standardization activities.

Within the framework of our project "Powerline Telecommunication", it is also planned to continue the further development of these measuring procedures.

BIOGRAPHY

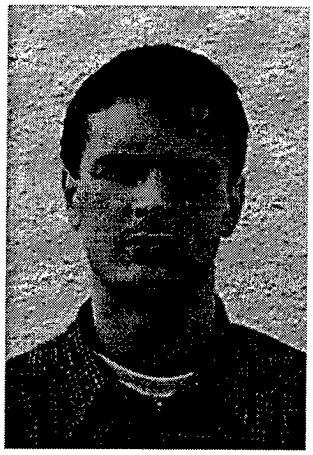

Ralf Kallenborn (age: 27) studied telecommunications in Trier, Germany and graduated as a Diplom-Ingenieur. His diploma thesis which he prepared in 1997 at GHMT in 1997 focuses on the development of measuring procedures to determine high-frequency infrastructure parameters of low-voltage networks.

Since mid of 1998, he is responsible for the project "Powerline Telecommunication" of GHMT as well as the qualification of municipal networks.

Mailing address

GHMT
Gesellschaft für Hochfrequenz-Meßtechnik mbH
In der Kolling 13

D 66450 Bexbach/Saar
Germany

Phone: ++49 / 68 26 / 92 28 – 31
Fax: ++49 / 68 26 / 92 28 – 99
e-mail: kallenborn@ghmt.com

Development of the dry type water blocking optical cables with SZ-slotted core and 2-fiber ribbons

Hirohito Watanabe, Naoki Okada, Masayoshi Yamanaka, Matsuhiro Miyamoto

Fujikura Ltd.
Telecommunication cable department Optical access network laboratory
1440, Mutsuzaki, Sakura-shi, Chiba, Japan

ABSTRACT

The newly designed dry type water blocking optical cables with SZ-slotted core and 2-fiber ribbons have been developed. The conventional water blocking optical cables contain jelly for the purpose of water blocking. The new type cables are not filled with jelly to simplify fiber joining work. In these cables, water swellable tape is wrapped around a slotted core to prevent the water penetration.

However, the fiber ribbon movement in case of severe environmental condition may occur in the non-jelly filled cable constructed by the conventional SZ-slotted rod. Then, from the view point of preventing the fiber ribbon movement, two types of cables have been designed and manufactured. One is the core put with cohesive elastomer intermittently to fix the 2-fiber ribbons, the other is the core structure of short SZ lay length.

Trial cables were tested and showed excellent transmission, mechanical and water blocking characteristics. Moreover, it was verified that the amount of the fiber ribbon movement can be kept small.

1. INTRODUCTION

In recent years, the optical subscriber networks are under construction. In order to construct subscriber networks economically, mid span access is frequently used.

In Japan the SZ-slotted core water blocking optical cables with 2-fiber ribbons are widely used in aerial and underground applications for easy mid span access.[1] But these cables are filled with jelly compound. And it is necessary to remove jelly from ribbons when splicing operation. So it is time-consuming and messy to wipe out jelly from 2-fiber ribbons. Demands of non-jelly filled cable are increasing for quick and clean mid span access operation. The non-jelly filled cable may degrade the reliability due to easier fiber ribbon movement against severe thermal and vibrational environments. We designed, fabricated and tested the dry type water blocking optical cables with SZ-slotted core and 2-fiber ribbons considering the prevention of fiber ribbon movement.

2. CABLE DESIGN

We designed new cable structure to accommodate 24, 48 and 128 fibers. These cables are composed with the SZ-stranding structure and non-jelly filled dry type water blocking structure.

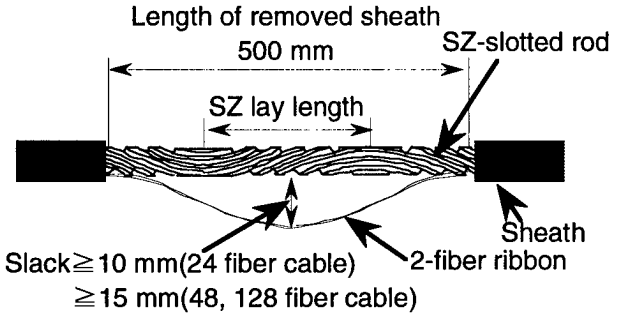

Fig. 1 Fiber slack of SZ-slotted rod cable

2.1 Requirements of cable structure

Following requirements are considered for new cable design.

(1) Mid span access operation

The necessary slack for mid span access operation is at least 10 mm (24 fiber type) or 15 mm (48,128 fiber type). This amount of slack has to be got from SZ-slotted core of 500 mm removed sheath length which is equivalent to the length of jointing closure as shown in Fig. 1.

(2) Water blocking

These cables are used in underground duct. Water blocking performance is required.

(3) Transmission, mechanical and temperature characteristics

(4) Reliability

Cables are sometimes installed under vibrational surroundings such as aerial application and cable routes near heavy traffic. Fiber movement from the cable core in the joint closure may cause small bend and loss increase. Stable fiber clinging are required under these condition.

Considering the requirement, we designed following three type of cables and compared them with the conventional cable. Dimensional parameter and cable cross section is shown in Fig. 2 and Table 1.

(a)Conventional jelly filled structure

Type (a) is the conventional jelly filled type cable structure which has 250 mm of the SZ lay length. This slotted core is filled with jelly to obtain water blocking characteristics and prevention of the fiber ribbon movement.

(b) Non-jelly filled structure

Type (b) is the non-jelly filled cable whose slotted rod is as same as that of conventional cable. In this cable, the water swellable tape is wrapped around a slotted core for the purpose of water blocking. This cable don't have any additional modification except for elimination of jelly.

(c) Intermittently bonding structure

Type (c) is the same structure as type (b) cable, but a small amount of cohesive elastomer is put intermittently to fix 2-fiber ribbons to SZ-slotted core for the prevention of the fiber ribbon movement. But this resin is soft but easily removable. In this cable, water swellable tape is wrapped around a slotted core for the purpose of water blocking.

(d)Short SZ lay length structure

Type (d) cable structure has short SZ lay length. The SZ lay length is 125 mm. In this cable, water swellable tape is wrapped around a slotted core for the purpose of water blocking. On the condition of the same stranding pitch radius, the fiber slack of this cable is lager than that of the conventional cable. Then, small diameter and light weight is achieved in this cable.

Fig. 3 shows the comparison of conventional

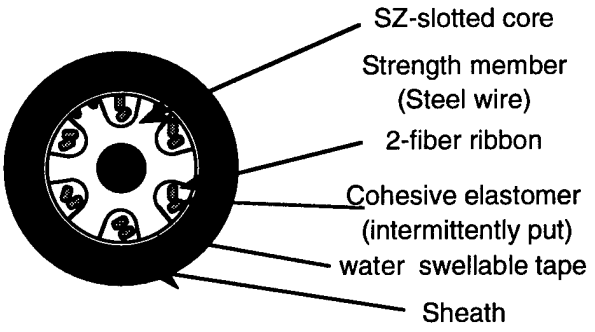

(c)Intermittently bonding type cable

Fig.2 Cross section of 24-fiber type cable

Table 1 Cable structure of 24-fiber type cable

	Cable diameter [mm]	Cable weight [g/m]	SZ lay length [mm]	Water blocking structure	Prevention of the fiber movement
(a) Conventional jelly filled structure	12.5	143	250	jelly filled	jelly filled
(b) Non-jelly filled structure	12.5	143	250	water swellable tape	none
(c) Intermittently bonding structure	12.5	143	250	water swellable tape	Cohesive elastomer put intermittently
(d) Small SZ lay length structure	11.8	121	125	water swellable tape	small SZ lay length

jelly filled type cable and newly designed short SZ lay length cable with 128 fibers. The outside diameter and weight of conventional cables and newly designed cables are shown in Table 2. The outside diameter and weight is reduced to be 17.0 mm and 220 g/m as shown in Table 2. The newly designed cable with short SZ lay length has smaller diameter by 8% and lighter weight by 18% than conventional one.

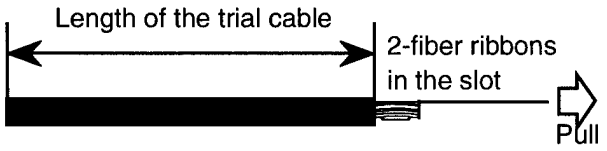

Fig.4 The measurement method of the pulling force of the fiber ribbon from the slot

3. CABLE CHARACTERISTICS

We manufactured trial cables such as (a) conventional jelly filled type cable, (b) non-jelly filled cable, (c) cohesive elastomer intermittently put cable, (d) short SZ lay length cable and we tested these cables.

Fiber ribbon moving resistance

We investigated the fiber ribbon moving resistance in the cable core. We examined the pulling force of the fiber ribbon from the slotted core to investigate the fiber moving phenomenon during mid span access operation. And we examined the vibration test and the galloping test to investigate the fiber moving characteristics in order to confirm the long-term reliability.

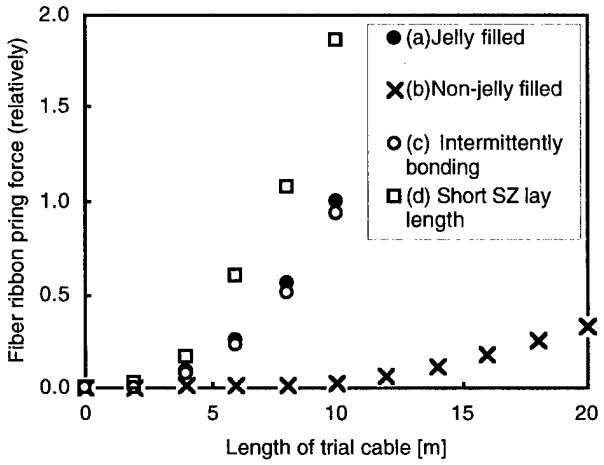

Fig.5 The results of pulling force of the fiber ribbon from the slot

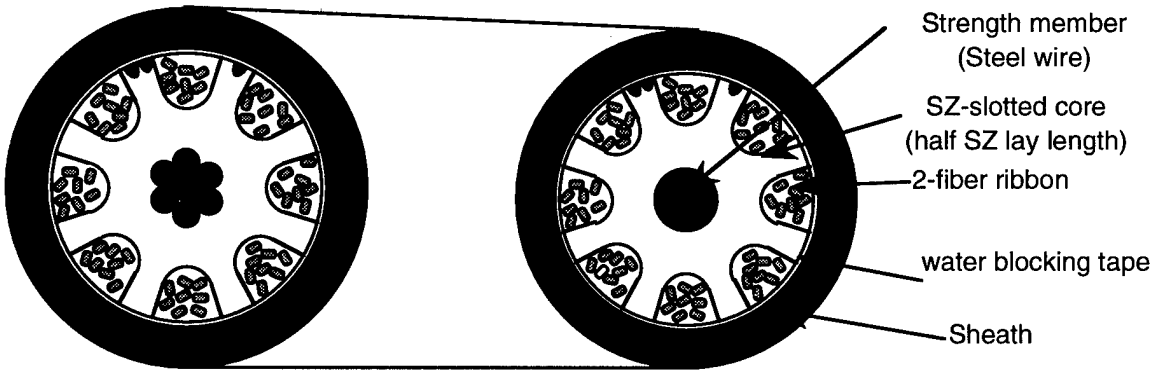

the outside diameter of the cable is 18.5 mm
(a) Conventional slotted core without jelly

the outside diameter of the cable is 17.0 mm
(d) newly designed slotted core type

Fig.3 Cross section of 128-fiber type cable

Table 2 Comparison of conventional cable and newly designed cable

	128 fiber cable		48 fiber cable		24 fiber cable	
	(a)Conventional cable	(d)Newly designed cable	(a)Conventional cable	(d)Newly designed cable	(a)Conventional cable	(d)Newly designed cable
Diameter [mm]	18.5	17.0	15.5	14.7	12.5	11.8
Weight [g/m]	270.0	220	191	174	143	121

We investigated the fiber ribbon moving characteristics of only 24 fiber cable. The fiber ribbons in 24 fiber cable has the smallest resistant to move among 24, 48 and 128 fiber count cables, because it has small stranding pitch radius.

(1) Pulling force of the fiber ribbon from the slotted core

The fiber ribbons in the groove are pulled and force of the fiber ribbon migration are measured as shown in Fig.4. The results are shown in Fig. 5. Compared with type (a) cable (conventional one), type (b) cable (conventional slot design without jelly) has the smallest pulling force of the fiber ribbon from the slotted core. The fiber ribbon pulling force of type (c) cable (intermittent bonding design) is as large as that of type (a) cable. On the other hand, the fiber ribbon pulling force of type (d) cable (Short SZ lay length) is about twice as much as that of type (a) cable.

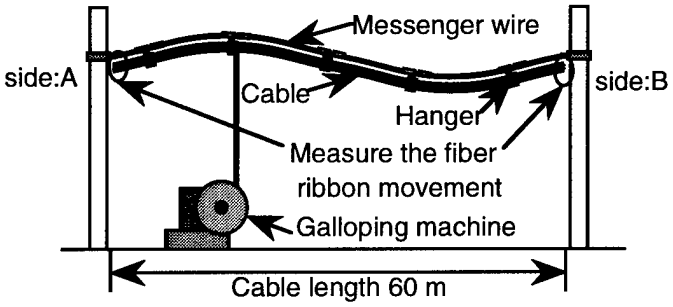

Fig. 6 Test procedure for cable galloping test

Table 3 Cable galloping test results

	Fiber ribbon movement[mm]					
	Side: A			Side: B		
Dancing time[min]	20	60	120	20	60	120
(a) Ordinary jelly filled cable	0	-1	-1	1	0	1
(b) Non-jelly filled cable	13	17	21	-14	-19	-23
(c) Intermittently bonding structure	-1	-1	0	1	1	1
(d) Small SZ lay length cable	-3	-5	-5	-5	-6	-6

(2) Cable galloping test

Under cable galloping condition, the fiber ribbon is easier to move longitudinally. Fig. 6 shows this test configuration. We installed these cables in aerial and the galloping was realized by forced vibration. Under this galloping condition, we measured the fiber ribbon movement at the cable end. Fiber is not fixed at the cable end and free . The results are shown in Table 3.

The obvious fiber ribbon movement was observed in type (b) cable. The fiber ribbon movement of type (c) cable were not observed. Type (d) cable shows small fiber ribbon movement. The amount was saturated as a function of dancing time.

(3) Vibration test

The cable was elongated and was subjected to vibration. We measured amount of the fiber ribbons migration in the SZ-slotted core as shown in Fig. 7. This examination simulates the vibrational condition near the railway and road.

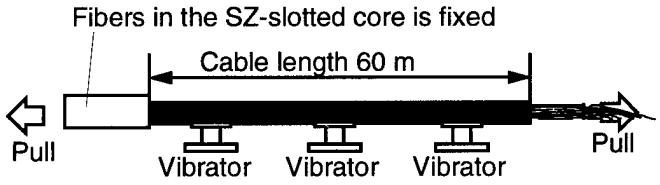

Fig. 7 The results of vibration test

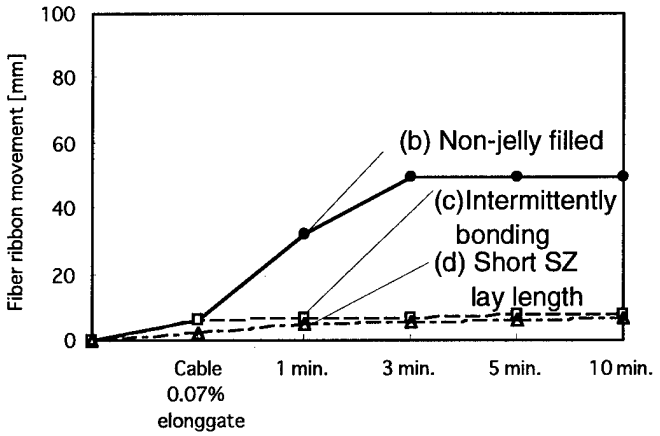

Fig. 8 The method of the vibration test

Table 4 Fiber ribbon moving characteristics

	(a) Conventional jelly filled cable	(b) Non-jelly filled cable	(c) Intermittently bonding structure	(d) Short SZ lay length cable
Pulling force of the fiber ribbon from the slotted core(relatively)	1	Less than 0.1	1	2
Cable dancing test	Very good	Negative	Very good	Good
Vibration test	Very good	Negative	Very good	Very good

Under this condition, the fiber ribbon moves easier under vibration. The results are shown in Fig. 8.

Type (b) cable showed the largest fiber ribbon movement. Type (c) cable and (d) cable didn't show any fiber ribbon movement.

Results of these three tests are shown in Table 4. The fiber ribbons of type (b) cable may move easily, but it is verified that the fiber ribbons of type (c) cable and type (d) cable have effective resistance to fiber ribbons movement.

We further investigated other cable characteristics such as the attenuation change in cable manufacturing process, temperature characteristics, several mechanical tests and water blocking test of the 128 fiber cables.

Attenuation change in cable manufacturing process

Fig. 9 shows the loss change of test cables at each manufacturing processes. The loss change were less than 0.02 dB/km at 1.55 μm. It is verified that these cables have stable loss characteristics in manufacturing processes.

Temperature characteristics

The cables were subjected to temperature tests. The temperature range is -30℃ through +70℃. Fig. 10 shows the temperature characteristics of all cables. The loss changes of all cables are less than 0.02 dB/km at 1.55 μm. Test result shows good temperature characteristics.

Several mechanical tests

The cables were subjected to tensile test,

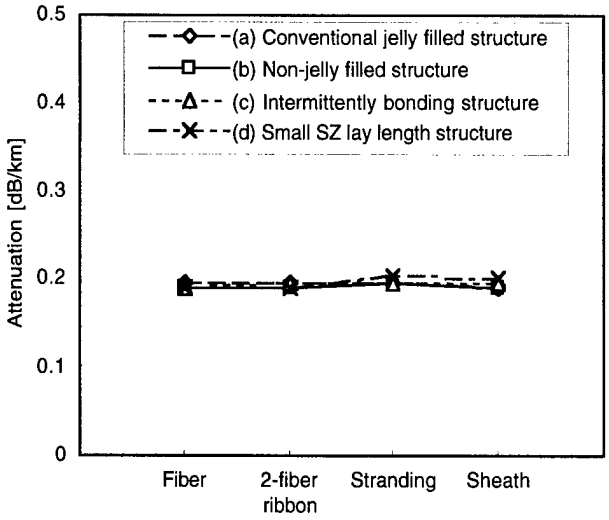

Fig. 9 Attenuation change in cable manufacturing process

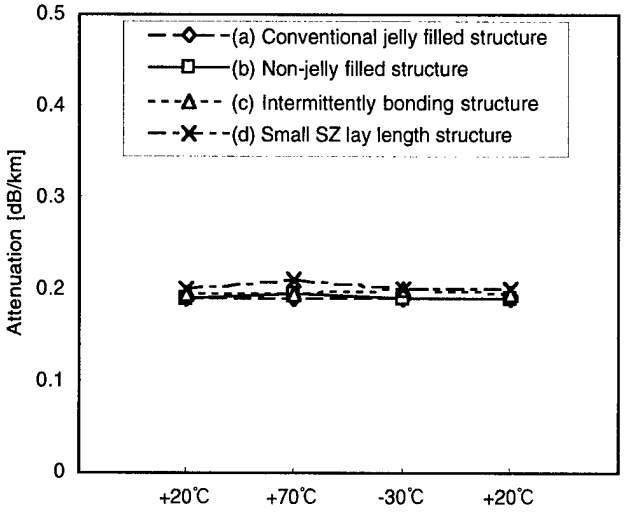

Fig. 10 Temperature dependence of attenuation change

Table. 5 Several mechanical test

Test item	test methods	Results
Tensil test	tensile strength:cable elongation 0.2%	Less than 0.02dB
Bending test	Bending dia.:r=6D(D:cable diameter) Bending angle:±90°	Less than 0.02dB
Compression test	Compression length:100mm Compression load:1960N	Less than 0.02dB
Impact test	Columnweight:1kg Impact height:1m	Less than 0.02dB
Twist test	Twist angle:±90° /m Tensile strength:25kgf	Less than 0.02dB
Squeezing test	Squeezing wheel radius:250mm Tensile strength:cable elongation 0.2%	Less than 0.02dB

loss measurement at 1.55 μm

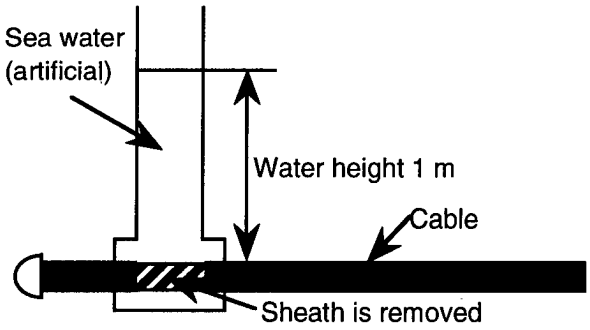

Fig. 11 Test procedure for water blocking

Table. 6 Water blocking test results

	Length of water penetration [m]
(a) Conventional jelly filled structure	Less than 3m
(b) Non-jelly filled structure	Less than 3m
(c) Intermittently bonding structure	Less than 3m
(d) Small SZ lay lengthstructure	Less than 3m

test, compression test, impact test, twist test, squeezing test as shown in Table 5. In each test, the loss change were not observed. As results, it was verified that these cables has an excellent mechanical characteristics.

Water blocking test

In these newly designed cables, the water swellable tape is wrapped around a slotted core for the purpose of water blocking. The test set-up of water blocking is shown in Fig. 11. Water blocking test results of newly developed cable are shown in Table 6. Good performance was obtained in every types of cables.

4. CONCLUSION

The newly designed dry type water blocking SZ-slotted core optical cables with 2-fiber ribbons have been successfully developed. We designed two types of cable structure from the view point of prevention of the fiber ribbon movement. Then we manufactured and examined these cables. Trial cables of two types showed excellent transmission, mechanical and water blocking characteristics. Moreover, the amount of the fiber ribbon movement can be kept small under severe vibrational condition. It is verified that both the intermittently fixed and the short SZ lay length structure are effective to prevent the fiber movement without degradation of transmission characteristics. And short SZ lay length structure realizes the small cables diameter and light weight.

REFERENCES

[1] N. Okada et al., "A SZ slot ribbon fiber cable for subscriber network", IWCS 1989

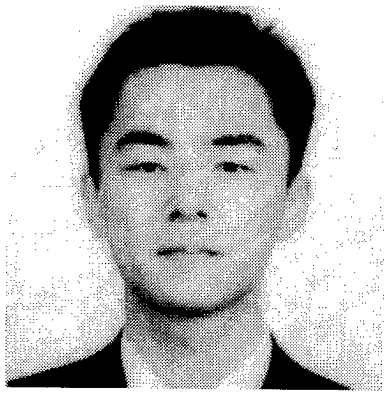

AUTHORS

Hirohito Watanabe
Fujikura Ltd.
1440 Mutsuzaki Sakura, Chiba, 285, Japan

Hirohito Watanabe was born in 1971. He joined Fujikura Ltd. after his graduation from Yokohama National University with a M.E. degree in 1996 and has been engaged in research and development of optical fiber cables. He is now an engineer in the Telecommunication Cable Department and a member of IEICE of Japan.

Naoki Okada
Fujikura Ltd.
1440 Mutsuzaki Sakura, Chiba, 285, Japan

Naoki Okada was born in 1964. Rejoined Fujikura Ltd. after his graduation from Chiba University with a B.E. degree in 1986 and has been engaged in research and development of optical fiber cables. He is now an engineer in the Telecommunication Cable Department and a member of IEICE of Japan.

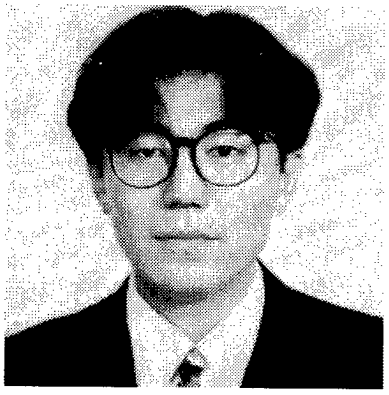

Masayoshi Yamanaka
Fujikura Ltd.
1440 Mutsuzaki Sakura, Chiba, 285, Japan

Masayoshi Yamanaka was born in 1966. He joined Fujikura Ltd. after his graduation from Tohoku University with a M.E. degree in 1992 and has been engaged in research and development of optical fiber cables. He is now an engineer in the Telecommunication Cable Department and a member of the IEICE of Japan.

Matsuhiro Miyamoto
Fujikura Ltd.
1440 Mutsuzaki Sakura, Chiba, 285, Japan

Matsuhiro Miyamoto was born in 1953. He graduated from Nagoya Institute of Technology with B.E. degree of electrical engineering. He joined Fujikura Ltd. after his graduation from Tokyo Institute of Technology with a M.S. degree in 1978 and has been engaged in research and development of optical fiber and optical fiber cables. He is now a manager of the Telecommunication Cable Department and a member of IEICE of Japan.

A STUDY ON STRAIN CHARACTERISTICS OF FIBER RIBBONS IN A SZ-GROOVED SPACER CAUSED BY CABLE BENDING

Akihito Makiyama, Jun-ichi Ohta and Akira Nishimura

Sumitomo Electric Industries, Ltd., Yokohama Japan

ABSTRACT

We have developed new aerial cable which consists of 4-fiber ribbons in a SZ-grooved spacer slotted rod.

We have investigated a strain of fiber ribbons in a SZ-grooved spacer cased by cable bending. Thus, we have obtained characteristics strain of 4-fiber ribbons in a SZ-grooved spacer different from the ones in S-grooved spacer.

In this paper, we describe characteristics of fiber strain dependence on cable bending diameter in S-grooved spacer rod and in SZ-grooved the ones.

INTRODUCTION

Recently fiber optics network has been extending into subscriber area, since, a production of the developed new aerial cable is increasing.

The cable characteristics own has been already investigated transmission properties, but has not reported a strain properties of fiber ribbons in a SZ-grooved spacer slotted rod by cable bending. However, measurement of characteristic strain by cable bending is important for considering long term reliability.

Generally in Japan, it is a popular cable design that 4- or 8-fiber ribbons are stranded in a S-grooved spacer. The characteristics of this type cable, such as fiber strain or transmission properties, has been well investigated. However the study is not sufficient yet, concerning characteristics of fiber ribbons in a SZ-grooved spacer.

Thus we have investigated strain characteristics caused by cable bending. At first, we considered two parameters; ① a bending diameter, ② a spiral radius of a ribbon in a straight cable, and compare the dependence on these parameters with a S-grooved spacer. A strain characteristics in a S-grooved largely depend on both a bending diameter of cable and a spiral radius of a ribbon. Including further studies, we intend to it clear whether a strain by cable bending depends on them or not, in a SZ-grooved spacer.

EXPERIMENT

STRUCTURE OF EXPERIMENTAL CABLE

We prepared aerial cables as shown Figure 1. These cables consists of messenger wire and cable core, which is stranding 4-fiber ribbons in SZ-grooved spacer, sheathed together polyethylene.

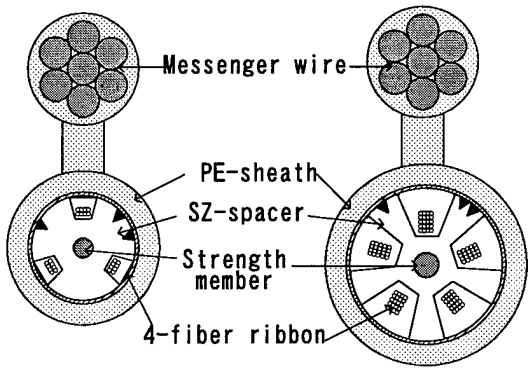

(a) 3-slot type (b) 5-slot type

Fig. 1 Experimental aerial cable cross-section

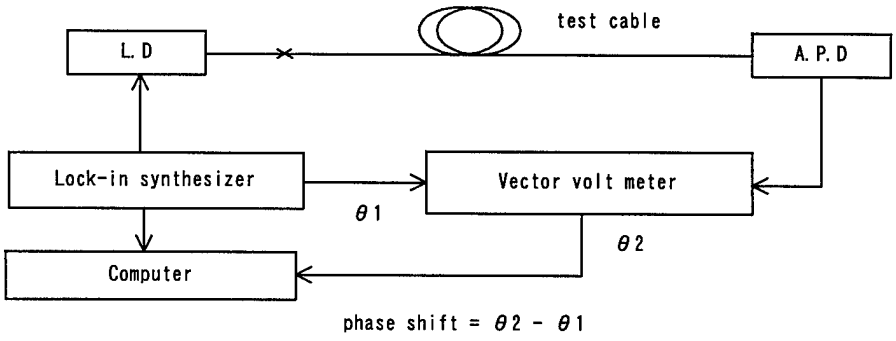

Fig. 2 Schematic diagram of phase shift method

Experiment cable dimensions are summarized in table 1. The first cable has a three SZ-grooved spacer and each groove contains two 4-fiber ribbons. The second has a five SZ-grooved spacer and each groove contains five 4-fiber ribbons. And third type cable, which isn't shown Fig. 1, has a ten SZ-grooved spacer. A 4-fiber ribbon size is 1.1 mm width and 0.3 mm thickness.

Table 1 Dimension of experiment cable

Groove number	3-slot	5-slot	10-slot
fiber count	24	100	200
Supporting wire	7/2.0 Steel wire		
Fiber ribbon	4-fiber ribbon		
Ribbon number	2/groove	5/groove	
Reversing angle	275 °		
SZ-pitch	300mm	340mm	500mm
Cable diameter	10mm	14mm	19mm

STRAIN OF FIBER MEASURING METHOD

We measure a strain characteristics by phase shift method. This measurement system consists of L.D, A.P.D, lock-in synthesizer, vector volt meter, and computer. The schematic diagram of the system is shown Fig 2. We measure the test cable on the condition that system is set up with frequency = 800 MHz. Resolution of fiber length is 0.898mm.

A measurement sample length is 10 ~ 14 meter. We consider two different ribbon in cable. One is a top ribbon in SZ-groove spacer. The other is a bottom ribbon in SZ-groove. (As shown Fig. 3)

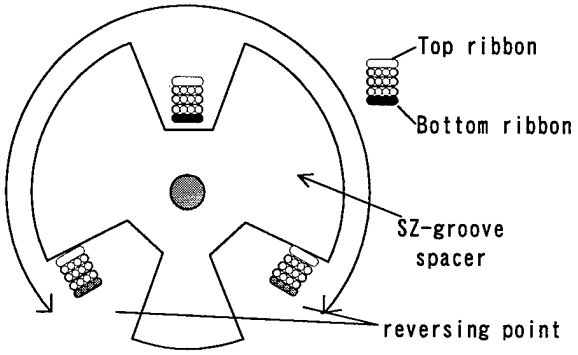

Fig. 3 Ribbon location of SZ-grooved spacer

The cables coiled around several mandrel (each ring diameter is 1200 mm, 1000 mm, 800 mm, 600 mm and 500 mm). For bent cable, two different groove location were considered. One is that the locus is on inside of the cable bent, and the other is that the locus is on outside. (As shown Fig. 4)

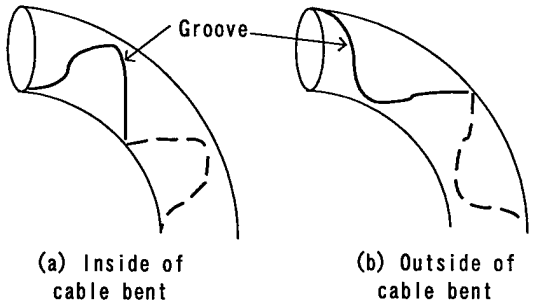

Fig. 4 The groove location of cable bent

RESULT AND DISCUSSION

EXPERIMENTAL RESULT

In this section, we describe the experimental result caused by cable bending. At first, we consider a condition that the groove locus is on inside of cable bent (ref. Fig. 4-(a)). Fig.5 shows relationship between strain of fiber and cable bending diameter. Fig. 5 is plotted on each property of both ribbon, top and bottom, in 3-slot, 5-slot, and 10-slot. In Fig. 5 we excepted bottom-ribbon in 10 slot.

We have found out that strain of fiber in a SZ-grooved spacer is dependence on cable bending diameter. However, two different behavior of top-ribbon and bottom-ribbon were observed.

One is that the behavior on top-ribbon is shrink strain in proportion to the reciprocal of cable bending diameter. The other hand is that behavior on bottom-ribbon is extend strain in proportion to the reciprocal of cable bending diameter.

Behavior on top-ribbon is considered influence on ribbon location in groove reversing point (ref. Fig.3). Since groove size design of SZ-spacer is possible for rotation of 2 or 5 ribbons stack, at reversing point a top ribbon puts on nearer inside-wall in groove than a bottom ribbon. As a result, different behavior on top-ribbon and bottom-ribbon is considered two causes, ① reversing angle on top-ribbon is smaller than on bottom-ribbon; ② both ribbons are able to remove at a narrow range in groove.

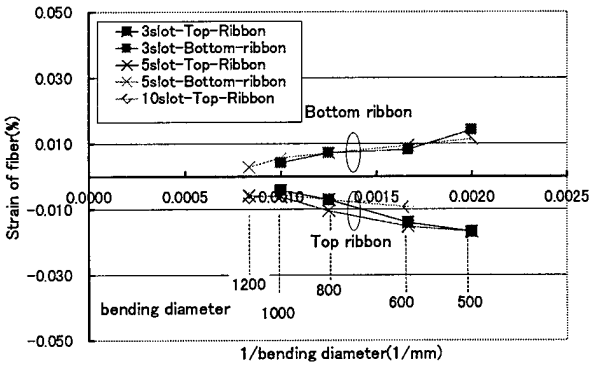

Fig.5 Strain of fiver vs. 1/bending diameter
3type SZ-spacer cable

Thus, SZ-grooved spacer cables, whose dimensions are in table 1, are obtained minute strain characteristics caused by cable bending. And, strain of fiber cased by cable bending got little dependence on cable diameter.

GROOVE LOCATION OF CABLE BENT

In this section, we describe the dependence on groove locus of cable bent (ref. Fig.4). We select cable 5-slot cable out of 3-type cable (ref. table1), because this cable structure is middle size of 3-type cables.

Two conditions are considered that groove locus is inside cable bent, and outside cable bent. Then cable bending diameters are considered similar to the former experiment. Fig.6 shows relationship between strain of fiber and cable bending diameter. Fig.6 is plotted on each property of both ribbon, top and bottom.

We guess that strain of fiber in a SZ-grooved spacer is little dependence on a groove position on cable bent. The strain of inside condition (ref.4-(a)) is smaller than the strain of outside (ref.4-(b)).

And in outside of cable bent the strain of fiber is dependent on cable bending diameter.

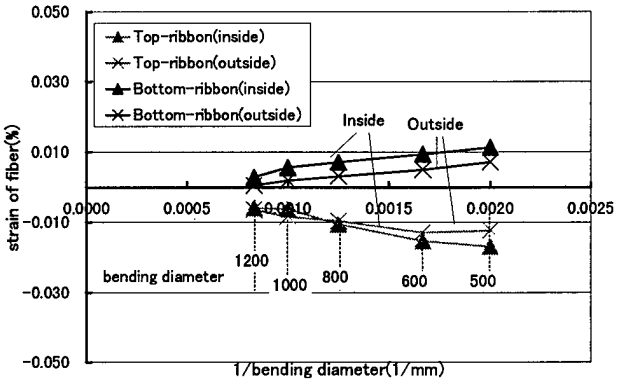

Fig.6 Strain of fiver vs. 1/bending diameter
A relationship that both groove locus
is on outside bent and on inside bent.
(5-slot cable of SZ-grooved)

COMPARISON S-GROOVED SPACER

In this section, we describe that we compare with the strain of fiber caused by cable bending, between in S-grooved spacer and in SZ-grooved spacer.

We select popular cable design that 4-ribbons are stranding in a S-grooved spacer, in Japan. The comparison cable design is cable diameter;12 mm, groove number;5, ribbon number;5/groove, S-pitch;500 mm, and fiber count;100.

Fig.7 shows relationship between strain of fiber and cable bending diameter. And this graph is indicated strain of fiber on two-type cables, one is S-grooved spacer cable and the other is SZ-grooved spacer with 5-slot cable (ref. table 1). The strain of SZ-grooved spacer are showed on condition that a groove locus is on inside of cable bent (ref. Fig.4-(a)).

We have found out two properties. One is similarity that the strain of fiber depend on cable bending diameter. The strain of fiber is in proportion to the reciprocal of cable bending diameter.

The other hand is that strain of fiber in SZ-grooved is more little than strain of fiber in S-grooved, caused by cable bending. The strain volume of fiber in SZ-grooved spacer is difference 1 figure smaller than the strain volume of fiber in S-grooved spacer. Thus, we obtain that the smaller strain by cable bending is content with considering long term reliability.

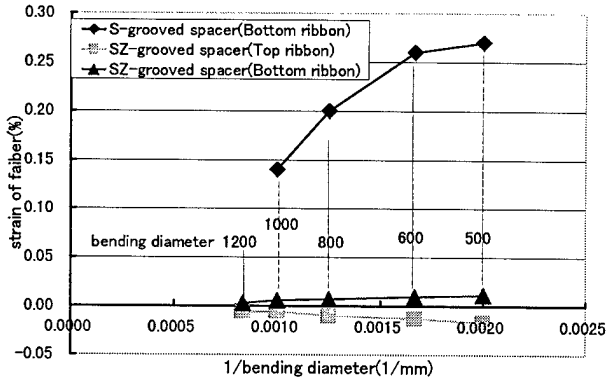

Fig.7 Strain of fiver vs. 1/bending diameter
A relationship that both S-grooved and SZ-grooved on cable bending.

CONCLUSION

We have investigated strain characteristics caused by cable bending. Thus, we found out five properties.

(1) The strain of fiber in SZ-grooved is dependent on cable bending diameter.
(2) The strain of fiber in SZ-grooved spacer is little dependent on cable diameter.
(3) The strain of fiber in SZ-grooved spacer cable has different behavior of top-ribbon and of bottom ribbon cased by cable bending.
(4) The strain of fiber in SZ-grooved spacer cable isn't dependent on location on cable.
(5) The strain of fiber in SZ-grooved spacer cable is very smaller than a strain of fiber in S-grooved spacer cased by cable bending.

References

[1] H.Iwata et al., in Proc. of IWCS, p10 (1997)
[2] H.Ishikawa et al., in Proc. of IWCS, p42 (1997)
[3] K.Niikura et al., Sumitomo Electric Tech. Review, No.29, p70 (1990)

Biographical Sketches of the Authors

Akihito Makiyama
Sumitomo Electric Industries, Ltd.
Engineering Department, Communications division

1, Taya-cho, sakae-ku
Yokohama, Japan

Akihito Makiyama received his B.E. degree from Kyushu Institute of Technologies in 1994.

He joined Sumitomo Electric Ind., Ltd. in 1994 and he is now an engineer of Communication Cable Division.

Jun-ichi Ohta
Sumitomo Electric
Industries, Ltd.
Engineering Department,
Communications division

1, Taya-cho, sakae-ku
Yokohama, Japan

Jun-ichi Ohta received his M.S. degree from Tokyo Institute of Technologies in 1987.

He joined Sumitomo Electric Ind., Ltd. in 1987 and he has been engaged in research and development of optical fibers. He is now a senior engineer of Communication Cable Division.

Akira Nishimura
Sumitomo Electric
Industries, Ltd.
Engineering Department,
Communications division

1, Taya-cho, sakae-ku
Yokohama, Japan

Mr.Nishimura received his M.E. degree from Kyoto University in 1984.

He joined Sumitomo Electric Ind., Ltd. in 1984.

Study of the SZ-stranded 2000-fiber cable with 8-fiber ribbons for underground access networks

Naoki Okada, Yoshiyasu Sato, Akimi Yamasaki, Matsuhiro Miyamoto

Fujikura Ltd.
Telecommunication cable department Optical access network laboratory
1440, Mutsuzaki, Sakura-shi, Chiba, Japan

ABSTRACT

The newly designed 2000-fiber optical cable is studied. This cable has composite structure with a central SZ-slotted rod and SZ-stranding U-grooves. The 8-fiber ribbons are used considering compatibility with ordinary 1000-fiber cables, and the dry type water blocking characteristic is achieved by water swellable wrapping tape. This cable structure has excellent mid span access performance because of its SZ-stranded and dry structure. The cable diameter is about 40mm which is as same as multi slotted rods type 1000-fiber cable, therefore high density of fiber packing is achieved, too.

In order to get easy mid span access operation and good cable characteristics, the special SZ-stranding method have been developed. And a prototype cable had been manufactured and its cable characteristics were investigated. As results, it is verified that this newly studied SZ-stranded 2000-fiber cables have not only the good cable characteristics but also the easy mid span access operation. Moreover, based upon these techniques, the 1000-fiber single SZ-slotted core cable has been developed. These cable structures are suitable for the underground ducts and its mid span access capacity is useful for the distributed subscribers in urban area.

INTRODUCTION

In recent years, the optical access networks are under construction to achieve the FTTH networks in the future. The aerial networks have been constructed with the new self-supporting SZ cables which had been reported on IWCS'97 [1,2]. In urban area, the telecommunication cables are installed in the under ground ducts in Japan. The single slotted core type 1000-fiber cables which had been reported on IWCS'95 are used in actual lines now [3]. This cable is the highest fiber count structure for commercial use in the world. However, higher count fiber cables more than 1000-fiber are demanded as the optical access networks are spreading. Therefore, we have tried to achieve the newly designed under ground cables in order to construct the future FTTH networks economically.

CABLE DESIGN

From the view point of the design of the cable structures, the following contents are most important.

1) High count and high density cable

In order to construct the new networks economically, the constructed ducts should be used efficiently, so the optical fibers should be packed in the ducts at high density. Therefore, high count and high density optical cables are demanded.

2) Mid span access

Availability of mid span access is important factor to construct the distributed networks. The networks can be constructed efficiently and economically with the easy mid span access technique.

In this paper, the design of new cable structure to accommodate high count fiber up to 2000 fibers is reported. This cable is based on the SZ-stranding structure in order to get the excellent mid span access performance. The special designed SZ-stranding method is proposed from the view point of not only good cable characteristics but also easy mid span access operation.

Design of cable structure

The newly designed 2000-fiber cable is composite structure with a central SZ-slotted rod and the SZ-stranding U-grooves as shown in Fig.1. The 8-fiber ribbons are used considering compatibility with ordinary 1000-fiber cables. The water blocking function can be obtained by water swellable tape. The dry structure is suitable for mid span access operation. This newly designed 2000-fiber cable is about 40mm in cable diameter which is as same as multi slotted cores 1000-fiber cable as shown in Fig.2 a). In case of 2000-fiber cable designed with multi slotted cores structure, the cable diameter become about 45mm as shown in Fig.2 b). Therefore, the composite structure with a central SZ-slotted core and SZ-stranding U-grooves is the best cable structure to get high count fiber cable at high packing density.

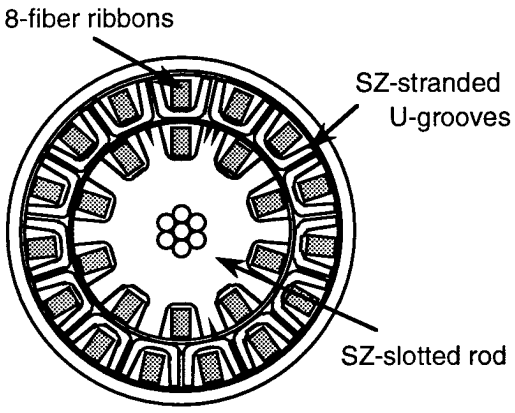

Fig.1 Cross sectional view of newly designed 2000-fiber cable

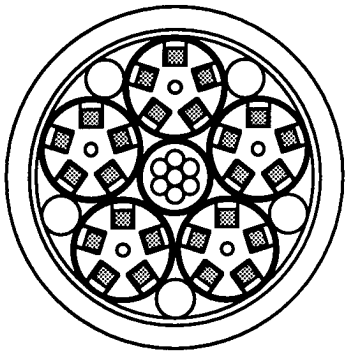

a)1000-fiber cable dia.= 40 mmϕ
b)2000-fiber cable dia.= 45 mmϕ

Fig.2 Multi slotted rods type cable

SZ-stranding method

At mid span access point, the sheath is removed for 700mm length which is almost equal to the length of jointing closure. The fiber can be picked out from the installed cable with the fiber slack as shown in Fig.3. It is necessary to get the target fibers from not only outer U-grooves but also inner SZ-slotted rod. The amount of fiber slack should be designed more than 20mm in order to obtain easy mid span access operations.

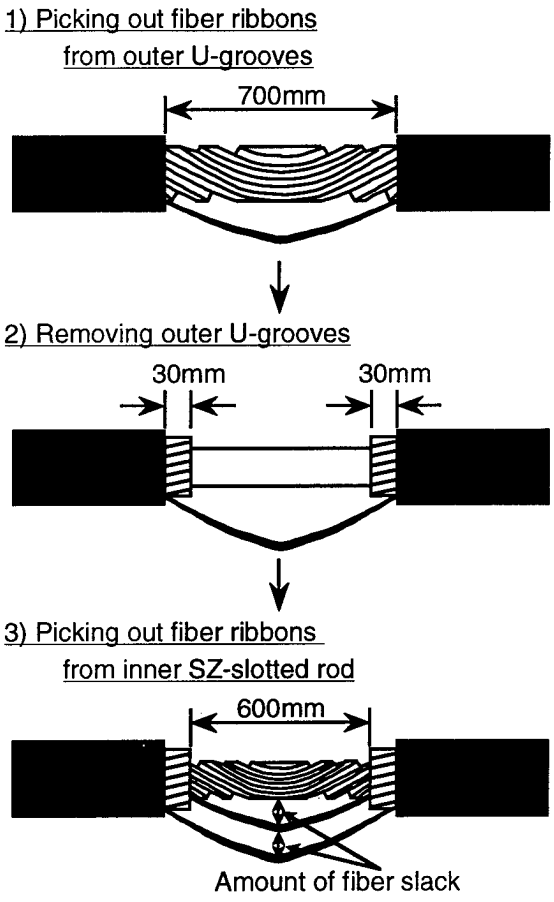

Fig.3 Mid span access of newly designed 2000-fiber cable

The fiber slack is influenced by SZ-stranding pitch, stranding pitch radius, and location of the

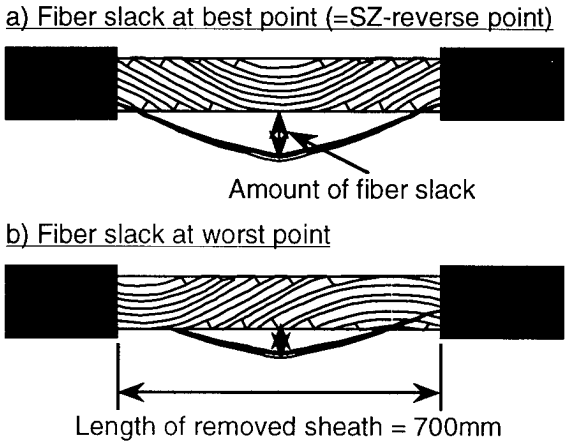

Fig.4 Fiber slack comparison at each point along installed cable

mid span access point along the installed cable. Short SZ-stranding pitch and large stranding pitch radius produce large amount of fiber slack. Moreover, the large fiber slack can be obtained in the case of mid span access at the best point where the SZ reverse point is just located at the center of the removed sheath as shown in Fig.4 a). Fig.5 shows the calculated and experimental results about the amount of fiber slack on the newly designed 2000-fiber cable. As results, in order to get 20mm of fiber slack at any location, the inner and the outer SZ-stranding pitch should be designed less than 380mm and 510mm respectively. On the other hand, if the mid span access point can be selected to meet the SZ-reverse point at the center of the removed sheath, the larger SZ-stranding pitch can be obtained. In that case, the inner and the outer SZ-stranding pitch are allowed up to 620mm and 940mm, respectively. This means that the stranding curvature radius of the fiber in the cable become larger as shown in Fig.6, so it may give easier ribbon stranding condition to obtain the good transmission characteristics.

We have developed new manufacturing method to achieve the latter structure. The SZ-stranding pitch of outer U-grooves is designed twice as that of inner SZ-slotted rod, and the outer U-grooves are stranded inspecting the stranding angle of the inner SZ-slotted rod. The special SZ-stranding method has been developed in order to correspond the inner and the outer SZ-reverse points. Moreover, in order to get the excellent transmission characteristics, the back-twisting of the stacked ribbons is needed.

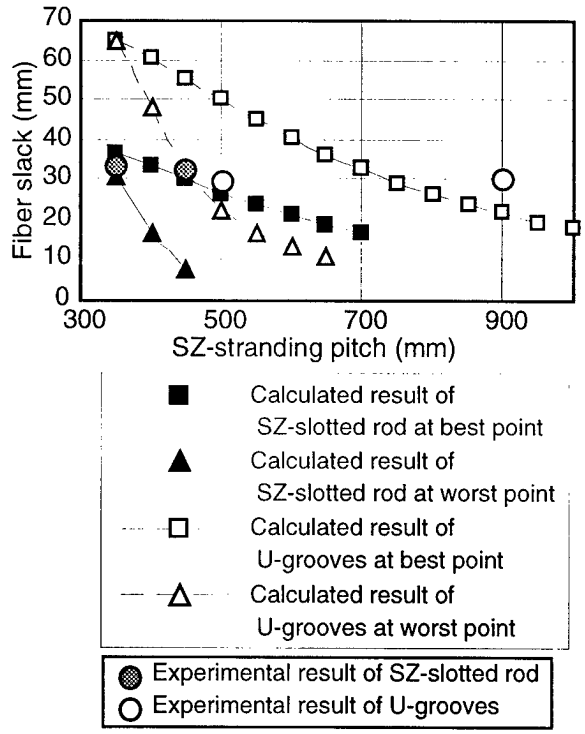

Fig.5 Calculated results of amount of fiber slack

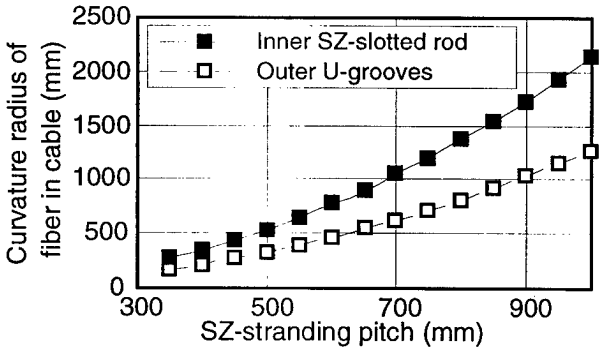

Fig.6 Calculated results of fiber curvature radius in cable

CABLE CHARACTERISTICS

In order to investigate the cable characteristics, the trial cables were manufactured in laboratory and tested.

Trial cable structure

The two types of cable structures which have different SZ-stranding pitch as shown in Fig.8 were studied. TNo.1 cable has larger SZ-stranding pitch. The SZ-stranding pitch of outer U-grooves is designed twice as that of inner SZ-slotted rod. The inner and the outer SZ-reverse points are corresponded, as a result, the mid span access is useful at the reverse point. On

the other hand, TNo.2 cable is designed with shorter SZ-stranding pitch, therefore mid span access can be performed at anywhere on the installed cables. The SZ-reverse points are not corresponded on TNo.2 cable.

The 480 fibers are accommodated in these trial cables as shown in Fig.7. The inner and outer slots inserted fibers are distributed around the cable, in order to investigate the transmission characteristics influenced by the drum winding condition.

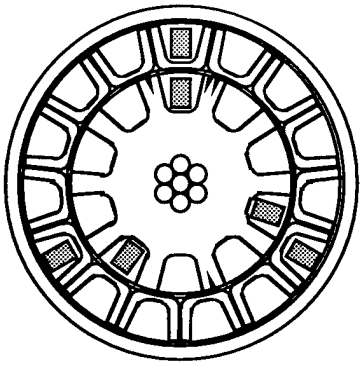

	Stranding pitch (relative value)	
	SZ-slotted rod	U-grooves
TNo.1	1.0	2.0
TNo.2	0.8	1.1

Fig.7 Cross sectional view and SZ-stranding pitch of trail cable

Transmission characteristics

The transmission characteristics were measured on each trial cables which were wound on 1400mmϕ barrel diameter at 1.55μm wave length. Fig.8-1 shows the results of the TNo.1 cable and Fig.8-2 shows the results of the TNo.2 cable. As results, the excellent transmission characteristics are obtained.

Temperature characteristics

The temperature characteristics of the trial cables were investigated. Fig.9 shows the results of the TNo.1 cable, and Fig.10 shows the results of the TNo.2 cable. Especially, the temperature characteristics of each slot in TNo.2 cable which have shorter SZ-stranding pitch are shown in Fig.11. The excellent transmission characteristics are confirmed on each cable and each slot in large temperature range, from -30 to 70℃.

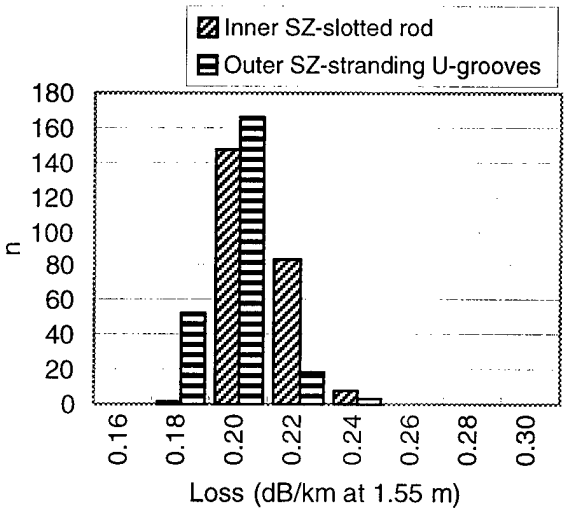

Fig.8-1 Transmission characteristics of TNo.1 cable

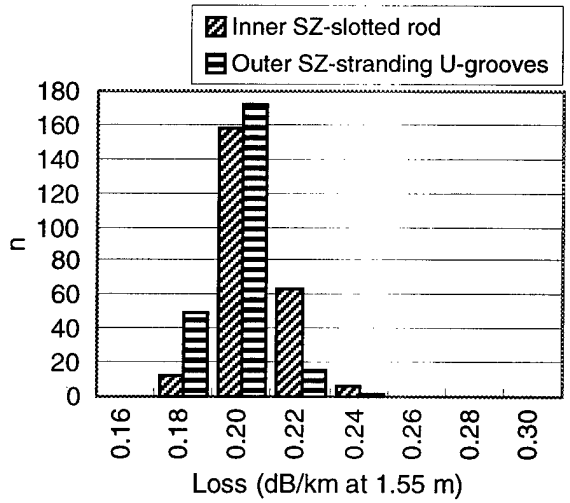

Fig.8-2 Transmission characteristics of TNo.2 cable

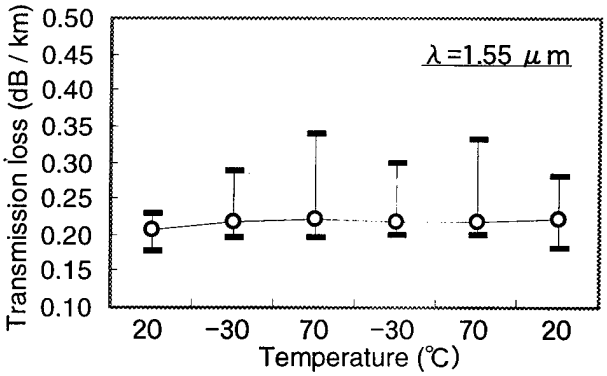

Fig.9-1 Temperature characteristics of SZ-slotted rod in TNo.1 cable

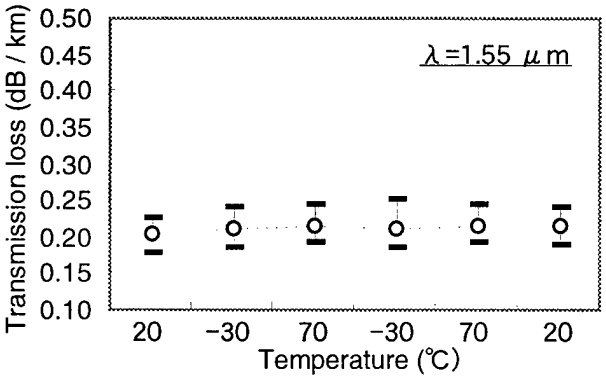

Fig.9-2 Temperature characteristics of U-grooves in TNo.1 cable

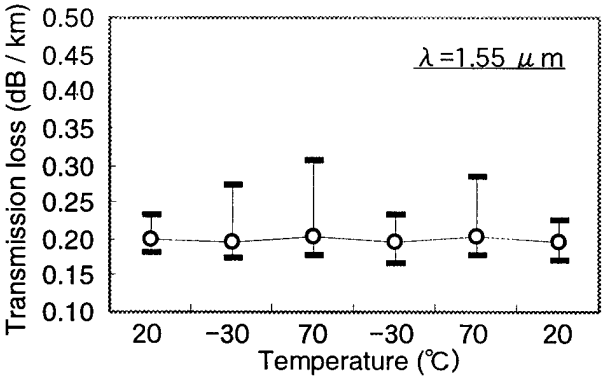

Fig.10-1 Temperature characteristics of SZ-slotted rod in TNo.2 cable

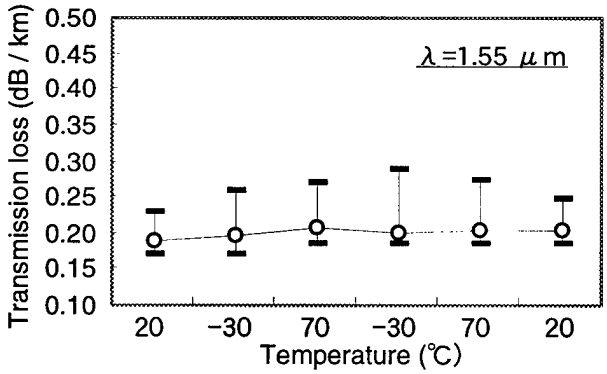

Fig.10-2 Temperature characteristics of U-grooves in TNo.2 cable

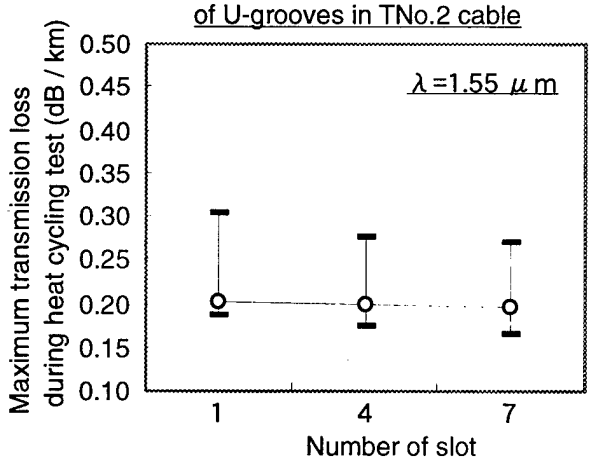

Fig.11 Temperature characteristics of each slot in TNo.2

Mechanical characteristics

The mechanical characteristics were investigated. The results are shown in Table 1. Good characteristics are obtained.

Table 1 Cable characteristics

Test items	Test conditions	Results
Bending	320 mmϕ ±90°	No change in loss
Lateral pressure	2 kN/100 mm	No change in loss
Tensile	10 kN	Less than 0.02 dB/100m
Squeezing	2 kN / 250 mmR-roller	Less than 0.02 dB/100m
Torsion	±90° / m	No change in loss
Impact	20 mmf ×1 kg×1 m	No change in loss

※ Measurement wavelength = 1.55 μm

Water blocking characteristics

The water blocking capability is demanded on the under ground cables. The newly developed cables are designed and manufactured using the water swellable wrapping tape in order to get the water blocking characteristics. Fig.12 shows the test set-up of the water blocking test. The full accommodated 2000-fiber cables were manufactured and used for the water blocking test. As results, the water penetration length was less than 8m. This results are almost same as ordinary slotted core cables, therefore good water blocking characteristic is confirmed.

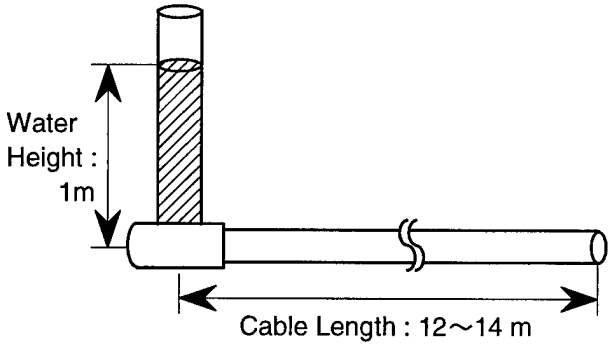

Fig.12 Water blocking test set up

Mid span access

The mid span access tests were performed as shown in previous Fig.3. The slack of fiber were measured at several access points which were located at the best point and the worst point

as shown in Fig.4. Table 2 shows the results of the mid span access tests.

In the case of TNo.1 cable, the enough fiber slack which is more than 20mm is gotten at only best access point. It is necessary to select the mid span access point. On the other hand, in the case of TNo.2 cable, the enough fiber slack is gotten at any points. This result means that the mid span access can be performed at any points of the installed cable. These results are almost corresponded to the calculated results.

Table 2 Fiber slack at mid span access

Cable		Relative SZ pitch	Best point	Worst point
TNo.1	Inner	1.0	30~33 mm	14~18 mm
	Outer	2.0	28~33 mm	10~12 mm
TNo.2	Inner	0.8	25~35 mm	24~34 mm
	Outer	1.1	41~53 mm	20~28 mm

Further studies

Based upon these techniques, the 1000-fiber single SZ-slotted core cable has been developed, too. Fig.13 shows the newly developed SZ 1000-fiber cable structure comparing ordinary 1000-fiber cable. The outer diameter of new cable is slightly larger than ordinary cable, however the mid span access capability is improved dramatically. The SZ-stranding pitch is designed in order that the enough fiber length is obtained at anywhere on the installed cable. Fig.14 and Fig.15 shows the transmission characteristics and temperature characteristics of the trial SZ 1000-fiber cable in which 480 fibers are accommodated. The excellent characteristics have been confirmed.

CONCLUSION

The newly designed 2000-fiber optical cable which has composite structure with a central SZ-slotted rod and SZ-stranding U-grooves has been studied. This cable has not only the good cable characteristics but also the easy mid span access capability. Moreover, the single SZ-slotted core 1000-fiber cable has been successfully developed. These cables are suitable for the underground ducts and its mid span access capability is useful for the distributed subscribers in urban area.

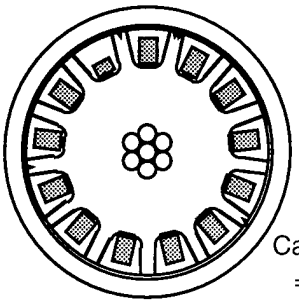

Fig.13-1 Newly studied SZ-slotted core 1000-fiber cable

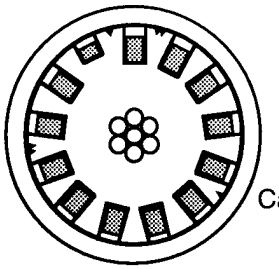

Fig.13-2 Ordinary helically slotted core 1000-fiber cable

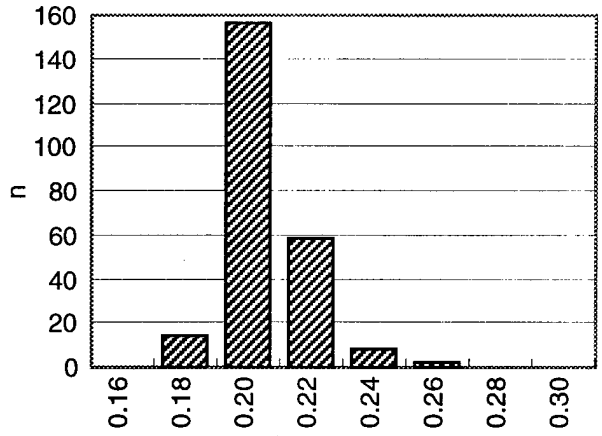

Fig.14 Transmission characteristics of SZ 1000-fiber cable

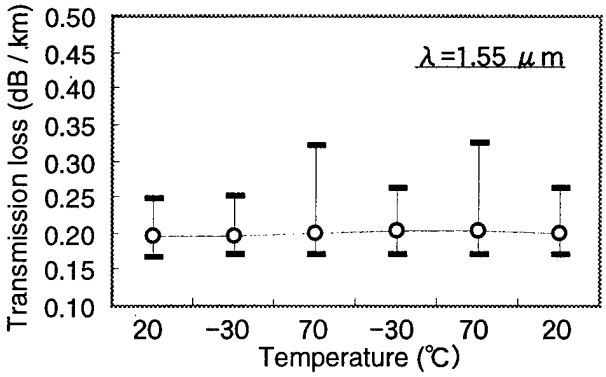

Fig.15 Temperature characteristics of SZ 1000-fiber cable

REFERENCES

[1] H. Iwata et al., "Design of Aerial Optical Fiber Cable System Suitable for Easy Branching", IWCS 1997

[2] N. Okada et al., "Study of the SZ-slotted rod type optical cable with 4-fiber ribbons for aerial applications", IWCS 1997

[3] N. Okada et al., "Development of single slotted rod type 1000-fiber optical fiber cable for subscriber loops", IWCS 1995

AUTHORS

Naoki Okada

Optical access network laboratory
Fujikura Ltd.

1440, Mutsuzaki,
Sakura-shi, Chiba,
285, Japan

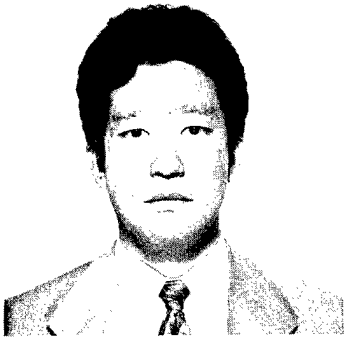

Naoki Okada was born in 1964. He joined Fujikura Ltd. after his graduation from Chiba University with a B.E. degree in 1986 and has been engaged in research and development of optical fiber cables. He is now an engineer in the Telecommunication Cable Department and a member of the IEICE of Japan.

Yoshiyasu Sato

Optical access network laboratory
Fujikura Ltd.

1440, Mutsuzaki,
Sakura-shi, Chiba,
285, Japan

Yoshiyasu Sato was born in 1969. He joined Fujikura Ltd. after his graduation from Tokyo Institute of Technology University with a M.E. degree in 1995 and has been engaged in research and development of optical fiber cables. He is now an engineer in the Telecommunication Cable Department and a member of the IEICE of Japan.

Akimi Yamasaki

Optical access network laboratory
Fujikura Ltd.

1440, Mutsuzaki,
Sakura-shi, Chiba,
285, Japan

Akimi Yamasaki was born in 1971. He joined Fujikura Ltd. after his graduation from Osaka University with a M.E. degree in 1997 and has been engaged in research and development of optical fiber cables. He is now an engineer in the Telecommunication Cable Department .

Matsuhiro Miyamoto

Optical access network laboratory
Fujikura Ltd.

1440, Mutsuzaki,
Sakura-shi, Chiba,
285, Japan

Matsuhiro Miyamoto was born in 1953. He graduated from Nagoya Institute of Technology with a B.E. degree of electrical engineering. He joined Fujikura Ltd. after his graduation from Tokyo Institute of Technology with a M.S. degree in 1978 and has been engaged in research and development of optical fiber and optical fiber cables. He is now a manager of the Telecommunication Cable Department and a member of IEICE in Japan.

Development of low skew optical fiber cable

Fumiki Hosoi, Masato Kosaka, Masami Hara,Yasuhiro Kamikura
The Furukawa Electric Co.,Ltd.
Ichihara,Chiba,Japan

Seiji Toda, Takayuki Watanabe, Osamu Suzuki
FUJITSU LIMITED
Kawasaki, Kanagawa,Japan

1.Abstract

Low-skew ribbon cable necessary for parallel optical transmission was developed. The cable was 288-fiber count slotted rod core design and 12-fiber ribbon were used.
First we investigated the causes of skew of 12-fiber ribbon, which are the difference in refractive index , dislocation of the fiber array and the residual strain among the fibers in the ribbon. Then we fabricated a prototype 12-fiber ribbon, good low-skew ribbons with SM fiber of 0.259 ps/m and MM fiber of 0.375 ps/m were obtained.
When the ribbon is stranded into a cable, each fiber in a ribbon suffers strain which results from the cable structure. This additional strain causes the increase of skew. We calculated the fiber strain distribution in a ribbon in the cable. In order to compensate such strain, we tried manufacturing a ribbon whose fibers have negative strain distribution. As a result, SM fiber cable with low skew of 0.520 ps/m was developed.

2.Introduction

In the field of recent computer systems, the development of distributed computing is in progress from the standpoint of ensuring high-speed processing and reliability. Distributed computing requires transmission of a large quantity of information from server to server in real time, and a parallel optical transmission system using a multiple-core optical fiber ribbon is a possibility for such an application. If a parallel optical transmission system is to achieve a bit-rate of a few Gbps to a few tens of Gbps, an allowable transmission skew is estimated to be less than 1 ps/m. First we investigated a low skew optical fiber ribbon. Second we calculated the fiber strain caused by cable structure. By controlling the fiber strain in the ribbon process, we realized an optical fiber cable with skew less than 1 ps/m.

3. Investigation of low skew optical fiber ribbon

3.1. Ribbon structure

The ribbon structure is shown in figure 1. It is 12 optical fiber ribbon coated with UV resin.

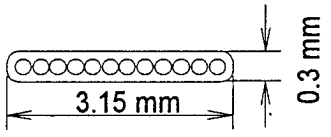

Figure 1 12 fiber Ribbon

3.2. First trial

The skew of the first prototype ribbon in the early stage of our development is shown in figure 2. In this case there was a significant difference in skew among the fibers. So we investigated the causes of ribbon skew.

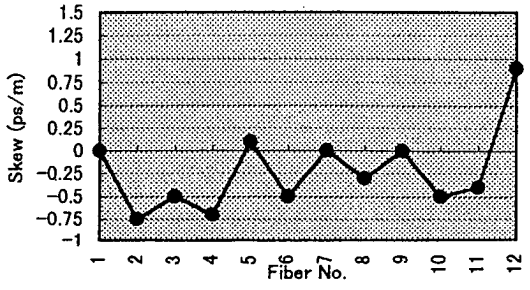

Skew 1.65 ps/m
Fig.2 Skew of initially developed ribbon (SM)

3.3. Causes of ribbon skew

The possible causes of ribbon skew are as follows:

(1) Difference in refractive index of each fiber from one fiber to another.
(2) Effect of dislocation in the ribbon array
(3) Difference in the residual strain of each fiber

The details are descrived below.

3.3.1. Difference of refractive index of each fiber

The effect of the difference in refractive index of each fiber can be reduced by employing the fibers drown from the same preform.

3.3.2. Dislocation in the ribbon array

The effect of dislocation in the ribbon array emerges when the ribbon is wound on the bobbin. When a ribbon with a dislocated array is wound on the bobbin, the dislocation generates a circumferential difference among the fibers, so the strain of one fiber will be different from that of another. This causes an increase of skew.

The skew arising from the dislocation in the ribbon array can be expressed by the following equation.

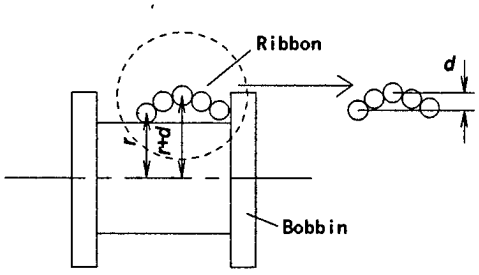

$$\Delta t = \kappa \left(\frac{Nd}{cr} \right) \qquad (1)$$

κ : Optical elastic coefficient
N: Refractive index
d: Dislocation of fiber array
r: Radius of bobbin
c: Velocity of light

Fig.3 Skew arising from dislocation of ribbon array

It is necessary to suppress the dislocation in the ribbon array.

3.3.3. Difference in the residual strain of each fiber

The skew arising from the difference in the residual strain of each fiber can be expressed by the following equation.

$$\Delta t = (\kappa - 1) \Delta \varepsilon \left(\frac{N}{c} \right) \qquad (2)$$

κ : Optical elastic coefficient
$\Delta \varepsilon$:Difference in the residual strain of each fiber
N: Refractive index
c: Velocity of light

The residual strain of each fiber depends on the supply tension of the fibers during ribbon production. Therefore, it is necessary to stabilize the supply tension of the fibers in order to control the skew.

3.4. Second trial

The second prototype ribbon is composed of same preform fibers. To suppress dislocation in the ribbon array, the ribbon coating die is modified. To reduce the residual strain of each fiber, we decreased the friction between fiber and parts of ribbon coating equipment.

Figure 4(a) shows the skew of the second trial ribbon made of SM fibers. A low-skew ribbon of 0.259 ps/m was obtained. The variation of skew was greatly diminished. A similar approach was made to MM fiber ribbon to reduce the skew to 0.375 ps/m.

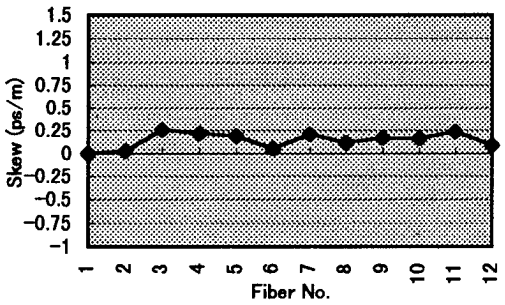

Skew 0.259 ps/m

Fig. 4 (a) Skew of second trial ribbon(SM)

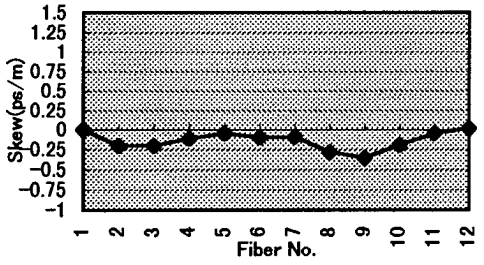

Skew 0.375 ps/m

Fig. 4 (b) Skew of second trial ribbon (MM)

3.5. Main cause of ribbon skew

The resultant ribbon was measured for the residual strain of each fiber. From the residual strain measurements, the skew of each fiber was calculated using equation (2).The results correspond to a case where each fiber has the same refractive index and the skew results only from the difference of the residual strain of the fibers. The extent of effect of residual fiber strain on the actual skew can be observed by comparing the calculated value with the measured skew. As shown in figure 5, the skew calculated from the residual strain of each fiber agreed well with the actually measured skew. It is evident from the above that, if the fibers of the same preform are used, the difference in refractive index of each fiber has little effect on skew but that the residual strain of each fiber is the main factor on which skew depends.

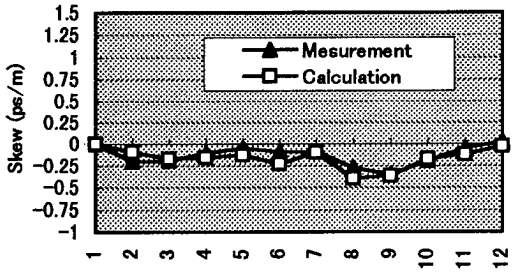

Fig.5 Comparison of Actually Measured Skew with Skew Calculated from Residual Strain (MM)

4. Investigation of low skew optical fiber cable

4.1. Structure of cable

Fig.1 shows the structure of a trial cable. This cable has slotted rod suitable for high fiber count. The cable was 288-fiber count slotted rod core design and 12-fiber ribbon were used.

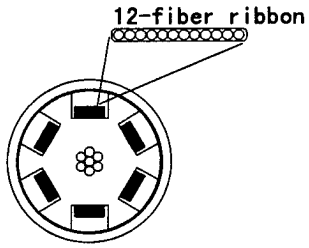

Fig.6 288-optical fiber cable for parallel optical transmission system

4.2. Increase of skew arising from cable structure

In the case of slotted core cable, the strain of each fiber is different depending on the fiber position in the ribbon. Propagation time is larger at the corner fibers because the length of the corner fibers are longer than the length of middle one. Fiber strain of a ribbon within the slotted rod is shown in the following equations.

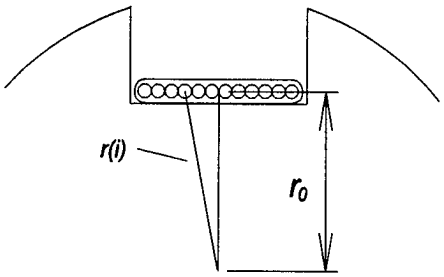

$$\Delta\varepsilon(i) = \frac{L(i) - L_0}{L_0} \quad (3)$$

$$L_0 = \sqrt{p^2 + (2\pi r_0)^2} \quad (4)$$

$$L(i) = \sqrt{p^2 + (2\pi r(i))^2} \quad (5)$$

$$r(i) = \sqrt{r_0^2 + \left[\left(\frac{M}{2} - i + \frac{1}{2}\right)d\right]^2} \quad (6)$$

$\Delta\varepsilon$ (i):Difference of strain between each fiber

p:Slotted rod pitch

i:Fiber Number in a ribbon

L(i): Length of No.i-fiber per length of one slotted rod pitch

M: Fiber count of a ribbon

d:Fiber diameter

Ribbon skew within the slotted rod is shown in the following equation.

$$\Delta t(i) = \kappa\, \Delta\varepsilon(i)\left(\frac{N}{c}\right) \quad (7)$$

κ :optical elastic coefficient

N: Refractive index of fiber

From equation (3) ~ (7), the increase of ribbon skew caused by cable structure is shown in figure 7 .

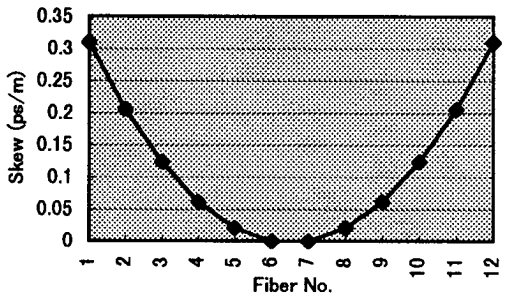

Fig. 7 Increase of ribbon skew caused by cable structure

Therefore, even if a low skew ribbon is obtained, an increase of skew occurs after cabling.

4.3. Compensation of the increase of ribbon skew

To realize the low skew cable, the fiber strain should be controlled to compensate the increase of skew after cabling process. Distribution of distortion shown in figure8 was given to a ribbon by applying larger tension to edge fibers than to middle fibers , so that the ribbon has the reverse distribution of skew.

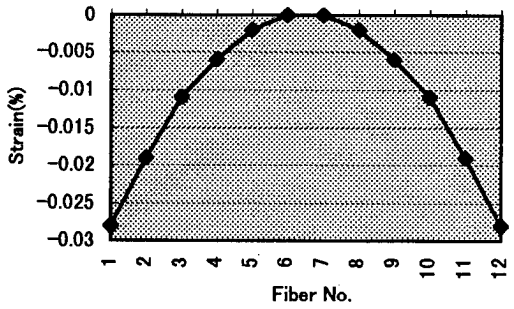

Fig.8 Fiber strain in a ribbon to compensate the increase of skew caused by cable structure.

4.4. Skew after cabling process

The ribbon with the reverse fiber strain was assembled into the cable, and ribbon skew was measured. The results are shown in Fig.9. Though a little variation is observed, this result shows that increase of skew at edge fibers are compensated by the reverse distribution of ribbon skew.

At this trial, ribbon skew of 0.52ps/m was

obtained for SM optical fiber cable.

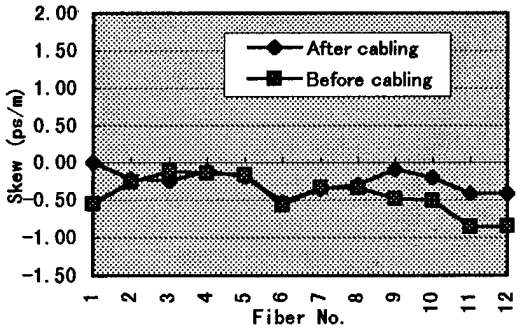

Fig.9 Ribbon skew before and after cabling process.

5. Conclusion

For development of low skew cable, firstly we investigated the methods to decrease the ribbon skew.

The causes of ribbon skew are difference in refractive index of each fiber from one fiber to another, effect of dislocation in the ribbon array and difference in the residual strain of each fiber. By investigating these causes, Low-skew ribbons with SM fiber of 0.259 ps/m and MM fiber of 0.375 ps/m were developed.

Increase of skew caused by cable structure occurs at cabling process. For this problem, the fiber strain was controlled to compensate the increase of skew after cabling process. As a result, a low-skew of 0.520 ps/m was obtained for SM optical fiber cable.

6. References

[1] K.Ieda and N. Kashima, " Effect of Cable Structure on skew in Optical Fiber Cables," IEICE B-10-30, p.491,1998

[2] N.Kashima "Evaluation of Skew and Parallel Transmission Distance in Single-mode Fiber ribbons," IEICE B-10-28, p489,1998

[3] F.Hosoi, M.Hara and Y.Kamikura " Development of low skew optical fiber ribbon," Proceeding of third OECC, 14p-53, p292,1998

[4] R.Matsuoka,Y.Shindo,N.Okada, N.Kume " Fabrication and Evaluation of 40-Fiber Array " Proceeding of 41 st IWCS , p384, 1992

Fumiki HOSOI

The Furukawa Electric Co.,Ltd
6,Yawata Kaigandori,Ichihara, Chiba,290-8555, Japan

Fumiki Hosoi received his M.E. degree in Physics engineering from Tokyo University in 1995. He joined The Furukawa Electric Co., Ltd and has been engaged in research and development of optical fiber cable. He is now a research engineer of optical fiber transmission research department, opto-technology laboratory.

Masato KOSAKA

The Furukawa Electoric Co., Ltd.
6, Yawata Kaigandori Ichihara, Chiba
290-8555, Japan

Masato Kosaka received his B.E. degree in Electronic Engineering from Ryukyu University in 1989. He joined The Furukawa Electric Co.,Ltd. in 1989 and has been engaged in the development of optical fiber and cables. He is now a engineer of Opto-Technology Laboratory. He is a member of the Institute of Electronics, Information and Communication Engineers of Japan.

Yasuhiro KAMIKURA

The Furukawa Electric Co.,Ltd
6,Yawata Kaigandori, Ichihara, Chiba, 290-8555, Japan

Yasuhiro Kamikura received his B.E. degree in Electronic Engineering from Tokyo University in 1975. He joined the Furukawa Electric co., ltd. in 1975 and has been engaged in the development of the optical fiber and cables. He is now a general manager of Opt-Technology Laboratory. He is a member of the Institute of Electronics, Information and communication Engineers of Japan.

Masami HARA

The Furukawa Electric Co.,Ltd
6,Yawata Kaigandori, Ichihara, Chiba,
290-8555, Japan

Masami Hara received his M.E. degree in Physics from Osaka University in 1987. He joined The Furukawa Electric Co., Ltd and has been engaged in research and development of optical fiber cable. He is now a research engineer of optical fiber transmission research department, opto-technology laboratory.

Seiji TODA

FUJITSU LIMITED

4-1-1 Kamikodanaka, Nakaharaku,
Kawasaki, Kanagawa 211 Japan

Takayuki WATANABE

FUJITSU LIMITED

4-1-1 Kamikodanaka, Nakaharaku,
Kawasaki, Kanagawa 211 Japan

Osamu SUZUKI

FUJITSU LIMITED

4-1-1 Kamikodanaka, Nakaharaku,
Kawasaki, Kanagawa 211 Japan

THE CHARACTERISTICS AND LONG-TERM RELIABILITY OF SEVERAL TYPES OF THIN OPTICAL-FIBER CORD

TSUYOSHI SHIMOMICHI, ETSUO INO, KATSUYOSHI ISHIDA, KEIJI OOHASHI, and MATSUHIRO MIYAMOTO

OPTICAL ACCESS NETWORK LABORATORY, FUJIKURA LTD.
1440, MUTUZAKI, SAKURA-SHI, CHIBA, 285-8550, JAPAN

Abstract

In order to enable higher-density wiring to be used in a central office, we have developed several types of thin cord and separable eight-cord ribbon. These cords possess not only adequate flexural rigidity, but also sufficient tensile strength for practical use in a central office. We have investigated the optical and mechanical properties of these cords under severe conditions for an extended period. No deterioration of the properties was observed under severe conditions. Good results were obtained for these cords in all evaluation tests.

1. Introduction

The demand for higher-density assembly of central office equipment has increased due to the spread of optical construction of the subscriber lines of optical transmission systems. In order to satisfy this demand, an optical-fiber cord that has a small diameter and can be used as wiring in or between items of central office equipment is required.[1],[2],[3] We have therefore developed two types of cord with a small diameter and two kinds of separable eight-cord ribbon. These cords possess not only adequate flexural rigidity, but also sufficient tensile strength for practical use. In this paper, we report about properties of these cords and their long-term reliability.

2. Samples of Optical Fiber Cords

We have produced two kinds of 0.9-mm single-core cord, a 0.25-mm single-core cord, and two types of separable eight-cord ribbon. The cross-sectional structures of these cords and cord ribbons are illustrated in Figure 1. Table 1 shows the construction of the single-core cords and Table 2 shows the construction of the eight-cord ribbons.

2-1. Single-Core Cords

(1) ϕ 0.9-mm cords

Figure 1-(a) shows the structure of ϕ0.9-mm single-core cords. Glass-fiber yarn is bundled around a conventional ϕ0.25-mm fiber and bound using UV resin. The resulting structure is then coated with UV resin. Since glass-fiber yarn

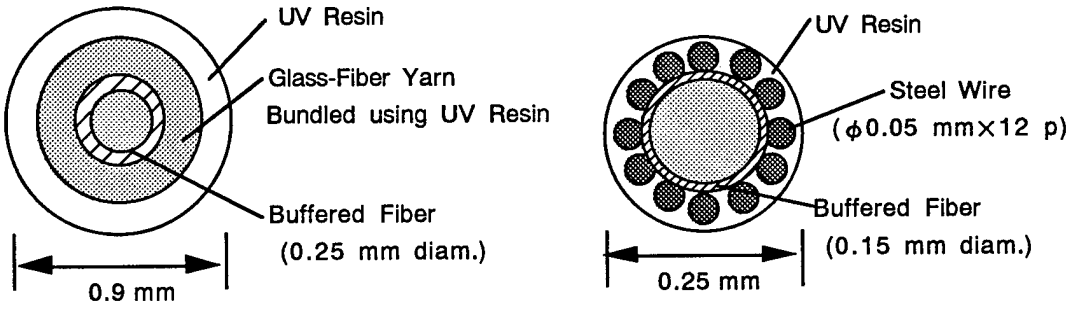

(a): 0.9-mm cord (b): 0.25-mm cord

Fig.1 Structure of the single-core cords.

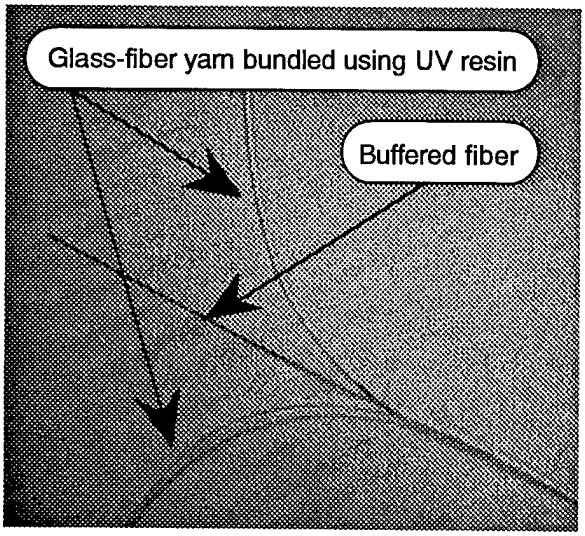

Fig.2 Separated buffered-fiber form the glass-fiber yarn.

has a high modulus of elasticity and is less expensive than aramido yarn, glass-reinforced cords are highly economical and easy to manufacture. The buffered-fiber in these cords can be separated from the glass-fiber yarn without difficulty(Figure 2). We prepared two kinds of ϕ 0.9-mm single-core cord using different types of glass-fiber yarn for the tension members (Type S and Type E). For type S cord, we used S glass-fiber yarn with high Young's modulus. The quantity of glass-fiber yarn used was 1200d. For type E cord, we used E glass-fiber yarn, which is commonly used as insulation. The quantity used was 2400d. Although S glass-fiber yarn has a higher modulus of elasticity than the E glass-fiber yarn, it is also more expensive. Applications that require high tensile strength justify the use of S glass-fiber yarn, and even higher strength can be achieved by increasing the amount of yarn used.

(2) ϕ 0.25-mm cords

The structure of ϕ0.25-mm single-core cord is shown in Figure 1-(b). The buffered fiber with a diameter of 0.15 mm, which was coated with a single layer of UV resin as the buffer layer, was used. Twelve steel wires with a diameter of 0.045 mm are bundled around the buffered fiber as tension members. Although the resulting cord has a very small diameter of 0.25 mm, it possesses not only adequate flexural rigidity, but also sufficient

Table 1 Properties of the single-core cords.

	ϕ0.9-mm cord		ϕ0.25-mm cord
	TYPE S	TYPE E	
Tension member	S-glass yarn	E-glass yarn	Steel wire
Amount of tension member	1200 denier	2400 denier	12 pieces
Diameter of the filament	ϕ7μm	ϕ7μm	ϕ45μm
Young's modulus of tension member	86 GPa (4.1 N/denier)	75 GPa (3.3 N/denier)	196 GPa (313 N/pieces)
Flexural rigidity	40.2 N•mm^2	39.2 N•mm^2	19.6 N•mm^2
Fiber strain at 68.6 N stress	1.02%	1.22%	1.50%
Transmission loss (at 1.30/1.55μm)	0.33/0.24 dB/km	0.33/0.22 dB/km	0.74/0.61 dB/km
Heat cycle test (-10 ~+40℃) (at 1.55 μm)	$\Delta\alpha$=0.05 dB/km	$\Delta\alpha$=0.04 dB/km	$\Delta\alpha$=0.22 dB/km
Crush test (490 N on 100 mm) (at 1.55 μm)	$\Delta\alpha$=0.12dB	$\Delta\alpha$=0.08dB	$\Delta\alpha$=0.15dB
Bending test (D=30 mm, 10 terns) (at 1.55 μm)	$\Delta\alpha$=0.21dB	$\Delta\alpha$=0.12dB	$\Delta\alpha$=0.05dB

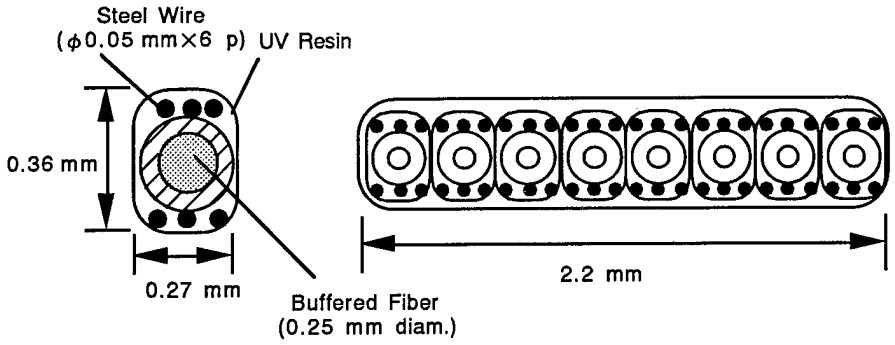

(a): Eight-cord ribbon (Type A)

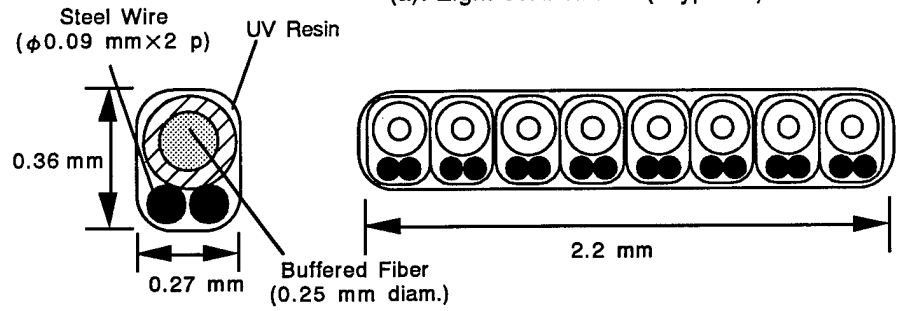

(b): Eight-cord ribbon (Type B)

Fig.3 Structure of the eight-cord ribbons.

Table 2 Properties of the eight-cord ribbons.

	Type A		Type B	
	Modified single cord	Cord ribbon	Modified single cord	Cord ribbon
Tension member	Steel wire			
Amount of tension member	6 pieces	6 × 8 pieces	2 pieces	2 × 8 pieces
Diameter of the filament	φ 45 μm		φ 90 μm	
Young's modulus of tension member	196 GPa (313 N/pieces)		196 GPa (1252 N/pieces)	
Flexural rigidity	5.1 N•mm^2	232.6 N•mm^2	10.6 N•mm^2	121.8 N•mm^2
Fiber strain at 68.6 N stress	2.35%	0.29%	1.90%	0.25%
Transmission loss (at 1.30/1.55 μm)	0.33/0.22 dB/km	0.33/0.22 dB/km	0.33/0.23 dB/km	0.33/0.20 dB/km
Heat cycle test (-10 ~+40℃) (at 1.55 μm)	Δ α <0.01 dB/km	Δ α <0.01 dB/km	Δ α <0.01 dB/km	Δ α <0.0 1dB/km
Crush test (490 N on 100 mm) (at 1.55 μm)	Δ α =0.47dB	Δ α <0.01dB	Δ α =0.02dB	Δ α <0.01dB
Bending test (D=30 mm, 10 terns) (at 1.55 μm)	Δ α =0.14dB	Buckling	Δ α =0.21dB	Δ α =0.20dB

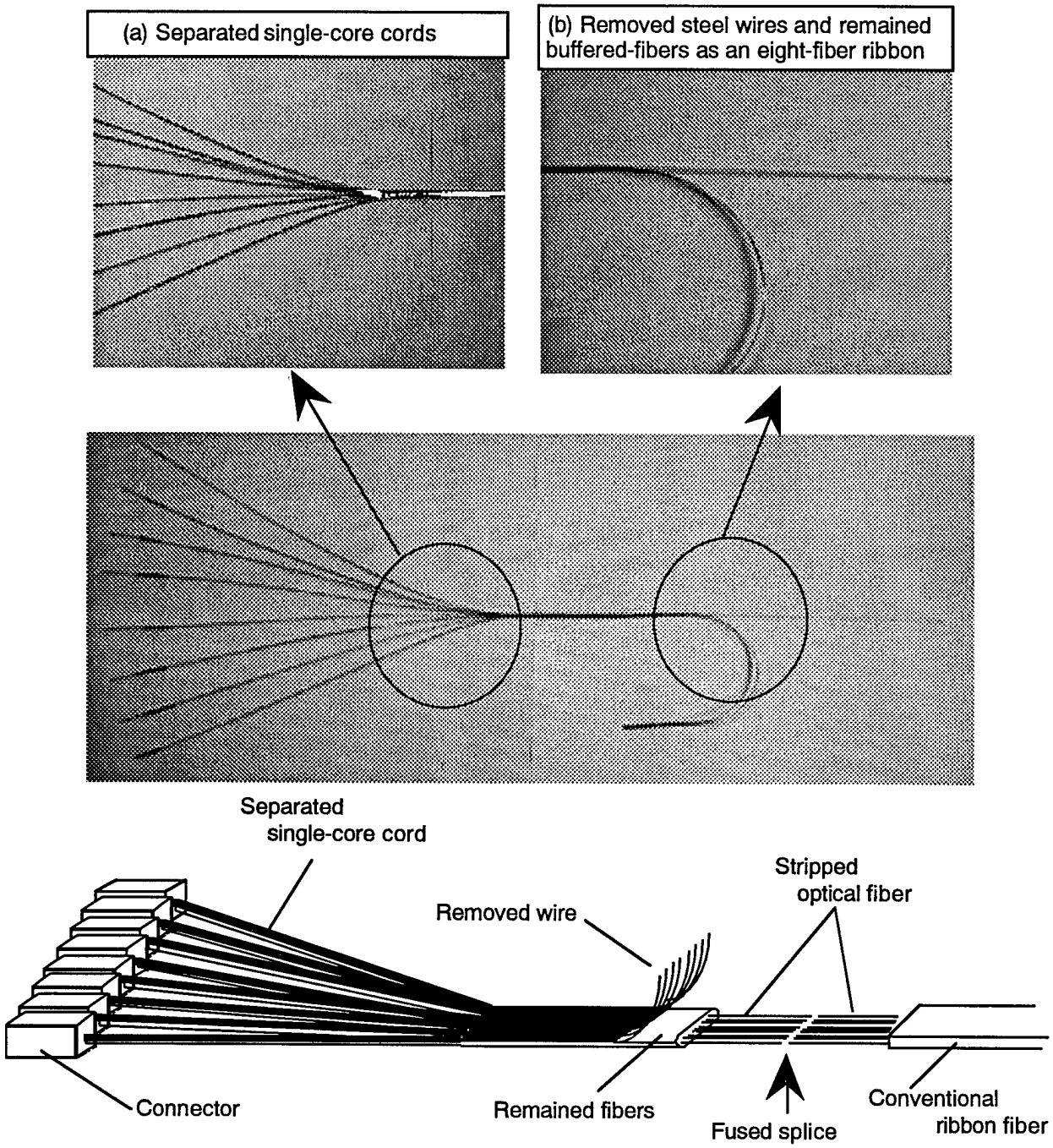

Fig.4 Functions of eight-cord ribbon.

tensile strength for use in a central office.

2-2. Eight -Cord Ribbon

We have produced two types of eight-cord ribbon (Type A and Type B) with different single-core cords. The single-core cords are rectangular with a small-side length of 0.27 mm and a large-side length of 0.36 mm. A steel wire is attached with a small-side length of 0.27 mm and a large-side length of 0.36 mm. A steel wire is attached vertically to one side or both sides of each cord. The rectangular shape of cords enables them to be positioned adjacent to each other, thereby allowing a uniform arrangement of the steel-wire surface. Therefore, the eight-cord ribbons are identical to a conventional eight-fiber ribbon in

Table 3 Test results of the single-core cords for long-term reliability .

Condition & Treatment time	Properties	φ0.9-mm cord		φ0.25-mm cord
		TYPE S	TYPE E	
Initial data	Mechanical Fiber strain at 68.6 N stress after treatment (%)	0.97	1.16	1.50
In air at 80 ℃ for 90 days		Same as above	Same as above	Same as above
In 95%- Rh air at 60 ℃ for 90 days		Same as above	Same as above	Same as above
In water at 20 ℃ for 90 days		Same as above	Same as above	Same as above
Initial dat	Optical Transmission loss after treatment (at 1.30/1.55 μm dB/km)	0.33/0.24	0.33/0.22	0.68/0.50
In air at 80 ℃ for 90 days		Same as above	Same as above	Same as above
In 95%-Rh air at 60 ℃ for 90 days		Same as above	Same as above	Same as above
In water at 20℃ for 90 days		Same as above	Same as above	Same as above

Table 4 Test results of the of the eight-cord ribbonsfor long-term reliability .

Condition & Treatment time	Properties	Type A		Type B	
		Modified single cord	Cord ribbon	Modified single cord	Cord ribbon
Initial data	Mechanical Fiber strain at 68.6 N stress after treatment (%)	2.42	0.18	1.94	0.36
In air at 80 ℃ for 90 days		Same as above	Same as above	Same as above	Same as above
In 95%- Rh air at 60 ℃ for 90 days		Same as above	Same as above	Same as above	Same as above
In water at 20 ℃ for 90 days		Same as above	Same as above	Same as above	Same as above
Initial dat	Optical Transmission loss after treatment (at 1.30/1.55 μm dB/km)	0.33/0.22	0.33/0.20	0.33/0.22	0.33/0.20
In air at 80 ℃ for 90 days		Same as above	Same as above	Same as above	Same as above
In 95%-Rh air at 60 ℃ for 90 days		Same as above	Same as above	Same as above	Same as above
In water at 20℃ for 90 days		Same as above	Same as above	Same as above	Same as above

identical to a conventional eight-fiber ribbon in terms of the pitch between optical fibers. The eight cord ribbon is 0.42 mm thick and 2.20 mm wide.

(1)Type A

The structures of the cord and Type A ribbon are shown in Figure 3-(a). Three steel wires are attached to both sides of a ϕ0.25-mm buffered fiber, and bound using UV resins. The outer diameter of each steel wire is 0.045 mm. Eight such cords are arranged in such a way that side is adjacent to, and bound using UV resin.

(2)Type B

The structures of the cord and Type B ribbon are shown in Figure 4-(b). Two steel wires are attached to either side of a ϕ0.25-mm buffered fiber, and bound using UV resins. The outer diameter of each steel wire is 0.09 mm. Eight such cords are arranged in such a way that the side is adjacent to, and bound using UV resin.

(3)Function of Eight-Cord Ribbon

Eight-cord ribbon has two main functions: jumpering due to its separability into single cords, and mass-fusion splicing.

Our eight-cord ribbon can be readily separated into single cords, which are reinforced with tubes and used as jumper cords (Figure 4-(a)).

In this eight-cord ribbon, the steel wires are arranged on either side or both sides of the cord-ribbon surface. This enables the layer of steel wire to be removed from the buffered fibers. Even after the steel wires are removed, the buffered fibers still remain as an eight-fiber ribbon. This ribbon is identical to a conventional eight-fiber ribbon in terms of the pitch between optical fibers, and enables easy mass-fusion splicing with other fiber ribbons (Figure 4-(b)).

3. Characteristics of Cords

We evaluated the properties of the cords and cord ribbons used in this study. The results obtained are summarized in Table 1 and Table 2. In the tensile strength test, we measured the elongation of each cord sample when a load was applied to the cord. Flexural rigidity was measured by the two-point bending method.[1] The bending loss test was conducted by measuring the transmission-loss increment per turn when the cord specimen was wound around a ϕ30-mm mandrel.

Low flexural rigidity of the cord may result in an abrupt increase in transmission loss during handling, while an excessively high flexural rigidity causes difficulty in handling. The properties of the ϕ0.25-mm single-core cords are inferior to those

the transmission-loss increment per turn when the cord specimen was wound around a ϕ30-mm mandrel.

Low flexural rigidity of the cord may result in an abrupt increase in transmission loss during handling, while an excessively high flexural rigidity causes difficulty in handling. The properties of the ϕ0.25-mm single-core cords are inferior to those of the other cords, presumably because the buffered fiber has a diameter of 0.15 mm and is coated with a single layer of coating material. For central office wiring, such cords are employed in applications that do not require long cords and in environments that are subject to small temperature changes. The ϕ0.25-mm single-core cords are therefore considered suitable for use in their intended applications. The rectangular cords, both Type A and Type B, were excellent in terms of transmission loss and transmission-loss temperature characteristics. For these prototype cords, conventional ϕ0.25-mm fibers are used for the buffered fiber. The cord ribbons proved to be separable into single-core cords. It was also possible to remove the steel wires collectively. In the case of the ϕ0.9-mm cords, the characteristics vary according to the type of yarn wrapped around the buffered fiber, the rigidity of the binding resin, and the yarn assembly method.

All of the cords can be used in practical applications.

4. Long-Term Reliability of the Cords

We evaluated the optical and mechanical properties of these cords under severe conditions for an extended period. For the evaluation of tensile strength, environmental loads were imposed on ϕ30-mm free coil samples. These samples were subjected to continuous application of bending distortion. Table 3 shows the results of long-term reliability tests. No deterioration of the properties was observed under the conditions used, which included air at 80 ℃, air at 60 ℃ and Rh of 95%, and water at 80 ℃. Good results were obtained for all the cords in all the evaluation tests.

5. Conclusion

With a view to increasing central-office wiring density, we have developed two kinds of 0.9-mm single-core cord, a 0.25-mm single-core cord, and two types of separable eight-cord ribbon. These cords possess not only adequate flexural rigidity, but also sufficient tensile strength for practical use in a central office. We have investigated the optical and mechanical properties of the cords under severe conditions for an extended period. No deterioration of these properties was

two types of separable eight-cord ribbon. These cords possess not only adequate flexural rigidity, but also sufficient tensile strength for practical use in a central office. We have investigated the optical and mechanical properties of the cords under severe conditions for an extended period. No deterioration of these properties was observed under severe conditions. Good results were obtained for these cords in all evaluation tests.

REFERENCES

[1]] M.Tachikura,H.Takemoto and N.Tomita , "Miniature optical fiber cords with high flexural rigidity", Technical Digest of 2nd Optoelectronics & Communications Conf.(OECC),pp.526-527, 1997.

[2] M.Sato,M.Tachikura,N.Tomita and S.Iwano, "A 1-mmϕ miniature optical fiber cord adaptable for MU-type connectors",Proc.of 45th IWCS,pp.378-380,1996.

[3] M.Tachikura, Y.Enomoto, S.Uruno, H.Takemoto, N.Tomita and H.Takasugi, "Optical fiber distribution system in central offices for the FTTH ERA",Proc.of 46th IWCS,pp.859-866, 1997.

Tsuyoshi Shimomichi

Optical access network laboratory Fujikura Ltd.

1440, Mutsuzaki, Sakura-shi, Chiba, 285, Japan

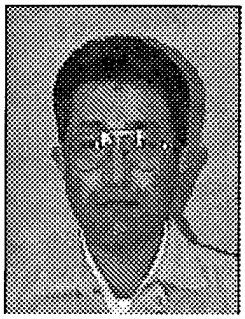

Tsuyoshi Shimomichi was born in 1960. He joined Fujikura Ltd. after his graduation from Nagasaki University in 1986 with an M.E. degree and has been engaged in research and development of optical fibers and optical fiber coatings. He is now a senior engineer for the Telecommunication Cable Department and a member of the IEICE of Japan.

Etsuo Ino

Optical access network laboratory Fujikura Ltd.

1440, Mutsuzaki, Sakura-shi, Chiba, 285, Japan

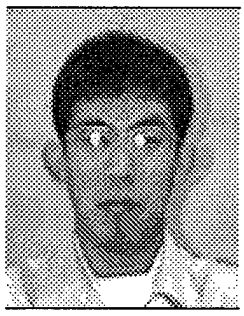

Etsuo Ino was born in 1970. He graduated from the Tohoku University in 1995 with a M.S. degree in chemistry and has been engaged in research and development of optical fibers.He is now an engineer in the Telecommunication Cable Material Section and a member of the IEICE of Japan.

Katsuyoshi Ishida

Optical access network laboratory Fujikura Ltd.

1440, Mutsuzaki, Sakura-shi, Chiba, 285, Japan

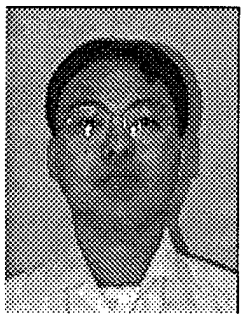

Katsuyoshi Ishida was born in 1967. He joined

Fujikura Ltd. after his graduation from Gunma University with a B.E. degree in 1991 and has been engaged in research and development of optical fibers. He is now an engineer in the Telecommunication Cable Material Section and a member of the IEICE of Japan.

Keiji Oohashi
Optical access
network laboratory
Fujikura Ltd.

1440, Mutsuzaki,
Sakura-shi, Chiba,
285, Japan

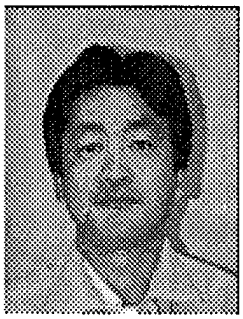

Keiji Oohashi was born in 1956. He graduated from the Tokyo Institute of Technology in 1980 with a B.E. degree in chemistry. After eight years of work as an engineer in the field of materials for motor vehicles, he joined Fujikura Ltd. in 1988. He has been engaged in research and development for optical fibers and optical fiber coatings. He is now chief of the Telecommunication Cable Material section and member of the IEICE of Japan.

Matsuhiro Miyamoto
Optical access
network laboratory
Fujikura Ltd.

1440, Mutsuzaki,
Sakura-shi, Chiba,
285, Japan

Matsuhiro Miyamoto was born in 1953. He graduated from Nagoya Institute of Technology with a B.E. degree of electrical engineering. He joined Fujikura Ltd. after his graduation from Tokyo Institute of Technology with a M.S. degree in 1978 and has been engaged in research and development of optical fiber and optical fiber cables. He is now a manager of the Telecommunication Cable Department and a member of IEICE in Japan.

PERFORMANCE AND RELIABILITY OF GRADED-INDEX POLYMER OPTICAL FIBERS

Lee L. Blyler, Jr., Todd Salamon, Whitney R. White, Michael Dueser, William A. Reed, Christopher S. Koeppen, Christine Ronaghan*, Pierre Wiltzius & Xina Quan

Bell Laboratories, Lucent Technologies
Murray Hill, New Jersey

***current address: Davis Standard Corporation**
Pawcatuck, Connecticut

ABSTRACT

We have developed a model that accurately predicts changes in index profile and fiber dimensions for graded-index polymer optical fibers under accelerated aging conditions. We also present initial results correlating differences in these physical characteristics to the optical performance of the fibers.

INTRODUCTION

Polymer optical fibers (POF) have long been considered and rejected for use in the telecommunications industry. Despite the potential for lower systems costs due to easy interconnection of large millimeter-sized fibers and for an extremely low-cost continuous manufacturing process, issues of high loss, low bandwidths, and long-term reliability have created insurmountable barriers to the use of POF in most applications.

In recent years, there have been major advances in the development of low-loss, graded-index polymer optical fibers (GI-POF). With the use of perfluorinated polymers, losses on the order of 50 dB/km have been obtained,[1,2] a significant improvement over the 150 dB/km losses observed with PMMA fiber.[1] In addition, through the diffusion of small dopant molecules in a polymer matrix,[3] it is now possible to reproducibly obtain graded-index profiles which has allowed the development of GI-POF with transmission capacity on the order of 2.5 Gb/s over 200m lengths.[4] These developments have led to renewed interest in the application of GI-POF as a high bandwidth medium for data transmission in local area networks. There are also potential applications in the interconnection of large telcom and computer systems.

Several issues must be resolved before the adoption of GI-POF in these demanding applications is possible. In addition to the obvious need for an assessment of long-term reliability and continued minimization of the loss, a better understanding of the anomalous optical performance observed to date in GI-POF is necessary. Unlike graded-index (or multimode) silica optical fiber, GI-POF appears to have unexpectedly robust transmission capacity with respect to deviations of the index profile from an ideal parabolic profile.[5] Thus, the bandwidths observed from perfluorinated GI-POF over a wide range of wavelengths are generally higher than would be predicted.

In this paper, we describe our work to model the long-term stability of the index profile of GI-POF and our preliminary efforts to understand how the profile relates to their optical properties.

LONG-TERM RELIABILITY

Perhaps the major obstacle in the acceptance of GI-POF is the perception that the use of small molecule dopants to create the index profile precludes the long-term stability of these fibers. We have developed a model which allows us to predict the short-term changes observed for GI-POF under accelerated aging conditions. The model requires the assessment of the diffusion kinetics of dopants in the polymer matrix

material of the fiber. Our goal is to use these kinetics to predict the degree to which the dopant remains immobilized in the polymer glass.

Assessment of Dopant Kinetics

Two methods have been developed to characterize the diffusion of small-molecule dopants in a polymer matrix near its glass transition temperature. In the first (described in detail elsewhere[6,7]), the index profile of a polymer fiber is measured directly as a function of time while it is immersed in a reservoir containing the dopant. The dopant has been diluted by a solvent that does not dissolve the polymer of the fiber. The second method uses dynamic light scattering to measure diffusion of dopant molecules homogeneously dispersed in a polymer matrix.

Immersion measurements. In this method, dopant molecules are diffused into a polymer fiber while tracking the resulting effect on the index profile of the fiber. The results described in this paper were measured on the PMMA/benzyl benzoate system using fibers approximately 400 μ in diameter. These were obtained by using a selective solvent to remove the cladding from step-index PMMA POFs manufactured by the Mitsubishi Rayon Corporation. The fibers were annealed at 150°C in Teflon tubing to allow the recovery of processing orientation and to stabilize their dimensions. They were then immersed in a mixture of a polybutene oil (a non-solvent for PMMA) with a low concentration of benzyl benzoate. Diffusion of the dopant was induced by subjecting the immersed fibers to temperatures ranging from 80 to 165°C. The index profiles of the fibers were characterized periodically using a Leitz Transmitted Light Interference Microscope in the transverse interference mode. Profiles such as those shown in Figure 1 were fit with a concentration-dependent diffusion coefficient having the functional form

$$D = D_o \exp [\alpha C]$$

where D_o and α are temperature-dependent parameters. For the 120°C data of Figure 1, D_o=1.9 x 10^{-11} cm^2/sec and α=56. We find that at elevated temperatures up to 50°C above the glass transition of the polymer, the diffusion kinetics are distinctly non-Fickian, requiring an exponential dependence of dopant diffusivity on concentration.

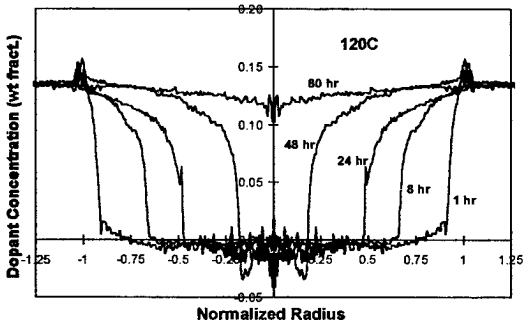

Figure 1: Concentration profiles in PMMA fiber aged at 120°C in 7.5%$_w$ benzyl benzoate mixture

Dynamic scattering measurements. Another approach to measuring the kinetics of dopant diffusion is through dynamic light scattering of homogenous dopant/polymer blends. In this technique, one measures the temporal correlations of the "speckle" pattern formed by a coherent light source impinging on a bulk sample. A schematic of the apparatus used in this work[8] is shown in Figure 2. The

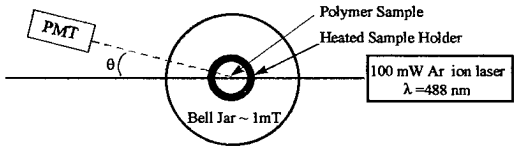

Figure 2. Schematic of dynamic light scattering apparatus.

temporal correlation function

$$g_2(\tau) = < I(t)\, I(t-\tau) > / <I(t)>^2$$

is associated with the relaxation of structure in the sample. In these experiments, the structure (and associated scattering) arise primarily from thermally excited fluctuations of the dopant concentration. In the case of purely diffusive motion of the dopant molecules, the correlation function has the functional form:

$$g_2(\tau) = 1 + \alpha \exp(-2\Gamma\tau)$$

where Γ is proportional to the diffusion constant D of the dopant molecules. This diffusive behavior is observed In the correlation function shown in Figure 3 for time scales exceeding 100 ms. At shorter times, one observes only a local,

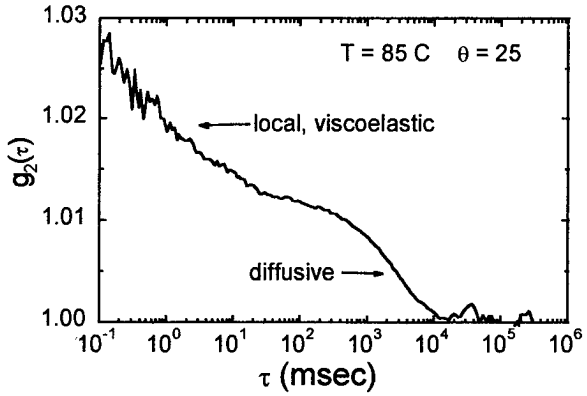

Figure 3. Correlation function for the motion of a proprietary dopant in a perfluorinated polymer matrix.

viscoelastic relaxation of dopant trapped in the fluoropolymer matrix.

From the diffusive model described above, the temperature and concentration dependence of the diffusion constant can be readily determined. An example set of data is shown below in Figure 4 for a proprietary dopant/perfluorinated polymer system.

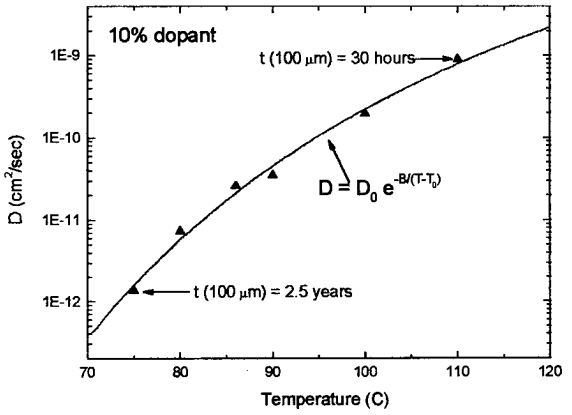

Figure 4. Temperature dependence of diffusion coefficients for a proprietary dopant in a perfluorinated polymer matrix.

Numerical simulations

With the diffusion kinetic data, we can use numerical simulations to predict the dopant concentration profile for a particular time-temperature history. Finite element modeling is used to simulate changes in the dopant concentration profile, axial contraction, and radial swelling of the fiber. The model incorporates an exponential dependence of dopant diffusivity on concentration since we find experimentally that the diffusion kinetics are distinctly non-Fickian. Details of the modeling algorithms are described elsewhere.[7] The Typical results showing excellent agreement between experiment and simulation are shown in Figures 5 and 6 respectively.

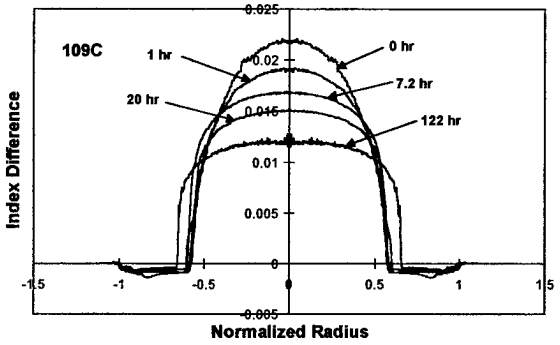

Figure 5. Experimental profile data for PMMA/benzyl benzoate fibers aged at 109°C.

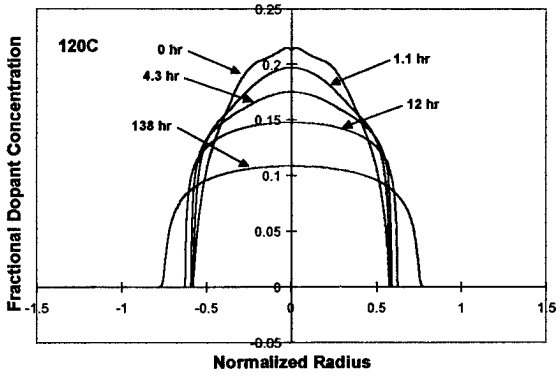

Figure 6. Simulation results for PMMA/benzyl benzoate fibers aged at 120°C

The model is valid for short-term aging conditions where the aging temperatures are near or above the glass transition temperature. Under these conditions, the profile flattens with time initially. At longer times, the doped behaves as a solvent for the undoped cladding, advancing as a front which locally swells and plasticizes the polymer matrix.

For conditions below the glass transition temperature, it is very difficult to obtain accurate diffusion data, even with the dynamic light scattering technique, because the time scales become excessively long. Our model is now being extended to simulate the lower temperature conditions where the non-Fickian diffusion behavior is even more pronounced by

extrapolating the diffusion kinetics data from higher temperatures.

OPTICAL MEASUREMENTS

In addition to the ability to predict the physical changes undergone by GI-POF as a result of exposure to various time-temperature histories, it is also necessary to correlate these physical parameters to the optical performance of the fiber.

A major concern in the use of GI-POF is possible degradation of the transmission bandwidth that can be supported by the fiber. In silica multimode fiber, the bandwidth is extremely sensitive to the shape of the index profile.[2] This is illustrated by Figure 7 which

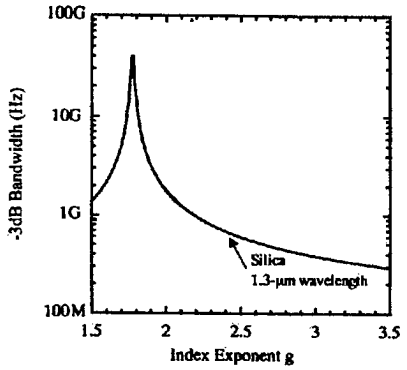

Figure 7. Effect of changes in index profile on bandwidth for silica multimode fiber (after Reference 2).

shows the bandwidth as a function of the index exponent g which describes the shape of the index profile as a function of the fiber radius r through the relations

$$n = n_1 [\, 1 - 2\,(r/a)^g \,\Delta\,]^{1/2} \quad \text{for } r < a$$
$$n = n_o \quad \text{for } r > a$$

where n is the refractive index, n_0 is the index of the cladding, n_1 is the index at the center of the core region, a is the radius of the core region, and

$$\Delta = (n_1^2 - n_0^2)/2n_1^2 = (n_1 - n_0)/n_1$$

With the major changes observed in the index profile of aged GI-POF illustrated above in Figures 1, 5, and 6, it is reasonable to expect that the transmission bandwidth of these fibers will be similarly affected.

To probe these issues, we have constructed the differential mode delay (DMD) apparatus shown in Figure 8.[9] In a DMD experiment, one excites a graded-index (multimode) fiber with a pulsed source having a spot size much smaller than the fiber core diameter. By varying the position of the source with respect to the fiber, one can launch power into different sets of modes carried by the fiber. With short pulses, we can also measure the time required for each input pulse to propagate through the fiber and the distortion of these pulses to determine the

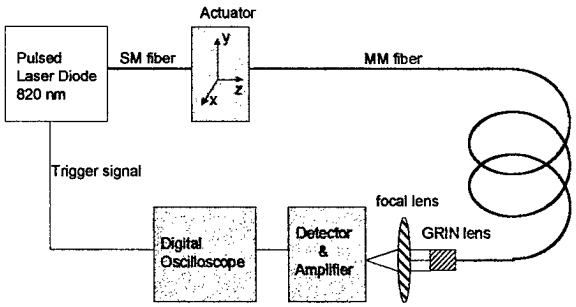

Figure 8. Differential mode delay (DMD) apparatus for polymer optical fiber.

intermodal dispersion and the bandwidth of the fiber.

Preliminary results from perfluorinated GI-POF have yielded surprising results. As seen in Figure 9, there is an extremely large central

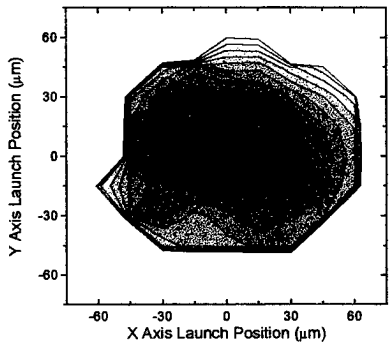

Figure 9. Variation of pulse delay with launch position for a 150 m perfluorinated GI-POF. Darker contours represent longer delay, and the spacing between contour levels is 40 ps.

region approximately 50% of the fiber core diameter over which there is very little variation in the pulse delay, despite the fact that the index profile is not ideal. This implies that the power input into a given mode in this region is very efficiently transferred to all the other modes in

the region. This coupling of the modes results in greater tolerance to the launch conditions and in higher observed bandwidths since the delays of all modes are effectively equalized.[10]

From cutback experiments and static light scattering measurements, the strong mode coupling would appear to stem from extrinsic sources. In the cutback experiments shown in Figure 10, the variations in pulse delay

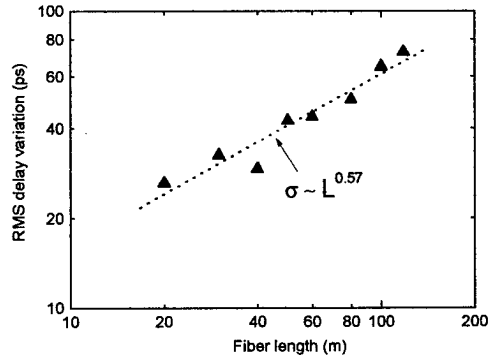

Figure 10. Dependence of delay variation on fiber length.

measured in the central region plotted against fiber length follows the relationship

$$\sigma \propto L^{0.57}$$

which is quite close to the square root dependence expected from a diffusive theory of mode coupling.[11] The relationship holds to the shortest length (20m) measured in these experiments, implying that the characteristic coupling length for this system is shorter than this length.

From static light scattering experiments, the intrinsic losses for the perfluorinated fiber system used in Figures 9 and 10 are on the order of 10 dB/km which would imply very weak mode coupling with a characteristic length on the order of 1 km. Thus it would appear that the mode coupling observed in these GI-POF arises from extrinsic sources of loss such as microscopic inhomogeneities in the GI-POF which produce strongly forward-directed scattering.

A major advantage of this extremely effective mode coupling in GI-POF is an improved tolerance of bandwidth to changes in the refractive index profile. Since the major effect of aging the fiber is initially a flattening of the profile in the central region, it is expected that the bandwidth of aged fibers should be relatively unaffected at short times. However, losses may still increase due to chemical degradation of the dopant. DMD experiments are underway to characterize the optical performance of GI-POF during aging.

CONCLUSIONS

We have reviewed the major issues concerning the long-term reliability of plastic optical fibers. A model is described that accurately predicts the changes observed in the index profile when aging GI-POF at or above the glass transition temperature of the fiber. Two techniques for measuring the diffusion kinetic data needed for the model are also outlined.

We also have discussed the measurement of differential mode delay in GI-POF and have shown how extrinsic loss mechanisms lead to extremely efficient transfer of power between modes in a large central region of the fiber. This high degree of mode coupling leads to an improved tolerance of the bandwidth to changes in the index profile. This, in turn, leads to a reduced sensitivity of the fiber to short-term aging, at least with respect to bandwidth.

[1] Y. Koike, T. Ishigure and E. Nihei, J. Lightwave Tech., **13**, No.7, p. 1475 (1995).

[2] E. Nihei, T. Ishigure, N. Tanio and Y. Koike, IEICE Trans. Electron., **E80-C**, No. 1, p. 117 (1997).

[3] N. Yoshihara, OFC '98, OSA Technical Digest Series Vol.2, Optical Society of America, Washington, DC, 1998. p308.

[4] Y. Koike, *POF Asia-Pacific Forum '96*, Tokyo, Japan, December 1996.

[5] T. Ishigure, A. Horibe, E. Nihei, and Y. Koike, *J. Lightwave Tech.*, **13**, 1686 (1995).

[6] L. L. Blyler, Jr., C. S. Koeppen, and H. E. Bair, *POF Asia-Pacific Forum '96*, Tokyo, Japan, December 1996.

[7] L. L. Blyler, Jr., T. Salamon, C. Ronaghan, and C. S. Koeppen, *MRS Symposium Proc., Reliability of Photonics Materials and Structures*, E. Suhir, C. R. Kurkjian, and M. Fukuda, Eds., in press.

[8] W. R. White and P. Wiltzius, POF Conference '97, Kauai, Hawaii, September 1997.

[9] M. Dueser, W. R. White, and W. A. Reed, Monterey, *IEEE Symposium on Organic*

Optics and Optoelectronics, California, July 1998.
[10] G. Jiang, R. F. Shi, and A. F. Garito, *IEEE Photonics Tech. Lett.*, **9**, 1128 (1997).
[11] D. Gloge, *Bell Syst. Tech. J.*, **51**, 1767 (1972).

AUTHORS

Lee Blyler is a Technical Manager in the Polymer and Chemical Engineering Department at Bell Labs, Lucent Technologies in Murray Hill, NJ. He received a PhD degree in Aerospace and Mechanical Sciences from Princeton University in 1966. He joined Bell Labs in 1965 and has carried out research in polymer engineering for application to lightwave systems over the past 25 years.

Todd Salamon was born in Bristol, CT in 1966. He received his PhD in Chemical Engineering from the MIT in the Fall of 1995. Todd is currently a member of the Scientific Computing Department of Bell Laboratories at Lucent Technologies.

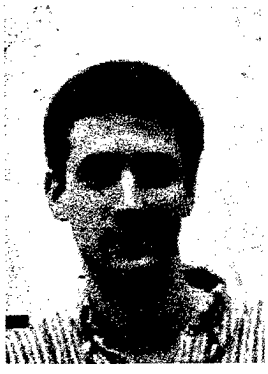

Whitney White is currently a Member of Technical Staff at Bell Laboratories in Murray Hill, NJ. He received his PhD in Applied Physics from Stanford. His primary research interests are optical properties and dynamics of polymer blends, and polymer optical fibers.

Michael Dueser was born in Menden, Germany in 1972. He has been working on measurements of multimode optical fibers as an intern in the Polymer & Chemical Engineering Research Department at Bell Labs. He is presently preparing his thesis on optical communications and optoelectronic devices to achieve the grade "Diplom-Ingenieur" in Electrical Engineering at the University of Dormund in Germany.

Bill Reed is a Distinguished Member of Technical Staff in the Optical Fiber Research Department at Bell Labs. His research interests include the optimization of optical performance through fiber design.

Chris Koeppen is currently a Member of Technical Staff at Lucent Technologies, Specialty Fiber Devices in Somerset, NJ. His work focuses on the development of fiber grating and rare earth doped - based fiber devices. He received his PhD in Physics from the University of Pennsylvania in 1997 where he researched various properties of plastic optical fiber, including rare earth doping, index profiles, dispersion, and mode coupling.

Christine Ronaghan studied diffusion of dopants in polymers as part of her MS thesis research while interning at Bell Labs. She received her BS and MS degrees in Chemical Engineering from Stevens Institute of Technology and currently works for the Davis Standard Corporation in Pawcatuck, CT.

Pierre Wiltzius received the degree of Diplomphysiker in 1976 and the degree of Dr. sc. nat. in 1981 from the E.T.H. in Zurich, Switzerland. He was a postdoctoral fellow in the Physics Department at the University of California in Santa Barbara and joined Bell Laboratories in 1984. He is currently the head of the Condensed Matter Physics Research Department. His research interests include soft condensed matter and complex fluids.

Xina Quan is the Head of the Chemical & Polymer Engineering Department at Bell Labs. She received BS and MS degrees from MIT and a PhD from Princeton, all in Chemical Engineering.

RECENT ADVANCES OF PLASTIC OPTICAL FIBER

Masaki Nishiguchi, Masanori Hattori, Seiji Takagi

The Furukawa Electric Co., LTD.
6 Yawata Kaigan-Dori, Ichihara-Shi, Chiba, Japan

Abstract

The standard of plastic optical fiber is established for LAN system and premises use.

The IEEE1394 integration wiring is paid to attention as a transmission system in this next generation's Home Network.

Some of makers are centered by using the plastic optical fiber to expand transmission distance, and the standard of 100Mbps/200Mbs-50m is being discussed with IEEE1394.b.

In the office LAN, the ATM standard of the plastic optical fiber is enacted in 1996 and the ATM router for the plastic optical fiber and the hub are introduced.

Various types of plastic optical fibers have been developed to meet requirements of varieties of applications.

I. Environment of plastic optical fiber

Although telecommunication services so far have been based on analog telephone services, new services such as Internet, digital broadcasting and CATV requires integration of broadcasting and telecommunication, and communication infrastructure for high-speed network, which realize new services, is being maintained.

In Japan, high-speed optical fiber network infrastructure based on PDS -ATM is being maintained by NTT, and new access networks is scheduled to be completed by 2005.

As for a new access infrastructure, many cost-reduction efforts have expand high-speed network service area such as INS64 (N-ISDN, 2B+D), OCN (a flat rate packet service, best effort type). And 2005 expect a new economical, high speed OCN service (10Mbps-packet service at a flat rate of ¥10.000/month).

Moreover, the experiment on B-ISDN is completed in various places, and the business service has already been being begun in part.

The personal computer, which has been used as a stand-alone unit, is connected as LAN in the office, and, in addition, the transmission capacity is increasing because of the upgrade of the amount of information, too. As a result, 100 Mbps Fast Ethernet, Gigabit Ethernet for floor wiring and truck line respectively, becoming popular, though 10 Mbps Ethernet and 100 Mbps FDDI were majority media only a few years ago.

Moreover, the personal computer is used and small-scale LAN is spreading also in a small and

medium-sized enterprise and a small-scale shop which up to now, is without relation to the personal computer. Moreover, this small-scale LAN connected with a public net (IPS etc) is used for various Internet services with the outside increases rapidly.

For home use, introduction of a lot of information appliances such as PC, DVD, digital video apparatus as well as new services, such as Internet, satellite digital broadcasting are expected to increase the capacity of transmission media up to several hundreds Mbps within years.

2. What is Plastic Optical Fiber?

The plastic optical fiber has been widely used from the optical fiber, which has a large numerical aperture with a large diameter, and easy handing characteristics, for the sensor, the illumination, and the decoration, etc. though the transmission loss is larger than a glass optical fiber.

The plastic optical fiber has the step index (SI type) structure, which composed of the core and the cladding plastic materials.

Those products available today are made from PMMA (Polymethlmethacrylate) as core material and fluoric resin as clad materials, because of its refractivity and transparency.

Recently, the plastic optical fiber has been paid to attention by upgrading the communication service as a short distance communication transmission line, for use premises or small office.

3. Various Communication Networks

Though glass optical fiber has a high bandwidth over 1Gbps, it's data link and connectors are extremely expensive because of the installation using fusion splice and processing. Therefore, glass optical fiber is suitable for long-distance, high-capacity network such as public network or backbone wiring for office building.

Metallic cables (twisted pair cable) is widely used for LAN network in the office floor and it's backbone at a speed of 156Mbps or 100Mbps as ATM or Fast Ethernet. However, it is necessary to equalize the data (to flatten signals over wide frequency range) when the data transmission of 100Mbps or more are required, and the problem of EMC grows additionally.

Because EMC problem which becomes a problem by the metal cable is free though the plastic optical fiber is restricted as a transmission distance within 50-100m, a connector and an optical data link are cheaper, and the connector processing is also easier, systems can be composed most cheaply in optical communications. Therefore, the plastic optical fiber is considered as the most suitable media for over 100 Mbps communication networks in premises, office LAN and automobile LAN.

The following table shows a comparison matrix of representative characteristics of communication media.

Table 1 Comparison matrix of transmission media

	UTP-5	POF	GI-GOF
Transmission rate	100Mbps	100Mbps~ 400Mbps	1.2Gbps
Transmission distance	100m	50m	2km
Cost of Transmission media approximately	¥60/m	¥50/m	¥200/m
Cost of transceiver approximately	¥700 and more	¥2.000 or less	¥20.000 and more
Outer Diameter	5.0mm	2mm~ 4mm	2mm~ 4mm
Connector type	RJ-45 IEEE1394-connector	F-07-pn、SMI RJ-45 MINI-MT	FDDI MT RJ-45 LC
Flexibility	Good	Good	Poor
EMC Problem	Fair	Good	Good
PL related problem	Good	Good	Poor

When EMC, the extendibility, and the cost are considered, it is thought that the plastic optical fiber is advantageous on the short distance high-speed signal transmission cable. As for transmission media used for home applications, PL (product liability) problem should be considered with no possibility of an injury caused by sharp edge from broken glass fiber. Further, safety disposal is required for the environment protection program, which are of interest to the society, especially in the future. Plastic optical fiber has neither disposal nor PL problems unlike glass optical fiber. So, plastic optical fiber is ideal for the household applications.

Hereafter, the application situation of the plastic optical fiber as the short distance high-speed transmission cable is described

(1) Premises Communication

As described before, the amount of data to be processed in premises and small offices are considered to increase rapidly. Factors, which cause are:

1) Ever-increasing nature of information (if e-mail as an example, the transmitted data has changed such stages. Simple text data (1st stage)-text data with attached file (2nd stage)-text data with attached file with picture (3rd stage) and so on.
2) Spread of information appliances (PC, DVD, Fax)
3) Popularization of Internet or Broadcasting etc.

The IEEE1394 integration wiring is paid to attention as a transmission system in this next generation's Home Network.

There are so many wiring systems today, such as broadcasting (coaxial cable), telephone (twisted pair), Audio Visual appliances (AV cables). IEEE1394 standard is expected as a connection between personal computer and peripheral information apparatus, to make common transmission paths by integrate complicated telecommunication and broadcasting interfaces together.

Thus IEEE1394 integrated system designed for to transmit different data with single cable by unifying telecommunication cables (telephone, Internet, PC) and those for broadcasting (CATV, satellite, DVD) by IEEE1394 interface.

Figure 1. shows this concept chart.

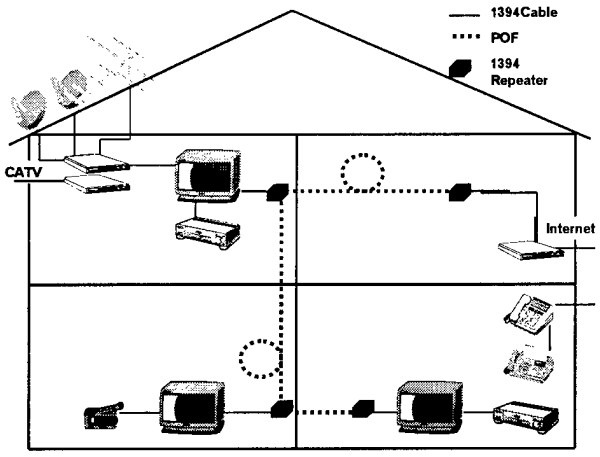

Fig.1 Home Network with IEEE1394 system

When a family wants to enjoy full services (VOD, Internet, Games etc.) in the home, tens of Mbps level will be expected in near future.

However, when the burst-character and the having degree of data are considered, the transmission capacity of 100Mbps or more is needed.

The IEEE1394 standard is shown below.

IEEE1394 standard

	IEEE1394-1995	IEEE1394-Longer
Transmission rate	100Mbps 200Mbps 400Mbps	100Mbps、200Mbps
Number of nodes which can be connected	63	—
Transmission medium	STP	POF,H-PCS
Isochronous transmission mode	Support	Support
Coding system	DS-LINK	Combination of 8B/10B and NRZI
Transmission distance	4.5m	50m
Transmission distance	4.5m	50m
Standardization	1995	1998

As shown in table 2, transmission distance of metallic cable is restricted within 4.5 meters, which may not enough inter-room data transmission.

Domestic consumer electric maker, the plastic optical fiber maker, and the connector maker are centered by using the plastic optical fiber to expand transmission distance, and the standard of 100Mbps/200Mbs-50m is being discussed with IEEE1394.b. It is expected to be standardized in March 1998. Moreover, the examination to transmit between a digital video camera, AV equipment such as DVD, and the personal computer with the plastic optical fiber is advanced.

(2) Office LAN

In the office LAN, 100Mbps Fast Ethernet has now driving 10 Mbps Ethernet, which has been the majority of office LAN until just 1-2 years ago. As for the plastic optical fiber, the approach from the extendibility to the office LAN is examined.

The ATM standard of the plastic optical fiber is enacted in 1996 and the ATM router for the plastic optical fiber and the hub are introduced.

While conventional plastic optical fiber is step index structure (SI type) and have bandwidth about 10 MHz-km, graded index structure (GI type) plastic optical fiber have higher bandwidth of 1GHz-km has been developed.

(3) Automotive LAN

The plastic optical fiber had been paid to

attention in the car field when environmental correspondence flowed. The metallic signal cables for quite a lot of signals are used in the car, becomes a problem in lightening the car. Moreover, the signal of the high capacity not compared has come to be transmitted up to now in the car such as the navigation system, VICS, Internet, and mobile telephones. The system of plastic optical fiber is evaluated by the automotive manufactures

On the other hand, it is development to deal with the generation control problem of carbon dioxide as for a hybrid car and the electric vehicle, etc. As for the electric vehicle driven by electricity, the noise problem grows very much though a lot of noise sources exist still in the car.

Therefor, the plastic optical fiber has such feature of flexibility for the compact wiring and excellent resistance to vibration. The plastic optical fiber which has very high thermal resistance in recent years is performed and development has been performed though thermal resistance of a usual plastic optical fiber is about 85℃.

4. Types of Plastic Optical Fibers

Various types of plastic optical fibers have been developed to meet requirements of varieties of applications.

1) Plastic optical fiber for communication

The plastic optical fiber for various communications has been developed aiming at above-mentioned in Home network and the office LAN.

Table 3 various types of plastic optical fibers for communication use

	Low NA SI-TYPE PMMA	GI-TYPE PMMA	SI-TYPE Modified PC	GI-TYPE All fluoride Resin
Attenuation	0.2dB/m	0.15dB/m Academy 0.8dB/m (MRC)	0.3dB/m	0.05dB/m Academy
Bandwidth	20 MHz·km	1.25 GHz·Km	20 MHz·KM	2GHz·km Academy
Light source	660nm Low-NA LED	660nm LD	780nm LD	1300nm LD
Transmission speed and distance	156Mbps-100m 200Mbps-70m	1.25GHz-100m Academy	156Mbps-100m 200Mbps-70m	1.25Gbps-200m 2.5Gbps-200m
Heat Resistance	85℃	85℃	125℃	Unknown
Fiber Price	Low	Medium	Medium	High
Link Speed(Light Source)	~200Mbps (~ Gbps LD)	Gbps Level	Gbps Level	Gbps Level
Link Price	Medium	High	Low	High
Main application	LAN(ATM-LAN) IEEE1394-Long	LAN(ATM-LAN) IEEE1394-Long	IEEE1394-Long	Dropping wire
Manufacturer	Mitsubishi-rayon Asahi-Chemical Toray	Mitsubishi-rayon	Furukawa	Asahi Glass

(1) Low NA-PMMA type plastic optical fiber

The plastic optical fiber used by the decoration and the sensor applications is about NA=0.5, and bandwidth is 7.5MHz·km. The bandwidth of 10MHz·km is necessary to communicate about 156Mbps/100m (prescribed by ATM) and 250Mbps/50m (prescribed by IEEE1394). The low NA PMMA fiber is fabricated to make NA = 0.3 by controlling the refractive index of the clad polymer in order to expand the bandwidth to

12MHz·km, which complies with both IEEE1394 and ATM.

(2) GI type PMMA plastic optical fiber

The GI type plastic optical fiber has a profile of refractive index which changes gradually from inside to the outer. The bandwidth is 1.25 GHz-km, which permit Giga bit level communications. And the one with very small transmission loss of 0.15dB/m has been reported though the transmission loss is an academy level.

(3) Modified polycarbonate type plastic optical fiber

While the wavelength window of the conventional PMMA plastic optical fiber is located at 660nm, the center of the transmission wavelength of modified PC fiber is located at the near infrared ray range of 780nm. The attenuation of this fiber is shown in Fig.2

The advantage of this fiber is that it can be use low-cost, high reliability semiconductor laser (LD), which is widely used for the CD and CD-ROM, in 780nm wavelength.

Further, this type of plastic optical fiber has a thermal heat resistance of about 145℃ as well as a thermal/humid resistance and is suitable to use automotive data transmission networks.

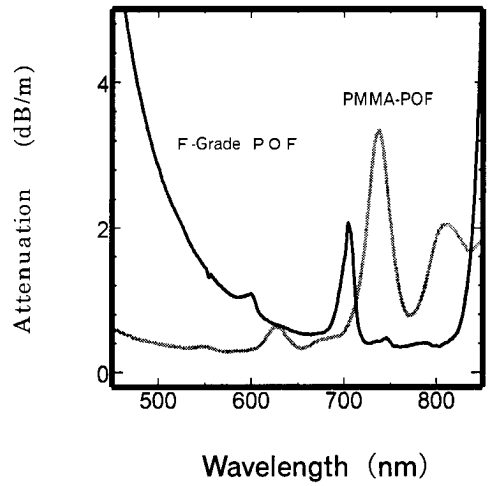

Fig.2 Attenuation loss of Modified polycarbonate type plastic optical fiber (PMMA is shown as a reference)

(4) All fluoride and GI type plastic optical fiber

Only the transmission loss of the plastic optical fiber was high up to now, and the application area was short distance transmission. This plastic optical fiber achieves 50dB/m with 1300nm band to which light has no transparency at all by a usual plastic optical fiber by using cyclic aliphatic and all per-fluoric non-crystalline resin without containing hydrogen at all for its core. This fiber achieved an extremely high bandwidth of 2.5GHz by introducing GI structure. This fiber is expected to expand the application field of plastic optical fiber in near future. However the fiber is difficult to apply in the practical wiring to use in office LAN yet because of raw materials is very expensive now

2) Heat resistance plastic optical fiber

Various types of plastic optical fibers are developed for automobile signal transmission network applications.

(1) Polycarbonate plastic optical fiber

It is a plastic optical fiber which uses a thermal resistance Polycarbonate resin as a core material, and a thermal resistance temperature is 125℃-135℃ (257-275 F)level.

The transmission loss greatly changes into a polycarbonate plastic optical fiber depending on the raw material and the manufacturing method. A polycarbonate plastic optical fiber of our company achieves a very low transmission loss of 0.4dB/m by a refinement and a new manufacturing method of the raw material.

(2) Modified polycarbonate plastic optical fiber

Our company developed the plastic optical fiber which had very high thermal resistance of 145℃ (293 F) by the molecular modification of the polycarbonate as a core material.

The fiber features not only no shrinkage to the high temperature but also the anti-oxidation characteristics, which allows the application continuous, high temperature circumstances.

Therefore, it is thought it is the best for the automotive applications, which require a high temperature for a long term.

Table 4 various types of plastic optical fibers used for Automobiles

Core material	Modified PC	PC	ARTON	Silicon resin
Attenuation	0.3dB/m (780nm)	0.4 ~ 1.2dB/m (660nm)	0.8dB/m (660nm)	0.8dB/m (660nm)
Heat resistant temperature	145℃	125℃ ~135℃	150℃	150℃
Life span	Good	Poor	UN-known	Good
Hot and humidity property	Good	Good	Good	Poor
Tensile strength	Good	Good	Good	Good
Property of low temperature	Good	Good	Good	Good

(3) Norvaline circular chain plastic optical fiber

A plastic optical fiber, which does not shrink up to a high temperatures about 150℃(302 F), has been developed by using non-crystalline resin (ARTON) to the core material. About 0.8dB/m of a polycarbonate average plastic optical fiber is achieved as for the transmission loss. A transmission loss of 0.8 dB/m is achieved which is an average polycarbonate plastic optical fiber level

(4) Silicone plastic optical fiber

While the conventional plastic optical fiber uses thermoplastic resin as the core material, this type of fiber is used silicone resin as core by liquid drawing techniques to achieve super high heat resistance.

However, as the nature of silicone, its hot humidity resistance is rather fair.

Conclusion

(Plastic Optical Fiber from Now)

Varieties of plastic optical fibers having different characteristics are developed in order to meet the requirements of various applications, though the plastic optical fibers in the past where only PMMA fiber. There are few results in the communication field though the research of the plastic optical fiber becomes very active. However, the short distance high-speed transmission media is about to become the necessity and indispensable by upgrading service. However, it is not avoided to become a competition with the metal cable so that the plastic optical fiber may become the kernel of this short distance high-speed transmission road. The points to be examined from now on for the spreading plastic optical fiber widely are described in the following.

(1) Low-cost data link

In order to compete with the metallic cable, development of a low-cost, high reliability data link is essential.

(2) Acknowledgment of plastic optical fiber

The acknowledgment degree in the communication field is very small though the plastic optical fiber came to rise to the topic greatly recently. It is important to advance the acknowledgment activity, and to be going to pile up results in the future.

(3) Connector

The plastic optical fiber should be equals level among optical fiber with the metal cable, which is very simple terminal processing. It will be necessary to examine connectors including the standardization in the future though a simple connector has been reported for these 1-2 years.

(4) Fiber cost

The market price of the metal cable, which has already been used, is very cheap. The cost of plastic optical fiber for communications use is comparatively expensive, even taking the small quantity into account. Cost reduction of the plastic optical fiber itself will be required in the future.

Reference

1) Y. Koike etc.:"Plastic optical fiber", Kyouritsu-syuppan

2) Y. Koike: processing of ECOC '96 MOB. 3.1.41(1996).

3) Asahi Glass: JP 04-213929

3) Y. Koike "Progress in Plastic Fiber Technology" ,OFC97

4) T. Fujimori, et al. :"An Introduction to An IEEE1394 Base Home Network",ATM Forum RBB SWG ,AF95-1378(1995)

5) S.Yamazaki, et al. :"A 2.5 Gb/s 100m GRIN Plastic Fiber Data Link at 650nm Wavelength " ,ECOC'95 TuL 2.5,pp337-343(1995)

AUTHORS

Masaki Nishiguchi
The Furukawa Electric Co., Ltd.
6,Yawatakaigan-dori Ichihara, Chiba, 290-8555
JAPAN

He was born in Osaka, Japan in 1963. He received his M.E. degree in material engineering from Tsukuba University in 1988. He joined The Furukawa Electric Co., Ltd. in 1988. He is now a senior research engineer of Opto-Technology Laboratory.

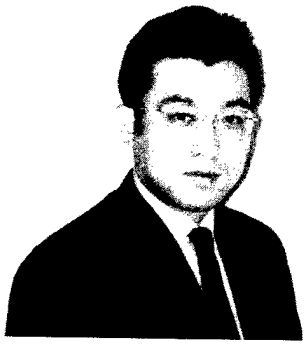

Masanori Hattori
The Furukawa Electric Co., Ltd.
6,Yawatakaigan-dori Ichihara, Chiba, 290-8555
JAPAN

He was born in Hokkaido, Japan in 1967. He received his M.E. degree in Applied Material Science from Muroran Institute of Technology in 1991. He joined The Furukawa Electric Co., Ltd. in 1991. He is now a research engineer of Opto-Technology Laboratory.

Seiji Takagi
The Furukawa Electric Co., Ltd.
6,Yawatakaigan-dori Ichihara, Chiba, 290-8555
JAPAN

He was born in Osaka, Japan in 1951. He received his M.E. degree in Industrial Chemistry from Kyoto University in 1976. He joined The Furukawa Electric Co., Ltd. in 1976. He is now a general manager of research department of Opto-Technology Laboratory.

PLASTIC OPTICAL FIBER AND OPTICAL LINK MODULE FOR SHORT HAUL HIGH-SPEED TRANSMISSION

Masanori Hattori, Masaki Nishiguchi and Seiji Takagi

The Furukawa Electric Co., Ltd. Opto-Technology Laboratory, Chiba, Japan

ABSTRACT

Targeting at short haul optical communication media for use in private homes and offices, we have developed a plastic optical fiber with low loss and high thermal resistance, using polycarbonate AF for the core material and an optical link with high dynamic range in combination with this plastic optical fiber.

It has been confirmed that the plastic optical fiber developed in this way permits low loss of 0.3dB/m and has excellent thermal resistance as high as 125 ℃ and very few transmission attenuation at a 780nm band on bending, and also is capable of transmitting up to 80m at 156Mbps. The eye pattern proved to be thoroughly open using the optical link consisted of a low-cost semiconductor LD and PIN-PD. The observed light detecting sensitivity after transmission of 80m was as large as -32dBm. Therefore, the home networks and LAN is expected to construct at low cost by using this plastic optical fiber and optical links.

INTRODUCTION

In these days, by the development and rapid spread of Internet services, personal computer serves as a multimedia terminal and its user comes to enjoy varieties of services of digital data more easily at home. At the same time, in the broadcasting field, CS broadcasting has already been digitized and terrestrial broadcasting is also expected to digitize until at least 2010 in Japan. Audio and visual appliances have been designed for codes offered as digital format such as CD, MD and DVD. Thus, as the amount of digital data is expected to increase rapidly even in home and small office, it comes to be possible to digital network with personal computer, which integrates personal computer, broadcasting and AV appliances in small office or each room in consumer's house. In those circumstances, POF is considered to be the most effective and suitable means to construct a short-haul network as a transmission media. Although the transmission distance is restricted to 50 to 100m because of its intrinsic higher loss characteristics at present, the plastic optical fiber has such advantages as free from

the EMC problems often encountered when the metallic cable is applied so far. Further, it permits rather economical construction of optical networks with low price optical data link and easy installing.

In correspondence to the development of plastic optical fiber of transmission optical signal over 100Mbps, IEEE1394.b was established in FEB. '98 which recommends the product capable of hot plugging and bandwidth as guaranteed. It is effective to construct multi-media network since it specifies the extension distance from 4.5m(metallic cable length defined in IEEE1394-1995) to 50m with POF.

By setting target of our POF to comply with IEEE1394.b, we have developed a plastic optical fiber with low loss and high thermal resistance, using polycarbonate AF for the core material and an optical link with a high dynamic range.

POF using PC(AF)

Since the polycarbonate AF has no saturated C-H bonding, there exists no absorption derived from the stretching vibration of C-H. Consequently, unlike polymethylmethacrylate and conventional polycarbonate (polycarbonate A), the polycarbonate AF provides lower absorption in the near infrared region. As regards the excellent physical characteristics, it has been confirmed that the polycarbonate AF has glass transition temperature as high as 165℃ and also has enough oxidation resistance as compared with that of conventional polycarbonate.[1]

We have developed a Step Index type plastic optical fiber with a fiber diameter of 0.5mm and NA of 0.35 and 0.53 using this polycarbonate AF for the core material, silicone resin for the clad material, and fluoro polymers for the protective layer. And we have also developed a cable of 1.2mm outer diameter by providing a jacket with thermoplastic covering layer. The POF cable features thin diameter and flexible, which allows easy wire installation in the room without deteriorating the interior appearance of the room.

We evaluated wavelength dependence of attenuation, thermal shrinkage property and thermal resistance property of the POF as a fiber and carried out transmission experiment of the POF cable using newly developed optical links.

Development of 780nm optical link

We have developed a links of 156Mbps transmitter and a receiver, whose package is of SONET with FC connector and receptacle. The transmitter and receiver consists of a light source a 780nm LD, whose relaxation frequency is 1.8GHz, and a Si-PIN photodiode, whose light detecting surface diameter is 0.8mm, cut off frequency is 0.5GHz. The transmitter output is set to -8dBm in compliance with IEC 825-1.

Result of experiment

Wavelength dependence of attenuation

The wavelength dependence of the attenuation of the POF cable is illustrated in Fig.1, while the loss level at individual wavelength is shown in

Table 1.

The wavelength dependence of attenuation was measured in 10m-1m cutback method, using a monochrometer connected with a halogen lamp as an incoming light source, and outgoing light from a multimeter as monitored the output signal. The POF of PC(AF) has a broader transmission window between 730nm and 820nm region than the conventional POF of PC(A) as there are not any saturated C-H bonding in the structure of PC(AF).

Another transmission window is seen at around 650nm, which allows the use of LED for conventional PMMA fiber.

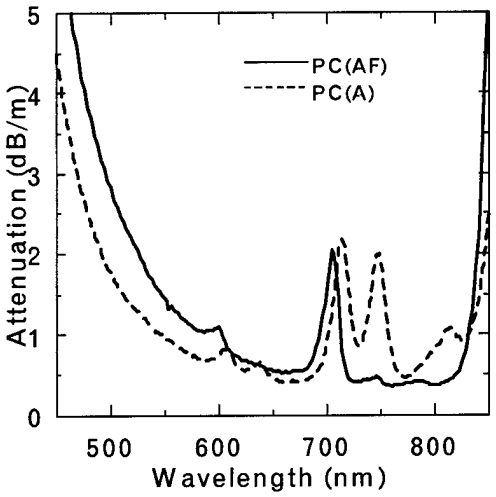

Fig.1 Wavelength dependence of attenuation

Table 1 Attenuation at varied wavelength

Wavelength (nm)	Attenuation (dB/m)
660	0.46
780	0.30
860	1.80
940	1.05

Transmission experiment

Bit error rate (BER) was measured by inputting random signals (125Mbps and 156Mbps NRZ, PRBS=2^{23}-1 and mark rate of 50%) by the use of 70311A Clock Source(16.1M～3.3GHz), 70841B Pulse Pattern Generator(0.1～3Gbps) and 70842B Error Detector (0.1～3Gbps) of Hewlett-Packard. The eye pattern was measured with the Ocilloscope of 54750A and 54751A of Hewlett-Packard.

We evaluated the transmission properties at 125Mbps and 156Mbps. The choice of the transmission speed is based on the reason that the transmission speed of 125Mbps is compatible to that of 100Mbps under the stipulation in IEEE1394.b (In IEEE1394.b, the data are scrambled and then coded using an 8B/10B block code).

The results of BER and the eye pattern diagram are illustrated in Fig.2 and Fig.3 respectively, and maximum transmission lengths of POF cable at BER of 10^{-12} are shown in Table 2.

In Fig.2, two marks(●,■) represent those of 125Mbps and 156Mbps transmission respectively. After 85m transmission at 125Mbps, a minimum received power of -32.35dBm was obtained at BER of 10^{-12}. As a result, a power margin of about 24dB was achieved at 125Mbps up to 85m by using 780nm LD. The eye pattern proved to be thoroughly open. Also a 156Mbps, it is confirmed that a power margin of about 23dB was achieved with eye pattern thoroughly open at the same condition.

We prepared an IEEE1394 repeater using this new links for transmission experiment complying with IEEE1394 protocol. By connecting a video camcorder and this repeater

using complied with IEEE1394-1995 DV-cable while two repeaters connected with a POF cable, the motion picture taken by one video camcorder was transmitted to the another camcorder with the POF cable of 50m length.

With those repeaters described above, the transmissions of motion pictures at 125Mbps were carried out well at 50m distance. In order to know the practical applicability of this POF cable wiring, the bend test complied with IEC794-1 was carried out by bending cable to a 90 degree at halfway. Loss of less than 0.24dB/m were observed.

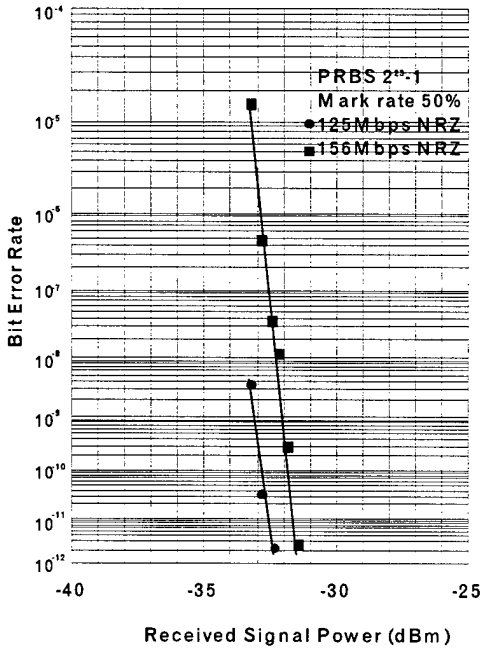

Fig. 2 Transmission property

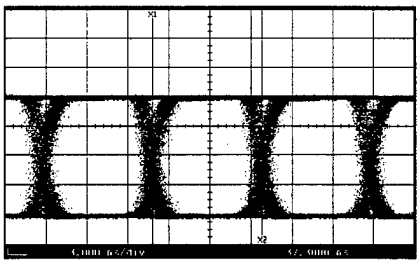

a) 125Mbps, transmission after 85m
(Time base scale:3ns/div)

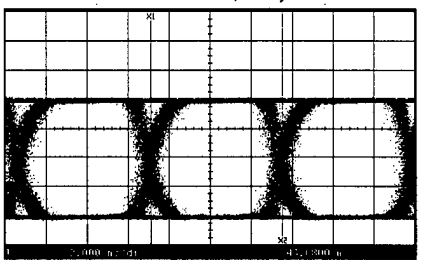

b) 156Mbps, transmission after 80m
(Time base scale:2ns/div)

Fig.3 Eye pattern diagram at BER of 10^{-12}

Table 2 Transmission distance

	Length	BER	Sensibility
125Mbps	85m	2.4×10^{-12}	-32.35dBm
156Mbps	80m	2.9×10^{-12}	-31.50dBm

Environmental properties

Thermal shrinkage property

Physical thermal resistance of plastic optical fiber depends on Tg of polymer as core material.

To evaluate the thermal shrinkage property of PC(AF) fiber, we prepared the samples of 100mm length and putting them into a thermostatic chamber heated at from 100 to 155℃, kept them for 240 hours, and observed the change of its length. The measurement was made at 5℃ intervals.

Fig.4 shows the result of rate of thermal shrinkage property at each temperature after 240 hours aging with the reference of PC(A)-POF. It

is confirmed that PC(AF)-POF does not deform up to around 150℃. By the application of PC(AF) for core material, the physical heat resistance of the fiber was improved by about 20℃.

Thermal resistance property

In general, polymeric material causes oxidative degradation when it is kept in the high temperature environment. The oxidative degradation is caused by the formation of carbonyl group, double bonding and cross-linking in core material. The increase of transmission loss of fiber is caused by the increase of the electron transition absorption occur to oxidative degradation and it will lead the electron transition absorption to shift to near infrared region. [2,3]

To evaluate the thermal resistance property of the fiber, we prepared the light source of 660nm LED and 760nm LED, and photodiode separated at a distance of 12m in order to avoid the excess loss by the heat of the chamber. Fiber of 10m length were put into thermostatic chamber at 125℃ while the 1m at both ends of the fiber were placed out of chamber.

The thermal resistance property of the fiber is shown in Fig. 5. It was observed that the increase of transmission loss due to heat aging proved to be less with 760nm than with 660nm. Transmission loss of the fiber after 300days aging at 125℃ increased to about 0.34dB/m at 760nm. It is confirmed that a considerable change in transmission loss has occurred due to electron transition absorption. From the above results, the POF was reliable for long term when it is used with a light source whose wavelength is over 660nm.

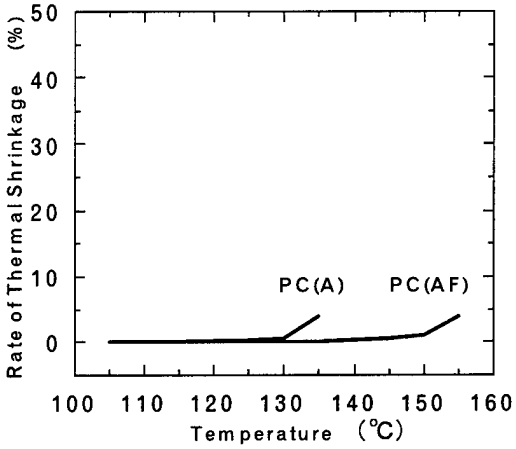

Fig.4 Thermal shrinkage property

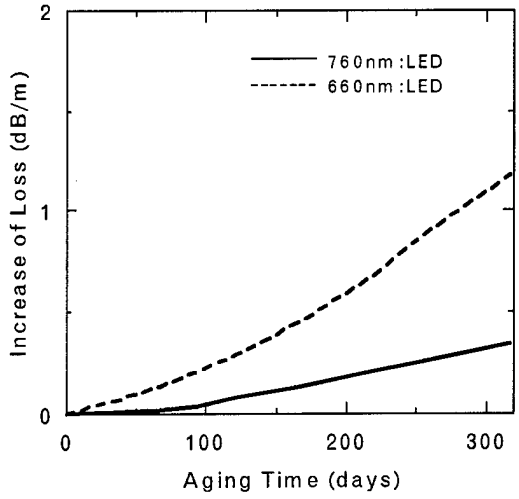

Fig.5 Thermal resistance property at 125℃

Conclusion

It is confirmed that this plastic optical fiber has not only transmission window near 660nm,

which is used conventional PMMA fiber but also has very broad transmission window from 730nm to 820nm, and minimum transmission loss exists at 780nm band. As the most suitable wavelength of the PC(AF) fiber is at around 780nm which corresponds to that of conventional semiconductor laser for CD and CD-ROM.

It is capable of transmitting about 80m at 156Mpbs and 85m at 125Mbps with 780nm wavelength band links. The fiber system of fiber and optical links are expected to construct a reliable and economical short haul network system in home or small office.

Reference

1. S.Irie and M.Nishiguchi: POF'94, Oct.27-28, Yokohama, P88 (1994)

2. Y.Takezawa et al. :J. Appl. Polym. Sci., 42 (10),2811-2817 (1991)

3. T.Yamashita, K.Kamada : Jpn. J. Appl. Phys., 32 2681 (1993)

AUTHORS

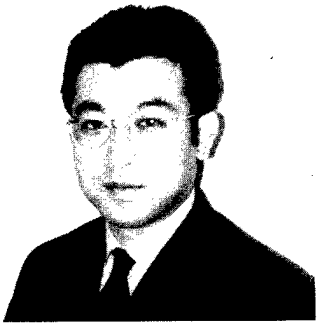

Masanori Hattori
The Furukawa Electric Co., Ltd.
6,Yawatakaigan-dori Ichihara, Chiba, 290-8555 JAPAN

He was born in Hokkaido, Japan in 1967. He received his M.E. degree in Applied Material Science from Muroran Institute of Technology in 1991. He joined The Furukawa Electric Co., Ltd. in 1991. He is now a research engineer of Opto-Technology Laboratory.

Masaki Nishiguchi
The Furukawa Electric Co., Ltd.
6,Yawatakaigan-dori Ichihara, Chiba, 290-8555 JAPAN

He was born in Osaka, Japan in 1963. He received his M.E. degree in material engineering from Tsukuba University in 1988. He joined The Furukawa Electric Co., Ltd. in 1988. He is now a senior research engineer of Opto-Technology Laboratory.

Seiji Takagi
The Furukawa Electric Co., Ltd.
6,Yawatakaigan-dori Ichihara, Chiba, 290-8555 JAPAN

He was born in Osaka, Japan in 1951. He received his M.E. degree in Industrial Chemistry from Kyoto University in 1976. He joined The Furukawa Electric Co., Ltd. in 1976. He is now a general manager of research department of Opto-Technology Laboratory.

HOW TO MEET THE REACH SPECIFICATION OF THE ISO 11801 WITH POF COMPARISON OF THE ATTENUATION WINDOWS ADVANTAGES OF GREEN LIGHT SOURCES

Olaf Ziemann, Torsten Ritter, Burkhard Gorzitza

Deutsche Telekom AG, TZ Darmstadt, Berlin/Germany
FHTW Berlin/Germany

ABSTRACT

The increasing demand for broadband networks in private and business environments gives a growing interest on Polymer Optical Fiber (POF) based transmission systems. The attenuation spectrum of today available PMMA based POF has its minima around the wavelengths of 520 nm, 580 nm and 650 nm. Due to the availability of low cost, high efficient and high speed LED in the red window, nearly all existing POF systems are working in these third attenuation window. In the ATM Forum[1], the use of 650 nm LED is specified. In the last few years, the development of InGaN technology[2] offers the possibility to produce high efficient and high bandwidth blue and green LED. The use of those LED for POF transmission systems was described[3] for bi-directional WDM POF systems. This paper will compare the different available LED sources with respect to their usability in POF systems.

INTRODUCTION

This year 1998 will bring a strong increase in the number of broadband access lines worldwide. A lot of projects with ADSL technology and broadband radio systems will offer the possibility for delivering data rates above 1 Mbit/s to the customer (for comparison: ISDN offers 128 kbit/s capacity). With VDSL and other systems, the available data rate will increase further in the very next future. This gives the need for high capacity, low cost installation options for building networks. As an example we look to a typical 15 stage building with 90 flats (details will be summarized[4]). Figure 1 shows the cable length distribution for the existing telephone cable system.

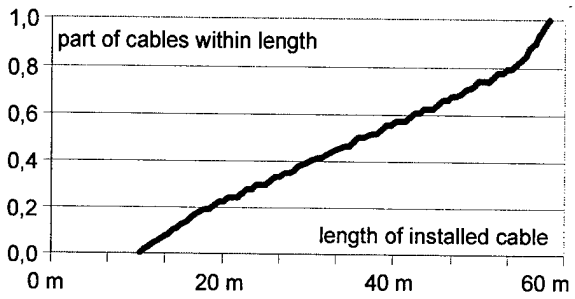

Fig.: 1: telephone cable length distribution

All cable lengths inside the building (between building distribution point and telephone outlets in the flats) are between 15 m and 57 m.
Within a number of national and international standards for building cabling systems, the reach requirement is 100 m. One example is the ISO 11801 for structured cabling. The use of category 5 twisted pair copper cables for data rates up to 100 Mbit/s enables these reach. The commercial available Polymer Optical Fiber (POF) does not allow a transmission over 100 m, if 650 nm LED are used, under worst case conditions. That's why the ATM Forum[1] has specified a reach limit of 50 m. This value fulfills the requirement of some groups, like the Full Service Access Network action, but an increased reach will be very helpful for the future application of POF. By the opinion of the authors, the best way for improving the reach value, is the use of green LED instead of the 650 nm red LED. In the next chapters, firstly the existing ATM Forum standard will by described. After this, we like to explain the possibilities of green LED in POF links.

Attenuation at 25°C, 50% RH, max. measured with 650 nm collimated light	[dB/50 m]	7.8 (156 dB/km)
attenuation increase at 70°C, 95% RH	[dB/50 m]	0,8 (16 dB/km)
loss increment due to source spectral distribution (660 nm center wavelength, 40 nm FWHM gaussian)	[dB/50 m]	3,4 (68 dB/km)
loss margin for launch NA up to 0,3	[dB]	0,5
loss for static bending 15 quarter turns with 25 mm bending radius	[dB]	0,5
worst case fiber loss	[dB/50 m]	13,0
worst case connection loss (PN connector = F07) 0,32 NA POF, Hot-Plate method, 65°C, 95% RH	[dB]	2,0
center wavelength min./max.	[nm]	640/660
spectral width FWHM max.	[nm]	40
average power (over life) min./max.	[dBm]	-8/-2
receiver sensitivity	[dBm]	-25
transmitter rise/fall time 10%-90% max.	[ns]	4,5
receiver rise/fall time 10%-90% max.	[ns]	5,0
signaling rate	[MBd]	155,5
link length	[m]	50

Tab. 1: ATMF-RBB Specification for POF-link

THE ATM FORUM POF LINK SPECIFICATION

In the ATM Forum, presently a specification for a 50 m POF-link with 155 Mbit/s is existent[1]. This specification contains the following parameters for the loss values. In figure 2 the main loss parts are shown graphically.

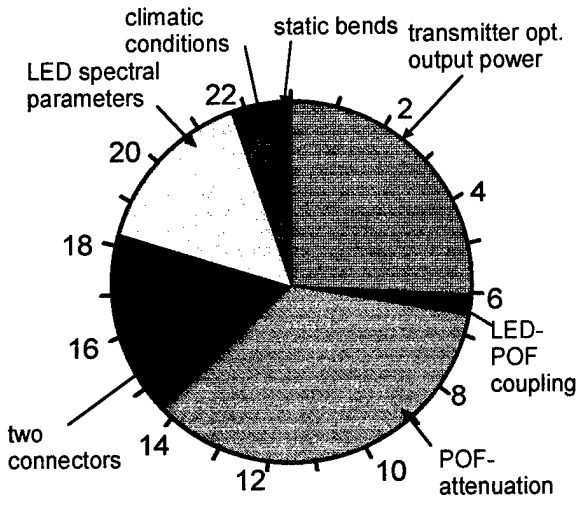

Fig. 2: Power budget for ATM Forum 50 m POF link specification

As can be seen, the POF attenuation at 650 nm needs only about a third of the whole power budget. Great parts of the power budget are reserved for connector loss, changes of optical source power and the influence of LED spectral parameters (spectral width and center wavelength).

If one likes to increase the system reach to 100 m, the budget has to be improved by the following values at least:

- fiber attenuation (156 dB/km): 7,8 dB
- excess loss by climatic conditions: 0,8 dB
- excess loss by source spectrum: 2,2 dB

That gives a total increment of 10,8 dB (assumed, that the same numbers of connectors and bends are allowed). The following chapters will explain some of the loss mechanism in more details.

REACH LIMITATION BY POF LOSS

The first parameter for the calculation of reach and capacity of any optical transmission system is the channel loss. The figure 3 shows attenuation spectra for some commercially available 1 mm diameter step index POF (based on PMMA[5, 6, 7 and 8]).

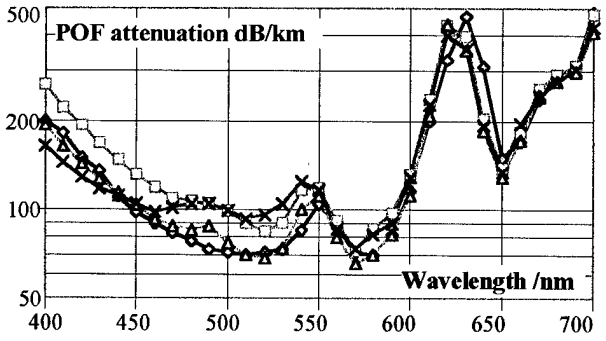

Fig. 3: Examples for spectral attenuation of different 1 mm step index PMMA POF

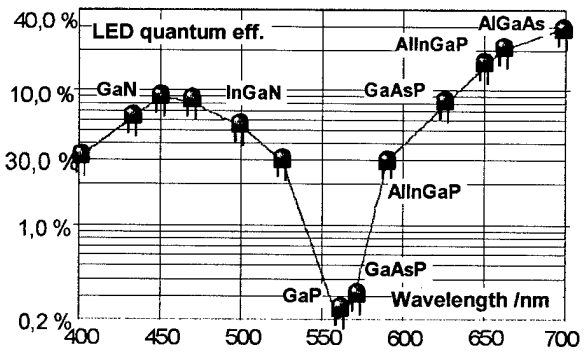

Fig. 4: quantum efficiency of available LED

As can be seen in the figure 3, there are three attenuation minima for green (around 520 nm), yellow (around 570 nm) and red (650 nm) light. A number of papers have proposed the use of green or yellow LED for POF systems[9,10], due to the small fiber attenuation. In laboratory, data rates of 10 Mbit/s were transmitted over 100 m step index POF. But all commercial available LED, based on AlInGaP or GaAsP have a small efficiency and small modulation bandwidth. The use of AlGaAs 660 nm LED, and some years later InGaAsP 650 nm LED was the only possible choice, due to the very good LED properties. The advantages of these LED in comparison to existing yellow and green LED predominated the disadvantage of a higher POF attenuation.

Since some years, LED made from new materials are on the market. The most important manufacturer of the InGaN LED is Nicha[2]. The external quantum efficiency of blue and green LED, made from GaN is about 10 % and 6 %, respectively. These are values very close to the data of the best red LED. Furthermore, GaN is a direct semiconductor, giving a very short carrier life time. This offers the possibility of high speed modulation. In figure 4, we have shown the external quantum efficiency of a number of commercial available LED. The quantum efficiency values were calculation from the values for emitting angle, center wavelength and luminous intensity (due to the not known far field distribution, the values can differ from the real number). The LED-signs represent available wavelengths. The points were connected virtually.

As can be seen, in the green, as well as in the red region, very bright LED are available. At the point of the lowest fiber attenuation around 570 nm, only low efficient LED exist. We have calculated the theoretical bandwidth for POF systems under the following assumptions:

- All LED work with the same LED current (here 30 mA)
- The spectral width of the LED was neglected (use of POF attenuation value at the LED center wavelength)
- calculation was done with maximum possible LED power or with a power limited to -2 dBm (Due to eye safety requirements, the maximum LED optical power may be limited. This limit is lower for shorter wavelengths, but the standards are in motion)
- The sensitivity of the receiver was assumed to be -25 dBm at 650 nm wavelength. For all other wavelength a constant quantum efficiency of the receiver was assumed.
- For additional losses (connectors, bends...) a margin of 9 dB was subtracted.

With these assumptions, the theoretical reach is shown in figure 5.

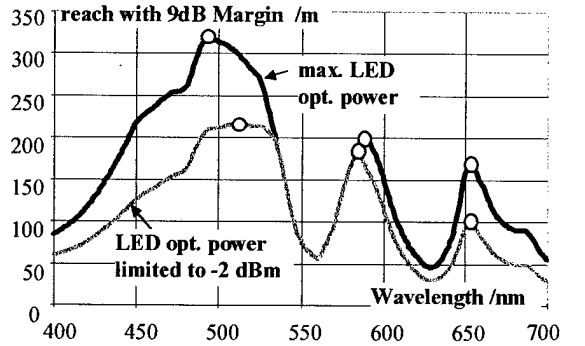

Fig. 5: Theoretical reach of POF links with different source wavelength.

One can see in this figure, that with the high efficient green LED a reach value of 300 m should be possible. The reach in the green and red window is about 200 m and 170 m, respectively. With limiting the LED optical power to -2 dBm, the reach values are about 220 m, 180 m and 100 m for the three windows. In both cases, the green LED offers the highest reach. The small efficiency of the yellow sources can not be compensated by the low attenuation of the POF.
In the ATM Forum specification the power budget besides the pure POF loss is 15 dB. If we take into account this value in the above presented calculation, we get the following reach values (see figure 6).

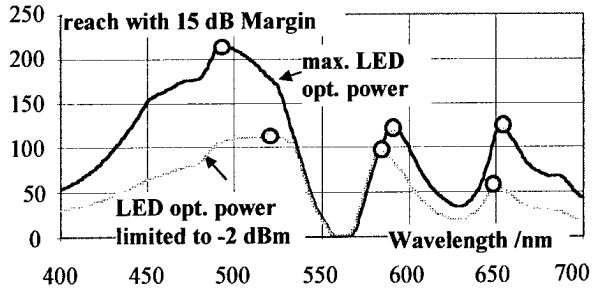

Fig. 6: Reach for POF systems with 15 dB margin addition to the attenuation

As can be seen, in the red window the reach is only 50 m with a limited LED power. The green LED, however, offers 100 m reach. But we will show in the next chapter, that the advantages of the green LED are not only the smaller POF attenuation.

MORE ADVANTAGES OF GREEN InGaN LED

Temperature behavior

According to the limits for eye safety, the optical power should not be higher than -2 dBm at all time. The transmitter must be designed in a way, that under all conditions, as aging, manufacturing tolerances and change of temperature (-20°C up to +70°C) this value will not be exceed. Taking into account the demand of low costs, no temperature stabilization or current regulation should be used. The specified minimal source optical power is given then as that value, which can be guaranteed under worst case conditions. The most important influence on the LED optical power is given by the temperature. Figure 7 shows the changes of the optical output power for three different LED according to reference[2].

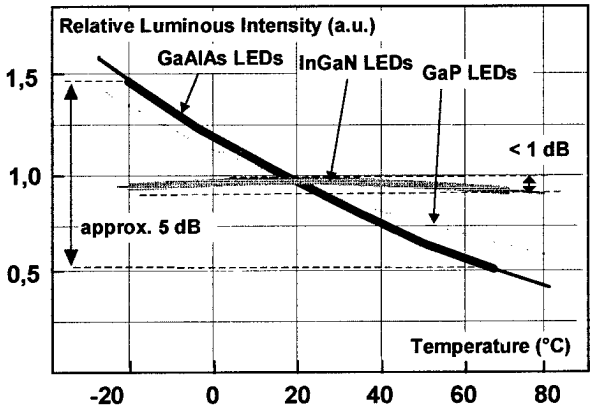

Fig. 7: Comparison of the temperature dependence of various LED

The optical power of red GaAlAs LED has a strong temperature dependence. Between -20°C and +70°C there is a difference of about 5 dB. GaN LED show, in contrast, much smaller changes in the optical output power. In ref.[2] a total change of 10% over the whole temperature range was indicated for GaN LED. The authors have measured a change of 1,2 dB for a 525 nm LED NSPG 500. This gives the possibility to specify a higher minimum source power with the same upper limit.

Influence of the source spectral properties

The attenuation window at 650 nm has very steep slopes. The following table shows the attenuation increase besides this minimum for a typical fiber.

wavelength deviation from 650 nm	attenuation increment (from 132 dB/km)
-20	229
-15	132
-10	52
-5	10
±0	0
+5	26
+10	67
+15	110
+20	140

Even deviations of 20 nm from the attenuation minimum cause an increment of loss up to >200 dB/km. Semiconductor diodes have a temperature dependence of the band gap in general. This gives a drift of the emission wavelength. Tanking into account the manufacturing tolerances, the ATM Forum has specified a center wavelength of 650 nm ±10 nm for that reason. Furthermore, semiconductor LED have a material dependent spectral width of some 10 nm. In fig. 8 it is shown, how the loss of a 50 m POF link (Toray fiber) is changed when using different LED parameters (gaussian shaped spectrum was assumed).
The attenuation window at 520 nm is much more flat. That's why changes of the center wavelength, or a high spectral width of the diode does not cause that great loss increments. In figure 9 the values for 100 m POF with a 525 nm InGaN LED NSPG 500 are shown.

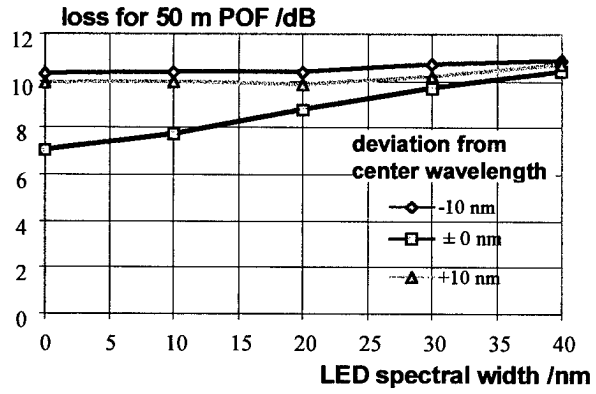

Fig. 8: Influence of source spectral properties to the link loss in the red window

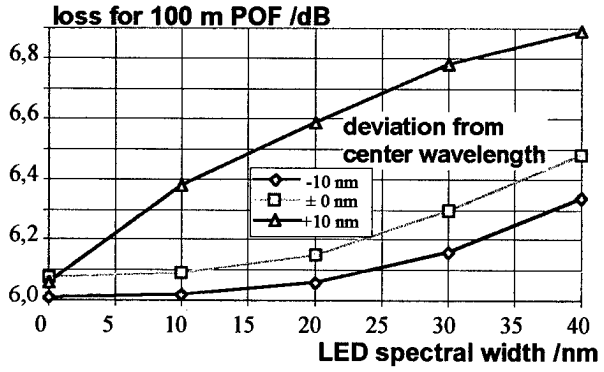

Fig. 9: Influence of source spectral properties to the link loss in the green window

While the attenuation for red LED increases by more than 3 dB for a 50 m POF link caused by source spectral parameters (±10 nm wavelength deviation and 40 nm width), the increment for a 100 m link with 525 nm LED is below 1 dB with the same source parameters. This further gives an improvement in the power budget when using green LED instead of red.

BANDWIDTH, LIFETIME AND OTHER PROBLEMS

A very important question is, whether the bandwidth of POF is the same in the green window, as specified in the red one. We have measured the bandwidth in all three windows with a very new arrangement (details will be published soon). First results are shown in figure 10.

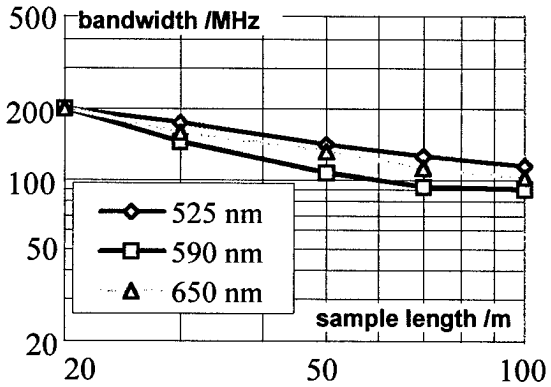

Fig. 9: Bandwidth of a Low-NA POF in the three windows

One can see, that the bandwidth of the POF is nearly equal for all three attenuation windows.
An other important point is the lifetime of the LED. In[2] a lifetime of more than 1.000.000 h was noted for GaN LED at typical current level. Taking into account the fact, that for POF links only a very small current is necessary, the lifetime is absolutely no problem.
The authors have also investigated problems of bend and connector loss, as well as the influence of the chromatic dispersion. No one of the points will disable the application of green LED for POF links, as we can see at the present time.

EXAMPLE FOR A LINK BUDGET AT 525 NM

Taking into account all the above mentioned points, we have calculated the power budget for a 100 m link with 155 Mbit/s data rate and 525 nm LED. The link budget is defined as follows.

- The maximum LED power is -2 dBm. The maximum decrease by temperature, aging and manufacturing tolerances id 3 dB, giving a guaranteed power of -5 dBm.
- The loss for LED coupling remains 0,5 dB.
- The specified POF attenuation at 525 nm was set to 90 dB/km (value accepted by POF manufacturer)
- The margin for 2 connectors is 4,0 dB (same value as in the 650 nm specification)
- The additional loss for the influence of the source spectral parameters is 0,8 dB (10 nm wavelength deviation, 40 nm spectral width)
- We estimated an influence of climatic conditions of 1,0 dB.
- For 10 static bends, a margin of 0,5 dB is reserved.
- The receiver sensitivity is -24 dBm (taking into account the higher photon energy with respect to 650 nm)

All these values are graphically shown in figure 11.

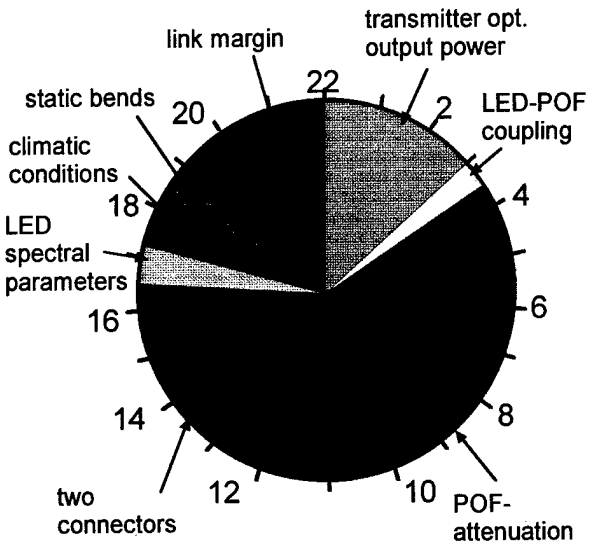

Fig. 11: Example for 100 m POF link with 520 nm LED

As can be seen, in spite of the little smaller link budget an the longer fiber length, and additional margin of 3 dB is possible. This shows very clear the advantages of green LED against the conventional red sources.

REFERENCES

1 ATM Forum: „155 Mbps Plastic Optical Fiber and Hard Polymer Clad Fiber PMD Specification", AF-PHY-POF155-0079.000, May, 1997

2 S. Nakamura, G. Fasol: "The Blue Laser Diode", Springer-Verlag Berlin Heidelberg New York, 1997

3 O. Ziemann: "Bi-Directional Transmission over Plastic Optical Fibers", POF'97, Kauai, 22.-25.Sept.97 pp. 48-49

4 R. Kramer: „Verkabelungstopologien für In-Haus-Netze", laufende Diplomarbeit am TZ der Deutschen Telekom, Berlin 1998

5 Laser Components Katalog, p. 55, 1 mm POF, Toray 1994

6 Low-NA (0,25)-POF, NC 1000, Luminous (Asahi chemical via Nichimen), 1996

7 ESKA PREMIER, ESKA MEGA, Plastic Optical Fibers for Data Communication, Mitsubishi 1997

8 Toray PMU-CD1002-22-E, Technical Bulletin 1997

9 J. Arrue, J. Zubla, J. Miscowitz (Lamda Opt. Comm.): „Components Choice to Lengthen Low Speed Plastic-Fiber-Optical Communications Links", POF'94, S. 78-81

10 K. Fukuoka, T. Iwakami (Toshiba), K. Schumacher (Toshiba Düsseldorf): "High-speed and long-distance POF transmission systems based on LED transmitters", POF'93, pp. 43-46

ABBREVATIONS

ADSL	Asymmetrical Digital Subscriber Line
ATM	Asynchronous Transfer Mode
FWHM	Full Width at Half Minimum
ISDN	Integrated Service Digital Network
ISO	International Standardization Organization
LED	Light Emitting Diode
POF	Plastic Optical Fiber
RH	Relative Humidity
VDSL	Very high speed Digital Subscriber Line
WDM	Wavelength Division Multiplexing

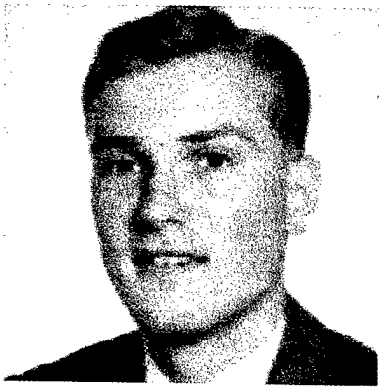

Dipl.-Ing. (FH) Burkhard Gorzitza was born in 1971 in Demmin (Mecklenburg-Western Pomerania). Having served an apprenticeship with measuring and industrial control technician, he went to work. His activities included dealing with measuring and control as well as maintaining biotechnological systems and building automation.
In 1998, he graduated at the Fachhochschule der Deutschen Telekom AG in Berlin in communication engineering as Diplomingenieur (a graduate in engineering). During his studies he concentrated on transmission technique.
Studying for his degree he was researching on Plastic Optical Fibers building an optical transmitter and receiver device for all POF attenuation minimum's.

Dipl.-Ing. (FH) Torsten Ritter was born in 1973 in Waren (Mecklenburg). In 1992 was his final examination. He has studied communication engineering at the Fachhochschule Berlin der Deutschen Telekom AG. His interesting was concentrate of transmission technique. The topic for his graduation was „Characterise measurement for POF transmission".

address:
Korsörer Str. 8/I
Berlin/Germany

Tel./Fax.: +49 30 448 92 97
e-mail: h0444jls@student.hu-berlin.de

Dr. Olaf Ziemann was born in 1965. He has studied Physics at the university of Leipzig. Between 1990 and 1995 he was a member of the Institute for Communication and Measurement a the Technical University of Ilmenau. He graduates in 1995 at the topic „Coherent optical transmission systems". In the same year, he joined the Technology center Darmstadt of the Deutsche Telekom in Berlin. His special interests are in the field of optical access network technologies and home wiring systems.
In 1996 O. Ziemann was involved in the foundation of the new sub committee „Polymer Optical Fibers" in the Information Technology Society (ITG-FG 5.4.1) and is still leading this group.
Presently O. Ziemann is engaged in research projects for the use of POF transmission systems in future broadband access systems, as investigated in the Full Service Access Network Initiative for example.

address:
Deutsche Telekom
Technologiezentrum Darmstadt, FZ 244a
Goslarer Ufer 35
D-10589 Berlin /Germany

Tel./Fax.: +49 30 3497 4442 /-4443
e-mail: ziemann@tzd.telekom.de

NEW POF-CABLE GENERATION WITH CORRUGATED MICRO TUBE (CMT) IN BUS SYSTEMS FOR AUTOMOBILES

Wolfgang Scheideler
ALCATEL
ke autoelectric GmbH
Floss-Germany

Helmut Steinberg
ALCATEL
ke autoelectric GmbH
Floss-Germany

Peter E. Zamzow
ALCATEL KABEL
Hannover-Germany

ABSTRACT

The development of polymer optical fibers (POF) with wide transmission bandwidths led to new aplications for automobiles.

The growing need for data handling within the car brought a continuous increase in cable lengths. A comfortable middle class passenger car requires about 1,800 m of cable in average. The POF bus system will reduce the need for additional cables for data handling.

Today's cables with copper pairs cannot be developed much further to meet in an economical way the increasing demands for data handling and safety.

A new and economical cable concept was developed for automobiles, with a POF bus system and with transmitters / receivers available on the market.

The employment of LEDs with different wave lengths permits several independent logical networks in one POF conductor.

A POF data line needs a direct mechanical primary protection. The system solution combines the POF with a corrugated laser-welded metallic micro tube with about 2.5 mm OD.

The corrugation of the micro tube gives a high compression strength, protects the POF conductor and provides sufficient plyability for the demanding installation in the car.

POF in automobiles

In the near future automobiles will have to have their own data highways because certain new requirements such as:

- integrated engine monitoring
- car diagnostic
- intelligent information systems
- opto-electrical displays
- reliability and safety

are expected features in a car with high image.

Conventional copper cable technics can be combined with POF systems and their components for advanced communication demands in piggyback manner (Fig. 1).

The 'intelligent' vehicle will have to provide ever more safety and comfort to the driver.

The first generation of entertainment and communication systems with POF technic was employed for:

- navigation (GPS)
- radio
- CD player, tape deck
- hifi systems
- telephone (GSM).

Car manufacturers will consider a communication network for the car only if it works in real time. Only then will the car meet all safety requirements. POF lines are not affected by EMV and thus warrant the real time performance of the communication lines.

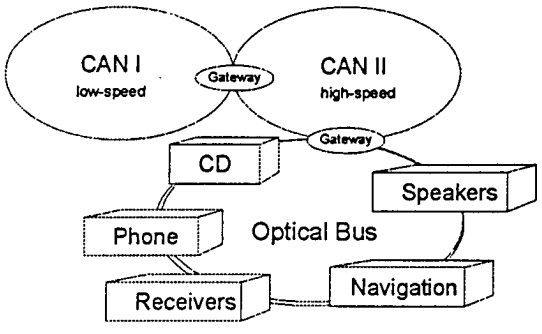

Fig. 1 Car network topology

The transmission properties of a cable are characterized by attenuation and bandwidth. A typical POF attenuation is 150 dB/100m. The data rate for a POF step-index profile is 50 Mbit/s for 100 m of fiber length (Fig. 2).

STANDARD COPPER SOLUTIONS FOR CARS

The growing amount of electronic components and the increasing number of optional equipment in the cars lead to an ever more complex board network. A separation into several cable strings with one central active switching point was sufficient in the past.[1] Future board networks will have to be of modular design with integrated technics (Fig. 1).

Line multiplex methods:

In a line multiplex system all receivers are connected to the central control unit by one single line. The messages for each station are encoded by the central control with an address. The station compares this address with it's own and, in case of agreement, takes action. Afterwards the action is confirmed to the central control.

Network for data communication

One data line connects all modules.

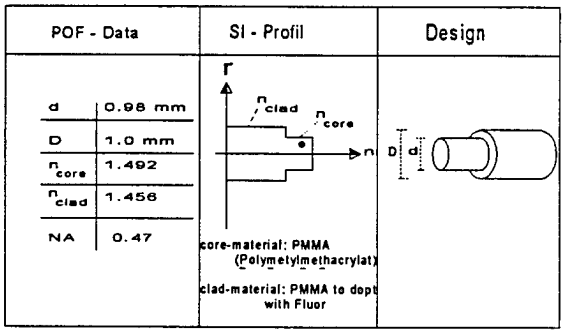

Fig. 2 Typical parameters of SI- POF

Small isolated solutions are combined into a network, able to
- provide controls for different systems
- prevent functional conflicts between individual systems
- reduces the number of sensors
- and, in case of emergency, utilizes data of another control device for emergency performance[2].

Adapter cables are used to connect different (high/low speed) systems. Recently developed communication networks such as the D2B (optical bus system) with transmission rates of >1 Mbit/s exceed the capability of conventional copper cables.

Further increase of bit flow would overtax the copper cables in cars. Cable networks of novel design in cars permit safe use of the mobile telephone GSM (global system for mobile telecommunication), and the navigation for street traffic GPS (global position system).

Symmetrical copper pairs, coaxial cables or CAN (controller area network) lines were designed for lower bit rates, and their limits are reached soon.

Safety has top priority in cars and any copper cable tree must be well protected against EMV.

COMUNICATION NEEDS AND SAFETY IN CARS

The introduction of catalytic converters triggered a tremendeous development of engine management in cars, which led to a substantial increase in data lines within the board network (Fig. 4).

The demand for additional communication paths in cars results from the growing amount of standard equipment in compact and mid-size cars, and also from optional features like mobile phones and navigation systems in upper mid-size and full-size cars.

Examples are:

- telephone
- radio, tape deck, CD player
- car sections control
- navigation
- information
- car motion control.

There are several ways to reduce the number of conductors and therefore the weight and volume of a cable [3, 4]. Considering the functional and geometrical arrangements of the sensors and actuators, there are three basic network structures:

- ring structure
- star structure
- bus structure.

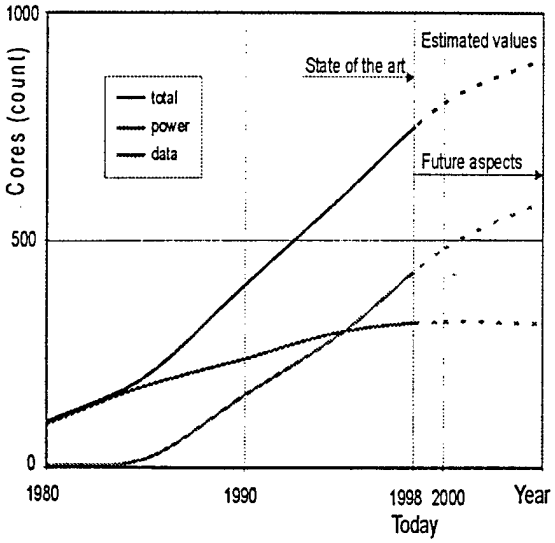

Fig. 3 Demand development of wire Harnesses

The areas in a car can be divided into three groups.

- internal area (passenger compartment and trunk),
- engine area (motor and AC compartment)
- external area (wheels, axles, brakes).

Each area presents certain requirements with respect to mechanical, thermal and chemical conditions for the cable to be installed there (Fig. 4).

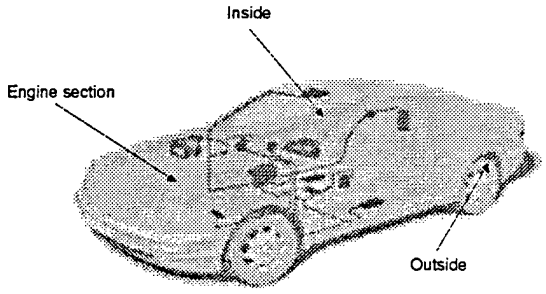

Fig. 4 Harness architecture in cars

If the cable harness is reduced to a point-to-point connection, e.g. sensor - control module - actuator, such a cable must fulfill all requirments, because it leads often through all three car areas.

Technical solutions for copper lines cannot be applied directly to optical fiber lines. One possibility to match the physical conditions in a car is offered with the CMT.

Special material combinations at the designers disposal permit well qualified technical solutions. POF conductors can be installed safely through all areas if they are protected by the CMT sleeve.

SOLUTIONS WITH POF

The POF fiber is larger than the regular glass fiber and therefore easier to handle (Fig 5).

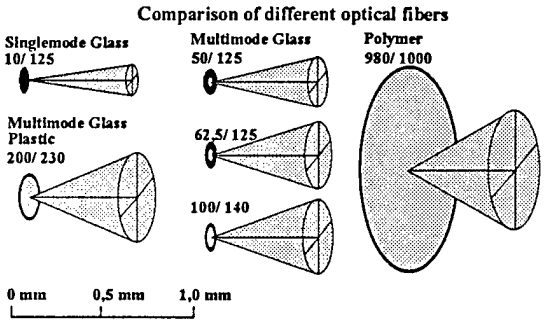

Fig. 5 Comparison of different optical fibers

The POF has essential advantages over the glass fiber:

- ease of handling
- higher flexibility at larger OD
- operation with visible light (red, green, yellow, etc.)
- simple monitoring
- easier light input
- easier fiber splicing
- attractive pricing for components with step-index profile

The improvement of the POF attenuation within the past ten years is shown in Fig. 6.

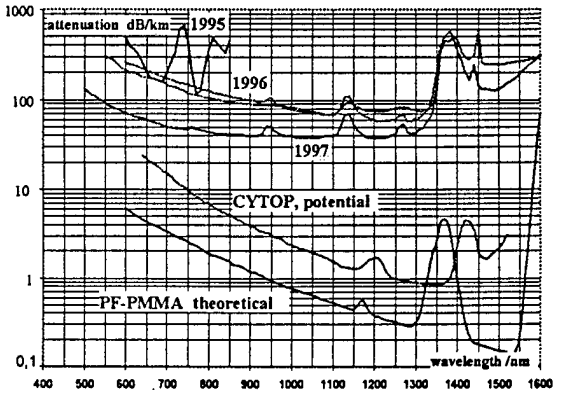

Fig. 6 Attenuation spectra of various POF designs

The good handling properties of a POF are proven by their bending behaviour under border case conditions, defined by total light emission.

It is essential that the POF cable never be bent over a radius smaller than 10 x core OD. This simple limit definition assures an optimized optical POF connection within the optical network.
The unprotected POF core performs between -20°C and 85°C. This must be considered for applications in a car.

Obviously, POF conductors will find applications in cars, because they are as easy to handle as an insulated copper wire and the large fiber OD assures simple connections [5].

Safety comes first in a car and the fober must be protected. The POF core gets mechanical and thermal protection from the laser-welded and corrugated micro metal tubes (Fig. 7).

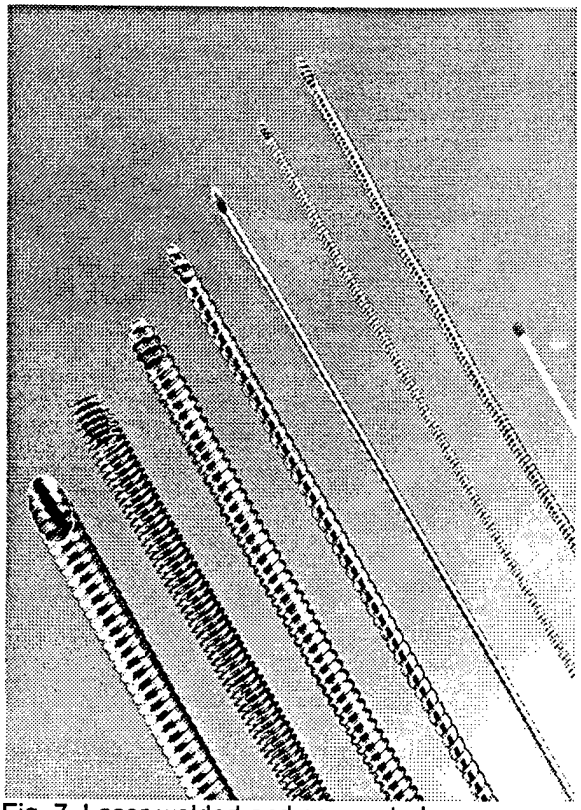

Fig. 7 Laser-welded and corrugated metal tubes (CMT)

The features of the CMT are:

- high resistance against transverse compression
- protection against high temperatures
- stability against various chemical agents
- resistance against vibrations
- high elastic tensile strength
- equalization of electrical potentials
- suitable for hybrid systems.

The laser-welded metallic corrugated micro tubes (CMT) give primary protection to the POF core and can be manufactured from various metals, e.g.:
- copper
- aluminum
- brass
- bronce
- steel
- stainless steels

Stainless steel tubes provide the best mechanical protection, including high transverse compression strength. Compared with smooth tubes, the compression strength of corrugated tubes is 5 to 10 times better. Tubes of stainless steel have walls from 150 □m to 200 □m thick.

The CMT have helical corrugation (Fig. 7). The degree of external stress has to be considered for the corrugation design, which can vary from deep and short to shallow and long.

Only in the range of elastic deformation is the CMT able to protect the POF core [6].

The transverse compression stability of CMT was subject of a presentation at the IWCS in Cleveland in June 1998 [6].

The axial deformation from tensile stress requires special attention.

Tests about the compression strength revealed an elastic (reversable) deformation of up to 12 %.

The POF core is no longer protected if the CMT suffers a permanent deformation. The outer shape of the CMT elements, the corrugation, enhances their flexibility and incorporates elasticity in axial direction.

The behaviour of samples under a tensile test (Fig. 8) is quite complex. Reliable results can be obtained only through test series. The here shown force-elongation results (Fig. 9) describe the mechanical reaction of CMT tubes.

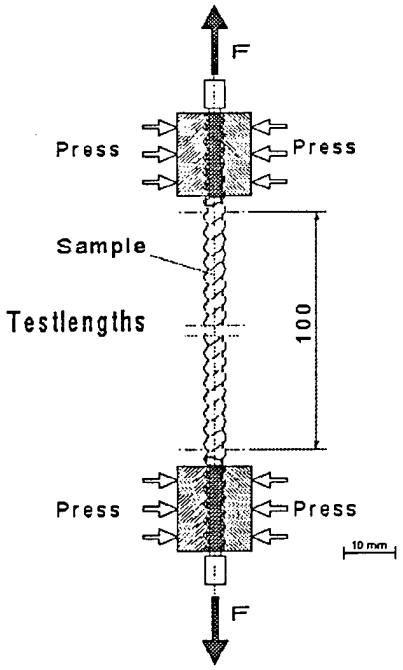

Fig. 8 Schematic of tension load equipment

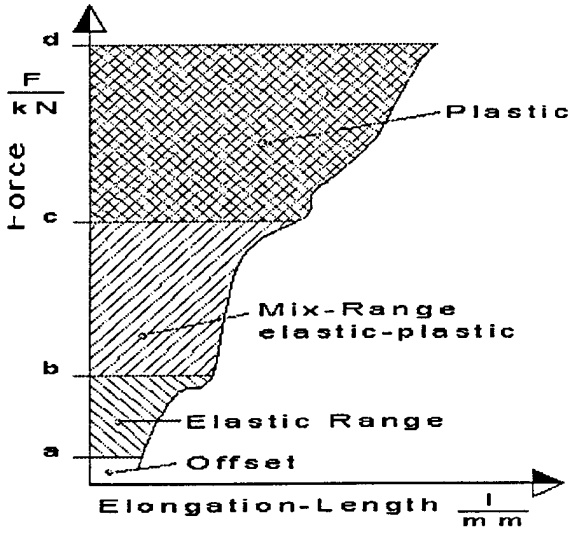

Fig. 9 CMT characteristic curve
F = f (elongation)

The typical force-elongation diagram shows the particularity of the CMT elements. There is a defined range a-b of reversible deformation in Fig. 9 where POF cores are safe.

The range b-c is transient while range c-d is purely irreversible, which means the corrugation is removed completely and the metal begins to flow.

The mechanical tensile forces in the purely elastic range (reversible deformation) lead to an elongation of 1% to 1.5%. This was observed with a CMT of < 5mm OD.

POF WITH CMT AND HYBRID SOLUTION

CMT are made in a continuous manufac-turing process [6, 7]. The manufacturing steps are:
- POF pay-off
- strip pay-off
- strip edge cutting
- tube forming
- core insertion
- laser welding
- split-clamp capstan
- corrugator for CMT configuration
- CMT take-up.

This process is done with a UNIWEMA ^{R} U 5L, which is designed to manufacture corrugated metal tubes with < 5 mm OD.
(UNIWEMA ^{R} is a trade mark owned by Alcatel Kabel AG & Co).

CMT protected POF conductors are shown in Fig. 10.

The parameters of the helical corrugation can be chosen to match the requirements of the application
- flexible corrugation
  -> short and deep grooves
- rigid corrugation
  -> long and shallow corrugation.

A wide choice of materials allows for optimized CMT and best protection for the POF core at a favourable cost.

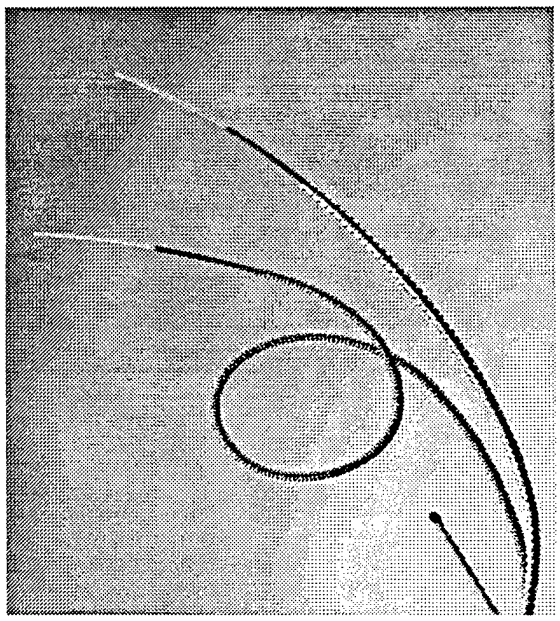

Fig. 10 Samples of Hybrid POF cores in CMT

Laser welded CMT offers mechanical protection for the POF conductor and shields it from environmental effects.

These special properties are utilized to achieve an economic cable tree for cars.

The new hybrid POF CMT cable, shown in Fig. 11 features:

- POF for optical transmission
- CMT with insulation, for electrical signals and for electrical power.

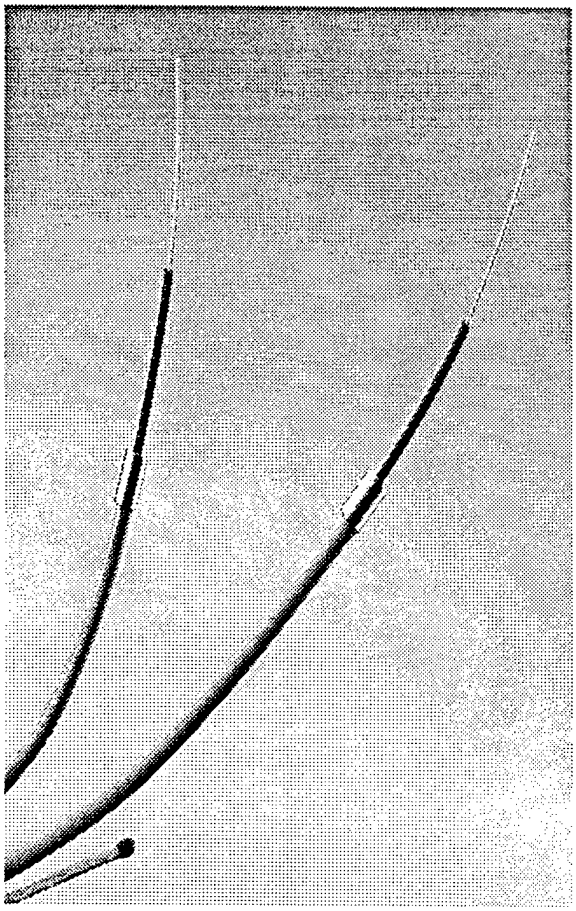

Fig. 11 Samples of hybrid POF CMT cables

The employment of two different optical frequencies (620 nm and 650 nm) permits a single cable solution (Fig. 12 a).

If only one frequency is used, the twin version of the POF cable must be chosen (Fig. 12 b).

The advantage of this hybrid POF CMT cable is that optical and electrial conductors are combined in one cable which reduces the harness cross sections while at the same time excellent mechanical protection is obtained.

Electrically the hybrid cable must have:

- 2.5 mm^2 conductor cross section
- copper conductivity 57 $m/\Omega\ mm^2$
- 2 kV surge voltage (insulated conductor against ground potential).

The CMT technic works with various metals, e.g.:

- copper
- aluminum
- brass

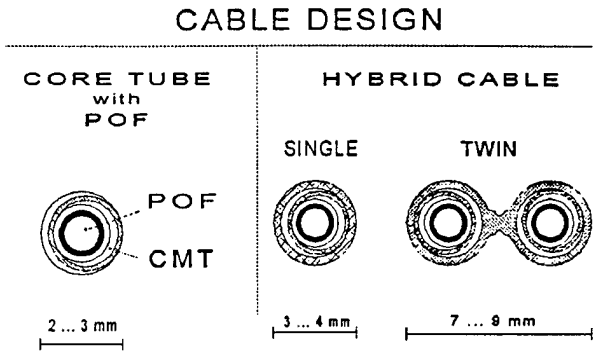

Fig. 12 New POF cable design with CMT basis element

Cables with low weight are preferred for cars. Aluminum alloys yield :

- low weight
- high compression resistance
- good electrical contacts
- primary POF protection
- economical solutions for hybrid networks
- high safety.

CONNECTING THE POF CMT CABLES

The growing information demand in cars leads automatically to more lines, connections, plugs, mounting elements etc.

For the installation and connection of the POF CMT cables, a special tool is needed to strip the corrugated metal sleeve off the POF core. A suitable sheath stripper is shown schematically in Fig. 13.

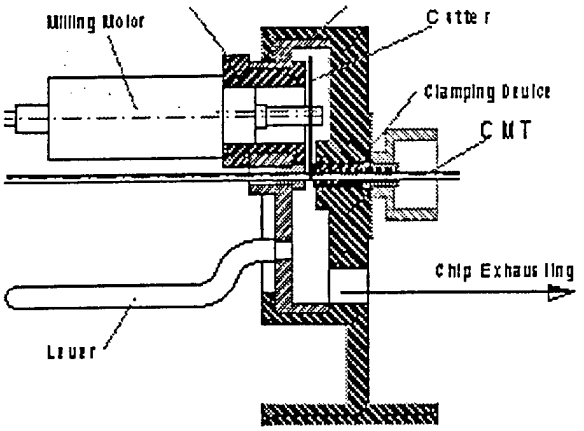

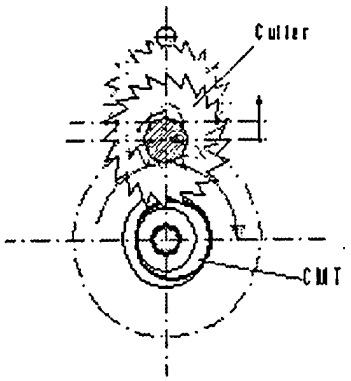

Principle of Cutting

Fig. 13 Schematic of an automatic hard cutting tool.

This hand tool enables the installer to quickly strip the POF CMT cable end , as shown in Fig. 13.

The CMT protects the POF during installation, as long as the minimum bending radius, defined before, is observed (Fig. 14).

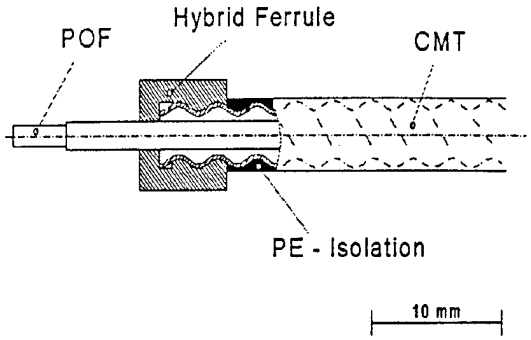

Fig. 14 Preparation of the hybrid POF CMT cable

A hybrid ferrule is crimped over the corrugated sleeve as termination. It makes the electrical contact and gives mechanical protection (tensile stress relief, torsion relief, swage prevention), while the POF as the optical conductor continues to the original optical splicing point.

The cable harness structure and it's volume change with this new technology. The number of conductors and the weigth go down while the number of interfaces goes up.

This concept allows to manufacture cable harnesses at favourable cost.

SYSTEM INTEGRATION

Fiber glass conductors as piggyback in harnesses for cars are tested under life-like conditions (Fig. 15). They are installed chiefly in the passenger compartment.

Copper cables however with their mechanical, thermal and chemical properties are installed through all three areas of the car [8]

An equivalent solution for POF cables is the CMT technic, suitable for piggyback as well as for single line systems. Using the metallic cable sheath of copper or aluminum or one of their alloys as electric conductor for power and the core for data makes a perfect hybrid cable.

As the CMT makes the electrical connection and the POF the optical transmission, this concept is superior to the piggyback system; the CMT protects the POF sufficiently at the cross-over points between the inner area, the engine area and the external area.

Only commercially available round rubber bushings are needed for the installation where the cable passes from one area into another.

Electric components for communication systems in cars will have to be more standardized in order to maintain reliablity and convenience. Hybrid POF CMT cables are a trend setting solution because of their quality, safety and economy in manufacturing.

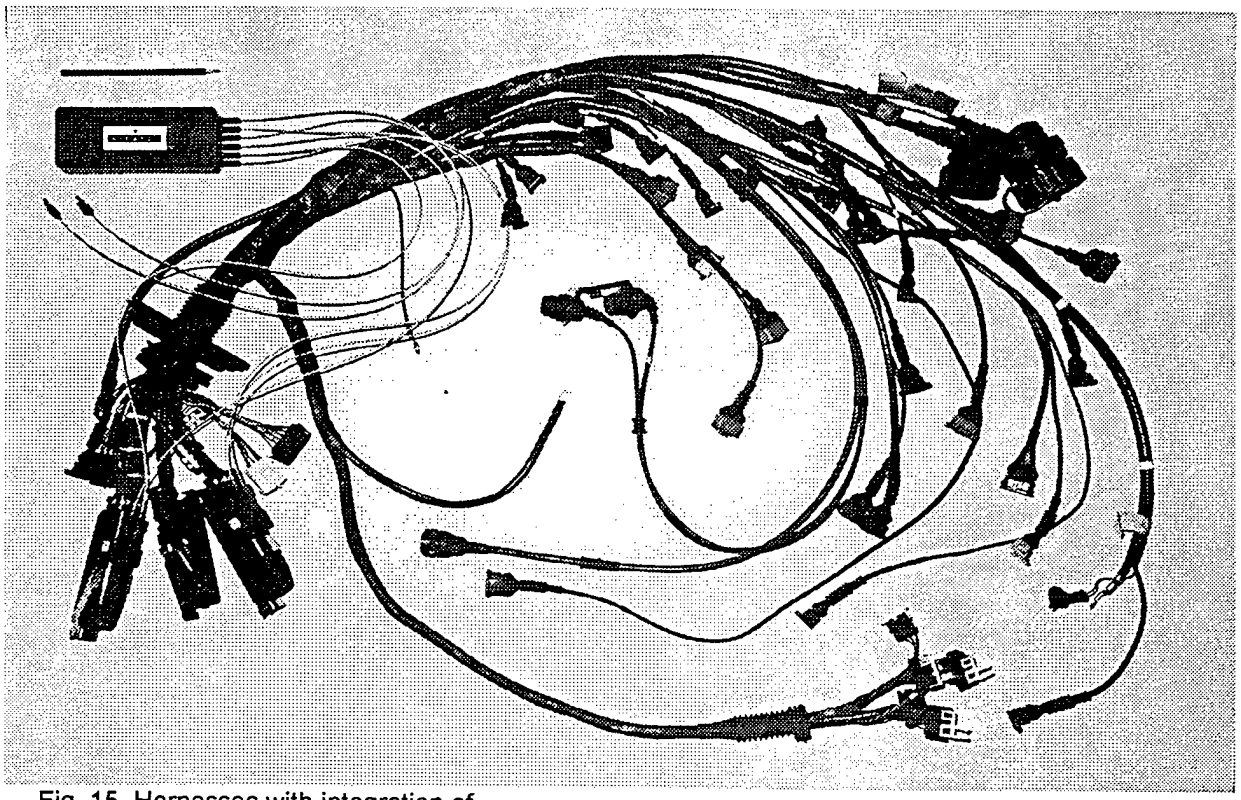

Fig. 15 Harnesses with integration of network system

OUTLOOK

The share of electronic parts in cars has grown substantially in recent years. The board network will grow more towards new tasks to support multi media services such as:

- satellite supported navigation
- navigation on roads
- internet communication
- mobile office
- communication in general etc.

Reliability and quality of future vehicles will depend even more on the harness design, which will become a key product in car production. It will influence the manu-facturing of cars worldwide.

The growing number of custom equipped cars of various types will lead to new cable concepts. The hybrid solution will serve to integrate complex harnesses and to optimize the cable in it's branches.

CONCLUSION

Tests were conducted with POF conductors in CMT for resistance against vibration, temperature shock and rhodent attacks, with positive results.

A new cable concept with hybrid POF - CMT for application in cars is presented.

A pilot bus system with a primary protection CMT was tested and the results are very favorable.

The potential for further developments of the POF lays with the gradient index (GI) profile POF. These GI profiles are produced with fluorized PMMA materials. Transmission attenuations of 1 dB/100 m can be expected. The bit transmission will be above 5 Gbit/s and system lengths of 100 m and more will be achievable.

References

[1] Beil, F; Pelz, N.
Eine bitserielle Universal-Schnittstelle nicht nur für Kfz-Anwendungen
Elektronik, Sonderdruck aus Heft 4, 1989
Franzis-Verlag München

[2] Ehlers, K.
Modularisierung und Module – Eindeutige Begriffe in der Automobilindustrie ?
Impulse 11, 1991, S. 5
Hauszeitschrift der VW AG

[3] Strauß, K.D.
Die Bedeutung von Datennetzwerken für das Kraftfahrzeug VDI Berichte Nr. 1009, S. 229 – 241
VDI-Verlag, 1992

[4] Polymer Optical Fiber Cables for both Automative and Customer Premises Application
Wolfgang Eickhoff, Helmut Haag, Dragan Stankovic, Peter Zamzow
International Wire & Cable Symposium Proceedings 1998

[5] Jürgen Krauser, Olaf Ziemann,
Polymer Optical Fiber Cables for In-house Cabling
ANCIT Workshop. Access Network construction and installation techniques, Volume 1,
Proceedings, Torino March 1998

[6] Haag, Hög, Staschewski, Peter Zamzow
Application of micro-spiral-corrugated welded tubes with optical fibres: Wire Association International 68th Annual Convention, Ohio, Cleveland, USA 1998

[7] Dr. Gerhard Wanser, Kabelmetal Hannover 1967, Cables with welded and corrugated metal sheaths.

[8] Schmitt, P: Schraft, R.D.
Kabelkonfektion – Quo vadis ? Trends in der Produktion von Kfz-Kabelsätzen,
Tagung 1997, München

Wolfgang Scheideler
ke autoelectric
Floss, Germany

Wolfgang Scheideler is engineering managing director of ke autoelectric in Floss.

In 1984 he completed his studies in Electrical Engineering at University of Paderborn. Afterwards he worked as R & D engineer and in 1989 he did a doctorate. In the same year he joined ke autoelectric. Floss, as head of technical acquisition. From 1992 to 1996 he was head of development and engineering department. Since July 1996 he has been engineering managing director.

Helmut Steinberg
ke autoelectric
Floss, Germany

Helmut Steinberg (35) is responsible for process development at ke autoelectric.

He received the Dipl-Ing-degree from the Technical University of Clausthal in 1990. From 1990 to 1995 he was a member of the Institute for welding techniques and he received the Dr-Ing. degree from the University of Clausthal in 1996. Since then he works on wire harness processing and especially on joining techniques for POF at ke autoelectric.

Peter E. Zamzow
Alcatel Kabel
Hannover
Germany

Peter E. Zamzow (58) is director of the Alcatel Kabel company.

He completed his post-graduate studies in telecommunications in Munich and Graz as Dipl-Ing. He joined AEG Kabel in 1970. He has been engaged in development and production of telecommunication cables. In 1980 he became head of the fiber optic division at AEG Kabel and in 1982 he was nominated as a senior engineer. From 1992 on he was plant manager of the new Optical Fiber Cable Plant Rheydt. Since July 1994 he is director, manager of the product group CATV, Telecommunication product line for Germany. Since 1998 responsible for Sales and Marketing in Division Licences and Production Lines world-wide.

THE IMPACT OF CONTAMINANTS ON WIRE COATING PROCESS

Maria A. Macip-Boulis

Alcatel NA Cable System, Inc., New Holland, Pennsylvania, USA

ABSTRACT

This paper will identify causes of structural defects introduced in insulated copper wire during the wire coating extrusion process.

The paper will demonstrate by the use of scanning electron microscopy, energy dispersive X-ray spectroscopy, and X-ray diffraction that the structural defects developed in the insulated copper wire during extrusion are caused by contaminants.

Results of the scanning electron micrographs, energy dispersive X-ray spectrums, and X-ray diffraction patterns, will show that the contaminants fall into several distinct groups: copper fines, copper fines-fibers aggregates, inorganic disperse particles, and metallic granular layers.

INTRODUCTION

There is a great demand for "twisted pair" based network cables that can transmit data at very high rates. Currently, there are cables that can transmit data greater than 1000 Mbps. Data transmission at higher rates however, are mainly limited by structural defects, which are introduced during the manufacturing of the cable or inherent in the wire conductor. These defects ultimately affect high rate transmission performance[1].

The manufacturing of twisted pair cables requires four independent operations: high speed wire plastic coating, primary pair twisting, cabling, and jacketing. During each operation structural defects could be introduced in the cable, but most likely during the wire coating operation, in which a thin coating of plastic is extruded around a copper wire conductor at speeds usually above 2000 m/min.[2] At these high speeds many extrusion and structural defects problems can arise. Among these are wire breaks, resin thermal degradation, irregular coating thickness, surges, surface roughness, and skips.

The purpose of this paper is to identify the origin of structural defects: imperfections developed in the coated wire during extrusion.

EXPERIMENTAL

Both the polymer insulation and the copper conductor from structural defects were characterized using electron microscopy, spectroscopy, and X-ray diffraction techniques. The electron microscopy included four types of scanning electron microscopes (SEM): the ISI DS-130 conventional (SEM), the ElectronScan E-3 environmental (E-SEM), the JEOL JSM-6300S field emission, and the Cameca SX-50 Electron Microprobe. Except for the E-SEM, all microscopes were equipped with an energy dispersive X-ray spectroscopy system (EDS). The Cameca microprobe was also capable of wavelength dispersive spectrometry (WDS). X-ray diffraction characterization was performed with a Philips multipurpose diffraction equipment.

For the plastic insulation, sample preparation was required when SEM, JOEL, and Microprobe were used. After the removal of the plastic insulation from the extruded defective areas, the insulation was immersed in liquid nitrogen, cut into two halves in the longitudinal and cross-section direction with a sharp blade under an optical microscope. Then, the samples were mounted in suitable sample holder to display their cross-sectional regions. Depending on the type of electron microscope used, the samples were finally coated with either gold or carbon.

For the copper conductor, sample preparation was not required. The wire samples were mounted on the sample holder vertically, where the wire was examined from all sides since surface quality is radial dependant. Surface examination around the wire gave the typical morphological features that characterize the average wire conductor surface.

RESULTS

Most of the structural defects in the insulated wire conductor were caused by contaminants. These contaminants are arranged into several distinct

groups: copper fines, aggregates of copper fines with fibers, inorganic particles, and metallic granular layers. Without exception, the contaminants were found on both sides of the insulation and conductor interface.

Copper Fines

The use of the Camera electron microprobe, the JEOL SEM, and the E-SEM to examine the wire surface and the inner surface of the insulation from irregular wall coating thickness samples revealed the presence of deposits of contaminants. These contaminants were contaminant are a byproduct of the wire drawing operation[3-5].

Copper Fines-Fiber Aggregates

Another structural defect on the coated wire were surges. In Figure 7, a surge is shown with large embedded contaminant aggregates. Higher magnification of the aggregate, Figure 8, and EDS elemental mapping depicted in Figure 9, show that the contaminant is composed of copper fines and fiber felt pad. During the wire coating operation

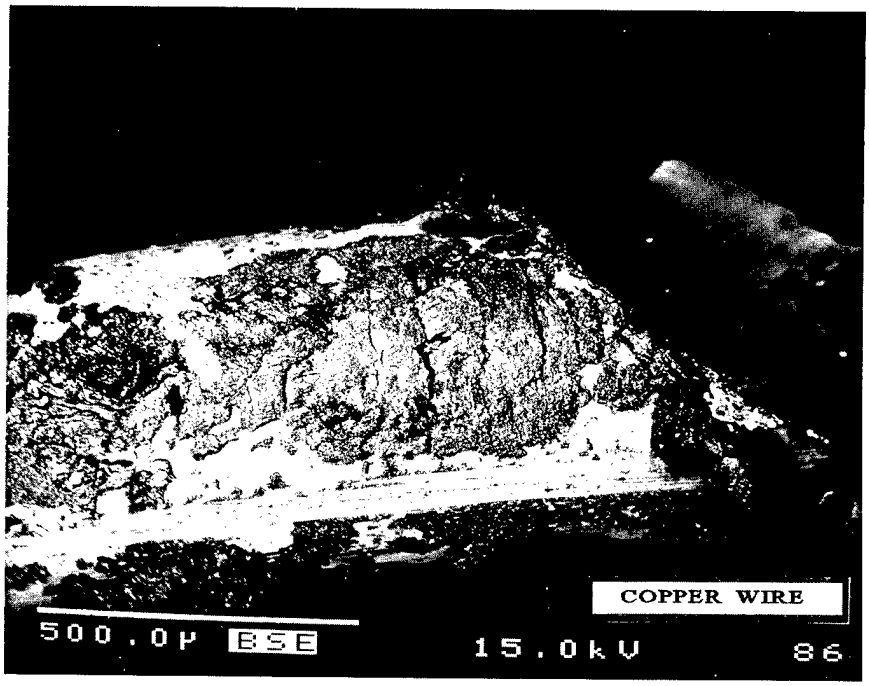

Figure 1. Copper fines aggregates

present as aggregates and discrete particles as shown in Figures 1, 2, and 3. To determine the nature of the contamination, elemental analysis was performed on the contaminants with the EDS in the electron microprobe and the JEOL field emission microscope. The major element in the contaminants was copper as shown in the EDS spectra, Figure 4 and 5. Further characterization of the contaminant removed from the wire conductor with the Philips X-ray diffraction indicated that the major crystalline phases in the sample were copper metal and cuppric oxide, Figure 6. These copper fines deposits present as the cleaning of the wire conductor surface after the pay off can be done by a different operation such as ultrasonic, electrolytic or mechanical. In this study, felt pads were used during the wire cleaning process thereby the copper fine and felt fiber blend.

Inorganic Particles

Individual and aggregate particles were also found on a structural defect known as "skip", which is the lack of insulation on the copper conductor. In the present study many of the characterized skips were caused by copper fines. However, many

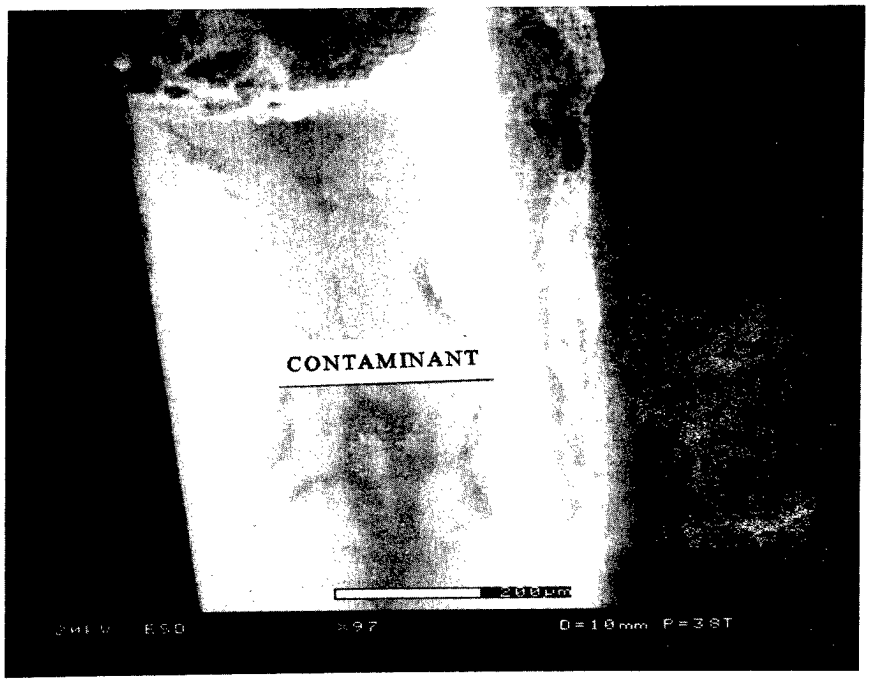

(A)

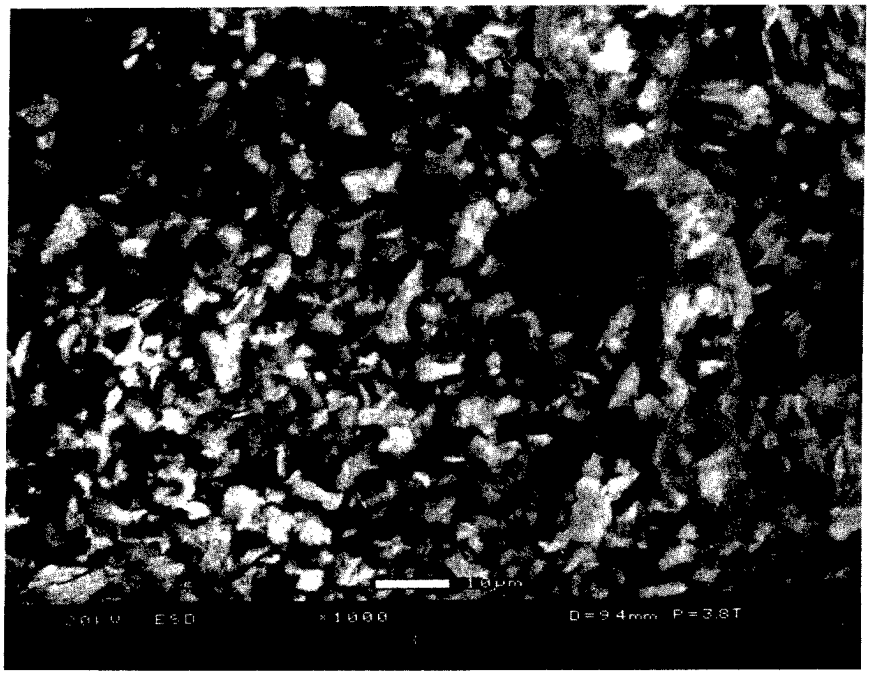

(B)

Figure 2. Contaminant present as discrete particles on the copper wire conductor
(A) E-SEM low magnification (B) E- SEM high magnification

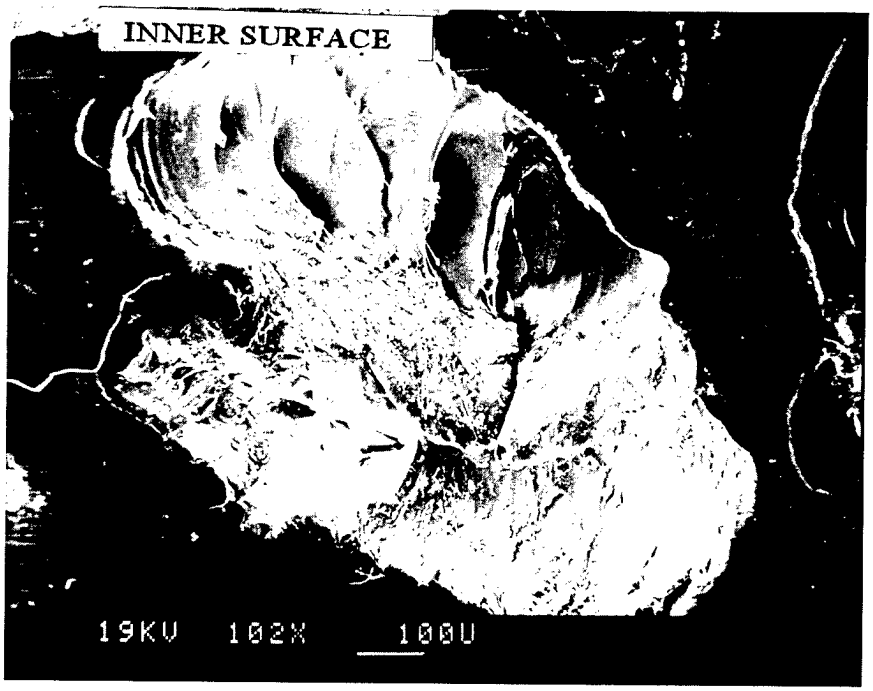

(A)

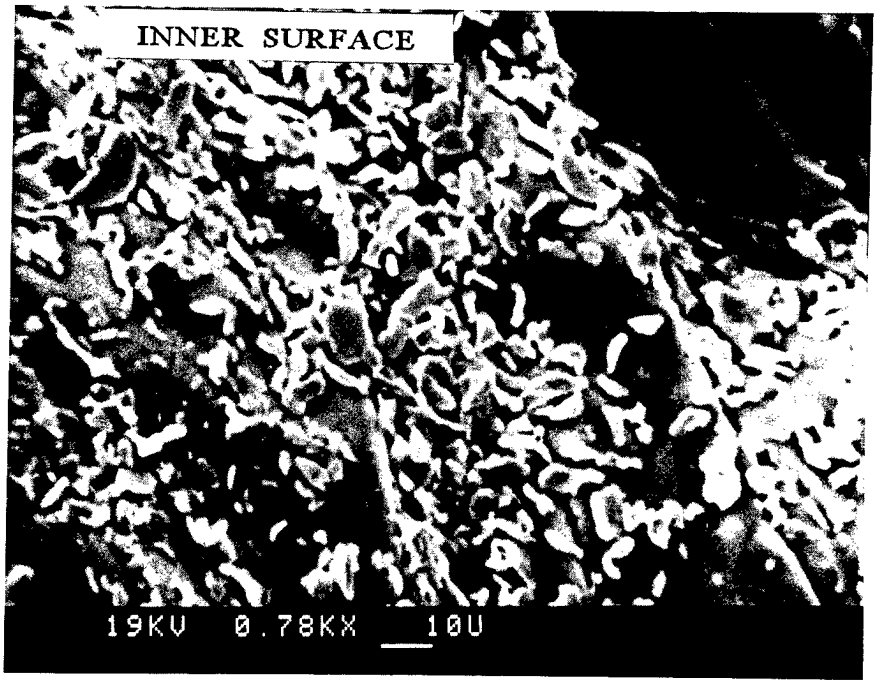

(B)

Figure 3. Discrete contaminant particles present on the inner plastic insulation surface
(A) Low SEM magnification (B) High SEM magnification

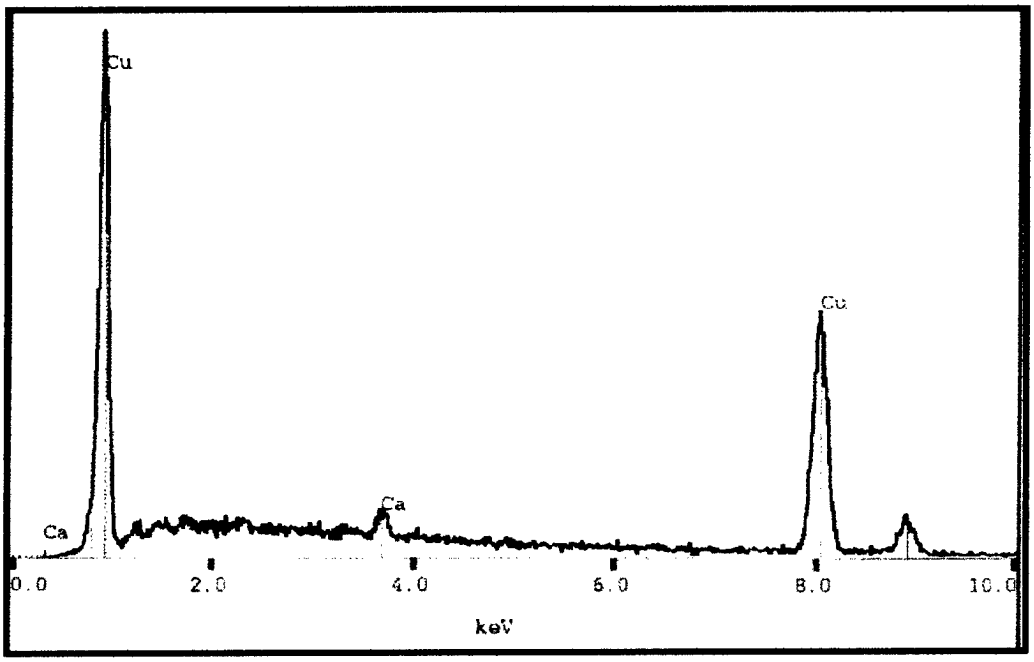

Figure 4. EDS spectra of copper fines shown in Figure 1

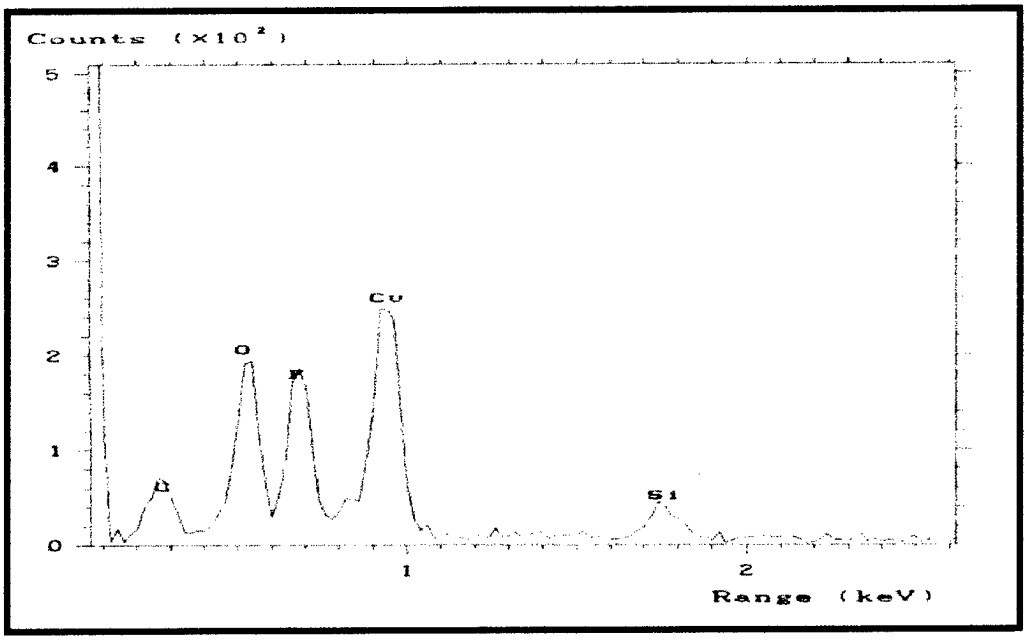

Figure 5. EDS spectra of discrete particles shown in Figure 3

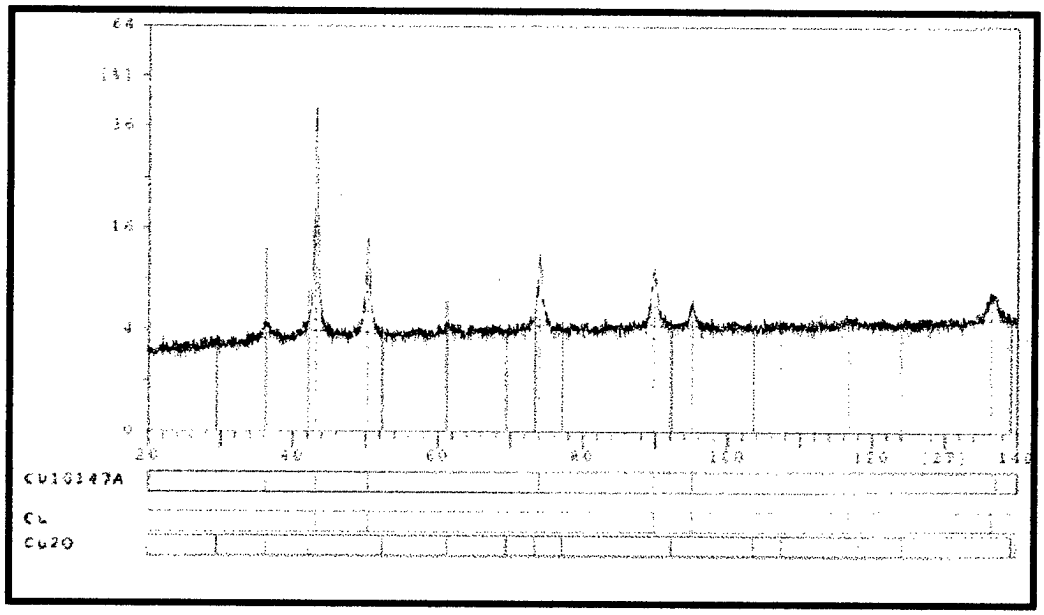

Figure 6. X-ray diffraction pattern of copper fines shown in Figure 1

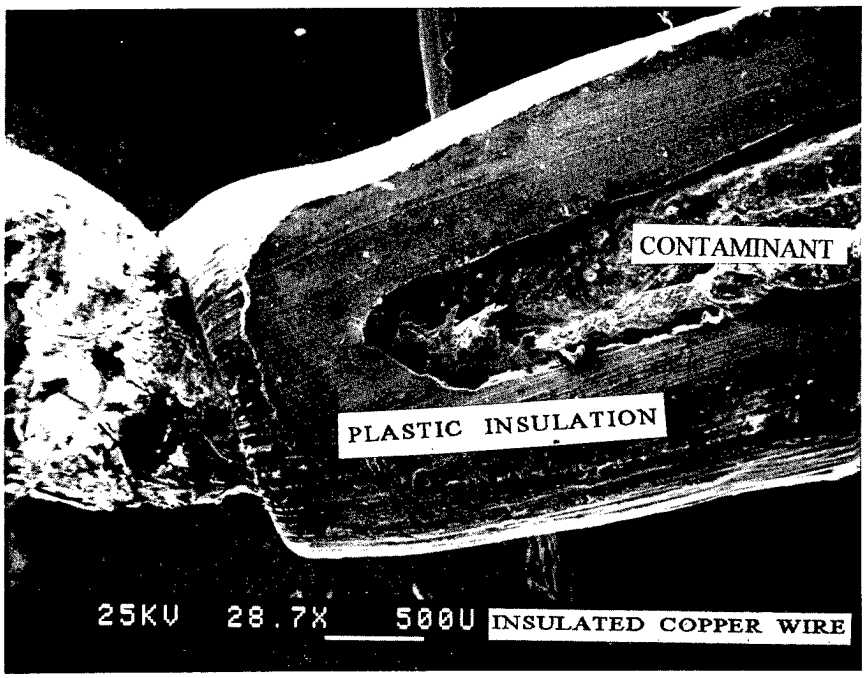

Figure 7. Metallic- fiber aggregate detected at the copper wire/ polymer insulation interface

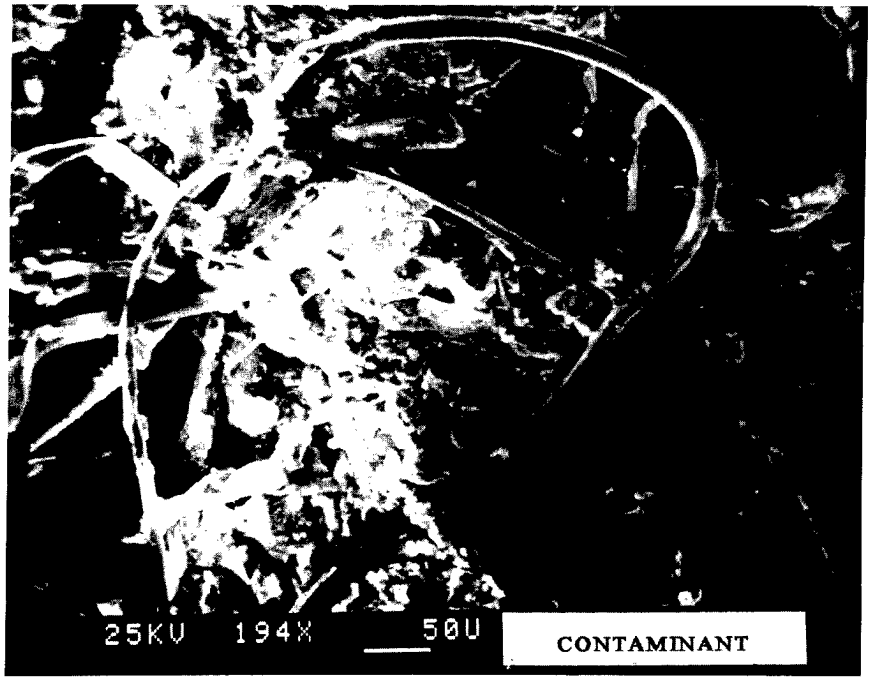

Figure 8. Metallic-fiber aggregate

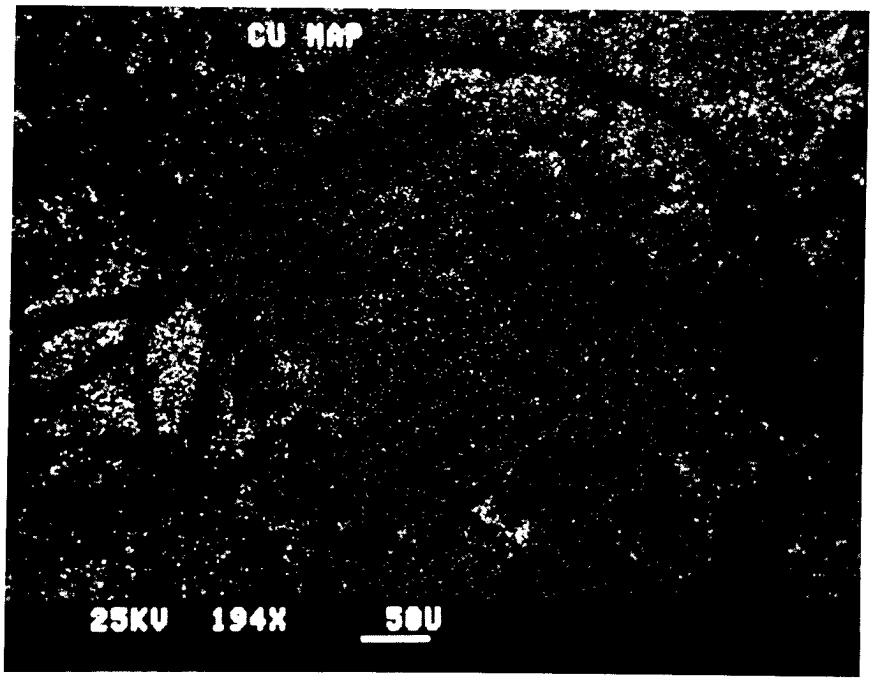

Figure 9. EDS copper mapping performed on the metallic-fiber aggregate

others skips were generated by particles other than copper fines, Figure 10. EDS elemental mapping performed on high magnification regions indicated that the particles are of metallic and non-metallic nature, Figure 11, 12, and 13. Iron and aluminum are the metallic components, while calcium is the major non-metallic component.

narrower processing windows, and more exacting product specification; secondly, cost of defective product; and thirdly, costly downtime. The data above has clearly shown that the origins of these contaminants are part and parcel of the manufacturing process. For example, copper fines come as a byproduct of copper extrusion into suitable gauges

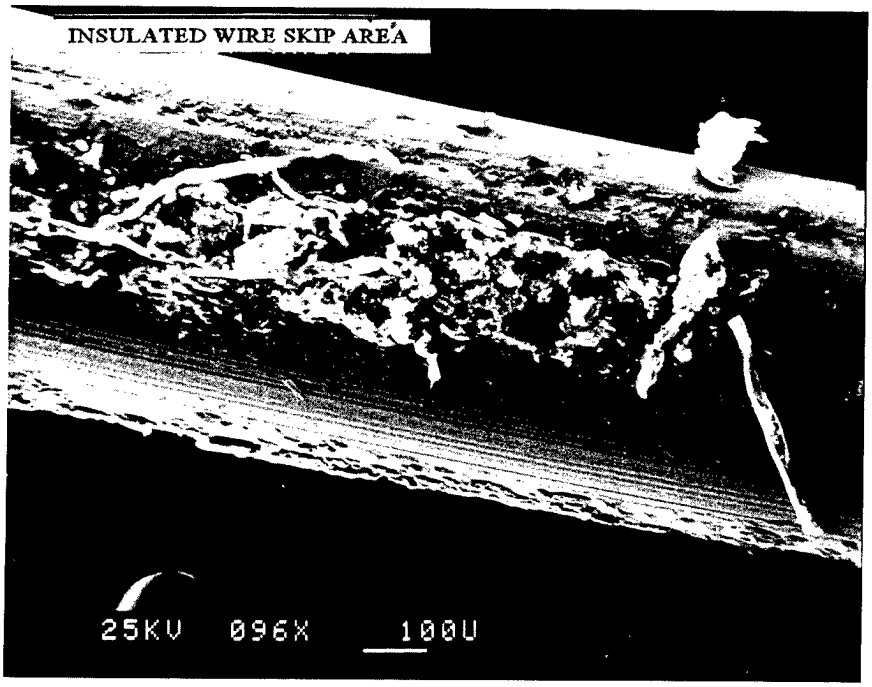

Figure 10. Skip region of an extruded coated copper wire sample

Metallic Granular Layer

Metallic granules were also found as a distinct thick layer on the inner surface of the polymer insulation, Figure 14. Higher magnification, Figure 15, shows the granular form of the layer. The layer is composed of copper particles mixed with particles of aluminum as mapped by the EDS, Figure 16.

DISCUSSION

Finding the source of the contaminants and devising methods to either minimize their impact or eliminate their presence is vital for several reasons: first, to meet

before coating it with a polymer insulation. Although the existence of copper fines byproduct was previously known, its impact on the wire coating process in general was not known.

Nevertheless, to minimize any potential impact on the coating process, copper fine by product were removed from the conductor by passing the conductor through felt pads. However, the presence of copper fine and fibers shown in Figures 7 and 8 indicates the cleaning process is a source for contaminants, which lead to further product defects.

Furthermore, the origin of metallic particles or debris,

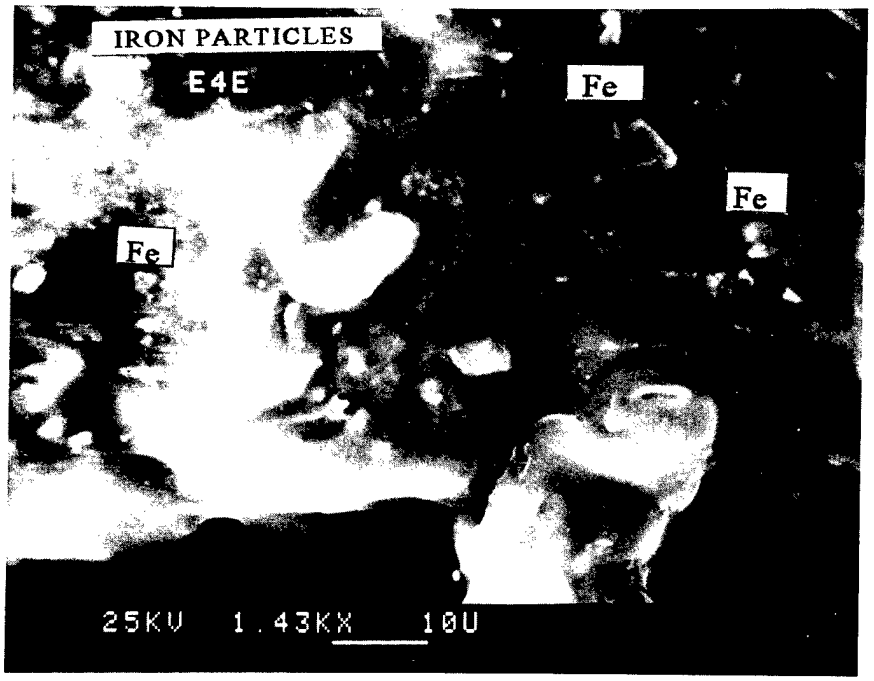

Figure 11. SEM high magnification of the center lower region shown in Figure 10

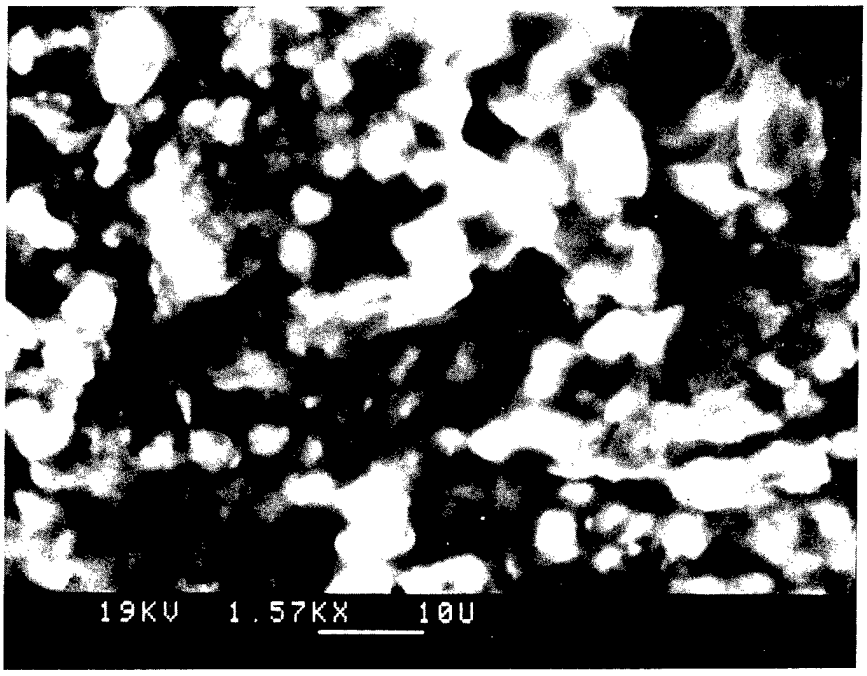

Figure 12. SEM high magnification of the center area shown in Figure 10

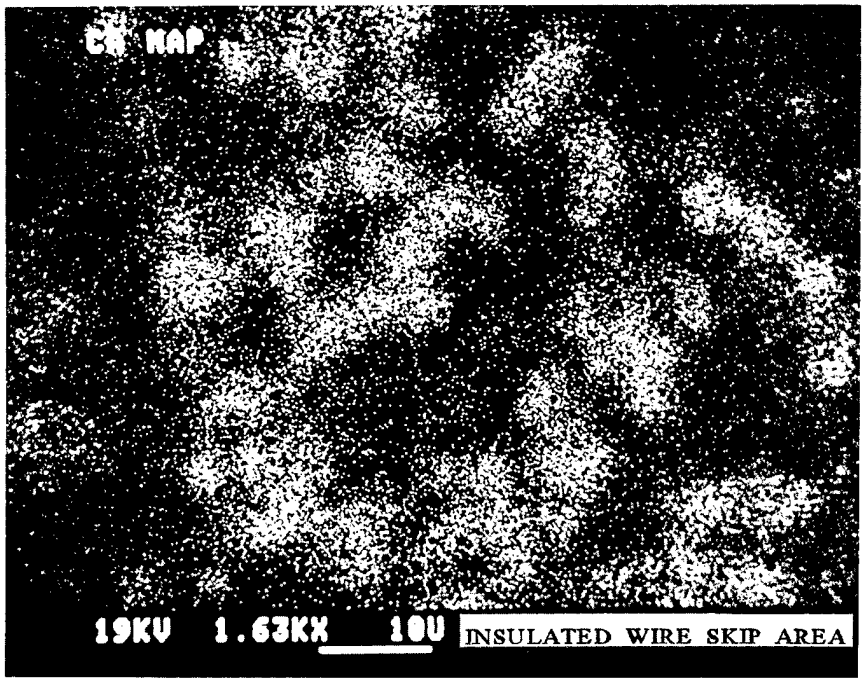

Figure 13. Calcium EDS mapping of the skip region shown in Figure 12

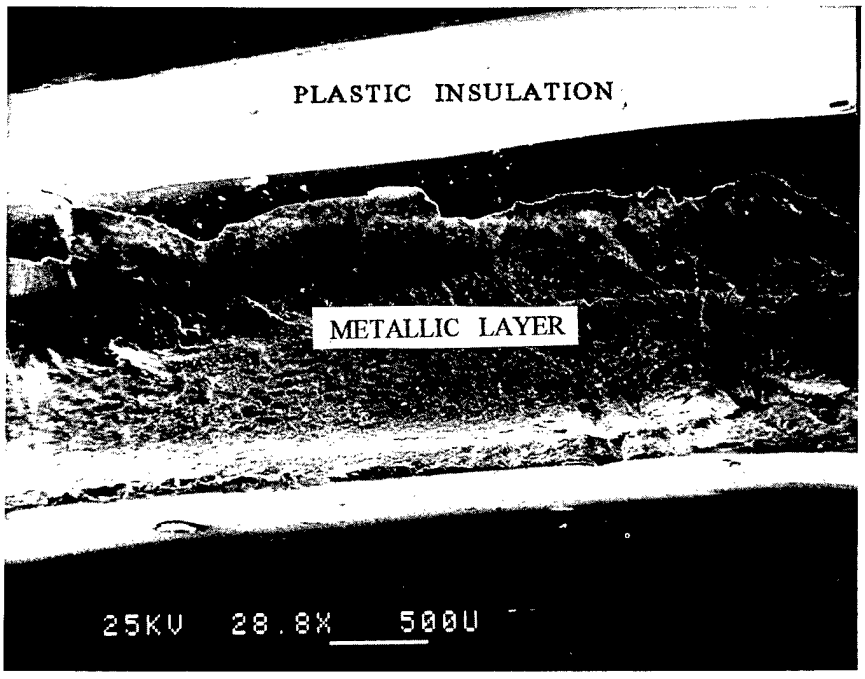

Figure 14. Metallic granular layer

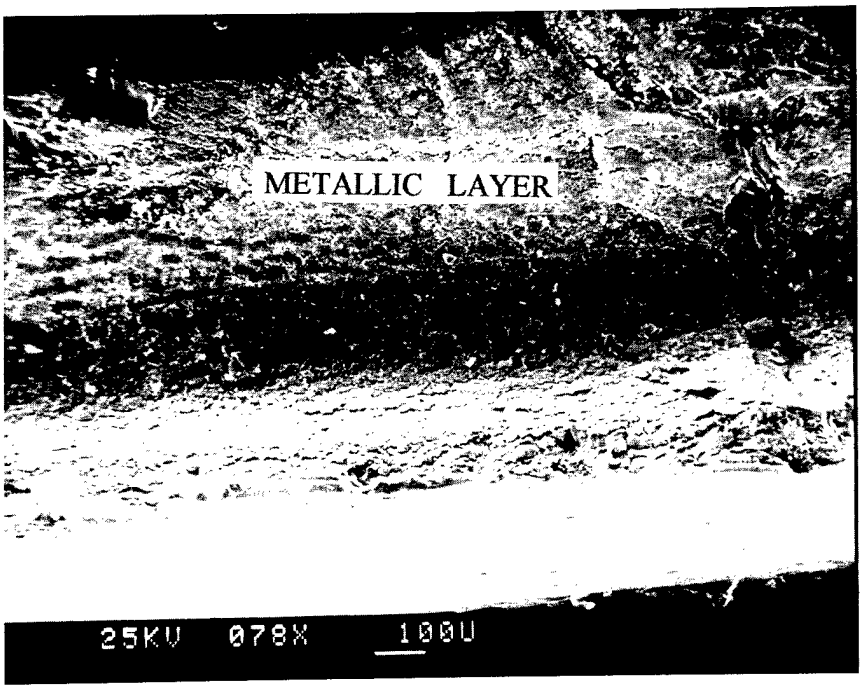

(A)

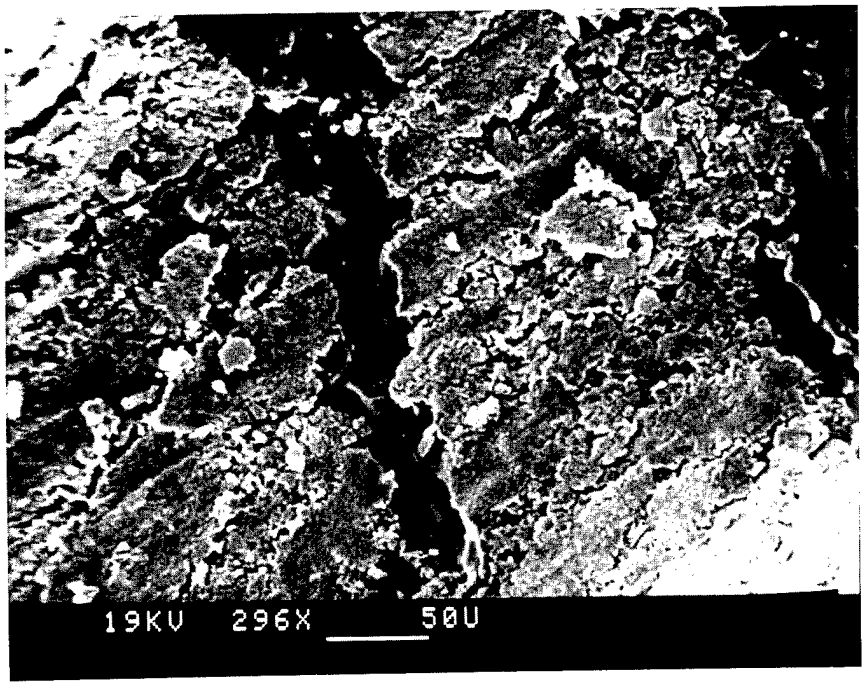

(B)

Figure 15. Metallic granular layer. (A) SEM low magnification
(B) SEM high magnification

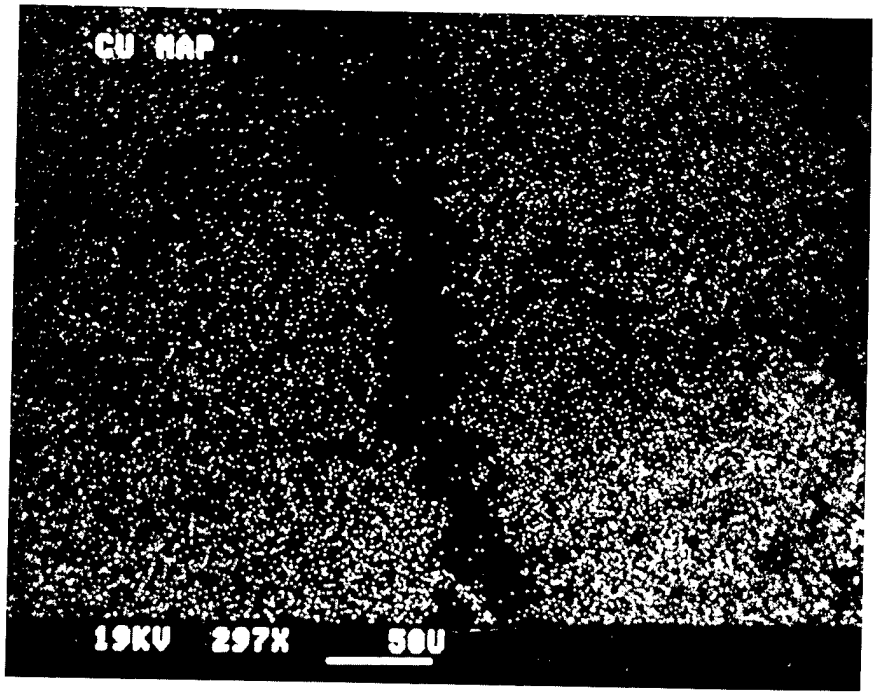

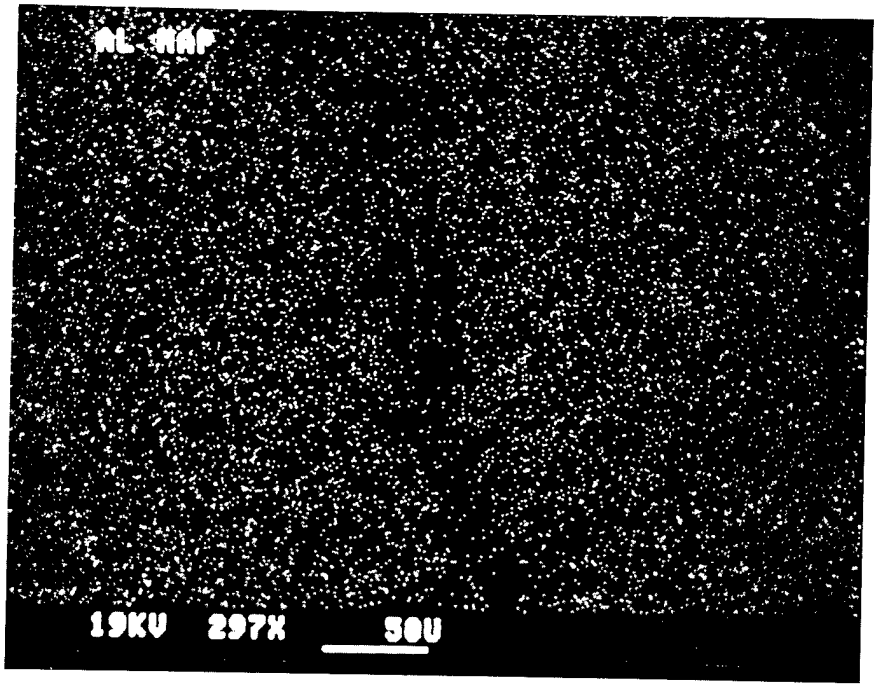

Figure 16. EDS mapping of metallic layer shown in Figure 15 (B)

i.e Iron and Aluminum, and the copper/aluminum metallic layers, is the wearing out of the wire drawing and extrusion line equipment. The drawing capstans are made of steel coated with a tungsten carbide, and the transfer pulleys used in the annealer and tension box in the draw and extrusion lines are made of aluminum coated with zirconium oxide. Once these ceramic coating are eroded, friction at the wire-steel and wire-aluminum interface would generate the Fe and A1 debris. Moreover, the source of non-metallic element or contaminant is the hard water in the oil/water emulsion lubricant primarily used to reduce friction at the copper wire drawing operation.

CONCLUSION

Structural defects in insulated wire conductor arise from contaminants, which are generated at the copper drawing lines and associated wire cleaning operation. Best example of these are the copper fines and copper-fiber aggregates. Further source of contaminants is the wear of the hauling and conveying secondary equipment in both the wire drawing operation and the wire coating process. In order to process a high quality insulated wire, contaminants must be reduced or eliminated. This can be accomplished by better design of wire cleaning operation and adhering to strict maintenance of secondary processing equipment

REFERENCES

1. Friesen, H. W., "An Evaluation of Measurement Techniques for Determining Copper Cable Structural Effects," International Wire & Cable Symposium Proceedings, 1991, p. 93.

2. Riekkinen A., and Ekholm, R.,"Plastic Insulating Of Telephone Wires at Ultra High Speeds," 24th International Wire & Cable Symposium, 1975, p. 43.

3. Chia, E. H. and Patel, G. R., " Characterization of Rod and Wire Defects Produced during The Manufacturing of Copper," Wire Journal International, June 1996, p. 50.

4. Baker, G. and Wright, R. N. " Speed Effects in Magnet Wiredrawing," Wire Journal International, October 1993, p. 58.

5. Meseha, G. M. and Garshasb, M., " Copper Wire Failure Classification Methodology Based on Rod and Wire Manufacturing Process," Wire Journal International, February 1997, p. 230.

Maria A. Macip-Boulis
132 White Oak Road
New Holland, Pennsylvania, 17557

Maria A. Macip-Boulis received her PhD in materials engineering from Drexel University. For 11 years as a Research Scientist and a Senior Research Scientist at Armstrong World Industries, she worked in the development of new products. In 1996, She joined Alcatel NA Cable System, Inc. at the New Holland manufacturing facility to be in charge of new materials development.

OSCILLATORY FLOW OF POLYPROPYLENE AND ITS EFFECT ON CONDUCTOR ECCENTRICITY

Jeff S. Borke

Equistar Chemicals, LP.
11530 Northlake Drive Cincinnati, OH 45249

Abstract

Centering of the conductor within the insulation for telecommunication constructions is critical to the electrical and physical properties of the cable. A phenomenon call oscillatory flow, which is observed in linear polymers, has been found to have a major contribution to the conductor being off-centered. In this study, processing variables such as melt temperature and die size are shown to have a direct influence on oscillatory flow of polypropylene and ultimately the eccentricity of the insulated conductor.

Background

Poor centering of the conductor (eccentricity) is a common problem in high speed wire insulation processes. For example, in the manufacturing of telecommunication singles, eccentricity can occur at line speeds as low as 150 m/min. In many instances maximum production speeds are limited because, of these eccentricity problems and soon become a major limiting factor to improving the economics of the wire insulating process.

Besides line speed limitations, eccentricity can also deteriorate the electrical and physical integrity of the final cable construction. Wall thickness variations can cause decreased signal performance due to capacitance effects. Also, since electrical breakdown failures are typically caused by pinholes or abrasions in the insulation surface, as wall thickness decreases the frequency of electrical breakdowns increase.

Knowing the problems that eccentricity creates, manufacturers have developed many ways of maintaining the concentricity of the conductor. For example, extruder design has a direct impact on conductor concentricity. For high speed insulating applications, wire coating heads, dies and guider tips are designed to center the conductor by distributing the pressure exerted by the polymer evenly around the diameter of the conductor to maintain concentricity (Figure 1). Also, rheological stabilizing forces of the polymer have been shown to have a considerable effect on concentricity [1]. This paper will concentrate on yet another rheological phenomenon known as oscillatory flow that has a dramatic effect on eccentricity.

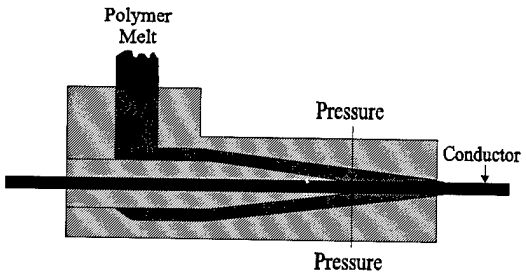

Figure 1.

Oscillatory flow can be classified as a type of extrudate distortion or melt fracture that occurs when polymer is being extruded through a die or capillary. Extrudate distortions can be subdivided into general categories that range from surface melt fracture (shark skin), to helical patterns to gross melt fracture. In the case of linear polymers such as linear low density polyethylene (LLDPE), high density polyethylene (HDPE) and polypropylene (PP), the extrudate can have a helical or rope-like appearance, while on a smaller but still visible scale the surface is smooth. Bergem [2] and Piau

et al. [3] have shown that this helical pattern is directly related to a swirling motion of the melt at the entrance to the capillary. Other work by Bersted [4] showed that the initiation site for oscillating flow is not in the die entrance region but rather the die itself. To date, the triggering criteria and the physical mechanisms governing the appearance of extrudate instabilities are still the subject of much controversy.

The objective of this paper is to correlate oscillatory flow to the amount of eccentricity that occurs in PP during a wire coating process. Furthermore, process variables such as melt temperature and die size will be evaluated as well to show what effect they have on the occurrence of eccentricity

Experimental Test Methods

All materials were extruded using a 2-1/2" 20:1 Davis Standard extruder equipped with a Maddock screw and Genca head, die and guider tip.

Wire was extruded onto 24 AWG solid copper wire.

The polypropylenes (PP#1 and PP#2) used in this experiment are classified as impact copolymers with a 2.5 MFR.

Results and Discussion

During high speed insulating processes, a cross-section of insulated wire is used to determine the amount of eccentricity. A common misconception when using this test method is to assume the center of the conductor is a continual distance from the center of the construction (Figure 2a). Upon closer examination during processing conditions that favor oscillatory flow, the conductor is forming a helical pattern within the insulating medium (Figure 2b), producing n% eccentricity at every cross-sectional point of the cable where:

$$\% \text{ Eccentricity} = \frac{\text{Min. Insulation Thickness}}{(OD_{Insulation} - OD_{Conductor})} \quad (1)$$

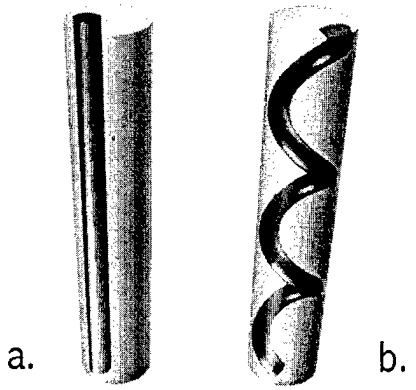

Figure 2.

Upon removal of the conductor from the process and extruding polymer directly onto the floor, a helical extrudate (Figure 3) is also observed under similar processing conditions. This helical flow is consistent with oscillatory extrudate distortion that occurs in linear polymers such as PP. With the conductor back in place and under extrusion conditions that produce oscillating flow, the conductor will again begin to oscillate.

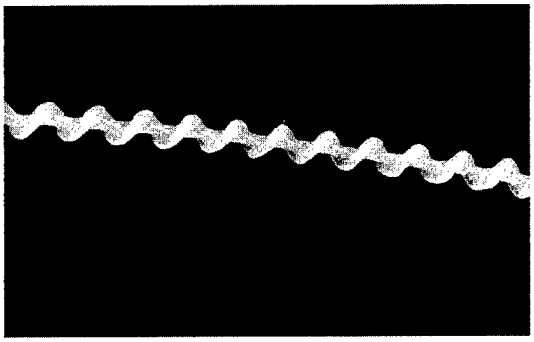

Figure 3.

Using the 'conductorless' method, the system is comparable to a large scale capillary rheometer in which the screw is providing the load to the melted polymer and the wire die is acting as the capillary. Capillary rheometers are used primarily to determine viscosity for a given shear rate range. To calculate viscosity, the wall shear stress and wall shear rate are needed. Equations 2, 3 and 4 describe viscosity (η), wall shear stress (σ) and wall shear rate (γ) for Newtonian fluids in a capillary where R is the capillary radius, Q is the flow rate, L is the capillary length and P is the driving pressure.

$$\eta = \sigma / \gamma \qquad (2)$$

$$\sigma = \frac{\Delta P \cdot R}{2L} \qquad (3)$$

$$\gamma = \frac{4Q}{\pi R^3} \qquad (4)$$

In a wire process, increasing the screw speed will increase the pressure and flow rate causing a growth in the wall shear rate and wall shear stress. Figure 4 shows the typical plot of P vs. Q and σ vs. γ for a polymer flowing through a capillary [5]. As a function of pressure or σ the extrudate goes through the typical melt fracture stages of a smooth surface, surface melt fracture (sharkskin), oscillatory flow and gross melt fracture.

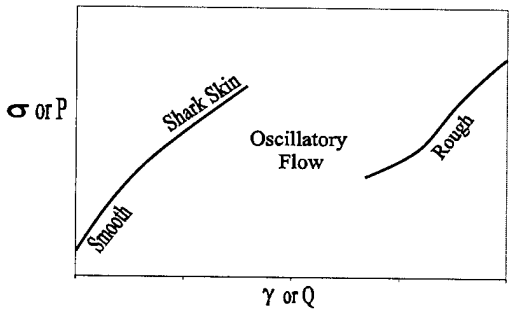

Figure 4

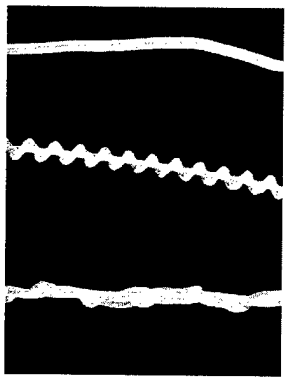

Figure 5.

To simulate the capillary rheometer, PP was extruded through the wire coating die without the conductor in place. Figure 5 shows the progression of extrudate formation from a smooth surface to gross melt fracture as the screw speed is increased. This confirms work by Bagley et al. [6] that in linear polymers flowing through tubes, the output surface becomes a function of the extrusion pressure (P) over a limited range of exit flow rates (Q).

To show oscillatory flow has a direct effect on eccentricity, two PP resins were evaluated using a Davis Standard 20:1, 2 ½" extruder. These PP resins differ in the point at which the onset of oscillatory flow occurs as well as the magnitude of oscillatory flow. Figure 6 shows the helical formation of PP#1 and PP#2 at four different screw speed. As can be seen in Figure 6, the onset of oscillatory flow in PP#1 occurs at higher screw speeds and the overall magnitude of oscillatory flow is less than PP#2. Each of these resins was then extruded onto wire at 400 m/min (the limit of the wire line take up system) with a screw speed of 47 RPM and eccentricity was measured. PP#1 showed a 75% improvement in eccentricity over PP#2 (Figure 7). This confirms the fact that the onset and magnitude of oscillatory flow have a direct effect on eccentricity.

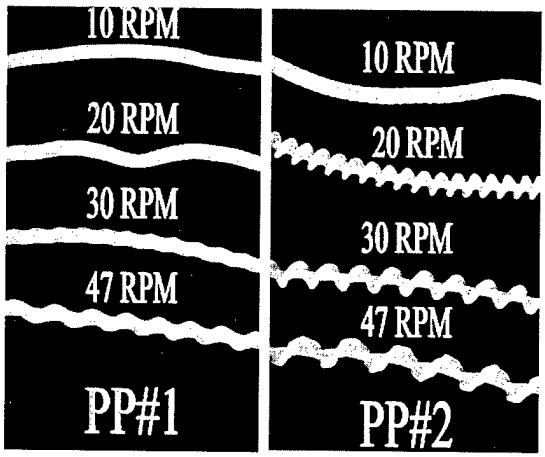

Figure 6.

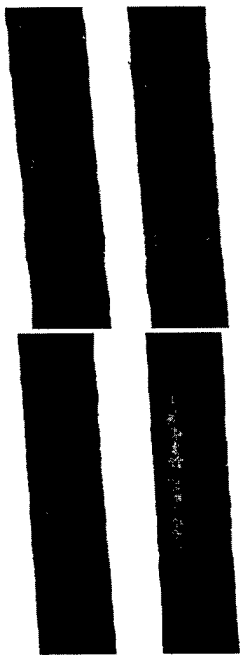

PP#1

%Eccentricity=5%

PP#2

%Eccentricity=80%

Figure 7.

Since the oscillatory regime is dictated by extrusion pressure, processing adjustments that can reduce head pressures were also examined. One method of reducing head pressures is to increase the melt temperature. Increasing the melt temperature reduces the viscosity of the polymer which ultimately reduces the overall head pressure. Figure 8 shows the effect of temperature on the onset of oscillatory flow. As can be seen in Figure 8, as temperature increases the onset of oscillatory flow occurs at higher screw speed. By using higher melt temperatures processors could reach higher screw speeds and in turn higher line speeds before eccentricity occurs.

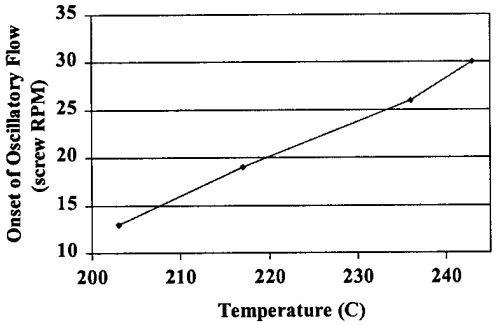

Figure 8.

Another way of reducing head pressures is to use over sized dies. Using oversized dies involves using a larger die than the final OD of the insulation construction and drawing down the insulation to the correct OD (Figure 9). By increasing the orifice diameter the pressure drop of the die is reduced, which will reduce the overall head pressure of the extrusion process. To show the effect of oversized dies on eccentricity, PP#2 was extruded on commercial extrusion lines at 1800 m/min using onsize and oversized dies. Using 33% oversized dies, PP#2 had an eccentricity of less than 10% which is a typical eccentricity specification maximum for an insulating process. Under the same processing conditions, on sized dies showed unacceptable eccentricity of greater than 10 percent.

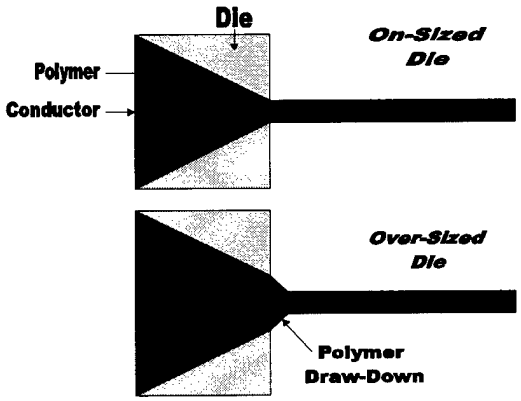

Figure 9.

Conclusions

There are many variables that affect the eccentricity of the conductor during the wire insulating process. A phenomenon known as oscillatory flow, which is seen in linear polymers such as HDPE, PP and LLDPE, has a direct affect on the centering of the conductor. Since pressure is proportional to the onset and magnitude of oscillatory flow, variables such as polymer melt temperature and die diameter can have a dramatic effect on eccentricity. Shown in this paper, increased melt temperatures and oversized dies reduced the onset and magnitude of oscillatory flow and ultimately reduced the eccentricity for a given construction. These practices can be implemented in the field to help combat the occurrence of eccentricity and ultimately increase line speeds for a more cost efficient process.

References

(1) Rheological Analysis of Stabilizing Forces in Wire-Coating Dies, Z. Tadmor & R.B. Bird, 1974, Polymer Engineering and Science, pp.124-136

(2) N. Bergem, Proc. VIIIth Int. Congr. Rheology, Gothenberg, 1976, p.50

(3) Influence of Upstream instabilities and wall slip on melt fracture and sharkskin phenomena during silicone extrusion through orfice dies, J.M Piau, published 1990.

(4) Investigation of the Oscillating Flow Phenomenon in High Density Polyethylene, B.H. Bersted, Journal of Applied Polymer Science, Vol 28, pp 2777-2791

(5) About the Origin of Sharkskin, A. Weill, Rheologica Acta, Vol 19, 1980, pp 623-632

(6) Baley, E.B., I.M. Cabot, D.C. West, J. Appl. Phys. 29, 109 (1958)

Jeff S. Borke

Research Engineer
Equistar Chemicals, LP.
11530 Northlake Drive
Cincinnati, OH 45249

Jeff Borke received his B.S. degree in Chemical Engineering from the University of Cincinnati in 1993. He joined Equistar Chemicals, LP. (formerly Millennium Petrochemicals Inc.) in 1993 and has worked in the Wire & Cable research and development group.

THERMAL AGING EFFECTS ON COAXIAL CABLE'S TRANSMISSION AND ITS LIFE EXPECTANCY

Lal M. Hore, and Orlando Chavez

Bellcore,
Morristown, New Jersey

ABSTRACT

Disc and air dielectric, and foamed dielectric coaxial distribution cables are aged at 80, 90 and 100°C. Periodically, the attenuation of the cables is measured. In the absence of any industry standard, a 7.5 percent increase in attenuation is selected as the failure criteria allowing determination of the failure points from each of the 80, 90 and 100°C attenuation data lines. Alternatively, 5% and 10% increases in attenuation are also considered to estimate the life expectancy of distribution coaxial cables. An Arrhenius projection to the expected life of the coaxial distribution cable is made by plotting the time (on a logarithmic scale) required for a selected percent change in signal attenuation to occur in aged cables as a function of the aging temperature, assumed in the range of 30 to 40°C.

INTRODUCTION

In the information super highway, coaxial cables are extensively used as an economical and readily available broadband link between the customers and the network. Cable television operators are major users of coaxial cables in their networks. Researchers in the past have published papers on the expected life of coaxial drop cables [1][2][3]. Hard-line coaxial distribution cables are designed either with foam dielectric or air and disc dielectric. They may have different ratios of air to solid polyethylene materials and different stabilizers in the dielectric. Both the above designs require the use of adhesive material on the center conductor of the coaxial cable to help ensure bonding to the dielectric.

The life expectancy of coaxial distribution cables depends largely on the long term consistency of the dielectric properties, i.e. dielectric constant (ε), and dissipation factor ($\tan \delta$) of the dielectric materials, stabilizers and adhesive coating materials over a wide frequency and temperature range. Unless the center and outer conductor materials of the coaxial cable are corroded, the aging of coaxial cables is not expected to produce any degradation in the transmission parameters, i.e. attenuation, structural return loss (SRL), characteristic impedance etc., attributable to changes in the metallic conductors alone. When coaxial cables are exposed to thermal aging, the stabilizers used in the dielectric are gradually depleted. As a result, the cable's dielectric properties are degraded and the coaxial transmission parameters can be adversely affected. Thermal aging of non-metallic components affects attenuation more than either SRL or impedance parameters. In the following design considerations, it will be evident that the dielectric materials play a significant role in the life expectancy of coaxial cable.

Test Methods on Coaxial Cables and Samples

In order to make a realistic prediction of the life of coaxial distribution cables under environmental aging conditions, a number of cable samples were selected for study. These 250 to 500 feet long cables were aged at 80, 90 and 100°C in forced air chambers. Before aging, attenuation of the cables was measured at room temperature. An HP 8753C Network Analyzer and an "S" Parameter 85046B Test Set were employed. The coaxial cables after aging for selected times were stabilized at room temperature for at least 24 hours before making any attenuation measurements between 5 MHz to 1 GHz at 51 individual frequency points.

The samples selected for the aging study were:

Disc and Air Dielectric Coaxial Distribution Cable - Sample A

Foam Dielectric Coaxial Distribution Cable - Sample B

Foam Dielectric Coaxial Distribution Cable - Sample C

ANALYSIS OF COAXIAL CABLE AGING DATA

Disc and Air Dielectric Cable Aging (Sample A) and Attenuation

Since attenuation is the primary transmission parameter that is most affected by thermal aging, this parameter was measured periodically at room temperature on aged samples. At the time of writing this report, measurements were completed for 68 weeks of aging.

Table 1 presents the average increase in attenuation in percent with respect to the initial values of Disc and Air Dielectric Coaxial Cable - Sample A in the frequency range of 5 to 1000 MHz for selected periods of aging.

Table 1. Percent Increase in Average Attenuation (α) of Disc and Air Dielectric Coaxial Cable vs. Aging Period - Sample A

Aging Temperature (°C)	Percent Increase in (α) After Aging (Weeks)			
Weeks	10	28	52	68
80	0.5	1.4	2.4	3.6
90	1.0	2.5	4.0	5.0
100	1.4	4.0	7.7	10.1

Foam Dielectric Coaxial distribution Cable (Samples B and C) and Attenuation.

Attenuation measurements were also carried out on two samples of foam dielectric coaxial distribution cables from two suppliers. The data were periodically collected after aging up to 68 weeks. Tables 2 and 3 provide data of the average attenuation increase in the frequency range of 5 to 1000 MHz for samples B and C for selected periods of aging.

Table 2. Percent Increase in Average Attenuation (α) of Foam Dielectric Coaxial Cable vs. Aging Period - Sample B

Aging Temperature (°C)	Percent Increase in (α) After Aging (Weeks)			
Weeks	10	28	52	68
80	0.7	1.9	3.6	4.5
90	1.2	3.3	5.3	7.1
100	2.1	5.1	8.8	11.8

Table 3. Percent Increase in Average Attenuation (α) of Foam Dielectric Coaxial Cable vs. Aging Period - Sample C

Aging Temperature (°C)	Percent Increase in (α) After Aging (Weeks)			
Weeks	10	28	52	68
80	0.4	1.6	3.2	3.8
90	1.0	3.8	5.3	7.4
100	1.5	4.4	8.7	11.6

ARRHENIUS PROJECTION OF CABLE LIFE

Disc and Air Dielectric Coaxial

In the industry, there is no precise requirement as to how large an increase in attenuation is permitted for any system design. In the absence of any industry standard, a 7.5 percent increase in attenuation is arbitrarily selected as the failure criteria in projecting the cable life. Linear regression lines are drawn through the percentage increase in attenuation points versus aging periods for 100, 90 and 80°C data points. By extrapolating these attenuation data lines, it is found that 52, 95 and 150 weeks correspond to the 7.5% increase in attenuation failure points for 100, 90 and 80°C aging respectively for Sample A (See Figure 1). If a 5% or 10% increase is considered as the alternative failure criteria, the corresponding crossover points for 100, 90 and

80°C become 33, 60 and 98 weeks for 5% or 68, 124 and 196 weeks for 10% increase respectively.

An Arrhenius projection to the expected useful life of the coaxial distribution cable can be made by plotting the time (on a logarithmic scale) required for a selected percent change in signal attenuation to occur in aged cables as a function of the aging temperature [$\log_{10}$T(time) vs. $^{o}K^{-1}$ (temp.)]. The effective operating temperature for the outdoor coaxial distribution cable is 30 to 40°C[5]. The actual temperature will however vary depending on the geographical location and plant types (aerial, buried etc.) of the installation. The Arrhenius projection of life of Disc and Air Dielectric coaxial cable is shown in Figure 2 for 5%, 7.5% and 10% failure points. The Figure shows that at 90°C, the slope of the projection line slightly changes. This observation, was also made by other researchers[6]. Table 4 provides the life expectancy data for the Disc and Air Dielectric Coaxial Cable for 5, 7.5 and 10% failure for 30, 35 and 40°C operating temperatures.

For air and disc dielectric coaxial cable sample A, the Arrhenius projection would predict a life expectancy of 38 years at 30°C or 22 years at 40°C. At 35°C, the expected life is 28 years. These projections are based on the assumption of 7.5% as the failure criteria of attenuation. For other failure criteria the expected life ranges from 25 to 14 years for 5% increase and 52 to 26 years for 10% increase respectively.

Table 4. Life Expectancy of Disc and Air Dielectric Coaxial Cable

Operating Temp. (°C)	Expected Life (Years) @ different Attenuation increase		
	5%	7.5%	10%
30	25	38	52
35	22	28	41
40	14	22	26

Foam Dielectric Coaxial

For foam dielectric coaxial cable samples B and C, similar procedures were followed to predict the life of the cables at an operating temperature range of 30 to 40°C. Considering the failure points limited to 5%, 7.5% and 10% increase in attenuation, we have estimated the life expectancy of the foam dielectric cable same as disc and air dielectric coaxial cable and presented in Table 5.

Table 5. Life Expectancy of Foam Dielectric Coaxial Cable

Operating Temp. (°C)	Expected Life (Years) @ different Attenuation increase					
	5%		7.5%		10%	
	Samp. B	Samp. C	Samp. B	Samp. C	Samp. B	Samp. C
30	17	22	25	29	33	43
35	14	17	22	23	25	31
40	10	12	14	18	19	23

For foam dielectric coaxial cable samples B and C, percent increase in attenuation versus aging period are plotted in Figures 3 and 5 for three aging temperatures, 100, 90 and 80°C. Using the crossover points for three failure criteria, e.g. 5, 7.5 and 10% increase in attenuation, Arrhenius projection of the life expectancy of coaxial cable samples B and C are made. These plots are shown in Figures 4 and 6.

For sample B, the Arrhenius projection for 7.5% attenuation increase, predicts a life expectancy of 25 years at 30°C, 22 years at 35°C and 14 years at 40°C. For 5% attenuation increase, the life expectancy ranges from 17 to 10 years and for 10% attenuation increase the corresponding periods are from 33 to 19 years (see Table 5).

For sample C, the projected life for 7.5% attenuation increase, ranges from 29 years at 30°C, 23 years at 35°C and 18 years at 40°C. The corresponding expected life ranges from 22 to 12 years for 5% attenuation increase, and 43 to 23 years for 10% attenuation increase within the operating temperature range of 30 to 40°C.

Figure 1. Percent Increase in the Attenuation of Disc and Air Dielectric Coaxial Cable (Sample A) Due to Aging

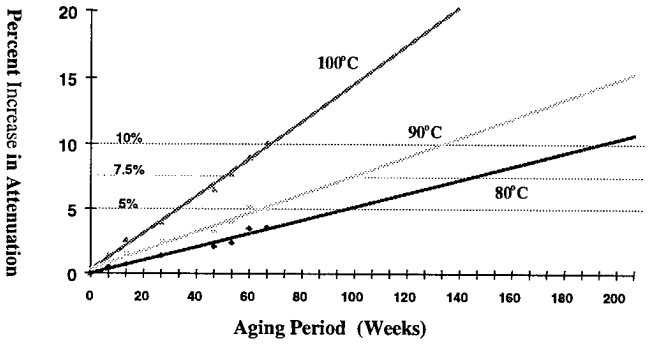

Figure 2. Arrhenius Projection of Life of Disc and Air Dielectric Coaxial Cable (Sample A) vs. Time of Degradation

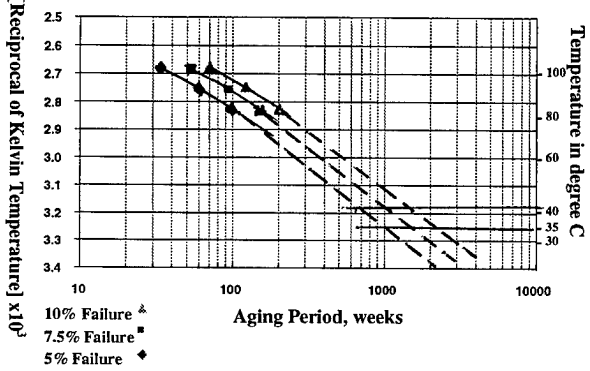

Figure 3. Percent Increase in the Attenuation of Foam Dielectric Coaxial Cable (Sample B) Due to Aging

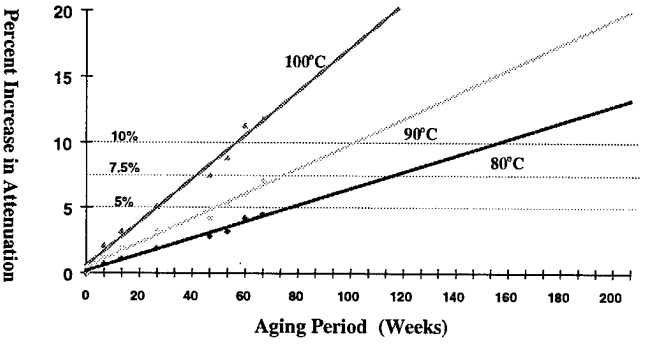

Figure 4. Arrhenius Projection of Life of Foam Dielectric Coaxial Cable (Sample B) vs. Time of Degradation

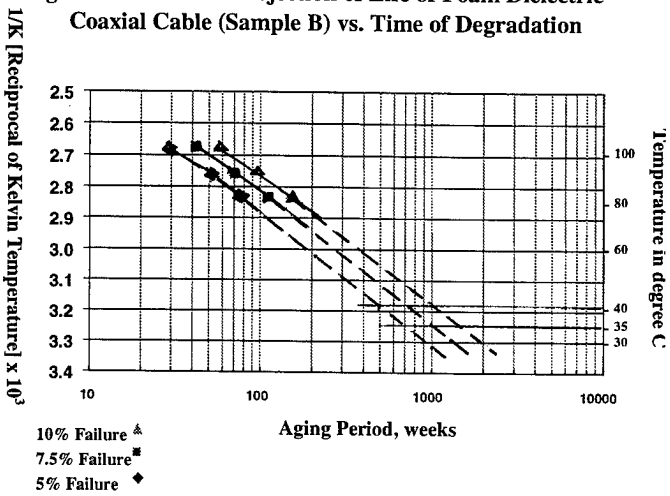

Figure 5. Percent Increase in the Attenuation of Foam Dielectric Coaxial Cable (Sample C) Due to Aging

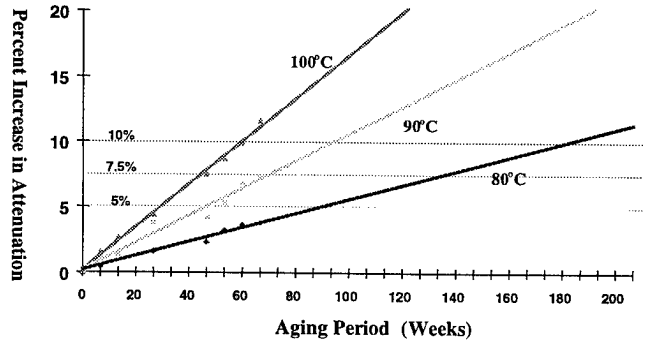

Figure 6. Arrhenius Projection of Life of Foam Dielectric Coaxial Cable (Sample C) vs. Time of Degradation

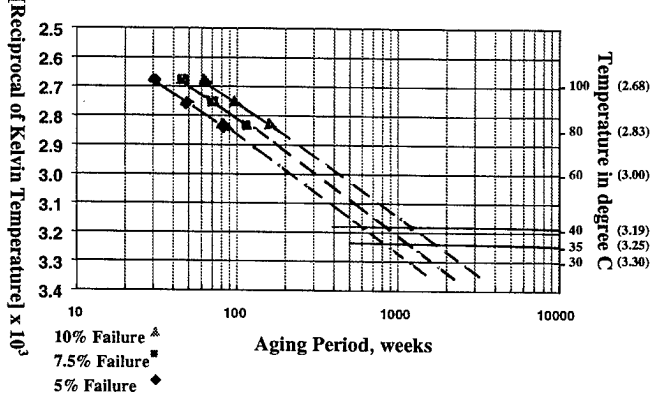

OXIDATIVE INDUCTION TIME (OIT) MEASUREMENTS

To ascertain the degree of stabilization of the cable dielectric, the concentration of stabilizers is determined by the High Pressure Liquid Chromatography (HPLC) Test Method, and/or by measuring the Oxidative Induction Time (OIT). The latter technique is commonly used by the industry[7] to determine the degree of stabilization.

In this series of tests, OIT data of the dielectric material from the distribution cable of three different manufacturers utilizing foam polyethylene or polyethylene disc and air dielectric were compared in accordance with ASTM D 4565[8]. On each of the three manufacturers' samples, OIT was measured on different samples that were unaged and also aged for 52 and 68 weeks at 80°C, 90°C and 100°C respectively. From each of these 3-foot cable samples, a specimen of the dielectric was cut from three places: 1) one end, 2) the opposite end and 3) the middle. A circular disc was cut from the dielectric and then a wedge cut along the radius of the disc. These wedges, which were used as the samples, weighed between 4 and 9 milligrams. They were weighed using a balance scale manufactured by E.H. Sargent, but with a control panel made by the Mettler Instrument Corp. Using a Dupont Thermal Analyzer in conjunction with a TA Instruments 2100 Thermal Analyst system, these samples were tested according to the procedure recommended by the ASTM method. Gas 1 was compressed nitrogen and Gas 2 was compressed oxygen. The equilibration temperature was 55.1°C + /- 0.1°C and the isothermal temperature was 181.7°C +/- 0.2°C.

The OIT was calculated using the heat flow vs. time curve generated by the Thermal Analyzer. The computer was used to draw a tangent to the portion of the curve parallel to the time axis and a tangent to the curve where it first changes its slope. The time at the intersection of these two tangents minus the time before oxygen was introduced into the chamber is the OIT.

The OIT measurements on PIC (Polyolefin Insulated Conductors) is traditionally used in telephone industry to ensure the life of the telephone cables. The hard-line coaxial cable's OIT requirements are less stringent in comparison to the telephone cables because of the coaxial cable's dielectric media being sealed under an aluminum shield conductor.

Figure 7. Stabilizer Retention in Percent of Original OIT [(a) 80°C Aging, (b) 90°C Aging, (c) 100°C Aging)]

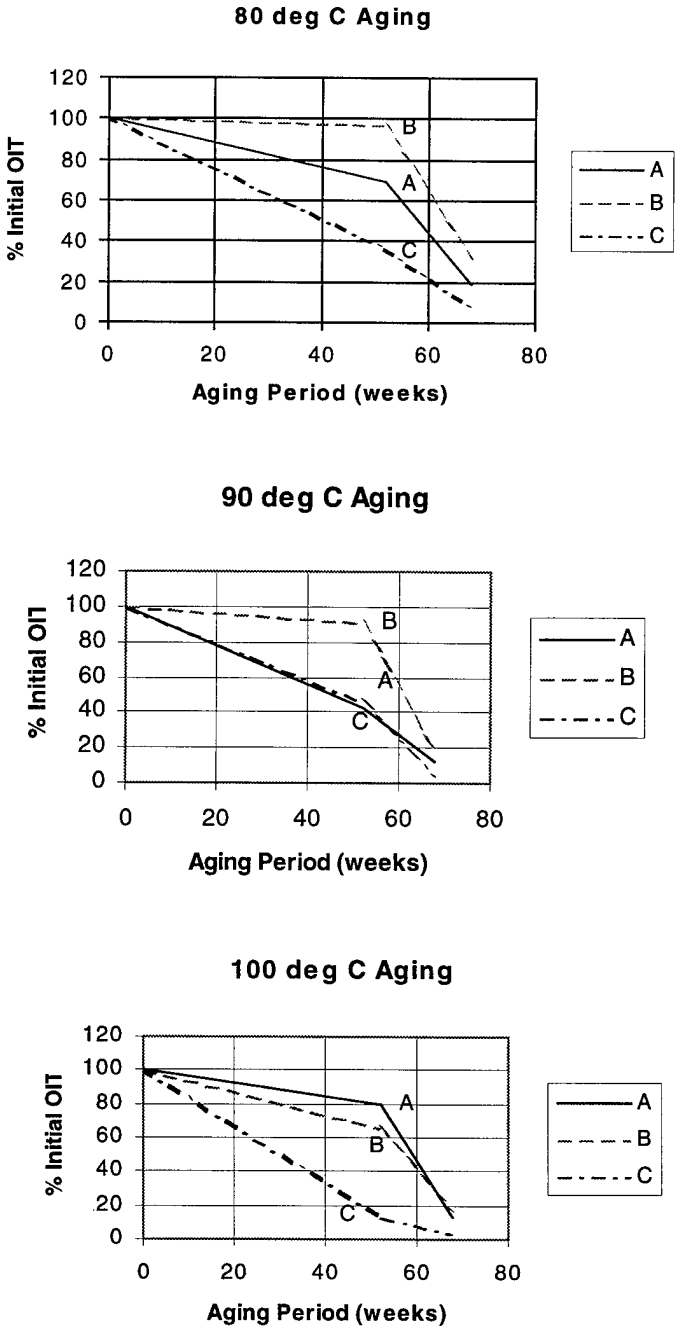

Figure 8. Stabilizer Retention in Percent of Original OIT [(a) Sample A, (b) Sample B, (c) Sample C)]

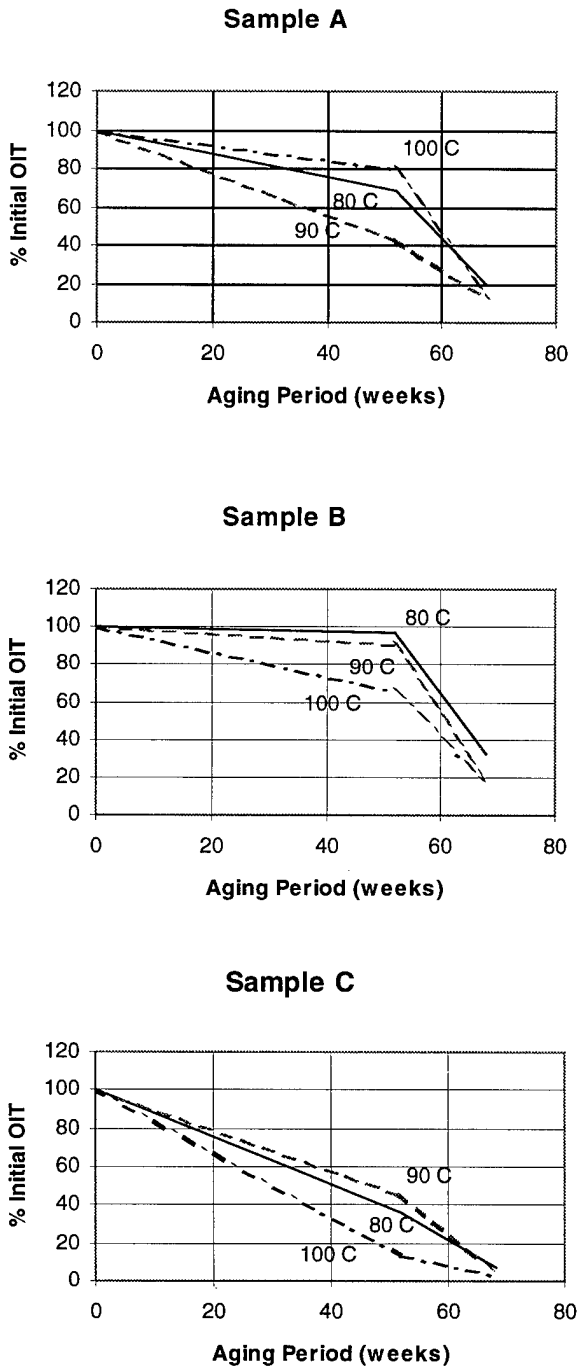

Figures 7 and 8 show stabilizer retention in percent of the original OIT values for samples A, B, and C after 52 and 68 weeks of aging at 80, 90, and 100°C. The OIT values show high degree of scattering up to 52 weeks. After 68 weeks the OIT values dropped significantly. The drop in the average value of OIT after 52 weeks of aging ranged from 13 to 80 percent for 100°C, 43 to 91 percent for 90°C, and 36 to 97 percent for 80°C aging. After 68 weeks, the OIT values ranged, from 3 to 18 percent for 100°C aging, 4 to 18 percent for 90°C aging, and 7 to 32 percent for 80°C aging. Even the same cable shows a wide spread of OIT values within a 3-foot section. For example, the 100°C aged sample A show 155, 119, 21 and 51 minutes as OIT values within a 3-ft sample. The wide variation of the stabilizer level between samples of the same cable section is a result of non-uniform stabilizer dispersion at the extruder line. After 52 and 68 weeks of aging, sample C suffered the maximum percentage loss of stabilizer at all three temperatures. The wide variation in the retention level of OIT values on the aged samples, might be related to changes in the cell structure and morphology of the polymer. These conditions could possibly be responsible for the degradation of the dielectric properties (i.e. ε, $\tan\delta$), and be partially responsible for the spread in the attenuation data. Since the production line extruder is not a high sheer mixer, there is every reason to believe that the stabilizers were dispersed non-uniformly throughout the dielectric media during the cable extrusion process.

CONCLUSION

Based upon the aging of distribution coaxial cables at elevated temperatures of 80, 90 and 100°C, followed by the measurements of attenuation and stabilizer levels of the cable dielectric materials, the following conclusions may be drawn:

1. The estimated life of disc and air dielectric coaxial cable based upon a maximum of 7.5% attenuation increase is 38 years at 30°C, 28 years at 35°C and 22 years at 40°C, assuming all temperatures represent the effective operating temperatures. For 5% allowable increase in attenuation, the expected life ranges from 25 to

14 years within the operating temperatures of 30 to 40°C. For 10% increase in attenuation, the corresponding expected life will range from 52 to 26 years (see Table 4).

2. The estimated life of foam dielectric coaxial cable, for a maximum of 7.5% attenuation increase, ranges from 25 to 29 years at 30°C, 22 to 23 years at 35°C, and 14 to 18 years at 40°C. For 5% attenuation increase, the expected life ranges from 22 to 10 years. For 10% attenuation increase, the corresponding periods are from 43 to 19 years, all within the constant operating temperature range of 30 to 40°C (see Table 5).

3. The oxidative induction time (OIT) data of the dielectric materials removed from the cables before aging show wide variation. This can possibly be attributed to non-uniform stabilizer dispersion at the extrusion line and use of different stabilizer in the three manufacturing samples. After 68 weeks of aging, the OIT data suffered the maximum drop of the 100°C aged samples. This was followed by the 90°C samples and next by the 80°C samples.

4. The trend in the drop of the OIT values of the dielectric can be correlated to the attenuation increase of the coaxial samples after aging (see Figures 1, 3, and 5). This observation confirms that the depletion of antioxidants from the dielectric is responsible for the attenuation increase in the coaxial cables.

ACKNOWLEDGMENTS

The authors thank William McLaughlin, a Summer Intern at Bellcore and Brent Christensen, Bellcore, for measuring the stabilizer levels of the dielectric materials from the cable samples. The authors also appreciate the efforts of Camille Berard for providing the graphical presentations of this report, and Lawrence Slavin for reviewing the report and offering valuable suggestions.

REFERENCES

[1] K. L. Smith, "Drop Cable RF Leakage Throughout 20 Years of Service", Cable-81 NCTA Annual Convention, Technical paper, 1981.

[2] P.L. Key, et el., "Reliability of Coaxial Drops in the CATV Industry", National Fiber Optics Engineers Conference, Technical Paper, 1994.

[3] J.N. D'Amico, et el., "The deterioration of Transmission Characteristics and Coaxial Cable Longevity", published in International Wire and Cable Symposium (IWCS) Proceedings (1995).

[4] Electrical Conductors Handbook, Published by Northern Electric Co; Ltd., 1968, page 167.

[5] G.A. Schmidt, "Life Prediction of Filled Cables in Pedestal Terminals", Proceedings of the 36th International Wire and Cable Symposium (1977).

[6] T.N. Bowmer, "Cracking of Foam-Skin Insulation in Pedestals", Proceedings of the 37th International Wire and Cable Symposium (1988).

[7] GR-1399-CORE, Generic Requirements for Coaxial Distribution Cable, Issue 1, July 1994.

[8] ASTM D-4565-94, Standard Method of Testing Physical and Environmental Performance Properties of Insulation and Jackets for Telecommunications Wire and Cable.

AUTHORS

Lal M. Hore is currently a Project Director responsible for development/updating of Bellcore's Generic Requiremtns for Outside Plant cables, coaxial cables and other wire products for voice, data and broadband applications. In addition, wire and cable analysis is also a part of his responsibility.

After receiving a M.Sc. Tech. degree in Applied Physics from the University of Calcutta and a Dr. Tech. Degree from the Technical University of Budapest in Electrical Engineering, he joined Bell Northern Research in 1970 to design and develop communications cables. In 1972 Lal moved to General Cable Company where he worked as a manager in the Communications Cable Section and next as a Staff Project Manager in the Applications Engineering Section until 1987 when he joined Bellcore.

Dr. Hore has authored numerous technical papers on dielectric materials and telecommunications wire and cable and holds a number of patents on telecommunications cables.

Orlando Chavez is a member of the Facilities and Components Group in Bellcore, Morristown NJ. He joined Western Electric in 1968 and worked at the Phoenix Cable Plant until December 1983. In 1984 he started work for Bellcore's CSO Quality Assurance Group. In May 1994 he joined the Distribution Network Components Group in Morristown. He is currently a team member who has responsibility for the test analysis of, Metallic Telecommunication Cable, Coaxial Components, Outside Plant Hardware, and Electrical Protection Devices.

NOVEL MATERIAL AND EXTRUSION TECHNOLOGY FOR HIGHLY EXPANDED INSULATION OF COAXIAL CABLES

Koji Ishihara, Yoichi Kawasaki, Toshio Sakamoto
Nippon Unicar Co. Ltd. Kawasaki, Japan

Sandra Maki
Union Carbide Canada Inc. Montreal, Quebec, Canada

ABSTRACT

We have been studying a combination technique of using both chemical foaming and physical gas injection to produce highly expanded insulation by a conventional extrusion line. The advantage of this system is that developed polyethylene compound can be processed to produce highly expanded insulation around 70-80% without installing sophisticated gas injection and extrusion equipment.

A unique blend of chemical blowing agent and other additive was used as a nucleating agent for this application. In addition, processing conditions were optimized by varying extrusion temperatures and gas injection conditions.
For modification of the existing extrusion line with a single screw for the chemical foaming, the screw type was redesigned for optimal mixing of polyethylene with nitrogen gas and a small nitrogen gas injection unit was equipped.
As a result of the investigation, the final CATV cable was found to have good electrical properties.

1. INTRODUCTION

Polyethylene materials containing chemical blowing agent have been successfully used to produce expanded insulation with expansion rates below 70% for coaxial cables. For high expansion rates i.e. over 70%, physically gas injected insulation is typically produced because of the lower signal transmission loss and easier processability. Fluorocarbons have been used in the past as the physical blowing agent, but today, nitrogen is being used as a substitute gas for fluorocarbons for environmental reasons.

However, nitrogen gas is more difficult to use for foaming to higher expansion rates. In addition, it is more difficult to achieve a homogeneous cell structure with nitrogen gas as compared with fluorocarbon gas.
On the other hand, a single stage extruder has been used for chemical foaming with around 50% expansion rate. It can be used for up to 70% expansion rate by increasing the quantity of chemical blowing agents.[1] However, as the increase of chemical blowing agent content in the insulation is increased, the electrical properties are worsened. Therefore, it would be very beneficial if highly expanded insulation (around 80%) could be achieved by processing using a conventional single stage extruder for chemical foaming apart from modification of a two-stage extruder for gas injection foaming.[2] This study considers the development of a unique compound and extrusion technology to allow highly expanded insulation to be produced without major modifications of a conventional single stage extrusion line for chemical foaming.

2.EXPERIMENTAL PROCEDURE

2.1. Materials

Base Resin. Three kinds of high density polyethylene (HDPE) and three kinds of low density polyethylene (LDPE) with low ε and $\tan\delta$ were selected as the components of the base resin for the

expandable insulation material. These are shown in Table 1 with basic properties. Melt tension was measured by capillary rheometer as an assessment of the foamability of the polyethylene.[3] High melt tension is usually preferred for the production of small foam cells. The different HDPE/LDPE ratios, as shown in Table 2 and 3, were examined to establish the optimum formulation for this application.

Blowing and Nucleating Agent. Chemical blowing agent and foam stabilizer were compounded with HDPE/LDPE blends together with other additive. Nitrogen gas was also used as the physical blowing agent. The basic properties of the chemical blowing agent and the foam stabilizer are shown in Table 4.

2.2. Extrusion Equipment

An outline of the extrusion equipment for the experiment is shown in Fig.1.

Extruder. As in the case of chemical foaming, a single stage extruder of 50mm ϕ (L/D=24/1) was used for extrusion of the expanded insulation layer.

Screw. Three screw designs were tested and they are shown in Fig.2. In order to achieve good mixing of molten polyethylene with nitrogen gas, modification was made on the screw configuration.

Gas Injection Device. A nitrogen gas tank, a pressure regulator, and mass flow controller of the gas were installed. Nitrogen gas was injected around a middle part of extruder cylinder through 0.10-0.23mm diameter inlet nozzle. Thinner diameter types of inlet nozzle were selected to increase the velocity of gas injection. The type of mass flow controller was chosen so as to operate precisely even at 5MPa higher than the pressure of molten polymer in the cylinder.

Die and Guider Tip. For extrusion of 7.3mm diameter insulation, the inner diameter of die was 3.4mm, and the outer diameter of guider tip was 2.05mm.

Cooling Trough. Cooling trough was divided into three zones to adjust the cellular structure of the expanded insulation and the roundness of core by controlling the cooling temperature at each zone. The first, second, and third zone were 3, 8, and 8 m long, respectively. In the experiment, the temperature was set at 60 ℃ in the first trough and at room temperature in the second and third trough.

2.3. Extrusion of Foamed Insulation

Fabrication tests of expanded insulation for the cable core were conducted using the extrusion line shown in Fig.1. For the inner conductor, a 1.8mm ϕ copper wire was used.
In order to obtain adequate adhesion between the foamed insulation and the conductor, L-LDPE having a low dissipation factor was coated 50 μ m thick on the conductor prior to foam extrusion. Expandable PE compounds were then extruded on the precoated conductor. The melt temperature, the amount of nitrogen gas injected and the cooling trough were adjusted to obtain the optimum cell uniformity.
The line speed was fixed at 15m/min. for the many extrusion variables studied. The expansion rate, extruded cell form uniformity, and surface appearance were evaluated for each experiment.

2.4. Manufacturing of Coaxial Cable

Coaxial cables of 10mm outer diameter, reflecting the requirements of the Japanese S-7C-HFL specification, were manufactured using the cable core having the best extrusion results. The core was wrapped with 0.2mm thick aluminum tape and then jacketed by LDPE based black compound (product diameter=10mm). Electrical properties such as capacitance, characteristic impedance, and attenuation were evaluated and the results were shown in Table 10. To examine resistance of the cable to heat aging and humid atmosphere,

a heat cycle test was conducted for three months under the following condition.
70℃ × 80%RH × 2hr ⇔ 20℃ × 80%RH × 2hr

3. RESULTS AND DISCUSSION

3.1. Materials

Base Resin. Several polyethylene blends using six different grades of polyethylene, shown in Table 1, were evaluated to establish the blend that would provide the best balance of foam properties: expansion rate, uniformity of cells and insulation smoothness.
As is shown in Table 2 and 3, there are significant differences between the different combinations. The blends (B-1 and B-2) with the highest melt mass flow rate (MFR) HDPE resulted in the largest cells. The blends (B-3 and B-4) with the lowest MFR HDPE and the blends (B-2 and B-6) with the lowest MFR LDPE exhibited a rough surface.
On the whole, it is thought that high MFR HDPE has a lack of melt tension causing a poor cell structure and that low MFR HDPE and LDPE show poor extrudability. Therefore, using this reasoning, the medium MFR HDPE (HD-2) was blended with the medium MFR LDPE (LD-2). The higher blend ratio of HDPE (B-9) showed poor uniformity of cell size, while the lower blend ratio of HDPE (B-8) showed better uniformity. However, it is preferable to make the cell strong by increasing the blend ratio of HDPE as high as possible. It was found that the best blend ratio was 50/50 (B-7).

Nucleating Agent. The evaluation results of foam extrusion are shown in Table 5. A higher quantity of chemical blowing agent (CBA=1.4%) caused larger cells to be produced, especially around the conductor, while a lower quantity of CBA (0.2%) showed a poor expansion rate. It was found that a moderate chemical blowing enhanced the expansion by nitrogen gas injection and that the addition of foam stabilizer contributed to uniformity of the cell size distribution.

3.2. Extrusion Condition

Extrusion Screw. Three types of screw designs illustrated in Fig.2 were used to establish the optimum screw design for achieving high expansion rates. The results of the foam extrusion evaluations are shown in Table 6. It was found that the screw-C with Dulmage mixing and a groove was the best for mixing molten polyethylene with nitrogen gas in the presence of a little amount of chemical blowing agent.

Gas Injection Nozzle. The pressure of gas injection was kept at 2-3MPa higher than that of molten polymer in the cylinder. Table 7 clearly shows that the smaller diameter nozzle produced a higher expansion rate and cell uniformity. This nozzle increased the velocity of gas injection, and the cell uniformity was thought to be brought about by the higher velocity without being affected by the pressure fluctuation of molten polymer in the cylinder. It was proved that nitrogen gas is desirable to be injected at higher speed and higher pressure through the smaller orifice for highly expanded insulation.

Extrusion Temperature and Gas Injection To optimize the extrusion temperatures, temperatures at the end of the extruder (C2, C3) and die head (H) were varied from 150℃ to 180℃. The quantity of nitrogen gas injection was also varied from 12Nl/hr. to 18Nl/hr.. The results were shown in Table 8 and 9. Because the resin temperature at die exit was higher by about 5℃ than the set temperature, the best temperature setting was around the lower peak of decomposition temperature of the chemical blowing agent. The optimal gas injection rate was about 15Nl/hr. and the excessive injection rate caused surface roughness. This is thought to be due to escape of gas from the surface of molten polymer.
By optimization of these extrusion conditions, 78% expansion rate of S-7C-HFL cable core with uniform cell was obtained as shown in Fig.3 (Screw-C).
Furthermore, 81% expansion rate was also

achieved in other commercial extrusion line for S-10C-HFL cable (product diameter=13mm).

3.3. Electrical Properties of Coaxial Cables

The electrical properties of the final product coaxial cable made by the best extrusion condition were measured and the results were shown in Table 10. The values measured met the Japanese specification for S-7C-HFL cable. The attenuation after heat cycle aging for three months was within 5% increase of the original value as shown in Fig.4 and 5 with Freon foaming and the specification limit.

4. CONCLUSION

The extrusion technology of highly expanded insulation with nitrogen gas injection for coaxial cables has been studied by the combination of the formulation optimization of polyethylene based compound and modification of a conventional extrusion line for chemical foaming.
The compound of HDPE/LDPE (ratio=50/50) with a little amount of chemical blowing agent proved to be good material to get highly expanded insulation around 70-80% by the optimized extrusion conditions. The electrical properties of the newly developed cable were maintained after heat cycle aging for three months.

5. ACKNOWLEDGMENTS

The authors wish to thank Mr. Yutaka. Nitta of Hijiri Manufacturing Ltd. and Mr. Hidetoshi Ota of Nippon Sanso Corp. for modifying the extruder and gas injection device, respectively.
The authors also wish to thank Mr. Takayasu Toshinaga of Shikoku Cable Co., Ltd. and Mr. Akihiko Umetani of Kansai Tsusin Densen Co., Ltd. for valuable assistance in manufacturing and evaluating the cable.

6. REFERENCES

1. S.Hashimoto et al.,"Highly Expandable Compound and Processing Technologies for Coaxial Cable", 41st International Wire and Cable Symposium (IWCS) Proceedings, pp. 506-510 (1992)

2. T.Higashikubo et al.,"Study on Highly Expanded Insulation Material for Coaxial Cables by Non-Fluorocarbon Foaming Technique", 45th International Wire and Cable Symposium (IWCS) Proceedings, pp.968-976 (1996)

3. T.Tanaka et al., " High Speed Transmission Coaxial Cable by A New Polyolefin Material ", 40th International Wire and Cable Symposium (IWCS) Proceedings, pp.270-276 (1991)

Table 1. Basic Properties of HDPE and LDPE

Properties	Unit	HD-1	HD-2	HD-3	LD-1	LD-2	LD-3
Density	kg/m^3	960	964	961	918	918	920
Melt Mass Flow Rate	g/10min	12.5	7.0	1.0	5.0	2.0	0.3
Melt Tension[1)]	g	0.3	0.7	1.1	10	12	20
Relative Permitivity[2)]	-	2.3	2.3	2.3	2.3	2.3	2.3
Dissipation Factor[2)] $\times 10^6$	-	18	14	23	55	58	77

1) at 160°C, Capillary ; L=8.0mm,D=2.1mm, Piston Speed ; 10mm/min, Drawing Rate=5m/min
2) at 1MHz

Table 2. Foam Extrusion Results of PE Blends[1)]

Resin Type	Unit	B-1	B-2	B-3	B-4
HDPE(HD-1)	-	50	50	-	-
HDPE(HD-3)	-	-	-	50	50
LDPE(LD-1)	-	-	-	50	-
LDPE(LD-2)	-	50	-	-	50
LDPE(LD-3)	-	-	50	-	-
Expansion Rate	%	61	66	60	62
Size Uniformity of Cells	-	BAD	BAD	GOOD	BAD
Surface Smoothness	-	GOOD	BAD	BAD	BAD

1) Each blend was extruded at 160℃ with N_2 gas injection (15Nl/hr)

Table 3. Foam Extrusion Results of PE Blends[1)]

Resin Type	Unit	B-5	B-6	B-7	B-8	B-9
HDPE(HD-2)	-	50	50	50	40	60
LDPE(LD-1)	-	50	-	-	-	-
LDPE(LD-2)	-	-	-	50	60	40
LDPE(LD-3)	-	-	50	-	-	-
Expansion Rate	%	67	70	73	70	65
Size Uniformity of Cells	-	GOOD	GOOD	GOOD	GOOD	BAD
Surface Smoothness	-	GOOD	BAD	GOOD	GOOD	GOOD

1) Each blend was extruded at 160℃ with N_2 gas injection (15Nl/hr)

Table 4. Properties of Chemical Blowing Agent and Foam Stabilizer

Properties	Unit	Chemical Blowing Agent	Foam Stabilizer
Form	-	powder	liquid
Color	-	yellow	yellow
Decomposition Temperature	℃	160-210	200<
Generated Gas	-	N_2,CO,CO_2,H_2O	-

Table 5. Foam Extrusion Results of Compounds[1)]

Test No.	Unit	C-1	C-2	C-3	C-4	C-5
Quantity of CBA[2)]	%	1.4	0.7	0.2	0.7	0.7
Foam Stabilizer[2)]	%	0.1	0.1	0.1	0	0.3
Expansion Rate	%	74	79	40	68	65

1) HDPE/LDPE=50/50 based compounds were extruded at 160℃ with N_2 gas injection (15Nl/hr).
2) Properties are shown in Table 4.

Table 6. Foam Extrusion Results by Screw Type[1)]

Screw Type		Screw-A	Screw-B	Screw-C
Expansion Rate	(%)	65	77	78
Size Uniformity of Cells	-	BAD	GOOD	GOOD
Fluctuation of O.D.[2)] of Core		MUCH	A LITTLE	VERY LITTLE

1) HDPE/LDPE=50/50 based compounds were extruded at 160°C with N_2 gas injection (15Nl/hr).
2) Outer Diameter of Cable Core

Table 7. Foam Extrusion Results by Nozzle Size[1)]

Inner Diameter of Orifice	(mm)	0.23	0.15	0.10
Expansion Rate	(%)	68	75	77
Size Uniformity of Cells	-	BAD[2)]	BAD	GOOD
Surface Smoothness	-	BAD[2)]	GOOD	GOOD

1) HDPE/LDPE=50/50 based compounds were extruded at 160°C with N_2 gas injection (15Nl/hr).
2) Fluctuation of O.D. of core occured.

Table 8. Extrusion Results at Different Temperature Conditions[1)]

Temperature Setting[2)]	(°C)	150	160	170	180
Expansion Rate	(%)	74	78	77	75
Size Uniformity of Cells	-	GOOD	GOOD	GOOD	BAD
Surface Smoothness	-	GOOD	GOOD	BAD	BAD

1) HDPE/LDPE=50/50 based compounds were extruded at each temperature with N_2 gas injection (15Nl/hr).
2) Temperature setting of C2, C3, and H zone

Table 9. Extrusion Results at Different Quantity of Gas Injection[1)]

Gas Injection	(Nl/hr.)	12	15	18
Expansion Rate	(%)	75	78	73
Size Uniformity of Cells	-	GOOD	GOOD	BAD
Surface Smoothness	-	GOOD	GOOD	BAD

1) HDPE/LDPE=50/50 based compounds were extruded at 160°C.

Table 10. Electrical Properties of Coaxial Cable Manufactured by the New Technology

			S-7C-HFL		
Constituent of 78% Expanded Insulation	Base Polymer		HDPE/LDPE		Specification
	Blowing Agent		Nitrogen, CBA		
	Nucleating Agent		CBA/FS[1]		
Cable Structure	Diameter of Inner Conductor (mm)		1.8		1.8
	Diameter of Core (mm)		7.3		7.3
	Outer Diameter of PE Jacket (mm)		10.2		10.0±0.5
			Original	After 90days[2]	
Electrical Properties	Capacitance (nF/km)		49	49	50±3
	Characeristic Impedance (Ω)		75.3	75.4	75±3
	Attenuation (dB/km)	220MHz	55.0	56.6(103%)	66> (57)[3]
		770MHz	107.9	111.2(103%)	132>(115)[3]
		1300MHz	143.4	149.6(104%)	173>(150)[3]
		1550MHz	160.7	168.3(105%)	204>(177)[3]
		1770MHz	174.6	183.1(105%)	220>(191)[3]

1) Chemical Blowing Agent／Foam Stabilizer
2) Heat Cycle Aging: 70℃ × 80%RH × 2hrs. ⇔ 20℃ × 80%RH × 2hrs.
3) The Standard Values are indicated in parentheses.

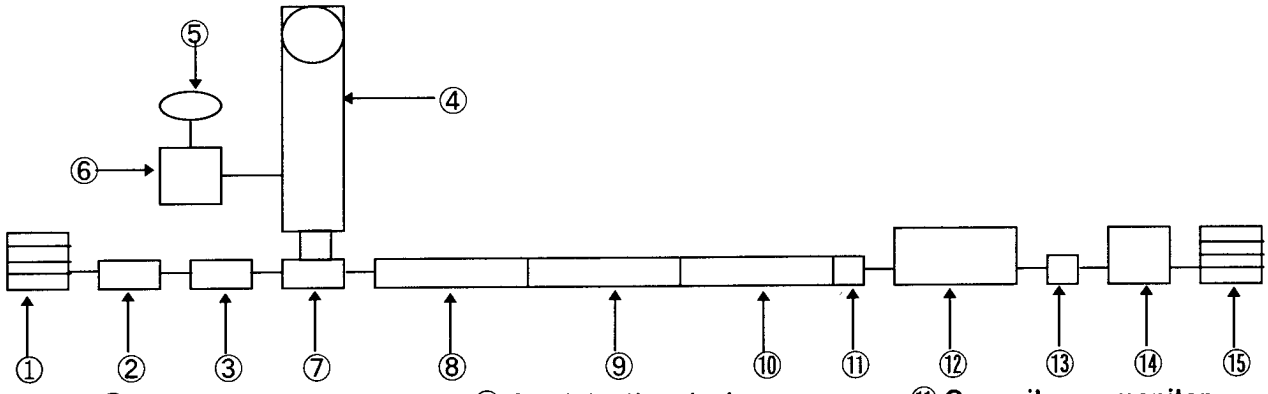

① Supply reel
② Pay-off capstan
③ Preheater
④ 50mm Φ Extruder
⑤ N2 gas tank
⑥ Gas injection device
⑦ Cross head
⑧ Cooling trough(No.1)
⑨ Cooling trough(No.2)
⑩ Cooling trough(No.3)
⑪ Capacitance monitor
⑫ Take-up capstan
⑬ Diameter monitor
⑭ Dancer roller
⑮ Take up reel

Fig.1 50mm Φ Extrusion Line for Experiments

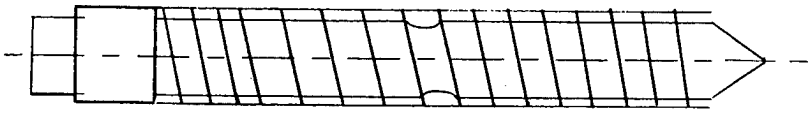

Screw-A : Full-Flighted Type Screw

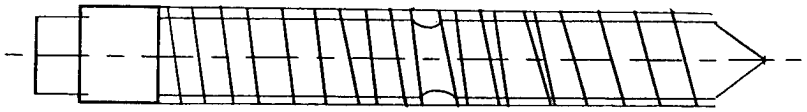

Screw-B : Double-Flighted Type Screw

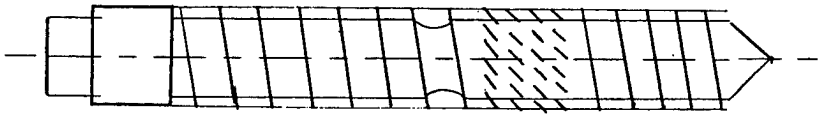

Screw-C : Dulmage Type Screw

Fig.2 Screw Designs for 50mm Φ Extruder

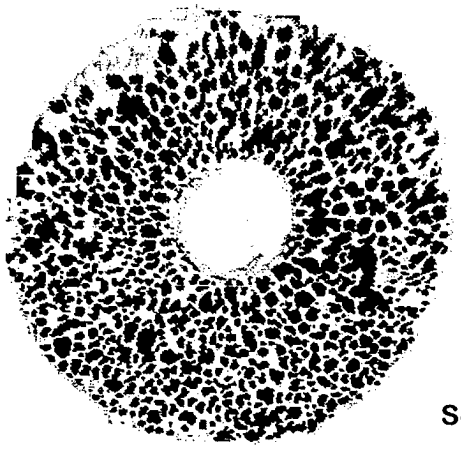

Screw-A

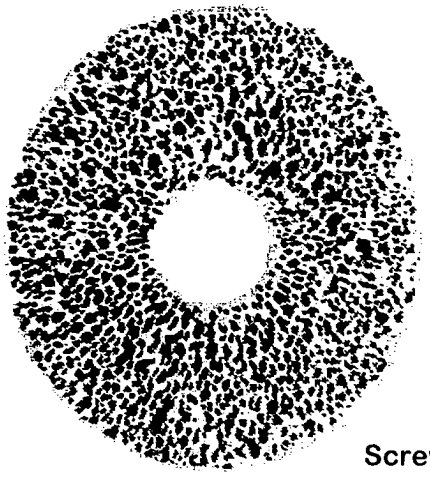

Screw-B

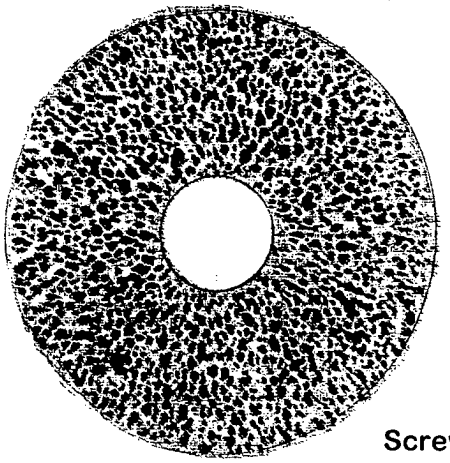

Screw-C

Fig.3 Cross-section of Expanded Insulation Obtained by Different Screw Types

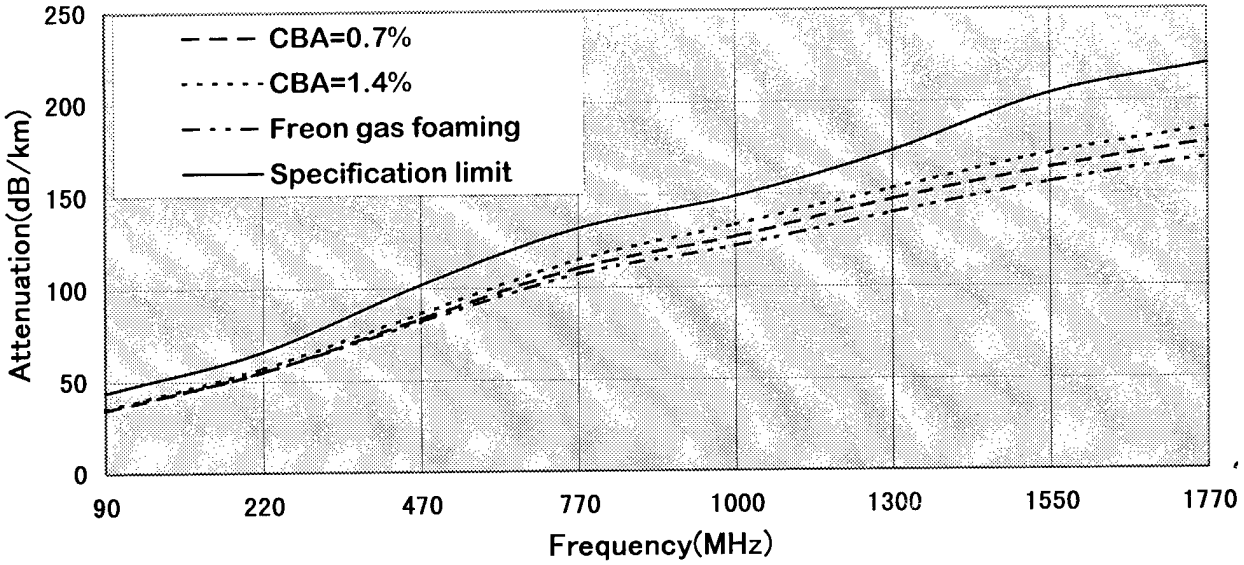

Fig.4 Attenuation of S-7C-HFL Cable(Original)

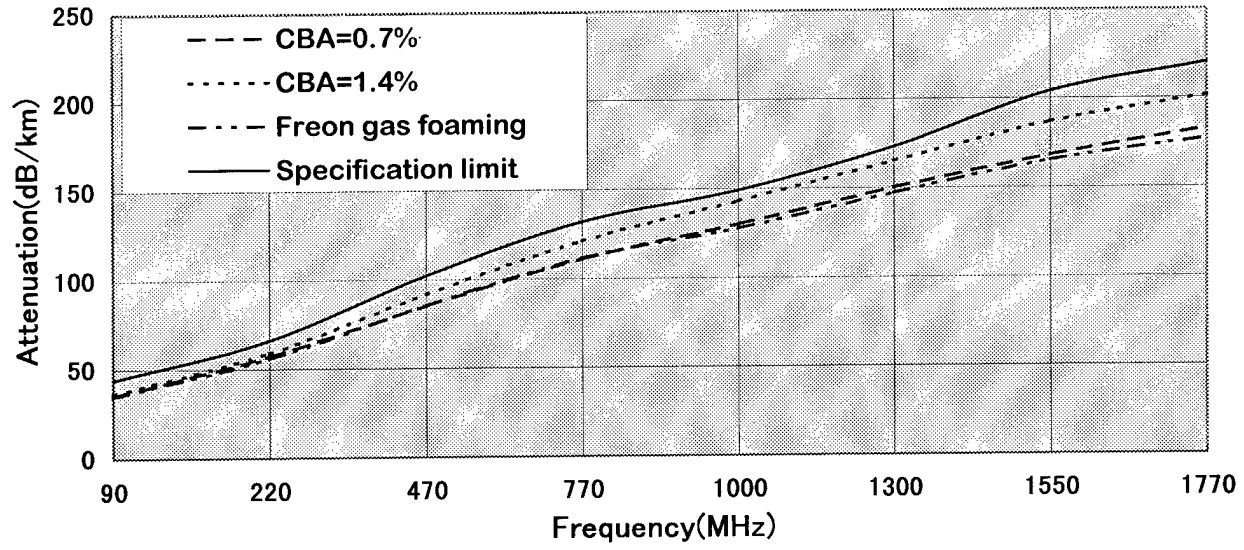

Fig.5 Attenuation of S-7C-HFL(after aging for 3months)

Koji Ishihara
Nippon Unicar Co. Ltd.
Polymer Research Laboratories
8-1, Ukishima-cho Kawasaki-shi
Kanagawa-ken, Japan

Mr. K. Ishihara received a B.S. degree of Petroleum Chemistry from Kyoto University in 1973. Then he joined Nippon Unicar Co. Ltd., where he has been engaging in research and development on wire and cable materials, and on other specialties of polyethylene. He is now Manager of Wire and Cable Group of Polymer Research Laboratory.

Toshio Sakamoto
Nippon Unicar Co. Ltd.
Polymer Research Laboratories
8-1, Ukishima-cho Kawasaki-shi
Kanagawa-ken, Japan

Mr. T. Sakamoto graduated from High School in Aomori Prefecture in 1959. He joined Nippon Unicar Co. Ltd. in 1962, where he has been engaging in research and development on wire and cable materials, especially in development on processing techniques in extrusion. He is now an engineer of Polymer Research Laboratory.

Yoichi Kawasaki
Nippon Unicar Co. Ltd.
Polymer Research Laboratories
8-1, Ukishima-cho Kawasaki-shi
Kanagawa-ken, Japan

Mr. Y. Kawasaki received a B.S. degree of Industrial Chemistry from Chuo University in 1964. Then he joined Nippon Unicar Co. Ltd., where he has been engaging in research and development on wire and cable materials, and on other specialties of polyethylene. He is now General Manager of Polymer Research Laboratory.

Sandra Maki
Union Carbide Canada
Specialty Polyolefins
10455 Metropolitain Blvd.
East, Montreal, Quebec, Canada

Sandra Maki received her B.Eng and M.Eng (Chemical) degrees from McGill University in Montreal (Canada) in 1986 and 1988 respectively. Upon graduation, she worked for DuPont Canada on the development of polyethylene films. Since 1989, she has been a Development Specialist for Union Carbide Canada working in the area of telecommunications cable. Her current research focuses on materials for coaxial cable.

GAS INJECTION COMPOUND for HIGH FREQUENCY INSULATION APPLICATIONS

Hans Eklind, Borealis AB, Stenungsund, Sweden
Hans-Bertil Martinsson, Borealis AB, Stenungsund, Sweden
Lars Westling, NOVA-BOREALIS Compounds LLC, Port Murray, NJ
Eric Brunner, NOVA-BOREALIS LLC Compounds, Port Murray, NJ

ABSTRACT

A polyethylene (PE) insulation compound with low dielectric loss at very high frequencies and extremely uniform cell structures has been developed. This paper discusses how the critical blend of High Density Polyethylene (HDPE) with a Low Density Polyethylene (LDPE) used as a property modifier, was achieved via viscosity and melt tension determinations.

The compound is coded EXP1

INTRODUCTION

The first links to the ground in an aerial telephone system are the antennae with their connecting cables. In the interest of packing as much information as possible into these links, the frequencies have been increased to circa 20 GHz.

Polyethylene is chosen as the cable insulation polymer since it has favorable electrical characteristics.

However, to satisfy the minimal signal losses and low dielectric constant required at these ever increasing frequencies, the polyethylene insulation must be foamed to a very high degree via gas injection to create the very small, numerous and uniform cell structures needed throughout the insulation matrix.

Depending upon the physical properties required of the insulation, various types of polyethylenes can be chosen such as Low Density (LD), Linear Low Density (LLD), Medium Density (MD) or High Density (HD). In the case of this paper, a HD grade with HD's inherent superior compression resistance (due to its higher stiffness modulus) was needed.

After choosing the required PE via density (i.e. for the major properties required), the viscosity of the material is then the next most important property in order to allow the material to be extrudable. The viscosity property used by resin suppliers to categorize materials is Melt Flow Rate (MFR).

- this viscosity value is more commonly referred to as Melt Index (MI) but MFR (@ 190°C and 2.16 kg conditions as per ASTM D1238, Condition E will be referenced in this paper.

Nevertheless, linear PE's be they LLD, MD or HD cannot easily be used as gas injection grades on their own. Melt strength and strain hardening are both very important in obtaining a homogenous cell structure during foaming. LDPE exhibits much more suitable values of these elastic-type properties than HDPE due to the inherently higher presence of long chain branching (LCB) .

- this comparison of LD to HD is particularly valid for the HD grades commonly used in Wire and Cable applications.

Therefore, the foam properties of HD can be improved by adding an appropriate grade of LD at a correct level to act as an elastic strength improver.

When dealing with polyethylene mixtures, it is essential to ensure that they are uniform so that consistency within a lot as well as from lot-to-lot is maintained. Therefore, in the case of our need to develop a nominally HD material from a HD and LD blend, the ability of the material to react with minimum variation throughout its extruded matrix to the introduction of the gas, is very important. The main theme of this paper therefore

stresses how critical blend composition is in order to create the correct balance of melt strength and strain hardening. Furthermore, the choice of MFR for the LD and HD components is also demonstrated.

EXPERIMENTAL WORK

Mixtures of HDPE and LDPE (i.e. the recipe of EXP1 and similar materials), were prepared in a Brabender kneader. The pure resins, a dry blend, the Brabender mixture and a full-scale produced mixture were then analyzed.

For viscosity measurements, a Bohlin CSM Rheometer was used to determine shear viscosity using the parallel plate fixture at 170°C with an applied shear of 1000 pascals (Pa).

For melt strength and strain hardening effects, extruded strands from a capillary rheometer (die L/D of 16:1 and 190°C melt temperature) were pulled at various rates, measuring the resistance to the tensile effect either at a constant haul-off speed or with increasing speeds until strand breakage.

- actually this test measures melt tension so in a way it can be referred to as a "dynamic melt strength" test.

RESULTS and DISCUSSION

a). Viscosity Measurements

Graphical Figure 1 shows the "compliance" J(t) of the pure constituents of EXP1, as well as EXP1 and 3 different "artificial" EXP1 mixtures (i.e. melt blended for different time periods).

- please note that the slope of each line is proportional to the inverse of the viscosity of the corresponding sample.

The viscosities for all 6 specimens are also reported as bar graphs in Figure 2.

As can be observed from Figures 1 and 2, the HD portion of EXP1 has a lower viscosity than the LD modifier. Also, you can note that the viscosity of each blend is dependent upon the mixing time as the 10-minute brabender exposure most closely approaches the viscosity of the in-house EXP1 compound.

Assuming that the viscosity of each constituent of the production-scale EXP1 is similar to the corresponding constituent of the Brabender mixtures, this indicates that the full-scale product is better homogenized than all the Brabender mixtures. This demonstrates the importance of obtaining a maximum homogenization in order to get the full effect of the LDPE portion.

Figure 3 and 4 illustrate how blend composition and MFR influence mixing viscosity. They show that the high MFR (low viscosity) of the HDPE portion strongly decreased viscosity of the mixture, despite the fact that the MFR of LDPE is reduced. Furthermore, the difference in viscosity of the samples with difference composition demonstrates the importance of having a constant mixing composition during all the production in order to keep the viscosity constant.

b). Haul-off Measurements

The influence of mixing conditions to melt strength is presented in Figure 5.

First of all, please note the wide disparity in the melt tensile resistance of the LDPE and HDPE components. The LDPE almost immediately i.e. at very low haul-off speed, has a resistance of 2 grams and breaks at under 3 grams at a speed of < 20 meters/min. In contrast, the HDPE component, being very linear (i.e. in molecular chain configuration) with relatively little side-chain branching very easily continues to stretch (orientate) with a very low resistance of < 0.5 grams and continues to orientate to a final breakage speed of > 160 fpm.

The production blend EXP1 exhibits a plateau value of > 1.0 grams and breaks at 75 m/min. If we consider this curve to be the ideal balance of melt elastic resistance (to produce consistent spherical cells) and orientability (minimize cell distortion), then the other methods shown in Fig. 5 suffer. The dry-blend and brabender melt mixes (10 seconds, 1 minute and 10 minutes) fluctuate and can be seen to be dominated by either the LD or HD phases when the mixing efforts are low.

This means that a badly mixed compound will produce very inhomogeneous foam.

Another way to present the data is via Figure 6 which shows the melt tension / melt strength at a given haul-off rate which in this case, is only 2 m/min.

Figures 7 and 8 illustrate the influence of mixing ratio and MFR on the melt tension behavior. When the LD portion is low, the compound behaves more like a pure HD, i.e. the melt strength is reduced, resulting in low melt tension. If the MFR of the HD is too high, similarly, the melt tension is low due to lower strain hardening effects availbable. Therefore, both a variation in composition and viscosity of the constituents will consequently have a strong effect on the foam properties.

The work in this paper results in a compound able to blow to an expansion level exceeding 80% with a very uniform distribution of cells. For a 7/8-inch RF cable, circa 5 % decrease in attenuation has been obtained at 2 GHz compared to commercially available cables,

At lower frequencies, little difference between the new compound and traditional cable materials is seen. However, the attenuation curves of cables made with the new material begin to demonstrate superiority above 200 MHz.

CONCLUSIONS

In order to have an optimum influence of the LDPE part of a HDPE/LDPE mixture on melt strength and strain hardening, it is essential to have sufficient homogenization. Experiments indicate that mixing in a Brabender kneader for up to 10 minutes gives a lower degree of homogenization than in the full-scale produced EXP1 compounds. Furthermore, in order to secure a consistent production and optimum foaming performance of EXP1, it is essential to have a constant mixing ratio as well as an optimum viscosity of the blend constituents.

REFERENCES

1. Eklind, H. : Report HED01902, 1998-07-07
2. Mandelkern, L., Alamo, R.G. and Stehling, F.C. : Trends Pol. Sci. 11, 377
3. Dordal, M. and Eggen, S. : Report HED01903, 1998-07-10

Figure 1: Influence of mixing conditions on compliance J(t) vs. time t.

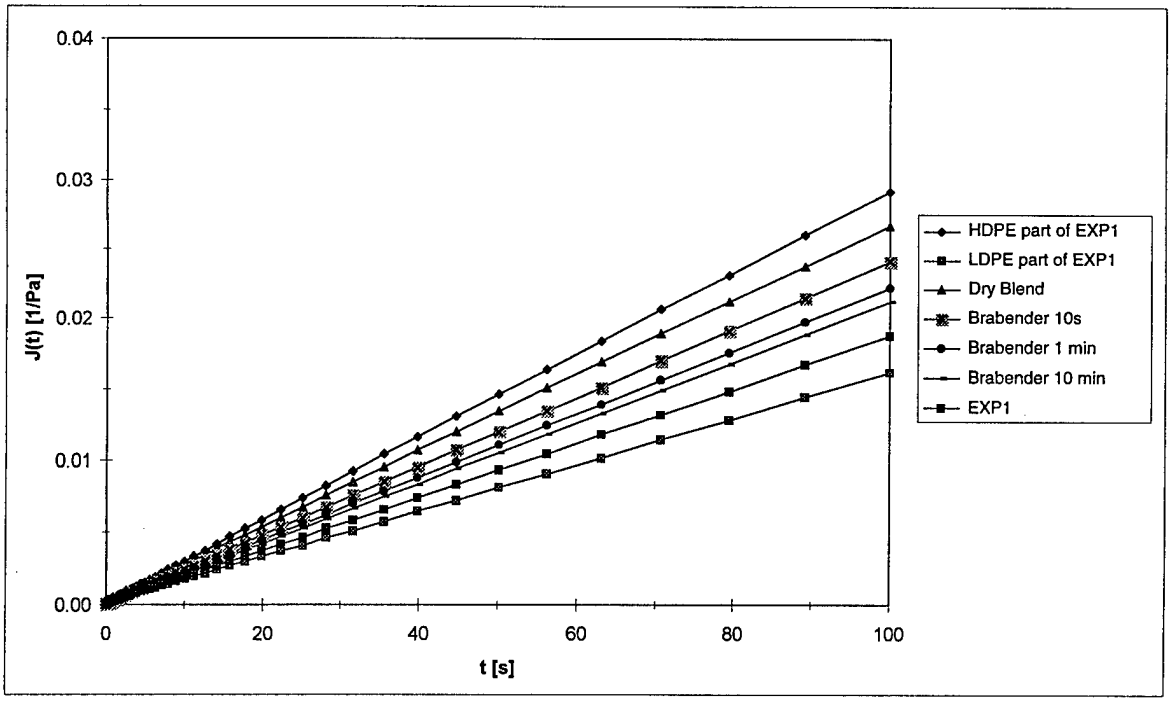

Figure 2: Influence of mixing conditions on shear viscosity η.

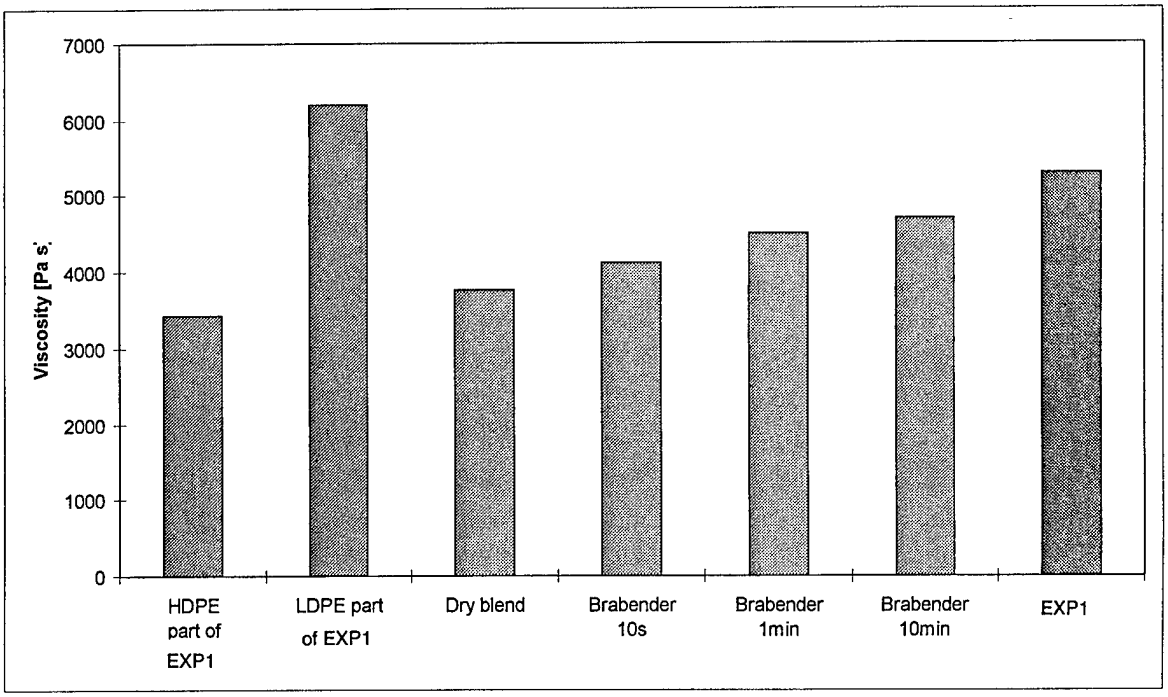

Figure 3: Influence of mixing ratio and MFR of the constituents on compliance J(t) vs. time t.

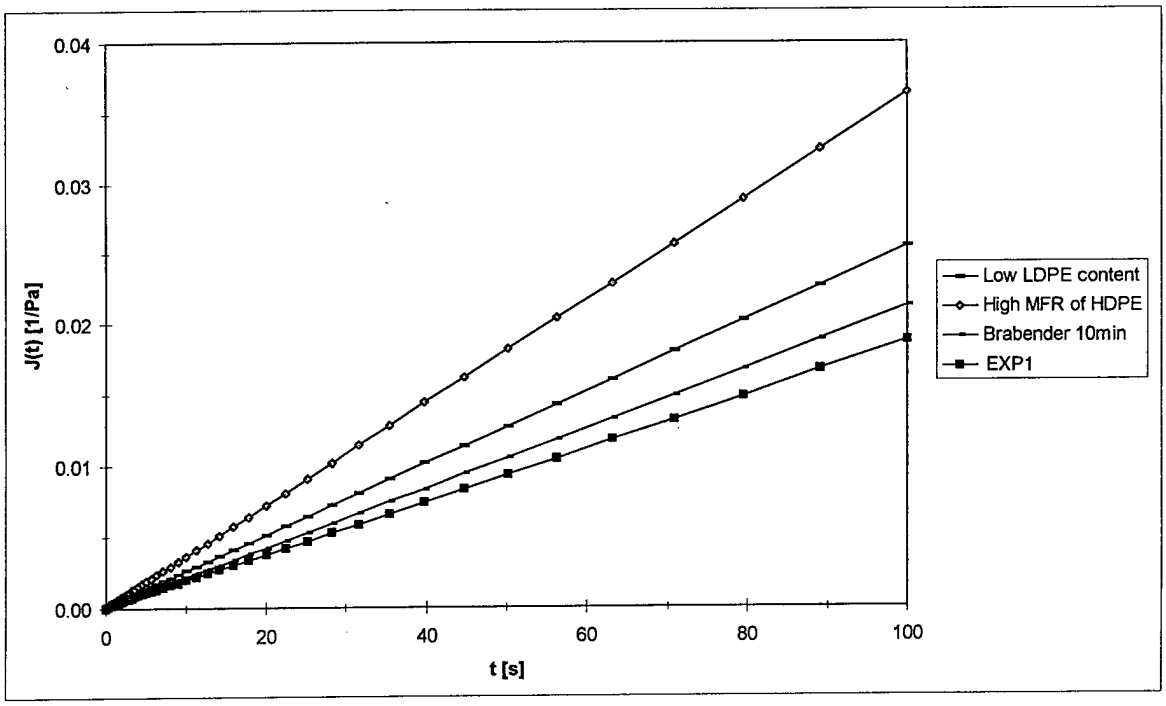

Figure 4: Influence of mixing ratio and MFR of the constituents on shear viscosity η.

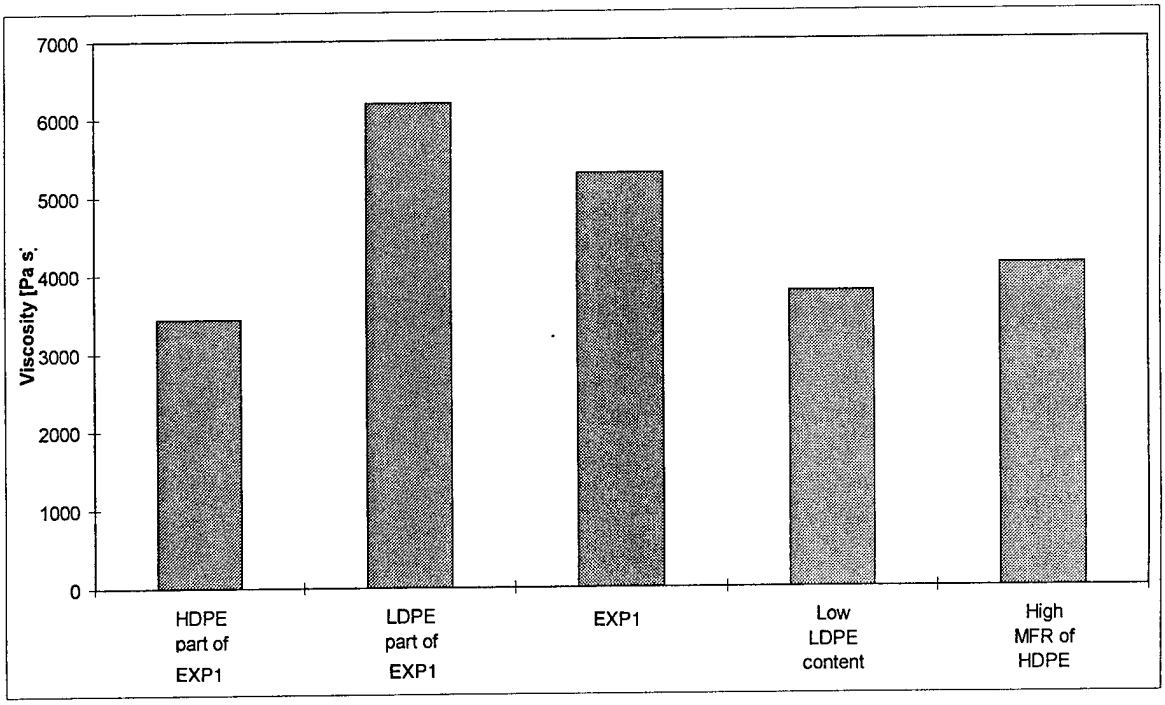

Figure 5: Influence of mixing conditions on melt strength vs. haul-off speed.

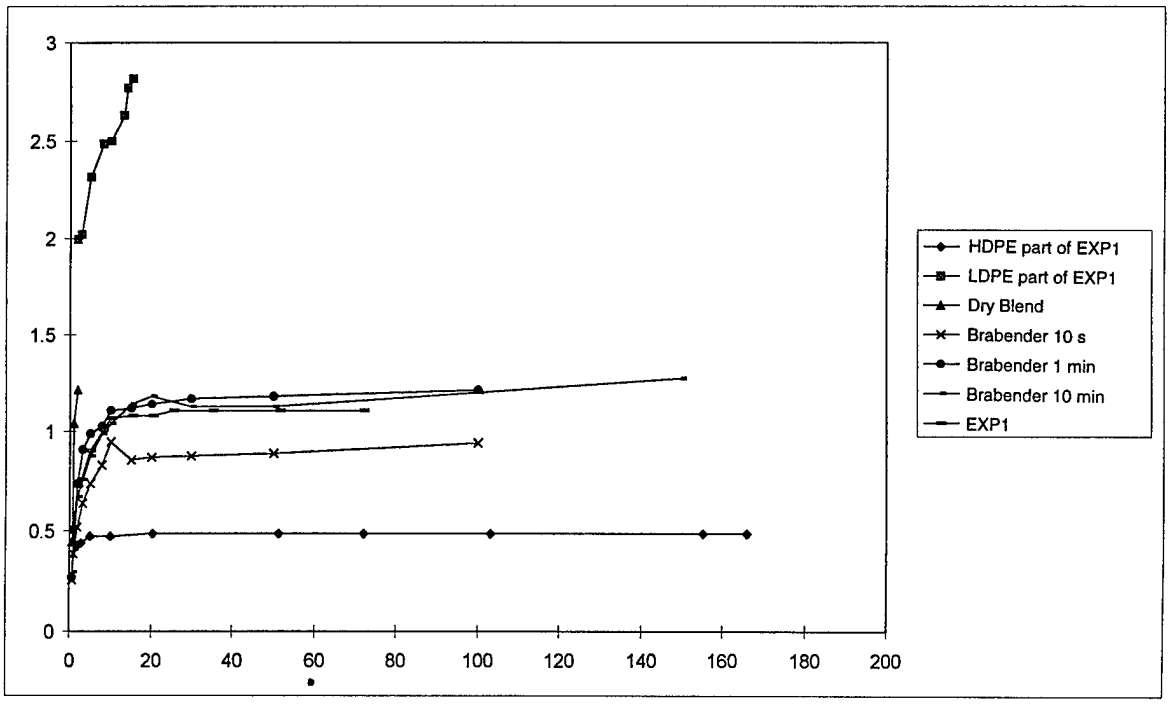

Figure 6: Influence of mixing conditions on the melt strength at a haul-off speed of 2 m/min

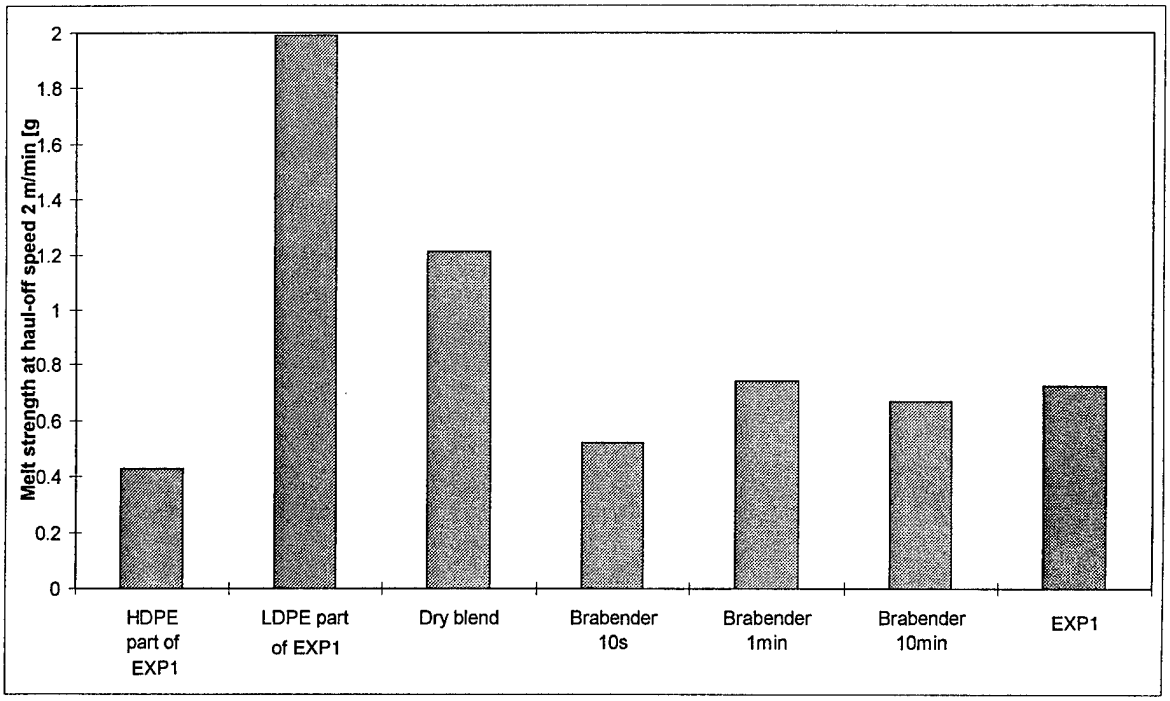

Figure 7: Influence of mixing ratio and MFR of the constituents on melt strength vs. haul-off speed.

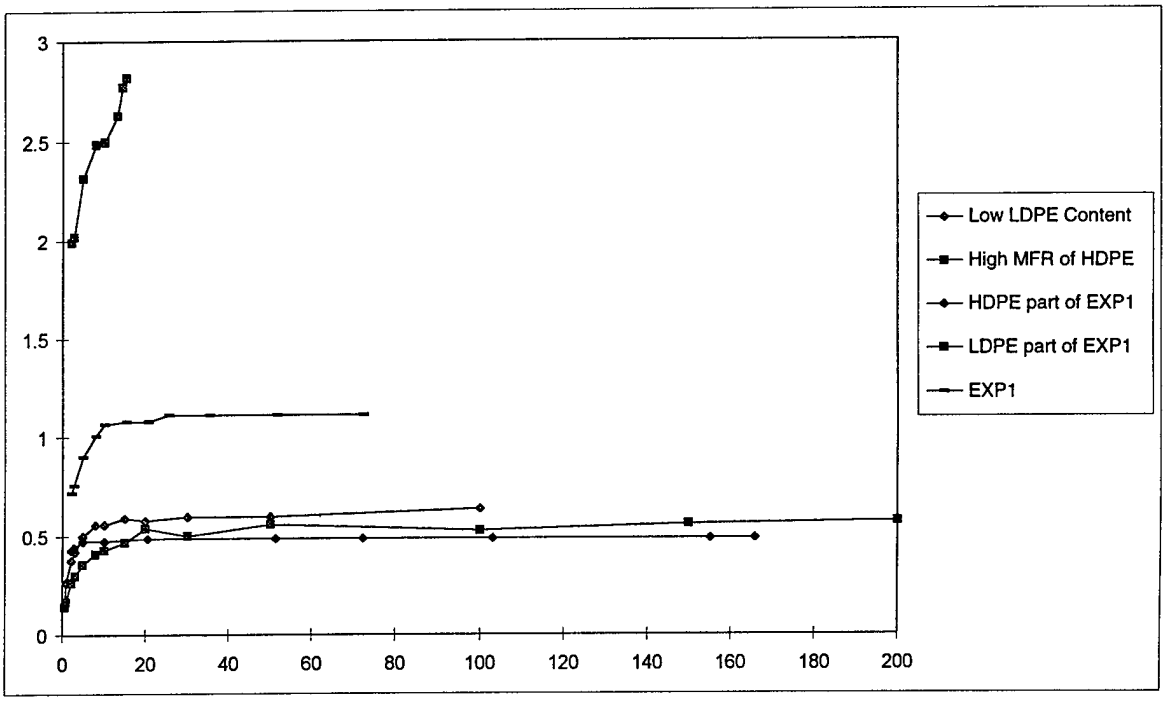

Figure 8: Influence of mixing ratio and MFR of the constituents on the melt strength at a haul-off speed of 2 m/min

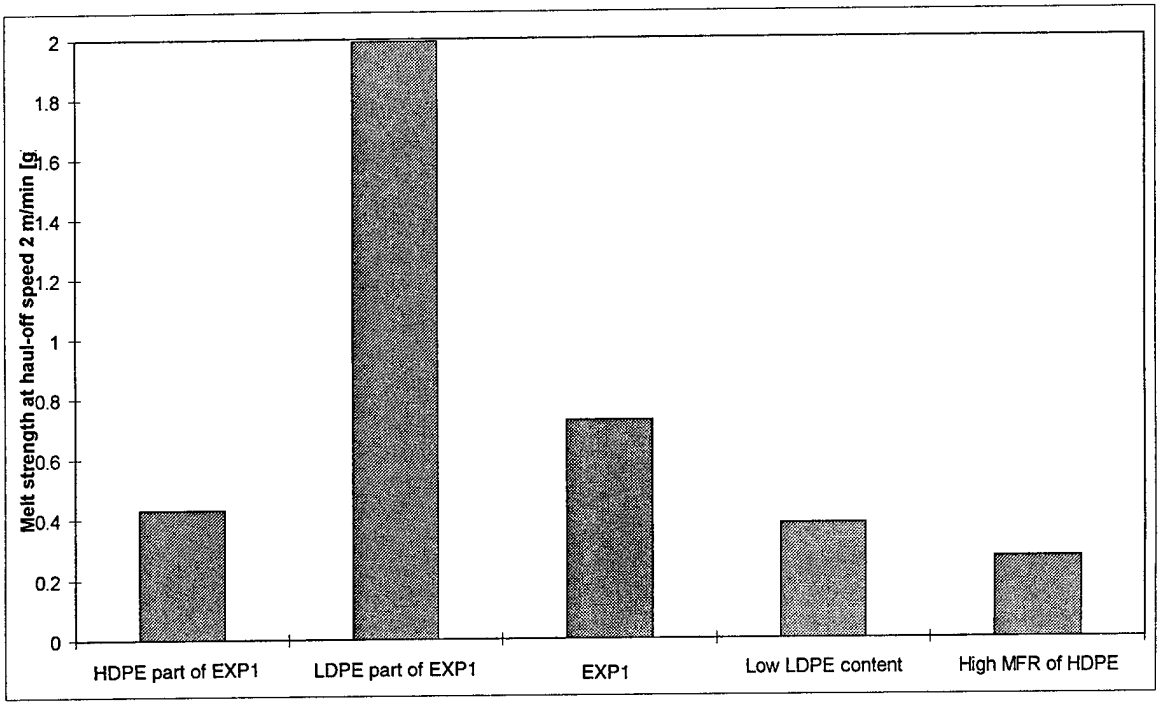

AUTHORS

Hans Eklind is a Senior Development Engineer at Borealis AB in Stenungsund, Sweden. After studying interphases in heterogeneous polymeric materials at Chalmers University of Technology, he earned his Ph. D. in Polymer Technology in 1996. He is currently working as a researcher and project manager in the area of flexible polyolefins with a special focus on materials for Wire and Cable.

Hans-Bertil Martinsson joined Borealis (formerly Unifos) in 1972 and has since 1988 been responsible for development of communication and jacketing grades for Wire and Cable.

Lars Westling is the Technical Center Manager of NOVA-BOREALIS Compounds LLC. He got his Master of Science in Chemical Engineering from Chalmers University of Technology in Gothenburg, Sweden in 1979. After a short stop over in the explosive industry which resulted in one patent, he has been working in the R&D organization of Borealis / Neste / Unifos. There he has worked with Molding, Film and Wire & Cable applications. Four years ago he left Europe for what is now NOVA-BOREALIS in the US.

Eric Brunner has been involved in Wire & Cable plastic materials first with DuPont Canada's SCLAIR® Linear Polyethylene Division and then through its acquisition by NOVA Chemicals of Calgary, Alberta. He has a Bachelors Degree in Applied Science (Mechanical Engineering) from the University of British Columbia at Vancouver, Canada and is currently on loan to NOVA-BOREALIS as a Senior Development and Technical Service Engineer specializing in Telecom applications requiring SCLAIR®, NOVAPOL®, Borealis, BORSTAR® and NOVA-BOREALIS resins and compounds.

Authors' addresses:
Borealis AB
444 86 Stenungsund, Sweden

NOVA-BOREALIS Compounds LLC
176 Thomas Road
Port Murray, NJ 07865

ANALYSIS OF THE PROCESSING OF FOAMED POLYETHYLENE FOR HIGH PERFORMANCE COAXIAL CABLE APPLICATIONS

Tong Chen[1], Rodney E. Ginger[2], James R. Leech[1], Sandra G. Maki[2]

Union Carbide Corporation
[1]Somerset, New Jersey, USA [2] Montreal, Quebec, Canada

ABSTRACT

Since their early use in the distribution of cable television, coaxial cable has developed into a vital component of today's networks, not just for television but for voice, Internet services, data and video. As wireless applications such as mobile telephony become more important, high performance coaxial cable used between the headend and the base station must provide increasingly reduced signal loss or attenuation as well as excellent physical integrity. The demand for these higher performance coaxial cables manifests itself in a need for improved quality dielectric foam. In this study, the processing of polyethylene foams is studied in an effort to explain differences in cell structure observed when physically expanded insulation of varying wall thickness are made with alternate nucleating agents. The insulation types compared are drop cable series 59 and 11 type, representing two extremes in dimensions for this specific cable design. A theoretical analysis is provided in an effort to explain these practical discoveries. For the system and processing conditions considered, the results show that under typical processing conditions, the cell size is not controlled solely by the heat transfer. Rather, the cell structure appears to be essentially determined by the nucleating agent material used.

INTRODUCTION

Coaxial cable is used in a wide variety of applications in today's rapidly changing telecommunications environment: e.g. conventional CATV cable, RF/microwave cable for mobile telephone communications, LAN cable, etc. The challenge to the cable manufacturer has been in achieving the demands for optimum physical integrity of the foam, while maintaining a consistent and uniform cell structure to ensure superior electrical performance i.e. structural return loss, impedance and capacitance uniformity.

Coaxial cable typically consists of two concentric conductors separated by a dielectric material. The signal attenuation α is a function of both the conductor and the dielectric materials used, as given in the following equation[1]:

$$\alpha = 0.002387 \frac{e^{0.5}}{\log \frac{D_o}{D_i}} \left[\frac{P_o^{0.5}}{D_o} + \frac{P_i^{0.5}}{D_i} \right] f^{0.5} + 1.506 \frac{f(df)e}{\log \frac{D_o}{D_i}} \quad (1)$$

where:
α = attenuation in db/100 feet
D_o = outside diameter of insulation in inches (inside diameter of outer conductor)
D_i = inside diameter of insulation in inches (outside diameter of inner conductor)
P_o = resistivity of outer conductor in micro-ohm-cm
P_i = resistivity of inner conductor in micro-ohm-cm
e = dielectric constant of insulation
f = frequency in megahertz
df = dissipation factor of insulation in radians

Therefore, the dielectric material chosen should have the lowest dissipation factor (df) and dielectric constant (e) possible. Polyethylene, with its excellent electrical properties (low df and e) and attractive value/performance is commonly used as the dielectric material. In order to further reduce the dielectric constant, the polyethylene is typically foamed either by

chemical or physical means. For high performance coaxial cable where high expansion levels are required, physically injecting an inert gas, such as nitrogen is the common means of producing foamed insulation. Figure 1 shows a schematic of the physical injection foaming process. There are five key phases:

- Polymer melting and mixing to achieve a uniform polymer melt
- Gas injection
- Polymer/gas mixing and heterogeneous nucleation for bubble formation
- Pressure release leading to bubble growth
- Cell stabilization and freezing of the insulation construction

These five phases each have important roles to play in ensuring optimized gas incorporation and cell structure. Further, the polymer and nucleating agent characteristics will greatly impact the expansion rate and cell structure achieved. A range of polyethylene compounds can be used ; however, blends of HDPE and LDPE are typically used to achieve a balance between foam structure toughness and cell structure quality. The nucleating agent also plays a critical role on the cell structure. Cell structure consistency can affect the stability of electrical properties such as impedance, SRL and capacitance.

Figure 1. Physical Gas Injection Line

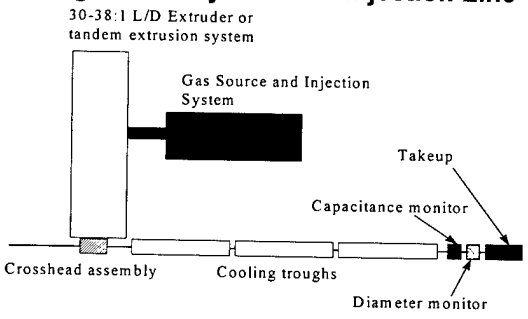

PROBLEM DEFINITION

It has been observed that the insulation wall thickness made affects the foam cell size and distribution. For optimized cable electrical performance, it is important that a uniform and consistent cell structure is achieved. In addition to the cell structure, the nucleating agent material used must offer a low dielectric constant and dissipation factor. Table 1 compares the electrical properties of masterbatches of the nucleating agent materials considered (10% concentration in LDPE).

Table 1. Comparison of Electrical Properties of 10% Nucleating Agent Concentration in LDPE

Nucleating Agent Particle Type	e at 1 MHz	df at 1 MHz
Azocarbonamide	2.36	0.0005
Organic nucleating agent	2.28	0.0001
Inorganic nucleating agent	2.34	0.00015

Azodicarbonamide is commonly used as a nucleating agent. However, for improved electrical performance, it is of interest to evaluate alternate nucleating agents.

Two foamed insulation constructions, a thinner wall RG59 (3.68 mm on 0.813 mm copper) and a thicker wall RG11(7.11 mm on 1.62 mm copper) type, were used to compare the cell structure produced. These represent two extremes in drop cable designs. Extrusion experiments were completed in an effort to understand the role of processing conditions on the observed cell structure and expansion rate for these two designs.

As mentioned, the specific nucleating agent characteristics have an important role to play in terms of the resulting cell structure. Hansen and Martin[2] studied the role of various nucleating agents on the cell structure and concluded that the reason azodicarbonamide was such an effective nucleating agent was that it produced heat which lead to a local viscosity decrease making bubble growth easier to achieve. The performance of the three nucleating agents in Table 1 were sought to be compared.

A more recent publication on the foaming of polyethylene sheet establishes that heat transfer is the primary parameter controlling the foaming process in thin sheeting[3]. The temperature decrease and hence the increase in polymer viscosity were found to control the

cell size achieved. It was expected that a change in processing conditions, which consequently changes the heat transfer rate, would affect the observed cell structure and expansion rate.

EXPERIMENTAL PLAN

In order to understand the parameters controlling the cell structure and expansion rate, the role of both nucleating agent materials and processing conditions was studied. Three nucleating agent types were considered:

- Chemical blowing agent (azodicarbonamide)
- Organic particle
- Inorganic particle

These nucleating agents had a similar average particle size but were quite different chemically. In addition, the particle shape was not exactly identical. Therefore, the nucleating agent material used was expected to affect the cell structure obtained.

Based upon previous research[2,3], heat transfer parameters were expected to have a significant influence on the observed cell structure. Cooling of the insulation increases the polymer viscosity and consequently is expected to inhibit cell growth. The three processing parameters that were chosen for the study were:

	Settings
• Air Gap:	0.15 and 1 m
• Water Temp:	25°C and 80°C
• Linespeed:	23 and 46 mpm

The output variables monitored were cell structure and % foam expansion:

$$\%\ Expansion = \left(1 - \frac{\rho_{FOAM}}{\rho_{SOLID}}\right) * 100\% \qquad (2)$$

A full factorial design was used to evaluate the effect of these parameters with the azo nucleating agent system. Two insulation constructions were made: RG59 (3.68 mm on 0.813 mm copper) and RG11 (7.11 mm on 1.62 mm copper) on a laboratory scale gas injection line using nitrogen. The formulations evaluated consisted of 70% HDPE/30% LDPE blend with 0.3% nucleating agent concentration (3% of a 10% concentrated masterbatch). A schematic of the line configuration used is shown in Figure 2. It is important to note that the water temperature was only controlled in the first water trough. The second trough used ambient air and the third cooling trough used 20°C water.

Figure 2. Schematic of Cooling Trough Setup for Extrusion Trials

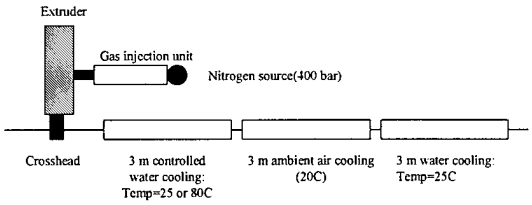

A melt temperature of 180°C was used throughout all the experiments. Further, the same insulation diameter and the same effective gas flow rate were targeted.

EXPERIMENTAL RESULTS

Figures 3-11 present the cell size analysis data for the RG59 and RG11 insulation. The foamed insulation density and, in turn, the foam expansion rate were also determined. For the azo based system, the foam expansions obtained were 71 ±3% and 65±4% for the RG11 and RG59 insulation respectively. A statistical analysis of the full factorial design data shows that the expansion rate is unaffected by process changes. This suggests that all of the gas added remains within the insulation and that likely, the primary cell growth phase is fairly short, i.e. completed within the air gap. This is what observed during actual extrusion where the insulation foams rapidly after exiting the die. Additional cell growth may actually be cell coalescence, resulting in essentially no further change in expansion rate.

Effect of Air Gap

Figure 3 shows the effect of changes in the air gap on the observed average cell size. The data obtained appears to show that the air gap has little effect on the resulting cell structure for the RG59 constructions. However, an air gap effect is noted for the RG11 insulation. This is likely because with the larger diameter RG11 insulation, there is less heat dissipation and the retained heat in the insulation results in lower

polymer viscosity, leading to continued cell "growth" or cell coalescence. As a result, the final cell size in the RG11 insulation is larger than in the RG59 case for the azo based system.

Figure 3

Effect of Air Gap on Cell Size (23 mpm, 80°C)

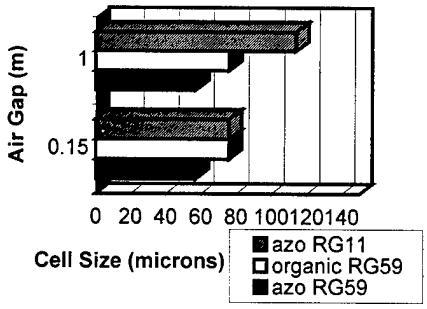

Effect of Water Temperature

Figure 4 shows the effect of cooling water temperature on the cell size. The results obtained were unexpected, since water temperature was anticipated to affect the cell structure. Note that this observation applies to

Figure 4

Effect of Water Temperature on Cell Size(23 mpm, 0.15 m)

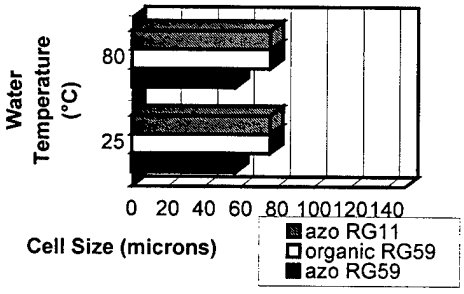

both the azo and organic nucleating agent materials. This observation seems to confirm that the majority of the cell growth occurs in the air gap.

Effect of Line speed

Figures 5 and 6 show the effect of line speed on cell size for the range of nucleating agents studied for RG59 and RG11 insulation, respectively.

In the case of the organic (RG59 and RG11) and inorganic (RG11 only) nucleating agents, line speed does appear to play a significant role on the cell structure. Specifically, as the line speed is increased, the cell size increases.

Figure 5

Effect of Linespeed on Cell Size for RG59 Air gap=1m, Water T=80°C

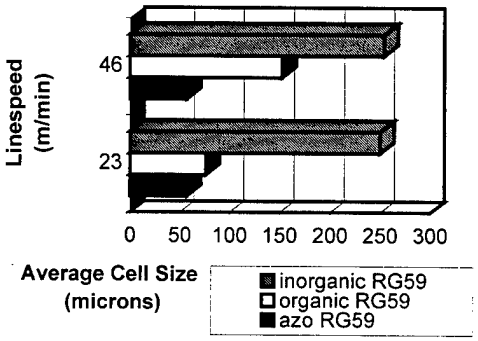

Figure 6

Effect of Linespeed on Cell Size for RG11 Insulation(1m, H20=80C)

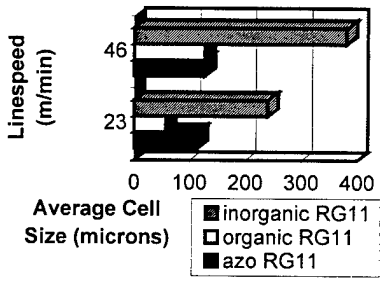

Photographs of certain insulation cross-sections are shown in Figures 7-11. A comparison of Figures 5 and 6 shows a wall thickness effect for the azo based blends. Cell size is almost twice as large in the RG11 insulation as in the RG59 insulation. As discussed, this may be related to the residual heat within the insulation which causes cells to continue growing or coalescing. This effect may be more pronounced with the azo based system because of its exothermic characteristics. In

the case of the organic nucleating agent, there appears to be an opposite effect i.e. cells are larger in the RG59 case.

It is evident from these comparisons that the key parameter controlling the cell size is the type of nucleating agent. The organic and azo based nucleating agents result in an acceptable cell structure while the inorganic nucleating agent does not. A possible explanation for this is there are lots of nuclei initiating bubbles but cell coalescence is greater. Another possibilility is that certain nucleating agents produces fewer active nuclei and consequently result in larger

Figure 7. Azodicarbonamide RG11 Effect of Air Gap (25°C water, 23 mpm)

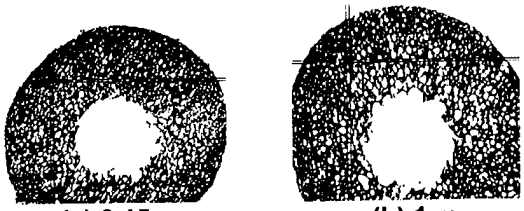

(a) 0.15 m (b) 1 m

Figure 8. Organic Nucleating Agent RG59 Effect of Line speed (1 m air gap, 80°C)

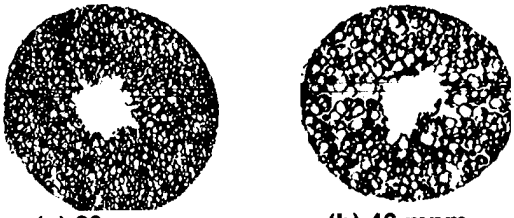

(a) 23 mpm (b) 46 mpm

Figure 9. Organic Nucleating Agent RG11 Effect of Line speed (1 m air gap, 80°C)

(a) 23 mpm (b) 46 mpm

Figure 10. Inorganic Nucleating Agent RG59 Effect of Line speed(1 m air gap, 80°C)

(a) 23 mpm (b) 46 mpm

Figure 11. Inorganic Nucleating Agent RG11 Effect of Line speed (1 m air gap, 80°C)

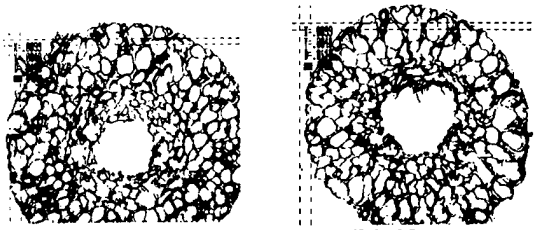

(a) 23 mpm (b) 46 mpm

cells. The tendency for cell coalescence may be greater with particle based nucleating agents, if they facilitate it by creating a weak spot between cells. This could explain why the azo nucleating agent, which does not have a particle after the exiting the die, results in mostly smaller cells. Furthermore, linespeed is a parameter that affects both the heat transfer as well as the shear and extensional deformation rates. It is plausible that higher line speeds increase the tendency for cell coalescence with particle nucleants, because of their increased motion in a higher deformation flow field.

HEAT TRANSFER ANALYSIS

The bubble growth is expected to be affected by the rapid cooling of the insulation, leading to an increase in the polymer viscosity. Heat transfer calculations are completed to explain experimental results. Assuming that one dimensional transient conduction is the predominant mode of heat transfer, a simplified analysis was completed to estimate the "thermal wave" boundary layer. For a semi-infinite body meeting certain boundary conditions, the temperature profile is given by[4]:

$$\frac{T(x,t)-T_s}{T_o-T_s} = erf\left(\frac{x}{2\sqrt{\alpha t}}\right) \qquad (3)$$

The boundary conditions that must apply are: (1) The surface temperature of the body suddenly changes from a value T_o to another temperature at time t, T_s i.e. $T(0,t)=T_s$ and that: (2) The temperature far from the surface remains the same, i.e. $T(\infty,t)=T_o$. For the water cooling, this equation was deemed to apply because of the short cooling times. The cooling in the air gap was estimated using analytical solutions for an infinite cylinder with heat transferred from the surface of the solid (insulation) by a fluid (air). In all of the calculations, the effect of the center conductor was neglected.

For this analysis, the thermal properties of the foam insulation were required. The thermal diffusivity for the foam is a function of the polymer and gas properties as well as the degree of foaming. The effective thermal conductivity is defined as[5]:

$$\lambda_{foam} = \lambda_{PE} + \lambda_{gas} + \lambda_{convection} + \lambda_{radiation} \qquad (4)$$

In our case, where the foam density is relatively low i.e. 0.3 g/cm^3, the convective thermal conductivity is negligible. λ_{PE} is defined as the product of the thermal conductivity of polyethylene and its volume fraction. Similarly, the thermal conductivity of the gas is the product of the thermal conductivity of nitrogen and its volume fraction. The radiative thermal conductivity is also assumed to be negligible at this range of foam densities (>0.1 g/cm^3). Using equation (4), the effective thermal conductivity of the polyethylene is calculated as approximately 0.10 W/m-K.

The thermal diffusivity, α, is defined as:

$$\alpha = \frac{\lambda}{\rho c_p} \qquad (5)$$

where λ is the effective thermal conductivity of the foam and ρ and c_p are the average density and heat capacity respectively. Using the parameters defined in Table 2, the thermal diffusivity for the foamed insulation is estimated as 1.7×10^{-7} m^2/s.

Table 2. Definition of Foam Thermal Properties

Parameter	Value
Thermal conductivity λ (W/m-K)	0.10
Average density ρ (kg/m^3)	300
Average heat capacity c_p (J/kg-K)	1800
Thermal diffusivity α (m^2/s)	1.7×10^{-7}

Using the calculated thermal diffusivity of the foam, the predicted insulation surface temperature after air cooling and the thermal "boundary layer" for the two constructions cooled in water can be calculated. The calculated heat transfer results obtained are shown in Table 3 (air gap) and Figures 12 and 13 (water cooling). Note that the key assumptions are expected to be valid because of the short cooling times. For all these calculations, the Fourier number was less than 1.

The results in Table 3 show that the air gap has little impact on the insulation cooling and therefore should not play a major role in the insulation cell structure. The centerline temperature is defined as the temperature in the center of the insulation i.e. r=0. Similar trends are observed for the temperature change at the midplane temperature (halfway between the insulation center and outer surface). In the thick wall case, the temperature does not change because of the high amount of retained heat in the insulation. This is what was observed in the extrusion trials where the air gap had an effect on the cell structure in the thick wall case.

Figures 12 and 13 show the predicted effect of water temperature on the midplane insulation thickness:

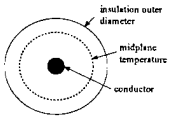

Calculations show that the predicted residence time for the insulation in the cooling trough is approximately 4 and 8 seconds for the two line speeds of interest. Despite this relatively short residence time, the polymer temperature at this midplane is observed to drop substantially in both the thin and thick wall insulation. All the calculated temperatures are below 150°C. At these temperatures, it is expected that the polymer viscosity reached will be high enough

Table 3. Effect of Air Gap on Insulation Temperature

Air Gap (m)	Linespeed (m/s)	Bi ($=h_c r/\lambda$)	Fo ($=\alpha t/r^2$)	Calculated Centerline Temp (°C)
	Thin wall insulation			
0.15	0.383	0.346	0.018	180
0.15	0.767	0.346	0.009	180
1.0	0.383	0.346	0.122	162
1.0	0.767	0.346	0.061	171
	Thick wall insulation			
0.15	0.383	0.44	0.0053	180
0.15	0.767	0.44	0.0026	180
1.0	0.383	0.44	0.035	180
1.0	0.767	0.44	0.0176	180
h_c = heat transfer coefficient, r=radius of insulation, t=time				

Figure 12

Calculated Change in Insulation Temperature (t/2) vs. Time Water Temperature=25°C

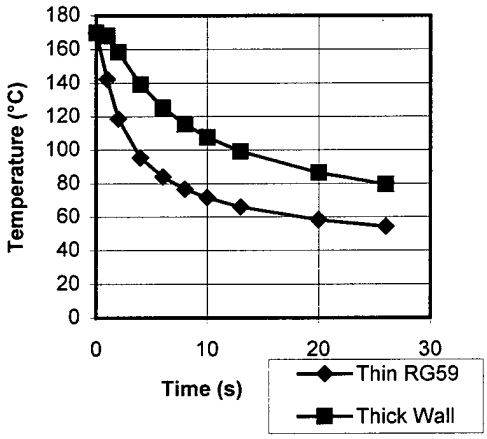

to greatly limit the cell growth or coalescence Therefore, the extrusion results obtained can be explained by the fact that the even with 80°C water, the polymer temperature drops so rapidly that cell growth cannot continue once the insulation enters the water. This appears to explain the lack of effect of the water temperature on the cell structure.

ANALYSIS OF CELL COALESCENCE

In the case of non-chemical blowing agent based nucleating agents, there is a significant effect of line speed changes on cell structure. The difference observed cannot be accounted

Figure 13

Calculated Change in Insulation Temperature (t/2) vs. Time Water Temperature=80°C

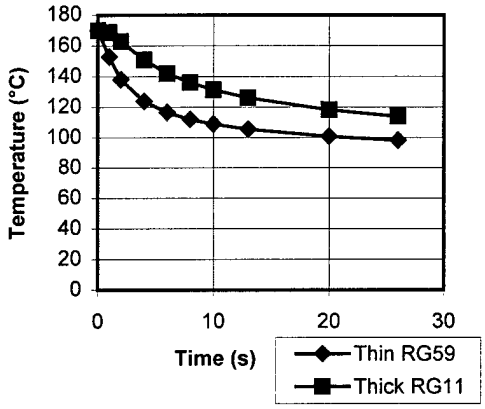

for by heat transfer alone. A possible theory relates to the effect of a combined change in the flow field due to line speed as well as an increase in the viscosity due to heat transfer. The change in the flow field may cause adjacent cells to interact and coalesce. A model to qualitatively assess this theory is proposed. The number of collisions between for by heat transfer alone. A possible theory relates to the effect of a combined change in the flow field due to line speed as well as an increase in the viscosity due to heat transfer. The change in the flow field may cause adjacent cells to interact and coalesce. A model to qualitatively assess this theory is proposed. The number of collisions between two spheres, N, per unit volume per unit time has been derived and is given by[7]:

$$N = \frac{16n^2r^3\gamma}{3} \qquad (6)$$

where γ is the rate of deformation, n is the number of spheres/cells per unit volume and r is the sphere/cell radius. These cell collisions will lead to a reduction in the number of bubbles, -dn/dt. For cells of uniform size:

$$n = \frac{3\phi}{4\pi r^3} \qquad (7)$$

where ϕ is the volume fraction of spheres. If a fraction of these collisions, β, result in cell coalescence, then the rate of change in the number concentration of particles, for constant ϕ, is:

$$-\frac{dn}{dt} = \frac{16\beta n^2 r^3 \gamma}{3} = -\frac{9\phi}{4\pi r^4}\frac{dr}{dt} \qquad (8)$$

Integration of this equation with initial conditions t=0, r=r_o gives:

$$\frac{r}{r_o} = \exp\left(\frac{4\beta\phi}{3\pi}\gamma t\right) \qquad (9)$$

This equation is proposed as a qualitative assessment of the cell coalescence phenomena. It shows that the final bubble size is controlled by the flow field (γ) as well as the time to freeze the polymer (t) to prevent further cell growth and coalescence. In addition, the efficiency of cell coalescence, β, will differ for various nucleating agents as was observed for the organic and inorganic nucleating agents.

ROLE ON NUCLEATING AGENT ON VISCOSITY

The data obtained show that the nucleating agent ultimately controls the observed cell structure. The cell size achieved is a function of the particle size, shape and surface characteristics of the nucleating agent. Another important parameter to consider is the effect of the nucleating agent on the shear viscosity. The shear viscosity of blends containing the azo and organic nucleating agents is compared. Figure 14 compares the shear viscosity characteristics of these two systems. These data were generated using an Instron capillary Rheometer (Model 4400, die=0.030, L/D=66.9). The results do not indicate any major differences between the alternate nucleating agent systems for test temperatures of 160 and 175°C. This suggests that alternate nucleating agents show comparable performance in terms of how they affect viscosity relative to azodicarbonamide based nucleants.

Figure 14

Apparent Shear Viscosity vs. Shear Rate for HDPE/LDPE Blends 70/30 with Different Nucleating Agents

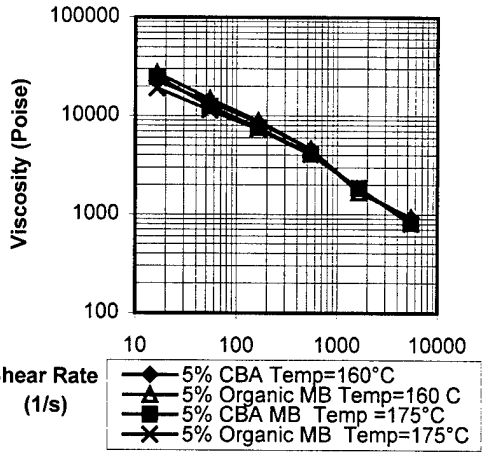

CONCLUSIONS

The results obtained show that the foaming of polyethylene is a complex process with the nucleating agent representing the primary factor controlling the formation and size of bubbles. Processing conditions play a lesser role in this regard. The choice of nucleating agent for coaxial cable applications is a question of balancing the electrical properties with the nucleation capabilities.

To summarize our key findings:

- Cell size is established in the air gap, since under typical processing conditions, the rate of water cooling is so great that the polymer viscosity rapidly increases, thereby preventing further cell growth/coalescence. It is proposed that the majority of the cell growth occurs very rapidly due to an observed lack of change in expansion rate with processing changes.
- In the case of thick wall insulation, the heat retained is much greater than in the thin wall case, leading to continued cell growth or coalescence. This was specifically observed for the azo based nucleating agent i.e. RG11 insulation results in larger cells than in the RG59 case. This is further compounded by the fact that this nucleating

agent is exothermic and locally increases the temperature at the cell site.

- A heat transfer analysis confirms that for the specific parameters studied, the cooling water causes a sudden drop in polymer temperature which prevents further cell growth/coalescence. The air cooling analysis predicts a larger cell size for the thicker insulation.
- For particle type nucleating agents, cell size is affected by the line speed. Line speed variations affect both the heat transfer rate and the strain rate. It is hypothesized that line speed increases cause the effective shear rate to increase and lead to cell coalescence. In the case of azodicarbonamide nucleating agents, which essentially do not leave "particles" after extrusion through the die due to exothermic decomposition, the line speed effect is minimized. Particles may increase the tendency for cell coalescence.

ACKNOWLEDGEMENTS

The authors wish to thank Dr. Martin Weber of McGill University for many useful discussions and guidance in the theoretical analysis. The diligent testing and extrusion work of Jean Guy Gagnon is greatly appreciated.

REFERENCES

1. L.S. Scarola, 46th Annual Convention of the Wire Association International, Chicago, Ill. October 6, 1976.
2. R.H. Hansen and W.M. Martin, I&EC Product Research & Development, vol 3., no.2 June 1964 pages 137-141.
3. S.T. Lee, N.S. Ramesh and G.A. Campbell, Polym.Eng. Sci, vol.36, no.19, October 1996 pages 2477-2482.
4. F. Kreith and W.Z. Black, Basic Heat Transfer, Harper & Row Publishers, 1980.
5. L.J. Gibson and M.F. Ashby, CELLULAR SOLIDS Structure and Properties, Pergamon Press
6. D. Klempner and K. Frisch, Polymeric Foams, Hanser Publishers, 1991.
7. R.F. Probstein, Physico-Chemical Hydrodynamics, 2nd. Ed. Ch. 8, Wiley Publishers, 1994.

Dr. Tong Chen
Union Carbide Corp.
1 Riverview Drive P.O. Box 450
Somerset, NJ 08875 USA
Tong Chen received his BS and M.Eng. in chemical engineering from Tianjin University and his Dr. of Science from MIT, also in chemical engineering, all with a polymer major. He has been with Union Carbide since 1991 working first in the Polymer Materials Science Skill Center and later in the Wire and Cable Skill Center as a research engineer. His current research effort focuses on new polymer material development for fiber optical cable applications.

Mr. James R. Leech
Union Carbide Corp.
1 Riverview Drive P.O. Box 450
Somerset, NJ 08875 USA
Since 1989, Jim Leech has been Technology Manager for Union Carbide's Telecommunications business. He has had almost 25 years in polymer research and development, the last 22 at Union Carbide. He holds an M.S. in Chemistry (University of Pittsburgh) and an M.B.A. in Chemical Marketing (Fairleigh Dickinson University). Jim was Chairman of the 1997 IWCS Symposium.

Mr. Rodney E. Ginger
10455 Metropolitan Blvd. East
Montreal East, Quebec
H1A 1B1 Canada
Rodney Ginger graduated from the University of Loughborough (UK) with a Master's degree in Polymer Science. He then worked for ICI (UK and Germany) where he was involved in polymer synthesis and process development. Subsequently, he was materials engineering material for BICC Cables (Canada). Since 1985, he has been the Wire & Cable Manager for Union Carbide Canada where he is involved in a range of research and development activities including power cable, telecommunications and flame retardant compound development.

Ms. Sandra Maki
10455 Metropolitan Blvd. East
Montreal East, Quebec
H1A 1B1 Canada
Sandra Maki received her B.Eng and M.Eng (Chemical) degrees from McGill University in Montreal (Canada) in 1986 and 1988 respectively. Upon graduation, she worked for DuPont Canada on the development of polyethylene films. Since 1989, she has been a Development Specialist for Union Carbide Canada working in the area of telecommunications cable. Her current research focuses on materials for coaxial cable.

A DECADE OF HTS MATERIAL ADVANCES

Paul C. W. Chu

Texas Center for Superconductivity and Department of Physics
University of Houston, Houston TX 77204-5932

High-temperature superconductivity (HSTy) is considered one of the most important discoveries in physics in decades. Over the last 12 years, more than 150 high-temperature superconducting (HTSg) compounds have been discovered with a record transition temperature (T_c) of 134 K at ambient and 164 K under high pressure. New and existing processing techniques have been developed and adapted to fabricate the materials in practical forms while retaining their superconducting properties. In the present talk, a brief review will be given about the material parameters that govern the behavior and performance of high-temperature superconductors (HTSrs), and the challenges that remain to turn HTSrs from materials of promise to materials of commerce.

Superconductivity was discovered in 1911 and has been one of the most studied physical properties of solids. The simultaneous occurrence of zero resistivity in and the ability to expel magnetic field from within a superconductor when cooled below its T_c have long fascinated scientists and technologists. Until the discovery of HTSy in 1986, superconductivity occurred mostly in intermetallic compounds and alloys with a highest T_c of 23 K. The phenomenon was explained rather satisfactorily within the framework of the Bardeen-Cooper-Schrieffer theory. The great technological promise of these low-temperature superconductors was not fully realized due to their low working temperature which requires aids of the rare, expensive, and difficult-to-handle liquid helium.

The situation suddenly changed in 1987 when superconductivity was discovered with a T_c = 93 K, above the boiling point of 77 K of plentiful and inexpensive liquid nitrogen. This made applications of superconductivity appear more practical than ever before. While the ensuing studies worldwide have produced unprecedented advancements in all areas of HTSy research from materials through science to applications, no comprehensive microscopic theory exists and commercialization of HTSy remains beyond our reach. This can be attributed to a large extent to material and related issues.

All known superconductors with a T_c above 30 K are cuprates which are physically intricate, chemically complex, and chemically unstable. They possess a layered structure consisting of many CuO_2-layers where supercurrent flows. To carry a large supercurrent, the CuO_2-layers have to be aligned. Some of these compounds exhibit graphite-like characteristics. The CuO_2-layers can be aligned by the so-called thermal mechanical deformation process for the fabrication of wires and cables. Unfortunately, the graphite-like behavior is a reflection of the weak coupling between the CuO_2-layers which results in weak flux-pinning and thus a reduced supercurrent carrying capability of these compounds at high temperatures and in high magnetic fields, *e.g.* $Bi_2Sr_2Ca_2Cu_3O_{10}$. Some cuprates do not have the graphite-like characteristics and show a large current carrying ability at high fields and temperatures, *e.g.* $YBa_2Cu_3O_7$. However, they have to be processed properly by the rather elaborated thin film techniques. They have also been shown to be very corrosive at their high processing temperatures and to degrade when exposed to humid air.

Improvements in existing materials and a broader material base would accelerate

progress in HTSy science and commercialization of the technology. For instance, a greater material base will enable us to test the generality of the proposed theoretical models; a higher T_c will reduce further the burden on our cryogenic technology for the operation of high-temperature devices, especially for large-current applications; a reduced anisotropy will enhance the interlayer coupling, improve the supercurrent carrying capability, and simplify the fabrication process; an improved chemical stability will enhance the life span of the devices; and simpler chemistry will make processing easier. Many of these will contribute to lowering the cost and improving the performance of high-temperature technology, two factors critical to the successful commercialization of any technology.

Biography

Paul C. W. Chu is the T. L. L. Temple Chair of Science, Professor of Physics, and Director of the Texas Center for Superconductivity at the University of Houston.

He received his B. S. degree from Cheng-Kung University in Taiwan, his M.S. degree from Fordham University in New York, and his Ph. D. degree from the University of California at San Diego.

In early January 1987, Chu's research group detected superconductivity at about -297°F, above the liquid nitrogen temperature (-321°F), in an impure and unstable sample. Two weeks later, he, his former student Mau-Kuen Wu, and their colleagues achieved stable superconductivity at -270°F. Later, in 1993, they again observed stable superconductivity under pressure at a new record-high temperature of -164°F.

Chu's research interests include superconductivity, magnetism, and dielectrics.

Chu has received numerous awards, including the National Medal of Science, the International Prize for New Materials, the Comstock Award, Texas Instruments' Founders' Prize, and the Bernd Matthias Prize. He is a member of the National Academy of Sciences; the American Academy of Arts and Sciences; the Chinese Academy of Sciences in Beijing, People's Republic of China; the Academia Sinica in Taipei, Taiwan, Republic of China; and the Third World Academy of Sciences. He has received honorary doctorates from a dozen universities.

THE STATUS OF SUPERCONDUCTING ELECTRIC POWER DEVELOPMENTS IN THE USA AND WORLDWIDE

James G. Daley and Christine E. Platt

U.S. Department of Energy, Washington, DC

ABSTRACT

Five years have passed since usable (100 meter) lengths of superconducting wire were made in 1993. Manufacture worldwide has since increased to several hundred kilometers per year.

The availability of superconducting wire, with 100 times the capacity of conventional wire, has spurred considerable interest in developing alternatives to a broad range of electrical equipment, including power cables, transformers, motors, generators, fault-current limiters and magnets. This new superconducting equipment would be half the size of conventional alternatives, and experience half the energy loss. Superconducting equipment will also have increased performance benefits, including reduced environmental impact, longer operating life, greater safety, and higher overload thresholds. Together, these new advantages could revolutionize electrical power as the use of fiber optics revolutionized electronic communications.

This paper examines the status of both superconducting wires and first-of-a-kind equipment development. Superconductivity is expected to play an important role in the electric power systems of the next century with initial adaptation beginning during the next ten years.

BACKGROUND

The electric power industry has experienced continuous innovation and improvement over the last hundred years, and the resulting electric grids found in major countries are the largest, most complex, and efficient "machines" ever made. Superconductivity will dramatically increase the capacity and efficiency of these highly developed systems.

Our building block for electric components is the copper or aluminum wires that transmit electricity, provide magnetic fields and create inductance. Superconductors carry current in a fundamentally different way from normal conductors. While normal conductors have a random electron flow, the flow of electrons in superconductors is very orderly. This ordered flow greatly increases the amount of current that can pass through a given cross-section of wire, and eliminates electrical resistance. Superconducting wires now being developed are expected to have 100 times the capacity of conventional wires.

This increased capacity makes possible electric power equipment that will be half the size of similarly powered conventional alternatives and will have half the energy losses. Superconducting electric system components such as generators, transformers, transmission cables and motors will have increased performance benefits, including reduced environmental impact, longer operating life, greater safety, and higher overload thresholds. They will increase existing substation capacity, and will be lighter and easier to site. Superconducting transmission cables have the potential to carry five times as much current as conventional cables with the same cross-section.

SUPERCONDUCTING WIRE PROGRESS

The wires now being developed are made from ceramic materials discovered ten years ago. These discoveries were rewarded by a Nobel prize in physics for the unforeseen "high" temperatures at which the superconducting state was achieved. Low-temperature

superconductors, which operate at much colder temperatures, were discovered in 1911, and are currently in use in the medical industry in magnetic resonance imaging (MRI) machines.

Top scientists around the world began to study the nature of these new materials, and found that these multi-component, granular ceramics were not well-suited for use in electrical wires. The new materials were even unlikely candidates for wire manufacturing when compared to conventional metallic conductors, or even the "intermetallic" niobium-titanium superconductors used in laboratory magnets since the 1960s.

Over the next ten years, painstaking worldwide research overcame the inherent obstacles to making wire out of these brittle superconductors. By 1993, long lengths of superconducting wires were available from several manufacturers around the world and engineers began prototype design. Ceramic superconductor wires are presently manufactured in a tape format that carries approximately 50 amperes. Figure 1 indicates the growth in U.S.-manufactured superconducting wire since 1990. Wire performance has continued to improved dramatically over the last five years, and is fast approaching the cost and performance characteristics desired for commercial application.

Powder-In-Tube (PIT) Wires

Until recently, most superconducting wire was manufactured by some variation on the powder-in-tube (PIT) method. The key elements of this method, shown in Figure 2, are the use of silver tubes that are initially packed with superconducting powder, and the processing steps that result in long lengths of flexible wires. Kilometer lengths are now routinely made, and are available from manufacturers in the U.S., Europe and Japan. Mature PIT wire is improving rapidly and has been used in the production of all pre-commercial prototypes of superconducting equipment. However, the PIT process also causes imperfections in the structure of the superconductor, which limits its current-carrying ability to a level far below its potential.

U.S. companies working closely with the Department of Energy to develop superconducting wire include American Superconductor Corporation, Intermagnetics General Corporation, and Oxford Superconductor Technology. Internationally, active manufacturers include Furukawa Electric Company, Nordic Superconductor, Siemens, and Sumitomo Electric Industries.

PIT Wire Status

Progress in wire development is measured by increases in the amount of electrical current that can be passed through a given cross-sectional area under specified conditions of temperature and magnetic field. This unit is the "current density," commonly expressed in terms of amperes per square centimeter. World record current densities are shown below, both for "shorts" (lengths of a few centimeters) and "longs" (lengths longer than 50 meters). For comparison, copper wires usually operate between 200 and 600 amperes per square centimeter.

Quoted Current Densities for PIT Multifilaments at 77 Kelvin and Self-Field * (Amperes per Square Centimeter)

Company	Filament Current Density in Short Lengths	Wire Current Density in Long Lengths (> 50 m)
American Superconductor	70,500	13,000
Furukawa	39,000	10,800
IGC	25,000	6,000
Nordic Superconductor	30,000	5,200

* Source: Presentation by G.N. Riley, USDOE Superconductivity Program Review, July 20-23, 1998, Washington DC

The difference between the filament current density values and overall wire current density values primarily reflects the fact that the superconductor occupies a relatively small percentage of the wire cross-section; silver occupies the majority. "Length effects" are still present in PIT wires in that the overall current density will be limited by the minimum value anywhere in a long wire length. A "weak spot" will adversely affect a measurement of current density. However, through improvements in process control, it is now possible to manufacture wire that is uniform over long lengths, and therefore less subject to length effects.

Several parallel lines of research are being followed to raise current densities within the superconducting filaments, and to reduce the manufacturing costs, especially by reducing the amount of silver needed.

Coated Conductors

Worldwide press coverage greeted the discovery of two entirely different wire manufacturing processes at the Department of Energy's Los Alamos and Oak Ridge National Laboratories in 1995 and 1996, respectively. Each laboratory developed a different approach to accomplishing the same result: preparing a flexible nickel template that, when coated with a superconductor, induces a near-perfect structure in the superconductor. The imperfections resulting from PIT processing are avoided and unprecedented amounts of current have been achieved.

These research breakthroughs take advantage of the high performance that is available through thin-film processing techniques. An additional benefit is that these approaches work with superconducting compounds that were not amenable to PIT processing, but which have intrinsically superior properties to the compounds now used in PIT processing. Since the Los Alamos and Oak Ridge announcements, researchers in other countries have greatly increased their activities on "coated conductors," and similar results are being obtained in Europe and Japan. A great deal of work needs to be done to develop practical manufacturing methods for preparing the underlying metal strip, as well as to develop suitable processes for applying the superconducting film coating.

One-meter lengths have begun to be made and continuous processing methods are being investigated. It appears possible to produce tapes that will transmit 1000 amperes at a reasonable manufacturing cost.

U.S. companies working closely with the Department of Energy to develop coated conductors include 3M, American Superconductor Corporation, Intermagnetics General Corporation, MicroCoating Technologies, Midwest Superconductivity and Oxford Superconductor Technology.

Coated Conductor Status

Current densities of one million amperes per square centimeter and greater are now regularly being measured in superconducting films on nickel substrates. The research is now focused on scaling up to longer lengths (1 m), and investigating low-cost industrial processes that can provide the same performance as the laboratory processes now being used. For example, pulsed- laser deposition is used now because it allows excellent control of processing conditions, but may not be economical for large-scale manufacturing. Electron-beam deposition is a commonly used industrial technique, yielding results equivalent to pulsed-laser deposition. Several other promising physical and chemical processes are being investigated.

A research roadmap developed by participants in the DOE program [*Research and Development Roadmap: Achieving Advanced Electrical Wires From Superconducting Coatings*, J.W. Muehlhauser, July 1997] calls for kilometer lengths of this new type of wire to be manufactured by the year 2002. Superconducting wire R&D in the U.S. often exceeds the aggressive schedule laid out in the roadmap: the poorest segments manufactured this year carry the same current as the best segments manufactured last year. Figure 3 shows the results of current density measurements in segments taken from a one-meter length.

THE SUPERCONDUCTIVITY PARTNERSHIP INITIATIVE

The Superconductivity Partnership Initiative (SPI) is the program's thrust toward early introduction and accelerated development of energy-saving electrical systems based on superconductivity. Vertically-integrated SPI teams include industry partners, national laboratories, and utility companies. This combination of perspectives and capabilities has led to outstanding materials performance, world-class competitive wire from program manufacturing partners, and systems designs which reflect the requirements of the ultimate consumer. While the average time from scientific discovery to prototype demonstrations based on that discovery is approximately 20 years, superconducting equipment prototypes are being built and tested just 10 years after the materials discovery. In 1996, three out of four of

the SPI projects exceeded output specifications by significant margins, and all set world performance records.

The SPI motor team, led by Reliance Electric Company (now Rockwell Automation), demonstrated a 200-hp prototype that tested at 60% higher power than originally specified. The demonstration was not limited by the superconducting technology, but reached the limits of the test apparatus itself. It was the first air-core synchronous motor with rotating superconducting field coils cooled by helium gas, and marks an important step toward developing ultra-efficient commercial superconducting motors.

Motors utilizing these rotor coils are expected to be half the weight and size of conventional motors and would provide greater operating efficiency. Since industrial electric motors consume most of the electricity used in a typical manufacturing operation, increased efficiency should yield significant savings in power costs. The cost premium of large superconducting motors, for example, would be reimbursed within two years by the cost of the energy saved, and the efficiency gains would exceed the total cost over the lifetime of the motor. Reliance worked with American Superconductor Corporation, Centerior Energy, Air Products & Chemicals, Sandia National Laboratories, and the Electric Power Research Institute on this project.

The SPI generator project, led by General Electric, concluded with the successful development and testing of the prototype racetrack superconducting rotor coil aimed specifically for superconducting generator application. The 34 A device was the world's largest racetrack coil. Almost 2 miles (2,400 meters) of superconducting wire were used for the coil, manufactured by team member Intermagnetics General Corporation. Other team members included Niagara Mohawk Power Corporation, and Argonne, Oak Ridge, and Los Alamos National Laboratories.

A fault-current limiter is designed to react to and absorb unanticipated power disturbances in the utility grid, preventing loss of power to consumers or damage to equipment. Lockheed Martin led the SPI team that tested a 2.4 kV fault-current limiter which reduced fault currents by 42% in the first cycle, in line with expected performance. This novel piece of equipment can be used for other valuable current-controlling functions. Southern California Edison, Intermagnetics General Corporation, and Los Alamos National Laboratory were partners in this effort.

Six new SPI teams are beginning new projects at the writing of this paper. A team led by ABB Inc.'s Power Transmission & Distribution Company will construct a 10 megavolt-amp, superconducting transformer. The transformer, a critical component in any electrical grid, would be installed at a utility in June 2001. Waukesha Electric Systems also expects to build and operate a 5 to 10 megavolt-amp prototype which will be installed on the Wisconsin Electric Power utility grid. This project is a follow-up to Waukesha's successful test of a 1 megavolt-amp transformer, which was also partially funded by the Department of Energy.

Superconducting transformers are expected to offer a number of improved features relative to conventional transformers as well as entirely new functionality with important utility systems benefits. In addition, superconducting transformers would replace the dielectric oil which surrounds the copper coils in today's power transformers with low-cost, environmentally-safe liquid nitrogen, which would eliminate the fire and spill risks associated with dielectric oil. This would allow indoor installation and other siting options that were previously too dangerous. The safer superconducting transformer is also expected to lower associated insurance costs and allow transformers to be installed closer to large load centers even within large cities. At half the size and weight of conventional transformers, superconducting transformers would increase existing substation capacity, and greatly relieve transportation challenges currently faced by electric utilities for conventional transformers.

Pirelli Cable Corporation will be demonstrating a three-phase, 120-meter cable system for continuous operation, including terminations and cryogenics. When completed, the cable system will be installed in an existing network of Detroit Edison. It was anticipated that Pirelli's previous SPI project would result in a 30-meter, 115 kV transmission cable that would carry 1200 amps; the flexible, 50-meter cable outperformed specifications by carrying 1800 amps. Pirelli will again be working with American Superconductor, Los Alamos National Laboratory, and the Electric

Power Research Institute.

In addition, the U.S.'s largest cable manufacturer, Southwire Company, will also develop, install, and test a 100-foot, three-phase, superconducting cable. This cable, and two others like it, will be used to supply power to two of Southwire's major wire plants and a large machine shop, by the end of 1999. These efforts include design of the cryogenic components and the cable terminations.

Underground power cables using superconducting wires have the potential to carry two to five times more power than cables of the same size made from copper wires, with half the losses. This would result in more efficient transmission, more effective use of existing rights-of-way, reduced environmental stress and cost-effective replacement of worn-out infrastructure with high-performance superconducting equipment. This is attractive to urban planners who need to retrofit aging infrastructures with increased power capacity, and to utility engineers nationwide who find it increasingly difficult to secure clearance for overhead transmission lines. At least two underground copper cables are required to replace one equally rated overhead transmission line, whereas a single superconducting cable could replace three conventional overhead lines of equal voltage. Moreover, the liquid nitrogen used to cool underground cables is less expensive and presents less environmental risk than the oil used to cool copper cables. It is expected that the first significant demonstration of utility networks utilizing superconductivity-based power transmission cables will occur in 2000.

The DuPont Company will build a superconducting reciprocating magnetic separator at one-quarter commercial scale. The technology is important to the chemical and materials industries, as well as having potential use in the separation of hazardous material. Boeing Phantom Works will develop a 10-kWh flywheel energy storage system for testing by Southern California Edison, based on existing superconducting bearing technology.

INTERNATIONAL COMPETITIVENESS

A recent report by the World Technology Evaluation Center of Loyola College assessed the relative competitiveness of the U.S. compared to Japan and Germany in the field of developing superconducting power and energy applications.[1] While it is now relatively routine to produce high-performance wire as long as 1 km, there are some striking differences between the relative standings of the U.S., Japan, and Germany.

In the United States, small start-up companies play a major role, and collaborations have been vital to the rapid progress that has occurred. Demonstration devices using superconductor technology are more widespread in the United States than in either Japan or Germany. The schedule for further scale-up is ambitious, but the actual implementation appears to depend strongly on a healthy federal- and utility-funded program. Assuming a continued commitment to coated conductors, WTEC anticipates that the U.S. program in YBCO tapes will lead both countries.

In the area of superconducting systems technology WTEC estimates that the United States is lagging Japan in generators, magnetic levitation, and fault-current limiters, and is lagging Europe (specifically, ABB Group) in transformers. It is believed that U.S. systems technology is level with Japan with respect to current leads, power cables, transformers, and flywheels, and is leading Japan and Germany with respect to motors and superconducting magnetic energy storage (SMES). The United States is also leading Germany in the area of power cables, current leads and fault-current limiters.

Superconducting Cable Projects (All Alternating Current)

Organization	Country	Comments
Furukawa/ Tepco	Japan	Testing 50 m, 66 kV, 1000 MVA cable
NKT	Denmark	10 m, 20 MVA cable
Pirelli Cable	United States	50 m, 115 kV, 400 MVA; full system testing end of 1998
Siemens	Germany	400 MVA, 100 kV; Design
Southwire Company	United States	30 m, 3-phase, 1250 A cable; testing tape and cryogenics
Sumitomo/ Tepco	Japan	Testing 50 m, 66 kV, 1000 MVA cable

Superconducting Transformers		
Organization	**Country**	**Comments**
ABB	Switzerland	3-phase/630 kVA; grid connected
Kyusha University/ Fuji Electric/ Sumitomo	Japan	3-phase/500 kVA
Waukesha Electric Systems	United States	

Superconducting Fault Current Limiters		
Organization	**Country**	**Comments**
ABB	Switzerland	1 MVA unit tested in power plant
Criepi	Japan	2.5 MVA unit tested
Lockheed Martin	United States	15 kV, 1200 A; assembly underway
Siemens/Hydro-Quebec	Germany/ Canada	100 kVA unit tested
Toshiba/Tepco	Japan	13.2 MVA LTS unit

Superconducting Generators		
Organization	**Country**	**Comments**
Super GM	Japan	70 MVA class LTS unit

CONCLUSIONS

Even though superconducting technology has made great strides in recent years, better performance and reduced costs are needed for superconducting wire technology to become widely commercially applicable. Another ten-fold decrease in the cost of superconducting wire and doubling of its performance during the next five years would strongly stimulate the availability of commercial devices. Within 10 years, superconducting wire is expected to be cost-effective for most applications.

With regard to electric power devices, it is imperative that resources remain focused on creating a robust, high-performance superconducting wire, and applying it to develop reliable and efficient equipment that addresses the needs of electric utilities and other customers. The electricity equipment in question is already highly efficient (usually over 90%) and the gain from superconductivity may only be a percentage point or two. It should be underscored, however, that over time this represents a great deal of energy and money because the equipment is typically very high-capacity and operates continuously. Widespread use of superconducting equipment could save as much as high as 7% of the U.S. electric bill, with associated savings of fossil fuels and reductions in greenhouse gas emissions.

The payoff of continued investment in superconducting technologies promises to be substantial. The International Superconductivity Industry Summit estimated the international market for superconducting electric power devices will grow to a value of $32 billion by 2020. The entire superconductor market, which includes applications for transportation, medicine, electronics and scientific research, was recently projected to be $122 billion by 2020.

ACKNOWLEDGMENTS

The authors would like to thank Joseph Badin and Audrey Lamanna of Energetics, Incorporated for their assistance in preparing this paper.

REFERENCES

[1] *Power Applications of Superconductivity in Japan and Germany*, WTEC, September 1997.

AUTHOR INFORMATION

Dr. James G. Daley holds a Ph.D. in Mechanical Engineering from the University of Connecticut. He is the Senior Manager of the Department of Energy's Superconductivity Program for Electric Power which he helped initiated in 1989. Prior to joining DOE, Dr. Daley was on the staff of Argonne National Laboratory where he worked on several advanced energy conversion projects as well as nuclear reactor component design. Previous employment included positions at General Electric's Transportation System Division and United Technology's Pratt and Whitney Aircraft Division. He has authored over 30 technical papers.

Dr. Christine Platt earned her Ph.D. in low-temperature physics from the University of Washington. She is the Manager of the Superconductivity Partnership Initiative, supervising the DOE's industrial partnerships to accelerate the development of superconducting electric power equipment. Prior to joining DOE, Dr. Platt served as Assistant Director for Corporate Programs and Principal Investigator at the Science and Technology Center for Superconductivity (STSC), where she helped build a number of collaborations between industry and STCS faculty. She holds the patent on lanthanum aluminate oxide as a substrate for thin-film superconductors, and has published primarily on the topic of high-temperature superconductors.

Both authors can be contacted at:

United States Department of Energy
1000 Independence Avenue, S.W.
EE-12
Washington, DC 20585

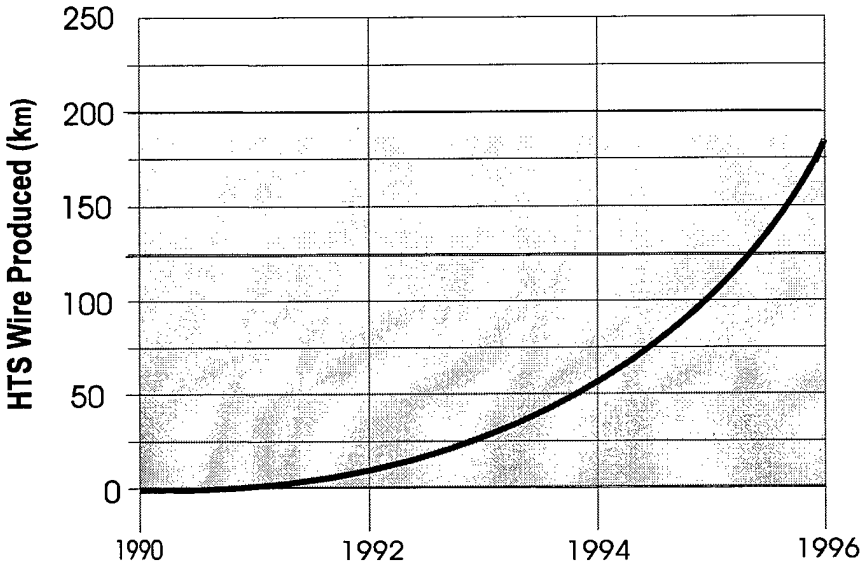

Growth in U.S.-manufactured superconducting wires since 1990. Worldwide production is 2 to 3 times greater.

Figure 1

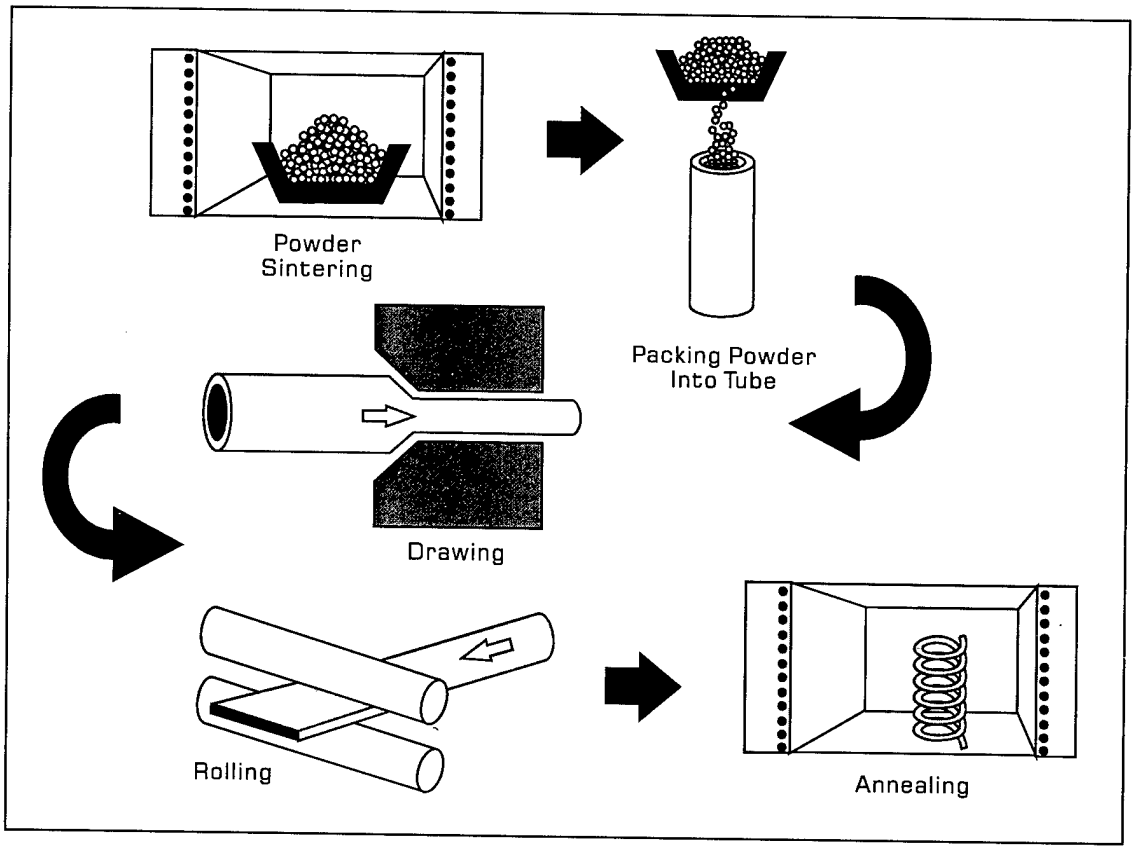

Figure 2 **OPIT Processing**

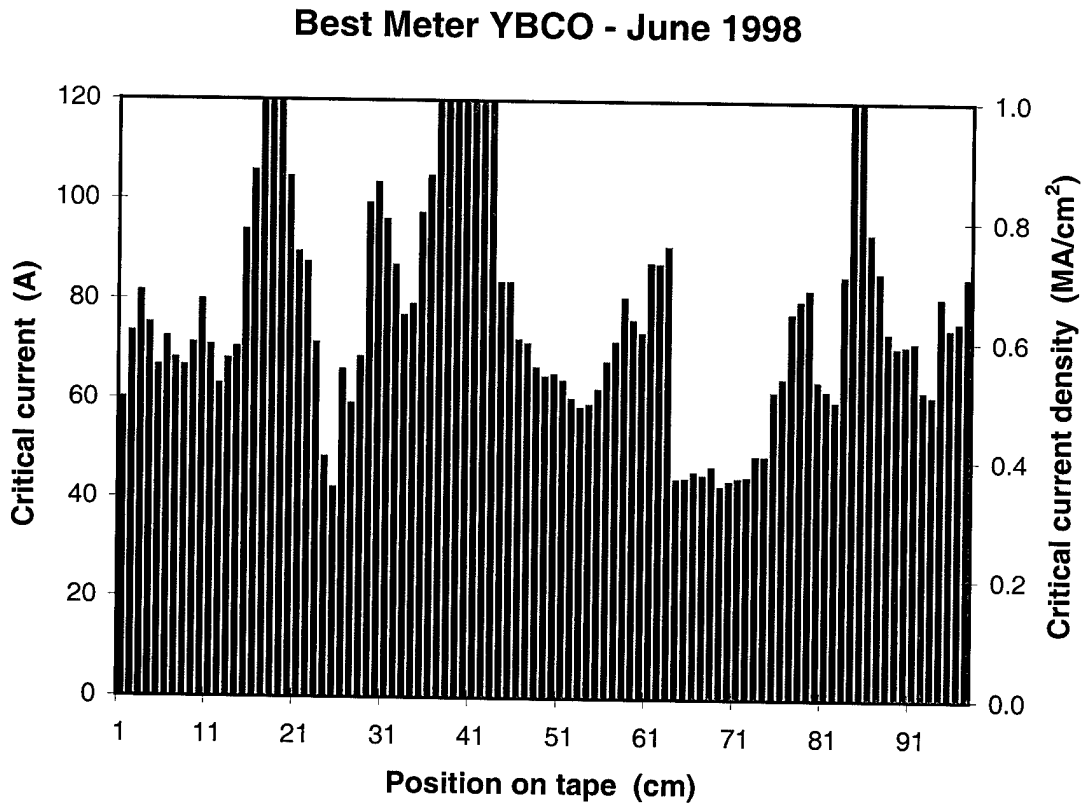

Figure 3 **IBAD Process, Los Alamos Superconductivity Technology Center**

THE HTS WIRE TECHNOLOGY: PRESENT AND FUTURE

Ken-ichi Sato

Basic High-Technology Laboratories, Sumitomo Electric Industries, Ltd., Osaka, Japan

ABSTRACT

Long and high current carrying High Temperature Superconducting (HTS) wires have been developed using bismuth-compound through powder-in-tube processing technology. Two breakthroughs, i.e. multifilamentary technique and thermomechanical processing, could make it possible. Towards actual application of HTS wires, many prototypes were developed. Typical application prototypes achieved to date are as follows: (1)7-Tesla magnet, (2)66kV power transmission cable system, (3)800kVA transformer, (4)100 Joule SMES coil, (5)current leads up to 14,500A. Among these prototypes, 2,000 A current leads and 7-Tesla magnet have been put for daily operation at present. Recent efforts are carried to develop specific wires for specific application such as high strength & high amperage conductor for large magnets and low-loss conductor for power application.

The other ongoing challenges are to develop the next generation HTS wires using Yttrium-based compounds. These includes a variety of processing technology development, i.e. PVD, CVD and LPE.

INTRODUCTION

In 1986, Bednortz and Muller discovered La-Ba-Cu-O compound having a higher critical temperature (Tc~30K) than those of any other superconducting materials so far reported.[1] After this discovery, Y-Ba-Cu-O (YBCO), Bi-Sr-Ca-Cu-O (BSCCO) and Tl-Ba-Ca-Cu-O (TBCCO) were discovered in 1987-1988.[2-4] The critical temperature (Tc) of these compounds are 90K, 110K and 125K. In 1993, Hg-Ba-Ca-Cu-O (HBCCO) was discovered and found to have a critical temperature of 135K, which is the highest Tc at present.[5] Because these compounds could show superconductivity at higher temperature than a boiling temperature of liquid nitrogen at atmosphere pressure (77.3K), there was a strong expectation to operate superconducting apparatus using liquid nitrogen as a coolant instead of liquid helium (4.2K) being used for cooling metallic superconductors. Liquid helium is expensive, easy to evaporate and hard to handle. Liquid nitrogen is cheap, hard to evaporate and easy to handle.

OVERVIEW OF HTS WIRE DEVELOPMENT

A great deal of efforts have been made to realize superconducting apparatus after the discovery of HTS materials. The key issue is a long HTS wire with high critical current density (Jc). Using BSCCO and powder-in-tube technique (PIT), 1,000m-long and high-Jc wires have been achieved.[6-8] A lot of demonstrators have been built and evaluated. Magnets and current leads were already implemented to equipment.

Table 1. Overview of HTS wire development.

Name	Material	Tc (K)	Present Status
YBCO	$Y_1Ba_2Cu_3O_x$	90	· Thin & Thick Film Processing Technique · 1m Long Wires · A Few Demonstrators
BSCCO (2223)	$(Bi,Pb)_2Sr_2Ca_2Cu_3O_x$	110	· Multifilamentary Configuration & Thermomechanical Processing Technique · 1,000m Long Wire · Implementation of Current Leads & Magnets · Lots of Demonstrators: Power Transmission Cables, Transformer, SMES Coil, & Fault Current Limiter
BSCCO (2212)	$Bi_2Sr_2Ca_1Cu_2O_x$	80	· Multifilamentary Configuration & Melt Processing Technique · Special Targeted Application at 4.2K
TBCCO	$Tl_2Ba_2Ca_2Cu_3O_x$ $Tl_1Ba_2Ca_2Cu_3O_x$	125 120	· Thin & Thick Film Processing Technique · Performance Needs to be Improved
HBCCO	$Hg_2Ba_2Ca_2Cu_3O_x$	135	· Thick Film Processing Technique · Under Research

Using YBCO and related compounds such as Nd-Ba-Cu-O and Sm-Ba-Cu-O, and film technique, so-called coated conductors are now being under development. YBCO is expected to have higher current carrying property under magnetic fields at 77.3K than BSCCO. A length of wire is limited up to 1m at present, and a few demonstrators were built. For TBCCO and HBCCO compounds, wire development stage is preliminary and needs further efforts. Table 1 summarizes an overview of HTS wire development status.

All these compounds are cuprate and brittle, and have two dimensional as electrical and magnetic properties. It is necessary to make flexible wire for application and to align crystals for obtaining high current carrying property.

BSCCO WIRE

Thermomechanical Processing

It was found that BSCCO crystals could be aligned by thermoplastic deformation technique, i.e. rolling and/or pressing, because BSCCO crystals were easy to cleave between their double Bi-O layers. Also, it was found that powder-in-tube technique could make it possible to obtain long length wires. Moreover, duplicating heat treatment and rolling process gave well-aligned and dense BSCCO microstructure, and, as a result, high current carrying properties.[9]

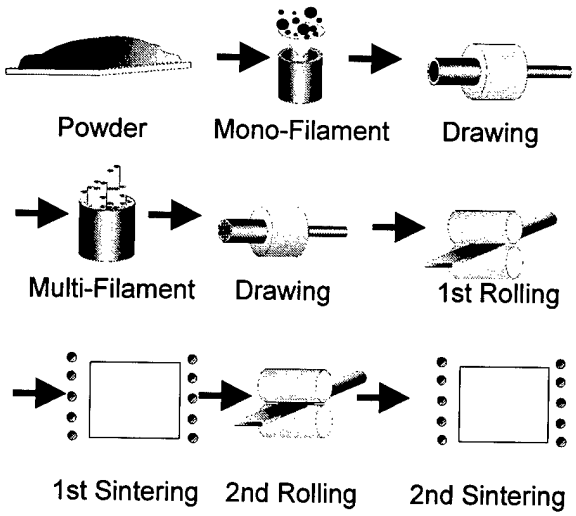

Fig. 1. Schematic procedure of thermomechanical processing technique of BSCCO wire.

Figure 1 shows a thermomechanical processing technique of BSCCO wires. The first rolling process is to align precursor powder, and the first sintering is to transform precursor to 2223 phase. The second rolling process is to align and make dense 2223 phase. The final step is the second sintering to bond 2223 phase strongly. This technique made it possible to obtain high current carrying wires. Figure 2 shows microstructures for (a) low current carrying wire and (b) high current carrying wire made by this technique.

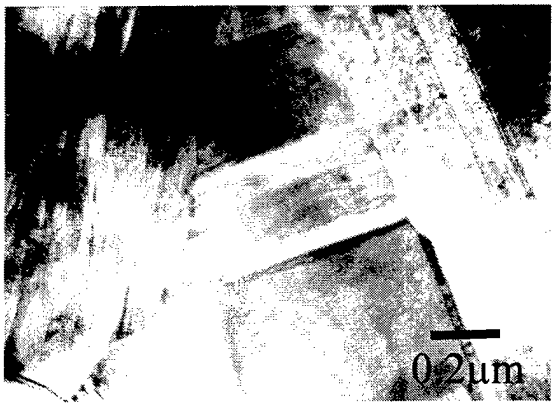

Fig. 2(a). TEM photograph of low current carrying wire. (Jc(77.3K)=5,000A/cm^2)

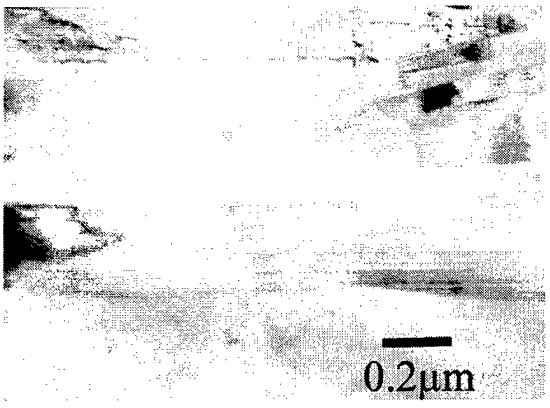

Fig. 2(b). TEM photograph of high current carrying wire. (Jc(77.3K)=54,000A/cm^2)

It is clearly shown in Fig. 2 that the high current carrying wire have well-aligned microstructure.

Multifilamentary Configuration

It is necessary to obtain flexible wires not only to apply these wires to magnets and cables, but also to fabricate long length wires. We needs to wind these wires to reel or spool in processing procedure. In this meaning, flexibility was crucial for a realization of HTS wires. Figure 3 shows a cross-sectional view of a mono- and a multifilamentary wire. Figure 4 shows bending properties of a mono- and multi-filamentary wire. The multifilamentary wire can tolerate against multiple bending procedure.

Fig. 3(a). Cross-sectional view of mono-filamentary wire.

Fig. 3(b). Cross-sectional view of multifilamentary wire.

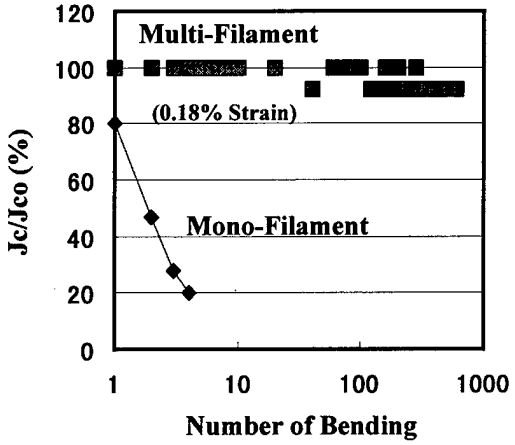

Fig. 4. Bending properties of mono- and multi-filamentary wire.

Table 2. Present status of BSCCO wire application.

Items	Present Status	Features
Current Leads[10-13]	·500A for 400kJ/SMES ·600A for MAGLEV ·2,000A for Synchrotron ·14,500A for ITER	·Implemented in 1993 ·Good against vibration ·Implemented in 1993 ·Reduce 70% power
Transformer[14]	·800kVA	·Non-flammable
SMES[15]	·100J Coil (77K) & 1kJ(35K)	·2Hz operation
Magnets[16-18]	·3T with 40mm RT bore ·4T with 50mm RT bore ·7T with 50mm RT bore ·0.19T with 280mm RT bore	·Fast cyclic operation ·4T in 10 seconds ·7T in 1 minute, and implemented in 1997 ·Active levitation, and implemented in 1997
Cables[19-22]	·7m & 1kA 3-Phase Cable ·50m & 3kA Conductor ·50m Model ·30m, 66kV & 1kA Cable	·Magnetic shielding ·Machine stranding ·66kV voltage evaluation ·Liq. N2 cooling system

Using this thermomechanical processing technology, flexible and long BSCCO wires over 1,000m length are now available. Figure 5 shows an example of long BSCCO wire.

Fig. 5. Outlook of long BSCCO wire.

APPLICATION OF BSCCO WIRE

Table 2 shows a present status of products and demonstration prototypes using BSCCO wires.

Present Product

Current leads and magnets are present products, which were already implemented to daily operated equipment. Current leads are used to transport current from power supply at room temperature to metallic superconducting coils in liquid helium, and to reduce liquid helium consumption because of no joule heating. Consumption of liquid helium can be reduced down to 1/3-1/4 of that of usual copper current leads.

Magnets are operated at around 20K, because BSCCO wires have high current carrying capability as same level as metallic superconductors such as Nb-Ti and Nb_3Sn. The other merit of operating at 20K is a high heat capacity leading higher stability than 4.2K operation. Superconducting magnets made of Nb-Ti and Nb_3Sn, are easy to lose superconducting state when a small heat

disturbance generated in coils due to mechanical movement of wires and ac losses. When magnets are energized, ac losses are generated due to magnetic field change. BSCCO wires have 100 times larger heat capacity at 20K than that of Nb-Ti at 4.2K. BSCCO magnets can be operated more stable and energized with higher ramp rate than metallic superconducting magnets. These features are the superior properties of BSCCO magnets. Figure 6 shows a example of BSCCO magnet, which could be generate 7 Tesla in one minute.

It is expected that stable operation and high ramp rate magnets will be strong tool for industrial application of magnetic field, such as magnetic separation of minerals, chemical reaction, single crystal pulling and continuous casting.

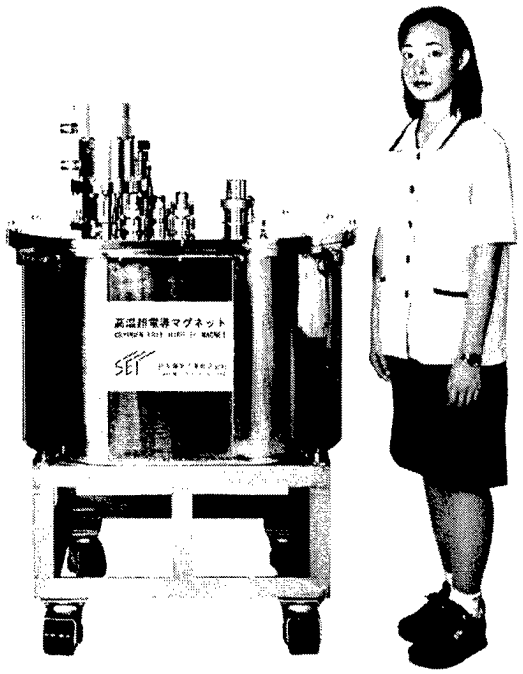

Fig. 6. Outlook of 7 Tesla BSCCO magnet, now daily operation for chemical reaction research.

Demonstration Prototypes

Among a number of proposed application of BSCCO wires, power apparatus is most expected one. Especially in Japan, power transmission cables are expected to be installed in metropolitan area for future power network. In metropolitan area, underground cables are usually used for transmission lines. Even at present, underground is already crowded with subways, communication cables, water pipes and gas lines, and it will be technically and economically difficult to dig new tunnels for future power transmission lines. Power cables with BSCCO wires will be compact enough to install in a small diameter ducts, i.e. 150mm diameter, to transport large electric power capacity of 500-1,000MVA with low voltage of 66kV.

Figure 7 shows a world first demonstration prototype of BSCCO cable with termination and liquid nitrogen forced flow cooling system. Its length was 30m and 1,000Arms loading test with 66kV was satisfactory performed. 60 pieces of BSCCO wires were wound on a 19mm diameter former in a shape of multilayer (4 layer) conductor by a dedicated stranding machine. The conductor after stranding experienced multiple bending procedure during building power cable, transportation and installation.

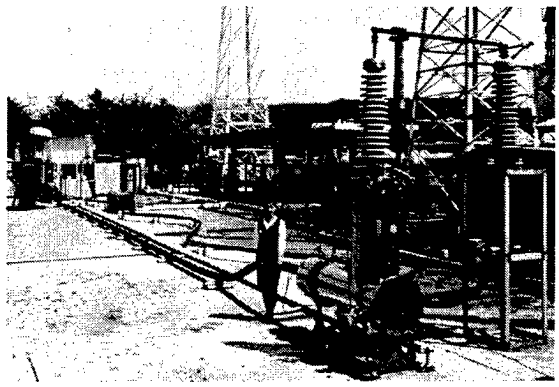

Fig. 7. Outlook of 30m BSCCO cable.

Table 3. Future issues and direction.

Material	Technical Issues	Direction
BSCCO	· High Strength for Large Magnet	· Ag Alloy Sheathing Technique
	· High Amperage for Large Magnet	· Large Sized & Flexible Conductor
	· Low AC Loss for Power Cables	· Transposed Conductor by Strands, Impedance Matched Multilayer Conductor
	· Low Ac Loss for Winding	· Decoupling of Filaments, Twisting
	· Higher Jc	· Superconducting Phase Homogeneity, Better Alignment, Improved Intergrain Connectivity
	· Pinning Site Creation	· Introduction of nm-scale Defects
YBCO	· Long Length Fabrication	· Verification of ~100m Length Wire
	· Reasonable Production Rate	· Development of Industrial Fabrication Method
	· Application Oriented Evaluation	· Prototype Making

FUTURE ISSUES AND DIRECTION

Table 3 shows a summary of future issues and direction of HTS wire development.

BSCCO Wire

Recent efforts are carried to develop specific wires for specific application. These efforts include high strength conductor and high amperage conductor for large magnets, and low ac loss conductor for power cables and windings. Further improvement for current carrying capability needs four major directions, i.e. (1) superconducting phase homogeneity, (2) better alignment of crystals, (3) improvement of intergrain connectivity and (4) introduction of pinning sites.

YBCO Wire

The other ongoing challenges are to develop the next generation HTS wires using Yttrium-based compounds. These includes a variety of processing technology development, i.e. PVD, CVD and LPE. Table 4 summarizes present results. YBCO material should be prepared to be single crystalline film to obtain high current carrying property. At present, only short length wires are demonstrated.

Table 4. YBCO wire results.

Process	Length (m)	Substrate	YBCO Deposition
ISD[23,24]	~m	Ni-alloy	PLD
IBAD[25]	~m	Ni-alloy	PLD, EB, CVD
Rabits[26]	~m	Ni, Ni-alloy	PLD, EB, CVD
LPE[27]	~cm	Ceramics	LPE

All these processes are challenged to obtain better crystalline structure of YBCO films. IBAD needs Ar-ion bombardment to get in-plane aligned buffer layer, such as YSZ to prevent inter-diffusion of nickel to YBCO and to get single crystalline YBCO structure. ISD (Inclined Substrate Deposition) is to incline substrate against plasma plume to obtain naturally forced in-plane deposition of YSZ buffer layer. Rabits is the process to obtain single crystalline substrate of nickel and nickel alloy, using thermomechanical treatment, i.e. rolling and heat treatment combination. LPE is liquid phase epitaxy process, and issues are a selection of substrate and high temperature processing because of melt technique. Future issues are (1) verification of long length wire possibility, (2) reasonable production rate processing technology development and (3) application oriented evaluation.

Diagnostic Issues

HTS wires needs precise material preparation of atomic scale and crystal alignment over 1,000m length. Superconducting property of 1,000m long wire is decided on a worst portion even if cm-order of defect. Two examples of diagnostic measurement are explained.

Figure 8 shows a result of overall length evaluation of critical current measurement for 1,000m long BSCCO wire, using usual four-probe method. Thus, superconducting property can be guaranteed.

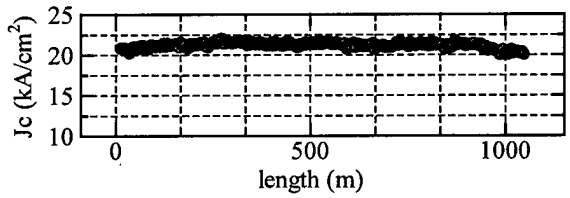

Fig. 8. Critical current measurement result over 1,000m long BSCCO wire.

The other example is an in-line monitoring of plasma plume when depositing YBCO thin film by a pulsed laser deposition.

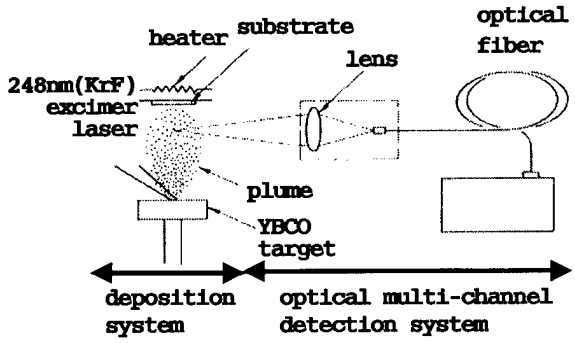

Fig. 9. Optical multi-channel diagnostic system of plasma plume of pulsed laser deposition.

With this system shown in Fig.9, a continuous control of deposition quality can be done, maintaining a number of YO and MgO ions at a fixed amount. Figure 10 shows an example of monitoring result.

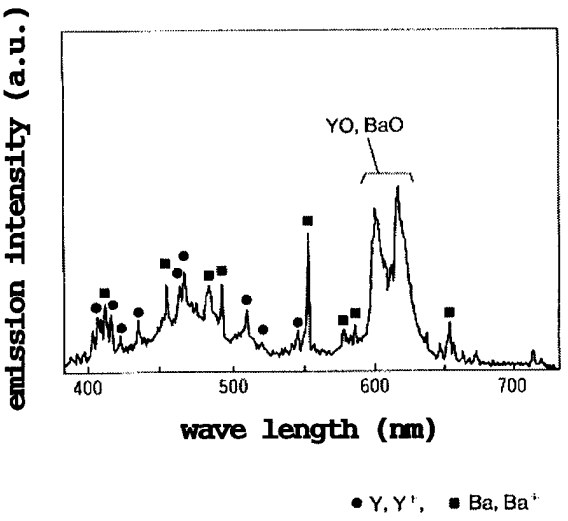

Fig. 10. In-line monitoring result of plasma plume.

CONCLUSIONS

Present status of HTS wire development is described. A lot of demonstrators are being built and evaluated, and current leads and magnets are already implemented to daily operated equipment, using BSCCO wires. Further improvements for application oriented direction are also summarized.

REFERENCES

1. J.G.Bednortz and K.A.Muller: Z.Phys. **B64**(1986)189.
2. M.K.Wu, J.R.Ashburn and C.W.Chu: Phys. Rev. Lett. **58**(1987)908.
3. H.Maeda, Y.Tanaka, M.Fukutomi and T.asano: Jpn. J. Appl. Phys. **27**(1988)L209.

4. Z.Z.Sheng and A.M.Hermann: Nature **332**(1988)138.
5. A.Schilling, M.Cantoni, J.D.Guo and H.R.Ott: Nature **363**(1993)56.
6. T.Hikata, T.Nishikawa, H.Mukai, K.Sato and H.Hitotsuyanagi: Jpn. J. Appl. Phys **28**(1989)L1204.
7. K.Sato et al.: IEEE Trans MAG **27**(1991)1231.
8. K.Sato et al.: Pro. 16th CEC/ICMC,(Elsevier Science, Oxford, 1997)1347.
9. for examples, USP5,639,714, EP356,969, USP5,516,753, EP066,172 etc.
10. for examples, USP5,114,908, EP412,442 etc.
11. T.Kato et al.: Adv. SuperconductivityⅨ, (Springer, Tokyo, 1997)1425.
12. E.Suzuki et al.: Submitted to Proc. EUCAS'97.
13. T.Ando et al.: Submitted to Proc. of MT-15, Beijing, China, October, 1997.
14. K.Funaki et al.: IEEE Trans. Appl. Superconductivity **7**(1997)824.
15. C.Suzawa et al.: Adv. SuperconductivityⅩ, (Springer, Tokyo, 1998)1293.
16. K.Ohkura et al.: Adv. SuperconductivityⅨ, (Springer, Tokyo, 1997)957.
17. J.Iannicelli et al.: IEEE Trans. Appl. Superconductivity **7**(1997)1061.
18. T.Kato et al.: .Adv. SuperconductivityⅩ, (Springer, Tokyo, 1998)877.
19. T.Hara et al.: Adv. SuperconductivityⅨ, (Springer, Tokyo, 1997)1331.
20. J.Fujikami et al.: Appl. Superconductivity **2**(1994)181.
21. K.Sato et al.: IEEE Trans. Appl. Superconductivity **7**(1997)345.
22. T.Shibata et al.: Adv. SuperconductivityⅩ, (Springer, Tokyo, 1998)1263.
23. K.Hasegawa et al.: Pro. 16th CEC/ICMC,(Elsevier Science, Oxford, 1997)1413.
24. K.Hasegawa et al.: Adv. SuperconductivityⅨ (ISS'96), (Springer, Tokyo,1997)745.
25. Y.Iijima et al.: Appl. Phys. Lett. **60**(1992)759.
26. A.Goyal et al.: Appl. Phys. Lett. **69**(1996)1795 .
27. M.Yoshida et al.: Appl. Phys. Lett. **65**(1994) 1714.

Ken-ichi Sato
Address: 1-1-3, Shimaya, Konohana-ku, Osaka, 554-0024 Japan
Superconductor R&D Department
Sumitomo Electric Industries, Ltd.

He majored in Physics, Dept. of Science, Kyoto University, and joined in Sumitomo Electric Industries, Ltd. in 1971. His expertise in Sumitomo Electric are development of non-ferrous alloys for electric conductors, superconducting materials and their application. He is a manager of Superconductor R&D Department.

THE ROLE OF HTS CABLES IN HIGH CURRENT CAPACITY NETWORK

Mujibar Rahman, Stephen Norman, Marco Nassi, Pierluigi Ladie'
Pirelli Cavi e Sistemi SpA, Viale Sarca 222, 20126 Milano, Italy

ABSTRACT

This paper identifies the role of High Temperature Superconducting (HTS) cables in future high current carrying electrical network. It also reports the status of developments of HTS cables in the field of Energy Transmission Cable system, dealing specifically with alternating current applications, even though future direct current applications can be also a possibility. An analysis of the main features, both in terms of expected performances as well as in terms of R&D requirements is presented for the two basic designs of HTS cables, namely Warm Dielectric and Cold Dielectric designs.
The general background to the most significant cable development programmes is summarized and more detailed information on the Pirelli HTS power cables developments is presented. The adopted method for defining the target performances needed to realize commercially viable systems is discussed. Finally, some considerations of the main advantages of HTS power cable systems and their potential benefits to the electrical power industry are summarized.

1. INTRODUCTION

The commercial implementation of liquid helium superconducting cable systems, which proved to be technically valid, has been judged to be impractical due to their excessive cost primarily due to cryogenic system-related expenses. The discovery in 1986 of High-Temperature-Superconductors (HTS) has greatly revitalized interest in superconducting cable systems. The availability of a less costly superconducting cable solution, cooled by Liquid Nitrogen (LN) and the need of high current carrying connections, are the driving forces behind various possible applications for HTS cables in electric energy transmission systems of tomorrow.

Traditionally, due to practical limitations of conventional cable sizes, network engineers have relied on increasing voltage to transmit higher amount of power. HTS cable with it's capability of carrying at least 2 to 5 times more current than the conventional cable with the same level of losses, provides network engineers for the first time with the option to transmit large amount of power with a reduced number of circuits or using higher voltage, as needed.

2. THE TWO BASIC CABLE DESIGNS

Two basic HTS cable designs are recognized worldwide as possible candidates for power transmission In one, the Warm Dielectric design (WD), only the HTS conductor is enclosed in a cryogenic environment (Fig. 1).The electrical insulation is applied over the cryostat which encloses the superconducting core and the LN coolant. In the other, Cold Dielectric Coaxial design (CDC), two concentric HTS conductors for each phase, separated by cryogenic insulation cooled by LN, are used. Moreover the CDC design can assume two different configurations depending on the position of the cryostat which can be over each core (Fig. 2) or over the assembled three-cores (Fig. 3). In both types of cables, the conductors may have one or more layers of HTS tapes carrying the current.

3. WARM DIELECTRIC CABLE DESIGN

The WD design is generally suitable for installation or retrofit in pipe or duct. As Fig. 4 shows, HTS cable of the WD design has the potential to carry more than twice the power of a conventional cable with approximately the same losses. Generally, it requires fewer HTS tapes than the CDC design but has higher lifetime operating costs because of its greater electric losses.

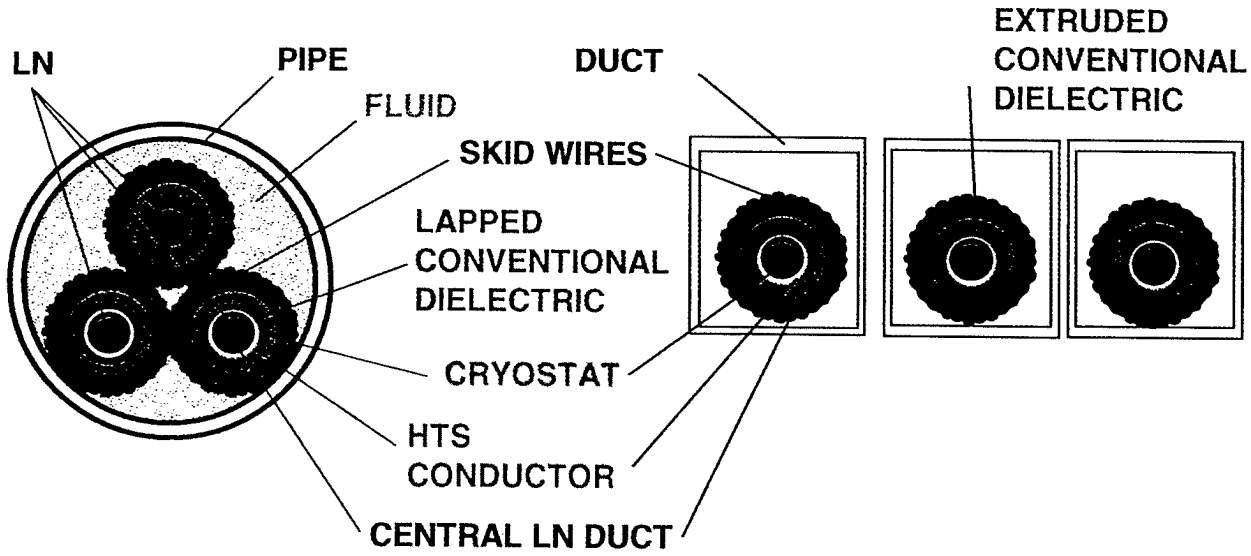

FIGURE 1
Schematic cross section of a WD design

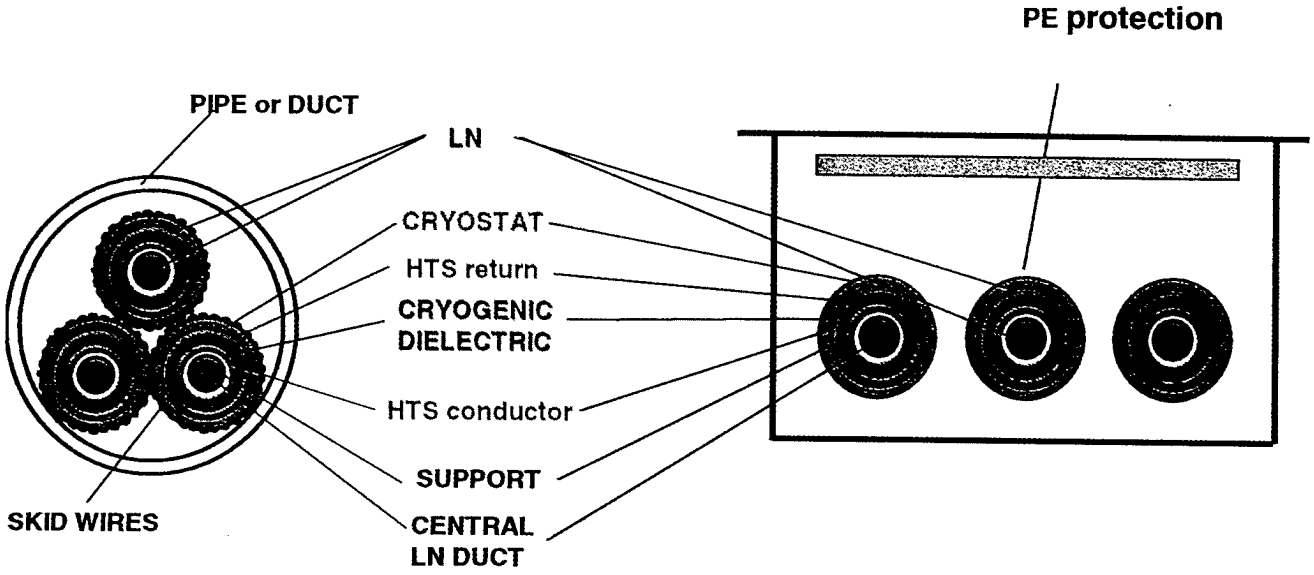

FIGURE 2
Schematic cross sections of CDC design in single-core configuration

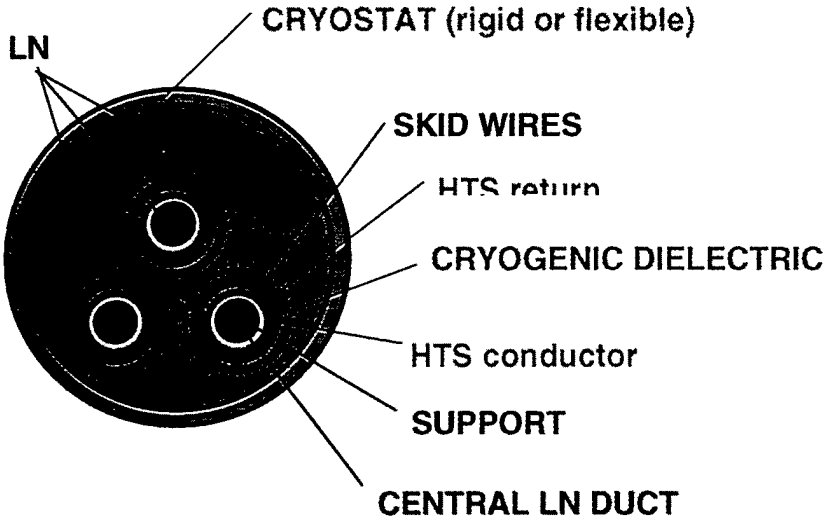

FIGURE 3
Schematic cross section of CDC design in three-core configuration

This design has several advantages such as:
- it has similar performance and requires similar installation procedures as compared to a conventional pipe-type cable;
- it uses existing, well-proven dielectric materials;
- accessories can be of simpler design: both termination and joints can be derived from conventional ones.

4. COLD DIELECTRIC COAXIAL CABLE DESIGN

The CDC cable design, in its single-core configuration, is provided with a flexible cryostat while, in the three-core configuration, it can be installed in either flexible or rigid pipes having cryogenic insulation to minimize heat losses. The more significant advantages of this design resides in its ability to transmit large amount of power with reduced losses in "compact" cable systems: up to five times the current of conventional cables at approximately two third of the losses (see Fig. 4). Its lifetime operational costs are lower than those of a WD design but its initial investment cost is higher because more HTS tapes are needed to provide for the concentric external conductor which acts as a return path for the current, furthermore the CDC design generally allows increased cooling distance (distance between two points on the cable before the LN must be replenished).
approximately 100 microjoules per meter[3]

5. R&D REQUIREMENTS

A major focus of the ongoing R&D effort is the development of long-length HTS tapes and related tape-manufacturing processes; these are essential requirements for HTS cable to be produced with the desired operating current and adequate mechanical and environmental performance. Today, the cable's fundamental building block is silver sheathed BSCCO-2223 tape comprising multiple ceramic filaments embedded in a silver matrix. With state-of-the-art tapes, retention of critical current (at 77 K) exceeding 95 % has been achieved when subjected to a tensile strain of up to 0.5 % or a stress of up to 300 MPa[1].

The chief challenges in HTS tape development and manufacturing are:
1. Increasing the critical current density of each tape;
2. Producing longer lengths of uniform tape;
3. Reducing the electrical losses for a.c. operation;
4. Achieving cost-effective and repeatable manufacturing processes.

On short samples of tape a DC critical current density of approximately 70.000 A/cm^2 at 77 K has been reported[2].
In a typical HTS tape with a DC critical current of 40 A (at 77 K), the AC losses in self field configuration in a tape carrying 30 Arms are.

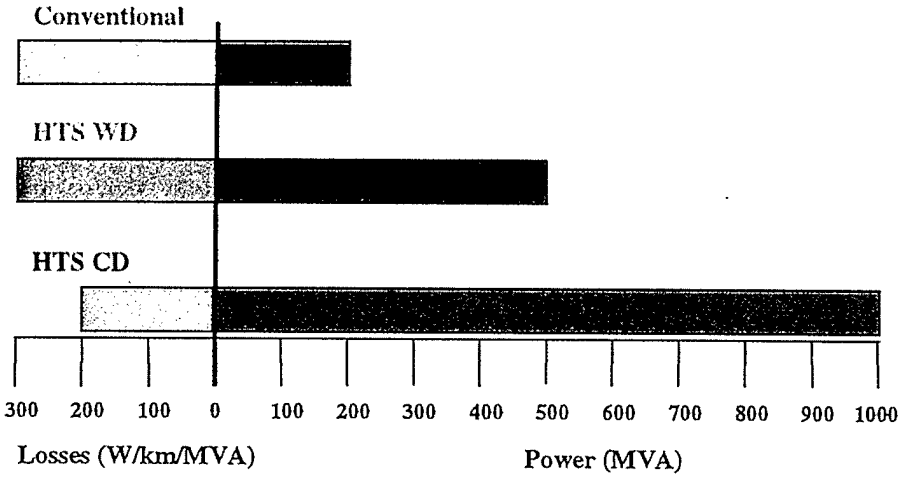

FIGURE 4
Losses and transmissible power for HTS and conventional pipe-type cables

The measurement of AC loss in an HTS cable is significantly more complex than for tapes. As best understood today, the conductor's AC loss in a given cable depends on such factors as the transport and critical current performance of the individual tapes, the number of tape layers and the conductor design. Finally, the phase configuration (single or three core) also has an impact when a WD design is used. Detailed understanding of these phenomena in each specific cable configuration is crucial and therefore much experimental (with both electrical and calorimetric measurement methods) and theoretical work has been planned for this purpose.

Reliability and operational life for superconducting cables of both basic designs, as for the conventional ones, are affected by the electrical insulation performance.

The WD design takes advantage of the decades of experience gained in the field of high and medium-voltage cable insulation technology; on the other hand it presents a special technological challenge because the insulation (whether it be lapped laminated tapes or extruded polymeric compound) has to be applied over the corrugated surface of the flexible cryostat.

In so far the CDC design is concerned, both lapped and extruded insulation exhibit superior electrical performance in a cryogenic environment than at room temperature, but mechanical performance can be challenging in terms of brittleness. Cryogenic dielectrics have a lower loss factor but the resultant a.c. heating effect is generated at LN temperature and has to be extracted by the cooling system.

For the CDC design, PPL (Polypropylene Paper Laminate) insulation appears to be one of the most promising solutions from both electrical and mechanical point of view. Specific R&D activities are now in progress with the aim of selecting optimized materials in order to achieve the best electrical and mechanical performance.

6. DEVELOPMENT PROGRAMS

The significant advances in HTS tape technology attained over the last ten years, particularly for BSCCO tape manufactured by the powder-in-tube method, have convinced some of the most important cable manufacturers and electric utilities to plan development programs with the objective of manufacturing and testing complete HTS cable system prototypes. These programs include both WD and CDC design cables and range from medium to high voltage as summarized in a recent report sponsored by the International Energy Agency[4].

In 1992, Pirelli completed the design of a 115 kV, 400 MVA cable of the WD type suitable for retrofit in existing 8 inch pipes[5,6]. Based on the conclusions of this feasibility and design study, the U.S. Electric Power Research Institute, the U.S. Department of Energy, and Pirelli undertook a program in 1995 to develop this cable design into an actual system prototype including joints, terminations and cryogenics[7]. HTS tapes for this project were supplied by American Superconductor Corp. who are collaborating jointly with Pirelli to develop

more advanced BSSCO tapes. In 1996 the 50 m HTS conductor was electrically tested to prove its current-carrying capability, and a DC critical current of 3300 A (1 μV/cm criteria, 77 K) was achieved. Subsequently, in 1997, a mock-up prototype cable (with Al tapes in place of the HTS tapes) was manufactured and electrically tested to verify the cable design. It withstood a lightning impulse voltage of 700 kV, well beyond the 550 kV BIL level required by the 115 kV voltage rating. To demonstrate its electrical insulation performance, a complete system comprising mock-up cable, accessories (terminations and joint) and cryogenics was assembled early 1998 in Pirelli's North America R&D facility and successfully tested at impulse up to 625 kV according to the same procedures as foreseen for the actual cable. Having thus successfully demonstrated the performance of the individual components, a full system incorporating the superconducting core will be assembled and tested during 1998 (in accordance with AEIC-CS2/90 and IEEE 48/96) by Pirelli. In the meantime $I_{C,DC}$ and AC loss measurements have been carried out in '98 on the actual 50 m cable. An $I_{C,DC}$ of 3200 A (77 K, 1 μV/cm criteria) was measured verifying a degradation less than 3% due to cabling process.

Pirelli is also involved in other HTS R&D system development programmes, each with distinct, specific goals ranging from design studies to experimental development of complete HTS cable systems. The approach adopted for all these programs has involved an initial feasibility study in order to analyse the suitability and effectiveness of various HTS system options within the context of a specific electrical transmission system under consideration, usually working in close collaboration with interested utilities.

A number of such feasibility studies have already been undertaken in collaboration with American utilities, demonstrating successfully that a joint approach facilitates the optimization of the system design to take into account cable and network constraints, whether it be for HV or MV pilot systems.

In September 1997 Pirelli and EDF (Electricitè de France) announced a development program for the design, construction and testing of a HTS system prototype suitable for high power transmission. In all probability a CDC solution at 90/225 kV will be the final choice.

Pirelli is also in the final negotiation phase for a contract by US Department of Energy (DoE) to install 120 meter three phase 25 kV cable and evaluate for continuous operation at Detroit Edison's down town network. Other partners in this program are: Electrical Power Research Instiute, Detroit Edison, American Superconductor Corporation and Lotepro.

7. TARGET PERFORMANCES

The definition of system performance targets commences with a thorough analysis of the required transmission capacity and installation configuration, to quantify the influence of the principal materials and system components upon performance, cost, and reliability[6]; an overall system specification is then defined. The approach taken was to consider state-of-the-art performance levels in specific fields such as HTS tapes, cryogenics systems, flexible and rigid cryostats and then to project forward anticipated advances in each area. The basic assumption in performing the analysis was that the main alternative competitor to a HTS cable system would be a conventional one both from a cost and a reliability point of view.

Several real applications of power transmission with different levels of voltage and length were selected. For all the selected applications a comparative benchmark was defined by analyzing or designing an equivalent conventional system, optimized for investment cost. For the corresponding HTS system solution, the relations between the main cost items such as HTS tapes, cables, accessories, installation and refrigeration plant were analytically described before proceeding to the system design based on several steps of optimization.

The results of the study demonstrated that for a certain number of applications, the specific cost of delivered power for a HTS system can be competitive with the specific cost of a conventional one, provided that the targeted performance improvements are successfully achieved.

It should also be mentioned that the competitiveness of HTS systems could be brought forward in terms of deployment time, if a total cost approach, including in the cost comparison not only the investment cost but also capitalized losses in subsequent operation, is considered.

Another essential area of development already underway is the work required to demonstrate the reliability of HTS cable systems, consisting of laboratory tests and in acquiring field experience with prototype installations.

8. ADVANTAGES AND OPPORTUNITIES

The major advantage of HTS technology resides in it's very interesting performance charachterstics[8]: it is the only power transmission system solution able to combine

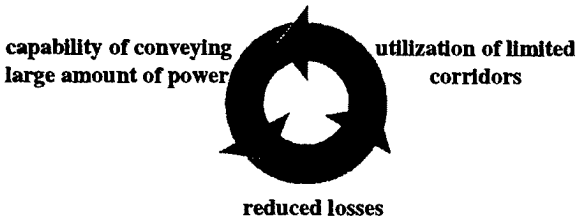

Fig 6. Three important benefits of HTS

in an effective way three important features (Fig. 6), namely the capability of conveying large amounts of power through limited corridors with reduced losses.
These technological benefits can offer particular advantages in applications such as:
- penetration in heavily congested urban areas;
- upgrading of existing underground circuits;
- one-to-one relocation of overhead lines into underground;
- elimination of transformation steps in urban feeders;
- increasing of transmission efficiency.

Furthermore HTS cables, in the coaxial Cryogenic Dielectric configuration, present several advantages in terms of environmental compatibility with respect to both underground cables and overhead lines.

Given their high current carrying capacity[9] and the above attractive characteristics, superconducting cables may open new options in network design (Fig. 7). Especially in congested urban areas, where demand for electricity is rising sharply but real estate and right-of-way are expensive and the installation of conventional transmission lines may be environmentally undesirable.
Prerequisites are that high-current-carrying HTS cable be compatible with existing network components, that it provides the electrical network with reliability at least as good as conventional cable and is cost effective.

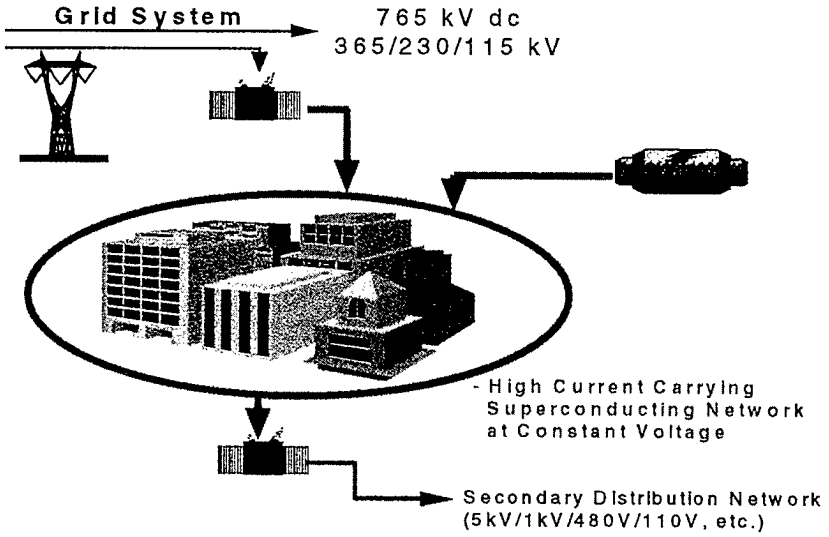

FIGURE 7
Future constant-voltage high current carrying superconducting network configuration

REFERENCES

1) W. L. Carter, G. N.Riley, A. Otto, D. R. Parker, C. J. Cristopherson, L. J. Masur and D. Buczek, Advances in the Development of Silver Sheathed (bi,Pb) 2223 Composite Conductors, The 1994 applied superconductivity conference, The Boston Marriott Copley Place, Boston, Massachusetts, Oct. 1994

2) Bart Riley, presentation at the DOE workshop in St. Petersburg, Fl, February 1998.

3) F. Gömöry, L. Gherardi, R. Mele, D. Morin, G. Crotti, PHYSICA C 279 (1997) 39-46

4) R. F.Giese, Directory of Superconducting Device Projects Bearing upon the Electric Power Sector, November 1997

5) D. W. Von Dollen, P. Metra and M. Rahman, Design Concept of a Room Temperature Dielectric HTS Cable, Proc. of the American Power Conference, Chicago, April 1993, p. 1206

6) D. W. Von Dollen et al., High Temperature superconducting cable technology, IEEE 3rd Conf. Power Cables, London, Nov. 1993

7) M. Rahman, M. Nassi, L. Gherardi and D. W. Von Dollen, Design, development and testing of the first factory-made high temperature superconducting cable for 115 kV - 400 MVA, to be presented in 1998 CIGRE meeting in Paris

8) F. Farneti, L. Lagostena, A. Bolza and P. Ladiè, Superconductive cable systems in electrical networks - Perspective and future use, IEA International Workshop on High-Tc Superconducting Power Transmission Cables, CISE, Apr. 1997

9) M. Rahman and M. Nassi, High-capacity cable's role in once and future grids, IEEE Spectrum, July 1997

AUTHORS

Mujibar M. Rahman since earning his engineering degrees from Bangladesh (1963),Germany (1967) and teaching at Berlin Technical University, held various engineering positions in R&D: in Telecommunication with Siemens Germany (1968) and in power cables with Siemens Austria (1971); in Fiber Optics with Canada Wire and Cable in Montreal (1977); in Fiber Optics with Pirelli Canada (1981). In 1986 he established Pirelli's north American fiber optic R,D&E in USA and was Pirelli's north American vice president & and chief engineer for Energy and Telecommunications R,D&E (1992). He directed Pirelli's worldwide research on HTS during 1996-98 and currently directs Pirelli's worldwide submarine optical cable products.

Stephen R. Norman is R&D Manager for HV cables and Superconductivity of Pirelli Cavi e Sistemi SpA. He is a fellow of the institution of Electrical Engineers and a graduate of the University of Southampton. He obtained his PhD in 1981 from the Electronics Department of the University of Southampton while doing post-graduate research for Pirelli in optical fiber telecommunications. Since joining Pirelli after graduation 1972, he has held a number of positions in R&D project management and operation management.

Marco Nassi earned a doctorate in engineering at the Polytechnic Institute of Milan in 1985. He has worked at the Italian National Council for Research in Milan, the Massachusetts Institute of Technology, Cambridge, and the Italian Agency for Alternative Energy Sources, Turin. Joining Pirelli in 1994, he is responsible for superconducting cable technology, design and applications.

Pierluigi Ladie' completed his Dr. Eng. Degree in Mechanical Engineering from Polytechnic Institute of Milan in 1976.In the same year he joined Pirelli where he was responsible for cable accessories design and project manager for submarine cable systems. He is currently responsible for Superconducting Cable Design.

A VISION FOR APPLICATIONS OF HTS TRANSFORMERS

V. R. Ramanan, Gilbert N. Riley, Jr.*, Lawrence J. Masur* and Steinar J. Dale

ABB Power T&D Company Inc., Raleigh, North Carolina
***American Superconductor Corp., Westborough, Massachusetts**

ABSTRACT

High temperature superconductor transformers (HTSTs) now provide a viable opportunity for significant improvements in operational and performance efficiencies in the electrical power delivery system. They bring well known benefits generally expected from superconductor transformers, such as low losses, absence of mineral oil, etc. However, when optimized as components in a utility power grid, the benefits HTSTs bring to the entire power system could be far greater. It is these power system benefits that will add the necessary value to HTSTs over conventional transformers, and enable their commercial acceptance and a large market penetration. To accomplish this in an HTST, the elements of transformer design, HTS wire performance design, and cooling system design must be optimized in combination. Such an optimized HTST will be a highly reliable, high performance device with a low total owning cost.

INTRODUCTION

Today's transformers, with their electrical steel cores and copper or aluminum windings, are very efficient devices (about 99.7% efficiency). They represent a mature technology, with little room for efficiency improvement. The possibility of significant efficiency improvements in transformers with superconductor windings has long been recognized. However, the high refrigeration costs associated with very low temperature (< 30 K) operation using helium have been a major barrier to the marketplace.

High temperature superconductors (HTS), with liquid nitrogen as the cryogen, directly address this barrier. Due to the considerable performance improvements in HTS wires over the last few years, the economic feasibility of an HTS transformer (HTST) is close to reality.

When compared with conventional transformers, the benefits from an HTST are: low losses (improved efficiencies), reduced size and weight, overloadability with minimal impact on transformer lifetime, and the favorable environmental impact derived from the absence of mineral oil. Table I below illustrates by example the potential extent of some of these benefits. In this Table, the HTS wire in a 100 MVA transformer is assumed to have a J_c of 100 A/mm^2 and an *ac* loss of 0.25 mW/Am in a parallel field of 0.1 T.

Table I

Certain key potential benefits of HTSTs over conventional transformers.

Transformer Characteristic	Ratio: (HTST/Conventional)
Total Losses	**31%**
Weight	**46%**
Total Owning Cost (*)	**77%**

(*) at 2.8$/W

Although the above cited benefits from HTSTs as stand alone devices are important, they alone would enable only niche application areas for HTSTs, in the context of increasing utility deregulation. As components integrated into a utility grid, HTSTs can bring vital added benefits to the operation and efficiency of the entire power system as discussed below. For acceptance in a broad marketplace, HTST applications must be differentiated from conventional transformers through these added benefits.

VISION FOR TRANSFORMER DESIGN: POWER SYSTEM BENEFITS FOCUS

Transformers offer protection to the power system by limiting large currents resulting from system faults, and they must be able to handle system overloads.

Table II

Examples of potential financial benefits available from HTSTs due to enhancements provided to power system performance and operation. The numbers provided are typical industry averages.

HTST Characteristic	Financial Benefits
Current Limiting Capability	
• Use conventional breaker instead of high current SF_6 breaker	$25,000 each
• Replace EHV breaker with circuit switcher	$25,000 each
• Use load break switches instead of breakers	$ 6,000 each
• Elimination of current limiting reactors	$20,000 each
Reduced Impedance(*): Impact on Power System	
• Reduced need for Load Tap Changer units (voltage regulation)	$75,000 per LTC
• Reduced system VAR requirements (Static VAR Compensation)	$50,000 per MVAR
• Reduction in capacitor banks (reduced reactive power losses)	$13,000 per 10 MVA
Reduced Transformer Impedance (*): Impact on Generation	
Example: 500 MVA Generator + Step-up Transformer	
• Reduced VAR requirements freed up for system, at $50/kVAR	$2.5 million
Additional available generator capacity from improved operation: **25 MW**	
1. Avoided capital cost, at $300/MW for gas turbine generator	$7.5 million
2. Additional revenue, at $0.04/kWh, **50%** capacity factor	$4.4 million (annual)

(*) Assumed: HTST impedance is 25% of that of conventional transformer

The greatest value of HTSTs is through their benefits to the power system. This is particularly congruent with the increasing utility focus on an improved overall power delivery infrastructure to deliver high quality power cost efficiently.

Reducing short circuit currents from faults in the power system, and protection from these currents are prime priorities in power systems design. As the nation's networks become increasingly interconnected, short circuit currents will continue to increase. Considerable investments are made in circuit breakers, protection relays, switches, etc. to limit their effects. To limit fault currents to acceptable levels, conventional transformers are designed with large impedances (typically 10%-16%), which can affect the voltage regulation and reactive power demand in the system.

As discussed in detail later, HTST coils possess an intrinsic current limiting capability. This capability will allow transformer designers to separate the transformer impedance from the system short circuit current requirements. With lower transformer impedance, more real and reactive power from existing generators are made available to the power system, and voltage regulation in the network is markedly improved. The need for on-load tap changers and capacitor banks for voltage regulation can thus be reduced, leading to considerable investment cost savings.

The dynamic current limiting of the HTST also can reduce the short circuit rating of the circuit breakers. Thus, the cost savings from use of circuit breakers with lower short-circuit current ratings could be significant. The need for additional current limiting devices with their costs, losses and space requirements can also be reduced or eliminated.

As illustrated in Table II, the potential power system benefits (efficiency improvements and financial savings) are quite sizable from HTSTs designed with a low impedance. Such devices, for example, can free up an additional 200 billion kWh of power, not now delivered from existing generators, over the typical lifetime (30 years) of each annual block of 30 installed generator step-up transformers rated above 500 MVA. Generation capacity expansions may thus be deferred.

It is clear that the potential current limiting capability in HTST coils must be exploited in the design of HTSTs.

VISION FOR HTS WIRE DESIGN:

OPTIMIZED CURRENT LIMITING CAPABILITY AND LOW LOSSES

In HTS wires and tapes the ceramic superconducting compound is contained within a silver alloy sheath. Among all available technologies for producing high temperature superconductors, the powder-in-tube (PIT) manufacturing technology for Bi-2223 HTS wires and tapes is the most proven and advanced, and, therefore, allows the most rapid advance toward full implementation of HTSTs in the power system.

High performance HTS wire optimized for transformers is critical to achieving the systems benefits described above. For superconducting transformers with an intrinsic current limiting capability, the HTS wire must meet performance targets in the areas of current carrying ability, mechanical robustness, *ac* losses and current limiting functionality. To assure economic competitiveness, such wire must ultimately be available at low cost. A US Department of Energy study[1] has defined this "low cost" to be around 100 $/kAm.

Currently, "filamentary" composite HTS wire based on Bi-2223 offers the most promise for realizing practical superconducting transformers. Although not yet optimized for transformers, mechanically robust composite Bi-2223 wire is already delivering high levels of superconducting performance. For example, at American Superconductor, critical current values of 100 A have been measured at 77 K and self field across long lengths of Bi-2223 wire.

Furthermore, because Bi-2223 has a high transition temperature relative to other HTS materials, it can be operated at liquid nitrogen temperatures. The cooling costs associated with Bi-2223 are likely to be relatively low. The remaining technical challenges for superconducting transformers are, therefore, related to achieving practical current limiting functionality and low *ac* losses.

A superconductor is a natural current limiter. At operating currents below the critical current, the effective resistance of a superconductor in a transformer is very low. However, if the current surges significantly above the critical current due to a system fault, the resistance of the superconductor increases dramatically, by many orders of magnitude. Therefore, the fault current is limited by the very large increase in resistance of the superconductor. Suitably optimized HTS wire could thus enable a transformer based on such current limiting capability. However, theoretical predictions suggest that currently available Bi-2223 wire with its silver matrix will not have sufficiently high electrical resistance to practically limit the fault current. As a result, the principal challenge is increasing the electrical resistance of the "matrix" material that surrounds the Bi-2223 in the composite wire. Substantial increases in matrix electrical resistance values have been demonstrated in short lengths of composite Bi-2223 wire fabricated at American Superconductor.

Although superconductors have no resistance in a *dc* application, certain physical mechanisms related to hysteresis within the superconductor and eddy currents within the normal metal matrix surrounding the superconducting filaments give rise to energy losses in the normal *ac* operation of the transformer. These losses are referred to as *ac* losses. Such losses lead to heating of the HTS wire, thereby increasing the cooling requirement of the transformer.

The principal challenge in developing HTS wire with low *ac* losses is fabricating wire in which hysteretic and eddy current losses are simultaneously minimized. Based on certain transformer design calculations, an *ac* loss target value of 0.25 mW/Am has been proposed for HTS wire optimized for commercial transformers[2]. Short lengths of composite Bi-2223 wire fabricated at American Superconductor have demonstrated performance near this target level.

Significant advances have already been demonstrated in each of the critical performance areas, in short lengths of composite Bi-2223 wire. However, important questions remain regarding the extent to which theory accurately predicts the behavior of such wires in an actual transformer. To answer these questions, tests on long lengths of prototype HTST wire are planned, under transformer operating conditions.

The experience gained through such activities should accelerate the development of low *ac* loss, current limiting HTS wire, manufactured in long lengths for commercial application.

VISION FOR COOLING SYSTEM DESIGN: RELIABILITY AND COST EFFICIENCY

The design for the cooling system to "deliver the cold" to the cryostat at the chosen operating temperature must be congruent with the complete transformer design. Such a design will be more cost and performance efficient than the adaptation of available refrigerators to the HTST application. This approach should yield a cooling system that is safe, highly reliable and efficient, allowing flexible operation over a wide range of transformer loads with minimal maintenance.

The design drivers for the cooling system are: power requirements, operating temperature, response to power system fault events, and a low maintenance schedule.

The power demands from the refrigerator can be considerable. Assuming a coefficient of performance (COP) of 0.05 (i.e., 20 W of power necessary to remove 1 W at 77 K), preliminary design calculations indicate that 12 kW of refrigerator input power is necessary at rated load for a prototype 10 MVA HTST under development. For a 100 MVA HTST at rated load, about 70 kW of input power will be required. Since a transformer can be exposed to a wide range of loads – from 50% to overloads of as much as 130% for a few hours – the cooling system operation must be flexible and cost efficient over such a range.

Using the Bi-2223 HTS wire and liquid nitrogen as the cryogen, the operating temperature for the HTST coils will be in the range 66 – 77 K. As the operating temperature is lowered, the HTS performance is improved and the safety margins are increased. On the other hand, refrigeration costs will increase. The selection of temperature will be an optimized balance between these two competing effects. A thorough evaluation and analysis is needed.

In the event of a system fault, the short circuit power could be several GVA! The cooling system must remove this power quickly and safely. Once the fault is cleared, a fast cool down of the HTS coils to the operating temperature is essential. A rapid return will enable the system to handle a larger frequency of fault events.

In a well designed cooling system, the maintenance schedules and costs must be comparable to existing utility practices. A three year maintenance interval and the possibility to perform this maintenance without interrupting the HTST operation should be the ultimate goals. Finally, the HTST cooling system must be supported by a reliable cryogen delivery infrastructure that is simple to manage and execute.

Based on the above discussion, it is apparent that accommodating a "simple" adaptation of available refrigerators in HTST design cannot be a viable long term application solution.

For a broad commercial applicability of HTSTs, the cooling system costs should be low, since HTSTs have to compete on investment costs with conventional transformers. It is thought that the cooling system costs should be less than about 20% of the total owning costs for an HTST. With this target, HTSTs can become competitive with conventional transformers on a total owning cost basis for transformer ratings greater than 40 MVA[3].

At a minimum, the investment in the refrigerator is covered by savings in the cost of losses in the transformer. This "zero sum" will not be acceptable to the HTST manufacturer or the customer: design flexibility in other HTST components is lost, and a large portion of the differentiating, added values in HTSTs are surrendered.

CONCLUSION

High temperature superconducting transformers can significantly improve the performance and operational efficiencies of power systems. Only an approach that stresses congruence in all the key design areas will ensure cost competitiveness and enable the commercial acceptance of HTSTs in the broad transformer marketplace over the long term. The widely deployed low impedance HTST, rated above 40 MVA, will employ HTS wires tuned for current limiting capability and low *ac* losses, and operate continuously through a cost and efficiency optimized cooling system.

REFERENCES

1. Superconductor Week, Oct. 1, 1997, p. 7
2. S. J. Dale, DOE Wire Development Workshop, 1997
3. S. J. Dale, V. R. Ramanan, and T. L. Baldwin, Proceedings of IEEE Winter Power Conference, 1998

Dr. V. R. Ramanan is Advisory Scientist and Magnetics Technology Team Leader at the Electric systems Technology Institute of ABB Power T&D Company in Raleigh, NC. He is the Program Manager for the anticipated DOE funded SPI project to develop and demonstrate a prototype 10 MVA HTST possessing the characteristics discussed above. Magnetics, materials, and sensors are other areas of interest for Dr. Ramanan.

Dr. Steinar J. Dale is Manager, Equipment & Materials Center at the Electric systems Technology Institute of ABB Power T&D Company in Raleigh, NC. The broad R&D portfolio in his Center includes insulation systems, magnetics, polymers and coatings, sensors and systems, electronics and instrumentation. A Fellow of IEEE, Dr. Dale is an expert in power systems and dielectrics research.

Dr. V. R. Ramanan or Dr. Steinar J. Dale

ABB-ETI
1021 Main Campus Drive
Raleigh, NC 27606

Dr Gilbert N. Riley, Jr. is Senior Technical Manager at American Superconductor Corp. in Westborough, MA. At ASC he has overall responsibility for all corporate R&D activities pertaining to HTS wires. Dr. Riley's background includes over ten years in materials processing, principally focused on composites materials.

Dr. Lawrence J. Masur is Senior Manager, Process Development, at American Superconductor Corp. He is responsible at ASC for transfer of HTS wire technologies from R&D to reproducible, long length manufacturing. As a Program Team Leader for the DOE SPI 10 MVA HTST project, Dr. Masur coordinates all ASC activities for the project.

Dr. Gilbert N. Riley, Jr. or Dr. Lawrence J. Masur

American Superconductor Corp.
Two Technology Drive
Westborough, MA 01581-1727

HIGH FIBER COUNTS IN AERIAL AND SUBMARINE OPTICAL CABLES WITH METAL TUBE DESIGN

Dr. C. Unger

NSW GmbH, Nordenham, Germany

Dr. G. Zeidler

Siemens AG, ÖN NK E, München, Germany

ABSTRACT

With the metal tube design it is currently possible to integrate up to 144 fibers in an optical ground wire cable and up to 48 fibers in an optical submarine cable. The investigations discussed in the paper (attenuation, tensile test, polarization mode dispersion, temperature cycling test, high-level short circuit current test on OPGW) demonstrate the performance of the cables in continuous operation.
Some 6000 km of cable of the presented LW MINISUB™CT submarine cable family have already been successfully installed. In the last project seven islands of the Azores were interconnected by means of an optical fiber ring; the longest section of the link being 386 km. It is thus by using the remote pumping technique one of the world's longest repeaterless submarine cable links.

INTRODUCTION

New telecommunication services are currently being introduced all over the world. It is the age of the computer and this, together with the growth in data communication, is leading to an explosion in the capacity required. All these services, such as Inter-/Intranet and multimedia applications, E-mail and video conferencing as well as other services still under development are demanding ever increasing transmission bandwidth with distribution extending close to end users.
This requirement for increasing capacity is currently being met in communication networks with the deployment of new cable designs. This paper presents rugged, high-fiber-count, wire-armored cables for arduous applications, that have currently been installed.
A distinction is made between optical ground wire cables with up to 144 fibers in central loose steel tubes and submarine cables with up to 48 fibers in central loose copper tubes.

The loose metal tubes provide an extremely flexible and durable structure for protecting and integrating the fibers in the cable.
Choosing the appropriate protective metal tube, e.g. aluminum or steel for ground wire cables is discussed with reference to the requirements placed on self-supporting optical aerial cables.

GENERAL DESIGN OF OPTICAL FIBER CABLES WITH METAL TUBES

There are various ways of integrating the optical fibers in the cable, but in most cases the fibers are located in a non-escaping filling compound and surrounded by a protective tube. There are two differing basic designs. In the one, the optical fibers are housed in a central, relatively large loose tube, in the other design they are housed in stranded, thin tubes / slots.

Manufacturing of the Metal Tubes

The metal tubes are formed from tape running longitudinally which is welded and then drawn down to the final diameter in reducing stages. The fibers or fiber bundles are introduced into the tube together with the filling compound during the welding operation.
The fiber excess length is produced with precision by the process selected [1].

OPGW design The choice of material (high-grade CrNi steel or aluminum) for the protective tube of the fibers is often a policy decision of the user. The central metal tubes can be up to 7.5 mm wide. The steel tubes employ a special grade steel which is protected against corrosion by a layer of special grease.
In principle the central steel tube, owing to its thinner wall of about 0.4 mm, can accommodate a larger number of fibers than the aluminum central tube.

So that, for example, an aluminum tube houses 36 fibers and a central steel tube 60 fibers with the same fiber excess length of 0.5 %.
The advantage of the Al tube is that it enlarges the conductive cable cross section for the short circuit current.
Under certain circumstances, it is possible to design highly compact OPGW cables with the aluminum central tube.
With high fiber counts the individual fibers are identified by a colored binder which is used to bundle for instance 6, 10 or 12 colored fibers into a single group. This avoids the problem of the user having to deal with a complicated marking scheme for the individual fibers (up to 144). However, since the fibers are still individually accessible they can be easily separated and fused at joints using conventional splicing machines.

Maximum Fiber Count in a Metal Tube

The maximum number of fibers in a central loose tube is limited by the fiber density (i.e. the ratio of the sum cross-sectional area of all the fibers relative to the inside area of the tube) and the fiber excess length (i.e. scope for the cable to vary in length without straining the fibers). An attempt has now been made to determine the additional losses as a function of a single parameter in place of these two characteristics. The criterion adopted to determine the maximum fiber density and fiber excess length is the force F_B with which the fiber is pressed against the inner wall of the central tube. This characteristic quantity is used to determine microbending losses which (for low stresses) are linearly proportional to the microbending force [2]:

$$\Delta \alpha_{Mikro} \propto p_0 \Leftrightarrow F_B \propto \frac{Rb - \sqrt{Rb^2 - \frac{\left(2\pi\rho_S{}^2 + S^2\right)}{64}}}{\sqrt{\left(2\pi\rho_S{}^2 + S^2\right)^3}}$$

The following parameters were used to calculate the force:
S - lay length,
ϱ_S - stranding radius
Rb - bend radius of the assumed circular bending of the fibers.

The bending force - normalized to the force resulting for a tube with an inside diameter of 4.3 mm, 20 fibers and 0.55 % fiber excess length - was then calculated.
If the measured attenuation values from a large number of test cables is plotted as a function of the normalized force, it is evident that the normalized force of the cable design must be less than 2.0 (Fig. 1)

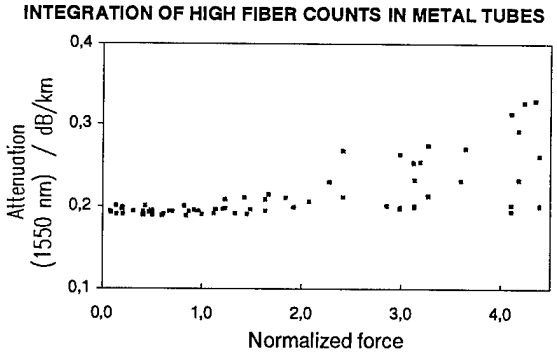

Fig. 1 Attenuation as a Function of the Normalized Force, Incremental Loss Increases with Fiber Count and Excess Length

With this characteristic parameter the cable designer is thus able to determine the optimum fiber tube diameter, maximum fiber count and largest possible fiber overlength. For the optical ground wires presented, with 96 and 144 fibers, the normalized force was 0.8 and 0.4 respectively.
It is furthermore necessary to take into consideration:
- the influence of the fiber
bending properties (MAC-value = mode field diameter / cut-off wavelength [2])
protection properties of the dual layer coating
- the protection by the filling compound due to the decoupling of external forces
- the influence of temperature due to the change of the properties of materials.

OPTICAL GROUND WIRE CABLE (OPGW)

Design of the OPGW

It is virtually impossible to judge the various concepts on their merits and demerits alone because the conditions encountered on the existing high-voltage facilities differ so widely. The different combinations of line-system and thermal requirements allow scope for differing designs. On the one hand, the optical fibers can be bundled inside a central tube of plastic or metal (steel or aluminum) with single or multi-layer wire armor on the outside (Fig. 2) or they can be housed in thin, stranded steel tubes taking the place of one or more wires in the inner layer of the armor. The choice of material (plastic, steel or aluminum) for the tube protecting the optical fibers is often a policy decision of the user.

Fig. 2 OPGW Cable with 96 and 144 Fibers

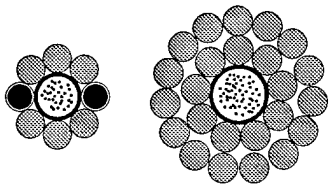

Fibers	96	144
Tube	d = 6.0 mm	d = 7.5 mm
Layers	single	double
Armouring	AY/AW 61/20 Al-Alloy + Al-clad steel wire	AY 265 only Al-Alloy
Cable	D=13.2 mm	D=22.5 mm

Fiber Excess Length

One of the main criteria for OPGW cables is adequate fiber excess length (selectable, normal to over 0.5 %). The optical fibers are housed helically in the central tube so that the fiber is longer than the cable. Tensile stressing of the cable - up to the point where the cable elongation equals the fiber excess length - does not affect the fiber (see Figs. 10 and 11 for the central tube in the submarine cable). The OPGWs can thus even survive storms and severe icing without fiber elongation.

Types of Armoring

In order to protect the optical fibers as far as possible from external influences, the OPGW cables are made up of one or more layers of armoring wires for strain relief and protection against buckling. The design of a cable depends basically on the current load it should withstand and the tensile strength that is required. These two factors determine the number and thickness of the armoring wires to be employed.
Figs. 2 shows various single and two-layer cables. These OPGW cables employ combinations of wires made from aluminum alloy (AY) and aluminum-clad steel (ACS, Stalum, alumoclad, AW). Aluminum alloy, comprising aluminum, magnesium and silicon, has twice the tensile strength of pure aluminum.
With the aluminum tube in particular there is an additional factor affecting the choice of armoring for the cable. The aluminum content of the tube enhances the electrical characteristics of the cable by carrying the short circuit current. Consequently, this function does not have to be performed by the armoring wires alone. It is thus possible for the armoring to have a smaller line cross section. Ultimately, this allows the OPGW cables to be made with only one layer of armoring but with a relatively high short circuit current rating. The design with only one layer of armoring and the fibers located in a central element is familiar particularly from Japan and the USA.

Test Results

The following section presents the main test criteria and the corresponding results for the two-layer and single-layer armored OPGWs with 144 and 96 fibers.

Attenuation Values OPGWs provide high transmission quality due to their very low attenuation of the transmitted optical signals. At an optical wavelength of 1550 nm the 144 fibers (of the cable previously discussed in Fig. 2) exhibited an attenuation of less than 0.21 dB/km (Fig. 3).

As a result it is possible to achieve average link losses for the fibers including all the splices below 0.21 dB/km (at an optical wavelength of 1550 nm) even on routes of more than 100 km.

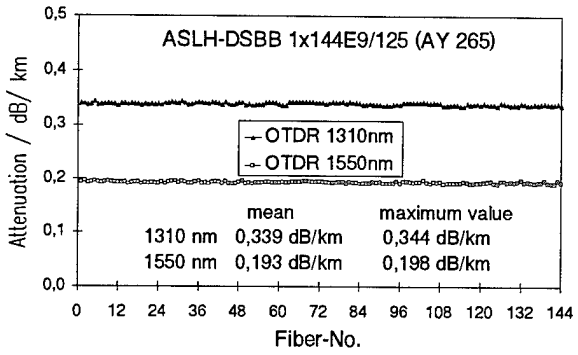

Fig. 3 Measurement of the Attenuation of an OPGW Cable (144 Fibers)

Polarization Mode Dispersion (PMD)

The measured values for PMD obtained with an interferometer for all 144 fibers at both wavelengths were significantly lower than the limit value of 0.5 ps/√km specified by some customers (Fig. 4). Critical for the PMD is the root mean square of the overall distance owing to the statistical nature of this parameter.

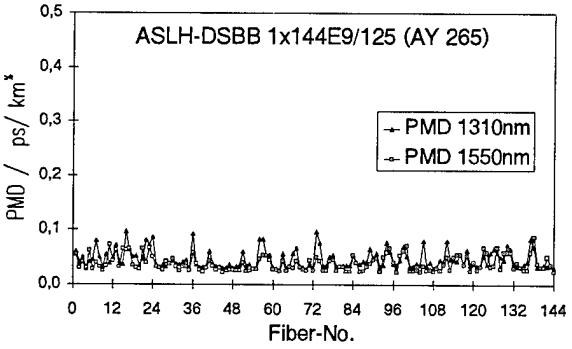

Fig. 4 Measurement of the PMD Values of an OPGW Cable with 144 Fibers

Response at Low Temperatures

Since OPGW cables must withstand extreme weather conditions without the transmission quality being impaired, the attenuation was measured at very low temperatures. Even at -40°C no changes in attenuation were detectable beyond the region of measuring uncertainty (Fig. 5), which means that these cables are suitable even for very cold climate regions.

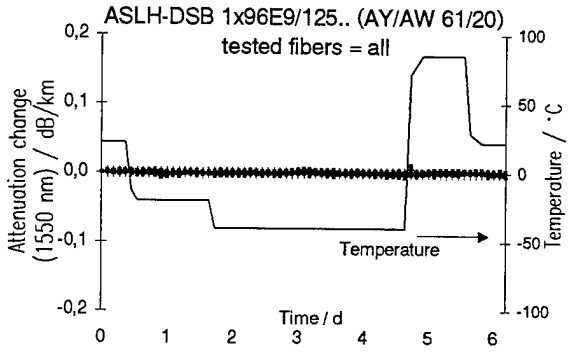

Fig. 5 Measurement of the Attenuation Variation in an OPGW Cable with 96 Fibers in the Temperature Cycling Test down to -40°C

High-Level Short Circuit Current Test

OPGW cables must withstand the high temperature stresses arising from short circuit currents on the high-voltage lines. In Germany OPGW cables must therefore be designed for temperatures up to 160 °C according to VDE requirements. Beyond this limit, which is used in tests as a reference value for the short circuit current, the tensile strength of aluminum and aluminum alloy decreases.

In tests with simulated short circuit currents the temperature rise in the armor layers was measured as well as the variation in attenuation of the fibers in the fiber tubes. When the reference value was reached (100 %), the temperature in the AY layer of the specimens under test rose to 120 °C and was thus still significantly below the upper limit specified by the VDE.

It only rose significantly (by more than 140 K) when the loading reached 130 % of the VDE-specified limit. However, despite such high overloading, no impairment of the fiber transmission quality could be detected. With a current load of 250 % the increase in attenuation in the most critical region - i.e. at 1550 nm - was only 0.03 dB/km (Fig. 6). All the attenuation changes were reversible.

The use of low-cost wires of galvanized steel in place of aluminum-clad steel produced virtually the same results.

In general terms, our OPGW cables are protected by a suitable combination of materials against overheating damage so that the optical fibers are not heated to an inadmissable level.

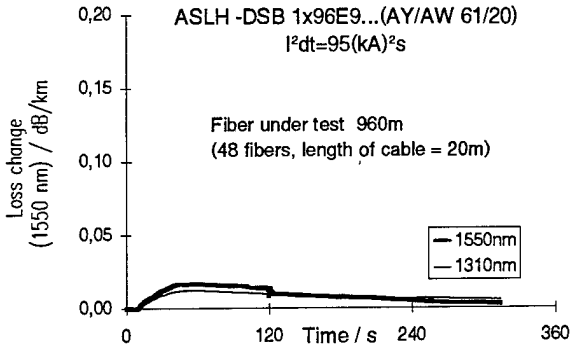

Fig. 6 Measurement of the Change in Attenuation of an OPGW Cable with 96 Fibers in the High-Level Short Circuit Current Test at 250 % VDE Loading

Theoretical Cable Model for the High-Level Short Circuit Current Test To establish a yardstick for designing OPGW cables to handle fault-current induced temperature rise, a theoretical model has been developed on the basis of experimental results for calculating the temperature characteristic. This model was adapted to practical requirements and verified by analyzing high-current tests on a wide range of OPGW cable types.

For the temporal temperature characteristic this provides a linked system of first-order linear differential equations that can be resolved numerically. The structure of the differential equation system varies of course according to the design of the OPGW cable (single, double-layer, one or two different materials in the inner layer).

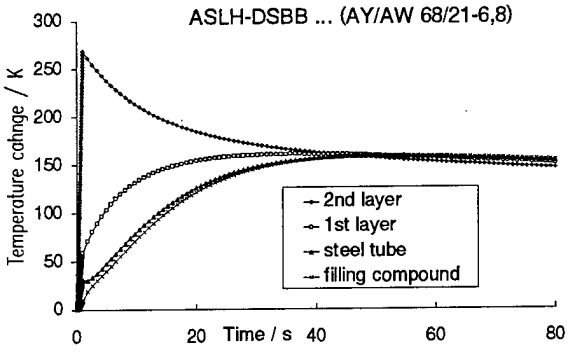

Fig. 7 shows the computed temperature characteristic in the various components of an OPGW ASLH-DSBB...AY/AW 68/21 for a short circuit current of 10 kA and 1s duration.

For these measurements an optical delay technique was used among others for the first time to determine the temperature in optical fibers.

From the speed at which information is transmitted in the optical fibers it is possible, by measuring over a sufficient length (> 100 m); to determine their temperature variation to an accuracy of ±5 °C (Fig. 8). At 100 % of the reference value the fiber temperature reached 80°C.

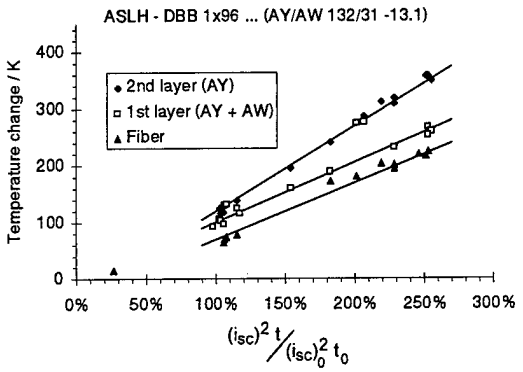

Fig. 8 Measurement of temperatures of optical fibers and armouring wires during the test of the short circuit current

Vibration and Corrosion Characteristics In order to test the performance of the OPGW cables in continuous operation, long-term tests were performed with wind-induced vibrations in conjunction with a salt fog spray test. These tests concentrated on OPGW cables with steel tubes. Three test pieces, each 27 m long, were vibrated in a salt spray chamber at a frequency of 20 Hz and a vibration angle of ± 20` through 100 million cycles. The subsequent examination revealed neither breaks nor increased attenuation. The steel tubes were not corroded, they merely had some slight abrasion on the surface. The test of mechanical self damping determines whether the particular OPGW cables need to be provided with dampers or not. The dampers are sized according to the damping performance found.

Installation (Torsion) The process of installing overhead wires calls for a rugged cable design which is highly crush resistant and largely free of torsion. In practical application cable designs with a central tube and two-layer armoring have proven to be particularly robust. Measurements of the rotation angle and torque during a tension test to 80 % of the rated tensile strength of the cable as well as installation trials with single-layer armored cables (with a significantly greater torsional tendency) were carried out successfully.

OPTICAL SUBMARINE CABLE MINISUB ™ CT

Design of the Submarine Cable with Copper Tube

To establish communication between islands, along the coast or across rivers there are submarine cables available incorporating the latest technology (Fig. 9). With these repeaterless "light weight" fiber-optic submarine cables it is possible to establish links without intermediate amplification up to 400 km long at installation depths of up to 6000 m.

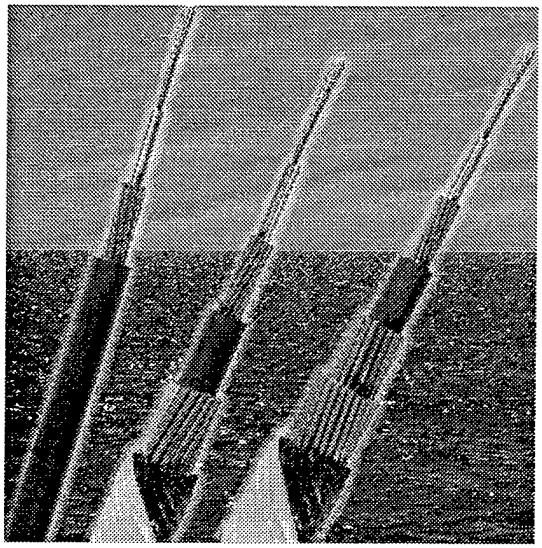

Fig. 9 Submarine Cables
LW (Light Weight) Minisub CT
SA (Single Armoured) Minisub CT
DA (Double Armoured) Minisub CT

The optical fibers are housed in a hermetically sealed central tube of copper (∅ 5 mm) providing the fibers with optimum protection against moisture and mechanical influences. The copper tube provides an extremely sound foundation for laying up the high-tensile steel wires in the first armoring layer which is then surrounded by a cable sheath (Fig. 9).
It is also possible to add a steel tape with a second HDPE-sheath on the light weight cable. This design is known as Light Weight Protected (LWP) cable. We are able to attach this second jacket on the whole length or on certain sections of the cable. The use of this LWP cable is policy decision of the user.
This cable family differs from the previous family, MINISUB 16C, in the following respect.

Whereas the foundation previously comprised a plastic central tube surrounded by a copper tube, the design of the new MINISUB CT cable omits the plastic tube [3]. The central copper tube, while smaller in diameter, provides more space for the fibers to isolate themselves from any mechanical influences acting on the outer cable layer.

For all projects, cables are used that incorporate the latest technology. Since only passive transmission devices are employed under water, there is no problem in using a high fiber count (e.g. 48 fibers). Systems, however, that incorporate repeaters (e.g. Transatlantic links) employ 6 fibers on average.
The transmission equipments are accommodated for easy access on land in existing exchanges or repeater stations. This facilitates replacement or expansion and makes maintenance significantly easier. A further advantage is the significant reduction in the cost and weight of the cable material through considerable savings in the copper and steel content, this weight reduction also resulting in simplification of the installation equipment.

Test Results

The fiber excess length reduces the risk of fiber damage particularly for high fiber-count cables. This is illustrated in Fig. 10 and 11 by the tensile test. In Fig. 10 it can be clearly seen that the cable elongates first until, at about 0.3 %, the fiber is slightly elongated. In Fig. 11 this behavior can be seen at up to 80 % of the rated tensile strength of 50 kN, with the fiber attenuation remaining virtually unchanged in the region of measuring uncertainty.

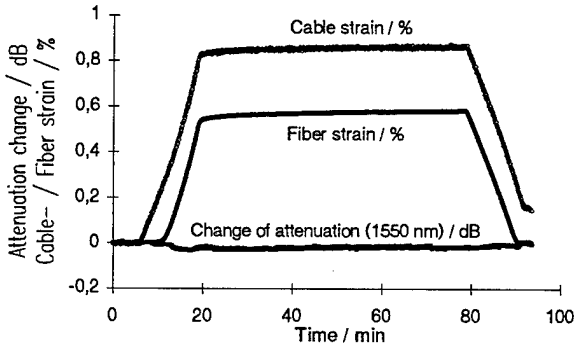

Fig. 10 Tensile Test on Submarine Cable LW Minisub CT to 80 % of Tensile Strength

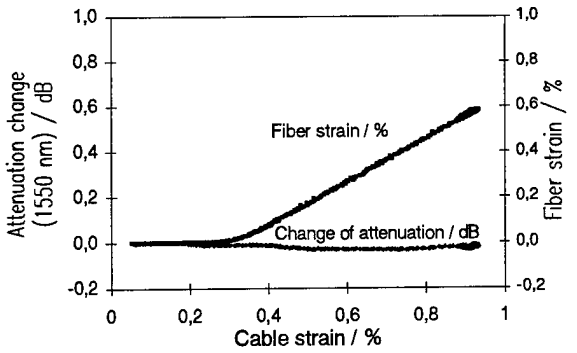

Fig. 11 Tensile Test on Submarine Cable LW Minisub CT to 80 % of Tensile Strength

Methods of Laying Submarine Cables

The compact yet lightweight MINISUB cables are relatively easy to install [4]. This enabled us to be the first company to use so-called flatback ships [3] for this purpose. These deepsea vessels are significantly less expensive to maintain than special-purpose cable-laying ships (Fig. 12).

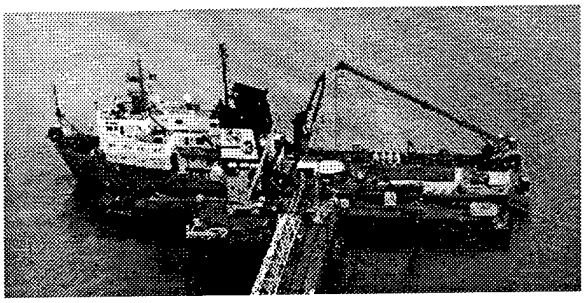

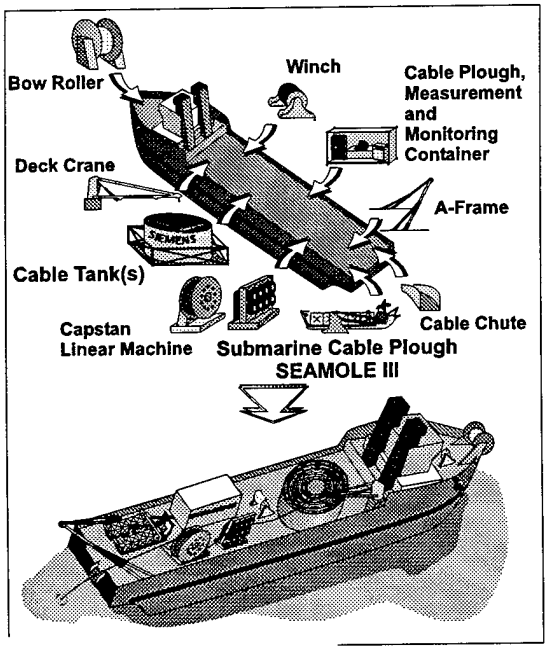

Fig. 12: Rigging of typical Supply Vessel used as Cable Laying Ship

In addition, they are more maneuverable, have a high towing capacity and provide adequate space on deck for the laying equipment.
The maximum weight of the transport tanks used for the purpose is up to 140 tons. (Fig. 13).

Fig. 13: Submarine Cable Tanks (up to 140 to) and Cable Drums for land sections

The submarine cables are plowed in at water depths of up to 500 m along the shore with computer-aided underwater cable plows (Fig. 14).

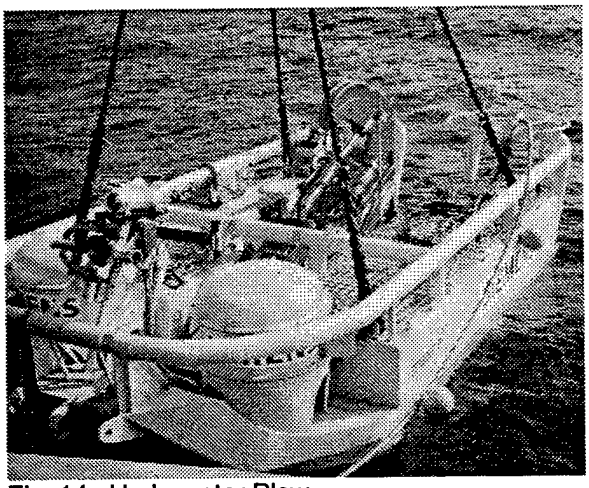

Fig. 14 : Underwater Plow

For this application the cables are generally protected by additional armoring layers (Fig. 9).
By using the smaller and stronger copper central tubes and reducing the steel wires in the first armoring layer the MINISUB CT cables are more compact than the previous family and have a higher density (3.4 g/cm³ as compared with 2.8 g/cm³). They thus sink deeper into the seabed so that there is little risk of sedimentary rock re-exposing the cables once they have been plowed in.

Practical Experience

Some 6000 km of the LW MINISUB™ CT submarine cable have already been successfully laid (Fig. 15).

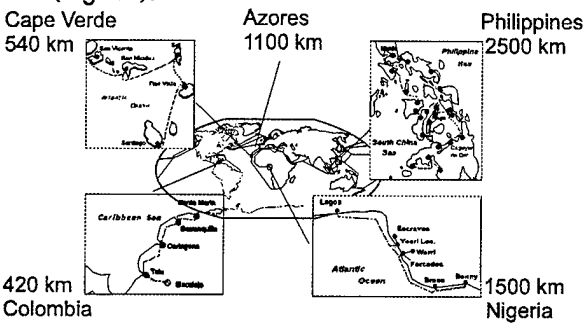

Fig. 15 Overview of Completed Projects with 6000 km of Submarine Cables Laid

In the latest project seven islands were interconnected by means of an optical fiber ring. Submarine cable totaling 1100 km was laid in the Azores; the longest section of the link being 386 km. It is thus one of the world's longest repeaterless submarine cable links (Fig. 16).
The entire link is administered by means of a modern SDH network management system. The new fiber-optic network is suitable not only for telephony but also for all other modern telecommunication applications, such as multimedia, Internet, video conferencing etc. The maximum transmission rate is 2.5 Gbit/s, this is roughly equivalent to the text of 150,000 DIN-A4 pages per second or some 32,000 simultaneous telephone conversations in digital quality.
For the 386 km long segment the remote pumping technique was employed with an erbium doped optical fiber located about 80 km from the end of the transmission link to amplify the signal after being attenuated over 300 km. The optical pump power is fed from the end of the cable via the fiber transporting the signal (1550 nm) but at a different wavelength of about 1470 nm. The pure silica core fibers employed were selected for this segment with reference to their:
- loss at 1470 nm and 1550 nm,
- mode field diameters to minimize splice losses,
- dispersion at 1550 nm so that all 12 fibers have approximately the same signal distortion which can be canceled with 12 dispersion compensating fibers.

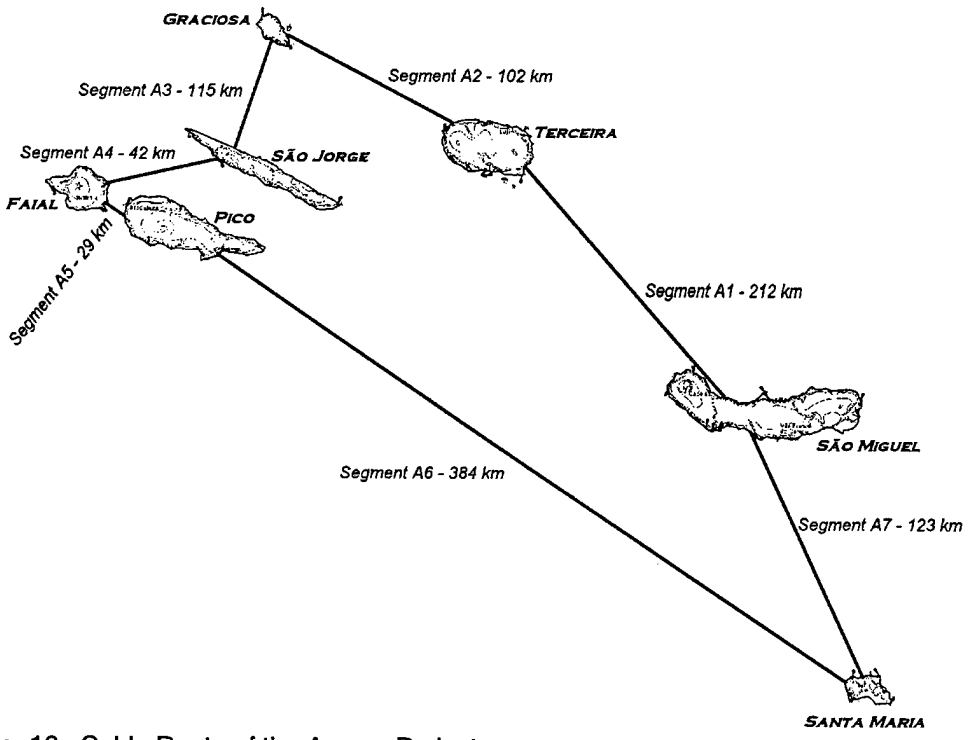

Fig. 16 : Cable Route of the Azores Project

The attenuation constant realized at a wavelength of 1550 nm was significantly smaller than 0.18 dB/km.
In order to measure this, special techniques were required because the erbium doped amplifier fibers absorbed the test signal at 1550 nm.
With this relatively small attenuation constant it is possible to implement links longer than 400 km.

CONCLUSION

With the presented cables with metal tubes we have set new standards in today's fiber optic cable technology.

The result, MINISUB, is a submarine cable specially designed for the use without repeaters. Due to its small outer diameter the MINISUB cable can be laid by small, general purpose ships, at high laying speed and provides low-cost maintenance.
The MINISUB system is suit for use at depths of up to 6000 m and for repeaterless distances of 400 km and more.
To meet the requirements of increasing transmission capacity in telecommunication networks, we developed submarine cables with up to 48 fibers.

The qualification of the new 96- and 144-fiber Optical Ground Wire Cables was presented. These cables with metal tubes fulfill all demands of OPGW, i.e., high strength, high short circuit current and best attenuation at low temperatures. Their excellent performance in practical use is guaranteed by the central tube design with the fiber excess length.

REFERENCES

[1] C. Unger, W. Stöcklein, A. Roller, W. Schweiker : Complete Range of Optical Aerial Cables with Plastic and Metal Tubes, ITG Conference, Cologne, 1996

[2] C. Unger: Characterizing the Optical Bending Properties of Single-Mode Fibers in Communication Cables, VDI-Verlag, series 10, No. 308, 1994, chapter 6.3

[3] D. Felicio: A non-repeteared achievement. telcom report, 19 (1996) No. 5

[4] H. Etzkorn, D. Koch: A non-repeated installation venture. SUBOPTIC, San Francisco, 1997

AUTHORS

Dr. C. Unger

NSW GmbH
Kabelstr.
D-26954
Nordenham
Germany

Fax:
04731-82-535,

Dr. G. Zeidler

Siemens AG
ÖN NK E
Kistlerhofstr. 170
D-81359
München

Clemens Unger was born in Blankenburg, Germany, in 1967. He received the degree in physics from the University of Jena, where he worked on fiber lasers and ultrashort pulse generation. He finished his Ph.D. work about micro- and macrobending behavior of cabled fibers at the Siemens Fiber Optic Cable Development Department in Neustadt/Coburg in 1994.
In 1995 he got the responsibility for a group at the Development Department of Siemens in Nordenham. He was especially involved in the progress of OPGW and fiber optic submarine cables of metal tube design.
In 1998 Dr. Unger joined the Norddeutsche Seekabelwerke GmbH as the Manager Sales and Development of Communication Cables.

E-Mail:
Clemens.Unger(a)p1.nhm1.siemens.scn.dbp.de

Dr. Günter Zeidler was born in 1940 in Rosshaupt, Germany. After his study of electrical engineering at the Technische Iniversität München he joined the Central Laboratory of Siemens & Halske where he worked on lasers in different positions.
Since 1969 he was responsible for a department in the Siemens research lab, working on fibers, integrated optics and fiber optic systems.
In 1976 he transferred to the business unit telecommunication cables, where he started to build up the fiber optic cable technology group.
Since 1992 he covers the position of the director of the development department.

E-Mail:
Guenter.Zeidler(a)mch400.siemens.scn.dbp.de

THE NEW 160 GIGABIT WDM CHALLENGE FOR SUBMARINE CABLE SYSTEMS

JF. LIBERT - JL.LANG - J. CHESNOY

ALCATEL SUBMARINE NETWORKS
536 Quai de la Loire -B.P. 849 - 62225 CALAIS FRANCE

ALCATEL SUBMARINE NETWORKS
Centre de Villarceaux - 91 625 NOZAY CEDEX FRANCE

1. ABSTRACT

Today's challenge is to design the 160 Gbit/s generation of undersea networks, before entering the Tbit/s era. Future technologies include new fibre, the Large Effective Area Fibre (LEA Fibre), new O/E components and 980nm pumps, for the submarine market, as well as new terrestrial interconnection. Once again undersea fibre optic cables are being called upon to enable this second WDM revolution.

2. INTRODUCTION

The emergence of optical amplification and SDH (Synchronous Digital Hierarchy) terrestrial networks have opened up a new range of networking opportunities in the submarine communication domain. WDM (Wavelength Division Multiplexing) technology combined with optical amplification has now become a reality for transoceanic networking. The first decision was made to go to utilise WDM at 4 to 8 times 2.5 Gbit/s and many new systems will implement this WDM technology beneath all oceans over the planet. Now a technology extension towards 16 wavelengths for large projects has been demanded.

Submarine cables have succeeded in meeting the demands of WDM technology through careful attention to the fibre properties needed for the satisfactory transmission of the signal. Dispersion management of the Non Zero Dispersion Shifted Fibre (NZ-DSF) needed in WDM systems has led to the development of new submarine cables. For example the 17mm OALC 4 cable (see figure 1) of Alcatel fully satisfies the constraint of maintaining low attenuation and low Polarisation Mode Dispersion (PMD) over the 25 year lifetime of an undersea system [1],[3].

For the next generation of systems, the same requirements that led to the development of 2.5 Gbit/s based systems for connection to the SDH STM-16 backbone terrestrial networks, has opened the way to the 10 Gbit/s basic bit rate and an n X 10 Gbit/s WDM aggregate. SDH STM-64 is thus the driver of this new terabit system [2]. Alcatel is now offering a OALW 160 family of undersea networks which has a capacity of 160 Gbit/s per fibre pair operating at 10 Gbit/s, making it suitable for use in future networks. This new system will be implemented on two large network loops, one in the Atlantic and one in the Pacific in the year 2000.

3. DEVELOPMENT

3-1 System evolution and constraints

3-1-1 WDM systems

The configuration of a WDM submarine system is described in Figure 2. The system is directly connected to the SDH equipment of the terrestrial networks.

The enabling key elements of WDM submarine technology are the following:

- broadband WDM amplification by erbium doped fibre amplifiers in the repeaters
- maturity of WDM active components (lasers and integrated laser modulators) in the terminals
- maturity of WDM filtering components and especially photorefractive filters for gain flattening in the repeater and for channels selection in the terminals.
- availability of digital STM-16 routing elements (ADM and crossconnects) that permit rerouting while using passive reliable submarine Branching Units (BU).
- properties of the WDM transmission fibre in the submarine transmission cable. The Non Zero Dispersion Shifted Fibre has low

attenuation and low PMD and, in order to decrease the interactions of the WDM channels during transmission, the dispersion is managed in the cable by alternating every 500 to 700km a cable section with standard Single Mode fibre (SMF) to keep the average dispersion close to zero.

3-1-2 10 Gbit/s transmission per channel

Recent discussions about submarine systems with an overall capacity of 160 Gbit/s have raised two questions:

- whether to use a 16 × 10 Gbit/s product, or a 32 × 5 Gbit/s system with the same overall capacity;
- whether the interface bit rate with terrestrial systems to be used at the beginning of the next millennium should be 2.5 or 10 Gbit/s.

The transmission of WDM channels at 5 Gbit/s has been successfully demonstrated over transoceanic distances for a number of years, but this is a non standard bit rate access. Various other factors have led Alcatel to choose a 16 × 10 Gbit/s solution together with 10 Gbit/s access for the new generation of systems. The main driver for this decision is the connection to the terrestrial network which will be SDH STM-64 (10 Gbit/s) following the deployment of the STM-16 (2.5 gbit/s). A key argument for using 10 Gbit/s access is that the equipment in the terminal stations will be 2 to 4 times less than that required at 2.5 Gbit/s.

WDM channels operating at 10 Gbit/s have to cope with additional transmission penalties measured by a Quality factor Q. Compared to operation at 2.5 Gbit/s, the signal to noise degrades by 6 dB and at the same time the ratio of nonlinear transmission penalty is increased by several dB. This means that the system has to be improved drastically compared to the present 2.5 Gbit/s WDM system to permit transoceanic distances based on 10 Gbit/s channel transmission. In addition to a reduction in repeater spans, evolution of the system will imply:

- return to Zero (RZ) modulation for improving the transmission of 10 Gbit/s channels.
- 980 nm pumping of the repeater (in place of 1480nm) to reduce the amplifier noise figure by 1 dB.
- digital signal processing to improve Forward Error Correction (FEC) technology, allowing a performance improvement of about 2 dB.
- 80 µm² effective area of the line fibre in order to increase the optimum output power by around 2 dB. Large Effective Area Fibre is a key improvement of the system.

Fig 3 summarises the benefits of the different technologies for the system. Considering that an optimised laboratory system demonstrates the limit of acceptable transmission (Bit Error rate 10^{-13}). An addition of 5 dB in the system margins are necessary for commercial systems (from industrial production margins to ageing margins). The different curves in figure 3 are positioned versus experimental results obtained on a transmission test bed in Alcatel. It is clearly seen that for different levels of achievement of the technology, different distances are realizable, from 4000km with the present technology (1480nm pumping, standard NZ-DS fibre) to 7000-8000km with the benefit of the above technology improvements.

3-2 Cable

3-2-1 Cabled fibre specifications

Not only are improvements in the effective area of the fibre important, but also a number of other fibre parameters have to be maintained or improved in order to gain the benefit of the effetive area increase :

- Large effective area is a key factor as discussed above. It allows an increase of the optical power in the line leading to a margin in proportion to the effective area: 2dB for 80 µm² versus 50 µm² Effective Area.
- Attenuation has to be maintained as close as possible to the 0.205 dB per km value. Increase by 0.04dB/km of the fibre attenuation completely neutralises the benefit of the increase of effective area from 50 to 80 µm². Figure 4 shows the compromise between attenuation and effective area. The benefit of the large effective area can be preserved for a hybrid section (50% LEA Fibre, 50% standard NZ-DS Fibre) and is also illustrated.
- The nonlinear coefficient n2 also has to be maintained or reduced when compared to the standard NZ-DS Fibre since the maximum optical power that can be launched is in fact propotional to Effective Area/n2. Thus the specific doping to get the increased Effective Area should not negatively impact the non linear coefficient.
- Polarization mode dispersion (PMD) must be reduced to values below 0.1 ps/sq(km).

This constraint on PMD is directly given by the constraint of having an overall cumulated PMD broadening in the line below 1/10 of the bit duration.

- Dispersion slope has to be as small as possible. A large slope results in the different channels having different compensation schemes in the terminals. It also reduces the efficiency of the in-line compensation for the side channels over longer distances.
- Stability of parameters during fibre production is an other important characteristic. For example, the in-line reperters can compensate for the attenuation slope (variation of the attenuation with wavelength), but only if the value is stable. In the same way the fibre attenuation must be low and stable. A paradox is that if the fibre has a better attenuation than specified, this improvement can not be used.

3-2-2 Experiment

Among all the parameters mentioned above, some of them are more critical than others in terms of stability. These are the attenuation loss and the attenuation slope within the signal wavelength range.
The other parameters, are either intrinsic to the fibre design (effective area, chromatic dispersion slope, non linear coefficient n2) and are quite stable, or their potential evolution is very well known, as zero dispersion wavelength with regard to temperature for instance, or as PMD with regard to cable induced stress.
In this section, we will focus on the stability of cabled large effective area fibre attenuation loss and attenuation slope. These two parameters result from a compromise between macro bending and micro bending fibre sensitivity and between macro bending and micro bending level induced by the cable structure.

Fibre Evaluation and Selection through macro bending and micro bending tests.

Fibre selection can be achieved in a number of ways. The most realistic is to evaluate fibres in cable trials, although this can take sometime. A less time-consuming alternative is to perform micro bending and macro bending tests on fibres at incoming stage and then set a limit value on sensitivity levels. The difficulty is to devise tests which are both accurate and as representative as possible of what the fibre will be submitted to during the cable manufacturing process, cable ship loading, cable laying and recovery, and in service life.
In order to overcome this difficulty, two tests are proposed.

1- Long length test on wire mesh (see fig. 5)

700 m of fibre are used for this test.
In stage one, the fibre is wound tension free in one layer on a bobbin of 400 mm outer diameter. The bottom of the bobbin is clean and smooth. After relaxation, spectral attenuation is performed within the range 1400 - 1600 nm.
In stage two, the same 700 m fibres are wound in one layer on a bobbin of 400 mm outer diameter under 80 gr take up tension. The bottom of the bobbin is covered with wire mesh. The size of the wires is 50 µm OD and the spacing between wires is 100 µm. After fibre winding, spectral attenuation results is performed again, within the range 1400 - 1600 nm.
Finally, the spectral attenuation result at stage one is substracted from the spectral attenuation result at stage 2. Figure 6 shows the results obtained. It should be noted that the difference between repeated measurements is better than 0.005 dB/km.

Principal points of interest in this test are:

- the long length of fibre tested
- the ability to repeat the measurements

In addition, the level of attenuation increase is quite low, 0.1 to 0.5 dB/km at 1550 nm, when compared to conventional tests performed on short length samples.

2 - Macro bending test (see Fig. 7)

In stage one a short fibre sample is optically measured with a 1550 nm laser emitter and receiver. The fibre sample is straight and stress free.
In stage two, the same fibre sample is submitted to a half loop in the middle. The radius of the loop can move in the range 7 mm - 18 mm in 1 mm increments from 7 mm up to 18 mm and then from 18 mm down to 7 mm.
At each increment, the measurement is performed three times.
Figure 8 gives an example of the result obtained with this test.
The main interest of this test is to give attenuation loss versus radius on the same fibre sample, on a continuous process. The limitation in the lower radius range is due to the dynamic of the E/R optical equipment ($\simeq$ 50 dB). The limitation in the higher radius range is due to the limit of detection of the E/R optical equipment ($\simeq$ 0.01 dB). It has to be noticed that an extrapolation can be made on higher radii than those measured.

Experiment on large effective area fibres

Experiments were carried out on five fibre designs ; types A,B,C,D,E. The effective area covered the range 50 μm^2 - 80 μm^2.
Table 1 gives typical characteristics of these five designs.

Fibre type	Aeff (µm2)	Cut off wave-length (nm)	Chromatic Dispersion at 1560 nm (ps/nm/km)	Macrobend sensitivity ϕ20mm at 1550nm (dB/m)	Wire mesh sensitivity at 1550nm (dB/km)
A	58	1290	-1.9	7	0.1
B	71 to 73	1400 to 1610	-1.76 to -3.3	10 to 90	0.2 to 2.2
C	80 to 83	1420	-1.1	19 to 20	0.09 to 0.12
D	70	1450	4.9	4 to 9	0.11 to 0.16
E	67 to 71	1480 to 1570	-0.48 to -1.9	2 to 10	0.3 to 0.66

Table 1 : Typical fibre characterisics

These five designs were submitted long length wire mesh, macro bending and cabling tests.

Figure 9 shows the results obtained from long length wire mesh testing.

Figure 10 shows the results obtained with microbending tests with a constant bending radius of 10 mm.

- Fibre design A exhibited the lowest attenuation increase. This was due mainly to the quite small effective area.
- With fibre design B the beneficial effect of the high fibre cut-off wavelength was very noticeable.
- Fibre design C had a quite high effective area (80μm^2). It exhibited very good performances, with regard to wire mesh test, but not very good macrobending performance.
- With fibre design E, it is interesting to note the dual beneficial effect of lower effective area and higher cut-off wavelength (67 μm^2, 1570 nm to be compared with 71 μm^2, 1480 nm).

Figure 11 shows the evolution in attenuation loss of the five fibre designs, after cabling.

It is interesting to note the correlation between results obtained from the wire mesh + macrobend tests with the results obtained from the cabling tests. The fibres exhibiting very poor performances in the wire mesh + macrobend tests give a very bad performance after cabling.

Figure 12 gives the attenuation slope within the system wavelength range [1547 nm, 1560 nm] for 2 fibres after cabling. One of these two fibres had good performance with regard to wire mesh and macrobending tests. In this case we can see that the attenuation loss slope is 0.0002 dB/nm/km which is similar to results on bare fibre.

The other fibre has very poor wire mesh and macrobending performances. The attenuation loss slope is < 0.0001 dB/nm/km which is very different from the result on bare fibre.

It is then possible to set some limits in wire mesh and macro bending performances, at fibre incoming stage, which guaranty a good behaviour and stability of the fibre after cabling.

4. CONCLUSION

The 160 Gbit/s WDM longhaul submarine system requires the use of new O/E components, 980 nm pumps, new terrestrial interconnections, and large effective area fibres.
Selection of fibres can be made trough a proposed cabled fibre specification in order to guarantee system perfomance.
In addition, the two proposed wire mesh and macrobend tests can be used as fibre incoming tests to ensure the stability of cabled fibre attenuation loss and slope.

5. REFERENCES

1- JF.LIBERT, JL. LANG, D. CURTIS and P. WORTHINGTON : Optical performance of Submarine Cables in optically amplified high bit rate systems, IWCS (1995)

2- J.CHESNOY and J.F.MARCEROU - Challenges and perspectives of the next generation of transoceanic networks Suboptic, San Francisco (1997)

3- Y. CHARLES, JF. LIBERT, P. WORTHINGTON, JL.LANG : A new high bit rate submarine product range . The OALC 4 cable, IWCS (1997).

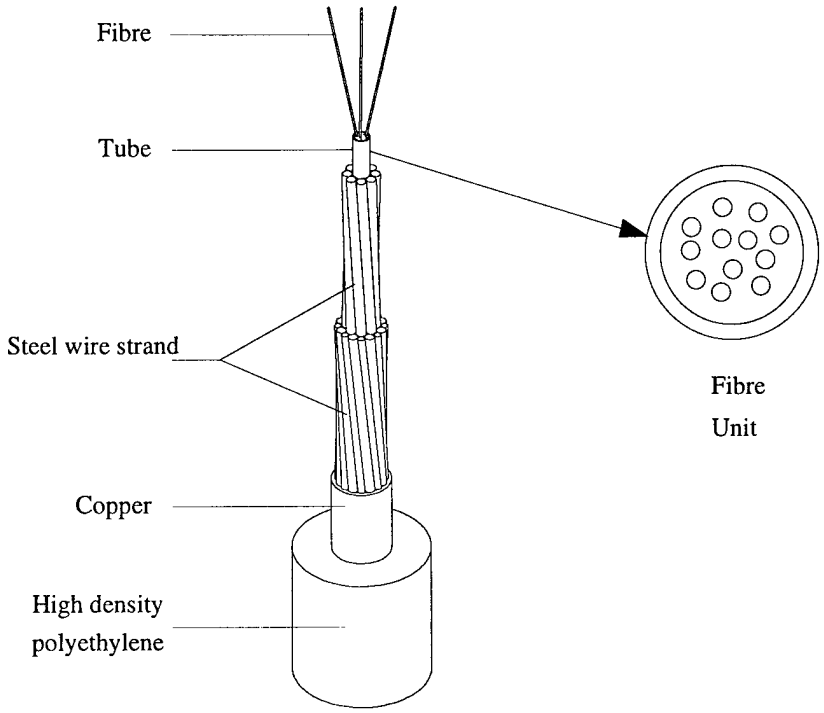

Figure 1 :
Description of the LW OALC 4 cable

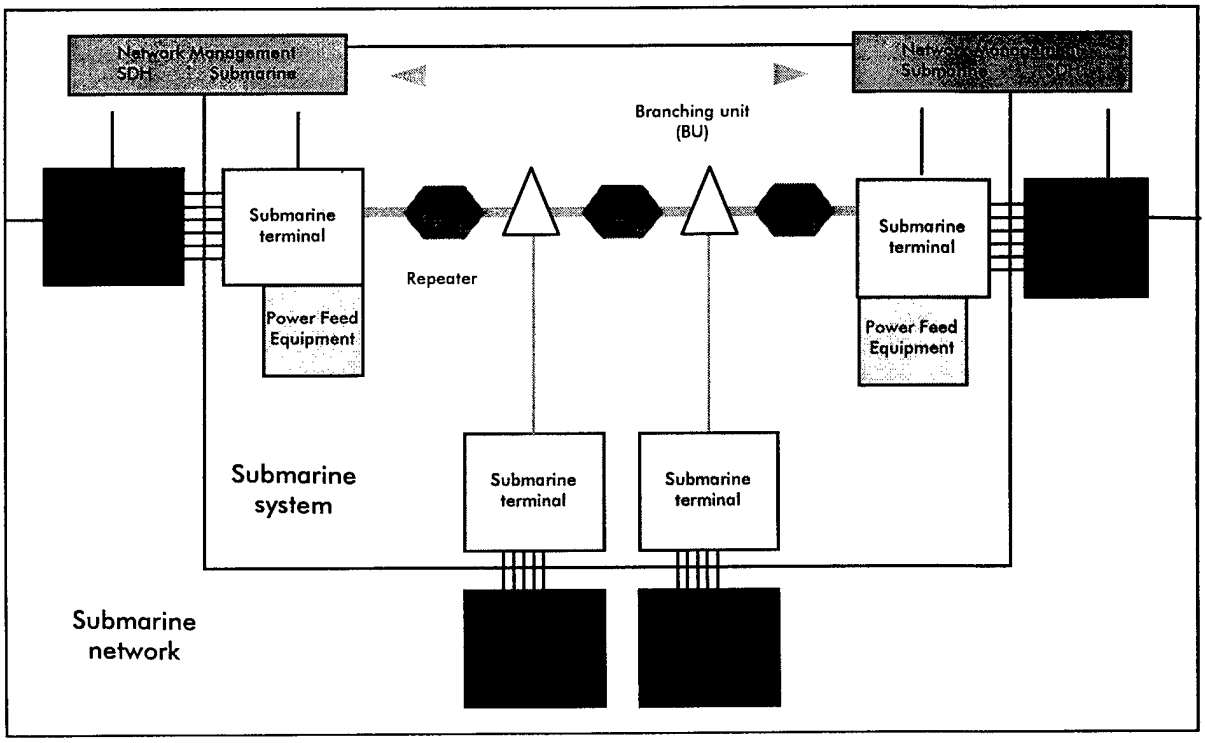

Figure 2:
Configuration of a WDM submarine system and related equipment.

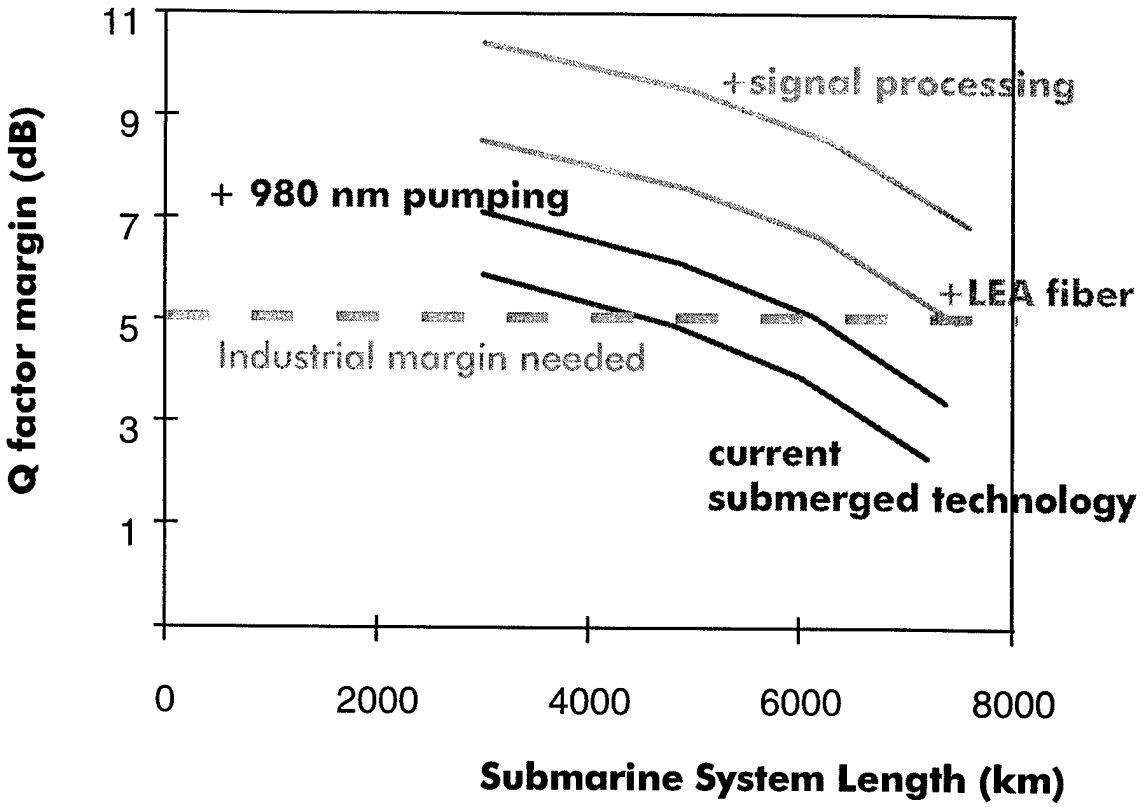

Figure 3
Achievable performances of 16 x 10 Gbit/s transmission for different technology implementations

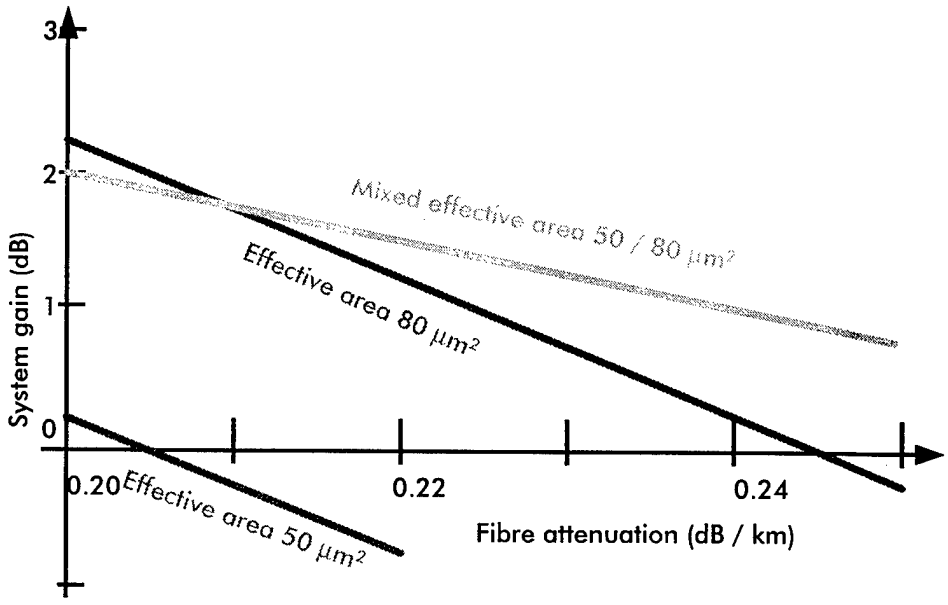

Figure 4 :
Compromise between attenuation and effective area of the fibre

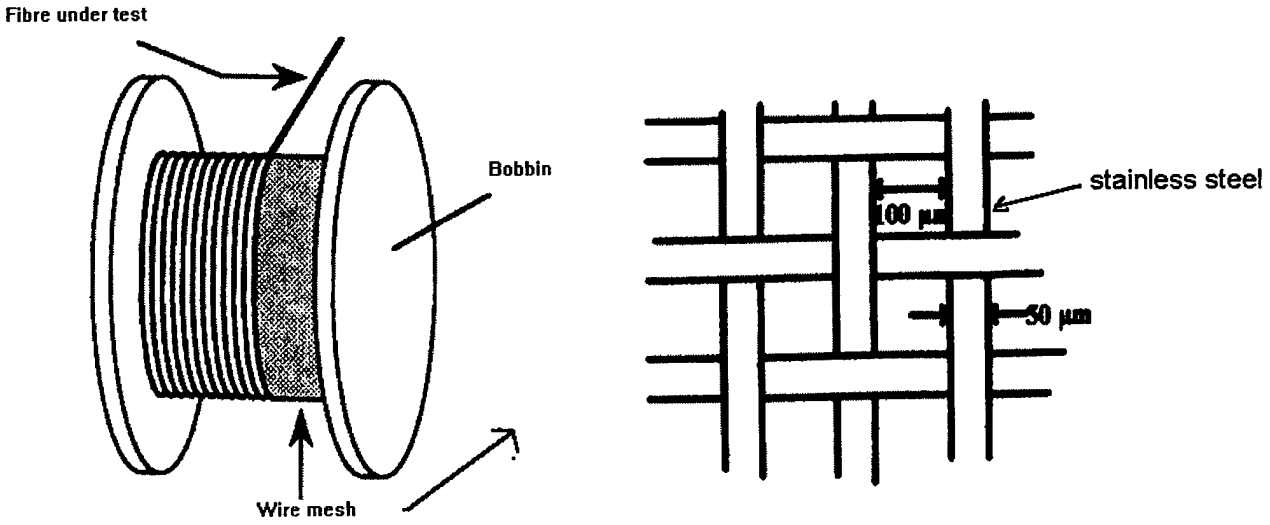

Fibre length under test : 700 m
Bobbin Diameter : 400 mm
Take up tension : 80 gr

Figure 5 :
Description of the long length wire mesh test

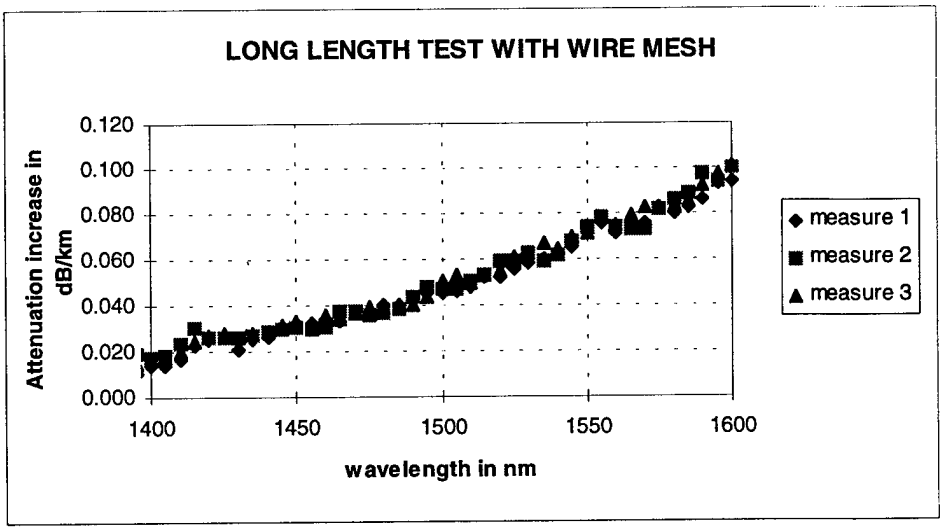

Figure 6 :
Comparisons of repeated long length wire mesh tests

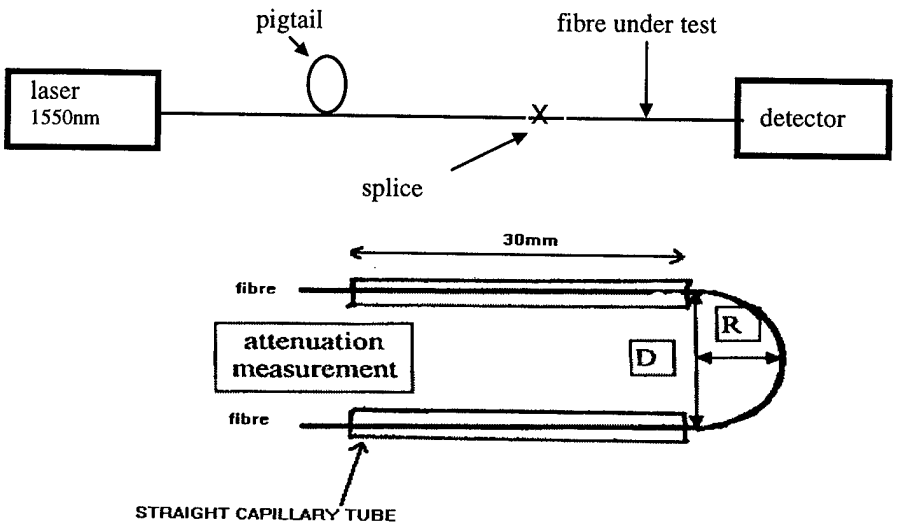

Figure 7 :
Description of the macrobending test

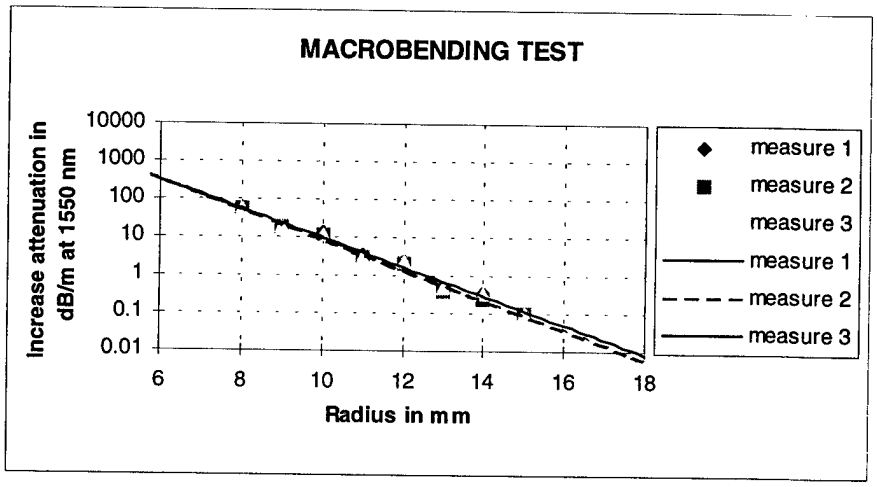

Figure 8 :
Repeated Macrobending test

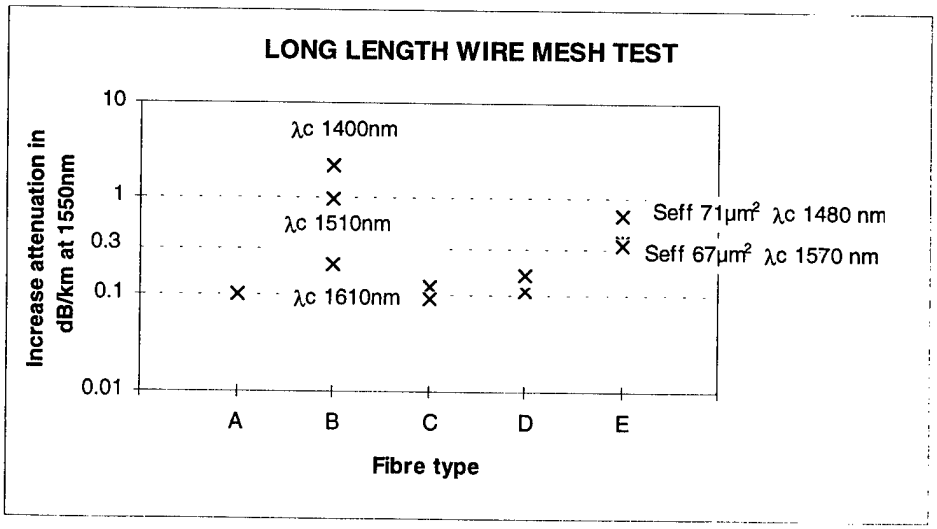

Figure 9 : Long length wire mesh test

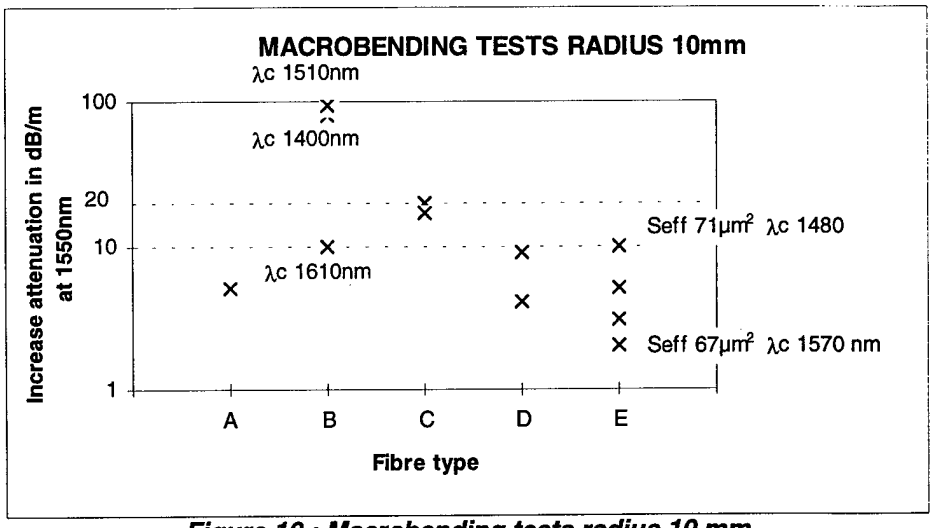

Figure 10 : Macrobending tests radius 10 mm

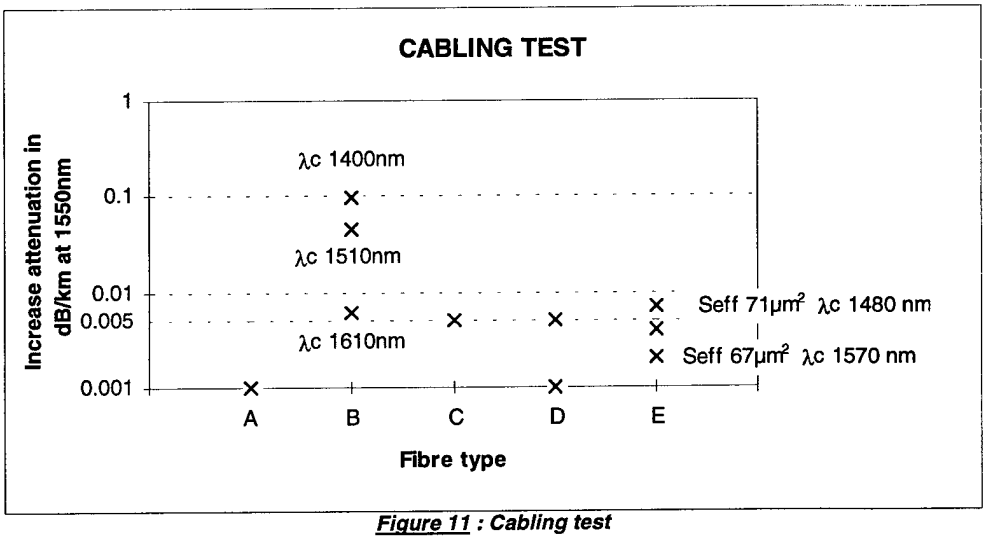

Figure 11 : Cabling test

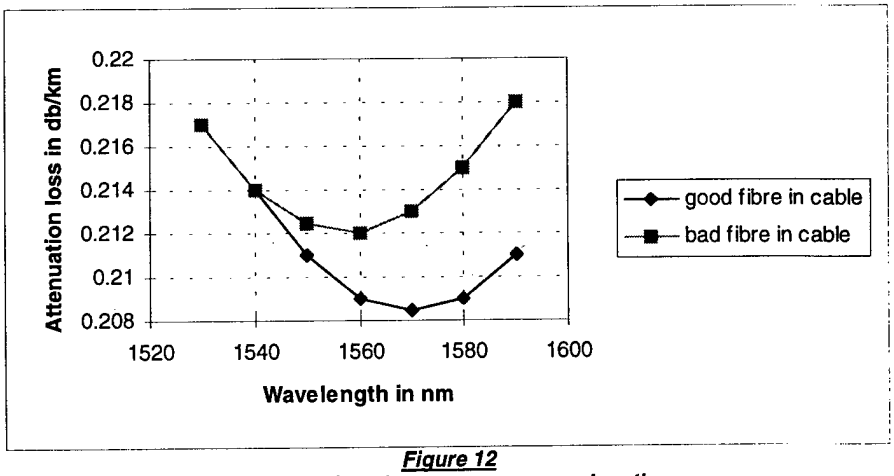

Figure 12
Attenuation changes versus wavelength

BIOGRAPHIES

José Chesnoy

Manager, Network and Systems Division,
Technical Directorate

Alcatel Submarine Networks

Born in 1954, José Chesnoy is a graduate of Ecole Polytechnique, Paris, (1974) and a Doctor of Sciences (Orsay 1981).

After beginning his career in the national research organisation CNRS in laser physics and non-linear optics, he joined Alcatel Alsthom Recherche in 1989 and became manager of the photonic and electronics division in 1990. In 1993, he was appointed manager of the fibre and photonic system department in Alcatel Alsthom Recherche. From 1991 to 1995 he was also responsible for the research activities on optical systems and fibres at the corporate Alcatel Alsthom level.

In 1995 Dr. Chesnoy joined Alcatel Submarine Networks as manager of the network and systems division within the technical directorate. Currently his principal work is on optical systems and networks for submarine applications.

Jean-Luc Lang

Manager of the Optical Transmission in the
Technical Department
Alcatel Submarine Networks

Jean-Luc LANG received his degree from the Institut Universitaire de Technologie of ORSAY (FRANCE). He joined Alcatel in 1975, and is currently working in Calais on optical transmission for undersea systems.

Jean-Francois Libert

Technical Manager, Optical Submarine Cable
Alcatel Submarine Networks

Jean-Francois Libert received his engineering degree from Hautes Etudes Industrielles of Lille (France). He joined Alcatel in 1984 and is currently based in Calais having responsibility for the design and development of fibre optic telecommunications cables for the undersea networks supplied by Alcatel.

STUDY OF ABRASION RESISTANCE BEHAVIOUR FOR DIFFERENT SUBMARINE CABLE PROTECTION METHODS

Yves CHARLES - Ian HOUGHTON - Jean-François LIBERT - Peter WORTHINGTON

ALCATEL SUBMARINE NETWORKS
536 Quai de la Loire - BP 849 - 62225 CALAIS FRANCE

1. INTRODUCTION

Today, more than 2 million simultaneous communications are carried in a single undersea canal; the submarine cable. Such capacities drive cable designers and system owners to consider optical cable system reliability as a key parameter.

High levels of confidence in cable integrity and routing have to be achieved. Cable failure is generally caused by extrinisic factors such as:

- fishing trawling gears
- anchor damage
- lightening surge
- self corrosion
- abrasion and chafing

This paper will focus on the last type of damage on the list, abrasion and chafing.

This type of damage is characterised by the fact that it is not depth limited. Abrasion may occur whatever the system depth, it is the type of chafing which changes. Figure one, from a survey of cable repairs, clearly shows that the percentage of cable failures due to abrasion is independent of depth.-
Hence this paper will consider abrasion phenomena in shallow water and in deep water. For each case it will propose solutions successfully designed and experimented. It will re-emphasise the efficiency of conventional methods to prevent cable abrasion like the selection of raw materials and basic cable design rules. It will also describe original solutions, like the DWP cable, specifically designed to prevent abrasion in deep water.

2. SHALLOW WATER

In shallow water cables have to provide protection both against abrasion and against the examples of external damage described in the introduction. Hence, a standard set of protection is normally provided i.e. armoured cables. These cables are characterised by the use of an overlay of galvanised armoured wires around the sheath of the lightweight cable (LW) which improves the cable resistance against abrasion.

For areas where the the sea bed is very rough extra protection can be provided :

- The double armour cable, in which a second overlay of larger galvanised steel wires is applied on the cable, improves the cable weight, stability and density and thus inhibits chafing.
- The rock armoured cable, characterised by its shorter pitch on the second overlay of galvanised steel wires to provide smaller bending stiffness and hence a better comformance to sea bed profile.
- The use of articulated ductile iron pipes in shallow water, especially in surf zones, eliminates abrasion damage and greatly increases weight and sea bed stability.

These types of protection (see fig 2) with some others like LWP and LWS cables are well-established and well-known in the submarine cable industry and hence are not the subject of this paper. The following focuses on deep water areas, where abrasion phenomena like sea bed stability and cable suspension have to be well understood in order to provide the appropriate cable design for protection from chafing.

3. DEEP WATER

3.1 SEA BED STABILITY

If a cable on the sea bed is subjected to transverse current, it will experience drag and lift forces which are resisted by the cable weight and friction. At a certain velocity, also called critical velocity, relative movement between the cable and the sea bed will take place. If the

current is cyclic (e.g. tidal), then the movement of the cable may take place on each cycle, leading to abrasion by the sea bed material. For stability, a small diameter and high weight in water (i.e. high density) are desirable. For comparing the stability of different cables, we can assume that the cable on the sea bed is affected by a transverse current with logarithmic profile of velocity or height (see fig 3).

The average current acting on the cable ($\overline{V}$) is approximately equal to the current at height $d/2$ above the sea bed. This produces lift and drag forces on the cable:

Lift $P_L = 0.5 C_L \rho d \overline{V^2}$ per unit length

Drag $P_D = 0.5 C_D \rho d \overline{V^2}$ per unit length

where C_L and C_D are lift and drag coefficients for a cylinder, and are both typically 1.2 at flow velocities of interest.

The cable is unstable (moves on the sea bed) if

$$P_D > \mu(w - P_L)$$

where
μ : friction coefficient
w : cable weight in water
d : cable diameter

or $$\overline{V} > \left\{ \frac{2w}{\rho d (C_L + C_D/\mu)} \right\}^{1/2}$$

$\overline{V}$ is the velocity at height $d/2$ over sea bed. For convenience it is the current at a standard height (1.0 m) which is used for comparison of cable stability.

$$V(1.0) = \frac{\overline{V} \ln(1.0/z_0)}{\ln(d/2z_0)}$$

where z_0 = sea bed roughness factor (typically 0.1 mm)

Modern fibre optic cables have a smaller diameter, a higher weight in water and a higher density than earlier cables (see fig 4 and fig 5). These factors result in a significantly improved stability on the sea bed in the presence of transverse currents. Fig 6 shows a comparison of the critical velocity (at 1m height above the sea bed) for a range of fibre optic and coaxial cables.

3.2. CABLE IN SUSPENSION

If cable is laid with insufficient slack over an uneven sea bed then cable suspensions will result. In this situation cable tension and the corresponding stress at contact points will increase with suspension length and the weight of cable in water. If there are sea bed currents present, then the force exerted on the suspended length may cause relative movement between the cable and the contact points.

In addition, the current may cause vibration or strumming of the cable which may increase its relative movement at the contact points. Strumming can occur when natural frequency of the cable suspensions are excited by the vortex shedding frequencies of the transverse current (see fig 7).

The vortex shedding frequency caused by a transverse current U flowing over a cable diameter d is

$$F_S = \frac{SU}{d}$$

when S = Strouhal number and is typically 0.2 for range of sea bed currents of interest.

The fundamental resonant frequency of a cable span of length L is :

$$F_1 = \frac{1}{2L}\left\{\frac{\pi^2 \overline{EI}}{m_e L^2} + \frac{T}{m_e}\right\}^{1/2}$$

$$F_1 = \frac{1}{2L}\left\{\frac{\pi^2 \overline{EI}}{m_e L^2} + \frac{T}{m_e}\right\}^{1/2}$$

$\overline{EI}$ = Bending stiffness
T = Cable tension
m_e = effective mass /unit length

Maximum amplitude of vibration will occur when $F_1 = F_s$, although there will be significant response if F_s is close to F_1, as the vortex shedding frequency tends to lock onto the fundamental resonant frequency of the span.

Note that both the resonant frequency of the cable span and the length of span are dependent on the cable tension T. For comparison of different cables, we assume the same geometry (sag to span ratio) and then:

$$T = \frac{wL^2}{8y_e}$$ y_e = Central sag of span.

Fig 8 shows a comparison of the relationship between the suspension length and the transverse current to excite the fundamental mode (F_1) for a coaxial cable (44 mm dia.) and a fibre optic cable (17 mm dia.). Note that the high bending stiffness of the large diameter coaxial cable means that it is more resistant to strumming for short span lengths. However, for longer spans (>10m), the difference is small.

The best way to avoid suspensions and their potential subsequent chafing problems is to prevent their appearance. Most of the time this is achieved by accurate pre-lay cable route surveys. These provide information like the slopes and the nature of the sea bed profile which enables the correct cable slack to be determined.

Furthermore, during cable-laying operations, software programs give 'real time' help to cable installers to avoid suspensions by the use of an accurate positioning of the cableship, and by a precise mastering of the cable bottom slack and cable tension.

Despite these precautions,hazardous areas remain where suspensions are unavoidable or where strong currents exist . For these areas a specific deep-water abrasion-resistant design has been designed the DWP (deep water protected) cable.

3.3. DWP Solution for Hazardous Areas

Normally in deep water only LW or LWP cables are used. However, the good behaviour of armoured cables in shallow water suggests their use at greater depths is possible in locations where the risk of abrasion is high.

The problem with these types of cables is their tendency to form loops and kinks due to the level of twist built into the cable during cable installation, especially in deep sea where cable tension may become high.

Hence, it was decided to develop an armoured design, suitable for deep-water installation.

The basis of this development was:

- Comparison of abrasion performance of steel versus polymers, in order to establish clearly the merits of the use of armoured cable in deep sea.
- Evaluation and characterisation of cable performances like twist, torque and recovery tension in order to reduce the tendency to form loops and kinks.
- Qualification of the product by mechanical test

This is described more in detail below.

3.3.1. Steel v Polymers in abrasion

Separate data is available on polymer abrasion resistance (e.g. from the Taber test) and steel abrasion resistance (e.g. from the rubber carrier wheel test ASTM G65). However, there was little data available comparing abrasion resistance of polymers and steels, in a way that enabled comparison between cable designs, needed when developing a cable for better abrasion resistance.

Since it was known that abrasion comparisons are highly dependent upon the method chosen, it was decided to give precedence to methods that simulated most closely the abrasion environment of concern.

The test sought was one that rapidly abraded polyethylene insulated lightweight cables, where the wear scar was similar to those recovered from the sea-bed in system repairs.

After some consideration of existing methods, it was decided to develop a specific test. Equipment was made that cycled a rigidly clamped 0.4 m length of cable at 96 cycles per minute on a 130 mm stroke, over a fixed abrasive block 50 mm wide, while immersed in salt water. (see fig 9)

Selection of the abrasive block material was a key issue. Natural sandstones proved too variable to give consistent results, so it was decided to use synthetic materials.

A synthetic abrasive was formulated for this test. This used a silicon carbide (SiC) based abrasive, with particle size 20 grit (relatively coarse), an open structure, and a ceramic bond between the particles, of adhesive grade Q (on a scale A - Z of increasing bond). The open structure assists with avoidance of clogging, particularly relevant to abrasion of plastics. Silicon carbide has sharp edges that rapidly abrade plastics, but become blunt more readily than aluminium oxide when used on steels. The bond grade was chosen with the intention that when used on steels the particles would slowly release, exposing fresh surfaces. However, this did not occur with the 9 kg load used, and the blocks polished instead. Two abrasive types were used.

A fixed load of 9 kg was used in this test. This was done on the basis that heavier cables are generally more stable, so would be expected to move less, which would offset to some degree their higher contact load. The tests were ended when sufficient insulation was removed to expose the cable's power conductor.

Abrasion tests were conducted on LW, LWP and SAL cable. After analysis, the following approximate comparative abrasion resistances were obtained :

Material	Relative Abrasion resistance per unit area
LDPE	1
LMDPE, M/HDPE	2
Steel Tape (370 MPa)	107
Steel armour wire (1500 MPa)	282

As would be expected, the results show that the inclusion of steel gives a large improvement in abrasion resistance, compared to that which can be achieved by polymers.

3.3.2. DWP design & evaluation

The lightweight unarmoured cables that are normally used in deep water offer only limited abrasion protection, and in some cases this may be insufficient.

Furthermore, the better steel performance clearly established confirmed that an armoured cable would be the ideal solution. An armoured cable which generates the lowest torque possible can be achieved by the use of a large number of small wires, but this leads to issues of manufacturing capability, and jointing problems. In addition, smaller wires are more vulnerable to corrosion.

So it was decided to adapt an existing design, the single armour light cable, using alternate wires and fillers to reduce weight. This cable design was given the descriptive name "Deep Water Protected" (DWP). (see fig 10)

This design generates half of the torque under load than standard armoured cable and passed an extensive qualification program. This program was built to check the cable's tensile performance, the stability of its composite structure made with fillers and armoured wires, and the improvement in abrasion resistance that it provides.

3.3.3. DWP qualification

The qualification of the DWP product (cable and joint) included:

- wire stability tests
- abrasion tests
- design study of installation capability
- Loop-kink
- Break load (258 kN) via joint and coupling anchorages
- Load v elongation at NTTS (175 kN)
- Fatigue test at 12 tonne (DWP cable and joint)
- 17 tonne cyclic 3 m sheave test (DWP cable and joint)
- 8 tonne tensile test of DWP connected to NL LWP
- 6 tonne crush test (similar to SAL)

This qualification also included a sea trial, in which a mini system, including joints, repeater and transitions with standard LW cables, was laid and recovered. In parallel, a final splice test was also successfully laid. By this, the successful use of this cable as a repair cable in areas where standard deep-water cables have been damaged was demonstrated and confirmed.

The DWP cable has been used on several systems at depths to 4 km, with over 700 km successfully installed.

4. CONCLUSION

Cable failures caused by chafe represent a small but nevertheless significant risk to cable systems. A theoretical study of the susceptibility of different submarine cables to abrasion indicates that the sea bed stability of fibre optic cables is superior to that of coaxial cables, making them less likely to abrade as a result of movement on the sea bed. Abrasion damage can be minimised by the optimum choice of insulation material. In addition, the presence of suspensions in high sea bed current chafing can be overcome by an increased protection — a very light armoured cable. Such type of optical cable has been developed and successully deployed in trials and system repairs in deep water.

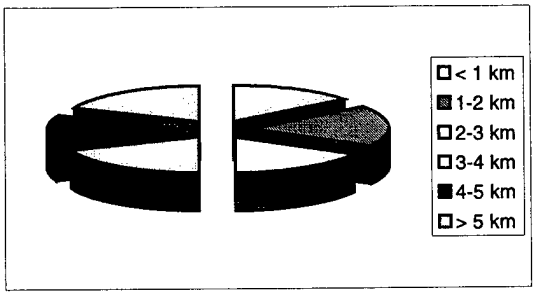

Figure 1 : Distribution of chafe fault by water depth

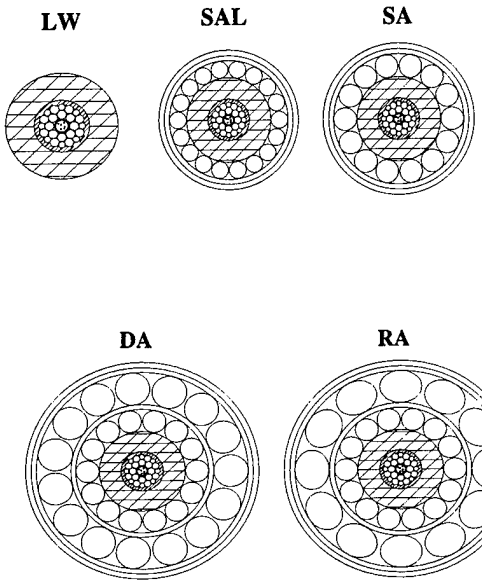

Fig. : 2 OALC 4 cable range and deployment depth

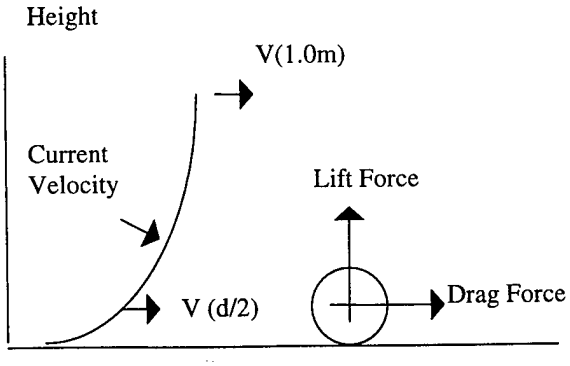

Figure 3 : Logarithmic profile of current velocity above sea bed

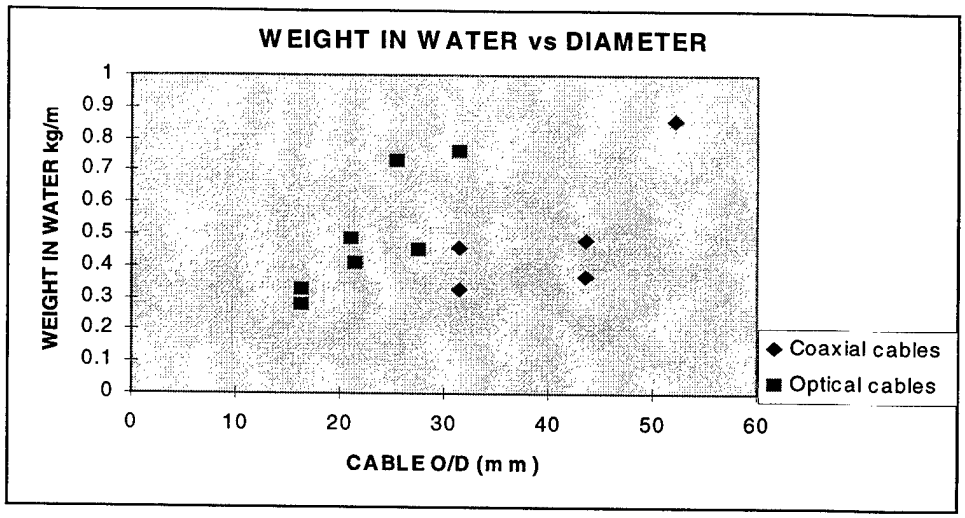

Figure 4 : Cable weight in water of fibre optic and coaxial cables

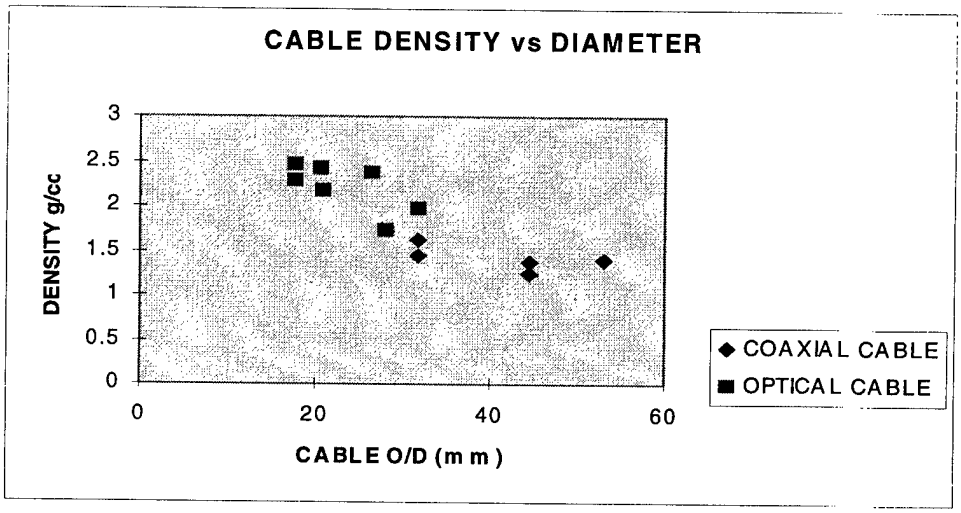

Figure 5 : Cable density of fibre optic and coaxial cables

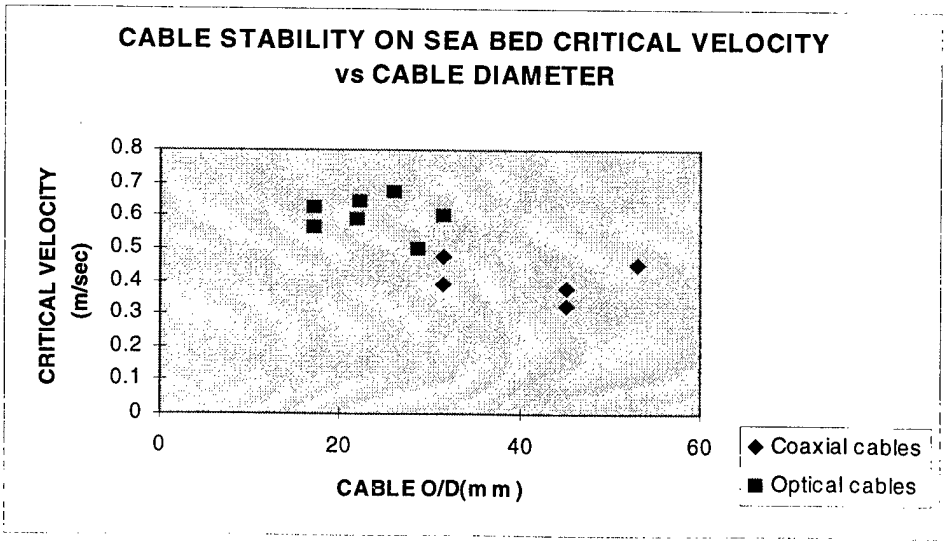

Figure 6 : Cable stability on sea bed of fibre optic and coaxial cables

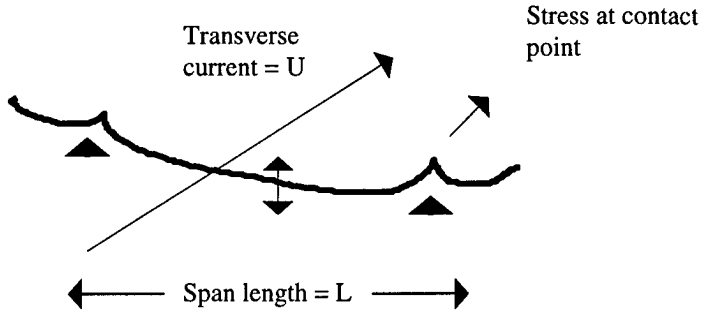

Figure 7 : Abrasion at contact points of cable in suspension

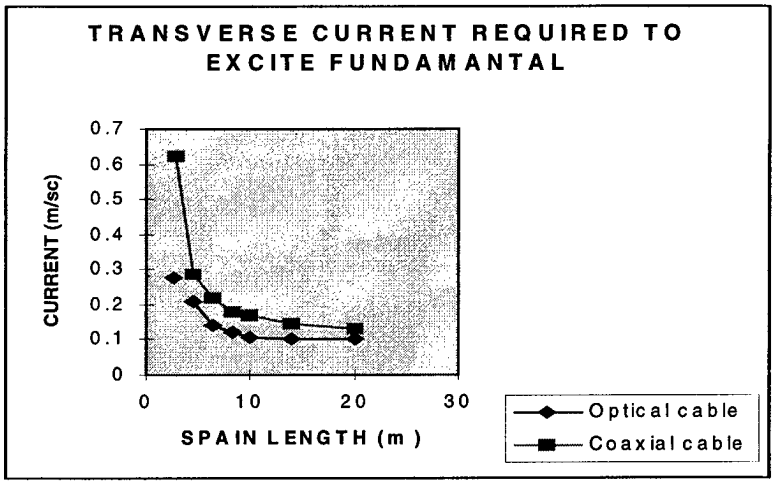

Figure 8 : Transverse current to stimulate strumming

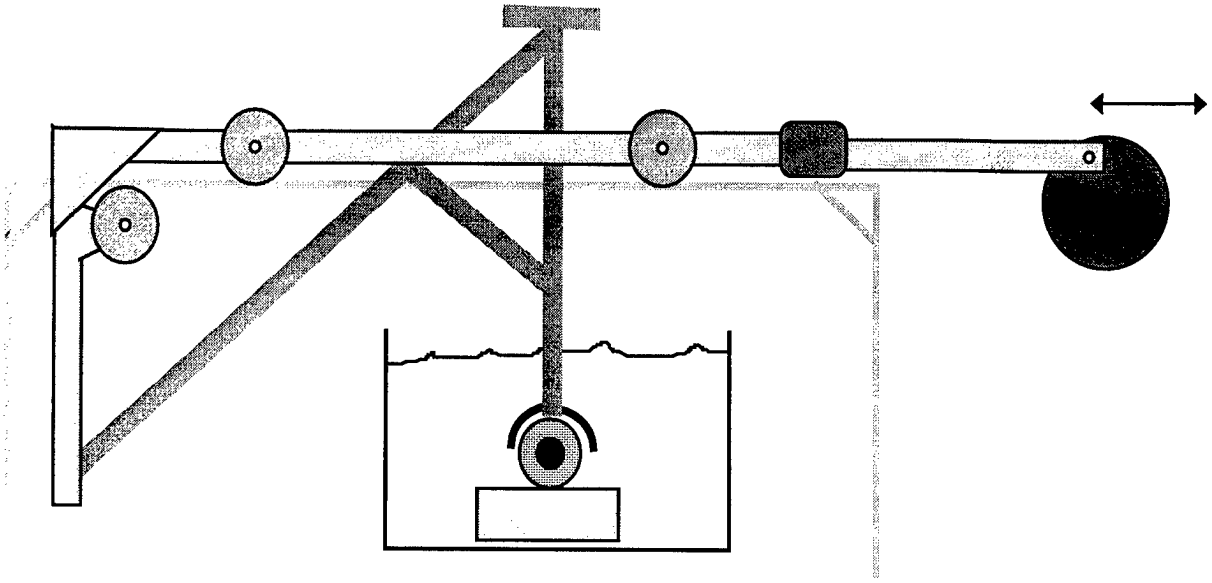

Figure 9 : Abrasion bench

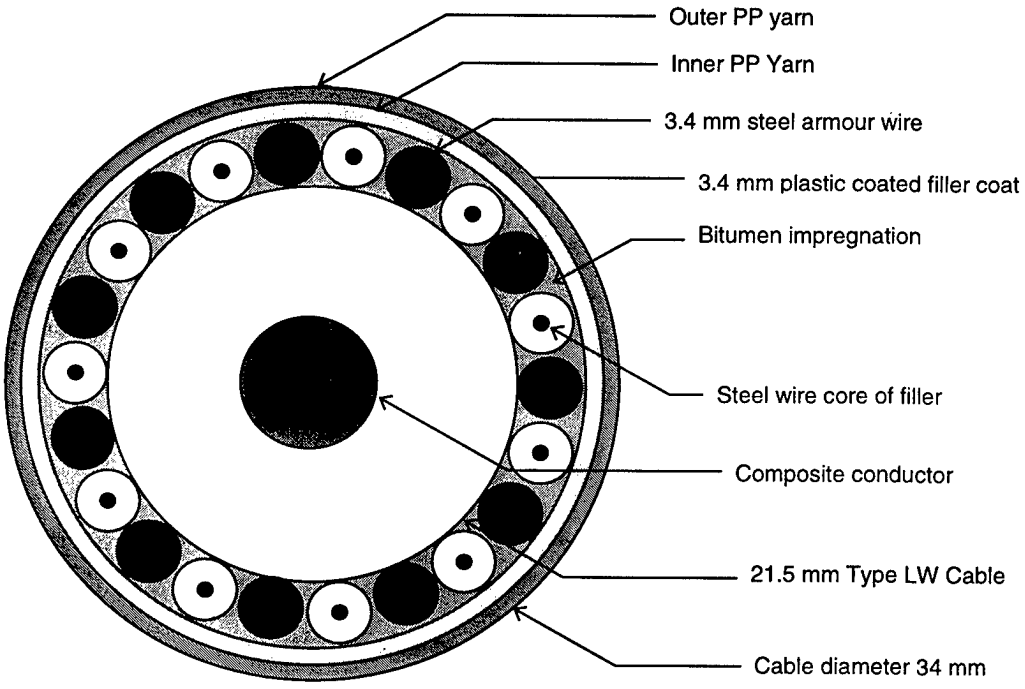

Figure 10 : DWP cable

BIOGRAPHIES

Y. CHARLES
Alcatel Submarine Networks
536 Quai de la Loire
62225 Calais Cedex

Yves CHARLES was born in 1967. He is graduated from Ecole Universitaire Des Ingénieurs de Lille (E.U.D.I.L.). He joined Alcatel in 1993 where he is in charge of cable design and product qualification in Calais, France.

J.F LIBERT
Alcatel Submarine Networks
536 Quai de la Loire
62225 Calais Cedex

Jean-François LIBERT received his engineering degree from "Hautes Etudes Industrielles" of Lille (FRANCE). He joined Alcatel in 1984. He is now Technical Manager for Optical Submarine Cable in Calais.

P. WORTHINGTON
Alcatel Submarine Networks
536 Quai de la Loire
62225 Calais Cedex

Peter WORTHINGTON is a development engineer in Alcatel Submarine Networks. He received a BSc in Electronics and Electrical Engineering from the University of Birmingham in 1971. Since 1977 he has been involved in the development of fibre optic cables for submarine systems.

Ian HOUGHTON
Alcatel Submarine Networks
Port Botany
Australia

Ian Houghton graduated from Sheffield University in 1981, with a BSc in Chemical Physics. Until 1984 he worked as a polymer technologist for Metal Box. He then joined STC, working on land and aerial optical fibre designs and manufacturing processes in Newport, Wales. In 1988 he joined Alcatel as Senior Cable Engineer, emigrating to Sydney to assist with setting up the submarine fibre optic cable factory at Port Botany. He has been involved with many fibre and cable developments, including joints, earthing systems, and cable protection systems. He has invented several novel patented cable designs, including the " DWP " design. He has been involved with land and sea cable installation and repairs, reliability and failure investigations, and fibre and system transmission testing, and standardisation issues.

EVALUATION OF MECHANICAL PROPERTIES OF VARIOUS FIBEROPTIC SUBMARINE CABLES IN BOTH ELASTIC AND PLASTIC REGIONS

T. C. Chu and R. J. Rue

Tyco Submarine Systems Ltd.
101 Crawfords Corner Road
Holmdel, New Jersey 07733

ABSTRACT

A theoretical model has been formulated to evaluate the mechanical properties of submarine cables in both the linear elastic and nonlinear plastic regions. This model has been successfully applied to the design of SL fiberoptic submarine cables at Tyco Submarine Systems Ltd. (formally AT&T Submarine Systems Inc.) The predicted tensile, torsional, and rotational properties for armorless cable, single armored cable, double armored cable, and rock armored cable agree very well with the test data for restrained and unrestrained cable ends.

FORMULATION

The present model is based on the linear theory of Cannon and Santana[1] in which the fundamental equations for the mechanical properties of a cable with helical strength members are:

$$M_t = C_1 \varepsilon_c - C_2 \phi \qquad (1)$$

$$T_t = C_3 \varepsilon_c - C_4 \phi \qquad (2)$$

where M_t and T_t are the resultant axial moment and tension applied at the cable ends, ε_c and ϕ are the cable strain and cable twist (radians per unit length) in the axial direction. The coefficients C_1, C_2, C_3, and C_4 are constants determined by the linear mechanical properties of the cable constituent materials and cable construction parameters as follows:

$$C_1 = \sum_{i=1}^{m} (\cos^2\theta_i - \nu_i \sin^2\theta_i) n_i E_{si} A_{si} R_i \sin\theta_i \qquad (3)$$

$$C_2 = J_c G_c + \sum_{i=1}^{m} \begin{pmatrix} n_i J_{si} G_{si} \cos^2\theta_i \\ + R_i^{\,2} n_i E_{si} A_{si} \sin^2\theta_i \cos\theta_i \end{pmatrix} \qquad (4)$$

$$C_3 = E_c A_c + \sum_{i=1}^{m} \begin{pmatrix} (\cos^2\theta_i - \nu_i \sin^2\theta_i)^* \\ n_i E_{si} A_{si} \cos\theta_i \end{pmatrix} \qquad (5)$$

$$C_4 = \sum_{i=1}^{m} n_i E_{si} A_{si} R_i \cos^2\theta_i \sin\theta_i \qquad (6)$$

n_i is the number of strength members in the i^{th} layer and m is the number of layers. E_{si} is the Young's modulus and A_{si} is the cross sectional area of a strength member in the i^{th} layer. R_i is the radius from the cable axis to the centerlines of the strength members and θ_i is the lay angle of a strength member in the i^{th} layer. ν_i is the radial contraction of the strength member in the i^{th} layer

$$\nu_i = \frac{1}{\varepsilon_c}\left(\frac{\delta R_i}{R_i}\right) \qquad (7)$$

J is the moment of inertia and G is the torsional rigidity. The subscript "c" refers to properties of all non-stranded cable components.

Equations (1) through (7) with constant mechanical properties are applicable to the linear elastic region where both cable strain ε_c and cable twist ϕ are small.

For cable under large applied tension and torque, such as during the recovery of submarine cable, the linear model is no longer adequate and nonlinear behavior of the cable has to be considered. The present nonlinear model has been formulated in four steps:

1. Conducted tensile test for each cable constituent material.

2. Applied nonlinear regression curve fitting method to the test data and established a functional relationship between the stress and strain for the material.

$$\sigma = F(\varepsilon) \qquad (8)$$

3. Derived the Young's modulus E and torsional rigidity G as function of strain ε from the above equation.

$$E(\varepsilon) = \frac{d\sigma}{d\varepsilon} = \frac{dF(\varepsilon)}{d\varepsilon} \qquad (9)$$

and

$$G(\varepsilon) = \frac{E(\varepsilon)}{2(1+\upsilon)} \qquad (10)$$

where ν is Poisson's ratio for the material.

4. Replaced the constants E and G with the above nonlinear functions $E(\varepsilon)$ and $G(\varepsilon)$ in the coefficients C_1, C_2, C_3, and C_4 of Equations (1) and (2) for each cable constituent and then integrated the resulting equations based on cable end conditions as follows:

If both ends are restrained, $\phi = 0$, then

$$M_t = \int C_1(\varepsilon_c) d\varepsilon_c \qquad (11)$$

$$T_t = \int C_3(\varepsilon_c) d\varepsilon_c \qquad (12)$$

If only one end is restrained and the other end is free to rotate, $M_t = 0$, then

$$T_t = \int \left[C_3(\varepsilon_c) - \frac{C_1(\varepsilon_c) * C_4(\varepsilon_c)}{C_2(\varepsilon_c)} \right] d\varepsilon_c \qquad (13)$$

$$\phi = \int \left[\frac{C_1(\varepsilon_c)}{C_2(\varepsilon_c)} \right] d\varepsilon_c \qquad (14)$$

Integration of Equations (11) and (12) or Equations (13) and (14) results in the desired mechanical properties of the cable in both the linear elastic and nonlinear plastic regions.

APPLICATIONS

The present model has been applied to evaluate the mechanical properties of various fiber optic submarine cable types. Depending on the ocean environment, submarine cable requires different classes of protection which results in various cable types. Typically, a long haul submarine communication system requires the cable types listed in Table 1.

Cable Type	Applicable Environment
Lightweight cable (LW)	Depth to 8000 meters, benign bottom
Special application cable (SPA)	Depth to 5000 meters, somewhat rocky bottom, risk of shark attack or abrasion
Light-wire armored cable (LWA)	Depth to 2000 meters, rocky terrain, risk of trawler damage
Single-armored cable (SA)	Depth to 1500 meters, very rocky terrain, high risk of trawler damage
Double-armored cable (DA)	Depth to 400 meters, surf zone, coral, volcanic rock, high risk of trawler damage
Rock-armored cable (RA)	Depth to 200 meters, Rocky terrain, high abrasion or crushing threat, high risk of trawler damage

Table 1 Submarine cable types

The configuration of Lightweight (LW) cable is shown in Fig. 1. The cable consists of a unit fiber structure protected by two layers of stranded high strength steel wires, a copper sheath, and a medium density polyethylene jacket. The unit fiber structure contains a copper clad steel wire (kingwire) with optical fibers helically wound and embedded in a buffering elastomeric material.

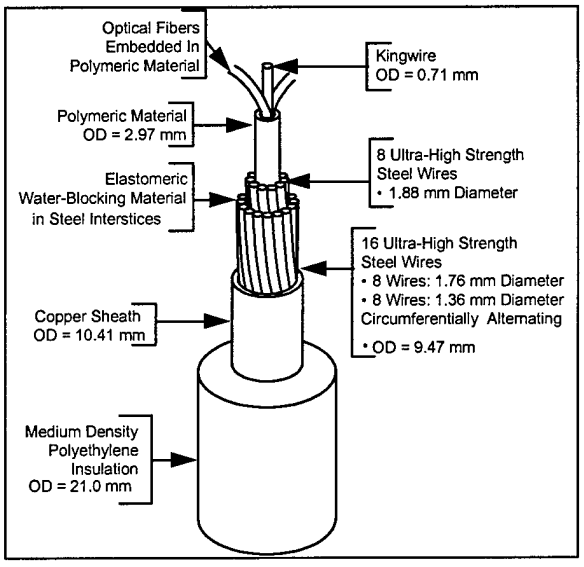

Fig. 1 Lightweight (LW) Cable

The configuration of Special Applications cable (SPA) is shown in Fig. 2. The SPA has an additional metallic tape and second polyethylene (HDPE) jacket over the LW cable to provide additional abrasion protection and hydrogen sulfide protection.

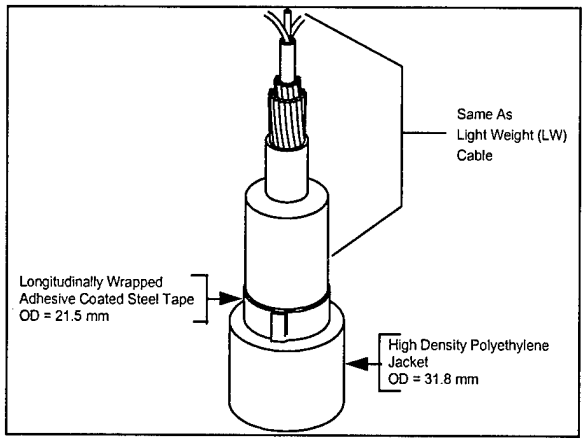

Fig. 2 Special Applications (SPA) Cable

The configurations of the Light-Wire Armored (LWA), Single Armored (SA) and Double Armored (DA) cables are shown in Fig. 3, Fig. 4 and Fig. 5 respectively. The LWA and SA have one armor layer applied over the Lightweight cable while the DA has two armor layers for additional protection.

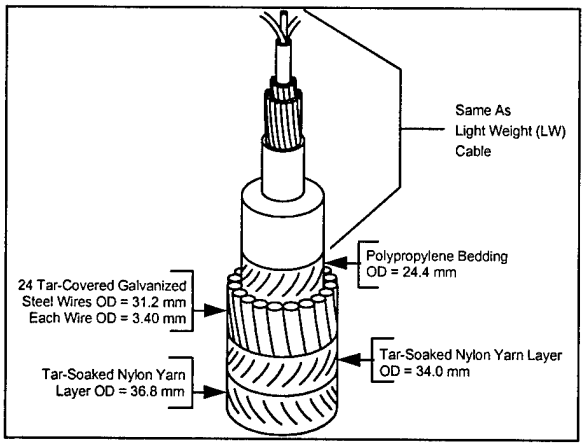

Fig. 3 Light-Wire Armored (LWA) Cable

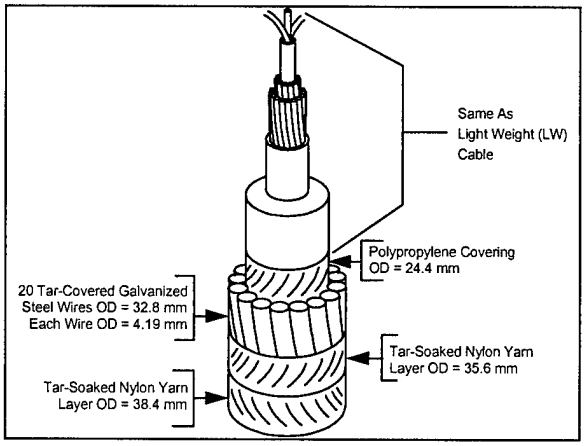

Fig. 4 Single Armored (SA) Cable

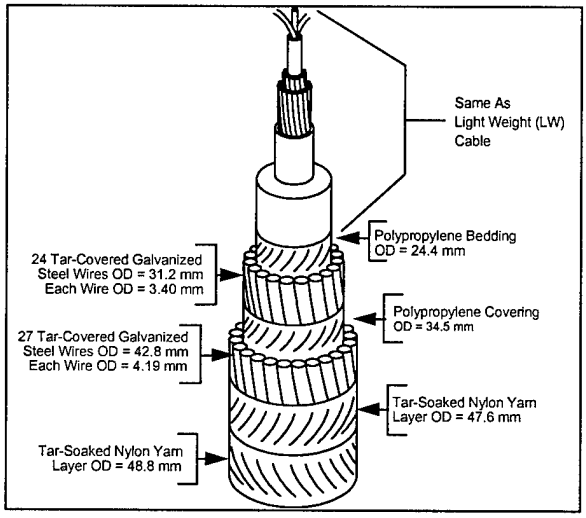

Fig. 5 Double Armored (DA) Cable

The configuration of the Rock Armor cable (RA) is shown in Fig. 6. A very heavy armor wire layer with very large lay angle (>50 degrees) is applied over the Single Armor cable for extra crush and abrasion protection.

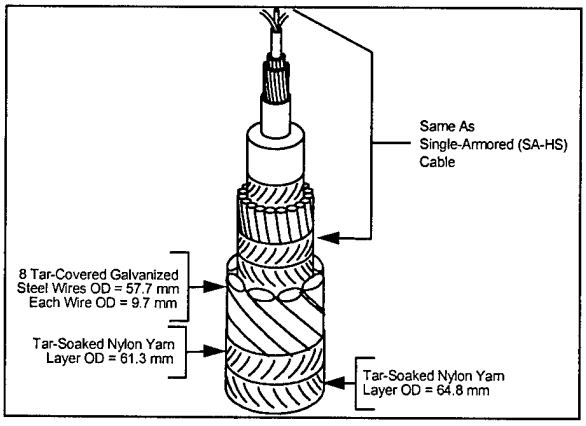

Fig. 6 Rock Armor (RA) Cable

In these cable types, the constituent materials that contribute most to the mechanical properties of the cable are the kingwire, stranded high strength steel wires, copper sheath, polyethylene, steel tape, and armor wires. These constituent materials were tensile tested and functional relations between stress and strain generated for them by applying nonlinear regression to the test data. Since the optical fibers used in these submarine cables are proof tested to 2% strain and the cables are designed to operate well below this limit, the functional relations that provide the best fit to the test data in the 2% strain range were selected. The following six order polynomial was found to be the best choice for the stranded high strength steel wires:

$$F(x) = \sum_{i=0}^{6} a_i x^i$$

The following exponential function fits well to the test data for the other cable constituent materials

$$F(x) = a_0(1 - \exp(-a_1 x)) + a_2$$

Functional relations and their corresponding test data for the high strength steel wire and medium density polyethylene are illustrated in Fig. 7 and Fig. 8.

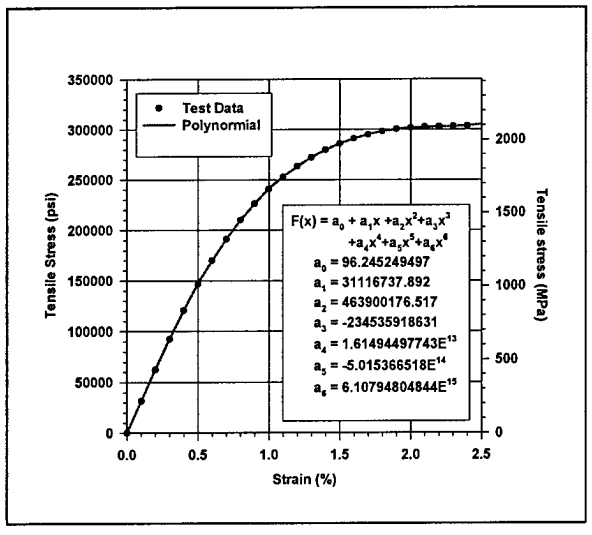

Fig. 7 Functional relation for stress and strain and test data for high strength steel wires

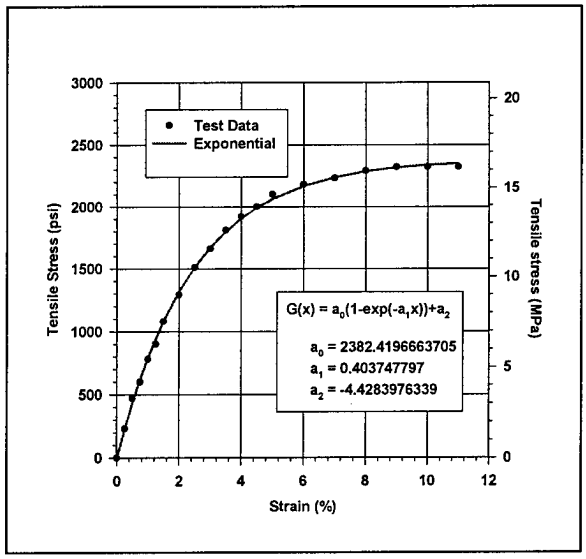

Fig. 8 Functional relation for stress and strain and test data for MDPE

Similar functional relations have been established for the other cable constituent materials. Differentiation of these functions gives the corresponding Young's modulus $E(\varepsilon)$ and modulus of rigidity $G(\varepsilon)$. The mechanical properties of the cable can then be obtained from Equations (11) to (14).

RESULTS

Theoretical properties have been evaluated from Equations (11) to (14) with $\nu_i = 0.5$. Tensile tests were conducted on a horizontal test bed as sketched in Fig. 9. The ram end of the test bed has a load cell to measure cable tension and torque and the other end of the cable is either fixed or attached to a swivel depending on the condition for restrained or unrestrained cable end. For the case of unrestrained end, the cable twist is measured by counting the number of rotations of the swivel that are required to reverse the torque reading at the load cell back to its initial value, close to zero. Test sample length was 100 m for the armorless LW and SPA cables and was 20 m for the four armored cables.

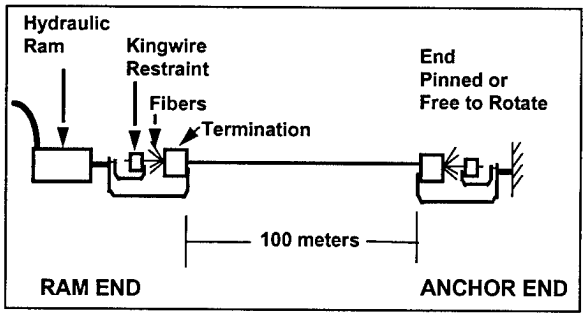

Fig. 9 Test Set-up

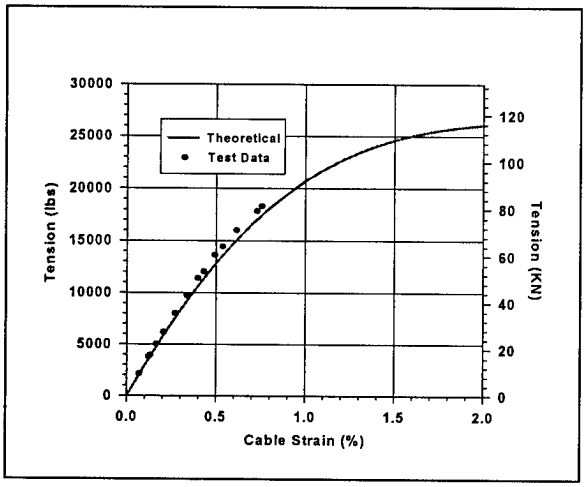

Fig. 10a Lightweight Cable tensile properties with both ends restrained

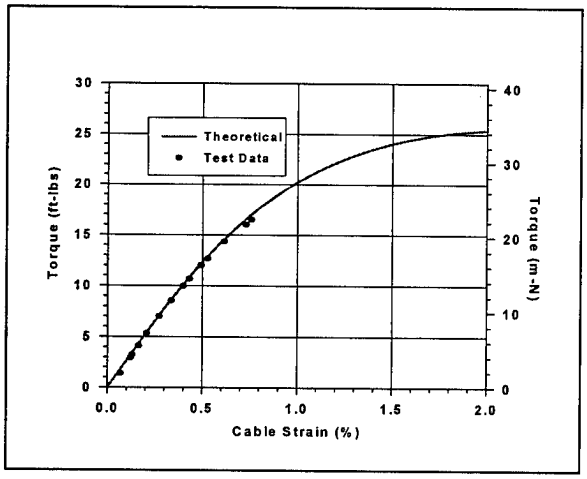

Fig. 10b Lightweight cable torsional properties with both ends restrained

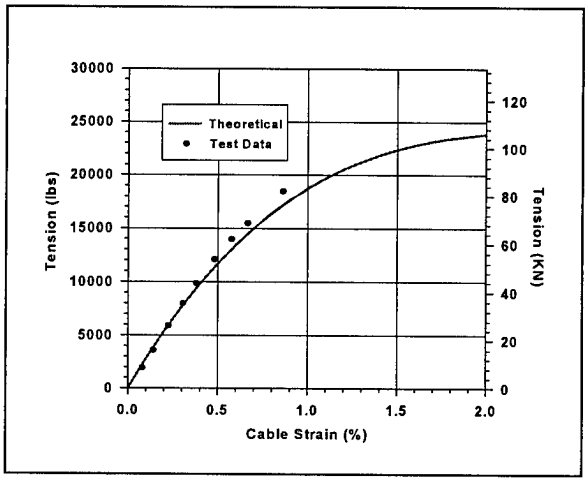

Fig. 10c Lightweight cable tensile properties with one end free to rotate

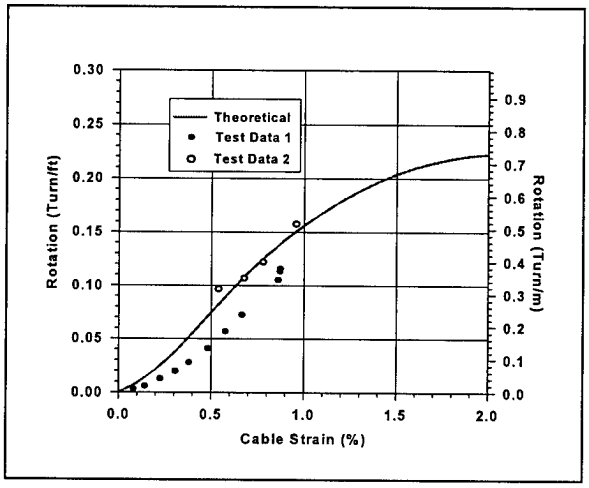

Fig. 10d Lightweight cable rotational properties with one end free to rotate

The above figures indicate good agreement between the theoretical values and test data for the LW cable, except for cable rotation measured from the horizontal test bed, "Test Data 1" in Fig. 10d. This deviation is believed caused by the horizontal test set-up. The long sample length (100 m) and associated friction force induced from the 1 m spaced supporting rods along the test bed could have affected the measurement. To eliminate the interference, a 15 m LW sample was tested vertically by hanging the cable from a crane and attaching heavy weight blocks at the lower cable end. The measured data points agree well with the theoretical curve as shown by "Test Data 2" in Fig. 10d. Similar results for the SPA cable for restrained and unrestrained end are shown in Fig. 11a through Fig. 11d, except for rotational test data. The rotational test remains to be done either by vertical hanging or other simpler method.

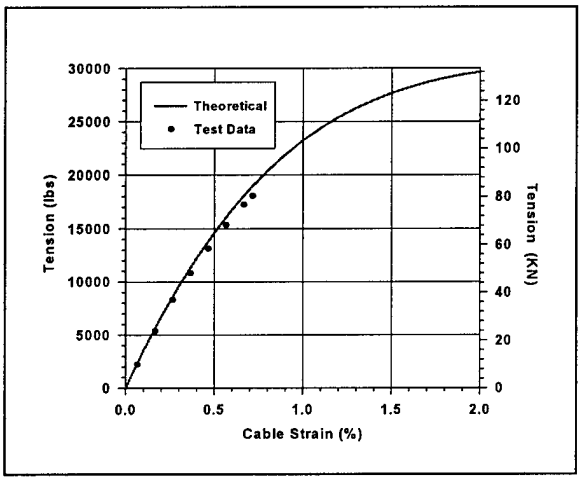

Fig. 11a SPA cable tensile properties with both ends restrained

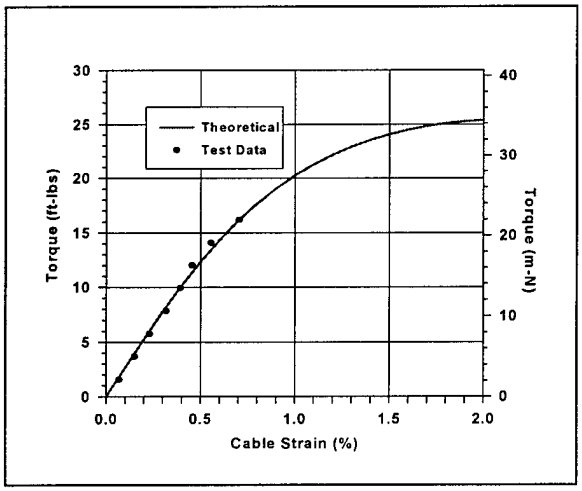

Fig. 11b SPA cable torsional properties with both ends restrained

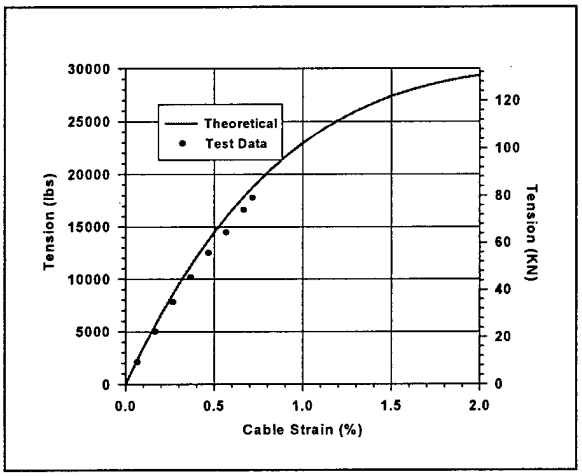

Fig. 11c SPA cable tensile properties with one end free to rotate

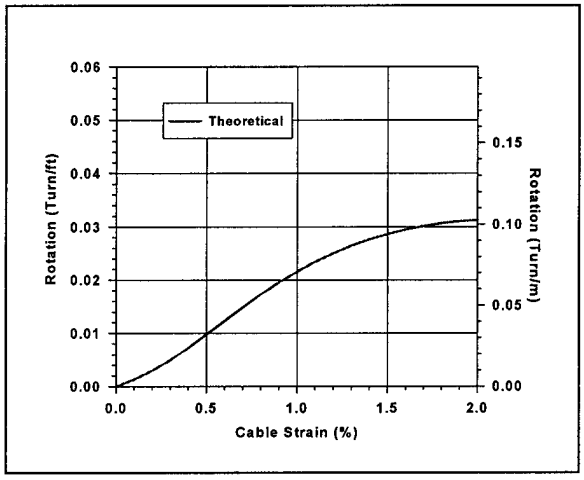

Fig. 11d SPA cable rotational properties with one end free to rotate

Theoretical results for armored cables are shown in Fig. 12a through Fig. 15d along with available test data. The armored cables were tensioned repeatedly up to their corresponding NTTS (Nominal Transient Tensile Strength - the maximum working load of the cable) for 10 cycles before loading to UTS (Ultimate Tensile Strength) during the 11th cycle. The test data denoted by "Test Data 1" in Fig. 12a through Fig. 15d represents the first tensile cycle. "Test Data 2" in Fig. 12a, 13a, 14a, and 15a represents the 11th cycle to the UTS. "Test Data 2" indicates higher tensile stiffness due to wire straightening and tightening of the armor package.

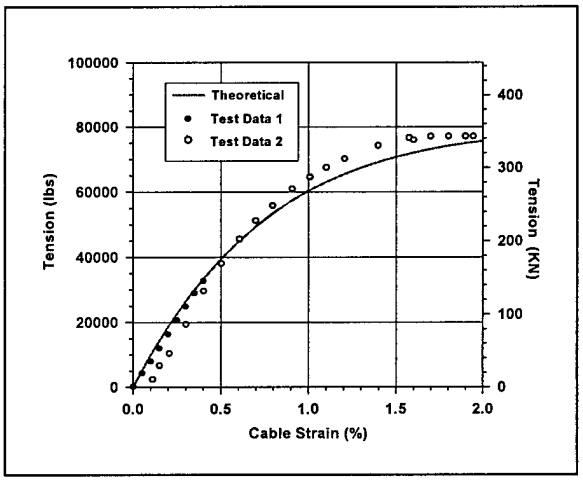

Fig. 12a LWA armored cable tensile properties with both ends restrained

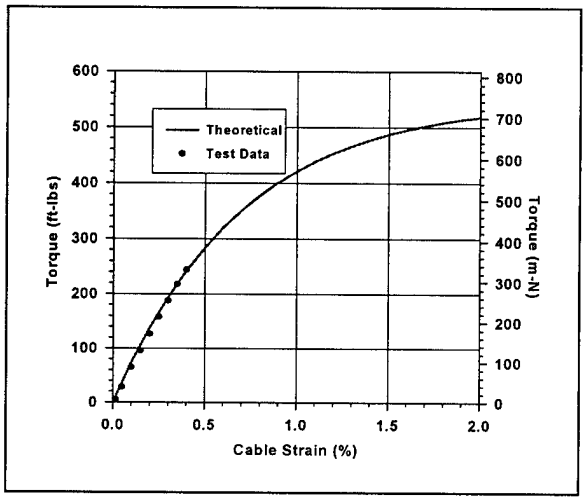

Fig. 12b LWA armored cable torsional properties with both ends restrained

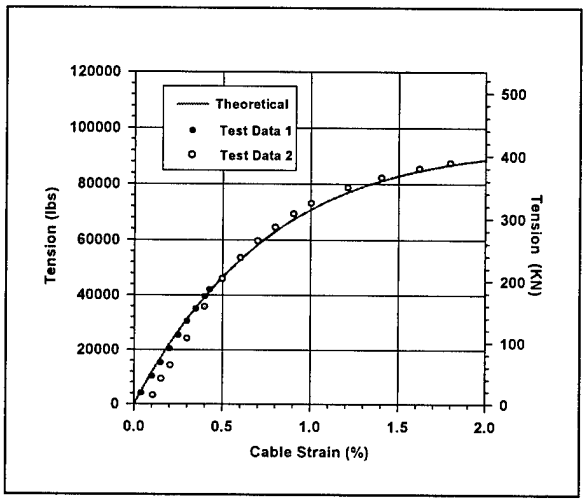

Fig. 13a SA armored cable tensile properties with both ends restrained

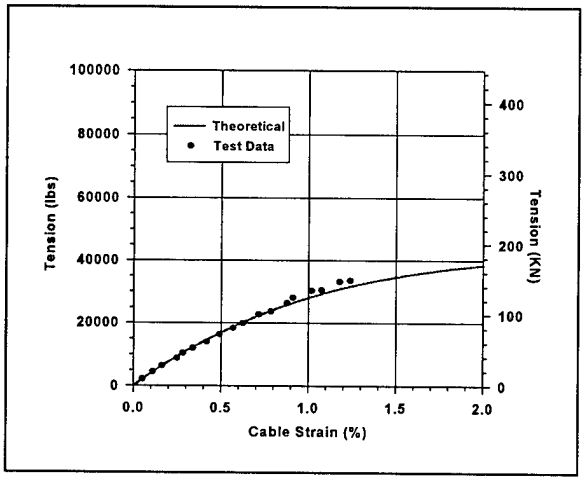

Fig. 12c LWA armored cable tensile properties with one end free to rotate

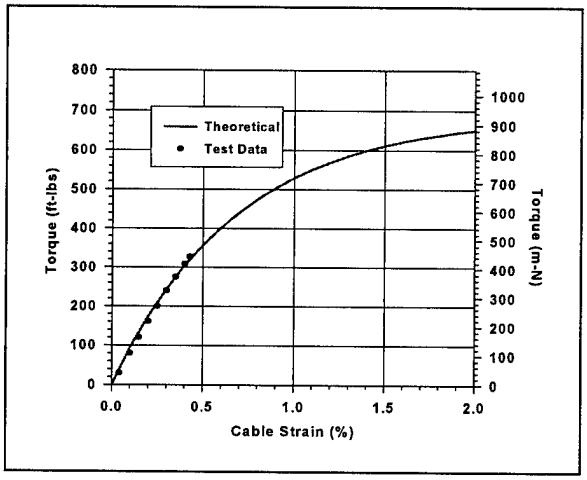

Fig. 13b SA armored cable torsional properties with both ends restrained

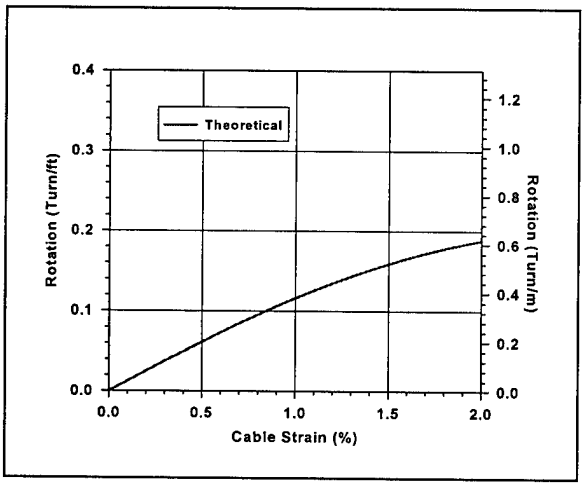

Fig. 12d LWA armored cable rotational properties with one end free to rotate

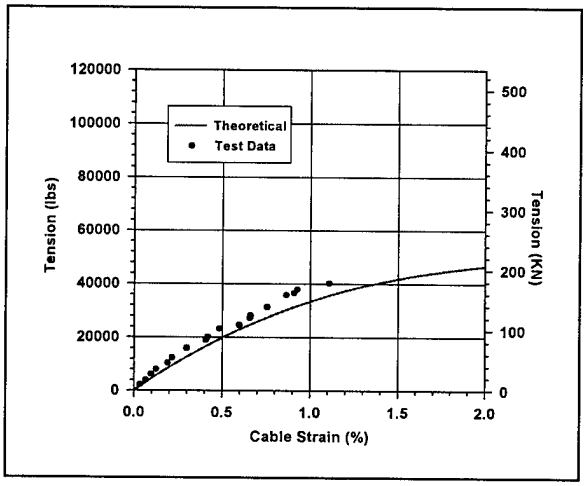

Fig. 13c SA armored cable tensile properties with one end free to rotate

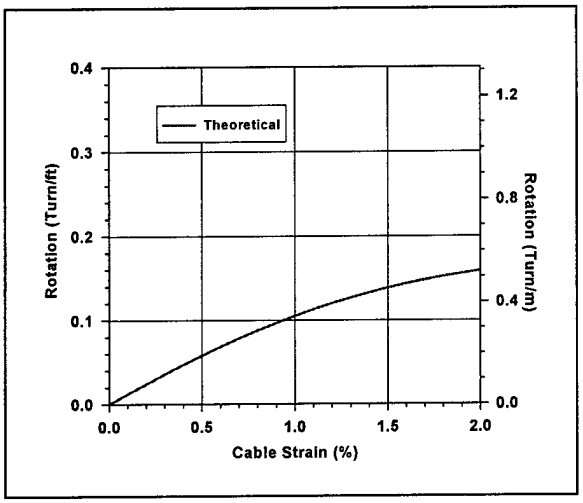

Fig. 13d SA armored cable rotational properties with one end free to rotate

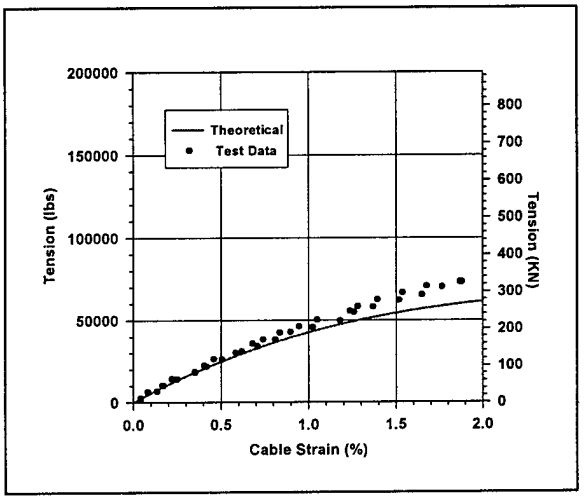

Fig. 14c DA armored cable tensile properties with one end free to rotate

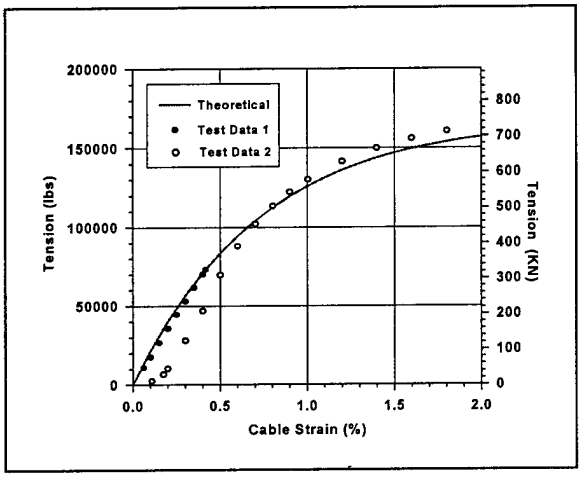

Fig. 14a DA armored cable tensile properties with both ends restrained

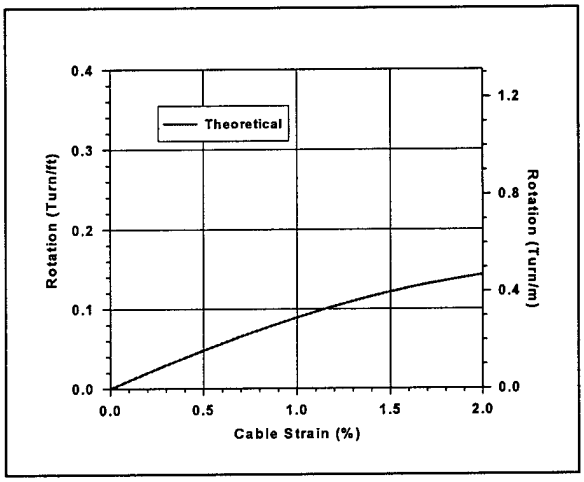

Fig. 14d DA armored cable rotational properties with one end free to rotate

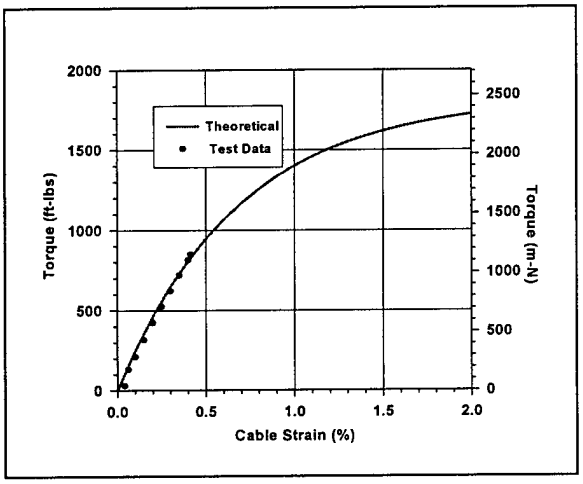

Fig. 14b DA armored cable torsional properties with both ends restrained

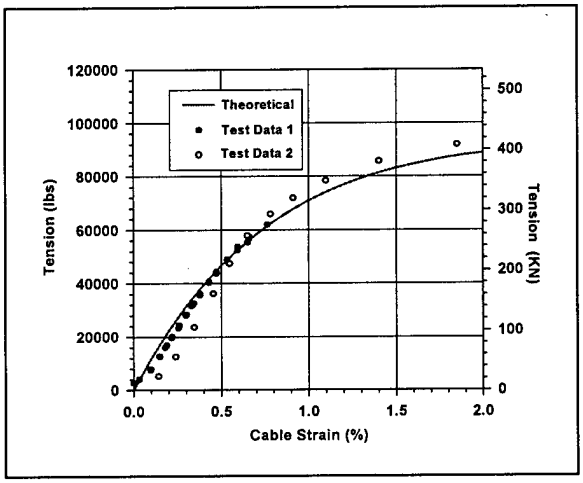

Fig. 15a RA armored cable tensile properties with both ends restrained

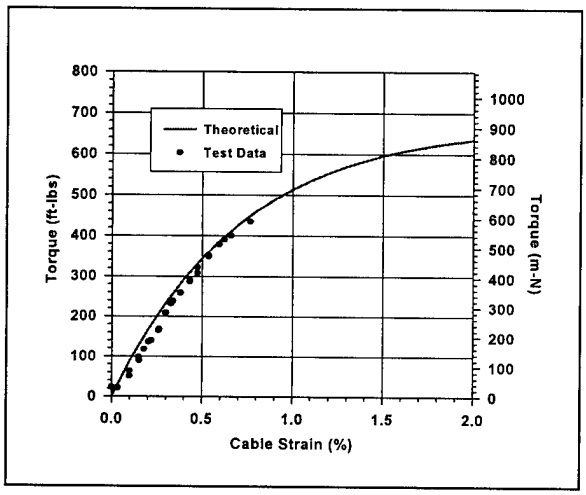

Fig. 15b RA cable torsional properties with both ends restrained

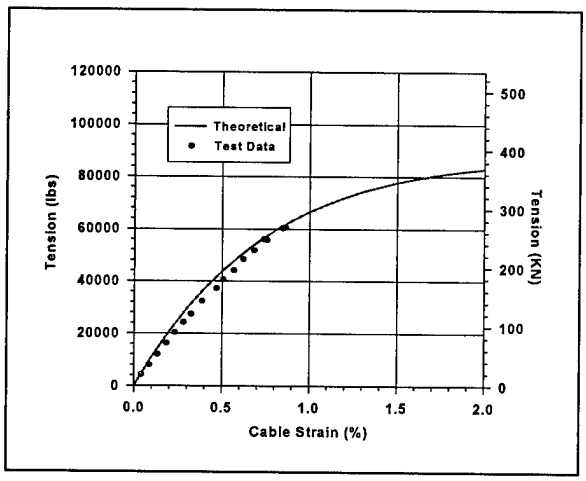

Fig. 15c RA cable tensile properties with one end free to rotate

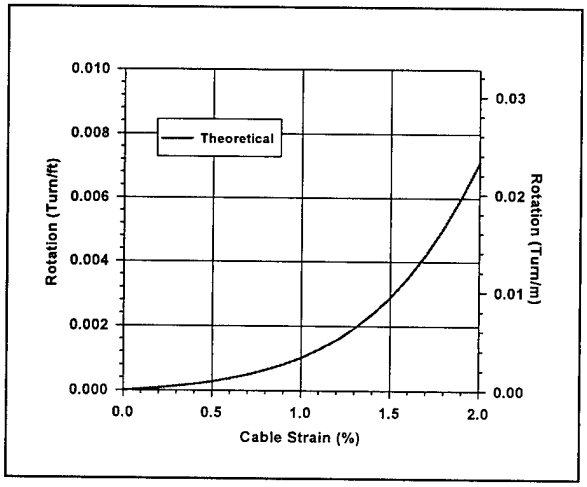

Fig. 15d RA cable rotational properties with one end free to rotate

CONCLUSIONS

A theoretical model has been applied to several fiber optic submarine cables to predict their mechanical properties in both the linear elastic and nonlinear plastic regions. Comparison between the theoretical and test data shows good agreement. However, more work is needed to configure a simple but accurate method to measure the rotational properties of these high strength and heavy weight cables. The model provides a valuable tool in optimizing a new cable design prior to the manufacture of costly prototype cable.

REFERENCES

1. T. C. Cannon and M. R. Santana, "Mechanical Characterization of Cable Containing Helically Wrapped Reinforcing Elements," Twenty-Fourth International Wire and Cable Symposium, 1975

BIOGRAPHY

T. C. Chu
Tyco Submarine Systems Ltd.
Holmdel, NJ

T. C. Chu received his B.S.M.E Mechanical Engineering from Cheng Kung University, Taiwan, 1964, M.S.M.E. Mechanical Engineering from Syracuse University, 1967 and Ph.D. Aerospace Engineering from Cornell University, 1971. He joined Bell Laboratories in 1972 and retired from AT&T Bell Laboratories in 1997. He was responsible for the design and development of AT&T's SL and SL100 fiber optic submarine cable. He is currently a technical consultant with the Cable Development Division of Tyco Submarine Systems Ltd.

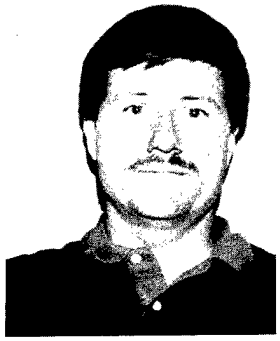

R. J. Rue
Tyco Submarine
Systems Ltd.,
Holmdel, NJ

R. J. Rue received his AAE-MET degree from Vermount Technical College, and his B.S-MET degree from Trenton State College. He joined the Undersea Systems Cable Development & Implementation Department at AT&T Bell Laboratories in 1984. His work has been focused on the development testing and analysis of fiber optic undersea cable designs and related hardware. He is currently a Senior Member of Technical Staff with the Cable Development Division of Tyco Submarine Systems Ltd. and is responsible for development and qualification testing of new cable and hardware designs.

THE RIBBON CONCEPT FROM THE MANUFACTURING PROCESS TO THE FIELD

Bertil Arvidsson	Jan Björkman	Juha Tanskanen
Ericsson Cables	Telia Network	Nextrom
Hudiksvall	Farsta	Vantaa
Sweden	Sweden	Finland

ABSTRACT

For many years the ribbon concept has been discussed in conferences, but still only some countries have fully adopted it. Leading countries have been USA, Japan, Italy and Sweden. In later years other countries have introduced ribbons, but still there is a wide-spread opposition. Here we discuss the process needed when higher volumes and therefore, faster process speeds and productivity are required. Specific questions deal with less scrap, lower costs and improved productivity.

Further, we discuss the reduced number of tests required for type testing a ribbon today compared with five years ago. The type of ribbon used in Sweden is the encapsulated design. Until now, mostly 4-fiber ribbons have been installed, but also the splittable 8-fiber ribbon has been introduced. For "Fiber-To-The-Whatever", i.e. FTTH a two-fiber ribbon is under evaluation. Virtually all cable designs have been the slotted core type.

Finally ten years of field experiences are presented with a discussion of installation techniques including splicing methods.

INTRODUCTION

With the abstract in mind we continue our study with the following introductory comment. Several years of customer contacts and discussions have made it clear that there still exist a number of misleading thoughts (1), but also positive ones (2) about the handling of ribbons.

Also discussed are specification issues about splice losses and one-way versus two-way OTDR measurements. In this context estimation values from the fusion splicer is also discussed. There are no changes in the transmission requirements for the cable nor for the splice due to the introduction of ribbons.

Some factors influencing the decision to introduce ribbons into Sweden were: high density fiber cables; easy to handle; robust and reliable; faster installation; cheaper cables, lower splicing costs.
The results of our study show a fast and easy production technique. Almost 10 years of type testing and process evaluations show that the number of tests can be reduced today for two reasons: The fiber has improved in quality and similarly for the processes. As a consequence of this work field measurements have also been reduced.

The field installations show similar splice results for single fiber splicing as for ribbon splicing. The installation technique being used in Sweden allow for one single fiber in a ribbon with a higher splice loss, which occurs very seldom. The exact specification is given in the paper and with this approach installation time is saved without jeopardizing the system requirements.

RIBBON PROCESSING

The ribbon process development and implementation have gone through several steps, because of different materials, testing procedures and requirements. By experience we know that to process a good quality ribbon it is necessary to know the mechanical and transmission properties. In addition, it is essential to know how to make the fiber for the ribbon, the fiber coloring process and the ribbon making itself. Material properties and selected combinations thereof play a very important role in each process step.

Reality today are high production speed, accurate geometrical dimensions and planarity, and excellent transmission properties. At present research is focusing on productivity and the economics of the ribbon production process. The main targets are to: reduce change and start up time, scrap minimization and preparation of the ribbon for the subsequent cabling process.

Fiber coloring for ribbon applications

The quality of the coloring is very important for ribbon properties. Sufficient amount of UV curing is needed to attain the optimum curing level for the fiber, especially when coloring at high speed. In practice, choosing between coloring parameters and other conditions is always a balance between two opposing ribbon properties: strippability and breakout. These are dependent on the UV curing dose, fiber materials, inks and nitrogen atmosphere in the irradiators. The maintenance of the curing system plays an important role in production. Figure 1 shows a comparison of the curing level of three different inks, but same color, with different UV dose at speed 1200 m/min.

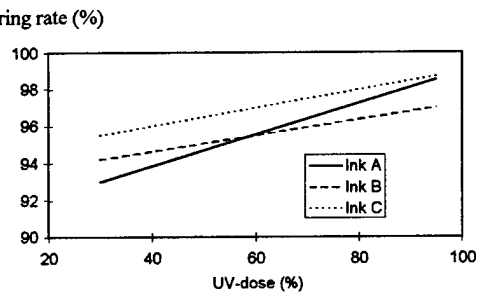

Figure 1. Curing rate for three different inks with different UV dose.

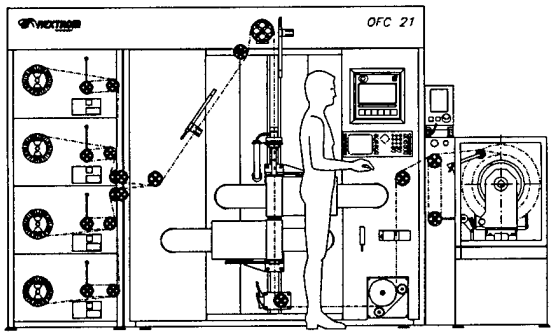

Figure 2. Layout of a 4-fiber ribbon line.

Ribbon manufacturing

The first requirement for good ribbon planarity is stable unwinding and guiding of the fibers. Other main requirements such as geometry parameters, strippability, breakout and ribbon curing are finalized during the coating and curing processes. A good quality take-up wind is important for the subsequent cabling process. Figure 2 shows a layout of a 4-fiber ribbon manufacturing system.

Productivity of the ribbon process

To improve productivity there are three main tasks: minimizing wastes, use preset toolings and change all unnecessary service and settings, so it does not interfere with the production time. This is a well understood philosophy and the same in many industries.

The heart of the process is a compact coating unit which is not disassembled between the runs.
The use of this wet-on-wet type of coater offers several benefits: constant quality between the runs, fast start-up and minimized cleaning and assembling time. This coating unit is interchangeable and is cleaned as a single unit in less than five minutes.

Optimizing start-up ramp

The start-up ramp is improved in three different ways: adjusting the speed according to the acrylate pressure (with optimum temperature), by selecting UV power increment of the system during ramps and by controlling pay-off tensions during ramp up. Using this scheme, the scrap length is shortened from 75 m to 35 m for a 4-fiber ribbon.

The following table (Table 1) gives a summary of the dimensional changes during ramp up. The first column describes the start-up length and the last the process speed. The others represent ribbon parameters.

Start m	Width µm	Height µm	Planarity µm	Speed m/min
15	1100	310	35	173
30	1130	300	34	244
45	1080	300	36	300
60	1110	310	37	346
75	1050	300	29	387
90	1100	280	21	400
105	1030	290	18	400
120	1040	290	17	400
after adjustments				
5	1150	320	34	141
10	1130	320	36	200
15	1180	310	29	244
20	1140	330	32	282
25	1150	300	34	316
30	1100	290	32	346
35	1080	290	25	374
40	1040	290	23	400
45	1020	280	15	400
50	1030	280	13	400
55	1010	290	11	400

Table 1. A particular case of optimizing start-up ramp for ribbon specifications:
width *1050 ± 50 µm*
height *280 ± 20 µm*
planarity *< 30 µm*

RIBBON PRODUCTS

In Sweden, we have developed, tested and installed 2-, 4-, 8- and 12-fiber ribbons, Fig. 3. They are all of the encapsulated type. Both single-mode and multimode fibers have been used.

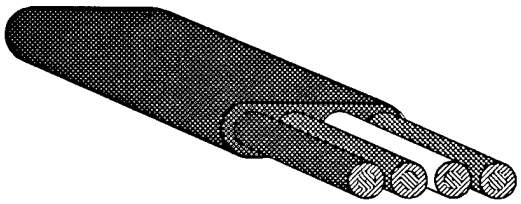

Figure 3. A typical 4-fiber encapsulated ribbon, where each fiber fulfils the coating dimension 242±7 µm and typically 250 µm colored. The ribbon itself is typically 1100 µm wide and 320-350µm thick. Glass diameter is 125±1 µm and the glass concentricity error between core and cladding is typically less than 0.4 µm.

For the 8- and 12-fiber ribbons the splittable concept has been adopted, i.e. the ribbon can be split in units of four fibers.

Geometry of the ribbon

About five years ago there were two main structures: edgebonded and encapsulated. The main difference was the thickness of the ribbon (edgebonded 280 - 300 µm, encapsulated 380 - 400 µm). Today for standardization, technical and economical reasons the two designs have moved closer towards a common thickness. This means that thickness is normally specified in the range of 300 - 350 µm.

MEASURING AND TESTS

When the ribbon concept was introduced in Sweden almost ten years ago, there was a great concern about the environmental behaviour of the ribbon itself, including the compatibility with other cable materials. Other important parameters were strippability and breakout. These parameters are connected to splicing of ribbons. The splicing issue will be further discussed below.

Another parameter creating some problems about five years ago was fiber curl (3). By rotating the bare glass fiber end it is possible to find out how straight the fiber is. The straighter the fibers are within a ribbon, the simpler the ribbon splice can be.
Today all major fiber manufacturers have this parameter under control. This means that it is not necessary to perform frequent curl measurements in the cable factory.

In general distribution of geometric parameters have become more accurate. Over the past 5 years typical values are somewhat tighter than those that are specified. One example is glass/core concentricity error with typical values less than 0.4 μm, but the specification is less than 0.8 μm (Swedish).

OTDR-measurements in the field are sometimes performed incorrectly. To get a true splice value it is necessary to measure from both ends. One-way measurements with an OTDR must be handled carefully, because of an apparent loss or "gainer" appearing at the interface (4). Good knowledge of the corresponding mode field diameter can help when using one-way field measurements.

The above comment about typical values and specifications does not mean that we should tighten specifications. It is more information useful at installations. The specifications should be written in a way such that the system performance is never jeopardized.

As outlined in (5) the number of different tests in evaluating changes in a ribbon or developing a new product have been reduced. At present we are concentrating on ribbon dimensions, water soak, strippability, separability and occasionally PMD and FTIR (5). A simple attenuation check is another logical choice.

Finally FEM-calculations have become a useful tool for optimizing a ribbon design (Figure 4). The picture shows a two-dimensional FE-model of one fourth of a 2-fiber ribbon. The contour plot in Figure 4 is the result of a linear elastic stress analysis and represents the stress distribution in the lateral direction, which simulates a crush test. Determination of the stress field can be helpful when explaining various phenomena, e. g. the differences in PMD between outer and inner fibers in a ribbon (6).

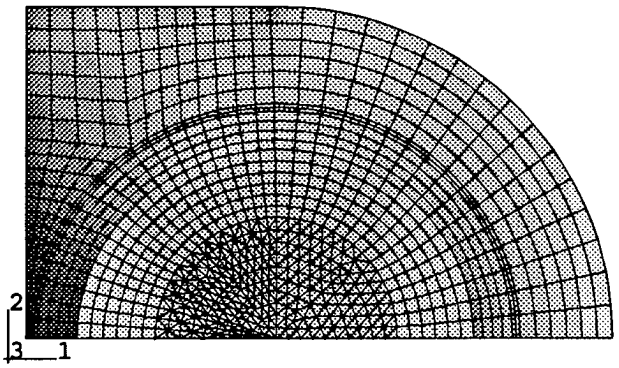

Figure 4. One fourth of a 2-fiber ribbon.

FIELD EXPERIENCE

Fiber optic cables were introduced into the Telia network with multimode fibers in 1979 and the breakthrough came in 1984 with single-mode. The first construction used, 1984-1987, was fibers in loose tube with one fiber in each tube. In the years 1988-1990 the slotted core construction was introduced with loose tube and with four fibers in each tube. In 1989 the 4-fiber ribbon was introduced with fibers in a slotted core and up to 96 fibers.

In the Swedish network, upto 1997, more than 40.000 km optical fiber cables containing more than 1.000.000 fiber kilometers have been installed.

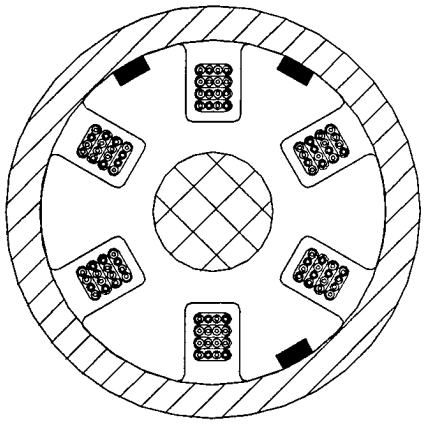
Figure 5. Typical Ribbon Duct Cable cross-section.

The cable constructions are

- non-metallic
- longitudinally water tight
- have a maximum pulling force 1,5 kN
- temperature range -40°C to +70°C.

When ribbons were introduced, no changes in the basic requirements for the fibers or the cables were made.

All cables fulfil the requirements in the European norms and the IEC norms.

Installation methods used for ribbon cables at Telia are:

- direct ploughing in split ducts
- cable caterpillar in ducts
- cable air blowing in ducts
- cable water blowing in ducts
- manual pulling

Considerations possible at installation:

- moisture
- variations in temperature
- cable bend
- cable bend at low temperature
- tensile force at installation
- radial load
- transport and handling of cable drums
- quality

Splicing methods used in Telia for ribbons:

- all permanent splicing performed with fusion splicing
- temporary splices with mechanical methods
- indoor flexibility points with connectors

The number of splices performed in Telia since 1985 is about:

Single fiber	4-fiber ribbon	8-fiber ribbon
1985-1990	1988-1997	1997-
50000	55000	500

Splice boxes
1985-1997
24500

Splice specifications in Sweden:
(results = mean of measured splice values)

1985-1996	1996- to date
max. 0.25 dB	max. 0.40 dB
	mean 0.10 dB
results 0.07 dB	results 0.07 dB

After installation all splices are measured from both directions and splices outside the requirements are respliced. Due to good experience, the splices are measured after the installation of the whole route. This has been done since 1990.

There are special requirements for underwater and submarine cables.

The philosophy behind the splicing approach is to allow for a fraction of splice values to be above the typical value (0.07), but within the specification. This means that installation time is saved and the system requirements are still fulfilled. Otherwise a lot of time would be spent in the field performing unnecessary resplicing.

Why ribbons?

- easy to handle
- lower splicing cost
- better service (faster installation)
- high density fibre cables with small diameter
- useable for transport network, access network, FTTB/C/H
- easy to make branch off
- robust and reliable

Improvements due to ribbons:

- lower splicing costs
- lower installation costs
- fiber curl
- more focus on coating material
- better strippability
- improvements of primary coating

CONCLUSION

We have followed the ribbon concept from the machinery, process, evaluation and into the field.

The basic conclusions can be summarized in three categories:

- the machinery is basically the same now as earlier, but several process improvements have been introduced, such as higher speeds, better winding quality and better curing control.
- several critical evaluation techniques have been identified: strippability, breakout and water-soak.
- overall field experience clearly explains the advantage of ribbon technology with faster installations to lower cost.

Finally good knowledge of fiber parameters and measuring techniques (two-way OTDR) are needed to enable preparation of a realistic system specification.

ACKNOWLEDGEMENTS

A special thank to Nils Artlöve, Telia Network Services for discussions. We kindly thank Lars Olof Nordin, Ericsson Cables for performing the FEM-calculations. We also thank Mats Eriksson, Ericsson Cables and Jari-Pekka Tiesmäki, Nextrom for discussions on the process.

REFERENCES

1 R. Foss, Direct in Ground Optical Nodes, EuroCable'98, Manchester, 1998.

2 H. Serrander, H. Olofsson, IWCS, Philadelphia, 1997.

3 K. Jonsson, A. Björk, Comparative Measurements of Curl and Splice Loss for an Optical 4-fibre ribbon, OFMC, Torino, 1993.

4 W. E. Beasley, Increasing Productivity of Single and and Mass Optical Fiber Splicing When Testing with One-Way OTDR, IWCS, St Louis, 1993.

5 B. Arvidsson, J. Tanskanen, Analysis of the Economics of On-line Colored Ribbon Manufacturing, IWCS, Reno, 1996.

6 K. Brising, Polarisation Mode Dispersion Field Measurements - A Survey of the Swedish National Network, IWCS, Reno, 1996.

AUTHORS

Carl Bertil Arvidsson,
Ericsson Cables AB,
Telecom Division,
S-824 82 Hudiksvall,
Sweden

Carl Bertil Arvidsson, manager of fiber optics at Ericsson Cables AB, Telecom Division, has been involved in optical fibers for many years. He is active in IEC and CENELEC with the standardization of optical fibers and cables. Prior to joining Ericsson in 1990, he worked as a technical project manager in Sweden, the United States and Switzerland. Before that he was a university lecturer in theoretical physics. He has a doctor degree in Theoretical Physics from Uppsala, Sweden.

Juha Tanskanen,
Nextrom,
P O Box 44,
FIN-01511 Vantaa,
Finland

Juha Tanskanen has a B. Sc. In Mechanical Engineering from Wärtsilä Polytechnic, Finland in 1984 and the M. Sc. In Computer Engineering from Tampere University, Finland in 1991. He joined Nokia-Maillefer as a development engineer in 1990 and is currently working for Nextrom as product manager for fiber coloring and ribbon lines.

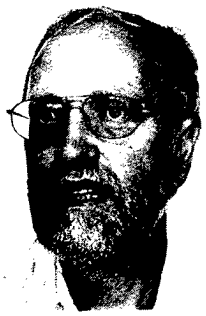

Jan Björkman,
Telia Network,
S-123 86 Farsta,
Sweden

Jan Björkman was born 1943. With a background in chemical engineering, he joined Telia 1977 and is since 1991 at Telia Network Services Outside Plant. He is now responsible for optical fibers and cables. He is also active in European and international standardisation on optical fibers and cables.

REVIEW ON THE CORRELATION OF THE OPTICAL LOSS WITH RIBBON TWIST

G.W.Seo, Y.H.Jeon, S.H.Kim, K.J.Lew, J.H.Oh, D.Y.Shin

Daewoo Telecom Co. Ltd.
531-1, Kajwa-dong, Seo-gu, Incheon, Korea

Samsung Chemical Paint Co. Ltd.
629-3, Sunggok-dong, Ansan City, Kyonggi-do, Korea

ABSTRACT

In general, when the optical fiber ribbon is twisted, each fiber in the ribbon experiences a difference strain force due to flat geometry of the ribbon. This strain difference causes the length difference of inner and outer fibers which induces the buckling and the optical losses. In this study, we show that the optical losses in the twisted ribbon have close relation with an adhesive force between the ribbon coating and fiber coloring resin in addition to mechanical properties of ribbon resin. We will suggest the basic properties that ribbon resin should have for making the ribbon keep the best condition even under an severe circumstances like ribbon twists.

1. Introduction

Designed as a method to increase the amount of fibers incorporated into a cable, ribbon is now becoming popular in fiber optic cable field with the lapse of time. The requirement for high-density cable has made a good many of loose tube cable substituted by ribbon cable recently and this present state will be continued for the time being. The mechanical property of ribbon, generally, is easy to come to be weaker than that of single fiber because of the fiber strain by difference in length of inner & outer fibers under a twisted condition. Our paper will show that the optical loss due to the twisted ribbon, chiefly, depends on the adhesion between ribbon and fiber coloring resin as well as the mechanical ones of ribbon coating resin in case that the mechanical properties of the first, the second coating and the coloring resin of fiber are same. Thus, to make ribbon keep optimum performance in harsh condition as a twists, ribbon resin with proper properties itself and proper adhesion with coloring resin should be very carefully selected. Namely, the ribbon thickness, Young's modulus and poisson's ratio of ribbon resin should be optimized to reduce optical loss when the cable is subjected to various mechanical & environmental conditions because the main goal of ribbon coating is generally to minimize the optical loss induced by the microbending and buckling of the fiber core. In this paper, in addition to mechanical properties of ribbon resin as mentioned above, it is evaluated that the adhesion between ribbon coating & fiber coloring resin is very important factor to improve the twists property of ribbon. We goes through procedures as follows for our paper. Firstly, fix the best process condition for ribbon making. Secondly, the one with the best mechanical & the environmental property among various ribbon resins is selected through the test. Thirdly, to make optical ribbons with various adhesive forces, we prepare five kinds of fiber coloring resin by combining properly silicon material with the existing coloring resin. At this time, we have to take good care lest other properties with the exception of the stripping property should be changed. Fourthly, the optical ribbons, which the new coloring resins and the one selected ribbon resin are applied, are made. Through the twists & bends test on the ribbons, we review whether its result has any correlation with the adhesion on the boundary between ribbon & fiber coloring resin. For analyzing their correlation, several experiments are done. Fifthly, to confirm whether the Young' Modulus of ribbon resin has an effect on the twisting & bending on ribbon, we make five kinds of ribbon resin that the adhesion with the fiber coloring resin, which is the best one, is same but Young's Moduli are different. Then, in the same way, we make ribbons with the new ribbon resins and the one kind of coloring resin with the best adhesion. Of course, several experiments on them are followed. In this paper, we are going to investigate the correlation of the twisted & bended ribbon with optical attenuation minutely and suggest the basic properties that ribbon resin should have for keeping the best ribbon condition under harsh circumstances like a twist.

2. Theoretical Background

2.1 Ribbon Manufacturing Process

The preparation of strain-free-ribbon should be preceded for getting more reliable data on the correlation the mechanical

property of ribbon resin with the optical property on ribbon bends & twists. That is, we need to prepare strain-free-ribbon because unstable state of ribbon with residual strain gives rise to an unexpected result on ribbon twists. Thus, we decided an ideal manufacturing condition of ribbon through several tests. The model and the derivation equations to be applied are as <Fig.1>, <Eq.1,2,3,4>. Namely, in ribbon process, the fibers inserted into the ribbon coating die basically have a constant incidence angle. Therefore, two fibers on each edge among 8 fibers in a ribbon to be touched on both sides of ribbon die suffer serious strain by lateral force and the others on inner side undergo serious vibration by static electricity and friction one another. Of course, the vibration has close correlation with ribbon property such as optical attenuation and ribbon geometry. Here, eq. (1),(2),(3) and (4) mean the incidence angle of each fiber into ribbon die, the lateral force to be added to each fiber during ribbon process, the residual strain of fibers in ribbon after ribbon process and the correlation factor to correct the difference of the residudal strains between experimental and theoretical data each. K factor is due to the vibration of fibers by electrostatic force among fibers and the hunting of fibers by minute vibration of equipment itself when pay-off tension is loaded. We manufactured ribbon with the working condition to be decided by equations to mentioned above.

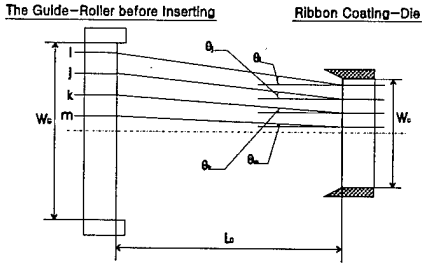

Fig.1 Schematic Diagram of Guide-Roller & Die

$$\theta = TAN^{-1}\frac{[\frac{(W_g - W_c)}{2} + \nu R_f - \nu(\frac{1}{2} \times \frac{W_g}{8})]}{L_o} \text{ -------- (1)}$$

i,j,k,m : Fiber identification
W_c : Width of ribbon coating die
W_g : Width of the last guide roller
L_o : Distance between coating die and the last guide roller
θ_{i-m} : Incidence angle
R_f : Radius of colored fiber
ν : 1,3,5,7 [i^{th} → m^{th} Optical fiber]

$$F_l = \sum_i^m F = \sum_i^m T_f \sin\theta \text{ ---------- (2)}$$

F_l : Lateral force
T_f : Back tesion loaded to fiber by pay-off

$$\varepsilon_i(\%) = K \cdot [\frac{T_f + \mu_{f-s}\sum_i^m F - \mu_{f-f}\sum_j^m F}{A_f E_f} \times 100] \text{ --- (3)}$$

ε_i : Strain of i^{th} fiber
A_f : Cross section of colored fiber
E_f : Young's modulus of colored fiber
K : Correlation factor of strain distribution
μ_{f-s} : Coefficient of friction, film to fteel
μ_{f-f} : Coefficient of friction, film to film

$$K = f(F_{Electrostatic}, F_V) \text{ ---------- (4)}$$

K : Correlation factor of strain distribution
$F_{Electrostatic}$: Electrostatic force among fibers
F_V : Force from fibers vibration caused by pay-off

2.2 Strains of Fibers in Ribbon

1) Under Ribbon Twists Condition only

In case that 8-fiber ribbon is twisted on Z-axis, the length of each fiber in ribbon will be calculated simply with eq. (5) and (6) to be induced from a model as <Fig.2>. These equations are applicable to a specific circumstances that ribbon gets twisted only and are expressed as helical functional relation of X-Y-Z.

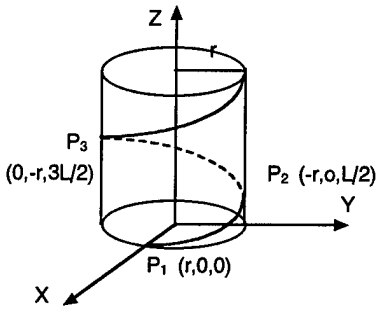

Fig.2 The length of helix on a twists

$$f(t) = r \cdot \cos t + r \cdot \sin t + t \cdot L/(2\pi) \text{ ---------- (5)}$$

$$L_{twist} = \int_0^{2\pi} \sqrt{f_x'^2(t) + f_y'^2(t) + f_z'^2(t)}\,dt \text{ --------- (6)}$$

Here, as r, P and L_{twist} mean the twisted radius, a point on helix and the length of fibers on helix on ribbon twist, x, y and z are expressed as follows each.

$$x = r \cdot \cos t = f_x(t)$$
$$y = r \cdot \sin t = f_y(t)$$
$$z = t \cdot L/(2\pi) = f_z(t), \quad 0 \le t \le 2\pi$$

Therefore, eq. (6) can be written as eq.(7).

$$L_{twist} = \int_0^{2\pi} \sqrt{r^2(\cos^2 t + \sin^2 t) + (L/2\pi)^2}\, dt$$
$$= \int_0^{2\pi} \sqrt{r^2 + (L^2/4\pi^2)}\, dt \qquad \text{---------- (7)}$$
$$= 2\pi\sqrt{r^2 + (L^2/4\pi^2)}$$

Thus, the difference in the length between outer fiber and inner fiber of 8-fiber ribbon can be calculated as eq.(8).

$$\Delta L = 2\pi\left[\sqrt{r_{out}^2 + \left(\frac{L^2}{4\pi^2}\right)} - \sqrt{r_{in}^2 + \left(\frac{L^2}{4\pi^2}\right)}\right] \qquad \text{--------- (8)}$$

Here, r_{out} and r_{in} are the distance of the inner fiber and outer fiber from the center of the ribbon.

2) Under Ribbon Twists & Bends Condition

As the cabled ribbon, generally, is easy to experience a twists and a bends together, we need to go deep into the study of them for making the better ribbon to keep good property under harsh surroundings. At this chapter, we are going to show a model and several expressions to induce the bended radius & the twisted strain of each fiber in ribbon under a specific circumstances. The model is as <Fig.3>.

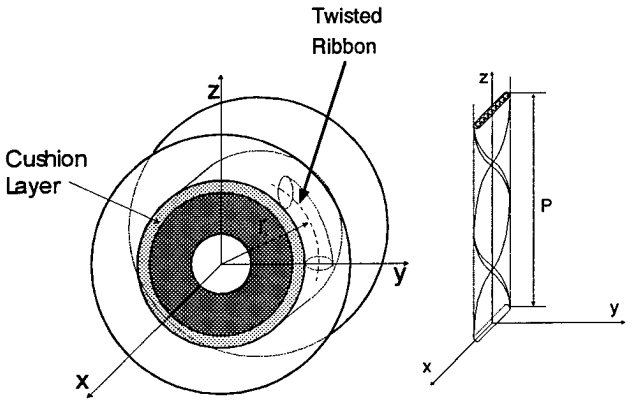

Fig.3 Schematic Diagram of the Twisted and Bended Ribbon on Drum

2-1) The Radius of Curvature

As the radius of curvature, chiefly, is written as eq. (9), curvature(κ) should be calculated first for getting it. Specially, we need to define the co-ordinate system because we regard the situation as the 3-dimentional when ribbon is winded with a twists on a drum. The co-ordinates are summaried in eq. (11).

Curvature (κ) = $|\, r''(s) \,|$
Radius of Curvature (r) = $1/\kappa$ ---------- (9)

$$|r''(s)| = \frac{\sqrt{(\dot{r}\cdot\dot{r})(\ddot{r}\cdot\ddot{r}) - (\dot{r}\cdot\ddot{r})^2}}{(\dot{r}\cdot\dot{r})^{3/2}} \qquad \text{------- (10)}$$

$$x = r_1 \cos\psi$$
$$y = r_2 \sin(P\psi/2\pi r_2) + r_1 \sin\psi \sin(P\psi/2\pi r_2)$$
$$z = r_2 \cos(P\psi/2\pi r_2) + r_1 \sin\psi \cos(P\psi/2\pi r_2) \qquad \text{------ (11)}$$

s : Path on helix
r_1 : Distance from the center of ribbon to the one of each fiber
r_2 : Distance from the center of bobbin to the one of each fiber
r : Positional vector on a plane or a space
$\dot{r}$: 1st differential for a twisted angle
$\ddot{r}$: 2nd differential for a twisted angle
ψ : Twisted angle
P : Twisted pitch
x,y,z : Position on a plane or a space
$\cdot$: Inner product

2-2) The Twisted Strain

It is said that the twists and the bends do harm on the property of the optical cable. The cable composed of many single fibers as loose tube cable is almost not influenced by the twists but the ribbon cable is much affected by it. Specially, the amount of the strain due to ribbon twists depends on positions of fibers in ribbon and, also, it is related to the adhesion between ribbon resin & coloring resin of fiber and mechanical properties of ribbon resin. The model for derivation of expressions to calculate the strain is introduced in <Fig.4>.

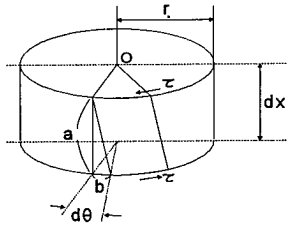

Fig.4 The schematic diagram on the twisted strain

The twisted ribbon can be expressed as eq.(12).

$$\gamma_i = \frac{b}{a} = r_0 \frac{d\theta}{dx} = \frac{2\pi r_0}{L_i} \quad (i=1,2,3\ldots8) = \frac{2\pi r_0}{\int_0^T \sqrt{\dot{r}_i \cdot \dot{r}_i}\, d\theta} \qquad \text{---------- (12)}$$

γ_i : Shear strain
a : Longitudinal twists length
b : Twists circular arc length
r_o : Diameter of fiber
$\dot{r}_i$: 1st differential for an angle
T : Twisted period
θ : Twisted angle
x : Longitudinal axis

The amount of the twisted strain of eq.(12) can be calculated from eq.(6) and (11).

3. Experiments and Analyses

3-1. Selection of Optimum Ribbon Resin

Among the existing several ribbon resin, we selected the optimal ribbon resin to have good properties as follows. Firstly, it has to have high Modulus, secondly, low T_g and high elongation, thirdly, low water absorption and shrinkage, fourthly, low surface tension of ribbon resin for improving slipping property and so on. Above all, we did test each sample under the same environmental condition and standards to get much more objective values because it is susceptible to circumstances at test. The test is done at 25°C and 65% R.H.. and its results are as follows.

Property \ Sample	A	B	C	D	E	F
Y.M. (kg/mm²)	43.14	35.2	28.83	15.57	31.04	25.95
Elongation (%)	7.18	6.42	8.05	6.80	7.00	6.9
Shrinkage (%)	6.1	13.7	13.7	13.4	15.3	12.0
Water Absorption (%)	0.2	0.5	0.2	0.8	0.4	0.4
Slip	107	266	180	114	115	113

Table.1 Comparison of main properties of each ribbon resin

From the <Table.1>, we knew the fact that the ribbon resin of A company has the best characteristics. In other words, it is estimated that the better slipping property comes from low liquid surface tension and low sharinkage is caused by relatively much more oligomer, generally having low shrinkage, in terms of analyses. Besides, it is desirable that it has high elongation in spite of high Y.M., which has an important effect on ribbon property. Here, to check if the better properties of resin could be kept after cabling or not, we selected three ribbon resins of A's, C's and D's companies having high, mean, low Y.M. values each and then made ribbon samples to have the least residual strain under the process condition deduced from Eq.(3). Loss change has been measured by periods as time goes by after ribbon insertion processs is finished. As expected, the ribbon coated with resin of A's company resulted in more stable characteristics as shown in <Fig.5>. Here, the reason that we focused on the property according to time than the one right after the ribbon insertion process is because of the movement of the inserted ribbons into more comfortable position in the slot, - which its extent depends on the properties of ribbon resin as Y.M. and elongation.

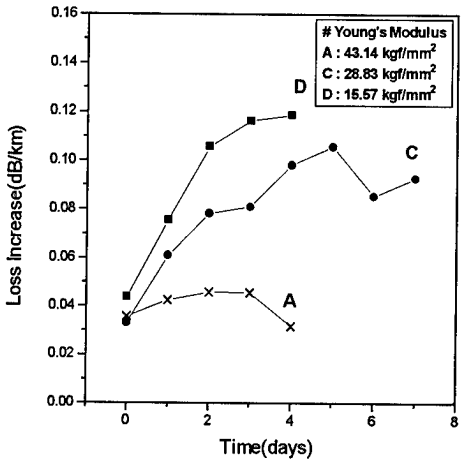

Fig.5 Loss change of each ribbon as time goes by

3-2. Preparation of coloring resin with silicone additives and adhesion test with ribbon resin

The stripped property of ribbon resin from coloring resin of fiber can be controlled by two methods to change the composition of ribbon resin or to modify the one of coloring resin. In this paper, the method by the latter will be introduced. At first, we tried to control the adhesion with ribbon resin by adding silicone additive, which is effective for lowering the surface tension of the target material, into coloring resin but we found out that its effect was not sufficient to modify it. By the way, when photoinitiators to have fast surface curing property were added with the silicon additive, the problem could be solved. That is, The proper mixing of two materials made an effect of increasing the crosslinking density of surface at UV-curing and, therefoe, the adhesion of ribbon resin on the surface of

coloring resin could be controlled property. These additives for adhesion modification were shown in <Table.2>. With using them ten kinds of coloring ink (5 kinds of Blue and White color individually) were manufactured and <Fig.6> & <Table.3> show the test method & results according to the standardand and procedure of JIS A 1613, K 6833, 6849.

Sample / Additive	A'	B'	C'	D'	E'
Polysiloxane (%)	2	2	3	3	3
Photoinitiator (%)	0	0.5	0.5	1	2

Table.2 Quantity of additive to control adhesion property

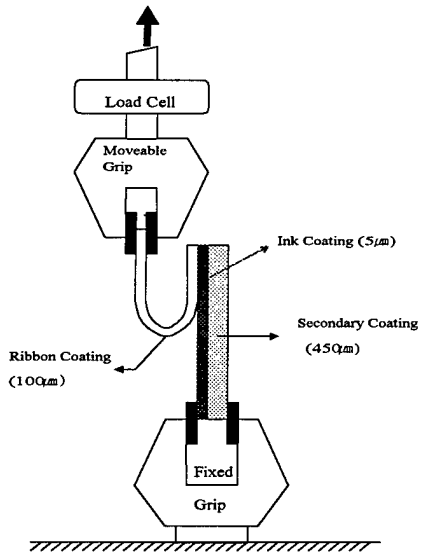

Fig.6 Adhesion test set-up

Sample / Item	White/Blue				
	A'	B'	C'	D'	E'
Adhesion (kgf/cm)	Out of Range	0.250 /0.243	0.162 /0.160	0.095 /0.087	Too Low
Surface Tension (mN/m)	37.34 /36.92	23.45 /23.85	23.50 /23.96	23.36 /23.42	23.0 /23.02

Table.3 Test results of adhesion and surface tension

From above adhesion test results it was impossible to measure adhesion force for both sample A', E' (White/Blue). In case of sample A', the delamination of ribbon resin from the adhesive surface could not be occured because of extremely complete adhesion and there was no adhesion force for sample E'. Sample B',C',D', however, showed the values that we wish to get through the proper combination. Merely there is some difference between the theoretical surface tension that we wanted to control intentionally and the real test result. It means that surface tension is much affected not by quantity of silicone but by existance of silicone. In fact, photoinitiator as well as silicone additives has an important on the adhesion.

3-3. Ribbon Making & Twisting/Bending Test [I]

Ribbon was manufactured with the colored fibers that slip-Improved coloring resin was coated on optical fiber with constant thickness and the ribbon resin of A's company selected in <3-1> paragraph. This process, also, was done under the optimal manufacturing condition decided Eq.(3). Then the bending and twisting test for 5 kinds of ribbon was executed and its method is simply expressed in <Fig.8>.

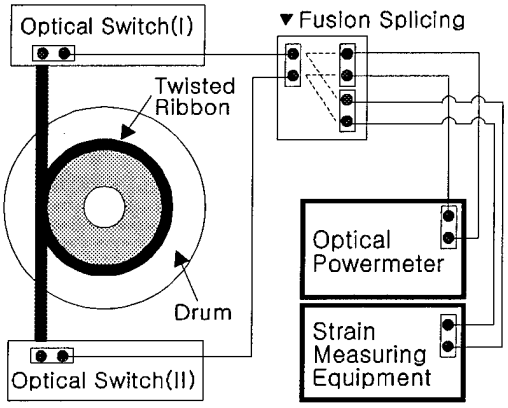

Fig.8 Schematic diagram of the bends and the twists test of ribbon

As shown in <Fig.8>, when ribbon was wound on drum of diameter ϕ77mm, curvature radius and shear strain could be calculated from Eq.(9) and Eq.(12). Also optical loss property was compared with strain according as ribbon was bended and twisted at each turn. To confirm more correctly the effect that the adhesion between fiber coloring resin & ribbon resin and Y.M. of ribbon resin influence upon the characteristics of ribbon on a bends & a twists, we have to mention two facts to occur regardless of their properties during the test. They were as follows. ; The first, there is little loss change until loss increases abruptly from 8-turn twist and, after 10-turn twist, ribbon resin is separated form coloring resin or the 1st, 2nd coating resin of fiber from its clad layer. But the latter is limited to fibers around the center of ribbon. The second, even though the curvature radius of outer fibers in ribbon is smaller than one of inner fibers, the optical loss of outer fibers is lower than the one of inner fibers. But above phenomena is natural on second thought. The difference of optical loss before and after 8-turn twist can be inferred and expected easily from

<Flg.9, 10>. We can know that the minimum curvature radius of ribbon at 8-turn twists is ϕ17.14mm (about ϕ 25mm at 7-turn twist) from <Fig.9> and this value is similar to the bending limit of normal fiber. In other words, the optical loss increases suddenly when bending radius becomes smaller than ϕ12.5mm which is the bending limit of normal fiber. In order to be certain of above fact, optical loss measuring test was carried out according to each bending radius for 4 kinds of normal single mode optical fibers used worldwide. Its result was shown in <Fig.10> and this shows that the optical loss starts to increase from the bending radius less than ϕ12.5mm (for the optical fiber used in this paper). However, if we inspect closely data, we could know easily that the variation of optical loss was appeared to be different not a few. Namely, when ribbon is bended with the radius of ϕ12.5mm without any twists, the optical loss increases to about 0.1dB but, if with a twists, it to about 0.3~1.8dB, in accordance with adhesion between coloring and ribbon resin, even in the radius of ϕ17.14mm.

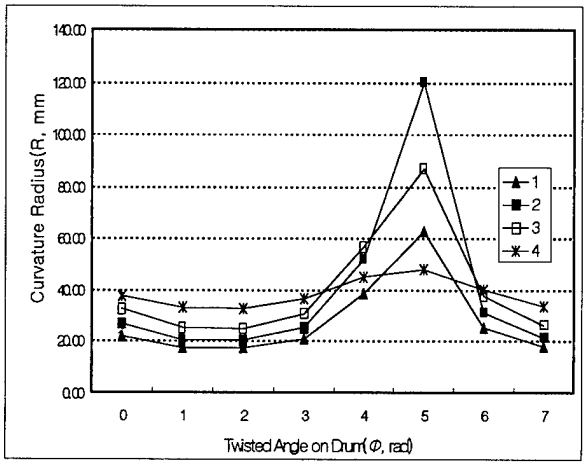

Fig.9 Comparison of curvature radius of each fiber in ribbon at 8-turn twists

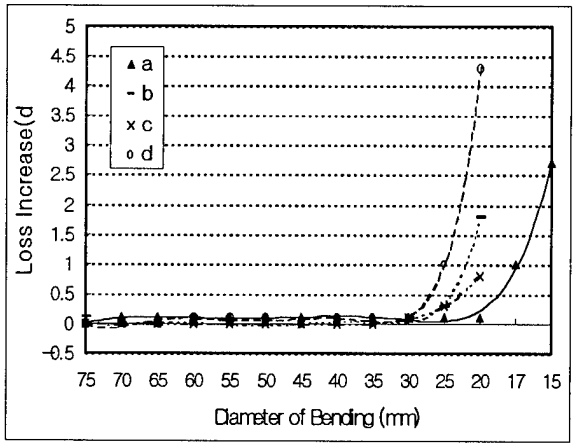

Fig.10 Loss change vs. bending diameter of optical fiber

Therefore, in this clause, the influence of adhesion between ribbon and coloring resin upon the optical property of ribbon will be concentrated on 8-turn twists which is considered as the worst environment to make optical loss increase extremely. From now the relationship between the adhesion and the optical property of ribbon under the twisting & bending test will be studied. At first, optical loss change for 5 kinds of ribbon, which have different stripping properties, is measured at 8-turn twists and ϕ38.5-radius-bends. Its result is as <Fig.11>. In this test the optical fiber a of <Fig.10> and the ribbon resin A of <Table.1> were used. The adhesion on boundary surface between ribbon & coloring resin becomes small in a following order A",B",C",D",E" in turn.

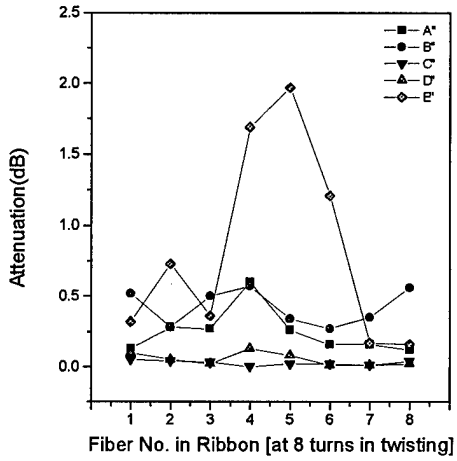

Fig.11 Loss change vs. adhesive property of riboon

From upper <Fig.11> ribbon sample C" and D" is affected little by torsion but sample A",B",E" is much. Especially for No. 4,5,6 fibers of sample E", optical loss changes are 4 times larger than ones of the others. Concerning above phenomenon, we can infer some causes to be much influenced by torsion in case of ribbons having higher and lower one as compared with ideal adhesion. The first, in case of higher adhesion, torsional effect was transmitted to the optical fiber directly. The second, in lower adhesion, as ribbon resin is easy to be delaminated from coloring resin under a twists condition, the twisted pitch on the delaminated point becomes decreased abruptly. Also, considering the affection of torsion, inner fibers in ribbon (No. 3,4,5,6) are more seriously influenced upon than outer fibers in ribbon (No. 1,2,7,8). It is thought that the shear strain of inner fibers is higher than one of outer fibers from Eq.(12) and its result is shown in <Fig.12>. Consequently the adhesion of about 0.087~0.162 kgf/mm^2 between ribbon & coloring resin is considered desirable. The stripping property of this extent of adhesion don't causes any trouble in ribbon property.

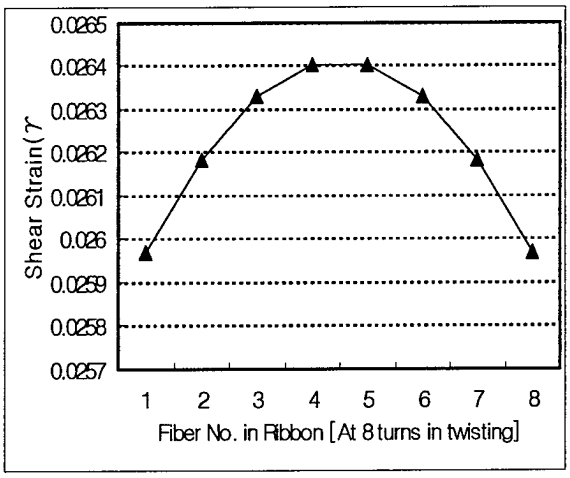

Fig.12 Shear strain of fibers in ribbon under the bended & twisted condition on drum

Moreover, to get a reliable data, strain measuring test was carried out with the same condition as the clausure of <3-3>. Its result is shown in <Fig.13> and shows the similar tendency to the one of <Fig.11>. Above all outer fibers in ribbon have (+) strain values and inner fibers (-) strain ones, namely, (-) strain values of inner fibers are caused by inflexible twisting. It is thought that this phenomenon is from the fact that the inner fibers are nearer to the central axis of torsion than the outer fibers.

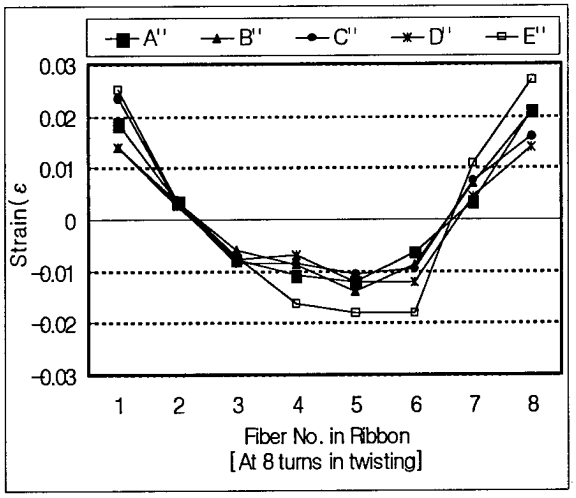

Fig.13 Measured strain of fibers in ribbon under the bended & twisted condition on drum

3-4. Ribbon Making & Twisting/Bending Test [II]

Up to now we focused on the effect of the adhesion between ribbon & and coloring resin upon the mechanical property of ribbon. Then, the influence of Y.M. of ribbon resin on ribbon twists will be investigated from now. For our experiment, we manufactured five kinds of ribbon resin that other properties excluding Y.M. are all same. In particular, to keep the fundamental properties (including the optimal adhesion with coloring resin) of ribbon resin except for Y.M. equally, we treated them very carefully. The Modification of Y.M. was achieved by controlling the crosslinking density of film with the quantity of the unsaturated Group of resin. That is to say, the composition of monomer and oligomer was controlled as <Table.4> for the tested ribbon. Here, for convenience' sake, when we set sample A of <Table.1> as 0% Y.M., the others can be expressed as the two higher ones (+20%,+10%) and the two lower ones (-20%,-10%) respectively.

Component \ Hardness	20%	-10%	0%	+10%	+20%
Oligomer	76	73	70	67	64
Monomer	19	22	25	28	31
Photoinitiator	5				
Total	100				

Table.4 Quantity of composition for controlling Y.M. of ribbon resin

Accordingly, after we prepared ribbon with 5 kinds of ribbon resin above, the twisting and bending test as <Fig.8> for them was executed and optical loss was measured at 8-turn twists. Its results are shown in <Fig.14,15>. Upon the results, the ribbon resin of our own selecting as a basis showed the best property. A little higher or lower Y.M. as compared with the basis resin makes bigger loss change and especially lower Y.M. have much more influence upon the optical of ribbon. It is considered that in the event of lower Y.M. of ribbon resin, it can't hold fibers tight effectively when ribbon is twisted.

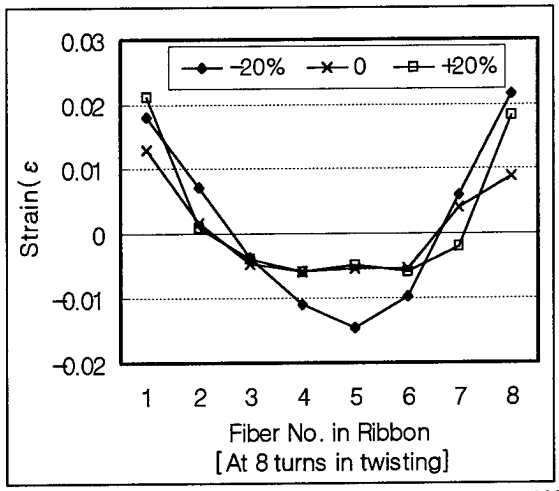

Fig.14 Loss change of fibers in ribbon according to Y.M. under the bended & twisted condition on drum

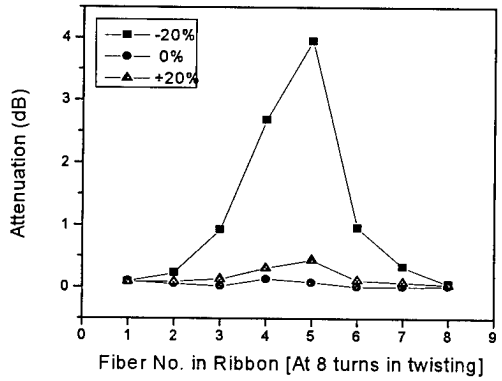

Fig.15 Measured strain of fibers in ribbon according to Y.M. under the bended & twisted condition on drum

4. Conclusion

Up to the present, we studied the correlation the optical loss on ribbon twists with the stripped property of ribbon resin & the Y.M. of ribbon resin itself. It was established that they have close relation with each other. In other words, in case that the properties to be required for the best ribbon as ribbon strip or Y.M. are unsuitable, fibers, when ribbon is twisted, come to be easy to experience buckling or microbending loss. Thus, we could know that it is essential to select ribbon resin with the proper Y.M. and adhesion with coloring resin of fiber for the best ribbon. From our experiments, we could say that ribbon resin with properties as A of <Table.1> and C' of <Table.3> should be selected for getting the better ribbon.

In conclusion, we could present the basic properties to be considered on the selection of ribbon resin through the theoretical & the experimental approach method. In particular, this will be a basis to make ribbon have good property even under the worst condition as a twists or a bends.

5. References

[1] G.W.Seo, Y.H.Jeon, S.H.Kim, "Review on the correlation between residual strain of fibers in ribbon and ribbon property", 46th IWCS, pp539-546, 1997

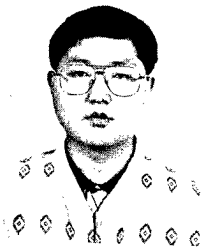

G.W.Seo
DAEWOOTELECOM Ltd.
531-1,Gajwa-Dong,Seo-Gu,
Inchon-City,Korea

He joined Daewoo Telecom.LTD. after graduating from Pusan University with M.S. degree in the inorganic material engineering in 1993 and, since then, has been engaged in Fiber Optic R&D Center. He is now senior engineer and is working as the cable designer.

Y.H.Jeon
DAEWOO TELECOM Ltd.
531-1,Gajwa-Dong,Seo-Gu,
Inchon-City,Korea

He is a senior engineer of Fiber Optic R&D Center. He graduated from KAIST with B.S. degree in the electrical material engineering in 1991 and joined it after military service in 1996. He is working as the cable designer in the optical cable part.

S.H.Kim
DAEWOO TELECOM Ltd.
531-1,Gajwa-Dong,Seo-Gu,
Inchon-City,Korea

He is now chief engineer of the optical cable part. He obtained bachelor's degree in the precision mechanical engineering from Hanyang University and joined DAEWOO TELECOM. LTD.in 1982. Since then, he has been engaged in Fiber Optic R&D Center. He is a member of CCITT(Study group 6).

K.J.Lew
DAEWOO TELECOM Ltd.
531-1,Gajwa-Dong,Seo-Gu,
Inchon-City,Korea

Now he is general manager of Fiber Optic R&D Center. He received bachelor's degree in electronic engineering from Hanyang University in 1980 and joined DAEWOO TELECOM. LTD. Since then, he has been engaged in Fiber Optic R&D Center.

J.H.Oh
Samsung Chemical Paint
Co. Ltd.
629-3,Sunggok-Dong,
Ansan-Ciity,
Kyonggi-Do,
Korea

He joined Samsung Chemical Paint Co. Ltd after graduating from Cornell University with M.S. degree in the material science & engineering in 1996 and since then, has been engaged in R&D Division. He is now general manager.

D.Y.Shin
Samsung Chemical Paint
Co. Ltd.
629-3,Sunggok-Dong,
Ansan-Ciity,
Kyonggi-Do,
Korea

He joined Samsung Chemical Paint Co. Ltd after graduating from Hanyang University with M.S. degree in the industrial chemistry in 1990 and since then, has been engaged in R&D Division. He is now senior engineer.

NON-DESTRUCTIVE MEASUREMENT SYSTEM OF FIBER ALIGNMENT FOR THE OPTICAL FIBER RIBBON

Ken Hashimoto, Yuichi Tamura, Masakazu Shigehara, Tomoyuki Hattori, Ichiro Tsuchiya

Sumitomo Electric Industries, Ltd., Yokohama, Japan

ABSTRACT

A non-destructive measurement system for fiber alignment of fiber ribbon has been newly developed. To measure the fiber position in the ribbon matrix coating, we modified the light-section method. In our method, a slit light is projected from one side of the ribbon surface, and images of the ribbon surface and the coloring layer of the fibers are obtained by two CCD cameras set in different angles. This system can calculate fiber alignment (planarity and horizontal separation) by processing these images. It enables us to evaluate fiber alignment in a fiber ribbon with an accuracy of 3μm and a measuring time as fast as 4 sec for eight- fiber ribbon.

1. INTRODUCTION

Fiber ribbons have been used in commercial optical fiber cable systems since they are advantageous for mass splicing as well as high-density package in cables. In a fiber ribbon, each fiber is surrounded by four layers: a primary coating, a secondary coating, a coloring layer, and a ribbon matrix coating.

To make splicing successful, it is necessary to have a good two-dimensional alignment of the fibers in a ribbon. If the alignment of fibers is not regular enough, glass fibers get damages when stripping all the coating layers around fibers at the same time.

Geometrical definitions in a cross section of a fiber ribbon are shown in Fig. 1. The values of Table 1 are examples of requirements for ribbon dimensional tolerances that are being considered in international standardization in IEC. [1]

It is easy to measure the outside dimensions, such as height (H) and width (W) with optical methods. On the other hand, for measurement of fiber alignment, that is horizontal separation and planarity, the microscope observation of cross section of a ribbon cut piece is often used. However, it requires so smooth end face that special care must be paid for sample preparation. Furthermore, it takes a lot of time to make samples, and it is impossible to measure all part of a ribbon because this method includes the destruction process.

We have, therefore, developed a novel apparatus for measuring fiber alignment by modifying the light-section method and realized a non-destructive measurement of fiber alignment applicable up to an eight-fiber ribbon.

Table 1 An Example of Ribbon Dimension Specification [1] (All values are maximum limit.)

Number of Fibers	Width W(μm)	Height H(μm)	Fiber Alignment: Horizontal Separation: Adjacent D(μm)	Fiber Alignment: Horizontal Separation: Extreme B(μm)	Fiber Alignment: Planarity P(μm)
4	1220	480	280	835	50
8	2300	480	300	1920	50

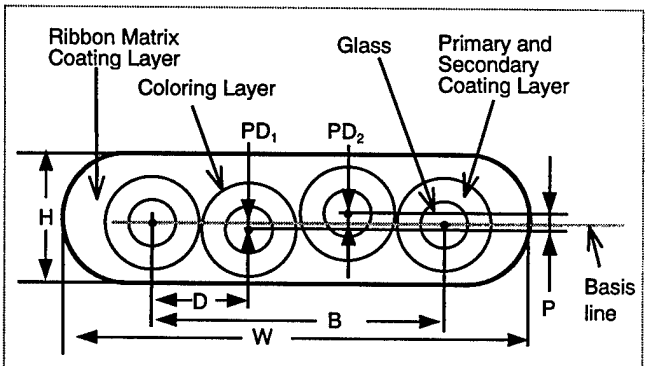

P : Planarity (PD_1 , PD_2 : Planarity Deviation)

D: Adjacent Fiber Distance

Fig.1 Cross Section of the Four-Fiber Ribbon and Fiber Alignment Parameters

2. PRINCIPLE

2.1 Light-section method

The light-section method, which is known as one of popular application of the triangulation surveying, is available for non-destructive measurement of three-dimensional position. It does not need large-scale apparatus and complicated data transactions compared with other internal measurement system such as X-ray CT. Therefore, we tried to apply the light-section method to fiber ribbon measurement.

To get the information of object surface more quickly, this method makes use of slit light for projection pattern instead of spotlight, because it reduces the line-scanning time. Figure 2 shows the general principle of the light-section method. A slit light is projected from one side of the object, and the reflected light image from the object can be detected using two-dimensional CCD camera. The height difference between surface 1 and surface 2 is obtained as follows.

$$H = D / (2 \cdot \tan\theta_p \cdot \cos\theta_d) \quad (1)$$

, where D, θ_p, θ_d are the measured distance between two reflected light from each surface in the observed image, the set angle of projection side and that of detection side in optical system, respectively. Generally, the projection side and the detection side are set in a symmetrical scheme. This setting makes it possible not only to get reflection light effectively but also to reduce complexity of the image processing for the measurement.

2.2 Measurement for objects under the transparent layer

The light-section method is only available for shape measurement of the object surface in most application. To evaluate the fiber alignment of a ribbon by the light-section method, it is necessary to measure the position of fibers inside the ribbon matrix coating. In case of a fiber ribbon, fibers could be observed through the ribbon matrix coating, because the resin is usually transparent material for an identification of fiber coloring layers.

Figure 3 shows the observation by the light-section method for the model object, which has a transparent layer. If the transparent layer above object has non-uniform thickness, the reflected light is observed at the different position because the projection light is refracted when it goes into the transparent layer.

Hence, we should consider correction of observed image of fibers considering the thickness and the refractive index of coating resin, 0because the thickness of coating resin layer of a fiber ribbon is not perfectly uniform.

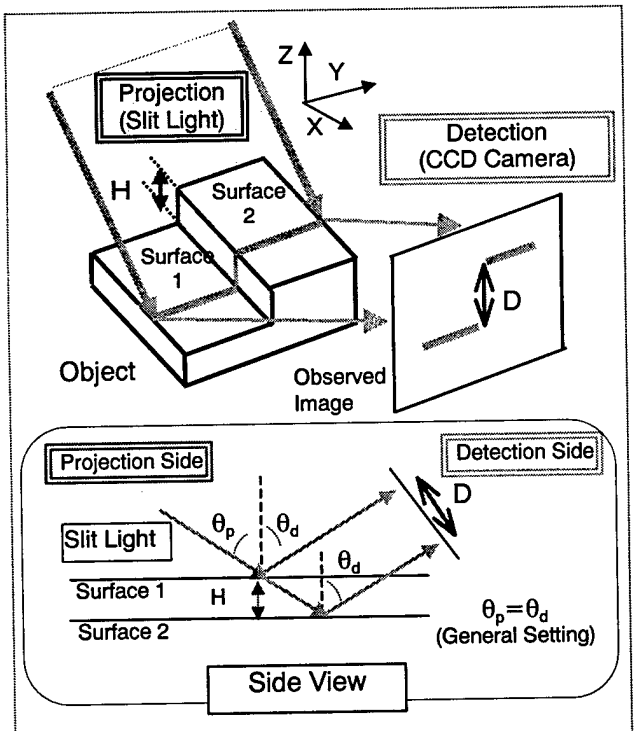

Fig. 2 General Light-section Method

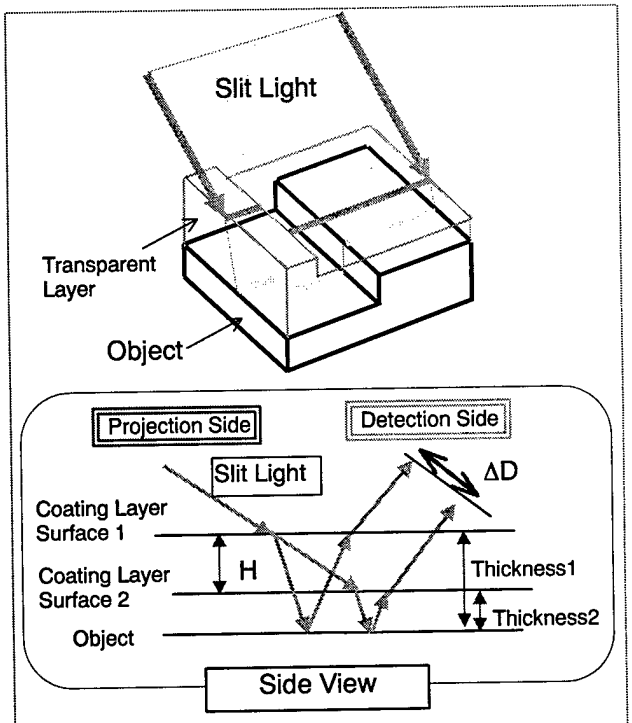

Fig.3 Measurement of the Object under the Transparent Layer

2.3 Setting for fiber ribbon measurement

When the light-section method is applied to a fiber ribbon, only the half side of fibers could be seen as circular-arc shape in an observed image as shown in Fig. 4. Therefore, the representative position of each fiber by the light–section method is defined to be the top position of the fiber as shown in Fig. 5.

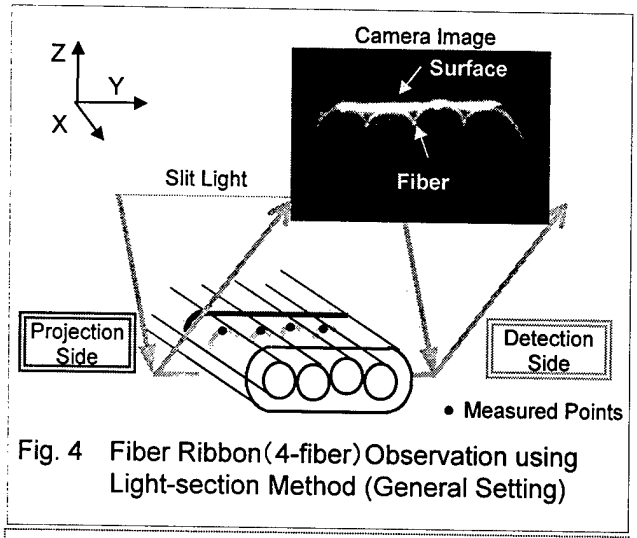

Fig. 4 Fiber Ribbon(4-fiber) Observation using Light-section Method (General Setting)

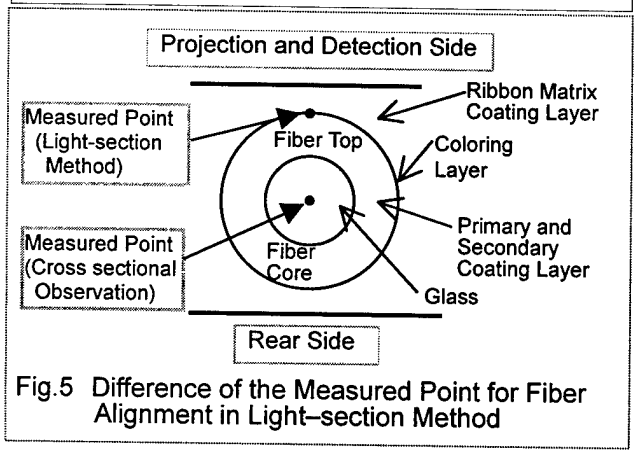

Fig.5 Difference of the Measured Point for Fiber Alignment in Light–section Method

However, the reflected light from ribbon surface is too bright to clearly see the image of top part of fiber coloring layer as shown in Fig. 4. Consequently, simply applying the light-section method to a fiber ribbon does not enable us to measure the each fiber, which is encapsulated in the ribbon matrix coating.

In order to overcome the limitation of the light–section method, we have compared the characteristics of the reflection light from the matrix coating layer surface with that of coloring layer of fibers. The direction of reflection light from the ribbon surface is restricted within a narrow angle, because there is large difference of refractive index between the ribbon matrix coating and air around fiber ribbon. On the other hand, the projected slit light is scattered at the coloring layer of fibers.

Therefore, we modified the setting of the light-section method. Setting of our optical system is shown in Fig. 6, where two CCD cameras are set in a different detection angle. A slit light is projected from one side of the ribbon surface. The reflected light image from ribbon matrix coating surface is detected by one camera and the scattered light image from coloring layer of encapsulated fibers is obtained by another camera.

As we need the difference of fiber positions under ribbon coating layer with non-uniform thickness, it is necessary to get both the image of ribbon matrix coating surface and the image of coloring layer of fibers.

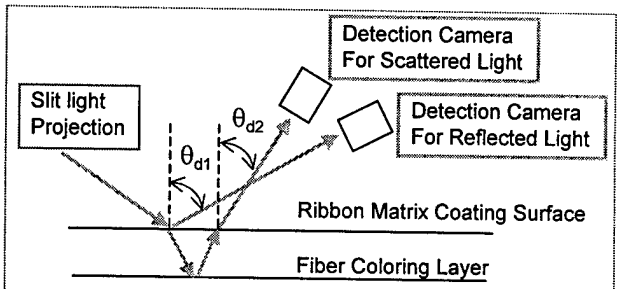

Fig.6 Modified Setting (Two Detection Angles)

3. NEW MEASUREMENT SYSTEM

3.1 System hardware

Based on the above consideration, a new measurement system has been built as shown in Fig. 7. It consists of an optical system and an image

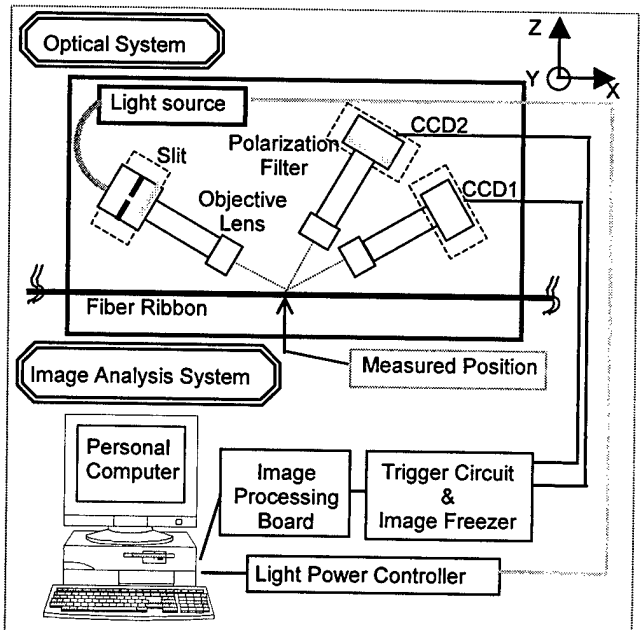

Fig. 7 Schematic View of the New Measurement System

analysis. In the optical system, the light projection apparatus and the two detection CCD cameras are set with a different angle, as is mentioned before.

In the image analysis system, a personal computer is used for the image processing for fiber alignment measurement of fiber ribbons as well as for hardware control.

Reflected light from ribbon surface (ribbon matrix coating surface) is detected with CCD1 in the opposite direction of the projection light. To detect the image of scattered light from fibers inside the ribbon matrix coating is set in a different angle. (For simplification, Image of CCD1 and CCD2 will be written as "surface" image and "fiber" image, respectively, below). Both CCD cameras have 640 x 480 pixels and one pixel is equivalent to about 5μm X 5μm area as a result of magnifying with objective lenses. Our system can be applicable up to 8-fiber ribbon observation. Figure 8 shows the example of images 8-fiber ribbon observed in our system.

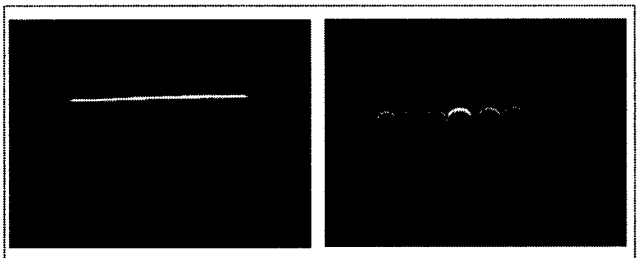

CCD1(Surface) Image CCD2(Fiber) Image

CCD1: Reflected light from ribbon matrix coating surface
CCD2: Scattered light from fiber inside ribbon matrix coating

Fig. 8 Example Image of 8-fiber Ribbon Observation

This optical system includes polarizing filters. "Fiber" image can be observed by modifying setting direction. However, reflected light from ribbon surface might be occasionally observed in the "fiber" image depending on the ribbon surface condition. It is preferable to isolate the information from two layers, for easy calculation of the image processing. To reduce this reflected light noise, polarization filters are set in both projection side and detection side with the polarization direction perpendicular to each other as shown in Fig. 9.

The status change of polarization of slit light at the ribbon surface is different from that of the fiber coloring layer. The ribbon surface rotates polarization angle by 90 degrees, while fiber coloring layer under the coating resin layer randomizes the polarization angle.

Accordingly, the reflected light from ribbon surface cannot pass through to the "fiber" image detection camera side with a set of polarizing filters, and only the scattering light image of fiber coloring layer can be obtained.

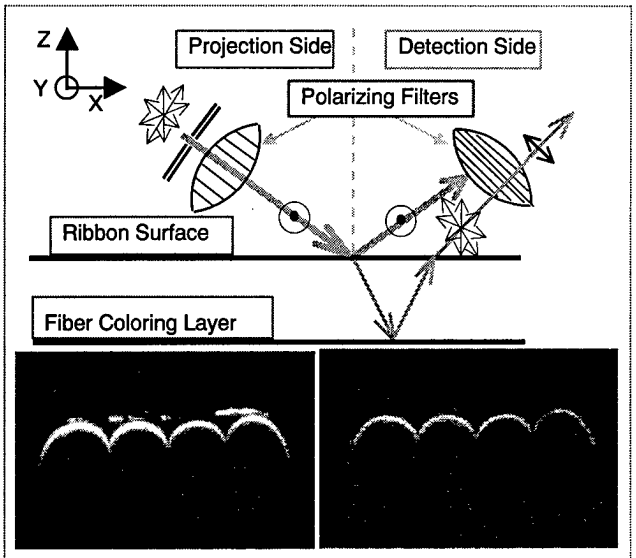

Fiber Image Without Filters Fiber Image With Filters

Fig. 9 Polarization Control for Fiber Observation

3.2 System software

Figure 10 shows the procedure of automatic measurement software in this system.

Bright area of acquired image is selected from initial "fiber" image for processing images effectively.

After light power is adjusted according as the brightness of observed images of the scattered light, a trigger signal is sent to the both CCD cameras. It is important to get the images at the same time when it is used for a continuous on-line monitoring during the manufacturing process.

Each horizontal line of processing area of the images are scanned and calculated the peak position of distribution pattern of the brightness data. The 2-dimentional precise position of "fiber" and "surface" can be obtained from these procedures. Correction of observed image of fibers should be performed according as coating thickness and refractive index of coating resin.

Figure 11 shows the schematic diagram of the light direction in the light-section method when the fiber positions and coating thickness are different.

When θ_p is projection angle and θ_d is detection angle, projection angle after refraction : θ_p' and detection angle before refraction: θ_d' can be defined as follows:

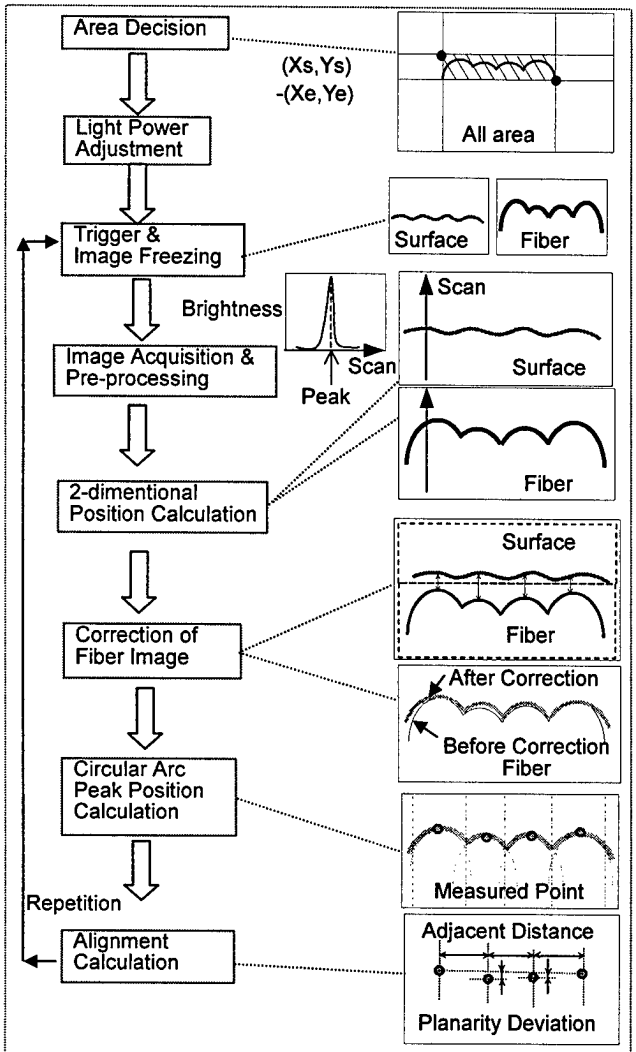

Fig. 10 Fiber Alignment Measurement Procedure

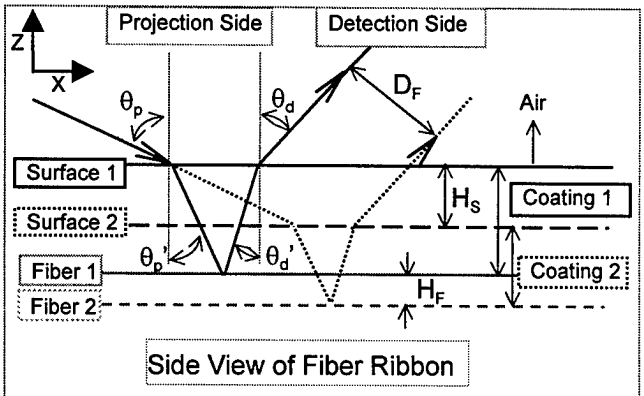

Fig.11 Light-section Method for the Fiber Ribbon Measurement

$$\theta_p' = \sin^{-1}(n_0 \cdot \sin\theta_p / n_1) \quad (2)$$
$$\theta_d' = \sin^{-1}(n_0 \cdot \sin\theta_d / n_1) \quad (3)$$

, where n_0 is refractive index of air, and n_1 is refractive index of coating resin.

Correction of the fiber coloring layer profile, as shown in the Fig. 11, can be calculated by

$$H_F = k_a \cdot D_F + k_b \cdot H_S \quad (4)$$
$$k_a = 1 / ((\tan\theta_p' + \tan\theta_d') \cdot \cos\theta_d) \quad (5)$$
$$k_b = 1 - (\tan\theta_p + \tan\theta_d) / (\tan\theta_p' + \tan\theta_d') \quad (6)$$

, where H_S is the difference of the coating surface profile and D_F is the fiber position difference which can be observed in the detection camera. H_S can be measured by the normal light-section method using the direct reflection image, and D_F can be observed in CCD camera.

The difference of thickness from one of the "surface" position, is enough for correction of the "fiber" position, because fiber alignment measurement is a relative evaluation. Therefore, the "fiber" image can be corrected using the "surface" position data.

The corrected "fiber " data is divided into the data of each fiber area. Using each circular-arc-like shape data, the peak point is calculated by fitting the parabolic function with a method of least squares. Fiber alignment can be calculated using this measured point of each fiber.

In final stage, fiber alignment is calculated based on the definitions shown in Fig. 1. The basis line goes through the top position of the first and the last fiber. The intersection points of basis line and orthogonal line from the top positions of each fiber are obtained. Using these intersection points, alignment parameters are measured. Horizontal separation (adjacent fiber distance) is defined as the distance between these intersection points and planarity deviation of each fiber is defined as distance between the intersection point and the top position of each fiber. Generally, planarity can be calculated as difference between the maximum and the minimum value of planarity deviations of all fibers within one fiber ribbon.

4. SYSTEM EVALUATION

We evaluated the repeatability of planarity deviation of each fiber and adjacent fiber distance in this system by measuring the same point of several samples ten times. As a result, repeatability measurement for the both parameters can be less than 2μm.

Furthermore, to make sure the absolute value, measured values by this system were compared with that by the microscope observation of cross

section of a ribbon. Samples are intentionally made to have various values of fiber alignment for this evaluation. As shown in Fig. 12, the measured value difference between two methods was confirmed to be below 3μm.

Figure 13 shows comparison of absolute values between two methods. Considering the destruction in the process of the cut piece of a ribbon in the microscope observation of cross section, the accuracy of the measurement with this system is enough for practical use.

This apparatus allows us easily to inspect all part of fiber ribbon products and to guarantee the quality of products.

The measurement time including data processing is as fast as 2 sec for a four-fiber ribbon, and 4 sec for an eight-fiber ribbon. This system is also available for continuous on-line monitoring of the fiber alignment during the manufacturing process of fiber ribbons.

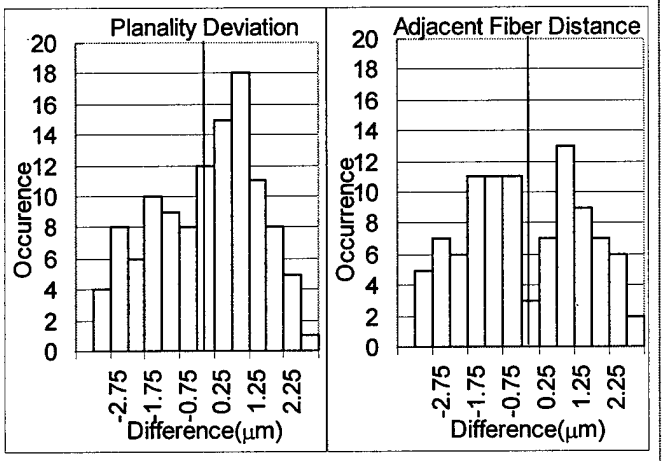

Fig.12 Difference of Fiber Alignment Data between Two Methods (Light-section Methods - Cross Sectional Observation)

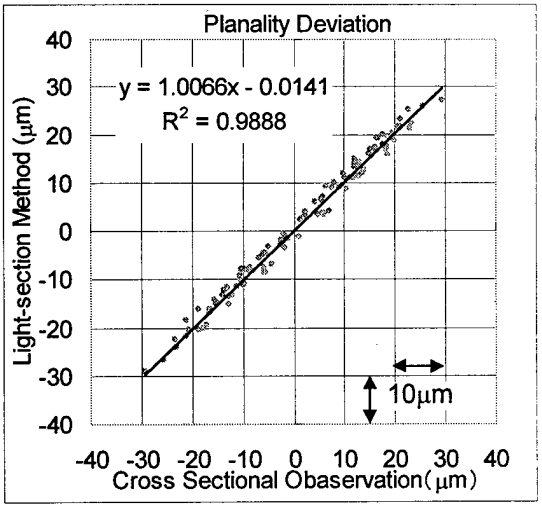

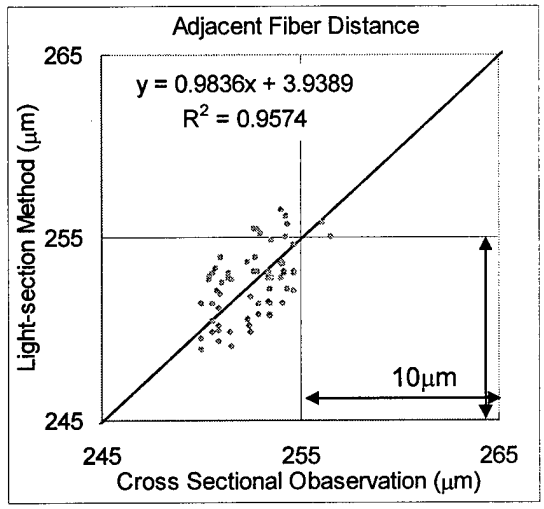

Fig.13 Comparison of Fiber Alignment Data of Two Methods
(Samples are intentionally made to be various values of fiber alignment for this evaluation.)

5. CONCLUSION

A non-destructive measurement system for fiber alignment of fiber ribbon has been newly developed, by modifying the light-section method. This system detects the coloring layers of fibers with correction for ribbon matrix coating thickness. Planarity and horizontal separation can be obtained by processing observed images and its accuracy is confirmed to be below 3μm.

REFERENCES

[1] Lauri Oksanen "Fiber Ribbon Measurements" D.D. Soares(ed), Trends in Optical Fibre Metrology and Standards, 415-427

Ken Hashimoto

Sumitomo Electric Industries, Ltd.

1, Taya-Cho, Sakae-ku, Yokohama, 244-8588, Japan

Ken Hashimoto received his M.S. degree in Precision machinery engineering from the University of Tokyo in 1994. He joined Sumitomo Electric Industries, Ltd. in 1994, and has been engaged in research and development of measurement technologies for optical fiber and optical devices. He is a member of Optomechatoronics R&D department in Yokohama Research Laboratories.

Yuichi Tamura

Sumitomo Electric Industries, Ltd.

1-1-1, Koya-kita, Itami, Hyogo, 664-0016 Japan

Yuichi Tamura received his M.S. degree in Precision engineering from Kyoto University in 1995. He joined Sumitomo Electric Industries, Ltd. in 1995, and has been engaged in research and development of measurement technologies and CAE(Computer Aided Engineering) technologies. He is a member of CAE Research Center.

Masakazu Shigehara

Sumitomo Electric Industries, Ltd.

1, Taya-Cho, Sakae-ku, Yokohama, 244-8588, Japan

Masakazu Shigehara received his M.S. degree in Electrical engineering from Tokyo Metropolitan University in 1988. He joined Sumitomo Electric Industries, Ltd. in 1988, and has been engaged in the research and development of measurement system for optical fiber and devices. He is a senior engineer of Optomechatoronics R&D department in Yokohama Research Laboratories.

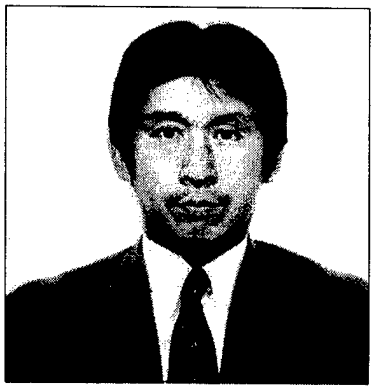

Tomoyuki Hattori

Sumitomo Electric Industries, Ltd.

1, Taya-Cho, Sakae-ku, Yokohama, 244-8588, Japan

Tomoyuki Hattori received his M.S. degree in Chemistry from Kyoto University in 1987. He joined Sumitomo Electric Industries, Ltd. in 1987, and has been engaged in the research and development of optical fiber and cable. He is a senior engineer of Transmission Media Department in Yokohama Research Laboratories and a member of the Institute of Electronics and Communication Engineer of Japan.

Ichiro Tsuchiya

Sumitomo Electric Industries, Ltd.

1, Taya-Cho, Sakae-ku, Yokohama, 244-8588, Japan

Ichiro Tsuchiya received his M.S. degree in Precision machinery engineering from the University of Tokyo in 1983. He joined Sumitomo Electric Industries, Ltd. in 1983, and has been engaged in research and development for optical fiber and cable technology. He is a Chief Research Associate of Transmission Media R&D department in Yokohama Research Laboratories.

NEW MICROBENDING TEST METHODS FOR FIBER OPTIC RIBBONS

Winfried Rutzen

Siemens AG, ÖN NK E SF, Nordenham, Germany

ABSTRACT

In this paper two new microbending test methods for ribbons will be presented.
Realistic "cable-like" conditions can be simulated with these test methods:

- Application of flat and lateral loads
- Long test lengths.

These advantages lead to reproducible microbending test results. We will also show the excellent correlation between the test results and the ribbon performance in SST (Super Single Tube) – cables.
For the first time, systematical investigations of the microbending properties of ribbons were possible. By using these new investigation methods, expensive cable tests can be avoided and considerable time and cost savings are achieved.

INTRODUCTION

To ensure lowest attenuation of cabled fibers, all mechanical loads, which act on the fibers, have to be minimized. Due to the very high packing density in ribbon cables, microbending losses can not be avoided.
For this reason it is important to optimize the microbending properties of fiber optic ribbons. Therefore powerful microbending test methods for ribbons are required.

THEORY

The microbending losses of ribbons are essentially determined by the following parameters:

1. Optical (glass) and mechanical (coating) fiber properties
2. Ribbon geometry
3. Mechanical properties of the ribbon coating
4. Roughness of the contact surface
5. Degree of mechanical load.

The parameters 1 to 3 are intrinsic ribbon properties, whereas the parameters 4 and 5 are determined by the microbending test.

MICROBENDING TEST METHODS

Two microbending test methods for ribbons have been developed:

Pneumatic expandable drum test

One ribbon layer is wound on a pneumatic expandable drum. The circumference of the drum can be evenly enlarged with the help of air pressure (see fig. 1). The ribbon is strained and pressed flat on the drum surface (see fig. 2). In that case the load acts on the complete width of the ribbon. The length under test is 100 m to 600 m and depends on the number of fibers per ribbon.

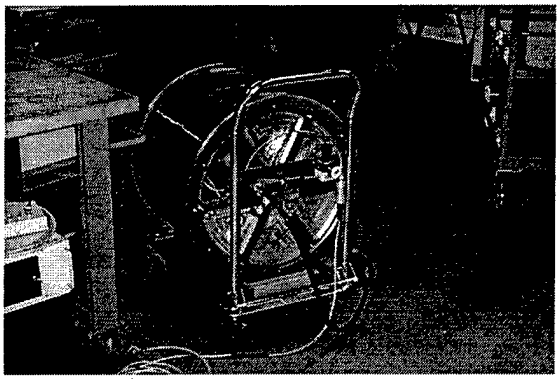

Fig. 1 Pneumatic expandable drum test setup

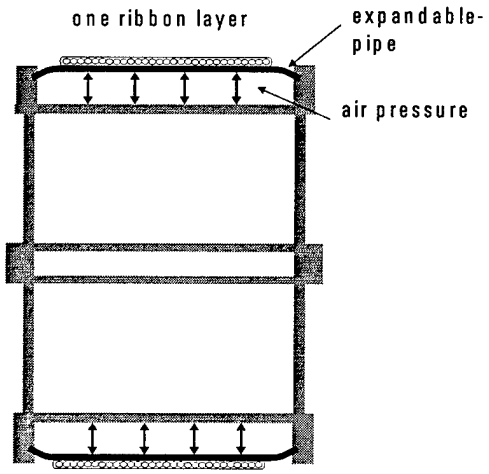

Fig. 2 Pneumatic expandable drum: cross section

Long length edge crush test

Several layers of the ribbon are put on each other to create a ribbon stack. This stack is placed between two plates, thus the flat ribbon surfaces are oriented perpendicular to the plates (see fig. 3). By moving one plate the stack is pressed together (see fig. 4). With this test configuration, especially the edge fibers of the ribbons will experience the highest load. The length under test is about 400 m.

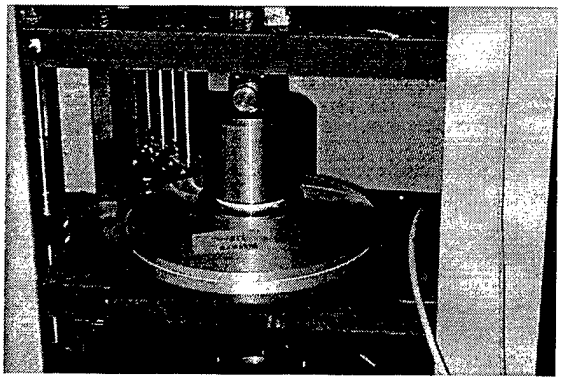

Fig. 3 Long length edge crush test setup

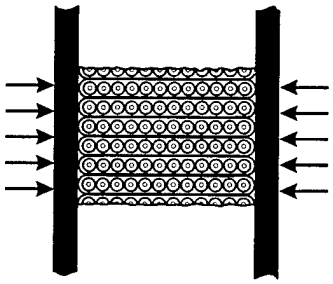

Fig. 4 Lateral load on the ribbon

PNEUMATIC EXPANDABLE DRUM TEST

Test procedure and results

The attenuation change as function of the load has to be measured. The air pressure will be increased from 0 bar to 1.5 bar and decreased form 1.5 bar to 0 bar in steps of 0.25 bar. The air pressure will be kept constant for 100 seconds. A multi channel power meter will monitor the attenuation change.

Figure 5 shows a typical result of a 4-fiber ribbon. It can be seen that the attenuation increases over time at constant air pressure levels. This is due to the creep of the glass in the primary coating.

Therefore the timing of the test is very important and has to be kept constant to achieve reproducible and comparable results.

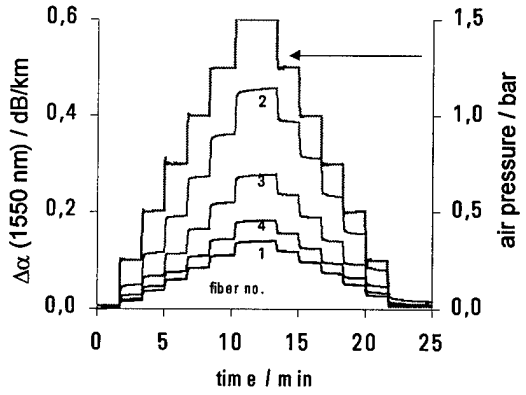

Fig. 5 Attenuation change and air pressure versus time

The calculation of the average attenuation change of each air pressure level leads to this figure:

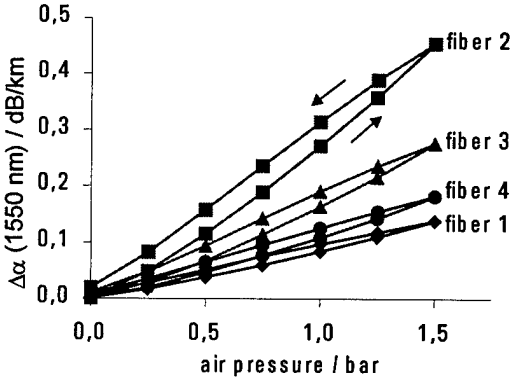

Fig. 6 Attenuation change versus air pressure

Now it can be easily seen that the attenuation change is almost direct proportional to the air pressure. The hysteresis is the result of the above-mentioned creep.

Now it is possible to calculate a regression line through the data points of a fiber.

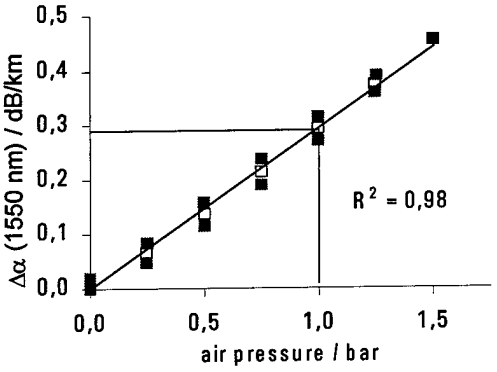

Fig. 6 Definition of the microbending factor k_{MB}

The slope of the regression line can be used to describe the microbending sensitivity of each fiber of a ribbon.
Therefore we define the **slope** of the regression line as **microbending coefficient k_{MB}**.
In this example (figure 6) this leads to k_{MB} = 0.29 dB/(km bar).
k_{MB} will be calculated for each fiber in a ribbon.

Further tests have shown that the reproducibility of k_{MB} is excellent. We repeated the complete test procedure (including rewinding the ribbon) and found an uncertainty of 2σ = 0,005 dB/(km·bar).

Air pressure as load parameter

The microbending coefficient uses the air pressure as load parameter. Measurements have shown that the fiber strain and also the tensile force at each pressure level is independent of ribbon type if the total fiber length (ribbon length times fiber per ribbon) is constant.

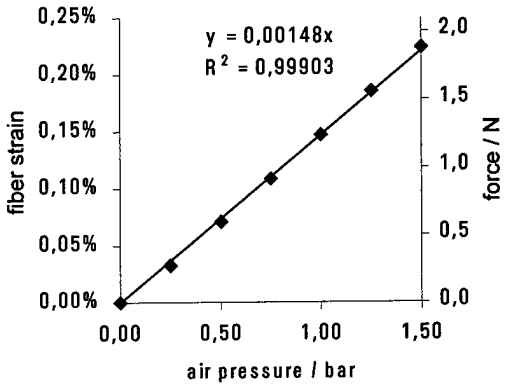

Fig. 7 Fiber strain / tensile strength during microbending test

We found a coefficient (slope of the regression line) m = (0.149 ± 0.004) %/bar for 4 – 24 fiber ribbons.

Influence of the ribbon geometry

With this test method the ribbon is flatly pressed on the drum surface. Figure 8 shows a 12-fiber ribbon with a very bad geometry.

Fig. 8 Cross section of a bad 12 fiber ribbon

Both sides of the ribbon have been tested:
Top side: k_{MB} = 0,35 dB/(km·bar)
Bottom side: k_{MB} = 0,10 dB/(km·bar)
(Average over all fibers)

Therefore it is very important to test both sides of a ribbon.
The variation of k_{MB} gives also an indication about the ribbon geometry.

LONG LENGTH EDGE CRUSH TEST

Test procedure and results

The test procedure is similar to the expandable drum test. The total lateral load will be increased to F_{max} = 1000 N. The typical length under test is 370 m.

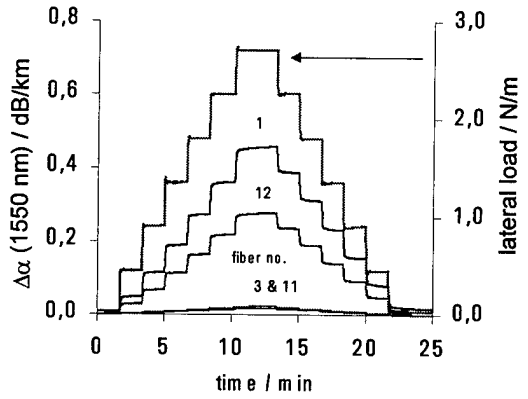

Fig. 8 Long length edge crush test of a 12 fiber ribbon

As expected, the maximum attenuation change appears on the edge fibers. The attenuation change of the next fibers is much smaller.
All further steps (definition of a microbending coefficient) are similar to the pneumatic expandable drum test.

COMPARISON OF THE MICROBENDING TEST RESULTS AND THE ATTENUATION INCREASE AFTER CABLING

For this comparison 4 different 12 fiber ribbon types have been manufactured. The thickness of the ribbon matrix material, line speed and other process parameters have been varied.
This ribbon has been tested with the pneumatic expandable drum (see figure 9).

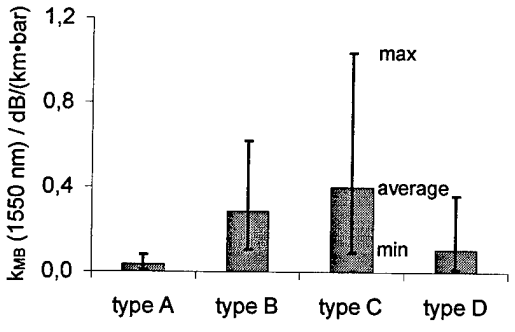

Fig. 9 Test results of 4 different ribbon types

The columns represent the average microbending coefficient of both ribbon sides and all 12 fibers. The error bars represent the minimum and maximum values of k_{MB}.

SST (Super Single Tube) – cables with 18 x 12 fiber ribbons have been manufactured with all 4 ribbon types (see figure 10).

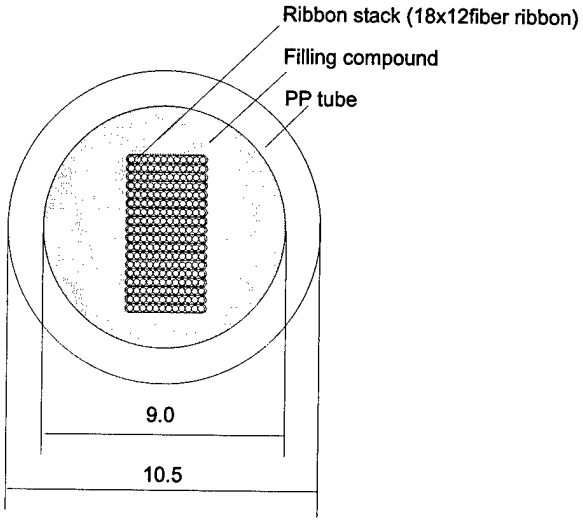

Fig. 10 Super Single Tube (SST) with 18 x 12-fiber ribbons

The attenuation increase (attenuation of cabled ribbon – fiber attenuation) has been measured.

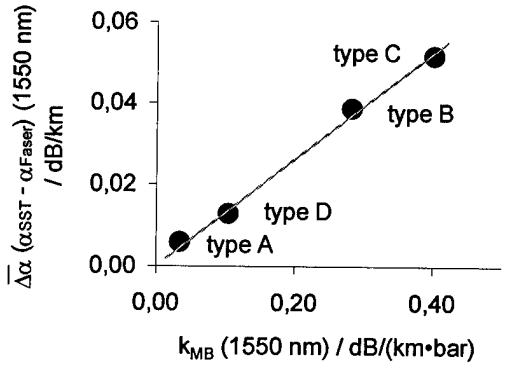

Fig. 11 Correlation between attenuation increase through cabling and microbending test

We found a good correlation between the average attenuation increase and the microbending coefficient from the pneumatic expandable drum test (see figure 11).

ADVANTAGES OF THE NEW TEST METHODS

The main advantages of the above mentioned test methods are the simulation of more realistic "cable-like" conditions:

- Application of flat and lateral loads
- Long test lengths.

The roughness of the contact surface can be changed by selection of appropriate polymer foils, which are applied on the surface of the drum or plates respectively. A multi channel power meter can easily measure the attenuation change.

These advantages lead to reproducible microbending test results.

Non-elastic deformations of the ribbon can be avoided by application of low mechanical loads, which typically occur in real cables.

The influence of individual ribbon parameters (e. g. the ribbon coating material) on the microbending sensitivity of ribbons has reliably been proven for the first time.

CONCLUSION

Two microbending test methods for fiber optic ribbons have been developed, which are used for the reliable characterization of the microbending properties of fiber optic ribbons. Comparable to the conditions in a cable, flat and lateral mechanical loads can be applied.

For the fist time, systematical investigations of the microbending properties of ribbons were possible. By using these new test methods, expensive cable tests can be avoided and considerable time and cost savings are achieved.

AUTHOR

Winfried Rutzen
Siemens AG
Kabelstrasse
26954 Nordenham
Germany

Winfried Rutzen was born 1969 in Coburg, Germany. He received his Dipl. Ing. (FH) from Fachhochschule Coburg in 1995. He joined to Siemens in 1994. He was engaged in the characterization of optical fibers, ribbons and cables. Now he is especially involved in the development of OPGW and fiber optic submarine cables of metal tube design.

ANALYSIS OF A MODULAR 24-FIBER RIBBON FOR THE DISTRIBUTION NETWORK

Scott A. McCreary, William E. Beasley, Stephen R. Stokes, Ronald G. Lindsay Jr.

Sumitomo Electric Lightwave Corp.
Research Triangle Park, North Carolina

ABSTRACT

A modular type 24-fiber ribbon was developed to optimize the packing density of optical fibers in a central tube design cable containing 432-fibers. The new ribbon can be easily split into two 12-fiber sub-ribbons at the end or in mid-span, and the 12-fiber sub-ribbons are completely compatible with standard optical ribbon mass fusion splicing equipment. A new tool was developed to cleanly, and consistently split the 24-fiber ribbon into its 12-fiber sub-ribbons without degrading the integrity of the 12-fiber sub-ribbons. Complete qualification testing of the ribbon and cable was conducted and is presented.

INTRODUCTION

With the rapidly increasing demand for bandwidth, new fiber optic technologies are being introduced to the market at a breakneck pace. These methods for increasing network capacity can be grouped into three generalized categories: installation of new fiber (overlay existing network or increase fiber counts), Time Division Multiplexing (TDM), or Wavelength Division Multiplexing (WDM). With the dropping prices of fiber, the one time cost to install a cable, and the future ability to lease fiber bandwidth, the option of installing higher fiber count cables continues to be a cost effective solution for short-haul distribution networks. Previous maximum fiber counts of 144 and 216 are no longer enough. To avoid pulling in multiple parallel cables, and to optimize usage of already overcrowded metropolitan duct systems, fiber counts up to 432 are now being sought in the U.S. market.

To meet these demands for higher fiber count cables, a new breed of "high count" cables have been introduced to the U.S. market over the past year. These cables, surpassing the previous maximum count of 216 fibers, are utilizing ribbon fiber technology to gain the highest fiber packing density possible.

As more fibers are placed in a single cable sheath, the ability to rapidly and cost effectively access and terminate fibers becomes a greater challenge. Cable accesses at end splice points as well as in midspan for customer add/drops need to be compatible with existing closure and splicing systems, while at the same time, employ non-service affecting procedures for live systems.

CABLE DESIGN

Several common high fiber count cable designs have evolved in the telecommunications industry. All utilize optical fiber ribbons which have been shown as the most efficient method of increasing fiber density.[7,1,4,3]

Slotted core cables popular in Japan have been well suited for the rapid increase in fiber counts up to 4000. Simple increases in cable core diameter permits additional deeper slots for stacking more ribbons.

Ribbon in loose tube cables were a natural progression in the U.S. due to the popularity of loose tube style cables. Enlargement of the

buffer tubes allows placement of stacks of 12-fiber ribbons in the multiple buffer tubes, which are then stranded around an enlarged central strength element.

The third type of ribbon cable currently used in the U.S. is a central buffer tube design with external strength elements. This style of cable has steadily gained popularity for fiber counts up to 216 due to its quick entry characteristics and easy taut sheath midspan accessibility.

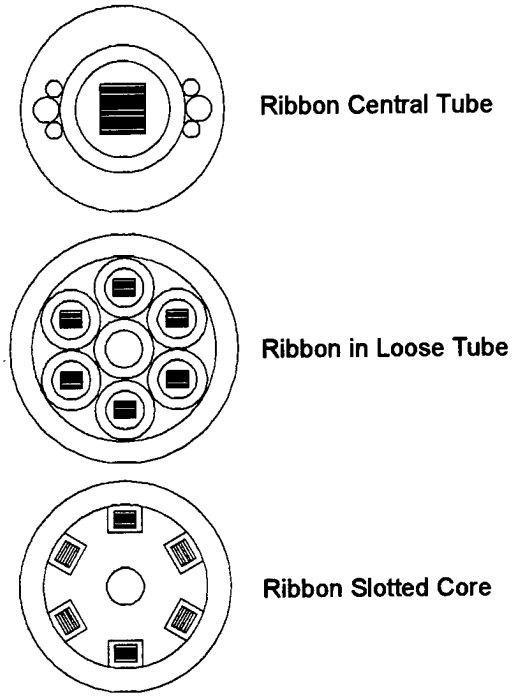

Figure 1. Various core construction options for high fiber count cables.

As a result of the steady increase in the volume of fiber optic applications, duct space availability has become a major concern in dense metropolitan areas.[2,3,4,6] By increasing the fiber density within a cable, duct space can be more efficiently utilized. In this way, higher fiber count cables take up less duct space and present a more economical solution than installation of multiple lower fiber count cables for a given fiber route.

Examination of the three different core constructions for high fiber count cables reveals that up to about 360 fibers, standard slotted core cables have slightly tighter fiber packing densities. However, as fiber counts increase to 432 and beyond, the central tube cable design out performs both the slotted core and ribbon in loose tube cables with smaller predicted diameters as shown in Figure 2.

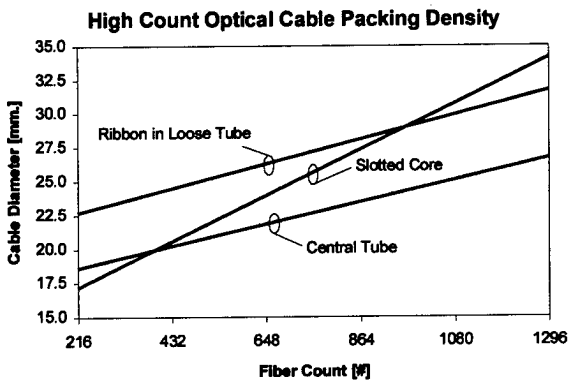

Figure 2. Fiber packing density trends for various high fiber count cable designs.

Not only is the cable diameter a key factor in the installation process, but the fiber preparation and splicing times are equally important. Fiber preparation time for splicing is a direct function of the cable type and studies have shown that ribbon fibers in a central tube design have the shortest preparation time when compared to other designs such as loose tube and fiber bundle cables.[9]

With the increasing fiber count trends, predicted packing densities, improved accessibility and familiarity of the craft with this style of ribbon cable, Sumitomo chose the central buffer tube design for the 432 fiber cable. Some key dimensions of Sumitomo's 432-fiber cable are listed in Table 1.

Table 1. 432 fiber cable dimensions.

Property	Value
Diameter:	20.8 mm (0.82 in)
Packing Density:	1.27 fibers/mm^2 (819 fibers/in^2)
Weight:	348 kg/km (234 lb/kft)

RIBBON DESIGN

In the U.S., 12-fiber ribbons have become the industry standard for telecommunications. Color coding schemes, mass fusion splicers, splice

closures, trays, and distribution panels are all based upon groups of 12 fibers. Therefore, it is highly desirable to continue to utilize 12-fiber ribbons in the high count cables.

However, in order to achieve a total of 432 fibers, thirty-six 12-fiber ribbons would need to be stacked and stranded in the central buffer tube. This tall stack would be very unstable and would have difficulty maintaining its orderliness during cable manufacturing and installation in the field. The solution is to redesign the ribbon to hold more than 12 fibers, making it wider and hence the stack shorter. The preferred design will use 12-fiber sub-ribbons to maintain the standard increment of 12-fibers.

Higher fiber count ribbon structures have been previously proposed to help address this stack stability issue.[1,11,12] These ribbon designs utilize 24 fibers, arranged in a single linear array with fibers #12 and #13 side-by-side in direct contact with each other. While this design offers superb packing density, separation of the 24-fiber ribbon into two 12-fiber ribbons for use with mass splicers, mass connectors or other commercially available ribbon accessories is difficult. Due to the small size of the individual fibers and their close proximity to each other, splitting of the ribbon by hand or even with a precision tool is nearly impossible without introducing reliability concerns to the underlying fibers as shown in Figure 3. Even if the 24-fiber ribbon is successfully split between the #12 and #13 fibers producing two 12-fiber ribbons, those edge fibers are no longer protected by an encapsulant layer and are at greater risk during handling and storage in splice closures. Furthermore, if peelable style ribbons are employed, the exposed edge fibers are susceptible to "falling out" of the ribbon structure.

Other ribbon structures have been proposed and were examined such as a notched ribbon structure. While these ribbons provided a low energy point for more easily splitting the ribbons at the desired points, these notches, or stress concentration points, provided a weak area in the ribbon structure, causing problems with handling robustness.

To address these issues, a modular style 24-fiber ribbon has been developed. Modular ribbons have been deployed in Japan with 4-fiber ribbon sub-units made into 8-fiber ribbons for increased fiber counts.

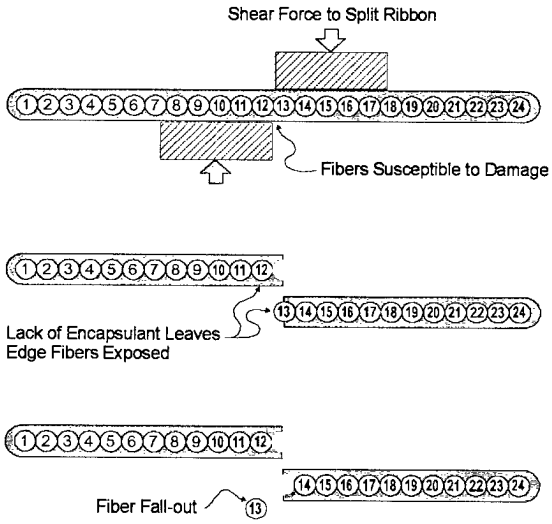

Figure 3. Non-modular style ribbons and issues with splitability.

Applying this technology, the modular 24-fiber ribbon utilizes standard encapsulated 12-fiber ribbons that have already demonstrated high reliability and strong field performance.[8] The standard 12-fiber ribbons contain 12 individually colored 250 μm optical fibers arranged in a flat linear matrix encapsulated by a UV cured acrylate material which has a peelable property for ease of individual fiber access in the field.

In the 24-fiber design, the two standard 12 fiber ribbons are joined together by a thinner secondary UV cured acrylate encapsulate layer to create a single 24 fiber ribbon as shown in Figure 4.

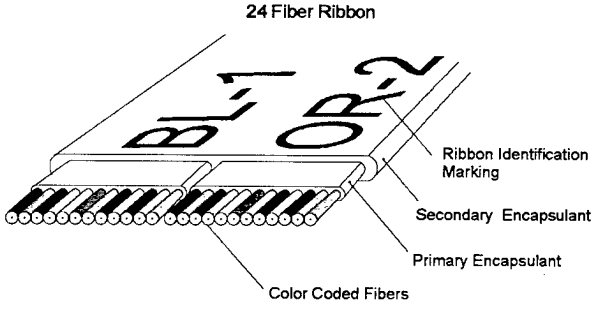

Figure 4. Construction of the modular 24-fiber ribbon.

Due to the thinness of the secondary encapsulate, its modulus had to be slightly increased to strengthen the structure of the 24-fiber ribbon. By keeping the secondary encapsulate thin, the impact on total cable packing density was minimized.

With the robust sub-structure of the modular 24-fiber ribbon, the two 12-fiber sub-units can be easily and safely separated by hand for end entry. A simple flex of the two halves in opposite directions will initiate the split, which can be continued down the length of the 24-fiber ribbon like a "zip-cord". The resulting 12-fiber sub-units are fully encapsulated, maintaining the integrity of an individual 12-fiber ribbon for handling, mass fusion splicing and standard field accessories.

Access to 12 fiber sub-units is quick and easy and can also be performed at mid-span with live fibers. By utilizing standard 12 fiber ribbons as the sub-units, the ribbons maintain excellent fiber alignment necessary for quality mass fusion splicing. Also, since the standard peelable 12-fiber ribbons are used, midspan access can still be easily achieved using standard glue and tape peeling methods already proven in the field.[8]

After splitting, each 12-fiber ribbon retains its own unique number marked on the ribbon surface. The U.S. industry standard ribbon marking scheme as specified in TIA–598 and TIA-359 remains unchanged for each of the 12 fiber modules as shown in Table 2.

Table 2. Ribbon identification marking scheme.

24 Fiber Ribbon #	Ribbon Marking	12 Fiber Ribbon #
1	SUMITOMO BL 1 SUMITOMO OR 2	1 2
2	SUMITOMO GR 3 SUMITOMO BR 4	3 4
⋮	⋮	⋮
17	SUMITOMO DD-YL 33 SUMITOMO DD-VI 34	33 34
18	SUMITOMO DD-RS 35 SUMITOMO DD-AQ 36	35 36

TOOL DESIGN

Buffer Tube Midspan Slitter

Midspan cable access to the ribbon fibers has been made easier and safer with the development of a tube slitter tool designed specifically for the high count central tube ribbon cables. As shown in Figure 5, the tube slitter is a clam shell design with two separate identical halves that fit together over the central tube. The separability of the tool halves is to facilitate cleaning, and for installation on to the cable tube. Each half of the tool has a blade running down the center that is set at a depth equal to the thickness of the central tube. Once the tool has been placed on the tube, the user slides the tool down the tube for the desired length. The central tube can then be easily removed in two pieces to expose the uncut fiber ribbons.

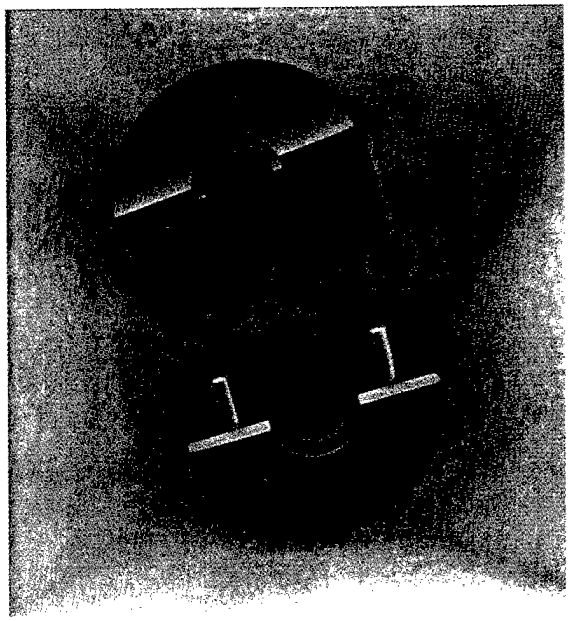

Figure 5. Detail of the buffer tube midspan slitter tool.

24-Fiber Ribbon Midspan Splitter

Separating the two 12-fiber ribbons at a cable end is easily done by hand. However, in midspan, where fibers are often live, more precision is desired. A simple low cost shearing tool to separate the 24-fiber ribbon into two 12-fiber ribbons at midspan has been developed.

The ribbon splitter tool breaks the outer layer of encapsulate leaving the two 12-fiber ribbons intact. Again, the retention of ribbon integrity provides easy mass splicing. Each of the 12 fiber ribbons can then be separated into individual fibers if necessary, using the industry recognized practice of glue and adhesive tape to peel the matrix.[8]

As shown in Figure 6, the 24-fiber ribbon splitter tool has a longitudinal slot along the top of the tool where the ribbon is placed. Two small clamps on the top of each end of the tool accurately position and secure the ribbon preventing any vertical movement. A sliding, controlled radius, disk in the center of the tool, imparts a shear force to divide the ribbon into two equally sized 12-fiber ribbons. This action cleanly and accurately separates the ribbon into two 12-fiber sub-units. The ribbon is then removed from the tool and the split is propagated by hand as needed. Attenuation measurements have verified this tool's performance for use with live systems.

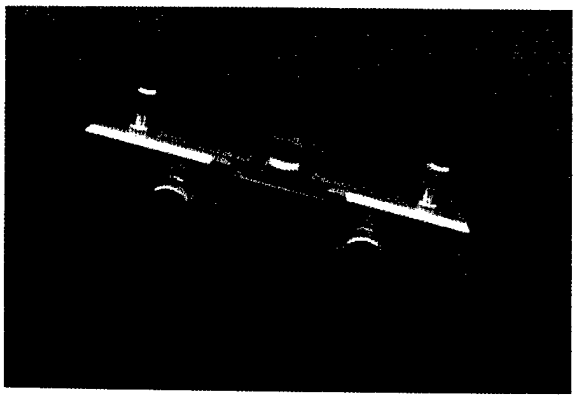

Figure 6. Detail of the 24-fiber ribbon splitter tool.

LABORATORY ANALYSIS

Mechanical & Environmental Tests

To ensure the robustness and integrity of the new 24-fiber modular ribbons and 432 fiber cable, complete testing against Bellcore's GR-20-CORE requirements has been conducted.[10] The cable and modular ribbon met or exceeded all applicable Bellcore & TIA specifications as shown in Tables 3 and 4.

Table 3. Summary of the key mechanical and environmental test results for the 24-fiber modular ribbon.

Test	GR-20 Requirements	Results	Test Procedure
Resistance to Twist (Aged, Unaged)	No separation of individual fibers after 20 cycles ±180°	Passed, 20 cycles ±180°	GR-20-Core 5.3.1
Ribbon Separation	Separation force not to exceed 13.4 N. Fibers maintain colorant.	Passed, all fiber peeled with full color retention	GR-20-CORE 5.3.2
Ribbon Flatness	Ribbon twist not to exceed 360° in 0.4 meter length.	Passed, twist did not exceed 360° in 0.4 meter length.	GR-20-CORE 5.3.3
Ribbon Strippability	Matrix and coating removed without damage to fibers	Passed, fully strippable with standard equipment	GR-20-CORE 5.3.4 FOTP-178
Tensile Strength	Tensile strength ≥ 3.0 Gpa for sample length of 0.5 m	Passed, Tensile strength ≥ 3.0 Gpa	GR-20-CORE 5.3.5 FOTP-28B

Table 4. Summary of the key mechanical and environmental test results for the 432-fiber cable.

Test	GR-20 Requirements	Results	Test Procedure
Low & High Temp. Bend (-30°C/+60°C)	≤0.05dB loss for 90% ≤0.15dB loss for 10%	100% of the fibers exhibited an attenuation increase ≤0.01dB at α_{1550}	EIA/TIA-455-37
Impact Resistance	≤0.05dB loss for 90% ≤0.15dB loss for 10%	100% of the fibers exhibited an attenuation increase ≤0.01dB at α_{1550}	EIA/TIA-455-25A
Compressive Strength	≤0.05dB loss for 90% ≤0.15dB loss for 10%	100% of the fibers exhibited an attenuation increase ≤0.01dB at α_{1550}	EIA/TIA-455-41A
Tensile Strength (600lb w/360°twist and 1 hr hold)	$\varepsilon_f \leq 0.60\%$ ≤0.05dB loss for 90% ≤0.15dB loss for 10%	Avg $\varepsilon_f = 0.054\%$ Max $\varepsilon_f = 0.063\%$ Avg $\Delta\alpha_{1550} = 0.00$dB Max $\Delta\alpha_{1550} = 0.07$dB	GR-20, Issue 1 GR-20-ILR, Issue 1B EIA/TIA-455-33A
Cable Twist	≤0.05dB loss for 90% ≤0.15dB loss for 10%	100% of the fibers exhibited an attenuation increase ≤0.01dB at α_{1550}	EIA/TIA-455-85
Cable Cyclic Flexing	≤0.05dB loss for 90% ≤0.15dB loss for 10%	100% of the fibers exhibited an attenuation increase ≤0.01dB at α_{1550}	EIA/TIA-455-104
Temperature Cycling (-40 to +70°C)	Avg increase ≤0.05dB/km Allow Max increase each fiber ≤0.15dB/km	100% of the fibers tested exhibited an attenuation increase ≤0.05dB/km at α_{1550}	EIA/TIA-455-3A
Cable Aging	Avg increase ≤0.10dB/km Allow Max increase each fiber ≤0.20dB/km±0.05dB repeatability error.	100% of the fibers exhibited an attenuation increase ≤0.06dB/km at α_{1550}	EIA/TIA-455-3A
Water Penetration (1m head, 1m sample)	No Leakage	No Leakage	EIA/TIA-455-82A
Jacket Shrinkage (Closure Test)	≤0.10dB loss for 90% ≤0.30dB loss for 10%	100% of the fibers exhibited an attenuation increase ≤0.01dB at α_{1550}	GR-20, Issue 1

Fusion Splicing

To ensure the 24-fiber ribbons and 12-fiber sub-ribbons are compatible with existing 12-fiber mass fusion splicing equipment, a splice analysis was completed using the new 24-fiber modular ribbons, and Sumitomo's T-63 mass fusion splicer. An OTDR, measuring the losses in both directions, was used to get actual splice losses (dB) for each fiber in the splice. The average splice loss was 0.034 dB as shown in Figure 7.

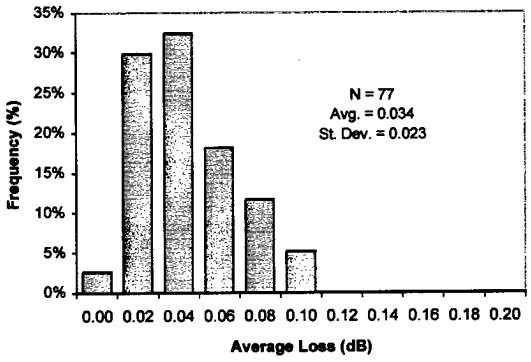

Figure 7. Average splice loss with mass fusion splicing

FIELD ANALYSIS

With an outer diameter of 20.8 mm (0.82 in), the cable can be easily installed in a standard 32 mm (1¼ in) innerduct. This was proven during a field trial where 1900 m (6200 ft) was installed into a smooth walled 32 mm (1¼ in) innerduct via a commercial cable blowing process. The innerduct path had an uphill section and also included one 90° turn. The cable was fitted on the leading end with a Kellems® pulling grip and a solid felt mouse slightly smaller than the inside diameter of the innerduct. The cable was fed through a blowing machine, and into the innerduct, at a rate of 81 meters/min (265 ft/min) for the entire 1900 meters (6200 ft), in a single direction taking less than one hour to complete the blowing process. Subsequent splicing of the fibers was also performed on the installed cable with equal success utilizing standard closures, splicers and procedures.

CONCLUSIONS

Modular style, dual encapsulate ribbons offer easy splittability and sub-unit robustness for handling and splicing. The use of standard 12-fiber ribbons in the modular structure ensures accurate fiber alignment, ribbon reliability, and compatibility with existing hardware. As cable fiber counts increase, central tube ribbon cables optimize packing density, provide ease of fiber entry at midspan, and offer the shortest splice preparation time when compared to loose tube and fiber bundle cables. Both the 24-fiber modular ribbon, and the 432-fiber cable fully passed all Bellcore GR-20 requirements and have been successfully installed in the field.

REFERENCES

1. Jackson, K.W.,Santana, M.R.,Sollenberger, N.W., Brown, R.J., Kroupa, K.M., Webb, S.H., "A Modular Ribbon Design for Increased Packing Density of Fiber Optic Cable", 42nd IWCS Proceedings, St. Louis, MO, 1993, pp. 20 - 27.
2. Legros, F., Roussel, Y., Brault, D., Guerin, J.Y., Louboutin, J.P., Boscher, D., "Optical Fiber Ribbon Cable Designs for a Wide Range of Applications as the Availability of FTTH is Realized", 45th IWCS Proceedings, Reno, NE, 1996, pp. 340 – 352.
3. McCallum, W.J., Light, M.C., Wagman, R.S., "Design and Development of a Compact High Fiber Count Ribbon Cable", 44th IWCS Proceedings, Philadelphia, PA, 1995, pp. 8 – 14.
4. Jackson, K.W., Sollenberger, N.W.,Gentry, S.P., Brown, R.J., Petisce, J.R., Santana, M.R., Taylor, C.R., Webb, S.H., "Optimizing Ribbon Structures for Performance and Reliability", 9th NFOEC, San Antonio, TX, 1993, pp. 205 – 213.
5. Konstadinidis, K., Sollenberger, N.W., Siddiqui, S., Jackson, K.W., Turnipseed, J.M., Au, T.W., DeFabritis, R.P., Taylor, C.R., "UV Color Coatings and Matrix Material Design for Enhanced Fiber Optic Ribbon Products", 46th IWCS Proceedings, Philadelphia, PA, 1997, pp. 274 – 280.
6. Ellwanger, M.R., Nave, S.D., McDowell III, H.R., "High Fiber Count Indoor/Outdoor Family of Ribbon Cables", 12th NFOEC, Denver, CO, 1996, pp. 371 – 380.
7. Keesee, J.R., Lochkovic, G.A., Smith, D., Toler, R., "A Comprehensive Approach to Ribbon Design With a Focus on Materials", 43rd IWCS Proceedings, Atlanta, GA, pp. 430 – 439.
8. Beasley, W.E., Neveux, P., Yamane, Y., "Meeting the Demands of the Local Loop With Improved Ribbon Fiber Midspan Access", 10th NFOEC, San Diego, CA, pp. 401 – 409.
9. Beasley, W.E., Canady, S.T., Karl, G., "Choosing the Right Cable for the Right Application, A Detailed Time Study of Cable Handling", 11th NFOEC, Boston, MA, pp. 491 – 501.
10. Bellcore GR-20-CORE, Issue 1, September 1994.
11. Gibson, D., Kemp, H., Kathiresan, K., Travieso, R., Karl, G., Mackie, G., "Field Deployment and Test Results for High Fiber Count Cables", 13th NFOEC, San Diego, CA, pp. 333 – 341.
12. Jackson, K.W., Brown, R.J., Kinard, M.D., Kroupa, K.M., Santana, M.R., Thomas, P.M., "Design and Performance of a High-Capacity, Compact, Modular Ribbon Cable Comprising 24-Fiber Ribbons", 45th IWCS Proceedings, Reno, NE, 1996, pp. 623 – 630.

Kellems® is a registered trademark of Hubbell Incorporated.

AUTHORS

Scott A. McCreary

Scott McCreary joined Sumitomo Electric Lightwave Corp. in 1998 as a Cable Applications Engineer. He holds a B.S. degree in Business Administration and Management from Virginia Commonwealth University, and a B.S. degree in Mechanical Engineering from North Carolina State University.

William E. Beasley

William Beasley is a 1990 graduate of Duke University where he received a B.S.E. in Mechanical Engineering and a B.A. in Mathematics. He joined Sumitomo Electric Lightwave Corp. in 1990 as a Product Design Engineer supervising the Fiber Optic Cable Testing Laboratories. William is currently Manager of Cable Applications Engineering.

Stephen R. Stokes

Stephen Stokes obtained a B.S. degree in Electrical Engineering from Virginia Polytechnic Institute and State University in 1988. He was employed by ITT Electro Optical Products Division and subsequently, Alcatel Cable Systems from 1980 to 1990 in the development of fiber optic measurement systems. From 1990 to 1991, Steve was employed by Galileo Electro-Optics Corporation as a Design Engineer in the development of light guide and imagescope products. He has been engaged in the research and development of fiber optic cables since joining Sumitomo Electric Lightwave Corp. in 1991. Steve is currently Manager of Product Design Engineering.

Ronald G. Lindsay, Jr.

Ronald Lindsay obtained a B.S. degree in Mechanical Engineering from North Carolina State University in 1989. He joined Sumitomo Electric Lightwave Corp. in 1990 as a Product Design Engineer for the optical fiber cable group. His primary responsibilities were design and development of optical fiber ribbons and ribbon cables. Ron is currently Manager of Passive Optical Components.

ATTENUATION , CHROMATIC DISPERSION AND POLARIZATION MODE DISPERSION PARAMETERS OF 40 000 KM OF STANDARD MONOMODE FIBERS IN THE OPTICAL NETWORK OF „DEUTSCHE TELEKOM AG"

Hartmut Gruhl and Joachim Vobian

Deutsche Telekom AG,TZ Darmstadt , Germany

Abstract: The attenuation , chromatic dispersion and polarization mode dispersion of 1500 installed standard monomode fibers - with about 40 000 km length in total - in the optical network of Deutsche Telekom AG have been measured and analyzed statistically in the second (1317 nm) and third (1556 nm) optical windows.
The attenuation has a mean value and standard deviation of (0.367 $\pm$ 0.015) dB / km at 1317nm and (
0.226 $\pm$ 0.013) dB / km at 1556nm . At 1317nm the chromatic dispersion is (- 0.14 $\pm$ 0.26) ps /(nm*km) and (16.66 $\pm$ 0.30) ps/(km*nm) at 1556nm. The PMD is between 0.05 ps / $\sqrt{km}$ and 6.3 ps / $\sqrt{km}$. The time dependence of the PMD was determined . This set of measured fiber parameters serves as a basis for general all-optical network design . The insertion loss of optical connectors and splices is measured , too.

1. Introduction. In the last few years all-optical network concepts have been investigated in detail world-wide. Laboratory record transmission experiments on standard monomode fibers have been performed, such as 10 Gbit/s over 2245 km standard monomode fibers [1], 40 Gbit/s over 150 km standard monomode fibers with no in-line amplifier [2], 10 x 20 Gbit/s wavelength device multiplexing over 1000 km standard monomode fiber with 100 km amplifier spacing [3], and others. However, the deployment of operational high-capacity systems in real networks has - by far - not yet reached that high technological level. A few 10 Gbit/s SONET terminals and some more N x 2.5 Gbit/s- wavelength device multiplexing systems (with the number of wavelength device multiplexing channels starting from N=4 and aiming at N=32 very soon) have been implemented in Japan and in the USA, respectively. In general, most network providers still rely on backbones of maximum data rates of 2.5 Gbit/s . On the one hand , this is due to commercial reasons regarding data traffic, fiber network infrastructure and prices of very advanced systems. On the other hand , there are several technical issues related to $\geq$10 Gbit/s systems, such as OAM and the physical system behaviour. While laboratory experiments can be optimized with respect to specific conditions , operational systems have to cope with the statistical distribution of fiber parameters in the network under consideration.

In this article , we report on the measured attenuation, chromatic dispersion (CD) polarization mode dispersion (PMD) of 1500 installed fibers with 40 000 km of total length in the optical network of the Deutsche Telekom AG . A statistical analysis of the data is presented .

2. Fiber Base under Investigation. The parameters of installed fibers were measured along nine links as shown in Fig. 1 , all links comprising 108 switching stations in total. The total length of all sections, the mean value and the standard deviation were 2843 km, 27.34 km and 9.13 km, respectively. On the average , 14 fibers per station were investigated , thus yielding a data set for more than 40 000 km of installed standard monomode fibers .

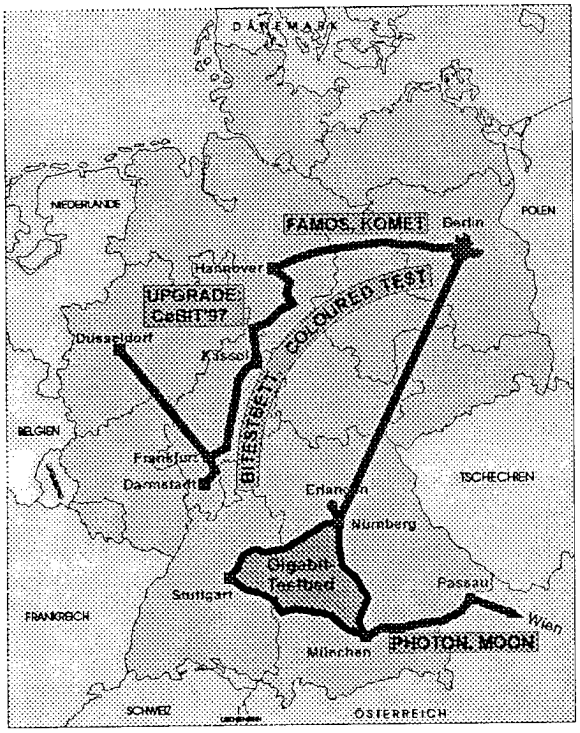

Fig. 1 Fiber base under investigation

3. Fiber Attenuation. Fiber attenuation was measured using several OTDRs from different manufacturers .
The accuracy of the measured attenuation values is 5% (relative error) .
Each fiber was measured in two directions and the attenuation is the arithmetic mean value of both measurements . This is very important in the case of the insertion loss of splices and connectors.
The main result is shown in Figs. 2 and 3. There the number of fibers is plotted versus the attenuation in intervals of 0.001 dB/km for two wavelengths, namely λ=1317 nm (Fig. 2) and λ=1556 nm (Fig. 3) .

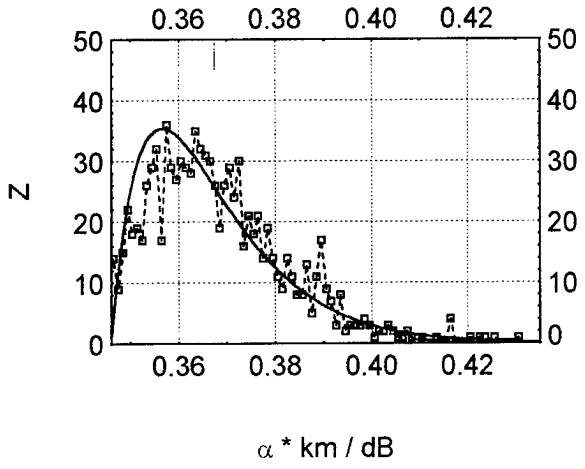

Fig. 2 Distribution of fiber attenuation of all fibers measured at 1317 nm

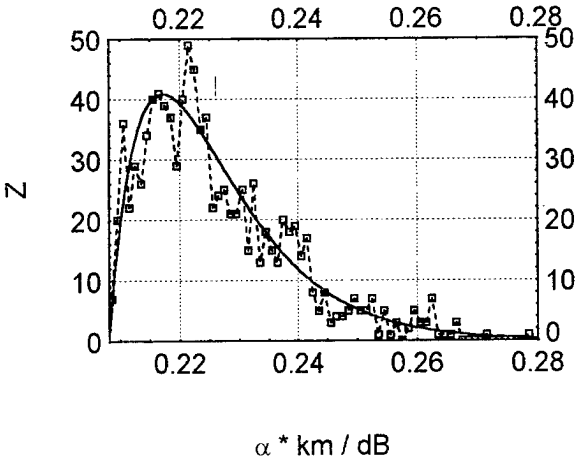

Fig. 3 Distribution of fiber attenuation of all fibers measured at 1556 nm

The distribution is asymmetric and of the form

$f(x) = b^* b * (x-x_0) * \exp(-b * (x-x_0))$ if $x>x_0$

$= 0$ if $x<x_0$.

$b = \sqrt{2} / \sigma$, $x_0 = \mu - \sqrt{2} * \sigma$

μ : mean value
σ : standard deviation

The peaks of the corresponding distributions are located at 0.356 dB/km and 0.217 dB/km. Due to the asymmetric distribution function the maximum is at an attenuation value less then the mean value. Along a few links, however, some older fibers exhibit an attenuation between 0.3 dB/km and 0.5 dB/km at 1556 nm .

The mean value and standard deviation was (0.367 ± 0.015) dB/km for λ=1317 nm while we found (0.24 ± 0.04) dB/km for the other wavelength including all fibers, and (0.226 ± 0.013) dB/km excluding those fibers with more than 0.3 dB/km at 1556 nm.

By a transmission method the spectral dependence of the fiber attenuation was determined between 1200 nm and 1700 nm . A typical result is shown in Fig. 4 .

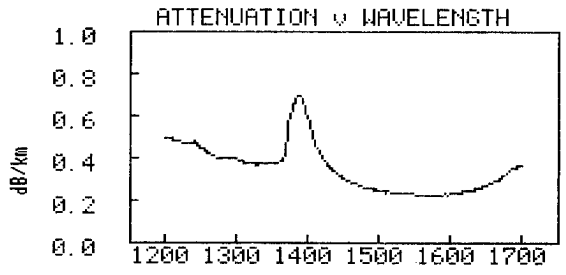

Fig. 4 Spectral dependence of fiber attenuation

This data is important for wavelength device multiplexing systems .

The insertion loss of optical connectors and splices is measured at four different wavelengths .
The results are presented in the following Table 1 :

	clean connector	non- cleaned connector
1317 nm	(0.53 $\pm$ 0.26) dB	(0.89 $\pm$ 0.59) dB
1556 nm	(0.425 $\pm$ 0.23) dB	(0.73 $\pm$ 0.47) dB

Table 1 Insertion loss of optical connectors

	splices
1317 nm	(0.088 $\pm$ 0.062) dB
1360 nm	(0.089 $\pm$ 0.061) dB
1410 nm	(0.100 $\pm$ 0.073) dB
1556 nm	(0.070 $\pm$ 0.065) dB

Table 2 Insertion loss of splices

As shown in Table 1 , it is important to clean the front surfaces of the connectors carefully .
A non - cleaned connector has a high back reflektion up to 3 % and this increases the bit-error rate in systems with data rates above 2.5 Gbit/s .

4. Dispersion measurements. The chromatic dispersion measurements were performed, making use of our field measuring set-up based on spectral group-delay measurements [5]. To increase the accuracy of the evaluation procedure, we have used different fit functions: the wellknown 5- term Sellmeier fit as well as a 4^{th}-order Legendre polynomial and cubic spline functions with different weight

	λ_0 in nm	$S(\lambda_0)$ in ps/km nm^2	σ in ps/km	D(1300nm) in ps/km nm	D(1550nm) in ps/km nm
5-Term-Sellm. Fit	1316.2	0.0864	2.6	-1.43	16.34
Orth.-Poly-nom. (4th)	1316.2	0.0870	2.8	-1.44	16.31
Splinefct. w = $2*10^4$	1316.6	0.0877	3.7	-1.49	16.35
Splinefct. w = $5*10^4$	1315.9	0.0878	2.3	-1.43	16.34

Table 3 Influence of the fit function on the calculated fiber parameters (ACTS UPGRADE project, Kassel - Trendelburg, L=36.7km)

factors [6]. Starting from the identical measuring points, the different fit functions result in different calculated dispersion parameters. Table 3 shows a typical example and demonstrates the influence of the choice of the fit function. The limits of accuracy of this measuring method are established.

The differences of the calculated parameters decrease with the number of measuring points and depend on their standard deviation values. In general, the accaracy of the zero-dispersion wavelength λ is about 1nm and a relatively good agreement can be achieved, making use of the 5-term Sellmeier fit and the 4th-order Legendre polynomial. Deviations occur in the case of cubic spline functions.

The histogram of λ shows two centers of gravity at ≈1308 and 1313nm. The range of λ extends from 1304 to 1318nm (14nm). An interesting parameter related to WDM is the slope $S(\lambda)$ at the zero-dispersion wavelength. In the vicinity of λ, $D(\lambda)$ can be approximated by the linear relation $D(\lambda) = S(\lambda)*(\lambda-\lambda)$. We found that $S(\lambda)$ does not vary very much in the case of standard fibers (0.085 to 0.090ps/km*nm^2). A slope larger than 0.090 (up to 0.096) can be regarded as an exception.

The mean dispersion data at 1310 and 1550nm are -0.14 and +16.7ps/km*nm, respectively. The minimum and maximum values of D(1310nm) are -0.68 and +0.51 ps/km*nm and those of D(1550nm) are 15.96 and 17.36 ps/km*nm. The standard-deviation values of the group-delay data are within the interval 2 to 12ps/km which can be regarded as a good accuracy, comparable to that of interferometric methods.

5. PMD measurements. For ultrahigh bit-rate systems working in the vicinity of the zero-dispersion wavelength, polarization-mode dispersion (PMD) cannot be neglected, in general. We measured the PMD in the time domain, making use of a Michelson interferometer, and in the frequency domain with the aid of a polarimeter. The polarimeter (Profile PAT 9000) combines 3 different modes – the Jones-Matrix Mode, the Arc-Angle Mode and the 3-Stokes Parameter Mode (Wavelength Scanning Method).

Within the framework of the ACTS PHOTON and UPGRADE projects we measured the PMD of fibers of buried

Telecom cables in Germany and Austria, between Darmstadt and Hannover and München – Passau – Wien. The total cable length investigated was 1472km, the repeater spacing varied between 16.4 and 56.5km. The number of the links was 46.
Fig. 5 shows the histogram of the measured normalized PMD values (in ps/km$^{1/2}$) for λ=1321nm. The histogram for λ=1546nm is very similar. Only a little difference of the PMD data at 1300 and 1550nm can be stated. More than 80% of the fibers under test have PMD values <0.5 ps/km$^{1/2}$ which means PMD values below the ITU limit, but 17% of the measured data are higher. This fact underlines the need for PMD measurements on installed cables for ultrahigh transmission systems.

difference we have observed in real Telecom cables. The consequence is dramatic. If an ultrahigh-bitrate system is to be installed, all fibers of the cable under discussion have to be measured to find the best one. The further consequence is the need to separate transmitter and analyzer in the case of field measurements.

It is an advantage of the Michelson interferometer that separate measurements can be performed without any problem; on the other hand, in the case of polarimeter measurements, a serious problem arises. In order to perform single-fiber measurements, a tricky procedure must be used. The Jones-Matrix Mode cannot be applied, generally. A prerequisite of

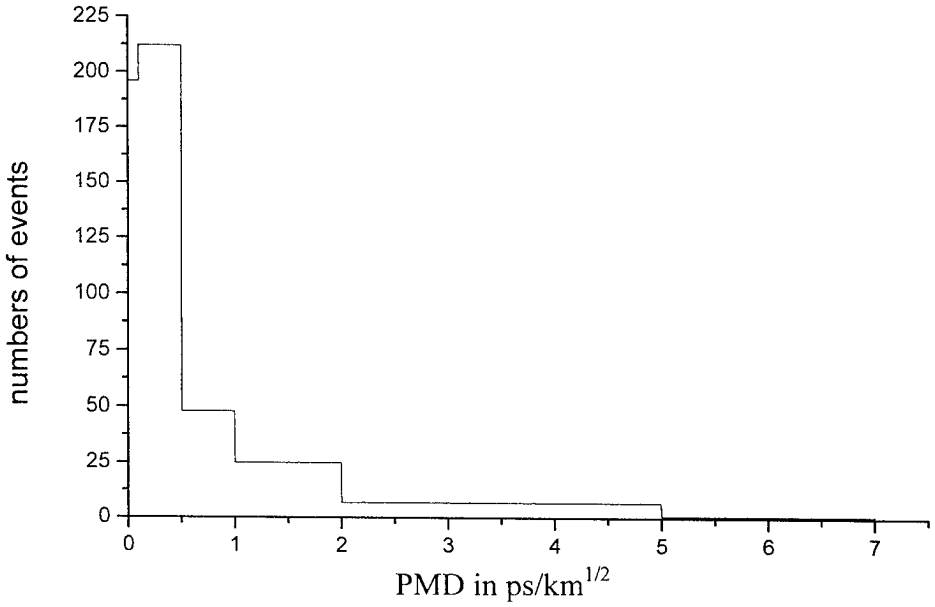

Fig. 5 Histogram of the measured normalized PMD in both optical windows

The PMD data of the fibers of one cable may show very large differences.
The results compiled in Tab. 4 impressively demonstrate this important effect. A factor ≥30 must be stated, up to now the largest

interferometric measurements in the time domain are incoherent radiation sources with high spectral bandwidths (Δλ≥50nm). The complementary polarimeter measuring method working in the frequency domain

Segment 1			Segment 2		
L =22.45 km			L =35.7 km		
Fiber	λ=1321nm	λ=1546nm	Fiber	λ=1321nm	λ=1546nm
27	10.85	11.39	7	4.54	14.54
28	9.75	8.05	8	1.25	1.58
29	2.92	3.90	11	4.50	2.66
30	8.43	6.28	12	5.40	4.68
31	4.27	4.21	13	4.41	3.22
32	6.82	5.60	14	2.97	2.59
33	1.20	1.39	25	2.12	1.91
34	13.78	11.11	26	4.91	16.77
37	6.68	5.19	27	9.72	6.98
38	2.93	4.32	30	1.04	0.97
39	7.35	6.98	31	>16.0	13.38
40	>30	11.93	32	5.53	5.52

Table 4 Michelson interferometer results (ps) obtained for two segments of the link 1.

demands coherent radiation sources. We use external-cavity lasers (linewidth about 200kHz) with spectral measuring ranges of 1260 – 1330 and 1470 – 1590nm, respectively

Fig. 6 shows, as an example, the PMD spectrum with very low PMD values, Nidda – Neustadt, (56.5km). In this case, the Arc-Angle Method (AAM) was used. Fig. 7 demostrates an example with very high PMD values (ps), segment 2 (35.7km) of link 1 , Arc-Angle Method.

It is a matter of course that the comparison of the results obtained in the time and frequency domains is a very interesting analysis. In Table 5 the results of some loop mesurements in both optical windows are compiled. The measurements were performed within the framework of ACTS PHOTON Passau – Wien. The agreement is satisfactory.

An important phenomenon is the wavelength dependence of the PMD which is demonstrated in Tab. 4 with Michelson interferometer results in both optical windows. In most cases, the PMD values do not depend on λ, deviations are within the range of accuracy. But – in many cables large differences of the PMD data can be stated in both directions, which means that PMD(1300nm) > PMD(1550nm) but also clearly PMD(1300nm) < PMD(1550nm). This strange phenomenon can be explained by taking into account the fiber-core ellipticity solving the vectorial Helmholtz equa-tion, making use of Mathieu functions.

The very high dynamic range of both devices (fiber lengths >200km) allows PMD measurements of chains of cable segments. Table 6 shows an example of

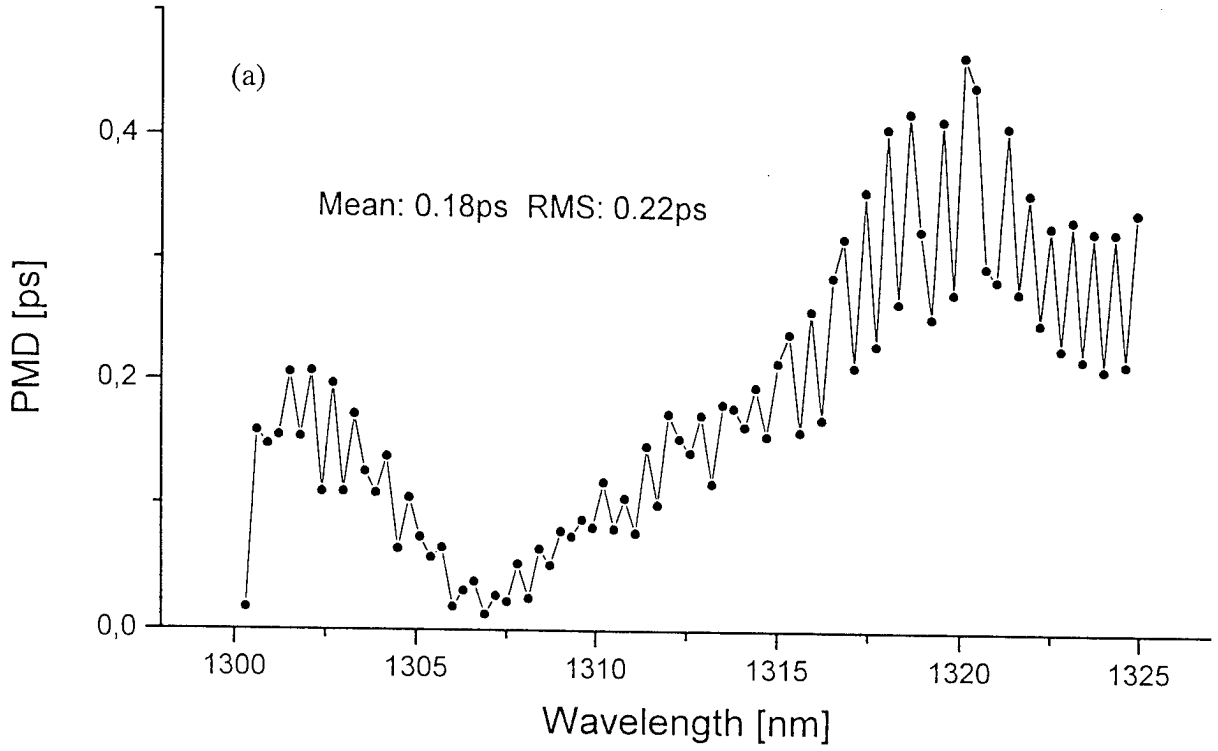

Fig. 6 PMD spectrum between Nidda and Neustadt (56.5km), ACTS UPGRADE project

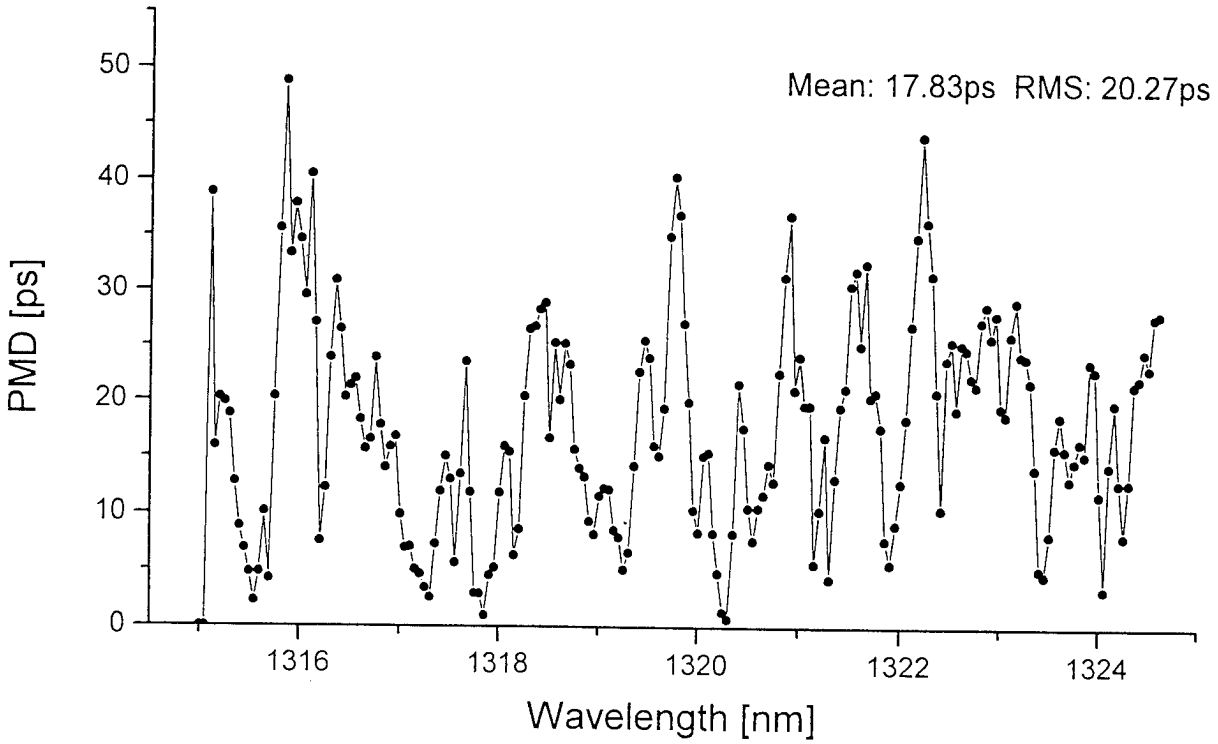

Fig. 7 PMD spectrum for segment 2 (35.7 km) of link 1

		Passau - Schärding - Raab-Schärding - Passau (91.7km)	St. Georgen - Linz -St.Georgen (36.2km)	Tulln - Wien - Tulln (88.7km)
1300nm	Michelson interferometer	0.52	0.77	3.08
	Polarimeter	0.64	0.94	2.49
1550nm	Michelson interferometer	0.59	0.59	2.83
	Polarimeter	0.57	0.81	2.35

Table 5 Comparison of loop results (ps) obtained in both optical windows, polarimeter and interferometer measurements

PMD in ps		1300nm				1550nm			
		13/25	14/26	15/27	16/28	13/25	14/26	15/27	16/28
Passau-Pocking 27.8km	Interfero-meter	2.94	2.41	3.25	2.70	3.11	2.27	2.78	2.90
	Polarimeter Arc-Angle	2.87	1.977	2.728	2.826	3.417	2.367	2.752	3.385
Passau-Simbach 64.7km	Interfero-meter	4.53	3.64	3.92	4.12	3.73	4.27	3.68	3.82
	Polarimeter Arc-Angle	4.04	3.922	3.321	3.78	3.43	4.643	4.193	4.186
Passau-Markt Schwaben 172.0km	Interfero-meter	-	-	-	-	3.78	4.18	3.46	3.73
	Polarimeter Arc-Angle	4.157	-	3.584	4.418	3.945	4.174	3.686	5.453
Passau-München 202.2km	Polarimeter Arc-Angle	4.679	4.553	4.007	-	5.343	4.667	3.853	3.539

Table 6 Chains of PMD measurements taken on the Passau - München link in both optical windows, polarimeter and interferometer measurements

these measurements. Again interferometric data are compared with polarimeter values. The square-root length dependence of the PMD is verified.

A very interesting comparison is shown in Table 7. The geometric sum of the PMD data of the single segments between Passau – Markt Schwaben (172km) are compared with the measured PMD value (ps) of the total link. Again the measurements were performed with the interferometer and the polarimeter in both optical windows.

PMD in ps		Σ segments 172km	Total measurements 172km
1300nm	Interfero-meter	4.32	-
	Polarimeter	3.83	3.58
1550nm	Interfero -meter	3.81	3.46
	Polarimeter	-	3.69

Table 7 : Segment PMD measurements (in ps) compared with the total link results (172 km)

6. Aspects of Network Design. The set of measured fiber parameters is a sufficient basis for the design of advanced optical transmission systems. The operation of advanced systems, such as 10 Gbit/s terminals or wavelength device multiplexing systems, has to be specified regarding additional fiber parameters besides attenuation, such as fiber chromatic dispersion and PMD.

It makes a significant difference whether a transmission system shall be optimized for one particular link or if it shall work at an arbitrary link in the network. The latter approach is of vital interest for a network operator. One has to accept the existing installed terrestrial fiber base as it is. System specification must cope with the statistical distribution of all fiber parameters - attenuation, λ_0, CD, PMD - and considerations of the impact of fiber nonlinearities. This task appears to be complicated at first sight. However, the moderate scattering of the attenuation figures (with the exception of very few old fibers) and the CD will most likely not cause fundamental problems for the design of advanced optical networks. It should be noted that the fiber attenuation may gradually increase during the lifetime of a fiber , partially due to additional splices - including repair of fiber cuts -, connectors, etc.. PMD might be a more serious problem and is still an object of current research.

7. Conclusion. In this article , more than 40 000 km of standard monomode fibers installed in the optical network of the Deutsche Telekom AG have been characterized in the two optical windows of interest for telecommunication, i.e. around 1.3 µm and 1.55 µm, respectively. The attenuation and chromatic dispersion (CD) was found to be in the range of α = (0.367 ± 0.015) dB/km and $D = -0.14 \pm 0.26$ ps / (nm · km) for λ=1317 nm. At 1556 nm we had α = (0.24 $\pm$ 0.04) dB/km for all fibers and α = (0.226 $\pm$ 0.013) dB/km if a few very old fibers above 0.3 dB/km attenuation were excluded. The chromatic dispersion is as large as $D = 16.66 \pm 0.30$ ps / (nm · km) at 1556 nm.

The zero dispersion wavelength λ_0 may range from 1304 nm to 1318 nm. However, the standard deviation of λ_0 of the fibers within one cable is much smaller, namely in the order of 2 nm. Thus , the zero

dispersion wavelength is one characteristic feature of the fibers in a particular cable. Another one is polarization mode dispersion (PMD). Fibers, especially in old cables can show a rather large PMD of several ps / $\sqrt{km}$.

Finally , the fiber data was briefly evaluated in the view of the design of advanced optical communication systems based on the installed fiber base. It is evident that the existence of PMD and its impact on network design is one of the most important issues.

8. Acknowledgement. The authors gratefully acknowledge the assistance of the colleagues at the various switching stations.

References

[1] N. Kikuchi, S. Sasaki, and K. Sekin, Electron. Lett., **31**, pp. 375-377, 1995.

[2] R. Ludwig, W. Pieper, H.G. Weber, D. Breuer, K. Petermann, F. Küppers, A. Mattheus, Electron. Lett., **33**, no. 1, pp. 76-77, 1997.

[3] D. Le Guen, F. Favre, M.L. Moulinard, M. Henry, G. Michaud, L. Macé, F. Devaux, B. Charbonnier and T. Georges, Proc. OFC'97, PD17, Feb. 16-21, Dallas, USA.

[4] J. Vobian, K. Mörl, W. Keilig, Proc. EFOC&N '94, pp. 174-179

[5] J. Vobian, G. Herchenröder, E. Unterseher, J. Opt. Commun., Vol. 6 (1985), 4, pp. 137-141

[6] J. Vobian, G. Herchenröder, R. Boness: Chro matic dispersion measurements – new challen ges, new approaches, Proc. OFMC'95, Sept. 1995, Liege, Belgium

Dr. Hartmut Gruhl
Deutsche Telekom AG
Post box 100003
D - 64307 Darmstadt ,
Germany

Hartmut Gruhl was born in 1954 . He received his diploma in physics in 1981 at the „Ludwig Maximilians Universität" in Munich . In 1987 he obtained a Doctor's degree (Dr. rer. nat.) at the Georg August Universität in Göttingen . Since 1987 he has been with Deutsche Telekom AG , responsible for Optical Transmission Techniques .

Dr. Joachim Vobian
Am Hang 6
D-64367 Mühltal
Germany

Joachim Vobian was born in 1935. He received his diploma in Physics 1961 at the Humboldt-Universität in Berlin. Since 1966 he has been with Deutsche Telekom AG, Research Institute, responsible for fiber-measuring technique. In 1992 he obtained a Doctor'degree (Dr. Ing.) at the Kaiserslautern University.

AN OPTICAL CABLE IDENTIFICATION SYSTEM BASED ON OPTICAL INTERFERENCE OF BACK-SCATTERED LIGHTS

Kyozo Tsujikawa, Koichi Matsuno, Koji Arakawa, and Koji Yoshida

NTT Technical Assistance & Support Center

Tokyo, Japan

ABSTRACT

We describe a new optical cable identification system that uses an optical interference of back-scattered lights. This system was applied to graded index multi-mode fiber cable and reliable identification was achieved.

This system will allow a reduction in manpower for cable maintenance, because it can accomplish quick identification using only one end of the cable.

1. INTRODUCTION

In support of new multimedia services, the optical subscriber network has been expanding, and quantities of optical fiber cables are being installed daily. For cable maintenance and replacement, it is often necessary to identify the required optical fiber cable among many others without slicing the cables open. Some methods have already been reported for solving this problem [1][2]. We previously proposed an optical cable identification system that used interference between two lights transmitted through two different fibers of an object cable [2]. The earlier system was economical and furnished reliable identification for single-mode fiber cable (SM cable) even at length exceeding 40 km. However, it required use of both ends of the cable. Cable identification from one end could reduce manpower even more.

Here, we describe a new system that can accomplish cable identification using only one end. This new system utilizes optical interference between two back-scattered lights in two different fibers. We applied it to identification of graded index multi-mode fiber cables (GI cables), some of which are currently being replaced with SM cables.

2. SYSTEM CONFIGURATION AND EXPERIMENTAL SETUP

Since many different optical modes exist in a multi-mode fiber, we think interference occurs between the different modes in one fiber [3]. Accordingly, first we investigated the effect of interference between different modes using the experimental setup shown in Figure 1(a). We used a distributed-feedback laser diode (DFB-LD) to provide a highly coherent cw light source with a wavelength of 1.55 μm, except in the case mentioned in section 3.2. A piezo-electric actuator with a signal generator was positioned on the cable. The input light was transmitted through the fiber and output light was detected by a photodetector. When a cable is vibrated by an actuator at a frequency *f*, optical phase variation is induced because of the changes in optical lengths [3]. A selective level meter was used to detect the fluctuation in optical power at the frequency *f* caused by optical interference. A SM optical fiber cord connected the cable and the photodetector to eliminate the noise of higher modes.

The configuration of the new cable identification system utilizing back-scattered lights is shown in Figure 1(b). In this system, we used either one or two fibers. When we used two fibers, the input light was divided by a 2x2 SM optical coupler and sent into them. The back-scattered lights were also mixed by the coupler and detected by a photodetector. To eliminate the higher modes, this system also incorporates a SM coupler and fiber cords. In consequence, it is applicable to SM cable as well as GI cable. The parameters of the tested GI cables are summarized in Table 1. We used two different types of cables. The far ends of the cables were fiber connectors, except in the case mentioned in section 3.3.

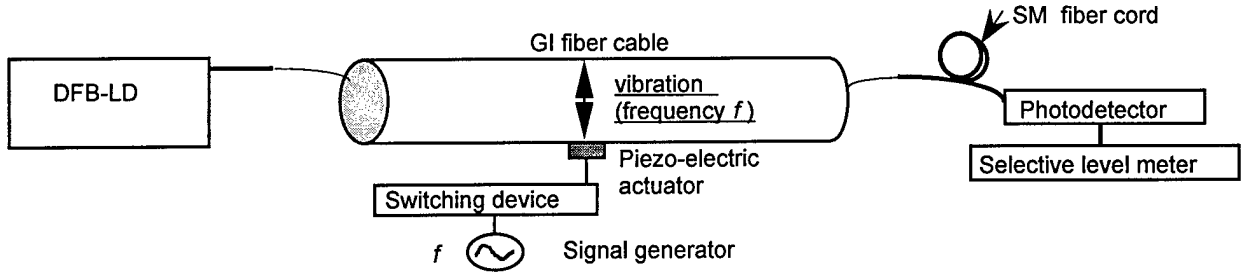

(a)Setup for investigation of the effect of interference between different modes.

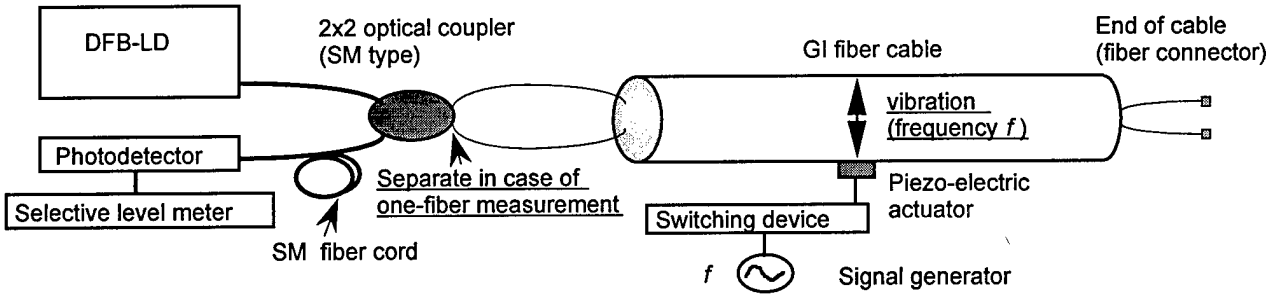

(b) Configuration of new optical cable identification system.

Fig. 1. Experimental setups.

Using these two system, we measured the S/N ratio, where S and N values were the optical power levels when the cable was and was not vibrated, respectively. The S and N values were estimated from an average taken from 10 measurements. S/N ratios above 10 dB are sufficient for identification of the object cable, because the changes in the N value are usually within ± 5 dB.

Table 1. Parameters of GI cables

	Cable A	Cable B
Cable	Unit type (8 units) Including 70-fibers Diameters of 28mm	Slotted-rod type Including 200-fibers Diameters of 18 mm
Fiber	Multi-mode for 1.31 μm Single fiber	Multi-mode for 1.31 μm 5-fiber ribbon

3. RESULTS AND DISCUSSION

3.1 Vibration frequency dependence

Figure 2 shows the relationships between the S/N ratio and the vibration frequency when we transmitted light through one fiber (Fig.1(a)). The S/N ratio obtained by the system without the SM fiber cord is also shown in Fig. 2. Figure 3 shows the relationships between the S/N ratio and the vibration frequency obtained using our new system (Fig. 1(b)). The mean values of four different fibers are shown. In these measurements, a 4-km length of cable A was vibrated in the middle at each frequency. We selected either one or two fibers in the same unit. We were able to confirm that interference between different modes occurred at specific frequencies in one GI fiber (Fig. 2).

We also found that the elimination of higher modes by the SM fiber was effective in increasing the S/N ratio. In Fig. 3, the S/N ratio for two fibers was higher than that for one fiber, although their frequency dependence were similar. We believe this is due to the effect of interference between the two lights back-scattered in two different fibers. The S/N ratio for two fibers was generally more than 10 dB between 1 and 5 kHz. In particular, we obtained an S/N ratio of more than 20 dB at 2 and 4 kHz using our new system. These values are sufficient for identification of the object cable.

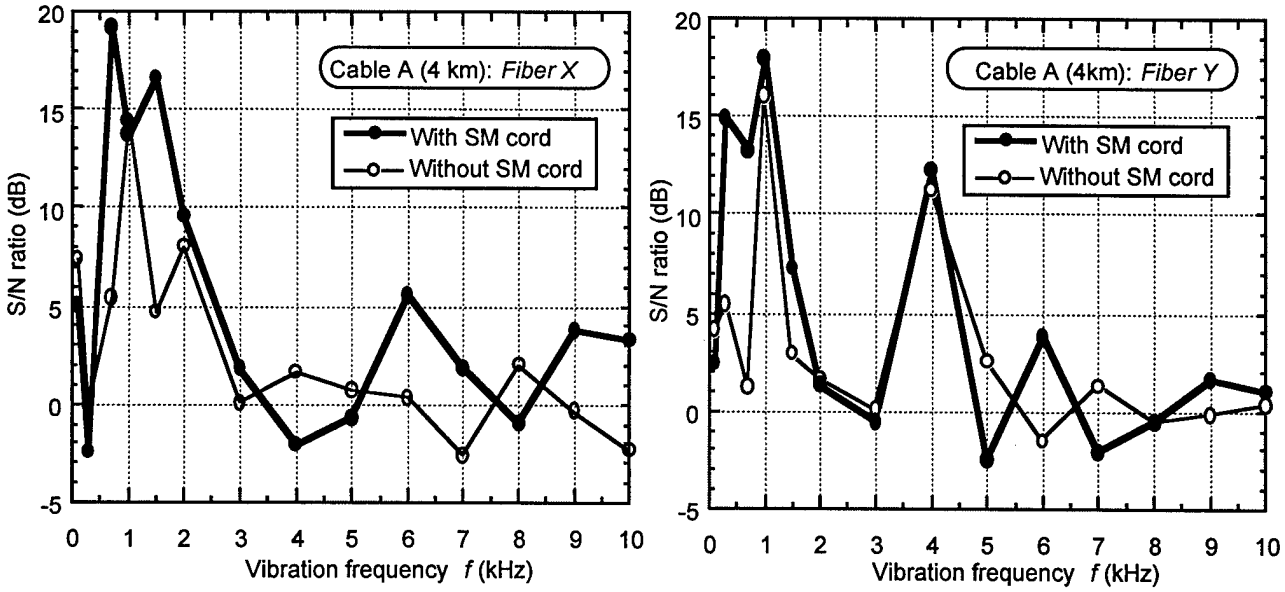

Fig. 2. S/N ratio versus vibration frequency
(two examples of different fibers obtained from transmitted light).

Next, to clarify the cause of the vibration frequency dependence, we used the new system to measure the S/N ratio every 0.1 or 0.2 kHz. In this measurement, 2-km lengths of cables A and B were vibrated near their far ends. We selected two fibers in the same unit of cable A, in the same ribbon of cable B, respectively. Figure 4 shows the relationships between the S/N ratio and the inverse of the vibration frequency. The frequencies of the S/N peaks are also shown. Assuming that the velocity of vibration is constant, the horizontal axis of Fig. 4 corresponds to the vibration wavelength. In short, high S/N ratios were obtained when basic or overtone vibrations were given. We also found that the S/N ratio of cable B was considerably higher than that of cable A. It exceeded 20 dB even when the vibration frequency was 6 kHz. As shown in Figure 5, the vibration of the actuator should be transmitted into the cable as waves and reflected by the metal fitting at the opposite side. Therefore, the cable can be expected to resonate at particular frequencies, that depend on the cable diameter. From the periodic change of S/N ratio in Fig. 4, we think that the S/N ratios obtained at these frequencies were high, because the optical fibers in the cable were vibrated at a large amplitude. Also, vibration should be transmitted more effectively in cable B because it is denser than cable A (Table 1). We think this is the reason the S/N ratio of cable B was higher than that of cable A.

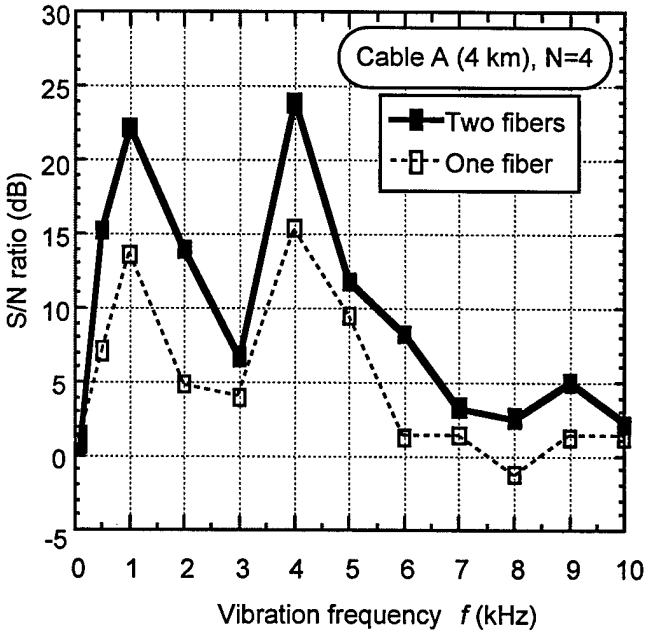

Fig. 3. S/N ratio versus vibration frequency
(obtained by new system).

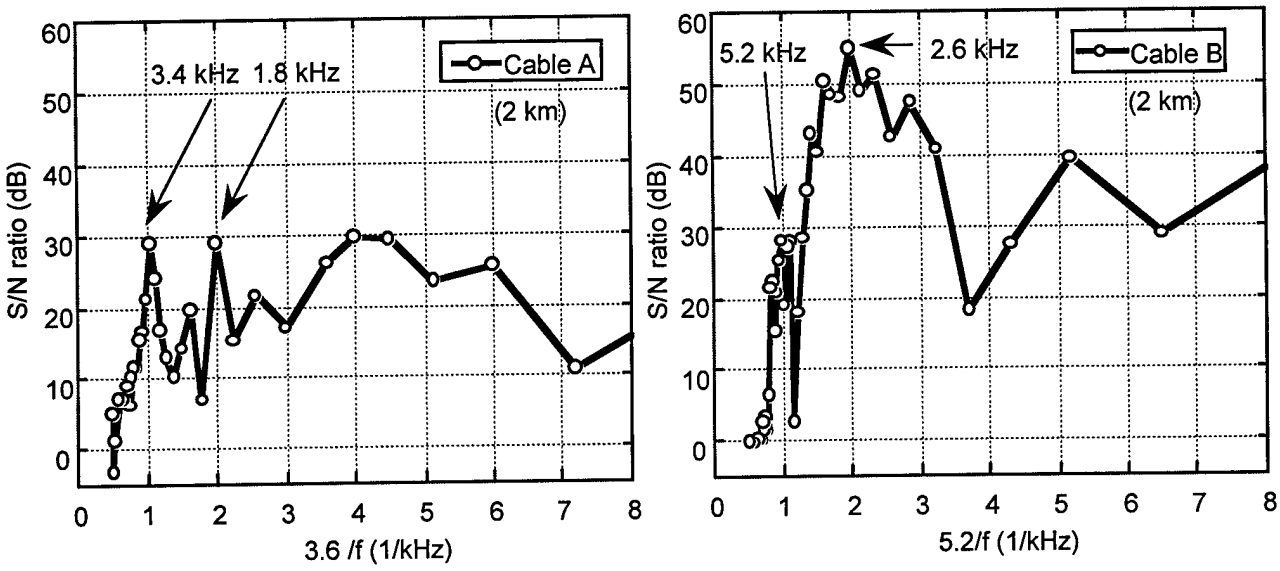

Fig. 4. S/N ratio versus inverse of vibration frequency

3.2 Light source characteristics and S/N ratio

We next investigated the relationships between the characteristics of light sources and S/N ratios at 3.4 kHz (cable A, 2 km). The light sources that we tested in the new system are described in Table 2. The coherence length Lc is estimated from equation (1), where λ is the center wavelength and $\Delta\lambda$ is the line width of the spectra.

$$Lc=\lambda^2/\Delta\lambda \qquad (1)$$

As we expected, the S/N ratio tended to increase as the coherence length increased. However, S/N ratio of DFB-LD with a wavelength of 1.31 μm is sufficient for identification. We also tested a Fabry-Perot laser diode, but did not obtain an S/N ratio (almost 0 dB).

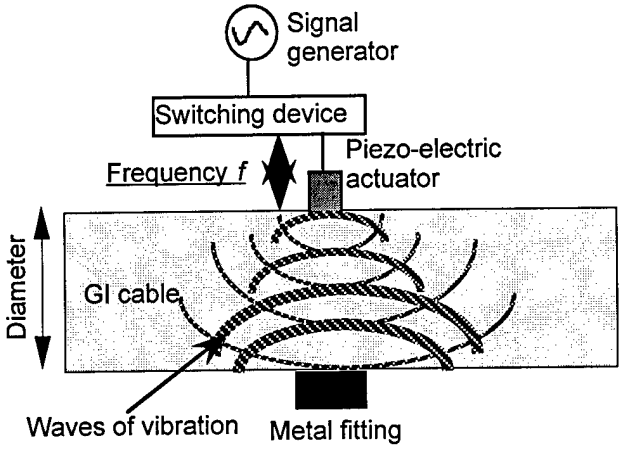

Fig. 5. Location of actuator and vibration transmission

Table 2. Characteristics of light sources and S/N ratios

No.	Type	λ (nm)	Δλ (nm)	Power (dBm)	Lc (mm)	S/N (dB)(*)
1	DFB-LD	1315.4	0.27	-6.3	6.4	16.2
2	DFB-LD	1549.7	0.30	-7.1	8.1	23.1
3	DFB-LD (Wavelength tunable)	1490.0	0.33	-5.0	6.7	30.6
		1570.0	0.27	-3.6	9.0	35.0

*Values at 3.4 kHz (cable A, 2 km)

Table 3. S/N ratios with different conditions of cable end

Condition of far ends of two fibers		Return loss (dB)(*)	S/N (dB)(**)	Identification
Fiber connector	Flat polished	17～18	22.6	OK
	Obliquely polished	51～53	0.1	NG
	Obliquely polished+Flat polished	16～18	23.5	OK
Bare fiber	Cut by dull edged cutter		0	NG
	Cut by fiber cutter		17.2	OK

* Values at 1.31 μm

* Mean values for 3.2 and 3.6 kHz (cable A, 2 km)

3.3 Influence of reflection from fiber ends

In our new system, we expected that the S/N ratio depends largely on the power level of reflection from the far ends of used two fibers. Accordingly, we next measured the S/N ratio of cable A (2 km) with several cable-end conditions. The results are summarized in Table 3. We measured the return loss of the ends of fiber connectors separately, and typical values are listed in Table 3. We were able to identify the cable having fiber connectors, even if they were obliquely polished types, by connecting them with the flat polished types. In cases where the cable end was cut by a dull edged cutter, the S/N ratio was not obtained. However, by newly cutting the ends of the fibers with a fiber cutter, we were able to identify the object cable.

3.4 Cable length dependence

Figure 6 shows the relationships between the S/N ratio and the cable length. Cables A and B with fiber connectors, were vibrated near their far ends. The most suitable vibration frequency for the individual cable was used. The S/N ratios of both cables decreased gradually as the cable lengths increased. However, the S/N ratios still exceeded 15 dB when the cable length reached 12 km. These values are sufficient for identification of the object cable.

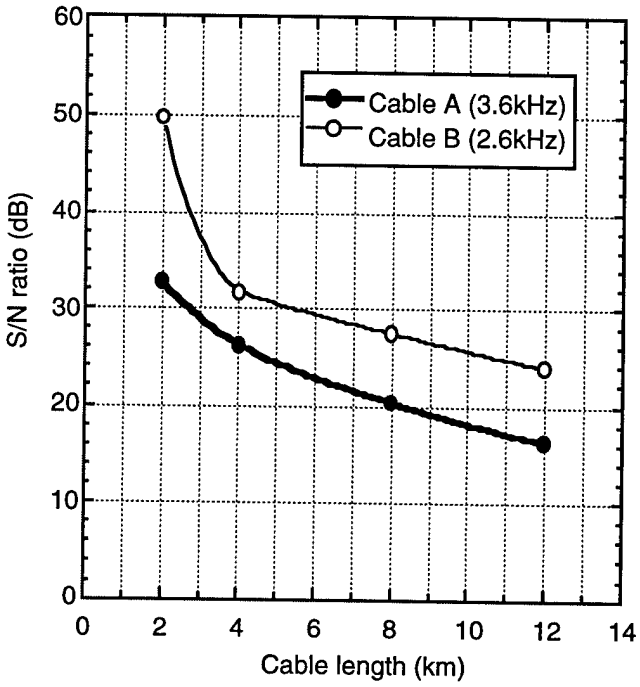

Fig. 6. S/N ratio versus cable length.

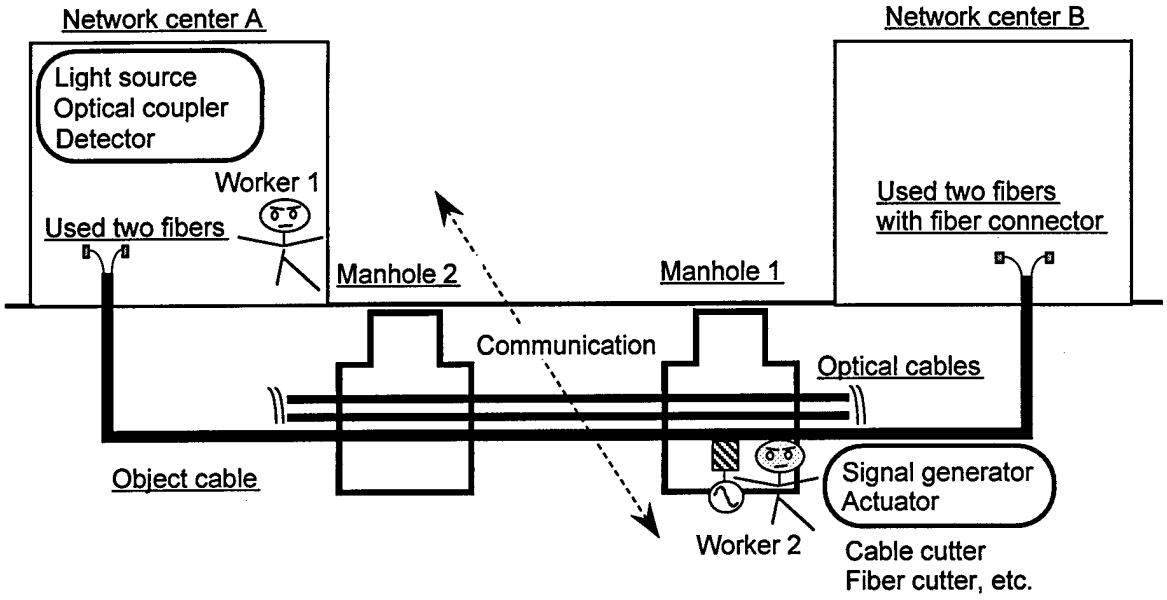

Fig. 7. Example of field application (removal of cable).

4. EXAMPLE OF FIELD APPLICATION

An example of field application of this system is illustrated in Figure 7. The cable designated for removal runs between network centers A and B with other optical cables. As most of the actual cases, we assume that the object cable have fiber connectors at the both ends.

First, at network center A, worker 1 positions a light source, an optical fiber coupler, and a photodetector. At manhole 1, worker 2 sets an actuator on one of the cables and vibrates it by means of a signal generator. Worker 1 communicates to worker 2 whether a vibration frequency is detected. If it is not , worker 2 sets the actuator on another cable. After identifying the object cable, worker 2 cuts it with a cable cutter and uses a fiber cutter to cut again the ends of the two measured fibers. Then worker 2 moves to manhole 2 and sets the actuator. This procedure is repeated until the removal the object cable is finished.

5. CONCLUSION

We have proposed an optical cable identification system based on the optical interference of back-scattered lights. This system achieved quick and reliable identification for GI cable at a length of 12-km from one end.

ACKNOWLEDGMENTS

The authors thank to Yuji Azuma and Masaru Kobayashi for their fruitful discussions and Masaaki Kawase for his continuous encouragement.

REFERENCES

[1] A. Fujisaki, H. Ogoshi, S. Sentsui, M. Kurokawa, M. Mizutani, and M. Miyazaki, "Optical talk set and optical identifier using polarised-wave-external-modulation method", 39th IWCS, pp. 418-423, 1990.

[2] Y. Azuma, K. Matsuno, K. Arakawa, and K. Yoshida, "An optical-cable identification system using optical interference between two optical fibers", 46th IWCS, pp. 650-657, 1997.

[3] S. A. Kingsley and D. E. N. Davies, "Multimode optical-fibre phase modulators and discriminators: I-Theory", Electronics Letters, vol. 14, pp. 322-324, 1978.

Kyozo Tsujikawa is a Research Engineer in the Technical Assistance and Support Center, NTT Maintenance Service and Operations Department . He joined NTT, after receiving his B.E. and M.E. degree in chemistry from Tokyo Institute of Technology in 1990 and 1992, respectively. He has researched low-loss optical fiber materials and engaged in the measurement of polarization mode dispersion and optical nonlinear effect. Mr. Tsujikawa is a member of the Institute of Electronics, Information and Communication Engineers of Japan.

Kyozo Tsujikawa
NTT Technical Assistance and Support Center
Midori-cho, Musashino-shi,Tokyo 180-8585, Japan

Koichi Matsuno is a Research Engineer in the Technical Assistance and Support Center, NTT Maintenance Service and Operations Department. He joined NTT in 1981. He has designed optical fiber cable identification systems and has developed optical fiber maintenance equipment. Mr. Matsuno is a member of the Institute of Electronics, Information and Communication Engineers of Japan.

Koichi Matsuno
NTT Technical Assistance and Support Center
Midori-cho, Musashino-shi,Tokyo 180-8585, Japan

Koji Arakawa is an Executive Engineer in the Technical Assistance and Support Center, NTT Maintenance Service and Operations Department . He joined NTT, after receiving B.E. degree in electrical engineering from Osaka Prefecture University in 1978. He has researched optical fiber cable reliability and has developed optical fiber maintenance equipment. Mr. Arakawa is a member of the Institute of Electronics, Information and Communication Engineers of Japan.

Koji Arakawa
NTT Technical Assistance and Support Center
Midori-cho, Musashino-shi,Tokyo 180-8585, Japan

Koji Yoshida is an Executive Engineer in the Technical Assistance and Support Center, NTT Maintenance Service and Operations Department . He joined NTT after receiving B.E. degree in communications engineering from Osaka University in 1973. He has developed optical testing instruments and researched optical fiber cable reliability. Mr. Yoshida is a member of the Institute of Electronics, Information and Communication Engineers of Japan.

Koji Yoshida
NTT Technical Assistance and Support Center
Midori-cho, Musashino-shi,Tokyo 180-8585, Japan

" APPROACH OF LOW PMD NON-ZERO DISPERSION SHIFTED SINGLE-MODE FIBER & CABLING TO ACHIEVE 40Gb/s DATA TRANSMISSION "

Kazumasa Ohsono Shinji Hinoshita Kotaro Tan
Yasunori Suzuki Yoshimi Nasuno

Hitachi Cable, Ltd. 5-1-1 Hitaka-cho, Hitachi-shi, 319-1411 JAPAN

ABSTRACT

We achieved that Low Polarization Mode Dispersion (PMD) Non-zero dispersion shifted single-mode fiber (NZDF) was obtained by Vapor Phase Axial Deposition (VAD) method without using a technology of the mode coupling such as spiral coating or span fiber. The achieved level of the average is 0.06 ps/$\sqrt{}$km, which extends the PMD-limited transmission distance(1dB PMD penalty) of about 800 km for STM-256 (40Gb/s) [1] .

INTRODUCTION

Long-haul multichannel transmission systems using optical amplifier have operated around the world. In this system, the industry is looking for high cost performance transmission line systems to increase the bit-rate speed over the longest distance [2] . The line systems constraints in increasing bit rates due to signal distortion are Four wave Mixing (FWM), Cross Phase Modulation (XPM), Self Phase Modulation (SPM), Chromatic Dispersion (CD) and Polarization Mode Dispersion (PMD) [3] . In this paper, PMD performance is analyzed because PMD is influenced by fiber birefringence and fiber mode coupling related to the cable structure with the manner of statistical random phenomena [4] [5] . PMD performance is very difficult issue, because using CD compensation to accumulated PMD is very difficult and unclear for the effect. Therefore , low PMD fiber for long distance amplified system cable is expected.

PREFORM PRODUCTION METHOD

Optical fiber has been fabricated by several method (VAD,OVD and MCVD) . VAD process itself has a great advantage in PMD performance because VAD process produces less birefringence compared with OVD or MCVD-rod-in methods. We investigated statistically fiber parameter for increasing PMD and limitation of manufacturing deviation to keep the low intrinsic PMD value of VAD process through coating and cabling processes without using the technology of the mode coupling such as span fiber [6] [7] . As a result we obtained a low-PMD fiber and cable.

PREFORM, FIBER & CABLE FABRICATION

The typical preform index profile for NZDF is

shown in figure 1. This profile type is dual shaped core. Germanium was doped in center and side core part. We fabricated this preform by VAD method. The fabrication of VAD for optical fibers is preferable method for PMD, because there is no preform-collapse process. The PMD of optical fibers is created by asymmetric structure of fiber and lateral stress for fiber. The asymmetric structure of fiber are core non circularity, core eccentricity and coating eccentricity etc..

Fiber Geometry Parameter vs. PMD

Fig.2 shows PMD as a function of core non circularity in core preform. Closed and open circle are production and experiment, respectively. From the analysis between core non circularity and PMD data plotting, the core non circularity was less than 0.4% case, the PMD of fiber was 0.06 ps/$\sqrt{}$km in average.

Fig.3 shows PMD as a function of the core eccentricity which occurred in outer-cladding process . In the case of the core eccentricity was less than 0.5 μ *m*, the PMD of fiber was 0.06 ps/$\sqrt{}$km in average.

Fig.4 shows PMD as a function of coating eccentricity which occurred in drawing process. In the case of coating eccentricity was less than 4 μm, the PMD of fiber was 0.06 ps/$\sqrt{}$km in average.

These results shows that the VAD method is effective fabrication for low-PMD fiber.

Cabling Process and PMD Change

Then we fabricated optical cable by adding the processes, coloring/tube-unit process, stranding process and sheathing process by using these low PMD fibers. Fig.5 shows the cross section of tube unit and cable. Tube unit consists of the required number of fibers, jelly compound and tube. The fibers have 0.05 % excess length than the tube length. The numbers of the tube are stranded around the central strength member in S-Z formation to form the cable core. The cable core is polyethylene sheathed.

Fig.6 shows the relation between fiber-PMD and unit-PMD. Unit-PMD average (0.075 ps/$\sqrt{}$km) is larger than fiber-PMD average (0.06 ps/$\sqrt{}$ km) . We analyzed the uncolored fiber received birefringence force due to the color ink coating, which might be derived from uneven thickness coating as unavoidable level of the vintage fibers, and the PMD was increased slightly.

Fig.7 shows the relation between fiber-PMD and cable-PMD. The cable-PMD values are consistent with the fiber-PMD values. We analyze the S-Z stranded tubes may give the residual mode coupling to the fibers and reduced the PMD value. The fibers are relaxed without receiving the lateral stress within the tube and the final cable-PMD showed the intrinsic PMD values of the fibers. Therefore we obtained low PMD cable which can use for ultra-high bit rate and ultra long distance translation system.

CONCLUSION

We achieved that Low Polarization Mode Dispersion (PMD) Non-zero dispersion shifted single-mode fiber (NZDF) was obtained by VAD method. We demonstrated the low PMD performance in high dispersion and rather complicated profile structure of NZDF with

the format of the final cabling. In addition, the method of the keeping the low PMD is to analyze the correlation between PMD and physical/dimension parameter of the each process in random access level. As final, cabled PMD was achieved 0.06 ps/$\sqrt{}$km in average level which promises the transmission of about 800 km, STM-256 (40Gb/s).

REFERENCES

[1] Draft new ITU-T Rec. G691,COM 15-R 5S-E APPENDIX I

[2] N.S.Bergano et al., J. Ligtwave Technol., vol.14, NO.6,(1996) pp.1299-1308

[3] A.Naka et al., J. Ligtwave Technol., vol.12, NO.2,(1994) pp.280-287

[4] C.D.Poole et al,Photon.Technol.Lett,3,1 (1991) pp.68-70

[5] C.D.Poole et al. ,J.Ligtwave Technol., vol.6,(1988) pp.1185-1190

[6] A.J. Barlow et al. Applied Optics 20:(1981) pp.2962

[7] M. Caiata et al. IWCS 1997 Proc.(1997) pp.617

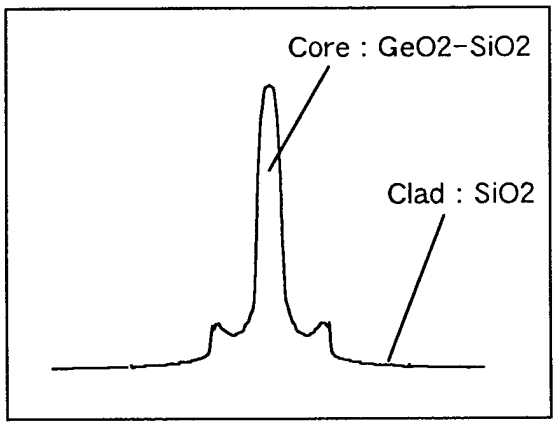

Fig.1 Typical preform index profile

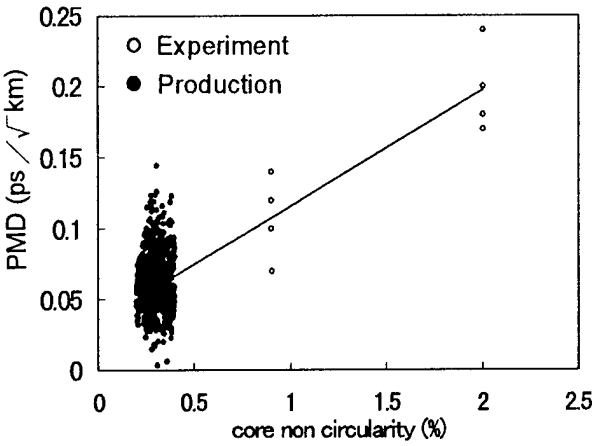

Fig.2 PMD as a function of core non circularity

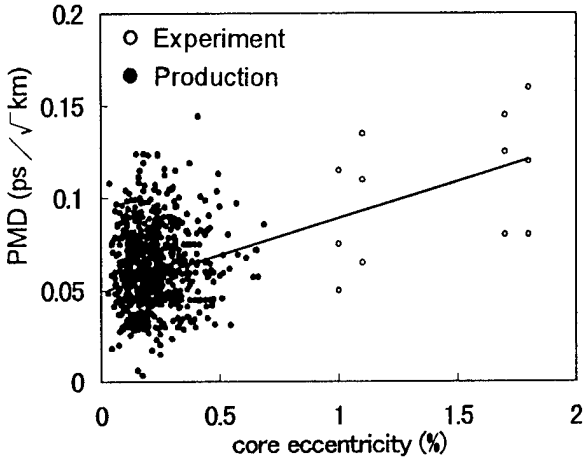

Fig.3 PMD as a function of core eccentricity

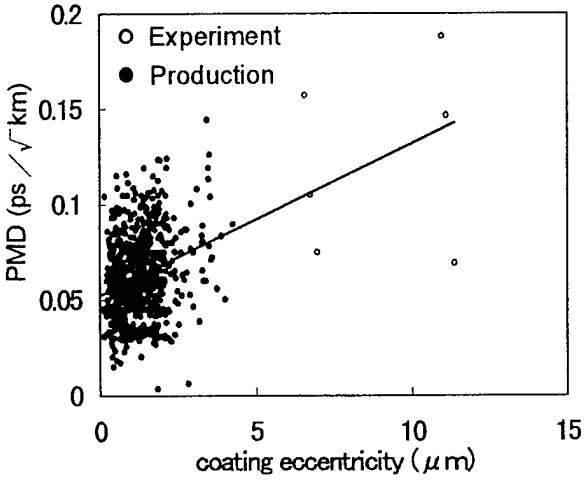

Fig.4 PMD as a function of coating eccentricity

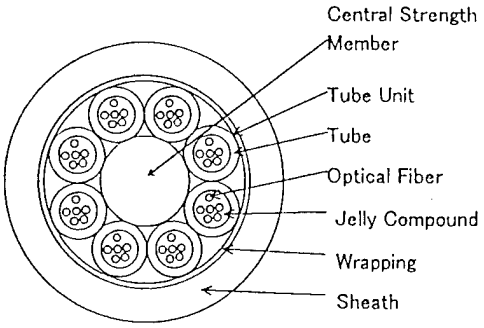

Fig.5 Cross section of tube unit and cable

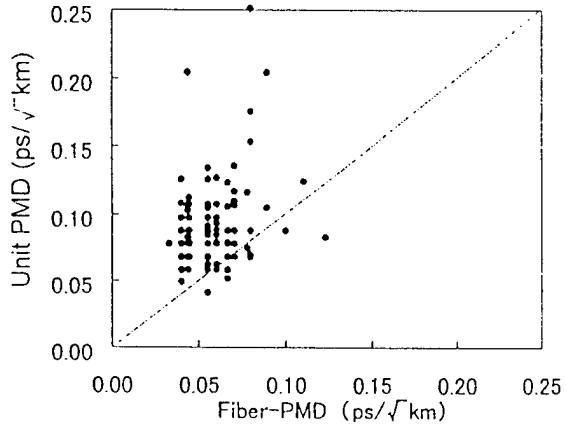

Fig.6 Relation between fiber-PMD and tube unit-PMD

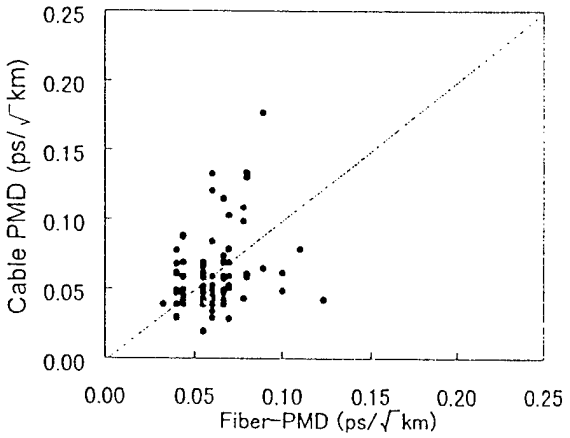

Fig.7 Relation between fiber-PMD and cable-PMD

Kazumasa Ohsono

Hitachi Cable, Ltd.

5-1-1, Hitaka-cho,
Hitachi-shi, 3191414
Japan

Mr. Ohsono received his B.E. degree in Mechanical Engineering from the Science University of Tokyo in 1982 and joined Hitachi cable, Ltd. He has been doing research work in optical fibers. He is now a senior researcher in the 4th Dept., Optroelectronic System Laboratory.

Shinji Hinoshita

Hitachi Cable, Ltd.

5-1-1, Hitaka-cho,
Hitachi-shi, 3191414
Japan

Mr. Hinoshita graduated in Electrical Engineerig from Kure National College of Technology in 1970 and joined Hitachi Cable, Ltd. He is currently responsible for the design and development of optical fiber and cable. He is now an executive senior engineer in the Telecommunications design Department.

Kotaro Tan

Hitach Cable, Ltd.

5-1-1, Hitaka-cho,
Hitachi-shi, 3191414
Japan

Mr. Tan received his B.E. degree in Electrical Engineering from the Chuo University in 1990 and joined Hitachi Cable, Ltd. He has been engaged in the design and development of optical fiber and cable. He is now an senior engineer in the Telecommunications Design Department

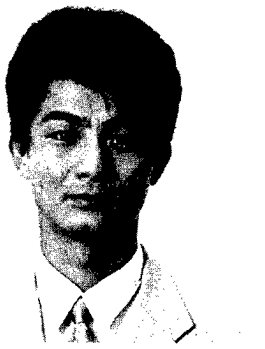

Yoshimi Nasuno

Hitachi Cable, Ltd.

5-1-1, Hitaka-cho,
Hitachi-shi, 3191414
Japan

Mr. Nasuno received his B.E. degree in Applied Physics from the University of Electro-Communications in 1991 and joined Hitachi cable, Ltd. He has been doing research work in optical fibers. He is now a senior researcher in the 4th Dept., Optroelectronic System Laboratory.

Yasunori Suzuki

Hitachi Cable, Ltd.

5-1-1, Hitaka-cho,
Hitachi-shi, 3191414
Japan

Mr. Suzuki graduated in Chemical Engineering from the Science University of Tokyo in 1991 and joined Hitachi cable, Ltd.
He has been engaged in the quailty assurance of optical fiber and cable. He is now a senior engineer in the Quality Assurance Sec. Ⅳ , Quality Assurance Department.

EFFECT OF TRANSIENT LOAD ON OPTICAL CABLE DURING LIFETIME

W. Griffioen

KPN Research, Leidschendam, The Netherlands

ABSTRACT

The effect of a transient load, e.g. due to installation or damage, on an optical cable during its lifetime is often questioned. In this paper the forces acting, and how they relax, are analyzed. Their effect on the most critical cable elements, like optical fiber, strength member and water-barrier, are estimated. It is concluded that for a cable surviving installation no significant risks are to be expected. After a dig-up a reparation length of less than 2x50 m (theoretical worst case), limiting reparation time, will be amply sufficient.

INTRODUCTION

Since the introduction of optical cables the installation in plastic (sub)ducts has become more and more popular. The number of these cables in ducts (or fiber members in small bores) is readily increasing, especially in the access network. Examples are blown fiber and JETNET®, a future (= fiber) proof copper network.[1,2] Ducted cables can slide easily over long lengths and have a risk of being stretched over these long lengths. The effect of a transient load on a cable during the rest of its lifetime is often questioned. Knowledge of this effect may be important for pulling of cables in ducts (or fiber members in small bores). Also dig-ups of ducted cable cause transient loads. Understanding of the forces acting, and how these forces relax, is needed to decide which length of cable must be replaced for reparation. This length shall be as short as possible (minimum of 20 m, set by modal noise)[3], e.g. to limit reparation time. In this paper the effect of peak- and residual-forces on the most critical cable elements will be analyzed.

The optical transmission must be maintained the entire lifetime of a cable. The most critical elements are, of course, the optical fibers themselves. They suffer from stress corrosion.[4] Residual stress after installation or a dig-up is a serious risk. In this case stress corrosion may result in delayed fracture of the fiber.

Another important cable element is the water-barrier (if present) which, if it ruptures, may lead to optical attenuation caused by hydrogen.[5] Also metal strength members can be critical, when yielding and permanent deformation occurs.[6]

First the choice to focus upon "duct cables" will be motivated: the still remaining questions about the actual service stress. Then these questions will be answered: the course of forces acting on the cable will be treated for installation of the cable in the duct and for damage (dig-ups) of cable and duct. For both situations the effects on the critical cable-elements will be examined.

CABLE

Two typical types of cable can be distinguished. The first type functions during service under about the same stress (or larger) as during installation. Such cables are direct-buried cables, submarine cables (both intended to be at about zero stress) and aerial cables (under permanent stress). They are supposed to be constructed such that they remain intact during their lifetime. In the second type the stress relaxes after installation. A typical example is a cable installed in a duct, very common for optical cables. The stress relaxation of such a cable is often questioned. Also the behavior of this type of cable during damage, e.g. dig-ups, needs some examination. This paper is limited to such "duct cables".

INSTALLATION

It will be assumed that installation of the cable occurs according to the rules, e.g. the maximum allowed pulling force will not be exceeded. No damage is expected then during this installation to optical fiber, strength member and water-barrier. The stress relaxation after installation,

however, is often questioned. This is especially important for the optical fiber where residual stress may lead to delayed fracture.

Stress Relaxation

The force F to pull a cable into a duct, with insertion force F_0, is given by:[7,8]

$$F = WR_b \sinh\left[f\theta + \sinh^{-1}\left(\frac{F_0}{WR_b}\right)\right] \qquad (1)$$

Here W is the weight of the cable per unit of length, f the friction coefficient between cable and duct, R_b the radius of curvature of the bent duct (characteristic for the trajectory: infinite for a straight trajectory; for a certain degree of tortuosity and some curves an effective value can be chosen) and θ the angle (hence length) over which the cable has been inserted (note: θ per unit of length is equal to $1/R_b$).[8] For zero insertion force the right-hand term between the brackets disappears. For a pull the maximum pulling force F_{pull} is at the end of the duct. After pulling this force drops to zero. In a trajectory where the curves are spread uniformly the maximum remaining force F_{max} will be in the middle of the trajectory (see Figure 1). From (1) it follows (the assumption of uniformly spread curves is not critical for this result):

$$\frac{F_{max}}{F_{pull}} = \frac{1}{\exp(f\theta/2)+\exp(-f\theta/2)} \qquad (2)$$

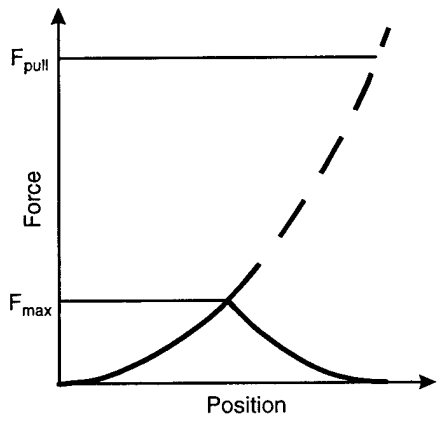

Figure 1 *Force relaxation after duct-installation.*

This ratio equals ½ for completely straight trajectories but far less for practical trajectories. Example: A cable with a weight W of 1 N/m and a friction coefficient f of 0.22 with the duct is pulled over 1000 m with a force of 2500 N. From (1) follows a total $f\cdot\theta$ of 4.7 resulting in a ratio of 0.1.

Note that for cables installed by blowing the previous calculation does not hold. Although the cable stress certainly drops after installation it is difficult to calculate how much. It also depends on the kind of trajectory and how was blown in. Fortunately cable stresses appearing with blowing are an order of magnitude less than with pulling.

Optical Fiber

When residual stresses remain after installation the only element which is critical is the optical fiber itself. Delayed fracture may occur due to stress corrosion caused by the residual stress.

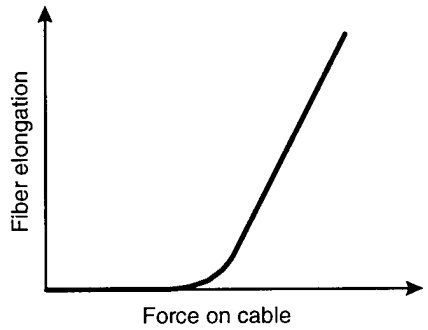

Figure 2 *Strain margin of an optical cable.*

In most cable constructions the fibers have a strain margin. Only from the force on the cable that corresponds to this margin the fibers start to elongate. If the maximum pulling force F_{pull} corresponds to a maximum fiber elongation it is easy to see, in Figure 2, that the fiber stress drops rapidly when the force on the cable relaxes. Not much fiber stress, or none at all, remains for duct cables, where the force on the cable drops to (far) less than half the maximum force at installation.

Even without strain margin, as is the case for pulled fiber members[9] of the "blown fiber" type, no serious problems are to be expected. The optical fiber survives more than 20 years when its service stress is less than one third of the proof-test.[10] Installation is usually done with the fibers not exceeding this stress. When the stress relaxes to less than half of this stress after installation the fibers survive much longer than 20 years. If installation is done at a higher stress a time of

flight measurement may be done to evaluate the maximum stress level (see Appendix). Note that usually the residual stress is far less than half the pulling stress, most likely also far less than one third (e.g. the practical example with factor already less than 0.1).

Conclusions for Installation

Residual stresses after installation drop far enough. Even delayed fracture of the optical fiber is not to be expected. When in doubt, optical "time-of-flight" measurements give sufficient information as basis for lifetime estimations.

DAMAGE

During dig-ups the cable may break at forces exceeding the specified maximum. There is, fortunately, a practical limit to this force. Lifting of the cable during dig-up will be limited to a reasonable height. The most critical elements are the strength member, the water-barrier and the optical fiber itself.

Length where Cable Specifications Exceeded

First it will be estimated over which length the cable might be stressed "over its specifications". The force F at a location somewhere in the duct follows from the maximum occurring force F_{break} at the location of damage, using (1) for relatively high forces (and/or dominant tortuousity of the duct trajectory):

$$F = F_{break} \exp(-f\theta) \tag{3}$$

Now θ represents the distance x from the location of damage, given by:[8]

$$\theta = \frac{8\pi \cdot A}{P^2} x \tag{4}$$

Here A and P are the amplitude and period, respectively, of the winding duct. For a completely straight duct (occurs rarely) the force F becomes:

$$F = F_{break} - fWx \tag{5}$$

A cable dig-up may stretch the cable until the maximum force F_{break} is reached or just cuts the cable at a lower force. Usually the latter is what happens when the cable breaks. Straining until the maximum force simply takes too much cable length, more than what is realistic for lifting. The elasticity of the cable is an important factor, characterized by the spring constant k:

$$F = k \cdot \varepsilon \tag{6}$$

The total pulled-out cable length l_ε is obtained by integrating twice (from two sides) over x the strain ε caused by the force F on location x. For a completely straight duct follows (integration until zero force F, assuming the tube is long enough):

$$l_\varepsilon = \frac{F_{break}^2}{kfW} \tag{7}$$

And for a winding duct (integrating to infinity, where the strain goes rapidly to zero):

$$l_\varepsilon = \frac{F_{break}}{k} \frac{P^2}{4\pi \cdot fA} \tag{8}$$

In the theoretical worst case situation the parameters are such that the cable breaks just when the maximum realistic value of l_ε is reached. If e.g. the friction is lower the cable will not break, if the friction is higher the length which is pulled out is smaller. For the straight duct the distance x_{max} over which the cable is loaded above its specified maximum F_{spec}, follows with (5) and (7):

$$x_{\max} = \frac{kl_\varepsilon}{F_{break}^2}\left(F_{break} - F_{spec}\right) \tag{9}$$

For the winding duct, with (3), (4) and (8):

$$x_{\max} = \frac{kl_\varepsilon}{2F_{break}} \ln\left(\frac{F_{break}}{F_{spec}}\right) \tag{10}$$

This equation is the most important one for estimation of the repair length. Note that this worst case result does not depend anymore on duct geometry and friction. The following practical numerical example will illustrate the above equations. A cable with a weight of 1 N/m and a friction coefficient f of 0.22 with the duct, having windings with amplitude A of 5 cm and period P of 10 m. This cable may not be loaded above its maximum specified force F_{spec} of 2500 N, breaks at a force F_{break} of 4500 N and has a spring constant k of 500 kN. The maximum length l_ε which is pulled out is 1.5 m (lifting of about 1 m).

For unlimited lifting it takes 213 m, from (3) and (4), before the 4500 N at break has dropped to 2500 N (for a straight duct even 9091 m!). The pulled out length is than 6.5 m, from (8). Limitation of lifting reduces the length over which the

cable is overstressed to 49 m, from (10). Note that the latter worst case situation occurs with lower friction of the cable than with the parameters above (changing the period P of the windings to 5 m would e.g. match this worst case situation). The general validity of this worst case result is illustrated also by the overstressed length for the straight duct of 74 m (same order of magnitude even here, occurring at unrealistic high values of the friction; high stresses are not to be expected at all in this case), from (9).

Note that the above theoretical reparation length is worst case indeed. Shorter reparation lengths than follows from (10) did, until now, not cause any problems.

Strength Member

Metal strength members show yield after initial elastic elongation. When the cable is constructed critical, i.e. the inelastic region is reached at the specified maximum load, the cable starts to deform permanently there.[6] This may change the strain margin, and hence the temperature window, of the cable, possibly resulting in excess signal attenuation of the fiber or even (delayed) fracture. Note that some permanent deformation does not necessarily lead to problems. Once installed no large strains and temperature changes are to be expected anymore.

Water Barrier

Another important cable element is the water-barrier (if present). When this barrier ruptures high concentrations of hydrogen may be generated and trapped.[5] This is caused by corrosion of the penetrating water at the inside (metal) cable elements, like the barrier itself. Excessive optical attenuation at 1300 nm and especially at 1550 nm may be the result. Note that for small leaks in the barrier hydrogen may accumulate while water-alarms do not beat. The hydrogen may spread all along the cable. Aluminum barriers, fortunately, can be stretched without breaking far more than the strains where cables usually break. Problems with the overlap are also not to be expected (supported by e.g. water-penetration tests after cable installation at high stresses)[11].

Optical Fiber

The nature of stress corrosion of an optical fiber is such that fracture occurs, or no weakening occurs at all (provided the primary coating of the fiber is not damaged). This is illustrated by the behavior of an optical fiber which fractures under a static stress σ_a applied during the time to fracture t_a. The decrease of the dynamic strength σ_d of this fiber with time t is given by:[12]

$$\frac{\sigma_d(t)}{\sigma_d(0)} = \left(1 - \frac{t}{t_a}\right)^{\frac{1}{n+1}} \qquad (11)$$

Here n is the corrosion susceptibility with a value of about 20 for optical fibers. In Figure 3 (a typical example of a pristine fiber, see [12]) the decrease in dynamic strength is given for applied stresses of 0.24 and 1.78 GPa, respectively, the latter stress (about one third of the dynamic strength) resulting in failure after 30 years. Note that in that case weakening from about 5 to 2 GPa occurs only 10 seconds before fracture (on a time-scale of 30 years!). This proves the statement that weakening is extremely bad luck.

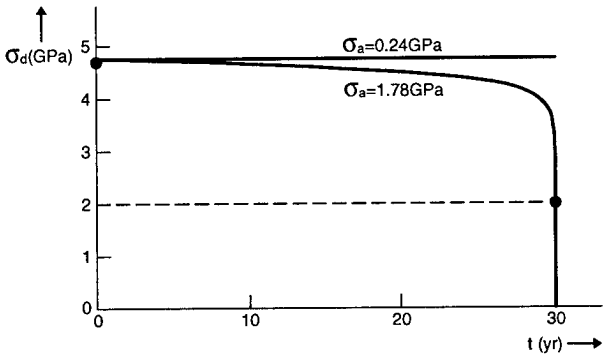

Figure 3 *Decrease of dynamic strength σ_d for a fiber under a stress σ_a of 0.24 and 1.78 GPa, respectively.*

The weak spots, just surviving the prooftest, which determine the mechanical tolerances for long lengths of fiber are believed to show a similar behavior as described above. If a transient stress during a dig-up does not result in fracture, no weakening of the fiber due to this stress is to be expected. And delayed fracture due to residual stress is not expected for the same reasons as for installation (the strain margin and the factor of only 0.1 for the stress relaxation of even the cable in the practical example).

Other Possible Problems

Another problem which may occur when the cable is stretched beyond its specified maximum load is longitudinal slip between its different elements. This can be caused by the fact that the load during the dig-up is transferred by other

elements than the outer jacket, which is in contact with the duct wall and experiences friction. Serious problems are not to be expected because the friction between the different elements will usually be larger than between the (lubricated) cable jacket and the duct wall.

Also the fibers may be pulled out at the dig-up. In cables where the fibers are stranded the fibers will only be stretched over a few meters. If the fibers lay in a straight tube the pull-out length might be rather long. The latter situation is comparable with pulling a cable which does not have a strain margin. The stress after the dig-up will in most cases drop below one third of the maximum stress during the dig-up. Where no break occurred during the dig-up no delayed fracture is to be expected. In doubt, again, optical "time of flight measurements" can be used.

In some cables half-isolated copper wires are used as a water-alarm. Excessive loads sometimes leads to malfunctioning.

Finally S-Z stranded tubes can be pulled "straight" during excess loads. No quantitative information is available, but also no problems of this kind have been reported.

Conclusions for Damage

Residual stresses after a dig-up drop far enough to prevent delayed fracture of the fibers. To replace all cable that has passed its specifications, e.g. to prevent yield of a metal strength member, a length of 2x50 m (worst case) is usually amply sufficient. This length can simply (by hand) be pushed into the duct, limiting reparation time.

CONCLUSIONS

Installation of optical cables in ducts (or fiber members in small bores) by pulling does not result in serious risks. "Time of flight" measurements of optical pulses, during and after installation may be used to confirm this. Respecting the maximum specified force on a cable after damage leads to a theoretical worst-case reparation length usually not exceeding 2x50 m. A length which can simply be pushed in by hand. The optical fiber is not weakened when it does not break. Also no delayed fracture is expected because the stresses usually drop by more than a factor of three after a dig-up or installation.

ACKNOWLEDGEMENTS

The author wishes to acknowledge Henk van Dusschoten and Piet Matthijsse of KPN Telecom, Arie van Wingerden of NKF and Onno Bresser of TKF for their valuable contributions.

REFERENCES

1. M.H. Reeve, S.A. Cassidy, "Installation of optical fibre units using viscous drag of air", *Proc. ECOC* (1983) 239-242.
2. W. Griffioen, H. Nijstad, A.T.M. Grooten, A. van Wingerden, G. Brown, D.F. Hawkins, G. Plumettaz, "A new, extremely versatile, access network cabling concept for migration to optical fiber", *Proc. 45th IWCS* (1996) 485-489.
3. *ITU-T Recommendation G.650* (previously "CCITT Recommendation"), Geneva (CH), 1993.
4. A.G. Evans, S.M. Wiederhorn, "Proof testing of ceramic materials - an analytical basis for failure prediction", *Int. J. of Fracture*, 10 (1974) 379-392.
5. W. Griffioen, "Water and hydrogen equilibrium for different cable constructions", *Electron. Lett., Vol.26, No.15* (1990) 1122-1123.
6. H. Murata, "*Handbook of optical fibers and cables*", Marcel Dekker, Inc., New York, 1996.
7. F.H. Buller, "Pulling tension during cable installation in ducts or pipes", *General Electric Review*, August 1949, pp. 21-23.
8. W. Griffioen, "*Installation of optical cables in ducts*", Plumettaz, Bex (CH) 1993.
9. P. Morris, "Development & design approval of two fibre, singlemode enhanced performance fibre unit (EPFU)", *Proc. 45th IWCS* (1996) 821-824.
10. W. Griffioen, "Mechanical lifetime of optical fibers", *Proc. 42nd IWCS* (1993) 471-475.
11. W. Griffioen, E. van Loenen, "Water and hydrogen equilibrium for different cable constructions", presented at *COST 218*, doc 218TD(89)038, Leidschendam (NL), 4-6 October 1989.
12. W. Griffioen, T. Volotinen, P. Wilson, A. Gouronnec, T. Svensson, "Handleability of aged optical fibers", *Proc. 44th IWCS* (1995) 857-864.
13. C.J. Sandwith, R.I. Odom, W.D. McCormick, J.A. Thornton, D.R. Wise, "Fiber-strain measurement using Brillouin optical-fiber time-domain analysis", *Proc. 45th IWCS* (1996) 415-427.

APPENDIX: TIME OF FLIGHT TECHNIQUE

Measuring the (total) strain Σ with optical "time-of-flight" techniques[9] means measuring the integrated strain ε over the length. This means that local excessive stresses in the fiber might be overseen. From (1) it follows, for zero insertion force:

$$\Sigma \propto \cosh(f\theta) - 1 \tag{12}$$

Using this it follows, with (1) again:

$$\frac{F_{\max}}{F_{pull}} = \frac{1}{2}\left(\frac{\Sigma_{pull}}{\Sigma_{\max}} - 1\right)^{-1} \tag{13}$$

F_{max}/F_{pull} is always smaller than ½, so this ratio between the (local) maximum force of the fiber remaining after pulling and the one at pulling will always be smaller than the measured ratio $\Sigma_{max}/\Sigma_{pull}$. Hence, no additional measurements of local strain (e.g. using Brillouin scattering techniques[13]) are needed.

BIOGRAPHY

Willem Griffioen received a MS degree in Physics and Mathematics from Leiden University (Netherlands) in 1980. Worked there until 1984. Joined KPN Research, St. Paulusstraat 4, 2264 XZ Leidschendam, The Netherlands. Responsibilities R&D of Outside-Plant and Installation Techniques. Worked at Ericsson Cables, Hudiksvall (Sweden) and at Telia Research, Haninge (Sweden) in the scope of exchange/joint projects with KPN Research. Received Ph.D. (Reliability of Optical Fibers) in 1995 from the Technical University of Eindhoven (Netherlands).

Verification of Optical Fiber and Cable Reliability

Kevin Houser - Corning Incorporated
Shirley Chahanovich - Pirelli Cables and Systems North America

Abstract

As environments are becoming increasingly harsh, the ability of optical fiber cable to withstand such environments is of the utmost importance to outside plant users. Laboratory accelerated aging environments have long been used as a measure to predict field performance of optical fiber and cables' ability to withstand harsh environments. However, there has been an issue in linking the laboratory environments with actual field exposure. To this end, actual field data from such a cable should provide real evidence of an optical fiber cable's ability to withstand these environments, thus providing the link between actual long-term reliability and laboratory tests.

In the present study, a 10 year-old field-aged cable was extracted from its deployed environment and tested to determine its resilience in withstanding mechanical and environmental conditions. In order to assess its resilience, a wide range of tests was performed on the aged cable and its components. The results of these tests were compared to test results obtained from unaged samples of the same era as well current data on the same design.

Surface roughness of the fiber was determined using an Atomic Force Microscope (AFM). Strength testing was conducted to verify failure probability. In addition, fiber strip force testing and Fourier Transform InfraRed (FTIR) analysis were conducted to determine the effect of aging on the coating materials.

Optical and material performances of the cable under mechanical stress were compared to historical test data on the single-armored, six-position, loose-tube cable design. These tests were performed in accordance to industry standard requirements. Testing results showed that there exists no significant degradation in the optical fiber cable's performance, which verifies laboratory testing and speaks to the true reliability of optical fiber cable.

Cable Design and History

The design is a single-armored, six-position cable (see Figure 1) which contains two live gel-filled 2.5/1.5 mm tubes with six fibers each, three soft fillers and one hard filler. The cable was manufactured in 1987 in compliance with Bellcore Specifications TR-TSY-000020, Issue 3 requirements. The fiber is Corning® SMF-28™ CPC3 standard single-mode optical fiber.

In 1987, the cable was installed in Oregon, at the base of the Cascade Mountain foothills, between the town of Medford and the Rogue River. The geography of the installation site indicates that it is a river valley surrounded by four mountain ranges. East of Medford are the Cascade Mountains with an elevation of 4,000(1219.5m) to 9,500 feet(2896m) and west of Medford are the Coast Range Mountains with an elevation of 3,500(921.1m) to 5,500 feet(1676.8m). North of Medford is the Umpqua Divide with elevations from 3,500(921.1m) to 5,500 feet(1676.8m) and south of Medford are the Siskiyous Mountains with elevations from 3,000(914.6m) to 7,600 feet(2317m).

The approximate mean annual temperature for Medford is 53°F(11.7°C) with recorded low temperatures of 0°F(-17°C) and high temperatures of 100°F(37°C). The mean annual precipitation averages 20.6-in(52.4 cm.) and average annual snowfall is 8.1 in (20.6cm). Because of it's geographical location, Medford is subjected to annual flooding and mudslides. A mudslide in 1997 was responsible for 200 feet

(61m) of this cable surfacing in a washout. The customer decided to reroute and replace the cable since the vicinity of a mudslide remains unstable for long periods. After rerouting the new cable, 86 feet of the 1987 cable was removed from a manhole and sent back to Pirelli Cable and Systems North America research facility for evaluation.

The 10-year-old field aged cable was an opportunity to benchmark and compare some of the mechanical, material and optical performances of a field-aged cable with original test results recorded on this 1987 cable design.

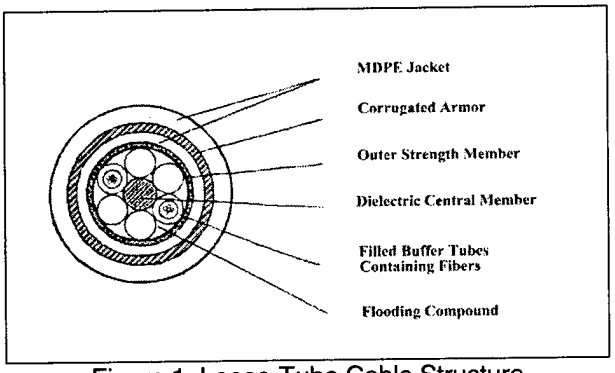

Figure 1. Loose-Tube Cable Structure

Cable Testing

Because only an 86 foot(26 meter) length of cable was available, it was necessary to limit the testing to the most significant areas of performance. Cable twist, flex, compression and impact, water penetration, compound flow, cable jacket shrinkage, tensile elongation of the outer jacket and fiber stripability were selected to be conducted at Pirelli's research facility. These tests would provide the information on cable performance after 10 years of field service and allow comparison with the original data acquired during the time of manufacture as well as with current requirements. Additional fiber tests were scheduled at Corning.

The cable was evaluated against the requirements of Bellcore specifications TR-TSY-000020 issue 3, GR-20-CORE issue 1, and the corresponding Electronic Industries Association (EIA-FOTP) test procedures with regard to mechanical and material performance.

Additional internal tests referred to as Product Capability Test (PCT) were performed upon completion of the tests, according to the requirements of the above Bellcore specifications. Cable performance in PCT provides important data by defining the capabilities of the cable design when tested beyond the requirements of the detailed specifications. It also provides valuable information when used to compare the field aged fiber optic cable performance with test data obtained for this design in the 1987 Initial Product Qualification.

PCT requirements are similar to Bellcore specifications with the exception that mechanical tests are more rigorous due to increased repetitions in the cable impact and cyclic flexing. Cable twist sample length was reduced from 4 meters to 2 meters. The PCT compressive strength test was performed with an increased load.

In the earlier Bellcore specification, the optical requirements for mechanical testing required measurements to be taken at the 1310 ± 20 nm wavelength for dispersion-unshifted single-mode fibers. The optical changes were based upon the total average change of at least four randomly chosen fibers. However, PCT and the current Bellcore specification require optical measurements at the 1550 nm wavelength and a minimum of 10 fibers for cables with six fibers per tube. Optical performance was monitored on all of the fibers in this twelve-fiber cable design.

The test setup required a minimum cable length of 18 meters with both cable ends stripped of the cable jacket for approximately 1 meter to expose the core components. The prepared length of the cable was placed through the mechanical test apparatus.

The 12 fibers were concatenated into a loop by fusion splicing. One end of the loop was fusion spliced to a 1000-meter pigtail connected to an Optical Time Domain Reflectometer (OTDR). The operational settings on the OTDR were based on 2 point dB loss with a 100 nanosecond pulse width. The horizontal and vertical scales were maximized in order to view all fibers under test on the OTDR display. Initial measurements before each test consisted of overall dB loss for the 12 fibers and individual measurements of each fiber. The fibers were identified by distance markers on the OTDR as shown in Figure 2.

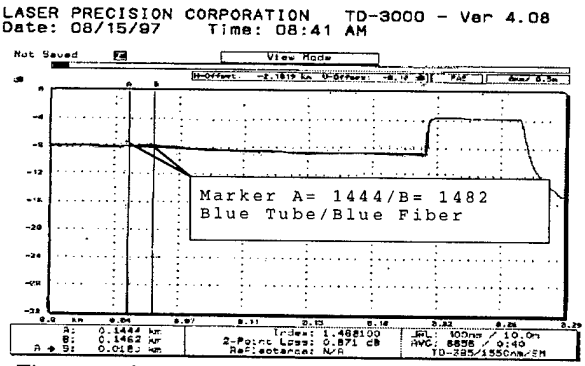

Figure 2: OTDR trace of fiber distance marking

The mechanical tests were performed according to the Bellcore specification followed by the PCTs. PCTs were performed in areas adjacent to the original test sites.

The cable was dissected upon completion of all tests to determine presence of mechanical damage. Examination of the jacket and armor was made under 10-x magnification at each test site.

The mechanical requirements of TR-TSY-000020, Issue 3, and GR-20-CORE, Issue 1 are shown in Table 1. Table 2 lists the mechanical test results obtained on the cable sample and Table 3 displays PCT requirements along with the performance of the test cable compared to these criteria. In both cases, the results show no evidence of deterioration in cable performance.

Based on the test results, there is no degradation in the optical or mechanical performance of the cable. The cable passed all the requirements of both Bellcore specifications (past and present) in Impact Resistance, Compressive Strength, Cable Twist, and Cyclic Flexing. The PCT results are comparable to data collected on similar cable designs.

Material Samples

All samples were conditioned according to the requirements of the Bellcore specification(s) and the EIA/TIA FOTP. The optional preconditioning cycle in compound flow allowed by the earlier Bellcore specification was omitted.

The summary of material requirements and results shown in Tables 4 and 5 also confirm that no cable degradation occurred.

An additional test was performed on the PBT buffer tubes due to concerns on the aging performance of this material. There is no apparent degradation of the PBT buffer tubes according to the comparison of the unaged and field aged test results in Table 6.

Fiber Testing and Results

While some of the cable was allocated for cable testing, a smaller section was reserved for fiber testing. Fiber samples were removed and subjected to a battery of fiber tests. The results from the field-aged fiber were compared to the appropriate recently manufactured fiber characteristics, and in accordance with relevant industry requirements. Fiber testing included strip force, atomic force microscopy, FTIR (Fourier Transform Infra-Red) analysis, dynamic fatigue, and strength testing.

Strip Force Testing

Strip force measurements give an indication of the fiber handler's ability to remove protective coating from the glass portion of the fiber without incurring damage. Strip force testing was conducted in accordance to FOTP-178 and EIA/TIA-455-178 "Measurements of Strip Force Required for Mechanical Removing Coatings from Optical Fibers." For this test, a total of 10 samples of each available fiber were tested for peak strip force (Newtons) and compared to a desired peak strip force range of 1.3N to 8.7N as outlined in Bellcore Document GR-20, issue 1.

Strip force testing results are summarized in Table 7. The aforementioned information shows that fibers dissected from the field-aged cable are comparable in strip force to those that were manufactured during the same time-period, but not cabled. The mean peak strip force average for both field-aged fibers is 3.09N.

Dynamic Fatigue and Strength Testing

Dynamic fatigue and strength testing were conducted to determine the effect of field aging on inherent fiber strength characteristics. Several samples were tested after having been pre-conditioned in a 23°C, 50% R.H. experimental environment. Due to the amount of fiber available, the samples were distributed equally among the four strain rates (0.025%, 0.25%, 2.5%, 25%) resulting in four fiber samples per strain rate.

Table 7 shows the results of the strength testing conducted on the fiber from the field-aged cable.

Figure 3 compares the Weibull distributions of the samples for aged and non-aged fiber at the 2.5%/min strain rate. The field-aged fibers had median strengths comparable to non-aged samples at the associated strain rates.

Figure 4 shows the results of dynamic fatigue testing. The results show that for dynamic fatigue, the field-aged fiber meets the proposed, GR-20 issue 2, Bellcore criteria of $n_d \geq 18$ with a n_d=19.4. Thus, testing has shown that no significant degradation in strength or dynamic fatigue characteristics has occurred to the tested fibers due to 10 years of environmental field aging.

Atomic Force Microscopy

Atomic force microscopy has been shown to be a useful technique for examining extremely small surfaces. For this reason, AFM testing was conducted to confirm the effect of field aging on the fiber.

AFM testing results are shown in Table 7 and three-dimensional images are provided in Figures 5 and 6. Results show that surface roughness values for the field-aged fiber bear a close resemblance to fiber of the same vintage that has been archived and fiber that was recently manufactured.

Based on this data, it can be deduced that the field-aging conditions did not seriously affect the surface roughness of the fiber.

Fourier Transform Infrared (FTIR)

FTIR scans of ink, inner primary and outer primary coatings were conducted to determine the effect of field aging on the chemical compositions of the aforementioned materials. The data shows that for both field-aged ink and coating samples, close matches were found with existing, known materials. The results show that the field-aged fiber has the same chemical characteristics as recently manufactured fiber with the same vintage CPC3 coating.

Summary and Conclusion

After significant aging in the field, the ability of this optical fiber cable to withstand harsh environmental conditions and remain in excellent condition was tested. As a result of the battery of testing that was conducted on this particular cable, it can be concluded that the reliability of optical fiber cables is such that reliability and lifetime models created to predict in-field service are more than suitable to accurately predict fiber and cable reliability. Optical and mechanical testing was conducted on both fiber and cable to verify performance after field aging. All testing indicates no degradation in fiber/cable performance. Thus, the reliability of optical fiber/cable has been verified.

Table 1: Bellcore Specifications Mechanical Test Requirements

	TR-20, Is. 3 Test Setup	GR-20, Is. 1 Test Setup
Impact Resistance	6.0 kg load 25x 150 mm drop distance	4.0 kg load 25x 150 mm drop distance
Compressive Strength	440 kg for 10 minutes	300 kg for 10 minutes
Cable Twist	4 m length 10 cycles of ± 180° twist	2 m length 10 cycles of ± 180° twist
Cable Cyclic Flexing	25 cycles on mandrel 20 x cable OD	25 cycles on mandrel 20 x cable OD

Table 2: Mechanical Test Results

Test	TR-20, Is 3 Specification	GR-20 Is. 1, Specification
Impact Resistance	Pass/ 0.05 dB @ both wavelengths	Pass/ 0.00 dB @ 1550 nm
Compressive Strength	Pass/ 0.05 dB @ both wavelengths	Pass/ 0.00 dB @ 1550 nm
Cable Twist	Pass/ 0.00 dB @ both wavelengths	Pass/ 0.00 dB @ 1550 nm
Cable Cyclic Flexing	Pass/ 0.00 dB @ both wavelengths	Pass/ 0.00 dB @ 1550 nm

No splits or cracks in cable sheath or armor under 10x magnification found at any of the test sites.

Table 3: Product Capability Test Requirements and Test Results

Test	Test Setup	Results
Impact Resistance	6.0 kg load increase # 30% 150 mm drop distance	Pass/ 0.02 dB @ 1550 nm
Compressive Strength	Increase load 30% for 10 minutes	Pass/ 0.05dB @ 1550 nm
Cable Twist	2 m. length 10 cycles of ± 180° twist	Pass/ 0.00 dB @ 1550 nm
Cable Cyclic Flexing	Increase cycles 30% on mandrel 20 x cable OD.	Pass/ 0.00 dB @ 1550 nm

No splits or cracks in cable sheath or armor under 10x magnification found at any of the test sites.

Table 4: TR-TSY-000020, Issue 3 Material Test Requirements

Test	Requirements
Water Penetration	No leaks in 1 meter sample for 4 hours
Compound Flow	No drips after 24 hours @ 65°C
Jacket Shrinkage	Shrinkage < 5% each specimen
Jacket Tensile Elongation	Min. yield strength = 11.0 MPa , Elongation %= 400
Fiber Strippability	Remove 50 mm of coating ≤ 13.4 N force.

Table 5: TR-TSY-000020, Issue 3 Material Test Results

Test	Results
Water Penetration	No leaks in 1 meter sample for 12 hours
Compound Flow	No drips after 24 hours @ 65°C
Jacket Shrinkage	Shrinkage < 4% each specimen
Jacket Tensile Elongation	Min. yield strength = 13.5 MPa, Elongation %.> 500
Fiber Strippability	Remove 50 mm of coating ≤ 3.4 N force.

Table 6: Internal Material Test Result Comparison

Test	1987 Test Results	1998 Test Results
Buffer Tube Tensile (PBT)	Unaged=5800 psi 250% Elong @ break	Aged = 6900 psi 325% Elong @ break

Table 7: Fiber Test Result Summary

	Field-Aged Fiber	Archived or Recently Manufactured Fiber
Peak Strip Force	3.09 N	3.18 N**
Median Strength	677 kpsi	649 kpsi*
Surface Roughness	.29 nm	.12-.49 nm*,**

* Archived, **Recently Manufactured

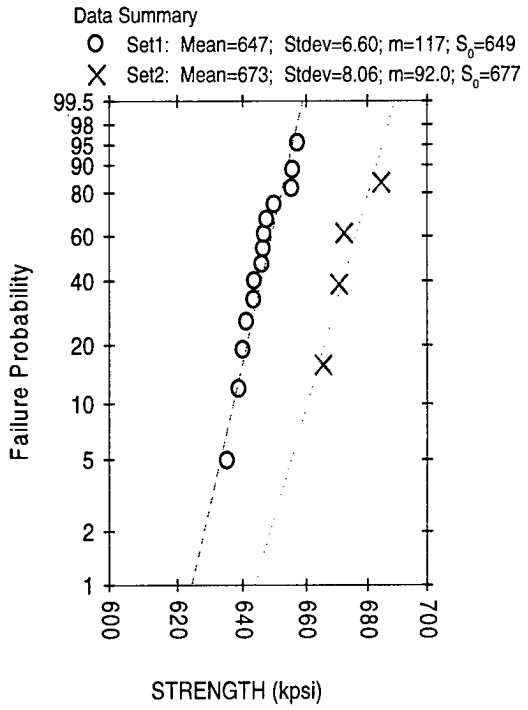

Figure 3: Comparison of field-aged fiber (Set 2) strength to non field-aged fiber (Set 1) strength.

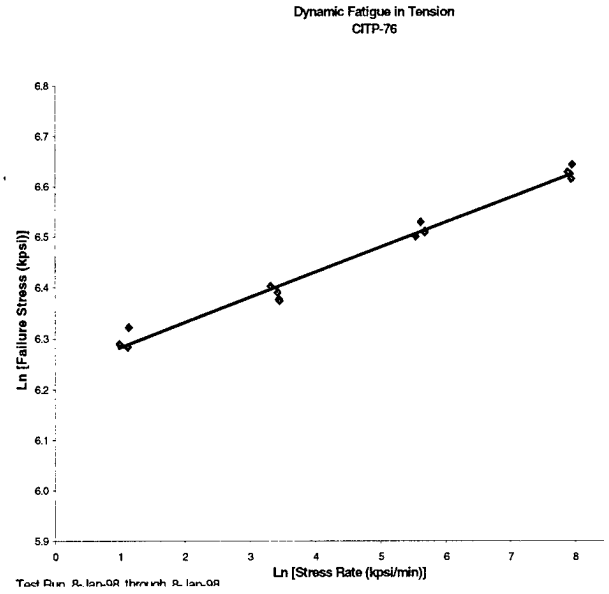

Figure 4: Dynamic Fatigue Data at each of the four strain rates (25, 2.5, 0.25, 0.025%/min)

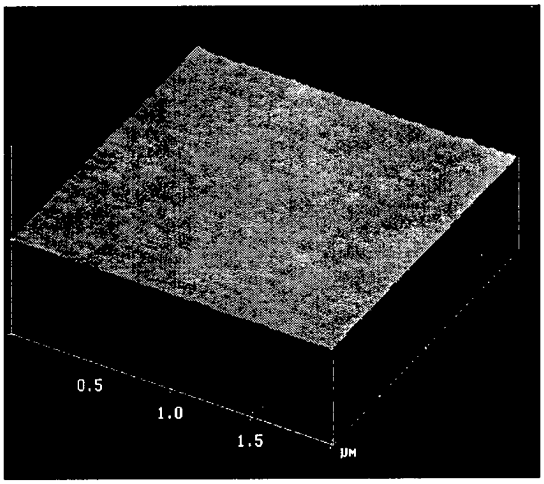

Figure 5: AFM scan for recently manufactured fiber with surface roughness of 0.12nm

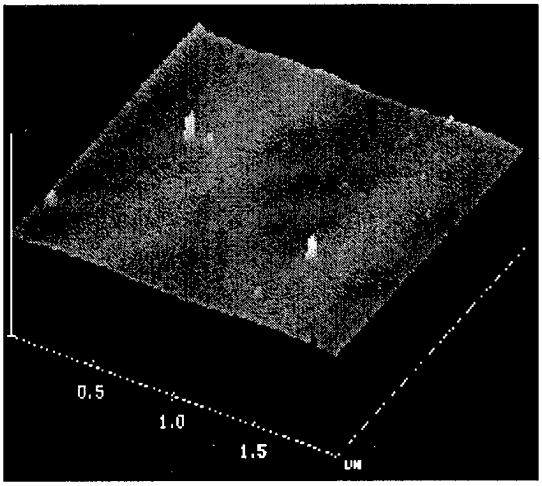

Figure 6: AFM scan of field-aged fiber with surface roughness of 0.29nm

Acknowledgements

The authors would like to thank the field engineers, design engineers, test engineers, technicians and laboratory personnel at Corning Inc. and Pirelli Cables and Systems North America for their assistance and research for the contents of this paper.

References

1. A. Dwivedi, G. S. Glaesemann, and C. K. Chien "Optical Fiber Strength, Fatigue and Handleability After Aging In A Cable," pp. 728-735 in the proceedings of the 43rd International Wire and Cable Symposium, 1994.
2. J. L. Smith, A. Dwivedi, and P. T. Garvey "Mechanical Behavior of Optical Fibers Removed From a Field-Aged Cable," pp.848-856 in the proceedings of the 44th International Wire and Cable Symposium, 1995.
3. M. L. Lundergan, B. D. Zimmerman, B. Waterman "Mechanical and Optical Functionality of Field-Aged Optical Ground Wire Cable," pp.449-458, NFOEC 1996 proceedings.
4. H. H. Yuce, et al., "Effects of the Environment on an Unprotected Reel of Optical Fiber," pp. 700-706 in the proceedings of the 40th International Wire and Cable Symposium, 1991.
5. H. H. Yuce, et al., "Fiber Reliability Study of Field Aged Optical Cables," pp. 705-712 in the proceedings of the 41st International Wire and Cable Symposium, 1992.

Shirley Chahanovich is a Senior Applications Technician and has been with Pirelli Cable and Systems North America since 1987. She spent the first three years of service in the fiber optic manufacturing facility. Since 1990, she has been a member of the Design and Test Engineering Department where she was responsible for product capability testing and fiber break source analysis. She joined the Application Engineering Department in 1997.

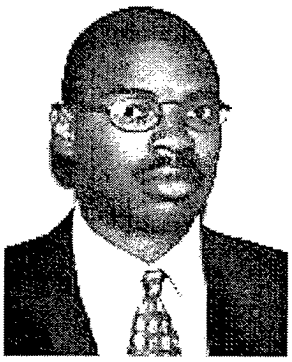

Kevin Houser is an Applications Engineer and has been with Corning Incorporated, Telecommunications Products Division since January 1997. He received his Bachelor of Science in Mathematics from Morehouse College in 1996 and his Bachelor of Science in Electrical Engineering from Georgia Institute of Technology also in 1996.

HYBRID FIBER-WIRELINE ACCESS TECHNOLOGIES

Dr. Tet Yeap

Bell Canada Advanced Research Laboratory, University of Ottawa
Ottawa, Ontario, Canada

Abstract

Deployment of Fiber to the Home (FTTH) architecture has been plagued by expensive port and installation cost. One approach to above problem is to bring high-speed data transmission into a neighborhood on a single optical fiber and route the data traffic to a home over an existing twisted-pair networks. This architecture is known as Hybrid Fiber Twisted Pair (HFTP) architecture or at times known as Very High Speed Digital Subscriber Loops (VDSL).

Current ADSL systems for transmission over existing twisted pair copper plant achieve 4 to 6 bits per Hertz data transmission. This is obtained using QAM and CAP single carrier technology. There is a need and a market for products offering higher data transmission speeds at VDSL rate (26 - 52 Mbps) over a 300 to 500 meters of existing copper plant; a data rate achieving 8 to 10 bits per Hertz bandwidth is desirable. The main problem is when a wideband signal is transmitted over a copper loop, the higher frequency components of the signal attenuate significantly more than the lower frequency components. In addition, narrowband interferers from AM or amateur radio signals also affect the transmission by destroying the signal in parts of the frequency band. Therefore, multicarrier transmission systems such as DMT or DWMT that could adapt to the channel response by placing more bits in subchannels with higher SNR and could avoid narrowband interferers altogether by turning off affected subchannels is required to optimize performance.

The development of transmission technology supporting the HFTP access networks is essential because most phone companies view the hybrid access networks as intermediate solutions towards a long term solution enabling the deployment of a full optical fiber high-speed network.

Dr. Tet Yeap
Bell Canada Advanced Research Lab
Universtiy of Ottawa
Ottawa, Ontario
Canada K1N 6N5
E-mail: tet@site.uottawa.ca

Tet Yeap is an associate professor of electrical and computer engineering at the School of Information Technology and Engineering, University of Ottawa, Canada. He is also a director of the Bell Canada Advanced Research Laboratory in Ottawa. He received the B.A.Sc. degree in electrical engineering from the Queen's University, Canada, in 1982, and the M.A.Sc. and Ph.D. degrees in electrical engineering from the University of Toronto, Canada, in 1984 and 1991, respectively. His research interests include broadband access architecture, neural networks, multimedia, parallel architectures, and dynamics and control.

LOOP PLANT ENVIRONMENT AFFECTING XDSL DEPLOYMENT AND PERFORMANCE

Craig F. Valenti

Bellcore, Morristown, NJ

Abstract

Many new digital subscriber line (DSL) loop transmission systems are being proposed, developed, and are nearing deployment. DSL is a high-speed telecommunications service that relies on existing standard twisted-pair copper wiring to deliver multimedia content.

A generic term for these systems is "xDSL." xDSL systems will require careful design and deployment strategies to ensure they do not interfere with one another or with existing services when deployed within the same or adjacent binder group[1] in the embedded loop plant. This issue has generated a number of topics that are generally referred to as "spectrum management" with associated "spectrum compatibility" studies and testing programs. The interference due to other systems inside the cable is known in the industry as crosstalk. The general nature and characteristics of crosstalk are described. The limitations that Near-End or Far-End Crosstalk (NEXT and FEXT) imposes on xDSL deployment will be addressed.

The configuration of the twisted-pair loop plant and how it affects xDSL transmission will also be discussed. The impact of bridged tap[2] on high frequency transmission systems (e.g., VDSL), in particular are singled out for study. Bridged tap with length equal to the quarter-wavelength of the transmitted signal can lead to severe nulls in the loop response function. These nulls may not allow transmission in this frequency range impacting VDSL deployment and operation. Results of loop simulations will be presented and possible strategies for remediation will be discussed.

Loop Transmission Parameters
NEXT & FEXT
Attenuation
Bridged Tap

Table 1: Some Loop Parameters Affecting Transmission

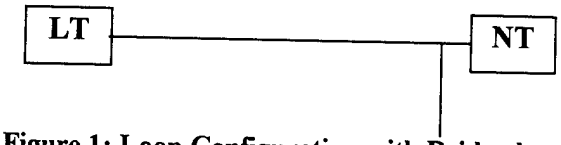

Figure 1: Loop Configuration with Bridged Tap

Craig F. Valenti, PhD
Senior Engineer
Bellcore
445 South St, 1J244G
Morristown, NJ 07960

Dr. Craig Valenti is a Senior Engineer in the Broadband Access Design and Engineering Group at Bellcore. He has over eighteen years experience both as a manager and as an individual contributor in the areas of high-speed copper loop transmission systems engineering, integration and testing. He has contributed to the development of physical layer requirements for Digital Subscriber Line technologies such as ISDN Basic Rate Access, High-bit rate Digital Subscriber Line (HDSL), Asymmetric Digital Subscriber Line (ADSL), and Very high-speed DSL (VDSL). He has been the primary force in the development of Bellcore's Access Test Bed Laboratory that is used for the prototyping, testing and integration of emerging xDSL access technologies. Dr. Valenti received a Ph.D. in Physics from the City University of New York in 1979.

[1] A binder group is a set of closely related pairs of wires in a cable. The binder group is most often 25 or 50 pairs twisted together into a group within the cable structure. The binder groups themselves may also be twisted among themselves within a cable.

[2] Bridged taps are open circuited stubs of cable pairs, which are intended for service deployment flexibility.

HIGH PERFORMANCE TWISTED PAIR PIC DISTRIBUTION CABLE (HPTP)

Jon . I . Green Norcom /CDT Kingston, Ontario Canada

ABSTRACT

This paper summarizes the CAT 5 transmission performance of 25 pair 24 AWG HPTP PIC Aircore Distribution Cable.

HPTP DESCRIPTION

High Performance Twisted Pair PIC Distribution Cables consist of 22 or 24 AWG balanced, precision engineered twisted pairs of polyolefin insulated copper conductors. These cables are available with either an air or filled core and standard industry sheaths.

Application

High Performance Twisted Pair PIC Distribution Cables are designed for distribution of broadband signals using ADSL, HDSL, or VDSL modem technologies. The superior transmission performance of these cables at high frequencies enables data transmission rates of 52 Mbps over 1,000 m (3,300 feet) or 26 Mbps over 1,500 m (5,000 feet), using VDSL modems. The excellent crosstalk isolation of these cables (min 20 dB better than conventional distribution cable) result in significantly reduced interference from other systems in the same cable or from outside noise sources. This reduced interference enables the use of both transmit and receive signals of different types (e.g., ADSL, VDSL, T1, etc.) within the same cable sheath. The extended reach capabilities of HPTP cables will allow up to 600 homes to be serviced from a single node, resulting in significant savings.

INTRODUCTION

The application of Broadband services in the outside plant , at this point in time, is envisioned to cover transmission rates of up to 52 Mbps. CAP, DMT and QAM modulating schemes have been developed that are capable of encoding up to a 52 Mbps transmission rate in a 10 MHz transmission bandwidth. This means that if a cable has suitable attenuation and crosstalk performance over a 10 MHz range, then a 52 Mbps transmission rate will be possible. Noting that attenuation is length dependent, it is evident that bandwidth availability will also be length dependent. The key factor is that at 10 MHz the attenuation of 22 AWG HPTP cable is slightly less than 50 dB/km, while the minimum near end crosstalk at the same frequency is also slightly less than 50 dB. In other words above 10 MHz the noise on the pair equals the receive signal level, hence the receive signal is not decipherable. The result being that a maximum 1 km length of 22 AWG HPTP cable will support 52 Mbps transmission. 24 AWG cables have a 24 % higher attenuation than 22 AWG cables, hence an 800 metre length of 24 AWG HPTP will support 52 Mbps transmission.

In the outside plant application the characterization of cables up to 30 MHz would give a suitable window above the required 10 MHz point. The 100 MHz measurements are an extension of the in building application, where for LAN networks a 100 MHz bandwidth over a 100 metre length is standardized and called CAT 5. Additionally for campus environments the HPTP cable can be used to extend LAN networks between buildings providing a 100 MHz bandwidth over 100 metres.

Commercial building Telecommunications standards such as TIA/EIA 568A cover transmission requirements for indoor cabling. A similar standard can be applied to outdoor PIC distribution cable. Currently ICEA are drafting ICEA S-98-688 titled "Broadband Twisted Pair Cable Aircore, Polyolefin Insulated, Copper Conductor". This specification has the same CAT 5 transmission performance requirements as described in the EIA/TIA 568A specification. The ICEA specification covers 24 AWG and 22 AWG cables and also includes far end crosstalk requirements.

This paper presents the results of testing carried out on 8 production runs of 25 pair 24 AWG A/C HPTP cable and compares the performance with the CAT 5 requirements. The transmission parameters covered include attenuation, power sum near end crosstalk, power sum equal level far end crosstalk, SRL and characteristic impedance.

Measurement

The measurements were made with a Network Analyzer & S-Parameter test set. A computer controlled switching matrix was used to switch through the 300 pair to pair crosstalk combinations present in each 25 pair cable. Measurements at 401 frequencies were obtained for each pair combination. The following graphs present the overall average for all 8 production

runs as well as the 1 % worse than (or 1 % greater than) envelope for each parameter. The envelope represents the 1 % worse than (or 1 % greater than) value measured at each of the 401 frequencies. Equations representing the least squares fit for PSUM NEXT and PSUM ELFEXT have also been generated.

Attenuation:

The CAT 5 performance standard for maximum attenuation is defined by the following equation:

1.967* SQR(F(MHz)) + 0.023* F(MHz) + 0.050/ SQR (F(MHz))

The average attenuation of the 24 AWG HPTP A/C cables was 12 % lower than this level. The maximum attenuation (calculated by averaging the maximum of the 8 runs) was 4.5 % lower than the CAT 5 requirement and the 1 % greater than envelope was 4 % lower than the CAT 5 limit.

FREQ	AVG	MAX	CAT 5 MAX
1.	1.8	2.0	2.0
4.	3.7	4.0	4.1
8.	5.2	5.7	5.8
10.	5.8	6.3	6.5
20.	8.2	8.9	9.3
25	9.2	10.0	10.4
31.5	10.3	11.2	11.8
62.5	14.8	16.1	17.0
100.0	19.3	20.8	22.0

Near End Crosstalk

The CAT 5 performance standard for minimum PSUM NEXT is described by the following equation:

CAT 5 MIN. NEXT = 62 -15 * LOG (F(MHz))

The average NEXT of the 24 AWG HPTP A/C cables can be described by the following equation :

AVG. NEXT = 76.1 - 13.3 * LOG (F(MHz))

The 1 % worse than NEXT of the 24 AWG HPTP A/C cables can be described by the following equation :

1 % W.T. NEXT = 69.1 - 13.7 * LOG (F(MHz))

At 10 MHz the HPTP cable 1 % W.T. NEXT performance is 8 dB above the Cat 5 requirement. The HPTP performance slopes off at 13.3 dB per decade, this is approximately 1.5 dB lower than the rate of 15 dB per decade specified for CAT 5 performance.

Freq (MHz.)	*AVG*	*1 % W.T.*	*FIT AVG*	*FIT 1 % W.T.*	*CAT 5 MIN*
1.	74.3	70.3	76.1	69.1	62.0
4.	68.2	60.8	68.0	60.8	52.9
8.	64.0	57.0	64.0	56.7	48.4
10.	62.4	53.2	62.8	55.4	47.0
20.	58.7	50.0	58.8	51.2	42.4
25.	57.6	49.6	57.5	49.9	41.0
31.5	56.3	46.9	56.1	48.5	39.5
62.5	52.5	44.0	52.2	44.5	35.1
100.	49.8	42.8	49.5	41.7	32.0

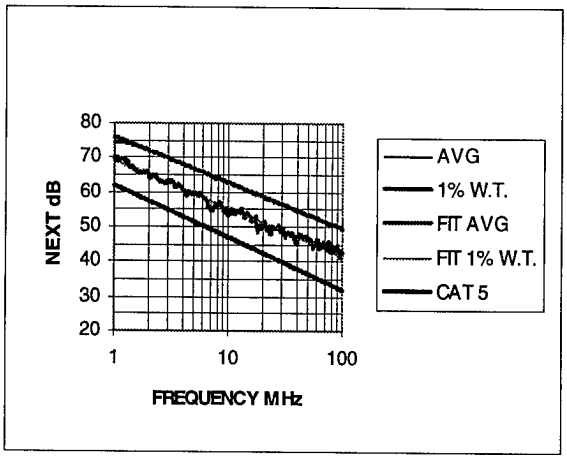

Equal Level Far End Crosstalk

The performance standard for minimum PSUM ELFEXT is described by the following equation:

61 -20 * LOG (F(MHz)) per 100 m.

The average ELFEXT of the 24 AWG HPTP A/C cables can be described by the following equation :

73.5 - 17 * LOG (F(MHz)) per 100 m.

The 1 % worse than ELFEXT of the 24 AWG HPTP A/C cables can be described by the following equation:

64 - 17 * LOG (F(MHz)) per 100 m

At 10 MHz the HPTP cable 1 % W.T. ELFEXT performance is 6 dB above the Cat 5 requirement. The HPTP performance slopes off at 17 dB per decade, this is 3 dB lower than the rate of 20 dB per decade specified for CAT 5 performance.

F (MHz.)	*AVG*	*1 % W.T.*	*FIT AVG*	*FIT 1 % W.T.*	*SPEC MIN*
1	71.9	64.8	73.5	64.0	61.0
4	63.5	53.9	63.3	53.8	49.0
8	57.9	48.2	58.1	48.6	42.9
10	56.4	46.6	56.5	47.0	41.0
16	52.8	42.9	53.0	43.5	36.8
20	51.2	41.2	51.4	41.9	34.9
25	49.5	39.7	49.7	40.2	33.0
31.5	48.1	38.1	48.0	38.5	31.0
62.5	42.8	33.9	42.9	33.4	25.0
100	39.5	30.9	39.5	30.0	21.0

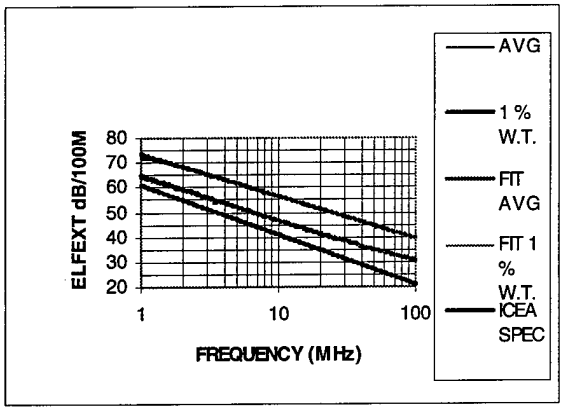

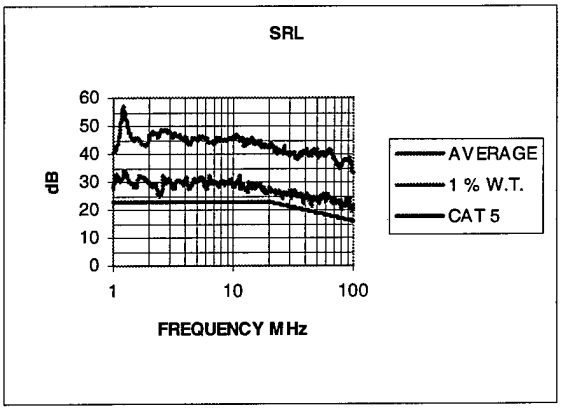

Impedance and SRL

The CAT 5 performance standard for minimum SRL is described by the following equation:

23 for 1 MHz to 20 MHz and

23 -10 * LOG (F(MHz)/20) for 20 to 100 MHz

The average SRL of the 24 AWG HPTP A/C cables is approximately 22 dB above this level, and the 1 % worse than SRL is approximately 6 dB above this level. CAT 5 requires that the characteristic impedance be between 85 and 115 ohms over the 1 to 100 MHz range. The average over the entire frequency range for the 24 AWG HPTP A/C cable was 104 ohms. The 1 % L.T. value was 98 ohms and the 1 % G.T. value was 109 ohms.

CHARACTERISTIC IMPEDANCE - OHM

Freq (MHz.)	*1% <*	*1 % >*	*AVG.*	*CAT 5 MIN*	*CAT 5 MAX*
1.	100	115	107	85	115
4.	97	110	104	85	115
8.	96	108	102	85	115
10.	96	108	102	85	115
16.	97	107	102	85	115
20.	97	106	103	85	115
25.	97	106	103	85	115
31.5	98	107	103	85	115
62.5	98	108	104	85	115
100.	98	109	104	85	115

SRL - dB

Freq (MHz.)	*AVG.*	*1 % W.T.*	*CAT 5 MIN*
1.	40.43	27.93	23
4.	45.81	31.31	23
8.	45.02	30.34	23
10.	46.20	29.07	23
16.	44.21	29.48	23
20.	43.03	28.11	23
25.	40.49	25.68	22.0
31.5	39.89	25.18	21.0
62.5	40.40	24.17	18.1
100.	33.64	21.78	16.0

Field Test Results

Several field tests with major Telco's in Canada and the U S A. are on going. In the trials the HPTP cable transmission performance was measured before and after installation. The effects of physical handling during installation, the use of connectors and splices were evaluated. The outcome was as follows:

-The performance of the cable was not changed due to standard installation practices.

-The attenuation was not effected by industry standard cable connectors.

-Crosstalk can be degraded if pair twist lays are not maintained.

-Splices may cause a discontinuity that can effect the impedance of a pair. The effect can be minimized by maintaining twist lays. Impedance discontinuities caused by splices had no noticeable effect on attenuation.

CONCLUSION

HPTP Cables provide a minimum 20 dB improvement in noise rejection and higher immunity to outside interference compared to conventional outside plant cables. HPTP Cables can be installed using generally the same practices as conventional outside plant cables, taking note to observe Category 5 cabling installation guidelines. Deployment of HPTP Cable between the fiber Node and Subscriber, with loop distances up to 1 km (3,300 feet) will allow for an evolution from POTS to Broadband services.

Biography

Jon Green received his B.Eng degree in electrical engineering from McGill University in 1981. Jon has worked in the telecommunications cable industry for 17 years, initially in the Research and Development group of Northern Telecom and currently in the Technology group of Norcom/CDT. He is currently senior engineer responsible for the in-building cable portfolio, electrical test methods and HPTP development.

FSAN INITIATIVE: ACCELERATING THE INTRODUCTION OF BROADBAND SERVICES TO THE HOME

Chris Taylor

Nortel Technology
Ottawa, Canada

Abstract

Three years ago a number of telecommunication network operators along with a leading group of equipment vendors came together to create requirement specifications for cost-effective access systems supporting a full range of narrowband and broadband services. This group of network operators represents about a third (310 million) of the one billion telephone lines worldwide. The main objective of this group, supported by the equipment vendors, is to accelerate the introduction of broadband services into the public network by developing a common approach to access networks. This has been achieved by specifying generic broadband network architecture and equipment requirements to obtain maximum worldwide volume through a common specification. One of the major challenges in FSAN has been to integrate the diverse requirements for broadband transport of various operators into a single specification. The hybrid fiber/copper architecture has been key in enabling system elements to be the same across several network variants. The activities of this organization have been grouped into three phases; currently phase three is being executed. In late 1998 and 1999 many trials are hoped to been seen employing the FSAN common architecture. FSAN is not a standard-ization activity. Instead, FSAN, is incorporating applicable standards where they exist, and members of FSAN are introducing their specifications into appropriate standards bodies. The hope is that through the achievement of the set of requirement specifications that the deployment of cost-effective full service access networks will be significantly advanced.

Biography

Chris Taylor graduated from the University of Ottawa with both a Bachelor's and Master's degrees in Engineering, 1989 and 1993 respectively. He has also obtained his Masters in Business Administration from the University of Ottawa in 1996. Chris began at Nortel in 1993 working largely in the fiber optic and electrical interconnect areas to support the development of Nortel products. For the past few years he has been engaged in the design and development of access network solutions, specifically in the ADSL, VDSL and DPL areas. He is currently a Manager in the Network Compatibility Group.

Chris Taylor, P.Eng.
Network Compatibility
Nortel Labs - Ottawa
E-mail: ctaylor@nortel.ca
Phone: (613) 763-9188 (ESN 393)
Fax: (613) 765-2173 (ESN 395)

ADSL DEPLOYMENT FOR BROADBAND SERVICES TO THE HOME

Ron Stein

Paradyne Corporation
Largo, FL

Topic

The topic, which we consider to be crucial to the adoption and mass deployment of DSL high-speed technology, is SERVICES CREATION AND REVENUE GENERATION OPPORTUNITIES USING HIGH-SPEED TECHNOLOGIES.

Providing xDSL services is about more than supplying a high-speed transport system, it is about effectively identifying the opportunities for generating revenue. By understanding the different audiences and their needs, it is possible to exploit the potential to create and provision value-added services and applications.

Presentation Summary

Speed alone does not drive the market for emerging access services, user demand sets the pace. In many cases, a multi-tier model of services based on different bandwidths will meet the wide variety of user requirements, but the fact remains, there are underlying reasons for the need for speed. Understanding these factors will allow service providers to carefully target market segments and develop services that drive profitable revenue. It is not enough to offer access lines of varying speeds to provide differentiation, it is necessary to explore new markets and expand the scope of service offerings to increase market share and build revenues. We must not take for granted that faster is better, but we should examine the different requirements of commercial users, residential recreational and small office, home office users and provide services to meet those requirements at a price to meet their budget.

As a service provider there are two primary ways to benefit from the market demand, by offering high-speed transport for Internet connection or high-speed transport with a range of value added services. Both of these have the potential to generate profitable revenue, but only by providing a bundle of attractive, value-added services can service providers attract a wider customer base. This is particularly true for the home office and small business market segments, who typically does not have the time, budget or expertise to manage a communications system and complex software solutions. They need a simple, cost effective, easy to maintain infrastructure that is reliable, and this is a major opportunity for service providers. Even carriers that are focused on providing wholesale copper will benefit from this understanding of the market.

Key Benefits The Presentation Would Offer

- Identify lucrative market segments
- Recognize market demand and accelerate market entry
- Recognize service opportunities which generate revenue
- Increase customer satisfaction
- Evaluate the practical considerations of service deployment

Biography

Ron Stein is Director of Marketing for Paradyne's Hotwire Digital Subscriber Line (DSL) and Multiple Virtual Lines (MVL) Products Division. In this role he is responsible for all Hotwire strategic and tactical marketing relationships and initiatives. With over twenty years of experience in engineering, business development, sales and marketing, Ron brings an extensive background in telephony, data communications and emerging collaborative technologies to Paradyne.

Ron brings a wide range of professional experiences to this role including previous assignments at Motorola, Racal-Datacom and VideoServer. His strategic guidance and insight into the practical application of technology have allowed him to successfully manage a number of diverse work groups and partnerships.

Ron holds a degree in electrical engineering from the University of Florida, has taught courses on Internet business strategies at Oglethorpe University in Atlanta, and is a frequent speaker at industry conferences and forums. Ron is a member of the Institute of Electrical and Electronics Engineers (IEEE) and the Central Florida Speakers Association.

Ron Stein
Director of DSL Marketing
Paradyne Corporation
8545 126th Avenue North
Largo, FL 33773
Tel: 813 530 2504
Fax: 813 530 2318
Email: Rstein@paradyne.com

COMBINATION FURNACE FOR DRAWING LARGE OPTICAL FIBRE PREFORMS AT HIGH SPEED

Markku Rajala*, Kai Asikkala*, Marko Mäkinen, Taneli Tuurnala** and Erkki Peltoluhta****

***ABR Innova Oy, Helsinki, Finland**
****Nextrom Oy, Vantaa, Finland**

ABSTRACT

Economical fabrication of optical fibre requires large preforms drawn into fibre at high speed. This can only be achieved if the drawing furnace meets the required specifications.

The first specification is that the furnace hot zone is both wide and long enough. The long hot zone is beneficial for decreasing the maximum furnace temperature needed to achieve the specified drawing tension. This not only increases the heating element lifetime but also decreases carbon sublimation from the graphite element thus decreasing aerosol and particle formation.

The second specification is a uniform gas flow inside the drawing furnace. Ideally the most stable drawing conditions are achieved when the fibre and gas velocities are equal.

The third specification is the slow radiative cooling of the fibre after it passes the hot zone which can be achieved either by passing the fibre through a tube which scatters the radiated power back to the fibre surface or by passing the fibre through a heated tube furnace.

This paper describes the parameters related to furnace design and relationship between furnace parameters such as temperature, drawing tension and speed and preform diameter.

The required furnaces parameters can be realised by either conductive or inductive heating of the graphite element. Induction heating is discussed in detail, because it provides simple furnace construction, good power efficiency, rapid furnace heating and excellent degree of freedom to construct the top gas supply system and the exit tube/furnace.

INTRODUCTION

Optical fibre formation in the drawing furnace depends on the furnace hot zone length and temperature, drawing tension and speed and preform size. This relationship can be approximated by an analogue to the basic formula for glass viscosity measurement using the fibre elongation method. When modified to fibre drawing the equation is:

$$\eta \propto \frac{\sigma \cdot l}{A \cdot v} \qquad (1)$$

where
η is viscosity
σ is drawing tension
l is hot zone length
A is preform area at hot zone
V is the drawing speed

With fused silica the temperature - viscosity relationship between 1600 to 2500°C is

$$\log\eta = -6.24 + (2.69 \times 10^4)/T \qquad (2)$$

where T is the absolute temperature

In optical fibre drawing the drawing tension should be fairly constant (and low enough) and the glass composition cannot be changed radically (so viscosity is close to the viscosity of silica). Thus in order to increase the drawing speed and preform size we have to play mainly with the hot zone length and furnace temperature.

Temperature increase will enhance carbon sublimation from the graphite surface and also increase SiO sublimation from the preform surface. These combined sublimation's will lead

to a situation which can generate various C-Si-O containing substances inside the furnace, at the furnace exit, on preform/fibre surface and both on and in the graphite element. A typical substance is SiC, which can cause problems both with fibre strength and with element lifetime. Thus increasing the furnace temperature should be minimised, if the hot zone length can be increased.

When the drawing speed increases it will be very important to have a stable drawing process, i.e. a drawing process which will not give fluctuations to the fibre diameter. The stability of the drawing process depends on several factors, two very important ones being the convective and radiative cooling.

The drawing process is divided into the neck-down and draw-down regions separately and mostly the draw-down region is considered in stability.

In this study the fibre cooling is divided into convective and radiative cooling. First the paper studies the stability of the process as a function of the convective cooling. This is done by introducing the Stanton number

$$\mathrm{St} = \frac{0{,}4 k_a L}{v_a \rho c_p v_0^{2/3} a_0^{5/3}} \qquad (3)$$

where
k_a is the thermal conductivity of gas
L is the length of the draw-down region
v_a is the gas velocity (compared to fibre
ρ is the gas density
c_p is the gas heat capacity
v_0 is the fibre velocity in the beginning of the draw-down region
a_0 is the fibre diameter in the beginning of the draw-down region

The drawing process is shown to be stable either at high Stanton numbers (> 0,017) or low draw-down ratios (<20). The draw down-ratio is $(a_0/a)^2$, where a_0 is the fibre diameter in the beginning of the draw-down region and a is the final fibre diameter. Thus with large preforms this becomes in practise too large (>100) for the process stability to be achieved by this way.

So stability is achieved by high Stanton numbers, which means (for large preforms and high drawing speeds) that

- the draw-down length L must be long (fibre cooled slowly)
- the gas velocity (with fibre surface as reference) should be low, which requires a downward draft of gas)
- gas should have high thermal conductivity

When radiative cooling is taken into account the region of stability is not monotonic, i.e. at a fixed draw-down ratio and Stanton number, radiative cooling first stabilises and then destabilises the fibre with increasing H. It was also noted that stable states of drawing would require lower radiative heat transfer coefficients that what would be the case in conventional fibre drawing.

Thus we are facing a dilemma: to have a stable drawing due to convection we would require a long draw-down area and to have a stable drawing due to radiative heat transfer we would require a short draw-down length.

If we look at the radiative heat transfer more carefully we note that the heat transfer is dependent on the coefficient H, but also on the temperature difference between the fibre and the far-field temperature seen by the fibre.

$$H = \frac{2L\varepsilon\sigma T_0^3}{v_0 \rho c_p a_0} \qquad (4)$$

$$q_r \propto H(\Phi_\infty^4 - \Phi^4) \qquad (5)$$

thus if we make the effective far-field temperature Φ_∞ close to the effective fibre temperature Φ we will depress the radiative heat transfer and overcome the stability problem with long draw-down lengths - and should end up with a stable drawing process.

The effective far-field temperature can be adjusted close to the fibre temperature by two ways:

- by having a heated extension tube where the temperature profile simulates the fibre temperature profile. This means that we

should have an approximately 300-500°C temperature gradient in the furnace.

- by having a reflecting tube, which would reflect most of the heat back to the fibre thus minimising the radiative heat transfer

We must also note that when the hot zone length and heating element diameter is increased, the thermal energy flow from the furnace is increased. This, together with the increased preform volume will increase the furnace power requirement. Thus it will both economical and easier engineering to design a drawing furnace working on inductive heating of graphite rather than on resistive heating.

INDUCTION HEATING OF THE GRAPHITE ELEMENT

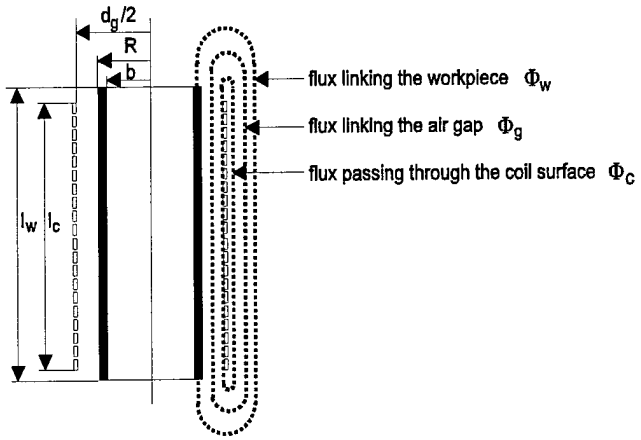

Figure 1. Schematic drawing of the configuration

The magnetic flux passes through the furnace components as shown in figure 1.

The parallel magnetic series can be transferred to an equivalent electronic serial circuit with the inclusion of the compensation capacitor.

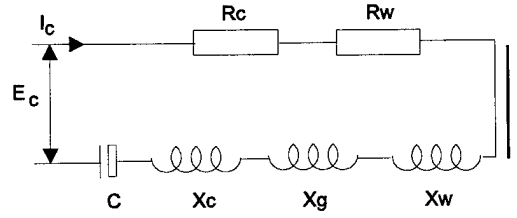

Figure 2. Equivalent circuit of the induction furnace. R refers to resistance, X to reactance and C to capacitance. The subsymbol c refers to coil, g to gap and w to work.

The coil is a single-layer winding, water-cooled to remove I^2R losses and the heat losses arriving from the workpiece.

The power loss in the element to be heated can be calculated from

$$P_w = \pi R^2 l H_s^2 \mu_r \mu_o 2\pi f p_{tube} \qquad (6)$$

P_w = power loss in the tube

R = tube outer radius

l = induction coil (tube) length

H_s = magnetic field strength

μ_r, μ_o = relative and absolute magnetic constants

f = frequency

p_{tube} = tube real power loss constant

$$p_{tube} + q_{tube} = \frac{2}{mR} \frac{\mathrm{Re}(I_0'(mR)) + j\,\mathrm{Im}(I_0'(mR))}{\mathrm{Re}(I_0(mR)) + j\,\mathrm{Im}(I_0(mR))} \times \frac{1 + \frac{B}{A} \frac{\mathrm{Re}(K_0'(mR)) + j\,\mathrm{Im}(K_0'(mR))}{\mathrm{Re}(I_0'(mR)) + j\,\mathrm{Im}(I_0'(mR))}}{1 + \frac{B}{A} \frac{\mathrm{Re}(K_0(mR)) + j\,\mathrm{Im}(K_0(mR))}{\mathrm{Re}(I_0(mR)) + j\,\mathrm{Im}(I_0(mR))}} \qquad (7)$$

where

$$\frac{B}{A} = -(2\ _r(\mathrm{Re}(I_0'(mb)) + j\,\mathrm{Im}(I_0'(mb))) - jmb(\mathrm{Re}(I_0(mb)) + j\,\mathrm{Im}(I_0(mb)))) / (2\ _r(\mathrm{Re}(K_0'(mb)) + j\,\mathrm{Im}(K_0'(mb))) - jmb(\mathrm{Re}(K_0(mb)) + j\,\mathrm{Im}(K_0(mb))))$$

I_0 is the modified Bessel function of the 0th kind

I_0' is the derivative of I_0

K_0 is another solution of the modified Bessel function, 0th order

K_0' is the derivative of K_0

b = tube inner radius

$$m = \frac{\sqrt{2}}{\delta}$$

δ = penetration depth, $\delta = 5000\sqrt{\frac{\rho(\Omega__)}{\mu_r f(\mathrm{Hz})}}\ cm$

FURNACE CONSTRUCTION

Based on the calculations from the equations shown previously the following furnace parameters were set:

- Total work power, P_w 30 kW
- Temperature of workpiece 2250 °C
- Work outer diameter, d_w 90 or 110 mm
- Work surface thickness, a_w 5 mm
- Work resistivity (@2300°C), ρ_w 15.5 μΩm
- Coil length, l_c 250 mm
- Coil inner diameter, d_c 170 mm
- Frequency, f 25 kHz
- Work relative permeability, μ_r 1
- Coil correction factor, k_r (assumed) 1.2
- Coil resistivity, ρ_c 0.033 μΩm (assuming the coil temperature to be 200°C)

The furnace was constructed from stainless steel. Concentrators and shields where used to focus the flux to the heating element.

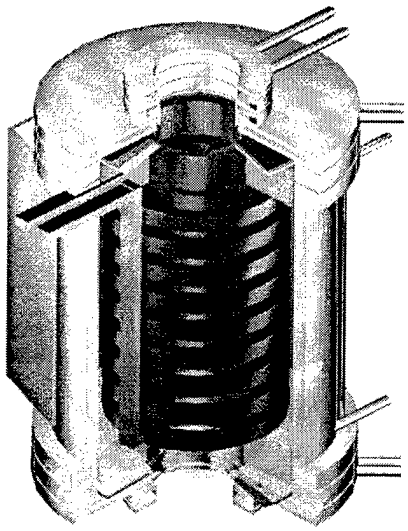

Figure 3. Inductively heated graphite furnace construction

A commercially available power supply unit capable of transmitting 44 kW power to the workpiece at 15-30 kHz frequency was used. This power unit uses solid state IGBT technology and self-tunes itself to the load with a pre-selected transformer ratio and compensation capacitance. The values obtained from the theoretical calculations were successfully used in pre-setting these values.

TEST RUNS

During the tests and additional, 1 m long extension tube was placed immediately below the fibre exit from the induction furnace to stabilise gas flows and fibre diameter during the tests. The tests were carried with 80 mm graphite element inner diameter.

The test results are shown in figure 4. It can be seen that increasing the furnace power (element temperature) rapidly decreases the fibre tension as expected and low fibre tensions can be achieved with moderate furnace power.

Most of the furnace power is actually consumed in heat losses through the insulation. When the preform diameter was decreased 23% (preform area decreased 40%), same fibre tension was achieved with only 5% less furnace power. Thus in order to decrease the furnace power it is essential to know the heat losses through different parts of the furnace.

The heat losses of the furnace were calculated by measuring the cooling water flows and input/output temperatures separately for the top and bottom plates, upper gas iris, furnace body, induction coil and power supply unit. Typical heat losses for a 35 kW furnace output power are shown in figure 5.

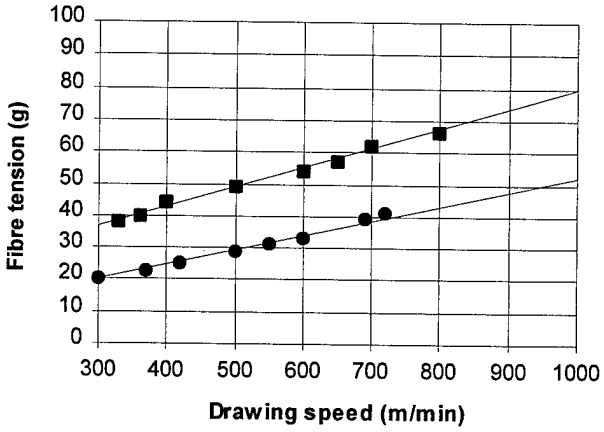

Figure 4. Fibre tension vs. drawing speed with two furnace input powers: 85% (■) and 90% (●).

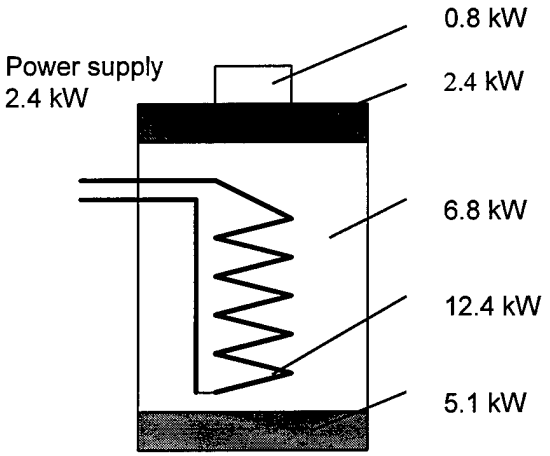

Figure 5. Typical heat losses from the induction heated graphite drawing furnace with 35 kW power supply output.

CONCLUSIONS

As conclusion, we can summarise the requirements for high-speed drawing of large preforms following:

- the furnace should have long hot zone
- the draw-down length L must be long (fibre cooled slowly)
- the gas velocity (with fibre surface as reference) should be low, which requires a downward draft of gas)
- gas should have high thermal conductivity
- radiative cooling of the fibre should be low, when fiber exits the hot zone

Inductively heated graphite furnace for optical fibre drawing is an attractive solutions especially when the preform size and hot zone length are increased. The basic induction heating theory can been used in calculating the power coupling in the fairly simple circular geometry of the fibre drawing furnace even if the heating element is not uniform.

Current IGBT power supplies make the tuning of the induction circuit extremely easy and theoretical calculations based on the workpiece and coil geometry (reactance and resistance) estimate the required compensation capacitance with good accuracy.

Test runs show that low drawing tensions and high drawing speeds can be achieved with moderate furnace power. The main requirement of the furnace power comes from the furnace heat losses through the insulation. Theoretical calculations show that the induction coil and heating element distance can still be increased without decreasing the power coupling too much and thus the insulation thickness can be increased to reduce the furnace power requirement.

ACKNOWLEDGEMENTS

Technology Development Centre (TEKES) is acknowledged for supporting this work. We are grateful to Ms. Anu Konkarikoski and Mr. Mika Immonen for their assistance during the test runs.

REFERENCES

1) F.T. Geyling & G.M. Homsy, Extensional instabilities of the glass fibre drawing process, Glass Technology, Vol. 21, No.2, April 1980, pp. 95-102

2) E.J.Davies, Conduction and induction heating, Peter Peregrinus Ltd, London, UK, 1990

AUTHORS

Markku Rajala received his M.Sc degree in physics from Tampere University of Technology, Finland, in 1984. He has worked with optical fiber manufacturing and ceramic materials and is currently general manager of ABR Innova Oy, a company specialized in high temperature applications.

Kai Asikkala is currently working as innovation manager of ABR Innova Oy and is specialized in design and R&D.

Marko Mäkinen received his M.Sc. degree in mechanical engineering and control engineering from Lappeenranta University of Technology, Finland, in 1990. He is working currently as team manager for Nextrom Oy and is in charge of the development of fiber drawing equipment.

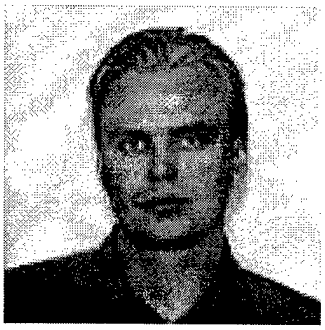

Taneli Tuurnala received his M.Sc. degree in physics from Helsinki University of Technology, Finland, in 1996. He has worked as process specialist and currently as project manager for optical fiber drawing equipment at Nextrom Oy.

Erkki Peltoluhta is working as a process specialist for Nextrom Oy. He joined the company in 1980, and since that has been engaged with the development of optical fiber manufacturing systems.

DESIGN OF RIBBON AERIAL CABLE STRANDED BY COPPER-CLADDED STEEL WIRE

S.C. Park, J.C. Cho, Y.I. Lee, H.J. Kang

Taihan Electric Wire Co., Ltd. Anyang-city, Kyungki-do, Korea

ABSTRACT

The application of metal-free self supporting aerial cable in power line network has been substantially increased during the last few years. But basically most metal-free materials such as plastic tube, aramid yarn and fiber reinforced plastic are expensive. Therefore, in order to satisfy the current tendency and design a economic cable, we try to make two kinds of compact new metallic aerial cables using of 48-fiber ribbon into central stainless tube with copper layer, having a strong resistance against lightning, although these cables consist of metallic element. This paper shows a new aerial cable to be designed for the central stainless tube with thin copper layer has excellent characteristics in comparison with the conventional metal-free aerial cable and optical ground wire.

INTRODUCTION

As the Fiber To The Home(FTTH) systems are being deployed, the aerial cables have become desirable due to low installation cost and easy maintenance. Thus, it is necessary to develop several kinds of economic and light aerial cables namely, all dielectric self supporting, 8-figure self supporting, OPGW and so forth. We have been taken into account metallic aerial cable instead of using expensive dielectric material. One construction is stranded by copper-cladded steel wires over the stainless tube and jacketed by XLPE(Cross-Linked Polyethylene) sheath. The other type consists of two layers of stranded wires with copper-cladded steel wires and Al alloys. The copper-cladded steel wire has better conductivity than that of aluminium-cladded steel wire. So, we can be able to decrease the cross-section of aerial cable and overall cable diameter. In addition, we consider the mass splicing efficiency by using of 8-fiber ribbon into stainless tube. The another focus of a newly developed cable will be on establishment of the long term reliability of the optical fibers using stainless tube with thin copper layer against fault current. The new aerial cable is conducted to evaluate its performance behavior in accordance with the electrical, mechanical and optical characteristics. Through the results of various investigations, we will describe the concepts of design and the characteristics of using of copper-cladded steel wire.

THEORY AND CABLE DESIGN

Cable Design

Fig. 1 shows the structure of 48-fiber

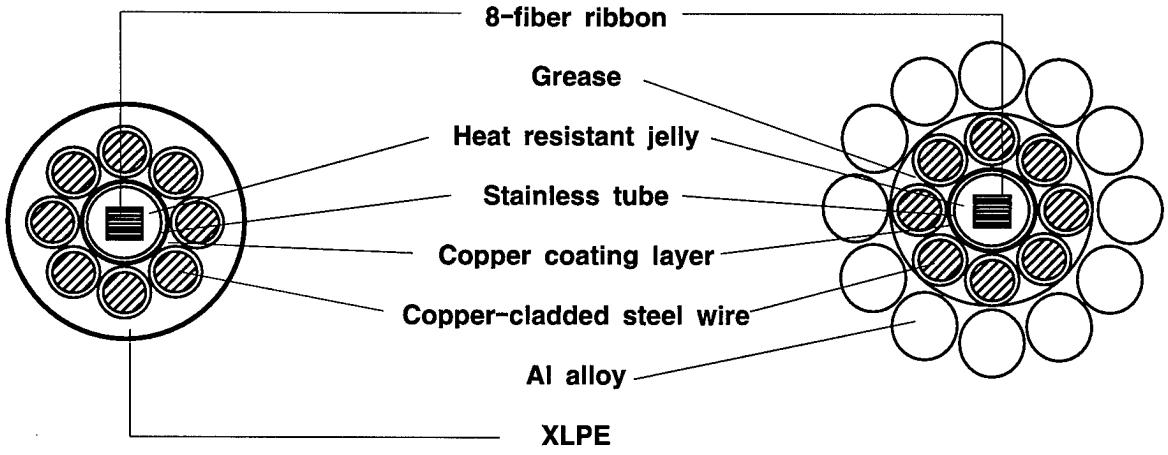

(a) Single layer type (b) Double layer type

[Fig. 1] Cross-section of two proposed cables

Items	Unit	Single layer	Double layer
Diameter of optical unit	mm	5.0	5.0
Overall diameter	mm	13.4	19.4
First wire type	-	copper-cladded steel	copper-cladded steel
No. of 1st wires	EA	ϕ 3.2mm×8	ϕ 3.2mm×8
Second wire type	-	-	Al alloy
No. of 2nd wires	EA	-	ϕ 4.0mm×12
Cross-section area	mm^2	60	220
Ultimated tensile strength	KN	70	90
Conductivity(Cu/Al alloy)	%	40	40 / 60
Sheath material	-	XLPE	-

[Table 1] Structure of aerial cable

aerial cable with the central stainless tube. The inner/outer diameter of central tube containing symmetrical 6-stack of 8-fiber thin ribbon is 4.5/4.9mm respectively. In order to give heat resistance to the optical fibers and physical contact between stainless inner tube wall and fiber, a high heat resistant jelly is filled in tube. The stainless tube is made in forming a stainless tape with thin copper layer and welding by a laser beam. And then, the copper-cladded steel wires and aluminium alloys are stranded around the stainless tube. Moreover, taking corrosion into consideration, the spaces between copper-cladded steel wires are filled by conductor protection with grease to give a corrosion resistance. Table 1 describes the main characteristics of the two proposed cable. Nevertheless, as the stainless tube has a merit of minimum dimensions to contain a desired number of fibers, we use the stainless tube with thin copper layer to be enhanced the heat resistant characteristic. In addition, the copper-cladded steel wires prevent in

duplicate conductance longitudinally superior to conventional aluminium-cladded steel wire against fault current. In case of single layer type, the XLPE layer provides reduction of inward heat penetration as well as mechanical strength. The double layer construction consists of a copper-cladded steel wires serving not only on tension elements but also on reduction of cable diameter and an outer layer of Al alloys serving mainly as electrical conductions.

Theoretical analysis

It is very important to evaluate the electrical test such as short circuit current because these new developed aerial cables are used in adjacent power lines. When a fault occurs in power lines or a lightning strike on the cable, a large amount of current may flow in the aerial cable. The short circuit current can be obtained using equation (1).

$$Im = \sqrt{\frac{C \cdot \log_e\left(\frac{\alpha \cdot \theta + 1}{\alpha \cdot \theta_0 + 1}\right)}{t \cdot \alpha \cdot Rdc(T) \times 10^{-5}}} \quad \cdots\cdots\cdots(1)$$

where,

Im	: short-circuit current
C	: heat mass (J/km · ℃)
α	: coefficient of resistance (/℃)
θ	: maximum temperature of cable during the short circuit (℃)
θ_0	: temperature of cable before short circuit (℃)
t	: duration time (sec)
Rdc(T)	: resistance at θ_0℃ (Ω/km)

The calculated values of short circuit current capacity are 64KA^2 · s and 617KA^2 · s respectively in 60mm^2 and 220mm^2 aerial cable at the same 40% conductivity. Considering the tensile strength of aerial cable for long-span and conductivity, we can design new developed aerial cables with a decreasing small diameter about 25% compared with that of conventional cable by using the copper-cladded steel wire. Also, the aerial cable stranded by copper-cladded steel wire withstands higher tensile strength than conventional cable stranded by aluminium-cladded steel wire at the same diameter and conductivity. Fig. 2 shows the relation of tensile strength versus conductivity about aluminium-cladded steel wire and copper-cladded steel wire at the same cable diameter. The tensile strength of the copper-cladded steel wire is about 40% stronger than that of aluminium-cladded steel wire. As a result, we can achieve the effect of reduction of overall cable diameter.

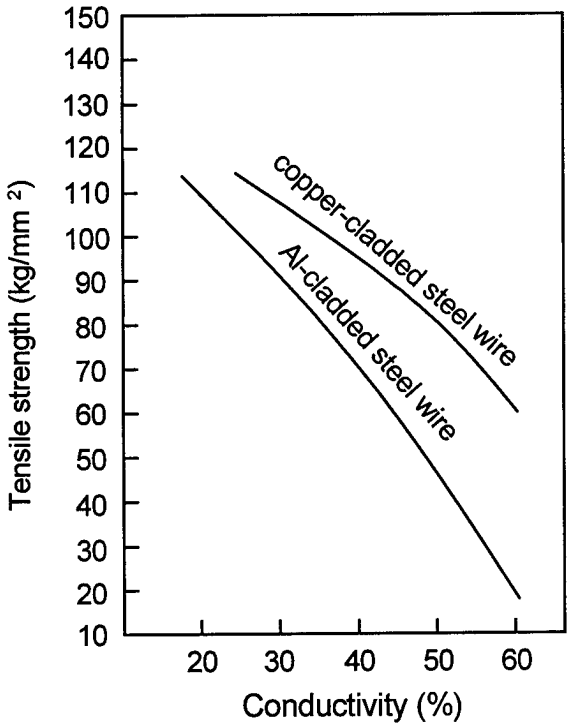

[Fig. 2] Comparison of tensile strength against conductivity

Short circuit test

In order to investigate the characteristics of single layer and double layer type in

response to a simulated short circuit current during a fault, we used a short-current generator to apply an instantaneous large current to the cable. Fig. 3 gives the increasing current intensity versus short circuit time for two kinds of cable type. The test current was applied to the cable according to the duration time. At that time, the temperature of the cable was increased up to 200℃. It was shown that both single and double layer type had a satisfactory heat resistant property. Moreover, no significant attenuation increase and mechanical damage of the cable element was observed.

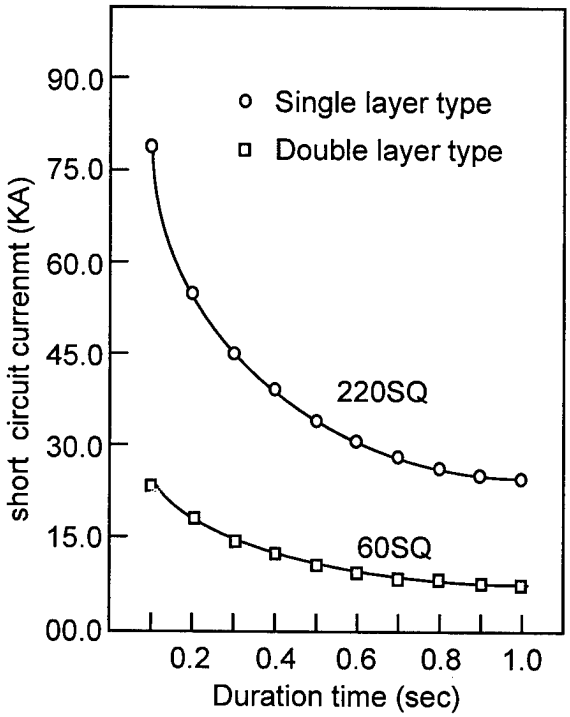

[Fig. 3] Relation between short circuit current and duration time

Tensile Test

The outer strand wires are significant element to the cable strength. Also, in order to minimize cable weight, the copper-cladded steel wire that will meet all the electrical and mechanical properties should be selected. The tensile performance of the cable was tested, and the changes in transmission loss and fiber strain that caused by application of tensile force were measured. Fig. 4 shows a plot of cable strain and fiber strain versus cable tension. There was no change in optical attenuation up to 50KN. At that time, the fiber strain reached up to 0.16% in single layer aerial cable. And, in case of double layer cable, the fiber strain has stable less than 0.12%.

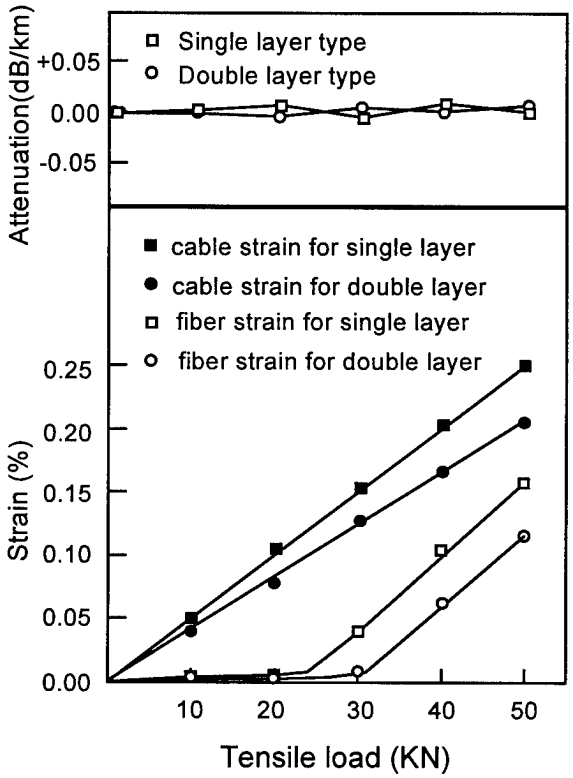

[Fig. 4] Attenuation and fiber strain versus tensile strength

Temperature Cycling Test

The transmission loss stability in the wide range temperature was experimentally investigated for stainless tube unit. The ribbon fibers in a 500m stainless tube sample were spliced in order to make a 2-km length sample. The range of temperature test from -30℃ to 100℃ was determined. Such conditions can lead to

degradation especially of plastic material. But, new aerial cable with stainless tube is less sensitive to temperature change in comparison to conventional aerial cable, because the temperature expansion coefficient of stainless tube is low. As a result, the change in attenuation at λ =1550nm was not more than 0.05dB/km as shown in Fig. 5.

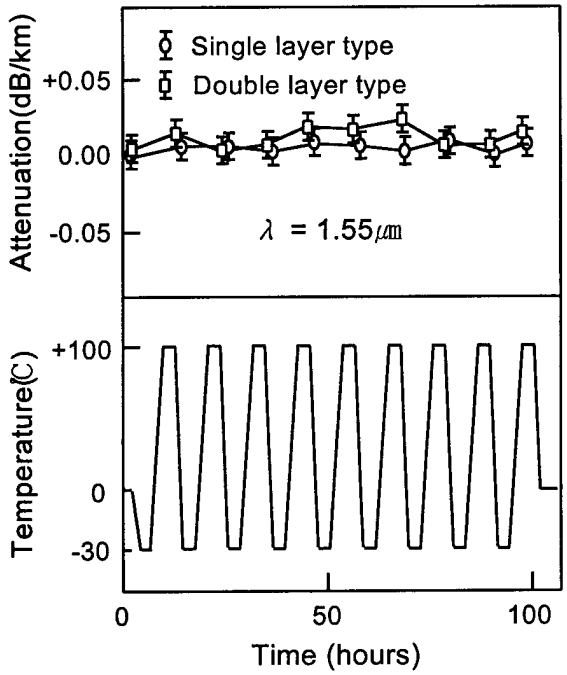

[Fig. 5] Temperature cycling test

Mechanical Test

Other various tests of the new aerial cable for practical use were carried out such as crushing, tensile load, vibration, twist, bend and squeezing test. It was confirmed that the new aerial cable has good characteristics equal to those of conventional OPGW or metal-free self supporting aerial cable as shown in Table 2.

CONCLUSION

The application of ribbon aerial cable for power utilities and pole has been carefully investigated. Based on metallic cable design, it was confirmed that both new developed ribbon aerial cables using stainless steel tube with thin copper layer were satisfied with the requirements for use of power and conventional metal-free self supporting cable lines. Especially, according to the various tests, we proved that the two kinds of aerial cables were capable of withstanding a high electrical current for a given duration and met the fault current rating without exceeding the design temperature. It was clarified that the proposed aerial cables have good mechanical properties less than 0.05dB/km enough to ensure optical reliability through tensile performance and other mechanical tests. The stainless with thin copper layer used for central tube had a excellent heat-resistance property to restrain inward heat flow compared to conventional pure stainless tube or aluminium, and the main advantages using of copper-cladded steel wire are good

Items	Test Condition	Results (dB)
Crush	• Plate width : 50×50mm • Force : 1000kg	< 0.05
Vibration	• Sample length : 30m • Tension : UTS 20% • Frequency : 10~55Hz	< 0.05
Twist	• Sample length : 30m • Tension : UTS 20% • 5 cycles each ±360°	< 0.05
Bend	• Bending diameter : 40,80,120mm • Bending angle : 180°	< 0.05
Squeeze	• Sample length : 20m • Tension : UTS 20% • Pulley diameter : ϕ 450mm	< 0.05

[Table 2] Various mechanical test

ground efficiency due to high conductivity, strong tensile strength and cost down effect without using of expensive metal-free materials. Therefore, the new ribbon aerial cable using stainless tube with thin copper layer and copper-cladded steel wire will anticipate to apply for the field in future.

REFERENCES

1. M. Amamiya, A. Ozawa, Y. Kimura "Development of Multicore OPGW with Tape-Coated Fibers" SEI Technical Review, Number 27, 1988

2. I. Matsubara, Y. Kitayama, S. Nishiyama, T. Kikuta, "Development of large-capacity composite fiber-optic ground wire", Conference of the Institute of Electric Engineers of Japan, 1065, 1986.

3. ASTM Designation B 452-88 "Standard Specification for Copper-Clad Steel Wire for Electronic Application"

4. ASTM Designation B 227-88 "Standard Specification for Hard-Drawn Copper-Clad Steel Wire"

BIOGRAPHIES

Sang-cheol, PARK

Taihan Electric Wire Co., Ltd. Korea

S.C. PARK received his B.A. degree from A-ju University in 1994. He joined Taihan Electric Wire Co., Ltd. and has been engaged in engineering department of optical fiber. Now he is a engineer of Fiber Optics Engineering Department.

Jin-cheol, CHO

Taihan Electric Wire Co., Ltd. Korea

J.C. CHO received his B.A. degree from Kwangun University in 1992. He joined Taihan Electric Wire Co., Ltd. and has been engaged in engineering department of optical fiber. Now he is a assistant manager of Fiber Optics Engineering Department.

Young-ik, LEE

Taihan Electric Wire Co., Ltd. Korea

Y.I. LEE received his M.S. degree from Yonsei University in 1981. He joined Taihan Electric Wire Co., Ltd. and has been engaged in engineering department of optical fiber. Now he is a assistant general manager of Fiber Optics Engineering Department, and a member of SG. 6, ITU-T sub-committee of Korea.

Hee-jeon, KANG

Taihan Electric Wire Co., Ltd. Korea

H.J. KANG received his B.A. degree from Hanyang University in 1979. He joined Taihan Electric Wire Co., Ltd. and has been engaged in engineering department of optical fiber. Now he is a general manager of Fiber Optics Engineering Department and a member of SG. 6, ITU-T sub-committee of Korea.

UV CURABLE MATERIALS WITH HIGH ADHESION TO COPPER

Masahito Mase, Hiroshi Abe, Zen Komiya, Takashi Ukachi

Tsukuba Research Laboratory, JSR Corporation, Tsukuba Japan

ABSTRACT

Adhesion properties of UV curable urethane acrylates were studied.
Relationship between surface profiles of copper plates and adhesion was investigated. The roughness of the copper surface had little effect on the adhesion whereas the presence of the oxidized copper on the surface showed increase in adhesion.
Some adhesion promoters were introduced to the coatings and the adhesion to the copper was evaluated. Among the adhesion promoters, γ-mercaptopropyltrimethoxysilane (MPTMS) was most effective.
It was also demonstrated that the viscoelastic property of the cured coating played an important role to the adhesion. Namely, as the increase in peeling speed, the coatings gave enhanced adhesion, when the coatings had low Young's modulus and relatively low glass transition temperature (Tg). In contrast, the one with high modulus and high Tg behaved differently. This behavior is explained by loss tangent (tanδ) curves of the coatings.

INTRODUCTION

Recent expansion of UV curable coatings to fiber optic application requires various specialized characteristics to the coatings. A number of different structures of cables for FTTH applications have been investigated. One of the newly evolved requirements for the coatings is high adhesion to metallic materials, especially to copper. Because it is used as a tension member of the cable and coated with the coatings. No investigation was reported on the control of the adhesion to copper of the coatings, although the adhesion of the coatings to glass has been widely studied.[1)]
In this paper, several factors which affect the adhesion of UV curable coatings to copper were evaluated. Controlling these factors, we can design highly adhesive coatings to copper.

EXPERIMENTS

1. Materials

1) Monomers

Acrylate monomers having glass transition temperatures (Tgs) of their corresponding homopolymers ranging from -3 °C to 175 °C were used.

2) Urethane acrylate oligomers

Polyether based urethane acrylate oligomer was prepared from diisocyanate and 2-hydroxyethyl acrylate and polyetherdiol.

2. Measurement

1) X-ray photoelectron spectroscopy

The surface of the copper plate was analyzed by using the X-ray photoelectron spectroscopy (XPS) to evaluate the amount of oxidized copper on the surface. The XPS analysis was made by using a take-off angle at 15 degree, which captures photoelectrons released from about 3 nm depth.

2) Surface roughness

Surface roughness of the copper plate was evaluated by using Dektak 3030. Dektak 3030 is a surface profile measurement system using a stylus.

3) Mechanical property

Young's moduli at 23 °C of films were measured by a standard method[2)] using films cured at UV dose of 1 J/cm^2 under ambient atmosphere with

about 200 μm thickness. The modulus was defined by 2.5 %-secant modulus.
Viscoelastic property was evaluated by using a viscoelastometer. The stretching frequency was 3.5 Hz. The temperature was raised from -100 °C to 200 °C at a ramping rate of 2 °C/min. Tg of cured coating was defined as the temperature at which loss tangent (tanδ) showed the maximum.

4) Peel strength

The coatings were drawn down on copper plates with a thickness of 100 μm and cured at UV dose of 0.3 J/cm^2 under nitrogen atmosphere. The cured coatings were conditioned for 24 hours at 23 °C, 50 % R.H. The resultant cured coating was cut into a strip in a size of 1 cm x 10 cm. The adhesion strength between the coating and the copper plate was evaluated by measuring the 90 degree peel strength at a peeling rate of 5 ~ 300 mm/min.

RESULTS AND DISCUSSION

Effect of surface profile to adhesion property

The adhesion of coating was evaluated using copper plate instead of copper wire. The plate surface was conditioned by four different ways.

1. No treatment : the copper plate was used as received.
2. Etched : the plate was treated with ammonium persulfate and sulfuric acid aqueous solution.
3. Burned : the etched plate was passed through a Bunsen burner flame.
4. Heated : the etched plate was placed in a muffle furnace at 800 °C for 45 minutes.

The conventional UV curable coating, S-1, was drawn on the plate and cured. The adhesion was evaluated by 90 degree peel strength. The results are summarized in Table 1. Etching did not affect peel strength, but burned or heated plates showed higher peel strength.

Table 1. Peel strength of coating (S-1) from copper plate

peel strength (g/cm)			
No treatment	Etched	Burned	Heated
10	9	18	18

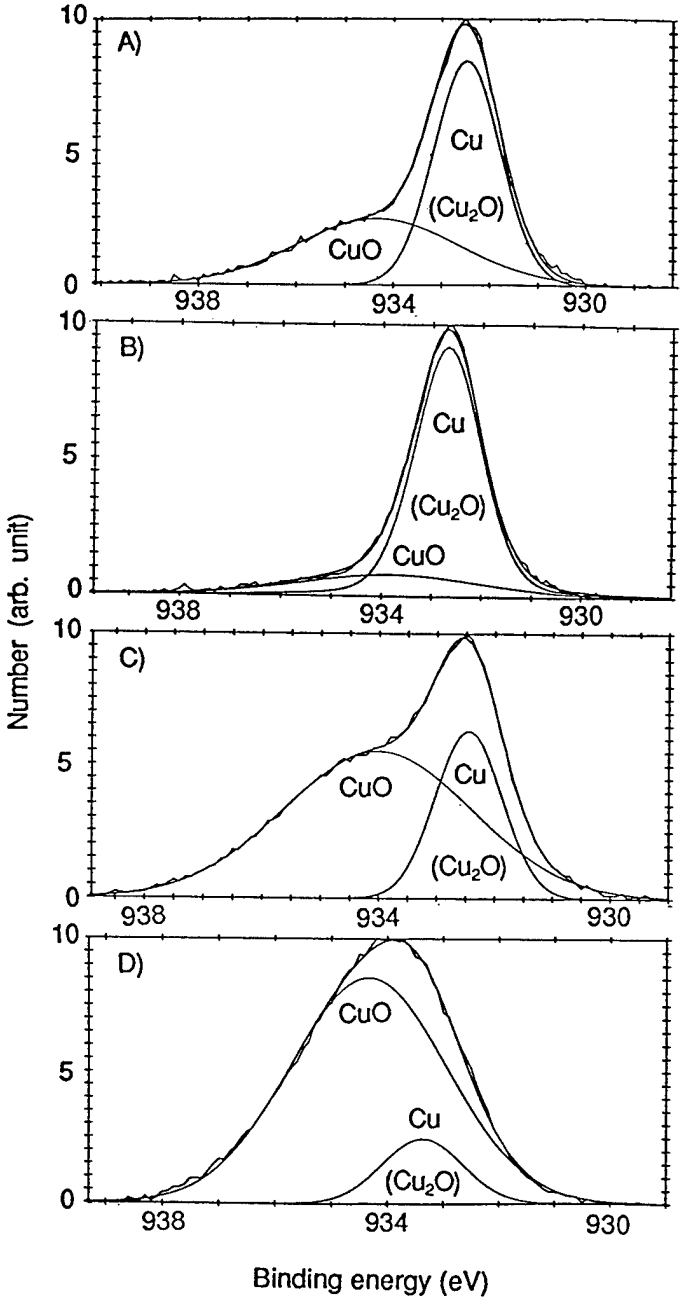

Figure 1. XPS spectra of the surface of the copper plate conditioned by the methods of A): no treatment, B): etched, C): burned by using a Bunsen burner flame, D): heated in a muffle furnace at 800°C for 45 minutes. Horizontal axis indicates binding energy and vertical axis correlates numbers of photoelectrons.

The surface of copper plates conditioned by the methods mentioned above was analyzed by XPS. Figure 1A shows XPS spectrum of the copper surface with no treatment. The spectrum was reduced to two peaks of which binding energies are about 932 eV and 934 eV. The peak at 932 eV is attributed to Cu and Cu_2O. The other peak correlates to CuO. Although Cu and Cu^I are not distinguishable, the oxidation states of the surface can be roughly estimated. Figure 1B clearly shows the etching process removed oxidized copper from the surface. The flame and furnace treatments of etched surface increased the amount of copper oxide dramatically as shown in Figures 1C and 1D. It should be noted that the amount of copper oxide of flame treated surface changed point to point, perhaps because of irregularity of the flame treatment. The XPS results indicate that the oxidation state of the copper correlates to the adhesion.

There was another possibility such as surface roughness. If the flame and furnace treatments made the surface rough, it might give higher adhesion. To confirm this, the surface roughness was evaluated. The results are in Figure 2. From the comparison of Figures 2A and 2B, etching increased the surface roughness. The surface profiles of the plates treated with flame and furnace are shown in Figures 2C and 2D showing comparable roughness to the etched surface. The XPS analysis and surface profile data indicate that the increase of the adhesion to copper plate was due to the amount of oxidized copper at surface not to the roughness.

Effect of adhesion promoters to adhesion property

Compounds having imidazole, mercapto, amino or phosphate groups are well known as adhesion promoter, because of their coordinating ability. We evaluated the effect of these compounds. The results are summarized in Table 2. The most effective one was mercaptosilane, γ-mercapto-propyltrimethoxysilane (MPTMS). The amino silane and phosphate enhanced in certain extent. However, imidazole and methacryloxy silane did not show remarkable effect on the adhesion.

In the case of glass, addition of MPTMS to the coating also enhanced adhesion due to the Si-O-Si bond formation between MPTMS and glass. However, it is not the case for the copper adhesion since other silane derivatives such as amino and methacryloxy silane gave moderate adhesion. The effectiveness of MPTMS could be due to the presence of mercapto group.

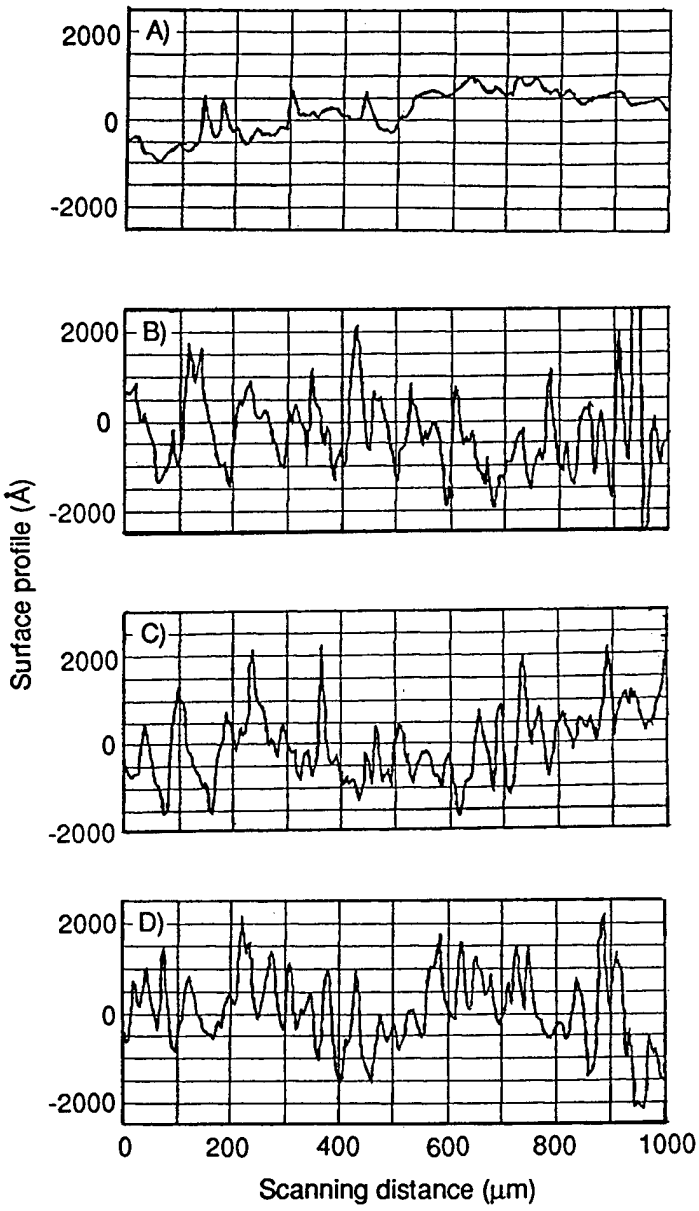

Figure 2. Surface roughness of the copper plates conditioned by the methods of A): untreated, B): etched, C): burned by using a Bunsen burner flame, D): heated in a muffle furnace at 800°C for 45 minutes.

Table 2 . Effect of adhesion promoters for adhesion to copper

Functional group of adhesion promoters	None	mercapto-silane	imidazole-silane	amino-silane	methacryloxy-silane	phosphate
Peel strength (g/cm)	10	73	12	20	9	40

1 wt% of adhesion promoters were added to the coating (S-1).

Effect of monomers to adhesion property

We have already found that the addition of high Tg monomers to the coating increased the adhesion to glass.[1] We thus applied this technique to increase the adhesion to copper. Table 3 shows several formulations with different Tgs controlled by employing monomers C, D, and E.

Table 3. Formulations of coatings with different Tgs

	S-2	S-3	S-4
Oligomer	69	69	69
Acrylate monomer			
Monomer A Tg= 75 °C	5	5	5
Monomer B Tg=175 °C	6	6	6
Monomer C Tg= -3 °C	10	5	5
Monomer D Tg= 94 °C	10	15	10
Monomer E Tg=145 °C	-	-	5
Property			
Young's modulus (MPa)	5.7	5.0	7.3
Tg (°C)	1	12	23
Peel strength (g/cm)	24	34	51

Each coating contains 3 wt% of photoinitiator and 0.1 wt% of MPTMS.

Increasing the Tg of the coating pushed up the peel strength as shown in Figure 3. The mechanism of adhesion to copper of these coatings can be understood in the similar manner which was reported in the literature 1), 3), and 4). Namely, as the Tg of the coating approaches the testing temperature, the adhesion increases. More precisely, the adhesion increases as the increase of tanδ values. Figure 4 demonstrates this relationship. Since S-4 has a higher tanδ value at 23 °C, it exhibits the highest peeling strength. Figure 5 also plots the peeling strength at different peeling speed. The faster the sample was peeled off, the higher the peeling strength became. This behavior is similar to the glass adhesion of the coatings.[1] Peeling speed can be interpreted to temperature. High peeling speed is attributed to the low temperature. For the coatings with lower Tgs than testing temperature, the tanδ value increases as the decrease in testing temperature.

S-5 is a coating with high Young's modulus (870 MPa) and high Tg (130 °C). Dependence of peel strength at 23 °C on peeling speed is shown in Figure 5. The coatings (S-2~S-4) showed high adhesion at high peeling speed, in contrast, S-5 exhibited lower peeling strength at higher peeling speed. Since S-5 has higher Tg than testing temperature, the increase in peeling speed, which equals the decrease in testing temperature, resulted in decrease of tanδ value. Hence it exhibited lower peel strength.

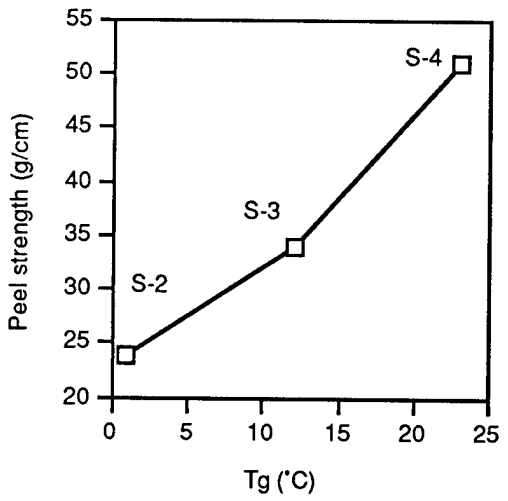

Figure 3. Peel strength plotted against Tg of the coatings.

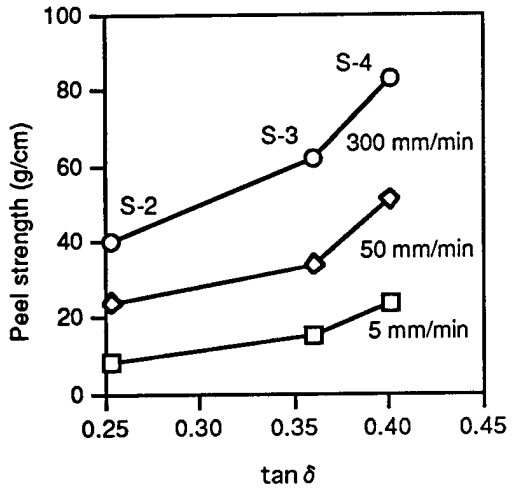

Figure 4. Peel strength plotted against tanδ at 23 °C. Peeling speed was varied from 5 mm/min to 300 mm/min.

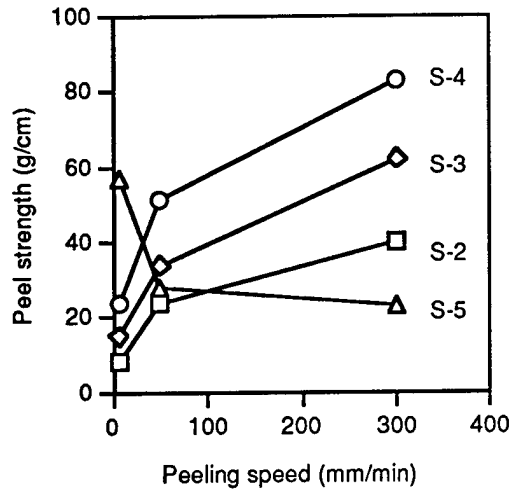

Figure 5. Peeling strength plotted against peeling speed.

CONCLUSION

The adhesion property of UV curable materials to copper was affected by three factors. The first factor was surface condition of the copper. From the results of XPS analysis and surface profile data, the increase of the adhesion to copper was due to the amount of oxidized copper at surface not to the roughness. The second was the functional group of adhesion promoters. Some of the adhesion promoters were examined and the compound functionalyzed with mercapto group was the most effective. This effect would be due to the coordination of mercapto group to copper. The third was viscoelastic properties. Addition of monomers with high Tg of their corresponding homopolymers to the coatings was effective to increase the adhesion to copper. This behavior is explained by loss tangent (tanδ) curves of the coatings. These three factors enable us to design highly adhesive coatings to copper.

REFERENCES

1) H. Takase, Z. Komiya, T. Ukachi, Proc. RadTech Asia **97**, 709 (1997).
2) T. Ukachi, A. Aoyama, Y. Naito, K. Igarashi, **41st** Proc. IWCS, 261 (1992).
3) M. Shimbo, M. Iwakoshi, M. Ochi, J. Adhesion Soc. Japan, **10**, 161 (1974).
4) M. Ukon, T. Takahashi, T. Ohtaka, T. Ukachi, Proc. RadTech Asia **95**, 295 (1995).

Masahito Mase
JSR Corporation, Tsukuba Research Laboratory,
25, Miyukigaoka, Tsukuba, Ibaraki 305-0841
Japan

Masahito Mase received his M. E. degree in Material Science from Nagoya Institute of Technology and joined JSR Corporation in 1991. He has been engaged in research and development of radiation curable materials for optical fiber coatings.

Zen Komiya
JSR Corporation, Tsukuba Research Laboratory,
25, Miyukigaoka, Tsukuba, Ibaraki 305-0841
Japan

Zen Komiya received his Ph. D. in Organic Chemistry from Hokkaido University and joined JSR Corporation in 1984. He was engaged in research and development of new transparent plastics and currently has been engaged in research and development of radiation curable materials.

Hiroshi Abe
JSR Corporation, Tsukuba Research Laboratory,
25, Miyukigaoka, Tsukuba, Ibaraki 305-0841
Japan

Hiroshi Abe received his M. E. degree in chemistry from Sophia University and joined JSR Corporation in 1996. He has been engaged in research and development of radiation curable materials .

Takashi Ukachi
JSR Corporation, Tsukuba Research Laboratory,
25, Miyukigaoka, Tsukuba, Ibaraki 305-0841
Japan

Takashi Ukachi received his B. E. degree in Biophysics and Bioengineering from Osaka University and Ph. D. in Material Science from Kyushu University. He started his professional carrier at JSR Corporation in 1976 and has been engaged in research and development of radiation curable materials.

Thermal Analysis of Buffer Tube Gels in Loose Tube Fiber Optic Cables

Michael T. Costello Ph.D.
Witco Corporation, 5777 Frantz Road, Dublin, OH 43017

Alan Eckard Ph.D. and William J. Thalman
Witco Corporation, 100 Bauer Drive, Oakland, NJ 07436

ABSTRACT

In loose tube fiber optic cables the buffer tubes are filled with hydrocarbon based gels to protect the optical fibers from water entry. These materials require mechanical and thermal stability and a comparison of the PE/PJ, ETPR, and gelled oil (GO) based filling and flooding compounds was undertaken using dynamic mechanical and thermal analysis.

Introduction

Recently a new class of filling compound has emerged which consists of low pour hydrocarbon carriers (either poly-α-olefin or mineral oil) combined with polymeric gelling agents. In a preferred formulation the gelling agent chosen is a block copolymer which is comprised of a rubber midblock and a styrene endblock. These formulations have the advantage of resistance to high temperature oil separation, improved compatibility with cable materials, and low temperature flexibility.[1,2] Additionally, these compounds can be cold filled due to their low room temperature viscosity. These compounds represent a new class of filling and flooding compounds which are thixotropic in character and possess physical properties which are difficult to measure by traditional methods. In this vane we have attempted to measure the visco-elastic properties of these materials using dynamic mechanical and thermomechanical analysis.

Previously, the viscoelastic properties of filling compounds have been studied using both dynamic mechanical thermal analyzers and rotational viscometers. Studies of filling compounds using DMA revealed that the storage modulus varied based on the composition of the gel and that there is a strong temperature dependence of the dynamic viscosity and storage moduli.[3] Studies of the visco-elastic properties of gelled oil compounds using a rotational viscometer confirm these findings and revealed that there is a weak correlation between drip performance and flowing point. In fact, it was concluded that a good filling compound should possess several properties including: a high storage modulus in the low shear stress region, a high flowing shear stress, and a low dynamic viscosity.[4] Other work has demonstrated the utility of DMA in understanding the compatibility of polymers exposed to flooding and filling compounds based on the changes in the storage and loss moduli of the polymer.[5]

In this paper we will investigate the rheological properties of the PE/PJ, ETPR, and gelled oil (GO) filling compounds using a variety of thermal and mechanical techniques. This is part of an overall investigation into the rheological properties of cable filling compounds. The glass transitions (T_g), storage modulus, loss modulus, and tan δ were measured in an attempt to obtain a deeper understanding of the phenomenon of oil separation, while the expansion coefficients and softening onset were measured with a thermomechanical analyzer to gain some understanding of void formation tendency.

Experimental

The dynamic mechanical measurements were made with a Perkin-Elmer DMA 7e with a frequency of 1.0 Hz, a dynamic control of -30mN,

and a static control of 120% of the dynamic set point between the temperatures -125 to +80°C. The experimental setup consisted of two (10mm diameter) parallel plates separated by 10mm gap distance. The stationary plate that holds the sample consists of a walled disc which is used to prevent the sample from flowing out from between the gap distance at high test temperatures.

The thermomechanical analyses (TMA) were made with a Perkin-Elmer DMA 7e fitted with a 0.5 mm radius spherical probe tip and a parallel plate stage. The measurements of the expansion coefficients of the filling and flooding compounds were measured using a 28-mm (large) furnace and a Large Quartz Dilatometer Accessory of approximately 1-cc volume. The method used was a modification of ASTM E831.

The compounds tested were comprised of polyethylene and petroleum jelly (PEPJ1 and PEPJ2), extended thermoplastic rubber (ETPR), polymer gelled poly-α-olefin (GO1), and polymer gelled low pour mineral oil (GO2).

Discussion

Dynamic Mechanical Analysis

The dynamic mechanical analysis of the five filling compounds studied was attempted, but due to methodology limitations the moduli curves for the PEPJ1 and PEPJ2 samples could not be obtained. It is recommended that an instrument that utilizes torsional (ω) stress would be more appropriate for these materials. The tan δ curves of GO1, GO2, and ETPR are included in Figures 1, 2, and 3, respectively.

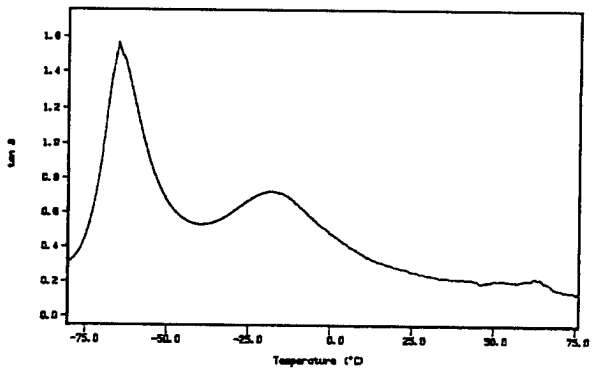

Figure 1. The tan δ curve of GO1 at 1Hz from -80 to +80°C.

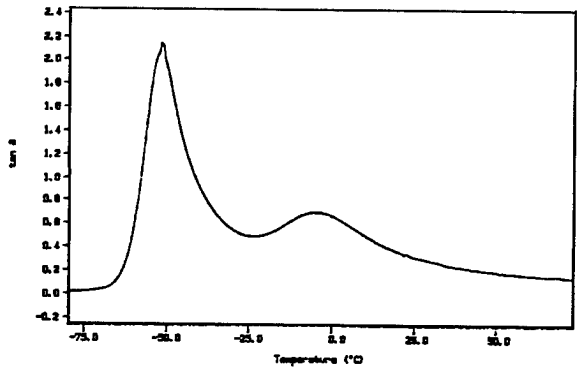

Figure 2. The tan δ curve of GO2 at 1Hz from -80 to +80°

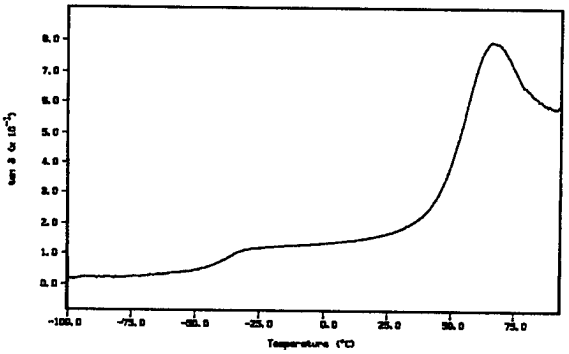

Figure 3. The tan δ curve of ETPR at 1Hz from -80 to +80°C.

Table 1. Glass Transitions and Onset Temperature

Sample	Tan δ Transitions (°C)		TMA (°C)
	$T_{carrier + rubber}$	$T_{styrene}$	T_{onset}
GO2	-50	-6	-43
GO1	-65	-18	-34
ETPR	-55[1]	+66	85
PEPJ1	-	-	76
PEPJ2	-	-	94

[1]this onset is tentatively assigned to the rubber block of the copolymer

As can be observed in the Figure 1 there are two main transitions for the blend GO1 in the tan δ curve. The blend GO1 possesses a low

temperature transition at -65°C, and a second smaller transition at -18°C. The onset of the pour point of the PAO is -65°C, while the T_g of the rubber domain of the gelling agent is -58°C, therefore the transition at -65°C is attributable to the pour point of the PAO combined with the glass transition of the rubber domain of the gelling agent. The higher transition at -18°C is due to the T_g of the styrene domain of the gelling agent.[6,7] With both transitions of the gelled oil well below room temperature, there is no danger of a large contraction during manufacture of the filling compound due to a phase transition.

In blend GO2 (see Figure 2) there are also two main transitions in the tan δ curve. The blend GO2 possesses a low temperature transition at -50°C, and a second smaller transition at -6°C. The transition at -50°C is attributable to the pour point of the low pour mineral oil combined with the glass transition of the rubber domain of the gelling agent, while the higher transition at -6°C is due to the T_g transition of the styrene domain of the gelling agent.[6,7] As with the PAO based gel (GO1) both phase transitions of GO2 are well below room temperature and, therefore, we would expect minimal contraction when filling a cable.

The tan δ curve for ETPR blend can be observed in Figure 3. This blend possesses two distinct transitions. The first onset transition at -50°C has not been assigned, but it is suspected that this may be a transition associated with the rubber mid-block of the polymeric gelling agent. The second T_g transition at +66°C is attributed to a transition of the styrene domain of the gelling agent.[6,7]

In an attempt to understand the effect of gelling agent concentration on the curve of gelled oils, several blends of the gelled poly-α-olefin and low pour mineral oil were prepared. These samples were run from -100 to +50°C with a static force of -20mN and an amplitude control of 5 μm. The results of five runs of the PAO based blends are overlaid on Figure 4, with a normalized tan δ axis for clarity. As can be observed in the figure, as the amount of polymer is increased the styrene transition temperature increases. This is indicative of an increase in size of the styrene domain as the gel becomes more concentrated and this glass transition will reach its maximum at the glass transition of the styrene of the pure polymer.

As can be observed in Figure 5 the glass transition of the styrene domain of the gelling agent in our system varies linearly with weight % concentration. This type of behavior has been observed in rigid PVC systems containing a variable amount of lubricant. In these systems the glass transition of the PVC varies linearly

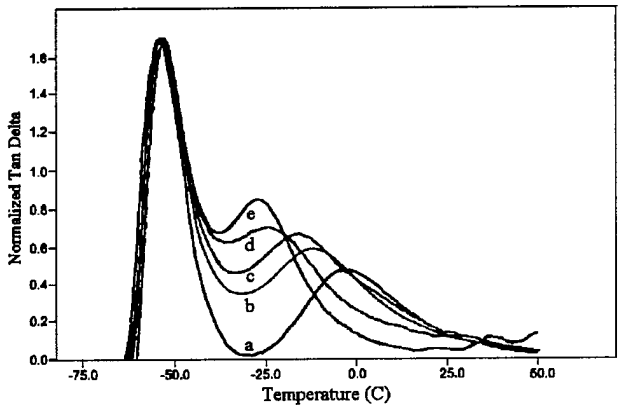

Figure 4. The normalized tan δ curves of blends of poly-α-olefin and (a) 4% (b) 8% (c) 12% (d) 16% and (e) 20% gelling agent at 1Hz from -80 to +80°C.

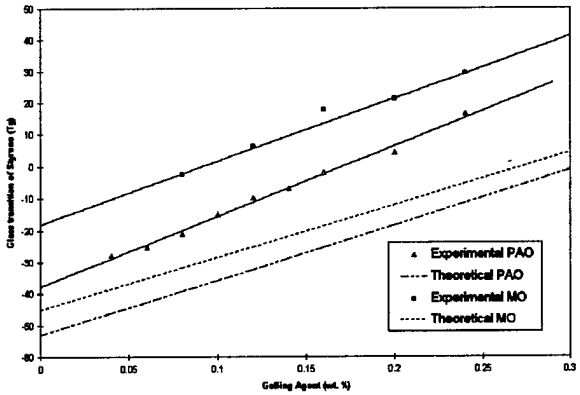

Figure 5. A plot of the styrene glass transitions vs. % gelling agent for both mineral oil and poly-α-olefin based blends.

with the addition of lubricant, until the system is saturated and the lubricant and PVC become two separate domains. At this point, since the saturation point has been reached, the glass transition of the PVC remains constant regardless of the amount of lubricant added.[8] Our system is clearly a polymer and oil blend which has not reached saturation, and therefore displays a linear correlation.

In a miscible polymer-polymer blend system the glass transition can be calculated using the Flory-Fox[9,10] equation ($T_{mix} = T_A V_A + T_B V_B$) which displays a linear correlation with volume % concentration. The theoretical regression lines using the Flory-Fox equation (and assuming volume % ≅ weight %) and substituting the pour point of the hydrocarbon oil and the glass transition of the styrene of the pure polymer are plotted on Figure 5. It can be observed that the theoretical line does not coincide with the experimental data since the weight percentage of polymer used does not closely approximate the volume percentage. In fact, the theoretical intercept for the glass transition of the polymer is 16°C smaller than the experimental prediction line for PAO and 27°C smaller than the experimental prediction line for mineral oil. Since the mineral oil is creating a larger apparent volume percentage than PAO the implication is that the mineral oil is more compatible than PAO and will possess a larger tendency to resist oil bleed.

Expansion Coefficients

The coefficients of expansion were measured and calculated using a quartz dilatometer. The results are listed in Table 2 and Figure 6. The highest expansion coefficients and therefore largest volume expansion was observed for PEPJ1 and PEPJ2, 7.9 and 5.8% respectively, while the ETPR and GO compounds were found to approximately half of the PE/PJ samples. In fact, the volume expansion of the ETPR compound was only slightly larger than the gelled oil, GO1 (4.2 vs. 3.9%). Of the gelled oils the GO1 formulated with a mineral oil carrier possessed a slightly larger value than the GO2 formulated with a synthetic poly-α-olefin carrier (3.9 vs. 3.2%). The low expansion coefficients for ETPR and gelled oil compounds indicate a smaller tendency to form voids (due to thermal contraction) during cable manufacture than traditional PE/PJ compounds.

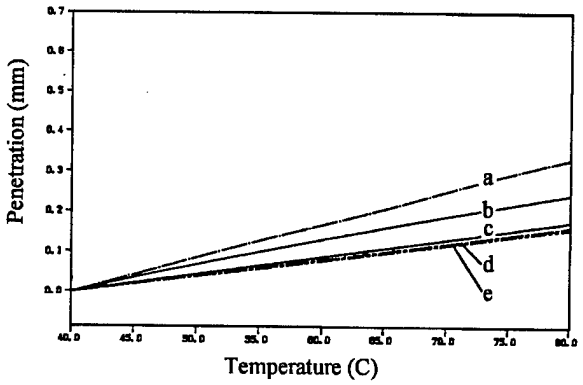

Figure 6. The thermal expansion curves for (a) PEPJ1 (b) PEPJ2 (c) ETPR (d) GO1, and (e) GO2 between +40 and +80°C.

Table 2. The coefficient of linear thermal expansion (α), coefficient of volumetric expansion (β), and % volume expansion (VE) between 40 and 80°C.

Sample	α (1/°C)	β (1/°C)	VE (%)
PEPJ1	0.035	0.00198	7.9
PEPJ2	0.026	0.00145	5.8
ETPR	0.018	0.00105	4.2
GO1	0.017	0.00098	3.9
GO2	0.014	0.00080	3.2

Thermomechanical Analysis

The onset of the softening points of the filling compounds are listed in Table 1 and Figure 7. As can be observed in Figure 7 the onset of the PEPJ1, PEPJ2, and ETPR1 were in the range of 70-90°C which is indicative of typical cable filling materials of these types. The onset temperatures of the gelled oil samples, GO1 and GO2 are -43 and -34, respectively. These

softening points are 100 to 130°C lower than typical cable compounds and reflect the low pour points associated with the hydrocarbon carriers used in their formulation, as well as, the low glass transition of the polymer gelling agent. These low softening points give these materials two improvements. First, since there is no phase transition between the manufacture and operating temperatures there is a low void formation tendency, and second the low softening point improves the low temperature flexibility.

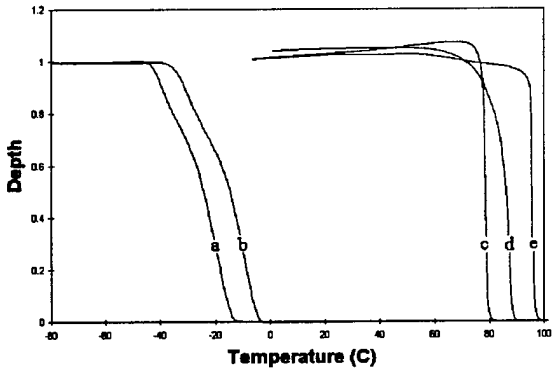

Figure 7. The TMA curves of (a) GO2 (b) GO1 (c)PEPJ1 (d) ETPR, and (e) PEPJ2 between -80 and +100°C

Conclusion

A comparison of the PE/PJ, ETPR, and GO based filling and flooding compounds was undertaken using dynamic mechanical and thermal analysis. It was found that the expansion coefficients of the materials decrease in the order PE/PJ>ETPR≈GO, and that the softening onset of the materials decrease in the order PE/PJ≈ETPR>>GO. This can be explained by the tan δ curves of these compounds which reveal distinct melting point transitions for the PE/PJ and ETPR compounds, while the GO displayed low temperature glass transitions for the styrene and rubber blocks of the copolymer gelling agent.

The low softening onset temperature coupled with the low coefficients of thermal expansion suggests gelled oils are ideal for cold filling operations. It would require handling a the high viscosity thixotropic material with special equipment, but the use of a material with phase transitions outside the normal filling and operating temperatures of a cable could serve to prevent excessive void formation which may lead to premature failures.

References

1. Costello, M.; Debska, A.; Eckard, A.; Thalman, W., Proceedings of the 44th International Wire and Cable Symposium, 479-483, **1995.**
2. Costello, M; Debska, A.; Eckard, A.; Thalman, W., Wire Journal International, 52-57, **1997.**
3. Gebizlioglu, O. S.; Plitz, I. M.; Zammit, M. J., Proceedings of the 44th International Wire and Cable Symposium, 457-462, **1995.**
4. Murata, A.; Oohashi, K.; Araki, S., Proceedings of the 45th International Wire and Cable Symposium, 570-574, **1996.**
5. Costello, M. T.; Debska, A.; Eckard, A.; Thalman, W., Wire Association International 1997 Conference Proceedings, 151-155, **1997.**
6. Wetton, R. E., Dev. Polym. Charact., 195, 5, **1986.**
7. Himes, G P.; Hansen, P. R.; Fulton, S. L.; Shafer, D. L., Proceedings of the TAPPI 1996 Hot Melt Symposium, 71, **1996.**
8. Bacaloglu, R.; Hegranes, B.; Fisch, M., J. of Vinyl & Additive Tech., 1-5, 3, **1997.**
9. Xue, G.; Dong, J.; Ding, J., Mater. Eng. (NY), 794-795, 9, **1995.**
10. Murayama, T., Encyc. of Polym. Sci. and Eng., 299-329, 5, **1982.**

Dr. Michael T. Costello has received his B.S. degree in chemistry from Virginia Polytechnic Institute in Blacksburg, Virginia and his Ph.D. degree from Purdue University in West Lafayette, Indiana. Dr. Costello has been involved in the pilot development of hydrogenation and sulfonation technologies and is currently developing improved cable fillers for the fiber optic market. He is employed as a Group Leader in the Performance Chemicals Group of Witco Corporation at their research center in Dublin, Ohio.

Dr. Alan D. Eckard has received his B.S. degree from Rensselaer Polytechnic Institute and his Ph.D. in physical chemistry from the University of Liverpool, England. After research fellowships at Keele University (UK) and the University of Toronto, Dr. Eckard has been involved in the development and application of industrial lubricants, coatings and surface treatment chemicals with several international manufacturers of these products for the over 20 years. He is currently Director of Research and Development for the Performance Chemicals Group of Witco Corporation at their research center in Oakland, NJ.

Mr. William J. Thalman has received his Masters degree in Chemistry from Montclair State College and is nearing completion of his Ph.D. degree in Physical Chemistry at Rutgers University. Mr. Thalman has been involved in the pilot development of dydrogenation and sulfonation technologies and is currently investigating methods to improve cable filler performance. He is employed as a Group Leader for the Performance Chemicals of Witco Corporation at their research center in Oakland, NJ.

LONG TERM HYDROLYTIC AGING STUDY OF A BLOCK COPOLY(ETHER ESTER) UNDERSEA CABLE BUFFER

Debra A. Simoff, Coralie A. Pryde†, Chester Gieniewski†

Bell Laboratories, Lucent Technologies, Murray Hill, New Jersey

ABSTRACT

Copoly (ether ester) elastomers are widely used, including use as buffers in undersea optical fiber cables. It is possible for the ester portions of such block copolymers to hydrolyze under certain conditions. We examined the propensity for hydrolysis to occur under worst case (immersion) conditions, and evaluated the impact of the hydrolysis on the mechanical reliability of the elastomer. We report here our results of a hydrolytic aging study for a particular elastomer, including water immersion times up to *9 years* at room temperature and accelerated aging at higher temperatures.

INTRODUCTION

Copoly(ether ester) elastomers have been widely used, including use as buffers in undersea optical fiber cables.[1] Despite the hydrolytic susceptibility of the ester blocks in these copolymers, few studies have been reported regarding their aging behavior in aqueous environments. We studied the aging behavior of a particular resin, Hytrel® G-4074, in both deionized water and synthetic seawater.

EXPERIMENTAL

Hytrel® G-4074 was obtained from E. I. du Pont de Nemours & Co., Wilmington, DE. Pellets and injection-molded bars were aged in deionized water and artificial seawater at 23-95°C. Melt flow rates (MFRs) of aged pellets were measured per ASTM D-1238, Condition FR-190/2.16. Tensile properties of aged bars were measured in an Instron tester. Infrared (IR) spectra were obtained on a Digilab FTS-60 Spectrometer: attenuated total reflectance (ATR) was used to examine molded bars and sample extracts; model compounds were examined as KBr pellets. NMR spectra were obtained using a Jeol FX90Q Fourier Transform NMR Spectrometer: unaged samples were scanned in $CDCl_3$; aged samples and model acid compounds required the addition of 15 vol % $DMSO_4$-d_6.

† Retired

RESULTS AND DISCUSSION

NMR Analyses.

^{13}C NMR analyses (Figure 1) indicated that the ester hard segment of Hytrel® G-4074 comprised poly(butylene terephthalate-*co*-isophthalate), while the ether soft segment was based on polypropylene oxide. The ratio of terephthalate to isophthalate was ~82:18 and the polymer comprised about 37% soft segment.

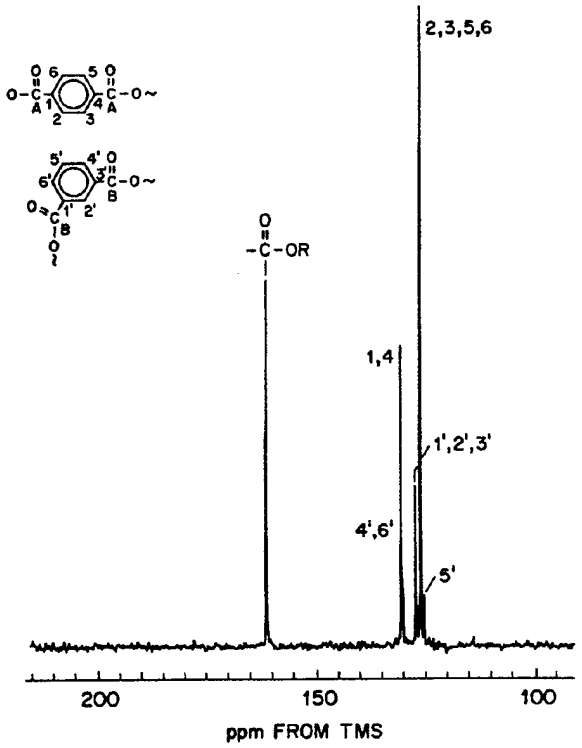

Figure 1 NMR spectrum of Hytrel® G-4074 -- aromatic region.

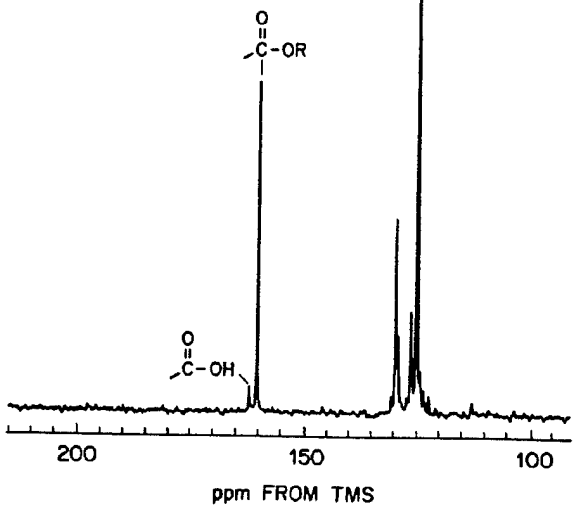

Figure 2 NMR spectrum of Hytrel® G-4074 bar aged 65 days in deionized water at 95°C.

Quantitative analyses of hydrolysis in aged samples were made by following changes in the aromatic carbonyl regions of the NMR spectra (Figure 2). Bars hydrolyzed at 95°C in water for aging times of 0, 27 and 65 days showed 0, 3.2 and 7.5% hydrolysis, respectively. These data are consistent with first-order kinetics (Figure 3). Oxidation was negligible in these samples, based on the absence of aldehyde and ketone absorptions at 205 ppm.[2,3]

Infrared Analysis

ATR spectra taken on portions of aged bars

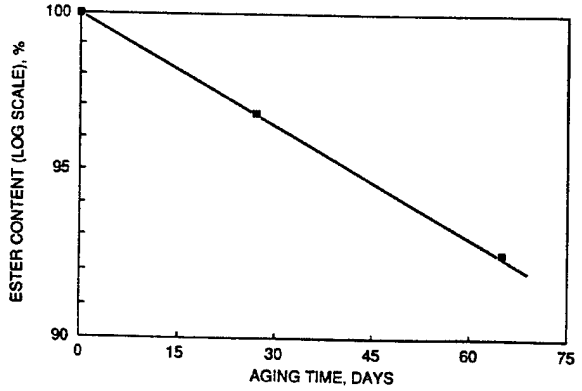

Figure 3 Plot of first-order equation for hydrolysis of Hytrel® G-4074 aged in deionized water at 95°C.

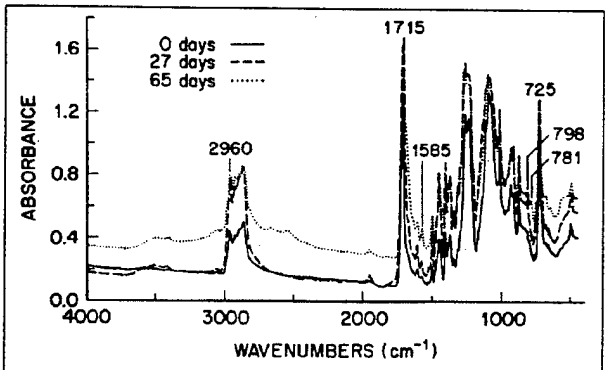

Figure 4 Infrared spectra of Hytrel® G-4074 after aging in 95°C water.

clearly reflected increases in hydrolysis, i.e., growth of hydroxyl and acid carbonyl bands, and changes in the C-O and aromatic substitution regions (Figure 4). Based on the spectra of model compounds (Figure 5 and Table 1), the latter three regions each comprise an envelope of several absorbances that can either decrease or increase at different stages in the hydrolysis, i.e., as mono-acids and di-acids are formed. Because of the complexity, these IR changes were not used to corroborate the NMR data on total scissions.

We observed that unaged samples of the Hytrel were soluble in chloroform, while bars that had aged significantly developed an insoluble fraction. Figure 6 shows the spectrum of the chloroform-soluble portion of a bar aged 65 days at 95°C, together with that from the sample's insoluble, gelatinous precipitate. Based on the sizes of peaks at 780 and 798 cm^{-1}, the precipitate contains a significant concentration of hydrolysis products, i.e., a large

Table 1 Infrared Bands in Model Compounds

	(cm^{-1})	(cm^{-1})	(cm^{-1})
Dimethyl esters:			
terephthalate	1728 strong	1504	814
isophthalate	1721 strong	1610	988
		1585 weak	
Monomethyl esters:			
terephthalate	1723	1572	798
	1695 v. broad	1508	
isophthalate	1730	1610	965
	1680	1585	
Acids:			
terephthalic	1700	1572	781
		1510	
isophthalic	1688	1612	690
		1584	

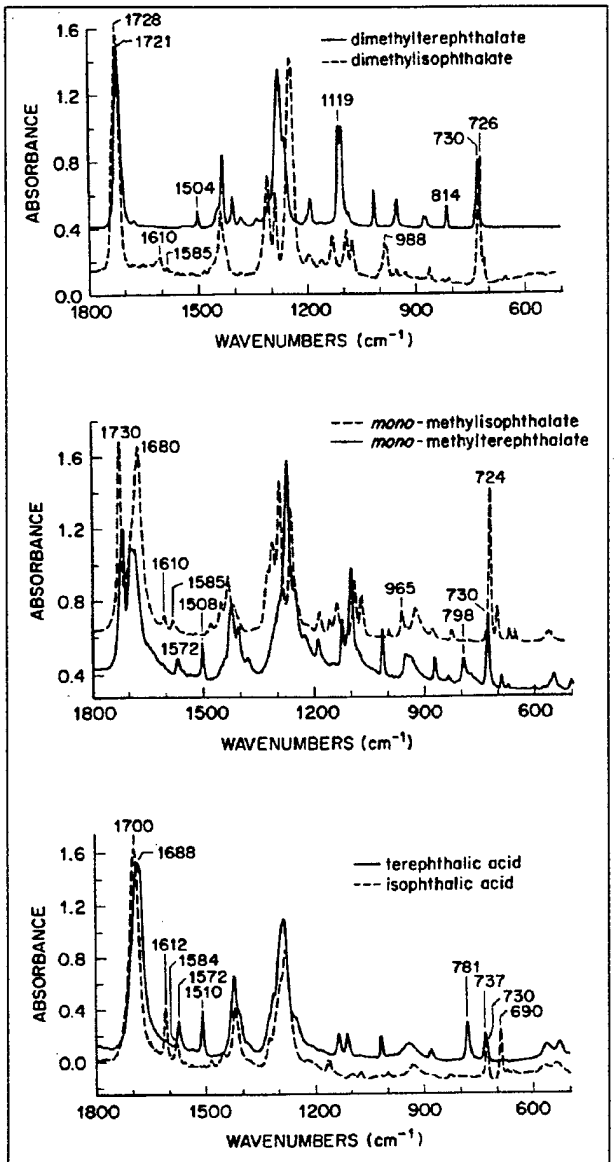

Figure 5. Infrared spectra of model compounds.

amount of terephthalic acid and a small amount of its monoester. In contrast, the spectrum of the soluble portion of the bar is very similar to that of unhydrolyzed material. Thus, the precipitation effected a relatively clean separation of hydrolyzed and unhydrolyzed material, suggesting that the scission was non-random.

Rheological and Mechanical Effects of Aging

Figures 7-9 show that melt flow rate and mechanical properties degrade with time upon water immersion at elevated temperatures. The changes in mechanical properties are

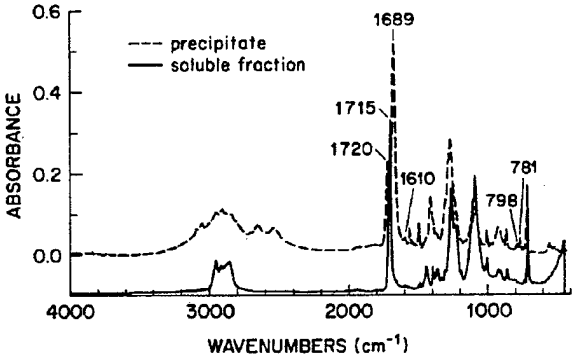

Figure 6. Chloroform fractionation of Hytrel® G-4074 bar aged 65 days in 95°C water.

manifested much later than those in melt flow rate. For example, after 27 days at 75°C, melt flow rate increases by 533%, while tensile strength and elongation decrease only ~10% and modulus shows little change. Synthetic sea salt does not accelerate the hydrolysis beyond that in deionized water, despite its slightly higher pH. If anything, the salt environment seems less severe.

Effects of Scission on Other Properties

We used our data to delineate relationships between percent hydrolysis and other properties. For example, comparison of Figures 3 and 7 shows that a large increase in MFR (from 5.7 to 25 gm/10 min) results from less than 0.5% ester hydrolysis. Cross-correlation among Figures 3, 8 and 9 shows that 3-5% hydrolysis corresponds to catastrophic failure. Comparison of our NMR results with GPC molecular weight data (not shown) suggests that ~15% reduction in M_n corresponds to ~0.8% scission of ester groups.

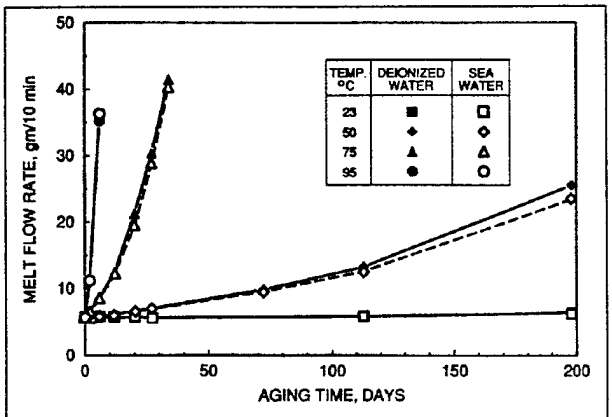

Figure 7 Melt flow rates of Hytrel® G-4074 pellets aged in deionized and salt water.

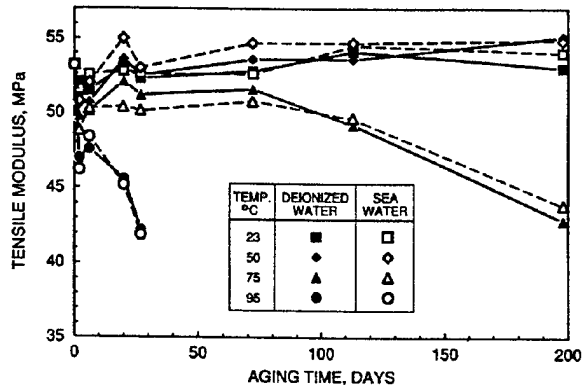

Figure 8. Tensile moduli of elastomer bars aged in deionized and salt water.

Ramifications

The useful lifetime of this elastomer is determined ultimately by the final application. However, one benchmark that has been used by the manufacturer is "tensile product half-life," i.e., the time for the product of tensile strength and elongation to decrease by half. Tensile product is roughly proportional to the energy required to break the material. It is a useful indicator of hydrolytic degradation, since strength, elongation, and tensile product half-life all decrease proportionally.

As seen in Figure 9, we observed the tensile product half-life for G-4074 to be 60 days at 75°C. At that point, we find this elastomer to be a very tough material, retaining an elongation of 380%. At twice this aging time, the material is still quite tough, with an extrapolated elongation

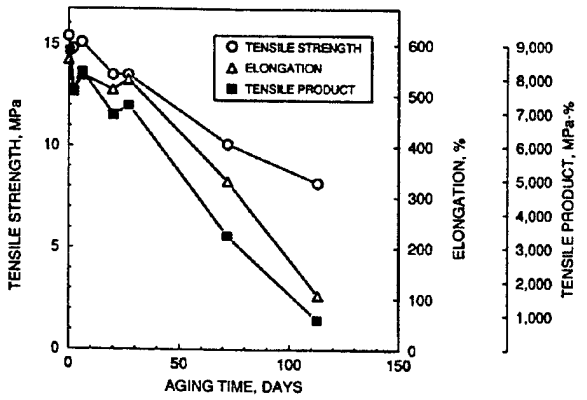

Figure 9. Tensile strength, elongation, and tensile product for elastomer bars aged in deionized water at 75°C.

of 80%. However, at roughly three times the "half-life," the elongation is projected to approach zero. At this point, modulus decays by ~20%; the material becomes cheesy and breaks easily upon handling. At still longer times, bars begin to delaminate and eventually fall apart.

While degradation of tensile properties was observed only at 75 and 95°C, sufficient melt flow rate data is available at lower temperatures to test whether the degradation follows an Arrhenius relationship over the ranges of time and temperature studied (Figure 10).

Above 50°C, the activation energy, E_a, as determined by either melt flow rate or the onset of delamination is 81-87 kJ/mol, while E_a computed for a 20% drop in modulus is 108 kJ/mol. The E_a computed from the manufacturer's data for tensile-product half-life of a similar elastomer is ~69 kJ/mol[4]. E_a reported for hydrolysis of poly(butylene terephthalate), which comprises the ester hard segment of G-4074, is 105-109 kJ/mol.[5,6]

The long-term (9 year) melt flow rate at room temperature was less than that predicted by extrapolation of high temperature data. Thus, such extrapolation over estimates the degree of hydrolysis that will occur at lower temperatures. One factor may be that poly(butylene terephthalate) has a T_g of ~50°C;[7] this 2nd order phase transition limits the hydrolysis that can occur in the glassy regions of the ester blocks.

SUMMARY AND CONCLUSIONS

We have conducted long term hydrolytic aging studies of Hytrel® G-4074, a block copoly(ether ester) elastomer. Degradation was first seen by an increase in melt flow rate, followed much later by decreases in mechanical properties. The addition of sea salt, which raises pH from 7 to ~8, did not significantly affect the degradation rate.

Ester hydrolysis was confirmed as the principal mode of degradation, with thermooxidation being negligible. The rate of disappearance of ester groups was consistent with first-order kinetics. The scission appeared to be non-random, occurring preferentially at or near end groups. Elongation approached zero after ~3% hydrolysis.

The temperature dependence for degradation of melt flow rate followed roughly an Arrhenius relationship at temperatures above 50°C, with an apparent activation energy of 81-87 kJ/mole. These data over-estimated the extent of hydrolysis that occurred at room temperature after aging for 9 years.

We conclude that, despite the susceptibility of the ester portions of the elastomer to hydrolysis, no significant degradation of mechanical properties due to hydrolysis should be expected over a period of 25 years at temperatures below 25°C.

ACKNOWLEDGEMENTS

We thank M. Spalding Stix, W. B. Wargotz, S. W. Kulba, C. A. Holden, H. E. Bair and F. M. Houlihan for their assistance, and we gratefully acknowledge John Engstrom, Ralph Fuller, and Frank Lewandowski of E. I. du Pont de Nemours & Co. for providing molecular weight analyses.

REFERENCES

[1] R. C. Mondello, U. S. Patent 4,156,104, May 22, 1979.
[2] R. S. Goglev and M. B. Neiman, *Polymer Sci. USSR* **9** 2351-2364 (1968) English Translation.
[3] E. Breitmaier and W. Volter, *Carbon 13 NMR Spectroscopy*, VCH Publishers, New York, 3rd Ed. p 217, 1987.
[4] "Hytrel 10-MS, A Hydrolytic Stabilizer Concentrate," Product Data Sheet HYT-114, Polymer Products Dept., E. I. du Pont de Nemours and Co.
[5] R. J. Gardner and J. R. Martin *J. Appl. Polym. Sci.* **25** 2353-2361 (1980).
[6] P. G. Kelleher, R. P. Wentz, and D. R. Falcone Polym. Eng. Sci. **22**(4) 260-264 (1982).
[7] G. R. Kriek "Polybutylene terephthalate: PBT" in *Modern Plastics Encyclopedia* **66**(11), Mid-October Issue (1989).

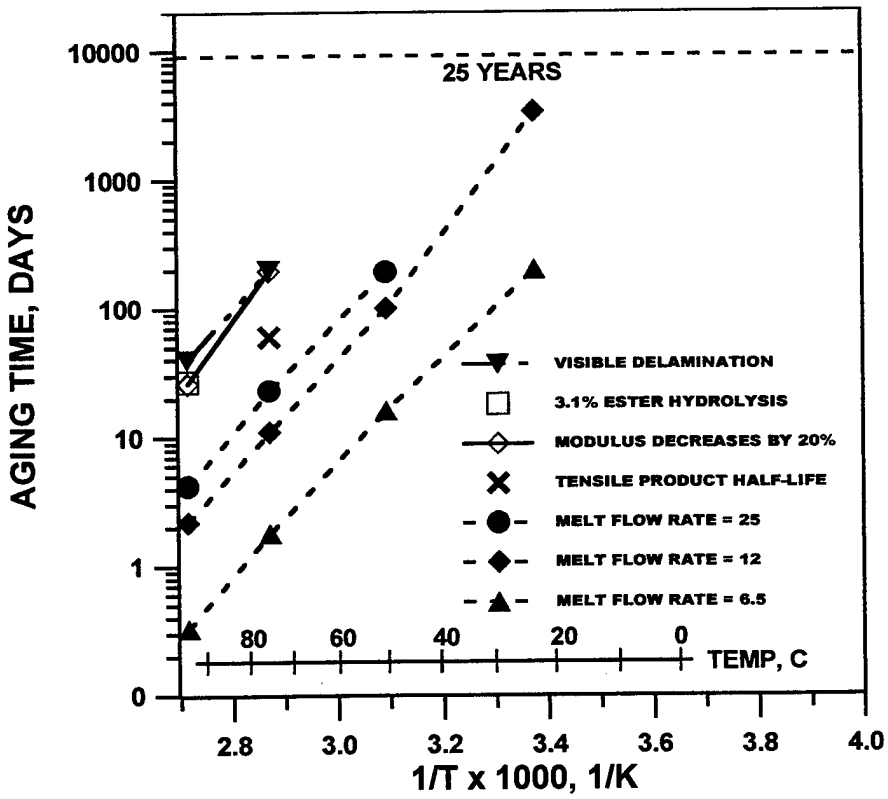

Figure 10. Arrhenius plot of the temperature dependence of property changes on aging in deionized water.

Debra Simoff
Bell Laboratories, Lucent Technologies
700 Mountain Avenue, Rm 7D-214
Murray Hill, NJ 07974

Debra Simoff is a Member of Technical Staff in the Polymer and Chemical Engineering Dept. at Bell Laboratories, Lucent Technologies, in Murray Hill, NJ. She conducts research on optical fiber coatings and other polymers used for telecommunications, and has earned an MS in Polymer Science and Engineering from UMASS Amherst.

FIBER GROUP INDEX MEASUREMENTS USING OPTICAL LOW COHERENCE REFLECTOMETRY

Gisella Marradi, Pier Giuseppe Peretta, Susanna Cattelan

SIRTI ,Cassina de' Pecchi (MILANO) ITALY

ABSTRACT

In this paper we describe a new method to measure the group refractive index n_g of optical fibers.
This method is based on a interferometric measurement realized by OLCR (Optical Low Coherence Reflectometer) device.
Measuring the ligth optical path of two different fibers of which one is the test fiber and the other is the reference one, we can measure n_g of the test fiber with a good precision.
We have measured n_g of Single Mode (SM), Multi Mode (MM), Disco and Doped fibers, using a SMR fiber as reference.

INTRODUCTION

Using high spatial resolution and large dynamic range Optical Low Coherence Reflectometry (OLCR), group refractive index n_g can be determined for the fibers which n_g unknown is. Group refractive index is an interesting parameter who allows us to measure the light optical path in a fiber and therefore its geometrical lenght.
In the following pages the theory of our relative measurement, the experimental setup and the results are described: group refractive index n_g is obtained comparing the light optical path between a test fiber sample and a reference one.

THEORY

In this section the theory on which the technique we used to measure n_g is based and the error analysis are described.
Our aim was to measure the group refractive index n_g of an l_1 lenght fiber using a known refractive index n_2 of l_2 lenght standard SMR fiber as a reference.
Using an OLCR device is possible to measure the light optical path x in a fiber.
Referring to the reference fiber we obtain :

$$x_2 = l_2 \cdot n_2 \qquad (1)$$

Refering to a test fiber:

$$x_1 = l_1 n_g \qquad (2)$$

Combining equations (1) and (2) we obtain:

$$\frac{x_1}{x_2} = \frac{l_1 \cdot n_g}{l_2 \cdot n_2} \qquad (3)$$

That is:

$$n_g = n_2 \cdot \frac{x_1}{x_2} \cdot \frac{l_2}{l_1} \qquad (4)$$

Supposing $l_1=l_2$ and knowing n_2 of the reference fiber, n_g can be easily calculated by means of the experimental measurement of the two optical paths.
At this point we have to define how much the length difference between the two fibers affects the ng value.
Let's modify equation (4) as follows:

$$n_g = \frac{l_1}{l_2} \cdot n_2 \cdot \frac{x_1}{x_2} = \bar{l} \cdot n_2 \cdot \frac{x_1}{x_2} \qquad (5)$$

The errors related the parameters in equation (5) are the followings:

$\bar{l} = l_1 / l_2 = 1 \pm \delta \bar{l}$ where $\delta \bar{l}$ is the cutting error;

$x_{1,2} + \delta x_{1,2}$; δx_1 and δx_2 can be considered equal as they depend on the OLCR precision which is $\geq 5um$;

$n_2 \pm \delta n_2 = 1.468 \pm 2 \cdot 10^{-3}$, according to the typical values for the third window supplied by SMR fibre manufacturers (see Table 1), and according to numerical simulation.

δn_g can be estimated according to the known error propagation equation.

Assuming $l_1 = l_2 \cong 1m$ we would obtain:

Case a) if $\delta \bar{l} = 10^{-3}$, that is $l_2 - l_1 = 1mm$, then $\delta n_g = 2.8 \cdot 10^{-3}$;

Case b)if $\delta \bar{l} = 10^{-4}$,that is $l_2 - l_1 = 0.1mm$, then $\delta n_g = 2 \cdot 10^{-3}$.

We conclude that by assuring a cutting error smaller than 0.1mm/m, we reach the reference fiber precision .

Fiber type	1300nm ng	1550 nm
SM-R	1.467	1.468
SM-DS	1.471	1.470

Table 1- Nominal values of n_2 of SMR and DS fibers

EXPERIMENTAL SETUP

All the group refractive index measurements have been performed with a OLCR implemented in the Sirti R&D labs [1]. Figure 1 shows the automated experimental test-bed, which uses low coherence sources (LEDs, ASE) to obtain a high resolution Michelson interferometer. The 3 dB coupler splits the light launched into the SMR fiber into two branches: the measurement and the reference one. Light is reflected by a mobile mirror placed at the end of the reference branch and in the measurement branch by the fiber under test connected at its end. We can calculate the optical path in the fiber under test by means of the interference peaks generated from both the fiber ends and the mirror at the detector interface. The dashed line in figure 1 shows that reference branch length can be varied, through special patch cords, in order to match different fiber lengths.

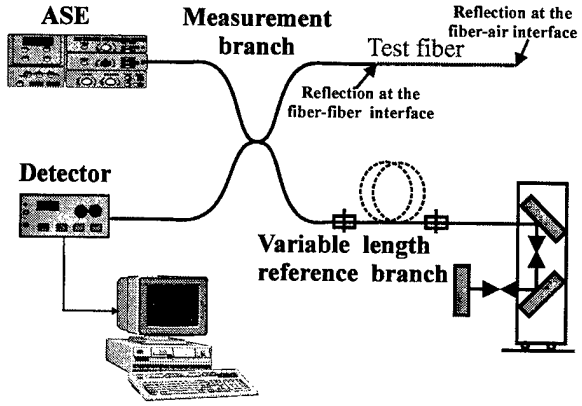

Figure1: Experimental setup of OLCR

MEASUREMENTS

Cutting error evaluation

By using two SMR fibers with known n_g one can easily find out the lenght difference from the distance between the interference peaks due to reflections generated at the fiber ends. In the ideal case of a perfect cut, the peaks overlap. Figure 2 shows the customised "double cleaver" developed in the Sirti R&D laboratories: it is based on two standard fiber cleavers and enables to cut the two fibers at the same time.

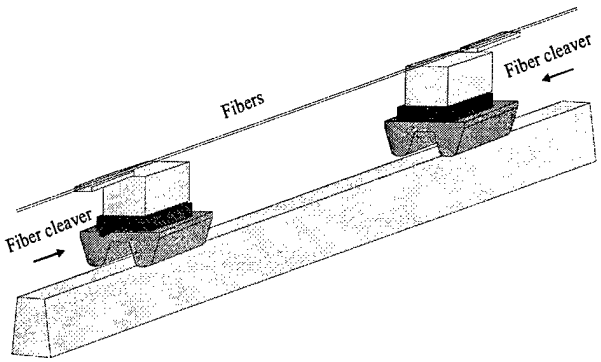

Figure 2: Double cleaver developed in Sirti R&D

OLCR measurements on several cutting trials showed that our double cleaver always keeps the length difference between the two fibers inferior to 0.1 mm/m. In this way the theorical

precision expected on n_g ($2x10^{-3}$) can be reached.

n_g measurements

After having verified the feasibility of the experimental method, we carried out a number of n_g measurements on different fibers: Single Mode fiber (SM), Single Mode- Dispersion Shifted fiber (DS), Multi Mode fiber (MM), Doped fiber, DISCO fiber.

The measurement procedure is the same as in the preceding paragraph ("Cutting error evaluation"), except that the two fibers are different. The first is a SMR fiber with a known n_g value; the second is the fiber under test with a n_g value which must be measured.

OLCR measures the optical path within each fiber: comparing these two values we can calculate the test fiber group refractive index (equation 4).

The mean values of the results are reported in Table 2. They are in agreement with the ones obtained using a numerical method [2,3].

Disco1	Disco 2	DS1	DS2
1.480	1.479	1.471	1.471

MM	Doped	SM
1.478	1.477	1.468

Table 2: mean values of n_g for seven fibers

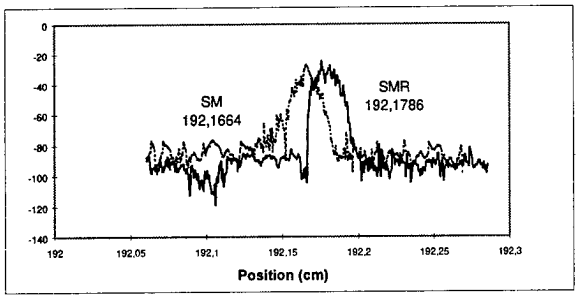

Figure 3a: position difference between the reflection at the test SM fiber-air interface and the reflection at the reference SMR fiber-air interface

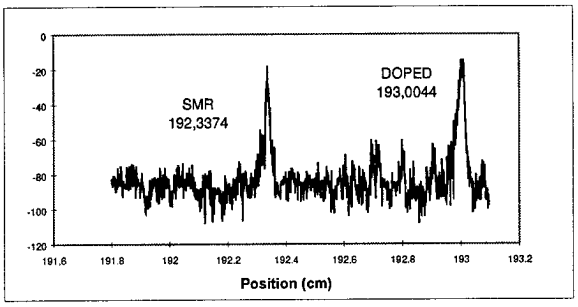

Figure 3b: position difference between the reflection at the test Doped fiber-air interface and the reflection at the reference SMR fiber-air interface

As an example we report in figure 3a and 3b some graphics showing the two interference peaks related to the fiber-air interface of the reference SMR fiber and the test DS (Doped,...) one.

CONCLUSIONS

This article demonstrates that we can use the Optical Low Coherence Reflectometry technique to measure the fiber group refractive index n_g with an error of $2x10^{-3}$. n_g is evaluated by measuring the optical path difference between the test and the reference fiber having a lenght difference inferior to 0.1 mm/m.

The n_g experimental measurements satisfy the theoretical previsions and are in agreement with literature results obtained through a different method [3].

The n_g precision cannot be better than $2x10^{-3}$, that is the known ng precision of the reference SMR fiber.

REFERENCES

[1] Bottanelli et al
"Wide range Optical Low Coherence Reflectometer for high resolution fault detection and component characterization", 45th International Wire and Cable Symposium -IWCS 96 (USA)

[2] W.V. Sorin, D. F. Gray
"Simultaneous thickness and group index measurement using Optical Low-Coherence Reflectometry", IEE Photonics technology letters, Vol. 4, No 1, January 1992

[3] S. Morasca et al
"Measurement of group effective index in integrated semiconductor optical waveguides", IEE Photonics technology letters, Vol. 5, No 1, pag. 40-42, 1993

Autors

Gisella Marradi was born in Pisa, Italy, in 1970. She received the doctor degree in Physics from Milan University in 1996.
After a period of tree years of work in CISE (during and after University), she joined R&D Dept. of SIRTI where she is currently engaged in optical fiber work. She is involved in national and international standard committes and had some papers published in national and international conferences.

Susanna Cattelan was born in Milan, Italy, in 1964. She receveid the bachelor in telecomunications in 1983.
From 1984 to 1988 she worked in the R&D Dept. of TELETTRA. Actually she is engaged in optical fiber work in the R&D Dept. of SIRTI, where she had some papers published in national and international conferences.

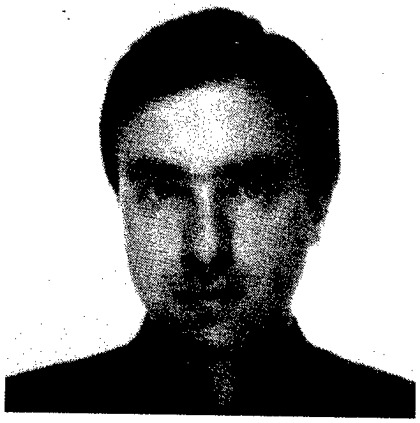

Pier Giuseppe Peretta was born in Turin, Italy, in 1965. He received the doctor degree in Electronic Engineering fron "Politecnico di Torino" in 1990. After a brief period of work in CSELT, he joined AET where he dealt with optical monitoring systems. In 1995 he joined R&D Dept. of SIRTI where he is currently engaged in passive optical components as a Senior Engineer. He is involved in national and international standard committes and had some papers published in national and international conferences.

Remote and Automatic 4,000-Fiber Optical Testing System

Hiroichi Katayose, Ken Sakuma, Kenji Yasuhara and Yoshikazu Numura
Fujikura Ltd. Optical Access Network Lab.,
Sakura-shi Chiba , Japan

Abstract

We have developed a compact Remote and Automatic 4,000-Fiber Optical Testing System. This system plays an indispensable role in the rapid expansion of optical fiber subscriber networks. It can be used for a 1,000-fiber cable installation test and remote fiber testing. The main components are a Optic Testing Control equipment(OTC) and 4 sets of 1,000-fiber Mechanical Optic Switches(FS). This system includes various test functions. These functions are :1.31/1.55/1.65 μ m 3-wavelength OTDR testing, 3-wavelength multi-fiber OTDR testing for up to 4,000 fibers, 3-wavelength light source function and optical power meter for in-line light checking. The OTDR testing has a fault-locating function, automatic checking of optic test result using cable database, test data storage and test results printing. Through the use of telephone line or LAN network, remote testing is also possible. OTDR testing time is less than 40 seconds for one fiber, and it has a dynamic range of 32 dB at 1.31 μ m wavelength and at pulse-width of 4 μ s. The dimension of the OTC is 480W x 250D x 145H(mm), and that of FS body is 580W x 290D x 65H(mm). Both the OTC and FS are compact and portable, and can be easily carried around. With all these functions, this system offers a complete testing environment for optical cable installation testing and optical cable maintenance testing.

1. Introduction

To provide high-speed and broad-band services, the use of optical fibers in subscriber networks has increased tremendously in these past a few years. It has become necessary to provide efficiency ways for 1,000-fiber optical cable installation testing and optical cable remote testing.

This paper describes the system for high-performance testing of 1,000-fiber optical cable. The system is known as configuration of "Remote and Automatic 4,000-Fiber Optical Testing System", which mainly consists of a optical test control system and four 1,000 fiber mechanical switches.

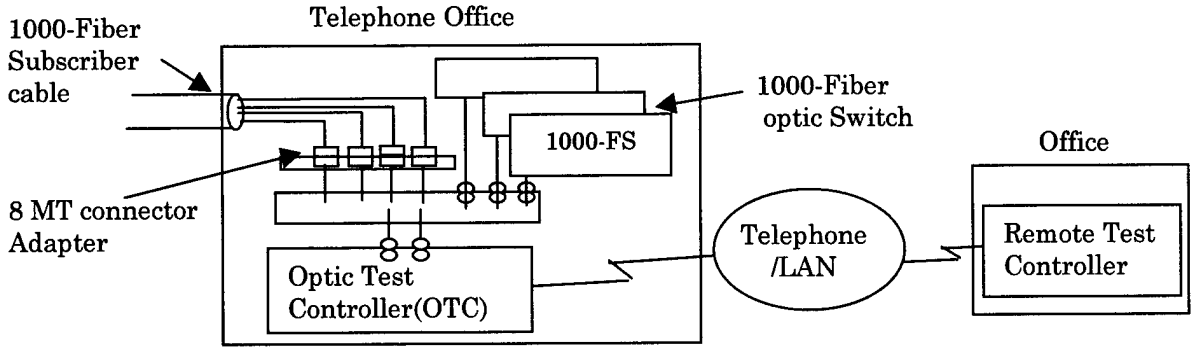

Figure 1. System Configuration

The introduction of the functions and the characteristics of each component and the configuration and the characteristics of the test program are also presented.

2. System Configuration

Figure 1 shows the system configuration of "Remote and Automatic 4,000-Fiber Optical Testing System". This system composes of an Optic Test Controller Equipment, 4 sets of 1,000-Fiber Switches and Remote Controller that provides remote test through telecommunication network. The 1,000 fiber-subscriber cable is connected to the FS using the 8-fiber MT Connectors. It is possible to test up to maximum of four 1,000 fibers cables using 4 sets of the FS.

2.1 Design of the OTC

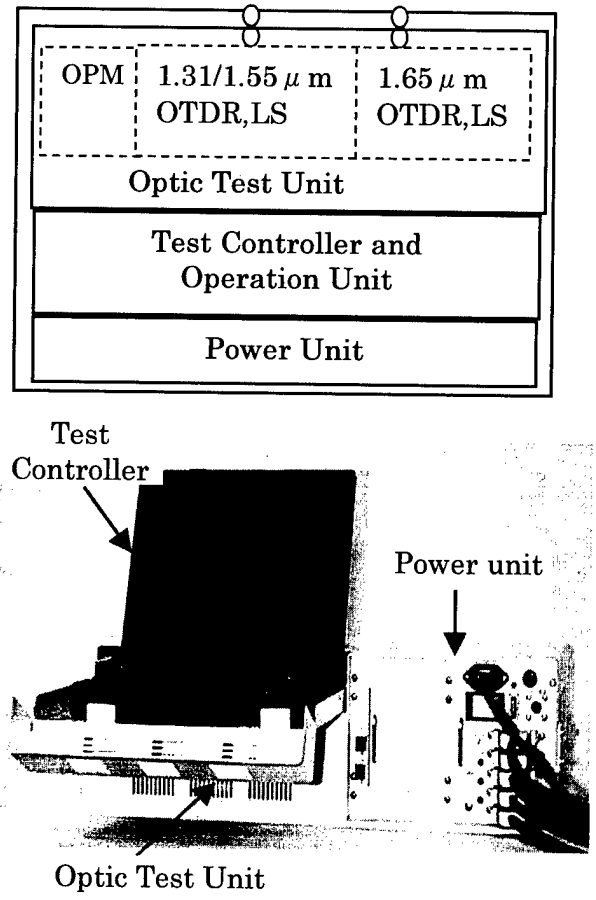

Figure 2 Construct of the OTC

Figure 2 shows the external view of OTC (Optic Test Controller). The OTC composes of Test Controller that is used for test operation and setting the test condition, Power Unit which is used to supply power to the OTC and 4 sets of the FS, and the Optic Test Unit for use in optical test. These units are built into the compact casing. The OTC is compact and portable, with the dimension of 480W x 250D x 145H(mm) and the weight of about 10kg.

Optic Test Unit has OTDR test function with testing wavelengths of 1.31 μ m/1.55 μ m/1.65 μ m, the light source function with wavelengths of 1.31 μ m/1.55 μ m/1.65 μ m. Optic Test Unit and F S are connected by the 2 fiber cords.

Two types of input power supply of the Power Unit, AC100V and DC48V, are provided.

2.2 Design of the FS

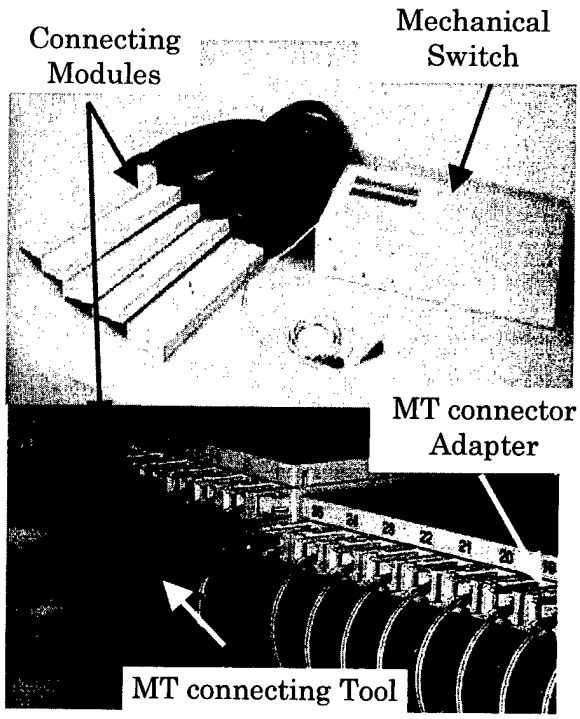

Figure 3 Construct of the 1,000-FS

Figure 3 shows the picture of the 1,000-Fiber Switch. It composes of the 1,000-Fiber

Mechanical Switch body and 5 sets of 200-Fiber Connecting modules. The 200-Fiber connecting modules has 25 sets of 8-Fiber MT connector adapter, the module casing and the tubing for 8-fiber ribbons. The 8-Fiber MT Connector Adapter has alignment pin and the coil spring, and it makes possible to perform the connection using the 8 M T connector in a short time. The FS is compact, with the dimension of 580Wx290Dx68H(mm). The main FS body is separated from the MT connecting modules. Therefore the space required for the FS is reduced. The weight is about 12kg, and it is easily transportable.

3. Functions and Characteristics

Table 1 shows the functions of the OTC and the 1,000-Fiber FS. The OTC has 4 main test functions, test data storage and test results printing functions.

Table1. Function of OTC and 1,000-FS

Item	Main Specification
OTDR test	Automatic OTDR test, wave shape analysis, fault location function, light source confirmation test 1310/1550/1650nm
Multi-fiber OTDR test	Automatic multi-fiber OTDR test for up to 4,000 fiber and 3 wavelength (Max 30 condition parameter) wave shape analysis and fault location function light source confirmation test
Loss test	Light source for loss measurement 1310/1550nm
Identific-ation test	Light source for fiber identification test1550/1650nm,
In-line optical test	OPM : 1310/1550nm checking Active-line :input power ≧ -50dBm
Remote	Remote testing for all test functions
Others	Test data storage and printing functions

Light source confirmation test is performed by selecting the test in the in-line optical test sub-menu in the OTDR test menu or loss test menu.

Table 2. Characteristics

Item	Characteristics
OTDR test	Wavelength : 1310±25nm, 1550±25nm, 1650±5nm
	Dynamic range : ≧32 dB (4 μ s pulse width, SNR=1, 1.31 μ m)
	Capacity : Monitor of 4,000 fibers / 4 sets of optical switch
	Distance : 5,10,25,50,100 km, pulse width : 20,100,500,1000,4000 ns Sampling resolution : minimum 1m (5km range)
	Testing time :about 40 sec/fiber (typical)
Loss test	Light source : ≧ -10dBm 1310±25nm, 1550±25nm 270Hz (pulse square)
Fiber Identification test	Light source : ≧ -10dBm 1550±25nm, 1650±5nm 270Hz (pulse square)
1,000-fiber FS	Switching time : ≦10 sec adjacent ports : ≦0.8 sec insertion loss : ≦ 1.3 dB

Table 2 shows the characteristics of each function. A 1,000 fiber optical subscriber cable is usually less than 25km in length and therefore 32 dB dynamic range of OTDR test function is adequate for use in optical subscriber cable installation testing. Remote testing function provides multi-fiber OTDR test and OTDR test. With all these functions, this system provides complete testing environment for optical subscriber cable installation testing and optical cable maintenance testing.

4. Test Software

The test program is running on Windows 95 operating system on a note type PC. Figure 4 shows Main Test function windows.

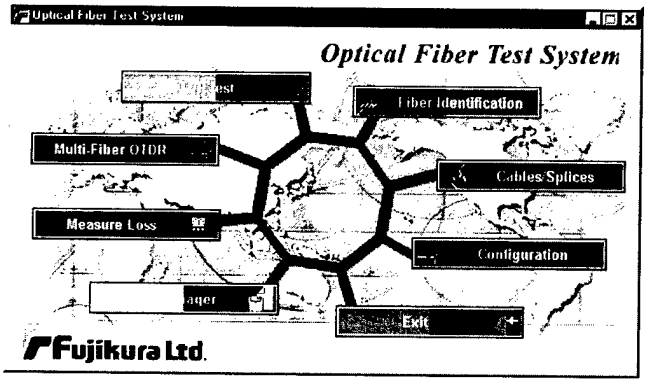

(1) Main Test function window

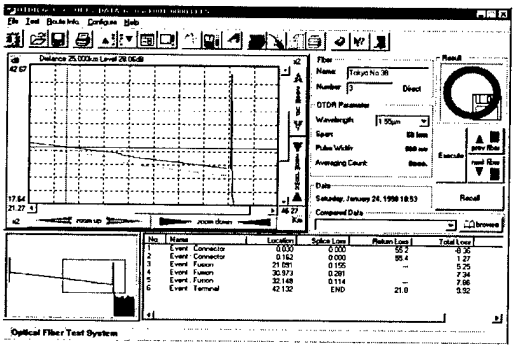

(2) OTDR Test window

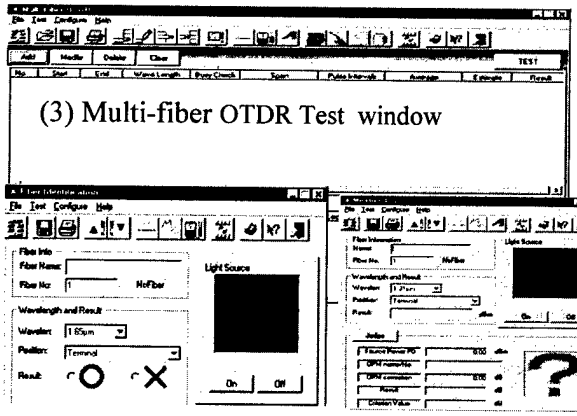

(3) Multi-fiber OTDR Test window

(4) Fiber Identification Test window

(5) Loss Measurement Test window

Figure 4 Test Program windows

- Support up to 4,000 fibers
- Easy to set up, measure and store data.
- Automatic or manual selection for OTDR setup parameters.
- Automatically measure and report splice and fault locations.
- The result waveform of OTDR can be displayed with reference waveform data overlapped.

5. Conclusion

We have described the Remote and Automatic 4,000-Fiber Optcal Testing System. This system consists of a Optical Testing Control equipment , 4 sets of 1,000-Fiber Mechanical optic Switch and a Remote Test Controller. The dimension of the OTC is 480W x 250D x 145H(mm), and that of the FS is 580W x 290D x 68H(mm), Both the OTC and the FS are compact and portable, and can be easily carried around. This system includes many test function : 1.31/1.55/1.65 μ m OTDR test, multi-fiber OTDR test, loss test, fiber identification test and in-line light checking . The OTDR test has fault locating function, automatic checking of optic test result. This system offers a complete testing environment for optical subscriber cable installation testing and optical cable maintenance testing.

6.References

[1] I.Nakanishi,N.Tomita and Y.Enomoto, "Optical Fiber Selector with a Fiber Moving Head and Multi-Fiber Array", Proceeding of the IEICE Communications Society Conference, B-651,pp.318, 1995.

[2] Furukawa,N.Tomita,N.Yamazaki and H.Suda, "Very Compact Optical Fiber Selector Using Fiber Transfer and Fiber Axis Alignment Techniques", Proceeding of the IEICE General Conference,B-986,1994.

[3] Hiroshi Furukawa , Yoshikazu Nomura and Hiroshi Yokosuka, "2×800 DIRECT FIBER TRANSFER OPTO-MECHANICAL SWITCH" Proceeding of the IWCS 1996, pp.900-905

Hiroichi Katayose

Optical
Access Network
Laboratory
Fujikura Ltd.
1440,Mutsuzaki,
Sakura-shi,Chiba,
285-8550,Japan

Hiroichi Katayose graduated in electronics engineering from Technological University of Nagaoka in 1983. He has been engaged in development of telecommunication cable and accessories. He is now an assistant manager of the Fiber and Cable Accessory Department within Optical Access Network Laboratory and a member of IEICE of Japan.

Ken Sakuma

Optical
Access Network
Laboratory
Fujikura Ltd.
1440,Mutsuzaki,
Sakura-shi,Chiba,
285-8550,Japan

Ken Sakuma graduated in materials science and metallurgy from The University of Tokyo in 1995. He is an engineer of the Fiber and Cable Accessory Department within Optical Access Network Laboratory.

Yoshikazu Nomura

Optical
Access Network
Laboratory
Fujikura Ltd.
1440,Mutsuzaki,
Sakura-shi,Chiba,
285-8550,Japan

Yoshikazu Nomura was born in 1951.He received the B.E.degee in mechanical engineering in 1975 from Shinsyu University.
He joined Fujikura Ltd. In 1975 and has been engaged in the research and development of telecommunication cable and accessories. He is now a manager in the Fiber and Cable Accessory Department within Optical Access Network Laboratory.

Kenji Yasuhara

Optical
Access Network
Laboratory
Fujikura Ltd.
1440,Mutsuzaki,
Sakura-shi,Chiba,
285-8550,Japan

Kenji.Yasuhara graduated electronics engineering in from Toyo University in 1987. He has been engaged in development of telecommunication cable and accessories. He is now an engineer of the Fiber and Cable Accessory Department within Optical Access Network Laboratory.

MINIMIZE NETWORK INSTALLATION COSTS BY SETTING APPROPRIATE MAXIMUM SPLICE LOSS VALUES

Peter Lindskog, Bernt Sundström*, Joanna Tyrcha, Rolf Sundberg****

Ericsson Cables AB, Sundbyberg, Sweden, *Ericsson Components AB, Kista, Sweden
*** Stockholm University, Stockholm, Sweden**

ABSTRACT

A mathematical method is presented that makes considerable time and cost savings possible, when installing fiber optic access networks. By setting maximum splice losses in accordance with these results, the specifications for maximum splice loss can be relaxed substantially. Much higher splice losses, up to 0.60 dB (for 16 splices), can be accepted, compared to 0.20 dB, which is typical today. Furthermore the results can be used in development of fusion splice machines in order to optimize cost, speed, simplicity and size. The four-parametric input function offers the possibility to make parameter fittings for most splice loss distributions. Appreciable installation time and cost can be saved, since resplicing can be minimized. As an example, a relaxation of the maximum splice loss value from 0.20 dB to e.g. 0.40 dB, would approximately reduce by 50 % the number of cable joints, where resplicing is necessary.

INTRODUCTION

As the demand for high bandwidth is growing, fiber cables are on an increasing scale installed in the access network. However, most existing fiber optical installation technologies have been developed for the transport network. In the access network the requirements on costs are considerably harder, and thus there is a growing demand for cost-effective installation methods.

Fiber ribbons are frequently utilized in fiber installations. Normally, ribbon splicing is impaired by higher splice loss than conventional splicing. Due to harder requirements on cost, speed, simplicity and size, future ribbon splice machines for access networks are also likely to suffer from higher losses.

However, splice loss requirements are normally set unnecessarily hard. In most cases there are many concatenated fusion splices between the transmitter and the receiver. In the network planning the maximum allowed splice loss value for one splice is often regarded as the maximum mean value for the splices in a link. Since it is very unlikely that all splices in a link get the worst permitted splice loss, the requirements can be relaxed considerably. Today, it is customary to resplice all splices with losses higher than a certain limit value, e.g. 0.20 dB. This limit value is also regarded as a maximum mean value for concatenated splices.

In this study more appropriate splice loss requirements are calculated by statistical analysis. The requirement on individual splices is chosen in such a way that the whole chain of splices get an appropriate splice loss distribution with respect to a specified maximum mean loss value, with a controlled low risk of exceeding this specified maximum value.

SPLICE LOSS DISTRIBUTION FOR ONE SPLICE

Splice loss due to core eccentricity

Fiber core eccentricities are due to a number of independent errors from manufacturing. Therefore the core center position can be seen as randomly distributed according to a rotation-invariant two-dimensional Gaussian probability distribution around the fiber-cladding center, with a variance parameter ν, say. In a splice situation we consider the relative positions of two more or less

eccentric core centers, independently positioned. Their difference in position is also a Gaussian vector in the plane, (x,y), but now with variance parameter $2v$.

The coupling loss u in the splice of two optical fibers is determined by the overlap integral of the assumed Gaussian mode fields. With a distance d between the core centers the splice loss u (in dB) is proportional to the squared distance $d^2 = x^2 + y^2$, more precisely it is given by $u = kd^2$, where $k = 10 \log e / w^2$ for a mode field radius w.

As well-known in probability theory, it follows from the Gaussian density for (x,y) that $u = k(x^2 + y^2)$ is exponentially distributed[1], with mean value $4kv$, that is the density for u is

$$f(u) = \frac{1}{4kv} e^{-\frac{u}{4kv}}, \quad u \geq 0. \qquad (1)$$

According to experience, this exponential is usually the dominating source of randomness in splice loss.

Splice loss due to other causes

However, several other small errors contribute differently to the total splice loss, e.g. mode field mismatch, core deformation, angular misalignment, measurement errors (an apparent loss). For small losses, the total loss in dB is approximately equal to the sum of the individual losses[2]. They are independent and consequently they will add up to an approximately Gaussian random loss contribution. When this is added to the exponential loss the total loss will have a distribution that is the convolution of the exponential and the Gaussian distributions. This was pointed out by Bonnedal[3]. This distribution depends on three parameters: the mean value (equal to the standard deviation) $1/\lambda$ of the exponential, where λ is the intensity parameter, and the mean μ and the standard deviation σ of the Gaussian component. Its density is given as

$$g(u) = \lambda \exp\left\{\frac{\lambda^2\sigma^2}{2} - \lambda(u-\mu)\right\}\Phi\left(\frac{u-\mu-\sigma^2\lambda}{\sigma}\right) \qquad (2)$$

where Φ denotes the standard Gaussian cumulative distribution function. In the notations of (1), $1/\lambda = 4kv$.

Ribbon splicing

When splicing ribbons, the fiber claddings are guided by V-grooves and are not aligned individually. Curl (bent fibers), diameter variations, non-circular claddings and dirt on fibers or in V-grooves will cause cladding offsets, that can vary considerably, and their distribution is unknown. Additionally, length differences between the individual fibers will give core deformations. All these factors affect the splice losses in a way that is difficult to predict. Figure 1 shows a histogram of 598 losses from ribbon splicing. By a modified maximum likelihood estimation method the parameters were estimated to be: $1/\lambda$ = 0.062 dB, μ = 0.017 dB and σ = 0.016 dB. Figure 1 can show that this distribution fits data well, except for occasional high losses.

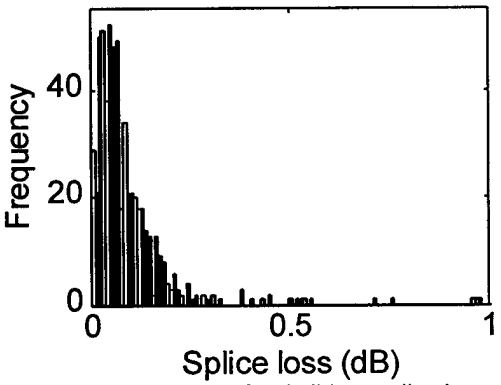

Fig. 1 Histogram of 598 ribbon splice losses from an installation in Stockholm.

Ribbon splicing is particularly vulnerable to occasional high losses, which do not follow any specific statistical distribution. Nevertheless they are important to allow for, since they can have a huge influence on the total loss. We incorporate them in the statistical model by specifying only the (typically small) frequency δ with which they occur. Thus the Bonnedal model (2) is modified by stating that individual losses belong to the distribution (2) with probability $1 - \delta$, and are unspecified high losses with probability δ. The probability δ is a fourth parameter that must be estimated from historical data or given a value in some other way. With the data shown in Fig. 1, δ = 3 % was judged reasonable, counting losses above 0.35 dB as high losses (up to a highest value of 1.2 dB).

Distribution for approved splices

When splices above a maximum tolerated loss value T are rejected and remade, it means that the distribution (2) is truncated at T. The truncated density $g_T(u)$ can also be expressed explicitly in terms of Φ and elementary functions:

$$g_T(u) = \frac{g(u)}{G(T)}, \quad u \le T \tag{3}$$

where

$$G(T) = \Phi\left(\frac{T-\mu}{\sigma}\right) - \exp\left\{\frac{\lambda^2\sigma^2}{2} - \lambda(T-\mu)\right\}\Phi\left(\frac{T-\mu-\sigma^2\lambda}{\sigma}\right)$$

is the cumulative distribution function corresponding to g, that is G(T)=Prob{splice is accepted}, given that it comes from distribution (2).

SPLICE LOSS DISTRIBUTION FOR CONCATENATED SPLICES

In this section we assume that distribution (3) holds, and defer the problem of occasional high losses to the next section. The probability distribution for the total splice loss for n concatenated splices is the convolution of n copies of the distribution for the individual splice. The convolution of g_T with itself cannot be explicitly given. Usually calculations for convolutions are made via Fourier transforms and Fourier inversion, since convolution of distributions corresponds to multiplication of their Fourier transforms. However, the truncated distribution (3) for the individual splice loss has no explicit Fourier transform.

Instead, the distribution for the total splice loss has been calculated by a saddlepoint approximation[4]. This is a very accurate distribution approximation in many situations. The saddlepoint approximation method uses the Laplace transform, and the Laplace transform $\varphi(\theta)$ of (3) can be explicitly calculated:

$$\varphi(\theta) = \frac{1}{G(T)(1-\theta/\lambda)}\left[b_1(\theta) - b_2(\theta)\right]$$

where

$$b_1(\theta) = \exp\left\{\mu\theta + \frac{\sigma^2\theta^2}{2}\right\}\Phi\left(\frac{T-\mu-\sigma^2\theta}{\sigma}\right)$$

and

$$b_2(\theta) = \exp\left\{\frac{\lambda^2\sigma^2}{2} + \lambda\mu + T(\theta-\lambda)\right\}\Phi\left(\frac{T-\mu-\sigma^2\lambda}{\sigma}\right).$$

The sum S_n of n losses has the Laplace transform $\varphi(\theta)^n$, with logarithm $K(\theta) = n \ln \varphi(\theta)$, the so called cumulant transform of S_n . Of special importance are its two first derivatives $K'(\theta)$ and $K''(\theta)$. Explicit expressions for these functions will not be given here, but are found separately [5].

We require a good approximation to the tail probability Pr (S_n>s) for the total loss to exceed a limit value s. For any such s the corresponding root $\hat{\theta} = \hat{\theta}(s)$ of the equation $K'(\theta) = s$ (the saddle point) has a crucial role. Here is the saddle point approximation to the tail probability formula (see (2.2.6) pp.27 [4]):

$$\Pr(S_n \ge s) = \varphi(\hat{\theta})^n \exp(-\hat{\theta}s + \tfrac{1}{2}\eta^2)[1-\Phi(\eta)] \tag{4}$$

where $\eta = \sqrt{n\hat{\theta}^2 K''(\hat{\theta})}$

A refinement is possible but was not found necessary[5].

As typical for many applications the saddlepoint equation $K'(\theta) = s$ cannot be solved analytically, although the solution $\hat{\theta}$ exists. The saddlepoint method can still be applied by solving the equation numerically. One possibility is to use Newton-Raphson type methods to calculate the saddlepoint. These methods will typically work well, because K' is an increasing function. The second derivative exists and is always positive. We have written a Matlab® computer program to perform these calculations.

The approximation has been checked in the special case of no Gaussian error contribution (σ= 0), when more exact calculations can be carried out by Fourier inversion. The approximation was found to be excellent. On theoretical grounds, there is no reason to believe that the approximation is worse with Gaussian error (σ> 0).

Modification to allow for "High Losses"

Here we show how the calculations can be modified to allow unspecified high losses with a

small frequency δ. We substitute with a worst case, in two steps. Some of these losses will probably fall outside the maximum tolerated loss value T. This proportion will of course depend on T. The worst case is that all fall within T, so they all contribute to the total loss. If so, the worst case is that they all equal T. This leads to the "worst case model": A (small) binomially Bin(n,δ)-distributed random number r of the n splices each contribute the loss T, together rT. The remaining $n - r$ losses follow the distribution (3). For fixed r the distribution of their loss sum S_{n-r} can be calculated by the saddlepoint approximation (4). In particular

$$\Pr(S_{n-r} > s - rT) \qquad (5)$$

can be calculated, and for fixed r this is equivalent with $\Pr(S_n>s)$. It only remains to calculate the mean value of (5) over all possible r-values, by weighting with the corresponding binomial probabilities and summing. Since δ is small, most weight will fall on $r = 0$, unless n is very large. Nevertheless, the modification is important when we aim at realistic values of small tail probabilities.

CALCULATION RESULTS

As an example appropriate maximum splice loss values have been calculated, based on splice loss data of a recent installation in Stockholm, (Fig. 1). In Fig. 2 the result has been plotted against the number of concatenated splices between transmitter and receiver. If maximum splice loss values are set as shown in Fig. 2, then the risk would be < 1 ‰, that any of the four fiber lines, in a 4-fiber ribbon link, should get a too high mean splice loss. Also plotted are the corresponding mean splice loss values for approved splices. These values are almost constant, i.e. very little affected by the maximum splice loss values.

For practical reasons maximum splice loss values should be a multiple of 0.05 dB, and therefore it is recommended that all calculated maximum splice loss values are rounded downwards to such values.

Fusion splices with too high loss values may be mechanically unstable. Consequently, there is an upper limit for the maximum splice loss values and these statistical results should be used with care.

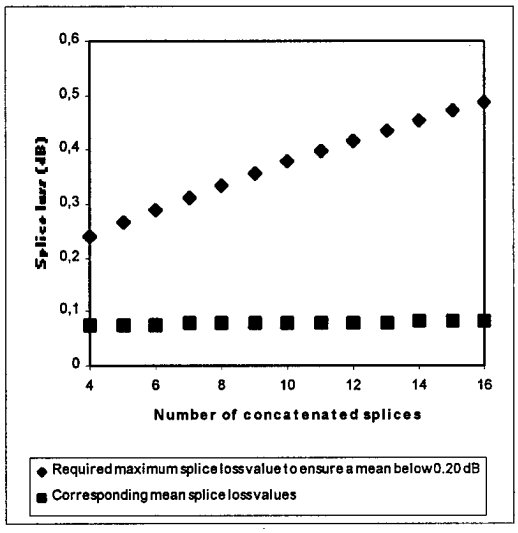

Fig. 2. Calculated maximum splice loss values plotted against the number of concatenated splices. The risk is less than 1‰, that any of the four fiber lines, in a 4-fiber ribbon link, exceeds 0.20 dB mean splice loss.

TIME SAVINGS

By relaxing the loss requirements as described here, much time can be saved, as fewer splices must be remade. Resplicing work is often expensive since it implies additional travelling to the cable joints, that access to the joint closures must be rearranged, that the joint closures must be reopened and reclosed etc. Furthermore, it is often a work for two persons, as one of them makes the resplicing work and the second one performs the OTDR measurements.

According to splice loss data from a recent installation, a relaxation of the maximum splice loss value from 0.20 dB to 0.40 dB, say, would approximately reduce by 50% the number of cable joints, where resplicing is necessary.

The main Swedish telecom operator Telia has for a period used relaxed splice loss requirements at some fiber network installations in rural areas. The result has been satisfactory and as a matter of fact very few splices have needed resplicing.

CONCLUSION

Field installation time and cost can be reduced substantially if higher individual splice losses are accepted, as long as the risk of exceeding a specified total loss value can be kept low. The

mathematical statistical method, using saddlepoint approximation, calculates the risk, that the total splice loss for the concatenated splices will exceed a specified maximum value, as a function of the maximum splice loss limit for the individual splice. By fitting input parameters to splice loss data, this method can easily be used for different loss distributions. The four-parametric splice loss distribution has not only been theoretically motivated but also found to fit data.

REFERENCES

[1] D.B. Payne, D.J. McCartney, Splicing and connectors for single mode fibres, Proc. Int. Conf. on Communications (ICC), Denver, 1981

[2] E.-G. Neumann, "Single-Mode Fibers", Springer-Verlag, Berlin 1988, p. 216

[3] D. Bonnedal, Statistical design of connector loss in local loop fibre optical transmission systems, EFOC/LAN London 1991

[4] J.L. Jensen, "Saddlepoint approximations", Oxford University Press 1995

[5] J.Tyrcha, R. Sundberg, Techn. report B:45, Mathem. statistics, Stockholm Univ. 1998

Peter Lindskog
Ericsson Cables AB
SE-172 65 Sundbyberg, Sweden
peter.lindskog@
eca.ericsson.se

Peter Lindskog is member of staff at Ericsson Cables AB, developing fusion splicing machines for optical fibers. He received his M.Sc. in Engineering Physics at Lund Institute of Technology 1994. He joined Ericsson the same year, and has worked in a research team, Fiber Network Application Laboratory, FiNAL, whose objective was to find competitive fiber solutions for tomorrow's access networks.

Bernt Sundström
Ericsson Components AB
SE-164 81 Kista, Sweden
ekabesu@eka.ericsson.se

Bernt Sundström received his Ph.D. in Semiconductor Physics (1981) from the Royal Institute of Technology (KTH) in Stockholm. He joined Ericsson in 1982 and has worked with optical fiber measurements, splicing, standards, education and reliability.

Joanna Tyrcha
Mathem. Statistics/SFG
Stockholm University
SE-10691 Stockholm, Sweden
joanna@matematik.su.se

Joanna Tyrcha received her Ph.D. in mathematics at the Jagiellonian University in Cracow in 1989. She worked for the Polish Academy of Sciences until 1992, when she moved to KTH, Stockholm. She has now a tenure position at Stockholm University as lecturer and in the departmental consulting group, SFG.

Rolf Sundberg
Mathem. Statistics/SFG
Stockholm University
SE-10691 Stockholm, Sweden
rolfs@matematik.su.se

Rolf Sundberg received his Ph.D. in 1972 from the dept of mathematical statistics at Stockholm University, where he is now professor. He works in both theoretical and applied statistics, including the departmental consulting group (SFG).

Optical and mechanical characteristics of optical cable after field aging and storage

Ting-chung Chang, Whei-Jen Chen, Chieh-Mei Hsiao, H.-F. Lin, His-Pai Hsu, Y.-c. Lin, Yuan-kuang Tu

OSP, Telecommunication Labs, Chunghwa Telecom Co., Ltd., Taiwan, ROC

Abstract

In this study, we investigate the optical properties and mechanical properties of fiber specimens that taken from the dismantled optical cable after field service. These test data of dismantled field service cable were compared with those of unaged fibers from the same vendor and fibers in loose tubes that stored in laboratory.

From the splicing test results among these field aged cable, we found that the increasing of fiber splicing losses were not due to the fiber itself but coming from the parameter setting of fusion splicer. Tensile measurements showed that the field environment is not the only factor that influences the fiber strength. The compatibility between the fiber coating and loose-tube filling compound also play an important role.

Introduction

The decreasing of fiber price and the increasing demand of bandwidth expected to provide voice, data, video, and multimedia services in future access networks has prompt the vast deployment of optical fiber cables. Virtually for every telecom service provider, their conduits are full of optical cables. Although there are no formal statistics data concerning the optical breakout that results to telecommunication outages, messages about fiber break in splice closures or in cables after a short time services remained keeping reporting by field people from time to time. Obviously, the mechanical and optical properties of optical cable are not as environment-proved as they are supposed to be, especially in a service area such as the subtropical weather zone with high temperatures and high humidity. There are abundant papers[1-7] that deal with the optical fiber strengths effected by laboratory accelerated aging, but most of these aging tests are based on uncabled optical fibers in hot water or in high humidity environment, which are not exactly the case of a real field experience.

As a result, there is always a need to actually take a look of the optical cable that has been deployed and under field aging for a certain time. It is necessary to establish some optical fiber cable performance after aging in field and correlate the data with the laboratory simulated test data.

In this study, we investigate the optical and mechanical properties of fiber specimens taken from 7 pieces of dismantled optical cables that under field service of 1-6 years to assess the effects of exposing the optical cables to the typical subtropical zone with high temperature and humidity environment. Originally, The field people were tried to rerouting the above cables due to an expansion of routs. They found that the fibers from these cables were hard to handle and the splicing losses were unexpectedly high.

In addition, the test data of dismantled field service cables were compared with those of unaged fibers from the same vendor and fibers in loose tubes, which stored in the laboratory environment. The cable structures included the loose-tube and mini-bundle cables.

Experimental

Sample

7 pieces of field service aged dismantled optical cables from 4 different manufacturers (A, B, C, D) and one piece of loose tube (E1, containing 6 fibers) as shown in table 1 were chosen for testing.

Table 1: Test samples

Sample	Field Service Time	Storage Time	Storage Environment
A1	Unknown	≤ 1 year	indoor
A2	unknown	≤ 1 year	indoor
A3	3 years	≤ 1 year	outdoor
A4	5 years	3 years	outdoor
B1	3 years	≤ 1 year	indoor
C1	6 years	3 years	outdoor
D1	1 year	≤ 1 year	indoor
E1		8 years	indoor

Note: ① A, B, C, and D are designated as dismantled cables from different supplier
② E is designated as the fiber removed from a loose tube

Fiber optical properties

All the fiber optical properties

such as cutoff wavelength, and mode field diameter were measured according to the description on FOTP-80 and FOTP-167. The splice loss of every spliced fiber was measured by OTDR in accordance with industry recommended test procedures.

Fiber tensile strength

Minimum of 30 specimens for each sample were measured by Universal Testing Machine using a gage length of 500 mm and a strain rate of 20 mm/min in a laboratory ambient environments of 23 ℃ and relative humidity of 60%.

Field aged dismantle optical cable splicing test

Splicing test were performed by splicing any two pieces of the fibers. The combination includes fibers with different geometry; cables with different manufacturers or vintage and fibers from the same cable etc.

Results and discussion

To evaluate the effects of MFD and cutoff-wavelength to the splice loss, the optical properties of fibers from the dismantled cables and splicing losses in between them were measured. Table 2 is a typical result.

Table 2: Fiber optical properties and splice loss between adjacent fibers

Fiber in blue loose tube(A2 cable)			
Fiber color	MFD(μm) 1310 nm	cutoff wavelength	splice loss (1310 nm)
B	9.15	1212	< 0.1dB
Y	9.27	1239	< 0.1dB
G	9.37	1219	0.19 dB
R	8.88	1218	0.15 dB
V	9.13	1216	< 0.1dB
W	9.11	1248	
Fiber in yellow loose tube(A2 cable)			
Fiber color	MFD(μm) 1310 nm	cutoff wavelength	splice loss (1310 nm)
B	9.15	1246	< 0.1dB
Y	9.20	1247	< 0.1dB
G	9.13	1233	0.14 dB
R	8.87	1210	0.13 dB
V	9.13	1197	< 0.1dB
W	9.17	1227	

From Table 2, the optical properties test results showed that the optical properties of all the field-served fibers appeared no change when comparing with those unaged fibers. It was also found that when the MFD differences of two fibers were smaller than 0.2 μm, the splicing loss would be within 0.1 dB. But when the MFD differences were larger than 0.2 μm, the splicing loss were in the range of 0.1dB to 0.2 dB.

We also carried out the inter-

cable and intra-cable splicing tests among these field aged cables to find out the cause for high splicing losses that were reported from the craftsman.

We chose 12 fibers from two loose tubes of each field aged cable to carry out 144 arc fusions for every simulated splicing test. The splicing combination include (a) splicing within the same cable (b) splicing of fibers from different manufactures but having the same fiber attenuation (c) splicing of fibers from the same manufacture but with different fiber attenuation and vintage (d) splicing of dissimilar fibers from different manufactures. The fusion yield was defined as " every step in fiber fusion process were success". These include fiber stripping, wiping, cutting, putting in the V-groove, and splicing loss less than 0.2 dB. Table 3--6 showed the results of each simulated splicing test.

Table 3: Splicing test within the same field aged cable

Cable	A2-A2	B1-B1	C1-C1	D1-D1	A3-A3
Mean splice loss	0.04 dB	0.03 dB	0.03 dB	0.04 dB	0.04 dB
Yield	97%	99%	96%	98%	80%

Table 4: Splicing test of fibers from different manufacturers but with the same fiber attenuation

Cable combination	☆0.4 dB A4 - 0.4 dB D1	0.5 dB A1 - 0.5 dB B1
Mean splice Loss	> 0.2 dB	0.05 dB
Yield	36%	98%

☆ : After re-adjusting the electrode rod position and re-making splice test, the mean splice loss decreased to 0.05 dB and the fusion yield increased to 94%

Table 5: Splicing test of fibers from the same manufacturers but with different fiber attenuation and vintage

Cable combination	☆0.5 dB A3 - 0.4 dB A4
Mean splice loss	> 0.2 dB
Yield	66%

☆ : After re-adjusting the arc power and re-making splice test, the mean splice loss decrease to 0.05 dB and the fusion yield increase to 92%

Table 6: Splicing test of dissimilar fiber from different manufacturers

Fiber	A2 - C1	B1 - C1
Mean splice Loss	0.06 dB	0.03 dB
Yield	95%	97%

Note: A; B are matched cladding fiber
C is depressed cladding fiber

From the simulated splicing test results, we could conclude that most of the mean splicing losses are in the range of 0.01 dB to 0.06 dB and are below the specification of our user requirement for splice losses cutoff(0.2 dB). But in some cases, the mean splicing losses were very high, we need to break and re-splicing again and again. When re-adjusting the fusion splicer parameters (such as electrode rod position; arc powers) and re-making the splice, the splicing losses dropped below 0.06 dB. Obviously, the high fiber splicing losses were not due to the fiber itself, but was due to the parameter setting of the fusion splicer. It is necessary for everyone that to check the fusion splicer parameter setting and to do arc test before carrying out a fusion work.

From table 3, the mean splice losses for fibers splicing within the same A3 cable were well below the fusion splice criterion of 0.2dB, but the fusion yields were below the acceptance value. Carefully inspecting the failure reasons of each splicing, we found that fiber stripping, cutting, and wrapping were the main causes of splice failures. Tensile measurements showed that the strength of A3 cable fiber was about 60% lower than that of its unaged original fiber. The tensile strength distribution appears to be very broad. In this case, fiber average strip force was 14 gw. We can even strip the fiber by hands, and the strip debris showed as a tube-off type. Evidently, the coating had lost its ability to protect the fiber surface. It must be noticed that the field environment of this case is not so harsher than that for other samples. The strength degradation may be caused by the interaction of filling compound and fiber coating. Similarly, the strength of fiber that was taken off from the loose tube which had stored in laboratory for about 8 years showed a drop of 52% of its unaged original fiber and a broad tensile strength distribution as shown in figure 1. The strip force behavior of the laboratory storage loose tube fiber was similar to that of the A3 cable fiber.

Figure 2 showed the AFM images of field aged A3 cable fiber and laboratory storage E1 fiber and was compared with the counterpart unaged fiber. The mean roughness and maximum height are tabled below:

Table 7: Roughness change of optical fiber after aging

Sample	Mean roughness (nm)	Maximum height (nm)
A3 cable fiber	8.72	65.87
E1 Fiber	8.53	63.73
unaged fiber	0.82	8.72

The increase of roughness on the fiber surface is proportional to the extent of strength drops. Therefore, based on the tensile strength, strip force measurement, and AFM examination, we could conclude that the diffusion of corrosive factors through loose tube filling compound that destroyed the adhesion between fiber and coating and corroded the glass surface was the main causes of tensile strength and strip force drop.

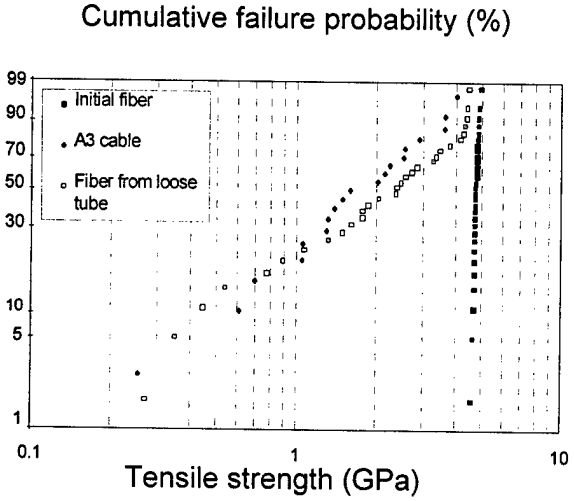

Figure 1: Tensile strength comparison of optical fibers before and after aging

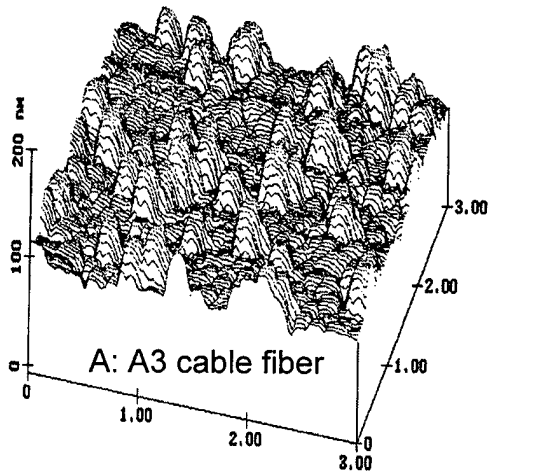

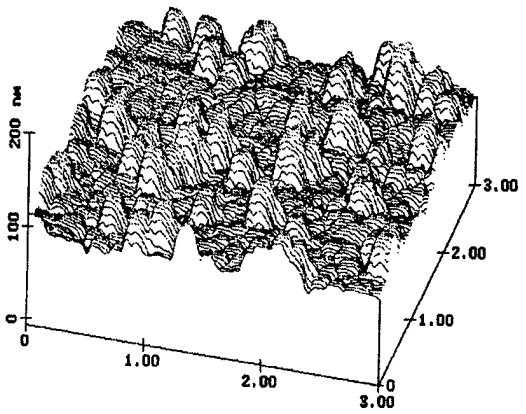

B: E1 fiber (fiber removed from the laboratory storage loose tube)

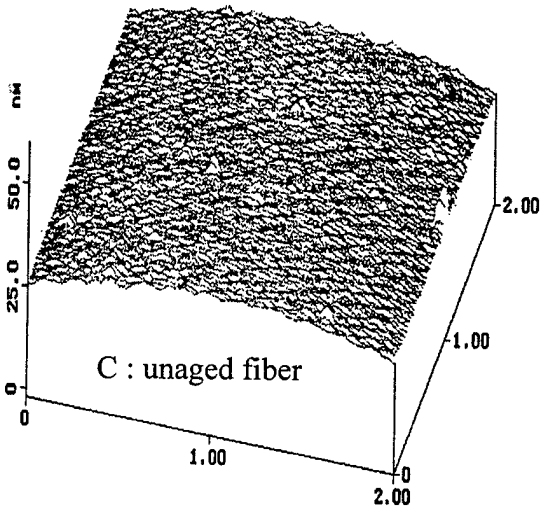

Figure 2: AFM images of optical fiber

This indicates that the field environment is not the only factor that

influence the fiber strength, the compatibility between the fiber coating and the loose tube filling compound also play an important role.

Figure 3 showed the tensile strength of cable fibers that were field-served up to 3 years. These cables were removed from field service for some reasons and stored in indoor environment. The tensile strength dropped by 5% to 10% when comparing to that of the unaged-recently-manufactured fiber. It is therefore concluded that the aging of these cables by the harsh subtropical environment has little degradation effect on the strength distribution of the fiber contained. The strength of these fibers is sufficient for common field handling scenarios during cable repair.

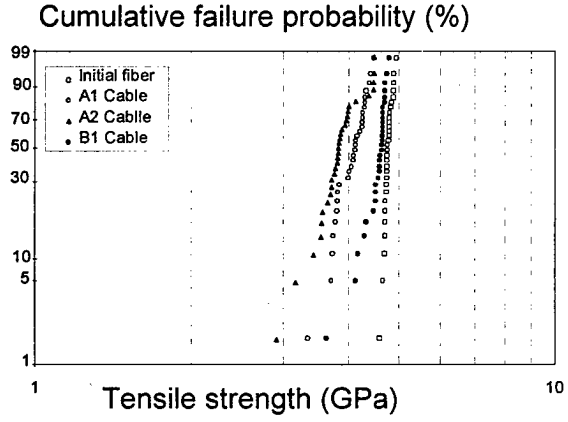

Figure 3 : Tensile strength comparison of optical fiber after field aging.

Conclusion

1. The high fiber splicing losses and handle ability problems that reported from the field people were not due to the fiber itself but due to the unsuitable inappropriate parameter setting of the fusion splicer. It is necessary to check the fusion splicer parameter setting and to do arc test before carries out a fusion work.

2. Tensile measurement showed that the field environment is not the only factor that influences the fiber strength. The compatibility of fiber coating and loose tube filling compound also play an important role.

3. Generally speaking, if the manufacturers choose the proper cable materials, real field aging of optical cable will not result in obvious degradation of the handling ability or mechanical strength of fibers.

Reference

1.H.C. Candan, D. Kalish, J.Am. Ceram. Soc., Vol.65 p171 (1982)

2.M.J. Matthewson, C.R. Kurkjian, J.Am. Ceram. Soc., Vol.71 p177 (1988)

3.H.H. Yuce, C. Wieczorek, A. DeVito Proc. 40th IWCS, p700 (1991)

4.C.R. Kurkjian, D. Biswas, H.H. Yuce, M.J. Matthewson, Proc. 11th NFOEC, p125 (1995)
5.J.J. Carr, Proc. 42th IWCS, p394 (1993)
6.A. Dwivedi, G.S. Glaesemann, C.K. Eoll, Proc. 43rd IWCS, p728 (1994)
7.D. Kalish, B.K. Tariyal, J.Am. Ceram. Soc., Vol.61 p518 (1981)

Biographies

Ting-Chung Chang
OSP, T.L.
Chunghwa Telecom
P.O. Box 6-48, Yang Mei
Taoyuan, Taiwan 326,
R.O.C.

Ting-Chung Chang received his M.S. degree in Applied Chemistry in 1984 from Tsing Hua University and then directly joined T.L.. He is now a research scientist and a member of outside plant laboratory in T.L..

Whei-Jen Chen
OSP, T.L.
Chunghwa Telecom
P.O. Box 6-48, Yang Mei
Taoyuan, Taiwan 326,
R.O.C.

Whei-Jen Chen received her M.S. degree in Applied Chemistry in 1991 from Tsing Hua University and then directly joined T.L.. She is now a research scientist and a member of outside plant laboratory in T.L..

Chieh-Mei Hsiao
OSP, T.L.
Chunghwa Telecom
P.O. Box 6-48, Yang Mei
Taoyuan, Taiwan 326,
R.O.C.

Chieh-Mei Hsiao received her M.S. degree in Chemical Engineering from Tsing Hua University. She joined T.L. in 1981 and presently worked as a research scientist and a member of outside plant laboratory in T.L..

Yih-chyuan Lin
OSP, T.L.
Chunghwa Telecom
P.O. Box 6-48, Yang Mei
Taoyuan, Taiwan 326,
R.O.C.

Yih-chyuan Lin received his Ph.D. degree in Photochemistry from Georgetown University. After working as a postdoctoral Fellow in the Institute of Materials Science at the University of Connecticut, he joined Telecommunication Laboratories in 1989 and presently is the project manager of O.S.P. materials and construction project.

Hsi-Pai Hsu
OSP, T.L.
Chunghwa Telecom
P.O. Box 6-48, Yang Mei
Taoyuan, Taiwan 326,
R.O.C.

Hsi-Pai Hsu is currently a project manager of the material group of Loop and Outside Plant Laboratory, Telecommunication Labs. . He received his Ph.D. degree in Chemistry in 1983 and has engaged in industrial materials research since then.

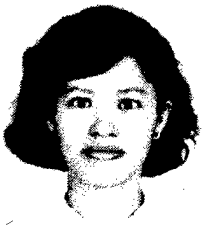

H. F. Lin
OSP, T.L.
Chunghwa Telecom
P.O. Box 6-48, Yang Mei
Taoyuan, Taiwan 326,
R.O.C.

H.F. Lin received her M.S. degree in Chemical Engineering from Tsing Hua University. She joined T.L. in 1981 and presently worked as a research scientist and a member of outside plant laboratory in T.L...

Yuan- kuang Tu
OSP, T.L.
Chunghwa Telecom
OP4423, 12, Lane 551,
Min-Tsu Road Sec. 5,
YangMei,Taoyuan, Taiwan
326, R.O.C.

Yuan-Kuang Tu received his BS, MS and Ph.D degrees in EE from National Taiwan University in 1977, 1979, and 1988. He joined T.L. in 1981 and worked for integrated optics, optoelectronic devices, and optical fiber communications. From 1990 to 1996, he was the project manager of Photonic Technology Research in Applied Research Lab. Now he is the Managing Director of the Outside Plant Technology Lab., and is in charge of the technology developments for access network. He is a member of IEEE/LEOS, IEEE COMSOC, ISHM ROC Chapter, Chinese Institute of Engineering, Optical Engineering Society of ROC, and Electronic Devices and Materials Association.

FAST MULTI-CHANNEL OPTICAL TRANSMITTANCE TESTING FOR OPTICAL CABLE QUALIFICATION

Arthur J Barlow, Danny Deogan, Mark Rendle and Tim G Arnold,

EG&G Fiber Optics, Wokingham, United Kingdom.

ABSTRACT

A new technique to detect optical transmittance in fibre cables and components is presented. The technique provides ultra-fast (50Hz) dual wavelength power monitoring in a large number of fibres (typically 160) with no moving parts. A system description and preliminary results are given.

INTRODUCTION

During the qualification and evaluation of optical components and cables, the measurement of optical transmittance is a common need. IEC-794 (EN18700) is the pertinent international standard, and specifies the use of optical transmission monitoring for testing and verifying the environmental performance of fibre cable under various influences, such as impact, flexure, crush, bending, temperature cycling etc.

The growing demand for higher fibre-count cables and more exacting quality standards within the industry, it is becoming necessary to perform measurements on many of the fibres within a cable qualification sample or component and possibly in both 1300 and 1550 nm windows at the same time. Moreover, it is frequently desirable to monitor the optical power during the impact strike, flexure cycle etc. This necessitates a power sampling-rate in excess of 10Hz for large numbers of fibre channels. Modern fibre cable and component testing requires dual wavelength, ultra-fast, high-count multi-channel power monitoring instrumentation.

This paper describes a new technique to monitor optical power transmission at 1310nm and 1550nm with typically minimum 50Hz sampling rate for up to 160 channels.

BACKGROUND

Optical transmittance loss may be determined by measuring the change in optical power output from the device using stable light source and power meter combination. For each fibre and wavelength to be monitored, at least one power meter and source is required, unless optical splitters are used. With fibre counts in optical cable now exceeding 144 fibres, equipment cost and complexity using this technique becomes prohibitive, and rarely is an integrated instrumentation and data acquisition package possible.

A common way to mitigate this cost and complexity is to use a single light source and detector, but to couple the light via optical switches or couplers to the test fibre channels. Each fibre can be monitored in turn by operating the fibre switches. The optical switching is typically accomplished by physically moving an input fibre into alignment with a chosen output fibre by mechanical means or by using integrated optical switches. Long-term source/detector drift (>1 hour time-scales) can be removed from the measurements by the use of additional fibre "reference" channels, which are not exposed to the test influences. However, mechanical switches require sub-micron mechanical accuracy and repeatability, in order to obtain better than 0.005 dB repeatability, and mechanical wear impacts the long-term durability and reliability of the switch. Typically, the optical switch will limit power measurement repeatability. Moreover, the optical switching time limits the overall monitoring speed to well below that required for cable testing.

NEW TECHNIQUE

To overcome the limitations of current methods, a new technique has been developed [1]. The technique is a combination of source time-division multiplexing into the test fibres and "spatial multiplexing" of the fibre output ends to different detectors. In this way, a very large number of fibre channels can be obtained using a modest number of sources and detectors, while simultaneously obviating the need for optical switches.

A typical system configuration using the new technique is shown in Figure 1. The optical sources are typically lasers or LEDs with optical filtering to provide narrower linewidths suitable for cable and component testing. Pairs of sources, for example at 1310 and 1550 nm respectively, are directed to (typically) sixteen test fibres via a 2x16 fibre-splitter. The entire array of sources are time multiplexed, each source being assigned a given time slot and energised only in that slot. The time slot signals are generated from an electronic clock within the measurement system. Each source is turned "on" in strict time rotation with the other sources in use. Thus for ten pairs sources there would be 20 time slots and 160 fibre leads used for connection to the test fibre cable inputs.

At the test cable output ends, there are typically sixteen large area detectors. Each detector is assigned *one* of the sixteen test fibre outputs from *each* source/splitter. Therefore up to ten fibres are combined using fibre splitters or bundled at the detector face. Each detector is read by a 16-channel data acquisition system, once per time slot. By arranging the fibres going to the sources and detectors as described, it is arranged that each test fibre be addressed uniquely during *one* time slot by *one* of the sources and *one* of the detectors. For ten pairs of LEDs, we have 160 fibre power -monitoring channels, each channel with dual wavelength monitoring.

Generalising this concept for a number, **m**, detectors and a number, **n**, sources, we can obtain a number, **[m x n]**, separate fibre readings (in one multiplex "cycle" of **n** sequential time slots). This provides a substantial cost saving on sources and detectors compared to the source-power meter combination method. The method described also eliminates optical switches and therefore offers a unique combination of higher power detection repeatability and overall speed or channel sample rate. Switching is replaced by source time division multiplexing.

In the configuration shown, a reference channel is not implemented. Because in this configuration, each fibre in the DUT uses a different source/detector combination (this is the key to the technique), no one fibre could be assigned as a reference channel and correctly compensate for the same light source *and* detector as any other test fibre channel. However, using modern electronic and thermal stabilisation techniques for both sources and detectors, adequate stability (~0.002dB/hour) for the short duration of the tests (impact, crush, flexing etc) for which this instrument is applicable has been achieved in practice. For longer term testing, we can exploit the fact that the dominant sources of drift are the LED sources, not the detectors, to obtain a partial referencing system. One detector is assigned as a reference, with its fibres (one coming from each splitter/LED pair) *not* exposed to the test regime. The power readings (collected as described above) from this detector are used to compensate for each respective LED drift. Typically ~0.002dB/24 hour stability is then achievable, permitting the unit to operate in temperature cycling applications also. This level of stability is close to state-of-the art.

The main features and advantages of the system are: -

- *No moving optical parts:* so improving power monitoring stability and maximising reliability and wear.
- *Lower cost for large channel counts:* to support **[m.n]** channels in the system, the required number of light sources is reduced from **[m.n]** in the standard method to **m** in this invention. Likewise the number of detectors is reduced from **[m.n]** to **n**. Thus for a 160-channel system (10.16), only 10 sources and 16 detectors would be required;
- *Time division multiplexing:* light sources are time multiplexed and injected via splitters to many fibres;

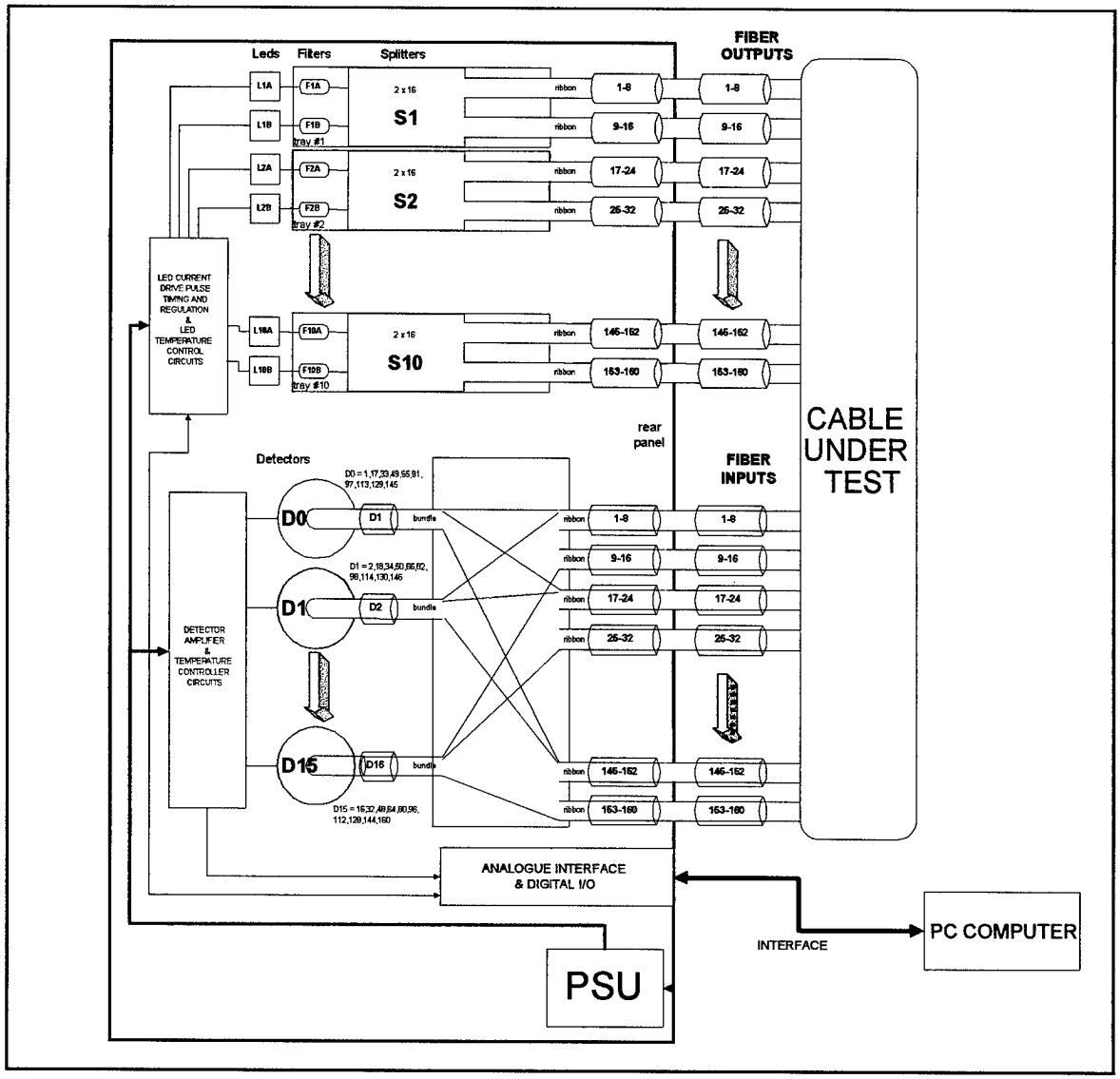

Figure 1: Multiplexed Power Monitoring System Architecture

- *Spatial Multiplexing*: detectors are connected to allow all fibres on source **m** to be arriving at each respective detector in parallel;
- *Flexibility:* the system can be configured with any **m** and any **n** values to allow cable testing, where the number of input ports is equal to the number of output ports;
- *Speed:* the system data logging speed is dictated by the bandwidth of the detector amplification, the system clock and the data logging sub-system. In our implementation, time slots 1ms in length are chosen giving a total cycle time for a 160-channel system of 20 ms (i.e. a complete "160-channel set" of power readings is obtained 50 times per second). The extremely short "cycle time" offered by this method is additional important in that it almost completely eliminates time skew between readings on different fibres on the time scales commensurate with the cable dynamics;
- *Single Integrated Package:* the entire system for up to 160 fibre channel counts can be housed within a 6U 19" cabinet, featuring internal temperature regulation, power supplies, input and output fibre management etc. A PC controls data acquisition, result presentation and storage.

RESULTS

A typical sample result is shown in Figure 2 using a commercially available instrument based on the technique described (EG&G Fiber Optics CPM500). The test sample was a simple group of bare ribbon fibres. Here 32 fibres (arranged in 4 8-way ribbons) are monitored simultaneously, with a 12 ms. sample interval for all channels. During the test time, some of the ribbon fibres were bent by hand with 1 cm. bend radius to introduce a bend loss. The fast data rate and low timing skew allows the fast fibre recovery to be faithfully recorded.

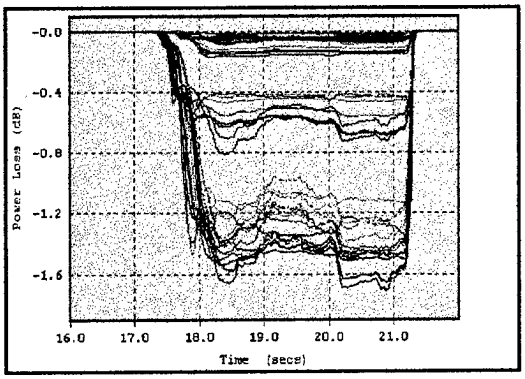

Figure 2: Typical Result for bent ribbon fibres (25 fibres in all)

A second result is shown in Figure 3. Here a sample of cable containing various fibre types from a number of vendors was subjected to a series of four crush test cycles, each with increasing load, at loads in excess of the standard IEC 794 levels. A deliberately slower rate of 1 cycle per second was used to allow for some data averaging. The relative performance of the different fibre types is clearly visible.

However, it is clear that individual fibre performance at each wavelength will depend critically on its inherent properties (micro-bending sensitivity, bend loss, MFD etc.), upon its position within the fibre ribbon, and the ribbon within the cable, as well as on the cable armouring design. Figure 4 shows the detail of the first crush cycle (numbered "1" in Figure 3), at 1550 nm. Note how some fibers react sharply to

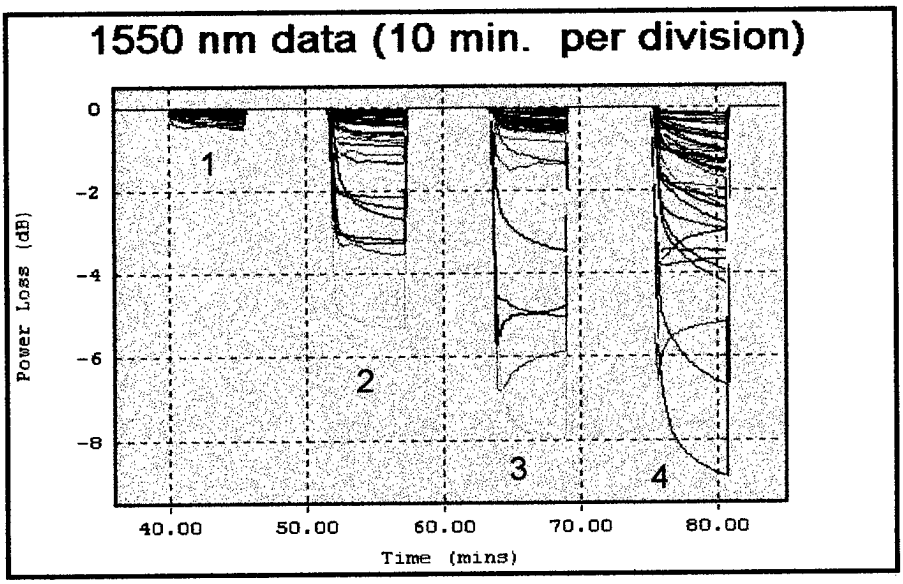

Figure 3: The response of a multi-vendor fiber cable to excessive crush/compression levels showing the response at 1550nm for four different compression force levels at a 1 second sampling rate.

the crush, while others react more gradually.

In Figure 5, we show the differing response at 1310 nm and 1550 nm of the same group of fibers at the same time, for the highest crush level of Figure 3 (the peak mark "4" in Figure 3). Note how the dual-wavelength readout allows the possible diagnosis of cable design issues and the very high data rate has enabled the recovery performance of the fibre cable to be assessed without distortion or significant timing skew between different fibres.

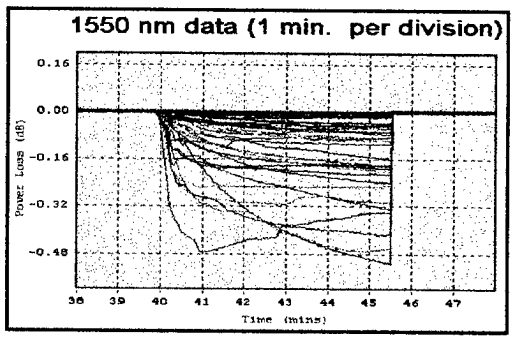

Figure 4: Detail of Figure 3 for peak #1 at 1550 nm

CONCLUSION

A new technique for optical power monitoring in multi-fibre components or cables has been presented. This technique uses a unique multiplexing method to provide ultra-fast (>50 Hz) sample rate in up to 160 fibres simultaneously, at 1310 and 1550 nm. The technique provides many advantages over more conventional environmental monitoring systems using optical switches and/or dedicated sources/power meters for each fibre monitored. The main advantages are speed of readout, high repeatability due to the elimination of optical switching devices, and lower cost for larger fibre counts. Additionally, the use of a reference channel can ensure excellent long-term stability. Preliminary results have been presented to demonstrate the high speed and performance of this technique. This ultra-fast power monitoring technique will assist in the development of high-quality fibre cables with high fibre counts.

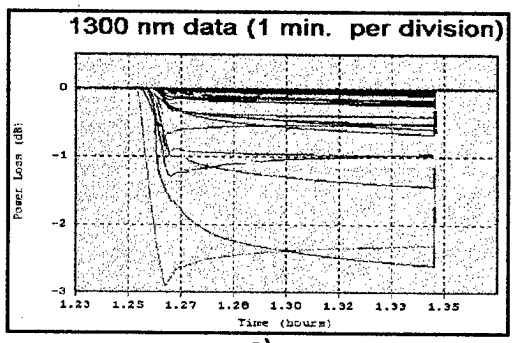

a)

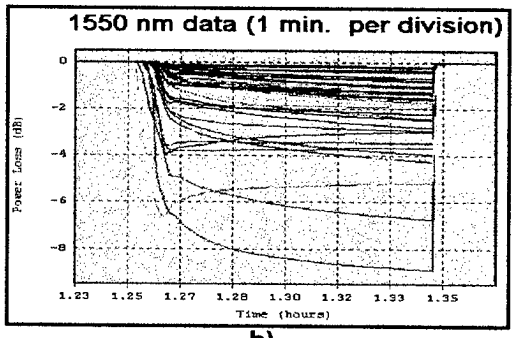

b)

Figure 5: Detail of Figure 3 for peak #4 a) 1310 nm and b) 1550nm.

ACKNOWLEDGEMENTS

The authors acknowledge the help and permission of Alcatel Cable, Claremont, USA and in particular T Voots, V Bourget and J Barker, to use the results of Figure 3/4/5.

REFERENCES

[1] EG&G Fiber Optics: Patent Applied For.

AUTHORS

EG&G Fiber Optics, Sorbus House,
Mulberry Business Park, Wokingham,
RG41 2GY, UNITED KINGDOM.

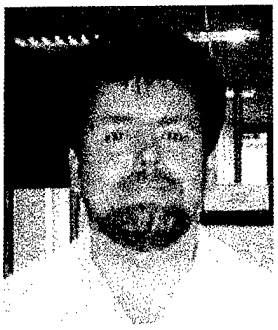

Arthur Barlow joined EG&G in 1985 and Is R&D Manager of the Fiber Optics Division, responsible for development of Fiber Optic Test Equipment. He holds a BSc degree in Applied Physics from Durham University, UK, and a PhD in Optical Fibre Communications from Southampton University, UK. His main interests are fiber measurements, opto-mechanical and instrumentation design. He holds several patents and has published many papers all the in the area of fiber optics and fiber/cable testing.

Danny Deogan joined EG&G in 1996 as a Design Engineer, responsible for electronic design work. He holds a BSc in Electronic Engineering from Glamorgan University, UK. He is currently involved in the development of the Power monitoring system.

Mark Rendle joined EG&G in 1996 as Senior Software Engineer, and has been responsible for software development of the power monitoring system. He is a Graduate of the Royal Society of Chemistry, UK.

Tim Arnold joined EG&G in 1986 and is currently Principal Engineer responsible for all aspects of electronic system design. He holds a BSc degree in Electronic Engineering from Hull University, UK. Tim specialises in analogue circuit design and system analysis.

A STUDY ON MID-SPAN ACCESSIBILITY FOR ULTRA HIGH COUNT SZ-TYPE OPTICAL FIBER CABLE

Hiroki Ishikawa, Yoshiyuki Suetsugu and Gen Morikawa

Sumitomo Electric Ind. Ltd., Yokohama Japan

ABSTRACT

In order to adequately design ultra high count SZ-type optical fiber cables which have good mid-span accessibility, we have first analytically calculated fiber slack length strictly considering slack length reduction caused by cable core and dependence on sheath removal position. The derived calculation method was verified through model experiment. Moreover, three approximation methods for slack length estimation were proposed, and their accuracy and available limits were examined. Using the result of the study, 2000-fiber SZ-type cable consists of 8-fiber ribbons was designed, manufactured and confirmed its good mid-span accessibility.

INTROCUCTION

Recently a demand for SZ-type ultra high count optical cable for example 2000-fiber, is increasing because of its good mid-span accessibility.[1] In order to achieve this kind of cable with high transmission property and enough mid-span accessibility, it is necessary to establish the method to estimate slack length accurately, because large slack length requires short SZ-pitch, but too short pitch stranding may cause optical attenuation increase.

However, it has not been established an accurate slack length estimation method but approximate calculation, because of its complexity.

In this paper, we present the strict slack length estimation method and its experimental validation. Three approximation methods are also proposed, and examined their accuracy.

SLACK LENGTH CALCULATION METHODS

In this section, we explain the derivation of strict slack length estimation method and three approximation methods. The approximation methods become rougher from Approx.-1 to Approx.-3, as described in the following, and their approximated points are summarized in table 1.

Table1 Summary of estimation methods

Method	Fiber Length Calculation	Diminish by Cable Core	Roundabout Route
Strict	Numerical Integration	Concerned	Concerned
Approx.-1	Numerical Integration	Concerned	Not Concerned
Approx.-2	Approx. Avg.	Concerned	Not Concerned
Approx.-3	Approx. Avg.	Not Concerned	Not Concerned

Strict Calculation

The fiber slack length, which is defined by d in fig. 1(a) has the maximum value when sheath removal length L is equal to SZ pitch P as shown in fig.1 (a). However, when L is not equal to P, d is diminished by two factors. One is that cable core's effect as denoted by g in fig. 1(b). The other is that fiber must take a roundabout route on cable core surface in section B-C in fig. 1(b).

In order to derive the strict slack length estimation method, it is necessary to clarify the fiber path from the point B to C in fig. 1(b). The path can be clarified by expanding cylinder surface to a plane which contains a straight line AB. On the plane, the fiber path A-B-C is on one straight line, because the fiber must take the short cut route. From this

premise, the relationship between fiber length, sheath removal length L and slack length d is denoted as eqs.(1). In eqs.(1), a and ϕ mean path radius of fiber and reversing angle, respectively.

$$\frac{L_f}{2} = \sqrt{a^2(\eta-\beta)^2+b^2} + \sqrt{(x^2-a^2)+(\frac{L}{2}-b)^2}$$

$$b = \frac{\frac{L}{2}a(\eta-\beta)}{\sqrt{x^2-a^2}+a(\eta-\beta)}$$

here $\beta = \cos^{-1}\frac{a}{x}$, $x = d + a$,

$$\eta = \frac{\phi}{2}\left|\sin\left(\theta_0+\frac{L}{P}\pi\right)-\sin\left(\theta_0-\frac{L}{P}\pi\right)\right|\Big/2 \qquad (1)$$

In eqs.(1), L_f means the laid fiber length in sheath removed section, and it is obtained by calculating eq.(2).

$$L_f = 2\int_{\theta_0}^{\theta_0+L\pi/P}\sqrt{1+\left(a\frac{\phi}{2}Cos(\theta)\right)^2}\,d\theta \qquad (2)$$

In strict sense, L_f depends on sheath removal position, thus it is necessary to calculate numerical integration for case by case. In eq.(2), θ_0 means the phase angle at the middle point of sheath removed section. Substituting the obtained L_f to eqs.(1), and solving the equation, the strict value of slack length d can be estimated. The eqs.(1) is so complicated that we solved them by using an aid of computer.

On the other hand, in the case of the fiber does not take the roundabout route, the slack length d is obtained by eq.(3). The second term of the equation denotes the slack length diminution by cable core.

$$d = \sqrt{\left(\frac{L_f}{2}\right)^2-\left(\frac{L}{2}\right)^2-(a\cdot\sin\eta)^2}-a(1-\cos\eta) \qquad (3)$$

Here, whether fiber takes roundabout route or not is distinguished by eq.(4). If the D, defined by eq.(4) is less than zero or η, defined as in fig.1(b) is greater than $\pi/2$, the fiber takes roundabout route on cable core surface.

$$D = \sqrt{\left(\frac{L_f}{2}\right)^2-\left(\frac{L}{2}\right)^2-(a\cdot\sin\eta)^2}+a\cdot\cos\eta-\frac{a}{\cos\eta} \qquad (4)$$

Approximation Method-1

The first approximation method is the same as strict one, but neglect the effect of taking roundabout route on cable core surface.[2,3] So the slack length is estimated by eq.(3) for any sheath removal position and for any SZ-pitch. This means that the estimated slack length by this method agrees with the strict value, in the case of that the fiber does not take the roundabout route.

This method is easier than the strict one and can be conducted analytically except for the numerical integration for L_f.

Approximation Method-2

In the second approximation method, an average fiber laid length L_{f2} is used instead of L_f used in eq.(3). The L_{f2} is obtained by eq.(5).

$$L_{f2} = L\left\{1+\left(\frac{a\pi\phi}{2P}\right)^2\right\} \qquad (5)$$

As seen from eq.(5), L_{f2} can be easily calculated. Thus in this approximation method, fiber slack length is estimated by whole analytical calculations. This point is the greatest merit of this approximation method.

Approximation Method-3

The third approximation method is the most popular and simplest one.[4] Here, an average laid fiber length L_{f2} is used and the two slack length reduction effects caused by cable core and fiber's roundabout route are neglected. In this method, the slack length is estimated by eq.(6).

As seen from the eq.(6), this method gives no dependence of slack length on sheath removal position.

$$d = \sqrt{\left(\frac{L_{f2}}{2}\right)^2-\left(\frac{L}{2}\right)^2} \qquad (6)$$

SLACK LENGTH CALCULATION RESULTS AND EXPERIMENTAL VERIFICATION

Calculation Results

We calculated the fiber slack length for the case of SZ-pitch is 800mm, path radius a is 15mm, and

reverse angle ϕ is 275°. Fig.2 shows the calculation results. In the figure, X-axis means the distance between the center of sheath removed section and the middle point in between reversing points of SZ-stranded fiber. Here, X=0 means that the middle point in between reversing points is on the center of sheath removed section, and θ_0 =0 in eq.(2). X=P/4 means that a reversing point is on the center of sheath removed section, and $\theta_0 = \pi/2$ in eq.(2). The calculation results denote that every method but approximation method-3 gives the minimum value when X=0. This result is naturally understood as that the reduction in slack length caused by cable core is maximized in this case.

In the cable design, it is necessary to assure the minimum slack length, so the minimum value has the most important meaning.

We also calculated the dependence of the minimum slack length on SZ-pitch. The calculation results for the case of sheath removal length is 500mm, path radius is 5mm and reverse angle is 275° are shown by fig.3. As seen from fig.3, the strictly estimated slack length is shorter than approximated value at longer SZ-pitch and it is relatively long under the condition $L = n^*P$, here n is an integer. At this SZ-pitch, the slack length reduction effect caused by cable core is minimized. Approximation method-3 gives most optimistic estimation result. The estimated slack length coincides with strictly estimated value under the condition $L = n^*P$, however at other SZ-pitch, the estimated slack length is longer than the strict value.

Approximation method-1 and -2 give estimated slack length which is very close to the strictly estimated value. The discrepancy from the strict value are only few millimeters at any point in calculated region.

Experimental Verification

In order to confirm the validity of our proposed strict estimation method, we conducted a model experiment. We drew an SZ path of SZ-pitch is 800mm on a cylinder whose diameter is 30mm, and put a coated fiber on the path with glue to stick on the cylinder surface. Then we removed the fiber for 500mm length of the cylinder and measured slack length. The measurement results is shown by filled circles in fig.2. They showed good agreement with the strictly estimated value. From this experimental result, the validity of our calculation method was confirmed.

ACCURACY EXAMINATION

The strict estimation is rather complicated and unable to be processed with pocket calculator. Therefore it is desirable to allow the approximation methods to use for cable design in some regulation or correction. In this section, the accuracy or the discrepancy of each approximation method from strict estimation method is examined.

In order to clarify the accuracy, we calculated slack length using strict and approximation methods for 250~1400mm of SZ-pitch, 500mm and 700mm of sheath removal length, and 2.5~20mm of path radius, but reverse angle was fixed to 275°. The calculation results were summarized in fig. 4 in which the ratio of P/L is taken for X-axis, and the ratio (approximately estimated slack length) /(strictly estimated slack length) is taken for Y-axis. From fig. 4, some knowledge can be drawn as follows.

At first, the ratio of each approximated value to strict value depends on only the ratio of sheath removal length to SZ-pitch, but has few dependence on path radius. In fig. 4, Approximation method-2 and -3 show variation of the ratio depends on path radius, and longer path radius gives larger discrepancy from strict value.

Approximation method-1 gives the most accurate estimation among the three methods. The estimated value exactly agree with the strict value when the ratio of SZ-pitch to sheath removal length is less than about 1.3. However, at the longer SZ-pitch which makes the ratio larger than 1.3, the estimated value is longer than the strict value.

Approximation method-2 gives the value very close to the strict one. The discrepancy of the estimated value from the strict one is less than 10% in the P/L range from 0.7 to 1.3. Consequently, in this range, the Approximation method-2 can be used for rough

estimation.
Approximation method-3 is the most rough estimation in the three methods. The estimated value coincides with the strictly estimated value only when the sheath removal length is equal to the SZ-pitch. This approximation method should not be used when above condition is not satisfied.
Of course, every method can be used with being corrected by use of the fig.4.

ULTRA HIGH COUNT SZ CABLE DESIGN

Using the strict slack length estimation method, we explained above, we designed and manufactured a trial 2000-fiber cable and measured fiber slack length on the test cable.
Fig. 5 demonstrates the cross section of our 2000-fiber cable. It had two layered structure, and consisted of 8-fiber ribbons. Inner layer was SZ slotted rod spacer which has ten slots and each slot contained ten 8-fiber ribbons. Outer layer was consisted of fifteen U-shaped plastic spacer units and each unit contained ten 8-fiber ribbons. The U-shaped spacer units were SZ-stranded. Both layers were wrapped with water-swellable tape. The outer diameter and the weight of the cable were 40mm and 1.1kg/m respectively.
The SZ-pitch of inner and outer layer were designed to make the slack length longer than 20mm for 700mm of sheath removal length, even if the center of sheath removal position was on the middle point in between reversing points. As the result of the calculation, the SZ-pitch of inner layer whose fiber path radius was 7.5mm was chosen to 700mm. And for the outer layer whose fiber path radius was 15mm, the SZ-pitch was chosen to 900mm.
On the other hand, according to the approximation method-2 and -3, the maximum SZ-pitch of outer layer was estimated 1,200mm and 2,800mm, respectively. However, these pitch would provide only 13mm and 1mm. It can be said that our derived strict slack length estimation method enabled adequate design of ultra high count cable with assuring the required slack length.
The measurement result of slack length on the trial 2000-fiber cable is summarized in table 2. As shown by table 2, the minimum slack length of both inner and outer layer are longer than 20mm. From this result, it was confirmed that our proposed design method of SZ cable was enough valid. The measured slack length longer than estimated value can be explained by ribbon excess length and/or ribbon movement in spacer.

Table 2 Slack length measurement result on 2000-fiber cable (700mm sheath removal)

	Min.	Avg.	Max.
Inner (N=10)	21mm	28mm	36mm
Outer (N=15)	20mm	28mm	37mm

SUMMARY

We derived a method to calculate slack length on SZ cable strictly, and verified the method experimentally. Moreover we examined the accuracy of three kinds of method to estimate slack length approximately, and found that the discrepancy of each approximated value from strict value are determined by only the ratio of SZ-pitch to sheath removal length.
Using the result of the study, we designed and manufactured 2000-fiber SZ cable, and confirmed the validity of our derived slack length estimation method by measuring the slack length on the trial 2000-fiber cable.

REFERENCES

[1] H. Iwata et al., "Design of high count optical Fiber cable suitable for mid-span access" in Proc. of the 1997 Comm. Society of IEICE Japan, B-10-3 p302 (1997).
[2] H. Ishikawa et al., "A study on behavior of fiber ribbons in SZ-grooved spacer and its application to aerial cable" 46th IWCS pp42-50(1997).
[3] H. Iwata et al., "Design of aerial optical Fiber cable system suitable for easy branching" 46th IWCS pp5-11(1997).
[4] Y. Ishibashi et al., "Development of aerial optical fiber cable with greater length of cable compared to supporting wire" 46th IWCS pp12-16(1997).

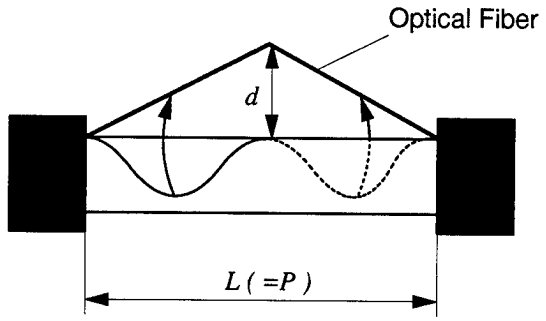

(a) L (sheath removal length) = P (SZ-pitch)

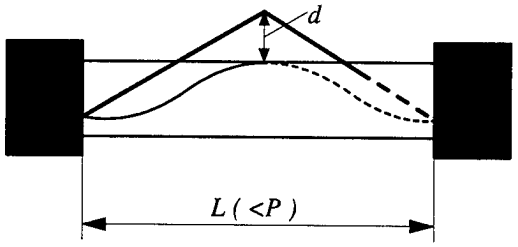

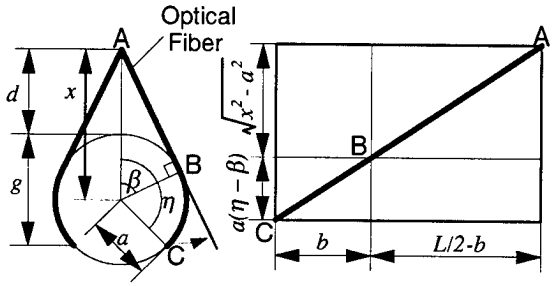

(b) L (sheath removal length) ≠ P (SZ-pitch)

Fig. 1 Mid-span accessibility

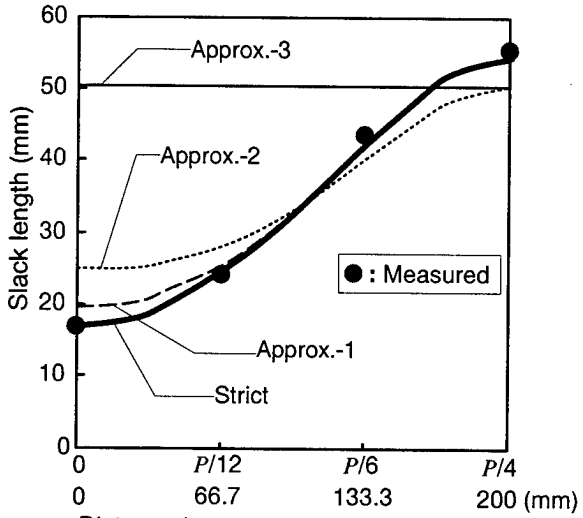

Fig. 2 Calculation results of dependence of slack length on sheath removal position and measurement results of model experiment

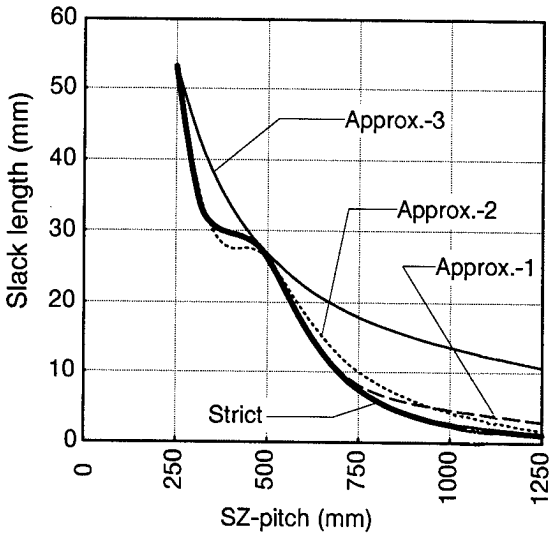

Fig. 3 Calculation results of dependence of slack length on SZ-pitch (500mm of sheath removal length L, 5mm of path radius a, and 275degrees of reverse angle ϕ.)

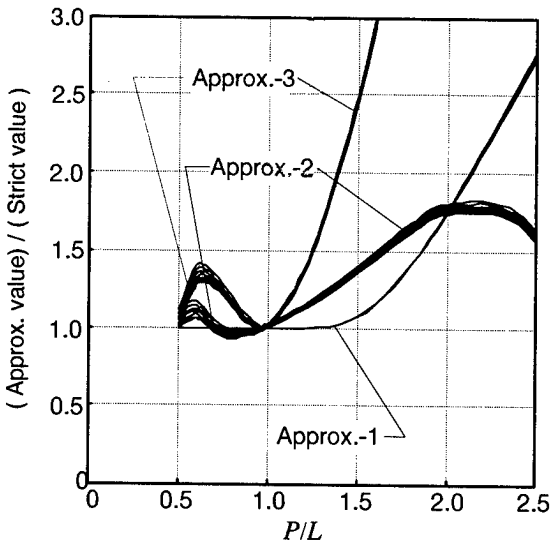

Fig. 4 Accuracy of each approximation method (Variation of the results is according to the path radius variety of a =2.5~20mm. Larger path radius causes larger discrepancy of approximated value from strict value.)

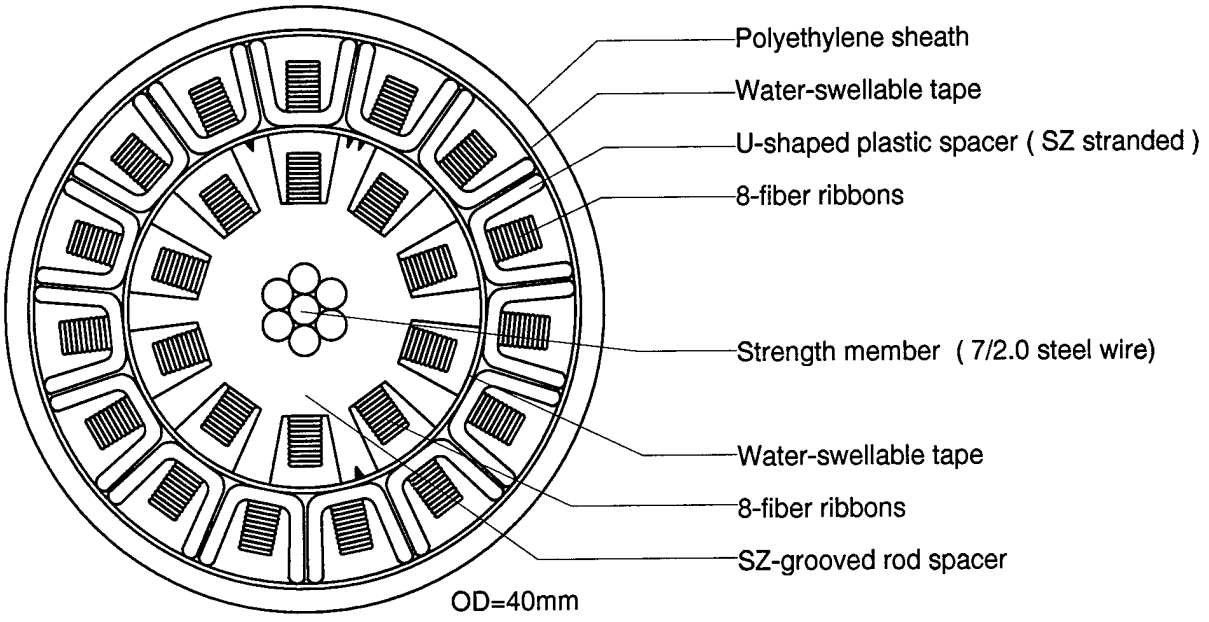

Fig. 5 Cross section of 2000-fiber SZ cable

Hiroki Ishikawa

Sumitomo Electric
Industries, Ltd.
1, Taya-cho, Sakae-ku,
244-8588, Yokohama,
Japan

Hiroki Ishikawa received his M.E. degree in applied physics from Tohoku University in 1990.
He joined Sumitomo Electric Ind., Ltd. in 1990 and he has been engaged in research and development of fiber-optic cables.
Mr. Ishikawa is a member of Communications R&D Department in Yokohama Research Labs. and a member of the IEICE Japan.

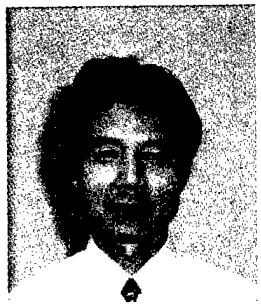

Gen Morikawa

Sumitomo Electric
Industries, Ltd.
1, Taya-cho, Sakae-ku,
244-8588, Yokohama,
Japan

Gen Morikawa received his M.E. degree in electrical engineering from Kyoto University in 1977
He joined Sumitomo Electric Ind., Ltd. in 1977 and he has been engaged in design and development of communication cables.
Mr. Morikawa is a chief research associate of Communications R&D Department in Yokohama Research Labs. and a member of the IEICE Japan.

Yoshiyuki Suetsugu

Sumitomo Electric
Industries, Ltd.
1, Taya-cho, Sakae-ku,
244-8588, Yokohama,
Japan

Yoshiyuki Suetsugu received his B.S. degree in physics and Ph. D. degree in applied physics from Tsukuba University in 1984 and 1996 respectively.
He joined Sumitomo Electric Ind., Ltd. in 1984 and he has been engaged in research and development of optical fibers and fiber-optic cables.
Dr. Suetsugu is a senior engineer of Communications R&D Department in Yokohama Research Labs.and a member of the IEICE Japan.

Reliability of Self-Supported Jelly-Filled Cables for Aerial Trial

C.-H. Hsieh, H.-F. Lin, S.-H. Chou, R.-C. Wang, Y.-H. Hwang,
C.-C. Pei, H.-P. Hsu, Y.-c. Lin, Y.-K. Tu

OSP, Telecommunication Laboratories, Chunghwa Telecom
P.O.Box 6-48, Yang-Mei, Taoyuan 326, Taiwan, R.O.C.

ABSTRACT

Self-Supported Jelly-Filled Cable has been successfully used for aerial route of being tested. The features of the cables used in aerial trials are jelly-filled cables instead of air-core cables and foam-skin insulation in place of solid one. Furthermore, the jelly compounds used in the aerial cables can meet the tighter jelly-dripping requirement. With the duration of 22 months, no unusual electrical properties of the pairs without customers was monitored. On the other hand, for the pairs with customers, no service calls due to cable-core problem occurred. Jelly-dripping and insulation crack both were not observed. Oxidative induction time and mechanical properties of insulation to evaluate the stability between jelly and insulation were also studied in this paper. The result is available to recognize the feasibility and reliability of self-supported jelly-filled cables used for aerial routes.

INTRODUCTION

Nonpressurized air-core aerial cables have been applied as telecommunication cables in many countries for a long time. Because of their exposure to a variety of dangers, such as storms, rodent attacks, and even bullets, external destruction resulted in great damage to the cable sheath, even affected the transmission performance of cable, such as crosstalk.[1-2] The most important issues in aerial route, which may cause cable-core problem, are the presence of water and heat. The former is due to cable destruction, while the latter is from daily exposure. An alternative cable used in aerial plant is jelly-filled one. Once external destruction caused broken cable sheath, air-core aerial cable must be replaced due to no jelly-protection. Jelly-filled cables can therefore reduce the administration and maintenance costs. Otherwise, jelly-filled cables can provide better service performance for aerial application than air-core cables.

Since 1972, most buried cables have been filled with oily hydrocarbon compound to protect them from water attack.[3-4] It is well known that jelly-filling can serve as a moisture-barrier. Whenever moisture is allowed to enter, it results in reducing the transmission performance, thus incurring the service complains from the customers. Although temperatures are cooler under ground, the daily exposure of aerial cables to high temperatures however can enhance jelly-insulation interactions.[2] As mentioned elsewhere,[3,5-6] jelly compounds have a tendency to extract stabilizers from the insulation materials. On the other hand, as the temperature increased, the mobility of jelly may increase. Therefore, the property of jelly compound used for buried cables may not meet the requirement to be used in the aerial route. Furthermore, the jelly compound should be compatible with the insulation material. It is clear based on the discussion that to improve the properties of jelly compound and insulation material is inevitable.

Jelly compound and insulation material both having good thermal stability are the major issues to improve. Jelly compound should be homogeneous, uniformly mixed, and contain a suitable antioxidant system. It should be compatible with the insulation, jacket, and the other materials in the cable. It should not affect tensile strength and elongation of the insulation too much.[7] Polyisobutene and petrolatum are usually used as jelly compounds.

The insulation materials of telecommunication cables are generally expected to have a lifetime of 40 years.[4,8] High density polyethylene (HDPE), one kind of polyolefins, is commonly used for insulation material and can be solid or foam-skin. A foam-skin HDPE was designed as cable insulation in 1976.[9] It consists of an inner coating of cellular HDPE with an outer skin of solid HDPE. Foam skin insulation instead of solid one can offer a weight reduction and high transmission properties.

Heat and physical stress are probably the two most major causes of HDPE degradation.[5,9] The stabilizer system most commonly employed in wire and cable insulation materials consists of an antioxidant and a metal deactivator. The effect of antioxidants on a polymer exposed to oxygen especially at high temperature is to inhibit oxidation. On the other hand, copper can be regarded as a catalyst to speed up the degradation rate of HDPE. Antioxidant and metal deactivator incorporated into the HDPE resins have

been proved to prevent thermal oxidation and cracking. Cracks appear preferentially at bends or stress points in insulations.

Bowmer et al. examined the effects of physical stress and stabilizer extraction on the aging of cable insulations.[4] Insulated wires stressed into tight wrapped coils were degraded 3-4 times faster than straight unstressed wires. Furthermore, extraction of stabilizers by jelly compound increased degradation rates by another factor of 3-4. Otherwise, jelly compounds extracted the stabilizers equally efficiently from both solid and foam-skin insulations.

The oxidative induction time (OIT) test is usually required to qualify insulation compound and jelly compound. It determines the time for oxidative degradation to begin at high temperatures (typically 200 ℃) in pure oxygen. Relative changes in OIT values represent changes in stability of polyolefins and/or stabilizer concentrations. However, Bowmer et al. suggested that very low OIT values of 2 minutes implied little or no stabilizer presented.[4]

Traditionally, the transmission performance of telecommunication line is estimated via the measurements of cable capacitance and insulation resistance in field trial. Cable capacitance is the effective capacitance between the two wires of a pair with all the other conductors, screen and sheath grounded.[7] The higher the dielectric constant of the insulation, the higher the cable capacitance. Good cable should state the meaning of low capacitance performance. The attenuation, both at voice and carrier frequencies, is directly proportional to the square root of cable capacitance.[10] Cable capacitance measurements can be used to monitor the transmission performance, even the effect of the jelly compounds upon the insulation.[11]

In this study, the jelly-filled aerial cables adapting improved jelly compounds and insulation materials have been used to examine the cable performance since 1995. The results during 22 months trial of the cables will be introduced in this paper.

EXPERIMENTAL

Four test sites at mountain areas in Taiwan, referred as area A, B, C and D, were selected for aerial trials of self-supported jelly-filled cables. Areas A, B, C to D are located in Taiwan from the south to the north and the distance between area A and area D is around 300 km. The jelly-filled cables deployed in the test routes were described in Table 1. These routes were designed to be without bridge-tap.

Table 1. Kinds of the jelly-filled cables deployed in the test routes

Service area	conductor diameter-# of pair-length
A	0.50 mm - 200 p - 1500 m 0.50 mm - 50 p - 1500 m 0.65 mm - 20 p - 300 m
B	0.50 mm - 50 p - 1000 m
C	0.50 mm - 200 p - 1000 m 0.50 mm - 100 p - 4000 m 0.50 mm - 50 p - 1000 m 0.65 mm - 20 p - 200 m
D	0.65 mm - 20 p - 3500 m

The electrical performance of these test routes was tested every three months. The trial items included TDR (time domain reflectometer), cable capacitance and insulation resistance.

ACR Data Loggers, model SR002, were placed in RA (ready access) or FA (fixed access) closures for each test route. The data of temperature and relative humidity were automatically recorded every 20 minutes and able to download to PC every several months with a period of 22 months for analysis.

Break load and elongation measurements, crack check and OIT test were used to evaluate the performance of insulation materials. Based upon regular methodology, before splicing, jelly compound has to be removed by solvent; therefore, the insulation in RA/FA closure was usually without jelly-protection. The insulation sample was removed from the cable sheath and the jelly compound was wiped off and removed by solvent. For field aging test, two sets of insulation samples, straight and twisted in pigtails, were put at RA/FA closures. For accelerating aging test, the samples were aged at 70 ℃, 85 ℃ and 100 ℃ in the ovens. Twisted insulated wires put at the closure were ready for crack check and OIT tests. Straight samples were used to measure elongation and break load.

Mechanical properties were measured with Instron model 1122 universal testing machine. Insulation was removed from the insulated conductor and tested for elongation and break load in accordance with ASTM D 638.[12] The speed of testing was 200 mm/min.

The OIT value of insulation sample was measured at 200°C with a Perkin-Elmer DSC-2C. The test procedure was in accordance with ASTM D 4565.[13] Degradation was observed as an exothermic reaction in the calorimetric trace. The time between the admission of oxygen and the onset of degradation was the OIT value. The datum for each sample was stated as the average of values at 3 measurements.

RESULTS AND DISCUSSION

The average temperature and the average relative humidity of each month were shown in Figure 1 and 2, respectively. The data indicated that four test sites had similar average temperature and average relative humidity in summer, but not in winter. Compared with areas B, C and D, area A had the highest average temperature and the lowest relative humidity around all recorded period. Furthermore, the average temperature difference between area A and the other sites was larger in winter than in summer. Therefore, the data conclude that area A has higher temperature and lower relative humidity (70 ~ 80%). However, the data showed that the mountain areas in Taiwan actually belong to highly humid region. Furthermore, the maximum instantaneous temperature recorded was 54.4 ℃ at area C. At area A, which located at the south of Taiwan, the maximum instantaneous temperature of each month was over 40 ℃, even up to 50 ℃. Therefore, the water penetration and the daily exposure of aerial cables need to be concerned in Taiwan.

Three kinds of cables were introduced and several features should be noted here. Self-supported jelly-filled cables and nonpressurized air-core aerial cables both are utilized in aerial plant. The third kind is original jelly-filled cables used in the conduit.

Self-supported jelly-filled cable is a new type of test cables. It has an integral steel messenger wire resulting in a "figure 8" cross-sectional profile and jelly-filled, and uses foam-skin insulation. Air-core aerial cables can provide two kinds of cross-sectional profile, "round" and "figure 8", is air-cores, and uses solid insulation. If the cables have the same cross-sectional profile, then without and with jelly-filled, the weight will have a 5 to 10% difference.

Normally, original jelly-filled cables used in the conduit have a "round" cross-sectional profile. In this study, by adding an integral steel messenger wire, this kind cable was used in aerial plant. However, due to terrible jelly-dripping problem, this cable is unsuitable to be used in aerial plant without any improvement. The result suggests that the requirement of jelly properties should be tighter for self-supported jelly-filled cables used in aerial plant. The improved jelly compound should meet the requirement for having a maximum drip amount of 0.5 gram during 24 hours at 80°C.

Self-supported jelly-filled cables used in all trial routes adapted improved jelly compound and insulation materials. Jelly dripping and insulation crack both were not observed in field trials with a duration of 22 months. It indicates that the performances of jelly compound and insulation material are made better and jelly compound is well compatible with insulation material.

The electrical performance of the test routes was tested every three months. TDR was used to measure the cable length, and also available to determine approximately the location of malfunction. Cable capacitance and insulation resistance of each pair are very helpful to identify the cable performance.

Customer's equipments will provide unusual electrical properties; therefore, the pairs without customer were utilized to measure the cable capacitance and insulation resistance. However, several unusual data were found out at test sites. For example, at area A, for a few pairs, the values of cable capacitance up to 80 nF/km and the values of insulation resistance down to only several hundreds MΩ were obtained. The location of malfunction was found by TDR measurement. One was due to rodent attacks, the other was improper connection. At area D, unusual electrical data were attributable to broken sheaths.

Cable capacitance were measured at a test frequency of 1000 Hz using capacitance meter. If the data of problemable pairs were put away, in the period of 22 months, the cable capacitances are below 55 nF/km. Compared with the initial data, the capacitance differences are within 5%, shown in Figure 3. On the other hand, the insulation resistances are greater than 5 GΩ-km, even up to 1 TΩ-km. Based upon the electrical data, it exhibits that self-supported jelly-filled cables can provide better service performance.

For the period of 22 months, the changes of break load and elongation are shown in Figure 4 and 5, respectively. The initial value of break load is 0.56 kgf and the elongation is 541%. Based upon the requirement of the specification, the break load and the elongation should not be less than 0.53 kgf and 300%, respectively. There are no significant change found. However, the relationship between mechanical property and crack problem has been studied in our previous work.[14] The conclusion was if the retention of elongation of insulation became less than 50% of the original values, cracking of insulation would begin to be created. The results of good mechanical properties and no crack formation showed that the insulation materials in aerial cables can still support good mechanical performance.

Compared with the initial OIT value, the changes of OIT values with the duration of 22 months are shown in Figure 6. The initial value of OIT was 29.8 minutes. As known, the OIT values decreased with an increase in

the deployment time. Furthermore, although the temperature and the relative humidity monitored were somewhat different, the changes of OIT values for these four test routes had similar tendency. Based upon our previous study,[14] even to the extent that the stabilizer has been completely depleted from the insulation. The insulation material still had good mechanical properties and no crack formation. However, the changes of OIT values by accelerating aging test are shown in Figure 7. As usually expected, the OIT values at high temperature decreased faster than at lower temperature. Based on the Arrhenius equation and accelerating aging result, it shows that after 7 years at 30 ℃ the stabilizer in the insulation will be completely used up at the mountain areas in Taiwan.

In the trial cables, to evaluate the status of the trial cables with customers was based on the customers' fault complaint record. After deploying the trial cables, several customers' lines were switched from original air-core cable to jelly-filled trial cable. Table 2 shows customer complaints of two kinds of cables and also cable-core problems. As mentioned above, higher complaint record at area A was due to improper connection and rodent attacks; however, not due to the malfunction of trial cable. On the other hand, at area C, compared with original air-filled cable, customer complaints of jelly-filled trial cable was higher. It was typhoon attack leading to the collapse of the poles. The result apparently shows that the performance of jelly-filled cables used for aerial state is much better than that of air-core cables. Furthermore, there is almost no cable-core problem in the system accompanied with jelly-filled cables for over 22 months.

Table 2. Customer complaints and cable-core problems for the ratio of jelly-filled trial cable (JF) and original air-core cable (AC)

service area	Customer complaints of JF:AC	Cable-core problems of JF:AC
A	0.53 : 1.00	0.64 : 1.00
B	0.14 : 1.00	0.00 : 1.00
C	1.80 : 1.00	0.00 : 1.00
D	0.28 : 1.00	0.00 : 1.00

CONCLUSION

With the duration of 22 months, self-supported jelly-filled cable successfully used for aerial route is the most important conclusion in this paper. Jelly-filled between the sheath and the insulation instead of air-core and foam-skin insulation in place of solid one are two major modification for the new type cables. The performance of jelly compound was characterized by jelly-dripping test, while the stability of insulation material was qualified by crack check, mechanical properties and OIT test. Otherwise, the status of transmission lines without customers were qualified by monitoring cable capacitance and insulation resistance; while ones with customers were identified based on the customers' fault complaint record. Replacing air-core cables by jelly-filled aerial cables, it can significantly reduce the amount of labor needed and lower the administration and maintenance costs.

REFERENCE

1. H.-F. Lin, C.-H. Hsieh, C.-C. Pei, Y.-H. Hwang, H.-P. Hsu, Y.-c. Lin and K.-Y. Chen, *Proc. 44th IWCS*, 599, 1995.
2. Dougherty and E. Gurney, *Proc. 42nd IWCS*, 126, 1993.
3. T. N. Bowmer, R. J. Miner, I. M. Plitz, J. N. D'Amico and L. M. Hore, *Proc. 39th IWCS*, 316, 1990.
4. T. N. Bowmer, E. P. Hjorth, R. J. Miner and O. S. Gebizlioglu, *Proc. 37th IWCS*, 490, 1988.
5. K. Tonyali, *Proc. 41st IWCS*, 304, 1992.
6. S.-I. Wang, H.-F. Lin, C.-H. Hsieh and D.-M. Fann, *Telecommunication Laboratories Internal Report,* 82-LL-055, 1993.
7. TR-NWT-000421, *Bell Communications Research, Technical Reference*, Issue 3, 1991.
8. F. K. Meyer and H. Linhart, *Proc. 32nd IWCS*, 94, 1983.
9. T. N. Bowmer, *Proc. 37th IWCS*, 475, 1988.
10. J. A. Olszewski and J. J. Woods, *Proc. 37th IWCS*, 504, 1988.
11. A. W. Stratton, T. J. Roessing and J. D. Burkhard, *Proc. 36th IWCS*, 322, 1987.
12. ASTM D 638-90, "Standard Test Method for Tensile Properties of Plastics".
13. ASTM D 4565-86, "Standard Test Methods of Physical and Environmental Performance Properties of Insulations and Jackets for Telecommunications Wire and Cable".
14. Unpublished results.

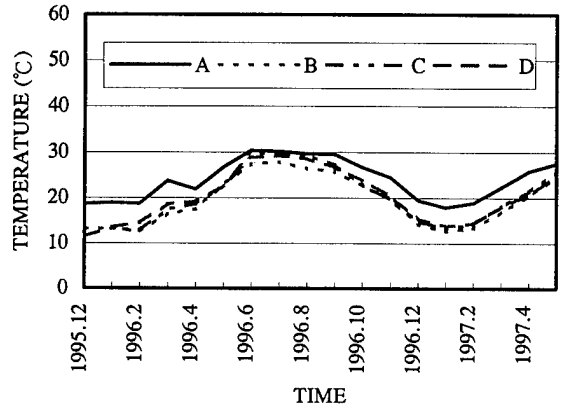

Figure 1. Average temperature of each month recorded in four test sites.

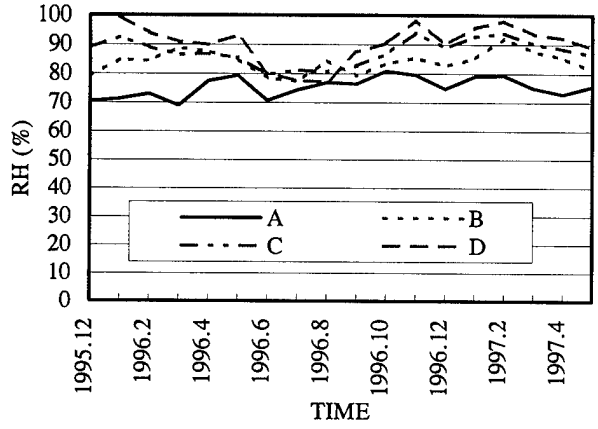

Figure 2. Average relative humidity of each month recorded in four test sites.

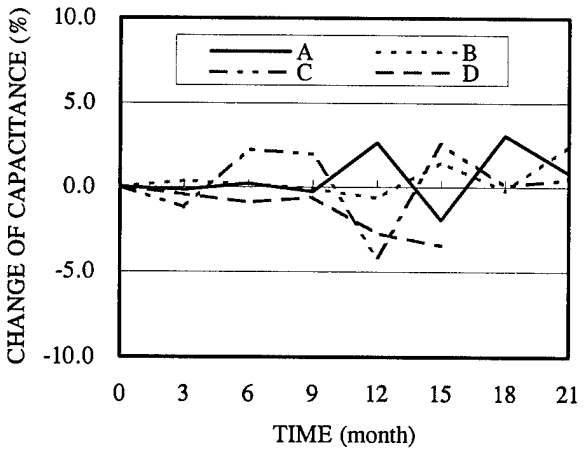

Figure 3. Change of cable capacitance compared with the initial value in four test sites.

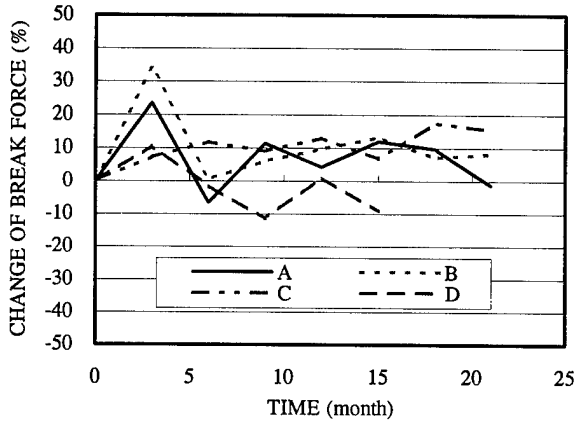

Figure 4. Change of break load compared with the initial value in four test sites.

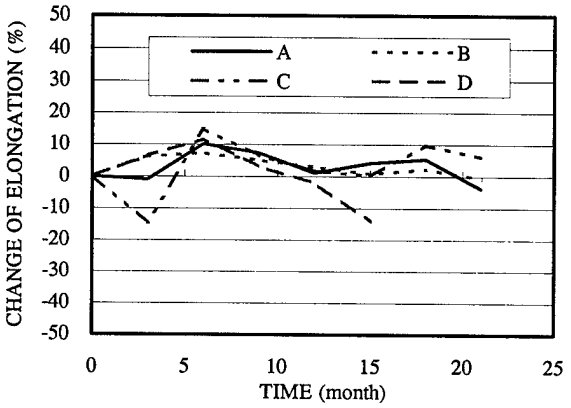

Figure 5. Change of elongation compared with the initial value in four test sites.

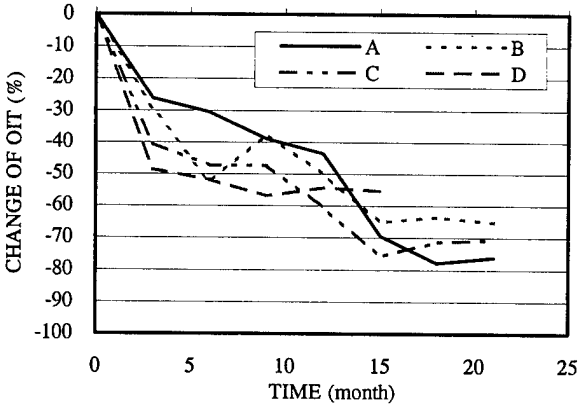

Figure 6. Change of OIT value compared with the initial value in four test sites.

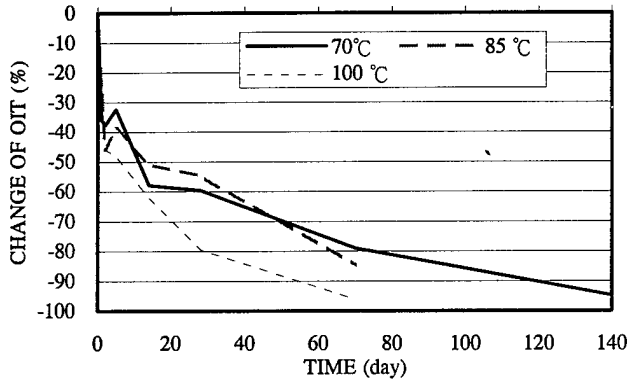

Figure 7. Change of OIT value compared with the initial value for accelerating aging at 70 ℃,85 ℃ and 100 ℃.

DELIVERING FIBER-TO-THE-DESK: A NEW LOW-COST SOLUTION

Daniel J. Rutterman

Siecor
Research, Development and Engineering
Hickory, NC

ABSTRACT

Historically, optical fiber cable designs have focused on backbone applications. The surging bandwidth requirements in LAN applications are now driving optical fiber closer to the desktop. The impetus for this capacity derives from the expanding voice, data, video, and telemetry/sensor applications. A cost-effective yet robust cable design to run from the telecommunications closet to the desktop has become a requirement for this application. These cables must combine conventional requirements, such as NEC flammability listing requirements, with the ability to support emerging connectorization technologies. This paper provides a discussion of an innovative Siecor design that meets all these requirements. These cables meet the performance requirements for riser and plenum distribution cables.

INTRODUCTION

Historically, optical fiber cable designs are used to meet the needs of fiber-to-the-desk (FTTD) applications. Tight-buffered cables are desirable for horizontal applications because of their ability to meet building fire codes as well as their increased physical flexibility, smaller bend radius, and easier handling characteristics in low fiber counts. Tight-buffered cables are also typically easier to terminate with field installable connectors. A typical horizontal FTTD cable is shown in Figure 1. These zipcord cables are distributed to each desk or application. At the desk, the cable is separated into two single-fiber cables for connectorization. Each fiber is then connectorized and plugged into individual data ports. These cables require costly aramid yarn for each unit of the zipcord. Using two separate connectors also unnecessarily increases space, material, and labor cost. A lower cost and more compact solution would serve desktop applications.

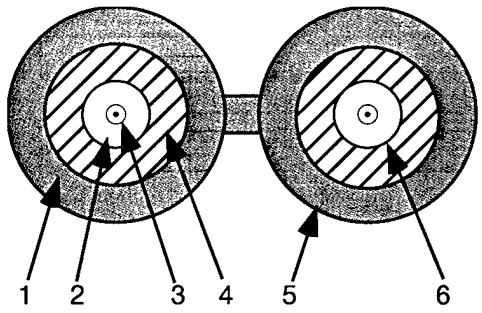

1. PVC Jacket
2. PVC Buffer
3. Optical Fiber
4. Aramid Yarn
5. 2.90 mm Outer Diameter
6. 0.90 mm Outer Diameter

Figure 1: Zipcord Cable with Tight-Buffered Fibers

CABLE DESIGN

A new cable design was engineered to reduce cable and connectorization costs of FTTD applications. The 2-fiber FTTD cable is shown in Figure 2. Compared to the standard zipcord cable, the non-fiber material cost of this new cable is significantly lower due to the smaller amount of aramid yarn and plastic used. The innovative buffer design encapsulates two optical fibers inside

one buffer. Instead of providing tensile strength for each fiber individually, which is the case for a zipcord cable, the two-fiber buffer design encompasses two fibers into one unit, thus reducing the amount of aramid yarn required for tensile strength. The amount of plastic is also reduced without sacrificing robustness. In fact, this cable meets the same environmental and mechanical requirements as standard riser and plenum distribution cables. These performance requirements are more stringent than those specified for interconnect cables like the zipcord cable.

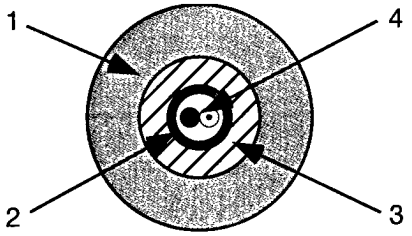

1. Outer Jacket
2. Loose Buffer
3. Aramid Yarn
4. 2 x Optical Fibers

Figure 2: 2-Fiber FTTD Cable

Since the new FTTD cable is more robust it can be used for both distribution and interconnect applications. The reduced amount of aramid yarn and plastics provide a smaller, more flexible cable with a smaller bend radius. The reduced bend radius will make the cable more user-friendly for installers. Connectorization space, material cost and labor cost are substantially reduced by terminating both fibers in a two-fiber connector instead of two, single-fiber connectors.

Although, the 2-fiber cable is used for most horizontal wiring applications, many system designers provide two spare fibers for redundancy and future growth. There are also systems that require 4-fibers such as token ring, SONET and dual attachment station FDDI networks. A 4-fiber FTTD cable is shown in Figure 3. An additional buffer is added to the 4-fiber design. The two buffers are stranded around a dielectric central member and covered with a layer of aramid yarn strength members and an outer jacket.

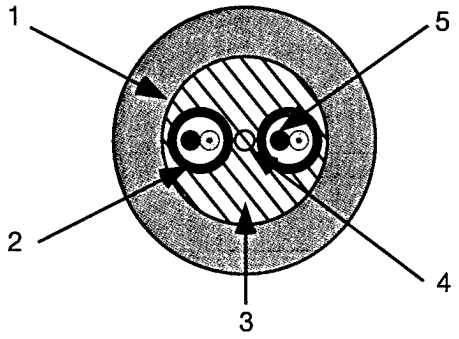

1. Outer Jacket
2. Loose Buffer (2)
3. Aramid Yarn
4. Dielectric Central Member
5. 2 x Optical Fibers

Figure 3: 4-Fiber FTTD Cable

The overall cable size and jacket materials of the riser, plenum and low-smoke zero-halogen (LSZH) cable design families are summarized in Table 1.

Table 1: Jacket Materials and Sizes

Cable	Riser	Plenum	LSZH
2-Fiber	3.2 mm PVC	3.0 mm PVC	3.4 mm FRPE
4-Fiber	3.5 mm PVC	3.3 mm PVC	3.7 mm FRPE

CABLE PERFORMANCE

Both the 2-fiber and 4-fiber cables meet the environmental and mechanical requirements of ICEA S-83-596 (reference Table 2), "Standard for Fiber Optic Premises Distribution Cable." The family of cables meets the flame and smoke requirements for the following tests: riser cables meet UL 1666, plenum cables meet UL 910, and LSZH cables meet UL 1666, UL 1685, IEC 332-3c and IEC 1034.

Compression Testing

The nature of the 2-fiber buffer design adds complexity when designing a cable to meet the requirements of the premises market. Specifically, fiber crossovers in the 2-fiber design can lead to compression failures unless the outer jacket is thick enough to withstand the compression without deflection, which would make the design cost

prohibitive (reference Figure 4). Siecor has developed a process to eliminate fiber crossovers within the buffer. Both the 2-fiber and 4-fiber designs meet ICEA S-83-596 compression specifications for the riser, plenum and LSZH design families. The test requires that 62.5 µm fiber delta attenuation not exceed 0.60 dB/km and single-mode fiber not exceed 0.40 dB/km when an 890 Newton force is applied onto 100 mm plates.

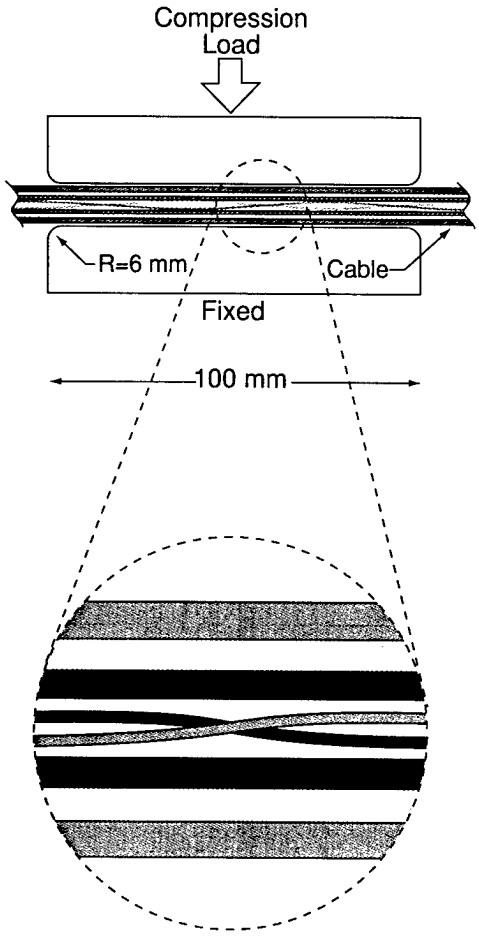

Figure 4: Compression Test Apparatus

Temperature Cycling

Riser, plenum and LSZH designs meet the environmental requirements of ICEA S-83-596. Figure 5 shows that 62.5 µm fiber easily meets the 0.60 dB/km delta attenuation specification. Single-mode fiber meets the 0.30 dB/km delta attenuation specification as shown in Figure 6.

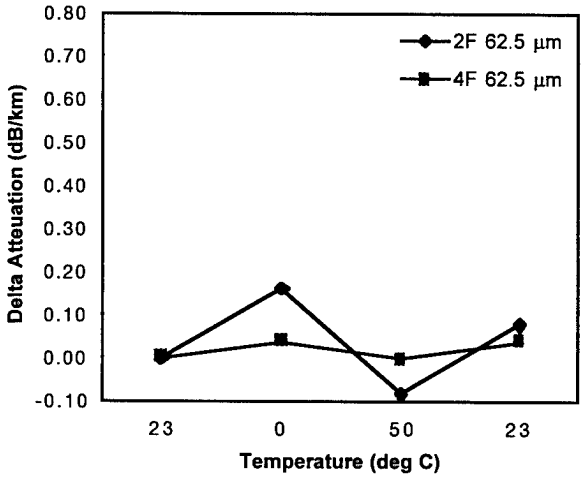

Figure 5: Temperature Cycling Results for 62.5 µm Fiber

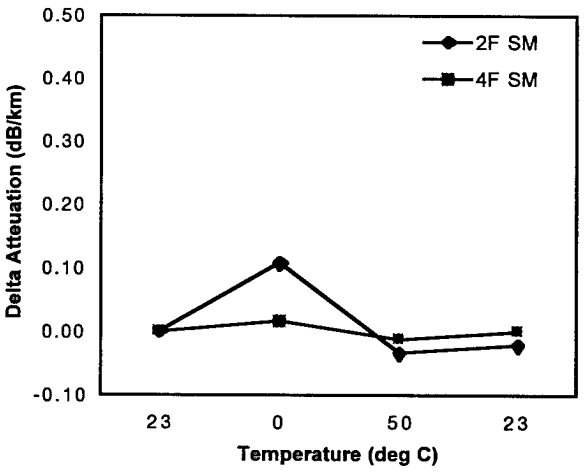

Figure 6: Temperature Cycling Results for Single-Mode Fiber

CONCLUSIONS

In conclusion, a cost-effective and robust cable design has been engineered specifically for FTTD applications. This cable meets the necessary mechanical, environmental, and flammability requirements for riser, plenum and LSZH applications. With its small size and innovative buffer, this cable delivers better performance and more versatility at a lower cost and occupies a smaller space compared to existing FTTD systems.

Table 2: 2-Fiber and 4-Fiber FTTD Cable Performance

Test	Single-mode Results*	62.5/125 μm Results**	Method
Temperature Cycling (0°C to 50°C)	Max. change < 0.3 dB/km	Max. change < 0.6 dB/km	FOTP-3
Tensile (440 N)	During load < 0.2 dB/km After load < 0.1 dB/km	During load < 0.5 dB/km After load < 0.2 dB/km	FOTP-33
Compression (890 N, 100 mm plate)	During load < 0.4 dB/km After load < 0.2 dB/km	During load < 0.6 dB/km After load < 0.4 dB/km	FOTP-41
Impact (10/20 cycles, 0.74 Nm)	Max. change < 0.2 dB/km	Max. change < 0.4 dB/km	FOTP-25
High Temperature Bend (50°C, 4 turns)	Max. change < 0.2 dB/km	Max. change < 0.5 dB/km	FOTP-37
Cold Temperature Bend (0°C, 4 turns)	Max. change < 0.2 dB/km	Max. change < 0.5 dB/km	FOTP-37
Cycle Flex (25 cycles, 20x OD)	Max. change < 0.2 dB/km	Max. change < 0.4 dB/km	FOTP-104
Twist Bend (10 cycles, 20x OD)	Max. change < 0.2 dB/km	Max. change < 0.4 dB/km	FOTP-91
Jacket Shrinkage (110°C, 2 hours)	< 5%		FOTP-86

* - Attenuation measurements at 1550 nm ** - Attenuation measurements at 1300 nm

ACKNOWLEDGMENTS

The author wishes to thank Mike McMillian, Dale Blevins, Jerry Wellman and Marvin Dockery for performing the testing for this paper and Todd Rhyne, Allen Dixon and Dave Kiel for their valued input.

Daniel J. Rutterman
Siecor
PO Box 489
Hickory, NC 28603
USA

Daniel J. Rutterman received a bachelor and master of science in mechanical engineering from Purdue University. He joined Siecor in 1993 as a process engineer. In 1995, he moved to a cable development engineering position in Siecor's Research, Development and Engineering department. Dan is currently a process engineering supervisor at the Siecor Specialty Cable Plant.

Development of High-Count Intra-Office Optical Fiber Cable with 8-Fiber Ribbon Cords,Fan-Out Fibers and SC2-Connectors

Nobuyuki Tuchiya,Kunihiko Kouda,Yoichi Nagase,
Hajime Tamura,and Masaaki Yoshida

Telecommunication Division,TOYOKUNI ELECTRIC CABLE CO.,LTD.
4125, Sakitama, Gyouda-City, Saitama, 361-8604Japan

Abstract

A compact and high-count optical fiber cable is effective for easy handling.Intra-Office Optical Fiber Cable has also been studied as a suitable structure for central telephone offices with fiber termination modules. In the 46th IWCS,We presented "Development of Small Size and High Performance Flat Intra-Office Optical Fiber Cable using Fiber Cord and Fiber Ribbon Cord" .

In this paper,we will introduce the newly developed High-Count Intra-Office Optical Fiber Cable with 8-Fiber Ribbon Cords,Fan-Out Fibers and SC2-Connectors,and its high and stable optical performances.

1.Introduction

Intra-Office Optical Fiber Cable has also been studied as a suitable structure for optical fiber distribution system in central telephone offices with fiber termination.

High-Count Intra-Office Optical Fiber Cable with 8-fiber ribbon cords,fan-out fibers and SC2-connectors has been recently required for optical fiber distribution system.

We have developed the 160-fiber core Intra-Office Optical Fiber Cable in which 8-fiber ribbon cords are stranded around a central tension member realizing stable optical perf-ormances.We also developed a simple fan-out fiber using 8-fiber ribbon cord with SC2-connector. We prepared a fan-out pipe to store 8-fiber ribbon cords and fan-out fiber all together for easy instruction and protect-ing from external force during installation.

The 8-single fibers after the fan-out have a protecting cord of 1.7mm diameter consisti-ng of polyamido resin,polyaramid tarns and a PVC resin. In this case,SC2-connectors are used. In this paper,the newly designed the 160-fiber core Intra-Office Optical Fiber Cable with 8-fiber ribbon cords,fan-out fibers and SC2-connectors is presented,and its high and stable characteristics are discussed.

2.Design of the Intra-Office Optical Fiber Cable

For the 160-fiber core Intra-Office Optical Fiber Cable design, following two matters have been carefully considered;

(1) Decrease of interaction between fiber ribbon cords and sheath
(2) Design of the cable to improve the performance & strength against lateral force since the cable is subjected to external force during production and installation

Figure 1 shows the design of the 160-fiber core Intra-Office Optical Fiber Cable using 8-fiber ribbon cords. The cable containing 20 fiber ribbon cords and a tension member has sheath diameter to be 20.3mm.

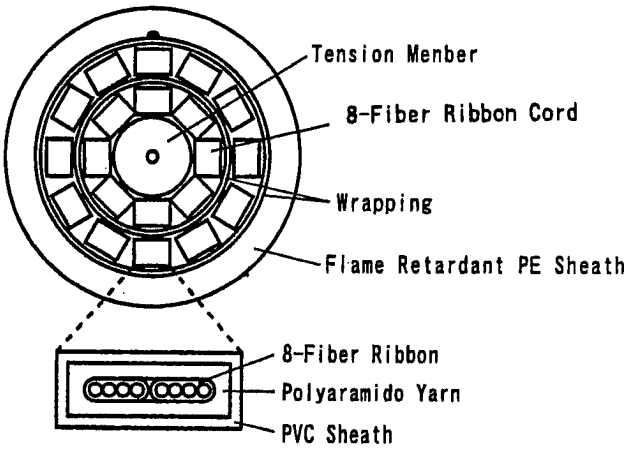

Figure 1 Design of 160-Fiber Core Intra-Office Optical Fiber Cable

The newly developed 8-fiber ribbon cord which consists of a 8-fiber ribbon,polyarami -do yarns and a PVC sheath has dimension to be 1.5×3.5mm. The 8-fiber ribbon in which singlemode fibers of 0.25mm coating diameter are used has dimension of common coating to be 0.30×2.1mm.Design of 8-fiber ribbon cord is shown in Figure1.The cable adopts a flame retardant PE sheath.

3. Mechanical Performance of the 160-Fiber Core Intra-Office Optical Fiber Cable

As summarized in Table 1,various kinds of mechanical tests and temperature cycling tests were conducted on the manufactured 160 -fiber core Intra-Office Optical Fiber Cable

Optical loss was continuousl monitored at 1550nm wavelength during those tests.

Stable and excellent results with no atten -uation increase are shown in Table 1.

Table 1 Summary of Tests and Results

Characteristics	Conditions	Results
Temperature Cycling	-10~40℃ 10 cycles 6 hours duration at each temperature	Less than 0.1dB/Km at 1550nm
Crush Resistance	9.8 N/mm 1 minute duration	Less than 0.1dB at 1550nm
Cable Bend	1 wrap on mandrel diameter 400mm (20×Dia.)	Less than 0.1dB at 1550nm

4.Design of the Fan-Out Fiber for 8-Fiber Ribbon Cord

Design of the fan-out fiber for 8-fiber ribbon cord is shown in Figure 2.The 8-fiber ribbon cord is separated to single fiber cord at the fan-out position. The single fiber cord is composed the fan-out tubing which provides excellent additional protecti -on for use with 250μm coated single-mode fibers. The tubing allows for the fanning out of fibers for easy connectorization. The tubing has a 1.7mm' outer diameter and a strength member(polyaramid yarn) is also included within the product for additional protection and strain-relief. The fan-out fibers are protected by a heat shrinkable tube.The spiral protective tube and SC2-connectors are used on this fan-out fiber as shown in Figure 2.

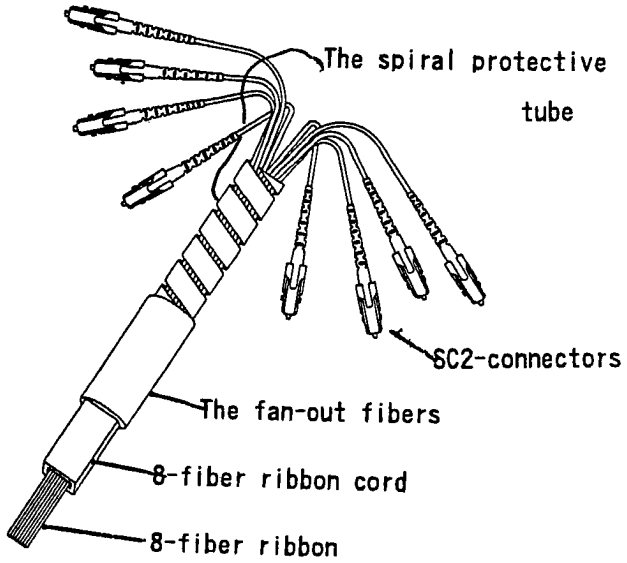

Figure 2,Design of the Fan-Out Fiber for 8-Fiber Ribbon Cord

5.Design of the Fan-Out Pipe for the 160-Fiber Core Inra-Office Optical Fiber Cable

Design of the fan-out fiber and the fan -out pipe for the 160-fiber core Inra-Office Optical Fiber Cable has been carefu -lly considered to improve the strength against lateral force of the fan-out pipe since the cable is subjected to external force during installation. The fan-out design and process for the 160-fiber core Intra-Office Optical Fiber Cable were carr -ied out almost same method of the Fan-Out Fiber For 8-Fiber Ribbon Cord shown in Figure 2.

Figure 3,Figure 4 and Figure 5 show the design and the fan-out process for the 160 fiber core Intra-Office Optical Fiber Cabl -e. The fan-out fibers which are protected by a heat shrinkable tube are separately allocated for getting small fan-out pipe

as shown in Figure 3.

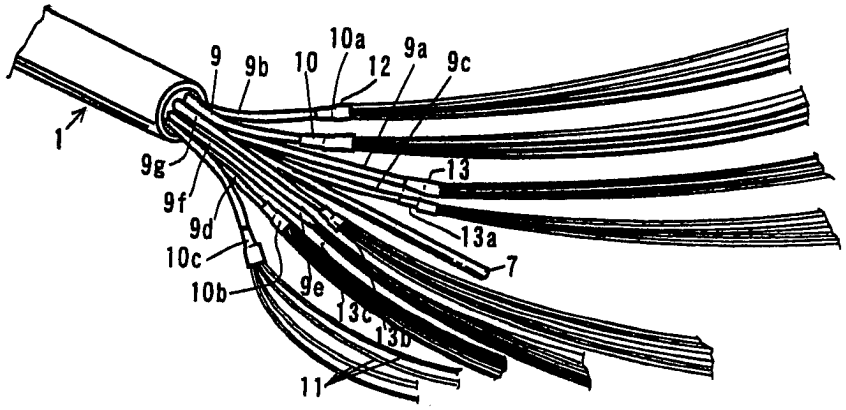

- 9, 9a~9g: 8-fibers ribbon cords
- 10, 10a~10c and 13, 13a~13c: fan-out fibers
- 11: single fiber cords
- 12: protective tube
- 7 : tension menber of cable
- 1 : 160-fibers core Intra-Office Optical Fiber Cable

Figure 3 One of the Fan-Out Process for Fiber Core Intra-Office Optical Fiber Cable

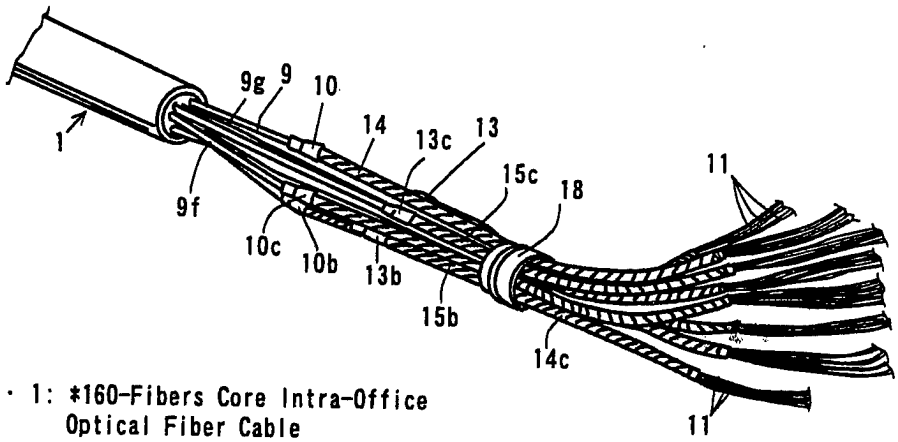

- 1: ※160-Fibers Core Intra-Office Optical Fiber Cable
- 9, 9g, 9f: 8-fiber ribbon cords
- 10, 10c, 10band13, 13b, 13c: fan-out fibers
- 14, 14c, 15c, 15b: spiral protective tubes
- 18: wrapping tape
- 11: single fiber cords

Figure 4 One of the Fan-Out Process for 160-Fiber Core Intra-Office Optical Fiber Cable

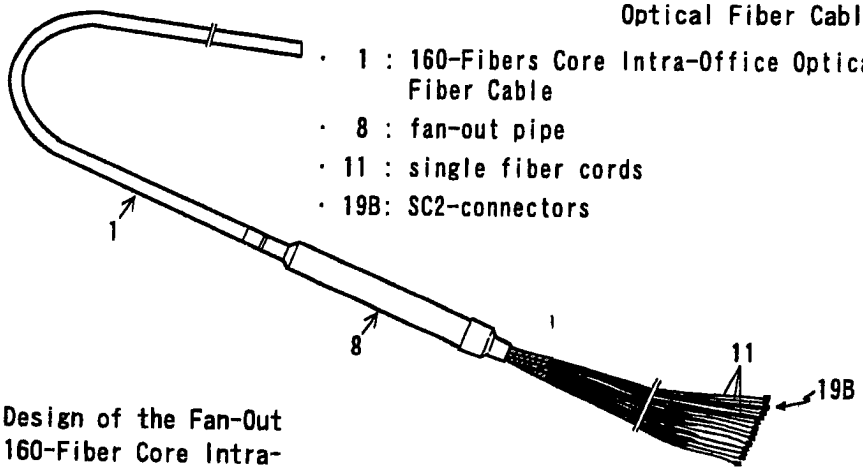

- 1 : 160-Fibers Core Intra-Office Optical Fiber Cable
- 8 : fan-out pipe
- 11 : single fiber cords
- 19B: SC2-connectors

Figure 5 The Design of the Fan-Out Pipe for 160-Fiber Core Intra-Office Optical Fiber Cable

The fan-out single fiber cords which have protecting cords of 1.7mm diameter consistin -g of polyamido resin, polyaramido yarn as a strength member and a PVC resin are protected by spiral protective tube and wrapping tape as shown in Figure 4

Figure 5 shows the final product and design of the fan-out pipe for the 160-fiber core cable. The fan-out pipe containing 8-fiber ribbon cords and fan-out fibers all together has the lengths of 300mm and the diameters of 50mm. This fan-out pipe can endure against more than 30Kg tensile streng -th similar to weight of 100m length 160-fiber core cable. Figure 6 shows tensile strength test method. An enough tensile strength of 45.8Kg was shown on this fan-out pipe.

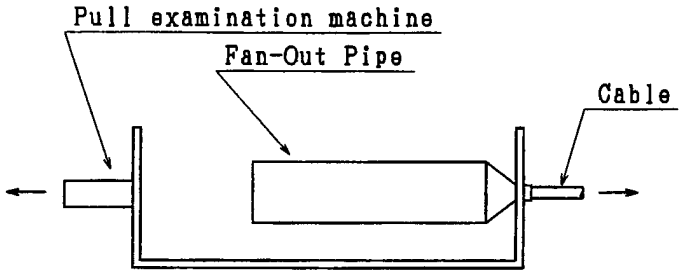

Pull speed:100mm/minute

Measurement value: 45.8kg

Figure 6 Tensile Strength of Fan-Out Pipe

Figure 7 shows the photograph of final product for the 160-fiber core Intra-Office Optical Fiber Cable. This Cable consists of a 160-fiber core cable, a fan-out pipe,160-single fiber cords and 160-SC2 connectors.

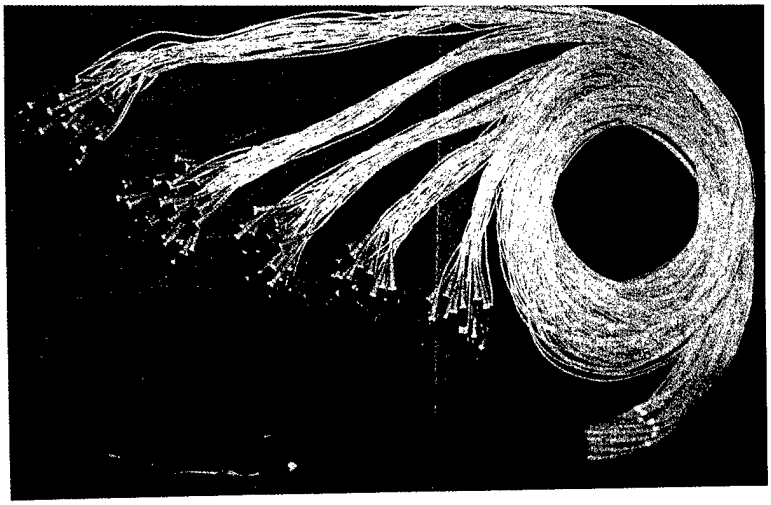

Figure 7 The photograph for the 160-Fiber Core Intra-Office Optical Fiber Cable

Figure 8 shows the characteristics of temperature cycling for the fan-out pipe (-10~40℃,6-hours duration at each temp.) Stable and excellent results with no attenuation increase have given the good prospect to the fan-out fiber and the fan-out pipe.

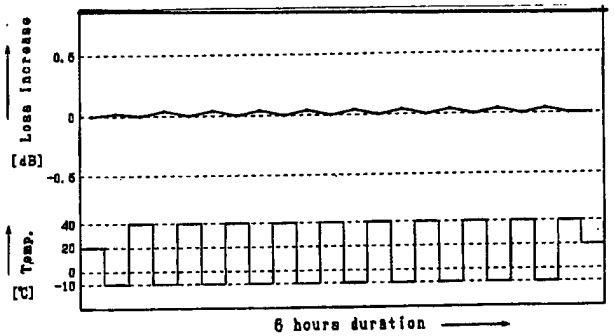

Figure 8 Temperature Cycling Test for The Fan-Out Fiber and The Fan-Out Pipe

6.Fiber Termination Module Frames

The 160-fiber core Intra-Office Optical Fiber Cable is installed in the fiber termi -nation module. Figure 9 shows one of the fiber termination module frames.The fan-out pipe is binded and is fixed in the termina -tion module,and fan-out single fiber cords with SC2 connector are installed on the tray in module. This frames are effective for easy handling.

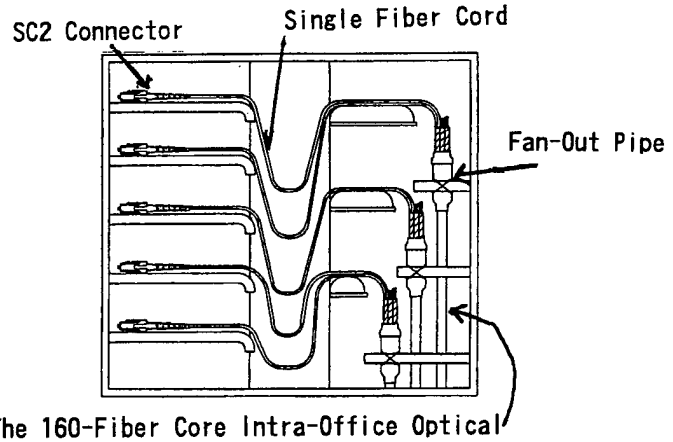

The 160-Fiber Core Intra-Office Optical Fiber Cable

Figure 9 The Fiber Termination Modules Frame

7.Conclusion

The newly designed and developed the 160-fiber core Intra-Office Optical Fiber Cable with 8-fiber ribbon cords ,fan-out fibers, and SC2 connectors was realized by the prop -er design.The stable and excellent results with no attenuation increase have given the good prospect to the Intra-Office cable

Nobuyuki Tsuchiya is a Member of Technical Staff in the Network & Fiber Optics Engineer -ing Department at Toyokuni Electric Cable Co.,Ltd.He is responsible for production engineering and development of Optical Fiber Cable.Mr.N.Tsuchiya joined Toyokuni Electric in 1983.He is a member of the Institute of Electronics, Information and Communication Engineers of Japan.

Kunihiko Koda is a Member of Technical Staff in the Network & Fiber Optics Engineering Department at Toyokuni Electric Cable CO.,Lt d.He is responsible for design and developme -nt of Fiber Optic Connector.Mr.K.Koda joine -d Toyokuni Electric in 1973.

Yoichi Nagase is a member of Technical Staff in the Network & Fiber Optics Engineering Department at Toyokuni Electric Cable Co.,Lt d.He is responsible for design and developme -nt of Optical Fiber Cable.Mr.Y.Nagase joine -d Toyokuni Electric in 1975.He is a member of the Institute and Communication Engineers of Japan.

Hajime Tamura is a Manager of the Network & Fiber Optics Engineering Department at Toyok -uni Electric Cable Co.,Ltd..He is responsib -le for design,development and process engin -eering for Optical Fiber Cable and Optical Connector.Mr.H.Tamura joined Toyokuni Electr -ic in 1969.He is a member of the Institute of Electronics,Information and Communication Engineers of Japan.

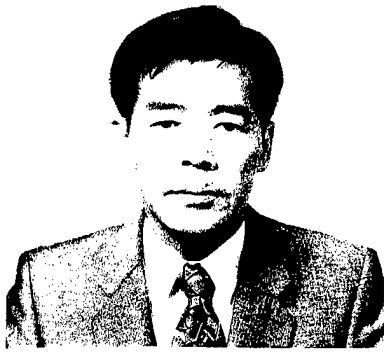

Masaaki Yoshida is a Director & Executive Manager of Research and Development Departme -nt at Toyokuni Electric Cable Co.,Ltd.. Mr.M.Yoshida joined Sumitomo Electric Indust -ries,Ltd.in 1966,and transfer & joined Toyo -kuni Electric in 1995.He is a member of the Institute of Electronics Information and Communication Engineers of Japan.

A UNIQUE SHEATHING SOLUTION FOR HALOGEN FREE, LOW SMOKE, FIRE RETARDANT FIBRE OPTIC CABLES

Mr Dudley Sawyer, Mr Joe Preston, and Mr Peter Holland

Scapa Polymerics Limited
Manchester
United Kingdom

Mr Vince Watson and Miss Jane Rhodes

Pinacl Communication Systems Limited
Denbighshire
United Kingdom

ABSTRACT

For decades polyolefinic materials such as polyethylene and polypropylene have been used in communication cables as non-metallic water barriers also termed water barriers. Polyolefin water barriers are now widely accepted in non-metallic constructions for data and telecommunication applications creating dry cables.

In more recent years, halogen free, low smoke, fire retardant compounds have become more widely accepted in communication constructions[1]. Such systems have traditionally required a double sheath construction to protect the cable from moisture and maintain the benefits of halogen free, low smoke, fire retardant materials.

Oversheathing with this new material enables replacement of the double jacket polyolefin/LSF system with a single "Universal" jacket. The compound is also UV stabilised and therefore can be used for both indoor and outdoor constructions. The new universal cables are not compromised in terms of fire performance or water barrier protection. A lighter, more flexible, more compact cost-effective construction is achieved.

The moisture resistant properties of the new sheathing compound will be characterised in detail. Its correlation and benefits to fibre optic cabling will also be indicated. Key properties have been characterised and compared to international standards in order to confirm its suitability for use in the manufacture of communication cables.

The fire properties have been measured along with the smoke generation, toxicity and acid gas emission. These are compared to the performance of typical polyethylene and PVC cable compounds. The processability of the new compound has also been assessed and is shown to be comparable to the latest generation of thermoplastic halogen free, low smoke, fire retardant cable compounds.

The paper demonstrates the development of a unique sheathing compound that will greatly benefit the manufacture of fibre optic cabling systems.

INTRODUCTION

The use of non-metallic polymeric water barriers in optical fibre cables has for many years been regarded by some as a "black art". Polyolefin materials such as polypropylene and polyethylene are known to possess good water barrier properties; this is known from experience gathered in the field over many years.

Many cable companies have offered a separate polyolefin water barrier sheath under a halogen free, low smoke, flame retardant sheath for cables intended for dual internal and external applications. Double sheathed versions are well suited to inter building and in building LAN applications where the cost of terminating a non flame retardant duct cable to an internal fire retardant cable can be avoided. Optical power budgets do not take a "hit" by doorstep termination through splice or connector losses.

There is a general trend in Europe towards the use of single jacketed cables in place of the traditional double jacketed cables. The authors set out to benchmark the water barrier performance of a standard polypropylene copolymer material by using the IEC 811-1-3 water absorption test[2]. This test gives the amount of water in mg/cm^2 absorbed by plaques soaked in water for 10 days at 70°C. The value obtained for the polypropylene copolymer was 0.5 mg/cm^2 (IEC 811-1-3). Values obtained for standard LSF systems were typically in excess of 6 mg/cm^2.

The target water absorption was $< 2\ mg/cm^2$ (IEC 811-1-3); this value was later reduced to $< 1\ mg/cm^2$. Compound S560 has been developed to meet this requirement having a measured value of less than 0.9 mg/cm^2. The fire performance of this

new material was also enhanced over the LSF material previously used in the double jacket design. Using the single Compound S560 sheath it became possible to change the design of a typical 4 fibre 900 μm internal/external cable from that given in Figure 1 to that given in Figure 2. The example of the 4 fibre distribution cable is used in this paper to demonstrate the design developments that have taken place due to the introduction of the new single jacket technology. The concept is equally applicable to both 900 μm buffered fibre cables, and loose tube cables in dry or gel filled loose tube forms.

Figure 1

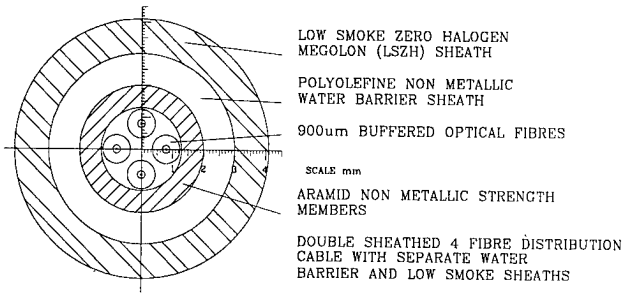

Figure 2

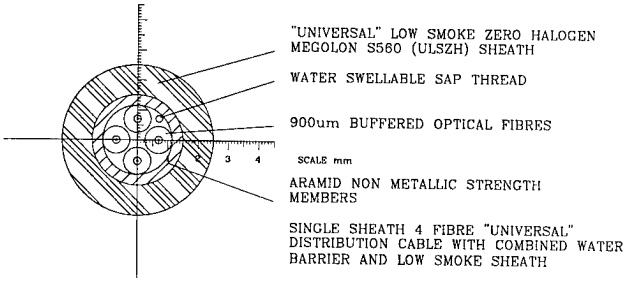

PHYSICAL PROPERTIES

Thermomechanical Properties

Recent work by CENELEC, the European Committee for Electrotechnical Standardisation, has resulted in the publication of a new harmonised specification covering halogen free, flame retardant, thermoplastic sheathing compounds for use in the construction of communication cables. In Table 1 we compare the thermomechanical properties of Compound S560 to the requirements of this specification which has been give the designation HD 624 Part 7[3]. Particularly interesting are the excellent high and low temperature performances of Compound S560 showing that the compound is eminently suitable for use in cables to be installed in environments of widely varying conditions.

Table 1 – Thermomechanical Properties.

Properties	HD 624 Part 7	Compound S560
Tensile Strength	9 MPa (minimum)	10.5 MPa
Elongation at Break	125 % (minimum)	155 %
After ageing for 7 days at 100°C :		
T.S. variation	±30 % (maximum)	+24 %
E@B value	100 % (minimum)	140 %
E@B variation	±30 % (maximum)	-10 %
Heat Shock 130°C for 1 hour	Pass (no cracks)	Pass (no cracks)
Cold Bend At –15°C	Pass (no cracks)	Pass (no cracks)
Cold Elongation At –15°C	20 % (minimum)	115%
Hot Pressure 80°C for 4 hours	50 % (maximum)	25 % at 90°C

Oil Resistance

It is customary to measure the performance of cable making compounds in both ASTM No 2 and Diesel oils at both ambient and elevated temperatures. These tests are not called for in HD 624 Part 7, but often form a part of the individual cable specifications. The results documented in Table 2 confirm that Compound S560 possesses the degree of oil resistance that is customary for a zero halogen, flame retardant sheathing compound.

Table 2 – Oil Resistance.

Oil	Retention of Tensile Strength	Retention of Elongation at Break
ASTM No. 2 7 days at 23°C	95 %	105 %
ASTM No. 2 4 hours at 70°C	80 %	95 %
Diesel 7 days at 23°C	75 %	85 %
Diesel 4 hours at 70°C	20 %	85 %

FIRE PERFORMANCE

Smoke Emission

The ASTM E662 test method[4] was used to assess the smoke emission of Compound S560. Figure 3 shows the results for the flaming mode and Figure 4 those for the non-flaming mode. Tests in both modes were carried out on 1.5mm thick plaque samples.

Figure 3 – Smoke (Flaming Mode)

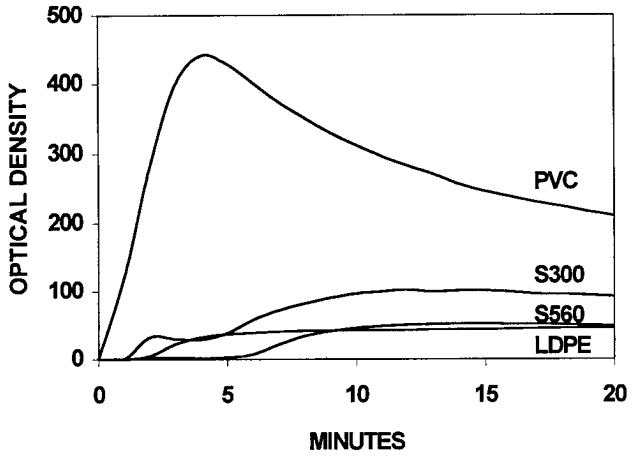

Figure 4 – Smoke (Non-flaming Mode)

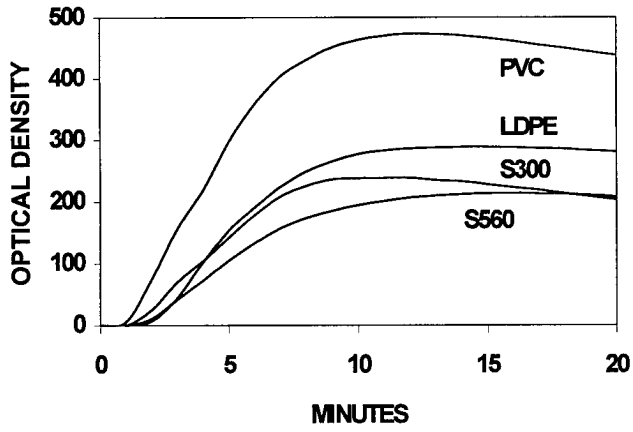

In both modes the smoke emission has been compared to a PVC sheathing compound, a low density polyethylene and a previous generation LSF sheathing compound (Compound S300). In the flaming mode Compound S560 exhibits excellent low smoke characteristics in line with those of LDPE. The improvements made over the earlier generation compound can also be seen. In the non-flaming mode Compound S560 shows superiority even over LDPE. Both figures clearly demonstrate the volume and rates of generation of smoke by PVC compound.

Combustion Gases and Toxicity Index

The most common methods of test for the quantities of acid and corrosive gases evolved during combustion are now grouped together in IEC 754[5]. The toxicity of the gases is evaluated using the NES 713 method[6]. The index produced is computed by measuring the concentrations of 12 selected gases evolved under the specified fire conditions. Table 3 shows the results of these tests ranged against the generally accepted cable industry standard. Again these demonstrate the superior level of performance of Compound S560.

Table 3 – Combustion Gases Analysis

Properties	S560	Standard
Acid gas emission (%)	zero	0.5 maximum
pH	6.2	4.3 minimum
Conductivity (μS/cm)	7	100 maximum
Toxicity Index	0.8	5 maximum

WATER ABSORPTION

A critical feature of Compound S560 is its water absorbance properties. As mentioned previously, a maximum level of 1 mg/cm^2 had been targeted for the compound when soaked in water for 10 days at 70°C as documented in IEC 811-1-3. The results of this test are shown in Figure 5 along with comparable results for a PVC sheathing compound, a low density polyethylene and two currently available LSF sheathing compounds (Compounds S300 and S530).

Figure 5 – Water Absorption

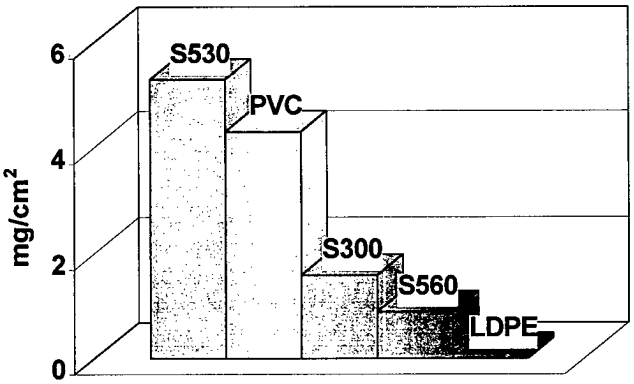

The results clearly demonstrate the advancements made with LSF technology in reducing the water absorption tendencies of this type of compound. Also of interest is the low value demonstrated by LDPE showing why the preferred option until now had always been to use a thin skin of PP or LDPE underneath a final LSF sheath.

ELECTRICAL PROPERTIES

Compound S560 was developed specifically for use as a sheathing compound for optical fibre cables. However, manufacturers of copper cables have recently started to take interest in the water absorption properties. For this reason a programme of electrical testing has commenced. Figure 6 shows a comparison of insulation resistances of a PVC sheathing compound, a low density polyethylene and a current generation LSF sheathing compound (Compound S530) over 21 days. For the purposes of this test, each material was extruded onto 1 mm^2 solid copper wire at a wall thickness of 0.6 mm (nominal).

Figure 6 – Insulation Resistance[7]

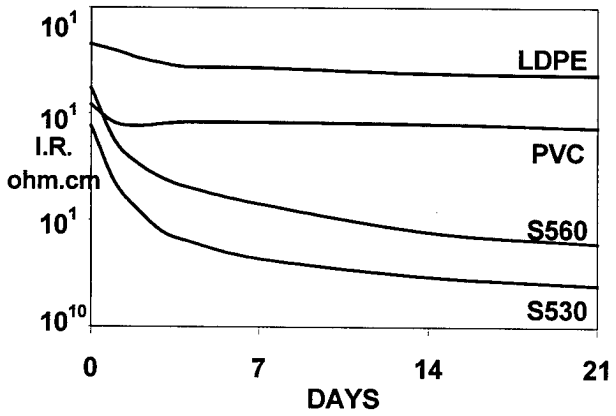

PROCESSING

The processing characteristics of Compound S560 were investigated on a 65mm 24 L/D extruder fitted with a constant pitch, low compression screw (a MEG screw). It was compared with a current generation LSF compound regarded as one of the more superior processing materials in its class (Compound S500[1]). As can be seen from Figure 7, volumetric outputs are almost identical until the higher screw speeds are reached. In practice, it would be rare to find screw speeds in excess of 40 rpm being used to process this type of compound. Melt temperatures are highly comparable, varying only by 3 or 4 degrees at any one screw speed (Figure 8). In fact, the greater the speed then the closer the temperatures become, suggesting that the melt viscosity of Compound S560 decreases with speed, thus making it suitable for higher outputs.

Figure 7 - Output

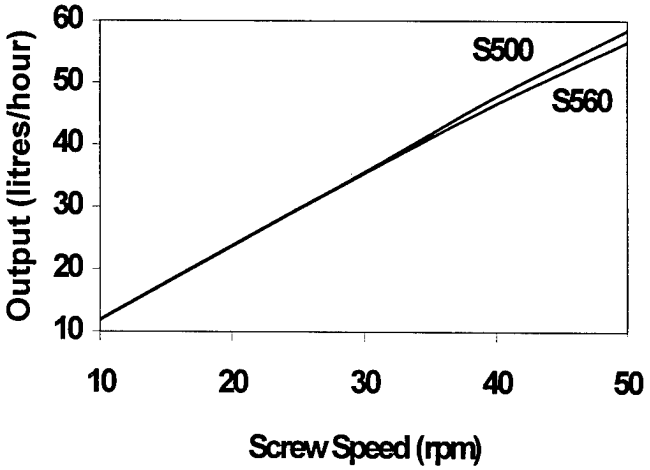

Figure 8 – Melt Temperature

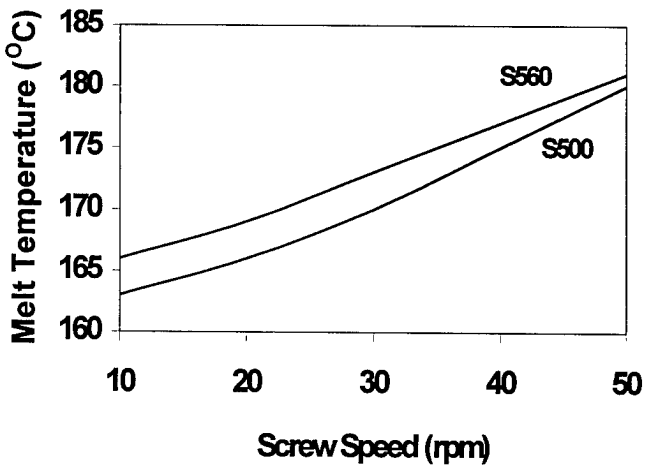

CABLE FIRE TESTS

Fire Tests

A 4 pair fibre Office Distribution Cable with a Compound S560 sheath was subjected to four different tests: -

IEC 332-1 single wire, vertical flame test[8] - **the maximum height of the cable charred or affected**

as measured from the point of flame application was 5.4 cms.

IEC 332-3 (category C, designation F) large scale vertical fire test for bunched wires or cables[9] - **the maximum height of the cable charred or affected as measured from the bottom of the burner was 68cms (in front of the cable group).**

IEC 754-1 acid gas evolution[5] - **the average gas yield expressed as hydrogen chloride was 5mg/g.**

IEC 1034 smoke density test (3 metre cube)[10] - **the minimum light transmission recorded was 90.3%.**

The results listed all meet the requirements of the international standards quoted.

Water/Moisture Tests

The effect of moisture on both singlemode and multimode optical fibres is being evaluated on a long-term basis. Listed below are the 30 days values.

Singlemode.
Water soak dependence of 9/125 singlemode optical fibres at 1310 μm and 1550 μm @ 20°C, induced attenuation is <= 0.05 dB/km.

Damp heat dependence of 9/125 singlemode optical fibres at 1310 μm and 1550 μm @ 85°C and 85% R.H., induced attenuation is <= 0.05 dB/km.

Multimode.
Water soak dependence of 62.5/125 and 50/125 multimode fibres at 850 μm and 1300 μm @ 20°C, induced attenuation is <= 0.2 dB/km.

Damp heat dependence of 62.5/125 and 50/125 multimode fibres at 850 μm and 1300 μm @ 85°C and 85% R.H., induced attenuation is 0.2 dB/km.

The continued evaluation of optical attenuation of the cable in relationship to water, which currently is looking favourable, will be maintained and be reported in a future paper.

CONCLUSION

The key properties required by international standards have been adhered to fully by this latest generation of sheathing material, confirming its acceptability in the halogen free, low smoke, fire retardant cable market. Compound S560 will enable the manufacturers of communication cables to produce a more cost-effective construction. The progress made allows a change from traditional double sheathed separate water barrier, and low smoke sheathed cables to more efficient single sheath "Universal" loose tube and 900 μm buffered cable designs with a high level of confidence.
The benefits of such a design change from the double jacket to the single jacket "Universal" type cables include the following. The new single jacket cable is smaller, lighter, more flexible and offers cost benefits over the previous double jacket design. Additionally and more importantly the water barrier performance is quantified.

REFERENCES

1. Dr J. Taylor, et al.: Sheathing power and telecom cables, IWCS, November 1992.
2. IEC 811:1993, Insulating and sheathing materials of electric cables - Common test methods.
3. CENELEC HD 624.7 S1, Materials used in communication cables. Part 7: Halogen free flame retardant thermoplastic sheathing compound.
4. ASTM E 662-83, standard test method for Specific Optical Density of Smoke generated by solid materials.
5. IEC 754-1:1982 and IEC 754-2:1991, Test on gases evolved during combustion of electric cables.
6. Naval Engineering Standard 713, Determination of the Toxicity Index of the products of combustion from small specimen of materials.
7. BS6746:1990, Specification for PVC insulation and sheath of electric cable.
8. IEC 332-1:1993, Tests on electric cables under fire conditions. Method of test on a single vertical insulated wire or cable.
9. IEC 332-3:1992, Tests on electric cables under fire conditions. Tests on bunched wires or cables.
10. IEC 1034-2:1991, Measurement of smoke density of electric cables burning under defined conditions. Part 2: Test procedure and requirements.

Dudley Sawyer
Scapa Polymerics Ltd
Columbine Street
Manchester M11 2LH
England

Dudley Sawyer joined Scapa Polymerics Ltd in January 1991 to work on the development of new zero halogen, flame retardant extrusion compounds for the electrical cable industry. He gained BSc (Hons) in Chemistry at the University of Manchester and he has extensive experience of the cable industry having previously spent 21 years with BICC Cables from 1969 - 1990, progressing from Assistant Chemist in the Wire and General Cables Division to Senior Material Technologist.

Joe Preston
Scapa Polymerics Ltd
Columbine Street
Manchester M11 2LH
England

Joe Preston joined Scapa Polymerics Ltd in 1970 as a Laboratory Assistant following 2½ years experience in the Plastics Industry. He studied chemistry at the North Trafford College of Technology. In 1977 he became responsible for the Quality Control function at Scapa Polymerics. He transferred his efforts in 1982 to Development, working on specialised cable tapes, and in more recent years, the Megolon range of low smoke, halogen free, fire retardant compounds. In 1991 he was appointed Technical Manager of Scapa Polymerics, responsible for all development and quality control functions.

Peter Holland
Scapa Polymerics Ltd
Columbine Street
Manchester M11 2LH
England

Peter Holland joined Scapa Polymerics in 1996 in a technical sales roll from the defence and aerospace industry. After having gained a BSc (1st class Hons) in Mechanical Engineering he worked in research, development and commercial environments, to achieve Chartered status. He is currently responsible for all product sales to the cable industry in UK and Ireland.

Vince Watson
Pinacl Communication
Systems Limited
Kinmel Park
Denbighshire
LL18 5TZ
Wales

Vince graduated from Staffordshire University with a BSc Hons in applied Science in 1989, and the University of Glamorgan with a MPhil in cable materials research in 1993. He is currently cable Development Manager with Pinacl.

Jane Rhodes
Pinacl Communication
Systems Limited
Kinmel Park
Denbighshire
LL18 5TZ
Wales

Jane graduated from Birmingham University with a B.Eng. (Hons) in Material Science in 1997. Since that time she has been working for Pinacl in the Cable Division as a graduate cable design engineer.

Quickly Assembling Technique for MT connector

Kazuhiro Takayama Masato Shiino

THE FURUKAWA ELECTRIC CO., LTD
6, Yawata-kaigandori, Ichihara-shi, Chiba, 290-8555, JAPAN
Phone: +81-436-42-1725 Fax: +81-436-42-9340 E-mail: ktakayama@ch.furukawa.co.jp

ABSTRACT

We have developed a new MT connector assembling technique which need no polishing process and realizes quick field installation. The new technique has enabled us to reduce assembly time to about three minutes.

MT connector assembled with this technique features the following characteristics:

average insertion loss : 0.19dB
minimum return loss : 48.8dB
average assembly time : about 3 minutes
insertion loss change in temperature cycling:
<0.2dB (-40 to 85 ℃; 10cycles)
insertion loss change in temperature and humidity cycling:
<0.2dB (-10 to 65 ℃, 93%RH; 10cycles)

It is demonstrated that MT connector assembled with the new technique maintains characteristics equal to that assembled with the conventional technique.

1. Background

Along with expansion of optical communication network, it is increasingly demanded to develop a new technology to reduce jointing time and jointing cost of ultra-high count optical fiber cables. Typical technique to connect optical fiber ribbons includes fusion splice and multi fiber connector such as MT. Low connection loss and stable environmental characteristics are required for the fiber joints. For ultra-high count cables, it is extremely important to complete connection in short time. In a bid to satisfy these demands, we have developed a quickly assembling technique for MT connector.

We set the following items as the targets of our development.

- No polishing required
- Quick assembly within three minutes
- Quick adhesion
- Optical performance equal to conventional MT connector
- Reliability equal to conventional MT connector

This paper presents the detail of the developed assembly method and the characteristics of quickly assembled 8MT connector.

2. Assembly method

Figure 1 shows the structure of MT connector.

Figure 2 describes the conventional sequence of connector assembly.

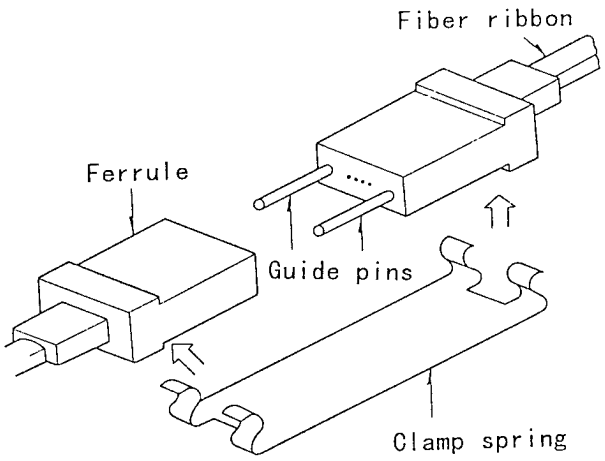

Fig.1 Structure of MT connector

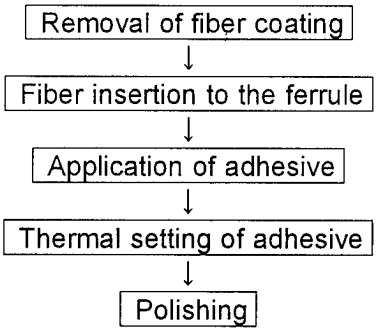

Fig.2 conventional assembly sequence

In the conventional sequence, much time was consumed in the adhesive setting and polishing. Therefore, we studied the application of quickly setting adhesive and the elimination of polishing process.

The new assembly sequence is shown in Fig.3.

(1) Removal of fiber coating

(2) Fiber insertion to the ferrule

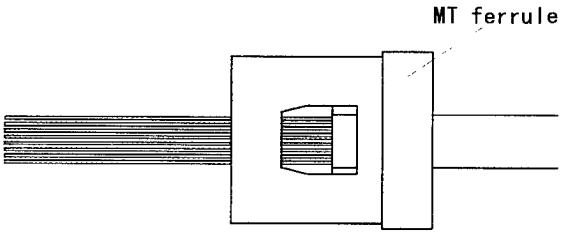

(3) Cut of protruded fiber ends

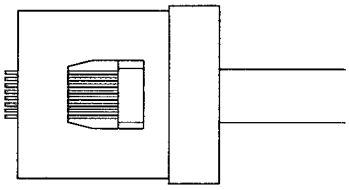

(4) Leveling of ferrule surface and fiber ends

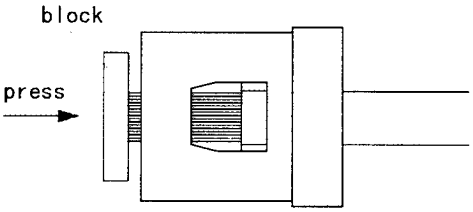

(5) Application and setting of adhesive

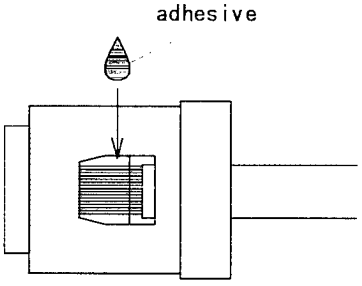

Fig.3 Quick assembly sequence

2-1. Removal of fiber coating and fiber insertion

In the conventional method, 10mm of fiber coating is removed and then fibers are inserted into the ferrule. In the newly developed method, about 30mm of fiber coating is removed because fiber ends are cut after fiber insertion.

2-2. Fiber insertion to ferrule

Because insertion fiber length is longer than conventional method, an insertion tool was developed so that fibers can be easily guided to the grooves of ferrule.

2-3. Fiber cutting

In order to eliminate the polishing process, fiber

ends are cut mirror surface and used as the contact surface. After the fiber insertion, fibers which are protruding from the ferrule end surface are cut. This method has an advantage of securing clean fiber ends, whereas if the fiber ends are cut prior to fiber insertion, the fiber ends may be contaminated with dust as they go through inside the ferrule.

2-4. Leveling of ferrule surface and fiber ends

Next step is to level the fiber end with the ferrule surface. In order to secure good optical performance and reliability, fiber end protrusion from the ferrule surface needs to be controlled. This is done by a special tool. The leveling of ferrule surface and fiber ends is done by pressing a flat block to the fiber ends until the block touches the ferrule surface. The protrusion of fiber ends from the ferrule surface is controlled within 5 μ m.Fig.4 shows an example of fiber protrusion from ferrule surface.

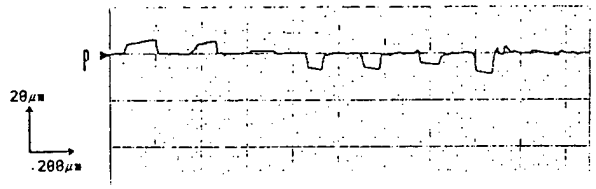

Fig.4 Leveling of ferrule surface and fiber ends

2-5. Application and setting of adhesive

In the conventional method, the adhesive was supplied and thermally set. In order to shorten the setting time, we investigated quickly setting adhesive. When the viscosity of the adhesive is too low, the adhesive may reach and contaminate the fiber ends. We selected an adhesive which has an appropriate viscosity to avoid the fiber end contamination.

3. Characteristics

3-1. Insertion loss

Fig.5 shows a histogram of insertion loss of 8MT connector assembled by the new method. Index matching material was applied on the fiber ends. The insertion loss was measured against a master 8MT connector. The average and maximum insertion loss at 1.3 μ m were 0.19dB and 0.54dB. At 1.55 μ m, they were 0.11dB and 0.35dB.

3-2. Return loss

Return loss at 1.3 μ m was 56.1dB in average and 48.8dB at minimum (n=20) .They were 54.0dB and 47.0dB (n=20) at 1.55 μ m.

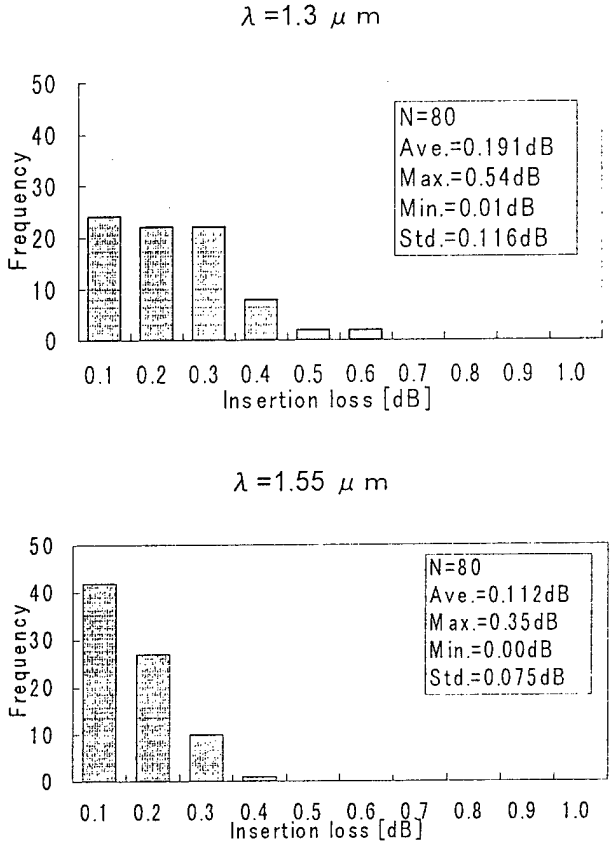

Fig.5 histogram of Insertion loss

3-3. Environmental Characteristics

3-3-1. Temperature cycling test

A result of temperature cycling test of -40 to 85 ℃ for 10cycles is shown In Fig.5. LED of 1.3 μ m was used as light source and good results were obtained with deviation from the initial loss of less than 0.2dB.

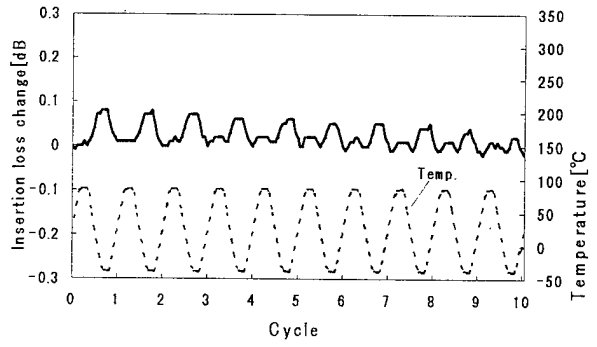

Fig.6 The insertion loss change in -40 to 80 ℃ temperature cycling test (λ =1.3 μ m)

3-3-2. Temperature and humidity cycling test

Fig.7 shows a result of Temperature and humidity cycling test of -10 to 65 ℃ (93%RH at 65 ℃) for 10 cycles. The deviation from the initial loss was well under 0.2dB.

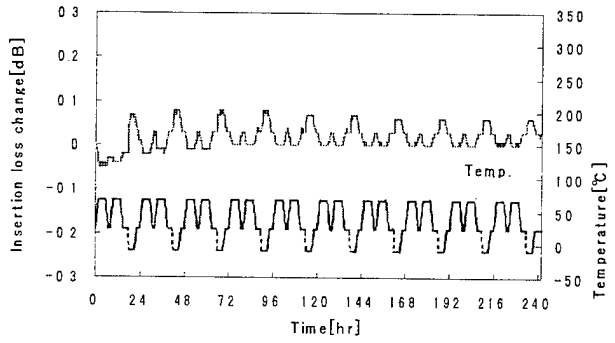

Fig.7 The insertion loss change in -10 to 65 ℃ temperature humidity cycling test (λ =1.3 μ m)

3-3-3. High temperature test

The loss variation under the high temperature test of +70 ℃ for 240 hours was less than 0.2 dB.

3-3-4. Low temperature test

Low temperature test of -40 ℃ for 240 hours showed a good result with loss change less than 0.2 dB.

3-4. Mechanical characteristics

3-4-1. Connection-disconnection test

One hundred times of connection and disconnection test was done. The loss change from the initial value was less than 0.2 dB.

3-4-2. Straight pull test

Loss change under a load of 5.9N was measured. Good result with loss change less than 0.2 dB was obtained.

3-4-3. Bend test

Bend test of ± 90 degrees for 10 cycles with a load of 0.5N was given.
The resultant loss change was less than 0.2 dB.

3-4-4. Vibration test

Vibration test of frequency of 10 to 55Hz for 2 hours. for each of three directions was carried out.
The loss change was less than 0.2 dB.

3-5. Assembly time

The assembly time of MT connector by the newly developed method was measured. The average time was about three minutes (n=30), which means the assembly time can be reduced to about one fifth of the conventional method.

Table 1 summarizes the results of the various tests mentioned above.

Table 1. Results of mechanical and environmental tests

Item	Conditions	Results
Insertion loss	against master n=80	Ave.0.19dB(1.3 μ m) Ave.0.11dB(1.55 μ m)
Return loss	n=80	Ave.56.1dB(1.3 μ m)
Temperature cycling	-40 to 85℃ 10cycles,n=6	loss change ≦0.2dB(1.3 μ m)
Temp.&humiditiy cycling	-10 to 65℃ 93%RH(at 65℃) 10cycles,n=3	loss change ≦0.2dB(1.3 μ m)
High temp. endurance	+70℃,240hours n=3	loss change ≦0.2dB(1.3 μ m)
Low temp. endurance	-40℃,240hours n=3	loss change ≦0.2dB(1.3 μ m)
Conection -disconection	100times n=3	loss change ≦0.2dB(1.3 μ m)
Straight Pulling	5.9N n=3	loss change ≦0.2dB(1.3 μ m)
Bending	0.5N,±90° 10times,n=3	loss change ≦0.2dB(1.3 μ m)
Vibration	10 to 55Hz,2hours Amp.1.5mm 3direction,n=3	loss change ≦0.2dB(1.3 μ m)
Assembly time	n=30	Ave.3min/pcs

4.Conclusion

We studied methods to shorten the assembly time of MT connector and developed a new method which can reduce the assembly time to one fifth of the conventional method. The new method uses a quickly setting adhesive and eliminates polishing process. Good optical and mechanical performances were obtained.

REFERENCE

1) S.Nagasawa et. al., "Mechanically Transferable Single-mode Multifiber connector", in Tech. Dig. IOOC'89. 21C2-1, 99. pp.48-49, 1989

2) M.Takaya, "Design and Development of Optical Fiber Jointing Techniques for Efficient Construction of Aerial Distribution Cable Systems", 46th IWCS, pp.500-505, 1997

3) S.Nagasawa, F.Asiya, T.Satake, "Optical Multifiber Connectors", MICROOPTICS NEWS. VOL.10, No.2, pp.49-55, 26 JUNE 1992

4) T.Ohta, Y.Kihara, T.Shigematsu, "High Quality Multiple-Fiber Connector", FURUKAWA ELECTRIC REVIEW. No.89, pp.9-14, December 1991

5) F.Asiya, T.Satake, S.Nagasawa, "Development of Multifiber Connectors and their Application", E-OFC'87, pp.303-308

Kazuhiro Takayama

The Furukawa Electric Co., Ltd.

6, Yawata-kaigandori, Ichihara-shi, Chiba 290-8555,Japan

He received the B.S. degree in physics from Ibaraki University, Ibaraki, Japan, in 1990.

He joined The Furukawa Electric Co., Ltd. in 1990. Since then he has been engaged in the research and development on optical component.

Masato Shiino

The Furukawa Electric Co., Ltd.

6, Yawata-kaigandori, Ichihara, Chiba 290-8555, Japan

He received the B.E. degree in electronic engineering from Chiba Institute of Technology, Chiba, Japan, in 1986.

He joined The Furukawa Electric Co., Ltd. in 1988. Since then he has been engaged in the research and development on optical component.

DEVELOPMENT OF SINGLE-MODE 2-FIBER MINI-MPO CONNECTOR USING INJECTION-MOLDED FERRULE

Yutaka Arai Naoko Shimoji Kazuhiro Takayama Koichi Maeno

Opto-technology Laboratory The Furukawa Electric Co., Ltd
6, Yawata-kaigandori, Ichihara-shi, Chiba 290-8555 JAPAN
Phone: +81-436-42-1725 Fax: +81-436-42-9340 E-mail: arayuta@ch.furukawa.co.jp

ABSTRACT

We developed Mini-MT ferrule injection molding method instead of conventional transfer molding. We also developed Mini-MPO connector using this ferrule to achieve lower cost. We studied wide range of ferrule materials and molding conditions, and realized exceedingly stable and accurate ferrule equal to transfer-molded ferrule. The prototype connector has high optical performance. The average insertion loss was 0.18 dB and the average return loss was 46.2 dB. Good mechanical and temperature characteristics were also obtained.

INTRODUCTION

In recent years, for the realization of multimedia society, transmission of large volume of data is absolutely necessary, for equipments such as high speed processing computers and large capacity data exchangers. Therefore optical fiber cables of high count and high fiber density are in greater demand, and so is the demand for multi-fiber optical connectors which can connect larger number of fibers.

Multi-fiber MT connector has been already used practically.[1] And also, MPO connector utilizing multi-fiber MT ferrule, which can connect and disconnect by push-on and pull-off actions, has been developed.[2] MPO connector is capable of connecting up to 12 fibers simultaneously.

Recently, Mini-MPO connector which is a smaller version of MPO connector has been developed for high density connection of up to four fibers. [3] [4]

For MPO and Mini-MPO connector, high-precision molded plastic ferrules are necessary to obtain required optical characteristics. MT ferrule needs to be made with submicron accuracy. Therefore, transfer molding technique using epoxy resin has been established as a suitable method to make high precision ferrule. [5]

Multi-fiber connectors such as MPO and Mini-MPO have drawn attention in data communication market and expected to be used in large quantities hereafter. These connectors are required lower cost and therefore need to be manufactured with high productivity.

For these reasons, we studied the application of injection molding technique, which is higher in productivity and lower in cost than transfer molding, to the manufacture of Mini-MT ferrule.

STRUCTURE

Fig. 1 shows the structure of Mini-MPO connector. Mini-MPO connector consists of two plugs and an adapter.

Fig. 2 shows the structure of Mini-MT ferrule which is a key part of the plug. The size of the endface of Mini-MT ferrule is 4.4 mm wide, 2.5

mm high. Plugs are aligned by two alignment pins. The pitch of the alignment holes is 2.6 mm.

The pitch of the alignment holes and the relative positions of the fiber holes to the alignment holes must be accurate in submicron order to obtain fine optical characteristics.

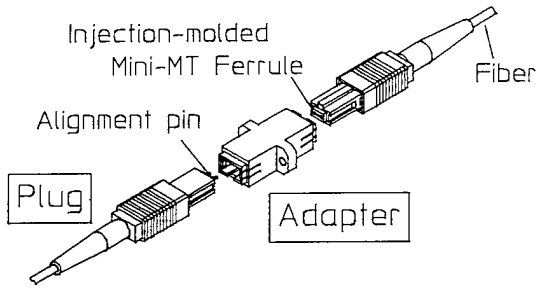

Fig. 1 Structure of Mini-MPO connector

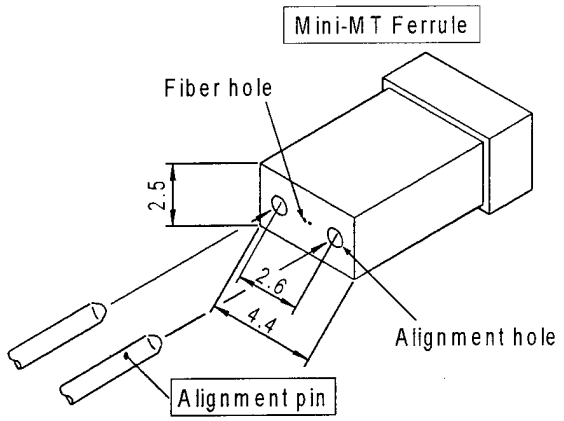

Fig. 2 Structure of Mini-MT Ferrule

INJECTION MOLDING TECHNIQUE

Development Concept

In plastic molded MT ferrule, optical characteristics depend on the diameter and the pitch of the alignment holes and the offset of the fiber holes. Today, in SC connector, which is widely used, the offset of the fiber hole against the ferrule periphery is severely controlled, and stable insertion loss of the order of 0.1 dB is achieved. For MT ferrule, even severer accuracy is required to obtain good performance for all the multiple fibers. Today, as a result of the development of thermally curable epoxy resin with low molding shrinkage and the advance in transfer molding technique, we have been able to obtain exceedingly stable MT ferrules with submicron order accuracy. Therefore MT connectors have attained fine optical characteristics which are close to those of mono-fiber connectors. Consequently, in recent years, MT connectors and MT connector families are paid much attention in data-communication field.

To cope with large demand expected hereafter, for MT and Mini-MT connectors, mass production technique and lower cost must be achieved. So we developed multi-fiber connector ferrule using injection molding technique.

Development of injection molding

We took a similar approach to develop injection molding as we did to transfer molding. However, in injection molding, it was difficult to obtain the resin which has the molding shrinkage rate similar to transfer molding resin. Also the molding shrinkage depended on fillers. Therefore it was difficult to obtain stable molding accuracy, so the application to single-mode fibers was not as easy as to multi-mode fibers.

We tried further approach to the optimization of molding materials and molding conditions. The molding shrinkage depends on the physical properties of the base resin and the form, size, and quantity of fillers, and the mold, and so on. As a result of much studies, we succeeded to achieve accuracy for injection molding equal to transfer molding. We could reduce the deviation of the alignment hole pitch to a few micrometer. And also, we realized uniform molding shrinkage and obtained high accuracy of the fiber hole position using isotropic filler. Therefore we could develop exceedingly stable submicron order accurate

ferrules equal to transfer molding and applicable to single-mode fibers. Moreover, the injection molding technique is superior to transfer molding in terms of continuous production and shorter molding cycle, so it enables us to obtain mass produced, and low cost ferrules.

CHARACTERISTICS

We constructed Mini-MT ferrules based on the above injection molding technique. With these ferrules, we assembled Mini-MPO connectors with single-mode 2-fiber ribbons. The ferrule endface is flat PC polished. Then, the following characteristics were tested without index-matching.

Optical Test Results

Fig. 3 and Fig. 4 shows the insertion loss and the return loss of single-mode 2-fiber Mini-MPO connectors using an LED operating at 1310 nm wavelength. The average insertion loss was 0.18 dB and the maximum insertion loss was 0.36 dB. And the average return loss was 46.2 dB and the minimum return loss was 40 dB. The results show that the injection-molded MT ferrule has sufficient accuracy in the alignment hole pitch and the relative positions of the fiber holes to the alignment holes.

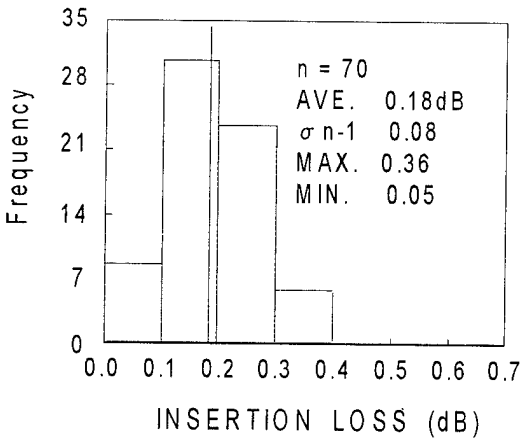

Fig. 3 Insertion loss for single-mode 2-fiber Mini-MPO connector using injection-molded ferrule

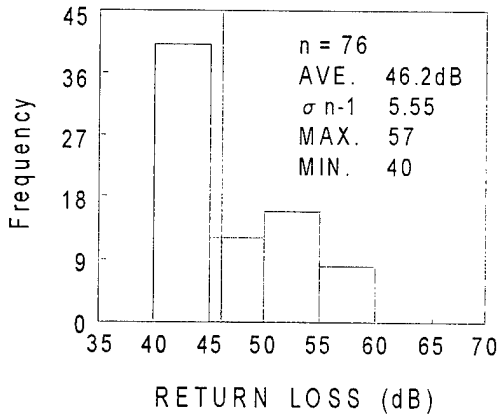

Fig. 4 Return loss for single-mode 2-fiber Mini-MPO connector using injection-molded ferrule

Mechanical and Temperature Test Results

Fig. 5 shows the insertion loss change of single-mode 2-fiber Mini-MPO connectors for 500 reconnections. The range of the maximum insertion loss change was less than 0.09 dB, and there was no damage to the connector.

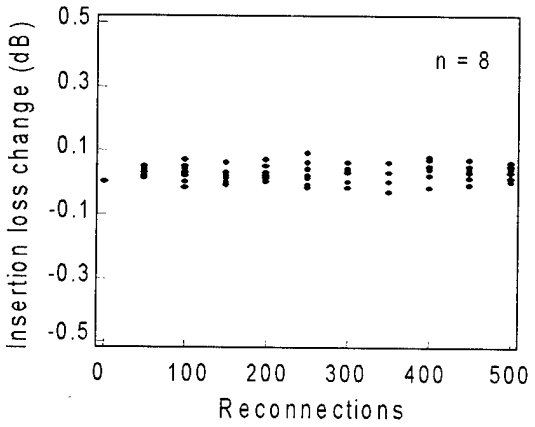

Fig. 5 Insertion loss changes of single-mode 2-fiber Mini-MPO connector using injection-molded ferrule for 500 reconnections

We also examined straight pull, side bend, side pull and temperature cycling characteristics.

At straight pull test, we applied a load of 68.6 N for one minute to the connectors which are attached to both ends of a fiber cord. The insertion loss change was less than 0.05 dB.

At side bend test, the fiber cord with connector was bent at 90 degree right and left to the fiber cord for 100 times with an applied load of 4.9 N to the fiber cord. The insertion loss change was less than 0.02 dB.

At side pull test, we applied a load of 20 N to normal to the axis of the connector. Fig. 6 shows the method of side pull test. The insertion loss change was less than 0.04 dB and the return loss change was less than 6 dB.

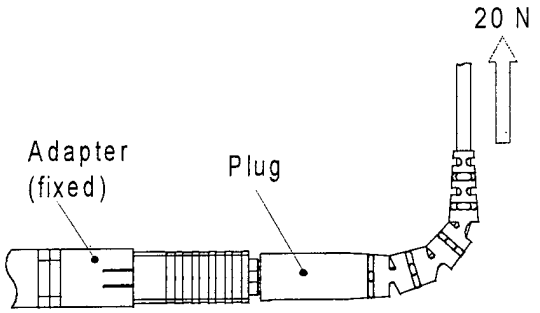

Fig. 6 The method of side pull test

Temperature cycling test from -25 to 70 ℃ was carried out for 10 cycles. The insertion loss change was less than 0.2 dB.

These results are summarized in Table 1.

Results of Mechanical and Temperature tests

Tests	Conditions	n	Results
reconnection	500 times	8	$\Delta i \leqq 0.09$ dB
straight pull	68.6 N × 1 min.	12	$\Delta i \leqq 0.05$ dB
side bend	4.9 N × 100 times	8	$\Delta i \leqq 0.02$ dB
side pull	20 N	10	$\Delta r \leqq 6$ dB $\Delta i \leqq 0.04$ dB
Temperature cycling	-25 ~ 70℃ 2.5 hours／cycle 10 cycles	6	$\Delta i \leqq 0.2$ dB

Δi: Insertion Loss Change Δr: Return Loss Change

Table 1 Results of mechanical and temperature tests on single-mode 2-fiber Mini-MPO connector using injection-molded ferrule

CONCLUSION

We developed Mini-MPO connector using injection-molded ferrule. The connector has flat endface and connects two single-mode fibers simultaneously. It has a low average insertion loss of 0.18 dB and a high average return loss of 46.2 dB at 1310 nm wavelength. We also carried out mechanical and temperature tests, and obtained good characteristics. The results shows that Mini-MPO connector using injection-molded ferrule have sufficient optical characteristics. We also confirmed that injection molding is suitable to supply large quantity of ferrules with low cost.

REFERENCES

1) Nagasawa et al, Proc. Iooc '89, paper 21C2-1, 1989, pp. 48-49

2) Nagasawa et al, IEEE Photon. Technol. Lett., Vol. 3, No. 10, 1991, pp. 937-939

3) Takaya et al, IEEE Photon. Technol. Lett., Vol. 10, No. 1, 1998, pp. 102-104

4) Shimoji et al, IWCS Proceedings 1997, pp. 510-515.

5) Yamakawa et al, Furukawa Review, No. 14, 1995, pp. 53-58

AUTHORS

Yutaka Arai

The Furukawa Electric Co., Ltd
6, Yawata-kaigandori, Ichihara-shi,
Chiba 290-8555 JAPAN

He received the B.E. degree in electronic engineering from Niigata University, Niigata, Japan, in 1986.

He joined The Furukawa Electric Company, in 1997. Since then he has been engaged in the research and development on optical component.

Kazuhiro Takayama

The Furukawa Electric Co., Ltd
6, Yawata-kaigandori, Ichihara-shi,
Chiba 290-8555 JAPAN

He received the B.S. degree in physics from Ibaraki University, Ibaraki, Japan, in 1990.

He joined The Furukawa Electric Company, in 1990. Since then he has been engaged in the research and development on optical component.

Naoko Shimoji

The Furukawa Electric Co., Ltd
6, Yawata-kaigandori, Ichihara-shi,
Chiba 290-8555 JAPAN

She received the B.S. and M.S. degree in physics from Chuo University, Tokyo, Japan, in 1991 and 1993, respectively.

She joined The Furukawa Electric Company, in 1993. Since then she has been engaged in the research and development on optical component.

Koichi Maeno

The Furukawa Electric Co., Ltd
5-1-9, Higashi-Yawata, Hiratsuka-shi,
Kanagawa 254-0016 JAPAN

He received the B.E. degree in applied chemistry from Hiroshima University, Hiroshima, Japan, in 1991.

He joined The Furukawa Electric Company, in 1991. Since then he has been engaged in the research and development on polymer processing and material.

A study on jointing work on the ground for the aerial optical cable installation

K. Kohga , H. Oizumi, M. Ueda, T. Kaneko
Mitsubishi Cable Industries LTD. Hyogo, Japan

Abstract

With the increase of high-count core optical fiber cables, the jointing work is more time consuming and costly than before. To reduce the time spent on jointing at the aerial location, we suggest a method which improves the environment for jointing works.

The improved method consists of doing the jointing work of the aerial optical fiber cables on the ground. We also developed an apparatus to store the extra length of cables. Jointing work on the ground using a 600-core optical fiber cable was tested in the field.

As a result, the jointing was done easier on the ground and reduced the time for the jointing by 15% compared to aerial work.

1. Introduction

Currently, with increasing demands of telecommunication line, high-count optical fiber cables are in great need. As the jointing includes numerous cores, much time is spent on cable installation. For cost reduction of the installation, the jointing workability must be improved, especially at the aerial location. To reduce the time on the jointing work, methods such as reducing the splice-count using ribbon fibers, speeding up the splice machine and improving the closure set to have easy assembly have been reported. However, we have not seen reports on improving the environment for jointing work at aerial locations.

In Japan , the jointing work of aerial cables are usually done on a aerial lift platform which is about 6m high from the ground.

This paper reports on the jointing work done on the ground to improve working conditions. After the splicing work is performed on the ground, the extra cable and closure is attached to a messenger wire at the aerial location.

2.Conventional methods and their problems

The jointing work includes sheath cutting and strength member stripping, splicing, closure assembly and attachment to the messenger. These work are done high above the ground on an platform of an aerial lift. (Fig. 1) The work is often interfered by:

1) weather (hot or cold, snow, rain, wind, humidity)
2) limit on the equipment weight and insufficient working space
3) swinging of the platform
4) time spent on moving material and men between the ground and the platform

3.The jointing method on the ground

a) Outline

First, sheath cutting and strength member stripping, splicing and closure assembly are done on the ground. Next, the closure and extra cable are attached to the messenger wire at the aerial location.

(Fig. 2) The merit of this method is that most of the work can be done on the ground. Its demerit is that it needs to store extra cable.

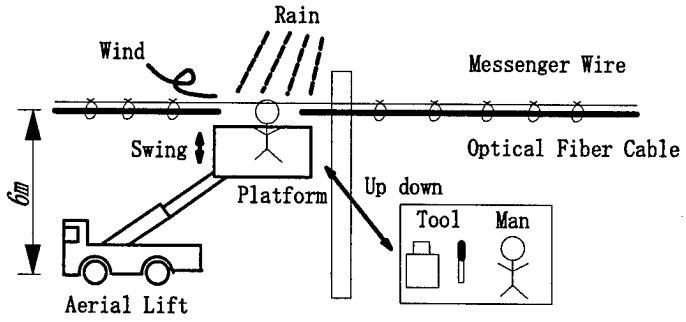

Fig.1 Conventional methods and their problems.

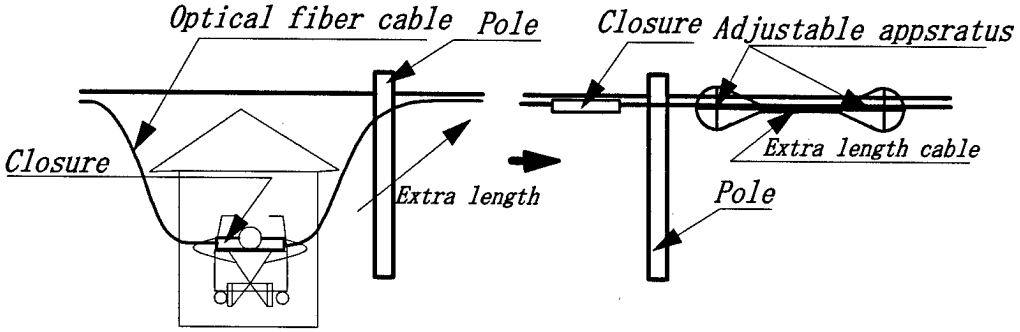

Fig.2 Jointing work on the ground

b) Method of storing extra cable

We choose a method of storing the extra length of cable in shapes of figure 8 on the messenger wire between the poles. (Fig. 3) Its features are as follows:

1) has enough storing capacity
2) does not interfere with the installation of other cable or equipment
3) neat appearance
4) does not interfere with the maintenance of power cables

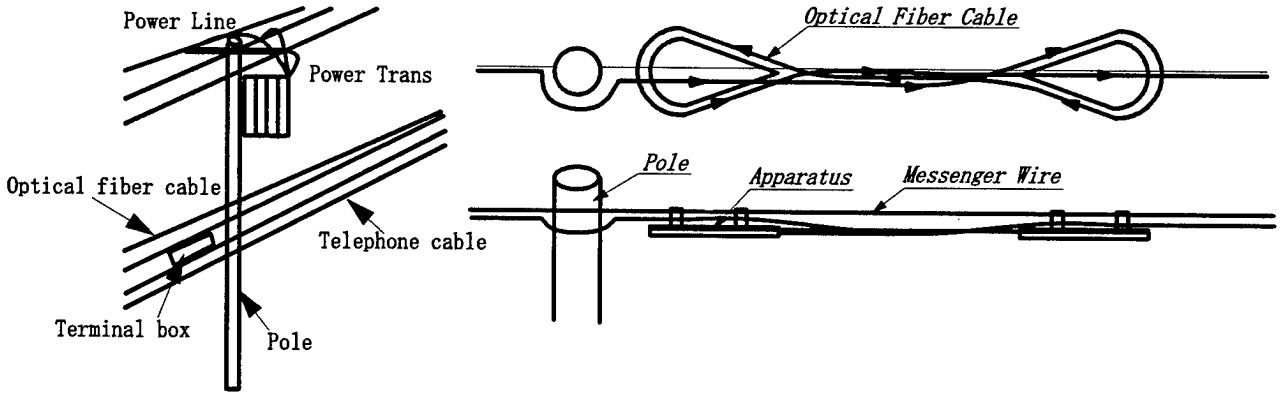

Fig.3 Method of storing extra cable

c) The apparatus specifications

The apparatus must maintain minimum radius at the bend of optical fiber cable. The apparatus has the following features and requirements.

1) Maintaining bending radius
   $R \geqq 10 \cdot D$ (D : cable diameter)
2) one apparatus can store up to a 600-core cable (D=25mm)
3) has enough strength
4) is simple in structure and made at a low cost
5) can be used over a long period of time

The structure and specification are shown in Fig.4 and Table.1. The apparatus consists of a cross-shaped frame, two messenger clamps and three adjustable arms. The bending radius can be adjusted by expansion and contraction of the three arms.

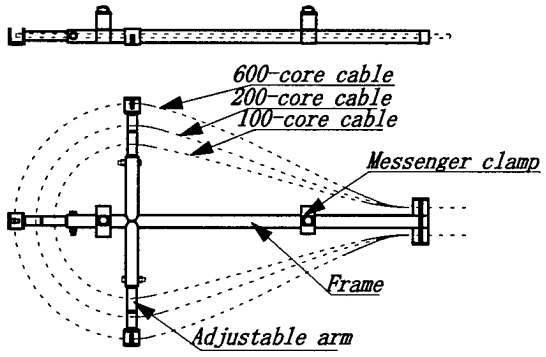

Fig. 4 Adjustable apparatus

Table 1 Specification

Fiber count (core)	Cable diameter D (mm)	Bending radius r (mm)
100	15	155
200	20	205
300	23	255
600	25	

4. Field test of the jointing work on the ground

We tested the jointing work in the field using a 600-core optical fiber cable with spacer slot. The weather at the field was fine. 200-cores of a 600-core fiber was spliced and evaluated. The time taken for jointing at aerial locations and the ground is shown in Fig 5.

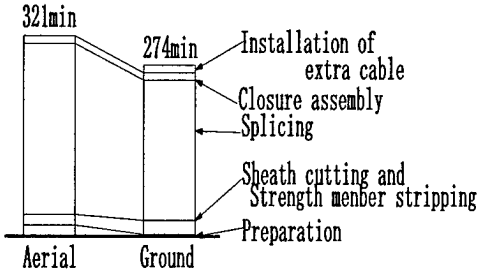

Fig 5. The time for jointing

5.Conclusion

We have developed a radius-adjustable apparatus to store extra cable of up to a 600-core optical cables at the splicing location. Using this radius adjustable apparatus, we demonstrated that jointing work for aerial optical fiber cables can be done on the ground.

As a result, by working on the ground we were able to reduce the time for jointing by 15% compared to aerial work.

References

[1] H.IWATA et al.," Development of Ultra-High Count Optical Fiber Cable Using 16 Fiber", IEICE Spring, 1996, B-1062

[2] S.HAYAMAI et al.," Study on Drop jointing using Fusion splicer", IEICE Spring, 1996, B-1083

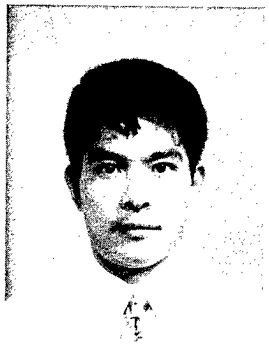

Kuniaki Kohga
MITSUBISHI CABLE INDUSTREIS, LTD.4-3
Ikejiri, Itami-city, Hyogo pref. ,
664-0027,Japan

Mr. Kohga, Senior Engineer of RF & Optical System Dept., has been engaged in design and development of termination box for optical fiber cable. He is now an engineer in development of optical fiber communication system. He received his M.S. degree in Communication engineering from Nagaoka University of Technology in 1986.

Masumitsu Ueda
MITSUBISHI CABLE INDUSTREIS, LTD.4-3
Ikejiri, Itami-city, Hyogo pref. ,
664-0027,Japan

Mr. Ueda , Engineer of Telecommunication Engineering Dept., is engaged in design and development of termination box for optical fiber cable. He received his B.S. degree in Precision Engineering from Osaka University in 1992.

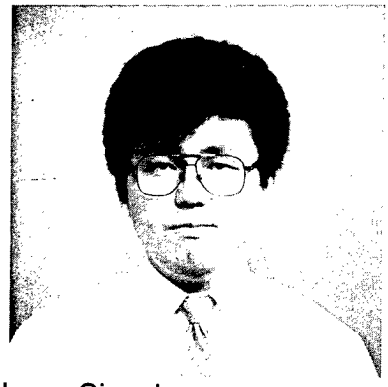

Haruro Oizumi
MITSUBISHI CABLE INDUSTREIS, LTD.4-3
Ikejiri, Itami-city, Hyogo pref. ,
664-0027,Japan

Mr. Oizumi, Engineer of Tele-communication Engineering Dept., is engaged in design and development of optical fiber cable. He received his B.S. degree in Applied Physics from Tohoku University in 1988.

Takashi Kaneko
MITSUBISHI CABLE INDUSTREIS, LTD.4-3
Ikejiri, Itami-city, Hyogo pref. ,
664-0027,Japan

Mr. Kaneko, Chief Engineer of Inspection Section, has been engaged in design and development of optical fiber cable. He is now a chief engineer in inspection of cable. He received his B.S. degree in Electrical engineering from Sophia University in 1974.

A NOVEL METHOD FOR TRUE SPLICE LOSS ANALYSIS BY USING ONE-END OPTICAL TIME-DOMAIN REFLECTOMETER INCORPORATED WITH THE MICROBENDER

Chien-Chung Lee, Tai-Jung Liaw, Fwu-Yuan Tsai, Ching-Shu Wang, Yuan-Kuang Tu

Outside Plant Lab., Chunghaw Telecom Lab., Taiwan, R.O.C.

ABSTRACT

By theoretical calculations and experiments, we demonstrate a simple and quick method based on microbending mechanism to analyze the true splice loss by only using optical time-domain reflectometer (OTDR) at one-end incorporated with the microbender. This method is also able to measure the distributed mode-field diameter (MFD) of the fiber. The true splice loss can be calculated by eliminating the MFD mismatch error that is measured by this method. The MFD measurement accuracy is within 7.5% with 2cm resolution.

INTRODUCTION

The splice losses of optical fibers are measured maturely by using optical time-domain reflectometry (OTDR). The measured error, caused by MFD and refractive index mismatch, is well known and can be eliminated by averaging the bi-directional measured splice losses. In practical field application, the bi-directional OTDR measurement can not be done until the whole fiber link is spliced completely. It costs a lot of time and money to open the protective closure and re-splice the fibers when the unqualified splice loss is found by averaging the bi-directional measured splice losses. Obviously, the averaging correction method is not suitable in field installation. The return-circuit method [1] was proposed to measure the true splice losses, but it is also time consuming to splice the return optical fiber link and switch OTDR back and forth for retrieving and averaging the bi-directional splice losses.

In this letter, we present a MFD error correction method by using the microbender and the unidirectional OTDR (UOTDR) technique to measure the true splice losses. The MFD mismatch is the major contributor to the splice loss error. For commercial single-mode step-index fibers, it has been proved that the effects of the refractive index and the Rayleigh loss mismatch are negligible when compare to MFD mismatch [1]. Therefore, the true splice loss can be retrieved by only eliminating the error induced by MFD mismatch. The procedure of our method is : first, we use the microbender to measure the microbending losses on fibers, then calculate the MFD ratio by using the relationship between MFD and microbending losses. Finally, we can retrieve the true splice losses by eliminating the MFD error. The theoretical analysis and experimental results are shown in the following sections.

THEORETICAL ANALYSIS

When fiber *#i* is spliced with fiber *#j*, the backscattering power P_{1i}, at the point immediately preceding the splice position, detected by OTDR from fiber *#i* is given by [2]

$$P_{1i} = \frac{1}{4}\left(\frac{\lambda}{\pi n_{1i} w_i}\right)^2 P_{in}\alpha_{si} D\frac{\upsilon}{2} e^{-2\alpha L} \qquad (1)$$

where λ is the optical probe wavelength, n_{1i} is the core refractive index of *#i* fiber, w_i is the Gaussian definition MFD of fiber *#i*, P_{in} is the power that enters into the fiber, α_{si} is the Rayleigh scatter loss of fiber *#i* in nepers per meter, D is the pulse-width of the transmitted light pulse, υ is the light velocity in the fiber, α is the loss in neppers per meter, and L is the fiber length. The backscattering power P_{2i}, at the point right after

the splice, detected by OTDR from fiber #*i* is given by

$$P_{2i} = \frac{1}{4}\left(\frac{\lambda}{\pi n_{1j} w_j}\right)^2 T_j T_{ji} P_{in} \alpha_{sj} D \frac{\upsilon}{2} e^{-2\alpha L} \quad (2)$$

where T_j is the splice transmission coefficient in the forward direction, and T_{ji} is the corresponding parameter in the reverse direction. The one-end OTDR splice loss α_i, which is measured from the fiber #*i*, is determined from the ratio of these two power levels, and given in decibels by

$$\alpha_i = 10\log\left(\sqrt{T_j T_{ji}}\right) + 10\log\frac{w_j}{w_i} + 10\log\frac{n_j}{n_i} + 5\log\frac{\alpha_{si}}{\alpha_{sj}}. \quad (3)$$

In Eq.(3), the first term describes the true splice loss. The second, third and fourth terms are the errors due to MFD, refractive index and Rayleigh-scatter loss mismatches, respectively.

Similarly, the one-end OTDR splice loss α_j measured from the opposite direction is given by

$$\alpha_j = 10\log\left(\sqrt{T_j T_{ji}}\right) + 10\log\frac{w_i}{w_j} + 10\log\frac{n_i}{n_j} + 5\log\frac{\alpha_{sj}}{\alpha_{si}}. \quad (4)$$

Obviously, the true splice loss α_t is obtained by averaging Eq. (3) and (4):

$$\alpha_t = \frac{1}{2}\left(\alpha_i + \alpha_j\right). \quad (5)$$

This MFD error correction method can estimate the true splice loss when the effects of the refractive index and Rayleigh-scatter loss mismatches are small. Therefore, the one-end OTDR splice loss α_i measured from fiber #*i* can be describedd by

$$\alpha_i \approx 10\log\left(\sqrt{T_j T_{ji}}\right) + 10\log\frac{w_j}{w_i}. \quad (6)$$

The microbending loss due to axial deformations has two loss sources, one arising from the permanent coupling between the LP_{01} mode and leaky or radiation modes, and another arising from the pure bending loss effect on the LP_{01} mode. By the proper microbender design and the bending-loss-insensitive wavelength selection, the microbending loss depends almost on the MFD. The microbending loss α_m of the SMF under-test can be described by [6]

$$\alpha_m = k' w^6, \quad (7)$$

where *w* is the MFD, *k'* is the constant determined by the microbender. Therefore, the MFDs at any points on the under-test fiber can be described as a function of the microbending loss at that point. After calibration with an MFD-known fiber, the MFD w_i at point *i* of the under-test fiber is given by

$$w_i = k\left(\overline{\alpha}_i - \alpha_i\right)^{\frac{1}{6}}, \quad (8)$$

where *k* is the calibration factor, $\overline{\alpha}_i$ is the loss measured by OTDR when the point *i* is clamped by the microbender, and α_i is the original loss at the point *i* measured by OTDR without the microbender. Therefore, by measuring the microbending loss ($=\overline{\alpha}_i - \alpha_i$) at each point (e.g., the points P1, P2, P3, and P4 in the fiber closures), the distributed MFDs of the optical fiber link can be obtained.

EXPERIMENTS AND RESULTS

The experimental setup is shown in Fig. 1. The under-test fiber is composed of a match-inner-cladding fiber of 2.1 km, a depressed-inner-cladding fiber of 2.1 km, and a dispersion-shift fiber of 2.1 km. The microbender, as shown in Fig.1, has two plates with periodic V-shaped grooves to create a microbend inducing structure and a clamping spring for constant deformation amplitude. The V-shaped grooves have a deformation period of 1 mm and a deformation length is 2 cm, which determines the measurement resolution. A 1310-nm OTDR is used to measure the microbending loss of under-test SMF clamped by this microbender. The microbending losses of different MFD fibers clamped by this microbender are measured as the step(1) shown Fig.1 for deriving the relationship between microbending loss and MFD. Fig. 2 illustrates the measured microbending losses (denoted as the label of "♦") for these three different MFD fibers. The variation of microbending-loss increases with the MFD value because of the increased macrobending-loss sensitivity. Therefore, we choose the smallest MFD fiber (here, the dispersion-shift fiber) as a calibration fiber, and thus the k value is, calculated by Eq. (1), about 14.87 ($=6.9/(0.01)^{1/6}$) for the known MFD of 6.9 μm and the measred microbending loss of 0.01dB. The dot-line in Fig.2

shows the k=14.86 calculated curve by using Eq. (1).Then, as the step(2) shown in Fig.1, the under-test fiber link is measured each time with the microbender located at the beginning, the splicing (both in front of and right after the splicing point), and the ending points of this SMF link. The measured OTDR traces for OTDR operated at ports A and B without microbender are shown in Fig. 3(a) and (b), respectively. Note that the MFD-mismatched points reveal the complementary behavior for the OTDR traces measured at A and B. The distributed MFDs of under-test fiber link, measured by OTDR at ports A and B incorporated with the microbender are shown in Fig. 3(c) and (d), respectively. The measurement results are in quite good agreement with the results using the destructive VAT method. The maximal difference between the proposed method and the VAT method is less than 7.5%.

As shown in Fig.4, the true splice losses were measured by using this microbending method and compared with the true splice losses measured by the bi-directional OTDR averaging method at 1310nm. The error of the estimated splice loss is defined by the difference between the splice loss of the microbending method and the bi-directional OTDR averaging method. From Fig. 4, we observe that the error is up to 0.32dB when the splice loss of fiber #1 and fiber #2 was measured from fiber #2. That is because that the measured MFD ratio error, which is equal to 7.5%, will induce about 0.31dB error for the estimated splice loss. Therefore, it is expected to reach the 0.1dB accuracy of the true splice loss by improving the accuracy of the MFD ratio measurement within 2.3%.

CONCLUSIONS

By theoretical calculations and experiments, we demonstrate a simple and quick method based on microbending mechanism to analyze the true splice loss by only using optical time-domain reflectometer (OTDR) at one-end incorporated with the microbender. This method is also able to measure the distributed mode-field diameter (MFD) of the fiber. The true splice loss can be calculated by eliminating the MFD mismatch error that is measured by this method. The MFD measurement accuracy is within 7.5% with 2cm resolution.

REFERENCES

1. *Amended/New Draft Recommendations of the G.600-series Submitted to the Xth CCITT Plenary Assembly*, Geneva, May 1992, pp.4 - 6.
2. Kapron, F. P., Adams, B. P., Thomas, E. A. and Peters, J. W.:'Fiber-Optic Reflection Measurements Using OCWR and OTDR Techniques',*Journal of Lightwave Technol.*,1989, vol. 7, pp.1234-1241.
3. BLANK, L. C., and SPIRIT, D. M., "OTDR enhancement through erbium fibre amplification," *Electron. Lett.*, 1989, vol. 25, pp. 1693-1694.
4. Souza, K. De, Wait, P .C. and Newson, T .P.:'Characterisation of Strain Dependence of the Landau-Placzek Ratio for Distributed Sensing',*Electron. Lett.*,1997, vol. 33, pp.615-616.
5. Sandeith, C. J., McCormick, W. D., Thornton, J. A., Wise, D. R. and Odom, R. I.:'Fiber-Strain Measurement Using Brillouin Optical-Fiber Tiime-Domain Analysis'.*International Wire & Cable Symposium (IWCS)*, Reno, Nevada, 1996, pp.415-427.
6. JEUNHOMME, L. B., *Single-Mode Fiber Optics*, Marcel Dekker Inc., New York, 1983, pp. 95-97.

Fig. 1. Experimental setup of distributed MFD measurement by using OTDR incorporated with a microbender.

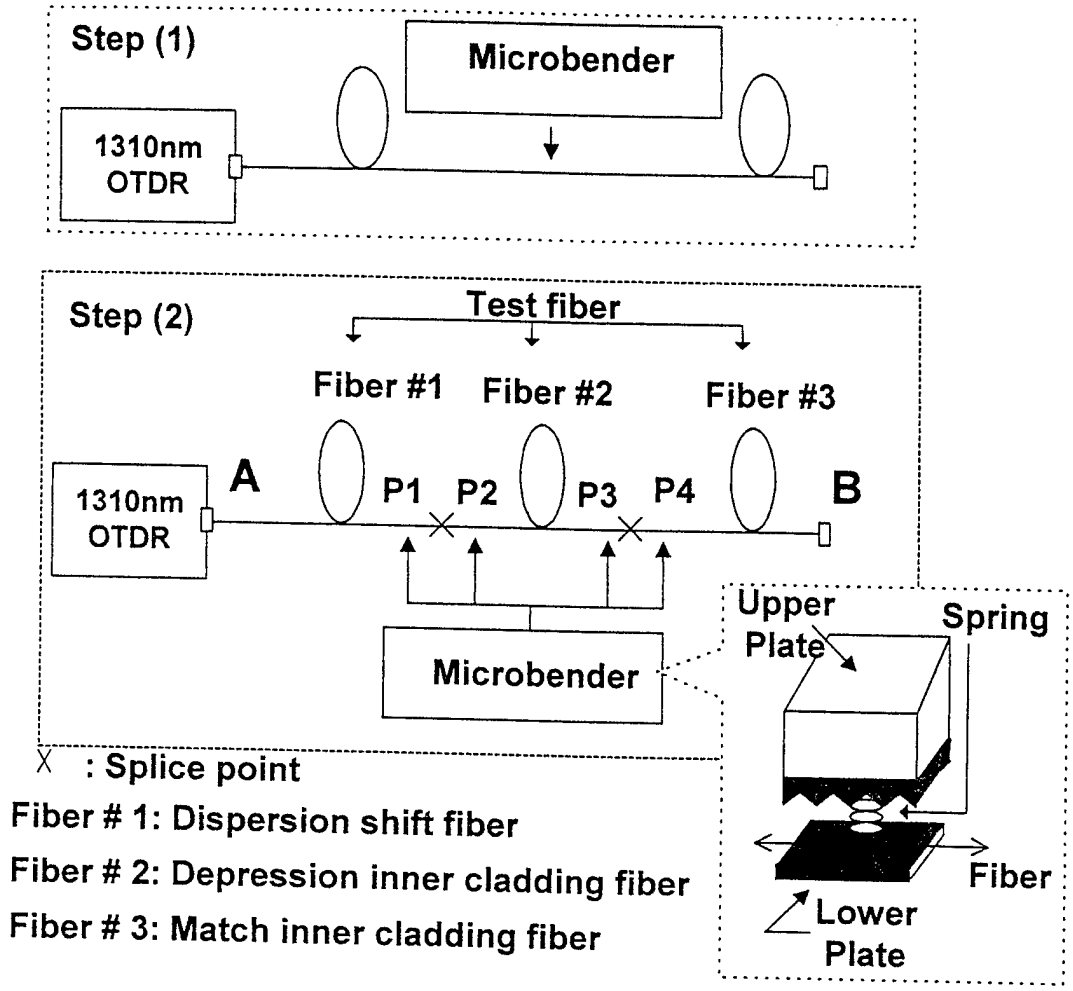

Fig. 2. The microbending loss versus the mode-field diameters (MFDs)of different fibers.

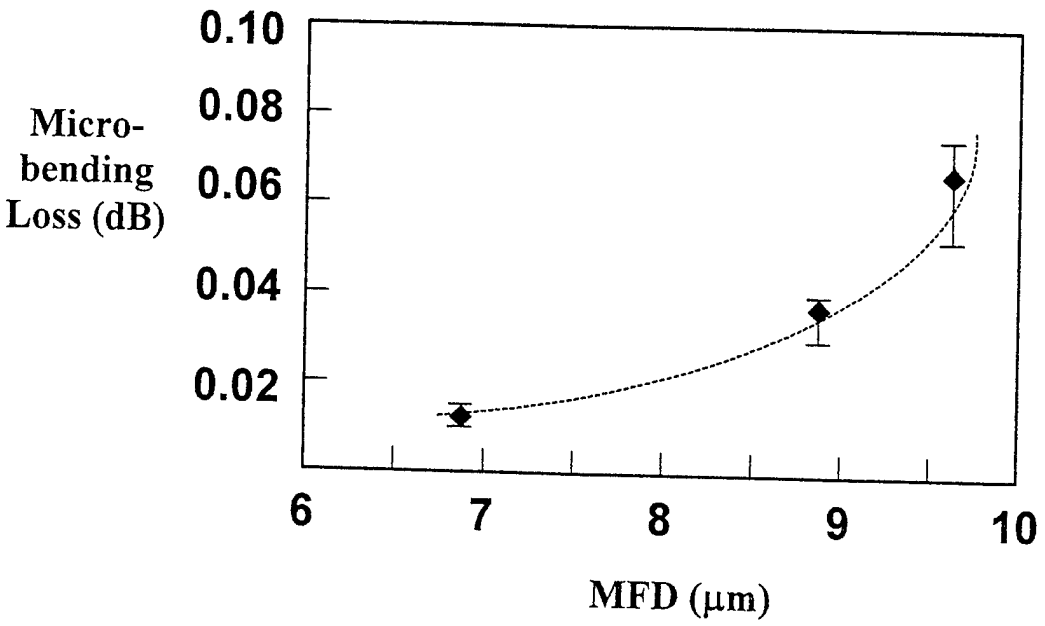

Fig. 3. The measured OTDR traces of under-test SMF links, measured by OTDR operated at ports (a) A and (b) B without the microbender. The distributed MFD of the under-test fiber links measured by an OTDR at ports (c) A and (d) B incorporated with the microbender.

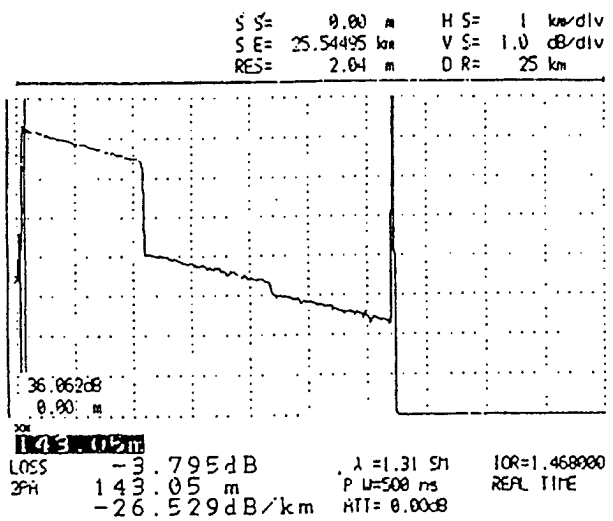

(a)

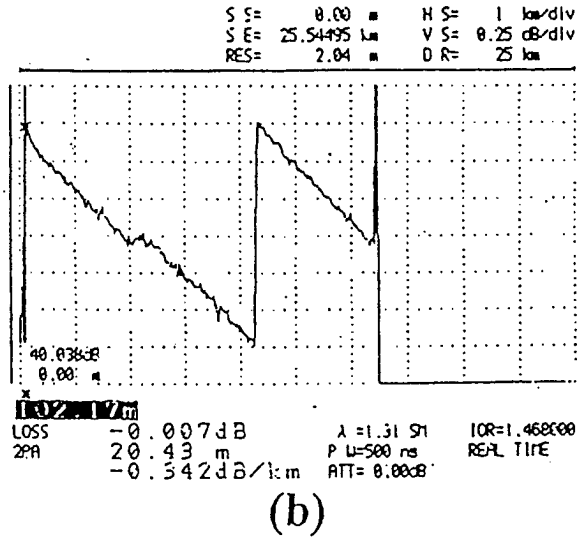

(b)

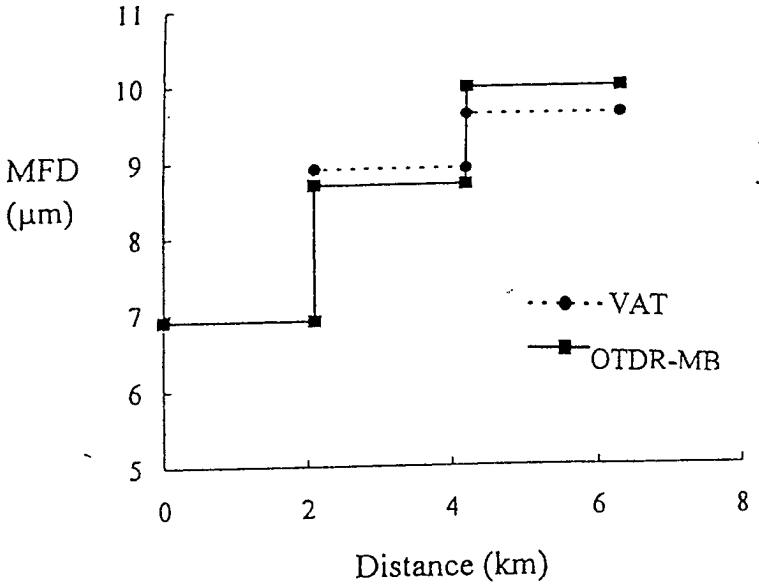

(c)

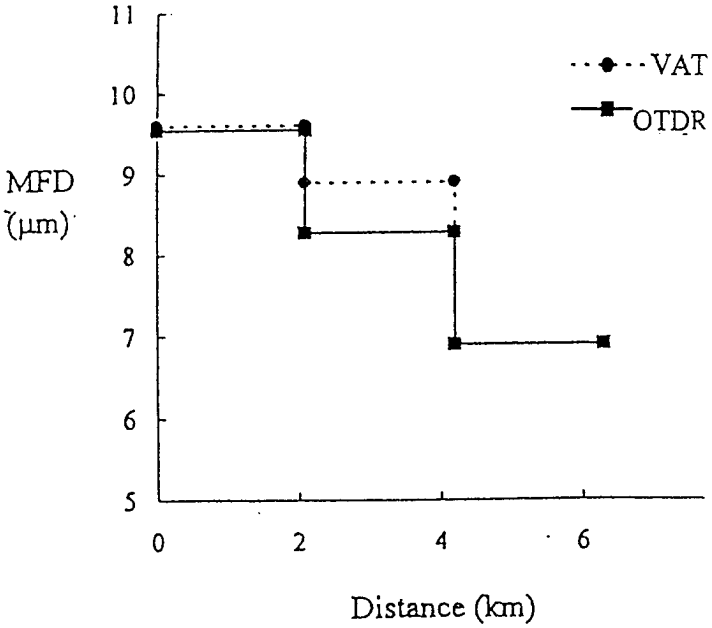

(d)

Fig.4. The measurement results for the splice losses at 1310nm by the microbending method. The measured splice losses are compared with the true splice losses which are defined by averaging the bi-directional OTDR splice losses.

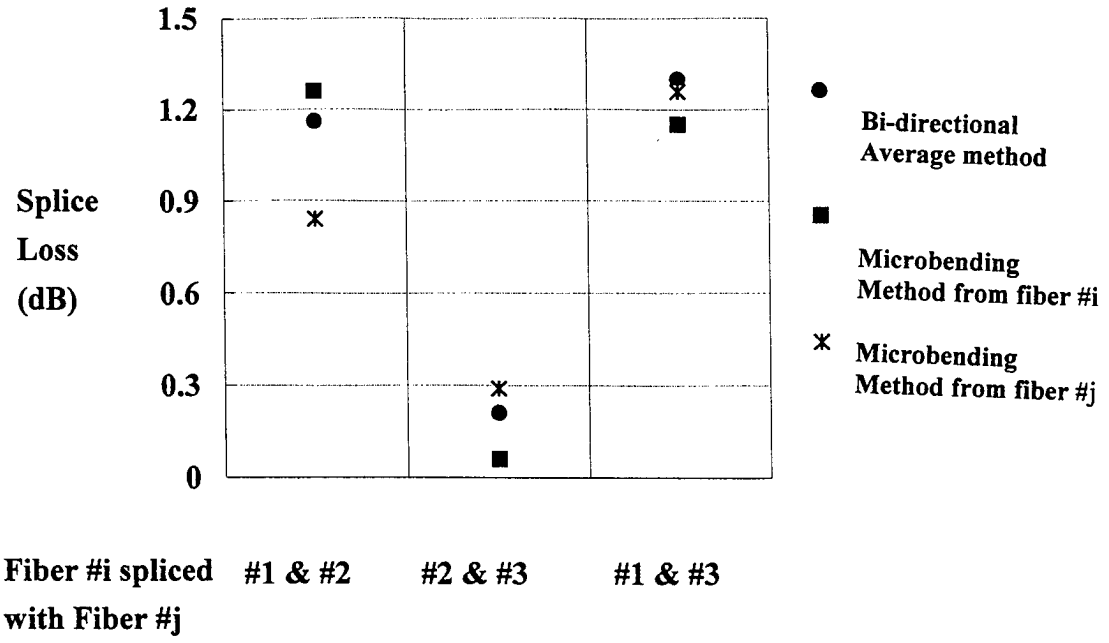

THE EFFECT OF PREPARATION CONDITIONS ON THE STRENGTH OF FUSION SPLICES I: USE OF AFM IMAGING

Joel D. Mann, Osman S. Gebizlioglu and Charles R. Kurkjian
Bellcore, 445 South Street, Morristown, N J. 07960

ABSTRACT

Certain splicing conditions are known to result in strength reductions from the initial fiber strength of 5.5 GPa. Particularly, mechanical damage and chemical contamination on the fiber surface may occur in the pre- and post-fusion splicing steps. The final strength of a fusion splice will be determined by how well a field splicing practitioner controls these steps. In this presentation, we report on the results of our evaluations of stripping techniques for modern fiber coatings and the associated risk of damage on the fiber surfaces by state-of the art microscopy techniques that include AFM (Atomic Force Microscopy) of bare fibers and their surfaces. Our results indicate that the cleanliness of a stripped fiber surface depends on the general type of stripping used, but even more importantly on the details of the stripping procedure.

INTRODUCTION

Fusion splicing of optical fibers has gained widespread acceptance as a reliable and efficient method of permanently joining optical fibers and fiber optic cables in the installation and maintenance of telecommunications outside plant. Fusion splicing operations today are carried out in fully-automated splicers which have built-in instruments to test splice quality, optical transmission, and tensile strength. An important step in successful fusion splicing is the preparation of fibers; this step involves cutting open the optical cable jacket and protective plastic tubes, and stripping back the fiber coating. In the next step, the fiber ends are cleaved and cleaned. After the fusion process, the last step consists of re-coating and/or protection of the fused fibers. It has been shown that fusion splices can be successfully made with essentially no degradation in strength of 5.5 GPa for an as-drawn fiber. In order to achieve this, the fiber surface must be pristine initially, and it must be kept clean in the pre- and post-fusion splicing steps. In other words, the fiber surface must remain damage-free and free from any contaminants, and the fusion of fibers must be carried out in the absence of water vapor in the fusion atmosphere. These conditions can rarely be met in the field, and even in the laboratory, they are seldom found. Many real-life conditions call for the use of mechanical stripping which is known to (1) damage the fiber surface and (2) to involve a cleaning process to remove residual polymer coating from the glass surface. While it is required that this 'cleaned' surface be clean to the naked eye, remaining microscopic contaminants may affect the final splice strength.

Work by Krause[1-5] has led to the development of rather sophisticated techniques for the control of fiber surface condition and heating sources which allow the fusion splicing of silica fibers with essentially no loss of mechanical strength relative to the as-drawn fiber (5.5 GPa or 800 ksi). While the ability to retain such strengths is interesting from a fundamental point of view and important in certain critical instances, the care and cost involved in the fabrication of such splices relegate their use only to a few critical applications. Normal applications are more likely to employ rather more ordinary, simpler, quicker and cheaper techniques. These techniques will usually involve mechanical stripping together with a solvent wipe for the removal of the polymer coating and cleaning of the fiber surface together with the use of an arc heating device for the fusion of two fibers. Issues concerning the effectiveness and reliability of fiber stripping and splicing are addressed in two documents: TR–NWT–000955[6] sets a strength requirement of 1.4 GPa and an objective of 2.8 GPa for mechanically stripped fiber, but GR–765-CORE[7] allows the strength requirement to drop to 0.35 GPa (1 lb.) upon fusion splicing of such a fiber. Because of this low strength requirement, such field splices are often strengthened with some type of splice protector. While these perform the protection role to some extent, they are bulky and show undesirable aging behavior. In an earlier paper,[8] we reported the initiation of a series of studies aimed at a fundamental understanding of this mechanical stripping process both from the point of view of the removal of the polymer coating and the resulting strength after stripping. In the present work, our primary aim has been the evaluation of the cleanliness of the glass surface after this stripping procedure. Both TR–NWT–000955[6] and the TIA/EIA Standard 455-178A (FOTP–178A)[9] require

that any residual coating left by the mechanical stripping operation be "completely" removed by wiping with a cloth or tissue moistened or soaked with isopropyl alcohol. The TIA/EIA document specifies that "any remaining coating residue visible to the naked eye be included in the recorded test results."

Figures 1-4 illustrate some of the history of fusion splice research and development. Figure 1 is from an earlier study[1] in which the importance of mechanical damage was simply demonstrated (curve b), and it was shown that the splice results published to that time (curve d) were controlled by such surface damage. In curve c of Figure 1, it can be seen that a strength distribution with a mean strength (σ) of ~ 450 ksi (~3.1 GPa) and a Weibull slope (m) of ~ 4 results if the silica surface is clean and undamaged. In this case the polymer coating was removed by the use of hot sulfuric acid without damage to the silica surface. This result was obtained using either a torch, arc or CO_2 laser. The strength reduction from the as-drawn level (5.5 GPa), is presumably the result of the interaction of the glass surface with water during splicing. When the reaction with water is eliminated, the strength distribution shown in Figure 2 is obtained.[2] These data indicate that fusion splicing can be accomplished with no strength degradation if extreme care is taken to eliminate mechanical damage and contamination with water and other foreign matter. As indicated above however, the attainment of such high quality conditions is difficult and costly. For this reason, most field fusion splicing is done with an electric arc heat source and the polymer coating is usually removed by means of a mechanical stripping tool. Early results which illustrate the strength degradation resulting from the stripping and subsequent arc fusion operations are shown in Figure 3[10]. A recent study[5] (Figure 4) shows that with more careful mechanical stripping and by certain optimization of the arc conditions, better results can be obtained ('mechanically stripped' curve in Figure 4). In fact, "by a refinement in processing which significantly reduces moisture and airborne particles at the fiber surface during fusion"[5] (including acid stripping), the curve labelled 'near pristine' in Figure 4 can be obtained.

Figure 5 presents data from a recent investigation[11] on the "strength after mechanical stripping" (SAMS). The strength reduction upon splicing a mechanically stripped fiber is normal and is thought to be due to residual polymer on the fiber surface. Krause, et al,[1-5] and Berg and Johansen[12] have stressed the importance of contaminants, either from the stripping procedure or the atmosphere, on the strength level obtainable in fusion splicing. Our aim in the present work is to understand this effect in more detail.

Two previous studies have employed atomic force microscopy (AFM) to investigate the extent and distribution of the residual polymer remaining on the surface of silica plates or fibers after mechanically removing the bulk of the polymer. Creuzet et al[13] applied a polyurethane coating to polished silica plates by hot pressing. The coating was then peeled off by hand. Zhong et al[14] used a mechanical stripper to remove an in-line applied, UV-cured urethane-acrylate coating from silica fibers. While both sets of investigators detected 'clumps' of residual polymer on the silica surface, larger clumps (1-μm wide and 20-nm high) were observed on the plates than on the fibers (35- to 60-nm wide and 3- to 6-nm high). More interestingly, Creuzet, et. al. found that the regions between the polymer clumps showed higher rms (root mean square) roughness than did the bare silica glass (0.6 nm vs 0.4 nm) which, they conclude, is due to a thin (~1 nm) continuous polymer film. The presence of such a film was substantiated by FTIR. Zhong, et. al. employed both contact and tapping mode AFM, but it is not clear whether the more sensitive tapping mode operation detected such a thin, continuous polymer film. Because of the interesting but somewhat contradictory results obtained in the AFM imaging studies just described, this tool has been employed here in an attempt to clarify these issues, and to evaluate the cleanliness of the fiber surface after different stripping and cleaning procedures.

EXPERIMENTAL

The coating of a commercial dual-coated single-mode fiber was removed in several different ways. The first is the most commonly used field technique that employs a mechanical stripping tool. In order to introduce some standardization in this procedure, the stripping was carried out while the fiber was mounted in the grips of a tensile testing machine. Following the stripping, a single alcohol wipe as specified in references 6 and 7 was used to remove the residual coating from the fiber surface. Alternate procedures involve soaking in either methylene chloride or acetone, with or without a final alcohol or acetone wipe. These fiber surfaces were imaged using an AFM.[15] The AFM employs an etched silicon tip to image the topography of the glass surface. As has been discussed,[13,14] these topographical results are not absolute, but depend on many factors, including the size of the area imaged and the digitization rate.

For this reason, the scans presented here have been standardized to a 2 μm by 2 μm area.

RESULTS AND DISCUSSION

Figure 6 is a 40X optical image of a fiber which has been mechanically stripped (bottom image), and mechanically stripped and cleaned with an alcohol-soaked cloth (top image). While,in the bottom image, there are large regions of the fiber which appear to have been stripped of the polymer coating, there are also lots of small bits of residual coating. The upper image is similar, but this time the fiber has been 'cleaned' by wiping once. This 'cleaning' is apparently effective since the image now appears featureless "to the naked eye"[7].

Figure 7 shows an AFM image of the fiber shown in the top of Figure 6 – the apparently 'clean' fiber. The extreme resolution, both lateral and vertical, clearly shows that quite a bit of polymer remains. The size and distribution of these polymer clumps are similar to those which Zhong et al[14] imaged, although somewhat larger. The AFM parameters are shown in Table 1. This sample has two quite large clumps: ~15 nm rms and ~ 250 nm in lateral extent with very tall (100's nm) spikes. There are also several smaller clumps, 2- to 10-nm high and ~ 50- to 150-nm wide. In the regions between these clumps, the rms roughness is quite small. As indicated in the experimental section, the rms value is dependent on the scan size. In the table, we have shown not only the overall roughness for the 2μ x 2μ scan, but the range of roughness for 500 nm x 500 nm square areas selected from this overall scanned region. It can be seen that the rms values for the regions between clumps compares favorably with that of the as-drawn fiber (this is a fiber which was taken from the draw tower before the coating operation). The values in column II for these two fibers are the same within experimental scatter.

An interesting behavior is shown in Figure 8. This fiber was mechanically stripped and cleaned by means of alcohol wipes as in Figure 7. In this case however, an attempt was made to more completely remove the residual polymer bits. This was done by employing several aggressive alcohol wipes rather than only one. As seen, the result is that the polymer clumps which were originally isolated 'hillocks', have been 'smeared' so that the entire surface is covered by a film with an rms roughness of 6.4 nm, substantially larger than that found by Creuzet et al.[13]

Figure 9 is an AFM image of a fiber which has been stripped by a chemical technique – in this case an acetone soak. While the rms roughness value is quite low, there are clearly very many regions of what appear to be residual polymer of quite large size (4-nm high and 50-nm wide). As in Figure 7, these polymer clumps are separated by apparently 'bare' fiber, although because of the density of the clumps a good measurement of rms roughness was not possible. Coating removal by means of a methylene chloride soak shows a similar behavior.

As indicated in the introduction, the recognized technique for complete removal of the polymer coating without the introduction of mechanical damage, is stripping in 'hot' concentrated sulfuric acid.[1-5, 12] This procedure is not trivial or foolproof either, however. Figure 10 shows two images of 'acid'-stripped' fiber. Clearly, as indicated in several publications,[1-5, 12] the care taken in the stripping as well as the cleanliness of the acid and rinsing solutions are of primary importance to the success of this procedure. On the left, residual polymer bits can be seen. This fiber was stripped in ~170°C sulfuric acid. Using acid at the recommended temperature of ~200°C has removed these lumps of polymer, but the remaining rms roughness of 0.744 nm is still significantly greater than that found for the fiber which had never been coated (~0.372 nm).

While the density of the polymer clumps which have been found here is in some cases similar to that of Zhong, et al,[14] in other cases very many more are found. In any event, it seems that there are regions on the fiber surface which show substantially greater adhesion to the polymer than the rest of the surface. In some cases the distribution of these regions is also similar to the distribution of the HF vapor etched pits developed by Inniss, et al.[16] (~ 5-10 per 2μx2μ square area). In their AFM experiment, an acid-stripped fiber was etched by holding it over an HF bath. Condensation at isolated positions on the fiber surface resulted in the etching of these positions by the condensed acid. Thus, it seems likely that certain positions on the fiber surface are in some way more reactive than others.

The preliminary work described here has reinforced earlier suggestions[13,14] that AFM imaging is a valuable tool for the study of the cleanliness of stripped fiber surfaces. The next step in the process of understanding this surface is the correlation of such images with the resultant splice strengths.

SUMMARY

In this work we have reviewed earlier fusion splicing studies. In view of the very large strength decrease

which was normally found to take place upon fusion splicing, our study has concentrated on the investigation of the reasons for this degradation. Primarily through the application of AFM imaging, it has been shown that both a thin continuous layer and isolated clumps of the polymer coating are retained. The amount and character of this residual polymer depends critically on the details of the procedure used to strip and clean the fiber surface. It is presumed that this residual polymer contributes to the loss in strength upon fusion splicing through carbonization of the coating and subsequent reaction of this carbonized material with the silica surface.[3] This process leads to strength reduction by the same mechanism (differential thermal expansion) as that involved in the reaction of a fiber surface with refractory particles during fiber drawing. Further work is being done to correlate the present findings with the strengths of fibers having the surface quality described here.

REFERENCES

1. J.T. Krause, C.R. Kurkjian and U.C. Paek, "Strength of Fusion Splices for Fiber Lightguides", *Elect. Letts*, **17**, *232-233 (1981).*

2. J.T. Krause and C.R. Kurkjian, "Fiber Splices with 'Perfect Fiber' Strengths of 5.5 GPa , $\nu < 0.01$", *Elec. Letts*, **21**, *533-535 (1985).*

3. J.T. Krause, G.W. Kammlott, S.G. Kozinski and R.S. Riggs, "Improved Strengths (3.7 GPa) of Arc Fusion Splices for High Yield Reliability", *19th European Conference on Optical Communication (ECOC '93), Montreaux, Switzerland (1993).*

4. J.T. Krause and D. Stroumbakis, "Factors Affecting Arc Fusion Splice Strengths", *SPIE*, 2611, *98-109 (1995).*

5. J.T. Krause, S.N. Kher and D. Stroumbakis, "Arc Fusion splices with Near Pristine Strengths and Improved Optical Loss", *22nd European Conference on Optical Communications, ECOC '96, Oslo, Norway, TuP 0.05 (1996).*

6. T.R.–NWT–000955, Generic Requirements for Single and Multi-Fiber Strippers, *Bellcore Morristown, N.J. 07960.*

7. G.R.–765–CORE, Generic Requirements for Single Fiber Single-mode Optical Splices and Splicing Systems, *Bellcore Morristown, N.J. 07960, (1995).*

8. J.D. Mann, M.R Ozgur, O.S. Gebizlioglu and C.R.Kurkjian, "Mechanical Stripping of Lightguide Coatings: Coating Morphology", *NFOEC Technical Proceedings, Vol.1,271 (1998).*

9. TIA/EIA–455–178A, FOTP–178, Measurements of Strip Force for Mechanically Removing Coatings from Optical Fibers, TIA, Arlington, VA (1996).

10. H.H. Yuce, P.L. Key and T. Wei, "Mechanical Reliability Considerations for Fusion Splices in Optical Fibers," *Proc. IWCS, 400-404 (1990).*

11. A. Dwivedi and J.L Smith, "Characterizing Field Handleability of Optical Fiber through the Measurement of Strength after Mechanical Stripping," *Proc. IWCS, 381 (1996).*

12. A, Berg and M. Johansen, "Arc Fusion Splices with Improved Strength (4.8 GPa) Approaching the Strength of the Fiber", *El. Letts, **31**, 308-309 (1995).*

13. F. Creuzet, G. Ryschenkov and H. Arribart, "A New Tool for Adhesion Science: The Atomic Force Microscope," *J. Adhesion, **40**, 15-25 (1992).*

14. Q. Zhong, D. Inniss, K. Kjoller and V.B. Elings, "Fractured Polymer/Silica Fiber Surface Studied by Tapping Mode Atomic Force Microscopy," *Surface Sci. Letts, **290**, l688-92 (1993).*

15. Digital Instruments, Santa Barabara, CA., Model Dimension 3000.

16. D. Inniss, Q. Zhong and C.R. Kurkjian, "Chemically Corroded Pristine Silica Fibers: Blunt or Sharp Flaws?," *J. Am. Ceram. Soc. **76**, 3173-3177 (1993).*

Table 1. Roughness Parameters

Sample	RMS 2μx2μ	RMS range 500 nmx500nm	P_N	P_{Ht}	P_W
As drawn	0.372	0.2-0.4			
M.S. 'wipe'	3.305	0.16-0.2	2 lge, 6 sm	2-10, 15	50-150, 250
M.S.'2-wipe'	6.4	0.7-2.3		25	1000
Acetone	0.340		50	4	100
L.T. acid	0.53	0.14-0.2	5	5	250
H.T. acid	0.744	0.3-0.6			

M.S. 'wipe' = mechanical strip with single alcohol wipe
M.S. '2-wipe' = mechanical strip with two alcohol wipes
Acetone = strip with acetone soak
L.T. acid = strip in sulfuric acid ~170°C
H.T. acid = strip in sulfuric acid ~ 200°C

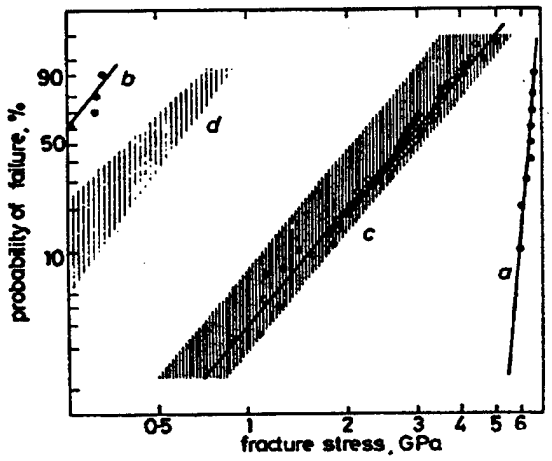

Figure 1. Splice strengths from the early work of Krause et al [1]. (a) an as drawn fiber ; (b) an acid-stripped fiber damaged by splicer grips; (c) acid stripped and fusion spliced in an arc, torch or laser; (d) compilation of other early results.

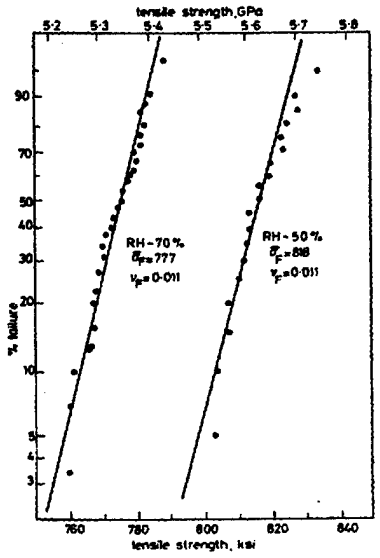

Figure 2. Strength of $(O_2 - Cl_2 - O_2)$ torch splicing of acid-stripped fiber.[2]

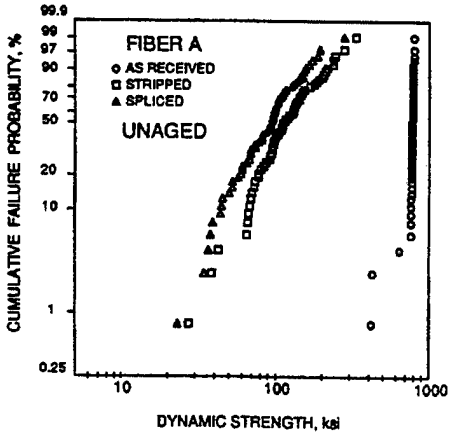

Figure 3. The effect of mechanical stripping and arc fusion splicing on fiber strength.[10]

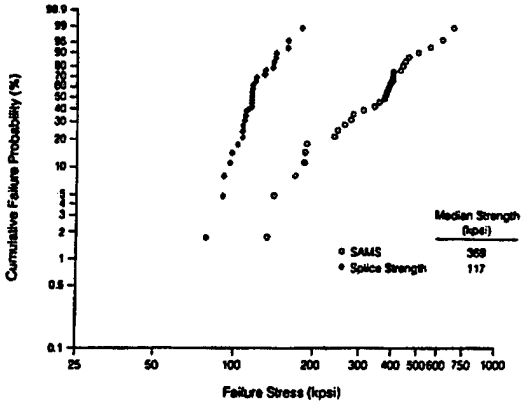

Figure 5. Recent data on strength after mechanical stripping (SAMS)[11]. Notice the increased degradation upon arc fusion splicing.

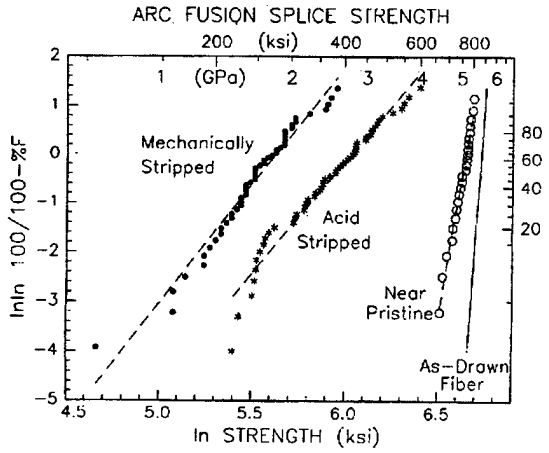

Figure 4. Effect of stripping and arc splicing conditions on fiber strength.[5]

Figure 6. Optical micrograph of (a) mechanically stripped (lower) and (b) mechanically stripped and alcohol-wiped (upper) fiber.

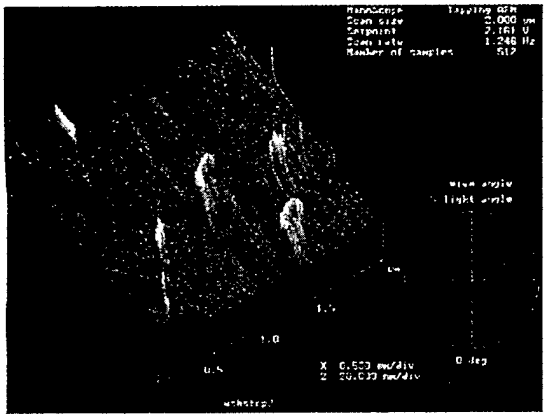

Figure 7. AFM image of fiber (b) in Figure 6. Roughness of mechanically stripped and wiped fiber (vertical scale 20 nm/div.)

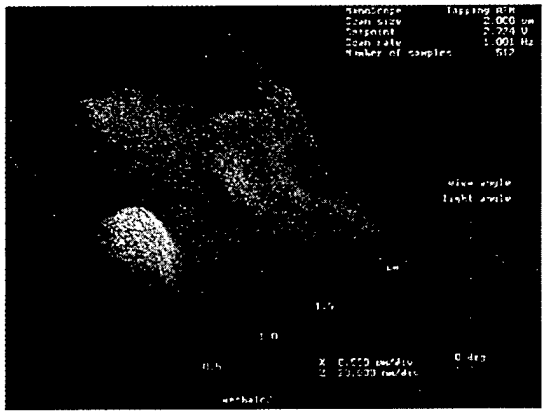

Figure 8. AFM image of fiber as in Figure 7, except with more aggressive wiping. (vertical scale 20 nm/div)

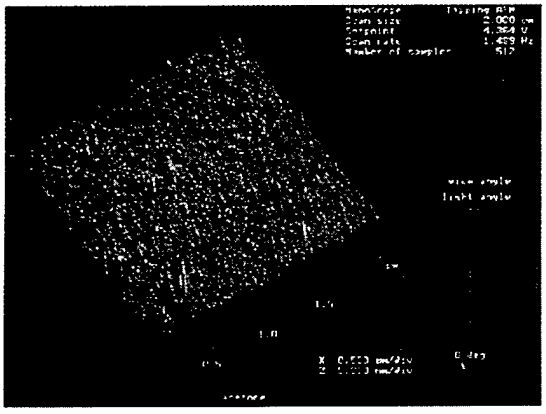

Figure 9. AFM image after removal of the coating by means of acetone soak (vertical scale 5 nm/div).

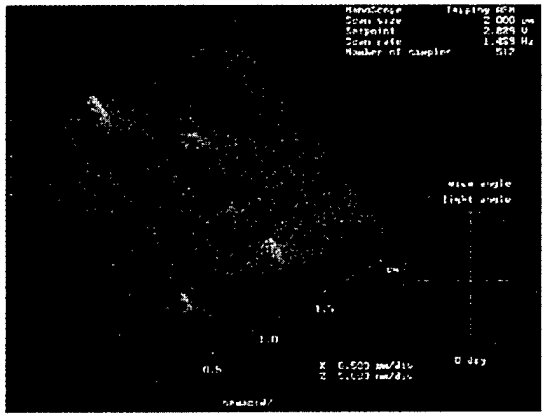

Figure 10a. AFM image of acid-stripped fiber. The acid temperature was too low ~ 170°C. (vertical scale 5 nm/div).

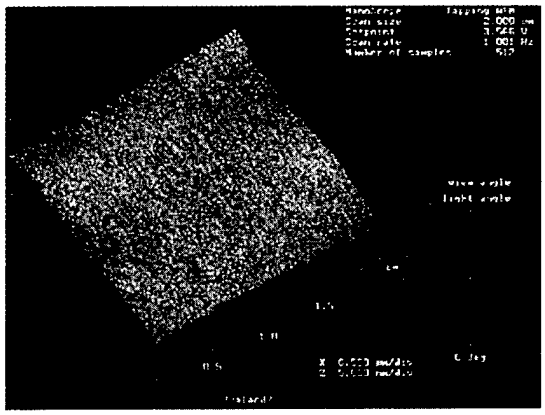

Figure 10b. AFM image of acid-stripped fiber. The acid temperature was 200°C(vertical scale 5 nm/div).

Joel D. Mann is a Member of the Technical Staff in the Optical Fiber & Components Group at Bellcore. Since he joined Bellcore in 1995, he has been involved in optical and mechanical characterization of fiber media and components. He has participated in numerous failure analyses of fiber optic components for clients from the global telecommunications industry and governments. Joel is expected to complete his studies toward a B.Sc. degree in Mechanical Engineering from the New Jersey Institute of Technology in 1999

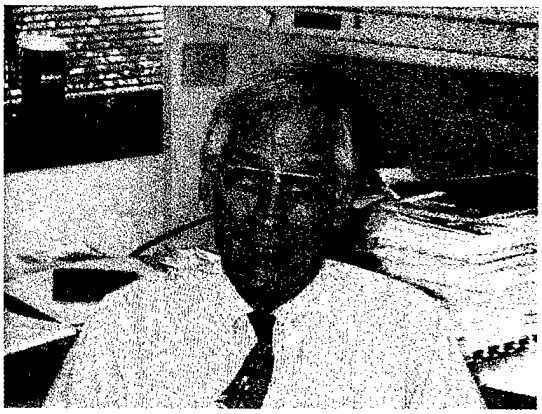

Charles R. Kurkjian received his B.Sc. from Rutgers in 1951 and his Sc.D from M.I.T. in 1955. In 1994 he retired as a Distinguished Member of Technical Staff from AT&T Bell Laboratories after 35 years of service. Since that time, he has been with Bellcore in the Optical Fiber & Components Group.

Osman S. Gebizlioglu is a Member of the Technical Staff in the Optical Fiber & Components Group at Bellcore. He holds B.Sc and M.Sc degrees in Chemical Engineering from the Middle East Technical University, Ankara, Turkey. After receiving his Ph.D in the Polymer Materials Program of the Chemical Engineering Department at Princeton University, Princeton, New Jersey, he was a Monsanto Postdoctoral Fellow in Mechanical Engineering at M.I.T, Cambridge, Massachusetts. Since he joined Bellcore in 1987, he has been involved in the investigations of performance / reliability problems in optical fibers, fiber optic cables, components and devices. He holds three US patents.

Anti-Rodent Type Portable Fiber Optic Cable for Safety Operation

Hiroshi Miyano, Makoto Katayama and Hisashi Tanji

Sumitomo Electric Industries, Ltd. ,Yokohama Japan

ABSTRACT

New design of anti-rodent type all-dielectric portable fiber optic cable has been developed by applying an animal repellent (microencapsulated synthetic capsaicin) in a jacket covered with a skin of normal polyethylene, which greatly improves operational safeness and handling easiness as well as anti-rodent performance. It has been confirmed that the anti-rodent PE jacket has no adverse influence on the cable characteristics including its flame-retardant property.

INTRODUCTION

A portable fiber optic cable is usually used temporarily in the field where rodents or brutal animals live. In order to maintain small diameter and light weight properties, the cable cannot accommodate armouring layer such as glass yarns or GRP rods [1]~[3]. Hence, the animal repellent such as a microencapsulated synthetic capsaicin, or food spices, could be a potential candidate as an ingredient for the jacket to realize anti-rodent type portable fiber optic cable that is environmentally safe (non-toxic). Such a material, on the other hand, might become an irritant to a human during its operation. Furthermore, such repellent material may drop its performance after exposure to outside environment for a long term duration. The optimum jacketing design carrying the anti-rodent performance, therefore, is required to solve these problems.

CABLE DESIGN

Conventional cable design

An all-dielectric portable cable with small diameter and light weight was reported in IWCS '85 [4]. This cable contains two tight buffer optical fibers housed in a flame-retardant grooved spacer together with aramid yarns as a strength member. The spacer is wrapped with a plastic tape and then covered with low density flame-retardant polyetylene. Besed on this original cable design, we have changed the jacket thickness from 0.65mm to 0.8mm (cable diameter 4.8mm) to prevent jacket break caused by trailing in the field and to enhance mechanical characteristics. We have studied an anti-rodent jacketing design for this conventional cable (Fig.1,D)

Design of anti-rodent jacket

Anti-rodent function was added to the conventional cable without increasing diameter and weight by mixing an animal repellent in the jacket. This repellent is a microencapusulated formulation of chemically synthesized capsaicin, which discourages gnawing of animal pests on the cable. Microencapsulation accelerates the activity due to concentration of the active ingredient, and mitigates irritation action for easy handling as well. The repellent is contained in the normal polyethylene master batch, which is then mixed to the based flame-retardant polyetylene (FR-PE) for extrusion. The microcapsule could be broken due to mixing at high temperature during jacket extrusion, hence we have selected based FR-PE which can be extruded at relatively low temperature.

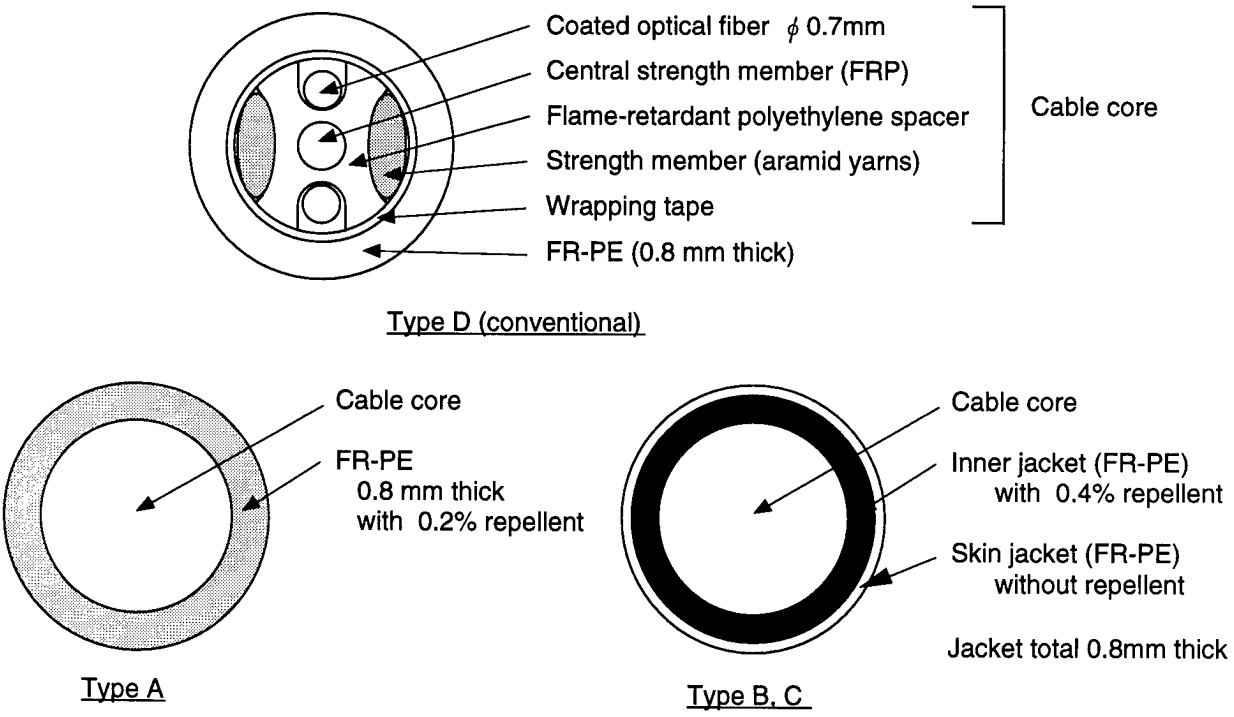

Fig. 1 Cross sectional-view of portable fiber optic cable

Three(3) types of anti-rodent jacketing structure, shown in Fig.1 and Table 1, have been manufactured and evaluated.

Cable A, shown in Fig 1, contains the repellent chemicals in the whole PE jacket. To keep the anti-rodent performance in outside environment for a long term duration, it is generally recommended that the dosage of the repellent in the jacket should be 0.4%,which is so high that irritation to humans might happen during cable handling. Taking into account that the portable cables are usually used intermittently in the field, we tried to reduce the dosage to 0.2%: half the recommended one, which is expected to maintain the anti-rodent performance for some years when the cable is continuously exposed to outside environment. The cable was tentatively used in the field and verified to have good anti-rodent performance: no serious damages were observed after installation for some months. However, careful handling and operation were still required due to irritation of the repellent chemicals.

Cables B and C have been developed to free the operator from this problem by encapsulating the anti-rodent jacket: external skin jacket of normal PE is applied over the anti-rodent PE. In order to maintain the good rodent resistance, the dosage of repellent in the inner jacket (0.4%) is two times higher than cable A, which is the originally recommended value. Keeping the whole jacket thickness of 0.8mm that is same as cable A, combination of inner and skin jacket thicknesses was varied between cables B and C to evaluate anti-rodent performance: ticknesses of skin are 0.1mm and 0.05mm for cables B and C, respectively.

ANTI-RODENT PERFORMANCE

Repellent dosage of PE jacket

The microcapsule of the repellent could break during extrusion and the active

Table 1 Anti-rodent jacketing design

Cable type	Jacket thickness (inner / skin) [mm]	Repellent dosage: active ingredient (inner / skin) [%]	Average dosage in total [%]		Microcapsule survival rate [%]
			expected	measured	
A	0.8 / -	0.2 / -	0.20	0.21	>60
B	0.7 / 0.1	0.4 / 0	0.34	0.35	>60
C	0.75 /0.05	0.4 / 0	0.37	0.36	>60
D	0.8 / -	0 / -	—	—	—

ingredient might migrate from the jacket or reduce its effect due to high temperature. We measured the actual dosage of active ingredient and survival rate of microcapsule in each jacket sample. The results (Table 1) show that enough active ingredient is contained in the jacket as expected. The survival rate of microcapsule is more than 60 %, which is considered to be sufficient to keep long term anti-rodent performance.

Rodent attack test

To evaluate anti-rodent performance of cables A~D, rodent attack tests were carried out on the following two conditions.

Test 1: Four cable samples (A, B, C and D) of approx. 20 cm long each were placed in a 40 x 22 x 18 cm cage together with three rats, which were 32 weeks old; the length of about 15cm and the weight 300g. The cables were simply exposed to the rodent attacks for four days. The rats were fed normally. Five(5) cages were tested. The test results (Table 2) indicate that all types of anti-rodent cable A, B and C have good rodent resistance, while the conventional cable D in all cages were bitten seriously; close to a cable cut. The difference in rodent resistance among cables A, B and C was not clear in the test.

Table 2 Rodent attack test results
(Test 1: Mixed cable types in a cage)

Class of cable damage	Quantity of cables (n = 5 for each cable)			
	A	B	C	D
#1	5	5	5	0
#2	0	0	0	0
#3	0	0	0	0
#4	0	0	0	5

Table 3 Rodent attack test results
(Test 2: Single cable sample in a cage)

Class of cable damage	Quantity of cables (n = 10 for each cable)			
	A	B	C	D
#1	8	7	9	0
#2	1	3	1	0
#3	1	0	0	0
#4	0	0	0	10

Class of cable damage

#1 Negligible: jacket scratched, not penetrated

#2 Fair: jacket penetrated, without damage to the spacer

#3 Danger: jacket penetrated, with damage to the spacer and optical fiber

#4 Horrible: close to cable cut

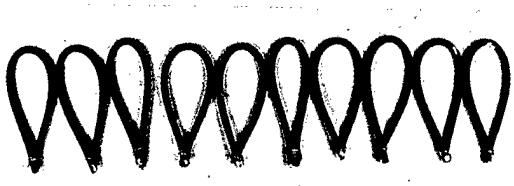

Type A

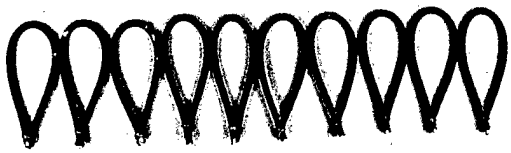

Type B

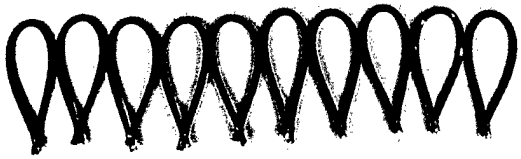

Type C

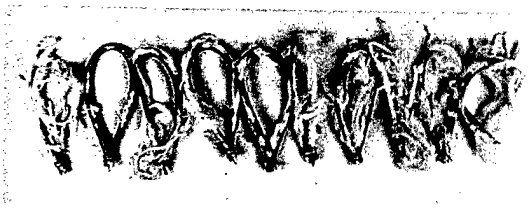

Type D (Conventional)

Photo 1 Cable samples after rodent attack test 2

Test 2: A single cable sample, instead of four samples, was placed in the cage and exposed to rodent attacks in the same manner as test 1. Ten(10) cages for each cable type were tested. The test results (Table 3 and Photo 1) show that cables B and C having higher dosage of the repellent are more resistant to rodent attacks than cable A. Furthermore, cable C is slightly better than cable B due to its thinner skin.

The conditions of the rodent attack tests above are considered to be severer than the actual field conditions. Noting that cable A verified the good anti-rodent performance in the field, cables B and C both could be adopted. From a safety operational viewpoint, we have finally selected the cable B that has thicker skin than C.

OTHER CABLE CHARACTERISTICS

Physical properties of jacket material

Physical properties of flame-retardant PE with/without the anti-rodent repellent were evaluated. Tensile strength and elongation of dosed PE maintained the high level though slight decrease was observed as the dosage increased (Table 4). Aging tests at 100℃ for two days showed no significant changes in the properties from the original sample. All samples, even the highest dosage of 0.4%, passed the impact test at -30℃. Melt flow index of dosed PE does not change

Table 4 Physical properties of flame-retardant PE with anti-rodent repellent

Item	Test method	Dosage of anti-rodent repellent		
		0	0.2%	0.4%
Tensile strength at break[MPa]	IEC 811-1-1	18.8	17.7	16.2
Elongation at break[%]	IEC 811-1-1	740	680	640
Tensile strength at break[%] after aging 2days, 100℃	IEC 811-1-2	-4	-8	-2
Elongation at break[%] after aging 2days, 100℃	IEC 811-1-2	-7	-9	+6
Impact test at -30℃	IEC 811-1-4	no breakage	no breakage	no breakage
Melt flow index (MFI)	IEC 811-4-1	0.188	0.192	0.207

significantly, indicating no adverse influence on the jacket extrusion.

Mechanical and flame-retardant properties

Mechanical and flame-retardant tests were carried out for cable B with good results as shown in Table5. In the Cable bend test at low temperature (-30℃), for example, no cracks were observed in the jacket after 10 cycles of repeated bend, maintaining good flexibility even with the anti-rodent PE jacket.

Table 5 Mechanical and flame-retardant properties (Cable B)

Item	Test method	Result
Cable bend at -30℃	IEC 794-1-E11 Mandrel dia.: 10 mm 10 cycles	No damage to the jacket
Crush	IEC 794-1-E3 Number of crush: 1 in 3 different places Load: 2kN/100mm	No damage to the jacket No loss increase
Impact	IEC 794-1-E4 Number of impact: 1 in 3 different places Energy: 10 J	No damage to the jacket No fiber breakage
Flame test	UL 83 Horizontal-specimen flame test	Passed the spec.

CONCLUSION

The new anti-rodent jacketing design of cable B greatly improves operational safeness and handling easiness as well as anti-rodent performance. It has been confirmed that the anti-rodent PE jacket has no adverse influence on the cable characteristics including its flame-retardant property. It also enhances the long term rodent resistance due to encapsulating structure besides high dosage of the repellent PE material.

References

[1] P. Gaillad et al., in Proc. of IWCS, p668 (1995)

[2] Paul J. P. Curado et al., in Proc. of IWCS, p711 (1996)

[3] H. J. Durigan et al., in Proc. of IWCS, p819 (1997)

[4] T. Ohsugi et al., in Proc. of of IWCS, p313 (1985)

Hiroshi Miyano

Sumitomo Electric Industries, Ltd.
1, Taya-cho, Sakae-ku, Yokohama, Japan

Hiroshi Miyano received his B. E. degree in electronic engineering from Tokyo Metropolitan University in 1996.

He joined Sumitomo Electric Ind., Ltd. in 1996 and has been engaged in design and development of fiber optic cables.

Makoto Katayama

Sumitomo Electric Industries, Ltd.
1, Taya-cho, Sakae-ku, Yokohama, Japan

Makoto Katayama received his M. E. degree in electronic engineering from Tottori University in 1993.

He joined Sumitomo Electric Ind., Ltd. in 1993 and has been engaged in design and development of fiber optic cables.

Hisashi Tanji

Sumitomo Electric Industries, Ltd.
4-5-33, Kitahama, Chuo-ku, Osaka,Japan

Hisashi Tanji received his M. E. degree in 1983 from Tohoku University.

He joined Sumitomo Electric Ind., Ltd. in 1983 and has been engaged in design and development of fiber optic cables.

THE VIBRATIONAL PROPERTIES OF ALL-DIELECTRIC, SELF-SUPPORTING (ADSS) FIBER OPTIC CABLES

Cristian Militaru

Alcoa Fujikura Ltd., Spartanburg, SC

Abstract

Over the past 10 years, there has been a tremendous amount of growth in the deployment of ADSS cables, typically on either electrical power transmission or distribution lines. This paper is an in-depth study of the vibration performance of ADSS cable, in an attempt to scientifically quantify the appropriate vibration protection needed. The following paper addresses three major purposes:

1) To establish a thorough method for self-damping power measurements of ADSS cable.

2) To compare the damper efficiency of a mass damper vs. an impact (spiral) damper and evaluate a method to determine the "k" value curves for ADSS cables.

3) To establish a set of vibration protection recommendations, for both mass and impact dampers, regarding location and number, as a function of the type of span: DE-DE, DE-S, S-S, span length, type of hardware: preformed or mechanical, dead-end or suspension units.

Self-Damping power tests

It is well known that ADSS cable provides a certain amount of self-damping of vibrational energy. The inherently difficult measurements of the self-damping power were performed in an Alcoa Fujikura Ltd. laboratory, using the DEAM system (see Fig.1). The method utilized additional elements in comparison to the standard used in the industry[1]. Due to the frictional force introduced when the cable is fanning the air, the aerodynamic damping power produced by this movement, p_a [mW/m] can be calculated using, for the first time as applied to ADSS cable, the following aerodynamic coefficient:

$\delta_r^a = Fct\left(\beta, \frac{Y}{d}\right)$ [-], where the ADSS cable is assumed to be a smooth cylinder as opposed to the rigid model. This coefficient resulted from an interpolation in the chart "sine-shaped" loop[2]. Additional assumptions:

air density: $\rho = 1.2044\left[N \cdot s^2/m^4\right]$

kinetic viscosity of air: $\upsilon = 156 \cdot 10^{-5}\left[m^2/s\right]$ (at STP)

V_w = laminar wind velocity (5 values were assumed):

$V_w = \{1.5;3;4.5;6;7.5\}$ [m/s]

Span length: L=49.53 [m]=162.5 [ft]

The ADSS cable test tension (3 values assumed):

$T = \{15\%;20\%;25\%\}\,RBS$ [N]

The Stoke's Number: β results from the relation:

$$\beta = \frac{(0.001 \cdot d)^2 \cdot f}{\upsilon} \text{ [-], where} \qquad (1)$$

d= cable diameter [mm];

f= vibration frequency [Hz], given by the Strouhal's equation: $f = 185 \cdot \frac{V_w}{d}$ [Hz]. (2)

The aerodynamic damping power is given in [mW/m] by :

$$p_a = \rho \cdot f^3 \cdot (0.001 \cdot d)^4 \cdot \left(\frac{\pi \cdot Y}{2 \cdot d}\right)^2 \cdot \delta_r^a \cdot 1000, \qquad (3)$$

where Y=the loop double amplitude at the antinode [mm]. For each one of the 5 values of wind velocity (and corresponding frequency), the test had 4 imposed values for Y:

$$Y = \left\{\frac{150}{f}, \frac{125}{f}, \frac{100}{f}, \frac{76.2}{f}\right\} \text{ [mm]} \qquad (4)$$

So, for each one of the 5 values of V_w , 4 values of p_a were determined, which were subtracted from the measured self-damping power, p, to determine the real ("reduced") self-damping power:

p_r : $p - p_a = p_r$ [mW/m] (5)

Test Set-Up

The Test set-up for the measurements of the self-damping power is presented in Fig.2.
The ADSS cable (48 fibers) tested had the following characteristics:
diameter: d=14.2 [mm]
mass: m=0.16 [kg/m]
strength: RBS=13514 [N]
The measured span length, L=49.53 m (162.5 ft) is constant, while the measured span between node 1 and node 2, L_{12}, is variable dependent upon the frequency (loop length): the bigger the wind velocity (frequency), the smaller the loop length and bigger L_{12}. The loop length is given by the relation:

$$l = \frac{1}{2 \cdot f} \cdot \sqrt{\frac{T}{m}} \quad [\text{m}] \qquad (6)$$

The transverse velocity: V , at the antinode (single amplitude) , near the shaker, is given by:

$$V = \pi \cdot f \cdot Y \cdot 0.001 \quad [\text{m/s}] \qquad (7)$$

where, Y is the loop double amplitude of the vibration, and,
$Y_1 \approx Y$ = loop double amplitude at antinode 1, measured close to the shaker, at the near end [mm]
$Y_2 \approx Y$ = loop double amplitude at antinode 2, measured at the far end [mm]
The power transfer from shaker at node 1 : P_1 , and from shaker at node 2 : P_2, are determined from:

$$P_1 = \sqrt{T \cdot m} \cdot \frac{V^2}{2} \cdot \frac{a_1}{Y_1} \quad [\text{W}] \qquad (8)$$

$$P_2 = \sqrt{T \cdot m} \cdot \frac{V^2}{2} \cdot \frac{a_2}{Y_2} \quad [\text{W}] \qquad (9)$$

where: $Z_0 = \sqrt{T \cdot m}$ [N·s/m] (10)
is the characteristic impedance of the cable, where
a_1 = loop double amplitude at node 1 [mm] (near the shaker)
a_2 = loop double amplitude at node 2 [mm] (at the far dead-end)
Thus, the power dissipated between nodes 1 and 2:

$$P = \sqrt{T \cdot m} \cdot \frac{V^2}{2} \cdot \left(\frac{a_1}{Y_1} - \frac{a_2}{Y_2} \right) \quad [\text{W}] \qquad (11)$$

and this power per unit length of ADSS cable is:

$$p = \frac{1000 \cdot P}{L_{12}} \quad [\text{mW/m}] \qquad (12)$$

From this measured value of the self-damping power: p, the calculated aerodynamic damping power, p_a, is subtracted to obtain the real ("reduced") self-damping power: p_r , given by rel. (5).

An important parameter in the test set-up is the shaker location. In order to minimize any effects of the shaker on the results, the shaker was placed at first antinode corresponding to the maximum wind velocity and minimum loop length and %RBS tested tension. Thus, the influence of the shaker on the measurements was practically zero. The DEAM system (see Fig.1) is measuring voltage:
TAO =Test A output [mV], so in order to determine the amplitude at nodes and antinodes 1 and 2 this DEAM system voltage is multiplied by a : K_f =Test A calibration factor [mils/mV], resulting: TAA =Test A amplitude: TAA= K_f·TAO·0.0254 [mm].
Finally, the system was calibrated to yield a factor of:

$$k_f = \frac{250 mils}{650 mV} = 0.384 \left[mils/mV \right] \qquad (13)$$

The wind power input: p_w [mW/m] is given by:

$$p_w = \rho \cdot f^3 \cdot (0.001 \cdot d)^4 \cdot \left(\frac{\pi \cdot Y}{2 \cdot d} \right)^2 \cdot \delta_r \cdot 1000 \quad [\text{mW/m}] \qquad (14)$$

where the aerodynamic coefficient was determined by using the formula corresponding to 5% wind turbulence[3]:

$$\delta_r = 7.9 - 5.7 \cdot \left(\frac{Y}{d} \right) + 17 \cdot e^{\left(-12 \cdot \frac{Y}{d} \right)} - 8 \cdot e^{\left(-14 \cdot \frac{Y}{d} \right)} \quad [-] \qquad (15)$$

The power to be dissipated by vibration dampers is p_w- p_r [mW/m], and the ratio which will be used, after the damper efficiency tests were performed is: $\frac{L \cdot (P_w - P_r)}{P_{max}}$ [-], where:

$$P_{max} = \frac{1}{2} \cdot \sqrt{T \cdot m} \cdot (2 \cdot \pi \cdot f)^2 \cdot \left(\frac{Y_{max}}{2} \right)^2 \quad [\text{W}] \qquad (16)$$

is the maximum theoretical dissipated power (resulting in no reflected wave) of the damper on an ADSS cable.

Conclusions for self-damping power tests

The test protocol had 3 possible outcomes:
case 1: $\frac{p_r}{p_w} \cdot 100 < 5\%$: p_r is negligible, it should not be taken into consideration in the power balance equation:

$$\frac{P_a - P_b}{P_{max}} > \frac{L \cdot P_w}{P_{max}} - \frac{L \cdot P_r}{P_{max}} \quad [-] \qquad (17)$$

damper dissipation power — wind power input — real("reduced") self-damping power

case 2: $\frac{p_r}{p_w} \cdot 100 > 5\%$: p_r is not negligible, it should be taken into consideration in the above power balance equation.

case 3: p_r curve [mW/m] crosses the p_w curve [mW/m]. The crossing point will establish the frequency (and corresponding wind velocity) from where the ADSS cable needs dampers.

The detailed test results are shown in Figures 3 through 13. In summary, the tests performed showed that self-damping power of the cable tested is not negligible, but small in comparison to either metallic conductors or optical ground wire, given the same diameter, mass, RBS, and tested tension. At T= 15% RBS, at higher frequencies the ratio $\frac{p_r}{p_w} \cdot 100$ decreases: from 32.30% (at V_w=1.5 m/s, Y=150/f=7.7 mm) down to 7.34% (at V_w=4.5 m/s, Y=76.2/f=1.3 mm), and then oscillates, stopping at about 11.60% (at V_w=7.5 m/s, Y=76.2/f=0.8 mm). As the tension increases to T=20% RBS, although the self-damping power is not negligible, it is smaller than at lower tensions. For both cases, T=15% RBS, and T=20% RBS, the test results meets the criteria for Case 2 and will need vibration dampers for the whole range of laminar wind velocities: [1.5....7.5] [m/s] and associated frequencies: [19.5...97.7] [Hz]. When the tension becomes 25%-30%RBS, the self-damping power is negligible for the whole range of frequencies, and should not be taken into consideration in the power balance equation(17).

For higher amplitudes, the curves shape goes asymptotically towards zero with a slowly decreasing slope (not an abrupt one). The reason for the curves shape is that even if for the higher amplitudes the self-damping power, p_r is increasing, the wind power input p_w, is increasing at a faster rate, given the same wind velocity and amplitude. From these extrapolated curves, the result is that the undampened amplitudes of the cable would be around Y_{max}/d=2.

It was mentioned earlier in the paper that the self-damping capability of the ADSS cable is lower than that of an equivalent metallic conductor. In the author's opinion, the self-damping power of the cable is a function of the "equivalent" stiffness of the two most important vibrational aspects of the cable, the aramid yarns and the outer jacket. Therefore, an "equivalent" modulus, E_{equiv}, can be used to determine the influence of these two elements upon ADSS cable self-damping. This equivalent modulus can be compared with the modulus of aluminum to determine which has more self-damping. For example, E_{Al} = 61824 N/mm2, and E_{aramid} = [1.5...1.7] E_{Al}. So, it is expected that the ADSS cable flexural rigidity (self-damping power) will be higher than that of aluminum. But, the contribution of outer jacket modulus, E_{OJ}=[0.005....0.008]E_{Al}, causes the total self-damping power of the cable to decrease considerably. Taking into consideration the cross-sectional area of the above elements of the ADSS cable,

$$E_{equiv} = \frac{\sum E \cdot A}{\sum A} = (0.165...0.180)E_{Al} \quad (18)$$

which is much smaller than that of aluminum, hence the self-damping power results. The second important factor is the position of these two elements relative to the surface of the cable. The element closer to the surface (outer jacket) will tend to decrease the cable's flexural rigidity, while the element closer to the center of the cable (aramid yarn) has less of a contribution, even if it's material properties would tend to increase the self-damping power. The third criteria to be considered is the loss factor of the outer jacket. The loss factor of the outer jacket will increase the self-damping of the cable, but its effects are less than that of the flexural rigidity of the cable. In general, as the aramid content of the cable increases, the self-damping will increase due to the inherent flexural rigidity of the material.

Damper efficiency tests

The efficiency of mass dampers as well as spiral vibration dampers was tested in conjunction with ADSS cable.

Test Set-Up

The damper efficiency test set-up is shown in Fig.14 and follows the ISWR method from the industry standard[4]. One exception is that the location of the damper is not clearly defined in the standard. As a result of the ambiguity of the standard, the first concern was the mass damper location. In order to improve damper efficiency, it was decided to locate the damper directly on the bare cable, and not on the hardware rods (SRL). The "stub length", or distance from the end of the hardware rods was selected to be less than the loop length at the frequency corresponding to rel. (2), calculated at the base wind velocity:V_w=15 mph (6.7 m/s). This resulted in a new design of the suspension clamp of the Alcoa damper, including a special cushion to protect the cable from wearing during vibrations. This will yield an increase in clamp mass, but the increase also occurs in the case of applying the damper over the rods. Placing the damper on the rods causes a larger overall diameter than placing the damper on the cable, so the increase in clamp mass will be bigger for the "damper over rods" than for the "damper over bare cable". The small increase in the clamp mass will increase the termination reactance at the damper location:

$X_T=X_D+X_S+X_M$ (19)

(where T=termination, D=damper, S=stub, M=clamp mass), because the clamp mass impedance is just a positive reactance, X_M. A higher reactance, keeping the resistance constant (which is only the damper resistance, $R_T=R_D$, because the stub impedance is also a positive reactance, $Z_S=jX_S$), will increase the reflection a small amount. This solution is better than locating the damper over the rods, which will need a bigger clamp mass (a bigger termination reactance), so a bigger reflection and lower absorption. Also, if a node occurs at the end of the rods, the characteristic impedance of the armored section, Z_{oa}, is bigger than the characteristic impedance of the bare cable Z_{ob}, because a bigger mass is present in the characteristic impedance equation,

$$Z_0 = \sqrt{T \cdot m} \tag{20}$$

in the armored section case, so,

$$Z_{oa} > Z_{Ob} \Rightarrow \left(\frac{P_r}{P_{\max}}\right)_b > \left(\frac{P_r}{P_{\max}}\right)_a \tag{21}$$

which means that the damping efficiency of the termination, as a whole, is smaller than the damping efficiency within the armored section, so the reflection will increase, and the absorption decrease. The preformed rods are very long, so it is expected that one or two vibration loops will be contained in the armored section at the highest frequency, resulting that, for lower frequencies than the highest one, a node might fall at the end of the armored section so the damper will be inefficient. The tests were performed for all harmonic frequencies, which are multipliers of the fundamental frequency, which corresponds for 1 loop in the entire span length: $l = L; n = 1$:

$$f_{fund} = \frac{1}{2 \cdot L} \cdot \sqrt{\frac{T}{m}} \quad [\text{Hz}] \tag{22}$$

For the particular cable tested: f_{fund}=1.14 Hz (T=15%RBS=456 lbs=2028 N) and the harmonic frequencies were spread between f_{min}=(11.66 Hz, V_{wmin}= 2 mph (0.9 m/s)) and f_{max}=87.48 Hz (V_{wmax}=15 mph (6.7 m/s) with increments of f_{fund}=1.14 Hz. The minimum loop length (corresponding to $V_{w\,max}$ and f_{max}) yields:

$$l_{\min} = \frac{1}{2 \cdot f_{\max}} \cdot \sqrt{\frac{T}{m}} = 0.644 \quad [\text{m}] \tag{23}$$

so damper spacing (location) resulted:

$$l_d = 0.7 \cdot l_{\min} = 45.06[cm] = 17.74[in] \tag{24}$$

from the dead-end, at the far end of the span. Using the same methodology proposed in the earlier section to minimize the impact of the shaker, the shaker was placed at

$$l_S = 0.5 \cdot l_{\min} = 32.18[m] = 12.67[in] \tag{25}$$

from the dead-end, at the near end of the span. The test was performed at a constant tension, T=15%RBS=456 lbs=2028 N, so the cable characteristic impedance during the test was

$$Z_0 = \sqrt{T \cdot m} = 18 \quad [N \cdot s/m] \tag{26}$$

The incident wind power [W/m], is given by:

$$p_w = \rho \cdot f^3 \cdot d^4 \cdot \left(\frac{\pi \cdot Y_{\max}}{2 \cdot d}\right)^2 \cdot \delta_r \tag{27}$$

where $\rho[N \cdot s^2/m^4], d[m^4]$ and δ_r is given by rel. (15) where Y is now designated Y_{max}. Y_{max} is measured by the DEAM system by measuring points "A" and "B", where $A_{voltmeter}=2 \cdot A$ and $B_{voltmeter}=2 \cdot B$. A= wave half amplitude, passing DEAM, going towards damper [m]; B= wave half amplitude, passing DEAM, after reflection from damper [m], therefore it can be determined:

$Y_{max}=2 \cdot A+2 \cdot B= A_{voltmeter}+ B_{voltmeter}$ [m] (28)

$Y_{min}=2 \cdot A -2 \cdot B= A_{voltmeter} - B_{voltmeter}$ [m] (29)

where: Y_{max} = double antinodal amplitude; Y_{min} = double nodal amplitude; the power dissipated by the damper is: $P_a - P_b$ [W] where:

$$P_a = \frac{1}{2} \cdot Z_0 \cdot \omega^2 \cdot A^2 \quad [\text{W}] \tag{30}$$

$$P_b = \frac{1}{2} \cdot Z_0 \cdot \omega^2 \cdot B^2 \quad [\text{W}] \tag{31}$$

and the wind power input to span is: $L \cdot P_w$ [W]. The maximum theoretical dissipated power (no reflection: B=0) is: $P_{\max} = \frac{1}{2} \cdot Z_0 \cdot \omega^2 \cdot \left(\frac{Y_{\max}}{2}\right)^2$ [W] (32)

where angular velocity is: $\omega = 2 \cdot \pi \cdot f[rad/s]$ (33)

The damper efficiency yields:

$$E = \frac{P_a - P_b}{P_{\max}} \cdot 100 \quad [\%] \tag{34}$$

and the damper is efficient as long as:

$$P_a - P_b > L \cdot (P_w - P_r) \quad [\text{W}] \tag{35}$$

or: $\frac{P_a - P_b}{P_{\max}} > \frac{L \cdot (P_w - P_r)}{P_{\max}}$ [-] (36)

where: Pr [W/m] is the real("reduced") self-damping power given by rel.(5) and whose values were determined for the same cable, tension, and wind conditions in the previously performed self-damping power tests.

Conclusions for damper efficiency tests

One Alcoa mass damper 1703-8 (with the special cushion insert inside the clamp) placed at one end directly on the bare cable, proved to be more efficient than one SVD (spiral vibration damper) placed at one end for all frequency ranges (11.66...87.48) [Hz], corresponding to laminar winds (2...15) [mph] = (0.9...6.7) [m/s] , for the same test rule:fY_{max}=3 inch/sec (76.2 mm/sec). This implies an allowable ratio Y_{max}/d between 0.460 (at f_{min}=11.66Hz) and 0.061 (at f_{max}=87.48Hz).

In general, it was found that a mass damper can dampen the vibrations in the above situation for spans up to 62 m=203 ft (efficiency: 18%.....41%). The spiral vibration dampers that were tested were effective for spans up to 50 m=164 ft (efficiency: 17%....32%). The results are shown in Fig.17.

One additional point that deserves discussion is that the cables are tested to millions of cycles of vibration and the vibration protection is not for the cable, per se, but to protect the hardware. More exactly, it is to protect the cotter pin of the extension link from the heliformed dead-end or the connection pin of the bail from the wedged mechanical dead-end. To address the vibrations seen by the hardware, it was decided to change the test rule to: fY_{max}=7 [inch/sec]=177.8 [mm/sec]. The test setup for this new rule is shown in Figure 14. Accordingly, a maximum allowable double (peak-to-peak) dampened amplitude at the antinode: Y_{max} was used equal to the diameter of the cable, d, corresponding to f_{min}(V_{wmin}=2mph=0.9m/s) at the start of test. The testing was started with a minimal wind load f_{min}(V_{wmin}=2mph=0.9m/s) and afterwards the dampened amplitude: Y_{max} decreased to 0.143·d, for f_{max} (V_{wmax}=15mph =6.7 m/s). The results of the test, with this new test rule, showed that one Alcoa mass damper, at one end, is efficient for all range of frequencies (11.66...87.48)[Hz] for spans up to 156 m (512 ft). See Fig. 15 for the efficiency curves. This maximum span of 156 m corresponds approximately to a factor: $K \cdot L_1 = 1800\left[ft^{3/2}/lbs^{1/2}\right]$. Repeated tests under the same conditions showed similar values with a maximum of 16% higher. Therefore, it was decided to go with a factor: $K \cdot L_1 = 2100\left[ft^{3/2}/lbs^{1/2}\right]$ for an initial stress at AAMT (-20° F) of 1 kpsi=6.89 N/mm^2. Based upon these test results, a method and an algorithm were established to determine the "K" values 4 curves for ADSS cables. The "K" value is used in conjunction with the damper to determine the overall amount of protection needed for a given span length: $K{\cdot}L_0$=no protection; $K{\cdot}L_R$=armor rods only; $K{\cdot}L_1$=dampers at one end; $K{\cdot}L_2$=dampers at both ends; taking into account factors as: wind derating guidelines (normal terrain, extremely flat, some vegetation, water crossing, etc.), initial tension at AAMT (-20° F) and final tension at AAT (60° F), the type of hardware, etc. Finally, a set of vibration protection recommendations were established:

a) for Alcoa mass dampers: location and number as a function of type of span (DE-DE, DE-S, S-S) and type of hardware, including preformed hardware (deadend or suspension units) or mechanical hardware (wedge deadends and bolted suspension units). 22 possible cases were investigated. Some examples are presented in Fig.16.

b) for impact (spiral) dampers: numbers as a function of: initial tension at AAMT (-20° F) and final tension at AAT (60° F), given as %RBS and span length.

Comparing this maximum "covered" span of this ADSS cable (using a mass damper) with the one for an OPT-GW of the same diameter, and same wind conditions and installation conditions, it can be noticed that it is smaller. The reasons for this performance are that 1) the cable has a smaller mass, and 2) lower tension, therefore the characteristic impedance of the ADSS cable is about 4-5 times less than that of an OPT-GW of a similar diameter. Hence, the maximum theoretical dissipated power, P_{max} (no reflection) of the damper on an ADSS cable is about 5-7 times smaller than P_{max} for OPT-GW of the same diameter at the same frequency and amplitude, because P_{max} it's a function of the characteristic impedance only, for a given f and Y_{max} (see rel.(16)), and this characteristic impedance is much smaller in the ADSS cable case than in the OPT-GW case. Also, the problem is that ADSS cable's P_{max} should cover an amount of wind power input which is in the same range for both ADSS cables an OPT-GW. Therefore, the "maximum span without dampers" and the "maximum span with one damper" will be smaller in the ADSS case than in the OPT-GW case, for about the same characteristics (diameter, mass, RBS) and maximum wind velocity (15 mph=6.7 m/sec).

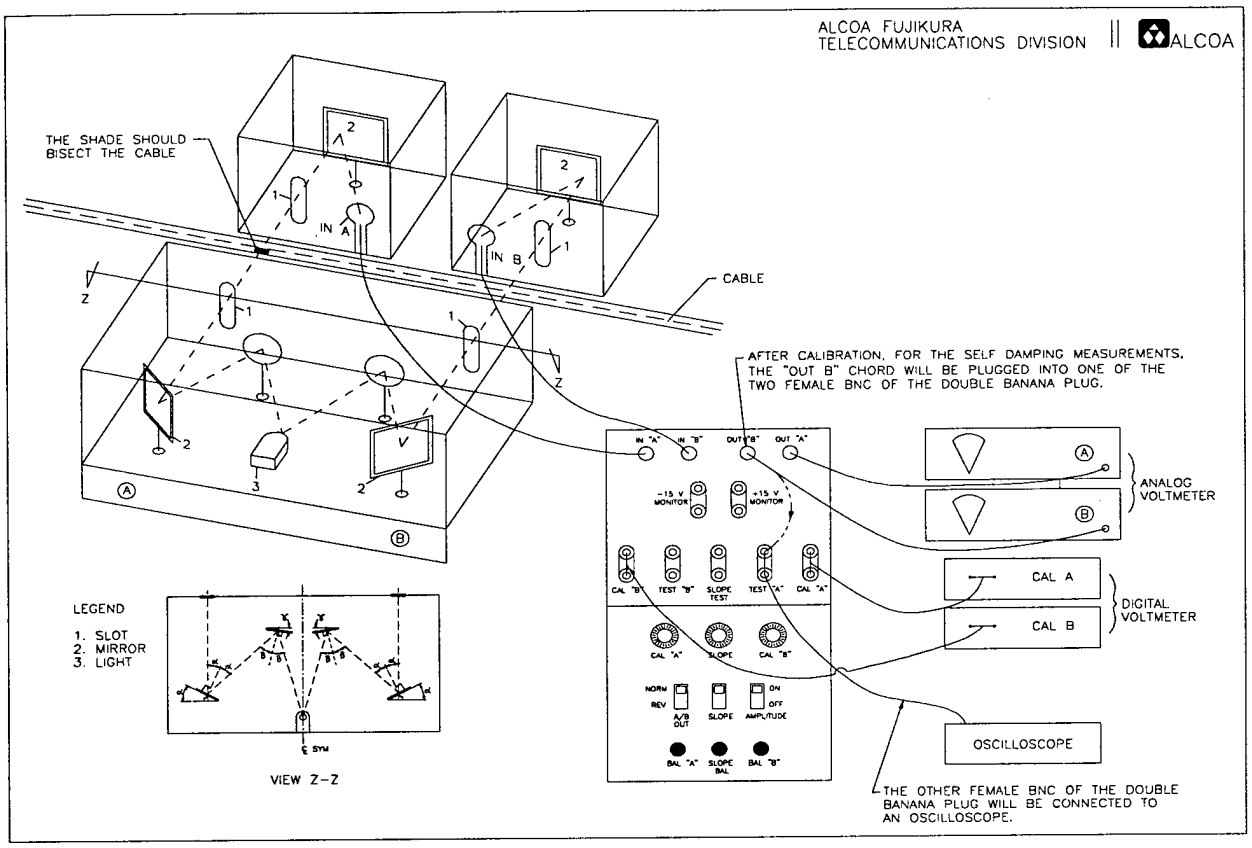

Fig. 1- DEAM (Damping Efficiency Amplitude Measurement) System

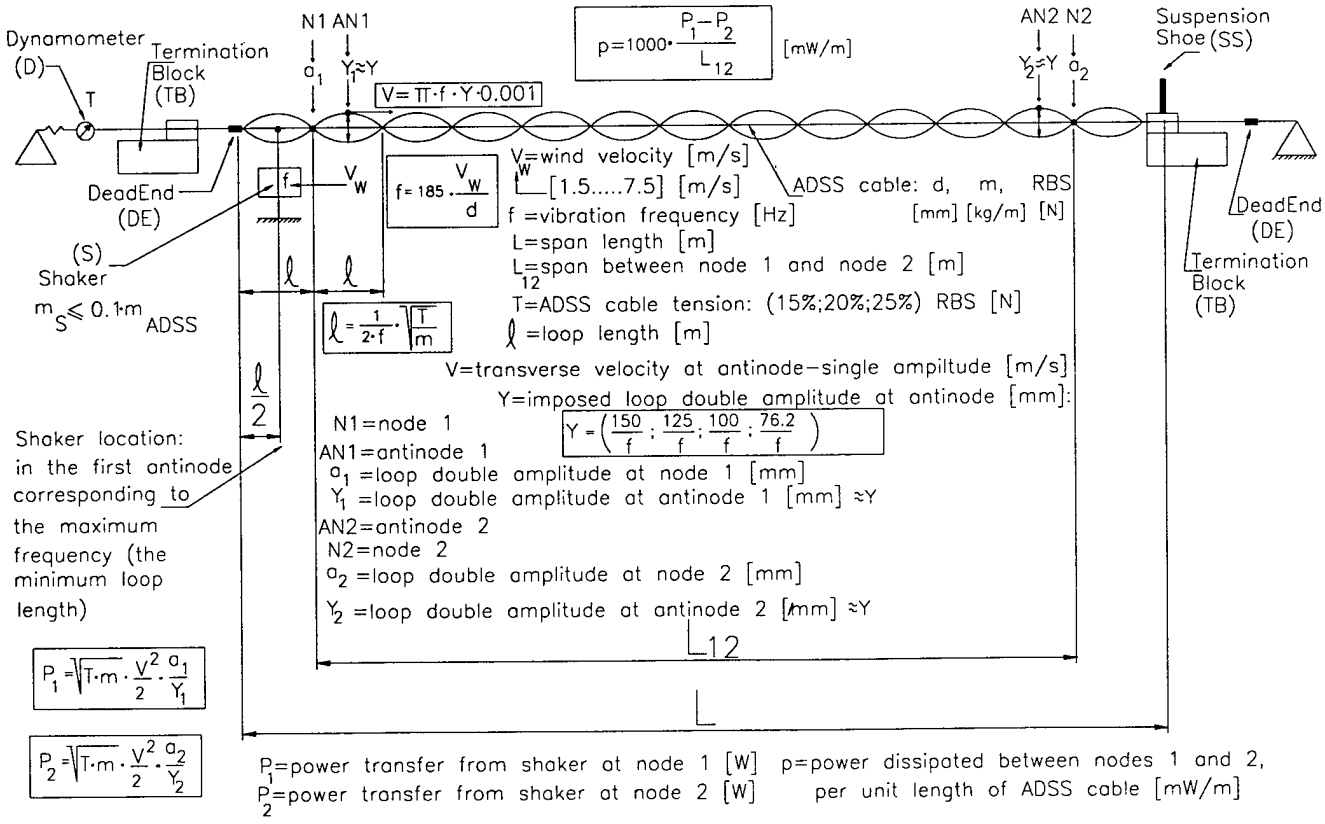

Fig. 2 - Self-damping measurements test set-up

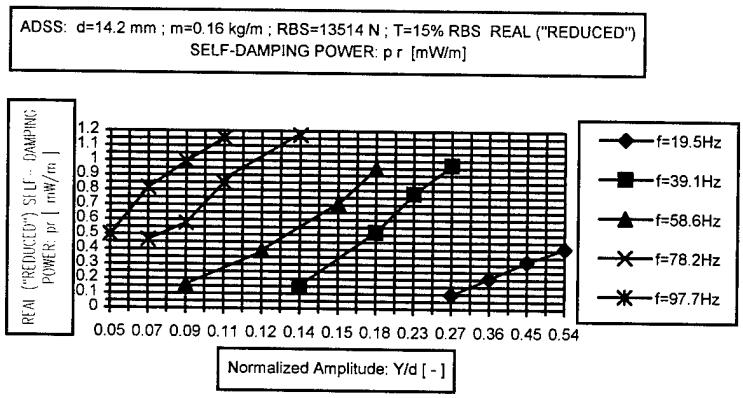

Fig.3 - p_r vs. Y/d at T=15 % RBS, parameter f

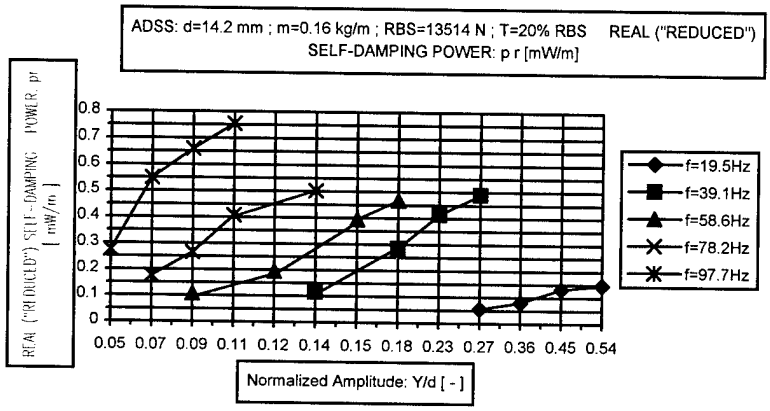

Fig.4 - p_r vs. Y/d at T=20 % RBS, parameter f

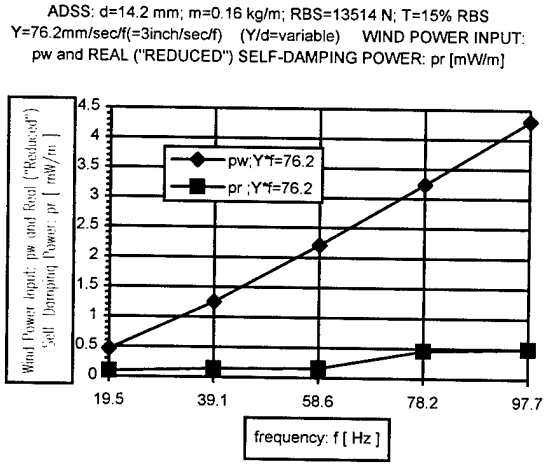

Fig. 5- p_w & p_r vs. f at T=15% RBS, parameter Y·f, Y/d variable

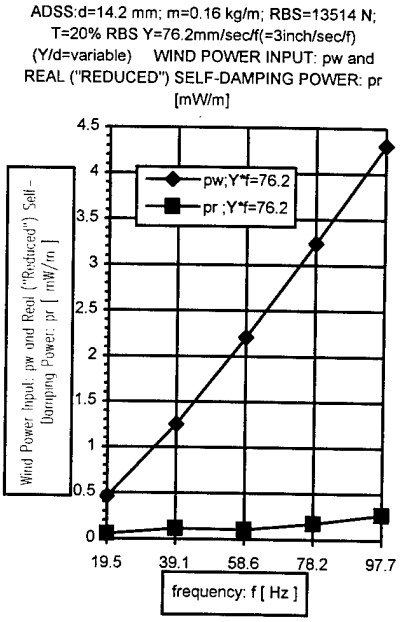

Fig. 6- p_w & p_r vs. f at T=20% RBS, parameter Y·f, Y/d variable

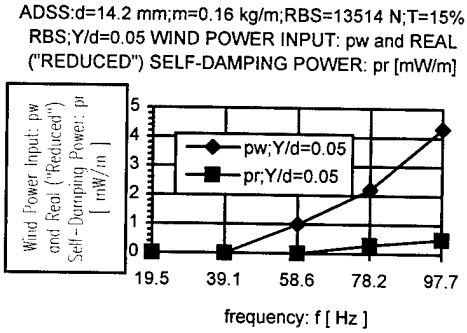

Fig. 7 - p_w & p_r vs. f at T=15% RBS, parameter Y/d =0.05

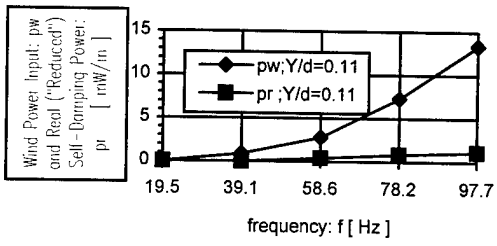

Fig. 8 - p_w & p_r vs. f at T=15% RBS, parameter Y/d =0.11

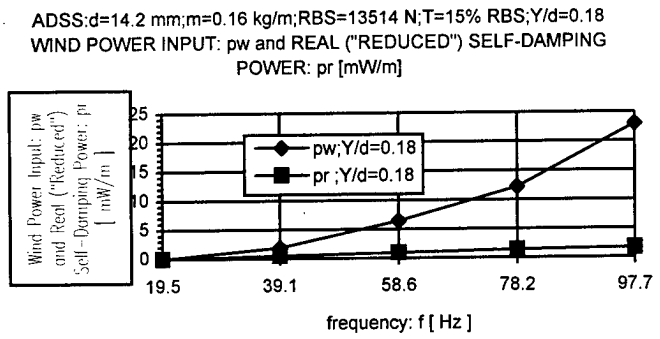

Fig. 9 - p_w & p_r vs. f at T=15% RBS, parameter Y/d =0.18

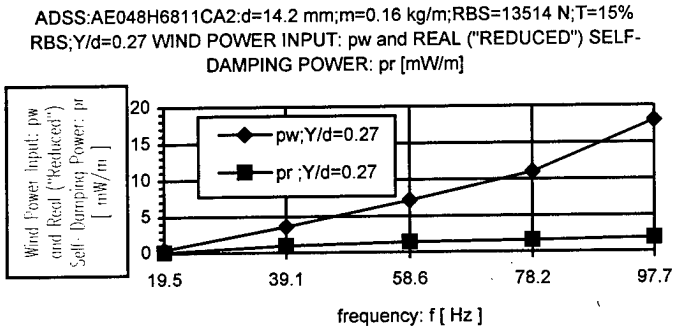

Fig. 10 - p_w & p_r vs. f at T=15% RBS, parameter Y/d =0.27

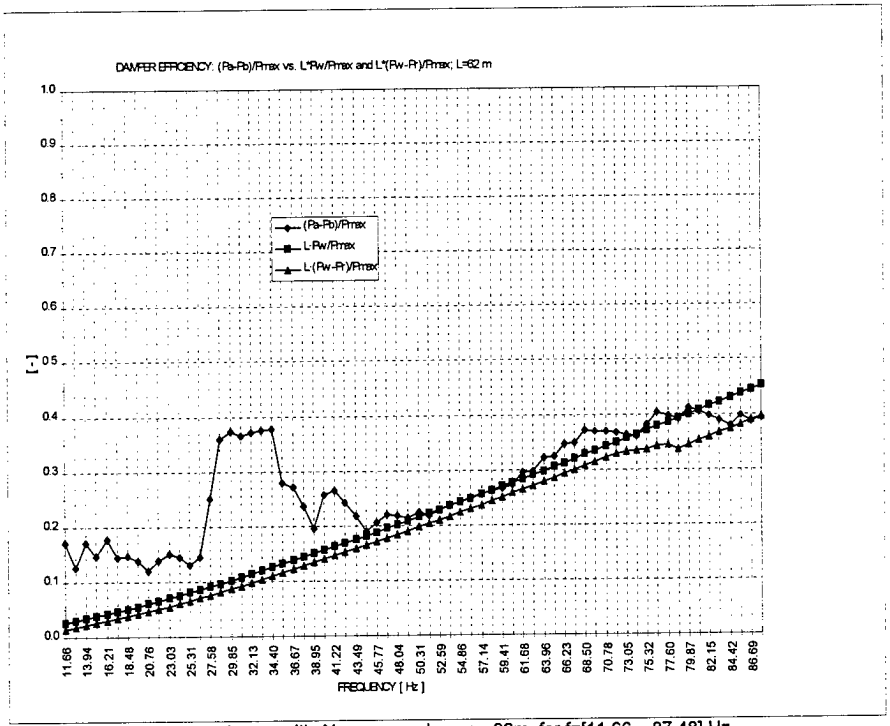

Fig. 17 - Maximum covered span with Alcoa mass damper: 62m, for f=[11.66....87.48] Hz, V_W=[0.9...6.7]m/s, Old Test Rule: f.Y_{max}=3 [inch/sec]

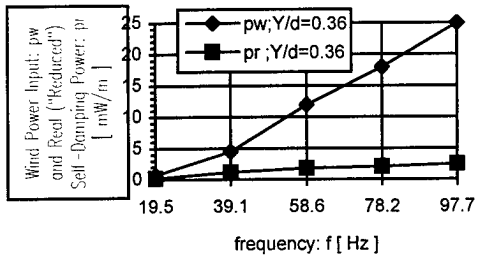

Fig. 11 - p_w & p_r vs. f at T=15% RBS, parameter Y/d =0.36

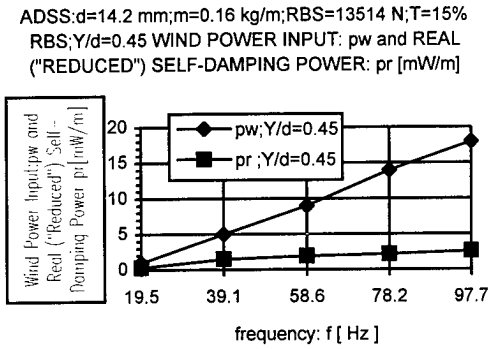

Fig. 12 - p_w & p_r vs. f at T=15% RBS, parameter Y/d =0.45

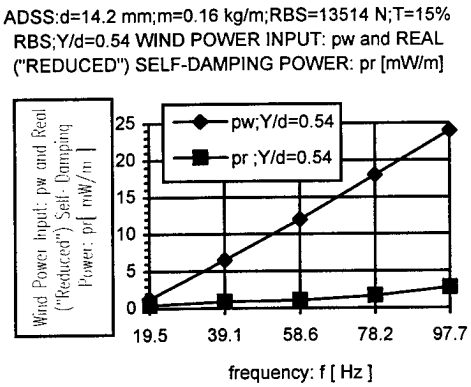

Fig. 13 - p_w & p_r vs. f at T=15% RBS, parameter Y/d =0.54

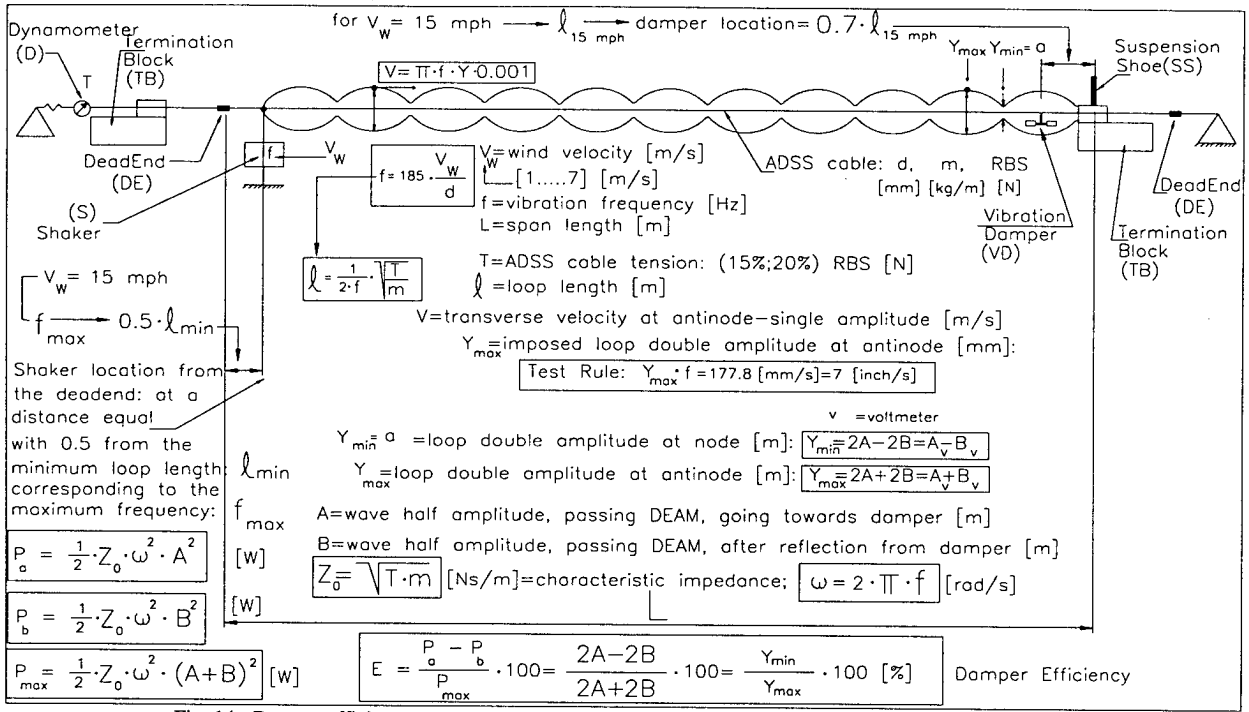

Fig. 14 - Damper efficiency measurements test set-up with the new Test Rule: f·Y_{max}=7 [inch/sec]

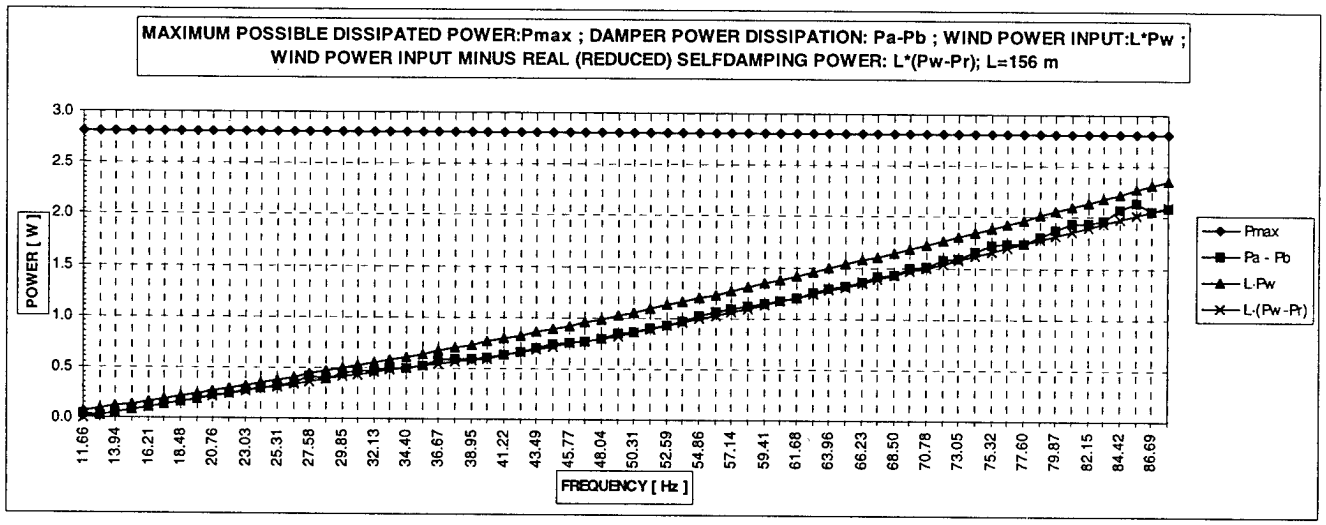

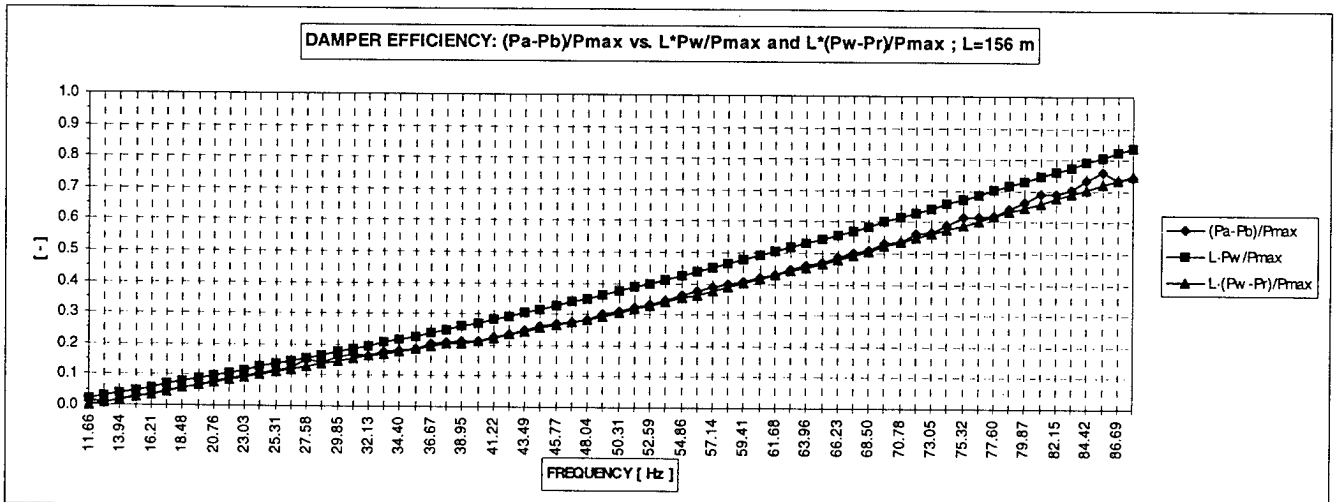

Fig. 15- Maximum "covered" span with Alcoa mass damper: 156 m, for f=[11.66.....87.48] Hz, V_w=[0.9.....6.7] m/s, New Test Rule: f·Y_{max}=7 [inch/sec]

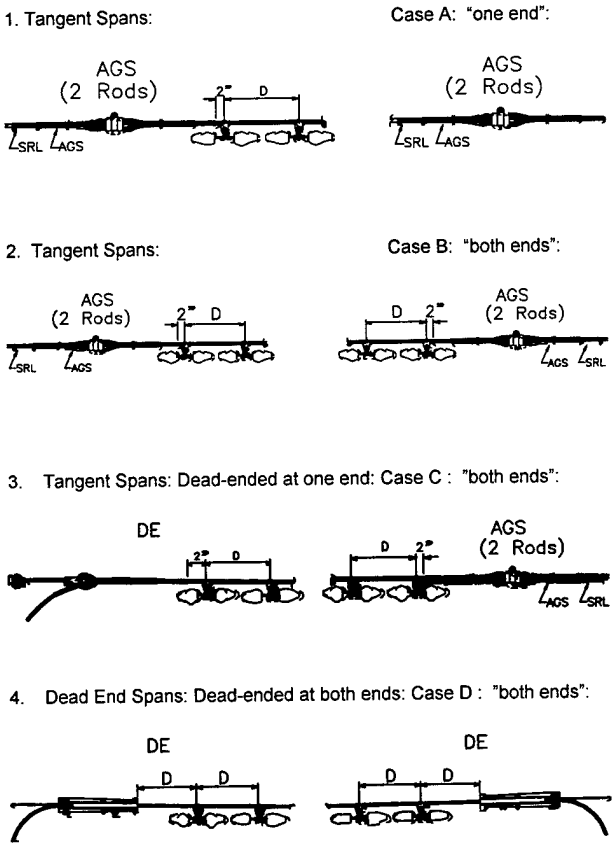

Fig.16- Mass damper location & number on ADSS cables

Dr. Cristian Militaru received MS degree (1980-1985) and Ph.D. degree (1990-1995) in Electrical Power Engineering from Polytechnic University of Bucharest, Romania. He worked for 11 years as a Transmission Design & Consultant Engineer in the power utility industry in Europe, Middle East and South-East Asia. Since 1996 he has been employed with Alcoa Fujikura Ltd., USA, as a Development Engineer in the OPT-GW & ADSS cable and hardware department.

References

1. IEEE 563-1978:Guide on conductor self-damping measurements.
2. C. Rawlins: ACPC technical paper no.27
3. Alcoa Electrical Products Div. Report nos. 93-82-1 and 93-83-3.
4. IEEE 664-1993: Guide for laboratory measurements of the power dissipation characteristics of aeolian vibration dampers for single conductors.

THE PHENOMENON OF AEOLIAN VIBRATIONS FOR ADSS CABLES

A.Ginocchio[1], E.Consonni[1], R.Sutehall[2], G.Diana[3], F.Resta[3], A.Manenti [4]

(1) Pirelli Cavi e Sistemi SpA, Milano, Italy
(2) Pirelli Communication Cables, Newport, U.K.
(3) Department of Mechanics, Politecnico di Milano, Italy
(4) Department of Mechanical Engineering, Universita' degli studi di Brescia, Italy

ABSTRACT

This paper is concerned with the study of the phenomenon of aeolian vibrations for innovative non-metallic optical cables known as ADSS (All Dielectric Self Supporting). It presents the general features of the phenomenon also in comparison with the behaviour of traditional metallic cables and traditional metallic Optical Ground Wires (OPGW). Analytical tools used to simulate cable dynamic behaviour are briefly recollected, together with some results relevant to this application. Two types of damping devices, suitable for application to these cables and for aeolian vibration amplitudes reduction, have been compared through tests on a laboratory span and analytical simulation.

INTRODUCTION

This paper, together with paper [1] also presented to this conference, deals with the dynamic analyses carried out to characterize the aeolian vibration behaviour of the All Dielectric Self Supporting optical cables.
The increasing demand for data transmission has recently given a great impulse to the study and manufacturing of optical cables. Newly built transmission lines are frequently equipped with traditional optical ground wires, while wrapped optical cables and ADSS cables are generally recommended for retrofit (on existing overhead power lines).
Traditional OPGWs generally consist of an aluminum tube containing buffer tubes with optical fibers, multiple layers of aluminum clad steel stranded wires; galvanized and steel wires may also be considered.

ADSS cables are innovative with respect to the materials used. Strength members generally consist of a central member of glass reinforced plastic and peripherical armour made of aramid yarn. Their mass per unit length is much lower than the one of traditional OPGWs and, as a consequence, the ratio T/w between tensile load and weight is sensibly higher. The small mass makes them suitable for retrofit but the high T/w value makes them more sensitive to aeolian vibrations.
The use of this type of optical cables for long span is relatively recent and, to our knowledge, no well documented field measurement relative to aeolian vibration amplitudes, nor a computational method to define the vibration amplitudes and the need for additional damping (damping devices) are available.
Some field measurement of bending amplitude has been reported to Cigré (Conférence Internationale des Grandes Réseaux Électriques à Haute Tension) [2] showing an intense aeolian activity of these cables but the correlation of bending amplitude to antinode amplitude is not easy to be defined.
As far as the fatigue limit vibration amplitudes of these cables are concerned, some tests already performed seem to indicate it is relatively higher than those of metallic standard cables for power distribution.
Moreover, no antinode vibration amplitude field measurements are available, so we choose the way to face and to manage the problem performing analytical simulations. Simulations need to define stiffness and damping data relevant to the cable and the energy input from the wind.
The research has been divided into two parts. The first one is devoted to define stiffness and damping of the cable through tests on a laboratory span and is described in paper [1].

Scope of the second part of the research, described in this paper, is to define the vibratory behaviour of these cables, also through comparison with metallic cables and traditional OPGWs, and to analyze which type of damping devices may be used to reduce aeolian vibration amplitudes and their efficiency.

AEOLIAN VIBRATIONS

For standard metallic cables it is used to define their behaviour with respect to aeolian excitation through simulation by suitable mathematical models [3][4][5]. The most simple and commonly used are based on the energy balance principle: at each one of the natural frequencies of the cable, the conductor vibration amplitude and the strains in any section of interest are evaluated through the balance between the energy input from the wind on the conductor and the energy dissipated by the conductor itself [6][7].
The computation requires the complete knowledge of energy input from the wind and all the mechanical characteristics of the cable: diameter, mass per unit length, flexural stiffness, self damping, tensile load.
As far as the energy input from the wind is concerned, many wind tunnel tests performed by various researchers are available [8][3]: they mainly refer to smooth cylinders in laminar flow, as the effect of stranding proved not to be relevant. All these data may be used also for simulations relative to ADSS cables in smooth flow or low turbulence conditions.
As far as cable stiffness and self-damping are concerned, many laboratory tests are available for standard stranded cables and these data can be derived from the conductor stranding through suitable semi-empirical relations [3][9]. ADSS cables, due to their structure and materials, need to be tested on a laboratory span to evaluate their flexural stiffness and damping properties.
Results of these tests are reported in [1] for the Pirelli ADSS cable whose main data are resumed in Table I.

Table I - Pirelli ADSS 72 FO cable main mechanical features

diameter	16 mm
mass per unit length	0.27 kg/m
Max Working Tension (MWT)	20 kN
Young modulus	15.3 kN/mm^2
Ultimate Tensile Strength (UTS)	62 kN
Every Day Tension (EDS)	11 kN (*)

(*) calculated for 350 m span, ice thickness 12 mm, wind 65 km/h and installation sag 1% of span

The cable self-damping versus non dimensional vibration amplitude u/D (u is the vibration amplitude, D is the cable diameter) is reported in fig.1. The self-damping is reported in the form of the non dimensional damping ratio r/r_c and has been obtained by the Inverse Standing Wave Ratio (ISWR) method [3][9].

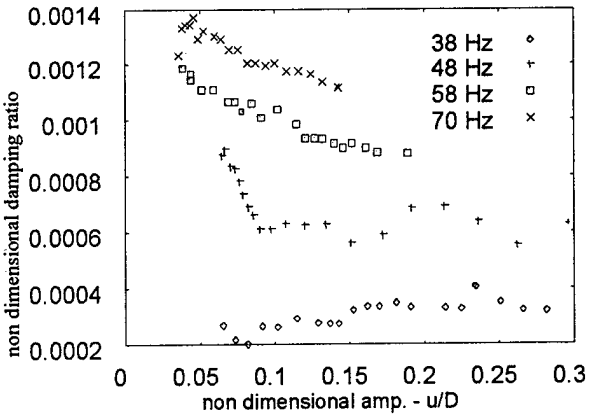

Fig.1 - ADSS self-damping ratio (r/r_c) versus non dimensional vibration amplitude.

The behaviour of this cable with respect to self-damping is not the same as traditional metallic OPGWs. In fact it can be seen that the r/r_c value is not increasing with vibration amplitude as usually assumed for metallic stranded cables, but it is almost constant with vibration amplitude. This means that the semi-empirical expression of the power dissipated by the cable derived from measurements [1] and used in the simulation programs:

$$P = k \frac{u^{\alpha} f^{\beta}}{T^{\gamma}}$$

contains the square power of the vibration amplitude (α=2), while for metallic cables this exponent is around 2.4. (f is frequency and T tensile load).

Taking into account the measured data, a simulation of the dynamic behaviour of the ADSS cable and of a traditional OPGW with respect to aeolian vibrations has been performed. The OPGW cable has nearly the same diameter (17.9mm) as the ADSS cable and the normal EDS value for this conductor is taken into account for computation: the ratio T/w between tensile load and weight is 1870 m for the OPGW and 4074 m for the ADSS cable and, as already observed the higher is T/w the more sensitive is the cable to aeolian vibrations.

.

The results of computations are reported in fig.2 as cable antinode vibration amplitude versus frequency.

As can be observed, the ADSS cable, in line with the T/w value, is more sensitive than the OPGW to aeolian vibrations: the frequency range passes from up to 80 Hz to up to 120 Hz and the vibration amplitude is two + three times in the range 30÷80 Hz.

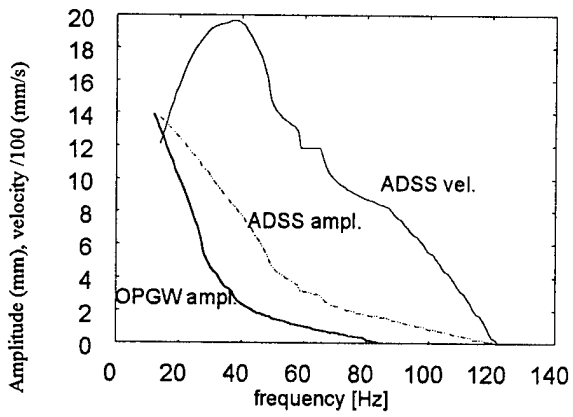

Fig.2 - ADSS cable - OPGW : aeolian vibration amplitudes (computed values). ADSS cable: vibration velocity (*100)

In particular, as far as the ADSS cable is concerned, it can be observed that the maximum vibration amplitude is around one diameter (i.e. the maximum amplitude excited by the aeolian vibration phenomenon) and that the frequency range extends up to 120 Hz.

Around 50 Hz the cable vibration amplitude is about 4 mm, which corresponds to a vibration velocity around 1400 mm/s (fig.2). This value is very high if compared to the value generally recommended for metallic cables (around 400 mm/s) and also if compared to the value (870 mm/s) set in the preliminary specifications prepared by Task Force 3 of Working Group 22-11 of Cigrè for this type of cables [10].

Moreover, problems of noise, of cable wear at the end fittings and of stress transmission to the tower members suggest to limit aeolian vibration amplitudes well below these values.

Aeolian vibration amplitudes may be limited by the use of suitable damping devices: it is necessary to analyze the available damping devices in relation to their efficiency with respect to this application.

DAMPING DEVICES

Damping devices already used for ADSS cables are spiral dampers and Stockbridge type (four resonances) dampers.

Spiral (impact) dampers

The spiral damper is a one piece PVC helical rod fitted loosely on the cable, except for one end, where the inner diameter has been reduced to grip the rods of the dead-end or suspension clamp. The damping mechanism is related to the fact that the damper vibrates and hits the cable.

Spiral dampers with respect to Stockbridge type dampers have the disadvantage that it is not easy to model the behaviour of cable + damper and so it is not possible to optimize their characteristics in relation to the required application.

The only way to check their efficiency is to test the damper itself on the cable on a laboratory span.

A spiral damper suitable for the ADSS 72 FO cable has been tested on a 46 m long laboratory span [9] to measure the power dissipated by the cable+damper as a function of frequency. The ISWR method , which needs the measurement of node vibration amplitudes, could not be used in this case because, due to the spiral damper damping mechanism, a single frequency cannot be excited and no stationary vibrations can be observed. It is easier to evaluate the power introduced by the shaker, using the Power Method (PM).

Fig.3a and 3b report the r/r_c value of the cable+damper as a function of the cable non dimensional vibration amplitude u/D for two frequencies in the range of interest of aeolian vibrations. The same figure reports also the values of the cable alone (also measured by the PM) for comparison.

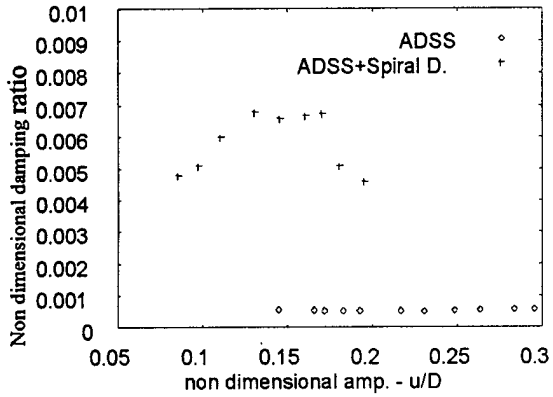

Fig.3a - Laboratory span. Non-dimensional damping r/roc for the cable alone and for the cable + spiral damper – 40 Hz

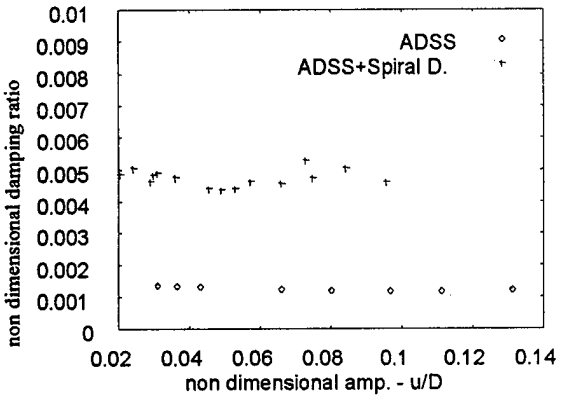

Fig.3b - Laboratory span. Non-dimensional damping r/r_c for the cable alone and for the cable+spiral damper – 60 Hz.

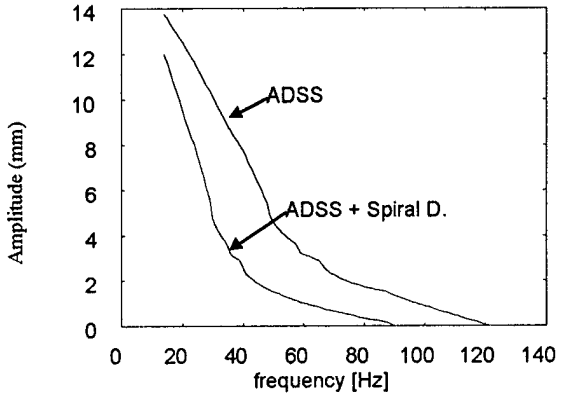

Fig.4a - 400 m span. ADSS cable alone and ADSS cable + two spiral dampers - aeolian vibration amplitude vs frequency

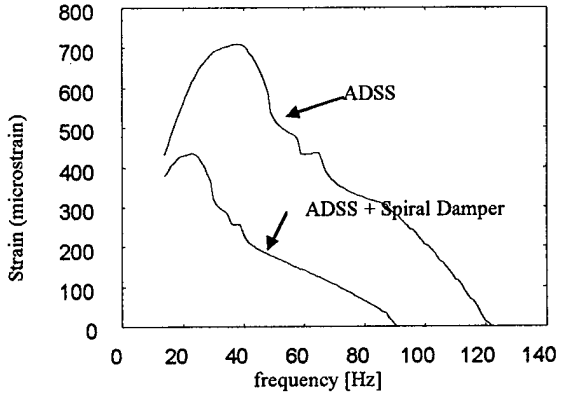

Fig.4b - 400 m span. ADSS cable alone and ADSS cable + two spiral dampers - strain on the cable at the suspension clamp vs frequency

It can be observed that the presence of one damper causes an r/r_c mean increment with respect to the cable alone around 300% for the laboratory span.

If a standard 400 m span equipped for example with two spiral dampers - one at each extremity - is taken into account, a self damping increment around 60% may be assumed.

Using this self-damping value, a simulation of the dynamic behaviour of the ADSS cable (400 m span) with two spiral dampers has been run. The results are reported in fig.4a,b in terms of cable vibration amplitude and cable strain at the suspension clamp vs frequency respectively.

The spiral dampers reduce vibration amplitudes; however the tests and computations performed cannot give any indication about design and optimization of the spiral dampers for different cables.

Stockbridge type dampers

Stockbridge type dampers are the most commonly used dampers and have the advantage that they can be tested on a laboratory span or, separately from the cable, on a shaker, thus defining their mechanical impedance (harmonic transfer function between clamp displacement and force transmitted to the cable) for different damper clamp vibration velocities of interest. The measured mechanical impedance is used to compute the energy dissipated by the damper as a function of the frequency and of the damper vibration amplitude, thus obtaining a mathematical model of cable + damper (based on the Energy Balance Principle) suitable for computation of the aeolian vibration amplitudes of the damped cable and for

optimization of the damper characteristics and position on the cable.

A first reference for the Stockbridge type damper choice is given by the result of the simulation of the dynamic behaviour of the cable alone subjected to aeolian excitation (damper operating frequency range) and by the formula [6] giving the damper optimum force as a function of frequency:

$$F_{opt} = 2\omega\sqrt{Tm} \qquad (1)$$

where:
F_{opt} is the damper optimum force per unit displacement of the damper clamp,
ω is the vibration frequency [rad/s],
T is the tensile load and
m is the cable mass per unit length.

The optimum damper force for this cable is very low and is reported together with the mechanical impedance of two types of dampers in fig.5b and fig.6b respectively.
The mechanical impedance have been measured on an electrodynamic shaker by imposing to the damper a frequency sweep at constant vibration velocity (100 mm/s) from 0 to 200 Hz and are reported in fig.5a and 5b respectively.
Damper 1 (fig. 5a,b) has a total mass of 2.7 kg, while damper 2 (fig. 6a,b) has a total mass of 1.2 kg.
As can be observed, damper1 is 'too heavy', while damper2 seems to fit the curve of the optimum force.

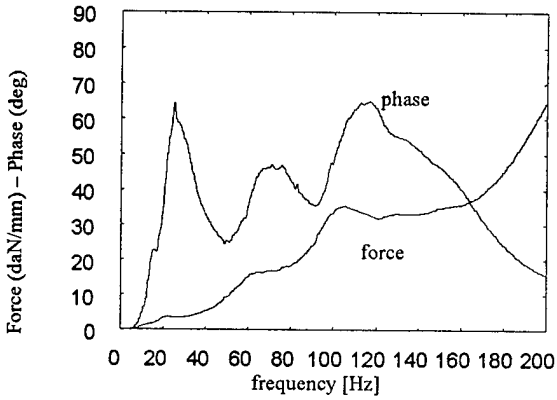

Fig.5a - Damper 1 mechanical impedance

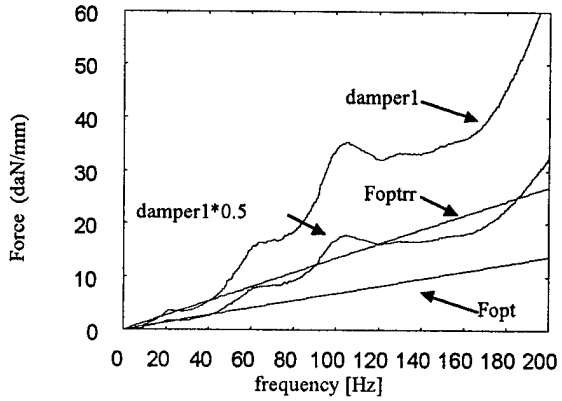

Fig.5b - Damper 1 mechanical impedance and optimum damper force for the cable alone (Fopt) and for the cable with reinforcing rods (Foptrr)

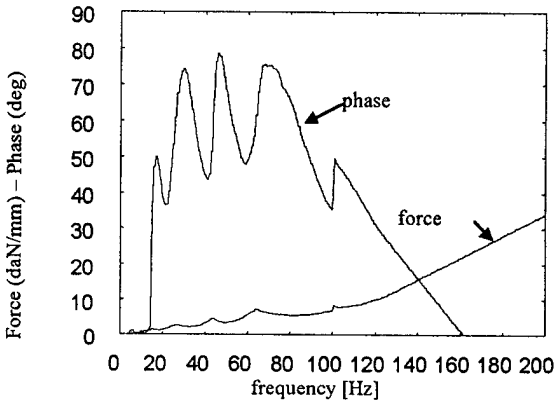

Fig.6a - Damper 2 mechanical impedance

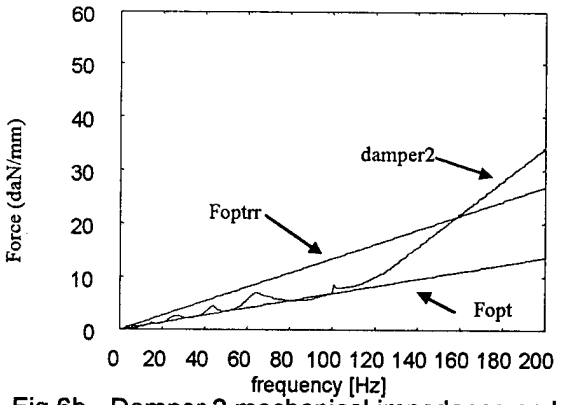

Fig.6b - Damper 2 mechanical impedance and optimum damper force for the cable alone (Fopt) and for the cable with reinforcing rods (Foptrr)

It is also to be taken into account that:
a) the presence of the damper on the cable locally modifies the cable mode of vibration and causes a damper lower efficiency ;
b) for this type of cables it is not possible to clamp the damper directly on the cable (problems of local compression and cable

damage), but it is better to put the damper on the reinforcing rods of dead ends or suspension clamps.

The presence of the reinforcing rods changes the mass and flexural stiffness of the cable, modifying the terms of the problem: the optimum damper force should increase because of the mass increasing; the cable local distortion due to the damper should decrease owing to the flexural stiffness increase and this last effect is the great advantage of using armour rods.
To evaluate these effects, tests on a laboratory span equipped with the cable with and without armour rods and damper have been performed, together with analytical simulation taking in to account the mentioned effects.
Also in this case, first, the system damping, always reported as the non-dimensional ratio r/r_C, has been evaluated through the PM. All the measurements being used to compare efficiencies of various dampers in various conditions, the end point losses, which contribute to the system damping in case of the PM method, are not important.
Fig.7 reports the measured cable+damper1 self damping as a function of u/D for the frequency of 60 Hz, both in the case that reinforcing rods are present or not. As it can be observed the damper1 efficiency improves when it is clamped on the armour rods.

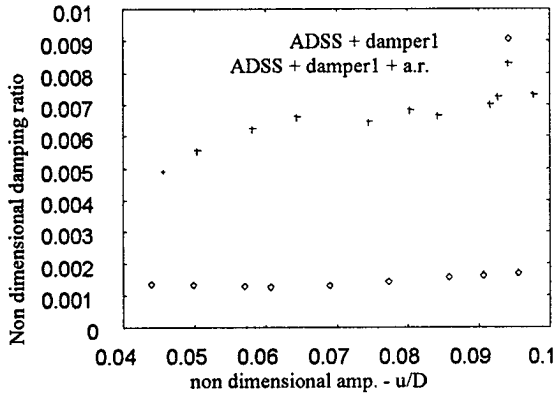

Fig.7 - Laboratory span: Damper 1 efficiency with and without reinforcing rods - non dimensional damping of the cable+damper vs u/D at 60 Hz

The results of the analytical simulation of the behaviour of the cable + damper1 are reported in Fig.8 as cable antinode amplitude of vibration both in the case that reinforcing rods are present or not. Also in this case it can be observed that the damper efficiency increase significantly over 50 Hz.

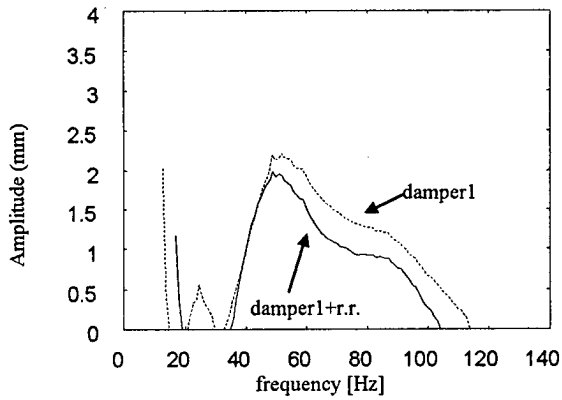

Fig.8 - Simulation of the aeolian vibration behaviour of the cable + Damper 1 with (+ r.r.) and without reinforcing rods - cable antinode vibration amplitude vs frequency

As the indication given by the damper optimum force seems to be in the right direction, we can try to use this criterion to define the optimum damper for this application.
As a first approximation, expression (1) has been used to evaluate the optimum damper force for the cable + reinforcing rods, simply taking into account the cable + reinforcing rods mass. Such optimum force has also been reported in fig.5b and 6b.
As it can be observed, damper1 force is closer to the newly defined optimum force but still remains too high, while damper 2 seems now to give a too low force.
In fig.5b it is also reported the force of a virtual damper characterized by half the force of damper1: its mechanical impedance fits the cable+armour rods optimum force above defined.
The simulation program has been used to check the efficiency of this virtual damper with respect to damper 1.
The results of the simulation are reported in fig.9 as cable antinode vibration as a function of frequency. The virtual damper effect is at least bad to that of damper 1.
This fact shows that the optimum damper force for the cable+armour rods computed by (1) cannot be used as the only criterion to optimize the damper.
On the other hand, the simulation program solves the motion equation of the cable taking into account all the different domains defined by the presence of the armour rods (different mass and stiffness) and of the dampers (complex force) with the relative end conditions (equilibrium and displacement, bending congruency)[11], thus defining the correct cable deflection shape for each mode of vibration.

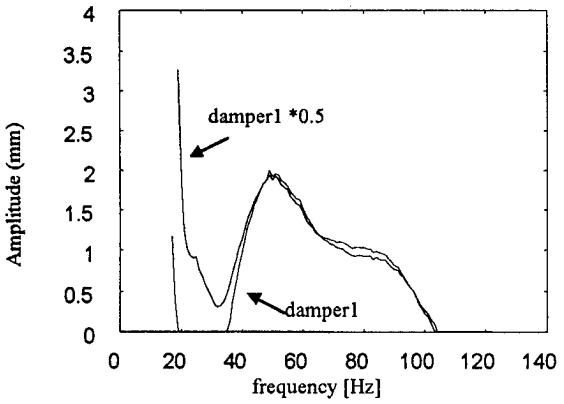

Fig.9 - Simulation of the aeolian vibration behaviour of the cable + damper1 and cable + virtual damper (damper1*0.5) - cable antinode vibration amplitude vs frequency

The analytical tool in our hands seems to be suitable to reproduce the behaviour of the system conductor + armour rods + damper to aeolian excitation, so it can be used to optimise the damper characteristics in relation to the proposed application.
A comparison between experimental and analytical findings is reported in the following for further validation of the mathematical model.
First, damper 1 and damper 2 have been tested on the laboratory span clamped on the reinforcing rods.

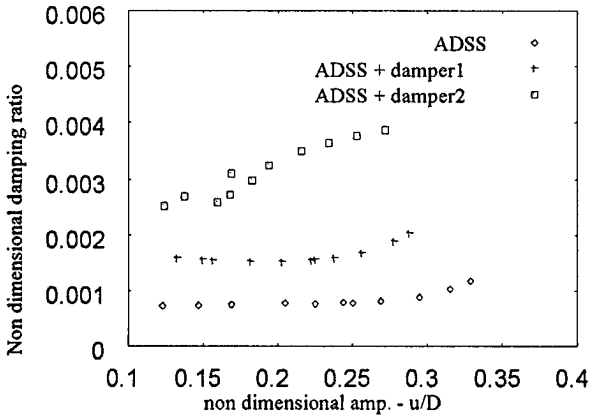

Fig.10a - Laboratory span: damper 1, damper 2 efficiencies on reinforcing rods - non dimensional damping of the cable+damper vs u/D at 40 Hz

The test results are reported as usual as non dimensional ratio r/r_c vs u/D for three frequencies of interest: 40 Hz (fig.10a), 60 Hz (fig.10b) and 80 Hz (fig.10c). The curve of the cable alone is also reported for reference.

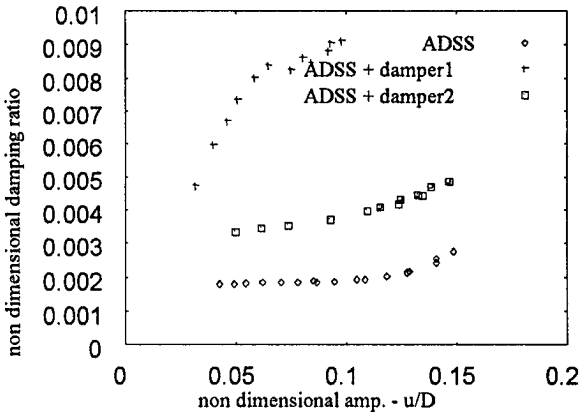

Fig.10b - Laboratory span: damper 1, damper 2 efficiencies on reinforcing rods - non dimensional damping of the cable+damper vs u/D at 60 Hz

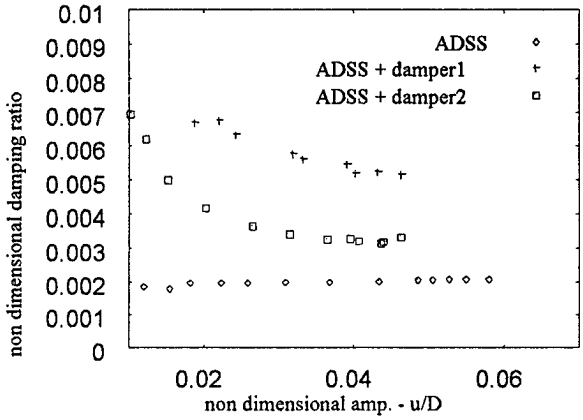

Fig.10c - Laboratory span: damper 1, damper 2 efficiencies on reinforcing rods - non dimensional damping of the cable+damper vs u/D at 80 .Hz

As it can be observed damper 1 is less efficient than damper 2 for frequencies approximately up to 50 Hz.
This is reproduced also by the simulation program, as shown in fig.11 in terms of strain on the cable at the suspension clamp vs frequency . The strain of the cable equipped with damper 1 is lower than the strain of the cable equipped with damper 2 approximately over 60 – 70 Hz.
This analysis points out that the damper optimization for ADSS cables is more complex than for traditional standard metallic cables since the low value of the $\sqrt{Tm}$ parameter requires the use of armour rods on the cable in correspondence of the damper clamp. This solution avoids:
- optical damages due to effects of local compression of the cable,

- too high local distortion of the cable (which compromise the damper efficiency) and, finally ,
- too low optimum damper forces.

The mathematical model introduces the effective mass, stiffness and extension of the reinforcing rods and is in condition of optimizing force and position of the damper for the required application.

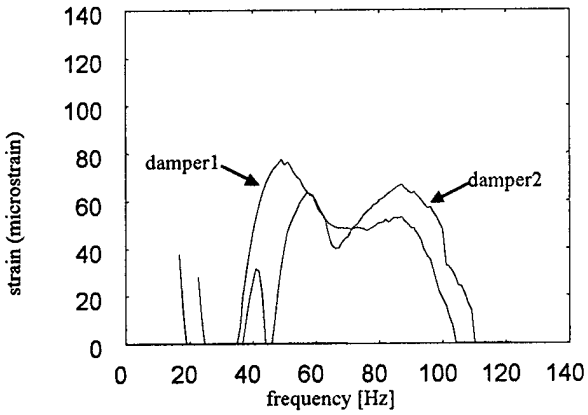

Fig.11 ADSS cable equipped with damper 1 and ADSS cable equipped with damper 2 - computed strain on the cable at the suspension clamp vs frequency

CONCLUSIONS

The dynamic behaviour of a 72 FO ADSS optical cable with respect to aeolian vibrations has been analyzed.

The damping devices used for these types of cables have been tested on a laboratory span, to evaluate their efficiency.

Experimentation has put in evidence the necessity to use reinforcing rods on the cable at the damper clamp. This makes the task of damper force optimization more difficult than in other cases.

An analytical tool to optimize Stockbridge type dampers with respect to force and position, taking into account of reinforcing rods, has been tested and validated.

References

[1] E. Consonni, P.Marelli, M. Falco, A. Cigada, M. Vanali – 'All Dielectric Self -.Supporting Cables: mechanical features and aeolian behaviour' – IWCS 1998

[2] A.D.Bartlett et al - 'Field testing of an ADSS optical fibre cable and damping devices in the UK - Cigré WG22-11 report 93 -1993.

[3] Cigré WG22-11 - TF1 - 'Modelling of aeolian vibrations of single conductors: an assessment of the technology' - to be published on Electra.

[4] Diana G. et al - 'Aeolian vibrations of overhead transmission lines: computations in turbulence conditions' - Jour of Wind Engineering and Industrial Aerodynamics 46 & 47 (1993) 639-648.

[5] Noiseux et al - 'Transformation of wind tunnel data on aeolian vibration for application to random conductor vibrations in a turbulent wind' - IEEE/PES 1986 Summer Meeting, Mexico City.

[6] R. Claren, G. Diana - "Mathematical analysis of transmission line vibration". IEEE Summer Power Meeting1967, 31 C 83

[7] Diana,G. et al. - 'Field measurement and field data processing on conductor vibration (comparison between exp. and anal. results)' - CIGRE' 1982 Sess.

[8] Diana, G. and Falco, M. (1971),"On the forces transmitted to a vibrating cylinder by a blowing fluid. (Exp.study and analysis of the phenomenon)". "Meccanica", n.1, 1971

[9] A.Cigada, A.Manenti - 'Sulla misura dello smorzamento proprio dei conduttori' - Atti del III Congr Naz di Misure Meccaniche e Termiche - Ancona 1997.

[10] Cigré WG22-11 - TF3 - 'Guide to fittings for optical cables on transmission lines - part 2 - testing procedures' - fifth draft, june 1998.

[11] M. Falco, M. Gasparetto, P. Nicolini, G. Di Giacomo - 'Comportamento vibratorio di lunghe campate di attraversamento, equipaggiate con conduttore singolo e con dispositivi smorzanti. (Verifica sperimentale sulla campata di attraversamento dello Stretto di Messina e messa a punto di un procedimento di calcolo per conduttori singoli equipaggiati con ammortizzatori di tipo Stockbridge)' - "L'Energia Elettrica" n.5, 1973

Biographies

Giorgio Diana: born 1936, mechanical Eng. Degree in 1961, Professor of Applied Mechanics since 1971. Actually he is a member of the Senato Accademico of Politecnico di Milano. His research works are in the field of fluidoelasticity, rotordynamics, vibration problems in mechanical engineering, railway vehicle dynamics, interaction between pantograph and catenary. Author of more than 100 papers at national and international conferences and reviews.
Member of Cigre (WG11-SC22- Chairman of TF1), president of the technical committee on rotordynamics of IFToMM.

Alessandra Manenti: born in 1958, mechanical Eng. Degree in 1982, PhD. in mechanical engineering in 1987, Researcher in Mechanical Measurements since 1986. Her research works are in the field of experimental and analytical behavior of overhead transmission line conductors, rotordynamics, statistical data analysis.

Ferruccio Resta: born in 1968, mechanical Eng. Degree in 1992, PhD. in mechanical engineering in 1996. His research works are in the field of experimental and analytical vibration problems in mechanical engineering, railway vehicle dynamics, interaction between pantograph and catenary, system control.

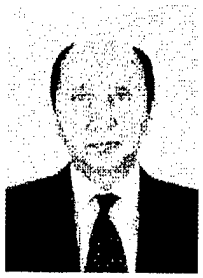

Alessandro Ginocchio was born in Milano in 1947. He graduated in Electrical Engineering from Politecnico di Milano in 1972 and joined Pirelli in 1974, where he was engaged in the research and development on submarine cable.
Since 1987 he has been responsible for the technological development of optical fiber cables.

Enrico Consonni was born in Seregno (Mi) in 1964. He graduated in Aeronautical Enginnering from Politecnico di Milano in 1991 and joined Pirelli in 1991, where he has been engaged in research and development of TLC cables, dealing mostly with environmental test, cable design and manufacturing technology.

Ralph Sutehall is a Senior Engineer with the Communication Division of Pirelli Cables in the UK, where he is responsible for installation development. He has been working with fiber optic cables for 24 years and is active member of the CIGRE working group on fiber optics.

ALL DIELECTRIC SELF-SUPPORTING CABLES: MECHANICAL FEATURES AND AEOLIAN VIBRATION

A.Cigada[2], E.Consonni[1], M. Falco[2], P.Marelli[1], R.Sutehall[3], M.Vanali[2]

(1) Pirelli Cavi e Sistemi SpA, Milano, Italy
(2) Department of Mechanics, Politecnico di Milano, Italy
(3) Pirelli Communication Cables Limited, Newport, U.K.

ABSTRACT

This paper deals with the dynamic analyses carried out to determine the aeolian vibration behavior of the All Dielectric Self Supporting Optical Cables (ADSS). The vibration numerical simulation usually requires two main tests giving the cable self-damping and the flexural stiffness EJ. Considering the long lasting experience gained on metallic cables, both the power method (PM) and the inverse standing wave ratio (ISWR) have been considered, in order to evaluate the cable self-damping. Some improvements, proven to be necessary in transferring the methods to the ADSS cables, are then described. Results from a standardized fatigue test are also shown and critically discussed.

INTRODUCTION

Although studies have already been carried out on ADSS cables, they lead to no consolidated and reliable background as in the case of metallic conductors or OPGW. Moreover, the ADSS cables present a number of innovative features in the construction materials and in the installation parameters (mainly the tensile strength) and, as a consequence, are characterized by a higher tension to weight ratio, if compared to the traditional metallic cables. The value of the tension to weight parameter determines the range of critical frequencies interested by the phenomenon, making ADSS cables more sensitive to the aeolian vibrations.

A new research is set-up to evaluate the maximum vibration levels induced by the wind on ADSS cables and to face the problem of the aeolian vibrations under an engineering point of view, also referring to the already existing wide literature concerning the metallic cables.

The more flexible approach to the problem is based on analytical simulations, that usually utilize [17] the so called Energy Balance Principle.

This method relies on an energy balance between the energy input due to the incoming wind and the energy output mainly due to the cable (+ damping devices, if present) dissipation. This energy balance, performed at each of the cable natural frequencies, leads to the estimation of the maximum vibration amplitude, as a function of the wind speed.

The wind energy input related to the vortex shedding has been deeply investigated, not only in air, but also in water and other fluids and can be represented by mathematical expressions which are nowadays of common use in simulation programs. Most of them, mainly derived from wind tunnel experimentation, can be reduced to the form:

$$P_w = f^3 D^4 \mathrm{fnc}\left(\frac{u}{D}\right) \qquad [1]$$

where f is the frequency of vibration, u is the amplitude of vibration, D is the cable diameter and fnc(u/D) is an empirical function based on the fitting of experimental results. Fig 1 shows the maximum energy introduced by the wind into a cable as function of the non-dimensional amplitude u/D (A is equivalent to u, D the cable diameter) obtained by various researchers by means of wind tunnel tests.

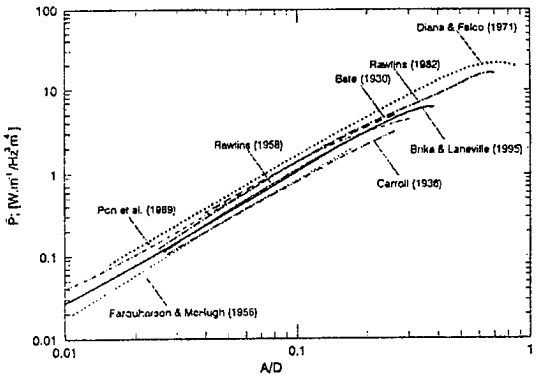

Fig 1 - Wind power input

A detailed analysis of the differences among the results of the various researchers is reported in [17]. While the energy input is rather well known, very little is available about the cable losses, in case of ADSS cables. Aim of the paper is, first of all, to define the cable self-damping together with

all those mechanical features (i.e. the EJ flexural stiffness value) needed for the numerical simulation of a real line.

Methods to define the cable self-damping are mainly derived from those already available from OPGW and ACSR cables and consist of experimentation on a laboratory span. They are fully described in the I.E.E.E.563-78 [2] standard and in the similar CIGRE-Electra n°62, 1979 [3] document and will be shortly summarized in the following.

These methods have proven to be effective when dealing with metallic cables: however it has to be investigated if this way of facing the problem can be transferred to the ADSS class of cables without any modifications or improvements. This research is also the occasion for a general critical review of the adopted methods and a first attempt to perform the uncertainty analysis related to the testing procedures.

The experimentation to get the cable losses has lead to interpolating expressions. The most common formula is in the form:

$$\frac{P}{L} = k\frac{u^l f^m}{T^n} \qquad [2]$$

where T is the tensile strength, k, l, m, n are constant that can be found in literature for the OPGW and ACSR cables; however, when going to the ADSS cables, it has to be verified if a formula like [2] will fit the experimental data and how to evaluate these constants, if a formula like [2] can be adopted. When the values of the k, l, m, n coefficients are known, simulation programs can give support in order to modify the line parameters in a cheaper and faster way, without performing new expensive tests.

The measurements presented in this paper are only a first approach, because only one cable has been considered and only one cable tension has been tested at different vibration frequencies and amplitudes.

Therefore, not being possible to get a complete law describing the cable losses, it has been stated that the damping ratio $h=r/r_c$ (where r is the damping constant and r_c is the critical damping) is the more efficient parameter to represents the cable damping, due both to its more immediate physical meaning and to the fact that, by comparing data on plots, scaling effects do not mask strong differences as it is the case of power plots required by the standards [1,2], which have logarithmic scales.

The first part of the paper will describe the different methods adopted for measuring the cable self damping: the power method (PM) and the inverse standing wave ratio method (ISWR) will be considered together with the decay, which, though not being considered in the above mentioned standards, is useful for a first approximation. In addition, the measurement set-up, which is similar to that adopted for metallic cables will be described.

The second part of the paper is focused on the modifications to the above mentioned methods required for testing ADSS cables and on some critical reviews of measurement aspects concerning the PM and ISWR methods, together with a first attempt to perform an uncertainty analysis on the gathered data.

The third part is about the definition of the cable flexural stiffness (EJ) and the final part describes a fatigue test (10^8 cycles) performed on a 72 fo ADSS cable according to a preliminary international standard proposal.

The prosecution of this paper, that is **"The Phenomenon Of Aeolian Vibrations For ADSS Cables"**, which could be considered as part two in the presentation of the research, is mainly aimed at defining the vibratory behavior of ADSS through numerical simulations, also tracing a path for the optimization of the efficiency of some damping devices.

CABLE DESCRIPTION

A typical ADSS cable design is illustrated below (fig.2).

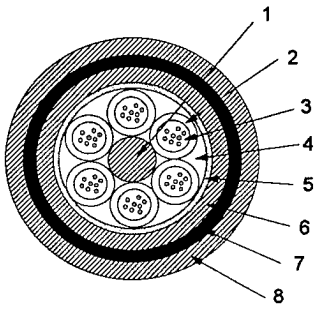

Figure 2 - ADSS 72 FO cable

1 - central strength member
2 - stranded loose tubes
3 - optical fibers in filling compound
4 - flooding compound
5 - wrapping tape
6 – inner sheath
7 – aramid yarns
8 - outer sheath

ADSS cables are innovative with respect to the used materials. Strength members generally consist of a central member of glass

reinforced plastic and peripherical armour made of aramid yarns. Their mass per unit length is much lower than in the case of traditional OPGW, while the ratio T/w between tensile load and weight is much higher. The small mass makes them suitable for retrofit but the high T/w value makes them more sensitive to aeolian vibration.

METHODS FOR MEASURING THE CABLE SELF DAMPING

The methods described in the standard to measure the self-damping of cables are substantially two: the Power method (PM) and the Inverse Standing Wave ratio method (ISWR). As these methods are widely described in [1,2,18] only a very brief summary will be given here; in any case some main aspects concerning the specific case of the ADSS cables will be discussed.

Before entering into details it is useful to examine the problem of measuring the energy dissipation on an experimental span [3].

Apart from the main energy loss due to the cable transversal motion, some other phenomena take place in the experimental span, also giving energy losses; these extraneous effects must be carefully evaluated and or eliminated.

Energy dissipation is mainly due to:

- cable clamping system at the span ends;
- local deformation induced by the device used to force it to vibrate;
- secondary transversal motion and or torsional vibration of the cable;
- cable motion in the air (aerodinamic drag)

In a real installation the contribution to the overall energy dissipation given by the span ends is less significant than in a laboratory testing span, due to the reduced length of an experimental span with respect to real ones.

Concerning the torsional and other transversal motion the way the cable is vibrating should be examined to ensure the absence of this kind of motion.

The aerodynamic dissipation should or should not be taken into account depending on the methods used to calculate the energy introduced in the line by the wind.

Power method

The cable is placed on the experimental span and, by means of an electrodynamic exciter, both amplitude and frequency controlled, is forced to vibrate at one of its resonance frequencies.

When a stationary condition is reached, considering one cycle of vibration, the energy introduced by the exciter in the line is equal to the one dissipated by the span, being the elastic and inertial forces conservative.

The energy introduced in the cable is calculated by measuring the force F exchanged between the cable and the exciter and the displacement of the forcing point μ_F; the result is then given by the formula:

$$E_{diss} = \pi F \mu_F \operatorname{sen}(\phi) \qquad [3]$$

The non dimensional damping coefficient h can be calculated dividing the energy introduced in the cable by the total kinetic energy of the cable:

$$h = \frac{1}{4\pi}\frac{E_{diss}}{E_{cin}} \qquad [4]$$

being the total kinetic energy of the cable given by the formula (l =span length, ω = circular frequency):

$$E_{cin} = \frac{1}{4} m l \omega^2 u^2 \qquad [5]$$

While the application of this method is quite simple, as it requires a limited number of measurements, all the external dissipation is part of the global computation of the cable self damping; special care must therefore be devoted to all the possible ways to reduce all these external loss sources.

Standing wave method

From an Electro-mechanical analogy (but also a mechanical re-formulation of the problem is possible [5]), the mechanical power P_i flowing in one section of the cable is given by:

$$P_i = \frac{V^2}{2} S_i \sqrt{Tm}$$

where:

- $V = \omega u$
- $S_i = \frac{a_i}{u}$ (inverse standing wave ratio - ISWR)

where a_i is the amplitude of vibration in a node.
The power dissipated between the node j and the node k will be:

$$P = P_k - P_j; \qquad [6]$$

And the power dissipated per length unit will be:

$$P_{diss} = \frac{P_k - P_j}{n_v \frac{\lambda}{2}} \qquad [7]$$

where n_v is the number of nodes between k and j and λ is the wave length.

Considering the kinetic energy of the portion of cable between the two nodes:

$$E_{c(max)} = \frac{1}{2} u^2 \omega^2 \frac{m}{4} \frac{1}{f} \sqrt{\frac{T}{m}}\, n_v \qquad [8]$$

the value of the non dimensional self damping coefficient is simply given by:

$$h = \frac{S_k - S_j}{\pi n_v} \qquad [9]$$

Advantage of this method is that the measured dissipation relates to the considered portion of cable only, therefore the estimated self-damping value is not affected by the above mentioned influence quantities (that is span ends and exciter-cable link).

The main problems the method presents are the correct estimation of the nodes position and the measurement of the node amplitude of vibration, which is normally 1/1000 the antinode amplitude, therefore a very small value, of the order of a few micrometers.

Decay

This method is not considered in the standards, however, if correctly employed, it can give a first approximation of the value of the self damping at all amplitudes in one trial.

This method is very quick and easy requiring in its simplest form just one vibration transducer measuring the decay after the exciter. The cable is forced to vibrate at one of his natural frequencies and then the exciter is stopped.

If a lightly damped system (h<<1) is left free to vibrate from a forced resonance condition it will undergo a stopping transitory that will look like figure 5.1.(decay).

Considering two successive peaks and defining δ as:

$$\delta = \ln\left(\frac{X_i}{X_{i+1}}\right) = \ln\left(\frac{e^{-h\omega_0 t}|X|\cos(\omega t + \phi)}{e^{-h\omega_0 t+T}|X|\cos(\omega(t+T)+\phi)}\right)$$

simplifying:

$$\delta = \ln\left(e^{h\omega_0 T}\right) = h\omega_0 T$$

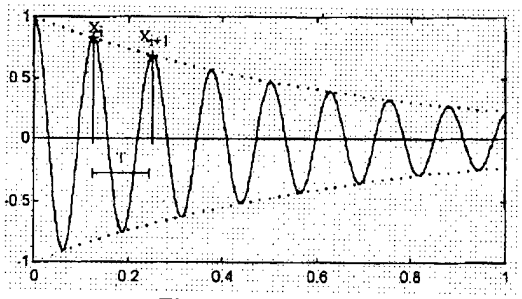

Figure 3: a decay

if h<<1, as in the case of cables, we can consider T as a function of ω_0, i.e. $T=2\pi/\omega_0$ giving:

$$h = \frac{\delta}{2\pi}$$

Applying techniques like the Hilbert transform (making easier the calculation procedure) it is very easy to compute the self damping just measuring the antinode vibration amplitude during a decay.

But, when the exciter is stopped, giving raise to the decay, it is not separated from the cable itself: this is the main concern the method presents because the exciter is an unwanted loss source.

To improve the results is therefore possible to compute the energy transferred from the cable to the exciter during the decay, with the same set-up already described for the power method. However this exciter loss is usually one order of magnitude less than the cable one.

It is therefore possible to get the cable self-damping out of the total dissipation, but the end losses are still included in the measurements.

MEASUREMENT SET-UP

Power method

The measurements have all been done on the experimental span whose main features are shown in the figure below:

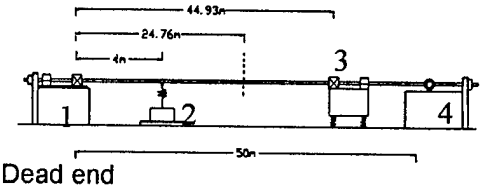

1. Dead end
2. Exciter
3. Seismic mass
4. Dead end

Figure 4 - Experimental span

The clamps used to hold the cables (Photo 1) are a combination of a pivot and a fixed clamp in order to minimize the dissipation at the dead ends and to produce reliable results with the power method.

Another advantage of this clamping method is that the dead end losses are kept constant with respect to the test frequency, allowing for data comparison under different conditions.

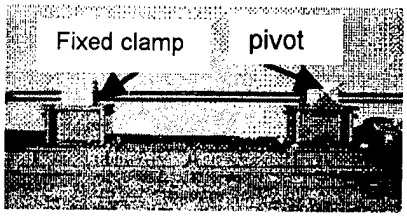

Photo 1 - Cable Clamps

To measure the exchanged force between the exciter and the cable a piezo load cell conditioned with a charge amplifier was used; on the top of the cable-exciter connection an accelerometer was fixed to measure the vibration

at the forcing point (being the superimposed motion a sinusoidal one, it was easy to get displacements out of the acceleration spectra via double integration).

Another accelerometer has been used to measure the vibration amplitude at the antinode.

As a completion of the measurement set-up a non contact laser displacement transducer has been used to duplicate the antinode vibration measurement; details about this point will be given in the following.

However, due to the fact that to distinguish the cable self damping from the extraneous losses the experimentation had to be doubled for two different span lengths, and due to the fact that, with the techniques described in [18] the accuracy of the ISWR method has been improved, it has been decided to use this latter, leaving the PM as a quick check and as an upper bound not to be trespassed by the ISWR results.

Standing wave method

The ISWR method requires the measurement of the vibration amplitude at two nodes of the cable. Amplitudes at the nodes are of the order of 1/1000 the amplitude at the antinode and also, due to the small non linearity of the system, the nodes keep on moving as the amplitude/frequency are corrected to maintain a resonance condition.

This makes nearly impossible to measure the amplitude at the two nodes by simply placing two transducers on them.

The problem has been solved by making two measurements, one on each side of the node, and interpolating the measurements with the theoretical equation of the vibrating cable given by the following formula [18]:

$$\frac{\varphi(x)}{u} = \sin\left(\frac{n\pi}{\ell}\sqrt{1-2ih}\ x\right) \qquad [10]$$

The first trials where made applying on the cable two accelerometers on the node sides, as previously done for the metallic cables (Photo 2). However due to the distortion produced by the presence of the sensors on the cable, it has been decided to substitute the accelerometers with non contact laser displacement sensors (Photo3).

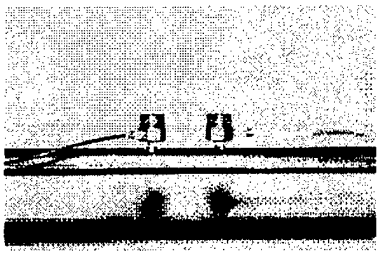

Photo 2 - Accelerometers at the node

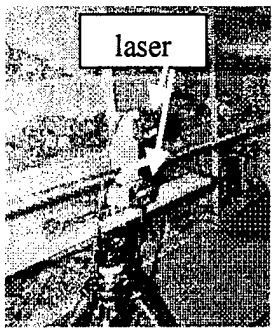

Photo 3 - Lasers at the node

CORRECTION OF THE SYSTEMATIC EFFECTS AND UNCERTAINTY ANALYSIS

The described measurement set-up provides good means for getting reliable results when dealing with metallic cables, as proven by several measurement campaigns, however some concerns have arisen in transferring the same methodology to the ADSS cables which have a lower mass per unit length. The presence of an accelerometer on the cable gives raise to a mass increment which is a higher percentage value for the ADSS cable than for the OPGW.

During the tests a reduction of the instrumented half wave vibration amplitude and length has been experienced, due to the fixing of the accelerometer on the cable; subsequent trials demonstrated that the added accelerometer mass reduced the measured vibration amplitude by an amount of about 30%, significantly changing the value of the computed self-damping: the presence of the accelerometer on the metallic cable didn't affect the results at all.

As a first step, a lighter accelerometer was used, in order to reduce this phenomena and some other tests were made employing a non contact triangulation laser displacement transducer. The comparison between different kinds of transducers at two different frequencies are shown in figure 5 for the case of the power method, even if this problem also affects the ISWR method. Concerning this latter method alone, the node vibration has been firstly measured by means of a couple of accelerometers. However, in this case too, it has been noted that the accelerometers sensibly distorted the cable modes of vibration: after the application of the accelerometers, the position of the node (kept under control by means of a non contact laser displacement sensor) dramatically changed, leading to uncertainties close to 50% of the estimated final value.

To solve this problem two triangulation non contact laser displacements were employed (Photo 3), their major cost and the reduced resolution are compensated by the adopted methodology which allows for measurements close to the node, but not exactly at the node, and

by the fact that no transducers are fixed to the cable at all (the same kind of transducers also measures the antinode vibration).

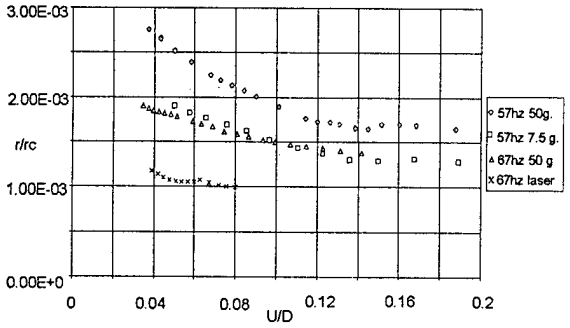

Figure 5 - Influence of the transducers on the PM measurements

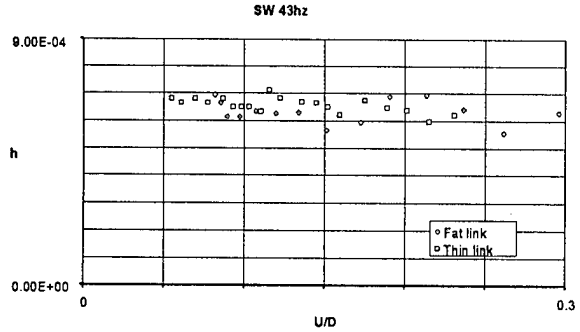

Figure 6 - Self damping with different links

This has also been the occasion for a critical review of some other aspects concerning the measurement method: some tests have been aimed at defining the influence of the exciter and its links to the cable. The link between the cable and the exciter has been created by means of a leaf spring: this should be soft enough to dynamically uncouple the cable from the forcing device, but stiff enough to give a proper excitation to the cable: in the case of the ADSS low stiffness beams were enough to give a good excitation: fig.6 shows a comparison between two beams with a 2:1 stiffness ratio for the frequency of 43 Hz with the ISWR method: it is noted that while the obtained h values are quite similar, the soft link does not allow for the reaching of sufficiently high amplitudes.

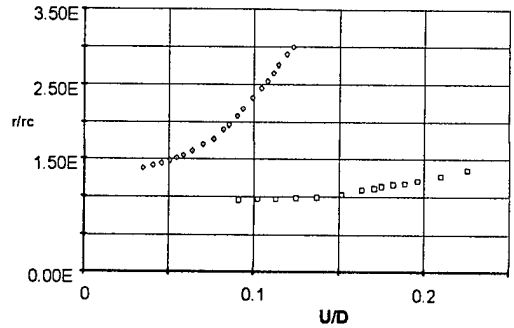

Figure 7 - PM influence of the exciter on the measurements

On the other hand the exciter itself could be a major part in the overall uncertainty. During the tests two different exciting devices have been used, the first was known to have a resonance around 50 Hz, the second which was a stiffer one exhibited no natural frequencies around 50 Hz: fig. 7 shows the comparison at the 51 Hz cable natural frequency (PM) in which a sharp difference is noted, leading to systematic effects which could get to dramatic differences greater than 300% between the two solutions.

A final step consists in a preliminary uncertainty analysis on the ISWR method aimed at knowing which could be the most critical measurement in the whole chain. At this first stage the analysis has been performed through analytical simulation of the real span by means of the model described in [12][18] and simulating measurements affected by reasonable uncertainties of one parameter at a time. In this case the analytical model has been considered the reference, affected by no uncertainty. The considered parameters have been the antinode position, the antinode vibration amplitude, the resolution of the laser displacement transducers, their distance. A time history corresponding to a virtual measurement has been generated starting from the numerical model described in [12] [18]; for each of the virtual sensors a known error has been introduced. The output of the numerical simulation has been passed to the normally used ISWR routine to analyze the results.

While the antinode position and the relative distance between the two sensor doesn't seem to affect the final result, in the next Table 1 is shown how an error on the antinode vibration amplitude significantly changes the self damping estimation.

Vibr. Mode	12	24	36
Error on the vibration Amplitude	Error on the self-damping		
-5%	+5%	+5%	+5%
-10%	+11%	+11%	+11%
-30%	+43%	+43%	+43%

Table 1

As can be seen from the table an uncertainty of 30% in the measure of the antinode vibration amplitudes leads to a more than 40% over estimation in the self damping which is not acceptable (the 30% uncertainty is the one estimated due to the presence of the accelerometer at the antinode).

The complete results of the standing wave method measurements will be shown in the next paragraph.

SELF DAMPING OF THE ADSS CABLES: RESULTS

Results concerning an ADSS and an OPGW cable will be shown for comparison. The main features of the two cables are reported in Tab.2. Results have been obtained for a constant tension, so the dependence from this parameter has not yet been investigated.

Cable	Mass [Kg/m]	Diam. [mm]	U.T.S. [kN]	E [kN/mm^2]
ADSS	0.27	16	62	15.3
OPGW	0.59	13.8	85.8	198.6

Tab 2 - Main features of the considered cables

According to the standard statements, Figure 8 shows the power dissipated per meter Vs non-dimensional vibration amplitude (i.e. the antinode vibration amplitude divided by de cable diameter) for the ADSS cable. For a comparison, the same value for an OPGW cable is shown (Fig.9). The diagram with logarithmic scales, however, compressing the measured values, seems to be not so suitable for giving the detailed trend of the cable self damping, as a function of frequency and amplitude. To get the same results in a more effective way, the non dimensional damping parameter has been plotted against the non dimensional vibration amplitude (u/D) in figure 10 for the ADSS cable, and in figure 11 for an OPGW.

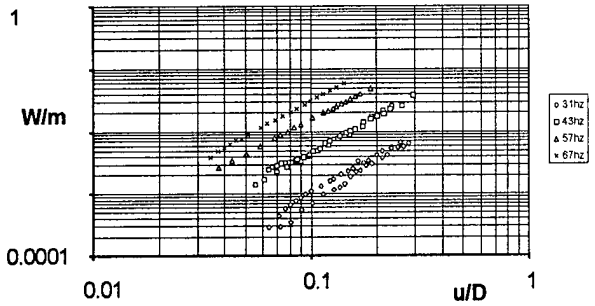

Figure 8 - ADSS Dissipated power Vs non dimensional vibration amplitude

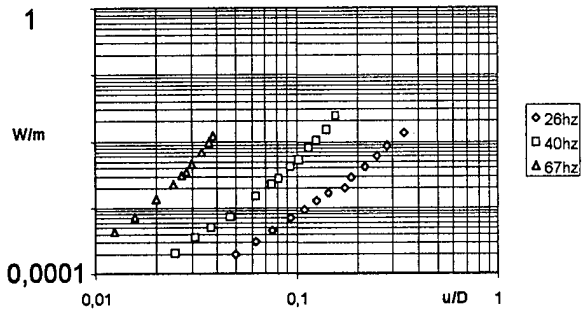

Figure 9 - OPGW Dissipated power Vs non dimensional vibration amplitude

As can be seen in the graph, the self-damping of the ADSS grows with frequency and tends to be constant with the antinode vibration amplitude. Although the order of magnitude is the same in the case of the ADSS and of the OPGW, the main difference consists in the fact that the ADSS damping has not a sharp dependence upon the antinode amplitude of vibration as in the case of the OPGW.

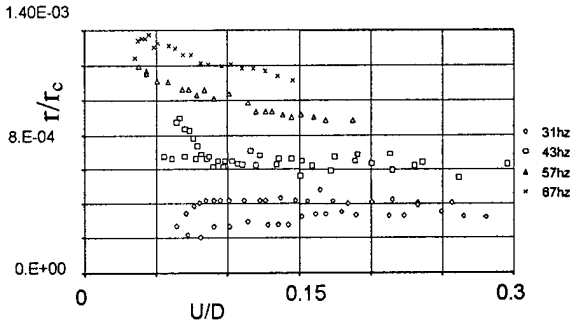

Figure 10 - ADSS Self damping h Vs u/D

Although the non dimensional damping is more or less the same for the ADSS and the OPGW, the energy dissipated by the ADSS cable is lower, due to its lower mass per unit length, as shown in the following formula:

$$P_{DISS} = \frac{1}{2} h m \omega^3 u^2 \qquad [11]$$

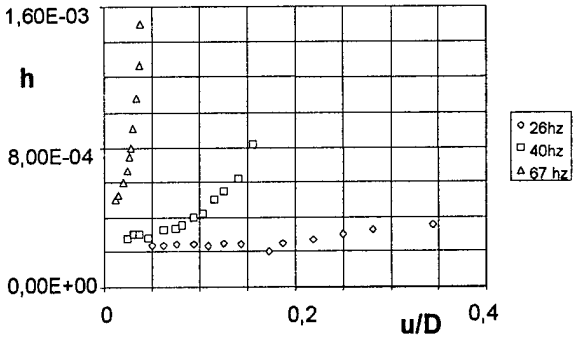

Figure 11 - OPGW Self damping h Vs u/D

As the energy due to the wind is a function of the cable diameter, while it is independent from its mass per unit length, the ADSS cable is expected to behave worse than the OPGW.

The first numerical simulation had therefore to be run: as the cable is modeled as a homogeneous tensioned beam, the flexural stiffness had to be estimated by means of proper experimentation (due to the particular kind of cable no numerical approximation has been considered possible).

ADSS CABLES MECHANICAL STIFFNESS

A set of experimental measurements has been performed to determine the ADSS flexural stiffness. Considering the cable as a tightened beam the natural frequencies of the span can be expressed in the form:

$$\omega_n = \omega_0\sqrt{(1+\alpha n^2)} \qquad [12]$$

where:

$$\alpha = \frac{EJ\pi^2}{Sl^2} \text{ and } \omega_0 = \frac{n\pi}{l}\sqrt{\frac{S}{m}}$$

By forcing the cable to vibrate under resonance condition, it is possible to get the needed EJ stiffness from the formula:

$$EJ = \frac{S}{\left(\frac{n\pi}{l}\right)^2}\left(\frac{\omega_n^2 m}{S\left(\frac{n\pi}{l}\right)^2} - 1\right) \qquad [13]$$

where the measured values are the tension S and the natural circular frequency ω_n.

The results of the tests performed on the ADSS cable are shown in the figure 12, together with the interpolation of the experimental data.

The EJ of this class of cables is very sensitive to frequency and this should be taken into account when calculating mechanical stresses.

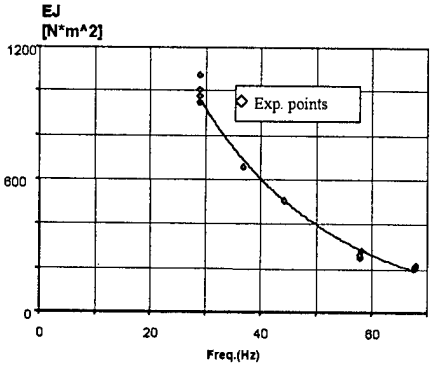

Figure 12 - EJ of the ADSS cables Vs frequency

Although a numerical simulation is going to be fully developed in the paper "**The Phenomenon of aeolian vibrations for ADSS cables**", some first results are considered here, before going to the essential results of a fatigue test. Having the needed EJ and damping it is possible to simulate the behavior of a real span 400 m long, where the only damping taken into account is the one of the cable, being the end span and armor rods losses a minor part of the global dissipation. The results of this simulation are shown in fig. 13 as amplitude of vibration Vs frequency, for a wind speed of 0-10 m/s.

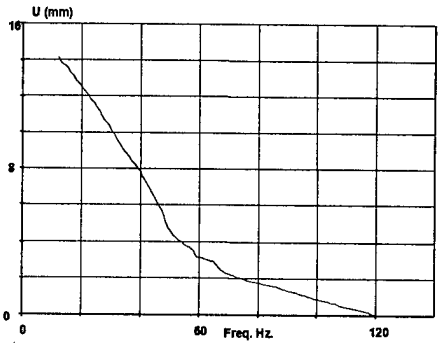

Figure 13 - Amplitude of vibration at antinode Vs frequency

The vibration levels are rather high; it is noted that for a frequency of approximately 55 Hz the vibration levels are of 4 mm, that is a peak-to peak level of about half diameter: this value is very close to that provided by the standard proposal IEEE P1222, about the fatigue test procedure for the ADSS cables.

FATIGUE TEST

The fatigue test has been run according to the proposed IEEE P122 standard. The cable has been kept vibrating for 10^8 cycles at ½ diameter peak-to peak. The testing span has been set-up according to the specification of the IEEE document and is represented in figure 14.

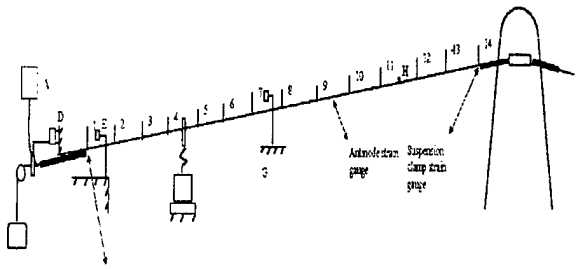

Figure 14 - Testing span

To fulfill the geometric requirements of the standard a suspension clamp was placed at the height of 190 cm to grant the correct inclination of 1.75±0.75 degrees with respect to the horizontal line.

The control parameter, that is the antinode vibration amplitude, has been kept constant through all the testing duration as can be seen from figure 15

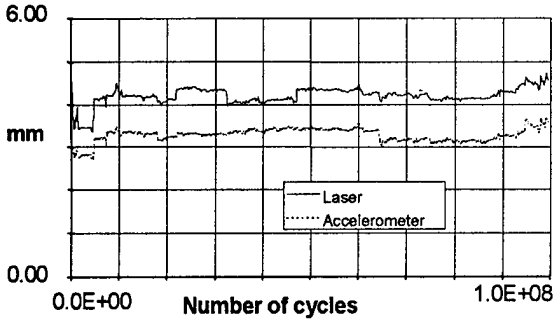

Figure 15 - Antinode vibration amplitude Vs number of cycles

To measure the strain level in the cable, three strain gauges were glued at the following position:

1. Immediately out of the preformed rods at the suspension clamp.
2. Antinode of the vibrating cable
3. Immediately out of the preformed rods at one span end

The strain levels observed during the test are shown in the next three graphs.(Figures 16-18)

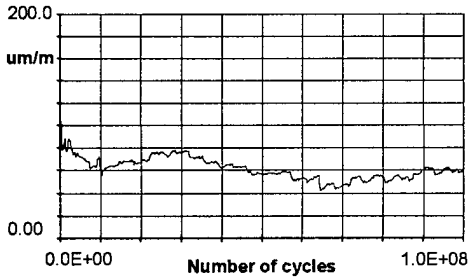

Figure 16 - Strain at the antinode

The optical performance of the cable has been monitored during all the test by means of a controlled light source and optical power meter.

The fibers were connected in a close loop to respect the minimum length required from the standards.

No significant attenuation change have been monitored during all the test duration.

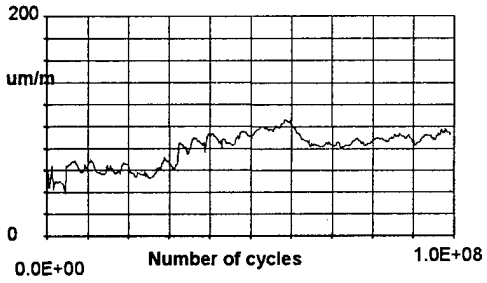

Figure 17 - Strain at the suspension clamp

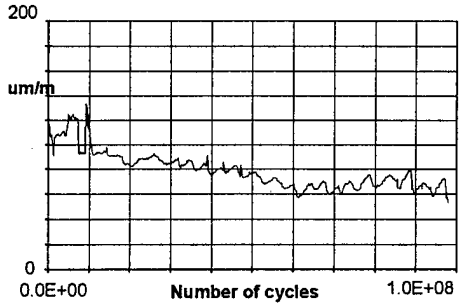

Figure 18 - Strain at the end clamp

Even if the cable fully passed the test it seems that the super imposed vibration amplitude is too severe. In a normal installation the damping introduced by the armor rods and other additional devices (Stockbridge dampers etc.) will reduce the vibration level the cable will be subjected to.

As a matter of fact the new proposal of standard recently discussed at the CIGRE meeting in Milan in June 1998, demands for testing at 870 mm/s antinode amplitude velocity (2.77 mm in displ. Amplitude at 50 hz) which is well below the 4 mm amplitude limit at which the described fatigue test has been carried out.

CONCLUSIONS

The dynamic behavior of ADSS optical cables is different from the behavior of traditional aerial metallic cables: this is mainly due to the ADSS higher rate of working tension to mass per unit length. A detailed study, with experimental test and numerical simulations, is performed on ADSS cables, in order to highlight the difference with metallic conductors. New methods to define the cable self damping have been considered to produce reliable and repeatable results, while the dynamic features of the cable are estimated by means of the natural frequency analysis.

The study confirms that the ADSS cables face the problem of aeolian vibrations caused by the vortex shedding phenomenon, but they have a range of critical parameters completely different from that of traditional metallic conductors or OPGW.

References

[1] IEEE -"Guide on Conductor Self-Damping Measurements-Std. 563-1978

[2] CIGRE WG22 -"Guide on Conductor Self-Damping Measurements-Electra N°62

[3] C.B.Rawlins-"Notes on the Measurements of Conductor Self-Damping"-Alcoa Report N°93-83-4

[4] D.U.Noiseux, S.Houle, R.Beauchemin -"Study of effective aeolian wind power imparted to single conductor spans"-CEA Project 146 T 328 - 1986 -

Proc.Int.Symposium on Overhead Conductor Dynamics - Toronto - 1981
[5] J.S.Tompkins, L.L.Merril, B.L.Jones -"Quantitative Relationships in Conductor Vibration Damping"-AIEE Winter General Meeting, New York, 1956 .Paper 56-212
[6] G.Diana, F.Cheli -"Dinamica e Vibrazioni dei Sistemi Meccanici"-UTET Libreria
[7] CIGRE WG11 -"Conductor Self-Damping"-August 1994
[8] R.Claren, G.Diana -"Mathematical Analysis of Transmission Line Vibration"- IEEE Summer Power Meeting 1967, Portland 1967, 31-C-83
[9] D.U.Noiseux -"Similarity Laws of the Internal Damping of Stranded Cables in transverse Vibrations"- IEEE T&D Conf.&Exp., Dallas, Sept.1991
[10] J.A.Nelder, R.Mead -"A Simplex Method for Function Minimization"- Computer Jnl - Vol.7, pp 308-313
[11] R.Claren, G.Diana -"Dynamic Strain Distribution on Loaded Stranded Cables"- from IEEE TRANSACTION ON POWER APPARATUS AND SYSTEMS Vol.PAS-88, N°11, Nov.1969, pp 1678-1690
[12] IEEE -"Standard Construction of Composite Fiber Optic Overhead Ground Wire (OPGW) for Use on Electric Utility Power Lines"- Std. 1138-1994
[13] IEEE -"Standard for All Dielectric Self Supporting Fiber Optic Cables"-Draft IEEE
[14] CIGRE SC22 WG11-TF1 Aeolian Vibration of single conductors
[15] Emil Simiu, R. H. Scanlan - "Wind Effects on Structures: Fundamentals and applications to design" – John Wiley and sons, 1996 N.Y.
[16] G. Diana, R. Claren "Vibrazioni nei conduttori", L'energia elettrica 1966
[17] CIGRE TF1 WG 22.11 "Modeling of aeolian vibration of single conductors: assessment of the technology.
[18] IEEE G. Diana M. Falco A. Cigada A. Manenti On The Measurement of Over Head Transmission Lines. Conductor Self-Damping. (to be published).

Authors

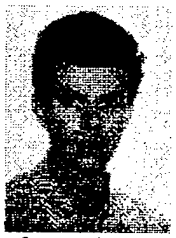

Alfredo Cigada: born in 1965, mechanical Eng. Degree in 1990, PhD in mechanical engineering in 1994, Researcher in Mechanical Measurements since 1992. His research works are in the field of fluidoelasticity, vibration problems of overhead transmission line conductors and railway vehicle dynamics, interaction between pantograph and catenary.

Marzio Falco: born in 1942, mechanical Eng. Degree in 1967, Professor of Applied Mechanics since 1983, Professor in Mechanical Measurements since 1993. He is responsible for the laboratory activities of the Department of Mechanics of Politecnico di Milano and director of the Calibration Center of the same University. His research works are in the field of fluidoelasticity, rotordynamics, vibration problems of overhead transmission line conductors and railway vehicle dynamics, dynamic behavior of undersea structures and interaction between pantograph and catenary. He is author of more than 50 papers in the above mentioned subjects.

Marcello Vanali: born in 1970, mechanical Eng. Degree in 1998 is attending the Department of Mechanics of Politecnico di Milano for researches concerning the cable dynamics.

Ralph Sutehall is a Senior Engineer with the Communication Division of Pirelli Cables in the UK, where he is responsible for installation development. He has been working with fiber optic cables for 24 years and is an active member of the CIGRE working group on fiber optics.

Paolo Marelli was born in Cantù (Como) in 1954. He graduated in Chemical Engineering from Politecnico di Milano in 1979 and joined Pirelli in 1980. Since 1987 he is involved in the Research and Development on terrestrial and aerial optical cables.

Enrico Consonni was born in Seregno (Mi) in 1964. He graduated in Aeronautical Engineering from Politecnico di Milano in 1991 and joined Pirelli in 1991,where he has been engaged in research and development of TLC cables, dealing mostly with environmental test, cable design and manufacturing technology

A NEW GENERATION OF OPTICAL MODULE : A COMPOSITE LOOSE TUBE

F.Legros, E.Kertscher, B.Buluschek.
SWISSCAB. Yvonand, Switzerland.

ABSTRACT

A new generation of optical module has been developed and its main advantages are reviewed. The processing conditions have been developed so to maximize reliability, productivity and flexibility.

The module consists in a composite (polymeric- metallic) loose tube which main advantage is that it permits to guarantee a very precise and regular control of excess length.

Several uses of this module may be expected but most interest arises from the Optical Power Ground Wire field.
In the frame of lowering costs of such optical cables, this design is a significant improvement since a single processing operation allows production of the optical core.
Reliability of optical cables is a crude point, especially when these are used in harsh environments. This is for example the case of OPGW cables, which are difficult to install, and subject to extremely severe environmental conditions (wind, ice, high temperatures due to lightening induced electrical currents,...). Consequences of lack of reliability are catastrophical especially because of cost of replacement.
The new design is a very efficient way to increase the level of reliability of such cables.

STRUCTURE AND ADVANTAGES OF THE NEW DESIGN

The module consists in a composite (polymeric- metallic) loose tube which main advantage is that it permits to guarantee a very precise and regular control of overlength. Inner layer is polymeric, outer layer is metallic. Conventional materials are used for the loose tube (PBT, PC). The two layers are bonded through the use of a thin layer of extrudable adhesive material. This induces that when the cable is subject to longitudinal mechanical sollicitations, probability of increase of attenuation, or even breakage of fibers [2] is much lower than in the other conventional designs. More advantages concern hydrogen effects, thermo-mechanical issues, bending properties, crush resistance. The efficiency of the design concerning bending properties is especially emphasized because handlability of cable on the field is a crude point.

APPLICATION TO OPGW CABLE

Overview of OPGW designs.

A considerable number of designs have been produced. Most of them are described in reference[1] and a global comparison has been made to clarify relative advantages.

Recent trend has been to focus on densification of fibers in cables [4,8,9] .This general trend is also valid in the OPGW context [3,6]. Since central tube permits such a densification, this has been the most significant observable evolution. A combination with the ribbon concept leads to very high densities of fibers.

New design applied to OPGW

Versatility of process permits to realize most advanced designs of modules. Two ways are to be considered : (i) fibers are grouped in bundles and identification is made by colored binders (ii) ribbons are stacked in matrix and identification is made by marking.

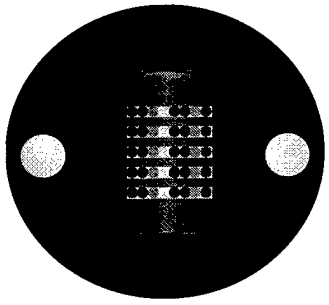

Fig.1. Densification of optical cables through central tube and ribbons (generic approach)

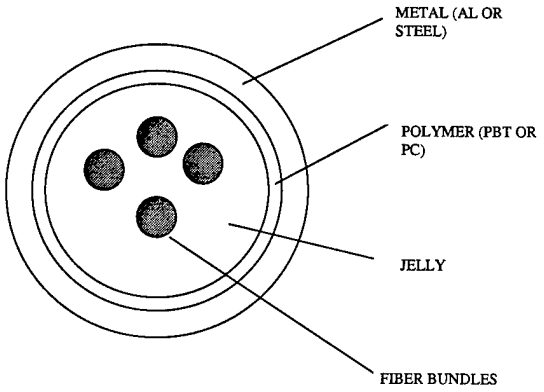

Fig.2. New optical module design (fiber bundle case)

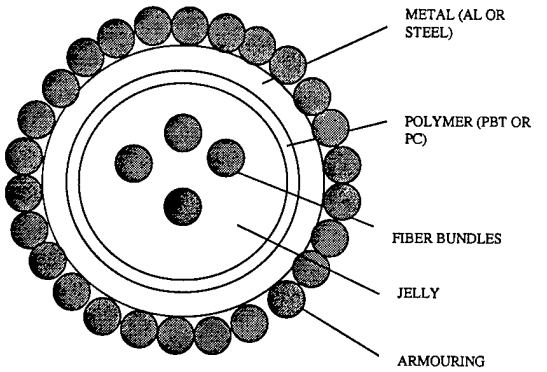

Fig.3. Outer armoring of OPGW new design (one layer case)

This central composite loose tube is armored so to respect OPGW specifications. Conventional armoring is made using of either one or two layers. In this last case :
- first layer : steel wires (galvanized steel wires or GALFAN or ACS)
- second layer : aluminum alloy

Processing conditions

The global idea is to superpose and combine major recent improvements in optical tube and forming-welding fields. The line simultaneously realizes the two following functions (i) extrude plastic tube with jelly and fibers (ii) cut, form and weld metal tape. The gluing material is co-extruded with plastic layer which constitutes the loose tube.

Comparison with available processing conditions

The main difficulty with metallic unitubes is to have under control overlength of fibers [1]. A considerable amount of energy has been spent so to achieve the necessary minimal dispersion of overlength. Use of SZ stranding of fibers, incorporation of the tube in the layer of ACS wires have been proposals so to get correct results. One difficulty focuses on the reliability of welding thin thickness of metal.

Welding. Influence on product

The ability to weld thin metallic pieces is most critical issue. Continuous processing and reliability of processing have been researched and all potential impact on product quality have been reviewed.
A smooth surface is required so that no breakage of fiber may occur. If welding results in remaining pieces of material breakage can occur. The fact that plastic layer is surrounding the optical fibers prevent risk of breakage due to sharp edges of metal.

The laser technique has proved to be very successful [5] in the composite tube application where thin metallic layers are involved (down to 0.1 mm of steel). This technology has been extended to optical composite unitubes. Moreover, handling of metallic tapes (cutting at precise dimensions, compensation of rotation effects of the edge to edge position) have been applied to processing equipment so to increase reliability of long lengths of optical modules production.

Cable specifications

In the OPGW field, major issues are :
- low attenuation
- crush resistance
- compacity
- reliability

Overlength of fibers

The excess length is the well known most critical issue in the optical cables. In the context of metallic loose tube, a precise control of overlength is known to be difficult. This question becomes to be critical with the central tube design since excess length has to be generated directly. A final value (measured on final cable) is searched up to 8 per mil, with a dispersion as low as possible around the average value.

The fundamental advantage of the new design is that overlength is generated in the plastic tube extrusion part of the process, where a very precise control is possible.

Moreover, contactless on-line overlength measurements are now available so that

overlength stability is checked at any time during the production process.

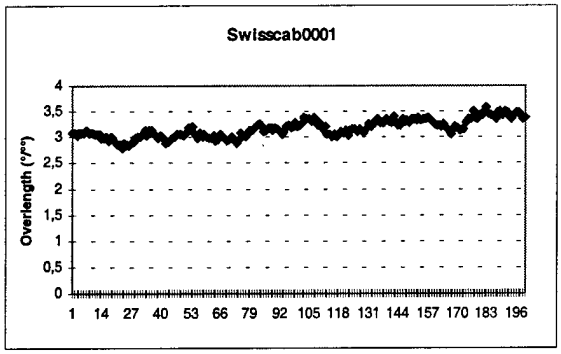

Fig.4. On-line excess length measurement process during optical module production

Mechanical properties of central loose tube

Several parameters have to be simultaneously optimized :
- compression resistance
- bending properties
- dilatation coefficient
- temperature resistance of tube

Aluminum or steel ?

Since wires have an aluminum superficial cover (typically an alumoweld composition is used), the use of Al for central tube is an advantage so to prevent from corrosion. Conventionally, nominal thickness of Al around 1 mm is available on the market (down to 0,4mm for steel) and this is considered as an advantage since a better protection of fibers is thus obtained. Technology is available so to either use Al or Stainless Steel. In last case, Steel may be sheathed with a superficial coating of Al. The new design permits to reconsider this point.

How to optimize compression resistance of central tube ?

Advantage of the new design is that it permits to tune physical performance of the central tube. A standard realization is illustrated hereinafter where 4 mm central tube has been considered for analysis. A PBT layer which thickness may be adapted is taken as reference.

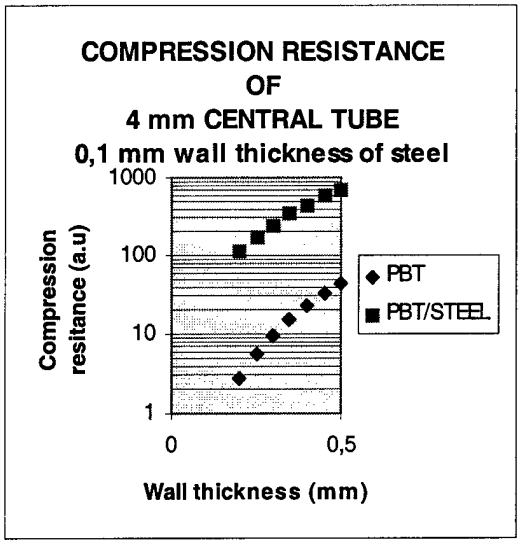

Fig.5. Compression resistance of 4 mm central tube

This is tested according to IEC 794-1 with goals up to 700 daN/100 mm.

Temperature due to short-circuit.

Determination of real temperature surrounding the fibers is a complex question. An interesting approach has been developed in including doped temperature dependent fibers [7]. Design with a XLPE sheath surrounding the optical module has been proposed with results up to 140 °C (20 kA rms for 450 ms) without increase of attenuation. Since PBT has a fusion temperature around 220 °C, a stronger behavior is expected. More stringent requirements may be also needed (up to 400 °C). However, such high temperatures are to be carefully studied especially because of risky effects on the cable sag. Nominal temperatures around 200°C are recommended for that reason. Simulation is based upon duration of heat transfer to materials, according to requirements deduced from lightening effect.

Jelly

Minimal requirements are similar to conventional optical cables : easy processability, viscosity range consistent with ability of fibers to move in the operating temperature range. Has to be added resistance to high temperature during short time. Jelly compounds are available on the market so to withstand flash point of more than 240 °C.

Hydrogen effects

This issue has been extensively studied [10] .On current basis, risk is minimal in a central tube

because fibers are surrounded by an isopotential voltage. No electrolytic effects are expected in the optical module.

Low attenuation

Since OPGW have to operate in a broad range of temperature, low attenuation, especially at low temperatures is required. The fact that polymer contracts may be a cause of high attenuation. In the case of the new design, polymer dilatation/contraction is canceled by adhesion to metal. The new design thus leads to very low attenuation changes, even at very low temperatures.

Following table summarizes advantages of the new design in an OPGW application.

Structure	Low attenuation	Reliability	Compacity	Crush resist.
Tight structure	--	---	++	-
Stranded polymeric loose tubes	++	+++	--	-
Polymeric slotted core	++	-	--	+
Central polymeric loose tube	++	+	++	-
Stranded steel loose tubes	++	+++	+	++
Central steel loose tube	+	+++	+++	++
Stranded polymeric loose tubes in aluminum slotted core	++	+++	+	+++
Central composite loose tube	+++	+++	+++	++

Table 1. Global comparison of OPGW cable structures (extended from [1]).

CONCLUSION

Use of the new design is **much more general than the OPGW case**. Direct buried cables, Industrial Network cables are examples of structures which can take advantage of this new optical module.

The composite loose tube:
- **increases reliability of cables**
- **permits to meet strongest requirements**
- **is consistent with cost reductions**
- **is broad range applicable**
- **is open to new generations of cables**

References

[1] Optical Ground Wire. A worldwide technical survey and comparison. Bonicel et al. Alcatel Cable. IWCS 1993, pp 42-47

[2] Fiber strength and lifetime. Siecor. 1997

[3] Design and test of a new metallic fibre-optic cable for aerial cable ways. A.Fargahi et al., IWCS 1993, pp 182-188

[4] Design and performance of a high-capacity, compact, modular ribbon cable comprising 24 fiber ribbons. IWCS 1996, pp 623-630

[5] Comparison of performances of welding processes. B.Buluscheck-F.Legros, Swisscab, May 1998

[6] Development and Design for Optimizing High-Count OPGW. IWCS 1997,C.H.Jung et al., pp 609-616

[7] Development and Characterisation of a New Dielectric Cored OPGW. Transfil Europe n°42, A.Stringer et al., pp 34-43

[8] Applications of Central Tube Designs in Fibre-Optic Cables, L.Faltin et al., Wire & Cable Asia, pp 79-82, January-February 1998.

[9] Optical fiber ribbon cable designs for a wide range of applications as the availability of FTTH is realized. IWCS1996. F.Legros et al. pp.340-352

[10] Hydrogen Effects In Optical Fiber Cables : a New Approach By Direct Pressure Measurement. IWCS 1991.B.Missout et al. pp 653-662.

François Legros is Industrial Development Manager in Swisscab. He previously worked as R&D Product Senior Manager in cable manufacturer Acome.

F.Legros
SWISSCAB S.A.
Rue de l'Industrie 5. CH-1462 Yvonand
Tel. +41 24 4300 104
Fax. +41 24 4300 124

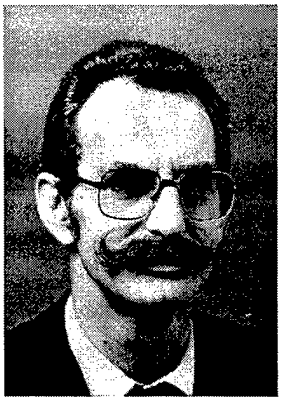

Bruno E. Buluschek graduated in mechanical engineering at the Technische Hochschule, Munich. In 1968, he started as a research engineer at the Federal Institute of Technology in Zürich, Switzerland, and received his Ph.D. in 1979. He joined Maillefer SA where he was in charge of the R&D Department and of Extrusion Department. In 1988 he started his own engineers office and is now working in the Industrial Development Department in Swisscab.

Dr.-Ing.Bruno E.Buluschek
SWISSCAB S.A.
Rue de l'Industrie 5. CH-1462 Yvonand
Tel. +41 24 4300 160
Fax. +41 24 4300 124

Eberhard Kertscher is Directing Manager of Swisscab, which he created in 1982. He previously worked in Maillefer SA and Rosendhal.

E.Kertscher
SWISSCAB S.A.
Rue de l'Industrie 5. CH-1462 Yvonand
Tel. +41 24 4300 120
Fax. +41 24 4300 124

Development of High Count Optical Wrap Cable around Overhead Ground Wire

Noboru Okada[1], Yoshiki Higashide[1], Yoshihisa Rintsu[1], Akihiko Ishikawa[1], Shigeru Ibuki [1],Shinichi Tanaka[2]

[1]THE FURUKAWA ELECTRIC CO., LTD.
Ichihara, Chiba, Japan
[2]CHUBU ELECTRIC POWER CO., INC.
Nagoya, Aichi, Japan

ABSTRACT

We have developed high-count optical cable to wind around overhead ground wire to cope with future increase in demand for communication.

The cable of 24fiber structure to use for the directly grounded neutral system has been applied as practical use so far.

We considered two types of optical fiber cables corresponding to the construction environment this time, and did the design of the 48fiber structure, manufacture and evaluation.

It could be put to practical use as for the production cable because of that there were good characteristics against each examination.

1. INTRODUCTION

As for optical wrap cable overhead ground wire, it points at a cable which exclusive winding machine is used to wind cable way around existing overhead ground wire.[1]

Therefore the cable is required the characteristics to withstand severe environment as same performance as OPGW.[2]

We have the design to realize high density, high count and restrained cable weight, which is no reinforcement of existing steel tower caused by increase of cable weight.

2. CABLE DESIGN

2.1 Cable diameter

A cable is considered with an influence on the steel tower strength due to the increase in the wind pressure load after the construction into consideration to use existing ground wire.

A wind pressure load to act on the ground wire can be found by the wind pressure load of around the unit area and the projection area of the ground wire.

However, the actual amount of increase in a wind pressure load in the utility territory is smaller than the calculation from the projection area.[3]

Therefore deciding a cable outside diameter, we researched the amount of increase of the wind pressure load by the wind tunnel experiment.[4]

Wind pressure load increase quantity (CD1/CD0) was found in the ratio with drag coefficient (CD0) only with the ground wire and drag coefficient (CD1) after a cable was wound.

Drag coefficient C is calculated the measurement value T of the wind pressure load by using equation (1).

$$C = \frac{2T}{\rho V^2 DL} \qquad (1)$$

Where:

T: Wind pressure load L: cable length
D: cable outside diameter ρ : air density
C: drag coefficient V: velocity of the wind

Figure 1 shows the result of the wind tunnel experiment when a cable is wound in the

ground wire (AC55mm ^{2}).

The amount of increase of the wind pressure load depends on the outside diameter and the winding pitch of the cable.

In a word, the upper limit 1.1 of the amount of increase in a wind pressure load is satisfied if the outside diameter of the cable is made 5mm and wound in less than a pitch 450mm.

In the case of the additional ground wire size (AC 260mm^2), the amount of increase in a wind pressure load is satisfied if the outside diameter of the cable is made 6mm and wound in less than a pitch 500mm.

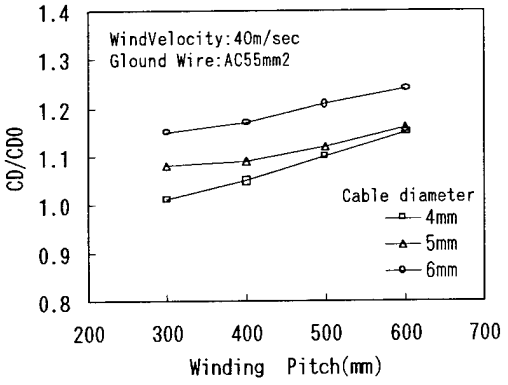

Fig.1 Wind load dependency on winding pitch

2.2 Ground wire and cable environmental temperature

It is necessary that the cable has an excellent transmission characteristic into high temperature and heat shock.

It is required that design of cable structure should be appropriate against two types of ground wire which is applied different temperature condition shown in table1.

Table1 Type of ground wire and temperature condition

Ground wire	AC55mm^2	AC260mm^2
Outside diameter	9.6mm	21.0mm
Maximum Temp.	120°C	300°C

As for resistance grounded neutral system that AC 55mm2 represents it, applicable temperature is low.

But, It must be made the cable thin because increase in a wind pressure load must be restrained.

As for directly grounded neutral system of AC 260mm^2, applicable temperature is high.

However, a cable outside diameter compared with resistance grounded neutral system can be made thick.

2.3 The structure of cable

The cable structure is applied the stranded unit type twisted 8 units which is consisted of 6 fibers in each unit to be common unit structure of existing cable.

The structure of the 48fiber cable is shown in figure 2.

The two types of cable is considered to satisfy a condition as below:

1st: Resistance grounded neutral system is used 0.25mm UV resins coated fiber to realize small outside cable diameter.

2nd: Directly grounded neutral system is used 0.4-mm silicon resin fiber to withstand severe high temperature compared with resistance-ground wire.

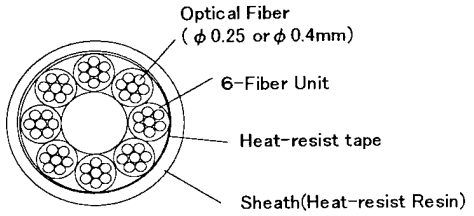

Fig2. The structure of the 48fiber cable

3 CABLE STRAIN

The cable is wound around the ground wire in accordance with direction of twist in the ground wire. Where, a strain is loaded 1 twist/1pitch in the cable.

The reliability of fiber is calculated by cable strain, which was applied after wound and environmental condition on the ground wire.

3.1 Winding strain after cable wound

The fiber strain ε to wind a cable is shown with the equation (2).

$$\varepsilon = \varepsilon_{et} + \varepsilon_{eb} + \varepsilon_{b} \qquad (2)$$

Where:

(ε_{et}) Shows elongation strain by twisted cable.

(ε_{eb}) Shows elongation strain by bent cable

(ε_{b}) Shows fiber bending strain.

The cable dimension is shown in figure 3.

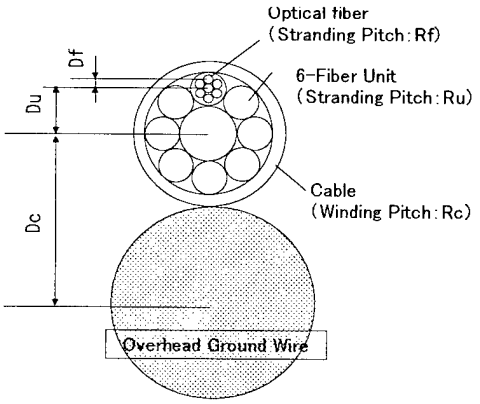

Fig.3 Cable dimension

3.1.1 Elongation strain by twisted cable

The stranding fiber pitch into unit and unit pitch into the cable is changed by cable wind around ground wire.

At this time, the elongation strain by twisted cable is calculated as below:

$$\varepsilon_{etu} = \left(\frac{p_u}{p_{u'}}\right)\sqrt{\frac{p_{u'}^2 + (2\pi D_u)^2}{P_u^2 + (2\pi D_u)^2}} - 1 \qquad (3)$$

$$P_{u'} = \frac{L_c}{\left(\frac{L_c}{P_u}\right) + 1} \qquad (4)$$

$$L_c = \sqrt{P_c^2 + (2\pi D_c)^2} \qquad (5)$$

Where:

ε_{etu} : Unit elongation strain by twisted cable

$P_{u'}$: Change of unit pitch after wind

L_c : Cable Length of 1 pitch

$$\varepsilon_{etf} = \left(\frac{P_f}{P_{f'}}\right)\sqrt{\frac{P_{f'}^2 + (2\pi D_f)^2}{P_f^2 + (2\pi D_f)^2}} - 1 \qquad (6)$$

$$P_{f'} = \frac{L_u}{\left(\frac{L_u}{P_f}\right) - 1} \qquad (7)$$

$$L_u = \sqrt{L_c^2 + (2\pi D_u)^2} \qquad (8)$$

Where:

ε_{etf} : Fiber elongation strain by twisted cable

$P_{f'}$: Change of fiber pitch after wind

The cable becomes short by twisted strength.

Therefore, elongation strain by twisted cable ε_{et} can be shown with the equation (9).

$$\varepsilon_{et} = (\varepsilon_{etu} + \varepsilon_{etb})\frac{\sum_j E_{u_j} S_{u_j}}{\sum_i E_{c_i} S_{c_i}} \qquad (9)$$

Where:

E_{u_j} : Young's modulus of the material which composes the unit

S_{u_j} : The area of the section which composes the unit.

E_{c_i} : Young's modulus of the material which composes the cable

S_{c_i} : The area of the section that composes the cable.

3.1.2 Elongation strain by bent cable

The elongation strain when the cable was bent is asked by the curvature of the cable and the unit.

Ideally the strain doesn't occur in fiber because the unit and fiber are moved in the stranding direction when the cable and unit are bent.

But, the cable and unit does not move perfectly, and the strain of a certain degree is left in it. (Effect on a strain relaxation: α)[5]

It define that this "effect on a strain relaxation" is used the value found from the experiment.

$$\varepsilon_{eb} = \alpha\left(\frac{D_f}{R_u} + \frac{D_u}{R_c}\right) \qquad (10)$$

Where:

R_u : The curvature of the unit

R_c : The curvature of the cable

3.1.3 Fiber bending strain

After the cable is wound, bending strain ε_b occurs on the surface of fiber.

This strain is calculated from the curvature of fiber after stranding pitch changes.

$$\varepsilon_b = \frac{1}{R_f}\left(\frac{d}{2}\right) \qquad (11)$$

Where:

R_f : The curvature of the fiber

3.2 Strain by the environment after the construction

The strain of the fiber, which an environment influence after the construction is presumed and which is added in the use period, was examined.

Though the reliability of the ground wire is designed as 36 years, cable wind is normally carried out 5 years passed since ground wire was constructed.

Table 2 shows the kind of the strain added after the construction.

Table2 Fiber Strain

Item (The kind of strain)		Strain AC55mm²	Strain AC260mm²	Time
Winding	Remaining	0.02	0.02	31y
	Elongation	εe	εe	
	Bend	εb	εb	
G.W. creeping		0.02	0.02	
Temp.	Always	0.056	0.081	31y
	Short time	0.078	0.161	345h
	Moment	0.111	0.322	410s 1900s
Weather condition	Max tension	0.098	0.068	31d
	Strong wind	0.198	0.115	1d
	Snow fall	0.196	0.065	3d

y: year, d: day, h: hour, s: second

3.3 Proof test

Screening level is designed from the strain of fiber, which it is added to after the cable construction.

Figure 4 shows winding pitch and screening level when the 5mm cable outside diameter was wound around the ground wire of AC 55mm ².

The winding pitch is more than 320mm if the upper limit of screening level equal to present OPGW (1.1 %).

On the other hand, winding pitch is less than 450mm in consideration of the load of the steel tower strength due to increase in wind pressure.

In a word, when it should be ensured 31-year reliability of the cable (fiber), the outside diameter of the cable makes 5mm if winding pitch is between 320mm and 450 mm.

It is estimated that the winding pitch was 500mm against the cable of 6mm outside diameter in case of AC 260mm ² ground wire by same way with AC 55mm ².

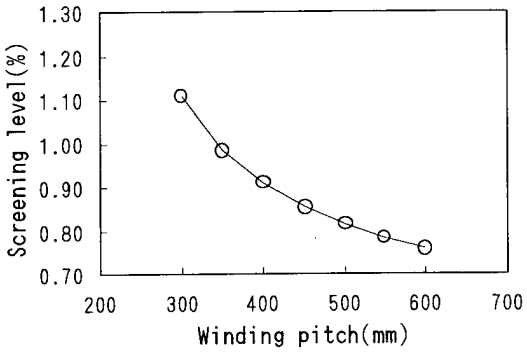

Fig.4 Relations between winding pitch and screening level

4 TEST RESULT

We carried out the evaluation, which is required from construction environment for two types of cables.

4.1 temperature characteristic

Especially, temperature characteristic is very important item in consideration of the construction environment of the cable.

Two types of specimen were a good result as shown in the table 3 even under each temperature condition.

Table3 Temperature test result

Item	Condition	Result(1310nm)
Heat Cycle	(U)-20°C～90°C (S)-20°C～150°C	Loss Increase < 0.1dB/km
High Temp.	(U)90°C 400hour (S)150°C 400hour	Loss Increase < 0.1dB/km
Low Temp	(U.S)-20°C 10hour	Loss Increase < 0.1 dB/km
Heat Shock	(U)120°C 1sec (S)300°C 1sec	Loss Increase < 0.1dB/km

U: Cable with UV Resin Coated Fiber
S: Cable with Silicone Resin Coated Fiber

4.2 Mechanical characteristic

A mechanical evaluation was carried out in consideration of the load to the cable expected of the construction.

Contents of a mechanical characteristic condition and the result are shown in the table 4.

It could confirm that it could be withstood against the mechanical load in the range of usual handling with the cable.

Table4 Mechanical test result

Item	Condition	Result(1310nm)
Tensile	0.5% Elongation	No increase Reversible
Crush	245N/50mmPlate	No increase Reversible
Bend	R150mm±180°Bend 5 Times	No increase
Twist	(1m/winding pitch) Times/m	No increase
Wind	200m Wrapping around ground wire	No increase
Vibration	Wrap around ground wire 50Hz100μm10^7Times	No increase No abrasion of sheath

4.3 Electric characteristic

Contents of an electric characteristic condition and the result are shown in the table 5.

As for which evaluation as well, it had a good result.

4.4 Thunder resist characteristic

Thunder resist characteristic of the cable is evaluated by the direct current arc examination.

Contents of a thunder resist characteristic are shown in the Table 6.

It confirmed that there was no problem about thunder resist characteristic.

Table5 Electrical test result

Item	Condition	Result
High voltage resist (Dry)	AC400kV/1.4m 1min	Good
Water resist (Wet)	Rising method	> AC222kV/1.0m
AC arc	(S) Arc current 31.5kA Arc time 0.3sec	Loss increase < 0.2dB/km No bit error
Short circuit resist	(U) Short circuit current 3.3kA 1sec G.W. temp. 120°C (S) Short circuit current 31.5kA 1sec G.W. temp. 300°C	Loss increase < 0.2dB/km No bit error

U: Cable with UV Resin Coated Fiber
S: Cable with Silicone Resin Coated Fiber

Table6 Thunder resist test result

Item	Condition	Result
DC arc	Electric charge 200C (Discharge)	Loss increase < 0.2dB/km No bit error

5 CONCLUSION

We developed that two types of cables complied with severe environment of overhead ground wire.

In view of the restrain of steel tower strength, these cable outside diameter were appropriate using 0.25mm UV coated fiber and 0.4mm silicon resin fiber.

In view of the severe high temperature condition, these cables were achieved the requirement considered with construction environment by proper cable structure.

These two types of cable could realize high density, high-count fiber and restrain of cable weight at this moment.

It is available that these cables could be supported increase in demand for multi-media communication in future.

6 REFERENCE

1 H. Yoshida et al., The Latest Techniques for OPGW, FURUKAWA Revue, 80,65,1987
2 Denkikyodoukenkyu, 45,6,1990
3 K. Yoshida et al.,:Winding Optical Fiber Cable onto Existing Ground Wire (IWCS1986)
4 A. Ikeda et al., Development of Ground Wire Optical Fiber Cable, FURUKAWA Revue, 76,43,1985
5 Y. Katsuyama et al., Bending Property and allowable Bending Radius for Unit-Type Optical Cable, J66-B, 2,203,1983

Noboru OKADA

The Furukawa Electric Co.,Ltd
6,Yawata Kaigandori,Ichihara, Chiba,290-8555, Japan

Mr. Okada received his B.E. degree in Physics from Shizuoka University in 1991. He joined The Furukawa Electric Co., Ltd and has been engaged in production engineering of optical fiber cable. He is now a engineer of the Production Engineering Section of Transmission systems Division.

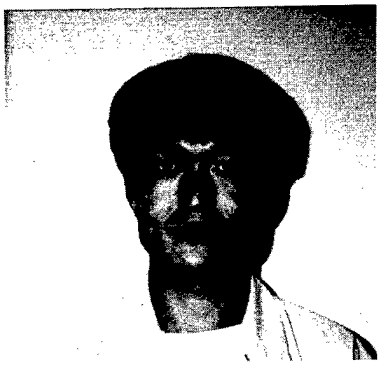

Yoshihisa RINTSU

The Furukawa Electric Co.,Ltd
6,Yawata Kaigandori,Ichihara, Chiba,290-8555, Japan

Mr. Rintsu received his M.E. degree in Applied Material Science from Muroran Institute of Technology in 1990. He joined The Furukawa Electric Co., Ltd and has been engaged in production engineering of optical fiber cable. He is now a engineer of the Production Engineering Section of Transmission systems Division.

Shigeru IBUKI

The Furukawa Electric Co.,Ltd
500,Kiyotaki,Nikkou, Tochigi,321-1444, Japan

Mr. Ibuki received his B.E. degree from Ibaragi University in 1972. He joined The Furukawa Electric Co., Ltd and he is now a engineer of the GWWOP Project Team of Bare Wire and Cable Division.

Akihiko ISHIKAWA

The Furukawa Electric Co.,Ltd
2-6-1,marunouchi, chiyoda-ku, Tokyo, 100-8322, Japan

Mr. Ishikawa received his M.E. degree in Department of Industrial Technology from Chiba Institute of Technology in 1991. He joined The Furukawa Electric Co., Ltd and has been engaged in engineering department. He is now a engineer of Transmission systems Division.

Shinichi TANAKA

CHUBU ELECTRIC POWER CO., INC.

1,Toshin-cho,Higashi-ku,Nagoya,Aichi,461-8680, Japan

Yoshiki HIGASHIDE

The Furukawa Electric Co.,Ltd
6,Yawata Kaigandori,Ichihara, Chiba,290-8555, Japan

Mr. Higashide received his M.E. degree Tokyo Institute of Technology in 1995. He joined The Furukawa Electric Co., Ltd and has been engaged in production engineering of optical fiber cable. He is now a engineer of the Production Engineering Section of Transmission systems Division.

FIBRE OPTIC LASHED CABLES ON HIGH VOLTAGE LINES

Ralph Böhme, Reinhard Girbig, Georg Hög

Alcatel Kabel AG & Co, Mönchengladbach, Germany

ABSTRACT

Worldwide Optical Ground Wire (OPGW) and All Dielectric Self Supporting cable (ADSS) have been established by power utilities as standard fibre optic cables for their networks on high voltage lines. The fast increasing demand for optical telecommunication cables has lead to new needs for inexpensive and fast installable fibre optic cables for applications on high voltage lines.

A possible solution is the attachment of optical fibre cable to ground wire or phase conductor, the so called Optical Attached Cable (OPAC). Out of the different solutions the All Dielectric Lashed cable (ADL) has been chosen due to its simple cable design and installation flexibility.

The paper presents the cable design, installation techniques including equipment and accessories and field experiences on 110 kV ground wire and 15 kV phase conductor installations.

INTRODUCTION

Deregulation and new services have increased the need for fibre optics everywhere. For power utilities planning new lines the best technical and economical solution is using OPGW or ADSS on lines without ground wire. Many high voltage lines are nowadays already equipped with OPGW and/or ADSS. As they were installed 4 or 5 years ago the fibre count of 6 to 12 of the early days is not sufficient any longer. Exchanging such an OPGW, which compared to its design lifetime of 30 to 40 years can be called new, is hardly economical. Very often the installation of additional ADSS is not possible due to ground clearance and load restrictions of the existing towers. This is one situation when OPACs can help. Installing OPAC on existing OPGW is an economical solution for fast and easy upgrade of fibre capacity without adding much additional load to the towers.

Furthermore, OPAC can be used on phase conductors when there is no ground wire, in the distribution network, as line inter-connections and as a fast installable optical link in case of line damage.

These are just a few scenarios where OPAC is a good and economical solution.

OPAC BASICS

The basic idea of OPAC on high voltage lines is to attach a light weight dielectric optical fibre cable to an existing rope, either ground wire or phase conductor.

Figure 1 shows an overview of excisting attachment techniques.[1-4]

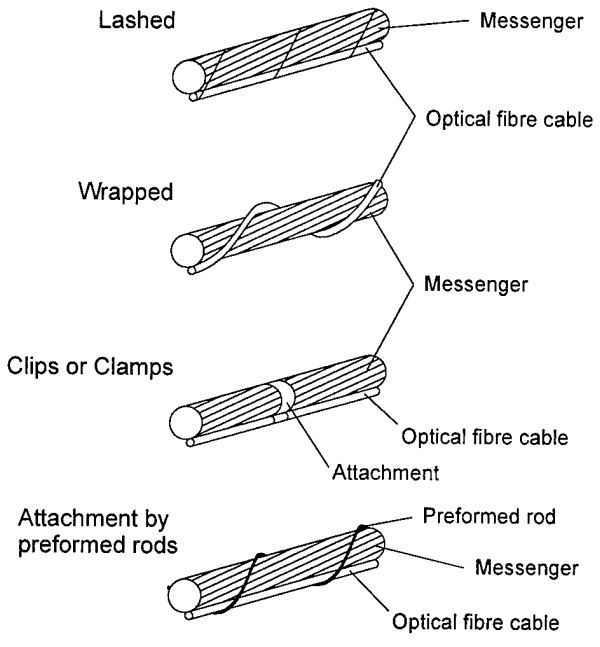

Fig. 1: OPAC Solutions

Out of these the lashed and wrapped technique are best suited for installation on ground wires, especially for long spans because the installation can be done with automative equipment.

The clipping or clamping can also be done by a machine but it has not proofed to be very reliable. Besides that the cable tends to slack which increases ice and wind load.

The use of preformed rods is very labour intensive as the rods have to be installed by hand and therefore this technique is mainly used on systems with low poles.

From the above techniques we have chosen the lashed cable technique to develop a complete system including cable, installation equipment and accessories. The main reason for this choice was that it offers more installation flexibility and allows for longer spliceless cable lengths than any other technique. Some of the major advantages are listed below:

- 3 to 6 km spliceless cable length, depending on installation technique and cable size
- Installation possible on weak poles
- Passing over lashed cable is possible
- Re-lashing possible e.g. in case of repair works
- No looping or slacking of cable over time ⇒ no increase of wind & ice load
- Good cable protection in case of lightning strike and bird attacks

In most cases the additional weight added by the cable is negligible. The wind load has no big impact on the overall load. With no wind the effective area of messenger and lashed cable is of course greater than the one for the bare messenger. This changes when the messenger swings out under wind: the effective area will decrease and will come close to the area for bare messenger.

For ice loading the situation is different. As the surface and overall diameter is increased, higher ice generation can be expected. An intense study on ice generation on a lashed system is planned for the coming winter. It will be performed at a very exposed location in the east of Germany at a test site with lots of experience on ice generation.[5]

Lashing Technique Overview

Lashing telecommunication cables to messenger ropes has been used since several years, e.g. in the U.S. mainly on specially installed steel ropes of around 10 mm diameter on low poles. All kind of telecom cables were and are attached to the messenger with stainless steel wires.

Lashing technique on high voltage lines, on the contrary, uses existing ropes and all dielectric cable and lashing binders.[6] This is because fault damage could result from broken lashing wire contacting a phase conductor along the cable route. Another reason to use dielectric lashing material is the higher tensile strength, light weight and the better resistance to corrosion and lightning strikes.

With our technique the optical cable will be lashed to the messenger with two dielectric lashing binders. Normally one binder would be sufficient, the second one is added for safety reasons. The binders are applied by a small device called Lasher.

At the beginning and end of each span the ADL cable is fixed on the messenger with a clamp which also serves as fixing for the two lashing binders.

A detailed description of the lashing devices and accessories will follow later in this paper.

CABLE DESIGN

Practically each small and light-weight dielectric optical cable could be used to be lashed to a messenger. The reason to chose a central buffer tube design is the resulting simple and cost effective cable. Taking into account the required cable performance and different installation methods a family of four cables has been developed with two different tube sizes for maximum fibre counts of 24 and 48 fibres, respectively and allowable tensile forces of 0.3 kN and 0.8 kN. Figure 2 shows the main characteristics for the two basic designs with 0.8 kN and maximum fibre counts.

The 0.3 kN type is used whenever the tensile load on the cable during installation is low, i.e. when the cable drum is in the air. For installation techniques where the cable drum is on the ground the 0.8 kN type is used to minimize the risk of cable damage. Higher tensile resistance is not advisable because the cable has to follow the messenger's movement and in the case of elongation a stronger lashed cable could cause problems.

Cable Type	ADL-D(ZN)9Y 1x24E9/125 0.8 kN	ADL-D(ZN)9Y 1x48E9/125 0.8 kN
Cross Section	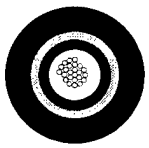	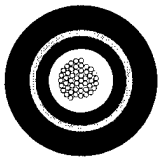
Fibre Count	24	48
Diameter [mm]	6.6	7.5
Weight [kg/km]	42	54
Rated Tensile Strength [kN]	5.3	5.3
Modulus of Elasticity [N/mm²]	102	104
Max. Perm. Working Stress (no fibre strain) [N/mm²]	216	216
Max. Perm. Working Tension (no fibre strain) [N]	800	800

Fig.2: ADL Cable Main Characteristics

Using a central buffer tube design the fibre excess length in the tube has to be adapted to the loading conditions of the messenger to reach the necessary strain window which varies from 0.3% to 0.35 %.

The use of the cable on high voltage overhead lines requires special jacket materials to withstand high temperatures either permanent in case of phase conductor or temporarely but much higher for ground wire applications during electrical faults.

For both applications appropriate jacket material has to be chosen. For phase conductor application with operational temperatures around 80 °C it is a special polypropylen blend. The same material can be used on ground wire when the resulting temperature rise during electrical fault is around 160 °C. For higher temperatures up to 300 °C a cross linked material is used.

LASHING BINDER

The lashing binder consists of multi-strand aramid yarns encased in a jacket of the same materials as used for the cable sheath for the different applications as discussed above.

It is weather-proof and U.V. resistant and has an outer diameter of 1.2 mm. Its tensile strength is 500 N.

INSTALLATION EQUIPMENT

This chapter describes the major parts of the installation equipment which consists of modified comercially available devices as well as specially developed ones. Depending on the chosen installation method they are used all together (Fig. 3) or separately. The major devices are presented as follows.

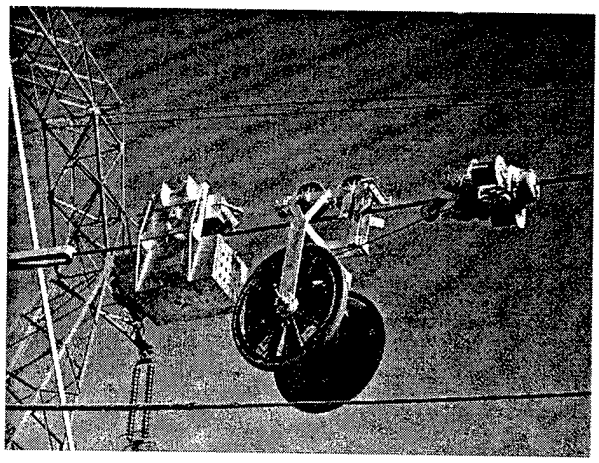

Fig. 3: ADL Installation Set on Ground Wire

Tug

Two tugs have been developed to pull the lasher and/or the cable reel. Both have gasoline engines, are remote-controlled and approved for application on high voltage lines. They are able to pass over ropes and mid-span joints of 8 mm to 50 mm diameter. Their weights are 32 kg and 58 kg capable of pulling loads of 100 kg and 300 kg, respectively.

Cable Reel and Reel Carrier

For installations where the cable reel has to be in the air, the ADL is delivered on a plastic reel. It is designed for multiple use, with a size of appr. 800 * 600 mm and a capacity of 2 km to 3 km cable length depending on the cable diameter. The specially designed Cable Reel Carrier serves as a pay-off for the ADL cable. The weight of the Reel Carrier is 30 kg.

Lasher

The Lasher is a comercially available model which has been modified to our special needs. It is capable of passing over 32 mm ropes and joints and is in the process of beeing upgraded to pass over 40 mm. It takes two spools of Lashing Binder with a capacity of appr. 1200 m, each. The overall weight including full spools is 25 kg.

The advantage of having three individual devices instead of an all-in-one is the lower weight for each individual device. This is important when moving the equipment from one side of a span to the other. Instead of lifting one very heavy equipment at a time it is easier and less dangerous to move three devices with less weight.

The other advantage is that one can use the devices independently for more installation flexibility.

Accessories

The following section lists the accessories needed for ADL installation:

- ADL Fixing Clamp
  The ADL Fixing Clamp is the general accessory used for lashed cable installation. It serves as cable and Lashing Binder fixation at the same time and is needed at least two times per span.
  It is a modified clamp approved for use on H.V. lines.

- Pole Protection Spiral
  Used to guide the lashed cable when bypassing a tower, especially a tension tower. It is a preformed spiral attached to a hook.

- Tower Downleading Accessories
  Depending on the tower type, splice closure location and/or customer requirements, different materials are used. For example, PE protection tubes, downleading clamps and heat-shrinkable materials.

  In the upper part of Figure 4 a typical ADL termination on ground wire with PE protection tube is shown.

Fig. 4: ADL Termination on Ground Wire (Upper Cable)

Furthermore, specially designed light weight accessories are used, as Gin Poles, Cradle Blocks and Lashing Binder Remover.

For the connection of ADL cables, all available splice boxes for optical aerial cables on H.V. lines can be used with the appropriate cable entry modification for the small diameters.

Lashing on phase conductors needs additonal accessories. Up to date these can be used up to 30 kV line voltage. A further upgrade to 150 kV is planned.

- Phase-To-Ground Termination
  It is used whenever the ADL cable has to go down from high to ground potential, i.e. at splice closures or line switches.

  The termination set consists of a plastic fixing rod, anti-tracking heat-shrinkable tubes and insulator caps. In combination with a Pole Protection Spiral two of the sets are used to by-pass a tower switch.

  Figure 5 shows a termination on a 15 kV line, Figure 6 an installation of a switch bypass on the same line.

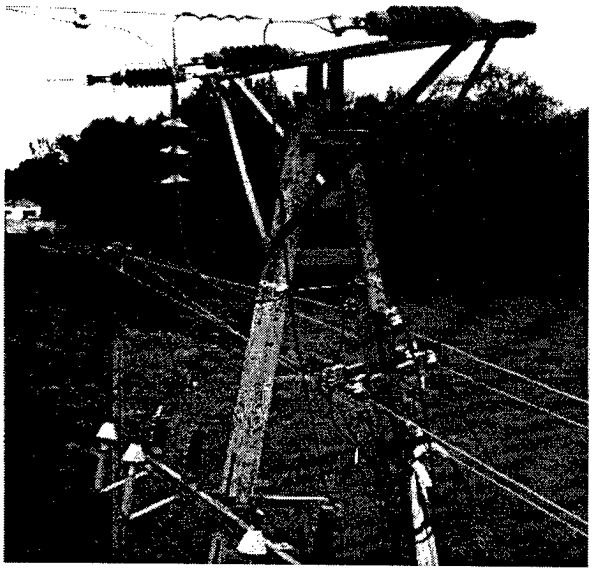

Fig. 5: Phase-To-Ground Termination

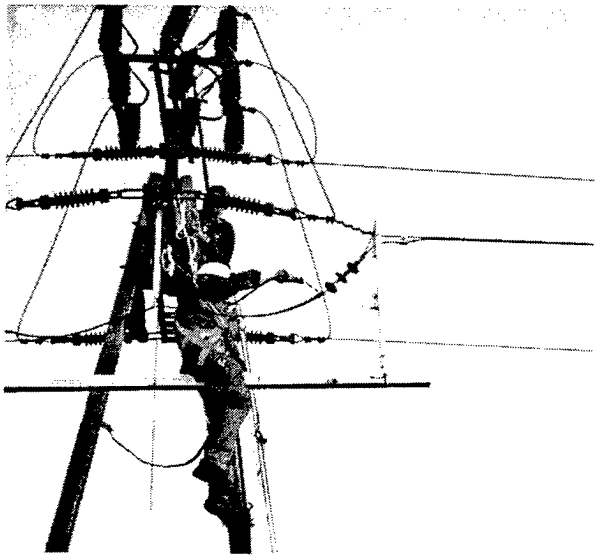

Fig 6: Installation of Tower Switch Bypass

TEST ON CABLE AND ACCESSOIRES

The ADL jacket materials have been selected after testing in our Material Competence Centre.

The ADL cables have passed all applicable tests according to prEN 187 200[7] including the following:

- Tensile test
- Thermocycling
- Cable bend
- Torsion

Although most of the accessories were already approved for use on H.V. lines, they have been tested in several installations before beeing used for customer installations.

To test the system under severe conditions, lightning strike as well as short-circuit tests with ADL cable lashed to OPGW have been performed.[8,9] The ADL cable, Lashing Binder and Fixing Clamps passed both tests with no significant damage. In case of lightning strike the cable jacket had slight imprints whereas some wires of the OPGW were severely damaged.

A self-damping test of an ADL lashed to a ground wire has been performed and compared to the behaviour of the bare ground wire [10,11]. The result shows that the vibration frequency for the lashed system is lower than for the bare conductor. This behaviour had been observed already during installation trials where the ground wire tended to vibrate but stopped vibration after lashing.

INSTALLATION TECHNIQUES

The installation of ADL cable can be generally split into three methods. Combination and modification of these basic methods are possible when required by line, terrain conditions or on customer demand.

Before starting an installation it is necessary to have as much as possible information about the line, towers used and terrain as well as special regulations regarding electrical safety to chose an appropriate installation method.

Under certain conditions live line installation is possible but it needs more careful planning and skillful and trained linesmen to do the installation.

Flying Reel Method

With this method the cable reel is in the air and both cable reel and Lasher will be pulled by a tug (Fig. 3). After completion of one span the equipment has to be moved to the next span. This is done by using a Gin Pole (Fig. 7).

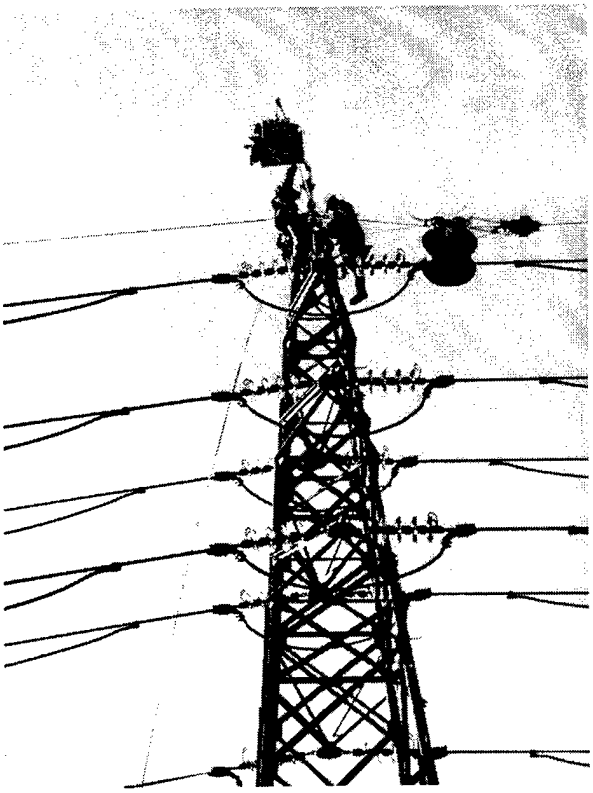

Fig. 7: Moving Equipment Across a Tower Top With a Gin Pole

This method is used mainly on ground wires on H.V. lines with strong towers able to carry the complete load of max. 225 kg.

For installation of long spliceless cable lengths with high fibre counts, the complete cable length can be delivered on two reels. Taking either one or two installation sets and starting from a central tower, the lashing is done in opposite directions. Using this operation, spliceless lengths of up to 4 km to 5 km for a 48 fibre cable can be achieved.

Back Pull Method

This is a two-step operation. In the first step the whole ADL cable length will be laid with cradle blocks pulled by a light weight tug or by hand; the cable reel stays on the ground. After completion of step one the Lasher will be connected to the first cradle block and while pulling back the cradle blocks together with the Lasher - into the direction of the cable reel - the ADL will be lashed to the messenger.

The pulling back of the cradle blocks, span by span, can be done either by hand or a winch.

This method takes more time than the Flying Reel method but in some cases, i.e. when there are difficult road, railway, river or line crossings or other obstacles in the way limiting the ground clearance, it is the only possible installation method.

Besides that, it is a technique well known to linesmen as it is often used for rope or conductor installation.

Moving Reel Method

When there is good access along the line either for a motor or hand vehicle this method can be used to lash the ADL to a phase messenger. The only restriction is that the messenger is not in the centre of the system.
The ADL cable is moved on the ground along the line while the Lasher is pulled by hand. The use of a tug or winch to pull the Lasher is possible as well.
This method is mainly used on lines with pole heights of 10 m to 15 m on the outer phase conductor. Ground wire installation is possible when the ground wire is the outermost wire of the whole system.

Installation Times

Giving installation times is always difficult as there are too many uncertainties depending on the chosen method, the line, terrain and weather conditions and the skillfulness of the linesmen.

As a rule of thumb and as an average for a link of 10 km to 20 km the laying speed per day is around 4 km to 5 km or one cable length.

FIELD TRIALS AND INSTALLATIONS

Field Trials

Before using the ADL Cable Technique in real installations, we performed several trials to check the cable, accessories and installation techniques.

The longest trial is running since November 1996. It is a 500 m one-span installation of a 12 fibre ADL cable. The test site at Minervois in southern France is a region strongly influenced by winds of the Mediterranean with wind speeds up to 160 km/h. Optical measurements show no attenuation change up to date.

Installations

Beginning in 1997 we sucessfully installed around 160 km of ADL cable ranging from 6 to 24 fibres on 15 kV phase conductor. Up to 800 km are planned until 1999.

In the same time frame we realized around 40 km with up to 48 fibres on ground wire on 110 kV lines in European countries like Poland, Norway and Switzerland.

Further installation are planned for this year on 20 kV phase conductor and 110 kV ground wire in Germany.

CONCLUSION

The installation of ADL cable is a fast and economical way of upgrading optical fibre networks on H.V. lines to fulfil the increasing demands of optical fibre telecommunications.

The advantage of the ADL technology over other OPAC solutions is the better performance and greater installation flexibility. The ADL technique should not be seen as a replacement of higher ranking technologies as OPGW, OPPC or ADSS, but used for special applications it can be the most economical way of optical fibre cable installation.

REFERENCES

1. Fuse, Shirasaka et al. 'Optical Fiber Cable Fastened To Overhead Ground Wire With Lashing Rod', International Wire and Cable Symposium Proceedings 1982, pp. 77 - 85

2. Cortines, Saez De La Maza et al. 'Digital Transmission System By Optical Fibers Lashed To The Ground Wire Of High Tension Lines', International Wire and Cable Symposium Proceedings 1984, pp. 380 - 387

3. Yoshida, Ikeya et al. 'Winding Of Optical Fiber Cable Onto Existing Ground Wire', International Wire and Cable Symposium Proceedings 1986, pp. 472 - 476

4. Dodd, McDowell III et al. 'Design And Test Considerations For Fiber Optic Aerial Cables', International Wire and Cable Symposium Proceedings 1990, pp. 166 - 175

5. Kloepper, Menze et al. 'Short- and Long-Span, Self-Supporting, Non-Metallic Aerial Fiber Optic Cable', International Wire and Cable Symposium Proceedings 1991, pp.186 - 194

6. Anonymous 'Fiber Upgrade In Oklahoma Includes A Record Aerial Span', Outside Plant July, 1986, pp. 48 - 52

7. prEN 187 200 'Sectional Specification: Optical cables to be used along electrical power lines (OCEPL)', Draft European Standard, 1998

8. Wiesinger, Zischank 'Lightning Current Tests of Optical Ground Wires', Test Report, 1996, pp. 16 - 18

9. FGH 'Optical Fibre Aerial Cables, Types SA/92-1/K, 9YI905 and LE 8087 Lashed To a Steel Reinfored Aluminium Conductor Type AA/ACS 85/36 - 9.2 With Lashing Line Type PS29-LL190', Test Report No.: LV 97011/1E, 1997

10. RIBE Engineering Services 'Vergleichende Messung der mechanischen Eigendämpfung am Erdseil Al/St 185/30 mm^2 - 19,0 mm∅ ohne und mit Lashed Cable ADSS 6,5 mm', VE-Bericht K 6676, 1998

11. RIBE Engineering Services 'Einfluß eines Lashed Cable auf das dynamische Verhalten eines Erdseils', Studie Bi-98/1-15, 1998

AUTHORS

Ralph Böhme
Alcatel Kabel
Bonnenbroicher Str. 2-14
41238 Mönchengladbach
GERMANY

Ralph BÖHME, born in 1954, received his Dipl.-Ing. degree from the Bergische Universität Wuppertal in 1986. He joined AEG Kabel in the same year. As a member of the engineering department for optical fibre cables he is responsible for the development and engineering of ADSS cables.

Reinhard Girbig
Alcatel Kabel
Bonnenbroicher Str. 2-14
41238 Mönchengladbach
GERMANY

Reinhard GIRBIG, born in 1954, received his Dipl.-Ing. Degree from the Ruhr University Bochum in 1982 and joined AEG Kabel in 1987. From 1993 to 1996 he worked as a project engineer and was responsible for the Transmission and Characterization Group in the Alcatel Optical Fiber Cable Competence Center in Bezons, France. He is now in charge of the engineering department in the Product Group Optical Aerial Cables within Alcatel Cable.

Georg Hög
Alcatel Kabel
Bonnenbroicher Str. 2-14
41238 Mönchengladbach
GERMANY

Georg HÖG, born in 1950, obtained his Dipl.-Ing. degree from the University of Aachen and joined AEG Kabel in 1977. After being engaged in the development of symmetrical telecommunications cables he became responsible for this group in 1980. In 1985 he became head of the Development Group for Optical Fibre Cables. He is now responsible for the Product Group Optical Aerial Cables within Alcatel Cable

THE SC-DC / SC-QC CONNECTOR

Karl M. Wagner, James P. Luther, David L. Dean

Siecor, Hickory, North Carolina

ABSTRACT

A new two or four fiber 2.5 mm ferruled connector in a standard SC package has been developed. The purpose of this paper is to present the connector and it's features and how they compare to current multi-fiber connector technologies. The unique alignment characteristics of the connector and its benefits will also be described. Single-mode data will be presented, showing an average attenuation loss of 0.33 dB with a max. of 0.72 dB. Side load performance, durability and temperature cycling are also summarized.

INTRODUCTION

With the evolving communication market new requirements for the next generation of multifiber connectors have emerged. Ideally the new connectors should be a familiar package, with high density to facilitate introduction into current and future wiring structures. A standard package would not require the end-user to purchase additional installation or polishing equipment. Furthermore it should be lower in cost and smaller than the current duplex SC interface.

With fiber approaching the desk, connectors have to be more user friendly and designed to accommodate both current single fiber cable designs as well as future cable structures. The SC-DC™ / SC-QC™ were designed to meet these requirements.

DC / QC FERRULE DESIGN

The SC-DC ("Dual Contact", two fiber version) and SC-QC ("Quattro Contact", four fiber version) are high density, SC-style connectors featuring a special ferrule (Figure 1). Connector designs support both single-mode and multimode applications.

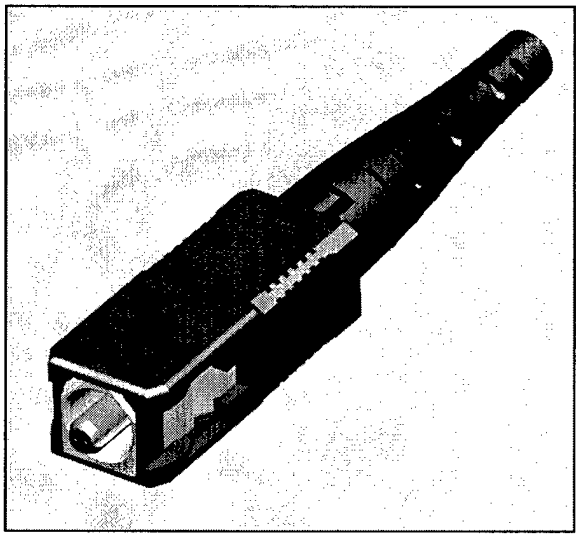

Figure 1 SC-DC / SC-QC connector

Traditionally multi fiber ferrules are square in shape and feature two guide-pin holes and several fiber holes molded in one plane (Figure 2). Guide-pins are used to achieve precise ferrule alignment. The guide pins are captured in the ferrule of one of the connectors, resulting in a non symmetric, male and female connector pairing.

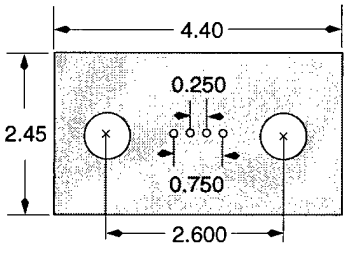

Figure 2 Mini-MT ferrule end-face [mm]

The new DC / QC ferrule design enables removal of the guide-pins from the connector into the coupler. Capturing the pins inside the coupler preserves the symmetric connector concept of the SC duplex.
The ferrule design maintains the traditional concept of molding alignment features and fiber holes in one plane. Major difference is the change from guide-pin holes to alignment grooves (Figure 3). The alignment grooves, 350 micron in radius, have a 2.6 mm center to center spacing; fiber holes are at a 750 micron (DC) or 250 micron (QC) center to center pitch.
The ferrule is cylindrical in shape, with an outer diameter of 2.5 mm, a standard for single fiber ceramic ferrule designs. Unlike the standard ceramic ferrule, ferrule and ferrule-holder are molded in one piece, reducing part and assembly complexity. The new design is molded using a thermoset process, providing tight dimensional control.

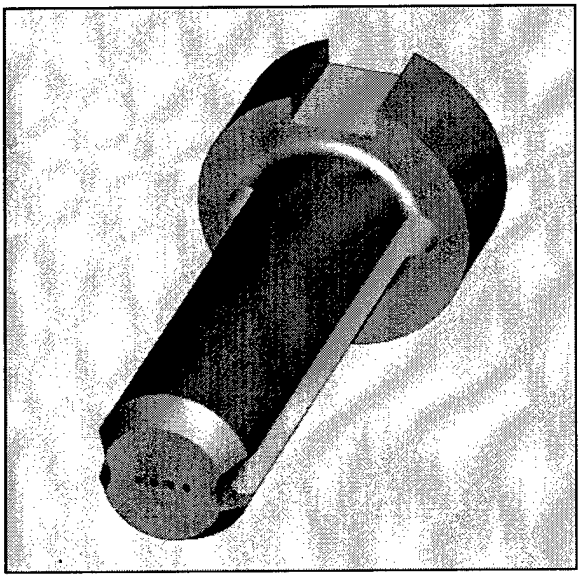

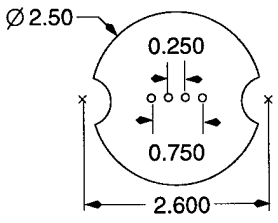

Figure 3 SC-DC / SC-QC ferrule design [mm]

The critical ferrule features are the alignment grooves and fiber holes. These features determine fiber alignment and hence connector performance. When two ferrules are mated inside a coupler, they are aligned axially and radially by ribs or pins inside the coupler sleeve. The ferrule groove-spacing and coupler pin-spacing are toleranced such that a light interference fit results. The ferrule outer diameter has clearance in the coupler sleeve and does not affect the alignment.
Figure 4 shows a direct comparison of the traditional hole-pin versus the groove-pin alignment performance. Single-mode MT ferrules were mated using guide pins and insertion loss performance was recorded. The same ferrules were then ground and modified to match the DC / QC ferrule design. Subsequently the modified ferrules where re-mated using a pin containing coupler prototype. No degradation of attenuation performance was found.

CONNECTOR HOUSING

To follow an easy migration path, the ferrule was packaged into standard SC hardware. The SC was chosen for its proven design with high density, easy push-pull insertion and customer familiarity. Because the ferrule OD is the industry standard 2.5 mm, all current assembly and polishing equipment may be used.
The connector is also available as a "Bag of Parts". To minimize assembly time the parts are preassembled, significantly reducing the amount of parts circulating the assembly floor, simplifying the process and minimizing the chance for errors (Figure 5).

Addressing the need for field installation, the SC-DC has also been developed in a field installable version. The SC-DC UniCam™ is based on proven technology, using the pre-stubbed fiber concept (1).
The UniCam concept eliminates the use of epoxy and polishing in the field, guaranteeing factory quality endface geometry and fast installation. A mechanical splice element aligns the pre-polished fiber stub with the installed fiber. To actuate the mechanical splice, a cam design is used. The cam compresses the top and bottom part of the splice, thus accurately aligning the fibers within v-grooves in the bottom splice part.

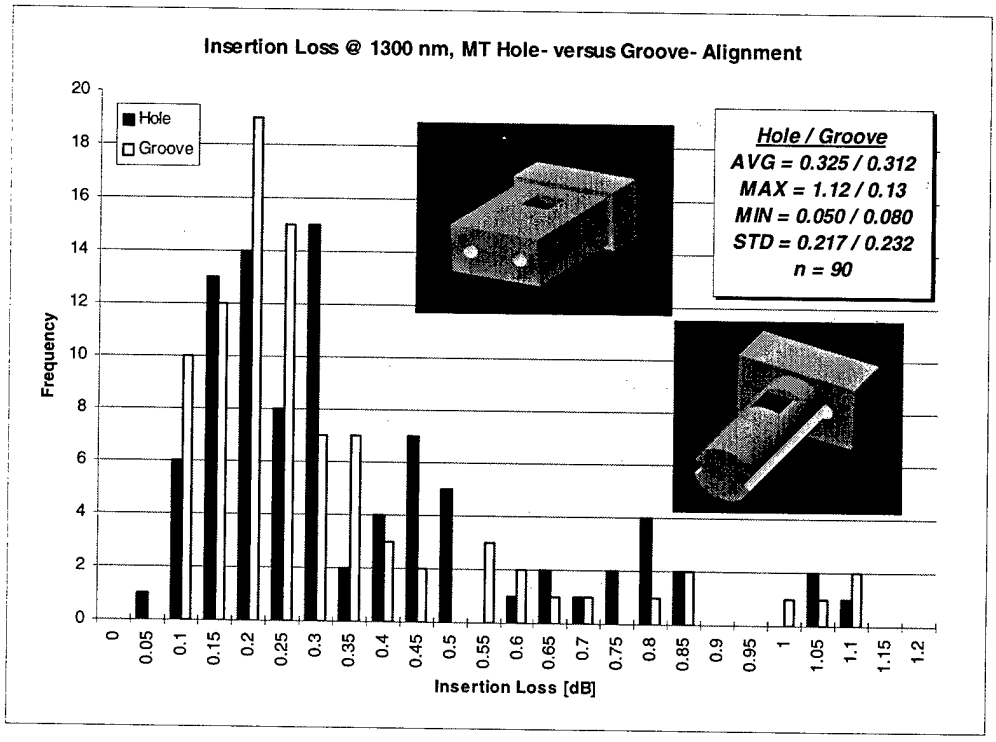

Figure 4 Insertion loss, hole versus groove alignment

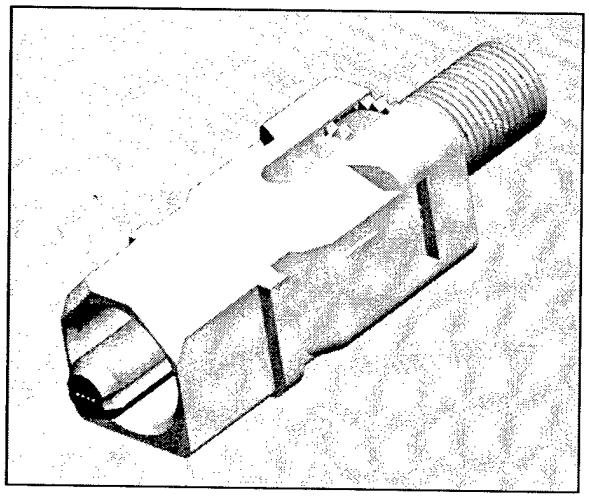

Figure 5 Preassembled connector hardware

COUPLER DESIGN

The SC-DC / SC-QC design differentiates between single-mode and multimode in the coupler insert. A one piece all-composite insert is used in the multimode coupler (Figure 6). The alignment features are precision molded ribs, located on the ID of the insert.

A single-mode coupler requires tighter tolerances and more accurate alignment. As a result the single-mode design uses four pieces (Figure 7). Guide-pins are captured in a floating subassembly, separating the alignment mechanism from external forces.

Alignment is based on the interference fit between the guide-pins and the ferrule groove. The actual force on the guide-pins is provided by the flexibility of the all-composite subassembly. To achieve maximum alignment accuracy of the ferrules, the guide-pins can float within the subassembly.

Both single-mode and multimode coupler inserts are captured within the SC type coupler housing, guaranteeing compatibility with current SC hardware and outlets.

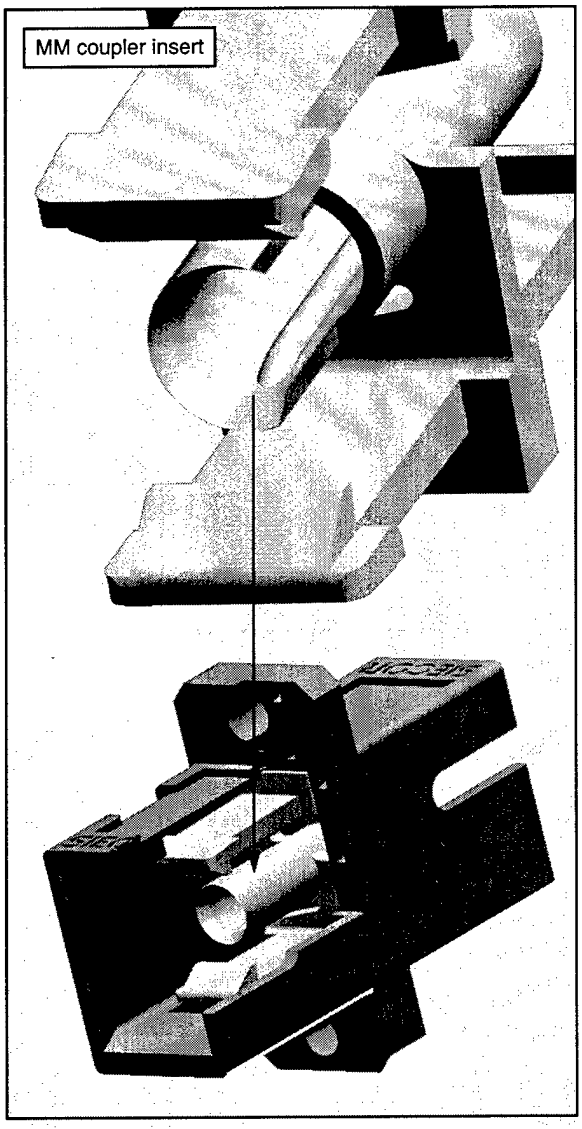

Figure 6 SC-DC/SC-QC mutimode coupler

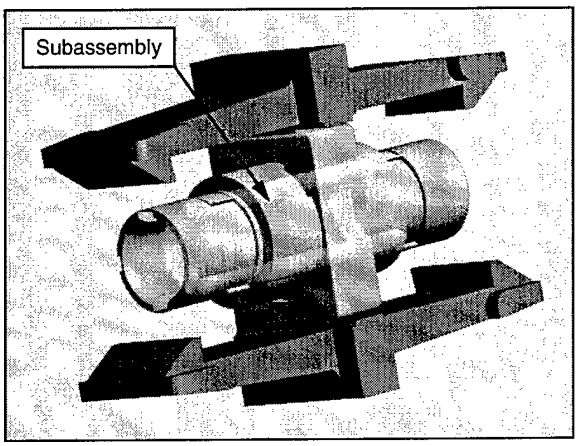

Figure 7 SC-DC/SC-QC single-mode coupler insert

CONNECTOR PERFORMANCE

Test results for SC-DC and SC-QC connectors demonstrate an average insertion loss of 0.33 dB for single-mode and 0.11 dB for multimode. Figure 8 shows a histogram of single-mode data for the SC-QC connector, along with sample size and statistical results of the measurement. The results were achieved with dry physical contact.

Capturing the pins (single-mode) or molded ribs (multimode) inside the mating sleeve provides maximum float of the ferrule within the SC connector and coupler hardware. This design de-couples the mated ferrules from external forces applied to the cable. Test results demonstrate stable insertion loss and return loss under loads up to 4.5 lb off axis pull @ 90 degrees. Figure 9 illustrates the side load performance, Figure 10 shows the return loss performance of the single-mode SC-DC per Bellcore GR 326 CORE test procedure.

Durability testing has been completed. Test results for the SC-DC / SC-QC connectors show no insertion loss degradation up to 500 re-matings. Figure 11 demonstrates SC-QC single-mode insertion loss performance of three connector pairs (12 fibers), per GR 326 CORE.

Temperature cycling demonstrated stable attenuation and return loss from - 40 to + 70 degree Celsius. The average change in attenuation was less than 0.1 dB, return loss delta was less than 3 dB.

INTERMATEABILITY

One of the design constrains of the DC / QC ferrule was plug to plug compatibility with the NTT Mini-MT ferrule. This constraint drove the selection of the 2.6 mm spacing and the 350 micron radius grooves. Figure 12 contains single-mode attenuation performance obtained by mating pin containing MT ferrules with the DC ferrule.

Test results show an average loss of 0.37 dB with a maximum of 0.56 dB. This underlines the flexibility of this new ferrule design, usable throughout future networks containing SC-DC or MT-RJ connectors.

CONCLUSION

A new multifiber optical connector for either two or four fibers has been developed. The connector features a completely symmetric design, eliminating system pre-engineering. Incorporating a standard 2.5 mm outer diameter ferrule in the SC package allows the use of current SC termination tools and procedures. The SC-QC achieves four times the density of the standard SC connector within the identical footprint. The critical ferrule dimensions are compatible with other evolving multifiber connector concepts, making the DC / QC ferrule a flexible solution for new network designs.

REFERENCES

1) M. DeJong, "Cleave and crimp fiber optic connector for field installation", Tech. Digest, Conf. on Optical Fiber Communications, paper ThA1, p. 139 (1990).

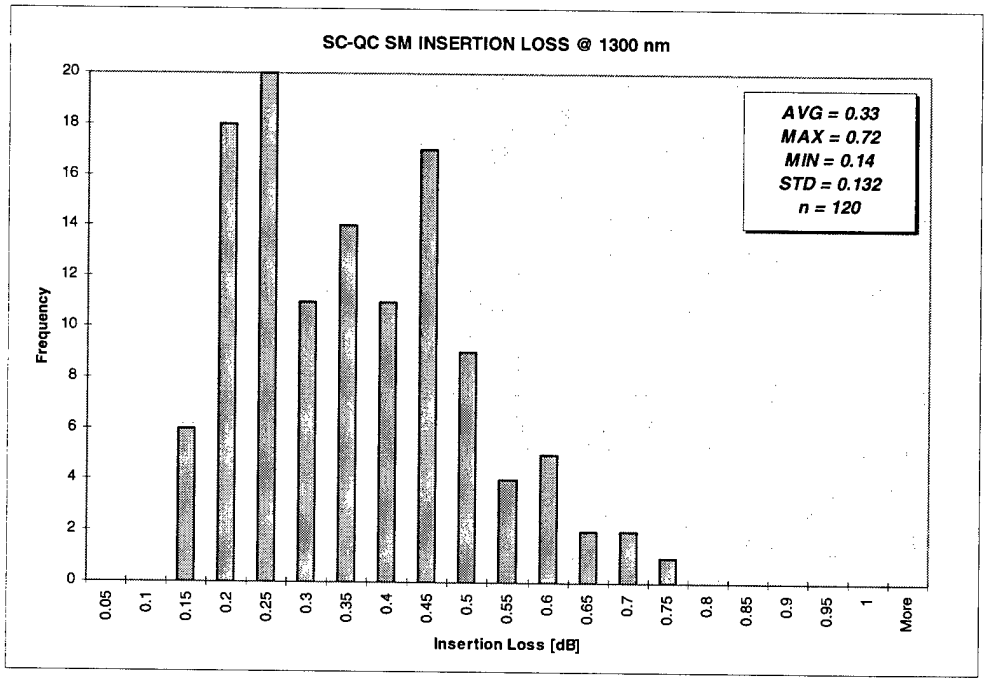

Figure 8 Single-mode insertion loss histogram for SC-QC

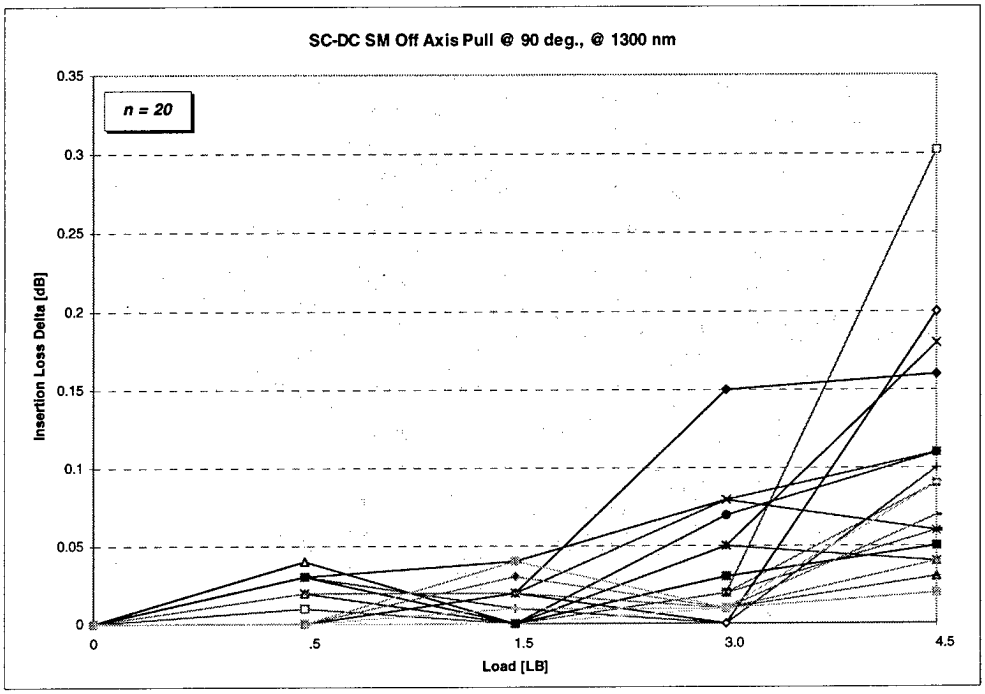

Figure 9 Single-mode insertion loss performance under load [90 ° off axis]

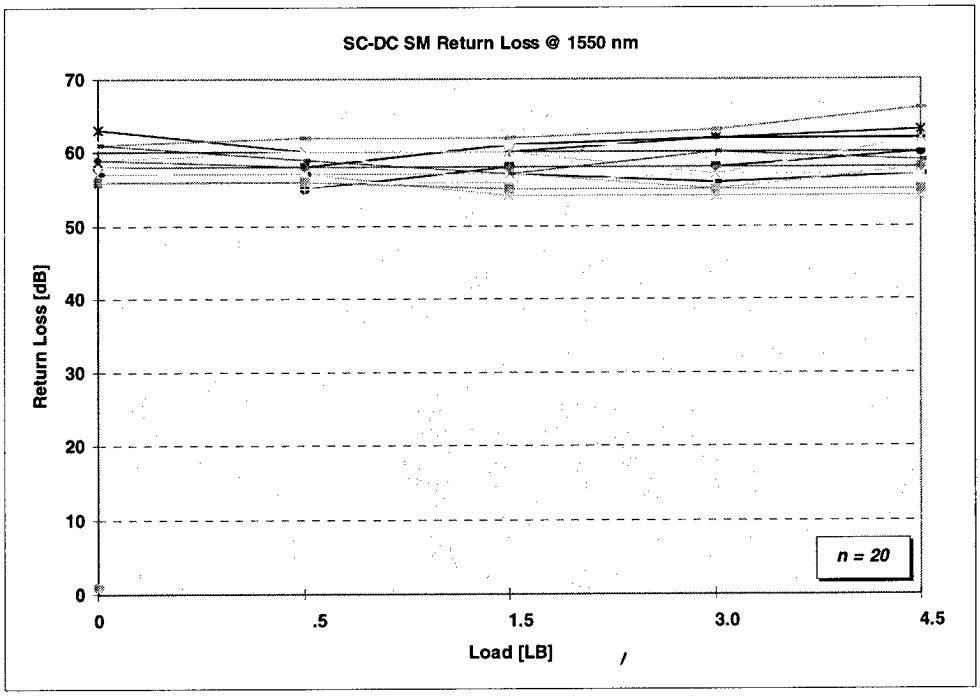

Figure 10 Single-mode return loss performance under load [90 ° off axis]

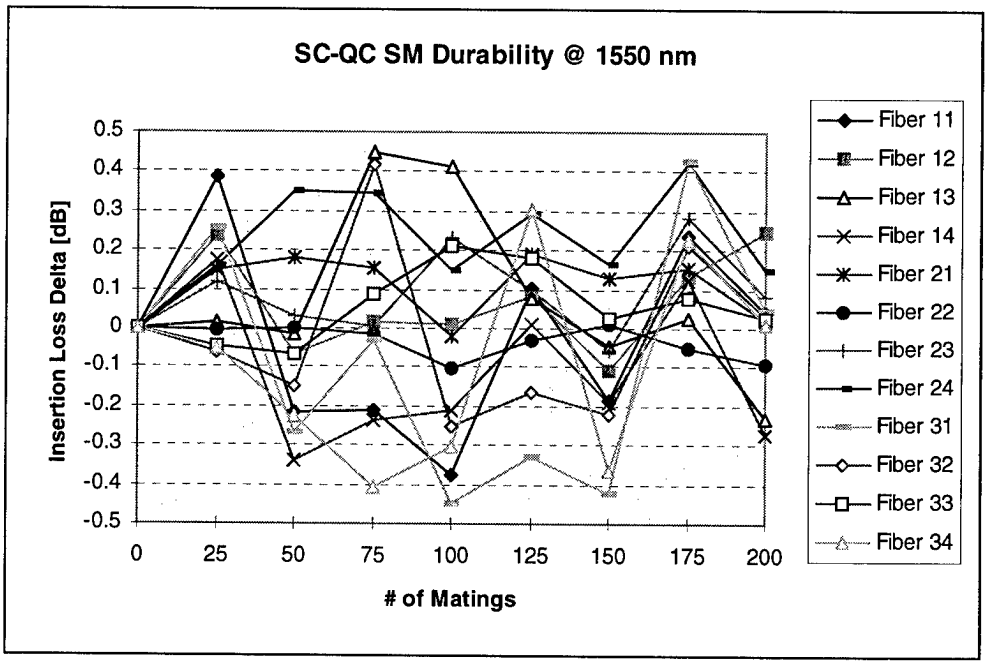

Figure 11 Single-mode durability performance

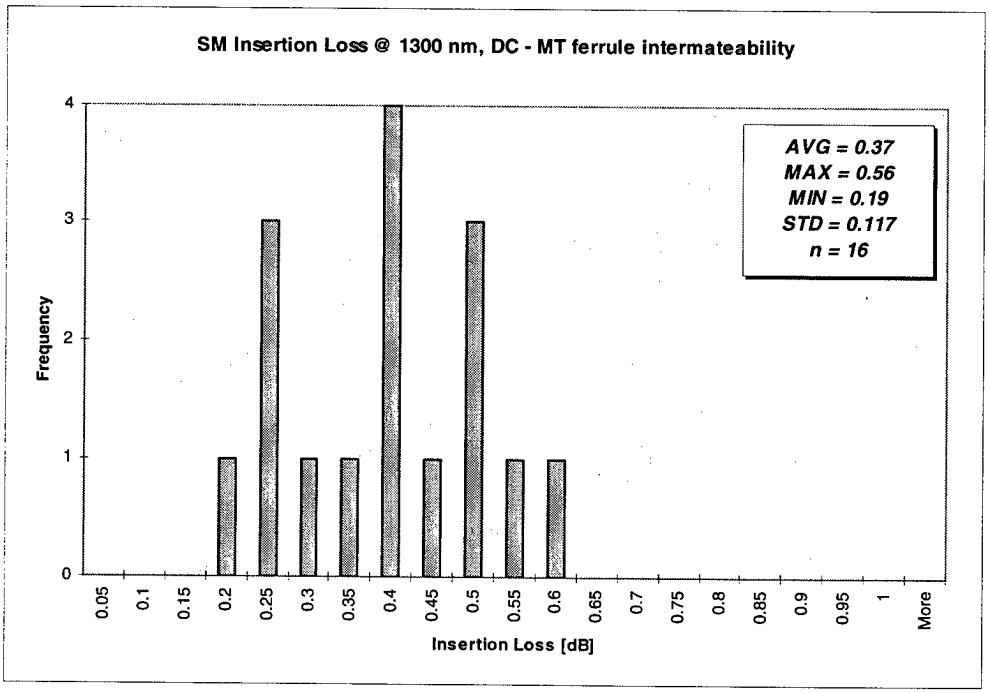

Figure 12 Single-mode insertion loss for DC - MT ferrule intermateability

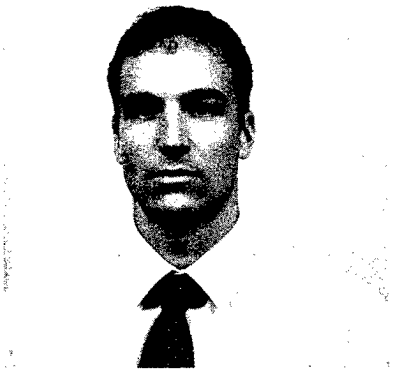

Karl M. Wagner received his Masters in Mechanical Engineering in March 1993 from the Technical University of Munich, Germany. After working in Italy and Germany, he joined Siecor in 1995 within the Hardware and Equipment division. He is presently product development engineer responsible for the SC-DC connector development.

David L. Dean received his Bachelors degree in mechanical engineering from NC State in 1983 and his Masters in mechanical engineering from MIT in 1985. He joined Siecor in 1985 and is presently the manager of the multifiber mold development group.

James P. Luther graduated from SUNY at Buffalo with a Bachelors degree in mechanical engineering. He has spent most of his 15 years at Siecor involved in process and product development. He is presently the manager of the cable assembly development group.

Development of MT Type Connector Using an Injection Molded Ferrule and a Quick Assembly Technique

Masaaki Takaya, Toshiaki Katagiri, Shinji Nagasawa, Yasuji Murakami

NTT Access Network Systems Laboratories
1-7-1 Hanabatake, Tsukuba-city, Ibaraki, 305-0805 JAPAN

Abstract

In this paper, we describe the design and performance of a newly developed single-mode multifiber connector which employs an injection molded mechanically transferable (MT) type ferrule and a quick assembly technique.

The injection molding technique makes the ferrule production process easier, and also contributes to cost effectiveness. The connector can be assembled without polishing or heating. The connector assembly time is only 3 minutes, which is about one-fifth that needed for the conventional MT connector. The connector ferrule has a structure compatible with the MT connector ferrule and the insertion loss of the fabricated connector is as low as that of the MT connector.

This connector will be useful for the economical construction of optical access networks for fiber to the home.

1. Introduction

It is essential to construct optical-fiber access networks to provide broadband services to customers over a wide area. It is important to develop a low cost, low loss, and high performance connector for this purpose. We have already developed the MT connector for practical use [1]. The MT connector is a multifiber array connector manufactured by plastic molding technologies. The centers of two guide-pins and optical fibers are precisely aligned on the same plane and low loss can easily be obtained after engaging a pair of ferrules simply by using the guide-pins and a clamp spring. Up to twelve fibers can be accommodated in a ferrule with a 7x3 mm cross-section.

However, there are some problems to be overcome before the MT connector can be more generally employed. The most important of these are its cost and assembly process. With the present techniques, it is more expensive to join fibers with a connector than by fusion splicing.

In this paper we first describe a quick assembly technique without polishing or heating for conventional MT type ferrules. Next we present a quickly assembled MT type connector which uses an injection molded ferrule.

2. Quickly assembling technique for MT type ferrule

A. Connector Assembly process

Figure 1 shows the structure of the quickly assembled multifiber connector. The basic

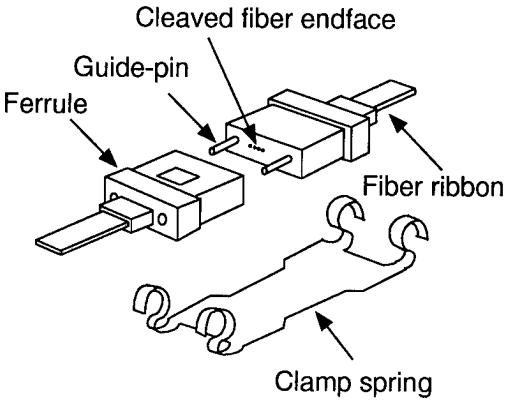

Fig. 1 Structure of the quickly assembled multifiber connector

structure of the connector is similar to that of the conventional MT connector. It consists of two ferrules, two guide pins and a clamp spring. The ferrules are aligned with two guide-pins and then held with a clamp spring. The ferrules can be disconnected after the clamp spring and guide pins are removed. Index-matching material is used between the ferrule endfaces. The quickly assembled connector is only 3 ×7 ×8 mm^3 in size and is compatible with the MT-type ferrule.

A feature of this connector is that the assembly process is shown in Fig. 2. Fibers with cleaved

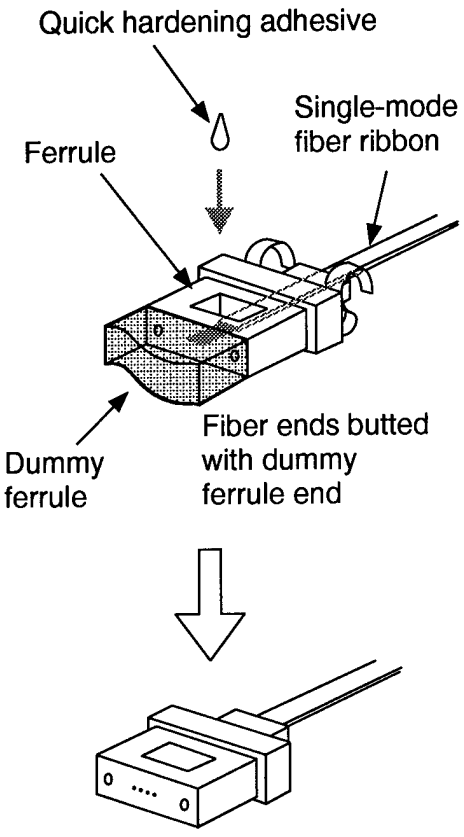

Fig. 2 Assembly process of the quickly assembled multifiber connector

endfaces are inserted into fiber-holes in the ferrule which is coupled with a dummy ferrule. The fiber endfaces make contact with the dummy ferrule's endface. The fiber endfaces are arrayed across the actual ferrule endface. These fibers are then fixed in place with a quickly hardening adhesive. The adhesive is hardened instantaneously using a solidifying medium. Detaching the dummy ferrule we obtain the assembled ferrule. This process eliminates the need for adhesive heating and endface polishing. The ferrule assembly time is 3 minutes, which is about one-fifth that with the conventional field assembly method.

B. Method of arranging fibers on the ferrule endface

We usually use a fiber ribbon when assembling a multifiber connector. When we cut fibers using a conventional fiber cutting tool, the positions of the fiber endfaces differ slightly. When we assemble the connector, the fiber endfaces must be arranged on the ferrule endface. The fibers are aligned on the ferrule endface when they are bent by the load which is applied during the fiber insertion process.

We consider the fiber to be a long slender column held in position at one end *O* and with an axial load *P* applied at the other end *A*, as shown in Fig. 3 (a). The material is assumed to be homogeneous and obeys Hook's law within the range of load. If we increase the load P, the fiber is bent, as shown in Fig. 3 (b). The load P_{cr} for bending the fibers is given by

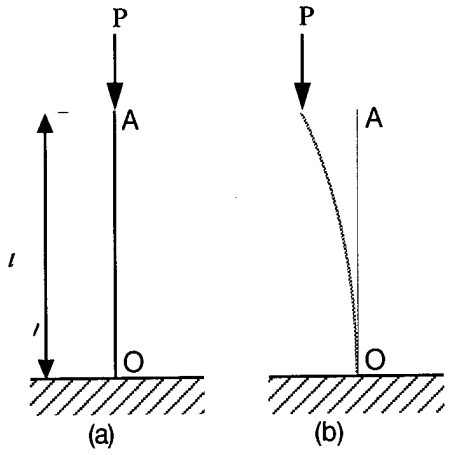

Fig. 3 A long slender column with an applied load P

equation (1) [2].

$$P_{cr} = \frac{\pi^2 E I}{4 l^2} \quad (1)$$

where E is the Young's modulus, I is a geometrical moment of inertia. This shows that a slight difference in cleaved fiber end position can be absorbed by bending the fiber with an appropriate force.

Figure 4 shows an example of the surface of the quickly assembled multifiber connector ferrule for 4-fibers when an appropriate force is applied to the fibers.

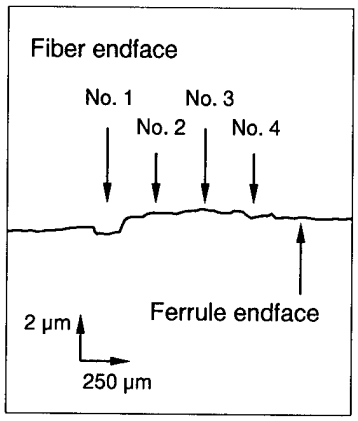

Fig. 4 Example surface of the quickly assembled multifiber connector ferrule

The above figure shows that the fiber endfaces are aligned on the ferrule endface.

C. Test results

We constructed a quickly assembled multifiber connector ferrule for 4-fiber ribbons based on the above design. The ferrule was a conventional MT type ferrule which we made from epoxy, (a kind of thermosetting resin) using the transfer-molding technique. The ferrule which we used in this connector was assembled with 1.3 μm zero-dispersion 4-fiber ribbons. The mode field diameter of the fiber was 9.5 μm. We then performed optical tests on the connector. The insertion losses were measured using an LED operating at 1.3 μm. Histograms of these insertion loses for are shown in Fig. 5.

We obtained an average insertion loss of 0.18 dB with a maximum value of 0.80 dB.

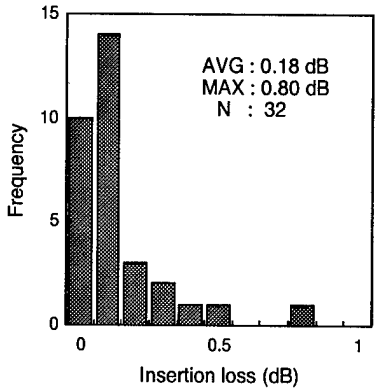

Fig. 5 Insertion loss histogram for the 4-fiber connector

We measured the return losses using an LD operating at 1.3 μm. Figure 6 shows return loss histograms for the connectors. The return losses were grater than 40 dB.

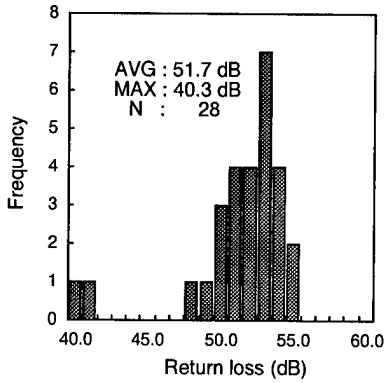

Fig. 6 Return loss histogram for the 4-fiber connector

We also examined connector durability as regards reconnection. Figure 7 shows the insertion loss changes of the connectors for 200 reconnections.

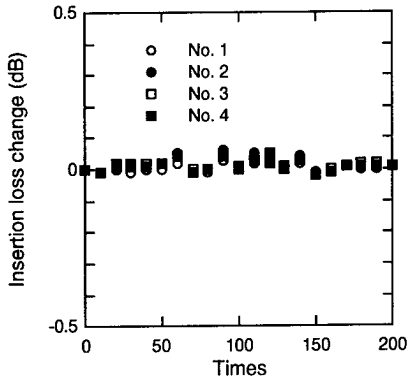

Fig. 7 Insertion loss changes of the connectors for 200 reconnections

The range of the maximum loss change was less than 0.2 dB, and there was no irreversible damage to the connector. This shows that the connector is stable as regards connection and reconnection.

Next we performed four environmental tests on the connector. They were a temperature change test (-40℃ to 70℃, 6h/cycle, 10 cycles), a temperature and humidity cycling test (93% at 65℃, 24h/cycle, 10 cycles), a high temperature endurance test (85℃, 240h), and a low temperature endurance test (-40℃, 240h).

The results are shown in Fig. 8(a)-(d). The connector characteristics were very satisfactory. The insertion loss changes were less than 0.2 dB during these tests for single-mode fibers.

These results indicate that the quickly assembled multifiber connector is stable as regards changes in temperature and humidity .

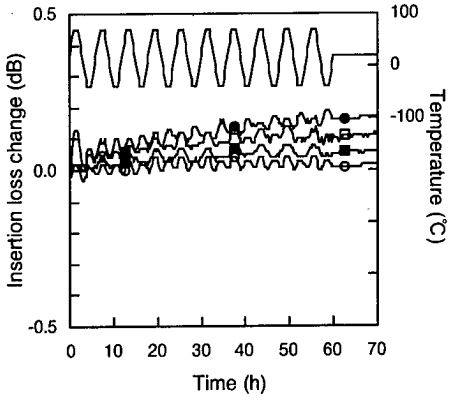

(a) Temperature cycle test
(-40℃ to 70℃, 6h/cycle, 10 cycles)

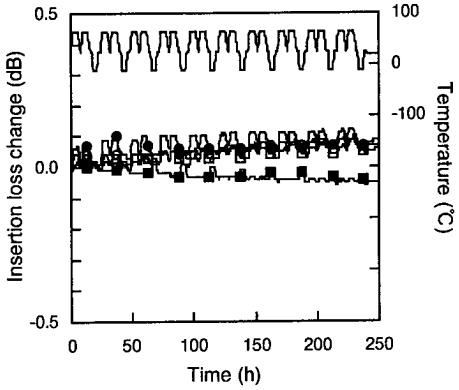

(b) Humidity cycle test
(93% at 65℃, 24h/cycle, 10 cycles)

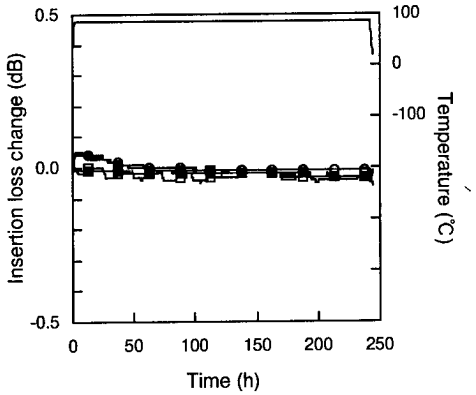

(c) High temperature endurance test
(85℃, 240h)

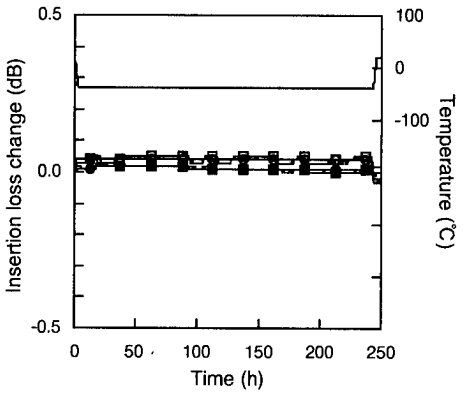

(d) Low temperature endurance test (-40℃, 240h)

Fig. 8 Environmental tests results on the connector

3. Quickly assembled multifiber connector using an injection molded ferrule

We have developed a modified version of the quickly assembled multifiber connector whose ferrule is made using injection molding techniques. We adopted thermoplastic resin as the ferrule material because of its suitability for mass production.

The injection molding technique using thermoplastic resin makes the ferrule production process easier than with the conventional transfer molding technique using thermosetting resin and is suitable for mass production.

The connector structure is the same as that of the quickly assembled multifiber connector which we described in section 2. It is compatible with the conventional MT connector. The connector assembly process is also the same as that of the quickly assembled multifiber connector.

We tested the trial connector for 4 and 8-fiber ribbons.

A. Test results

We constructed this connector based on the above design. We adopted polyphenylenesulfide (PPS), a kind of thermoplastic resin, because it has advantages of malleability, and resistance to heat, water and chemicals. The ferrules which we used in this connector were assembled with 1.3 μm zero-dispersion 4-fiber ribbons. The mode field diameter of the fiber was 9.5 μm. We then performed optical tests on the connector.

We measured the insertion and return losses at a wavelength of 1.3 μm using an LED and a backreflection meter. The average insertion loss was 0.22 dB, and the return loss was greater than 40 dB as shown in Figs. 9 and 10, respectively.

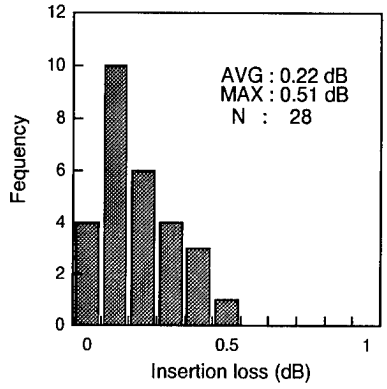

Fig. 9 Insertion loss histogram for the 4-fiber connector

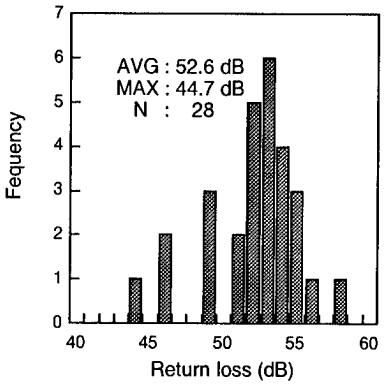

Fig. 10 Return loss histogram for the 4-fiber connector

We also fabricated and tested an 8-fiber connector. The test results are shown in Figs. 11 and 12.

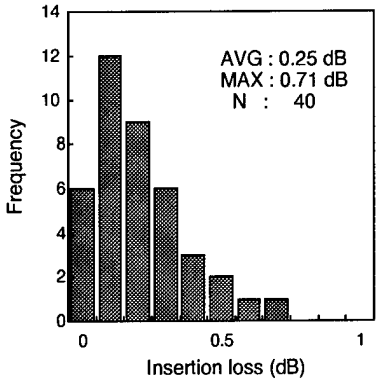

Fig. 11 Insertion loss histogram for the 8-fiber connector

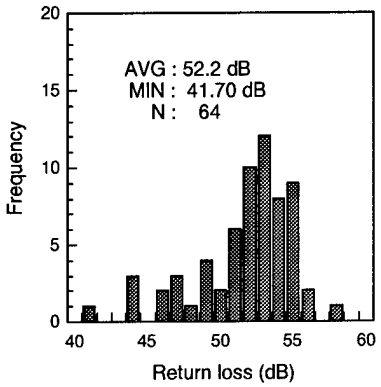

Fig. 12 Return loss histogram for the 8-fiber connector

The fabricated 8-fiber connectors exhibited an average insertion loss of 0.25 dB and the return loss was greater than 40 dB. These values are as low as those obtained for 8-fiber joints with the MT connector.

These optical tests results for the connector are as excellent as those of the conventional MT connector.

We also examined reconnection durability. Figure 13 shows the insertion loss changes of the 4-fiber connector for 200 reconnections.

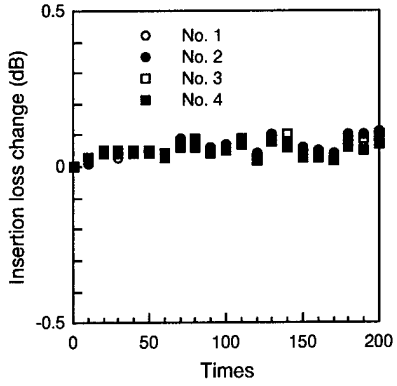

Fig. 13 Insertion loss changes of the connector for 200 reconnections

The range of the maximum loss change was less than 0.2 dB, and there was no irreversible damage to the connector. This shows that the connector is stable as regards connection and reconnection.

B. Cause of the insertion loss

There are three main factors which cause losses when we join fibers. They are fiber core offset, fiber axis tilt, and fiber endface separation. In an MT connector, the main source of the insertion loss is misalignment of the fiber core position of the connector ferrule.

To clarify the origin of the insertion loss of the quickly assembled multifiber connector with the injection molded ferrule, we estimated the connection loss caused by misalignment of the fiber core position of the connector and compared it with the measured insertion loss.

Figure 14 shows the endface geometry of the ferrule. The origin for the endface geometry is defined as the midpoint on a straight line between the centers of two guide-holes. The designed core centers are arranged along the line at intervals of 250 μm. The core centers of the ferrule are aligned usihg two guide-pins. Connection losses occur when the core positions deviate from their designed positions.

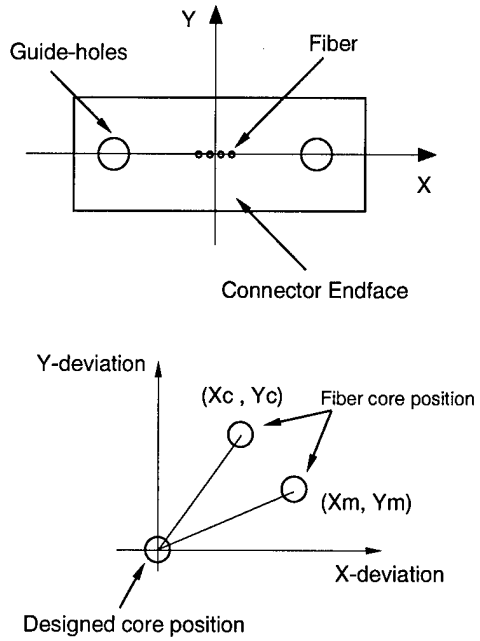

Fig. 14 Endface geometry of the ferrule

The distances between a designed core position and an actual core position are defined as X-deviation and Y-deviation in the X and Y-axis directions, respectively.

The estimated loss α is calculated from the misalignments *d* [3], which correspond to the distance between the two deviations of each core in the ferrules. The equation is given by,

$$\alpha_i\,(\mathrm{dB}) = 4.34 \times \left(\frac{d_i}{\omega}\right)^2 \qquad (2)$$

$$d_i^{\,2} = (X_{ic} - X_{im})^2 + (Y_{ic} - Y_{im})^2$$

where *i* is the number of cores in the ferrules. *Xic* and *Xim* are X-deviations of cores *i* in the ferrules. *Yic* and *Yim* are Y-deviations, ω is the mode field radius of the fibers.

We measured each core position deviation in the ferrules. We employed a noncontact measurement technique using a microscope with a high resolution CCD camera [4]. The estimated losses were calculated using the measured values and equation (2). Here, we used a value of 4.75 μm as the mode field radius. Figure 15 shows the relation between the actually measured insertion losses and calculated losses from the measured fiber core deviation.

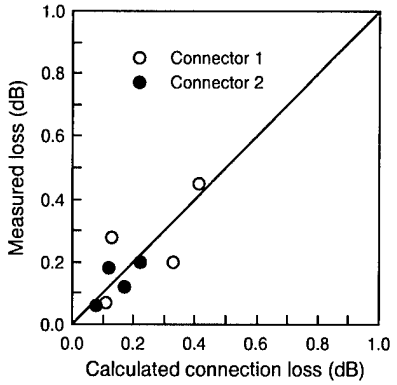

Fig. 15 Relation between the measured insertion losses and calculated insertion losses

All the results are in good agreement. This shows that the connection losses of the connectors are mainly caused by positional deviation of the cores. This is analogous to the case of the MT connector.

5. Conclusion

We have developed a quickly assembled multifiber connector with an injection molded ferrules. This makes it possible to achieve high productivity, and also contributes to cost effectiveness. The ferrule assembly time is 3 minutes, which is about one-fifth that with the conventional field assembly method.

We measured the insertion and return losses of these connectors. We obtained a low average insertion loss of 0.25 dB and a return loss of greater than 40 dB for an 8-fiber connector.

We have already developed various MT-based connectors for telecommunication and data communication use. Our new connector exhibits good levels of performance and will be employed with these connectors. They are promising with regard to upgrading the access networks for fiber to the home.

References

[1] F. Ashiya, T. Satake, and S. Nagasawa,

"Development of Multifiber Connectors and their Applications," E-FOC '87, pp. 304-308, 1987.
[2] J. N. Cernica, "Strength of Materials," Holt, Rinehart and Winston, Inc., 1966
[3] D. Marcuse, "Loss analysis of single-mode fiber splices," The Bell System Technical Journal, vol. 56, No. 5, pp. 703-718, 1977.
[4] N. Matsumoto, and S. Nagasawa, "Study on Reference Multifiber Connector," in Nat. Conv. Rec. IEICE, Japan, paper B-1034, 1985.

Masaaki TAKAYA

NTT
Access Network Systems Laboratories
1-7-1, Hanabatake, Tsukuba-City, Ibaraki, 305-0085 JAPAN

Masaaki Takaya is a research engineer at NTT Access Network Systems Laboratories.

He joined NTT in 1992. Since 1993 he has been engaged in the research and development of multifiber connectors.

Mr.Takaya is a member of IEICE of Japan.

Toshiaki KATAGIRI

NTT
Access Network Systems Laboratories
1-7-1, Hanabatake, Tsukuba-City, Ibaraki, 305-0085 JAPAN

Toshiaki Katagiri is a senior research engineer at NTT Access Network Systems He joined NTT in 1974. Since 1982, he has been engaged in developmental research on optical fiber joint and switching technology.

Shinji NAGASAWA

NTT
Access Network Systems Laboratories
1-7-1, Hanabatake, Tsukuba-City, Ibaraki, 305-0085 JAPAN

Shinji Nagasawa is an executive research engineer at NTT Access Network Systems Laboratories.

He joined NTT in 1976. He has been engaged in the research and development of multifiber connectors.

Mr. Nagasawa is a member of IEEE.

Yasuji MURAKAMI

NTT
Access Network Systems Laboratories
1-7-1, Hanabatake, Tsukuba-City, Ibaraki, 305-0085 JAPAN

Yasuji Murakami is an executive research engineer at NTT Access Network Systems Laboratories.

He joined NTT in 1975. He has been engaged in the research and development of optical fiber cable and optical fiber joint.

Field-installable Connector for Optical Fiber

Kazuhiro Takizawa, Toru Arikawa, Yasuhiro Tamaki and Hiroshi Yokosuka

Fujikura Ltd. Optical Access Network Laboratory
Sakura-shi, Chiba, JAPAN

ABSTRACT

We have developed the field-installable single fiber connector (SC-type and ST-type) and field-installable mini-MPO (Multi-fiber Push-On) connector, which are designed to be easily assembled in the field. These connectors can also be installed in the field without polishing and resin bonding process.

The field-installable SC-type connector, which is used for single-mode fiber, has a mean connection loss of 0.15 dB and a return loss of higher than 40 dB.

The average insertion loss of field-installable mini-MPO connector (SM) is 0.25 dB. The test results confirm that these connectors could be successfully employed in the field.

1. Introduction

The implementation of optical fiber network enhances the construction of flexible and efficient information exchange and transmission systems1)2)3). Optical connectors play an important role in these optical connectivity systems. The ease of installing and assembling these connectors in the field has been the main emphasis and the topic of discussion4)5)6).

We have developed the field-installable single fiber connector (SC-type and ST-type) and field-installable mini-MPO (Multi-fiber Push-On) connector which can be easily and quickly assembled in the field. In this paper, we will present the structures and the optical performance of the field-installable connectors.

2. Field-installable single fiber connector

2.1 Field-installable SC-type connector

2.1.1 Structure of field-installable SC-type connector

Fig.1 shows the structure of the field-installable SC-type connector. The connector section is similar to the conventional SC connector, with the mechanical splice section designed at the back. In addition to that, fiber is assembled in the connector ferrule during production and the endface is polished to high precision. To reduce the reflection loss at the mechanical splice, index matching grease is inserted into the splice section beforehand. Polishing, bonding resin and electrical power supply are thus not needed in the field, and field assembly is easy and can be achieved in a short time.

This connector is available for the fibers shown in table 1.

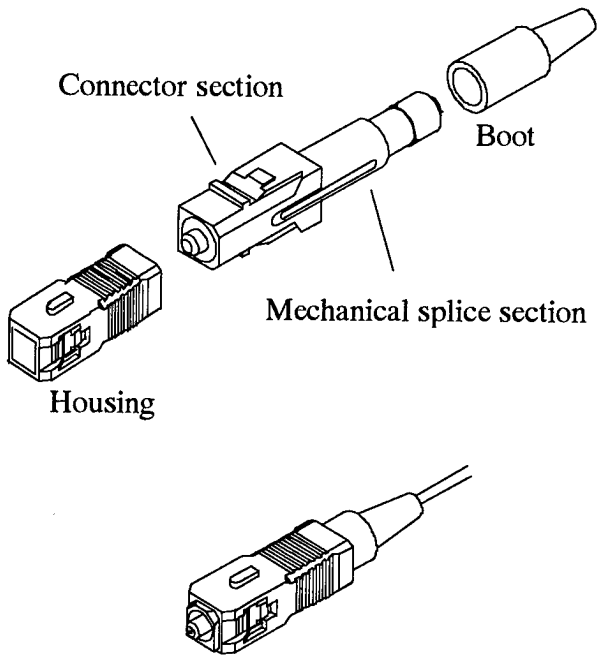

Fig.1 Structure of field-installable SC connector

Table 1 The fiber to apply to field-installable SC-type connector

Core diameter(μm)	9(SM) 50(GI) 62.5(GI)	
Cladding diameter(μm)	125	
Coating diameter(mm)	0.25	0.9
Code diameter(mm)	1.5	3

2.1.2 Assembly method of field-installable SC-type connector

Assembly method of field-installable SC-type connector is shown in Fig.2. To install this connector, the wedge is inserted into the mechanical splice part to open it slightly, so that the connecting optical fiber can be inserted. When the wedge is removed, the fibers are jointed and connector is assembled. By using the tool which is shown in Fig. 3, the assembly can be performed easily.

The average time taken to strip the fiber jacket, perform splicing at the mechanical splice and finally to assemble the connector, is less than 2 minutes.

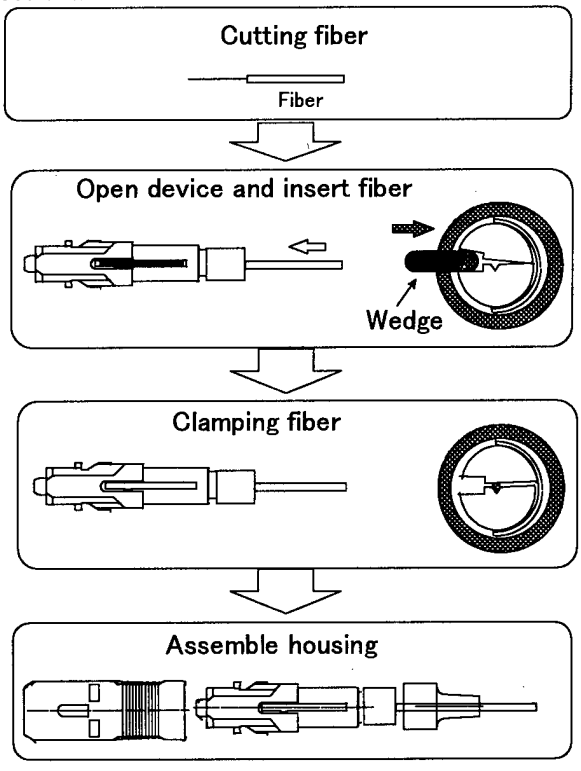

Fig.2 Fiber assembly process of field-installable SC connector

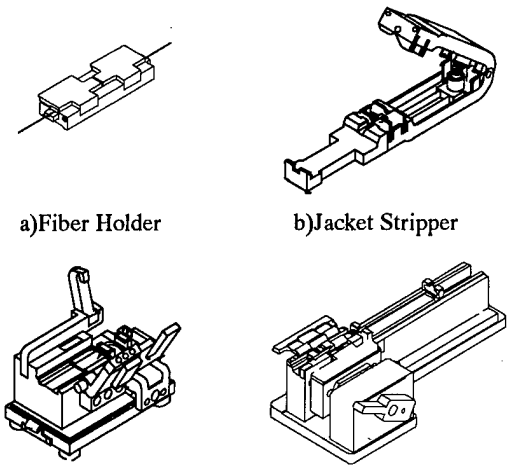

Fig. 3 Tool kit for field-installable SC connector

2.1.3 Characteristics of field-installable SC-type connector

1) Insertion Loss

Fig. 4 shows the results of the insertion losses of field-installable SC-type connectors for single-mode fiber. The measurement was conducted at a wavelength of 1.31 μm without the use of refractive index matching materials. The average insertion loss is 0.15 dB. The result confirmed the excellent connection loss performance of the field-installable SC-type connector.

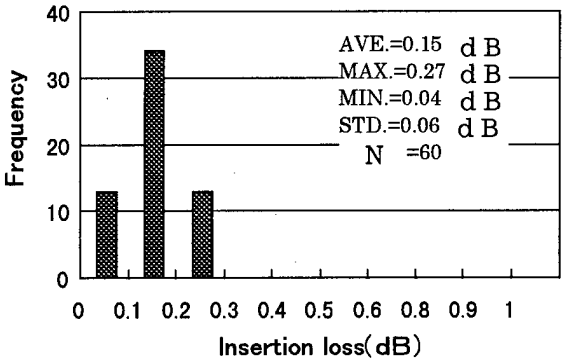

Fig. 4 Insertion loss of field-installable SC-type connector

2) Return loss

The return loss of the single-mode field-installable SC-type connector was measured when mated with a reference connector. The histogram of the test results is shown in Fig. 5. The return losses are higher than 40 dB.

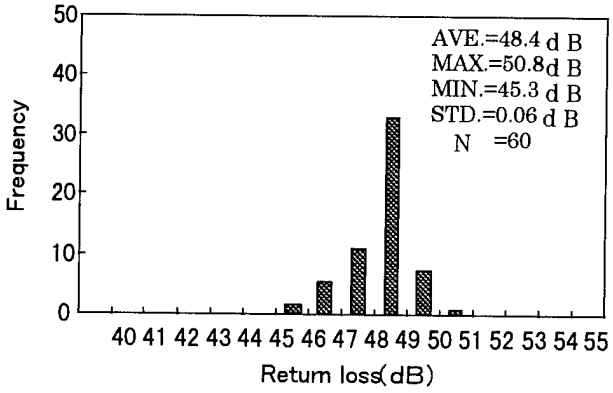

Fig. 5 Return loss of field-installable SC-type connector

3) Reliability test

The insertion loss fluctuation of the connector was measured for ten cycles with the temperature of each 6-hour cycle varies from -40 °C to 70 °C . The results of the measurement are shown in Fig. 6. The loss fluctuation during the test is within 0.1 dB.

The results of reliability test for SM fiber are also shown in Table 2. The data show the average values for the loss changes for 8 samples for each test. The results of each test demonstrate the stability and reliability of the connector and its suitability for actual implementation in the field.

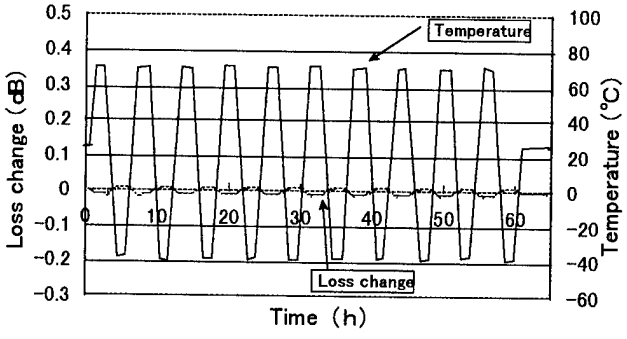

Fig. 6 Temperature cycling test result of field-installable SC connector

Table 2 Characteristics of the field-installable SC-type connector

Item	Test conditions	Characteristics
Insertion loss	SM fiber	Avg.: ≦0.2dB
	GI(62.5/125) fiber	Avg.: ≦0.1dB
Optical return loss	SM fiber	≧40dB
	GI(62.5/125) fiber	≧35dB
Repeatability	500 times re-connection	Change: ≦0.18dB
Temperature cycling	-30 ~ 70 °C /6h × 10 cycle	Change: ≦0.11dB
Condensation	-10 ~ 25 ~ 65 °C 93%RH/24h × 10 cycle	Change: ≦0.10dB
High temperature	70°C 240h	Change: ≦0.10dB
Low temperature	-40°C 240h	Change: ≦0.12dB

2.2 Field-installable ST-type connector

Fig.7 shows the structure of the field-installable ST-type connector. It is composed of the connector part, which is compatible with the ST connector ,and mechanical splice part. The basic principle of the construction method of the ST-type connector is same as that of the field-installable SC-type connector.

The optical performance of the field-installable ST-type connector is similar to that of SC-type connector.

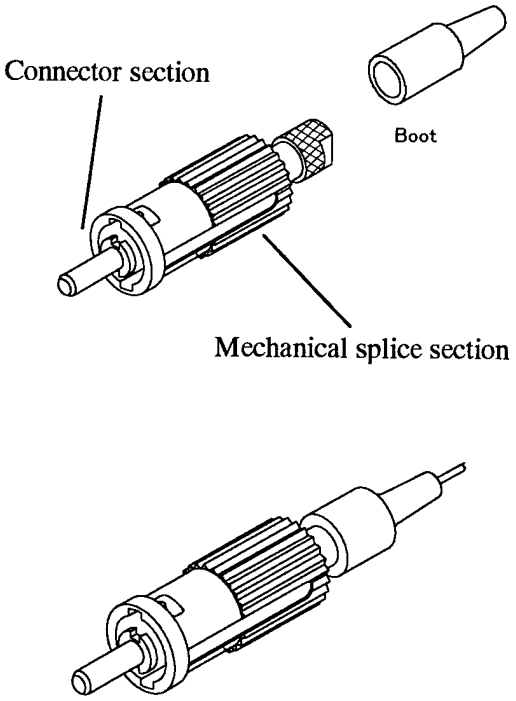

Fig. 7 Structure of field-installable ST connector

3. Field-installable mini-MPO connector

3.1 mini-MPO connector

In order to realize efficient fiber optic subscriber networks and optical computer networks, it is necessary to connect high density fibers and equipments easily1)2). The MPO (Multi-fiber Push-On / Pull-Off) connector, which is an extension of the multi-fiber MT (Mechanically Transferable) connector, is suitable for the fiber counts ranging from 2- to 12-fiber and is used widely. We have successfully developed the 2- and 4-fiber mini-MPO connector which has a higher packaging density than the conventional 2-fiber MPO connector or the 2-fiber connector which uses zirconia ferrule.7)8)9)10).

Fig. 8 shows the structures of the mini-MPO connector and the conventional MPO connector. The principle structure of the mini-MPO connector is same as that of MPO connector. The connection principle lies in the structure obtained by polishing the MT ferrule end face diagonally or perpendicularly so as to make the fiber tips protrude out. The fibers can therefore be mated directly with PC(Physical Contact) resulting in a low return loss. The cross section area of the mini-MPO connector is approximately 70 % of that of the conventional MPO connector.

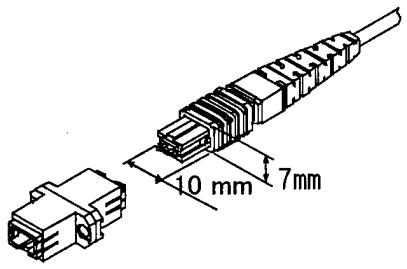

(a) Mini-MPO connector

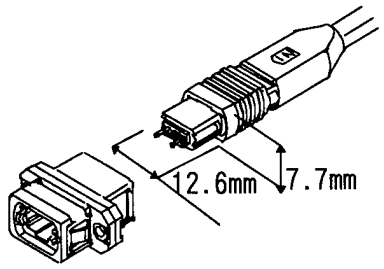

(b) MPO connector

Fig. 8 Structures of mini-MPO connector and MPO connector

3.2 Structure and assembly method of field-installable mini-MPO connector

We have developed the field-installable mini-MPO connector for easy assembly in the field.

Fig. 9 shows the structure of the field-installable mini-MPO connector. The connector is composed of MT ferrule section, mechanical splice section and housing parts. The MT ferrule section contains factory-installed fibers and the end surface is polished.

Assembly method of field-installable connector is shown in Fig.10. The wedge is inserted externally into the mechanical splicing part to open it slightly, and bare fibers which have been cut with a mirror end-face are inserted. After the connecting optical fibers come into contact with the fibers in the ferrule, the wedge is removed and then the fibers are mated. The average assembly time is about 2 minutes.

3.3 Characteristics of field-installable mini-MPO connector

Fig.11 and Fig. 12 show the results of the insertion loss and return loss of field-installable mini-MPO connectors for single-mode fiber. The measurement was conducted at a wavelength of 1.31 μm without the use of refractive index matching materials. The average insertion loss is 0.25 dB and the return losses are higher than 40 dB.

The test results confirm that the connector could be successfully employed in the field.

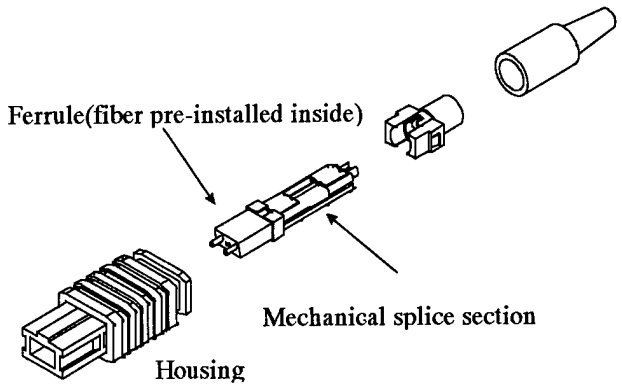

Fig. 9 Structure of field-installable mini-MPO connector

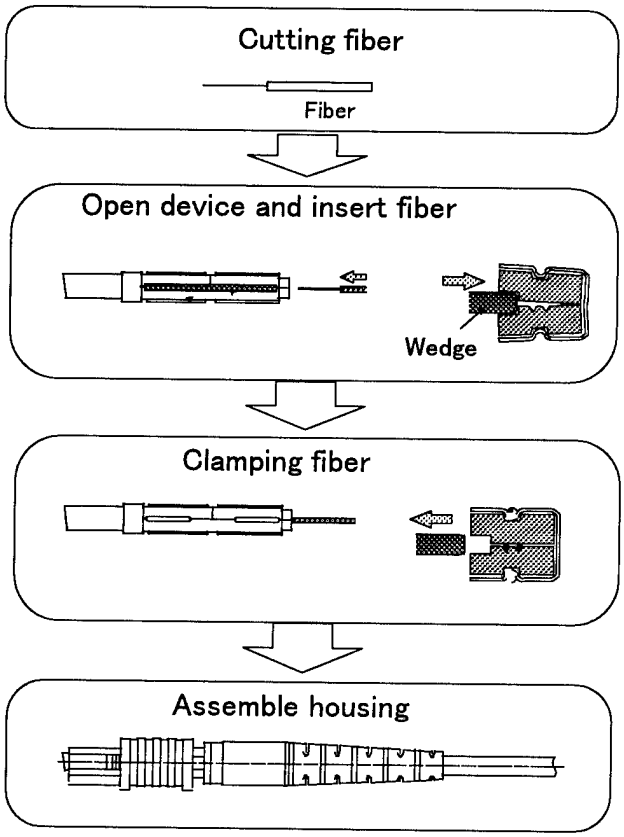

Fig. 10 Fiber assembly process of field-installable mini-MPO

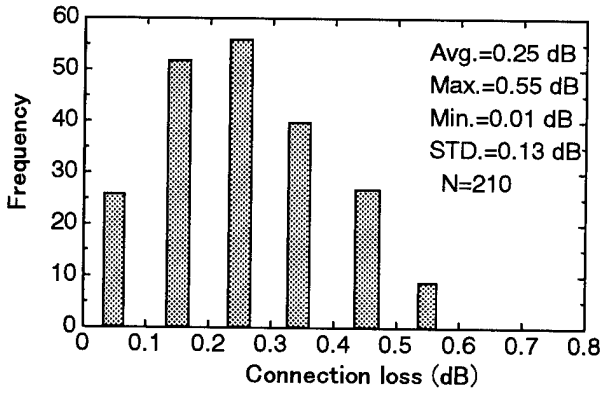

Fig. 11 Insertion loss of field-installable mini-MPO

4 .Conclusions

We have developed the field-installable single fiber connector (SC-type and ST-type) and field-installable mini-MPO connector which can be installed in the field without polishing and resin bonding process. The practical implementation of these connectors has also been confirmed.

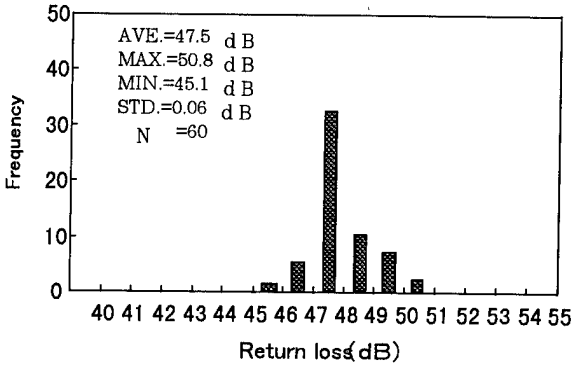

Fig. 12 Return loss of field-installable mini-MPO connector

References

1)S.Nagasawa, et al.:Single-Mode Multifiber Connectors for Future Large Scale Subscriber Networks, ECOC'93, MoP1.5,pp.29-32,1993

2)S.Tomita, et al.:Ultra High-Density Optical Fiber Cable with Thin Coated Fibers and Multi-Fiber Connectors, 42nd IWCS,1993

3)K.Takizawa, et al.:Reference Multifiber Connector, 44nd IWCS,1995

4) K.Takizawa, et al.: Study on High Speed MT-connector Assemble Method, Proceedings of the IEICE general conference, B-1069, 1996

5) K.Hogari, et al.: Field-installable Single-fiber Connector, Electronics Letters, vol.33, No.12, pp1072, 1997

6))K.Takizawa, et al.:Development of Field-installable Single-fiber Connector, Proceedings of the IEICE general conference,B-10-29,1997

7) K.Takizawa, et al.: Development of Mini-MPO Connector, Proceedings of the IEICE general conference,B-10-32,1997

8)K.Takizawa, et al.:Development of Mini-MPO Connector, 46nd IWCS,1997

9)N.Iimazu , et al.: Development of Mini-MPO Connector, ECOC'98,14C3-2 ,1998

10)M.Takaya et al : Designed Performance of a Miniaturized MPO type Connector for High-Density Optical Duplex Connection, IEEE Phton. Technol.Lett.,vol.10,No.1, pp102-104,1998

Kazuhiro Takizawa
Fujikura Ltd.
1440 Mutsuzaki Sakura,Chiba,285-8550,
Japan

Kazuhiro Takizawa was born in 1968. He graduated from Yokohama National University with an M.E. degree in 1993. He joined Fujikura Ltd., and has been engaged in the research and development in the Fiber and Cable Accessory Department of the Optical Access Network Laboratory. He is a member of the IEICE of Japan.

Yasuhiro Tamaki
Fujikura Ltd.
1440 Mutsuzaki Sakura,Chiba,285-8550,
Japan

Yasuhiro Tamaki was born in 1955. He received a B.E. degree in mechanical engineering in 1977 from Saitama University. He joined Fujikura Ltd. in 1982. He is now a general manager in Fiber and Cable Accessory Department of the Optical Access Network Laboratory and a member of the IEICE of Japan.

Toru Arikawa
Fujikura Ltd.
1440 Mutsuzaki Sakura,Chiba,285-8550,
Japan

Toru Arikawa is a manager of Fiber and Cable Accessory Department in Optical Access Network Laboratory. He received B.E. and M.E. degrees in image science engineering from Chiba University in 1982 and 1984, respectively. He joined Fujikura Ltd. after his graduation, and has been engaged in the research and development of optical fibers, components and accessories.

Hiroshi Yokoasuka
Fujikura Ltd.
1440 Mutsuzaki Sakura,Chiba,285-8550,
Japan

Hiroshi Yokosuka graduated in mechanical engineering from Tokyo Metropolitan Technical Junior College in 1967. He has been engaged in development of telecommunication cables and accessories. He is now a general manager of Optical Access Network Laboratory. He is a member of IEICE of Japan.

OPTICAL CONNECTORS RELIABILITY AT FOUR DIFFERENT CLIMATIC CONDITIONS: RELEVANT MEASUREMENTS AND MOST COMMON FAILURES MODES

Sergio Bianco [(1)], Diego Suino [(1)], Marco Ughetti [(1)], Francesco Montalti [(2)]

[(1)] CSELT Via R. Romoli 274, Torino, Italy; [(2)] Telecom Italia Via Val Cannuta 250, Roma, Italy

ABSTRACT

The reliability of the SC-APC connector has been investigated through a complete set of measurements and tests including a 5000 hours ageing test performed at four different climatic conditions. The results of this work improve the current state of knowledge about the failure modes and mechanisms of a ferrule physical contact optical connector. Particularly, our reliability test shows that the most common failure modes are the increase of the attenuation and the degradation of the coupling mechanism. These failure modes are due to two main failure mechanisms: fiber breakages and relaxation of the latch inside the adapter. This test reveals also that the return loss seems not to be affected by the high value of fiber undercut found after the ageing. This is because even very high value of undercut are not enough to produce a lack of physical contact on APC connector. Moreover an unexpected deformation of the ferrule surface has occurred.

INTRODUCTION

As optical connectors are more and more getting widely used in the distribution networks and consequently in not controlled environments it is important to address reliability issues and possibly to improve our knowledge about the life time of these components.

It is widely recognized that presently no well defined test and analytical methods for estimating the reliability of fiber optic connectors are available. Consequently this problem is addressed within the activities of several Standardization Bodies at international level. For example: IEC 86B WG 5 "Reliability of fiber optic interconnecting devices and passive components", COST 246 WG 2 "Material science and reliability of optical connection and branching devices".

Anyway this is not an easy issue because of many reasons, particularly:

- the wide range of service conditions (temperature and humidity) and the associated variety of failure modes;
- the ageing works in different ways on the different materials of the component (zirconia, epoxy, plastic).
- the expected life of the connector depends on the handling, that is how many times it is connected or disconnected and how it is cleaned during its life;
- a field failure statistics is still lacking.

The aim of this work is to review, in general terms, basic reliability concepts referred to optical connectors, give the results of a reliability test performed at CSELT on SC-APC connectors and explore the applicability of these results to improve the current state of knowledge about the failure modes and mechanisms of these devices. This test is specially focused to assess the reliability of a ferrule physical contact optical connector during its static life, that is a life without many mating operations.

The reliability of a component is the ability of the component itself to perform a required function under stated conditions for a stated period of time.

The basic elements of a reliability test plan are:

- identification of all possible failure modes;
- identification of the failure mechanisms and the relevant test to accelerate them;
- find the correct life-stress model and determine the acceleration factor;
- determine the overall failure rate (FIT) through applying statistical model to the sperimental data.

For the reasons listed above, at this moment, it is not possible to estimate the real lifetime of optical connectors from the test data.

Table 1 summarizes the current state of the knowledge about the failure modes, failure mechanisms and their causes or accelerating factors referred to optical connectors. **Failure modes** are the change of optical or mechanical characteristics that reveals a functional anomaly; **failure mechanisms** are the first stage factors which causes the failures modes; **causes** are mechanical or environmental stress that produce or accelerate the failure mechanisms.

An other critical issue regarding optical connectors reliability is the end of life (or failure) criteria that is the criteria used to consider an optical connector dead (not working any more) and so to count it as a failure. The selection of failure criteria must be based on system requirements and is consequently system dependent.

Table 2 shows the of end of life criteria for SC-APC connectors followed in our work; these criteria are very similar to those proposed by COST 246 WG 2 (Copenhagen, March 1997). *"A connection is considered failed when one of the three parameters of*

the first column of Table 2 is changed over the limits given in the second column.

Table 1 Failure modes failure mechanisms and causes for physical contact optical connectors

Failure mode	Failure mechanism	Causes
Insertion Loss increase Reflection increase Degradation of coupling mechanism	Fiber break Contamination of endface Break or Deterioration of endface Deterioration of adhesive High undercut Alignment sleeve crack Deterioration of the latch	High humidity HighTemperature Temperature variation Cable or fibre pulling Torsion Flection Vibration

Table 2 End of life criteria

Parameter	**End of life (failure)**
Attenuation	Variation > 0.3 dB
Return loss	< 55 dB
Coupling mechanism	< 40 Newton

TEST PLAN

The overall sample under test consists of 45 SC-APC patchcords (90 plugs) and 45 SC-APC adapters (with the sleeve made of zirconia) from different suppliers. As all suppliers use the same technology to produce this connector we have not performed an analysis aimed to point out the different performances of the components of each supplier. However, in this paper it will be specified if a particular kind of failure mode or failure mechanism occurres only on components from a particular supplier or if it is common to all suppliers.
Before the ageing test, the following measurements have been performed:

- visual inspection of the ferrule endface by a microscope;
- geometrical parameters (curvature radius, endface angle, undercut and apex offset);
- attenuation at 1550 nm on 189 random connections;
- return loss on open plugs;
- return loss on 189 random connections;
- spectral attenuation on 189 random connections.

Then, the sample was split in 4 groups formed by 11 patchcord and 11 adapters each.
Three groups were put in three different climatic chambers at three different climatic conditions (see table 3); the fourth group was stored at ambient conditions.

Table 3 The four climatic conditions

Groups	1	2	3	4
Temp. [°C]	75	45	25	Ambient
RH [%]	85	85	75	Ambient

Figure 1 shows the specimen's disposition that is the same for each of 4 groups: a chain of six patchcords connected by five adapters, four patchcord connected two by two, a free patchcord and four free adapters.
The ageing test lasted 5000 hours, but the following measurements have been performed after 1000, 2000 3000 and 5000 hours of ageing on the components of each group:

- visual analysis by microscope;
- geometrical parameters;
- attenuation (40 connections with plugs and adapters of the same group);
- return loss (open plugs and 40 connections with plugs and adapters of the same group);
- spectral attenuation (40 connections with plugs and adapters of the same group).

As the chains have been opened only at the end of the 5000 hours of ageing only the attenuation of the chain and the return loss of the connections have been measured at 1000, 2000 and 3000 hours.
After the ageing the same measurements performed before the test have been repeated.
Moreover, after the optical and geometrical measurements, the cable pulling test and the strength of coupling mechanism test have been run; these mechanical tests are aimed to check the degradation of component's mechanical performances after the ageing.
All optical, geometrical and mechanical measurements or tests have been performed following the IEC –61300 series procedures.

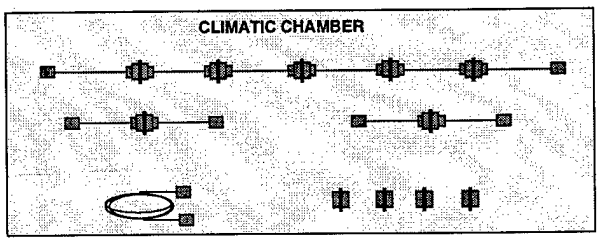

Figure 1 Scheme of the specimens disposition

TEST RESULTS

General view of the failures occurred

Table 4 gives the total percentage of failures found in the components of each group after the tests. This percentage is calculated as the number of components (plugs and adapters) failed with respect to the total number of components of each groups, that is 22 plugs and 11 adapters.

Table 4 Total percentage of failures at 5000 hours

	75°C 85%RH	45°C 85%RH	75°C 25%RH	ambient
Attenuation	37.5%	6%	0%	12%
Return loss	0%	18%	0%	0%
Coupling mechanism	100%	18%	14%	0%

The following paragraphs analyze in a detailed way each failure mode and the correlate failure mechanisms.

Attenuation

Figure 6 show the results of the attenuation measured at 1550 nm on 189 random connections (involving all tested plugs) before the ageing test and on the 130 still working connections after the ageing test. These measurements have been performed mating in a random way all plugs under test without taking into account the different climatic conditions during the ageing. This, to have a general view of the behavior of this parameter on a significant number of connections. The results are briefly summarized on Table 5.

We can observe a slight degradation of the attenuation, particularly the mean value rises to 0.25 dB. We have to point out that in Figure 6 only still measurable connections after the ageing test, that is still working connection, are considered. In fact, at the end of the 5000 hours a number of not working connections (without optical continuity) that are not considered in the graph but that have to be considered as failures have been found. The total percentage of failures is 34% (all suppliers are involved). This percentage is calculated as the number of failed connections referred to the number of measured connections. Particularly, 31% is the percentage of not working connections and 3% is the percentage of still working connections at the end of the ageing test showing a variation in the attenuation more than 0.3 dB (end of life criteria for attenuation).

In order to assess the behavior of each group at each climatic condition the attenuation has been measured during the ageing (at 1000 h, 2000 h, 3000 h and 5000 h) on 40 connections for each group done connecting the 5 patchcords and the 6 adapters not used to build the chains. 40 is the number of connections obtained connecting every plug not involved in the chains with every other plugs (as the number of plugs is 10, every plugs has been connected with other 8 plugs).

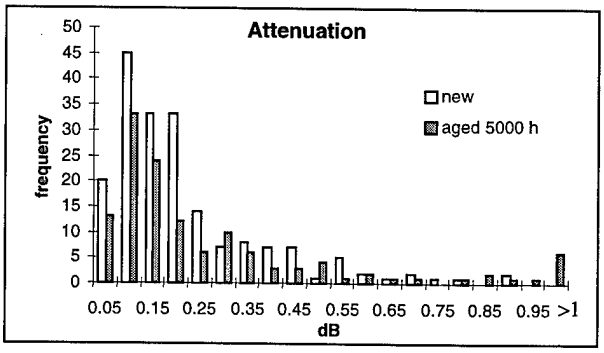

Figure 6 Attenuation on random connections

Table 5 Attenuation on random connections: summary of the results

Attenuation	N.	Mean [dB]	Max [dB]	Failures [%] (Var> 0.3 dB)
Before	189	0.19	0.89	34 (31+3)
Aged 5000 h	130	0.25	1.43	

Figure 7 gives the number of failures occurred at each time for each group. In order to calculate the number of failures referred to the single plug, the average value of the attenuation of each plug has been evaluate as the sum of the values of the attenuation obtained connecting each plug with the other 8 plugs divided for the number of measurements (8). A failure is considered when a plug shows a change in this average value of the attenuation over 0.3 dB. A failure is considered even when a plug or an adapter is not working any more.

As far as the chains are concerning, 1 failure at 1000 h on the chain aged at 75°C, 85% RH and 1 failure at 3000 h on the one aged at 45°C, 85% RH have occurred. Both of them are due to the fiber breakage in one of the patchcords.

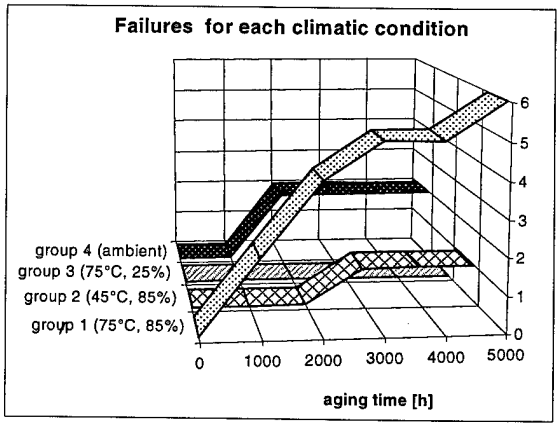

Figure 7 Number of failures occurred on each group during the ageing test

Failure mechanisms The observed failures regarding the attenuation that have just been discussed are due to two main failure mechanisms: fiber breakage and adapter breakage. Figure 8 gives the number of fiber breakages occurred during the ageing test whereas Figure 9 gives the percentage of broken fibers found after all tests and measurements (particularly after the mechanical tests).

Measurements performed by a low coherence interferometric reflectometer revealed that most of the fiber breakages occurred at about 1 cm from the ferrule endface that is in the weakest zone of the fiber where the coating has been removed during the assembling of the connector (Figure 10). As most of the broken fiber occurred in groups aged at high humidity (group 1 and 2) it is thought that the high humidity produces the growing of little cracks already present in the zone pictured in Figure 10. Moreover, as most of the fiber breakages before the mechanical tests occurred in group 1 (75°C, 85%RH) it is believed that even the shrinking of the cable at high temperature is an important factor. As this kind of failure occurred even on the patchcords of the chains aged at high humidity (group 1 and 2) it seems that even components not handled during the test are inclined to the fiber breakage.

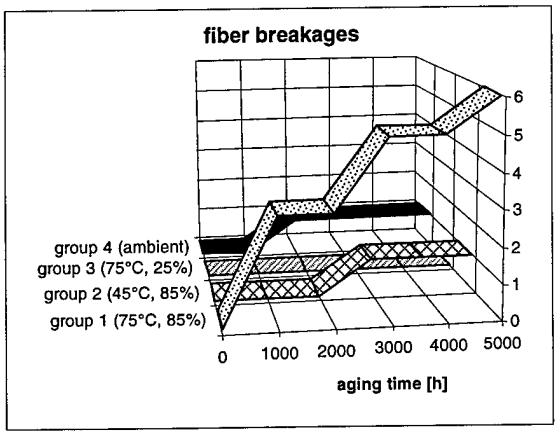

Figure 8 Fiber breakages during the ageing test

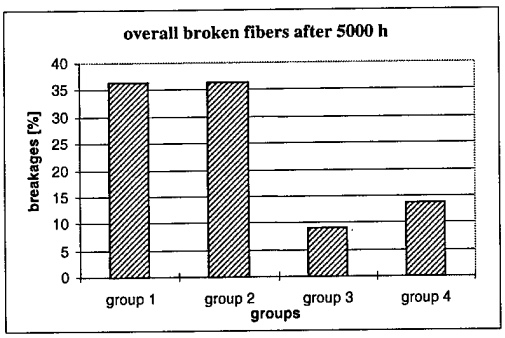

Figure 9 Percentage of broken fiber in each group at the end of the tests

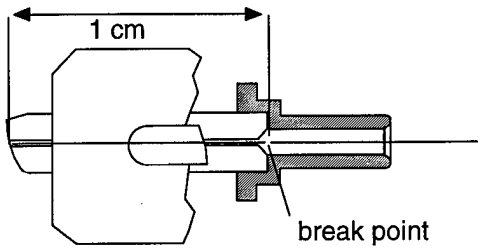

Figure 10 Scheme of the plug showing the break point position

Figure 11 gives the number of adapter breakages occurred in each climatic conditions during the ageing. An adapter breakage is consider when the adapter is not able any more to align the two fiber cores or to maintain the two fiber cores mated.

The adapter breakages are mainly due to the relaxation of the adapter latch and also to the degradation of the plastic material causing the breakage of the adapter's body itself (a supplier has been particularly involved). These kind of failures occurred particularly at high temperature and humidity. The relaxation of the latch will be further discussed in the paragraph regarding the coupling mechanism.

It must be highlighted that the 3% of the connections showing an increase of attenuation over 0.3 dB (see Table 5) involve 5 plugs that revealed the breakage of the fiber after the mechanical tests.

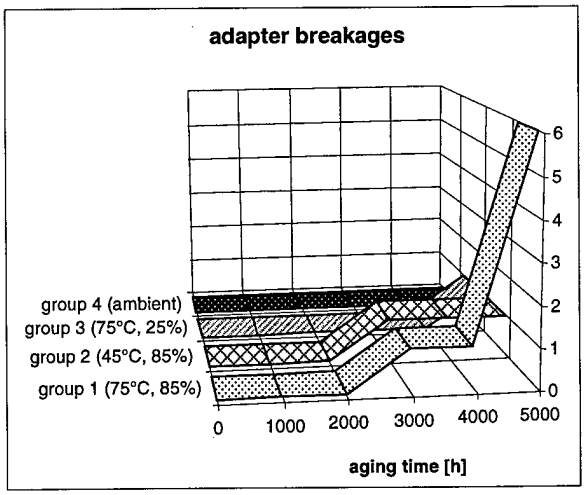

Figure 11 Adapter breakages during the ageing test

It is possible that a little crack in the fiber was already present at the end of the ageing test which resulted in an increase of the attenuation. The degradation of the attenuation involved also a plug with a plastic endface deformation (see the paragraph "visual inspection").

Return Loss

Figure 12 shows the results of the return loss measured at 1550 nm on 189 random connections (involving all tested plugs) before the ageing and on the 133 still working after the ageing test. These measurements have been performed mating in a random way all plugs under test without taking into account the different climatic conditions during the ageing. This, as for the attenuation, to have a general view of the behavior of this parameter on a significant number of connections. Figure 13 shows the results of the return loss measured at 1550 nm on the 90 open plugs before the ageing test and on the 76 still working open plugs after the ageing test. These results are briefly summarized on table 6.
Only a slight degradation of the return loss of connected plugs has occurred. A failure is considered when the return loss of a connection or an open plug is < 55 dB after the ageing (if it was ≥ 55 dB before the ageing test). The total percentage of failures in the return loss of connected plugs is only 3%. This percentage is calculated as the number of failed connections referred to the number of connections measured after the ageing test. The total percentage of failures in the return loss of open plugs is 5%. This percentage is calculated as the number of failed plugs referred to the number of plugs measured after the ageing test.

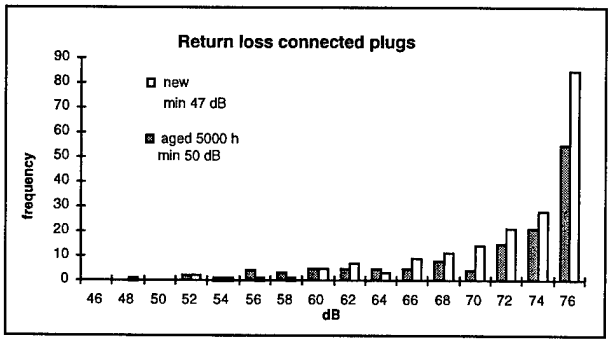

Figure 12 Return loss on random connections at 1550 nm (before and after 5000 h of ageing)

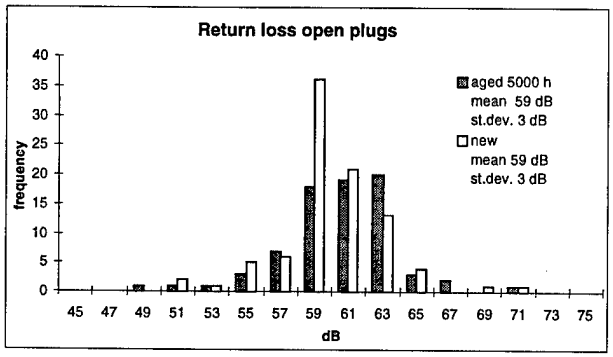

Figure 13 Return loss on open plugs (before and after 5000 h of ageing)

Table 6 Return loss: summary of the results

	Return loss	N.	Min [dB]	Failures
connected	Before	189	47	3%
	Aged 5000 houres	133	50	
open	Before	90	49	5%
	Aged 5000 houres	76	47	

Figure 14 gives the number of failures occurred at each time for each group. Only 4 failures occurred at 5000 hours on plugs of group 2, aged at 45°C and 85% RH.

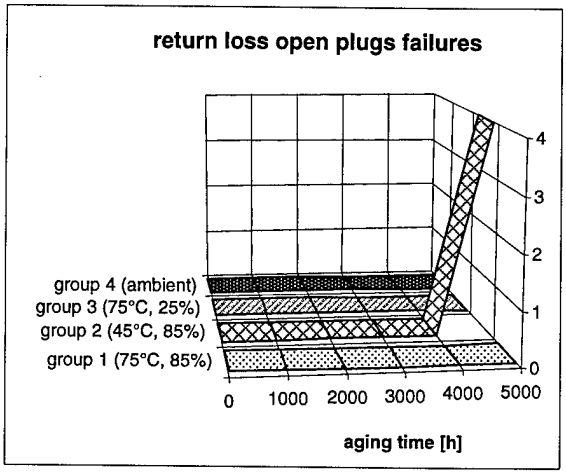

Figure 14 Return loss failures

Failure mechanisms It is widely believed that a factor affecting the return loss on physical contact optical connectors is the fiber undercut. In fact, in this kind of component the geometrical characteristics of the ferrule are critical. In particular a good geometry of the polished ferrule end surface is important to guarantee the physical contact between the two fiber cores. As far as reliability is concerned the fiber undercut is particularly important because it is affected by ageing and temperature variation. Fiber undercut is defined as the average distance between the fiber surface and the circular arc fitting the ferrule surface at the both sides of the fiber. The fiber undercut arises from the polishing process and from fiber movements in the ferrule due to thermal and mechanical stresses. High values of undercut (> 150 nm) can cause the lack of physical contact between the two fiber cores producing a

decrease of the return loss of the connection due to the high reflection arisen in glass-air transition. Previous tests and measurements showed that this is true in case of PC connectors (not angled). Fiber undercut has been measured by an interferometric device following the IEC procedure.

Figure 15 and 16 show the comparison between the undercut measurements results obtained before and after the 5000 h ageing test on all tested plugs. Figure 15 gives the distributions of the results obtained on plugs connected in the climatic chambers whereas Figure 16 gives the same for plugs open in the climatic chambers. These results show that the fiber undercut have been risen up values of about 300 nm for the plugs connected in the climatic chamber; the distribution of the results on connected plugs has shifted towards higher values of fiber undercut; instead the distribution of the results on open plugs shows both high values of protrusion and undercut. Figure 17 and 18 show how the fiber undercut has changed on plugs of different groups, during the ageing, respectively on open plugs and on connected plugs in the climatic chambers. As for connected plugs (Figure 17) the undercut of plugs of groups 1 and 3 (high temperature) has increased very soon whereas the undercut of the plugs of groups 2 (high humidity) has increased more slowly.

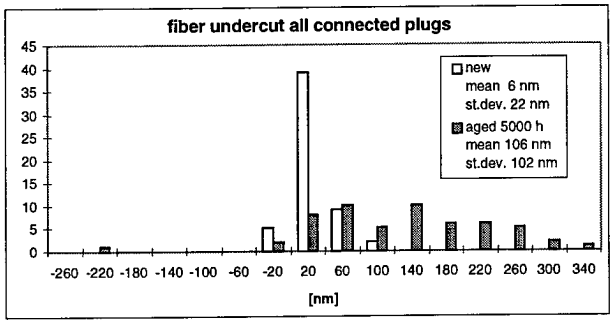

Figure 15 Undercut results on plug connected in the climatic chambers

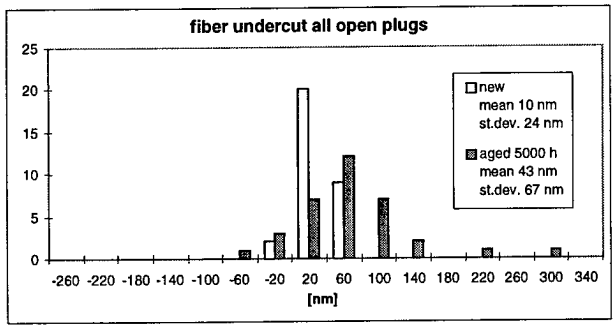

Figure 16 Undercut results on plug open in the climatic chambers

These results confirm that the ageing test affects in a very strong way this parameter producing both very high values of protrusion and of undercut, above all on plugs aged at high temperature. The increased fiber undercut in the mated connectors is due to the pressure on the fiber produced by the ferrule end face elastic deformation associated with the high temperature. The comparison with the data collecting during a previous ageing test performed on PC connectors shows that the increased undercut is particularly evident in case of angled connectors. This because their curvature radius (5-10 mm) is less than the curvature radius of a PC connectors (10 mm-25 mm) and so the pressure pushing force on the fiber is higher.

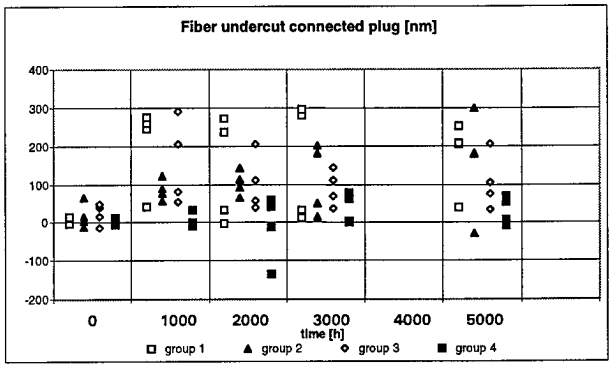

Figure 17 Undercut results of measurements repeated every 1000 hours (open plugs)

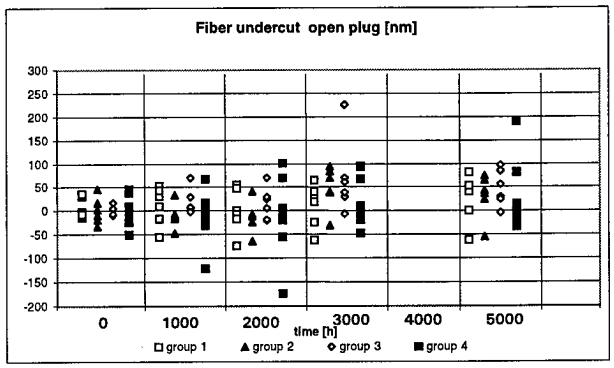

Figure 18 Undercut results of measurements repeated every 1000 hours (connected plugs)

Anyway, as very few failures in the return loss parameter has occurred, it seems that these high values of undercut measured after the ageing are not enough to produce the lack of physical contact on APC connectors. In fact Figure 19 states that there is not a connection between the return loss and the undercut.

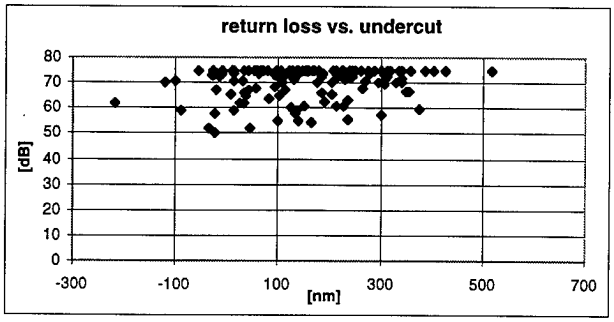

Figure 19 Return loss measured at 5000 hours of ageing as a function of the sum of the undercut of the two plugs.

This graph shows the return loss measured after the end of the ageing test on connected plugs (133 connections) as a function of the sum of the undercut of the two plugs involved in the connection. In order to verify that on APC connectors very high values of undercut do not affect the physical contact, a measurement of return loss during a thermal cycling on a connection involving two plugs with more than 200 nm of undercut have been performed (Figure 20).
As no significant variation related to the temperature has been observed it seems that even at 70° C (probably with values of undercut of about 250 nm for each plug) the fibers of the two plugs are still in physical contact.

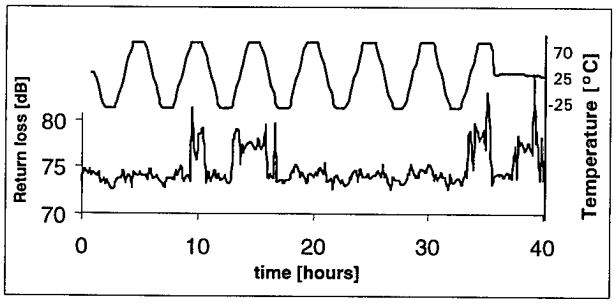

Figure 20 Return loss measured during a thermal cycling on a connection with high undercut

An other measurement useful to assess the physical contact is the spectral attenuation. Spectral attenuation is a measurement suitable to assess the physical contact between the two fibers of the two plugs involved in the connection when it is not easy to determine it by return loss measurement as in the case of angled connectors that show very high value of return loss even in the open plug configuration. The spectral attenuation has been performed (between 1400 nm and 1600 nm) on 189 connections before the ageing and on the 130 still working connections after the ageing. Moreover it has been performed on a number of connections made with plugs belonging to the same group at 1000 h, 2000 h, 3000 h and 5000 h. After the end of the ageing test the spectral attenuation has been performed also at high temperature (70 °C) on some connections involving plugs with very high values of undercut. The results confirm the ones obtained by the return loss measurement: all connections were in physical contact. This means that in case of angled connectors even very high values of undercut (300 nm) do not affect the physical contact between the two fibers. Probably, this is due to the curvature radius of APC connectors that is less than the curvature radius of PC connectors so the elastic deformation of the ferrule end face is able to recover an higher value of undercut.
As the fiber undercut is not the failure mechanism responsible for the failures observed in the return loss, it is believed that they are due to damages on the ferrule or on the fiber surface (see the paragraph "visual inspection").

Coupling mechanism

The strength of coupling mechanism test (40 Newton for 2 minutes) has been performed after the ageing on 82 connections (plug-adapter) involving plugs and adapters belonging to the same group. The aim is to check how the ageing test affects the mechanical proprieties of the adapters and plugs. The results (Figure 21) show that most of the failures occurred on connections made by plugs and adapters aged at high temperature and humidity (group 1). Failures occurred both on connections involving adapters connected in the climatic chamber ("conn" in the Figure 21) and on connection involving open adapters ("open" in the Figure 21).

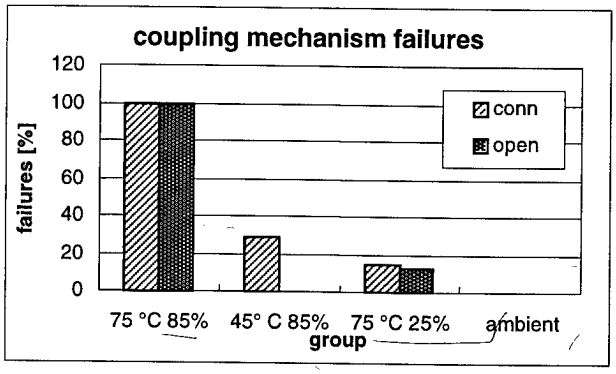

Figure 21 Strength of coupling mechanism test results

Failure mechanisms The decreased strength of the coupling mechanism seems to be caused by the relaxation of the adapter latch.
The relaxation of the adapter's latch is believed to be caused by the decrease of the Young's modulus of the latch at temperature of about 70 °C.

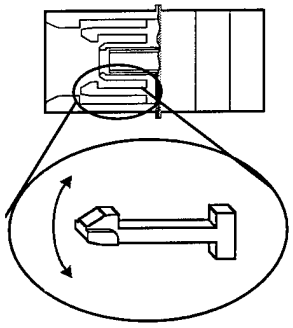

Figure 22 APC adapter and magnification of the adapter latch

In fact previous measurements performed on adapters of the same kind revealed that the Young's modulus of the latch falls at about 1/3 of his value when the temperature rises in the range 60°C-70°C. It is believed that after the ageing the latch remains in a wider position causing the adapter to break (see the paragraph "Attenuation") and the decrease of the strength of coupling mechanism. This is particularly true for adapter connected in the climatic chamber.

Additional Tests

Pulling test. The pulling test has been performed after the ageing test on all plugs still working (67 plugs).
The pulling test consists in applying 100 N to the cable for 2 minutes keeping the plug still.
This test is aimed to check how the ageing affects the mechanical proprieties of the cable and of the fiber inside the cable.
During these tests, as shown in Figure 23, many failures due to the breakage of the fiber occurred particularly in plugs aged at high humidity (groups 1 and 2)

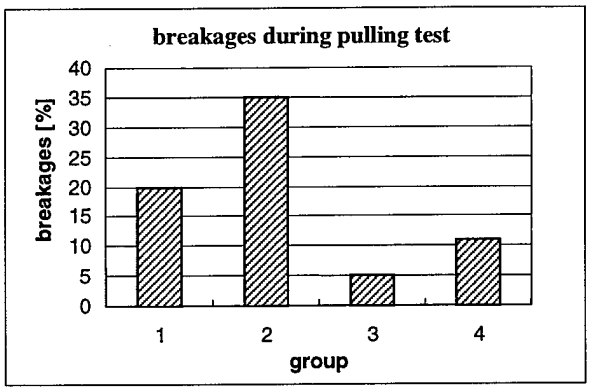

Figure 23 Fiber breakages occurred during the pulling test

Visual inspection A visual inspection of the ferrule has been performed before the ageing test, after 1000 h, 2000 h, 3000 h, and at the end of the ageing test by an interferometric microscope. Many damages have been observed (only some suppliers were involved). They include growing of grains on the zirconia surface, holes, scratches and plastic deformation of the ferrule endface.
Figure 24 shows the total number of ferrule endface damaged for each group. Figure 25 gives the number of ferrule endface for each group with something affecting the polishing of the endface like grains or holes.
Figure 26 gives the number of ferrule endface for each group that showed a plastic deformation of the ferrule near the fiber in the contact zone. This kind of plastic deformation occurred only on plugs connected in the climatic chamber.
Figure 27 shows the images of a ferrule endface without damages (a), a ferrule endface with holes (b) and two ferrule endfaces with a plastic deformation (c, d).
The plastic deformation of the endface of the zirconia ferrule is believed to be caused by phase shifting of the crystal structure of zirconia. Under physical pressure and in a humid environment it is possible that the crystal structure changes from tetragonial into monoclynic which might cause the reported observations.

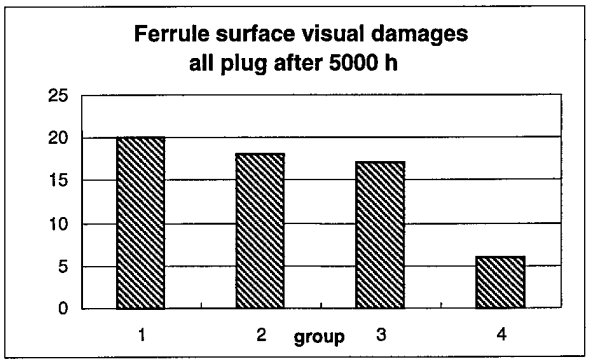

Figure 24 Number of ferrule surface damaged (all kind of damages)

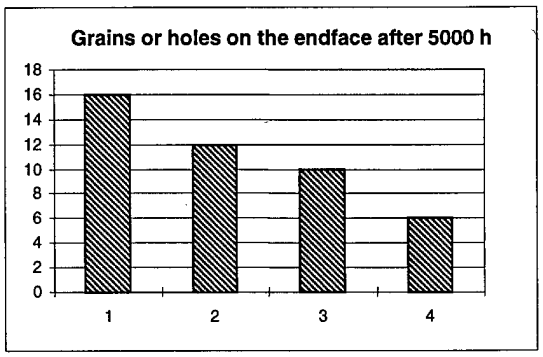

Figure 25 Number of ferrule surface showing grains or holes

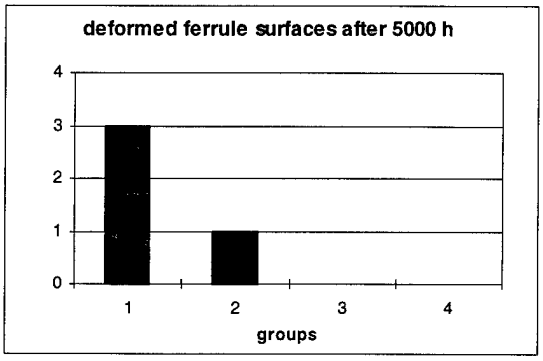

Figure 26 Number of ferrule surfaces showing a plastic deformation

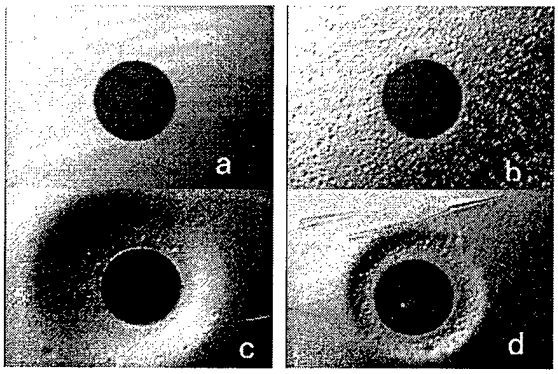

Figure 27 Images from a microscope showing: a) good ferrule surface b) ferrule surface with holes c) e d) ferrule surfaces deformed

It is important to highlight that further investigations are necessary to understand how this kind of phenomena affects the long term performances of the component.

SUMMARY

In order to try to draw some conclusions from the very large amount of data discussed in this paper, Figure 28 gives the total percentage of components (plugs and adapters) failed during the test whereas Table 7 gives a summary of the failure modes occurred, the failure mechanisms believed to produce that failure mode and the causes believed to accelerate that failure mechanism.

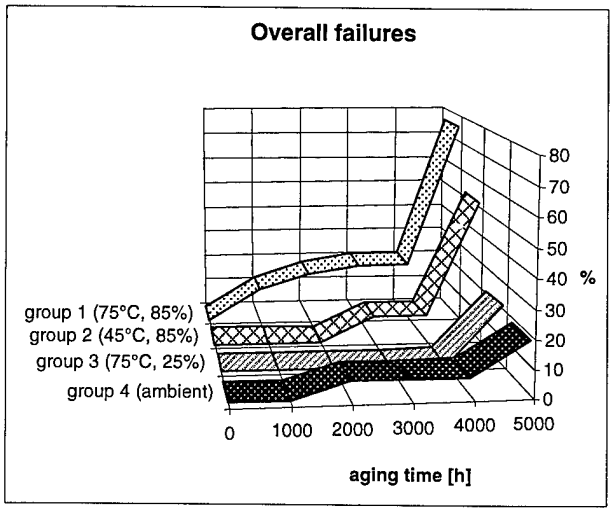

Figure 28 Total percentage of components (plugs and adapters) failed

Particularly, it seems advisable to focus on the following points:

- The increase of the attenuation is a very common failure mode due to two main failure mechanisms: fiber breakages and adapter breakages.
- Fiber breakage seems to be accelerate mainly by the high humidity (producing a growing of little crack already present) and even by the high temperature (shrinking of the cable).
- Adapter breakage seems to be due to the relaxation of the adapter latch and the degradation of the adapter body at high temperature; particularly the combination of high temperature and high humidity (75°C, 85% RH) seems to be a too stressful test condition for the adapters.
- Return loss is not a very common failure mode and seems to be affected only by the degradation of the ferrule endface whereas is not affected by the undercut. In fact, even very high values of undercut do not affect the physical contact on APC connectors.
- The degradation of the coupling mechanism is a very common failure mode on components aged at high temperature and humidity.
- An unexpected zirconia instability in high humidity conditions has been revealed by this test.

Future work could be focused on a more quantitative analysis of the expected life time of this kind of connector in order to obtain a FIT (Failure in Time) number. This attempt could be done by considering the effect of one failure mechanism at a time.

Table 7 Summary of failure modes, failure mechanisms and causes occurred during the test

Failure modes	Failure mechanisms	Causes
Attenuation increase	Breaking or Deterioration of the ferrule endface	High humidity and zirconia instability
	Fiber breakage	Growing of little crack at high humidity and shrinking of the cable at high temperature
	Adapter breakage	Relaxation of the adapter latch at high temperature
Return loss	Degradation of the polished surface?	Zirconia instability
Coupling mechanism	Relaxation of the adapter's latch	Change of the elasticity of the latch at high temperature

ACKNOWLEDGEMENTS

The authors whishes to tank A. Piccirillo (CSELT) for her fruitful help on reliability issues, T. Bolhaar (AMP) for sharing information about zirconia issues, L. Chiaro, G Grego (CSELT) for their work on the mechanical proprieties of the adapter latch, E. Ripamonti and P. Motta (CSELT) for their kind help in testing.

REFERENCES

[1] M. Ughetti "Optical connector reliability" Proceeding of Third COST 246 Workshop, Rome, 1996

[2] IEC WG5 Reliability of fibre opric interconnecting devices and passive components (draft)

[3] LeFevre "Failure mechanism and reliability of fibre optic connectors and splices" SPIE, 1973

AUTHORS

Sergio Bianco was born in Turin, Italy, in 1952. In 1971 he joined CSELT where he works in the Physical Carrier Qualification group at the study and development of measurement technique on optical fiber and passive optical component. His activity includes the development of the software used to control measurement set up.

Diego Suino was born in Turin, Italy, in 1962. He received his doctorate in Physics from the University of Turin. In 1989 he joined CSELT where he works in the Physical Carrier Qualification group engaging at the study and development of measurement technique on optical fiber and passive optical component. His activity includes also passive optical component specification and characterization. Moreover his present responsibilities include IEC WG86B activities.

Marco Ughetti was born in Turin, Italy, in 1967. He received his doctorate in Physics from the University of Turin. In 1995 he joined CSELT where he works in the Physical Carrier Qualification group engaging at the study and development of measurement technique on optical fiber and passive optical component. His activity includes mainly optical connectors specification and characterization and testing on copper cables. Moreover he is involved in CECC TC86BXA activities.

Francesco Montalti was born in Florence, Italy, in 1953. He received his doctorate in Physics from the University of Rome in 1976. In 1979 he joined Face Standard (Italian ITT branch) Research Center where he did research on optical fibers, optical components and thin film technologies. In 1985 he joined SIP (now Telecom Italia) Headquarters where he was involved in the development of optical and copper cables as well as the related hardware (splicing, closures, connectors). From 1994 he is in charge of the Cables Specifications in the "Outside Plant Technologies" section of Telecom Italia Network Division.
His responsibilities include the activities of ITU-T SG 6 (Outside Plants), IEC TC86B, CECC TC86BXA. He lectures at "Scuola Superiore Guglielmo Reiss Romoli"

Optical Fiber Cord with SC-type Optical Connector Integrated with Fiber Bragg Grating

Kazuaki Morita, Shigeru Suzuki, Yuichi Morishita, Kozo Kiyotake, Kazunari Sugi and Ken-ichi Muta

SHOWA ELECTRIC WIRE & CABLE CO., LTD.
4-1-1, MINAMIHASHIMOTO, SAGAMIHARA, KANAGAWA, 229-1133, JAPAN

ABSTRACT

Broadband chirped fiber Bragg gratings at 1.65 μm-band were prepared and assembled in the zirconia ferrules of SC-type connectors.Insertion loss of rejection band at 1.65 μm was over 30dB and rejection bandwidth was 15 nm. Insertion loss of transmission windows around 1.31 and 1.55 μm was below 1 dB. Environmental characteristics of the SC-type connectors with fiber Bragg gratings and thermal stability of fiber Bragg gratings was tested with good results.

BACKGROUND

It is important to maintain and manage the subscriber network at low cost because the cost is the most important issue in terms of realizing fiber to the home (FTTH). The optical fiber line remote testing system using optical time domain reflectometry(OTDR) is attracting much attention in Japan because the system allows to identify the point of failure in the optical line[1].In this system, a filter which reflects and rejects only the OTDR light is inserted before the optical network unit (ONU) to make it possible to carry out the OTDR test during on-line service.

Conventionally, dielectric multilayer thin film filters have been used as such rejection filters. The connectors using dielectric multilayer thin film filters have disadvantage as to production cost and mass-producibility because the connector with that filter consists of more parts and requires highly delicate aligning.

The connectors using FBG filters, on the other hand, have advantage because they realizes a fiber type device which is (1) extremely simple construction and (2) very easy and reliable to connect to the optical line. The number of components and the fabrication processes are greatly reduced by the employment of FBG filters, and it becomes possible to produce high-performance connector with filter at low cost.
This connector is a very simple and highly reliable device because the construction that the FBG is housed in connector ferrule eliminates the necessity of an extra construction for FBG reinforcement.

FABRICATION

The fiber Bragg grating was fabricated by the phase mask method[2] irradiating a convenient single-mode fiber with KrF excimer laser light(λ=248nm). A phase mask with linear chirp was used to obtain broadband filters, and the length of FBG was 13mm.

Target characteristics of grating were transmission loss of over 30 dB at the rejection wavelength region of 1650 $\pm$7.5 nm and transmission loss of below 1 dB and return loss of over 35dB at transmission windows (1310$\pm$ 20nm and 1550$\pm$30nm). The fabricated FBG was annealed, before assembling, for the purpose of assuring long-term stability of FBG characteristics. The annealed FBG (13mm long) was inserted and fixed with adhesive in a zirconia ferrule (16mm long).

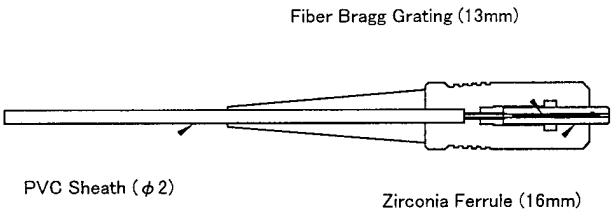

Fig. 1 *Construction of SC-type connector with FBG filter*

OPTICAL CHARACTERISTICS

Twenty samples of SC-type connectors with FBG filter were prepared, and transmission and reflection spectra shown in Fig. 2 and 3, respectively, were observed and transmission losses at transmission windows shown in Fig. 4 were measured. The spectra were observed using broadband light sources and an optical spectrum analyzer, and insertion and return losses at transmission windows were measured using Fabry-Perot laser diode and an optical power meter. In addition, the histogram of center wavelengths, transmission losses, and 30-dB bandwidths at the rejection band obtained from spectrum data are shown in Fig. 5, 6 and 7, respectively.

Characteristics at the rejection band were the center wavelength of 1648.3 nm, the transmission losses of over 36 dB and the mean bandwidth of 15.4 nm. Characteristics at transmission windows, in addition, were the insertion loss of less than 1 dB and the return losses of over 35 dB, which are satisfactory for practical use.

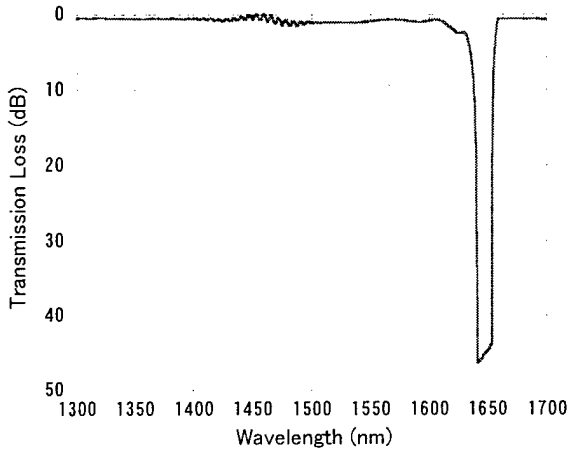

Fig. 2 *Example of transmission spectrum*

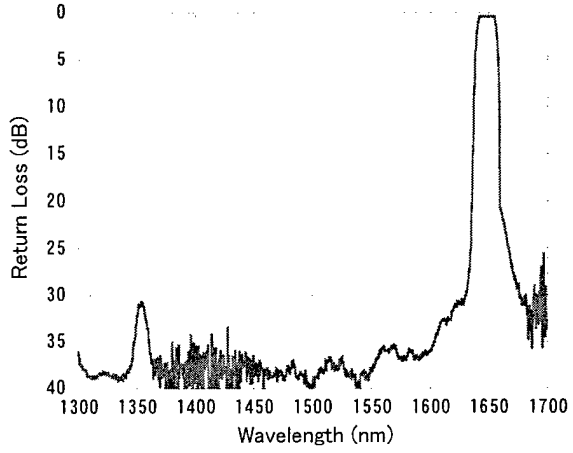

Fig. 3 *Example of reflection spectrum*

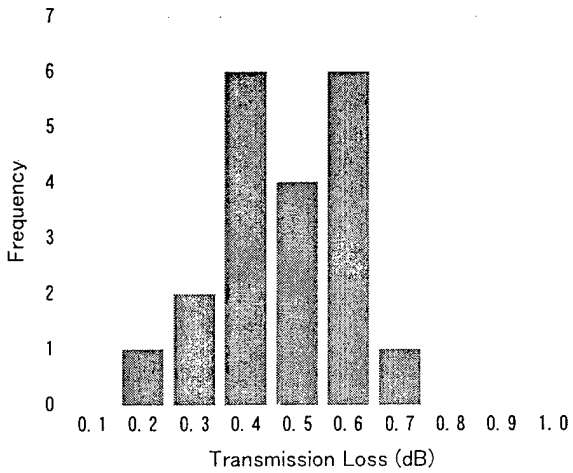

λ	1310 nm
Avg.	0.51 dB
Std.	0.21 dB

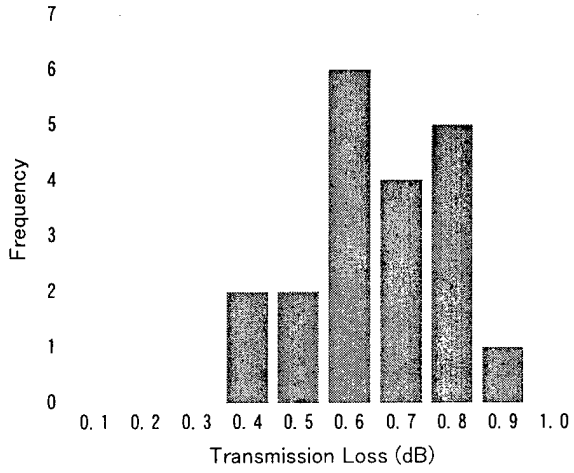

λ	1550 nm
Avg.	0.67 dB
Std.	0.16 dB

Fig. 4 *Histograms of transmission losses at transmission windows*

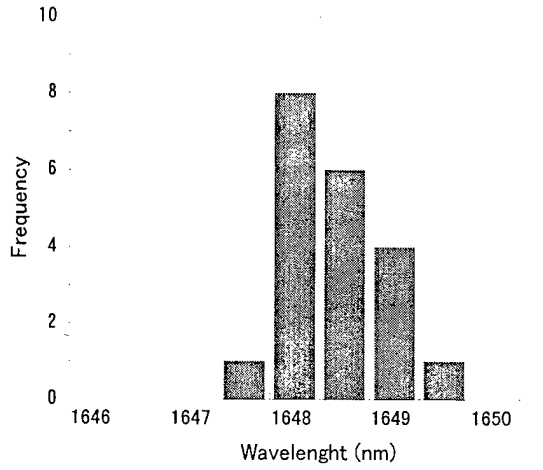

Avg.	1648.31 nm
Std.	0.52 nm

Fig. 5 *Histogram of Center Wavelength*

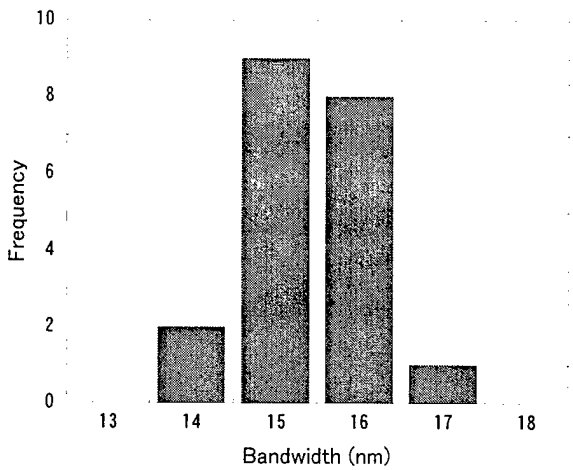

Avg.	15.39 nm
Std.	0.81 nm

Fig. 7 *Histogram of 30-dB Rejection Bandwidth*

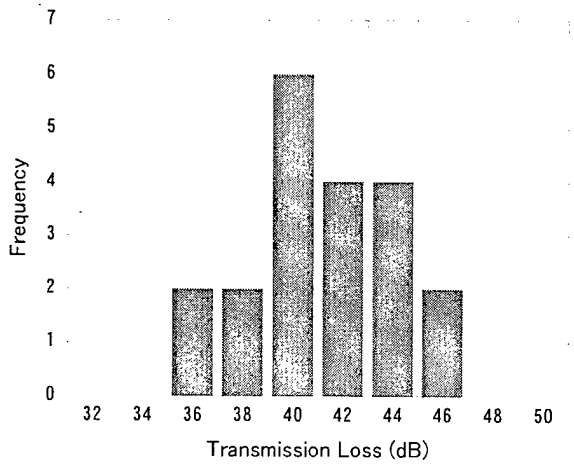

Avg.	42.86 dB
Std.	3.80 dB

Fig. 6 *Histogram of transmission loss at rejection wavelength region.*

ENVIRONMENTAL CHARACTERISTICS

Temperature cycling tests(-40 to +75℃, 336 hours), high temperature storage tests(80℃, 336 hours) and low temperature storage tests(-40℃, 336 hours) were carried out to evaluate environmental characteristics of the connector. Changes in characteristics before and after the test are shown in Table 1.

Changes in insertion loss at transmission window and center wavelength were recorded during the temperature cycling test, and results are shown in Fig. 8 and 9, respectively.

Table 1 *Changes in Characteristics before and after Environmental Test*

Item	Change in insertion loss			Change in wavelength
	1.31 μm	1.55 μm	1.65 μm	
High temperature storage test	< 0.1 dB	< 0.1 dB	< 1.0 dB	< 0.2 nm
Low temperature storage test	< 0.1 dB	< 0.1 dB	< 1.0 dB	< 0.2 nm
Temperature cycling test	< 0.1 dB	< 0.1 dB	< 1.0 dB	< 0.2 nm

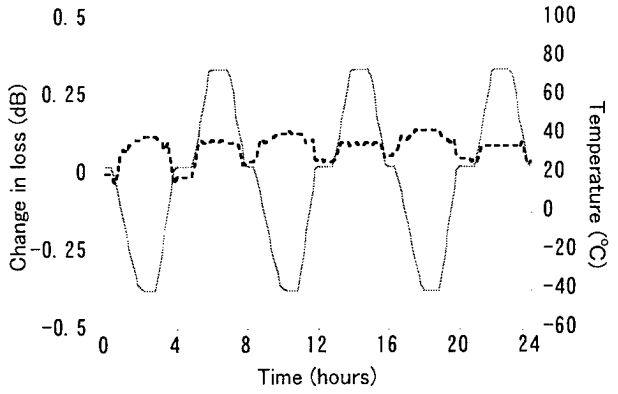

Fig. 8 *Changes in insertion loss during temperature cycling test*

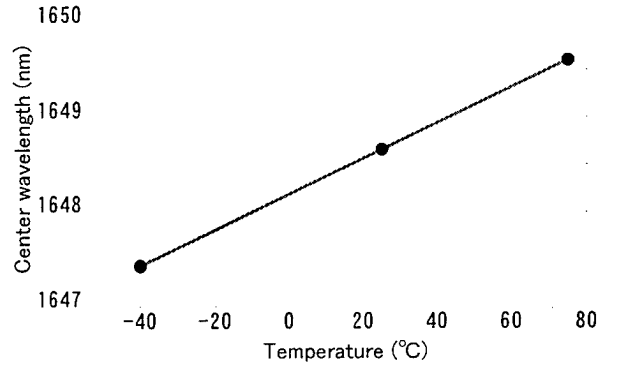

Fig. 9 *Temperature dependence of Bragg wavelength during temperature cycling test.*

The temperature coefficient of the Bragg wavelength in the temperature range of the temperature cycling test was 1.9×10^{-2}nm/℃, which is consistent with the value estimated from the temperature coefficient of refractive index of silica glass(1.2×10^{-5}/℃) and the thermal expansion coefficient of zirconia(8.3×10^{-6}/℃).

EVALUATION OF THERMAL STABILITY

Long term reliability of this connector components other than FBG filter has been well-established through many applications. The long term reliability of the connector with FBG was therefore evaluated through thermal stability tests on the rejection characteristics of the FBG filters. Samples used in the test were those which were recoated with covering resin after annealing. Thermal stability was evaluated by analyzing the time-depend deterioration of rejection characteristics by the aging curve approach.[3]

Samples were held for 20 hours at three temperature levels of 120, 160 and 200℃, and changes in rejection were recorded during the test.

Decay, relations between storage time t and normalized rejection ratio Rs(t), is shown in Fig. 10, where $Rs(t)=R(t)/R_0$, R_0 is initial rejection ratio of sample, and R(t) is that of sample at storage time t.

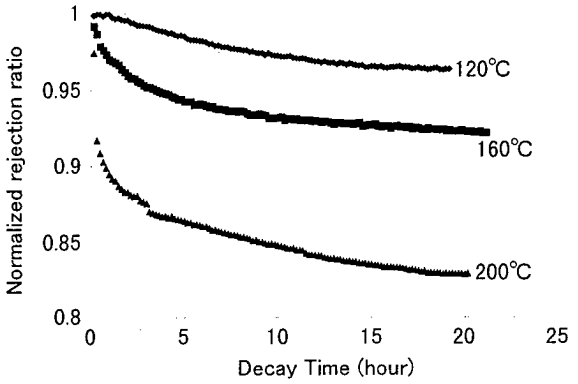

Fig.10 *Decay of the FBG at three different temperature levels of 120, 160 and 200℃*

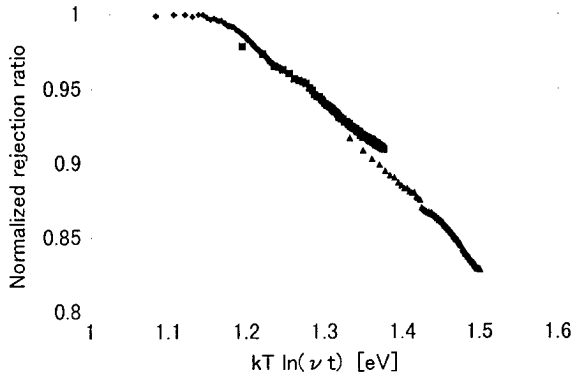

Fig. 11 *Aging curve obtained from decay of Fig.11.*

Figure 11 shows normalized rejection ratio plotted against $kT\ln(\nu t)$, where k is Boltzmann's constant, T is test temperature, ν is frequency term (attempt frequency) and t is storage time.

Deterioration in rejection during 25 years at 70℃ is predicted from the aging curve as shown in Fig. 12. This figure shows that the FBG filter fabricated under the condition of this experiment retains over 90% of its original rejection even after 25 years at 70℃, indicating that the FBG filters have the thermal stability which is satisfactory for practical use.

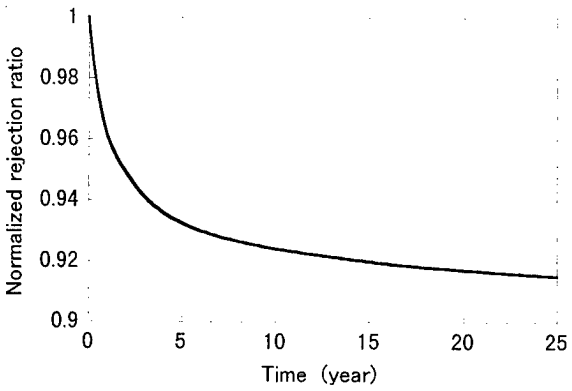

Fig. 12 *Predicted thermal stability of FBG based on accelerated aging tests(Fig.12).*

CONCLUSION

Optical fiber cord with SC-type connector, integrated with a broadband 1650nm rejection filter of fiber Bragg grating housed in zirconia ferrule, was developed and demonstrated good performance.

Optical characteristics of the device were center rejection wavelength of 1650nm, rejection of over 30 dB and 30dB bandwidth of over 15nm, and those at transmission windows(1310 and 1550 nm) were transmission loss of less than 1 dB and return loss of over 35 dB, which are fully satisfactory for practical application.

According to environmental tests of temperature cycling test, high temperature storage test and low temperature storage test, changes in loss between before and after the test were less than 0.1 dB and those in center wavelength were less than 0.2 nm.

In addition, the estimated deterioration in rejection after 25 years at 70℃ was less than 10 % according to thermal stability tests conducted on fiber Bragg grating elements, indicating that the device stability is satisfactory for practical use.

REFERENCES

[1] N. Tomita, Y. Enomoto, K. Tanaka, T. Kurashima, K. Hogari, S. Furukawa and N.Nakao, Technical Report Of IEICE Japan, OCS97-25, pp. 1-7 (Japanese)

[2] K. O. Hill, B. Maro, F. Bilodeau, D. C. Johnson and J. Albert, *Appl. Phys. Lett.*. **62** (1993) 1035J

[3] T. Erdogan, V. Mizrahi, P. J. Lemaire and D.Monroe, *J. Appl. Phys.* **76** (1994) 73.

AUTHORS

Kazuaki MORITA was born in Tokyo, Japan, in 1969. He received the B.E. and M.E. degree in Organic Materials Science from Tokyo Institute of Technology in 1993 and 1995 respectively. In 1995, he joined Showa Electric Wire & Cable Co., Ltd.(SWCC), Kanagawa, Japan. He has been engaged in development of optical fiber devices.

Kozo KIYOTAKE was born in Fukuoka, Japan, on Jun 27, 1965. He received the B.E. degree in Applied Chemistry from Kumamoto University, Kumamoto, Japan, in 1989. In 1989, he joined Showa Electric Wire & Cable Co., Ltd. (SWCC),Kanagawa, Japan. He has been engaged in development of optical fiber devices.

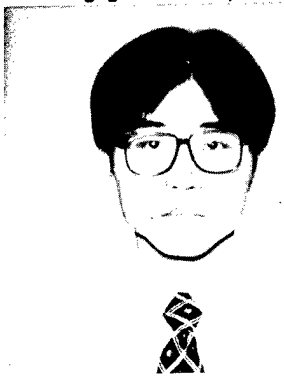

Shigeru SUZUKI was born in Aichi, Japan in 1970. He received B.E. and M.E. degree in Applied Physics from Hokkaido University in 1993 and 1995 respectively. In 1995, he joined Showa Electric Wire & Cable Co., Ltd.(SWCC), Kanagawa, Japan. He has been engaged in development of optical fiber devices.
Mr. SUZUKI is a member of the Institute of Electronics Information and Communication Engineers (IEICE) of Japan.

Kazunari SUGI was born in Tokyo, Japan, on December 24, 1954. He received the B.E. degree in Mechanical Engineering from Waseda University, Tokyo, Japan, in 1976. In 1985, he joined Showa Electric Wire & Cable Co., Ltd.(SWCC), Kanagawa, Japan. He has been engaged in development of optical fiber devices.
Mr. SUGI is a member of the Institute of Electronics, Information and Communication Engineers (IEICE) of Japan.

Yuichi MORISHITA was born in Tokyo, Japan, on March 28, 1965. He received the B.E. degree in Applied Physics from Science University of Tokyo, Japan, in 1988. In 1991, he joined Showa Electric Wire & Cable Co., Ltd.(SWCC), Kanagawa, Japan. He has been engaged in development of optical fiber and optical fiber devices.
Mr. MORISHITA is a member of the Institute of Electronics, Information and Communication Engineers (IEICE) of Japan.

Ken-ichi MUTA was born in Nagasaki, Japan in 1950.He received B.E., M.E. and Ph.D. degree in Organic Materials Science from Tokyo Institute of Technology in 1974, 1976 and 1980 respectively. In 1980, he joined Showa Electric Wire & Cable Co., Ltd.(SWCC), Kanagawa, Japan. He has been engaged in development of optical fiber and optical fiber devices.
Dr. MUTA is a member of the Institute of Electronics Information and Communication Engineers (IEICE) of Japan, Applied Physics and Ceramics Society.

DEVELOPMENT OF FUNCTIONALITY OF ARAMID YARNS AS OPTICAL FIBER CABLE REINFORCEMENT

H.A.M. Stuut, O. Grabandt and J.H. van Leeuwen

Akzo Nobel, Aramid Products VoF, P.O. Box 9300, 6800 SB Arnhem, The Netherlands

ABSTRACT

As a result of ongoing efforts by Aramid Products aiming at valuable improvements of the performance characteristics of Twaron aramid yarns, major progress at several fronts has been achieved. In this paper important developments regarding the primary mechanical properties like specific strength and modulus, the additional functionality provided by customized surface properties, now resulting in an "anti-tracking" finish and processability, especially improvement of bobbin stability are addressed.

INTRODUCTION

As a result of its favorable intrinsic properties, Aramid yarn presently is the predominant reinforcing material for Optical Fiber Cables, especially for long span ADSS cables. In the early days of the ADSS technology Aramids appeared to have an edge over the alternative reinforcing materials mainly as a result of its superior specific modulus, and since then it has become the preferred reinforcing material. A survey of the main types of Twaron aramid applied in these area's is presented in the table below.

Table 1: Survey of Twaron types and its main applications

Twaron type	Modulus range [GPa]	Main Applications
1000	65 - 70	Pulling tape, Ripcord
1111	80 - 90	Indoor Optical cables, Dropwire
2200	100 - 110	OFC general, Aerial OFC, Dropwire
1055	110 - 120	Aerial OFC, Central rods

In the first part of this presentation the primary mechanical properties of aramid yarns will be discussed in relation with the underlying structure and the means to improve them by upgrading the spinning process.
The second part deals with additional functionality provided by the customized properties of the yarn surface. Topical information is presented regarding the development of a semi-conductive finish to be applied on the reinforcing yarns for ADSS optical cables mounted on towers of high voltage power lines. The customized conductivity contributes to remedies against tracking damage caused by dry-band arcing.
Processability of the yarn is the subject of the final part, with emphasis on bobbin stability. Requirements regarding bobbin stability are becoming more and more severe as modern servers allow higher rotational speeds and OFC-producers tend to demand heavier bobbins. A novel approach aiming at improvement of bobbin stability is presented.

PRIMARY MECHANICAL PROPERTIES RELEVANT FOR THE REINFORCEMENT OF OFC'S

Introduction

The macro-molecular structure of the p-aramid (P-pPTA), as it results from the polymerization process, and the para-crystalline conformation arising during the spinning process, largely determine the main physical and mechanical properties of the aramid yarns. These properties also include the physical and mechanical properties which are of importance for its successful application as reinforcing material for ADSS cables. Both the chemical and physical structure and the relation between the relevant structural elements and the physical and mechanical properties are thoroughly documented elsewhere [1]. In order to facilitate an indication of the realized improvements of the yarn properties, some elements of the relations between structure and properties will be worked out to some extent herein.

Process, structure, property relations

The production of aramid yarns starts with polymer chemistry. The polymer P-pPTA is characterized by a given molecular weight and weight distribution. These

characteristics, which are controlled very carefully, determine the limits of the attainable yarn strength. The stable polymerization process is rather mature and developments are focused on further improvements of quality maintenance.

Steric hindrance within the macro-molecule results in a semi-rigid chain structure and as a result, the spinning solution has a (lyotropic) liquid crystalline nature. In the spinning process, which hinges on mechanical and physical properties, not on chemistry, this solution is transformed into a highly oriented para-crystalline solid having a well defined yarn geometry. The main structural parameter which can be influenced intentionally by adjusting settings in the spinning process is the orientation distribution of the chain direction. This is of paramount importance because the modulus of the yarn, which is the most essential performance characteristic of the OFC-reinforcement, is directly determined by the width of the orientation distribution, the chain modulus and a shear modulus. The latter are material constants and both theoretical estimates and experimental results point to a value of about 200 GPa for the chain modulus (e_c) and about 2 GPa for the shear modulus (g_0). By using a simple but powerful series model [2], see equation [1], the yarn modulus E_y can be predicted as a function of a well established orientation parameter [3] ($<\sin^2\varphi>$), as is shown in Figure 1.

$$\frac{1}{E_y} = \frac{1}{e_c} + \frac{\langle \sin^2 \varphi \rangle}{2g_0} \qquad [1]$$

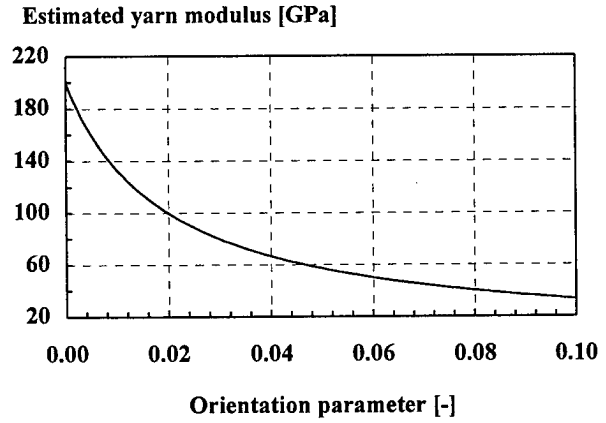

Figure 1: Yarn modulus in dependence of orientation parameter, based on series model and literature values for elastic constants.

By assuming a Gaussian distribution, the values of the orientation parameter can be transformed into half width heights; the values 0.01, 0.02 and 0.03 of the orientation parameter (see X-axis labels in Figure 1) transform into 4.0, 5.7 and 7.0 degrees. An intention to improve the yarn modulus calls for a reduction of the width of the orientation distribution, which already is rather narrow.

Process developments

A reduction of the width of the orientation distribution can be achieved by subtle optimizations in several stages of the yarn spinning process. The main factors being the draw ratio in the spinneret and air-gap above the coagulation bath and time, temperature and tension of the hot stretching during the drying stage. An element still to be mentioned is the role of water. The solvent of the spinning solution, sulfuric acid, is largely replaced by water in the coagulation bath. In the neutralizing and washing stages the remainder of the acid is removed thoroughly, but the yarn is soaked with water when entering the drying sections. The adhering water is removed completely, but the absorbed water still acts as a plasticizing agent, which facilitates further reduction of the orientation, whereas the available space for absorbed water decreases during this process. Summarizing it can be stated that the modulus target is attained by adjusting the width of the orientation distribution. This is to be achieved by controlling:

- the draw ratio in spinneret and air gap;
- the reduction rate of the water content during drying;
- the exposure to temperature and tension during drying.

Ongoing upgrading of production equipment, aiming at increased versatility in these respects, will soon result in the ability to supply an Twaron yarn having a modulus higher than 120 GPa.

The relation between strength, structure and process settings is rather complex and will not be addressed herein. However, process developments meant to improve the yarn characteristics are not implemented unless it has been proven that the target value of the strength is maintained. Other physical properties, like density and dielectric constant are hardly affected by modest changes in orientation and can be considered to be material constants. On the other hand, increase of modulus, while maintaining the strength, inevitable results in a decrease of ultimate elongation.

ADDITIONAL FUNCTIONALITY RESULTING FROM SURFACE ADDITIVES

Introduction

In addition to the main functions of the reinforcing yarns, i.e. providing the required mechanical strength and stiffness, several other useful functions can be performed by the yarns simultaneously. A well known example is the water-blocking finish [4]. This water-blocking function of the yarn is in particular successful thanks to the position of the reinforcing yarns underneath the outer jacket, as is usual in the predominant designs of ADDS cables. New is the development of a finish with customized conductivity. By applying this finish, the electrical resistance of the Aramid reinforcing yarns can be decreased by three to five decades. This development was triggered by reports about tracking problems occurring at ADSS cables strung on overhead power lines. Although they are being developed separately, an integration of the water-blocking and anti-tracking function is envisaged. The application of this finish requires an after-treatment and is, as a matter of course, connected with additional process costs.

Requirements on ADSS cables installed on high voltage overhead power lines

Capacitive coupling of the cable to ground and to phase conductors creates a potential on the cable, which in turn can cause an electrical current directed toward the earthed fittings of the cable, when the cable is wet and dirty. The risk for evoking damaging electrical phenomenon at the cable surface, becomes substantial in case of system voltages exceeding 150 kV. The current density at the cable surface of a wet cable, which increases towards the towers, gives rise to Joule-heating, and consequently can cause a dry-band. The conductive wet surface layer is interrupted and the potential gradient changes into a potential step which can evoke arcing. When the conditions stabilize the location and size of the arc, the heating can cause serious tracking damage in short time. These phenomena are intensively studied and appear to be understood quite well [5,6]. A wide variety of solutions are proposed; the following classes of remedies can be distinguished:

- Selecting the suspension position for the ADSS cable connected with the lowest electrical field strength;
- Developing and applying tracking resistant sheath material;
- Developing and applying arc control devices;
- Utilizing controlled cable impedance.

The newly developed finish with customized conductivity fits in the latter class. Increased conductivity of the cable facilitates discharging and will therefore result in reduced potential and potential gradients. This also holds if the semi-conducting layer is applied directly beneath the outer jacket [7,8]. In this case discharging of the outer surface is enabled by a capacitive coupling between outer surface and semi-conductive substrate. So, reinforcing yarns provided with a customized conductivity could be a suitable solution [9].

Both safety requirements and the risk for Joule heating of the cable call for a lower bound of the cable impedance. From studies analyzing the usefulness of a semi-conductive layer beneath the jacket it appears that the resistance should have a value within the range of 10^1 - 10^3 MΩ/m [8,9].

Development of a semi-conductive aramid yarn

At a certain stage in the yarn production process a spin finish has to be applied in order to enable further processing. The finish primarily acts as a lubricant and secondly as an antistat. From a physical point of view an antistat is closely related to an agent providing (semi-)conductivity. So, the starting point for this development was to explore surfactants which already have proven to perform well as finish component. As this is a matter of primary interest for a yarn producer, considerable expertise and knowledge could be allocated for the present development.

From the several classes of surfactants, the anionogenic ones appeared to be the most suitable for application in yarn finishes. Within this class the phosphates and phosphonates are the most effective surfactants. Assessment of the thermal and oxidative stability is part of the screening procedure and also in this respect phophates and phosphonates appeared to fulfill the requirements holding for finish components. As a provisional target for the resistance of the layer of reinforcing aramid yarns, the geometric mean of the aforementioned lower and upper bounds of the cable resistance, being 10^2 MΩ/m, has been chosen. The resistance of the cable is considered to be the substitute value for the parallel arranged resistances of the yarns. The number of yarns, however, depends on the strength level of the ADSS cable. Some characteristics of the yarns are given in table 2 and the

estimated values of the required yarn resistance for a range of OFC-strength classes in table 3.

Table 2: Characteristics of the yarn

Characteristic	units	typical value
Nominal Linear density	dtex	1610
Number of filaments	-	1000
Filament diameter	m	12×10^{-6}
External surface	m^2/m	0.038
Net cross sectional area	m^2	0.12×10^{-6}

Table 3: Models of peripheral Twaron aramid reinforcement for three OFC strength classes

Characteristic	units	Class A	Class B	Class C
Actual Linear Density	dtex	1720	1720	1720
Number of yarns	-	50	100	200
Net cross sectional area	m^2	$6x10^{-6}$	$12x10^{-6}$	$24x10^{-6}$
Required resistance per yarn	MΩ/m	$5.0x10^3$	$10x10^3$	$20x10^3$

The results of resistance measurements of a selection of Twaron aramid and reference yarns are shown in table 4. Apparently, the regular finishes on the Twaron types already have a considerable effect on the resistance of the yarns. Depending on the type of yarn, the reduction still to be realized only amounts one to three decades.

Table 4. Results resistance measurements on some yarn types

Material type *)	Finish content	Resistance measured at [MΩ/m]		
	[%]	10 kV/m	20 kV/m	60 kV/m
Twaron -**)	0.0	$6.0x10^9$	$5.9x10^9$	$5.4x10^9$
Twaron 2200	0.9	$4.1x10^5$	$3.6 x10^5$	$2.0x10^5$
Twaron 1055	0.6	$5.3x10^6$	$5.5 x10^6$	$5.8x10^6$
Twaron 1052	3	$9.3x10^4$	$9.0 x10^4$	$1.0x10^5$
E-Glass	0.3	$2.8x10^8$	$3.0 x10^8$	$2.9x10^8$

*) Twaron in 1610 dtex and E-glass in 680 dtex

**) An experimental yarn produced without applying any finish ("clean yarn")

The next step was to test the effect of some existing, proprietary anti-static finish types on the Twaron types shown in table 4. These finishes, which contain the aforementioned anionogenic surfactants, are normally not applied on these yarns. The results are plotted in Figure 2.

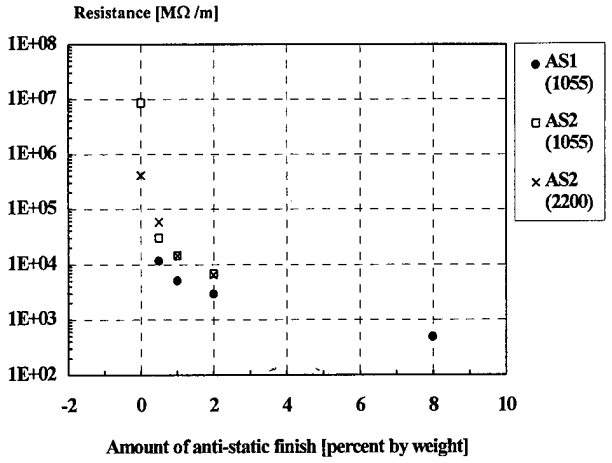

Figure 2: Effect of finishes containing surfactants on resistance of yarns

The observations shown in Figure 2 appear to fit very good with a power function like: $R = a * x^b$. The insert in Figure 2 shows the parameters and the R-squared value obtained from a least square fit. The effect of these finishes on the sample yarns is reviewed in table 5. The resistance at a finish concentration of 1% (C=1) is given by the parameter "a" as shown in the insert in Figure 2. Apparently finish type AS1 is more effective as a resistance reducing agent. Finish type AS2 is less effective on Twaron 2200 than on Twaron 1055, most likely as a result of the lower initial resistance level of Twaron 2200. From these results it can be concluded that the resistance of yarns can be changed significantly by applying finishes containing surfactants. This justifies a further search for more effective candidates to be applied in dedicated finish formulations.

Table 5: Effect of anti-static finishes on the resistance of commercial yarns

Yarn type	Finish type	Resistance at C = 1 [MΩ/m]	Reduction factor *)
Twaron 1055	AS1	5.5×10^3	1700
Twaron 1055	AS2	1.4×10^4	625
Twaron 2200	AS2	1.7×10^4	24

*) Resistance at C = 0 divided by resistance at C = 1

On the bases of earlier evaluations of commercial available surfactants for application in spin finishes, four candidates have been tested in experimental finish formulations. Concentration series of these experimental finishes were applied on clean yarn. The results of the resistance measurements on these yarns are plotted in Figure 3.

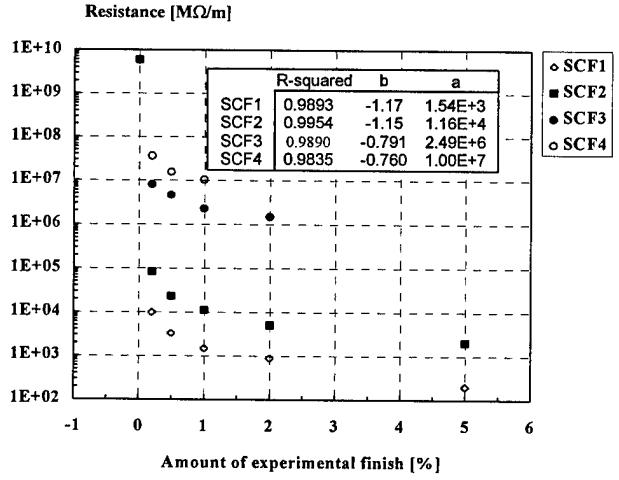

Figure 3: Yarn resistance versus amount of experimental semi-conductive finish

Also in this case, the responses can be modeled quite well using a power function. The obtained values of the parameter "a" again gives a good indication of the effectiveness of the experimental finishes, see table 6. Obviously SCF1 and SCF2 outperform the other two experimental finishes. Taken into account additional data about thermal and oxidative stability, SCF1 is selected for further exploration and testing on some commercial yarns, which already are provided with a regular finish, see Figure 4. For reference purpose the data for SCF1 on clean yarn, taken from the previous figure, also are shown in Figure 4.

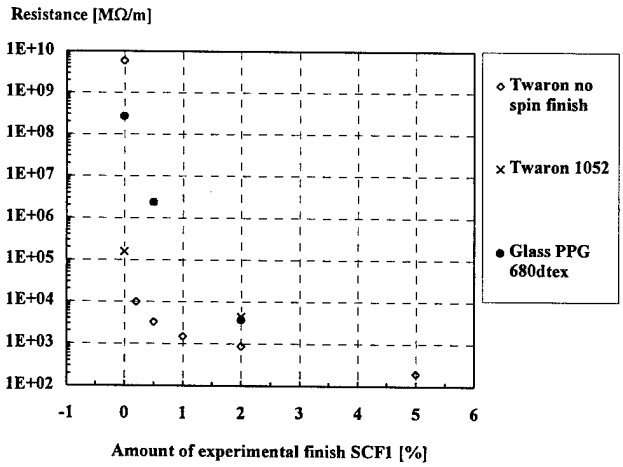

Figure 4: Resistance of various yarns versus the amount of experimental semi-conductive finish

Table 6: Effect of experimental finishes on the resistance of a clean yarn

Experimental finish	Resistance at C = 1 [MΩ/m]	Reduction factor (see note at table 4)
SCF1	1.5×10^3	1.8×10^6
SCF2	14×10^3	0.43×10^6
SCF3	2.4×10^6	2.5×10^3
SCF4	10×10^6	0.59×10^3

Summarizing it can be stated that not only the target level for the yarn resistance can be attained quite easily, but that there is sufficient flexibility to attain higher or lower levels. In addition, the cable manufactures have the disposal of another degree of freedom as they can mix semi-conductive yarns with regular yarns.

The matter of thermal and oxidative stability of the semi-conductive finishes still has to be addressed. The candidate semi-conductive finishes indicated above, have been selected from a set of thoroughly tested surfactants. As to thermal and oxidative stability, the surfactant applied in the experimental finish labeled SCF1 shows superior behavior. Nevertheless, the endurance of electrical resistance had not yet been looked at, so far. Therefore some additional experiments with heat-treated yarn samples have been carried out. Yarn samples obtained by applying SCF1 on Twaron 1055 were treated during 2, 5, 10, and 20 minutes at temperatures of 90, 120 and 220°C. The lower temperatures represent extreme situations during service, whereas the highest value that of the production step were the outer jacket is added by extrusion. The heat treatments at 90 and 120°C caused no effect at all; that at 220°C resulted in an increase of resistance after 20 minutes. The latter observation, however, is connected with evaporation of the basic finish applied on Twaron 1055, not with a deterioration of the surfactants.

Discussion and outlook

It has been shown that Aramid yarns which are used as peripheral reinforcing members in ADSS cables can be given a resistance value in the range required to limit the risk for dry band arcing. This can be achieved by applying suitable surfactants in the finish. The obtained resistance value is shown to be largely independent of the voltage applied during the measurements. The compounds responsible for the semi-conductive behavior of the developed yarn have an excellent thermo-oxidative stability.

Major progress has been achieved with respect to the problems imposed by the risk for dry-band arcing. A semi-conducting reinforcing yarn which provides the cable with a stable controlled impedance, when it is applied as peripheral strength member, has been developed. The concept of applying a specialized finish for this purpose, gives the opportunity for customizing the conductivity of the yarns to the needs of the OFC industry.

Regarding the water-blocking function touched upon earlier in this chapter, some interesting developments can be disclosed briefly. The present water-blocking finish has proven to fulfill customer needs and its quality is generally appreciated. Nevertheless, a next generation water-blocking finish, which shows superior temperature stability and, moreover, has advantages as to processability, is being developed.

PROCESSING CHARACTERISTICS AND BOBBIN STABILITY

Introduction

The OFC application environment determines the OFC cable length and amount of reinforcing material in the OFC. Realization of the design requires choices as to yarn count and yarn length on bobbins in order to enable full utilization of the available server capacities. Moreover, highest OFC production efficiency requires excellent bobbin stability and yarn processability during fast server operation. These considerations are connected with a collection of additional requirements which the yarns and the bobbins have to meet:

- Bobbin stability should be maximized as the OFC-producers tend to require higher yarn length, i.e. heavier bobbins, and tend to increase production speed;
- Yarn have to be assembled when high yarn counts are required. This requires specialized equipment in order to minimize yarn length differences and to optimize yarn coherence;
- Yarn finish and surface additives should not give rise to formation of deposits on yarn guides.

These requirements with respect to processing characteristics have prompted several developments. Bobbin stability will be addressed in some depth.

Bobbin stability; kinetics of stranding (or serving)

During OFC production the peripheral reinforcing yarns are helically wrapped around the optical core by using a server or strander. The optical core is fed along the central axis of the server, while the aramid yarns are drawn of from the bobbins which are mounted on a large disk which revolves on the server axis. The geometry of the revolving system is given schematically in Figure 5. By using elementary physics and mathematics the following expressions for the acceleration of a point at the circumference of a bobbin are derived.

$$a_r = -\frac{R_s^2\omega_s^2 + R_b^2(\omega_s+\omega_b)^2 + R_sR_b(\omega_s^2+(\omega_s+\omega_b)^2)\cos(\omega_b t+\psi)}{\sqrt{R_s^2+R_b^2+2R_sR_b\cos(\omega_b t+\psi)}} \quad [2]$$

$$a_t = -\frac{R_sR_b((\omega_s+\omega_b)^2-\omega_s^2)\sin(\omega_b t+\psi)}{\sqrt{R_s^2+R_b^2+2R_sR_b\cos(\omega_b t+\psi)}} \quad [3]$$

where

a_r, a_t = acceleration in radial and tangential direction

R_s, R_b = radius of server revolving disk and of bobbin respectively

ω_s, ω_b = angular speed of server revolving disk and bobbin respectively

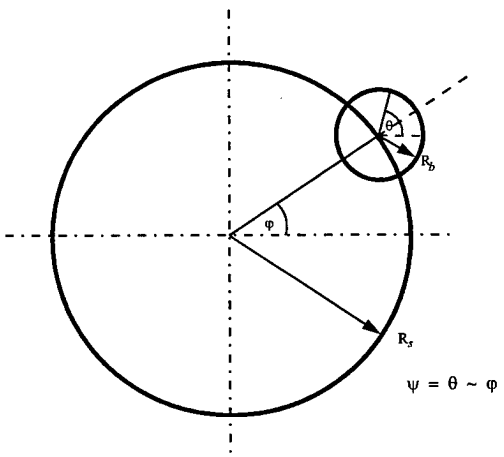

Figure 5: Geometry of server revolving system

Before having a general look at these equations, it is noticed that two main modes of server operation, with respect to yarn take-off, are in use:

- the yarn is drawn off overend, or;
- the yarn is drawn off from a bobbin revolving on its own axis.

From practical experience it is known that the former mode appears to be considerably less demanding as to bobbin stability than the latter.

When the yarn is drawn off overend, the angular speed of the bobbin (ω_b) equals zero and the expressions [2] and [3] reduce to:

$$a_r = -\omega_s^2 \sqrt{R_s^2 + R_b^2 + 2R_s R_b \cos(\psi)} \qquad [4]$$

$$a_t = 0 \qquad [5]$$

When these equations are compared with equations [2] and [3] it can be noticed that in this case any point at the bobbin circumference (defined by the value of the angle ψ) experiences a constant centripetal acceleration and no tangential acceleration or deceleration. The experience that this operation mode hardly cause stability problems, is explained by these mild conditions.

A large majority of the servers operates with yarn take-off from revolving bobbins. Figure 6 shows a graphical representation of the equations [2] and [3] for this case, i.e. it depicts the acceleration / deceleration experienced by a point at the bobbin circumference defined by:
$0 \le \omega_b t \le 2.4*\pi$ and ψ = constant = 0, and using the following values for radii and angular speeds: R_s = 0.505 m; ω_s = 20.9 s^{-1} (200 rpm); R_b = 0.11 m; ω_b = 7.4 s^{-1} (70 rpm).

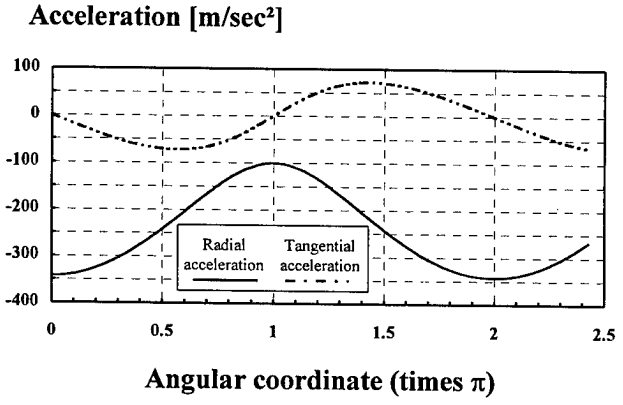

Figure 6: Acceleration of any point at bobbin circumference for given values of geometry and revolving speed, see text

Probably any point at the circumference experiences simultaneously a cyclic changing radial and tangential acceleration with a phase shift of about $\pi/2$. In this example the maximum centripetal acceleration is about 340 m/s^2, i.e. about 35 times g. The combined action of these accelerations can be seen as a continual, massage of the bobbin. The intensity of the massage depends on the design of the server (mainly the disk radius R_s), the applied angular speeds and, as a matter of course, on the mass of the bobbin. So far, the bobbin mass has not been taken into consideration, but it will be evident that the inertial forces in the yarn packages resulting from these accelerations are the very cause for unwanted deformations of the bobbins. Figure 7 gives an impression of a type of deformation occurring in a yarn package after the onset of bobbin instability.

Aspects of bobbin stability

The present general stability level of the cross-wound Twaron bobbins is sufficient in nearly all end-use area's, but some OFC-producers report that the limits of bobbin stability are reached when the high speed levels of the modern servers are exploited. The request for heavier bobbins, which enable longer production runs, gives rise to additional stability requirements.

The topic of bobbin stability has been addressed several times[10] and many of the factors affecting bobbin stability are known and understood quite well. The first factor to be addressed is the possibility for unwanted, uncontrolled change of the moisture content of the yarn bobbin in the time between delivery and processing. In the production process the target for moisture content equals the equilibrium for the given type. Decrease of moisture content of a completed bobbin is connected with decrease of linear density and, consequently, with a decrease of the cross-sectional area of the yarn on the bobbin. This causes a reduction of the density, hardness and stability of the bobbin.

Regarding bobbin stability, the yarn producer has to make choices as to the type of winding technology, taking into account the process speed and yarn characteristics on the one hand and the process costs on the other hand. When certain a technology is installed, the winding process has to be controlled properly. The controls to be set on the winder are: yarn tension, contact force and winding ratio. The effect of yarn tension and contact force are straightforward. An increase of either of them results

in increased hardness, package density and improved bobbin stability. Unfortunately, the available ranges of both the yarn tension and the contact force of the existing winders are rather limited and the stability levels, required in the near future, can't be attained by simply adjusting the setting of these controls. Therefore the remaining control, the winding ratio, is addressed in an intensive study as well.

For a given tube dimension, the winding ratio completely determines the winding pattern. But, the relation between winding ratio and geometrical effects in the winding pattern are rather intricate and the effects of small changes of the winding ratio are hard to predict. Nevertheless, several non-commercial computer programs dealing with this relation quantitatively and graphically, exists. Experts in the field of winding technology discern several aspects of the geometry of a winding pattern, and, regarding opinions on their possible effects on bobbin stability, several schools can be distinguished. In order to arrive at an useful starting point for an experimental design, an analysis of all of the relevant geometrical aspects was made. Using the estimated ranking of their relative importance, four factors have been selected. These factors not only completely define the winding ratio, but they also enable a statistical experimental design. Table 7 lists the factors and an indication of their settings on which the design of the experiment is based. In order to get information about possible interactions, if any, the yarn tension and the contact force are included in the design. The total number of settings is 144, whereas the statistical approach allowed a reduction to 28. A collection of experimental bobbins have been wound from one Twaron type with given linear density according to this design and subsequently tested using a modern commercial server. The main response is the growth of the bobbin in axial direction as depicted in Figure 7, as a result of a test run at about 200 rpm of the main server disk and about 70 rpm of the bobbins.

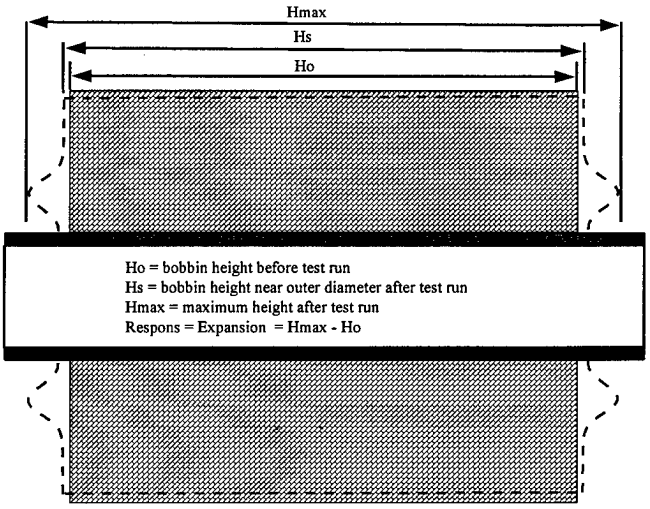

Figure 7: Typical response mode of a tested bobbin

A clarification of the factors in table 7 which are marked with an asterisk, requires a short description of some geometrical features of the winding pattern. Based on the correspondence in shape we can recognize a cylinder circumference and cylinder ends at a bobbin; the cylinder circumference will be named "face" and the cylinder end "shoulders". During winding the yarn is laid on the face by a traverse guide, which moves to-and-fro between the shoulders at a frequency which is directly related to the angular speed of the bobbin. The number of revolutions per double stroke of the traverse guide is called the winding ratio; its value must deviate from integers and simple fractions. After one double traverse stroke the angular position of the turning point at the shoulder, differs considerably from the starting position. The relative angular position of the next turning point relates to the factor "Type of shift". If this second angle is positive with respect to the first one, then the setting is "After", else it is "Pre". The angular shifts of turning points corresponds with shifts at the face . The shift or lay distance is measured along the face in a direction perpendicular to the yarns. The completion of a winding pattern requires several double strokes. Each of the consecutive pairs of double strokes is connected with a lay distance. The "distribution factor" is related to a pair of double strokes giving rise to a lay distance which approximately equals the yarn width, and the position of that pair in the sequence of double strokes defining one complete winding pattern. The "yarn width to lay distance ratio", which has just been indicated, can be controlled. The setting "medium" of this factor corresponds to a value 1, i.e. the yarn width equals the lay distance.

Table 7: Factors and settings in experimental design	
Factors	Settings
Yarn tension (winding tension)	Low, high
Contact force	Low, high
Crossing angle	Low, medium, high
Ratio of lay distance to yarn width *)	Low, medium, high
Distribution factor *)	S2, S3
Type of shift *)	"Pre", "After"

*) See text for clarification

A statistical analysis of the collection of response values in relation to the applied settings of the winding factors, has yielded a clear-cut result consisting of a set of significant parameters describing the sensitivities and the interactions. When making use of these parameters, response surfaces can be plotted in order to visualize the quantitative results. Figure 8 shows an example of such a response surface illustrating the strong and non-linear effect of the crossing angle and the ratio of lay distance to yarn width (width ratio). Various results have been obtained from these experiment. The known effect of yarn tension is confirmed convincingly. In addition a modest positive interaction with the contact angle is found. The direct effect of the contact force appeared stronger than expected. Moreover, a rather strong interaction with the width ratio, distribution factor and type of shift were found. The crossing angle both has a rather strong linear and quadratic effect and, in addition, an interaction of similar magnitude with the distribution factor. In case of the width ratio a small linear and a surprisingly strong quadratic effect was found; moreover, a modest interaction with the type of shift emerged. The majority of these observations looks plausible, some of them are not yet fully understood. The most valuable findings of this first step in a series of investigations can be summarized as follows:

- the winding ratio can be addressed successfully in a systematic study;
- the importance of taken into account the yarn width carefully has become evident;
- in order to obtain the highest possible bobbin stability, several parameters have to be controlled simultaneously.

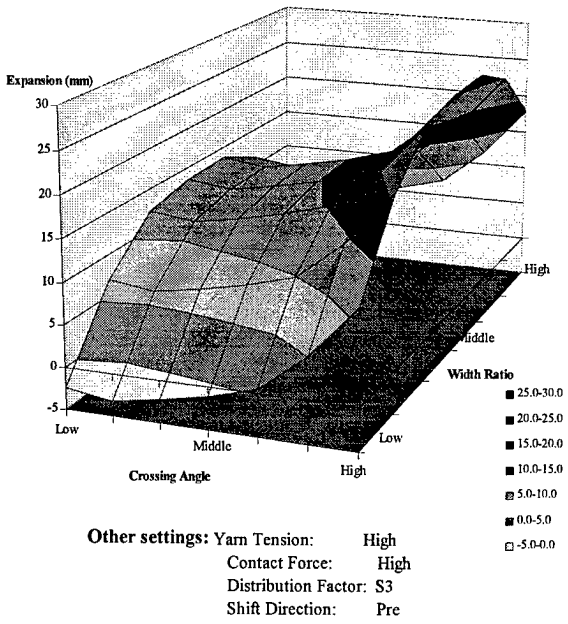

Figure 8: Axial bobbin expansion in dependence of crossing angle and width ratio; calculated result based on parameters obtained from regression analysis of observed reponses

FINAL CONSIDERATIONS

From the viewpoint of the OFC-designer this expansion of the available modulus range offers the opportunity to optimize the amount of Aramid yarns in OFC's.

The combination of strength element, element ensuring protection against water and element providing a required impedance in the Twaron reinforcing yarns, is a result of the strategy of Aramid Products to focus development efforts on opportunities to attain functional integration. This functional integration provides the OFC industry with opportunities for substantial cost efficiency.

The insight gained in the effect of winding parameters will be used to improve the stability of the Twaron bobbins in order provide the OFC-producer with bobbins which can be processed in a more profitable way.

REFERENCES

1. M G Northolt and D J Sikkema, Lyotropic Main Chain Liquid Crystal Polymers; Chapter 6 in "Liquid Crystal Polymers From Structures to Applications", Edited by A.A. Collyer, Elsevier Applied Science, 1992
2. M G Northolt and R v d Hout, Polymer, 1985, **26**, 310
3. M G Northolt and J J Van Aartsen, Journal of Polymer Science: Polymer Symposium 1977, **58**, p283 - 296
4. O Grabandt, S Willemsen and J H van Leeuwen, IWCS Proceedings, 1992, **41** p. 392 - 297
5. Carter C N, Waldron M A, "Mathematical model of dry-band arcing on self-supporting, all-dielectric, optical cables strung on overhead power lines", IEE Proceedings-C, 1992, 139 (3), pp. 185 - 196
6. Carter C N, "Dry Band Electrical Activity on Optical Cables Separately Strung on Overhead Power Lines", Proc. 37th IWCS, 1988, pp. 117 - 121
7. Peackock A J, Wheeler J C G, "Development of aerial fibre optic cables for operation on 400 kV power lines", IEE Proceedings-A, 1992, 139 (6), pp. 304 - 314
8. Berkers A G W M, Wetzer J M, "Electrical Stresses on a Self-Supporting Metal-Free Cable in High Voltage Networks", Proceedings of the 5th DMMA, Canterbury, 1988, IEE Conf. Pub. No. 289, pp. 69 - 72
9. Oestreich U H P, Nassar H M, " Self-Supporting Dielectric Fiber Optic Cables in High Voltage Lines", Proc. 37th IWCS, 1988, pp. 79 - 82
10. J J Bensink and A L van den Bos, How Improvement in Aramid Package Stability Can Lead to Higher Production Speed in Optical Fiber Cables, Proc. 40th IWCS, 1991, pp. 526 - 530

Ir. H.A.M. Stuut (1946) received a B.Sc. degree in mechanical engineering and a M.Sc degree in materials science from the Technical University of Delft. In 1975 he joined Akzo Nobels research laboratories and worked on structure - property relations of fibers and electro-deposits. Presently he is an end use development engineer at Akzo Nobel Aramid Products.

Dr. O. Grabandt (1957) received his Ph. D. in physical chemistry from the University of Amsterdam. He joined Akzo Nobel in 1988 and worked on carbon and aramid fibers. Presently he is technical account manager within Akzo Nobel Aramid Products.

Ir. J.H. van Leeuwen (1941) moved after 5 years of experience in applied physics within Akzo Nobel to a group studying the possibilities of industrial fibers in New Applications. At present he is technical service and development manager within Akzo Nobel Aramid Products

ADVANCED IMPACT POLYPROPYLENE BUFFERING MATERIAL FOR SUPERIOR LONG TERM HYDROLYTIC AND THERMO-OXIDATIVE STABILITY

Brian G. Risch, Jeff Auton, and Olivier Tatat

Alcatel
O.F.C.C.C
P.O. Box 39,Claremont, NC

ABSTRACT:

A grade of impact modified polypropylene with a specially formulated, proprietary, antioxidant package which gives it much greater thermo-oxidative stability and long term reliability than standard polypropylenes is presented in this study. This material is compared to other grades of impact modified polypropylene, as well as several grades of stabilized, and unstabilized PBT in terms of reliability in accelerated testing. Various tests including oxidative induction time (OIT) testing combined with oven and humidity aging and mechanical testing were used to evaluate the long term reliability of specially stabilized impact modified polypropylene, general purpose grades of impact modified polypropylene, and PBT for buffer tube applications. The type and quantity of antioxidants dramatically effect the aging performance of impact modified polypropylene as well as estimated lifetime. The dramatic superiority in the hydrolytic stability of impact modified polypropylene over PBT is also illustrated as a function of aging in a high humidity environment.

INTRODUCTION:

Resistance to degradation due to oxidation or hydrolysis is an important requirement for buffer tube materials. The need for hydrolytic stability of buffer tubes is increased as dry waterblocking materials based on superabsorbent polymers replace conventional flooding compounds in a cable design. These materials may entrain water within a cable and replace a layer of protective gel over the buffer tubes thereby causing a greater risk of hydrolytic degradation.

The assurance of long term reliability of fiber optic telecommunications cables and fiber optic telecommunication cable components is of paramount importance in the fiber optic industry. For fiber optic telecommunications cables, the requirements for polymer stability are among the toughest for polymer applications due to harsh environments and long service lifetimes. Poly(butylene terepthalate) (PBT) has seen use in fiber optic buffer tube applications for a number of years. PBT shows relatively good thermo-oxidative stability under normal use conditions, but is extremely sensitive to hydrolysis due to ester groups within the polymer backbone.[1] Hydrolytic degradation of PBT fiber optic buffer tubes is well documented in the wire and cable literature.[2,3, and 4] Recently the use of polypropylene impact copolymers (i-PP) has offered an alternative to PBT for buffer tube materials which offers dramatic improvements in terms of hydrolytic stability.[5,6,7,8, and 9]

The improvements in hydrolytic stability of i-PP over PBT are due to the fact that there are no groups in the polypropylene backbone which are subject to hydrolytic attack as well as the fact that water has a much lower solubility in i-PP than in polyesters, polyamides, or polycarbonates. In PBT water can react with an ester linkage producing alcohol and acid end groups. [10]

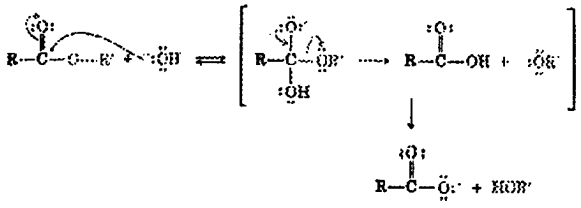

The acid endgroup can catalyze further reaction. Additionally, the lower molecular weight byproducts can plasticize the PBT, reducing the T_g and increasing the rate of reaction. Polypropylene lacks hydrolyzable groups and therefore is not sensitive to moisture. The improved hydrolytic stability of i-PP over PBT can lead to improved reliability of buffer tubes especially in cables, breathable enclosures, or pedestal enclosures where temperature and humidity are uncontrolled.

Although polypropylene is highly resistant to hydrolytic decomposition, its oxidative stability is highly dependent on the stabilizer package used in the formulation and may vary greatly from grade to grade of material. This report summarizes a series of comparative tests which have been conducted on PBT and impact-modified polypropylene (i-PP) buffer tubes in order to determine the relative resistance to thermo-oxidative and hydrolytic decomposition. The results of dry heat aging tests as well as hydrolytic stability tests on standard PBT, hydrolytically stabilized PBT, and various grades of impact polypropylene buffer tubes are compared in order to estimate buffer tube reliability and lifetime modeling.

EXPERIMENTAL:

Dry Heat Aging:

Buffer tube samples were wrapped in 3.5" coils for 10 turns and placed in ovens at 150°C, 145°C, 140°C, 135°C, 125°C, 110°C, 100°C, and 85°C. The temperatures of these ovens was periodically monitored with thermocouples.

Hydrolytic Stability Testing:

Buffer tube samples were wrapped in 3.5" coils for 10 turns and placed in controlled humidity ovens at 85°C and 85% R.H.

Tube Tensile Elongation:

Buffer tube tensile elongation was determined using a procedure as described in ASTM 348 except that the buffer tubes did not have a gauge section of reduced diameter. Machining of the tubes could not be done without causing defects in the tubes that could cause premature breakage. An Instron model 4468 mechanical tester was used for all tests. A gauge length of 20mm was used with a crosshead speed of 50mm/min. 2.5mm and 3.0mm buffer tubes were used in all tests. Grip adapters with tube inserts were used which insured that tubes were not crushed in the grips.

OIT Determination:

OIT determinations were carried out according to ASTM D3895[11] except that aluminum sample pans were used instead of copper since copper has been shown to catalyze some degradation reactions in polyolefins resulting in reduced OIT values as well as variability of test results depending on the state of oxidation of the pan's surface.[12,13, and 14] A TA 910 DSC was used for OIT (Oxidative Induction Time) determination. OIT values were determined at 200°C.

RESULTS:

Table 1 shows the conditions used for dry heat aging tests. The partial pressure of H_2O during the tests was approximately 0.18 psi. In order to calculate the relative humidity during the tests the partial pressure of water is divided by the pressure of saturated water vapor at the given temperature. Table 1 illustrates the aging temperature, the vapor pressure of saturated H_2O at each temperature (100% Hunidity), and the relative humidity of each test condition.

Table 1: Conditions For Dry Heat Aging Tests:

Temperature (°C)	$P^{Sat.}$ (H_2O) psi.	R.H. %
85°C	8.57	2.1%
100°C	14.7	1.2%
110°C	20.8	0.87%
125°C	33.1	0.55%
135°C	44.7	0.41%
140°C	52.4	0.35%
145°C	60.0	0.30%
150°C	69.0	0.26%

Effects of dry heat aging tests of specially stabilized impact polypropylene and PBT at various temperatures are illustrated in Figure 1. It is evident that under the various dry heat conditions investigated, the specially stabilized impact polypropylene performed as well as or superior to PBT.

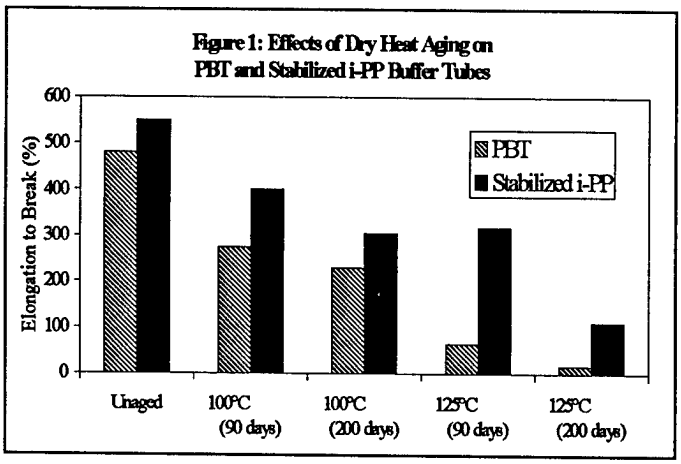

Under conditions of high humidity, the performance of impact polypropylene relative to PBT is far superior. The hydrolysis resistance of PBT can be improved through the use of hydrolytically stabilized grades of PBT, but even hydrolytically stabilized PBT offers lower resistance to hydrolysis when compared to impact polypropylene. Figure 2 illustrates the effects of aging impact polypropylene, standard PBT, and two grades of hydrolytically stabilized PBT at 85°C and 85% R.H. The failure criteria is when brittle cracking is seen in the tubes which corresponds to a reduction in average elongation to break of below about 10%. The use of a hydrolytically stabilized grade of PBT significantly extends the time to failure from approximately 23 days to about 50 days doubling the expected service lifetime in conditions of high humidity. Impact polypropylene, however, can be aged under these conditions for over 135 days with no measurable changes in properties.

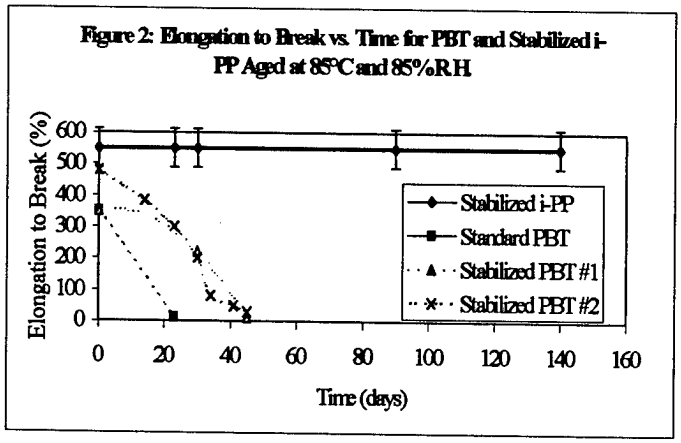

In addition to the samples which were aged for Figure 2, nine different grades of PBT were tested for hydrolytic stability by aging at 85°C and 85%R.H. for 45 days. These specimens were then tested for ultimate elongation at 10mm/min. and 50mm/min. At a crosshead speed of 50mm/min. only 3 out of 9 PBT samples retained an average ultimate elongation of over 10%. At a crosshead speed of 10mm/min. 5 out of nine retained an average ultimate elongation of greater than 10%. These results indicate variability from grade to grade of PBT as well as the effect of strain rate on mechanical properties. A summary of the test results is given in Table 2.

Table 2: Effects of Aging on Mechanical Properties of PBT Buffer Tubes:

	10mm/min. Crosshead Speed		50mm/min. Crosshead Speed	
Material	% Change in Yield	Elong. @ Break	% Change in Yield	Elong. @ Break
A	14	430%	30	78%
B	21	87%	15	130%
C	40	5%	*	2%
D	21	425%	32	435%
E	16	4%	20	4%
F	14	375%	6	411%
G	-5	375%	27	4%
H	47	5%	*	2%
I	15	390%	*	5%

*Sample broke at or before yield point.

The dramatic effect of humidity on service lifetime that is present in both standard and hydrolytically stabilized PBT, is not present in polypropylene since polypropylene is not susceptible to hydrolytic decomposition. The actual in service lifetimes which these hydrolytic stability tests simulate vary widely depending on the actual in-service temperature and humidity. Gebizlioulu and Plitz[15] have estimated that the failure points of standard PBT and hydrolytically stabilized PBT would correspond to a service lifetime of about 10 years for standard PBT and about 20 years for hydrolytically stabilized PBT at 40°C and 60% relative humidity. In tropical or subtropical environments where average relative humidity can commonly be over 90%, lifetimes could be reduced below these values especially if non-stabilized PBT is used.

An interesting note is that impact polypropylene will actually perform better under conditions of extreme humidity since the partial pressure of H_2O is so high under these conditions that the partial pressure of oxygen is reduced. For example, at 85°C and 85% R.H. the partial pressure of H_2O is 8.57psi. Since one atmosphere is 14.7psi at sea level, the partial pressure of oxygen under these conditions is reduced by 58%. Since the primary degradation mechanism for impact polypropylene is oxidative degradation, which is dependent on the partial pressure of oxygen, the lifetime of the tubes may actually be extended under these conditions. Table 3 illustrates the reduction in OIT for stabilized i-PP various under various aging conditions. Note that the reduction in OIT is substantially less under conditions of high humidity. This phenomenon can be totally explained by the reduction in the partial pressure of oxygen under these conditions. It is not surprising that no change in buffer tube elongation was seen during the course of the test. This effect, of course ,is reduced at lower temperatures where the partial pressure of H_2O is reduced.

Table 3: Comparison of residual OIT After Various Aging Conditions for Stabilized i-PP.

Condition:	OIT Results
Before Aging	> 90 minutes
85°C/85%RH (30 days)	60 minutes
85°C (30 days)	30 minutes

Other factors which can effect elongation and aging performance of buffer tubes are processing conditions such as linespeed and cooling rate. Since the glass transition temperature of PBT is about 60°C, this material can be quenched below its T_g if cooled too quickly. A combination of high linespeed and cold water quenching of PBT buffer tubes can result in greatly reduced elongation relative to buffer tubes which are slowly cooled. A variation in elongation at break of 100% or more can be caused by variation in process conditions. If buffer tubes are cooled extremely quickly, all ductility may be lost during high speed testing.

In order to investigate the effects of cooling rate on buffer tubes, buffer tubes were processed with identical line configurations except for variation in linespeed. A fast and slow linespeed were used with the fast linespeed being 5x that of the slow linespeed. Elongation to break and break stress were then measured on buffer tube samples. An additional PBT buffer tube was produced (High Speed PBT #2) with high linespeed, reduced melt temperature, and cold water temperature in order to produce the most rapid cooling. Although these process conditions would not be used in normal production of PBT buffer tubes, the elongation and tensile strength of this PBT buffer tube showed the most dramatic reduction illustrating the possible range of effects. Although there was a strong effect on mechanical properties due to processing , this grade of PBT easily exceeded the Bellcore requirement for buffer tube elongation with all processing conditions.

The same processing experiment that was performed on PBT buffer tubes was performed on i-PP buffer tubes. Since i-PP has a glass transition below room temperature, post-extrusion crystallization and ductility are not reduced due to processing at high linespeeds. Although some variation can be seen in initial modulus as a function of linespeed,[16] no noticeable effects are seen in the ultimate elongation or yield strength of i-PP for the range of linespeeds used in this study. The results of processing experiments for i-PP and PBT are shown in Table 4.

Table 4: Effects of Cooling Rate on Buffer Tube Mechanical Properties:

Buffer Tube Description	Break Strength (Mpa)	Elongation @ Break
PBT Low Speed	66	419%
PBT High Speed	46	297%
PBT High Speed #2	25	160%
i-PP Low Speed	35	>600%
i-PP High Speed	35	>600%

Although there is no risk of buffer tube failure due to hydrolysis with i-PP, oxidative degradation resistance of i-PP must be known in order to obtain an estimation of service lifetime. To obtain this oxidative degradation resistance data, dry heat aging tests were performed under the conditions specified in Table 1. Data has been collected on the i-PP buffer tubes which were first introduced in 1995.[5,6,7,8,and 9] The grade of i-PP from which these buffer tubes was compounded contained a

proprietary additive package which was specially developed for buffer tube applications. Although some aging test data has been presented on this material already, an extensive report on materials reliability has not been presented due to the very long time to oxidative failure for this particular grade of polypropylene. Arrhenius data has been compiled showing that the buffer tube lifetime can be extrapolated to over 50 years at temperatures of 40°C, 30°C, and 20°C. From the Arrhenius data an activation energy of 19 Kcal/(mol*°K) with a regression coefficient of 0.986 has been determined for the degradation of stabilized polypropylene.

Figure 3: Arrhenius Plot For Lifetime Estimation of Stabilized Impact Polypropylene Buffer Tubes

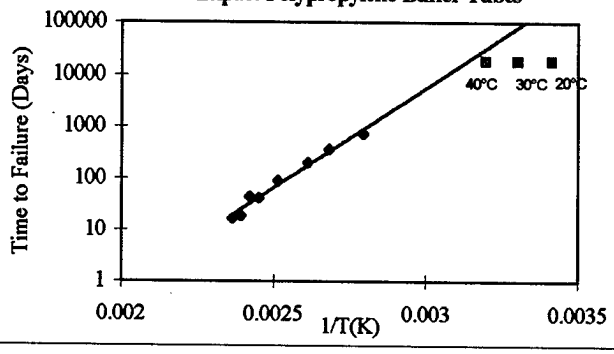

An Arrhenius plot obtained by examining the time to failure of stabilized i-PP buffer tubes placed in a coil of 10 loops around a 4" mandrel under the conditions identified in Table 1 is included as Figure 3. For reference points, lifetimes of 30 years at 40°C, 30°C, and 20°C are plotted as squares. Since the Arrhenius curve lies well above these squares, a lifetime of well over 30 years can be expected at actual operational temperatures. Buffer tubes retained their ductility after over two years of continuous exposure to dry heat aging at 85°C. The two year exposure point is indicated as the failure point since this is the amount of aging time at the time of writing.

These specially stabilized impact polypropylene buffer tubes can offer improved reliability over buffer tubes made out of other more standard grades of impact-modified polypropylene. Although buffer tubes made of alternative grades of impact-modified polypropylene should possess inherently good hydrolytic stability due to the absence of hydrolyzable polymer backbone units, these materials may not exhibit the superior thermo-oxidative stability of the specially stabilized grade. The specially stabilized grade contains a proprietary additive package that gives it oxidative stability far superior to standard grades of impact polypropylene. Figure 4 illustrates the OIT results of the specially stabilized grade and three other grades of impact modified polypropylene. From these results it is evident that the thermo-oxidative stability of the buffer tubes with the proprietary stabilizer package is several times greater than that of other grades of impact-modified polypropylene. These results indicate that the lifetime of such buffer tubes would be greatly reduced relative to that predicted for the impact polypropylene buffer tube material which was originally developed especially for fiber-optic buffer tubes.

Figure 4: OIT Results for Various Grades of Impact Polypropylene

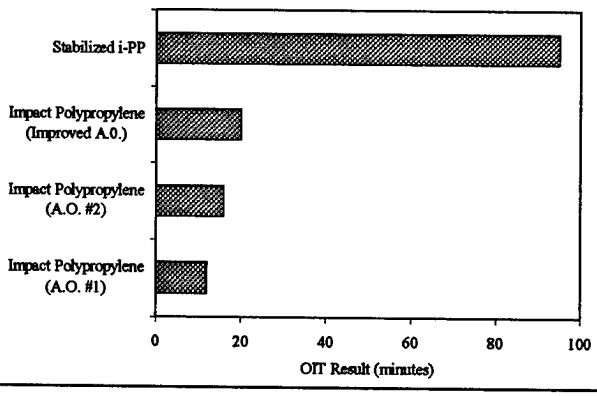

CONCLUSIONS:

Both PBT and stabilized impact polypropylene offer good thermo-oxidative stability. PBT, however, is also sensitive to hydrolytic decomposition. The improved hydrolytic stability of impact polypropylene over PBT can lead to improved reliability of buffer tubes especially in cables or pedestal enclosures where temperature and humidity are uncontrolled and can reach extreme conditions. The specially stabilized grade of polypropylene discussed can also offer improved long-term cable reliability in areas of high temperature and humidity. Impact modified polypropylene may also offer advantages in overall buffer tube reliability due to the fact that the mechanical properties of i-PP are not as sensitive to processing conditions as PBT. Alternative grades of impact modified polypropylene may not possess the same level of thermo-oxidative protection that is present in the grade of impact polypropylene which was originally developed for fiber optic buffer tubes and introduced in 1995. Although there are several grades of impact modified polypropylene available today which may be suitable for buffer tube production and short-term use. Commodity grade impact polypropylenes do not have a sufficient level of antioxidants to ensure long-term reliability for buffer tube applications in warm climates. In order to provide 20 or 30 years of service life in warm environments, an OIT value in excess of the 20 minute Bellcore requirement may be necessary.

ACKNOWLEDGEMENTS:

We would like to thank Jim Holder, Tracy Overcash, and Bill Brewer for producing the polypropylene buffer tubes used in this study. Additionally, we would like to thank Bob Stulpin for his assistance in manufacturing PBT buffer tubes.

REFERENCES:

[1] Gachter, R., and Muller, H, (eds.) "Plastics Additives Handbook", 3rd. ed.,(1990) Hanser.
[2] Parris, D. and Warner, B., "Testing of Fiber Optic Materials After Accelerated Heat and Humidity Aging", *International Wire and Cable Symposium, 39th IWCS Proceedings*, 1990, 237-42.
[3] Eickholt, J. "Reliability Testing of Fiber Optic Loose Buffer Tubes", *International Wire and Cable Symposium, 42nd IWCS Proceedings*, 1993, 476-78.
[4] Gebizlioglu, O.and Plitz, I. "Monitoring Accelerated Aging of Polyester Buffer Tubes in Fiber Optic Cable", *International Wire and Cable Symposium, 42nd IWCS Proceedings*, 1993, 509-515.
[5] Adams, M., Holder, J., McNutt, C., Tatat, O., and Yang, H., "Buffer Tubes- The Next Generation", *International Wire and Cable Symposium, 44th IWCS Proceedings*, 1995, 16-21.
[6] Shepley, J. and Holder, J., "Field Application of Advanced Buffer Tube Material"
[7] Holder, J. and Power, R., *Lightwave* 1995
[8] Yang, H.M., Holder, J.D., and McNutt, C.W., "Polypropylene-polyethylene Copolymer Buffer Tubes for Optical Fiber Cables and Method for Making the Same", International Patent Application Number wo 96/23239, August 1, 1996.
[9] Yang, H.M., Holder, J.D., and McNutt, C.W., "Polypropylene-polyethylene Copolymer Buffer Tubes for Optical Fiber Cables and Method for Making the Same", U.S. Patent Serial Number 08/377,366, January 24,1995.
[10] McMurry, John, *Organic Chemistry,* Brooks/Cole (Pacific Grove, CA) 1988, 760-62.
[11] ASTM Method D 3895, "Test Method for Oxidative Induction Time of Polyolefind by DSC", American Society for Testing and Materials.
[12] Kuck, V.J., *Proc. 6th Intern. Conf. Plastics in Telecomm.* 1992, **3**, 1-10.
[13] Patterson, G.H., and Riga, A.T., *Thermochim. Acta.* 1993, **226**, 201-210.
[14] Riga, A.T., *Proc. 20th North Amer. Therm. Anal. Soc., Conf.* 1991, 517-521.
[15] Gebizlioglu, O.and Plitz, I. "Monitoring Accelerated Aging of Polyester Buffer Tubes in Fiber Optic Cable", *International Wire and Cable Symposium, 42nd IWCS Proceedings*, 1993, 509-515.
[16] Risch, B.G. "Influence of Nucleating Agent and Melt Flow Index on Impact Polypropylene Fiber Optic Buffer Tubes", *56th Annual SPE ANTEC Conf. Proceedings*, 1998, 1016-20.

Brian G. Risch
Alcatel OFCCC
2512 Penny Rd.
P.O. Box 39
Claremont, NC 28610

Brian G. Risch is a Senior Materials Scientist at Alcatel Telecommunications Optical Fiber Cable Competence Center. He holds a B.A. degree in Physics from Carleton College and a Ph.D. in Materials Science and Engineering from Virginia Polytechnic Institute and State University. His Ph.D. research was in the area of polymer crystallization and structure property relationships in polymers. Directly after he finished his Ph.D. he worked for ORD laboratories in the area of optical polymers developing new polyurethane and polythiourethanes for high performance ophthalmic lens applications. Since 1996 Brian has worked for Alcatel's Optical Fiber Cable Competence Center (OFCCC) in the area of thermoplastic cable materials. His specialization has been in the area of processing and crystallization behavior of polyolefins for cable applications.

Jeff Auton
Alcatel OFCCC
2512 Penny Rd.
P.O. Box 39
Claremont, NC 28610

Jeff Auton received his B.S in Biology from Lenoir-Rhyne college in 1984. He worked as a QA Chemist in other industries prior to joining Alcatel in 1989. He has been with Alcatel for 9 years in materials development. Currently Jeff is working at Alcatel's O.F.C.C.C. as a Materials Specialist.

Olivier Tatat
Alcatel OFCCC
2512 Penny Rd.
P.O. Box 39
Claremont, NC 28610

Olivier Tatat received his engineering degree from the Institut des Sciences de l'Ingenieur de Montpellier (ISIM) in 1982 and joined Les Cables de Lyon, now Alcatel Cable in 1985. He has been working in the Alcatel Optical Fiber Cable Competence Center in Bezons, France for 5 years as a project leader. He his now the Material Technology Manager of the OFCCC located in Claremont, USA .

CONTROLLED JACKET BOND COATED STEEL ARMORING FOR FIBER OPTICAL CABLES

Felix Achille
Kenneth E. Bow
William F. Busch

The Dow Chemical Company, Midland, Michigan

ABSTRACT

This work was undertaken because of the need for easy access to the fibers at breakout points along the cable span. With the movement of fiber systems into feeder and subscriber applications, it is frequently required that a larger fiber count distribution cable, for example, be spliced to a relatively smaller breakout cable. This means that the distribution cable must be opened, a splice made, and then the breakout point secured for environmental protection. The industry has approached the need for more rapid breakouts by moving to "dry" cable to eliminate the cleaning and difficulties associated with jelly filled cables. This move has reduced splicing time significantly. One other area where further improvements could be made was in stripping the jacket of armored cable to gain access to the cable core. When a bonded jacket with standard coated steel armor is used, there is extreme difficulty in removing the jacket. However, bonded jackets provide many benefits in terms of cable protection. To maintain these benefits and to add a new benefit of easy strippability, a new controlled jacket bond coated steel was required. This paper will describe the development of this product.

INTRODUCTION

There has been a movement away from filled and flooded cable designs so that today the standard method globally for blocking fiber optical cable from the longitudinal flow of moisture is to use water blocking tapes, powders, and yarns. These so called "dry" designs have several benefits in fiber optical cable. First, they greatly reduce the amount of time required for splicing the cable.[1, 2] Second, the use of water swellable tape facilitates the manufacture of the bonded sheath cable.[3] Third, the use of the dry design reduces cable manufacturing costs.[4] These benefits will be expanded upon in the following paragraphs.

The traditional way to water block fiber optic cables is to incorporate a jelly-like filling compound within the core to prevent migration of water into and along the cable core. The ability of the filler to accomplish this 100% of the time is a concern. Void spaces can exist in the filler due to difficulties in the filling operation during cable manufacture. Mechanical factors associated with handling of the cable can displace the filler and create void spaces that act as channels for longitudinal water flow. Aging of the cable during storage and after installation can cause the filler to be absorbed by the plastic materials in the cable. This in turn also leaves voids that form water paths in the core and sheath interfaces.[5] Furthermore, by elimination of synthetic oils, floodants, and jellies within the core and sheath interfaces, there is a profound effect on reducing the time required to clean these materials from the cable components during splicing. The end-user benefits of easier splicing, easier training of personnel, and reduced cost have accelerated the move to dry cable.

A typical metallic armored fiber optical cable uses coated steel 0.15 mm (6 mils) thick to protect the operating core of the cable from rodents, other wildlife, moisture, and to allow for accurate location and real time monitoring of the integrity of the sheath. The coated steel is bonded to the cable jacket, or plastic oversheath, during the extrusion of the cable jacket or plastic oversheath. The resulting sheath structure is called a laminate or bonded sheath. It is congruent with the dry cable concept because a bonded sheath offers moisture resistance to the fiber optical cable in

several ways. Among them are a longitudinal water blocked interface between the jacket and armor. With a sealed overlap, the metallic armor is integrated into the sheath as a metallic moisture barrier effective against both radial and longitudinal moisture penetration. The use of water swellable tape over the core of a fiber optical cable also benefits the manufacture of a fiber optical cable with coated steel armor. By using the water swellable tape under the coated steel, the core of the cable is free of floodants which could contaminate the surface of the tape and interfere with bonding of the jacket or sealing of the overlap.

The manufacturing costs of cable with dry cable versus filled and flooded cable have been extensively documented.[6] Only a summary will be given here. The essential finding of the study was that the differences in raw material costs between cable with petro-jelly or synthetic fillers and floodants and dry cable is small in both absolute and relative terms. Any difference in material costs is more than compensated for by cable manufacturing efficiencies. One of these efficiencies is reduced process set-up times, which can be 50% less with dry cable. Likewise, the material changeover times on tube stranding lines can be one-third of those with petro-gel filled cables. Processing speeds can be increased because they are not rate limited by the need to heat, pump, and cool the petro-gel. The capital outlay is significantly less for equipment to handle water swellable tapes versus fillers and floodants. Power costs are subsequentially less with dry designs since there are no heating and cooling requirements. The material handling and logistics costs are also significantly less since drums or bulk handling of the filler is not required. Capital costs associated with equipment for handling heavy drums are also eliminated. No special handling of the dry fillers are required which in turn eliminates safety and ergonomic concerns. Factory maintenance costs are significantly reduced with elimination of equipment associated with the melting and pumping of fillers. In the case where reprocessing of the sheath is required, the stripping costs can be 60% less with dry cable. A significant cost reduction with dry cable is the cost associated with routine testing of the cable. Since no cleaning of the fillers is required, testing time is about 50% less with the dry cable. Overall, the dry cable is the most cost effective way to manufacture a water blocked cable.

PRODUCT DEVELOPMENT

As the applications for fiber optical cables move into the feeder and subscriber loop, there are more and more requirements for mid-span entry and easy access to the core of the cable. There is also a need for armored cable because of the mechanical and environmental hazards associated with these applications. The traditional way to make a bonded sheath is to maximize the bond between the coating on the steel and the jacket. However, a high level of bonding creates difficulty in easy access to the cable core. Gaining access more easily means easier splicing and shorter splicing times in line with the benefits of dry cable. The paradox is that there is a direct relationship between the level of jacket bond in a bonded sheath cable and the mechanical performance of the cable in various industry tests such as cable flexing, twist, bend, and crush resistance.[7] However, to design a bonded sheath that facilitates stripping of the cable jacket means that some sacrifice must be made in jacket bond which, in turn, could affect performance. The challenge is to design a coating on the tape that meets both the need for easy jacket removal and still meets the industry requirements for mechanical performance of the sheath. A further challenge is to design this coating so that there is basically no difference in cable processing relative to a standard type of coating. In line with the need for easier splicing and the evolution of fiber optical cable to the local loop, a "controlled jacket bond" coated steel armor has been developed. The jacket adhesion has been controlled to a level that permits easy stripping of the jacket yet at a high enough level to allow retention of the benefits of the bonded sheath.

The development of a coated steel armor with a controlled jacket bond had to meet several key criteria - 1) be a solution that would provide a reliable, consistent level of controlled bond regardless of the processing conditions for the cable sheath, 2) be at a level of bond strength that could be stripped by hand, 3) be at a level of bond that would maintain the mechanical properties of the cable, 4) be such that a plastic layer is always maintained on the surface of the metal for corrosion protection.

There were several alternatives considered. The one chosen was one in which the controlled bond was built into the composition of the coating on the steel. The product concept is to

Table 1
Comparison of Adhesion Properties of Standard Bond and Controlled Jacket Bond Coated Steel After Water Aging at 70°C

		Adhesion* in N/m (lb/in)		
	Specification	Initial	7 Days	14 Days
Standard Peel Strength	610 (3.5)	876 (5.0)	876 (5.0)	876 (5.0)
Controlled Bond Peel Strength	610 (3.5)	701 (4.0)	701 (4.0)	701 (4.0)
Standard Seal Strength	1750 (10.0)	4030 (23.0)	5081 (29.0)	5081 (29.0)
Controlled Bond Seal Strength	1750 (10.0)	2103 (12.0)	1928 (11.0)	1928 (11.0)

* Peak Values

Table 2
Jacket Bond Strength of Standard and Controlled Jacket Bond Steel after Water Aging at 70°C

	Jacket Bond Strength* in N/m (lb/in)		
Coated Steel Tape	Initial	7 Days	14 Days
Standard Bond	5958 (34.0)	5783 (33.0)	5783 (33.0)
Controlled Bond	3505 (20.0)	3330 (19.0)	3330 (19.0)

*Peak Values

have a multilayer coating and have one of the layers act as a bond control layer. By correctly manipulating the compositions of the layers it was possible to control the jacket to steel bond strength of the cable sheath at the desired level. A comparison of the coated steel adhesion properties is shown in Table 1. These data were gathered using the procedures of ASTM B736 for peel strength and heat seal strength. After determination of initial bond strength, the strips prepared previously were placed in deionized water at 70°C. The coated steel with the controlled jacket bond coating meets the requirements of ASTM B736 for Type 1, Class 2 polyolefin coated metal.

The jacket bond values were obtained using Dow Test method CM-4. In this test method a plaque of jacketing resin (medium density polyethylene) is bonded to a sheet of the coated metal in a platten press at 180°C. The plaque is then cut into 25.4 mm (1 inch) strips and tested for adhesion between the steel and the oval jacket, using an Instron testing machine with a cross head speed of 50.4 mm/min (2 inches/min).

After determination of initial bond strength, the strips prepared previously were placed in deionized water at 70°C. Table 2 shows the initial bond strength of water aging on jacket bond. The data indicates that the controlled jacket bond has about 60% of the adhesion of the standard coating on steel. At this level it is below the maximum limit it can be (about 75%) and still allow a user friendly cable to be manufactured. As can be observed the bond is not showing a sensitivity to water. This type of performance is consistent with long cable life. The jacket bond must not show water sensitivity in order to maintain its benefits of corrosion, moisture and rodent protection.

Tests for corrosion resistance were run in accordance with Dow Test Method CM-5. This method used 0.1N HCl as the test medium. A coupon of the coated metal is place in the solution for 20 days. The amount of edge corrosion is measured and a rating assigned according to ASTM D1654. The results of the tests are shown in Table 3. The coated steel with the controlled jacket bond coating is showing equivalent corrosion resistance to the coated steel with the standard coating. The special feature in the design of the controlled bond coated steel is that a layer of copolymer remains on the surface of the steel after the jacket is removed. This feature is consistent

Table 3
Corrosion Resistance after 20 Days Immersion in 0.1N HCl

Coated Steel Tape	Corrosion Rating*, ASTM D1654
Standard	9
Controlled Bond	9

*Rating System: 9-10 = Excellent; 8 = Very Good; 6-7 = Good; 5 = Fair; 3-4 = Poor; 0-2 = Very Poor.

with the need to protect the steel from corrosion at splices and terminations. This allows the connector to maintain a stable resistance versus time.

The finished cable must meet performance criteria established for armored sheaths in various industry specifications. The most important of these criteria are those related to mechanical tests because the use of an armored sheath enhances the mechanical properties of a fiber optical cable. Some mechanical properties that are improved with a bonded sheath are bend performance (tighter bends around smaller mandrels), side wall bearing pressure, crush resistance, impact resistance, puncture resistance, buckling resistance, and resistance to thermal cycling. There are also test requirements that measure the resistance of the cable sheath to the environment. These also must be met.

The cable armored with the controlled jacket bond coated steel was extensively tested to various mechanical requirements. These tests were high temperature bond (60°C, FOTP-37), low temperature bond (-30°C, FOTP-37), impact (FOTP-25), compression (FOTP-41), tensile strength (FOTP-33), cable twist (FOTP-85) and cyclic flex (FOTP-104). The environmental tests were temperature cycling (FOTP-3), cable aging (85°C, FOTP-3) cable freezing (FOTP-181). All performance levels were met and dynamic properties of the cable as observed for impact, cyclic flex and twist were exceptional.[8]

FIELD PERFORMANCE

The following information is a summary showing the effect on fiber optic cable termination and splicing time of using cable with the controlled jacket bond coated steel tape. It must be kept in mind that the major time factor in splicing a fiber optical cable is the amount of time it takes to splice the fibers. Although the minor part of the time is spent on opening the sheath, maintaining electrical continuity of the armor and closing the sheath, the convenience and ease of doing these operations is still an important time factor. Typically a larger fiber count cable, in this study, a 144 fiber cable, is opened and spliced to a smaller fiber count cable, in this study, a 12 fiber cable. The type of cable is also an important factor in splicing time, i.e., whether the cable is of the loose tube, ribbon fiber or fiber bundle design.

Table 4 reports the added time for cable end preparation when the cable is armored with a coated steel armor tape. It should be noted that the time is increased by a few minutes for mid-span entry due to the need of a second grounding clamp. Times are longer for the loose tube cable design because this cable has two jackets whereas the ribbon and bundle cable designs have only one.

A field test has confirmed the value of using cable with the controlled bond feature.[9] In this test 10 cm (4 inches) of outer jacket was removed from cable having armor with either the standard coating or the controlled jacket bond coating. The cables were of identical construction with 6 buffer tubes. Three craft personnel were used in an identical situations of mid-span entry. The times to remove the jacket were recorded. On the average the time to remove the outer jacket of the cable having steel armoring was 7:45 minutes. The time to remove the outer jacket of the cable when using the controlled jacket bond coated steel armor was only 1:20 minutes. This is a significant time savings in favor of the use of the coated steel armor that gives the controlled jacket bond.

There are three types of cable of interest, the loose tube (LT) design, the ribbon (R) fiber design, and the fiber bundle (FB) design. Splicing times have been reported for three combinations of mid-span entry in which a 144 fiber distribution cable is spliced to a 12 fiber

Table 4

Preparation Time for Armored Cables Maximum Bond to Jacket

	Time for Preparation	
	Maximum Bond	**Controlled Bond**
Loose Tube Design	9 minutes cable end	2 minutes cable end
	12 minutes cable mid-span	3 minutes cable mid-span
Ribbon Design	5 minutes cable end	1 minute cable end
	8 minutes cable mid-span	2 minutes cable mid-span
Fiber Bundle Design	5 minutes cable end	1 minute cable end
	8 minutes cable mid-span	2 minutes cable mid-span

Table 5

Comparison of Total Single Fiber Splicing Time Between with Standard and Controlled Jacket Bond Coated Steel

Cable Types*		Total Splicing Times, Minutes			Increased Time for Splicing, %	
144F	12F	Fibers	Standard Coated Steel	CJB Coated Steel	Standard Coated Steel	CJB Coated Steel
LT	LT	126	147	131	17	4
LT	R	114	131	118	15	4
LT	FB	128	145	132	13	3
R	LT	111	128	115	15	4
R	R	99	112	102	13	3
R	FB	113	126	116	12	3
FB	LT	118	135	122	14	3
FB	R	106	119	109	12	3
FB	FB	120	133	123	11	3
Average		115	131	119	14	3

*LT - Loose Tube Fiber Optical Cable Design
*R - Ribbon Fiber Optic Cable Design
*FB - Fiber Bundle Fiber Optic Cable Design

breakout cable.[10] These combinations are: 1) distribution cable with loose tube design to breakout cable with loose tube or ribbon, or fiber bundle design, 2) distribution cable with ribbon design to breakout cable with loose tube or ribbon, or fiber bundle design, and 3) distribution cable with fiber bundle design to breakout cable with loose tube or ribbon or fiber bundle design. These data were also gathered for single (S) fiber splicing and mass (M) fiber splicing.

To obtain Table 5, the data of Table 4 were combined with the data on cable splicing. The data in Table 5 show the total splicing time for opening a 144 fiber count cable mid-span and then splicing it to a 12 fiber count cable. Various combinations of loose tube, ribbon or fiber bundle 144 fiber count and 12 fiber count cables were single fiber spliced together. The table presents data on these various combinations by first comparing the absolute time to splice the fibers in the core of a cable and then to make a splice to the cable sheath with coated steel having either the standard or controlled bond. The percentage of time required for splicing is then calculated and is shown in columns 4 and 5.

As can be observed in the fourth column, the percent increase in time due to the use of

Table 6

Comparison of Total Mass Fiber Splicing Time Between Cable with Standard and Controlled Jacket Bond Coated Steel

Cable Types* 144F	Cable Types* 12F	Total Splicing Times, Minutes: Fibers	Total Splicing Times, Minutes: Standard Coated Steel	Total Splicing Times, Minutes: CJB Coated Steel	Increased Time for Splicing, %: Standard Coated Steel	Increased Time for Splicing, %: CJB Coated Steel
LT	LT	95	116	100	22	5
LT	R	75	92	79	22	5
LT	FB	97	114	101	18	4
R	LT	69	86	73	25	6
R	R	49	62	52	27	6
R	FB	71	84	74	18	4
FB	LT	87	104	91	20	5
FB	R	67	80	70	19	4
FB	FB	89	102	92	15	3
Average		78	93	81	21	5

*See Table 5.

standard coated steel armor shows a range of time increase for overall cable splicing time from 11 to 27%. The fifth column shows the additional preparation time when cable having coated steel with the controlled jacket bond technology is used. The increase in time for splicing the overall cable ranges from 3 to 6% depending on the cable design.

An analysis of Table 5 shows that the cable splicing time by use of the controlled jacket bond steel versus the standard coated steel ranges from 8 to 13% less. The average reduction is 9% for all the different combinations. Obviously the saving in time is less when cables having the same core construction are spliced together because of the relative ease in splicing the fibers.

Table 6 shows the same type of data for mass spiced cable. Here the use of mass splicing reduces the time splicing the fibers on the average of 37 minutes or 32% versus single splicing of the fibers as shown in Table 5. The time savings associated with the opening of the cable at mid-span through use of the controlled bond steel are even more pronounced because of the overall reduction in fiber splicing time. The reduction in splicing time ranges from 12 to 21% less for the controlled jacket bond steel versus the standard steel. The average reduction is splicing time through use of the controlled bond steel is 16% for all the different combinations of cable core constructions.

This analysis shows that the use of the controlled jacket bond coated steel armor tape significantly reduces the amount of time spent in the field in the preparation and grounding of the coated steel armor. It is also obvious by comparing Table 6 to Table 5 that the use of mass splicing greatly reduces the splicing time versus single fiber splicing.

GROUNDING PRACTICES

There is a need to ground the metallic armor of a fiber optical cable because it can act as a conductor for lightning, other transients, or induced currents. Normally exposure or cable with metallic components to induced currents is low but must be considered in order to avoid potential danger to personnel and electronic equipment. As a result a number of specifications have been developed including the ITU/CCITT series K and L recommendations. The intent of these specifications and other locally specific specifications is to create a low impedance path from the cable armor to all other local cable armors and earth ground. This low impedance path will dissipate lightning or other

induced currents thereby reducing voltages that may endanger equipment or personnel. In general the specifications state that all metallic components, including the armor, should be grounded. Armors at splice points should be bonded together to provide electrical continuity and keep all the metallic components at the splice point at the same electric potential. The use of controlled jacket bond steel can facilitate the grounding process by allowing a quick separation of the jacket to install grounding clips or connectors.

At the entrance point to a building the armor should be grounded to the building ground. The use of an "insulating joint" allows the cable to be run into the building. Once inside the building the ground to the building ground is made through a protection grounding device containing surge protectors. An insulating joint is installed to break the continuity of the armor and the cable proceeds to the patch panel. Using this method eliminates the need for a splice closure on the building at the cable entrance. Local fire codes can be met by installing the cable in conduit. By using lightning surge protectors to ground the armor, there is provision for the use of long range tone location and sheath monitoring equipment. These are invaluable tools for cable locating and preventative maintenance. These tools take advantage of the armor on an armored cable to increase system reliability.[11]

The CCITT standard states that the resistance to ground through the connecting conductor should be low enough to carry the current necessary to dissipate the maximum expected voltage. For armored fiber optical cable in the outside plant, the grounds are generally designed for a ground resistance of 25 ohms. This may not be practical in areas where the soil conditions are rocky or dry and sandy. Special chemical grounds may be needed to lower ground resistance in these areas.

The same issues related to the grounding of the armor are also inherent in the grounding of the electronics used in the system. The experience with lightning strokes to fiber optical cable systems indicates that the electronic components of the system are most susceptible to the stroke. Field data indicate that the electronic grounds become the entry path for the lightning currents into the cable system (versus the other way around). The impedance, not the resistance, of the ground system becomes the key factor to consider for preventing damage. In particular the key parameter is the inductance of the grounding system because transients from lightning or ground faults consist of fast changing currents that contain a wide range of frequencies.[12] Under fault conditions, the inductive reactance of the system affects transient voltage levels in the network much more than the resistance of the grounding conductors. It is necessary to minimize the inductance of the ground paths even when the dc resistance is low. All conductors must follow the most direct route possible with a minimum of sharp turns. Excess lengths of wire at the termination points must be removed. Coiling or twisting of the ground wires should be avoided. Lengths should be shortened and as straight as possible. When high voltages are present the electrostatic field is concentrated near bends or loops or coils because of the abrupt change in the direction of the field.

Discontinuities such as connectors can change the characteristic impedance of the ground path. These changes can cause the transient energy to be reflected back toward its source instead of being drained to ground. The reflections of the transient disturbance and resulting voltages are several orders of magnitude higher than those of the transient that caused the disturbance in the first place. The other issue is resonance. These incident and reflected pulses may end up in phase, and the voltage at that point will be magnified further. So splices and ground branches should be selected such that their reflectivity is negligible. Use of low profile connectors, for example, can reduce reflectivity.

An evolution in the design of connectors has resulted in connectors suitable for armored fiber optical cable with (or without) bonded or laminate sheaths. These connectors do not require the jacket to be stripped. They are slipped over both the jacket and coated metal. They use small tangs ("crocodile teeth")to lock into the jacket and to penetrate the plastic coatings on the inner side of the armor. The primary function of the connectors is to pass currents associated with electrical interference to grounding locations. Therefore, electrical stability of the connections is essential. Sophisticated test requirements have been developed by the Rural Utility Services (RUS, an agency of the US Government) to assure reliable performance. Generally, the following types of tests must be

Table 7
Effects of Environmental Testing on Connector Resistance[1]

		Change in Milliohms From Initial Value[2]		
Sample	Initial Value Milliohms	Thermal Cycling[3]	Corrosion[4]	Surge Testing[5]
A	2.22	2.30	0.48	-0.41
B	2.61	0.97	0.01	0.52

1. Connectors used with coated steel armored bonded sheath fiber optical cable.
2. RUS Specification PE-33 requires that the total change be less than 5 milliohms.
3. Thermal cycling consisted of exposing each sample to 25 temperature cycles. One cycle ranges from -40 to +60°C. Each cycle lasted 4 hours with a transfer time of 30 minutes between temperatures.
4. Samples were exposed to a salt fog test per ASTM B-117-73/79 for a period of 72 hours. Initial connection resistance of each sample must not exceed 5 milliohms, with post test values of below 10 milliohms.
5. Connectors must withstand one 30 kA surge without damage and connection resistance must not change more than 5 milliohms from pretest values.

successfully passed for acceptance: 1) connector resistance; 2) environmental requirements, temperature cycling, salt fog exposure; 3) endurance tests--fault current and current surge.

Table 7 shows test data for two connectors commonly used. All meet the requirements of less than 5 milliohm change after thermal cycling, exposure to salt spray (corrosion), and a simulated lightning surge. These three tests are the most critical in determining the field performance of a connector.

CONCLUSIONS

A new coated steel has been developed for fiber optical cable to facilitate the breakout process. This coated steel has a controlled jacket bond which allows for easy stripping of the jacket at access points while maintaining the mechanical properties, moisture resistance, and rodent resistance associated with armored fiber optical cables with bonded sheaths.

The coated steel with the controlled jacket bond armor meets all industry requirements for adhesion. The cable with the controlled jacket bond armor meets all industry requirements for mechanical and environmental performance.

The bonded sheath with the controlled jacket bond armor is consistent with the concept of dry cables. The bond of the coating on the steel to the cable jacket forms a longitudinal water block between the jacket and armor that is effective after handling of the cable during manufacturing, and installation and after aging in the environment. The combination of coated steel with a sealed overlap and the bonded jacket forms a radial and longitudinal water block for the cable core.

The design of the controlled jacket bond coating results in a layer of copolymer coating that remains on the steel after stripping of the jacket. This coating protects the steel from corrosion at splices and terminations. Connecting devices have been developed that provide easy installation on the armor and stable electrical properties after exposure to the environment. The controlled jacket bond facilitates the installation of these connecting devices.

REFERENCES

1. P. Gaillard, C. McNutt, J. Holder, A. Bouvard, and O. Tatat, "Significant Improvement of Loose Tube Cable Spliceability Based on New Cable Dry Design," Proceedings of the 45th International Wire and Cable Proceedings, 1996, pp 353 - 358.
2. Richard G. Gravely III and Stephen R. Stokes, "An Improved Loose Tube Cable with Dry Water Blocking Elements," Proceedings of the National Fiber Optic Engineers Conference, June 11-22, 1995, Boston, MA, pp 367-375.

3. K. E. Bow, DG Pikula, B. D. Stevens, "Techniques to Obtain a Bonded Jacket, Fully Filled Cable," Proceedings of the SPE 45th Annual Technical Conference and Exhibit, Antec 1987, pp 397-399.
4. S.W. Czupryna, " A High Performance, Cost Effective Alternative to Viscous Filling and Flooding Compounds for Optical Cables", GECA-TAPES, February, 1998.
5. Ibid., Bow, Pikula, and Stevens.
6. Ibid., Czupryna.
7. W.F. Busch, K. E. Bow, D. C. Pikula, " Effect of Sheath Processing Parameters on Cable Performance" Proceedings of the 38th International Wire and Cable Symposium, 1989, pp 427-431
8. Clinton E. Clyburn III and Catharina L. Tedder, "A New Generation Craft-Friendly Cable for Outside Environments," Proceedings of the 45th International Wire and Cable Symposium, 1996, pp 359-368.
9. Ibid, Clyburn.
10. W. E. Beasley, S. T. Canady, and G. Karl, "Choosing the Right Cable for the Right Application" Proceedings of the National Fiber Optic Engineers Conference, June 11-22, 1995, Borton MA.
11. J. Chamberlain and D. Vokey, "Grounding Practices for Fiber Optic Cable Outside Plant," *Outside Plant*, August 1996, pp 25-26.
12. J.F. Rodrigues, "Grounding Network Components," *TE&M*, June 1, 1992, pp 102-105.

AUTHORS

Felix Achille
Dow Chemical Co.
200 Larkin Center
1605 Joseph Drive
Midland, MI 48674

Felix Achille received a B.S. degree in Chemistry in 1977 from Illinois State University. He joined The Dow Chemical Company in 1978 as a chemist and is now a Research Leader for the Dow Fabricated Products Business, Films and Engineered Laminates group. Since 1994, he has been active in the development and implementation of new plastic coated metal for use in fiber optic telecommunication cables.

Kenneth E. Bow
Dow Chemical Co.
200 Larkin Center
1605 Joseph Drive
Midland, MI 48674

Kenneth E. Bow received a B.S. degree in Electrical Engineering from Michigan State University in 1962. He then joined The Dow Chemical Company, Midland, MI, where he has been involved in the research and development of materials for the wire and cable industry for more than 30 years. He is currently the Chief Scientist for the development of polymer and coated metal products for wire and cable applications. He is responsible for the global development of cable technology associated with plastic-coated metallic shielding and armoring tapes.

William F. Busch
Dow Chemical Co.
200 Larkin Center
1605 Joseph Drive
Midland, MI 48674

William F. Busch received a B.S. degree in Chemical Engineering from the State University of New York at Buffalo in 1977 and a M.S. degree in Chemical Engineering from the University of Virginia in 1979. He is currently the Team Leader of the Engineered Laminates R&D Department of The Dow Chemical Company. He is involved with product and application development of coated metal laminates for the wire and cable industry.

A New Approach to Fiber Strength Reliability Mechanism Against Heat-Damp Aging.

Hideyuki Suzuki Ikuo Seki Shinji Hinoshita
Hideki Shimane Kodo Yamada Takahiro Yamazaki

Hitachi Cable, Ltd. 5-1-1 Hitaka-cho, Hitachi-shi, 319-1414 JAPAN

1. Abstract

The gradual deterioration in the fiber strength of optical fiber under a high-temperature and high-humidity environment was found to vary greatly depending on the organic functional group of the silane coupling agent.

It was also found that the effect of differences in the organic functional group on heat and humidity resistance was more likely caused by differences in the bonding characteristics between the silane coupling agent and the glass surface than by differences in reactivity with moisture or in migration characteristics within the coating layer. Continued study of these bonding characteristics should make it possible to achieve an optical-fiber structure with an even higher level of reliability.

2. Introduction

It is well-known that the strength of optical fiber gradually deteriorates under a high-temperature and high-humidity environment. The cause of this problem is thought to be the penetration of moisture into the interface between the glass and coating layer resulting in erosion of the glass layer and peeling of the coating layer. This phenomenon has a damaging effect on long-term reliability and has therefore become a serious issue.1)-7)

The authors have found that a silane coupling agent added to the coating layer is a major factor affecting deterioration in fiber strength. In this regard, we report on a new approach to clarifying the mechanism behind strength deterioration by comparing the performance of different coupling agents that can and cannot prevent such deterioration.

3. Experimental Coating Materials and Evaluation Method

3.1 Experimental materials

The materials used for optical-fiber coating in this report are all ultraviolet-curable resins of the urethane acrylate family, namely oligomer (prepolymer), monomer, photo initiator, and other

antioxidants. The material compositions for both the primary and the secondary coatings were fixed to ensure uniform evaluation conditions. Silane coupling agents were added to the primary coating and their effects were investigated with the drawn coated fibers.

3.2 Evaluation method

HDA (Heat-Damp Aging)

Fibers were stored in a high-temperature and high-humidity environment with no stress applied (zero-stress aging). Unless otherwise indicated, all experiments were 30 days duration and were conducted at 85℃ and 85% humidity.

Fiber tensile strength and m-value calculation

Tensile strength:

Fiber strengths at the time of tension fracture were measured, and results were analyzed on a Weibull probability chart. From this, a comparison could be made of the fiber strength distribution.

m value:

The Value of m represents the distribution slope in a weibull probability chart as shown in Fig.1.

AFM (Atomic Force Microscope) observation

The coating layer of the optical fiber was chemically removed in order to allow observation of the glass surface of the fiber using an AFM. We could then observe the AFM image and analyzed the AFM data scan chart to evaluate the roughness of the surface of the glass in relation to fiber strength.

Pull-Out-Force measurement

The pull-out force of pull-out-length 10-mm between the glass and the coating layer of the fiber was measured. In this process, a 10-mm section length of the fiber was first bonded over the coating with the fixing sheet. The glass was then pulled out at the cutting point of the coating by pulling the fiber with a tensile tester.

EPMA (Electron Prove Material Analyzer)

Electron beams were irradiated on the object of analysis in order to generate wavelengths and intense characteristic X-rays. By measuring these the name of chemical elements and their amount in the target material could be ascertained. Samples were adjusted by burying the fiber in resin, polishing a cross section, and performing metal vapor deposition.

4. Experimental Results

Three types of silane coupling agents (A, B, and C) were chosen with the aim of analysing their effects on fiber strength. The general formula for these silane coupling agents is shown in Fig. 2. The functional groups of these three silane coupling agents are referred to as Ya, Yb, and Yc. The same amount of these silane coupling agents were used to form the urethane-acrylate-based ultraviolet-curing resin of the optical fiber, and a series of

experiments and observations were performed.

Table 1 shows the comparison of fiber strength and m-value data for the optical-fiber samples before and after HDA. As shown, silane-coupling-agent type A exhibits little strength deterioration. It also has a sufficiently large m value after HDA, and has sufficient humidity (water) resistance. From these three silane coupling agents, we selected A and C for comparison purposes and then proceeded with the study.

Table 2 compares the 10-mm pull-out force between samples A and C before and after HDA. Although there is no change in pull-out force when aging the samples at 21℃ X 50%, sample A increased and sample C decreased in pull-out force for aging at 85℃ X 85%. In both cases, measurements were taken after drying the samples for 24 hours in a room at 21℃ X 50%.

Figure 3 shows an AFM image of the glass surfaces for samples A and C obtained through AFM observations. For (1)A of Figure 3, the morphology of the residual polymer may be imaged as droplet-like islands which shall be disregard when seeing the roughness of the glass surface. Fig. 4 is an AFM data scan chart showing the roughness of these surfaces for three positions line scan. Sample A shows no major change in surface condition after HDA when disregarded the ghost noise derived from the droplet-like islands. Sample C exhibits a growth in roughness (1-2 nm level) due to the penetration of moisture into the interface between the coating layer and glass. These results correspond with the evaluation result of pull-out force (Table 2). It is therefore understood that silane coupling agent C cannot sufficiently increase adhesion strength between glass and the coating layer under a high-temperature and high-humidity environment.

5. Discussion

A number of theories have been put forward 8)-15) on the mechanism behind the effects of silane coupling agents. When using such an agent in a fiber coating layer, it is thought that the functional group bonds with the matrix of the primary coating material while the other side of the chain end of the agent that brings about hydrolysis interacts in some way with the glass surface. It is believed that this interaction causes a hydrogen bond or an Si-O-Si covalent bond. In short, there are thought to be 2 main results in using a silane coupling agent to strengthen the adhesion between an inorganic surface like glass and an organic matrix:

1) The organic matrix bonds with the functional group; and

2) The -OH of the inorganic surface and the -OH of the silane coupling agent become connected through either a

covalent bond or a hydrogen bond.

Referring again to the AFM image of Fig. 3, it appears that moisture has penetrated the interface between the glass surface and the coating layer in the case of fiber C. This leads us to infer that silane coupling agent C has weaker bonding capabilities with a glass surface compared to silane coupling agent A. Since the only difference between agents A and C is the structure of the functional group, we made the following three hypotheses as possible factors behind the effect of this group.

(1) Reactivity of the silane-coupling-agent's hydrolytic group with moisture

(2) Migration characteristics of the silane coupling agent towards the glass surface

(3) Bonding characteristics between the silane coupling agent and glass surface

Based on the above inferences, we conducted an experiment to examine these possible factors.

With regard to (1), in view of the difficulty involved in taking direct quantitative measurements of the silanol group in the materials, it was instead decided to compare the reactivity with moisture of agent A with that of agent C by a model experiment. In this experiment, the same amounts of agents A and C were added to the same basic material and the same amount of water was added to each sample. Table 3 shows the results of this experiment by comparing the amounts of remaining moisture after certain periods of time.

These results reveal no significant difference between agents A and C. This leads us to conclude that reactivity with moisture cannot in itself explain the influence of a silane coupling agent on heat and humidity resistance.

With regard to (2) above, the migration characteristics of coupling agents A and C were compared. This was done by examining a fiber cross section after a sufficient period of time following the fiber manufacture. In this way we could determine the amount of Si on the outer side and inner side of the primary coating layer, as shown in Fig. 5. We wish to point out here that it is not possible to accurately quantify the content of Si in the primary resin because of less accuracy due to less quantity containment. However, since it is only the silane coupling agent that contains Si among the primary coating layer, we should be able to measure the differences in Si molecule concentration to know the differences in concentration of the silane coupling agent. Table 4 shows the results of this comparison using EPMA measurements of Si reactivity. As shown, In the table 4,relative index of Si concentration data are shown. The relative index number of the oouter layer of the primary coating of each fiber (A & C) is indicated "100" respectively.We observe

the same level migration to the inner side within the primary coating layer between the coupling agent A and C as shown in Table 4.

It was also confirmed that among the same sample fibers used in these measurements, the fiber using silane-coupling-agent C showed a fiber strength degradation after HAD. This result indicates that migration characteristics of silane coupling agents have little effect on heat and humidity resistance.

A major difference could therefore not be found between silane-coupling-agents A and C in terms of their reactivity with moisture and their migration characteristics toward the glass surface. There is a strong probability that the difference between the functional group causes a difference in bonding characteristics between the glass and the coating. This becomes dominant factor in trying to improve the fiber strength.

6. Conclusion

The following conclusions are made on the basis of the above experiments.

1) Differences in fiber strength after HDA due to differences in silane-coupling-agents A and C are governed by the adhesive characteristics of the coupling agent with the glass surface. The fiber strength deterioration is a significant factor when the coupling agent, which degrades the pull-out force due to the moisture,is used.

2) Although the only difference between coupling-agents A and C is their organic functional group, this difference does not produce a great effect on reactivity with moisture before coating and on migration characteristics to the glass surface after coating. On the other hand, we can conclude that "bonding characteristics of a silane coupling agent with glass are a major factor in the deterioration of fiber strength after HDA."

Further studies will focus on clarifying the mechanism of chemical bonding with glass and finding a method for strengthening the chemical bond in order to manufacture optical fiber with an even higher level of reliability.

References

1) M.Vyas, E.Buckland and P.Neveux,Jr., *Proc.of* IWCS,40 55 (1991)

2) H.H.Yuce, J.P.Varachi, J.P.Kilmer, C.R.Kurkjian and M.J.Matthewson OFC'92, Tech Digest,Postdeadline Paper - PD-21 (1992)

3) D.Innis, Q.Zhong and C.R.Kurkjian, J.Amer. Ceram. Soc.,76,3173 (1993)

4) James J. Carr *Proc.of* IWCS,42 394 (1991)

5) Kariofilis Konstandinis, Neil W.Sollenberger, Shahab Siddiqui, Ken W.Jackson, John M.Turnipseed, T.W.Au, Raymond P.DeFabritis, and Carl R.taylor *Proc.of* IWCS,46 274 (1997)

6) J.L.Armstrong, M.J.Matthewson,

C.R.Kurkjian, and C.Y.Chou *Proc.of* IWCS,46 902 (1997)

7) Tomoyuki HATTORI, Akira URANO, Nobuhiro AKASAKA, and Yasuo MATSUDA *Proc.of* IWCS,44 865 (1995)

8) Dipak R.Biswas, Charles R.Kurkjian and Osman S.Gebizlioglu *Proc.of* IWCS,45 456 (1996)

9) H.A.Clark, E.P.Pluddemann: 18th SPI 20-C (1963)

10) G.E.Vogel, O.K.Johanson, F.O.Stark, R.M.Fleischmann: 22th SPI 13-B (1967)

11) D.J.Tutas: 19th SPI 21-C (1964)

12) W.A.Zisman: 19th SPI 21-B (1964)

13) J.G.Vail: Soluble Silicate Vol.1, 171 Reinhold Publihsing Corp., New York (1952)

14) E.P.Pluddemann: Mod. Plast., 40, 133 (1963)

15) E.P.Pluddemann: Comps. Mater., 74(6), 173-216

Hideyuki Suzuki
Hitachi Cable, Ltd.
5-1-1,Hitaka-cho,
Hitachi-shi,
319-1414
Japan

Mr. Suzuki received his B.E. degree in Chemical Engineering from Ibaraki University in 1993 and joined Hitachi cable, Ltd. He has been engaged in research work on ultra-violet curable material used for wire and cables. He is now a researcher in the 2nd Dept., Power System laboratory.

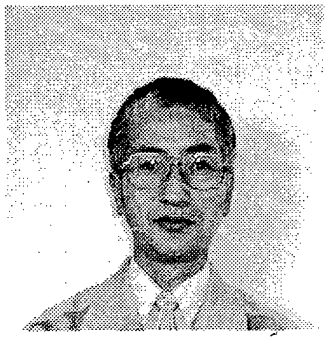

Ikuo Seki
Hitachi Cable, Ltd.
5-1-1, Hitaka-cho,
Hitachi-shi,
3191414
Japan

Mr. Seki received his B.E. degree in Organic Chemistry from Gunma University in 1971 and joined Hitachi cable, Ltd. He has been doing research work in optical fibers. He is now an executive senior researcher in the 2nd Dept., Power System Laboratory.

Shinji Hinoshita
Hitachi Cable, Ltd.
5-1-1,Hitaka-cho,
Hitachi-shi,319-1414
Japan

Mr. Hinoshita graduated in Electrical engineering from Kure National College of Technology in 1970 and joined Hitachi Cable, Ltd. He is currently responsible for design and development of optical fiber and components of mobile access networks. He is now an executive senior engineer in the Telecommunications Design Department.

Hideki Shimane
Hitachi Cable,
Ltd.
5-1-1,Hitaka-cho,
Hitachi-shi,
319-1414
Japan

Mr. Shimane received his B.E. degree in Electrical Engineering from Shibaura Institute of Technology in 1993 and joined Hitachi cable, Ltd. He has been engaged in the design and development of optical fiber cables and telecommunications cables. He is now an engineer in the telecommunications Design Department.

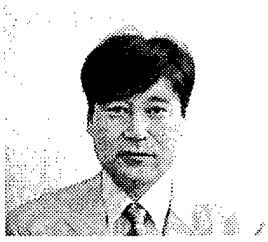

Takahiro Yamazaki
Hitachi Cable,
Ltd.
5-1-1,Hitaka-cho,
Hitachi-shi,
319-1414
Japan

Mr. Yamazaki received his B.E. degree in Electrical Engineering from Ibaraki University in 1982 and joined Hitachi Cable, Ltd. He has been engaged in the development and production of optical fiber cable. He is now a senior engineer in the Optical Fiber and Communications Cable Department.

Khodo Yamada
Hitachi Cable,
Ltd.
5-1-1,Hitaka-cho,
Hitachi-shi,319-1414
Japan

Mr. Yamada received his M.E. degree in Chemical Engineering from the Science University of Tokyo in 1984 and joined Hitachi Cable, Ltd. He has been engaged in the development andproduction of optical fiber cable. He is now a senior engineer in the Optical Fiber and Communications Cable Department.

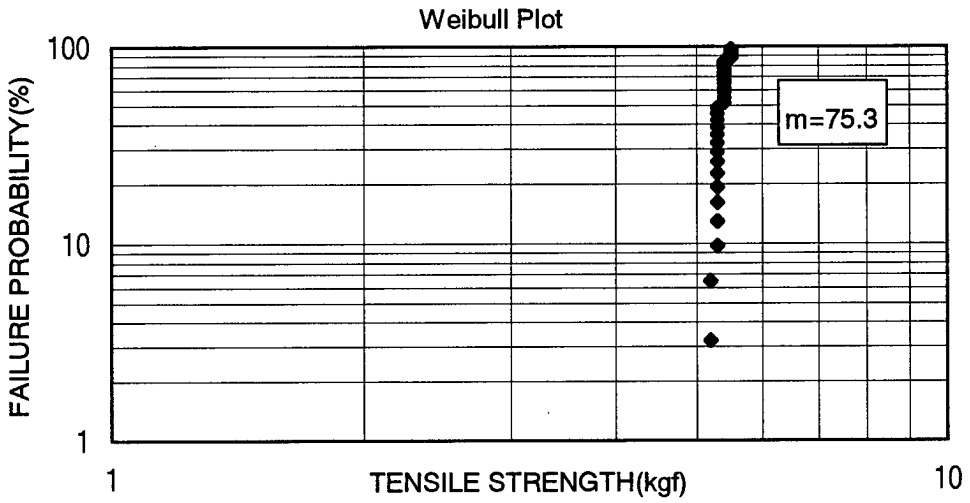

Figure 1 m value

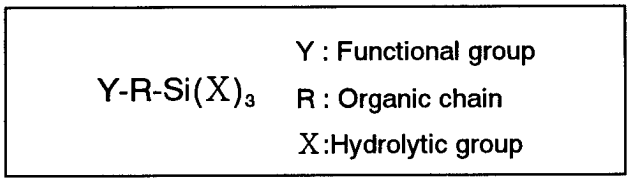

Figure 2 General formula for silane coupling agents

Table 1. Relationship between functional-group types and strength

Samples (Silane coupling agent)			A	B	C
Y (functional group)			Ya	Yb	Yc
Fiber format	initial	Tensil strength median (kgf)	6.0	5.8	5.7
		m value	90.9	99.0	75.6
	After aging (85°C x 85%, 14 days)	Tensil strength median (kgf)	4.7	4.9	4.3
		m value	50.3	9.3	10.7

Table 2 Pull-out force

Silane coupling agent		A	C
Initial		100	100
After aging	21°C x 50% x 30 days	100	100
	85°C x 85% x 30 days	140-160	60-70

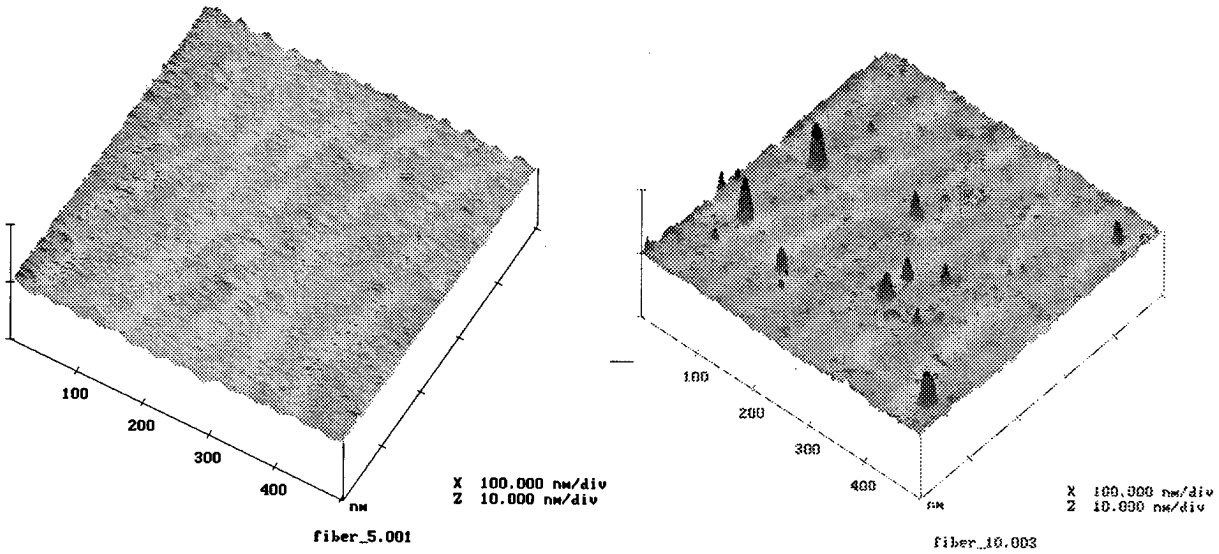

initial

After aging (85°C x 85%, 30 days)

(1) A

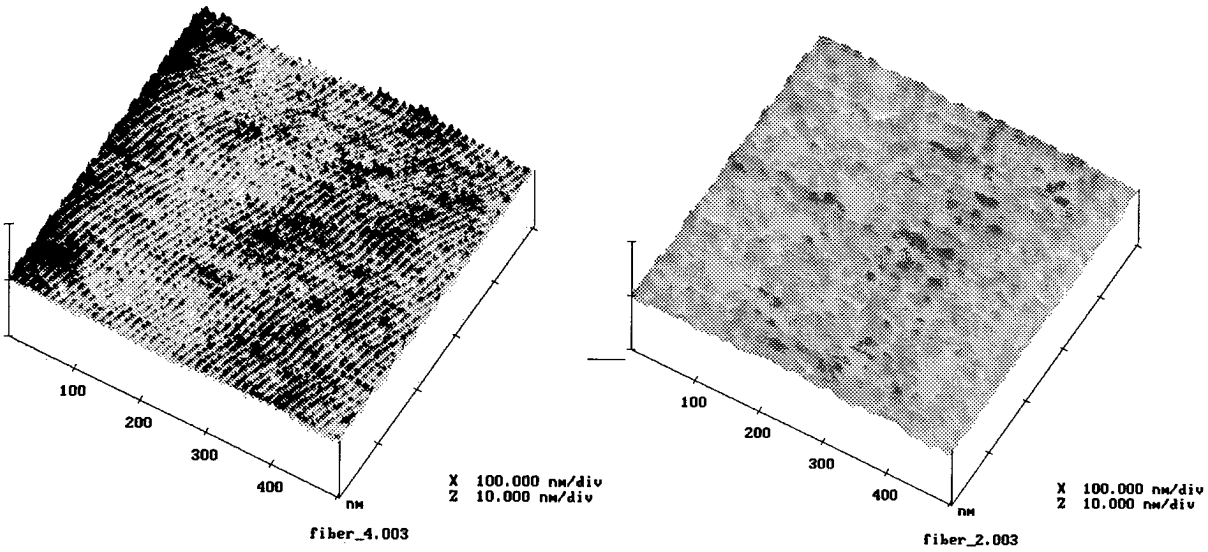

initial

After aging (85°C x 85%, 30 days)

(2) C

Figure 3 AFM image of glass surface (samples A and C)

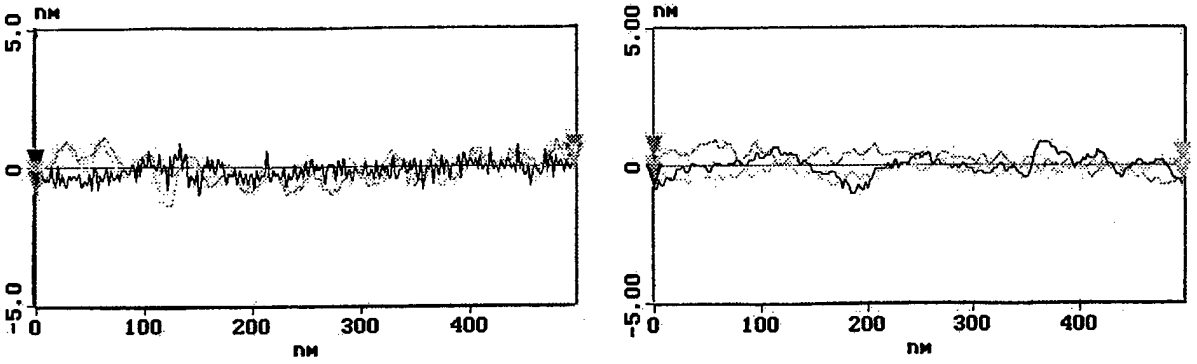

initial

After aging (85°C x 85%, 30 days)

(1) A

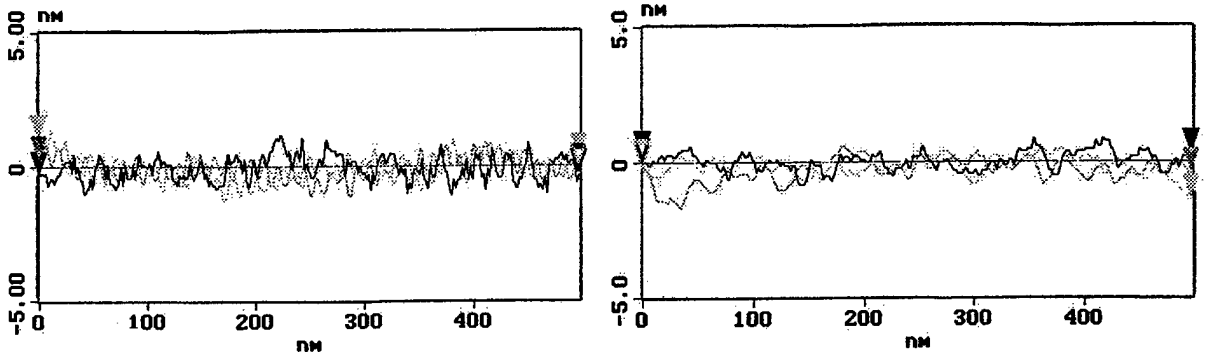

initial

After aging (85°C x 85%, 30 days)

(2) C

Figure 4 AFM data scan chart to show roughness

Table 3. Reactivity between silane coupling agent and moisture

Coupling agent		A	C
Amount of moisture (%)	initial	100	
	after 1 hour	100	100
	after 4 hours	90	95
	after 4 days	50	50

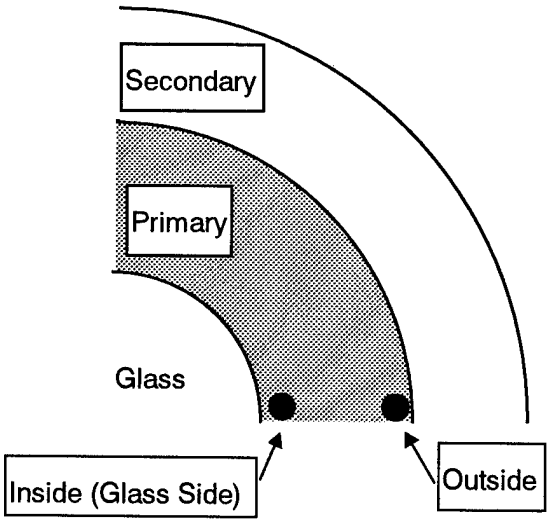

Figure 5 Measurement locations of Si concentration

Table 4 Comparison of Si concentration

	A	C
outside	100	100
inside (glass side)	240	250

MECHANICS OF DELAMINATION RESISTANCE TESTING

P. L. Tabaddor, C. J. Aloisio, C. H. Plagianis, C. R. Taylor
V. Kuck* and P. G. Simpkins*

Lucent Technologies Inc., Bell Laboratories
2000 NE Expressway, Norcross GA 30071
*** 600-700 Mountain Avenue, Murray Hill, NJ 07974**

ABSTRACT

A significant challenge in the design of fiber optic coating systems is the need to balance the delamination resistance with the ability of the coating to be easily removed when necessary. Delamination resistance, a measure of the integrity of the glass primary interface and fiber robustness, is an important property during fiber manufacture, handling and processing in the field. Two different methods for measuring the delamination resistance are presented in this paper. The impact of changing the mechanical properties of the primary and secondary coating on delamination resistance is also examined.

INTRODUCTION

In the various stages of fiber processing, it is necessary to maintain the integrity of the interfacial bond between the glass and the primary coating. The failure of this bond, referred to as a delamination, can result in severe performance degradation or, at the very least, a negative customer perception. The strength of this bond is dependent upon the coating composition and its mechanical properties. The optimization of the coating's mechanical properties allows not only for improved delamination resistance, but also ensures product robustness under a variety of field and aging conditions.

This paper examines the relationship between mechanical properties of the primary and secondary coatings and delamination resistance. Specifically, the impact of primary-glass adhesion, and the modulus of the primary and secondary coatings on delamination resistance is investigated. Two methods of testing are discussed: (1) compressive loading of a fiber not under tension, and (2) a rewind proof-tester configuration, where the tension and/or the loading rate can be varied.

DELAMINATING TESTING METHODOLOGY

Two methods developed to evaluate the delamination resistance of the fiber samples are described below. The first method was developed to simulate handling situations where, the fiber is subjected to a low longitudinal tension and a crushing normal force. In the second method, developed to re-create delaminations associated with fibers passing over pulleys during manufacture, a high longitudinal tension/one-sided low normal force is applied.

Compressive loading method: Figure 1 illustrates the test setup used for this method of measuring delamination resistance. A 3 inch piece of optical fiber is gently pulled to remove any curvature and taped on to a glass slide. The slide is then fixed to an aluminum block on the delaminator in such a way that the fiber is aligned with the center. A free floating plate connected to a 1/4" diameter rod is loaded with a desired test weight and lowered at a speed of 1.7 mm/sec onto the fiber.

The loaded rod is allowed to rest on the fiber for 5 seconds and then raised off the sample. The block is manually moved 1/8" to expose a new test region, and the test is repeated. After 10 sites have been impacted, the slide is removed from the delaminator, and an index matching liquid, such as glycerine, is applied to the fiber. The impacted areas are visually examined with an optical microscope operated at 400X magnification. The percent delamination is then calculated from the ratio of the number of damaged sites to the total possible (i.e. 10).

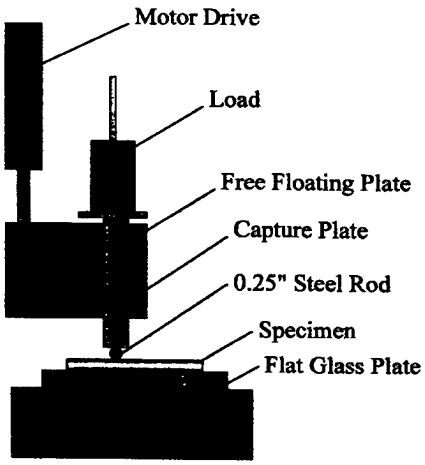

Figure 1. Test setup for delamination resistance by the compressive loading method

Dynamic testing method in tension: A rewinder/proof-tester configuration is used to study the impact of tension and loading rate on the resistance to delamination. The test uses a 76mm diameter pulley with five, 200μ delaminators/pins under tensions of 500 and 1000g at testing speeds of 0.1, 0.2, 0.5, 1, 3, 6 and 10m/sec. The mechanical arrangement is such that the fiber is in contact with the pulley for 180 degrees. Once the entire length to be tested has been pulled through the rewinder assembly (i.e. the fiber is impacted 16 times), the number of delaminations created is determined by examining the fiber under a microscope. The percent delamination is then calculated as a ratio of the number of delaminations created to the total number of delaminations possible (i.e. 16).

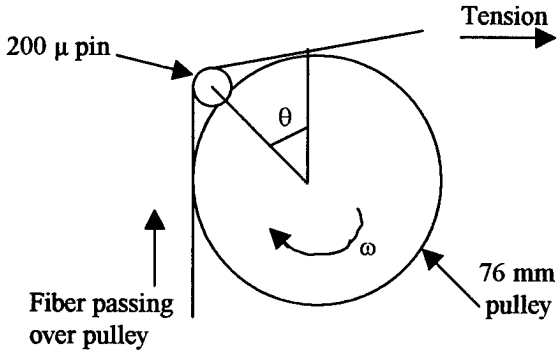

Figure 2. Schematic for dynamic test method in tension

In the dynamic testing method with tension, the total time that the fiber is in contact with the pulley and the delaminating pins is an important consideration. The pin size and the pulley diameter define the initial contact angle, which influences the rate at which the load is applied to the fiber. As shown in Figure 3, T_r is the 'rise' time from the instant the fiber leaves the pulley surface, due to the 200μ diameter and T_d is the 'dwell' time due to the wrap of the fiber around the pulley.

The total time the fiber is in contact with the pin can be derived as

$$T_t = (2\pi/3 + 2\theta)/\omega \qquad (1)$$

where θ is the angle between the pin and the fiber contact point with the pulley (Figure 2) and ω is the angular velocity of the pulley.

The 'rise' and 'fall' times of the loading are given by

$$T_r = 2\theta/\omega \qquad (2)$$

Consequently the 'dwell' time during which the load is constant is given by

$$T_d = T_t - 2T_r = 2/\omega(\pi/3 - \theta) \qquad (3)$$

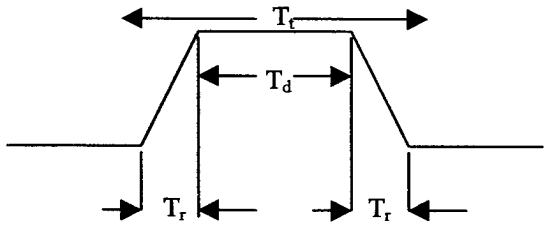

Figure 3. Illustration of the fiber path over the pulley

The longitudinal speed of the fiber over the pulley determines the loading rate, which in turn modifies the mechanical response of the primary and the secondary coatings. The deformation rate, "F", in the dynamic test is a function of the "rise" time and is given by

$$F = 1/T_r \qquad (4)$$

In addition to longitudinal tension, a one-sided normal force is applied to the fiber as it passes over the pin. Using the string approximation for a 200μ pin, the normal force on the fiber can be calculated.

The normal force at 500 and 1000 grams tension is determined to be 44 grams and 88 grams, respectively. These tensile loads are significantly lower than the normal forces applied in the compressive test for measuring delamination resistance.

MECHANICS OF DELAMINATION: Theory

Figure 4 shows a typical primary-glass interface failure referred to as a delamination. Note that the failure occurred without any visible damage to the secondary outer surface.

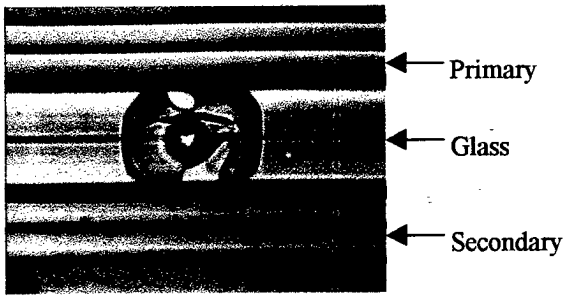

Figure 4. Typical primary-glass interface failure

When a coated fiber passes over a perturbation, as in the dynamic test, the extent to which the coating is deformed depends on the longitudinal speed of the fiber. At greater speeds, the modulus of the secondary coating is higher which diminishes the impact on the primary coating and the primary-glass interface. At very low speeds, the secondary can be permanently deformed without causing a delamination. In the intermediate speed zone, the residual radial tensile stresses resulting from processing can couple with the recoil of the secondary coating to provide the stresses and conditions needed to create the delamination.[1, 2] Adjacent to the delamination (Figure 4 also), tears or puckers are occasionally observed. Tearing relates mostly to the strength of the bond between the primary coating and the glass. During the deformation/damage process, the multi-axial stress field tries to raise the primary coating from the glass. If the glass-primary bond is strong, the primary will tear. If it is weak, the coating will pucker or, as a worse case, catastrophically delaminate. Tearing is also observed in the compressive loading test and is dependent mostly on the chemical composition of the primary coating. At the higher loads, more tearing is observed.

Besides the modulus and the temperature dependent relaxation behavior of the secondary coating, the resistance to delamination can be impacted by the modulus and tear strength of the primary coating, and the strength of the adhesion at the primary-glass interface. In subsequent sections, the relationship between the primary coating properties and delamination resistance will be investigated. The effect of varying the glass transition temperature and relaxation behavior of the secondary coating has not been included here, but will be presented at the symposium.

DYNAMIC MECHANICAL ANALYSIS

The dynamic mechanical behavior for the primary coatings was observed with a Rheometric Scientific RSA-II at a frequency of 1 rad/sec and a heating rate of 2°C/min. The storage modulus (E'), the loss modulus (E") and tan δ curves were obtained from the isotherms performed at temperatures ranging from –75 to 25°C at intervals of 10°C. Using the data obtained at 25°C as the reference, a master curve was generated by time-temperature superposition. The mechanical properties of the primary coating over the frequency range used in the delamination under-tension test could then be determined from the master curves.

THE EFFECT OF CHANGES IN THE PRIMARY COATING PULL-OUT ON DELAMINATION RESISTANCE

The strength of the primary-glass interface can affect the resistance of the fiber to delamination. The fiber pull-out test measures the adhesion between the primary coating and the glass.[3] Here, a tensile force is applied to a dual coated fiber specimen mounted on a rigid tab with a cyanoacrylate adhesive. The force required to separate the glass fiber from 1 centimeter of the primary coating is then measured.

To study the impact of primary-glass adhesion using the pull-out test on delamination resistance, three model formulations were prepared with the *in-situ* modulus held constant.

The *in-situ* modulus is a measure of the crosslink density of a coating material and corresponds to the plateau or equilibrium modulus on the E' curve. For the same family of coatings, the *in-situ* modulus typically reflects the pull-out behavior i.e. as the pull-out force increases, so does the *in-situ* modulus. In this study, the coatings were designed to keep the *in-situ* modulus constant, so that the effect of changing the primary-glass adhesion on delamination resistance alone could be observed. Table 1 summarizes the targeted values for the pull-out force and relative *in-situ* modulus values for the three model formulations. Note that in the design of these coatings, the pull-out was successfully varied while keeping the *in-situ* modulus reasonably constant.

Table 1. Pull-out and *in-situ* modulus values for three model formulations

Formulations	Pull-out (lb./cm)	*In-situ* modulus ratios
A (pull-out)	High	1.02
B (pull-out)	Nominal	1.00
C (pull-out)	Low	0.96

Delamination resistance testing was done on all three samples using both the dynamic method in tension and the compressive method. Figures 5 and 6 shown below, illustrate the dependence of delamination resistance on the pull-out force.

Both methods indicate that there is no clear relationship between delamination resistance and pull-out force. In other words, the delamination resistance does not decrease with decreasing pull-out force as one would expect. In fact, the fiber with the lowest pull-out value shows the highest resistance to delamination by the compressive loading method (Figure 6).

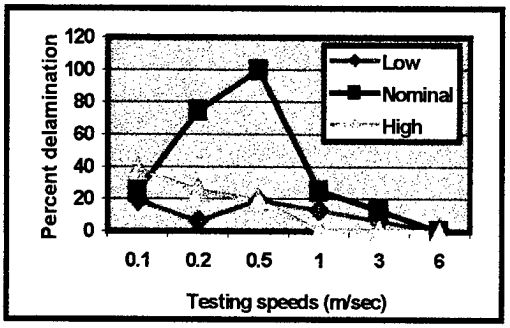

Figure 5. Delamination resistance data by the dynamic tension method (effect of varying pull-out)

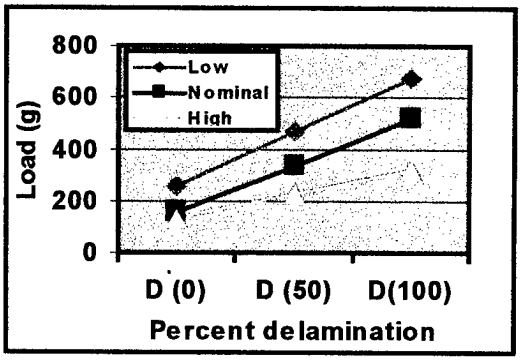

Figure 6. Delamination resistance measurements by the compressive loading method (effect of varying pull-out)

EFFECT OF VARYING THE *IN-SITU* MODULUS OF THE PRIMARY COATING ON DELAMINATION RESISTANCE

The *in-situ* modulus, which is a diagnostic measure of the low-strain shear modulus of the primary coating, can be used to determine the cure characteristics independent of the adhesion[4]. The test procedure calls for the measurement of the filar displacement of the glass relative to the polymer coating as various loads from 10 to 70 grams are placed at the end of the fiber strand. The modulus is then obtained from a plot of the load versus the filar displacement.

Three model primary coating formulations were prepared to investigate the effect of varying the *in-situ* modulus on delamination resistance. Fiber was drawn using these model formulations while keeping the secondary coating chemistry constant. Table 2 summarizes the relative *in-situ* modulus values obtained for the three model formulations.

Table 2. *In-situ* modulus for the model formulations

Formulation	Relative *In-situ* modulus	Pull-out (lb./cm)
A (modulus)	0.75	Low
B (modulus)	1.0	Nominal
C (modulus)	1.25	High

The delamination resistance of the samples was measured using both the dynamic and the compressive loading methods. In the dynamic method, the number of delaminations created under 500 and 1000g tensions was measured at testing

speeds of 0.1, 0.2, 0.5, 1.0, 3.0 6.0 and 10.0m/sec. Figure 7 is a plot of the delamination resistance (measured at a 1000g tension) versus line speed for primary coatings with varying *in-situ* modulus.

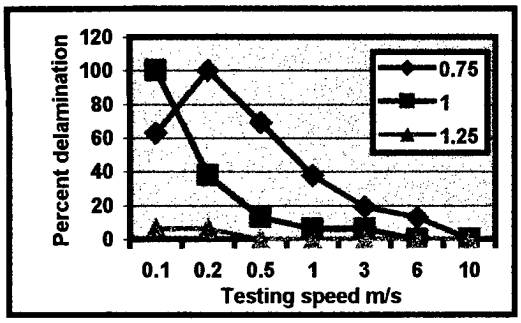

Figure 7. Delamination resistance vs. line speed at 1000g tension, dynamic test method

Two of the three curves in Figure 7 are characterized by a high percent delamination at low testing speeds and a low percent delamination at high speeds. The greater the *in-situ* modulus of the primary coating, the greater the delamination resistance. It also appears that an increase in the *in-situ* modulus shifts the time scale of the response of the coating system to lower speeds. In other words, the higher the modulus of the primary coating as measured by the *in-situ* modulus test, the lower the effective rate experienced at the primary-glass interface where delaminations are formed. Therefore, the characteristic peak seen in Figure 7 shifts to lower speeds. The effect is illustrated in Figure 8 where a delamination resistance master curve is constructed using graphically determined *in-situ* modulus shift factors and the 0.75 modulus ratio curve as a reference.

In a separate plot (Figure 9), using an estimate of loading frequency based on the pulley's angular rotational speed, the elastic component of the primary coating modulus is overlayed on the same delamination data. Between 0.1 m/s and 10 m/s, the elastic modulus of the primary coating increases considerably making the coating more resistant to delamination. In other words, the visco-elastic properties of the primary coating play an important role in the delamination process. The storage modulus of the secondary coating can also increase in the frequency range discussed above, thus offering increased protection to the primary-glass interface. However, since the fibers prepared with the three model formulations had the same secondary coating, the trends in the delamination resistance indicated in Figure 9 can be attributed mostly to changes in the primary coating i.e. increasing *in-situ* modulus.

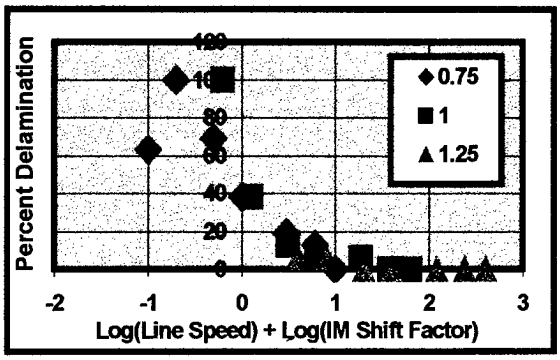

Figure 8. Delamination resistance master curves obtained by shifting curves in Figure 7

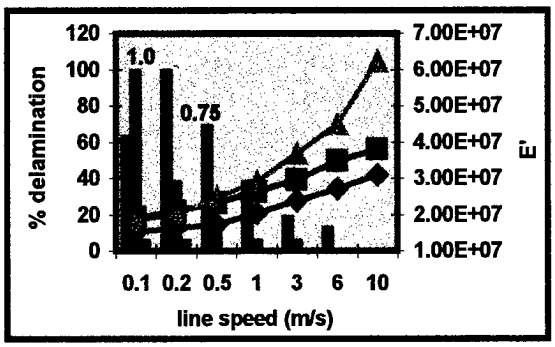

Figure 9. Effect of changing E' on delamination resistance

For these model formulations, the pull-out force is seen to increase as the *in-situ* modulus increases (Table 2). It is therefore difficult to exclude the possibility that greater primary-glass adhesion, does not improve delamination resistance. However, the model formulations prepared by varying the pull-out force alone showed no clear correlation with delamination resistance. Perhaps, some method other than the pull-out test, can clarify the influence of primary-glass adhesion on delamination resistance.

In the compressive test method, a stationary fiber strand held against a rigid surface is subjected to increasing loads until delaminations are observed. Here also, the greater the *in-situ* modulus of the primary coating, the greater the load it requires to create an equivalent percentage of delaminations. In fact, this relationship between the primary coating *in-situ* modulus and the load required to create 100% delaminations is linear. Figure 10 illustrates the change in delamination resistance with *in-situ* modulus as obtained by the compressive test method.

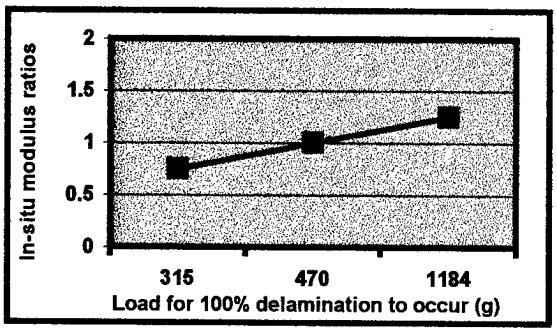

Figure 10. Effect of primary *in-situ* modulus on D(100)

CONCLUSIONS

Delamination resistance of several model coating formulations was measured by two different methods developed to simulate typical handling operations during processing and manufacturing. The model formulations were designed to vary *in-situ* modulus of the primary coating and the strength of the primary-glass interface as measured by the pull-out test. While the delamination resistance was clearly dependent on the *in-situ* modulus of the primary coating, there was no clear correlation with the pull-out force.

ACKNOWLEDGMENTS

The authors gratefully acknowledge the supplier's help in preparing the model formulations and testing support by Daniel Harper, Modhurima Ahmad and Matthew Montelone.

REFERENCES

1. W. W. King and C. J. Aloisio, "Thermomechanical Mechanism for Delaminations of Polymer Coatings from Optical Fibers," *Journal of Electronic Packaging, Transactions of the ASME*, pp, 133-137, June 1997, Vol. 119.
2. C. J. Aloisio, W. W. King and R. C. Moore, "A Viscolelastic Analysis of Thermally Induced Residual Stresses in Dual Coated Optical Fibers," *Proceedings 44th International Wire and Cable Symposium, 1995,* pp. 139-145.
3. C-K Chien, "Investigation of Pullout Force for Coating Adhesion in Optical Fiber," *Proceedings 45th International Wire and Cable Symposium, 1996,* pp. 558-560.
4. B. J. Overton and C. R. Taylor, *Proc. of SPE ANTEC*, p392, April 18-21, 1988

BIOGRAPHIES

Priya L. Tabaddor
2000 NE Expressway, Norcross, GA 30071

Priya Tabaddor received her Ph.D. in Polymer Chemistry from Virginia Polytechnic Institute and State University in May 1995. She is currently a Member of the Technical Staff in the materials technology Group at Bell Laboratories working on the development of materials for optical fiber applications and related products. She is active in the Fiber Coatings Working Group of the Telecommunications Industries Association.

Charles J. Aloisio
2000 NE Expressway, Norcross, GA 30071

Charles Aloisio began his career with Bell Laboratories in 1952. He worked in the Materials Group with Bell Labs in Indianapolis from 1967 to

1972, while obtaining his MS and Ph.D. from Purdue University. He is currently a Distinguished Member of the Technical Staff in the Material Technology Group and has worked on applying rheology and viscoelasticity to a variety of materials such as polypropylene and polyethylene for cable sheathing and DEPIC insulation, copper and optical fiber coatings.

Claire H. Plagianis
2000 NE Expressway, Norcross, GA 30071

Claire Plagianis joined the Materials Technology and Quality Engineering group in September, 1990. She is a Senior Technical Associate at Bell Laboratories working on analysis and development of materials for fiber optic applications. She received her B.S. in Chemistry from Carnegie-Mellon University in 1975.

Carl Taylor
2000 NE Expressway, Norcross, GA 30071

Carl R. Taylor is currently Bell Laboratories Technical Manager of the Materials Technology and Quality Engineering Group at Lucent Technologies' main Fiber Optic Manufacturing site in Atlanta. Prior to joining Bell Laboratories in 1977, he earned a B.S. in Chemistry from the College of Wooster in Ohio and a Ph.D. in Physical Chemistry from the University of Wisconsin in Madison. He holds nineteen patents and has authored or co-authored 29 publications.

Valerie Kuck
600-700 Mountain Avenue, Murray Hill, NJ-07974

Valerie Kuck is a Member of Technical Staff in the Polymer and Chemical Engineering Dept. at Bell Labs in Murray Hill, NJ. She has conducted materials development in a variety of areas including optical fiber coatings and polyethylene wire insulation. She received an MS in chemistry from Purdue University.

Peter G. Simpkins
600-700 Mountain Avenue, Murray Hill, NJ-07974

Peter Simpkins is a Distinguished Member of the Technical Staff in the Polymer and Chemical Engineering Department at Murray Hill, N.J. He is a graduate of California Institute of Technology (MS) and of Imperial College of Science and Technology, London (Ph.D.), specializing in Aerodynamics. His current research is concerned with the mechanics of coating and coating defects.

Moisture Penetration Through Optical Fiber Coatings

Janet L. Armstrong,[1] M. John Matthewson,[1] Charles R. Kurkjian [2]

[1] Rutgers University, Piscataway, New Jersey
[2] Bell Communications Research, Morristown, New Jersey

ABSTRACT

A new technique for measuring the diffusion coefficients of water vapor through optical fiber polymer coatings has been developed which uses the relationship between the fiber strength and the water concentration at the glass surface. This technique is verified by comparison with standard weight gain/loss measurements performed on freestanding polymer films. A detailed analysis using an axisymmetric solution of the diffusion equation has been applied to the coated fiber geometry. A much simpler solution for a planar sheet was also used which gives similar results for the fiber, but is only an accurate analysis for the flat polymer films. In all of these cases Fickian diffusion has been assumed and is justified by the good agreement between the experiment and theory. The diffusion of water vapor both into and out of the polymers was investigated, and a slight difference in the behavior was observed for one coating.

INTRODUCTION

Since, the strength of polymer coated fibers depends on the water activity at the polymer/glass interface, the requirements for today's coatings is not only to provide mechanical protection, but also supposedly to prevent moisture from penetrating the coatings. It is believed that the coated fiber's lifetime will increase if water transport can be slowed. Studies are usually conducted on polymer films in order to determine the permeability or diffusion coefficients of water in the polymer coatings. This is a convenient and simple way of making these measurements, but the curing conditions for the polymer when coated on the fiber and when cast as a freestanding film are different and may result in a different permeability.

A different approach to determining the diffusion coefficient for the polymer coatings is to monitor the strength of the fibers as a function of time after changing the ambient humidity in the test environment.[1] This is a novel way of sensing humidity because the strength of the fiber is dependent on the concentration of the moisture at the glass/coating interface. This technique not only measures diffusion coefficients, but also determines the equilibration time needed for the test environment to fully reach the glass/polymer interface. There are some published data of this sort by Bouten,[2] and Kurkjian *et al.*.[1] Bouten measured the strength as the fiber equilibrated on moving from 60 to 100% relative humidity and drying from 42% to a vacuum of 10^{-4} Pa. He found the diffusion coefficients for those two experiments were not the same, but his drying range extended past the observed discontinuity in the strength *versus* humidity behavior reported by Duncan *et al.*.[3] Therefore, his drying experiment might be spanning two different kinetic regimes.

As mentioned earlier, most of the work performed in this field has been on polymer film samples. There are numerous techniques for determining diffusion coefficients in polymer films; one of the most popular and simplest ways is to measure the film's weight change as a function of time after it has been immersed in a particular environment.[4] Another technique[5,6] is to use infrared evanescent fields to determine the concentration of the diffusing species. This technique is feasible as long as the optical intensity is known as a function of concentration of diffusant.

Figure 1 shows the two geometries that are investigated here. For the case of a planar film of thickness $2l$, the time dependent solution to the diffusion equation, where both surface concentrations are constant, $C(|x| = l, t) = C_1$, and the initial concentration distribution within the film, $C(|x| < l, t = 0) = C_2$, is uniform, the concentration profile is given by:[7]

$$\left(\frac{C(x,t)-C_2}{C_1-C_2}\right) = 1 - \frac{4}{\pi}\sum_{n=0}^{\infty}\frac{(-1)^n}{2n+1} \times \cdots$$
$$\exp\left\{\frac{-D(2n+1)^2\pi^2 t}{4l^2}\right\}\cos\left(\frac{(2n+1)\pi x}{2l}\right). \quad (1)$$

While Eq. 1 is directly applicable to the planar film, it can be used as an approximate solution for the cylindrical coating, Figure 1b, where $l = b - a$, and the glass/coating interface is at $x = a$.[1]

Diffusion coefficients in polymer films can be measured by simply recording the weight of the film as a function of time after the environment is suddenly changed. The accumulated mass of the diffusing species at time t, M_t, is given by:[7]

$$\frac{M_t}{M_\infty} = 1 - \sum_{n=0}^{\infty}\frac{8}{(2n+1)^2\pi^2}\exp\left(\frac{-D(2n+1)^2\pi^2 t}{4l^2}\right), \quad (2)$$

where M_∞ is the mass that has entered after infinite time.

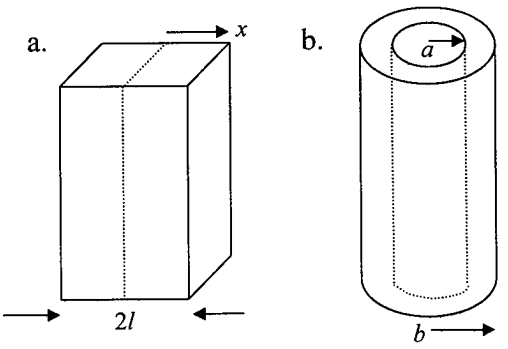

Figure 1: The geometry for the (a) polymer film and (b) coated fiber.

For completeness, the full solution of the diffusion equation in cylindrical symmetry has also been used. Assuming the outside concentration is a constant, $C(r = b, t) = C_1$, and that glass/polymer interface is impermeable, $\partial C(r = a, t)/\partial r = 0$, the solution to the diffusion equation is:[7]

$$1 - \frac{C(r,t)}{C_1} = \pi\sum_{n=1}^{\infty}\exp(-D\alpha_n^2 t)J_1(a\alpha_n) \times \cdots$$
$$J_o(b\alpha_n)\left(\frac{Y_o(r\alpha_n)J_1(a\alpha_n) - J_o(r\alpha_n)Y_1(a\alpha_n)}{J_o(b\alpha_n)^2 - J_1(a\alpha_n)^2}\right), \quad (3)$$

J and Y are the Bessel functions, and α_n is the nth positive root of:

$$J_1(a\alpha)Y_o(b\alpha) - J_o(b\alpha)Y_1(a\alpha) = 0. \quad (4)$$

In order to obtain a diffusion coefficient, the concentration at the polymer/glass interface, $C(r = a, t) = C_0$, has to be known as a function of time. A simple way of measuring this concentration is to determine the strength of the fiber as a function of time after the ambient humidity is suddenly changed. Since the strength of the fiber depends on the amount of the water vapor present at the interface, the effective concentration or humidity can be obtained from these results.

The above model is based on the assumption that Fickian diffusion is taking place. Polymers show considerable variability in their permeability to various diffusing species and the diffusion is often not Fickian.[5] Some polymers will tend to

absorb the diffusing species and form clusters within their structure in which case the concentration profile for diffusion in and out of the polymer will not be symmetrical. In this paper, the water vapor diffusion coefficients in both polymer films and coatings are measured and compared to show that measuring the strength of the fiber is a valid and useful technique. The symmetry of the diffusion both in and out of the coating was used to evaluate the importance of accumulation. Finally, a special strength enhancing fiber coating is studied to determine if it shows different permeability characteristics.[8,9]

EXPERIMENTAL PROCEDURES

Diffusion into freestanding polymer films was studied by using two humidity chambers. A computer controlled precision balance was placed inside one of the humidity chambers that were controlled at 25 ± 0.1°C and either 20 or 95 ± 1.0% relative humidity. The films were left overnight in the other humidity chamber that was controlled to 25 ± 0.1°C and either 95 or 20 ± 1.0% relative humidity respectively. For example, if the film was left overnight in 25°C and 20% relative humidity, the chamber with the balance in it was set to 25°C and 95% relative humidity. Then the film was placed in the high humidity chamber and the weight was measured as a function of time. This particular experiment measures diffusion of water vapor into the film. The reverse experiment measures diffusion of water vapor out of the film. Polyimide and acrylate films were studied.

A two-point bend apparatus[10] was used to measure the strength of the fiber and was operated with a constant faceplate velocity of 5000 μm/s. These experiments were conducted in the same manner as the weight change experiments; namely, the fiber was equilibrated overnight in one humidity chamber before being broken in a second. Specimens were broken until an equilibrium strength was reached. This produced the strength of the fiber as a function of time in the test environment. In order to determine diffusion coefficients the strength data have to be converted to an equivalent concentration or humidity at the glass surface. This conversion is performed by measuring the equilibrated strength as a function of humidity in the range of 25 to 95%. This was achieved by leaving the fibers overnight at 25°C in a set humidity in order to ensure the fibers were equilibrated with their test environment. Twenty samples were broken in each humidity.

The fiber coatings investigated here were a single layer of UV-acrylate (125 μm glass diameter and 250 μm overall diameter) and a polyimide (220 μm glass diameter and 245 μm overall diameter). Also, two dual layer UV-acrylate coated fibers were studied which were identical except that one had 3 wt.% of silica particles incorporated in the secondary coating (125 μm glass diameter, 185 μm primary coating and 250 μm overall diameter).

RESULTS AND DISCUSSION

The results of the weight change experiments of the acrylate and polyimide freestanding films are shown in Figure 2. For clarity, the normalized weight change is shown:

$$W_n = \frac{W_t - W_{dry}}{W_{wet} - W_{dry}}, \qquad (5)$$

where W_t is the weight at time t, W_{dry} is the weight in the drier environment, (20%), and W_{wet} is the weight in the wetter environment, (95%). The normalized accumulated weight is then equal to Eq. 2. The diffusion coefficients for the films were found by fitting the data to this equation. Measured values of $D = (5.17 \pm 0.12) \times 10^{-13}$ m^2/s for diffusion into, "wetting", and $(5.79 \pm 0.13) \times 10^{-13}$ m^2/s for diffusion out of, "drying", the acrylate film were found. A value of $(9.40 \pm 0.35) \times 10^{-13}$ m^2/s was found for wetting and $(9.24 \pm 0.29) \times 10^{-13}$ m^2/s for drying of the polyimide film. The errors represent a 95%

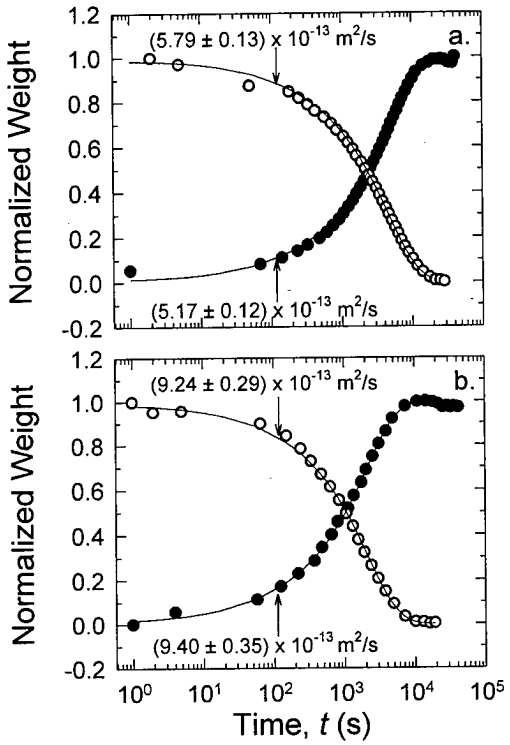

Figure 2: The predicted fit (solid lines) from Eq. 2 and the diffusion into (•) and out of (○) (a) acrylate film and (b) polyimide film.

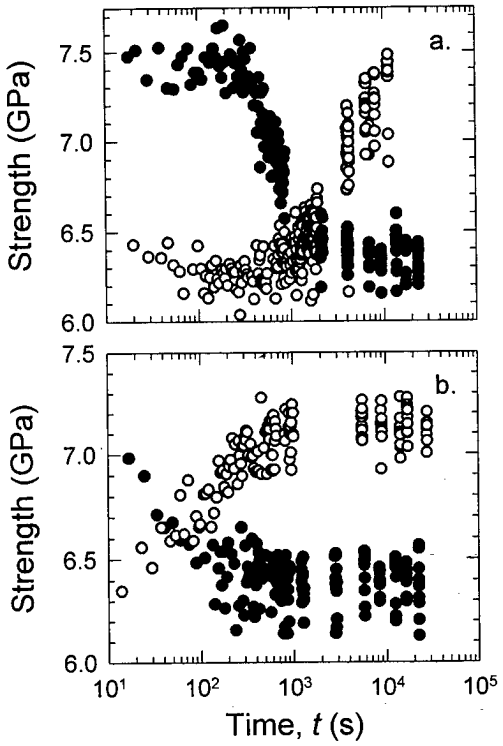

Figure 3: Diffusion into (•) and out of (○) (a) acrylate coated fiber and (b) polyimide coated fiber.

confidence interval. There appears to be a slight accumulation in the acrylate layer, since the diffusion coefficients for drying and wetting within 95% confidence are slightly different.

Figure 3 shows the raw strength data for the acrylate and polyimide coatings. The diffusion coefficients cannot be directly obtained from this graph. The strength must be converted to the corresponding effective humidity at the glass/polymer interface. This conversion was performed by fitting the equilibrated strengths at various humidities to the following empirical equation:

$$\sigma = A + B\,e^{-CH}, \qquad (6)$$

where σ is the strength, A, B, and C are constants, and H is the relative humidity expressed as a percentage. Figure 4 shows Eq. 6 fitted to the strength data for acrylate and polyimide coated fibers. This equation is then used to map the results in Figure 4 into the normalized humidity, defined by:

$$RH_n = \frac{RH_t - RH_{low}}{RH_{high} - RH_{low}}, \qquad (7)$$

where RH_t is the relative humidity at time t, RH_{low} is the lowest relative humidity, and RH_{high} is the highest relative humidity. The results are shown in Figure 5. If a planar geometry is assumed for the coating, the normalized humidity is given by equation 1. This equation has been fitted to the data (dashed lines), and the best-fit diffusion coefficients were obtained by regression analysis. The cylindrically symmetric solution, Eq. 3, has been calculated for the same best fit values of the diffusion coefficients and is shown (solid lines) in Figure 5. The difference between the two solutions is dependent on the ratio of the outer and inner radii of the coating. This ratio is small for the polyimide coating so the difference between the planar and cylindrical solutions is negligible. That ratio is approximately two for the

acrylate coating, but the difference is still relatively small. For bigger radii ratios, the planar solution will not provide an adequate description.

Similar values for the diffusion coefficients were found both when weighing the freestanding films (Figure 2) and from the strength measurement technique (Figure 5). The diffusion coefficient was found to be slightly higher in the polyimide for both techniques. This validates the strength measurement technique, and it should be noted again that this technique determines the *in situ* diffusion coefficient for the real coating, rather than a model sheet specimen. However, the diffusion coefficient is not measured as accurately with this technique because of the inherent variability in the strength. This makes it harder to measure small changes in strength, whereas small changes in weight can be measured accurately. This is aggravated by only having a limited experimental time before the half-life of the diffusion (where the normalized humidity is 0.5) is reached. As a result the standard error in the estimates of the diffusion coefficients are approximately three times higher than for the gravimetric technique. However, the ~ 10% error is acceptable for most purposes. Figure 5b illustrates a limitation in the strength measurement technique. Since the polyimide is so thin (12.5 μm) the diffusion does not allow enough time to make many measurements before the half-life. As a result the half-life is not well defined and fitting to the data did not produce reliable error estimates in this case. The stress measurement technique is therefore not useful for a half-life below about 50 s.

Another result shown in Figure 5a is that the diffusion in and out of the coating is not

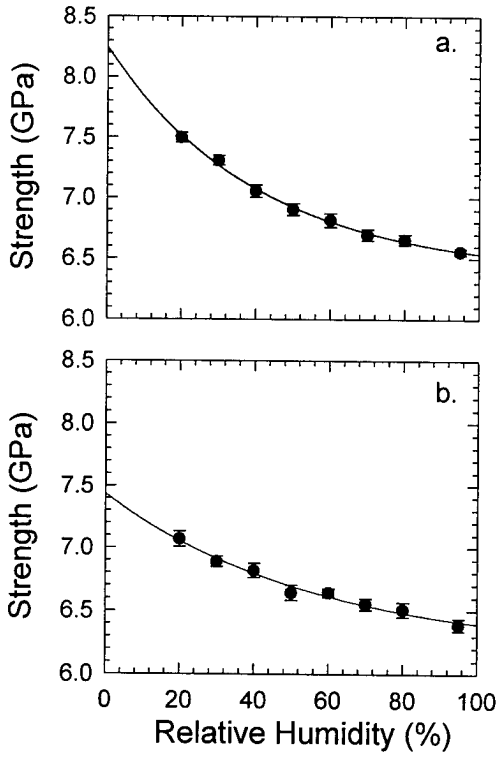

Figure 4: The equilibrium strength (at 25°C) as a function of humidity for (a) acrylate coated fiber and (b) polyimide coated fiber.

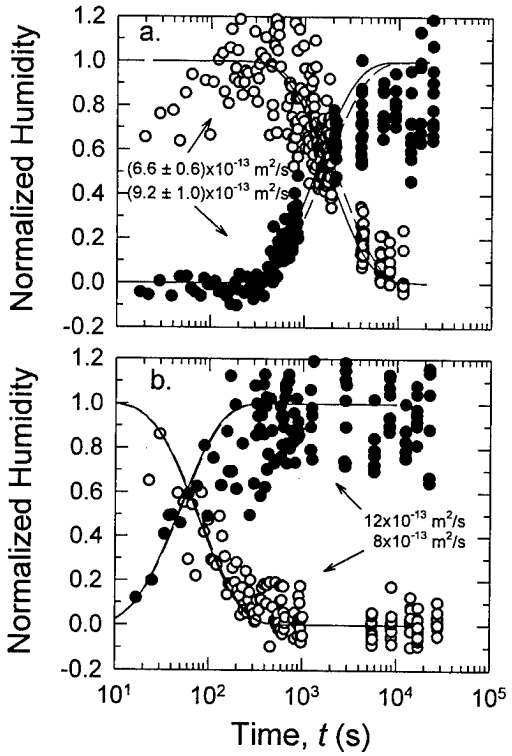

Figure 5: A cylindrical fit, Eq. 3, (solid lines), and a planar fit, Eq. 1, (dashed lines) to the diffusion into (•) and out of (○) (a) acrylate coated fiber and (b) polyimide coated fiber.

symmetrical. There is some slight deviation. This implies that the water vapor may be interacting with the polymer. Slight asymmetry was also observed in the planar films (Figure 2a), but the sense is reversed. It is not clear whether this asymmetry is significant. The polyimide films (Figure 2b) appear to be symmetrical, but because of the large error found in Figure 5b for the strength technique, no conclusions can be drawn.

Effect of silica particles in coating

We have studied the affect of having colloidal silica particles incorporated in the outer layer of the dual coated fiber. In previous work, the silica particles were found to have a beneficial effect on fiber reliability by greatly delaying the onset of the fatigue and aging "knees".[8,9] The particles preferentially dissolve in moisture thus reducing the activity of the water at the glass surface, which results in a reduction of the corrosion rate of the glass. One possible mechanism that has been suggested for the particles is that they simply absorb the ambient moisture, thus keeping the fiber surface drier. However, Rondinella *et al.*[8,9] argue that the quantity of silica in the coating is inadequate to explain the dramatic increase in lifetime. We provide direct evidence for this assertion here, since if the silica particles were absorbing significant amounts of water, the diffusion through silica-loaded coating would appear much slower using the strength measurement technique. We have compared two fiber specimens; one with 3 wt.% of silica particles in the secondary coating and a second identical specimen, drawn at the same time using the same polymer, but without the silica particles. Since both specimens have a dual coating, it is only possible to determine an effective overall diffusion coefficient for both layers.[1] However, if the diffusion coefficient of the second layer is substantially changed by the presence of the silica particles, this would be readily apparent. The normalized humidity *versus* time for both of these specimens is shown in Figure 6. The data were fitted to the cylindrically symmetric solution of the diffusion equation (3) and for both specimens the diffusion in both directions is the same; namely $D = 3 \times 10^{-12}$ m^2/s. Since the silica additive has no effect on the rate of diffusion, this shows that the silica does not act as a sink for water. As suggested in the earlier work, this shows that the mechanism by which the powder delays the onset of fatigue and aging knees does not involve gettering the water.[8,9]

CONCLUSIONS

Diffusion coefficients for water in polymer coatings on optical fiber can be measured by monitoring the strength of the fibers as a function of time after the ambient humidity is suddenly changed. This technique gives comparable diffusion coefficients to the more commonly used film weighing technique. It is however, more

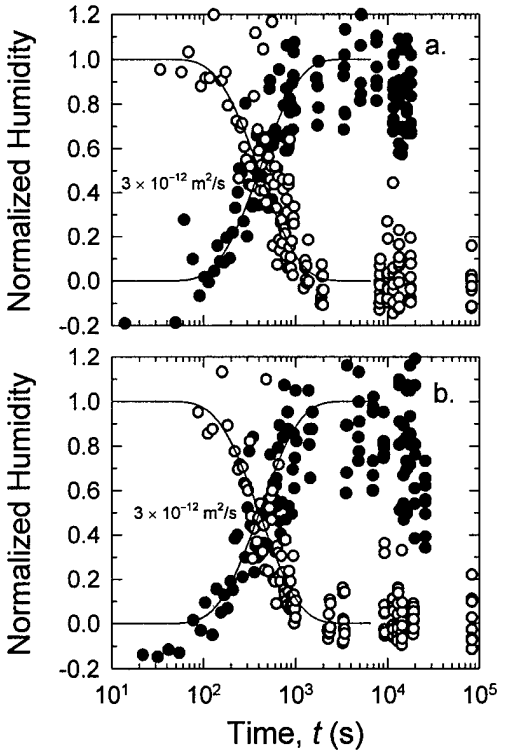

Figure 6: The diffusion, in the range from 30 – 95% *RH* at 25°C, into (•) and out of (○) a dual coated fiber with (a) 0 wt% silica and (b) 3 wt% silica added to the secondary coating.

meaningful because it is an *in situ* measurement that does not rely on the assumption that the film has seen the same cure conditions (and hence has the same properties) as the real coating. However, the precision with which the diffusion coefficient can be determined is somewhat lower and is limited to coatings with diffusion times greater than about 50 s.

For all of the coatings studied here, moisture penetrates on a time scale of $\sim 10^2$ to 10^3 seconds. It is therefore unlikely that water permeability in the coating is a controlling factor in how the coating influences the fiber reliability on the time scale of $\sim 10^9$ s (~25 years).

Here we have used the cylindrically symmetric solution to the diffusion equation to accurately describe diffusion through the cylindrical shell. However, a simple planar sheet solution gives results with acceptable precision for coating outer to inner diameter ratios of less than approximately two.

Under the conditions used here, the diffusion is accurately described by Fickian behavior. We also show that the diffusion is not affected by a few weight percent of colloidal silica particles in the coating, which has significance for how these particles improve fiber reliability.

ACKNOWLEDGEMENT

We would like to thank Bell Communications Research – Morristown, N. J. for their financial support of this research.

REFERENCES

1. C. R. Kurkjian, J. L. Armstrong, M. J. Matthewson and I. M. Plitz, "Diffusion of water through lightguide coatings," *Proc. Nat. Fiber Optic Engineers Conf.,* **2** 133-138 1996.
2. P. C. P. Bouten, "Lifetime of pristine optical fibres," 1987.
3. W. J. Duncan, P. W. France and S. P. Craig, "The effect of environment on the strength of optical fiber" in "Strength of inorganic glass," ed. C.R. Kurkjian, 309-328 Plenum Press, New York, 1985.
4. T. Ogawa, T. Nagata and Y. Hamada, "Determination of diffusion coefficient of water in polymer films by TGA," *J. Appl. Polymer Sci.,* **5** 981-987 1993.
5. N. E. Schlotter, "Diffusion of small molecules in glassy polymer thin films studied by waveguide raman techniques," *J. Phys. Chem.,* **94** 1692-1699 1990.
6. N. E. Schlotter and P. Y. Furlan, "Small molecule diffusion in polyolefins monitored using the infrared evanescent field," *Vibrational Spectroscopy,* **3** 147-153 1992.
7. J. Crank, *The mathematics of diffusion,* OUP, Oxford, UK, 1975.
8. V. V. Rondinella, M. J. Matthewson and C. R. Kurkjian, "Coating additives for improved mechanical reliability of optical fiber," *J. Am. Ceram. Soc.,* **77** [1] 73-80 1994.
9. V. V. Rondinella, M. J. Matthewson, P. R. Foy, S. R. Schmid and V. Krongauz, "Enhanced fatigue and aging resistance using reactive powders in the optical fiber buffer coating," *Proc. Soc. Photo-Opt. Instrum. Eng.,* **2074** 46-51 1993.
10. M. J. Matthewson, C. R. Kurkjian and S. T. Gulati, "Strength measurement of optical fibers by bending," *J. Am. Ceram. Soc.,* **69** [11] 815-821 1986.

Janet L. Armstrong
Rutgers University
Dept. of Ceramic and Materials Eng.
Brett & Browser Road
Piscataway, New Jersey 08855

Janet Armstrong received her BS and MS in Ceramic Engineering from Rutgers University in 1995 and 1997 respectively. She is currently pursuing her PhD in Ceramic Engineering at Rutgers University. Her thesis work consists of investigating the mechanical reliability of optical materials. She has been jointly working at Bellcore in Morristown, NJ and Rutgers University.

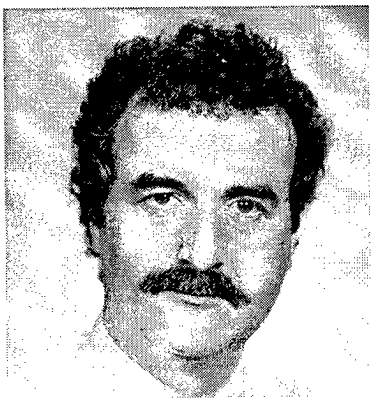

Dr. M John Matthewson
Rutgers University
Dept. of Ceramic and Materials Eng.
Brett & Browser Road
Piscataway, New Jersey 08855

John Matthewson received his BA degree in Theoretical Physics in 1975 and his MA and PhD degrees in Physics in 1978, all from Cambridge University. Since then he has worked in the Cambridge University Computer Laboratory, AT&T Bell Laboratories and IBM Almaden Research Center. He is now an Associate Professor in the Fiber Optic Materials Research Program at Rutgers University where his research group is concerned with strength and fatigue of optical materials in general and oxide and non-oxide fibers in particular.

Dr. Charles R. Kurkjian
Bell Communications Research
445 South Street
Morristown, New Jersey 07960

Chuck Kurkjian is a member of the Fiber Media and Components Reliability Group at Bellcore in Morristown, NJ. He spent 35 years at Bell Labs involved in various aspects of glass and glass fiber research, and since joining Bellcore in 1994 he has concentrated on issues of mechanical reliability of lightguide fiber, cable, and optical components. He graduated from Rutgers University in 1952 and M.I.T. in 1955 with degrees in Ceramics.

OPTICAL CABLE RECYCLING

Tsuneo Konaka, Masaki Shima, Teruhiko Hara, Shiro Nishi, Ikuo Imoto

Nippon Telegraph and Telephone Corporation, Tsukuba Ibaraki, Japan

ABSTRACT

We have examined the possibility of recycling cable sheath material, of using optical cable scrap to produce cement and of recycling plastic cable core materials as feed-stock using a supercritical water method.
Over 1 km of optical cable with a sheath made of recycled material was stably extruded and its performance was similar to that of currently used cable. We have already started to recycle optical cable scrap as part of a cement production process and about 45 tons was recycled in 1997. This involves decomposing plastic optical core materials in supercritical water to obtain useful chemical components such as benzene, phenol and aniline.

INTRODUCTION

Recycling can reduce the environmental pollution caused by waste disposal and allow us to use natural resources effectively. This makes it an important subject in relation to sustainable development. Currently, optical cable waste amounts to about 500 tons in NTT and it is estimated that will grow to more than 10,000 tons in future. The method we use for optical cable recycling is the same as that used for plastic recycling because optical cable is mainly composed of plastic materials. Various issues related to the recycling of plastic telecommunication scrap have already been raised and discussed (1-3). Legal restrictions and cost are the main factors determining whether waste is disposed of in landfills, incinerated or recycled. In many cases plastic scrap recycling is difficult because of cost considerations and it is then mainly disposed of via landfill or incineration. However, the costs of landfill and incineration will become higher than that of recycling in the future, because they are increasing with the strengthening of legal controls and the reduction in the landfill number of sites. Optical cable recycling is important in that it can reduce both the environmental impact and the cost of waste disposal.
At the 46th IWCS we reported the excellent performance of recycled sheath material and recycled sheath optical cable (3). In this paper, we describe the production reproducibility and performance of recycled sheath optical cable, the environmental impact of sheath material recycling, the recycling of optical cable scrap for cement production and the potential for the feed-stock recycling of cable core materials.

CABLE SHEATH RECYCLING

We have already reported on the possibility of producing recycled sheath optical cable (3). However, there are various difficulties to overcome if we are to achieve this. These include problems related to production stability, reproducibility, the construction of an economical recycling system and finding a way to guarantee the quality of the recycled material.
We studied production stability and the reproducibility of recycled sheath optical cable. We collected sheath materials from NTT cable scrap at three copper recovery companies. The collected materials were comminuted, washed, dryed, extruded and pelleted. These pellets were then used to produce a 300-fiber SM optical cable of 1 km in length at three cable companies.

The recycled material was stably extruded as cable sheath in each case. The sheath properties at the beginning, middle and end of the cable were almost constant and similar to those of new material except for an increment in the melt index (MI) as shown in Table 1. Slight decomposition at high molecular weight caused the increase in the MI but had no serious adverse effect on the other properties (3). No unusual roughness was observed on the sheath surface. The performance of the three recycled optical cables were similar to that of current cable as shown in Table 2. These results show that optical cable can be produced stably and reproducibly using recycled sheath materials.

Table 1 Properties of new and recycled materials

Properties	Pellet		Recycled cable sheath		
	New	Recycled	Beg.	Middle	End
Melt index	0.15	0.21	0.24	0.26	0.27
Tensile strength (MPa)	16.9	19.7	18.5	18.9	18.4
Elongation at break (%)	700	730	700	722	696
Thermal aging 100 ^{o}C, 48 hrs					
Tensile strength retention (%)	100	98	100	96	94
Elongation retention (%)	100	107	105	103	90
Brittleness temperature F_0 (^{o}C)	<-60	<-60	<-60	<-60	<-60
Stress crack resistance 500 hrs	0/10	0/10	0/10	0/10	0/10

Table 2 Performance of optical cable with recycled sheath

Properties	Recycled sheath
Crush (dB)*	< 0.1
Squeezing (dB)*	< 0.1
Torsion (dB)*	< 0.1
Impact (dB)*	< 0.1
Repeated bending (dB)*	< 0.1 (no damage)

*Optical lLoss increment

ENVIRONMENTAL IMPACT OF SHEATH MATERIAL RECYCLING

The sheath material recycling process is shown in Fig. 1. The sheaths were removed from cable scrap using a slotting machine. Then the sheaths were comminuted into pieces of about 10 mm which were washed and dried. They were molded into rods of about 3 mm in diameter by using an extruder and the rods were cut into 3 mm pellets. We examined the energy expended during these processes. From these data we estimated the amount of CO_2 and NO_x generated in the sheath recycling process. In Fig. 2, these data are compared with the amount of CO_2 and No_x generated during the production of new sheath material and during the disposal of sheath scrap by incineration. The recycling process generated the smallest amounts of CO_2 and NO_x. This result shows that sheath material recycling is effective in reducing environmental impact.

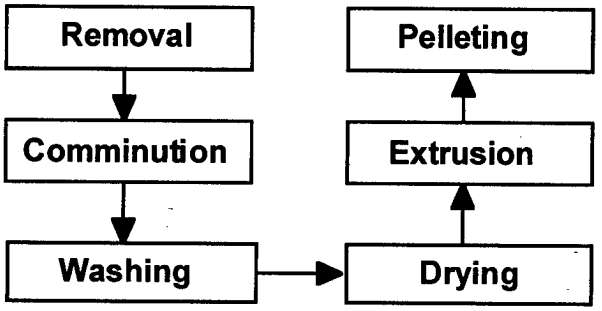

Figure 1 Cable sheath scrap recycling process

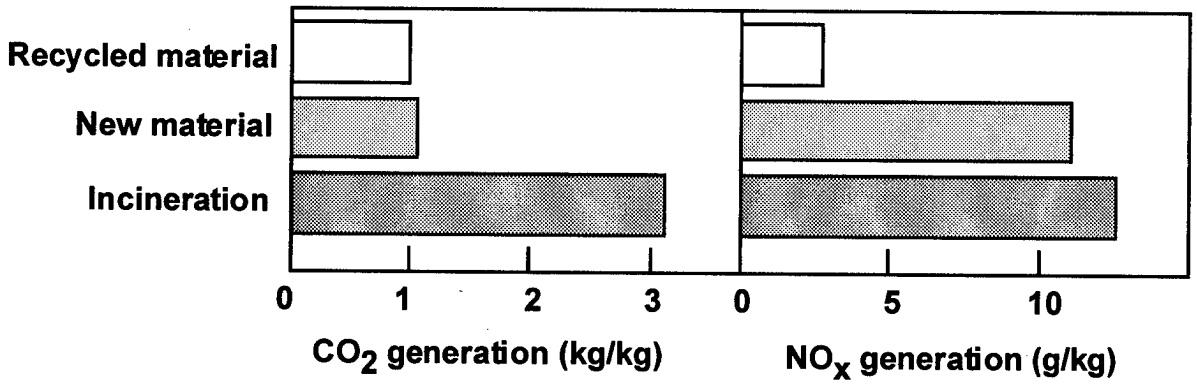

Figure 2 Environmental impact of recycled sheath material, new sheath material and incineration disposal of sheath scrap

CEMENT PROCESS RECYCLING

The cement production process is shown in outline in Fig. 3. The main components of cement are CaO, SiO_2, Al_2O_3 and Fe_2O_3 and the main raw materials are quartzite, clay, limestone and gypsum. A mixture of quartzite, clay and limestone is calcined in a rotary kiln at a high temperature of 1800℃ where clinker is produced. A mixture of clinker and gypsum are milled and becomes cement. Many kinds of waste such as discarded tires or sludge containing cement components, are used as raw materials or fuel. The poisonous gases from the waste decompose during the cement production process because of the high calcination temperature. Therefore, recycling in the cement production process does not generate more waste or poisonous gases. Optical fiber cable consists of plastics and other materials such as Fe, Al and SiO_2. We recycled the optical cable scrap in the same way as discarded tires. The cable scrap must be cut into pieces with a length of less than 35 cm to allow it to be introduced stably into a rotary kiln. Moreover, no polyvinyl chloride sheath cable is included because it would raise the chloride content of the cement raw materials above the required level. The optical cable scrap is chopped into pieces about 30 cm long and mixed with chopped up discarded tires. The mixture is combined with cement raw materials at the entrance to a rotary kiln as shown in Fig 3. Figure 4 is a photograph of the mixture being transported on a belt conveyer into the rotary kiln. The plastics are used as a heat source for cement calcination, and Fe, Al and SiO_2 become cement components. About 45 tons of cable scrap were recycled via cement production in 1997.

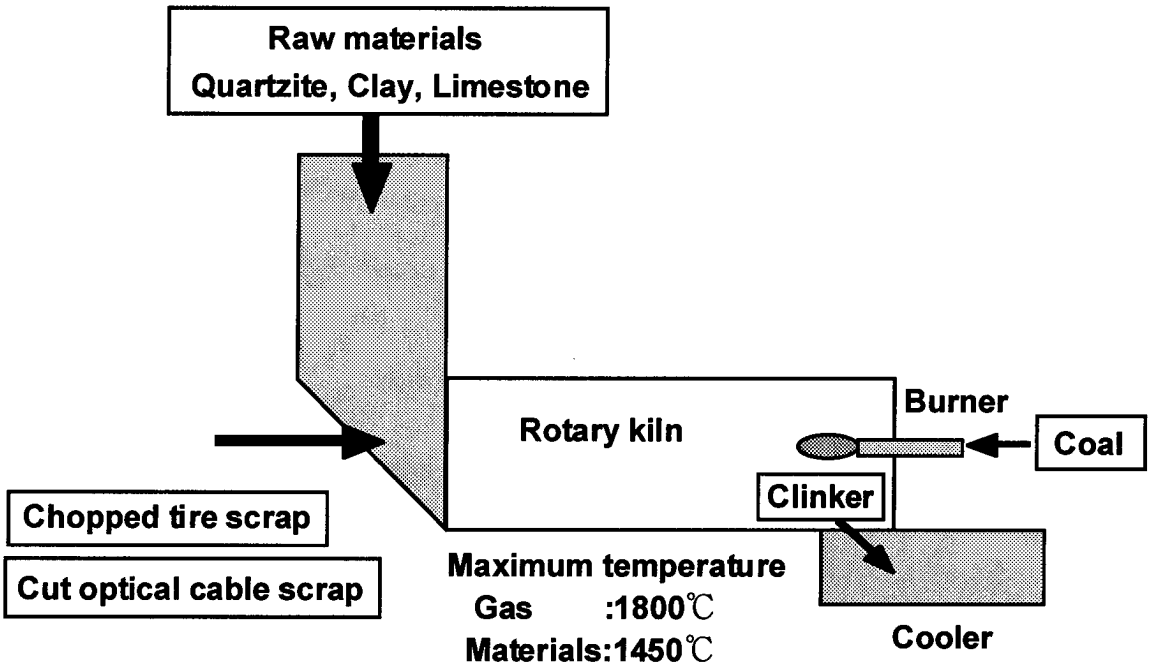

Figure 3 Optical cable recycling in cement production process

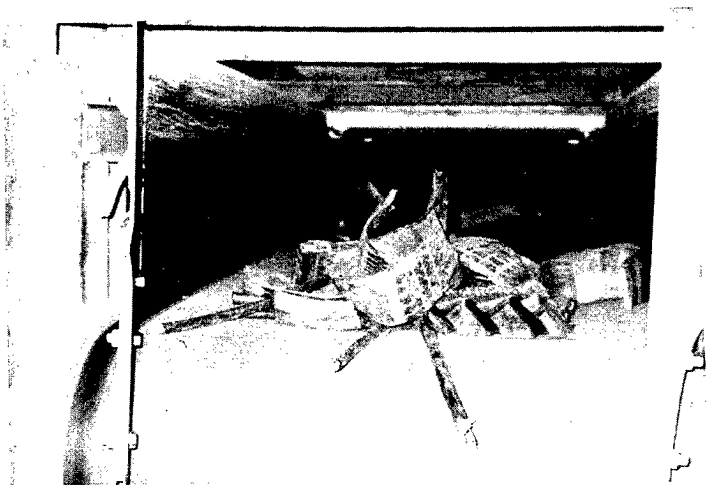

Figure 4 Chopped optical cable and discarded tires on belt conveyer

Table 3 Components of products from plastic cable core materials

Conditions	Slotted rod	Wrapping tape	Ripcord	Fiber ribbon
400 ℃ 37 MPa 1h	Ethylhexanol t-Butylphenol (about 70% undecomposed)	Benzene Toluene	Phenylene -diamine	Tetrahydrofurane Butanediol SiO_2
600 ℃ 60 MPa 1h	Acetic acid Phenol	Benzene Ethylhexanol Phenol	Aniline	Phenol SiO_2

FEED-STOCK RECYCLING

Optical cables contain many kinds of plastic. Studies have been undertaken on the decomposition of various compounds by using supercritical water technology (4). We have started to decompose plastic cable core materials in supercritical water to determine whether or not the decomposition products contain useful components (5). The slotted rod, wrapping tape, ripcord and fiber ribbon were cut into pieces of about 1 mm in size. Each specimen was placed in supercritical water in a tubular cell for 1 hr at either 400℃ and 37 MPa or 600℃ and 60 MPa. The products were identified by a gas chromatograph mass spectrometer. The results are summarized in Table 3. The components of the products depend strongly on the supercritical water conditions. There are some useful products, such as phenol, benzene and aniline. These results show the potential for the feed-stock recycling of plastic cable core materials.

CONCLUSION (DIRECTION OF OPTICAL CABLE RECYCLING)

To reduce the environmental impact of optical cable, we need to consider its whole life cycle when we develop new optical cables and the demand to do this is increasing every year. Recycling is one of the most important subjects to be considered. We summarize the direction of optical cable scrap recycling based on our results. We believe that recycling will develop in three steps as shown in Fig. 5. In the first step optical cable scrap will be recycled at the same or lower cost than waste disposal. In this step, it is necessary that any pretreatment for recycling should be simple and cheap. In the second step the sheath will be recycled as new cable sheath. There is a possibility that this sheath recycling will result in a profit. The third step is a recycling process which makes the most of the individual characteristics of each component.

Step 1

All optical cable scrap is recycled for cement production. The advantages are that the pretreatment is simple and cheap and it is possible to recycle large amounts of scrap. The cost is already lower than that of disposal by incineration.

Cable with a polyvinyl chloride sheath can not be recycled for cement production.

Step 2

The sheath from cable scrap is recycled as a new cable sheath and the core part is used for the cement production process. There is a possibility that the cost of the recycling process will become less than the cost of recycled pellets. This possibility is very high in the case of nonhalogenated sheath recycling because nonhalogenated pellets are expensive. Most of the metal cable sheath which is removed to recover copper is disposed of in landfills or by incineration. There is also the possibility of recycling metal cable sheath scrap economically as a new optical cable sheath because we can obtain this scrap cheaply. However, pretreatment is needed to separate Al from the sheath because the most widely used metal cable sheath is an laminated Al polyethylene sheath.

Step 3

We can separate the optical cable into its individual components using existing technologies. However, the separation cost is very high and there is currently no appropriate recycling target for such separated components. Once legal controls have been strengthened and the cost of waste disposal become very high, there will be a strong demand for individual component recycling. It is therefore now important to begin a variety of studies on optical cable recycling. The decomposition of optical cable components by using supercritical water technology is one of such studies. One study has already suggested employing fiber ribbon scrap as plastic reinforcing material thus making good use of the high tensile strength of optical fiber (6).

Polyvinyl chloride sheath cable

It is very difficult to recycle this type of cable, because many are thin and sheath separation is very costly. There is a steadily increasing demand for an alternative sheath material that has an acceptable price, does not generate poisonous gases and can be recycled via cement production.

REFERENCES

(1) P.Peuch, "Plastics in telecommunications and the environment," PIT 7th, London, p.131, (1995)

(2) A.C.Dixon and M.Endean, "Recycling of consumer products," PIT 7th, London, p.145, (1995)

(3) T.Konaka, S.Murai and S.Nishi, "Recycling of plastic scrap from outside plant in NTT," 46th IWCS, Philadelphia, p.443, (1997)

(4) M.Modell, J.Larso and S.F.Sobczynski, "Supercritical water oxidation of pulp mill sludges," Tappi J. June, p.195, (1992)

(5) Y.Sato, K.Takeshita, S.Nishi and T.Konaka, "Recycling of optical fiber cable," Niohonkagakukai Yokoshu, Vol.73, 1D701, (1997) (in Japanese)

(6) J.Takahashi, M.Takeda, M.Nomura, H.Tsuda, K.Kenmochi and H.Fukuda, "Strength of optical fibers," Proceedings of The 75th ISME Spring Annual Meeting, Vol.11, No.98-1, p.98, (1998) (in Japanese)

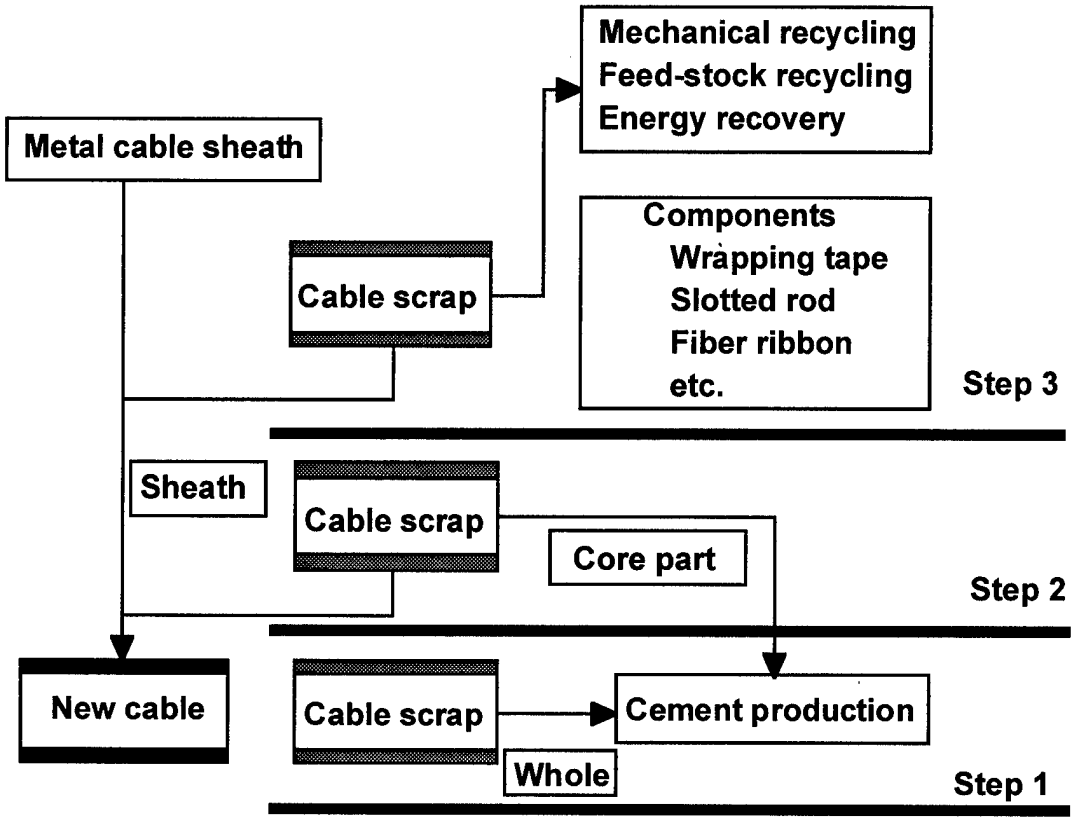

Figure 5 Direction of optical cable recycling

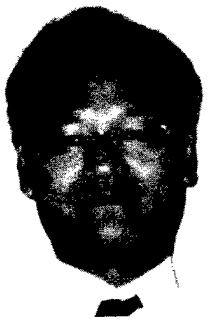

Tsuneo Konaka
NTT Access Network Systems Laboratories
1-7-1 Hanabatake, Tsukuba, Ibaraki, 305-0805 Japan
Tsuneo Konaka is a senior research engineer. He was born in 1949 and received B.S. and M.S. degrees in nuclear engineering from Hokkaido University in 1972 and 1974.
He joined NTT in 1974. Since 1994 he has engaged in research on recycling and environmental matters related to outside plant.

Masaki Shima
NTT Access Network Systems Laboratories
1-7-1 Hanabatake, Tsukuba, Ibaraki, 305-0805 Japan
Masaki Shima is a research engineer. He was born in 1971 and received B.S. and M.S. degrees in physics from Chiba University in 1996 and 1997.
He joined NTT in 1997. Since 1997 he has engaged in research on recycling and environmental matters related to outside plant.

Teruhiko Hara
NTT Access Network Systems Laboratories
1-7-1 Hanabatake, Tsukuba, Ibaraki, 305-0805 Japan
Teruhiko Hara is a senior research engineer supervisor. He was born in 1957 and received B.S. and M.S. degrees in civil engineering from the Tokyo Institute of Technology in 1980 and 1982.
He joined NTT in 1982. Since 1997 he has engaged in research on recycling and environmental matters related to outside plant.

Shiro Nishi
NTT Science and Core Technology Laboratory Group
3-9-11 Midori-cho, Musashino, Tokyo, 180-0012Japan
Shiro Nishi is a senior research engineer supervisor. He was born in 1957 and received B.S. and M.S. degrees in macromolecular science from Osaka University in 1980 and 1982.
He joined NTT in 1985. Since 1996 he has engaged in research on the recycling of plastics.

Ikuo Imoto
NTT Kansai Procurement & Supply Department
3-15 Baba-cho, Chuo, Osaka, 540-0007 Japan
Ikuo Imoto was born in 1955 and graduated at Tachiki High School in 1974.
He joined NTT in 1974. Since 1995 he has belonged to the Kansai Procurement & Supply Department.

MODELING UTP CABLING: RETURN LOSS, CAT 5 AND BEYOND

John W Kincaid, Paul Z Vanderlaan

Belden Wire and Cable Company
Richmond, Indiana

ABSTRACT

A uniform model for the Cat 5 differential mode unshielded twisted pair cable (UTP) is presented in equation format. Reflection coefficients and input impedance are defined for arbitrary terminations. Return loss and insertion loss deviation are defined and shown to be a function of the intrinsic cable parameters as well as source impedance, load impedance and cable length. A cabling channel is modeled as multiple two port segments of uniform cable and connector hardware components. Channel return loss and insertion loss deviation are determined by solving a cascade of two port equations for voltage, impedance and reflection coefficient. Basic cable and channel model results are compared to empirical results. Performance characteristics at frequencies greater than 100 MHz are considered.

INTRODUCTION

The TIA/EIA standards organization has been instrumental in developing requirements[1] for UTP Category 5 premises cabling (also known as structured cabling). This activity has taken place over a number of years and standardization work is continuing in stride with market place demands for greater bandwidth and connectivity. This is resulting in the enhancement of certain standards (for example Cat 5) as well as consideration of requirements for even higher categories of performance (Cat 6,7).

The return loss parameter has recently been identified as important for IEEE 802, 1000 BASE T operation and is being considered for standardization.

Return loss was chosen as the theme of this paper because it is a parameter that describes an important basic characteristic of cabling. As a relatively new and unfamiliar requirement for Cat 5 cabling there is also a need to explain the characteristics of this parameter. Over the past year simulation and performance evaluation of cabling links and channels has been the subject of many contributions to TR41.8.1 working group meetings. A contribution by Adriaenssens of Lucent discussed a basic modeling approach.[2] This was followed by numerous other contributions[3,4,5,6] using similar or related techniques that have confirmed the practical usefulness of modeling. This paper discusses a modeling technique and certain results that have been presented at TIA TR41.8.1 working group meetings.

The paper concludes that the particular modeling technique used is reasonably accurate and is a valuable tool for analysis of the impact of cable and connecting hardware on channel return loss performance.

UNIFORM CABLE MODEL, CAT 5

A uniform model for the Cat 5 differential mode UTP cable is given below in equations (1)-(5). The model explicitly covers the secondary (γ, Z) transmission line constants and assumes a limited range of primary constants ($\mathbf{R}$, $\mathbf{L}$, $\mathbf{G}$, $\mathbf{C}$) that meet the criteria for a uniform line with negligible unbalance or common mode.

Time delay, nanoseconds per meter;

$$\tau = 534 + 36/\sqrt{f} \quad \text{.....(1)}$$

Phase constant, radians per meter;

$$\beta = 2 \cdot \pi \cdot f \cdot \tau / 100000 \quad \text{.....(2)}$$

Attenuation constant, Nepers per meter;

$$\alpha = (1.967 \cdot \sqrt{f} + 0.023 \cdot f + 0.05/\sqrt{f}) \cdot 0.01/8.686. \quad (3)$$

Propagation constant, radians per meter;

$$\gamma = \alpha + j \cdot \beta \quad \text{.....(4)}$$

Characteristic impedance, Ohms;

$$Z_o = Z_{hf} / 100((100 + 5.5/\sqrt{f}) - j \cdot 5.5/\sqrt{f}) \ldots\ldots (5)$$

In equation (5) the term Z_{hf} represents the high frequency asymptote of the impedance.
The variable f is frequency in MHz and the operator j is sqrt of –1.

CABLING RETURN LOSS

Cabling return loss is often measured with a network /S parameter analyzer setup as shown in figure 1. The balun and load characteristics are chosen in accordance with the frequency range and application of interest.
Return loss may be interpreted as an indicator that is inversely proportional to the magnitude of signal reflection that may exist on a cabling system. Thus, small values of return loss imply the existence of possibly undesirable high levels of signal reflection. The reflections are caused by impedance mismatches that occur in the system. Sources of reflection are impedance variations in the cable, the connecting hardware and the termination impedances. Generally, the larger the mismatch the greater the reflection and the smaller the return loss. However, resonant peaks or levels of signal reflection will occur at ¼ wavelength frequency intervals determined by connecting hardware characteristics, cable length and delay values.
Return loss is calculated directly from the magnitude of the input reflection coefficient,

$$RL = -20 \cdot \log_{10} |\rho_n| \ldots\ldots (6)$$

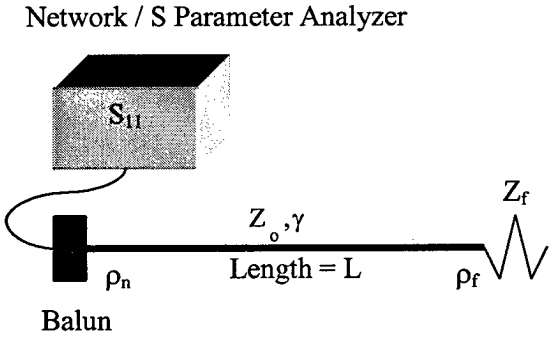

Figure 1. Basic Return Loss Measurement Setup

Uniform Cable Return Loss Model, Cat 5

This model is based on the cable equations (1)-(5) and does not take into account the physical nonuniformities which are present to some degree in all physical cables. Structural nonuniformities will be covered in a later section of the paper.
The uniform cable model is a natural benchmark to gauge the performance potential of physical cables. In the model, the input reflection coefficient ρ_n, is defined by the relationship given in equation (7) and is seen to be a function of the source impedance, Z_n, and the cable input impedance, Z_{in}, defined in equation (8).

$$\rho_n = (Z_{in} - Z_n) / (Z_n + Z_{in}) \ldots\ldots (7)$$

$$Z_{in} = Z_o \cdot (1 + \rho_f \cdot \varepsilon^{-2 \cdot L \cdot \gamma}) / (1 - \rho_f \cdot \varepsilon^{-2 \cdot L \cdot \gamma}) (8)$$

The cable input impedance is a function of the cable length L, the propagation constant γ, the cable characteristic impedance Z_o and the output reflection coefficient, ρ_f, defined in equation (9).

$$\rho_f = (Z_f - Z_o) / (Z_f + Z_o) \ldots\ldots (9)$$

Z_f and Z_n are the load and source impedances respectively.

The uniform model makes it clear that cable return loss is affected by more than just the cable characteristics. The dependence on length, source and load impedance causes cable return loss to be a system or applications parameter rather than strictly a cable parameter. Thus care must be exercised when configuring a measurement setup such as in figure 1 to ensure the measurement system parameters are consistent with the application-system parameters.

The solution of equations (1)-(9) was implemented with a commercially available mathematical analysis software package[7] for PC's. The software requires minimal programming skill and complex variable equations are analyzed in their natural form basically as written above. The software also provides graphical capabilities that were used to produce the figures.

Dependence on Z_o. The cable characteristic impedance enters the model through equations (8) and (9). As defined in equation (5), the impedance magnitude frequency response is shown in figure 2 for Z_{hf} = 100 Ω, 106 Ω and 109 Ω.

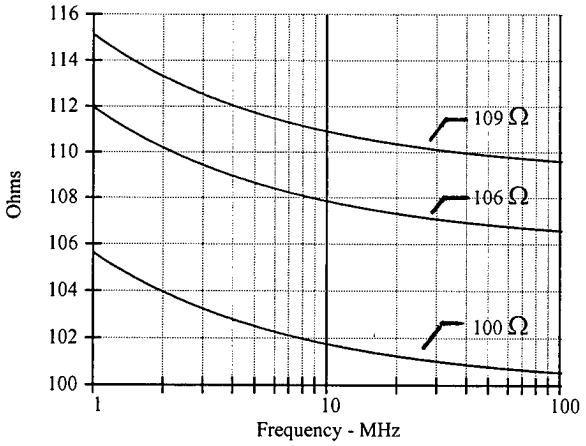

Figure 2. Characteristic Impedance vs. Frequency.

For Z_{hf} = 100 Ω the impedance amplitude is considerably greater than 100 Ω at low frequencies and asymptotically decreases to about 100 Ω. The 109 Ω plot increases to a value of about 115 Ω at 1 MHz.

Equation (8) indicates that with negligible output reflection coefficient the input impedance becomes equal to the characteristic impedance. In this situation the return loss is determined primarily by the difference between source impedance and the characteristic impedance as indicated by equation (7).

Figure 3 illustrates the return loss performance of 30 meter lengths of 100 Ω, 106 Ω and 109 Ω cable. The source and load impedances are equal to 100 Ω. The cyclic troughs in the plots indicate the presence of ¼ wavelength resonance effects. At 100 MHz there is approximately a 20 dB return loss penalty associated with a 9 Ω offset from 100 Ω.

The specification limit corresponds to 1000 BASE T requirements for cabling.

Dependence on L. The length parameter L enters the model through equation (8) and is a multiplier on the propagation constant. The length and the attenuation constant act together as a divisor and reduce the impact of the output reflection coefficient ρ_f. For long enough cable lengths the attenuation will make the output mismatch negligible at low frequencies and thus the mismatch becomes more important for shorter lengths. However even with a negligible load mismatch the deviation of input impedance from the source impedance determines the input reflection coefficient in equation (7).

Return loss behavior for 15, 30 and 60 meter lengths of 109 Ω cable is shown in figure 4. The source and load impedances are equal to 100 Ω. The return loss at 100 MHz is improved approximately 4 dB for the 60 meter length compared to the 15 meter length.

The trough frequencies are seen to be length dependent and form envelopes of increasing return loss with increasing frequency.

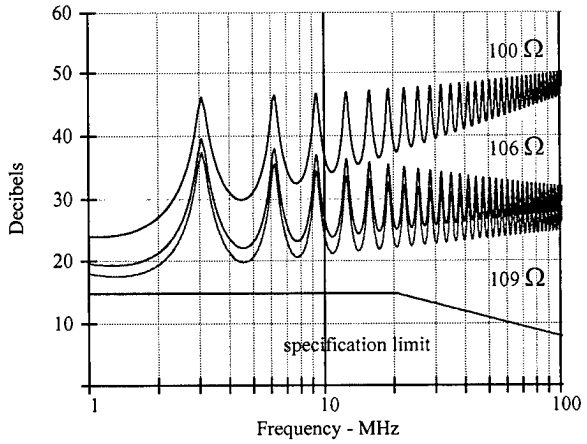

Figure 3. Return Loss vs. Frequency.

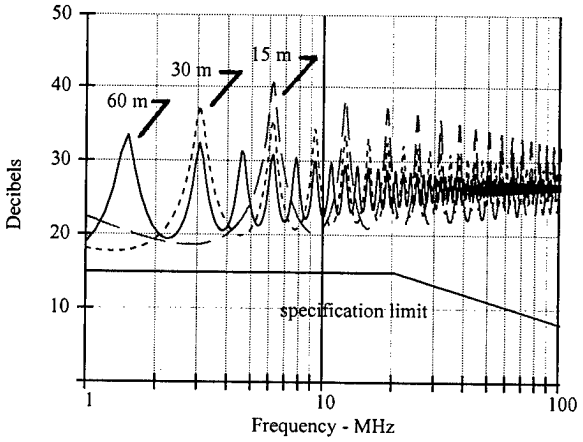

Figure 4. Return Loss vs. Frequency.

The lowest frequency trough location is seen to change from 3 MHz to about 2 MHz to less than 1 MHz as the length increases from 15 to 60 meters. The low frequency troughs for short lengths come closest to the specification limit.

Dependence on Z_f and Z_n. The source and load impedances enter the model through equations (7) and (9). Figures 5, 6, and 7 compare return loss for 10 % deviations from 100 Ω for the 109 Ω cable. Figure 5 compares return loss for the 30 meter length with 100 Ω source and load impedance to that for a 90 Ω load. Slightly more degradation is evident in figure 6 for a 90 Ω source impedance. However variations in both source and load shown in figure 7 result in a degradation which causes the specification limit to be exceeded.

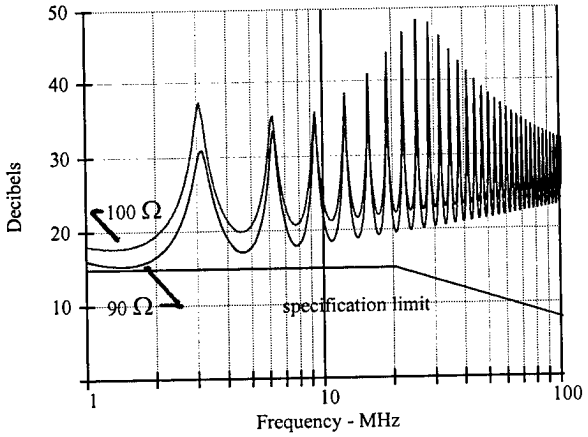

Figure 5. Return Loss for the 109 Ω cable of figure 2. Load impedance indicated on chart. Source impedance = 100 Ω.

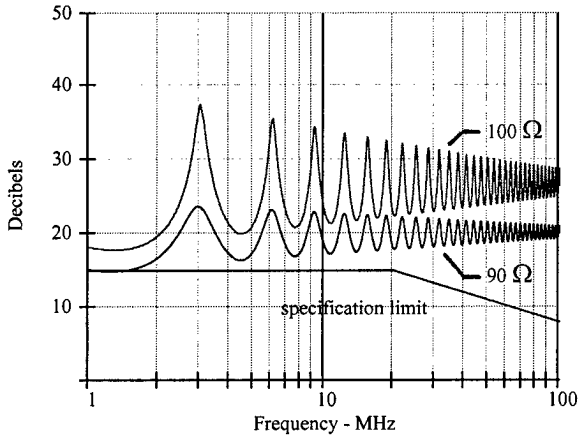

Figure 6. Return Loss for the 109 Ω cable of figure 2. Source impedance indicated on chart. Load impedance = 100 Ω.

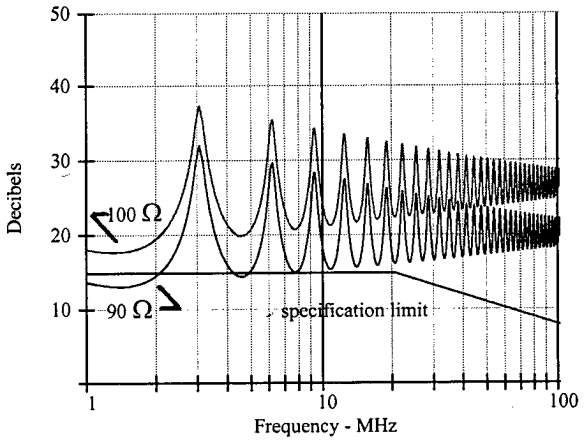

Figure 7. Return Loss for the 109 Ω cable of figure 2. Source impedance = Load impedance. Values indicated on chart.

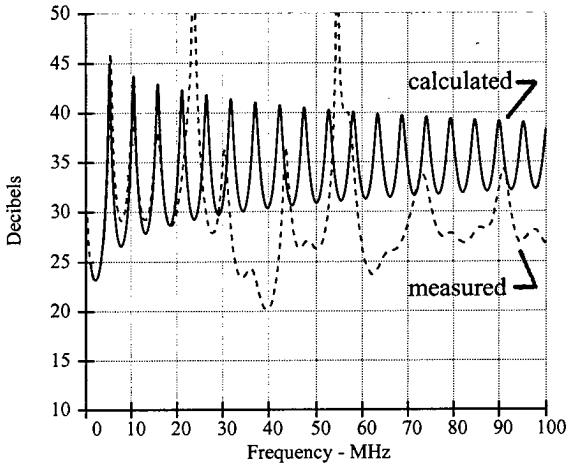

Figure 8. Return loss comparison:calculated vs. measured for 20 meter cable length.

Measured Results. Figure 8 compares modeled performance with measured performance of a 20 m length of 103 Ω cable with delay of 470 ns/ 100 m. Measured response follows the model but evidence of impedance nonuniformity or structural roughness is quite evident above about 25 MHz. The cable length is too short to produce significant resonant return loss due to a periodic impedance structure. The random structural variations are seen to be slightly modulated by the resonant trough characteristic.

Figure 9 is a plot of performance for a 100 m length of the same cable plotted in figure 8. The model resonant trough effect dies out at the higher frequencies where there is some evidence of periodic structural return loss. Here return loss is degraded about 4 dB's compared to the 20 m length. The measured return loss is actually greater than the model prediction for certain bands at both high and low frequencies. This is due to phase cancellation associated with the periodic structural return loss.
The model data indicates the measured data, while not poor, could theoretically be improved about 10 db's. To achieve this the twisted pair must be made to closer dimensional tolerances and approach the structure of the uniform model.

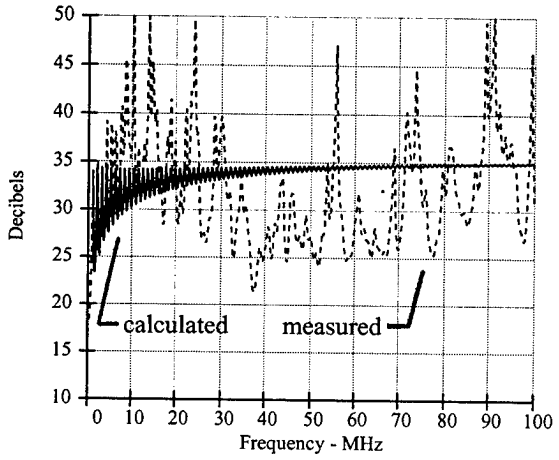

Figure 9. Return loss comparison: calculated vs. measured for 100 meter cable length.

Uniform Cable Insertion Loss Deviation

Insertion loss[8] is closely related to attenuation. However, insertion loss takes into account the effects of source and load impedance mismatch relative to the cable characteristic impedance. Insertion loss will be greater than cable attenuation, α, when there is a mismatch.
Insertion loss deviation for the setup of figure 1 is given below.
The load voltage[9] (V_f) is related to the voltage at the input to the cable (V_{in}) by equation (10).

$$V_f = V_{in} \cdot (\varepsilon^{-\cdot L \cdot \gamma}) \cdot (1 + \rho_f) / (1 + \rho_f \cdot \varepsilon^{-2 \cdot L \cdot \gamma}) \quad (10)$$

The input voltage is defined by source voltage (V_n) division between the source impedance (Z_n) and the cable input impedance in equation (11).

$$V_{in} = V_n \cdot Z_{in} / (Z_{in} + Z_n) \quad (11)$$

Insertion loss (IL) is then found from equation (12).

$$IL = -20 \cdot \log_{10} |2.(V_f / V_n)| \quad (12)$$

Insertion loss deviation (ILD) is defined by equation (13).

$$ILD = IL - \alpha \quad (13)$$

Insertion loss deviation for the uniform cable with Z_{hf} = 109 Ω is shown in figure 10. Two families of curves are presented. The lower family is for source and load impedances equal to 100 Ω and includes plots for 100m, 30m and 15m cable lengths. The other family of plots covers the same lengths but is for source and load impedances equal to 90 Ω.
These deviations from cable attenuation are quite small and could be neglected. However the deviation becomes more significant when connecting hardware components are considered later in the paper.

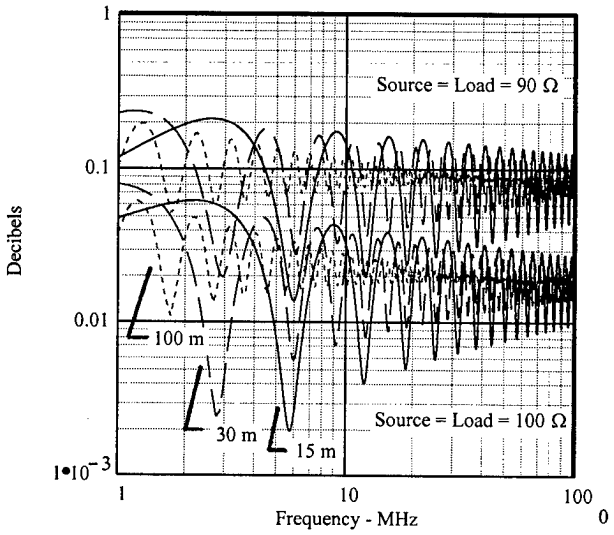

Figure 10. Insertion Loss Deviation vs. Frequency.

CONNECTOR HARDWARE MODEL

The connecting hardware is modeled as a very short length of uniform cable. This is based on the

secondary transmission line constants (γ, Z) and has proven satisfactory for the purposes of evaluating return loss and insertion loss. The model is given below in equations (14)-(18).

Time delay, nanoseconds per meter;

$$\tau = 570 \quad \ldots\ldots (14)$$

Phase constant, radians per meter;

$$\beta = 2 \cdot \pi \cdot f \cdot \tau / 100000 \quad \ldots\ldots (15)$$

Attenuation constant, Nepers per meter;

$$\alpha = (0.4 \cdot \sqrt{f}) \cdot 8.686 \quad \ldots\ldots (16)$$

Propagation constant, radians per meter;

$$\gamma = \alpha + j \cdot \beta \quad \ldots\ldots (17)$$

Characteristic impedance, Ohms;

$$Z_o = Z_{cx} / 100((100 + 5.5/\sqrt{f}) - j \cdot 5.5/\sqrt{f}) \quad \ldots\ldots (18)$$

The variable f is frequency in MHz and the operator j is sqrt of –1.
In equation (18) the term Z_{cx} along with the connector length L_x are selected to give connector return loss values given in Table 1.

These are arrived at by solving equations (6)-(9) using the connector model equations (14)-(18) along with 100 Ω source and load impedances.

Table 1. Connecting Hardware Return Loss at 100 MHz.

Return Loss Decibels	L_x = 0.03 m Z_{cx} - Ω	L_x = 0.06 m Z_{cx} - Ω
14	408	235
15	366	216
18	275	176
20	232	158

CHANNEL MODEL

The channel is modeled as a cascade interconnection of uniform cable and connector hardware elements as shown in figure 11. The elements are characterized by the appropriate equations discussed earlier. The equations for reflection coefficient, input impedance and voltage at each interface between cable and hardware are determined from equations (7)-(10). It can be seen that the 4-connector channel model involves 29 complex variable interface equations.

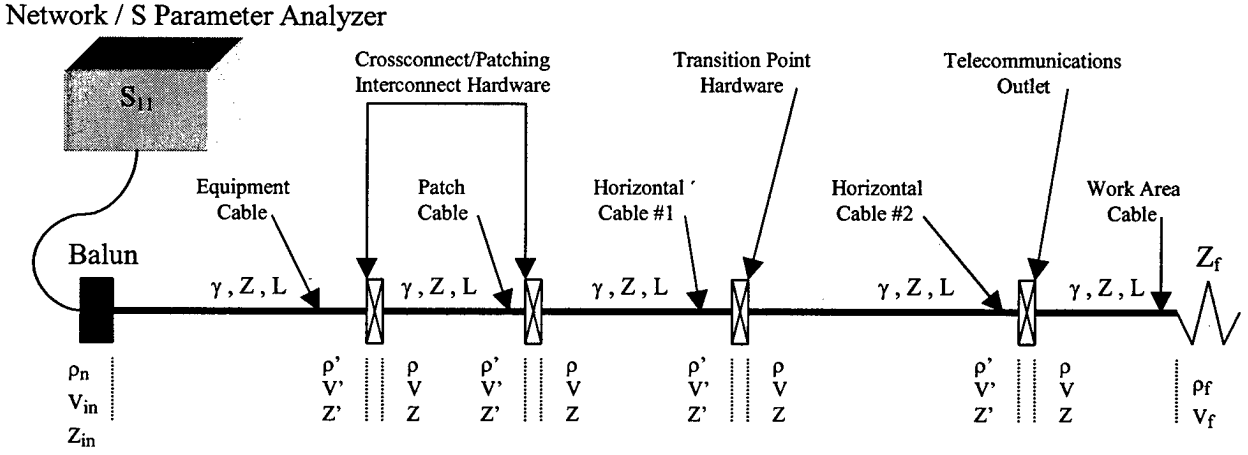

Figure 11. Cascade interconnection of uniform cable and connector hardware elements.

The input reflection coefficient and return loss are found by sequentially solving the equations starting with the output reflection coefficient equation. The insertion loss and insertion loss deviation are found by sequentially solving the equations starting at the input voltage equation. Two examples comparing measured and calculated channel performance will be discussed below.

Two Connector, Single Cable Example

In this example one cable is fitted with a connector at each end. The connectors were measured to have 15 dB of return loss at 100 MHz. In the model 15 dB was obtained by adjusting the length to 0.03 m with impedance of 366 Ω . The cable is the same as given in figures 8 and 9. Figures 12 and 13 compare measured and calculated performance for 20 m and 100 m lengths of channel respectively.

The connectors return loss is seen to dominate the performance of the channel return loss. Comparing figures 9 and 13 it is seen the channel return loss at

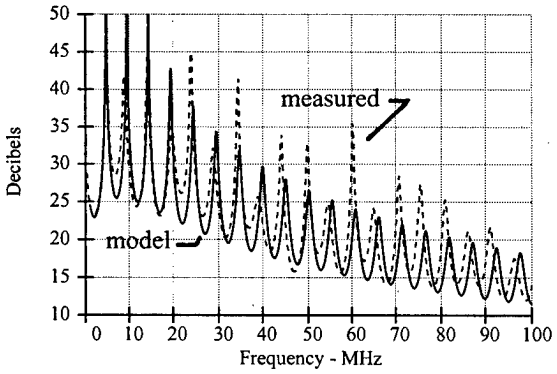

Figure 12. Channel return loss comparison: model vs. measured for 20 m length.

100 MHz is degraded about 20 dB compared to cable return loss. Improvement in the cable return loss would have negligible impact on the channel return loss in this case. Figure 14 shows just the channel and cable model results for the 100 m length.

Three Connector, Four Cable Example

This example is similar to the setup in figure 11 without transition point hardware. The equipment, patch and work area cables lengths are 1 m, 2m, and 7 m respectively. The cable time delay constant term is 490 in equation (1) and the cable Z_{hf} is 100 Ω in equation (5). The attenuation constant is according to equation (3). The connectors are the same as used in the first example.

Channel length = 25 meters. Figure 15 compares modeled and measured performance for horizontal cable length of 15 m. Return loss for 25 m of cable is plotted at the top of the graph. The narrow trough spacing in the channel response corresponds to the 15 m length of horizontal cable and not the end-to-end 25 m channel length. A wide trough which corresponds to the 2 m patch cable length is also apparent.

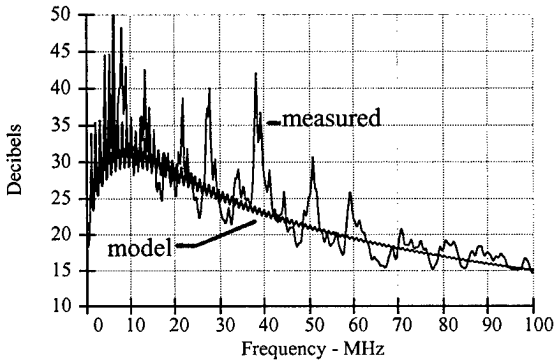

Figure 13. Channel return loss comparison: model vs. measured for 100 m length.

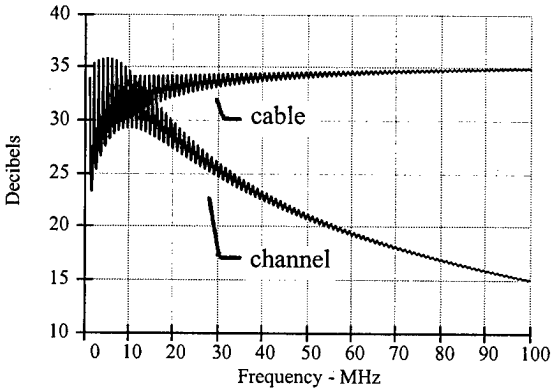

Figure 14. Return Loss: uniform cable vs channel with 15 dB connectors.

Channel length = 100 m. Figure 16 is similar to figure 15 except now the horizontal cable length is 90 m. Here the dominant feature is the wide trough.

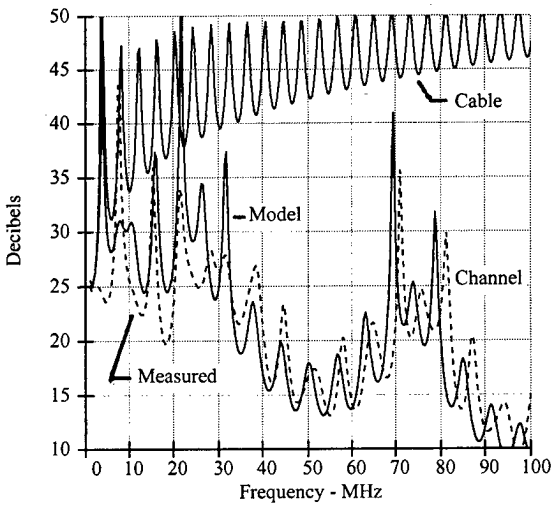

Figure 15. Return loss comparison; 25 m channel loaded with 3 connectors vs. unloaded 25 m cable length.

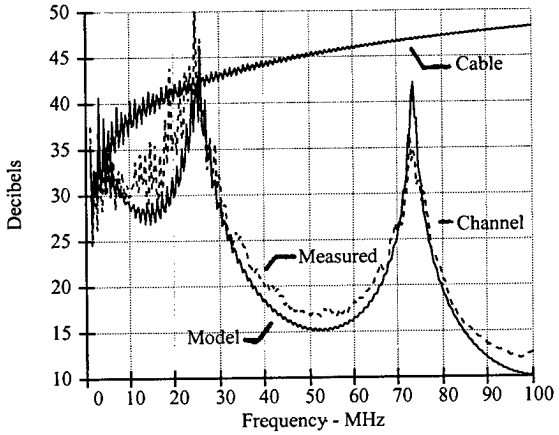

Figure 16. Return loss comparison; 100 m channel loaded with 3 connectors vs. unloaded 100 m cable length.

Figure 17 presents the modeled insertion loss deviation performance for the 25 m and 100 m channels presented above. Insertion loss deviation is the difference between insertion loss for a channel with cable and connecting hardware compared to a channel of the same length containing only uniform cable. The deviation at 100 MHz is about 1decibel for each channel. The trend shown in the figure is the deviation increases with increasing frequency. The

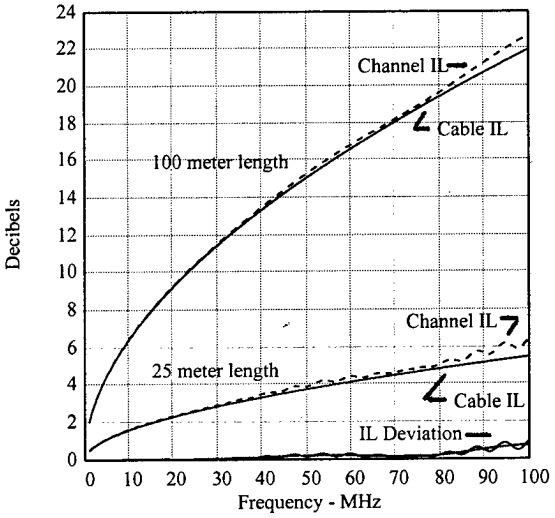

Figure 17. Insertion loss deviation comparison; 25 m and 100 m channels.

deviation is basically caused by resonance (troughs) of the return loss that occurs at certain frequencies depending on cable construction and the spacing of connecting hardware components. The reflected signal levels (return loss) cause a decrease in the signal level delivered to the load. This results in higher attenuation or higher insertion loss than would be expected. At least up to a frequency of 100 MHz the wide trough due to the 2 m patch cord is negligible. However the narrow return loss troughs seen in the 25 m channel cause a ripple in the 25 m channel insertion loss response.

Four Connector, Four Cable Model Results

The channel model of figure 11 provides for transition point hardware. Return loss performance for 4 horizontal cable length configurations are presented below. Otherwise, cable and connector parameters are the same as in the 3-connector examples. The configurations are given in table 2.

Table 2. Horizontal Cable Length Configurations

Configuration	Horizontal Cable Length meters	
	#1	#2
a	90	0
b	15	75
c	15	15
d	15	2

With horizontal cable #1 equal to 15 m the return loss in figure 18 is seen to have narrow width troughs similar to the 25 m channel performance of figure 15. Horizontal cable # 2 length variation from 2 m to 75 m does not alter the basic narrow trough characteristic.

The channel return loss is considerably degraded compared to cable performance of the same length. The trend is increasing degradation with increasing frequency.

The connecting hardware return loss performance must be improved to achieve improved channel performance at frequencies below 100 MHz and improvement is a prerequisite beyond 100 MHz.

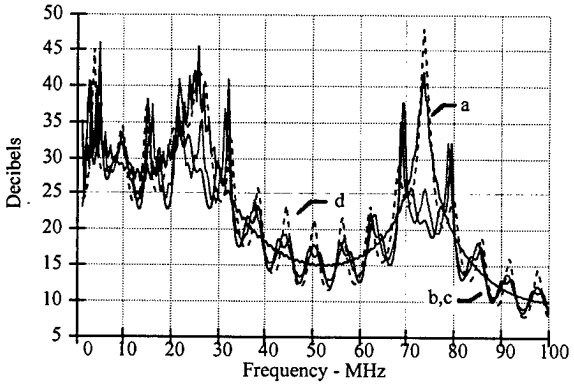

Figure 18. Return loss comparison; 100 m channel with transition point per table 2.

BEYOND CAT 5

To achieve acceptable channel performance beyond Cat 5 both cables and connecting hardware, which have appropriate return loss characteristics, are required. Cables that exceed Cat 5 performance have been commercially available for some time and are now the subject of intense standardization activity. These cables are manufactured with tighter dimensional tolerances and control than the typical Cat 5 cable.

Figure 19 compares a uniform cable model performance to 250 MHz with measured performance (sample impedance was 101 Ω). It is seen the low frequency performance follows the model up to about 35 MHz. At higher frequencies there is about 10-15 dB deviation from the model and some evidence of structural roughness and periodic type return loss. There is still room for improvement compared to the model.

Comparing figures 9 and 19, the 250 MHz cable shows an improvement of about 6 dB or greater up to 100 MHz and about the same performance at 250 MHz.

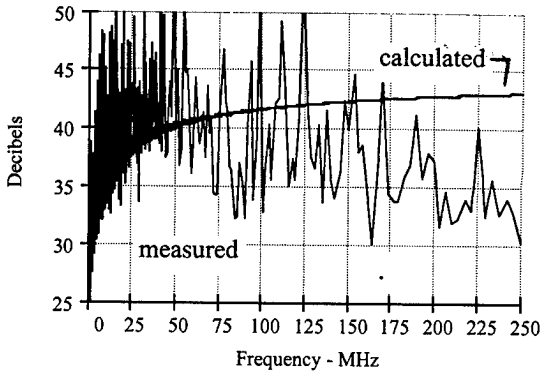

Figure 19. Return loss comparison; calculated vs. measured, 100 meter cable length.

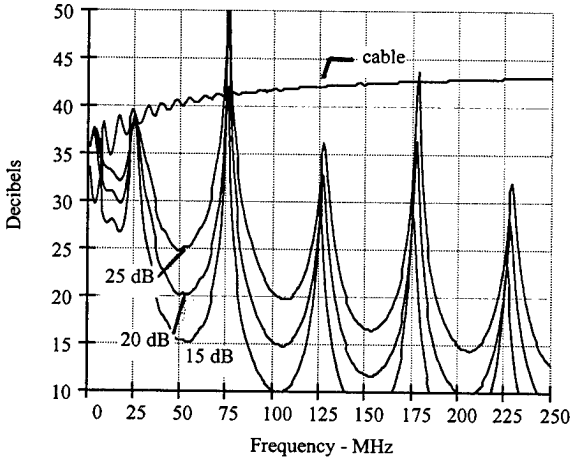

Figure 20. Return loss comparison; 100 m channel with 15 dB, 20 dB and 25 dB connecting hardware.

Figure 20 shows modeled channel performance up to 250 MHz. The channel configuration is similar to figure 15 with 101 Ω cable and time delay constant equal to 480 in equation (1). Connector return loss of about 22 dB at 100 MHz is required to obtain similar channel return loss at 250 MHz.

CONCLUSION

This particular modeling technique is reasonably accurate and is a valuable tool for analysis of the impact of cable and connecting hardware on channel return loss performance.

REFERENCES

1. *Commercial Building Telecommunications Cabling Standard*, TIA/EIA-568A-1995.
2. TIA TR41.8.1 contribution *A Close Look at Parameters Affecting Link Return Loss*, L. Adriaenssens, Lucent Technologies .
3. TIA TR41.8.1 contributions on SRL Channel Model Results, D. Hawkins, Lucent Technologies.
4. TIA TR41.8.1 contributions on Channel Simulation Results, P. Kish(Nordx/CDT), C. DiMinico(CDT).
5. TIA TR41.8.1 contributions on cable and channel return loss modeling, J. Kincaid and P. Vanderlaan, Belden Wire and Cable.
6. Belden modeling and measured results, page 13 of IEEE 802 Tutorial on 1000 BASE T.
7. Mathcad7 Professional published by Mathsoft Inc.
8. L. N. Dworsky, *Modern Transmission Line Theory and Applications*, John Wiley & Sons, 1979
9. J. I. Potter and S. Fich, *Theory of Networks and Lines*, Prentice-Hall, Inc., 1963

Paul Vanderlaan

Paul is a Product Development Engineer at the Belden Engineering Center. He holds a BSEE degree from Purdue University and has over 5 years experience with Belden developing high performance premises cables. He holds one patent. Paul represents Belden at TIA standardization meetings and is well known in the premises community. He has presented several papers at BICSI Conferences as well as at the IWCS Symposium.

(PO Box 1980; Richmond, IN, 47375)

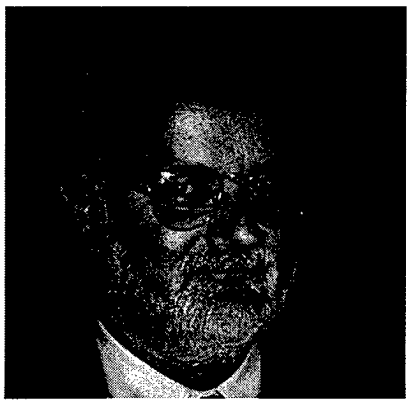

John Kincaid

John is a Senior Product Engineer at the Belden Engineering Center. He holds BSEE and MSEE degrees from the University of Oklahoma and has over 25 years experience with Belden. His experience encompasses engineering management and product development positions in the USA as well as in Europe. He holds nine patents. John is active in IEC and TIA cable standardization activities. He is the US Technical Advisor to IEC SC 46A on coaxial cables, and is Convenor of IEC SC 46A/WG3 on data and CATV cable. He is an expert on working groups 5 and 7 dealing with shielding and premises cabling issues.

(PO Box 1980; Richmond, IN, 47375)

Development of Equal Level Far-End Crosstalk (ELFEXT) and Return Loss Specifications for Gigabit Ethernet Operation On Category 5 Copper Cabling

Christopher T. Di Minico
Cable Design Technologies (CDT) Corporation, Massachusetts

Paul Kish
NORDX/CDT, Montreal, Canada

ABSTRACT

1000BASE-T, a Gigabit Ethernet Physical layer specification for 1000 Mb/s, is designed to operate on 4-pair 100 ohm Category 5 balanced copper cabling as specified in ANSI/TIA/EIA-568-A. During the development of 1000BASE-T it was recognized that the 1000BASE-T link segment transmission parameters of equal level Far-End crosstalk (ELFEXT) loss and return loss needed to be added to the transmission parameters of attenuation and Near-End crosstalk (NEXT) as specified in ANSI/TIA/EIA-568-A for Category 5 cabling. This paper provides a description of the development of these parameters.

The 1000BASE-T link segment transmission parameters include insertion loss, NEXT loss, ELFEXT loss, return loss, link delay, and characteristic impedance. The link segment transmission parameter limits are specified to ensure 1000BASE-T operation on a Category 5 link segment of at least 100 meters constructed of cable and connecting hardware that meet the minimum requirements of the Category 5 specification, i.e., the components are worst case.

Category 5 cabling as specified in ANSI/TIA/EIA-568-A consists of cable, connecting hardware, and recommended topology[1] (Figure 2). The transmission characteristics of the ANSI/TIA/EIA-568-A cabling channel are specified for NEXT loss and attenuation.

Validation of 1000BASE-T operation on Category 5 was performed with simulation software that used the cabling measurements of NEXT loss, FEXT loss, and insertion loss as input, and then output the signal-to-noise margin based on the design constraints. Link segments using minimally compliant components were constructed and measured. Some of the measured data, falling short of worst case, were scaled to touch the limit line.

BACKGROUND

Ethernet standards are developed by the 802.3 working group of the IEEE LAN-MAN Standards Committee. In the spring of 1997, a task force called 802.3ab was formed to work on a copper cabling solution for Gigabit Ethernet. The 802.3ab Gigabit Ethernet copper solution, now termed 1000BASE-T, is specified to operate on 4-pair, 100 ohm Category 5 balanced copper cabling as defined in ANSI/TIA/EIA-568-A.

A 1000BASE-T Link segment consists of 4-Pair 100 ohm Category 5 Cabling as illustrated in Figure 1. Each of the 4-Pairs is a full duplex channel supporting an effective data rate of 250 Mb/s simultaneously in both directions achieving an aggregate data rate of 1000 Mb/s. Five-level Pulse Amplitude Modulation (PAM5) is employed for transmission over each wire pair. The PAM5 baseband signaling of 125 Mbaud is used on each of the wire-pairs to constrain the width of the transmit signal spectrum below 80 MHz.

[1] Category 5 cabling channels as specified in ANSI/TIA/EIA-568-A exclude the equipment connectors and may include a transition point. The building cable is referred to as horizontal cable.

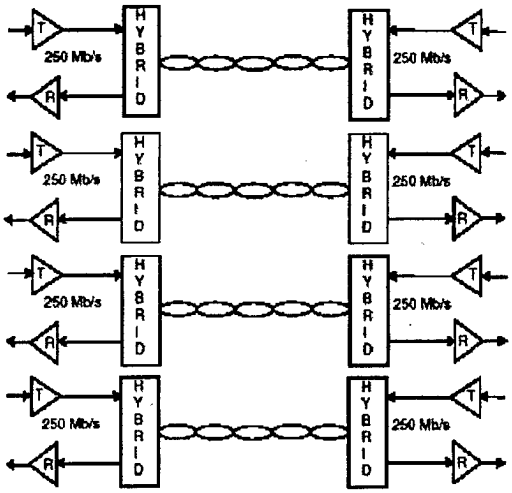

Figure 1

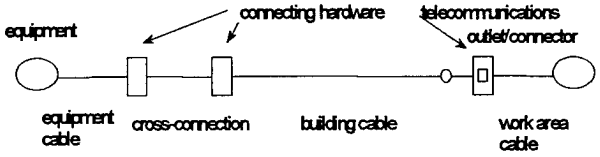

Figure 2

Full-duplex bi-directional transmission. Full-duplex bi-directional transmission consists of transmitting and receiving data simultaneously in both directions on each of the four wire pairs. Hybrid circuits are needed to enable bi-directional transmission over single wire pairs. Bi-directional transmission allows FEXT to combine with NEXT and echo at the receiver (Figure 3).

Cancellation in a Digital Signal Processor (DSP). The most significant impairments in a 4-pair Category 5 transmission system are those caused by Echo (combined effect of the cabling return loss and the hybrid function), NEXT and FEXT. Since the sources of all these impairments are known to the receiver (transmitted symbol sequence, received symbol sequence), it is possible to employ Digital Signal Processing (DSP) cancellation techniques to mitigate the effect of these impairments on the receiver.

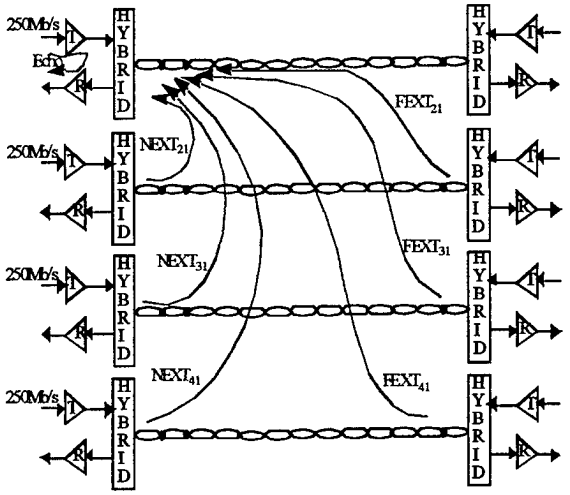

Figure 3

The characteristics of the impairment signals are learned in order to implement the necessary cancellation. A pulse is transmitted while the receive signal is monitored. The receive signal is sampled and a digital filter with a finite impulse response is constructed with the negative of these sampled values as the coefficients. The filter impulse response is constructed to have a pulse response that is the exact opposite of the pulse response of the received impairment and therefore, adding the output of this filter to the received signal will result in the necessary cancellation. In practice, the difficulty in cancellation is determining the coefficients in the presence of transmission from the far end.

ELFEXT

Development of Cable FEXT limits based on Cable NEXT limits. ANSI/TIA/EIA 568-A standard specifies the NEXT loss and the attenuation limits for Category 5 cables and connectors that comprise a worst case Category 5 channel up to a frequency of 100 MHz. The FEXT loss requirements are not specified but can be derived from the NEXT limits. This is because both NEXT and FEXT are mathematically related to the coupling function

between two pairs over the length of cable. This section provides a methodology for deriving the worst case FEXT limits and substantiates the results based on empirical data. Additional theoretical information on ELFEXT simulation is provided in Annex C.

Figure 4 below illustrates the coupling between two pairs for a cable of length (l) composed of (n) sections, where each section represents an incremental cable length (Δx). The equation for the coupling function $(\delta_k)^1$ depends on the capacitance unbalance (Cu) and the mutual inductance unbalance (M) for each section of cable. (δ_k) is the coupling function for NEXT or FEXT. In the case of NEXT, the coupling function (δ_k) is the sum of the capacitance unbalance and the mutual inductance unbalance terms. In the case of FEXT, the coupling function δ_k is the difference between the capacitance unbalance and the mutual inductance unbalance terms.

The coupling current at section (k) divides in two and travels toward the near end (inxt) and toward the far end (ifxt). For NEXT, the current starts at the near end of the disturbing pair, travels a distance x, is coupled into the disturbed pair at section (k), and travels back to the near end of the disturbed pair. The total distance traveled is (2x). The coupling current (inxt) experiences an attenuation and phase delay of $(e^{-2\gamma x})$ relative to the input signal. The equations for NEXT, based on Figure 4, are:

$$NEXT = 10\log\left[\sum_k \left|\frac{i_{nxt}}{I_o}\right|^2\right] \quad \text{(eq 1)}$$

$$NEXT = 10\log\left[\sum_k \left|\frac{\delta_k e^{-2\gamma x}}{2}\right|^2\right] \quad \text{(eq 2)}$$

In a similar mariner, for FEXT, the current starts at the near end of the disturbing pair, travels a distance x, is coupled into the disturbed pair at section (k), and travels toward to the far end of the disturbed pair. The total distance traveled is (l). The coupling current (ifxt) experiences an attenuation and phase delay of $(e^{-\gamma l})$ relative to the input signal. The equations for FEXT, based on Figure 4, are:

$$FEXT = 10\log\left[\sum_k \left|\frac{i_{fxt}}{I_o}\right|^2\right] \quad \text{(eq 3)}$$

$$FEXT = 10\log\left[\sum_k \left|\frac{\delta_k e^{-\gamma l}}{2}\right|^2\right] \quad \text{(eq 4)}$$

$$FEXT = 10\log\left[\sum \left|\frac{\delta_k}{2}\right|^2\right] + 10\log\left[\left|e^{-\gamma l}\right|^2\right] \quad \text{(eq 5)}$$

$$FEXT = ELFEXT + Attenuation \quad \text{(eq 6)}$$

NEXT & FEXT Model

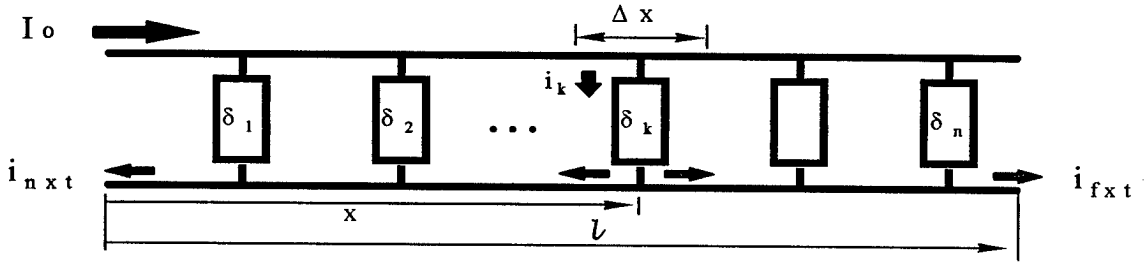

Figure 4

$$\delta_k = \frac{i_k}{I_o} = \frac{Cu_k Z_o}{8} \pm \frac{M_k}{2Z_0} \quad \text{(eq 7)}$$

A Mathcad model was developed for an n-section transmission line, which incorporates the above equations 1 thru 7 . The attenuation equation for the cable was taken per TIA/EIA 568-A and the propagation delay was taken per TIA/EIA 568-A1. The coupling function (δ_k) was varied until the corresponding NEXT limit of 32.3 dB was reached at 100 MHz.

The coupling function for FEXT is the difference between the capacitance unbalance and the mutual inductance unbalance terms in the equation for (δ_k). To obtain the worst case FEXT, it is assumed that one or the other term is dominant, in which case the same function (δ_k) can be used to derive both NEXT and FEXT. The result of these calculations is illustrated graphically in Figure 5.

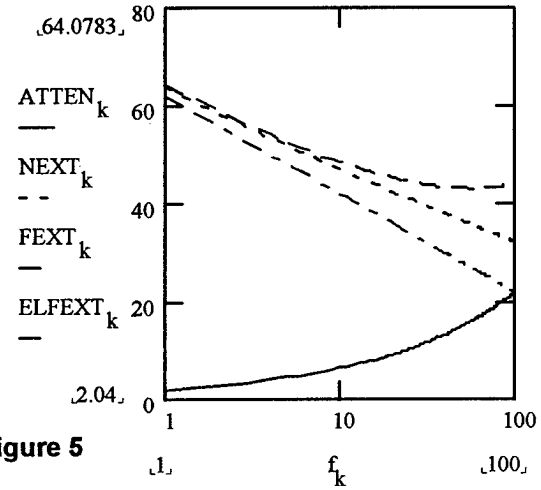

Figure 5

From Figure 5 above it is evident that at low frequencies (less than 4 MHz) the NEXT and the FEXT limits in dB are roughly equal. At high frequencies, FEXT is much less than NEXT because of the signal attenuation over 100 meters of cable.

ELFEXT is defined as the difference between FEXT and attenuation in dB as developed in equations 3 through 6. ELFEXT is a function only of the couplings between cable pairs. Unlike NEXT, which is mostly affected by unbalance couplings close to the end of the cable, ELFEXT is equally affected by unbalance couplings anywhere along the cable. In the above analysis, a uniform coupling function was assumed. However, the same analysis can be performed using any desired coupling function.

ELFEXT follows a 20 dB per decade slope as a function of frequency whereas NEXT follows a 15 dB per decade slope. The value of ELFEXT at 100 MHz for worst case Category 5 cable is 22 dB and FEXT is 44 dB. The modeling results agree closely with FEXT measurements taken on a worst case cable, as illustrated in Figure 6.

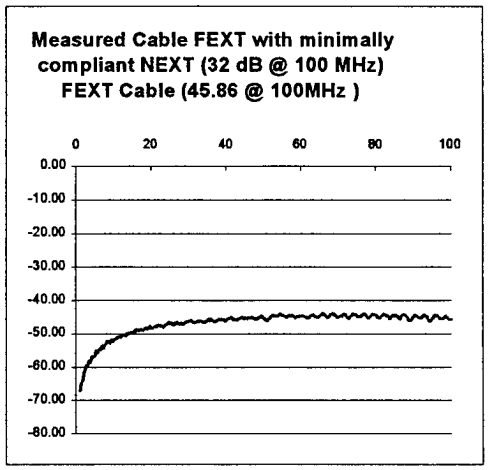

Figure 6

Development of Connector FEXT contribution to the link. The objective in this section is to characterize the connecting hardware FEXT contribution to the overall link crosstalk performance. With an understanding of the connector FEXT contributions, and the cable, the worst case cabling performance can be determined by calculation using worst case component specifications and cabling configurations i.e., numbers of connectors and cables.

Modeling and measurements determined the FEXT contribution of the connecting hardware to the link segment. The measurement configurations shown in Figure 12-Annex B were constructed of cable with crosstalk loss >65 dB in order to isolate the connecting hardware contribution. The number of connectors were varied as well as the distances.

The configurations 1-3 illustrated in Figure 12-Annex B were measured in sequence in order to determine the incremental connector FEXT contribution. Simulation results show good agreement to the measurement (Figure 13). Measurements and simulation show expected slope of 20 dB per decade. Values at 100MHz are provided in Table 1.

Table 1

Configuration (4 connector)	Measured FEXT (dB) @100Mhz	Calculated FEXT (dB) @100MHz	Measured ELFEXT (dB) @100Mhz	Calculated ELFEXT (dB) @100MHz
Concatenated 4 ft and 35 ft	18.73	18.74	15.79	16.12

Development of Channel ELFEXT limits based on Cable ELFEXT and Connector ELFEXT. Comparisons were made between vector summation and a power summation of the cable and connecting hardware contributions, and the simulated link segment. The graph of Figure 14-Annex B shows good agreement between a voltage summation and the simulated ELFEXT of the link segment.

Based on the analysis, a link limit was calculated using a voltage summation of minimally compliant cable and connecting hardware.

$$ELFEXT_{cablink(f)} \geq -20\log\left(10^{-\frac{ELFEXT_{cable}}{20}} + 10^{-\frac{FEXT_{connector}}{20}}\right) \text{ dB} \quad \text{(eq 8)}$$

1000BASE-T (Draft 4) specifies that the worst pair ELFEXT loss between any two duplex channels (any two pairs) shall be greater than:

$$ELFEXT_{loss(f)} \geq 17 - 20\log(f/100) \text{ dB} \quad \text{(eq 9)}$$

Where f is the frequency over the range of 1 MHz to 100 MHz.

1000BASE-T (Draft 4) also specifies a power sum ELFEXT (PSELFEXT) limit in order to simplify a multiple disturber ELFEXT field test. The PSELFEXT between a duplex channel (a pair) and the three adjacent disturbers shall be:

$$PSELFEXT_{loss(f)} \geq 14.4 - 20\log(f/100) \text{ dB} \quad \text{(eq 10)}$$

Where f is the frequency over the range of 1 MHz to 100 MHz.

Return Loss

Development of Link Return Loss Limit Based on Component Values. The objective of this section is to characterize the connecting hardware return loss contribution to the overall link performance. With an understanding of the connector contributions, the worst case cabling performance can be calculated based on worst case component specifications and the cabling configurations, i.e., numbers of connectors and cables.

Modeling and measurements determined the return loss contribution of the connecting hardware. The measurement configurations are shown in Figure 8-Annex A, and Figure 9-Annex A .

Return Loss is a measure of the reflected signal energy in dB. The return loss is affected by the impedance mismatch between the cabling and the far end termination and between the various components comprising a channel, including horizontal cables, patch cables and connectors. The impedance matching between cables and connectors are particularly important at higher frequencies.

The model for return loss is illustrated in Figure 7. It consists of a series of concatenated transmission lines where each component is modeled by its own transmission matrix $[T_k]$. The Return Loss is determined from the resultant transmission matrix using the equations shown in Figure 7.

RETURN LOSS MODEL

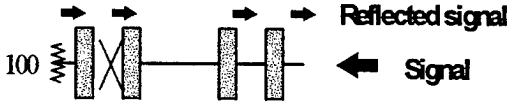

$$\begin{bmatrix} A & B \\ C & D \end{bmatrix} = \prod_k [T_k] \qquad Z_{in} = \frac{A + \frac{B}{100}}{C + \frac{D}{100}} \qquad RL = -20\log\left|\frac{Z_{in} - 100}{Z_{in} + 100}\right| \quad \text{(eq 11)}$$

Figure 7

Return Loss Modeling Results. A Mathcad model was developed for modeling a worst case channel including up to four connectors. The worst case return loss occurs for a short length channel where the magnitude of the far end reflections are the greatest. Figure 11-Annex A illustrates the modeling results for the channel configuration shown in Figure 9-Annex A for manufacturer 2.

The predicted return loss trace in Figure 11-Annex A closely matches the measured data (Figure 10-Annex A). The peaks occur at the same frequencies of approximately 50 MHz and 90 MHz. The modeling results were generated using connecting hardware having 15.6 dB return loss (practical worst case) and a mismatch of 10 ohms between the patch cable and the horizontal cable impedance.

The graph also illustrates another transmission parameter, labeled as Roughk. This transmission parameter is the insertion loss deviation (ILD) of the channel, also called roughness. Insertion loss deviation is quite pronounced at higher frequencies. Insertion loss deviation is a new parameter under study by the TIA TR 41.8.1 working group. Insertion loss deviation needs to be taken into account in the overall channel budget for insertion loss. It can also be considered as excess noise and can contribute to jitter in digital systems.

The return loss limit for 1000BASE-T is shown as the lower dotted line in Figure 10-Annex A. The return loss for a 1000BASE-T (DRAFT 4) link is specified as:

$$\text{Return_Loss}(f) \begin{cases} 15 & (1\text{-}20\ \text{MHz}) \\ 15\text{-}10\log_{10}(f/20) & (20\text{-}100\ \text{MHz}) \end{cases} \text{(dB)}$$

where f is the frequency in MHz. The reference impedance shall be 100 ohms.

The return loss specifications for an "Enhanced Category 5 Cabling" (currently balloting in TIA/EIA) is a 2 dB improvement over the specifications of ANSI/TIA/EIA-568-A. This limit is shown as the upper dotted line in Figure 10-Annex B. The improvement in return loss can be achieved using the "Enhanced Category 5" connecting hardware and cable.

CONCLUSION

The transmission parameters of ELFEXT loss and Return Loss have been developed to characterize cabling as specified in ANSI/TIA/EIA-568-A in order to validate 1000BASE-T operation on Category 5 cabling. Two-connector topologies minimally compliant with TIA/EIA-568-A are expected to meet these limits. Other Category 5 topologies can be implemented as long as they meet the ELFEXT loss and return loss limits.

"Enhanced Category 5 Cabling" (currently balloting in TIA/EIA) will sufficiently characterize the cabling components to ensure a compliant four-connector topology.

Annex A: Return Loss Test Configurations and Measurements

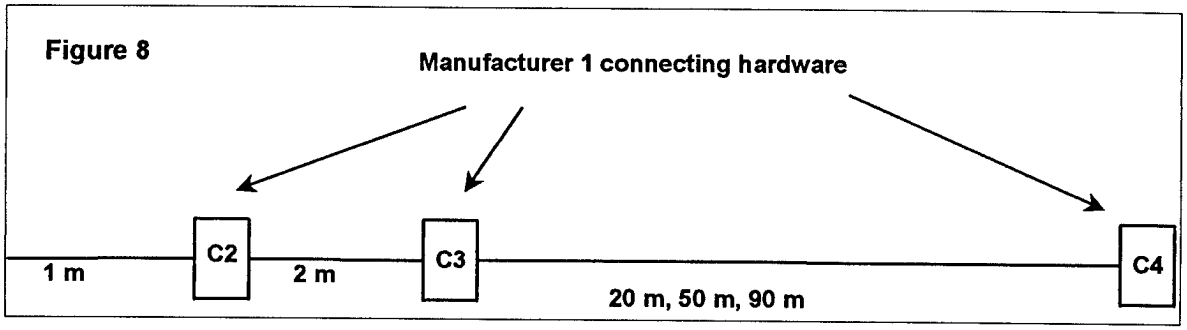

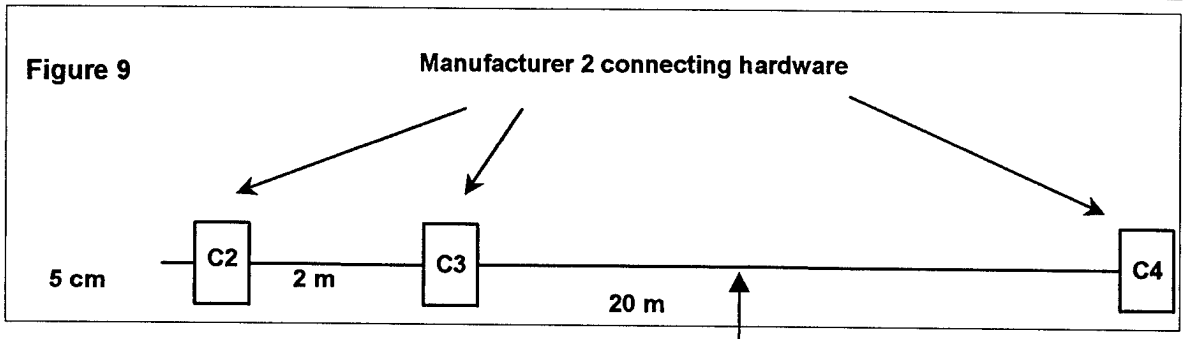

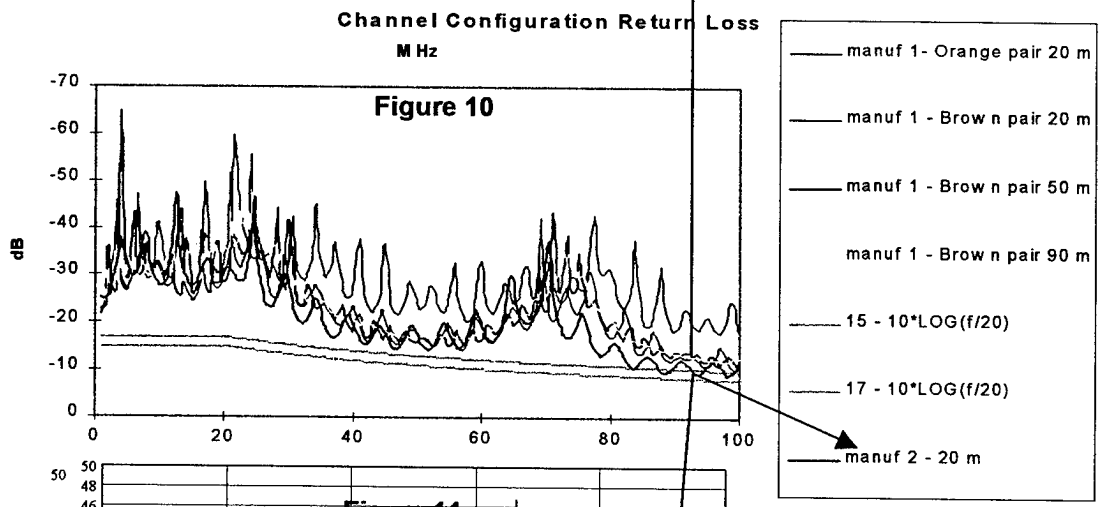

Figure 10

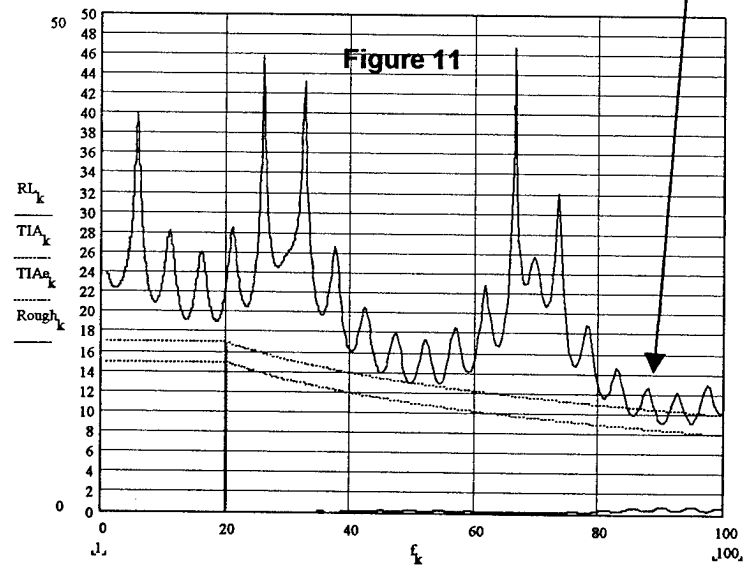

Figure 11

Annex B: ELFEXT Configuration and Measurements

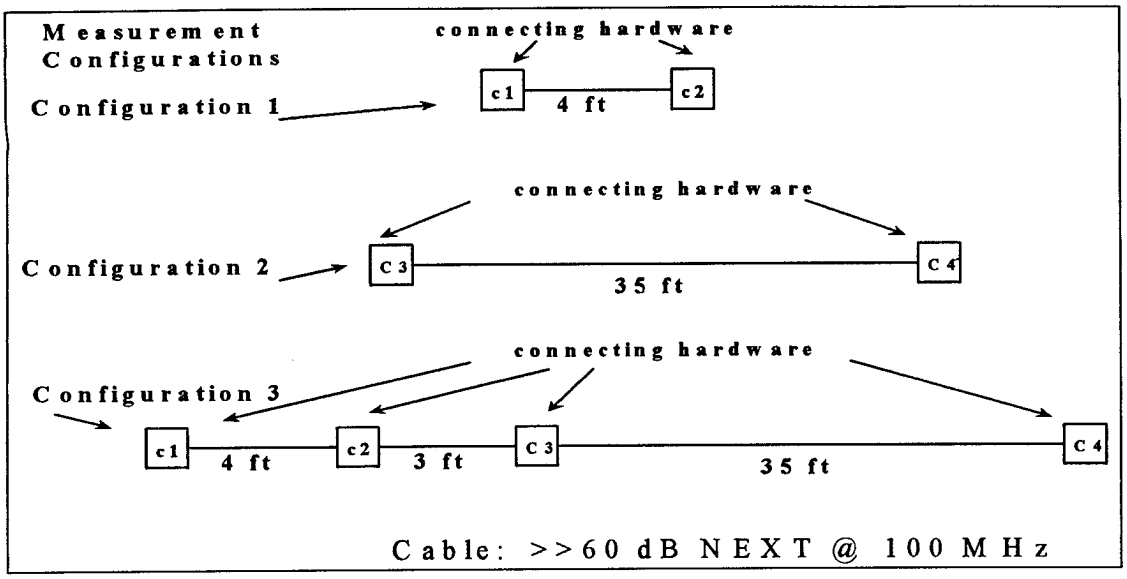

Figure 12

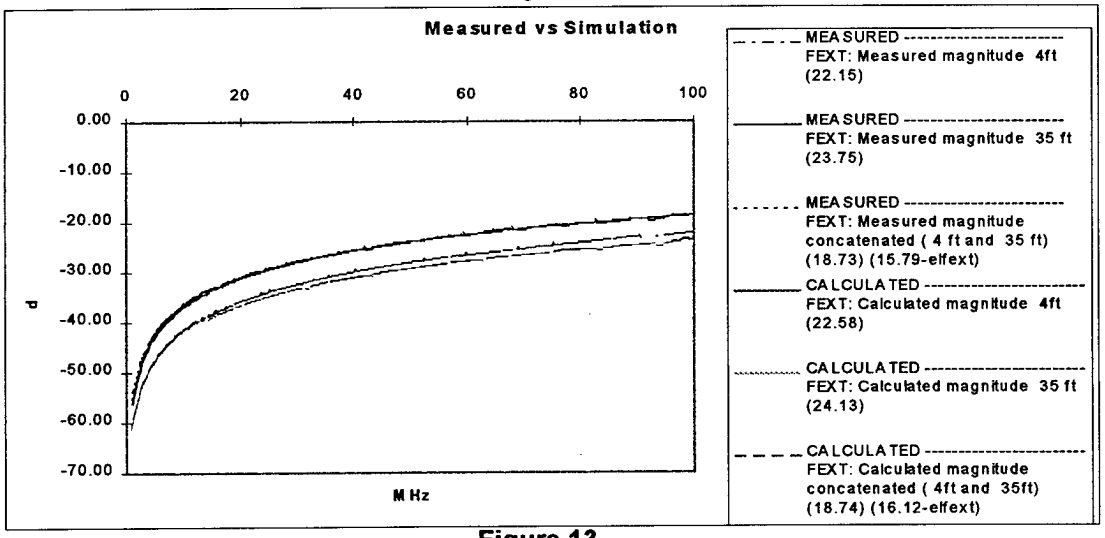

Figure 13

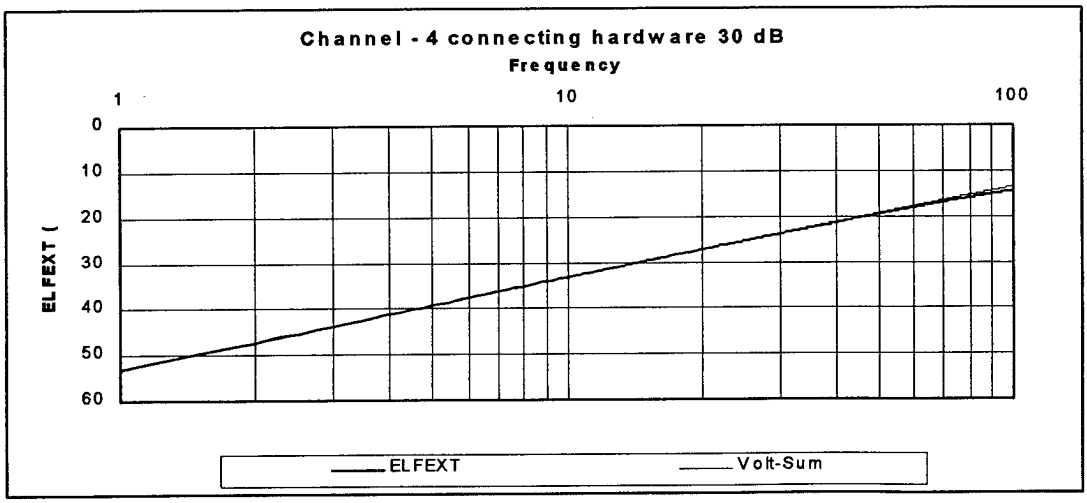

Figure 14

ANNEX C: ELFEXT SIMULATION

H. Cravis and T.V. Crater evaluated the expression for Far-End Crosstalk between two pairs when one considers two pairs of propagation constant, $\gamma(f)$, in a cable section of length l. Their expression for the incremental crosstalk current dI on the disturbed pair at the receiving end, due to the incremental length of cable dx at some distance x, is given by

$$\frac{dI}{I_0} = \left(\frac{Z_0 Y}{16} - \frac{Z}{4 Z_0} \right) e^{-\gamma l} dx \quad [3]$$

where Z is defined as the mutual impedance unbalance between pairs per unit length at a distance x from the signal source, Z_0 is the characteristic impedance of both pairs – assumed to be equivalent, and Y is the unbalance admittance between pairs per unit length. The bracketed expression above, when Z, Z_0, and Y are independent of frequency, is the unbalance per unit length, commonly called the crosstalk coupling function $C_t(x)$. A more exact expression for the above can be developed when one considers different propagation constants for the send and receive pairs. If we let γ_1 be the propagation constant for the send pair and γ_2 be the constant for the receive pair, then the above equation can be rewritten as follows:

$$\frac{dI}{I_0} = \left(\frac{Z_0 Y}{16} - \frac{Z}{4 Z_0} \right) e^{-\gamma_1 x} e^{-\gamma_2 (l-x)} dx$$

The final equation for the equal level Far-End crosstalk (ELFEXT), $E(f)$, is found by integrating the ratio dI/I_r in x, where I_r is the current on the disturbing pair at the receiving end of the cabled pairs, and being similar to the equation provided by the before-mentioned authors[4], is given by:

$$E(f) = i 2\pi f \int_0^l C_r(x) e^{-(\gamma_1 - \gamma_2)x} dx$$

The above equation is pivotal in modeling the ELFEXT between two arbitrary pairs in a cable. With appropriate assumptions made for the propagation constants, I let $C_t(x)$ be normally distributed in amplitude as a function of x, with zero mean, and with a variance to drive the resultant $E(f)$ toward some desired level as a function of frequency.

In order to model the ELFEXT of a channel, one must include the contributions of different cabling segments as well as connecting hardware in the channel. This is accomplished by using piece-wise integration; whereby, the contributions of previous segments are appropriately phased and attenuated as a function of x before being added to other expressions further along in the channel. A simple model for each connecting hardware contribution is developed and is provided for completeness, as follows:

$$E(f) = i 2\pi f C_c(x_0) e^{-\gamma_c dx} dx$$

where γ_c is the propagation constant for a connector, dx is the incremental length (set to the span of a single connector in a channel), and where $C_c(x_0)$ is the coupling function between pairs in the connecting hardware at some arbitrary distance, x_0, in the channel and over an incremental span dx.

BIOGRAPHIES

Christopher T. Di Minico: With Cable Design Technologies (CDT) Corporation, Director of Network Systems Technology. Member of IEEE, TIA TR41.8.1, and the US advisory group for international cabling standards development. B.S.E.E. at Northeastern University with over 30 years experience in the cabling industry both in design and installation.

Paul Kish: Graduate M.A.Sc Electrical Engineering from University of Waterloo (1972) with 25 years experience in the cabling industry. He has held positions as the Manager of the cabling design and cable

development laboratories at NORTEL. Currently, Senior Product Manager at NORDX/CDT responsible for the IBDN System and telecommunication standards. Chairman of the TIA Telecommunication Standard Subcommittee for User Premises Cabling.

AKNOWLEGEMENT

Dave Hawkins, Lucent Technologies, provided the ELFEXT simulation analysis in the development of the connector and cable ELFEXT contribution to the cabling as well as the simulation description in Annex C.

REFERENCES

[1] Transmission Systems for Communications (BELL LABS)

[2] THE BELL LABS SYSTEM TECHNICAL JOURNAL, MARCH 1963, page 476, APPENDIX B.

[3] THE BELL LABS SYSTEM TECHNICAL JOURNAL, MARCH 1963, page 476, APPENDIX B, EQUATION (35)

[4] THE BELL LABS SYSTEM TECHNICAL JOURNAL, MARCH 1963, page 476, APPENDIX B, EQUATION (36)

Power Sum, Integral Power Sum and Vector Sum - Crosstalk

M. Belanger, J.- F. Richard and J.- H. Walling

NORDX/CDT, Montreal, Canada

Abstract

We show that, by the use of power splitters, direct measurements of power sum crosstalk - we call it the integral power sum crosstalk - are feasible. Our proposed method allows the measurement of power sum NEXT and Input-to-Output FEXT with sufficient accuracy for quality control purposes.

It is not our intention to build multiple pair test sets. Hence our work has to be understood as a challenge to the test set manufacturing industry to develop some innovative solutions to speed up testing cycles. This is even more important with increasing demand for broadband cables.

Testing times can be shortened to a time of approximately 15 minutes for a 25 pair cable, as compared to approximately 3 ½ hours required on an HP Z-2010 for full testing. The HP Z-2010 has been choosen as being an excellent representation of the multiple pair test sets, currently commercially available. This incidentally requires working with the full potential of the computers used to control the network analyzer/S-parameter test-set, such that only the raw, uncalibrated S-parameters are transferred from the network analyzer/S-parameter test-set to the computer, where all calibration calculations are done.

Background

For multiple pair cables, i.e. 25 pair cables, the majority of current wire and cable standards specify the worst pair power sum crosstalk. This is also increasingly required for four pair cables.

Therefore testing cables for their power sum crosstalk performance is increasingly required. However, these measurements are time consuming, especially for multiple pair cables, since the number of pair combinations to be measured increases substantially.

To date the power sum NEXT requires the testing of 300 pair combinations for a 25 pair cable, whereas the power sum FEXT requires the measurement of total of 600 pair combinations. The time required for these measurements is in the order of 3 ½ hours, which is not acceptable from a manufacturing point of view.

Our objective is to indicate ways to substantially reduce testing times.

To achieve this we use power splitters to energize all disturbing pairs simultaneously, and we call the power sum crosstalk thus measured the integral power sum.

Such a measurement gives us a direct measure of the power sum, which has only to be measured as many times as the number of pairs in the cable.

In an automated test system the pair-to-pair crosstalk measurement can also be made without increasing the complexity of the switching. This is required in order to assess which pair combination or combinations may eventually lead to a failure of the power sum crosstalk.

For multiple pair cables we propose the use of active power splitters, in order to obtain sufficient power levels in the disturbing pairs. This will of course limit to some extent the possibilities for calibration of such a system but it would be more suitable for higher pair count cables. In this paper we will not explore the use of active power splitters.

Introduction

To simplify our work we limit the present reporting to 4 pair cables only which are fully tested. Our intent is only to evaluate the proposed method and therefore we can neglect that the time saving on four pair cables is negligible, because of the low pair count.

For our tests we use three different kinds of passive power splitters, i.e. :

- M/A-Com DS-4-4
- M/A-Com PD 25-0010-SMA
- Pulsar PS -04-452/4S

These power splitters have all four output ports in order to simulate the conditions prevailing in a 50-Ohm switch with twice as many baluns as pairs under test.

The baluns we use are from BH Electronics. We use these baluns because they have the same connectors as the power splitters. Additionally they simplify our task regarding the ease of connecting the pairs to the baluns.

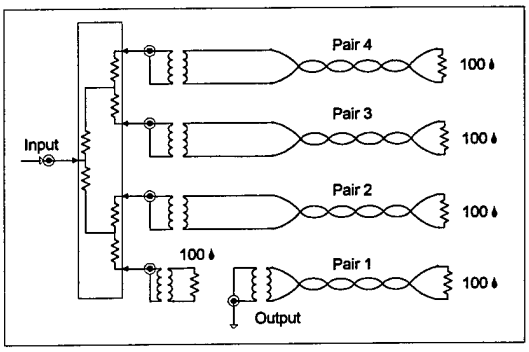

Fig. 1 : Set-up of Power splitter for measuring power sum NEXT for pair # 1

For the measurement of the integral power sum NEXT we use the set-up shown in Fig. 1, whereas for the integral power sum FEXT we use the set-up according to Fig. 2.

For termination of the baluns and the pairs we use resistors supplied by JC Electronics Corp, which are especially designed for testing.

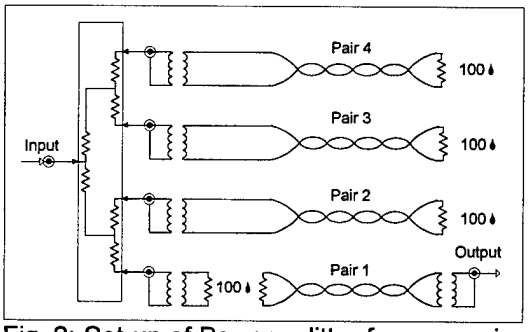

Fig. 2: Set-up of Power splitter for measuring power sum FEXT for pair # 1

Methodology and Calculations

Though we are losing some information concerning the S-parameters through the use of the power splitters, we can devise different ways to calibrate the set-up shown in the Fig. 1 and Fig. 2. We indicate these in the following.

- We can calibrate the network analyzer with the S-parameter test set just prior to the power splitter. The losses for each path must to be measured. Both losses, i.e. the loss of the pair position on which the integral power sum is being measured and the power sum loss for the remaining positions, where the disturbing pairs are being connected, must be subtracted from the result obtained.

- Alternatively we can terminate all the baluns of the disturbing pairs with a 100 Ohm termination, and calibrate on the path for the disturbed pair. In this case only the power sum of the remaining position needs to be subtracted from the result obtained.

We explored both alternatives, and compare the results obtained with the power sums calculated from pair-to-pair measurements, which are taken directly, using two baluns on the network analyzer/S-parameter test-set.

Additionally we measure the crosstalk for each pair combination on each path through the power splitter, and calculate also the power sum for each pair.

We generally measure between 3 and 350 MHz with linear frequency division of this interval. We use 1601 points per sweep.

Results

Fig. 3 shows the losses for the different positions on the power splitter, including the losses of the corresponding baluns. These losses are obtained by simple transmission measurements at the different positions, when the calibration has been done directly ahead of the balun connection plane. In this case the results obtained on one position have to be decreased by the loss indicated for this position, and the power sum loss of the remaining positions.

Fig. 4 indicates the losses for each position on the power splitter, when the calibration is done on one specific position of the power splitter. In the example given, this is done for the position #1 on a M/A-Com DS-4-4 power splitter. In this case the loss obtained for the calibration position

is virtually zero, whereas the losses of the other positions have to be measured and their power sum subtracted from the obtained integral power sum measurements.

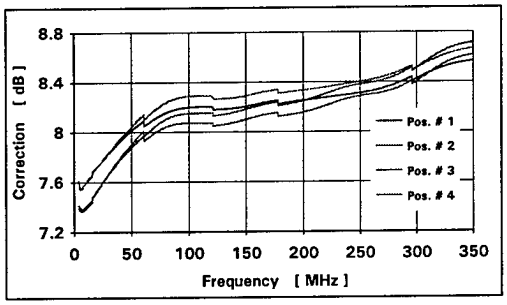

Fig. 3 : Calibration before power splitter. Loss for the different power splitter positions, including the balun loss, while remaining positions are terminated at the balun with 100 Ohm. Power splitter: M/A-Com DS-4-4

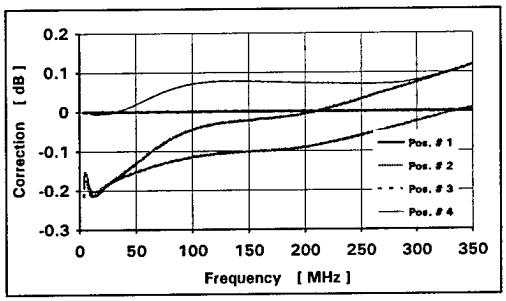

Fig. 4 : Calibration after power splitter. Loss for the different power splitter positions, when calibrated at position 1, while remaining positions are terminated with 100 Ohm. Power splitter: M/A-Com DS-4-4

In Fig. 5 we have the power sum NEXT measurement, obtained from pair-to-pair measurements compared to the integral power sum NEXT measurement, when the calibration is done before the power splitter. In this case the power splitter is also a M/A-Com DS-4-4 power splitter.

Fig. 6 to Fig. 9 indicate the results of the power sum and integral power sum NEXT and FEXT for two pairs, respectively. For these pairs the pair-to-pair crosstalk is measured and also their integral power sum crosstalks when calibrated before and after the power splitter.

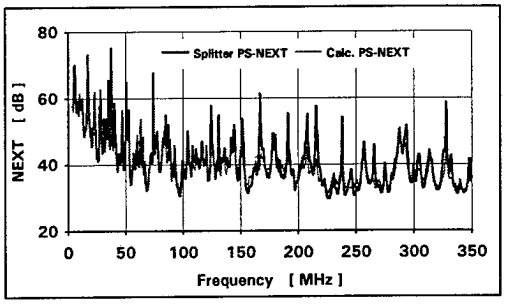

Fig. 5 : Direct measured power sum NEXT compared to the calculated power sum NEXT resulting from individual measurements. Calibration before power splitter

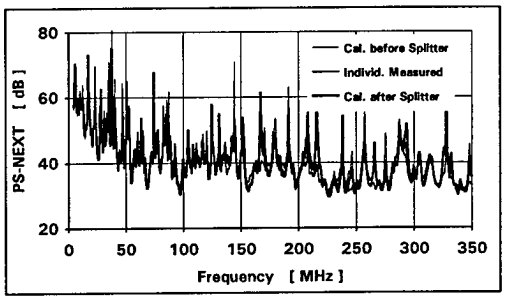

Fig. 6 : Comparison of the integral power sum NEXT of a pair, when calibrated before and after the splitter to the power sum NEXT calculated from individual pair-to pair measurements

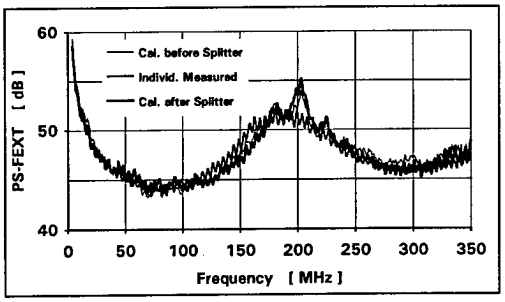

Fig. 7 : Comparison of the integral power sum NEXT of the same pair as in Fig. 6, when calibrated before and after the splitter to the power sum FEXT calculated from individual pair-to pair measurements

Fig. 10 and Fig. 11 show the integral power sum NEXT and FEXT curves

of one pair compared to the vector sum calculated from the individual pair-to-pair measurements. So far, all reported measurements are made using a M/A-Com DS-4-4 power splitter. But all the measurements are made as well with the two other power splitters, mentioned earlier.

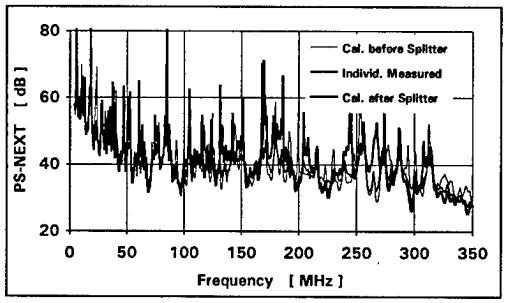

Fig. 8 : Comparison of the integral power sum NEXT, when calibrated before and after the splitter to the power sum NEXT calculated from pair-to pair measurements

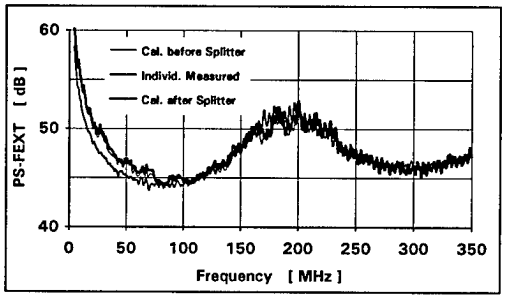

Fig. 9 : Comparison of the integral power sum NEXT of the same pair as in Fig. 8, when calibrated before and after the splitter to the power sum FEXT calculated from individual pair-to pair measurements

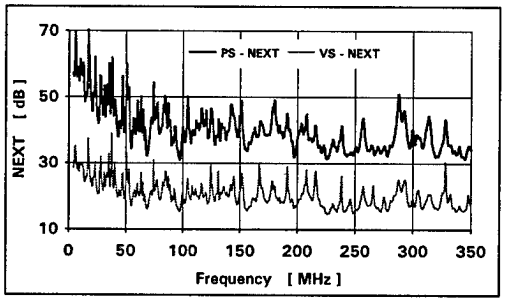

Fig. 10 : Integral power sum NEXT compared to the vector sum NEXT based upon pair-to-pair NEXT

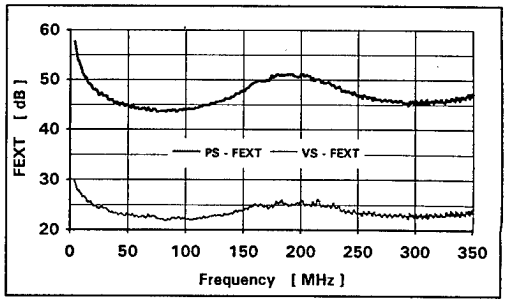

Fig. 11 : Integral power sum FEXT compared to the vector sum FEXT based upon pair-to-pair FEXT

In Fig. 12 and Fig. 13 we have the integral power sum NEXT and FEXT for the same pair, when using the same baluns, but different power splitters.

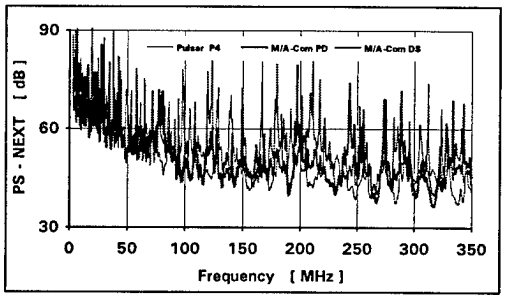

Fig. 12 : Comparison of the integral power sum NEXT of one pair, when measured using different power splitters

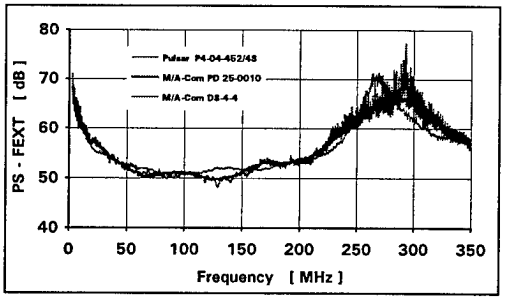

Fig. 13 : Comparison of the integral power sum FEXT of one pair, when measured using different power splitters

Discussion of Results

Fig. 3 and Fig. 4 clearly indicate that it is feasible to attain reasonably

small deviations of the losses for each path. In fact, it seems to be realistic to strive for well balanced power splitters, eventually in conjunction with one preamplifier, yielding errors of less than 0.1 dB of the integral power sum crosstalk. As an alternative to passive power splitters used in combination with one preamplifier, it is also possible to use an amplifier directly for each path. In this case these amplifiers should be well balanced with respect to their power output and phase.

We prefer to use a calibration before the power splitters to maintain the integrity of the S-parameters. Power sum NEXT measurements of one pair using such a calibration in comparison to the traditional power sum NEXT, resulting from individual pair-to-pair measurements, is shown in Fig. 5. It shows that it is feasible to obtain results with a sufficient degree of accuracy.

Fig. 6 to Fig. 9 show the integral power sum NEXT and FEXT, respectively, with calibration before and after the power splitter, in comparison to the power sum NEXT and FEXT, resulting from individual pair-to-pair measurements, for two pairs, respectively.

The results indicate that the integral power sum NEXT measurements yield acceptable results with both calibration methods. The deviations observed for the FEXT measurements are in the order of approximately 1 dB, if we omit the spikes observed in Fig. 7. Though this can be considered acceptable, some work may be necessary to improve the FEXT measurements. The deviations seem to be due to minor phase offsets in the power splitters, and eventually to some reflections.

In order to obtain an idea of the accuracy which we may expect using the proposed method, we calculate the vector sum of the measured pair-to-pair crosstalk values. The results are shown in Fig. 10 and Fig. 11. We compare the vector sum NEXT and FEXT to the integral power sum NEXT and FEXT values, respectively, obtained with a calibration after the power splitter. The ratio of integral power sum to vector sum ought to be two for equal phase and varying magnitudes. Hence, the deviation from this value gives a measure of the obtained accuracy.

Table 1 shows a compilation of the deviations, in percent, of all the measured points. Though we can use a scatter plot to assess the accuracy, we preferred here to take the average of all 1601 points measured for each case, and used this average for comparison purposes.

Ratio of Powersum to Vectorsum						
	Calculated		Measured		Deviation [%]	
	NEXT	FEXT	NEXT	FEXT	NEXT	FEXT
Pair 1	1.94	1.94	1.97	1.93	1.47	0.16
Pair 2	1.96	1.99	1.98	2.00	0.76	0.85
Pair 3	1.97	1.98	1.95	1.99	1.03	0.15
Pair 4	1.98	2.00	1.97	1.98	0.46	1.11

Table 1

We see that the accuracy is in the order of approximately 1.5 %. These

values have been confirmed also using the loss curves used in the calibration itself.

Nevertheless, we should strive for a better balanced power splitters in respect to equal power output while maintaining an equal phase.

Summary and Conclusion

We demonstrate that is feasible to measure the power sum crosstalk of a single pair in a multiple pair cable in only one measurement. This method requires the use of power splitters to inject the disturbing signal into all the adjacent pairs simultaneously. As all the disturbing signals have to be in phase the power splitters must be well balanced.

The main advantage of such a method is to reduce the total number of measurements, and with it the testing time. Thus for instance the power sum NEXT and FEXT measurement of a 25 pair cable requires 900 individual pair-to-pair measurements, and requires lengthy calculations to obtain the final results.

In our proposed method, this would be replaced by simply measuring 25 integral power sum values each for NEXT and FEXT respectively.

The total testing time will be considerably reduced using a power splitters in addition to a 50 Ohm switch, to energize all disturbing pairs at the same time, and measure the combined effect on the disturbed pair (integral power sum). The switching should be done prior to the baluns, though it might be also feasible to devise power splitting on the 100 Ohm side. This may also require amplifiers after the balun to obtain sufficient power levels, though the calibration may become difficult.

The testing time increases with the present method very rapidly, i.e. proportional to the square of the paircount. The testing time for our proposed method increases only linearly with the pair count of the cables. It is estimated that the testing time of a 25 pair cable for NEXT alone can be reduced from the current 3 ½ hours to less than 15 minutes.

It is evident, that more work has to be done in this direction, mainly to boost the accuracy, and to expand the method proposed here to more than four pairs.

Such an effort is well justifiable, as the time savings for the wire and cable industry are very appreciable.

Authors

Martin Bélanger received his B.E. in Electrical Engineering in 1992 from University of Sherbrooke. He joined the Technology Cable Group of Northern Telecom Canada Limited, now Nordx/CDT, in 1992. He was initially responsible for cable design and electrical test methods. Then his responsibilities shifted to the manufacturing aspects of data grade cables, quality assurance and new manufacturing test facilities. He is at present working in the IBDN Systems and Applications Group.

Jean-François Richard received his bachelor's degree in Electrical Engineering from the Ecole Polytechnique in Montreal in 1991.

From 1991 to 1995 he worked both at the "Ecole Technologique Superieure" and at the Ecole Polytechnique as a Research and Teaching Assistant. In 1995 he joined Nordx/CDT in the Engineering Department, and works since on a continuous quality improvement program.

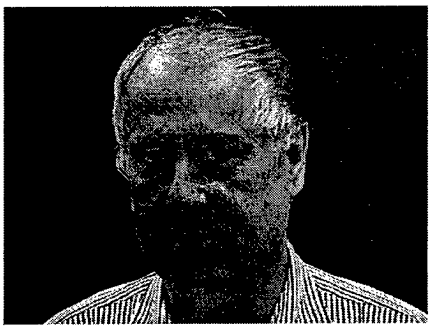

Jörg-Hein (Jo) Walling received his diploma in Mechanical Engineering in 1966 at the Technical University of Berlin. In 1974 he obtained a Doctor's degree (Dr.-Ing.) at the same University. In 1974 he joined Northern Telecom in the Research and Development department. Since 1976 he has been senior engineer at the Nortel, now Nordx/CDT, Lachine Cable Plant, responsible for the design of Outside Plant and Data Grade Wires and Cables.

HIGH GRADE COPPER DATA CABLES AND CONNECTING HARDWARE FOR GENERIC CABLING

Helmut G. Haag, Paul E. Gregor, Mike Voigt, Dietmar Seidel

Alcatel Kabel AG & Co, Mönchengladbach, Berlin, Germany

ABSTRACT

More than ever a remarkable tendency towards broadband transmission resp. higher data rates on copper cables for the international defined tertiary level for LAN technologies is going on seriously.

Cable networks for transmission of voice, data, text, image and video grow together in practice, on national level worldwide and within international standardisation bodies, for instance regarding "Small Office Home Office" (SOHO) and "Command Control and Communications for Buildings" (CCCB)-Technologies, i.e. installation of generic cabling for all applications.

This contribution summerises the necessary design considerations particular for high grade cables and connecting hardware enabling real generic cabling according to the scope of IS 11801.

Additionally components have been connected together to built up a channel configuration in order to examine the relevant channel characteristics.

Finally various applications have been adopted to the cabling in order to obtain evidence that simultaneous operation over one cable is possible without serious electrical interference.

As an overall result evidence has been achieved that cable sharing as defined within ISO/IEC 11801 is possible generally, however certain transmission qualities for channel components are necessary to be installed employing adequate workmanship for erecting the cabling.

INTRODUCTION

According to the scope of IS 11801 generic cabling shall be able to carry different services including voice, data, text, image and video via a cable simultaneously.

Therefore components needed to built up the cabling, like cables and connecting hardware have to meet a sufficient electrical quality up to a frequency of about

1000 MHz in order to be prepared for the coming future applications considering the already made proposals on international level for a second edition of IS 11801.

Since the life expectancy of the cabling shall be more than ten years design of components have to fulfil logically the increasing demands of transmission technologies as a matter of required high economy. Additionally high stability of electrical characteristics of cables after installation procedure have to be obtained.

More than ever a considerable compromise between acceptable economy and future oriented design and production philosophy for components is necessary.

Among several construction criteria for cabling components particular importance should be placed upon:

- High transmission quality up to a frequency of 1 GHz (achieveable upon the state of technique)
- Possibility regarding cable sharing using all relevant transmission applications
- EMC, ability for usage in severe environmental conditions

▼ Detection safety

▼ Conformance respecting fire rating on international base

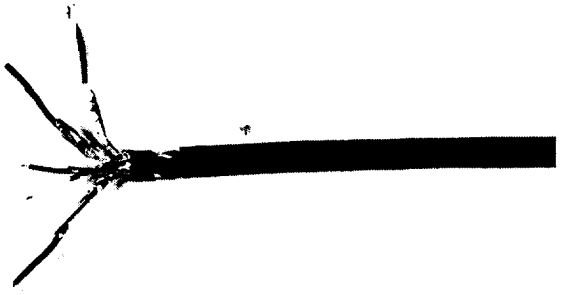

Fig. 1: 4-pair cable sample with individual shielded pairs

DESIGN CRITERIA FOR COPPER DATA CABLES

Generally cable design intended for use as generic cabling at present has to approach a compromise between high grade electrical and mechanical performance on the one hand and favourable economy on the other hand.

Solid copper conductors are insulated with special polyethylene foam skin compound in order to get low mutual capacitance values resp. low attenuation level. Relating the desired homogenity of transmission circuits basically high accuracy of copper conductor concentricy within insulation, cylindricity of core and pureness of dielectric material are most important to be met.

Such technology can be achieved by employment of modern extrusion lines working computer controlled full automatically. Individual shielded pairs with relatively short pitch lengths present electrical stable stranding elements which can be manufactured most economical.

Normally four pair design constitute the cable core, each pair individually shielded with a longitudinal aluminium tape to avoid crosstalk between transmission circuits. The cable core is eventually covered by an overall tinned copper braiding considering the specified transfer impedance.
For jacket material special plastic compound (LSZH) is extruded in order to meet the requirements of IEC 332 regarding flammibility, fume and toxic gases release in case of fire.

Cable design in general shall be a compromise between high grade transmission characteristics and minimized cable dimensiones.

The following table 1 exhibits the most important production, design data and the reasons to apply:

cable design criteria	technical reason
foam skin PE-insulation	lower attenuation/high phase velocity
relativ short lay lenght of pairs	• high crosstalk attenuation • immunity against electrical interference • stability of transmission characteristics after laying procedure • low delay skew values
individual shielding of pairs	• remarkable improvement of crosstalk attenuation/ACR • improvement regarding cable sharing • no/reduced electrical influence respecting different environment conditions • improvements with respect to EMC
copper braiding	• lower transfer impedance • robust cable design • stability of transmission parameters • EMC • firm mountability
plastic jacket	• LSZH, low smoke emission, zero halogen

Table 1: Production and design data for cables

ELECTRICAL CHARACTERISTICS OF DATA CABLES

DC and VF-properties

The tests have been performed on regular delivery lengths of 1000m within a temperature range of 18 deg.C and 22 deg.C. Measurements are normally carried out by using automatic testing equipment with the exeptions regarding insulation resistance and dielectric strength.

characteristic at 20°C	requirement acc. to ISO/IEC 11801	test result	IEC test method
DC loop resistance of conductor [Ω/km]	≤ 192	144	189-1
DC insulation resistance 100 V, 60 sec. [GΩ x km]	≥ 150	≥ 5000	189-1
DC resistance unbalance [%]	≤ 3	0.2	ffs
mutual capacitance at 800 Hz [nF/km]	not specified	45	189-1
capacitance unbalance pair to ground at 800 Hz [pF/km]	≤ 3400	720	189-1
dielectric strength cond./cond. cond./shield	1 kV; 1 min. DC or 2.5 kV; 2 sec. DC or 700 V; 1 min. AC or 1.7 kV; 2 sec. AC	passed	189-1

Table 2: DC and VF characteristics of data cables

High frequency characteristics of data cables
Measurements have been executed generally by using IEC test methods as far as available at present.

Attenuation. The following attenuation values for a 100m cable length have been taken for a frequency range between 1 MHz and 1000 MHz employing a network analyser, type HP 4396 A, operating automatically.

Figure 2 shows in graphic configuration typical obtained values for attenuation in comparison to the values proposed internationally within ISO/IEC resp. German draft specification DIN E 44312-5.

In order to detect undesired attenuation peaks sufficiently about 1200 frequency points have been tested. The achieved attenuation curve follows as expected approximately the square root law.

Due to the selected low copper conductor diameter and specific shielding performance obtained attenuation level meets the proposed limits without a huge safety margin but together with an economical lower cable diameter.

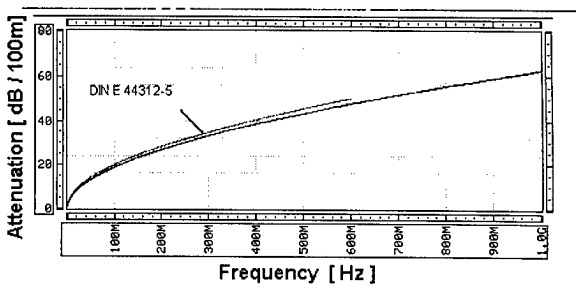

Fig. 2: Obtained attenuation values of data cables

Near End Crosstalk attenuation. The measurements have been executed within a frequency range of 1 MHz up to 1000 MHz on cable lengths of 100m from both ends. In fact of the frequency dependence a sufficient high number of tests (>1200) within the examined frequency range have been used. All possible circuit combinations have been tested. Pairs not under test have been terminated with the nominal characteristic impedance All possible circuit combinations have been performed.

Figure 3 exhibits the achieved NEXT level compared to proposals on ISO/IEC-level resp. German Draft specification DIN E 44312-5.

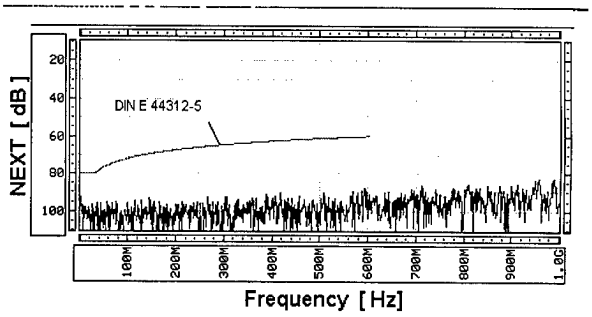

Fig. 3: Near End Crosstalk Attenuation of data cables

Due to the special individual shielding of pairs high NEXT-values can be realized in order to guarantee future applications with increased requirements. This comparison shows more than 20 dB NEXT worst case at 600 MHz above limits under discussion.

In fact of this particular high NEXT-level achieved by a special shielding design no Far End Crosstalk measurements (ELFEXT) have been carried out with respect to the capability of testing equipment.

Attenuation to Crosstalk Ratio (ACR). ACR values as a result of calculations on NEXT and attenuation figures (figures 2 and 3) show very clearly the ability of such a cable construction to be used for generic cabling with sufficient safety limits.
In figure 4 a comparison of obtained results to values of and ISO/IEC proposals resp. DIN E 44312-5 show the outstanding quality of the here examined cable lay out.

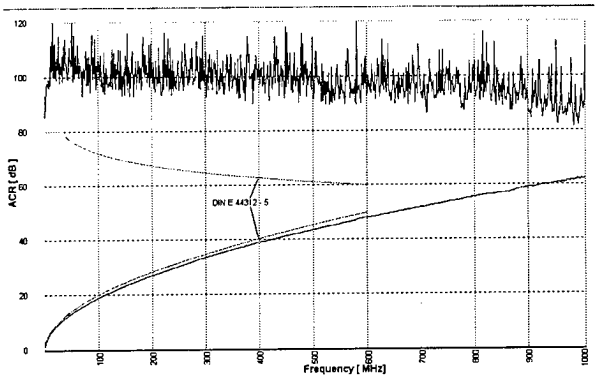

Fig. 4: Attenuation to Crosstalk Ratio of data cables

Characteristic impedance. Measurements between 1 MHz and 1000 MHz using the open/short circuit method have been performed. Figure 5 shows typical test values together with the limits under discussion internationally and German Draft specification DIN E 44312-5. The achieved results are within the specified tolerance of 100 ± 15 Ω.

The recorded curves present the typical homogenous character for individual shielded pairs in contrary to unshielded stranding elements.

The slight increase of curve at higher frequencies are caused by the termination procedure resp. unshielded part of test pair.

As stipulated internationally no return loss measurements shall be performed for cables since the criteria characteristic impedance including tolerances describe the necessary homogenity of the circuit sufficiently. In case of any dispute calculations into return loss values are to be done.

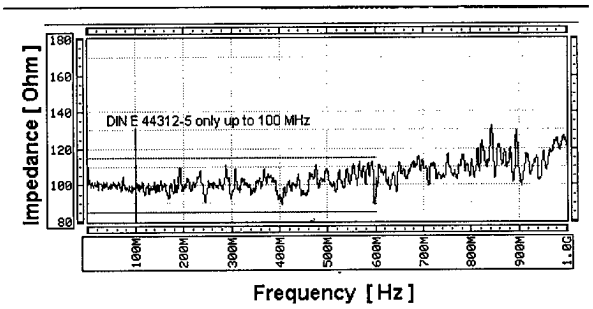

Fig. 5: Characteristic impedance of data cables

Phase velocity of propagation. The velocity of propagation has been calculated based upon the open/short circuit test method between 1 MHz and 600 MHz. As shown in figure 6 the quotient "V(Ph)/Co" approaches asymtotical towards an almost constant factor of approximately. "0,77" corresponding to a velocity of 231.000 km/sec.

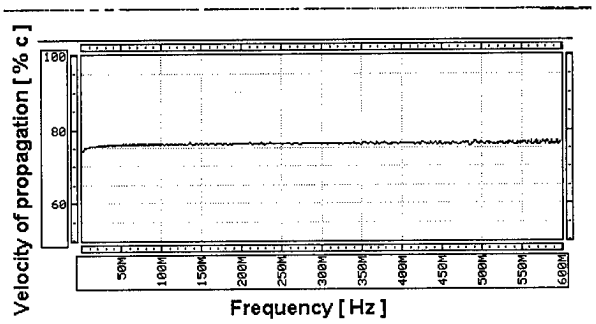

Fig. 6: Phase velocity of propagation of data cables

Delay skew. For the examined 4-pair cable construction delay skew has been found below 5 nsec/100m. It expresses the well selected lay length configuration of this cable technology. Within prEN 50288-5-1:1998 a maximum value of 40 ns/100m at 100 MHz has been listed up.

Longitudinal conversion loss (LCL). The tests have been performed upon the IEC procedure for shielded cables within a frequency range of 1 MHz to 100 MHz.
The results are drawn graphically in figure 7 which exhibits clearly the desired homogenity of this

generic cable design. Compared to the proposed values to be specified the recorded results meet fully these requirements for a frequency range up to 100 MHz.

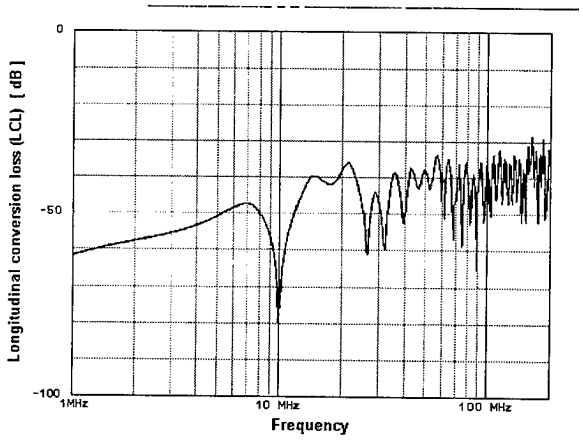

Fig. 7: Longitudinal Conversion Loss for data cables

Screening attenuation. In figure 8 screening attenuation has been drawn for a frequency range between 30 kHz and 1000 MHz using symmetrical powering on a 1m cable sample. This curve shows a comparison to requirements of prEN 50288-5-1.

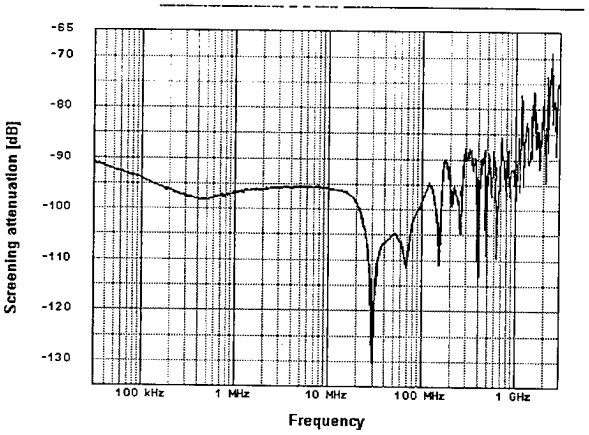

Fig. 8: Screening attenuation of data cables

Coupling attenuation. In order to describe the capability for such a shielded cable design totally the so called screening attenuation has to be added to the longitudinal conversion loss from the physical point of view in order to achieve as a final expression the coupling attenuation.

The sum of both criteria leads to a remarkable coupling attenuation level above 135 dB for the relevant frequency range. Figure 9 presents a comparison of the calculated coupling attenuation on the one hand and the relevant provisions within prEN 50288-5-1:1998.

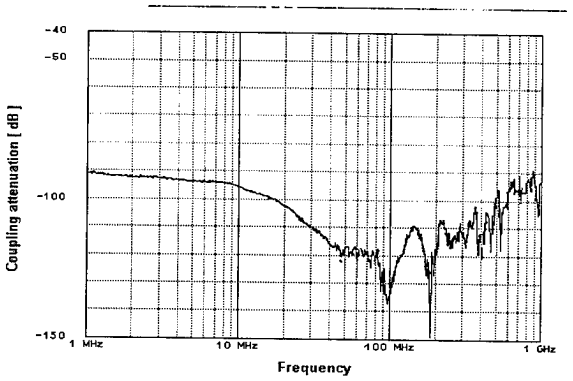

Fig. 9: Coupling attenuation of data cables

Transfer impedance. Based upon the IEC test procedure transfer impedance has been measured up to a frequency of 10 MHz with respect to the test equipment dimensions. The results are recorded in figure 10 in comparison to ISO/IEC 11801 limits.

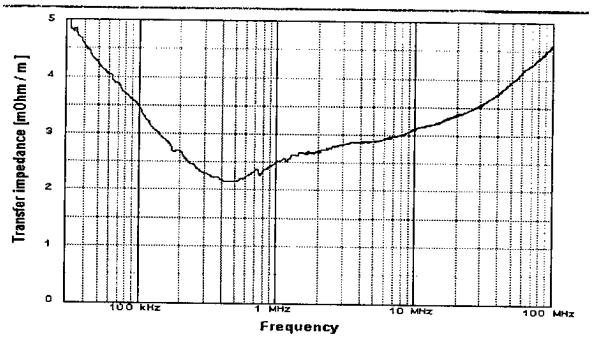

Fig. 10: Transfer impedance of data cables

DESIGN PARAMETERS FOR CONNECTING HARDWARE

Since the planned system applications consider a frequency range at least up to 600 MHz all the components within the transmission path have to present a certain high electrical quality. The poorest component dictate the overall per-

formance of the total channel obviously. The connecting hardware has to meet this defined quality, too. Typical crosstalk attenuation values are more than 70 dB at 600 MHz.

TRANSMISSION CHARACTERISTICS OF CHANNEL CONFIGURATION

Even if highest qualities for link components have been used it is of fundamental importance to install the products necessary for a transmission channel with great accuracy and workmanlike.

Upon the completed channel configuration (figure 11) relevant tests have been executed to collect evidence of a sufficient high quality enabling fully generic cabling.

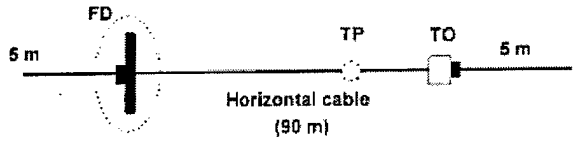

Fig. 11: Channel Configuration for Interconnect-Environment

Attenuation of channel

Figure 12 presents a comparison between the collected results of the channel under test up to a frequency of 1000 MHz and the proposed future requirements of ISO/IEC resp. German Draft specification DIN E 44312-5 The obtained attenuation level meets with a safe distance the limits under discussion.

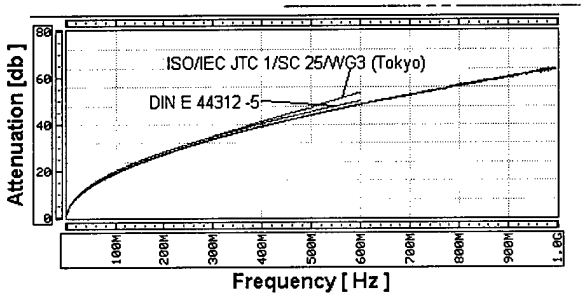

Fig. 12: Attenuation of channel configuration

Near End Crosstalk Attenuation of channel

NEXT measurements have been carried out up to a frequency of 1000 MHz from both ends of the channel. The achieved NEXT-level have been found remarkable above the specified values as an confirmation of the well prepared make up of cables and connecting hardware.

As mentioned under tests for cables a sufficient high number of frequency points have to be taken in order to detect undesired peaks for the whole observed range.

Figure 13 shows the collected values in comparison to the international proposed NEXT requirements.

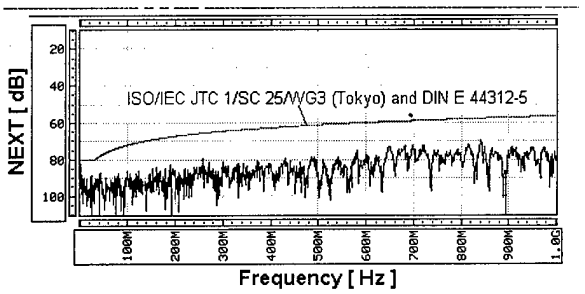

Fig. 13: Near End Crosstalk Attenuation for a channel

Attenuation to Crosstalk Ratio of channel

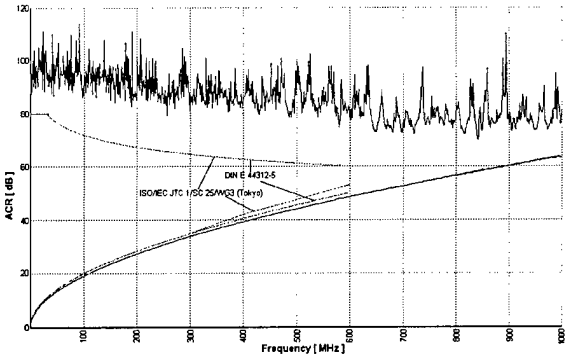

Fig. 14: Attenuation to Crosstalk Ratio of channel

Figure 14 exhibits the calculated ACR-values up to a frequency of 1000 MHz in comparison to the ISO/IEC-proposals resp. the German Draft Standard DIN E 44312-5. The obtained ACR-level presents even at 1000 MHz a positiv value > 4 dB.

Return Loss of channel

On the international level it has been decided that the return loss property should give indication about the homogenity of the transmission channel. The characteristic impedance will be guaranteed only by design of components.

In figure 15 return loss values are drawn up to a frequency of 1000 MHz. Compared to the proposals on international scale this channel configuration delivers a sufficient safe distance.

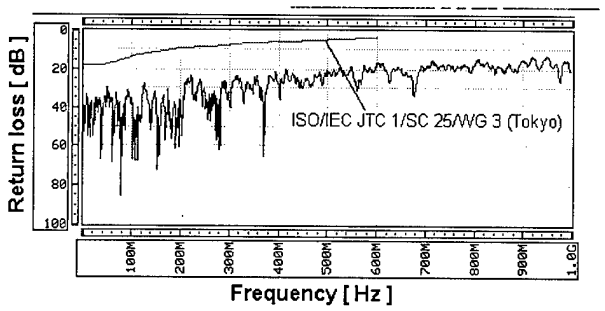

Fig. 15: Return Loss of channel

OPERATION WITH DIFFERENT TRANSMISSION APPLICATIONS

The presented high performance cabling has been taken under practical operation to obtain evidence for possible cabling sharing capability.

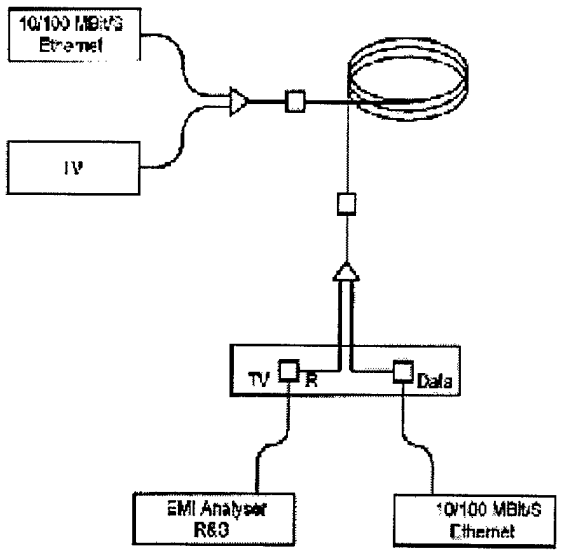

Fig. 16: Transmission configuration in principle

In figure 16 the transmission configuration indicating the various applications are drawn in principle. The 4-pair cable uses one pair for TV distribution, two pairs for data communication and the remaining pair could be adopted to *a suitable* telephone circuit.

Results of transmission tests with generic cabling

Tests have been concentrated on parallel operation of TV signals and data services. Regarding the TV signals a frequency range between 5 and 862 MHz has been taken into account. For the data transmission systems with 10 Mbit/s and 100 Mbit/s have been adopted.

Within the test configuration 70m and 90m data cable lengths plus 5m flexible cords at both sides including balun for the TV application have been connected together

As a first result of tests it has been confirmed that TV transmission is possible via distances up to 90 m using balanced cables and TV-equipment available on market. Received TV-signals have been registered without any quality degredation.

A corresponding calculation is given in following table 3 as a confirmation of the practical transmission results.

link component	budget for link component	
	450 MHz	600 MHz
CATV amplifier output	110 dBµV	110 dBµV
signal splitter	0 dB	0 dB
patch cord incl. balun	2.5 dB	3 dB
category 7 cable	39 dB	43 dB
wall outlet incl. balun	2.5 dB	3.0 dB
CATV outlet level	66 dBµV	61 dBµV

Table 3: Calculation of link budget for TV-transmission

Within a second test cycle the electromagnetic interferences between simultaneous operating transmission circuits have been examined. Figure 17 and 18 show as examples diagramms of

detected electrical interactions of the TV-pair caused by the parallel working 10 Mbit/s (100 Mbit/s) system for a frequency range of 5 to 105 MHz (45 to 200MHz). The small peaks shown have no significant influence on to the TV picture quality.

In order to minimize electrical interference of this particular data system on the TV path the output power level of the TV transmitter could be increased accordingly.

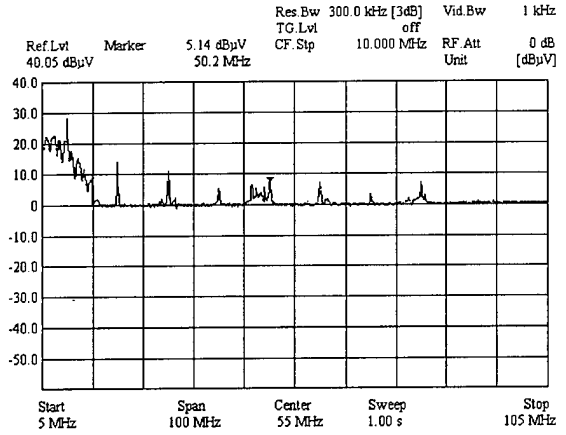

Fig. 17: Voltage level of a TV channel transfered by a 10 Mbit/s Ethernet data transmission circuit

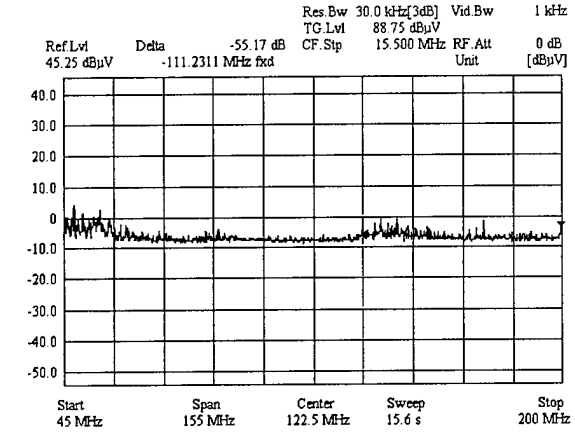

Fig. 18: Voltage level of a TV transmission circuit caused by parallel operating 100 Mbit/s data system

In figure 18 such a TV transmission link with a parallel operating 100 Mbit/s fast ethernet data channel is shown regarding the frequency range 5 to 200 Mhz. The transfered level is low enough for an interference free TV operation. For higher frequencies no negativ electrical influences have been observed.

CONCLUSION

Operation of multiple applications working simultaneously within a 4-pair cable consisting of high grade category 7 components has been brought evidence that generic cabling respectively cable sharing is possible.

Depending from the link attenuation primarily caused by cables adequate amplifiers and equalizers which compensate typical cable attenuation are necessary for further improvement of TV-transmission basically using known technologies.

Since individual shielded pairs constitute modular stranding elements increase of pair count for future application purposes is easy to be realized.

Generic cabling systems, including SOHO and CCCB intelligent home applications, at present under discussion internationally can be realized by using the described cabling technology in order to achieve an acceptable economy.

REFERENCES

1. ISO/IEC IS 11801 Generic Cabling for Customer Premises

2. Gregor, Tholen, Knop 'Data cables and system components for the use up to 100(300)MHz', International Wire and Cable Symposium Proceedings 1994

3. DIN E 44312-5, August 1996, Anwendungsneutrale Verkabelungssysteme ("600 MHz"), Beuth Verlag Berlin

4. Richter, Lehan 'Copper Cables for Local Area Networks with Very High Bit Rate Data Transmission', International Wire and Cable Symposium Proceedings 1993

AUTHORS

Helmut G. Haag
Alcatel Kabel
Bonnenbroicher Str. 2-14
41238 Mönchengladbach
GERMANY

Helmut G. Haag was born in 1948. He is Managing Director of Telecommunication in ALCATEL KABEL, Germany and member of the board of KABELRHEYDT, Germany. After reaching his Dipl.-Physiker from Stuttgart University he joined KABEL RHEYDT (which was taken over by ALCATEL in 1992) in 1975. There he had different positions in Development, Production, Marketing and Sales. He took his present position in 1997 resp. July 1998. Since long he is member of national and international standardisation bodies UIT, IEC, CENELEC and DKE.

Paul E. Gregor
Alcatel Kabel
Bonnenbroicher Str. 2-14
41238 Mönchengladbach
GERMANY

Paul E. Gregor was born in 1941. After study at Ingenieurschule Duisburg, Germany, he joined AEG KABEL, today ALCATEL KABEL Mönchengladbach where he had been involved in development projects for special symmetrical and coaxial telecommunications cables. About for a decade he took over the responsibility as head of design department for cable design technology. At present he is responsible for the technical sales department and is acting as a member in national and international standardisation bodies, like DKE resp. ISO/IEC.

Dietmar Seidel
Alcatel Data Cable
Sonnenallee 228
12057 Berlin
GERMANY

Dietmar Seidel was born in 1949, Profession Electrical Mechanic, finished his studies as an Electrical Engineer 1974 in Berlin, Germany. Since January 1991 he is with ALCATEL Data Cables, Berlin. Before ALCATEL he spent time with two other big companies, also in the high frequency field. At present he is responsible for Quality Control department.

Mike Voigt
Alcatel Data Cable
Sonnenallee 228
12057 Berlin
GERMANY

Mike Voigt was born in April 1967, Profession Electrical Mechanic, finished his studies as an Electrical Engineer 1993 in Berlin, Germany. Since January 1994 he is with ALCATEL Data Cables, Berlin. At present he is responsible as a Product Manager for shielded products within the company.

EFFECTS OF PRODUCTION-SPECIFIC INTERFERENCE SIGNALS ON TRANSMISSION CHARACTERISTICS OF 600 MHZ DATA CABLES

Andreas Obst – Jörg Bör

GHMT mbH, Bexbach, Germany – Kerpenwerk GmbH & Co., Stolberg, Germany

ABSTRACT

The manufacturing process of high-quality Category 6 and Category 7 cables is, among others, determined by two cost originators that are closely related, i. e. the rate of defects occurring both during the extrusion or stranding of wires and the application of foils which requires an above-average amount of work for assuring the quality by means of measurements.

This lecture presents the sources of defects which occur in the course of the manufacturing process and provides information on concepts allowing to minimize these defects. The correlation between the constructive cable features and the resulting electrical transmission characteristics is in the foreground of the discussion.

NECESSITY OF HIGH-PERFORMANCE DATA CABLES

In parallel with the rapid development of signal processors and with respect to operational and memory-specific performance features, the information technology sector as well experienced a similar growth in the past few years. Notwithstanding the ever increasing interconnection of global IT networks, the data transfer rate also rose exponentially in the end-user area, i.e. in local area networks.

Figure 1: Chronological development of data transmission

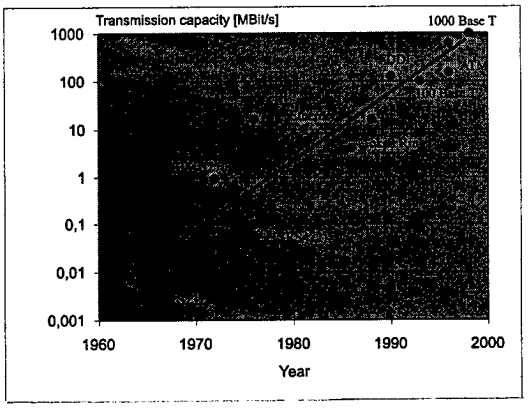

This trend that is represented in the above figure will also be continued in the next few years.

In order to realize transmissions with a high degree of information packing density, so far two solution approaches have been examined for the tertiary transmission channel.

1. Approach: Data Compression

Standardized, unshielded Class D copper cables are currently dominating on a worldwide basis. The 100 MHz bandwidth of these cables will only be suitable for future information packing densities, if the active side uses data compression procedures. For that purpose, however, the used Category 5 copper cables must provide a high system reserve at lower bandwidth.

Within the framework of this approach, solutions are being discussed which will split the transmission channel as has been planned e.g. for transmissions via Gigabit Ethernet. However, in case of four-pair data cables, such solutions would, on principle, mean the loss of the universal multi-service capability.

The international introduction of the two new cabling section classes E and F will point the way to the future. With the probable bandwidths of 200 MHz and 600 MHz respectively, these classes will guarantee secure data transmissions even for future applications. Since the 25th session of the ISO/IEC held in Tokyo in May 1998, this extension of the bandwidth has gained international acceptance.

Figure 2: Cabling classes
in accordance with the draft of ISO/IEC 11801

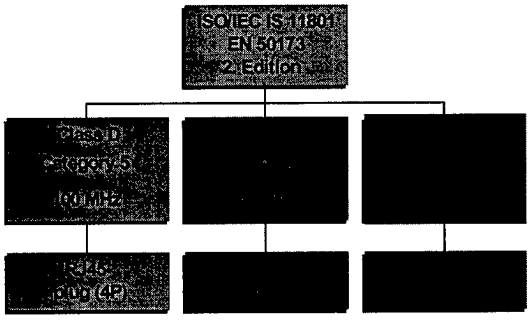

2. Approach: Extension of Bandwidths

Several European manufacturers of data cables have already propagated this concept that is of growing importance – and, meanwhile, has been taken into account by international standards – for four years because of strategic reasons and to give security for further applications. Already in 1996, the German draft standard E-DIN 44312-5 provided preliminary limits (by way of information) up to 600 MHz for cables, plug-and-socket connectors as well as cabling sections, which led to a restructuring of cabling throughout Germany. To date, more than 100,000 kilometers of 600 MHz data cables have been installed in Germany alone.

Table 1: Sales figures of LAN data cables in Germany

Length in km	1996	1997	1998	Total
Symmetrical copper cables	344	401	447	1,192
S/STP cables	92	130	154	376
600 MHz S/STP cables	9	40	72	121

The decision in favor of 600 MHz cables ensures, in particular, a high degree of protection for the relevant investments. Considering that installed data cables have an average service life of approximately 15 years, Figure 1 clearly shows that especially manufacturers of data cables have to offer high-performance products already now. At the moment, the vision of transmitting future network protocols only via optical media has somewhat been put into the background.

Another enormous market potential, i.e. the cabling of households and domestic users, can be realized as soon as cable television is incorporated in the concept of a multi-service-capable, structured cabling. For that purpose, data cables will be available before long which distinctly exceed a minimum ACR of 10 dB at a cable length of 100 m and a bandwidth of more than 1 GHz. At the beginning of this year, GHMT already certified this high-performance for prototypes which today reached production stage.

DEVELOPMENT OF COSTS FOR HIGH-PERFORMANCE DATA CABLES

The high market acceptance which S/STP cables have gained in Germany is not only reflected in the volume of manufactured cables but can also be recognized by the development of prices for the top-of-the-range product.

In spite of the current saturation stage, the crumbling of prices for 600 MHz installation cables will continue also in 1999 because market analyses forecast a increasing demand of large volumes within the construction industry.

Figure 3: Crumbling of prices in case of 600 MHz cables (Basis: 50 km; 1 US$ = 1.80 DM)

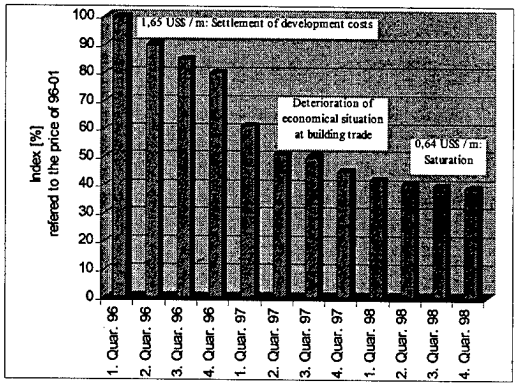

The technical advantages of wide-band cabling are, however, realized by sophisticated and thus costly design and production measures. Cable manufacturers can only counter this upward spiral of prices by optimizing the production of cables with respect to material and manufacturing costs. The minimization of rejects by means of an analytical detection of faults within the course of the manufacturing process is an additional point of departure regarding cost reductions. Only when production quality is ensured in all manufacturing phases through well thought-out and reproducible criteria will it be possible to reduce the extent of measurements and hence provide an economic cost framework for both 200 MHz and 600 MHz cables.

A comparison of the current cable prices shows that European S/STP cables can certainly hold their own with American UTP cable if the respective benefits of these cables are compared. The weighting of these benefits should be oriented towards the primary purpose of the product.

Table 2: Comparison of costs of S/STP and UTP data cables (status: October 1998; basis: 50 km; 1 US$ = 1.80 DM)

	S/STP data cables	UTP data cables (Plenum)
Benefits:	• Very high bandwidth on all four pairs with an excellent system reserve. • Optimal EMC characteristics regarding immunity to interference. • Good environmental compatibility and good resistance to fire due to the utilization of flame-retardant and non-corrosive materials.	• Easy installation because of small cable diameters and simplified laying procedure. • Very good characteristics with respect to resistance to fire due to the utilization of Teflon.
Price:	640 US$ per km (of cable).	580 US$ pro km (of cable).

FAULTS IN TRANSMISSION CHARACTERISTICS OF DATA CABLES

In spite of the enormous cost pressure, the transmission characteristics of high-quality 600 MHz data cables must be kept at a high level. In this connection, cable faults may occur both in the course of production development and production.

Table 3: Possible anomalies in case of data cables

Faults occurring within product development	• On account of incorrectly defined parameters for braided shields, the optimal shielding characteristics are not reached. • The reduction of return losses requires an individual matching of mechanical, chemical, and electrical material properties on the extrusion systems. • The calculation of optimal length-of-lay combinations must be verified by production-type tests for all stranders that are used. • The attenuation may gradually rise as a function of time on account of aging effects occurring in a wire insulation material that is not suitable for this frequency range.
Faults occurring within the production process	• Impedance faults may be caused by deposits on copper lines (oxidation, emulsions, mechanical compressions). • *Inhomogeneous strands may cause a frequency-selective suppression of signals.*

The tight integration of design specifications applicable to cable production and cable characteristics which are of importance for the actual application requires that potential sources of faults are already taken into account in the development phase. In particular, any errors which may possibly arise during the production process must be considered already in the development phase and avoided by selecting appropriate machines and defining corresponding process parameters.

Another prerequisite for the production of data cables with a constantly high level of quality are well controlled and reproducible manufacturing processes.

By taking the last item of Table 3 as an example, we would like to demonstrate that a high level of production quality is indispensable when the frequency limit of Category 5 is exceeded.

Within the framework of a quality assurance program, GHMT has carried out measurements on cables since the beginning of 1996. Simultaneously, the cable manufacturer Kerpenwerk has optimized and stabilized its manufacturing quality through plant tests before launching the 600 MHz cables. Parts of these results achieved by both enterprises will be presented in the following.

Frequency-Selective Suppression of Signals

When a test cable was produced in order to run in a wire extrusion system, the operational attenuation which to date has been known as a stable parameter in manufacturing processes showed a frequency-selective blocking response (cf. Figure 4, curve B).

Figure 4: Registered frequency responses of operational attenuation

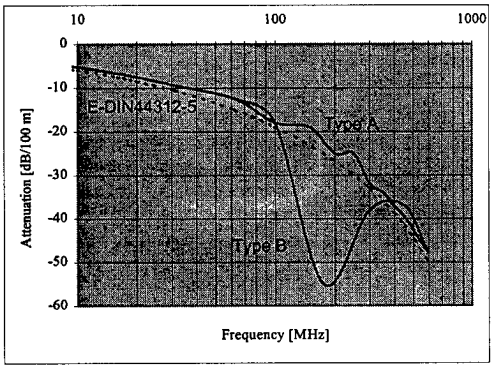

While curve A shows a periodically oscillating course of the attenuation which is caused by approximately regular differences of the coaxial capacitance, curve B represents a typical, wide-band frequency-selective blocking response owing to random differences of the capacitance. The tolerance characteristic in accordance with E-DIN 44312-5 has been indicated as a dotted line.

Fault Analysis

The stepwise analysis of the individual coaxial wire capacities of the faulty pair showed an irregularly oscillating course of the capacity of one wire.

Figure 5: Coaxial wire capacities of previously stranded wires with wide-band increase of operational attenuation

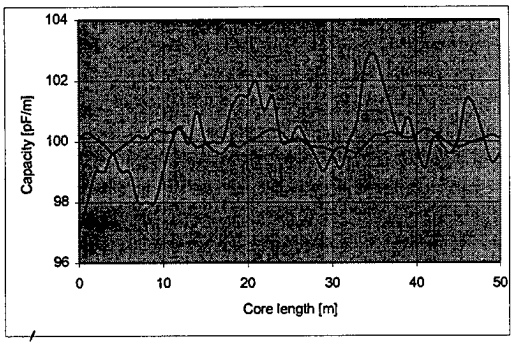

The resulting assumption that a stochastically occurring difference of the coaxial capacitance could be regarded as the cause has been confirmed by extrusion tests which were carried out by Kerpenwerk. For that purpose, wires with predetermined aperiodic, coaxial capacitance

changes were extruded. The frequency responses of operational attenuation which were measured on stranded pairs were correlated with the production parameters by means of mathematical procedures.

At the same time, extrusion tests were carried out with periodic modulation. On account of the high manufacturing speed and the stable automatic control process, the intentional periodic impression of coaxial capacitance differences is, however, problematic. It requires a lot of work to produce capacity changes in small time intervals allowing to prove a narrow-band distortion of the transmission function within the operating frequency range.

Practical Simulation

The effect on the operational attenuation can be demonstrated without any extensive mathematical calculations for the specific case of a locally restricted, periodic change of the coaxial capacitance.
A periodic change of the coaxial capacitance was impressed on an S/STP cable – which previously had been tested and shown as free from faults – by soldering 25 discrete capacitors of 4 pF each between the wire "a" and the foil shield on this cable. At equidistant distances of $\Delta z = 2$ m and a cable-specific nominal velocity of propagation amounting to NVP = 0.76, the mono-frequent distortions of the transmission function were in accordance with

$$f_n = \frac{NVP \cdot c_0}{2n \cdot \Delta z}$$

at 57 MHz ($n=1$) and the integer multiples. By measuring the operational attenuation, it was possible to prove discrete increases of the attenuation up to the seventh harmonic.

TECHNICAL ANALYSIS OF FAULTS IN THE PRODUCTION PROCESS

Manufacturing faults such as the attenuation rises described above must be recognized as early as possible. In the event that eight-wire data cables include a defect wire, the damage will be limited if only a replacement for the faulty wire must be manufactured. However, if a faulty wire is inserted into a cable, the entire product will be faulty. For that reason, the technical analysis of faults is indispensable for the manufacturing phase of wire extrusion. Possible faults occurring in this production stage are:

1. Inhomogeneities of the wire insulation

- Emulsion residues of the wire-drawing process reduce the wringing fit of the conductors.
- The insulation material must be homogeneous during the entire extrusion process. This applies in particular to wires with foamed insulation materials.
- Inhomogeneities of the wire insulation lead to partial differences of the coaxial capacitance. Depending on the cause, these differences can be stochastic or periodically distributed.

2. Deviations from the wire geometry

- Changes of the wire diameter and changes of
- the wire centricity within the wire insulation lead to differences of the coaxial capacitance.

3. Effects of the manufacturing process

- Irregularities of the conductor temperature lead to uncontrolled shrinkage. This effect may be caused both by wire preheating and by environmental influences.
- Fluctuations in the automatic line control, e.g. in case of an unstable process point, have a considerable effect on the electrical characteristics of the wires.

However, a well controlled production of wires does not yet guarantee high-quality cables. The subsequent manufacturing phases can damage even a perfect wire to such an extent that transmission characteristics are considerably reduced. In this connection, the following points should be observed – among others:

- The combination of two unequal wires should be avoided for the production of wire pairs.
- Inhomogeneous tensile loads during the stranding process lead to capacity differences.
- Periodic fluctuations during the application of foils may cause an equidistant mechanical load of the pairs.

Considering this background, the manufacturing process should be optimized through theoretic calculations and practical tests before a product is launched on the market.

THEORETICAL MODEL

Within the framework of a research project, it will developed a simulation program which allows an in-depth examination of the described irregular transmission characteristics. Since the analytical solution of wave propagation with inhomogeneous line characteristics requires a high amount of mathematical work and is only valid for special cases, the degrees of freedom of the simulation would be restricted. That is why an interpolation approach[1/2/3] is favored which furnishes sufficiently exact results at the available processing capacity. The solution approaches are now briefly presented.

In order to derive the propagation coefficient from the transmission line constants, an equivalent circuit must be used that allows to describe the real conditions – and deviates from the known coaxial calculation form. For that purpose, a line model is suitable which represents the electrical effects of environmental conditions (e.g. a metallic cable conduit, adjacent pairs) or of a cable screen on the transversal fields. In the further course of the analysis, only the capacitive and magnetic couplings to the external reference potential will be taken into account. To maintain the general validity of the derivation both for S/STP cables and for UTP cables, ohmic and inductive losses of an optional screen are not included. As each real screen is sufficiently thick vis-à-vis the penetration depth of the electromagnetic field in the relevant frequency range beyond 10 MHz, this negligence is justified. All propagation processes are based on a time function of exp(jωt) which is not described specifically in the following.

Figure 6: Two-wire line with asymmetric transmission line constants

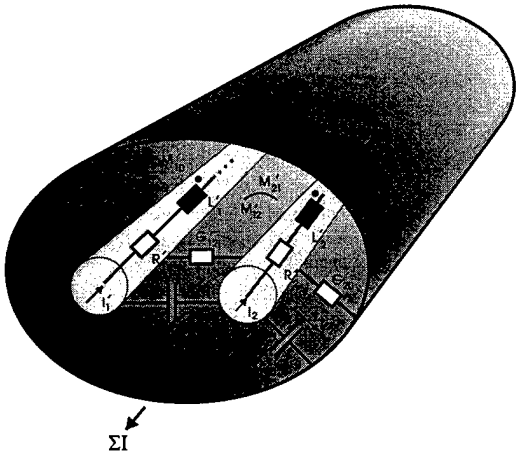

After establishing Kirchhoff's laws by taking into account the longitudinal resistance values per unit length, the transverse conductance, and the magnetic couplings

$$-\frac{dU_1}{dz} = \{R_1' + j\omega\cdot(L_1' - M_{10}')\}\cdot I_1 + j\omega\cdot(M_{12}' - M_{10}')\cdot I_2$$

$$-\frac{dU_2}{dz} = j\omega\cdot(M_{21}' - M_{20}')\cdot I_1 + \{R_2' + j\omega\cdot(L_2' - M_{20}')\}\cdot I_2$$

$$-\frac{dI_1}{dz} = (G_{10}' + j\omega C_{10}')\cdot U_1 + (G_{12}' + j\omega C_{12}')\cdot(U_1 - U_2)$$

$$-\frac{dI_2}{dz} = (G_{12}' + j\omega C_{12}')\cdot(U_2 - U_1) + (G_{20}' + j\omega C_{20}')\cdot U_2$$

a second-order differential equation system results for the line-to-line voltages

$$\frac{d^2}{dz^2}\begin{pmatrix}U_1\\U_2\end{pmatrix} = \begin{pmatrix}a_{11} & a_{12}\\a_{21} & a_{22}\end{pmatrix}\cdot\begin{pmatrix}U_1\\U_2\end{pmatrix}$$

with the propagation matrix ||A||, as a rule, no longer being symmetric. In order to solve the equation, the mutual coupling must be eliminated. Therefore the matrix ||A|| must be transformed into a diagonal matrix whose elements correspond to the propagation coefficients of the respective waves along the lines. Hence we obtain the characteristic quantities of natural waves in this system – without having to leave the quasi-stationary line equations through field statements of higher order. To achieve this, the voltage vector (U) is linearly transformed into the voltage vector (W):

$$(U) = \|V\|\cdot(W)$$

In order to diagonalize the coefficient matrix ||A||, a transformation matrix ||V|| must be determined having the property:

$$\|V\|^{-1}\cdot\|A\|\cdot\|V\| = \|\Gamma^2\| = \begin{pmatrix}\gamma_1^2 & 0\\0 & \gamma_2^2\end{pmatrix}$$

This homogeneous system of linear equations has a non-trivial solution, if its coefficient determinant is equal to zero. A conversion leads to the following equation:

$$\sum_{j=1}^{2}\left\{\|A\| - \gamma_j^2\cdot\|E\|\right\}\cdot(v_j) = \|0\|$$

We obtain two systems of equations with two values for γ_j^2 and two column vectors (v_j), which together form the transformation matrix. By solving the polynomial equations, the following equation results:

$$\gamma_{1,2}^2 = \frac{a_{11}+a_{22}}{2} \pm \sqrt{\frac{(a_{11}+a_{22})^2}{4} - a_{12}a_{21} - a_{11}a_{22}}$$

Now the elements of the transformation matrix ||V|| can also be determined with the exception of a constant factor which is selected in such a way that the individual column vectors form two-dimensional unit vectors.

$$v_{11} = \frac{a_{22}-\gamma_1^2}{\sqrt{(a_{22}-\gamma_1^2)^2 + a_{12}^2}} \qquad v_{12} = \frac{-a_{21}}{\sqrt{(a_{11}-\gamma_2^2)^2 + a_{21}^2}}$$

$$v_{21} = \frac{-a_{12}}{\sqrt{(a_{22}-\gamma_1^2)^2 + a_{12}^2}} \qquad v_{22} = \frac{a_{11}-\gamma_2^2}{\sqrt{(a_{11}-\gamma_2^2)^2 + a_{21}^2}}$$

The derivation has shown that there is – for each propagation matrix ||A|| consisting of the transmission line constants – an eigenvector matrix which transforms the voltage vector (U) into the new voltage vector (W) and simultaneously uncouples the system of wave equations.

The independent voltages w_j represent natural waves with the propagation coefficients γ_j of the asymmetric two-wire line whose wave equations are solved by means of the customary exponential statement.

The physical significance of this transformation into natural waves in order to solve the coupled wave equation consists in the fact that an asymmetric two-wire line is energized at the begin, and natural waves propagate along an interference-free line without any interaction with different propagation coefficients. In case of the symmetric two-wire line, the matrix ||A|| will be symmetric, and the natural waves w_j are the well-known common-mode wave w_1 and the normal-mode wave w_2.

Any further simulation requires powerful computers because the simplified assumption of the symmetric loss-free or distortion-free two-wire line is then not admissible. To simulate real-world conditions, it must additionally be assumed that all transmission line constants are dependent on the frequency. The theoretic derivation[4] of the frequency dependence is known for various line types. However, this does not affect the solution of the wave equation.

To date, we had to assume that the medium is homogeneous in the direction of propagation. This restriction was necessary in order to solve the wave equation of the natural waves from the system of differential equations. The asymmetric two-wire line of the length *l* will now be broken down into *n* segments of the length Δz and having different transmission line constants. The chain parameter matrix of the transmission function of the voltage vector (W) can now be calculated separately for each segment by means of the derived equations – subject to the prerequisite that the transmission line constants are homogeneous in longitudinal direction.

We proceed from the assumption that the longitudinal resistance values per unit length R_i, L_i and M_i which are homogeneously distributed in all chain parameter matrices have the same frequency responses. The same applies to the distributed leakage G_i whose frequency responses are ideally determined through measurements on the used polyethylene because the material parameters cannot be calculated analytically. The partial capacitance values per unit length C_i are adjusted to the curves of coaxial capacitance differences that have been measured under practical conditions.

The transmission function of the asymmetric two-wire line is calculated by multiplying the individual chain parameter matrices with a mode coupling[2] taking place between the natural waves at each contact point between segments of different transmission line constants. The mode coupling is also represented in chain form and included in the interconnection. Using a sufficiently large number of line segments, it can be expected that the simulation maps the attenuation rises occurring under practical conditions and thus supports the test results which to date are based on phenomenological findings. By embedding numerical program routines [5] (FORTRAN is to be preferred) which have been optimized with respect to the processing time, the simulation can be carried out on PCs.

ACCEPTANCE MEASUREMENTS PERFORMED ON 600 MHZ CABLING SECTIONS

The quality of an installed high-speed cabling section is decisively limited by the value of the used plug-and-socket connectors and their installation technique. Under certain circumstances, however, the data cable, too, f.e. after mechanical stress of installation, shows poorer electrical characteristics than those that have been determined by the type certification in a neutral test laboratory. How will it then be possible to document the performance of a network for the end users?

In order to determine the quality of a cabling section, among others, the operational attenuation and the near-end crosstalk (NEXT) attenuation must be measured.

The mobile network scanners which are currently available have – independently of the different measuring procedures – a maximum test bandwidth of 155 MHz at an insufficient level-specific, dynamic range of measurement amounting to 65 dB. Even in 1999, no measuring units will probably be available which – in the range beyond 300 MHz – are able to determine the transmission characteristics of 600 MHz cabling sections.

A major field of the lab has been the provision of measuring services for LAN acceptance measurements. The measuring equipment which in part has been developed by the company itself allows a level-specific, dynamic range of measurements of 110 dB at a bandwidth of 750 MHz. Meanwhile more than 20,0000 of the cabling sections installed in Germany have been measured and recorded by our site-survey department.

Figure 7: Acceptance measurement performed on a 600 MHz cabling section

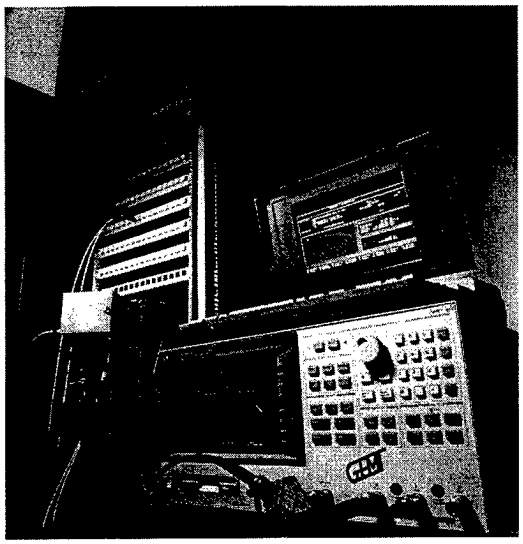

CONCLUSION

Transmission-specific faults which are only recognized through on-site acceptance measurements and can be attributed to the data cable constitute avoidable damages for the cable manufacturer. By means of a consistent fault analysis in the production process, the cable manufacturer can, however, ensure the quality of its products even at a very high transmission bandwidth.

Using simulations, it will in the future be possible to optimize further the cable design by taking into account high-frequency aspects and adapt it to the manufacturing conditions. The extending of this interesting business area will be continued by our develop department in 1999 as well.

The increasing requirements of the market to commission only Class F (600 MHz) local area networks which have been documented through measurements clearly show the quality awareness of end users and the task of cable manufacturer to meet the same requirements. Particularly in case of high-speed networks, a well controlled and reproducible manufacturing process will be necessary and a sophisticated measuring technology will be indispensable to ensure a system performance in compliance with the future requirements.

REFERENCES

[1] Multiple lines and line couplers
Marquardt, J.
Universität Hannover, 1986

[2] Calculation of mode couplings on waveguide transitions
Obst, A.
Universität Hannover, 1994

[3] Transmission-line properties of parallel strips separated by a dielectric sheet
Wheeler, H. A.
IEEE Trans. on microwave theory, 1965

[4] The electromagnetic screen in telecommunication and high-frequency technology
Kaden, H.
Springer-Verlag, Berlin,1950

[5] Numerical recipes - The art of scientific computing
Press. W., Flannery B., Teukolsky, C.

[6] "Installation von Datenkabeln"- "Symmetrische Kabel für zukunftssichere Netze
Gerhard, G.
Expert Verlag, Reihe Kontakt & Studium

BIOGRAPHIES OF THE AUTHORS

Andreas OBST (age: 32) is head of the laboratories for EMC and transmission measurements of LAN components at GHMT.

In 1993, he graduated at Technische Universität Hannover majoring in high frequency engineering. In the course of his diploma thesis at kabelmetal electro company in Hanover, he optimized elliptical shaped waveguides with corrugated sheath.

In 1994, he entered the product-engineering department of Alcatel Cable in Berlin. There he has been responsible for design, testing and quality features of symmetrical high-speed data cables.

At the beginning of 1997 he joined GHMT in his present position.

Mailing address

GHMT
Gesellschaft für Hochfrequenz-Meßtechnik mbH
In der Kolling 13

D 66450 Bexbach/Saar
Germany

Phone: ++49 / 68 26 / 92 28 - 0
Fax: ++49 / 68 26 / 92 28 - 99
E-mail: obst@ghmt.com

Jörg Bör was born in Hamburg, Germany in 1965. Following his studies of electrical engineering at RWTH Aachen and his graduation as Diplom-Ingenieur in 1991, he started his professional career as a design engineer at Kerpenwerk GmbH & Co.

His activities at Kerpenwerk focus on the further development of symmetric copper data cables and the improvement of electrical transmission characteristics up into the gigahertz range.

Currently, Jörg Bör is group leader of electrical development at Kerpenwerk GmbH & Co.

Mailing address

Kerpenwerk GmbH & Co.
Zweifaller Straße 275 – 287

D 52224 Stolberg
Germany

Phone: ++49 / 24 02 / 17 – 440
Fax: ++49 / 24 02 / 75 – 154
E-mail: Joerg.Boer@kerpen.com

TECHNOLOGY AND EVOLUTION OF OPTICAL CABLES IN BRAZIL

Paulo José Pereira Curado; Ronaldo Arruda
CPqD - Campinas - SP - Brazil

ABSTRACT

In this work, the stage of development of optical cable in Brazil will be presented, showing the usual alternatives for optical cables adopted. Stress will be given to several specific solutions for cables in duct, buried and aerial applications and some particular solutions for domestic conditions.

Also optical subscriber network evolution will be showed, including new models of cables under study and development outlooks.

INTRODUCTION

The development of optical communications in Brazil started in the mid-70's with the effort of Telebrás – a holding of Telecommunications operating companies – in research and development of laser, optical fibers and optical equipment. This effort was part of the Brazilian government strategy to boost the industry.

In this program, multimode and singlemode optical fibers were developed. The technology developed was applied to the industry and a series of equipment, among which cables, couplers, splitters and optical amplifiers that contemplate specific Brazilian particularities and conditions. Moreover, capabilities in human resources were developed in the area.

At first, systems were developed for local trunkings in multimode fibers travelling in 850 nm and 1,310 nm, with signals travelling at 34 and 140 Mbit/s. This technology was quickly replaced by singlemode fiber cables in 1,310 nm and 1,550 nm at 622 Mbit/s and already in SDH hierarchy.

In large cities, networks in SDH rings are already implanted, and the great regional rings of each state connected to the Embratel nationwide network are at the last stage of completion.

Most systems work with singlemode fiber in 622 Mbit/s. Few are working on singlemode fiber with shifted dispersion. The application of multiplexed systems in wavelength (WDM) is already a reality and systems at 2.5 Gbit/s are already in commercial operation.

TRUNKING NETWORKS

Optical fiber applications in local and long-distance trunking networks are mature in the country and since 1988 all trunkings have been made with optical networks.

In terms of infrastructure, most urban links are made through duct-installed cables, with only small portions installed with aerial and buried cables. For long-distance trunkings, buried cables and optical fiber ground-wires (OPGW) prevail.

In the beginning, for long-distance links in Brazil, practically there was no experience in the use of cables. All links were made with radio systems. There was no telecommunication physical structure linking large cities.

By means of agreements among telecommunication companies and highway or railroad franchisees, it was possible to install cables using the infrastructure and areas belonging to these companies. Most cables were buried, with some duct lines. Another type of widely used infrastructure is that of electricity companies, both

with the use of dielectric cables in poling and in optical ground-wire cables in transmission lines.

Embratel connections between the capitals of the Northern states is made by a submarine cable that follows the country's northern coast.

The Embratel national network is a wide one, with over 10,000 kilometers of cables already implanted that connect the main cities in the country. Currently, some connections to some state capitals and alternative routes are being installed.

CABLES FOR TRUNKING NETWORKS

The loose conception is used as the basic technology to build optical cables and craftperson is trained to install this type of cables. This technology was developed by 8 domestic manufacturers supported by the Research & Development Center (CPqD).

The development started with cables with metallic components. Despite their good performance, these cables had some inconveniences as to lightning. For this reason, fully dielectric cables were adopted.

In Brazil, there is a large supervision infrastructure of metallic cables by pressurization, and dry core cables were always used. An attempt was made to use the same philosophy and infrastructure for optical cables, but the difficulties to set up and develop an optical fiber supervision system (SRO) led to the adoption of jelly-filled cables for protection against moisture.

As to arrangement, cables with 2-72 optical fibers are used, in three basic arrangements:

- cables with 1-12 optical fibers, with six units of 6 optical fibers;
- cables with 18-36 optical fibers, with six units of 6 optical fibers;
- cables with 48-72 optical fibers, with twelve units of 6 optical fibers;

From these basic premises, specific cables were developed for each application shown below:

Cables in ducts

The cable for duct application is a fully dielectric, loose, jelly-filled cable, with maximum capacity of 72 optical fibers, in the previously described arrangements.

They are installed mostly in 100 mm-PVC ducts. Multiple subducts with four pipes with an internal diameter of 25 mm are used. Maximum diameter of this cable is 19 mm in this case.

Figure 1 shows the cross-section of a typical arrangement.

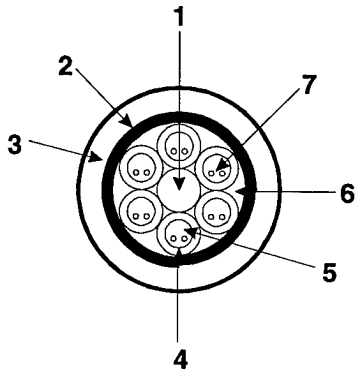

1- Central member
2- Strength member
3- Jacket
4- Loose tube
5- Jelly
6- Jelly
7- Fiber Optic

Figure 1 - Duct cable.

The cable has as basic mechanical characteristics an installation load equal to twice the weight of the cable by km (minimum 2,000 N) and minimum static bending radius 10 times the external diameter of the cable. The other mechanical characteristics are consistent with those found in international specifications. The cable is designed for use between -20°C and +65°C. The external coating is made of polyethylene with a minimum absolute thickness of 1.4 mm.

Buried cables

These optical cables are applied in direct contact with the ground, buried at a minimum depth of 1.20 mm. Usually they are installed along highways or railroads by automatic installation processes.

The options of cables are used:

a) Directly buried cables.

These are fully dielectric cables installed in direct contact with the ground, in loose, jelly technology, with maximum capacity of 72 optical fibers, in the arrangements previously described.

Their main characteristic is high mechanical resistance provided by a double external polyethylene coating, with a minimum thickness of 4 mm and an additional Polyamide coating for protection against attack by insects, which is the result of specific studies.

Initially this protection was designed to be located outside the cable, but in its applications, it was found that it could be damaged, particularly at crossings where installation in ducts is required, which makes it ineffective against attack by insects. This way, the application of the Polyamide layer between two 2-mm coats was developed, as seen in figure 2.

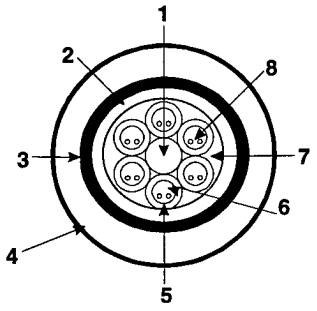

1- Central member
2- Inner Jacket
3- Poliamide
4- Outer Jacket
5- Loose tube
6- Jelly
7- Jelly
8- Fiber Optic

Figure 2 – Directly buried cable.

The mechanical characteristic of this cable is maximum installation load equal to 1,000 N, considering that the cable is designed to be deposited, and minimum static bending radius 10 times the external diameter. The other mechanical characteristics are consistent with those found in international specifications. The cable is designed for use between -20°C and +65°C.

b) Cables directly buried and protected against rodent attack

These optical cables have the same characteristics as the directly buried cables, except that they have an additional protection against rodent attack, developed in a specific study .

This protection can be either a fiberglass tissue or rods placed along the perimeter of the first external coating, as can be seen in the example in figure 3.

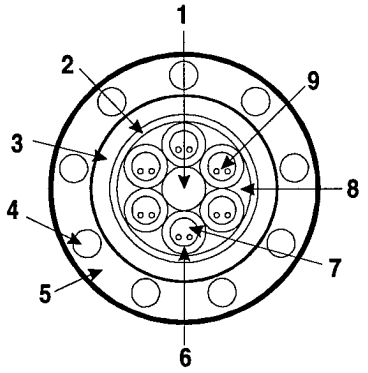

1- Central member
2- Waterblocking Tape
3- Inner Jacket
4- Glass fiber rod
5- Outer jacket
6- Loose tube
7- Jelly
8- Jelly
9- Fiber Optic

Figure 3 – Directly buried cable, protected against rodent attack.

c) Protected and buried optical cable

In this model, on a duct optical cable with a Polyamide protection, a protection duct is applied with a minimum thickness of 4 mm that forms an assembly that is installed in direct contact with the ground.

The advantage of this type of cable is its high mechanical resistance and the possibility to move it. This possibility is used in case the cable needs to be repaired, thus minimizing maintenance work, or for replacement of the cable due to obsolescence or failure.

A cross-section of this cable can be seen in figure 4.

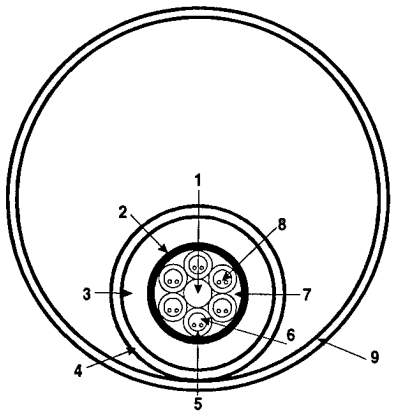

1- Central member
2- Strength member
3- Jacket
4- Poliamide
5- Loose tube
6- Jelly
7- Jelly
8- Fiber Optic
9- Duct

Figure 4 – Protected and buried optical cable.

The cable has the same characteristics as a duct cable. The assembly follows the characteristics of the buried cable.

Removing cables in assemblies of up to 2 km long is possible, and due to this function, the ratio between the diameter of the cable and the duct should be greater than 1.8, besides a very low friction.

The external diameter of the assembly is approximately 30 mm for the arrangement of up to 12 optical fibers, 35 mm for arrangements of up to 36 optical fibers and 40 for the arrangement with up to 72 optical fibers.

Aerial optical cables

A type of cables that is extensively used in the country is the aerial optical cable. These are self-supported, fully dielectric cables with loose technology and maximum capacity of 12 optical fibers. Lately, the use of greater capacity cables has been enhanced, ranging from 36 to 72 optical fibers.

Due to the amount of damage caused by lightning and problems with the power network, a fully dielectric cable was adopted. To conform to the poling of electric power networks in the country, cables were standardized for maximum spans of 80 m, 120 m and 200 m.

Figure 5 shows a typical cable cross-section, where the supporting element is distributed along the perimeter of the coating.

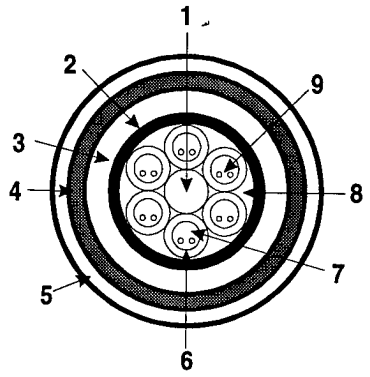

1- Central member
2- Waterblocking tape
3- Inner jacket
4- Strength member
5- Outer jacket
6- Loose tube
7- Jelly
8- Jelly
9- Fiber Optic

Figure 5 – Aerial optical cable

The characteristics of tensile strength of the cable are the function of its weight and application span. The other mechanical characteristics are consistent with those found in the international standardization. Special attention is given to cable creep, due to the high temperatures found and the wind vibration. The galloping vibration is not taken into account. These cables are projected for use both in a local and a long-distance environment, with temperatures ranging between -20°C and +65°C.

As agricultural burning is a frequent incident close to the installation of aerial cables, these have fire-retardant characteristics, so as not to become an agent spreading fire to non-affected areas.

The standardization of cables for spans above 200 m is being discussed, for application in determined areas of the country where topography is favorable, and there is the possibility to use the network of high voltage transmission lines.

Indoor cables and cords

The optical cords adopted in the country are compatible with international standards. They are made of an optical fiber with an adhesive secondary coating protected by aramide filaments and an external coat made of a fire-retardant material with a 3-mm external diameter.

Because of the network implantation philosophy that makes use of many splice frames, indoor cables are not very much used. Two models are standardized:

a) Cord indoor cable: Cable with a maximum of twelve cords, protected by a fire-retardant coating.

b) Basic unit indoor cable: Cable with the core of an external cable, protected by a coat made of a fire-retardant material.

Several models of indoor optical cables are being discussed. They will be shown further on in this work.

Ground wire cables with optical fibers

Brazil has highly favorable characteristics to increase the implantation of cables in transmission lines. Almost all power in Brazil is generated by hydroelectric dams, and transmission lines connect the main cities of the country. Several routes have been implanted in partnership among power and telecommunications companies, but the installation by the owner of the transmission line and its exploitation is becoming increasingly popular.

Cable capacities vary greatly and there is no standardization in terms of models. Totally different technologies coexist, such as technology with extruded pipe, with welded pipe, slotted core with protected by tape or pipe, among others.

Evolution of the Technology

The technology adopted for trunking network cable has kept pace with international developments and local needs.

Among these developments, the following can be highlighted:

- Increased capacity of duct cables to meet certain specific needs and high demand areas.

- Dry core cable, to optimize splicing operations and some types of transition cables (indoor and outdoor use).

- Cables with metallic protection: In certain situations, problems with electric protection can be minimized and the use of cables with this protection against rodent attack is indicated, taking the required dimensional and mechanical characteristics into consideration.

- Aerial cables for long spans: These are cables for use in transmission lines in spans of up to 1,000 m. Besides their mechanical conception, the coating materials with resistance to tracking are under development.

SUBSCRIBERS OPTICAL NETWORK

In Brazilian telecommunications, two extremes coexist: on the one hand a great unmet demand for basic telephony services in limited areas, and on the other hand a great amount of subscribers in need of increasingly sophisticated services. This calls for the evolution of the network by means of optical cables.

The subscriber optical network evolution is planned to occur in the following stages:

- Serving great subscribers: Service to great subscribers is conducted by specific dedicated optical cables. For great concentrations, integrated network solutions are used.
- Opticalization of the feeding network: Expansion of the network for telephony services started with the setting of optical cables in the feeding network, both in active and passive networks, parallel to current metal networks. Equipment is implanted in one distribution node, where conversion of optical signals into electric signals is made, and the distribution network continues to be made of metal.
- Hybrid Fiber / Coaxial Networks: some telephony operating companies are setting these networks to supply cable TV services, for future partnership with companies rendering this type of service. Optical fibers are implanted up to a convenient location in

the network. From this place on, analog TV signals are distributed by coaxial cables.

- Optical Network in FTTCab configuration (Fiber-to-the-Cabinet): In this network set-up, the optical network is expanded to a location as close to the subscriber as possible, so new services can be supplied via metallic network through metallic pair network, using xDSL technology.
- Optical Network in FTTC configuration (Fiber-to-the-curb): As the demand for higher rate signals increase, optical networks will be expanded to get close to the user's location, in a point that typically serves 16-48 subscribers.
- Optical Network in FTTH Set-up (Fiber-to-the-home): In an objective network, subscribers will be served by dedicated optical fibers.

With this forecast of growth of optical networks to serve subscribers, new families of optical cables are being proposed, with different arrangements and technologies that will be shown below.

CABLES FOR SUBSCRIBERS NETWORK

In the evolution of the subscribers network, the first step, in which the great subscribers are served, the same telecommunications infrastructure and materials used in the trunking networks are also used. In many cases they are considered trunkings. An important remark is the existence of an increased use of aerial cables.

For applications of opticalization of the feeding network and fiber / coaxial network, the use of a minimum of six optical fibers by distribution point was defined. A careful analysis of the network status showed that in the most critical cases, 15-20 distribution points are found per route.

Taking these points into account, and the fact that most companies work with loose technology, a fully dielectric subscriber cable with a maximum of 144 optical fibers and loose technology was proposed, with the basic arrangements of trunking cables plus a cable arrangement of 84-144 optical fibers of 12 optical fiber units.

It should also be considered that the metallic pair subscriber networks are usually built as an underground network in ducts to the feeding network and aerial network to the distribution network.

The concept of derivation splice without interrupting of the other fibers by means of a mid-span access was also introduced. Another key aspect was the development of dry-core cables, with protection against humidity provided by waterblocking materials.

The cable is used in duct networks and can also be used in the aerial network lashing in a metallic messenger

Figure 6 shows the cross-section of an arrangement of this cable.

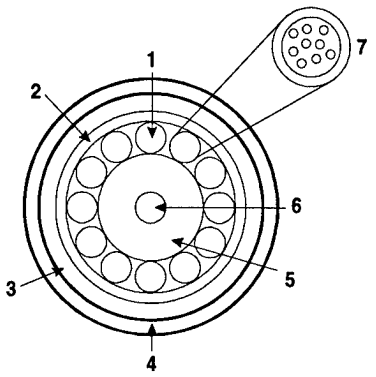

1- Loose tube
2- Waterblocking tape
3- Strengnt member
4- Jacket
5- Str. Member coating
6 – Central member
7 – Loose tube (12 fibers)

Figure 6 – Cables for subscriber networks.

With the introduction of this cable arrangement and the use of overlapping networks, it is necessary to develop indoor cables for use in telephone exchanges.

A family of indoor cables comprising the following models was proposed and is under development:

a) Indoor cord cables: made of 36 2-mm thick optical cords, with characteristics suitable for indoor use (flexible, fire-retardant, etc).
b) Cables made of optical elements: made of 36 or 72 optical elements (fibers with adhesive secondary coating) with the same characteristics for indoor use.
c) End cables: Cable made with a maximum of 144 fibers, in the same arrangements as the outdoor cable. They have the same characteristics as the cable for outdoor use

and for indoor use. Used in situations requiring elimination of the transition splice.

Besides these cables that are required for setting the first stages of the evolution, some proposals of evolution for FTTx set-ups are being discussed, with the introduction of ribbon technology cables. The table 1 shows a proposal for a set of cables.

This proposal is based on the following points:

- Use of greater capacity cables to better exploit the existing infrastructure.
- Compatibility with existing networks.
- Use of overlapping networks.
- International standardization.

Stress should be given to the possibility to use mixed cables, with coaxial conductors and symmetrical pairs. This can make evolution easier and reduce implantation costs in the evolution of the network.

STANDARDIZATION AND CERTIFICATION SYSTEM

Standardization

For many years Telebrás held the monopoly of telecommunications in Brazil. And it was the greatest buyer. Therefore its business standardization was considered as valid documents nationwide for many years.

In the late 80's, with the commercial opening and the organization of the Brazilian standardization in the Telecommunication area through the ABNT (Brazilian Association for Technical Standards), Telebrás started to support the Brazilian study commissions in charge of developing the standards. In this work, the Brazilian standard now effective were discussed and agreed upon.

These standards are developed by the study commission including participation of all segments involved (producers and consumers) and neutral agencies. The commission issues a base text that is submitted to national voting. Any individuals or agencies can participate. The resulting document is published as a National Standard.

In the area of optical cables, the commission in charge is CE 86.1, optical cables and fibers. During the last few years it has issued several standards, among which we must mention:

– Singlemode optical fibers
– Multimode optical fibers
–Dielectric underground optical cable – including duct cables and dielectric buried cables.
– Aerial optical cable
– Optical cords
– Indoor optical cables
– Underground cables with metal guard (LAP cover).
– Ground-wire cables with optical fibers (OPGW)

The standard for long span aerial cables, subscriber network underground cables (up to 144 optical fibers) and underground cables with rodent-resistant metallic protection are in the process of being voted.

The test methods are developed in the same system by the CE 86.2 commission that has issued over 40 standard in the last few years, covering mechanical, optical and thermal tests, among others.

It is interesting to note that all this standardization is in harmony with the one existing in international agencies such as IEC and ITU-T.

	Indoor	Feeder	Distribuition	Acess	Subscriber
Fibers	144/720	144/720	24/144	4/24	2/4
Tecnology	Ribbon	Ribbon	Loose	Loose	Tight
Aplication	Indoor	Underground	Underground /aerial	Underground/ aerial	aerial
Main caracteristics	handling	Compactness	Individual Access	Robustness	Robustness

Table 1 – Proposal Optical cables for subscriber Network

Certification

For many years the certification system applied was the one used by Telebrás, that issued qualification certifications for determined products, one of which was the optical cable.

The Telebrás qualification system includes supplier's plant assessment, laboratory assessment of products in accordance with Telebrás or National specifications and on-going assessment of product performance.

With the reorganization of the Brazilian telecommunications system now under way, the law determines the type of products for which certification is required. The voluntary certification by companies is being discussed.

CONCLUSIONS

This work showed a view of the optical cable technology developed, used and produced in Brazil, and the evolution of the domestic Telecommunications network.

Furthermore, the advancements under way were shown, as well as proposals for evolution of cable technology more suitable for domestic conditions both related to the telephone network and the labor available to build the network.

Paulo José Pereira Curado
CPqD
Campinas, Brazil

Paulo José Pereira Curado was born in 1962. He graduated in Mechanical Engineering from Campinas State University (UNICAMP) in 1985 and in that year he joined Telebrás Research and Development Center in the Outside Plant Department. He has been engaged in research and development of optical fiber cables for trunk lines. Presently he is working with Optical Subscriber Networks in Outside Plant area. He is coordinator of Fiber Optic and Optical Fiber Cable Study Commission of Brazilian Standartization Association (ABNT).

Ronaldo Arruda
CPqD
Campinas, Brazil

Ronaldo Arruda was born in 1947. He graduated in Electrical Engineering from PUC/MG in 1971 and have been working in Telebrás System since them. He worked in metallic cable development and was in a charge to introduce optical fiber systems in Telebrás companies. Presently is responsible for standardization area in CPqD. He is the coordinator of Fiber Optics Technical Commission of Brazilian Standartization Association (ABNT) and delegate of Brazilian Administration on ITU Study group 6.

VENI, VIDI, PROBÁVÍ (I CAME, I SAW, I QUALIFIED) AIR BLOWN FIBER IS TESTED AGAINST THE STANDARDS

Terri L. Dixon and Keith Quistorff

Sumitomo Electric Lightwave Corp., Research Triangle Park, NC

ABSTRACT

Qualification against industry standards is imperative for new products entering the market. Unfortunately, there is an inherent lag between the introduction of new technologies and applicable standards. So how does one qualify a product that the standards are not designed for like an air blown optical fiber (ABF) cabling system? Simply ignoring standards because they are not one hundred percent compatible is not an option. This paper discusses the challenges faced and how they were overcome in qualifying the indoor cables of the Sumitomo ABF system, as well as recommendations for future standards development.

INTRODUCTION

The question of how to properly qualify ABF cable to industry standards has been difficult to answer. Existing fiber optic cabling standards are intended to ensure the optical quality of cables before, during, and after installation. But, unlike conventional cables, ABF cables consist of two separately installed components which experience completely different loading conditions during and after installation. One must consider the intent of each specification in the standard to determine which component(s) should be tested.

AIR BLOWN FIBER FUNDAMENTALS

An ABF system is a flexible cabling network used in campus cabling installations. This system is composed of tube cables, fiber bundles, distribution and termination hardware, and fiber bundle installation equipment.

A typical ABF system starts with installation of a network of tube cables. These cables are packaged with up to nineteen tubes per cable (see Figure 1). They replace the innerduct and/or cable sheath of conventional cabling systems and are available in riser, plenum, and outdoor designs to accommodate all potential environments that a network designer may be faced with.

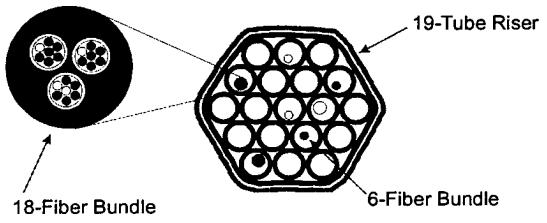

Figure 1: ABF Tube Cable and Fiber Bundle Examples

The tubes are connected with push-fit connectors to create point to point pathways. The tube interconnections are generally protected by an enclosure, also known as a Tube Distribution Unit (TDU). TDUs are designed for either indoor or outdoor environments and serve not only to protect the tube interconnections but also to allow for tailored routing of individual tube pathways. Because the tube cable network provides point-to-point pathways, all fiber splices can be eliminated. In addition, since standard 250 micron coated fiber is utilized, fiber terminations do not require any special hardware or equipment over conventional cabling systems.

Once the tube cable network is in place, fiber bundles can be installed as needed. The fiber bundle installation equipment involves a dry air (or nitrogen) source, payoff stand, motor controls, and blowing head (see Figure 2). The

Table 1: A listing of U.S. cabling standards

Standard Number	Standard Title
UL 910	Test for Flame Propagation and Smoke-Density Values for Electrical and Optical Fiber Cables Used in Spaces Transporting Environmental Air.
UL 1666	Test for Flame Propagation Height of Electrical and Optical Fiber Cables Installed Vertically in Shafts
RUS 7 CFR 1755.900 (Rural Electrification Administration)	Specification for Filled Fiber Optic Cables
Bellcore GR-20-CORE	Generic Requirements for Optical Fiber and Fiber Optic Cable
Bellcore GR-409-CORE	Generic Requirements for Premises Fiber Optics Cables
ANSI/ICEA S-83-596-1994	Standard for Fiber Optic Premises Distribution Cable
ANSI/ICEA S-87-640-1992	Standard for Fiber Optic Outside Plant Communications Cable

fiber bundles are inserted into the tubes through the blowing head, which controls the speed of installation.

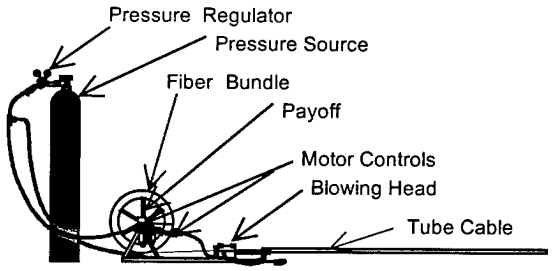

Figure 2: Fiber bundle installation equipment

Fiber bundles are available in 2-, 6-, 12-, and 18-fiber arrangements which are comprised of either single-mode, 50 μm multimode, or 62.5 μm multimode fibers. Arrangements up to six fibers are combined with a rip cord when required and covered with either a nylon or UV acrylate coating to form a unit. For the higher fiber count bundles, multiple fiber units are combined. Fiber units are then covered with a foamed polyethylene jacket to provide mechanical protection to the fibers and give the bundle specific aerodynamic properties (see Figure 1).

CABLING STANDARDS OVERVIEW

Several decades ago, building codes and standards did not include requirements for telecommunications equipment (The Telecommunications Distribution Methods Manual). With the rapid advancements in communication technology since that time, it has become necessary to include provisions for telecommunications equipment in codes and standards. Today, various building codes and standards govern the installation practices and materials used in the construction of telecommunications facilities.

Standards are designed to address minimum product requirements. Consumers want some knowledge of the lowest common denominator to which a given set of products will perform. They are established as a way to compare and judge similar products against certain criteria. The purpose of standards is to ensure quality of construction as well as protecting lives and property. Standards also "ensure that all network elements can coexist" (Engel, p. 32).

As table 1 shows, there are a number of different standards which telecommunications grade fiber optic cables may be tested against. Upon detailed review and comparison of each cabling standard, it was concluded that the S-83-596-1994 (Standard for Fiber Optic Premises Distribution Cable) and S-87-640-1992

(Standard for Fiber Optic Outside Plant Communications cable) standards developed by the Insulated Cable Engineers Association, Inc. (ICEA) were appropriate for qualifying ABF cables. This conclusion was based on the ICEA standards' overall market acceptance and use of industry standard TIA test procedures.

QUALIFICATION OF INDOOR AIR BLOWN FIBER CABLES

ICEA qualification testing can be divided into three basic categories of testing: material, environmental, and mechanical testing. Materials testing examines the properties of the components which comprise the cable. This testing is done to ensure that cable materials will meet specific guidelines such as ultimate elongation and tensile strength. Environmental testing examines the flammability characteristics and the qualities of the cables at varying temperatures. Mechanical testing explores how a cable stands up to physical stress, such as being crushed, twisted, and pulled.

Since air blown fiber cables perform the same basic function as conventional cables, ABF cables are expected to meet the same service load conditions as their conventional counterparts. Material and environmental tests are typically included in the standards to represent long term service conditions, so these tests are fully applicable to ABF cables.

Unlike conventional fiber optic cable, ABF fiber bundles are installed with negligible mechanical loading. This results in installation conditions which are significantly different from conventional fiber optic cables. Since the mechanical testing requirements generally represent installation loading conditions, a major question faced in qualifying Sumitomo's air blown fiber product was determining how to properly apply a conventional cabling test plan to the ABF system.

When a conventional cable is installed, it may be put under tension, crushed, bent, and twisted. Various fiber optic test procedures are designed to simulate these cases. If a cable can pass these types of tests, then the assumption is made that the cable will function in a similar manner in the field, and any signal losses will be kept to a minimum.

In an ABF installation scenario, the tube cables are installed with no optical fiber component. As a result, any potential stresses resulting from cable installation loading will not be seen by the optical fibers. Most of the mechanical test procedures require optical monitoring of the fibers during the test. Even though this is not indicative of an ABF installation, it is possible to justify some of the tests from the standpoint of long term service conditions. In order to reduce doubt and ambiguity during testing, it was decided to test the air blown fiber products with the fiber installed in order to conform as closely as possible to the qualification standards.

Test Specimens

It is not necessary to test every combination of tube cable and fiber bundle in a product line for qualification purposes. The worst case scenario for each product class should be chosen to represent its group. It was decided that, in any instance, the largest count fiber bundle would be the worst case for the fiber component. It was then necessary to determine which tube cables would represent worst case scenarios for the riser and plenum environments.

Riser cables are available in three standard sizes: 2-tubes, 7-tubes, and 19-tubes per cable. For some tests, the smallest cable would be worst case, and in other instances, the largest cable would be worst case. Therefore, all tests were applied to both the 2- and 19-tube riser cables. Each cable had both a single-mode and multimode 18-fiber bundle installed for testing. For the 19-tube cable the fiber bundles were placed in tubes on the outside edge of the cable.

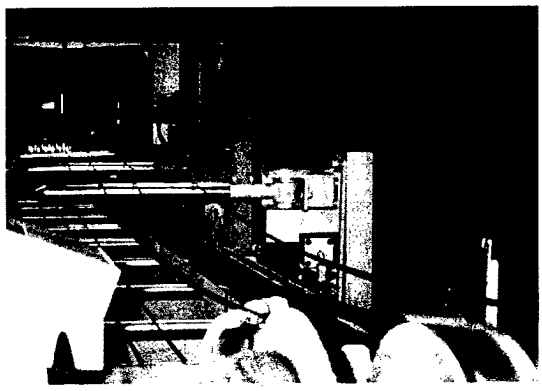

Figure 3: Plenum cable on tensile machine

Table 2: Air Blown Fiber Riser Qualification Results

	Test	Requirements	2-Tube Riser	19-Tube Riser	Service Conditions	Installation Conditions	Appropriate for ABF
Material	Cable Jacket Thickness (ASTM D 4565)	85% nominal thickness ≤ ave. thickness ≤ 115% nominal thickness. No point less than 70% nominal.	Pass	Pass	X	X	X
	Jacket Tensile Strength and Ultimate Elongation (FOTP-89A)	Tensile strength unaged ≥ 13.8 MPa, ultimate elongation ≥ 100%, tensile strength aged ≥ 85% original, ultimate elongation aged ≥ 50% original	Pass	Pass		X	X
Environ.	Temperature Cycling (FOTP-3)	SM < 0.3 dB/km, MM < 0.6 dB/km	Pass	Pass	X		X
	Flammability (UL 1666)		Pass	Pass	X		X
Mechanical	Low & High Temperature Bend Test (FOTP-37A)	SM < 0.2 dB/km, MM < 0.5 dB/km	Pass	Pass		X	
	Repeated Impact Test (FOTP-25A)	SM < 0.2 dB, MM < 0.4 dB	Pass	Pass	X	X	X
	Compressive Loading Test (FOTP-41)	SM < 0.4 dB during loading, SM < 0.2 dB after loading, MM < 0.6 dB during loading, MM < 0.4 dB after loading	Pass	Pass	X	X	
	Tensile Loading and Bending Test (FOTP-33A)	SM < 0.2 dB during loading, SM < 0.1 dB after loading, MM < 0.5 dB during loading, MM < 0.2 dB after loading	Pass	Pass		X	
	Twist-Bend Test (FOTP-91)	SM < 0.2 dB, MM < 0.4 dB	Pass	Pass		X	
	Cyclic Flexing Test (FOTP-104)	SM < 0.2 dB, MM < 0.4 dB	Pass	Pass		X	
	Cable Jacket Cold Bend Test (UL 444)	No visible cracks	Pass	Pass		X	X
	Cable Bend Test (ASTM D 4565)	No visible cracks	Pass	Pass		X	X

The plenum cable is a single tube design, resulting in only one choice of cable for worst case scenario. Two plenum cables were tested; one with a single mode 18-fiber bundle and the other with a multimode 18-fiber bundle.

Cable Testing

The riser cable test plan, results, and applicability of each test is shown in Table 2. Similar information for the plenum cable is shown in Table 3.

Table 3: Air Blown Fiber Plenum Qualification Results

	Test	Requirements	Plenum	Service Conditions	Installation Conditions	Appropriate for ABF
Material	Cable Jacket Thickness (ASTM D 4565)	85% nominal thickness ≤ ave. thickness ≤ 115% nominal thickness. No point less than 70% nominal.	Pass	X	X	X
	Jacket Tensile Strength and Ultimate Elongation (FOTP-89A)	Tensile strength unaged ≥ 24.1 MPa, ultimate elongation ≥ 100%	Pass		X	X
	Flexibility Test (UL 444)	No cracks on surface	Pass		X	X
Environ.	Temperature Cycling (FOTP-3)	SM < 0.3 dB/km, MM < 0.6 dB/km	Pass	X		X
	Flammability and smoke resistance (UL 910)		Pass	X		X
Mechanical	Low & High Temperature Bend Test (FOTP-37A)	SM < 0.2 dB/km, MM < 0.5 dB/km	Pass		X	
	Repeated Impact Test (FOTP-25A)	SM < 0.2 dB, MM < 0.4 dB	Pass	X	X	X
	Compressive Loading Test (FOTP-41)	SM < 0.4 dB during loading, SM < 0.2 dB after loading, MM < 0.6 dB during loading, MM < 0.4 dB after loading	Pass	X	X	
	Tensile Loading and Bending Test (FOTP-33A)	SM < 0.2 dB during loading, SM < 0.1 dB after loading, MM < 0.5 dB during loading, MM < 0.2 dB after loading	Pass		X	
	Twist-Bend Test (FOTP-91)	SM < 0.2 dB, MM < 0.4 dB	Pass		X	
	Cyclic Flexing Test (FOTP-104)	SM < 0.2 dB, MM < 0.4 dB	Pass		X	
	Cable Jacket Cold Bend Test (UL 444)	No visible cracks	Pass		X	X

Materials and environmental testing, including flammability requirements, were all deemed appropriate for ABF cables and completed successfully. Mechanical testing proved to be more challenging. The referenced test methods for several mechanical tests were deemed inappropriate for ABF tube cables since the cables are installed with no optical component. These tests represent installation loading conditions where the pass/fail criteria are based on optical characteristics. Rather than simply substitute a more appropriate test, it was decided to follow the test plan as specified, with fiber bundles installed, and also perform additional testing to determine whether the function of the tube cable was impaired.

Tube cables need to remain free of obstructions in order to permit the free flow of air and fiber bundles. For those mechanical tests simulating installation conditions, it is appropriate to test for tube cable obstructions rather than optical characteristics. To determine whether or not obstructions occurred during the mechanical tests, it was decided to remove fiber bundles from the test cables after testing was completed. Any obstructions would be observed through the inability to remove fiber bundles from the cables.

In no instance were difficulties encountered removing the fiber bundles, so it was concluded that the riser and plenum cables did not incur any obstructions which would prevent the functionality of the cables.

Testing the indoor ABF cable products with the fiber bundles installed proved to be a success. The riser and plenum ABF cables passed every test requirement of ICEA S-83-596-1994 as well as the additional obstruction tests.

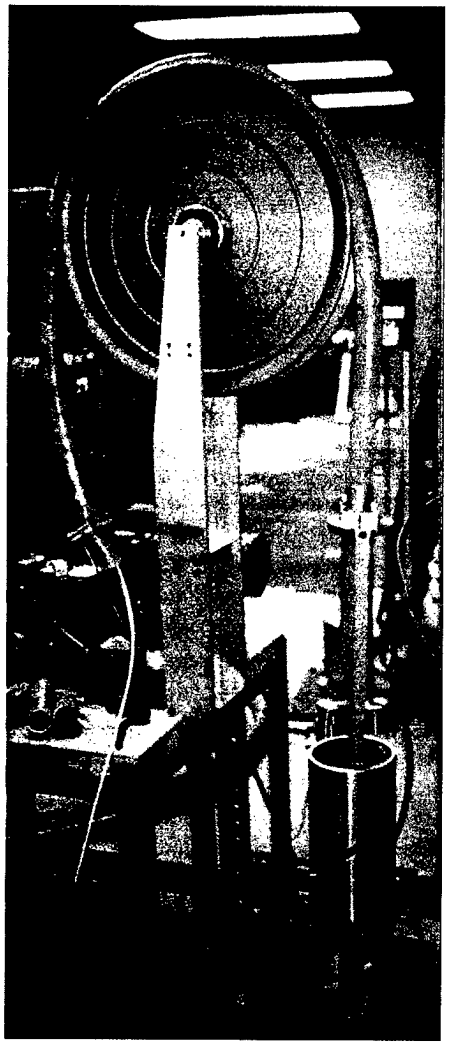

Figure 4: 19-Tube Riser on Twist-Bend Machine

SHOULD CABLING STANDARDS BE CHANGED?

Air blown fiber systems and other emerging cabling technologies are quickly gaining market share in the telecommunications industry. As a result, current standards are no longer capable of meeting the broad spectrum of cable designs available to satisfy all of today's cabling scenarios. As new technologies and the resulting products evolve, the limits of current standards are pushed beyond their intended scope. The standards should be modified to readily adapt to new technologies.

On the other hand, one must consider the purpose of standards – to address minimum product requirements in order to ensure the performance of similar products against certain criteria. If there are limited similarities between conventional and emerging products, perhaps the primary purpose of the standards would be defeated by making them readily adaptable to a broader range of products.

The best solution may require a compromise resulting in standards evolving to reflect what might be appropriate for installation and in-place testing requirements for a limited group of products. One way to do this may be to provide guidelines that allow the manufacturers to apply specific test requirements to alternative products as deemed appropriate. The purpose of standards should not change – they must continue to ensure the performance of similar products against certain criteria. However, the criteria should reflect a given product's actual installation methods and requirements, resulting in meaningful data that ensures a manufacturer's system will work after installation is complete. For a conventional cabling system, perhaps that means performing the tests as they are currently stated in the standards. For other systems, it may be different. For an air blown fiber system, it is inappropriate to perform many of the mechanical tests with fiber installed. This does not simulate actual installation conditions. Instead of monitoring fiber attenuation, a more appropriate test would verify the integrity of the tubes during and after loading conditions are applied.

Presently, cabling standards do an excellent job of ensuring that conventional cables that fall

within limited design parameters will display satisfactory performance during and after typical installation loads are applied. However, emerging technologies must also be addressed appropriately. Because these technologies are not properly addressed, it is proposed that current standards for conventional cables allow modified test plans for products similar in function but not in design.

SUMMARY

Sumitomo's riser and plenum ABF cabling products were tested against and passed ANSI/ICEA-S-83-596-1994, Standard for Fiber Optic Premises Distribution Cable. The fact that ABF tube cables are installed without optical fiber required forethought to ensure meaningful results from tests that simulate installation conditions.

The challenges faced in qualifying ABF products bring to light the fact that the current revision of the standards is not sufficient to address emerging cabling technologies. Increased adaptability of the cabling standards is required to better keep up with innovations in the marketplace.

Increased adaptability is accomplished by continually examining existing specifications and ensuring new cable designs are taken into consideration. Pacesetting standards organizations can maintain industry leadership by taking these measures into account.

BIBLIOGRAPHY

Engel, F. "Put your money where your mouth is." *Communications News* (35:7), July 1998, pp. 32-33.

Standard for Fiber Optic Premises Distribution Cable (ANSI/ICEA S-83-596-1994). Insulated Cable Engineers Association, Inc. Second Edition, June 1994.

The Telecommunications Distribution Methods Manual. BICSI, 1995.

ACKNOWLEDGEMENTS

The authors would like the acknowledge and thank the members of Sumitomo's Lightwave Lab, Materials Lab, and Machine Shop for all their help during the qualification testing of the air blown fiber cables.

ABOUT THE AUTHORS

Terri L Dixon
Sumitomo Electric Lightwave Corp.
78 Alexander Drive
Research Triangle Park, NC 27709

Terri L Dixon is an Applications Engineer for ABF cabling systems at Sumitomo Electric Lightwave Corp. She received a bachelor's in electrical engineering from The Pennsylvania State University and a master's of applied science in management sciences from the University of Waterloo. She is a recipient of the J. William Fulbright Foreign Scholarship.

Keith Quistorff
Sumitomo Electric Lightwave Corp.
78 Alexander Drive
Research Triangle Park, NC 27709

Keith Quistorff is a Senior Product Design Engineer at Sumitomo Electric Lightwave Corp. He received a bachelors of science degree in mechanical engineering from North Carolina State University in 1987. His professional experience includes over six years of design & development work with air blown fiber products.

OPTICAL FIBER DISTRIBUTION IN CENTRAL OFFICES AND TESTING METHODS FOR COMMERCIAL FTTH SYSTEM

Kenichi TOMITA, Kenji YOSHIOKA, Naoki NAKAO, and Nobuo TOMITA

NIPPON TELEGRAPH AND TELEPHONE CORPORATION, Makuhari, Chiba, Japan

ABSTRACT

Nippon Telegraph And Telephone Corporation (NTT) introduced the fiber to the home (FTTH) in Yokohama in 1997, and started to offer the commercialized services. In this area, we are providing a CATV as video service, N-ISDN and POTS as telecommunication services. These services are realized with passive double star (PDS) topology and wavelength division multiplexing (WDM) components.

This paper describes a novel optical fiber distribution method in central offices and a remote fiber testing system (RFTS) AURORA (Automatic Optical Fiber Operation Support System) which has a new maintenance and fiber identification wavelength of 1650 nm. These technologies have already been introduced in the FTTH system in the Yokohama area. We have confirmed that they provide good performance in the field.

INTRODUCTION

In 1995, we conducted fiber to the home (FTTH) trials at three sites in the suburbs of Tokyo. The trials included the provision of CATV and video on demand (VOD) as video services, and also N-ISDN as a telecommunication service. These systems use two optical wavelengths 1310 nm and 1550 nm over one fiber to take advantage of optical fiber characteristics and to maximize the efficiency of fiber plants. [1]

In July 1997, NTT started to offer commercial services in the area of Yokohama shown in Fig. 1 via the FTTH system that we realized by using passive double star (PDS) topology and wavelength division multiplexing (WDM) components.
We focus on an optical fiber distribution method for use in central offices and testing methods and show how they are used in the commercial FTTH system in Yokohama (Yokohama FTTH system).

We discuss the fiber distribution configuration in a central office in terms of splitter and filter location and describe the structures of a high density splitter, splitter frame and indoor cable.

We also describe a new version of AURORA [2] with a maintenance wavelength of 1650 nm and an ID tester as a fiber identifier.

FIBER DISTRIBUTION IN CENTRAL OFFICES

Splitter and filter position

Figure 2 shows the single star network architecture and access methods for testing. Test access modules (TAMs) [3] are used to insert the test light into optical fibers. A TAM consists of an 8 ch coupler and filters for protecting the optical line terminals (OLTs) from the reflected test light. These filters have to be put between the couplers and the OLTs.

As regards splitter and filter position, we considered 3 possible patterns for the PDS network architecture, as shown in Fig. 3. We selected pattern I-B as the most suitable by taking ease of system maintenance and cost reduction into consideration. [4]

Configuration of Yokohama FTTH system

We decided on of the Yokohama FTTH system configuration shown in Fig. 4 based on the above considerations.

Splitters configuration. We have adopted splitters which employ planar lightwave circuits (PLC) with wavelength insensitive couplers as shown in Fig. 5. Because the PLC is advantageous in terms of high-density and mass production.

This splitter has 4 input ports for 1310 nm, 2 input ports for 1550 nm and 32 output ports. The insertion loss requirement form port A to port B is $\leq$ 19.5 dB at 1310 nm, the requirement from port C to port B is $\leq$ 15.4 dB at 1550 nm, and the required isolation between 1310 nm and 1550 nm is $\geq$ 50.0 dB.

High-density splitter frame. We installed a frame to accommodate the splitters between the OLTs and FTMs to relieve congestion of the distribution as shown in Fig. 6.

The structure of splitter frame is shown in Fig. 7. This frame consists of 7 shelves which can accommodate 50 splitters with 32 output ports and 11,200 fibers on the downstream side. And this frame is 1.6 m (W) x 0.6 m (D) x 1.8 m (H).

High-density indoor optical cable. We increased the density of the indoor optical cables between the splitters and the TAMs to simplify the distribution.

The structure of this cable which contains 160 fibers is shown in Fig. 8. The cable diameter is approximately 20 mm. The required insertion loss is ≤ 0.7 dB at 1310 nm.

We confirmed that the above requirements were satisfied in manufacturing trials.

TESTING METHODS

Configuration of AURORA

Figure 9 shows the system configuration of AURORA. It is composed of test control modules (TCM), fiber selectors, TAMs, termination cords with a communication light pass filter which cuts off the maintenance light. The TCM consists of test and measurement equipment and an N x M fiber selector which can connect any piece of test and measurement equipment such as an OTDR, a light source, or a power meter.

Test light wavelength for maintenance

We have selected a wavelength of 1650 ± 5 nm for maintenance, because this wavelength meets to the following requirements.

- It should be more sensitive than service wavelengths for the purpose of detecting abnormal events easily before the events affect services. This requires a longer wavelength than that used for telecommunication.

- It should be at least 100 nm from service wavelengths to prevent interference.

- It should have narrow range so that either a dielectric multilayer interference filter or a fiber grating filter [5] [6] can be used as a termination cord. The fiber grating filter is more inexpensive than a dielectric multilayer interference filter, however its cutoff range is narrower.

Termination cord with a filter

We used not only dielectric multilayer interference filters but also fiber grating filters for the termination cord in the customer's building. The FTTH system requires many termination cords, so we have to reduce the filter cost. Therefore, we have decided to use the fiber grating filter which will be suitable for mass production and reduce the cost more.

The required insertion losses are ≤ 1.1 dB at 1310 nm and 1550 nm, and ≥ 20 dB at 1650 nm. The required reflection losses are ≥ 35 dB at 1310 nm and 1550 nm, and ≤20 dB at 1650 dB.

ID tester for fiber identification

Conventional ID testers detect the 1550 nm wavelength, so we have made ID testers which detect only the 1650 nm wavelength by modifying the curvature radius of the fiber bending unit.

The required insertion losses of the fiber bending unit are ≤ 0.5 dB at 1310 nm and ≤ 2.5 dB at 1550 nm.

We confirmed that the above requirements were satisfied in manufacturing trials.

CONCLUSIONS

We have proposed a new configuration for optical fiber distribution in central offices with a high-density splitter frame which accommodates a maximum of 11,200 fibers and a high-density indoor optical cable which contains 160 fibers.

We have also described AURORA and an ID tester with a 1650 nm wavelength test light which are designed to test optical fiber lines in subscriber loops. These technologies have already been introduced in the Yokohama FTTH system. We confirmed that they provide good performance in the field.

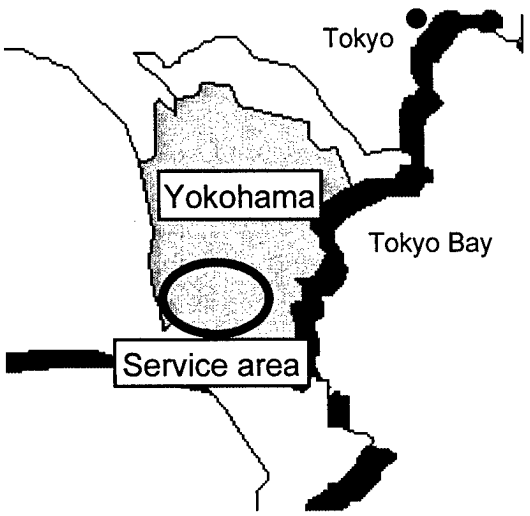

Fig. 1 Service area of Yokohama FTTH system

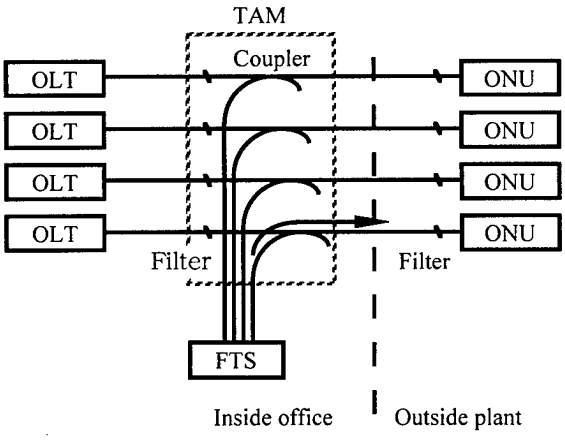

OLT : Optical Line Terminal
ONU : Optical Network Unit
TAM : Test Access Module
FTS : Fiber Test System

Fig. 2 Single star network architecture

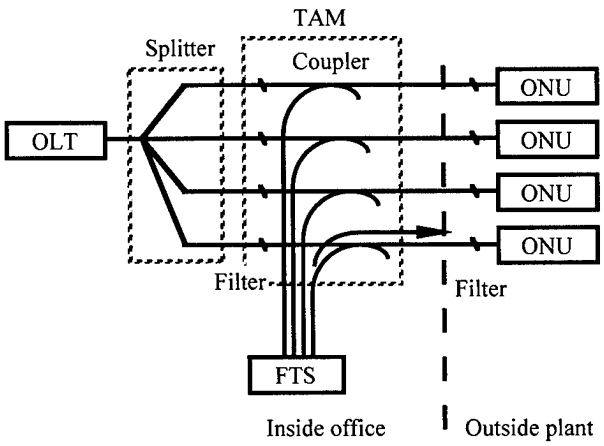

Pattern I-A : PDS networks with splitters inside the office and filters inside the TAM

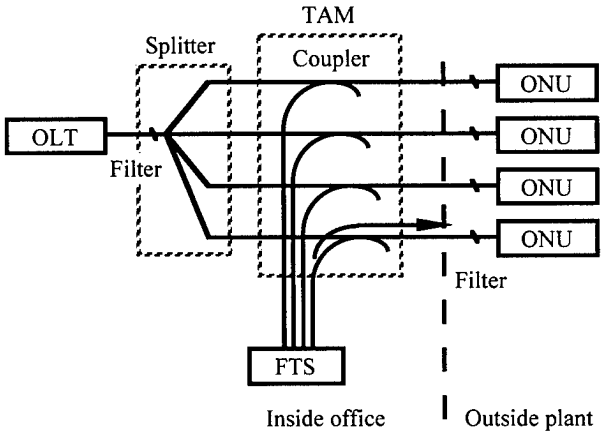

Pattern I-B : PDS networks with splitters inside the office and filters inside the splitter

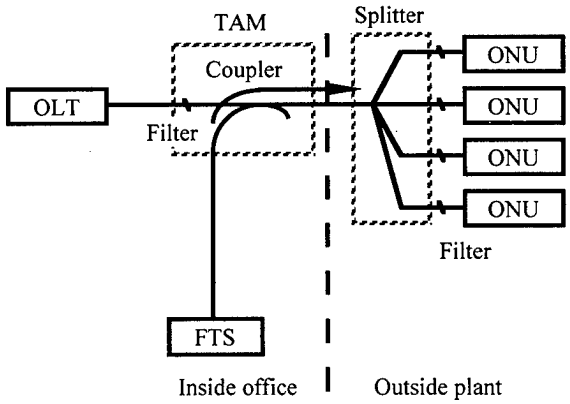

Pattern II : PDS networks with splitters outside the office

Fig. 3 Patterns of PDS network architecture

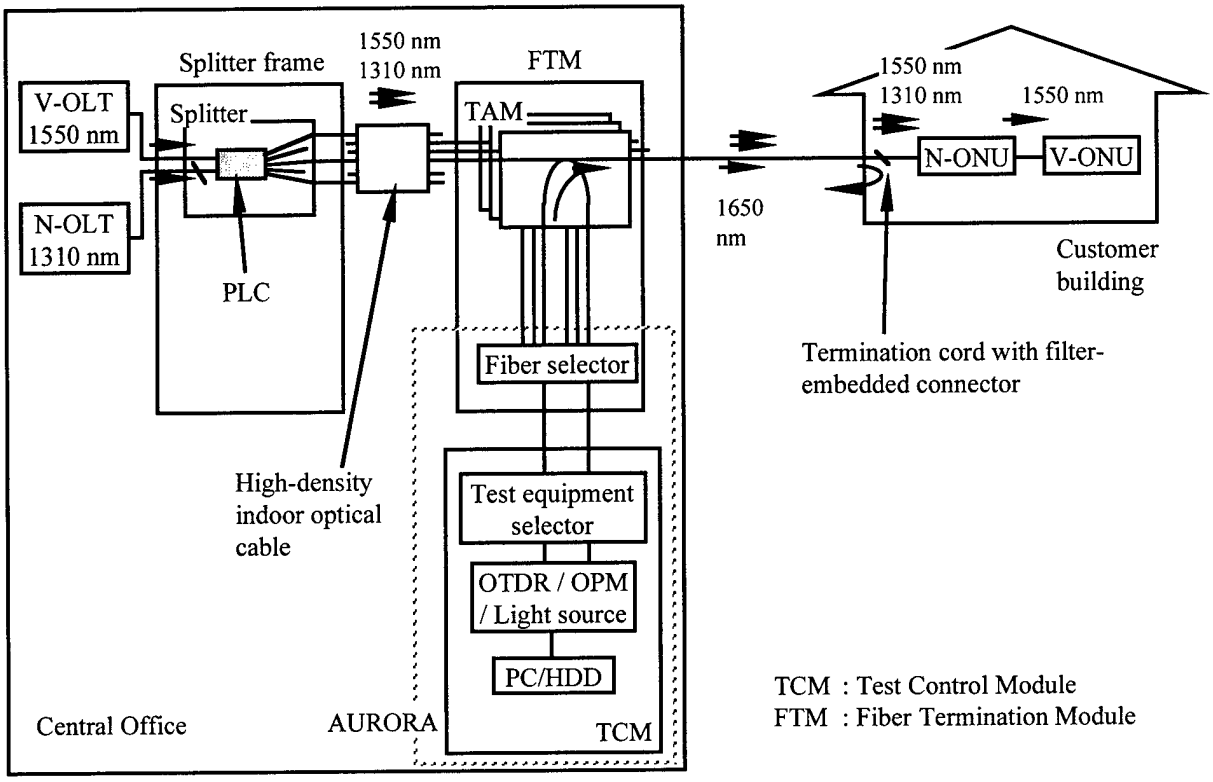

Fig. 4 Configuration of Yokohama FTTH system

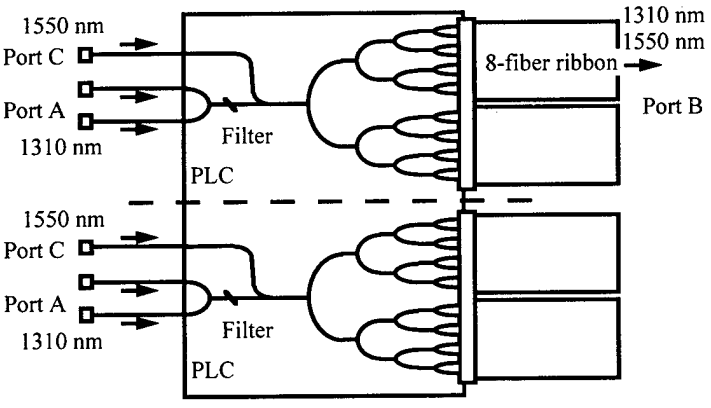

Fig. 5 Configuration of a PLC-type splitter

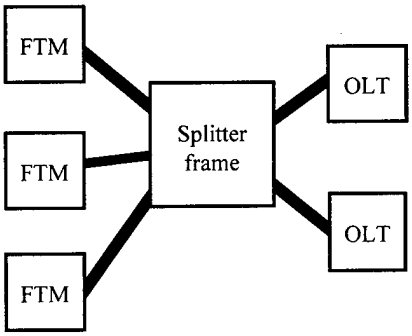

Fig. 6 Splitter frame position

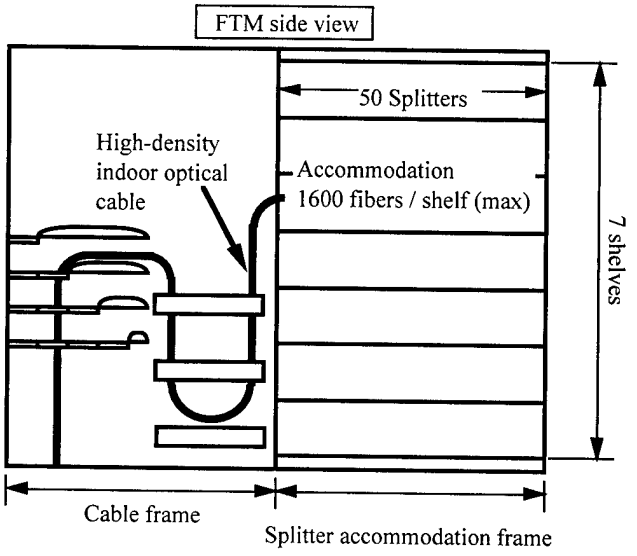

Fig. 7 Structure of splitter frame

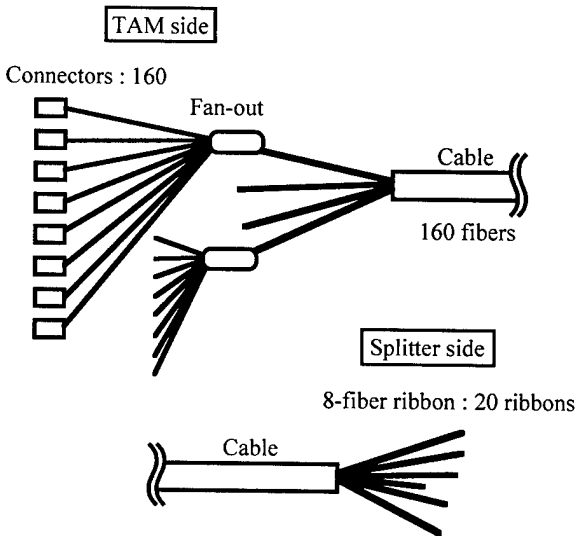

Fig. 8 Structure of high-density indoor optical cable

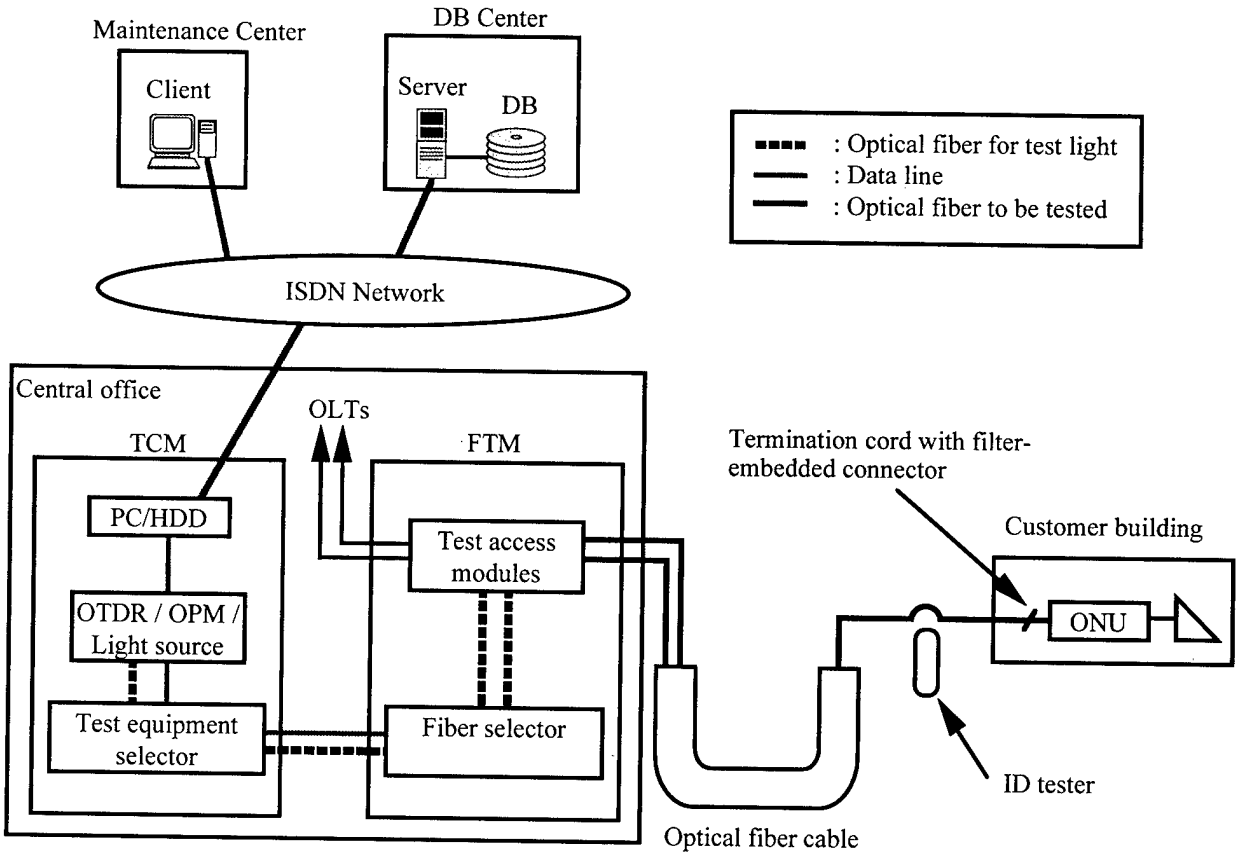

Fig. 9 System configuration of AURORA

ACKNOWLEDGMENTS

We thank Atushi Hariki, Shinichi Sugiura and Masato Kuroiwa for their encouragement.

REFERENCES

(1). Y. Yoshii, K. Tomita, K. Omoto, N. Nakao, and M. Kuroiwa, "Remodeled Automatic Fiber Testing System for FTTH Trials", 45th IWCS Proceedings, pp. 396-401, 1995.

(2). T. Ebihara, N. Nakao, and M. Kuroiwa, "Novel Automatic Remote Fiber Line Testing System and New Fiber Termination Module for Expanding Local Subscriber Loops", 22nd ECOC Proceedings, pp. 69-42, 1996.

(3). T. Oguchi, N. Takato, H. Hanafusa, N. Tomita, Y. Enomoto, and N. Nakao, "Design and Fabrication of Highly-Dense Optical Components for In-Service Fiber Testing and Monitoring in Subscriber Loops", IEICE TRANS. ELECTRON., VOL. E80-C, NO. 1, pp. 123-129, January 1997.

(4). N. Nakao, T. Enomoto, and M. Kuroiwa, "Splitter Positions and Testing Wavelength for Optical Fiber Access Network", 22nd ECOC Proceedings, pp. 269-272, 1996.

(5). K. Tomiyama, K. Hogari, S. Furukawa, Y. Miyajima, N. Tomita, and M. Ohashi, "Application of Broad-Band Fiber Grating Filters to Termination Cables", in Nat. Conv. Rec. IEICE, , SB-11-8, pp. 749-750, March 1996.

(6). K. Tomiyama, S. Furukawa, K. Hogari, and N. Tomita, "Studies on 1.65 μm Fiber Grating Filters to Termination", in Nat. Conv. Rec. IEICE, , B-10-45, p. 344, September 1997.

AUTHORS

Kenichi TOMITA
NTT-Makuhari Building 1-6 Nakase Mihama-ku Chiba-shi, Chiba 261-0023 Japan

Kenichi Tomita graduated from Tomakomai National College of Technology in 1988.

After joining NTT in 1988 he engaged in constructing outside telecommunication plants. He is currently a technical staff member of the Access Network Systems Laboratories, and is engaged in the development of operation systems for optical access networks.

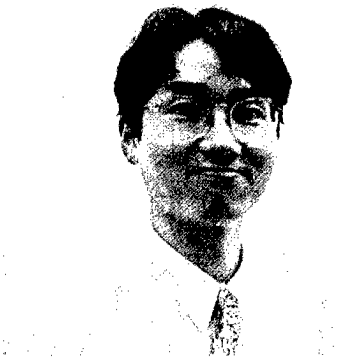

Kenji Yoshioka
NTT-Makuhari Building 1-6 Nakase Mihama-ku Chiba-shi, Chiba 261-0023 Japan

Kenji Yoshioka received his Bachelor's degree in science from Hokkaido University in 1990.

After joining NTT in 1990, he engaged in the development of fiber optic cables. He is currently an Engineer in the Access Network Systems Laboratories, and engage in the development of operation systems for optical access networks.

He is a member of the Institute of Electronics, Information and Communication Engineers of Japan.

Naoki NAKAO
NTT-Makuhari Building 1-6 Nakase Mihama-ku
Chiba-shi, Chiba 261-0023 Japan

Naoki Nakao received his Bachelor's degree and Master's degree in electrical engineering from Okayama University in 1985 and 1987, respectively.

After joining NTT in 1987, he engaged in the development of splicers for copper pairs. He is currently a Senior Engineer in the Access Network Systems Laboratories, and is responsible for the development of operation systems for optical access networks.

He is a member of both the Institute of Electronics, Information and Communication Engineers of Japan, and the Institute of Electrical and Electronics Engineers, Inc.

Nobuo TOMITA
NTT-Makuhari Building 1-6 Nakase Mihama-ku
Chiba-shi, Chiba 261-0023 Japan

Nobuo Tomita received his Bachelor's degree and Master's degree in electrical engineering from Kumamoto University in 1972 and 1974, respectively, and his Doctor's degree in information engineering from Kyushu University in 1988.

After joining NTT in 1974, he engaged in research on broadband and digital subscriber loops and in the development of optical fiber cable components. He is currently a Senior Research Engineer and a Supervisor of the Access Network Systems Laboratories, and is responsible for the development of optical fiber distribution systems in central offices and operation systems for optical access networks.

Dr. Tomita is a member of both the Institute of Electronics, Information and Communication Engineers of Japan, and the Institute of Electrical and Electronics Engineers, Inc.

A VERY INNOVATIVE TECHNOLOGY FOR RIGHT OF WAY APPLICATION

J.P. Bonicel[1], H. Costa-Elias[2], P. Vertuaux[3], P. Gaillard[4], R. Newman[5], M. Rivard[6]

[1]Alcatel - TPLE - France, [2]SANEF - France, [3]ADPS - France,
[4]Alcatel - OFCCC - USA, [5]MKI - France, [6]Marais - France,

ABSTRACT

In Europe, the liberalization of Telecommunications is ongoing and new Telecom Operators are investigating all the possibilities to find new right of ways, allowing the installation of long distance fiber optic cables in a very short period of time, with the minimum initial capital investment. This challenging target generates many innovative ideas and we intend to present in this paper a very innovative technology that we have developed to install metal-free, fiber optic cables along motorways.

In standard fiber optic installations, for example to install fiber optics in ducts, the civil works and cable laying represents 8 to 10 times the price of the optical cable. These works are very time consuming, and must be reduced for safety reasons; therefore a completely new system has been developed. This new system will enable the installation of around 10 km per day and per team, of an optical cable specially designed for this application.

Quick to install, this new technology will provide the opportunity to divide the cost of the complete installation compared to a standard one by about a factor of 4.

To reach this target, a full range of products and equipment have been developed in order to install a special metal free cable of 8 mm diameter with 60 single mode fibers, into a small groove dug in the asphalt of the motorway. The automatic laying machine digs the groove, cleans the groove, dries the groove (if necessary), lays the cable in the groove and pours into the groove a special flexible bituminous compound stable vs. temperature and compatible with the optical cable.

After different field experimentation, and many laboratory tests that demonstrate the reliability of this new technology, it has been decided to install around 1600 km of optical cable containing 60 optical fibers.

1. INTRODUCTION

Besides traditional Telecom operators (TELCOs), new Telecom operators want to create their own optical networks starting with the long distance links and going deeper and deeper into cities. The main concerns of creating these new optical networks are :

. Implementation of the network in a limited period of time.
. Low cost network, particularly for civil works.
. High reliability.

TELCOs have built their networks for years by installing cables in ducts (1)(2) or using directly buried cables. New operators must find alternative solutions to install quickly and at low cost their networks. They are ready to use all possible solutions and right of ways (ROW). A lot of ROW are possible such as :

. Railways (3)
. High voltage lines (4)(5)
. Phase conductors (6)
. Micro civil works (7)
. New trend in civil work and construction (8)
. Sewer tubes (9)
. Rivers
. Motorways.

Motorways have been used for a long time for traditional installation of optical cables (cables in ducts or directly buried).

Some motorways do not have ducts preinstalled. In such cases, due to heavy traffic and safety concerns, the traditional installation technique of optical cables is not possible because it is too slow and very expensive.

Based on all this analysis, an innovative technology has been developed to enable the

quick implementation of a long distance telecommunication motorways network.

2. NETWORK PROJECT

2.1. Optical Network on Motorways : Why ?

In France a large part of the motorway network is operated by private or state owned companies. But all of them act like private ones.

There are two reasons to install an optical network on motorways.

The first one is that the development of ITM (Intelligent Traffic Management) increases the bandwidth which is needed to operate motorways (video, toll, automatic accident detection, etc...). Optical networks are a good solution for this need.

The second reason concerns the deregulation of the telecommunication market.

Before July 96, nobody except the operator of the motorway, could install a duct along motorways. The motorway company could do it under the condition that the duct was necessary for its mission.

The law that organizes the liberalization of telecommunications modifies that principle, and telecom operators (TELCOs) are now also allowed to install their ducts on motorways. Motorway companies can't oppose a demand from a TELCO.

Motorway companies do not want various TELCOs to dig along the road. They find it dangerous and embarrassing for their clients.

For these two reason, motorway companies planned to install optical network on motorways. So they can answer their needs, and they can lease dark fiber to TELCOs.

TELCOs are interested as they would spend much less money in leasing the number of dark fibers they really need, which is generally one pair, compared to the construction of a network over hundreds of kilometers. On a single pair of fiber, the total bit rate on use between Paris and Calais is currently 20 Gbit/s.

2.2. Constrains and advantages compared to other ROW

In France, except on roads, there are few solutions to install long distance telecommunication networks :

. The railway company (SNCF)
. The electricity company (EDF)
. The water ways

None of them have an obligation to answer the demand of TELECOs.

2.3. Targets of the project

The targets of the project for SANEF (motorways in the north and east part of France) are :

1. Realize the work in the quickest and least embarrassing manner for the traffic.
2. Decrease the costs so that a business could be developed.
3. Sign contracts with TELCOs before the beginning of the works in order to secure the project financial viability.

To be able to meet the first 2 targets, a new installation technique was proposed and developed using the strong competencies of the companies involved in this project. The basic idea was to develop a fast technique to be able to have a small 60 optical fiber cable automatically laid in a groove made at the surface of the road and to fill the groove with bituminous compound to provide the cable a good protection. Fig. 1 gives a schematic presentation of the optical cable in the groove.

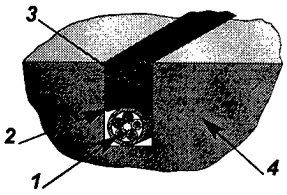

1. Cable
2. Slot
3. Bituminous filling compound
4. Bitumen (road)

Figure 1, Motorway cable laying technique

3. OPTICAL CABLE AND SPLICE BOXES

3.1. Optical cable

The optical cable used for this project is described in detail in the cable design session (10).

A cross section drawing of the cable is shown in fig. 2 and performances are given in table 1

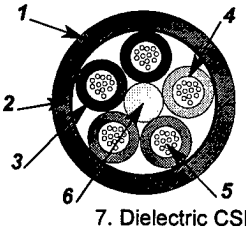

Loose tube design

1. Outer sheath
2. Dielectric reinforcement
3. Core wrappings
4. Loose tube
5. Filling compound
6. Optical fiber

Figure 2, Cable structure

ITEM	GOAL
Cable OD	maximum 8.5 mm
Tensile strength	70 daN (short term)
Crush resistance	20 daN/100 mm
Impact resistance	5 N.m
Bending diameter	100 mm (static)
Temperature range (operation)	-40°C / + 70°C

Table 1 : Optical cable performances

A fully dielectric design has been chosen because of its immunity to electromagnetic hazards, which is a key advantage for long distance applications or a use in linear networks such as links laid along motorways. Often high voltage lines are running in parallel with motorways and induced voltages may be of big concern if the optical cable includes a metallic component.

All environmental constrains that the cable should be able to support during the laying operation or in normal service have been investigated and some of them are reported in (10). The loose tube structure chosen provides the fibers the lowest stress/strain level and gives the best long time reliability.

3.2. Splice boxes

Lynx WTC 48 splice boxes are installed in small premanufactured man holes. The size of these man holes are 1000 x 500 x 300mm. A total coiled cable length of a round 10 m is stored in the man hole.

3.3 Field experimentation before network deployment

One of the basic questions regarding the optical cable environment was to understand if the fiber attenuation would be stable in all circumstances, particularly when cars and trucks run on the groove containing the cable.

In a normal installation, the groove is made on the emergency stopping lane where normally no cars or trucks are present. However, to be sure that pressure applied by tires including when braking will not create problems on the optical cable, extensive field experiment has been performed.

An optical cable as described in paragraph 31 was installed at different depths (25, 40, 50, 60 mm) for 350m in different paths but always on the running lanes and not on the emergency stopping lane

. Parallel to the lanes
. Perpendicular to the lanes
. Sinusoïdal pattern

A schematic presentation of the cable layout is given in fig. 3.

This installation was made near a turnpike where it was easy to analyse over a long period of time that braking would not create problems to the cable. Different tests were performed as presented here after and during tests fibers were looped and constantly monitored to be sure to catch all potential change in attenuation. Measurements were made using last data aquisition equipment HP 8153A / HP 81554SM to catch all transient changes in attenuation.

3.3.1. Short term test :

. ***Running test :*** a truck with 13 tons on each axle is running several times on the cable.

. ***Crush test :*** 6/10mm gravels were poured on the bituminous compound on the groove. A truck with 13 tons on each axle run, brakes, changes sharply the direction while running on the groove with gravels.

During all these tests there was no variation in attenuation at 1310 and 1550 nm.

3.3.2. Long term test

On the same length of cable a long term test was performed to check the attenuation stability

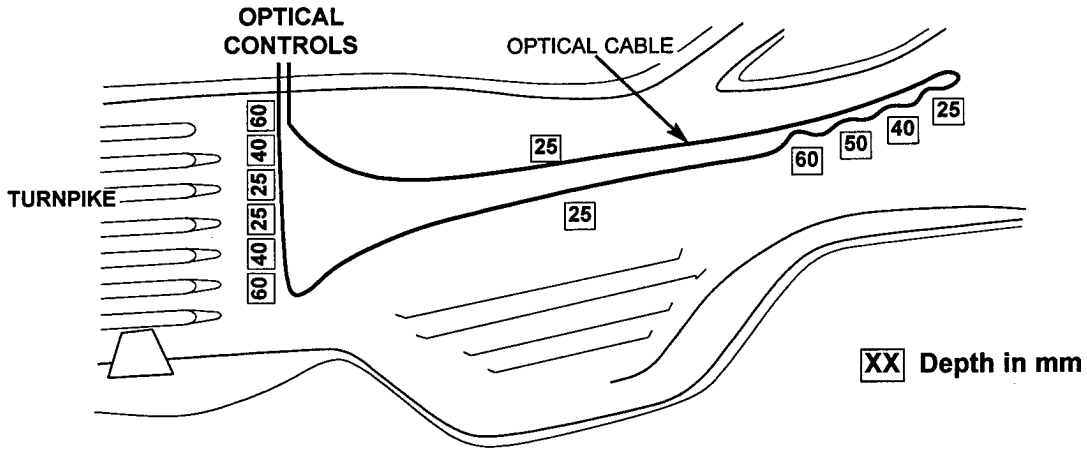

Figure 3 : Cable lay out in groove near the turnpike

when cars and trucks were running all day over different parts of the cable. Two different pieces of control equipment were used :

- A control with a computerized transmission equipment according to fig. 4.

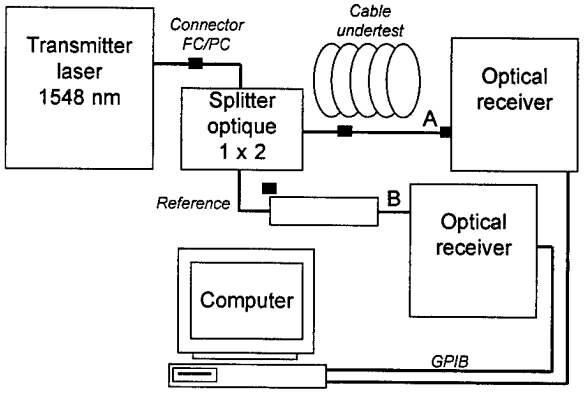

Figure 4 : Computerized transmission bench

- A control with telemonitoring OTDR Helios / Atlas equipment from Wavetek according to fig. 5 .

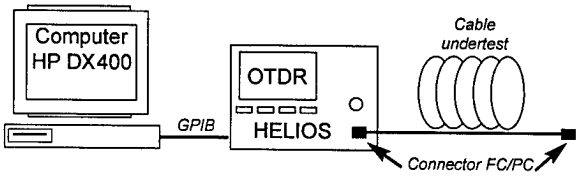

Figure 5 : Computerized telemonitoring bench

During 32 days all fibers were continuously monitored in transmision or with OTDR and no change in attenuation at 1310 or 1550 nm was identified by the data acquisition systems.

3.4. Freezing test in man hole

Due to the risk of water accumulation in man holes and frost during winter time a test was performed in the laboratory. Ten meters of cables were spliced using a splice box LYNX WTC 48. The looped box and 10 m of cable were placed in the man hole which was filled with water. The man hole was put in a chamber at -30°C and the attenuation of fibers was monitored.

No change in attenuation was noted during the test.

4. AN INNOVATIVE INSTALLATION TECHNIQUE

During the first phase all tests performed on the new cable, splice boxes and cable installed in a groove have demonstrated the good level of reliability of this new technology.

During the second phase, it was necessary to industrialize this technology to be able to install the cable at a high rate.

4.1. Installation : General constraints

The overall project management of the SANEF outwork was taken on by M.K. International who had, at the owners request, to take into account a number of constraints in order to reduce the motorway downtime to a minimum.

These constraints were as listed below :

1. The overall operating length of the moving site was not to exceed 300m.

2. Climatic constraints

- . Temperature above -5°C.
- . Rainfall at less than 5mm/h.
- . Visibility at more than 300m.

3. Laying of a minimum 5 km in 8h.

4. The plant must give a computerised record of the line trace in relation to the motorway's white lines or the security barriers with a tolerance of +/- 5 cm. Also permit the localization in relation to hectometre markers.

5. Continuous cable tension control maintaining tension below maximum allowable.

6. Placing of cable drums must be rapid and permit the delivery of the necessary cable lengths to ensure the installations of junction boxes at their agreed positions.

7. Machines must not be more than 2m wide.

8. The installation groove must, when possible, be carried out dry and without tearing or uploft.

Before backfilling, the groove must be clear of dust and gravel and perfectly dry.

Dimensions will be :

- . Width 10 +/- 2mm
- . Depth 25 +/- 5mm
- . Bending Radius 500 +/- 50mm

9. Suction of debris must be filtered so as not to cause any pollution.

10. Cable guides between the drum carrier and the cable layer also a guide into the bottom of the cable groove.

11. Resin backfill.

12. Smooth finish (no resin overflow).

13. A slight sanding of the resin to ensure adherence for vehicle tires.

4.2. Process

The fiber optic cable is buried in a small groove cut into the asphalt coating of the emergency stopping lane. Immediately after laying, it is covered with a cord of elastomer product applied in the hot liquid phase. This cord fills the groove. Accordingly, as soon as the cord has cooled and hardened, the road is returned to traffic.

Taking into account the coefficent of thermal expansion of the road asphalt coating, the optical cable and the elastomeric product, the cable is particularly well protected. Mathematical

simulations have demonstrated that the cable is held "cocoon-like" in the filled groove.

Continuous sections of cable are between 6 and 8 km long on average. At the intersection points, the two cables terminations are connected in sealed chambers installed in protected areas on the other side of the safety barrier.

Operational terminations are installed at the toll gates in the motorway management districts.

4.3. Laying methodology

To meet the demands of the SANEF the laying methodology had to be :

. Fast
. Without any major obstruction into the lanes used for traffic,
. Without any destructive impact on the running structure.

Accordingly, the idea of a punch discharging the content of the groove towards lower courses soon became evident as the only valid method. Obviously, this could only be achieved for :

. A hot asphalt coating above 8°C which is particularly malleable because it consists of an assembly of small size aggregates bonded together by an asphalt binder. By applying a load to the aggregates, they are dispersed into the basic binder which is softened by heat and accepts the migration with ease.

. Because of the small dimensions of the groove to be made, this migration only concerns small volumes and therefore has little effect on the remainder of the wearing course. Beyond a depth of 40mm, no anomaly can be detected in the structure of the wearing course.

On the basis of this observation, confirmed by a number of tests, MARAIS developed a simple machine consisting of a punching disk onto a variable load of between 5 and 10 tons is applied by hydraulic means, depending on the nature and temperature of the coating. To prevent immediate creepage towards the surface of the volume removed from the groove, two plates press the wearing course either side of the punch disk.

The opening thus formed has the following dimensions :

. Width : From 10 to 12 mm
. Depth : Between 25 and 30 mm

However, this solution will not allow a continuous groove to be cut because of a number of particular points often encountered on motorways : access ramps, emergency stopping lane heterogeneous coating, heavy vehicle lane instead of an emergency shoulder on steep gradients, etc.

Accordingly, the machine is provided with a second tool for forming a groove according to the dry sawing method while preserving the small sizes imposed initially. This method produces chips and a vacuum attachment is hitched behind the system in order to pump the chips produced and to keep the groove clean.

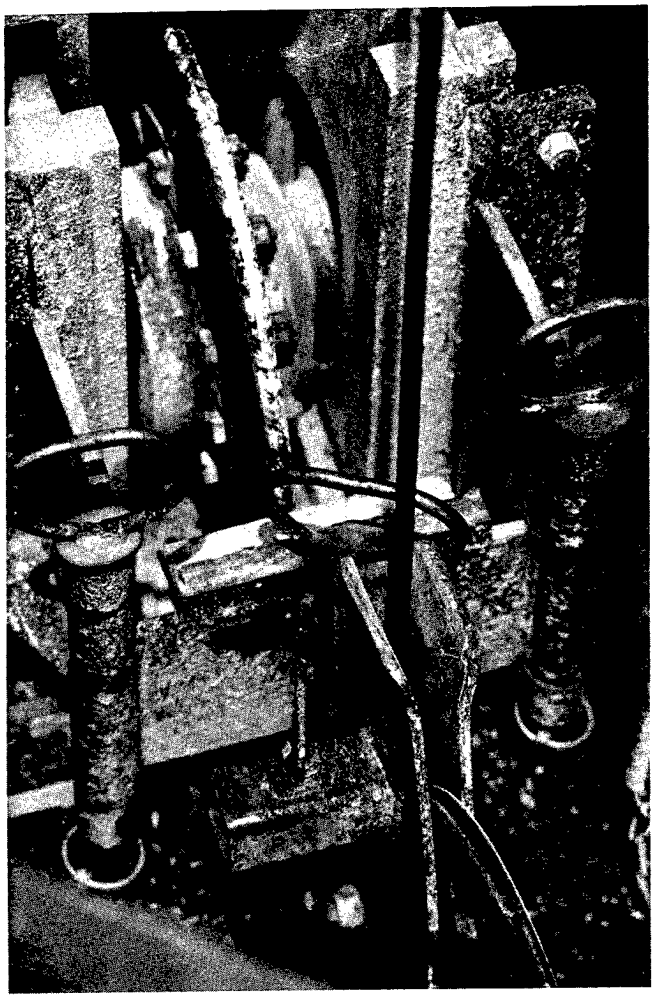

Figure 7 : Laying machine : Punching device

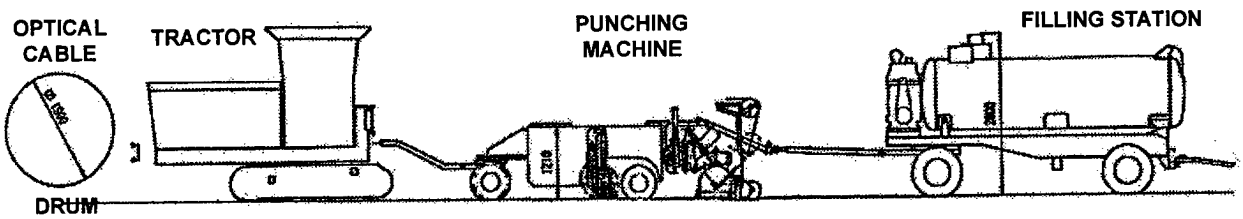

Figure 6 : Overwiew of the automatized laying equipment

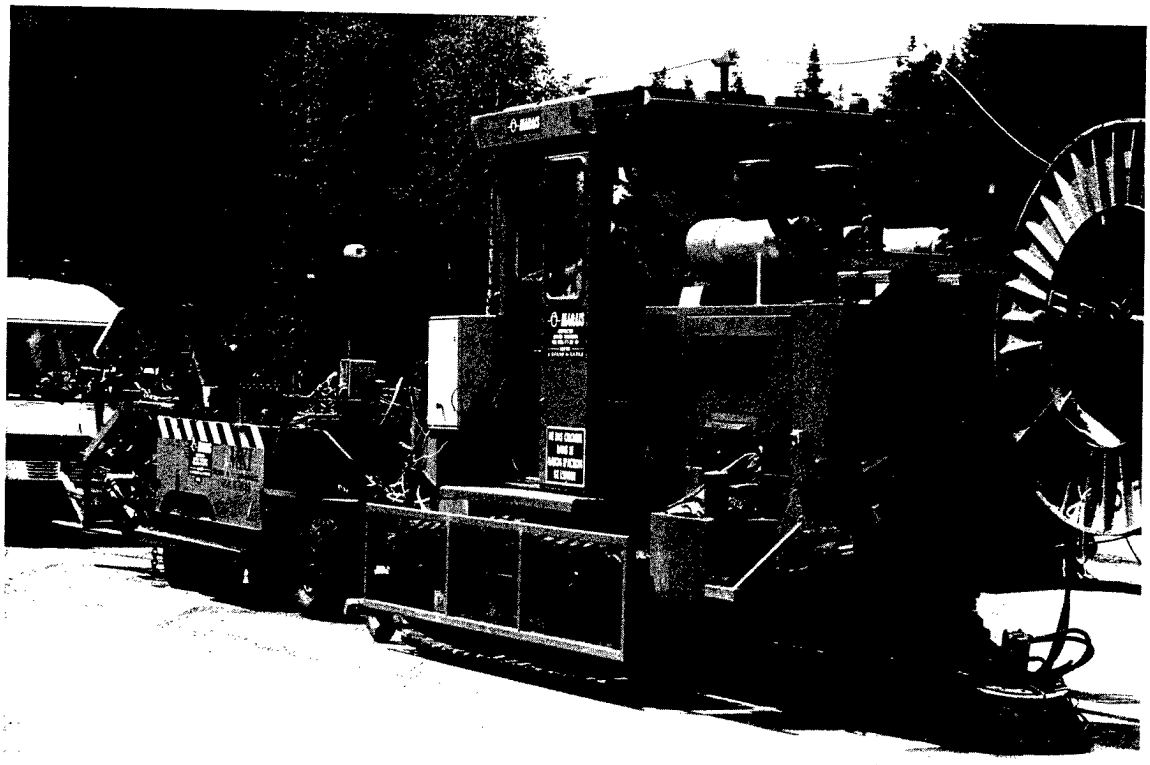

Figure 8 : Picture of the automatized laying technique

At the rear of each tool, a set of sheaves and a laying wheel deposits retains the cable at the bottom of the opening as the system moves forward.

In this way, the fiber optic cable, carried at the front of the laying gear, is placed at the bottom of the groove behind the machine.

Subsequently, a trailer deposits the filling cord into the groove.

The road surface can be used within 15 minutes of cable laying.

Fig.6, 7 and 8 give an overview of the automatized laying equipment.

4.4. Rates

On open roadways, when there are no obstacles to be crossed, each machine can operate at 2000 m/hour.

On an average given day, allowing for the obstacles encountered, a basis of 10 km per machine is regularly observed for a working period of 8 hours.

4.5. Constraints

. Coating temperature

This is the main limiting factor. Indeed, if the coating is not at the right temperature, it is almost totally deprived of plasticity and, in this case, the groove is not cleanly cut. This leads to:

- Either the collapsing of the groove sides causing cable crushing and potentially breakage or attenuation increase of the optical fibers it contains.
- Or the tearing away of the filling cord by passing vehicles, causing the optical fiber cables to be laid bare.

That is why it is necessary to work with a coating with a temperature at the heart exceeding 25°C, spread uniformly over a depth of 40 mm.

To do this, there are two possibilities :

- Ensuring the laying work when the ambient temperature is at least equal to 20°C.
- Otherwise, completing the site by a heating system which raises the coating temperature just ahead of the laying machine.

. Climatology

During rainy weather, even if the groove is well cut, the adhesion of the filling compound is random. In addition, run-off water tends to flow into the groove.

4.6. Argument

. Economy

1. *ABSENCE* of waste.

It is possible to lay, in one operation, a cable comprising 60 fibers or more in a groove without generating any waste to be evacuated and handed : a real revolution compared to the current sleeve technique.

2. High laying *RATE.*

Laying a fiber cable at a rate of 10 km/day and per machine is quite a stake to win

when traditional sleeve laying only advances at the rate of 2 km per day and per machine.

3. *LOW COST* of filling product because the volumes needed are particularly small.

. Safety

A site implementing small gauge machines advancing quickly is always more safe than a slow-moving site with bulky machinery.

As soon as the machines have finished their work, the road can be returned to normal traffic.

. Structural preservation

Cutting a 10 x 25 mm groove into a plastic coating does not cause any damage to the emergency shoulder. In addition, the mark merges into the road surface in the course of time.

5. NETWORK INSTALLATION

5.1. Project Management

Project management and planning are conducted using appropriate software for drawing and as builts tied in with existing services.

Fibre test using reflectometre for recording curves for use with an emulation software on P.C.

5.2. Feasibility Tests

Two feasability tests were carried out :

1. Laboratory tests.

These tests were used to judge the different products or methods simultaneously and to validate the solutions.

a). Chemical tests on resins, effects of hydrocarbons, salt, frost, heat and thermal differences.

b). Mechanical tests on the aging model in relation to the roads mechanical constraints and wear and tear of the slot.

c). Tests on core samples having been subjected to punch loads.

This test was carried out on a 30 km section on the A26 between Arras and Reims and enabled the verifications of service quality, the project management procedures, the installations plant and resources. Productivity levels were checked at rates of 1200 m/hour during two consecutive days of six hours.

The impact of weather conditions and the impact on motorway traffic, housekeeping maintenance and safety have also been checked.

5.3. Installation

Due to the very positive tests described in paragraphs 3 and 6.2. it was decided to install a network of 1600 km of 60 fiber cable. Prior line trace marking on the ground using hectometric markers and traffic lines and specific points like joint boxes, slip road crossing and toll barriers were taken by survey and translated to paper and numerically.

Post project cable reconnaissance enables the easy locating of the cable.

As built drawing complete with automatic photographs every 500m as well as photos at every particular point (joints, crossing etc.). These photos were numerised and supplied on a CD ROM to the owner for chronological archives. The photos show the site conditions during installation and the line marker.

The installation was carried out using 8 different project work crews :

1. Line schedule : Laying out the longitudinal line trace for the cable and setting joint and diversion positions.

2. Lower pass : Carring out of the installation of covered metal guttering for passing bridges in advance of the main cable laying crew.

3. Toll gates, district offices, pylons and rest areas : Preparation and installation of joint boxe diversions and preparation for cable passage.

4. Slotting : Prepare the cable slot, lay the cable and lay resin backfill.

5. Finishing : Clean up and check network continuity, joint and chamber access.

6. Cable engineering : Fixing all passive telecoms equipment. Pre-cabled junction boxes were not allowed for at connection boxes every 2 km.

7. Cable connection : At each junction and diversion.

8. End connections : Installation of all passive equipment at network heads, network nodes and in all the districts.

5.4. Commissioning and Handing Over.

This was carried out in 2 phases :

1. For each segment of fibre optic cable with bi-directional reflectometre at 1310nm and at 1550nm. The attenuation was less then 0.25 dB/km at 1550nm and 0.38 dB/km at 1310nm.

Maximum chromatic dispersion 20ps/nm km.

Maximum mode polarisation dispersion **0.5ps/$\sqrt{\text{km}}$ (typical < 0.2 ps/$\sqrt{\text{km}}$)**

2. For each loop, partial handing over, reflectometric tests in both directions at 1310nm and 1550nm and a power test on the loop. The average attenuation on the loop and the attenuation of each splice gave the following values for :

A(dB) = (L x aF) + (NE x aE) + (NC x aC)

Where L = length of fibre
aF = fibre attenuation factor
NE = number of splice
aE = average splice attenuation
NC = number of connections
aC = average connector attenuation

With the following factors :

	1310nm	*1550nm*
aF dB/km	0.38	0.25
aE dB	0.10	0.10
aC dB	0.50	0.50

6. ECONOMICAL ANALYSIS

The main objective of this inovative installation technique was to drastically reduce the cost compared to a traditional process where plastic tubes or cables are laid in a trench.
Table 2 presents the relative cost of these 2 techniques and points out the strengths of the new one.

PARAMETER	RELATIVE COST	
	TRADITIONAL	NEW TECHNOLOGGY
Trench and other civil works	360	36
Cable 60 fibers G652	43	43
Engineering and splicing	21	21
TOTAL	424	100

Table 2 : Relative cost of the 2 techniques

The costs of the new technology should be doubled, at it is suitable to install two cables, one on each side of the motorway to have a 100% redundant system.

RETURN ON EXPERIENCE

Since October 1997, SANEF operates an optical network 1.600 km long, along 800 km of motorways.

This network was built in 5 months.

All the operators customers of SANEF have chosen to lease secured pairs of fibers : one pair on each side of the motorway.

Due to the system redundancy (one cable on each side of the motorway) the disponibility of the service is 100 %.

7. Conclusion

Following methodologic analysis we have developped and carefully tested new products and very innovative technique for the installation of optical cables along motorways. After detailled lab and field experimentations a network of 1600 km of 60 fibers cable was installed in 5 months. Associated to this high speed project there are dramatic advantages in installing telecommunication networks along this right of way (ROW) that is motorways. In particular this innovative technology divides the cost of a complete installation by about four compared to a standard one . Using the right products (optical cables, splice boxes...) and with a redundant installation (one cable on each side of the motorway) the reliability of the system is 100 %. This network gives the opportunity to implement on this reliable network high bit rate systems at 2.5 or 10 Gbit/s TDM or n x 2.5 or 10 Gbit/s WDM on each pairs of fibers.

REFERENCES

(1) Automatic long length optical fiber cable installation system J. Sogame . NTT - EURESCOM - Torino, 30 - 31 March 98

(2) Current Developments in Cable-in-Duct Blowing Techniques - W. Griffioen, KPN Research, Leidschendam, The Netherlands; G. Plumettaz, Plumettaz SA,Bex, Switzerland, IWCS 97 - p. 363

(3) Aerial Fiber Optic Cable for Railway Applications Metallic or Dielectric Solutions - J.P. Bonicel, O. Tatat, G.Couvrie, Alcatel Cable, Bezons Cedex, France; L. Rapebach, SNCF, France; P. Zamzow, Kabel Rheydt, Mönchengladbach, Germany; J. Rauchs, Opticable, Belgium; and C. Vergez, Alcatel Contracting, France, IWCS 95 - p.368

(4) (1) Bonicel (J.P.), Cortines (C.G.), Delomel (J.C.), Hog (G.), Pouilly (S.), Tatat (O.), Zamzow (P.E.), "Optical Ground Wire A Worldwide Technical Survey and Comparison". International Wire & Cable Symposium Proceedings, 1993.

(5) Aerial optical cables along electrical power lines by J.P. Bonicel and O. Tatat, Alcatel.REE : Revue de l'électricité et de l'électronique, March 98.

(6) Optical Phase Conductor for Medium Voltage Overhead Power Lines - R.Böhme, G. Hög, M. Hoffart, U. Jansen, K. Nothofer, Kabel Rheydt AG, Mönchengladbach, Germany, IWCS 96 - p. 43.

(7) A New Application of Air Pulled Cable in Microduct for the Local Loop - P. Lesueur, D. Lecoq, G. Le Goff, A. Pecot, J. Le Rouzic, France Telecom, Lannion, France, IWCS 95 - p.382

(8) New trend in civil work and construction EURESCOM - Torino, 30 - 31 March 98.

(9) FAST - The optical fiber cabling system for cable plants in sewer tubes - W. Liese Alcatel. Eurescom - Torino 30 - 31 March 98.

(10) Optimization of loose tube cable designs : The next step.
P. Gaillard, O. Tatat, Alcatel Cable - OFCCC - Claremont, NC; K. Nothofer, Dr A. Weiss, Alcatel Kabel - Germany; D. Benzel, Alcatel Cable - France. IWCS 98.

AUTHORS

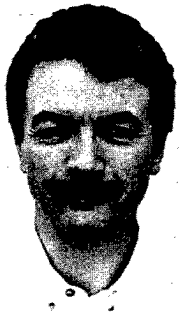

Jean-Pierre Bonicel
Alcatel
30 rue Pierre Bérégovoy
92111 Clichy
France

Jean-Pierre BONICEL (46) received his engineering degree from the Institut des Sciences de l'ingénieur of Montpellier (ISIM) in 1976. He joined Les Cables de Lyon, now Alcatel, in 1977. After being Manager of the Alcatel Optical Fiber Cable Competence Center (Claremont, NC), he is now Product Marketing Manager for the Telecom Product Line in Europe (TPL-E).

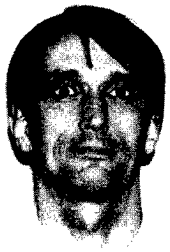

Pierre GAILLARD
Optical Fiber Cable
Competence Center
Alcatel
Claremont, North Carolina
USA

Pierre GAILLARD received his engineer degree from the Ecole Catholique des Arts et Métiers (ECAM) in 1980. He joined Les Cables de Lyon, now Alcatel, in 1983. He is now Resources and Technology Manager of the Alcatel Optical Fiber Cable Competence Center.

Philippe VERTUAUX
Sté ADPS
37 rue Pierre Lhomme
92400 Courbevoie
France

Philippe VERTUAUX was born in 1958, He obtained his degree in Economics and Commercial Science from the ISSEC Institute.
He began his career within the THOMSON-CSF Group, where he successively exercised as Project Manager and Department Manager on telecommunication systems for the National Defense. As assistant to the Fixed Networks Department's manager in the RCC Department (Réseaux Communication Commandement) he was in charge of the transit network for the InterArmy needs and satellite communications (SOCRATE and "SYRACUSE III" projects). Then he took in charge the commercial activities of this department.
In July 1993 he created the new Company A.D.P.S. (Assistance aux Directions de Projects et aux Systèmes) of which he is the Chairman and Managing Director.

Rod NEWMAN
MKI
14, Rue des Sorins
92000 Nanterre
France

Rod NEWMAN was born in 1953, studied building and civil engineering at the South Bank Polytechnic in London.

He worked for multinational construction companies in Europe until the end of 1995, when he "started-up" MKI in France.

MKI is today one of the world's leading turnkey project managers to the telecommunication industry, with offices in all major European cities, far East and Australia, offering specific knowledge and expertise in the field of optical fibre system.

Rod NEWMAN is now Managing Director for MKI France.

Hélidéo COSTA-ELIAS
SANEF (North and EAST of France turnpike)
100 Avenue de Suffren
75015 Paris
France

Hélidéo COSTA-ELIAS, born in 1957, received his engireering degree from the national school of civil ingineering (ENPC) in 1981. In 1982 he founded a software company and sold his shares in 1991. He joined SANEF as director of the modernisation and developpement, in charge of all the technological projects, espacially in the software and telecommunication area. He totally renewed the telecommunication network of SANEF, and developped a new business in SANEF with the optical cables. His activity now represents 20 M$ and 3% of the turn over of the company with a very high profitability. He was elected in France, "Manager of the year 1997" for telecommunication and network.

Daniel RIVARD
Marais
Le Clos du Moulin
49330 Mire
France

Daniel RIVARD, born in 1948, is a self made man. He has been designing, manufacturing and selling trenching and laying equipment from 1976 to 1992 in his own factory. Since 1993 he is running one hundred of highly specialised engineers and technicians in mechanized laying of power and telecom cables. Currently he owns more than 60 pieces of specific equipment which he has designed.

OPTICAL FIBRE CABLE LINKS WITHIN DRINK WATER PIPES AS AN ALTERNATIVE TELECOMMUNICATIONS ROUTE TECHNOLOGY

Paul E. Gregor, Helmut G. Haag, Werner Braun*

Alcatel Kabel AG & Co, Mönchengladbach, Germany
*** Kellner Telecom, Korntal-Münchingen, Germany**

ABSTRACT

The high cost level for underground cable installations require with a strong increasing tendency alternative laying technologies like incorporation of optical fibre cables into existing drink water supply ducts instead employment of conventional burial procedures in order to improve economy for erection of telecommunication cable plants.

A further reason to use alternative cable route solutions is the disadvantage of high density of cables and ducts particular in narrow city areas which constitute serious difficulties for additional new installations.

This contribution describes basically the design considerations for link components like cables and pipe flanges necessary and the special laying technique for broadband cables.

INTRODUCTION

At present the erection of fibre cable links by private enterprises is increasing remarkable in Germany caused by the liberalization of the telecommunication services since the beginning of 1998.

More than 50% of the total costs to build up cable links have to be considered for make up of the cable route. Consequently huge measures are taken seriously to reduce this unfavourable cost portion by employment of alternative procedures.

Since existing pipeline networks constitute a huge grid of about 500.000 km for drink water supply within Germany, particular respecting the regional and municipal range a challenge has been occured to use these ducts for dual functions, a symbiosis for water and communication transmission.

Further advantages for the alternatives are the fast installation time, strong reduced organisation work for relevant traffic regulations to be done normally and reduced problems regarding questions of ownership for new cable route decisions.

This contribution describes a typical overall alternative technology for integration an optical fibre link into a drink water pipeline including all necessary access components, equipments, tools and installation methods based upon a project of about 3.4 km link extension within a northwest German city.

The decision for this concrete project has been placed since existing cable routes were already occupied by other infrastructure elements and the required fast realisation time avoiding any heavy traffic organisation measures.

THE DRINKING WATER DUCT

The high expenditures for a conventional cable route performance had to be reduced significantly by using an existing drinking water duct. The duct consisted of a 200 mm diameter steel pipe and for a certain distance of a 300 mm diameter cast iron type.

A number of water pipe slide valves have been located along the pipeline section. At these points the optical fibre cable had to be led through a special by-pass device. The operating water pressure in the pipe ranged between 3 and 5 bar depending on the actual water consumption.

OPTICAL FIBRE CABLE DESIGN

For transmission of broadband signals resp. high data rates single mode fibres and cable design have been performed according international specification IEC 793/IEC 794, european provisions EN 187000/EN 188000 and additional German national standard DIN VDE 0888.

The cable core consists of six filled buffer tubes each containing eight SM-fibres. Stranding of tubes has been carried out in SZ-technique around a metalfree central strenght member. In order to obtain longitudinal watertightness and to improve impact resistance the interstices of the cable core have been filled continously with a suitable jelly compound.

To achieve the necessary cable tensile strength a certain number of aramid yarns have been wrapped helically around the core. Those yarns are combined with a special hot melt material in between and to the following sheath construction to realize the desired pulling strength.

To increase the mechanical protection behaviour and to get a permanent vapour barrier a laminated aluminium polyethylene sheath (LAP) has been manufactured, which consists of a both side coated aluminium tape with a thickness of 0.2 mm sealed to the special polyethylene jacket. Such a sheathing design constitute a high impact resistance which is needed for later cleaning measures of the water pipeline.

The described cable type A-DF(ZN)(L)2Y 6 x 8 E9/125 0,36F3,5 is shown in figure 1.

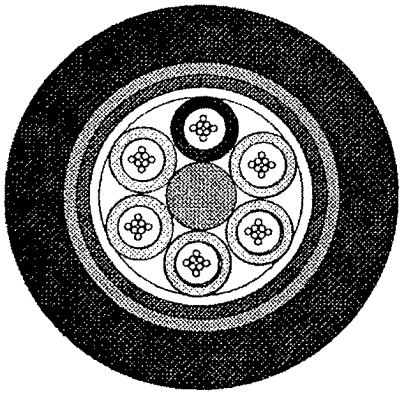

Fig. 1: Optical fibre cable A-DF(ZN)(L)2Y 6 x 8 E9/125 0,36F3,5 / 0,25 H19

ACCEPTIBILITY OF CABLE MATERIALS

The chemical neutrality of all cable materials and especially of the sheathing compound to drinking water is important to be met. The optical fibre cable had to fulfil the stringent Federal Public Health Authorities requirements in Germany (BGA-Kommission, 1.und 2. Mitteilung des Bundesgesundheitsamtes./ Bundesgesundheits-blatt 20-1977-S.10 bis 60 bzw. 124 bis 129 /KTW-Specification) and DVGW document W 270 for hygienic and microbiological technologies.

Test protocols had to be submitted recognizing the cable lay out for employment in contact with drinking water according to the requirements of Federal Health Authorities.

Furthermore, adequate measures were to be taken to exclude all risks regarding infection or other microbiological contamination during the cable laying work. The pulling rope and the cable had to be cleaned thoroughly. To remove contaminations which might have penetrated into the pipeline during the laying process despite all preventive measures, the duct was rinsed sufficiently after the cable installation.

The contractor has been declared responsible for all changes towards unallowed water quality. The final acceptance test did not reveal any cause for complaint.

DESIGN PERFORMANCE OF PIPE FLANGE FOR OPTICAL FIBRE CABLE ENTRIES

One of the innovative tasks of this project was to overbridge the pipe slide valves without effecting its optical properties and mechanical intactness. A water pipe flange with a slide valve ensures that after the drilling of a hole into the pipe and closing the slide valve, the pipe can maintain water supply until the optical fibre cable has to be pulled into the pipe.

In figure 2 design of the cast iron flange for cable entries and exits is shown in principle. It consists of an upper and a bottom part. Within the upper part the sealing

device is located which consists of special drink water proved hard rubber rings being pressed against the cable and the inner flange surface with a suitable pressure. In order to find the necessary mounting conditions for the sealing device

adequate examinations have been made in laboratory consequently.

In case of a later damage of cable caused for instance by excavation work respectively pulling the cable far above the allowed pulling strength cable has to break before sealing system becomes destroyed.

To avoid cable damage within the flange below the the sealing component and to lead the cable to the safer bottom of the pipe a stainless steel tube with a suitable bending radius has been incorporated. The steel tube has been modified with special perforations close to the entrance of sealing elements in order to avoid any permanent air concentration.

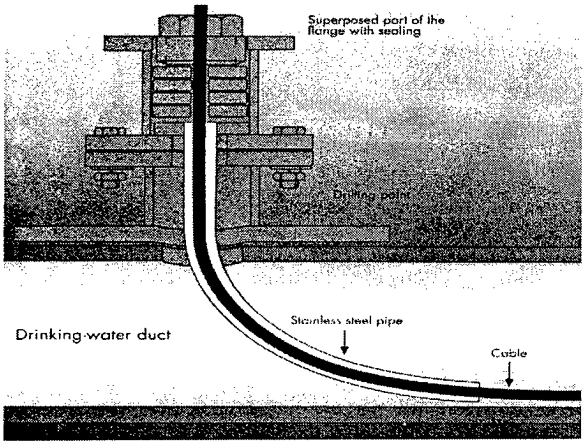

Fig. 2: Water pipe flange with sealing device in principle

In figure 3 the original flange construction mounted onto the pipe is shown.

The special sealing device chosen guarantee the almost triple pressure level compared to the operational water pressure in practice without deterioration of cable characteristics.

To achieve this, the cable manufacturer ran a series of tests providing pressures of 15 bar. The optical fibre was introduced and fixed into the flange equipped with a sealing system on both sides, each consisting of six sealing elements and a spanning nut.

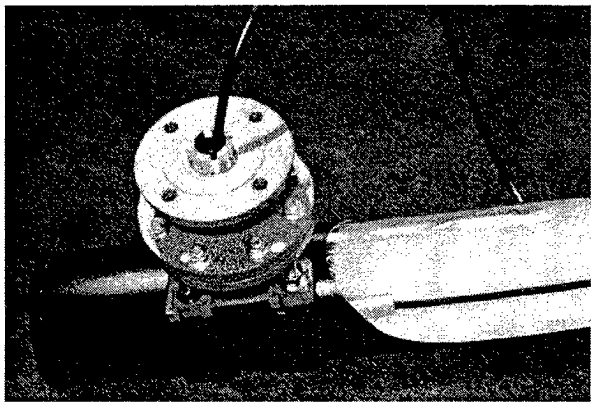

Fig. 3: Mounted water pipe flange in original performance

Figure 4 exhibits the special test set-up, in which the appropriate mechanical tension for the sealing elements had been adjusted. The mechanical and optical properties of the cable and the tightness of the total flanges have been examined within a time period of 72 hours of exposure to pressure.

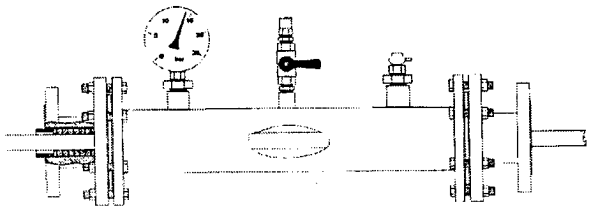

Fig. 4: Test set-up for cable and flange technology under water pressure

This examinations expressed, that

- the introduction of the cable into the sealing elements causes no problems
- the sealing systems works safe and reliable when mounted correctly
- no increase of optical attenuation occur
- no deformation of the cable occur

STRUCTURE OF ENTRIES AND EXITS ALONG A TYPICAL URBAN PIPELINE

Generally there are two reasons that cables have to leave the pipeline at unregular distances along the drink water pipeline, which are drawn in priciple in figure 5. That is the need to overbridge existing slide valves along the link. The second reason is to incorporate in certain cases subscribers into the telecommunication cable network under preparation. At overbridging and subscriber branching points additional cable lengths is necessary to be layed to enable easy performance of jointing sleeve in case of for instance repair work upon water pipeline.

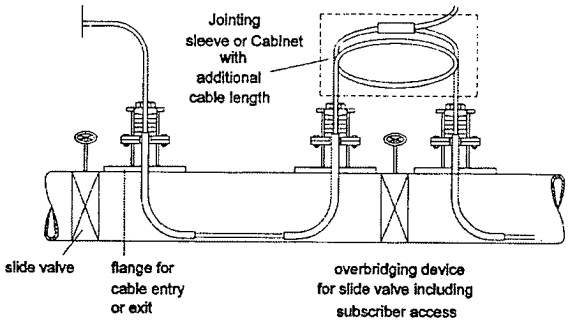

Fig. 5: Overbridging devices for water pipeline slice valves along an optical fibre cable link

CABLING LAYING PROCEDURE AND MOUNTING OF FITTINGS

As a first installation step holes have to be drilled into the water pipes at all cable entries and exits. In this case of a typical urban area the cable has to overpass a high number of slide valves. Therfore, the cable lengths that could be pulled directly into the pipeline without any branching or overbridging points had been relatively short with distances between 150m and 250 m as an average value. Normally cable pulling has been executed from an exit location point into both directions.

Accordingly the number of holes to be drilled and fittings to be installed was here exceptionally high. The fittings used for the holes drilled into the pipes were standard pipe clamps and slide valves with seals and retaining clips. The drilling of holes into the pipe has been carried out under operation of pipeline. An impression of the pneumatic drilling process in practice is given in figure 6. In order to perform a precise drilling a special platform has been mounted firm between slide valve and drilling device.

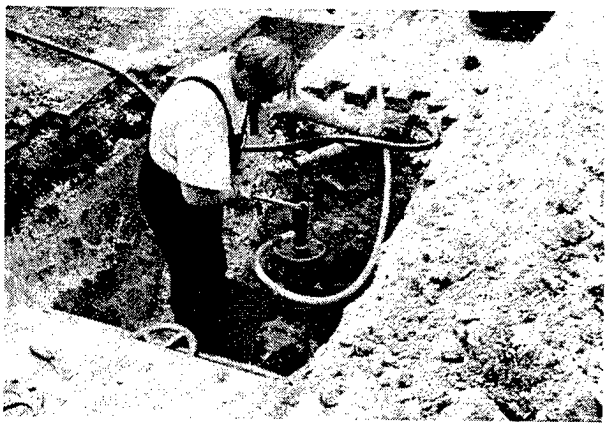

Fig. 6: Execution of drilling process on water pipeline

The hole diameter was selected as big as possible with 100 mm in order to simplify the later introduction of the go-devil. The holes were sealed until cable pulling by means of blind flanges mounted on slide valves which themselves were fastened with conventional pipe clamps (figure 7).

Fig. 7: Flange installed on the water pipe before cable pulling

The water supply was interrupted by sections during the introduction of the plastic rope and for the cable pulling procedure. Therefore, most of the work has been done during the night and week ends.

After closing the water supply, the slide valves installed on the pipe clamps were removed and

replaced by the superposed bottom flange with its sealing system. Then, the go-devil connected to the plastic rope was introduced into the hole and flooded forward into the pipe by progressive opening of the water shunt. In a second step the optical fibre cable was attached to the rope and pulled through the section. Figure 8 shows the superposed bottom part of the flange with the arriving optical fibre cable protected by a plastic tube temporarily.

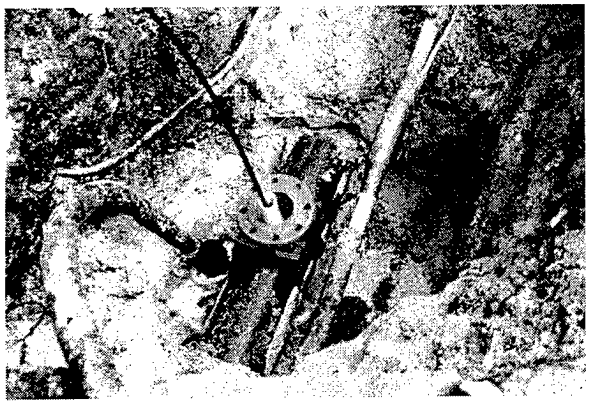

Fig. 8: Superposed bottom part of the flange with arriving optical fibre cable

The cable entries have been closed safely by the sealing system. After complete installation of the flange and refilling the pipe water tightness was controlled. The cable exits at the superposed flanges were sealed by a flexible plastic tube and protected against mechanical loads by cover plates, a necessity since all fittings were installed directly into the ground.

At each overbridging point for slide valves and at potential subscriber branch-offs, cable overlenghts in ring shape have been installed. This will allow a future maintenance, extension or cable jointing and branching measures.

Due to the short cable length per section the installation of additional closures could not be avoided. The following components were implemented for cable jointing and termination applications:

- 19" main distribution cabinets with high return loss (HRL) fibre connectors..
- Single fibre splice management and patch closures in cross-connects cabinets on the section ensuring optimal modularity for future extensions (Points of Presence).

  In one of the cross-connection cabinets presently the terminations of three cables, eight fibres of one buffer tube of each cable core were terminated with HRL-connectors allowing a later connection to further subscribers to be carried out with appropriate jumpers.

- Jointing sleeves for burial applications at connection points without potential future subscriber branch-offs.
- A typical branch-off-point to a subscriber is shown in figure 9 where the optical fibre cable has been installed between a slide valve and the subscriber premises. The OF cable is normally covered by a plastic tube to achieve sufficient protection against undesired mechanical impacts

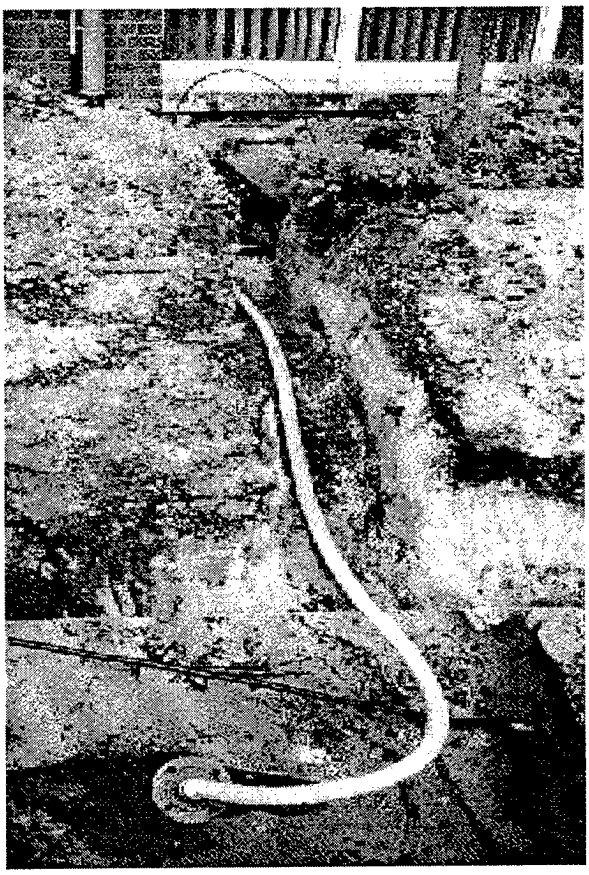

Fig. 9: Typical branch-off-point of drink water OF cable link

TESTING OF COMPLETED LINK

After installation of all link components each fibre was tested with special attention to all pipe sealing locations. No increase of optical attenuation has been registered caused by transversal pressure on the cable.

Further test results on completed link were:

- Insertion attenuation at 1310 nm wavelength to evaluate the fibre the overall link quality including all connections. The average attenuation of 1,7 dB has been tested significantly below the specified maximum limits.

- OTDR measurements at 1310 nm and 1550 nm wavelenghts from both fibre ends to indicate homogenity of link including the fibre splice quality.
  The average attenuation for fibre splices have been found below 0,05 dB.

CONCLUSION

A new installation technology for integration of optical fibre cables into supply ducts, like drink water pipelines has been taken into practice with an already strong increasing tendency to be used.

Appropriate components to build up such a new technology are available.

Sufficient knowledge of this alternative cable laying technique is available, however important measures are necessary to be performed without any compromize for instance regarding laws, recommendations, provisions, regulations, instructions and guide lines of responsible health authorities. Cleanness of drinking water pipes including components to be integrated into the pipes has to be taken as the very first law.

The most important reasons to apply this technology are:

- Considering a pipeline section without any slide valves or other devices within the line reduction of necessary investment can be put down to a remarkable level compared to conventional installation methods.
  In figure 10 a typical overall cost situation is shown considering conventional laying procedure and increasing number of slide valves along the link.

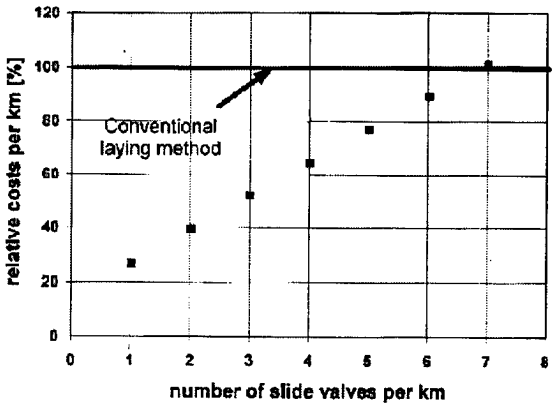

Fig. 10: Comparison of installation costs regarding conventional and alternative cable laying procedure

- Depending of increasing numbers of pipeline slide valves, to be overbridged by additional equipment economy becomes influenced unfavourable.

  Based upon an already existing pipeline infrastructure and considering a typical city environment time reduction for cable installation into supply pipelines has been found up to a favourable factor 5:10 compared with conventional laying methods.

- Minor problems regarding difficult route conditions with crowded and narrow underground environment.

- Optical fibre lenghts up to 3000 m (one lenght) have been flooded into a water pipeline section without intermediate slide valves.

- Reduction of the water supply capacity has been calculated between 4 and 6 % considering the here described dimensions of cable and pipeline.

- In case of repair work upon pipelines, slide valves or flanges with integrated cable intensiv cleaning with suitable chemicals and water is important to be executed. Finally verification of drink water quality is necessary as normally done permanently.

- In order to reduce time for repair work it is useful to store spare material, particular a pair of flanges for the ingoing and outgoing cable.

REFERENCES

1. DIN VDE 0888: Optical fibres for telecommunications and data processing installations, Berlin Offenbach: vde-verlag
2. DIN EN 187000: Specification of optical fibre cables, Berlin Offenbach: vde-verlag
3. DIN EN 188000: Specifications of optical fibres, Berlin Offenbach: vde-verlag
4. IEC 793-1: Optical fibres, Part 1: Generic Specification, Berlin Offenbach: vde-verlag
5. IEC 794-1: Optical fibre cables, Part 1: Generic Specification, Berlin Offenbach: vde-verlag
6. 'Construction of Telecommunication Cable Plants-Engineering Criteria' Telecom Cables & Networks, Alcatel Kabel 1/96
7. 'A cityNet Project - Engineering, Installation and Operation' Telecom Cables & Networks, Alcatel Kabel 2/96
8. Gregor, Stolz, Naumann 'Optical Fibre Cable Plants along Gas Pipelines', etz 10/1997
9. Jänker, Gregor, Röhr 'A Medium Voltage Power Cable Plant Integrating Optical Fibres', Elektrizitätswirtschaft, issue 26/1997, pp 1560 - 1565

AUTHORS

Helmut G. Haag
Alcatel Kabel
Bonnenbroicher Str. 2-14
41238 Mönchengladbach
GERMANY

Helmut G. Haag was born in 1948. He is Managing Director of Telecommunication in ALCATEL KABEL, Germany and member of the board of KABELRHEYDT, Germany. After reaching his Dipl.-Physiker from Stuttgart University he joined KABEL RHEYDT (which was taken over by ALCATEL in 1992) in 1975. There he had different positions in Development, Production, Marketing and Sales. He took his present position in 1997 resp. July 1998. Since long he is member of national and international standardisation bodies UIT, IEC, CENELEC and DKE.

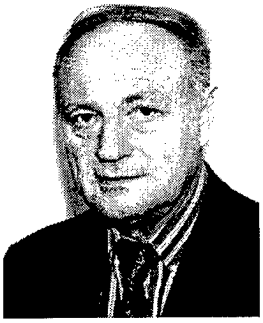

Paul E. Gregor
Alcatel Kabel
Bonnenbroicher Str. 2-14
41238 Mönchengladbach
GERMANY

Paul E. Gregor was born in 1941. After study at Ingenieurschule Duisburg, Germany, he joined AEG KABEL, today ALCATEL KABEL Mönchengladbach where he had been involved in development projects for special symmetrical and coaxial telecommunications cables. About for a decade he took over the responsibility as head of design department for cable design technology. At present he is responsible for the technical sales department and is acting as a member in national and international standardisation bodies, like DKE resp. ISO/IEC.

RETENTION OF STRENGTH IN OPTICAL FIBRES UNDER STRAIN IN A WARM, MOIST FIELD-INSTALLED ENVIRONMENT

Peter Ostojic, David Coulson, Ken Clarke, Alfred W. Kruijshoop

Telstra Research Laboratories, Telstra Corporation, Clayton, Victoria, Australia

ABSTRACT

As a result of a route upgrade, fibres retrieved from a cable that had been subjected to high humidity, temperature and an applied stress for 13 years were examined. The dynamic stress corrosion susceptibility parameter (n_d) and the strength of the fibres was determined and both were found to be high for all fibres. Presented is some 'real world' evidence to indicate that the vast majority of fibre in a network enjoying less severe conditions, can be expected to have the desired long service life.

1.0 INTRODUCTION

Owing to the importance of telecommunications in today's society, the reliability of telecommunications networks is one of the prime concerns not only to carriers but also to users of such technology. Improving overall network reliability was one of the major considerations in the adoption of optical fibres for use in telecommunications since they are not prone to many of the problems affecting copper wire.

Although not subject to the same problems as copper, optical fibres are not entirely problem free. Of particular relevance to fibre reliability is static fatigue. Static fatigue[1] is the term used to describe the interaction between glass subjected to an applied tensile stress, and water. That interaction results in the formation/extension of flaws on the glass surface with the rate of interaction increasing as the tensile load, humidity and/or temperature increases.[2, 3] In optical fibre the process of static fatigue can result in surface flaws growing to such an extent that: (i) handleability problems occur because the fibre cannot withstand even gentle handling without breaking or, in the worst case (ii) spontaneous fibre breakage occurs. It is that event that has resulted in the finite (approximately 40 year) design lifetime of optical fibres.

The challenge of incorporating static fatigue into a viable fibre lifetime model has been met with considerable success and currently there are some 15 fibre lifetime models available. Not surprisingly, much contention exists as to which model is the most accurate, the relevance of the underlying assumptions of many of the models to modern-day fibre and the methods of obtaining and analysing data from fibres in order to determine certain fibre lifetime parameters.[4] It is however, generally accepted that regardless of which path fibre lifetime theory follows, certain fundamental fibre parameters will be needed to make use of that theory. One such parameter is believed to be the stress corrosion susceptibility parameter (n) and it is also generally accepted that as the value of n increases, so too does the fibre lifetime.

A value of n greater than about 20 has been suggested as desirable to achieve a satisfactory fibre lifetime[5]. Improvement in manufacturing technology has resulted in the virtual elimination of extrinsic (processing-induced) flaws as well as significantly reducing the severity of intrinsic (inherent) flaws, on the fibre surface and so current production (new) fibres easily meet that value. Earlier production (old) fibres however, contain both extrinsic and (comparatively) large intrinsic flaws and so would be expected to have not only a lower n-value than current production fibres, but a lower tensile failure stress as well.

Most of the work on fibre lifetime has been carried out in the laboratory and the results assumed to translate into 'the real world'. Owing to the costs involved in installing, monitoring and recovering optical fibre cable from the field with a significant service life history, little work appears in the

literature addressing the validity of that assumption[6].

Following a route upgrade that fortuitously involved ploughing new optical fibre cable along exactly the same path as an old existing cable, Telstra was recently able to obtain samples of old fibre from cable that had been in-service since 1985. That cable, which had no moisture barrier, was from the tropical latitudes of the Northern Territory of Australia and so was subjected to both high ground temperatures and, owing to monsoonal rains, high humidity (typically 98% RH minimum). The entire service history of the cable was known and no fibre failures had been recorded.

Testing of cable prior to when cut-over indicated the fibres to be under a tensile load, but within specification, a finding subsequently verified by Brillouin scattering techniques. A 1530 nm Brillouin Optical Time Domain Analyser (BOTDA) instrument developed in our research laboratories was used to measure the levels of strain on the installed fibres. The various Brillouin frequency shifts of all 8 fibres in the cable were taken in-situ before any excavation work was undertaken. These measurements were later compared with reference measurements made on the same fibres once they had been removed from the recovered cable to ensure there were no residual strains present. Further corrections were made for the different temperatures of the fibres while in the soil (31°C) and when the reference traces were taken back in the laboratory (21°C). In this way the fibres were all found to have been under strains in the range 0.097% to 0.110% (corresponding to frequency shifts of around 50 MHz). Since fibre from duct-hauled cables along the same route also exhibited these values, it can be assumed the cores of these fibres were under such strains since cable manufacture in 1985.

Thus, fibres from the recovered cable samples contained both extrinsic and ('large') intrinsic flaws and had been subjected to high temperatures, high humidity and some applied tensile stress for a period in excess of some 13 years. According to fibre lifetime theories, those conditions are particularly detrimental to fibre and so provide a 'worst case' scenario for the overall reliability of the optical fibre network. This work reports on the failure stress and *n*-values of those recovered fibres and discusses the implications of the findings to network reliability and fibre lifetime theory.

2.0 METHOD

To ensure all fibres were at the same initial state prior to testing, all retrieved fibre samples were dried for a minimum of 5 days at 30°C before testing and stored at that temperature until testing was complete. To ensure all fibres were at the same state during testing, all tests were performed with the fibres submerged in de-ionised water maintained at 40°C. In order to make comparisons, current production fibre was also included in this work and it too was tested at 40°C.

Fibre coatings were analysed using Fourier Transform Infra-Red (FTIR) spectroscopy.

Since the mechanism of static fatigue involves water at the crack tip[7], it might be expected that for a fibre loaded slowly in an aqueous environment, water has much time to interact with the glass. As a consequence microcracks in a slowly loaded fibre are more likely to be extended by static fatigue resulting in a reduced fibre failure load when compared with the same fibre loaded at a faster rate. This is observed in practice and forms the basis of the dynamic method for determining the stress corrosion susceptibility parameter (n_d). It was this method that was employed in the current work. Fibres were tested in 2-point bend, for such tests fibre samples some 35 mm long are bent into a C-shape and placed between machined faceplates (jaws) grooved to hold 30 fibres simultaneously. The two jaws are then driven together at a user-defined rate by a computer-controlled stepper motor. As the jaws move together the stress on the fibres increases until they break. The breaks are detected by an acoustic emission transducer mounted on one of the jaws and a computer records the jaw separation at failure. That information is then used to determine failure stress.[8]

Pre-conditioning time in the test environment has been shown to influence the value of the failure stress particularly at high loading rates where it is thought that the environment has insufficient time to diffuse through the fibre coating. This, in turn,

can result in an inaccurate determination of the stress corrosion susceptibility parameter and so it has been suggested that a suitable conditioning time be experimentally determined for the fibre/coating system under test.[9] One fibre was selected at random from the cable and its pre-conditioning time was determined by mounting samples of that fibre in the 2-point bender and soaking the samples in de-ionised water at 40°C for various times before driving the jaws together at a rate of 5 μm/sec. A plot of Soak-time vs Failure Stress was determined and an appropriate pre-conditioning time identified (see Figure 1). An identical procedure was used to establish the pre-conditioning time for the current production fibre.

In the absence of formal guidelines, four faceplate velocities (υ) were arbitrarily chosen to determine the dynamic stress corrosion susceptibility parameter (n_d). Those values were 0.5, 5, 50 and 500μm/sec.

It is assumed that failure data from experiments such as these fit a 2-parameter Weibull distribution. The required parameters are the shape parameter (also called the Weibull modulus, m) and the scale parameter (also called the characteristic value, σ_o). In order to determine the Weibull modulus to within 10% of its true value, a minimum sample size of 30 fibres was used in this work[10] for each of the four faceplate velocities, as well as in determining the appropriate pre-conditioning time. The accuracy in the scale parameter is dependent on both the Weibull modulus and the sample size.[11]

For the various fibres tested, the shape and scale parameters of the data sets for each of the four loading rates were determined using the maximum likelihood estimate of Thoman *et al.*[12] The use of a small sample of data to determine the Weibull modulus of the parent population can introduce a bias into that calculated value which can be off-set by the use of appropriate unbiasing factors. Unbiasing factors for the maximum likelihood estimate of the Weibull modulus have been determined [12] and were used in this work.

For lifetime studies, it has been suggested that the median value of failure stress ($\sigma_{0.5}$) ie. the value below which 50% of fibres will fail, is suitable and that value was used in this work.[13] The 96% confidence intervals for $\sigma_{0.5}$ at each loading rate were determined from published tables at the appropriate sample sizes.[12]

Linear regression was used to fit a line to the ln(Median Failure Stress) vs ln(Faceplate Velocity) data and the dynamic stress corrosion susceptibility parameter was derived from the slope of that line [13] according to: [9]

$$n_d = 1 + 1/\text{slope}.$$

All fibres tested were assumed to have a diameter of 125 μm and a coated diameter of 250 μm.

3.0 RESULTS AND DISCUSSION

Figure 1 shows the (typical) effect of soak time in de-ionised water at 40°C on the median (Weibull) failure stress for one of the fibres tested. Unlike the graph shown in Figure 1, failure stress usually decreases as soak time increases, eventually reaching a constant value. The decrease in failure stress is associated with diffusion of the external environment through the polymeric fibre coatings to the fibre surface and its subsequent interaction with that surface.

The fact that the fibre tested did not display that characteristic prompted further study. It was found that even after drying for a minimum of 5 days at 30°C, the polymeric coating surrounding the fibre did not adhere to the fibre surface. That lack of intimate contact presumably allowed water to quickly travel along the gap at the coating/glass interface from the ends of the fibre, rather than diffusing through the coating. Upon examination, it was found that the remaining seven fibres also evidenced coating delamination.

On the basis of that finding and Figure 1, a pre-conditioning time of 24 hours was deemed suitable and subsequently applied to all retrieved fibres tested. A pre-conditioning time of 1008 hours (42 days) was deemed suitable for current production fibre, which did not appear to de-laminate.

Table 1 shows the dynamic stress corrosion susceptibility parameter (n_d) for each of the fibres tested in this work and the median Weibull failure

stress ($\sigma_{0.5}$) of the fibres tested at a faceplate velocity of 0.5 µm/sec.

The table shows the stress corrosion susceptibility parameter for all retrieved fibres to be in excess of 20 and the strength of the fibres to be high.

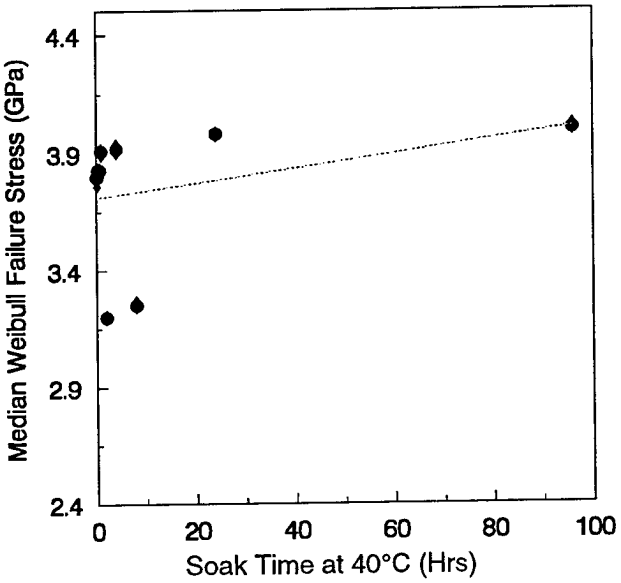

Figure 1: Median (Weibull) Failure Stress vs Soak Time at 40°C for one of the field-recovered fibres. The figure is typical of all fibres tested. Diamonds represent 96% confidence intervals.

On the basis of both their n_d and $\sigma_{0.5}$ values then, these old, stressed, delaminated fibres subjected to years of high-humidity and high-temperature still display lifetime characteristics that, even by today's standards[5], would be accepted as satisfactory for ensuring a long service life.

4.0 CONCLUSIONS

Generally, estimations of fibre lifetime are made from studies of pristine fibre, laboratory-aged under assumed in-service conditions. While such studies are both necessary and valuable in advancing fibre lifetime theory, the validity of the assumptions made is always contentious and leads to the possibility of either over- or under-estimating fibre lifetime. In the current work, field recovered fibres that had been subjected to extreme conditions of high humidity, temperature and applied stress for 13 years, were examined. Those 'old' fibres were found to display neither a low dynamic stress corrosion susceptibility parameter nor a low tensile strength (brittleness). There is now some 'real world' evidence to indicate that in-service optical fibres subjected to quite severe operating conditions have a lifetime in excess of 13 years. The vast majority of fibre in a network should enjoy far less severe conditions and so could be expected to have a lifetime greatly in excess of that figure.

Table 1: Dynamic stress corrosion susceptibility parameter (n_d) and median Weibull failure stress at a faceplate velocity of 0.5 µm/sec ($\sigma_{0.5}$). For comparison, Bellcore[5] suggestions for those values are also shown as are the values for a current production fibre.

Fibre Colour	n_d	$\sigma_{0.5}$(GPa)
Blue	28.0	3.4
Orange	24.8	3.4
Green	26.6	3.6
Brown	21.5	3.3
Grey/Slate	29.5	3.6
White	25.0	3.4
Red	23.9	3.4
Black	26.2	3.4
Current Production (Natural)	41.3	4.3
Bellcore[5]	> 20	> 3.1

These findings confirm the confidence telecommunications organisations have in employing optical fibres as their prime transmission medium.

5. ACKNOWLEDGMENTS

The permission of the Director, Telstra Technology Strategy and Research, to publish this paper is acknowledged. The authors acknowledge the assistance of Dr. Ed Johansen, National Manager (Access Technologies) and Les Kiss, Project

Manager (Cable Technology) both from the Network Technology Group and Multimedia, Telstra Corporation, Melbourne, Victoria, Australia for providing the samples and encouragement to complete this work. The assistance of Ray Boast, Project Leader (TRL), in managing the administrative aspects associated with this project is also gratefully acknowledged. Special thanks to Kevin Moseley, Principal Telecommunications Technical Officer (TRL), for his efforts in obtaining the data from which n_d and $\sigma_{0.5}$ were determined.

5.0 REFERENCES

1. T. C. Baker; F. W. Preston:
J. Appl. Phys. **17** 170 (1946).

2. R. J. Charles:
J. Appl. Phys. **29** 1549 (1958).

3. S. M Wiederhorn; S. W. Freiman;
E. R. Fuller; C. J. Simmons:
J. Mater. Sci **17** 3460 (1982).

4. P. Ostojic: *J. Mater. Sci.* **30** 3011 (1995).

5. Bellcore Generic Requirement
GR-20-ILR, Issue 1B (1996)

6. A. Gouronnec, R. Goarin, G. LeMoigne,
M. Baptiste: *SPIE* **2290** 191 (1994)

7. T. A. Michalske; S. W. Freiman:
Nature **295** 511 (1982)

8. 2- Point Bend Apparatus User's Manual
Fiber Sigma. New Jersey. USA

9. V. V. Rondinella; M. J. Matthewson:
J. Am Ceram. Soc. **76** 139 (1993)

10. J. C. Glandus; P. Boch:
J.Mat Sci Lett. **3** 74 (1984)

11. J. E. Ritter; N. Bandyuopadhyay; K. Jakus:
Am Ceram Soc Bull. **60** 798 (1981)

12. D. R. Thoman; L. J. Bain; C. E. Antle:
Technometrics **11** 445 (1969)

13. F. P. Kapron; H. H. Yuce:
Optical Eng. **30** 700 (1991)

AUTHORS

Postal Address for all Authors: Telstra Research Laboratories, 770 Blackburn Road, Clayton 3168, Victoria, Australia

Dr Peter Ostojic (p.ostojic@trl.oz.au)
Ken Clarke (k.clarke@trl.oz.au)
David Coulson (d.coulson@trl.oz.au)
Alfred W. Kruijshoop (a.kruijshoop@trl.oz.au)

HIGH DENSE OPTICAL FIBER UNIT FOR EXTENDING FLEXIBILITY OF AIR BLOWN FIBER SYSTEM

Yoko Taira, Nobuyuki Suzuki, Junichiro Hanai, Shinya Takaoka, Masaharu Saeki, and Hiromi Kato

Sumitomo Electric Industries, Ltd. ,Yokohama Japan

ABSTRACT

A new optical fiber unit for the Air Blown Fiber (ABF) system has been developed for enhancing the product advantages. This new optical unit can accommodate 18-core (18-c) optical fibers, the highest fiber count available in current ABF units, while the diameter is two third of the current 18-c unit. Due to its dense design, this new 18-c optical unit shows similar performance as the standard 6-c optical unit. Hence, the new 18-c unit can be applied to the ABF system with any tube sizes applied. Furthermore, increasing the fiber density drastically with improving the blowing performance, this new optical unit enables us to utilize the ABF system with higher flexibility.

1.Introduction

The ABF system, in which compressed air propels an optical fiber unit into an empty polyethylene (PE) tube, was introduced at major optical markets for its high flexibility and feasibility to system expansion or reconfiguration. For enhancing this product's advantages to follow the major market stream, an increase in fiber density is required. A current 18-c optical unit is one option available for covering such a demand. However, the current 18-c optical unit is applicable to a tube that has a 8.0mm outer diameter (OD) and a 6.0mm inner diameter (ID), not for a smaller tube (OD/ID = 6.0mm/4.5mm) as shown in Fig. 1. This constraint comes out of the dimension of the conventional 18-c unit: it is 50% larger in diameter and 125% higher in weight than the current 6-c optical unit. Moreover, the current 18-c unit does not have the same blowing performance as the standard 6-c unit in the standard tube due to its large dimension.

This paper covers our newly developed high dense 18-c optical unit that shows the similar blowing performance as the current 6-c optical unit with regardless of tube sizes.

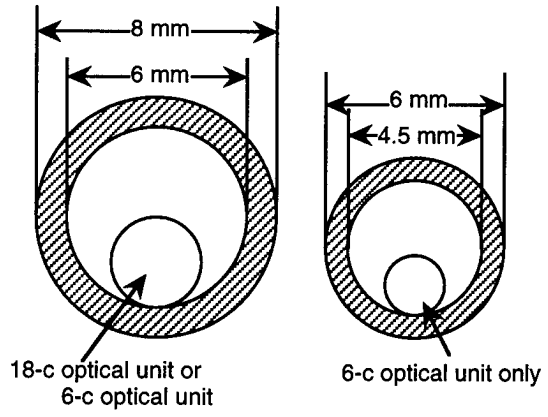

Fig.1 Current optical units and PE tubes

2. Design of new 18-c optical unit

The development of the new optical ABF unit was aimed at expanding applicability of a high fiber count unit to various tube sizes. For this concept, the new

Unit type	Standard 6-c unit	Conventional 18-c unit	**NEW 18-c UNIT**
Unit structure	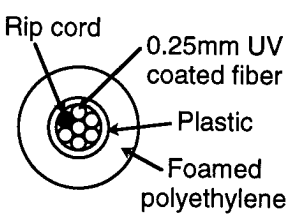	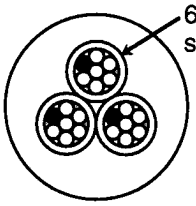	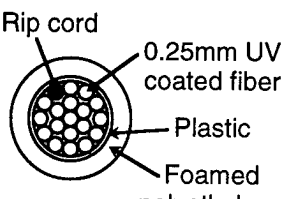
Diameter	2.0 mm	3.0 mm	2.0 mm
Weight	2.0 g/m	4.5 g/m	2.1 g/m
Fiber density	1.9 c/mm^2	2.6 c/mm^2	5.7 c/mm^2

Fig.2 Optical fiber unit structures

18-c fiber unit needed to be smaller in diameter and lighter in weight. One of the target designs was the standard 6-c fiber unit, the most popular unit in the ABF system. Based upon this downsizing concept, the new 18-c optical unit has been designed as shown in Fig. 2. It has a dual layer of optical fibers while the conventional 18-c unit consists of three sets of 6-fiber sub-unit. This means the new 18-c unit has the densest design available for a 18-c unit. Furthermore, a production innovation enables us to design thinner jacketing layers. As a result, the new 18-c unit realizes almost the same dimension as the current 6-c unit: the fiber density becomes more than twice of the conventional 18-c unit and more than three times of the 6-c unit.

3. Attenuation after cabling and during temperature cycling

Three major fibers, singlemode fiber, 50 μm core multimode fiber, and 62.5 μm core multimode fiber, were used for trial productions. All fibers showed stable attenuations during unit productions. Attenuations of singlemode fibers were less than 0.4dB/km and 0.3 dB/km at 1310nm and 1550nm wavelengths respectively after the production. Those of 50 μm multimode fibers and 62.5 μm multimode fibers were less than 0.7 dB/km and 0.9 dB/km at 1300nm wavelength, as shown in table 1.

A temperature cycling test from -30℃ to +60℃ was conducted to this new optical unit as shown in table 1. All types of fibers showed stable temperature performances similar to the current optical units. Attenuation variations of singlemode fibers were less than 0.05dB/km at both 1310nm and 1550nm wavelengths. Those of multimode fibers were less than 0.2 dB/km at 1300nm wavelength.

Table 1. Attenuation after cabling and during temperature cycling

Fiber type	Attenuation after cabling	Attenuation variation in temperature cycling (-30℃～+60℃)
Singlemode	≦0.4 dB/km (λ=1310nm) ≦0.3 dB/km (λ=1550nm)	Δ≦0.05 dB/km (λ=1310nm) Δ≦0.05 dB/km (λ=1550nm)
50 μm multimode	≦0.7 dB/km (λ=1300nm)	Δ≦0.2 dB/km (λ=1300nm)
62.5 μm multimode	≦0.9 dB/km (λ=1300nm)	Δ≦0.2 dB/km (λ=1300nm)

4. Blowing performance

4-1) In case of a horizontal route.

For evaluating distance blowing performance, the new 18-c optical unit was blown into two types of PE tubes. One was a standard tube: this is a popular tube size and suitable for a constructing distance optical network. Another was a smaller tube: this is a new tube size suitable for indoor or short distance optical network constructions due to its small dimension. Based upon application areas of these two tubes, we evaluated the blowing performances of the three different units - a standard 6-c unit, a conventional 18-c unit, and the new 18-c unit - by the use of either 1000 meters standard tube or 500 meters small tube.

Fig. 3 shows the blowing performances of the optical units blown into a standard 1000 meters tube under the different air pressures. All types of the optical units achieved 1000 meters blowing installations successfully with 882 kPa pressurized air as shown in Fig. 3-1. A conventional 18-c unit, however, took the longest time with more than 50 min. Fig. 3-2 shows the same 1000 meters blowing installation but lower pressurized air of 686 kPa was applied. In this testing condition, the conventional 18-c unit could not be blown with more than 600 meters. These test results prove that the new 18-c unit can be applied to distance optical networks with a standard large tube, showing similar performances as the standard 6-c optical unit.

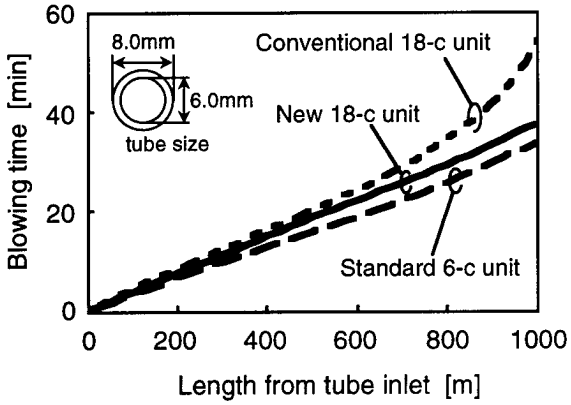

Fig. 3-1 Blowing performance
of a horizontal route
(1000m standard tube / P=882kPa)

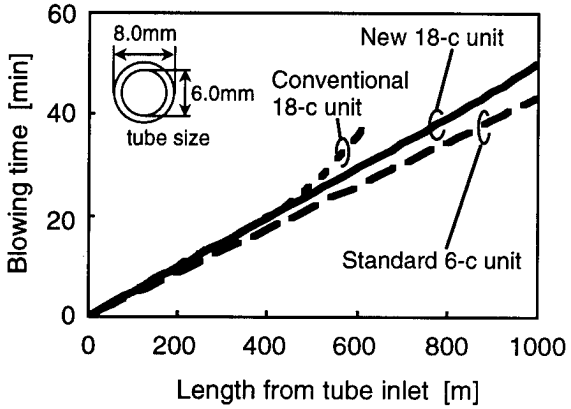

Fig. 3-2 Blowing performance
of a horizontal route
(1000m standard tube / P=686kPa)

Fig. 4 shows the performances of the optical units blown into a 500 meter small tube. The conventional 18-c optical unit could not be blown successfully on this testing condition even with 882 kPa of air pressure applied. This test result indicates that the new 18-c unit can be available even with the small tube applied.

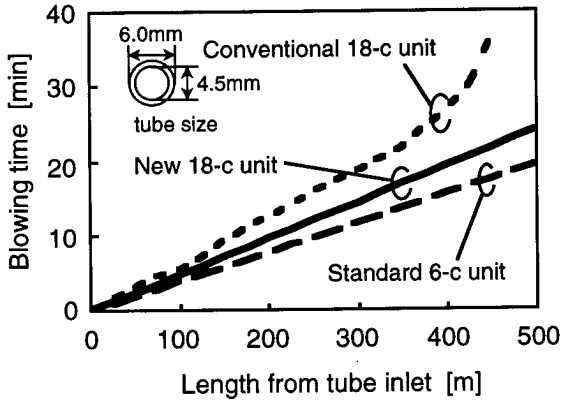

Fig. 4 Blowing performance
of a horizontal route
(500m small tube / P=882kPa)

Reviewing these test results, the new 18-c unit shows superior blowing performance compared to the conventional 18-c unit, and the performance is almost comparable to the standard 6-c unit. As a result, this new optical unit increases the fiber density drastically with improving the blowing performance.

4-2) In case of a horizontal and vertical combination route.

A current optical system where the ABF system is applicable indicates that the optical unit will be blown into a more complex route due to the market expansion.[1],[2] Therefore, we evaluated the unit performance blown into a horizontal and vertical combination route. This test assumes a more severe blowing condition than the simple horizontal route discussed in a previous section 4-1. Moreover, a theoretical approach will become more important to assure a unit blowing under such a complex route. Therefore, we performed the unit installations blown into a horizontal and vertical combination route. Fig. 5 shows a route configuration of this blowing test: each route of which total length is between 120 and 420 meters contains a 20 meters vertical portion. A route is made of either standard or small tubes. We also compared the test results with the theoretical ones.

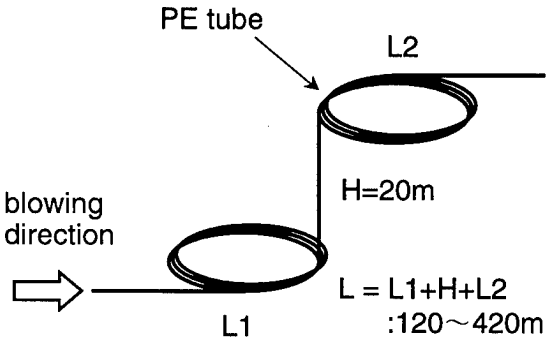

Fig.5 Tube configuration contain vertical part

Fig. 6 shows one blowing test result with a 420 meter standard tube: a vertical route is located in the middle of a route. In this test, the conventional 18-c unit stopped in the middle of the route while both the 6-c and new 18-c units succeeded in the installation. Table 2 summarizes the blowing performances by standard tubes of which the maximum distance were 420 meters. In these tests, both the new 18-c unit and the standard 6-c unit succeeded all blowing tests while the conventional 18-c unit fail the longest 420 meter installations.

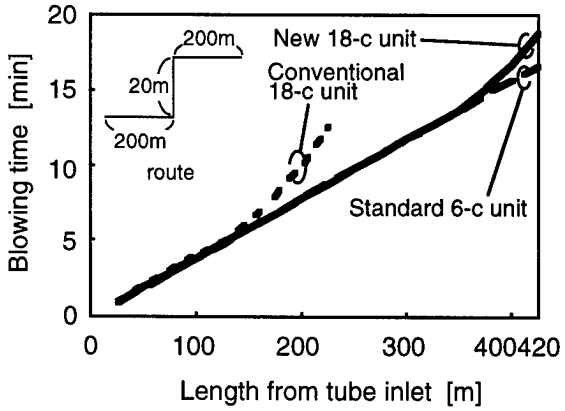

Fig. 6 Blowing performance
(Standard tube / horizontal and vertical route)

Table 2 Test result of blowing unit installation
(standard tube/horizontal and vertical route)

(unit : min.)

Route configuration \ Unit structure				Standard 6-c unit	New 18-c unit	Conventional 18-c unit
L [m]	L1 [m]	H [m]	L2 [m]			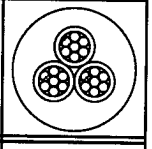
220	100	20	100	8'48	8'55	8'50
320			200	12'39	12'49	13'29
420			300	16'17	23'03	Fail *(1)
320	200		100	12'35	12'18	14'33
420			200	17'42	18'50	Fail *(2)
420	300		100	16'15	16'07	Fail *(3)

* Note : stopped at (1) 300m, (2) 225m, (3) 400m

Fig. 7 shows a test result of a unit installation blown into a small tube: the conventional 18-c unit failed in this installation. Table 3 summarizes the blowing test results by small tubes of which maximum distance was 220 meters. These results also indicate that the new 18-c unit has almost the same blowing performance as the standard 6-c unit.

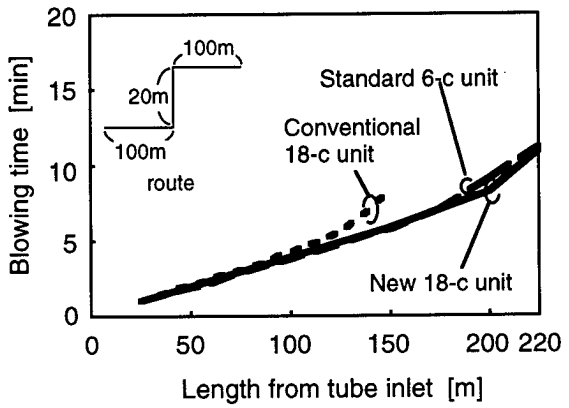

Fig. 7 Blowing performance
(Small tube / horizontal and vertical route)

Table 3 Test result of blowing unit installation
(Small tube/horizontal and vertical route)

(unit : min.)

Route configuration / Unit structure				Standard 6-c unit	New 18-c unit	Conventional 18-c unit
L [m]	L1 [m]	H [m]	L2 [m]			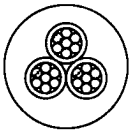
120	0	20	100	5'06	5'21	6'05
170	100		50	6'42	6'37	9'44
220			100	11'09	10'58	Fail *

* Note : stopped at 160m

Theoretical approaches were conducted to assure that the experimental results followed the blowing theory. The blowing theory has been established through our previous technical papers.[3],[4],[5],[6] Hence, we applied this established blowing theory to the experimental results.

F(l), a blowing force per unit length at a point "l", is expressed as the following equation.

$$F(l)=\frac{\pi d_1 d_2}{8}\left(\frac{P_{out}^2-P_{in}^2}{L}l+P_{in}^2\right)^{-\frac{1}{2}}\frac{P_{in}^2-P_{out}^2}{L}$$

In this equation, "d_1" and "d_2" indicate the inner diameter of the tube and the outer diameter of the optical unit respectively. "L" is the tube length. "P_{in}" is the absolute pressure value at the tube inlet, and "P_{out}" is the pressure value at the tube outlet. This equation shows that the air pressure gradient becomes smaller as long as the point "l" is closer to the tube inlet: then the viscous drag force becomes smaller.

At a vertical route, the unit weight is the resistant force. Therefore, the unit can be blown as long as F(L1), the blowing force at the starting end of the vertical portion, exceeds the optical unit weight per length.

Fig. 8-1 summarizes calculation results by this blowing theory: the horizontal axis shows a horizontal route length (L1) and the vertical axis shows a total route length (L1 + H + L2). In this figure, each unit can succeed a blowing installation into a route of which configuration is located under the calculated line. This figure shows that the new 18-c unit has very similar in blowing performance to the standard 6-c unit. Figures 8-2 through 8-4 show comparisons between theoretical results and experimental results. In these figures, we classified blowing results into four categories, "excellent", "good", "worse" and "worst". "Excellent" indicates a successful blowing condition with a stable speed, and <good> indicates a successful blowing result with slowing a blowing velocity. "Worse" indicates a failed test condition in which the optical unit went through a vertical portion, and "worst" indicates a failed test condition in which the unit couldn't reach the end of the vertical route. All of the experimental results

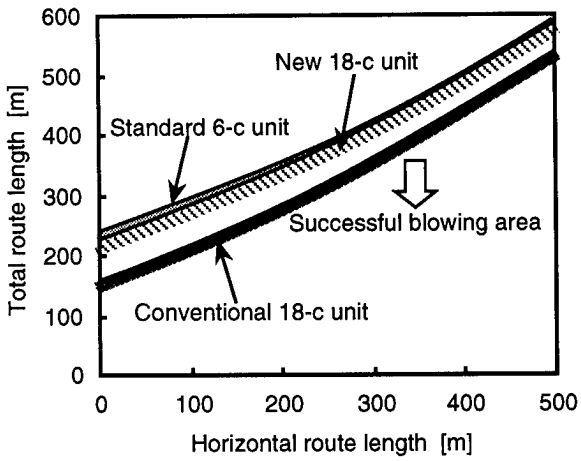

Fig.8-1 Successful blowing area by calculation

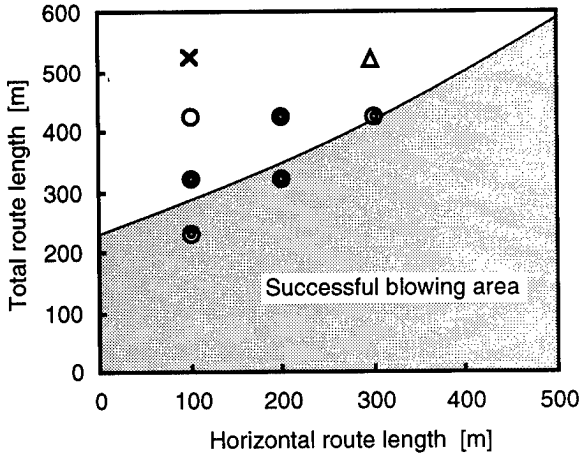

Fig.8-2 Standard 6-c unit

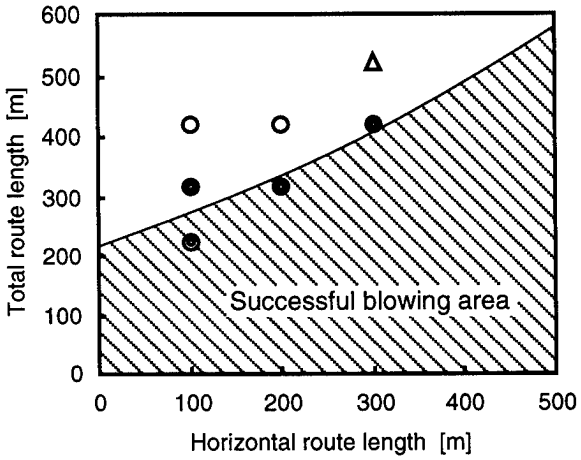

Fig.8-3 New 18-c unit

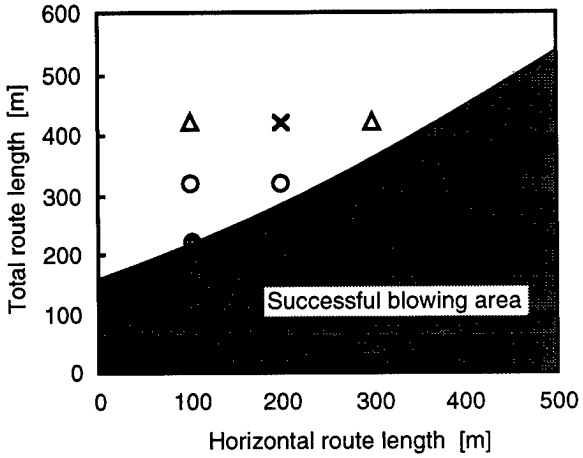

Fig.8-4 Conventional 18-c unit

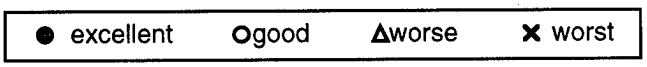

Fig.8 Calculation and experimental results of unit blowing performances

follow the calculated result. However, the experiments show the better blowing results than the calculation ones. This bias implies that the actual blowing carries other positive factors that are not considered in the theory. We assume that one positive factor that assists better blowing is a surface condition: an actual optical unit upon which is a rough surface can receive a larger pressurized air than a theoretical one. By reviewing these experiment and theoretical results, we obtain a basic approach to predict a unit blowing performance under a complex route.

5. Conclusion

A new high fiber count optical unit has been developed and evaluated the experimental and theoretical blowing performances. The new optical unit behaves with almost the same blowing and environmental performances as the standard 6-c optical unit. The new optical unit increases the fiber density drastically with increasing the blowing performance: hence, the new optical unit gives more flexibility to the ABF system.

References

[1]S.Konno et.al., "New composite cable applying the air blown fiber technique" proceedings of IWCS'89, pp344-350

[2] Y.Matsumoto et.al., "Evaluation of the ABF-multiplex installation technique and its application in customer access optical fiber network" proceedings of IWCS'96, pp835-844

[3]S.A.Cassidy and M.H.Reev, "A radically new approach to the installation of optical fibre using the viscous flow of air," proceedings of IWCS '83, pp250-254

[4] Y.Terasawa et.al., "Prediction of blowing velocity and distance in air blown fiber cabling system" proceedings of IWCS'90, pp299-305

[5] H.Sano et.al., "Performance of improved air blown fiber system" proceedings of IWCS'93, pp570-577

[6] I.Sakabe et.al., "A study of air blown fiber for a long distance tube" proceedings of IWCS'97, pp341-347

Yoko Taira

Sumitomo Electric
Industries, Ltd.
1, Taya-cho, Sakae-ku,
Yokohama,244-8588, Japan

Yoko Taira received the B.E. degree in electorical engineering from Hokkaido University in 1993 and joined Sumitomo Electric Industries, Ltd. She has been engaged in development and design of optical fiber cables in the Fiber Optics Division.

Shinya Takaoka

Sumitomo Electric
Industries, Ltd.
1, Taya-cho, Sakae-ku,
Yokohama,244-8588, Japan

Shinya Takaoka received his M.S. degree in electorical engineering from Shizuoka University in 1986 and joined Sumitomo Electric industries, Ltd. in the same year. He has been engaged in designing and developing optical fiber cables. He is a senior enginner of the Fiber Optics Division.

Nobuyuki Suzuki

Sumitomo Electric
Industries, Ltd.
1, Taya-cho, Sakae-ku,
Yokohama,244-8588, Japan

Nobuyuki Suzuki received his B.E. degree in engineering from University of Electoro Communication in 1987 and joined Sumitomo Electric Industries, Ltd. He has been engaged in development and design of optical fiber cables in the Fiber Optics Division. He is a senior enginner of the Fiber Optics Division.

Masaharu Saeki

Sumitomo Electric
Industries, Ltd.
1, Taya-cho, Sakae-ku,
Yokohama,244-8588, Japan

Masaharu Saeki graduated from Kyushu Institute of Technology in 1974 and joined Sumitomo Electric Industries, Ltd. He has been engaged in development and design of optical fiber cables in the Fiber Optics Division. He is a manager of the 1st Fiber Optics Engineering Section.

Junichiro Hanai

Sumitomo Electric
Industries, Ltd.
4-5-33, Kitahama,
Chuo-ku,
Osaka, 541-0041, Japan

Junichiro Hanai received his B.E. degree in engineering from Tokyo University in 1986 and joined Sumitomo Electric Industries, Ltd. He has been engaged in development and design of optical fiber cables in the Fiber Optics Division. He is a senior enginner of the Fiber Optics Division.

Hiromi Kato

Sumitomo Electric
Industries, Ltd.
4-5-33, Kitahama,
Chuo-ku,
Osaka, 541-0041, Japan

Hiromi Kato was born in 1957 in Shimane, Japan and graduated in civil engineering from Matsue Technical College in 1978 and joined Sumitomo Electric Industries, Ltd. He has engaged in communication cable construction section in the Communication Division. He is a senior enginner of the Communication Engineering Division.

THE MODULAR DESIGN AND EVALUATION OF BLOWABLE ACRYLATE MULTI-FIBRE UNITS

D. Pendleton, S.R.Dodd, A.P.J. Cadden

Optical Fibres

Second Avenue, Deeside Industrial Park,
Deeside, Flintshire, CH5 2NX, UK
Tel: +44 1244 281281 Fax: +44 1244 287287

ABSTRACT

This paper details the design and evaluation of 8 and 12 fibre blowable acrylate multi-fibre units. The paper describes the kinds of network that give rise to demands for such units and the evaluation of each unit design for mechanical, optical and installation performance. Each design is based on a ribbon sub-unit structure with the size of the ribbon and hence the unit sizes being dictated by the customer's requirement. At the time of writing the 8F and 12F units are undergoing product qualification testing. This data will be presented at the conference.

INTRODUCTION

History

The techniques of blowing fibres into a duct are well established[1]. Traditional blown fibre units are made from a buffer type material to protect the fibres and a foamed polyethylene skin to provide a lightweight rough surface against which the air could drive.

In the late 1980's Optical Fibres developed single blowable buffered units based entirely on UV acrylate coating systems and a blowing method that allowed several fibres to be blown into a small duct simultaneously[2]. In this case the low friction and roughness of the outer coating is achieved by introducing lightweight particles into the outer coating. Optical Fibres has extended this technology to develop 4 fibre bundles (initially with BT) again based entirely on UV acrylate coatings. The Enhanced Performance Fibre Unit (EPFU) has the advantage of being both lighter and smaller than the previous polyethylene units allowing ducting and connector systems to also reduce in size.

Initially customer requirements were for 2 and 4 singlemode fibre units and 4 fibre multi-mode units. However, interest in blown fibre technology has increased and, with it, demands for higher fibre count units. The requirement is now for different fibre counts at different points in the network.

Network Requirements

The use of Blown Fibre in the access network provides a network owner with a number of benefits. There is enhanced flexibility to readily expand and upgrade the network, and improved customer service through just-in-time installation. Significant cost savings can also be made by optimising the investment in installed fibres and deferring fibre roll-out.[3,4,5].

The deployment of optical fibre in the access network can be considered in three portions; loop, distribution and drop. Typically, the loop is a high fibre count ring, several kilometres in length that originates and terminates in the local exchange. The distribution part of the network routes fibres from the loop to the point from which the drop is made to individual subscribers.

Access networks being installed today increasingly require high fibre counts in the loop

and distribution parts of the network. Generally, optical fibre local loops have required from 48 to 96 fibres. More recently, demand has been seen for higher counts of up to 288 fibres. In response to this demand, it was necessary to design higher fibre count units and higher count tube bundles for the Blown Fibre system. It was recognised that the combination of high count fibre units containing eight or twelve fibres and high count tube bundles containing 19 or 24 tubes, would provide the required capacity increases. Combination systems could also be designed with high fibre count units for an active ring deployed in the central tube(s) of a tube bundle, and lower fibre count units for a passive drop, installed in the outer tubes.

The modular design of multi-fibre units allowed the fibre count to be increased whilst optimising the unit size. This also enabled increased fibre counts to be installed into existing duct systems, minimising investment and disruption.

Unit Design

In order to accommodate this new requirement Optical Fibres has developed a range of higher fibre count UV acrylate units based on a ribbon sub-unit structure allowing the fibre count to be increased with ease while minimising the increase in unit weight and size. Typical designs for 8F and 12F multi-fibre units are detailed in Figures 1 and 2.

The design of blowable acrylate fibre units has been discussed previously[6]. Typically they consist of a soft buffer layer to protect the fibres and an outer layer containing particles, e.g. hollow glass micro-spheres in this case to provide a low friction rough surface to promote good blowing performance and special anti-static additives to enhance the unit blowing performance in dry environments.

Optical Performance

From previous design work on the smaller fibre count units, it is known that an insufficient buffer layer can cause attenuation increases due to inadequate protection of the fibres. It was found that the corner fibres of the ribbon sub-unit package were sensitive to attenuation increases for the same reason. A similar effect is experienced when the corner fibres of ribbon packages are exposed to lateral forces in a cable[7].

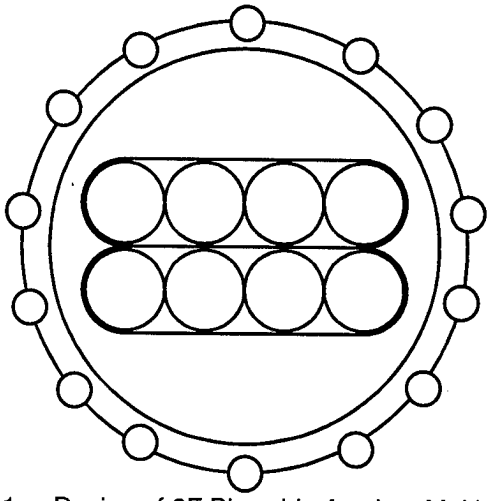

Fig 1. Design of 8F Blowable Acrylate Multi-Fibre Units

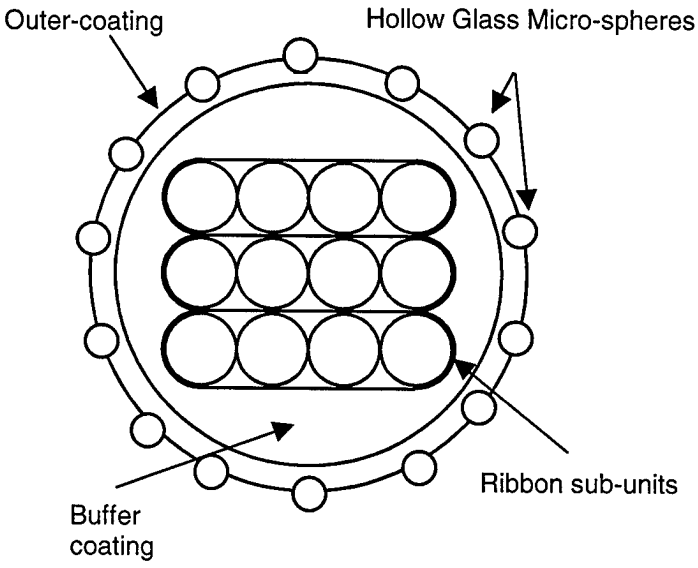

Fig 2. Design of Blowable 12F Acrylate Multi-Fibre Units

In order to optimise the product design for corner fibre attenuation effects three unit designs with varying diameters of buffer layers were evaluated. The effect of the thickness of the buffer layer versus 1550nm attenuation increment of corner fibres is given in Figure 3. It can be seen that the increment penalty for these fibres reduces as the diameter of the buffered layer increases.

It can also be seen that the attenuation increment for all other fibres within the ribbon sub-unit package are considerably lower than the corner fibres and remain unaffected by buffer coating diameter changes.

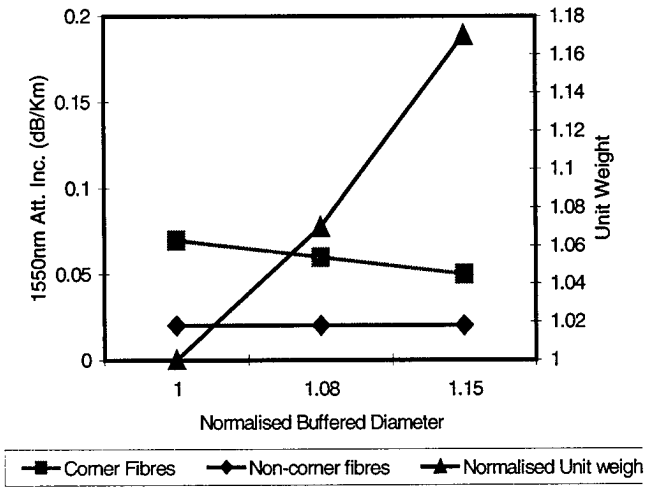

Fig.3 The Effect of Buffer Coating Diameter on Corner Fibre Attenuation and Unit Weight

Unit Weight

The weight of the unit is known to have a direct effect on the forces that resist blowing as well as pulled installation performance[8]. The increase in unit weight with the increase in buffer coating diameter is also presented in figure 3. It can be seen that an increase of 15% in the buffer-coating diameter increases the unit weight by 17% and yields only a 0.02dB/Km reduction in the corner fibre attenuation increment.

The unit selection criteria required a design that would optimise both the unit weight, and therefore resistance forces to blowing and pulling, and also the optical performance of the corner fibres of each unit.

Eight and twelve fibre designs that gave optimal installation and optical performance were chosen for product qualification testing.

Unit Characteristics

Unit Strippability

The requirement is to remove the coating from 2 metres of each individual fibre in a time equivalent to 1 minute per fibre. Units were stripped after pre-conditioning at 0°C, 20°C and 40°C.

Using a stripping tool the outer coatings could be easily removed providing access to the ribbon sub-units. The fibres could be easily broken out of the ribbon sub-units by hand. Optical Fibres has recently developed the IRIS range of coloured fibre inks that promote good breakout from encapsulated products. Hot-strip of ribbons was not a consideration during the fibre access trials.

Unit Coiling

Blown or pulled fibre installation can take place from either a spool or a blown fibre pan, the preferred method used by BT. The unit is placed into a pan using a coiler that induces a half-twist in the unit as it is placed in a rossetted coil. Packaging the unit in this way has several advantages:

1. It allows centre blowing – a technique that enables the installer to double the installation distance by blowing from a central access point.

2. Onward blowing – another technique that allows increased installation distances.

3. Easy recovery of unit when removing from a blowing duct.

Both the 8F and the 12F unit performed well during their panning operation.

Temperature Dependant Attenuation (TDA) Performance

The environmental performance of EPFU designs is well documented[6]. The Temperature Dependant Performance of the 8F and 12F units are shown in Figures 4 and 5. It can be seen that both unit designs exhibit good stable performance throughout the temperature cycle.

Installation Performance

The results of the installation tests are shown in Figure 6. The installation performance of the units was assessed using a 500m reference-blowing route. This consisted of a blow duct with an internal diameter of 3.5mm and an external diameter of 5mm and three 450° bends of 0.5m diameter. The outer acrylate coating designed and used by Optical Fibres ensures excellent blowing performance.

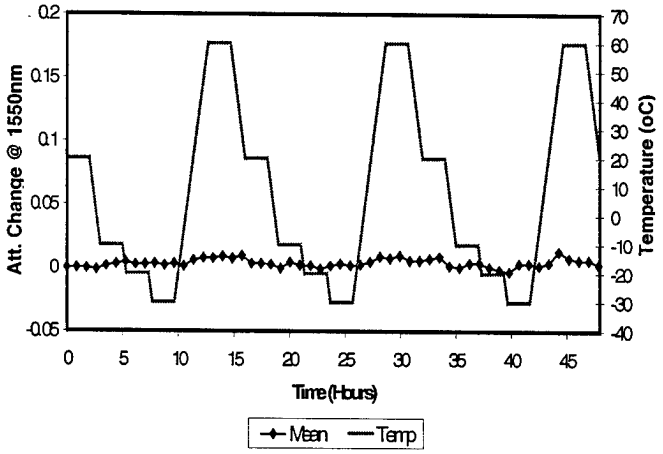

Fig. 4 TDA performance of 8F Unit

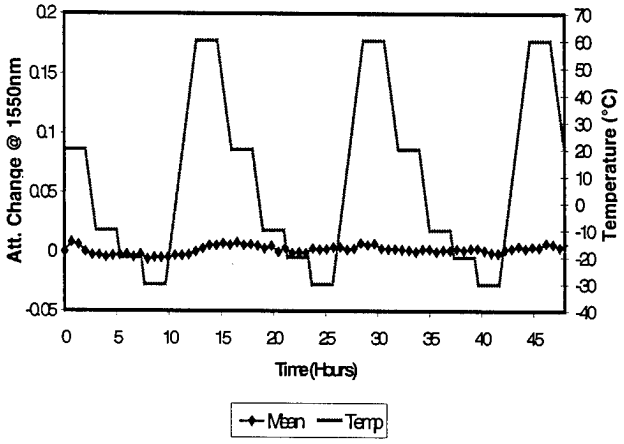

Fig. 5 TDA Performance of 12F Unit

The units were installed without problem at an average speed of 35m/min for the 8F unit and 34m/min for the 12F unit. No attenuation increase was observed following installation. Further blowing work with these units has indicated that blowing distances in excess of 2Kms are possible with modified installation techniques[9].

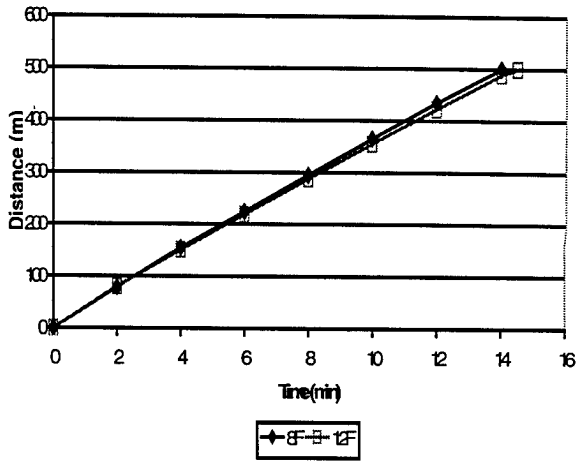

Fig. 6 Installation Performance of 8 and 12 fibre Units

Conclusion

Optical Fibres has designed and tested 8F and 12F blowable acrylate fibre units based on a 4F-ribbon sub-unit.

It was found that the buffer coating diameter has an impact both on corner fibre attenuation of the ribbon sub-unit package and the overall unit weight and that the design must be optimised to ensure both acceptable optical and installation performance. Further work on minimising the corner fibre attenuation continues.

The coatings used are based on the successful EPFU design allowing easy access to individual fibres and ensured that the outer surface of the unit is optimised for installation performance.

Both of the 8F and 12F unit designs are now undergoing an extensive qualification programme.

Further work on other modular designs is envisaged to meet differing customer requirements.

Acknowledgements

The authors wish to thank Sheila Williams, Christine Jones, Simon Tomlinson, Mark Holland and Gary Rogers for their help during this work

References

1. S A Cassidy M H Reeve,
   INSTALLATION OF OPTICAL FIBRE UNITS USING VISCOUS DRAG OF AIR
   9th European Conference on Optical Communications (1983), pp 239-42

2. A Sadler,
   BLOLITE BLOWN FIBRE SYSTEM PERFORMANCE
   EFOC Proceedings (1991), pp 92-96

3. A Mayhew, J Mellis
   BLOWN FIBRE AS A REDUCED COST NETWORK PLANNING SOLUTION,
   Eurescom ANCIT Workshop (1998)

4. H Wilderjans, L Cauwenberghs, G Jordens
   ECONOMIC AND FIELD EVALUATION OF MODULAR CABLING TECHNIQUES IN THE BELGACOM NETWORK.
   Eurescom ANCIT Workshop (1998)

5. G Azzarello
   IMPACT OF NEW CABLING TECHNIQUES ON ITALIAN ACCESS NETWORK
   Eurescom ANCIT Workshop (1998)

6. A P Morris
   DEVELOPMENT AND DESIGN APPROVAL OF TWO FIBRE, SINGLEMODE ENHANCED PERFORMANCE FIBRE UNIT (EPFU)
   IWCS Proceedings (1996), pp 821-827

7. S. Tomita, M. Matusmoto, S. Nagasawa, T. Tadatoshi
   ULTRA HIGH-DENSITY OPTICAL FIBRE CABLE WITH THIN COATED FIBRES AND MULTIPLE CONNECTORS
   IWCS Proceedings (1993), pp 5-15

8. J P Wells, A Cadden, G Brown, P Clayton
   A NOVEL METHOD FOR THE INSTALLATION OF LIGHTWEIGHT OPTICAL FIBRE UNITS INTO TUBING
   IWCS Proceedings (1996), pp 828-834

9. C Barrow
   INSTALLATION TECHNIQUES FOR FIBRE BUNDLES IN MICRO-TUBES
   Eurescom ANCIT Workshop (1998)

BIOGRAPHIES

David Pendleton has been with Optical Fibres for 7 years and is currently Senior Development Engineer, Value Added Products. He received his B.Sc. honours degree in Applied Physics from Liverpool John Moores University in 1987.

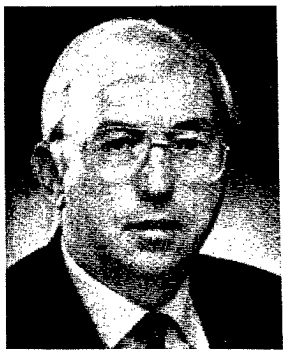

Aidan Cadden has been with Optical Fibres for 13 years and is a Development Engineer with the Value Added Products Department. He received his B.Sc. honours degree in Applied Chemistry (Polymer and Colour Science) from Queens University Belfast in 1970.

Stephen Dodd has been with Optical Fibres for 13 years and is currently Product Manager, Access Networks, with responsibility for the promotion of Blown Fibre Technology world-wide. He received his BSc in Physics and Electronic Engineering from Manchester University in 1985.

LIFETIME OF HIGH-STRENGTH SPLICED FIBERS

Marco Zimnol, Bernt Sundström*, Torbjörn Svensson**

Ericsson Cables AB, Sundbyberg, Sweden, *Ericsson Components AB, Kista, Sweden, **Telia Research AB, Farsta, Sweden

ABSTRACT

Mechanically stripped acrylate-coated standard single-mode fibers were high-strength spliced and recoated. From dynamical tensile testing with a specially designed expander tester, the *n*-value of splices was determined. This was used to estimate the splice lifetime under tension, adopting the standard power law model. It is shown that the lifetimes of these splices are sufficiently long for normal applications. The measurements made, indicate that an alternative use of acid stripping implies no advantage with respect to the *n*-value of splices.

INTRODUCTION

The limited space available in submarine cable splice closures and the densification of telecommunication equipment such as WDM transponders call for physically reducing the mechanical protection of splices and the size of fiber bends. A tendency therefore, is to use unsupported fiber splices in such devices. However, the unsupported splices can be subjected to bends and axial tensile stresses that affect their reliability.

It has been shown previously[1] that fiber splices can be stressed without limiting the service lifetime, if they are made with a high-strength technique using acid stripping. In this paper, the effects from use of mechanical stripping for the high-strength splicing is studied. In both cases the same high strength-splicing technique has been used, by which any contact of the bare fiber with solid objects is avoided.

The lifetime of splices under tension has been calculated with the standard power-law model[2] using the values of the stress corrosion susceptibility parameter (*n*-value) obtained in dynamic tensile tests. For comparison, the lifetimes of splices when using the different stripping procedures have been estimated for various bend diameters.

THEORY

In many applications, the only mechanical stress on fiber originates from bending of fiber. The maximum tensile stress of a bent fiber is calculated according to:

$$\sigma = E\frac{d}{D}, \qquad (1)$$

where

E = 72.2 GPa (Young's modulus of glass),
d = 125 μm (fiber glass diameter),
D = bend diameter.

Empirically, it is usually found that the strength, S, of fiber during dynamic testing at constant stress rate, $d\sigma/dt$, follows a relation $\ln(S) = const_1 + \ln(d\sigma/dt)/const_2$. See the straight line in Figure 2. In principle, an empirical relation on this form is sufficient, though it is useful to refer to the power law theory of crack propagation[2], in which the factor $const_2$ above equals $n+1$, and n is referred to as the stress corrosion susceptibility parameter. While employing the power law in the case of slow tensile tests the relation reads in detail:[3]

$$\ln S = \frac{\ln\left((n+1)BS_i^{n-2}\right)}{n+1} + \frac{\ln(\mathrm{d}\sigma/\mathrm{d}t)}{n+1}. \qquad (2)$$

The unspecified factor BS_i^{n-2} is in common with the case of static stress below, and will be eliminated in the forthcoming. The time to failure in the dynamic tensile test, $t_{f,dynamic}$, is related to the time to failure at static stress, $t_{f,static}$:[4]

$$t_{f,dynamic} = (n+1)\,t_{f,static}. \qquad (3)$$

Applying this to equation (2) leads to

$$\ln t_f = -n \ln S + \ln\left(BS_i^{n-2}\right) \qquad (4)$$

where t_f is the time to failure at static stress. The n-value and the term containing BS_i^{n-2} are known after having plotted the experimental data according to equation (2) in Figure 2. This expression can be used to predict the spliced fibers' lifetime under a known static stress, for example caused by bending according to equation (1).

EXPERIMENTS

Standard single mode fibers (coating diameter 250 µm, glass diameter 125 µm) were mechanically stripped using a special stripper. Owing to the stripper design, the fiber glass surface is not touched and mechanical damages of the fiber by the stripper blades are mainly avoided. After stripping, the fibers were high-strength spliced and recoated, followed by storage in a constant climate room, where they were kept one week and finally dynamically tensile tested using a specially designed expander tester.[5] This equipment enabled simultaneous testing of several splices at very low stress rates.

Five sets of splices were measured at the following stress rates:

- $3.5 \cdot 10^{-6}$ GPa/s
- $3.5 \cdot 10^{-5}$ GPa/s
- $3.5 \cdot 10^{-4}$ GPa/s
- $3.5 \cdot 10^{-3}$ GPa/s
- $3.5 \cdot 10^{-2}$ GPa/s .

Each set consisted of 30 splices, positioned at equal distance along a continuous fiber of about 20 m length in total.

The tensile test results for the different strain rates are shown in the Weibull plot (Figure 1).

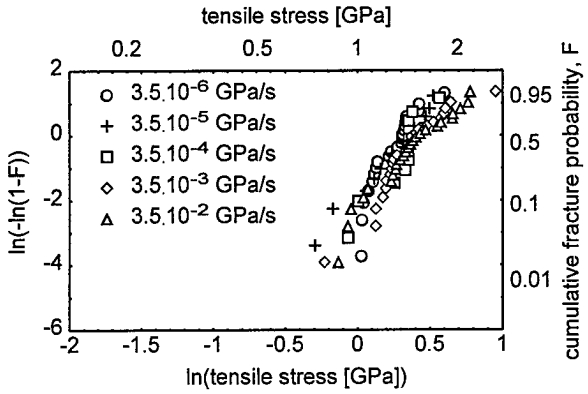

Figure 1 Weibull plot of the tensile test results

Data from failure events obviously originating from the fiber but not from splices have been excluded. Such superfluous events could be identified as belonging to a higher strength mode having a steep Weibull slope.

RESULTS

In Figure 2, the measured strength values at different stress rates are plottet in logarithmic co-ordinates.

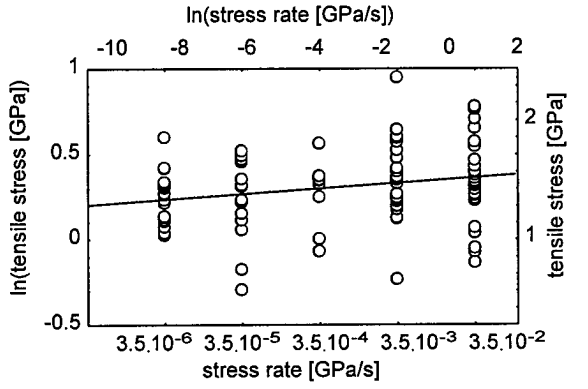

Figure 2 Tensile test results and regression line

Linear regression gives slope and intercept of the regression line:

slope = 0.014 and *intercept* = 0.356.

These values are used to calculate the *n*-value

$n = 70$ ($n = 1/slope - 1$)

and the constant term in equation (4).

This *n*-value is considerably higher than for the pristine fiber (n = 20 to 25) but generally, a high *n*-value is typical for flaws in weak silica fiber, such as fibers aged in water, and at the low stresses typical for static tests.[4] As the above result originates from fiber glass involving melting zones as well as mechanically stripped portions of glass (with degraded strength), the apparently high *n*-value observed here should very well be expected. Correspondingly, the susceptibility of splice flaws to stress corrosion is low, and further degradation of splice strength during service will be slow (the exact rate is determined by factors as the initial strength and the applied tensile stresses).

Using equation (4), it is now possible to estimate the lifetime (time to failure, t_f). Some examples of such lifetimes of splices in circular bends as a function of bend diameters are listed in Table 1. For comparison, corresponding lifetimes resulting from earlier tests on acid stripped and spliced fibers[1] are also given. From Table 1 follows that for all reasonable bending diameters the stress-limited lifetime of average splices will surpass the service lifetime of any equipment. Proof testing may be employed in order to make the lifetime of every splice coincide with the average values shown.

For safety reasons, a conservative approach based on the use of the lowest possible value of n = 14 was made in ref (1). A less conservative approach is made here, implying the inclusion of all the data from acid stripped fiber splices in ref (1). This leads to a value of $n = 29$ which is compared here with the value $n = 70$ for mechanically stripped fiber in this study, Table 1. Both the values are evaluated by linear regression of all the available series of tensile tests, without exceptions, and the corresponding lifetimes at varying bend diameters is calculated, for the two types of splices.

Table 1 Estimated average lifetime of fiber splices under bending

bend diameter [mm]	tension [GPa]	lifetime, mechanical stripping, $n = 70$	lifetime, acid stripping,[1] $n = 29$
6	1.50	$3 \cdot 10^{-2}$ sec	520 min
7	1.29	24 min	27 days
8	1.13	190 days	3 years
9	1.00	2000 years	90 years
10	0.90	10^6 years	1800 years

In the cases under study, the fiber strength will be limited more probably by defects from the fusion splicing than from mechanical or chemical stripping. Although mechanical stripping may be detrimental to the fiber's initial strength when compared with acid stripping in general, a combination of mechanical stripping with a proof test of splices will exclude any splice being too weak. In this way, the mechanical stripping should result in expectedly safe splices having lifetimes being competitive with those of splices in fibers stripped in acid. This statement is further supported by the high *n*-value observed here in mechanically stripped fiber. A mechanical stripping procedure, which surpasses the fusion process used with regard to residual strength of fiber, is needed for a good yield.

CONCLUSION

The *n*-value of splices in mechanically stripped fiber is significantly higher than in pristine fiber and also exceeds the value found in acid stripped fibers. Calculations show that lifetimes of unsupported high-strength fusion splices being made after mechanical stripping of the fiber is long enough to be safely used in equipment, provided that the tensile forces are limited to reasonably low values.

ACKNOWLEDGEMENT

The authors are grateful to Dr Leif Stensland, Ericsson Components AB, for critical reading of the manuscript, to Ola Hultén, Ericsson Cables AB, for continuous support and to Ralf Björklund, Telia Network Services, for performing the measurements.

REFERENCES

[1] M. Zimnol, B. Sundström and T. Svensson, "Lifetime of Splices under Tension", submitted to European Conference on Optical Communication '98 (ECOC), Madrid (1998)

[2] S. M. Wiederhorn, Symp. on Fracture Mechanics in Ceramics, Vol. II, p. 613, N. Y. USA: Plenum (1974).

[3] F. P. Kapron and H. H. Yuce, "Theory and measurement for predicting stressed fiber lifetime", Optical Engineering, Vol. 30, No. 6. pp.700 (1991).

[4] A. Breuls, "A COST 218 comparison of n-values obtained with different techniques", 2nd Optical Fibre Measurement Conference (OFMC '93), pp. 9-12 (Sept. 1993).

[5] J. Björkman and T. Svensson, "Quick Access to Fracture Statistics at Ultra-Wide-Range Tensile Test of Optical Fibers", Proc 39th IWCS, p 373 (1990).

Bernt Sundström was born in 1946. He received his Ph.D. in Semiconductor Physics (1981) from the Royal Institute of Technology (KTH) in Stockholm. He joined Ericsson in 1982 and has worked with optical fiber measurements, splicing, standards, education and reliability.

Marco Zimnol
Ericsson Cables AB
SE-172 87 Sundbyberg,
Sweden
marco.zimnol@
eca.ericsson.se

Marco Zimnol was born in 1970. He studied physics at the Martin-Luther-University in Halle, Germany, and joined Ericsson after his graduation in 1996. He is a member of the technical staff developing fusion splicing machines for optical fibers and has also worked with reliability issues.

Torbjörn Svensson
Telia Research AB
SE-123 86 Farsta,
Sweden
torbjorn.k.svensson@telia.se

Torbjörn Svensson received his M.Sc. and Ph. D. from the Royal Institute of Technology, in Stockholm, Sweden. He joined Telia 1985 where he was employed due to his experience in material related matters. His engagements have been in quality assurance, developing new techniques for testing fibers and cables and studying splicing technology, often contributing his findings at the IWCS, SPIE, MRS, COST, and other fora. He is currently focussing on fiber access networks and the reliability of optical transmission systems, at Telia Research.

HIGH QUALITY FIBER OPTIC SPLICES AND SIGNIFICANTLY IMPROVED SPLICE LOSS MEASUREMENT ACCURACY

Bert Zamzow[1], Gervin Ruegenberg[1], Marty Anderson[2], Helmar Krupp[3]

[1]Siemens AG, Munich, Germany
[2]Siecor Corporation, Hickory, North Carolina
[3]RXS Kabelgarnituren GmbH, Hagen, Germany

ABSTRACT

Fusion splicing is used to join optical fibers with low splice loss, low reflection and high long-term stability. The operators of the fusion splicers want:

- fast and inexpensive fiber preparation
- fully automatic operation of the fusion splicer without the need to adjust parameters
- precise splice loss measurement on-site

This paper shows how to accomplish these needs by new measurement techniques and their application in fusion splicers. It describes improvements in splice loss performance and estimation accuracy. Also the ability to remove guesswork in the field will be discussed. The operator will benefit from these new enhancements that include:

- accurate cleave angle measurement and compensation for poor cleaves by adjusting fiber feed automatically; splice loss is improved by minimizing high losses (>0.1 dB) by 60 %
- automatic detection of the fiber type being spliced
- improved loss measurement accuracy (|Measured Loss - Real Loss|) from 0.030 dB down to 0.018 dB.

INTRODUCTION

The process of joining optical fibers by fusion splicing takes several steps. For a better understanding of the following sections these steps are explained briefly below.
First the fiber ends need to be prepared. The coating is removed by a stripping tool and the fiber is cleaned with alcohol. Next the fiber end is cleaved to create a perpendicular and flat end surface.
After this the fiber is inserted into the splicing machine. Fig. 1 shows a typical commercial fusion splicer.

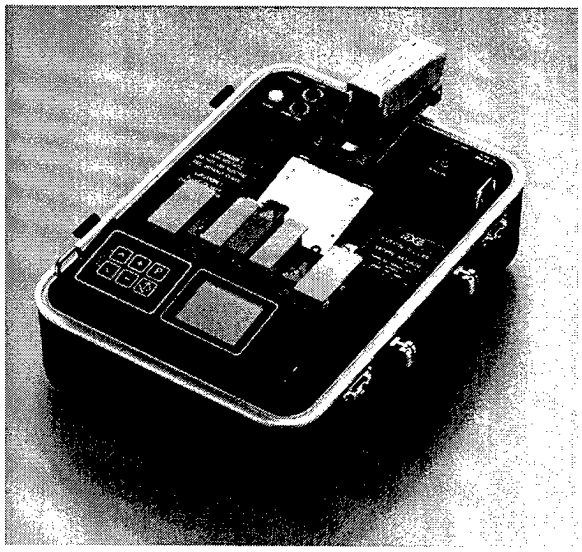

Fig. 1: Commercial Fusion Splicing Machine

The next steps are usually performed automatically. First the fibers are positioned for perfect alignment of the fiber cores. Next the fibers are melted together. Finally the splice loss is evaluated.

Although it sounds easy to perform a fusion splice there are some things to be considered, if a minimal splice loss is the goal. These issues are discussed below.
As the tools used to prepare fibers become worn with use, the quality of the prepared fiber suffers,

resulting in poor cleaves and ultimately poor splices. To avoid unnecessary downtime, e.g. for repairing the cleaver, the operator needs a compensation for poor cleaves.
Also, the user must know which fiber type is being spliced in order to select the right splicing program. However, the fiber type may be unknown because of insufficient information about the fibers used in the cable. To avoid the trial and error process of identifying the correct parameters, the user needs a fiber type detection on site.
Finally, the operator needs to leave the job site knowing confidently that the loss of the completed splices is within his acceptance criteria. Many fusion splicers include a splice loss estimation; however, most of these estimators work best only when the splice is actually good. The user needs a reliable splice loss evaluation to identify both good and bad splices.

In the next sections the techniques and application are introduced, that provide solutions to the problems mentioned above. First the principles of the locally injected light and power-through splice loss measurement are discussed. Next the new measurement methods are explained. In the following section the application of these techniques is shown. Finally the benefits for the operator are listed.

SPLICE LOSS EVALUATION

To evaluate the splice loss, two methods are commonly used.
The first is to measure the core misalignment via image analysis. Specific parameters like core offset, core bending, etc. can be determined. The loss is calculated from these parameters using an empirically acquired formula. This technique is not able to cover all the loss mechanisms of the splice, because it is limited to the few parameters describing the splice. This shortcoming usually leads to a too optimistic splice loss evaluation, especially when incorrect parameters are used or the actual loss is high. Because the loss value is based on the assumed values on the basis of the parameters this approach is called splice loss estimation.
A direct method and hence a real measurement technique can be accomplished using the Local Injection and Detection (LID) method[1]. Light is launched into the fiber in front of the splice and detected behind the splice as illustrated in Fig. 2. Usually bend couplers are used to provide easy fiber insertion and removal. They are specially designed to minimize fiber stress and so to prevent the fiber from any damage.

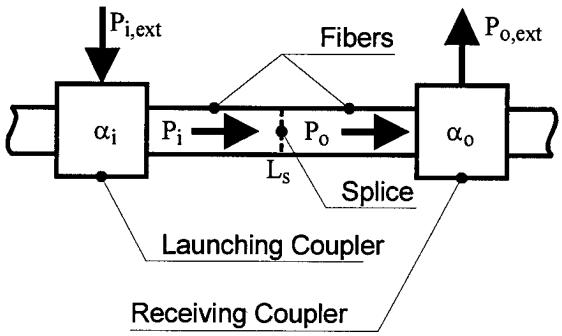

Fig. 2: Measuring the Splice Loss with a LID-System

An external power $P_{i,ext}$ is launched into the fiber via a bend coupler leading to power P_i inside the fiber. After a splice with loss L_s the power P_o remains in the fiber. P_o is coupled out of the fiber as an external power $P_{o,ext}$ also by means of a bend coupler. External powers and internal powers correspond according to

$$P_i = \alpha_i P_{i,ext}$$

$$P_{o,ext} = \alpha_o P_o$$

with the coupling efficiencies α_i and α_o. The splice loss

$$L_s = 10 \log \frac{P_i}{P_o}$$

is calculated from the internal powers. Unfortunately it is not possible to determine the internal powers, even if the external powers are known. This is because the coupling efficiencies vary strongly with the coating type and color.
To determine the splice loss the coupling efficiencies must be eliminated from the calculation. This requires a known loss L_{ref} at the splice point. The loss of the air gap between the unspliced fibers can be used as a reference value (Fig. 3).

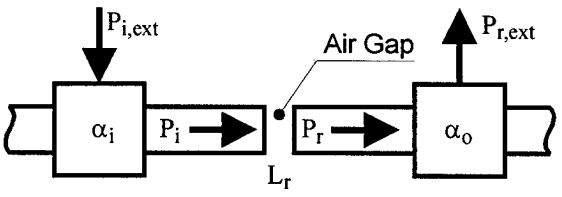

Fig. 3: Measuring the Loss of the Air Gap Loss as Reference Value

The loss of the air gap has a fixed value of 0.30 dB if the gap is very small and the fibers are aligned for maximum transmission[2].
The air gap reference is measured just before the fibers are melted together. In this situation the fibers are already perfectly aligned. The external input power $P_{i,ext}$ is the same during reference value measurement and splice loss evaluation. The efficiencies α_i and α_o are constant too, because the fiber position in the couplers is not modified during the whole splicing cycle. This means, that P_i is also the same as in Fig. 2.
Only the received external power has altered to

$$P_{r,ext} = \alpha_o P_r ,$$

because L_r usually differs from L_s. If the reference value

$$L_r = 10\log\frac{\alpha_o \alpha_i P_{i,ext}}{P_{r,ext}}$$

is known, the loss can be calculated as

$$L_s = L_r + 10\log\frac{P_{r,ext}}{P_{o,ext}}.$$

This means, that if the reference value is known, the loss can be determined from the ratio of the detected external powers $P_{r,ext}$ and $P_{o,ext}$.
Although it sounds easy to obtain the reference value, there are quite a few problems if a high precision loss measurement is needed. The loss of the air gap depends mainly on the following parameters:

- the angle of the two fiber axes
- the cleave angle of the fiber ends
- the diameter of the mode field radius

Measurement techniques to determine these parameters are explained in the next section. The subsequent section shows how the reference value is adapted to these parameters.

MEASUREMENT TECHNIQUES

Axis Angle Detection

As explained in the above, an accurate method for the measurement of the axis angle is necessary to determine the reference value.
The axis angle detection and later the cleave angle detection is performed via image analysis. Most common fusion splicers already have an optical system that is designed for the demand of fiber positioning. A widespread method for obtaining an image of the fiber is shown in Fig. 4.

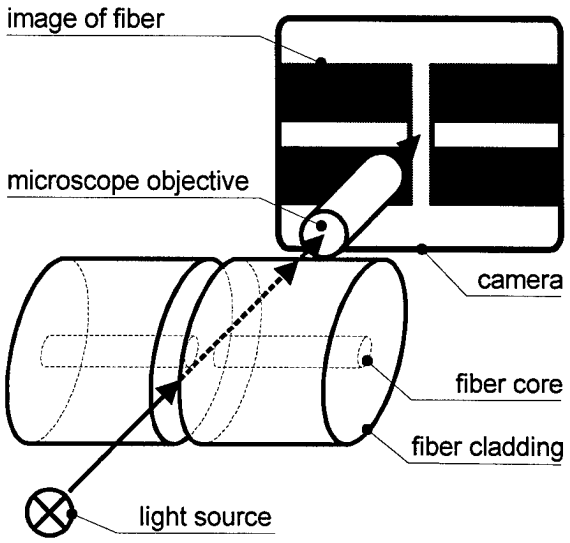

Fig. 4: System to Project a Fiber Image onto a Camera

The image of the fibers is projected onto a camera chip. A microprocessor reads it from the camera and performs the image evaluation. There are two of these systems delivering images from orthogonal axes to get a three-dimensional overview of the fiber positions.
In the following only the x- and z-axis are depicted. The y-axis is handled in an analog way. The final overall angles or offsets are calculated via Pythagora's theorem.
A simple way to obtain the angle of a fiber is illustrated in Fig. 5. The fiber position in x-direction is measured at two detection columns. The distance between the columns is Δz. The offset in x-direction is Δx.

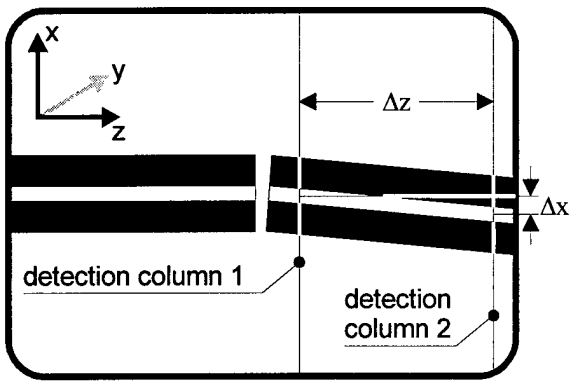

Fig. 5: A Simple Method to Measure the Axis Angle of a Fiber

The angle is calculated as

$$\alpha_{ax} = \arctan\left(\frac{\Delta x}{\Delta z}\right).$$

This method is very simple, but has some disadvantages that make it unsuitable for accurate adaptation of the reference value. The disadvantages in detail are:

- A tilt of the camera is seen as an angle of the fiber.
- Distortions of the optical system can lead to the problem, that a straight fiber appears bent. This affects the accuracy of the angle measurement.
- Inhomogenities of the illumination can lead to the same effects as caused by distortions.

These drawbacks can be reduced by using different locations for the detection columns in the sampled image. To eliminate them an apparent solution is to measure only with one detection column.

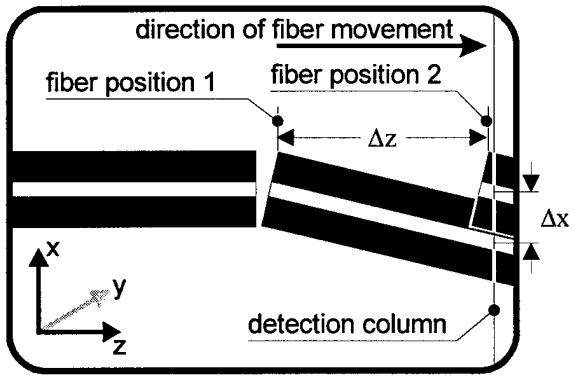

Fig. 6: Enhanced Method for Measuring the Axis Angle

Instead of using two different detection columns the fiber is moved past a single column. The direction of movement is given by the mechanical setup and is free of tilt errors. The offset Δx in x-direction between the fiber in position 1 and in position 2 is measured. With the distance Δz that the fiber has moved the angle is again calculated as

$$\alpha_{ax} = \arctan\left(\frac{\Delta x}{\Delta z}\right).$$

With this technique the axis angle for the left and right fiber are both measured in each axis. Due to the independence of optical distortion an accuracy of 0.05° can be achieved.

Cleave Angle Detection

Both splice loss performance and loss measurement accuracy depend on the quality of the fiber endfaces. The predominating factor is the cleave angle. The goal is to measure the cleave angle accurately without additional hardware effort.

As mentioned previously the optical system in common fusion splicers is mainly designed for fiber positioning. These optical systems have a resolution of approx. 1 µm limited by diffraction effects in the visible wavelength range. Additionally every optical system has distortions and slight illumination irregularities. That does not affect fiber positioning and video loss estimation.

An obvious method to find out the cleave angle is to determine the z-position of the fiber end for each video line in the image. After the edge of the fiber is detected that way, the cleave angle can be determined by calculating the angle of it relative to the video lines.

However such a direct detection of the cleave angle is too inaccurate for adaptation of the LID reference value.

Commercial fusion splicers are actually equipped with a far more precise system than the video system. The trick is to use it for cleave angle measurement.

Most splicing machines have a high precision mechanism to adjust the fibers' positions before splicing. This mechanism is needed to align the fiber cores in transverse directions and to perform the fiber feed during the fusion process.

The fiber movement along its axis (z-direction) is done by a high resolution actuator e.g. by means of a piezoelectric device. Therefore it is possible to perform extremely small steps in z-direction

(e.g. 5 nm compared to the resolution of approx. 1 µm of the optical system). Although this resolution seems quite sufficient, how can it be used for cleave angle detection?
The recipe is simple and can roughly be described in three sentences. First the gap between the fibers is reduced as much as possible. Then the distance between the fibers is increased again slowly. Simultaneously the point at which the light from the light source is able to pass through the gap between the fibers is monitored.
Due to diffraction effects at a small gap (approx. around 3 µm) between the fiber ends, the light is prevented from travelling trough the gap even if the fibers have no physical contact.
Keeping this in mind it is possible to define two virtual fibers that are slightly longer, than the real fibers.

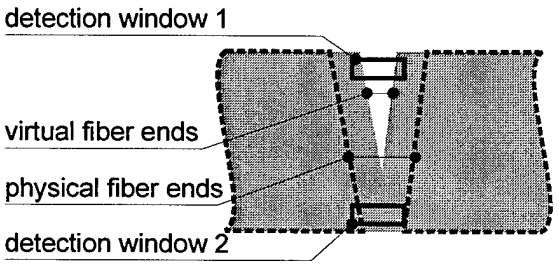

Fig. 7: Definition of Virtual Fiber Ends

Fig. 7 shows the physical and virtual fiber ends. Reduction of space between the two fibers is possible until the physical fiber ends get into contact. The virtual fibers overlap in this situation. The intensity of light that passes the gap is monitored by the two detection windows.
If the fibers have physical contact, an image similar to Fig. 8 is recorded by the camera. Remember, that the physical fiber ends can not be seen on the image. They are depicted in Fig. 8 only by way of illustration.

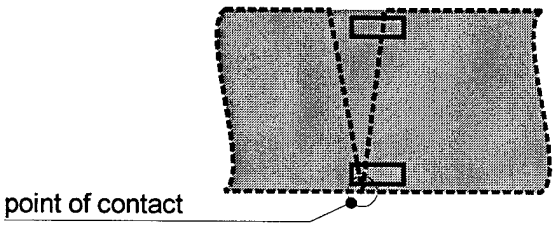

Fig. 8: Two Fibers Having Physical Contact

The gap between the fibers is closed, because of the totally overlapping virtual fibers. The detection windows recognize the darkest brightness level that is possible.
The fiber ends should be as close as possible, but without forcing the fibers to bend. They have physical contact only in a single point due to their cleave angles. The location, where the fibers have physical contact is marked in Fig. 8.
The distance between the fibers is now increased step by step. This is done with a resolution beyond that of optical systems working in the visible wavelength range. While the space between the fibers is increased, the brightness in the two detection windows is observed.

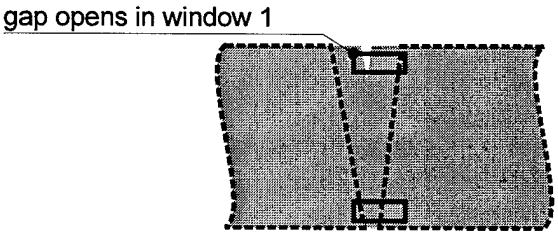

Fig. 9: Detection Window 1 Registers, that the Gap Starts to Open

After several steps the gap starts to open like in Fig. 9, which means that it is now possible for the light emitted by the light source to pass through the gap between the fibers. If there is a cleave angle, there is no concurrent opening of the gap. The opening starts at the location, where the distance between the endfaces is the largest.
The extension of the fiber gap can be stopped, when it is opened totally. This means that the gap is transparent for light in its whole transversal extension which is illustrated in Fig. 10.

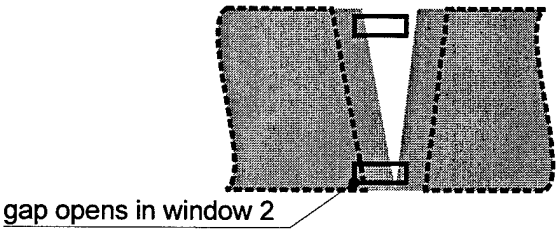

Fig. 10: Detection Window 2 Registers, that the Gap has Opened Totally

During the whole process of increasing the gap, the brightness at the two detection windows is monitored. After the gap is opened totally, the two data arrays of the detection windows are evaluated. They contain the sampled brightness

inside the detection windows for a certain distance between the physical fibers.

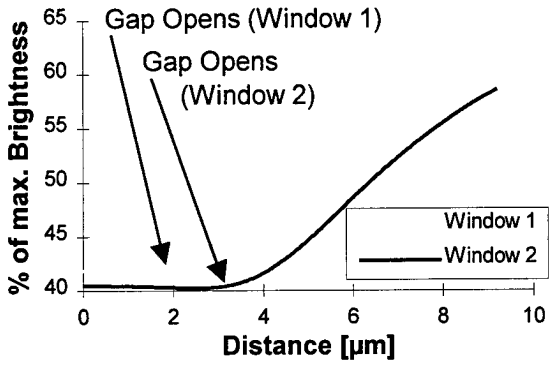

Fig. 11: Sampled Brightness of Detection Windows

Typical curves of the brightness are depicted in Fig. 11. Starting at a distance of 0 µm the brightness level for both detection windows is invariant at first.
At approx. 1.8 µm the curve of window 1 starts to rise significantly. That means, that the gap is now opening at the location corresponding to window 1.
At about 3.2 µm the curve of window 2 also starts to rise. So window 2 also has detected that the gap opens at the corresponding location.
The different starting values are created by the illumination inhomogeneities caused by the optical system. Due to the fact that only the change in gradient is used to calculate the angle, the inhomogenious illumination does not affect the measurement accuracy.
To calculate the cleave angle the distance between the opening in window 1 and window 2 (1.5 µm in the example above) and the distance in transversal direction between the two windows is needed.
The angle measured by this technique is the overall cleave angle of both endfaces. A differentiation of the individual angles is not necessary, because the angles are small and hence this produces only a neglectable error.
The accuracy of this method is about 0.1°.

Automatic Fiber Type Detection

After the axis and cleave angles are determined the last parameter missing to adapt the reference value is the mode field diameter of the fibers to be joined.

Although the mode field diameter varies from fiber to fiber, it is sufficient to distinguish between four fiber types:

- dispersion shifted (DS)
- standard singlemode (SM)
- multimode with 50 µm core diameter (MM50)
- multimode with 62.5 µm core diameter (MM62.5)

There are two different detection methods for singlemode and multimode fibers.

DS and SM Type Detection. The mode field is measured before the fibers are spliced. While the transmitted light is measured via the LID system, the transverse offset of the fibers is varied (Fig. 12).

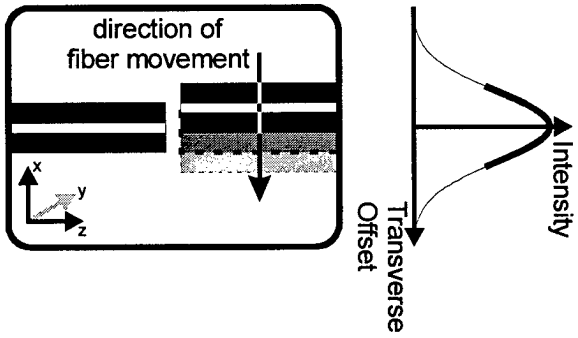

Fig. 12: Mode Field Diameter Measurement Method

If the distance between the fiber ends is sufficiently small, a gaussian like intensity distribution is measured.
The mode field radius can be read off as the transverse offset, where the transmitted power has decreased by a factor of 1/e relative to the maximum.
This method is normally used for measuring the spot size of a fiber and is know as the Transverse Offset Method[3].

MM Type Detection. If the previous method is applied to multimode fibers, a strongly varying pseudo mode field diameter between 16 µm and 30 µm is measured. There is no correlation between diameters and multimode fibers with a larger core of 62.5 µm.
The mode field diameter of MM fibers is related to the stationary mode field of the fiber. This means that the power interchanged between the individual modes of the fibers is balanced. Each mode receives the same power as it emits.

The bend coupler launches an asymmetrical power distribution into multimode fibers. As a result the power launched into the individual modes differs from the stationary distribution. Due to a small free fiber length the distance between the launching LID-coupler and the position of the air gap is very short. This length of fiber does not allow the modes to fill the multimode fiber core completely.
Without a completely filled multimode core the distribution of power in the individual modes is greatly influenced by the coupling conditions, such as coating fiber color or core position. When a multimode fiber is tested, this sensitivity to the coupling conditions leads to a strong varying mode field diameter if the method for detecting DS and SM fibers is used .
To distinguish between a MM50 and a MM62.5 a large transverse offset is needed. Because MM fibers have a core diameter that is significantly larger than the wavelength, there is no evanescent electromagnetic field outside the fiber core in contrast to SM fibers[4]. Therefore the power is concentrated inside the core diameter. Thus the transmitted power at a large transverse offset can be used to identify the different MM fibers (Fig. 13).

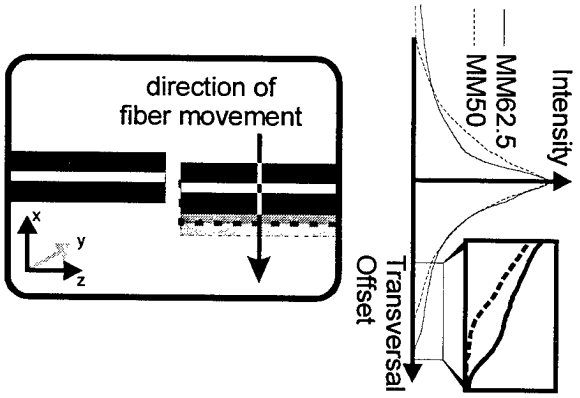

Fig. 13: Method to Identify Different Multimode Fibers

For a 50 µm fiber, the transmitted intensity at a transverse offset between 40 and 60 µm is significantly lower than for a 62.5 µm fiber.

APPLICATION OF MEASUREMENT TECHNIQUES

Splice Process Improvement

In addition to the adaptation of the reference value, the measured cleave angle can be used to enhance the fusion process itself.
When two fibers are spliced a forward movement (feed) in the axial direction (z-axis) is applied. This is needed to compensate for unevenness and small defects of the endfaces.
If fibers with large cleave angles are to be joined, it is likely that there is an angle between the endfaces. This has the effect, that a certain amount of material is missing when the fibers are pushed together. This is illustrated in Fig. 14. The overall cleave angle α_{cl} produces a material deficit of volume V_m.

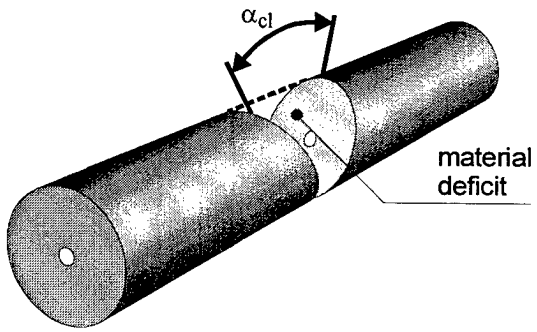

Fig. 14: Material Deficit Caused by Cleave Angles

During fusion of the fibers this deficit induces a material flow. The flow also affects the fiber core and causes it to bend. This results in an increased loss.
To reduce this effect a higher feed is needed to balance the material deficit. Hence the cleave angle α_{cl} is measured (primarily to adapt the reference value) and an accommodated z-feed can be applied to achieve minimum loss. For a fiber of diameter d the additional z-feed Δz_{af} is calculated from the volume of the missing material

$$V_m = \tfrac{1}{2}\pi\left(d/2\right)^2 d \tan\alpha_{cl}$$

and the volume

$$V_d = \pi\left(d/2\right)^2 \Delta z_{af}$$

that is delivered by increasing the z-feed by Δz_{af}. To balance these volumes an extra z-feed of approximately

$$\Delta z_{af} = {}^{d}/_{2} \tan \alpha_{cl}$$

should be applied.

Loss Measurement Improvement

To adapt the reference value for the LID-based loss measurement, the air gap loss under ideal conditions is taken as a starting point. Ideal conditions mean, that the fiber core axes are parallel, have no offset and the endfaces are perpendicular to the axes. This air gap loss is the ideal air gap loss $L_{r,id}$.

If light is emitted by a fiber end with a cleave angle the direction of the emitted light differs from that of the fiber axis. The angle between the direction of the light and the axis depends on the cleave angle and the refractional index distribution of the fiber. Conversely a light beam should be launched into the fiber at the same angle to achieve optimum efficiency.

The consequence of this is, that even if two fibers have parallel axes, the emitted light ray and the optimal launch ray build an angle. This results in an increased air gap loss. Fig. 15 depicts the situation, if both cleave angle α_{cl} and axis angle α_{ax} are considered.

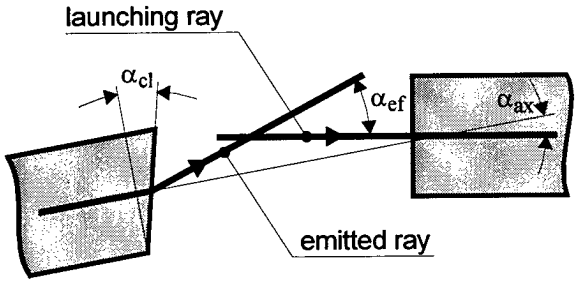

Fig. 15: Effective Angle Composed of Cleave and Axis Angle

Normally both fibers have different cleave angles. But if the angles are small like in splicing reality, it is possible to define an overall cleave angle that is located only at one fiber. Under these circumstances the emitted and the launching ray form an effective angle

$$\alpha_{ef} = \alpha_{cl} - n(\alpha_{ax} + \alpha_{cl}).$$

The actual air gap loss increases with the effective angle. To adapt the reference value to the effective angle, a correction loss

$$L_{r,c} = 10 \frac{1}{\ln 10} \left(\frac{\pi}{\lambda} w \sin \alpha_{ef} \right)^2$$

is added to the ideal air gap loss. λ is the operating wavelength of the LID system and w is the mode field radius of the measured fiber.

With the adapted reference value the splice loss is calculated as

$$L_s = L_{r,id} + L_{r,c} + 10 \log \frac{P_{r,ext}}{P_{o,ext}}.$$

OPERATORS BENEFITS

In this final section the benefits for the operator from these new techniques are described. The user benefits from

- fiber type detection
- splice loss improvement
- splice loss measurement improvement

Fiber Type Detection

Due to the new automatic fiber type detection fiber there is no need for the user to know about the type of the spliced fibers. The best splicing process parameters set is chosen by the splicing machine itself.

This minimizes errors caused by operators mistakes of choosing the wrong process setup. Moreover it is unnecessary to instruct the operator about the fiber types he is working on.

Another positive effect is that a fiber type determination can be performed in the field. No laboratory testing is needed.

Splice loss improvement

As a result of the splice process adaptation to the cleave angles the amount of high losses (≥ 0.1 dB) is reduced by about 60%. The diagram Fig. 16 shows testing data from various splices.

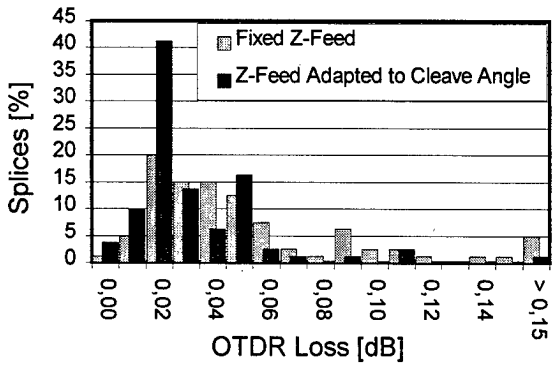

Fig. 16: Distribution of Splice Losses (Eccentric and Concentric Fibers, New and Worn Fiber Cleavers)

The data consists of 80 splices. 62.5 % were made with a high eccentric (0.8 µm) SM fiber, the rest was done using a commercial standard SM fiber. Three different fiber cleavers were used, each in different stages of wear (new, used, ready for service).
This shows, that a significant improvement is achieved by compensation for bad cleaves. This allows to prolong cleaver service intervals and avoids unnecessary downtime for repairs.

Splice Loss Measurement Improvement

The correction of the LID loss measurement reference value leads to a significant improvement in loss measurement.

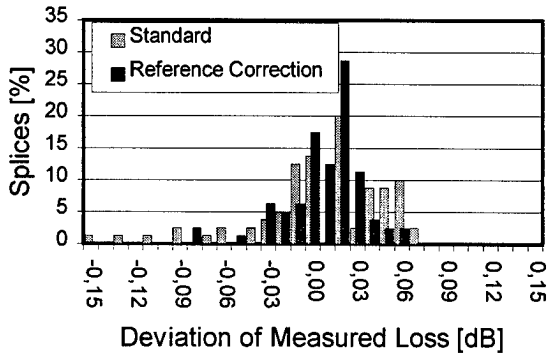

Fig. 17: Deviation of Measured Loss (Eccentric and Concentric Fibers, New and Worn Fiber Cleavers)

The splices were made under the same conditions as in Fig. 16. The deviation is defined as measured loss by the machine minus real loss (measured bi-directional by an OTDR).

Without a correction of the reference value an average absolute error of 0.030 dB is achieved. This error is reduced to 0.018 dB by the adaptation of the reference value.
Especially the number of splices that are measured much too optimistic (deviation < -0.05 dB in Fig. 17) is dramatically reduced by 60 %. This provides extra security so that undetected bad splices are not in the fiber system. That means the user can leave his job site in confidence of really not having exceeded his acceptance criteria.

CONCLUSION

This paper has introduced a set of new techniques that will improve common fusion splicers. Not only the loss measurements accuracy was increased, but also the fusion process itself was enhanced to minimize the number of splices with high losses. Furthermore the automatic fiber type detection extended the possibilities of a LID system beyond fiber positioning and loss measurement. All this requires no hardware effort and is therefore available not only for new machines, but also older machines can easily be upgraded.
Because these measurement techniques are quite new there is still room for further improvements. A further decrease of measurement error seems also possible like a more detailed fiber type differentiation for the automatic type detection. Also time optimization of these new techniques is a subject of current research.

REFERENCES

1 "Microprocessor-Contolled Fusion Splicer", Reinhard Engel, Siemens Telecom Report, pp. 268, 5/86

2 "Messung und Analyse der Resonatoreigenschaften von Einmodenfaserverbindungen zur Abschätzung und Reduzierung der Dämpfung thermischer Spleiße", Th. Eder, Fortschritt-Berichte Reihe 21 Nr. 54, 1989, VDI-Verlag

3 "Single-Mode Fibers - Fundamentals", E.-G. Neumann, 1988, Springer-Verlag

4 "Optische Nachrichtentechnik", H.-G. Unger, Teil 1, 1992, Hüthig Buch Verlag

AUTHORS

Bert Zamzow
Siemens AG, OEN NK E VT
Hofmannstr. 51
81 359 München, Germany
bert.zamzow@oen.siemens.de

Dipl.-Ing. Bert Zamzow graduated as engineer of telecommunications at the Technische Universität Hamburg-Harburg. He joined the splicing machines development department at Siemens in 1996. He is currently working on software design and process enhancements for future fusion splicers.

Gervin Ruegenberg
Siemens AG, OEN NK E VT
Hofmannstr. 51
81 359 München, Germany
gervin.ruegenberg@oen.siemens.de

Dipl.-Ing. Gervin Ruegenberg received his diploma of electronics from the University of Kaiserslautern. He joined Siemens in 1984 as a development engineer for optical transmitter and receiver modules. Today he is responsible for development of fusion splicing technique for optical fibers.

Marty Anderson
Siecor Corp.
853 22nd Street Place, SE
Hickory, NC 28602, US
marty.anderson@siecor.com

Marty Anderson is currently a Product Specialist for splice equipment at Siecor, providing technical and marketing support. As a field engineer he gained extensive experience installing fiber systems for Telco, CATV and LAN applications. Marty is a graduate of North Carolina State University where he received a B.S. in Electrical Engineering.

Helmar Krupp
RXS Kabelgarnituren GmbH
MP 3
Profilstrasse 4
58 093 Hagen, Germany
helmar.krupp@rxs.de

Helmar Krupp was born in 1969. He received his engineer degree in telecommunications from the Hochschule Bremen in 1993. In 1995 he joined RXS in Marketing and Productmanagement for Fiber Optic Products. Currently he is the Product Manager for Fusion Splice Equipment.

A NEW CHEMICAL STRIPPING METHOD FOR OBTAINING HIGH STRENGTH SPLICES OF UV COLORED OPTICAL FIBERS

Shahab Siddiqui, Louis R. Pritchett, John R. Szwec, Carl R. Taylor,
Robert J. Brown, Jr., and Harish C. Chandan

Bell Laboratories, Lucent Technologies, Inc., 2000 Northeast Expressway, Norcross, GA 30071

ABSTRACT

A new two-step chemical stripping method for coating removal, which provides high strength splicing of optical fibers colored with ultra-violet (UV) curable inks containing titanium dioxide, is described. The use of concentrated sulfuric acid heated to 185± 5°C, is an industry standard for chemically removing coatings from uncolored fibers. However, this method can not be used to obtain high strength splices, 200 Kpsi or greater, if the fiber is color coated with a titanium dioxide pigmented ink. In this report we describe an innovative approach designed to chemically remove any insoluble ink ingredients as well as the coatings efficiently in two sequential steps. In the first step, the colored layer is removed completely by using a controlled immersion time in dilute acid held at temperatures much lower than 185°C. In the second step, the fiber coatings are removed using standard conditions to give a clean glass surface. This new method consistently provides high strength splices.

INTRODUCTION

Fused silica, the material of optical fiber, has the unique property of having very high pristine strength (>800 Kpsi), which is stronger than steel and perfectly elastic up to its breaking point[1]. Its pristine strength is retained by the polymer coating layers surrounding the glass, which protects it from mechanical damage. However, it can be greatly degraded during the fiber jointing (splicing) procedure which is done mainly by thermal fusion. Fiber splicing is a way of increasing the fiber length indefinitely and/or branching off new origination points at any fiber location. Splicing is unavoidable and involves complete removal of the polymer coating prior to fusion of the two glass ends. The ultimate objective is to have splices with high enough strength and low optical loss at each splice. Depending on the requirement for specific splice strength and loss, the polymer coating can be removed by mechanical or chemical means. For moderate to high strength splices, the polymer coating must be removed chemically to avoid mechanical damage to the glass surface prior to fusion splicing to give a simple, permanent and low loss connection.

High strength splicing of optical fibers (200 Kpsi or greater) is critical for some applications such as undersea cables. For an uncolored fiber, obtaining high strength splices is not a problem when the fiber coatings is chemically stripped using the industry standard hot concentrated (conc.) sulfuric acid (H_2SO_4) prior to cleaving and splicing of glass fibers. However, for a colored fiber made with pigmented inks, high splice strength is not consistently attainable using the standard sulfuric acid technique. Most likely, pigments in the inks are not completely removed in the chemical dissolution or the subsequent arc fusion splice process thereby causing to make weak splices at these fiber joints. These weak fiber links can be fatal for any system requiring robust and reliable long-term usage as in the submarine fiber optic cable deployment.

The outermost layer of optical fibers is generally colored for identification purpose. Fibers are, in general, colored using pigmented polymer coatings (inks). Pigments usually are colored, insoluble organic materials which are used in the ink formulation for providing a number of discernible color shades. Insolubility is a highly desirable characteristic in the pigment for color durability and stability. In addition to the colored pigments, a white inorganic pigment namely titanium dioxide (TiO_2) is invariably used in the color coating formulation for imparting

whiteness, brightness and most importantly opacity to the color coating layer. TiO_2 is notoriously insoluble in major solvents and quite abrasive in the solid state. It is slowly soluble in hot and conc. H_2SO_4 but readily soluble in hydrofluoric acid (HF)[2].

The overall cleanliness of the glass surface[3] as well as the surface texture or morphology is very critical for high strength splices. Many conditions must be strictly met for high quality splices. Firstly, the polymer coating on the fiber must be chemically removed from the glass surface without any mechanical damage. Secondly, low particulate grade acid and solvent rinses are required with frequent replenishing to avoid contaminant deposition/ re-deposition on the glass. Thirdly, the arc fusion electrodes (in arc fusion splicing) must be kept clean consistently to avoid cross-contamination of the clean bare glass surface. There are some additional factors that affect strength also but not to the extent as the above.

In this paper, we present an innovative modification of the sulfuric acid method for stripping color as well as fiber coatings from colored fibers. The new method is a two-step sulfuric acid dip procedure and it consistently gives high strength splices (>200 Kpsi) in acceptable yields (>60%) for all colored fibers. In the first step, the colored layer is removed completely without significantly attacking the fiber coatings by using diluted sulfuric acid at a relatively lower temperature and a well-controlled immersion time. In the second step, the fiber coatings are removed in a separate concentrated sulfuric acid bath (@ 185± 5°C) to give a clean glass surface. This new technique is a significant development of the chemical stripping method for obtaining high strength splices of colored fibers for use in critical applications as in undersea cable systems.

EXPERIMENTALS

Acid-Base Titration

Equipment

- GPD Titrino Titrator made by Metrohm LTD with a Electrode probe 6.0232.100 combine pH glass input 1, Eppendorf auto pipette .25 ml, Barber-colman series 10 controller, Heating Jacket (Metal), 50 ml Teflon test tube, 150 ml beaker, 50 ml pipette, Magnetic stir bar, and 100 ml & 50 ml Graduated cylinders, etc.

Method

50 ml of sulfuric acid (of known initial strength) was pipetted into a dry clean Teflon tube. The test tube was then brought to a fume hood and placed in a metal jacket. The jacket was then heated to the desired temperature by using a temperature controller. The acid temperature was checked periodically with a mercury thermometer and a correction factor was used on the controllers if necessary. After the solution in the Teflon tube had been heated for the desired time it was removed and carefully poured into a 50 ml graduated cylinder and measured to determine how much evaporation had occurred during the heating process. The cylinder was then covered with aluminum foil and allowed to cool for 1 hour. After the solution had cooled to room temperature it was poured into a clean dry 150 ml beaker. A 0.25 ml sample was then pipetted into a beaker containing approximately 100 ml of nano- pure water and a magnetic stir bar. This solution was then titrated using a 1.0 N standard solution of NaOH to determine the final acid concentration.

Coatings Removal Method for Splice Preparation

Equipment and Chemicals.

- Aluminum heating mantle, Type J or K thermocouple, heater controller, heat resistant block, teflon tube, test tubes, watch glasses, a thermometer, a timer, magnetic stainless steel holding block, a magnetic strip to hold fibers, acid and heat resistant gloves, etc.
- Concentrated sulfuric acid, methanol (electronic grade), alcohol pad and blue pad

Coatings Removal Method

Step 1. *Preparation*

The teflon test tube containing 50 mL of sulfuric acid (of known initial strength) was placed in the aluminum heating mantle. It was gradually heated within ± 2° C of the target temperature (temperature of the acid). The acid must be

allowed to stabilize approximately for one hour at this temperature before use.

Step 2. *Color Removal Procedure*

The colored fiber was placed in the groove of the stainless steel holding block, so that it is centered on, and perpendicular to the wide edge. Approximately 3 inches of it was allowed to extend beyond the edge. It was secured in position with the magnetic strip and the perpendicularly was rechecked. The fiber end was immersed in the sulfuric acid maintained at target temperature for 40 ± 10 seconds. Care was taken not to let the fiber touch the test tube walls and overexpose it to the acid for longer than recommended above. The fiber was removed from the acid and immediately immersed in methanol at ambient temperature for ~5 seconds to rinse off the acid. A rubbing action was applied on the acid immersed portion of the fiber with an alcohol pad or equivalent until the colored layer wipes off cleanly.

Step 3. *Fiber Coatings Removal Procedure*

After the color is removed from the fiber ends, standard concentrated (36N) sulfuric acid was used routinely @ 185± 5°C to remove the fiber coatings (20 ± 10 seconds) keeping the color/clear interface above the surface of the acid. Care was taken not to bring the colored part of the fiber to touch the acid. After rinsing off the acid in electronic use grade methanol for 25 seconds, the clean glass ends were then cleaved and fusion spliced using standard techniques. The splice was re-coated and verified for splice loss and strength requirement.

RESULTS

The One- Step Standard Sulfuric Acid Method For Removing Color Coatings. The use of standard concentrated (conc.) hot sulfuric acid (@ 185± 5°C) is a widely accepted method for removing coating, prior to splicing optical fiber. In fact, both the pigmented color coatings and the fiber coatings can be removed, in the same immersion, under the above conditions, by slightly increasing the immersion time. After the appropriate rinses, the glass surface is clean enough to produce: high strength, low loss and high reliability splices.

Routinely, fusion splices with median strengths from 290 to 300 Kpsi or above can be obtained when uncolored fibers (see Figure 1) or fibers colored with non-TiO_2 inks are prepared for splicing using the "One-step "process.

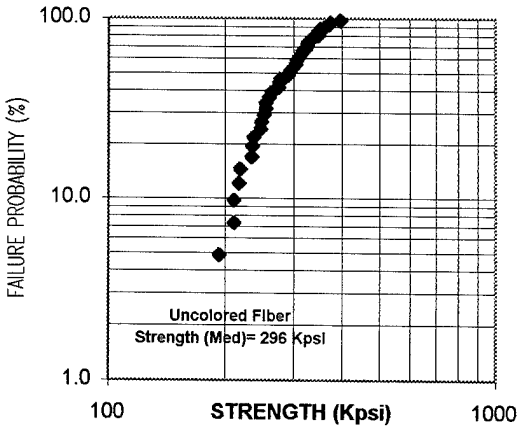

Figure 1. Splice Strength of Uncolored Fibers

When the "One-step" process was applied to fibers colored with inks containing titanium dioxide (TiO_2), fusion splice strengths were consistently lower (~ 100-150 Kpsi), for a 0% yield. Figure 2 is a comparison of splice strength results for fibers colored with blue inks: with and without TiO_2. As the figure illustrates: under identical splicing conditions, a colored fiber produces much higher splice strengths, when the opacifier, TiO_2 , is not in the formulation of the ink (median strength of 332 Kpsi w/o TiO_2 vs 142 Kpsi w/ TiO_2 for the same color).

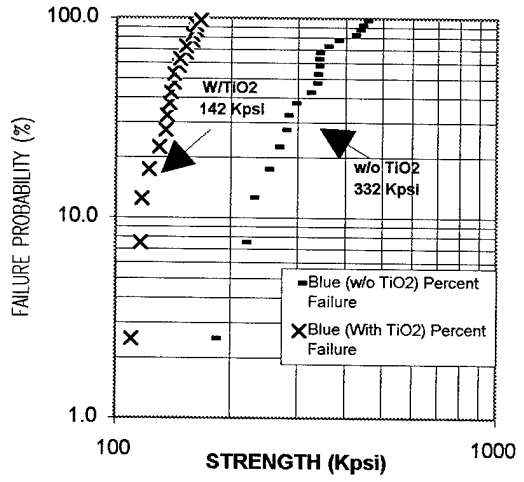

Figure 2. Effect of Titanium Dioxide on Splice Strength

The above experimental results were reproducible for all colors of ink containing TiO_2 despite the various precautions taken prior to splicing. It appears that the bare glass surface is contaminated with some residual impurity following the acid dip and the solvent rinses. Most likely, titanium dioxide (TiO_2 in some form or another) is the root cause of the problem since substituting TiO_2 (as in non-TiO_2 inks, see below in Figure 3) solves the problem. Although reportedly known to be soluble in hot and conc. sulfuric acid[2], it is possible that TiO_2 is not completely dissolved in the immersion time and thus not removed entirely. Apparently then, the SiO_2 (glass) forms some kind of bond with the TiO_2 (presumably because of high affinity of fine residual TiO_2 to freshly clean glass surface). Because of the different rates of shrinkage upon cooling following thermal fusion, cracks are induced due to stress concentration, which lowers the strength of the glass.

Attempts to detect titanium in any form on the bare glass by EDAX (Energy Dispersive X-Ray Analysis) have failed. There was no apparent presence of titanium, within the limits of detection, by the SEM method. This suggests that some other contaminant other than titanium is the culprit, or that the titanium concentrations are lower than the SEM detection limit. However, very careful EDAX analysis, in limited cases, showed the presence of more organic compounds (high concentration of carbon) on bare glass, from colored fiber samples containing TiO_2, than from uncolored samples. This suggests incomplete removal of coatings, by the acid, from TiO_2 pigmented colored fibers for unknown reasons. The root cause of, such a low concentration of, titanium's effect on splice strengths will be pursued in the future by more sensitive analytical tools.

As long as TiO_2 is absent in the colorant, the splice strength is consistently 200 Kpsi or higher. For example, in non- TiO_2 colored fibers the median strength is ~300 Kpsi (see Figure 3). These inks are specially colored pigment formulations made with a substitute opacifier, instead of TiO_2, which is proprietary.

The next section describes an approach to resolving the deleterious effects that titania has on splice strengths of TiO_2- colored fibers.

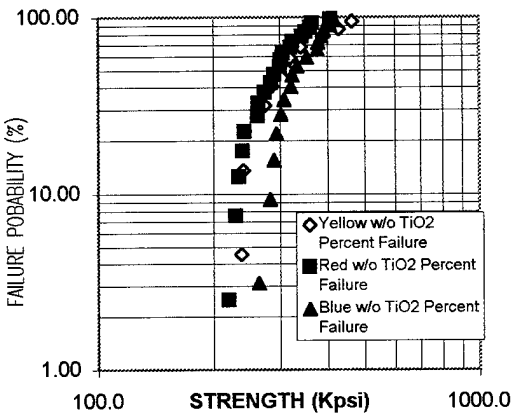

Figure 3. Splice Strength with non- TiO_2 Inks

A Two-step Sulfuric Acid Method For Completely Removing Coatings. Since the above straight-forward one-step method for removing color coatings as well as fiber coatings did not work to produce high-strength splices for TiO_2-pigmented colored fibers, it was decided to use an entirely different sulfuric acid bath to remove the color coated layer prior to removing the clear fiber coatings in another acid bath. The rationale for doing this was to keep the contaminant away from coming in contact with the bare glass in the final coatings removal step.

It was shown that using hot conc. (36N) sulfuric acid (@ 185± 5°C for a short time (10 seconds or less) to remove the coloring layer first also attacked the fiber coatings simultaneously. This phenomenon is uncontrollable and unpredictable. The situation varies from color to color, colored layer thickness differences, etc. In extreme cases, the fiber gets fully exposed to the bare glass while the intent was to remove only the color. All these produce low strength splices most likely because of the undesirable glass surface contamination presumably by TiO_2.

Since the action of the hot conc. acid on the fiber coatings is so aggressive, the temperature of the acid was lowered as an attempt as to selectively remove the color coatings only. After experimentation it was found that using the concentrated sulfuric acid at a temperature range of 60 ± 2 °C in the first acid bath seemed to selectively remove color coated layers. Later, upon removal of the fiber coatings using the standard acid bath in a second and

separate bath gave acceptable yield of high strength splices. Presumably the cross-contamination of the exposed glass surface is minimized by this technique. Figure 4 shows graphically the mean break strengths obtained by this method for seven representative pigmented colors containing TiO_2. As shown, the average strength in each case is above 200 Kpsi comparable to that for the eighth ink- black color which does not contain TiO_2 (see Figure 4, below).

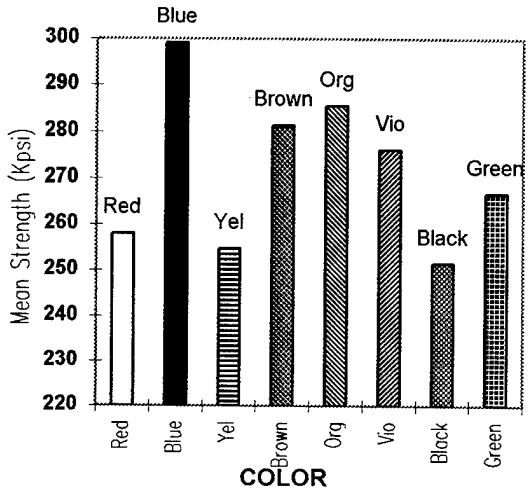

Figure 4. Mean Splice Strength of Colored Fibers using Sulfuric Acid for Color Removal at 60±2°C

The color removal step as described above, however, requires visual inspection and careful handling for high success rate. As soon as the color is removed, the fiber needs to be withdrawn and acid rinsed off thoroughly. Otherwise, the secondary coating fiber surface seemed to be attacked undesirably in the first step thereby increasing the chance of glass contamination. Thus the method above is not very robust from user's point of view. First and foremost, the strength plummets if enough care is not exercised during the color removal process, most likely due to glass contamination. Secondly, what makes it complicated and frustrating is the wide variation in time it takes to remove the various colors. Figure 5 shows the wide dipping time variation for color removal for the above eight colors. As shown in the figure, some colors take much longer than others to come off. In this experiment, red color took 50 seconds on the average for color removal whereas blue took 21 seconds under the same conditions using the same acid bath. Also, a

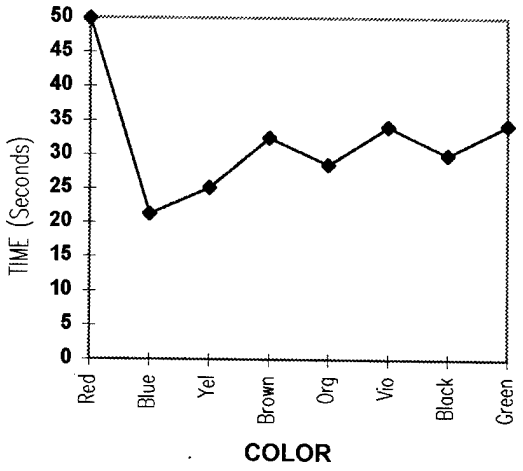

Figure 5. Average Immersion Time Variation for Color Removal Using Sulfuric Acid at 60±2°C

specific color may take longer sometime than the same color at other times. For example, red in one trial took 32 seconds; the same fiber in another trial took 85 seconds for color removal. This is a complex phenomenon and depends on many factors such as colored layer thickness, the colorant itself, adhesion of the ink to the secondary fiber surface, etc. The method can also be operator dependent. As a obvious next step for controlling time of color removal, the operating temperature was further lowered. Unfortunately the color removal process is not effected predictably at temperature lower than 55°C. Either the color is not removed uniformly or it takes unacceptably too long for the removal process at lower temperatures. Overall, the above process is on the very narrow edge of processing window for all practical purposes.

A Modified and Improved Two-step Sulfuric Acid Method For Completely Removing Coatings. The above method can not be used reliably since the operating temperature window for the color removal process is very narrow. Also, the most concentrated form of sulfuric acid straight from the manufacturer's bottle erratically attacks the secondary fiber coatings even at low temperature while attempting to remove the color coding layer (as discussed above). As an effective compromise to balance the two issues

at hand (wide variation in color removal time and premature attack on optical fiber coatings) which impact strength adversely, an attempt was made to remove the color layer by using a diluted version of the sulfuric acid but at a slightly elevated temperature when compared to the above method (that is, higher than 60°C). Naturally, the temperature in this step should be much lower than 185°C since it is known that the fiber coatings would invariably be attacked at that high of a temperature.

After carrying out a number of screening experiments in the laboratory, it was determined that a dilute sulfuric acid solution (of wide concentration range) at an optimized temperature T (60°C<T<185°C) works quite reliably to remove the color coded layer of an optical fiber without attacking the secondary coating fiber surface. The color is removed completely in the first step in a reasonable time frame (40-50 seconds). In the second step, the fiber coatings are removed using the nominal sulfuric acid procedure. This modified two-step process provides high strength splices consistently with high yields (that is, with high rates of success) presumably because the bare glass contamination by TiO_2- pigmented coloring inks is much less to non-existent in this new methodology. Also, this method works uniformly for all available UV- curable colors (12 colors) used in this study.

Scope of the Selective Color Removal Process. Like mentioned above, in this new procedure the color removal uses an acid which is already in use in the splicing industry for chemically removing fiber coatings. However, it is noteworthy to mention that the acid used here for removing colors is of reduced concentration (18-24 N). Also, the process temperature (105-125°C) is much lower. All these are attractive features in terms of personal and environmental safety. The main performance attribute of this method, however, is that it more or less takes about the same time for color removal (40-50 seconds) for all the colored fibers tested so far. However, significant variation in thickness and degree of cure for the colored layer are likely to seriously affect the above performance attribute.

The first step selectively removes the color layer containing titanium dioxide (TiO_2) or any unidentified harmful component of the pigmented ink in the isolated bath. This greatly reduces the chance of contaminating the glass since it is not exposed at this stage. The fiber acrylic coatings are removed in the second step using conc. sulfuric acid at 185± 5°C. This produces a pristine surface on the exposed glass, a proper color/fiber interface and a coating/glass interface (see Figure 6).

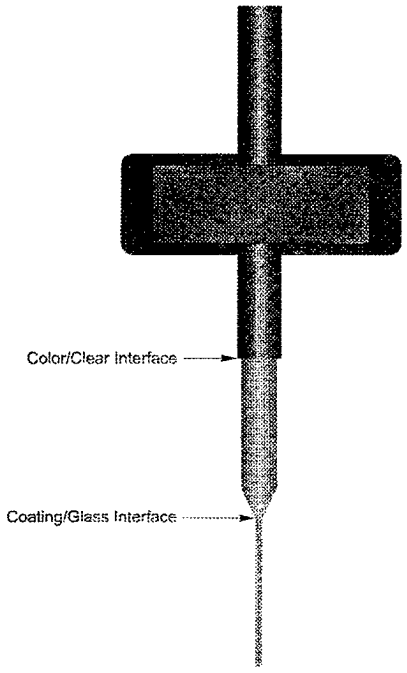

Figure 6. A Clean Glass Ready for Cleaving and Splicing

In Table 1 is summarized median strength results for all colored fibers obtained by this method.

Table 1. Median Splice Strength and % Rate of Success for UV Colored Fibers

Color	Median Strength (Kpsi)		% Rate of Success (% Strength >200 Kpsi)	
	Virgin	Cabled	Virgin	Cabled
Green	315	321	82	100
Yellow	297	278	90	88
Brown	362	269	100	100
Blue	308	217	94	72
Orange	305	288	90	78
Red	314	325	100	100
Violet	264	299	91	91
Black	349	293	100	90

These splices were all proof-tested to failure. This table compares splicing results of cabled and uncabled (virgin) fibers. Also, it summarizes the rate of success (which is % of splices with strengths greater than 200 Kpsi) for the above fibers. The above table definitely shows that colored fibers whether virgin or retrieved from a cable produce indistinguishable results.

Figures 7-9 show Weibull plots for all available colors which show high strengths (>200 Kpsi) and high splice yields (>>60%) regardless of color. This is a very important result since each color has a different concentration of TiO_2 in the ink formulation. For example, TiO_2 concentration in white, rose, aqua, and slate inks are typically higher than that in other colors. Despite that, all colors produce high strength splices (compare figure 9 with figures 7-8).

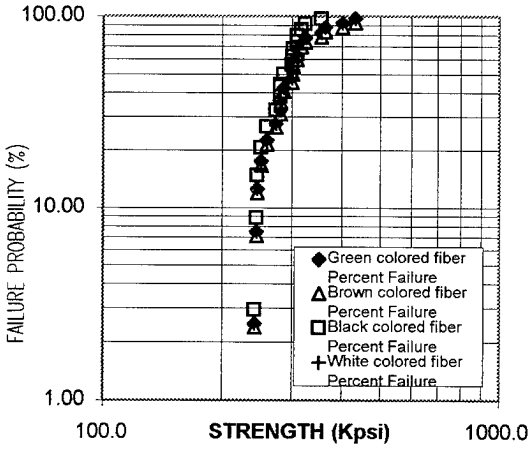

Figure 7. Splice Strength of Colored Fibers (Green, Brown, Black and White)

One potential concern in this method is the constant water evaporation of the dilute sulfuric acid over time which would greatly affect the performances. Ideally, one would like to use the dilute acid bath for color removal over an extended period of time for continued operation. However, it is not practical since the acid is continuously evaporating with change in concentration. Eventually the concentration of acid will increase to a point when it would attack the fiber coating prematurely during the color removal process. In fact, Figure 10 illustrates a case in point where the highly concentrated acid eventually attacked the fiber coatings prematurely.

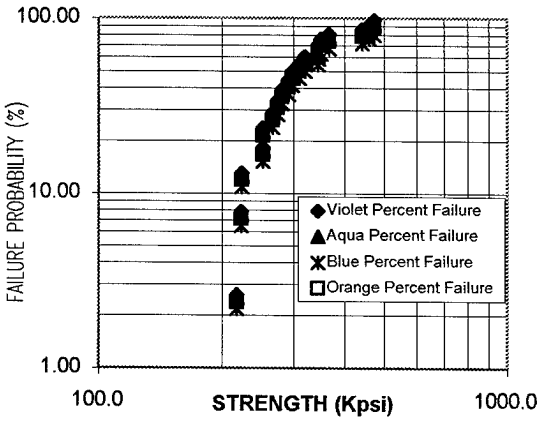

Figure 8. Splice Strength of Colored Fibers (Violet, Aqua, Blue and Orange)

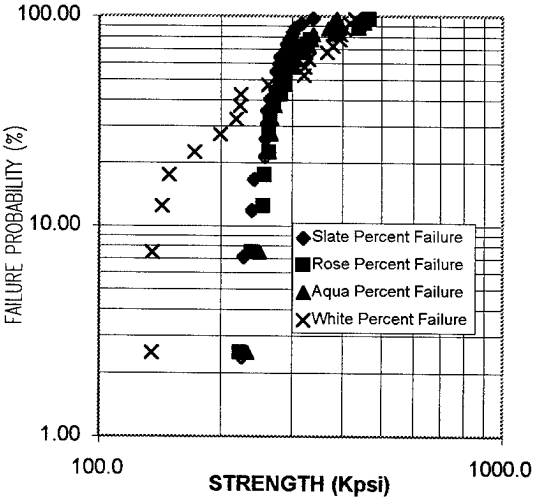

Figure 9. Splice Strength of Colored Fibers with Relatively Higher TiO_2 Concentration (Slate, Rose, Aqua and White)

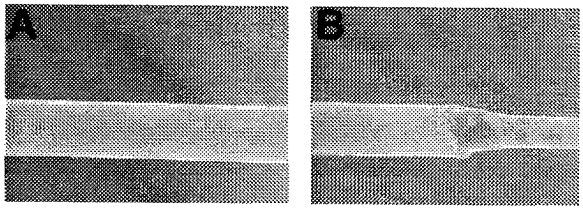

Figure 10. SEM Pictures of Fiber Surfaces @ 100x Magnification: **'A'** shows no surface attack by acid right after color removal and **'B'** shows undesirable attack by acid while removing color.

This likely contaminates any bare glass with TiO_2 thereby adversely affecting splice strengths. It is to be emphasized here once again that the preparation of clean glass without contamination is critical for successful high strength splices.

Optimization of the Selective Color Removal Procedure. The selective color removal step has been demonstrated to be dramatically improved by using a dilute sulfuric acid (of wide concentration range) and lower temperature (than 185°C). The actual color removal time varies with these two important factors. However, at an optimized acid concentration and a temperature range, the color removal time remains quite constant for all twelve pigmented colors used in this study. We carefully studied this ubiquitous evaporation phenomenon with many temperature and acid concentration profiles in order to design the most effective color removal procedure with a large processing window for extended life of this acid bath. Figure 11 shows a representative example of such a drastic increase in acid concentration with time at two different temperatures.

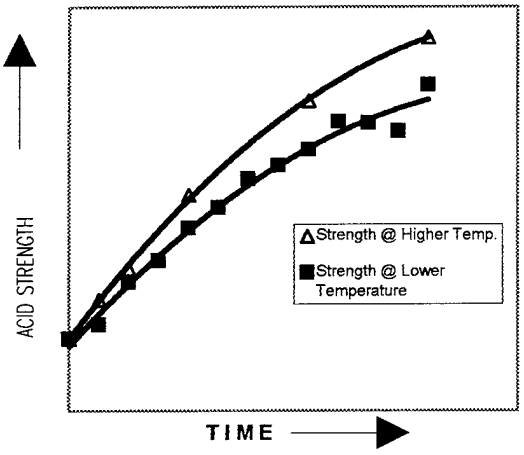

Figure 11. Change of Acid Strength With Temperatures

For a given acid concentration, the color can be removed earlier at higher temperature than that at lower temperature; however, the latter has longer bath life and a larger operating window. By properly adjusting and maintaining the acid concentration and temperature, we were able to effectively prepare colored optical fibers for high strength splices with acceptable yields[4].

CONCLUSION

This work has demonstrated that by properly adjusting the temperature and the strength of sulfuric acid, the color coded layer of an optical fiber can be selectively removed within an acceptable time frame. This is highly effective in producing high strength robust splices.

In this work we have used fibers colored with twelve different UV curable inks from one specific ink supplier. The color removal procedure described here has been developed for fibers colored with these inks. How this will behave when we use it for another set of inks from a different supplier will have to be studied later. However, we believe the method is quite general and can be used for any set of inks by optimizing various conditions or factors affecting ink cure and interfacial adhesion such as ink type, fiber type, thickness of colored layer, and ink processing parameters, etc.

ACKNOWLEDGEMENT

The authors gratefully acknowledge help from Mr. Celestino Rey, Ms. Ella Shmukler, Mr. Robert G. Towns, Mr. Ron D. Parker, Mr. Kelly Hopkins, several production specialists and Ms. Beverly Rodriguez while completing this work.

REFERENCES

1. J. T. Krause and C. R. Kurkjian, *Elect. Lett.*, 1985, 21(12), pp.533-535.
2. The Merck Index, Tenth Edition, Published by Merck & Co., Rahway, NJ, USA, 1983, pp. 9301-9302.
3. J. Suzuki, S. Yaguchi and M. Yushinuma, *Proccedings of the 46th International Wire and Cable Symposium,* 1997, pp.457-461.
4. L. R. Pritchett, Jr., S. Siddiqui, and J. R. Szwec, "Preparation of Colored Optical Fiber for Splicing", filed for a U. S. patent in March, 1998.

BIOGRAPHIES

Shahab Siddiqui
2000 NE Expressway, Norcross, GA 30071

Shahab Siddiqui is a Member of Technical Staff in the Materials Technology and Quality Engineering group at Bell Laboratories of Lucent Technologies Inc., in Norcross, GA. He joined AT&T Bell Laboratories in 1984 and worked in many areas of both fundamental and applied polymer chemistry at Bell Labs in Murray Hill, Princeton and Richmond. Currently he is responsible for the design and development of UV curable inks and other related materials for fiber optic applications at Norcross. He received a Ph.D. degree in Physical Organic Chemistry from the University of Kentucky in 1982. He is the author/ co-author of over thirty scientific publications in his field of expertise.

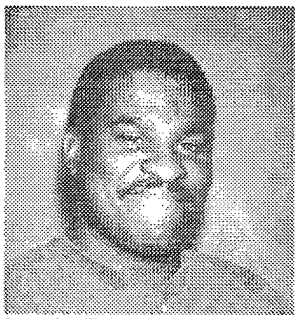

Louis R. Pritchett
2000 NE Expressway, Norcross, GA 30071

Louis Pritchett received a BSMET from Southern Polytechnical Institute and a MS in Engineering from Steven's Institute of Technology. He joined Bell Laboratories, then AT&T and now Lucent Technologies, in 1987. While working for AT&T, Mr. Pritchett was responsible for the assembly and testing of optical repeaters. Currently, he is responsible for the manufacture, measurement, and processing of submarine optical fiber.

John R. Szwec
2000 NE Expressway, Norcross, GA 30071

John R. Szwec graduated from Georgia State University with a Bachelor of Science Degree in Chemistry in August of 1994. He first joined Lucent Technologies Bell Labs in October of 1994 as a contract employee. Then John was hired by Lucent Technologies as a Senior Technical Associate in Bell Laboratories in 1996. He is involved in many research and development projects for materials development for terrestrial as well as submarine light-guide applications.

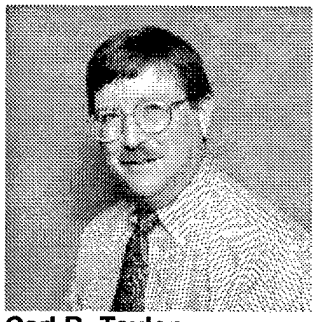

Carl R. Taylor
2000 NE Expressway, Norcross, GA 30071

Carl R. Taylor is currently Bell Laboratories Technical Manager of the Materials Technology and Quality Engineering Group at Lucent Technologies' main Fiber Optic Manufacturing site in Atlanta. The group has responsibility for the design and engineering of materials used in fiber optic cable and apparatus products as well as responsibility for the quality of all incoming materials and components. He has previously been Supervisor of the Plastics Engineering and Characterization Group in Atlanta and Supervisor of the Polymer Materials Research, Engineering, and Applications Group at Bell

Laboratories in Murray Hill, NJ. Prior to joining Bell Laboratories in 1977, he earned a B.S. in Chemistry from the College of Wooster in Ohio and a Ph.D. in Physical Chemistry from the University of Wisconsin in Madison. His graduate work focused on the physical and viscoelastic properties of polymers. He holds nineteen patents and has authored or co-authored 29 publications.

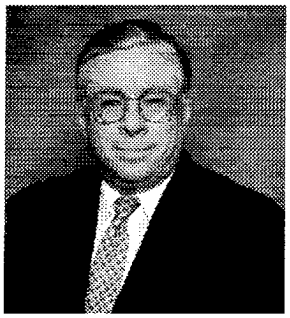

Robert J. Brown, Jr.
2000 NE Expressway, Norcross, GA 30071

Robert J. Brown, Jr. is currently Bell Laboratories Technical Manager of the Post Draw Technology Engineering Group at Lucent Technologies' main Fiber Optic Manufacturing site in Atlanta. The group has responsibility for the design and engineering of high-speed coloring and rewinding of optical fiber as well as design of the processing of long fiber sets for submarine fiber applications. He has previously been the Technical Program Manager for AT&T's Telstar 4 satellites as well as manager for the Bell Labs group that designed the communications payload and propulsion subsystem for the Telstar 3 series of satellites. He was also responsible for the design of AT&T's first satellite data communications network using VSATs (Very Small Aperture Terminals). Prior to joining Bell Laboratories in 1971, he earned a BS, MS, and Ph.D. in Electrical Engineering from The Georgia Institute of Technology. He has authored or co-authored 9 publications.

Harish C. Chandan
2000 NE Expressway, Norcross, GA 30071

Harish C. Chandan is a Distinguished member of Technical Staff at Lucent technologies Inc., Bell Laboratories, Norcross, Georgia which he joined in 1977. He manages the Fiber Qualification Laboratory. His other activities include mechanical reliability of fibers, polymer coatings and glass processing. Dr. Chandan holds a Ph. D. in Ceramic Science from Pennsylvania State University. He is active in the Fiber Reliability Working Group in the Telecommunications Industries Association.

EFFECT OF pH ON THE STRENGTH AND FATIGUE OF FUSED SILICA OPTICAL FIBER

Andrew T. Taylor, M. John Matthewson

Rutgers University, Dept. of Ceramic and Materials Eng., Piscataway, New Jersey

ABSTRACT

The fatigue behavior of both bare and polymer coated silica optical fiber has been determined in various buffered pH solutions. Bare and polymer coated fibers were studied to distinguish any coating effects. Numerical integration techniques were utilized to fit the data to three kinetics models, and the fatigue parameters were calculated together with their corresponding confidence ellipses.

The apparent reaction order for the reaction between the OH^- ion and SiO_2 between pH 4 and pH 10 was determined to be ~ 0.3 and this value is independent of the kinetics model used to fit to the data. The relationship between fatigue and pH is nonlinear; indicating different mechanisms at high, low, and intermediate pH.

INTRODUCTION

The current industry accepted model for strength and reliability calculations is a combination of an empirically derived rate law for crack extension:[1,2]

$$\dot{c} = \frac{dc}{dt} = v = AK_I^n , \qquad (1)$$

and the well-known Griffith equation:

$$\sigma_a = \frac{K_I}{Y\sqrt{c}} , \qquad (2)$$

where v is the slow crack growth velocity, A is a constant depending on the environment, σ_a is the applied stress, K_I is the stress intensity factor, and n is the stress corrosion susceptibility parameter, which is often treated as a constant. Eq. 1 is mathematically simple to manipulate and was useful in providing the initial basis for the theory of subcritical crack growth but "has outlived its usefulness and now represents an obstacle to further progress."[3] Koa[4] determined that A followed an Arrhenius temperature dependence and that the activation energy depended on the applied stress.

For convenience, the power law, designated model 1 here, may be rewritten as:[5]

$$\text{Model 1: } \frac{dc}{dt} = A_1 \left(\frac{K_I}{K_{IC}} \right)^{n_1} , \qquad (3)$$

where K_{IC} is the critical stress intensity factor. If, as is commonly assumed, n_1 is a material constant, then all the environmental dependence of fatigue must be in A_1. Under these conditions A_1 is expected to depend on both an Arrhenius term and the concentration of the chemical species causing the crack growth. While this species is normally assumed to be water, here we will examine only the dependence on the hydroxyl ion concentration. It is well known that silica is weaker and fatigues faster in high pH.[4,6,7]

We can rewrite A_1 as:

$$A_1 = \nu [OH^-]^x \exp \frac{-Q}{RT} , \qquad (4)$$

where ν is a frequency factor, x is the apparent reaction order, Q is the activation energy, and R and T have their usual meanings. One can predict the time to failure, t_f, under a constant applied stress, σ_a, by combining Eqs. 2 and 3 and integrating:

$$t_f \sigma_a^2 = \frac{2K_{IC}^2}{Y^2 A_1 (n_1 - 2)} \left(\frac{\sigma_a}{\sigma_i} \right)^{2-n_1} , \qquad (5)$$

where σ_i is the inert strength. In this model, the activation energy is stress independent. Eq. 5 may be rewritten in a simplified form:

$$t_f \sigma_a^2 = B_1 \left(\frac{\sigma_a}{\sigma_i} \right)^{2-n_1}, \quad (6)$$

where the so-called "B parameter" is:

$$B_1 = \frac{2K_{IC}^2}{Y^2 A_1 (n_1 - 2)}. \quad (7)$$

B_1 is considered a constant for any material and environment. In this form evaluation of K_{IC} and Y is avoided. One problem with this simplification is that the value of B_1 is highly sensitive to the value assumed for the inert strength.

Other crack growth velocity models based on chemical kinetics have been proposed and are designated model 2:[8]

$$\text{Model 2:} \quad \frac{dc}{dt} = A_2 \exp n_2 \left(\frac{K_I}{K_{IC}} \right), \quad (8)$$

and model 3:[9]

$$\text{Model 3:} \quad \frac{dc}{dt} = A_3 \exp \left[n_3 \left(\frac{K_I}{K_{IC}} \right)^2 \right]. \quad (9)$$

These three models have been compared by Jakus, *et al.*[5] and Bubel and Matthewson.[10]

In model 1 above, the activation energy is independent of the applied stress, despite experimental evidence to the contrary.[4,11] In model 2, the stress affects the activation energy of the chemical reaction via an activation volume and is linear with stress intensity.[8] In model 3, the activation energy of the chemical reaction is by the strain energy density at the crack tip as a chemical potential and is quadratic with stress intensity.[9]

Predicted lifetimes are highly sensitive to the form of the stress dependence of the kinetics and model 1 yields the most optimistic lifetime predictions.[5,12] Models 2 and 3 cannot be explicitly integrated for dynamic fatigue and therefore numerical techniques are necessary. Similar to model 1, the B-parameters can be defined for models 2 and 3 as:

$$B_2 = \frac{2K_{IC}^2}{Y^2 A_2 (n_2)}, \quad (10)$$

$$B_3 = \frac{K_{IC}^2}{Y^2 A_3 (n_3)}. \quad (11)$$

In general, fatigue data appear to give the best fit to model 1.[12,13] However, in all three models the stress dependence is determined by the n_i (i = 1, 2, 3) while the environmental dependence is contained within the A_i. An alternative means of testing the appropriateness of the kinetics model is to determine the trends in the fatigue parameters with changing environmental conditions, such as humidity,[14,15] or pH.

In this research, we have determined the fatigue behavior of both bare and polymer coated silica optical fiber in various buffered pH solutions. For purposes of describing the data it was assumed that fatigue of silica involves the chemical reaction with OH^- ions only, as described by Eq. 4. Therefore, the slope of a $\log A_i$ *vs.* pH plot gives the *apparent* reaction order x with respect to OH^- ions.

EXPERIMENTAL PROCEDURE

Dynamic fatigue experiments were performed using a two-point bending technique on bare and coated fused silica optical fiber in temperature controlled 25±0.2°C standard pH buffer solutions (Fisher Scientific, Fair Lawn, NJ) in the range pH 1 to 12 from Fisher Scientific. In two-point bending,[16,17] the fiber is held between two faceplates which are brought together at a controlled rate by a computer-controlled stepper motor until the fiber breaks, as shown in figure 1. When the fiber breaks the event is detected acoustically by a transducer. The failure strain, ε_f, is calculated from the separation distance at failure, D, as:

$$\varepsilon_f = \frac{1.198\, d_f}{D - d_c + 2d_g}, \quad (12)$$

where d_f is the fiber diameter, d_c is the diameter of the fiber with coating, and d_g is the depth of the groove.

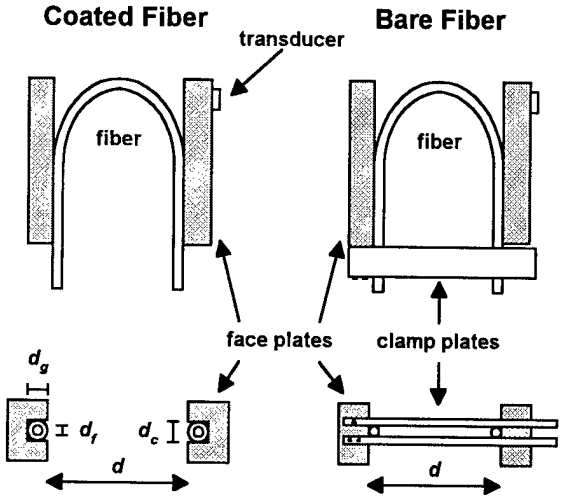

Figure 1. Two-point bending apparatus for bare and coated optical fiber.

Bare fiber specimens were prepared by stripping the polymer coating by immersing in hot sulfuric acid (~ 200°C) for about 30 s followed by rinsing with water and then acetone. This stripping method does not degrade the strength of the fiber.[18] After stripping, the bare fiber was immersed in the pH environment for 30 s before breaking. Coated fiber was soaked for at least two weeks before breaking to fully equilibrate with the test environment. A preliminary investigation of the diffusion of ionic species through the polymer coated specimens was done to substantiate the aforementioned soaking time by monitoring strength as a function of time after immersion in the test environment. The dynamic fatigue data for bare fiber was for 12 specimens per rate, at four loading rates spanning 1.5 decades, while for the coated fiber 20 specimens per rate were used at nine loading rates spanning 5 decades.

In this work, strain was converted to stress, σ, using the following expression:[19]

$$\sigma = \varepsilon_f E_0 (1 + 2.125\varepsilon_f), \qquad (13)$$

where the Young's modulus, E_0, is 72.2 GPa. This equation will not be valid at high strains because the modulus will eventually decrease with strain since the tangent modulus ($d\sigma/d\varepsilon$) must approach zero at the theoretical strength of the material.

RESULTS AND DISCUSSION

The effect of loading rate and pH is seen in figure 2 for bare fiber. These results loosely correlate with published data for the pH dependence of the dissolution rate in aqueous solutions, as seen in figure 3.[20] We also tested coated fused silica fiber and found results similar to the bare fiber data, as seen in figure 4. The error bars in figures 2 and 4 represent 95% confidence intervals. Typical Weibull moduli were in the range of 70 to 90 for both bare and coated fiber.

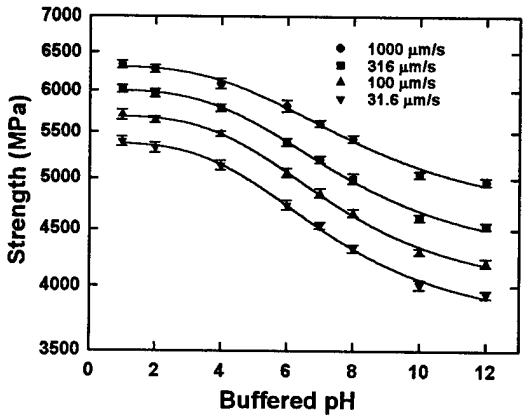

Figure 2. Strength of bare fiber in two-point bending at 4 loading rates in various 25°C pH buffer solutions.

Numerical methods were utilized to find the fatigue parameters from the dynamic fatigue data. The observed trends in the calculated parameters and the size of the error bars make it difficult to interpret the fatigue behavior. The error bars for the fatigue parameters are large because these parameters are correlated with one another. For example, figure 5 shows the ellipses for the bare fiber in pH 7. The ellipses are all narrow and the area of the normalized ellipses are a measure of the uncertainty, *i.e.*, the smaller the ellipses, the better the fit. In figure 5, model 1 had the best fit while model 3

clearly had the worst fit. Although model 1 fits best here, model 2 also had a good fit. At low pH, model 2 had the smallest ellipses while at high to moderate pH, model 1 had the smallest ellipses.

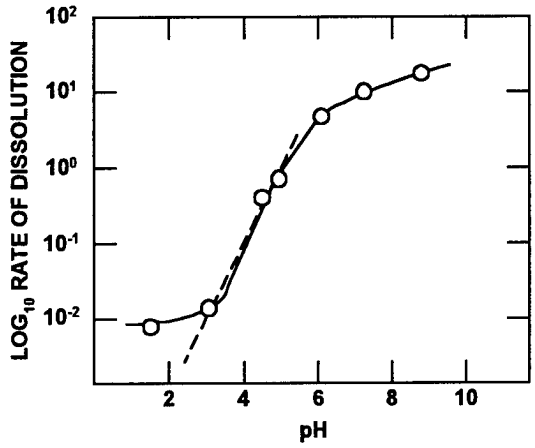

Figure 3. Dissolution rate vs. pH for fused silica.[20]

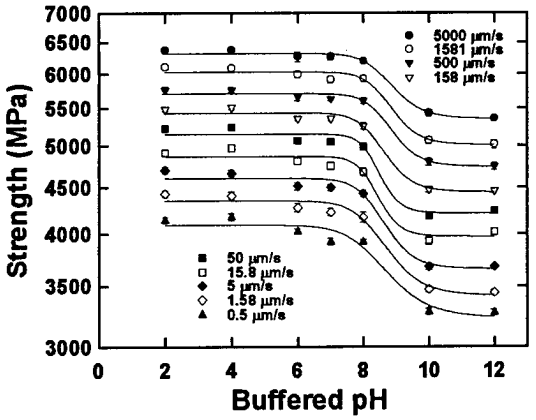

Figure 4. Strength of coated fiber in two-point bending at 9 loading rates in various 25°C pH buffers.

Figures 6 and 7 show the fatigue parameters, n_i, for bare and coated fiber, respectively. By examining these figures we see that n_i is not constant with changing environment. The trends in the data are modest compared with the size of the error bars. It was therefore decided to use the assumption that n_i is constant and re-examine the data. This was accomplished by calculating the weighted average n_i for each model. Since an underlying assumption of the models is that all the environmental effect should be in A_i, *i.e.*, n_i is constant, this constraint on n_i is reasonable. The effect of constraining n_i on the A_i value is shown in figure 8. The error bars for the constrained fit are substantially smaller. Model 2 shows the least change in n_i with pH. Only model 2 showed the same trends in A_i with pH for constrained and unconstrained n_i.

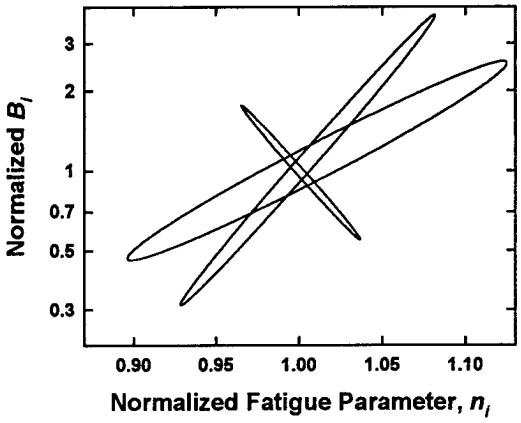

Figure 5. B_i and n_i confidence ellipses calculated for bare fiber in pH 7 at 25°C and normalized to the best fit values.

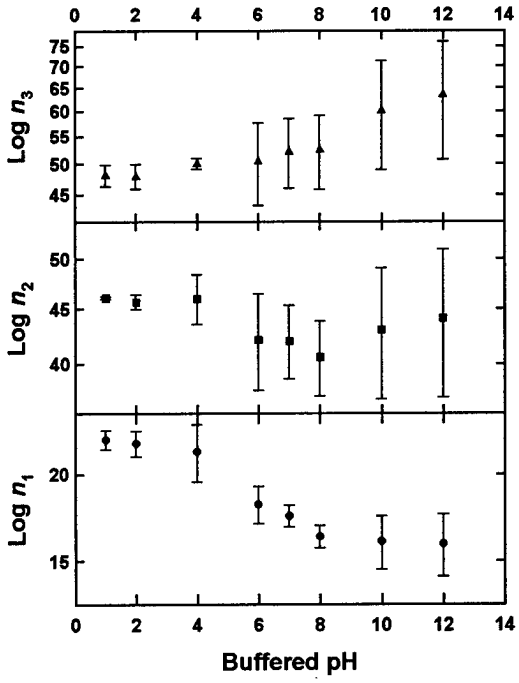

Figure 6. Fitted fatigue parameter n_i vs. pH for bare fiber.

A simple chemical kinetics model was used that assumed that the fatigue of silica involves the chemical reaction with OH^- ions, as written in Eq. 4. It is certain that a reaction with molecular water is occurring simultaneously. In the buffer solutions, the activity of water is essentially unity and constant. If the simple chemical kinetics model were correct, the slope of a log A_i *vs.* pH plot would give the true reaction order x with the OH^- ion. The *apparent* reaction order between pH 4 and pH 10 is ~ 0.3, as seen in figure 8, and this value is independent of the kinetics model used to fit to the data.

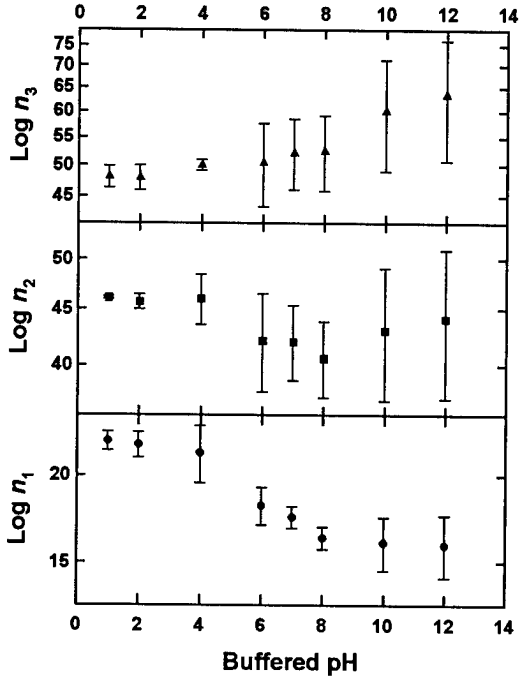

Figure 7. Fitted fatigue parameter n_i vs. pH for coated fiber.

CONCLUSIONS

The various kinetic models were fitted to fatigue data for both coated and bare fiber. It was found that both the power law, model 1, and the exponential, model 2, describe the stress dependence equally well. Trends in the fatigue parameters with pH favors model 2, which therefore gives the best overall description of the behavior. Since predicted lifetimes are highly sensitive to the kinetic form of the stress dependence of fatigue and model 1 is the most optimistic in lifetime predictions, one should use a more conservative and logical kinetic form, such as model 2. This model is based on physical principals, rather than model 1, which is empirical in nature.

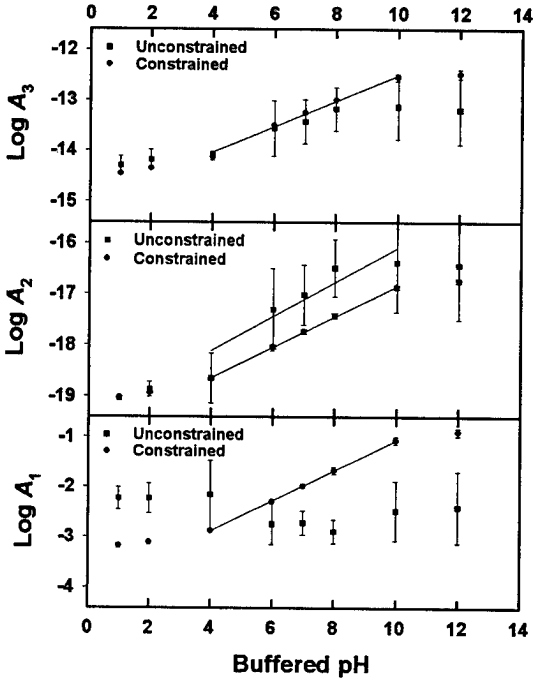

Figure 8. Log A_i *vs.* pH for models 1, 2, and 3 for bare fiber at 25°C showing both as fitted and constrained values.

The apparent reaction order with respect to the OH^- ion between pH 4 and pH 10 was found to be ~ 0.3 and is approximately zero outside this range, i.e., fatigue is substantially independent of pH at high and low pH. It is likely that the behavior between pH 4 and 10 is more complex and might show a stronger $[OH^-]$ dependence over a more limited range.

ACKNOWLEDGEMENTS

We thank the Corning Foundation for their support with a Corning Foundation Fellowship.

REFERENCES

1. W. Griffioen, "Evaluation of optical fiber lifetime models based on the power law," *Opt. Eng.*, **33** 488-497 1994.
2. F. P. Kapron and C. R. Kurkjian, "Reliability and standards in photonics," *Proc. XVIII Int. Cong. Glass,* C6-28-37 1998.
3. I. Scanlan, "The constants associated with the process of crack growth in silica in water as a function of stress and temperature," unpublished work.
4. C. K. Kao, "Optical fibre and cables" in "Optical fibre communications," eds. M.J. Howes and D.V. Morgan, Wiley, 1980.
5. K. Jakus, J. E. Ritter, Jr. and J. M. Sullivan, "Dependency of fatigue predictions on the form of the crack velocity equation," *J. Am. Ceram. Soc.*, **64** [6] 372-374 1981.
6. S. M. Wiederhorn, "A chemical interpretation of static fatigue," *J. Am. Ceram. Soc.*, **55** [2] 81-85 1972.
7. G. S. White, S. W. Freiman, S. M. Wiederhorn and T. D. Coyle, "Effects of counterions on crack growth in vitreous silica," *J. Am. Ceram. Soc.*, **70** [12] 891-895 1987.
8. S. M. Wiederhorn and L. H. Bolz, "Stress corrosion and static fatigue of glass," *J. Am. Ceram. Soc.*, **53** [10] 543-549 1970.
9. B. R. Lawn, "An atomistic model of kinetic crack growth in brittle solids," *J. Mat. Sci.*, **10** 469-480 1975.
10. G. M. Bubel and M. J. Matthewson, "Optical fiber reliability implications of uncertainty in the fatigue crack growth model," *Opt. Eng.*, **30** [6] 737-745 1991.
11. Y. S. Shiue, "Strength degradation of silica optical fibers: chemical kinetics and coating effects," 1998.
12. M. J. Matthewson, "Fiber lifetime predictions," *Proc. Soc. Photo-Opt. Instrum. Eng.*, **1580** 130-141 1991.
13. M. J. Matthewson, "Chemical kinetics models for the fatigue behavior of fused silica optical fiber," *MRS Proc. Spring Meeting,* in press.
14. J. L. Armstrong, M. J. Matthewson, C. R. Kurkjian and C. Y. Chou, "Kinetics models for fatigue of high-strength fused silica optical fiber," 902-909 1997.
15. J. L. Armstrong, M. J. Matthewson and C. R. Kurkjian, "The humidity dependence of high-strength fused silica lightguides," *J. Am. Ceram. Soc.* submitted.
16. P. W. France, M. J. Paradine, M. H. Reeve and G. R. Newns, "Liquid nitrogen strengths of coated optical glass fibres," *J. Mat. Sci.*, **15** 825-830 1980.
17. M. J. Matthewson, C. R. Kurkjian and S. T. Gulati, "Strength measurement of optical fibers by bending," *J. Am. Ceram. Soc.*, **69** [11] 815-821 1986.
18. M. J. Matthewson, C. R. Kurkjian and J. R. Hamblin, "Acid stripping of fused silica optical fibers without strength degradation," *J. Lightwave Tech.*, **15** [3] 490-497 1995.
19. W. Griffioen, "Effect of nonlinear elasticity on measured fatigue data and lifetime estimations of optical fibers," *J. Am. Ceram. Soc.*, **75** [10] 2692-2696 1992.
20. H. Baumann in "The chemistry of silica," R. K. Iler, p. 65, Wiley, New York, 1979.

Andrew Thomas Taylor
Rutgers University
Dept. of Ceramic and Materials Eng.
607 Taylor Road
Piscataway, New Jersey 08854-8065

Andrew Taylor received his BS and MS in Ceramic and Materials Engineering from Rutgers University in 1993 and 1995, respectively. He was awarded the Corning Foundation Fellowship at Rutgers University from 1995-1997. He is currently pursuing his PhD in the Fiber Optic Materials Research Program at Rutgers University investigating the strength and reliability of optical fibers.

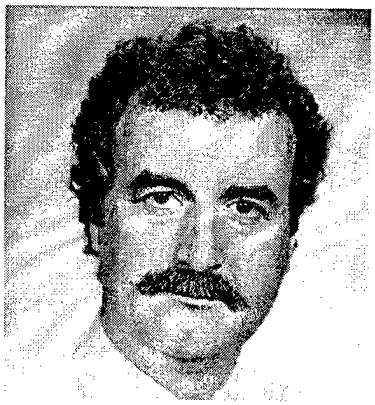

Dr. M. John Matthewson
Rutgers University
Dept. of Ceramic and Materials Eng.
607 Taylor Road
Piscataway, New Jersey 08854-8065
mjohnm@fracture.rutgers.edu

John Matthewson received his BA degree in Theoretical Physics in 1975 and his MA and PhD degrees in Physics in 1978, all from Cambridge University. Since then he has worked in the Cambridge University Computer Laboratory, AT&T Bell Laboratories and IBM Almaden Research Center. He is now an Associate Professor in the Fiber Optic Materials Research Program at Rutgers University where his research group is concerned with strength and fatigue of optical materials in general and oxide and non-oxide fibers in particular.

MECHANICAL BEHAVIOR AND B-VALUE OF AN ABRADED OPTICAL FIBER

T. Volotinen", A. Breuls*, N. Evanno+, K. Kemeter#, C. Kurkjian¤, P. Regio, S. Semjonov§, T. Svensson×, all participants of COST 246 SG4, and S. Glaesemann++**

"OFCON Optical Fiber Consultants AB, Hudiksvall, Sweden;
***Plasma Optical Fibre, Eindhofen, The Netherlands;**
+France Telecom CNET, Lannion, France;
#Siecor GmbH, Neustadt, Germany;
¤Bellcore, Morristown, NJ U.S.;
****CSELT, Torino, Italy;**
§FORC, Moscow, Russia and Bellcore, Morristown, NJ U.S.;
×Telia Research, Farsta, Sweden;
++Corning Inc, Corning, NY U.S.

ABSTRACT

The mechanical behavior of high strength and abraded (proof test level) optical fibers have been tested by joint experiments at nine laboratories in a wide range of dynamic stress rates and on static stresses. The answers to the open questions about B-value magnitude, measurement method and life time estimation were found (see Conclusions). Although measurement results diverge slightly because of accuracy problems and environmental conditions, the results show that the one-region power-law model cannot describe the test results, but the two region power law theory[1-6] can. Both n- and B-values are dependent on dynamic stress rate and static stress level. For long term life time estimations of optical fibers the B and n-values of Region I shall be used, and they should be evaluated from the test results on fiber weak spots at low stress rates or from static fatigue tests, by using the two region power law theory.

1. INTRODUCTION

The European research action COST 246 was established in 1993 with the scope to provide joint work on problems of reliability and life-time estimations of optical fibers, cables, passive components and optical amplifiers. In this paper the results for one of the topics - the B-value problem and optical fiber life time estimation- are presented. Other papers, such as the ones published by S. Semjonov et. al[4] and M. Bubnov et.al[5] including the cube corner indentation-work[6] on fibers to be presented at this IWCS-conference, have been effectively stimulated by the COST 246 initiative.

The work of this paper was stimulated by the European participants of IEC standardization group on optical fiber reliability, who asked COST 246 for a recommendation for measurement methods of B-value, together with a wish to simplify and qualify the power-law based lifetime report of IEC[7] for standardization. There has been a continuing controversy in the optical fiber community over the magnitude of the B-value (strength preservation parameter). While it has been studied mainly on high strength fibers, it is of greater immediate importance for fibers with 'proof test' level flaws, because the life time is defined by the fractures at these. In order to study this, a special abraded fiber (J-fiber) was prepared by S. Glaesemann of Corning, Inc. for study by COST 246. In this paper, the round robin tests on Fiber J together with a theoretical analysis are presented.

The earlier reliability action COST 218 (1987 - 1992, A. Breuls, T. Svensson, W. Griffioen and others) started the studies on life time theories of fibes[8-9], and concluded with the suggestion that the well known one-region power law theory is appropriate, and, in particular, the Mitsunaga-approximation of it for the life time estimation of fibers in cable networks, in the case B-value is negligible. However, no final agreement was found about the B-value magnitude (whether it is negligible or not) or about a reliable measurement method for it. It was not completely understood either, why the high speed measurements on high strength fibers showed a much higher B-value (above 0.001 GPa^2s) than

the values predicted from the inert strength and ambient environment fatigue tests (below 10^{-5} GPa^2s).

It was suggested that these problems be avoided by measuring the factor β ($\sim BS^{n-2}$, where S is the inert strength and n is the n-value) from static fatigue or dynamic fatigue measurements of the weak spots. This method has practical limitations.

An eight decades range of variation exists in the reported[5,2-4] values of B (fracture preservation parameter) for silica glass optical fibers, ranging from $2 * 10^{-8}$ GPa^2s to 0.5 GPa^2s. The high values, above 0.001 GPa^2s, have been obtained from high speed tensile tests[10,11,5] on pristine high strength fibers by direct fitting the well-known one-region power law model to the test data. On the other hands, the low values, below 10^{-5} GPa^2s, are obtained by combining the fatigue test data from ambient conditions with inert strength measurements at liquid nitrogen temperature or under high vacuum conditions, on high strength fibers[5,12,13].

So far, five unsolved problems have existed:
- A) to decide which of these magnitude levels of B-value is correct for the long term static fatigue of the weak spots in installed fibers in cable networks.
- B) to verify whether the mechanical behavior parameters (n-value and B-value), which are measured on high strength fiber, are valid for static fatigue of weak spots.
- C) to find a reliable measurement method for B-value.
- D) to find how much larger the initial (= inert) strength is than the measured strength at room conditions, in order to know the relevant start-length of the surviving flaws after a proof test, for life time estimation.
- E) to find an explanation for why the n-value of high strength fibers is dependent on loading time, as earlier found in the round robin test of high strength fibers by COST 218[16].

Solutions to these problems are found in this work by measuring the static and dynamic fatigue of an abraded fiber at eight laboratories and comparing the data with the two- region theory.

Optical fiber life time

The controversy in the magnitude of B-value raises two questions regarding life time estimation. IEC[7] suggests that the life time t_f of optical fibers (i.e. the time–to-reach-a-given-fracture-probability of a fiber under a given small static tensile stress) can be approximated by the known Mitsunaga equation[14].

The exact one-region power-law lifetime equation has different approximations depending on the level of B-value[7-9]. Mitsunaga-approximation agrees with the exact equation[7-9], only if B-value is below 10^{-5} GPa^2s. For significantly higher B-values than 10^{-5} GPa^2s an exact equation should be used.

One approximation for the one-region power law is the so called *minimum life time equation*[1,7], which also is used to calculate the lifetime of fibers. A requirement is that the initial strength of it, S_{pmin} (~ initial length of the crack) is known. Sometimes a "rule of thumb" $t_{fmin} \approx (B/\sigma_p^2)(\sigma_p/\sigma_a)^n$ is used (σ_p is proof stress)[7].

The minimum life time equation gives very short life times, if B-value is below 10^{-5} GPa^2s, n-value is around 20 and the initial strength of the weakest crack, S_{pmin}, is approximated to be only as large as the proof test stress σ_p. --It has been proposed to solve this problem by missing out this equation from the life time standard report[7]. However, it is similar to the definition of B-value. Furthermore, it is used for the evaluation of the effect of a proof test, which is as important as life time estimation.

Definition of B-value

Strength preservation parameter, B-value, (as well as fatigue parameter, n-value) is defined[7] by equation which describes the weakening of fiber strength

$$S^{n-2}(t) = S^{n-2}(0) - \frac{1}{B}\int_0^t \sigma^n(t)dt, \quad (1)$$

where $S(0)$ is the initial strength in the environment, $S(t)$ is the strength to which the crack has weakened under the tensile stress σ applied for a time t. Inert strength (initial strength at an inert environment) S is 1.3 - 2.5 times higher than the measured strength at room conditions depending the stress rate[5,12]. B (B - value) is[7]

$$B = \frac{2K_{Ic}^{2-n}}{(n-2)AY^2} = \frac{2K_{Ic}^2}{(n-2)V_cY^2}, \quad (2)$$

where the parameters are given earlier. The latter, normalized formula of Eq. 2 is preferred, because they define a clear meaning for the crack growth velocity V_c. V_c is dependent on the material structure and environment[7], but the critical stress intensity K_{Ic} is independent on the environment. Y, the geometrical shape factor of the crack. The fatigue parameter n is also dependent on the material and environment. Thus B is strongly dependent on the environment and material.

2. THE TWO REGION MODEL

It has been known from studies[1,17] of silica and glass materials that the crack growth process includes three regions, however, it has been until recently assumed that the crack growth of optical fiber weak flaws can be approximated by the function of Region I, neglecting Region II. However, this assumption has raised the problem of B-value and initial strength. It has not been realized either that depending on the level of B- and n-values, which both are dependent of the environment (humidity, temperature, chemicals, etc.), the measured n- and B-values and static behaviors may not be usable for long term application, because the measurement range is too close to the transition between the regions.

In the following numerical simulations, we use the same basic formulae of the two-region power law model with the parameters used in ref.4. The two region model[4, 19] is described

$$\frac{da}{dt} = V_1\left(\frac{K_I}{K_{IC}}\right)^{n_1} \qquad \text{for } K_I \le r\,K_{IC} \qquad (3)$$

$$\frac{da}{dt} = V_2\left(\frac{K_I}{K_{IC}}\right)^{n_2} \qquad \text{for } K_I \ge r\,K_{IC} \qquad (4)$$

where V_1, V_2, n_1 *and* n_2 are the parameters of the respective regions and $V_1 = V_2 r^{(n2-n1)}$. Eqs. 3 and 4 can be rewritten in strength degradation terms for a dynamic fatigue test by using S_i is initial strength, S_r and σ_r are the strength and applied stress at the transition, σ_f is the fatigue strength for the stress rate:

$$S_i^{\,n_1-2} = S_r^{\,n_1-2} + \frac{\sigma_r^{n_1+1}}{B_1(n_1+1)\dot{\sigma}} \qquad (5)$$

for the crack growth through Region I, and

$$S_r^{\,n_2-2} = \sigma_f^{\,n_2-2} + \frac{\sigma_f^{n_2+1} - \sigma_r^{n_2+1}}{B_2(n_2+1)\dot{\sigma}} \qquad (6)$$

for crack growth through Region II, and where[19]

$$B_2 = \frac{2\cdot K_{IC}^2}{(n_2-2)\cdot V_2\cdot Y^2}, \text{ and} \qquad (7)$$

$$B_1 = B_2 r^{n_1-n_2}\frac{(n_2-2)}{(n_1-2)}. \qquad (8)$$

In Figs. 1 and 2 we consider two cases: static fatigue (σ = const) and dynamic fatigue ($\sigma = \sigma' t$). Calculations are made both for abraded fibers (initial strength = 1 GPa) and for high strength fibers (initial strength = 12 GPa). For the static and dynamic graphs in Figs. 1 and 2 the parameters used in ref. 4 are used: n_1 = 21, B_1 = 4.5 x 10^{-5} GPa^2s, n_2 = 4.5, B_2 = 0.0082 GPa^2s, r = 0.645. The transition from Region I to Region II occurs $rK_I = K_c \approx 0.6$ MPa$\sqrt{m}$.

For high strength fibers, in particular in Region I, typically measured fracture times and strength values at ambient conditions are significantly lower than the theoretical curves shown in Figs 1a and 2a. Curves at two decades lower level, which would represent a lower B-value (or larger cracks), would be in better agreement with normal high strength fiber test results. Crack growth velocity (i.e. B- and n- value) both in Region I and II is highly dependent on the chemical environment as well as on the temperature[2,17,19]. High strength fiber parameters may also slightly differ from the parameters of large weak flaws[9,18].

3. COMPARISON OF THE ONE AND TWO-REGION MODELS

Effect on static and dynamic fatigue

Two interesting practical conclusions can be drawn from the dynamic fatigue curves (Fig. 2). A flat transition regime on the level of ~0.6 of the initial inert strength is observed for abraded fibers in the range of stress rates between 10^{-3} and 1 GPa/s. This region is normal for standard testing machines. Thus, an usual dynamic test gives incorrect fatigue parameters for abraded fibers because of the transition between the regions. Only testing machines with an extended stressing rate region can be used for measuring the correct

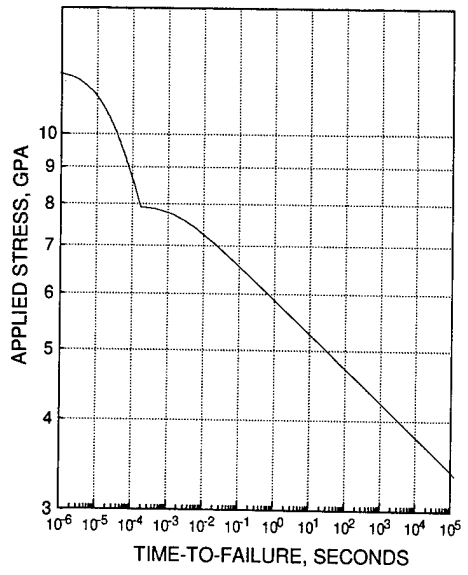

Fig. 1a. Theoretical static fatigue plot for high-strength fiber[4]. Initial strength 12 GPa is used.

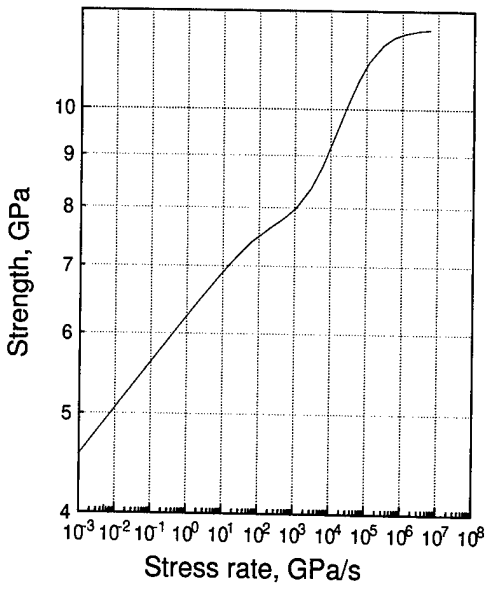

Fig. 2a. Theoretical dynamic fatigue plot for high-strength fiber[4]. Initial strength 12 GPa is used.

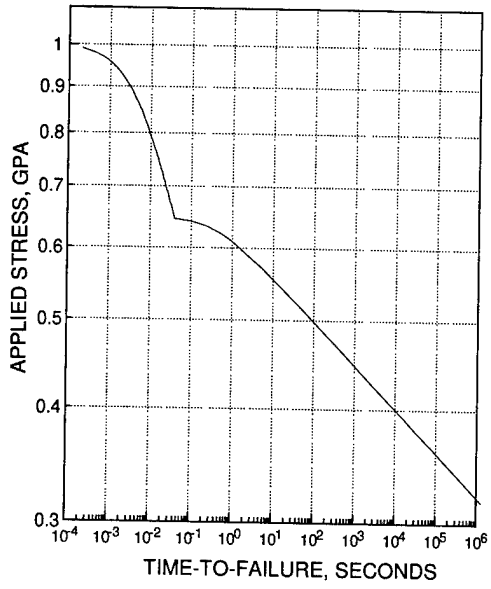

Fig. 1b. Theoretical static fatigue plot for low-strength fiber[4]. Initial strength 1 GPa is used.

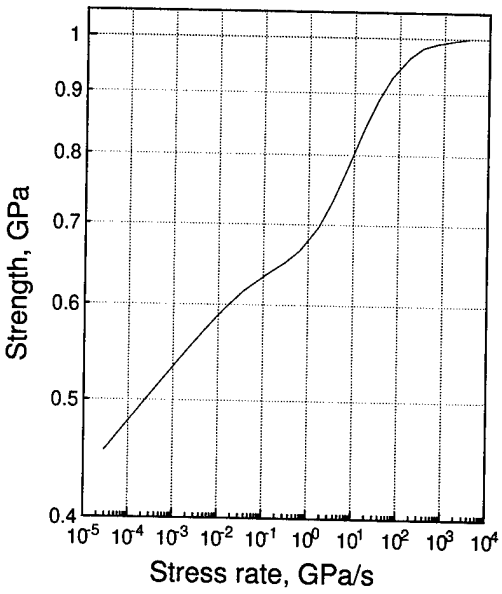

Fig. 2b. Theoretical dynamic fatigue plot for low-strength fiber[4]. Initial strength 1GPa is used.

value of n_1 and B_1. Static fatigue testing at sufficiently long times can also be used. For high strength fibers, the flat transition regime is observed in Figs. 1a and 2a at stress rates exceeding 1 GPa/s. So, for these kind of fibers a standard testing machine can be used for measuring n- and B- parameters of Region I. But in the case where B_1-value is very low and n_1 relatively high (25 - 40), the flat transition regime (and a high, intermediate n-value) can be found at the stress rates used in fatigue tests.

The transition was found by S. Sakaguchi et al[2] at the K_I = 0.61 MPa$\sqrt{m}$ for fused silica rod, and very recently by G.S. Gleaseman et al[19] also at. 0.61 MPa$\sqrt{m}$ (r = 0.81 with K_{Ic}= 0.75 MPa$\sqrt{m}$) in abraded fibers similar to Fiber J.

Differences between high strength and weak fibers

If we assume that the only difference in the behavior of the dynamic fatigue curves for strong and weak fibers is due to the two-region model and that the crack growth rates are the same for both fiber types, we could use the results from high-strength fiber testing to predict the lifetime of weak fibers. If this theoretical result was to hold for fibers, static fatigue testing of a strong fiber for a few months would be equivalent to static fatigue testing of an abraded fiber for 25 years, because the crack sizes in high strength fibers are smaller by about 10^2.

However, it has not been shown in this work, and to our knowledge elsewhere either, whether the results on high strength fibers are directly applicable to the behavior of weak spots of fibers. Some published test data on weak or abraded fibers[18], as well as some theoretical studies[9], indicate that the fatigue and aging of weak spots can differ from high strength fibers.

Furthermore, it can be concluded that the high speed tests are applicable only to weak fibers, not to high strength fibers. To measure Region II for high strength fibers, tensile testing equipment much faster than 1000 GPa/s (strain rate over 1600 %/s) would be needed. The speed of voice (mechanical wave speed = maximum possible speed for elongation) in silica glass is of the order of 5000 m/s. This phenomena gives an absolute limit for the high speed testing of fibers.

Effect on weak spot distribution and life time

In Fig. 3 we qualitatively demonstrate the theoretical effect of the two-region power law to the weak spot distribution surviving a proof test[5]. The curves are strongly dependent on the n- and B-values of the fiber, but the principle is clear. At the relatively high fracture probabilities, i.e. less than 10^{-3} below the original fracture probability before proof test, the one region power law gives a too high estimation for the fracture probability.

But at the very weakest points and lowest fracture probabilities, i.e. more than 10^{-3} below the original fracture probability, the two region model gives a higher fracture probability. The crossing point of curves B (one region model) and C (two-region model) is highly dependent of the B-value and n-value at the low stress rates, i.e. in Region I.

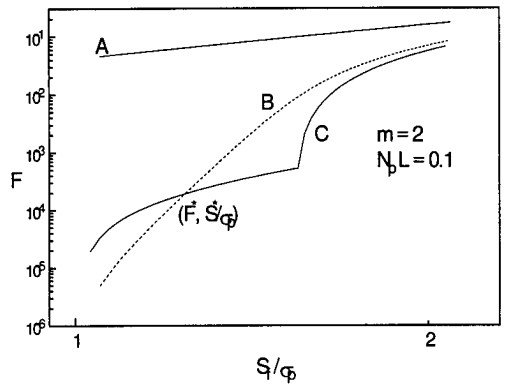

Fig. 3. Theoretical Weibull-plots of the fiber inert strength distribution before (A) and after proof testing: non-modified (B) and modified with regard for the two-region crack growth (C)[5]. B = 4.5×10^{-5} GPa^{2}s and n = 21 were used for non-modified plots A and B. $B_1 = 4.5 \times 10^{-5}$ GPa^{2}s; n_1 = 21; $B_2 = 8.2 \times 10^{-3}$ GPa^{2}s; n_2 = 4.5 and r = 0.645 were used for modified plot C.

4. EXPERIMENTS

The round robin test results

High stress rate measurements were carried out on this fiber at Corning, Inc., France Telecom and Telia. Also 'normal' and low stress rate dynamic and static fatigue measurements have been made in several laboratories. From the test results (Figs. 4 and 5) the following conclusions can be drawn for abraded Fiber J:

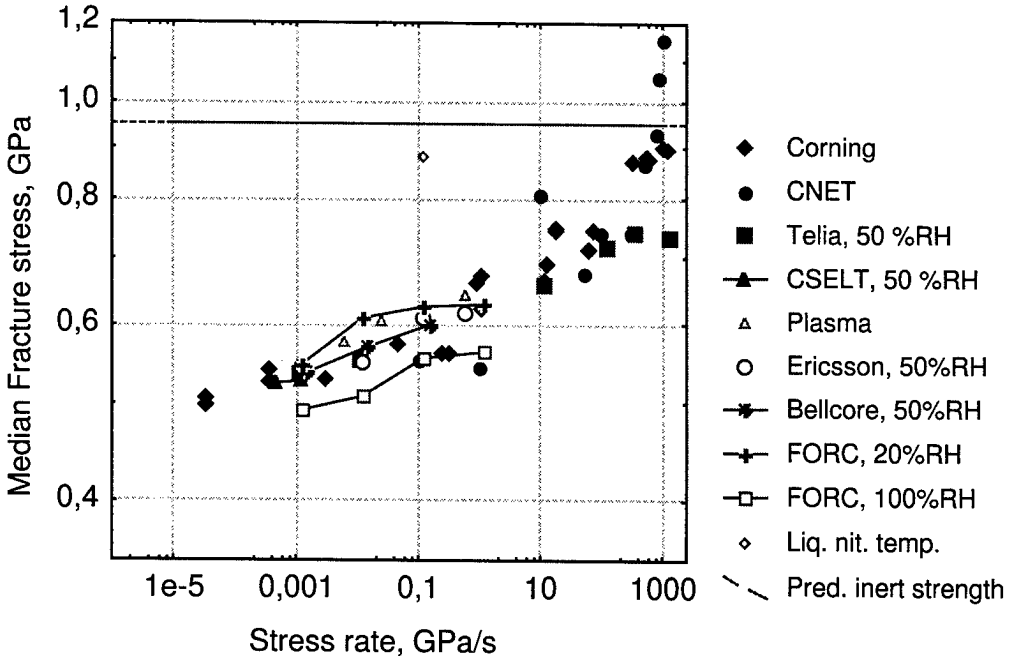

Fig. 4. The measured dynamic fatigue results of the round robin tests for abraded Fiber J measured at eight laboratories. Each point presents a median value of 20 - 30 samples. Gauge length was 500 mm except for one of the labs which had 100 mm.

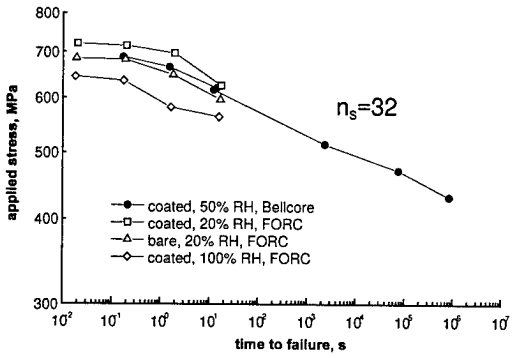

Fig. 5a. Dynamic and static fatigue of Fiber J.

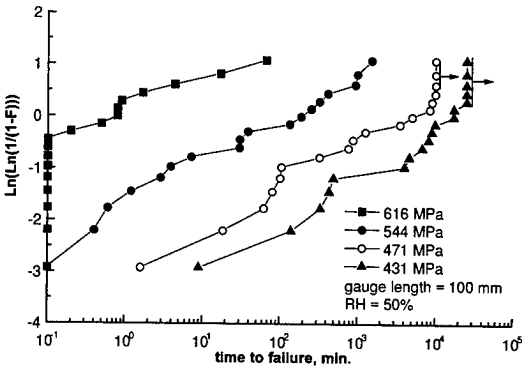

Fig. 5c. Static fatigue of Fiber J.

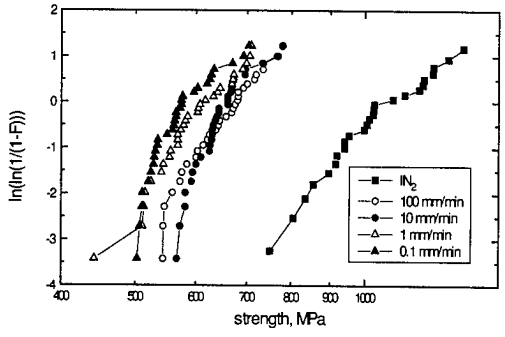

Fig. 5 b, Dynamic fatigue of Fiber J

- The low m-value (~12) makes it necessary to test a large number of samples.
- The n_1-value for Fiber J was 32 at the static tests (Fig. 5 a) and 40 at the lowest stress rates in Region I (Fig.4.); 40 - 50 at the intermediate stress rates 0.01 - 1 GPa/s, and very low, only 2 - 7, at the high stress rates in Region II.
- The predicted values by fitting the two-region power-law to the Corning data are the following: $B_1 = 1.4*10^{-10}$ GPa^{2}s; $B_2 = 0.0091$ GPa^{2}s, $n_1 = 45$, $n_2 = 2.3$ and $r = 0.737$ (with $K_{IC} = 0$ 0.75 MPa$\sqrt{m}$). The prediction to the other data of Fig.4

(excluding FORC's data at 100 %RH and data from CNET) gave similar parameters.
- Inert strength 0.89 GPa was measured at liquid nitrogen temperature. Initial strength, predicted from Corning data by fitting the two region theory was slightly higher, 0.94 GPa in average.
- Thus the shift inert strength/strength at room conditions σ_I/σ_{RT} ~ 1.5 - 1.6 at the stress rate 0.01 GPa/s (~ 1%/min) and 1.3 - 1.4 at 0.1 GPa/s (~ 10 %/min).

The variation of the test results is caused partly by the different humidity of the test environment, and partly by measurement accuracy. The tensile test difference (shift) between laboratories, defined in earlier COST 246 comparisons on high strength fibers, is below ± 0.05 GPa. Also the scatter in the strength of Fiber J (low m) is causing a variation to the median values.

Comparison with other low strength fibers studied within COST 246

Different kinds of weak spots exist in optical fibers: surface abrasions caused by contact with drawing tower parts, imbedded particles of impurity materials, surface particles sublimated from oven material, crystallized particles such as silica, etc. etc. COST 246 earlier studied four types of abraded fibers[16], with imbedded chromium oxide metal particles inside the fiber glass, with zirconium particles on the fiber surface and abrasion against coating applicator dye of copper.

Fiber J of this work was abraded by drawing in contact with a crossing glass fibers. A similar fiber has been studied[16] earlier and the results are in good agreement with the results in this paper. A similar fiber has been studied by G. S. Glaesemann in ambient conditions and humid conditions[19]. The predicted parameters for ambient conditions (n_1= 28, n_2= 2.25, r = 0.81, B_1= 1.86 10^{-7}GPa^{2}s, B_2=4.39 10^{-3} GPa^{2}s, V_1= 0.187 m/s and V_2= 8.25 10^{-4} m/s) differed only slightly from the predicted parameters of this paper. At the 100 % RH the n-values are the same, B-values are lower and the critical crack growth velocities are higher.

Very recently dynamic and static fatigue was also measured[6] for a flat fiber which had been indented by using a cube-corner shaped diamond with an applied load of 1 gram. This fiber showed quite a narrow strength distribution (m ~ 50–70) and a very clear two- region behavior was found, with n-value ~44 (30 to 80) at intermediate stress rates and n_1 ~ 21 (17 to 25) at long times.

In addition, T. Volotinen reported at MRS Spring -98 conference results for a test fiber abraded by drawing the bare fiber, prior to coating applicator, around small Teflon-coated wheels. The results indicated two-region behavior, similar to Fiber J of this paper.

Inert strength of weak spots

In theory, the initial strength (~ the length of a crack) at any environment is equal to the strength at inert environment. The critical stress intensity factor K_{Ic} (0.75 - 0.789 MPa$\sqrt{m}$)[15,12] is a material structure constant, which is thought to be independent of the environment. It is always reached at the border of Region 2 and 3 prior to a fracture of the fiber. However, the crack growth velocity V_c at the fracture is different depending on the environment, and the fracture can occur at different stress because of the crack growth.

The shift between inert and ambient strength is strongly dependent on the environment and both B- and n- values, as well as on the stress rate at which the inert strength and ambient strength are compared. In European countries it is usual to measure thestrength of fiber at 10 %/min strain rate (≈ 0.1 GPa/s), and in U.S. at a much lower strain rate 1%/min (≈ 0.01 GPa/s). Thus the published data must be compared with care.

Test results for fiber J show that the strength measured at liquid nitrogen temperature is only 1.3 - 1.4 times the strength at 0.1 GPa/s stress rate (≈ 10 %/min strain rate) whereas for the indented fiber it was about 1.5[6]. Other laboratories have reported shifts 1.3 - 2.0 for low strength fibers and 1.9 - 2.5 for high strength fibers. Thus, according to the worst case approximation[5], the strength of weakest surviving flaw after a quick (10 - 100 ms) proof test in ambient conditions is of the order 0.9 of proof test stress. Thus, the inert strength S_{pmin} of it is at least 1.2 - 1.4 of the proof test stress σ_p.

5. DISCUSSIONS

Limitation of the high speed measurements

The J-fiber data do not really show agreement in detail over the whole stress rate range. What they do show is that all laboratories show a

reasonable agreement in the low stress rate regime and the three laboratories that did high rate testing, Corning, Telia and CNET, show that at high stress rates a second region appears. For the cube-corner indentation fiber[6], essentially the liquid nitrogen strength (~90%) was reached, at the highest rates, which is an indication that the data is close to the truth.

The very large, eight decades spread in B-values, which is continually referred to, is the result, primarily of the Telia and France Telecom data on high strength fibers. However, it can now be understood why there is this curvature in the dynamic fatigue curve at the stress rates 10 - 1000 GPa/s. The measurement data and the curvature are qualitatively correct. However, the assumption that the initial strength is at the level of the curvature is not correct. The curvature only indicates the transition between Regions I and II.

It is now clear from Fig. 2 of S. Semjonov et al[4] that obtaining inert strengths at room temperature on high strength fibers would require stress rates three decades of magnitude higher than presently available at any laboratory. We see large disagreement between the three laboratories' data at the high stress rates (Fig.4) for Fiber J. COST 246 also analyzed the technical aspects of the pieces of equipment used and the reasons for the possible accuracy problems internally.

For the determination of the B- and n-value of Region I, fatigue tests at low stress rates together with inert strength measurements can be used. In order to reach the inert strength of weak fibers by high stress rates measurements, equipment with adequate accuracy is required.

Life time estimation of optical fibers in real service environment

20 years of experience from the field all over the world with over 100 million kilometers of optical fibers installed, has shown that the fibers do not seem to fracture frequently. Partly this is due to the fact that the applied stresses in the fibers are on average significantly lower than 1/4 of proof test stress. Furthermore, this suggests that the static fatigue of fiber weak spots is not very well estimated with the one-region power-law approximation by using n-value measured on high strength fibers and B-value assumed to be negligible.

The test results of this work show that the B-value for long term static fatigue is low, below 10^{-5} GPa^2s. Therefore the first doubt regarding the Mitsunaga model is solved. However, the minimum life time equation can be used only if the accurate B- and n-value of Region I and the inert strength (= initial length of the crack after proof test) of the weakest spot are known. To calculate the effect of a quick proof test, the two-region model with Region II parameters is needed.

The two-region model can explain the delayed fatigue (the distribution of cracks after proof test is better than assumed, the n_1- and B_1-values of the weak spots can be more favorable for long life), as well as the dependency of n-value on loading time and both high and low B-values obtained.

For the life time calculation of fibers in cable networks, the n- and B- values of Region I must be used. They should be measured on weak spots in the service environment by using very long loading times, far away from the transition between Regions I and II.

The accuracy of the estimations made by using one-region model based Mitsunaga- equation is very much dependent on the distribution of the weak spots and of the B-value (assumes it being negligible) and n-value. The parameters of the surviving weak spot distributions are affected by the two region behavior, and both too conservative or too optimistic estimations can be made depending on the allowed maximum fracture probability.

There are indications[18], but it is not yet completely shown, that both B_1-value and n_1-value of weak spots are different from the values measured for high strength fibers. This subject should be studied further.

The discussion in this paper does not consider the possible long term changes in the static fatigue, which can be caused by any kind of aging, or reaching of a chemical equilibrium of the dissolution reaction of silica, or by a change of the chemical or physical environment.

6. CONCLUSIONS

The mechanical behavior of high strength and abraded (proof test level) fibers have been tested by different laboratories at a wide range of dynamic stress rates and on static stresses. This

was done in order to find answers to the questions about the B-value magnitude, measurement method and about the life time estimation methods. Although measurement results diverge slightly, the results show that the one-region power-law model can not describe the test results, but the two region power law can. The differences of the results at the highest stress rates are due to the testing accuracy and the test environment rather than the fiber.

Studies on an indented and some other weak fibers also show a two -region behavior. However, studies on other specific types of weak spots should be carried on in order to draw final conclusions about general behavior of weak spots in optical fibers.

The answers to the problems are the following:
- A) The low value levels of B-value, below 10^{-5} GPa^2s are correct for the long term static fatigue of the weak spots of fibers. Also the n-value is dependent on stress rate, and thus it must be ascertained that both n- and B-values used for the life time calculations represent Region1.
- B) The mechanical behavior parameters (n-value and B-value), which are measured on high strength fibers in Region I, i.e. at low stress rates or in static tests at low stresses are probably usable. However, the very best are the values of Region I measured directly on the weak spots of the fibers.
- C) The recommended method to predict B-value of a fiber for life time estimation includes two steps: to measure inert strength of weak spots at liquid nitrogen temperature or high vacuum, and to measure dynamic or static fatigue of the weak spots at the environment of application in Region I (at very low stress rates or static stresses). The high speed measurements can also be used, if the accuracy is ascertained. The B-value of Region II of weak fibers can be obtained from the high speed tests. It is needed for estimation of the effect of proof test. None of the available instruments can reach the high stress rates necessary to reliably measure the inert strength of high strength fibers.
- D) The initial strength of fiber weak spots (the proof test level cracks) is about 1.5 times the measured strength at low stress rate, 0.01 GPa/s $\approx$ 1 %/min strain rate, under room conditions.
- E) The crack growth process of fiber weak flaws can be described by the two-region model, and both B- and n-value of fibers are dependent on the loading time and the environment. Because the B-value is strongly dependent on the environment, the transition from Region I to II may occur at the stress rates normally used. Thus both too low and too high n-values can be reached, if the prediction is done by assuming only one-region behavior. The intermediate transition regime between Regions I and II explains the leveling of fatigue curves measured by high-speed tests on high strength fibers, - not the reaching of the initial strength.

7. ACKNOWLEDGEMENTS

The authors thank Corning Inc. for abraded fiber J and the support to this work. The colleagues at COST 246 SG4 and WG1.1 are acknowledged for the valuable comments and discussions. Dr. F. Kapron, Bellcore, and the European members of the Optical Fiber Reliability Group of IEC SC86A WG1 are gratefully thanked for the challenging task and help in discussions.

8. REFERENCES

1. E.R. Fuller et al., J. Mat. Sci. Vol 15 (1980) 2282.
2. S. Sakaguchi et al., J. Mat. Sci., Vol 17 (1982) 1982.
3. T. Hanson et al., J. Mat. Sci. Vol.32 (1997) 5305.
4. S. Semjonov et.al., to be published MRS Spring Meeting, DD-conference (1998).
5. M. Bubnov et al., to be published MRS Spring meeting, DD-conference (1998).
6. S. Semjonov et. al., ibid (IWCS 1998).
7. IEC- Technical Report on power-law, ver. May 1998.
8. W. Griffioen et al. SPIE Vol. 1791 (1992) 190.
9. W. Griffioen, Doctoral Thesis, Eindhoven University of Technology (1994).
10. T. Svensson et al., SPIE Vol. 1791 (1992) 117.
11. A. Gouronnec et al., Proc. IWCS (1996) 906.
12. C. Kurkjian et al., SPIE Vol. 2611 (1995) 56.
13. J. Armstrong et al., Proc. IWCS (1997) 902.
14. Y. Mitsunaga et al., Electron. Lett., Vol. 7, No. 16 (1981) 567.
15. R. C. Bradt et.al., Fractography of Glass, Plenum Press, NewYork (1994).
16 T. Svensson et al., SPIE Vol. 2290 (1994) 211.
17. A. K. Varashneya, Fundamentals of Inorganic Glasses, Academic Press, Inc., London (1994).
18. G.S.Glaesemann, Proc. IWCS (1992) 698.
19. G.S. Glaesemann, et al., to be published MRS Spring Meeting, DD-conference (1998)

BIOGRAPHIES

Photo was not available.

Tarja T. Volotinen received her Ph. D. in physics in 1991from Helsinki University. She worked for Nokia Cables 1979 - 1986, with the measurement technique and quality control of optical fibers and cables; and for Ericsson Cables at Hudiksvall in Sweden 1986 -1997,

with cable manufacturing problems and optical fiber reliability. At the moment she works for the consulting company. (Chairman of COST 246)

Photo was not available.

Anton H. E. Breuls received his M. Sc. degree in applied physics in 1982. He worked for PTT Research 1982 - 1984 and for Philips Glass Division 1984 -1987. Since 1987 he has worked for Plasma optical Fibre B. V., since 1990 as the manager of the research and development. (Member of COST 246 MC and SG4)

Noella Evanno graduated from the University of Rennes I. She joined France Telecom -CNET in 1996, where her research work includes reliability studies of optical fibers.(Member of COST 246 SG4)

Photo was not available.

Karsten Kemeter received his M. Sc and Ph. D. in theoretical physics in from the University of Gottingen, Germany, and joined Siecor GmbH, Germany in 1996, as an application and product engineer for optical fibers. He is responsible for standardization, product qualifications and customer support. The influence of non-linear effects of optical fibers on long-haul high bit-rate transmission systems is one of his special topics. (Member of COST 246 SG4).

Charles R. Kurkjian received his B.Sc. from Rutgers in 1955 and his Sc. D. from M.I.T. in 1955. In1994 he retired as a Distinguished Member of Technical Staff from A.T.&T. Bell Labs after 35 years service. Since that time he has been with Bellcore in the Fiber Media and Components Group. (Member of COST 246 SG4).

Photo was not available.

Paola Regio received her degree in Physics from the University of Torino in 1993. She prepared her thesis In CSELT on the mechanical properties of fibers and joined CSELT. At the moment she is working on the reliability of the passive components of the optical networks. (Member of COST 246 SG4)

Sergei L. Semjonov graduated from the Moscow Physical -Technical Institute in 1982 and received his Ph. D. in physics from the General Physics Institute in 1997 ,and since 1982 he has been employed by the Fiber Optics Research Institute of the Russian Academy of Sciences in Moscow. It has since been transformed into the Fiber Optics Research Center (FORC). He is head of the fiber drawing group. (Member of COST 246 SG4)

Photo was not available.

Torbjörn K. Svensson received his M.Sc and Ph.D. from the Royal Institute of Technology in Stockholm, Sweden. He joined Telia 1985. He has worked with quality assurance, development of new techniques for testing of optical fibers, cables, and splicing technology. He is currently focussing on fiber access networks and reliability of optical transmission systems at Telia Research. (Member of COST 246 MC, SG4..)

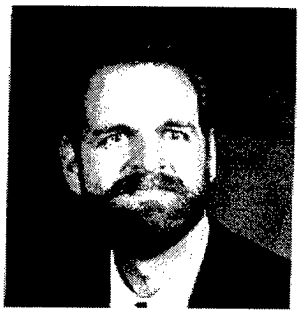

G. Scott Glaesemann is a senior development engineer at Corning's Sullivan Park technology center and has been with Corning since 1986. He received his M.S. and Ph.D. from the University of Massachusetts and his B.S. from North Dakota State University.

SPLICE LOSS IN NON-ZERO DISPERSION-SHIFTED FIBERS

Mary E. White
Sheila A. Cooper

Corning Incorporated
Corning, New York

ABSTRACT

As non-zero dispersion-shifted fibers (NZ-DSF), and the more recently introduced optimized type of NZ-DSF with large effective area, Corning® LEAF® fiber become more prevalent in the marketplace, system designers need access to accurate information regarding splice loss. This paper examines laboratory splice loss data, modeled field performance data, and splice loss measurement considerations. Fusion splicing practices and equipment set-up are also examined.

All NZ-DSF designs, including LEAF fiber require a renewed understanding of splice loss measurement. This paper provides an understanding of the issues outlined above with the objective of providing insights on how carriers can achieve consistent low loss splices.

INTRODUCTION

With fifteen years of experience deploying standard single-mode optical fiber (SMF) in their networks, carriers and other end users have developed a practical understanding of the challenges associated with splicing optical fibers. However, new opportunities in long-distance high data rate applications have raised the question of the use of non-zero dispersion-shifted fibers (NZ-DSF) which now are the fibers of choice for these applications. In addition, a recently introduced optimized type of NZ-DSF with large effective area, Corning® LEAF® fiber, also must be considered.

Large effective area fiber permits more power to be transmitted, resulting in longer distances, higher TDM rates and better system performance either through higher Signal-to-noise ratio (SNR) or lower Bit-error-rate (BER), than standard NZ-DSF. One important factor in network design that needs to be considered is splice loss budget. To better understand the effect on splice loss budget modeled data for both passive alignment systems, which mechanically align the fibers, and active alignment systems, which line up the fiber cores to minimize loss, will be provided.

LEAF fiber installation allows longer distances (10% to 15%) between repeaters without degrading system transmission performance versus NZ-DSF with small effective area. Most systems would typically be made up of cables ranging from 6 km to 12 km in length. This would translate into between 8 cable splice points and 15 cable splice points. By using LEAF fiber, overall system splice loss would be lower than that of standard NZ-DSF.

Laboratory Splice Loss Data

Laboratory data shows acceptable splice loss results for active alignment splicing. A study using six LEAF fibers was completed at Corning's Center for Fiber-Optic Testing. This study included six splices between each of the fifteen combinations of LEAF fibers available. An active alignment splicer was used. Limited data from subsequent studies show substantially lower splice loss results. The fibers selected for the study included a wide range of mode-field diameters and core/clad offsets as shown in Table 1.

Table 1: Characteristics for fiber used in study

	Mode Field Diameter (μm)	Core/Clad Offset (μm)
Fiber #1	9.92	0.19
Fiber #2	9.65	0.18
Fiber #3	9.48	0.33
Fiber #4	9.88	0.11
Fiber #5	9.48	0.12
Fiber #6	9.65	0.33

A summary of the results is shown in Table 2 and the distribution is shown in Figure 1.

Table 2: Laboratory LEAF fiber splice loss study results

	Active Alignment Results
Number of Splices	90
Average Splice Loss(dB)	0.05
Standard Deviation (dB)	0.02
Maximum Loss(dB)	0.08

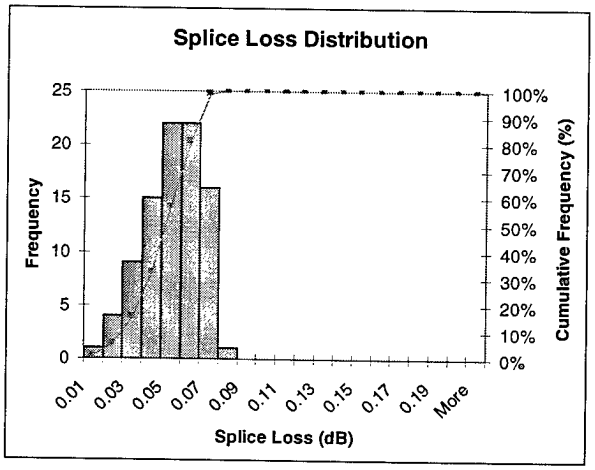

Figure 1: Laboratory Splice Loss Study Distribution

Modeled Splice Loss Data

When predicting splice loss for two fibers, there are two important factors: the size of the light carrying portion of the fiber and the location of the light carrying portion of one fiber with respect to the other. Typically, the size of the light carrying portion of the fiber is described by the mode-field diameter. The location of one fiber with respect to another is accounted for in the splice loss equations. These equations account for lateral offset, angular misalignment, and end separation.

For standard single-mode fibers as well as the dispersion–shifted family of fibers, equations derived from theoretical models have been quite accurate in predicting splice loss. Through the use of Monte Carlo techniques, splice loss distributions can be predicted for wide ranges of mode-field diameters and core-clad offsets.

Use of the standard equations is still an excellent predictor of splice loss performance for LEAF fibers. With Monte Carlo techniques and standard splice loss equations, a distribution of the expected splice losses for LEAF fiber to LEAF fiber splicing can be created. These Monte Carlo results represent the expected distribution of losses for passive alignment splicers. Since active alignment splicers are commonly used for high data rate systems, an active alignment splice loss model was also developed.

The active alignment splice loss model is based on worst case actual laboratory data. This data has few splice losses less than 0.02 dB and shows that the degree of alignment achieved between any given pair of fibers varies from splice to splice. Using this information, a transform using a distribution of degrees of alignment is applied to the theoretical splice loss distribution. The result is a predicted distribution of splice losses for active alignment splicing.

The Monte Carlo simulations were performed using mode field diameters ranging from 9.0 μm to 10.0 μm and core-clad offsets as large as 0.8 μm. Every effort has been made not to under-predict splice loss distributions with this model. As specifications are tightened, particularly for core-clad offset, splice performance will improve. The LEAF fiber Monte Carlo results for

both passive and active alignment systems are shown in Figure 2 and Figure 3.

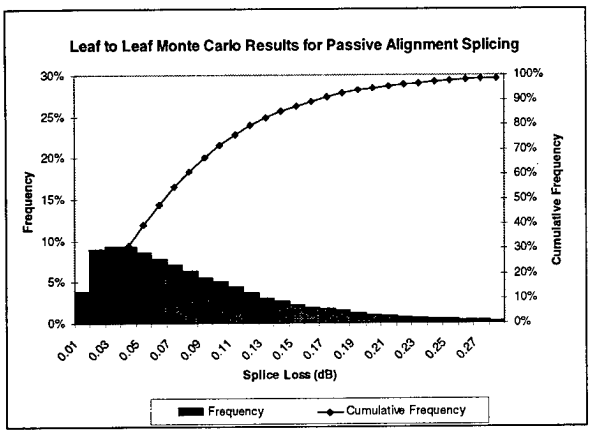

Figure 2: LEAF Fiber Monte Carlo Results for Passive Alignment Splicing

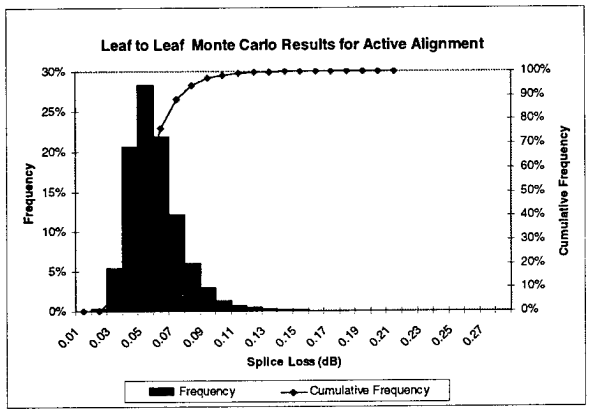

Figure 3: LEAF Fiber Monte Carlo Results for Active Alignment Splicing

The impact of the splice loss distribution on system budgets and installation costs can be very large. The difference between active and passive alignment yields are shown in Table 3and Table 4.

Table 3: Span Yields vs. Number of Splices for Passive Alignment Splicing

Passive Alignment Span Yields					
Criterion	**Single Splice Yield**	**Span with 4 splices**	**Span with 7 splices**	**Span with 10 splices**	**Span with 15 splices**
Budget (dB)	0.20	0.80	1.40	2.00	3.00
≤0.20 dB	94.7%	99.6%	100%	100%	100%
≤0.15 dB	87.6%	97.8%	99.5%	100%	100%
≤0.10 dB	71.7%	79.9%	84.5%	88.2%	91.6%

Table 4: Span Yields vs. Number of Splices for Active Alignment Splicing

Active Alignment Span Yields					
Criterion	**Single Splice Yield**	**Span with 4 splices**	**Span with 7 splices**	**Span with 10 splices**	**Span with 15 splices**
Budget (dB)	0.20	0.80	1.40	2.00	3.00
≤0.20 dB	99.99%	100%	100%	100%	100%
≤0.15 dB	99.9%	100%	100%	100%	100%
≤0.10 dB	98.4%	100%	100%	100%	100%

For active alignment splicing, even with a ≤ 0.10 dB splice loss budget, single fiber splicing should result in 98.4% yield. For series of four or more splices, the overall yield is predicted to be 100%. The need to break and remake a splice typically will be a result of fusion splicing practices as opposed to fiber parameters. Use of splicer estimated loss or uni-directional OTDR measured loss need to be understood in light of these results.

Splice Loss Measurement

As early experience with SMF and recent experience with standard NZ-DSF indicated, uni-directional OTDR measurement of splice loss may be deceiving. To obtain accurate, reliable splice loss values, bi-directional measurements must be made. The uni-directional measurement error is primarily a function of the differences in the mode-field of the two fibers. This effect will be slightly more pronounced in all standard NZ-DSF designs, due to the smaller

mode field diameter (MFD) than in LEAF fiber. The measurement error is shown in Figure 4.

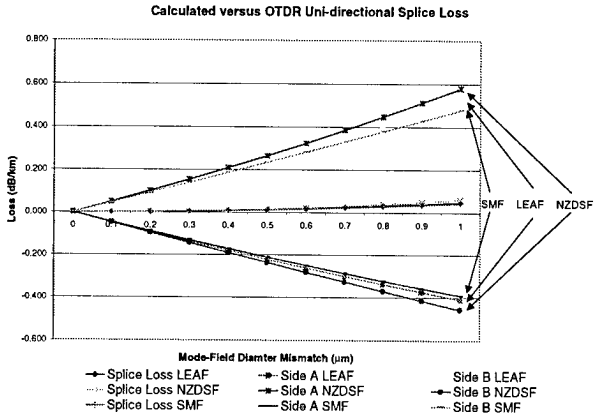

Figure 4: Error Associated with Uni-directional Splice Loss Measurement

Fusion Splicing Practices

Splicing conditions have a much greater impact on splice loss when splicing NZ-DSF. These more complex fiber designs are more sensitive to critical parameters such as clean splicing conditions, the end angle of the cleave, and splicing procedures. Additional attention needs to be given to both the equipment and the work area to achieve consistently low splice loss.

There are a number of things to keep in mind when preparing the fiber for splicing. Cleanliness plays an important part in achieving quality splices. The work area and all splicing tools should be kept clean and free of debris such as cable filling compound stripped coating or fiber ends. The stripper and cleaver should be cleaned frequently so that the fiber is not damaged during splicing preparation. Multiple passes with the stripping tool can also damage the fiber, possibly causing it to break during cleaving, splicing or installation. The splice equipment should be kept clean and dust free. Debris in the fiber alignment area (V-grooves) may cause fiber misalignment that would result in a poor quality splice.

After stripping, the fiber should be wiped clean using an alcohol wipe. Make sure all coating and debris are removed before inserting the fiber into the cleaver. Once cleaved, the fiber end should not be wiped clean. Wiping may place debris on the fiber end face that could cause problems with splicing. For best results, insert the cleaved fiber into the splicer alignment holder before repeating the process for the other fiber.

Equipment maintenance is also important. The stripper should be in good condition and the proper size. The cleaver should have a sharp blade that is perpendicular to the fiber axis. If more than a few bad cleaves are noted, the cleaver blade may need to be cleaned, rotated or replaced.

Splice loss is more sensitive to cleave end angle when splicing NZ-DSF compared to standard single-mode fiber. Laboratory studies show that end angles greater than 2 degrees can more than double the splice loss as compared to standard single-mode fiber, as indicated in Figure 5.

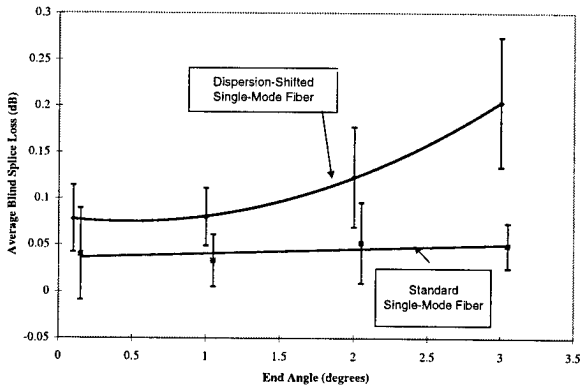

Figure 5: The Effect of End Angle on Splice Loss

As high data rate applications have evolved, splice equipment manufacturers have continuously improved the equipment they provide so that it is capable of splicing the new, more complex fiber designs. Adjusting machine settings to optimize results as well as developing algorithms to provide more accurate splice loss estimations are just two improvements available to the end-user.

There are many manufacturers of splicing equipment. Two equipment manufacturers recommendations are included below. Other

splicing equipment manufacturers should be contacted directly for specific recommendations.

Profile alignment splicers optically align the cores of the fibers to be spliced. The set-up of the splicer can be adjusted to improve performance. For older models such as the Fujikura FSM-20CS and FSM-20CSII, there are two switches that may be changed that will improve splicer performance with NZ-DSF. The first switch changes the cleave angle alarm threshold from 5° to 3°, which is the smallest end-angle alarm available for this model. Tightening this parameter will decrease distortions of the fiber cores at the splice point, thereby minimizing the associated splice loss. The second switch changes the splice loss estimation algorithm to account for the smaller core and mode-field diameter of NZ-DSF (in comparison to standard single-mode fibers). The splice loss estimation algorithm does not affect actual splice loss; it does, however, provide the user with a more accurate estimation of actual splice loss. Corning recommends bi-directional OTDR splice loss measurement.

For newer models such as the Fujikura FSM-30S, one needs only to select the DS AUTO fiber splicing mode and change the cleave angle alarm threshold to optimize splicer performance. In this mode, the splicer automatically monitors and adjusts the arc power, which may be helpful in field conditions. The splice loss estimation algorithm is also automatically updated to account for the more complex fiber design. The user also can select the cleave angle alarm threshold; 2° is the recommended threshold for NZ-DSF.

For Siecor's M90 fusion splicer with local injection and detection (LID®) system, there are no changes to the splicer set-up required for single-fiber fusion splicing. These splicers optimize the transmitted power through the splice and the fuse time during splicing. Each works equally well with standard single-mode and dispersion-shifted fiber. Good cleaving is of course important, and the LID system has a built-in alarm to indicate high end-angles (angles > 1.6°).

Of particular value to the installer are the choices available for splice loss estimation. With these options, a more accurate estimate of splice loss is available for the NZ-DSF designs. For the M90 splicer, Table 5 shows how to choose the best option for splice loss estimation.

Table 5: Settings for Siecor's M90 Splicer

Settings Available			For LEAF choose:
SMF			SMF
SMF	**DS**		DS
SMF	DS	**LS**	LS

The splice loss estimation algorithm does not affect actual splice loss. The same low loss splices can be achieved using splicers that have only the SMF option. Bi-directional OTDR splice loss measurement is recommended.

CONCLUSIONS

LEAF fiber can consistently provide lower loss splices with active alignment systems than other NZ-DSF designs. With attention to splicing practices and equipment set-up, LEAF fiber offers the same ease of installation as standard single-mode fiber designs. System designers can feel confident that they can take advantage of all the benefits of the LEAF design in their high data rate systems and still achieve excellent splice performance.

ACKNOWLEDGEMENTS

The authors wish to acknowledge Doug Duke from Alcoa Fujikura Ltd. and Todd Rhyne from Siecor for their helpful information and advice.

REFERENCES

1. Sheila A. Cooper, J. Jeff Johnson, Randy L. McClure and Mary E. White, "Splicing Non-Zero Dispersion-Shifted Fiber", Outside Plant, December, 1997, pp. 31 –37.

2. Alcoa Fujikura Ltd., "Splicing Guidelines for Dispersion-Shifted Fibers or Non-Zero Dispersion-Shifted Fibers", Alcoa Fujikura Splicing Applications Notes, OFSP-AN-002.

BIOGRAPHIES

Mary E. White is a 1991 graduate of Auburn University where she received a B.S. in Mechanical Engineering. She joined Corning Incorporated in 1995 as an Applications Engineer in the Telecommunications Products Division responsible for providing technical support to optical fiber cable and end-user customers. She has published several other papers on applications in telecommunications and her experience includes cable manufacturing and field applications.

Sheila A. Cooper is a Senior Product Engineer in Corning Incorportated's Telecommunications Products Division (TPD). She received her B.S. in Physics from Michigan Technological University. She has worked in TPD since 1988, and in her current position is the principal statistician for the Product Engineering Department. Her experience includes optical, environmental, mechanical and field applications testing.

Analysis of Multimode Fiber Behavior with Laser Sources in the Development of the Gigabit Ethernet Fiber Optic Specifications

John S. Abbott, Michael J. Hackert, Douglas E. Harshbarger
Corning Incorporated, New York

David G. Cunningham, Hewlett-Packard, United Kingdom

Christopher T. Di Minico, Cable Design Technologies (CDT) Corporation, Massachusetts

Ian H. White, University of Bristol, United Kingdom
Bristol, England

ABSTRACT

During September 1997 it was demonstrated that technical issues remained to be solved to achieve the targeted Gigabit Ethernet multimode fiber (MMF) operating distances for type 1000BASE-LX (Long Wavelength Laser) and for type 1000BASE-SX (Short Wavelength Laser). The issues were related to the use of laser sources with multimode fiber.

At that time, jitter measurements demonstrated eye-closure not accounted for by the link model used to calculate operating distances. The additional jitter contributions not accounted for in the link model were attributed to the affect of a source mode power distribution (MPD) and fiber differential mode delay (DMD). Source mode power distribution is a measure of the intensity profile of the laser. Differential mode delay is the difference in propagation time of different mode groups of the multimode fiber. Worst case DMD occurs when equal power is launched into the fastest and slowest fiber mode groups appearing as pulse-splitting in the impulse response or nulls in the frequency response.

To mitigate the affect of the differential mode delay (DMD) related jitter and achieve acceptable multimode fiber optic operating distances, additional specifications have been added to Gigabit Ethernet. These include a mode conditioning patch cord, fiber optic transmitter launch conditions, fiber optic receiver jitter tolerance, and fiber optic receiver bandwidth.

This paper provides an overview of the DMD related jitter contribution and addresses specific areas of analysis related to the development of the Gigabit Ethernet fiber optic specifications. The emphasis will be on the validation of the usage of the mode conditioning patch cord to produce appropriate launch conditions for 1000BASE-LX, and the development of worst case statistical models to characterize modal bandwidth and jitter performance using measured DMD profiles and source mode power distributions.

The laser source, receiver, and the fiber can contribute to jitter. The quantitative effect of different kinds of "jitter" on system performance is not fully understood and the standards specifications reflect this in how system penalties are allocated to different parts of the system.

BACKGROUND

In January 1996 the IEEE Computer Society LAN MAN Standards Committee approved a project to develop a supplement to the Ethernet Standard to support operation at a data rate of 1000 Mb/s. Referred to as Gigabit Ethernet, a primary objective of the standard is to leverage available technology and provide higher data rate backbones which are interoperable with existing 802.3 topologies i.e., 10 Mb/s and 100 Mb/s Ethernet LANs. The standard's physical layers, based on Fibre Channel (FC-PH): ANSI X3.230-1994 Fibre Channel Physical and Signaling Interface standard, include 1000BASE-SX, a short wavelength transceiver (850 nm) which uses two multimode fibers, 1000BASE-LX,

a long wavelength transceiver (1300 nm) which uses two multimode or singlemode fibers (SMF), and 1000BASE-CX, which uses two pair of specialized balanced copper cabling.

The elements of a Gigabit fiber optic transmission link are the fiber optic transmitter (laser), fiber optic media, and fiber optic receiver as shown in figure 1.

Test points TP1 through TP4 are for system conformance testing. The fiber optic media type, modal bandwidth, and operating distance currently in the standard are provided in Table 1 and Table 2 for both 1000BASE-SX and 1000BASE-LX.

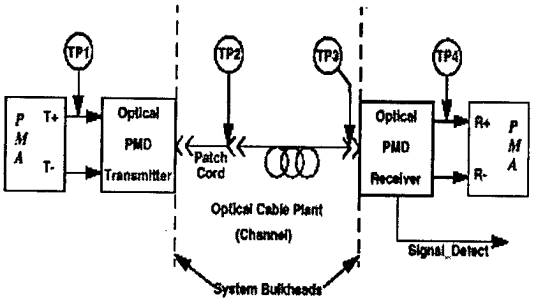

Figure 1

Table 1. Operating Range 1000BASE-SX For Each Fiber Type

Fiber type	Modal bandwidth (MHz.km)	Minimum range (meters)
62.5 μm MMF	160	2 to 220
62.5 μm MMF	200	2 to 275
50 μm MMF	400	2 to 500
50 μm MMF	500	2 to 550+
10 μm SMF	N/A	Not supported

Table 2. Operating Range 1000BASE-LX For Each Fiber Type

Fiber type	Modal bandwidth (MHz.km)	Minimum range (meters)
62.5 μm MMF	500	2 to 550+
50 μm MMF	400	2 to 550+
50 μm MMF	500	2 to 550+
10 μm SMF	N/A	2 to 5000+

Fundamental Concepts. Multimode fiber information carrying capacity is typically rated in terms of a bandwidth length product (MHz-km) which can be used to determine how far a system can operate at what bit rate[1]. A simple intuitive model for the bandwidth characteristics considers the fiber to consist of a number of discrete delay lines, each of which corresponds to a particular mode[2,3,4]. A conceptual model is shown in figure 2. In the figure, the low order modes (LOM) correspond to the modes or rays propagating down the center of the fiber; the high order modes (HOM) propagate near the core / clad interface; and the intermediate modes propagate in between. Although somewhat counter intuitive, the intermediate modes carry most of the power.

In an ideal fiber, all of the delays are tuned to be identical. Thus, when a temporally narrow pulse of light is launched into the fiber, its shape is maintained at the output. However, as the example in figure 2 shows, the over exaggerated delay error causes the output pulse to be broadened. The high order mode power arrives late relative to most of the power (in the intermediate modes), and the low order modes arrive early. Thus, the bandwidth is reduced and the information carrying capacity is limited.

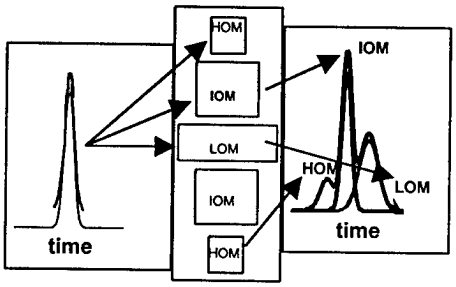

Figure 2 - Conceptual Model for Multimode Bandwidth

This model then explains why bandwidth is launch dependent. The output pulse given in figure 2 corresponds to an overfilled launch where all of the modes are excited with the maximum amount of power they can carry. This launch is defined by standards[5]; and a typical source that this might correspond to is an LED. If the launch

power distribution is now reduced so that only the lower and intermediate modes are excited, the power in the late peak of the pulse disappears, the pulse width decreases, and the bandwidth goes up. The analogy can be extended equally as well where the launch is restricted to just the lowest order modes and the output pulse becomes very narrow. Thus, if all of the modes of a multimode fiber are not tuned perfectly, the bandwidth can change as the launch power distribution changes.

The tuning of these modes is measured by the differential mode delay (DMD) measurement. The DMD is a process-tuning tool which measures the delay of each of the modes. It has never been standardized since it is difficult to implement, costly to run, and not a functional input measure for system modeling. Bandwidth, on the other hand, is functional and is used in system modeling[1]. It consists of recording the mean delay as a spot of light formed by a single-mode fiber is scanned across the input of the fiber. The typical technique for this measurement is a variation of the time domain bandwidth measurement[5] in which a high-speed pulse is used. The US National Institute of Standards and Technology (NIST) recently reported on improved resolution using a frequency domain technique which allows measurement of short lengths (approx. ten meters or ±0.3 ps/m)[6]. An example is given in figure 3 where delay (given in ps/m or ns/km) is plotted versus offset of the singlemode spot where positive delay corresponds to increased time.

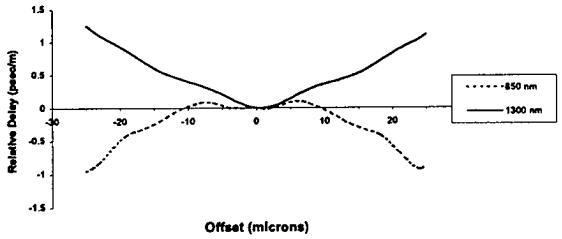

Figure 3 - Differential Mode Delay for TIA TG 2.2 Round Robin Cable (Fiber 7)

The DMD measurement is effectively a very precise measure of the graded index of a multimode fiber. Measures of the index such as the Refracted Near-field (RNF) measurement[5] fail to have sufficient resolution to observe the delay errors, which are significant for tuning a multimode fiber. Figure 4 shows an example of a perfect alpha profile and a perturbed profile that

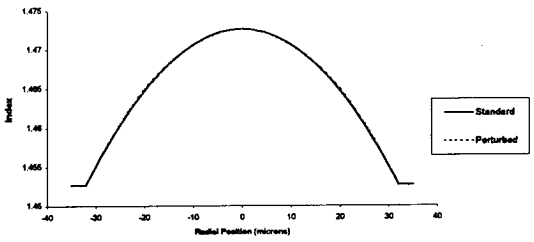

Figure 4- Theoretical Bandwidth Impact to Index Perturbation

reduced the modal bandwidth by approximately a factor of two. It is evident from the figure that the difference is barely perceptible. Typical RNF measurement equipment has insufficient resolution to measure this small difference (just another challenge to tuning for increased bandwidth). Fortunately, a theoretical foundation to model bandwidth from DMD data was completed during early fiber development[2,3,4]. The models provide sufficient accuracy to estimate average performance when empirical adjustments are made. However, the precision is somewhat limited.

At the wavelength of peak bandwidth, the DMD profile for an ideal fiber is flat. For FDDI grade 62.5 µm fiber this occurs near 1300 nm. However, as we move off this peak wavelength, e.g., to 850 nm for FDDI grade 62.5 µm fiber, the DMD profile shifts. The shift is upward to greater delays for shorter wavelengths and downward to lower delays for longer wavelengths. The intuitive model given in figure 2 corresponds to the latter, longer wavelength case. This wavelength relationship suggests that for restricted launches produced by lasers, the 850 nm bandwidth should increase relative to the overfilled launch for 62.5 µm fiber. Both wavelengths should increase for 50 µm fiber. Exploitation of this characteristic has been a topic of standards development for the last couple of years and its investigation is ongoing.

The mechanism by which restricting the launch from LED-like overfilled conditions to laser-like restricted conditions improves 850 nm operation on FDDI grade 62.5 μm fiber is not present for 1300 nm. However, in order to achieve the 1 Gigabit per second digital data rate, very fast source devices are required. One must use a laser with its restricted launch, regardless of its wavelength and its impact on system bandwidth. For that reason, source characteristics like the degree of launch restriction, launch offset, overshoot, and ringing become just as important as fiber index profile.

Sources with highly restricted launches can excite fibers in such a way that only HOM and LOM of figure 2 are present. This phenomena, called pulse splitting, occurs primarily with 1300 nm dual-purpose singlemode/multimode lasers connected using multimode quality connectors. An example of the rising edge of the digital signal exiting a link is given in figure 5. The stair step formed on the rising edge is caused by two discreet delays occurring in the fiber and the ringing in the source. An example of the DMD of a fiber showing this effect is given in figure 5. The DMD is flat

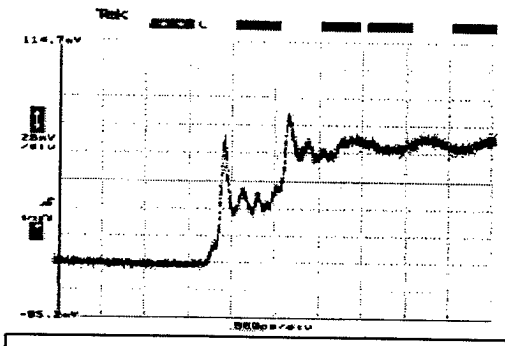

Figure 5 – Rising Edge of Digital Signal Showing Plateauing

over most of the radial extent of the fiber, but shows a large delay error for the lowest order modes on center, such as might be caused by a center line dip in the index profile. The overfilled launch (OFL) bandwidth for this fiber is high since most of the power is carried in the intermediate modes that are well tuned. Thus, this fiber works as desired for overfilling sources such as LEDs (for which 62.5 μm fiber was designed) but runs into this issue when ultra restricted, singlemode

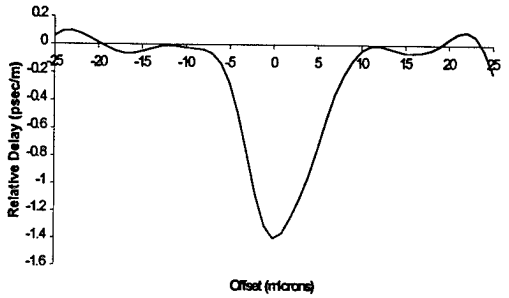

Figure 6 - DMD at 1300 nm , Fiber with Centerline Perturbation

launches such as those generated by the 1300 nm SMF Fabra Perot (FP) laser. The offset of 3 – 7 mm introduced by a MMF connector is also necessary and is typically present on the jumper connecting the source to the cable plant.

One solution to this problem is to control the launch distribution produced by the source. After evaluating various launch specifications and control mechanisms, it was agreed that sources must meet a coupled power ratio (CPR) requirement and that 1300 nm operation would require an offset launch patch cord.

CPR measurement is described in OFSTP 147 and consists of taking the ratio of the power coupled into SMF compared to MMF. The requirement ensures that a source launches a power distribution, which is fairly overfilled. The offset patch cord achieves a significantly over filling power distribution by launching from a singlemode fiber into a multimode fiber through a controlled offset created by a special connector. The source must be designed to couple efficiently into the SMF launch fiber. By controlling the source launch conditions as well as adding a receiver bandwidth requirement and reallocating the jitter budget, agreement was achieved on the lengths in the current standard.

Effect of different modal power distributions on bandwidth and jitter modeling development and results.

A model is developed here to understand and characterize the fiber bandwidth and the jitter in relationship to the relative power in a mode group and the mode delay of the group relative to the weighted average. The model, which has been verified over many years for overfilled launches and the offset launch used in the DMD measurement, can be applied to understand and characterize the wide variety of sources that can meet, and possibly extend, the operating distances of Gigabit Ethernet.

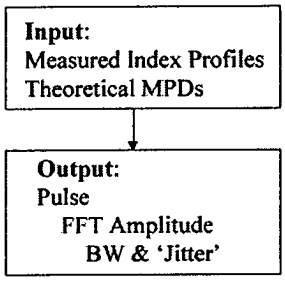

Assumptions used by the model include discrete modes and strong coupling within degenerate mode groups. The calculated pulse to be analyzed for bandwidth and jitter is given by

$$P(t) = \sum P_m \, \delta(t-\tau_m) \qquad [1]$$

Here P_m is the relative power in mode group m and τ_m denotes the mode delay of the group relative to the weighted average. The mode delays are determined by the profile index error and for this model were numerically calculated from a set of 237 index profiles. The profiles were chosen to thoroughly demonstrate various perturbations but do not represent a typical distribution or statistical sample. These profiles meet the modal bandwidth requirements of the fiber specified in FDDI and Gigabit Ethernet of 160 MHz.km at 850 and 500 MHz.km at 1300 nm.

In contrast, the mode power distribution P_m that was used was purely theoretical and was chosen to model a wide variety of conceivable launches, not all of which might be easily achievable in practice. P_m was modeled as a '2-sided' parabola with a maximum at mode group m_{max}, and which decreased parabolically to zero at $m_1$and m_2 (the broadness of the parabola was allowed to vary on each side and m_1 was allowed to be negative to model centered launches). Examples are shown in figure 7. 1162 distinct mode power distributions and the 237 index profiles were studied.

Figure 7. Examples of Launches used in the Bandwidth Simulation.

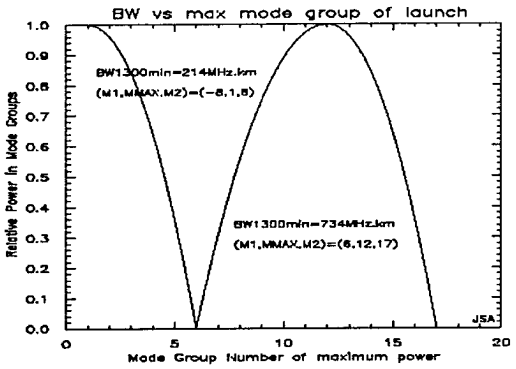

The bandwidth is calculated in the usual way taking the Fourier Transform of P(t) and determining the frequency f where the transform amplitude A(f) decreases to 0.5.

A jitter metric to quantify the multipulse character of P(t) was constructed by looking at oscillations in the transform amplitude A(f). The frequency and amplitude of a local minimum are denoted by (f_{min}, A_{min}) and the next local maximum by (f_{max}, A_{max}). As a metric to quantify which of the profile/launch combinations gave rise to multipulse structure, we tracked the parameter $J=A_{max}-A_{min}$. A typical receiver has its own maximum bandwidth and both A_{min} and A_{max} were truncated at the appropriate frequency.

Example bandwidth results presented at an IEEE 802.3 working session in Boston in January 1998 are shown in figures 8 and 9. Figure 8 shows the minimum 1300 nm bandwidth over all 237 profiles as a function of the mode group with maximum power m_{max}. Note that when m_{max} is in the range 7-15, the minimum 1300 nm bandwidth is above 250 MHz.km for all launch widths studied and that for some launches, the minimum bandwidth remained above 500 MHz.km. When m_{max} is in the range 11-13

the minimum bandwidth is above 300 MHz.km for all launches and a significant portion of the launches exceed 500 MHz.km for all profiles. This study suggests that it is relatively rare for a launch to bring the minimum bandwidth down to 250 MHz.km, and that this is associated with some of the mode power distributions peaked at groups 1 and 2.

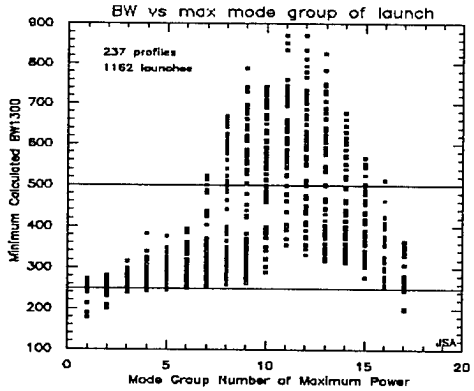

Figure 8. Minimum Bandwidth vs. mode group of maximum power. Each dot represents the minimum BW for 237 profiles.

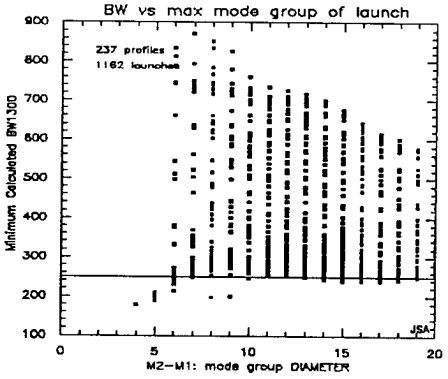

Figure 9. Minimum Calculated Bandwidth vs. the mode spread M_2-M_1. Each dot represents the minimum bandwidth over 237 profiles.

Figure 9 shows the minimum 1300 nm bandwidth as a function of the 'spread' in mode group number (m_2-m_1). Plotted this way it is clear that while the maximum BW_{min} increases as the mode spread decreases, the lowest BW_{min} is associated with small spot spread. From figure 8, one sees it arises from small spots near the center.

Figure 10 shows the 'jitter metric' A_{max}-A_{min} versus the mode group with maximum power m_{max}. Note that 'jitter' is insignificant for all launches with m_{max} greater than about 8, which is consistent with the guidelines for BW_{min} in figure 8.

Figure 11 shows the 'jitter metric' as a function of the mode group spread M_2-M_1. Again, the potential for higher jitter increases with a portion of the launches as the mode group spread decreases, and figures 8, 9, 10, 11 together suggest that only a small portion of launches are expected to show bandwidth or jitter issues. These are associated with narrow mode power distributions concentrated in the lowest order modes.

This summarizes modeling results for 62.5 μm fibers at 1300 nm. Analogous modeling was done for 850 nm and 50 μm fibers. The 850 nm results have been extended to the use of actual sources rather than theoretical distribution [2].

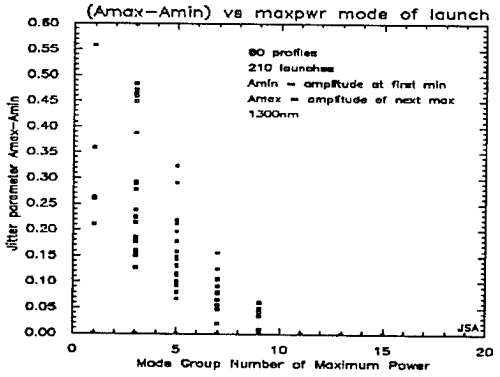

Figure 10. Maximum Calculated Jitter Metric A_{max}-A_{min} vs mode group of maximum power Mmax. Each dot represents the maximum 'jitter' over 80 profiles.

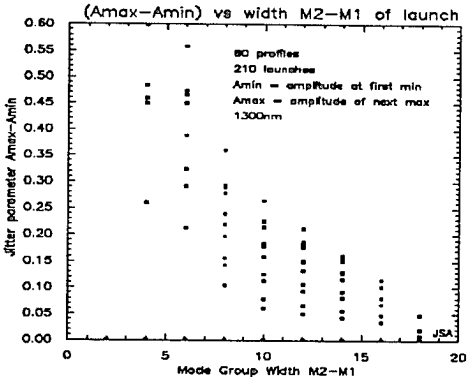

Figure 11. Maximum 'Jitter metric' A_{max}-A_{min} vs. mode group spread M_2-M_1.

Experimental and theoretical validation of the offset launch patch cord for 1000BASE-LX Gigabit Ethernet multimode fiber links.

During the final stages of the Gigabit Ethernet standardization, it was discovered that there existed a small but statistically significant population of fibers for which the bandwidth with laser excitation was lower than the bandwidth when measured with an overfilled launch. This was found to be true at operating wavelengths near both 850 nm and 1300 nm. The Gigabit Ethernet committee and the associated ad hoc Modal Bandwidth Investigation (MBI) group investigated the cause of the observed decrease in modal bandwidth with laser operation.

In this section we will concentrate on the use of an offset launch (mode conditioning) patch cord for 1000BASE-LX. A summary of the important results of the MBI will be presented. These results were used by the Gigabit Ethernet committee to generate the specifications for the offset launch patch cord and to confirm that it would maintain at least the overfilled launch bandwidth for at least 99% of installed 62 MMF (assuming a 160/500 MHz.km modal bandwidth for the 62 MMF).

Laboratory and field testing by various members of the MBI indicated that for unconditioned 1000BASE-LX on the order of 10% of installed multimode fiber cables could suffer the bandwidth collapse with typical 1000BASE-LX transceivers. It was also discovered that small connector offsets in range of only 3 μm to 7 μm could exacerbate the bandwidth reduction and associated jitter.

Theoretical studies confirmed this but also indicated that an offset singlemode to multimode fiber launch could solve the problem by maintaining a high bandwidth due to a mode conditioning effect. Figure 12 illustrates the bandwidth as a function of the launch position of a singlemode spot for a fiber investigated by the MBI. For small offsets this fiber clearly exhibits the bandwidth collapse effect but, as expected from theory, an offset in the range 17 μm to 24 μm restores the bandwidth to greater than its overfilled launch value.

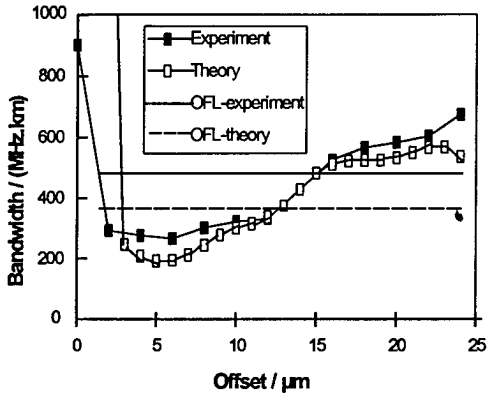

Figure 12. Plot of link bandwidth versus offset position for a 1.3μm wavelength 62.5 μm MMF link. Also shown is the OFL bandwidth obtained from measurement and simulation

The Offset Launch technique for 1000BASE-LX 'offset' launch is implemented by offsetting a singlemode fiber radially from the core center of the MMF. This launches a singlemode spot of light into the core of the multimode fiber as shown in figure 13.

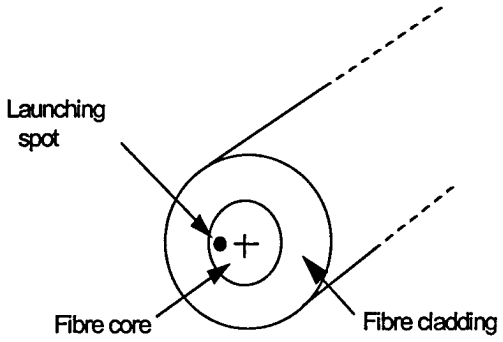

Figure 13. Illustration of offset launch technique showing a small single- mode spot of light launched with a radial offset from the center of the MMF core

By illuminating a region of the MMF radially displaced from the core center only a subset of the propagating modes are excited at the launch. The enhancement of bandwidth results from this selection of launched modes. Although the offset launch creates an underfilled launch it nevertheless excites a relatively large number of high order modes. Hence, the 'offset' launch technique

is relatively insensitive to modal noise, to fiber microbending and to mechanical agitation.

Statistical Analysis of the Launch.

In the laboratory and in field trials, the MBI established that the offset launch maintained at least the overfilled launch bandwidth in all fibers that exhibited the bandwidth collapse. However, because of logistical and cost issues only a relatively small number of fibers could be experimentally tested. It was therefore recognized that a theoretical study was required to generate a larger set of statistical data.

To carry out the statistical analysis of the 'offset launch', a detailed numerical model was developed [7]. To model the range of performance levels expected in the installed fiber base, a series of simulations were carried out. For the simulations the fibers were assumed to have characteristic defects in their core refractive index profiles that could occur during the fiber manufacturing process. These defects include (i) peaks or dips in the refractive index distribution at the center, (ii) variations at the core/cladding interface including spikes and abrupt cut-offs and (iii) changes in the index profile along the fiber radius. Figure 14 shows a schematic diagram of the different types of MMF profiles that were included in the simulations.

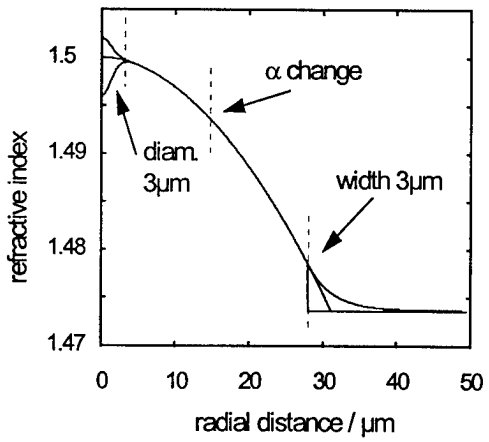

Figure 14. Schematic diagram of the refractive index profiles with characteristic central index and core/cladding interface defects. These perturbations are used by the simulation to create 81 different MMF profiles.

The center defects were modeled with a gaussian shape having a FWHM of 3μm and index amplitudes of +0.002 and -0.004 for peaks, and dips, respectively. The defect amplitude for a peak has been chosen as smaller than a dip since it is believed that, by only affecting the propagation time of the fundamental mode, central peaks result in more severe bandwidth degradation. The values used for the power-law coefficient are α=1.89, 1.97, and 2.05. These were chosen so that both near optimum (α=1.97) profiles can be studied along with both overcompensated and undercompensated ones.

On this basis simulations at 1300 nm for a range of offset injections have been carried out for 81 different 62.5 μm and 81 different 50 μm diameter MMFs. The 81 profiles are composed of the three possible center distortions, the three different core/cladding interfaces, the three different profile parameters for the inner part of the profile and the three possible profile parameters for the outer section of the fiber core. It is important to ensure that the performance characteristics of the 81 fibers represent 'worst-case' fibers in the field. To ensure this we used the following procedure; the overfilled launch bandwidth and DMD were calculated for each profile, the DMD's were then scaled to the DMD value characteristic of the worst case 5 percentile level. If the scaling caused the OFL bandwidth to fall below 500 MHz.km then the DMD was only scaled by the factor required to set the OFL bandwidth at 500 MHz.km. By scaling the DMD and bandwidth in this way one can obtain a statistical estimate for the performance of the worst case 5% of installed fibers. The MBI assumed that the 5 percentile DMD value was 2ns/km for 62MMF at operating wavelengths near 1300 nm.

The results of the simulations are summarized in figure 15 where the percentage of link failures (bandwidth less than OFL bandwidth) that occur at each offset position are shown for both 62.5 μm and 50 μm MMF.

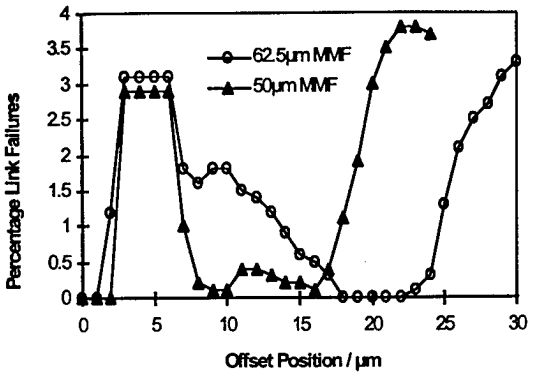

Figure 15. Percentage of link failures (offset launch bandwidth less than OFL bandwidth) that occur at each offset launch position for both 62.5 µm MMF and 50µm MMF with operation at 1300 nm

It can be seen that although no link failures occur with precise center launch this very rapidly rises to around 3% for small offsets. For both 62.5 µm and 50 µm MMF cases the percentage of failures then dramatically falls from over 3% of all fibers for 0 to 5µm offsets down to 0% for larger offset values. By setting the acceptance criteria such that a small number of failures are allowed, it can be seen that 99.7 % of all 62.5 µm MMF thought to occur in the field have the required link bandwidth in the offset range 17µm to 23 µm (i.e. 4 failures out of the 81 profiles (~5% of the 5% 'worst-case' fibers). For the 50 µm MMF case it can be seen that 99.6% of all fibers maintain at least the OFL bandwidth for the offset range 10µm–16 µm.

Modulation Performance of Offset Launch Schemes.

The 3 dB fiber bandwidth only provides part of the information necessary to determine whether link failures are likely to occur. In addition, if ripples occur in the frequency response, unacceptable levels of jitter and eye closure can result. Figure 16 shows the frequency response of all the 81, 62.5 µm, fibers at an operating wavelength of 1300 nm for a transmission length of 500 m with offsets of 17µm to 23 µm. Since Gigabit Ethernet supports a signaling rate of 1.25Gb/s, the frequency range up to 1.5 GHz is considered.

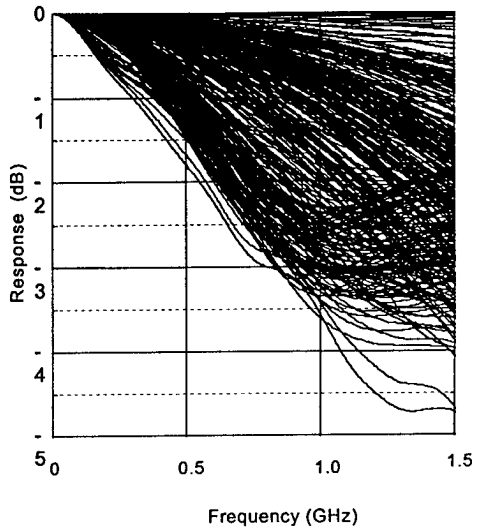

Figure 16. Frequency response of 81 62.5 µm MMF (length 500 m) at an operating wavelength of 1300 nm for offsets positions 17 to 23µm.

It was found that for frequencies up to 1.5GHz there are no troughs in the frequency response that have amplitudes >1 dB. This indicates that the eye quality and jitter values will be acceptable.

Eye diagrams were calculated for the fibers which exhibited the largest ripples in their transfer functions. The calculated eye diagrams for one limiting case are illustrated in figure 17 where the received eye diagrams are shown for four different launch conditions. The particular profile chosen has a peak at its center and this case is very similar to the fiber of figure 1 investigated by the MBI. Clearly the eye is open for the range of offsets used by the offset launch patch cord.

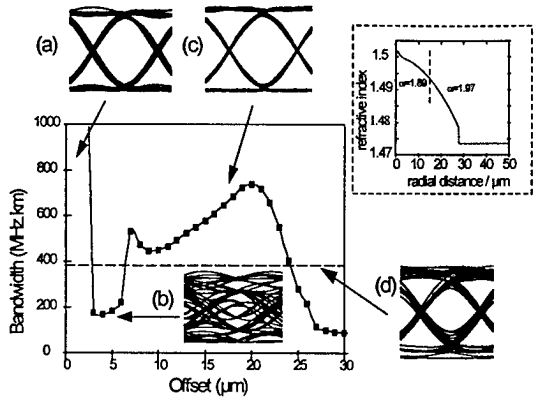

Figure 17. Transmission performance of a 62.5 μm fiber with a central index peak, an abrupt core/cladding interface, an inner profile parameter of 1.89 and an outer profile parameter of 1.97. The received eye diagrams after 500 m at 1.25 Gb/s are shown for launch positions of (a) 0 μm (b) 4 μm (c) 18 μm and (d) OFL conditions at an operating wavelength of 1300 nm .

As was stated earlier all experimental and field trial results confirmed that the offset launch maintained at least the overfilled launch bandwidth, adequate eye opening and resulted in good system performance.

CPR specifications for offset launch patch cords.

Simulations were also used to calculate the coupled power ratio (CPR) and bandwidth as a function of the offset position for the 81 scaled profiles. In figure 18 for 62.5 μm MMF the CPR is plotted as a function of the link bandwidth.

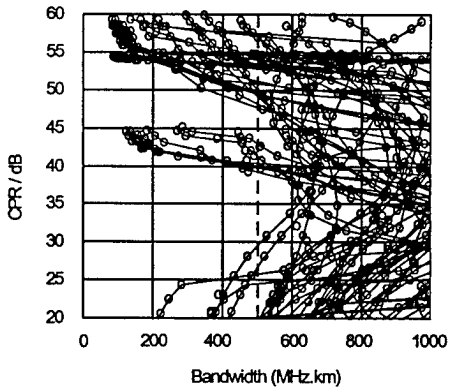

Figure 18. CPR plotted against offset bandwidth for 62.5 μm MMF.

From figure 18 it can be seen that for 62.5 μm MMF a region exists between 28 dB and 40 dB for which at least 500 MHz.km is achieved. Similar calculations were done for the 50 μm MMF case which showed that the CPR range which maintains at least the overfilled launch bandwidth is 12 dB to 20 dB.

The Gigabit Ethernet committee adopted a CPR test as a conformance test specification for the offset patch cord. The committee also specified that the physical offset of the singlemode to multimode fiber should be permanent. The specification for the physical offsets and CPR values were derived using figures 15 and 18. The specified offsets were as follows: for 62.5 μm MMF 17 μm to 23μm, for 50 μm MMF 10μm-16 μm.

CONCLUSIONS

This paper provides an overview of the DMD-related jitter contribution and addresses the validation of the usage of the mode conditioning patch cord to produce appropriate launch conditions for 1000BASE-LX as well as the development of worst case statistical models to characterize modal bandwidth and jitter performance using measured DMD profiles and source mode power distributions. This analysis led to the validation of the allowable operating distances for 1000BASE-SX and 1000BASE-LX.

REFERENCES

1) Bandwidth model developed for IEEE P802.3z Specification for 802.3 Full Duplex Operation Supplement to Carrier Sense Multiple Access with Collision Detection (CSMA/CD) Access Method and Physical Layer Specification for 1000 Mb/s Operation.

2) Mammel & Cohen, 'Numerical Prediction of fiber transmission characteristics from arbitrary refractive-index profiles', Appl. Optics 21 (1982) 4/pp 699-703.

3) Petermann, K., 'Simple Relationship between Differential Mode Delay in Optical Fibres and the deviation from optimum profile', Elec. Lett. 14 (1978) 24/pp 793-4.

4) Olshansky, R., 'Pulse broadening caused by deviation from the optimal index profile', Applied Optics 15 (1976) 2/pp 782.

5) TIA References: Fiber Optic Test Procedures (FOTPs) - TIA-455, Optical Fiber System Test Procedures (OFSTPs) - TIA-526, and Informative Test Methods (ITM) - TIA-TSB62.
6) S.E. Mechels, J.B. Schlager, D.L. Franzen. "High-Resolution Differential Mode Delay Measurement in Optical Fibers using a Frequency-Domain Phase-Shift Technique," Photonics Technology Letters, vol. 9, no. 6, June 1997, pp. 794-6.
7) L.Raddatz et al.,: "An Experimental and Theoretical Study of the Offset Launch Technique for the Enhancement of the Bandwidth of Multimode Fiber Links", IEEE Jour. Lightwave Tech. 16, 3, pp324-331, 1998
8) Pepeljugoski et al., "Effect of Launch Conditions on Power Penalties in Gigabit Links Using 62.5 μm Core Fibers Operating at Short Wavelength", NIST Symposium on Optical Fiber Measurements, Sept. 1998.

BIOGRAPHIES

John S. Abbott: With Corning Incorporated since 1979, John is an Engineering Associate in the Telecommunications Products Division engaged in modeling the optical fiber manufacturing process as well as light propagation in the finished fiber. A graduate of Caltech (B.S. mathematics, 1974) and MIT (Ph.D., mathematics, 1979), John has patents in various areas of optical fiber manufacture and measurement.

David G. Cunningham: With HP Laboratories at Bristol, England since 1987, David Cunningham is Department Scientist in the Extended Enterprise Laboratory. A graduate of The Queens University of Belfast, he has a BSc degree in physics (1981) and a PhD degree in laser and atomic spectroscopy (1985). He is the HP Laboratories project manager for Gigabit Ethernet. His previous projects include the 100VG-AnyLAN standard, the Serial HIPPI standard, and an FDDI physical network layer. His work has produced various patents in the areas of integrated optics, optical signal processing, coding and communication systems.

Douglas E. Harshbarger is the Market Development Engineering Manager, Premises Systems for Corning's Telecommunications Products Division. He is responsible for analyzing optical fiber and optical LAN system components for the premises market. Recently he led Corning's Gigabit Ethernet standard development team in their work in IEEE. Prior to joining Corning Incorporated, Harshbarger spent seven years as an engineering officer in ther United States Air Force. He holds a BS in electrical engineering from the University of Virginia and an MS in electrical engineering from the University of Nevada, Las Vegas. He is also a BICSI registered communications distribution designer.

Michael J. Hackert is an Electro Optic Measurement Project Engineer working at Corning's Center for Fiber Optic Testing. He joined Corning after receiving his MSEE degree from Stanford University in 1982.
He began his work in fiber at Catholic University where he received a BSEE. Throughout his career, Mike has supported the advancement of fiber through the development of new fiber designs and metrology needed to test them. He has published numerous papers on measurements and actively participates in standards. He currently chairs the TIA FO-2.2 task group on modal dependence of bandwidth and IEC TC86 WG4 on calibration.

Christopher T. Di Minico : With Cable Design Technologies (CDT) Corporation, Director of Network Systems Technology. Member of IEEE, TIA TR41.8.1, and the US advisory group for international cabling standards development. B.S.E.E. at Northeastern University with over 30 years experience in the cabling industry both in design and installation.

Ian H. White: Ian is currently Head of the Department of Electrical and Electronic Engineering, University of Bristol, and Deputy Director of its Centre of Communications Research. Ian graduated from the University of Cambridge, England, with an M.A. degree in 1980 and a Ph.D. degree in 1984. After academic posts in Cambridge and Bath Universities, he moved to Bristol University in 1996. His main research interests are now in diode laser components for applications in optical communications and sensing. Ian has in excess of 100 journal publications, has contributed to several books and holds 10 patents. He is editor of Optical and Quantum Electronics.

OPTIMIZING THE EMBEDDED FIBER PLANT USING DENSE WAVELENGTH DIVISION MULTIPLEXING

Paul L. Scrivener

Pirelli Telecom Systems Division, Lexington, South Carolina

ABSTRACT

Proposed transmission networks of the future will incorporate more advanced optical technology enabling the transition to the all-optical network. In pursuit of the all-optical network, new "enabling" technologies have enabled the realization and introduction of Hyper Dense Wavelength Division Multiplexing (H-DWDM), advanced Erbium Doped Fiber Amplifiers (EDFA) and enhanced transponder technology including features such as optical and system performance monitoring.

With the latest optical technologies, low loss, densely spaced optical channel multiplexers and demultiplexers allow us to increase the number of multiplexed channels. Only a few years ago, the first four channel WDM system was introduced, since then, the number of wavelength division multiplexed channels has been increasing due to market demand for ever greater capacity. Systems at 8, 32, and 64 channels have been tested and deployed, with planned upgrades to 128 channels

Optimization of the EDFA for H-DWDM applications, such as the introduction of automatic power control and by the use of multiple stages in the EDFA allow the inclusion of dispersion compensation and optical add drop multiplexing modules, providing additional features for H-DWDM systems.

The limitations of H-DWDM and EDFA systems due to non-linear effects, dispersion and PMD will be discussed relative to the different deployed fiber types along with the evolving H-DWDM technologies that are emerging to overcome these issues.

INTRODUCTION

Fuelled by the growth in Internet traffic in the last few years we have seen an explosion in the requirement for capacity. 15 years ago traffic was largely voice with defined growth rates of 4 to 5 % per year.[1] Today voice traffic is still growing at 8 to 10 % per year, however data traffic is driving the requirement for greater capacity. IP traffic dominates the data market with IP growing at 4 to 10 times per year. However data service revenues are rising at a far less rate than the traffic. Therefore a major factor determining the technology deployed to satisfy the growing capacity requirement is cost.

The ability to supply this extra capacity has been limited by fiber exhaust in today's networks. This paper will discuss the economic limitations of installing new fiber, and the technical issues associated with deploying Time Division Multiplexed (TDM) and WDM systems, such as network architecture, available technology and the impact of the different deployed fiber types.

SOLUTIONS TO FIBER EXHAUST

Multiple solutions to fiber exhaust include installation of new fiber, higher bit rate TDM, DWDM, and a combination of these solutions.

The ideal solution is also dependent on the type of network. For example the economics are different for metropolitan (metro) type applications where distances are limited to less than 100 km, typically 10 to 30 km, and long haul applications where distances can range from 400 km to 6000 km.

Metro applications

In metro applications the driving factor is cost. With the current cost of high bit rate TDM and WDM equipment it is still more economic to install new fiber if there is room in existing conduit. However in Metro areas if the conduit is exhausted and new conduit needs to be installed the use of TDM, WDM or both to relieve capacity constraints becomes viable. As an example a cost analysis shows that to expand capacity by 16 x OC-48 channels on a metro

route of less than 70 km, typical of most metro routes, and there is existing space in conduits it is more cost effective to install new fiber. However, if new conduit needs to be installed and if the route is longer than 3 km it is more cost effective to deploy WDM.

Additionally, in these shorter distance applications higher rate TDM over WDM can be rapidly deployed without the limitations set by fiber constraints such as PMD, dispersion and non-linearities which can distort signals and limit the performance of long haul systems.

Long haul applications

Economical considerations in long haul systems are more straightforward than in metro applications. The combination of high channel count Hyper Dense Wavelength Division Multiplexing (H-DWDM) systems and high bit rate TDM makes the economical advantages of increasing the capacity of the existing embedded fiber plant very attractive.

In these long haul systems careful system design is required to overcome signal degradation due to fiber non-linear effects, dispersion and PMD.

FIBER NON-LINEARITIES

In high bit rate H-DWDM systems the three main non linear distortions that impact system performance are Self Phase Modulation (SPM), Cross Phase Modulation (XPM) and Four Wave Mixing (FWM). SPM acts as a negative chirp, which increases with system length and amplifier power level. The effect is to cause spectral broadening which reduces the dispersion tolerance window. XPM acts as a cross talk penalty, which increases with increasing power and system length and with decreasing channel spacing. To first order, XPM penalty is independent of dispersion; it causes spectral broadening which will reduce the operating dispersion tolerance window. The impact that these non-linear distortions have on the performance of the system is dependent on the fiber type. Fibers having an effective area greater than 75um^2 such as standard SM fibers and some NZD fibers, allow for lower power densities, and therefore, reduced non-linear distortion. Both SPM and XPM can be controlled via dispersion compensation management. In particular the penalties from these non-linear distortions can be minimized by distributing dispersion compensation at each line amplifier site. By compensating only at the terminal ends, there will be residual eye closure penalty.

FWM penalties are worst for channels near the dispersion zero where the dispersion is low and phase matching occurs. FWM penalties **cannot** be dispersion compensated.

FWM causes interchannel crosstalk and is worst case for equally spaced WDM channels. If the channel spacing is equal to within +/- 10 GHz, FWM acts as a coherent crosstalk, and the penalty can be severe. The FWM penalty can be minimized by employing fiber with high local dispersion and by using an unequal WDM channel plan. The dispersion characteristics of the fiber and the per channel power determine the maximum channel count on a particular fiber type by limiting the minimum channel spacing.

In figures 1, 2 and 3a/b you can see the effect of FWM on dispersion shifted, standard NZD and NZD fibers with a large effective area respectively. The channels are on a nominal 100 GHz frequency plan and the plots were taken after approximately 500 km of fiber with four in-line amplifiers.

In figure 1, for the dispersion shifted fiber case, the power per channel and the channel frequency are chosen such that the generated FWM components do not fall on the signal channels. The FWM components can be clearly seen. With dispersion shifted fiber the maximum channel count is severely restricted as the dispersion zero falls within the operating window of the amplifier.

For the NZD fiber in figure 2 the zero dispersion is nominally greater than 1560 nm and some evidence of FWM components can be seen in this region.

In figure 3a and 3b no evidence of FWM components can be seen. The nominal zero dispersion for large effective area NZD fibers is below 1530nm. Because of the lower power density and the non-zero dispersion the channels can be more densely spaced therefore a higher channel count can be deployed.

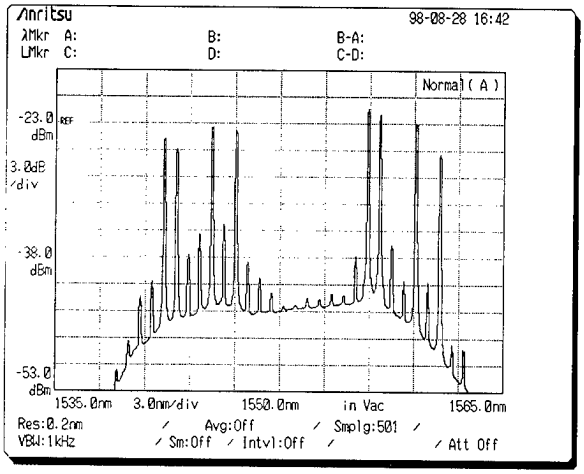

Figure 1: FWM generation in dispersion shifted fiber.

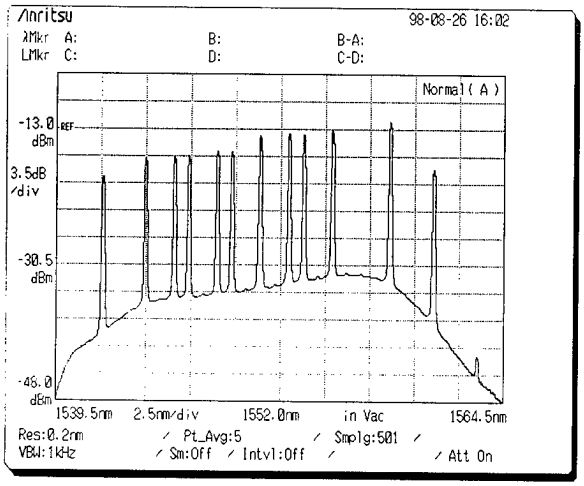

Figure 2: FWM generation in NZD fiber.

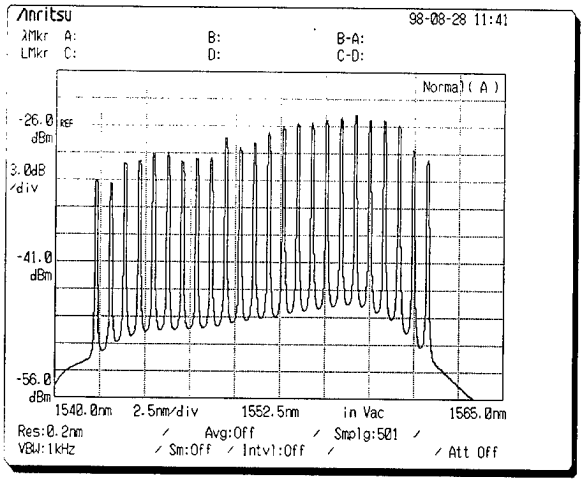

Figure 3a: FWM generation in large effective area NZD fiber.

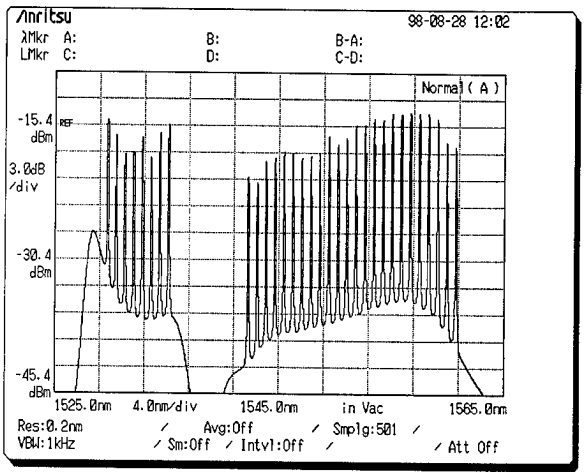

Figure 3b: FWM generation in large effective area NZD fiber.

INFRARED (IR) BAND OPERATION.

FWM limits the maximum channel count dependent on fiber type due to minimum channel spacing constraints. However, recent progress in erbium doped fiber amplifier design has enabled the available gain bandwidth to be extended out past 1600 nm effectively doubling the available bandwidth. This has enabled commercial systems to increase channel counts up to 128 channels and allow for potential terabit/s operation. However this longer wavelength region is more susceptible to fiber bending, cabling losses and environmental stresses. Even so, the incrementally higher losses around 1600 nm do not preclude the use of this region. By flexible and modular amplifier design it is possible to optimize the EDFA for this region.

DISPERSION AND PMD

Other than non-linear effects, dispersion and PMD are the two fiber characteristics that particularly impact the deployment of TDM terminals at bit rates above OC-192 in long haul H-DWDM applications. The dispersion limited transmission distance reduces quadratically as the bit rate is increased.

By the use of dispersion compensating fiber or gratings the resultant end-to-end dispersion in the system can be managed. Ideally the compensation should be distributed along the system length in order to maximize the distance before regeneration and to reduce penalties. Compensation can be distributed along the system length without impacting span budgets if

in-line amplifiers with mid-amplifier-access are used. Mid-amplifier-access is achieved by having a two-stage amplifier enabling a "lossy" component to be inserted between the two stages without impacting the noise figure of the amplifier and therefore the span budgets. This "lossy" component can be a dispersion compensating module or add/drop multiplexer.

Using lumped dispersion compensation at the terminals cannot fully compensate for distortion of the optical eye pattern and so introduces a penalty or a limit to the maximum transmission distance.

PMD also limits the transmission distance for OC-192 and higher bit rates. For OC-192 an upper limit of mean differential group delay (DGD) of 14 ps has been proposed to keep the power penalty below 2dB. Assuming a 5 span, 6 amplifier system the mean DGD allocation for the fiber would be 11 ps equating to a PMD value for the fiber of 0.45 ps/√km. For recently installed fiber this is an achievable figure however for older fiber the value can be considerably higher thereby severely limiting the transmission distance at bit rates of OC-192 and above.

DISPERSION MANAGED SOLITONS

PMD compensators are under development but are not yet commercially available. An alternative approach to reduce the impact of PMD is the use of dispersion-managed solitons whose RZ pulses are more robust than NRZ pulses. The higher peak power of the soliton pulse induces a self-trapping effect, which reduces the PMD induced pulse spreading. This effect improves the robustness to PMD by 2 to 3 times. Additionally the requirement for precise dispersion management through dispersion compensation is relaxed.

Dispersion-managed solitons were transmitted over a commercial network route of 900 km of single mode -28 fiber.[2] The fibers were selected for their high PMD coefficients. The mean DGD of the system fiber was measured at 26.9 ps or a PMD coefficient of 0.9 ps/√km. The bit error rate after 900 km transmission showed a penalty of less than 2 dB. In figure 4a and 4b the transmitted and received eye diagrams are shown. Note the RZ format of the eyes and that the received eye after 900 km shows little intersymbol interference. The noise on the eye is from the amplified spontaneous emission generated by the EDFA amplifiers.

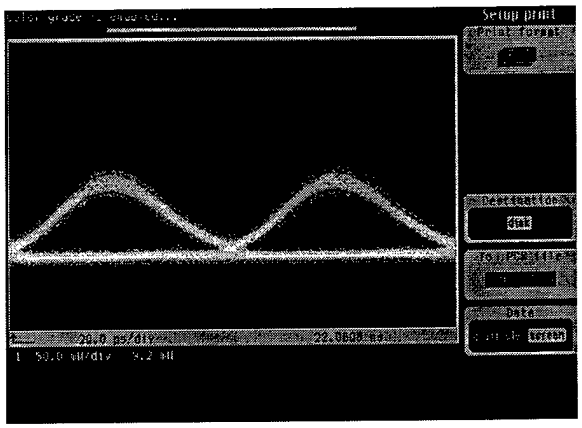

Figure 4a: Transmitted soliton eye.

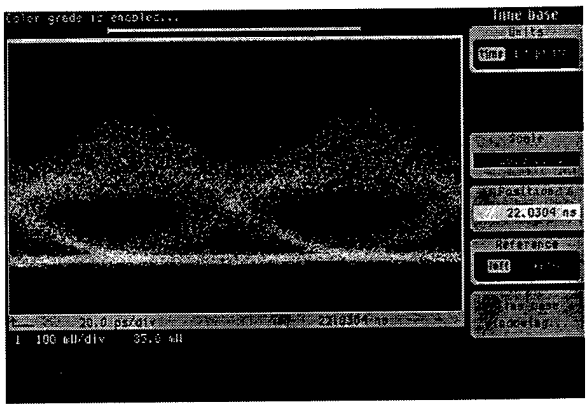

Figure 4b: Received soliton eye after 900 km.

Soliton transmit transponders were used for wavelength conversion to match the channel plan of the WDM system and for converting the commercial OC-192 line terminal NRZ signal format to the RZ soliton pulse format. Then after transmission through the WDM system and 900 km of fiber receive transponders were used for converting the received soliton pulses back to NFZ format for the OC-192 receiver.

CONCLUSION

By the use of high bit rate TDM and H-DWDM it is possible to optimize the embedded fiber plant to enable above terabit/s transmission over a single fiber. However there are limitations, dependent on the fiber type deployed, to the maximum channel count allowable due to the impact of non-linear distortions, most notably FWM.

Limitations on the use of high bit rate TDM over WDM systems due to dispersion can be minimized by the use of dispersion compensation. Additionally transmission systems can be made more robust to the higher PMD coefficients on older deployed fiber by the use of dispersion-managed soliton systems.

REFERENCES

[1] Mathew Steinberg, "The high capacity explosion," in NFOEC '98, Orlando, FL, 1998, pp. 19-38.

[2] Niall Robinson, Gary Davis, John Fee, Giorgio Grasso, Pierluigi Franco, Adriano Zuccala, Alessandro Cavacuiti, Mauro Macchi, Alessandro Schiffini, Luca Bonato and Raffaele Corsini, "4 x SONET OC-192 field installed dispersion managed soliton system over 450 km of standard fiber in the 1550 nm erbium band," in OFC'98, San Jose, CA, 1998, PD19.

The author **Paul Scrivener** joined Pirelli in the UK in 1979, starting in the fiber fabrication field. Through the 1980's, he was responsible for developing rare earth doped fibers for use in Pirelli's optical amplifier systems. In 1991, Paul moved to the research and development of Pirelli's DWDM and EDFA systems in Milan, Italy. Since 1995, he has been based in Lexington, South Carolina responsible for optical engineering and system integration.
Email: paul.scrivener@us.pirelli.com

OPTIMIZATION OF LOOSE TUBE CABLE DESIGNS: THE NEXT STEP

P. Gaillard[1], O. Tatat[1], K. Nothofer[2], Dr. A. Weiss[2], D. Benzel[3]

1. Alcatel OFCCC, Claremont, NC, USA, 2. Alcatel TPLE, Germany, 3. Alcatel TPLE, France

ABSTRACT

This paper discusses basic concepts for the design of loose tube optical fiber cable and introduces the next step in cable design optimization.

A loose tube cable containing up to 60 fibers, with an outer diameter of less than 8.5 mm, and a central tube cable containing up to 72 fibers, with an outer diameter of less than 8.0 mm, have been developed. These optimized designs are intended to be installed in protected environments, such as a rigid trench or ducts, and are particularly well fitted to some new emerging rights of way, such as motorways, or to blowing techniques for duct laying.

The cable structures are presented as well as the results obtained during the qualification test program. Some extended tests, such as long-term aging and evaluation of crush resistance at high temperature have been performed. Test results are presented and discussed.

Designs for other fiber counts are presented as well.

INTRODUCTION

The need exists to reduce cable installation costs, which can be achieved by using optical fiber cables having reduced diameter, higher fiber density and better handleability. To ensure fiber reliability, cable performance must be matched to the installation/operating conditions. Historically, very conservative cable designs have been used to anticipate the potential for harsh installation/operating conditions over the lifetime of the cable and because the actual stresses placed on the cable during its lifetime were not well understood. A better knowledge of the stresses/strains induced in the cable over its lifetime will allow optimization of cable designs while maintaining good reliability. Selection of less harsh environments for cable deployment allows for more optimized designs which offer excellent performance and reliability.

For this optimization process, there are advantages to continue working with the loose tube design (either stranded or central tube design), which is popular throughout the world. These advantages apply to both the customer and the cable manufacturer as follows:

- these designs exist now and have been widely used for several years (more than 15 years for the loose tube design);
- their reliability is based on a strong background regarding manufacturing and field experience gained so far (the first experiences having taken place nearly 20 years ago), as well as regarding the concept itself (loose design allowing the fibers to be free of strain with the exception of bending strain due to cabling);
- such designs have been manufactured for years, and corresponding machinery, tooling and processes are well known. They have been used and continuously improved in the cable industry;
- the same background exists for splicing, handling accessories and tools for these designs, and their adaptation or the development of a new family range of products is easy.

In addition it is important to remember that in long distance or trunk and/or high bit rate applications, reliability is a key point. Consequently, it is necessary to make sure that fiber break or loss increase risks are as limited as possible, which can be realized by providing a very high degree of protection to the fibers.

Cable design optimization considerations

The optimization of a cable design generally results from a compromise between two opposite types of considerations:

- improve the product and its manufacturing process, i.e. selection of better materials, reduction of the cable size, adaptation of the manufacturing processes... These are obvious optimization actions, well known and widely used;
- maintain a sufficient level of performance on the completed cables to be assured the specifications will be met given reductions in design safety factors (margin limits, etc.) in conjunction with limited process and material variation in manufacturing within "best commercial practice".

The first set of considerations has limited furture optimization opportunity with current fiber designs, manufacturing capabilities and stringent performance specifications based on potentially harsh environments. The consequence is that if the optimization process has to continue, the next step that comes to mind is to rework the cable performances (i.e. to review the product specification). This can be done either through a more accurate estimation of the real strains the cable will have to face during its installation and through its lifetime, or through the implementation of installation techniques which provide the cable a more protected environment, or a combination of both. These kinds of considerations are reinforced by the result of cable field failure analysis. This analysis reveals that the primary cause of outage is due by far to external causes such as civil/works soil digging.

Another solution would consist of using resistant fibers, which exhibit improved bending and microbending sensitivity and higher stress resistance compared to that of current fibers.

Two examples of a next step optimization

To illustrate this concept and to answer a particular need, we have developed a loose tube and a central tube cable design intended to be installed in protected environments (the cable being surrounded by a stable and rigid protection), such as a rigid trench, a cable trough, or a conduit. This is particularly well fitted to some new emerging rights of way such as road networks (and more particularly motorways[1]). In this instance the cable can be installed in a small trench or slot which has been dug directly into the road asphalt (see Figure 1), This design can also be used in a duct network using blowing techniques.

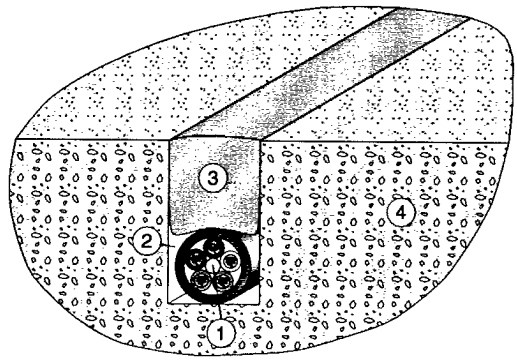

1- Cable
2- Slot
3- Bituminous filling compound
4- Asphalt (road)

Figure 1, Motorway Cable Laying Technique

The cable can be considered protected (particularly regarding mechanical strains, to some extent) by its immediate environment, according to the following considerations:

- the cable installation location can be considered relatively stable in dimension (i.e., no significant occurrences of displacement or deformation), and hard enough to act as a mechanical barrier for the cable vs. external radial aggressions such as crush, impact, or rodent bites[2]... In addition, the cable laying conditions do not require strong tensile resistance, if the cable were simply paid off from its reel and installed into its housing with a near to zero effort;
- a duct which is buried in the ground or laid in an existing infrastructure (tunnel, sewer or a building) acts also as a protection for the cable, due to the hardness and free space provided around the cable. Although duct pulling may require stronger cable tensile resistance, the light weight and small diameter of the cable together with the use of blowing techniques will allow a limited tensile force requirement.

Consequently, the degree of protection ensured by the cable can be lowered, thus leading to a lighter and cheaper optimized cable design.

As another example, existing specifications issued years ago include technical requirements, the level of which can be now recognized as too high, based on the experience gained and technical studies conducted in this matter. If so, the cable design can be reconsidered, and as a consequence its structure further optimized vs. said parameter.

Optimized cable designs

The developed cable designs basic descriptions are as given in Table 1.

Table 1: Cable Designs

Cable Type	Loose Tube	Central Tube
Structure	Fully dielectric	Fully dielectric
Nominal OD	8.2mm	7.9 mm
Fiber capacity	60	72
Reinforcement	CSM, Dielectric yarns	Dielectric yarns
Outer sheath	PE, 0.8mm nominal	PE, 1.4mm nominal

Based on identical mechanical and environmental requirements, the stranded loose tube design offers the better known cable structure with a higher potential regarding fiber excess length. Identification and organization of the fibers in the splice box is easier. The central tube design offers a better fiber density with good mechanical robustness, while fiber identification and fiber organization in the splice box is more time-consuming.

The nominal cable diameters lead to a cabled fiber density of approximately 1.15 to 1.47 fiber/mm^2. This value can be compared with standard loose tube design, in which the density ranges from typically 0.35 for "low" fiber count (36 fibers) to typically 0.8 for higher fiber count (144). Furthermore, the level of fiber density reached on this cable is comparable to those obtained for distribution cables (e.g. ribbon cables, microtube cables) with a much higher fiber count, typically several hundreds of fibers.

A cross section drawing of the cables is shown in Figure 2.

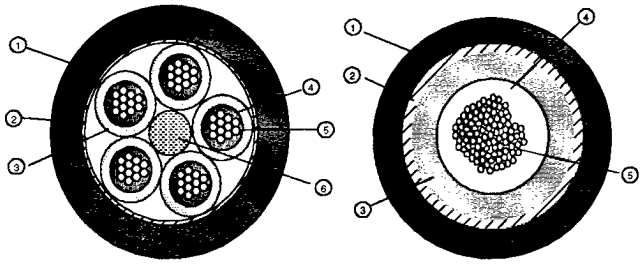

1- Outer sheath
2 - Dielectric reinforcement
3 - Loose Tube
4- Filling compound
5- Optical fiber
6- Dielectric CSM

Figure 2, Cable Structures

The following considerations have been made in building these cable designs:

- the fully dielectric design has been chosen because of its immunity to electromagnetic hazards, a key advantage for long distance applications or for use in linear networks such as links installed along motorways;
- the 12 fiber tube has been chosen for the loose tube design in order to have a very compact and dense design. The tube OD is similar to existing sizes, allowing to fit easily with available access tools and splicing accessories. With the central tube design, the fiber bundles are identified using a special identification code based on 12 colors and additional ring markings;
- light mechanical reinforcement has been applied around the loose tube cable core in order to increase the cable tensile resistance brought by the dielectric CSM and to strengthen the outer sheath, so as to provide sufficient resistance to tearing during cable handling;
- the loose tube cable sheath thickness has been reduced as much as possible, providing reasonable cable core protection during laying and extrusion capabilities. The sheath material can be either polyethylene (high density being preferred due to its better mechanical properties) or higher performance materials, such as polyamide, for applications in which more stringent requirements are needed in terms of

temperature, crush resistance or tear resistance;
- although the targeted tensile resistance (70 daN, which corresponds roughly to the force that can be applied manually) is relatively low due to installation techniques not inducing too much stress on the cable. It has been found useful to design the loose tube cable so as to obtain a high tensile strain free window in order to provide enhanced reliability. This will allow the cable to face relatively large elongation, for example due to ground movements.

The main performances targeted for these designs have been established as given in Table 2.

Table 2 , Design Targets

Item	Goal
Cable OD	Max. 8.5 mm
Tensile strength	70 daN (short-term)
Crush resistance	20 daN/100 mm
Impact resistance	5 Nm
Bending diameter	100 mm (static)
Temperature range	-40°C / + 70°C

Standard testing results

In order to verify that such designs are capable of meeting targeted performances, qualification cable lengths have been submitted to an extensive testing program conducted according to IEC 794-1 test methods.

The tests made and the results obtained are presented in Table 3 (all attenuation measurements were made at 1550 nm, level of performance obtained); the column "comments" gives further details on the test results.

Table 3, Test Results

Item	LT Results	CT Results	Comments
Cable OD	8.2	7.8	
Linear weight (kg/km)	51	43	
Tensile strength (daN)	140	80	No meas. strain on the fibers, no meas. loss increase
Static bending radium (mm)	80	80	No meas. loss increase during the test
Dynamic bending radium (mm)	150	120	No meas. loss increase during the test (bending under tension)
Kink radius (mm)	Down to 25 mm	Down to 40 mm	No kink
Crush (daN/cm)	Up to 40	Up to 40	No meas. loss increase after the test
Cut through (daN)	Up to 40	Up to 40	No meas. loss increase after the test; loss began ~20daN
Impact (Nm)	Up to 15	Up to 25	No meas. Loss increase during the test
Torsion (turns)	1m ± 1	1m ± 1	No meas. loss increase during the test
Operating temp. range (°C)	-40 / + 70	-40 / + 70	$\Delta\alpha < 0.05$ dB/km

These results are fully in compliance with initial targets, and even out perform requested performances for some items, which demonstrate the capability of the products. It can be particularly noted that despite the light design, these cables exhibit very good resistance against radial loads. Additionally, the central tube design exhibits a thermal behavior comparable to that of the loose tube design, despite the absence of rigid reinforcement elements.

Extended testing results (loose tube cable)

Since such a design is less ruggedized than current structures, dedicated investigations have been conducted to check behavior vs. "permanent" or exceptional stresses due to

particular mechanical situations or due to environmental conditions.

For this purpose further testing as been performed and the results are presented below.

Long-term accelerated aging

The purpose of this test was to simulate long-term aging, and to check for evidence of adverse effects after aging. A 60 OF cable was placed in an aging chamber, and maintained at 85°C for two months. A sampling of 30 optical fibers was measured in spectral attenuation between 1200 and 1700 nm before and after the test, including the intermediate point between the two periods. The results summary is given in Table 4 (max. attenuation change, dB/km), showing the behavior of the cable vs. long term aging.

Table 4, Long-Term Aging

	1310nm	1550nm
After 1 month	< 0.05	< 0.05
After 2 months	< 0.05	< 0.05

In addition the cable was submitted to a standard thermal cycling (two consecutive cycles between -40°C and +80°C) at each step of the test. No significant difference in the results compared with the initial thermal test was noted.

Extended tensile strength test

In order to determine the cable design margin vs. tensile stress, and to check the design ability to sustain higher tensile loads or elongation, the cable has been submitted to an extended tensile strength test.

The result obtained during this test is given in Figure 3 (stress/strain curves on the cable and the fibers). It can be seen on these curves that the typical fiber overlength (value for which the cable can be elongated without applying tensile strain on the fibers) is approximately 0.6 %, which provides as targeted a very good safety margin regarding the possible external strains the cable can be submitted to. As a consequence this elongation corresponds to a cable tension (140 daN) much higher than the targeted value, the cable ES being approximately 260 daN/%. This tension value could of course be reduced e.g. through a stranding pitch increase, thus providing further design optimization.

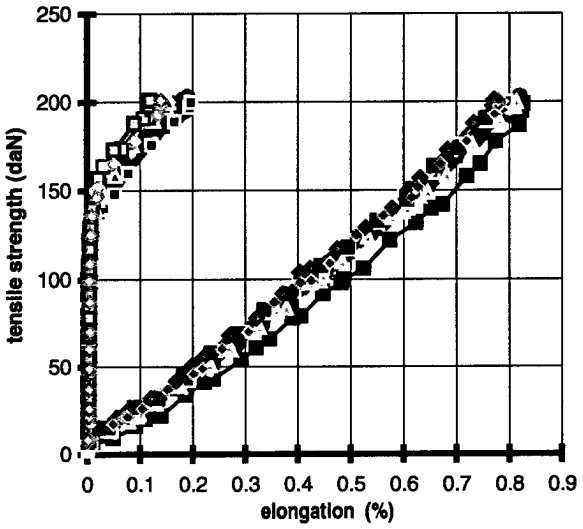

Figure 3, Tensile Strength Test

Extended crush strength test

The purpose of this test is to further investigate cable resistance to crushing, to simulate a situation in which the cable is submitted to a permanent crush and to investigate possibilities of creep of the cable structure under this load at high temperatures. For this a 10 m long, 60 OF cable sample has been submitted to a series of different levels of crush strains at different temperatures; during the test 24 looped fibers were monitored in attenuation at 1550 nm. The test conditions and obtained results are given in Table 4; for the tests realized at high temperature the crushing effort has been maintained for at least one hour in order to let the structure creep.

Table 4, Extended Crush Test

Test #1	Crush (daN/ cm)	Temperature	Result
1	30	Ambient	No meas. Loss increase during the test
2	40	Ambient	No meas. loss increase after the test
3	10	40°C	No meas. loss increase during the test
4	10	60°C	No meas. loss increase after the test

The analysis of the results shows that at ambient temperature, loss increase occurs at approximately 34 daN/cm, while at high temperature structure internal creep limits under moderate (10 daN/cm) crush load remains acceptable for most situations. In any case no measurable residual attenuation was noted after load release.

Long term static bending at high temperature

In order to check the cable ability to sustain static bending for a long time, a cable sample length was coiled around three different diameters (70, 80 and 100 mm bending radius, two loops) and stored in an oven at 85°C for three months. No cable break (kink) has been noted after this 90 day aging for any of the tested bending radii, and the cable dissection has not revealed any visual degradation of the different cable components.

Short term high temperature

In some special situations, there may be a requirement that the cable sustain a high temperature for a short time (e.g. if there is a need to apply a special sealing or water tightness compound over the cable). In this situation the light outer protection of the cable might be a concern. In order to investigate this point, such conditions have been simulated by pouring compound at high temperature (>180°C) on a cable sample that was installed in a slot made with a U-shaped aluminum tape, buried into a sand bedding. During the test the cable sheath temperature was measured and the cable sample was dissected after the test.

A typical curve of cable sheath temperature is given in Figure 4, showing that the maximum temperature experienced by the cable does not exceed 100°C. In addition the dissected cable sample did not show any visible degradation of the cable components. A cable laying field test under actual conditions has confirmed these results.

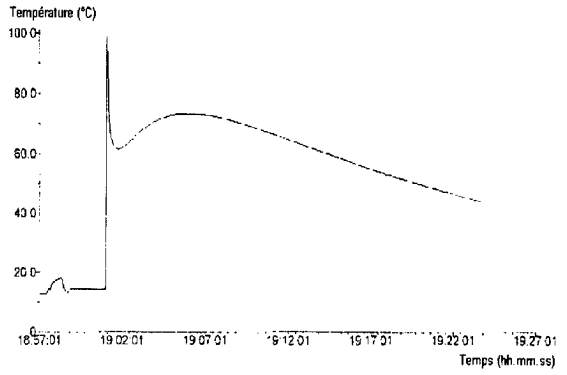

Figure 4, Short Term, High Temperature Test

Extension to other fiber counts

This philosophy can be extended to different fiber counts. A theoretical analysis has been conducted for up to 216 fibers for duct type, dielectric designs. The results are presented in Table 5 in terms of cable OD, linear weight and bending performance. These results correspond to a cable design having a tensile resistance with two times the cable linear weight and a minimum of 0.4% for the nominal tensile strain free window. The bending diameter is related to the capability of the CSM. It is important to note for these designs that the crush resistance may vary according to the cable size. The outer sheath thickness has been adapted according to the cable OD, to approximately 10% of its value.

Table 5: Extension to Higher Fiber Counts

Cable Type	OF Count	OD (mm)	Weight (g/m)	Density (f./mm^2)	Bending dia. (mm)
LT	60	8.2	50	1.15	100
LT	72	10	85	0.92	150
UT	72	7.9	45	1.47	160
LT	96	12	115	0.85	170
UT	96	8.4	52	1.73	170
LT	144	15	200	0.81	170
UT	144	9.3	65	2.12	190
LT	216	16	200	1.22	170

These results show substantial advantage over the standard design. The fiber density in the cable being minimized for intermediate higher fiber counts (one layer of cables having more than 6 tubes) due to the nature of the structure (need to upjacket the CSM to strand the tube, which is lost space). For these medium count ranges, however, such a solution seems less attractive in terms of density than the designs commonly proposed for distribution cables (ribbon or microtube structures).

For the central tube design, a limitation of the fiber count is given by the identification limits due to the ring marking code. Up to 144 fibers were cabled using a 6 mm central tube corresponding to 9.3 mm OD, which leads to a fiber density of 2.12 fiber/mm^2.

CONCLUSION

A cable design optimization process can be further enhanced to a new level, selecting less harsh environments for cable deployment and considering that cable performance needs to be matched to the installation/operating conditions.

To illustrate, a loose tube and a central tube cable containing up to 60 or 72 fibers, with an outer diameter of less than 8.5 mm have been developed and have shown excellent performance while offering very small and compact designs. These optimized designs are intended to be installed in protected environments, such as a rigid trench or ducts using blowing techniques and are particularly well suited to some new emerging rights of way.

REFERENCES

(1) "A very innovative technology for right of way application", JP. Bonicel et al. 1998 IWCS proceedings

(2) "Rodent protected dielectric cables: where is the solution?", P. Gaillard et al., 1995 IWCS proceedings

AUTHORS

Pierre Gaillard
Optical Fiber
Cable Competence
Center
Alcatel
Claremont,
NC - USA

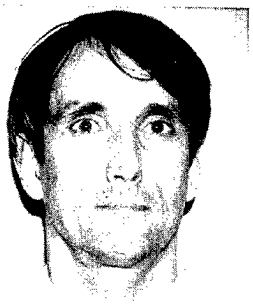

Pierre Gaillard received his engineer degree from the Ecole Catholique des Arts et Métiers (ECAM) in 1980. He joined Les Câbles de Lyon, now Alcatel, in 1983. He is now Deputy Manager with responsibility for the Design Technology Group.

David Benzel,
Alcatel
536 quai
de la Loire
62225 Calais
Cedex, FRANCE

Dave J. Benzel born in Buffalo, NY, USA in 1965, received his B.S. degree in Electrical Engineering from Clarkson University in 1987. He has held several positions in Field Engineering, Plant Engineering and Product Development after joining Alcatel in 1991. Since May of 1997 he has held the position of Technical Manager for the manufacturing facility in Calais, France.

Olivier Tatat
Optical Fiber
Cable Competence
Center
Alcatel
Claremont,
NC, USA

Olivier Tatat received his engineering degree from the Institut des Sciences de l'Ingénieur de Montpellier (ISIM) in 1982. He joined Les Câbles de Lyon, now Alcatel, in 1985. He now works as Technology Manager, in charge of the Materials Group, in the Alcatel Optical Fiber Cable Competence Center.

Klaus Nothofer,
Alcatel
Bonnenbroicher
Strasse 2-14
41048
Mönchengladbach
Germany

Klaus Nothofer obtained his Dipl.-Ing. Degree from the Fachhochschule Düsseldorf and joined AEG Kabel, now Alcatel, in 1981. He is head of the engineering for telecommunication cables of Alcatel TPLE. He is responsible for the coordination of the engineering of the Alcatel European optical fiber cable factories.

Dr. Alexander Weiss
Alcatel
Bonnenbroicher
Strasse 2-14
41048
M önchengladbach
Germany

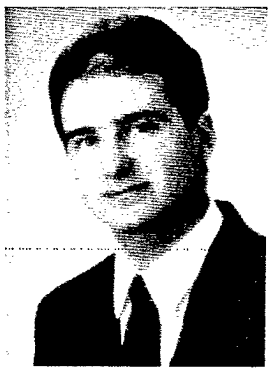

Dr. Weiss obtained his degree of graduated chemist from the University of Tübingen in 1990. He joined AEG Kabel in 1990, now Alcatel. He is in charge of optical fiber cable development and is responsible for the materials engineering for the Alcatel European optical fiber cable Units.

Development of Optical Fiber Ribbon Units for Fiber Blowing

Masato Kosaka, Ichiro Kobayashi, Fumiki Hosoi,
Hideaki Kanzaki, Hideyo Hiramatsu, Yasuhiro Kamikura

Opto-Technology Laboratory, The Furukawa Electric Co., Ltd.
6, Yawata Kaigandori, Ichihara, Chiba, Japan

Abstract

Higher fiber density and lower cost are demanded of the optical fiber units for fiber blowing as of other optical fiber cables. Besides, good workability such as easy unit jacket removal without any tool is desired.

In order to satisfy these demands, we designed, manufactured and evaluated 8, 16, 20 and 24 optical fiber units for fiber blowing, using 4-fiber ribbons. The units can be efficiently and economically spliced by mass-fusion splicing technique. As for the fiber density, the units we developed have one of the highest fiber density and the 24-fiber unit is the highest fiber count which has been reported. As for the low cost, these units can be economically manufactured from ribbon fibers by one process, because the unit jacket are all made of thermoplastic materials.

Excellent results were obtained in the evaluation of not only temperature, mechanical and installation characteristics but also long-term reliability. It was verified that the developed units are suitable for practical use.

1. Introduction

Fiber blowing is to feed an optical unit into a tube of a pre-installed tube cable by the flow of gaseous medium. (The fiber blowing technique configuration is shown in figure 1.) This technique can be applied to various applications, such as optical local area networks in buildings and distribution networks.

The units using fiber ribbons are superior to the units using mono-coated fibers in term of fiber density, low cost and mass splicing.

Therefore we developed the fiber ribbon units.

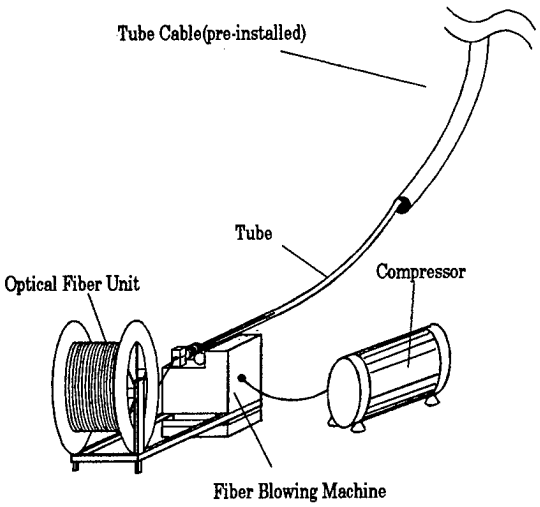

Figure 1. The fiber blowing technique configuration

2. Units Design

We designed the units taking into account the following points.

(1)Use of fiber ribbons to realize higher fiber density, highest fiber count, low cost and mass splicing

(2)One process manufacturing in order to realize low cost

(3)Considerations of materials and structure of coating in order to achieve its easy removal without tools

(4)Structure to attain low fiber strain when the unit is wound on a reel

As to (1), we used 4-fiber ribbons whose width is 1.1mm and thickness is 0.3mm.

As to (2), we realized one process manufacturing, by selecting thermoplastic jacket materials

As to (3), we improved the jacket removal by selecting special jacket materials and by providing notches on unit surface. (figure 4) As results of these improvements, we could remove the unit jacket for more than 1m along the notches from the unit end. The jacket removal takes two steps. First, a small cut was made to the end of the unit on the notches by scissors and then the cut jacket halves are pulled apart. (figure 2) Besides, the unit jacket can be also removal for mid-span access using a special tool.

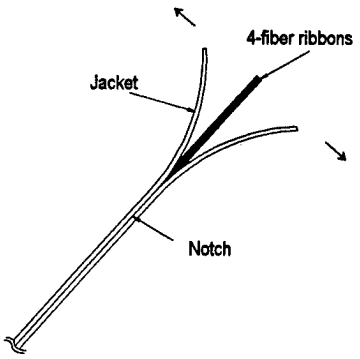

Figure 2. Jacket removal

As to (4), we decided not to strand the ribbon stack after the following considerations.

Figure 3 Shows the different positions of the ribbon stack relative to the reel surface. In this case, the ribbon stack of 20 fibers is stranded clockwise. The fibers which suffer the most bending strain among those positions are shown by black dots at position B and D, where the diagonal of the ribbon stack is perpendicular to the reel surface, the edge fibers marked by black dots suffer the most bending strain because the distance to the bending center of the ribbon stack becomes the farthest for these fibers. Besides the bending strain, fibers also suffer the strain caused by the stranding torsion.

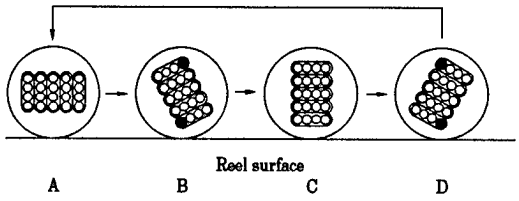

Figure 3. Ribbon stack positions of stranding unit (20-fiber unit)

Figure 4 shows the typical ribbon stack positions when the ribbon stack is not stranded. In this model, the ribbon stack relative to the ribbon surface is assumed not to change throughout the whole unit length. The fibers of most strain for each position are also shown by the black dots.

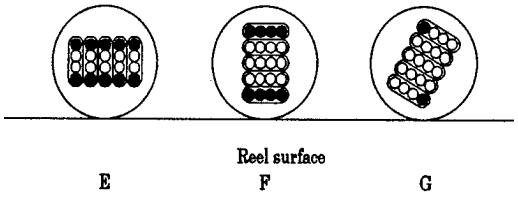

Figure 4. Ribbon stack positions of non-stranded unit (20-fiber unit)

The maximum fiber strain was calculated at different ribbon stack positions for the two types of units, one being the stranded type, the other being

the non-stranded type. The results are shown in table 1.

Table 1. Fiber strain at the strain maximum position (%)

	Stranded			Non-stranded		
	Pitch (mm)			Condition (fig.4)		
	100	500	1000	E	F	G
8	0.62	0.35	0.34	0.27	0.11	0.29
16	0.77	0.49	0.48	0.27	0.34	0.43
20	0.87	0.59	0.58	0.27	0.45	0.53
24	1.00	0.69	0.68	0.27	0.57	0.63

We confirmed that the non-stranded unit suffers smaller strain than stranded unit because of the lack of the stranding torsion. For the 8-fiber unit, the optimal position is F where each ribbon is placed parallel to the reel surface. For the unit with more than 16 fibers, the optimal position is E where each ribbon is placed perpendicular to the reel surface.

3. Units Structures

The developed units consist of stacked 4-fiber ribbons, jacketed with thermoplastic materials such as foamed polyethylene. The structures of the developed 8-, 16-, 20- and 24-fiber units are shown in figure 5.

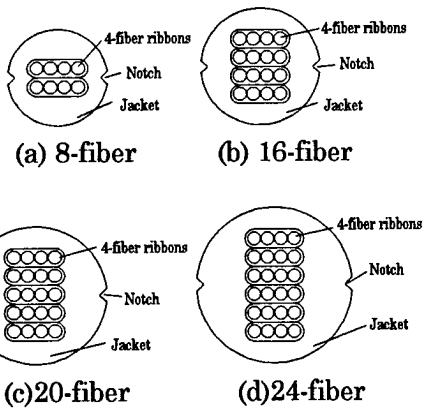

(a) 8-fiber (b) 16-fiber

(c)20-fiber (d)24-fiber

Figure 5. Structure of developed units

The unit diameters, weight and fiber density are shown in table 2. As for the fiber density, the units we developed have one of the highest fiber density and the 24-fiber unit is the highest fiber count which has been reported

Table 2. Unit diameters, weight and fiber density

	diameter (mm)	weight (g/m)	density (F/mm^2)
8	1.8	2.2	3.1
16	2.2	3.4	4.2
20	2.5	4.3	4.1
24	2.9	5.4	3.6

4. Characteristics

4.1 Attenuation, Temperature and Mechanical Characteristics

The attenuation and temperature and mechanical characteristics of each unit were evaluated. The results are shown in table 3. Excellent results were obtained for each test.

Table 3. Attenuation, temperature and mechanical characteristics

Item	Condition	Result(1550nm)
Attenuation	OTDR	≦0.22dB/km
Temperature cycling	-30～70℃ 10cycles	<0.03dB/km
Crush	150N/20mm	No change
Bend	R=25mm	No change
Torsion	±360° /1m	No change

*No. of fibers in unit: 8, 16, 20 and 24

4.2 Jacket Removability

The jacket removability tests were carried out by the method explain in section 2. The results are shown in table 4. We confirmed that the units have a good jacket removability.

Table 4. Results of jacket removability

No. of sample	20
Removal length	1m
Removal time	<30sec.
Sample condition	No fiber breakage
	No ribbon peeling

*No. of fibers in unit: 8, 16, 20 and 24

4.3 Installation Characteristics

4.3.1 Installation into a cable on a reel

Each unit was installed by fiber blowing technique into a 10-tube cable which is composed of 4.5mm in inner diameter and 6.0mm in outer diameter tubes. The cable is 500m long and wound on a 1m diameter reel. The initial installation speed was about 20m/minutes. The installation time and the attenuation (at 1550nm) of each unit were measured after installation. The results are shown in figure 6. It was found that all the units were completely installed in less than 25 minutes without a loss of installation speed and that their attenuation after the installation was not increased from the initial state at all.

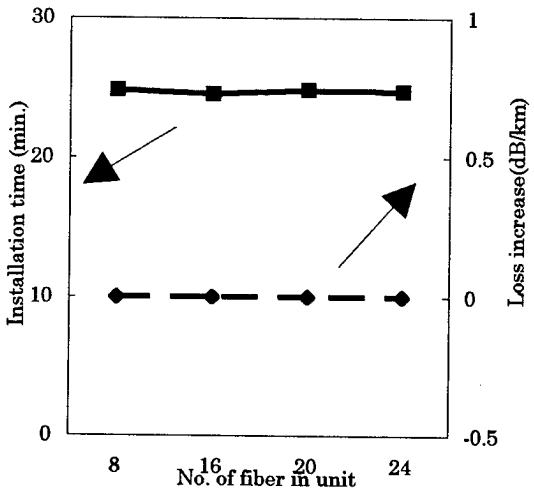

Figure 6. Results of installation into a cable on a reel

4.3.2 Installation into a long tube

The 24-fiber unit was installed by fiber blowing technique into a single tube (4.5mm in I. D. and 6.0mm in O. D.). 1000m long was wound on a 1.6m diameter reel. The initial installation speed was about 20m/minutes. The installation time and the attenuation (at 1550nm) of the unit were measured after installation. The result is shown in figure 7. It was found that the unit was completely installed in about 66 minutes and that its attenuation after the installation had remained unchanged from the initial state.

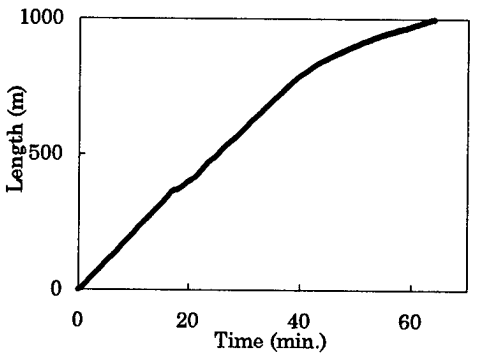

Figure 7. Result of long tube installation (24-fiber unit)

4.3.3 Installation into a vertically pre-installed cable

Each unit was installed into a 10-tube cable, 85m long, vertically pre-installed in a building, which is equivalent to 25-story. The initial installation speed was about 20m/minutes. The installation time of each unit was measured. The results are shown in figure 8. It was found that all the units was completely installed without a loss of installation speed.

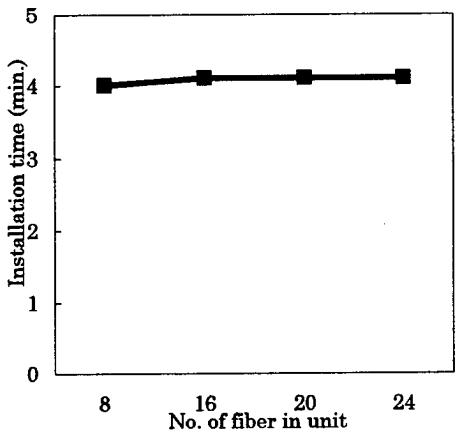

Figure 8. Results of installation into a vertically pre-installed cable

4.4 Long-term Reliability

The 24-fiber unit wound on a reel and the 10-tube cable wound on a 1m diameter reel were subjected to 100 cycles of temperature from -30 to +70℃. We compared the installation performance of different combinations of units and cables which have or have not gone through the temperature cycling. The installation time and the attenuation (at 1550nm) of the unit were measured after installation. The results are shown in table 5. We confirmed that the installation performance is excellent and stable even after temperature cycling is given to both unit and cable.

Table 5. Results of long-term reliability

		Cable given temp. cycle	
		0-cycle	100-cycle
Unit given temp. cycle	0-cycle	24.7 ≦0.22	24.5 ≦0.22
	100-cycle	24.5 ≦0.22	24.9 ≦0.22

The upper: installation time (min.)
The lower: attenuation after installation (dB/km)

5. Conclusions

We designed, manufactured and evaluated high density, high fiber count, low cost 8, 16, 20 and 24 optical fiber units for fiber blowing using 4-fiber ribbons. Excellent results in various characteristics tests and good unit jacket removability were obtained. We conformed that the developed units possess suitable characteristics for practical use.

6. References

(1)S. Furukawa et al., 2nd Optoelectronics & Communications Conference technical digest, 9EP-21, 1997
(2)M. Kosaka et al., Proceedings of the 1997 IEICE society conference, B-10-13
(3)M. Kosaka et al., Proceedings of the 1998 IECE general conference, B-10-54
(4) M. Kosaka et al., 3rd Optoelectronics & Communications Conference technical digest, 13D2-5, 1998

Authors

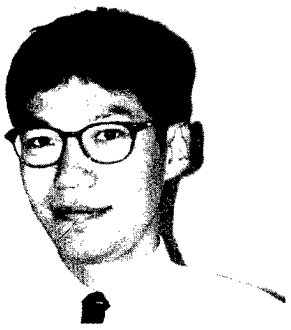

Masato Kosaka
The Furukawa Electoric Co., Ltd.
6, Yawata Kaigandori Ichihara, Chiba
290-8555, Japan

Masato Kosaka received his B.E. degree in Electronic Engineering from Ryukyu University in 1989. He joined The Furukawa Electric Co., Ltd. in 1989 and has been engaged in the development of optical fiber and cables. He is now a research engineer of Opto-Technology Laboratory. He is a member of the Institute of Electronics, Information and Communication Engineers of Japan.

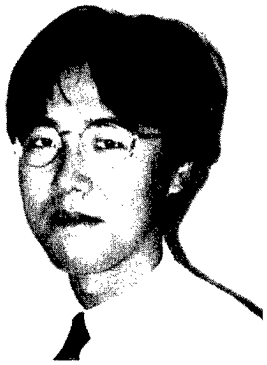

Fumiki Hosoi
The Furukawa Electoric Co., Ltd.
6, Yawata Kaigandori Ichihara, Chiba
290-8555, Japan

Fumiki Hosoi received his M.E. degree in Physics Engineering from Tokyo University in 1995. He joined The Furukawa Electric Co., Ltd. in 1995 and has been engaged in the development of optical fiber and cables. He is now a research engineer of Opto-Technology Laboratory. He is a member of the Institute of Electronics, Information and Communication Engineers of Japan.

Ichiro Kobayashi
The Furukawa Electoric Co., Ltd.
6, Yawata Kaigandori Ichihara, Chiba
290-8555, Japan

Ichiro Kobayashi received his B.S. degree in Physics from Chuou University in 1986. He joined The Furukawa Electric Co., Ltd. in 1986 and has been engaged in the development of optical fiber and cables. He is now a senior research engineer of Opto-Technology Laboratory. He is a member of the Institute of Electronics, Information and Communication Engineers of Japan.

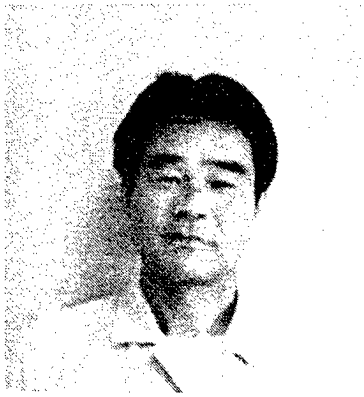

Hideaki Kanzaki
The Furukawa Electric Co.,Ltd.
6,Yawata Kaigandori Ichihara, Chiba
290-8555, Japan

Hideaki Kanzaki joined The Furukawa Electric Co., Ltd. in 1969 and has been engaged in research and development of optical fiber cables. He is now a senior research engineer of Opto-Technology Laboratory. He is a member of the Institute of Electronics, Information and Communication Engineers of Japan.

Hideyo Hiramatsu
The Furukawa Electoric Co., Ltd.
6, Yawata Kaigandori Ichihara, Chiba
290-8555, Japan

Hideyo Hiramatsu received his B. E. degree in Electronic Engineering from Kyoto University in 1984. He joined The Furukawa Electric Co., Ltd. in 1984 and has been engaged in research and development of optical fiber cables. He is now a senior research engineer of Opto-Technology Laboratory. He is a member of the Institute of Electronics, Information and Communication Engineers of Japan.

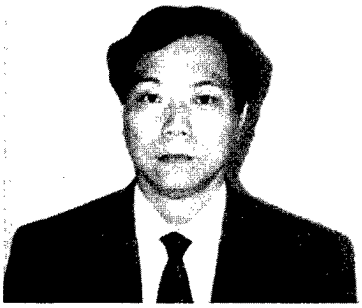

Yasuhiro Kamikura
The Furukawa Electric Co.,Ltd.
6,Yawata Kaigandori Ichihara, Chiba
290-8555, Japan

Yasuhiro Kamikura received his B.E. degree in Electronic Engineering from Tokyo University in 1975 . He joined The Furukawa Electric Co., Ltd. in 1975 and has been engaged in the development of optical fiber and cables. He is now a general manager of Opto-Technology Laboratory. He is a member of the Institute of Electronics, Information and Communication Engineers of Japan.

MODELING OF PROOF TEST LEVEL FLAWS USING CUBE CORNER INDENTS

S.L. Semjonov*^, G.S. Glaesemann#, C.R. Kurkjian+ and M.M. Bubnov*

*FORC, GPI, Russian Academy of Sciences, Moscow, Russia
#Corning, Inc, Corning, New York 14831
+Bellcore, Morristown, New Jersey 07960
^Work performed while on leave at Bellcore

ABSTRACT

Proof test level flaws in lightguide fibers have been modeled using radial cracks in flat silica fibers. These cracks were produced using a diamond cube corner indenter with loads from 0.2 to 10 grams. Room temperature strengths (σ_{RT}) from 150 to 500 MPa with Weibull m-values of 30-70 were obtained (stress rate ($\dot{\sigma}$) = 0.12 GPa/s). It was found that $\sigma_{RT} \sim P^{-1/3}$ as predicted theoretically. The ratio of liquid nitrogen to room temperature strengths ($\sigma_{IN_2}/\sigma_{RT}$) was found to be approximately 2. The strengths of these indented fibers were measured at high stress rates. In these tests the strength appears to saturate at approximately the liquid nitrogen value at approximately 10^4 GPa/s). The full strength/stress rate curve can be approximated by a two-region semi-log plot. This indicates that the two regionmodel suggested by Glaesemann et al[1,2], is real.

INTRODUCTION

Most standard telecommunication lightguide fibers now are proof tested at 700 MPa. This strength corresponds to a flaw size of ~1 μm. The high quality fibers produced today rarely have such flaws and thus it is difficult to study them in detail. However, since an understanding of these flaws is important for the prediction of the lifetime of such fibers, synthetically produced flaws usually are employed. Such flaws have been produced both by abrasion[3,4] and by the fusion of refractory particles[5,6] onto the fiber surface. Both techniques show a rather broad distribution of strengths and therefore they contain a broad distribution of flaw sizes. While it has been suggested that real production fibers may in fact contain a very wide distribution of flaw behavior[7], it is necessary to study simple flaw types separately in order to understand their behavior fully. For these reasons, we have chosen to study a well- characterized proof test level flaw – one produced by indentation with a diamond cube corner indenter. Using indenting loads from 0.2 to 10 grams we are able to span the range of strengths of interest.

The normal model for the study and prediction of fiber lifetimes is a single region power law model. Recently Glaesemann, et al.[1,2] have suggested the existence of a region II-like behavior in abraded (~700 MPa) fibers. This gives rise to two values of n (the stress corrosion susceptibility factor) and B (the strength retention factor). It is very important to verify this finding since it has substantial impact on the lifetime predictions of such fibers.

EXPERIMENTAL

Fibers with two flat sides were drawn especially for these experiments in order to simplify the indentation process. The polymer coating was removed with hot sulfuric acid from 2-3 cm of the center of the fiber sample and a single indent was made. Indentations were made using a low load indentation instrument[8] and a diamond cube corner indenter[9]. This indenter produces a triangular-shaped impression with radial cracks extending from the three corners. The indentation was made so that one of the radial cracks was perpendicular to the fiber axis. A drop of ink on the fiber surface near the indent enabled one to locate the position of the indentation. Tensile strength measurements at moderate stress rates were made with a commercial tensile tester[10] and static fatigue measurements were made using a set-up as described by Krause[11]. The high stress rate measurements were made with the instrument described by Glaesemann[2,12].

RESULTS

Figure 1 shows a Weibull plot of room temperature strength ($\dot{\sigma}$~ 0.12 GPa/s) for various indentation loads. Figure 2 is a plot of strength versus indentation load. As indicated earlier[13], loads which result in a given strength are two orders of magnitude less with a cube

corner indenter than with a Vickers indenter. It can be seen that the theoretically expected[14] $\sigma \sim P^{-1/3}$ relation is obeyed. Figures 3 and 4 show AFM and SEM images of these indents. Figure 5 is a combined plot of dynamic and static fatigue at room temperature and approximately 50 % relative humidity. This is a power law (log-log) plot and indicates that within experimental error two n-values are required. While it might be expected that a semi-log (exponential) plot would give a single straight line, this was found not to be the case (see Figure 9). Figures 6 and 7 are the data obtained with the high stress rate equipment described earlier by Glaesemann[2,12]. As can be seen, while the log-log plot of these data seems to require three regions, a semi-log plot can be satisfactorily fit with two regions. The fit to an exponential law is in agreement with the results of Muraoke and Abe[15]. As indicated earlier however, they did not find region II behavior in tests on 50 μm flaws. In Figure 8, data on fibers with two different strength levels (1 and 2 gram indents) have been shifted and are found to coincide. In Figure 9, all of the data on 1 gram indented fibers have been combined on a semi-log plot. In this plot, the open circles and open squares represent the data shown earlier in Figure 5.

DISCUSSION

As can be seen from the above data, the use of a cube corner indenter gives strengths which correspond roughly to the proof test levels currently employed. The fit of the data to a single $\sigma \sim P^{-1/3}$ line indicates that all of these indentation loads produce post-threshold flaws. Flaws resulting in inert strengths of approximately 700 MPa require a load of approximately 0.5 grams, while the development of room temperature strengths of this order requires loads of only approximately 0.06 grams. With these latter loads it is likely to be difficult to get good uniformity in the indentation process. In addition, modifications to the present tensile testing technique may be needed to maintain the mounting damage below that of the indentation damage. In this case, bending techniques as used by Lin and Matthewson[14] might be used. As pointed out earlier, the development of 'proof test' level flaws at such low indentation loads also emphasizes the need for extreme care in the handling of bare silica fibers.

In the regime of 'ordinary' times to failure, 1 to 100,000 seconds for fibers with strengths approximately 200 – 300 MPa, it was found that two n-values (44 and 21) are required to fit the data within experimental error (a bend also was present in an exponential plot). At this strength level, the transition from one n-value to another occurs at t ~ 50 seconds, but will be found to shift to shorter (longer) times for stronger (weaker) fibers. This may at least partly explain the variability found in the n-values for 'low strength' fibers[16,17,18]. Since the indents that produced the cracks studied here result from irreversible deformation, there are residual stresses associated with these cracks. Ordinarily this is expected to affect the magnitude of the n-value observed[19,20]. It is not clear whether such an effect is influencing the results observed here. While the exact representation of the moderate stress rate range are somewhat in doubt, the appearance of a second regime, a so-called 'region II – like' behavior, seems to be definitely confirmed.

Thus, in addition to the illustration of the advantages of such indentation techniques, this work reinforces the findings of Glaesemann, et al.[1,2], that a second region appears in the strength-stress rate curves at a stress rate of ~ 1 to 10 GPa/s for fibers having strengths of ~ 200 to 700 MPa. While these data actually appear to indicate a third region at intermediate stress rates ($\dot{\sigma} \sim 10^{-1}$ GPa/s), on an exponential plot this region is eliminated.

CONCLUSIONS

We have shown that by using a cube corner indenter, strengths of the order of normal proof test levels can be obtained, with tight distributions (Weibull m ~ 30-70). The fatigue behavior of such indented fibers (σ ~ 300 MPa) indicates a transition in behavior at moderate stress rates (failure times ~ 50 seconds) and may partially explain the apparent variability in the reported n-values for such low strength fibers.

High stress rate experiments show an apparent 'region II' behavior and a saturation of the strength at ~ 90% σ_{IN_2} for a stress rate of ~ 10^4 GPa/s. This indicates that the 'two-region' model of Glaesemann, et al.[1,2] must be considered in evaluating proof test parameters. Additional studies are required in order to fully predict long time behavior .

REFERENCES

1. T.A. Hanson and G.S. Glaesemann, J. Mat. Sci., **32**, 5305 – 5311 (1997).
2. P.T. Harvey, T.A. Hanson, M.G. Estep and G.S. Glaesemann, Proc. IWCS, 883- 888 (1997).
3. G.S. Glaesemann, Proc. IWCS, 698-704 (1992).
4. M.M. Bubnov, E. M. Dianov and S.L. Semjonov, Mat.Res. Soc. Symp. **244**, 97-101 (1992).
5. D.J. Wissuchek, MRS Proc. #531 (1998).
6. T. Breuls and T. Svensson SPIE, **2074**, 78 (1994).
7. C.R. Kurkjian, Mat.Res.Soc. Proc. **531** (1998).
8. Leco, Model M-400-G3, St. Josephs, MI 49085-2396.
9. Nano Instruments, Oak Ridge, TN 37830.
10. Instron, Canton, MA 02021.
11. J. T. Krause, and C. Shute, Adv. Ceram. Matls.,**3**, 118-121 (1988).
12. G. S. Glaesemann, Proc. SPIE, **2611**, 38-44 (1995).
13. C.R. Kurkjian S.L. Semjonov and O.S. Gebizlioglu, Proc. NFOEC, 73-80 (1997).
14. B. Lin and M. J.Matthewson, Phil. Mag., **74**, 1235-1244 (1996).
15. M. Muroake and H. Abe, Mechanics and Materials for Electronic Packaging, **1**, 141, ASME (1994).
16. C.R.Kurkjian, J.T. Krause and M.J. Matthewson, J. Lightwave Tech. **7**, 1360-1370 (1989).
17. M.M. Bubnov and S.L. Semjonov, Proc. MRS #531 (1998).
18. D. B. Marshall and B. R. Lawn, J. Am. Ceram. Soc., **63**, 532 (1980).
19. B.L. Symonds, R. F. Cook and B.R.Lawn, J. Matls,. Sci, **18**, 1306 (1983).

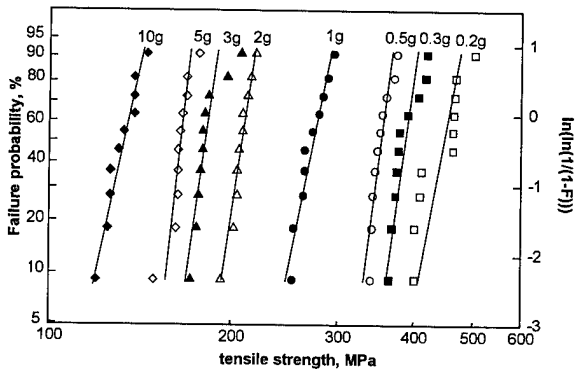

Figure 1. Strength of indented fibers at different indentation loads. Stress rate ~ 0.12 GPa/s; relative humidity ~ 50%.

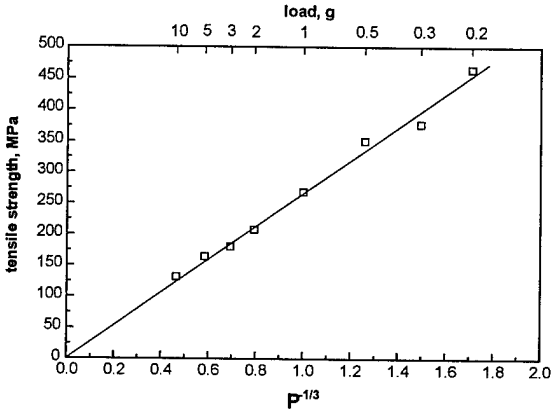

Figure 2. Dependence of median strength of indented fibers on indentation load.

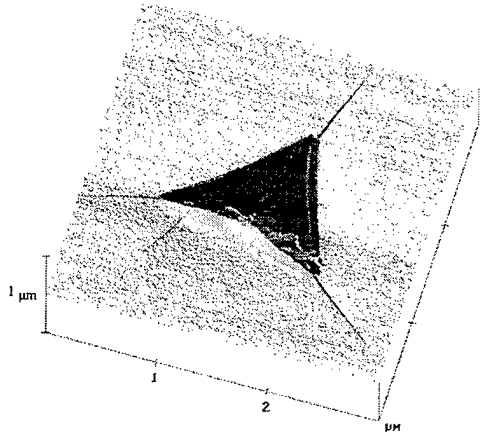

Figure 3. AFM image of 1 gram indent.

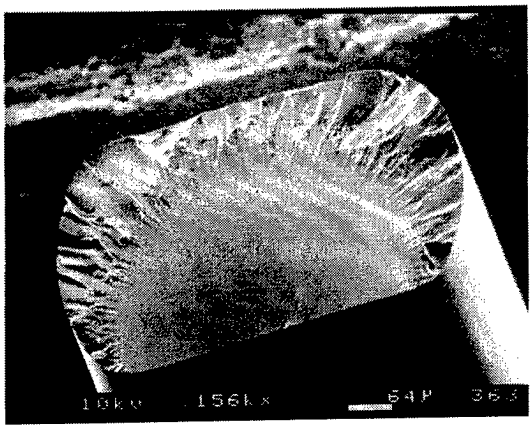

Figure 4. SEM image of fiber indented with 10 gram load.

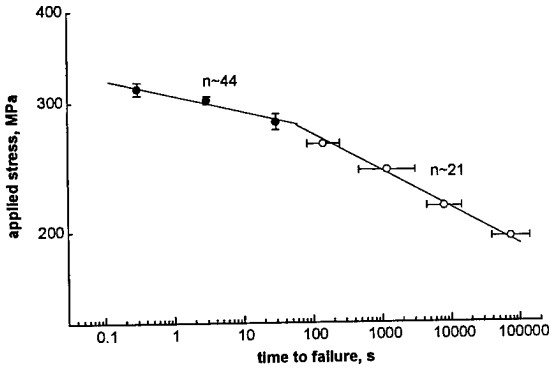

Figure 5. Combined plot of dynamic and static fatigue of 1 gram indented fiber at room temperature and ~ 50% RH (● - dynamic fatigue; ○ - static fatigue).

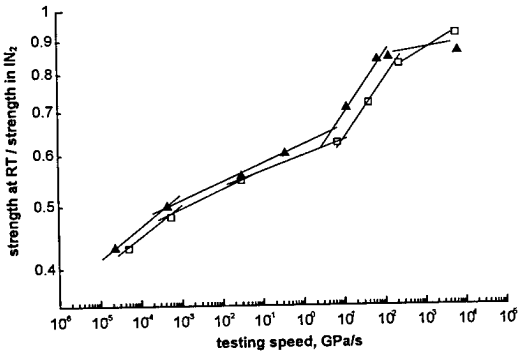

Figure 6. Median strength of indented fibers with high speed tester. (log-log plot).
□ - 1 gram indent; ▲ - 2 gram indent.

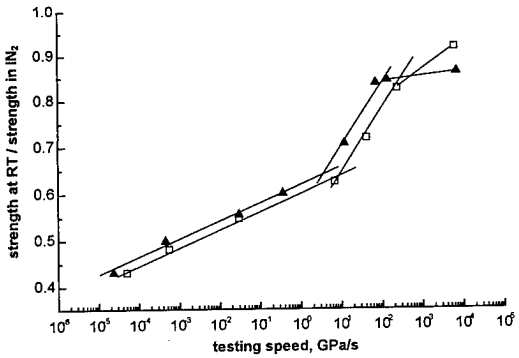

Figure 7. Median strength of indented fibers with high speed tester (semi-log plot).
□ - 1 gram indent; ▲ - 2 gram indent.

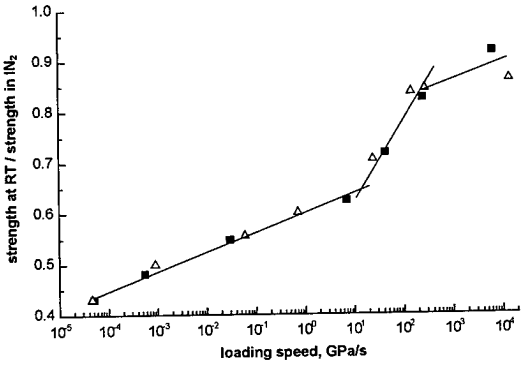

Figure 8. Median strength of indented fiber with high speed tester (semi-log plot). □ - 1 gram indent; ▲ - 2 gram indent (recalculated).

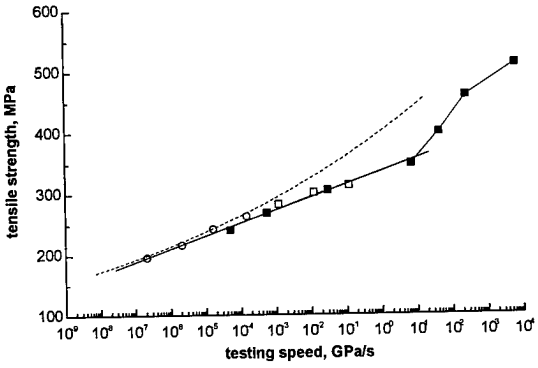

Figure 9. Combined plot of dynamic and static fatigue and high speed testing for 1 gram indented fiber. ■ - high speed; □ - dynamic fatigue; ○ - static fatigue; - - - - n = 21.

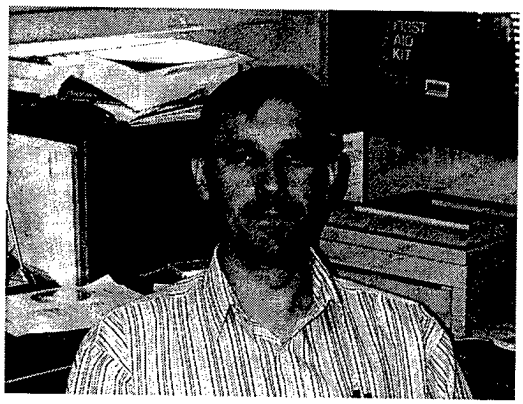

Sergei L. Semjonov graduated from the Moscow Physical -Technical Institute in 1982 and received his PhD in physics from the General Physics Institute in 1997. Since 1982 he has been employed by the Fiber Optics Research Institute of the Russian Academy of Sciences in Moscow. It has since been transformed into the Fiber Optics Research Center (FORC). He is head of the fiber drawing group.

Charles R. Kurkjian received his B.Sc. from Rutgers in 1955 and his ScD from M.I.T. in 1955. In 1994 he retired as a Distinguished Member of Technical Staff from A.T.&T. Bell Labs after 35 years service. Since that time he has been with Bellcore in the Fiber Media and Components Group.

G. Scott Glaesemann is a senior development engineer at Corning's Sullivan Park technology center and has been with Corning since 1986. He received his M.S. and Ph.D. from the University of Massachusetts and his B.S. from North Dakota State University.

Mikhail M. Bubnov graduated from Moscow State University in 1970 and in 1978 received the Candidate of Science degree in physics from the P.N. Lebedev Physical Institute of the Academy of Sciences of the USSS. He is currently head of the fiber group at (FORC).

BREAK SOURCE ANALYSIS: ALTERNATE MIRROR MEASUREMENT METHOD

Linda K. Baker and G. Scott Glaesemann

Corning Incorporated, Corning, New York

ABSTRACT

Break source analysis (BSA) refers to the methods used to determine the cause of failure in optical fiber. Integral to this assessment is the determination of the magnitude and mode of stress at failure. It is common to use the measured mirror radius to calculate the stress at failure. However, bending and torsional stresses can alter the mirror shape, thereby introducing significant uncertainties to the stress determined by this method. This paper describes an alternate mirror measurement technique and associated mirror constant that reduces uncertainties in the calculated failure stress.

Optical fibers of varying diameters (80, 125, and 250 microns) were abraded and tensile tested to failure. The break ends were inspected under an optical microscope and the mirror radii were measured using the traditional method and the chord method. These mirror dimensions were plotted as a function of breaking stress. This study shows that the radius determined by the mirror chord measurement follows a similar relationship as the traditional radius measurement, but is less influenced by non-tensile stresses.

INTRODUCTION

Fracture behavior in glasses has been studied extensively, and the use of break source analysis to determine the mode of failure is common practice. During the fracture process, the crack grows from its original flaw size until it approaches terminal velocity, at which point the surface becomes increasingly roughened by mist, hackle, and eventually crack branching.[1] The mirror region is the smooth portion of the crack surface that is surrounded by the mist and hackle.[2] This behavior is well documented in the literature,[3-5] and illustrated in Figure 1.

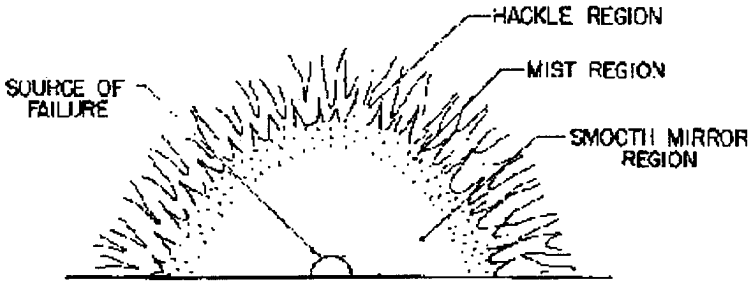

Figure 1. Schematic of fracture surface.[5]

The distance from the origin to the mirror-mist boundary can be related to the level of stress on the material at failure. It has been shown that the following equation describes the relationship between the mirror size and fracture stress:[6]

$$\sigma_f = \frac{A}{\sqrt{r}} \qquad (1)$$

where σ_f is the fracture stress, r is the mirror radius, and A is the mirror constant. Mirror constants have been measured for many materials,[1] and have been shown to be independent of the rate and mode of loading.[3] If the fracture data is gathered from testing under constant stress, then good agreement is found between various investigators for the mirror constant.[7] For silica, the mirror constant has been measured to be 2.1 $MPa \cdot m^{1/2}$ to 2.23

$MPa \cdot m^{1/2}$.[5,8] In the case of optical fiber the mirror radius, r, traditionally is taken as the distance from the origin to the mirror-mist boundary on a line from the origin through the center of the fiber as shown in Figure 2. The mirror constant for this measurement technique on optical fiber is 1.89 $MPa \cdot m^{1/2}$.

It has been noted[6] that bending causes non-uniform stress gradients in the sample, and therefore, distortion in the mirror shape can occur. For this reason, it was suggested that the mirror radii must be measured along the tensile surface in order to avoid stress gradients.[3] However, other researchers have advised against measuring the mirror radius along a free surface of the sample since surface damage and edge effects can alter the radius measurement.[2,7] This work seeks to validate the use of the chord method of mirror measurement for optical fiber, which does reference the edge of the specimen, as well as to determine the effect of bending stress on this measurement technique.

EXPERIMENTAL PROCEDURE

Single-mode silica-clad optical fibers of three diameters (80, 125, and 250 microns) were drawn and coated with a standard polymer coating. In order to obtain strengths in the region of interest, fibers were abraded either by particle abrasion or a sharp blade before loading to failure in tension. Prior to abrasion a 10 cm length of the polymer coating was chemically removed using methylene chloride. The 80 and 250 micron fibers were used to expand the range of observable mirrors. The 250 micron fiber allows for better resolution in the low strength region and the 80 micron fiber was found to have more surviving mirrors at elevated strength levels than the 125 micron fiber. A total of 123 specimens were tested at a strain rate of 25%/min. This strain rate allows a significant amount of fatigue before failure, thereby minimizing any influence of contact residual stresses on the fracture mirror. The mirror radius measurements were performed using magnifications of 200x, 400x, 600x, or 1000x. The mirror size determined the maximum magnification possible while still viewing the full mirror. Mirror measurements were collected using the traditional radius measurement method, illustrated in Figure 2, as well as the chord measurement method, illustrated in Figure 3.

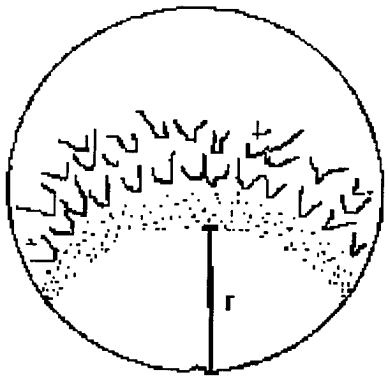

Figure 2. Traditional radius measurement.

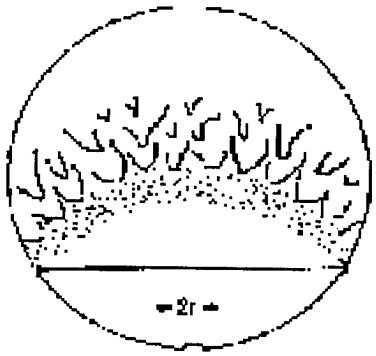

Figure 3. Chord radius measurement. (Radius = Chord/2)

In order to investigate the effect of both tensile and bending stresses on the fracture surface, samples of 125 micron fiber were chemically stripped as before, then the stripped portion was wrapped around a 41 mm diameter mandrel, resulting in 213 MPa (31 kpsi) maximum bending stress. A static weight was applied to the hanging portion of the fiber in order to supply the tensile stress. A flaw then was introduced on the stripped section of the fiber using a razor blade; care was taken to ensure the flaw was placed in the region of the fiber that would be exposed to the maximum bending stress. The sample was allowed to hang until the fiber broke via fatigue. Fracture surfaces were examined and the mirrors measured using the same equipment and techniques described earlier. Fifteen samples were obtained, with tensile stresses ranging from 221 to 517 MPa (32 to 75 kpsi).

RESULTS AND DISCUSSION

The results for the tensile testing are shown in Figure 4. The radius measured using the traditional method is labeled *traditional*, while the radius measured using the new chord method is labeled *chord*.

The mirror constants were determined for both measurement techniques by determining the mirror constant for each specimen according to Equation (1) and selecting the median value. The mirror constants determined by this method are shown in Table 1. The predicted strength versus mirror curves have been added to Figure 4 for both mirror measurement methods.

Table 1.

	Median $MPa \cdot m^{1/2}$ ($kpsi \cdot \mu m^{1/2}$)	**Standard Deviation** $MPa \cdot m^{1/2}$ ($kpsi \cdot \mu m^{1/2}$)
Traditional Method	1.96 (284.0)	0.13 (18.4)
Chord Method	1.72 (249.5)	0.15 (21.9)

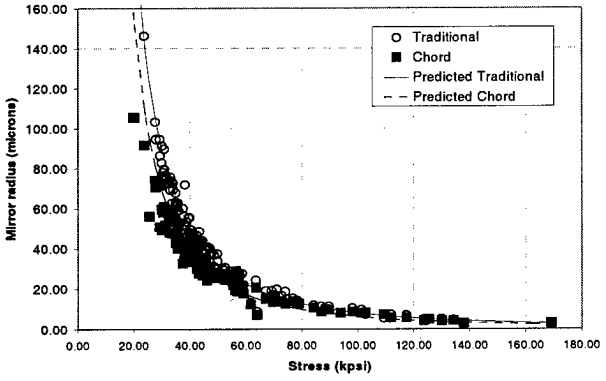

Figure 4. Measured strength versus mirror radius as measured by the traditional and chord techniques.

Figure 4 shows that the chord method results in a radius that is consistently smaller than the traditional measurement method. Consequently, the mirror constant for the chord method is significantly lower than that determined by the traditional method. For the case of pure tension, either measurement technique will suffice provided the correct mirror constant is used. Furthermore, the chord measurement was not affected by edge effects.

In their deployed state fibers are commonly subjected to combined tension and bending loads. Figures 5 and 6 show examples of fracture surfaces of fibers subjected to such loading conditions. The well known distortion of the mirror is clearly evident, especially in the lower strength specimen in Figure 6.

Figure 5. Fracture surface obtained from 213 MPa (31 kpsi) bending and 276 MPa (40 kpsi) tensile stresses.

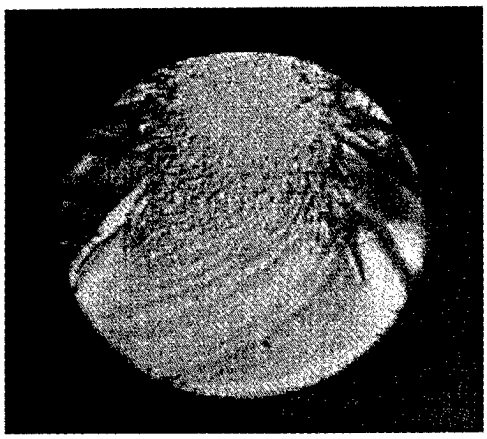

Figure 6. Fracture surface obtained by 213 MPa (31 kpsi) bending and 221 MPa (32 kpsi) tensile stresses.

The maximum stress on the fiber surface, obtained by adding the tensile and maximum bending stresses, is plotted versus the mirror radius for both methods in Figure 7. The predicted curves for pure tension also are

shown. For both mirror measurement methods, the actual mirror measurement was greater than the predicted mirror measurement. The effect of bending is to enlarge the mirror radius for both measurement methods beyond that for pure tension. However, the chord measurement method is less sensitive to the bending stress profile.

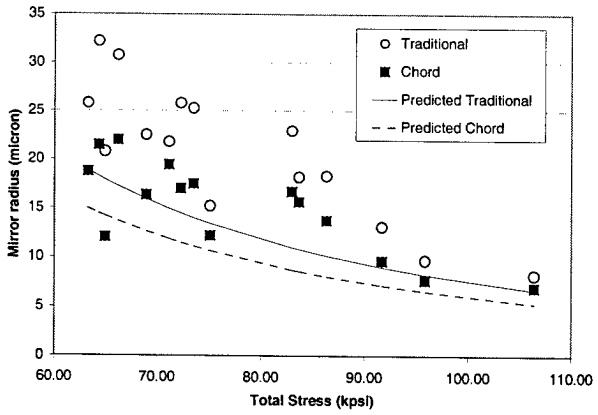

Figure 7. Total combined tensile and 213 MPa (31 kpsi) bending stresses. Associated mirror measurements using both traditional and chord measurements.

These results indicate that the use of Equation (1) to estimate the fracture stress in the presence of bending can lead to an underestimation of the actual applied stress at failure. In this case, 31 kpsi bending stress results in the underestimation of the total failure stress by 20% for the traditional mirror measurement method and 15% for the chord measurement method. Note that for lower bending stresses this underestimation will be significantly less. Future work will focus on obtaining the dependency of the mirror constant on bending stresses for the case of combined tension and bending loads.

The results of this study highlight the need for knowledge of the stress state at failure. Some practical recommendations can be made:

1. Before removing a broken fiber from its packaged state, attempt to measure the state of bending of the broken fiber or of the surrounding fibers if any are present.
2. Determine the location of the failure origin with respect to the axes of the bending stress. This is important in determining the bending stress acting on the flaw that failed.
3. Examine the shape of the fracture mirror for signs of bending.
4. Use the chord mirror measurement, as it is less sensitive to bending than the traditional method.

Finally, residual stresses generated during fiber manufacturing were not taken into account in this study. Due to the fact that they are small compared to typical fracture stresses, this omission is warranted.

CONCLUSIONS

The chord method of obtaining a mirror radius from an optical fiber fracture surface is valid for determining tensile stresses using the appropriate mirror constant. In instances where bending stress as well as tensile stress are present, the chord method results in a predicted stress closer to the actual fracture stress. However, when bending is present the failure stress will be underestimated for both measurement techniques. Therefore, when dissecting a broken fiber one must take every opportunity to determine the level of bending on the fiber at the time of failure.

REFERENCES

1. S. W. Freiman, "Brittle Fracture Behavior of Ceramics", *Ceram. Bulletin*, **67** [2] 392-402 (1988).

2. V. D. Frechette, *Failure Analysis of Brittle Materials*, in the Advances in Ceramics Series, Vol. 28, 1990.

3. E. B. Shand, "Breaking Stresses of Glass determined from Fracture Surfaces," *The Glass Industry*, April 1967.

4. T. A. Michalske, "Quantitative Fracture Surface Analysis", in *Ceramics and Glasses*, Engineered Materials Handbook, Vol. 4, S. J. Schneider, Jr., Chairman, ASM 652-662 (1991).

5. J. J. Mecholsky, "Fracture Surface Analysis of Optical Fibers", in *Ceramics*

and Glasses, Engineered Materials Handbook, Vol. 4, S. J. Schneider, Jr., Chairman, ASM 663-668 (1991).

6. E. B. Shand, "Breaking Stress of Glass Determined from Dimensions of Fracture Mirrors", *J. Am. Ceram. Soc.*, **42** [10] 474-477 (1959).

7. J. J. Mecholsky, S. W. Freiman, "Determination of Fracture Mechanics Parameters Through Fractographic Analysis of Ceramics," in *Fracture Mechanics Applied to Brittle Materials*, S. W. Freiman, editor, ASTM STP 678, (1979).

8. J. J. Mecholsky, R. W. Rice, and S. W. Freiman, "Prediction of Fracture Energy and Flaw Size in Glasses from Measurements of Mirror Size", *J. Am. Ceram. Soc.*, **57** [10] 440-443 (1974).

Linda K. Baker
MP-RO-03
Corning Incorporated
Corning, NY 14831

Linda K. Baker is a senior market development engineer for the Telecommunications Products Division. She is responsible for providing engineering support to select cable customers, and for managing the current technical issues surrounding the mechanical reliability of optical fiber. Baker joined Corning in 1990 as a process engineer, and has worked for several years in manufacturing. She holds a bachelor's degree in ceramic engineering from Alfred University and a master's degree in material science from the University of Florida.

G. Scott Glaesemann
SP-DV-01-08
Corning Incorporated
Corning, NY 14831

Scott Glaesemann is a senior development engineer responsible for the optical fiber mechanical testing laboratory at Corning's Sullivan Park technology center and has been employed by Corning for 12 years. He received his master's degree and doctorate in mechanical engineering from the University of Massachusetts, and a bachelor's degree in mechanical engineering from North Dakota State University.

CHARACTERISTICS OF TIN-CODOPED GERMANOSILICATE FIBER BRAGG GRATINGS WRITTEN THROUGH AN UV-TRANSPARENT COATING

Tadahiko Nakai, Kazuo Imamura, Yasuhide Sudo, Yoshiyuki Imada

Mitsubishi Cable Industries, LTD. , Itami, Hyougo, Japan

ABSTRACT

Fiber Bragg gratings which uses the photo induced refractive index change of the core of optical fibers are being largely studied in optical communications and fiber sensor systems. Generally, the coating is removed when fabricating fiber Bragg gratings. In this paper we report on a direct fabrication of a narrow-band reflective fiber Bragg gratings without removing the coating, using a tin-codoped germanosilicate fiber and an UV transparent coating. The optical transmission characteristic of the fabricated fiber Bragg grating had maximum reflectivity of more than 99%, FWHM:0.12nm and side-robes suppression of more than 25dB on grating length of 24mm. We also tested the mechanical strength of the fabricated fiber Bragg gratings. The average breaking stress was 4.9GPa, n value was 20.

INTRODUCTION

In recent years, fiber gratings and its applications are widely studied in optical communications and fiber sensor systems. The technology is ready to be tried in practical uses. The fabrication of fiber gratings was first demonstrated by Hill et al in 1978[1]. At first, gratings were fabricated by using stable waves of the laser beams induced into the fiber core. Next, the two-beam interferometric method which fabricates the gratings by a side exposure of the fiber became the widely used. The most commonly used method now is exposure by an simple phase mask method which uses ±1 diffracted order beams. Fiber Bragg gratings create a periodic refractive index modulation lengthwise to the fiber using the photo induced refractive index change of the core. Therefore the fiber grating functions as a reflective filter for a particular wavelength in the same cycle as the refractive index modulation. Usually, the fabrication of a fiber Bragg grating consists of mechanically and chemically removing the coating. This process weakens the fiber at the gratings[2]. Large amounts of UV rays irradiated during fabrication of the fiber grating is also thought to increase the refractive index and tensile stress at the core[3]. On the other hand, fibers grated by an in-line single pulse have been confirmed to have no deterioration in strength. However, the reflectivity does not increase because the increase of the refractive index is small[4,5]. A method which directly exposes UV rays on the coating can increase the productivity. The fabricated fibers would have long-term reliability as it would not require re-coating and makes packaging simple. For such a method, an UV transparent resin was used to coat a high sensitive fiber to obtain satisfactory transmission characteristics and the mechanical strength[6,7,8,9]. In this paper we report on the characteristics of a tin-codoped germanosilicate fiber having an UV transparent coating with fiber gratings fabricated by a direct exposure of UV-rays on the coating.

SAMPLE FIBERS

Fiber parameters

The tin-codoped germanosilicate fibers used in the experiment was made by the VAD method and solution-doping techniques. Table 1 shows the fiber parameters. To enhance the photosensitivity during irradiation of UV-rays, along with Ge, the core of the optical fiber was codoped with Sn and Al at concentrations 15000ppm and 900ppm respectively.

Table 1: Tin-codoped germanosilicate fiber parameters

Relative index difference Δ, %	0.97
Sn concentration , ppm	15000
Al concentration , ppm	900
Mode field diameter , μm	5.55
Cutoff wavelength , μm	1.27
Cladding diameter , μm	125
Coating diameter , μm	200

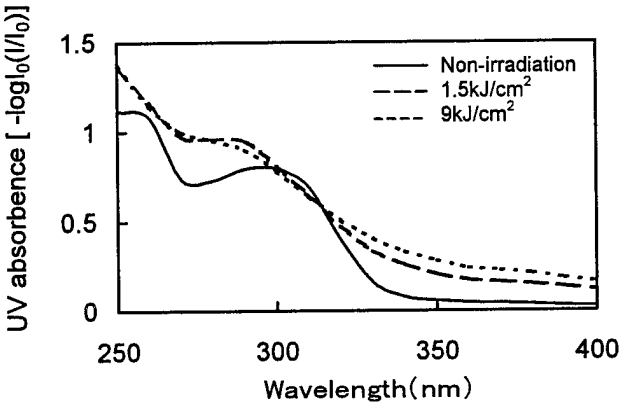

Fig.1 UV-absorbance spectra change of 60 μm thick sheet of UV-transparent UV-curable resin depending on incident energy

Coating materials

When fabricating fiber gratings on a common communication fiber, it is necessary to mechanically or chemically remove the coating as the coating cures by absorbing UV-rays. We used a UV transparent UV curable resin as the coating material to prevent loss of incident optical energy. The absorbance of the UV transparent resin had absorbance of 0.16 at wavelength 266nm at 10 μm thickness. Figure 1 shows the change in absorbance of the UV transparent UV curable resin against the density of the UV irradiation. UV was irradiated under the same conditions as in actual fabrication of gratings. 266nm wavelength was used, evaluations were made on a 60 μm thick sheet. Figure 1 shows that at wavelengths 250～300nm the absorbance is around 1. We obtained good results of under 1 around wavelength 266nm even when the irradiation energy density reached 9kJ/cm^2

FABRICATION OF FIBER BRAGG GRATINGS

In common communication fibers, the photo induced refractive index change is very small because the refractive index difference Δ by Ge is below 1%. Generally, measures such as high pressure hydrogen treatments are made to enhance the photosensitivity. To continuously increase the photo induced refractive index change, it is effective to increase the Ge concentration or codope such elements B and Sn. It is more effective to codope elements such as B and Sn as increased Ge concentration may not match the refractive index when connecting to common communication fibers. Figure 2 shows change of reflectivity with the time of tin-codoped fibers with or without high pressure hydrogen treatment. The experiment was carried out with the coating removed. Figure 2 shows that tin co-doped fibers have better sensitivity compared to DSF(Dispersion Shift Fiber). Direct exposure of UV rays on the coating prevents the optical incident power from reaching the fiber core as the resin coating absorbs the UV rays. To make up for the transmittance loss of UV rays by the coating when fabricating gratings directly on the coating, a UV transparent resin was used to coat the high

photosensitive tin-codoped fiber. The fiber was put under high pressure hydrogen treatment of 20MPa for two weeks.

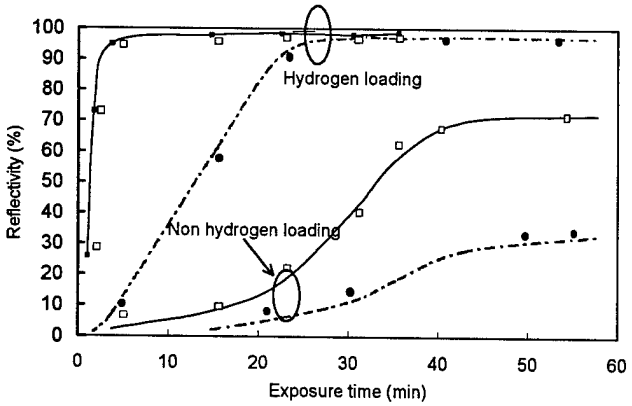

Fig.2 Change of reflectivity with the time of tin-codoped fibers with or without high pressure hydrogen treatment.

- □ Tin-codoped germanosiricate fiber
- ● DSF(Dispersion Shift Fiber)

OPTICAL SOURSE AND FABRICATION SYSTEM

Figure 3 shows the structure of fiber grating fabrication system. As a UV coherent optical source, a beam of wavelength 266nm which has frequency quadrupled Q-switched Nd-YAG lasers was used. The laser had maximum average power of 100mW. 10Hz performance was possible at pulse width 50n. After the irradiation beam was expanded with a beam- expander and made into a parallel beam, a portion with even power was slit. The slit beam was reflected at 90 degrees with a movable mirror and was condensed with a cylindrical lens. From the condensed area, the beam was transmitted through a phase mask and irradiated on the optical fiber. The condensed beam can be moved in the fiber lengthwise by moving the mirror. The average incident power on the phase mask was 10mW.

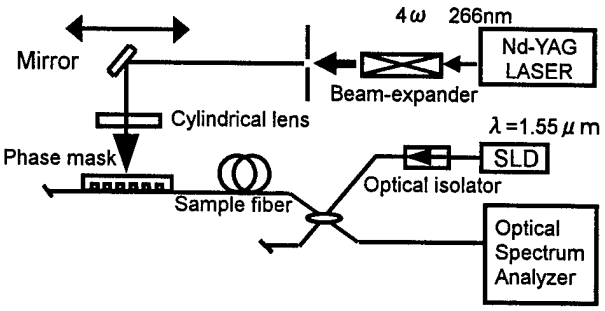

Fig.3 Structure of fiber grating fabrication system

FIBER BRAGG GRATINGS CHARACTERRISTICS

Transmission characteristics

Figure 4 shows the reflective spectral of narrow band reflective fiber grating with a grating length of 24mm. The irradiated energy density on the fiber coating was 1.5kJ/cm^2. In this experiment we succeeded in obtaining a maximum reflectivity of 99% on a grating length 24mm. The center resonance wavelength of this fiber grating was 1544.6nm, the FWHM was 0.12nm, and side-robes suppression of more than 25dB was possible at the center wavelength band by apodization. The surface of the coating was in a good state with no visible yellowing or damages.

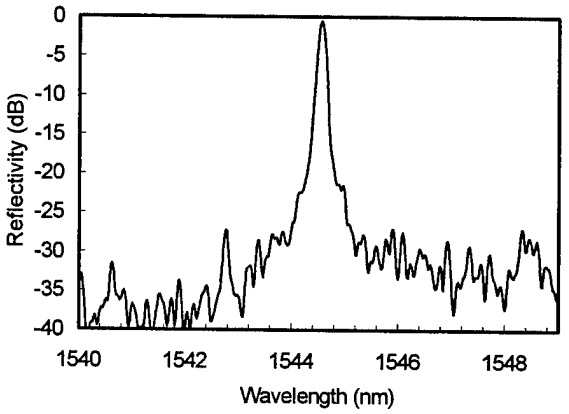

Fig.4 Reflection spectrum of 99% reflectivity of fiber Bragg gratings written through an UV-transparent coating(FWHM ; 0.12nm、L=24mm)

Mechanical strength characteristics

Mechanical strength of fiber gratings irradiated under same conditions were evaluated. The temperature and humidity in the laboratory for the experiment was controlled to be 22℃ and 50% RH respectively. The results are shown in the Weibull plots in Figure 5. Tensile was tested on 100mm gage, tensile speed was 100mm／min. The breaking stress of fiber gratings were : maximum 5.42GPa, minimum4.4GPa, average 4.9GPa. The tensile speed was changed in three stages 1%/min, 10%/min,and 100%/min. The dynamic fatigue was evaluated taking the average value of the breaking stress of each stage. Figure 6 shows the results of dynamic fatigue characteristics. The results show that dynamic fatigue modulus n of fibers without gratings were n=23, dynamic fatigue modulus n of fibers with gratings were n=20. Judging from these experimental results, we concluded that the fiber grating we fabricated had sufficient reliability.

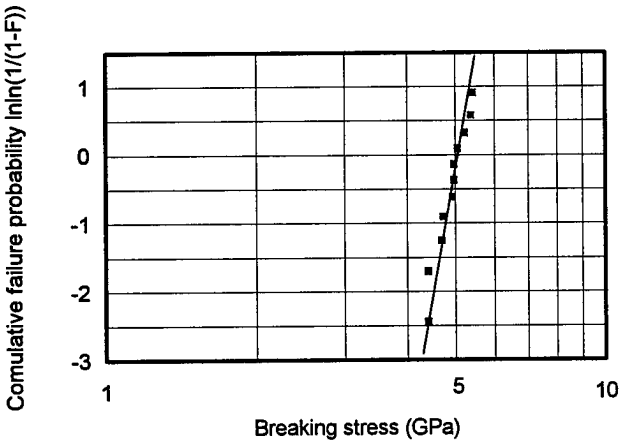

Fig.5 Weibull plots for fiber Bragg gratings

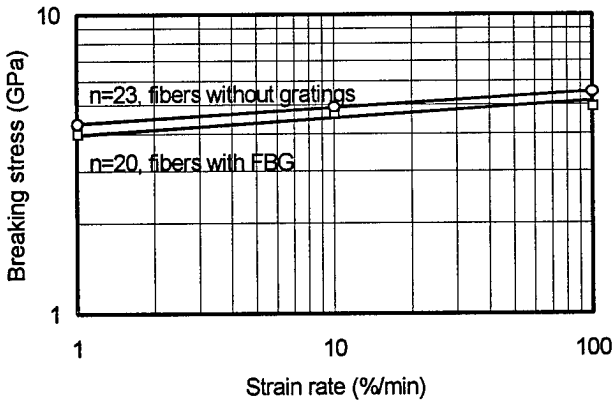

Fig. 6 Dynamic fatigue characteristics for fiber Bragg gratings

Coating material

One important factor in evaluating the fiber coating is the modulus. The modulus of the coating of the fiber grating portion fabricated to have good fiber strength was evaluated. A sample was taken from a small part of the fiber coating (cylinder shaped) which was divided lengthwise in two parts, the irradiated front side and the back side. Tensile was applied in the fiber axial direction for a gage length of 15 mm at a velocity of 1mm/min. Table 2 shows the evaluation results of the modulus dependency to the energy density. The modulus was tested up to a 2.5 %strain stress. The modulus increased with the irradiation time. The energy intense front side of the irradiated surface changed more than the back side. In the actual process of fabricating the gratings, the increase of the modulus of both the front and back sides of the coating layer remains within 20 % as the energy density is around 1.5kJ/cm^2. This is a satisfactory level as a coating material.

Table 2:Change in modulus of coating layer after UV-irradiation

Irradiated time, min	0	20	50
Incident energy, kJ/cm^2	0	3	7.5
Front side modulus, MPa	459	540	601
Back side modulus, MPa	459	533	540

CONCLUSION

A narrow band reflective fiber grating having a maximum reflection of more than 99%, FWHM of 0.12nm, side-robes suppression of more than 25dB was fabricated by direct UV ray exposure on the coating of an tin-codoped germanosilicate fiber. The mechanical strength characteristics had a average breaking strength of 4.9GPa, n value of 20. This grating method which does not remove the coating, prevents weakening of the fiber strength and simplifies the manufacturing process. High strength fiber gratings can be used not only for communications but for sensor systems as well.

REFERENCES

1. HILL,K.O., FUJII, Y., JOHNSON,D.C., and KAWASAKI, B. S. : 'Photosensitivity in optical fibre waveguides : Application to reflection filter fabrication ', Appl. Phys. Lett., 1978, 32, pp. 647-649.

2. FECED, R., ROE-EDWARDS, M. P., KANELLOPOULOS, S. E., TAYLOR, N. H., and HANDERK, V. A. : ' Mechanical strength degradation of UV exposed optical fibres ', Electron. Lett., 1997, 33 pp.157-159.

3. FONJALLAZ, PY., LIMBERGER, H. G., SALATHE, R, P., COCHET, F., and LEUENBERGER, B. : 'Tension increase correlated to refractive-index change in fibers containing UV-written Bragg gratings ', Opt. Lett., 1995, 20, pp 1346-1348

4. ASKINS, C. G., PUTNAM, M. A., PATRICK, H. J., and FRIEBELE, E.J. : ' Fibre strength unaffected by on-line writing of single-pulse Bragg gratings ', Electron. Lett., 1997, 33, pp. 1333-1334

5. DONG, L., ARCHAMBAULT, J.-L., REEEKIE, L., RUSSELL, P. ST .J., and PAYNE, D. N. : 'Single pulse Bragg gratings written during fibre drawing', Electron. Lett., 1993, 29, pp. 1577-1578

6. DONG, L., CRUZ, J. L., REEEKIE, L., XU, M. G., and PAYNE, D. N. : 'Enhanced photosensitivity in Tin-codoped germanosilicate optical fibers', IEEE Photonics Technol. Lett., 1995, 7, pp. 1048-1050

7. ESPINDORA, R.P., ATKINS, R.M., SIMOFF, D. A., NELSON, K. T., and PACZKOWSKI, M, A.: 'Fibre Bragg gratings written through a fiber coating'. OFC '97 Tech. Dig., 1997, Postdeadline paper PD-4

8. SIMOFF, D. A., PAXZKOWSKI, M. A., RAGAN, R., INNISS, D., STRASSER, T. A., BORICK,J.M., PEDRAUANI, J. R., ESPINDOLA, R. P., ATKINS, R.M., NELSON,K. T., ASPELL, J., and Kuck, V. J.: 'Coatings having enhanced UV transparency for the fabrication of optical fiber gratings'. IWCS '97 Track1, Session 2-7, 1997, pp. 86-93

9. IMAMURA, K. , NAKAI, T. , MORIURA, K. , SUDO, Y. , and IMADA , Y. : 'Mechanical strength characteristics of tin-codoped germanosilicate fibre Bragg gratings by writing through UV-transparent coating '.Electron. Lett., 1998, 34, pp. 1016-1017

Tadahiko Nakai
Mitsubishi Cable Industries, Ltd.
4-3, Ikejiri, Itami, Hyougo, 664-0027, Japan

Mr. Nakai, staff engineer of RF & Optical System Engineering Section, is engaged in design and development of optical system. He received his B.E. degree in Electrical Engineering from Osaka University in 1995. He is a member of The Japan Society of Applied Physics.

Yasuhide Sudo
Mitsubishi Cable Industries, Ltd.
4-3, Ikejiri, Itami, Hyougo, 664-0027, Japan

Mr. Sudo, manager of RF & Optical System Engineering Section, is engaged in production and development of optical transmission equipments and subscriber equipments . He received his M.S. degree in Electrical Engineering from kyoto University in 1975.

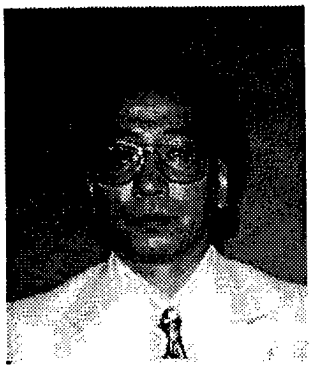

Kazuo Imamura
Mitsubishi Cable Industries, Ltd.
4-3, Ikejiri, Itami, Hyougo, 664-0027, Japan

Mr. Imamura, senior research engineer of Electronics & Communication Research Dept., is engaged in design and development of optical subscriber systems and optical components. He received his M.S. degree in Electrical Engineering from Osaka University in 1983. He is a member of The Institute of Electrical Engineers of Japan and The Japan Society of Applied Physics.

Yoshiyuki Imada
Mitsubishi CableIndustries, Ltd.
4-3, Ikejiri, Itami, Hyougo, 664-0027, Japan

Mr. Imada, manager of Electronics & Communication Research Dept. He received his B.E. degree in Electrical Engineering from Osaka University in 1967. He is a member of IEEE.

THE ANALYSIS AND RESEARCH OF CHIRPED BRAGG FIBER GRATING THEORY ON DISPERSION COMPENSATION

Zou liu-juan[1], Zhou Zhi-min[1], Xiao Long-pan[1], Zou Dao-Wen[2]

[1]Huazhong University of Science and Technology, Wuhan
Hubei; 430074, P. R. China
[2]Jiang Xi Normal University, Nanchang, jiangxi 330027, P. R. China

Liu Shuihuo, Lin Bing, Zhao Zisen

Wuhan Research Institute of Posts and Telecommunication, Wuhan, Hubei 430074, P. R. China

ABSTRACT

This paper, based on the general theory of linear Chirped Bragg fiber grating, discusses some parametres including different chirped values and quasi-gauss coupling function relating with the reflectivity coefficient dispersion compensation .

The result shows that selecting larger chirped value and appropriate qusi-guass coupling function can improve the dispersion compensation while ensuring high reflectivity. The concept of "figure of merit" in the microwave field is introduced to quantize the equalizing power of the dispersion compensator.

1. INTRODUCTION

Because of the appearance of Erbium-doped fiber amplifier, the overall optical fiber communication of long distance and the high speed has realized. However, the optical signal in 1.55μm wavelength is amplified by the Erbium-doped fiber amplifier and the distortion of optical signal is amplified as well. The transportable distance of optical signal is greatly shortened. Therefore, many ways have been attempted in solving the problems caused by dispersion.[1,2] The linear chirped Bragg fiber grating is the least in volume, the highest in egualizing power dispersion compensation device of all. Recently it is a focus of study in this respect.[3,4]

This paper gives a qualitative analysis of the dispersion characteristics of chirped Bragg fiber grating, Using the coupled mode equation we derive the matrix type of its resolution. We got the response characteristics from numerical analysis. Then the concept of "figure of merit" in the microwave field is introduced to quantize the equalizing power of the dispersion compensator.

2. THE PRINCIPLE AND OMPUTATION METHOD OF CHIRPED BRAGG FIBER GRATING ON DISPERSION COMPENSATION.

grating is shown in Fig.1. The refraction index distribution along the axis is in quasi-period:

Fig.1: The structure Figure of Linear Chirped Bragg Fiber Grating

$$n = n_0 + \Delta n\left[1 + \cos\left(\Omega_0 Z + FL_g^{-2}\left(Z/L_g\right)^2\right)\right] \quad (1)$$

$$-L_g/2 < Z < L_g/2$$

$$\Omega_0 = 2\beta_0 \quad (2)$$

Where $\beta_0 = \Omega_0/2$ is the center wave number of the grating, F the chirped coefficient, L_g the length of the grating. In order to meet the matching condition of phase, the corresponding optical components in different position of chirped Bragg fiber grating satisfy the formula as follows:

$$\Omega_0 + FZ - 2\beta = 0 \quad (3)$$

If the center frequency of chirped Bragg fiber grating is ω_0, the corresponding center wave nunber is β_0, then at the first class approximation it can be got that:

$$\beta = \beta_0 + \left.\frac{\partial\beta}{\partial\omega}\right|_{\omega=\omega_0}(\omega - \omega_0) \quad (4)$$

If the group velocity of optical pulse is V_g, then the delays for optical pulse to generate in propagation of chirped Bragg fiber grating can be shown approximately as follows:

$$\tau = 2L_g/V_g \quad (5)$$

Let (4) take the place of β in (3), according to the above formula we can get:

$$FL_g^{\,2}\theta = \tau\Delta\omega \quad (6)$$

$$-1/2 < \theta = Z/L_g < 1/2, \Delta\omega = \omega - \omega_0$$

If the freguency bandwidth needing compensation is δν, from (6) We can get

$$FL_g^{\,2} = \tau\delta\omega = 2\pi\tau\delta\nu \quad (7)$$

Where, FL_g^2 is chirped coefficient. In Linear approximation we can get the relationship between chirped coefficient and dispersion as follows:

$$\ddot{\phi} = \frac{\delta t}{\delta\omega} = \frac{\tau}{2\pi\delta\nu} = \frac{\tau^2}{FL_g^{\,2}} \quad (8)$$

The above formula has theoretical significance for design of chirped Bragg fiber grating. In 1.55μm band fiber loss is generally 20PS²/km. According to formula (8), to design the chirped Bragg fiber grating for compensation distance of 100km, dispersion of 2000 PS², bandwidth of 20GHZ, its delays should be is approximately 251PS.

It should be noted that the above discussion is in approximation. In order to get the relationship between dispersion and frequency in detail, we must solve the following coupled mode equation.[5]

$$\frac{dA}{d\theta} = KB\exp(i\sigma\theta) \quad (9)$$

$$\frac{dB}{d\theta} = KA\exp(-i\sigma\theta) \quad (10)$$

Where $\sigma = (\Omega - 2\beta)L_g$ (11)

A and B are the compounding amplitude of the forward wave and backward wave, K is coupled coefficient. When Kand σ are a constant, the resolution of equation (9) and (10) can be expressed as following matrix:

$$\begin{bmatrix} A0 \\ B0 \end{bmatrix} = \begin{bmatrix} \cosh(r\theta) - i(\theta/2\gamma)\sinh(r\theta) & K\sinh(r\theta)/r \\ K\sinh(r\theta)/r & \cosh(r\theta) + i(\theta/2\gamma)\sinh(r\theta) \end{bmatrix} \begin{bmatrix} Ai \\ Bi \end{bmatrix} \quad (12)$$

Where $r = \sqrt{K^2 - \sigma^2/4}$

A0 and B0 refer to output at the right end of

chirped Bragg fiber grating, A*i* and B*i* input at the left end of the grating. If the linear chirped Bragg fiber grating is considered to be a series of connections of even period Bragg fiber grating with different period , then K and σ of each small band even period Bragg fiber grating are a constant, and they can be expressed as formula (12) type. At the same time, each small band output corresponds to a left small band input of the fiber grating. Thus we can get response characteristics of overall chirped Bragg fiber grating. The initial condition is set at $(1\ 0)^T$ when computing. Finally we get the reflectivity and dispersion.

$$R = \left| B^2 / A^2 \right| \tag{13}$$

$$\phi = \frac{d^2\phi}{d\omega^2} \tag{14}$$

$$\phi = arctg(B/A)$$

In general, the Guass shape coupling function plays a level and smooth part in reflectivity spectrum and dispersion compensation characteristics.[6] In the following computation, we have selected quasi gauss function.

$$K(Z) = K_0 \exp(-m \times \left| Z / L_g \right|^n) \tag{15}$$

Where K_0, m and n are an adjustable parameters.

3. COMPUTATION AND ANALYSIS

From fregoing computation, we can obtain that the refractivity δn of linear Chirped Bragg fiber grating changes along propagative direction of axis Z, as shown in Figure 2:

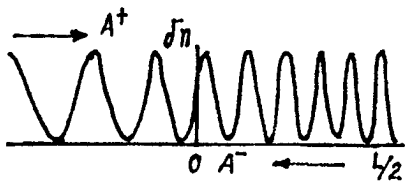

Fig.2: The Linear Chirped Bragg Fiber Grating Changes Along Propagative Direction of Axis Z

We can get separately the reflection spectrum figure of linear chirped Bragg fiber grating by approximate method from Section 2 of this paper under KL=5 for chirped coefficient F=50, F=100, and F=150, as shown in Figure 3.

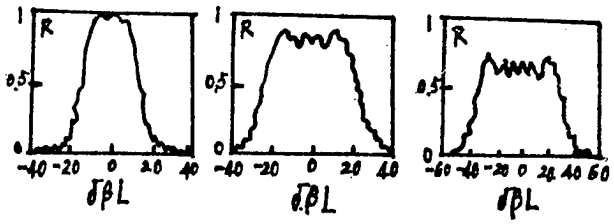

(a) F=50 (b) F=100 (c) F=150

Fig.3: The Reflection Spectrum Figure of Linear Chirped Bragg Fiber Grating under KL=5

A conclusion can be drawn from the fact which precedes. In the situation of the same KL value the maximum reflectivity value is decreased for reflection spectrun to increase the bandwidth. If we require not only wider bandwidth, but also bigger reflectivity for chirped Bragg fiber grating , then we must increase the value of KL. The KL is expressed as the coupled degree of propagating optical wave in chirped Bragg fiber grating. If the value of KL is the bigger, then the couple of forward wave and backward wave is ampler, the reflectivity is bigger.

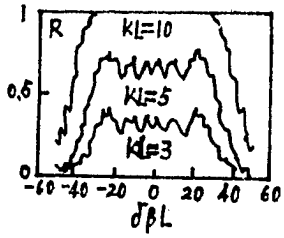

Fig.4: The Reflective Spectrum Figure of chirped Bragg Fiber Grating in the Value of Different KL

When the value of KL is increased at F=150, not only the reflectivity of the chirped Bragg fiber grating is raised, and the reflectivity bandwidth of the grating is also increased to a certain extent, a shown in Figure 4.

4. FIGURE OF MERIT

When we use the Bragg fiber grating or other dispersion compensators in the fiber communication system, we must remember that the spectral breadth response of the dispersion compensator devices must be wider than the signal spectral breadth. However dispersion is always contradictory to the response spectral breadth. The narrower the spectral breadth response, the larger the dispersion value. So we need to introduce a measurement for the equalizing power of the dispersion compensator, which considers two quantities of the dispersion and the spectral breadth response at the same time. We call it the "figure of merit" of a dispersion compensator. It was first introduced into the microwave field by Priest and Giallordnzi.[7] It is instructive to the design of the dispersion compensator. For example, the unchirped Bragg fiber grating, although it has a large dispersion, has a very narrow spectral breadth response , and a small fignre of merit, which makes it useful as a dispersion compensator.

4.1 Figure of Merit

Let us consider the propagation of a signal having an amplitude A(o,t) at Z=0, i.e., at the input end of the fiber. This signal propagates along the fiber at a group velocity V_g, we define a normalized time as $T=t-z/V_g$ and a normalized amplitude U(Z, T), that takes into account the fiber loss (given by the coefficient α).

$$A(Z,T)=\sqrt{P_0}e^{(-\alpha z/2)}U(Z,T) \qquad (16)$$

Where p_o is the power in the mode. The propagation of the normalized amplitude is then given by

$$\frac{\partial U}{\partial Z}=-i\frac{\beta_2}{2}\frac{\partial^2 U}{\partial T^2} \qquad (17)$$

where $\beta_2=\partial^2\beta/\partial\omega^2$ is the dispersion of the fiber. β being the propagation constant of light in the fiber. In the angular frequency domain, the second derivative becomes a multiplication by $(-\omega^2)$. The angular frequency ω should be taken here as the detuning with respect to the central frequency of the pulse. We then find that the Fourier transform

$\tilde{U}(L_f,\omega)$,after propagation along a fiber length L_f, becomes

$$\tilde{U}(L_f,\omega)=\tilde{U}(0,\omega)\exp(i\beta_2\omega^2 L_f/2) \qquad (18)$$

Now, let this pulse pass through a dispersion compensator with a complex frequency response $g(\omega)e^{i\phi(\omega)}$. The resulting pulse is

$$\tilde{U}(L_f,\omega)=g(\omega)\tilde{U}(0,\omega)\exp[i(\beta_2\omega^2 L_f/2+\phi(\omega))] \qquad (19)$$

The phase of the frequency response of the dispersion compensator can be expanded as a Taylor series:

$$\phi(\omega)=\phi_0+\dot{\phi}+\ddot{\phi}\omega^2/2+\cdots\cdots \qquad (20)$$

The effect of the dispersion compenstor is thus to modulate the spectrum amplitude through $g(\omega)$, to add a constant phase shift Φ_0 ,a time delay $\dot{\Phi}$, and a dispersion proportional to $\ddot{\Phi}$. The total dispersion is thus the sum of the fiber dispersion and the compensator dispersion , If we assume that the amplitude response $g(\omega)$ is constant across the bandwidth of the signal ,and if we drop the time delay introduced by the compensator ,we find that

$$\tilde{U}_f(L_f,\omega)=\tilde{U}(0,\omega)\exp[i(\beta_2 L_f+\ddot{\phi})/2]\omega^2 \qquad (21)$$

To define the figure of merit , we now consider the broddening of a Gaussian pulse after propagation through an optical fiber of length L_f. The full-width at half-maximum(FWHM)of the input pulse

is τ_0. The pulse normalized amplitude is then

$$U(0,t) = e^{-4Ln2(t/\tau_0)^2} \qquad (22)$$

By taking the Fourier transform of U(o,t), insertion in (6), and taking the inverse transform, one gets the output pulse width τ_1, This is given by the well-known expression

$$\tau_1 = \tau_0\sqrt{1+(\frac{4Ln2\beta_2 L_f}{\tau_0^2})} \qquad (23)$$

From (44), we see that when a dispersive compensator is added, the dispersion $\beta_2 L_f$ is replaced by the total dispersion $\beta_2 L_f t\ddot{\phi}$. Therefore the pulse width after the compensator is

$$\tau_2 = \tau_0\sqrt{1+\left[\frac{4Ln2(\beta_2 L_f + \ddot{\phi})}{\tau_0^2}\right]} \qquad (24)$$

For perfect dispersion compensation, we must have $\ddot{\phi} = -\beta_2 L_f$, and the compression ratio achieved by the compensator is:

$$\tau_1/\tau_0 = \sqrt{1+\left(\frac{4Ln2\ddot{\phi}}{\tau_0^2}\right)} = \sqrt{1+M^2} \qquad (25)$$

Where M is the figure of merit defined by

$$M = \ddot{\phi}(\delta\omega)^2/4Ln2 \qquad (26)$$

Where $\delta\omega = 2\pi\delta\nu$ is the bandwidth of the pulse.

4.2 Calculation Example

Let us now consider a practical example. When designing a despersion compensator, one usually starts with a given value of dispersion to compensate. The dispersion of our compensator is calculated by taking the second derivative of the phase of their frequency response with respect to angular frequency ω ,and therefore has units of S^2, A more convenient unit is PS^2. Historically, dispersion of an optical fiber D has often been expressed in units of PS/nm ·Km. In order to work with more compatible units, we will use the fiber dispersion parameter β_2 expressed in units of PS^2/Km. The conversion factor between these units depends on the wavelength and is given by

$$\beta_2(PS^2/Km) = 5.31\times10^{-7}\lambda^2(nm)D(PS/nm\cdot Km)$$

At 1.55μm, the conversion factor is 1.27. A typical value of fiber dispersion at this wavelength is 20 PS^2/Km. Let us say we want to compensate for 100 Km of fiber, The total dispersion is then 2000 PS^2. The next important parameter is the bandwidth required. A 2.5Gb/s signal from a directly modulated laser diode may extend over as much as 30 GHZ because of frequency chirping. The compensator required should then have a dispersion $\ddot{\Phi} = 200PS^2$ over a bandwidth $\delta\nu = 30GHZ$`. The required value of τ can be:

$$\tau = 2\pi\ddot{\Phi}\delta\nu = 370PS$$

The value of the chirped coefficient of the compensator is then given by

$$FL_g^2 = 2\pi\delta\nu T = 70$$

The corresponding figure of merit is M=25.2

5. CONCLUSION

From the above study we get:

(a) If the chirped value increases, We can get smoother dispersion compensation curve. If the value of n increases to a certain extent, we can raise the range of dispersion compensation curve.

(b) Design of chirped Bragg fiber grating can be realized by increasing bandwidth and chirped value and selecting appropriate parameter of quasi-gauss modulation function, we can get reflectivity and dispersion compensation in accordance with our demand at requested bandwidth (20~30 GHZ /channel).

(c) From the expression of M, it can be seen

that the delay τ and chirped coefficient FL_g^2 can change independently. This means that we can get the expected value M, and then can design the dispersion compensator with demanded dispersion in the constant spectral breadth.

REFERENCES

1 T.0zeki, "Optical equalizers", Opt. Let., Vol.17, pp.375-377, 1992.

2. I.J. Cimini, E. J. Greensrein, and A. A. M. Saleh, "Optical equalization to combat the effect of laser chirp and fiber dispersion", J. Light wave Technol., Vol.8, PP.649-659, 1990.

3. Jose E. Roman and kim A. Winick "wave guide grating filters for dispersion compensation and pulse compression", IEEE J. Quantun Electron, Vol.29, PP.975-982, 1993.

4. F. Ouellete, "ALL-fiber filter for efficient dispersion compensation" Opt. Lette., Vol.16, PP. 303-305, Mar.1991.

5. A. W. Snyder and J. D. Love, Optical waveguide Theory. New york: chapman and Hall, 1983, ch.27.

6. F. Ouellette, "Dispersion concellation using linear chirped Bragg grating filters in optical waveguides ", Opt. Lett., Vol.12, PP. 847-849, Oct.1987.

7. R. G. Priest and T. G. Giallorenzi, "dispersion compensation in coherent fiber optic communication", Opt, Lett., Vol.12, PP 622-625, 1987.

BRIEF BIOGRAPHICAL SKETCH

Zou Liu-juan, Female; Associate Professor; Date of birth:March 10,1946; Nationality: chinese, Place of birth: Shanghai, P. R. China. Graduated from Department of Nuclear phgsics of Peking University, Beijing, P. R. China at 1970.

In 1970~1983, worked in Bo Hai Shipbuilding Factory of China's ships and Vessels Industrial Compang, engaged in radioactive measurement and protection of nuclear reactors. Since 1983, working in the Huazhong University of Science and Technology. Engaged in research of the application of the Positron annihilation technology in Material Science. Publications: published more than 30 papers both at home and abroad. From March, 1993 to July 1994,worked for a new and high technology company (i.e. OPCOM) in KUALA Lumpur of Malaysia upon invitation, engaged in manufacturing the preform of Optical fiber with M. C.V. D. equipment from NOKIA Company of Finland. Since 1994,doing scientific research on optical fiber communication.

PACKAGING SOLUTIONS FOR A MULTIWAVELENGTH IN FIBER BRAGG GRATING BASED CHROMATIC DISPERSION COMPENSATOR

Francesco Pozzi, Raffaella Vinzio, Andrea Marcone

Sirti S.p.A. - Cables and Optical Technologies
Cassina de' Pecchi (MI) - Italy

ABSTRACT

We describe two active packaging solutions for thermal compensation and mechanical protection of multiwavelength in fiber Bragg grating based chromatic dispersion compensators. We propose a linear housing for up to five 10 cm long chirped gratings and a circular one which overcomes any limitation in grating number or length. In particular, we will describe how the circular package design has been tailored in order to neglect PMD degradation due to bending induced birefringence. The reliability of the two packages has been demonstrated through transient and steady state climatic sequences. Both solutions have a thermal uniformity within 0.6°C, power consumption figures lower than 1.2 Watts and ensure a wavelength shift reduction by a factor of ten. A 2.488 Gbit/s point-to-point link has been also implemented for system performance evaluation. Device optimisation in the presence of group delay ripples has been obtained exploiting the attractive feature of package tunability.

INTRODUCTION

It is a matter of fact that long haul multiwavelength links operating at bit rates of 10 Gbit/s and more must provide for chromatic dispersion compensation in order to avoid strong penalties in system performance: one of the most promising and cost-effective techniques to achieve this scope is based on the use of in fiber chirped Bragg gratings in combination with optical circulators. As a drawback, fiber gratings are terribly sensitive to environmental conditions changes concerning temperature and mechanical stress which makes it necessary to realize a thermally compensated and strain-free package whenever they are used in the field.
In the case of DWDM (Dense Wavelength Division Multiplexing) links it will be necessary to compensate different wavelengths at the same time and this would be efficiently achieved by packaging all the fiber gratings within a single housing, that is making up a new DWDM device named multiwavelength chromatic dispersion compensator.
Here we report of two different active packaging solutions based on Peltier cells.
The first fits for about 10 centimeters long gratings and relies on a linear design that locates them into parallel thermalised grooves, the second is a compact round package design which fits for all grating lengths and organizes the excess fiber as well.
Laboratory measurements have been performed to validate both packaging solutions: iterative climatic sequences confirmed a reliable and stable behaviour over time in all temperature conditions that may be encountered in a central office environment (i.e. 10°C-40°C).
Climatic sequences were perfomed in both stationary and transient conditions recording the optical, thermal and electrical characteristics of the packaged device. Once attested the performance of the packages, we made system measurements over a point-to-point link operated with two wavelengths testing the packaged dispersion compensator under field environment conditions.
In this paper we first report of the main packaging conception issues taken into account together with the thermal characterisation results obtained for the two packages; in the followings we will describe the system experimental testbed made up for the functional testing of the multiwavelength chromatic dispersion compensator under operating conditions and the conclusions driven about the performance of the packages.

PACKAGE DESCRIPTION

The multiwavelength chromatic dispersion compensator consists of a three port circulator

and two commercial chirped fiber gratings spliced together in series as shown in the figure below.

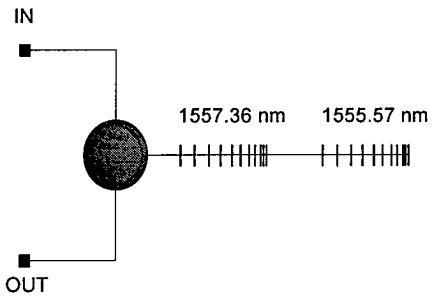

Figure 1 - Two wavelength chromatic dispersion compensator

As is well-known the central wavelength shift imposed on in fiber Bragg gratings by temperature changes is as high as 0.1nm/10°C. Therefore the gratings must be thermalised to assure a reliable and stable behaviour over time and this can be achieved by using either an active or passive packaging technique.
We discarded the passive solution not only because it suits better for short grating lengths and our chirped gratings are 10 cm long, but because of the intrinsic 'freezing' effect experienced by the optical properties which are stuck to the grating packaging condition.[1] This prevents the optimisation of the compensator in the presence of strong group delay ripples or in case of high detuning between the source and the grating. While ripples can be reduced by a careful apodization process, the grating tunability seems to be the unique solution to lasing source mismatch.
We believe that an active package represents the simplest and most reliable way to perform tunability of a series of long gratings. To keep a compact size all the gratings will be tuned at the same time and the optimum compensating condition will be achieved considering the intersection wavelength range between the grating effective bandwidth and the source linewidth. In case of direct modulation at 2.488 Gbit/s the source linewidth is about 0.3 nm which, for an effective bandwidth of 0.5 nm, turns to a useful tunable range of 0.2 nm (i.e. 20°C).
We designed two packages with different geometries able to satisfy the requirements for a stable and reliable DWDM device suitable to operate in a Central Office environment. The thermal characterisation of the packages was performed by means of an automatic laboratory testbed made up of an amplified spontaneous emission source, a climatic cell, a package temperature controller (ILX) and an optical spectrum analyser.

The main design features, the results of the climatic test sequences and the electrical power consumption figures for the two packages are reported hereafter.

Linear package

The core of the linear package is an aluminum bar with five parallel grooves 12.6 cm long able to host one chirped grating each. The temperature sensor is a 10 kΩ NTC thermistor positioned in the middle of the bar, inside a cavity underneath the grooves. Three Peltier cells connected in series are used to heat/cool the bar as shown in the schematic of figure 2.

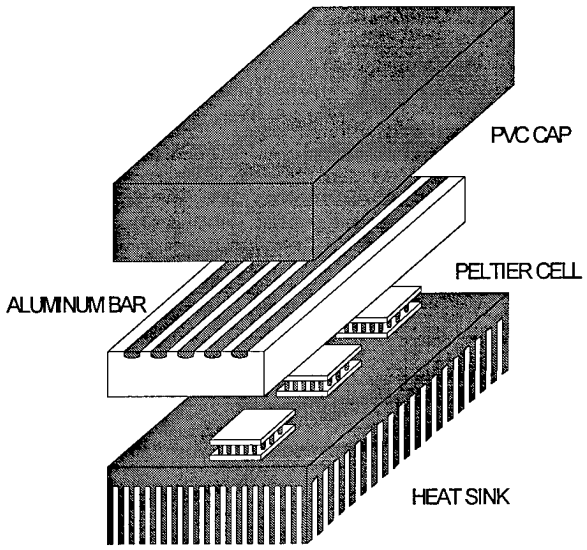

Figure 2 - Linear package

An additional thermistor was placed at the bar edge and sample uniform gratings were layed down the grooves in order to monitor the temperature uniformity of the aluminum bar as well as the central wavelength stability of the gratings with respect to climatic cell temperature variations at a fixed package temperature.
The measured central wavelength thermal drift was less than 0.01nm/10°C for all the sample gratings over the climatic cell temperature range of 0°C-45°C for a package temperature set to 25°C. In this case the temperature distribution was uniform within 0.6°C and the maximum power consumption figures were 1.2 Watt at 40°C and 2.5 Watt at 45°C.
Later measurements were performed with the package temperature set to 30°C to evaluate the power consumption figures for different climatic cell temperatures as summarized in table 1: this time the environment temperature was varied from 10°C to 40°C and the worst case

temperature fluctuation of the feedback thermistor was 0.6°C as shown in figure 3.

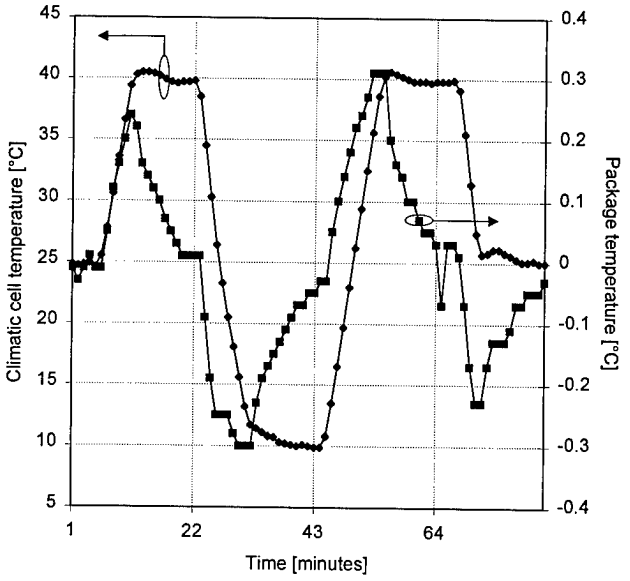

Figure 3 - Linear package thermal characterisation

Circular package

The circular package has a 1 cm large aluminum groove in which all the gratings, the splices and the excess fiber are layed down together. Three Peltier cells provide the heat/cool function and are disposed at the vertices of an equilateral triangle as shown in figure 4.

The winding diameter is included between 8.6 cm and 9.6 cm in order to minimize package size as well as PMD degradation caused by bending induced birefringence. In fact, this is given by: [2]

$$\delta n_{bend} = n_e - n_o = 0{,}133\left(\frac{r}{R}\right)^2$$

where n_e and n_o are the extraordinary and ordinary stress induced indices, r is the fiber radius and R is the bending radius.

Here the package worst case induced birefringence is about 2.81×10^{-7} which is negligeable compared to the typical intrinsic birefringence value affecting chirped fiber gratings (much higher than 10^{-6}).

All the climatic tests were performed setting the package temperature to 30°C: this was chosen to be the optimum operating temperature during the system measurements, as we will show in the next section.

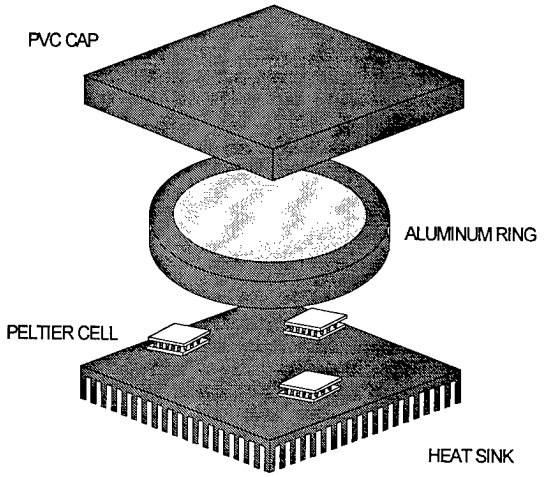

Figure 4 - Circular package

Two thermistors and two uniform sample gratings were monitored during consecutive cycles in which the climatic cell temperature was varied from 10°C to 40°C: the thermal uniformity was kept within 0.4°C and the worst case temperature fluctuation of the feedback thermistor was 0.6°C as shown in figure 5 and 6, respectively. The central wavelength drift experienced by the gratings was less than 0,01nm/10°C as expected in the event of a temperature variation smaller than 1°C.

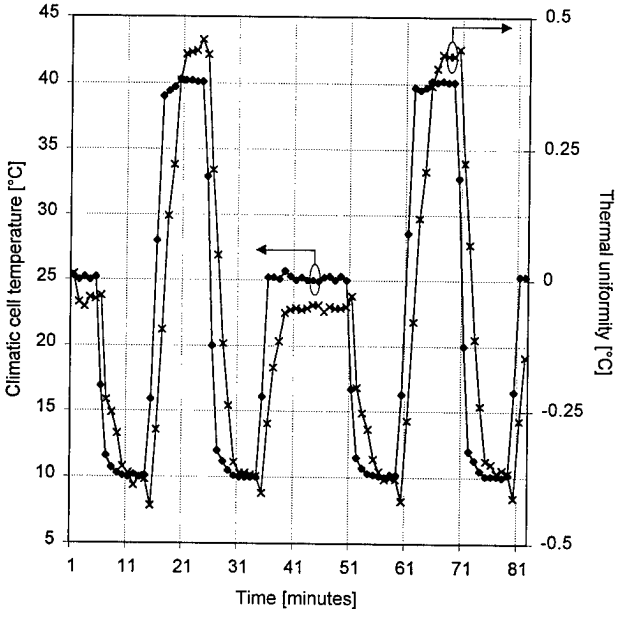

Figure 5 - Circular package: thermal uniformity during two consecutive climatic cycles (25-10-40-10-25°C)

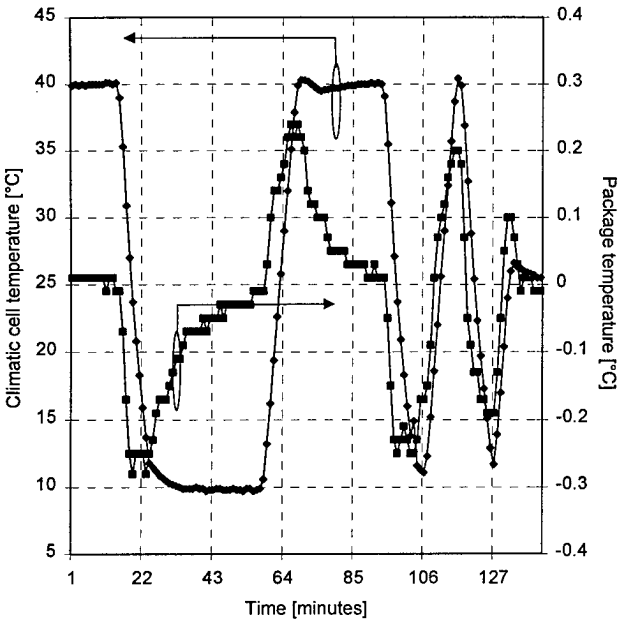

Figure 6 - Circular package thermal characterisation

Package comparison

From the thermal point of view the two packages are equivalent as they show practically the same temperature stabilization characteristics, tunability range as well as power requirements. Nevertheless both structures exhibit pros and cons which should be considered with regards to the specific application.

A critical point to assure the correct operation of the linear package is that the gratings must be carefully glued at the edges of the grooves: this offers the attractive opportunity to recover undesired wavelength detuning on each single grating thanks to pretension (obviously just in case an upwards wavelength shift is required).

In addition, it intrinsically does not introduce bending induced birefringence. As a drawback the number and the length of the gratings represent the design parameters and cannot be modified later on. Another weak point is that the excess fiber needs to be collected by an external splice organizer therefore increasing the package overall dimensions.

The circular solution is compact, does not need any additional support to organize the excess fiber and the splices and the gratings are not fixed to the groove. Moreover, the circular package allows immediate upgrade such as the increase of the number of gratings or the insertion of components longer than 10 cm such as very long broadband compensators, even if such components do not need thermal compensation and could be packaged into the aluminum ring alone without Peltier cells.

Table 1 - Power consumption @Tpackage = 30°C

Climatic cell temperature [°C]	Electrical power consumption [Watt]	
	Linear package	Circular package
10	1	1.2
15	0.6	0.7
20	0.3	0.3
25	0.07	0.08
30	0	0
35	0.1	0.1
40	0.4	0.5

There are still the following drawbacks: gratings are not immediately accessible and no pretension can be imposed on them.

SYSTEM VALIDATION

The system measurement setup shown in figure 7 was made up in our laboratories in order to assess the package performances in a two wavelength 2.488 Gbit/s point to point transmission link.

The aim of the trials was twofold: we wanted to explore the system penalty within the package tunability range and carry out comparative transmission error measurements employing both the linear and the circular packaging solutions.

Such a two wavelength link represents a minimum configuration for WDM applications, nevertheless will satisfy the purpose of testing our packages under operating conditions.

Testbed description

The core of the experimental setup is a commercial 2.488 Gbit/s SDH transceiver from

Wandel&Goltermann into which a 140 Mbit/s PDH tributary has been inserted and extracted to test bit error rate performance at different granularity levels.

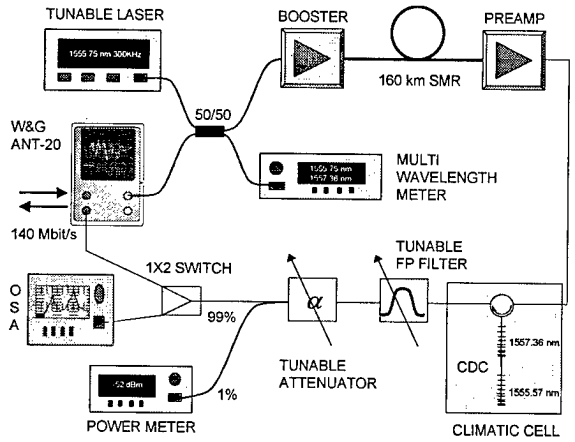

Figure 7 - System testbed

The transmitter is a stabilised DFB laser source at 1557.36 nm directly modulated at the STM-16 rate and is classified as the Long Haul interface L-16.2 according to the ITU G.957 recommendation. The tunable laser supplies a CW wavelength at 1555.75 nm externally modulated (300 KHz) in order to suppress stimulated Brillouin scattering. Both wavelengths are boosted by a EDFA at a power level of +16dBm, guided into a 160km G.652 fiber span, preamplied and dispersion compensated according to the post-compensation scheme.

The packaged chromatic dispersion compensator has been put into the climatic cell in order to simulate a typical central office environment. As the cell temperature was varied between 10°C and 40°C the package temperature was kept constant by means of an ILX temperature controller (not drawn on the figure).

Several test points have been arranged at the transmitter and receiver end: the multiwavelength meter monitored the wavelength stability over time, the power meter measured the total received optical power, the optical spectrum analyser (OSA) was used to record the received signal power as well as the optical spectrum shape and the SDH receiver displayed the performance analysis in terms of B1, B2sum, B3 and TSE in compliance with the ITU G.707 and G.783 specifications.

The two way opto-mechanical switch was used to avoid connection repeatability uncertainty.

Optical spectra

At the end of the trials we recorded the optical spectra at the preamplifier output, at the CDC output and at the receceiver input (Fabry-Pérot tunable filter output).

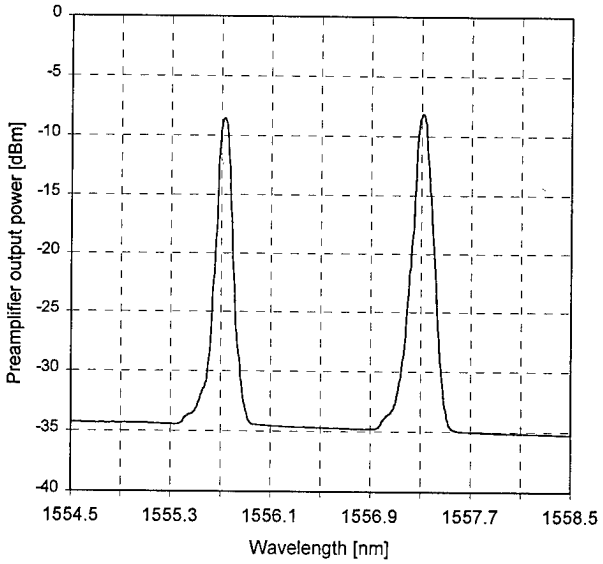

Figure 8 - Optical spectrum at the preamplifier output

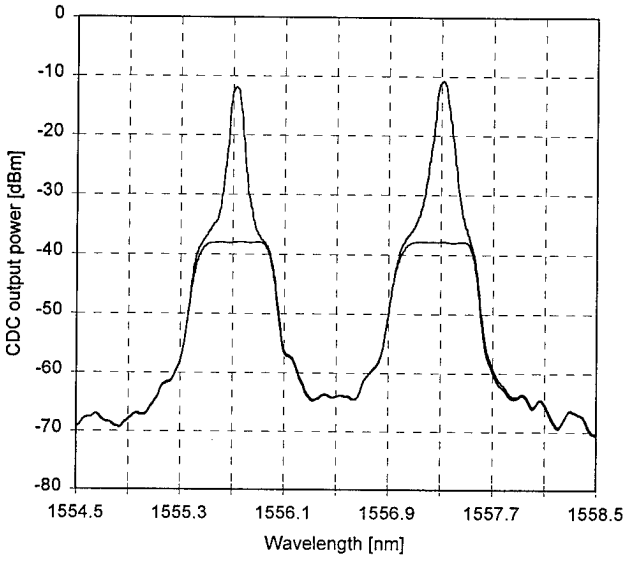

Figure 9 - Optical spectrum at the CDC output

As shown in figure 8 the signals are equalized within 1 dB. Figures 9 and 10 display the signals as well as the gratings reflection spectra.

The post-compensation scheme with the CDC placed between the receiver and the preamplier

allows for both device insertion loss compensation and amplified spontaneous emission (ASE) filtering.

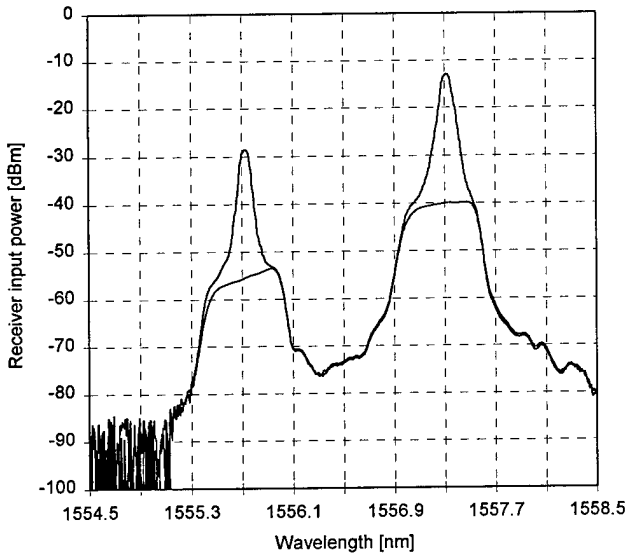

Figure 10 - Optical spectra at the receiver input

Device characterisation

The multi-wavelength chromatic dispersion compensator is made of two commercial 10 cm long chirped gratings centered at 1557.2 nm and 1555.7 nm with a bandwidth of about 0.5 nm and an out of band isolation higher than 25 dB.

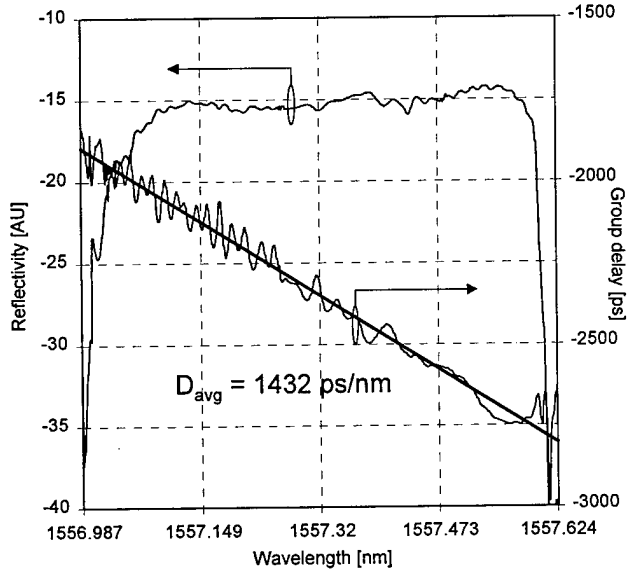

Figure 11 - Group delay and amplitude response of the 1557.2nm chirped grating with the package tuned at 30°C

A complete amplitude and phase characterisation of the 1557.36 nm chirped grating was performed in order to investigate the system performance in relation to the effective grating bandwidth, the group delay ripples and the grating temperature.
The amplitude and group delay responses have been measured with a typical experimental setup made up of a tunable laser source, a Mach-Zehnder external amplitude modulator driven by a 100 MHz sinusoidal RF signal and a network analyser.
The results are given in figure 11: the mean square estimate of the grating dispersion coefficient is 1432 ps/nm and the group delay curve appears highly rippled.
The typical chromatic dispersion coefficient of single mode step index fiber at 1550 nm is as high as 17 ps/nm/km; in the case of a perfectly linear group delay curve, the amount recovered by the grating should correspond to a fiber length of about

$$L = \frac{D_{grating}}{D_{fiber}} \cong 84km$$

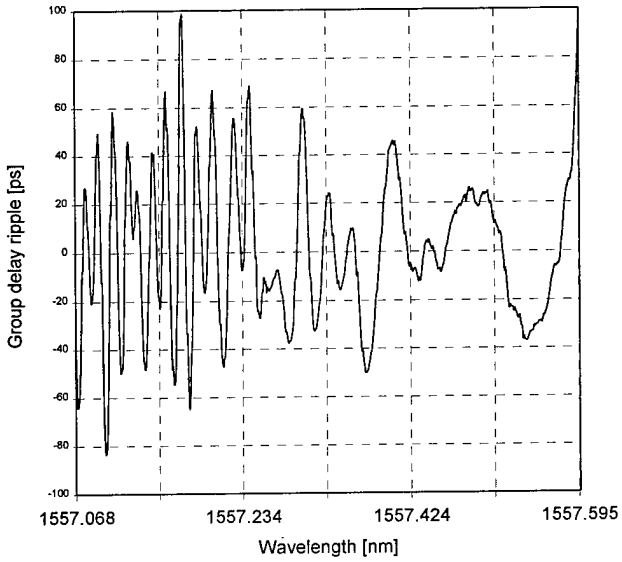

Figure 12 - In band group delay ripple amplitude of the 1557.2nm chirped grating with the package tuned at 30°C

As it can be clearly seen in figure 12, the grating is affected by strong ripples within the 3dB bandwidth: this will impair the compensator performance and modify the dispersion coefficient effectively seen by the optical signal, especially during operation in the shorter wavelength side.
The same measurement was performed with the compensator packaged into both the linear and

circular housings and no variations were noticed concerning the grating spectral properties. During the measurements the package temperature was set to 30°C as this was the temperature tuning condition chosen to carry out the system measurements as we will discuss in the next subsection.

Package tunability

Previous to extensive system characterisation, we carried out a useful performance analysis to get insight on the grating effective dispersion coefficient variation within the package tunability range.

The package temperature was varied from 10°C to 40°C with a 5°C step for a fixed received signal power of –30.5 dBm and a cell temperature of 25°C.

The results are shown in table 2 where the back to back and the uncompensated 160 km G.652 fiber span figures are also given for comparison.

When the package temperature is set to 10°C the CDC compensates the whole 160 km fiber length and the system recovers the back-to-back situation; at 15°C and 20°C, the device approaches its nominal condition and compensates for about 80 km. Further temperature increase shifts the group delay curve to longer wavelengths at a rate of 0.1nm/10°C so the signal enters more and more the highly rippled region leading to unpredictable operation. The performance degrades excepted at 30°C where there is a penalty minimum: this temperature was chosen to carry out the system measurements.

We discarded the 10°C temperature because the tunability range edges represent the failure threshold for the package reliability: in fact, the thermal uniformity cannot be assured anymore and the package might not guarantee the expected stable performance over time.

Performance analysis

As already pointed out, the 2.488 Gbit/s transceiver is able to display the defect/anomalies at different granularity levels.

In particular we report the results concerning the multiplex section error monitoring at the STM-16 level (B2sum) and the bit error rate (TSE) of the PDH 140 Mbit/s tributary.

Figures 13 and 14 display the error rate curves for the back to back, the 160 km uncompensated fiber span as well as the compensated (with CDC) configurations.

The compensated link curves are six: they are given for both the linear and the circular housings in the case of three different stationary cell temperatures (10°C, 25°C and 40°C).

The compensated curves overlap regardless of the package type or the cell temperature for both the anomaly parameters.

Table 2 - Chromatic dispersion compensator performance within the package tunability range

$T_{package}$	B2sum	TSE
10°C	1.02E-7	1.29E-7
15°C	1.43E-6	1.69E-6
20°C	3.48E-6	4.11E-6
25°C	1.69E-5	2.01E-5
30°C	7.63E-7	9.02E-7
35°C	4.43E-5	5.11E-5
40°C	2.28E-5	2.52E-5
B_to_b	1.47E-7	1.59E-7
160 km	1.03E-4	1.2E-4

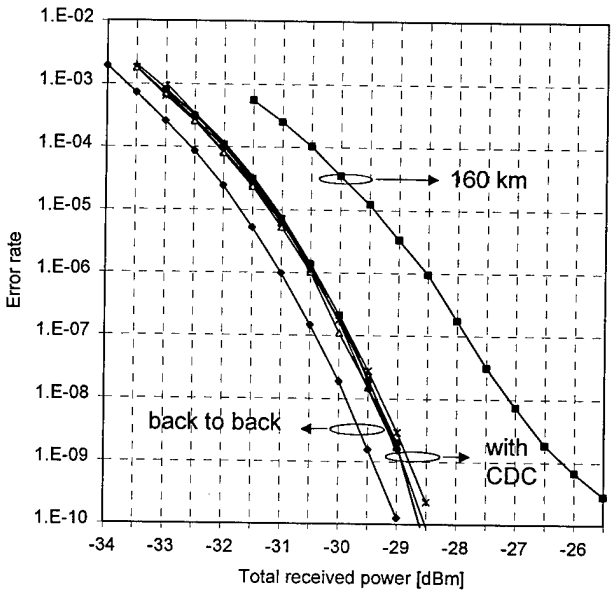

Figure 13 - B2sum curves versus total received power

As it is clearly visible the grating temperature set to 30°C enables a fiber length compensation much higher than 80 km. As a consequence, the system penalty @BER=10^{-9} is dramatically reduced from 3.5dB to 0.5 dB and the BER floor

of the uncompensated curve is completely eliminated.

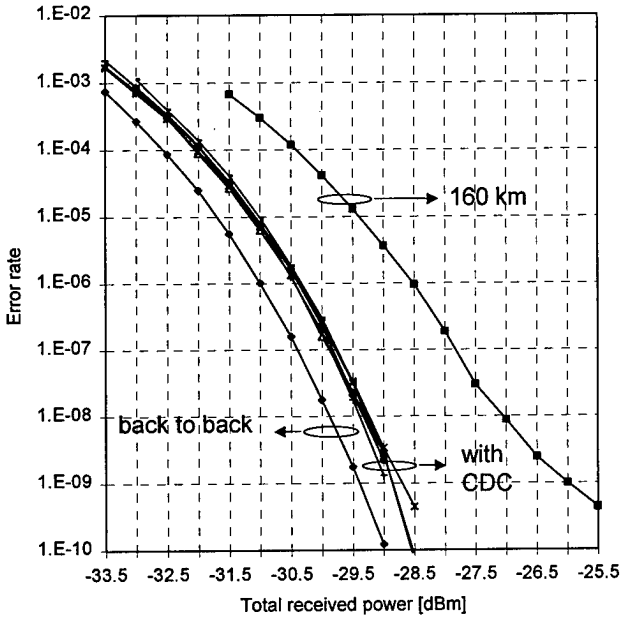

Figure 14 - TSE curves versus total received power

CONCLUSION

We have reported of two different packaging solutions designed for multiwavelength chromatic dispersion compensators.
A reliable and stable performance over time has been demonstrated by means of consecutive climatic cycles. Both packages reduce in fiber Bragg gratings wavelength thermal drift by a factor of ten and show low power requirements.
The 2.488 Gbit/s point to point system validation has showed that in case of highly rippled chirped gratings, the effective dispersion coefficient can be optimised thanks to package tunability. This feature is extremely wanted to recover grating/source mismatch. Finally the performance analysis at the STM-16 and at the 140 Mbit/s granularity levels confirmed that the two packages are suitable to operate in a Central Office environment (10-40°C).

ACKNOWLEDGEMENTS

This work was partially supported by the ACTS A046 PHOTOS project.

REFERENCES

[1] Fiber Gratings: Temperature and Mechanical Sensitivity of Narrow Band Transmission Filters Using Different Packaging Solutions – S.Pitassi, F. Pozzi, A. Marcone, V. Spano, Proceedings IWCS 1996
[2] Single-Mode Fibre Fractional Wave Devices and Polarisation Controllers – H.C. Lefevre, Electronics Letters, vol. 16, no. 20, 1980
[3] Fiber Grating Based Chromatic Dispersion Compensators: Packaging and System Performances – P.G. Peretta, F. Pozzi, M. Signorelli, Proceedings IWCS 1997

AUTHORS

Francesco Pozzi F.Pozzi@sirti.it

Francesco Pozzi was born in 1968 and received the doctor degree in Electronic Engineering from "Politecnico di Milano". He joined the R&D Dept. of SIRTI in 1995 where he is currently engaged in optical components as well as in testing of equipment based on WDM-SDH-ATM technology and networking as a Senior Engineer. In particular he has been working on optical amplifiers, fiber grating based components as well as high capacity communication systems. He is involved in ACTS PHOTOS and PROMETEO project with Telecom Italia and had some papers published in national and international conferences.

Raffaella Vinzio R.Vinzio@sirti.it

Raffaella Vinzio was born in 1971 in Varallo Sesia (Italy). She graduated in Electronic Engineering from Politecnico of Torino, Italy, and from Ecole Supérieure d'Electricité (SUPELEC), France, in 1996. She joined the R&D Dept. of SIRTI in 1997 where she is currently engaged in DWDM optical components and systems as a Junior engineer.

Andrea marcone A.Marcone@sirti.it

Andrea Marcone was born in Genova, Italy, in 1962. He received the doctor degree in Mechanical Engineering from "Politecnico di Milano". At the beginning of 1991 he joined R&D Dept. of SIRTI where he has been engaged in the project and development of accessories for telecommunications systems as a Senior Engineer.

DEVELOPMENT OF FLAT FLEXIBLE ERBIUM-DOPED FIBER-COIL SHEETS (EDF-SHEETS)

Katsuaki Kondo, Minoru Yoshida, Kazuo Imamura, Tatsuhiro Kawamura, Yasuhide Sudo, Yoshiyuki Imada, *Atsushi Toyohara

Mitsubishi Cable Industries, LTD. , Itami, Hyougo, Japan
*** NEC Corporation, Kawasaki, Kanagawa, Japan**

ABSTRACT

This paper reports on the development of flat flexible erbium-doped fiber-coil sheets (EDF-sheets). EDF-sheet is EDF arranged in a flat coil like alignment and laminated with resin for protection.

To assemble the EDF in small spaces inside the EDF amplifiers(EDFAs), we developed one-layer-EDF-sheets (1L-EDF-sheets) consisting of a layer of short EDFs and two-layer-EDF-sheets (2L-EDF-sheets) which consists of long EDFs stacked in two layers. The thickness of EDF-sheets are combined thickness of EDF coils and the laminating sheet. They are thinner than 1mm and flexible.

We made two samples, one was a 97mm × 65mm × 0.45mm sized 1L-EDF-sheet having EDF of erbium concentration of 984ppm, 11.2m long, and the other was a 105mm × 73mm × 0.7mm sized 2L-EDF-sheet having EDF of 320ppm, 34.4m long.

We confirmed that the amplifying characteristics of the EDF-sheets were the same as those of EDFs inputting high and low power signals of wavelength 1520 ~ 1580nm were input. From these experimental results we expect the EDF-sheets will be important for miniaturized EDFAs.

Introduction

EDFs play an important role as a amplifying medium of amplifiers of 1550nm band optical fibers for communications. [1],[2] Though the length differs depending on the erbium concentration, excitation light and the necessary amp gain settings, usually more than 10m of EDFs are necessary for highly efficient EDFAs used for communications. EDFs are wound to EDF-Reels(EDFRs) and assembled inside them.

Presently, the miniaturized EDFA has lead to the necessity of fitting optical and electronic parts in smaller spaces. However, reducing the space or fitting parts in narrow spaces is difficult with the EDFR which is hollow at the middle of the reel and has collars making dead spaces. Furthermore, the EDFR does not have the flexibility to be placed in open spaces of compact devices and can only be used in large open places.

There are methods which wind the EDF inside the device without using EDFRs. However, this method bends the EDF causing it to break. It is also difficult and time consuming to align the EDF inside.

To fit inside miniaturized EDFA and to make more spaces for other EDFR parts, we have developed the EDF-sheet which a flat coil of EDFs laminated with a resin protector.

EDF-sheets

EDF-sheets are EDFs aligned flat coil like without twisting, bending or crossing and laminated with resin for protection.

We completed an 1L-EDF-sheet consisting of one layer of short EDFs and a 2L-EDF-sheet which consists of long EDFs stacked in two layers. With the long EDFs, the EDF coil area is large because of the flatness of the coils. The 2L-EDF-sheets are stacked in two layers to keep the sheets from spreading out too large. The size of the 2L-EDF-sheets are thicker than one-layer sheets by an EDF coating diameter but can carry twice the length of one layer types. However, flat coils stacked in many layers to minimize the area will limit the flexibility of the EDF-sheets.

In this paper we report on 1L-EDF-sheets consisting of one layer of short EDFs and 2L-EDF-sheets which consists of two layers of long EDFs. Figure 1 and 2 show the coil shape inside of EDF-sheets of 1-L- and 2L-EDF-sheets respectively.

A reel with 0.25mm mandrel which is the outer diameter of EDF for 1L-EDF-sheet coating and a 0.50mm mandrel which the size of two EDFs for the 2L-EDF-sheet were used to wind the EDF into a flat coil. The mandrel of the reel has a cross section shaped like a track and has grooves so the EDF can be set in the shape of a letter S. EDF was wound to the reel at a 1N tension. EDF coils wound on the reel was fixed temporarily with an UV-curable resin which is the same resin as the EDF coating. The temporarily fixed EDF coils were taken off from the reel and laminated into EDF-sheets. The laminating material used was an environmentally safe, flexible fluororesin, 0.1mm thick.

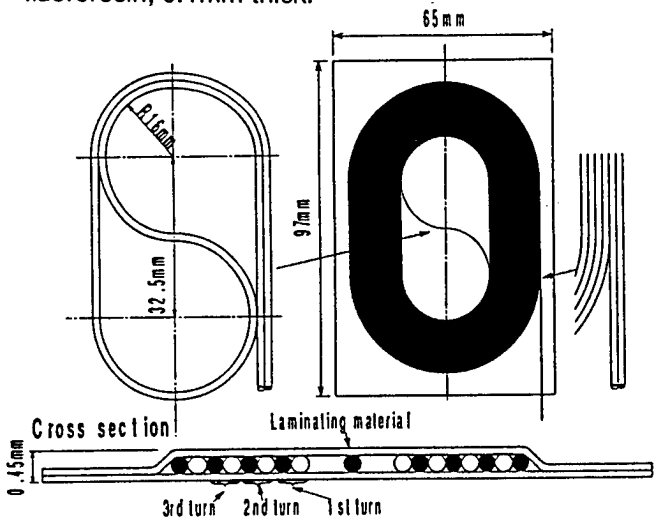

Figure 1 The structure of an 1L-EDF-sheet

Used EDF have erbium concentration of 984ppm, length 11.2m, and CL product 11kppm·m. The sheet size was 97mm × 65mm × 0.45mm.

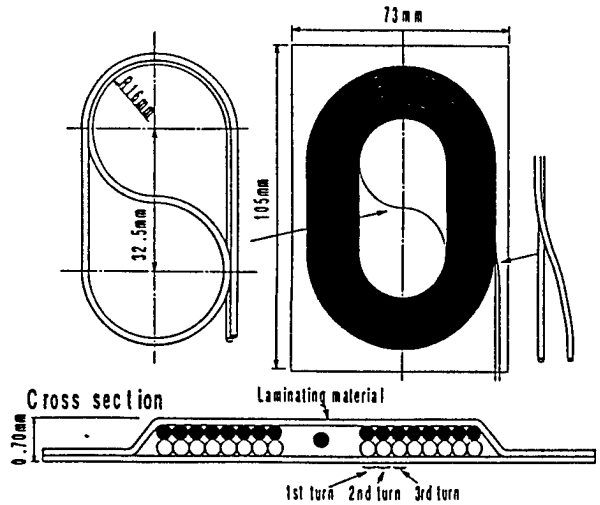

Figure 2 The structure of an 2L-EDF-sheet

Used EDF have erbium concentration of 320ppm, length 34.4m, and CL product 11kppm·m. The sheet size was 105mm × 73mm × 0.7mm.

The thickness of the sheets are the combined thickness of 0.25mm of EDF coil with 1L-EDF-sheet, 0.50mm with the 2L-EDF-sheets, to the thickness of the front and back laminated materials, each 0.1mm. The sheets are very thin, with the thickness of 1L-EDF-sheet at 0.45mm and the 2L-EDF-sheet at 0.7mm. EDF coils inside EDF-sheets had least bending radius of 16mm, the linear length of the track was 32.5mm. Sheet sizes differ depending on the length of the coil. The laminated sheet is a rectangle having 2mm spaces around the coil.

The relations with length of EDF and sheet sizes and ratio of sheet volume to EDFR volume with EDF-sheets are shown in Figure 3. The sheet size is represented by the length of the long side. The short side can be obtained by subtracting 32.5mm, the length of the linear length of the track, from the length of the long side. Compared to EDFR (Mitsubishi design: collar ϕ 40mm, thickness 8mm) when carrying less than 50m of EDF, EDF-sheets reduces the volume by 70%. The thin and flexible EDF-sheets can be easily assembled in the open spaces inside the device.

Not only is the EDF-sheets superior to EDFR because it has smaller volume but it is also superior because of its easiness to assemble into the EDFA.

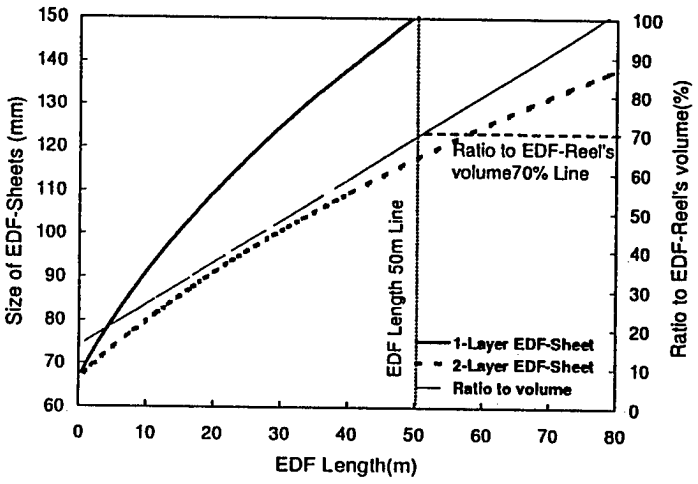

Figure 3 The relations of length of EDF and sheet sizes and ratio of sheet volume to EDFR volume with the one and two-layers EDF-sheets

EDFR which we compared with EDF-sheets is Mitsubishi design EDFR(collar ϕ 40mm, thickness 8mm).

Sample of EDF-sheets

We made samples of one and 2L-EDF-sheets. 1L-EDF-sheets used EDF having erbium concentration of 984ppm, length 11.2m, and CL product 11kppm·m. The sheet size was 97mm × 65mm × 0.45mm. The 2L-EDF-sheets used EDF having erbium concentration of 320ppm, length 34.4m, and CL product 11kppm·m. The sheet size was 105mm × 73mm × 0.7mm. The fiber parameters used are shown in Table 1. Figure 4 shows a completed 1L-EDF-sheet.

Table 1 The fiber parameters of EDFs which the 1L-EDF-sheets and the 2L-EDF-sheets used.

Fiber Parameter		1L-EDF-Sheets	2L-EDF-Sheets
Al	(ppm)	5000	10000
Er	(ppm)	984	320
Δ	(%)	1.42	1.34
λc	(μm)	0.98	0.87
MFD	(μm)	4.32	5.78

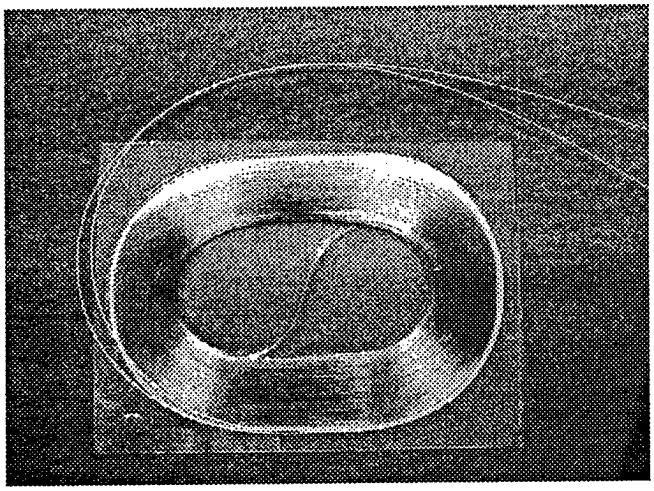

Figure 4 Picture of a completed 1L-EDF-sheet

Evaluation of the characteristics

The following items confirmed that there were no deterioration in the characteristics of the EDFs by their fabrication into EDF-sheets.

1. No change in the transmission loss characteristics when heat cycle was applied.

2. No difference in the spectral loss characteristics to EDF at room temperature.

3.No difference in the amplifying characteristics compared to EDF.

For tests 2 and 3, the 1L-EDF-sheet and the EDF from the same lot as those inside of the EDF-sheet stated in section 3 was used for comparison.

This EDF was tested in a loose state without any bends or twisting. We refer to this EDF from the same lot as "EDF for comparison" here after.

Temperature cycling test

The erbium doped on the EDF has absorbance at bandwidth 1550nm. This absorbance characteristic is temperature reliant. For this reason, when putting the EDF-sheets under heat cycling test, it is necessary to separate the temperature reliance of the erbium absorbance with the temperature reliance of transmission characteristics caused by fabrication in to flat coils and sheets.

To remove the temperature reliance of the erbium absorbance, we did the heat cycle test with a flat optical fiber coil sheet using a non-doped single mode fiber having the similar fiber parameter as EDF.

The conditions for the heat cycling test was as follows; temperatures: -40℃ to 75℃, transition rate: 1℃/min, dwell time at extremes of -40℃ and 75 ℃ : 15min., cycles:8. We evaluated the characteristics of the flat optical fiber coil sheet by analyzing the change in the transmission loss at wavelength 1550nm. The results are shown in Figure 6. The change in the transmission loss of flat optical fiber coil sheets are a mere±0.02dB, small enough to ignore. From these results we conclude that there are no temperature reliance of the transmission characteristic caused by fabrication into flat coils or sheets.

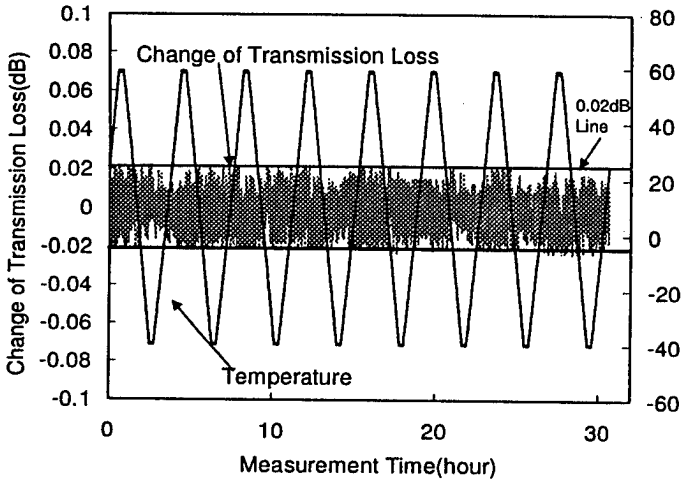

Figure 6 The change in the transmission loss at wavelength 1550nm. of the flat optical fiber coil sheet for the heat cycling test

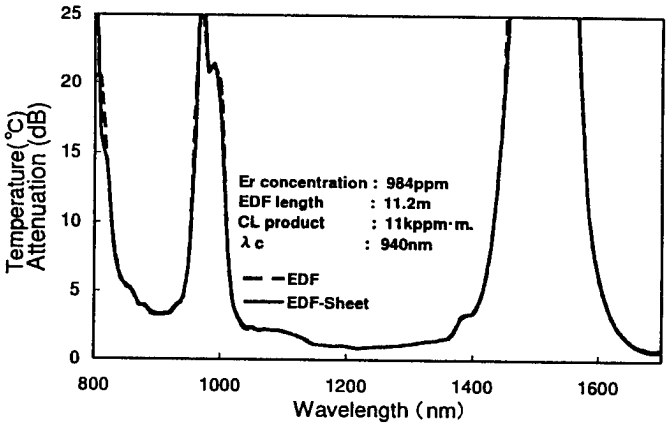

Figure 7 The spectral loss of EDF-sheets and EDF

Spectral loss

Using a white light source in the wave length band of 800~1700nm , the spectral loss of EDF-sheets and EDF for comparison was compared by a Spectrum analyzer.

The results are shown in Figure 7. The spectral loss of EDF-sheets and EDF for comparison was less than 0.02dB up to wavelength 1700nm. The results show EDF has not changed by fabrication into sheets as there was no increase in the loss.

Amplifying characteristics

1550nm band amplifying characteristics of EDF-sheets and EDF for comparison was compared. The excitation system of EDF used an LD-optical source of wavelength 1480nm with rear excitation of 70mW. The input power signal wavelengths were 1520nm ~ 1580nm, the gain wavelength reliance during input of high and low power signals of EDF-sheets were analyzed. Figure 8 shows the results of gain dependencies of EDF-sheets on wavelength of input signals and the difference in amplification with EDF for comparison . Input powers of low power signals is –39.5dBm, and those of high power signals is –3.5dBm. The EDF-sheets had the same level of amplification as EDF for comparison (± 0.11dB) during input of both low and high power signals. The results show that the amplification characteristics of the EDF- sheets have not changed by fabrication into sheets.

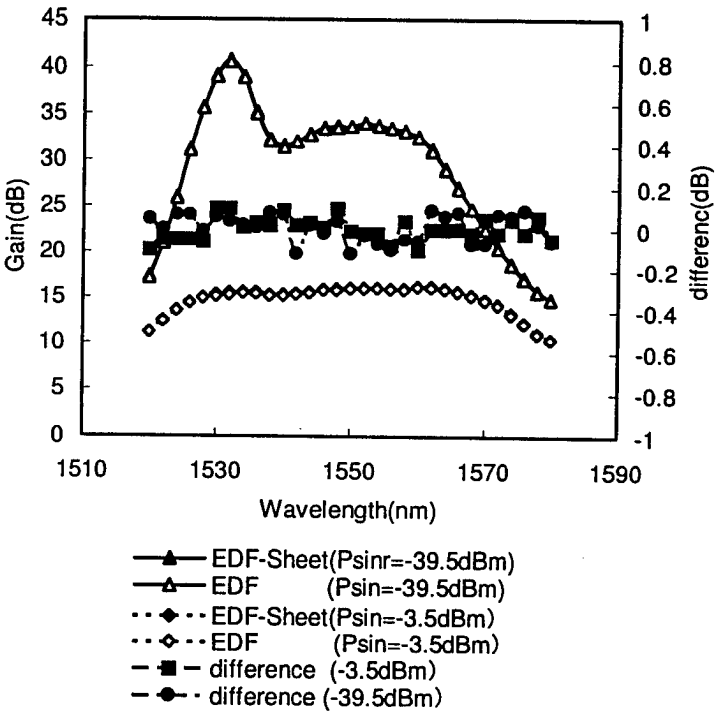

Figure 8 Gain dependencies of EDF-sheets on wavelength and the difference in amplification with EDF for comparison during input of –3.5dBm and –39.5dBm signals。

Conclusion

The EDF-sheets we developed can carry EDF in a small volume, minimizing the volume of EDFR more than 70%. The EDF-sheets are thin and can be easily assembled into open spaces of EDFA. We evaluated the EDF-sheets for their characteristics and found that there are no temperature reliance of the transmission characteristic caused by fabrication into flat coils or sheets. There were no difference in the spectral loss compared to EDF before fabrication into sheets and the amplification characteristics of the EDF-sheets did not deteriorate at the 1.55μm band. EDF-sheets have the same characteristics as the conventional EDFR which winds the EDF on reels, but has a smaller volume and can make the assembly of EDFAs smaller and easier. EDF-sheets are expected to play an important role as a device for high-efficient compact amplifiers for communications.

Reference

(1) M. Yoshida, et. al., "Development of compact Er^{3+} -doped fiber amplifiers for practical applications", in Technical Digest on Optical Amplifiers and their Applications, **13**, pp.282-285 (1990)

(2) M. Nakazawa, et. al.,"Efficient Er^{3+} --doped fiber amplifier pumped by 1.48μm InGaAsP laser diode", Appl. Phys. Lett., 54, pp.295-297(1989)

Authors

Katsuaki Kondo
Mitsubishi Cable Industries, Ltd.
4-3, Ikejiri, Itami, Hyougo, 664-0027, Japan

Mr. Kondo, staff research engineer of Electronics & Communication Research Dept., is engaged in design and development of optical components. He received his M.S. degree in Electromagnetic Energy Engineering from Osaka University in 1996.

Minoru Yoshida
Mitsubishi Cable Industries, Ltd.
4-3, Ikejiri, Itami, Hyougo, 664-0027, Japan

Minoru Yoshida received his M.S. degree in Electromagnetic Energy Engineering from the institute of Laser Engineering of Osaka University in March 1985. His research for his master's thesis was related to laser-induced microscopic lithography and machining for laser fusion. Currently, he is working for Electronics & Communication Research Dept. of Mitsubishi Cable Industries, Ltd., specializing in the optical fiber communication field. He is interested in optical amplifiers for optical fiber communication and fiber lasers by the rare-earth doped optical fibers.

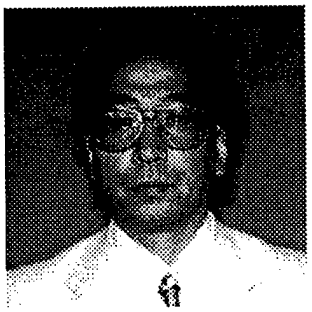

Kazuo Imamura
Mitsubishi Cable Industries, Ltd.
4-3, Ikejiri, Itami, Hyougo, 664-0027, Japan

Mr. Imamura, senior research engineer of Electronics & Communication Research Dept., is engaged in design and development of optical subscriber systems and optical components. He received his M.S. degree in Electrical Engineering from Osaka University in 1983. He is a member of The Institute of Electrical Engineers of Japan and The Japan Society of Applied Physics.

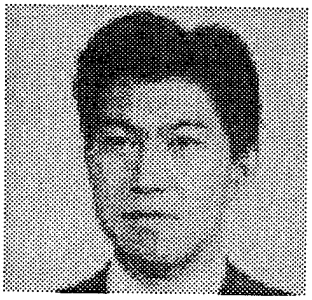

Tatsuhiro Kawamura
Mitsubishi Cable
Industries, Ltd.
4-3, Ikejiri, Itami,
Hyougo, 664-0027,
Japan

Mr. Kawamura, staff engineer of RF & Optical System Engineering Section, is engaged in design and development of optical system. He received his B.E. degree in Communication Engineering from Waseda University in 1993. He is a member of The Institute of Electrical Engineers of Japan .

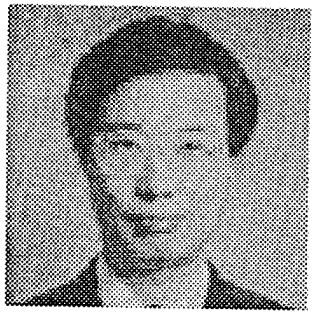

Yasuhide Sudo
Mitsubishi Cable
Industries, Ltd.
4-3, Ikejiri, Itami,
Hyougo, 664-0027,
Japan

Mr. Sudo, manager of RF & Optical System Engineering Section, is engaged in production and development of optical transmission equipments and subscriber equipments . He received his M.S. degree in Electrical Engineering from kyoto University in 1975.

Yoshiyuki Imada
Mitsubishi Cable
Industries, Ltd.
4-3, Ikejiri, Itami,
Hyougo, 664-0027,
Japan

Mr. Imada, manager of Electronics & Communication Research Dept. He received his B.E. degree in Electrical Engineering from Osaka University in 1967. He is a member of IEEE.

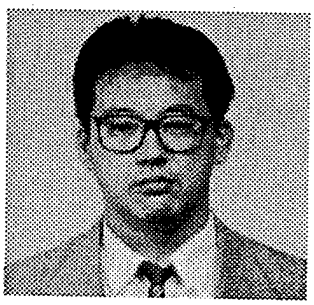

Atsushi Toyohara
NEC Corporation
1753 Shimonumabe,
Nakahara-ku,
Kawasaki Kanagawa,
211-8666 JAPAN

Atsushi Toyohara received the B.E. degree in electro-communication engineering from Osaka Electro-Communication University in 1987. He joined NEC Corporation in 1987, and is now Assistant manager of the 1st Development Department, Transmission Devices Division. He is engaged in the development of optical fiber amplifiers. Mr. Toyohara is a member of the Institute of Electronics, Information and Communication Engineers.

A new technique for measuring the parameters of channels, cables, and connecting hardware.

Clifford R. Curry

Leviton Telcom, Bothell, Washington

ABSTRACT

When evaluating the performance of an unshielded twisted pair cable, channel, or connector, extensive measurements are needed. The four wire-pairs in the device must be measured from both the near and far ends in order to determine the NEXT, FEXT, attenuation and return loss. This requires an eight port measuring device, which is expensive and not readily available. In this paper, I describe a method to characterize the entire device with four port measurements from only one side of the device. This is performed by taking multiple measurements from one side of the device while the other side is loaded with various known standards. In this way, for example, the FEXT of a channel may be evaluated without ever measuring at the far end of the cable. The cable, channel, or connector is modeled as a reciprocal eight port network. Finally, the measurement technique is verified by comparing eight port measurements of a twisted pair cable with results derived from five four port measurements of one end of the cable. Results show that the technique has promise, although more work is required to achieve the level of accuracy needed for cat 5 measurements.

1.0 INTRODUCTION

This measurement technique is derived in these steps: first, the equations that relate the four by four scattering matrix at one side of the device under test to the loading present at the other side are formulated so that the 64 parameters of the device under test enter into the equations in linear fashion. The linear equations theoretically allow solution for the 64 unknowns up to an arbitrary scaling factor. This unknown scaling factor is found by requiring that the final scattering matrix derived for the device under test be symmetrical.

Although the solution of a set of linear equations is a theoretical possibility, the question remains as to how many and what kinds of simple loads provide sufficient information for a unique solution to be determined. This is resolved by extensive computer simulations of the problem using various combinations of simple, 4 port loads created from throughs, shorts, opens and loads. Taking all through combinations, all 2-load and 2-short combinations, and all 2-load and 2-open combinations, as well as all shorts, all opens, and all loads, 264 combinations of five loads were found to provide sufficient information. All of these combinations involve two through-type four ports and three open-short-load type four port loads. Since the problem has been formulated as a linear system, sufficiency of information can be resolved by using the singular value decomposition technique.

Many N-port networks can be naturally divided into an input side and an output side, each of which has N/2 ports. This is definitely true of Cat 5 style UTP (unshielded twisted pair) cable and connecting hardware, which consists of four channel pairs. The 8 by 8 matrix describing the channel interaction has 64 entries. Cables and connectors are reciprocal devices, so that their terminal behavior can be described by a symmetrical, 8 by 8 matrix. In the following, we will use a number scheme for 8-ports as shown in Figure 1.

Figure 1: Numbering scheme used in this paper for eight port networks

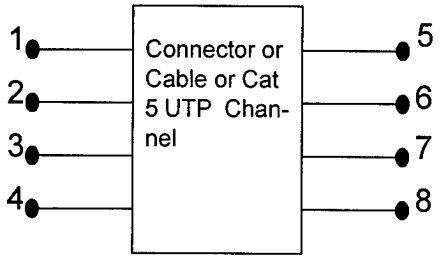

There are 36 unique numbers that describe such an eight port. The unique entries in the scattering matrix description of the network are as shown in equation 1. Because the matrix is symmetrical about the diagonal, only the upper right half is shown.

$$S = \begin{bmatrix} rl & nxt1 & nxt1 & nxt1 & atten & fext & fext & fext \\ & rl & nxt1 & nxt1 & fext & atten & fext & fext \\ & & rl & nxt1 & fext & fext & aten & fext \\ & & & rl & fext & fext & fext & atten \\ & & & & rl & nxt2 & nxt2 & nxt2 \\ & & & & & rl & nxt2 & nxt2 \\ & & & & & & rl & nxt2 \\ & & & & & & & rl \end{bmatrix} \quad \text{(EQ 1)}$$

In equation 1, the symbol rl stands for the 8 return loss measurements of the device, $nxt1$ stands for the 6 values of next from side one, $nxt2$ stands for the 6 values of is the next from side two, $atten$ stands for the 4 attenuation measurements, and $fext$ stands for the 12 values of far end crosstalk.

A direct measurement of FEXT requires that a source be connected to a channel on one side of the device, and the crosstalk be measured at the other side of the device. However, it is possible to determine all 36 of the parameters of the device (including FEXT) without measuring or driving any of the ports on the second side.

When measuring from one side, the 4 by 4 input scattering matrix of the device under test consists of four return loss's and the six nexts from side one. This is measured by loading the output ports of the device with four, uncoupled, 100 ohm resistors. When the output of the device is loaded with other than this standard load, the measured scattering matrix at the device's input depends on more than just these 10 parameters: every single one of the s_parameters of the device under test effects the input measurement. It is this fact that allows multiple input measurements, under different output loading conditions, to be used to derive all the device parameters.

2.0 THE PROPOSED TECHNIQUE

Breaking the eight by eight scattering matrix of the device under test into four quadrants,

$$Smat = \begin{bmatrix} s_{11} & s_{12} \\ s_{21} & s_{22} \end{bmatrix}, \quad \text{(EQ 2)}$$

allows the 4 by 4 input scattering matrix measured at the input of the device under test to be expressed as a function of the load connected at its output [1]:

$$S_{in} = s_{11} + s_{12} S_{load} (1_{4x4} - s_{22} S_{load})^{-1} s_{21} . \quad \text{(EQ 3)}$$

In equation 3, the symbol 1_{nxn} stands for the n by n identity matrix.

By terminating the device under test with several different known loads, and measuring S_{in}, many equations in the 64 unknowns s_{11}, s_{12}, s_{21}, and s_{22} can be written. Unfortunately, these equations are nonlinear, and can be difficult to solve.

By reformulating equation 3, a set of linear equations in the unknowns can be written. This is done by transferring the parameters of the device under test into a so called "chain-s matrix" [2]. This chain-s matrix is defined in this way:

$$Chain = \begin{bmatrix} c_{11} & c_{12} \\ c_{21} & c_{22} \end{bmatrix} = \begin{bmatrix} s_{12} - s_{11} s_{21}^{-1} s_{22} & s_{11} s_{21}^{-1} \\ -s_{21}^{-1} s_{22} & s_{21}^{-1} \end{bmatrix} . \quad \text{(EQ 4)}$$

The s matrix can be derived from the chain-s matrix using

$$Smat = \begin{bmatrix} c_{12}c_{22}^{-1} & c_{11} - (c_{12} - c_{22}^{-1}c_{21}) \\ c_{22}^{-1} & -c_{22}^{-1}c_{21} \end{bmatrix}. \quad \text{(EQ 5)}$$

Linear equations for the chain-s parameters of the device under test, equivalent to equation 3, are then [2]

$$S_{in}(c_{21}S_{load} + c_{22}) - (c_{11}S_{load} + c_{12}) = 0 . \text{(EQ 6)}$$

When equation 6 is multiplied out, the terms multiplying each of the 64 entries of the chain-s matrix can be gathered in a matrix of known numbers. Each measurement of a four port load results in 16 equations in 64 unknowns of the form

$$\begin{matrix} \longleftarrow 64 \longrightarrow \\ \uparrow \\ 16 \\ \downarrow \end{matrix} \begin{bmatrix} Coefficients \end{bmatrix} \begin{bmatrix} c1 \\ c2 \\ \dots \\ c64 \end{bmatrix} = 0 . \quad \text{(EQ 7)}$$

In equation 7, the coefficients are expressions that contain the entries of S_{in} and S_{load}. The unknown vector consists of the sixty four entries of the chain-s matrix, here denoted as c_1 through c_{64}. When equation 7 is solved, the chain-s matrix is known, and so the scattering matrix of the device under test is known.

The solution of equation 7 lies in the null space of the coefficient matrix. After one measurement, 16 equations are known, after 2 measurements, 32 equations are known, and so on. Theoretically, measurement with 4 different loads would provide 64 equations in 64 unknowns, and the null space of the coefficient matrix (in this case a 64 by 64 matrix) would be one dimensional. Therefore the solution vector, $\begin{bmatrix} c1 & c2 & \dots & c64 \end{bmatrix}^t$, would be known up to an arbitrary complex scaling factor. In order to find this scale factor, additional information must be used.

Since connecting hardware or cabling systems are reciprocal devices, this fact can be used to solve for the scaling factor. Once the entries of the chain-s matrix are found using equation 7, the scaling factor that multiplies the chain-s matrix in order to result in a symmetric s_matrix is the solution of

$$k^2 [1_{4x4}] = (c_{22}^{-1})^t (c_{11} - c_{12}c_{22}^{-1}c_{21}) . \quad \text{(EQ 8)}$$

Unfortunately, there are two solutions to equation 8. The sign ambiguity must be resolved with still even more information. The effect of choosing a positive or negative k in equation 8 is to change the sign of the attenuation of the device under test. At low frequencies, there is very little phase shift in a connector or cable channel, so that the sign of k that produces a positive real part of the attenuation can be chosen. As the frequency rises, the attenuation will change phase in a smooth, periodic fashion. Therefore, the appropriate sign of k is that which leads to a continuous attenuation phase as frequency increases.

Although theoretically the solution of equation 7 can be found with only four loads, simulations have shown that five or more arbitrary loads are needed. This has not been proven rigorously, although my investigations agree with another researcher's recently published conclusions[3]. In fact, there are only a few loads that are practical to construct: those consisting of opens, loads, shorts, and throughs. Simulations involving 18 different simple open, short, load, and through four port loads have shown that 264 combinations of the loads taken 5 at a time will lead to a solution of equation 7. All of those solutions involve two different through type four ports and three open-short-load combinations.

For example, all the parameters of a four pair UTP cable channel can be found by measuring at only one side, while loading the other end consecutively with the five loads in figure 2.

Figure 2: Five loads that allow determination of attenuation, FEXT, and NEXT from both sides of a four pair cable channel from measurements at one side only

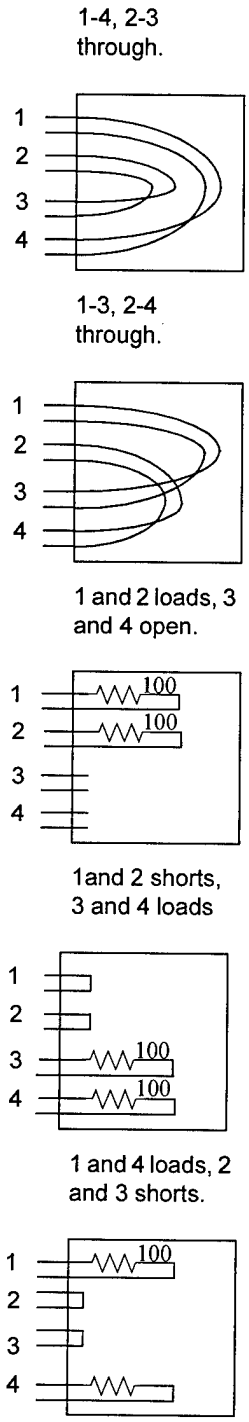

The five loads are figure 2 have the scattering matrices of equation 9.

$$S_{I1} = \begin{bmatrix} 0 & 1 & 0 & 0 \\ 1 & 0 & 0 & 0 \\ 0 & 0 & 0 & 1 \\ 0 & 0 & 1 & 0 \end{bmatrix} \qquad S_{I2} = \begin{bmatrix} 0 & 0 & 1 & 0 \\ 0 & 0 & 0 & 1 \\ 1 & 0 & 0 & 0 \\ 0 & 1 & 0 & 0 \end{bmatrix}$$

$$S_{I3} = \begin{bmatrix} 0 & 0 & 0 & 0 \\ 0 & 0 & 0 & 0 \\ 0 & 0 & 1 & 0 \\ 0 & 0 & 0 & 1 \end{bmatrix}$$

$$S_{I4} = \begin{bmatrix} 0 & 0 & 0 & 0 \\ 0 & -1 & 0 & 0 \\ 0 & 0 & -1 & 0 \\ 0 & 0 & 0 & 0 \end{bmatrix} \qquad S_{I5} = \begin{bmatrix} -1 & 0 & 0 & 0 \\ 0 & -1 & 0 & 0 \\ 0 & 0 & 0 & 0 \\ 0 & 0 & 0 & 0 \end{bmatrix}$$

(EQ 9)

Equation 7 is solved with the numerical technique called the singular value decomposition[4]. After measuring the five loads of figure 2, the coefficient matrix has 5*16=80 rows and 16 columns. A basis for the null space of the coefficient matrix as derived from the singular value decomposition is just a single vector, of length 64. This is the $[c1\ c2\ \ldots\ c64]^t$, solution of equation 7. The scale factor is then solved for using equation 8. Finally, the scattering matrix of the cable channel is found from equation 5. Thus, by making five, four port measurements, the entire eight by eight scattering matrix of the cable channel is found.

3.0 EXAMPLE

Two, four pair, UTP channels were measured with this technique, and the computed results compared with the direct measurement of the eight port s-parameters. Measurements of the balanced parameters of the pairs were made with an eight port s-parameter test set, connected to eight baluns. Measurements of one side of the channels were made with the first four ports of the test set. The five loads of figure 2 were made from integrated circuit sockets, with chip resistors soldered between the pins for the loads, and short wires for the throughs and shorts.

The first channel consisted of a pigtail of twisted pairs, a jack, a three meter patch cord, a second jack, 90 meters of high quality UTP cable, a third jack, a second three meter patch cord, a fourth jack, and another pigtail of wires.

One hundred fifty points were taken from 1MHz to 100MHz, logarithmically spaced. For this measurement, no attempt was made to determine the correct phase of the calculated s-matrix, as only the magnitudes were of interest in this case.

Figure 3 shows a graph of the attenuation of pair one. The calculated attenuation, derived from the five four port measurements agrees well with the directly measured attenuation value.

Figure 3: Attenuation, pair 1 Measured directly, and computed from measurements of one side

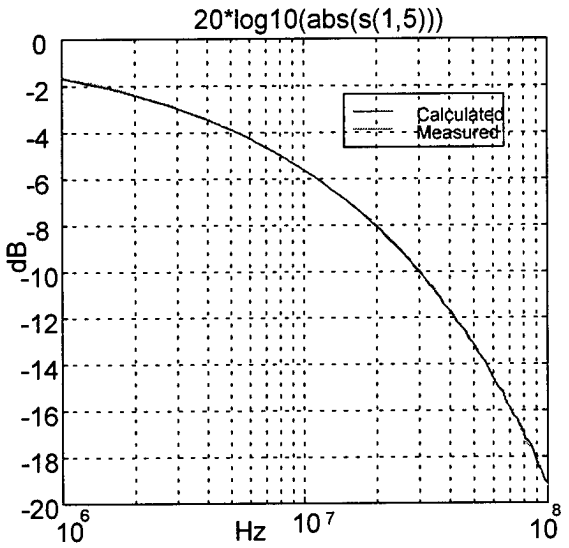

Figure 4 shows a FEXT calculation, and the direct measurement. The FEXT as derived from the calculations differs significantly from the directly measured FEXT. The calculated value exhibits more noise-like variation, and there are large deviations between the measured and calculated values at high and low frequencies. Best results are obtained in the middle frequencies, where the attenuation and the FEXT of the channel are both in the mid range.

Figure 4: FEXT comparison, direct measurement and calculation, pairs 1 to 3.

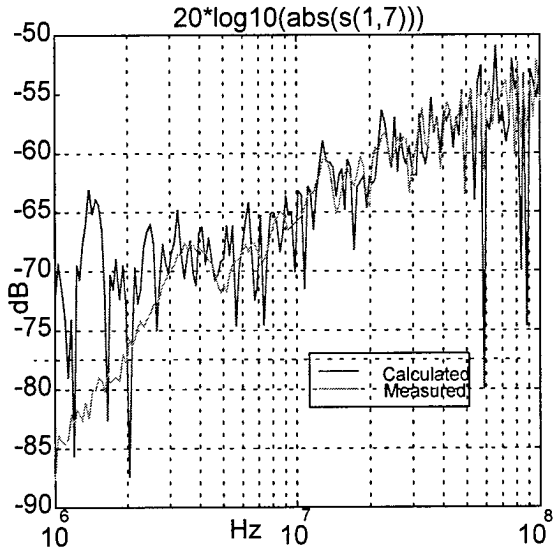

Figure 5 shows the Next from the far side between pairs 3 and 4. Noise and dynamic range problems are evident in the computed responses, especially at low frequencies where the Far side Next is very small.

Figure 5: Far side Next from calculation and from measurements, pairs 3 and 4.

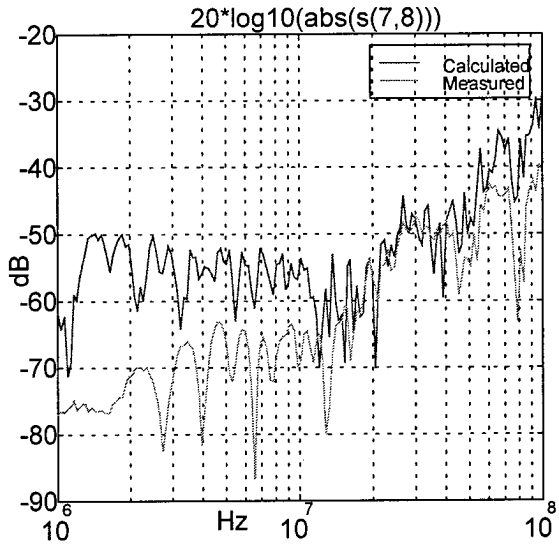

A second channel was measured. This one, too, was a channel of approximately 100 meters in length, using advanced cat 5 cable. For this channel, both the magnitude and phase

of the calculated data are compared to the eight port measurements.

To decide on the sign of the solution to the quadratic of equation 8, both solutions were taken as a possible correct solution: then a straight line approximation of the past (unwrapped) phase of the transfer function of channel 1 was formed. The possible correct solution that was closest to the extrapolated linear phase was taken as the true solution. For this to work, the phase of the transfer function must be sampled with sufficient fineness so that it does not change too much from sample to sample. Since the speed of signals on a cable is about 3/4 the speed of light, one would expect the phase to change 1.60 degrees per megahertz in a one meter length of cable, or 160 degrees per megahertz for the channel.

For this data, 333 evenly spaced points were take over the 100 MHz frequency range of the measurement. This amounts to an expected 50 degrees of phase shift between frequency samples, so that it was easy to unwrap the phase into a linear progression. Measurements of this channel were made with a smaller I.F. bandwidth on the network analyzer, (300Hz), in an attempt to improve the signal to noise ratio of the measurement.

Figure 6 shows the magnitude of the attenuation of pair 1 in the channel. The calculated response shows considerable error at high frequencies. The source of this error is undetermined.

Figure 6: Magnitude of pair 1 attenuation, calculated from measurements, and directly measured.

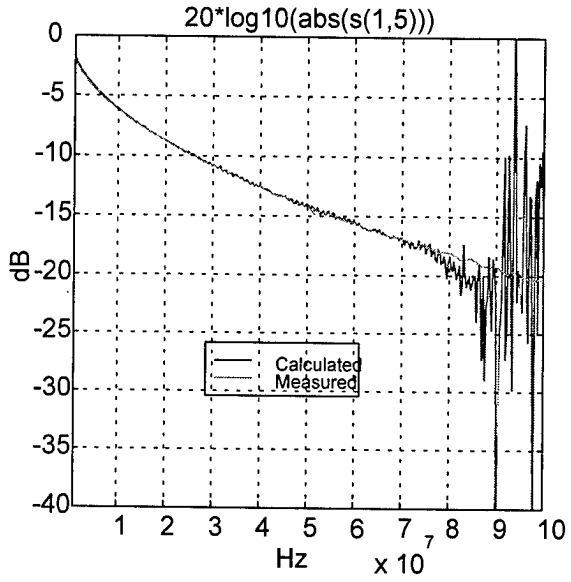

Using linear extrapolation on the unwrapped phase is an effective method for choosing the sign of the root of equation 8, as shown by the calculated and measured phase shift of the pair 1 attenuation, figure 7.

Figure 7: Phase of the pair 1 transmission, calculated from near end measurements, and measured directly.

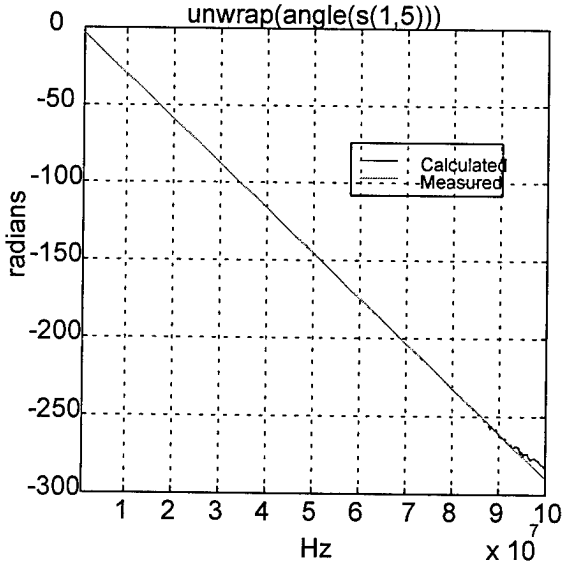

At lower frequencies, the two curves of figure 7 are indistinguishable. At high frequencies, where the magnitude error shown in figure 6 is large, the phase error is appreciable, also.

Determination of FEXT on this channel is shown in figures 8 and 9, showing the magnitude and phase, respectively.

Figure 8: FEXT measured from both ends, and calculated from near end measurements only

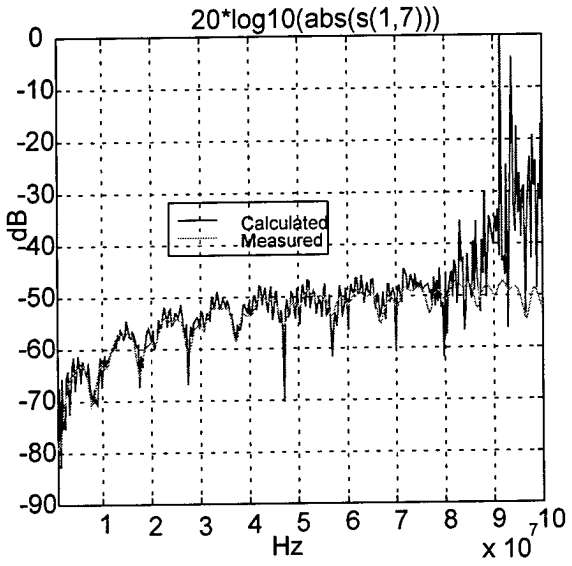

As in figure 6, figure 8 shows some problems in calculation of the parameters at frequencies greater than 80 MHz.

Figure 9: Phase of FEXT, pair 1 to 3, calculated from one sided measurements, and measured directly.

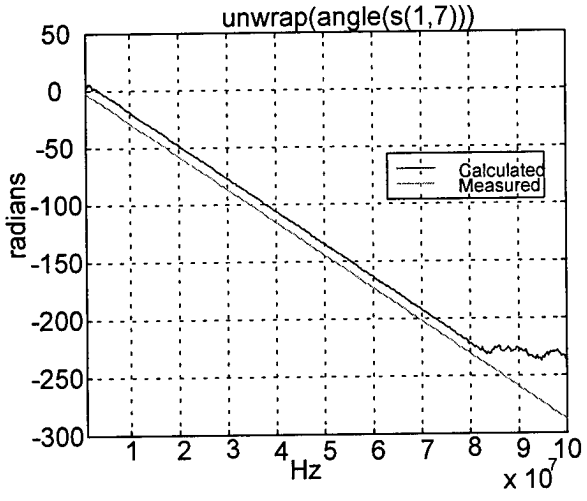

A graph of the unwrapped phase estimate of the measured and calculated FEXT, figure 9, indicates two problems with the simple linear extrapolation scheme for determining the correct sign of the quadratic root of equation 8. At start-up, the extrapolation is subject to errors due to the measurements error and the small amount of data available. Then at high frequencies, errors in the measurement can cause the linear extrapolation to get off track, making wrong decisions about the sign of the quadratic root.

4.0 CONCLUSION

A new technique for evaluating 4-pair cables, channels, and connecting hardware has been presented. The technique involves a test set with half the number of ports that a direct measurement would require. Active measuring instrumentation is only needed at one side of the device. Results show that careful measurements must be performed to make the technique accurate. It is easier to determine attenuation with this technique than to estimate for FEXT and Next of a channel. Although careful measurements and more work at perfecting measurement methodologies are needed, the technique shows promise as a method that reduces the hardware needed to make multiport measurements.

5.0 REFERENCES

[1]R. W. Newcomb, *Linear Multiport Synthesis*. New York: McGraw-Hill, 1964.

[2]K. Silvonen "LMR 16- A Self Calibration Procedure for a Leaky Network Analyzer", *IEEE Trans. on Microwave Theory and Techniques,* Vol. 45, No. 7, pp. 1041-1049, July, 1997.

[3]D.E.Bockelman, and W.R. Eisentatdt, "Calibration and Verification of the Pure-Mode Vector Network Analyzer," *IEEE Trans. on Microwave Theory and Techniques,* Vol. 46,No. 7, pp. 1009-1012, July, 1998.

[4]G. H. Golub, and C.F.Van Loan, *Matrix Computations*, Baltimore: John Hopkins, 1989.

Clifford R. Curry, Ph.D.
Electrical Engineer
Leviton Telcom
2222 222nd Street SE.
Bothell, WA. 98021-4422

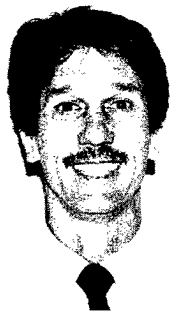

Clifford R. Curry was born in Wichita, KS. He received the B. S. E. E. degree from the University of Illinois in 1975, the M. S. E. E. degree from Wichita State University, Wichita, KS., in 1977, and the Ph.D. degree in Electrical Engineering from the University of Washington, Seattle, WA. in 1997.

From 1978 to 1980 he was a Design Engineer at John Fluke Manufacturing Company in Everett, WA. From 1980 to 1984 he designed ultrasonic imaging medical equipment for Advanced Technology Laboratories in Bellevue, WA. From 1985 to 1990 he was Principal Engineer at Quinton Instrument Company in Seattle, WA, designing patient monitoring instrumentation for cardiology applications. Since 1997 he has been an Electrical Engineer at Leviton Telcom in Bothell, WA, where he is responsible for design of advanced connectors for data communications.

HOW EFT DISTURBANCES AFFECT FAST ETHERNET PERFORMANCE IN MULTICHANNEL PLASTIC AND METAL RACEWAYS

Mirek Michalak

The Wiremold Company, West Hartford, Connecticut

ABSTRACT

Wire and cable management systems increase workstation flexibility by integrating power, voice, and data cabling in a multi-channel raceway. However, in a typical commercial building, power lines carry transients, which could potentially affect the integrity of the data transmitted on communications cabling located in the same raceway.

Statistics show that Ethernet is the most popular physical layer LAN (local area network) in use today. Therefore, this document focuses on the effect of electrical fast transient (EFT) disturbances, on Fast Ethernet (100Mbps) performance. It also evaluates the effect of physical separation of power and data cabling on high-speed network performance. Furthermore, the differences in LAN performance in plastic and metal raceways, with respect to EFT disturbances present on power lines, are presented.

With Gigabit per second transmissions soon becoming a reality, many cable manufacturers offer the next generation of UTP cable (referred in this document as Gbps) with improved performance. The immunity to noise of category 5 and Gbps UTP cables is compared.

INTRODUCTION

EFT is a class of electromagnetic interference that is characterized by a burst of repetitive (nonperiodic or periodic) and relatively short duration pulses. Of particular concern are EFT disturbances most often caused by transient currents (commonly called arcing) during a make or break of an electrical contact, and the sudden changes in magnitude and direction of currents of everyday office equipment, such as copiers, pencil sharpeners, power switches, etc. The resulting arcs generate EFT disturbances. What makes this phenomenon of particular significance to data transmission is that the frequency spectrum of the transient (MHz range) is in the vicinity of the frequency band within which information-carrying signals of the high-speed LAN protocols are transmitted on copper media.

Two types of surface mounted raceways are available on the market today: plastic and metal. Plastic, unlike metal, is completely transparent to the electromagnetic fields. In a typical multi-channel raceway, communications cabling runs parallel to power lines in adjoining compartments - in some instances over significant distances (90 m maximum). Furthermore, the most commonly used media for network wiring is unshielded twisted pair (UTP). In this scenario, EFT disturbances present on the power lines transfer over by capacitive and inductive coupling. Previous work related to this subject [1] provided information about the common and differential mode voltages in category 5 UTP cables coupled from parallel power lines.

If EFT disturbances are strong enough, they could possibly corrupt data signals or impair the operation of computers and any information technology products. In the

present work, a real network environment is used to check how transients affect data transmission.

CONFIGURATION AND TEST PROCEDURES

The test-bed was constructed of 90 m of non-metallic (plastic) three-compartment raceway, and 90 m of metal two-compartment raceway. The raceways were supported in a serpentine fashion on wooden scaffolding as shown in Figure 1. The configuration was such that adjacent raceway sections were always separated by at least 2 ft (0.6 m).

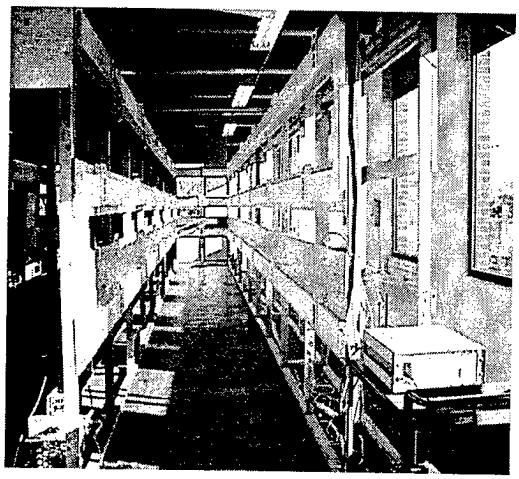

Figure 1. Photograph of the 90 m raceway test bed.

In the raceway, one of the outer compartments housed a single-phase, 3 loose conductor, 20 Amp rated unshielded power cable as depicted in Figure 2. Power outlets were spaced along the raceway 8 feet apart using typical installation techniques. The adjacent compartment housed the data cable under test (category 5 or Gbps) at either 0 or 2-inch (5.1-cm) separation. This cable arrangement was typical to plastic and metal raceways. The metal raceway was grounded at the near end (the end nearest the EFT generator).

Numerous previous tests [1] have demonstrated that once the distance over which the power and data cables are held in close parallel proximity to each other exceeds approximately 12 feet (3.7 m), additional length has a negligible effect on the level of voltage coupling observed. Since the coupling length ceases to be a factor

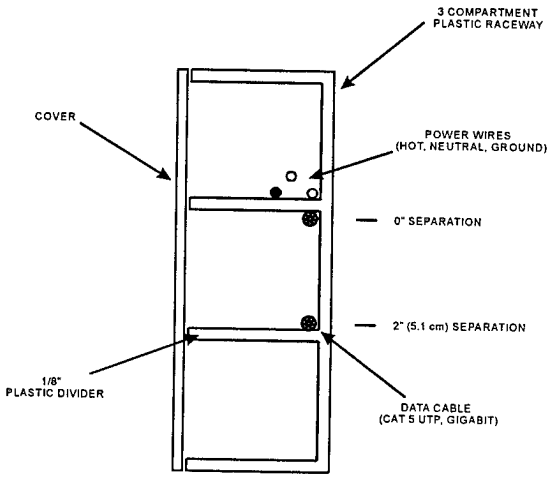

Figure 2. Plastic raceway cross section.

beyond this approximate threshold, the 0 separation was retained for 50 ft (15 m) starting at near end and left at 2 in. (5.1 m) for the remaining length.

Each data cable was terminated at both ends with a modular data jack of equivalent category (commonly known as RJ-45). A cable tester was used to test the wire map, impedance, length, attenuation, and NEXT of each cable.

A Fast Ethernet LAN was assembled by locating a PC based workstation, equipped with 100 Base-TX Network Interface Card (NIC), at each of the two ends of the raceway (refer to Figure 3). Two category 5 patch cords were used to connect the workstations to the 90-m data link. To simplify the test, the network configuration did not include any hubs. However, one of the patch cords was modified to provide a crossover of the transmit and receive twisted pairs. Microsoft networking in Windows 95 was utilized to interface the workstations.

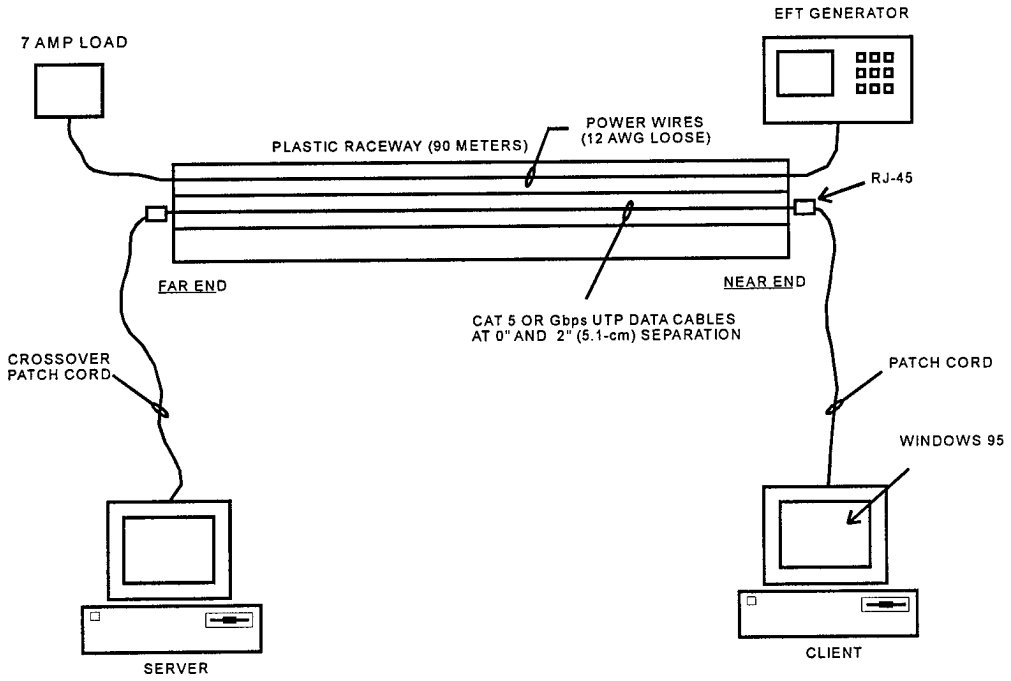

Figure 3. Test arrangement.

An EFT generator with characteristics and performance prescribed by the International Electrotechnical Commission IEC 1000-4-4 standard for electromagnetic compatibility testing [2], was chosen as a controlled means for introducing a defined electrical disturbance onto the power lines. The particular waveform used is depicted in Figure 4.

The EFT generator output was applied to the active power line at near end. The far end of the power line was terminated with a 7 Amp resistive load.

Tests by others [3] have indicated that pulses from ordinary office sources such as fluorescent lights, electric pencil sharpeners, and paper punchers are less severe than the IEC Level 1 noise imposed on power lines (500 V, 5 nsec). Therefore, the 500 V transient amplitude is a reasonable representation of the maximum electromagnetic interference from typical disturbers found in an office environment.

To test the most severe condition, the EFT generator output was varied between 0 and 2,000 V.

FAST ETHERNET PERFORMANCE TEST

Network Error Check

The first method used to evaluate Fast Ethernet performance was to measure the number of network errors by utilizing LAN analyzer software running in both workstations.

The software in conjunction with a certified NIC card was capable of detecting the CRC (Cyclic Redundancy Check), alignment errors, and lost packets during data transmission from server to client.

The CRC is a method of error detection. Using a standard algorithm that performs a calculation on the packet, the transmitting station generates a number that in turn is inserted into the header of the transmitting packet. When the receiving station receives the packet, the algorithm is applied again and the new number is compared with the transmitted number. A match indicates that

the data was received as sent. A mismatch indicates a data transmission error.

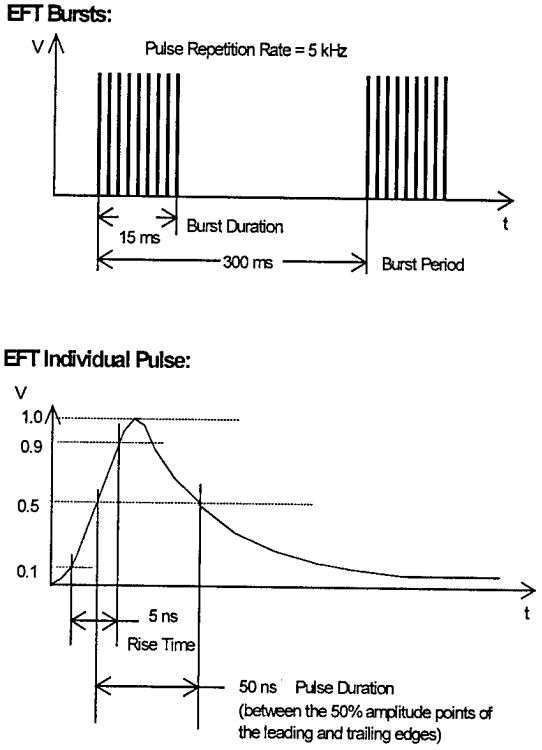

Figure 4. Controlled fast transient waveform.

Alignment errors occur when a received frame's total number of bits is not divisible by eight.

Lost packets appear when a packet never reaches its destination or arrives in unrecognized form (completely distorted). The packet counter of the LAN analyzer located in the receiving station allows detection of lost packets.

To generate traffic, the LAN analyzer located in the server (far end) was programmed to send 300,000 packets of data, each 768 bytes long, with no delay between packets. This configuration resulted in about 20% network utilization. At the same time, the EFT generator was turned on, and the network traffic was monitored by the analyzer located in the client (near end) and connected to the network through the noisy link of 90 m cable. The analyzer was able to detect lost packets and network errors caused by the noise coupled from the power lines.

Transfer Time Test

A more important test for the LAN end-user is to measure file transfer time in the presence of EFT disturbances. By executing a file copy command in Windows 95, a directory of program files (66 MB) was transferred between server and client. During each transmission, the files are divided by the transmitting station into packets and sent one at a time to the other workstation.

Ethernet LAN utilizes a class of random access algorithm, called carrier sense multiple access (CSMA). It uses hardware at each station to sense if the channel is busy. Having transmitted a packet, a station then determines whether the packet has reached its destination successfully. If the transmitting station does not receive a positive acknowledgment, it waits for a randomly chosen length of time before retransmitting the packet. Multiple retransmissions and a busy channel result in increased transfer time. Transfer time is the time required for transferring the entire file from station to station.

TEST RESULTS

Network Error Test Results

Figure 5 shows the difference between the number of Fast Ethernet errors in plastic verses metal raceways, and category 5 verses Gbps UTP cables. It indicates that category 5 cable, located in plastic raceway at zero separation from the power cables, provides good noise immunity from typical office disturbers. The number of network errors remains zero until the EFT generator output reaches 700 V. The physical characteristics of category 5 cable and the principles of balanced signal transmission along a pair of twisted wire contribute to good noise immunity of Fast Ethernet data transmission. The improved balance of Gbps cable increases the magnitude of the tolerable noise level to 800 V.

By separating the data cable from the power cables by 2 in., the no-error condition is

Figure 5.
Effect of EFT Disturbances on Network Errors
{100 Base-T Ethernet}

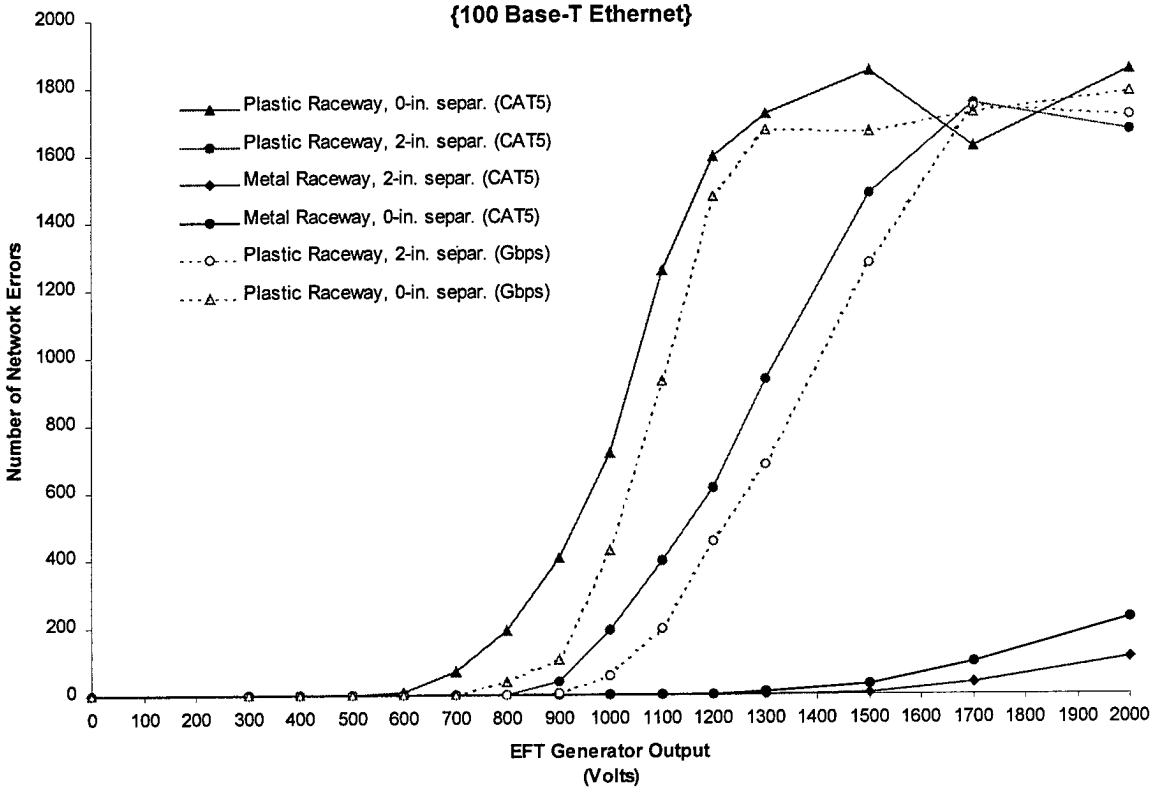

shifted to 900 V for category 5 cable and 1,000 V for Gbps cable.

Each of the plastic raceway graphs in Figure 5, regardless of separation or type of cable, consist of three distinctive sections.

The first section is a response with no network errors or lost packets present. It results from the differential mode voltages coupled to data cable lower than the actual signal carrying data.

However, as the noise increases to the level that it changes the content of transmitted packets, the CRC and alignment errors start to appear. Further increase in the noise magnitude causes collisions with data signals and corruption of additional packets beyond their recognition resulting in lost packets (the LAN analyzer does not retransmit lost packets in traffic generating mode). This results in a high slope (almost vertical line) of the graph.

After reaching its peak, the graph levels off at about 1800 network errors and remains constant. This phenomenon can be explained by the fact that the EFT generator sends a burst of pulses with the duration of 15 ms while the burst period is 300 ms (refer to Figure 3). This means that a window of 285 ms free of noise is available in every burst cycle. Once all packets transmitted during the 15 ms duration are affected by the noise, additional increase in magnitude of the EFT generator has no effect on LAN errors.

Figure 5 depicts also how LAN errors vary as a function of EFT magnitude in category 5 cable located in a metal raceway grounded at near end. It can be seen from the obtained data, that in this test the metal raceway outperformed the plastic in regard to immunity to higher EFT magnitudes. Plastic, unlike metal, is transparent to electromagnetic waves and does not provide any shielding. As mentioned before, UTP cables in a non-metallic raceway rely on

Figure 6.
Effect of EFT Disturbances on Network Transfer Time
{100 Bas-T Ethernet, 60Mb File Transfer}

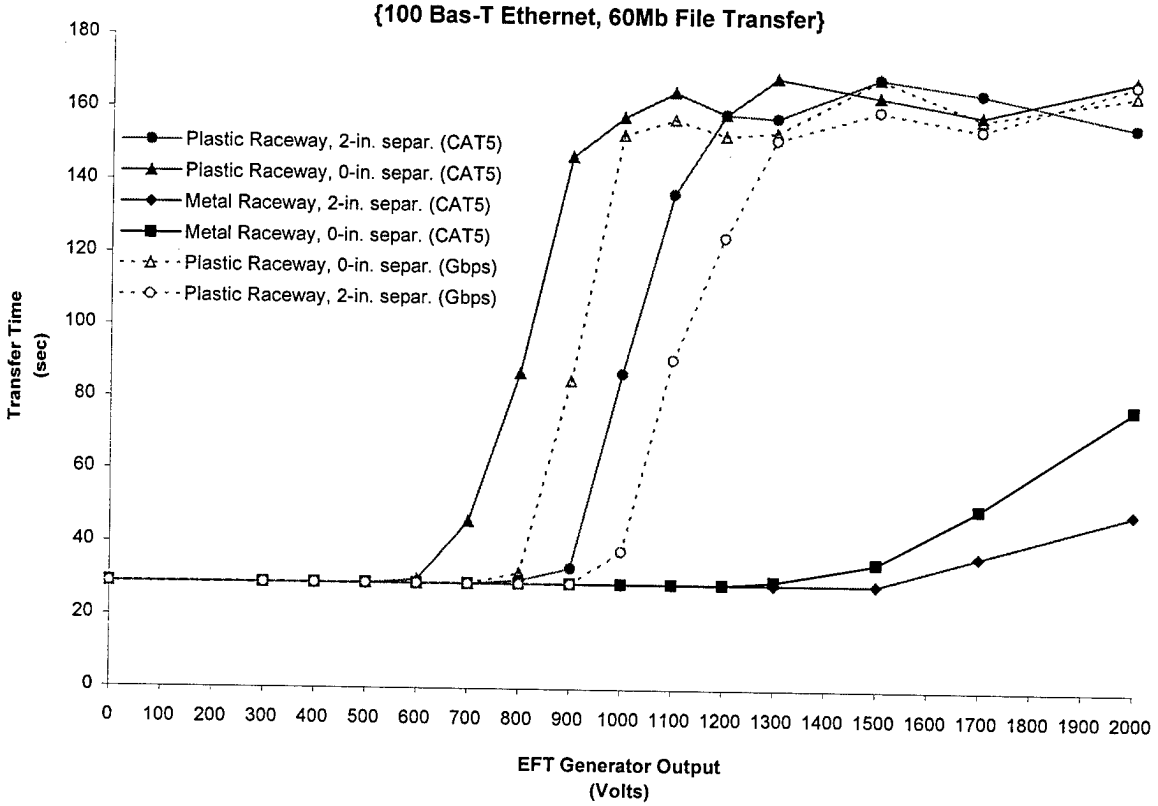

good cable balance to minimize noise interference.

TRANSFER TIME TEST RESULTS

The results obtained by performing the transfer time test (Figure 6) follow the same trend and confirm the same findings as the network error test data.

With category 5 cable in plastic raceway, the transfer time remains constant at about 30 seconds until the transient noise reaches 700 V level at 0 separation, and 900 V at 2-in. (5.1-cm) separation. Transfer time for the Gbps cable starts increasing at EFT generator output set to 800 V with 0 separation and 1,000 V with 2-in. (5.1-cm) separation. On the other hand, noise amplitudes reaching as much as 1,500 V do not affect transfer time in the metal raceway.

CONCLUSIONS

The test results illustrate that category 5 cable located in a non-metallic raceway in a compartment adjacent to the power cables provides satisfactory Fast Ethernet performance in the presence of EFT voltages from typical office disturbers such as pencil sharpeners, copiers, and light switches.

Metal raceway with its shielding properties improves the noise immunity even further.

As predicted, better-balanced Gbps cable shows improved immunity to noise over category 5 cable.

REFERENCES

[1] Hashim A., Makwinski M., "Coupling of Electrical Fast Transients from Power Cables to Parallel UTP Cables in Close Proximity", presented at International Wire

and Cable Symposium, November 13-16, 1995, Eatontown, New Jersey.

[2] International Electrotechnical Commission International Standard IEC 1000-4-4: Electromagnetic Compatibility (EMC) Part4: Testing and measurement techniques - Section 4: Electrical fast transient/burst immunity test.

[3] George Weller, "Measurement of Electrical Noise from Common Office Sources" - A contribution to TR41.8.3 Pathway Separation Task Group, March 1, 1995.

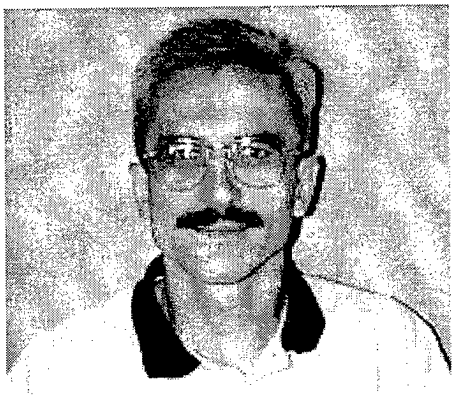

Mirek Michalak
The Wiremold Company
60 Woodlawn Street
West Hartford, CT 06110

Mirek Michalak is a senior Electrical Engineer with The Wiremold Company involved in the electromagnetic compatibility testing of wire management systems. He received his B.S. degree in Electrical Engineering from University of Hartford.

EMC WITHIN SYSTEMS AND INSTALLATIONS

Dirk Wilhelm
Dr. Peter Schulz
GHMT mbH, Bexbach/Saar, Germany

ABSTRACT

The rising integration of electronic data processing with the day-to-day operations of a business as well as the constantly increasing degree of networking of the individual systems enormously increase the dependence of enterprises on properly working data networks. The calculated damages which can be caused by such failures range from $ 100,000 per hour for medium-sized companies to $ 5,000,000 per hour for large banks or industrial groups. A study that had already been prepared in 1987 pointed out even more dramatically that many organizations are vitally dependent on their DP environments. According to findings of this study, banks would survive a complete breakdown of their IT systems for only 2 days while the survivability of insurance companies would amount to 5.6 days.

For that reason, many businesses decided to dimension their systems in such a way that they include a certain degree of redundancy.

These redundancy considerations should also include electromagnetic compatibility (EMC). However, it often happens that fundamental measures are not taken into account in the design and construction phases.

This paper discusses the constraints that affect the electromagnetic compatibility of systems and installations and how such constraints must be taken into account when planning and implementing IT facilities.

INTRODUCTION

Within the territory of the European Union, the electromagnetic compatibility of devices is regulated by the 89/336/EEC directive as well as national adoptions of this directive. Devices meeting the relevant requirements are externally marked by the so-called CE sign (Communauté Européenne). In other countries, the compliance with EMC regulations is similarly examined by using other measures, e.g. the execution of tests to FCC standards (emissions only) and application of FCC labels.

Initially, scarce attention was given to the fact that these standards deal – almost exclusively – with devices and only insufficiently with the interconnection of these devices.

Standards may ensure that certain products are also standardized. However, the large variety of systems existing e.g. in a building is currently still reflected in standards that are frequently conflicting with one another.

It is then difficult for both design engineers and users of such complex systems to find and implement the applicable standards. Electromagnetic compatibility of systems, however, is dependent on much more factors than the EMC of devices alone. Based on a large number of troubleshooting activities carried out for facilities whose proper operation was disturbed by electromagnetic interference, the authors were able to gather crucial information which is presented in the following five-column model.

The EMC response of a system consists of the following individual factors:

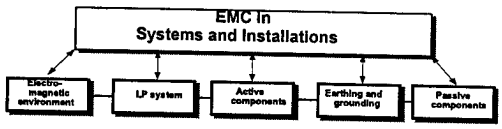

Figure 1: Five-column model

As can be seen in the above diagram, the EMC of devices which is dealt with in the relevant EMC regulations is only a part of the overall system. In spite of this, many users live in the belief that an installation of devices whose EMC has been tested would be enough to meet the enormous safety requirements of their overall system.
The following sections describe the boundary conditions that are actually of importance in order to ensure that the EMC of a system is protected.

ELECTROMAGNETIC ENVIRONMENT

When planning an IT installation, the sources of interference existing on site should be analyzed before certain active and/or passive components are selected. These sources of interference constitute, in their entirety, the electromagnetic environment. It is very useful to know the ranges of the working frequencies (of the installation to be designed) already during this analysis because environment-induced sources of interference should be regarded as particularly critical – although this must not be interpreted in such a way that the remaining frequency range can then be neglected. For example, 10BaseT services (central frequency: 10 MHz) can be disturbed very much by neighboring FM stations (f = 87.5 ... 108 MHz). In addition to the working frequency along the transmission route, the internal clock frequency of the device (e.g. on the backplane) which is often several times higher must also be taken into account.

Any influencing factors which exceed the range of customary EMC tests with respect to the amplitude or also the frequency range must likewise be taken into account and require an appropriate modification of the relevant EMC test regulations.

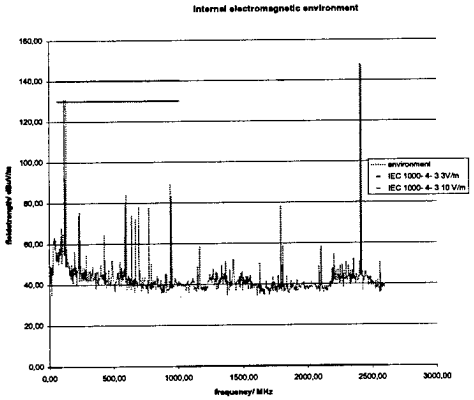

Figure 2: Electromagnetic environment

Thus a neighboring radio station may require an increase of the test field strength over and beyond the customary values of 3 V/m (domestic and office environments) and 10 V/m (industrial environments) to ensure the interference immunity against radiated electromagnetic fields, while the standard frequency range to be tested (80 – 1,000 MHz) should be extended if a radar station (e.g. f = 2.4 GHz) is located in the neighborhood.

The same applies analogously to conducted influencing factors in case of a mains supply with a large extent of transients or CW or also to the discharge of static electricity if unfavorable floor coverings are used. Even if the analysis of the electromagnetic environment does not show any particularities in the pre-operation phases, the standardized test procedures must be applied completely because the boundary conditions may change during the service life of an installation. Flashes of lightning constitute another factor of the electromagnetic environment. On account of their significance they are dealt with in a separate section.

LIGHTNING PROTECTION

The probability of nearby and/or direct lightning strikes depends on the respective geographical location. Critical parameters of the lightning currents to be expected for the installation under review are the:

- lightning current rise rate di/dt_{max} (inductive overvoltages);
- lightning current amplitude $\hat{I}_{max}$ (potential rises);
- charge (quantity of electricity)
  $Q = \int i(t)dt$ (melt out);
- resistance-specific energy
  $W / R = \int i^2(t)dt$
  (heating up of conductors)

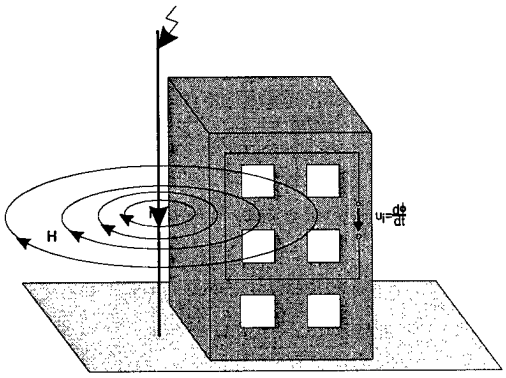

Figure 3: Influence of lightning

Traditional lightning protection measures comprise the external lightning protection consisting of air terminations and down conductors and only prevent damages to buildings and human beings.

Disturbances and failures of IT installations which are caused by overvoltages can only be avoided by implementing a consistent lightning protection zone concept taking into account the electromagnetic compatibility. This will be illustrated by a concrete example later on.

Using a lightning protection zone concept, any work and resources which are required in order to protect installation components of differing significance (e.g. servers and data centers on the one hand and offices on the other hand) can be planned efficiently. Components with especially high demands on failsafe operation can be included in the lightning protection zones 2 and 3 (LPZ) while components of less importance may be included in LPZ 1.

LPZ 1 is realized by using the existing steel reinforcements of concrete buildings or, if we have a building without reinforcements, by installing ring circuits in false floors or suspended ceilings. Cabinets, panels, and in part also peripherals are then connected to these ring circuits using low-resistance lines.

LPZ 2 comprises specific screening measures which protect against transient magnetic fields caused by neighboring lightning strikes. For example, screen grids with corresponding fine mesh sizes can be installed. Earthing leads for an adequate connection of components should also be planned.

If required, LPZ 3 can be established by using specifically screened data cabinets or specially shielded data cables.

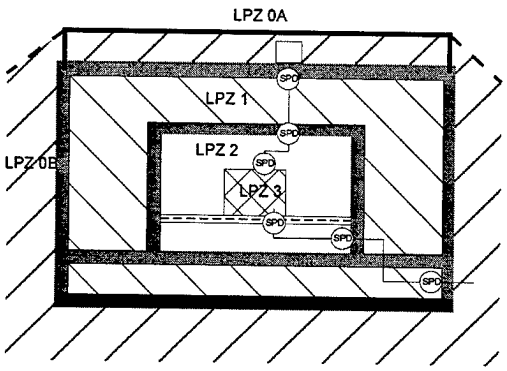

Figure 4: Lightning protection arrangement

EARTHING AND GROUNDING

In the event that a protection zone concept as described in the section above has been realized, we already have a favorable starting position for planning an earthing and grounding concept which is suited for the installation of high-performance IT systems.
In this connection, the term "earthing" comprises all measures serving to protect human – beings and avoid e.g. hazardous contact voltages on metallic housings of devices. For that purpose, the housings are connected to the potential equalization bar of the building by means of PE lines.

The term "grounding" denotes all measures in order to create reference potentials and to discharge parasitic currents injected by electromagnetic sources of interference (by inductive, capacitive or radiated coupling). As such parasitic currents may be characterized by very high frequencies, the grounding system must be realized with as low impedances as possible – unlike protective circuits which are merely dimensioned to discharge interference currents with power network frequencies. In case of installations in already existing or insufficiently designed buildings, these requirements are often difficult to meet.

The IT installation will be especially susceptible to faults, if the power supply of the DP system and of the other loads is provided through a common TN-C network. In such a case, the protective conductor PE and the neutral conductor N are combined (PEN conductor), and operating currents also occur in the protective circuit. As shown in Figure 5, screens of the installation cables which are included in the earthing and grounding system are then used as unwanted paths for reverse currents.

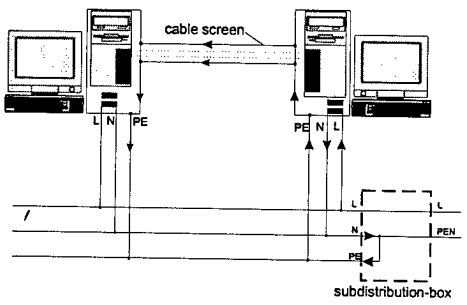

Figure 5: TN-C installation

This may affect the traffic of data communication as has been shown by the analysis of disturbed systems on site.

Such interference can be eliminated by the consistent introduction of a five-wire system (TN-S network), in which there is only one connection between N and PE at the feeding point into the building. Within a second phase, a low-impedance grounding concept should be realized to connect the shielding system to the earth of the building.
Especially in case of high-speed data networks with bandwidths of up to one or several GHz, the star-type earthing arrangement which was previously favored in order to avoid loops should be discarded, and a meshed concept with as many meshes as possible should be realized because signal-transmitting wires serve as a coupling path for high frequencies (Fig. 6).

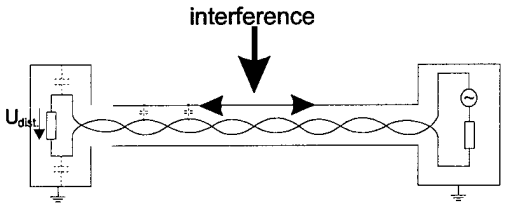

Figure 6: Shield connected at one side only and resulting problems

In case of high frequencies, the impedance to earth – and hence the undesired voltage drop – increases in part systems of the earthing installation on account of the rising inductive percentage of PE conductors with small cross sections. Furthermore, the star-type earthing mutates (in case of high frequencies) through capacitive couplings into an undefined meshed system with large loop areas.

As already mentioned at the beginning, an existing lightning protection zone concept provides a suitable basis for a HF-capable, meshed earthing and grounding concept because the steel reinforcements of floors and walls can be used in such a case to connect the system screens several times to the earth of the building and can also be used to establish multiple meshes of small sizes, as shown in Figure 7. In the event that such large-surface grounded facilities are not available yet, they should be installed subsequently, if possible. Due to their reduced self-inductance, strips or foils are better suited than litz wires which, however, are easier to lay.

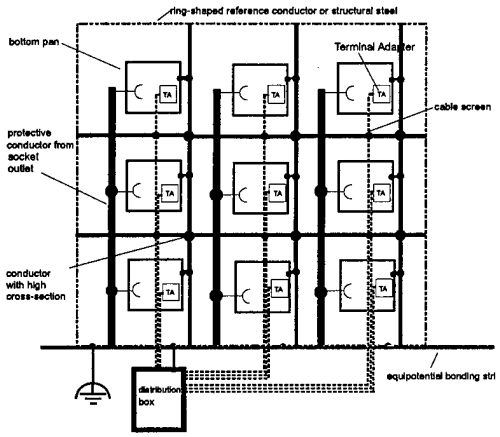

Figure 7: Meshed grounding with an arrangement of bottom tanks

ACTIVE COMPONENTS

As soon as the constraints with respect to the building itself and the electromagnetic environment have been identified, the requirements applicable to the active components of the IT system can be specified. A modified course of action would also be possible if the components have already been selected at the start of the project. In such a case, the requirements on the building structure (lightning protection concept, power supply, and degree of screening) must be defined in such a way that the disturbance variables to be expected within the building do not exceed the interference thresholds of the system. It should be emphasized that the interference thresholds refer to the overall system and NOT to the individual components.

Although the EMC directive of the European Union permits the assumption that the protection requirements of an installation are complied with if its components meet the protection requirements (i.e. sufficiently high immunity to interference and sufficiently low emitted interference) and the installation guidelines of the manufacturers have been observed, this course of action termed as "modular approach" has proved to be inadequate under practical conditions. That is why this modular approach should not be used for safety-relevant systems or systems whose failure would cause enormous costs.

Since peripherals and the cabling of devices significantly influence the EMC response, a model of the systems which is as similar to the real systems as possible should be examined in the EMC laboratory in a preliminary phase. Although a worst-case scenario is difficult to real-

ize in a lab, it should be attempted nevertheless. When setting up such a model, the actual later application should be taken into account in any case. A mistake that is frequently made when active LAN components are tested consists in tests without any cables or with cables of reduced lengths. In such cases, the necessarily increasing signal attenuation and the decreasing screen attenuation do not influence the result of EMC tests very much. In practice, however, lengths of up 90 m are used, and the signal-to-noise ratio is then distinctly worse than the result of a lab test with a cable of 3 m (Fig. 8).

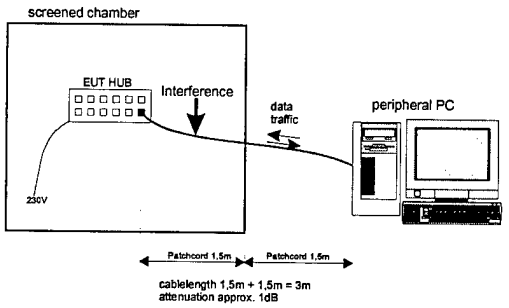

Figure 8: Measuring arrangement that is not suitable for the determination of the system characteristics

The interference immunity tests to be carried out in the lab should serve both to simulate typical interference phenomena occurring within the electromagnetic environment and to check their effects on the specimen (i.e. the model system). The test regulations of the applicable product standards (e.g. prEN 55024, Immunity ITE) refer to so-called basic standards which in turn describe a suitable arrangement in order to simulate interference phenomena. In case comprehensive results are to be obtained for the basic interference immunity of a system (i.e. the immunity which can be achieved in an ideal lab environment), all parameters listed in Table 1 should be checked, if possible.

During the on-site installation of the system, we should then aim at reproducing the ideal lab environment – for example by ensuring adequate earthing and grounding conditions.

The amplitudes of the applied disturbance variables depend on the respective place of utilization (cf. section "Electromagnetic Environment" above) and the safety requirements of the operator. In case of an environment subject to these disturbances, the frequency range of the tests should be extended to ensure that at least the already existing external sources of interference (e.g. radar equipment) and their effects on the specimen are recorded.

Test standard	Disturbance parameter	Test level
IEC 1000-4-2	Electrostatic discharge	4/8 kV
IEC 1000-4-3	Radiated electromagnetic field (80 ... 1,000 MHz)	3/10 V/m
IEC 1000-4-4	Fast transients (burst)	1/2 kV
IEC 1000-4-5	Slow transients (surge)	0,5/1/2/4 kV
IEC 1000-4-6	Conducted CW (0.15 ... 80 MHz)	3/10 V
IEC 1000-4-8	Magnetic field (50 Hz)	3/30 A/m
IEC 1000-4-9	Transient H field	100..1000 A/m
IEC 1000-4-10	Damped oscillating H field	10..100 A/m
IEC 1000-4-11	Voltage dips / interruptions	30 (60)%, 10 (100) ms

Table 1: Basic immunity standards

PASSIVE COMPONENTS

Passive components such as panels, plugs, outlets, cables, etc. – particularly in case of copper connections – have a significant influence on the EMC characteristics of the overall system. Their interaction among one another (e.g. possible connection of a component to the screen and cable shield) as well as with active components and peripherals must carefully be dimensioned (by taking into account suitable reserves) because installation and site-specific conditions must always be included in reality.
EMC-relevant parameters of passive components are, for example, transfer impedance, longitudinal conversion loss, screening effectiveness and coupled noise attenuation.
To date, these parameters are required in the applicable standards (e.g. ISO IEC 11801) only for component tests and not for link tests. However, experience has shown that cables with excellent properties and high-quality panels or outlets do not necessarily guarantee a link with excellent EMC characteristics. Therefore several approaches are available in order to submit suitable measuring procedures to the standardization committees.
The following example shows the simple line-injection method that can always be applied in order to test the compatibility.

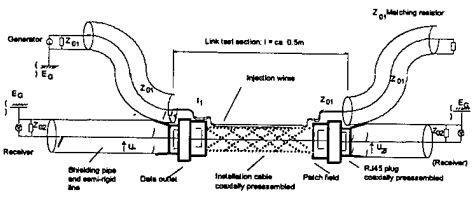

Figure 9: Measurement of the transfer impedance on a combination of data cables and components

CONCRETE EXAMPLE

To illustrate the course of action for the realization of an EMC-safe, distributed system, the calculation of a lightning protection concept is presented in the following.

A concept ensuring an interference-free operation is to be developed for the data center of a bank. On account of their functionalities, the active components have already been determined. First of all, it should be examined whether a lightning protection concept of adequate quality can be realized by connecting the components to the steel reinforcements of the building.

Prerequisites:

Rating in safety class 2: 95 – 98% of all neighboring lightning strikes should be survived without any damages.

General building characteristics:

- air terminations with a mesh width of 10 m existing;
- realizable mesh width of steel reinforcement in the data center: w = 0.15 m;
- diameter of steel reinforcement: d = 0.8 cm;
- permeability of steel reinforcement: μ_r = 200;
- immunity to interference of used devices to IEC 1000-4-9: 100 A/m;
- immunity to interference of used devices to IEC 1000-4- 10: 10 A/m;
- setup of the devices with a safety clearance of $d_{S/0,5}$ = 0.5 m from the external wall of the building.

Assumption derived from the rating in safety class 2:
lightning current $i_{0/f/max}$ = 150 kA, first stroke;
lightning current $i_{0/s/max}$ = 37.5 kA, second stroke.

Medium distance from the lightning strike into the air terminal to the shielded volume s_o = 6.5 m.

Average magnetic field effective in zone 0 across the shielding volume: $H_{0/f/max}$ resulting from the first stroke:

$$H_{0/f/\max} = \frac{i_{0/f/\max}}{2*\pi*s_0} = \frac{150kA}{2*\pi*6{,}5m} = 3672{,}8A/m$$

Average magnetic field effective in zone 0 across the shielding volume: $H_{0/s/max}$ resulting from subsequent strokes:

$$H_{0/s/\max} = \frac{i_{0/s/\max}}{2*\pi*s_0} = \frac{37{,}5kA}{2*\pi*6{,}5m} = 918{,}2A/m$$

Resulting screening factor SF resulting from the steel reinforcements of the building in the data center (worst-case):

$$SF = 20*\log\left[(8{,}5/w)/\sqrt{1+18*10^{-6}/(0{,}5*d)^2}\right] = 34dB$$

Safety distance $d_{S/0,5}$ from the screen grid within the shielding volume:

$$d_{s/0,5} = \frac{w*SF}{10} = \frac{0{,}15*34}{10} = 0{,}51m$$

Effective field in zone 2 within the safety distance $d_{S/0,5}$: $H_{2/f/max}$ resulting from the first stroke.

$$H_{2/f/\max} = \frac{H_{0/f/\max}}{10^{SF/20}} = \frac{3672{,}8}{10^{34/20}} = 73{,}3A/m$$

Effective field in zone 2 within the safety distance $d_{S/0,5}$: $H_{2/s/max}$ resulting from the subsequent strokes.

$$H_{2/s/\max} = \frac{H_{0/s/\max}}{10^{SF/20}} = \frac{918{,}2}{10^{34/20}} = 18{,}3A/m$$

Evaluation:

First stroke:
A system immunity to interference of 100 A/m to IEC 1000-4-9 (without taking into account coupling effects in conductor loops) is sufficient if the safety clearance of $d_{S/0,5}$ = 0.5 m is met.

Second stroke:
A system immunity to interference of 10 A/m for the second stroke (similar to IEC 1000-4-10) is not sufficient because a field of 18.3 A/m can occur.

For that reason the safety clearance to the external wall of the building should be enlarged.

With respect to the selected clearance of 1 m the following value results due to the fact that the field decreases by at least 1/d:

$$H_{2/s/\max/1m} = \frac{H_{2/s/\max/0,5m}*0{,}5m}{d_{S/1}} = \frac{18{,}3*0{,}5}{1(!)} = 9{,}2A/m$$

The observation of an immunity to interference of 10 A/m to IEC 1000-4-10 is sufficient in case a safety clearance of $d_{S/1}$ = 1 m is provided between the devices and the external walls of the data center.

Within a second stage, a conductor loop installed in the data center and the resulting induced voltage should be taken into acount.

Prerequisites:

- width of the conductor loop: b = 5 m;
- length of the conductor loop: l = 6 m;
- self-inductance of the loop: L = 25.4 µH;
- transfer impedance of the link: Z_T = 800 mΩ;
- distance between shield wall and the next point of the conductor loop: $d_{S/1}$ = 1 m;
- rise time T_f of the magnetic field for the first stroke: 10 µs;
- rise time T_s of the magnetic field for the second stroke: 0.25 µs.

The conductor loop is fully permeated by B, i.e. vertically to the direction of the field with B being constant and maximal across the entire area of the loop.

Regarding the open-circuit voltage $U_{0c/f/max}$ of the loop, the following applies for the first stroke:

$$U_{0c/f/max/1m} = \mu_0 * b * l * H_{2/f/max/1m} / T_f$$
$$= 1{,}25 * 10^{-6} * 5 * 6 * 36{,}5 / 10 * 10^{-6} = 137 \text{ V}$$

Regarding the open-circuit voltage $U_{0c/s/max}$ of the loop, the following applies for the second stroke:

$$U_{0c/s/max/1m} = \mu_0 * b * l * H_{2/s/max/1m} / T_s$$
$$= 1{,}25 * 10^{-6} * 5 * 6 * 9{,}2 / 0{,}25 * 10^{-6} = 1380 \text{ V}$$

Regarding the short-circuit current, the following applies for the first stroke taking into account the self-inductance L of the loop:

$$i_{Sc/f/max/1m} = 1{,}25 * 10^{-6} * b * l * H_{2/f/max/1m} / L$$
$$= 1{,}25 * 10^{-6} * 5 * 6 * 36{,}5 / 25{,}4 * 10^{-6} = 54 \text{ A}$$

Same for the second stroke:

$$i_{Sc/s/max/1m} = 1{,}25 * 10^{-6} * b * l * H_{2/s/max/1m} / L$$
$$= 1{,}25 * 10^{-6} * 5 * 6 * 9{,}2 / 25{,}4 * 10^{-6} = 13{,}58 \text{ A}$$

By taking into account a transfer impedance of Z_T = 800 mΩ, the following voltage U_L results between the screen and the inner conductor:

$$U_{L/f} = Z_T * i_{Sc/f/max/1m} = 800 \text{ mΩ} * 54 \text{ A} = 43{,}2 \text{ V}$$
$$U_{L/s} = Z_T * i_{Sc/s/max/1m} = 800 \text{ mΩ} * 13{,}58 \text{ A} = 10{,}9 \text{V}$$

Evaluation:

In the worst case, the voltage coupled into the signal path may cause a short interruption of the data communications. A destruction of the connected devices can, however, be excluded.

The voltage coupled into the signal path can be reduced further by using symmetric cables and the resulting LCL (as a rule: 60 dB). The probability that data communications are affected will then be minimized as well.

CONCLUSION

In order to assure a maximum availability, the above measures should be taken into account already at an early stage. Although existing installations can be modified in this respect, the described ideal conditions can then only be realized with considerably higher expenses.

EMC tests which only focus on the devices are not sufficient in case of complex facilities and systems if a maximum availability is to be ensured. For that purpose, all parameters listed above must properly be taken into account when designing and installing such systems.

BIOGRAPHIES OF THE AUTHORS

Dirk WILHELM (age: 31 years) studied telecommunications in Kaiserslautern, Germany and graduated as a Dipl.-Ingenieur.

He is general manager of GHMT mbH, an independent test laboratory for the global certification of cables, components and active devices of LANs and WANs.

His diploma thesis prepared in 1993 at GHMT mbH dealt with the development of a measuring procedure in order to examine EMC characteristics of symmetric data cables. Meanwhile this measuring procedure has been accepted as the German proposal for an international standard on this issue.

His technical field of responsibilities at GHMT mbH comprises the appraisal and analysis of electromagnetic compatibility of distributed facilities and systems.

Mailing address

GHMT
Gesellschaft für Hochfrequenz-Meßtechnik mbH
In der Kolling 13

D 66450 Bexbach/Saar
Germany

Phone: ++49 / 68 26 / 92 28 - 0
Fax: ++49 / 68 26 / 92 28 - 99
E-mail: wilhelm@ghmt.com

Dr. Peter Schulz (age: 31 years) studied telecommunications in Kaiserslautern, Germany and did his doctorate there in 1998 as a Dr.-Ingenieur. His thesis focused on the subject "Reduction of work and expenses caused by the evaluation of conformity to EMVG by means of a new multiple carrier procedure".

His field of responsibility at GHMT mbH comprises the appraisal and analysis of electromagnetic compatibility of distributed facilities and systems.

Mailing address

GHMT
Gesellschaft für Hochfrequenz-Meßtechnik mbH
In der Kolling 13

D 66450 Bexbach/Saar
Germany

Phone: ++49 / 68 26 / 92 28 - 0
Fax: ++49 / 68 26 / 92 28 - 99
E-mail: schulz@ghmt.com

Balance measurements on UTP and STP cables

J.- H. Walling and O. Saad *

* NORDX/CDT, Montreal, Canada

Abstract

With different baluns, we measure the balance of UTP, FTP and STP cables, i.e. the longitudinal conversion loss (LCL, called also coupling attenuation near end) and the longitudinal conversion transfer loss (LCTL, called also coupling attenuation far end). The baluns are first characterized, using three baluns, where two baluns are connected back to back, in order to determine their intrinsic loss. Different test setups are verified, such as the

a.) use of a resistor network for LCL measurements, with the center tap (common mode termination) terminated to ground. We use basically three terminations on the center tap, i.e. 25 Ohm, 50 Ohm and 75 Ohm.

b.) use of baluns terminated in 50 Ohm as terminations for LCL measurements, where the common mode port is differently terminated, while the unbalanced port is terminated in 50 Ohm.

c.) use of minimum loss impedance matching pads, as proposed for instance in an ASTM proposal [1]. For this purpose the loss of the impedance matching pads has been determined also, using three different min. loss pads.

The objective of our study comprises four issues:

- to come up with some reliable balance requirements which could be taken as a base for standardization within IEC 46C for the revision of IEC-61156-1 [2] or similar cable standards.
- to simplify the test method, using preferentially 50 Ohm terminations in conjunction with a balun, thus that the method is easily adaptable to automated test systems.
- to establish reliably a reference ground plane. This is essential for UTP cables. Towards this purpose we use, besides grounding the adjacent pairs not under test, a threaded metallic drum, which is grounded as well. We propose, aside of the above mentioned threaded drum, the use of a 3/8 inch copper tube, 100 m long total, into which the cable under test can be pulled.
- to verify those baluns with common mode port, readily available for their suitability to assess balance parameters of cables, and to come up with an estimate of error, using different baluns.

Background

In previous articles we asses the performance requirements of baluns and their impact on the measurement of balance parameters of cables [3];[4]. In these articles we conclude that baluns have to meet minimum requirements to measure balance of data grade cables.

The ITU Recommendation 0.9 and the IEEE Standard 455-1985 indicate different tests to measure LCL in a low frequency range [5];[6]. Few recent articles deal with higher frequency ranges of up to and exceeding 100 MHz [7].

For the definitions of single and two-port network balance measurements and the corresponding parameters, we refer to the ITU - Recommendation G.117 [5];[8]. We note that IEC adopted in the IEC 61156-1 draft, the terms coupling attenuation near-end and coupling attenuation far-end, which were introduced by L. Halme [10]. Though this coupling attenuation is not a power ratio in the usual sense, the analogy to the crosstalk behavior of cables becomes evident, primarily with regard the coupling attenuation far-end, as we will see later on.

To date there are several baluns available to measure the balance of cables. These baluns are, at least within their specified performance range acceptable for balance measurements.

We compare, nevertheless, balance results obtained with different baluns.

Characterization of the Baluns

We measure first the balance parameters of the baluns, i.e. the LCL of individual baluns and the LCTL of a matched pair of baluns.

For the LCL of the baluns, we use a standard with an impedance of 100 Ohm and an infinite LCL. For the LCTL measurement both baluns are connected back to back on the 100 Ohm terminal, while the remaining ports are terminated with 50 Ohm termination plugs. In both cases, i.e. for LCL and LCTL we calibrate directly before the balun connection plane and subtract the intrinsic balun losses and the turns ratio from the results obtained.

The obtained curves are the balun limit curves, which indicate the maximum attainable balance measurements of the devices under test. Beyond these limits, the results are mostly covered by the balance of the balun(s).

We use four different kinds of baluns. these are listed in Table 1.

Balun	Type	Freq. MHz Min.	Max.
Analog-Elektr.	SMB-61	0.1	350
North Hills	0322 BF	1	100
North Hills	0322 BFA1	1	100
BH Electronics	BH	3	350

Table 1

Methodology

For each balun type, we determine the intrinsic balun losses, and add to it the turns ratio. To do this we use three baluns and measure the intrinsic loss for all balun combinations. This way the loss for each balun can be determined separately. Incidentally, the same procedure we use also to determine the loss of the minimum loss matching pads. It has to be mentioned, that the commercially available minimum loss matching pads are modified, in order to have 50 Ohm coaxial connectors also on the 75 Ohm sides. Incidentally, the same is true also for the terminations,

which are made generally using 50 Ohm coaxial connectors. This modification is dictated mainly by the connector types used for the common mode port of the baluns.

As the S-Parameter test set is calibrated just before the balun connection plane, the sum of intrinsic and turns ratio loss is subtracted from the obtained results in order to obtain the LCL and the LCTL of the device under test.

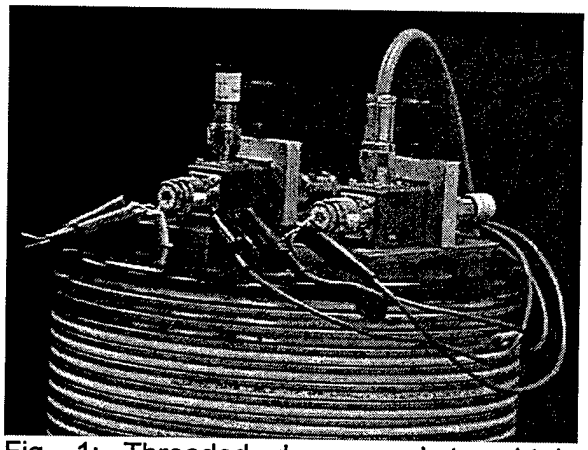

Fig. 1: Threaded drum used to obtain repeatable ground plane conditions for balance measurements. Pairs not under test are grounded as well

For balance measurements the reference ground plane is of utmost importance. We use, therefore, a threaded bronze drum, which is grounded. The top of this drum, with a winding capacity of 100 m of cable is shown in Fig. 1. including the baluns.

The cables are wound into the grooves of the thread. Even, using such a drum, we ground the adjacent idle pairs, i.e. the pairs not under test, with grounding clips. They are also visible on the Fig. 1.

Note: The ends of the cable are fed through into the center of the drum and guided in tubes to the top plate, where the baluns are located. Several feed throughs have to be provided, at least at one end of the cable on the drum, in order to compensate for the varying diameters of the cable. Alternatively, we propose the use of a 3/8 inch copper tube, approximately 99.5 m long, with spiral sleeves over the ends, such that the shield can be extended directly up to the balun. This tube can be mounted straight with a single relatively large loop in the middle of the length of 100 m.

We also measure the same cable stretched out and suspended, where only the adjacent pairs are grounded. The wires are suspended straight after taking them from the drum. Consecutively the cable is coiled and re-measured for balance in coil form, again with the adjacent pairs grounded.

LCL Measurements: For the LCL measurements we use a direct input to the common mode port of the balun, while measuring at the 50 Ohm port as schematically shown in the Fig. 2. Additionally we use an input over a minimum loss pad, as proposed recently for a revision of ASTM D-4566 [1](see Fig. 3). The minimum loss pad is said to be required to accommodate a common mode impedance of the DUT of 75 Ohm approximating the common mode impedance of an UTP cable.

We terminate the DUT at the far end with different terminations. We use a center tapped resistor network, as stipulated in the proposed revision of ASTM D-4566 (see Fig. 3 and Fig. 4) or baluns, which are terminated with 50 Ohm at their 50 Ohm ports, whereas the common mode ports are terminated either with 25, 50 or 75 Ohm, in order to approximate the common mode impedance of STP, FTP and UTP,

respectively. The schematics used is shown in Fig. 2. Additionally we make measurements, leaving the common mode port at the far end open.

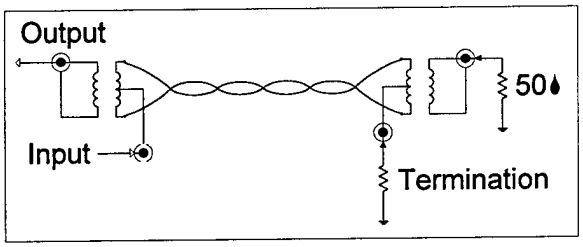

Fig. 2 : LCL test measurement set-up as proposed with a 50 Ohm termination

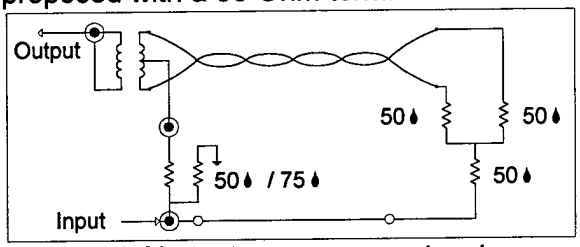

Fig. 3 : LCL test measurement set-up as proposed in ASTM D-4566

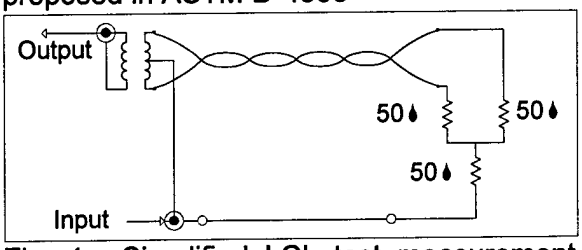

Fig. 4 : Simplified LCL test measurement set-up

LCTL Measurements: For the LCTL measurements we use a minimum loss pad at the input to the common mode port of the balun, as stipulated in the proposed revision of ASTM D-4566 and shown in Fig. 5. Alternatively we use a simplified circuit where we inject the signal directly into the common mode port of the balun. At the far end we use again 25, 50 or 75 Ohm terminations at the common mode port of the balun, in order to approximate the common mode impedance of STP, FTP and UTP respectively (see Fig. 6). Again we make measurements, leaving the common mode port at the far end open.

The 50 Ohm port of the balun at the input is always terminated with a 50 Ohm load.

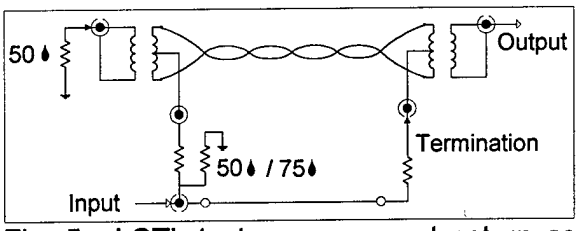

Fig. 5 : LCTL test measurement set-up as proposed in ASTM D-4566

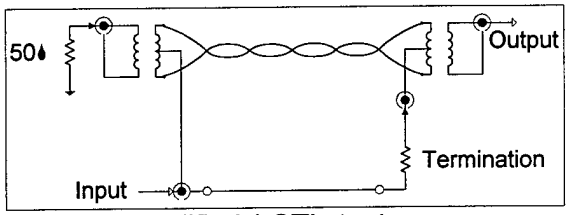

Fig. 6 : Simplified LCTL test measurement set-up

Results

All our measurements are made with the cable on the drum, unless otherwise mentioned.

LCL Measurement Results: Fig. 7 shows the intrinsic loss, including the turns ratio for three baluns of the same kind as an example. We use only the baluns # 1 and # 3, whereas the third balun is only required to separate the losses for each balun individually.

Fig. 8 shows the loss of the minimum loss pad used for the measurements. Here only the loss of the pad, which we use is shown. The losses of the other pads, are very similar.

The Fig. 9 indicates the LCL limit of the balun used for the LCL measurements.

As already mentioned, all values measured, exceeding this limit line, are strongly influenced by the balun balance itself.

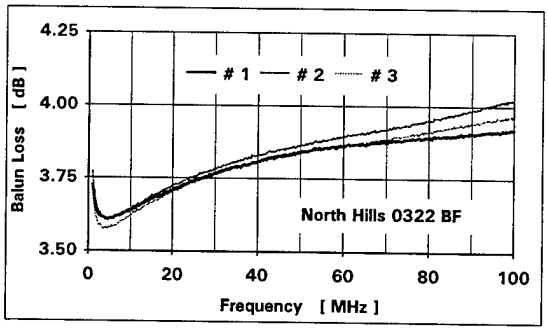

Fig. 7 : Balun intrinsic and turns ratio loss

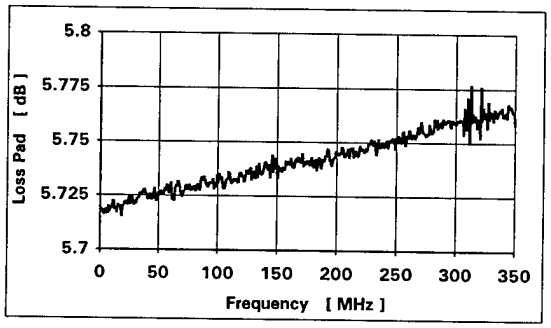

Fig. 8 : Loss of the used minimum loss pad

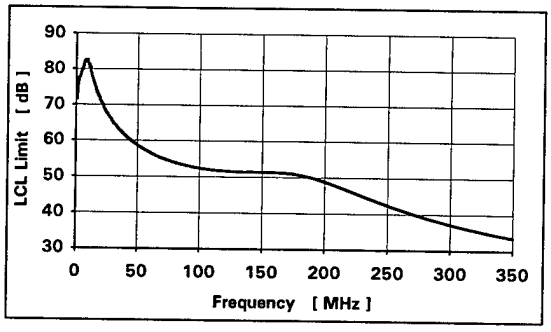

Fig. 9 : LCL limit due to balun (Balun: Analog Elektronik SUR-61)

In Fig. 10 we have the measurements of an UTP pair, using a resistor network at the far end. The results are compared with or without a min. loss pad at the input side, according to Fig. 3 and Fig. 4.

Fig. 11 shows the compares the LCL, using different terminations of the common mode port at the far end upon the LCL of an UTP pair. Here we use different terminations, and also a center tapped resistor network, though only the results with the 50 Ohm termination are shown.

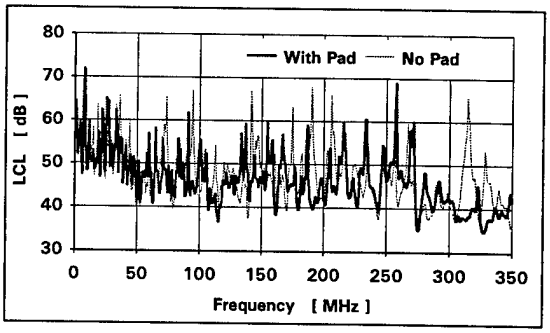

Fig. 10 : Comparison of the LCL of an UTP pair measured in accordance with Fig. 1 and Fig. 2

In Fig. 12 we have the balance of an UTP pair measured with different baluns. For comparison purposes the frequency range is limited to 100 MHz.

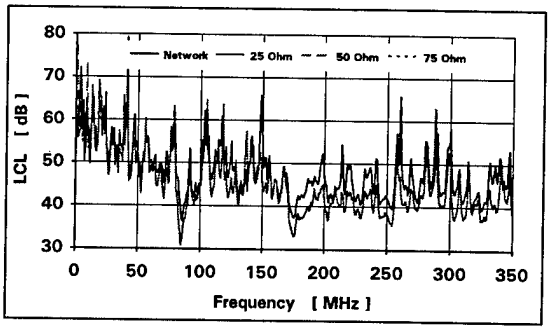

Fig. 11 : LCL of an UTP pair, measured in accordance to Fig. 2 and Fig. 3, with different common mode terminations

In Fig. 13 we have the results of the balance of an UTP pair, when measured on the drum in comparison to the same cable suspended straight.

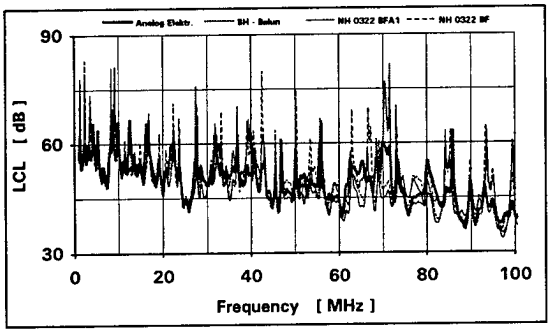

Fig. 12 : LCL of an UTP pair measured with different baluns

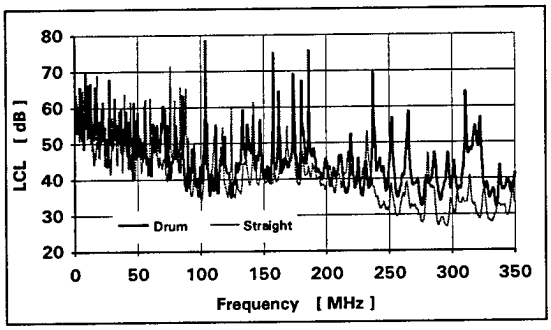

Fig. 13 : LCL of an UTP pair measured on a drum compared to the results of the straight suspended cable

In Fig. 14 we have the balance of a pair of a high performance UTP cable. Here the comparison covers the cable on the drum, straight suspended and also extends to the cable in coil form.

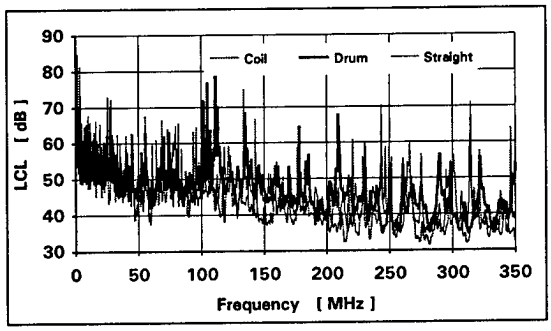

Fig. 14 : LCL of a pair of a high performance UTP cable measured with the cable in coil form, on the drum and straight suspended

In Fig. 15 we have the LCL of a FTP pair, with different common mode terminations on the far end. Here, additionally, to the grounding of the adjacent pairs, also the overall shield has been grounded. In Fig. 16 we have the LCL for all pairs of a FTP cable with a 50 Ohm termination on the far end.

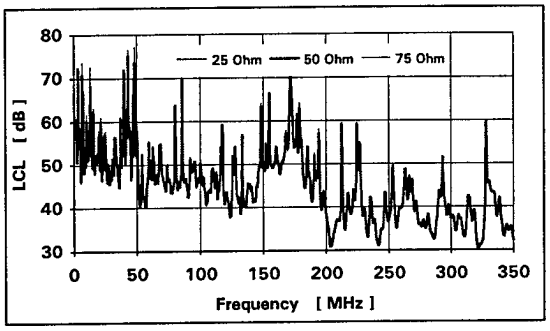

Fig. 15 : LCL of a pair of foil shielded cable (FTP) according to Fig. 3, measured with different common mode terminations

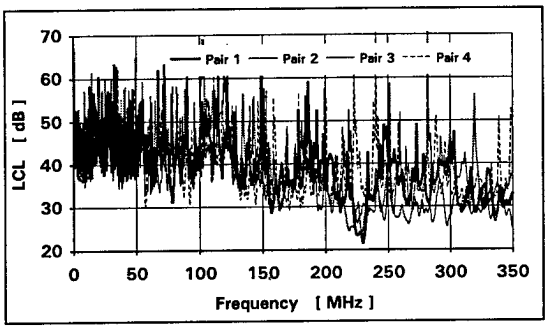

Fig. 16 : LCL of a pair of foil shielded cable (FTP) according to Fig. 3, with 50 Ohm common mode terminations

In Fig. 17 we have the LCL of a STP cable. Here the individual shields and the pairs not under test are grounded. The far end is terminated on the common mode port with a 50 Ohm termination according to Fig. 3. In Fig. 18 one pair of a STP cable is shown, where the common mode port at the far end is terminated with different terminations or is left open.

LCTL Measurement Results: Fig. 19 indicates the intrinsic and turns ratio loss

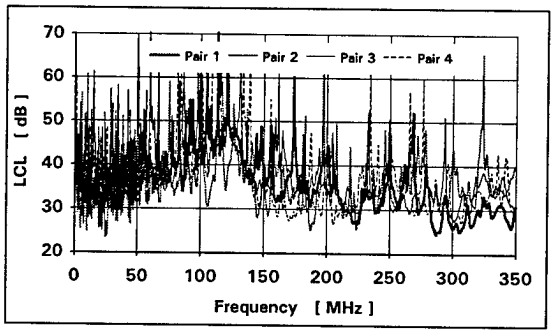

Fig. 17 : LCL of a pair of shielded cable (STP) according to Fig. 3, with 50 Ohm common mode terminations

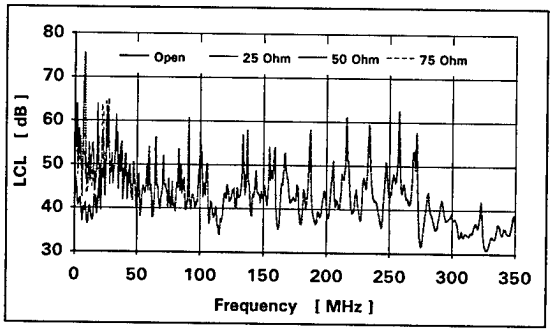

Fig. 18 : LCL of a pair with different common mode terminations on the far end.

of one of the matched balun pairs used for our measurements. Again, this is a limit curve, beyond which the balance measurements become very much influenced by the baluns themselves.

In Fig. 20 we have for one pair of an UTP cable the LCTL, measured with and without a minimum loss pad at the input. Fig. 21 shows for the same pair the measurements with different terminations at the common mode port of the far end.

In Fig. 22 we have the LCTL results for one pair of an UTP cable obtained with different baluns. Here, again, the frequency is limited, for comparison purposes to 100 MHz.

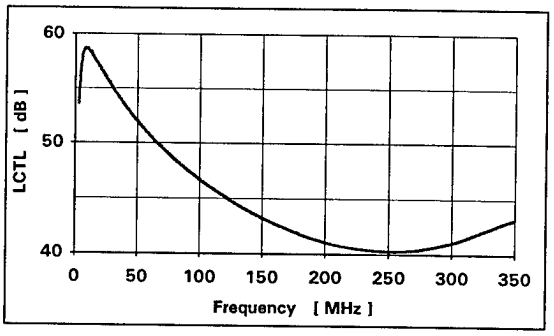

Fig. 19 : LCTL limit due to the baluns (Baluns: Analog Elektronik SUR-61).

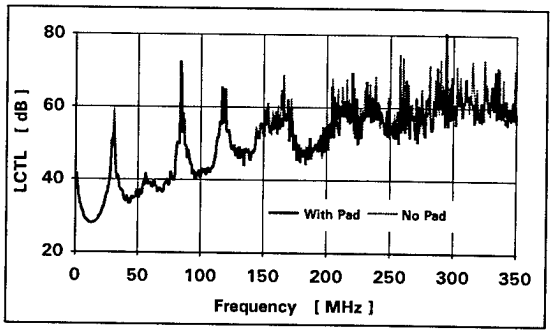

Fig. 20 : LCTL according to Fig. 5 and Fig. 6, with 50 Ohm termination on the far end

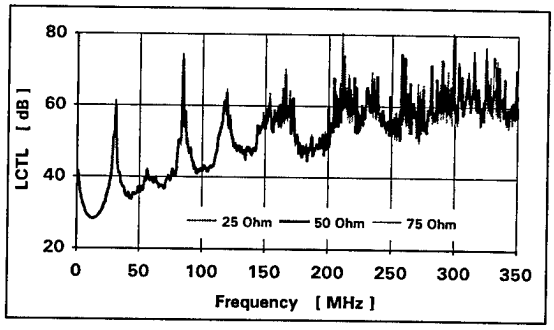

Fig. 21 : LCTL of an UTP pair with different common mode terminations at the far end

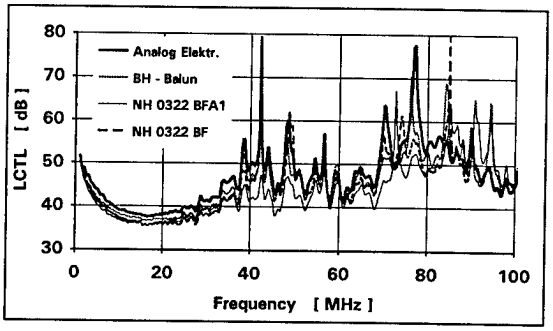

Fig. 22 : LCTL of an UTP pair measured with different baluns

The LCTL measured on the drum and straight suspended is shown for one pair of an UTP cable in Fig. 23. Fig. 24 indicates the LCTL results for one pair of a high performance UTP cable, in coil.
form, on the drum and stretched out straight.

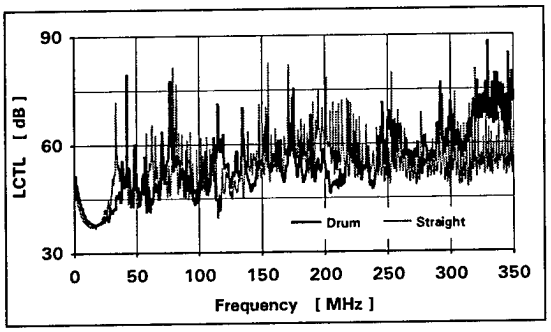

Fig. 23 : LCTL of an UTP pair measured on a drum as compared to the results of the straight suspended cable

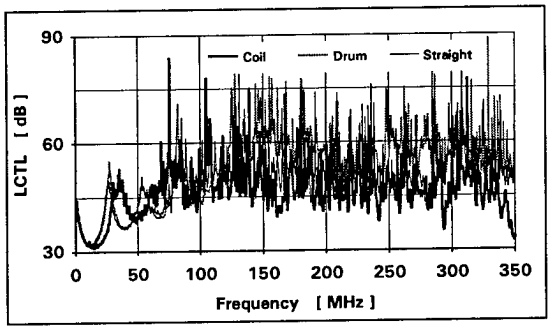

Fig. 24 : LCTL of a high performance UTP cable measured with the cable in coil form, on the drum and straight suspended

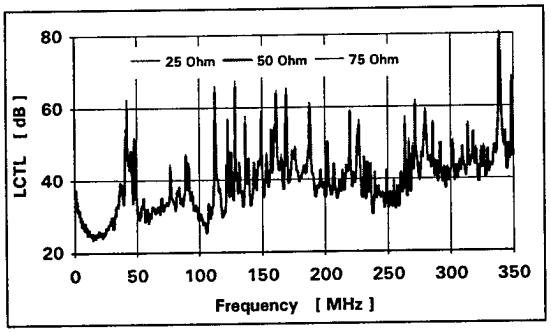

Fig. 25 : LCTL of a foil shielded cable (FTP), measured with different common mode terminations on the far end

In Fig. 25 we have the LCTL of a pair of a foil shielded cable (FTP), with different terminations at the common mode port of the balun at the far end. In Fig. 26 we have the LCTL of the four pairs of a foil shielded cable.
Fig. 27 shows the LCTL of one pair of an individually shielded twisted pair cable (STP), again with different terminations of the common mode port of the balun at the far end. In Fig. 28 we have the LCTL of the four pairs of a foil shielded cable.

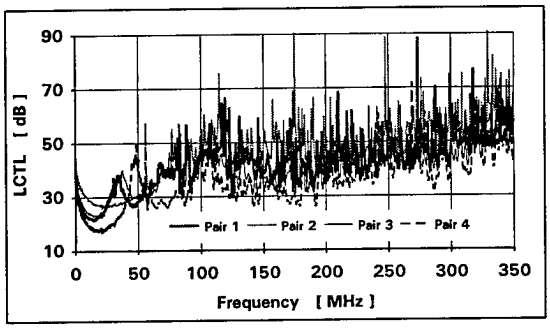

Fig. 26 : LCTL of a foil shielded cable (FTP) with 50 Ohm terminations on the far end

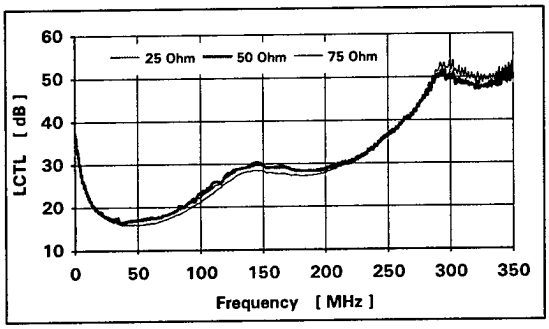

Fig. 27 : LCTL of a pair of a shielded cable (STP) with different common mode terminations on the far end

In Fig. 29 is shown the LCTL of one pair, as measured and the LCTL limit line of the baluns used for this measurement.

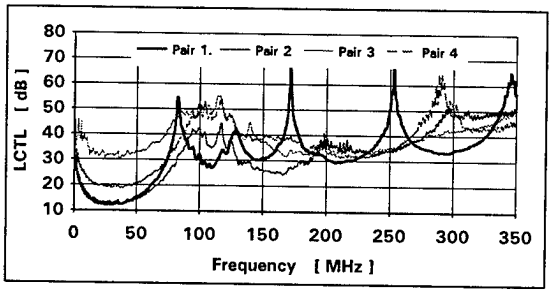

Fig. 28 : LCTL of a shielded cable (STP) with 50 Ohm terminations on the far end

Finally in Fig. 30 we have the LCTL of an individually shielded twisted pair with open common mode port at the far end, in comparison to the results obtained with different terminations.

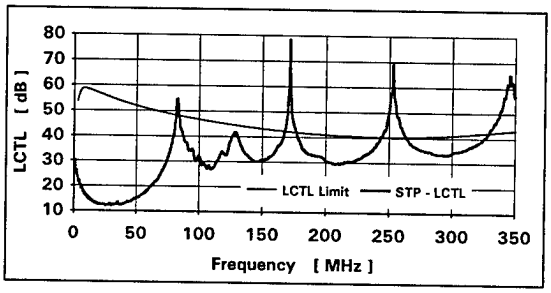

Fig. 29 : LCTL of a pair of a shielded cable with the LCTL limit of the baluns used

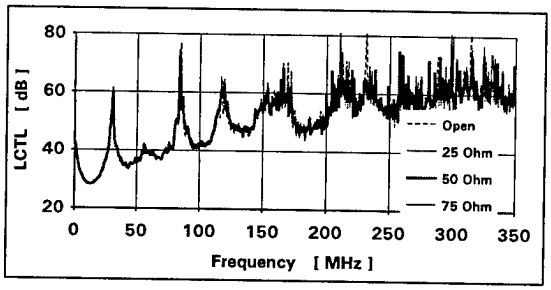

Fig. 30 : LCTL of a pair of a shielded cable with open common mode port and different common mode terminations at the far end

Discussion of Results

The results we report indicate very clearly, that the use of minimum loss matching pads at the input of the baluns is not required (see Fig. 10 and Fig. 20).

We compare the use of a balanced center tapped resistor network for LCL measurements with the use of a balun, which is terminated at its differential port with 50 Ohm. We use different terminations on the common mode port or the center tap of this resistor network or of this balun, respectively. The results indicate that they are insensitive to the resistance value of the termination at the center tap or common mode port. This is also true for foil shielded and individually shielded twisted pairs, i.e. FTP and STP cables. However, the measurements with the center tapped resistor network have to be repeated, with the resistor connections poled. We have to take the average of both measurements, as in general the balance of the resistor networks is not high enough, to get away with one measurement only.

In fact, even using no termination at the common mode port of the far end balun, we obtain acceptable results, though the LCL measurements are slightly affected at lower frequencies, in the range of up to approximately 20 MHz (see Fig. 18). The LCTL measurements are not affected at all, as can be seen in Fig. 30.

Our results indicate an acceptable repeatability, when using different baluns, as can be seen from the Fig. 12 and Fig. 22. Here the measurements are limited to 100 MHz, as some of the baluns used, were limited to this maximum frequency (see Table 1).

All our results indicate a very good repeatability, if the cables are measured on the drum. It seems that the provision of additional well defined groundplane is

substantially superior for balance measurements, than to simply ground the adjacent pairs.

Generally we find the LCL values for Cat. 5 UTP cables to be better than 30 dB. The LCTL measurements yield, at least at lower frequencies slightly lower values, which improve toward higher frequencies.

We find also that high performance UTP cables, as those recently introduced into the market by some manufactures, yield slightly better LCL values, but that a specification limit of 40 dB is definitely too tight.

In fact, on LCTL we observe the same phenomenon of a minimum at intermediate frequencies, as for Input-to-Output FEXT. In the case of FEXT this is due to the attenuation of the pair, whereas in the case of LCTL this is due to the common mode attenuation. If there is a reliable and repeatable method to measure the common mode attenuation, then we can define an equal level LCTL, or EL-LCTL. However, this requires additional work.

Therefore, we can to date only recommend to specify any LCTL value up to frequencies of 100 MHz.

Summary and Conclusion

Our results indicate that it is adequate to terminate the cable using a balun, which is terminated on its differential port with 50 Ohm. For all balance measurements it is sufficient to terminate generally the baluns on their common mode ports with 50 Ohm. We find this holds very precisely for all kinds of cables, i.e. for UTP, FTP and STP cables, and this both for LCL and LCTL measurements.

Hence, we propose a test circuit for LCL measurements according to Fig. 2 with a 50 Ohm termination on the common mode port.

We propose, additionally, the use of either a threaded, grounded metal drum for measuring the balance of UTP cables, or alternatively the use of a metal tube, which is not substantially larger in its inside diameter than the cable outside diameter. It has to be noted, however, that we did not yet make any measurements with such a tube. Therefore, this option, though very attractive from a user point of view, will have still to be investigated further.

We propose for UTP cable as a specification value 30 dB of LCL and 35 for high performance cables, and this in the frequency range up to 100 MHz. We strongly urge to abstain from the introduction of any heuristic equation to discribe the frequency dependence of LCL and LCTL as there is no physical justification available.

For LCTL we propose a value of 25 dB for Cat.5 UTP cables and 28 dB for the high performance UTP cables and this also flat for a frequency of up to 100 MHz. Beyond this frequency we do not have yet enough reliable results to suggest any specification values.

References

[1] NN: Proposal for inclusion of a test method for LCL and LCTL in ASTM D-4566

[2] NN: Multicore and Symmetrical Pair/Quad Cables for Digital Communications.
IEC - 1156-1 (1994), called after revision IEC - 61156-1.

[3] J.- H. Walling et al.: Crosstalk Measurements as a Means to Characterize the Balance of Data Grade Wires.
45th IWCS, 1996, p. 751-761

[4] J.- H. Walling et al.: Performance Assessment of Baluns
46th IWCS, 1996, p. 698-707

[5] NN: Measuring Arrangements to Assess the degree of Unbalance about Earth
CCITT Recommendation 0.9 (Geneva 1972, amended at Malaga-Torremolinos, 1984 and at Melbourne, 1988)(Revision 1996 : see [8])

[6] NN: IEEE Standard Test Procedure for Measuring Longitudinal Balance of Telephone Equipment Operating in the Voice Band.
ANSI/IEEE Std 455-1985

[7] L. Staschover: Measurements Unbalance to Ground of Balance Systems.
North Hills Electronics
Contribution to JTC1/SC25/WG3 in Munich (Green Paper 25)
45th IWCS, 1996, p. 751-761

[8] NN: Transmission Aspects of Unbalance about Earth
ITU-T Recommendation G.117 (2/96)

[9] NN: Unbalance about Earth of Telecommunication Installations
ITU-T Recommendation K.10 (3,93)

[10] L. Halme: Personal communication

Authors

Jörg-Hein (Jo) Walling received his diploma in Mechanical Engineering in 1966 at the Technical University of Berlin. In 1974 he obtained a Doctor's degree (Dr.-Ing.) at the same University.

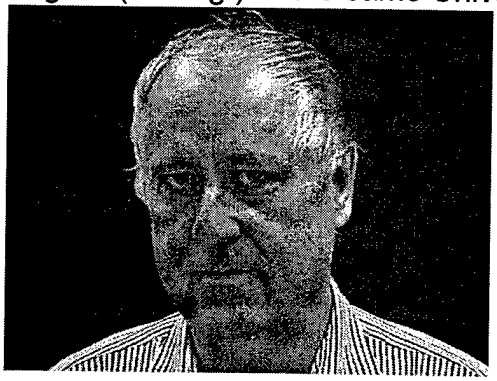

In 1974 he joined Northern Telecom in the Research and Development department. Since 1976 he has been a senior engineer at the Nortel, now Nordx/CDT, Lachine Cable Plant, responsible for the design of Outside Plant and Data Grade Wires and Cables.

Omar Saad received his B. Sc. A. in Electrical Engineering in 1991 from the "Ecole Polytechnique de Montreal". In 1994 he obtained at the same University his Masters degree (M. Sc.A.), also in Electrical Engineering. In 1997 he joined Nordx/CDT in the Research and Development Department, where he is currently working on cable design of data grade cables.

IMPLEMENTATION OF IEC 61196-1 SHIELDED SCREENING ATTENUATION TEST METHOD

John W. Kincaid, Carl W. Dole

Belden Wire and Cable
Richmond, Indiana

ABSTRACT

The physical design and electrical characteristics of coaxial cable screening attenuation (shield effectiveness) test fixtures, which meet the guidelines of IEC 61196-1[1], are presented. Two test fixtures are considered: one for large diameter cable (for example RG-6 type CATV cable) with an upper frequency limit greater than 2 GHz and another for smaller diameter cable with an upper frequency limit greater than 4 GHz. The test procedure is reviewed. Advantages and limitations are discussed. Screening attenuation performance results for a selection of coaxial cable are presented.

INTRODUCTION

This paper describes a practical test fixture that has been developed for the measurement of shielded screening attenuation (also known as shield effectiveness) of coaxial cable. The theoretical basis of the fixture is contained in the draft Amendment 1[1] to International Electrotechnical Commission (IEC) Standard 61196-1 and the original German development publications[2].

A number of test methods and devices have been developed and used by industry to characterize the shielding performance of shielded cables in the RF and microwave bands. Among these are found the absorbing clamp, various shield effectiveness test fixtures, surface transfer impedance test fixtures, the mode stirred chamber, the TEM cell and the open field antenna site. The shielded screening attenuation test is a new addition to this wealth of test methods.

The fixture uses commercially available transmission line hardware, is low in cost, and is easily assembled for utilization in a general laboratory or production environment.

TEST FIXTURE DESIGN

The test fixture housing is a metallic cylinder that forms a triaxial test configuration with the cable sample shield and center conductor. A breakdown drawing of the fixture showing dielectric supports and cable under test is shown in figure 1.

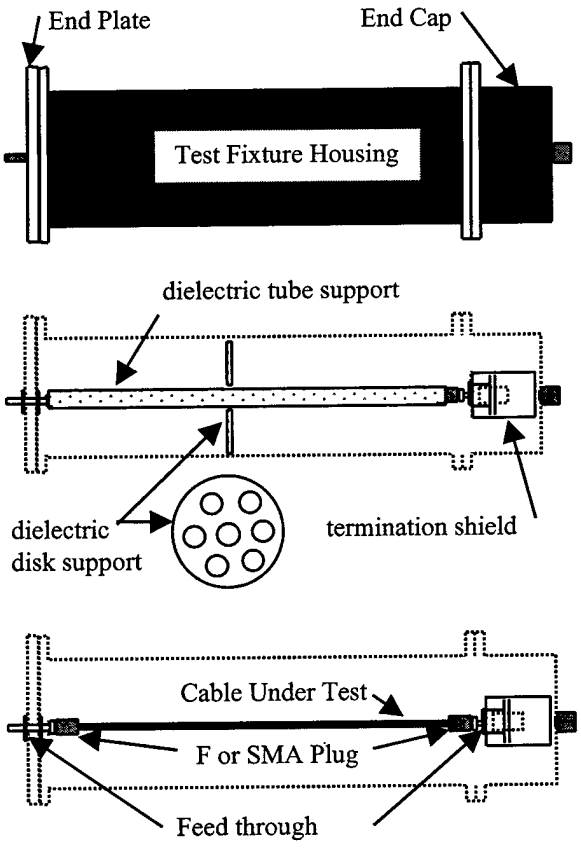

Figure 1. Test Fixture Construction Details

The test fixture housing is one or more sections of standard 50Ω rigid transmission line outer conductor fitted with coupling flanges at each end. Fixtures were constructed with 38.7mm and 76.5mm diameter lines. The 38.7mm fixture was 1.5m long and the 76.5 mm fixture was made in 1.5m, 3m and 6.7m lengths using cascaded sections.

The 38.7mm fixture was fitted with 50Ω SMA type feed-throughs and terminating resistive load.

The 76.5mm fixture was fitted with 75Ω F type feed-throughs and terminating resistive load.

An end plate closes the housing at one end and an end cap encloses the other. A feed-through connector is mounted in the center of the end plate. The end cap is fitted with a 50-ohm type N feed-through connector. The center pin of the N feed through connects into one end of an anchor connector. The sample termination shield consists of a split anchor connector that is mated to the end cap anchor connector. One side of the split anchor connector is fitted with a feed-through connector and the mated pair encloses and shields the cable sample termination. This arrangement provides for terminating the cable sample under test with a shielded resistive load and for connecting the shield to the center pin of the N feed through.

The cable sample under test is fitted with a plug type connector at each end and is connected between the feed-through connectors respectively located in the end plate and the split anchor connector. The cable sample under test is centered by PTFE dielectric tube and disk supports.

Electrical Characteristics

The test fixture is electrically composed of two regions; the test chamber, which is located between the cylindrical housing and the cable sample shield, and the cable sample.

Test chamber. The test chamber portion is viewed as a transmission line with center conductor (the cable sample shield) short circuited to the end plate at one end. At the other end is the 50Ω N feed-through connector. The chamber electrical characteristics depend on length, diameter, dielectric, and cable under test.

Table 1 gives the chamber cut-off frequency, nominal impedance and percent velocity characteristics for three cables that were tested in the fixtures. The cut-off frequency is the upper test frequency limit and is a function of the housing diameter, cable shield diameter, and chamber dielectric material. The nominal impedance is also a function of housing and cable shield diameters as well as the effective dielectric constant of the cable jacket and PTFE support material.

Table 1.
Test Chamber Electrical Characteristics

Cable #	Fc - GHz	Z_o - Ohms	% VP
2	2.1	149	91
8	4.1	132	92
9	4.3	138	96

Figure 2 presents the chamber return loss (cable #2) measured at the end cap N connector of the 1.5m long 76.5mm diameter fixture. The theoretical cutoff frequency is about 2.1 GHz.

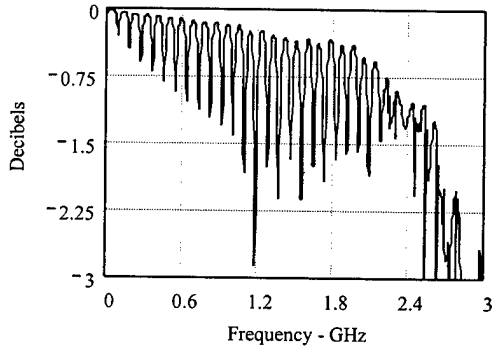

Figure 2. 76.5 mm chamber return loss.

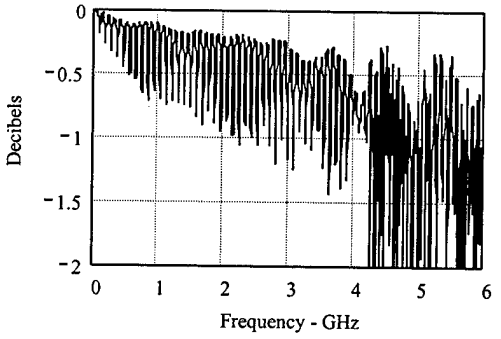

Figure 3. 38.7 mm chamber return loss.

A higher upper frequency limit is obtained with the smaller diameter fixture. Figure 3 presents the chamber return loss (cable #9) for the 1.5m long 38.7mm diameter fixture. The theoretical cutoff frequency is 4.3 GHz.

The input impedance to the chamber consists of resonant peaks corresponding to length and %VP, which are difficult to measure with a network analyzer. Figure 4 shows one such peak reaching an amplitude of some 50,000Ω. An equivalent frequency resolution of 5 kHz was required to properly capture the peak.

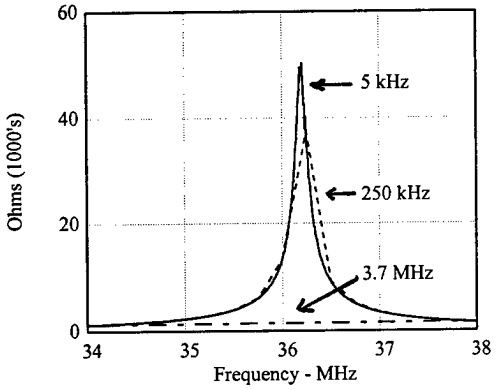

Figure 4. Chamber input impedance resonance peak variation with frequency resolution.

The cable sample jacket is part of the dielectric material present in the test chamber. Figure 5 indicates that at least to a frequency of 3 GHz the PVC jacket material causes less than 1 decibel loss.

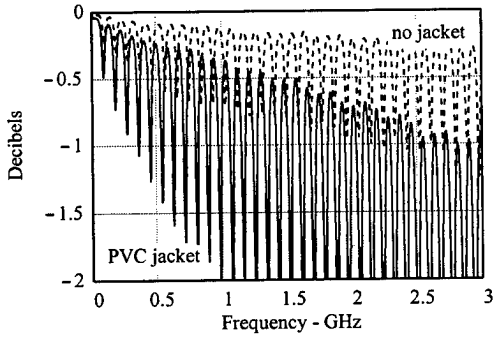

Figure 5. 38.7 mm chamber return loss effect of PVC jacket.

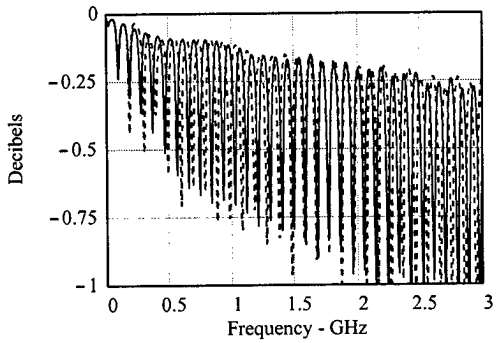

Figure 6. 38.7 mm chamber return loss. Effect of dielectric support.

Another factor in the test chamber is the dielectric tube and disk PTFE support material. Figure 6 compares chamber return loss for cable 9 measured with one disk support versus two disks and tube support. There is minimal amplitude change due to the low loss nature of PTFE but the phase and hence the %VP is significantly affected. With only two disks (dotted line plot) the %VP is about 99%. Addition of the tube (solid line plot) reduces the %VP to about 96 % at 1.5 GHz.

The test chamber diameter ratio determines the upper frequency test limit and the lower frequency limit is determined by the length of the cable sample. The sensitivity of the test method is limited by contact resistance where the cable sample shield forms a short circuit with the cylindrical test fixture end plate and by leakage from the cable sample termination which is located within the fixture test chamber. These factors have been minimized to achieve a measurement capability greater than 140dB over the 1-3000 MHz frequency range.

Cable sample. The cable sample portion is a terminated transmission line that is terminated in a resistive load closely matching its characteristic impedance.

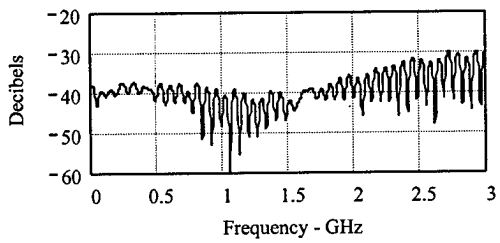

Figure 7. Cable sample return loss.

The cable sample return loss (cable # 9) measured as installed in the test fixture housing is given in figure 7. The results include the effect of end plate and anchor connector feed throughs, the resistive load and the cable itself.

Figures 8 and 9 give the magnitude and phase of the sample input impedance measured at the end plate feed through. Impedance amplitude and phase of the resistive termination are also plotted. Small impedance mismatches in the connection hardware and the cable cause the ringing in figures 8 and 9.

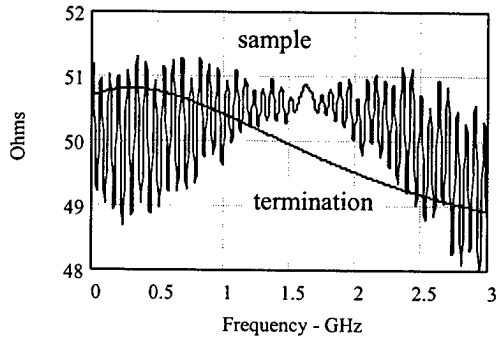

Figure 8. Cable sample input impedance magnitude.

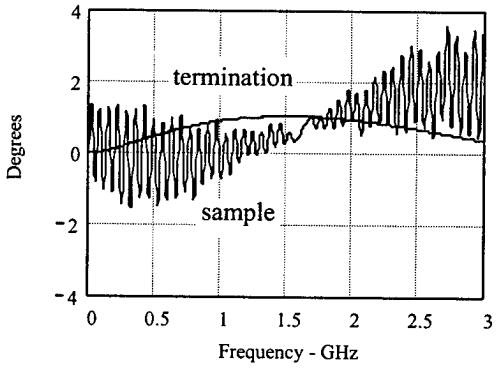

Figure 9. Cable sample input impedance phase angle.

TEST PROCEDURE

The shielded screening attenuation test is closely related to the absorbing clamp test. With both of these methods the sample under test is energized and a signal which is proportional to the resulting leakage field is measured. However, with the shielded screening attenuation method, the leakage field is contained or shielded within a cylindrical metallic tube.

Screening attenuation is derived from the difference in power levels (insertion loss) between the end plate (energized sample) and the end cap (chamber).

The equipment setup is given in figure 10 and the equipment is listed in table 2.

Normally the sample under test is powered and leakage is measured from the chamber. However the direction of power flow may be reversed and practically the same insertion loss is measured due to reciprocity. This is useful when the resistive termination is limited to a low power rating.

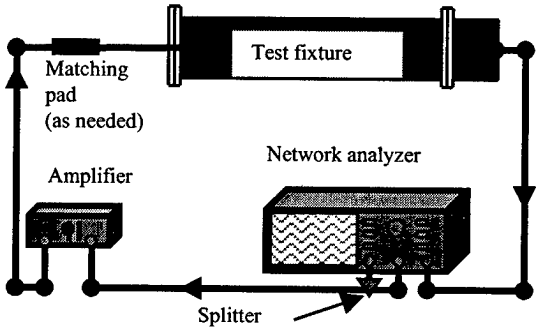

Figure 10. Test Equipment Setup

Table 2.
Screening Attenuation Measurement
Test Equipment

Network Analyzer: HP8753B, +10dBm output, 10 Hz res. bandwidth HP 8510B
Power Splitter: HP11850C, 9.5 dB loss nominal, DC-3 GHz
Matching pad: HP11852B, 5.7dB loss nominal, DC-2 GHz, 50Ω-75Ω, type N connectors
Power Amplifier: HP8347A, 25 dB gain nominal, 100 kHz-3 GHz HP8447D, 27 dB gain nominal, 100 kHz-1.3 GHz
Resistive Termination in Anchor Connector: 75Ω type F for CATV fixture 50Ω SMA for microwave fixture

DESCRIPTION OF SAMPLES TESTED

Several constructions of RG-6 type and RG-59 type coaxial cable[3] were tested in the 76.5mm fixture and are designated #'s 1-6. (#1 is RG-59 type and #'s 2-6 are RG-6 type cables)
Smaller 50 Ω samples were tested in the 38.7mm fixture and are designated #'s 7-9. (# 7 is RG 58 type, # 8 is RG-223, and # 9 is RG-402 type cable) The construction details for the samples are shown in Tables 3 and 4.

Table 3.
Test Sample Construction

#	Foil (inner)	Braid / Angle	Foil	Braid/Angle (outer)
1		95% b. c. /23°		
2	a	40% Al /38°		
3	a	60% Al 27°		
4	a	80% Al /27°	b	
5	a	95% Al /42°	b	
6	a	60% Al /27°	a	40% Al /20°
7		95% t. c. /23°		
8		95% Ag-Cu /28°		95% Ag-Cu /40°
9	.0122mm polyester/ .0178 mm Cu	92.5% t. c. Tin Dipped 64°		

Table 4.
Aluminum Foil Description

	Layer Thickness (mm)			
Foil Type	Al Foil	Polyester	Al Foil	Width (mm)
a	.00889	.02286	.00889	19.05
b	.0254	.02286		25.4

TEST RESULTS

Cable #'s 1-6 were tested in the 76.5mm fixture with a length of 6.7m. The results are plotted in figure 11 with an upper frequency of 100 MHz. The first resonance peak in the response is at about 20 MHz and subsequent peaks are spaced at about 20 MHz intervals. The screening attenuation is found from an envelope curve (not shown) formed by the peaks. The peak frequencies depend on sample length and %VP.

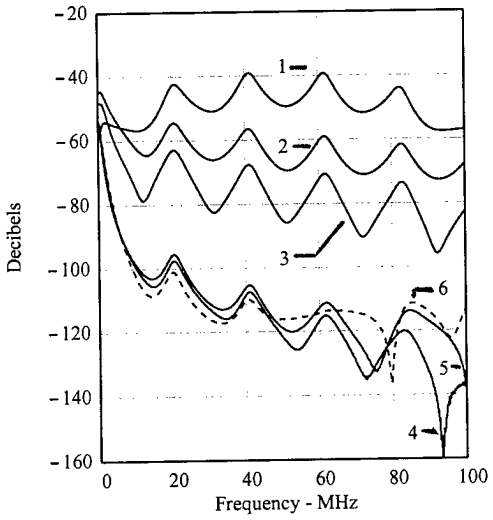

Figure 11. Screening attenuation results; 6.7 m fixture.

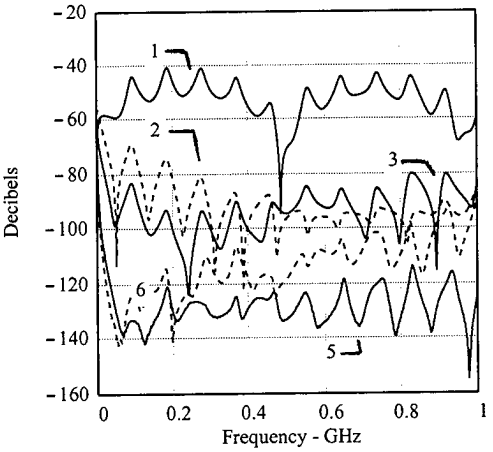

Figure 12. Screening attenuation results; 1.5 m fixture.

Figure 12 plots results measured in the 1.5m long 76.5mm fixture. The upper frequency is 1 GHz and the first peak resonance frequency is about 100 MHz. Note the peaks have not been connected by envelope curves for clarity. The 1.5m fixture is not long enough to resolve screening attenuation below 100 MHz.

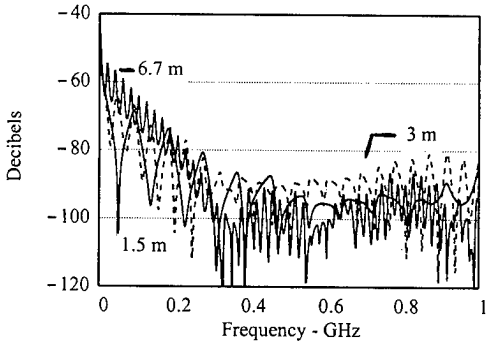

Figure 13. Screening attenuation, cable 2; 76.5 mm fixture, 3 lengths.

Figure 13 plots results for 1.5m, 3m and 6.7m long fixtures. The 6.7m fixture gives better resolution below about 400 MHz. Above 400 MHz the 6.7m and 1.5m fixtures give similar performance. The 3m fixture gives slightly more pessimistic results. This is thought to be due to sample variance.

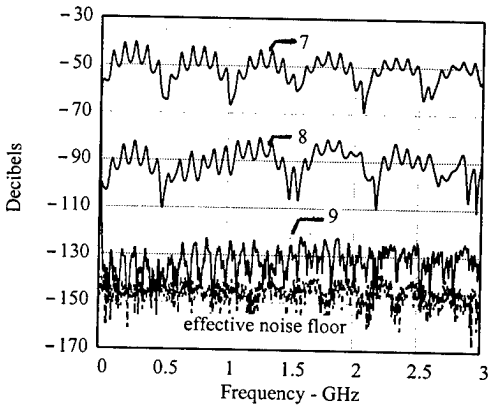

Figure 14. Screening attenuation; 38.7 mm fixture.

Cable #'s 7-9 were tested in the 38.7mm fixture with a length of 1.5m. The results are plotted in figure 14. The effective noise floor is due to the analyzer noise floor in combination with the amplifier(s) used to increase the measurement range.

CONCLUSION

The new test method has characteristics that make it very attractive. These advantages are however accompanied by certain disadvantages.

Advantages

Low cost: Required hardware can be purchased and assembled for an estimated $1000.
Results are expressed in decibels.
Covers a wide frequency range, 20 MHz - 4 GHz
Cable and connector can be tested together.
Cable shields with non-metallic outer layers can be tested.
The shielded or enclosed nature of the test. This makes it feasible for general laboratory or even production environments and the possibility of a greater range of shielding effectiveness.
The method is being standardized by the IEC.

Disadvantages

Length of fixture required to cover frequencies as low as 20 MHz.
Some variability may result in interpreting the position of the screening attenuation envelope and assigning values of performance.

References

1. IEC 61196-1 Generic Standard for Coaxial Cable. IEC Committee Draft for Vote: 46A/320/CDV, closing date for voting 6/30/98.

2. Breitenbach, O; Hahner, T; Mund, B: "Screening of Cables in the MHz to GHz Frequency Range Extended Application of a Simple Measuring Method", ", IEE Colloquium on Screening Effectiveness Measurements, Savoy Place, London, May 6, 1998.

3. Kincaid, J; Dole, C; "Test Fixture Design and Shielded Screening Attenuation Performance of CATV Coaxial Cable", IEE Colloquium on Screening Effectiveness Measurements, Savoy Place, London, May 6, 1998.

John Kincaid

John is a Senior Product Engineer at the Belden Engineering Center. He holds BSEE and MSEE degrees from the University of Oklahoma and has over 25 years experience with Belden. His experience encompasses engineering management and product development positions in the USA as well as in Europe. He holds nine patents. John is a member of the IEEE and is active in IEC and TIA cable standardization activities. He is the US Technical Advisor to IEC SC 46A on coaxial cables, and is Convenor of IEC SC 46A/WG3 on data and CATV cable. He is also an expert on working groups 5 and 7 dealing with shielding and premises cabling issues.

(PO Box 1980; Richmond, IN, 47375)

Carl Dole

Carl is an Associate Product Engineer at the Belden Engineering Center and has been with Belden eight and one-half years. He graduated with highest distinction with an A.S. degree in Electrical Engineering Technology from Purdue University and is a senior pursuing a B.S. degree in EET, also from Purdue University. Prior to joining Belden, Carl worked 10 years in television broadcast engineering and has a FCC General Class Radiotelephone License. Presently he is working on developing improved test methodologies for shielding and other tests at Belden.

(PO Box 1980; Richmond, IN, 47375)

AUTHOR INDEX

Name	Page
ABBOTT, J. S.	897
ABE, H.	495
ACHILLE, F.	705
AKIMOTO, H.	34
ALOISIO, C. J.	725
ANDERSON, M.	854
ARAI, Y.	574
ARAKAWA, K.	450
ARIKAWA, T.	666
ARMSTRONG, J. L.	732
ARNOLD, T. G.	536
ARRUDA, R.	793
ARVIDSSON, B.	404
ASIKKALA, K.	483
AUTON, J.	698
BAKER, L. K.	933
BARLOW, A. J.	536
BASTIDE, C.	25
BEASLEY, W. E.	432
BELANGER, M.	768
BENZEL, D.	913
BIANCO, S.	672
BING, L.	944
BIZEUL, J. C.	57
BJÖRKMAN, J.	404
BLELL, B. M.	10
BLYLER, JR., L. L.	241
BÖHME, R.	642
BONICEL, J. P.	57, 815
BÖR, J.	785
BORKE, J. S.	294
BOURGET, V.	57
BOURHIS, J.-F.	81
BOW, K. E.	705
BRAUN, W.	825
BREULS, A.	881
BREULS, T.	66
BROWN, JR., R. J.	864
BRUNNER, E.	317
BUBNOV, M. M.	928
BULUSCHEK, B.	631
BUSCH, W. F.	705
BUSH, H. M.	92, 103
CADDEN, A. P. J.	845
CATTELAN, S.	513
CHAHANOVICH, S.	468
CHANDAN, H. C.	864
CHANG, T.-C.	527
CHARLES, Y.	385
CHAVEZ, O.	299
CHEN, T.	325
CHEN, W.-J.	527
CHESNOY, J.	375
CHO, J. C.	489
CHOU, S.-H.	548
CHU, P. C. W.	335
CHU, T. C.	394
CIGADA, A.	621
CLARKE, K.	832
COMBELLACK, R. A.	176
CONSONNI, E.	612, 621
COOPER, S. A.	891
COPE, K. E.	111
COSTA-ELIAS, H.	815
COSTELLO, M. T.	501
COULSON, D.	832
CUNNINGHAM, D. G.	897
CURADO, P. J. P.	793
CURRY, C. R.	965
DALE, S. J.	360
DALEY, J. G.	337
DAO-WEN, Z.	944
DEAN, D. L.	650
DEBBAN, H. P.	103
DEI, Y.	34
DEOGAN, D.	536
DI MINICO, C. T.	758, 897
DIANA, G.	612
DIXON, T. L.	801
DODD, S. R.	845
DOLE, C. W.	999
DUESER, M.	241
ECKARD, A.	501
EKLIND, H.	317
ELISSON, P.	25
ERICSSON, K.	147
EVANNO, N.	881
FALCO, M.	621
GAILLARD, P.	815, 913
GARCIA, M.	57
GEBIZLIOGLU, O. S.	589
GIENIEWSKI, C.	507
GINGER, R. E.	325
GINOCCHIO, A.	612
GIRBIG, R.	642
GLAESEMANN, G. S.	928, 933
GLAESEMANN, S.	881
GORZITZA, B.	264
GOSSIAUX, M.-G.	81
GRABANDT, O.	688
GREEN, J. I.	477
GREGOR, P. E.	776, 825
GRIFFIOEN, W.	462
GRUHL, H.	440
GRUHN, J. D.	126
HAAG, H. G.	776, 825
HACKERT, M. J.	897
HANAI, J.	837
HÄNNINEN, M.	147
HARA, M.	41, 227
HARA, T.	740
HARSHBARGER, D. E.	897

Name	Page
HASHIMOTO, K.	420
HATTORI, M.	248, 257
HATTORI, T.	420
HESS, D.	192
HIGASHIDE, Y.	636
HINOSHITA, S.	457, 714
HIRAMATSU, H.	41, 49, 921
HIRVENSALO, M.	147
HJERTBERG, T.	147
HÖG, G.	642
HOLLAND, P.	563
HORE, L. M.	184, 299
HOSOI, F.	49, 227, 921
HOUGHTON, I.	385
HOUSER, K.	468
HSIAO, C.-M.	527
HSIEH, C.-H.	548
HSING, K. V.	184
HSU, H.-P.	527, 548
HWANG, Y.-H.	548
IBUKI, S.	636
IMADA, Y.	938, 959
IMAMURA, K.	938, 959
IMOTO, I.	740
INO, E.	233
ISHIDA, K.	233
ISHIHARA, K.	307
ISHII, N.	4
ISHIKAWA, A.	636
ISHIKAWA, H.	542
IWAKURA, D.	41
IWATA, H.	34
JEON, Y. H.	411
KALLENBORN, R.	201
KAMIKURA, Y.	41, 49, 227, 921
KANEKO, T.	579
KANG, H. J.	489
KANZAKI, H.	41, 921
KATAGIRI, T.	658
KATAYAMA, M.	597
KATAYOSE, H.	517
KATO, H.	837
KAWAMURA, T.	959
KAWASAKI, Y.	307
KELLER, D. A.	17
KEMETER, K.	881
KERTSCHER, E.	631
KIM, S. H.	411
KINCAID, J. W.	748, 999
KINOSHITA, T.	85
KISH, P.	758
KIYOTAKE, K.	682
KOBAYASHI, I.	41, 49, 921
KOEPPEN, C. S.	241
KOHGA, K.	579
KOMIYA, Z.	495
KONAKA, T.	740
KONDA, E.	49
KONDO, K.	959
KOSAKA, M.	227, 921
KOUDA, K.	558
KRUIJSHOOP, A. W.	832
KRUPP, H.	854
KUCK, V.	725
KURKJIAN, C.	881
KURKJIAN, C. R.	589, 732, 928
KUZUSHITA, H.	85
LADIÉ, P.	353
LANG, J.-L.	375
LEE, C. D.	161
LEE, C.-C.	583
LEE, Y. I.	489
LEECH, J. R.	325
LEGROS, F.	631
LEW, K. J.	411
LIAW, T.-J.	583
LIBERT, J.-F.	375, 385
LIN, H.-F.	527, 548
LIN, Y.-C.	527, 548
LINDSAY, JR., R. G.	432
LINDSKOG, P.	522
LIU-JUAN, Z.	944
LONG-PAN, X.	944
LOUBOUTIN, J. P.	57
LUPIA, J. A.	117
LUTHER, J. P.	650
MACIP-BOULIS, M. A.	281
MAENO, K.	574
MAKI, S.	307
MAKI, S. G.	325
MÄKINEN, M.	483
MAKIYAMA, A.	215
MANENTI, A.	612
MANN, J. D.	589
MARCONE, A.	950
MARELLI, P.	621
MARRADI, G.	513
MARTINSSON, H.-B.	317
MASE, M.	495
MASUR, L. J.	360
MATSUNO, K.	450
MATTHEWSON, M. J.	732, 874
MATTHIJSSE, P.	170
MCCREARY, S. A.	432
MCLAUGHLIN, W.	184
MICHALAK, M.	973
MIHALACOPOULOS, G. D.	73
MILITARU, C.	602
MIYAMOTO, M.	208, 220, 233
MIYANO, H.	597
MONTALTI, F.	672
MORIKAWA, G.	542
MORISHITA, Y.	682
MORITA, K.	682
MORIURA, K.	85
MUNDAY, S.	17
MURAKAMI, Y.	658
MUTA, K.	682
NAGAI, M.	85
NAGASAWA, S.	658

Name	Page
NAGASE, Y.	558
NAKAI, T.	938
NAKAJIMA, F.	4
NAKAO, N.	808
NASSI, M.	353
NASUNO, Y.	457
NEWMAN, R.	815
NISHI, S.	740
NISHIGUCHI, M.	248, 257
NISHIMURA, A.	215
NORMAN, S.	353
NOTHOFER, K.	913
NUMURA, Y.	517
OBST, A.	785
OH, J. H.	411
OHSONO, K.	457
OHTA, J.	215
OIZUMI, H.	579
OKADA, M.	34
OKADA, N.	208, 220, 636
OOHASHI, K.	233
ORCEL, G.	57, 81
OSTOJIC, P.	832
PARK, S. C.	489
PATEL, N. I.	136
PEI, C.-C.	548
PELT, M.	192
PELTOLUHTA, E.	483
PENDLETON, D.	845
PERETTA, P. G.	513
PLAGIANIS, C. H.	725
PLATT, C. E.	337
POZZI, F.	950
PRESTON, J.	563
PRITCHETT, L. R.	864
PRYDE, C. A.	507
QUAN, X.	241
QUISTORFF, K.	801
RAHMAN, M.	353
RAJALA, M.	483
RAMANAN, V. R.	360
REED, W. A.	241
REGIO, P.	881
RENDLE, M.	536
RESTA, F.	612
RHODES, J.	563
RICHARD, J.-F.	768
RICHTER, S.	57
RILEY, JR., G. N.	360
RINTSU, Y.	636
RISCH, B.	17, 25
RISCH, B. G.	698
RITTER, T.	264
RIVARD, M.	815
RONAGHAN, C.	241
ROSKO, J.	17
RUE, R. J.	394
RUEGENBERG, G.	854
RUTTERMAN, D. J.	554
RUTZEN, W.	427
SAAD, O.	988
SAEKI, M.	837
SAKAMOTO, T.	307
SAKUMA, K.	517
SALAMON, T.	241
SATO, K.	345
SATO, Y.	220
SAWYER, D.	563
SCHEIDELER, W.	271
SCHULZ, P.	980
SCRIVENER, P. L.	908
SEIDEL, D.	776
SEKI, I.	714
SEMJONOV, S.	881
SEMJONOV, S. L.	928
SEO, G. W.	411
SHIGEHARA, M.	420
SHIINO, M.	569
SHIMA, M.	740
SHIMANE, H.	714
SHIMOJI, N.	574
SHIMOMICHI, T.	233
SHIN, D. Y.	411
SHUIHUO, L.	944
SIDDIQUI, S.	864
SIMOFF, D. A.	507
SIMPKINS, P. G.	725
SOGAME, J.	34
STEIN, R.	481
STEINBERG, H.	271
STEVENS, J. B.	25
STOKES, S. R.	432
STUUT, H. A. M.	688
SUDO, Y.	938, 959
SUETSUGU, Y.	542
SUGI, K.	682
SUINO, D.	672
SULTAN, B.-Å.	147
SUNDBERG, R.	522
SUNDSTRÖM, B.	522, 850
SUTEHALL, R.	612, 621
SUZUKI, H.	714
SUZUKI, N.	837
SUZUKI, O.	227
SUZUKI, S.	682
SUZUKI, Y.	457
SVENSSON, T.	850, 881
SZWEC, J. R.	864
TABADDOR, P. L.	725
TAIRA, Y.	837
TAKAGI, S.	4, 248, 257
TAKAOKA, R.	49
TAKAOKA, S.	837
TAKAYA, M.	658
TAKAYAMA, K.	569, 574
TAKIZAWA, K.	666
TAMAKI, Y.	666
TAMURA, H.	558
TAMURA, Y.	420
TAN, K.	457
TANAKA, S.	636
TANJI, H.	597

Name	Page
TANSKANEN, J.	404
TARDY, A.	57
TATAT, O.	698, 913
TAYLOR, A. T.	874
TAYLOR, C.	480
TAYLOR, C. R.	725, 864
THALMAN, W. J.	501
TODA, S.	227
TOMITA, K.	808
TOMITA, N.	808
TOMITA, S.	34
TOYOHARA, A.	959
TSAI, F.-Y.	583
TSUCHIYA, I.	420
TSUJI, K.	85
TSUJIKAWA, K.	450
TU, Y.-K.	527, 548, 583
TUCHIYA, N.	558
TUURNALA, T.	483
TYRCHA, J.	522
UEDA, M.	579
UGHETTI, M.	672
UKACHI, T.	495
UNGER, C.	365
VAIDYA, D. S.	73
VALENTI, C. F.	476
VAN BERGEN, A. H.	66
VAN LEEUWEN, J. H.	688
VANALI, M.	621
VANDERLAAN, P. Z.	748
VERTUAUX, P.	815
VINZIO, R.	950
VOBIAN, J.	440
VOIGT, M.	776
VOLOTINEN, T.	881
WAGNER, K. M.	650
WALLING, J.-H.	768, 988
WANG, C.-S.	583
WANG, R.-C.	548
WATANABE, H.	208
WATANABE, T.	227
WATANABE, Y.	4
WATSON, V.	563
WEISS, A.	913
WESTLING, L.	317
WHITE, I. H.	897
WHITE, M. E.	891
WHITE, W. R.	241
WILHELM, D.	980
WILTZIUS, P.	241
WORTHINGTON, P.	385
YAMADA, K.	714
YAMANAKA, M.	208
YAMASAKI, A.	220
YAMAZAKI, T.	714
YASUHARA, K.	517
YEAP, T.	475
YODER, R.	17
YOKOSUKA, H.	666
YOSHIDA, K.	450
YOSHIDA, M.	558, 959
YOSHIOKA, K.	808
ZAMZOW, B.	854
ZAMZOW, P. E.	271
ZEIDLER, G.	365
ZHI-MIN, Z.	944
ZIEMANN, O.	264
ZIMNOL, M.	850
ZISEN, Z.	944

REPRODUCTION QUALITY NOTICE

This document is the best quality available. The copy furnished to DTIC contained pages that may have the following quality problems:

- Pages smaller or larger than normal.
- Pages with background color or light colored printing.
- Pages with small type or poor printing; and or
- Pages with continuous tone material or color photographs.

Due to various output media available these conditions may or may not cause poor legibility in the microfiche or hardcopy output you receive.

☑ If this block is checked, the copy furnished to DTIC contained pages with color printing, that when reproduced in Black and White, may change detail of the original copy.